Solvent Extraction:
Fundamentals to Industrial Applications

Proceedings of ISEC 2008
International Solvent Extraction Conference

Editor-in-Chief

Bruce A. Moyer
Chemical Sciences Division
Oak Ridge National Laboratory

A Publication of The
Canadian Institute of Mining, Metallurgy and Petroleum
Xerox Tower, 855 - 3400 de Maisonneuve Blvd. West
Montréal, Québec, Canada H3Z 3B8
http://www.metsoc.org

ISBN: 1-894475-80-1 (Volume I)
ISBN: 1-894475-81-X (Volume II)

Printed in Canada
Copyright ©2008

All rights reserved.
This publication may not be reproduced in whole or in part,
stored in a retrieval system or transmitted in any form or by any means,
without permission from the publisher.

ISEC 2008 ASSOCIATE EDITORS

Pascal Baron
CEA Valrho-Marcoule
Bagnols, France

Alexandre Chagnes
ENSCP–CNRS–Université Paris
Paris, France

Peter M. Cole
TWP Matomo Process Plant (Pty) Ltd
Johannesburg, South Africa

Gérard Cote
ENSCP–CNRS–Université Paris
Paris, France

Mark L. Dietz
University of Wisconsin-Milwaukee
Milwaukee, WI, USA

T. Alan Hatton
Massachusetts Institute of Technology
Cambridge, MA, USA

E. Philip Horwitz
PG Research Foundation
Darien, IL, USA

E. Susana Pérez de Ortiz
Imperial College London
London, UK

Gordon M. Ritcey
Gordon M. Ritcey & Associates
Nepean, Ontario, Canada

David Robinson
CSIRO Minerals
Perth, Australia

Robin D. Rogers
The Queen's Univ. of Belfast, N. Ireland, UK
Univ. of Alabama, Tuscaloosa, AL, USA

Kathryn C. Sole
Anglo Research
Johannesburg, South Africa

Peter A. Tasker
University of Edinburgh
Edinburgh, UK

Terry A. Todd
Idaho National Laboratory
Idaho Falls, USA

Michael J. Virnig
Cognis Corporation
Tucson, AZ, USA

ISEC 2008 SPONSORS

FOREWORD

The North American industry has employed major solvent-extraction processes to support a wide range of separations including but not limited to chemical, metallurgical, nuclear, biochemical, pharmaceutical, and petroleum applications. The knowledge enabling these separations has been obtained through fundamental studies in academe, government and industry. In recognition of these activities, the International Solvent Extraction Committee decided at the March 2002 meeting in Cape Town, South Africa to hold the ISEC 2008 Conference in North America. The ISEC 2008 Organizing Committee selected Tucson, Arizona as the site because of the mining industry in the region.

The International Solvent Extraction Conferences have been and continue to be a major gathering of scientists, engineers, operators, and vendors from around the world, who present new findings since the last meeting, exchange ideas, make business contacts, and conduct collegial discussions. Historically, the first solvent extraction conference was held on nuclear separations at Gatlinburg in 1962. Several ISEC-type conferences followed at Brussels in 1963, Harwell in 1965, Goteborg in 1966, and Jerusalem in 1968. The first ISEC organized by the Society of Chemical Industry was held in The Hague in 1971. Since then, ISECs have been held in Lyons (1974), Toronto (1977), Liege (1980), Denver (1984), Munich (1987), Moscow (1988), Kyoto (1990), York (1993), Melbourne (1996), Barcelona (1999), Cape Town (2002), and Beijing (2005). It was fitting that more than two decades after the Denver conference, North America is the host of the ISEC 2008 in Tucson, Arizona, USA.

The ISEC 2008 program emphasizes fundamentals to industrial applications of solvent extraction, particularly how this broad spectrum of activities is interconnected and has led to the implementation of novel processes. The oral and poster sessions have been organized into seven topics: Fundamentals; Novel Reagents, Materials and Techniques; Nuclear Fuel Reprocessing; Hydrometallurgy and Metals Extraction; Analytical and Preparative Applications; Biotechnology, Pharmaceuticals, Life-Science Products, and Organic Products; and Process Chemistry and Engineering. Over 350 abstracts were received, resulting in more than 260 manuscripts published in these proceedings. Five outstanding plenary presentations have been identified, with five parallel sessions for oral presentations and posters. The plenary speakers are truly experts in their specific fields of solvent extraction and consist of Hans-Jörg Bart, Bernard Boullis, Gary Kordosky, Franz Schmidtchen, and Hitoshi Watarai. Originally, Georges Wipff had accepted our invitation to present a plenary lecture but unfortunately was unable to attend the conference. We elected to retain his contribution in the proceedings in view of the growing importance of molecular simulations in understanding liquid-liquid extraction. Hitoshi Watarai was gracious to step forward in this situation to prepare and present a plenary lecture on a similar topic. Keynote speakers have been

invited to lead each session and two honorary sessions, one recognizing the major contributions of Henry Freiser over his career and a memorial session for H.R.C. Pratt, have been organized. The conference papers traverse a broad range of topics at the highest level of scientific and engineering acumen. For example, of scientific interest, papers in fundamentals use state-of-the-art molecular dynamic modeling to describe molecular transport from one phase to and through an interface to the second phase; whereas, at the other end of the spectrum, in the area of plant operation, process flow-sheet optimization models are shown to implement extraction kinetics models in extractor design equations to optimize throughput in existing plants. Also, the resurgence of interest in nuclear fuels reprocessing is represented in this Conference through sessions dedicated to this area.

To provide the opportunity for attendees and students to be exposed to the basic concepts in solvent extraction over a broad spectrum, a preconference Solvent Extraction Short Course has also been reinstituted at the ISEC 2008. In four sessions on the Sunday and Monday before the Conference, the topics of Fundamentals, Hydrometallurgical Extraction, Topics in Extraction, and Equipment Selection have been explored. International experts in solvent extraction, mass transfer, thermodynamics, and equipment and plant design presented approximately 14 lectures to the participants.

In addition to the broad-range technical program presented, the Organizing Committee is pleased to offer a Post-Conference Technical Tour to the participants. The Copper SX Technical Tour in Arizona features visits to large and small copper SX plants and a bus tour through the scenic wonders of the Southwest United States desert. This tour promises to be a highlight of the conference complimenting the many papers dealing with copper extraction. In addition, local tours of the Tucson area in the beautiful Southwestern United States are available for spouses and attendees during the week of the meeting.

The ISEC 2008 would not have been possible without the generous support provided by our Gold Sponsors and the other major sponsors. The Organizing Committee thanks them for their recognition of the importance of this meeting through their financial and other contributions.

I take this opportunity to graciously thank all the members of the ISEC 2008 Organizing Committee, the Editor of the proceedings, the Topical Chairs, the Session Chairs, the reviewers of manuscripts, the members of the Secretariat, and the Organizing Committee Administrative Assistant. Their enormous efforts and dedication over the past six years made the ISEC 2008 a tremendous success. Thanks also are due to the authors, technical exhibitors, and delegates for their significant contributions to, and participation in, the Conference.

I am certain that the ISEC 2008 will have a lasting impact on solvent extraction through the Conference Proceedings and that the Conference has inspired our participants to develop exciting contributions for their profession and the next ISEC.

Enjoy the meeting: learn, exchange ideas, describe your products, renew acquaintances, and make new friends!!

L.L. Tavlarides
Chair: Organizing Committee

PREFACE

The proceedings of the International Solvent Extraction Conferences (ISECs) and its predecessor conferences represent an all-inclusive archive of progress in the field of solvent extraction (SX), and we have attempted herein to maintain this great tradition! As before, a remarkable diversity of chemical topics is covered. In recognition of the major role SX plays in the hydrometallurgical and nuclear industries, these proceedings begin with sections focusing on hydrometallurgy, process chemistry, and engineering. More fundamental topics follow, including sections on novel reagents, materials, and techniques, featuring novel applications in analytical and biotechnology areas. Despite the diversity of topics and ideas represented, however, the primary focus of the ISEC community continues to be metals extraction. Although extraction of organic compounds is the topic of a significant number of papers, contributions related to the petrochemical, pharmaceutical, food, and other industries that employ solvent extraction are, however, not as extensive as we initially had hoped, especially in view of their economic importance. Sessions on petrochemical applications, for example, could not be organized, because of the lack of papers. Perhaps in the future, it would benefit progress in the field of SX as a whole to find greater synergy between the extraction of metals and organic compounds, as many of the same principles and techniques apply, and shared insights may spark unexpected advances.

As a whole, these proceedings serve as a guidepost to future directions in the field of SX. For the last several decades, SX has been regarded as a mature industrial technology, and the foundation for this status can be seen in developments especially since the start of the nuclear era in the 1940s. Historians even find uses of solvent extraction well into the early 1800s. But if there has been the recent danger of perception that the field has reached a plateau destined for only incremental improvements, perusal of these proceedings can lend reassurance that quite substantial advances are occurring, even ones that might be looked upon as true paradigm shifts. One shift that has already taken place is the impact of supramolecular chemistry. Highly organized molecules such as crown ethers and calixarenes, once thought to be prohibitively expensive for applications other than in analytical laboratories, are now incorporated into both accepted industrial SX processes for cleanup of nuclear waste and ongoing research for more efficient reprocessing. Supramolecular chemistry has also unlocked mysteries regarding the nature of third-phase formation, revealing this phenomenon to be one of self-assembly of extractant molecules and their complexes into organized structures. In many respects, the limitations posed by third-phase formation in SX are responsible for the peculiar structures found to be optimal for extractant molecules and for use of modifiers in solvent systems, all of which are defining characteristics of the art of SX but without much fundamental understanding. While the impact of supramolecular chemistry has actually been unfolding over the 40 years since crown ethers were first reported, a more recent paradigm shift is occurring in the use of computational techniques. One may find papers reporting on computations at different spatial and time scales, from molecular

design to dynamics of metals crossing interfaces to fluid dynamics in equipment to flowsheet and plant design. It may be expected that future SX practitioners only a decade from now will approach research tasks at any of these scales or at perhaps all scales in one comprehensive model with the aid of computational tools to guide and shorten the path to a research goal previously attained only through inspired but time-consuming experimental efforts. Finally, evident in many papers is the remarkable energy devoted by researchers to finding and developing new extractants possessing new types of selectivity and improved properties, especially as driven by the needs of nuclear, analytical, and niche applications. This energy has never really abated, as one would expect for fundamental research, despite arguments at previous ISECs that no new reagents were needed. Granted, the appearance of new reagents has been slower for hydrometallurgical applications, owing to more stringent economics, but nevertheless new reagents continue to be marketed by suppliers and evaluated by researchers. Certainly, even conservative hydrometallurgists would still have to admit that a new nickel-selective reagent, still yet to be found, would be quite attractive commercially.

In approaching the daunting task of putting these proceedings together in the unprecedented timeframe of three months from receipt of manuscripts to delivery of ca. 260 peer-reviewed and edited papers to our publisher, we made some changes more than methods used in the past. An internet-based system set up by our Secretariat was employed to collect abstracts and manuscripts, thereby avoiding labor- and mail-intensive handling of camera-ready hard copies and allowing a rapid means for our editors and reviewers to electronically access the manuscripts from their locations in several countries. As before, manuscripts received a rigorous peer review by 1 or 2 independent reviewers. However, we broke with tradition and decentralized the peer-review process by involving 15 Associate Editors in much the same way that journals operate. In this way, and taking advantage of the internet, it was possible to obtain international participation in putting the proceedings together in a short amount of time without the entire burden falling on a few individuals as has been the case in the past. Associate Editors each had responsibility for overseeing the distribution of manuscripts from the central web site to reviewers (almost exclusively by email), returning review comments to authors, and judging the acceptability of revised manuscripts, which were then uploaded to a central web site for final editing and electronic transmittal to the publisher. It may be noted that the completely electronic means of assembling the proceedings continues to develop from the past few ISECs and will hopefully make this task easier for future proceedings. In the present case, it was possible to complete the task in a much shortened timeframe, to involve a wide representation of our SX community, and to deliver diverse set of papers spanning the state of our art.

I personally thank each of our Associate Editors for their devotion and generous efforts in coordinating the peer review of the ISEC manuscripts, and I also wish to thank our reviewers for lending their critical eyes to improving the manuscripts and ensuring their high quality. Mihaela Gurau is thanked for acting as Editorial Assistant for the ionic-liquids papers. Becky Maggard of Oak Ridge National Laboratory provided excellent assistance in the final editing phase and provided the design of the cover and

layout of the front matter. The help and guidance of Ronona Saunders with CIM was indispensable in the final assembly of the book. Finally, we are indebted to our authors for their excellent contributions and enthusiastic participation!

Bruce A. Moyer
ISEC 2008 Technical Program Chairman

ISEC 2008 ORGANIZING COMMITTEE

Chair: Organizing Committee	〉	Lawrence L. Tavlarides, *Syracuse University*
Co-Chair	〉	Gary Kordosky, *Cognis Corporation*
Treasurer	〉	Andrew Nisbett, *Cognis Corporation*
Chair: Technical Program	〉	Bruce Moyer, *Oak Ridge National Laboratory*
U.S. Representative	〉	Terry Todd, *Idaho National Laboratory*
Canadian Representative	〉	George P. Demopoulos, *McGill University*
Conference Secretariat	〉	A6 Consultants LLC, *Tucson, Arizona*
Administrative Assistant	〉	Dawn M. Long, *Syracuse University*
Members	〉	Lætitia Delmau, *Oak Ridge National Laboratory*
	〉	T. Alan Hatton, *Massachusetts Institute of Technology*
	〉	R. Scott Herbst, *Idaho National Laboratory*
	〉	David Hobbs, *Savannah River National Laboratory*
	〉	Jeffrey Kanel, *J.S. Kanel & Associates, Inc*.
	〉	Kwadko Osseo-Asare, *Penn State University*
	〉	Gordon Ritcey, *G.M. Ritcey & Associates, Inc.*
	〉	Robin D. Rogers, *The University of Alabama*
	〉	Costas Tsouris, *Oak Ridge National Laboratory*
	〉	Vincent Van Brunt, *University of South Carolina*
	〉	Jack Watson, *Oak Ridge National Laboratory (retired)*

INTERNATIONAL COMMITTEE ON SOLVENT EXTRACTION

Prof. Geoff W. Stevens, *University of Melbourne, Australia* (Chairman)
Prof. Hans-Jörg Bart, *University of Kaiserslautern, Germany* (Secretary)
Dr. E. Susana Ortiz, *Imperial College London, United Kingdom* (Treasurer)
Dr. Jeaneth S. Benedetto, *Campus da UFMG, Brazil*
Mr. Peter Cole, *TWP Matomo Process Plant, South Africa*
Prof. Weiyang Fei, *Tsinghua University, China*
Prof. Masahiro Goto, *Kyushu University, Japan*
Dr. Baruch Grinbaum, *Bateman Litwin, Israel*
Dr. Gary A. Kordosky, *Cognis Corporation, USA*
Prof. Kenneth L. Nash, *Washington State University, USA*
Dr. Hans Reinhardt, *MEAB Metallextraktion AB, Sweden*
Mr. Gordon M. Ritcey, *Gordon Ritcey and Associates, Inc., Canada*
Prof. Lawrence L. Tavlarides, *Syracuse University, USA*
Prof. Hitoshi Watarai, *University of Osaka, Japan*
Prof. Eugeny V. Yurtov, *Mendeleev University of Chemical Technology, Russia*

ISEC 2008 TECHNICAL REVIEW PANEL

Keith Barnard
Pascal Baron
Hans-Jörg Bart
Suzanne Belanger
Jack Bender
Laurence Berthon
Cyril Bourget
Michel Burgard
John Campbell
Jesus de Casas
Alexandre Chagnes
Marie-Christine Charbonnel
Ji Chen
Jing Chen
Chu Yong Cheng
Violina Cocalia
Peter Cole
David Cordes
Gérard Cote
Michael Cox
Guillermo DelCul
Auwer Den
Mark L. Dietz
Simon Donegan
Christian Ekberg
María Elizalde
Alain Favre-Reguillon
Angus Feather
Kevin Felker
Douglas Flett
Robert Fox
Walter Furst
Andreas Geist
Karsten Gloe
Jürgen Gnoinski
Richard Grant
Eric Guibal
Philippe Guilbaud
Antje Hansmeier
Juris Harlamovs
T. Alan Hatton
David Henderson
R. Scott Herbst
Clement Hill
John Holbrey
E. Philip Horwitz
Michael J. Hudson
Don Ibana
Jie Ke
Vladimir Kislik
Gary Kordosky
Marthie Kotze
Shekhar Kumar
Jack Law
Michael Lecomte
Gary Leeke
Deqian Li
Leonard Lindoy
Murdoch MacKenzie
Pascale Maldivi
Philippe Mandin
Marcelo Mansur
Leigh Martin
Katarzina Materna
Daniel McAlister
David Meikrantz
Manuel Miguirditchian
Graeme Miller
Bruce Mincher
Michael Moats
Giuseppe Modolo
Philippe Moisy
Ron Molnar
Jean-Paul Moulin
Bruce Moyer
Anja-Verena Mudring
Richard D. Noble
S.A.F. Onink
Alena Paulenova
Patricia Paviet-Hartmann
Candido Pereira
Manuel Nunes da Ponte
E. Susana Perez de Ortiz
Dean Peterman
Jean Pierre Simonin
John Preston
Gordon M. Ritcey
David Robinson
Eduardo Robles
Mario Avíla Rodrigues
Hector Rodriguez
Robin D. Rogers
Tracy Rudisill
Yuji Sasaki
Stefan Schlosser
Tim Simmance
Igor Smirnov
Kathryn C. Sole
Christian Sorel
Barry Spencer
Moncef Stambouli
Ron Swart
Peter A. Tasker
Nick Tatalias
Robin Taylor
John Thomas
Owen Tinkler
Terry A. Todd
George Vandegrift
Michael J. Virnig
Ann Visser
Arjan Westra
Maciej Wisniewski
David Woodhead
Jacolien Wyethe

ISEC 2008 ACKNOWLEDGMENTS

A special thank you to Syracuse University for donating the time of Mrs. Dawn Long and the use of their facilities in support of ISEC 2008.
A special thank you to Becky R. Maggard, Administrative Assistant for Dr. Bruce Moyer, and Oak Ridge National Laboratory for support of ISEC 2008.

Table of Contents

Proceedings of ISEC 2008
International Solvent Extraction Conference

Associate Editors iii
Sponsors iii
Foreword v
Preface ix
Organizing Committee – International Committee xiii
Technical Review Panel xiv
Acknowledgments xiv

PLENARY LECTURES

Development of Solvent-Extraction Processes for Metal Recovery—
Finding the Best Fit between the Metallurgy and the Reagent 3
G.A. Kordosky

Column Design—Where Do We Go? 17
H.-J. Bart

Future Nuclear Fuel Cycles: Prospects and Challenges 29
B. Boullis

Ions and Their Complexes at Liquid-Liquid Interfaces: Nanoscopic
Views from MD Simulations 43
A. Chaumont, G. Chevrot, N. Galand, N. Sieffert, R. Schurhammer and G. Wipff

The Role of Entropy in the Design of Molecular Hosts 59
F.P. Schmidtchen

Complex Formation and Aggregation at Liquid-Liquid Interfaces 83
H. Watarai

HYDROMETALLURGY & METALS EXTRACTION

Developing High-Performing Copper Solvent-Extraction Circuits:
Strategies, Concepts, and Implementation 93
A. Nisbett, S. Peabody and G. Kordosky

Stripping Equilibrium Modification Based on the Chemical Structure of Equilibrium Modifiers 101
J.T. Bender and M. Virnig

Copper Solvent Extraction from Waste Cyanide Solution by a Solvent Mixture of a Quaternary Amine and Nonylphenol 107
F. Xie and D.B. Dreisinger

Reagent Stability in Synergistic SX Systems Incorporating LIX®63 Oxime and Versatic 10. Part I. Oxime Degradation Products and Oxime Isomer Analysis 113
K.R. Barnard

Reagent Stability in Synergistic SX Systems Incorporating LIX®63 Oxime and Versatic 10. Part II. The El Boleo Case Study 119
K.R. Barnard and N.L. Turner

Reagent Stability in Synergistic SX Systems Incorporating LIX®63 Oxime and Versatic 10. Part III. Nickel Laterite Case Study 125
K.R. Barnard and N.L. Turner

Processing of African Copper-Belt Copper-Cobalt Ores: Flowsheet Alternatives and Options 131
P.M. Cole and A.M. Feather

Copper and Cobalt Solvent-Extraction Process Developments at Chambishi Metals PLC 139
R. Minango, H.P. Singh, C. Kapambwe, E. Bwalya and D. Bukunkwe

Improvement in Copper and Cobalt Production Due to Inclusion of Solvent Extraction of Copper at Mopani Copper Mines PLC'S Nkana Cobalt RLE Plant 145
B. Mwakila, R. Silwamba, G. Miller and G.C. Chisakuta

Copper Removal from a Cobalt Sulfate Stream using pH-Controlled Solvent Extraction 151
S.A. Scott

Development of Process Flowsheet for Recovery of High-Purity Cobalt from Sulfate Leach Liquor of Waste $LiCoO_2$ 157
B. Swain, J. Jeong, J-C. Lee and J-S. Sohn

Separation of Cobalt and Zinc from Manganese, Magnesium and Calcium using Synergistic Solvent Extraction Consisting of Versatic 10 and LIX 63 163
C.Y. Cheng, W. Zhang and Y. Pranolo

Evaluation of Versatic 10 and Versatic 10/Nicksyn Synergistic Systems for Nickel-Calcium Separation on the Tati BMR Hydrometallurgical Demonstration Plant 169
H. Masiiwa, O. Mathe, S. Donegan, G. Nel, R. du Preez, M. Kotze and N. Ireland

Separation of Copper, Iron and Zinc from Cobalt and Nickel with Mixed CYANEX 272 and LIX 84 Extractants 177
W. Zhang, C.Y. Cheng, M. Rodriguez and Y. Pranolo

Interfacial Tension and Nickel Stripping Kinetics with Versatic 10 and LIX 63 Synergistic Systems 183
W. Zhang, R. Narendranathan, C.Y. Cheng and Y. Pranolo

Characterization and Dissolution of Hybrid Electric Vehicle (HEV) NiMH Batteries for the Development of a Hydrometallurgical Recycling Method 189
K. Larsson, C. Ekberg and G. Skarnemark

Life-extension of Electroless Nickel Plating Bath by Removing Phosphite Ions with Amine Extractant 195
M. Tanaka, H. Narita, Y. Sato and Y. Saiki

Highlights and Hurdles in Zinc Production by Solvent Extraction: The First Four Years at Skorpion Zinc 201
J. Gnoinski, K.C. Sole, D.R. Swart, R.F. Maluleke, G. Díaz and F. Sánchez

Zinc Solvent Extraction in the HydroZinc™ Process 209
J.R. Harlamovs and S. Bélanger

Separation of Zinc from Iron(II) in Spent Pickling Effluents Produced by the Hot-DIP Galvanizing Industry by Liquid-Liquid Extraction 215
C.A. de Morais, D.H. Carvalho, S.D.F. Rocha and M.B. Mansur

Separation of Zinc and Copper from Sulfuric Acid Liquor Obtained in the Leaching of Zinc-Industry Residues by Liquid-Liquid Extraction 221
L.R. Gouvea and C.A. Morais

Selective Extraction and Recovery of Copper from Zinc Leaching Liquor 227
A. Deep, S.M.C. Santos, R.M. Machado and J.M.R. Carvalho

Solvent-Extraction Separation of Zinc, Manganese, and Cobalt in Sulfate Solutions by D2EHPA 233
A.R. Eivazi Hollagh, D. Moradkhani, E.K. Alamdari and D. Darvishi

Effect of TBP on the Thermodynamics of Zn, Cd, Co and Mn Extraction with D2EHPA 239
D. Darvishi, D.H. Fatmehsari, S. Etemadi and E.K. Alamdari

Use of Solvent Extraction Technique in Brazillian Uranium Mills – An Overview 245
L.A. Gomiero and C.A. Morais

Expansion Capacity of an SX Unit in Uranium Process Pilot Tests 251
B. Courtaud, F. Auger, P. Morel and M. Sanoussi

Extraction of Uranium: Comparison of Stripping with Ammonia vs. Strong Acid 257
B. Moldovan, B. Grinbaum and A. Efraim

Solvent-extraction and Purification of Uranium(VI) and Molybdenum(VI) By Tertiary Amines from Acid Leach Solutions 263
A.M.G. La Gamma, E.T. Becquart and M. Chocron

Degradation Problems with the Solvent Extraction Organic at Rössing Uranium 269
B. Munyungano, A. Feather and M. Virnig

Role of Vanadium(V) in the Aging of the Organic Phase in the Extraction of Uranium(VI) by Alamine 336 from Acidic Sulfate Leach Liquors 275
A. Chagnes, G. Cote, B. Courtaud and J. Thiry

The Degradation of the Ketoxime LIX 84-I and its Impact on the Solvent Extraction of Palladium 281
S.F. Woollam and R.A. Grant

Liquid-Liquid Extraction of Gold(III) by 2-Ethylhexanol and its Application to Emulsion Pertraction Technology 287
C. Vargas, F.J. Alguacil, E.G. Palacios, I. Corona, F. Chavez, M. Alonso, F. Lopez and A. Lopez-Delgado

Recovery of Silver and Gold from Thiourea Leach Liquors by Di(2-ethylhexyl)dithiophosphoric Acid 293
Z. Gamino Arroyo, M. Stambouli, A. Buch, D. Pareau, J. El Bekri and M. Avila Rodriguez

Thermodynamic Models for Gold and Silver Extraction from Copper-Ammonia-Thiosulfate Solutions 299
P. Mendoza-Muñoz, G.T. Lapidus and M. Ávila-Rodríguez

Extraction, Separation, and Recovery of Pt(IV) and Rh(III) using CYANEX Extractants 305
B. Gupta and I. Singh

Influence of Gold and Zinc on Free Cyanide Extraction from Alkaline Solutions using Trioctylphosphine Oxide 311
G.C. Guimarães, M.B. Mansur and A.H. Martins

Recovery of Indium from Spent Flat-Panel Display with Solvent-Impregnated Resins 317
K. Inoue, M. Nishiura, H. Kawakita, K. Ohto and H. Harada

Liquid-Liquid Extraction of Hg(II) from Hydrochloric Acid Solutions by CYANEX 923 323
F. de M. Fábrega and M.B. Mansur

Production of High-Purity Ammonium Metavanadate by Solvent Extraction: Pilot-Plant Evaluation 329
K.C. Sole, K. Field, R. Maluleke, J. Schulze-Messing, K. Viljoen and D.F. Dutton

Solvent Extraction of Tantalum from Synthetic Concentrates 335
R.P. Singh Gaur

The Recovery of Sulfuric Acid from Nickel Electrolyte by Solvent Extraction: Pilot-Plant Evaluation 341
K. Viljoen, K.C. Sole, B.K. Ferreira and L.J. Bryson

Extraction of Mineral Acids and Metal Salts with Binary Extractant Based on Dinonylnaphthalenesulfonic Acid 347
S.A. Kulichenkov, V.V. Belova, A.I. Kholkin, A.A. Voshkin and T.I. Zhidkova

Recovery of Heavy Metals from WPA Phosphoric Acid 353
M.P. Elizalde, A. Ocio, A. Almela and B. Menoyo

PROCESS CHEMISTRY & ENGINEERING

Successful Design of Agitated Liquid-Liquid Extraction Columns via Pilot Plant Testing 361
D.J. Glatz and W.L. Parker

Modelling of Copper Extraction in a Pulsed Sieve-Plate Column 367
M.L.F. Gameiro, S. Agarwal, M.R.C. Ismael and J.M.R. Carvalho

Comparison of Disk and Doughnut and Sieve-Plate Internals in Pulsed Columns at Extreme Phase Ratios 373
B. Grinbaum and G. Stevens

Design of Passive Decanters for SX Columns 379
B. Grinbaum

SX Purification of Fertilizer-Grade Phosphoric Acid using BPC: Laboratory Scale to Industrial Plant 385
A. Efraim and R. Movsowitz

Pilot-Scale Studies of an Electrostatically Agitated Solvent-Extraction Column 391
M.J. Steffens and D.C. Ibana

Transient Drop Behavior of Single Drops in Reactive Extraction 397
M. Kalem and A. Pfennig

CFD-Supported Design in Liquid-Liquid Extraction 403
T. Gurker, T. Haderer and R. Marr

Dynamic Model for a Mixer-Settler System 409
E.F. Gomes, G.A. Pinto, M.M.L. Guimarães and L.M. Ribeiro

Development of a Computer Simulation of the Platinum Solvent Extraction at Precious Metals Refiners (PMR) 415
R.A. Grant and S.F. Woollam

Stability of the Dispersed Band in a Shallow-Layer Settler 421
M.M.M. Ribeiro, E.V. Soares, M.M.L. Guimarães and A.M.A. Fiúza

Optimization of the Design of Mixer-Settlers in Zn Solvent Extraction 427
D. Martín, F. Sánchez, M. Frades and A.B. Mejías

Copper Solvent Extraction—2007 World Operating Data 435
T. Robinson, M. Moats, W. Davenport, G. Karcas, S. Demetrio and E. Domic

A Simple Model for Predicting Zinc-DEHPA Extraction Isotherms 441
J.R. Harlamovs

Operational Practices for CYANEX® 272 Extractant Circuits 447
C. Bourget and B. Jakovljevic

Aspects of the Design of SX Plants for the Modern Hydrometallurgical Refinery 453
E. Robles, I. Cronje, S. Poulter and R. Haywood

Modelling Cobalt Extraction with CYANEX 272 459
H.A. Evans, P.A. Bahri, J.A. Rumball and K.R. Barnard

Solvent Stability Testing in Development of Liquid-Liquid Extraction Processes.....467
Z. Gross and O. Lerner

Some Practical Aspects for Impurity and Crud Control in Solvent-Extraction Processes.....473
H. Laitala, E. Ekman and G. Karcas

A New Technology for Treating Wastewater Produced in the Oil Industry: A Semi-Industrial Scale Operation.....479
W.E. Fernandes Jr., J.B.A. Paulo, N.A. Moraes and G.S. Medeiros

Innovations in the Configuration of a Pinned-Bed Clarifier for Clarification of a Zinc Leach Liquor.....485
M. Langton, H.F. Fuls, K.C. Sole, A. Rampersad, C. Blaauw and B. Martinson

Improved Organic Recovery with Hydrocyclones at Freeport-McMoran Copper and Gold Morenci Operations.....491
M.A. Thumberg and E.P. Kramer

Operation of a Flottweg Tricanter® Centrifuge for Crud Treatment at Bwana Mkubwa Solvent-extraction Plant 497
A. Mukutuma, N. Schwarz and A. Feather

Crud Treatment and Clay Treatment with One Multipurpose Solid Bowl Centrifuge 503
T. Hartmann

NUCLEAR FUEL REPROCESSING

Key Features of the TALSPEAK and Similar Trivalent Actinide-Lanthanide Partitioning Processes.....511
K.L. Nash

Partitioning of Trivalent Actinides from a PUREX Raffinate using a TODGA-Based Solvent-Extraction Process.....521
G. Modolo, H. Vijgen, R. Malmbeck, D. Magnusson and C. Sorel

Complexation of Lanthanides and Actinides by Acetohydroxamic Acid 527
R.J. Taylor, S.I. Sinkov and G.R. Choppin

Americium/Europium Separation by Synergistic Extraction Mixtures of Bis-tetrazolyl Pyridines with Chlorinated Cobalt Dicarbollide 533
I.V. Smirnov, V.A. Babain and A.V. Chirkov

Lanthanide and Actinide Extractions using Functionalized Cobalt Bis(dicarbollide) Ion Derivatives Substituted with Metal Ligating Functions..... 539
M. Lučaníková, P. Selucky, J. Rais, B. Grüner and M. Kvíčalová

A Comparative Study of Some BTP and BTBP Class Ligands 545
T. Retegan, C. Ekberg, A. Fermvik, M.R.S. Foreman and G. Skarnemark

The Effect of Irradiation on Extraction of Various Metals by C5-BTBP..... 551
A. Fermvik, C. Ekberg, M.R.S. Foreman, T. Retegan and G. Skarnemark

Improved Separation of Am(III) from the Light Lanthanides using a Soft-Donor Synergist..... 557
D.D. Ensor and M.H. Zimmerman

The Behavior and Importance of Lactic Acid Complexation in TALSPEAK Extraction Systems 563
T.S. Grimes, M. Nilsson and K.L. Nash

Separation of Lanthanides from Trivalent Actinides, the Role of Aqueous-Phase Soft-Donor Complexing Agents..... 569
M. Nilsson, C. Hoch, G.P. Meier and K.L. Nash

Bis-diglycolamides (BIS-DGA) as New Extractants for An(III) and Ln(III) from Aqueous High-Level Wastes Issued from the PUREX Process..... 575
A.G. Espartero, M.T. Murillo, M. Almaraz, J. Sánchez-Quesada, M. Segura, J.C. Iglesias-Sánchez, P. Prados and J. de Mendoza

Modified PUREX First-Cycle Extraction for Neptunium Recovery..... 581
B. Dinh, P. Moisy, P. Baron, J-N. Calor, D. Espinoux, B. Lorrain and M. Benchikouhne-Ranchoux

Plutonium Purification Cycle in Centrifugal Extractors: From Flowsheet Design to Industrial Operation 587
P. Baron, B. Dinh, J. Duhamet, F. Drain, F. Meze and A. Lavenu

Partitioning of Eu(III) between Acidic Aqueous $Al(NO_3)_3$ and Tri-*n*-Octyl Phosphine Oxide 593
J.C. Shafer, R.C. Harrington and K.L. Nash

Modeling of Distribution and Speciation of Plutonium in the UREX Extraction System 599
A. Paulenova, P. Tkac, G.F. Vandegrift and J.F. Krebs

Investigating the use of Bismuth(V) for the Oxidation and Subsequent Solvent Extraction of Americium(VI) 605
L.R. Martin, B.J. Mincher and N.C. Schmitt

Studies on the Stripping of Transuranic Elements from Loaded TRPO by N,N-dimethyl-3-oxa-glutaramic Acid 611
J. Chen, J. Wang and W. Duan

Solvent-Extraction Purification of Neptunium 617
E.A. Kyser and S.L. Hudlow

Simultaneous Recovery of All Actinides from Spent Nuclear Fuel by Carbamoylmethylphosphine Oxide in Fluorinated Diluents 623
M. Ozawa, T. Iwai, V. Babain and A. Shadrin

Studies on the Stripping of Cerium from the Loaded TBP-Kerosene Solution 629
S.E. Rizk, N. Abdel Rahman, J.A. Daoud and H.F. Aly

Next-Generation PUREX Flowsheets with Acetohydroxamic Acid as Complexant for FBR and Thermal-Fuel Reprocessing 635
S. Kumar and S.B. Koganti

Study on the Properties of Saline HLLW in China 641
J.F. Liang, X.G. Liu, C.L. Song and R.Z. Jiao

Actinide Extraction from Simulated and Irradiated Spent Nuclear Fuel using TBP Solutions in HFC-134a 647
A. Shadrin, V. Babain, V. Kamachev, A. Murzin, D. Shafikov and A. Dormidonova

Development of a Process for the Extraction of ^{137}Cs from Acidic HLLW Based on Crowncalix Extractant—Use of Dialkylamide Modifier 653
J. Alexová, M. Šírová, J. Rais, S. Suzuki, M. Hirata, T. Kimura and S. Tachimori

Simultaneous Separation of Cesium and Strontium from Spent Nuclear Fuel using the Fission-Product Extraction Process 659
J.D. Law, D.R. Peterman, C.L. Riddle, D.A. Meikrantz and T.A. Todd

Radionuclide Partitioning in the Modified UNEX Process 665
V. Babain, I. Smirnov, M. Alyapyshev, T.A. Todd, J.D. Law, R.S. Herbst and A. Paulenova

The Radiation Chemistry of Cs-7SB, a Solvent Modifier used in Cs and Sr Extraction 671
B.J. Mincher, S.P. Mezyk, L.R. Martin and G. Elias

The Radiation Chemistry of CCD-PEG, a Solvent-Extraction Process for Cs and Sr from Dissolved Nuclear Fuel 677
B.J. Mincher, R.S. Herbst, R.D. Tillotson and S.P. Mezyk

A Study of Radiolytic Stability of 25,27-Bis(2-propyloxy) calix[4]-26,28-crown-6 (iPR-C[4]C-6) 683
J. Wang and C. Song

Dramatic Improvements in Caustic-Side Solvent Extraction of Cesium through More Efficient Stripping 689
L.H. Delmau, E. Bazelaire, P.V. Bonnesen, N.L. Engle, M.G. Gorbunova, T.J. Haverlock, B.A. Moyer, D.D. Ensor, V.M. Meadors, B.W. Harmon, R.A. Bartsch, M.A. Surowiec and H. Zhou

An Overview of Spent-Fuel Processing in the Global Nuclear-Energy Partnership 695
J.J. Laidler

Development and Application of Centrifugal Contactors in China 703
P. Cao and W. Duan

Industrial Application of GNEP Solvent-Extraction Processes 709
S.T. Arm, C. Phillips and A. Dobson

Technical Feasibility of the DIAMEX Process 715
C. Sorel, M. Montuir, D. Espinoux, B. Lorrain and P. Baron

Extraction of Uranium(VI) by N,N-di-(2-ethylhexyl)isobutyramide (DEHiBA): From the Batch Experimental Data to the Countercurrent Process 721
M. Miguirditchian, C. Sorel, B. Camès, I. Bisel and P. Baron

Mass-Transfer Testing of a 12.5 cm Rotor Centrifugal Contactor 727
D.H. Meikrantz, T.G. Garn, J.D. Law, N.R. Mann and T.A. Todd

Hydraulic and Clean-in-Place Evaluations for a 12.5 cm Annular Centrifugal Contactor at the INL 733
T.G. Garn, D.H. Meikrantz, N.R. Mann, J.D. Law and T.A. Todd

Catalog Solvent Extraction: Anticipate Process Adjustments....739
S.G. Campbell, E.A. Brass, S.J. Brown and M.W. Geeting

Extraction of Actinides by Multidentate Diamides and their Evaluation with Computational Molecular Modeling....745
Y. Sasaki, Y. Kitatsuji, M. Hirata, T. Kimura and K. Yoshizuka

Chemical Interaction Matrix between Reagents in a PUREX Based Process....751
R.K. Brahman, W.P. Hennessy and P. Paviet-Hartmann

Studies on Reaction Runaways for UREX/PUREX Solvent-Nitric Acid and Red-Oil Synthesis....757
S. Kumar, R. Kumar and S.B. Koganti

Development of Novel Contactor for Nuclear Solvent Extraction....763
S. Kumar, R. Kumar, D. Sivakumar, M. Balamurugan and S.B. Koganti

Extraction of Protactinium-233 and Separation from Thermal Neutron-Irradiated Thorium-232 using Crown Ethers....769
M.G. Jalhoom, D.A. Mohammed and J.S. Khalaf

ANALYTICAL AND PREPARATIVE APPLICATIONS

Chiral Recognition by Molecular Aggregation at Liquid-Liquid Interface....779
H. Watarai

Partition Behavior of Several Extractants and Their Iron(III) Complexes in Some Micellar Systems....787
K. Inaba, T. Doi, J. Noro and H. Naganawa

Analysis of Binding Reactions of Ionic Substances to Nonionic Surfactant Micelles....793
T. Takayanagi, Y. Takimoto, A. Ikuta and S. Motomizu

Tetraalkylphosphonium Polyoxometalates as Novel Ionic Liquids....799
M.L. Dietz, P.G. Rickert, M.R. Antonio, M.A. Firestone, J.F. Wishart and T. Szreder

Effect of Solvent on the Extraction of Chromium(VI)-with Quaternary Ammonium Ions....805
J. Noro and Y. Komatsu

Extraction Equilibrium of Lanthanides(III) with 2-Thenoyltrifluoroacetone in the Water-1-Propanol-Chloroform Ternary Solvent System....811
A. Ohashi, T. Hashimoto, H. Imura, T. Hori and K. Ohashi

Quantitative Separation of Alkaline Earth Metal Ions Combining Two Kinds of Solvent Extraction 817
S. Oshima, J. Noro, K. Fujinaga, H. Kokusen, S. Tsurubou and Y. Komatsu

The In Situ Extractant Formation Method as a Useful Tool for Developing a New Functional Chelate Reagent: Piperidinedithiocarbamic Acid Forming System 823
K. Fujinaga, A. Yamauchi, Y. Seike, Y. Komatsu and M. Okumura

Smart-Level Solvex: A New Instrument for Quantifying Phase Disengagement 829
M. Dann, M.B. Songo and K.C. Sole

Analytical Applications of Ion-Transfer at a Liquid|Liquid Interface Illuminated with an Ultraviolet Laser Beam 835
T. Hinoue and T. Kimoto

Solvent Extraction as a Tool for Design of Sulfonamide-derived Pb(II) Sensors 843
K. Kavallieratos, R.J. Alvarado and J.M. Rosenberg

Cellulose Triacetate Based Novel Optical Sensor for Uranium Estimation 849
J.M. Joshi, P.N. Pathak, A.K. Pandey and V.K. Manchanda

Liquid Phase Headspace Microextraction into a Single Drop of Water 855
A.Y. Nazarenko

Intensification of Liquid-Liquid Reaction and Separation Processes with Miniaturization 861
G.S. Luo, J.H. Xu, S.W. Li, K. Wang and J. Tan

The Intensification of Mass Transfer Performance of Liquid-Liquid Dispersed System in Microchannels 867
J.H. Xu, J. Tan, S.W. Li and G.S. Luo

Protein Extraction to Ionic Liquids and its Change of Biological Function 873
M. Goto, K. Shimojo and F. Kubota

Extraction of Amino Acids and Dipeptides by Calixarene Carboxylic Acid Derivatives 879
T. Oshima, A. Irie, K. Ohto, K. Inoue, H. Kodama, T. Ishii and Y. Baba

Spectrophotometric Determination of Ultra-Trace Beryllium after Separation and Preconcentration using Quinalizarine-Modified Magnetic Microparticles 885
P. Ashtari, K. Wang, X.H. Yang, K. Ashtari and A. Khanchi

Preparation of Binuclear Complexes by Solvent Extraction and their Photophysical Properties 891
Y. Hasegawa, S. Tamaki, M. Inoue and H. Yajima

Neptunium Estimation in Dissolver and High-Level-Waste Solutions 897
P.N. Pathak, D.R. Prabhu, A.S. Kanekar and V.K. Manchanda

The Use of Voltamperometry in the Determination of the Active Components of Commercial Extractants 903
M.P. Elizalde, M.S. Rúa, A. Almela and M. Huebra

Aqueous in Organic Entrainment Analysis 909
K.R. Barnard

Determination of Indium by Solvent Extraction Spectrophotometrically 915
D.D. Malkhede, Y.S. Thakare and S.M. Khopkar

BIOTECHNOLOGY, PHARMACEUTICALS, LIFE-SCIENCE PRODUCTS, AND ORGANIC PRODUCTS

Continuous Production of Biodiesel Via an Intensified Reactive/ Extractive Process 923
C. Tsouris, J. McFarlane, J.F. Birdwell Jr. and H.L. Jennings

Purification of Biofuels using Ionic Liquids 931
F. Santangelo, A.E. Wentink, A. Górak, W. Pitner and M. Schulte

Extractive Catalyst Recovery in an Ionic-Liquid Process for the Production of 2,5-Dihydrofuran 937
J.S. Kanel, S.N. Falling, J.R. Monnier, G.W. Phillips and S.A. Godleski

Study of Vanillin Extraction from Solutions of Lignin Oxidation 943
V.E. Tarabanko, Y.V. Chelbina, K.L. Kaygorodov, N.V. Tarabanko and N.V. Koropachinskaya

Extraction Characteristics of Phthalic and Trimellitic Acid with 1-Octanol and 10 % TRPO/Kerosene 949
Z. Zhou, W. Qin and Y. Dai

Extraction of *Linum usitatissimum* L. Using Supercritical CO_2 and Organic Solvent 955
E.L. Galvão, H.N.M. Oliveira, L.A.G. Gonçalves, A.V.B. Moreira and E.M.B.D. Sousa

Extraction of Triterpenes – Oleanolic and Ursolic Acid from Sage.....961
M. Schmidt and H.-J. Bart

Extraction of Levulinic Acid to Increase the Selectivity and Efficiency of the Carbohydrate Acid-Catalyzed Conversion.....967
V.E. Tarabanko, M.A. Smirnova and M.Y. Chernyak

Purification of Cyclitols using Bioextraction.....973
A.E. Wentink, J. Micović, K. Gerlach and M. Raventos

Continuous Enantioselective Extraction of Amino Acids in a Highly Intensified Centrifugal Extractor.....979
B. Schuur, J.G.M. Winkelman and H.J. Heeres

CENTREK® Centrifugal Extractors in Biotechnology and Pharmaceutics.....985
G.I. Kuznetsov, A.V. Kosogorov, A.A. Pushkov, Z.I. Kuvaeva and A.V. Mikulich

Reversed-Micelle Size-Driven Solubilization and Stripping of α-Amylase with Weak Net Charge.....991
K. Tonova and Z. Lazarova

Development of Inorganic Microcapsules for the Oral Delivery of a Hydrophilic Drug.....997
E. Toorisaka, M. Hirata and T. Hano

Rationalization of the Emulsification Process of Emulsions used for Detoxification of Chloroquine.....1003
M. Grosber-Manon, D. Pareau, M. Seiller, A. Buch, J. el Bekri, J-L. Grossiord and M. Stambouli

FUNDAMENTALS

Toward the Computer-Aided Design of Ion Sequestering Agents.....1011
B.P. Hay

Aggregation of Organic Extractant Phases: Consequences on Extraction Properties.....1017
L. Berthon, Y. Meridiano, S. Lagrave, X. Crozes, C. Sorel, N. Zorz, F. Testard and T. Zemb

From Databases to *In Silico* Design of Novel Metal Binders.....1023
A. Varnek

Extractant Aggregation as a Mechanism of Metal Ion Selectivity.....1029
M.P. Jensen, T. Yaita and R. Chiarizia

Effects of Hydration and Solvation of Metal Complexes on Separations of Metal Ions by Solvent Extraction 1035
J. Narbutt

Thermodynamic and Structural Description of Europium Complexation in 1-Octanol Solution 1043
M-C. Charbonnel, T-H. Vu, N. Boubals, L. Couston and F. Arnaud

Polyamines as Oxoanion and Chlorocomplex Receptors 1049
M.G. Sánchez-Loredo, M. Wenzel, K. Gloe, K. Gloe, M. Grote, H.-J. Holdt and A. Kelling

Comparison of Cloud Point and Solvent Extraction of Gd(III) from Aqueous Solutions 1057
A. Favre-Réguillon, D. Murat, A. Chagnes, G. Cote, J. Foos and M. Draye

Synthesis and Evaluation of Sterically Focused Tetradentate Nitrogen Ligands Containing the 2-Methylpyridyl Moiety for the Separation of An(III) from Ln(III) 1063
M.D. Ogden, G.P. Meier and K.L. Nash

Atomistic Simulation of Water/Tributylphosphate-dodecane Interface 1069
S. Cui, V. de Almeida and B. Khomami

Experimental Data and Regressions Concerning the Evaluation of 1,2-Propylene Glycol as a New Solvent for Aromatic Hydrocarbons Liquid-Liquid Extraction from Catalytic Reformer Products 1075
F. Oprea and O.A. Guțu

Origins of *f*-Element Selectivity in Solvent Extraction 1081
M.P. Jensen

Prediction and Optimization of the Separation Selectivity Between Metallic Elements with Similar Chemical Properties 1087
S.C. Belair and P. Dannus

Anion-Exchange Extraction of Carboxylates 1093
A.L. Gulevich, T.N. Kiyko and V.A. Kovalevich

Synergistic Extraction of Trivalent Lanthanides and Actinides from Acidic Chloride Media by Tetra(*n*-octyl)diglycolamide 1099
D.R. McAlister and E.P. Horwitz

Synergistic Extraction Mechanism of Samarium with Alkylphosphoric Acids as Main Extractant 1105
K. Kondo, T. Watanabe, E. Kamio and M. Matsumoto

Calorimetric Investigations of Metal Extraction for Two-Phase Systems 1111
P.R. Zalupski and K.L. Nash

The Effect of Aqueous-Phase Composition on the Separation of Hafnium and Zirconium from Acidic Chloride-Sulfate Media by Extraction with Alamine 336S in Benzene 1119
N.M. Rice and R. Lee

Software "EXTREQ-2" for Mathematical Modeling of Multicomponent Extraction Equilibria.....1127
K.A. Slavinskiy, A.M. Chekmarev and S.I. Stepanov

Complexation of Americium with α-D-isosaccharinate.....1133
S. Allard, C. Ekberg, R. Jolsterå, A. Knutsson and A. Ödegaard-Jensen

The Thermodynamics of Extraction of Bismuth by P,P'-di(2-ethylhexyl)ethylene- and Methylene-diphosphonic Acids 1139
C.G. Otu and E.O. Otu

Thermodynamic Study of Extraction of Cr(III) from Aqueous Solutions by Bis(2-ethylhexyl) Phosphoric Acid (DEHPA) 1145
R.G. Turriza Cruz, R. Navarro, T.I. Saucedo, P. Gonzalez, M. Stambouli, D. Pareau and M. Avila-Rodriguez

Comparison of the Coordination Behavior of Cu(II) and Fe(III) with Organophosphorous Acids and Hydroxyoxime-Based Ligands in Aqueous and Nonaqueous Media 1151
I. Van de Voorde, K. Latruwe, L. Pinoy, E. Courtijn and F. Verpoort

Spectroscopic Study on the Solvent Extraction of Chromium(VI) and Vanadium(V) by Primary Amine.....1159
X. Lin, H-B. Cao, Y-P. Li and Y. Zhang

Dispersed Phase Holdup in Karr Reciprocating Columns.....1165
R. Arunachalam, T. Bowser and G.W. Stevens

CFD Modeling of Pump-Mixers.....1171
K.K. Singh, S.M. Mahajani, K.T. Shenoy and S.K. Ghosh

CFD-PBM Coupled Model using the Finite Pointset Method and the SQMOM.....1177
C. Drumm, S. Tiwari, M.M. Attarakih, J. Kuhnert and H.-J. Bart

Numerical Approach to the Marangoni Convection-Enhanced Mass Transfer of Single Moving Drops 1183
J. Wang, C. Yang and Z-S. Mao

Kinetics of Scandium Solvent Extraction by N-(2-hydroxy-5-nonylbenzyl)-β,β-dihydroxyethylamine Under Non-Stationary Phase Contact Surface 1189
S.A. Semenov and A.M. Reznik

Extraction and Separation of Thorium(IV) from Lanthanides(III) with Room-Temperature Ionic Liquids Containing Primary Amine N_{1923} 1195
Y. Zuo, J. Chen, Y. Bai and D.Q. Li

The Kinetics of Cu(II) Extraction by 5-nonyl-2-hydroxybenzaldoxime (P50) in a Micelle System 1201
S. Glasson, G.W. Stevens and J.M. Perera

Modeling of Mass-Transfer Induced Instabilities at Liquid-Liquid Interfaces 1207
S. Miroshnichenko and A. Pfennig

Numerical Study of a Rising Droplet using Commercial CFD Software 1213
T. Atmakidis and E.Y. Kenig

Numerical Approach to the Three-Dimensional Marangoni Effect in a Two Liquid Layer System 1219
Z-S. Mao, P. Lu, G. Zhang and C. Yang

Scale-Up of Karr Reciprocating-Plate Extraction Columns 1225
K.H. Smith and G.W. Stevens

Experimental Investigation of Droplet-Droplet Coalescence in Liquid-Liquid Systems 1231
R.T. Eiswirth and H-J. Bart

Reliable Design of Physical and Reactive Extraction Based on Simple Lab-Scale Experiments 1237
A. Pfennig

Modeling of Unit Operations by Molecular Simulations 1243
D. Babic and A. Pfennig

Pseudo-Equilibrium State of the System Zr–HNO_3–TBP–Diluent 1249
O.A. Sinegribova, O.V. Muraviova and K.T. Win

Extraction of Some Rare Earth Elements by D2EHPA in Systems with Artificial Mechanical Disturbance 1255
N.F. Kizim and E.N. Golubina

NOVEL REAGENTS, MATERIALS, AND TECHNIQUES

Separations, Coordination, and Solvation in Ionic Liquids; What is There That is Unique? 1263
G. Gurau, V.A. Cocalia and R.D. Rogers

Complexation Studies of F-Elements in Ionic Liquids 1271
A.V. Mudring

Preliminary Investigation of the Kinetics of the Separation of Yttrium(III) using Cyanex 923 in Ionic Liquids 1277
H.L. Yang, J. Chen and D.Q. Li

Zinc and Iron Extraction with Mixtures Containing Phosphonium Ionic Liquids 1283
M. Regel-Rosocka and M. Wiśniewski

Reactive Extraction in Acidic Ionic Liquid Systems 1289
D. Naydenov and H-J. Bart

Extractive Removal of Palladium(II) from Chloride Media with Pyridinecarboxamides and Phosphonium Ionic Liquids 1295
A. Cieszyńska, M. Regel-Rosocka and M. Wiśniewski

Gas Sorption using Ionic Liquids 1301
R.D. Noble, D.L. Gin, J.E. Bara, B. Voss, A. Finotello and T. Carlisle

New Sorbents Based on the Immobilization of Cyphos IL-101 (Trihexyl(tetradecyl)phosphonium Chloride) in Alginate Gel Beads for Gold Recovery from HCL Solutions 1307
K. Campos, T. Vincent, P. Bunio, A. Trochimczuk and E. Guibal

Recovery of Cd(II) Ions from Aqueous HCl Solutions using Cyphos IL 101 (Trihexyl(tetradecyl)phosphonium Chloride) Immobilized in Alginate Gel Beads 1313
R. Navarro, L.A. Arias, I. Saucedo, M. Avila and E. Guibal

Efficient Removal of Dicyclopentadiene Impurities from Cyclohexane using Ionic Liquids 1319
P. Ruiz, A. Ruiz, D. Gorri and I. Ortiz

Selective Removal of Nitrogen-Containing Compounds from Straight-Run Diesel Feed using ILs 1325
L-L. Xie, A. Favre-Reguillon and M. Lemaire

Improved Ionic Liquids for the Extraction of Aromatic Hydrocarbons from Naphtha 1331
A.R. Hansmeier, G.W. Meindersma and A.B. de Haan

Ionic Liquids in Extraction Operations: Comparison of Rotating Disc Contactor Performance Between [4-mebupy]BF^4 and Sulfolane® for Aromatics Extraction 1337
S.A.F. Onink, G.W. Meindersma and A.B. de Haan

Solvent Impregnated Resin for Isolation of U(VI) from Industrial Wastes 1343
M. Karve and R.V. Rajgor

Hollow-Fiber Supported Liquid Membrane (HFSLM) for the Separation of Lanthanides and Actinides 1349
P.K. Mohapatra, C.B. Patil, S.A. Ansari, A. Bhattacharyya and V.K. Manchanda

Carrier-Mediated Transport of Actinide Ions using Supported Liquid Membranes Containing TODGA as the Carrier Extractant 1355
S. Panja, P.K. Mohapatra, A. Dakshinamoorthy, S.K. Munshi, P.K. Dey and V.K. Manchanda

Recovery of Uranium from Dilute Solution using Liquid Emulsion Membrane System 1361
S. Mukhopadhyay, S.K. Ghosh and V.A. Juvekar

Improving the Performance of Supported Liquid Membranes 1367
M. Fritz, M. Siebenhofer and R. Marr

Separation of Co(II) and Li(I) by Supported Liquid Membrane and Solvent Extraction using CYANEX 272 as an Extractant 1373
B. Swain, J. Jeong, J-C. Lee, K. Yoo and M-S. Kim

Evaluation of the Dependency of Phase Composition on Indium(III) Permeability in CYANEX 272 / NPOE PIM-Based Systems 1379
E. Rodríguez de San Miguel, J.C. Aguilar, M. Muñoz and J. de Gyves

Phenol Removal from Dilute Aqueous Streams using Solvent-Impregnated Resins 1385
B. Burghoff, E.L.V. Goetheer and A.B. de Haan

Extractant Impregnated Resin Technology for the Recovery of Aldehydes from Aqueous Streams 1391
K. Babić, A.G.J. van de Ham and A.B. de Haan

Displayed "End Effects" for Extraction with Emulsion Liquid Membranes: Mass-Transfer Model of Extraction of Zinc with D2EHPA in Single-Drop Apparatus 1397
J.F. le Bon, A. Buch, D. Pareau, C. Leroi, J. El Bekri and M. Stambouli

Removal and Separation of Organic Acids by Membrane-Facilitated Solvent-Extraction Techniques 1403
Z. Lazarova and S. Boyadzhieva

Membrane-Based Solvent Extraction as an Alternative to Conventional Processes in the Treatment of Hot-Dip Galvanizing Processes 1409
J.A. Carrera, E. Bringas, M.F. San Román and I. Ortiz

Converting Membrane-Based Solvent-Extraction Networks into Sustainable Processes: Remediation of Groundwater Polluted with Cr(VI) as Case Study 1415
E. Bringas, M.F. San Román and I. Ortiz

Synergistic Extraction of Rare Earths with a Mixture of CALIX[4]arene Carboxylic Acid and Primary Amine N1923 1421
W.W. He, W.P. Liao, D.Q. Li and C.J. Niu

Separation of Minor Actinides from Lanthanides by Dithiophosphinic Acid Extractants 1427
D.R. Peterman, M.R. Greenhalgh, R.D. Tillotson, J.R. Klaehn, M.K. Harrup, T.A. Luther, J.D. Law and L.M. Daniels

Selective Extraction of U(VI) and Some Other Metals from Nitric Acid Media by Polyphosphine Polyoxides 1433
M. Nogami, K. Maruyama, Y. Sugiyama and Y. Ikeda

Extraction of Metal Ions from Chloride Media: Can Malonamide Derivatives be Useful? 1439
A.P. Paiva, P. Malik, A.M. Rosa, C. Castro and M.C. Costa

Separation of Palladium in Hydrochloric Acid Solution with Sulfide-Containing Amide Compounds 1445
H. Narita, M. Tanaka and K. Morisaku

Polytopic Salicylaldimine Ligands for the Recovery of Zinc Chloride 1451
T. Lin, V. Gasperov, K.J. Smith, C.C. Tong and P.A. Tasker

Anion Recognition: The Selective Extraction of $[PtCl_6]^{2-}$ 1457
K.J. Bell, J. Chartres, R.J. Ellis, D.J. Robinson, C.C. Tong, R.J. Warr, A.N. Westra, M. Schröder and P.A. Tasker

Design of Extraction Reagents of High Selectivity Based on Steric Factors 1463
S. Umetani, Y. Fukui and K. Uezu

A Search for New Copper Solvent-Extraction Reagents: Acylpyrazolones and Phenoxypyrazoles 1469
J. Campbell, R.M. Swart, S. Owens, P.A. Tasker and L.J. Stewart

Polyacidic Extractants to Improve Mass Transport Efficiencies of Base Metals 1475
R.J. Gordon, J. Campbell, D.C.R. Henry, R.M. Swart, P.A. Tasker, F.J. White, J.L. Wood and L.J. Yellowlees

Solvent Extraction of Several Metal Ions with a Novel Tripodal Type of Carboxylic Acid 1481
K. Ohto, Y. Fujimoto, H. Furugou, H. Kawakita, H. Harada and K. Inoue

Next Generation Extractants for Separation of Cesium from High-Level Waste 1487
R.A. Bartsch, H. Zhou, L.H. Delmau and B.A. Moyer

Liquid-Liquid Extraction Studies with Bis-β-diketones 1493
M. Wenzel, D.J. Bray, J.K. Clegg, K. Gloe, K. Gloe, L.F. Lindoy and G.V. Meehan

4,5-Bis(diphenylphosphinoyl)-1,2,3-triazole: A Novel Ligand for Metal Extraction 1499
H. Mukai, S. Kobayashi, S. Butoh, S. Ikegami, A. Minami, Y. Maruyama, Y. Matsuo, J. Murakami, S. Mae, T. Sasamori, N. Tokitoh and S. Trofimenko

Optical-Response Extraction of Gold(III) by *cis-trans* Photoisomerization of Bis(2,2'-dipyridinyl-6-YL)diazene 1505
K. Takeshita, N. Sawai and Y. Okada

The Potential Use of Hydrocarbon Magnetic Liquids in Solvent Extraction 1513
L.L. Vatta, K.R. Koch and K.C. Sole

Study and Application of Modified Rotating-Disc Contactors 1519
W. Fei and Y. Wang

Thin-Layer Extraction 1525
R. Lavie

Controllable Preparation of Nanoparticles by Drops and Plugs Flow in a Microchannel Device 1531
S. Li, J. Xu, Y. Wang and G. Luo

Preliminary Experimental Study of Butyl Acetate Separation by Air-Assisted Solvent Extraction 1537
Y. Ma, Z. Chang, B. Xiao, S. Shen and H. Liu

Ultra-Fast Extraction of an Ethyl Ester of Docosahexaenoic Acid with Silver Ion Using Slug Flow 1543
E. Kamio, Y. Seike, H. Yoshizawa and T. Ono

Fundamentals and Potential Applications of Cloud-Point Extraction 1549
M.A. Ensor and K.L. Nash

Cloud Point (Two-Aqueous Phase) Extraction of Heavy Metal Salts 1555
L.J. Nogueira Duarte and J.P. Canselier

A Membrane Process to Recover Extractants from Residual Phases 1561
S. Wang, W. Qin and Y.Y. Dai

Potential of Liquid Membranes for the Treatment of a Phenolic-Resin Plant Effluent 1567
S. Agarwal, M.T.A. Reis, L.M. Ferreira, P.F.M.M. Correia and J.M.R. Carvalho

Separation and Purification of EOPO2500 Copolymer in Three-Liquid-Phase Extraction Systems 1573
S.F. Shen, Z.D. Chang, H.Z. Liu, Y.C. Ma and X. Hu

Functionalized Organo-Ceramic Adsorbents for Germanium Separations 1579
H.J. Park and L.L. Tavlarides

Poly-*N*-isopropylacrylamide with Incorporated Thioether Units as an Extraction Media for Soft Metal Ions 1585
K. Chayama, Y. Morita and S. Iwatsuki

Extraction of Copper from Phosphoric Acid Solutions Using Alginate Beads Containing LIX 622 1591
F. Mijangos, A. Ocio, M.P. Elizalde and A. Almela

Microemulsion Leaching of Metals 1597
E.V. Yurtov and N.M. Murashova

Novel Dextran Gel Formation by Enzymatic Reaction to use for Solid-Phase Extraction 1603
H. Kawakita, H. Seto, K. Ohto, H. Harada and K. Inoue

Partitioning of Modified Merrifield Resins Microparticles in Aqueous Biphasic Systems 1609
Y.F. Deng, D.L. Zhang, L.L. Zhu and J. Chen

Tartaric Acid-Based Complexing Surfactants for Micellar Enhanced Ultrafiltration: A Green Way for Metal Removal 1615
L. Dupont-Leclercq, S. Giroux, S. Parant, B. Henry and P. Rubini

Stabilized Metal and Metal Sulfide Nanoparticles Prepared by the Two-Phase Liquid-Liquid Method 1621
G. Sánchez, R. Tovar, J. Aguilera, F. Ruiz and G. Martínez

Back-Extraction of Metal Species from Supercritical Carbon Dioxide Modified with Tri-*n*-butyl Phosphate 1627
Y. Enokida, K. Sawada and Y. Katakami

Plenary Lectures

DEVELOPMENT OF SOLVENT-EXTRACTION PROCESSES FOR METAL RECOVERY—FINDING THE BEST FIT BETWEEN THE METALLURGY AND THE REAGENT

Gary A. Kordosky

Cognis Corporation, 2430 North Huachuca Drive, Tucson, AZ. USA 85745
Corresponding author email address: gary.kordosky@cognis.com

ABSTRACT

A solvent-extraction process for metal recovery fits between a feed solution carrying the metal or metals of interest and one or more metal-effluent streams from which the metal product or products are produced. The technical and economic success of the total metal-recovery and production process is dependent on the success of each unit operation and on how well the chemistry of the leaching and metal-production processes fit with the chemistry of the solvent-extraction reagent. Metal-recovery processes for copper, uranium, and nickel are examined from the perspective of how well both the chemistry of the metal-leaching and metal-recovery processes fit with the chemistry of the existing reagents and what must be done to develop the total metal-recovery and production process.

INTRODUCTION

The chemical literature has many references for the use of solvent extraction (SX) as a separation technique in analytical chemistry, and a large amount of fundamental knowledge in solvent extraction, particularly in the areas of solution chemistry and organic extractants, comes from analytical chemistry [1]. Solvent extraction as a technique for the recovery and purification of a metal goes back to at least 1842 when Peligot extracted uranyl nitrate into ethyl ether [2].

The first reasonably large-size use of SX as a unit operation in hydrometallurgy was in the Manhattan project for the production of pure uranium using the technique described by Peligot [3]. In the 1950s, SX was applied on a large scale for the recovery of uranium from solutions generated by sulfuric acid leaching of uranium ores [4]. Today many metals are recovered by SX including copper, uranium, molybdenum, vanadium, palladium, cobalt, and germanium among others, but copper, with about 3.3 million tonnes production by SX in 2007, is by the far the metal recovered in the greatest tonnage.

In order to address the development of an SX process for metal recovery, it is important to understand that SX is only one unit process in a series of unit processes needed to win metal from ore and other sources. The SX process must therefore be compatible with, and complimentary to, the leaching process that precedes it and the

final metal-recovery process that follows (Figure 1). The success of the whole process is dependent on the success of each individual unit process and on how well the unit processes fit together.

Solvent extraction as part of an overall metal-recovery and production process has three main objectives:

1. Purification of a metal(s) from impurities either by extracting the desired metal(s) from the impurities or by extracting the impurities from the desired metal(s).
2. Concentration of metals in order to reduce downstream processing costs.
3. Conversion of the aqueous matrix to a form that simplifies and allows for more efficient downstream processing.

In any given solvent-extraction process one, two, or all three of these objectives may be accomplished.

To have a commercially successful metal-recovery process that includes SX, the metal-containing streams entering and exiting the SX plant and the economics of the process must be fully taken into consideration. Most commonly, the metal-containing solution feeding an SX plant, often called the pregnant leach solution (PLS), arises from a metal-leaching process for ore or concentrate, but scrap metal, recycled material, and waste streams are also possible sources of metal. The final metal product is most often a metal, but metal salts are also produced. The aqueous stream exiting the SX plant from which the final product is produced is often called the pregnant strip solution.

To fully take the metal feed solution entering the SX plant into consideration, the following should be known about the solution: the concentration and oxidation states of metals, the anions and their concentration, polar organic contaminants and their concentrations, the temperature, the suspended-solids content, any remaining leaching agents such as oxidants, and the pH. In order to take the pregnant strip solution fully into consideration, the metal-production process and the requirements of this process must be also known.

There are many technically and commercially successful metal-recovery and production processes that use SX. Three SX metal recovery processes will be addressed in this paper; copper recovery, uranium recovery using amines, and nickel recovery. The total metal-recovery process, from leaching to metal product, is addressed to show how the particular SX process fits into the overall metal-recovery process. For copper it will be seen that the SX process fits the overall metal-recovery process extremely well, while with uranium and nickel the fit is not as good, and one or more of the individual unit processes has to be adapted to the properties of the available SX reagent.

COPPER PRODUCTION BY LEACH/SOLVENT EXTRACTION/ELECTROWINNING (L/SX/EW)

Copper recovery by SX was commercialized when the Ranchers Bluebird plant started in March 1968 using the hydroxyoxime reagent LIX® 64 (LIX® is a registered trademark of Cognis) in the acid leach/solvent extraction/electrowinning (L/SX/EW) generic flowsheet shown in Figure 1 [5].

Copper oxide ores are leached with sulfuric acid, because it is readily available and the lowest-cost mineral acid. Leaching reactions for Malachite and Azurite follow:

$$CuCO_3 \cdot Cu(OH)_2 + 2H_2SO_4 \rightarrow 2CuSO_4 + CO_2 + 3H_2O \quad (1)$$

$$(CuCO_3)_2 \cdot Cu(OH)_2 + 3H_2SO_4 \rightarrow 3CuSO_4 + 2CO_2 + 4H_2O \quad (2)$$

Leach solutions resulting from leaching copper oxide ores have pH values in the range of 1.1 to 2.2 and contain <1 to ~20 g/L Cu, depending on the leaching characteristics of the ore, the copper grade of the ore, and the leaching technique used.

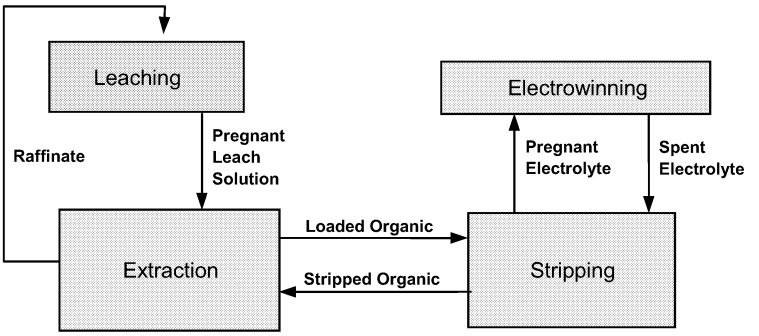

Figure 1. Generic flowsheet for the recovery of copper from oxide ores using acid leach/solvent extraction/electrowinning.

The net reaction for electrowinning copper from an aqueous solution follows:

$$Cu^{2+} + H_2O \rightarrow Cu + 2H^+ + \tfrac{1}{2}\, O_2 \quad (3)$$

High-quality copper is electrowon from aqueous solutions having ~35 g/L Cu and ~160 to 190 g/L H_2SO_4. This solution is used to strip copper from the loaded reagent.

A simplified extraction ⇌ stripping reaction for the hydroxyoxime copper SX reagents based on the general structure in Figure 2 is given directly below:

$$2RH_{(org)} + Cu^{2+} + SO_4^{2-} \underset{\text{Strip}}{\overset{\text{Extract}}{\rightleftharpoons}} R_2Cu_{(org)} + 2H^+ + SO_4^{2-} \quad (4)$$

Note how well the extraction and stripping reactions for copper solvent extraction fit the overall L/SX/EW process. Protons generated in electrowinning copper are carried in the spent electrolyte to the strip mixers, where these protons strip copper from the copper-loaded reagent. These protons are then carried to extraction by the unloaded SX reagent molecule, where copper is extracted by the unloaded SX reagent molecule with concomitant release of these protons to the aqueous raffinate. These protons are then carried to leaching by the recycled raffinate, where they leach more copper. At the same time, copper leached from the ore by these protons is carried by the solvent-extraction reagent from the leaching solution to the pregnant electrolyte from which copper is electrowon, and in the process, more protons are generated. With respect to copper and

proton transfer, hydroxyoxime-based copper SX reagents are a perfect fit with the oxide copper L/SX/EW process. Furthermore, because the extractive strength of these reagents can be tailored, a reagent can be selected such that the copper extraction-stripping equilibrium lies well toward extraction under typical extraction conditions and well toward stripping under typical stripping conditions.

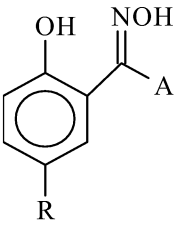

R	A
$C_{12}H_{25}$	C_6H_5
C_9H_{19}	C_6H_5
C_9H_{19}	CH_3
C_9H_{19}	H
$C_{12}H_{25}$	H

Figure 2. General structure for hydroxyoximes used in copper solvent-extraction reagents.

These reagents are also highly selective for copper over most ions present in a copper leach solution, extracting only molybdenum(VI) and small amounts of Fe^{3+} from typical copper oxide leach solutions. Iron does not deposit during copper EW, but it does reduce current efficiency. However, the Fe^{3+}/Fe^{2+} couple keeps the oxidation potential of the EW solution in a suitable range; thus, in a copper solvent-extraction plant, some iron transfer from the leach solution to the stripping solution is beneficial. Today's copper SX reagents fit this requirement nicely in that some reagents are more selective over iron than others. This allows plant operators to choose a more-or-less selective reagent depending on the needs of the particular plant or leach solution. Interestingly, on loading, copper "crowds" molybdenum from copper SX reagents, and molybdenum is not stripped by typical copper stripping solutions. Thus, if a small amount of molybdenum is extracted, that molybdenum simply remains at a minor steady-state concentration in the organic phase with little effect on the overall copper leach/SX/EW process.

Finally, copper solvent-extraction reagents have less than 1 ppm water solubility, and they are quite stable in typical copper SX plants. These properties help keep reagent consumption low, which is important to the commercial success of the process.

The technical and economic success of the copper oxide L/SX/EW process led to research in leaching secondary copper sulfide ores, and there are now many L/SX/EW plants operating on secondary copper sulfide ores. Fortunately, the copper and proton balance across L/SX/EW for secondary copper ores is the same as for copper oxide ores. The impurities in these leach solutions are also similar to the impurities in copper oxide leach solutions, and the pH of these leach solutions is in the same range as the pH of the copper oxide leach solutions.

The copper L/SX/EW process for producing high-quality copper from oxide and secondary sulfide ores is an example of a great fit between the needs of the process and the properties of commercially available SX reagents. No doubt this is one of the key reasons for the technical and economic success of this process and also one of the key reasons much effort has gone into improving not only copper SX reagents but also the leaching and electrowinning processes. For example, there are now several plants that leach copper concentrates instead of sending them to a smelter. Copper electrowinning is

now common at current densities > 300 amps/m^2 instead of the 180 amps/m^2 used in the Ranchers plant, thus significantly reducing the capital cost for EW per unit of copper plated. Unfortunately, such a great fit of the reagent properties to the overall metal-recovery process is rare.

URANIUM PRODUCTION BY LEACH/SOLVENT EXTRACTION/PRECIPITATION (L/SX/P)

As previously mentioned, metal recovery by solvent extraction was first applied on a large scale to recover uranium from solutions generated by sulfuric acid leaching of uranium ores [4]. Di-2-ethylhexylphosphoric acid (DEHPA) was the SX reagent used in these plants. Within a short period of time, Alamine® 336 (Alamine® is a registered trademark of Cognis), a tertiary amine made from an approximate 3/2 blend of C_8/C_{10} alcohol, became the preferred reagent for this use and remains so today.

The process starts with a sulfuric acid leach of uranium ore in the presence of an oxidant, typically oxygen, manganese dioxide, or sodium chlorate, often at temperatures of 40 to 80 °C and at an oxidation potential of 400–500 mv relative to a saturated calomel electrode. These conditions result in a relatively aggressive, nonselective leach for uranium(VI), with the following equilibria governing the uranium species in solution:

$$UO_2^{2+} + 2SO_4^{2-} \rightleftharpoons UO_2(SO_4)_2^{2+} \quad (5)$$

$$UO_2(SO_4)_2^{2-} + SO_4^{2-} \rightleftharpoons UO_2(SO_4)_3^{4} \quad (6)$$

Impurities may include soluble silica, Fe^{2+}, Fe^{3+}, chloride, nitrate, phosphate, thiocyanate, organic acids, and metals such as tungsten, molybdenum, vanadium, zirconium, thorium, arsenic, and antimony. Some of these metals are present as anions and some as both anions and cations. The pH typically varies from about 1 to 1.8. Each of the impurities can bring its own unique problems to uranium production.

The process finishes with the precipitation of a final product that is acceptable to the market or that can be calcined at the plant to U_3O_8. In most plants, the precipitate is ammonium diuranate [$(NH_4)_2U_2O_7$], often called yellow cake, or UO_3.

DEHPA as the Extractant

Under the conditions of the typical uranium leach liquor, DEHPA will extract uranium, iron(III), Al(III), vanadium(IV and V), zinc, Mo(VI), and possibly other metals. Iron loading on DEHPA can be controlled by reducing Fe(III) prior to solvent extraction with DEHPA, but this is expensive, since more oxidant is needed when the raffinate is recycled back to leach. While the extraction reaction for uranium is shown as reversible, stripping uranium from DEHPA with acid is not practical, and the preferred stripping method used either ammonium or sodium carbonate.

Problems using DEHPA for uranium extraction include the extraction of impurities, the water solubility of the sodium and ammonium salts of DEHPA, and the need to use a third-phase modifier such as TBP because of the limited solubility of the uranium, sodium, and ammonium salts in the organic diluent. In addition, stripping

uranium from DEHPA with base can result in co-extracted iron and aluminum, forming insoluble hydroxides. This will cause severe operating problems because of stable emulsions and crud generation. Simply said, DEHPA was used for uranium extraction from sulfuric acid leach solutions, because there was no other acceptable extractant commercially available at the time. This fact drove development of Alamine 336, the first commercial tertiary amine extractant for uranium from sulfuric acid leach solutions.

Alamine 336 as the Extractant

The recovery of uranium from sulfuric acid leach solutions using a tertiary amine such as Alamine 336 proceeds according to the simplified protonation and extraction equations given below:

$$2R_3N_{(org)} + H_2SO_4 \rightleftharpoons [(R_3NH^+)_2SO_4^{2-}]_{(org)} \quad (7a)$$

$$R_3N_{(org)} + H_2SO_4 \rightleftharpoons [R_3NH^+HSO_4^-]_{(org)} \quad (7b)$$

$$4[(R_3NH^+)HSO_4^-]_{(org)} + UO_2(SO_4)_2^{2-} \rightleftharpoons [(R_3NH^+)_4UO_2(SO_4)_3^{4-}]_{(org)} + 2H_2SO_4 + SO_4^{2-} \quad (8)$$

$$2[(R_3NH^+)_2SO_4^{2-}]_{(org)} + UO_2(SO_4)_3^{4-} \rightleftharpoons [(R_3NH^+)_4UO_2(SO_4)_3^{4-}]_{(org)} + 2SO_4^{2-} \quad (9)$$

Since amine protonation with sulfuric acid is complete at pH < 2.2, the aqueous solution to be treated by the amine should have a sufficient acid concentration to protonate all the amine without the pH rising above ~2.2. If the pH of the solution to be treated rises above 2.2 during extraction, acid can be added to the aqueous solution to be treated, or a pre-protonation stage can be inserted ahead of extraction to ensure that there is sufficient acid to fully protonate the amine.

Tertiary amine acid and metal complexes have limited solubility in typical SX diluents and will form a third phase that usually settles between the diluent phase and the aqueous phase in the settler. To avoid third-phase formation, a modifier such as tridecanol is added to the amine organic phase.

Uranium is stripped from a protonated amine in two ways, either with a base that deprotonates the amine, or by anion exchange with an anion that competes favorably with uranium for the protonated amine:

$$[(R_3NH)_4UO_2(SO_4)_3]_{(org)} + 4NH_3 \rightarrow 4R_3N_{(org)} + UO_2(SO_4)_2^{2-} + 4NH_4^+ + SO_4^{2-} \quad (10)$$

$$[(R_3NH)_4UO_2(SO_4)_3]_{(org)} + xA^- \rightleftharpoons 4(R_3NH^+A^-)_{(org)} + UO_2(SO_4)_2^{2-} + SO_4^{2-} + (x\text{-}4)A^- \quad (11)$$

The most common stripping method is deprotonation of the amine with ammonia gas, which is injected into the mixers of three to five countercurrent strip stages over a pH range of 3.5 to 5. The first strip stage has the lowest pH, and the pH is gradually raised in each successive stage. This ensures that pregnant strip solution, which has the highest uranium content (~25 to 100 g/L U), is in contact with an aqueous solution of a relatively low pH to limit precipitation of yellow cake during stripping, and that uranium

strip solution having the lowest uranium content is in contact with an aqueous solution having the highest pH, thereby ensuring good stripping. If a plant operator wants to produce a strip solution containing a uranium concentration on the high side while avoiding yellow cake precipitation in the strip mixer settlers, the pH needs to be controlled from the first to the last strip stage over the range 3.5 to 4.5. Since a local high pH must be avoided in all strip mixers, gaseous ammonia used in stripping is diluted with air.

Under the conditions of a typical uranium sulfuric acid leach solution, the only other metal normally co-extracted to any great extent by tertiary amine is molybdenum. Even though most other common metals are either not extracted, or only extracted to a small extent, many uranium amine circuits will scrub the loaded organic in one to three stages using a 10 to 20 g/L sulfuric acid solution. The scrub stages help ensure low carryover of either extracted or entrained impurity metals to the uranium pregnant strip solution, and as a result, a high-purity uranium product can be produced.

If molybdenum is co-extracted with uranium, the uranium can be selectively stripped with an acidified chloride solution having 80 to 100 g/L chloride. Molybdenum is then stripped with ammonia/ammonium chloride or sodium carbonate at pH ~9.5. Frequently in amine SX plants where molybdenum is co-extracted, a blue-to-green sludge or crud forms in the extraction settlers. If it forms in large quantities, it can be very troublesome, as it will tie up significant quantities of amine and may even shut a plant down until it is cleaned out. The chemistry of molybdenum cruds can be complex [6].

A third stripping method uses ~400 g/L sulfuric acid. The pregnant stripping solution can be built to over 150 g/L uranium, with the final strip solution having a g/L acid to g/L uranium ratio of about 1.5. Some of the acid is recovered and the remainder neutralized prior to precipitation of high-purity uranium oxide with hydrogen peroxide.

Since the protonated amine is the active extractant, completely deprotonating the amine will completely strip any metal (e.g., Mo) or any nonmetal anion (e.g., organic acids) from the amine. This offers an easy and effective way to keep the amine organic phase in good shape. For this reason most amine SX circuits have an amine regeneration stage where either all, or a portion of, the stripped organic is contacted with an aqueous solution at pH about 10.5 to 11.

The fit between the properties of the tertiary amine extractant Alamine 336 and the requirements of a uranium SX circuit, while not ideal, is still quite good. Tertiary amines strongly extract uranium under the conditions presented by typical sulfuric acid uranium leach solutions, and even though the protonated amine is not as selective for uranium as might be desired, most impurities that are extracted can be removed from the loaded solvent using wash stages. If molybdenum is co-extracted, uranium can be selectively stripped using an acid chloride solution. Stripping uranium with aqueous ammonia is efficient and produces a strip solution from which high-purity ammonium diuranate product can be precipitated simply by adding excess ammonia. Other stripping agents, such as acidified chloride or concentrated sulfuric acid, offer flexibility should it be needed. If sulfuric acid is used to strip uranium, the amine will transfer acid from stripping to extraction, thereby reducing the amount of acid that needs to be neutralized prior to precipitating uranium with hydrogen peroxide.

Alamine 336, which will load about 1.2 g/L U under ideal conditions, has been used at concentrations up to ~10 vol %. This is a sufficient concentration to handle most uranium leach solutions. While the acid and metal-loaded amine complexes have limited solubility in typical SX diluents and will form a third phase, the addition of a commercially available, low-cost modifier such as isodecanol avoids this problem.

Tertiary amines are quite stable under typical uranium leach solution conditions, but a high oxidation potential will cause amine degradation. There are certain conditions under which amine degradation can be very fast, for example, in the presence of nitrate with some chloride and a high oxidation potential. Fortunately, this condition is rare, and where it may occur, precautions can be taken [7].

Amine SX circuits tend to be more sensitive to the phase continuity in the mixer than copper SX plants running hydroxyoxime SX reagents. The reasons for this are thought to be that the active amine extractant is charged, many uranium leach solutions contain relatively high levels of solids or soluble silica, and solids may precipitate during extraction. Specifically, most, but not all, amine circuits need to run organic-continuous in the mixers in order to achieve good phase separation and low entrainment.

Finally, extraction and stripping kinetics of amines are very rapid; therefore, small mixers and relatively gentle mixing can be used. Alternatively, equipment such as columns or in line mixers, where drop size can be controlled, may be used. This could reduce the capital to build the SX plant and theoretically reduce entrainment, thereby making the process more economical.

Nickel Production by Leach/Solvent Extraction/Nickel Reduction (L/SX/NR)

Nickel production by SX/NR was commercialized in 1971 when SEC Corporation used SX to recover nickel from a copper refinery bleed stream followed by electrowinning nickel from the pregnant nickel strip solution [8]. Refinery bleed stream was diluted with water and then subjected to copper solvent extraction using pH control with ammonia. The copper-free raffinate was taken to pH ~8 to 8.5 with gaseous ammonia, and after settling and filtration of iron and aluminum hydroxides, the nickel was extracted using LIX 64N. The loaded organic first passed to a wash stage controlled at pH ~5.5 with sulfuric acid to remove ammonia and then to nickel stripping with spent electrolyte solution containing ≥80 g/L Ni and 5 g/L free sulfuric acid. A pregnant strip solution containing ~1 g/L free acid and about 83 g/L Ni was produced. The pregnant Ni strip solution advanced to electrowinning to produce Ni metal. While this small plant was technically and economically successful, today some 37 years later, Ni solvent extraction is still not widespread. There are several reasons for this, one of the most important being the lack of a solvent-extraction reagent for nickel that fits well with the various hydrometallurgical routes to recover nickel from ores and to produce high-quality nickel product.

Nickel is found in nature as either an oxide (laterite ores and sea nodules) or a sulfide. Cobalt is usually found with nickel, often at ~10% of the nickel concentration, so any nickel solvent-extraction circuit always includes some consideration of cobalt solvent extraction. There are a number of ways to put nickel, along with cobalt and other metals, into solution from either oxide or sulfide ores. Examples include high-pressure

sulfuric acid leach (HPAL) of laterite ores, autoclave leaching of nickel sulfide concentrate or high-grade nickel sulfide ore, ammonia leaching of nickel sulfide concentrate, reductive roasting of nickel laterite ore followed by ammonia leaching, heap leaching of NiS ore, and heap leaching of nickel laterite ores with acid. The leach solutions resulting from these leaching techniques often go through various process steps to remove iron, aluminum, and other metals if possible, depending on the ore and the metals dissolved in the leaching process. Interestingly, the use of any of the leaching techniques above followed by Fe and Al removal on the leach solutions results in only two aqueous solutions from which nickel needs to be recovered and concentrated, a dilute sulfuric acid solution at pH about 2.5 or an ammonia solution.

The final nickel products of greatest acceptance produced by hydrometallurgy are high-purity nickel metal and high-purity nickel oxide (NiO). Nickel metal is produced from an aqueous solution by either hydrogen reduction or electrowinning. In either case, the aqueous solution from which nickel is reduced must be of very high purity, contain a relatively high concentration of Ni (>70 g/L), and have virtually no free acid (pH > 3.5). Protons generated by hydrogen reduction of nickel must be neutralized as they are produced or nickel reduction will cease. This is normally done with ammonia; thus, a nickel plant producing nickel metal by hydrogen reduction also produces an equimolar tonnage of ammonium sulfate. Protons generated in Ni electrowinning at the anode must be kept out of the cathode solution. This is done using a diaphragm in the electrowinning cell. NiO is obtained by pyro-hydrolysis of a high-purity, high-concentration nickel chloride solution or by roasting $NiCO_3$ in a kiln. NiO can be reduced to produce Ni metal.

A nickel solvent-extraction circuit should produce one of three high-purity solutions, an aqueous sulfate solution containing at least 70 g/L Ni at pH ≥3.5, an aqueous ammonia solution containing a high nickel concentration (~80 g/L) from which nickel carbonate can be precipitated by distilling the ammonia, or an aqueous acid chloride solution containing a high nickel concentration (~80 to 110 g/L Ni).

Therefore, an ideal nickel solvent-extraction reagent would:

1. Strongly and selectively extract nickel in the presence of copper, zinc, cobalt, manganese, and calcium from either a sulfate solution at pH ~ 2.5 or from an ammonia solution.
2. Be stripped to produce one of the three high-purity nickel solutions mentioned above from which nickel metal or nickel oxide are produced.

The fact that one wants an ideal reagent to do certain things does not mean that it is possible for a reagent to do those things. For example, extracting Ni from a solution at pH ~2.5 and stripping nickel from this reagent with sulfuric acid to obtain a Ni solution having a nickel concentration of ≥70 g/L at pH ~3.5 does not seem possible. However, extracting Ni from a dilute ammonia solution and then stripping Ni with sulfuric acid to obtain a concentrated Ni solution at pH 3.5 is not only possible, it has been run commercially in the SEC plant and in the Cawse nickel project in Australia [9].

Consider the commercially available reagents that extract nickel. Organo phosphoric, phosphonic, and phosphinic acids extract many metals more strongly than Ni including Fe^{3+}, Zn, Cu, Co, Mn, Ca, Mg, and Cd, and nickel is not fully extracted until the pH reaches the 5 to 6 range [10]. The organothiophosphinic acid Cyanex 301 extracts

Cu, Zn, and Fe^{3+} more strongly than Ni. Co is extracted under about the same conditions as Ni, but significantly, Ni and Co^{2+} are extracted more strongly than Mn, Mg, and Ca [10]. Versatic acids extract Fe^{3+}, Cu, and Zn more strongly than Ni, while Cd, Co^{2+} and Mn^{2+} are extracted over a similar pH range as Ni, but Versatic acids are selective for Ni over Ca and Mg [11]. Oxime copper extractants extract Cu and Fe^{3+} more strongly than Ni, while they extract Co^{2+} at about the same pH as Ni. They do extract Zn and Mn at a higher pH than Ni [12]. Combinations of some of the above reagents with certain other reagents are synergistic with respect to the extraction of Ni and Co, thus allowing selective extraction of these metals over Mn, Mg, and Ca, but usually not over Fe^{3+}, Cu, and Zn [13]. Depending on the combination of reagents and synergist, pH may or may not need to be controlled during extraction. These synergistic reagents have not been applied on a commercial basis and will not be further discussed.

It is obvious that none of the reagents mentioned above have all the properties of an ideal nickel extractant. In fact, most of them have very few of the properties of an ideal nickel extractant.

Organo Phosphorous-based Reagents

With the organophosphorous-based acid extractants, Fe^{3+}, Cu, Zn, Co^{2+}, Ca, and Mg need to be removed prior to Ni extraction, and nickel extraction must be pH-controlled at 5 to 6 to achieve high nickel recovery. The only advantages of these extractants are that they can produce a strip solution from which Ni^{2+} can be reduced to Ni metal or from which pyro-hydrolysis could produce NiO, and they are commercially available. These types of extractants have been used to remove metals such as Zn, Co^{2+}, Cu, Mn, and Fe^{3+} ahead of Ni solvent extraction, but they have not been used as the primary Ni extractant [14].

Cyanex 301 extracts Ni and Co at relatively low pH (pH_{50} about 0.9), so this reagent can be used without pH adjustment to obtain high Co and Ni recovery from sulfate leach solutions at pH 2.5. However, Ni is not extracted selectively over Co^{2+}, and stripping is only accomplished with a relatively high acid concentration; thus, this reagent will not produce a strip solution from which high purity Ni can be electrowon or hydrogen-reduced. In addition, this reagent extracts iron and Zn more strongly than Ni or Co^{2+}, and it irreversibly extracts copper at very low pH. In spite of these shortcomings, Cyanex 301 has been incorporated into the Goro flowsheet for co-extraction of Ni and Co followed by four stages of stripping with ~6 M HCl at about 60 °C to produce a solution containing 80-110 g/L Ni, 6–10 g/L Co, ~1 g/L Zn and very low levels of Mn, Mg, and Ca [15]. This stripping solution will advance to Co extraction with tri-isooctyl amine prior to Ni recovery by pyro-hydrolysis to produce NiO as product and HCl for recycle to stripping.

Versatic Acids

Versatic acid has been used commercially for Ni extraction coupled with Ni EW, but it is certainly not an ideal nickel extractant [14]. Cu, Zn, Fe^{3+}, Co^{2+}, and Mn need to be removed from the aqueous solution prior to Ni extraction, and Ni extraction must be

pH-controlled at 6.5 to 7 in order to achieve high nickel recovery. Because Versatic 10 acid reagent is somewhat water soluble at the extraction pH, the raffinate is pH-adjusted to about 2 and then the Versatic acid is recovered for the raffinate using diluent in one stage of extraction. On the positive side, Versatic acid extractants are commercially available, and they can produce a strip solution from which metallic nickel can be produced or from which pyro-hydrolysis could produce NiO. Versatic 10 has been used as a primary nickel extractant, where, as expected, most metals were removed from the leach solution ahead of nickel extraction [14].

Ketoxime Reagents

Ketoxime-based copper solvent-extraction reagents have been used to extract Ni from ammonia leach solutions at several Ni plants [8,9]. LIX 84-INS, a relatively strong extractant for Ni from ammonia leach solutions having little free ammonia, and from which a sulfate strip solution containing ≤150 g/L Ni at pH 3.0 to 3.5 can be produced, is the reagent of choice for this application. LIX 84-INS can be modified with tridecanol or other modifiers to allow stripping of the Ni with an ammonia solution containing about 210 g/L ammonia and 180-200 g/L carbon dioxide to produce a strip solution containing about 80 g/L Ni. Thus, the use of this reagent for Ni extraction from an ammonia leach solution offers the plant a choice to produce either Ni as metal or as NiO.

Unfortunately, the above-described solvent-extraction process is not trouble free for several reasons. Co^{2+} present with Ni in the leach solution will be extracted and stripped with Ni. However, some of the extracted Co^{2+} oxidizes to Co^{3+} which does not strip with Ni, and over time cobalt will poison the reagent, thus lowering the Ni transfer capacity of the organic phase [9]. For this reason, all the Co^{2+} in an ammonia leach solution needs to be oxidized to Co^{3+} prior to Ni extraction. Cobalt(III) can be removed from the organic phase by reduction with a more active metal (Zn or Fe powder) in the presence of dilute acid, but this process is messy and results in some reagent degradation.

Cu^{2+} in an ammonia leach solution is very strongly extracted by ketoxime-based reagents, and the Ni stripping method dictates how the copper must be dealt with. In a circuit with a concentrated ammonia strip for nickel, copper will build up in the solvent to a steady-state concentration, and any copper that loads above this level will then report to the Ni pregnant strip solution. If the copper level in the Ni pregnant strip solution is too high, it must be removed from this solution prior to producing the final Ni product. In a circuit with an acid strip, where a solution from which Ni metal can be electrown or hydrogen-reduced is produced, no measurable copper is found in the nickel pregnant strip solution. The copper concentration in the organic phase is controlled by taking an appropriate bleed of the Ni-stripped solvent to a copper strip stage where some Ni also strips. The copper can be electrowon to produce a nickel-free, high-quality copper cathode, while the Ni is returned to the overall metal-recovery circuit somewhere ahead of solvent extraction by bleeding the copper strip solution.

Fresh LIX 84-INS is highly selective for Ni over Zn. However, degradation products, which reduce Ni selectivity over Zn, build over time in the organic phase, and zinc that loads during Ni extraction from an ammonia solution must be dealt with. In Ni SX circuits, where Ni has been extracted from an ammonia solution and where a sulfuric

acid strip is used to strip Ni, a pH-controlled wash stage is always present to remove ammonia from the organic phase and thus limit ammonia transfer to the pregnant strip solution. About 50 to 60% of the loaded zinc will be removed in this wash stage. If too much loaded zinc passes through the wash stage, it will report to the nickel pregnant strip solution from which it will need to be removed. Typically, this is done by ion exchange or solvent extraction with one of the organophosphorous based reagents.

On the positive side, LIX 84-INS transfers protons in the nickel ammonia system from stripping to leaching in an analogous way to proton transfer in the copper oxide leaching system. Consider the ammonia leaching of $Ni(OH)_2$, which is one intermediate product resulting from acid leaching of Ni laterite ores, and the leaching of Ni metal according to the equations below:

$$Ni(OH)_2 + 2NH_4^+ + 4NH_3 \rightarrow Ni(NH_3)_6^{2+} + 2H_2O \quad (12)$$

$$Ni + 2NH_4^+ + 4NH_3 + \tfrac{1}{2}\, O_2 \rightarrow Ni(NH_3)_6^{2+} + H_2O \quad (13)$$

Now consider the chemical equations for extracting Ni from an ammonia solution and for stripping Ni with either sulfuric acid or a concentrated solution of ammonia and carbon dioxide:

$$Ni(NH_3)_6^{2+} + 2RH_{(org)} \rightleftharpoons R_2Ni_{(org)} + 2NH_4^+ + 4NH_3 \quad (14)$$

$$R_2Ni_{(org)} + H_2SO_4 \rightleftharpoons NiSO_4 + 2RH_{(org)} \quad (15)$$

$$R_2Ni_{(org)} + 4NH_3 + 2[NH_4HCO_3] \rightleftharpoons Ni(NH_3)_6^{2+} + 2HCO_3^- + 2RH_{(org)} \quad (16)$$

Note that protons generated by electrowinning Ni, or by the formation of ammonium carbonate in a concentrated solution of ammonia and carbon dioxide, are transferred from stripping to leaching by the reagent during the extraction and stripping operations.

While ketoxime-based reagents will extract Ni from acid solution at pH ~4 they are not used for this purpose because of slow extraction kinetics.

CONCLUSIONS

No matter the metal to be recovered, building a flowsheet incorporating solvent extraction always involves understanding the metallurgy of the desired metal or metals and the accompanying impurities, along with understanding the properties of the available solvent-extraction reagents.

The fit between the properties of the available extractants and various metal recovery processes can range from the near-ideal fit of the copper hydroxyoxime-based reagents to the reasonable fit of tertiary amines for uranium recovery to the very poor fit with reagents for nickel recovery. In the case of copper, a great deal of research and development has gone into finding ways to put copper into solution so as to take advantage of copper SX with the available copper SX reagents and the very high-purity cathode copper that is produce in EW. The same certainly cannot be said for nickel. In many cases, a company selects the Ni product to be produced and then builds a flowsheet around producing that product from the ore that is available. Or a company builds a

flowsheet around an ore resource using processes they have experience with. Because of the variety of nickel ores, the various leaching methods, the impurities that report to the leach solution, the final desired product, and the lack of a nickel extractant that fits well with a wide range of nickel recovery technologies, there are almost as many hydrometallurgical nickel-recovery flowsheets as there are hydrometallurgical nickel plants.

As an additional note, the solvent-extraction community needs to understand that it is likely more effort in the future will go into finding ways to fit commercially available extractants into metal-recovery flowsheets than to developing new extractants that fit the metallurgy as well as oxime copper extractants fit the L/SX/EW flowsheet for copper. The reasons for this are economic: the high cost to develop new reagents and the manufacturing process for a new reagent, the high cost to register new chemicals, and the lack of metals that have the potential to be recovered by hydrometallurgy in the quantities that copper and uranium are recovered. Perhaps zinc would be a good target, but are there any others?

REFERENCES

1. G. Morrison and H. Freiser, Solvent Extraction in Analytical Chemistry, John Wiley and Sons, Inc., New York, 1957.
2. E. Peligot, *Ann, Chim. Phys*., (3), **5**(1) (1842).
3. D. W. Bridge and J. B. Rosenbaum, "Metallurgical Application of Solvent Extraction; Fundamentals of the Process," U.S. Dept. of the Interior, Bureau of Mines information circular 8139, 1962.
4. A. M. Ross, "Solvent Extraction, Newcomer to the Colorado Plateau," AIME Annual Meeting, New Orleans, February, 1957.
5. K. L. Power, "Operation of the First Commercial Copper Liquid Ion Exchange and Electrowinning Plant," AIME Annual Meeting, New York, February, 1970.
6. B. A. Moyer and W. J. McDowell, "Characterization of Molybdenum Interfacial Crud in a Uranium Mill that Employs Tertiary Amine Solvent Extraction," in Hydrometallurgy: Research, Development, and Plant Practice, K. Osseo-Asare and J. D. Miller, Eds., The Metallurgical Soc. of AIME, New York, 1983; pp. 503-516.
7. A. Feather, B. Munyungano, and M. Virnig, "Degradation Problems with the Solvent Extraction Organic at Rossing Uranium," Proceedings of the International Solvent Extraction Conference (ISEC 2008), Tucson, Arizona, September, 2008.
8. R. D. Eliasen and E. Edmunds, Jr., "The S.E.C. Nickel Process," *CIM Bulletin*, February, 82–86 (1974).
9. M. Mackenzie, M. Virnig, and A. Feather, "The Recovery of Nickel from HPAL Laterite Solutions using LIX 84-INS and Some Possible Impurity Control Strategies," ALTA 2005 Nickel/Cobalt Conference, Perth, May 2005.
10. P. M. Cole and K. C. Sole, "Zinc Solvent Extraction in the Process Industries," *Mineral Processing and Extractive Metallurgy Review*, **24**(2), 91–137 (2003).
11. G. M. Ritcey, "Solvent Extraction, Principles and Applications to Process Metallurgy," Revised 2nd ed., Volume 1, 2006; pp. 99–103.
12. MCT Redbook, "Solvent Extraction Reagents and Applications," Cognis Corporation, 2007; pp. 7–8.
13. C. Y. Cheng, K. Barnard, and M. Urbani, "Application of Synergistic Solvent Extraction for Metal Recovery," ALTA 2005 Nickel/Cobalt Conference, Perth, May 2005.

14. S. Donegan, “Direct Solvent Extraction of Nickel at Bulong Operations,” *Minerals Engineering*, **19**(12), 1234–1245 (2006).
15. I. Mihaylov, E. Krause, D. F. Kolton, Y. Okita, J.-P. Duterque, and J. J. P. Perraud, “The Development of a Novel Hydrometallurgical Process for Nickel and Cobalt Recovery from Goro Laterite Ore,” *CIM Bulletin*, **93**(1041), 124–130 (2000).

COLUMN DESIGN—WHERE DO WE GO?

H.-J. Bart

Lehrstuhl f. Thermische Verfahrenstechnik, TU Kaiserslautern
Postfach 3049, 67653 Kaiserslautern, Germany
Corresponding author email address: bart@mv.uni-kl.de
Web page: www.uni-kl.de/LS-Bart/

ABSTRACT

This paper reviews the progress in column design in comparison to the state of the art using pseudohomogeneous dispersion or backmixing models. The use of standardized lab-scale cells for determination of droplet rise, breakage, and coalescence as well as mass transfer on single-droplet versus continuous mini-plant experiments will be discussed. Combined with droplet-population balancing, the small-scale experiments serve as basis to replace pilot-plant experiments by computer simulations. Finally it will be shown that coupling of CFD and population balances gives independence from geometrical constraints and is only limited by the computational costs. It is a way to a more straightforward and saver design of industrial-size columns and allows one to evaluate costs of process design in an early stage.

INTRODUCTION

Chemical, pharmaceutical, and related industry is driven by a "fast-time-to-market" pressure, which is a problem with long-term planning and extensive operation on pilot-plant scale. In the distillation field, this has been accomplished when apparatus and process layout in an early stage (feasibility studies, etc.) are dominated by "in-silico" design on the computer using only a thermodynamic database or little experimental input. A "go-stop" decision for a process development comprising distillation compared to an extraction is thus usually easier achieved.

Additionally, there is some reluctance of process people to apply extraction, since there is the disadvantage of the usage of a solvent, where phase losses always result in discussions about product purity. An advantage with solvent extraction is the possible usage of reactive carriers, which counterbalances the disadvantages of using solvents (entrainment, emulsion formation, etc.). Chemical reactions enhance selectivity dramatically and intensify process performance. Commercial liquid ion exchangers (one binding site) can be used to extract anions, cations, and even neutral compounds [1,2]. In order to enhance selectivity, chelating ion exchangers (two binding sites) are known, and chiral carriers (three-dimensional carriers, including three and more binding sites) allow affinity separations according to the “host-guest” principle (molecular recognition) [3].

The engineering apparatus design work is strongly dominated by tedious and costly pilot-plant experiments with extraction columns at about 150 mm in diameter. The pilot data are analysed on the basis of the HTU-NTU concept taking dispersion effects into account. The height of a dispersion unit, HDU, can be related to a dimensionless Bodenstein number [4], being derived from the dispersion model, first proposed by Langmuir [5]. An alternative is the usage of the backflow model, where again one backflow parameter accounts for axial dispersion, giving an equivalent description [6]. The flow is resolved only in axial direction and a pseudo-homogeneous dispersed phase is characterized by a mean Sauter droplet diameter. This is a hydraulic diameter, which will not reflect if the droplets are rigid, circulating, or oscillating. These hydrodynamic simplifications make it necessary to rely on correlations specific for any column geometry in mind. This also leads to problems in the further scale-up procedure to industrial-size columns (diameter > 0.5 m), since local flow conditions (local hold-up, velocities, droplet-size distribution, etc.) will change with increasing column diameter. Generally spoken, the models are too simple to depict the real hydrodynamic behavior. This is one of the reasons why with the installment of a process using extraction columns costly continuous pilot-plant experiments are a must.

DROPLET POPULATION MODELLING

The ongoing call by industry for a more straightforward, reliable, and money-saving design procedure can be met when using droplet-population balance models (DBPM), with their origin in crystallization [7]. The population balance so far has been used to model the complex hydrodynamic behavior of the dispersed phase of different types of agitated extraction columns [8-11]. The population-balance equation for a differential height, ∂z, of an extraction column was first formulated by Casamatta [12] based on a droplet-volume distribution:

$$\frac{\partial P(v)}{\partial t}+\frac{\partial [u_d P(v)]}{\partial z}=\frac{\partial}{\partial z}\left(D_d \frac{\partial P(v)}{\partial z}\right)+R(v)+\delta(z-z_d)u_{d,\text{sup.}}f(v) \tag{1}$$

D_d is the axial dispersion coefficient, $f(v)$ is the volumetric inlet distribution, and the source term R represents the net droplet volume production due to coalescence and breakage per unit time as first formulated by Valentas and Amundson [13] and given here in terms of a droplet volumetric distribution:

$$\begin{aligned} R(v)=&\underbrace{\frac{v}{2}\int_0^v \omega(v-v',v')\frac{P(v-v')}{v-v'}\frac{P(v')}{v'}dv'}_{\textit{formation by coalescence}} - \underbrace{v\int_0^{v_{\max}} \omega(v,v')\frac{P(v)}{v}\frac{P(v')}{v'}dv'}_{\textit{loss by coalescence}} \\ &+\underbrace{\int_v^{v_{\max}} \vartheta(v')v\beta_n(v\,|\,v')\Gamma(v')\frac{P(v')}{v'}dv'}_{\textit{formation by breakage}} - \underbrace{\Gamma(v)P(v)}_{\textit{loss by breakage}} \end{aligned} \tag{2}$$

In the above Equation 2, Γ and ω are the frequency functions for breakage and coalescence respectively, β is the daughter droplet distribution resulting from the breakage of a mother droplet having volume v`, and ϑ is the number of daughter droplets formed by breakage.

Similar solute balances are also written for the dispersed and continuous phases [14,15]:

$$\frac{\partial P(c)}{\partial t} = -\frac{\partial [u_d P(c)]}{\partial z} + \frac{\partial}{\partial z}\left[D_d \frac{\partial P(c)}{\partial z} \right] + R\{P(c)\} + \frac{S(v)}{v} k_c P(c_x - m\bar{c}_y) + \delta(z - z_d) u_{d,\mathrm{sup}} f(v) \delta(c_y - c_{in}) \qquad (3)$$

The new variable $P(c)$ is given by $P(c) = \bar{c}_y P(v)$, where $\bar{c}_y$ is the average solute concentration of all the droplets having volume in the range $(v, v+dv)$ at any level z in the column, k_c is the overall mass-transfer coefficient, c_x is the solute concentration in the continuous phase, S is the surface area of droplet of volume v, and m is the distribution ratio for the solute between the two phases. The source term R is similar to that in Equation 1, but it is modified to include mass-transfer and thus has a more complex form. The solute balance for the continuous phase reads:

$$\frac{\partial [(1-\phi) c_x]}{\partial t} = \frac{\partial [u_c (1-\phi) c_x]}{\partial z} + \frac{\partial}{\partial z}\left[D_c \frac{\partial [(1-\phi) c_x]}{\partial z} \right] - \int_{v_{\min}}^{v_{\max}} \frac{S(v)}{v} k_c P(c_x - m\bar{c}_y) dv \qquad (4)$$

where ϕ is the hold-up of the dispersed phase that is given by:

$$\phi = \int_{v_{\min}}^{v_{\max}} P(v) dv \qquad (5)$$

and D_c is the dispersion coefficient of the continuous phase. Note that $v_{\min}$ and $v_{\max}$ are the minimum and maximum droplet volumes. The above system of equations, with the appropriate initial and boundary conditions derived by special balances at both ends of the column, completely define the hydrodynamics and mass-transfer in a liquid-liquid extraction column. The equations are quite general and could be easily modified to special types of columns by only modifying the set of geometrically dependent functions such as droplet-rise velocity, mass-transfer, and the axial-dispersion coefficients.

In order to complete in an early design stage with other unit operations, fast and reliable column simulations are mandatory. In a network research activity of RWTH Aachen, TU München, and TU Kaiserslautern, this has been demonstrated, when using DPBM for simulating pilot-plant column behavior in silico. Columns of different types and sizes could be successfully simulated based on correlations for droplet rise and breakage, etc., determined in standardized laboratory cells (see Figure 1) [16]. Using DPBM, one now can easily simulate the hold-up, Sauter diameter, and the concentration profiles along the column height. The result is either in optimal operating conditions for a certain separation problem or in optimized apparatus internals for a specific separation task (see Figure 2). This approach brings fast judgement of pilot-plant behavior without

being subject to approval of any governmental agency, and additionally only a low amount of chemicals and feed material is necessary. This saves time and costs considerably and is recently validated with industrial examples [17].

A short review will be given here to identify the different design steps and parameters necessary during the design procedure. As with any separation problem, one basically needs information for phase equilibria and if necessary for mass transfer, reaction kinetics, and chemical equilibria. So far, these parameters are also needed in a conventional design.

The state of the art to characterize two-phase flow in extraction columns is the slip-velocity concept after Gayler et al. [18]. Correlations are available to correct the predictable terminal velocity of a single droplet in an empty tube taking into account the influence of average hold-up and column-internals geometry. For backmixing, droplet-size-dependent parameters were evaluated by Garthe for pulsed and stirred columns [19]. Fortunately, dispersion coefficients approach similar values for both phases and become independent on droplet-size at high specific throughputs and power input [10,20], which simplifies calculations.

The most sensitive parameter for column performance is the droplet size, which strongly depends on breakage and coalescence. DPBM allows the calculation of droplet and hold-up profiles with numerical methods either based on moments or droplet classes [10,21]. The breakage in agitated columns depends on the physicochemical system properties, the geometry of the internals, and the energy input. The breakage mechanism is either due to oscillatory breakage when colliding with turbulent eddies [22,23] or due to shear stress [24-26].

Following the approach of Gourdon et al. [10], the breakage frequency required in the DPBM can be calculated from the droplet-residence time in a compartment τ_m and the breakage probability p (d), derived from the model:

$$\Gamma(v) = p(d)\frac{u_y(d)}{H_c} = \frac{p(d)}{\tau_m} \tag{6}$$

The coalescence rate $\omega(v,v')$ in fluid systems is either from empirical or semi-empirical models [27], where in the latter it is a product of coalescence efficiency $\lambda(v,v')$ and coalescence rate $h(d, d')$:

$$\omega(v,v') = h(v,v') \cdot \lambda(v,v') \tag{7}$$

The collision of droplets is affected by local turbulences, circulating flows, and different droplet velocities and physicochemical parameters, like surface tension, density, charge of the surface, etc. and mass-transfer direction [10]. Analogous to the kinetic gas theory, the collision rate of two droplets can be set proportional to the mean-square fluctuation velocities [23]. The coalescence efficiency is high if the kinetic energy of the colliding droplets is higher than the surface energy (energy model) [28] or if the droplet contact is sufficiently long for film drainage between the drops (drainage model) [29,30]. The most recommendable model is from Coulaloglou and Tavlarides [23], where two coalescence

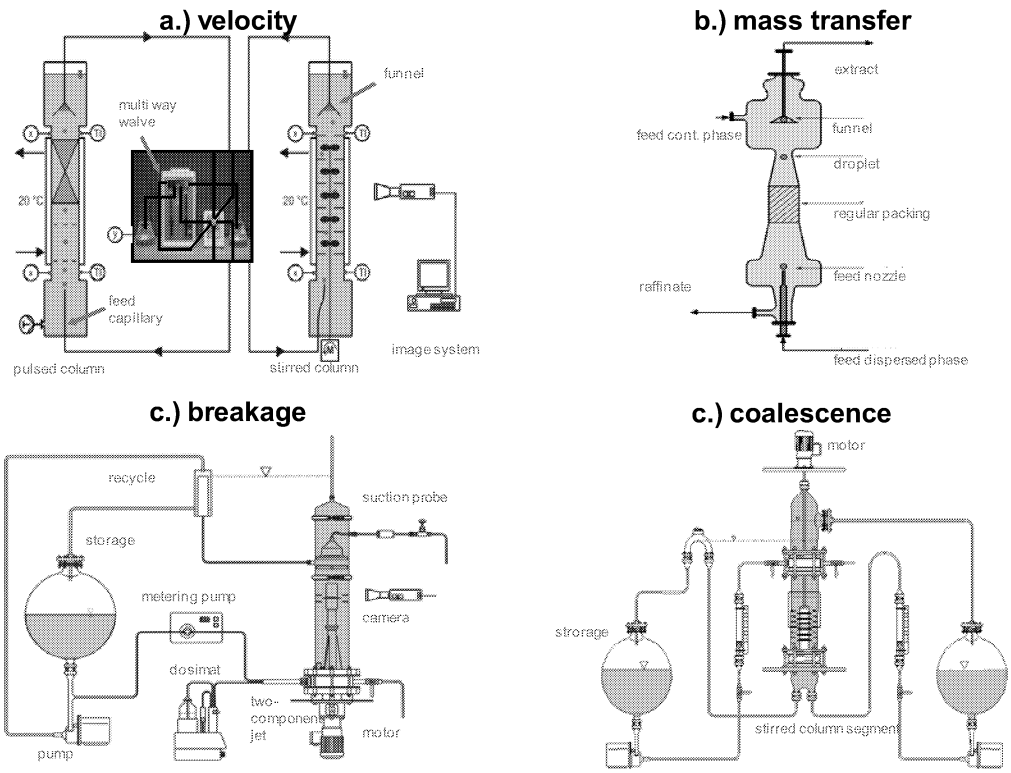

Figure 1. Lab-scale cells [16].

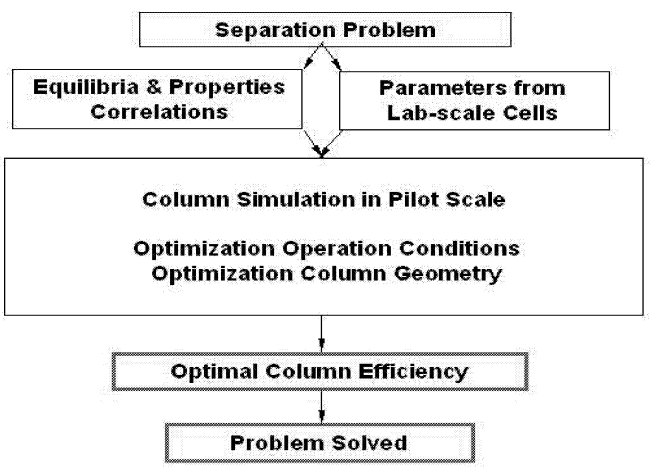

Figure 2. New design methodology [16].

parameters have to be estimated experimentally. They can be determined in a standardized lab-scale apparatus containing usually five column compartments to reduce inflow/outflow effects (see Figure 1c). Since backmixing and breakage are known from experiments or correlations, the deviation from simulated droplet-size distribution is due to coalescence effects, which allows parameter estimation through a mean least-square sum-of-errors optimization procedure [31].

If we sum up at this point, we do have all equilibria and mass-transfer information from literature data banks or experiments, droplet motion from correlations, and droplet breakage and coalescence from correlations or small lab-scale experiments. As shown in Figure 3, with a Windows-based computer program called liquid-liquid extraction column module (LLECMOD), a user-friendly input/output can be generated for different column types and working conditions [32]. A screenshot is given in Figure 3, and predicted column profiles compared with experimental data are given in Figure 4, as discussed in detail by Schmidt et al. [33]. The mean relative error between predicted and measured Sauter diameter and hold-up is at about 15%. A higher deviation of about 20% was with the concentration profiles, which are very sensitive to the concentration jumps at the inlet, which are difficult to measure (see Figure 4).

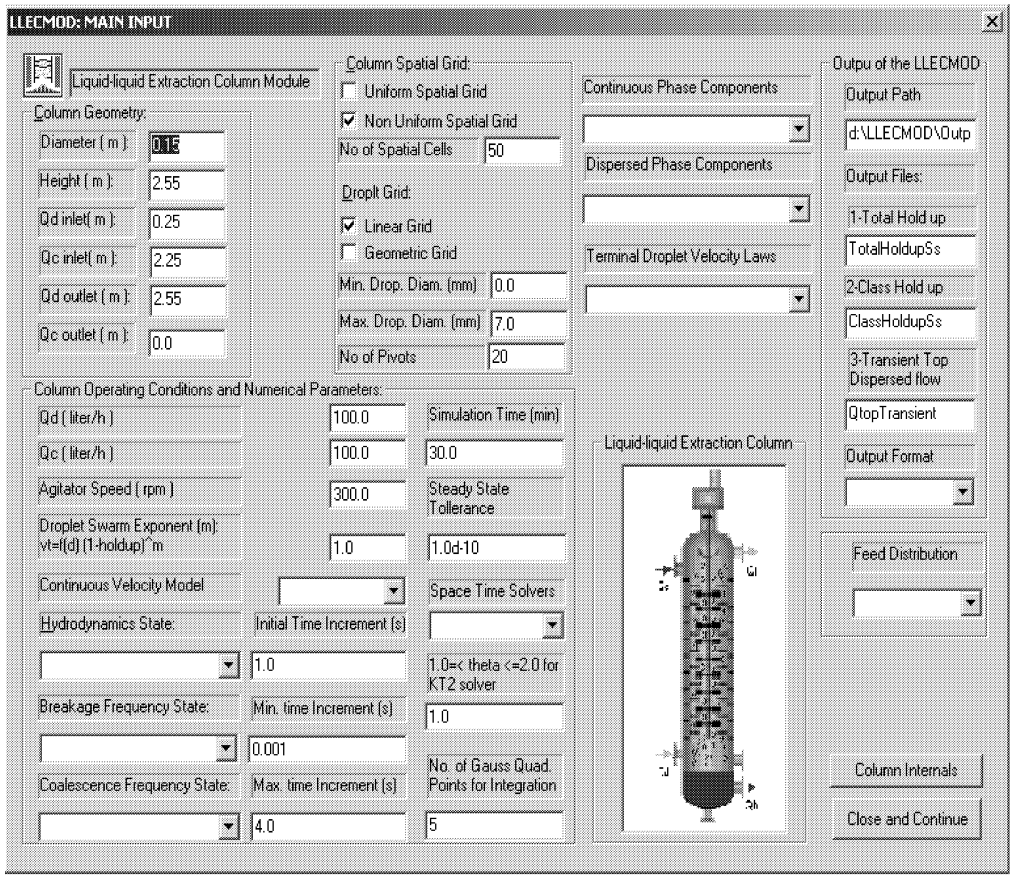

Figure 3. Screenshot of the Windows-based computer program LLECMOD.

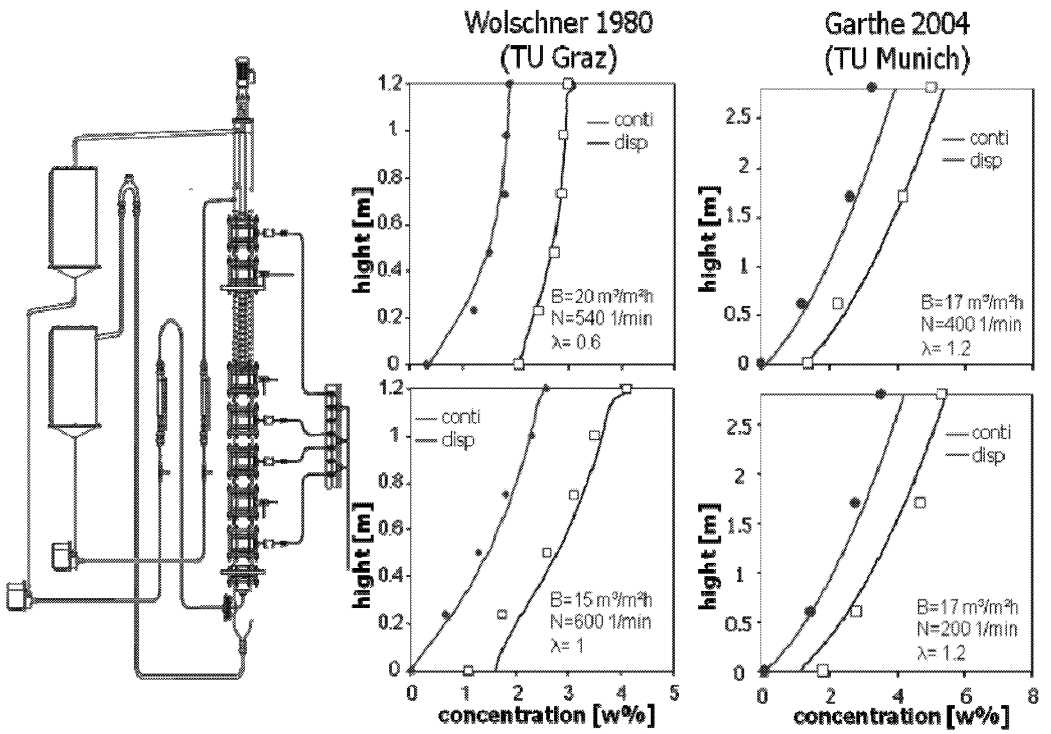

Figure 4. Concentration profiles (RDC DN80 [19], DN100 [34]).

THE ALTERNATIVE APPROACH

When processing a totally new design task, it is difficult to cover all effects in a solvent-extraction column induced by change in wetting performance, enrichment of impurities, crud formation, etc. As a rule, continuous pilot experiments are performed prior to industrial installation of a new process. The alternative is to use lab-size mini-plant extraction-column experiments for the detection of the coalescence parameters and long-term process stability. Additionally the mass-transfer-efficiency can be already validated by the DPBM approach at this scale, and small product samples can be obtained. The mini-plant replaces the coalescence cell (see Figure 1d), and the performance of a pilot-scale column can be computed "in silico" (see Figure 2). The computed results are then the basis of the industrial design.

Steinmetz [35] showed, that a scaling from mini-plant to pilot-plant scale is possible when using DPBM. However, the value held constant was droplet distribution and hold-up, which is not easy to achieve. As state-of-the-art, either the stirrer tip velocity or otherwise the specific power input is recommended to be held constant. The first approach scales rpm to the first power, the latter to the third power. He found that the same specific energy distribution, where the rpm are squared, is the adequate scaling condition. Errors in the predicted concentration profiles in the best case of less than 5% and worst case of less than 20% could be obtained [33] under the assumption of similar

specific throughputs and a variation in compartment geometry (as is compartment height) to achieve the same droplet residence times τ_m, and thus same droplet breakage probabilities. The coalescence rate is the same in the pilot- as in the mini-plant, since we have similar hold-up and droplet-size distributions. This methodology has been proved with several industrial examples [36] and is currently validated by industry.

WHERE DO WE GO?

Local specific energy dissipation can be resolved by CFD (Computational Fluid Dynamics) methods. Current research in the last years tried to improve the predictability of the PBM when coupling it with CFD [37]. The link can, on the one hand, eliminate the simplifications and shortcomings of the dispersion model by giving a local resolution of the two-phase flow and, on the other hand, save at least some of the small lab-scale experiments. The pseudo-homogeneous conditions can be removed and, therewith, also the simple dispersion model, since CFD can account for hydrodynamics and turbulence of the fluid. The models for coalescence and breakage of the droplets usually need the local turbulence, more precisely the turbulent energy dissipation, which can be applied by the turbulence model, also locally resolved. There is no longer the need to use averaged values [36], as with DPBM relying on the dispersion model formulation for any droplet class and the continuous phase. Additionally, this linkage of CFD and DPBM is totally independent from geometrical constraints and will allow a detailed 3-D simulation of industrial-sized columns, insofar as the computational load is bearable.

However, the coupling of these two methods encounters obstacles and limitations to be overcome. First, publications have adopted this approach with simplifications when only using a one-way coupling. This means that only the result of the flow simulation is used for the calculation of the drop-size distributions, while the influence of the drops on the flow field is neglected. A multi-block approach, where the investigated geometry is subdivided into subregions, is another alternative in that respect [38]. These simplifications in the coupling procedure can be reduced by implementing the population-balance equations in a CFD code [39]. As an example, the velocity profile in the middle of a RDC compartment is given in Figure 5. Iso-optical fluids were used to validate the CFD calculation of two-phase flow with PIV (particle image velocity) measurements. The realizable $k-\varepsilon$ model in the CFD calculations gave quite good accordance also at other measuring positions [40]. Figure 6 depicts the local hold-up for the same conditions as in Figure 5, and in Figure 7 is a qualitative comparison for 10% hold-up in the toluene/water system. For better visibility, the organic droplets are marked out, and a good accordance with CFD calculations can be seen.

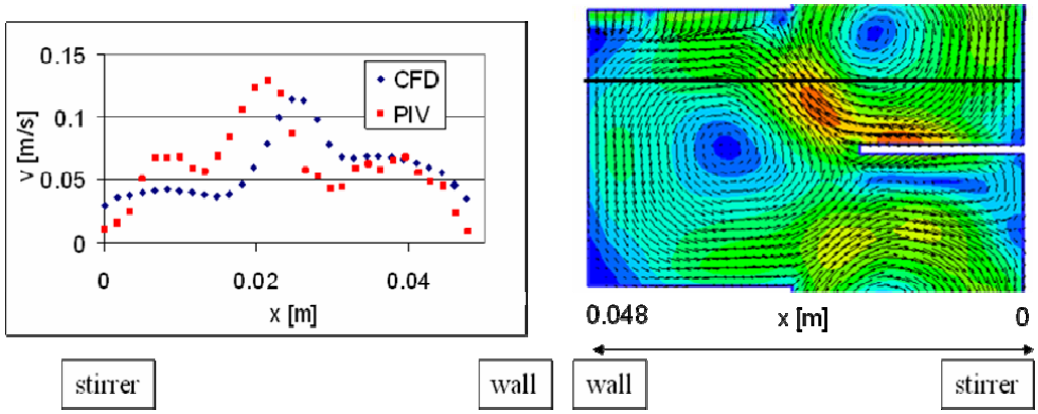

Figure 5. CFD vs. PIV at 85 L/h heptane, 180 L/h iso-optical fluid, and 150 rpm (measuring plane: solid line at half-distance rotor-stator).

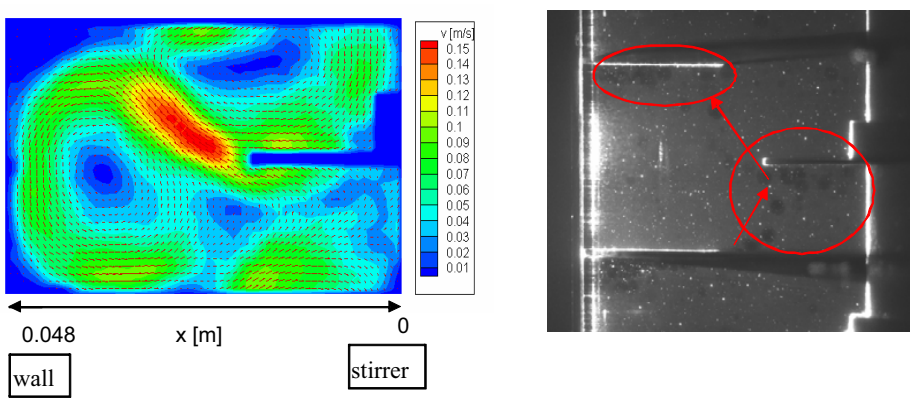

Figure 6. CFD vs. PIV, local hold-up (conditions as in Figure 5).

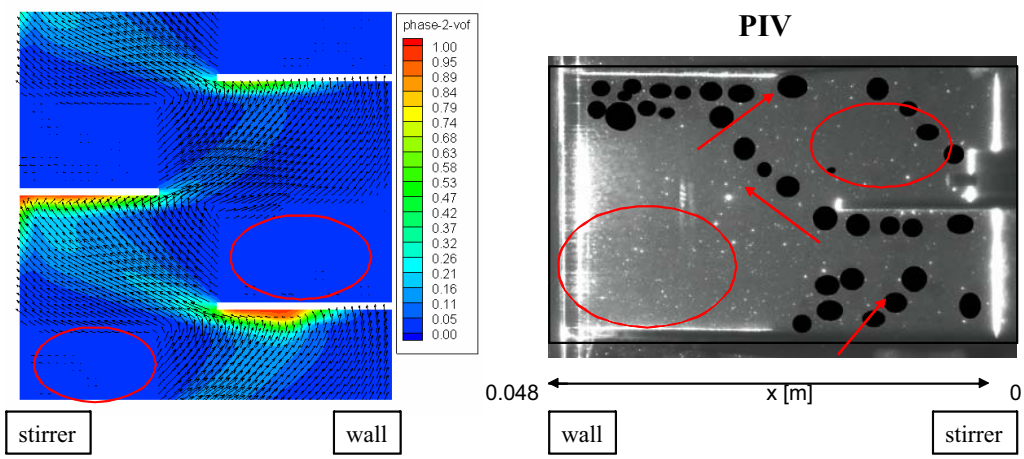

Figure 7. CFD vs. PIV, local hold-up (toluene 5 m/h, water 5m/h, 300 rpm).

In a final statement, we may draw the following conclusions:

- Standardized lab-scale cells allow monitoring of single-droplet behavior.
- Mini-plant extraction-column experiments resemble pilot-plant-scale effects.
- The gap between single-droplet/mini-plant scale to pilot scale can be closed with DPBM modelling.
- A decisive parameter is local energy distribution in the scale-up of columns.
- A combination of CFD and DPBM is a promising way to analyze and predict industrial-scale column behavior.
- CFD can resolve two-phase flow and local energy distribution in any geometry.
- Droplet breakage and rise can be predicted from CFD results.
- Predictive droplet coalescence models exist already but need further refinement.

ACKNOWLEDGMENTS

The author wishes to thank the DFG (Deutsche Forschungsgemeinschaft), Bonn, the AiF (Arbeitsgemeinschaft industrieller Forschungungsvereinigungen "Otto von Guericke" e.V.), and BMWA (Bundesministerium für Wirtschaft und Arbeit), both Berlin, KTI (Kommission für Technologie und Innovation), Bern, as well as Kühni AG, Allschwil/Basel, Novartis, Basel, Roche, Basel, DSM Nutritional Products, Sisseln, and Lonza, Visp, all Switzerland, for their financial support.

NOMENCLATURE

c	concentration
D	axial dispersion coefficient, $m^2\ s^{-1}$
d	diameter, m
$f(v)$	inlet distribution, m^{-1}
H_c	column height, m
h	collision rate, $m^3 s^{-1}$
k_c	mass-transfer coefficient, $m\ s^{-1}$
m	distribution ratio
P	probability function, m^{-1}
$p(d)$	breakage probability
R	source term, $m^{-1}\ s^{-1}$
S	area, m^2
t	time, s
u	velocity, $m\ s^{-1}$
v	droplet volume, m^3
z	height, m

Greek letters

β	daughter droplet distribution, m^{-1}
δ	Dirac delta function
ϑ	number of daughter droplets
Γ	breakage frequency, s^{-1}
λ	coalescence efficiency
ϕ	hold-up
τ	residence time, s
ω	coalescence frequency, $m^3\ s^{-1}$

Indices

c,x	continuous phase
d,y	dispersed phase
m	mean
max	maximum
min	minimum
n	number
sup.	superficial

REFERENCES

1. T. C. Lo, M. H. I. Baird, and C. Hanson, Handbook of Solvent Extraction, Wiley Interscience, New York, 1990.

2. H.-J. Bart, "Prozessintensivierung durch reaktive Carrier bei Reaktivextraktion und -sorption," *Chem. Ing. Techn.*, **77**, 1773-1783 (2005).
3. A. B. de Haan, "Affinity Solvents for Intensified Organics Extractions: Developments, Challenges and Prospects," *Tsinghua Sci. Technol.*, **11**, 709-717 (2006).
4. S. Stemerding and F. J. Zuiderweg, "Axial mixing and its influence on extraction efficiency," *Chem. Engineer*, **168**, 156-160 (1996).
5. I. Langmuir, "The velocity of reactions in gases moving through heated vessels and the effect of convection and diffusion," *Z. Phys. Chem.*, **61**, 422-436 (1908).
6. H. R. C. Pratt and G. W. Stevens, "Axial Dispersion," Science and Practice in Liquid-Liquid Extraction, Charedon Press, Oxford, 1992; pp. 416-491.
7. H. M. Hulburt and S. Katz, "Some Problems in Particle Technology," *Chem. Eng. Sci.*, **19**, 555-574 (1965).
8. S. D. Al Khani and C. Gourdon, "Dynamic and steady-state simulation of hydrodynamics and mass-transfer in liquid-liquid extraction columns," *Chem. Eng. Sci.*, **44**, 1295-1305 (1989).
9. T. Kronberger, A. Ortner, W. Zulehner, and H.-J. Bart, "Numerical simulation of extraction columns using a drop population model," *Comp. Chem. Eng.*, **19**, 639-644 (1995).
10. J. C. Gourdon, G. Casamatta and G. Muaret, "Population Balance Based Modelling of Solvent Extraction Columns," Liquid-Liquid Extraction Equipment, John Wiley & Sons, New York, 1994; pp. 137-226.
11. M. Henschke, "Auslegung pulsierter Siebboden-Extraktionskolonnen," Professorial Dissertation, RWTH Aachen, Aachen, 2003.
12. G. Casamatta, "Comportement de la population des gouttes dans une colonne d'extraction: transport, rupture, coalescence, transfer de matière," Institute National Polytechnique de Toulouse, Toulouse, 1981.
13. K. J. Valentas and N. R. Amundson, "Breakage and Coalescence in Dispersed Phase Systems," *Ind. Eng. Chem. Fundam.*, **5**, 533-542 (1966).
14. E. Ramkrishna, Population balances: Theory and applications to particulate systems in engineering, Academic Press, San Diego, 2000.
15. S. D. Al Khani, C. Gourdon, and G. Casamatta, "Simulation of hydrodynamics and mass-transfer of disks and rings pulsed column," *Ind. Eng. Chem. Res.*, **27**, 329-333 (1988).
16. H.-J. Bart, D. Garthe, T. Grömping, A. Pfennig, S. Schmidt, and J. Stichlmair, "Vom Einzeltropfen zur Extraktionskolonne," *Chem. Ing. Techn.*, **78**, 543-547 (2006).
17. G. Sieder, W. Bäcker, T. Grömping, and A. Pfennig, "Vom Einzeltropfen zur Extraktionskolonne: Ergebnisse aus der Anwendung in der industriellen Praxis," VDI/GVC Fachausschuss "Extraktion", Würzburg, 2006.
18. R. Gayler and N. W. Roberts, "H.R.C. Pratt, Liquid-liquid extraction. A further study of hold-up in packed columns," *TransEChemE*, **31**, 57-58 (1953).
19. D. Garthe, "Fluid Dynamics and Mass-transfer of Single Particles and Swarms of Particles in Extraction Columns", Verlag Dr. Hut, Munich, 2006.
20. G. Modes, "Grundsätzliche Studie zur Populationsdynamik einer Extraktionskolonne auf Basis von Einzeltropfenuntersuchungen," Shaker Verlag, Aachen, 2000.
21. M. M. Attarakih, H.-J. Bart, and N. Faqir, "Solution of Population Balance Equation using the Sectional Quatrature Method of Moments (SQMOM)," *Chem. Eng. Sci.*, submitted (2007).
22. C. Tsouris and L. L. Tavlarides, "Breakage and coalescence models for drops in turbulent dispersions," *AIChEJ*, **40**, 395-406 (1994).

23. C. A. Coulaloglou and L. L. Tavlarides, "Description of interaction processes in agitated liquid-liquid dispersions," *Chem. Eng. Sci.*, **32**, 1289-1297 (1977).
24. V. Cauwenberg, J. Degreve, and M. J. Slater, "The Interaction of Solute Transfer, Contaminants and Drop Break-up in Rotating Disc Contactors: Part II. The Coupling of the Mass-transfer and Breakage Processes via Interfacial Tension," *Can. J. Chem. Eng.*, **75**, 1056-1066 (1997).
25. V. Cauwenberg, J. Degreve, and M. J. Slater, "The Interaction of Solute Transfer, Contaminants and Drop Break-up in Rotating Disc Contactors. Part I. Correlation of Drop Breakage Probabilities," *Can. J. Chem. Eng.*, **75**, 1046-1066 (1997).
26. G. Narsimhan and J. P. Gupta, "Model for Transitional Breakage Probability of Droplets in Agitated Lean Liquid-Liquid Dispersions," *Chem. Eng. Sci.*, **34**, 257-265 (1978).
27. M. J. Prince and H. W. Blanch, "Bubble coalescence and break-up in air sparged bubble volumns," *AIChEJ*, **36**, 1485-1499 (1990).
28. H. Sovova and J. Prochazka, "Breakage and coalescence of drops in a batch stirred vessel-I Comparison of continuous and discrete models," *Chem. Eng. Sci.*, **36**, 163-171 (1981).
29. A. K. Chesters, "The modelling of coalescence processes in fluid-liquid dispersions. A review of current understanding," *TransEChemE*, **69A**, 259-281 (1991).
30. R. H. Davies, J. A. Schonberg, and J. M. Rallison, "The lubrification force between two viscous drops," *Phys. Fluids*, **1**, 77-81 (1989).
31. M. M. Attarakih, H.-J. Bart, and N. Faqir, "Numerical solution of the spatially distributed population balance equation describing the hydrodynamics of interacting liquid-liquid dispersions," *Chem. Eng. Sci.*, **59**, 2567-2592 (2004).
32. M. M. Attarakih, H.-J. Bart, L. Lagar, and N. Faqir, "LLEDMOD: A windows-based program for hydrodynamics simulation of liquid-liquid extraction columns," *Chem. Eng. Proc.*, **45**, 113 (2006).
33. S. A. Schmidt, M. Simon, M. M. Attarakih, L. Lagar, and H.-J. Bart, "Droplet-population balance modelling - hydrodynamics and mass-transfer," *Chem. Eng. Sci.*, **61**, 246-256 (2006).
34. B. H. Wolschner, "Konzentrationsprofile in Drehscheibenextraktoren," Dissertation, TU Graz, Graz, 1980.
35. T. Steinmetz, "Tropfenpopulationsbilanzgestütztes Auslegungsverfahren zur Skalierung einer gerührten Miniplant-Extraktionskolonne," Dissertation, TU Kaiserslautern, Kaiserslautern, 2006.
36. T. Steinmetz and H.-J. Bart, "Hydrodynamic scaling of mini-plant extractors on energy-dissipation based population balances," *Chem. Eng. Techn.*, submitted (2007).
37. A. Vikhansky, M. Kraft, H.-J. Bart, M. Simon, and S. A. Schmidt, "Droplets Population Balance in a Rotating Disc Contactor: An Inverse Problem Approach," *AIChEJ*, **52**, 1441-1450 (2006).
38. V. Alopaeus, J. Koskinen, and K. I. Keskinen, "Simulation of population balances for liquid-liquid systems in a non-ideal stirred tank. Part 1: Description and qualitative validation of the model," *Chem. Eng. Sci.*, **54**, 5887-5899 (1999).
39. S. Lo, "Application of population balance to CFD modelling of gas-liquid reactors," Trends in numerical and physical modelling for industrial multiphase flows, Corse, 2000.
40. C. Drumm and H.-J. Bart, "Coupling of CFD with DPBM for a RDC Extractor," 3rd International Conference on Population Balance Modelling, Québec, Canada, 2007.

FUTURE NUCLEAR FUEL CYCLES: PROSPECTS AND CHALLENGES

Bernard Boullis

Commissariat à l'Energie Atomique, Direction de l'Energie Nucléaire,
Centre de Saclay, 91191, Gif-sur-Yvette cedex-France.
Corresponding author email address: bernard.boullis@cea.fr

ABSTRACT

Solvent extraction has played, from the early steps, a major role in the development of nuclear fuel cycle technologies, both in the front end and back end. Today's stakes in the field of energy enhance further than before the need for a sustainable management of nuclear materials. Recycling actinides appears as a main guideline, as much for saving resources as for minimizing the final waste impact, and many options can be considered. Strengthened by the important and outstanding performance of recent PUREX processing plants, solvent-extraction processes seem a privileged route to meet the new and challenging requirements of sustainable future nuclear systems.

INTRODUCTION

Nuclear energy—it's day after day more obvious—should play an outstanding role in the future. Many facts (economics, fossil-resource possible rarefaction, fears about climate change, etc.) lead us today to consider that nuclear energy should bring a significant, a reliable, and a sustainable contribution to meet the drastically increasing energy needs of the global community.

Nuclear energy encompasses both nuclear power plants and the associated fuel cycle, with many diverse steps, from mining to final waste management. And the fuel-cycle policy, the management we decide for nuclear materials, is a key point when we address either near-term development or obviously long-term sustainability issues. The front end of the nuclear fuel cycle has focused a lot of work, notably in order to optimize enrichment technologies. And we do observe today a renewed interest into the preliminary steps of mining, milling, uranium extraction, and purification, as a strong "nuclear renaissance" is expected to be confirmed in the next decades, drawing increased needs for fresh nuclear fuels.

But it's mostly the back end which has been on the spot in the recent years, in the last decade! And this has been drawn by both waste concerns and resource issues. It appears rather clearly now that long-lasting nuclear options should be actinide recycling options.

The stakes, the driving forces appear more and more distinct: on one hand, saving uranium resources leads to recycling uranium and plutonium into reactors able to take full advantage of these elements; and on the other hand, decreasing the amount, long-term toxicity, and residual heat of the waste constitutes an important stake that calls for actinide recycle, too [4]. The general direction appears rather clear, but still many options are open:

- Recycle which actinide? Only major ones? Or all actinides?
- Recycle actinides, how? Diluted in the fuel, in a homogeneous mode? Or for some of them in dedicated devices? In dedicated fuels, in a dedicated strata?
- And what processes to recover actinides from spent fuel? Solvent extraction has been from the fifties up to now the leading technology in this field (PUREX is the reference for spent-fuel processing worldwide); and it seems very likely it will be the same in the next decades, even if heavier actinide separation gives rise to specific issues and thereby could bring up innovative processes.

Thus, many relevant answers are possible to these questions, depending both on the respective weight given to the different criteria to be taken into account or on the timescale looked at. We propose here to try to give a brief overview of the main guidelines for fuel-cycle development, starting from today's status (and mentioning as an example the French experience in the field), and to highlight some technical or scientific challenges to be surmounted.

RECYCLING URANIUM AND PLUTONIUM INTO LIGHT-WATER REACTORS

Reprocessing uranium oxide (UOX) spent fuel unloaded from light-water reactors (LWRs) has been proving up to now a very efficient way to allow a rational development of a fleet of nuclear power plants.

If we consider the French case, where more than 75% of the electricity supply is nuclear electricity, we can measure the benefits of a recycling policy. Uranium oxide spent fuels (about 850 metric tons per year) are reprocessed in the La Hague plants, and the total amount of recovered plutonium is reused as MOX fuel, successfully loaded (and burned) into 20 power plants within the French fleet (see Figure 1).

Reprocessing and recycling operations can be seen today as mature, efficient, safe, clean, and cost-effective technologies. This is testified by the feed-back from more than fifteen years of operation of the La Hague and MELOX plants, where thousands of metric tons of spent fuel and tenths of tons of plutonium oxide have respectively been reprocessed and recycled. In the La Hague plants, where an advanced form of the PUREX process is operated (see Figure. 2), both recovery yields and purification levels are very high (up to 99.9% of uranium and plutonium recovered and decontamination factors about 10^6 or more). The amount of technological secondary waste, the level of radioactivity released, the worker's radiation exposure have all been drastically lowered during the last two decades, although at the same time throughput was increased a lot!

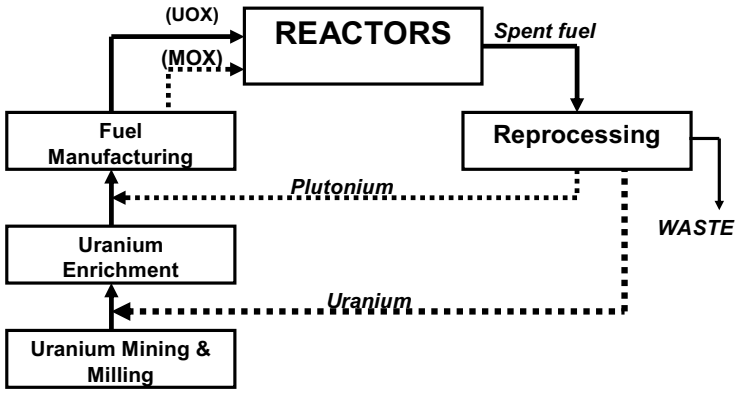

Figure 1. The closed nuclear fuel cycle.

Reprocessing UOX spent fuel and recycling plutonium into MOX fuel for LWRs provide significant benefits:

- *Natural uranium savings* (possibly up to 15%, compared with the "once-through" option).
- Enrichment *energy savings*.
- It drastically *decreases not only the volume* amount but also *the long-term radiotoxicity of the final waste* (spent-fuel radiotoxicity after some centuries is mainly borne by its plutonium content).
- It opens the way to waste-form optimization: *immobilization of fission products and minor actinides into glass canisters is today an international standard for high-level and long-lived waste conditioning*. And recent studies performed in France for the assessment of deep repository of these glass canisters in clay confirm a very late and very low impact (residual estimated dose three orders of magnitude less than the natural radioactivity level, and not before a hundred thousand years!).
- It provides effective *burning of fissile plutonium*.

This confirms we have today an available, quite modern, well-proven technology, which can be considered in several respects (diverse criteria, either economical or ecological ones) as the state-of-the-art option for the back end of the nuclear fuel cycle. We will probably have to face, if the so-called *"renaissance" of nuclear energy* (as very probably) comes to be confirmed during the next decades, a large amount of unloaded spent fuel that we will have to make sure we will be able to manage efficiently and safely. *It seems maybe important in this respect to avoid worldwide spent-fuel accumulation, and reprocessing and recycling already appears as a relevant strategy, mature at industrial scale.*

Moreover, these "today well-proven technologies" have in the recent past years been subject to improvements. This is the case for light-water reactors: "Generation 3" will bring first improved safety, but it has also been designed, too, in order to burn more efficiently and to a larger extent plutonium-bearing MOX fuels.

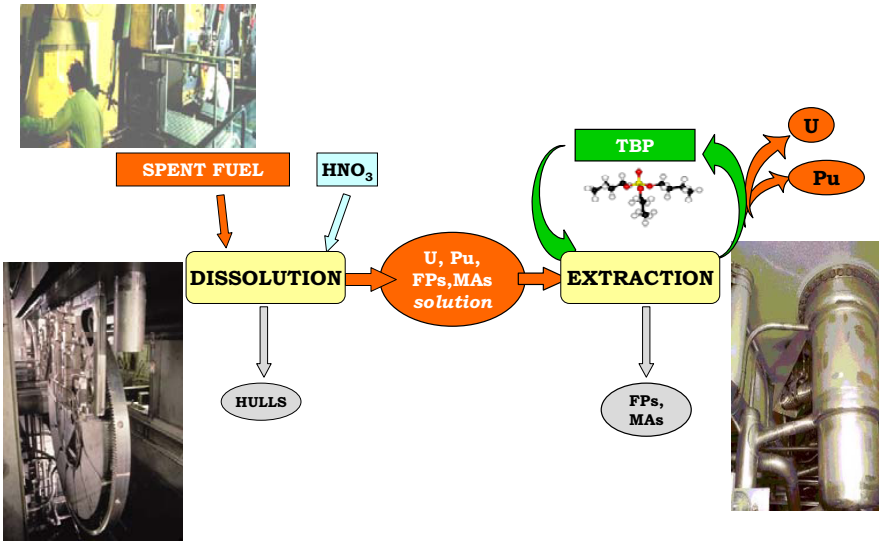

Figure 2. Principle of the PUREX process.

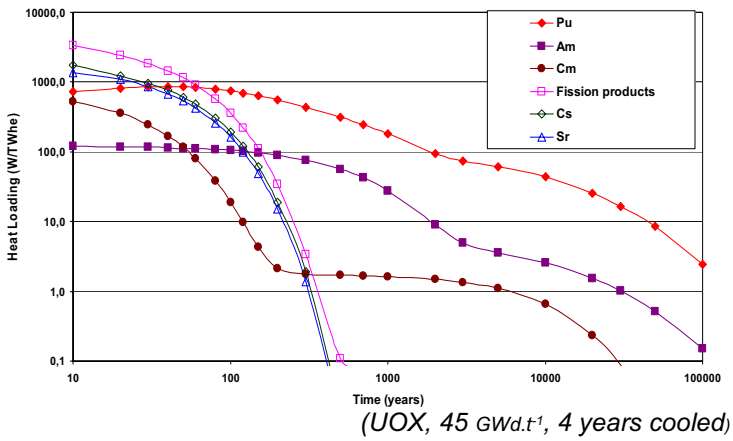

Figure 3. Final waste residual heat.

This is the case for PUREX process, too: *the COEX concept*, *based on the co-processing of both uranium and plutonium* all along the recovery operations (from dissolution, followed by joint extraction, to co-conversion and solid new fuel from solution) could bring significant simplifications and an improved resistance, too, vs. plutonium-diversion risks. To a large extent, the basic technologies remain unchanged, and only the way we combine them is different from the previous well-proven process.

MULTI-RECYCLING URANIUM AND PLUTONIUM

The sustainability issue is obviously a key issue when addressing the long-term perspective: the need to optimize the use of available natural resources, for instance,

becomes more acute again. This emphasizes the need for recycling options as an absolute necessity at this farther horizon; but it points also to some changes in the different components of the recycling strategy. The main point is that we have to evolve from today's light-water reactors to new reactors, able to take advantage at best of the energetic potential of the initial uranium.

Only less than 1% of the total potentiality of uranium is efficiently burned in LWRs, even after plutonium recycle in MOX fuels. *Fast neutron reactors (FR) could be far more efficient*: from the same initial quantity of natural uranium, one could get, by recurrent recycling of plutonium and uranium, more than fifty times more energy than from today's LWR fuel cycle. This seems to be the main guideline for future nuclear fuel cycles: go on recycling uranium and plutonium (using, for instance, the COEX process) into fast reactors able to burn with an increased efficiency the recycled materials.

RECYCLING MINOR ACTINIDES TOO?

Recycling options could be completed into a more sophisticated way to meet other requirements or challenges. Recycling minor actinides (neptunium, americium, and curium) in order to make easier the management of the final waste has been focusing a large amount of research work in several countries during the last decade, for example, the UREX concept in the United States [5-6] and the NEXT process in JAPAN [7]. It's well established now that the PUREX solvent, based on tri-*n*-butylphosphate, is able to extract neptunium with uranium and plutonium, and reprocessing flowsheets can be modified in order to recover it [1]; but almost no potentialities exist for americium and curium recovery. In France, too, additional steps to PUREX or COEX, using innovative extracting molecules, were designed and successively tested some years ago at the laboratory scale. These complementary steps, so-called DIAMEX (for both actinide and lanthanide co-extraction) and SANEX (for actinide from lanthanide separation), could open the way of minor-actinide recovery for recycle [2-3]. And transmutation experiments have been launched, often within an international frame, to check the ability of fast reactors to burn these elements, too.

But many questions, many options are here still opened, as for instance:

- *Which actinide do we need to recycle and why?* Minor actinides, if immobilized into glass, according to French studies, don't move in a significant way through a clay repository (but we know that it can be quite different for other repositories under oxidizing conditions, where neptunium, for instance, is more mobile and can be a significant dose-contributor). The incentives for minor-actinide recycle could be decreasing long-term (1000–10,000 years) radiotoxicity (due first to americium and then to curium) (see Figure 5) or decreasing heat emission during the first millennium (due mainly to ^{241}Am) (see Figure 3) or decreasing accessibility to recycled uranium and plutonium (by adding other radioactive emitters?).
- *And how to recycle the selected minor actinides?* Altogether, with plutonium and uranium in a homogeneous mode (but with drawbacks on the downstream operations to be further analyzed)? Or in dedicated

fuels or targets, disposed in an appropriate manner in the fast reactors? (Heavier technical issues, but on a small part of the fuel)? Or into dedicated transmutation systems (see Figure 6)?

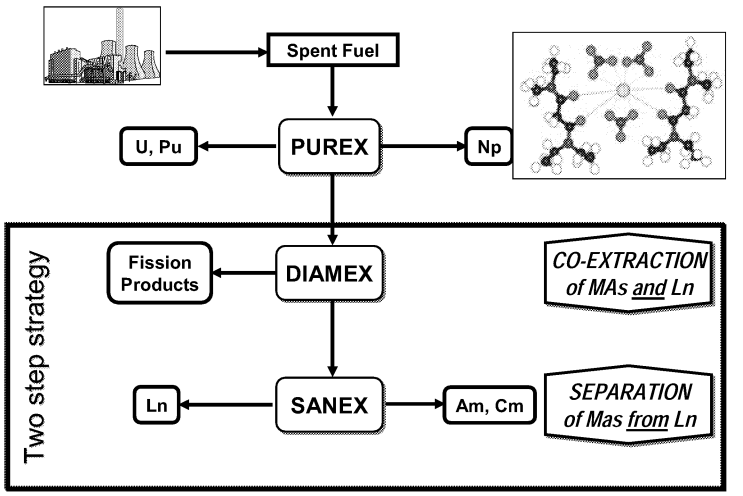

Figure 4. Minor-actinide recovery via the CEA general flowsheet.

These questions call for further investigations, need further research in order to assess the different options and to finalize the best technical solutions. In France, we intend to perform pilot-scale experiments in the future "fast-reactor prototype," whose project is to be commissioned by 2020 using new fuel-cycle facilities to be built at La Hague (for core and experimental, minor actinide-bearing, assemblies fabrication).

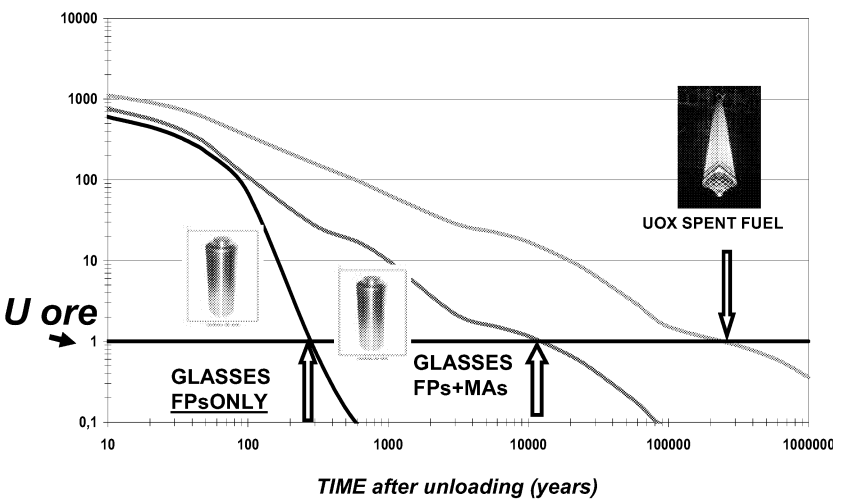

Figure 5. Final waste radiotoxicity.

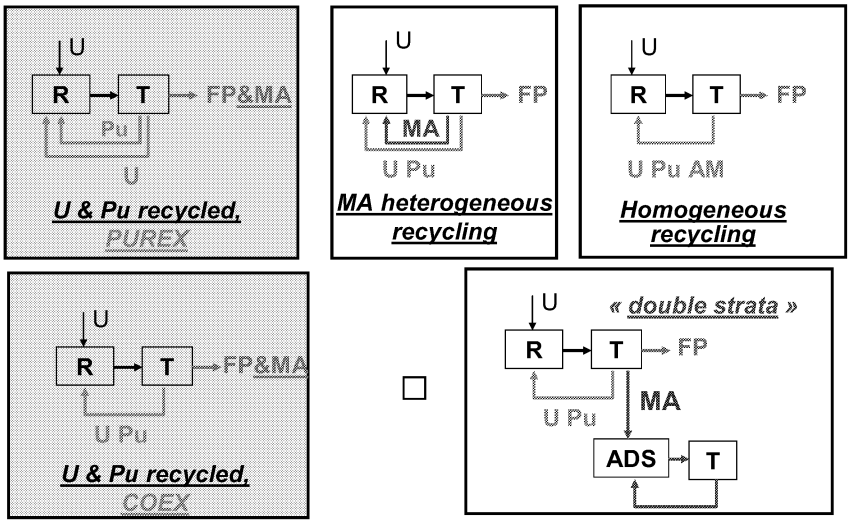

Figure 6. Actinide-recycling options.

But we can present the following guidelines for the R&D about the diverse possible options: There are some incentives for removing all the minor actinides from the ultimate waste, but it's questionable that neptunium, americium, and curium should inevitably be seen as a whole. When neptunium's potential mobility isn't an issue, americium seems to be the first main target, because a) its potential radiotoxicity is far above the others; b) americium is the main contributor to residual heat after a century (obviously if plutonium has been removed!); and c) curium, whose long-term toxicity is not so high (even if we have to take into account an increased amount of curium following americium recycling), seems maybe more difficult to handle in the near term.

If the goal remains to recycle all actinides, it may appear simpler and, to some respect, more efficient to manage and recycle them all together in a "homogeneous" way. This has been the basis of recent developments in the U.S. (UREX concept [4-5]) or in France (GANEX concept [3]). With such concepts, all the transuranics and a part of uranium are managed as a whole all along the processes, from recovery steps to recycling steps, and this can be seen as providing an increased resistance to proliferation risks by decreasing the "accessibility" to fissile materials. But such options, if they are probably the most elegant ones in a very long-term prospective, also present some drawbacks in the nearer term. Namely, they would need, if deployed, a significant "reset" of the reprocessing processes and cannot be simply added to a pre-existing uranium and plutonium recycling option. Another possible drawback could be difficulties to deliver recycled new fuel for both thermal and fast reactors, which probably will still be present all through this century in "symbiotic" nuclear fleets.

- So, a possible option could be a "heterogeneous" recycling of the minor actinides, where uranium, plutonium, and possibly neptunium go into the core fuel and americium and curium go into dedicated "targets," which could be multi-recycled. These targets could also be in fact the uranium "blankets" around the core of fast reactors

without any added inert material, allowing the possibility of efficient breeding under safer conditions, considering the proliferation concerns, and efficient burning for minor actinides, both core and blankets being processed for recycle in the same plant (see Figure 7).

- And another option could be to separate completely into two distinct strata, on one hand the electric power generation (with only uranium and plutonium recycle) and, on the other hand, the long-lived waste-burning operations (with dedicated minor-actinide bearing fuels, dedicated reactors—for instance, accelerator driven systems—and dedicated processing and recycling devices).

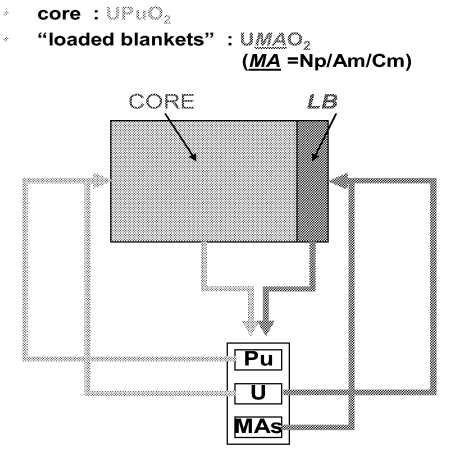

Figure 7. MA recycle in blankets.

WHAT KIND OF SEPARATION PROCESSES?

Up to now, solvent-extraction processes have been the "reference technology" for fuel processing at commercial scale, and this has been true for about fifty years. Why such a long-lasting success? Many reasons could be presented, but the main ones seem to be the following:

- First, as testified by PUREX operation experience, solvent-extraction processes are able to provide, in the nuclear field as in other fields, extremely high separation yields, considering both recovery and purification yields.
- Second, as seen in modern PUREX plants, these high yields are obtained without generating an important amount of secondary technological waste. And this is obviously very important in the nuclear industry.

Besides the above "intrinsic" attractive properties of solvent-extraction processes, one must mention the fact that a very heavy work has been achieved up to the recent decades in order to better master the technology and large-scale operation. And even if alternative processes are thinkable, are surely possible options for future nuclear-fuel

processing plants, and provide in some cases very encouraging results, it will be a very long road to bring them from laboratory to commercial-plant scale. So, starting from this "state-of-the-art" solvent-extraction technology, able today to recover and recycle uranium and plutonium from spent oxide fuels unloaded from water reactors, how can we progress in order to meet tomorrow's requirements?

We have seen above that many management options are still open for actinide recycle, opening the way to many process options with either complementary steps or quite new extraction processes. Here, we find many examples in what is studied and proposed by many research teams all around the world. But there is another key factor for the design of fuel-cycle processes: it's the nature of the fuel itself! And here we could observe some changes, maybe important ones, in the next decades, leading to changes in the processing media (molten salts have been already experimented for metallic fuels, up to pilot scale!) or maybe in the nature of the process itself! But there is really no evidence that solvent extraction would not be the best option again, owing the reasons detailed above.

A very abundant work has been undertaken in many countries in order to design new extractants able to selectively recover americium and curium [2-7]. These extractants have to cope with many requirements and constraints: affinity, selectivity, (obviously), easy reversibility (for an operable process), stability (both chemical and radiological), favorable kinetics, harmlessness of byproducts, easy on-line removal, etc.

Thus, plenty of innovative molecules have been designed, synthesized, and checked. Among this large diversity, some main guidelines emerge: as trivalent actinide cations are "harder" than lanthanide ones, soft-donor ligands are used for actinide-from-lanthanide separation, especially nitrogen-bearing extractants in order to selectively extract actinide ions or selective aqueous complexants in order to keep actinide cations unextracted, while lanthanide ones are extracted. Many difficulties are encountered, like, for instance, competition of actinide cations with protons, requiring low acid concentrations in the aqueous phase for an efficient selectivity. Various such difficulties lead to rather sophisticated flowsheets involving, for example, accurate operation parameters and reagent needs for buffers, salting-out reagents, and synergistic mixtures of extractants, solvating or acidic ones. And such a complexity, added to the fact that some of the fission products could present a parasitic effect on the operation, leads generally to proposed two-step processes (see Figure 4):

- A first step, using hard-donor ligands (CMPO, diamide, etc.) to co-extract and then co-back-extract both trivalent actinide and lanthanide ions (and thus to get rid of other fission products);
- A second step, using soft-donor ligands (e.g., bispyridinyltriazines as actinides-specific extractants, HEDTA as actinide-specific aqueous hold-back complexant, etc.) in order to achieve under "cleaner" chemical conditions the actinide-lanthanide separation.

As it is seen, the goal of minor-actinide-selective recovery implies today rather complex processes. The recent experiments performed in diverse countries show that it is achievable, with high yields and satisfying correctly most of the requirements. But there still is a real incentive, a real need for further improvements, in order to try *to simplify today's proposed flowsheets* and to optimize them with respect to the diverse recycling

goals we could have (all actinides or part of them, homogeneous or heterogeneous, etc.). A big challenge is to design a "one single-cycle process," allowing directly from selective actinide recovery; attempts are ongoing for this purpose, already with encouraging results (see Figure 8). But there is obviously room for further progress and even for real breakthroughs maybe in the near future.

Besides these main guidelines, many other developments are in progress. One is to recover some fission products, especially Cs and Sr, to decrease the final waste residual heat, using for instance functionalized calix-crowns [8]. Among other developments is to optimize the conversion of the recovered actinides from solution to solid new fuel (mainly oxide but other metallic or ceramic forms also).

A very strong advantage of hydro-processes is that we can say, as testified by modern PUREX plant operation, that operating the solvent-extraction technology at commercial-plant scale for nuclear-fuel processing purposes is today well mastered, thanks to the huge work performed in the field until now. And this huge experience is directly applicable to the design of minor-actinide recovery facilities. In a schematic way, the challenge here, aiming at industrial facilities and starting from PUREX, is to design new molecules and new processes at laboratory scale. The transposition to larger throughputs shouldn't be so difficult of an issue.

And here is a big difference with other processes, like for instance pyro-processes, using high-temperature molten salts. The principle of such processes is, in some cases, for some fuels or some global strategies, very attractive: very low radio-sensitivity of the reagents and compactness in the principle. There is precedent in successful checks at laboratory and, for some of them, at pilot scale [9]. But operating commercial plants addresses specific issues, and there are still many questions about some important items, like for instance generation and management of technological waste. This requires heavy development work, and pyro-commercial plants shouldn't be seen within the same time schedule as solvent-extraction based plants.

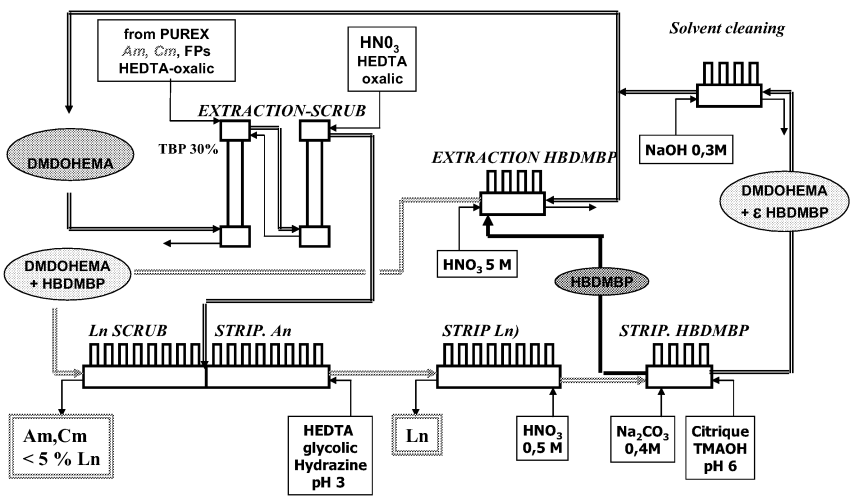

Figure 8. A possible "single-cycle" flowsheet.

A NEED FOR BASIC RESEARCH

If we are able to design a lot of interesting, maybe outstanding, processes, it's evident that we haven't fully understood the basic mechanisms involved! And this could be an important drawback for future developments. Some recent results can illustrate this above assumption.

The DIAMEX process can be seen as a success of nuclear research in recent years, where an extensive work has been done to select and to optimize the malonamide extractants. And a large series of hot runs with genuine spent fuel testify to the validity of the process. But experiments using small-angle X-ray scattering drastically changed the picture we had in mind about extraction mechanisms. Solvates seem not to be homogeneously dispersed in the organic phase at the concentrations used in the process but rather form aggregates with a polar core containing metallic ions. This result was quite new, and even if here not directly correlated with extraction results, it's very important in order to understand and then to anticipate potential "third-phase" formation. Recently, Yaita et al. published interesting results about another diamide extractant, the so-called TODGA (TetraOctylDiGlycolAmide), which is a very promising extractant because it presents very high distribution ratios, especially for trivalent cations [10].

Here again, aggregates in the organic phase have been observed. But, in addition, this seems clearly related to the distribution ratio of americium. So, solvation phenomena, which are essential for solvent-extraction processes, seem to be in such cases not so well mastered. And this situation points out the interest, the importance, of performing more basic research in the field, even if efficient processes have already been designed.

Another example, about what can be seen as *the* key point in partitioning, is *selectivity*. The goal is to extract one or some elements among many others, sometimes with very close chemical properties, a situation that distinguishes nuclear reprocessing from other hydrometallurgical separation problems. And, as mentioned above, it's for instance difficult to separate trivalent actinides from lanthanides, which has been focusing a very important part of the research in minor-actinide partitioning programs, and many new molecules were designed and tested.

When Kolarik discovered in 1998 (in the frame of the EU "NEWPART" research project) the fantastic properties of bis(triazinyl)pyridine molecules (BTPs), this was a big surprise [11] (see Figure 9). Before that, we had experimented with many other pyridinic compounds, with some results concerning selectivity, but otherwise rather poor results in that very low nitric acid concentrations were required together with the obligatory use of a lipophilic anion to get a synergistic effect. Such a gap remains today not fully explained, and investigations following various routes have been undertaken.

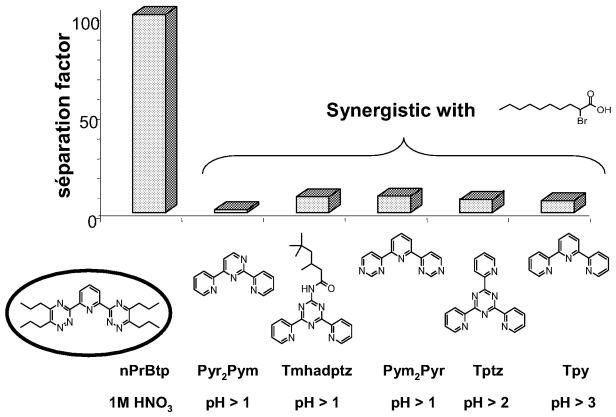

Figure 9. Actinide/lanthanide separation factors for BTPs and other extractants.

CONCLUSIONS

Nuclear fuel-cycle options are of major importance for the future of nuclear energy. Actinide recycling appears as a main guideline for the design of sustainable roads.

Starting from today's available technologies, it could be possible to evolve to different processes, designed to fit different strategic options (uranium and plutonium co-processing, minor-actinide recycling, all-actinide grouped management, etc.). This could give us a very welcome *flexibility*, probably necessary for fuel-cycle plants that should have to serve symbiotic reactors fleets. And such *a progressive approach* for the improvement, the completion of today's well-proven technologies should be very valuable to adapt, at each time, recycling processes to the evolution of recycling needs.

Many routes will probably be explored, taking obviously into account the possible changes in the nature of the fuel itself. But solvent extraction will surely hold a great role. It has proven for decades its ability to recover very efficiently diverse elements from spent fuel, at commercial plant scale, in a very reliable way and with a low amount of technological waste. And these can be seen as key points when thinking to future processes.

New strategies, probably new recycling needs, innovative fuels, and new constraints will obviously require important developmental work in order to improve, to complete, and to adapt existing solvent-extraction processes. And this calls both for a better in-depth understanding of the basis of partitioning processes and for an exploration of new promising concepts: herein lie important scientific and technical challenges.

REFERENCES

1. P. Baron, M. Lecomte, B. Boullis, and D. Warin, "Separation of the long-lived radionuclides: Current status and future R&D Program in France," Global 03, New Orleans, USA, 2003.
2. X. Heres, E. Ameil, I. Martinez, C. Hill, and P. Baron, "Extractants separation in DIAMEX-SANEX process," Global 07, Boise, USA, 2007.

3. M. Miguirditchian, L. Chareyre, and C. Hill, "GANEX: adaptation of the DIAMEX-SANEX process for the group actinide separation," Global 07, Boise, USA, 2007.
4. U.S. DOE report to congress: Spent nuclear Fuel Recycling Program Plan, 2006.
5. G. F. Vandegrift, et al., "Designing and demonstration of the UREX+ process using spent nuclear fuel," Atalante 04, Nimes, France, 2004.
6. E. D. Collins, et al., "Hot test evaluation of the reverse TALSPEAK process," Global 05, Tsukuba, Japan, 2005.
7. H. Funasaka, "Perspective and current status on fuel cycle System of Fast Reactor Cycle Technology Development Project in JAPAN," Global 07, Boise, USA, 2007.
8. J. Law, D. Peterman, C. Riddle, D. Meikrantz, and T. Todd, "Advances in Development of the fission product extraction process for the separation of cesium and strontium from spent nuclear fuel," ICEM, Bruges, Belgium, 2007.
9. G. E. Benedict et al., "Pyroprocess programs at Idaho National Laboratory," Global 07, Boise, USA, 2007.
10. YAITA, *Solvent Extr. Ion Exch.*, **22**(4), 553-571 2004.
11. Z. Kolarik, C. Madic, et al., "New partitioning techniques for minor actinides," Final Report, NEWPART, EUR 191 49EN, 2000; p. 286.

IONS AND THEIR COMPLEXES AT LIQUID-LIQUID INTERFACES: NANOSCOPIC VIEWS FROM MD SIMULATIONS

A. Chaumont, G. Chevrot, N. Galand, N. Sieffert, R. Schurhammer, and G. Wipff

Laboratoire MSM, UMR CNRS 7177, Institut de Chimie
4 rue B. Pascal, 67 000 Strasbourg (France)
Corresponding author email address: wipff@chimie.u-strasbg.fr

ABSTRACT

Classical molecular-dynamics "MD" simulations of ions, extracting ligands, their complexes, and their counterions at liquid-liquid interfaces provide dynamic pictures that can be viewed as realistic nanoscopic models or, at least, as stimulating mental pictures that allow us to better understand "what happens at the interface" in assisted ion extraction. An important expected outcome is the high surface activity of most partners involved in the extraction process, leading to locally enhanced concentrations at the nanoscopic level. Furthermore, there is a deep relationship between the surface activity and the tendency of aggregation in water, with marked counterion effects in both cases. The case of classical molecular organic liquids, SC-CO_2, or ionic liquids as receiving phases will be considered.

INTRODUCTION

Much of what we know of the structure of liquids and of their solvation properties comes from computer simulations, mainly of the molecular-dynamics "MD" type [1]. Earlier, we have been interested in the modelling of solvation in the context of ion complexation in host-guest supramolecular systems, a field of choice to test and develop state-of-the-art computational methodologies that are also used to study recognition processes in bigger and more complex systems (e.g., in biology) [2]. The simulations showed that the solvent determines the conformation of macrocylic extractants, like 18-crown-6, the *222* cryptand, or calixarenes, and markedly contributes to their recognition properties towards cationic or anionic guests [3]. The question of ion extraction was first addressed by simulating these species in "oil" solutions, where oil was modelled by chloroform. A next step has been to simulate ligands and their complexes in biphasic water/oil systems to see whether they spontaneously partition as anticipated from the experimental observations, that is, towards the oil phase [4].

It was, however, a puzzling discovery to us that they in fact did not partition to the bulk organic phase, but instead adsorbed at the interface, as found first with calix[4]arenes and their Cs^+ complexes [4]. Even the "spherical" cryptands and cryptates that lack the amphiphilic topology were found to be surface active [5]. Meanwhile,

computational evidence of their surface activity has been accumulated, based on the comparison of different solvent models, different initial situations (e.g., juxtaposed liquids versus randomly mixed liquids) [6], or the calculation of the free energy ΔG profiles for interface crossing by the complex or the ligand [7]. Experimental data (e.g., kinetic models, surface-tension measurements, surface spectroscopy, and electrochemical data) also support the view that extractant molecules and their complexes are surface active. In this paper, we illustrate some recent directions for computational research and modelling in the field of ion extraction, involving salts, ligands, additives (see Figure 1 with the acronyms of ligands and ions) in binary water/oil solutions. More details about each system can be found in the cited references.

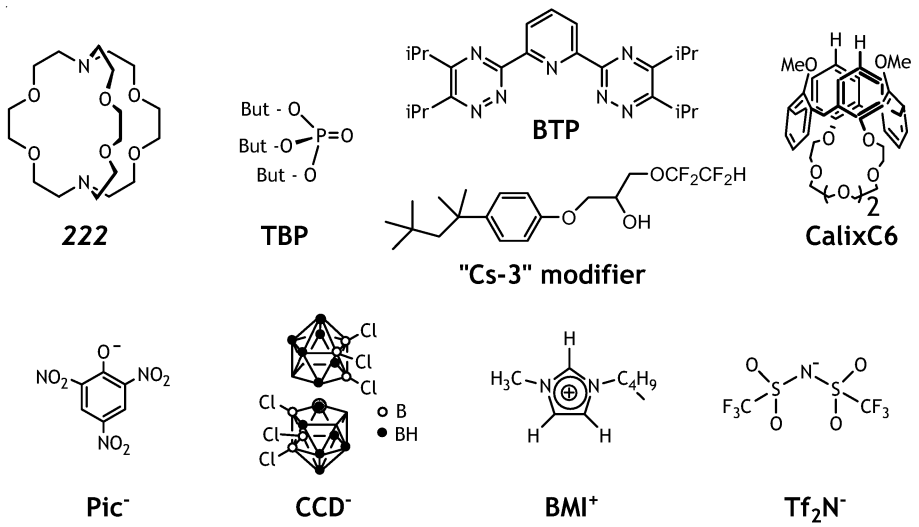

Figure 1. Acronym of simulated species: cryptand *222*, TBP, BTP (*i-Pr* derivative), CalixC6, picrate Pic^-, chlorinated dicarbollide CCD^-, the "Cs-3" modifier, BMI^+, and Tf_2N^- ions (ionic liquid).

METHODS AND COMPUTATIONAL FEATURES.

Nanoscopic Representation of Binary Systems

Typically, biphasic systems are built from adjacent "cubic" boxes of water and oil (of ca. 5 nm side each) into which the solutes are immersed. The resulting box is simulated with 3D periodic boundary conditions, that is, surrounded by 26 identical boxes obtained by translation, as are the unit cells of crystals. Thus, the juxtaposed liquids are represented as alternating slabs of ca. 5 nm width, and simulated in selected thermodynamic ensembles, like the (*NVT*) ensemble where the number of particles *N*, the volume *V*, and the temperature *T* are maintained constant.

Molecular Dynamics

The trajectories of all particles (N atoms) are assumed to be governed, like those of macroscopic objects, by the Newton's equation of motion $F_i = m_i\, a_i = -\text{grad}_i\, U$. Their calculations require an "accurate" representation of the potential energy U, from which the force F_i acting on each atom i can be calculated. In practice, U is described by an empirical force field, based on a ball-and-stick representation of the system. Atoms are "soft balls" connected by harmonic springs, and their noncovalent interactions are described, for example, via pairwise additive 1-6-12 potentials (coulombic + van der Waals interactions). This model implies that the number of "covalent bonds" remains constant during the simulations, and thus, bond-formation or -breaking processes cannot be simulated. The atomic charges are generally determined by quantum-mechanical "QM" calculations, and their performance can be tested by comparing force field to QM-calculated small prototypes, or by simulations on condensed phases (e.g., pure liquids). The treatment of "long-range" forces is an important issue, especially in the case of ionic solutes or ionic liquids. Whereas the first MD studies were achieved with an abrupt cut-off distance to calculate these interactions (typically 12 to 15 Å), the more recent ones use more satisfactory procedures, like the Ewald summation or the Reaction Field correction at the boundaries.

In practice, due to computer-time limitations, a reasonable compromise has to be found between the size of the system to simulate, the simulated time t, and the "accuracy" of the representation of the potential energy U. For instance, accounting for polarization effects scales up the computer demands by a factor of ca. 5 to 10. Methods based on a QM representation of U, like the Carr-Parrinello CPMD method are limited to small systems (e.g., 18-crown-6 and its hydrates) [8] for ca. 5 to 100 ps. Our first MD simulations on interfacial systems involved ca. 5,000 atoms, and were run for 10 to 100 ps, requiring ca. one month of CPU on supercomputers. Today, one can simulate solutions with 30,000 atoms for 1 to 100 ns in a few days or weeks with a cluster of PCs. The simulation times have to be long enough to allow for an efficient sampling of the configurations of the solution and thus depend on its nature, relaxation time, and diffusion coefficients. For instance, a binary water-oil mixture, initially randomly mixed, separates in less then 1 ns with chloroform as oil component but is still incomplete after 10 ns or more when octanol [9] or an hydrophobic ionic liquid constitutes the oil phase [10]. Big and heavy solutes (e.g., metal complexes, CCD^- anions) also diffuse more slowly than small and light ones and require longer simulations.

SOME RESULTS

Each study corresponds to consistent sets of computer MD experiments on model systems, generally of increasing complexity, allowing us, via pair-wise comparisons, to observe some specific effects. In essence, the systems are dynamic, complex, and quite difficult to display. The few pictures presented are selected snapshots that are representative of the statistical distributions. These are often quite poor representations, however. In the future, it will be desirable to deposit the trajectories in databases, to allow the user free examination on interactive computer-graphics systems.

The Neat Water-"Oil" Interface with Different "Oil" Liquids

A first important computational result concerns the water/oil binary mixtures and the characteristics of the liquid-liquid interface, where oil is an organic liquid-like alkane or aromatic derivatives.[11] For instance, a "randomly mixed" nanosolution of water and chloroform has been found to demix in less the 0.5 ns, leading to a well-defined biphasic system where the two phases are separated by a narrow interface (less than 1 nm) [6].

Comparisons with MD results with other liquids like supercritical fluids (SC-CO_2), organic liquids like nitrobenzene [12], octanol, or hydrophobic ionic liquids [13] reveal that the size, the polarity of the interface, and properties like solvent ordering at the interface and intermiscibility of the two liquids, are modulated by the nature of the oil phase. Generally speaking, the more polar the oil phase is, the more hygroscopic it is, and the slower is the simulated demixing of the "randomly mixed" liquids (see Figure 2 with octanol and the hydrophobic [BMI][Tf_2N] ionic liquid as "organic" liquids that all form a distinct phase with water at the macroscopic scale). The demixing simulation of the [BMI][Tf_2N]/water "random mixture" takes ca. 50 to 100 ns, depending on the theoretical representation of the ionic liquid [10,14]. With octanol as the organic component in a 50:50 volumetric ratio with water, the phases separate in ca. 15 ns, forming in fact octanol bilayers alternating with water nanoslabs. Other octanol patterns can be found, depending on the box shape and solvents ratio and thus on the confinement of the solution [9].

An important conclusion from these simulations is that, in reality, water and oil do not mix at the microscopic level but delineate liquid-liquid interfaces. Interfaces do not only concern liquids at rest, but also their metastable mixtures formed, for example, in agitation conditions, or in the course of mechanically driven separation processes (centrifugation, gravitational forces), and therefore containing oil-in-water or water-in-oil droplets, or microemulsions.

Recent Developments on the Cs^+ Complexation and Extraction by CalixC6

Extraction of $Cs^+ NO_3^-$ by CalixC6 to Chloroform: Why Does the Solvent Modifer "Cs-3" Promote Extraction [15]?

Most academic studies on solvent extraction use lipophilic counterions like Pic^-, but real solutions (e.g., irradiated nuclear fuel dissolved in nitric acid) may contain large amounts of hydrophilic anions like NO_3^-, requiring the addition of co-solvents like the fluorinated alcohol "Cs-3" (Figure 1) to promote extraction. MD simulations of CalixC6 and its $Cs^+NO_3^-$ complex provide microscopic views that may explain the synergistic effect of Cs-3. First, simulations of the chloroform + Cs-3 mixture show that Cs-3 enhances the solvation of all partners, and especially of the NO_3^- counterion, via strong hydrogen bonds (Figure 3). Furthermore, the calculations predict that NO_3^- should be co-extracted as loose contact ion pairs, rather than dissociated ion pairs.

Looking at the water/oil interface, one sees that Cs-3 molecules are surface active and concentrate at the aqueous interface (either flat or curved interface; see Figure 3), thereby lowering the interfacial pressure and facilitating the interface crossing by the complexed ion. Also note that the asymmetrical structure of the Cs-3, compared, for

example to octanol, prevents the formation of interfacial layers ("films") that would hinder interface crossing. The same behavior is found at "flat interfaces" and at the surface of spherical water droplets formed during mechanical agitation in an oil-rich system.[15]

Extraction of Cs^+ by CalixC6 to a Room Temperature Ionic Liquid "IL"

Why is extraction with an IL more efficient than with chloroform? What is the origin of the Cs^+ versus Na^+ extraction selectivity [16,17]?

Ionic liquids like [BMI][Tf_2N] based on the butylmethylimidazolium cation BMI^+ and the Tf_2N^- anion ($(CF_3SO_2)_2N^-$) can be used as receiving phase in ion extraction with higher efficiency compared with classical organic solvents [18,19]. Inspired by the experimental studies of Luo et al. [20], we simulated the free M^+ alkali ions, the ligand L (CalixC6) and its Cs^+ complex in the [BMI][Tf_2N] IL, as well as at the IL/water interface. These simulations reveal important features:

- All species, and especially the NO_3^- counterion and the complex, are better solvated by the IL than by an organic molecular solvent like chloroform.
- At the water/IL interface, some M^+ (Na^+ or Cs^+ ions) or NO_3^- ions come into contact with IL ions of opposite charge (Tf_2N^- and BMI^+, respectively) and are therefore close to the extractant molecules at the interface. When chloroform is the receiving phase, such ions are "repelled" by the interface, preventing their complexation via a least-motion pathway with free ligands adsorbed at the interface.
- At the interface, a few BMI^+ cations of the IL migrate to water, which is favorable for a cation-exchange mechanism (BMI^+ for M^+), precluded with a neutral molecular solvent.

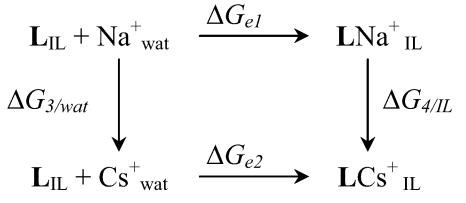

Scheme 1

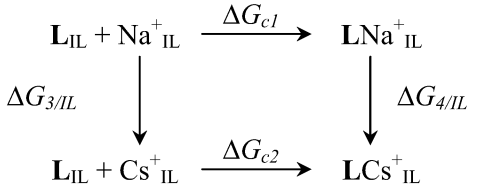

Scheme 2

- The question of ion-extraction selectivity was addressed via the stepwise "alchemical mutation" of Na^+ to Cs^+ in their free states in water ($\Delta G_{3/wat}$) and in their complexed states in the IL receiving phase ($\Delta G_{4/IL}$). The corresponding changes in free energies were calculated using the thermodynamics perturbation theory. The extraction selectivity, determined experimentally as $\Delta\Delta G=\Delta G_{e1}-\Delta G_{e2}$, has been obtained computationally via the thermodynamic cycle (Scheme 1) as $\Delta\Delta G=\Delta G_{3/wat}-\Delta G_{4/IL}$, correctly predicting that Cs^+ will be better extracted than Na^+. Likewise, calculations predict that M^+ complexation by the calixarene L in a monophasic IL system (Scheme 2) would also favor Cs^+, as in pure water. In a chloroform solution, however, the selectivity would be inversed, according to the

simulations, Na^+ being preferred over Cs^+. Thus, although inherently polar, the IL behaves as chloroform as receiving phase but more like water as far as complexation in a single phase is concerned [16,17].

Tests with an Improved Methodology

We have reconsidered the case of Cs^+ extraction by CalixC6 to chloroform, using improved treatments of electrostatics, namely including polarization of the solvents and solutes, and accounting for long-range interactions. The results confirm our conclusions drawn 10 years ago on the surface activity of the Cs^+CalixC6 complex and of its Pic^- counterion at the chloroform/water interface, be it flat (50:50 water:oil ratio) or curved (90:10 oil:water ratio) [21]. Likewise, simulations of single ions at aqueous interfaces show that accounting for polarization effects enhances the surface activity [22]. These results thus validate those obtained with the less expensive methodology based on 1-6-12 potentials without polarization and confirm the importance of interfacial adsorption in processes like ion extraction or phase-transfer catalysis [23].

Hydrophobic Ions Are Surface Active and Also Tend to Aggregate in Water with Marked Counterion Effects: The Case of Dicarbollide Anions and of 222 Cryptates

Surface Activity

It was early shown by MD simulations that anions like Pic^- that are commonly used in extraction systems are surface active and tend to stack in water and at the interface [24]. The case of chlorinated cobalt dicarbollide CCD^- anions is interesting, because they are very hydrophobic, nonprotonatable, stable under radiolysis, and have been used as synergistic agents in conjunction with classical extractant molecules to extract cations like Cs^+, Sr^{2+}, and trivalent actinides An^{3+} or lanthanides Ln^{3+} [25]. They can be used as additives or covalently linked to complexing moieties (crown ethers, phosphoryl containing groups like CMPO, and calixarene derivatives).

When simulated at the water/chloroform binary system, CCD^- anions are found to concentrate at the interface, thereby attracting their counterions (M^+, UO_2^{2+}, and Eu^{3+}) close to the organic phase (see Figure 4) [26]. Thus, again, although lacking the classical amphiphilic topology, they behave like surfactants, and their surface activity is modulated by the hydrophilic/hydrophobic balance of their counterions. For instance, the salts are more surface active with Cs^+ than with Na^+ as counterion [26].

Cation complexes can be viewed as big hydrophobic ions and, according to the MD simulations, are also surface active, with marked counterion effects. For instance, the $K^+\subset$ 222 cryptates, although quasi "spherical," adsorb at the water/SC-CO_2 interface, and their surface activity increases when the X^- counterions evolve from Cl^- to Pic^- and CCD^- [27]. The same feature has been found computationally for model spherical ions (of ca. 5 Å radius) [28], or for tetrahedral ions like $AsPh_4^+$ or BPh_4^- [29]. The smaller ClO_4^- anions, although less hydrophobic, also approach closer to the interface than the NO_3^- or Cl^- ones [30], and this is in keeping with their tendency to promote third-phase formation. A fortiori, less "spherical" complexes formed with, for example, calixarenes, are more surface active. Likewise, we anticipate bulky hydrophobic ions (e.g., polyoxometallate anions) to be also surface active, with marked counterion effects. Even

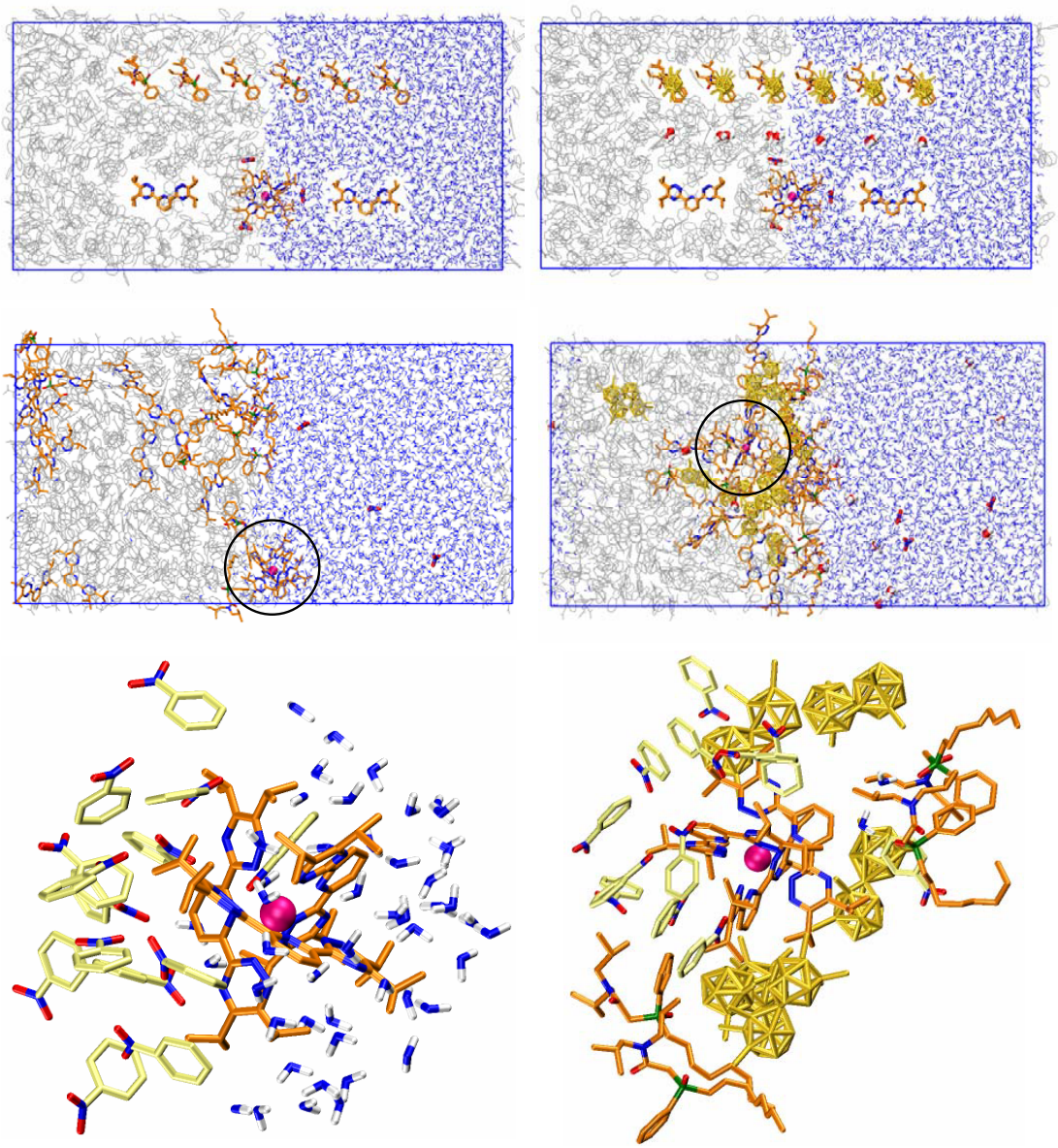

Figure 5. The $Eu(BTP)_3^{3+},3NO_3^-$ complex in the presence of 12 CMPO + 12 BTP ligands at the nitrobenzene-water interface, without CCD^-s (*left)* and with 12 CCD^- H_3O^+ added ions (*right*). From top to bottom: Initial and final views (15 ns), with typical snapshots of the $Eu(BTP)_3^{3+}$ complex adsorbed at the interface (*left*) or extracted (*right*).

(iii) as co-solvent (improving the solvation of the extracted complexes). The modelling of such systems points to the importance of correctly accounting for the complexity of the system and for concentration effects that deeply modify the characteristics and the supramolecular organization of the solution.

Acidic solutions are more difficult to model by classical MD, because this would require an a priori knowledge of the nature and concentration of the different forms of the acid. Furthermore, the p*Ka* is stressed to be different in the interfacial region, the organic phase, and in bulk aqueous solution. Our approach with nitric acid has been to consider an equimolecular mixture of the HNO_3 and H_3O^+ NO_3^- forms, showing that the former is highly surface active and partitions more, as expected, to the organic phase [49]. Furthermore, in the case of uranyl extraction by TBP, we have found that the acid induces local mixtures of "oil," acid, water, and $UO_2(NO_3)_2(TBP)_2$ complexes, which can be viewed as the early step of third-phase formation [49].

PERSPECTIVES

There is always something to be learned from "in silico" computer experiments on ion extraction, where solvents are explicitly represented. Some results seem obvious to experimentalists, others remain somewhat provocative or seem irrelevant, because the simulated system is too simple in terms of constitution or representation. Modelling does not merely consist of applying computational techniques but first requires one to analyze a complex process, and to decide and test to which extent it can be simplified and reduced in terms of complexity, size, time scale, and empirical representation of its energy. Ideally, one could dream of starting the simulation like the real experiment with the salts in water and the extractants in the oil phase to see whether complexation will occur and whether the complex will finally be extracted. This is presently hardly feasible, because it would require excessively long simulations as well as to activate the process along some selected "reaction coordinate" (see, for example, the complexation pathway of Cl^- into a macrocylic host in water [52]). One exception concerns the case of uranyl nitrate extraction by TBP from acidic water to chloroform or to SC-CO_2 [53]. During the demixing simulation of a random mixture of solvents, TBP, and $UO_2(NO_3)_2$ molecules, we have indeed observed the spontaneous formation of the $UO_2(NO_3)_2(TBP)_2$ complex and its partitioning in the oil phase. This occurred, however, only when the TBP concentration was high enough, as achieved experimentally [53], pointing to the importance of the complexity of the system, which is supramolecular in nature. As in the case of charged amphiphiles, the concentration and the medium (counterions and additives) determine the nature of the assemblies and of its function. Extracted complexed ions are in essence hydrophobic and surface active, and we believe that computer simulations of related complex heterogeneous solutions will contribute to improve our understanding of the deep relationship between the surface-active character of the complexes and of their counterions, the third-phase formation in solvent extraction, and the Hofmeister's classification of salts [54].

$Ba^{2+}\subset$222,2Pic^- cryptates with divalent cations are surface active, partly due to the concentration of Pic^- anions at the interface (Figure 4). Also noteworthy is the case of acids that are often present in extraction systems. Simulations have correctly predicted that nitric acid is surface active (in its neutral form HNO_3) [31] and that other acids (like carboxylic acids) should be a fortiori more surface active, possibly promoting the extraction of M^{n+} by exchanging their protons and stabilizing the co-extracted anion via hydrogen-bonding interactions.

Implications Concerning the Mechanism of Assisted Ion Extraction

The fact that the studied extractant molecules and their complexes are surface active strongly suggests that the ion complexation takes place "right at the interface," that is, in a very thin domain (of the nanometer size) of the solution. It is thus crucial that highly hydrophilic species (e.g., M^{3+} cations) can approach close enough to the interface to meet the ligand, and this may be facilitated by suitable counterions that are hydrophobic and surface active enough to induce a locally enhanced concentration of cations. The importance of the liquid-liquid interface in solvent-extraction chemistry has been pointed out in the literature based, for instance, on surface-tension measurements [32,33], the interpretation of kinetic results [34-37], interfacial electrochemistry [38-41], or surface spectroscopic results [42-44] on various systems. The MD simulation results are fully consistent with this view and provide detailed nanoscopic representations of the interfacial landscape.

Hydrophobic Aggregation of Ions in Water

When simulated in pure water, the CCD^- anions do not disperse, but tend to aggregate, due to "hydrophobic attractions," with again clear counterion effects; for example, there is more aggregation with Cs^+ than with H_3O^+ as counterion [26]. The simulated aggregates are dynamic in nature, and their size, on the order of 2 nm, fluctuates with time, involving some anion exchanges between the "cluster" and "bulk" water domains. These results are fully consistent with those of light-scattering studies on aqueous solutions of concentrated sodium and cesium dicarbollide salts [45]. It was concluded that about 80% of ions form large aggregates (of up to 115 nm), and a small fraction of molecules dissolve molecularly or form small aggregates. The behavior of nanoaggregates is fairly complex and depends on the concentration and aging of the solutions and on the counterions. Computational and experimental results, although dealing with systems of different sizes, are thus consistent with each other.

With big cationic solutes ($K^+\subset$222 cryptates), one also observes a clear tendency for aggregation in water, and this is more pronounced with Pic^- than with Cl^- as counterion, in keeping with the self-aggregation of the Pic^- anions themselves in water [46]. Divalent cryptates like $Ba^+\subset$222, 2Pic^- also make short contact in water, because the complexed cations act as counterions of negatively charged $(Pic^-)^n$ columns (Figure 4). When the liquid is not polar enough to solvate the salt well, the cryptates and their counterions collapse into a big droplet of "molten salt" type [46]. This has indeed been observed computationally with $K^+\subset$222, Pic^- cryptates [46], as well as with the CCD^- Cs^+ salt in chloroform [26]. In more polar solvents, the ions dilute more randomly; see,

for example, the simulations of the Cs^+CCD^- salt in nitrobenzene [12] or octanol solutions [9], and of monocharged cryptates in acetonitrile [46].

Importance of the Nature of the Organic Phase and of Synergistic CCD^- Anions in the Eu(III) Extraction by BTP Ligands

The case of cation extraction by BTP ligands is important from the experimental point of view, because these ligands display an interesting actinide(III)/lanthanide(III) extraction selectivity [47]. The $Eu(BTP)_3^{3+}$ extracted complex has been characterized experimentally by various structural methods and by titration, showing that the cation is well shielded from the solvent by the three BTP ligands. Experimentally, extraction takes place in acidic conditions, using for example, TPH (a mixture of branched alkanes) and octanol or pure octanol as receiving phase and is markedly enhanced when dicarbollide salts are added to the system. Aromatic solvents like nitrobenzene can also be used for academic experiments but not for industrial processes. We have simulated biphasic water/oil solutions containing some key solutes involved in that process, modelling the cation by Eu(III), similar in size as Am(III) or Cm(III). We wanted to investigate under which circumstances the complex, once formed, partitions towards the oil phase: what is the influence of synergistic CCD^- anions, and how important is the choice of the organic phase from the practical as well as from the computer-modelling points of view. Most simulations have been performed with three solvents, chloroform, octanol, and nitrobenzene, as receiving phase, with different amounts of added CCD^- counterions. The main results have been published [9,12], and selected snapshots are shown in Figure 5.

With the three tested organic solvents, the $Eu(BTP)_3^{3+}$ complex is found to strongly adsorb at the interface, attracted by water dipoles. It can thus hardly be extracted to either of the studied organic phases. Even when its three NO_3^- counterions have been replaced by three CCD^- anions, it remains trapped at the interface with its counterions, without undergoing migration to the oil phase. This contrasts with the case where CCD^- anionss are in excess: the complex has lost any contact with the water phase at the microscopic level and can thus be considered as "extracted". The key issue is to quit the interface, and the simulations clearly show that this process is promoted by the CCD^- anions when they are in excess. That is, they partition between the interface and the organic phase and surround and neutralize the $Eu(BTP)_3^{3+}$ complex, whose hydrophobic periphery is mainly solvated by organic molecules (octanol or nitrobenzene), without attracting water. With chloroform as organic phase, no extraction takes place in the same simulated conditions, presumably because this solvent is not polar enough to properly solvate the complex and its counterions. It thus becomes clear that synergistic agents like CCD^- anions have to be concentrated enough to promote extraction. The same feature has been found by MD simulations on uranyl extraction by diketonate ligands to SC-CO_2 [48] or on uranyl extraction by TBP to chloroform or SC-CO_2 [49-51]: a high concentration of TBP has to be added to the solution (both experimentally and computationally) because, according to the simulations, TBP acts (i) as ligand or co-ligand of the metal (making the complex more hydrophobic), (ii) as a surface active amphiphilic species (promoting the formation of microemulsions and interfaces), and

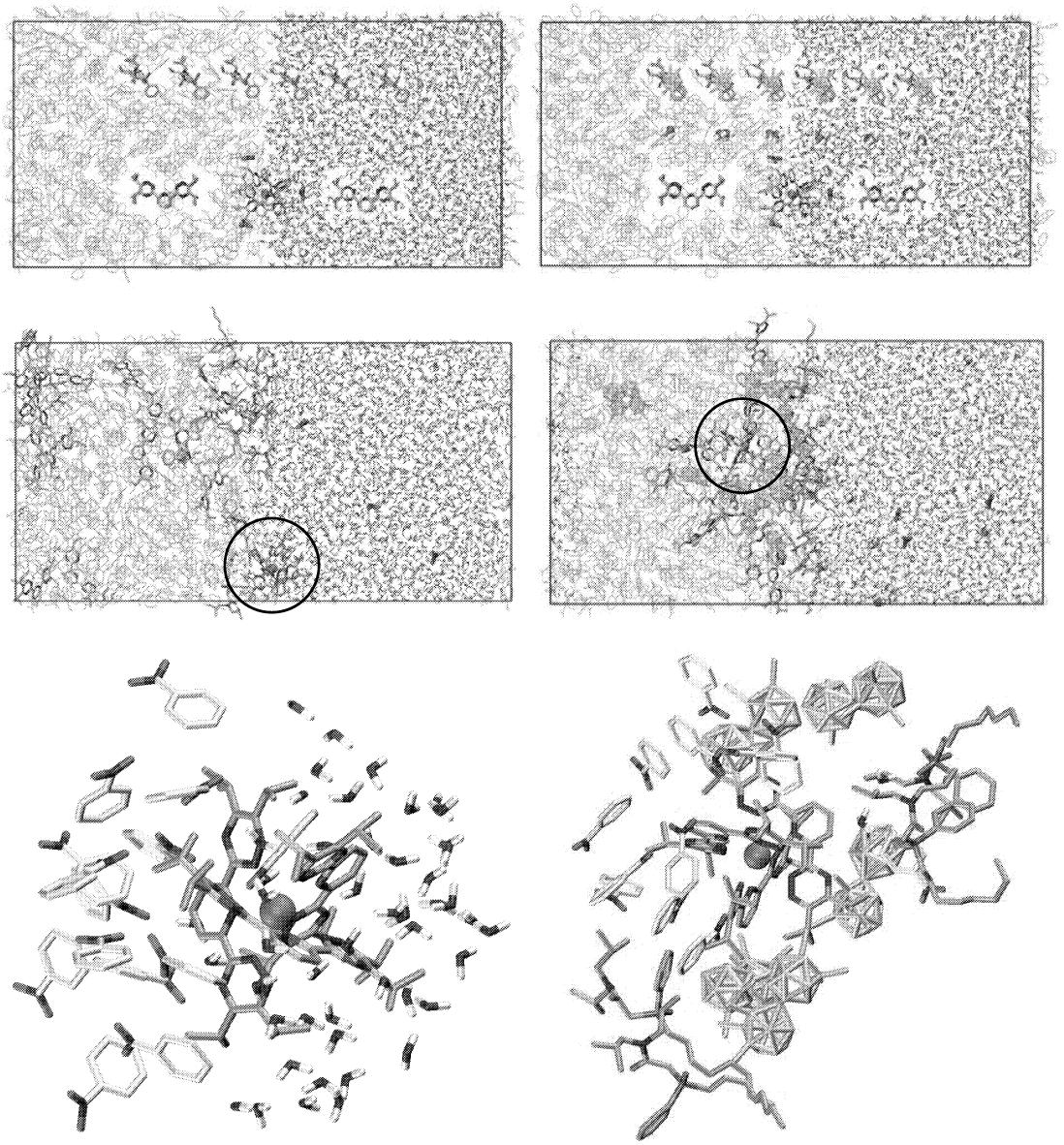

Figure 5. The $Eu(BTP)_3^{3+}$,$3NO_3^-$ complex in the presence of 12 CMPO + 12 BTP ligands at the nitrobenzene-water interface, without CCD^-s (*left)* and with 12 CCD^- H_3O^+ added ions (*right*). From top to bottom: Initial and final views (15 ns), with typical snapshots of the $Eu(BTP)_3^{3+}$ complex adsorbed at the interface (*left*) or extracted (*right*).

(iii) as co-solvent (improving the solvation of the extracted complexes). The modelling of such systems points to the importance of correctly accounting for the complexity of the system and for concentration effects that deeply modify the characteristics and the supramolecular organization of the solution.

Acidic solutions are more difficult to model by classical MD, because this would require an a priori knowledge of the nature and concentration of the different forms of the acid. Furthermore, the p*Ka* is stressed to be different in the interfacial region, the organic phase, and in bulk aqueous solution. Our approach with nitric acid has been to consider an equimolecular mixture of the HNO_3 and H_3O^+ NO_3^- forms, showing that the former is highly surface active and partitions more, as expected, to the organic phase [49]. Furthermore, in the case of uranyl extraction by TBP, we have found that the acid induces local mixtures of "oil," acid, water, and $UO_2(NO_3)_2(TBP)_2$ complexes, which can be viewed as the early step of third-phase formation [49].

PERSPECTIVES

There is always something to be learned from "in silico" computer experiments on ion extraction, where solvents are explicitly represented. Some results seem obvious to experimentalists, others remain somewhat provocative or seem irrelevant, because the simulated system is too simple in terms of constitution or representation. Modelling does not merely consist of applying computational techniques but first requires one to analyze a complex process, and to decide and test to which extent it can be simplified and reduced in terms of complexity, size, time scale, and empirical representation of its energy. Ideally, one could dream of starting the simulation like the real experiment with the salts in water and the extractants in the oil phase to see whether complexation will occur and whether the complex will finally be extracted. This is presently hardly feasible, because it would require excessively long simulations as well as to activate the process along some selected "reaction coordinate" (see, for example, the complexation pathway of Cl^- into a macrocylic host in water [52]). One exception concerns the case of uranyl nitrate extraction by TBP from acidic water to chloroform or to SC-CO_2 [53]. During the demixing simulation of a random mixture of solvents, TBP, and $UO_2(NO_3)_2$ molecules, we have indeed observed the spontaneous formation of the $UO_2(NO_3)_2(TBP)_2$ complex and its partitioning in the oil phase. This occurred, however, only when the TBP concentration was high enough, as achieved experimentally [53], pointing to the importance of the complexity of the system, which is supramolecular in nature. As in the case of charged amphiphiles, the concentration and the medium (counterions and additives) determine the nature of the assemblies and of its function. Extracted complexed ions are in essence hydrophobic and surface active, and we believe that computer simulations of related complex heterogeneous solutions will contribute to improve our understanding of the deep relationship between the surface-active character of the complexes and of their counterions, the third-phase formation in solvent extraction, and the Hofmeister's classification of salts [54].

ACKNOWLEDGMENTS

The authors are grateful to IDRIS, CINES, Louis Pasteur University, and the GDR-PARIS for computer resources, to the European Union EUROPART project (FI6W-CT-2003-508854) for financial support, and to E. Engler for assistance. GC, NS and NG thank the French Ministry of Research for a PhD grant.

REFERENCES

1. M. P. Allen and D. J. Tildesley, Computer Simulation of Liquids, W. F. van Gunsteren, and P. K. Weiner, Eds., Clarendon Press, Oxford, 1987.
2. G. Wipff, Computational Approaches in Supramolecular Chemistry, Kluwer, Dordrecht, 1994.
3. P. Auffinger and G. Wipff, "Hydration of the Bicyclic 222 Cryptand and 222 Cryptates Studied by Molecular Dynamics Simulations," *J. Am. Chem. Soc.,* **113**, 5976-5988 (1991).
4. M. Lauterbach and G. Wipff, in Physical Supramolecular Chemistry, L. Echegoyen and A. Kaifer, Eds., Kluwer, Dordrecht, 1996; pp. 65-102.
5. P. Jost, N. Galand, R. Schurhammer, and G. Wipff, "222 Cryptand and its Cryptates at the Water/Chloroform Interface: Molecular Dynamics Simulations of Concentrated Solutions," *Phys. Chem. Chem. Phys.,* **4**, 335-344 (2002).
6. N. Muzet, E. Engler, and G. Wipff, "Demixing of Binary Water- Chloroform Mixtures Containing Ionophoric Solutes and Ion Recognition at a Liquid-Liquid Interface: A Molecular Dynamics Study," *J. Phys. Chem. B,* **102**, 10772-10788 (1998).
7. M. Lauterbach, E. Engler, N. Muzet, L. Troxler, and G. Wipff, "Migration of Ionophores and Salts through a Water-Chloroform Liquid-Liquid Interface: Computer MD-PMF Investigations," *J. Phys. Chem. B,* **102**, 225-256 (1998).
8. R. Schurhammer, P. Vayssière, and G. Wipff, "18-Crown-6 and its Hydrates: Bridging, but Versatile Hydrogen Bond. A Theoretical Study of Static and Dynamic Properties," *J. Phys. Chem. A,* 11128-11138 (2003).
9. G. Chevrot, R. Schurhammer, and G. Wipff, "Synergistic Effect of Dicarbollide Anions in Liquid–Liquid Extraction: A Molecular Dynamics Study at the Octanol–Water Interface," *Phys. Chem. Chem. Phys.,* **9**, 1991-2003 (2007).
10. G. Chevrot, R. Schurhammer, and G. Wipff, "Molecular Dynamics Simulations of the Aqueous Interface with the [BMI][PF_6] Ionic Liquid: Comparison of Different Solvent Models," *Phys. Chem. Chem. Phys.,* **8**, 4166-4174 (2006).
11. I. Benjamin, "Theory and Simulation of Solvation and Chemical Reactions at Liquid Interfaces," *Acc. Chem. Res.,* **28**, 233-239 (1995).
12. G. Chevrot, R. Schurhammer, and G. Wipff, "Molecular Dynamics Study of Dicarbollide Anions in Nitrobenzene Solution and at its Aqueous Interface. Synergistic Effect in the Eu(III) Assisted Ion Extraction," *Phys. Chem. Chem. Phys.,* **9**, 5928-5938 (2007).
13. A. Chaumont, R. Schurhammer, and G. Wipff, "Aqueous Interfaces with Hydrophobic Room-Temperature Ionic Liquids. An MD Study," *J. Phys. Chem. B,* **109**, 18964-18973 (2005).
14. N. Sieffert and G. Wipff, "The [BMI][Tf_2N] Ionic Liquid/Water Binary System: A Molecular Dynamics Study of Phase Separation and of the Liquid-Liquid Interface," *J. Phys. Chem. B,* **110**, 13076-13085 (2006).
15. N. Sieffert and G. Wipff, "The Effect of a Solvent Modifier in the Cesium Extraction by a Calix[4]arene: A Molecular Dynamics Study of the Oil Phase and the Oil–Water Interface," *Phys. Chem. Chem. Phys.,* **9**, 3763-3775 (2007).

16. N. Sieffert and G. Wipff, "Comparing an Ionic Liquid to a Molecular Solvent in the Caesium Cation Extraction by a Calixarene: A Molecular Dynamics Study of the Aqueous Interfaces," *J. Phys. Chem. B,* **110**, 19498-19506 (2006).
17. N. Sieffert and G. Wipff, "Alkali Cation Extraction by a Calix[4]crown6 to Room Temperature Ionic Liquids. The effect of Solvent Anion and Humidity Investigated by Molecular Dynamics Simulations," *J. Phys. Chem. A,* **110**, 1106-1117 (2006).
18. A. E. Visser, R. P. Swatloski, S. T. Griffin, D. H. Hartman, and R. D. Rogers, "Liquid/Liquid Extraction of Metal ions in Room Temperature Ionic Liquids," *Sep. Sci. Technol.,* **36**, 785-804 (2001).
19. A. E. Visser and R. D. Rogers, "Room-Temperature Ionic Liquids: New Solvents for *f*-element Separations and Associated Solution Chemistry," *J. Solid State Chem.,* **171**, 109-113 (2003).
20. H. Luo, S. Dai, P. V. Bonnesen, A. C. Buchanan III, J. D. Holbrey, N. J. Bridges, and R. D. Rogers, "Extraction of Cesium Ions from Aqueous Solutions Using Calix[4]arene-bis(*tert*-octylbenzo-crown-6) in Ionic Liquids," *Anal. Chem.,* **76**, 3078-3083 (2004).
21. N. Sieffert, "Importance des Interfaces Liquide–Liquide: de l'Extraction d'Ions à la Catalyse par Transfert de Phase. Etudes par Dynamique Moléculaire avec des Solvants Moléculaires et des Liquides Ioniques," Thesis, 2007, Université Louis Pasteur Strasbourg, France.
22. L. X. Dang, "A Mechanism for Ion Transport Across the Water/Dichloromethane Interface: A Molecular Dynamics Study Using Polarizable Potential Models," *J. Phys. Chem. B,* **105**, 804-809 (2001).
23. N. Sieffert and G. Wipff, "Importance of Interfacial Adsorption in the Biphasic Hydroformylation of Higher Olefins Promoted by Cyclodextrins: a Molecular Dynamics Study at the Decene - Water Interface," *Chem. Eur. J.,* **13**, 1978-1990 (2007).
24. F. Berny, N. Muzet, L. Troxler, and G. Wipff, in Supramolecular Science: where it is and where it is going; R. Ungaro and E. Dalcanale Eds., Kluwer Acad. Pub., Dordrecht, 1999; pp. 95-125.
25. J. Rais and B. Grüner, in Ion Exchange and Solvent Extraction; Vol. 17, Y. Marcus, A. K. SenGupta, and J. A. Marinsky, Eds., M. Dekker, New York, 2004; pp. 243-334.
26. G. Chevrot, R. Schurhammer, and G. Wipff, "Surfactant Behavior of "Ellipsoidal" Dicarbollide Anions. A Molecular Dynamics Study," *J. Phys. Chem. B,* **110**, 9488-9498 (2006).
27. A. Chaumont, N. Galand, R. Schurhammer, P. Vayssière, and G. Wipff, "Accumulation of Host-Guest ion Complexes at the Water / SC-CO_2 Interface with Different Counterions: a Molecular Dynamics Study," *Russ. Chem. Bull., Internat. Ed.,* **53**, (2004).
28. B. Schnell, R. Schurhammer, and G. Wipff, "Distribution of Hydrophobic Ions and their Counterions at an Aqueous Liquid-Liquid Interface: a Molecular Dynamics Investigation," *J. Phys. Chem. B,* **108**, 2285-2294 (2004).
29. R. Schurhammer and G. Wipff, "Are the Hydrophobic $As\phi_4^+$ and $B\phi_4^-$ Ions Equally Solvated? A Theoretical Investigation in Aqueous and Non Aqueous Solutions using Different Charge Distributions," *J. Phys. Chem. A,* **104**, 11159-11168 and **105**, 292 (2000).
30. F. Berny, R. Schurhammer, and G. Wipff, "Distribution of Hydrophilic, Amphiphilic, and Hydrophobic Ions at a Liquid-Liquid Interface: a Molecular Dynamics Investigation," *Inorg. Chim. Acta,* **300-302**, 384-394 (2000).
31. R. Schurhammer and G. Wipff, "Interfacial Activity of Nitric Acid at the Water / SC-CO_2 Interface: a Molecular Dynamics Investigation," *New J. Chem.,* **26**, 229-233 (2002).

32. Z. Yoshida and H. Freiser, "Mechanism of the Carrier-mediated Transport of ¨Potassium ion across Water-Nitrobenzene Interface by Valinomycin," *J. Electroanal. Chem.,* **179***,* 31-39 (1984).
33. J. Szymanowski, "Kinetics and Interfacial Phenomena," *Solvent Extr. Ion Exch.,* **18***,* 729-751 (2000).
34. P. R. Danesi, in Principles and Practices of Solvent Extraction; J. Rydberg, C. Musikas, and G. R. Choppin, Eds., Marcel Dekker, New York, 1992; pp. 157-207.
35. H. Watarai, "What's Happening at the Liquid-liquid Interface in Solvent Extraction Chemistry?" *Trends in Analytical Chem.,* **12***,* 313-318 (1993).
36. G. A. Yagodin and V. V. Tarasov, "Interfacial Phenomena in Liquid-Liquid Extraction," *Solvent Extr. Ion Exch.,* **2***,* 139-179 (1984).
37. G. F. Vandegrift and E. P. Horwitz, "The Mechanism of Interfacial Mass Transfer of Calcium in the System: Di(2-Ethylhexyl)Phosphoric Acid in Dodecane-Dilute Nitric Acid," *J. Inorg. Nucl. Chem.,* **39***,* 1425-1432 (1977).
38. H. H. Girault and D. J. Schiffrin, in Electroanalytical Chemistry, A. J. Bard, Ed., Dekker, New York, 1989; pp. 1-141, and references cited therein.
39. J. Koryta, "Ion Transfer across Water/Organic Boundaries and Analytical Applications," *Ion Selective Electrode Rev.,* **5***,* 131-164 (1983).
40. P. Vanysek, W. Ruth, and J. Koryta, "Valinomycin Mediated Transfer of Potassium Across the Water/Nitrobenzene Interface. A Study by Voltammetry at the Interface between Two Immiscible Electrolyte Solutions," *J. Electroanal. Chem.,* **148***,* 117-121 (1983).
41. A. N. Popov, in The Interface Structure and Electrochemical Processes at the Boundary Between Two Immiscible Liquids, V. E. Kazarinov, Ed., Springer Verlag, Berlin, 1987; pp. 179-205.
42. M. Fujiwara, S. Tsukahara, and H. Watarai, "Time-resolved Total Reflection Fluorometry of Ternary Europium(III) Complexes Formed at the Liquid-Liquid Interface," *Phys. Chem. Chem. Phys.,* **1***,* 2949-2951 (1999).
43. K. B. Eisenthal, "Liquid Interfaces Probed by Second-Harmonic and Sum-Frequency Spectroscopy," *Chem. Rev.,* **96***,* 1343-1360 (1996).
44. L. F. Scatena and G. L. Richmond, "Isolated Molecular Ion Solvation at an Oil/Water Interface by Vibrational Sum-Frequency Spectroscopy," *J. Phys. Chem. B,* **108***,* 12518-12528 (2004).
45. P. Matejicek, P. Cigler, K. Prochazka, and V. Kral, "Molecular Assembly of Metallocarboranes in Water: Light Scattering and Microscopic Study," *Langmuir,* **22***,* 575-589 (2006).
46. P. Jost, R. Schurhammer, and G. Wipff, "Supramolecular Interactions of Cryptates in Concentrated Solutions. The effect of Solvent and Counterions Investigated by MD Simulations," *Solvent Extr. Ion Exch.,* **25***,* 257-271 (2007).
47. A. Geist, C. Hill, G. Modolo, M. R. S. J. Foreman, M. Weigl, K. Gompper, and M. J. Hudson, "6,6'-Bis(5,5,8,8-tetramethyl-5,6,7,8-tetrahydro-benzo(1,2,4)triazin-3-yl)(2,2') bipyridine, an Effective Extracting Agent for the Separation of Americium (III) and Curium(III) from the Lanthanides," *Solvent Extr. Ion Exch.,* **24***,* 463-483 (2006).
48. N. Galand and G. Wipff, "Uranyl Extraction by β-Diketonate Ligands to SC-CO_2: Theoretical Studies on the Effect of Ligand Fluorination and on the Synergistic Effect of TBP," *J. Phys. Chem. B,* **109***,* 277-287 (2005).
49. M. Baaden, F. Berny, and G. Wipff, "The Chloroform / TBP / Aqueous Nitric Acid Interfacial System: a Molecular Dynamics Investigation," *J. Mol. Liquids,* **90***,* 3-12 (2001).

50. M. Baaden, F. Berny, N. Muzet, L. Troxler, and G. Wipff, in Calixarenes for Separation. ACS Symposium Series 757, G. J. Lumetta, R. D. Rogers and A. Gopalan, Eds., American Chemical Society, Washington DC, 2000; pp. 71-85.
51. M. Baaden, M. Burgard, and G. Wipff, "TBP at the Water–Oil Interface: the Effect of TBP Concentration and Water Acidity Investigated by Molecular Dynamics Simulations," *J. Phys. Chem. B,* **105***,* 11131-11141 (2001).
52. A. Chaumont, E. Engler, and G. Wipff, "Halide Anion Capture and Recognition by a Tetrahedral Tetraammonium Receptor in Water: A Molecular Dynamics Investigation," *Eur. J. Chem.,* **9***,* 635-643. (2003).
53. M. Baaden, R. Schurhammer, and G. Wipff, "Molecular Dynamics Study of the Uranyl Extraction by Tri-*n*-butylphosphate (TBP): Demixing of Water/'Oil'/TBP Solutions with a Comparison of Supercritical CO_2 and Chloroform," *J. Phys. Chem. B,* **106***,* 434-441 (2002).
54. M. G. Cacace, E. M. Landau, and J. J. Ramsden, "The Hofmeister Series: Salt and Solvent Effects on Interfacial Phenomena," *Quart. Rev. Biophys.,* **30***,* 241-277 (1997).

THE ROLE OF ENTROPY IN THE DESIGN OF MOLECULAR HOSTS

Franz P. Schmidtchen

Department of Chemistry, Technical University of Munich, Lichtenbergstrasse 4
D-85747 Garching, Germany
Corresponding author email address: schmidtchen@ch.tum.de

ABSTRACT

Tuning selectivity in two-phase extraction necessitates command over the individual preferences of the ions in focus for their molecular environment. On this terrain, a bold threshold is set by the interaction with the solvent, which extends not only to the direct mutual enthalpic stabilization experienced by all compounds in condensed phases. Rather, solvation encompasses also the structural rearrangements felt in the solvent and surfaces as the observable entropy, which frequently dominates the overall energetics in associations. These solvation influences need to be overcome and differentially outmatched by additives acting as molecular ligands (i.e., hosts). Traditionally, the design and construction of such hosts took the maximization of attractive interactions with the guest species (the ions) as the prime goal (cf. the fit, as in the lock-and-key metaphor), which included the dedicated preorganization of the respective anchoring functionalities within the host structure. Though such structuring also touches on the entropic aspects of binding, it addresses only some fraction of the overall effect. The present lecture focuses on the role of entropy in molecular associations and its accounting and implementation into the design of molecular hosts

INTRODUCTION

Molecular interactions resulting in the trade of energy and momentum between molecules are ubiquitous and unavoidable. Art comes into play when such interactions are to be guided to afford a preference over what must be expected anyway as a result from such fundamental energetic exchange. In fact, the governance over these processes is at the heart of all chemical sciences and spans from the choice of simple solvation conditions (“similia similibus solvuntur”; lat.: like dissolves like) to the erection of highly sophisticated supramolecular networks (e.g., the DNA doublehelix, folded proteins, membranes, ribosomes, the cytoskeleton, light-harvesting antennae, molecular machinery, etc.) that constitute and characterize all living matter. Inspired by these examples, the focus of scientific attention currently shifts from the classic construction of covalently connected frameworks, which have arrived at a respectable level of maturation already, to the elaboration of noncovalent assemblies [1]. The promiscuous ambivalence, fragility, and sensitivity towards reversible rearrangements in such systems

present demanding challenges, which are well recognized, indeed [2,3], but not at all solved to any reasonable satisfaction.

Of prime concern towards this goal is the development of dedicated structures that would interact selectively with a certain molecular target to perform a peculiar function such as to effect its transfer across a liquid-liquid phase boundary. We will call such compounds molecular hosts irrespective of their chemical nature, size, mode of action, or preparation. The common denominator just refers to the reversibility of interaction with the binding partner in a dynamic and kinetic sense, which limits its absolute magnitude to a regime <80 kJ mol^{-1} and to a selectivity feature characterizing the capacity of the host to determine the fate of the specific guest, leading to its discrimination over all potential competitors. In this respect the mere host-guest association event in the thermodynamic ground state constitutes a necessary prerequisite defining a binding selectivity that may, however, only set the stage for a subsequent kinetic process. The kinetic selectivity emerging from the latter step need not necessarily enforce the discrimination seen in the binding step but may follow a different pattern [5]. Thus, it is rational to treat both steps distinct from one another.

This article concentrates on the initial binding process and the options to influence the selectivity outcome by designing the host structure. Of course, thermodynamics will ultimately dictate the selectivity facet, yet it is important to discern two divergent goals requiring distinctly different energetic signatures in realization: Thermodynamic selectivity may target the maximization of the binding free energy leading to high affinity systems as they are required, for example, in drug development in the blocking of enzyme active sites. The precise molecular layout there is of minor concern as long as the uptake of the substrate into the active site is efficiently prevented. Alternatively, the molecular association could aim at the generation of a unique host-guest complex structure. A well-defined structural platform is indispensible, for instance, in the build-up of molecular architectures in nanotechnology or for catalyses requiring fixed stereoelectronics. For purposes of extraction from aqueous solution, the structure to be attained is one that presents a hydrophobic exterior of the associated complex ensemble to the solvent environment. The outer lining should be devoid of sites capable of interacting with water molecules that would otherwise impede the “pushing out” of the complex from the aqueous phase. As a corollary, then, the first decision in host design must address the function envisaged. The result of this decision then defines a pattern of thermodynamic state functions suggesting a strongly negative association enthalpy concomitant with a negative entropy component for creating structural uniqueness.

More relaxed enthalpy requirements along with positive entropies are desirable for optimizing affinity (see below). A collateral incidence of such signatures is the prediction that the association-dissociation kinetics is likely to possess a steeper temperature dependence in the former case owing to a larger $\Delta H^{\neq}$ of activation necessary in the more robustly structured system to escape from the deep enthalpic well founding the host-guest complex. Aside from kinetics, the absolute and relative stability (with respect to potential competitors) of this complex was in the focus of supramolecular chemistry even decades before this term was coined [6]. Following an intriguing pictorial metaphor introduced by Emil Fischer more than a century ago [7], generations of chemists looked upon host-guest binding as an act of recognizing geometrical

complementarity (and much later also complementarity of charges, chemical functions, etc.) between the interacting partners in much the same way as a mechanical key fits into a corresponding lock, enabling selective entrance to the keyholder. Despite the fertility and success of this idea for the explanation of a plethora of association phenomena, the exclusive emphasis on the enthalpy (attraction/repulsion) of the interaction partners in the lock-and-key model promotes a misleading perspective of host-guest binding in general [2,3,8]. An unbiased view of the simple complementarity models of host-guest association will immediately trace their failures (examples of which are presented later in this review) to the omission of the entropy component that, according to fundamental thermodynamics, must contribute to the observed affinity, yet is either totally dropped from consideration in the original model or only fractionally incorporated in the more elaborate "induced-fit" model of molecular recognition [9].

One can speculate on the origin of such obvious disregard. Major reasons may be "the low level of common intuition about entropy" in the chemical community [3,10] or the easier and more straightforward division of enthalpy into dominant and negligible contributions. This is hard to achieve with the entropic state function, as all components of the associating system including solvent background electrolytes, counterions, solubility adjuvants, or others are intimately involved. At present, we are still unable to quantitatively account for individual entropic contributions required as input parameters in the rational design of host compounds. However, we realize the necessity to expand the current conceptual models by including at least some aspects of entropy. The recent progress of computational and experimental calorimetric methods foster our hope to put entropic reasoning on a solid quantitative footing in the foreseeable future.

SOME FUNDAMENTALS

Host-guest chemistry for the sake of selectivity must address the high-end regime of molecular interaction energetics, because the free-energy differences $\Delta\Delta G^o$(A,B) = RT ln K_{eq}(B)/K_{eq}(A) on binding substrates A or B to a host compound can only become large if the individual association free energies ΔG^o(A) and ΔG^o(B) are even greater. For isothermal binding processes depicted in Scheme 1, the position of the equilibrium, as transmitted by the association constant K_{eq}, is governed by two fundamental equations (2 and 3) which can be combined to give Equation 4.

Scheme 1

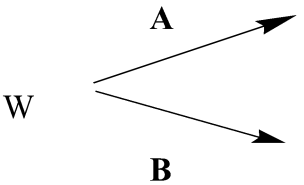

{A⊂W} $$K_{eq}(A) = \frac{[\{A \subset W\}]}{[A] \times [W]} \quad (1a)$$

{B⊂W} $$K_{eq}(B) = \frac{[\{B \subset W\}]}{[B] \times [W]} \quad (1b)$$

Interestingly, this rearranged form of the familiar Gibbs-Helmholtz Equation 3 reveals the affinity of the two binding partners as a consequence of balancing two

entropy components: The entropy change in the system ΔS^o and the entropy change in the rest of the universe $\Delta H^o/T$. The latter term denotes the heat reversibly exchanged with the environment divided by the temperature of the isothermal process as defined for an entropy change. There is no better way to illustrate the importance of entropy in molecular association than by Equation 4.

$$\Delta G^o = - R\,T \ln K_{eq} \tag{2}$$

$$\Delta G^o = \Delta H^o \quad - \quad T\,\Delta S^o \tag{3}$$

$$R \ln K_{eq} \quad = \quad \Delta S^o \quad - \quad \frac{\Delta H^o}{T} \tag{4}$$

Traditionally, this notion has been underappreciated, as the subject of host design was focused on discovering the strongest binding partner for a given guest, which is equivalent to finding the most enthalpically stable host-guest pair. Except for the exotic situation of studying binding near absolute zero temperatures ($T\,\Delta S^o \rightarrow 0$) or the adventitious case where ΔS^o equals zero, such approaches can be severely misleading, because entropy as an essential component of the energetics is deliberately disregarded. Even the most simple associative process between molecular species in the gas phase does involve a nominal decrease in entropy, since three degrees each of translation and overall rotation are sacrificed to form a rigid complex [11]. However, the extent to which the system's entropy suffers from this effect can vary within vast limits [12]. Incomplete arresting of relative motions between the bound partners and the initiation of novel vibrational modes in the complex could counterbalance the expected entropy loss. On top, it is conceivable that entropy is even produced on guest association if a gain in molecular flexibility (i.e., conformational entropy) outmatches the translational/rotational restriction of binding. For instance, a well-organized host could diminish or partially lose its structural integrity on guest association, furnishing a more positive entropy contribution than was required to make up for the putative loss occurring on merging two independently moving particles into one. Examples suggesting such an explanation have been observed in ligand binding of some proteins. A corresponding design would open a novel target for tailoring the entropy component in artificial host compounds.

Beyond doubt, interaction enthalpy is an important contribution to overall host-guest affinity, yet it may not be the decisive one. Figure 1 qualitatively illustrates two extremes for the dependence of enthalpy on a structural parameter in the complex (distance, a dihedral torsion, or the

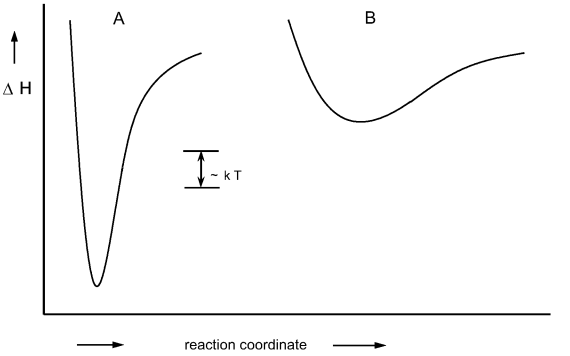

Figure 1. Illustration of the different shapes of enthalpy wells.

like). Optimizing the enthalpic interaction ΔH would target the deepest enthalpic well (A), whilst the shallower, yet broader, enthalpy dip B characterizes a host-guest pair that is inferior to A with respect to enthalpy but outmatches this complex in binding free energy ΔG, due to a much more favorable entropy component. Affinity maximization using an energy-minimization strategy fails to return the correct candidate in this scenario [13]. We conclude that host design following common docking procedures [14], even if guided by X-ray crystal structures showing a concrete supramolecular interaction motif [15], does not rightly address the essence of host-guest recognition. The design of molecular hosts based on enthalpy alone is at risk to fall victim to oversimplification.

Some remedy can be expected from the regard of entropy in design considerations. The step to take involves a translation of the quite abstract macroscopic state functions into a molecular context [16]. Ludwig Boltzmann built a bridge that allows crossing this gap by a formula relating the entropy S (based on the 3rd law of thermodynamics, this is the entropy change from zero Kelvin to the temperature of measurement ΔS) to the number of energetically accessible microstates W (Equation 5) [17], namely the number of ways to distribute the total energy onto the energy levels held by the system's components.

$$S = R \ln W \tag{5}$$

There is little doubt that W is dramatically dependent on the structural context. However, backtranslation, the deconvolution of W or its representation ΔS into a set of concrete structures is not possible. For all real systems, the number W and also its change in binding processes is intractably huge. A good reflection of entropy that is handier to supramolecular chemists is the dynamics of the system, namely the positional, configurational, conformational, and vibrational space visited by the components in time. The space is filled with enthalpic wells of varying deepness and shape separated by barriers of different heights, and this rugged landscape is populated by the system's atoms. At equilibrium, the populations of the individual wells and their interconversion rates contain information about some facets of the total entropy that are relevant in host design and can be accessed using, for example, specialized NMR techniques [18].

INSPECTING THE BARE BONES OF MOLECULAR ASSOCIATION: THE LOCK-AND-KEY MODEL

A first approximation to the qualitative estimation of entropy could take the sketch depicted in Figure 2 as a basis. The host and guest partners generally interact in multiple ways to form a variety of one-on-one aggregates featuring various conformations of the partners interacting in a variety of topologies (binding modes). In addition, depending on concentration, higher-order complexes are formed consisting of more than one copy of the same partner binding to its counterpart or even including another molecular species (counterion, specific solvent molecule, buffer species, etc.). Many of these host-guest configurations will be of low and comparable energy ($<10\ kT$) and thus will be populated side by side at equilibrium to create a structural ensemble. Other configurations are only transiently visited or exhibit a weak correlation of enthalpy

and structure (they float on a flat or very shallow extended area on the potential-energy surface). Whether a single spatial arrangement represents a distinct host-guest complex or just a transient variant of some parent configuration is arbitrary to some extent and depends on both the kinetic barrier separating them and an energetic threshold value corresponding to the thermal energy available. Viewed from the point of host design, the latter is an input parameter dictated by the prospected function and thus is not subject to deliberate tailoring. The sketch in Figure 2 illustrates the simple notion that the number of accessible microstates (the entropy) increases with the number of host-guest spatial arrangements and consequently with the diversity of the structural ensemble.

A logical consequence to boost host-guest affinity would call for the accumulation of identical binding sites, each one interacting with a monovalent guest with the same noncooperative affinity. Simple statistical reasoning (see Equation 5) leads to the conclusion that the presentation of five identical anchor sites on one host molecule augments guest affinity by an order of magnitude over the individual parent interaction. Of course, the precise topological correspondence of host and guest structure is lost unless host symmetry leads to structural degeneracy in the complexes. The general strategy "enforce stickiness by means of fuzziness" is solely based on entropy and exceedingly successful in biology (e.g., in viral cell adhesion, streptavidin-biotin click connection, or even in sexual mating), however, it is not particularly efficient in terms of atom economy or synthetic expenditure, two important cornerstones in host design. Furthermore, the overall selectivity is not enhanced, but rather diminished, since all competitors would experience the same basic boost of their affinities, and the likelihood for unintentional adjuvant interactions exclusively open to a few of the many potential competitors increases (e.g., by optional multivalent interactions).

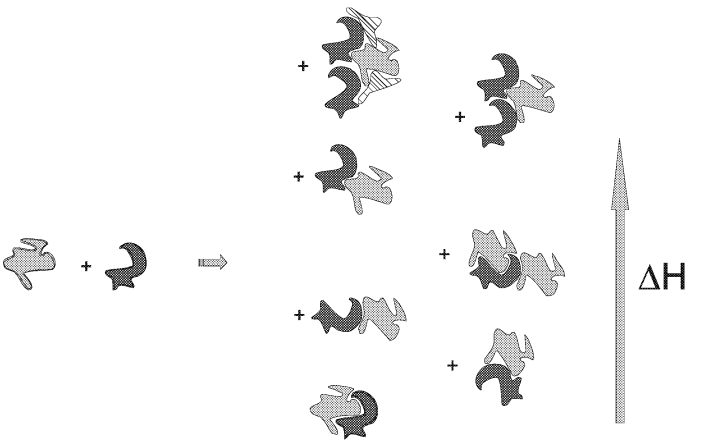

Figure 2. An illustration of the structural ensemble arising from host and guest association (shaded platelets) sorted according to enthalpy.

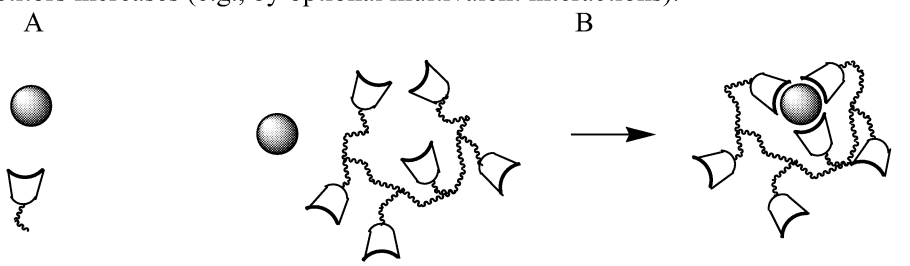

Figure 3. Schematic representation of host-guest complexation by a monovalent (A) versus a multivalent host (B).

The urge to improve selectivity can be served in this strategy by allowing cooperative action of the anchor sites on the host binding the guest at more than one site of interaction. Such multivalent binding [19,20] assumes an intermission by a nonbinding moiety linking the anchor groups that are actively interacting with the guest species. The concept breaks down the closer the anchoring functions are spaced and as the bridging units get more and more involved in the direct interaction with the guest and the anchor groups alike. Finally, the properties of the parent binding sites are distorted due to their vicinity such that their effect on binding cannot be delineated from their original structure anymore. Then the further use in host design mandates the definition of a new binding moiety combining the parent functions and linkers, yet possessing a completely new set of properties. At any rate, the covalent combination of anchoring functions represents a restriction of their mobility that emanates as a bonus in the entropy of binding, since the fixations of the second and all other anchor groups to the guest occur as intramolecular (first order) processes in contrast to the initial intermolecular (second-order) binding step. Supplementing the entropy-based benefit that was already identified in the chelate effect by early coordination chemists [21], the motional restriction seen in multivalent binding also has bearing on enthalpy. The influence can be attributed to the dissymmetric shape of the familiar Lennard-Jones pair potentials of common van der Waals interactions. A gain in enthalpy on binding a second anchor group can arise if the motional amplitudes due to clipping shorten the average distances of nonbonded substructures. This tightening can be rationalized as a slide on the outer branch of the Lennard-Jones pair-potential curve towards the enthalpy minimum. Because this move encompasses all interaction pairs, the entire complex structure, rather than a single group, is compacted [22]. Recent experimental evidence stemming from a trend analysis of binding several series of linear-chain substrates to bovine carbonic anhydrase supports this view [23].

Chemical intuition calls for some kind of compensatory effect between enthalpy and entropy in supramolecular associations, since stronger binding (more negative ΔH) is expected to limit the relative motility of the binding partners and thus should diminish entropy (more negative ΔS). The most obvious result of such enthalpy-entropy compensation (EEC) phenomena is the striking invariance of the affinity ΔG from structural modification within a series of homologous compounds. In fact, early analyses could explain the observations [24,25] graphing the ΔH versus $T\,\Delta S$ dependency as a curved plot that only in the regime of low interaction strength is almost linear, but approaches a limiting value at high ΔH (Figure 4).

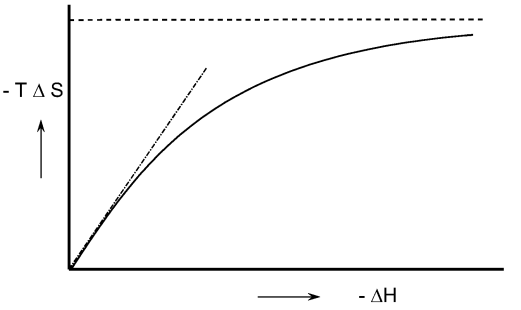

Figure 4. Tentative enthalpy-entropy compensation curve [22].

An important consequence of this model is the expectation that, once a host-guest system has reached the limit, any additional incorporation of binding functionality should no longer suffer from entropic counteraction but be fully translated into binding affinity. The model, however, assumes that the width of the enthalpic well relating to the amplitude of molecular vibrations correlates inversely with its deepness. At first glance,

the connection of binding energy ΔH (viz., the deepness of the well) and the tune of molecular vibrations seems reasonable. However, no such relation has been confirmed for covalent bonds, and there is no argument why supramolecular interactions should be different in this respect [26]. Moreover, fundamental bare-bones theoretical models using calibration to experimental observables arrive at $\Delta H/T\Delta S$ anticompensation relationships that are incompatible with EEC being a constitutive ingredient of all supramolecular interactions [27]. As there is also no strong evidence for the curvature of the $\Delta H/T\Delta S$ plot (Figure 4) implying a maximum limit for the entropy loss, the meaning and extent of EEC to host design must be considered an open question.

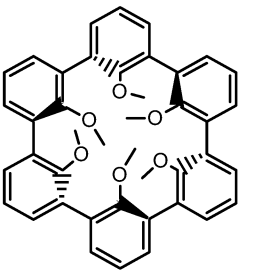

spherand

Empirically, the concept of host preorganization [28] that touches on a similar balance of enthalpy and entropy components features a success story. The covalent connection of binding functions to furnish a molecule that can satisfy all binding needs of a supramolecular guest species and on top cannot escape from presenting this optimal molecular directional layout can be looked upon as the igniting spark to the study of molecular recognition. Initially, the much improved affinities and guest discrimination capacities of rigidly preorganized hosts were exclusively assigned to the freezing of all conformational degrees of freedom in the host structure as is exemplified in the spherand series of alkalimetal cation complexands [29]. The basic idea of minimizing entropy loss by rigidification followed the motto: “what is not there in the first place cannot be lost subsequently.” Meanwhile, consensus is reached that steric congestion caused by the tight covalent connectivity in this host series promotes metal ion complexation enthalpically, too. The cation binding ether atoms are rigidly held in positions and at distances that are conducive to complexation, yet would be relaxed to a less favorable arrangement, if it were allowed by the framework. The benefit of preorganization in this scenario resembles a spring-loaded situation that as a whole cannot be accounted for by an entropic bonus alone.

PUTTING FLESH TO THE BONES: THE REAL CASE REQUIRES THE INCLUSION OF SOLVATION

Contrasting the so-far discussed, somewhat fictitious case of a host compound complexing some guest in free space with no other interaction partner around, the real situation one must address and accommodate the presence of other molecules in much higher abundance, as they are present in all experimentally testable conditions in condensed phases. A true appreciation of the role played by the solvent must respect the “granular character” of such an environment that is dissent from any continuum representation. The difference originates from the anisotropic discontinuity at the molecular level and is reflected in the quite variant standard entropies of the solvents. Most important is the notion that the solvent molecules not only mediate a field effect on the host-guest interaction in focus, for instance, by attenuating the electric field by virtue of their dielectric permittivity and readjust the relative contributions of enthalpic components (coulombic versus van der Waals versus strain, etc.). Rather they are active

participants influencing and competing in all processes and on all levels of the molecular scenery. As a corollary, the overall outcome sensed macroscopically by some physical method is as much a consequence of the action of solvent molecules as it is the result from the direct mutual interaction of the binding partners. The selectivity of molecular recognition is tied to the entire system and is definitely not a molecular property of the host compound. Without the due specification of the environmental conditions (solvent, counterions, buffer, background electrolytes, etc.) the frequently heard claims of the discovery of a novel specific host for some peculiar guest lacks a serious foundation [30].

The individuality of solvent extends beyond the structure of the single molecule to the interaction pattern seen in the entire ensemble and ultimately shows up in the macroscopic state functions. The structuredness of the solvent persists in spite of rapid time averaging, and from its physical basis, it is a component of the solvent entropy. Trouton recognized early on that the entropy of transfer from the liquid to the gas phase at the boiling point T_m (the entropy of evaporation $\Delta H_{evap}/T_m$) is little changed for a number of simple solvents (Trouton's rule). Many other solvents, especially the more useful polar ones including water, show strong deviations from this rule. Obviously, the latter fraction must differ from the former in the entropy of the condensed phase if the approximation of the vapor phase as an ideal gas is valid. An inspection of the solvation entropies of transfer of a solvent molecule from a fixed position in the gas phase to a fixed position in the pure liquid solvent (the so called Ben-Naim standard transfer; the process is devoid of the change in translational entropy and picks up the change in solvation entropy most directly [30]) in general corroborates this expectation (Table 1 [31]). When allowance is made for molecular size and flexibility, the more polar solvents show the more negative transfer solvation entropies, indicating more restricted molecular motility and thus enhanced structuredness. Water occupies no extreme position in this series although, according to many other criteria, it certainly is one of the most structured solvents known. The tiny size of the water molecule and its small molar volume compared to other structured solvents like DMSO or sulfolane may make up on the balance sheet to raise water to a unique position among the solvents.

Table 1. Molar standard entropies of solvation ΔS^* (J K^{-1} mol^{-1}) of solvent molecules by their liquid phase (Ben-Naim standard, transfer of a mol of solvent molecules from a fixed position in the ideal gas phase to a fixed position in their their own solution [32]).

Solvent	$-\Delta S^*$	Solvent	$-\Delta S^*$	Solvent	$-\Delta S^*$
water	66.2	acetonitrile	47.8	tetrahydrofurane	52.4
methanol	62.7	nitromethane	58.8	dimethylsulfoxide	75.2
acetone	49.8	dichlormethane	47.6	dimethylformamide	73.9
chloroform	51.3	1,8-eucalyptol	34.4	N-methylacetamide	53.7
hexane	53.6	sulfolane	126.1	ethylenecarbonate	40.2
benzene	54.9	diethyl ether	47.2	1,1,1-trichlorethane	34.5

Solvent entropy is an important issue in molecular recognition as this value sets a limit to what can be gained on host-guest association. On physical contact of the binding partners, solvent molecules must be stripped off from the interface and join the bulk solvent interactions. Undoubtedly, this desolvation comes along with an entropy change

that is determined by the characteristics of the solvent layer covering the interface areas in both binding partners and the level of entropy in the receiving bulk phase. Only the latter is known with decent certainty, whilst the interfaces themselves may vary widely in their entropy features, and therefore offer a great chance for solvation design. Improving host-guest stickiness certainly mandates the alignment of shape and chemical functionality at those substructures buried on binding and excluded from solvation, (steps A1, and A2 in Scheme 2), yet the prudent confection of the host-guest interface in terms of entropy tailoring has hardly been tried.

Such notion comes as a surprise since the quite variant response of solvation within a homologous series has long been recognized. For instance, in the Hofmeister series derived 120 years ago, the salting-out effect of ions on proteins in water is classified. Contrasting the naive expectation based on fundamental electrolyte theory, which treats all ions in water alike based on their charges and sizes, the Hofmeister series reports on a bias for the ion that must arise from the individual interaction pattern with solvent water. Instrumental techniques like neutron diffraction can directly observe these peculiarities [34] and come up with rationalizations for the dramatic differences found. The Hofmeister bias for anions covers almost 12 orders of magnitude [35], and a great share of this span must be attributed to the anions' effect on water structure, that is, on the entropy of solvation. Recently arguments have also been presented that connect the profound energetic differences in the anion series to genuine changes in chemical ion-water bonds [36].

The design of solvating molecular surfaces as an entry to exploit entropy contributions for boosting affinity or structural uniqueness necessitates a quantitative, or in the first instance, at least a qualitative measure of the balance of the desolvation processes A1 and A2 in Scheme 2 and the reunification of the number (n + m) of water molecules with the bulk (Step B2). In terms of entropy, this balance can be summed up as solvent entropy change as distinct from the change in solute entropy comprising the conformational/configurational entropy differences experienced by the host-guest partners themselves (Step B1). Both fractions must necessarily add up to the experimentally observed entropy of association ΔS_{assoc}.

Scheme 2

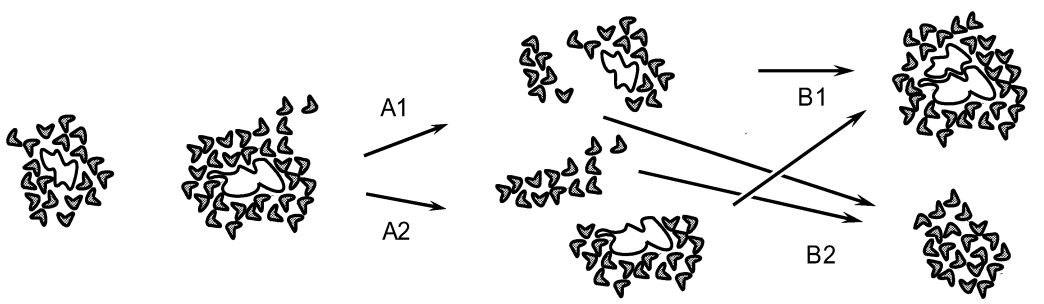

Parsing the observable entropy in the solute and solvent parts is, of course, a completely artificial move that is solely justified to ease the comprehension and at best allow a rough estimate, which of both shares is primarily addressed by a structural

modification introduced in design. There is no exact experimental way to arrive at such dissection, because the delicate interconnection of structure and solvation transmits even the smallest changes at one substructure to the entire rest of the molecule. Thus, there is no modification possible that a priori can be regarded as being innocent, enabling a general correlation of a structural versus the entropic change. The dependency on context is much more pronounced than for structure–enthalpy correlations, where conditions that quantify the impact of a structural modification on the overall energetics can be found with reasonable fidelity.

The problem in evaluating entropy contributions derives, both from the adaptability of the solvent to solvate a structural variant of the parent using a rearrangement of its molecular ensemble and to extend this change via its own structure to more remote parts of the solute. This mechanism accounts for the marked nonadditivity in entropy-structure correlation and has also been called to rationalize solvophobic interactions [37]. When this adaptive solvation is blocked due to unsuitable size relations of host and solvent, as they can occur on solvation of concave cavities such as in macrocyclic hosts, a respectable enhancement of affinity can be achieved even with non-polar solvents capable of very limited energetic exchange only [38].

Currently, the role of entropy of solvation on host-guest binding is best illuminated taking water as a solvent, though this solvent certainly occupies a very special place among the media for molecular recognition. Due to its importance in the biological world, the vast majority of studies aiming at the energetics and molecular mechanisms of solvation have been conducted in water, and we trust that the general outlines of the possible facets can be seen using water as the example. A short catalog of interaction possibilities and their entropic consequences for supramolecular association are collected in Table 2.

Table 2. Empirical qualitative energetics of the aqueous solvation of solute structural moieties at ambient temperatures

Entry	Interaction type	Prototypical moiety	ΔH of hydration	$T\,\Delta S$ of hydration	Entropic effect when replaced in the course of host-guest association
1	hydrophobic	CH_2, aryl-	moderately exothermic	negative	favorable
2	hydrophilic	peptide, sugar	exothermic	weak, variable	weakly unfavorable
3	hard metal cation	Li^+, Na^+, Zn^{2+},	strongly exothermic	negative	favorable
4	soft cation	K^+, guanidinium	exothermic	distinctly positive	unfavorable
5	hard anion	phosphate	exothermic	negative	favorable

The most stunning situation in aqueous solvation happens when there is a minimum of solute-solvent interaction because of incompatible interaction modes. This situation is met when hydrocarbon moieties incapable of any hydrogen bonding interaction are brought into contact with water. The thermodynamic signature of the so-called hydrophobic effect is well established and features a dominant negative entropy

term that is in part counterbalanced by a favorable negative enthalpy contribution at room temperature [32]. On raising the temperature, the relative proportions of both components change due to a strong positive heat capacity change rendering the hydrophobic effect enthalpy-driven and entropy-opposed at temperatures greater than ~ 60 ^{o}C. It is relevant to note the dependence of hydrophobicity on molecular size: small molecules show a different pattern than extended surfaces [37], which in turn also modulate the interaction by their geometrical profile on the molecular scale [39]. Despite the clear-cut experimental energetics, there is no consensus on the molecular origin of these effects [37,40-42]. In the absence of an unambiguous molecular picture of the hydrophobic effect, any theoretical attempt at translating a desired entropic outcome into some concrete covalent structural motif as required in host design may prove futile.

Another scenario expands when host or guest partners form moderately strong enthalpic interactions with water (Table 2, entry 2). Typical examples are represented by sugar moieties, the surfaces of globular proteins at large, or the helical grooves formed by B-DNA. In those cases, the solute surface can intervene with the hydrogen bonding network of bulk water, thereby distorting its regular pattern and dynamics. The hydration layer surrounding, for example, the covalently connected hydroxy functions of a saccharide is perturbed by strong hydrogen bonding to these hydrophilic groups. The cause is a misalignment (nonoptimal spacing) of the H-bond donor and acceptor sites of the solute and solvent networks. This misfit results in an energized state of the hydration shell relative to the bulk solution that is relaxed when a fraction of this layer is merged with the bulk water on association [43]. In comparison to the hydrophobic effect, the adhesion of water molecules to hydrophilic surfaces involves an exothermic enthalpy output and a small positive entropy contribution. Many sugar derivatives have been examined in their binding energetics to protein receptors (lectins), and the variation with the peculiar pattern of decoration of the amphiphilic surface leaves little doubt that there is an intimate connection of structure and energy governing this relationship. Thus, a foundatory platform indispensible for host design appears to be in operation.

With respect to solvation entropy, quite a broad range is covered in examples taken from the biological world. Many saccharides exert a mild destructering effect on the water H-bonding network, resulting in the inhibition of freezing (ice crystallization) by glass formation [44] or in the increase of rotational freedom around the glycosidic bonds in sugar polymers [45]. Such observations point to a moderate lift of the system's entropy that is, however, reversed on molecular association. On the other hand, a strong reduction in hydration entropy may result if certain spatial boundary conditions apply, as is true in the hydration of the major and minor grooves in B-DNA [46]. Only the minor groove harbors a string of several well-ordered layers of water molecules (the "spine of hydration"), which owe their existence to the hydrogen-bond capacity of nucleotide sequences rich in A-T pairs at the bottom of the groove. A hydrogen-bonded chain of water molecules is then formed on top of this base by virtue of the walls of the sugar phosphate backbone, forming a furrow that prevents transversal movement of the chain. The dynamics of water exchange in this environment is significantly reduced as read from dedicated NMR-experiments. The entropy balance of minor-groove binding guests in turn is expectedly tuned by the actual binding mode: specific binders that replace the spine of hydration generate a more positive contribution of desolvation entropy than

similar guests interacting with the major groove or binding unspecifically at the minor groove (replacing the top water layers only) [47]. As is true for the hydrophobic effect also, the hydrophilic hydration cannot be rationalized to any satisfaction in quantitative terms. However, judged from the stringent qualitative interrelation of structure and solvation entropy, there is hope that entropy features can be incorporated in host design on an empirical basis using polyamphiphilic building blocks.

Similar to hydrophilic interactions, the hydration of charged centers marks a prominent position because of its strength. As already mentioned electrolyte theory could indeed rationalize many physical properties that are primarily based on coulombic interactions between an ion and the dipolar solvent molecules, furnishing a solvation shell of radially defined dimensions. Owing to the relatively weak diminution of the electrostatic energy with distance ($\sim r^{-1}$) a far-reaching orientational effect on solvent dipoles was postulated that should apply to all ions but depend in magnitude on the charge of the central ion. The restructuring influence should be visible remote from the ion's position and show up in the single-ion state functions like entropy or heat capacity. Even before the inauguration of electrolyte theory, Hofmeister had discovered the distinct individuality of the anions in particular and suggested to arrange their efficiency in salting out basic proteins in a sequence [33]. Later this series proved to underly quite a variety of phenomena in aqueous solution chemistry but resisted an all encompassing comprehension [48-50].

With the advent of differential neutron- and X-ray diffraction techniques offering a direct experimental look at the water structure surrounding the ions, it became clear that the anticipated long-distance influence on water structure does not exist [51-53]. Rather, for monovalent cations the distortion of the solvent structure occurs in the first hydration layer immediately contacting the ion only. The cations of high charge density (Li^+, Na^+) exhibit a structuring influence, whereas the larger alkali cations (K^+, Rb^+, and Cs^+) and all organic cations, in particular those occurring in proteins (primary ammonium, guanidinium, but also tetraalkylammonium), show structural blurring. Only small multivalent cations like Mg^{2+} and Cr^{3+} extend their influence beyond the first hydration layer.

A similar basic pattern is seen in the anion series. Among the halides, only fluoride achieves a well-structured first hydration shell, whilst all others progressively lose the capacity to organize their solvent shells with decreasing charge density. Gratifyingly, the picture is continued with multicharged anions like sulfate, carbonate, or thiosulfate and thus appears coherent with the Hofmeister series [49,50]. Anions of high charge density (so called

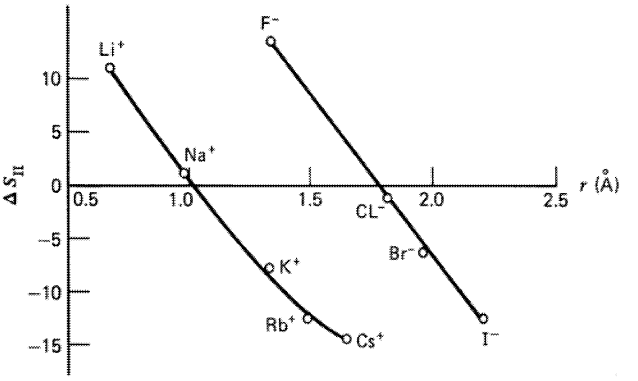

Figure 5. Dependence of the excess entropy of the water in the hydration shell on the crystal radius of the halide ions [75].

cosmotropes like F^-, SO_4^{2-}, and CO_3^{2-}) arrange their first hydration shells well (but not the water structure at large), and in this respect, they oppose the larger ones (Cl^-, I^-, SCN^-, and ClO_4^-, the chaotropes) that eventually lack such structure completely. The absence of long range effects, however, requires that all differences seen between the ions must emerge from the direct interactions of the ion itself with the first-layer water molecules that now must invoke extra electrostatic bonding types [51] modulating the enthalpic component of the interaction. Good candidates could be dispersion forces [54] or hydrogen bonding itself, since this type of interaction may consist of variable, yet substantial covalent character as can be inferred from spin coupling between fluoride and protons of the host structure in certain abiotic receptor compounds [55]. Of course, the extent of ordering in the solvation shell must also be apparent in the entropy term, and a respective plot is shown in Figure 5. The excess entropy of water near the ion over the bulk level is depicted versus the anion crystal radius for the halides. Only fluoride, but not all the heavier halides, shows a negative value leading to a positive entropy contribution on desolvation or binding by some host, respectively.

The important lesson to learn for host design in this case calls for an encapsulation host. The total replacement of the hydration shell by the host structure would yield an entropy gain for fluoride in contrast to the higher halides. For these, the relaxed positioning of water in direct contact to the ion as compared to the situation in the bulk solvent contributes an unfavorable share to host-halide complexation. A direct corroboration of this entropic effect can be deduced from the selectivity of anion complexation by some encapsulation hosts resembling molecular oysters [56]. The negatively charged guest there is sequestered into a molecular cavity formed from two peptidic macrocycles thereby requiring extensive desolvation of both partners. Sulfate, one of the most powerful cosmotropes, is found to be the much preferred guest species in an aqueous DMSO solvent, suggesting a decisive role of the desolvation entropy in the definition of binding selectivity in this case.

The inverse scenario is met on association to a guanidinium cation, which is a popular building block in abiotic anion receptors. Here the dehydration on binding a supramolecular partner adds a negative entropy share to the total diminishing the affinity on this basis. A prudent strategy for the design of guanidinium receptors acting in water should aim at utmost hindrance of hydration of this site not only for the reason of limiting the enthalpic cost of stripping off the solvent, but also for the sake of minimizing entropy loss emerging from the return of hydration shell water molecules to the bulk. In this sense, qualitative considerations on the impact of entropy may guide the basic directions on how to construct molecular receptors. Such strategic masterplans are more than welcome to avoid fundamental pitfalls that cannot be repaired even by the best-fitting host design.

THE ROLE OF ENTROPY BY COMPUTATIONAL AND EXPERIMENTAL APPROACHES

Compared to the rich body of information on the mutual enthalpic interactions between molecules or individual functional groups, we must currently state a paucity of information on the corresponding entropy part that surely hampers or impairs the rational

design of host-guest systems. Alleviation of this situation is sought on two fields, the computational simulation or the direct experimental evaluation of prototypical models. Both approaches appear still in their infancy at present, yet they have the capacity to mutually enforce each other. The experimental approach provides a bold frame of results to which theoretical predictions can be checked and iteratively improved. Computational modelling in turn can identify the relevant questions to be answered by experiment. Though modern computational chemistry in principle already provides the framework for entropy studies of host-guest association, the methodological detail has not yet evolved to a state of general utility for molecular-design purposes. It is well appreciated that all the information on entropy is contained in molecular dynamics (MD) run on systems comprising the binding partners and maybe not-so-innocent bystanders (buffer, counterions, etc.), not to speak of phase boundaries, surfaces, nano containments, etc., all soaked in a sufficient amount of solvent. The complexity of such systems notwithstanding, host-guest affinity representing free-energy differences between the dissociated and complexed state can be calculated with reasonable accuracy (~4 kJ mol^{-1}) by free energy perturbation (FEP) or thermodynamic integration (TI) approaches [58].

In contrast, the calculation of entropy differences or absolute entropies suffers from errors that may be larger by an order of magnitude [59,60] and thus is devoid of any predictive value in design. The difficulties arising in calculating entropies [61] derive both from the particular force fields employed, which in most cases are parameterized to reproduce structures rather than thermodynamic values of state functions, and on convergence problems that relate to sufficient sampling of the phase space expanded by the multiparticle system. Modern methodological developments address both aspects [59,61-65]. Above all, they aim at the reduction in complexity either by exploitation of symmetry features specifically of the solvent [62], or by calculating individual components of the total entropy, such as solute/solvent entropies [59], translational/rotational entropies [66], or configurational entropy [63-65].

These studies furnished the important message that the host-guest configurational entropy, at least in some cases, is of the same order of magnitude as the total enthalpic interaction, invalidating any approach to score host-guest binding exclusively on the basis of enthalpy minimization (fit) [63]. Moreover, calculations based on the mining minima (M2) concept showed the shape of conformational minima in flexible hosts to contribute more to the entropy outcome than their sheer number [63]. Simple counting of stable conformations apparently is not an appropriate means to grasp configurational entropy. This result compromises the dominant role of host preorganization in entropy-based affinity enhancement.

On the empirical terrain, the progress in NMR-techniques furnished a direct access to measure configurational entropies from molecular dynamics [66,67]. Now there is evidence that proteins may trade entropy shares across their structures, allowing a ligand to bind selectively at a binding site concomitant with a substantial loss in local entropy, however, at the expense of structural order and an increase in entropy somewhere more remote from the binding site. By this mechanism, the overall entropy balance can be positive and favorable for binding due to overcompensation. Such a process requires a molecular machinery capable of coupling a preorganized, yet noncomplementary host binding site (with respect to the specific guest) to the binding

event and transducing the structural change to some other substructure. An adaptation of this principle that may not be rare in biology [68] has appeared in the literature [69]. The release of entropy on binding to a host rotaxane (axle-wheel system) is there rationalized by motional relaxation of the mechanically interlocked system. Since the thermodynamic evidence presented derives from van't Hoff analyses of (quite unspecific) fluorescence quenching in a structurally diverse series of host compounds, the conclusions and claims advanced on this basis are less compelling.

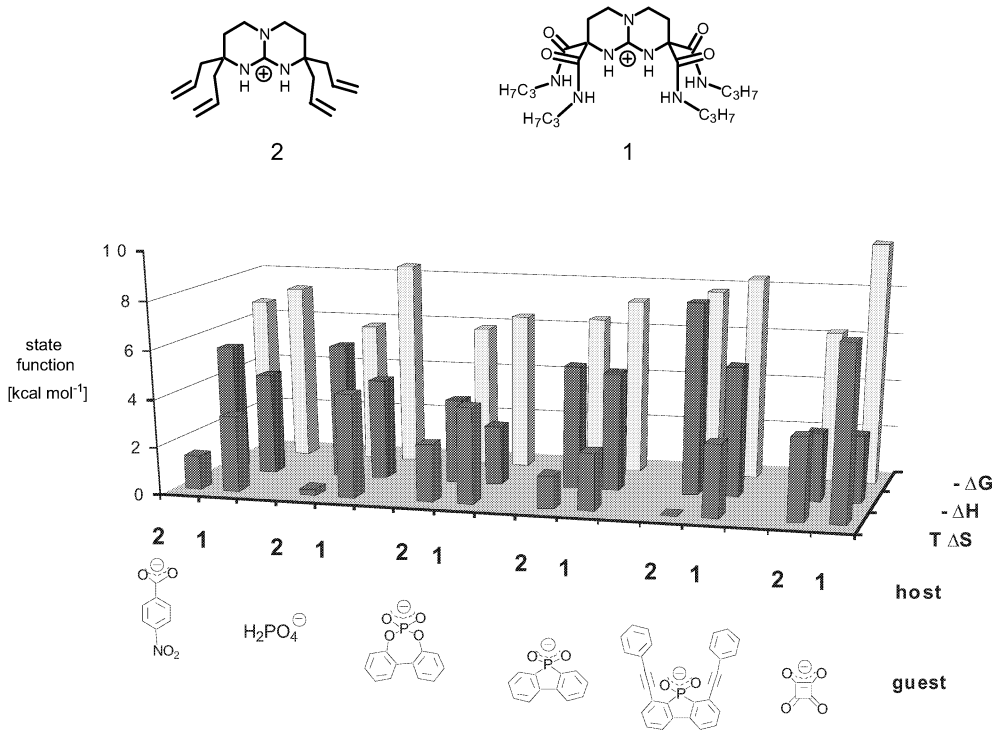

Figure 6. Energetics by ITC of oxoanion binding to guanidinium hosts in acetonitrile at 298 K. The improved affinity (ΔG^{o}) of the carboxamido host **1** versus the allylguanidinium salt **2** lacking additional anchoring functions is due to enhanced entropy rather than enhanced enthalpic interaction. [72]

More reliable evidence is collected by the direct measurement of heat effects on changing the relative and/or absolute host and guest concentrations. In this respect, modern microcalorimetry opened a door to provide and inspect the enthalpy and entropy components to the free energy of associating systems [70-72]. For instance, the origin of the affinity improvement found with the guanidinium carboxamide anchorgroup **1** complexing oxoanions in acetonitrile compared to the alkyl-substituted analog **2** (Figure 6) was traced to an augmentation in the entropy output rather than to an enhancement of the interaction enthalpy [73]. Contrary to the expectation that was based on the traditional advice to add supplementary binding functionality (the secondary carboxamido groups) to the parent guanidinium moiety, the goal of affinity enhancement

was reached indeed, yet for a different reason requiring the revision of the original concept of oxoanion binding. Even simple and purportedly well-established anchor functions may reveal an unforeseen face if probed by the most suitable physical method.

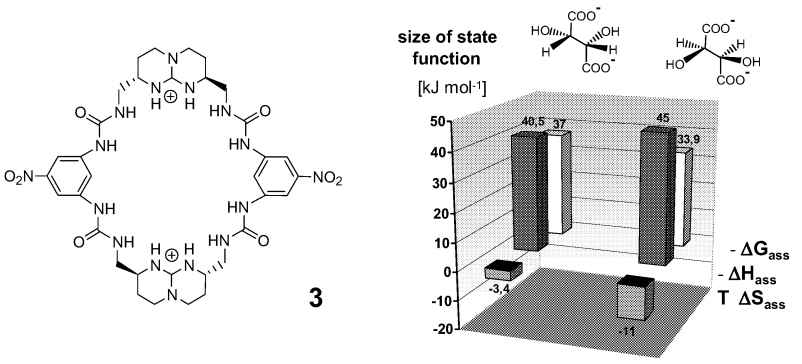

Figure 7. Energetics of enantiorecognition of tartrate by the macrocycle **3** in acetonitrile at 298 K. Though L-tartrate (right) displays weaker affinity (less negative ΔG^{o}), it better fits to the macrocycle as indicated by the more negative binding entropy [73].

Calorimetry was also instrumental in pin-pointing the best structural base for enantiorecognition. For this purpose the uniqueness of molecular interaction rather than overall affinity must be addressed, because the specific distinction of geometrical arrangements in two molecular species is interrogated that do not differ in chemical nature, size, conformation/flexibility or solvation properties. Taking dianionic tartrate as enantiomeric substrates binding to the macrocyclic host **3** as an example, the better fit in the respective diastereomeric host-guest complexes surfaced in the energetic signature as determined by isothermal titration calorimetry. Interestingly, the more stable host-guest complex (with L-tartrate) featured the distinctly more positive entropy of association. Provided the reasonable presumption of near identical solvation in both complexes holds, the more positive entropy relates to a

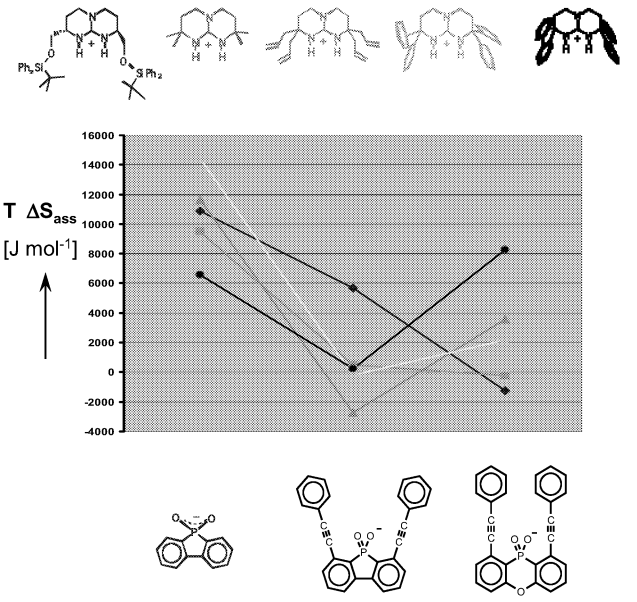

Figure 8. Correlation of association entropy with the stringency of binding. In each series of cations or anions, there is one pairing that exhibits minimum experimental entropy, suggesting a unique fit in this combination only [74].

greater structural fuzziness in this complex species compared to its counterpart. Recognition of the geometrical form (i.e., the fit) is better for the D-tartrate complex despite its weaker affinity. As this example shows, the free energy of binding or its translation, the association constant, cannot be taken as an indicator of host-guest binding uniqueness. A better and more direct measure of singularity could be represented by the association entropy if other contributions to this quantity are negligible or kept constant by the proper choice of conditions.

Decisions on the binding uniqueness are necessary beyond the distinction of enantiomers, for example, when best-fitting supramolecular partners for selfassembly systems are to be found. Towards this goal, trend analyses in a series of guanidinium-phosphinate host-guest binding partners differing in binding-site accessibility have been undertaken, employing entropy as a probe of configurational integrity. As observed by ITC, the matrix of pairing of both ensembles in acetonitrile (see Figure 8) showed great variation of the absolute entropy contributions ($T\,\Delta S^{o}$ up to 16 kJ mol^{-1}) to the total free energy output. However, for each member of the guanidinium ensemble, there was just one phosphinate partner exhibiting a minimum in entropy production. The respective pairings all fall into the same regiment of association entropy in absolute terms, suggesting that these combinations, but not all others, represent the instance of a unique fit. Gratifyingly, the flagged host-guest pairs correlate perfectly with the geometric stringency of the binding site accessibility in the cationic and anionic series. This result questions the a priori and general assumption of a unique complex structure formed on host-guest association that still dominates the literature of supramolecular binding.

CONCLUSIONS

The design of supramolecular interactions implies a purpose that mandates accounting of all relevant influences. In this respect, the role of entropy is as yet severely underestimated, though its qualitative involvement and substantial magnitude is plain to see in the association energetics. A major obstacle in the adoption of entropy arguments in design stems from its resistance to dissection into individual contributions assignable to structural moieties. Thus, for entropy there is no additive scheme available that proved so successful for the estimation of enthalpy.

A helpful step in this direction, though not backed by general experimental realization, is parsing the total entropy change into two fractions: the entropy change attributable to the solute partners as opposed to the change related to solvent rearrangement. Solute entropy change describes the direct interaction in analogy to the gas-phase process and the respective arguments concerning the trade of degrees of freedom of translation/rotation into vibrational ones are valid for either case. Biological examples have sharpened the view that solute preorganization in the sense of optimal positioning and motional confinement is not the ultimate choice in maximizing host-guest affinity. We recognize the real possibility to preorganize the host structure in a way to furnish a gain rather than a loss in entropy on guest complexation. Because enthalpy-entropy compensation is real, but not complete, this gain could even make up for an investment in enthalpy emerging from the anticipated less-than-optimal geometric and functional complementarity in such host compounds. The necessity to limit the entropy

gain at the actual site of guest binding in order to conserve the selectivity properties adds to the challenge of constructing abiotic hosts according to this mechanism.

Analyzing and using solvent entropy change for design meets with even higher hurdles. The problems arise from the notion that the state of solvation (and consequently the entropy) of those parts of the binding partners constituting the interface in the final complex (the problems are compounded if an ensemble of complex structures is formed) has a dramatic effect on the outcome. In cases allowing a serious estimate (e.g., binding of sugar residues to lectins), up to 100% of the observable energy change can emerge from solvent entropy (as $T\Delta S$). Solvation and its constitutive components differ with the chemical nature and decoration pattern of molecular surfaces, yet at the state of the art, no rationalizations that could satisfy moderate quantitative ambitions are available. Qualitative considerations referring to the entropy contributions of hydrophobic, hydrophilic, or ionic patches of the structure can be used as an input for design and surely will prove profitable and novel, as they have received little attention so far.

In prospect, there are two lines of research that may alleviate the situation: One can hope for the due progress in the methods of computational chemistry, which in combination with the extrapolated improvement of the calculation capacity, might furnish a remedy from the convergence problems that haunt present day entropy calculations. On the other hand, the availability and wide-spread use of reliable calorimetric instrumentation can be expected to substantially broaden the experimental basis in supramolecular energetics. A better paved experimental platform would serve the development of the theoretical background underlying solvation entropy and at the same time fill the arsenal of entropy data ready to use in an incremental approach to host construction. At the state of the art in host design, we are just beginning to rationally incorporate entropy-based concepts and ideas that are well recognized as fundamental ingredients of all molecular interactions for over a century. It is about time to get them accommodated in thoughtful respect.

ACKNOWLEDGMENT

The support of this work by Deutsche Forschungsgemeinschaft und Hans-Fischer-Gesellschaft, München, is gratefully acknowledged.

REFERENCES AND NOTES

1. G. M. Whitesides, “Revolutions in Chemistry,” *Chem. Eng. News,* **85**, 12-17 (2007).
2. F. P. Schmidtchen, “Reflections on the Construction of Anion Receptors: Is there a Sign to Resign from Design?” *Coord. Chem. Rev.,* **250**, 2918-2928 (2006).
3. G. W. Whitesides and V. M. Krishnamurthy, “Designing Ligands to Bind Proteins,” *Quart. Rev. Biophys.,* **38**, 385-395 (2005).
4. The designation which of the binding partners in a host-guest system is the host is arbitrary and physically meaningless. Contrary to traditional usage, which commonly nominates the larger partner as the host, we here adopt the viewpoint of the molecular designer: The modifyable partner is considered the host, though it may be the smaller participant in the supramolecular interaction. Conversely, for the sake of consistency the

guest is always the component with a given invariant structure, let it be a small anion or a protein receptor site.

5. F. P. Schmidtchen, "Selectivity: Thermodynamic and Kinetic," Encyclopedia of Supramolecular Chemistry, (J. Atwood, J. Steed, Eds.), Marcel Dekker, New York, 2004; pp. 1225-1230.
6. The term goes back to a suggestion by J.-M. Lehn in 1978.
7. E. Fischer, "Einfluss der Configuration auf die Wirkung der Enzyme," *Ber. Dtsch. Chem. Ges.,* **27**, 2985 (1894).
8. a) M. Berger and F. P. Schmidtchen, "Artificial Host Molecules for Anions," *Chem. Rev.* **97**, 1609-1649 (1997); b) W. Peschke and F. P. Schmidtchen, *Tetrahedron Lett.,* **36**, 5155-5158 (1995).
9. S. Günther, K. Rother, and C. Frömmel, "Molecular Flexibility in Protein-DNA Interactions," *BioSystems,* **85**, 126-136 (2006).
10. G. Ercolani, "Comment on Using a Convenient Quantitative Model for Torsional Entropy to Establish Qualitative Trends for Molecular Processes that Restrict Conformational Freedom," *J. Org. Chem.,* **64**, 3350-3353 (1999).
11. M. I. Page and W. P. Jencks, "Entropic Contributions to Rate Accelerations in Enzymic and Intramolecular Reactions and the Chelate Effect," *Proc. Nat. Acad. Sci.,* **68**, 1678-1683 (1971).
12. B. Lu and C. F. Wong, "Direct Estimation of Entropy Loss Due to Reduced Translational and Rotational Motions upon Molecular Binding," *Biopolymers*, **79**, 277-285 (2005).
13. W. F. van Gunsteren, D. Bakowies, R. Baron, I. Chandrasekhar, M. Christen, X. Daura, P. Gee, D. P. Geerke, A. Glättli, P.H. Hünenberger, M. K. Kastenholz, C. Oostenbrink, M. Schemk, D. Trzesniak, N. F. A. van der Vegt, and H. B.Yu, "Biomolecular Modelling: Goals, Problems, Perspectives," *Angew. Chem. Int. Ed.,* **45**, 4064-4092 (2006).
14. We refer here to static energy minimization including structural relaxation (induced fit) and environmental solvent models.
15. A. M. Davis, S. J. Teague, and G. J. Kleywegt, "Application and Limitations of X-ray Crystallographic Data in Structure-based Ligand and Drug Design," *Angew. Chem. Int. Ed.*, **42**, 2718-2736 (2003).
16. F. L. Lambert, "A Modern View of Entropy," *Chemistry*, **15**, 13-21 (2006).
17. A. H. Jungermann, "Entropy and the Shelf Model," *J. Chem. Educ.,* **83**, 1686-1694 (2006).
18. S. W. Homans, "Probing the Binding Entropy of Ligand-Protein Interactions by NMR," *ChemBioChem*, **6**, 1585-1591 (2005).
19. V. M. Krishnamurthy, L. A. Estroff, and G. W. Whitesides, "Multivalency in Ligand Design," Fragment-based Approaches in Drug Discovery, W. Jahnke, and D. A. Erlanson, Eds., Wiley-VCH, Weinheim, Germany, 2006, pp. 11-53.
20. G. M. Whitesides, B. Bilgicer, and D. T. Moustakas, "A Synthetic Trivalent Hapten that Aggregates anti-2,4-DNP IgG into Bicyclic Trimers," *J. Am. Chem. Soc.,* **129**, 3722-3728 (2007).
21. R. Breslow, S. Belvedere, L. Gershell, and D. Leung, "The Chelate Effect in Binding, Catalysis, and Chemotherapy," *Pure Appl. Chem.,* **72**, 333-342 (2000).
22. a) D. H. Williams, E. Stephens, D. P. O'Brien, and M. Zhou, "Understanding noncovalent interactions: Ligand binding energy and catalytic efficiency from ligand-induced reductions in motion within receptors and enzymes," *Angew. Chem. Int. Ed.,* **43**, 6596-6616 (2004); b) D. H. Williams, M. Zhou, and E. Stephens, "Ligand Binding

Energy and Enzyme Efficiency from Reductions in Protein Dynamics," *J. Mol. Biol.*, **355**, 760-767 (2006).

23. V. M. Krishnamurthy, B. R. Bohall, V. Semetey, and G. M. Whitesides, "The Paradoxical Thermodynamic Basis for the Interaction of Ethylene Gklycol, Glycine, and Sarcosine Chains with Bovine Carbonic Anhydrase II: An Unexpected Manifestation of Enthalpy/Entropy Compensation," *J. Am. Chem. Soc.,* **128**, 5802-5812 (2006).
24. J. D. Dunitz, "Win Some, Lose Some: Enthalpy-Entropy Compensation in Weak Molecular Interactions," *Chem. Biol.,* **2,** 709-712 (1995).
25. D. H. Williams and M. S. Westwell, "Aspects of Weak Interactions," *Chem. Soc. Rev.,* **27**, 57-63 (1998).
26. D. Cremer, A. Wu, A. Larsson, and E. Kraka, "Some Thoughts about Bond Energies, Bond Lengths, and Force Constants," *J. Mol. Model.,* **6**, 396-412 (2000).
27. D. M. Ford, "Enthalpy-Entropy Compensation is Not a General Feature of Weak Association," *J. Am. Chem. Soc*. **127**, 16167-16170 (2005).
28. D. J. Cram, "Preorganization – from Solvents to Spherands," *Angew. Chem.,* **98**. 1041-1060 (1986).
29. E. Marverick, D. J. Cram, "Spherands – Hosts Preorganized for Binding Cations," Comprehensive Supramolecular Chemistry, G. W. Gokel Ed., Elsevier, Oxford, UK, 1996; pp. 213-243.
30. For a full list of parameters required to specify conditions of molecular interactions consult: *Nature Biotech*. **25**, 894-898 (2007).
31. Y. Marcus, "The Properties of Solvents," Wiley, Sussex, UK, 1998; pp. 37-42.
32. B. Lee, "Analyzing Solvent Reorganization and Hydrophobicity," *Methods Enzymol.,* **259**, 555-576 (1995).
33. Y. Zhang and P. S. Cremer, "Interactions between Macromolecules and Ions: The Hofmeister Series," *Curr. Opin. Chem. Biol.,* **10**, 658-563 (2006).
34. G. W. Neilson, P. E. Mason, S. Ramos, and D. Sullivan, "Neutron and X-ray Scattering Studies of Hydration in Aqueous Solution," *Philos. Trans. R. Soc. London Ser. A,* **359**, 1575-1592 (2001).
35. R. Custelcean and B. A. Moyer, "Anion Separation with Metal-Organic Frameworks," *Eur. J. Inorg. Chem*., 1321-1340 (2007).
36. K. D. Collins, G. W. Neilson, and J. E. Enderby, "Ions in Water: Characterizing the Forces that Control Chemical Processes and Biological Structure," *Biophys. Chem*. **128**, 95-104 (2007).
37. a) L. R. Pratt, "Molecular Theory of Hydrophobic Effects: She is Too Mean to Have Her Name Repeated," *Annu. Rev. Phys. Chem*., **53**, 409-436 (2002); b) H. S. Ashbaugh and L. R. Pratt, "Contrasting Nonaqueous against Aqueous Solvation on the Basis of Scaled-Particle-Theory," *J. Phys. Chem. B,* **111**, 9330-9336 (2007).
38. K. T. Chapman and W. C. Still, "A Remarkable Effect of Solvent Size on the Stability of a Molecular Complex," *J. Am. Chem. Soc.,* **111**, 3075-3077 (1998).
39. B. D. Isbister, P. M. St. Hilaire, and E. J. Toone, "Spatial Organization versus Total Surface Area as a Predictor of Protein Hydrophobicity. The Hydrophobicity of the Concanavalin A Binding Site," *J. Am. Chem. Soc.,* **117**, 12877-12878 (1995).
40. J. K. Shah, D. Asthagiri, L. R. Pratt, and M. E. Paulaitis, "Balancing Local Order and Long-Ranged Interactions in the Molecular Theory of Liquid Water," *J. Chem. Phys.,* **127**, 144508(1)-144508(7) (2007).
41. J. L. Li, R. Car, C. Tang, N. S. Wingreen, "Hydrophobic Interaction and Hydrogen-Bond Network for a Methane Pair in Water," *Proc. Nat. Acad. Sci.,* **104**, 2626-2630 (2007).

42. M. Rodnikova and J. Barthel, "Elasticity of the Spatial Network of Hydrogen Bonds in Liquids and Solutions," *J. Mol. Liq.* **131-132**, 121-123 (2007).
43. R. U. Lemieux, "How Water Provides the Impetus for Molecular Recognition in Aqueous Solution," *Acc. Chem. Res.,* **29**, 373-380 (1996).
44. L. Cordone, G. Cottone, and S. Giufridda, "Role of Residual Water Hydrogen Bonding in Sugar/Water/Biomolecule Systems: A Possible Explanation for Trehalose Peculiarity," *J. Phys. Condens. Matter,* **19,** 205110 (2007).
45. M. M. Kuttel and K. J. Naidoo, "Free Energy Surfaces for the α(1→4)-Gycosidic Linkage: Implications for Polysaccharide Solution Structure and Dynamics," *J. Phys. Chem. B* **109**, 7468-7474 (2005).
46. P. L. Privalov, A. I. Dragan, C. Crane-Robinson, K. J. Breslauer, D. P. Remeta, and C. A. S. A. Minetti, "What Drives Proteins into the Major or Minor Grooves of DNA?" *J. Mol. Biol.* **365**, 1-9 (2007).
47. B. Jana, S. Pal, P. K. Maiti, S. T. Lin, J. T. Hynes, and B. Bagchi, "Entropy of Water in the Hydration Layer of Major and Minor Grooves of DNA," *J. Phys. Chem. B,* **110**, 19611-19618 (2006).
48. P. Lo Nostro, B. W. Ninham, S. Milani, A. Lo Nostro, G. Pesavento, and P. Baglioni, "Hofmeister Effects in Supramolecular and Biological Systems," *Biophys. Chem.,* **124**, 208-213 (2006)
49. S. Shimizu, W. M. McLaren, and N. Matubayasi, "The Hofmeister Series and Protein-Salt Interactions," *J. Chem. Phys.,* **124**, 234905/1-234905/4 (2006).
50. Y. Koga, "What Some Anions Do to H_2O? Towards Understanding the Hofmeister Series," *Netsu Sokutei,* **34**, 3-13 (2007).
51. M. Y. Kiriukhin and K. D. Collins, "Dynamic Hydration Numbers for Biologically Important Ions," *Biophys. Chem.,* **99**, 155-168 (2002).
52. A. K. Soper and K. Weckström, "Ion Solvation and Water Structure in Potassium Halide Aqueous Solutions," *Biophys. Chem.,* **124**, 180-191 (2006).
53. P. E. Mason, G. W. Neilson, J. E. Enderby, M. L. Saboungi, C. E. Dempsey, A. D. MacKerell, Jr., and J. W. Brady, "The Structure of Aqueous Guanidinium Chloride Solutions," *J. Am. Chem. Soc.,* **126**, 11462-11470 (2004).
54. S. Rossi, P. Lo Nostro, M. Lagi, B. W. Ninham, and P. Baglioni, "Specific Anion Effects on the Optical Rotation of a-Amino Acids," *J. Phys. Chem. B*, **111**, 10510-10519 (2007).
55. S. O. Kang, M. A. Hossain, and K. Bowman-James, "Influence of Dimensionality and Charge on Anion Binding in Amide-based Macrocyclic Receptors," *Coord. Chem. Rev.* **250**, 3038-3052 (2006).
56. C. Reyheller, B. P. Hay, and S. Kubik, "Influence of Linker Structure on the Anion Binding Affinity of Biscyclopeptides," *New J. Chem.*, **31**, 2095-2102 (2007).
57. C. Chipot, "Free Energy Calculations in Biological Systems. How Useful are they in Practise?" Lecture Notes in Computational Science and Engineering, **49,** 185-211 (2006).
58. T. Kristof and G. Rutkai, "Chemical Potential Calculations by Thermodynamic Integration with Separation Shifting by Adaptive Sampling Monte Carlo Simulations," *Chem. Phys. Lett.*, **445**, 74-78 (2007).
59. J. Carlson and J. Åqvist, "Calculations of Solute and Solvent Entropies from Molecular Dynamics Simulations," *Phys. Chem. Chem. Phys.*, **8**, 5385-5395 (2006).
60. S. Z. Wan, R. H. Stote, and M. Karplus, "Calculation of the Aqueous Solvation Energy and Entropy, as well as Free Energy, of Polar Solutes," *J. Chem. Phys.*, 121, 9539-9548 (2004).

61. D. Trzesniak and W. F. van Gunsteren, "Pathway Dependence of the Efficiency of Calculating Free Energy and Entropy of Solute-Solute Association in Water," *Chem. Phys.*, **330**, 410-416 (2006).
62. F. Reinhard and H. Grubmüller, "Estimation of Absolute Solvent and Solvation Shell Entropies via Permutation Reduction," *J. Chem. Phys.*, **126**, 014102/7 (2007).
63. C. E. Chang and M. K. Gilson, "Free Energy, Entropy, and Induced Fit in Host-Guest Recognition: Calculations with the Second-Generation Mining Minima Algorithm," *J. Am. Chem. Soc.*, **126**, 13156-13164 (2004).
64. M. K. Gilson and H. X. Zhou, "Calculation of Protein-Ligand Binding Affinities," *Annu. Rev. Biophys. Biomol. Struct.*, **36**, 21-42 (2007).
65. B. J. Killian, J. Y. Kravitz, and M. K. Gilson, "Extraction of Configurational Entropy from Molecular Simulations via an Expansion Approximation," *J. Chem. Phys.*, **127**, 024107/16 (2007).
66. S. W. Homans, "Water, Water Everywhere – Except Where It Matters?" *Drug Discovery Today*, **12**, 534-539 (2007).
67. S. W. Homans, "Dynamics and Thermodynamics of Ligand-Protein Interactions," *Top. Curr. Chem.*, **272**, 51-82 (2007).
68. a) K. K. Frederick, M. S. Marlow, K. G. Valentine, and J. Wand, "Conformational entropy in Molecular Recognition by Proteins," *Nature*, **448**, 325-329 (2007); b) S. Arumugam, G. Gao, B. L. Patton, V. Semenchenko, K. Brew, and S. R. V. Doren, "Increased Backbone Mobility in β-Barrels Enhances Entropy Gain Driving Binding of N-TIMP-1 to MMP-3," *J. Mol. Biol.*, **327**, 719 (2003).
69. J. Zhu and D. B. Smithrud, "Host-Rotaxane Model Proteins that Promote Ligand Association Through a Favorable Change in Configurational Entropy," *Org. Biomol. Chem.*, **5**, 2992-2999 (2007).
70. F. P. Schmidtchen, "Isothermal Titration Calorimetry in Supramolecular Chemistry," in Encylopedia of Supramolecular Chemistry, J. Atwood and J. Steed, Eds., Marcel Dekker, New York, 2007, DOI 10.1081/E-ESMC-120041528.
71. F. P. Schmidtchen, "Artificial host molecules for the sensing of anions," *Top. Curr. Chem.*, **255**, 1-29 (2005).
72. V. D. Jadhav and F. P. Schmidtchen, "Surprises in the design of anion receptors: Calorimetry prevents false reasoning," *Org. Lett.*, **11**, 331-3314 (2005).
73. a) V. D. Jadhav and F. P. Schmidtchen, "Judging on host-guest binding mode uniqueness: Association entropy as an indicator in enantioselection," *Org. Lett.,* **12**, 2329-2332 (2006); b) V. D. Jadhav and F. P. Schmidtchen, "A novel synthesis of chiral guanidinium receptors and their use in unfolding the energetics of enantiorecognition of chiral carboxylates," *J. Org. Chem.*, in print.
74. M. Haj-Zaroubi and F. P. Schmidtchen, "Probing Binding Mode Diversity in Guanidinium-Oxoanion Host-Guest Binding," *Chem. Phys. Chem.*, ***6***, 1181-1186 (2005).
75. O. Y. Samoilov, "Residence times of Ionic Hydration," Water and Aqueous Solutions: Structure, Thermodynamics and Transport Processes, R. A. Horne, Eds., Wiley, New York, 1972; p. 597.

COMPLEX FORMATION AND AGGREGATION AT LIQUID-LIQUID INTERFACES

H. Watarai

Department of Chemistry, Graduate School of Science
Osaka University, Toyonaka, Osaka 560-0043 Japan.
Corresponding author email address: watarai@chem.sci.osaka-u.ac.jp

ABSTRACT

Development of experimental techniques to measure the interfacial reaction and the features of interfacial reactions is reviewed. Firstly, in the complex-formation kinetics at the interface, the catalytic effect of the interface is concluded. Secondly, the interfacial aggregation of the complex has been found as a general feature of liquid-liquid interfacial reaction, and the mechanisms are analyzed with a help of molecular dynamics simulation in some cases.

INTRODUCTION

The liquid-liquid interface is an extremely thin mixed-liquid state with about one nm thickness, in which the properties such as cohesive energy density, electrical potential, dielectric constant and viscosity are drastically changing. Solute molecules adsorbed at the interface can behave like a two-dimensional gas, liquid, or solid depending on the interfacial concentration. Microscopically, the interfacial molecules exhibit local inhomogeneity. Therefore, various specific chemical phenomena that are rarely observed in bulk liquid phases can be observed at liquid-liquid interfaces [1-3]. However, the nature of the liquid-liquid interface and its chemical function are not fully understood. These situations are mainly due to the lack of experimental methods required for the determination of the chemical species adsorbed at the interface and for the measurement of chemical kinetics at the interface [4,5]. Chemical reactions at the liquid-liquid interface are the most fundamental subject in solvent-extraction chemistry. In the beginning of 1980s, the high-speed stirring (HSS) method was invented by Watarai and Freiser [6,7]. Recently, some new methods have been invented in our laboratory [8], which will bring a break through in the study of interfacial reactions. In this paper, some typical results on the complexation and aggregation at liquid-liquid interfaces by using above methods will be summarized as well as some insight on the molecular pictures obtained by a molecular dynamics simulation.

MEASUREMENT OF LIQUID-LIQUID INTERFACES

High-Speed Stirring Method

The HSS method made it possible to measure both an interfacial concentration and an extraction rate for the first time by a simple principle. When a two-phase system is highly stirred or agitated in a vessel and the interfacial area is extremely extended, the interfacial amount of an adsorbed compound is increased, and its the bulk concentration in the organic phase is decreased. In the original HSS method, the concentration decrease in the organic phase caused by an agitation was measured spectrophotometrically using a PTFE phase separator and a spectrophotometer. Furthermore, the extraction rate could be measured by this method simultaneously. The measurements were usually carried out by employing 50 mL for each phase at the stirring speed of 5000 rpm under high-speed stirring conditions and 200 rpm in a phase-separation condition. The flow rate is 10-20 mL/min. The concentration change of the extracted complex or consumed ligand was used for the kinetic analysis of the extraction or interfacial complexation. The HSS method is very useful both for the determination of adsorptivity in a dilute concentration of weakly adsorbed molecules and for the study of extraction kinetics, because of its high sensitivity.

Centrifugal Liquid Membrane Method

Both requirements of a high specific interfacial area and a direct spectroscopic observation of the interface were attained by the centrifugal liquid membrane (CLM) method [9]. A two-phase system containing about each 100 μL of organic and aqueous phases is introduced into a cylindrical glass cell whose height and inner diameter were 3.3 and 1.9 cm, respectively. The cell is rotated at the speed of 7000-10,000 rpm. By this procedure, a stacked two-liquid membrane with each thickness of 50-100 μm is produced inside the wall, which attains the specific interfacial area over 100 cm^{-1}. UV/Vis spectrometry and other spectrometry were used for the direct measurement of the interfacial species as well as those in the bulk phases. This method was excellently applicable for the measurement of interfacial reaction rate as fast as the order of sec.

Two-Phase Stopped Flow Method

Analogous to the stopped-flow method used in the study of solution kinetics, rapid stopped-flow mixing of organic and aqueous phases is an effective way to produce a dispersed system within a few ms. The specific interfacial area of the dispersion attained as high as 700 cm^{-1} and the interfacial reaction in the dispersed system can be measured by a photodiode array spectrophotometer during the period of ca. 200 ms. This method is applicable for rather fast interfacial reactions such as diffusion rate-limiting reactions [10].

Interfacial Reflection Spectrometry

By the total internal reflection (TIR) condition at the liquid-liquid interface, one can observe interfacial reaction in the evanescent layer with a thickness of ca. 100 nm. Fluorometry is the most sensitive method for detection of interfacial species and its dynamics. Time-resolved laser spectrofluorometry is a powerful tool for the elucidation of rapid dynamic phenomena at the interface [11]. Time-resolved total reflection fluorometry can be used for the evaluation of rotational relaxation time of octadecylrhodamin B and thus the viscosity of the interface [12]. Laser excitation can produce excited states of the adsorbed compound at the interface. As an example, the decay of the triplet state of porphyrin was observed at the interface [13].

Micro-Two-Phase Sheath Flow Method

The measurement of fast chemical reactions at the liquid-liquid interface is very difficult. The micro-two-phase sheath-flow method is the only method that can measure such fast interfacial reactions finishing within 100 μs. An inner organic micro-flow was generated in an outer aqueous-phase flow from the tip of a capillary (i.d. 10 μm) with the same linear velocity. The fluorescence spectrum at the interface was observed as a function of the distance from the tip of the inner capillary, which was the starting point of the reaction. The distance from the tip was converted to the reaction time. This technique enabled the detection of a fast interfacial reaction of the order of 10 μs. The rate of the lactone cleavage reaction of octadecylrhodamine B (C_{18}RB) was investigated with the micro-two-phase sheath flow/two-photon excitation microscopy. The formation of the fluorescent forms of C_{18}RB was confirmed from the two-photon excitation fluorescence spectra at the toluene/water and heptane/water interface during 80 μs after the contact of two phases [14]. This method was applied for the measurement of luminescence lifetime of samarium(III) complex with 2-thenoyltrifluoroacetone and the synergic extraction rate at the interface [15].

Raman Spectroscopy of the Interface

Raman scattering spectrometry has some advantages over infrared (IR) spectrometry in the sensitivity, the spatial resolution, and the applicability to aqueous solution. It can attain high sensitivity, when it is performed under the resonance condition, or under the surface-enhanced condition, where silver or gold nanoparticle is used as a source of plasmon. The combination of resonance Raman microscope spectrometry and the centrifugal liquid membrane (CLM) method is a powerful technique to observe directly the Raman spectra of the liquid-liquid interface and the bulk phases by traveling the focal point of an objective lens. It was demonstrated that this method was highly useful for the kinetic measurement of the interfacial reaction [16].

Nano-sized silver colloids have been used as substrates of surface-enhanced Raman scattering (SERS), with high signal enhancement by a factor of over 10^5. With the resonance Raman condition, one can further attain a high signal enhancement. SERS

from oleate-stabilized silver colloids with 5-nm in diameter adsorbed at the toluene/water interface was measured under total internal-reflection (TIR) condition [17].

Optical Chirality Measurement of the Interface

Optical chirality of molecules is a characteristic measure of stereochemical properties of biological, pharmaceutical, and metal coordination compounds. Chiral structures of amino acids, proteins, DNAs, and various drugs in solutions have been determined from the measurement of circular dichroism (CD). The CD spectra of molecules at liquid-liquid interfaces have been measured for the first time by the CLM/CD method [18] and SHG/CD method [19]. The centrifugal liquid membrane cell was combined with the circular dichroism spectropolarimeter to measure the CD spectra of the liquid-liquid interface. This method can be applied to any optical active species formed at the liquid-liquid interface.

The most selective technique to measure the optical chirality at the interface is the second harmonic generation-circular dichroism (SHG-CD) spectroscopy, as demonstrated by a pioneering work of Hicks and co-workers [20,21]. SHG is advantageous relative to other spectroscopic techniques in its inherent high interfacial selectivity due to the second order nonlinear susceptibility and in its high sensitivity afforded by the resonance effect in an adsorbed dye molecule [22,23]. Therefore, SHG spectroscopy can provide specific information relating to the electronic state of complex molecules, which are present only at the interface. Recently, the nonlinear optical activity spectra of the liquid-liquid interface adsorbed by an aggregate of achiral molecules has been observed in our laboratory.

Single Molecule Probing at the Interface

A single-molecule probing is an ultimate method for measuring the behavior of molecules and the properties of the nano-environment of the liquid-liquid interface. The first observation of the single-molecule behavior at the liquid-liquid interface has been accomplished by means of the total internal-reflection fluorescence microscopy and a special micro cell [24,25]. A pinhole, 50 μm in diameter, was attached just in front of an avalanche photodiode, to restrict the observation area at the interface to a diameter of 830 nm. Time-resolved photon counting was carried out using a multichannel scalar. The overall detection efficiency of fluorescence at the interface was calculated to be 3.3%.

A demonstration of the single-molecule detection at the liquid-liquid interface was reported for the fluorescent probe of 1,1'-dioctadecyl-3,3,3',3'-tetramethyl-indocarbocyanine (DiI), which is a monovalent interfacial active cation with two C_{18} alkyl-chains. The influence of two kinds of surfactants, sodium dodecyl sulfate (SDS) and dimyristoyl phosphatidylcholine (DMPC), on the lateral diffusion dynamics of DiI at the interface was investigated. The observed interfacial viscosity was only slightly affected by the coexistence of SDS, but DMPC had a remarkable effect. The DMPC molecule has two alkyl chains fixed to the polar head group. This will be the cause of the stiffness of the monolayer of DMPC molecules. These results demonstrated that the

single-molecule probing method could successfully measure the hydrodynamic properties of the interfacial monolayer.

Magnetic Susceptibility Measurement of the Interface

Magnetophoretic force is used to measure the magnetic susceptibility χ_p of an individual microdroplet [26]. The size and the migration velocity of a microdroplet are directly measured with a microscope, and then the magnetic susceptibility is obtained. By using a high magnetic field generated with a superconducting magnet (10 T), this technique allowed us to measure a volume magnetic susceptibility of 10^{-6} level for a single microdroplet [27]. In the case of pure 2-fluorotoluene in water, the velocity was in agreement with the calculated one using $(\chi_p - \chi_m) = 0.82 \times 10^{-6}$. When the organic droplets contain lauric acid and are dispersed in a dilute Dy(III) aqueous solution, the observed χ_p of the single droplet depended on the radius. From an analysis, the interfacial concentration of dysprosium(III) (mol m^{-2}) was determined as well as the interfacial magnetic susceptibility (m^3 mol^{-1}). This technique is now the only method to be able to measure the interfacial magnetic susceptibility of a single droplet. Magnetophoretic force could be used to accelerate the extraction rate of a lanthanide ion, which was observed by a fluorescence microscopy.

INTERFACIAL COMPLEXATION AND AGGREGATION

Most attractive features of the liquid-liquid interfacial reaction are the catalytic effect in the solvent extraction or interfacial complexation, and the aggregation of hydrophobic dyes and metal complexes.

Interfacial Catalysis in Metal Extraction Kinetics

The extraction kinetics of Ni(II) and Zn(II) with *n*-alkyl-substituted dithizone (HL) in chloroform was the first system, which was studied by the HSS method. The observed extraction rate constants were linearly proportional to both metal ion concentration in the aqueous phase $[M^{2+}]$ and ligand concentration in the organic phase $[HL]_o$, and inversely to the hydrogen ion concentration $[H^+]$ in the aqueous phase. In this case, the rate-determining step was usually thought to be an aqueous-phase complexation of a 1:1 complex. However, the observed extraction rate constant did not decrease with an increase in the distribution constant, K_D, with the increase of the *n*-alkyl chain. Furthermore, the HSS method revealed the dissociated form of the *n*-alkyl-dithizone adsorbed at the interface generated by the vigorous agitation. From these experimental results, the contribution of the interfacial reaction was concluded, and the observed extraction rate constant k' was represented as,

$$k' = \left(k + k_i K_L' \frac{A_i}{V} \right) \frac{K_a}{K_D} \tag{1}$$

where A_i/V refers to the specific interfacial area, k and k' are the formation rate constants in the aqueous phase and interface, respectively, and K_L' the adsorption constant of L^-

from the aqueous phase to the interface. Under the conditions of $k \ll k_i K_L' A_i/V$, the interfacial reaction governed the overall extraction rate and $\log(k_i / M^{-1}s^{-1}) = 8.08$ for the Zn^{2+} system and $\log(k_i / M^{-1}s^{-1}) = 5.13$ for the Ni^{2+} system were determined [7].

From this study, one can understand that the liquid-liquid interface has a role of catalyst in the extraction rate through the adsorption of extractants like a solid catalyst. A primary criteria of the interfacial adsorption of the ligand is whether the interfacial ligand concentration shows an adsorption isotherm or not. Many extractant systems of 2-hydroxy oxime, β-diketone, 8-hydroxyquinoline derivatives, 1,10-phenanthroline, and so on obeyed the Langmuir isotherm,

$$[HL]_i = \frac{aK'[HL]_o}{a + K'[HL]_o} \tag{2}$$

where $[HL]_i$ and $[HL]_o$ refer to the concentrations at the interface and organic phase, respectively, a the saturated interfacial concentration, and K' the interfacial adsorption constant defined by $K' = [HL]_i/[HL]_o$ under the condition of $[HL]_o \rightarrow 0$.

The adsorptivity and the orientation of the 2-hydroxyoxime molecules were well simulated by the MD simulations [28]. The polar groups of -OH and =N-OH of the interfacially adsorbed P50 molecule is accommodated in the aqueous phase side of the interface so as to react with Ni(II) ion at the interfacial region [29]. The diffusive behavior of LIX65N around the interface was also simulated for 1 ns. The result clearly shows that LIX65N is more stable at the interface than in the heptane phase. This is thought to be the reason why the reaction rate constants of Ni(II) at the heptane/water interface have almost same magnitude with those in the aqueous phase.

Pyridylazo-ligands have been widely used in the extraction photometry of various metal ions. For example, 1-(2-pyridylazo)-2-naphthol (Hpan) is one of the most well known reagents, but it shows a slow extraction rate for some metal ions such as Ni(II) and Pd(II). 2-(5-Bromo-2-pyridylazo)-5-diethylaminophenol (5-Br-PADAP) is more sensitive than Hpan for Cu(II), Ni(II), Co(II), and Zn(II), giving metal complexes of molar absorptivity in the order of 10^5 $M^{-1}cm^{-1}$. 5-Br-PADAP showed a significant adsorption at the heptane/water interface, but the adsorptivity at the toluene/water interface was very low. Hpan did not adsorb at the toluene/water interface at all. The adsorption constants of 5-Br-PADAP (HL) at the heptane/water and toluene/water interfaces were obtained as $\log K' A_i$ (cm^3) = 1.64 and $\log K' A_i$ (cm^3) = -0.367 [30]. The solvent effect on the adsorptivity of the ligand affected directly the interfacial reaction rate. In the heptane system, the Ni(II) complex was not extracted into the heptane phase. On the other hand, in the toluene system the complex was extracted very slowly. The extraction rates of Ni(II) and Zn(II) with 5-Br-PADAP were studied by means of CLM [31]. The molecular dynamics simulation of the adsorptivity of 5-Br-PADAP in heptane/water and toluene/water interfaces suggested that 5-Br-PADAP could be adsorbed at the interfacial region more closely to the aqueous phase, but 5-Br-PADAP in the toluene/water interface was still surrounded by toluene, which might lower the probability to react with aqueous Ni(II) ions [30].

The fast reaction rate between Zn(II) ion with 5-octyloxymethyl-8-quinolinol (Hocqn) at the 1-butanol/water interface was measured by the two-phase sheath flow

method [32]. The formation of a fluorescence complex at the interface was measured in the period less than 5 ms after the two-phase contact.

A typical kinetic synergism has been observed for the catalytic effect of *N*,*N*–dimethyl-4-(2-pyridylazo)aniline (PADA) on the extraction of $Ni(pan)_2$ [33]. The extraction rate of $Ni(pan)_2$ into toluene is very slow even under a high-speed stirring conditions. By comparison, the addition of PADA at the diluted concentration as 10^{-5} M can accelerate the extraction rate about ten times. The observed extracted species was only $Ni(pan)_2$, and no net consumption of PADA was observed after the extraction, while a significant interfacial adsorption of PADA was observed during the extraction under the high-speed stirring condition. These results were analyzed by the mechanism of the interfacial ligand-substitution reaction.

Interfacial Aggregation at Liquid-Liquid Interface

Another specific feature of the interfacial reaction is the formation of aggregates of metal complexes and other solvophobic interfacial molecules. As reported in many interfacial adsorption systems, the saturated interfacial concentration of molecules is usually the order of 10^{-10} mol/cm^2, which can be attained even under an extremely low bulk phase concentration. This means that the liquid-liquid interface is ready to be saturated to form a two-dimensionally condensed state for the adsorbate. In solvent-extraction processes for metal ions, we used to find formation of some precipitate at the interface, called crud. Therefore, the study of interfacial aggregation is important to control the interfacial reaction met in the industrial solvent-extraction systems.

Many interfacial aggregation systems have been studied, for example, the protonated tetraphenylporphyrin (TPP) at the toluene or dodecane/aqueous acid solution interface, and the aggregation of the Pd(II)-tetrapyridylporphine (tpyp) complex and Pd(II)-5-Br-PADAP (PdL) complex. The molecular recognition ability of the Pd(II)-5-Br-PADAP for the isomers of diazine derivatives has been evaluated. The aggregation kinetics of nickel(II)-5-Br-PADAP complex at the heptane-water interface has been studied by using centrifugal liquid membrane (CLM) spectrophotometry [34]. The interfacial aggregation between ligands in NiL_2 complexes was observed as the growth of a remarkably intense and narrow absorption band (J-band) at 588 nm, showing a bathochromic shift from the absorption maximum of the monomer complex (569 nm), accompanied by a decrease of the absorbance of the free ligand at 452 nm. The formation of the aggregate was initiated at the time when the interfacial concentration of the monomer complex exceeded the critical aggregation concentration (cac) of 2.4×10^{-10} mol cm^{-2}. Recently, the second harmonic generation–circular dichroism (SHG-CD) method has been applied, for the first time, to the measurement of the CD spectra of the interfacial complex [19]. Interfacial aggregation of tetra-*p*-sulfonatophenylporphyrin (TPPS) induced by the co-existence of a chiral ion was studied using the SHG-CD method. This study enabled the chirality measurements of the interfacial complex and the interfacial aggregates, which were very difficult to be measured using ordinary CD spectroscopy due to the very low interfacial concentrations.

REFERENCES

1. H. Watarai, N. Sawada, and T. Sawada, Interfacial Nanochemistry, Kluwer Academic/Plenum Publishers, New York, 2005.
2. A. G. Volkov and D. W. Deamer, Liquid-Liquid Interfaces, Theory and Methods, CRC Press, New York, 1996.
3. A. G. Volkov, D. W. Deamer, D. L. Tanelian, and V. S. Markin, Liquid Interfaces in Chemistry and Biology, John Wiley and Sons, New York, 1998.
4. J. Rydberg, C. Musikas, and G. R. Choppin, Principles and Practices of Solvent Extraction, Marcel Dekker, New York, 1992.
5. H. Watarai, *Trends in Anal. Chem.*, **12,** 313 (1993).
6. H. Watarai and H. Freiser, *J. Am. Chem. Soc.*, **l05,** 189 (1983).
7. H. Watarai and H. Freiser, *J. Am. Chem. Soc.*, **l05,** 191 (1983).
8. H. Watarai, S. Tsukahara, H. Nagatani, and A. Ohashi, *Bull. Chem. Soc. Jpn.*, **76,** 1471 (2003).
9. H. Nagatani and H. Watarai, *Anal. Chem.*, **70,** 2860 (1998).
10. H. Nagatani and H. Watarai, *Anal. Chem.*, **68,** 1250 (1996).
11. M. Fujiwara, S. Tsukahara H. Watarai, *Phys. Chem. Chem. Phys.*, **1,** 2949 (1999).
12. S. Tsukahara, Y. Yamada, T. Hinoue and H. Watarai, Bunsekikagaku, **47,** 945 (1998).
13. S. Tsukahara and H. Watarai, *Chem. Lett.*, **89,** (1999).
14. T. Tokimoto, S. Tsukahara and H. Watarai, *Langmuir*, **21,** 1299 (2005).
15. T. Tokimoto, S. Tsukahara and H. Watarai, *Analyst*, **129,** 1099 (2004).
16. A. Ohashi and H. Watarai, *Chem. Lett.*, **32,** 218 (2003).
17. S. Yamamoto, K. Fujiwara, and H. Watarai, *Anal. Sci.*, **20**, 1347 (2004).
18. S. Wada, K. Fujiwara, H. Monjushiro, and H. Watarai, *Anal. Sci.,* **20**, 1489 (2004).
19. K. Fujiwara, H. Monjushiro, and H. Watarai, *Chem. Phys. Lett.*, **349**, 353 (2004).
20. T. Petralli-Mallow, M. T. Wong, J. D. Byers, H. I. Yee, and J. M. Hicks, *J. Phys. Chem.*, **97**, 1383 (1993).
21. J. M. Hicks, T. Petralli-Mallow, and J. D. Byers, *Faraday. Discuss.*, **99,** 341 (1994).
22. R. M. Corn and D. A. Higgins, *Chem. Rev.*, **94**, 107 (1994).
23. P-F.Brevet, Surface Second Harmonic Generation, Presses Polytechniques et Universitaries Romandes, Lausanne, 1997.
24. F. Hashimoto, S. Tsukahara, and H. Watarai, *Anal. Sci.*, **17**, i81 (2001).
25. F. Hashimoto, S.Tsukahara, and H.Watarai, *Langmuir*, **19**, 4197 (2003).
26. M. Suwa and H. Watarai, *Anal. Chem.*, **73**, 5214 (2001).
27. M. Suwa and H. Watarai, *Anal. Chem.*, **74**, 5027 (2002).
28. Y. Onoe and H. Watarai, *Anal. Sci.*, **14**, 237 (1998).
29. H. Watarai and Y. Onoe, *Solvent Ext. Ion Exch.*, **19** 155 (2001).
30. H. Watarai, M. Gotoh, and N. Gotoh, *Bull. Chem. Soc. Jpn.*, **70**, 957 (1997).
31. Y. Yulizar, A. Ohashi, and H. Watarai, *Anal. Chim. Acta*, **447**, 247 (2001).
32. T. Tokimoto, S. Tsukahara, and H. Watarai, *Bull. Chem. Soc. Jpn.*, **76**, 1569 (2003).
33. Y. Onoe, S. Tsukahara, and H. Watarai, *Bull. Chem. Soc. Jpn.*, **71**, 603 (1998).
34. Y. Yulizar and H. Watarai, *Bull. Chem. Soc. Jpn.*, **76**, 1379 (2003).

Hydrometallurgy & Metals Extraction

DEVELOPING HIGH-PERFORMING COPPER SOLVENT-EXTRACTION CIRCUITS: STRATEGIES, CONCEPTS, AND IMPLEMENTATION

Andrew Nisbett, Stephen Peabody, and Gary Kordosky

Cognis Corporation, Mining Chemicals Technology, 2430 N Huachuca Drive, Tucson, Arizona, USA. Corresponding author email address: andy.nisbett@cognis.com

ABSTRACT

An aspect of copper solvent-extraction plants that has been addressed by Cognis in recent years involves optimizing circuit configurations and staging to enhance the performance of the circuit. This results in the solvent-extraction plant being able to transfer more copper at higher overall recovery with less reagent inventory in the circuit. The economic benefits of this can be significant for the plant operator. This paper will demonstrate by means of laboratory-scale operational data how a high-performing copper solvent-extraction circuit can be designed by implementing a few strategies and concepts. Generally, these concepts require little or no additional capital investment for a new operation and can be easily retrofitted to an existing operating plant.

INTRODUCTION

It is estimated that in excess of 3.4 million metric tons of copper are produced annually via the leach/solvent-extraction/electrowinning (L-SX-EW) route. The earliest commercial plant of this nature was at the Ranchers Bluebird operation which was designed to produce about 5,000 tons per year [1]. Since 1968, many more of these facilities have been commissioned around the globe with production capabilities from as low as 1,000 tons to as high as 380,000 tons per annum of copper.

Early copper solvent-extraction reagents required multiple stages of extraction and stripping and also placed a limit on the pH and copper tenor of the leach solution (PLS) they could treat. With the advent of stronger, more selective reagents, a wide range of leach solutions can now be treated very successfully [2], and today a simple circuit containing two extraction stages and one strip stage is common. Computer-based modeling tools such as the Optiform™ formulation model [3], can predict an ideal reagent blend based on the characteristics of the solution being treated, the plant staging and the requirements of the plant operator.

Often, the staging of the SX plant is largely dictated by the capital constraints of the project, requiring much emphasis to be placed on reagent development and selection. There are, however, a number of simple concepts that can be implemented with regard to circuit design that will more fully utilize the thermodynamic properties of the reagent.

This improved performance lowers operating costs, often with little or no increase in capital requirements.

EVOLUTION OF SX PLANTS

A common trend in the design of a plant treating a heap-leach solution is a simple two-extract by one-strip (2E x 1S) design, also known as a series circuit. Depending on the project and the total volume of pregnant leach solution (PLS) to be treated, the design engineer may choose to construct one train consisting of large mixer-settlers or two or more mirror-image trains with smaller mixer-settlers. Miller [4] suggests that recent corporate risk-management studies have identified the provision of two SX trains as a prime driver towards reducing the business-interruption risk from an SX fire event. The improvements that can be made to this most basic circuit design are shown in Figure 1.

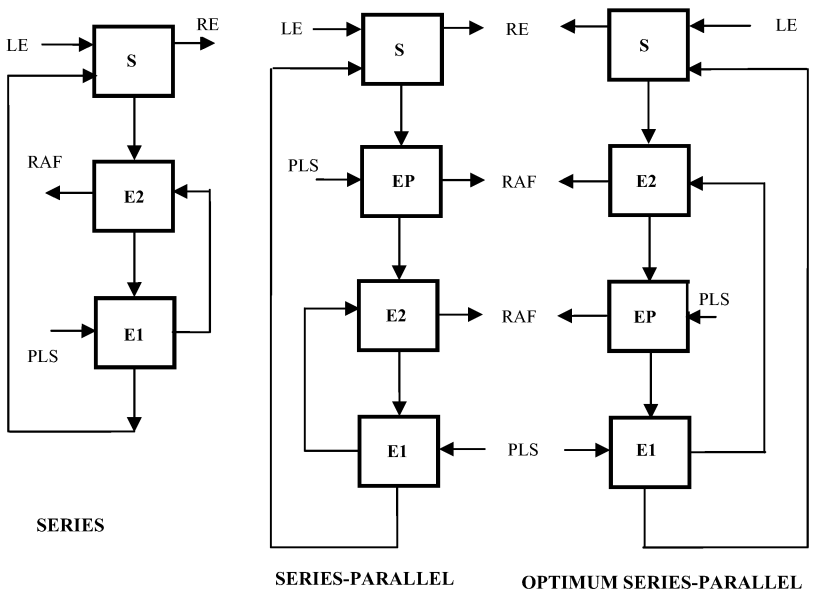

Figure 1. Illustration of different SX configurations.

Improvement 1: Series-Parallel Configuration

An evolution of the series circuit is a series–parallel (S/P) configuration (2E x 1P x 1S) that was first introduced to the industry by Cognis during the 1970s (Figure 1). This configuration does not improve the performance of the reagent in the SX circuit but is an improvement in that it does allow the SX train to treat double the amount of aqueous flow with only one additional stage being required. This results in significant capital savings. Common current practice, especially with high-producing plants, is to initially design the SX plant with a series-parallel configuration and thus utilize the savings in capital at the start of the project.

Improvement 2: Optimum Series-Parallel Configuration

Hein [5] has described the development and merits of the Cognis Optimum Series-Parallel Configuration (OSP) in some detail (Figure 1). In essence, the OSP configuration transposes the E2 and EP stages relevant to advance organic flow. The OSP improvement to the conventional S/P SX circuit requires little or no additional capital for a new plant. For an existing operation, some additional piping is required, the cost of which must be offset against the operational improvement the OSP configuration offers.

Improvement 3: Cross-Strip Concept

The composition of the electrolytes (in terms of acid and copper content) in the SX-EW process are largely dictated by the requirements of the tankhouse in producing high-quality copper. Increasing electrolyte acid concentration to favour SX performance may be to the detriment of tankhouse operation and final metal quality.

However, the availability of two or more SX trains offers the opportunity to implement the cross-strip concept. The total Lean Electrolyte (LE) flow, normally divided evenly to the strip stages of A and B Trains, is introduced in its entirety to the strip stage of A Train. The partial Rich Electrolyte (RE) produced in this stage then reports to the strip stage of B Train which in turn produces the final RE. Because the total electrolyte flow remains constant, the compositions of both the LE and final RE do not change. The advantage of the cross-strip concept is that the partial RE exiting A Train is higher in acid and lower in copper than the RE exiting Train B; thus, the copper tenor of the SO is also lower than Train B. The schematic in Figure 2 illustrates the concept.

Implementing the cross-strip concept into a new plant design would in most instances be relatively simple, involving only a few piping changes, and an additional pipe would need to be installed between the two trains.

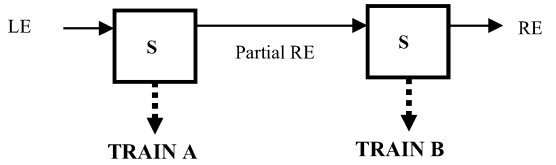

Figure 2. Cross-strip concept.

Improvement 4: Variable Temperature in Strip

The extraction/strip chemical-equilibrium equation for oxime extractants is shown in Equation 1:

$$2RH + Cu^{2+} \leftrightarrow R_2Cu + 2H^+ \quad (1)$$

An increase in temperature shifts the copper extraction equilibrium to the right, thereby making extraction more favorable and stripping less favorable [6]. Therefore,

decreasing the temperature in stripping will shift the equilibrium left and will thus produce a lower stripped organic (SO).

Depending on the project or plant, the SX operator may be fortunate enough to have access to a waste source of heat or energy. An example of this could be waste heat from a roaster, sulfur burner, or autoclave. Should such a fortunate scenario exist, it may be possible to implement a variable-temperature-in-strip concept which would enhance the performance of the SX process. The LE prior to solvent extraction is cooled by heat exchanging with the PLS. The SX generated RE is then re-heated prior to electrowinning by the waste heat source.

LABORATORY-SCALE EVALUATIONS

In order to illustrate the concepts and improvements described above that could be applied when designing copper SX circuits, a series of laboratory-scale continuous SX circuit campaigns were performed. A leach solution containing 2.70 g/L Cu at a pH of 1.86 was used together with solvent containing 15 vol % LIX® 984N. The LE contained 35 g/L Cu and 178 g/L acid, and in all the test campaigns the targeted RE composition was 50 g/L Cu. The aim of the testwork was to quantify the benefits the improvements offer and to extrapolate the results into a generic case study for a commercial production facility designed to produce around 100,000 tons of Cu annually. Because of the high PLS flow required to meet this production, the base case is two trains of SX, each operating in series parallel.

In the laboratory-circuit campaigns the temperature in the extraction stages was ambient (~25 °C). The temperature in the strip stages were controlled at 36 °C, apart from the low-temperature-in-strip testwork, when this was lowered to 27 °C. The results of the testwork are detailed in Table 1.

DISCUSSION AND SUMMARY OF RESULTS

- Net transfer (expressed as g/L Cu per volume percent reagent) measures the efficiency of the organic phase in transferring Cu. While the plant operator would like to maximize net transfer, an inverse relationship exists between Cu recovery and net transfer. For the S/P configuration with this PLS, a slightly higher net transfer would be expected in view of the overall recovery obtained. This suggests that the PLS has a low total sulfate concentration and thus offers low buffering during the solvent-extraction process
- In this study the OSP configuration offers only an unusually small increase in recovery over the S/P configuration. In previous OSP configuration investigations by Cognis, increased recoveries of between 2 and 4 percent were reported. There is a second benefit to the OSP configured circuit. A characteristic of OSP circuits is that the E2 raffinate is much lower and the EP raffinate somewhat higher in comparison to the conventional S/P circuit. If the plant operator is able to keep the two raffinates separate, he can apply these solutions to different areas of leaching. For example, the low-tenor (E2) raffinate could be applied to more mature heaps, which would ultimately result in a lower inventory of copper

present in the solution contained in these heaps. The higher-tenor (EP) raffinate could in turn be applied to newer heaps.

Table 1. Complete laboratory-circuit data to simulate two trains of SX

Configuration / Improvement	S/P (Base Case)	OSP	Cross Strip + OSP	Cross Strip + OSP + Low Strip Temp	All Improvements Base Case Recovery
Train A					
O:A E1	1.52	1.53	1.51	1.52	1.08
O:A EP	1.51	1.50	1.52	1.52	1.07
S.O (g/L Cu)	3.20	3.20	2.72	2.46	2.46
E2 Raff (g/L Cu)	0.28	0.13	0.09	0.07	0.13
EP Raff (g/L Cu)	0.33	0.45	0.34	0.27	0.47
Overall Rec. (%)	88.8	89.4	92.3	93.7	89.1
Net Transfer	0.221	0.223	0.228	0.230	0.304
Train B					
O:A E1	1.52	1.53	1.53	1.52	1.22
O:A EP	1.51	1.50	1.50	1.52	1.22
S.O (g/L Cu)	3.20	3.20	3.20	2.92	2.89
E2 Raff (g/L Cu)	0.28	0.13	0.13	0.11	0.11
EP Raff (g/L Cu)	0.33	0.45	0.45	0.36	0.43
Overal Rec. (%)	88.8	89.4	89.4	91.4	90.0
Net Transfer	0.221	0.223	0.223	0.227	0.272

- The cross-strip concept gives a marked decrease in the value of the SO for Train A. This translates into achieving higher recoveries in both the E2 and EP stages.
- Decreasing the temperature in the strip stages results in a further lowering of the copper tenor of the SO, which enables both trains to achieve higher recoveries from both the E2 and EP extraction stages.
- The recovery benefits of the cumulative improvements over the series-parallel recoveries are around 5 and 2.5 percent for A and B Trains respectively. This is achieved with a small increase in net transfer of the organic phase.

PLANT OPERATING CONSIDERATIONS

If the plant operator wanted to increase the base case recovery to the recovery achieved using the improvements, he would have to significantly increase either the reagent concentration or the organic flowrate. This in turn would result in an increase in operating costs. The plant operator may also choose to accept the “base-case” recoveries of ~89%, but use the improvements to decrease the base-case reagent concentration. In order to illustrate this, the laboratory circuit with all the improvements was operated with reduced organic flows to target base-case recoveries. Results are reported in Table 1.

A drop in the advance O:A from about 1.52 to about 1.08 represents a decrease in reagent concentration of about 24 percent. A drop in advance O:A from about 1.52 to about 1.22 represents a decrease in reagent concentration of about 19 percent.

FINANCIAL EVALUATION

In order to illustrate the financial benefits the SX circuit improvements offer, a rough financial analysis was performed based on the generic case study. On the assumption that the plant operator only wished to achieve the base-case recoveries, it follows that he could make the choice between either reducing the organic flow or maintaining the organic flow and reducing the reagent concentration. If the latter option is chosen, it is calculated that the volume percent reagent could be reduced to 10.8 and 12.2 for A and B Trains, respectively, or an average concentration of 11.5 vol %for the two trains. Table 2 below is an illustration of the initial-fill costs of the organic phase for both the base-case circuit and a circuit incorporating the improvements.

Table 2. Summary of initial-fill organic costs

	S/P (Base Case)	With Improvements
Total organic inventory (m^3)	5500	5500
Reagent concentration (volume %)	15.2	11.5
Volume reagent (m^3)	836	633
Volume diluent (m^3)	4664	4867
Cost reagent ($million @ $ 9.0/L)	7.52	5.70
Cost diluent ($million @ $ 1.0/L)	4.66	4.87
Total organic cost ($million)	12.18	10.57
Savings ($million)		1.61

The savings in the capital cost of the organic phase offered by the improved SX circuit design needs to be offset against any additional capital equipment the improvements require:

- Different piping for the OSP configuration – negligible, if any, required.
- Additional piping for the Cross-Strip concept.
- Heat exchangers and piping necessary for cooling and re-heating of the electrolyte.

The improvements also realize savings in operating costs since any organic lost from the circuit by entrainment will contain less reagent (by concentration) when compared to the base case circuit.

CONCLUSIONS

Laboratory-circuit data shows that the improvements made to the base-case circuit significantly improve the performance of the solvent-extraction circuit by more fully utilizing the inherent thermodynamic properties of the extractant. The improvements can be implemented individually or collectively depending on the circumstances of each unique project. The actual benefit of each improvement will be specific to each plant, leach solution, and reagent type and would need to be evaluated on an individual basis.

The Optimum Series-Parallel configuration and Cross-Strip concept offer no risk in implementation and would require little or no additional capital for a new project. For an existing plant, the retro-fitting capital requirements need to be evaluated against future

operating cost savings. The low-temperature-in-strip concept is fairly unique and will probably only be applicable to a select few projects. Nevertheless, the design engineer should be vigilant for these opportunities should they occur, since they can offer performance benefits to the SX plant.

REFERENCES

1. G. A. Kordosky, "Copper Recovery Using Leach/Solvent Extraction/Electrowinning Technology: Forty Years of Innovation, 2.2 Million Tons of Copper Annually," International Solvent Extraction Conference 2002, K.C. Sole, P. M. Cole, J. S. Preston, and D. J. Robinson, Eds., South African Institute of Mining and Metallurgy, Johannesburg, South Africa, 2002; pp. 853−862.
2. J. A. Tumilty, G. W. Seward, and J. P. Massam, "The Accorga P-5000 Series in the Solvent Extraction of Copper: Performance Characteristics and Implications for Plant Economics," International Solvent Extraction Conference 1977, CIM Special Volume 21, 1979; pp. 542−55.
3. H. Hein and G. Araya, "Reagent Blend Formulated Upon Copper Solvent Extraction Plant Requirements," HydroCopper 2007, Vina del Mar, Chile, 2007; pp. 239−246.
4. G. M. Miller, "SX Fires – Their Initiation and Propagation," ALTA SX Fire Protection Summit, ALTA Metallurgical Services, Melbourne, Australia, 2005.
5. D. Ibaceta, J. Garrido, H. Hein, and G. Araya, "SX Developments at Dos Amigos in Northern Chile," ALTA 2003, ALTA Metallurgical Services, Melbourne, Australia, 2003.
6. G. Kordosky, M. Virnig, and B. Boley, "Equilibrium Copper Strip Points as a Function of Temperature and other Operating Parameters: Implications for Commercial Copper Extraction Plants," International Solvent Extraction Conference 2005, Beijing, China, 2005.

STRIPPING EQUILIBRIUM MODIFICATION BASED ON THE CHEMICAL STRUCTURE OF EQUILIBRIUM MODIFIERS

Jack Thomas Bender and Michael Virnig

Cognis Corporation, Mining Chemicals Technology, Tucson, AZ, USA
Corresponding author email address: jack.bender@cognis.com

ABSTRACT

Equilibrium modifiers are used to improve the net transfer of copper from extraction to stripping with strong extractants such as the salicylaldoximes. These equilibrium modifiers function by hydrogen bonding to the phenoxy and oxime functional groups of the hydroxy oximes. Equilibrium modifiers containing a variety of functional groups and degree of functionalization were evaluated with regard to their impact on the net transfer. The impact of the nature of functional groups and the overall chemical structure of the modifier on modification will be discussed.

INTRODUCTION

Equilibrium modifiers have long been used to modify 5-alkyl-salicylaldoxime (aldoximes) reagents in copper solvent extraction [1-3]. Modification of the aldoximes is necessary because of the very high stability of the copper chelate. Without modification, the concentration of acid necessary to effectively strip the copper creates a solution that is unsuitable for electrowinning. The first generation of aldoxime reagents was modified with 4-nonylphenol (ACORGA® P series). Using 4-nonylphenol produced a viscous reagent that increased crud formation, phase separation times, and oxime degradation [1]. A variety of equilibrium modifiers have since been employed with aldoximes used in copper solvent extraction-electrowinning (SX-EW) to improve the ease of copper stripping while minimizing the adverse affects to the system. Currently, the modifiers commonly used are alcohols, ketones, esters, or 5-nonyl-2-hydroxyacetophenone oxime (ketoxime). Many articles and reviews have been referenced regarding the behavior and properties of these modifiers by Kordosky, Szymanowski, and Sastre [1,3-4].

No detailed study of the relationship between the structure of equilibrium modifiers and their properties has been carried out. The functional groups and the molecular geometry of equilibrium modifiers have an affect on the ease with which copper can be stripped from the loaded aldoxime reagents [3]. The stripping data for a variety of modifier candidates have been determined, and there is a definite trend in modification strength, which increases as the polarizability of the functional group increases. In addition, bifunctional modifiers (compounds with two of the same

functional group) have at least twice the modification strength as monofunctional compounds, assuming the functional group for both compounds is the same. Space-filling molecular models of the bifunctional compounds having the highest per-molecule modification strength were used to show that the hydrogen-bond-accepting functional groups of the modifier fit in a "lock-and-key" type mechanism with the hydrogen-donor sites of the aldoxime reagents.

EXPERIMENTAL

The following general procedure was used to determine the modifier strength for each chemical compound. To a series of 50 mL volumetric flasks was added a constant amount of LIX® 860N-I (5-nonyl-salicylaldoxime/kerosene) (~4.9 mL). Each flask was then charged with a different amount of modifier, which could range from 0.1 g to 2.0 g of material. The volumetric flasks were then brought up to volume with Conoco 170 Exempt diluent. A QC copper max load value [5] and a QC equilibrated stripped organic value [5] were determined using standard techniques on a Perkin-Elmer AAnalyst 300 series atomic absorption spectrometer using a Lumina series lamp. The effective strip points were then plotted versus the amount of modifier. An effective strip point was then calculated by dividing the QC equilibrated stripped organic value by the QC copper max load and multiplying by 5.6 (see Equation 1). An equation was then generated that can be used to determine the amount of modifier necessary to deliver a formulation with a desired extractive strength.

$$\text{Effective Strip Point} = \frac{(\text{QC equilibrated stripped organic value})(5.6)}{(\text{QC copper max load})} \quad (1)$$

In the case of the amide modifiers, which depressed the extraction loading capacity significantly, a small amount of oxime (<2%) was added to achieve a copper max load of 5.6 g/L.

DISCUSSION

There are many chemical interactions that are involved in the intramolecular and intermolecular hydrogen bonding of species in the organic phase and in the chelation of copper by aldoxime reagents. While a complete understanding of the interplay of these interactions is not well defined, we are able to discuss some of the more important factors which affect hydrogen bonding in the solvent-extraction system. Specifically, we will be looking at the intramolecular hydrogen bonding of 5-nonyl-salicylaldoxime (LIX 860N-I), the intermolecular hydrogen bonding between aldoximes, and the intermolecular hydrogen bonding of the aldoximes and equilibrium modifiers. The aldoximes are hydrogen-bond donors/acceptors (they have labile hydrogens and polarized oxygen bonds), while the modifiers can be either a hydrogen-bond donor/acceptor or merely a hydrogen bond acceptor (having no labile hydrogens). While an in-depth discussion of hydrogen bonding is beyond the scope of this work, it is important to note that the

hydrogen bonds formed by the compounds in the organic phase are mainly the result of electrostatic interactions.

Aldoxime reagents form hydrogen bonds in order to stabilize the polar functional groups in the hydrocarbon diluent (Figure 1). These hydrogen bonds are either intramolecular or intermolecular [3]. The orientation of the intermolecular hydrogen bonding in aldoximes is analogous to the bonding of the copper-loaded aldoxime chelate. Intra and intermolecular hydrogen bonding shifts the equilibrium of the extraction and stripping reactions towards the copper free aldoximes. This shift in equilibrium is relatively small; therefore, equilibrium modifiers can be added to shift the equilibrium to the left (Figure 1). This shift in equilibrium makes it easier to strip copper from the complex. If the effect is large, there is the potential to also affect extraction.

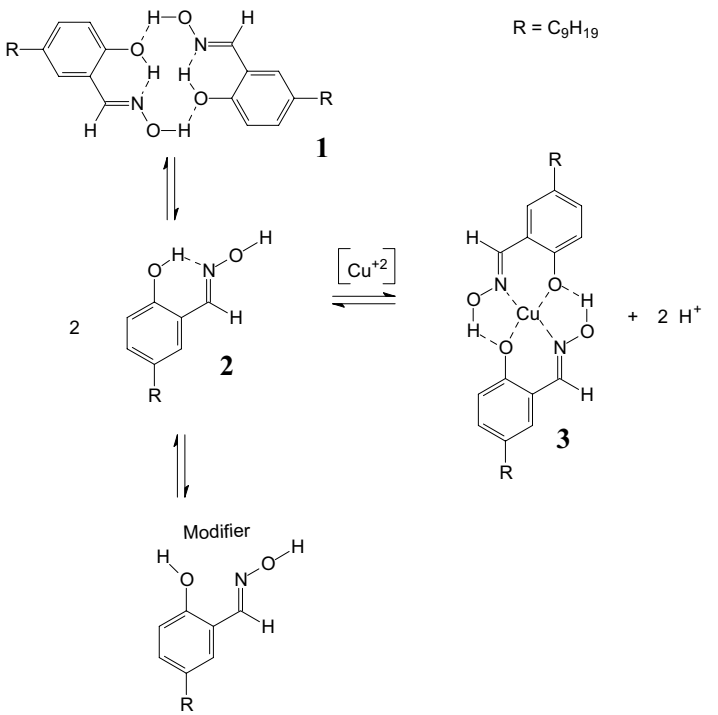

Figure 1. Reaction equilibrium for the intermolecular hydrogen bonding, chelation, and modification of aldoximes. Spatial representations of the bonding found for intramolecular (**1**) and intermolecular (**2**) hydrogen bonding of aldoximes and the copper chelate of aldoximes (**3**).

Modifiers with various functional groups have been tested for their modifier strength. For the purpose of our discussion, modifier strength is equivalent to the degree of equilibrium shift. We determine this shift in equilibrium by determining the amount of modifier necessary to reach the equilibrium strip point corresponding to a desired extractive strength for a particular reagent formulation.

We have tested more than 50 monofunctional and multifunctional compounds. A partial list of these compounds can be found in Table 1. The compounds in Table 1 have been sorted according to the mole-equivalent amount of modifier needed to reach a specified equilibrium strip point. The strongest modifiers are bifunctional ethers, esters, and monofunctional amides, while the weakest modifiers are monofunctional ethers and esters. Based on the data, we can conclude that for monofunctional species the trend in modifier strength is the same as the trend in bond polarity. The relative order for polarity of chemical bonds can be found in Figure 2. While the trend of monofunctional modifier strength can be explained by bond polarity, it does not explain the much higher modifier strength of bifunctional modifiers. In the case of modifiers with ether functional groups, the monofunctional compounds need more than twice the mole quantity of modifier than the bifunctional compounds to reach the desired strip point. In addition, the bifunctional ethers are better modifiers than any monofunctional species. Molecular models of the bifunctional compounds show how the geometry of the polar functional groups interact with the hydrogen-bonding sites of the aldoxime. The bifunctional groups with the highest modifier strength have a "lock-and-key" relationship with the aldoxime phenoxy and oxime groups. The lock-and-key mechanism is based on interactions that are shape-specific. In the case of aldoximes, the orientation of the functional groups is relatively fixed due to the rigidity of the aromatic ring and the intramolecular hydrogen bonding. Once the first hydrogen bond is formed, the second functional group of the bifunctional modifier is in the correct orientation to form the second hydrogen bond. Pictures of the functional-group interactions using molecular models of an aldoxime with 2,2,4-trimethyl-1,3-pentanediol diisobutyrate (TXIB) (Figure 3) and *t*-butoxy-*n*-butoxy hexane (Figure 4) illustrate how this lock-and-key mechanism work. Bifunctional ether modifiers with a linear and a branched end tend to be stronger modifiers, because the more accessible end helps to initially break the chelate or intermolecular hydrogen bonding, which allows the copper to be stripped, and then the less accessible end comes around to complete the lock-and-key mechanism.

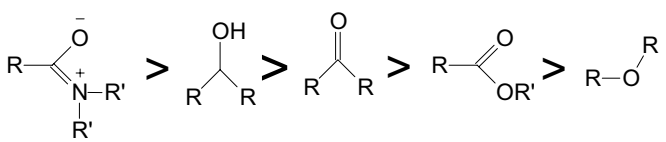

Figure 2. The relative order of bond polarity: amide > alcohol > ketone > ester > ether.

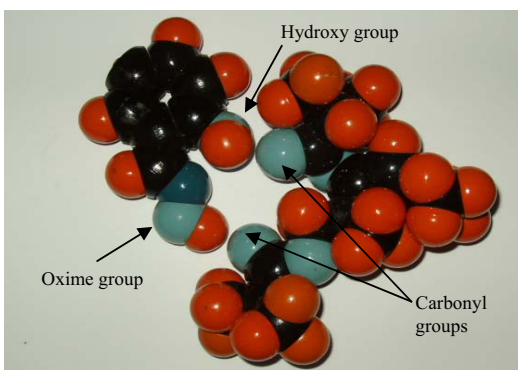

Figure 3. This is a representation of the interactions between the hydrogen-bond acceptor/donor groups of the hydroxy oxime and the carbonyl groups of the TXIB. Because of the large alkyl groups in the backbone of the TXIB and the branching of the alkyl ends, the carbonyl groups are forced into a conformation that allows it to interact very well with the phenoxy hydrogen and oxime hydrogen.

Table 1. A list of equilibrium modifiers tested for modifier strength. The compounds are sorted according to the per-mole equivalent modification at various equilibrium strip points.

Modifier	Functional group	MW	Equivalent modification (mole) at desired copper strip point			
			2.05	1.8	1.65	1.4
1,6-Di-*t*-butoxy hexane	Diether	230.39	0.37	0.51	0.62	0.82
N,N-Dimethyldecanamide	Amide	199.34	0.40	0.52	0.59	0.72
Di(ethylene glycol) dibutyl ether	Diether	218.34	0.43	0.57	0.68	0.89
N,N-Dimethyldecanamide	Amide	199.34	0.44	0.55	0.63	0.78
N,N-Diethyldodecanamide	Amide	255.44	0.46	0.59	0.67	0.81
N,N-Diethyl-2-ethyl hexanamide	Amide	199.34	0.47	0.59	0.67	0.80
1,4-Bis-*t*-butoxy butane	Diether	202.34	0.54	0.66	0.76	0.96
2-Ethylhexyl succinimide	Imide	211.30	0.57	0.76	0.88	1.10
1-*t*-Butyoxy-2-*n*-butoxy ethane	Diether	174.28	0.57	0.71	0.82	1.06
4-*t*-Butylcyclohexanone	Ketone	154.25	0.58	0.82	0.99	1.30
Ferrimod 100	Diester	258.36	0.64	0.83	0.97	1.28
Isodecyl alcohol	Alcohol	158.28	0.69	0.91	1.08	1.43
Dodecanol	Alcohol	186.34	0.69	0.97	1.16	1.52
TXIB	Diester	300.44	0.71	0.95	1.11	1.40
TDA	Alcohol	200.38	0.72	1.00	1.18	1.53
Exxal 10 alcohol	Alcohol	158.28	0.74	1.00	1.19	1.57
7-Ethyl-2-methyl-undecanol	Alcohol	214.39	0.75	1.01	1.16	1.42
Trimethyl nonanol	Alcohol	186.34	0.76	1.01	1.16	1.42
4-Isopropyl cyclohexanone	Ketone	140.23	0.84	1.10	1.27	1.59
p-*sec*-Butyl cyclohexanone	Ketone	154.25	0.85	1.11	1.28	1.58
t-Butyl octyl ether	Ether	186.34	0.89	1.20	1.40	1.77
3-Isopropyl cyclohexanone	Ketone	140.23	0.90	1.18	1.36	1.70
3,3,5-Trimethyl cyclohexanone	Ketone	140.23	0.91	1.19	1.38	1.72
5-Ethyl-2-nonanone	Ketone	170.30	0.95	1.28	1.50	1.90
p-*t*-Amyl cyclohexanone	Ketone	168.28	0.96	1.24	1.42	1.75
2-Ethyl hexyl lactate	Ester	202.39	0.96	1.26	1.45	1.78
t-Butyl decyl ether	Ether	214.39	0.96	1.26	1.46	1.81
2-Ethyl butyl caproate	Ester	228.38	0.99	1.33	1.56	1.97
Heptyl caproate	Ester	242.40	1.01	1.33	1.54	1.91
3,3-Dimethylbutyl caproate	Ester	228.38	1.12	1.43	1.62	1.96
6-Undecanone	Ketone	170.30	1.13	1.50	1.74	2.18
Heptyl 2-ethylbutyrate	Ester	214.35	1.13	1.51	1.75	2.19
2-Ethylbutyl caproate	Ester	228.38	1.15	1.55	1.80	2.27
3-(Cyclohexyl)-propionitrile	Nitrile	137.22	1.16	1.52	1.73	2.09
Di-*n*-octyl ether	Ether	242.45	1.17	1.48	1.67	1.98
Di-*n*-hexyl ether (distilled)	Ether	186.34	1.18	1.63	1.94	2.52
Heptyl 3,3-dimethylbutanoate	Ester	214.35	1.26	1.72	2.02	2.58
t-Butyl-2-ethylhexyl ether	Ether	186.34	1.52	2.00	2.31	2.87

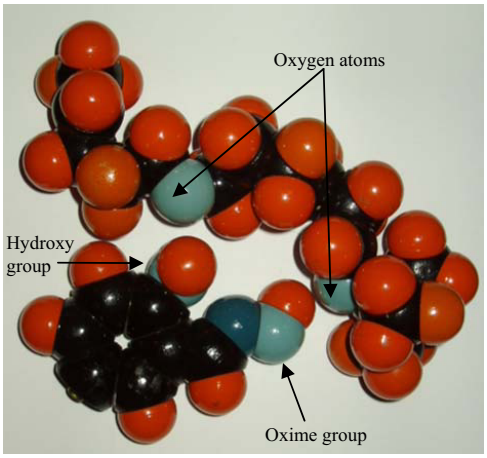

Figure 4. This is a representation of the interactions between the hydrogen-bond acceptor/donor groups of the hydroxy oxime and the oxygen atoms on the ether. Because the backbone of the di-ether compound is very flexible (all of the carbons can freely rotate), the oxygen atoms can adopt a conformation that allows it to interact very well with the phenoxy hydrogen and oxime hydrogen. This di-ether also has the advantage of being able to take a two-step approach to the lock-and-key mechanism by first having the more accessible oxygen break a chelate bond and then the other oxygen atom can move over to complete the lock-and-key mechanism.

CONCLUSIONS

Based on the results of this work, a structure-property relationship has been determined for the hydrogen bonding between equilibrium modifiers and aldoximes. The modifier strength of monofunctional species is equivalent to the trend in bond polarity. Thermodynamic modifiers interact with the copper extraction system through a complex system of bonding, and additional work will be necessary to elucidate these relationships.

REFERENCES

1. G. A. Kordosky and M. J. Virnig, “Equilibrium Modifiers in Copper Solvent Extraction – Friend or Foe,” Fifth International Conference of Professor Ian Ritchie, Volume 1: Leaching and Solution Purification, C. A. Young, A. M. Alfantazi, C .G. Anderson, D. B. Dreisinger, B. Harris, and A. James, Eds., The Minerals, Metals and Materials Society, Warrendale, PA, 2003; pp. 905−916.
2. G. A. Kordosky, “Copper Recovery Using Leach/Solvent Extraction/Electrowinning Technology: Forty Years of Innovation, 2.2 Million Tonnes of Copper Annually,” Proc. ISEC 2002, Vol. 2**,** K. C. Sole, P. M. Cole, J. S. Preston, and D. J. Robinson, Eds.; Cape Town, South Africa, 2002; pp. 853−862.
3. A. M. Sastre and J. Szymanowski, “Discussion of the Physiochemical Effects of Modifiers on the Extraction Properties of Hydroxyoximes. A Review,” *Solvent Extraction and Ion Exchange,* **22**(5), 737−759 (2004).
4. R. Swart, K. Cramer, O. Castro, P. Tasker, and R Forgan, “Evolution of Copper Solvent Extraction Reagents,” HydroCopper 2007, D. M. Menacho and J. M. Casas de Prada, Eds, Vina del Mar, Chile, 2007; pp. 42−44.
5. “Standard Cognis Quality Control Test for LIX® Oxime Reagents,” Technical Bulletin, Cognis Corporation.

COPPER SOLVENT EXTRACTION FROM WASTE CYANIDE SOLUTION BY A SOLVENT MIXTURE OF A QUATERNARY AMINE AND NONYLPHENOL

Feng Xie and David B. Dreisinger

Department of Materials Engineering, University of British Columbia, 309-6350 Stores Road, Vancouver, BC, Canada V6T 1Z4.
Corresponding author email address: drei@interchange.ubc.ca

ABSTRACT

The recovery of valuable metals and cyanide from gold-mill effluents is a matter of interest from both environmental and economic points of view. Current recovery methods are either costly or still underdeveloped. The use of a solvent mixture of a quaternary amine and nonylphenol to extract copper from waste cyanide solution was proposed, and some fundamental studies have been carried out. The results showed that variation of the type of diluent or the temperature produced little effect on copper extraction. Lower pH and CN/Cu mole ratio favored the extraction of copper. The presence of $NaNO_3$ and NaCl in solution significantly depressed copper extraction, but the addition of Na_2SO_4 to solution had no impact on copper extraction.

INTRODUCTION

The cyanidation process has been the dominant gold-ore treatment process for more than 100 years. A critical problem associated with the process is the treatment of the large volume of cyanide-contaminated effluents. Environmental constraints require that the concentration of free cyanide and the WAD (weak-acid-dissociable) cyanide species discharged into the tailing should be controlled below a strict limit. The presence of copper minerals in a gold ore may worsen this situation, since the reactivity of common copper minerals with cyanide is substantial [1]. The destruction and removal of high levels of cyanide and copper using the INCO SO_2/Air, hydrogen peroxide, or Caro's acid oxidations techniques could severely decrease the profitability of the process [2]. Acidification, Volatilization, and Recovery (AVR) and some modifications thereof have been developed and practiced in some gold operations. The main drawback associated with these processes is the high operational cost due to high reagent consumption [3]. The use of activated carbon and ion-exchange resins were studied extensively for the recovery of the cyanide species from effluents, but none of them have been successfully practiced, either due to low adsorption capability or high cost [4,5].

An alternative technology involves the application of solvent extraction as a pre-concentration step, and copper cyanide species may be further recovered by electrowinning or the AVR process [6]. The need for clarified feed solution for solvent

extraction will not be a limitation while targeting heap-leaching solutions or dam-return water. However, for operations using carbon-in-pulp (CIP) for the recovery of gold, it will be necessary to thicken and wash the solids in order to produce a clarified feed solution for solvent extraction. In this work, some fundamental studies on the extraction of copper from copper cyanide solution by the mixture of a quaternary amine were carried out under different experimental conditions, and their potential influence on copper recovery was examined.

EXPERIMENTAL

The extractant LIX® 7820 (mixture of Aliquat® 336 and nonylphenol) was supplied by Cognis. Synthetic copper cyanide solutions were made up from CuCN and NaCN at different ratios. The extraction experiments were carried out in a sealed 200 mL beaker at 20 ± 2 ºC. Initially, 50 mL of organic solution were contacted with 50 mL of aqueous solution, and the mixture was agitated magnetically until equilibrium was reached. Equilibrium pH was controlled by direct addition of concentrated H_2SO_4 or NaOH solution. The copper content in the aqueous solution was analyzed by atomic absorption spectrophotometry (AAS), and Cu in the organic phase was calculated by mass balance. Analysis of the loaded organic samples by AAS confirmed that an average accuracy of 97% between analytical and calculated results could usually be obtained.

RESULTS AND DISCUSSION

Effect of Diluent

The effect of different organic diluents on copper extraction was determined at different pH values (Figure 1). No remarkable difference on copper extraction was observed while changing the diluents, although diluents could have a major effect on phase separation. These results also indicated that copper cyanide species could be extracted from weak alkaline cyanide solutions (pH < 11) by the extractant and might be effectively stripped off at high alkali concentrations (pH > 13). Hence, this reagent would be effective for recovery of anionic cyanide species from gold plant effluents, which are generally at pH values > 10.5.

Effect of Extractant Concentration

Figure 2 shows the variations of copper extraction against equilibrium pH in aqueous solution under different extractant concentrations. As expected, when the extractant concentration was increased, enhanced extraction was observed. The initial copper concentration also influenced the extraction efficiency of copper (lower initial copper resulted in higher copper extraction), as the extraction efficiency is determined by the anionic capacity of the solvent mixture. Results suggested that higher extractant concentrations would allow more efficient extraction at higher pH values, but this would cause the stripping to be somewhat more difficult (higher pH or more stripping stages).

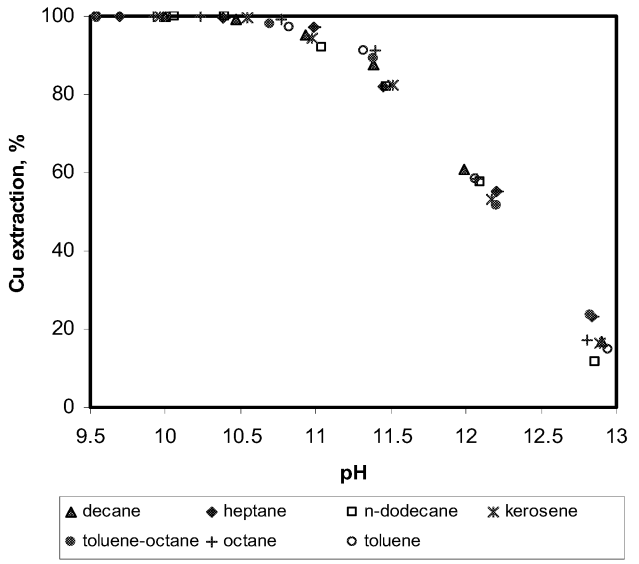

Figure 1. Effect of different diluents on copper extraction
Org.: 20% v/v LIX 7820. Aq.: initial Cu, 1.0 g/L; CN_T:Cu = 5:1.

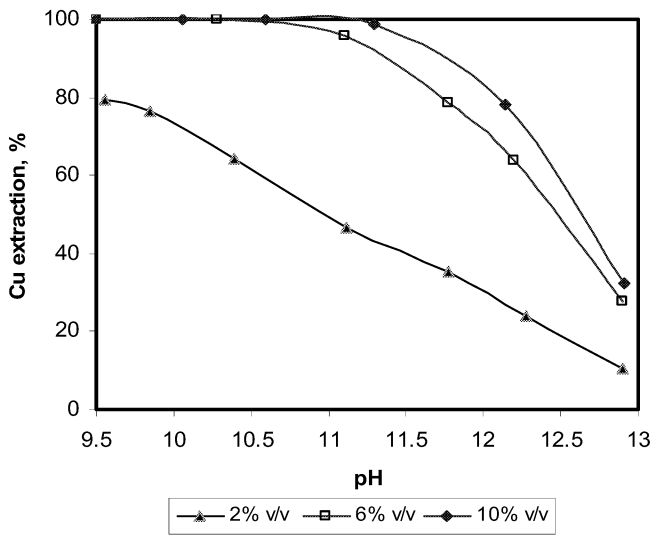

Figure 2. Effect of the extractant concentration on copper extraction
Org.: LIX 7820 in *n*-octane. Aq.: initial Cu, 0.25 g/L, CN_T:Cu = 5:1.

Effect of CN/Cu Ratio

The variations of copper extraction against pH under different initial total cyanide to copper ratios (CN_T/Cu) are shown in Figure 3. The adsorption equilibrium isotherms

at different initial CN_T/Cu ratios are shown in Figure 4. The loading of copper was strongly influenced by the CN_T/Cu ratio, and higher cyanide levels tend to suppress copper extraction. This was due to the fact that a relatively high CN/Cu ratio favors the formation of $Cu(CN)_4^{3-}$ over $Cu(CN)_3^{2-}$ in solution, which would require three Aliquat 336 molecules per copper for extraction, while $Cu(CN)_3^{2-}$ would only require two. White precipitates were found in the organic phase when tests were carried out on the solution with an initial CN_T/Cu below 3 (equilibrium pH at 10.50 ± 0.05). Under CN-deficient conditions, the precipitate CuCN and insoluble complex of polymeric copper cyanide species with quaternary amines might form.

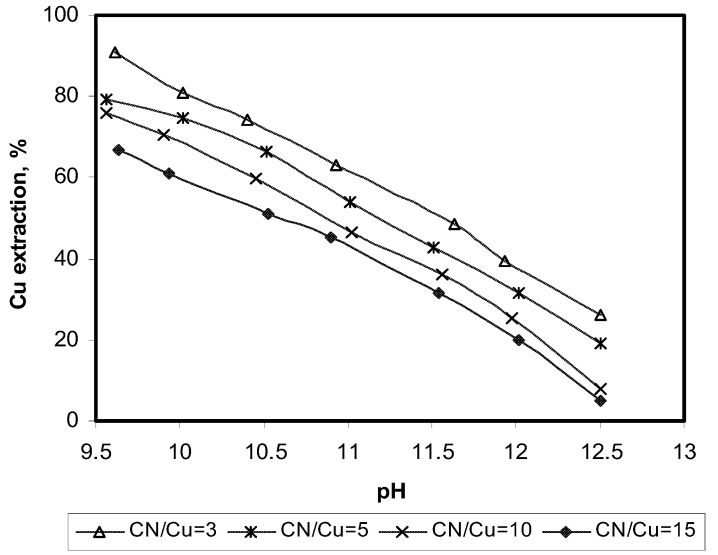

Figure 3. Effect of the cyanide-to-copper ratios on copper extraction
Org.: 2% v/v LIX 7820 in *n*-octane: Aq.: initial Cu, 0.25 g/L, CN_T:Cu = 5:1.

Number of Stages and A/O Ratios

Based on the equilibrium isotherms presented in Figure 4, a simple McCabe-Thiele diagram was constructed, indicating 2 stages of extraction would be sufficient to recover copper to 98% from a starting concentration of 150 mg/l of Cu at an A/O ratio of 1:1.

Effect of Common Anions

The effect of common anions on the extraction of copper is shown in Figure 5. Copper extraction decreased slightly with an increase in the concentration of sulfate anions, but it was significantly suppressed with the addition of chloride and nitrate ions. Charge density is probably the key factor. Sulfate has a higher charge density and tends to have a tighter solvation shell than either chloride or nitrate. Therefore, it prefers staying in the aqueous solution to the organic phase. The studies on the effect of three

monovalent cations (Li^+, Na^+, and K^+ as chloride) showed little difference on copper extraction.

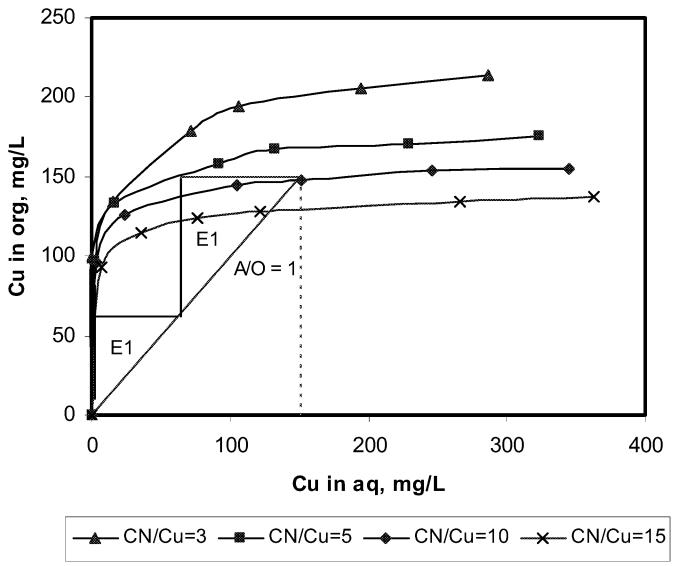

Figure 4. Equilibrium adsorption isotherm at different cyanide-to-copper ratios
Org.: 2% v/v LIX 7820 in *n*-octane: Aq.: equilibrium pH at 10.50 ± 0.05.

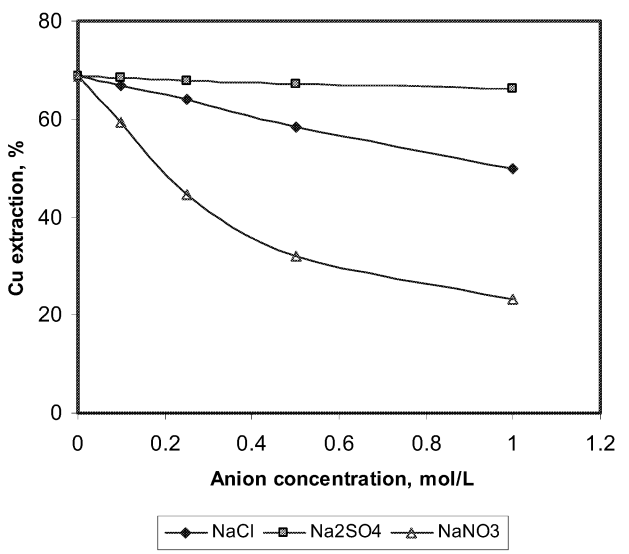

Figure 5. Effect of the common anions on the copper extraction.
Org.: 2% v/v 7820 in *n*-octane: Aq.: initial pH at 10.5, CN_T:Cu = 5:1,Cu = 0.25 g/L).

CONCLUSIONS

The solvent extraction of copper from synthetic copper cyanide solutions has been investigated using a modified quaternary amine. The choice of diluent has little influence on the extraction of copper. The extraction of copper is favorable at high extractant concentration and low equilibrium pH. The high cyanide-to-copper ratio suppressed the extraction of copper due to the increase of less extractable $Cu(CN)_4^{3-}$ in the solution. The presence of chloride and especially nitrate ion significantly suppressed the extraction of copper and sulfate ion showed little influence.

ACKNOWLEDGMENT

The authors wish to acknowledge Dr. Berend Wassink for his generous help on the project, and Cognis is thanked for providing laboratory samples of reagents.

REFERENCES

1. W. H. Jay, "Copper Cyanide Recovery System," Cyanide: Social, Industrial and Economic Aspects," A. A. Young, L. G. Twidwell, and C. G. Anderson, Eds., The Minerals, Metals and Materials Society, Warrendale, PA, 2001; pp. 317-340.
2. J. R. Goode, J. McMullen, J. A. Wells, and K. G. Thomas, "Cyanide and the Environment; Barrick Gold Corporation's Perspective," Cyanide: Social, Industrial and Economic Aspects, A. A. Young, L. G. Twidwell, and C. G. Anderson, Eds., The Minerals, Metals and Materials Society, Warrendale, PA, 2001; pp. 12-15.
3. J. Barter, G. Lane, D. Mitchell, R. Kelson, R. Dunne, C. Trang, and D. Dreisinger, "Cyanide Management by SART," A. A. Young, L. G. Twidwell, and C. G. Anderson, Eds., The Minerals, Metals and Materials Society, Warrendale, PA, 2001; pp. 549-562.
4. M. D. Adams, "Removal of Cyanide from Solution using Activated Carbon," *Minerals Engineering*, **7**(9), 1165-1177 (1994).
5. V. A. Leao and V. S. T. Ciminelli, "Application of Ion Exchange Resins in Gold Hydrometallurgy, a Tool for Cyanide Recycling," *Solvent Extraction and Ion Exchange*, **18**(3), 567-582 (2000).
6. D. B. Dreisinger, B. Wassink, F. P. De Kock, and P. West-Sells, Solvent Extraction and Electrowinning Recovery of Copper and Cyanide – Recent Developments," Randol Gold '96, Randol International, Golden, CO., 1996; pp. 315-319.

REAGENT STABILITY IN SYNERGISTIC SX SYSTEMS INCORPORATING LIX®63 OXIME AND VERSATIC 10. PART I. OXIME DEGRADATION PRODUCTS AND OXIME ISOMER ANALYSIS

K.R. Barnard

The Parker Centre (CSIRO Minerals), P.O. Box 7229 Karawara, WA 6152, Australia
Corresponding author email address: Keith.Barnard@csiro.au

ABSTRACT

The combination of LIX 63 oxime with a carboxylic acid such as Versatic 10 is the basis of two synergistic solvent extraction systems that each exhibit desirable metal separation properties. However, sufficient reagent stability is also a necessary prerequisite for commercial use. This paper briefly reviews the chemistry of LIX 63 oxime, including a summary of isolated and characterized degradation products, factors known to cause oxime degradation, and development of an analytical method to observe oxime isomer inter-conversion in these fascinating systems.

INTRODUCTION

The α-hydroxyoxime-containing reagent LIX® 63 was the first attempt to develop an organic copper extractant which could be incorporated into a leach/solvent extraction/ electrowinning operation [1]. Although it was never used for this purpose in its own right, it was used in catalytic quantities alongside LIX 65 benzophenone oxime in the first commercially applied copper solvent extraction (SX) reagent, LIX 64. In terms of copper extractants, this reagent combination has since been superseded by the phenolic oxime reagents. Nowadays the commercial use of LIX 63 is restricted to one or two small, niche applications.

That is about to change. LIX 63 is expected to enjoy a commercial renaissance as a core component in patented synergistic systems which combine LIX 63 with the carboxylic acid extractant Versatic 10 and, where nickel is present, tributylphosphate (TBP) as a kinetic accelerator. The TBP-containing synergistic system is capable of separating Ni, Co, Cu, and Zn from gangue metals such as Mn, Mg, and Ca [2]. It is well-suited to treating heap-leach nickel laterite solutions without the need for an intermediate precipitation/releach step, that is, it is a direct SX, or 'DSX' process. This system is soon to be or currently is being tried by several companies, suggesting it has the potential for mainstream application. However, the commercial revival of LIX 63 will initially commence with the TBP-free DSX system, which is capable of separating Co, Cu, and Zn from Mn, Mg, and Ca. This system is to be utilized by Baja Mining as a main process-plant component at their El Boleo (Boleo) project [3].

However, the proven and desirable metal separation properties of these reagent systems are not the only consideration where any potential commercial application is concerned. The organic combination also needs to be sufficiently chemically robust under expected operating conditions in order for the process to be economically attractive, as has been achieved for the Boleo system. Work has therefore been undertaken to better understand the chemistry associated with these systems, particularly LIX 63 oxime. This paper is the first of three on this topic presented here. The latter two papers focus on aspects of work performed specifically under Boleo and synthetic nickel laterite conditions. The present paper summarizes the "current position" regarding LIX 63 oxime degradation in these synergistic systems and presents the development of an analytical method to observe discrete *syn* and *anti* LIX 63 oxime isomers.

LIX 63 DEGRADATION

The active agent in LIX 63 is 5,8-diethyl-7-hydroxydodecan-6-oxime ('oxime', Figure 1). It can exist in either the *syn* or *anti* form, with both forms present in LIX 63 [4]. Due to its stereochemistry, only the active *anti* isomer and not the inactive *syn* isomer is capable of metal chelation. Of the organic reagents in these synergistic systems, it is the most expensive and the most chemically reactive.

Until recently, little was known about degradation of this oxime. Two postulated mechanisms were hydrolysis and Beckmann rearrangement to form hydroxyketone (also known as acyloin) and an amide, respectively [5]. Whewell *et al.* [6] found gradual degradation of LIX 63 occurred in the presence of >100 g/L sulfuric acid at 28 °C and accelerated with increasing temperature and acidity. Oxime hydrolysis to form acyloin was inferred from infra-red analysis. Hydrolysis is well established for current aromatic-based commercial SX oxime reagents [7]. Indeed, this is the only degradation mechanism of note for these reagents under typical copper operating conditions.

Accelerated degradation of oximes when in the presence of strong organic acids such as di(2-ethylhexyl)phosphoric acid (D2EHPA) and sulfonic acids has been observed [8-10]. Hydrolysis and Beckmann rearrangement were suspected, based on limited spectroscopic evidence [8].

The interest in the current DSX systems has seen the chemistry of LIX 63 oxime revisited, particularly when in the presence of a carboxylic acid such as Versatic 10 [11-13]. Different degradation mechanisms have been found to predominate under extract and strip conditions, with oxime degradation occurring more readily under extract conditions. Two 'new' oxime degradation products have been isolated and spectroscopically characterized: 5,8-diethyl-6,7-dodecanedione (diketone, Figure 1) [11] and 5,8-diethyldodecan-6-oxime-7-one (keto-oxime) [12]. The generation of acyloin as a degradation product has also been confirmed [11], although no evidence supporting amide formation has been uncovered. In addition a 'potential' degradation product, 5,8-diethyl-6,7-dodecanediol (diol), has also been isolated and characterized [12]. None of these species have any clear adverse effect on phase disengagement time or metal selectivity. These species and conditions favouring their formation are briefly described below.

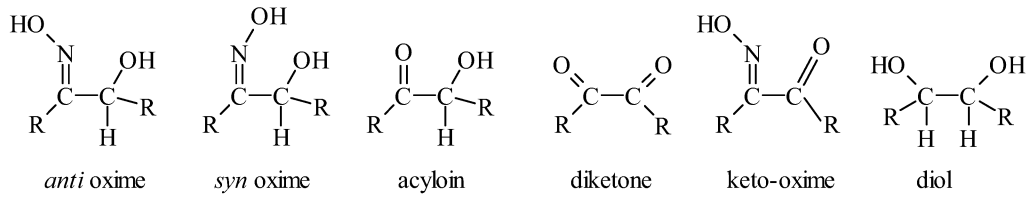

Figure 1. Structures of *anti* and *syn* oxime, acyloin (hydroxy-ketone), diketone, keto-oxime, and diol (R = 1-ethylpentyl group).

Isolation and Characterization of Oxime Degradation Products

Diketone

Diketone, formed via degradation of oxime in the presence of D2EHPA under strip conditions at 60 °C, was isolated via repeated column chromatography on a silica gel column using hexane as eluant [11]. It has been characterized using proton and carbon NMR, FT-IR, microanalysis, GC-MS and UV-visible analysis.

This species has been observed to readily form in systems containing Versatic 10 (pK_a 7.33) or D2EHPA (pK_a 3.01) [11], but not in organic acid-free systems [11,13]. Diketone formation in the metal-free synergistic system also occurs in the absence of an aqueous phase [13], directly implicating Versatic 10 in this degradation reaction. Increasing the pK_a of the organic acid resulted in faster oxime loss and a greater molar proportion reporting as diketone [11]. Subsequent studies have found diketone forms via degradation of acyloin in the presence of organic acids Versatic 10, D2EHPA or $CHCl_2COOH$ (pK_a 1.25) at 60 °C. This mechanism requires oxidation of the acyloin hydroxyl group to a carbonyl group. Additional mechanisms cannot be discounted. Degradation of diketone to acyloin in the presence of $CHCl_2COOH$ does not occur.

As diketone is formed as a result of the presence of the organic acid, it is generated under both extract and strip conditions. The proportion of diketone formed as a function of oxime consumed increases as a function of temperature under both extract and strip conditions, indicating diketone is a thermodynamically preferred degradation product [13]. However, diketone itself also appears to degrade under suitable conditions [11]. Decreasing operating temperature reduces oxime loss and diketone formation.

Keto-oxime

Keto-oxime was synthesized by both permanganate and chromite oxidation of oxime [12]. It was purified using column chromatography followed by preparative scale HPLC and characterized using proton and carbon NMR, FT-IR, microanalysis, GC-MS and UV-visible analysis. Only low yields (<15%) of the highly purified material were obtained.

Although some keto-oxime can be formed under strip conditions, it is most readily formed under extract conditions where, under the conditions used to date, it is typically the major identified degradation product. It is believed to be formed via metal (particularly manganese) complex-catalysed oxidation. Minimizing manganese loading under Boleo conditions resulted in reduced oxime degradation and keto-oxime formation.

Regeneration of oxime from keto-oxime via borohydride reduction after removal of Versatic 10 by alkaline extraction has been demonstrated [12].

Diol

Acceptably pure diol was synthesized in good yield (82%) by borohydride reduction of acyloin [12]. It was characterized using proton and carbon NMR, FT-IR, microanalysis, GC-MS and UV-visible analysis. To date, only trace quantities of diol have been observed in any operating solutions [12], and so it is not currently considered to be an important degradation product. However, it would become commercially relevant if borohydride-based regeneration of oxime from keto-oxime was employed, as any associated diketone and acyloin impurities would be converted to diol.

Acyloin

A 93% pure solution of acyloin was kindly supplied by Cognis Corp., the manufacturer of LIX 63. This impure material was analyzed using FT-IR and GC-MS. Some diketone was present.

Acyloin is generated from oxime as a result of the presence of Versatic 10 and therefore would form under both extract and strip conditions [13]. To date, net generation of acyloin has only been observed under strip conditions.

Comparison of Infra-red Spectra

The Fourier Transform infra-red (FT-IR) spectra of *anti* oxime and the related products are compared in Figure 2. Where present, absorbances associated with hydroxyl and carbonyl stretching are highlighted. Only species with an oxime moiety have a peak around 1415 cm^{-1} (*anti* oxime 1406 cm^{-1}; keto-oxime 1421 cm^{-1}). Similarly, only species with a non-oxime hydroxyl group have a peak around 1030 cm^{-1} (*anti* oxime 1036 cm^{-1}; diol 1026 cm^{-1}; acyloin 1032 cm^{-1}).

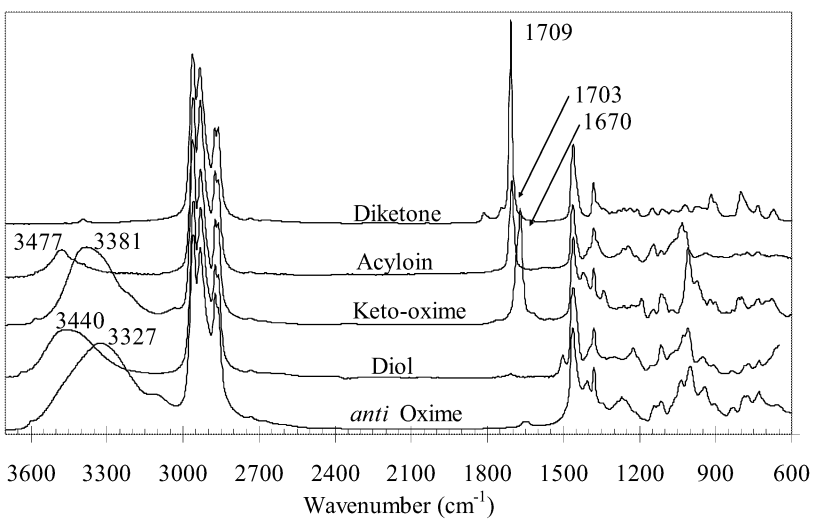

Figure 2. FT-IR spectra of *anti* oxime and related products.

OXIME ISOMER ANALYSIS AND INTERCONVERSION

Besides degradation, another major issue affecting these synergistic systems was the potential for *syn*/*anti* oxime isomer interconversion. Unlike benzophenone oxime in LIX 65 [14], no analytical procedure enabling the analysis of discrete *syn* and *anti* isomers of LIX 63 oxime had been published. Previous gas chromatography (GC) and/or high-pressure liquid chromatography (HPLC) analyses of LIX 63 had only ever observed one oxime isomer [14,15]. Development of a chromatographic method to observe both isomers was therefore undertaken.

An HPLC-based method using a C18 reverse-phase column and isocratic elution with an 80:20 mixture of HPLC grade acetonitrile and 1.0% v/v acetic acid in milliQ water has been developed. Detection of the discrete oxime isomers and degradation products is possible using a photodiode array (PDA) detector. Initially, an evaporative light scattering detector (ELSD) was also used as a second detector. Unlike the PDA, this detector had the advantage of being able to detect oxime but not diluent, which elutes close to oxime. Use of the ELSD and a pure *anti* oxime reference enabled assignment of the *syn* and *anti* oxime peak sets, which in turn allowed the optimum PDA oxime detection wavelength (200 nm) and suitable elution conditions to be determined. Figure 3 highlights the superiority of oxime detection at 200 nm relative to 220 and 240 nm.

Assuming similar molar absorbtivities of the isomers at 200 nm, the oxime in LIX 63 is approximately 60% *anti* and 40% *syn*. If, as suspected, the *syn* isomer plays no role in metal complexation, then only about 60% of the oxime present in a freshly-prepared solution containing LIX 63 would be immediately capable of metal complexation.

As metal extraction effectively removes only the *anti* isomer, a non-equilibrium condition between the residual, uncoordinated oxime isomers results. Re-establishment of the equilibrium by gradual interconversion of *syn* oxime isomers to the *anti* configuration over several days has been observed, resulting in a greater proportion of the active *anti* isomer. In contrast, inter-conversion is not favoured under strip conditions.

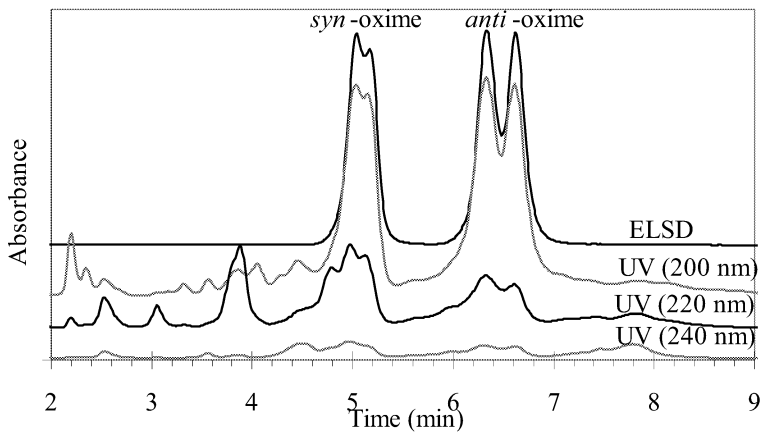

Figure 3. HPLC chromatograms of LIX 63 in ShellSol D70 diluent using ELSD detection and UV detection at 200, 220, and 240 nm.

REFERENCES

1. G. A. Kordosky, "Copper Recovery Using Leach/Solvent Extraction/Electrowinning Technology: Forty Years of Innovation, 2.2 Million Tonnes of Copper Annually," Proc. Int. Solvent Extr. Conf. 2002, K. C. Sole, P. M. Cole, J. S. Preston, D. J. Robinson, Eds., South African Institute of Mining and Metallurgy, Johannesburg, 2002; pp. 853-862.
2. C. Y. Cheng, "Solvent Extraction of Nickel and Cobalt with Synergistic Systems Consisting of Carboxylic Acid and Aliphatic Hydroxyoxime," *Hydrometallurgy*, **84**, 109-117 (2006).
3. W. J. A. Yeo, J. Wyche, M. Holmes, E. Norton, D. Hunter, T. Ross, S. Britton, and G. Bosworth, "Baja Mining Corp. El Boleo Project Feasibility Study Summary Report," Report 43-101, at http://www.bajamining.com/boleo/dfs_update/, accessed 10/10/2007.
4. T. T. Tammi, "Separation of the Isomers of the Commercial α-Hydroxyoxime LIX 63," *Hydrometallurgy*, **2**, 371-380 (1977).
5. R. R. Swanson, "Liquid Ion Exchange: Organic Molecules for Hydrometallurgy," Proc. Int. Solvent Extr. Conf. 1977, CIM Spec. Vol. 21, B. H. Lucas, G. M, Ritcey, and H. W. Smith, Eds., Can. Inst. Mining Metall., Montreal, 1979; pp. 3-8.
6. R. J. Whewell, H. J. Foakes, and M. A. Hughes, "Degradation in Hydroxyoxime Solvent Extraction Systems," *Hydrometallurgy*, **7**, 7-26 (1981).
7. J. A. Tumilty, G. W. Seward, and J. P. Massam, "The ACORGA P-5000 Series in the Solvent Extraction of Copper: Performance Characteristics and Implications for Plant Economics," Proc. Int. Solvent Extr. Conf. 1977, CIM Spec. Vol. 21, B. H. Lucas, G. M, Ritcey, and H. W. Smith, Eds., Can. Inst. Mining Metall., Montreal, 1979; pp. 542-551.
8. A. J. Oliver and V. A. Ettel, "LIX®65N and Dowfax 2AO Interaction in Copper Solvent Extraction and Electrolysis," *Can. Metall. Quart.*, **15**(4), 383-388 (1976).
9. M. E. Keeney, "Chemical Properties of Selected Nickel(II) and Copper(II) Hydroxyoxime Solvent Extraction Systems," Ph.D. Thesis, Penn. State University, 1981.
10. K. Inoue, P. Zhang, Y. Koga, and H. Eguchi, "Development of Synergistic Solvent Extraction System for the Recovery of Nickel and Cobalt from Spent Hydrodesulfurization Catalysts," Nickel-Cobalt '97 Volume I: Hydrometallurgy and Refining of Nickel and Cobalt, W. C. Cooper and I. Mihaylov, Eds., Canadian Institute of Mining, Metallurgy and Petroleum., Montreal, 1997; pp. 221-233.
11. K. R. Barnard and M. D. Urbani, "The Effect of Organic Acids on LIX®63 Stability Under Harsh Strip Conditions and Isolation of a Diketone Degradation Product," *Hydrometallurgy*, **89**, 40-51 (2007).
12. K. R. Barnard, "Isolation and Characterisation of the LIX®63 Degradation Product 5,8-diethyl-6,7-dodecandione monooxime (Keto-oxime) and 5,8-diethyl-6,7-dodecanediol (Diol) and Regeneration of Hydroxyoxime from Keto-oxime," *Hydrometallurgy,* http://dx.doi.org/10.1016/j.hydromet.2007.10.005
13. K. R. Barnard, "LIX®63 Stability in the Presence of Versatic 10 Under Proposed Commercial Extract and Strip Conditions, Part I: Operation at High Temperature," *Hydrometallurgy*, http://dx.doi.org/10.1016/j.hydromet.2007.11.002
14. W. Sowa, B. H. Licht, and I. J. Itzkovitch, "Gas Chromatography and High Pressure Liquid Chromtaography of Commercial Hydroxyoxime Copper Extractants," *J. Chrom*., **116**, 197-200 (1976).
15. A. W. Ashbrook, I. J. Itzkovitch, and W. Sowa, "Losses of Organic Compounds in Solvent Extraction Processes," Proc. Int. Solvent Extr. Conf. 1977, CIM Spec. Vol. 21, B. H. Lucas, G. M, Ritcey, and H. W. Smith, Eds., Canadian Institute of Mining and Metallurgy, Montreal, 1979; pp. 781-790.

REAGENT STABILITY IN SYNERGISTIC SX SYSTEMS INCORPORATING LIX®63 OXIME AND VERSATIC 10. PART II. THE EL BOLEO CASE STUDY

K.R. Barnard and N.L. Turner

The Parker Centre (CSIRO Minerals), PO Box 7229 Karawara, WA 6152, Australia
Corresponding author email address: Keith.Barnard@csiro.au

ABSTRACT

The stability of LIX®63 oxime in the presence of Versatic 10 under Baja Mining's El Boleo proposed extract operating conditions was investigated to assess the effect of anaerobic operation at 30 and 40 °C, and the effect of pre-reducing the feed solution using sulfite, zinc metal, and nitrogen purging. Operation at higher temperatures resulted in more rapid loss of oxime. Anaerobic operation provided no clear benefit relative to aerobic operation. Use of zinc pre-reduction provided no clear benefit. Sulfite pre-reduction had a major and immediate adverse effect on oxime levels. Aerobic operation at low temperatures is recommended.

INTRODUCTION

The active agent in LIX®63 hydroxyoxime is 5,8-diethyl-7-hydroxydodecan-6-oxime ("oxime", Figure 1). Both inactive *syn* and active *anti* isomeric forms are present in LIX 63 [1]. The combination of this oxime with a carboxylic acid such as Versatic 10 affords a synergistic solvent extraction (SX) system capable of directly separating Cu, Co, and Zn from Mn, Mg, and Ca [2]. From a metal selectivity perspective, this reagent combination is suitable for application at Baja Mining Corporation's El Boleo (Boleo) copper/cobalt project in Mexico [3]. Indeed, this direct SX (or 'DSX') process is to be a main process plant component in the Boleo project [4]. However, the decision to use this system was only taken after demonstrating that oxime degradation could be controlled and minimized under Boleo conditions. Oxime degradation could virtually be eliminated (as reported in the fully integrated pilot campaign on the Boleo process [4]) by operation at low temperature and by minimizing manganese loading via tight pH control. But determining these parameters was not straight forward. Three Boleo-specific papers (in addition to this one) outlining how the key factors affecting reagent stability were determined and overcome will be published on this topic, with one already available [6].

Initial stability studies had found considerable degradation of oxime occurred at high operating temperatures (>40 °C), particularly under Boleo extract-stage conditions [5,6]. Two major degradation products were diketone and keto-oxime (Figure 1) [5,7]. Conditions leading to these products have recently been summarized elsewhere [8]. The rate of oxime degradation observed in the initial studies was very high and needed to be

addressed. The generation of keto-oxime and diketone, both oxime oxidation products, suggested that operation under anaerobic conditions and/or pre-reduction of the manganese-rich Boleo aqueous feed solution could be of benefit. The current paper summarizes work performed to assess the effect of these two options.

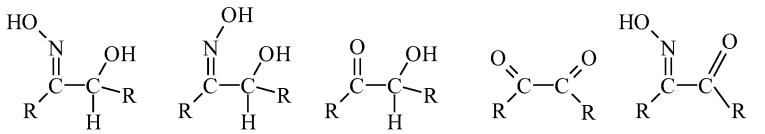

Figure 1. Structures of *syn* and *anti* oxime and the known degradation products acyloin, diketone, and keto-oxime (R = 1-ethylpentyl group).

EXPERIMENTAL

Organic solution containing 0.40 M oxime as LIX 63 (assuming 70% w/w oxime; 0.31 M if 55% w/w [6]) and 0.50 M Versatic 10 in Shellsol D70 was prepared. A sulfate-based Boleo synthetic aqueous solution containing Co (0.3 g/L), Cu (0.03 g/L), Mg (14.9 g/L), Mn (45.1 g/L), Zn (1.11 g/L), Ca (0.22 g/L), Na (9.26 g/L), Fe (0.01 g/L), Al (0.01 g/L), and Cr (0.002 g/L) was prepared.

Eight tests were performed under conditions summarized in Table 1 in 1.7 L cylindrical glass containers (11 cm diameter x 18 cm height) sealed with a flanged lid. The lid was clamped to the container and lid openings were sealed with subseals. In each system, organic and aqueous phases were mixed vigorously using a 60 mm Teflon coated magnetic stirrer bar. Organic solutions were loaded at the required A:O ratio and adjusted to pH 4.50. Organic solutions to be maintained under anaerobic conditions (experiments 2-6) were deoxygenated by nitrogen purging (30 min) prior to anaerobic metal loading.

Table 1. Test conditions

	Temp (°C)		Atmosphere		A:O ratio		Aqueous Pretreat		
Expt	30	40	N_2	Air	1:1	2:1	N_2	sulfite	Zn
1		■		■		■			
2		■	■			■	■		
3		■	■			■		■	
4a	■		■			■		■	
4b	■		■			■		■	
5		■	■			■			■
6		■	■		■			■	
7	■			■		■			■

Oxime was determined using a Shimadzu LC10 high-pressure liquid chromatography (HPLC) instrument via the method described previously [8]. Underivatized samples were also analyzed by gas chromatography (GC) using an AT-5MS fused silica capillary column to assess the presence of oxime degradation products.

For experiments 2-7, aqueous pre-treatment involved purging with nitrogen for 30 min. In addition, where used, sodium sulfite was added to a concentration of 2.0 g/L.

Where used, zinc (5 g/L) was added with stirring (15 min) before being allowed to settle (30 min) prior to careful decantation of the aqueous solution. Gas (either high-purity nitrogen or air) pre-saturated by passage through a dreschel bottle containing water and diluent was continually passed over the systems. Organic samples were taken by syringe, stripped (100 g/L sulfuric acid, A:O ratio 5:1), washed (H_2O, A:O 1:1), dried (Na_2SO_4), and stored (4 °C) prior to oxime analysis.

RESULTS AND DISCUSSION

Oxime Degradation

Results from oxime analyses are summarized in Table 2. Rate constants associated with weekly oxime consumption and oxime half lives were determined as described previously [5]. The rate plots (Figure 2) did not include the day 0 data-point. As a result, calculated half lives are indicative of ongoing oxime loss in systems but do not reflect the marked initial loss of oxime which occurred in some systems.

Examination of the results from the eight experiments revealed the following:

- All experiments with sulfite pre-reduction and a 2:1 A:O ratio (i.e., high metal loading levels) showed very high (>25%) initial oxime loss.
- All experiments conducted at 40 °C had half lives less than 0.5 years regardless of the pre-treatment and/or atmospheric conditions used, whereas all experiments conducted at 30 °C had half lives greater than 0.5 years.
- Aerobic operation at 30 °C (with initial zinc reduction, expt 7) resulted in the longest oxime half-life.
- The half-life under nitrogen with no pre-reduction (expt 2) appears particularly short at 40 °C, especially relative to the aerobic expt (1).
- If expt 3 (sulfite addition) is used as a standard reference to assess the merits of pre-reduction and each reductant used, then we get the following:
    - Use of a 1:1 A:O ratio (expt 6) gave a similar half-life, but initial oxime loss was not as marked, suggesting increased loading of one or more metals accelerates initial oxime degradation in the presence of sulfite.
    - Use of Zn pre-reduction (expt 5) resulted in a shorter half-life, but markedly less initial oxime loss.
    - Use of no pre-reduction and an aerobic atmosphere (expt 1) resulted in a slightly shorter half-life, but markedly less initial oxime loss.
    - Use of an inert atmosphere and nitrogen pre-reduction (expt 2) resulted in a markedly shorter half-life, and markedly less initial oxime loss.
    - Longer half lives were obtained operating at lower temperature (expts 4a, 4b).

The present results clearly indicate the use of sulfite under anaerobic conditions is detrimental to oxime and should be avoided completely. Interestingly, anaerobic operation, either with or without zinc pre-reduction, also appears to be detrimental, or at least showed no clear benefit, relative to aerobic operation. This suggests that the rate of oxime degradation was not dependent upon the presence of gaseous oxygen. Minimizing oxime degradation was best achieved by operation at lower temperatures without any pre-reduction.

Table 2. Oxime content (%) relative to the initial concentration in the different systems, rate constant, half-life and day-3 oxime isomer ratio

Expt	Temp		Atmos.		Aq.		Pretreat			Weeks of operation*								Rate const.	Half life	Day 3 *anti/syn*
	30	40	N_2	Air	1:1	2:1	N_2	sulf	Zn	0.4	2.0	2.9	3.0	4.4	6.0	7.4	9.4			
										Oxime content (%)								(per wk)	(yrs)	ratio**
1		▒		▒		▒				99	98	95	94	92	82	77	67	0.042	0.32	3.0
2		▒	▒			▒				100	84	73	73	65	57	53	41	0.093	0.14	2.0
3		▒	▒			▒		▒		57	61	55	57	54	48	44	45	0.034	0.39	3.1
4a	▒		▒			▒		▒		72	64	61	61	58	49	51	57	0.024	0.54	3.0
4b	▒		▒			▒		▒		71	68	60	60	62	59	57	58	0.020	0.67	3.0
5		▒	▒			▒			▒	98	92	87	82	76	68	62	61	0.061	0.22	1.7
6		▒	▒		▒			▒		99	87	79	77	74	68	71	66	0.034	0.40	1.9
7	▒			▒		▒			▒	98		94		95	89	88		0.016	0.84	3.0

* For experiment 7, sampling times (in weeks) were: 1.0, 2.6, 4.0, 6.0, 7.0.
** Ratio in fresh organic was 1.5 Expt 7 ratio is after 7 days.

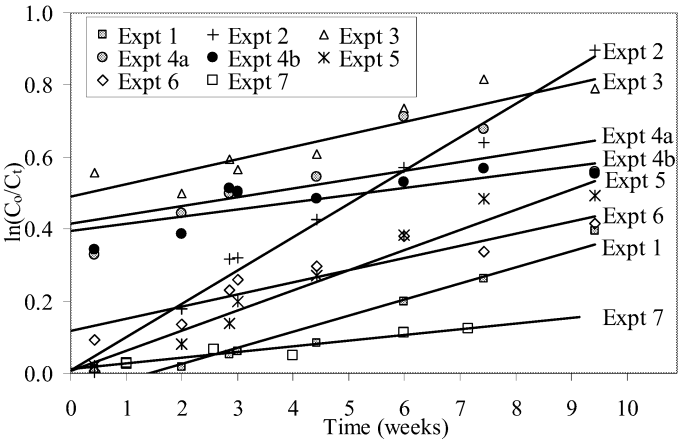

Figure 2. First-order rate plots of oxime loss in the eight experiments. The steeper the gradient, observed the shorter is the oxime half-life.

Analysis of Degradation Products

The eight organic samples were analyzed by GC (e.g., Figure 3) to assess compositional changes in each sample with time. These analyses revealed that:

- Anaerobic addition of sulfite at high A:O ratios (expts 3, 4a, 4b) resulted in the rapid formation of diketone, acyloin, and species at 8.5 min (doublet) and 9.0 min (multiplet), consistent with the observed marked, initial oxime loss in these systems. Analysis of the 9.0 min peak set revealed it to be a nitrogen-containing, non-derivatizable species with a parent ion at M/Z 367, suggesting this could be an alkylated keto-oxime. Hydrolytic degradation of oxime and reductive alkylation of amines by reaction with sulfite or dithionite has been noted previously [9].
- Diketone formation (initial and ongoing) occurred regardless of atmospheric conditions at 40 °C (aerobic, anaerobic; expts 1, 2 and 5). Aerobic operation at 30 °C resulted in little diketone being formed throughout the trial.

- Only aerobic operation resulted in a clear increase in keto-oxime concentration throughout the trial, with increased levels observed at the higher operating temperature. The formation of keto-oxime only under aerobic conditions is indicative of this being an oxygen-based oxidation process.
- Acyloin gradually decreased with time in all systems, suggesting it is not a stable species under the conditions used. Subsequent investigation has revealed acyloin degradation results in diketone formation [8].
- Differences in degradation products observed under aerobic (expt 1) and anaerobic (expt 2) conditions were apparent, indicating that different oxime degradation mechanisms dominate under aerobic and anaerobic conditions.

These results indicated that some diketone formation would be unavoidable upon contact of organic with aqueous, particularly at higher temperatures. Diketone formation can be minimized by operation at lower temperatures. Keto-oxime appears to be generated via an oxidation mechanism and so can be avoided (or minimized) by operation under anaerobic conditions, again preferably at lower temperatures. Sulfite addition under anaerobic conditions results in multiple degradation products.

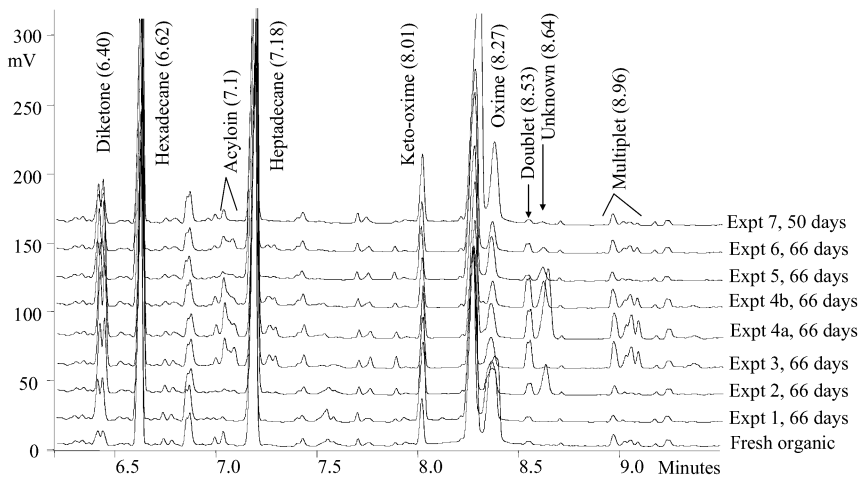

Figure 3. GC traces (6.2-9.5 min region) of the organic samples at the conclusion of the trial.

Observation of *Syn* and A*nti* Oxime Isomers

HPLC analysis allows the observation of discrete *syn* and *anti* isomers. Only the *anti* isomer forms metal complexes [1]. Oxime in LIX 63 is approximately 60% *anti* and 40% *syn* [8]. Inspection of the oxime isomer levels in the day-3 samples (Table 2) revealed an increase in the *anti*/*syn* ratio. This was attributable to *syn* to *anti* isomer inter-conversion, with >100% *anti* oxime (relative to fresh LIX 63) observed in the relatively undegraded day-3 samples (expts 1, 2, 5, 6, 7). Of these five samples, the two aerobic samples (expts 1, 7) had large *anti*/*syn* ratios (3.0), whereas the anaerobic sample ratios were all less than 2.0. The reason for this is currently unknown. However, given the nil benefit of working anaerobically, investigation of this effect is not planned.

CONCLUSIONS

Operation at 40 °C showed unacceptable rates of oxime degradation, regardless of the pre-treatment or atmospheric conditions used. In contrast, longer half-lives were observed for systems operating at 30 °C. Keto-oxime was only formed under aerobic conditions, whereas diketone was formed under both aerobic and anaerobic conditions.

No beneficial effect associated with operation under anaerobic conditions, with or without zinc pre-reduction, was noted. The use of sulfite as a pre-reductant under anaerobic conditions had a clear detrimental effect on oxime and should not be used.

Differences in the relative amounts of degradation products formed under aerobic and anaerobic conditions were apparent, suggesting different degradation mechanisms.

The present results led to subsequent oxime stability studies on manganese loading being performed aerobically at 30 °C, which was found to be the remaining 'key' that Baja Mining required to control reagent degradation in this system.

ACKNOWLEDGMENT

Dr. David Dreisinger (Vice President-Metallurgy, Baja Mining Corporation) is thanked for permission to publish this work.

REFERENCES

1. T. T. Tammi, "Separation of the Isomers of the Commercial α-Hydroxyoxime LIX 63," *Hydrometallurgy*, **2**, 371-380 (1977).
2. C. Y. Cheng, "Solvent Extraction of Nickel and Cobalt with Synergistic Systems Consisting of Carboxylic Acid and Aliphatic Hydroxyoxime," *Hydrometallurgy*, **84**, 109-117 (2006).
3. C. Y. Cheng, K. R. Barnard, and M. D. Urbani, "Improving Plant Operations using Synergistic Solvent Extraction Technology and Organic Monitoring," Proc. First Extractive Metallurgy Operators' Conference, AUSIMM, Victoria, 2005; 59-66.
4. W. J. A. Yeo, J. Wyche, M. Holmes, E. Norton, D. Hunter, T. Ross, S. Britton, and G. Bosworth, "Baja Mining Corp. El Boleo Project Feasibility Study Summary Report," Report 43-101, 11 July 2007 at http://www.bajamining.com/boleo/dfs_update/, accessed 10/10/2007.
5. K. R. Barnard and M. D. Urbani, "The Effect of Organic Acids on LIX®63 Stability Under Harsh Strip Conditions and Isolation of a Diketone Degradation Product," *Hydrometallurgy*, **89**, 40-51 (2007).
6. K. R. Barnard, "LIX®63 Stability in the Presence of Versatic 10 Under Proposed Commercial Extract and Strip Conditions, Part I: Operation at High Temperature," *Hydrometallurgy*, http://dx.doi.org/10.1016/j.hydromet.2007.11.002.
7. K. R. Barnard, "Isolation and Characterisation of the LIX®63 Degradation Product 5,8-diethyl-6,7-dodecandione monooxime (Keto-oxime) and 5,8-diethyl-6,7-dodecanediol (Diol) and Regeneration of Hydroxyoxime from Keto-oxime," *Hydrometallurgy,* http://dx.doi.org/10.1016/j.hydromet.2007.10.005.
8. K. R. Barnard, "Reagent Stability in Synergistic SX Systems Incorporating LIX®63 Oxime and Versatic 10, Part I: Oxime Degradation Products and Oxime Isomer Analysis", Proc. Int. Solvent Extr. Conf. 2008, CIM, Montreal, 2008.
9. P. M. Pojer, "The Use of Soduim Dithionite for the Reduction of Imines and the Cleavage of Oximes," *Aust. J. Chem.*, **32**, 201-4 (1979).

REAGENT STABILITY IN SYNERGISTIC SX SYSTEMS INCORPORATING LIX®63 OXIME AND VERSATIC 10. PART III. NICKEL LATERITE CASE STUDY

K.R. Barnard and N.L. Turner

The Parker Centre (CSIRO Minerals), P.O. Box 7229 Karawara, WA 6152, Australia
Corresponding author email address: Keith.Barnard@csiro.au

ABSTRACT

The effect of operating temperature on LIX®63 oxime stability in the presence of Versatic 10 and tributyl phosphate (TBP) under synthetic nickel laterite extract operating conditions has been assessed. At 30 °C the half life of LIX®63 oxime was almost two years. This decreased to eight weeks at 60 °C. The operating conditions resulted in accrual of diketone and keto-oxime, and the loss of acyloin.

INTRODUCTION

Solvent extraction processes to separate Ni, Co, Cu, and Zn from Mn, Mg, and Ca using synergistic SX technology have recently been developed [1]. A benefit of such systems is that they have the potential to recover nickel and cobalt from laterite leach solutions via 'direct solvent extraction' (DSX), that is avoiding the need for intermediate precipitation and releach steps. It is achieved by using an organic solution containing Versatic 10, the α-hydroxyoxime LIX® 63 (5,8-diethyl-7-hydroxydodecan-6-oxime, Figure 1), and tributylphosphate (TBP). The presence of TBP distinguishes it from the solvent used in the essentially nickel-free El Boleo operation [2]. Its presence is essential for treatment of nickel-containing solutions, as it acts mainly as a nickel strip modifier (accelerator).

However, desirable metal separation properties are not the only consideration where any potential commercial application of a reagent system is concerned. The organic combination also needs to be sufficiently chemically robust under expected operating conditions in order for the process to be economically attractive. Initial studies have highlighted the potential for degradation of LIX 63 hydroxyoxime ("oxime") when used under harsh or inappropriate operating conditions [2-4]. A summary of known oxime degradation products is presented elsewhere [5]. Although oxime degradation can now be controlled in the El Boleo system, the nickel laterite system presents a totally new set of conditions—the presence of TBP in the solvent and, most importantly, a different aqueous extract solution. Reagent degradation rates have been found to be very

dependent on aqueous-phase composition. The current paper provides an interim update on work currently being performed under synthetic nickel laterite extract conditions to assess the impact of operating temperature on oxime stability under nickel laterite conditions.

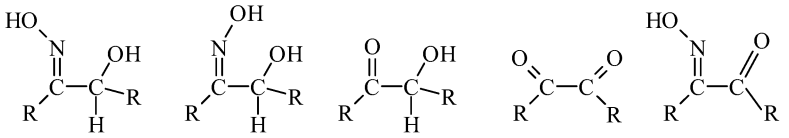

Figure 1. Structures of *syn* and *anti* oxime and the known degradation products acyloin, diketone and keto-oxime (R = 1-ethylpentyl group).

EXPERIMENTAL

An organic solution containing 0.50 M oxime as LIX 63, 0.50 M Versatic 10, and 0.50 M TBP in ShellSol D70 was prepared and washed four times using a 50 g/L sodium sulfate solution (A:O 1:4). For consistency with earlier work, LIX 63 was assumed to contain 70% w/w oxime rather than 55% w/w as found recently [3].

A synthetic nickel laterite feed solution based on that used in [1] containing 3.0 g/L Ni, 0.30 g/l Co, 0.20 g/L Cu, 0.21 g/L Zn, 1.9 g/L Mn, 10.1 g/L Mg, and 0.50 g/L Ca was prepared.

Tests under laterite extract conditions were performed at 30, 37, 45, 52, and 60 ± 2,°C in square glass jars (70 mm width x 75 mm height) with Halar-coated lids located in glycol baths maintained at the required temperature. Organic (200 mL) was initially loaded with metal by mixing with the aqueous laterite solution (200 mL) whilst maintaining the pH at 5.50.

Each sample was then mixed vigorously at the appropriate temperature for 9 weeks using a 3.5 cm Teflon coated magnetic stirrer bar and an IKA RCT Basic magnetic stirrer/hotplate and IKA ETS-D4 temperature controller. The pH in all systems was monitored intermittently during the stability trial and adjusted back to pH 5.50 as required. No aqueous solutions were replaced during the trial. Organic samples were taken after 2, 5, 21, 43, and 64 days and stripped (100 g/L sulfuric acid, A/O 5:1, 40 °C), washed (distilled water), dried (Na_2SO_4), and stored at 4 °C prior to gas-chromatography (GC) analysis.

GC analyses were performed using a Varian 3800 gas chromatograph fitted with a flame ionization detector and an SGE BP-1 fused silica capillary column (30 m x 0.32 mm i.d., 0.50 μm film thickness). Helium (1.7 ml/min) was used as the carrier gas. The injection and detector ports were held at 260 °C and 280 °C, respectively. After sample injection at 150 °C, the oven temperature was held (one minute), then increased to 220 °C at 5°C/min, then to 320 °C at 50 °C/min where it was held for two minutes. To enable the detection of the oxime extractant, samples (90 μL) were dissolved in 400 μL of a 1:1 dimethylformamide:toluene solution and derivatised by adding Sylon BFT (BSTFA containing 1% TMCS, 200 μL, Supelco) and heating (80 C) for one hour.

RESULTS AND DISCUSSION

Oxime Degradation

The operating conditions used resulted in essentially complete nickel, cobalt, copper, and zinc loading and low manganese loading (between 0.1 and 0.3 g/L) in all samples. Oxime levels determined throughout the trial for the organic samples agitated under extract conditions at the various temperatures (expressed as a percentage of their initial, day-0 concentration), rate constants and half-lives are presented in Table 1.

Rate constants associated with weekly oxime consumption were determined by the method of integration, assuming a first-order rate of reaction [4]. The resulting rate plots are shown in Figure 2. The lines of best fit, from which each rate constant was determined, were not forced through the origin. Oxime half lives were calculated from the corresponding rate constant as follows:

$$\text{Half-life (weeks)} = \ln 2/(\text{weekly rate constant}) \quad (1)$$

Table 1. Summary of oxime content seen in the samples

Experiment	Day 5	Day 21	Day 43	Day 64	Rate const (w)	Half life (weeks)
	Oxime (%)					
Extract, 30 °C	99	96	95	93	0.007	99
Extract, 37 °C	97	93	91	87	0.013	51
Extract, 45 °C	97	89	83	77	0.029	24
Extract, 52 °C	97	88	80	70	0.038	18
Extract, 60 °C	92	76	59	46	0.083	8

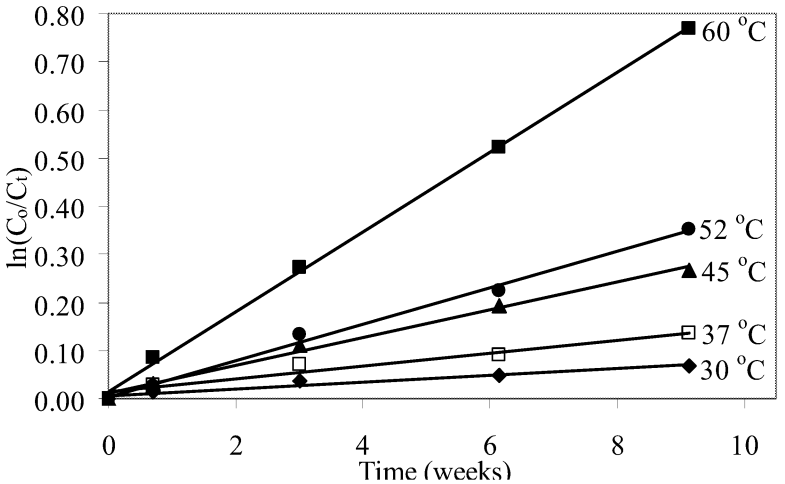

Figure 2. First-order rate plots of oxime loss at various temperatures. The gradient equals the rate constant. The steeper the gradient observed, the more rapid isthe rate of oxime loss.

These interim results clearly demonstrate the detrimental effect of increasing temperature on oxime stability under synthetic laterite extract conditions. Although such a trend was expected, the actual half-lives at any given temperature were previously unknown. On that basis, the results serve to highlight the relative ruggedness of this synergistic system when operated at or below 37 °C. In addition, the operating parameters used in system, specifically reagent composition and extraction pH, are yet to be optimized from a reagent stability perspective. Such changes were successfully employed to minimise oxime degradation in the El Boleo system.

The present synergistic systems do suffer from some ongoing degradation during both extract and strip conditions [3], due partially to the necessary presence of Versatic 10. This 'unavoidable' degradation is minor at low temperatures (e.g., <40 °C), but occurs more rapidly with increasing operating temperature [3]. However, to date most degradation seen in these synergistic systems occurs under extract conditions [3,5]. For example, the observed extract stage half-life of eight weeks at 60 °C is much lower than the 34 weeks observed under synthetic strip conditions at 60 °C [4]. Given this, it is of interest to benchmark the current oxime half-life under laterite conditions to other, commercially-used SX reagents. Although not strictly comparable for reasons discussed above, the calculated oxime half life at 45 °C (24 weeks) is similar to those determined for commercially used nonyl (half-life 16 weeks) and dodecyl (half-life 31 weeks) aromatic aldoxime copper extractants when continuously mixed under synthetic copper strip conditions at 45 °C in the presence of 180 g/L sulfuric acid and 30 g/L copper [6]. The 30 °C result also compares favourably to the laboratory-determined half life for the optimised El Boleo system at the same temperature. This, coupled with operation at lower temperatures (ideally <40 °C) and the knowledge that initial stability issues were encountered and overcome in the El Boleo system, suggests this yet-to-be-optimized system would be sufficiently chemically robust under these conditions so as to be economically attractive. However, as reagent-degradation rates can be very dependent on aqueous-phase composition, any intended application of this system at a given site would require stability trials to be conducted under site-specific operating conditions.

This work and an additional study focussing on the impact of metal-loading levels under the same synthetic laterite conditions at 45 °C are continuing.

Oxime Degradation-Activation Energy

The temperature-related oxime data was used to calculate the activation energy (E_a) for oxime degradation under synthetic laterite extract conditions by using the Arrhenius equation,

$$k = A \exp(-E_a/RT), \quad (2)$$

Where k is the rate constant, A is the pre-exponential factor, R is the gas constant (8.314 J/(K mol)), and T is temperature (in Kelvin) and is the rate constant at infinite temperature. The pre-exponential factor can be looked upon as a "collision effectiveness" value, being a product of collision rate and collision efficiency.

Determination of E_a is most readily achieved by taking the logarithm of each side of this equation which then becomes

$$\ln(k) = \ln(A) - (E_a/RT). \quad (3)$$

The Arrhenius plot based on the available interim data gave a good fit (Figure 3). From this plot, A is 2.55 x 10^9 per week, and E_a was calculated to be 67 kJ/mol. These values were used to calculate expected oxime half life at different operating temperatures (Figure 3).

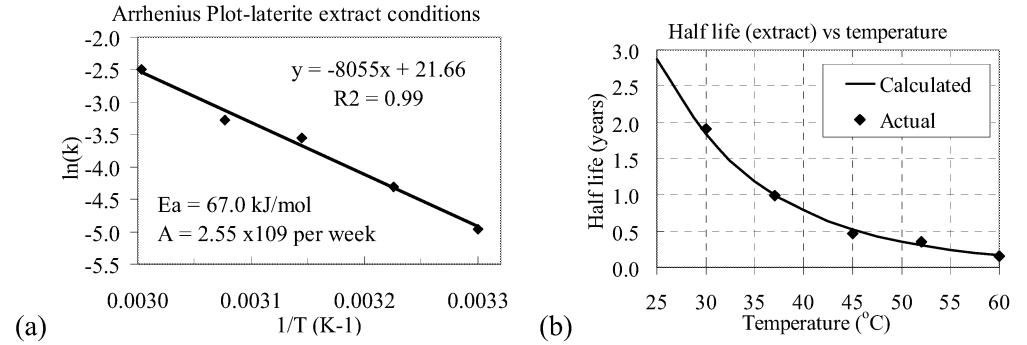

Figure 3. (a) Arrhenius plot of the rate constants for oxime loss in the synergistic organic system under synthetic laterite extract conditions. (b) Calculated and actual oxime half life as determined from the present data as a function of temperature under laterite extract conditions.

Degradation-Product Analysis

GC traces of 60 °C organic samples taken over the first 64 days of the trial (Figure 4) highlight the major compositional changes observed in these systems. Under extract conditions at all temperatures, diketone and keto-oxime (Figure 1) were observed to increase with time, whereas acyloin concentration decreased. Increasing operating temperature accelerated diketone and keto-oxime formation and acyloin loss. Future quantitative analysis of these species is planned.

As the presence of these species in the El Boleo system do not have any adverse effect on metal extraction isotherms and phase disengagement [7], they are also considered unlikely to have any material effect here.

CONCLUSIONS

The effect of operating temperature on LIX 63 oxime stability in the presence of Versatic 10 and TBP under non-optimized synthetic nickel laterite extract operating conditions has been assessed. At 30 °C the half-life of LIX 63 oxime was almost two years. This decreased to eight weeks at 60 °C. Ongoing operation also resulted in accrual of diketone and keto-oxime and the loss of acyloin.

The level of oxime stability exhibited under the synthetic laterite conditions below 40 °C under non-optimized conditions is promising from a commercial perspective.

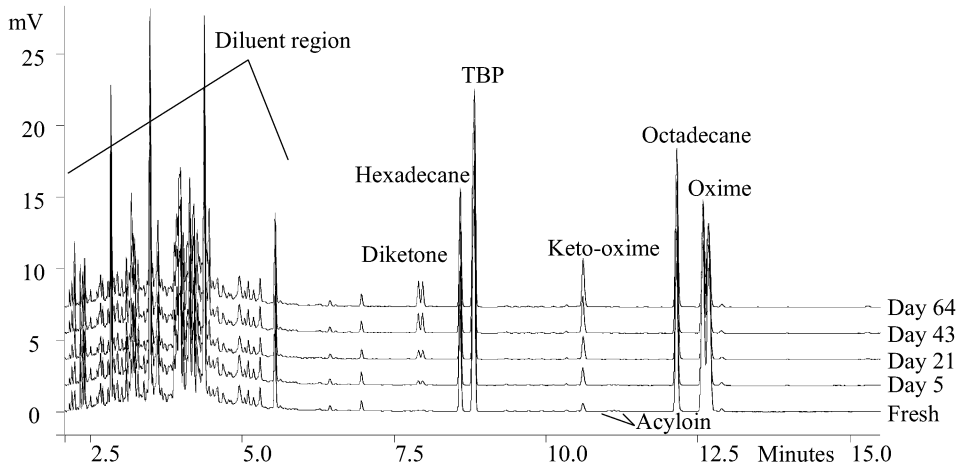

Figure 4. GC traces highlighting major changes observed in diketone, keto-oxime, acyloin, and oxime content in the 60°C extract system with time.

REFERENCES

1. C. Y. Cheng, "Solvent Extraction of Nickel and Cobalt with Synergistic Systems Consisting of Carboxylic Acid and Aliphatic Hydroxyoxime," *Hydrometallurgy*, **84**, 109-117 (2006).
2. K. R. Barnard and N. L. Turner, "Reagent Stability in Synergistic SX Systems Incorporating LIX®63 Oxime and Versatic 10, Part II: The El Boleo Case Study", Proc. Int. Solvent Extr. Conf. 2008, Canadian Institute of Mining, Metallurgy and Petroleum, Montreal, 2008.
3. K. R. Barnard, "LIX®63 Stability in the Presence of Versatic 10 Under Proposed Commercial Extract and Strip Conditions, Part I: Operation at High Temperature," *Hydrometallurgy*, http://dx.doi.org/10.1016/j.hydromet.2007.11.002.
4. K. R. Barnard and M. D. Urbani, "The Effect of Organic Acids on LIX®63 Stability Under Harsh Strip Conditions and Isolation of a Diketone Degradation Product," *Hydrometallurgy*, **89**, 40-51 (2007).
5. K. R. Barnard, "Reagent Stability in Synergistic SX Systems Incorporating LIX®63 Oxime and Versatic 10, Part I: Oxime Degradation Products and Oxime Isomer Analysis", Proc. Int. Solvent Extr. Conf. 2008, Canadian Institute of Mining, Metallurgy and Petroleum, Montreal, 2008.
6. G. Kordosky, "Copper SX Circuit Design and Operation-Current Advances and Future Possibilities," Proc. ALTA SX/IX World Summit, ALTA Pty. Ltd., Melbourne, 2003.

PROCESSING OF AFRICAN COPPER-BELT COPPER-COBALT ORES: FLOWSHEET ALTERNATIVES AND OPTIONS

P.M. Cole[1] and A.M. Feather[2]

[1]*TWP Matomo Process Plant (Pty) Ltd, P.O. Box 5100, Rivonia 2128, South Africa*
[2]*Cognis Corporation, P. O. Box 361, Honeydew 2040, South Africa.*
Corresponding author email address: pcole@twpmatomo.co.za

ABSTRACT

The Central African Copper Belt has one of the world's last large deposits of copper and cobalt. Favorable developments in the region have led to new projects assessing various flowsheets for the recovery of copper and cobalt. The recovery of copper in these treatment routes is well understood. The recovery of cobalt is complex, and a wide range of processes are considered in choosing a flowsheet. Particularly challenging is the complex nature of the deposits, as the region is known for high levels of manganese and magnesium. Solvent extraction often features prominently for copper and cobalt recovery options. Since over one third of world cobalt reserves are in the African Copper Belt and prospects under development there project large tonnages of cobalt production into a relatively small market, cobalt market dynamics will dictate cobalt recovery decisions in the region. It is likely that all the larger projects will consider only copper revenues, or greatly reduced cobalt revenue, in financial analyses.

INTRODUCTION

The Central African Copper Belt, host to extensive high-grade copper-cobalt mineralization, is at present receiving much interest from the international mining industry [1] that is driven by the current metals boom, by political stability, and the new 2003 Mining Code in the Democratic Republic of Congo (DRC), and by privatization of the mining industry in Zambia. Since the 2006 general election in the DRC—the first free election in 40 years—many large mining companies have returned to the region. Major new African Copper Belt projects in advanced stages of development are listed in Table 1. The Muliashi project is in Zambia and the others are in the DRC. State-owned Gécamines, guardian of the DRC's copper and cobalt interests, has actively wooed investors as partners in the rehabilitation of run-down existing plants and the development of dormant and new mining projects. All of the projects listed will see the installation of new processing plants. The copper recovery flowsheets feature solvent-extraction (SX) and electrowinning (EW) technology to ensure that high-grade copper cathode is produced. The situation for cobalt is more complex, with the trend towards minimizing risk by limiting capital expenditure in the cobalt circuit.

Table 1. New Cu-Co projects in the African Copper Belt (adapted from [2])

Project Name	Expected Completion	Copper (t/a)	Cobalt (t/a)
Muliashi	Q1 2008	60,000	–
Ruashi	Q2 2008	45,000	3,500
Luita	Q4 2008	100,000	12,000
KOV	Q4 2009	250,000	27,500
Tenke-Fungurume	Q4 2009	115,000	8,000
Kolwezi (Phase1/Phase2)	2009	42,000/70,000	4,200/8,400
Kinsevere	Q1 2010	60,000	–

TYPICAL CHARACTERISTICS OF AFRICAN COPPER BELT ORE

The Central African Copper Belt, one of the world's great metallographic provinces, stretches a distance of 500 km from Kolwezi in southern DRC to Luanshya in Zambia. The listed projects are initially targeting surface oxide ore bodies, although significant sulfide deposits also exist. The Kolwezi project treats oxide tailings accumulated from the prior flotation of high-grade ore. Secondary supergene minerals dominate the oxide ore bodies–malachite ($Cu_2(CO_3)(OH)_2$) for copper and heterogenite (CoO(OH)) for cobalt, which give way to sulfide phases such as chalcocite (Cu_2S) and carrollite ($CuCo_2S_4$) at increasing depths. Grades vary between 0.7 and 6% for copper and up to 1.03% for cobalt. Oxide copper leaches readily in dilute sulfuric acid; secondary sulfides require oxidative conditions, and cobalt, present as Co(III), requires reductive conditions to ensure good recoveries.

Common impurities are Fe, Mn, Zn, Mg, Al, Ca, sometimes Ni, and occasionally Cd and U. Manganese levels are higher in ore from the DRC compared with Zambia. Some ores feature up to 150 kg/t gangue acid consumption (GAC) and are blended to give economically acceptable GACs of around 40 kg/t of ore.

NEW COPPER-COBALT PROJECT FLOWSHEET DEVELOPMENT

When examining the economics of projects, mining companies and their financial backers are increasingly considering the revenue from copper and cobalt individually. Medium- to long-term prospects for favorable copper prices are good. The future price of cobalt is uncertain, with the region holding 37% of the world's reserves of cobalt and the total cobalt production represented by the projects listed in Table 1 approaching the current world demand of 65,000 t/a. When any one of the larger projects starts refining and selling cobalt associated with the copper recovered, the cobalt price will be affected. For cobalt products other than cathode, marketing becomes more difficult, and revenues may depend on finding niche-market customers. For this reason, most projects now require that the revenues from copper are sufficient to pay back the project capital expenditure.

Common sense dictates that projects initially bring copper-recovery circuits on line and produce an intermediate cobalt precipitate for storage, sale, or toll refining. This limits initial capital expenditure and reduces the complexity of the operation in a region

deficient in technical skills. This trend is exemplified in the evolution of the Ruashi project's cobalt refining strategy, where a complex flowsheet aimed at premium cobalt products has given way to a revised circuit to produce cobalt intermediate precipitates. Furthermore, sale of intermediate product may be problematic because of the focus of local mining authorities on maximizing beneficiation of resources. A sensible strategy for mining companies is to start copper production as soon as possible and then finance the cobalt-recovery circuits from copper revenues. Stockpiling of intermediate cobalt precipitates for future treatment is an option which may prove to be more acceptable to mining authorities.

Copper Recovery Circuit

At the Luilu and Shituru refineries in the DRC and Chambishi in Zambia, copper is electrowon directly from liquor derived from leaching with spent electrolyte. This technology was rejected for the new projects because of poor overall recoveries and compromised cathode quality. Instead, leach-SX-EW technology is used. While some of the ore at the Luita and Muliashi projects will be treated by heap leach, agitation leach is the predominant leaching method chosen for the new project flowsheets. Agitation leach-SX-EW technology is widely practiced in the Zambian Copper Belt and is well understood in the region [3]. The SX step interfacing between the leach and EW circuits allows production of LME Grade A copper cathode.

The main issues in developing a suitable copper-recovery flowsheet are:

- Leach conditions chosen to maximize recovery and minimize costs;
- Solid/liquid (S/L) separation;
- Soluble loss of copper and acid to tailings;
- Water balance;
- Preparation of a suitable bleed stream for a cobalt-recovery circuit.

Figure 1 shows a typical copper-recovery flowsheet. The leaching circuit design must aim to maximize metal extraction from all mineral components of the feed: copper oxide, cobalt oxide, and sulfides if present. Thus for the KOV design [4], an upfront oxidative leach (atmospheric pressure and 60 ºC) targets the copper oxide and secondary sulfide minerals, followed by a reductive leach using SO_2 to reduce Co^{3+} present in the cobalt oxide. The oxidant is Fe^{3+}, generated using an air-SO_2 mixture. Combining the oxide and sulfide leaches in this way has been adequately demonstrated at the Sepon copper plant in Laos [5]. Unleached sulfide in the tailings may be recovered by flotation. Increasing quantities of primary sulfides are expected with depth in the ore body. Copper will be recovered from the concentrate using an oxidative pressure leach with autoclave conditions that generate sulfuric acid for use in the atmospheric leach.

Capital and operating costs and ease of operability and maintenance are factors that influence the choice between filters and countercurrent decantation (CCD) for post-leach S/L separation. Some leach slurries separate poorly and contain fines and silica. CCD is favored for Copper Belt projects because of a perceived advantage in ease of operability and lower maintenance costs. Some projects may use a combination of the two, an option which provides maximum process benefit but prohibitive capital costs.

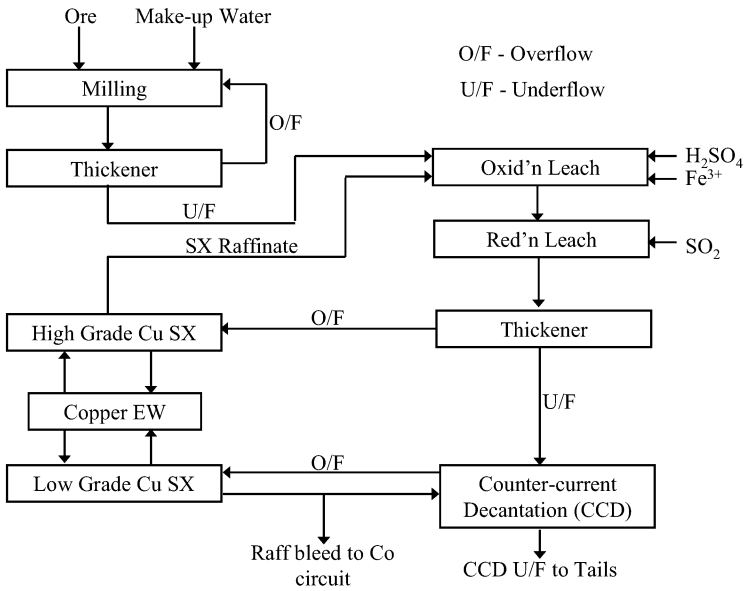

Figure 1. Copper recovery flowsheet for treatment of Copper Belt Cu-Co oxide.

Soluble losses of copper and acid in discarded leach tails result in lost copper revenues and acid credits for the leach. With copper prices of greater than 6,000 US$/t and the high cost of acid, it is vital to minimize these losses. The advantages of the Split Circuit™ for the minimization of soluble copper and acid losses from circuits have been well tested and is widely used in the Zambian Copper Belt [6]. Figure 1 shows the split-circuit flow scheme incorporated into a typical copper recovery flowsheet. Leach slurry fed to a primary thickener produces a high-grade copper overflow stream, and the underflow reports to the CCD wash circuit. Exiting washed residue contains reduced levels of soluble copper and acid, and the overflow is a low-grade copper stream. Treating the high- and low-grade copper streams in separate SX circuits allows high-grade raffinate to be returned to leach, maximizing acid recycle and reducing the quantity of acid and copper that reports to the wash residue. The efficacy of the split-circuit concept depends on how well the leached ore responds to the primary S/L separation step and enables the copper SX to be configured to produce a feed to the cobalt circuit with a low copper tenor.

It is crucial to minimize liquid discharges to tails and the input of fresh water, an important consideration in a high-rainfall region like the DRC. Water-balance maintenance is greatly eased by decreasing the volume of water that enters with the milled ore. Two ways to achieve this are by high-compression thickening of preleach solids and milling in SX raffinate. The latter practice, successfully used at Sepon, requires expensive materials of construction in the pre-leach circuit [5].

The relatively high levels of manganese in the DRC Copper Belt ores are potentially problematic. Manganese, transferred via entrainment into the advance electrolyte from the SX circuit can be oxidized at the anodes in the EW circuit. The

oxidized species can cause degradation of the SX organic phase. Minimizing manganese transfer to the EW circuit is done by selecting an extractant that exhibits good physical phase-separation and minimal crud generation properties or by including an organic wash stage in the SX configuration.

Cobalt Recovery Circuit

Table 2 compares a typical copper-circuit bleed stream (feed to the cobalt-recovery circuit) with the specifications for an upgraded stream suited for EW of high-grade cobalt metal and a purified stream suited for producing premium-grade chemicals (i.e., cobalt sulfate crystal).

Table 2. Comparison of typical Co circuit feed and suitable product streams

Element	Co Circuit Feed (mg/L)	Electrolyte for Co EW (mg/L)	Stream for high-grade chemicals (mg/L)
Co	6,000	60,000	60,000
Ni	100	60	< 25
Cu	150	1.8	2
Zn	50	3	2
Fe	1,200	3	2
Mn	1,400	2,000	10
Al	700	1,500	2
Mg	1,500	< 10,000	10

The need for substantial removal of impurity species is clearly indicated. Various techniques for removing impurities are employed. A cobalt-recovery circuit to produce cobalt metal or pure chemicals is likely to feature a number of these upgrading steps. A variety of such cobalt-recovery circuits have been extensively investigated for the Kolwezi, Tenke-Fungurume, and Ruashi projects. Since production of premium-grade cobalt products requires significant capital investment some of the new copper-cobalt projects (e.g., KOV [4] and more recently Ruashi) have opted to produce cobalt intermediates for storage or sale. In the case of Ruashi, a more complex flowsheet, developed to produce a range of cobalt products, has reached an advanced stage of design which may be used in the future if upgraded cobalt products are required. This type of conceptual cobalt-circuit flowsheet is shown in Figure 2.

The most likely route for iron removal is by oxidation to ferric and precipitation as an insoluble hydroxide by raising the solution pH. To achieve <1 mg/L residual iron with minimum cobalt loss, a two-stage precipitation process using sequential pH adjustments is required. Increasing temperature, if waste heat is available, is beneficial for the reaction and improves filterability of the iron precipitate. Air, air/SO_2 gas mixtures or other suitable reagents may be used as oxidants. At the pH 5 to 5.5 needed to minimize cobalt loss, aluminium is slow to hydrolyze and precipitate, making its removal by precipitation more difficult than that of iron.

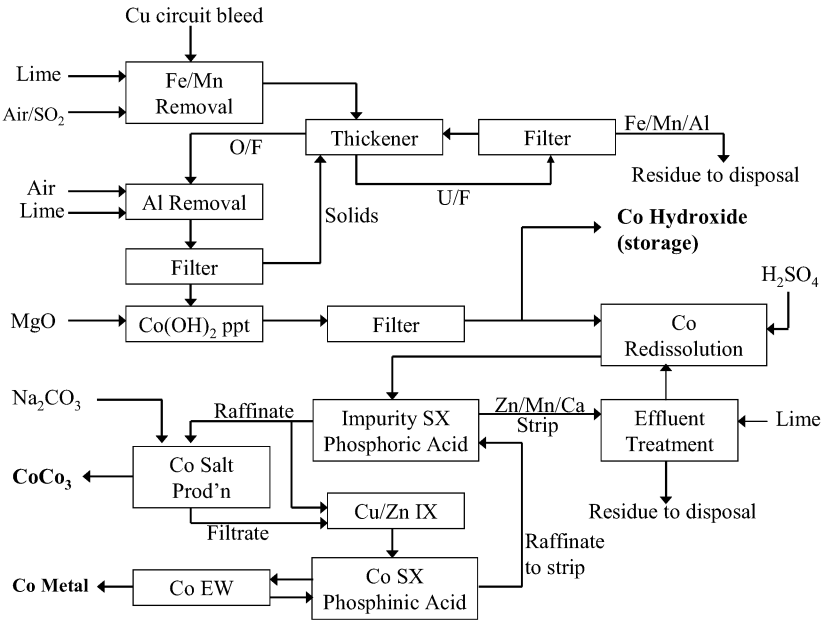

Figure 2. Cobalt recovery flowsheet for treatment of Copper Belt Cu-Co ores.

The bulk of the manganese entering the cobalt circuit needs to be removed. This can be achieved by oxidative precipitation or by SX, preferably using primary and polishing removal steps. For complete removal by oxidation with air/SO_2 mixtures, co-precipitation of cobalt is likely to occur. Air/SO_2 mixtures are suited for moderate manganese-removal duties and can be considered in conjunction with the iron-removal step. Use of air/SO_2 mixtures for large manganese-removal duties is shown to be impractical due to the large gas volumes required [7]. Manganese removal by SX using a phosphoric acid extractant (di(2-ethylhexyl)phosphoric acid, D2EHPA) is possible, although co-extraction of zinc, iron, aluminium, and calcium need to be considered [8]. Ferric ion requires strong HCl and longer residence times for stripping, and gypsum precipitation is an issue when sulfuric acid stripping solution is used. The latter problem is alleviated if the raffinate of a subsequent SX step is used for make-up of the D2EHPA strip liquor. A similar flow scheme pertains to the Impurity and Co SX steps of Figure 2. Co EW provides some manganese-removal capacity [8]. Up to 2 g/L Mn is required in the electrolyte for depolarizing the anodes during EW, and oxidation of Mn^{2+} at the anode results in precipitation of MnO_2 that, in reasonable quantities, is easily removed by physical means.

Ion exchange (IX) can be used, employing an aminophosphonic chelating resin to remove low levels of copper and zinc in a single step [9]. SX can be used to remove high levels of copper and zinc, but a scavenger IX step may be necessary to achieve low-level specifications. Oximes can be used for copper SX, provided the extraction pH is adjusted [10], but care needs to taken to ensure that Co^{2+} co-extraction is minimized. Both D2EHPA and phosphinic acid extractants can be used for zinc SX [11]. Commercial

supply of phosphinic acid extractant is dominated by CYANEX® 272 (Cytec). Ionquest® 290 (Rhodia) and LIX® 272 (Cognis) are recent additions to the industry.

Calcium, magnesium, and nickel can be rejected by SX. The selectivity for cobalt over nickel, calcium, and, to a lesser extent, magnesium for a phosphinic acid extractant is understood from its unique selectivity series: Fe^{3+} > Zn > Cu > Co > Mg > Ca > Ni. CYANEX 272, noted for its high cobalt-over-nickel separation factor, is now widely applied for cobalt separation from nickel [2], with an extended application base resulting from the factor of selective cobalt extraction over calcium and magnesium. As magnesium levels of 10 g/L can be tolerated in cobalt EW, low levels of magnesium co-extraction, reduced in part by organic scrubbing, are acceptable. Indeed, some magnesium will have positive benefits on the conductivity of the electrolyte.

The use of cobalt-selective SX as a primary upgrading step to a cobalt EW electrolyte, favored in the early Kolwezi flowsheet scenarios, is replaced in most of the latest flowsheet options with primary upgrading via $Co(OH)_2$ precipitation. Cobalt hydroxide precipitation is with active magnesia (MgO), followed by redissolution of the filtered hydroxide with spent cobalt EW electrolyte. While this provides rejection of soluble calcium and magnesium, unreacted MgO will report to the electrolyte. Since nickel follows cobalt in this process route, a specific nickel removal step is required. IX using resin with bis-picolylamine functionality is the preferred process.

Metal extraction by SX results in the displacement of protons that then need to be neutralized. Sodium or ammonium hydroxide is typically used, resulting in the generation of dilute sodium or ammonium sulfate waste solutions, disposal of which requires containment in an on-site certified repository or, alternatively, recovery of the salt by crystallization for ultimate disposal off site. This issue, exacerbated by a positive net water balance, undoubtedly greatly influenced the shift from cobalt upgrading with SX to precipitation.

The decision to rehabilitate the existing Luilu refinery that uses outdated inefficient technology producing subgrade cobalt metal for the Kamoto project (not listed in Table 1) is based on capital cost. An economic assessment of a modern flowsheet featuring SX and EW to produce premium-grade metal was shown to be extremely positive, due largely to improved cobalt recoveries and pointed towards implementation of the upgraded circuit in the future [12].

Plant Utilities

Due to the high cost of sulfuric acid delivered into the region (250 US$/t and higher) and delivery uncertainties caused by difficulties with transport logistics, many of the new projects plan to install an on-site acid plant. These facilities produce 98 wt % H_2SO_4 and are a source of SO_2 that is used in the reductive leach and potentially for iron and manganese removal.

CONCLUSIONS

All of the new Cu-Co projects currently under development for implementation in the African Copper Belt feature modern SX-EW copper recovery flowsheets. Copper

SX-EW is well established in the region and well understood. The trend for cobalt is to limit initial capital expenditure by producing cobalt intermediates, with a view to future financing of the cobalt refinery circuits from copper revenues. The development of the mines and refinery operations in areas impoverished by years of civil war and political instability will contribute significantly to the economy of the region and the upliftment of its people.

REFERENCES

1. G. Kordosky, "The Copper of Africa – A Renaissance in Copper Hydrometallurgy," HydroCopper 2007, Santiago, Chile, 2007; pp. 31–40.
2. O. Tinkler, D. Flett, and C. Bourget, "Flowsheet Considerations for Copper-Cobalt Projects in the DRC," ALTA 2007, ALTA Metallurgical Services, Melbourne, 2007.
3. J. A. Holmes, A. D. Deuchar, L. N. Stewart, and J. D. Parker, "Design, Construction and Commissioning of the Nchanga Tailings Leach Plant," Extractive Metallurgy of Copper, J. Yannopoulos and J. Agarwal, Eds., Metallurgical Society of AIME, Littleton, CO, Vol. II, 1976; pp. 907–925.
4. L. Treadgold and J. Parker, "The Re-development of the KOV, Kananga and Tilwezembe Copper-Cobalt Deposits in the DRC," Copper 2007, Vol. IV, P. A. Riveros, D. G. Dixon, D. B. Dreisinger and M. J. Collins, Eds., Canadian Institute of Metallurgy, Montreal, 2007; pp. 61–75.
5. K. Baxter, D. Dreisinger, and G. Pratt, "The Sepon Copper Project: Design of a Flowsheet," Hydrometallurgy 2003, Vol. 1, The Minerals, Metals and Materials Society, Warrendale, PA, 2003; pp. 1487–1502.
6. G. M. Miller and A. R. Nisbett, "Use of Split Circuit™ SX Plants for High Copper Recovery and Low Operating Costs," ALTA 2007, ALTA Metallurgical Services, Melbourne, 2007.
7. J. van Rooyen, S. Archer, and M. Fox, "Manganese Removal from Cobalt Solutions with Dilute Sulphur Dioxide Gas Mixtures," Fourth Southern African Conference on Base Metals, South African Institute of Mining and Metallurgy, Johannesburg, 2007; pp. 365–376.
8. J. Preston, A. M. Feather, D. Dreisinger, T. O'Kane, P. Cole, G. Iorio, and S. Burkes, "Process for Recovering Cobalt from Solutions," DRC Patent No. ND/5/EXT/99, 10 February 1999.
9. J. P. Wyethe and M. H. Kotze, "Impurity Removal by Fixed Bed Ion Exchange from Cobalt Electrolyte Derived from the Kakanda Tailings Dump," ALTA SX/IX 2000, Vol.1, ALTA Metallurgical Services, Melbourne, 2000.
10. S. A. Scott, "Copper Removal from a Cobalt Sulphate Stream using pH-controlled Solvent Extraction," International Solvent Extraction Conference 2008, Canadian Institute of Mining, Metallurgy and Petroleum, Montreal, in press.
11. P. M. Cole and K. C. Sole, "Zinc Solvent Extraction in the Process Industries," *Mineral Processing & Extractive Metallurgy Review,* **24**, 91–137 (2003).
12. L. M. Roux, E. Minnaar, P. J. Cilliers, M. Bellino, and R. Dye, "Comparison of Solvent Extraction and Selective Precipitation for the Purification of Cobalt Electrolytes at the Luilu Refinery, DRC," Fourth Southern African Conference on Base Metals, South African Institute of Mining and Metallurgy, Johannesburg, 2007; pp. 343–363.

COPPER AND COBALT SOLVENT-EXTRACTION PROCESS DEVELOPMENTS AT CHAMBISHI METALS PLC

R. Minango, H.P. Singh, C. Kapambwe, E. Bwalya, and D. Bukunkwe

Chambishi Metals Plc, P. O. Box 21151, Kitwe, Zambia
Corresponding author email address: robertm@chambishi.com.zm

ABSTRACT

In the existing circuit at Chambishi Metals Plc, Zambia, copper is recovered as copper cathode and sludge/powder from the roaster and pressure leach plant solutions by electrowinning and electrostripping. A copper-free cobalt-rich solution is produced, which is purified and concentrated in the cobalt purification circuit by precipitation of metal hydroxides through controlled addition of either calcium carbonate or calcium oxide, followed by redissolution. Zinc and nickel are removed from the cobalt liquor by solvent-extraction and ion exchange, respectively. An alternative process route was developed to treat the roaster and pressure leach plant copper-rich cobalt solutions using solvent-extraction and electrowinning to produce hig-purity copper and cobalt cathodes. A cobalt solvent-extraction pilot plant, using CYANEX 272 was operated to control or reject impurities from the copper solvent-extraction raffinate (copper-free-cobalt rich solution). A concentrated cobalt electrolyte, suitable for the electrowinning of high-purity cobalt cathode, was produced.

INTRODUCTION

Laboratory copper solvent-extraction studies [1,2] were conducted with a view to installing copper solvent-extraction (SX) ahead of the copper electrowinning and electrostrip tank house in order to increase production capacity of copper and produce high-purity copper cathodes. LIX® 984 N-C supplied by Cognis Corporation was used as the extractant. The performance of conventional extractants and circuit configuration for concentrated copper streams is well-documented [3].

A laboratory study [4] was also conducted in order to assess the purification and concentration of the copper-free cobalt-rich solution by cobalt SX using a phosphinic acid extractant, CYANEX® 272 supplied by Cytec. CYANEX 272 is selective for cobalt over magnesium, calcium, and nickel, which are some of the impurities in the Chambishi solutions. CYANEX 272 is being used or has been tested for similar application [5-9]. The benefit of implementing the cobalt solvent-extraction flowsheet at Chambishi include improved cobalt recovery, higher current efficiency, and the ability to handle feed materials with higher zinc, nickel, and magnesium concentrations.

CHAMBISHI PROCESS FLOW DIAGRAM

The simplified current and proposed flowsheet for Chambishi Metals Plc is given in Figure 1. The proposed solvent-extraction process is in dotted lines.

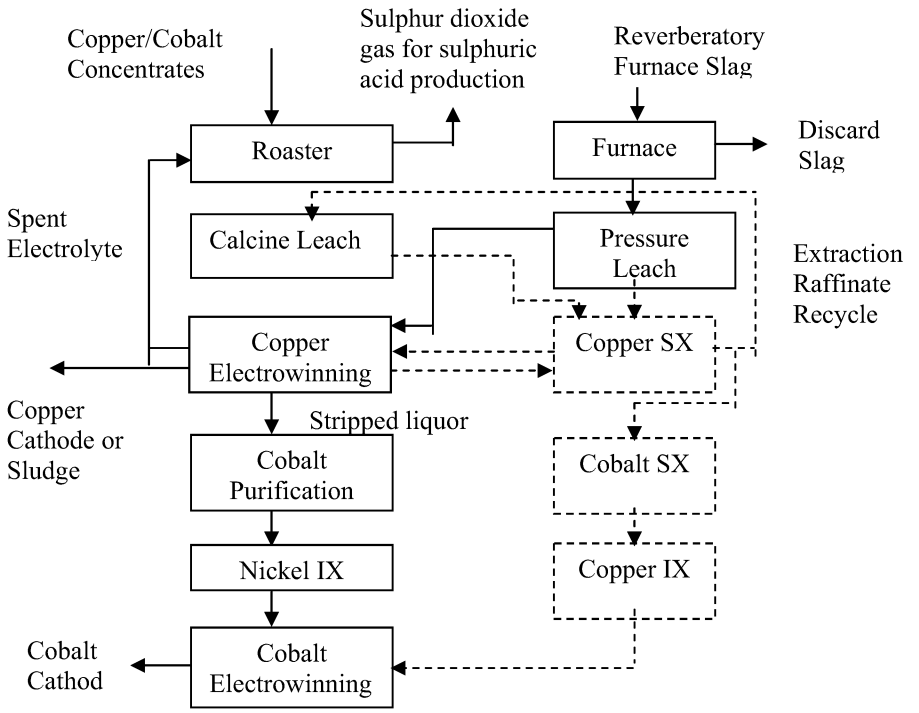

Figure 1. Current flowsheet for Chambishi Metals Plc (solid lines, 2007) and the proposed solvent-extraction process (dotted lines).

COPPER SOLVENT-EXTRACTION PROCESS DEVELOPMENT

Copper SX tests were carried out in box-type mixer-settler units with an active volume of 1 L. Three copper SX circuits were operated, namely the primary SX circuit on Roaster Solution and Pressure Leach Solution, as well as a secondary SX circuit on the combined raffinate from these circuits. The combined raffinate was neutralized with calcium carbonate prior to SX. The chemical composition of these streams is listed in Table 1. The organic phase in the three circuits comprised 32% v/v LIX 984 N-C in Shellsol 2325. The circuit configuration, operating conditions, and results are summarized in Table 2.

Table 1. Chemical composition of Cu SX feed solution (PLS), g/L

PLS	Cu	Co	Fe	Zn	Ni	Mn	Mg	Ca	H_2SO_4
Roaster	35	8	2.43	0.056	0.034	0.630	9.30	0.62	11.5
Pressure leach	30	20	3.0	0.010	0.100	0.024	0.425	0.20	3.0
Combined raffinate	5−6	12.6							5−6

Copper concentrations in the secondary SX circuit were consistently reduced to less than 100 mg/L. A low copper concentration in the raffinate is essential for an effective down-stream process. Cobalt losses to the copper stream (strip raffinate) and impurity co-extraction were negligible. Copper concentrations in the strip raffinate were adequate for copper electrowinning. obtained from the existing cobalt purification circuit at Chambishi Metals Plc. The block diagram for the pilot-scale testwork to purify and concentrate cobalt from PLS using CYANEX 272 is given Figure 2.

Table 2. Pilot-plant copper solvent-extraction operating conditions

Parameter	SX1 Roaster Solution (Cu/H_2SO_4), g/L	SX1 Pressure Leach Solution (Cu/H_2SO_4), g/L	SX2 Roaster & Pressure Raffinate (Cu/H_2SO_4), g/L
Configuration	2E, 2S	2E, 2S	4E, 2S
Extraction O/A ratio	3	3	2.5
Extraction Raffinate	5–6 /57.0	4.5/44.1	<100 mg/L /11.8
Strip Feed	35.1/180	36 /182.8	30 /180
Strip Raffinate	50.1/ 156.6	52.7 /159.7	33.4/74.5
Strip O/A	1.7	1.7	1.7

COBALT SOLVENT-EXTRACTION PROCESS DEVELOPMENT

Cobalt SX was conducted using 30% v/v CYANEX 272 as an extractant, and 5% v/v tributylphosphate, as a phase modifier, in SSX 210, an aliphatic diluent supplied by Sasol. Prior to extraction, the extractant was subjected to 60% saponification using sodium hydroxide. The average chemical composition of the expected feed to the CoSX circuit (ferric thickener overflow solution (PLS)) is given in Table 3. The solution was

Table 3. Composition of ferric thickener overflow solution (PLS), g/L

Co	Cu	Fe	Zn	Ni	Mn	Mg	Ca	pH	Temp, ^oC
10.2	0.40	0.054	0.130	0.051	0.502	3.30	0.336	3.75−4.6	30−40

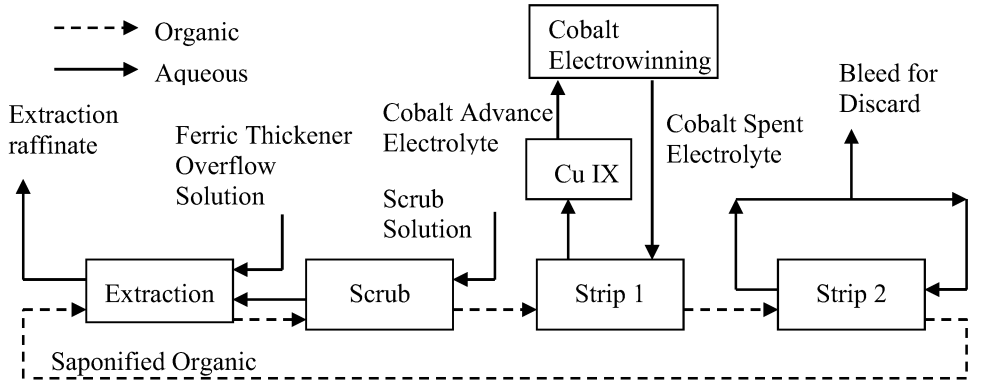

Figure 2. Block flow diagram for cobalt solvent-extraction.

The pilot-plant circuit configuration and operating conditions are given in Table 4. The average cobalt concentration in the extraction raffinate varied between 6 and 20 mg/L. The extraction efficiencies are given in Table 5. Calcium co-extraction was negligible. The loaded organic was scrubbed with a solution containing 29 g/L cobalt and at pH 1.2–1.8. The scrub raffinate contained 24 g/L cobalt and at pH 4.4–5.2. Nickel and manganese were not scrubbed.

Table 4. Operating conditions for the pilot plant for cobalt solvent-extraction

Extraction		Scrubbing	
No. of stages	4	No. of stages	4
O:A ratio	1	O:A ratio	15−20
pH range	4.38−5.9	pH range	4.4−5.2
Co extraction	99.8%	Scrub efficiency	66% Mg, 9 % Ca
Strip 1		**Strip 2**	
No. of stages	4	No. of stages	2
O:A ratio	0.33	O:A ratio	5
pH range	1.4−4.6	Strip solution	200 g/L H_2SO_4
Co strip efficiency	99.8%		

Table 5. Extraction efficiency, %

Co	Cu	Fe	Zn	Ni	Mn	Mg
99.8	99.9	97.5	98.7	16.3	99.9	21.7

Although the cobalt concentration in the stripped solvent in Strip 1 was about 20 mg/L, the cobalt loss was about 1.6%. This could have been due to recycling the Strip 2 strip solution and due to problems associated with pH control in the first stripping circuit. The operating conditions for Strip 1 will require optimization in order to produce a

purified cobalt electrolyte with minimum cobalt loss. The composition of the Strip raffinate (A/E) generated in Strip 1 is given in Table 6.

Table 6. Composition of strip 1 feed and raffinate, mg/L

PLS	Co	Cu	Fe	Zn	Ni	Mn	Mg	Ca	pH
Feed	33420	< 0.1	0.27	< 0.1	5	1610	355	8	1.4−2.0
Raffinate	37750	126	0.37	3	22	1796	411	28	4.1−4.6

The copper and residual zinc in the Strip 1 raffinate were removed by ion exchange using Duolite® C467 resin in a single-stage column producing an advance electrolyte with an average chemical composition shown in Table 7. The relative affinity of this resin for various cations decreases in the order $Pb^{2+} > Cu^{2+} > Zn^{2+} > Mg^{2+} > Ca^{2+} > Cd^{2+} > Ni^{2+} > Co^{2+} > Sr^{2+} > Ba^{2+}$. Although copper was reduced to less than 0.1 mg/L, the ion exchange conditions or parameters will require further optimization.

Table 7. Composition of cobalt advance electrolyte, mg/L

Co	Cu	Fe	Zn	Ni	Mn	Mg	Ca	pH
37586	< 0.1	0.36	< 0.1	6	1670	408	29	4.0−4.8

The zinc and iron in the organic exiting the final Strip 1 stage were stripped with 200 g/L sulfuric acid. The zinc and iron stripping efficiencies were 88 % and 85 %, respectively.

CONCLUSIONS

The copper and cobalt in the Chambishi Metals Plc liquors can be purified and concentrated by SX, producing copper and cobalt electrolytes suitable for electrowinning of high-purity copper and cobalt cathodes. The operating conditions for selective stripping of cobalt from CYANEX 272 (Strip 1) and copper ion exchange require further optimization in order to guarantee production of a purified cobalt electrolyte with minimum cobalt loss.

ACKNOWLEDGMENT

Acknowledgment is due to the management of Chambishi Metals Plc, numerous staff, and others who contributed to the success of the projects.

REFERENCES

1. R. Minango, E. Bwalya, D. Bukunkwe, and B. Grinbaum, “Development of a Novel Three-Step SX Process to Recover Copper from an Acidic Solution,” Third Southern African Conference on Base Metals, South African Institute for Mining and Metallurgy, Johannesburg, 2005; pp. 337–352.
2. D. Cowie, T. Gittins, R. Minango, and E. Bwalya, “LIX 984N Solvent-extraction Study,” Chambishi Technical Services, Report No.TS/CM/014–2002.

3. K. C. Sole, “Solvent-extraction of Copper from High Concentration Pressure Acid Leach Liquors,” Proceedings of the International Solvent-extraction Conference 2002, South African Institute for Mining and Metallurgy, Johannesburg, 2002; pp.1033–1038.
4. D Cowie, T Gittins, R. Minango, and E. Bwalya, “CYANEX 272 Solvent-extraction Study,” Chambishi Technical Services, Report No.TS/CM/013–2002.
5. M. J Dry, G. Iorio, D. F. Jacobs, P. M. Cole, A. M. Feather, K. C. Sole, J. Engelbrecht, and K. C. Matchett, “Cu/Co Tailings Treatment Project, Democratic Republic of Congo,” ALTA 1998 Nickel/Cobalt Pressure Leaching and Hydrometallurgy Forum, ALTA Metallurgical Services, Melbourne, 1998.
6. E. G. Liranza, A. M. Daudinot, R. V. Martinez, and B. R. Ba’rzaga, “Separation of Cobalt and Nickel by Solvent-extraction from Sulphate Liquors obtained by Acid Leaching of a Product from the Caron Process,” International Solvent-extraction Conference 2002, South African Institute for Mining and Metallurgy, Johannesburg, 2002; pp. 952–957.
7. A. Feather, W. Bouwer, A. Swarts, and V. Nagel, “Pilot-Plant Solvent-extraction of Cobalt and Nickel for AVMIN’S Nkomati Project,” Proceedings of the International Solvent-extraction Conference 2002, South African Institute for Mining and Metallurgy, Johannesburg, 2002; pp. 946–951.
8. K. C. Sole, A. M. Feather, and P. M. Cole, “Solvent-extraction in Southern Africa: An Update of Some Recent Hydrometallurgy Developments,” *Hydrometallurgy*, **78**, 52–78 (2005).
9. L. M. Roux, E. Minaar, P. J. Collier, M. Billion, and R. Dye, “Comparison of Solvent-extraction and Selective Precipitation for the Purification of Cobalt Electrolyte at the Luilu,” Fourth Southern African Conference on Base Metals, South African Institute for Mining and Metallurgy, Johannesburg, 2007; pp. 343–363.

IMPROVEMENT IN COPPER AND COBALT PRODUCTION DUE TO INCLUSION OF SOLVENT EXTRACTION OF COPPER AT MOPANI COPPER MINES PLC'S NKANA COBALT RLE PLANT

B. Mwakila,[1] R. Silwamba,[1] G. Miller,[2] and G.C. Chisakuta[3]

[1]Nkana RLE Cobalt Plant, Mopani Copper Mines Plc, Kitwe, Zambia.
[2]Miller Metallurgical Services, Corinda, QLD, Australia. [3]Cognis Corporation, Chingola, Zambia. Corresponding author email address: bmwakila@mopani.com.zm

ABSTRACT

Nkana Cobalt Plant Roast-Leach-Electrowin produces cobalt from cobalt concentrates from the Nkana Concentrator by roasting to convert insoluble metal sulfides into soluble sulfates and oxides. The soluble sulfates and oxides (calcine) are then leached, getting the cobalt into solution along with copper and other impurities. Until December 2006, advance electrolyte was routed to copper tankhouse for electrowinning and electrostripping of copper as a first step in impurity removal. Stripped liquor was then sent to a cobalt purification circuit for classical precipitation by automated pH control. This process has been modified to include copper solvent extraction to first remove copper from calcine leach solution. This paper discusses how inclusion of solvent extraction has resulted in increased productivity.

INTRODUCTION

The Nkana Cobalt Roast-Leach-Electrowin (RLE) Plant was commissioned in 1982 to produce cobalt as a by-product of a copper-producing metallurgical complex, receiving its cobalt concentrates from Nkana Concentrator [1]. The cobalt is associated with a copper ore as a carrolite. The resultant cobalt concentrate has the following typical assay grades: 1.6 % Co, 9.0% Cu, and 21.0% S.

When the plant was designed in the 1980s, solvent-extraction (SX) technology was not immediately adopted as a means of copper impurity separation because most of the copper SX reagents at that time were mainly meant for very dilute solutions (max. 0.5-7 g/L Cu in the pregnant leach solution (PLS)) and were quite sensitive to pH [2]. Separation of copper from the cobalt-bearing solution thus continued to be via electrochemical means.

Copper-bearing cobalt solution was initially sent to an electrowinning copper tank house where copper was subjected to electrowinning, then electrostripping. Copper produced from these processes was treated as scrap copper suitable for doping in converters at the smelter. Resultant stripped solution, relatively free of copper, was

routed to the purification circuit, where classical pH precipitation methods are, up to today, used to remove other impurities from the cobalt solution.

The process of electrowinning and electrostripping had posed serious production constraints, as it required meticulous blends to be prepared with a Cu:Co ratio of 4:1 in the roaster feed. There was also a limit placed on the resultant copper advance electrolyte to the electrowinning tank house. Average acceptable concentrations were 20–25 g/L Cu. Concentrations above these were a serious process constraint.

To remedy this, SX was re-examined. With development of SX technology, stronger and more powerful reagents capable of handling very high copper concentrations in the region of 25-30 g/L Cu in the PLS had become available. After pilot-plant trials, the circuit was successfully modified to include copper SX as a first step in impurity removal, and a SX plant was commissioned in January 2007. The process modification is shown in Figure 1 along with the original circuit.

PROCESS DESCRIPTION OF MODIFIED CIRCUIT

Copper SX was included between calcine leach and iron removal. To remove copper to the desirable level, the copper SX plant was designed with a two-stage extraction circuit, namely Primary and Secondary extraction [3]. The configuration used is shown in Figure 2, and Table 1 shows typical design parameters.

Primary Solvent Extraction

Primary SX comprises three extraction mixers-settlers (E1, E2, and E3) that lower the concentration of copper in calcine leach solution (CLS) from 25 g/L Cu to 2.7 g/L Cu. The resulting primary raffinate is pumped back to the leaching circuit, and about 60 m^3/h is bled off to the ferric cascade for iron removal by lime precipitation. The resulting ferric thickener overflow from iron removal is pumped back to secondary SX.

Secondary Solvent Extraction

There are two smaller mixer-settlers (E4 and E5) that make up the secondary extraction circuit. Ferric thickener overflow from iron precipitation enters E4 and exits E5 after residue copper from primary raffinate has been recovered. Final raffinate from E5 is pumped to the cobalt purification circuit where classical pH precipitation techniques are employed to remove other impurities such as zinc in the clean-up cascade circuit. The cobalt purification circuit produces an advance electrolyte for cobalt electrowinning.

Stripping of Loaded Organic

After loading copper from cobalt solution in secondary extraction, and from calcine leach solution in primary extraction, the organic is stripped in two stages (S1 and S2) to produce an advance electrolyte that feeds the copper electrowinning tankhouse. In total, the SX plant has a design capacity to transfer 20,000 t copper per annum.

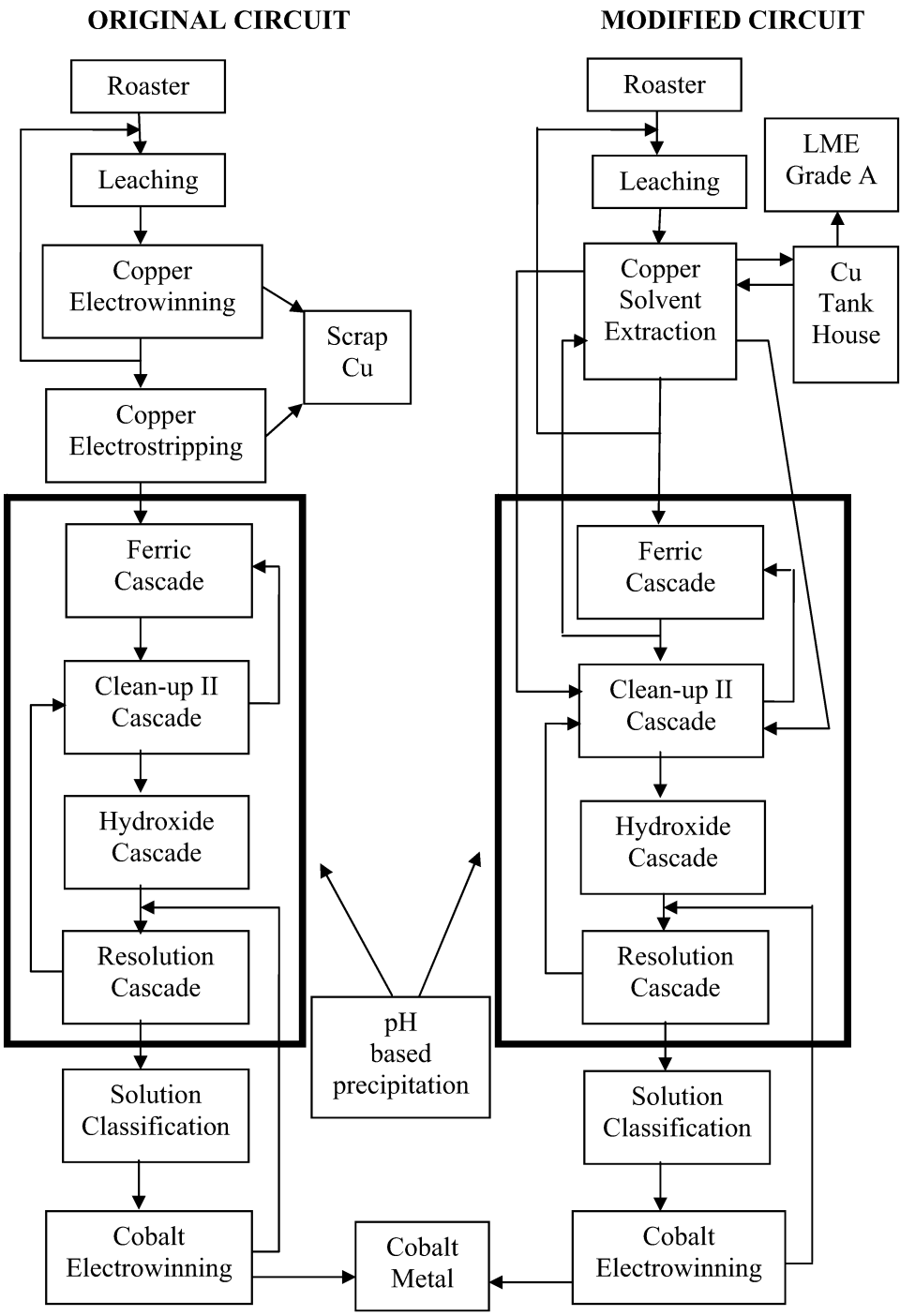

Figure 1. Comparison of the original and the modified circuits.

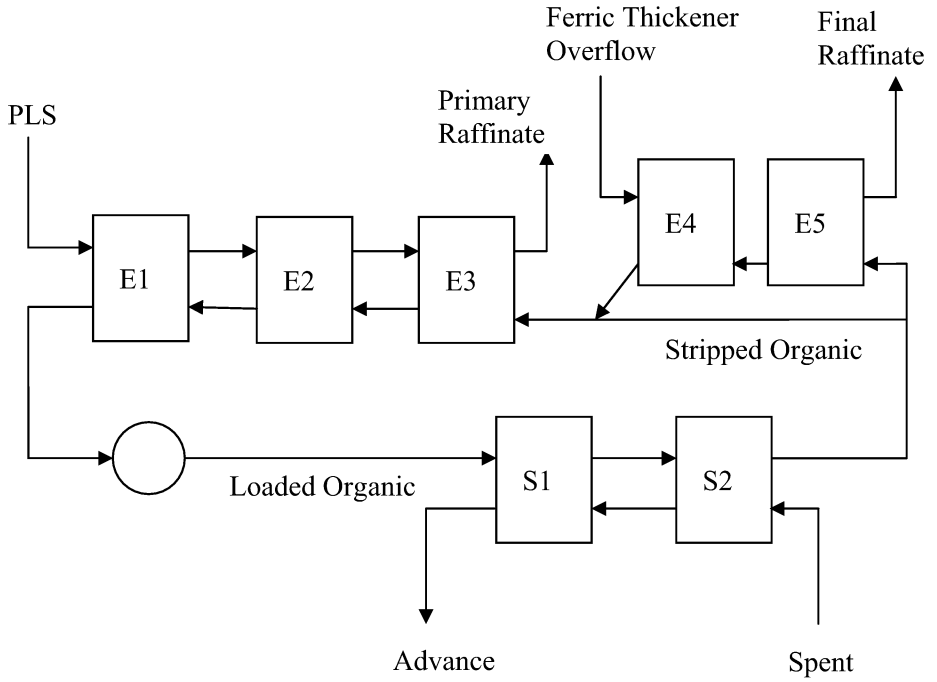

Figure 2. Configuration of the SX circuit at Nkana RLE Cobalt Plant.

Table 1. Design parameters of the SX at Nkana RLE Cobalt Plant

Solution	Parameter	Value
PLS	Cu tenor (g/L)	25.0
	Co tenor (g/L)	10.0
	Flow (m^3/h)	127
	pH	0.7
	Recovery (%)	89
Primary Raffinate	Cu tenor (g/L)	2.7
	Co tenor (g/L)	9.5
	Flow (m^3/h)	60
	pH	3.5
	Recovery (%)	97
Loaded Organic	LIX 984N conc. (%v/v)	23
	Flow (m^3/h)	350

DISCUSSION

Nkana Cobalt Plant has derived significant improvements in productivity following this circuit modification. The constraint placed on roaster blend to limit copper input to the circuit has been removed, as the copper tankhouse now operates as a separate entity that picks up copper, not directly from CLS, but from SX to produce LME grade A copper. Figure 3 shows copper input, copper production as well as cobalt metal production, both before and after the modification. Copper input into the circuit and corresponding production has gone up. Copper production has increased from an average 800 t of copper per month to 1,300 t. Similarly, cobalt production at an average of 160 t per month is above the previous average of 140 t. Production of LME grade copper from electrowinning has reduced costs and has freed up smelter capacity.

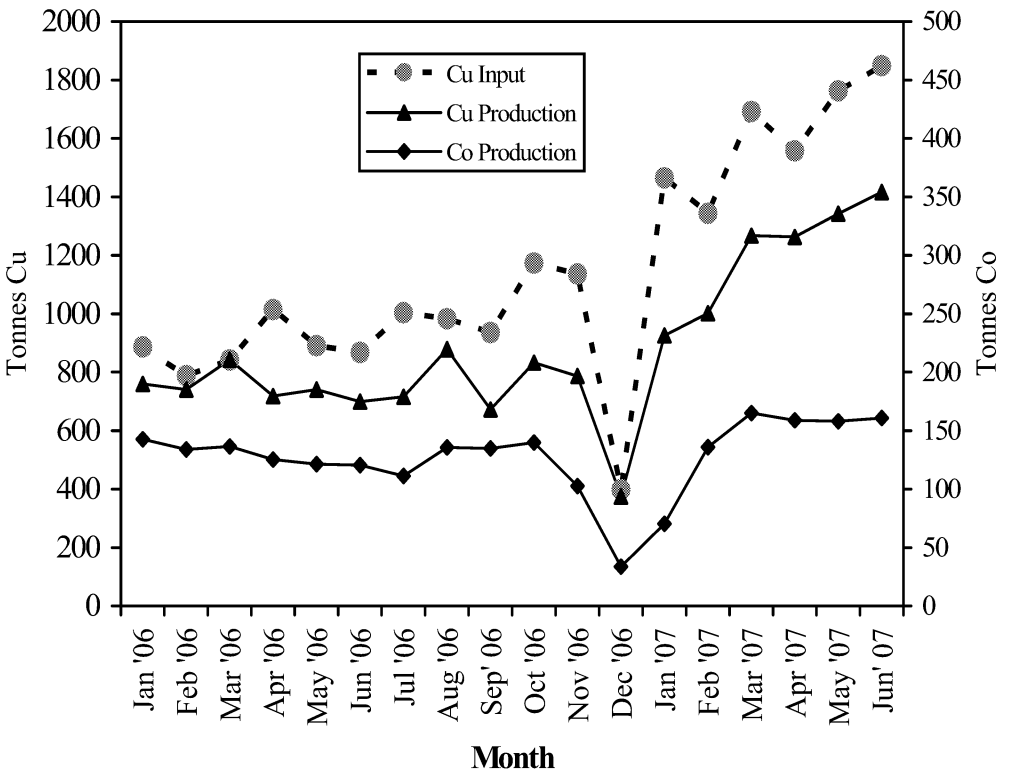

Figure 3. Historic trends of copper/cobalt input and production.

CONCLUSION

Use of SX of copper to remove copper as an impurity from cobalt solution while producing LME grade copper has been successfully implemented at Nkana Cobalt plant. Major benefits of this have been (1) reduction of roaster constraint, which means higher copper inputs can now be handled; (2) double handling of scrap copper from electrowinning and electrostripping has been eliminated; and (3) a consistent production of cobalt can be sustained.

ACKNOWLEDGMENTS

The authors would like to thank Mopani Copper Mines Plc, especially Management and Staff at Nkana Cobalt Plant, for their permission and support in writing this paper. Our special thanks also go to Shankar Aburi Rao for proof reading the manuscript and offering invaluable critique to the technical content of the presentation.

REFERENCES

1. J. Aird, R. S. Celmer, and A. V. May, “New Cobalt Production from R.C.M.’s Chambishi Roast-Leach-Electrowin Process,” *Mining Magazine*, 320−323 (October 1980).
2. T. C. Lo, M. H. I. Baird, and C. Hanson, Handbook of Solvent Extraction, John Wiley & Sons, New York, pp. 650−657, 1985.
3. G. M. Miller and A. Nisbett, “Decreasing Operating Costs and Soluble Loss in Copper Hydrometallurgy with Use of Innovative Solvent Extraction Circuits,” First Extractive Metallurgy Operator’s Conference, Brisbane, QLD, Australia, 2005.

COPPER REMOVAL FROM A COBALT SULFATE STREAM USING pH-CONTROLLED SOLVENT EXTRACTION

Sean A. Scott

Mintek, Private Bag X3015, Randburg, South Africa
Corresponding author email address: seans@mintek.co.za

ABSTRACT

A number of copper-cobalt projects are currently being developed in Zambia and Democratic Republic of the Congo, which have an integrated leach solvent-extraction electrowinning circuit for the recovery of copper. A bleed stream of the raffinate is generally taken from this circuit for the recovery of cobalt. The permissible copper concentration in this stream is stringent if it is targeted at the production of cobalt cathode. Ion exchange has previously been considered for this application, but, more recently, interest has been shown in the use of solvent extraction. The inclusion of either of these process technologies in a generic Cu/Co recovery flowsheet was considered on the basis of risks associated with each to consistently produce a suitable advance electrolyte for the production of LME grade Co cathode.

INTRODUCTION

Several copper-cobalt projects currently being developed in Central Africa have an integrated leach solvent-extraction (SX) electrowinning circuit for the recovery of copper [1,2]. A bleed stream of the raffinate is generally taken from this circuit for the recovery of cobalt. The permissible copper concentration in this stream is stringent if it is targeted at the production of cobalt cathode. Ion exchange (IX) has previously been considered for this application, but, more recently, interest has been shown in the use of SX.

Mintek has previously investigated copper removal from a cobalt stream containing ~3 g/L Cu and ~8 g/L Co to 0.3 mg/L in the raffinate by pH-controlled SX on a pilot-plant scale. One of the operating conditions identified that most affected the consistent achievement of this specification was the mixing intensity employed during extraction. The organic phase employed was 30% v/v LIX® 984N in an aliphatic diluent, and it was thought that, by lowering the concentration of extractant and hence the viscosity of the organic phase, improved mixing (mass transfer) and stage efficiencies could be achieved.

The aim of this testwork was to compare the effects of mixing intensity, pH, and residence time on the Cu SX raffinate produced using 10 and 30 % v/v LIX 984N. These data were used to technically compare SX versus ion exchange (IX) as options for copper removal to the levels required for the production of LME grade cobalt cathode.

EXPERIMENTAL

Extraction Equilibrium Isotherms

Since residence time and mixing were factors identified as influencing the extent of extraction achievable, extraction isotherms were generated on both batch and continuous bases. Batch tests were performed conventionally by contacting aqueous and organic phases at various phase ratios in a stirred beaker while controlling the pH at the value desired. Continuous isotherms were generated by feeding aqueous and organic phases into a stirred mixer while controlling the pH. The combined flowrates of the phases were varied to achieve specific residence times in the mixer. A swept-vane pumping impeller was used for mixing.

Feed Solution

The composition of the feed solution used for all tests is given in Table 1. The composition reflects a typical solution after Fe, Al, and Mn removal. Ca was at saturation since these processes usually employ lime or limestone as the neutralizing reagent.

Table 1. Synthetic SX feed solution composition (mg/L)

Mg	Al	Si	Ca	Cr	Mn	Fe	Co	Ni	Cu	Zn	Pb	S	As
2800	< 2	25	576	< 2	94.5	< 2	10150	< 2	482	< 2	< 2	8650	49

RESULTS AND DISCUSSION

Extraction Equilibrium Isotherms

The batch extraction equilibrium isotherms are shown in Figure 1. The 30% LIX 984N displayed the steepest isotherm, which would minimize stage and phase-ratio requirements. At pH 1.8 and a phase ratio (O/A) up to 1, the isotherm generated using 10% LIX 984N was comparable to that for 30% LIX 984N, and raffinate concentrations of 0.02 mg/L Cu were measured for each of the contacts. At pH 1.5, raffinate concentrations of <0.3 mg/L Cu could only be achieved with the lower concentration reagent when the O/A ratio was increased to 10.

Extraction isotherms generated on a continuous basis are compared in Figure 2. The isotherms compared are those generated at impeller tip speeds of 0.68 m/s. The continuous isotherms were relatively similar and were dependant to a greater extent on the extraction pH rather than the extractant concentration.

The effect of increased impeller tip speed on the achievable raffinate Cu concentration is illustrated in Figure 3. The raffinate Cu concentrations varied from 59 mg/L at an impeller tip speed of 1.6 m/s (400 rpm) down to 0.12 mg/L at an impeller speed of 4.1 m/s (1039 rpm).

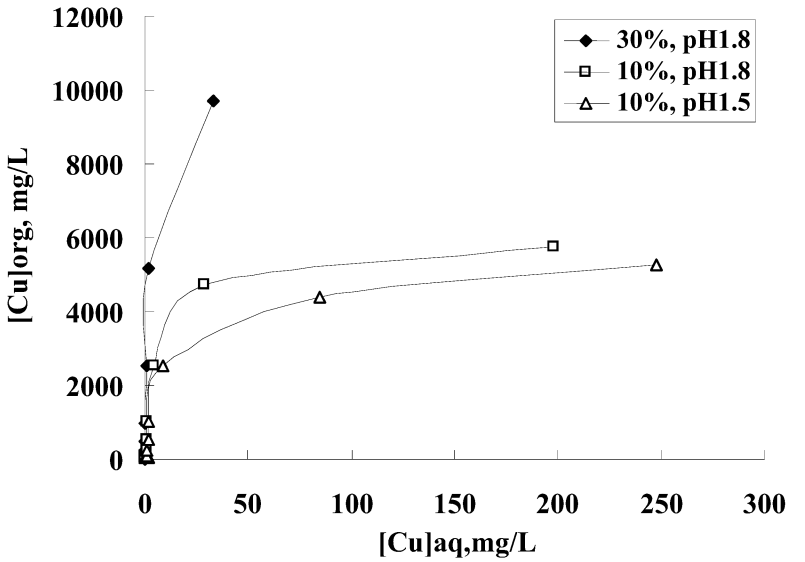

Figure 1. Batch extraction equilibrium isotherms for 10% and 30% LIX 984N organic phases.

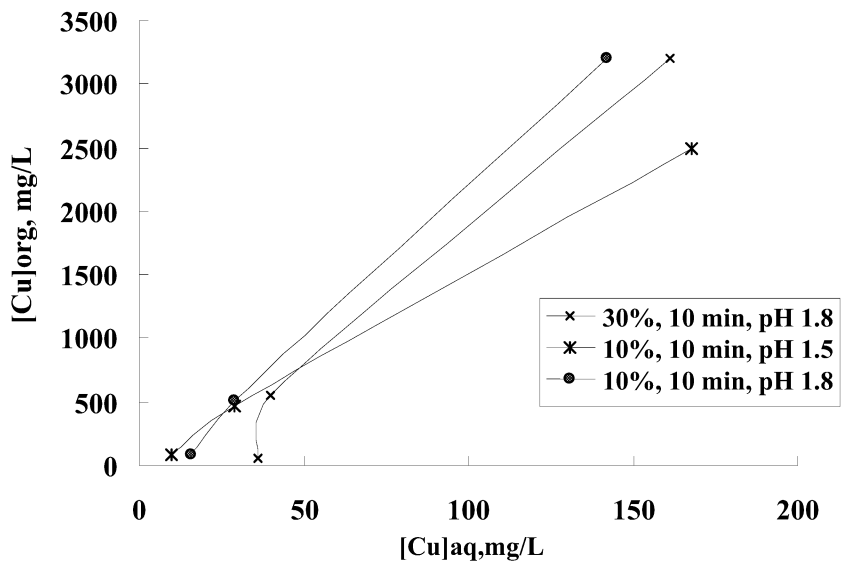

Figure 2. Continuous extraction equilibrium isotherms for LIX 984N organic phases.

When 30% LIX984N was employed, raffinate concentrations of <1 mg/L Cu could not be achieved even at tip speeds of 4.1 m/s, and it was not practically possible to operate at higher impeller speeds. The impeller speed was thus kept constant at 3.14 m/s

(800 rpm), and the mixer residence time varied. A mixer residence time in excess of 10 min was required to achieve a raffinate concentration of <1 mg/L Cu, with 0.25 mg/L achieved with a 15 min residence time. Further increase in the residence time did not improve the extent of extraction.

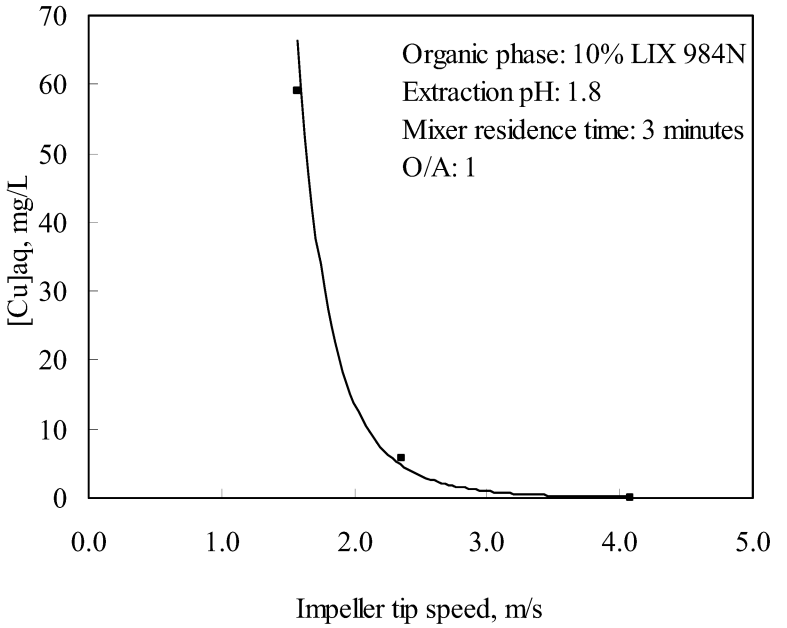

Figure 3. Effect of impeller tip speed on raffinate Cu concentrations: 10% v/v LIX 984N.

The extent of Co co-extraction measured during the batch isotherm tests is shown in Figure 4. The 10% LIX 984N organic phase loaded ~0.6 mg/L Co over the range of phase ratios tested, with a slight decrease in loading at O/A of unity. The 30% LIX 984N organic loaded up to 1.3 mg/L Co, which again decreased when subjected to a 1:1 contact with the aqueous phase. Viscosity measurements of the organic phases contacted at various ratios with the aqueous phase showed the same trend, with the highest viscosity measured at a phase ratio of unity. It is thought that the increased loading at the 1:1 phase ratio was directly related to the increased viscosities, which would negatively affect mixing characteristics and mass transfer between phases.

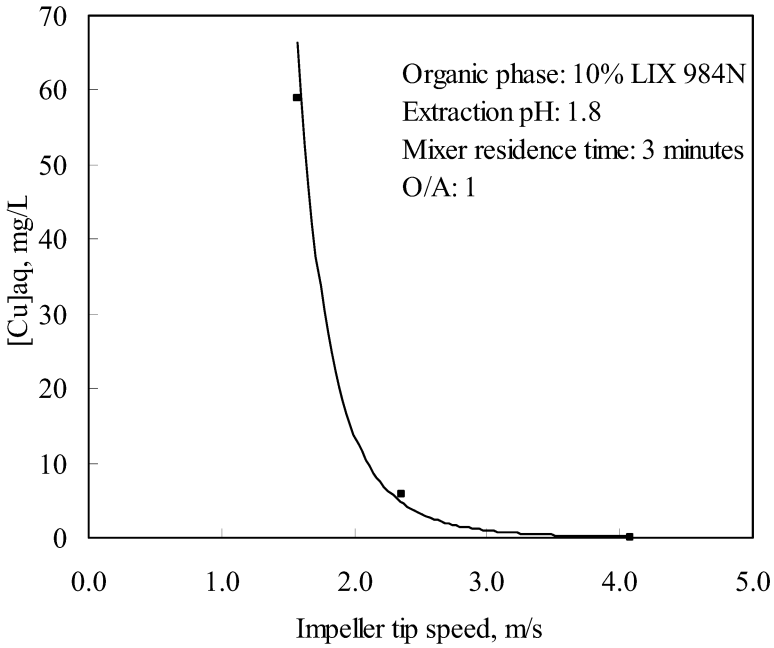

Figure 4. Loaded organic Co concentrations: batch extraction isotherms at pH 1.8.

SX/IX COMPARISON

From the results obtained, operational considerations associated with both an SX and IX circuit for the removal of Cu to a final concentration of <0.3 mg/L were compared.

SX Considerations

- Since an extractant concentration different to that employed for the primary Cu SX circuit is used, the secondary Cu SX circuit is a stand-alone circuit requiring organic make-up and reservoir tanks separate to that of the primary circuit.
- Maintenance of impeller speeds of >4 m/s is vital, and reliable monitoring and immediate corrective action in the event of any failure is key to consistent operation. The same applies to pH monitoring and control, with a deviation below the target pH resulting in higher than tolerable Cu in the raffinate, while a deviation above setpoint results increased Co co-loading.
- Co loading seems inevitable with pH-controlled operation and may require reductive conditions for stripping or, at worst, organic fouling to an extent that requires replacement.
- The NaOH addition required for pH-controlled operation increases the Na load in the circuit and ultimate generation of Na_2SO_4, requiring environmentally safe disposal.

IX Considerations

- Inherent with all IX operations is additional water usage that leads to a positive water balance.
- Co-loaded Co can be selectively eluted but has to be reprocessed by recycling to upfront unit operations for recovery. The associated sites require neutralization.
- Due to the high affinity of the resin for Fe(III), an upfront Fe removal step that consistently produces a low Fe content barren solution is required, as Fe fouling of the resin requires reductive elution conditions.
- An increased Na load as result of the regeneration step also applies as for the SX option but is worse due to Co co-loading.
- IX does not require the stringent adherence to operational set points to consistently produce barren solution at the specified Cu concentration as does SX.

CONCLUSIONS

Achieving Cu tenors in Co electrowinning advance electrolyte that comply with those required for the production of LME grade Co cathode was shown to be possible by controlling the pH of extraction in a Cu SX circuit using a conventional Cu extractant. Key operating conditions for the secondary Cu SX impurity removal circuit were the intensity of mixing and extraction pH. The degree of mixing required was identified to be a function of the extractant concentration. Dilute organic phases achieved similar extraction efficiencies to the more concentrated organic phase conventionally used in a primary/secondary SX configuration.

Although consistent performance of the pH-controlled SX circuit is completely dependant upon strict adherence to key operating conditions, this process is comparable, in terms of the extent of Cu extraction possible and low associated Co co-loading, to the IX option. Although a precipitation route may produce similarly low Cu concentrations, the associated Co co-precipitation results either in a significant valuable metal loss or large internal recycle with the associated reprocessing reagent consumption and cost.

REFERENCES

1. M. J. Dry *et al.*, “The Recovery of Cobalt from Copper Solvent-Extraction Raffinate in the Democratic Republic of the Congo,” ALTA 1998 Nickel/Cobalt Pressure Leaching and Hydrometallurgical Forum, ALTA Metallurgical Services, Melbourne, Australia, 1998.
2. P. M. Cole and A. M. Feather, “Flowsheet Alternatives for Processing African Copper Belt Copper Cobalt Ores,” International Solvent Extraction Conference ISEC 2008, Canadian Institute of Mining, Metallurgy and Petroleum, Montreal, 2008; in press.

DEVELOPMENT OF PROCESS FLOWSHEET FOR RECOVERY OF HIGH-PURITY COBALT FROM SULFATE LEACH LIQUOR OF WASTE $LiCoO_2$

Basudev Swain, Jinki Jeong, Jae-chun Lee, and Jeong-Soo Sohn

Minerals and Materials Processing Division, Korea Institute of Geoscience and Mineral Resources (KIGAM), Daejeon, 305-350, Korea.
Corresponding author email address: jinkiz@kigam.re.kr

ABSTRACT

A new hydrometallurgical process flowsheet for the recovery of high-purity Co(II) sulfate solution/salt from waste $LiCoO_2$ cathodic active material is described. Co(II) was recovered as Co(II) sulfate from sulfate leach liquor by solvent extraction using CYANEX 272. A mathematical model to determine optimum conditions for quantitative extraction of Co(II) was developed, and metal extractability correlated with CYANEX 272 concentrations and O/A volume ratio. From the model, the extraction mechanism and McCabe-Thiele extraction isotherm were derived and compared with obtained results. Cobalt sulfate of 99.99% purity was produced.

INTRODUCTION

According to the Cobalt Development Institute, demand for Co(II) for rechargeable batteries increased from 700 to 5000 t/a last decade. It is estimated that battery applications accounted for nearly 25% of total Co demand, namely about 12,000 t [1]. Worldwide rechargeable battery demand is predicted to reach 4.6 billion cells by 2010 [2]. The projected demand for mobile phone rechargeable batteries ensures steadily increasing demand, and the waste generated from these could cause serious environment problems. In next five years; popularity for hybrid vehicles is expected to increase demand for Co in rechargeable batteries. The waste generated, increasing energy demand for Co, rapid decrease in primary resources, strict environmental legislations such as the European Union's Waste of Electrical and Electronic Equipment (WEEE) and Restriction of Hazardous Substances (RoHS) directives and the extended producer responsibility (EPR) system in Korea provide additional motivation for $LiCoO_2$ waste recycling [3,4].

EXPERIMENTAL

Materials

Black amorphous waste $LiCoO_2$ generated from the lithium ion battery (LIB) industry was supplied by a Korean industry having the following characteristics: particle

size 8.3 μm, 60.2 wt % Co(II) and 7.09 wt % Li(I). All the chemicals used were analytical grade reagents. CYANEX 272 was used without further purification.

Method

Partially saponified CYANEX 272 (up to 65%) with 5 vol. % phase modifier (tri-*n*-butylphosphate) was used as the extractant. Leach solution (pH 5.0) was used for solvent extraction. Suitable volumes of organic and aqueous phases were equilibrated for 10 min followed by phase separation. The concentrations of Co(II) in the feed, raffinate, and stripped solution were determined by titration with 0.05 M EDTA in the presence of Murexide indicator. For low mg/L range Co(II) solutions, the concentrations of Li(I) were determined using atomic absorption spectrometry (AAS).

RESULTS AND DISCUSSION

The leach liquor generated under optimized conditions contained 44.72 g/L Co(II) and 5.43 g/L Li(I) at pH 5.0. From our investigation it was observed that the best separation factor as well as best Co(II) extraction were observed at equilibrium pH = 5.35 which corresponds to initial feed pH 5.0. At this equilibrium pH, only 8.23% Li(I) was co-extracted along with 51.23% of Co(II). The dependency of log *D* (distribution ratio) vs. equilibrium pH for Co(II) is a straight line. The best straight line fitted to data can be expressed as $y = 1.02x - 5.27$, $R^2 = 0.97$. The slope of 1.02 suggests that the extraction of Co(II) occurs through exchange of one mole H^+ with one mole Co(II) [3].

Effect of Concentration and Volume of CYANEX 272

Extraction conditions were optimized in terms of extractant concentration and volume ratio at initial pH 5. The concentration of CYANEX 272 was varied from 16 to 64 vol. % at different O/A volume ratios. It was observed that the extraction of Co(II) increases as a truncated S-shaped curve when the O/A varies from 1 to 4. For efficient use of CYANEX 272 and quantitative extraction of Co(II), a model is proposed. The proposed model is constructed on the assumption that the transfer of metal species into the organic phase occurs through a nonlinear sigmoid phenomenon, where volume of extractant, V_{org}, is the forcing variable and the metal extraction percentage is the response.

Metal Extractability Behavior and Modeling

Percentage of Co(II) extracted (*E*) is considered as a response to the active extractant percentage in the fresh solvent system. The extracted Co(II) percentage exhibits a truncated sigmoid-shaped trend with insignificant lower part as a function of CYANEX 272 volume for a particular concentration. A nonlinear modified sigmoid function was proposed to predict *E* in terms of V_{org} in Equation (1).

$$E = 100 - (Ae^{-V_{org./B}}) \quad (1)$$

where the unstructured parameters A and B were estimated by a multivariate nonlinear regression analysis using Trust-Region algorithms [5]. For all extractant concentrations, namely, 16 to 64 vol. %, the percentage of Co(II) extraction from the aqueous phase was predicted and compared with observed values. These were compared graphically by plotting E versus V_{org} as shown in Figure 1a, where symbols denote experimental points. Similarly, the co-extracted Li(I) percentage limited towards a truncated sigmoid trend with significant lower part as a function of CYANEX 272 volume for a particular concentration of CYANEX 272. For Li(I), a nonlinear modified sigmoid function was proposed to predict E in terms of V_{org} in Equation 2:

$$E = 100-(A_1 e^{-V\text{org}*B1}) \quad (2)$$

where the unstructured parameters A_1 and B_1 were similarly estimated by a multivariate nonlinear regression analysis using Trust-Region algorithms [5]. For all CYANEX 272 concentrations, the percentage of Li(I) extraction from aqueous phase was predicted and compared graphically by plotting E versus V_{org} (Figure 1b). The MATLAB® 6.5 Interactive Curve Fitting procedure was used for prediction and comparison for each case. The curves were generated by the use of estimated parameters in a generic model equation. The best fitted parameters were estimated using nonlinear least-squares method, Trust-Region algorithms and LAR robust method for performing the minimization of the objective function given by the sum of squares due to error (SSE) $\sum_i e_i^2$. The error (e) is the difference between the observed and predicted responses for metal extraction (E). The predicted responses are fitted values obtained by evaluating the best fit equation at the observed values of independent variable V_{org}. The 95% confidence interval value is calculated for each case. The parameters estimated are given in Table 1. The random patterns of the residuals indicate that the model is free of systematical errors.

Table 1. Estimated model parameters and goodness of fit

Estimated model parameters and goodness of fit for Co(II)						
CYANEX 272, Vol %	A ± SE	B ± SE	SSE	R^2	Adj. R^2	RMSE
16	129.30 ± 7.60	20.40 ± 1.730	21.22	0.9965	0.9958	2.06
24	119.70 ± 20.27	14.98 ± 3.350	98.03	0.9864	0.9837	4.428
32	124.90 ± 47.80	10.06 ± 4.611	244.00	0.9601	0.9521	6.985
40	125.9 0± 38.03	5.70 ± 2.571	75.01	0.9841	0.9810	3.873
48	140.60 ± 67.74	10.06 ± 2.534	81.28	0.9787	0.9744	4.032
56	115.40 ± 38.86	5.70 ± 1.770	26.70	0.9885	0.9861	2.311
64	93.76 ± 28.29	5.70 ± 1.586	14.15	0.9905	0.9886	1.682
Estimated model parameters and goodness of fit for Li(I)						
CYANEX 272, Vol %	A_1 ± SE	B_1 ± SE	SSE	R^2	Adj. R^2	RMSE
16	97.7 ± 0	-6e-14 ± 7e14	poor	poor	poor	poor
24	112.2 ± 22.81	0.0144 ± 0.008	452.80	0.8184	0.7820	9.516
32	110.8 ± 16.28	0.0185 ± 0.006	206.20	0.9259	0.9111	6.421
40	110.1 ± 13.09	0.0244 ± 0.006	115.10	0.9653	0.9583	4.799
48	130.1 ± 32.51	0.0466 ± 0.018	411.80	0.9470	0.9364	9.075

SE = Standard errors

RMSE = Root mean squared error

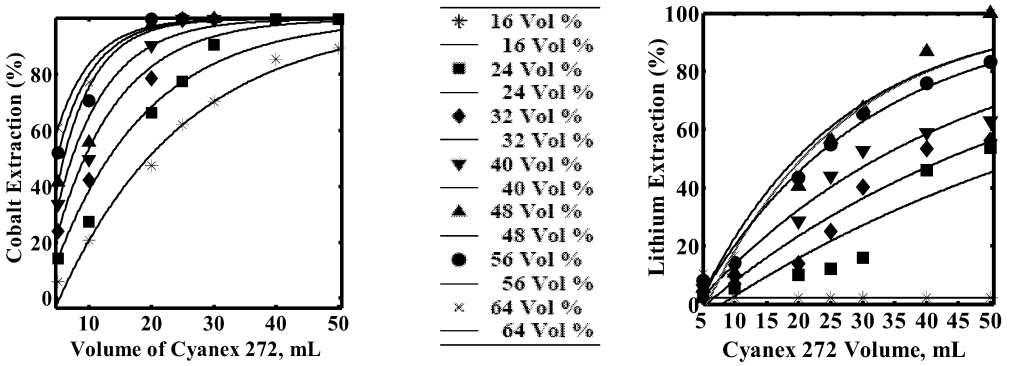

Figure 1. Extraction of (a) Co(II) and (b) Li(I) at different [CYANEX 272] from leach liquor, the best fitted line generated by model equation.

Determination of the Nature of the Extracted Complex

The dependency of log *D* on log [CYANEX 272] for cobalt was plotted for both calculated values from proposed model and observed experimental values. The plot is a straight line having slope of 1.95 for the experimentally observed values. The slope value calculated from the proposed model was 2.18. Both the calculated and observed slope values of nearly 2 indicated the association of two moles of extractant for one mole of cobalt. This complex formation has been studied in our earlier work. The reliability of the proposed model for a cation exchange reaction mechanism is verified, and it agrees reasonably with the proposed mechanism in our earlier fundamental study [3].

McCabe-Thiele Extraction Isotherm

From our proposed model the concentration of Co(II) in the aqueous and organic phases and distributions were calculated for different phase ratios. Theoretical maximum loading of CYANEX 272 was also calculated for two selected concentrations, *i.e.*, 32 and 48 vol. %, based on mechanism. For construction of McCabe-Thiele diagrams the organic and aqueous Co(II) concentrations were calculated from the model. The extraction isotherms are plotted in Figure 2 to determine the number of stages required for the quantitative extraction of Co(II) using 32 and 48 vol. % CYANEX 272. The pH of the leach liquor was adjusted to 5. The O/A ratio was varied from 1/5 to 5/1 keeping the total volume of the organic and aqueous phases constant. The McCabe-Thiele diagram for 32 vol. % CYANEX 272 (Figure 2(a)) indicated two stages are required for quantitative extraction of Co(II) at a phase ratio O/A = 2/3 under these conditions both for the calculated model and experimental results. The McCabe-Thiele diagram for 48 vol. % CYANEX 272 (Figure 2(b)), indicated two stages are required for quantitative extraction of Co(II) at a phase ratio O/A = 2/3. It also requires the same two stages for both calculated model and proposed model, but at a different operating ratio of O/A=0.85. Both studies indicated that two stages are required for quantitative extraction of Co(II) at a phase ratio O/A = 2/3 for both concentrations of CYANEX 272 studied.

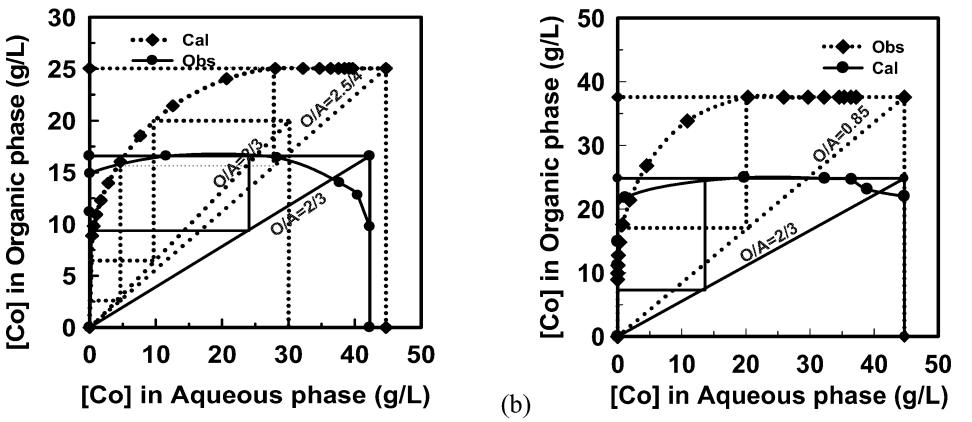

Figure 2. McCabe-Thiele isotherm for extraction of cobalt from leach liquor using (a) 32 vol. % and (b) 48 vol. % CYANEX 272 at pH 5.00. (Dotted lines indicate calculated line and dark lines indicate the observed results.)

Counter-Current Batch Simulation Studies for Co(II) and Li(I) Separation

In order to achieve quantitative extraction of Co(II), a two-stage countercurrent batch simulation study was carried out using 32 and 48 vol. % saponified CYANEX 272 at O/A = 2/3. For 32 vol. % CYANEX 272 only 60.8% but in case of 48 vol. % CYANEX 272, 99.99% Co(II) was extracted along with 15.6% and 35.5% of Li(I) contamination, respectively. The 48 vol. % CYANEX 272 was used for further studies.

Recovery of Pure Co(II)

The loaded organic phase (48 vol % CYANEX 272) after two-stage countercurrent extraction contains 44.719 g/L Co(II) and 1.93 g/L Li(I). Scrubbing studies were carried out using 0.1 M Na_2CO_3 with an O/A of 1/5 to 5/1. The scrubbing isotherm indicated that about three stages of scrubbing are required at O/A ratio of 2.5 for achieving quantitative scrubbing. From purified Co(II) loaded organic, pure Co(II) sulfate was easily stripped by contact with 5 M H_2SO_4 at an O/A ratio of 5. The purity of the stripped Co(II) sulfate was 99.99%. If required, the Co(II) sulfate hexahydrate may be readily crystallized from such a strip liquor. The Co(II) may be also readily recovered as high-purity electrolytic Co(II) by electrowinning. Since the Li(I) concentration in the scrubbed solution is low, it can be extracted by an environmentally friendly adsorption process using MnO oxide as adsorbent, which has been prepared and studied in our laboratory.

CONCLUSIONS

Co(II) sulfate with 99.99% purity can be recovered from LIB industry waste using CYANEX 272 by solvent extraction from the leach liquor by managing different process parameters such as pH of the leach liquor, CYANEX 272 concentration, O/A volume

ratio, and suitable extraction, scrubbing and stripping isotherms. The proposed model simulates the percent extraction values (E) values related to organic volume (V_{org}) within acceptable confidence. The process flowsheet is effective for converting the $LiCoO_2$ waste to value-added wealth through a simple hydrometallurgical process, to support environment policies and conservation of the natural resources. An overall process flowsheet is suggested in Figure 3 based on the experimental investigations.

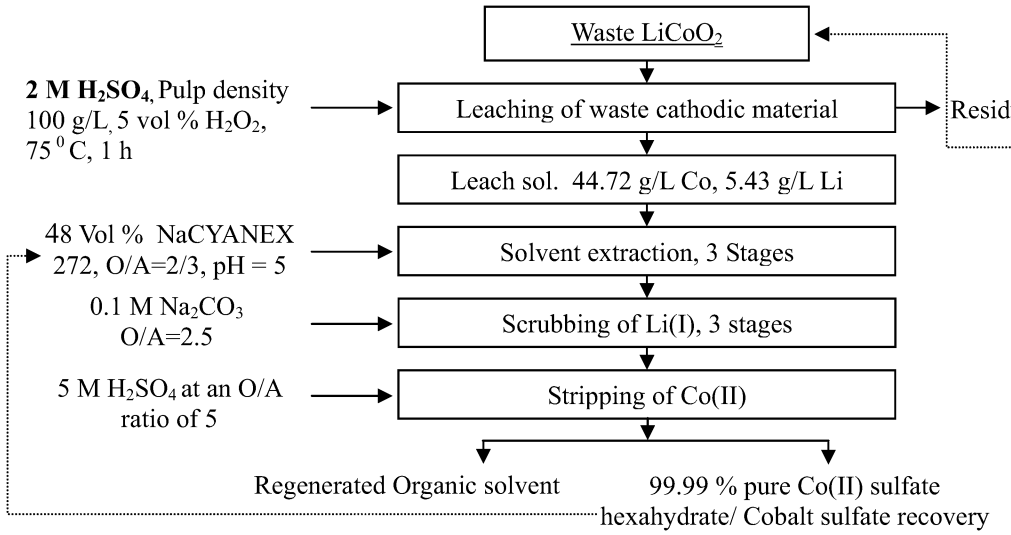

Figure 3. Flowsheet for recovery of high pure Co(II) from waste $LiCoO_2$.

ACKNOWLEDGMENTS

This research was supported by the Korea Institute of Geoscience and Mineral Resources funded by the Ministry of Science and Technology of Korea.

REFERENCES

1. http://www.thecdi.com/cdi/images/documents/facts/COBALT_FACTSElectronics.pdf, accessed May 12th 2007.
2. P. V. D. Bossche, "The Current Legislative Development in the EU Waste Policy: Challenge or Opportunities for Metal Industry," Cobalt Development Institute, 2006, **06**/1**,** 1−14.
3. B. Swain, J. Jeong, J. C. Lee, and G. H. Lee, "Separation of Cobalt and Lithium from Mixed Sulfate Solution using Na-Cyanex 272," *Hydrometallurgy*, **84**(3-4), 130−138 (2006).
4. A. Gottberg, J. Morris, S. Pollard, C. Mark-Herbert, and C. Matthew, "Producer Responsibility, Waste Minimization and the WEEE Directive: Case Studies in Eco-Design from the European Lighting Sector," *Sci. Total Env.,* **359**(1–3), 38–56 (2006).
5. W. S. Cleveland, "Robust Locally Weighted Regression and Smoothing Scatterplots," *J. Am. Stat. Ass.*, **74**, 829−836 (1979).

SEPARATION OF COBALT AND ZINC FROM MANGANESE, MAGNESIUM AND CALCIUM USING SYNERGISTIC SOLVENT EXTRACTION CONSISTING OF VERSATIC 10 AND LIX 63

Chu Yong Cheng, Wensheng Zhang, and Yoko Pranolo

The Parker Centre / CSIRO Minerals, PO Box 7229, Karawara, WA 6152, Australia
Corresponding author email address: chu.cheng@csiro.au

ABSTRACT

By adding 0.4 M LIX 63 to 0.5 M Versatic 10 in Shellsol D70, large synergistic shifts were obtained for Cu (ΔpH_{50} 2.45), Co (ΔpH_{50} 4.24) and Zn (ΔpH_{50} 1.62). After a single contact at pH 4.5, the separation factor of metals over manganese reached over 42,000 for Cu, over 6,000 for Co, and over 380 for Zn, indicating excellent separation of Cu and Co and good separation of Zn from Mn, Mg, and Ca, and selective stripping of Zn over Co is possible. The system was further optimized with the modified synthetic Boleo pilot-plant solution. It was found that, at an A/O ratio of 2:1 with 0.33 M Versatic 10 and 0.30 M LIX 63 in Shellsol D70, the composition approached optimum. The pH_{50} difference of Co over Zn reached 1.4 pH units, indicating a good selective stripping to obtain separate Co and Zn products. At pH 5.5, the extraction of Co and Zn was 93% and 70% in a single contact, respectively, while the Mn extraction was only 0.28 g/L.

INTRODUCTION

The Boleo Cu-Co-Zn Project of Baja Mining Corp. is situated in the Baja Peninsula of Mexico [1]. After oxidation and reductive leaching, copper solvent extraction (SX), and iron removal, the pregnant leach solution (PLS) contains large amounts of manganese. Due to the very high manganese concentration, it is very difficult to separate Co and Zn from Mn, Mg, and Ca using conventional SX processes. The SX Group of the Parker Centre/CSIRO Minerals has developed novel direct solvent-extraction (DSX) processes to directly separate Ni, Co, Cu, and Zn from Mn, Mg, and Ca without precipitation and releach using synergistic solvent-extraction (SSX) systems with commercially available reagents [2-4]. Since 2004, the group has conducted preliminary batch tests (pH isotherms) for the selection of a SSX system, selective stripping tests for the possible recovery of Co and Zn as separate products, and further tests to optimize the selected SSX system with the synthetic Boleo leach solution.

SELECTION OF AN SSX SYSTEM

Metal pH Isotherms

The synthetic (expected) Boleo solution contained (in g/L) 0.195 Co, 0.145 Cu, 1.16 Zn, 44.6 Mn, 25.7 Mg, and 0.46 Ca. The high Mn concentration indicated the difficulty of separation of Co and Zn from Mn. Several organic compositions were tested to select the most efficient SSX system. It was found that 0.5 M Versatic 10 and 0.4 M LIX® 63 in Shellsol® D70 at an A/O ratio of 2:1 performed the best.

The metal pH isotherms with the system containing 0.5 M Versatic 10 acid alone and the SSX system containing 0.5 M Versatic 10 acid and 0.4 M LIX 63 are shown in Figures 1 and 2, respectively. The pH_{50} values of Cu, Co, and Zn decreased from 4.40, 7.35, and 5.45 pH units (Table 1) with Versatic 10 alone to 2.10, 3.30 and 4.08 pH units with the SSX system, respectively. The ΔpH_{50} values (pH_{50} differences without and with the addition of LIX 63) of Cu, Co, and Zn for the SSX system compared with Versatic 10 alone were found to be 2.30, 4.05, and 1.37 pH units, respectively.

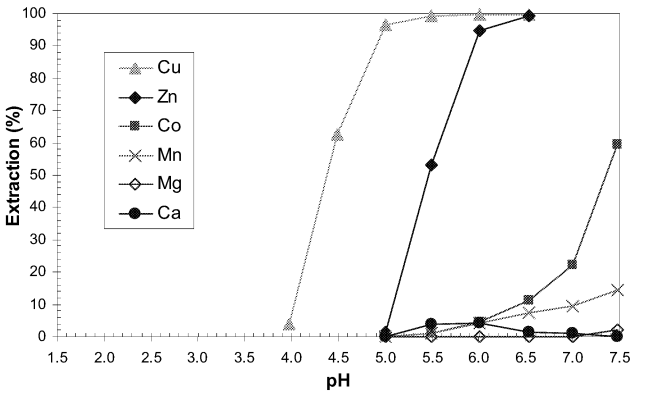

Figure 1. Metal pH isotherms with 0.5 M Versatic 10 alone in Shellsol D70.

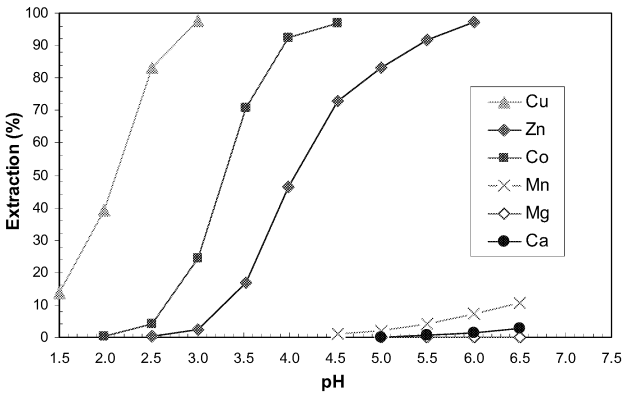

Figure 2. Metal pH isotherms with the SSX system.

Separation of Co, Cu, and Zn from Mn, Mg, and Ca

Although the $\Delta pH_{50(Mn-M)}$ (M denotes Cu, Co, and Zn) cannot be determined without pH_{50} values of manganese, the separation of Cu, Co, and Zn from Mn can be indicated by their separation factors over manganese at a certain pH value. At pH 4.5 and an A/O ratio of 2:1 after a single contact with the SSX system, the extraction reached almost 100% for Cu, 98% for Co, 80% for Zn, and only 1.55% for Mn. Almost no Ca and Mg were extracted. The separation factors for Cu/Mn and Co/Mn were greater than 72000 and 3000, respectively, suggesting an easy and complete separation of copper and cobalt from manganese with the selected SSX system. The separation factor of Zn over Mn was found to be above 250, suggesting a good separation.

Table 1. pH_{50} and ΔpH_{50} of metals for the two systems

Organic solution composition	pH_{50}			ΔpH_{50}		
	Cu	Co	Zn	Cu	Co	Zn
0.5 M Versatic 10	4.40	7.35	5.45	—	—	—
0.5 M Versatic 10/0.4 M LIX 63	2.10	3.30	4.08	2.30	4.05	1.37

Selective Stripping

Selective stripping tests were conducted counter-currently at an O/A ratio of 10:1 in a mini mixer-settler. Temperature was controlled at 40 ± 2 °C by circulating hot water in a water jacket. The batch loaded and scrubbed organic solution and a slightly acidic aqueous solution were counter-currently pumped into the rig and the pH controlled at 3.8, 3.5, 3.25, and 3.00. At pH 3.00, the zinc stripping efficiency reached 68.5% while only 11.7% Co was stripped. Table 2 shows that at pH 3.25 and an O/A ratio of 10:1 in two stage of stripping, the Zn concentration in the organic solution decreased largely while the Co concentration kept almost unchanged. It is concluded that selective stripping of Zn over Co is possible.

Table 2. Metal concentrations in organic solution in stripping stages

Metal	Concentration in organic solutions (g/L)		
	Scrubbed organic	Strip stage 1	Strip stage 2
Co	0.378	0.351	0.334
Zn	2.591	1.408	0.816

SSX SYSTEM OPTIMIZATION

Metal pH Isotherms

Due to a subsequent change in the composition of the Boleo pilot-plant leach solution, it was necessary to optimize the CSIRO SSX system to suit the composition. The synthetic Boleo pilot-plant solution contained (in g/L) 0.29 Co, 0.002 Cu, 1.90 Zn, 0.25 Ni, 15.8 Mn, 0.015 Fe, and 0.51 Ca. A number of pH isotherms tests were conducted by varying the Versatic 10 and LIX 63 concentrations at A/O ratios of 2:1. It was found that with 0.33 M Versatic 10 and 0.30 M LIX 63 (Figure 3), the pH_{50}

difference between cobalt and zinc reached 1.4 pH units, indicating very good zinc selective stripping could be obtained. At pH 5.5 after a single contact at 30 °C, the extraction of cobalt and zinc were 93% and 70%, respectively, while the manganese extracted was only 0.28 g/L. This indicates that the SSX system consisting of 0.33 M Versatic 10 and 0.30 M LIX 63 approached optimum.

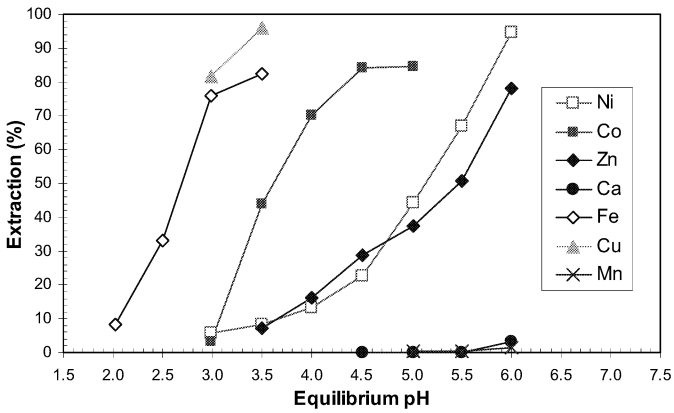

Figure 3. Metal pH isotherms with the optimized SSX system at an A/O ratio of 2:1 and 30 ˚C.

Extraction Kinetics

The extraction kinetics of Fe, Cu, Zn, Co, Ni, Mn, and Ca with the optimized DSX system at 30 ˚C were determined (Table 3). The extraction kinetics of iron and copper were very fast. Within 30 s, over 97% of the iron and copper were extracted, and almost all the iron and copper were extracted within 2 min. The extraction of cobalt and zinc was also fast. Over 86% Co and 84% Zn were extracted within 30 s. Both cobalt and zinc extraction peaked after 1 min of mixing, with cobalt extraction 95% and zinc extraction 84%. Their extraction slightly decreased due to the extraction of nickel, although the nickel extraction kinetics was slow. Within 2 min, only 13% Ni was extracted. Its extraction slowly increased to 81% after 10 min of mixing. This also caused the slight decrease in extraction of calcium, although its extractions were very small. This means for an industrial operation with 2 min residence time, a small amount of Ni would be co-extracted with Fe, Cu, Co, and Zn.

Distribution pH Isotherms

The distribution isotherms of Zn, Co, Ni, and Mn were determined using the system containing 0.33 M Versatic 10/0.30 M LIX 63 in Shellsol D70 and the synthetic Boleo pilot-plant solution. At an A/O ratio of 2:1, three theoretical stages are needed for Zn to obtain a raffinate containing 20 mg/L Zn with 100% stage efficiency.

Stripping Kinetics

The stripping kinetics of Fe, Cu, Zn, Co, and Ni were determined using the optimized DSX system with 30 g/L H_2SO_4 solution at an A/O ratio of 1:1 and 30 °C (Table 4). The stripping kinetics of zinc was very fast. Within 30 s, more than 99% of the zinc was stripped while nearly 99% Co was stripped after 2 min mixing. The stripping kinetics of copper was reasonably fast, that of iron(III) and nickel was slow. Only 32% Ni was stripped within 2 min and 54% after 10 min mixing. Therefore, this DSX system is not suitable for the recovery of both Co and Ni. Iron and nickel can be stripped with a higher acidity solution. In a plant operation, a bleed stream may be needed to keep iron and nickel at a low level.

Table 3. Metal extraction kinetics with the optimized SSX system

	Extraction (%)						
Element	0 min	0.5 min	1.0 min	2.0 min	3.0 min	5.0 min	10.0 min
Ni	0.0	7.3	10.4	13.3	28.3	43.7	81.3
Co	0.0	86.5	95.2	95.1	94.3	93.7	93.5
Zn	0.0	83.7	83.8	83.4	82.0	80.8	80.0
Mn	0.0	2.3	2.2	2.1	1.91	1.8	1.7
Fe	0.0	98.3	98.9	99.3	99.9	99.9	>99.9
Ca	0.0	1.2	1.1	0.9	0.8	0.7	0.6
Cu	0.0	97.8	98.7	99.1	99.9	99.9	>99.9

Table 4. Metal stripping kinetics with the optimised SSX system

	Stripping (%)						
Element	0 min	0.5 min	1.0 min	2.0 min	3.0 min	5.0 min	10.0 min
Ni	0.0	43.1	37.1	32.4	37.6	53.9	54.3
Co	0.0	77.1	93.0	98.9	99.4	99.5	99.6
Zn	0.0	99.1	99.9	99.9	>99.9	>99.9	99.9
Fe	0.0	25.9	10.6	35.4	58.8	79.2	89.6
Cu	0.0	85.6	67.8	50.9	85.4	86.2	82.9

DSX CIRCUIT PERFORMANCE IN PILOTING

Baja Mining conducted two pilot-plant operations in 2004 [1,5] and in 2006 [6,7] with very good performance of the DSX circuit. A news release from Baja Mining in December 2004 says “the CSIRO DSX circuit for cobalt and zinc recovery performed very well. The advantage of the DSX circuit for Boleo plant design is that cobalt and zinc are separated from manganese and magnesium in the Boleo leach solutions. In the Lakefield pilot plant, cobalt and zinc were recovered with overall efficiency >95% to produce a concentrated zinc sulphate solution and a concentrated cobalt solution”. The CSIRO circuit performed even better in the pilot-plant operation at Lakefield Research, July 2006. The overall recovery of cobalt and zinc reached over 99% with a raffinate contained only 4.2 mg/L Zn and 0.95 mg/L Co. The DSX circuit showed no sign of reagent degradation after the pilot-plant operation of three months [8].

CONCLUSIONS

By adding 0.4 M LIX 63 to 0.5 M Versatic 10 in Shellsol D70, large synergistic shifts were obtained for Cu, Co, and Zn at 40 °C and an A/O ratio of 2:1. After a single contact at pH 4.5, the extraction reached almost 100% for Cu, 98% for Co, 80% for Zn, and only 1.55% for Mn. Almost no Ca and Mg were extracted. The separation factor of metals over manganese reached over 42,000 for Cu, over 6,000 for Co and over 380 for Zn, indicating excellent separation of Cu and Co and good separation of Zn from Mn, Mg and Ca. In selective stripping at pH 3.00, the zinc stripping reached 68.5%, while only 11.7% Co was stripped, indicating that selective stripping of Zn over Co is possible.

The SSX system was further optimized to reduce the co-extraction of Mn with the synthetic Boleo pilot-plant solution. It was found that, at an A/O ratio of 2:1 with 0.33 M Versatic 10 and 0.30 M LIX 63 in Shellsol D70, the SSX system composition approached optimum. The pH_{50} difference of Co over Zn reached 1.4 pH units, indicating a good selective stripping to obtain separate Co and Zn products. At pH 5.5 in a single contact, the extraction of Co, and Zn was 93% and 70%, respectively, while the Mn concentration in the organic solution was found to be 0.28 g/L. The extraction and stripping kinetics of Cu, Co, and Zn were fast. The CSIRO DSX circuit has been tested in two integrated pilot-plant trials with excellent results.

ACKNOWLEDGMENTS

The authors would like to thank Mr. Peter Miovski and Mr. Mark Urbani for conducting the first and second stages of the test work. Shell Chemicals provided Versatic 10 and the Shellsol diluents and. Approval to publish this paper by Baja Mining is gratefully acknowledged.

REFERENCES

1. D. Dreisinger, W. Murray, K. Baxter, M. Holmes, H. Jacobs, and R. Molnar, "The Metallurgical Development of the El Boleo Copper-Cobalt-Zinc Project," ALTA Copper 2005, ALTA Metallurgical Services, Melbourne, Australia.
2. C. Y. Cheng and M. D. Urbani, "Solvent Extraction Process for Separation of Cobalt and/or Manganese from Impurities in Leach Solutions," Patent No. WO 2005/073415 A1.
3. C. Y. Cheng and M. D. Urbani, "Solvent Extraction Process for Separation of Cobalt and/or Nickel from Impurities in Leach Solutions," Patent No. WO 2005/073416 A1
4. C. Y. Cheng, "Solvent Extraction of Nickel and Cobalt with Synergistic Systems consisting of Carboxylic Acid and Aliphatic Hydroxyoxime," *Hydrometallurgy*, **84**, 109-117 (2006).
5. Anon., "Boleo Pilot Plant Program at SGS Lakefield Research Successfully Completed," News release, Baja Mining Corp., Toronto, December 2004.
6. D. Dreisinger, K. Baxter, and R. Molnar, "New Development in the Boleo Copper-Cobalt-Zinc-Manganese Project," ALTA Copper 2006, ALTA Metallurgical Services, Melbourne, Australia.
7. Anon., "Baja Mining Phase 2 Pilot Plant Program Successfully Completed," News release, Baja Mining Corp., Toronto, July 2006.
8. D. Dreisinger, Private communication, 2006.

EVALUATION OF VERSATIC 10 AND VERSATIC 10/NICKSYN SYNERGISTIC SYSTEMS FOR NICKEL-CALCIUM SEPARATION ON THE TATI BMR HYDROMETALLURGICAL DEMONSTRATION PLANT

Huziel Masiiwa,[1] Osefelepelo Mathe,[1] Simon Donegan,[1] Gerhard Nel,[2] René du Preez,[3] Marthie Kotze,[3] and Neil Ireland[4]

[1]Botswana Metal Refinery, Francistown, Botswana. [2]Norilsk Nickel Africa (Pty) Ltd, Johannesburg, South Africa. [3]Mintek, Randburg, South Africa. [4]Norilsk Process Technology, Perth, Australia.
Corresponding authors email address: hmasiiwa@bmr.co.bw, renedp@mintek.co.za

ABSTRACT

Mintek recently tested on a laboratory scale the use of mixtures of Versatic 10 (V10) and a synergist (Nicksyn) for the extraction of nickel from leach liquors obtained in the refining of sulfide concentrates. These were then tested at the Tati Botswana Metal Refinery Hydrometallurgical Demonstration Plant nickel solvent-extraction circuit. The trial showed that the V10/Nicksyn blend improved nickel recovery and reduced the number of extraction stages and water consumption. For the commercial plant, these benefits would yield a payback period of less than 18 months. The synergist caused an increase in phase-disengagement time in all the stages of the circuit. The degradation rate of the synergist relative to V10 could not be accurately defined.

INTRODUCTION

Tati Botswana Metal Refinery Hydrometallurgical Demonstration Plant (BMR HDP) was constructed in 2004 to demonstrate the feasibility of the Activox® process. The plant employs three solvent-extraction circuits to separate copper, cobalt, and nickel from pregnant leach solution (PLS). Limestone is used to precipitate iron from the PLS before the cobalt (CoSX) and nickel solvent-extraction (NiSX) circuits, resulting in a calcium-saturated solution. An overview of the process description is given by Kloiber et al. [1]. Plant results confirmed that the process was technically and commercially viable, and this led to approval for construction of the first commercial-scale Activox refinery.

The Tati BMR HDP NiSX circuit was commissioned using Versatic 10 (V10) as the extractant. Although target recoveries were achieved, the extraction circuit required tight pH control for optimum Ni-Ca separation, as well as PLS dilution with filtered water to avoid calcium saturation. It was considered that the introduction of a synergist would result in improved selectivity for nickel over calcium, thus leading to improved recoveries, less stringent pH control, and reduction or complete elimination of dilution water requirements. In addition, significant savings on capital costs would be realized

through reducing the number of extraction stages required. Mintek has developed various synergistic systems based on mixtures of carboxylic acids (such as V10) and different viable synergists with a view to designing a hydrometallurgical process for the recovery of nickel from dilute acidic leach liquors, as previously described [2].

Mintek evaluated the V10/Nicksyn™ (the Mintek developed synergist) blend extensively in order to determine the advantages/disadvantages of this system over the use of V10 alone [3]. This led to a plant trial using this system at the Tati BMR HDP. The paper gives an overview on laboratory test work carried out at Mintek, the results of the plant trial at the Tati BMR HDP, and a preliminary techno-economic evaluation of the use of the synergistic system at the BMR commercial plant.

LABORATORY TEST WORK

Experimental

The Mintek-developed synergist (Nicksyn), in different combinations with V10 and diluted with Shellsol D70, was evaluated to optimize nickel recovery and Ni-Ca separation from a CoSX raffinate stream at Tati BMR HDP. The stream contained 20 g/L Ni, 500-600 mg/L Ca, and 540 mg/L Mg. Cu, Zn, Mn, Fe, and Co were <2 mg/L in solution as a result of their effective extraction in the upfront Cyanex 272 circuit.

Metal-distribution equilibria were obtained with regard to pH versus extraction, and extraction and stripping isotherms, as described previously [3]. Tests were done to determine the stability of Nicksyn mixed with V10 over a period of 90 days.

Results and Discussion

Curves of pH versus extraction with 1.0 M V10 only and mixed with 0.20-1.00 M Nicksyn in Shellsol D70 at 35 ºC, showed that synergistic shifts in the pH_{50} values (the pH value at which 50% of the metal originally present in the aqueous phase is extracted under a given set of conditions) for the extraction of nickel increased from 0.90 to 1.45 units when Nicksyn addition was increased from 0.20 to 1.00 M, respectively, whilst the extraction of calcium was insignificantly affected. The separation between nickel and calcium ($pH_{50}^{Ca\text{-}Ni}$) increased from 1.32 pH units (V10 only) to 2.83 pH units (1.0 M V10/1.0 M Nicksyn). Molar ratios of V10:Nicksyn of 5:1 and 4:1 were considered for the demonstration plant to optimize the benefit relative to cost.

Maximum loading experiments indicated that about 20 g/L nickel loading could be achieved using 1.25 M V10/0.31 M Nicksyn in Shellsol D70 (V10:Nicksyn = 4) at pH 6.0 and 35 ºC. These conditions were applied in generating the extraction isotherm.

The McCabe-Thiele construction confirmed that a nickel loading of about 20 g/L could be achieved in three countercurrent extraction stages at an O:A phase ratio of 0.9, with calcium loading on the organic phase being below the detection limit. These operating conditions were therefore recommended for the extraction circuit on the demonstration plant.

The distribution isotherm and McCabe-Thiele construction generated for stripping of nickel from batch-loaded 1.25 M V10/0.31 M Nicksyn in Shellsol D70

(containing about 20 g/L Ni) at 35 ºC, using synthetic spent electrolyte containing 61 g/L Ni and 40 g/L H_2SO_4 as strip solution, indicated that nickel could be stripped in two countercurrent stripping stages at an O:A phase ratio of 1.2 and at 35 ºC. Loaded strip liquor containing about 86 g/L Ni was obtained, as would be expected based on the acid content of the synthetic strip liquor.

Stability tests were carried out using organic phases containing 1.25 M V10 mixed with 0.31 M Nicksyn, simulating extraction and stripping conditions. Samples taken of the organic phases at chosen time intervals (15, 29, 45 and 90 days for stability tests representing stripping conditions and 90 days for a stability test representing extraction conditions) were then used (separately) to determine the pH versus extraction curves for nickel and calcium from Tati CoSX raffinate at 35ºC. The pH_{50} values as well as $pH_{50}^{Ca\text{-}Ni}$ obtained for nickel and calcium are given in Table 1, together with those obtained using the fresh organic phase. Variations in pH_{50} values of Ni (4.57 to 4.63) and Ca (6.55 to 6.67), and therefore variations in $pH_{50}^{Ca\text{-}Ni}$ (1.97 to 2.05) were insignificant over the 90-day period of the stability tests. It can be concluded that the organic-phase mixture was stable under the given conditions for a period of 90 days.

Table 1. pH_{50} and $pH_{50}^{Ca\text{-}Ni}$ values for nickel and calcium extraction by 1.25 M V10/0.31 M Nicksyn in Shellsol D70 (fresh and after use in stability tests) at 35 ºC

	$pH_{50}Ni$	$pH_{50}Ca$	$pH_{50}^{Ca\text{-}Ni}$
Stripping conditions:			
Fresh	4.57	6.55	1.98
15 days	4.61	6.58	1.97
29 days	4.63	6.66	2.03
45 days	4.59	6.60	2.01
90 days	4.60	6.58	1.98
Extraction conditions:			
90 days	4.62	6.67	2.05

PLANT TRIAL

Plant Set-Up

For the V10 trial, data gathered between January and July 2006 (2558 operating hours) were used, while for the V10/Nicksyn trial, data from March to June 2007 (2810 h) were used.

The V10 trial operated on a 5 extract, 1 scrub, 2 strip, and 1 stripped organic after-settler arrangement. The extraction pH was typically controlled at 6.95 to 6.35 using aqueous ammonia. The extraction advance O:A phase ratio was used to control nickel extraction in order to achieve the target recovery of 99.3%. With high nickel loadings, calcium saturation was observed.

The V10/Nicksyn trial operated on a 4 extract, 1 scrub, 2 strip, and 1 stripped organic-wash arrangement. The circuit ran on a flat extraction pH profile of 5.5 across the four extraction stages. The extraction advance O:A phase ratio was used to control nickel extraction in order to achieve recoveries above 99.8%. A summary of the performance of the two trials is shown in Table 2.

Table 2. Comparison of operating conditions

		V10	V10/Nicksyn
V10 concentration	M	1.57	1.31
Nicksyn concentration	M	0	0.27
Typical organic nickel loading	g/L	21	14
Typical PLS grade	g/L Ni	14.2	13.7
Advance O:A phase ratio	Extract	0.7	1.4
	Scrub	4.4	35
	Strip	0.96	1.5
Phase disengagement time, s	Extract	53	82
	Scrub	96	116
	Strip	51	94
Nickel recovery	%	99.3	99.8

Results and Discussion

The V10/Nicksyn plant trial was carried out at a lower Nicksyn concentration than initially recommended [2] to optimize operating costs. Initially, the extraction pH values were maintained at a relatively high level to give the same loading as for the V10 trial, but due to the need to fully exploit the synergist's nickel-calcium separation, pH values were gradually reduced, with a resultant drop off in loading to 14 g/L nickel compared with 21 g/L for the V10 trial. The extraction advance O:A phase ratio had to be increased from 0.7 to 1.4 to maintain the required nickel-transfer rate. Increasing Nicksyn concentration to increase loading was not considered due to the associated increase in viscosity, phase disengagement time, and costs. Raising extraction pH values to increase loadings could not be tested due to time limitations.

The increased nickel extraction by the V10/Nicksyn blend is clearly indicated in some profiles generated on a weekly basis (as indicated in the legend) during the campaign and shown in Figure 1. For the V10/Nicksyn trial, the bulk of the nickel was extracted in the first two stages, while the V10 system required all 5 stages due to the need to control calcium co-extraction.

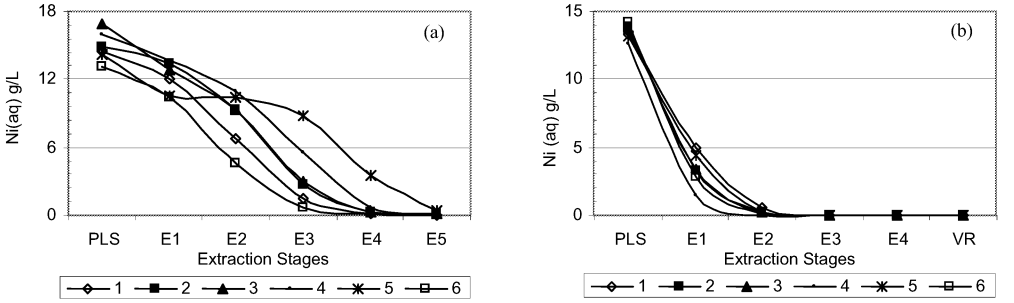

Figure 1. Extraction nickel aqueous concentration profile. (a) V10 and (b) V10/Nicksyn.

Despite high nickel extraction by the V10/Nicksyn blend, calcium loading was minimal as shown in Figure 2 (chosen profiles were generated on a weekly basis as indicated in the legend). This was in contrast to loadings of >100 mg/L in E5 for the

V10-only system, which required tight pH control to avoid calcium saturation. These results indicate that there is potential to drop another extraction stage for the V10/Nicksyn trial and still achieve target recoveries.

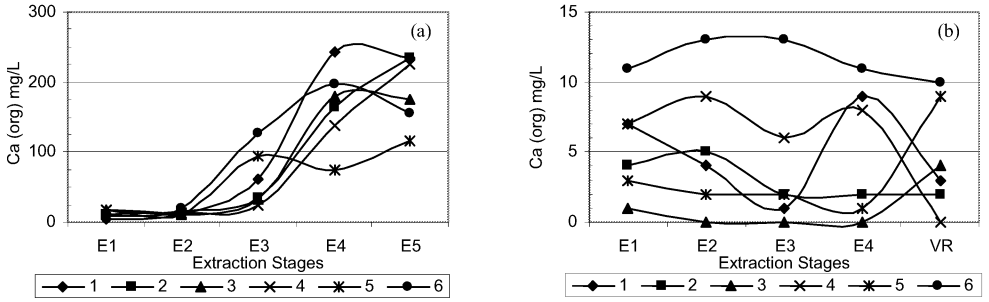

Figure 2. Extraction calcium organic concentration profile. (a) V10 and (b) V10/Nicksyn.

The introduction of Nicksyn caused a significant increase in phase-disengagement time across the circuit (Table 1). The strip stages were particularly affected, as this resulted in relatively high levels of entrainment in the stripped organic. Washing of the stripped organic proved necessary due to the use of spent electrolyte as strip solution, and the need to obtain very low levels of nickel in the raffinate. The difference in organic physical properties did not appear to have any detrimental effect on the extraction circuit.

For the V10 trial, filtered dilution water was required to reduce calcium concentration. This additional flow would have led to a 10% increase in the size of the full-scale NiSX plant for a similar nickel production. This requirement was significantly reduced by the V10/Nicksyn trial as the scrub advance O:A phase ratio was increased to 35 compared with 4.4 for the V10 trial. Despite the reduced dilution water requirements for the V10/Nicksyn system, crud formation was minimal. Analysis of the crud also showed insignificant levels of calcium (<0.25%), indicating that it was not related to gypsum precipitation. This shows that it is possible to operate the circuit without scrubbing, but a stage would still be required to wash low levels of chloride entrainment.

A comparison of the reagent make-up for the two trials is given in Table 3. The lower reagent losses experienced with the V10/Nicksyn trial are ascribed to the lower crud levels which were achieved due to operation at a lower pH and the elimination of occasional gypsum precipitation. Furthermore, a lower V10 concentration was used in the V10/Nicksyn trial, contributing to the lower V10 loss. Importantly, the V10:Nicksyn make-up ratio closely matched the ratio maintained in the organic phase, indicating no preferential loss of either component. This confirms that the major cause of loss was due to crud formation and entrainment.

Table 3: Reagent make-up

Make-up (L/m^3)	V10	V10/Nicksyn
Diluent	1.84	1.5
V10	0.40	0.28
Nicksyn	0	0.13

TECHNO-ECONOMIC EVALUATION

The prelimary techno-economic evaluation of the V10 and V10/Nicksyn systems for the Tati BMR Commercial Refinery was based on the following assumptions:

- A commercial plant throughput and consumptions as summarized in Table 4.
- Increased Ni recoveries in NiSX using V10/Nicksyn from 99.3 to 99.8%.
- Long-term US$ exchange rate of ZAR 7.2/US$ and Ni metal price of US$ 4.5/lb.

Table 4. Commercial plant throughput and consumptions

Throughput:			V10	V10/Nicksyn
Flowrates:	PLS	m^3/h	130	122*
	Organic	m^3/h	91	170**
Reagent consumptions:	Diluent	t/a	74	138***
	V10	t/a	45	37
	Nicksyn	t/a	0	8

* Reduction in Ni PLS due to 7% decrease in scrub liquor flowrate.
** Advance organic flowrate based on 1.4 O:A ratio.
*** Higher diluent consumption for V10/Nicksyn due to increased settler area requirements with longer phase-disengagement time.

Increased diluent consumption and higher reagent costs for the Nicksyn reagent increased the NiSX plant reagent costs by 4% but improved nickel recoveries by 0.5%. Higher loading can be achieved with further optimization of the extraction pH profile, thereby lowering the advance organic flowrates and ultimately saving on reagent costs.

The capital cost for the NiSX plant was 35% higher for the V10/Nicksyn system. The higher phase-disengagement time with the V10/Nicksyn reagent doubled the settler areas. Some of the additional capital was offset against the reduction in extraction stages from 5 to 4 and the elimination of the standby extraction stage for the V10 system (the BMR plant design allowed for a standby extraction stage to cater for periods when one of the extraction stages are taken off line during descaling).

The payback on the additional capital for the V10/Nicksyn system is less than 18 months. Using a V10/Nicksyn extractant in NiSX simplifies the NiSX operation, minimizes the scaling risk, reduces pH dependency on the extraction step, and improves nickel recoveries. The long-term reagent degradation rates and impact of possible degradation products (if any) on the reagent selectivity and phase disengagement are still under investigation.

CONCLUSIONS

1. The V10/Nicksyn system has proved to be very robust, and the circuit operation was simpler than the V10 circuit. It was easy to achieve recoveries of >99.8% without co-extracting calcium.
2. The V10/Nicksyn system was operated with 4 extraction stages yielding a 0.5% increase in nickel recovery, and results showed that it was possible to drop another extractant stage and still achieve target recovery.

3. Water consumption was reduced by at least 90% by operating on the V10/Nicksyn system. Scrubbing of co-extracted elements was not required; however, a single stage was retained primarily for washing low levels of aqueous chloride entrainment.
4. Phase-disengagement time across all the stages increased with the V10/Nicksyn system, and this was a limiting factor in achieving even higher recoveries.
5. Replacing V10 with a V10/Nicksyn system increased the NiSX capital and reagent costs by 35% and 4%, respectively, but improved nickel recoveries by 0.5%. The payback on the additional capital for the commercial plant is less than 18 months.
6. Further process optimization will be carried out with a view to improving extraction nickel loading and thus yield more savings on reagent costs and further strengthen the business case for the use of Nicksyn. The long-term reagent-degradation rates and impact of the degradation products on the reagent selectivity and phase disengagement are still under investigation.

ACKNOWLEDGMENTS

The authors would like to thank the staff of Mintek and BMR who contributed to the success of the lab test work and the plant trial, respectively. We are grateful to the management of BMR and Mintek, the plant owner Norilsk Nickel Africa, and Norilsk Process Technology for providing resources and for permission to publish this paper.

REFERENCES

1. O. Kloiber, G. Johnson, C. Palmer, A. Swarts, and J. Brits, “Tati Hydrometallurgical Demonstration Plant Project,” ALTA 2005 Ni/Co, 16-18 May 2005.
2. A. C. du Preez and J. S. Preston, “Separation of Nickel and Cobalt from Magnesium and Manganese by Solvent Extraction with Synergistic Mixtures of Carboxylic Acids,” *J. S. Afr. Inst. Min. Metall.*, **104**(6), 333−338 (2004).
3. R. du Preez, M. Kotze, G. Nel, S. Donegan, and H. Masiiwa, “Solvent Extraction Test Work to Evaluate a Versatic 10/Nicksyn™ Synergistic System for Nickel-Calcium Separation,” Fourth Southern African Base Metal Conference, South African Institute of Mining and Metallurgy, Johannesburg, 2007; pp. 193−210.

SEPARATION OF COPPER, IRON AND ZINC FROM COBALT AND NICKEL WITH MIXED CYANEX 272 AND LIX 84 EXTRACTANTS

W. Zhang,[1] C.Y. Cheng,[1] M. Rodriguez,[2] and Y. Pranolo[1]

[1]*The Parker Centre / CSIRO Minerals, PO Box 7229, Karawara, WA 6152, Australia*
[2]*Minara Resources Ltd., Level 4, 30 The Esplanade, Perth, WA 6000, Australia*
Corresponding author email address: chu.cheng@csiro.au

ABSTRACT

With a mixed extractant system consisting of CYANEX 272 and LIX 84 in Shellsol D70 and an A/O ratio of 5:1 in a single contact, the separation factors of Cu, Zn, and Fe over Co and Ni reached over 3×10^5, indicating a very easy and excellent separation of Cu, Zn, and Fe from Co and Ni. In semi-continuous extraction tests at A/O ratio 5:1, the extraction of Cu, Fe, and Zn reached almost 100%, and their concentrations in the raffinate were below 0.2 mg/L (the detection limit). In a pilot-plant operation, with the plant solution from Minara Resources containing (g/L) 126 Ni, 8.1 Co, 0.17 Cu, 1.83 Zn, and 0.03 Fe, the concentrations of Cu and Fe in the raffinate were below 0.3 mg/L, from which a high-quality cobalt product containing <50 mg/L Cu and Fe could be achieved. At a wide A/O ratio range of 2 to 7, the target <0.3 mg/L Cu and Fe in the raffinate were consistently achieved. A reasonably wide operating pH window in pH control and A/O ratios was identified. The scrubbing efficiencies of cobalt and nickel, under well-controlled conditions, were >90% and >85%, respectively. The stripping efficiencies were 96−99% for copper and zinc and in the range of 50−90% for iron.

INTRODUCTION

In recent years, the Solvent Extraction (SX) Technology Group of the Parker Centre/CSIRO Minerals has developed novel synergistic and mixed extractant solvent extraction systems [1−6]. One of the systems is for the separation of Cu, Fe, and Zn from Ni and Co with mixed CYANEX 272 and LIX 84 extractants [7−8].

In Minara's Murrin Murrin operation, the solution from leaching the mixed nickel and cobalt sulfides contains small amounts of iron, copper, and zinc impurities. After iron removal by neutralization, the copper is precipitated as copper sulfide with nickel sulfide, and then the zinc is separated from cobalt and nickel in SX circuit 1 using CYANEX 272 (di(2,4,4-trimethylpentyl)phosphinic acid). The cobalt is separated from nickel in SX circuit 2, again using CYANEX 272. Due to incomplete removal of copper, the cobalt product cannot be qualified for a premium grade. Currently, no commercial SX extractant has been highly selective for the separation of Cu, Zn, and Fe from Ni and Co in a single SX circuit. The ion-exchange route is less viable due to its large capital investment and the difficulty of removing both copper and iron. Development and

commercialization of a new and highly selective extractant for this purpose would be very expensive. Therefore, the development of an effective organic system with commercially available extractants is an attractive alternative.

The development of a new organic system for upgrading the Minara cobalt product has passed batch, semicontinuous and fully-continuous tests (pilot operation) stages using plant leach solutions. The pilot-plant operation was successfully completed in May 2006 with excellent results and all project goals being achieved. This paper reports and discusses the major test results of the different development stages.

EXPERIMENTAL

Batch tests were performed in 1-2 L rectangular boxes immersed in a water bath to achieve desired temperatures. Solution pH was manually adjusted by adding dilute ammonia or sulfuric acid. The plant aqueous solution contained (g/L) 124 Ni, 10.5 Co, 0.42 Cu, 1.05 Zn and 0.2 Fe. The plant organic solution containing 20% v/v CYANEX 272 in Shellsol 2046 was stripped with 100 g/L sulfuric acid before use. The mixed organic system was made by adding LIX 84 (2-hydroxy-5-nonylacetophenone oxime) to the original Minara plant organic solution to yield an organic solution containing 15% v/v LIX 84 and 17% v/v CYANEX 272 in Shellsol 2046. Semi-continuous extraction, scrubbing and stripping tests were separately conducted using a mini rig (0.2 L mixer and 0.4 L settler) at 50 ± 2 °C to determine the best operating conditions. The loaded organic solutions in the extraction tests were used as feed for scrubbing tests and the scrubbed organic solutions as stripping feed. Fully continuous tests were carried out using mixer-settlers (0.5 L mixer and 1.2 L settler) at 50 ± 2 °C. The aqueous feed solution from Minara contained (g/L) 126 Ni, 8.1 Co, 0.17 Cu, 1.83 Zn, and 0.03 Fe. To observe the behavior of iron, technical grade $Fe_2(SO_4)_3$ was added to obtain 30 mg/L Fe in the feed solution. The pilot plant consisted of two extraction, one scrubbing and two stripping stages.

BATCH TESTS

Metal pH Isotherms

Metal pH isotherms were determined at 55 °C with A/O ratio 5:1. Compared with the organic system with CYANEX 272 extractant alone (Figure 1), the organic system with the mixed CYANEX 272 and LIX 84 extractants resulted in about a 3.5 pH_{50} shift for Cu and no observable effect on the pH_{50} of Fe and Zn (Figure 2). Over 97% Cu and Zn and 100% Fe were extracted at pH 3.5 while the co-extractions of Co and Ni were less than 2.5%. The separation factor of Zn over Co was larger than 8.8×10^3 and that of Cu over Co reached over 11×10^3, suggesting an easy and complete separation of Zn, Cu, and Fe from Co and Ni.

Metal Distribution Isotherms

Metal distribution isotherms were carried out at pH 3.5 with A/O ratios varying from 3 to 10. The Zn extraction increased with increasing A/O ratio from 79% to >99.9%

with separation factors β(Zn/Co) from 10^3 to 10^5, and the Cu extraction from 94.6% to >99.9% with β(Cu/Co) from 0.3×10^5 to 3×10^5. This range of separation factors indicates a very high selectivity for Zn and Cu over Co. At an A/O ratio of 9 and pH 3.5, only two stages of extraction are needed for achieving raffinate solution containing a few mg/L of Zn and Cu, based on the McCabe-Thiele diagrams.

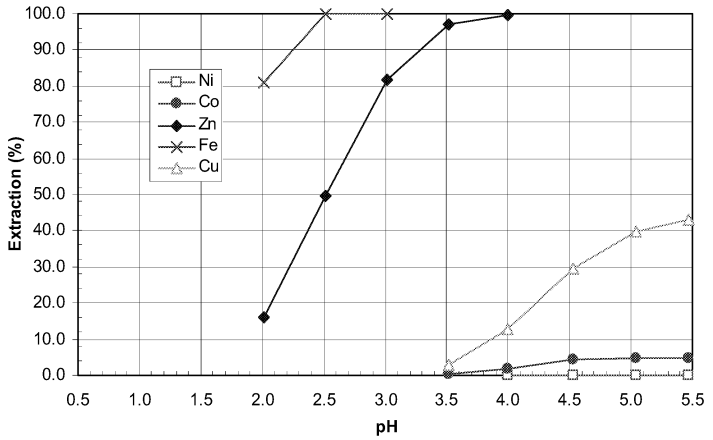

Figure 1. Metal pH isotherms with Minara CYANEX 272 organic system.

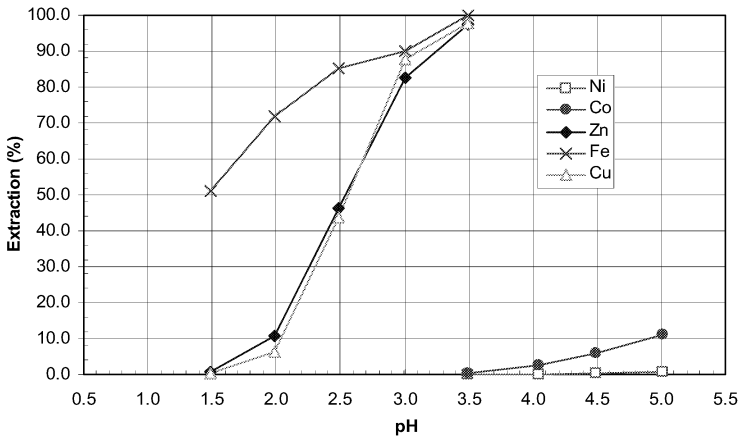

Figure 2. Metal pH isotherms with the mixed system consisting of CYANEX 272 and LIX 84.

Extraction Kinetics

Metal extraction kinetics of the mixed organic system were measured at pH 3.5 and A/O ratio of 5:1 at time intervals from 0.5 to 5 min. All iron and > 97% of Cu and Zn were extracted within 30 s, indicating fast extraction kinetics for the elements concerned.

Stripping Kinetics

The organic solution loaded at pH 3.5 and an A/O ratio of 5 was used for determination of the metal-stripping kinetics. The loaded organic solution was then stripped with 30 g/L sulfuric acid at an A/O ratio of 1:1 and 55 ˚C. More than 99% of Cu and Zn were stripped within 1 min. In comparison, the Fe stripping was slow, with only 12% Fe stripped within 2 min. With 100 g/L sulfuric acid, over 97% Fe was stripped within 2 min, indicating that an organic bleed treatment with a high acid concentration solution may be needed in a plant operation to strip the iron.

SEMI-CONTINUOUS TESTS

Semi-Continuous Extraction

The effects of pH and A/O ratios on metal extractions with two extraction stages are given in Table 1. The extractions of Cu, Zn, and Fe showed an increasing trend with increasing pH in the range of 3.3 to 3.7. However, the behaviors of metals with A/O ratios were different due to competing extractions. Copper was completely extracted at pH 3.5-3.7 and A/O ratios from 5 to 9. However, Zn extraction decreased remarkably at A/O above 7 due to limited capacity of the organic system for Zn at higher A/O ratios. Iron should be completely extracted as expected based on its pH isotherm. The incomplete Fe extraction indicated that the plant solution could contain some Fe(II) instead of Fe(III). Complete Fe extraction at pH 3.7 and an A/O ratio of 7 was achieved after addition of 30% v/v H_2O_2 to oxidize Fe(II) to Fe(III).

Table 1. Effect of pH and A/O ratios on metal extractions (%)

pH	Metal	A/O 5:1	A/O 7:1	A/O 9:1
3.3	Fe	25.2	26.7	22.8
	Cu	91.7	100.0	98.8
	Zn	79.1	82.4	73.0
	Co	0.02	0.02	0.01
	Ni	0.00	0.00	0.00
3.5	Fe	36.9	37.0	25.5
	Cu	100.0	100.0	100.0
	Zn	94.7	93.4	77.2
	Co	0.04	0.03	0.01
	Ni	0.00	0.01	0.00
3.7	Fe	82.7	58.4	34.0
	Cu	100.0	100.0	100.0
	Zn	100.0	99.4	88.4
	Co	0.25	0.05	0.02
	Ni	0.03	0.01	0.01

Overall, the optimum extraction conditions were A/O ratio 5-7 and pH 3.7 for achieving complete extraction of Zn and Cu with <0.2 mg/L (below detection limit) in the raffinate, and complete Fe extraction if all Fe(II) was oxidized to Fe(III). Co-

extraction of Ni and Co was as low as 147 and 85 mg/L, respectively, which can be easily scrubbed off in the scrubbing stage.

Semi-Continuous Scrubbing

Three semi continuous scrubbing tests were carried out at 50 ± 2 °C, pH 3.3 and A/O ratio 1:5 in a single scrubbing stage using three different scrub solutions containing Zn and Cu to scrub Ni and Co in the loaded organic. Cobalt was completely scrubbed with all three scrub solutions while about 4-6 mg/L Ni remaining in the scrubbed organic, which is less than 0.001% of Ni loss based on extraction A/O ratio of 5 and 96 g/L Ni in the feed solution.

Semi-Continuous Stripping

Three semi continuous stripping tests were carried out at 50 ± 2 °C and A/O ratio 1:5 in two stages with the pH in strip stage 1 being controlled at 1.7, 1.5, and 1.3, respectively. The best stripping results were obtained at pH 1.3 with over 99% Zn and Cu, and 60% Fe stripping efficiencies. Bulk stripping for Fe(III) was tested using 100 g/L sulfuric acid at an A/O flow-rate ratio of 1:5 with Fe stripping efficiency being 85%.

FULLY CONTINUOUS TESTS

The primary objectives of the fully continuous tests were to optimize extraction, scrubbing, and stripping conditions and to obtain operating windows for commercial plant design and operation. Less than 0.3 mg/L of Cu and Fe and 0.2-0.5 mg/L Zn in the raffinate were achieved by controlling pH above 3.7 (best between 3.7 and 4) in extraction stage 2 (Table 2). In extraction stage 1, it was key to control pH below 3.7 (best between 3.5 and 3.7) to minimize co-extraction of Ni and Co in the range of 0.04-0.1% and 0.04-1.0%, respectively. The optimum A/O ratios were in the range 4 to 7. Below A/O 4, Co co-extraction increased significantly; above A/O 7, the organic became viscous due to overloading, resulting in significant aqueous entrainment.

Table 2. Effect of pH and A/O flow ratio on extraction of metals

Element	Operating windows		Concentration (mg/L)	Extraction (%)
Cu	E2 pH: 3.7 - 4.0	A/O: 2 - 7	<0.3 in raff	>99
Fe	E2 pH: 3.7 - 4.0	A/O: 2 - 7	<0.3 in raff	>99
Zn	E2 pH: 3.7 - 4.0	A/O: 2 - 6	0.2-0.5 in raff	>99.5
Ni	E1 pH 3.5 - 3.7	A/O: 2 - 7	<200 in organic	0.04 - 0.10
Co	E1 pH 3.5 - 3.7	A/O: 4 - 7	<100 in organic	0.04 - 1.0

Scrubbing worked well with 85-90% Ni and >90% Co scrubbing efficiencies at pH 2.8-3.3 and a wide range of A/O ratios from 1:2 to 1:7. The stripping efficiency was in the range of 96 to 99% for Cu and Zn, and 50 to 90% for Fe at pH 1.2-2 in most cases. Total metals in the stripped organic recycling to the extraction was less than 200 mg/L which occupied less than 2% of the total organic capacity. Ni and Co in the loaded strip liquor were, on average, 246 mg/L and 22 mg/L, respectively, corresponding to <0.01%

Ni and <0.015% Co, respectively. With 30 mg/L Fe in the aqueous feed, only 50-100 mg/L Fe remained on the stripped organic, indicating that bleeding and bulk stripping of the organic for the loaded Fe may not be necessary in plant operations.

CONCLUSIONS

The batch, semi continuous and fully continuous test results demonstrated that the new organic system of mixed CYANEX 272 and LIX 84 extractants is suitable for the separation of Cu, Fe, and Zn from Ni and Co to upgrade the Minara Co product. The primary goal to obtain a product solution containing <0.3 mg/L Cu and Fe was achieved so that the cobalt product can be upgraded to premier grade. The system offers a wide range of operating windows in pH control and A/O ratios with very small loss of Co and Ni in the overall circuit. It is recommended to advance to a larger scale or commercial operation using the new organic system.

ACKNOWLEDGMENTS

Mr. Mark Urbani, Mr. Peter Miovski, and Mr. Russell Pennifold are acknowledged for carrying out the testwork. The authors thank Minara Resources Ltd. and CSIRO Minerals for permission to publish this paper.

REFERENCES

1. C. Y. Cheng, "SX Application for Nickel and Cobalt: Pros and Cons of Existing Processes and Possible Future Development," Proceedings ALTA SX/IX World Summit, ALTA Metallurgical Services, Perth, Australia, 2003.
2. C. Y. Cheng, "Solvent Extraction of Nickel and Cobalt with Synergistic Systems consisting of Carboxylic Acid and Aliphatic Hydroxyoxime," *Hydrometallurgy*, **84**, 109-117 (2006).
3 C. Y. Cheng and M. D. Urbani, "Purification of Laterite Leach Solutions by Direct Solvent Extraction," TMS Annual Meeting, Vol. 3, The Minerals, Metals and Materials Society, Warrendale, PA, 2003; pp. 251-265.
4. C. Y. Cheng and M. D. Urbani, "The Recovery of Nickel and Cobalt from Leach Solutions by Solvent Extraction: Process Overview, Recent Research and Development," ISEC 2005, Beijing, P. R. China, 2005; pp. 503-526.
5. C. Y. Cheng, K. B. Barnard, and M. D. Urbani, "Application of Synergistic Solvent Extraction for Metal Recovery," Proceedings ALTA 2005 Nickel/Cobalt Conference, ALTA Metallurgical Services, Perth, Australia, 2005.
6. C. Y. Cheng, K. B. Barnard, and M. D. Urbani, "Improving Plant Operation using Synergistic SX Technology and Organic Monitoring," First Extractive Metallurgy Operators' Conference, AusIMM, Brisbane, Australia, 2005; pp. 59-66.
7. C.Y. Cheng and M. D. Urbani, "Synergistic Solvent Extraction Process". WO Patent No. 2006032097, 2006.
8. C. Y. Cheng, W. Zhang, and M. Rodriguez, "Separation of Copper, Iron and Zinc from Cobalt and Nickel in Minara Process Liquor by Synergistic Solvent Extraction: Pilot Plant Operation," ALTA Ni/Co, ALTA Metallurgical Services, Perth, Australia, 2007.

INTERFACIAL TENSION AND NICKEL STRIPPING KINETICS WITH VERSATIC 10 AND LIX 63 SYNERGISTIC SYSTEMS

W. Zhang, R. Narendranathan, C.Y. Cheng, and Y. Pranolo

The Parker Centre / CSIRO Minerals, P.O. Box 7229, Karawara, WA 6152, Australia
Corresponding author email address: chu.cheng@csiro.au

ABSTRACT

The nickel stripping kinetics for synergistic organic systems containing Versatic 10 and LIX 63 are slow and significantly improved in the presence of tributylphosphate (TBP). Interfacial tension (IFT) was measured during stripping to identify any connection between the interfacial properties and the nickel stripping kinetics for various organic compositions. A typical IFT curve for the mixed organic systems as a function of stripping time was characterized by an initial rise within two minutes, when most of the loaded metal complexes were stripped into the aqueous phase, followed by a decreasing trend or levelling-off, which corresponded to a slow stripping of nickel. This indicates that IFT may be related to both amount and types of the metal-organic complexes at the interface. In comparison, there were virtually no changes in the IFT values over the whole stripping time for the systems containing Versatic 10, featuring a high IFT value, or LIX 63 alone, featuring a low IFT value, due to the fact that very little metal was loaded at pH 5.0 with the two systems. In the range of 0.5-1.0 M TBP, the IFT values decreased strongly, corresponding to a remarkable improvement in the nickel stripping kinetics. It is proposed that more TBP may be involved in the Ni-LIX 63 complexes at higher concentrations which makes the complexes more surface active and thus improves the nickel stripping kinetics.

INTRODUCTION

The Solvent Extraction Technology Group of the Parker Centre/CSIRO Minerals has developed novel synergistic solvent-extraction (SSX) systems for separation and recovery Ni and Co from leach solutions [1-2]. In the SSX system consisting of Versatic 10 and LIX® 63, the stripping kinetics of nickel are slow [3]. The presence of tributylphosphate (TBP) significantly improved the stripping kinetics. It was proposed that Versatic 10 functions as an extractant for Co with LIX 63 as the synergist, and vice versa for Ni [3]. A study by Flett et al. [4] for the system containing a hydroxyl oxime and lauric acid mixture in hexane suggested that the slow stripping rate of nickel from the organic system may be due to specific interfacial effects. The slow stripping of nickel could be related to the formation of hydrophobic Ni-LIX 63 complexes that limit the reaction rate at the interface. It is well known that the interfacial tension (IFT) can be used for estimation of equilibrium concentrations of the organic components at the

interface for a well-defined organic system. Several isotherms have been established, including the Gibbs, the Langmuir-Gibbs, the Szyszkowski, the Frumkin, and Temkin isotherms [5-7]. However, due to the complex nature of the current organic system involving two extractants and TBP modifier under dynamic conditions in stripping, an initial investigation focused only on the measurement of IFT in stripping from the organic systems consisting of different concentrations of Versatic 10, LIX 63, and TBP in Shellsol® D70. The aim of this study was to identify any connection between the behavior of nickel stripping and the interfacial properties of the above organic system and the effect of TBP on IFT and Ni stripping kinetics.

EXPERIMENTAL

A synthetic nickel laterite leach solution containing (g/L) Ni 3, Co 0.3, Cu and Zn 0.2, Mn 2.0, Mg 10, and Ca 0.5 was used for loading the organic solution at 30 ± 1 °C and pH 5. All the metals in the aqueous samples and the stripped liquor were assayed by inductively coupled plasma atomic emission spectroscopy. The strip solution used for the stripping kinetic study contained 5 g/L Ni and 10 g/L sulfuric acid. Prior to each test, the strip solution and the loaded organic solution were preheated separately in a water bath to a desired temperature. Keeping the aqueous solution stirred, the organic solution was poured in and timing started. The stirring stopped at a specified time, and the two phases were separated and centrifuged to remove any entrainment. The aqueous solution and then the organic solution were poured into a dish with a water jacket. The IFT measurement started immediately using a DuNuoy ring interfacial tensiometer. Each measurement was duplicated, and a correction factor for the densities of the liquids and the diameter of the ring was applied accordingly [8].

RESULTS AND DISCUSSION

Effect of TBP Concentration

The metal stripping kinetics from the loaded organic solutions without TBP and with 1.0 M TBP are compared in Figure 1. The presence of TBP significantly improved the Ni stripping kinetics. The variations of IFT with stripping time at different TBP concentrations are shown in Figure 2a. A typical IFT curve at a fixed TBP concentration is characterized by an initial rise (one IFT unit) within 2 min. followed by a decreasing trend or levelling off. The initial rises in IFT corresponded to the period when most of the loaded metals except for nickel were stripped into the aqueous phase, suggesting that the IFT values measured reflect the changes in the amount of the metal-organic complexes at the interface. An increase in IFT with a decreased population of the complexes at the interface indicates that these metal-organic complexes are more surface active. This agrees with the observation by Staszak and Prochaska [5] for Cu(II) complexes with hydroxyoxime chelating ligands under equilibrium conditions. The loaded nickel was only partially stripped within 2 min. The decreasing trends with an extension of stripping time (Figure 2a) appears to resemble the stripping curves of Cu and Zn (Figure 1a and 1b) rather than to reflect the slow stripping behavior of nickel.

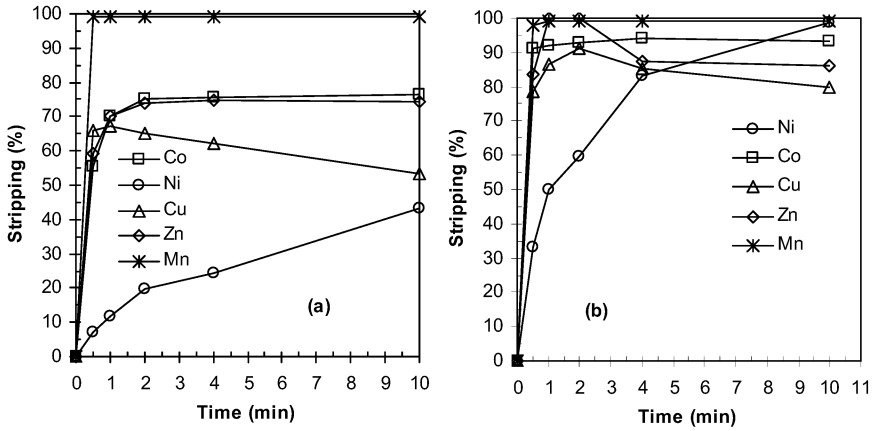

Figure 1. Comparison of the metal stripping kinetics from the loaded 0.5 M Versatic 10/0.5 M LIX 63 in Shelsol D70 without TBP (a) and with 1.0 M TBP (b) at 30 °C.

The effect of the TBP concentration on IFT can be clearly seen in Figure 2b. The IFT values generally increased by about one IFT unit with increasing TBP concentrations up to 0.5 M and then decreased rapidly (by >2.5 IFT units) with further increase in TBP concentrations from 0.5 to 1.0 M. This marked decrease in IFT coincidentally corresponded to a significant improvement in the nickel stripping kinetics.

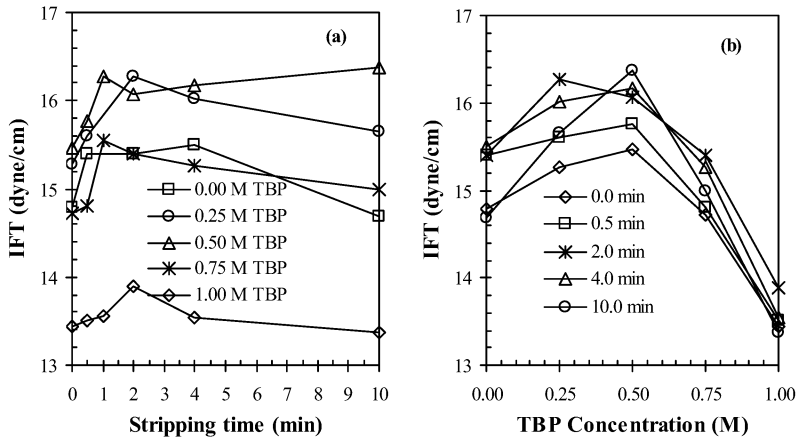

Figure 2. Variations of IFT with stripping time and TBP concentration during the stripping from the loaded organic systems containing 0.5 M Versatic 10/0.5 M LIX 63/0-1.0 M TBP.

Effect of Versatic 10 Concentration

The variations of IFT with stripping time from the loaded organic system containing different concentrations of Versatic 10 (0-1 M) are shown in Figure 3a. It is interesting to note that there is virtually no initial rise in the IFT for the system containing 0.5 M of each LIX 63 and TBP without Versatic 10 (Figure 3a) due to the fact that only small amounts of metals (mainly Cu) would be loaded at pH 5 and thus fewer

metal complexes formed based on the metal pH isotherms obtained in the previous studies [3]. This observation supports the view that the initial rises in the IFT actually corresponded to the amount of metal complexes at the interface.

The effect of Versatic 10 concentration on the IFT is shown in Figure 3b. It clearly shows that the IFT values increased almost linearly by more than 4 IFT units with increasing Versatic 10 up to 0.5 M and then levelled off. Since the IFT reflected the interfacial concentrations of the metal-extractant complexes, the big changes in the IFT suggest that the complexes involving Versatic 10 may dominate in the interface. The levelling-off effect at higher Versatic 10 concentrations may be related to the formation of Versatic 10 dimers.

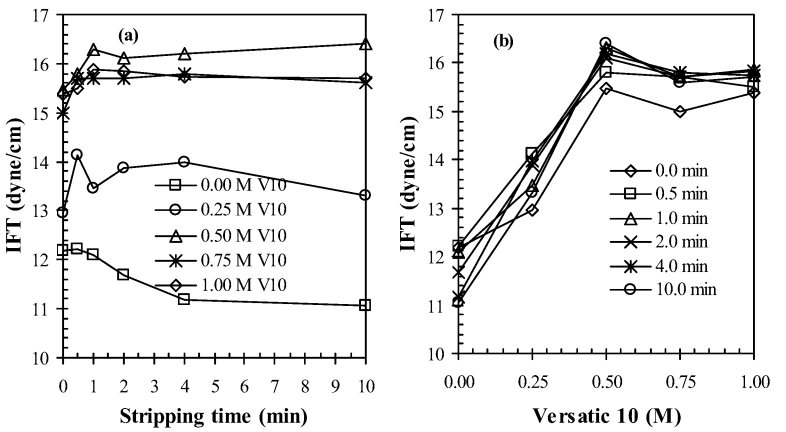

Figure 3. Variations of IFT with stripping time and Versatic 10 concentration during stripping from the loaded organic system containing 0-1.0 M Versatic 10/0.5 M LIX 63/0.5 M TBP.

Effect of LIX 63 Concentration

The variations of IFT with stripping time for the loaded organic system containing different concentrations of LIX 63 are shown in Figure 4a. The IFT curves in Figure 4a, which are similar to previous IFT curves, are again observed with an exception for the organic system containing only 0.5 M of each Versatic 10 and TBP without LIX 63 which showed an almost constant IFT value over the whole stripping period due to little metal loading [3].

In contrast to the effect of Versatic 10 concentrations, an increase in LIX 63 from 0.0 M to 0.25 M resulted in a decrease in IFT by more than 4 IFT units and then fluctuated at 0.5 M with a general decreasing trend as the LIX 63 concentrations increased further to 1.0 M (Figure 4b). These changes in IFT could be related to the formation of different metal-extractant complexes, particularly Ni-LIX 63 complexes. The variations of IFT with higher LIX 63 concentrations could be due to the formation of LIX 63 dimers and synergistic mix of reagents consisting of bifunctional bonding to metal by two LIX reagents or combination with TBP and Versatic 10 reagents.

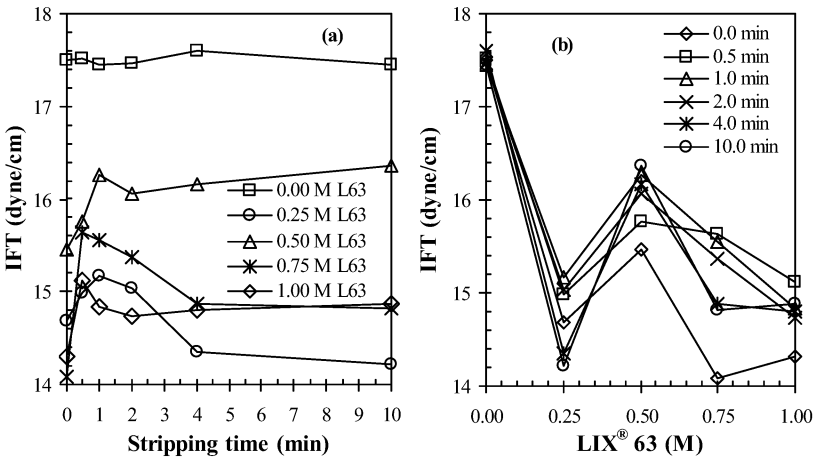

Figure 4. Variations of IFT with stripping time and LIX 63 concentration during the stripping from the loaded organic system containing 0.5 M Versatic 10/0 - 1 M LIX 63/0.5 M TBP.

Comparison of the Effects of Versatic 10, LIX 63, and TBP

The above results suggest that the measured IFT values could be related to the activities of the extractants, the types and amounts of metal-organic complexes at the interface. With the organic system containing 0.5 M LIX 63 alone, without Versatic 10 (Figure 4a), the average IFT value is about 12 dyne/cm compared to 17.5 dyne/cm for the organic system containing 0.5 M Versatic 10 extractant alone, without LIX 63 (Figure 3a). In the absence of TBP, the IFT of the organic system containing equal 0.5 M Versatic 10 and LIX 63 was about 15 dyne/cm, which is very close to the mean IFT values (14.75 dyne/cm) of the first two systems. With 0.5 M TBP in the mixed system, the average IFT value rose to about 16 dyne/cm, suggesting that TBP at lower concentrations may be more involved in metal-Versatic 10 complexes. With a further increase in TBP to 1 M, the averaged IFT falls to 13.5 dyne/cm, suggesting that more TBP at higher concentration may be involved in Ni-LIX 63 complexes and make the complexes more surface active and thus improve the stripping kinetics.

CONCLUSIONS AND RECOMMENDATIONS

The measured IFT during the stripping may reflect the amount and type of metal-organic complexes distributed at the interface. The presence of TBP at lower concentrations in the range of 0-0.5 M resulted in virtually no increase in IFT values. The IFT value decreased with higher TBP concentrations in the range of 0.5-1.0 M. The degree of the change deceased in the presence of excess of either LIX 63 or Versatic 10. This may be related to the capacity of LIX 63 and Versatic 10 to form dimers while TBP does not. The synergistic system appears to be quite complex. A fundamental study on the metal-organic complexes and synergistic mixed reagent species is recommended for better understanding the mechanism of the improved stripping kinetics in the presence of TBP.

ACKNOWLEDGMENTS

The authors thank Dr. Keith Barnard for his assistance in using the tensiometer and Dr. Matthew Jeffery for reviewing this paper and providing valuable comment.

REFERENCES

1. C. Y. Cheng and M. D. Urbani, "Solvent Extraction Process for Separation of Cobalt and/or Manganese from Impurities in Leach Ssolutions," International Patent Publication No. WO 2005/073415.
2. C. Y. Cheng and M. D. Urbani, "Solvent Extraction Process for Separation of Cobalt and/or Nickel from Impurities in Leach Solutions," International Patent Publication No. WO 2005/073416.
3. C. Y. Cheng, "Solvent Extraction of Nickel and Cobalt with Synergistic Systems consisting of Carboxylic Acid and Aliphatic Hydroxyoximes," *Hydrometallurgy*, **84**, 109-117 (2006).
4. D. S. Flett, M. Cox, and J. D. Heels, "Extraction of Nickel by a Hydroxyloxime/ Carboxylic Acid Mixture," International Solvent Extraction Conference (ISEC 74), A. Naylor, Ed., Lyon, France, 1974; pp. 2560-2575.
5. K. Staszak and K. Prochaska, "Interfacial Activity of Copper(II) Complexes with Chelating Ligands and Individual Hydrophobic Extractants in Model Extraction Systems I. Study of Equilibrium Interfacial Tension at the Hydrocarbon/Water Interface for Systems with Copper(II) Complexes with Chelating Ligands and Individual Hydrophobic Extractants," *Journal of Colloid and Interface Science*, **280**, 184-191 (2004).
6. H. Freiser, "Metal Complexation at the Liquid-Liquid Interface," *Chemical Review*, **88**, 611-616 (1988).
7. J. Szymanowski, Hydroxyoximes and Copper Hydrometallurgy, CRC Press, London, 1993.
8. H. H. Zuidema and G. W. Waters, "Ring Determination of Interfacial Tension," *Industrial and Engineering Chemistry*, *Analytical Edition*, **13** (5) 312-313 (1941).

CHARACTERIZATION AND DISSOLUTION OF HYBRID ELECTRIC VEHICLE (HEV) NiMH BATTERIES FOR THE DEVELOPMENT OF A HYDROMETALLURGICAL RECYCLING METHOD

Kristian Larsson,[1] Christian Ekberg,[1] and Gunnar Skarnemark[2]

[1]Industrial Materials Recycling. [2]Nuclear Chemistry, Department of Chemical and Biological Engineering, Chalmers University of Technology, 412 96 Göteborg, Sweden
Corresponding author email address: kristian.larsson@chalmers.se

ABSTRACT

This paper deals with a study of the chemistry behind and the development of a hydrometallurgical method specifically targeted to recycle Hybrid Electric Vehicle (HEV) type NiMH batteries. The batteries are characterized through ICP-OES, SEM, and XRD to determine phases and metal content. Different dissolution techniques are utilized and their respective effect on the subsequent solvent extraction process is discussed. Thus the selection of dissolution method is closely linked to the extraction and the selective stripping of the metals.

INTRODUCTION

There are a large number of Hybrid Electric Vehicles (HEV) with nickel metal hydride batteries (NiMH), which will need an effective recycling process, preferably with a strong environmental perspective minimizing waste in the process. With rising metal prices, stronger legislation concerning waste, and increasing public awareness of environmental issues, manufacturers of these products will need well-developed recycling methods.

The main body of this paper will deal with better characterizing the starting material. The principal element in the batteries is Ni with lesser amounts of Co, Mn, Al, Zn and Y (which are added to change the properties of the battery). The hydrogen absorbing alloy consists of a mix of lanthanides (La, Ce, Nd, Pr) and Ni. Earlier work in the literature includes dissolution of the electrode materials and suggested paths for solvent extraction for some different NiMH battery types [1-6].

The anode material is often not separated in suggested processes for recycling, because it can be difficult, but the quantity and uniformity of HEV batteries when they can be gathered from a single source in large numbers makes the separation of constituents feasible. There is also the question of how the material should be handled, either through regeneration as in work by Wang *et al.* [7] or by recycling the material into pure metals. However, as the development of batteries continues, the interest in reusing the alloy diminishes (especially with the current focus on Li-ion batteries).

The object of this study is also to make the metals used in these batteries available for other uses, so the recycling process should produce pure metal products. To minimize the secondary wastes from a potential process, all materials in the batteries should be considered for recycling.

EXPERIMENTAL

Mechanical Separation

Panasonic Prismatic 6.5 Ah NiMH Module 7.2 V batteries (plastic casing) for HEVs were used in the experiments. The batteries were discharged with a constant current down to a low voltage, and then the top of the plastic casing was cut open and the six cells of the battery removed (see Figure 1). The electrodes are rectangular and attached to steel side plates alternating between anode and cathode plates. Cutting the side plates off separated the individual electrode plates. A polymer separator covered the cathode plates and thereby protected the plates from contaminating each other.

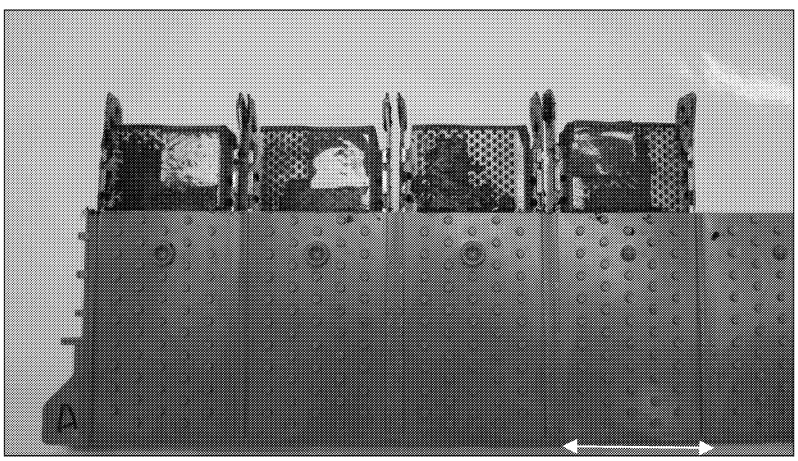

Figure 1. A HEV battery with opened plastic casing showing four cells.

The experiments were performed on samples that were washed with distilled water and dried at 50 ºC to remove the electrolyte (KOH). The anode paste material was removed by twisting the plate and lightly scraping the surface (the active material was fairly brittle when dry). The cathode material is pasted to a mesh substrate. Removal of this material from the mesh is difficult with a mechanical process.

Individual cells weighed 150 g and consisted of 13 cathode and 14 anode electrodes, which had a dry weight on average of 3.83 g and 3.60 g, respectively.

X-ray Powder Diffraction (XRD)

A Siemens D5000 diffractometer employing a Cu K_α source and a scintillation detector was used to determine the phases of the anode and cathode materials, using a step

size of 0.05 degrees. The JCPDS-ICDD database [8] was used to identify phases. The method was used to gain qualitative information (as there was mainly one large phase present).

Scanning Electron Microscopy (SEM)

A FEI Quanta 200 ESEM FEG was used with an Oxford Inca 300 Energy Dispersive X-ray (EDX) system for chemical analysis. Images were taken mainly with 15 kV operating voltage in high vacuum mode. No sample preparation was necessary.

Digestion and Chemical Analysis

Aqua regia (one part conc. HNO_3, three parts conc. HCl) was used for total dissolution of the samples. The different parameters of interest were the acid-to-solid ratio, the temperature, the digestion time, and the concentration of the added acid.

A Thermo iCAP 6500 Inductively Coupled Plasma Optical Emission Spectrometer (ICP-OES) was used to determine the elemental composition of the digestion solutions.

RESULTS AND DISCUSSION

X-ray Powder Diffraction (XRD)

The XRD results shown in Figures 2 and 3 differed slightly from reported diffractograms of other NiMH batteries [2,9]. There was no metallic nickel or NiO detected in the cathode powder after it had been removed from the supporting mesh. The hydrogen absorbing alloy of the anode was identified as being of the $LaNi_5$ type with substitutions of the La with different lanthanides and substitutions of Ni with Co, Al, and Mn. The different combinations of substitutions gives very similar diffractograms, so the exact alloy could not determined by XRD alone, but the chemical analysis was more indicative. Figures 2 and 3 show that the starting material is very homogeneous.

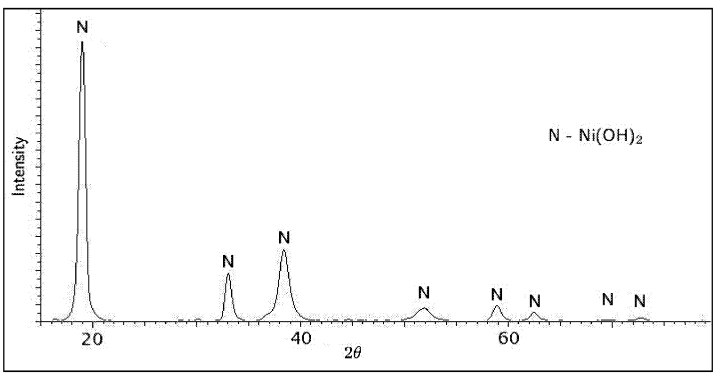

Figure 2. Cathode material diffractogram.

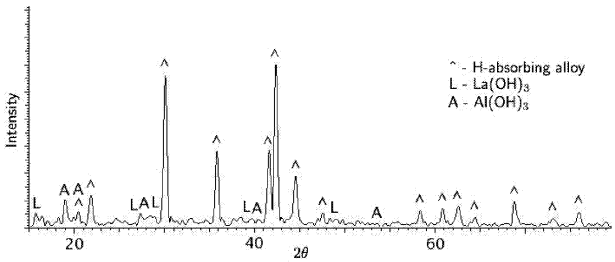

Figure 3. Anode material diffractogram.

Scanning Electron Microscopy (SEM)

The advantage of SEM is that the elemental composition of the material can be observed as well as the microstructure, and the size of individual particles can be estimated.

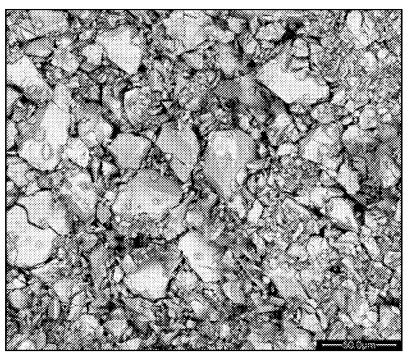

Figure 4. SEM image of anode material.

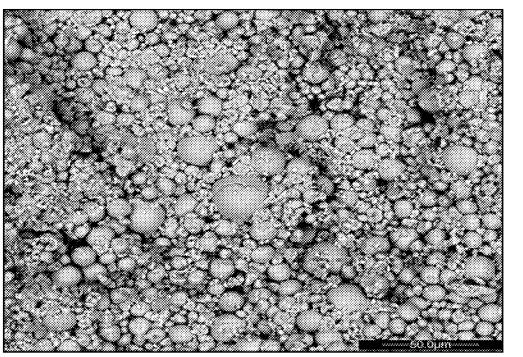

Figure 5. SEM image of cathode material.

Figure 4 shows how the surface of the anode active material has particles of varying sizes with angular and more irregular shapes. This contrasts with Figure 5, an image of the cathode material showing $Ni(OH)_2$ spheres embedded amongst smaller particles that are generally shards of broken spheres or irregular particles with a higher content of cobalt or yttrium. These aspects can influence the dissolution behaviour.

Dissolution and Solvent Extraction

Total Dissolution

The results of the aqua regia dissolutions (20 ºC, 10:1(cathode), 30:1(anode) liquid:solid) are shown in Table 1. The cathode dissolution includes the nickel metal substrate.

Table 1. Total dissolution (% of total content), 3 days

	Ni	Co	Mn	Al	Y	Zn	La	Ce	Nd	Pr
Anode	55.9	5.1	5.6	2.5	0.8	0.14	20	8.2	0.75	0.48
Cathode	88.7	5.6	0.3	0.1	0.6	3.10	-	-	-	-

Anode Dissolution

Leaching the anode alloy in 0.25 M HCl (20 ºC, 15:1 liquid:solid) (Table 2) gave low nickel dissolution but high yields for the lanthanide and yttrium content and some cobalt leaching. Interestingly the Ni, Al, and Zn content in the solution decreases with time, probably due to precipitation when the pH increases in the solution as a result of the dissolution reactions.

Table 2. Selective leaching of anode (% of each element), 0.25M HCl

	Ni	Co	Mn	Al	Y	Zn	La	Ce	Nd	Pr
18h	5.3	23.4	36.0	5.1	50.1	7.1	38.4	38.7	35.8	37.0
166h	2.4	26.0	50.8	1.9	68.6	2.2	54.4	56.5	52.7	53.7

Solvent Extraction from Total-Dissolution Liquor

In the literature, there are a few studies dealing with extracting different metals from complete-dissolution liquors. Zhang *et al.* [6] used D2EHPA in kerosene for separating the lanthanides from Ni and Co that were separated with trioctylamine in kerosene. In later work [10], CYANEX 272 was used for the separation of Ni and Co. The metals were precipitated with oxalic acid, achieving a purity of 99.8% for nickel and 99.6% for cobalt. Pietrelli *et al.* [4] precipitated the lanthanide content as sodium lanthanide double sulphate salts.

Solvent Extraction from Selective-Dissolution Liquor

The cathode material can be leached in acidic or basic media [2], but the main interest is what form is the best for separating the Zn and Co from Ni. The conditions should be such that the substrate mesh is not dissolved, as it is relatively pure Ni and need not be dissolved with the nickel hydroxide. The most important separation in the resulting liquor is of Ni and Co, which is studied to some extent in the literature [5, 10-12].

The lanthanides in the anode material can be separated during the leaching process as shown in Table 2 and then the elements in the resulting solution, mainly Mn, Y, Co, and lanthanides, can be separated by precipitation or liquid-liquid extraction. By actively controlling pH of the solution, the dissolution of Ni, Al, and Zn could potentially be reduced, which would lead to one less separation step compared to total dissolution, as the separation of lanthanides with D2EHPA could be avoided. The remaining material could be handled in a scheme similar to that for the total dissolution treatment route.

CONCLUSIONS

The anode material primarily consists of 55.9% Ni, 5.6% Mn, 5.1% Co, 2.5% Al, 0.8% Y, 20% La, 8.2% Ce, 0.75% Nd, and 0.48% Pr as shown by aqua-regia dissolution and ICP-OES determination. This is mainly a metal hydride alloy as shown by the XRD measurements. Aqua-regia dissolution of the cathode material gave a composition of 88.7% Ni, 0.3% Mn, 5.6% Co, 0.6% Y, 3.1% Zn, and 0.1% Al. The cathode material is mainly $Ni(OH)_2$.

Stepwise dissolution for the anode material is a possibility when considering the total process of recycling HEV NiMH batteries. The characterization and dissolution of HEV

NiMH batteries indicates that dissolving the cathode and anode material separately can be beneficial as they have different dissolution behavior, and a separation can be achieved by leaching of the anode material. Therefore, the complexity and cost of separations could potentially be reduced using selective dissolution as compared to the total dissolution option. Future work will concern developing the method further.

ACKNOWLEDGMENTS

We would like to acknowledge the economical support from Stena Metall AB and our appreciation of the support from the team at Nuclear Chemistry at Chalmers.

REFERENCES

1. D. P. Mantuano, G. Dorella, R. C. A. Elias, and M. B. Mansur, "Analysis of a Hydrometallurgical Route to Recover Base Metals from Spent Rechargeable Batteries by Liquid-Liquid Extraction with Cyanex 272," *J. Power Sources*, **159**(2), 1510-1518 (2006).
2. M. Miyake and M. Maeda, "Dissolution of Nickel Hydroxide in Ammoniacal Aqueous Solutions," *Metallurgical and Materials Transactions B*, **37**(2), 181-188 (2006).
3. L. Pietrelli, B. Bellomo, D. Fontana, and M. Montereali, "Characterization and Leaching of NiCd and NiMH Spent Batteries for the Recovery of Metals," *Waste Management*, **25**(2), 221-226 (2005).
4. L. Pietrelli, B. Bellomo, D. Fontana, and M. R. Montereali, "Rare Earths Recovery from NiMH Spent Batteries," *Hydrometallurgy*, **66**(1-3), 135-139 (2002).
5. N. Tzanetakis and K. Scott, "Recycling of Nickel-Metal Hydride Batteries. I: Dissolution and Solvent Extraction of Metals," *J. Chem. Tech. and Biotech.*, **79**(9), 919-926 (2004).
6. P. Zhang, T. Yokoyama, O. Itabashi, Y. Wakui, T.M. Suzuki, and K. Inoue, "Hydrometallurgical Process for Recovery of Metal Values from Spent Nickel-Metal Hydride Secondary Batteries," *Hydrometallurgy*, **50**(1), 61-75 (1998).
7. R. Wang, J. Yan, Z. Zhou, X. Gao, D. Song, and Z. Zhou, "Regeneration of Hydrogen Storage Alloy in Spent Nickel-Metal Hydride Batteries," *J. Alloys and Comp.*, **336**(1-2), 237-241 (2002).
8. *Powder Diffraction File*, Joint Committee of Powder Diffraction Standards – International Center for Diffraction Data.
9. D. A. Bertuol, A. M. Bernardes, and J. A. S. Tenorio, "Spent NiMH Batteries: Characterization and Metal Recovery through Mechanical Processing," *J. Power Sources*, **160**(2), 1465-1470 (2006).
10. P. Zhang, T. Yokoyama, O. Itabashi, Y. Wakui, T. M. Suzuki, and K. Inoue, "Recovery of Metal Values from Spent Nickel-Metal Hydride Rechargeable Batteries," *J. Power Sources*, **77**(2), 116-122 (1999).
11. D. Darvishi, D. F. Haghshenas, E. K. Alamdari, S. K. Sadrnezhaad, and M. Halali, "Synergistic Effect of Cyanex 272 and Cyanex 302 on Separation of Cobalt and Nickel by D2EHPA," *Hydrometallurgy*, **77**(3-4), 227-238 (2005).
12. K. Sarangi, B. R. Reddy, and R. P. Das, "Extraction Studies of Cobalt (II) and Nickel (II) from Chloride Solutions using Na-Cyanex 272. Separation of Co(II)/Ni(II) by the Sodium Salts of D2EHPA, PC88A and Cyanex 272 and their Mixtures," *Hydrometallurgy*, **52**(3), 253-265 (1999).

LIFE-EXTENSION OF ELECTROLESS NICKEL PLATING BATH BY REMOVING PHOSPHITE IONS WITH AMINE EXTRACTANT

Mikiya Tanaka,[1] Hirokazu Narita,[1] Yumiko Sato,[1] and Yukinori Saiki[2]

[1]National Institute of Advanced Industrial Science and Technology (AIST), 16-1 Onogawa, Tsukuba, Ibaraki 305-8569, Japan. [2]Japan Kanigen Co., Ltd., 1-35-11 Miyagi, Adachi, Tokyo 120-0047, Japan.
Corresponding author email address: mky-tanaka@aist.go.jp

ABSTRACT

During electroless nickel plating, the bath is repeatedly used by supplying nickel ion and hypophosphite ion as a reducing reagent. With increasing repetition, however, phosphite ion, formed by the oxidation of the hypophosphite ion, accumulates in the bath, which causes deterioration of the plating performance. In order to reduce the emission from the plating plants, a bath life-extension process is proposed in which the removal of the phosphite ion and the supply of the hypophosphite ion are simultaneously done. The results of the initial feasibility study using di(2-ethylhexyl)amine are presented.

INTRODUCTION

Electroless nickel plating is an indispensable surface-finishing technology in fields such as the automobile and electronic industries [1]. During the electroless nickel plating operation, the plating bath is repeatedly used by supplying nickel ion and hypophosphite ion as a reducing agent. With increasing repetition, however, the plating performance is degraded because of the accumulation of the phosphite ion formed by the oxidation of hypophosphite ion. The plating bath is therefore discarded when the phosphite ion concentration exceeds 1 kmol m^{-3}.

In order to reduce emissions from plating plants, a recycling process is proposed in which nickel in the spent bath is recovered as nickel sulfate solution using solvent extraction and reused in the plating process [2-3].

Another approach to reduce the emission is to extend the bath life [4]. The most effective method to realize this would be to remove phosphite ion from the bath. Amine extractants can extract undissociated acids and thus extract phosphite ion as undissociated phosphorous acid at a sufficiently low pH region. Kawano *et al.* [5] proposed a process in which phosphorous compounds and organic acids in the electroless nickel plating bath were removed using solvent extraction. Although this process was proposed mainly for the removal of the phosphorous compounds and organic acids in the spent bath, they claimed that the process is also applicable to the bath before disposal in

order to extend its lifetime. In this case, however, the decrease in the concentrations of the valuable components due to dilution and the accumulation of the sulfate ion are unavoidable, because a large amount of sulfuric acid must be added for the pH adjustment.

In the present study, a bath life-extension process is proposed in which the removal of phosphite and the supply of hypophosphite are simultaneously done.

PROCESS DESCRIPTION

A conceptual diagram for the bath life-extension process is shown in Figure 1. Initially, free amine is mixed with hypophosphorous acid in order to form amine hypophosphite (acid treatment). The amine hypophosphite is then mixed with the plating bath in order to extract phosphite ion, which is present in the bath in high quantity and at the same time to allow the organic phase to release hypophosphite ion (extraction). The formed amine phosphite is finally mixed with sodium hydroxide in order to regenerate the free amine (stripping).

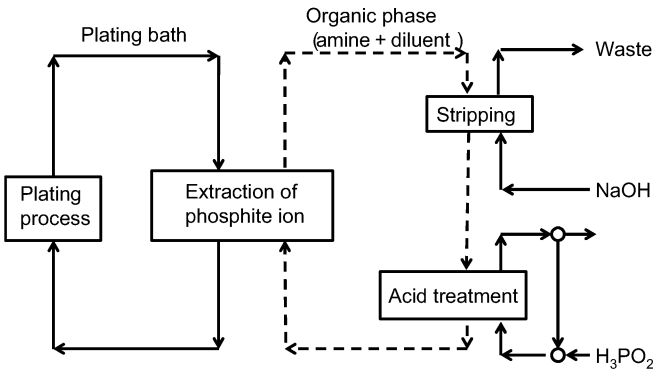

Figure 1. Conceptual diagram for the bath life-extension process using phosphite removal.

In the actual process, coexisting organic acid anions and sulfate ion in the bath are also extracted to some extent, and these ions are transferred to the aqueous phase during the stripping stage.

EXPERIMENTAL METHOD

A model bath with pH 4.8 was prepared from analytical-grade reagents so that its composition became close to that of the real bath. The composition and the pH of the model bath are shown in Table 1.

Table 1. Composition of the model spent bath

Component	Conc./kmol m^{-3}	Component	Conc./kmol m^{-3}
Na_2SO_4	0.35	Na_2HPO_3	0.70
$NiSO_4$	0.078	Lactic Acid	0.30
NaH_2PO_2	0.24	H_2SO_4	0.20

The organic phase was prepared by dissolving the specified amount of di(2-ethylhexyl)amine (DEHA) (Tokyo Kasei, purity > 98%) into butyl acetate (Wako).

Equal volumes of the aqueous and organic phases were poured into a separatory funnel and vigorously shaken for 10 min by a shaker at room temperature (297 K) in order to attain equilibrium. Two phases were then allowed to settle and were separated.

The concentrations of hypophosphite and phosphite were determined by iodometry, while that of lactate was done by capillary electrophoresis. Sulfate was determined by ICP-AES.

RESULTS AND DISCUSSION

Figure 2 shows the relationship between the initial aqueous hypophosphorous acid concentration, $C(H_3PO_2)_{init}$, and the equilibrium organic hypophosphorous acid concentration, $C(\overline{H_3PO_2})$, where C and the overbar denote the molar concentration and the organic phase, respectively. This figure indicates that it is possible to form a desired concentration of amine hypophosphite by adjusting $C(H_3PO_2)_{init}$.

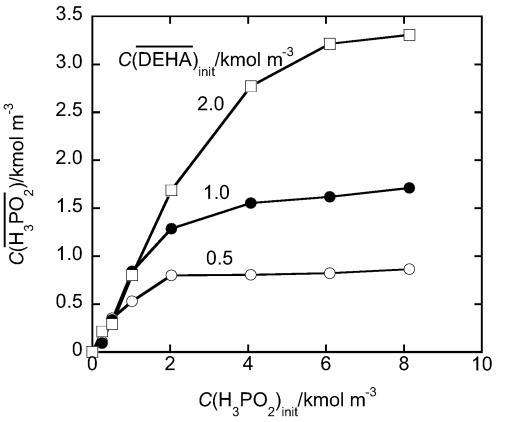

Figure 2. Relationship between $C(H_3PO_2)_{init}$ and $C(\overline{H_3PO_2})$ for the acid treatment.

The molar ratio, $C(\overline{H_3PO_2})/C(\overline{DEHA})_{init}$, was 1.7 regardless of the initial DEHA concentration when the initial hypophosphorous acid concentration was sufficiently high. This suggests that the hypophosphorous acid extraction with DEHA in butyl acetate is expressed by the following two equations:

$$\overline{DEHA} + H_3PO_2 \rightleftharpoons \overline{DEHA \cdot H_3PO_2} \quad (1)$$

$$\overline{DEHA \cdot H_3PO_2} + H_3PO_2 \rightleftharpoons \overline{DEHA \cdot (H_3PO_2)_2} \quad (2)$$

This result is in agreement with the previous one for hypophosphorous acid extraction with trioctylamine dissolved in toluene [6].

The organic phases formed in the experiment of Figure 2 were mixed with the model bath. Figure 3 shows the relationship between $C(H_3PO_2)_{init}$ in the acid treatment and the percentage extraction of phosphite ion. When the initial DEHA concentrations were 1 and 2 kmol m^{-3}, more than 30% and 53% of the phosphite ions were extracted, respectively.

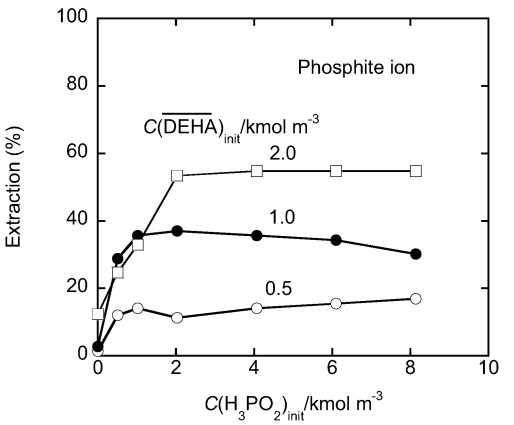

Figure 3. Relationship between $C(H_3PO_2)_{init}$ in the acid treatment and the percentage extraction of phosphite ion from the model spent bath.

Figure 4 shows the relationship between $C(H_3PO_2)_{init}$ in the acid treatment and the percentage extraction of lactate ion. In the region in which $C(H_3PO_2)_{init}$ > 2 kmol m^{-3}, when the concentration of DEHA was 1 and 2 kmol m^{-3}, 50-60% and 60-75% of the lactate ions were extracted, respectively. Because lactate was added as a complexant in order to stabilize the bath, the loss of lactate is undesirable. If the overall merit due to the bath life extension becomes greater, however, such a loss would be acceptable.

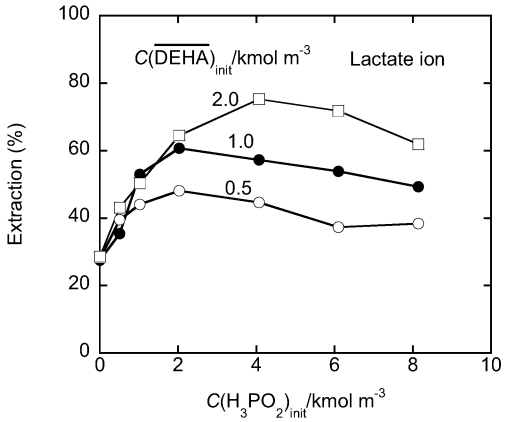

Figure 4. Relationship between $C(H_3PO_2)_{init}$ in the acid treatment and the percentage extraction of lactate ion from the model spent bath.

Figure 5 shows the relationship between $C(H_3PO_2)_{init}$ in the acid treatment and the percentage extraction of sulfate ion. The percentage extraction, which was less than 20% at a DEHA concentration lower than 1 kmol m^{-3}, markedly increased to 49% at a DEHA concentration of 2 kmol m^{-3}. Sulfate ion accumulates in the bath because nickel ion is supplied as nickel sulfate during the repeated use of the bath, which tends to result in Glauber's salt deposition. In this sense, the extraction of sulfate ion is favorable.

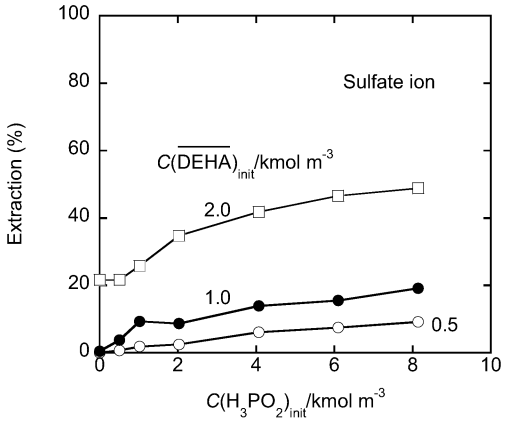

Figure 5. Relationship between $C(H_3PO_2)_{init}$ in the acid treatment and the percentage extraction of sulfate ion from the model spent bath.

Figure 6 shows the relationship between $C(H_3PO_2)_{init}$ in the acid treatment and the hypophosphite concentration in the aqueous phase after extraction, C(hypophosphite). The dotted line denotes the hypophosphite concentration in the initial model bath. The hypophosphite concentrations were significantly increased after the extraction, which indicated that the hypophosphite ion was released into the aqueous phase during the extraction.

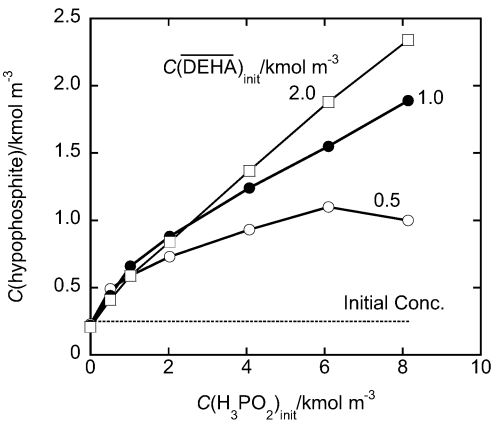

Figure 6. Relationship between $C(H_3PO_2)_{init}$ in the acid treatment and C(hypophosphite) for extraction from the model spent bath.

Table 2 shows the results of a stripping test from 2 kmol m^{-3} DEHA using 2, 3, and 4 kmol m^{-3} sodium hydroxide solutions. Stripping of phosphite and hypophosphite ions was complete regardless of C(NaOH), while that of lactate ion was complete when C(NaOH) ≥ 3 kmol m^{-3}.

Table 2. Stripping of anions with sodium hydroxide solution using 2 kmol m^{-3} DEHA

C(NaOH)/kmol m^{-3}	Stripping (%)			pH after stripping
	Phophite	Hypophosphite	Lactate	
2	100	100	69	7.4
3	100	100	100	13.6
4	100	100	100	14.0
$C(\overline{\text{anion}})_{\text{init}}$ /kmol m^{-3}	0.27	0.95	0.15	

CONCLUSIONS

A bath life-extension process has been proposed that removes phosphite ion from the electroless nickel plating bath and simultaneously supplies hypophosphite ion to the bath using an amine extractant. Initial experimental results have confirmed its feasibility, although the operation conditions should be optimized in order to obtain a higher removal efficiency of phosphite ion and the appropriate hypophosphite concentration in the extraction raffinate.

REFERENCES

1. R. E. Miller, “Trends in the Electroless Nickel Industry,” *Plating & Surface Finishing*, **74**(12), 52−56 (1987).
2. M. Tanaka, M. Kobayashi, and T. Seki, “Recovery of Nickel from Spent Electroless Nickel Plating Baths by Solvent Extraction,” Proceedings ISEC 2002, South African Institute of Mining and Metallurgy, Johannesburg, South Africa, 2002; pp. 787−792.
3. M. Tanaka, H. Narita, and Y. Sato, “Improvement of the Extraction and Stripping Rates of Nickel in the Solvent Extraction System with LIX 84I,” *Metall. Rev. MMIJ*, **18**(2), 27−41 (2007).
4. M. Tanaka, Y. Saiki, K. Hagisawa, and H. Narita, “Bath Life Extension during Electroless Nickel Plating by Solvent Extraction,” Proceedings ISEC 2005, China Academic Journal Electronic Publishing House, P. R. China, 2005; pp. 1374−1379.
5. Y. Kawano, K. Shiomori, and T. Sana, “Treatment Method of the Waste Water from Electroless Plating,” Japanese Patent Application, No. 2005-42183, 17 Feb. 2005.
6. T. Sana, K. Shiomori, and Y. Kawano, “Extraction Equilibria of Hypophosphorous, Phosphorous and Phosphoric Acids by Toluene Solution of Tri-n-octylamine,” *Ars Separatoria Acta*, **2**, 125−138 (2003).

HIGHLIGHTS AND HURDLES IN ZINC PRODUCTION BY SOLVENT EXTRACTION: THE FIRST FOUR YEARS AT SKORPION ZINC

J. Gnoinski,[1] K.C. Sole,[2] D.R. Swart,[1] R.F. Maluleke,[1] G. Díaz,[3] and F. Sánchez[3]

[1]*Skorpion Zinc, Rosh Pinah, Namibia*
[2]*Anglo Research, a division of Anglo Operations Ltd, Johannesburg, South Africa*
[3]*Técnicas Reunidas, Hydrometallurgy and Electrochemistry, Madrid, Spain*
Corresponding author email address: jgnoinski@skorpionzinc.com.na

ABSTRACT

The keystone of the Skorpion Zinc process, in which zinc is refined directly from a silicate ore, is the solvent-extraction circuit. Using a novel flowsheet based on the Modified Zincex process, first metal was produced in mid-2003 and full refinery production of 150,000 t/a special high grade zinc (>99.995% Zn) was achieved during 2005. Some operating and process challenges encountered through commissioning, ramp-up, and two years of full production are described.

INTRODUCTION

Skorpion Zinc, located in southern Namibia, is the first plant to produce zinc cathode directly from ore. The process involves atmospheric leaching of silicate ore, upgrading and purification of the pregnant leach solution (PLS) by solvent extraction (SX), and zinc recovery by electrowinning (EW) [1-3]. The SX process is the heart of the flowsheet, serving to produce an advance electrolyte (AE) of purity such that special high-grade (SHG) zinc (>99.995% purity) can be consistently produced. First metal was produced in May 2003, and the refinery has been operating at full production of 150,000 t/a Zn since 2005. The refinery output now routinely exceeds design capacity, confirming expectations for the use of SX technology for industrial zinc projects [4].

The SX process, based on the Modified Zincex™ process supplied by Técnicas Reunidas, uses di(2-ethylhexyl)phosphoric acid (D2EHPA) to purify and upgrade the PLS from 35 g/L to >100 g/L Zn in the AE. The key advantage of SX is that, in addition to the rejection of base-metal and other cationic impurities, halides (which are present in the ore) can also be rejected, thereby avoiding their highly detrimental effects in EW.

During the first four years of operation, understanding of critical operational parameters for the SX circuit has advanced significantly. Many of the challenges that have faced the operation were not identified during extensive upfront laboratory studies and piloting of the process, and have required innovative adaptations to maintain consistent product purity. Some of the operational challenges and learning points are discussed.

SKORPION ZINC SOLVENT-EXTRACTION CIRCUIT

As shown in the simplified SX flowsheet (Figure 1) [1,2], Zn is extracted in three stages using 40 vol % D2EHPA in Escaid® 100, loading the organic phase to ~14 g/L Zn. Co-extracted impurities and contaminants from aqueous entrainment are removed in three wash/scrub stages. Zinc is stripped from the organic phase using spent electrolyte (SE) from EW, generating an AE containing ~115 g/L Zn. A stripped organic (SO) bleed is regenerated with 6 mol/L HCl to avoid poisoning by iron and other trivalent cations. Aftersettlers are installed on the raffinate and AE lines to limit organic entrainment losses to the aqueous phases leaving the circuit.

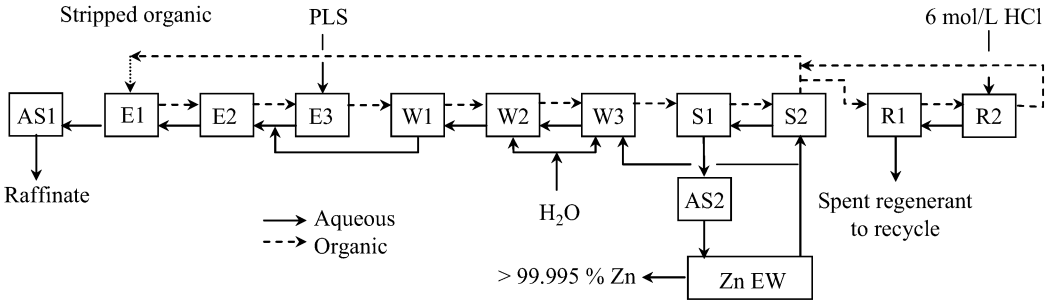

Figure 1. Schematic of the Skorpion Zinc SX flowsheet.

OPERATIONAL CHALLENGES AND LEARNINGS

The SX circuit serves to upgrade and purify the leach liquor, producing an electrolyte suitable for production of SHG zinc. Operational efficiency (production throughput and product purity) is impacted by a variety of physical and chemical factors.

Operating Philosophy

Extraction performance in 2007 is shown in Figure 2. The PLS contained 38 ± 3 g/L Zn. The advance O:A ratio was controlled to extract 25 g/L Zn, yielding a 13 g/L Zn raffinate. At this zinc loading, co-extraction of impurities is minimized and consistent zinc transfer (445 t/d) sustained. Overall SX plant availability was 97%.

Since start-up, the PLS has varied from 25 to 40 g/L Zn due to variability in ore grade and production strategy. The design operating philosophy required that the organic phase flowrate be modified according to the PLS Zn concentration to maintain constant Zn transfer to EW. This was achieved by routine tuning of process parameters (including PLS, organic, wash-water, and SE flowrates; pump mixing and degree of agitation; recycle flowrate; and overflow levels within the mixer and settlers) by the operators. In practice, this caused wide flowrate fluctuations, lack of stability, and difficulties with control. In combination with better control of ore grade through mining and blending strategies, and hence a more consistent PLS composition, a constant zinc loading on the organic phase is now targeted. This allows other operating parameters to be held constant for extended periods, permitting equilibration of the settler hydrodynamic flow patterns and minimizing interfacial turbulence and upsets.

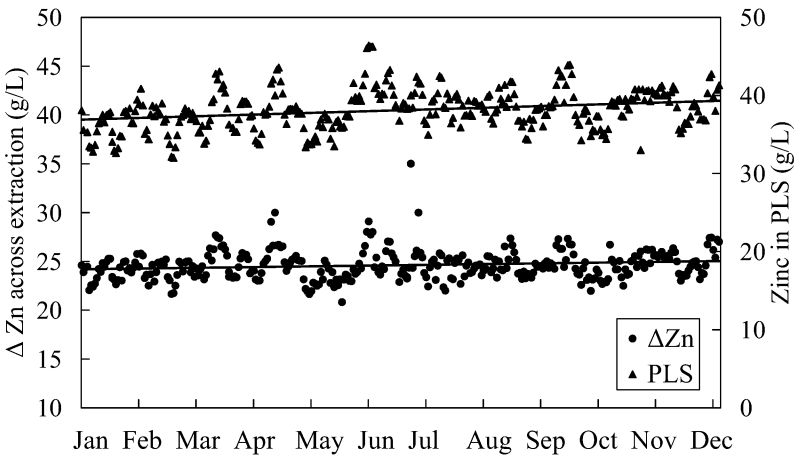

Figure 2. Zinc extraction from PLS (daily data from January to December 2007).

Impurity Deportment to Advance Electrolyte

Figure 3a shows the typical variation in PLS concentrations of critical impurities. Although these vary widely, very tight specifications on their concentrations in the AE are required (<50 μg/L) to avoid potentially catastrophic consequences in the cell house. After more than 15 months of stable operation, a significant excursion of metal impurities (Cu, Ni, Cd, and Co) in the EW circuit forced an unscheduled shutdown of the refinery in August 2006, with a fire originating from impurity-related hydrogen evolution at the cathodes. After restarting the refinery, intermittent impurity transfer across SX continued to impact the EW performance and refinery output. A salient feature was that the intermittent impurity excursions occurred as well-defined spikes against otherwise steady background levels (Figure 3b), rather than as an overall increase in the impurity background, suggesting a physical rather than chemical transfer mechanism. In addition to co-extraction, transfer of impurities from the PLS across the SX circuit may occur by aqueous entrainment in the loaded organic phase, via occlusion or surface adsorption on crud, or by another mechanism involving degradation of the extractant or diluent.

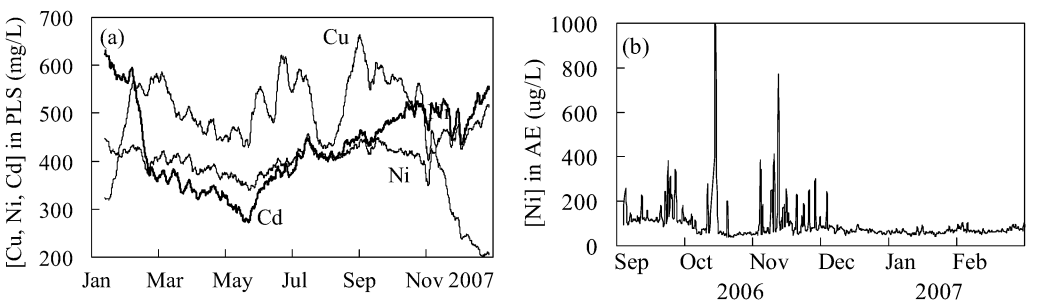

Figure 3. (a) PLS and (b) AE concentrations of critical impurities.

Health of Organic Phase

Within two years, design production had been achieved, and the operating focus had shifted from production ramp-up to cost control and reagent optimization. Extractant consumption had been reduced considerably by implementing better process and operating control, and routine replenishments were far less frequent than during ramp-up. The longer lifetime of the organic components in the circuit implied a steadily changing composition of the organic phase due to evaporation and degradation. One of the issues identified was an excessive diluent consumption. In particular, the lower molecular mass components of the diluent were being preferentially lost due to their higher volatility. This consumption is promoted by four main factors: (1) the mixer-settlers are open in a covered building, (2) the extraction temperature of 40 ^{o}C, (3) local humidity in the Namib desert is extremely low—all promoting diluent evaporation—and (4) crud formation.

During an in-depth analysis of the organic phase following the fire events, it was established that the viscosity and density of the SO were considerably higher than expected and that several trivalent cationic species had irreversibly accumulated on the SO. With high organic consumptions during commissioning and ramp-up, the routine solvent replacement had kept the effects of these factors under control. As reagent losses decreased, their influence became apparent, manifesting as stable emulsions, increased phase disengagement times, and impurity spikes to the electrolyte.

Loading of Trivalent Cations onto Organic Phase

D2EHPA is a strong extractant for Fe(III), but iron is not stripped by H_2SO_4. Most iron in the leach liquor is removed by precipitation, but small amounts (<5 mg/L) inevitably report to SX, leading to a slow build up on the SO. The original process design aimed to maintain organic-phase iron loading below 300 mg/L by treating an intermittent organic bleed with 6 mol/L HCl, where stripping of Fe(III) occurs by the formation of relatively stable ferri-chloro complexes and regenerating the organic phase (RH) [8]:

Extraction: $$Fe^{+3} + 3\ RH_{(org)} \rightarrow R_3Fe_{(org)} + 3\ H^{+} \quad (1)$$

Regeneration: $$x\ R_3Fe_{(org)} + y\ HCl \rightarrow 3\ RH_{(org)} + Fe_xCl_y^{3x-y} \quad (2)$$

Somewhat unexpectedly, analysis of the SO also showed the accumulation of up to 1 g/L rare earth elements (REE). REE had not been previously detected in the Skorpion ores (although they were subsequently identified in an adjacent sulfide deposit). Although below the detection limit in the PLS, the closed-loop nature of the SX-EW circuit means that any of these trivalent cations extracted from the PLS are not bled from the circuit. The chondrite-normalized plots of the REE concentrations in the SO and AE (Figure 4) show remarkable consistency over a two-year period. The electrolyte chondrite pattern has a negative Eu anomaly, attributed to Ca substitution of Eu in feldspar, an alteration product of which is sauconite (a major component of the Skorpion ore). The SO plots show a complementary effect, with high concentrations at each end of the REE range and low concentrations in the mid-REE region. It is evident that the

process is enriching the middle REE at the expense of the light and heavy REE. It is well known that D2EHPA is a strong extractant for REE. Under the Skorpion operating conditions, the light and heavy REE report to the SO, while the middle REE report to the electrolyte. In both cases, this results in a circulating and gradually accumulating levels of REE in the circuit.

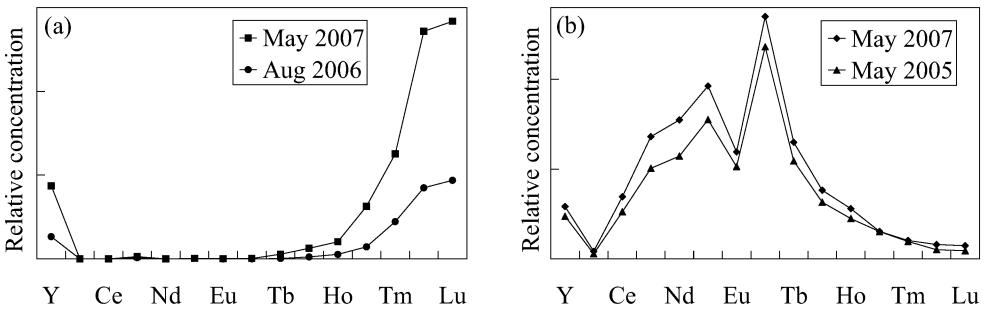

Figure 4. Chondrite-normalized plots of REE concentrations in (a) SO and (b) AE.

In the original design, an organic bleed treated 1.5% of the total organic flow. With the regeneration circuit operated at an O:A of 7, an iron-removal efficiency of ~30% per pass or 1.5 kg/h Fe was obtained. This proved inadequate to control the build-up of other trivalent cations, including Al(III) and REE. The regeneration circuit is now run continuously, treating 3% of the total organic flow at an O:A of 11.2. This maintains the total metal loading on the organic returning to the extraction circuit at <150 mg/L.

Crud Formation and Deportment

Crud formation has been a major problem since commissioning, causing both organic losses and impurity carryover. The main reasons for crud formation were established as (1) the presence of suspended solids in the PLS and (2) the presence of air entrainment, produced in the mixer siphon breakers and settler overflow launders.

The total suspended solids (TSS) profile in the PLS has been statistically correlated with the corresponding Al and Si concentrations (Figure 5) [5]. During 2007, TSS averaged 45 mg/L, compared to the target specification of <10 mg/L. During the impurity excursions, a change in the physical appearance of the crud occurred, from coarse bottom crud to voluminous, highly gelatinous floating crud. Floating crud has often been associated with fine clays and silica, both of which are present in the Skorpion ore [2]. The predominance of Si analyzed among the contaminants and crud solids left little doubt that it was the main contributing factor in the crud formation [5]. Floating crud passes with the organic phase through the washing and scrubbing stages. Under the strong acid regime of the strip, the crud partially breaks down, releasing the entrapped PLS into the electrolyte, and thereby introducing contaminants to the EW circuit.

The original process design employed sand filters for PLS clarification, but these suffered frequent gypsum blockages. PLS ponds, subsequently installed downstream of the thickeners, provided some improvement in PLS quality by allowing additional settling time for solids. In 2006, an Ishigaki-Fiber Washikimizu filter was tested for

solids removal [6]. Although pilot results were good, the anticipated operating costs due to routine replacement of the filtration media were prohibitive. A pinned-bed clarifier (PBC) was then evaluated and, under optimized conditions, consistently removed solids from this PLS to <10 mg/L TSS [7]. The feasibility study of installing a full-scale PBC treating 1500 m^3/h PLS is underway. A Flottweg centrifuge will also be installed during 2008 to assist in the treatment of crud and effective recovery of the organic phase.

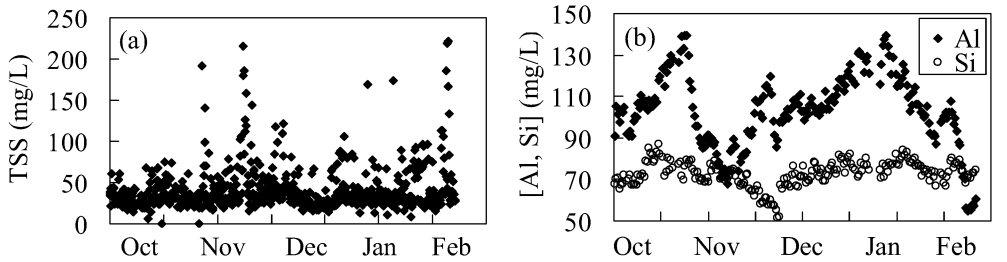

Figure 5. Variation in (a) TSS and (b) Si and Al in PLS (Oct 2006 to Feb 2007).

Equipment and Process Improvements

Excessive air entrainment, which promotes crud formation, resulted from the particular pump-mixer design. Two of the four installed mixers in the extraction stages are now permanently switched off to avoid over-mixing and emulsion formation. Settler overflow launder levels were increased as normal operating strategy to avoid a "waterfall" effect at the end of the settler, the aerosols from which also contributed to organic losses. This practice has additional benefits in terms of fire-risk reduction. Automation of the pump-mixers, interface-level control in the settlers, and installation of automated siphon breakers further contributed to smoother running of the circuit.

While installation of PLS ponds had a beneficial effect in reducing TSS values, seasonal problems were introduced from the significant variation in ambient temperature. The extraction reaction is endothermic, and so extraction efficiency drops off rapidly below 40 ^{o}C. This necessitated the installation of a heat exchanger on the PLS line ahead of the SX circuit to maintain the PLS temperature during the winter months.

Improved pH control in the upstream leach and neutralisation circuits, continuous removal of crud from the extraction stages, and increased runtime of the regeneration circuit has resulted in significant process improvement. The cumulative effect of the various modifications reduced the frequency of cleanout of the extraction mixer-settlers from six times per year in 2005 to twice in 2007. Impurity concentrations are closely monitored and installation of additional AE holding capacity allows a quarantine period for analysis before the electrolyte enters the cell house. No further electrolyte impurity excursions have occurred.

COMPARISON OF DESIGN AND ACTUAL PERFORMANCE

Considerable improvement has been made to the operation of the Skorpion Zinc SX circuit as a result of better understanding of critical parameters. As indicated in Table

1, the plant is today successfully operating well beyond many of the original design parameters. Typical PLS, AE, and cathode compositions are compared in Table 2.

Table 1. Comparison of design and actual SX operating parameters (October 2007)

Parameter	Design	Actual
Operating temperature (^{o}C)	40	43
D2EHPA consumption (kg/t Zn)	1.1	0.9
Diluent consumption (kg/t Zn)	3.8	10.1
ΔZn across extraction (g/L)	20	25
ΔZn across stripping (g/L)	40	70

Table 2. Typical compositions of SX process streams and zinc cathode

Element	PLS (mg/L)		AE (mg/L)		Zinc cathode (ppm)	
	Design	Actual	Design [2]	Actual	Design*	Actual
Al	300	82		190		
Pb					30	25
Sn					2	2
Ca	650	664		54		
Cd	100	330	<0.05	0.01		
Cl	5000	1031	<100	50		
Co	100	18	<0.05	0.02		
Cu	700	504	<0.05	0.09	10	7
F	200	43	<20	7		
Fe	5	1.5	<5	<5	20	3
Mg	200	1040				
Mn	500	2120	3000	2200		
Ni	800	328	<0.05	0.08		
Si	40	67				
Zn	30,000	38,000	>90,000	117,000		

* LME specification for SHG zinc cathode.

CONCLUSIONS

The performance of the Skorpion Zinc SX circuit has demonstrated the efficiency of the Modified Zincex process for industrial SHG zinc production. Although a variety of problems were encountered during the start-up and ramp-up of the refinery, SHG zinc cathode was consistently produced, indicating the flexibility and robustness of the process in coping with PLS variations. The major mechanism of impurity transfer across the SX circuit has been attributed to intermittent episodes of aqueous entrainment associated with the accumulation and release of crud in the extraction and stripping stages, respectively. Degradation and/or deterioration of the organic phase also caused conditions conducive to impurity transfer. Several abnormal upstream operational conditions were identified that promote crud formation through ingress of excessive solids. Improving pH control in the leach and neutralization circuits, continuous removal

of crud from the extraction stages, and increased runtime of the regeneration circuit resulted in significant process improvements with no impurity excursions. Further process and operating cost improvements are expected with installations of solid-liquid separation technology such as pinned-bed clarification, which will ensure low TSS values in the PLS and a tricanter centrifuge for organic recovery from crud.

Skorpion Zinc is also proud that their excellent production record is matched by an exceptional safety record. No lost time incidents were reported from October 2005 to July 2007, and Skorpion received the Chief Executive's Award in 2007 for the best safety record in the Anglo American Group worldwide.

ACKNOWLEDGMENTS

The sustained commitment of the management and staff of Skorpion Zinc, and support of Anglo Base Metals, in achieving the excellent results to date is acknowledged. This paper is published by permission of Skorpion Zinc.

REFERENCES

1. P. M. Cole and K. C. Sole, "Zinc solvent extraction in the process industries," *Miner. Proc. Extr. Met. Rev.*, **24**, 91-137 (2003).
2. H. Fuls, K. C. Sole, and T. Bachmann, "Solvent Extraction in Zinc Production from a Primary Source: The Skorpion Zinc Experience," International Solvent Extraction Conference 2005, Chinese Academy of Science, Beijing, China, 2005; pp. 1223−1228.
3. J. Gnoinski, T. Bachmann, and S. Holtzhausen, "Skorpion Zinc: Defining the Cutting Edge of Zinc Refining," Lead-Zinc 2005, T. Fujisawa, J. E. Dutrizac, A. Fuwa, N. L. Piret, and A. H.-J. Siegmund, Mining and Materials Processing Institute of Japan, Tokyo, Japan, 2007; pp. 1315−1325.
4. M. A García, F. S. Ruiz, A. B. Mejias, and M. Frades, "The Skorpion Zinc Plant: Zincex™ Solvent Extraction. The Best Expectations Confirmed after Commissioning," Lead-Zinc 2005, T. Fujisawa, J. E. Dutrizac, A. Fuwa, N. L. Piret, and A. H.-J. Siegmund, Mining and Materials Processing Institute of Japan, Tokyo, Japan, 2007; pp. 1327−1336.
5. J. Gnoinski, "Skorpion Zinc: Optimisation and Innovation," Africa's Base Metals Resurgence, Southern African Institute for Mining and Metallurgy, Johannesburg, 2007; pp. 329−342.
6. H. F. Fuls and K. Nong, "Piloting of the Ishigaki Fibre-Wakishimizu (Fibre Media Rapid Filtration Equipment) at Skorpion Zinc," Africa's Base Metals Resurgence, Southern African Institute for Mining and Metallurgy, Johannesburg, 2007; pp. 223−240.
7. M. Langton, H. Fuls, K. C. Sole, A. Rampersad, C. Blaauw, and B. Martinson, "Innovations in the Configuration of a Pinned-Bed Clarifier for Clarification of a Zinc Leach Liquor," International Solvent Extraction Conference 2008, Canadian Institute for Mining and Metallurgy, Montreal, 2008; in press.
8. E. A. Roux, M. J. Sechemane, and S. Holzhausen, "Iron Removal in the Skorpion Process," Iron Control Technologies, J. E. Dutrizac and P. A. Riveros, Eds., Canadian Institute of Mining, Metallurgy and Petroleum, Montreal, 2006; pp. 491−500.

ZINC SOLVENT EXTRACTION IN THE HYDROZINC™ PROCESS

J.R. Harlamovs[1] and S. Bélanger[2]

[1]*Teck Cominco Metals Ltd., Applied Research and Technology, Trail, BC, Canada*
[2]*Teck Cominco Metals Ltd., Trail Operations, Trail, BC, Canada*
Corresponding author email address: juris.harlamovs@teckcominco.com

ABSTRACT

The recovery of zinc using solvent extraction is an integral part of the HydroZinc process. This paper describes the key aspects of the process. The pilot-plant operation is described in detail, particularly the extraction, scrubbing, stripping, and galvanic iron removal steps. The scrubbing performance, which is critical to electrowinning special high-grade zinc, is reviewed. The performance of a galvanic iron removal process, an alternative method of removing iron from the solvent, is also discussed. Control of entrainment, crud, and biomass, as well as operational issues of running a large solvent-extraction pilot plant, are outlined.

SOLVENT EXTRACTION CIRCUIT DESCRIPTION

The overall HydroZinc™ integrated heap-leach pilot plant is described elsewhere [1,2]. The solvent-extraction circuit consisted of two extraction stages, three scrubbing stages, and two stripping stages (Figure 1). The extractant, di(2-ethylhexyl)-phosphoric acid (DEHPA) was diluted to 20% by volume with Orfom SX 11. Zinc was extracted in two countercurrent stages, generating an acidic raffinate, which was recycled to the heap. Different methods of solvent removal from the raffinate and the advance electrolyte were evaluated.

The loaded solvent was washed and scrubbed with dilute spent electrolyte. Scrub raffinate solution was either recycled to the heap or to extraction, depending on the plant operating strategy. Zinc was stripped from the scrubbed solvent with spent electrolyte. Entrained solvent was removed from the advance electrolyte using dual-media filtration and activated carbon. To avoid solvent poisoning by ferricions, a portion of the stripped solvent was contacted with metallic zinc shot to reduce ferric to ferrousions.

The mixer-settlers were constructed of 316 stainless steel. Standard pump-mix impellers (Lightnin R320 and A310) were used to contact the liquid phases in two mixers. The total mixer retention time was typically about 2 min. The settler had a reverse-flow configuration and an area of 2.6 m^2. Typical SX feed and solvent flows were 4 and 5 m^3/h, respectively. The iron removal column, 0.3 m diameter, contained 40 L to 80 L of 6 mm leaded zinc shot. The contact time in the zinc shot bed was less than one minute.

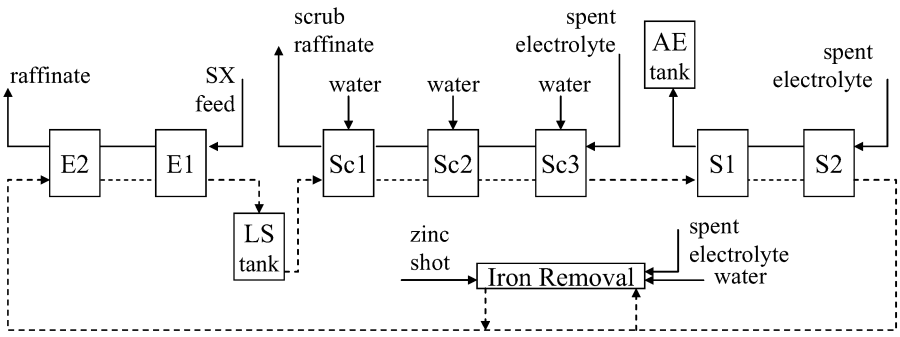

Figure 1. Schematic of the solvent extraction circuit.

SOLVENT-EXTRACTION PERFORMANCE

Extraction

A typical SX feed (pH 3.5) assayed 20 g/L Zn, 0.8 g/L Mg, 0.8 g/L Cd, 0.6 g/L Ca, 0.6 g/L Fe, 0.2 g/L Al, 0.2 g/L SiO_2, 0.02 g/L Mn, 0.08 g/L Co, and 0.04 g/L Ni. The solvent-to-aqueous (O:A) ratio in extraction was controlled to extract about 10 g/L Zn. At a given solvent ratio, the zinc extracted increased linearly with the zinc content of the SX feed (Figure 2). Increasing the external O:A at a given zinc concentration in the SX feed increased zinc pick-up, but the lower solvent zinc concentration promoted minor element co-extraction. About half of the zinc was extracted in each stage. Laboratory tests showed that zinc extraction was complete in thirty seconds; this corresponds to a stage efficiency of about 97% for a mixer retention time of 2 min.

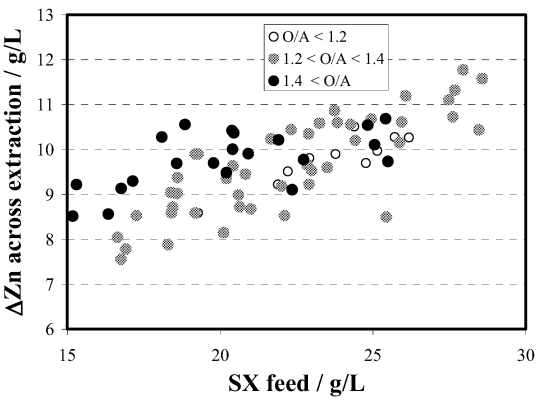

Figure 2. Zinc extracted from SX feed (data from July 2001 to December 2002).

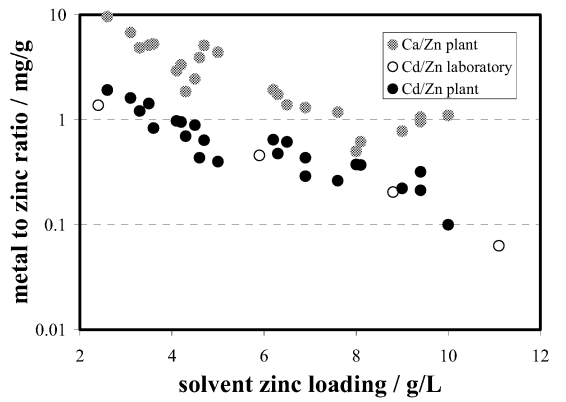

Figure 3. Decrease in cadmium and calcium extraction with zinc loading.

Only cadmium and calcium co-extracted appreciably. Calcium co-extracted more than cadmium (Figure 3). In the narrow concentration range tested (0.5 to 0.6 g/L Ca; 0.4 to 0.9 g/L Cd), co-extraction was independent of the concentration of these elements in

the SX feed. Co-extraction decreased with zinc loading. To minimize co-extraction of calcium and cadmium, the solvent should be loaded to at least 8 g/L Zn. An excessively high loading increases the viscosity of the solvent, slowing down phase disengagement. Thus, a compromise between a high zinc loading and an acceptable viscosity must be sought.

Scrubbing

Approximately 1.5 L/min of water were added to each of the three scrub mixer-settlers and 1.5 L/min of electrolyte to scrub 3. This gives a blend of washing and chemical stripping of impurities in scrubbing. Given the inherent error in scrub efficiency measurements, the best long-term indicator of scrubbing efficacy was the quality of the advance electrolyte. Calcium is the most difficult minor element to scrub in this system; consequently, optimizing calcium scrubbing results in optimization of all scrubbing. The strategy for maintaining electrolyte quality was to control the calcium concentration below 100 mg/L in the advance electrolyte by varying the aqueous scrub feeds.

The removal of entrainment in the three scrub stages was estimated at 94% to 97%. This was based on metals that are very weakly extracted by DEHPA. The removal of entrainment was independent of the volume or acidity of the scrubbing solutions.

The chemical scrubbing effectiveness could not easily be calculated, because the calculation relies on very accurate measurement of minor-element concentrations. Qualitatively, overall about 60% of the co-extracted calcium was removed in Sc1, about 25% was removed in Sc2, and about 10% was removed in Sc3. The corresponding values for cadmium are 85% in Sc1 and 15% in Sc2. Removal was below the detection limit in Sc3.

Stripping and Electrolyte Quality

The external O:A in stripping ranged from 5:1 to 10:1 and was adjusted to maintain the target zinc concentration in the advance electrolyte. More than half of the loaded zinc was stripped from the solvent in the first stage. Zinc concentration in the stripped solvent was typically below 0.5 g/L.

Table 1. Summary of advance electrolyte composition for the SHG run

	Concentration / (g/L)				Concentration / (mg/L)			
	Zn	H_2SO_4	Mn	Al	As	Ca	Cd	Co
average	110	71	2.5	0.4	<0.010	52	0.3	0.5
min-max	100-120	50-100	1.3-3.3	0.3-0.6		30-80	0.2-0.5	0.2-0.7
	Concentration / (mg/L)							
	F	Fe	Hg[a]	Mg	Ni	Pb[b]	SiO_2	Sb
average	12	21	7	10	0.2	0.6	35	0.02
min-max	9-17	3-30	2-15	6-17	0.1-0.3	0.1-1.9	15-50	<0.01-0.02

[a] µg/L [b] total lead

For the last three months of the campaign, the pilot plant produced special high-grade (SHG) zinc at the design production rate (~1 t/d Zn). Table 1 shows the advance electrolyte quality over this period. The electrolyte was of high quality; calcium could easily be maintained under 100 mg/L and cadmium in the cathode was ~3 g/t. The cobalt concentration was a little higher than desirable but current efficiency was about 90%.

Iron Removal

The iron-removal column was simple to operate, upflow or downflow (aqueous or solvent continuous). The column typically treated 50% to 100% of the total solvent flow. About 1 L/min of diluted electrolyte was dispersed into the solvent. The iron loading rate was determined by turning off the flows to the iron removal column and monitoring the iron concentration in the bulk of the solvent (Figure 4). The depletion of iron was then monitored in the plant when the column was operated downflow (solvent continuous).

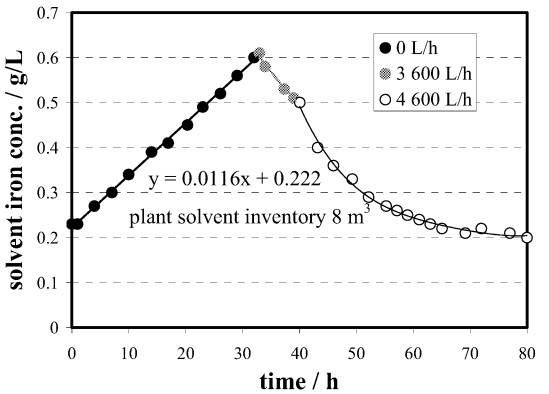

Figure 4. Solvent iron concentration profile during the iron loading and removal tests.

The concentration of iron increased linearly with time with the iron removal column offline. The loading rate was about 1.5 g/min; at steady state this is equal to the iron removal rate. Figures 5a and 5b show zinc shot and acid consumption over time.

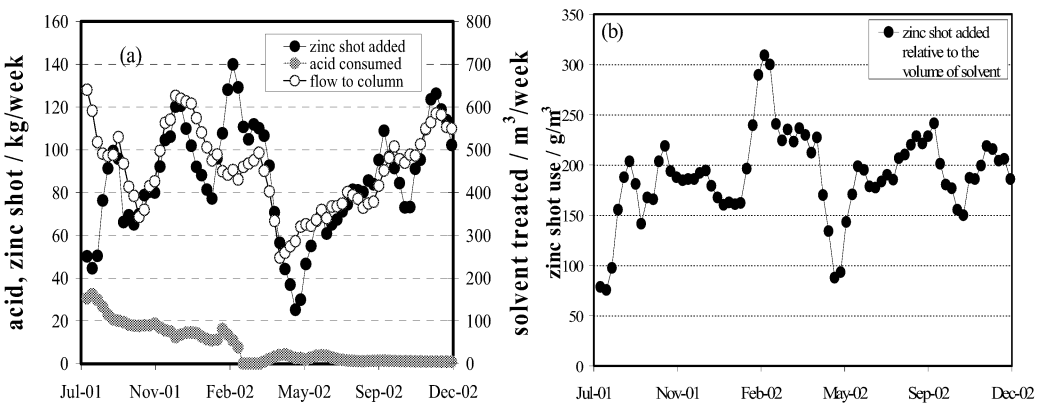

Figures 5a and 5b. Iron removal column acid and zinc shot four-week average consumption.

The iron removal shows a first-order behavior and is consistent with earlier work [3,4]. Zinc shot consumption tracked with the volume of solvent fed to the iron-removal column (Figure 5a). The iron stripped did not account for the zinc shot consumed. Zinc reacting with acid would generate about 3 L/min of hydrogen. This was not observed. The zinc shot consumption averaged about 170 g/m^3 solvent treated for the upflow configuration and about 190 g/m^3 solvent for downflow operation (Figure 5b). About 50 mg/L of oxygen dissolved in the solvent would be required to consume 190 g/m^3 of zinc shot. The solubility limit of oxygen in kerosene, at one atmosphere, is about 150 mg/L to 200 mg/L [5]. There is therefore approximately enough oxygen solubility in the kerosene to account for the bulk of the zinc shot consumed.

Entrainment

Solvent continuity was maintained in mixer-settlers where raffinate and advance electrolyte exited the circuit (E2, S1). Mixers E1 and S2 were maintained aqueous-continuous to minimize the carryover of impurities into scrubbing, and to minimize loss of electrolyte in S2. Initially, the target continuity was aqueous in all three scrub stages to minimize entrainment and impurity transfer to electrowinning. Scrub mixer-settlers 1 and 2 were tested with both continuities. Electrolyte quality was marginally better running solvent continuous in Sc1 and Sc2, but the improvement was too small to have a measurable impact on the quality of the (already pure) advance electrolyte.

Aqueous-in-solvent entrainment was monitored primarily in E1 and Sc3. The largest factor in decreasing entrainment was increasing the impeller size, so the agitation speed could be reduced. Figures 6a and 6b show the effect on the aqueous entrainment.

Switching to the larger impellers also reduced the solvent-in-aqueous entrainments dramatically. With the smaller impellers, the entrainments in the raffinate and advance electrolyte were typically 30 mL/m^3 and ~150 mL/m^3, respectively. Increasing the impeller size to 15 cm reduced the solvent entrainments to ~20 mL/m^3 and <30 mL/m^3. Coalescers, a flotation cell, and dual-media filters were evaluated for solvent removal from raffinate; dual-media filters were the most effective, but cost effectiveness of treating the raffinate needs to be evaluated further.

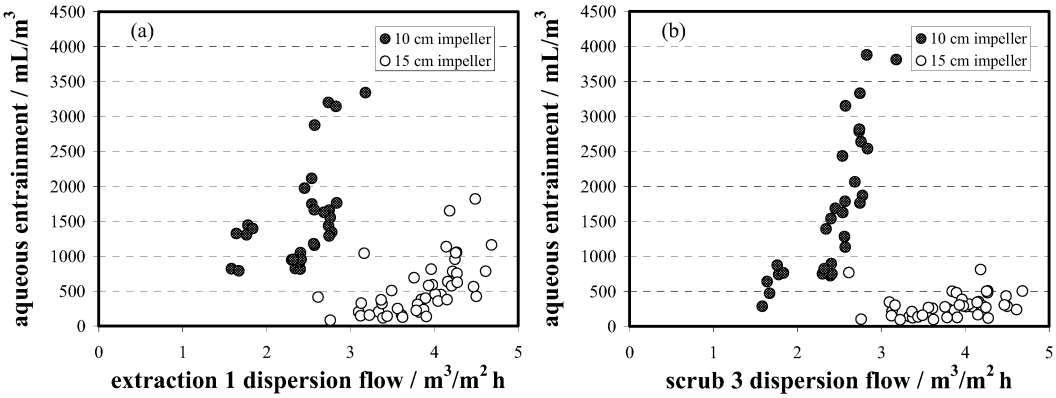

Figures 6a and 6b. Effect of impeller size on aqueous-in-solvent entrainment.

Crud and Solvent Loss

Crud generally was not an issue in the plant, especially after the operation of the clarifier and polish filter, ahead of SX, stabilized. The plant did experience significant fungal growth in the mixer-settlers, raffinate after settler and tank [6]. The fungal growth was increased dramatically when the raffinate was aerated during flotation tests. The mixer-settlers E1 and Sc1 had the fastest rates of crud accumulation. Although the fungal growth may have made washing impurities more difficult, its most significant deleterious effect was downstream, clogging emitters in the heap leach. Over 26 months of operation, 12.3 m^3 of solvent were added as make-up. This total solvent loss was equivalent to 200 mL/m^3 of raffinate treated. This includes spills and periods of poor operation with incorrectly sized impellers. The estimate for solvent consumption for the full-scale plant is 2.7 L/t of zinc electrowon (30 mL/m^3 of raffinate).

CONCLUSIONS

Solvent extraction of zinc from a neutralized heap leach solution proved to be technically feasible. The primary elements of concern, calcium, and cadmium, were kept out of the advance electrolyte. Stripping of iron with zinc shot was a simple and convenient method of keeping iron loading at low concentrations.

ACKNOWLEDGMENTS

The authors would like to thank Teck Cominco Metals Ltd. for permission to publish this paper. We would like to acknowledge many talented people, who made this project possible and successful.

REFERENCES

1. H. M. Lizama, J. R. Harlamovs, S. Bélanger, and S. H. Brienne, “The Teck Cominco HydroZinc™ Process,” Hydrometallurgy 2003, Fifth International Conference in Honor of Professor Ian Ritchie, Vol. 2: Electrometallurgy and Environmental Hydrometallurgy, The Minerals, Metals and Materials Society, Warrendale, PA, 2003; pp. 1503–1516.
2. J. R. Harlamovs *et al.*, “A Heap Bioleaching Process for Zinc,” United States Patent, No. 6,736,877, 18 May 2004.
3. B. Belew, J. R. Harlamovs, T. J. O'Keefe and J. L. Watson, “Reductive Stripping of Iron (III) from Di(2-ethylhexyl)phosphoric Acid,” Proceedings of the Milton E Wadsworth (IV) International Symposium of Hydrometallurgy, Society of Mining, Metallurgy and Petroleum Engineers, Littleton, CO, 1993; pp. 801–816.
4. T. J. O’Keefe, “Method for Stripping Metals in Solvent Extraction,” United States Patent, No. 5,228,903, 20 July 1993.
5. A. Seidell and W. F. Linke, “Solubilities of Inorganic and Metal-Organic Compounds,” Vol. 2, 4th ed., American Chemical Society, Washington, D.C., 1965; pp.1235 and 1236.
6. N. Callao *et al.*, “Biological Degradation of Solvent Extraction Circuit Plant Organic,” Hydrometallurgy 2003, Fifth International Conference in Honor of Professor Ian Ritchie Vol. 1: Leaching and Solution Purification, The Minerals, Metals and Materials Society, Warrendale, PA, 2003, pp. 1003–1022.

SEPARATION OF ZINC FROM IRON(II) IN SPENT PICKLING EFFLUENTS PRODUCED BY THE HOT-DIP GALVANIZING INDUSTRY BY LIQUID-LIQUID EXTRACTION

Carlos A. de Morais,[1] Diogo H. Carvalho,[2] Sônia D.F. Rocha,[2] and Marcelo B. Mansur[2]

[1] Centro de Desenvolvimento da Tecnologia Nuclear, CDTN/CNEN Av. Presidente Antônio Carlos, 6627- Campus da UFMG – Pampulha, CEP 310270-901, Belo Horizonte, MG, Brazil. [2] Universidade Federal de Minas Gerais, R. Espírito Santo, 35, Centro, CEP 30160-030, Belo Horizonte, MG, Brazil.
Corresponding author email address: marcelo.mansur@demet.ufmg.br

ABSTRACT

The separation of zinc from iron(II) in pickling effluents produced by the zinc hot-dip galvanizing industry was investigated by contacting an industrial effluent (37.2 g/L Zn, 119 g/L Fe^{2+}, 1.9 g/L Mn, 0.085 g/L Cr, 0.078 g/L Ni, and 0.038 g/L Cu) with an organic solution containing 90% v/v of TBP (tri-*n*-butyl phosphate) dissolved in Exxsol D-100. Batch-scale studies showed that TBP selectively separates Zn from Fe(II) from acid solutions ($[H^+] \approx 1.45$ mol/L). Pilot-scale tests using pulsed columns in continuous operation pointed out it is a feasible method to recover zinc and iron(II) for reuse, thus avoiding metal precipitation as sludge that would be disposed in landfills as commonly done industrially in the conventional treatment of such effluents.

INTRODUCTION

Metal-plating processes involve the combination of several deposition and finishing operations. In the case of zinc-plating or zinc hot-dip galvanizing process, a layer of zinc is deposited by immersing steel goods in molten zinc to provide corrosion protection or decoration. High-quality zinc layers require appropriate pretreatment of the surface to be coated (washing, degreasing, rust removal, and fluxing steps), so several types of effluents can be generated by the mixture of the various washing waters and the saturated solutions which are substituted regularly. Such solutions, commonly referred to as pickling effluent, are normally hydrochloric acid media, as the use of HCl offers some advantages over H_2SO_4, as it produces a more even and cleaner surface, requires lower liquor temperatures, and it can be regenerated [1].

Pickling effluents generated by the zinc-plating industry normally contain high concentrations of zinc and iron (mainly Fe^{2+}) dissolved in HCl solution, and many other metals at lower concentrations like chromium (from the passivation step), nickel, copper, etc. Such effluents are normally treated by precipitation using soda or lime as

precipitating agents [2,3]. In fact, precipitation is an efficient method to produce a treated solution but both acid and metal content confined to the sludge are not reprocessed. In addition, the amount of precipitating agents required for treatment and the cost for the safe disposal of sludge produced can be high, so there is some interest in developing new treatment processes which allow the reduction of the quantity of wastes and also the recovery of valuable products to be recycled or reused in other applications.

A comparative study using neutral (tri-*n*-butylphosphate (TBP)) and acidic (CYANEX 272, CYANEX 301, and CYANEX 302) extractants to separate zinc from iron(II) in pickling effluents by liquid-liquid extraction showed that TBP and CYANEX 301 are very selective reagents for zinc over iron(II) at acid conditions ($pH \leq 1$) [4]. However, as iron(III) was found to be extracted by both reagents, a previous iron-reduction step was recommended, as stripping was not found to be a selective process. In addition, as zinc complexes with CYANEX 301 are very stable, thus requiring concentrated acidic stripping solutions, and also dithiophosphinic acids are not too stable in the presence of iron(III) [5], TBP seems to be the preferred reagent for the zinc-iron separation step in the present context. In this paper, the extraction of zinc over iron(II) from HCl pickling effluents with TBP as reagent has been highlighted, aiming to recover valuable metals and treat final effluents.

EXPERIMENTAL

The pickling effluent used in this study was generated by a zinc-plating company located at Minas Gerais, Brazil, containing 37.2 g/L zinc, 119 g/L iron (mostly ferrous ion), 1.9 g/L manganese, and small quantities of chromium (0.085 g/L), nickel (0.078 g/L), and copper (0.038 g/L) dissolved in HCl media ($[H^+] \approx 1.45$ mol/L). It was previously filtered to remove oil and suspended solids. The organic phase consisted of TBP dissolved in Exxsol D-100 at various concentrations. No modifier agent was used in the solvent phase, and all other chemicals used were of reagent-grade quality. The study was carried out at room temperature and it consisted of bench- and pilot-scale tests.

The bench-scale testing used a 100 mL glass reactor. Both liquids at defined aqueous/organic volumetric ratio were stirred magnetically for 10 min (equilibrium was reached within 3 minutes). Firstly, preliminary tests using TBP of different grades (commercial grade with 98% purity and analytical grade with 99% purity supplied by Merck) were carried out to compare its ability to extract both zinc and water after successive contacts of extraction and stripping. In these tests, a synthetic aqueous solution (20 g/L zinc and 2 mol/L HCl) was contacted with same volume of TBP (30 mL); the loaded organic phase was contacted with the same volume of water for zinc stripping and then contacted ten times with the synthetic solution. The volume of both phases after equilibration was measured using a graduated cylinder, and all aqueous phases were analyzed by atomic absorption spectrometry for zinc content. Secondly, the effect of the TBP concentration on the zinc extraction was evaluated by contacting the industrial pickling effluent with organic phases at concentrations ranging from 70% to 100% v/v commercial TBP. Finally, zinc extraction and stripping isotherms were obtained using the successive contact method.

The pilot-scale tests were carried out using a countercurrent pulsed column (height 1500 mm and shell diameter of 26 mm made of borosilicate Pyrex glass, 51 perforated plates made of Teflon). The bottom settler of the column had 350 mm height and 52 mm diameter, while the top settler had 300 mm height and 52 mm diameter; both polyethylene settlers. Liquids were fed to the column using piston pumps (Omel) with variable amplitude and frequency. In all extractions tests, amplitude and frequency were kept constant at 25 mm and 60 pulses/min, respectively. In the stripping experiments, the amplitude was 25 mm, while the frequency was 40 pulses/min. Extraction and stripping runs were carried out by contacting the industrial effluent with an organic phase containing 90% v/v commercial TBP at changing flow-rates and different contacting times. In extraction and stripping experiments numbered 1 and 2 (runs E1, E2, S1 and S2), the contact time was 25 min., while in the third extraction and stripping experiments (runs E3 and S3), the contact time was 35 min. In the extraction step, TBP was the continuous phase, while in the stripping step the stripping aqueous solution was the continuous phase. When steady-state was reached, zinc and iron concentrations were determined by atomic absorption spectrometry in both phases. The organic phase output from the first stripping experiment was used in the other runs.

RESULTS AND DISCUSSION

In preliminary tests, the effect of TBP grade on the solvation of water molecules and also on the zinc extraction from concentrated HCl solutions by successive contacts of extraction and stripping stages was evaluated. With regard to the water solvation by TBP, the relative variation of the organic-phase volume did not exceed 10% for both reagents (analytical and commercial grade). In fact, a relatively higher volume variation was observed only after the first contact stage, stabilizing within 4% maximum from the second to the tenth contact. Both reagents become saturated with water in the very first contact, so their volumes did not change significantly in the subsequent contacts. With regard to zinc extraction, analytical-grade TBP extracted 6.5% more zinc (in average, varying from 2.5% to 13.7%) than commercial-grade TBP (see Figure 1). Despite relatively better extractions obtained by analytical-grade TBP, the commercial-grade reagent was selected for the continuing tests.

Figure 2 shows the effect of the extraction of zinc from the effluent at changing concentration of TBP in the organic phase. As expected, a higher metal extraction was obtained with the increase on the concentration of TBP. Comparing results shown in Figures 1 and 2, it can be verified that TBP is a very effective reagent for zinc extraction, as it was quantitatively extracted in a single contact stage (zinc extractions higher than 50% for all conditions investigated). The relatively lower extraction of zinc verified in Figure 1 is due to the higher acidity of the aqueous phase that negatively affects zinc extraction.

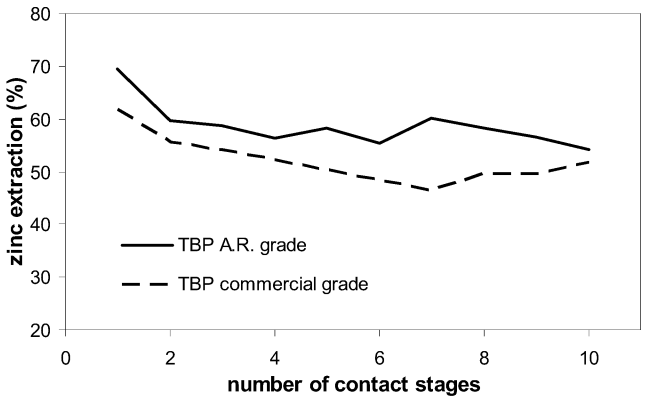

Figure 1. Extraction of zinc using TBP of different grades.
Aqueous phase: 20 g/L Zn, 2 mol/L HCl. Organic phase: 100% v/v TBP, A/O ratio = 1.

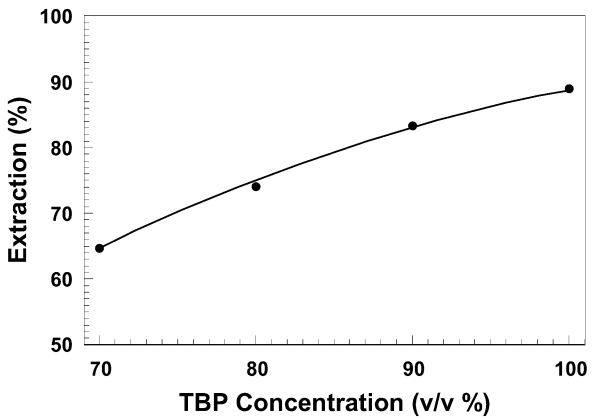

Figure 2. Effect on the extraction of zinc with the concentration of TBP (A/O ratio = 1).

Figure 3 shows the isotherm of zinc extraction with commercial TBP from industrial effluent. The organic phase was fully loaded at ~38 g/L of zinc. According to the McCabe-Thiele method, just three theoretical countercurrent stages are necessary to obtain a raffinate containing 0.73 g/L of zinc (98% extraction), resulting in a loaded phase with 34 g/L of zinc (89.5% saturated). The concentration of iron in the extract was 2.3 g/L (1.0% extraction). Figure 4 shows the isotherm of zinc stripping using water as stripping solution. It can be seen that maximum loading of zinc in the aqueous phase obtained in this study was 44 g/L.

The results of the pilot-scale pulsed column tests are summarized in Table 1. Three extraction runs (E1, E2 and E3) and three stripping runs (S1, S2, and S3) were carried out at different flow rates. For the extraction runs, around 98% of zinc was extracted with less than 2% extraction of iron, so this step was quite selective, but the concentration of zinc and iron in the extract phase was relatively low compared to those predicted by the McCabe-Thiele construction. For the stripping runs, around 98% of zinc was stripped, but the concentration of iron in the strip liquor was considered too high,

thereby corroborating previous studies that stripping is not very selective, and all iron(III) present in the effluent has to be reduced to iron(II) prior to the liquid-liquid extraction step. The change in the volume for both phases was around 10% (average for all runs), a bit higher than obtained in the saturation experiments. In the extraction tests, the volume of the aqueous phase decreased, while the volume of the organic phase increased; contrary behavior was observed for the stripping runs. The increase of volume coincides with the direction of zinc transfer. In fact, water molecules around zinc atoms are solvated by the molecules of TBP, so both metal and water are transferred between liquid phases.

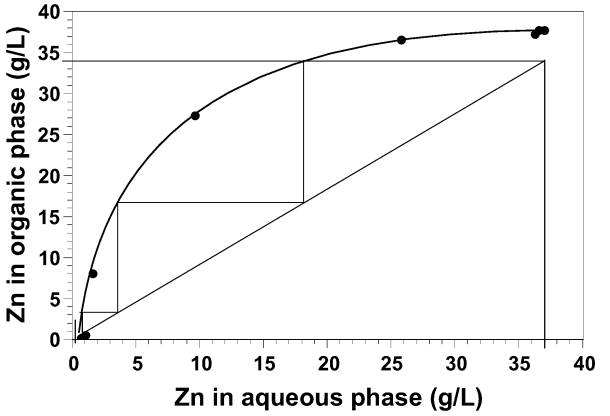

Figure 3. Isotherm of zinc extraction from the effluent with commercial TBP
Aqueous phase: effluent. Organic phase: 90% v/v TBP, A/O ratio = 1.

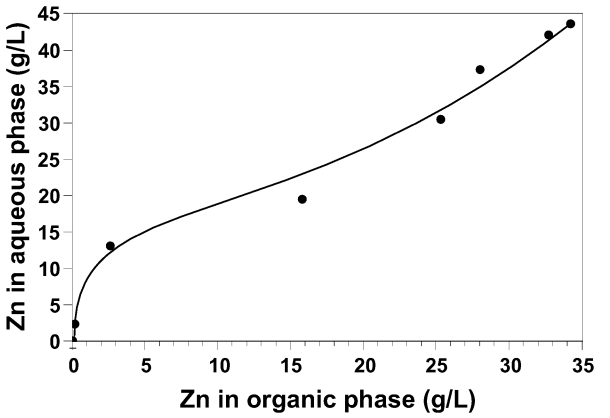

Figure 4. Isotherm of zinc stripping from the loaded organic phase
Aqueous phase: water. Organic phase: zinc-loaded 90% v/v TBP, A/O ratio = 1.

The average content of other metals in the raffinate was 1.8 g/L Mn, 0.003 g/L Cu, 0.074 g/L Ni, and 0.08 g/L Cr.

Table 1. Experimental conditions of pilot-scale tests in the pulsed column

Run*	Aqueous phase (Input / Output)			Organic phase (Input / Output)		
	Flowrates (mL/min)	[Zn] (g/L)	[Fe] (g/L)	Flowrates (mL/min)	[Zn] (g/L)	[Fe] (g/L)
E1	16.0 / 14.4	37.2 / 1.0	119 / 131	17.0 / 18.3	0.0 / 29.3	0.0 / 1.0
E2	14.6 / 13.4	37.2 / 0.4	119 / 127	18.5 / 21.8	0.0 / 31.0	0.0 / 1.5
E3	10.3 / 9.1	37.2 / 1.0	119 / 137	13.4 / 14.2	0.0 / 24.0	0.0 / 2.6
S1	16.1 / 17.2	0.0 / 32.5	0.0 / 1.1	16.3 / 16.1	28.0 / 0.5	1.5 / < 0.005
S2	14.1 / 15.8	0.0 / 29.6	0.0 / 1.8	18.5 / 16.8	27.5 / 0.8	1.0 / < 0.005
S3	10.0 / 11.2	0.0 / 25.1	0.0 / 3.0	13.1 / 11.4	28.0 / 0.7	1.5 / < 0.005

* E means “extraction run”; S means “stripping run”.

CONCLUSIONS

This study shows that solvent extraction with TBP is a feasible method to separate zinc from iron(II) from spent pickling effluents. In contrast to precipitation methods that are commonly used to treat such effluents, solvent extraction may allow the reuse of metals, thus avoiding the generation of toxic sludges that would be disposed in landfills. The process still needs to be optimized, and the reduction of iron(III) to iron(II) seems indispensable to reduce the contamination of iron in the final solution, thus making the recovery of a high-grade zinc product possible.

ACKNOWLEDGMENTS

Sincere thanks to CNPq, CAPES, FINEP, and FAPEMIG for financial support.

REFERENCES

1. J. M. Magalhães, J. E. Silva, F. P. Castro, and J. A. Labrincha, “Physical and Chemical Characterisation of Metal Ffinishing Industrial Wastes,” *J. Environ. Man.*, **75**(2) 157-166 (2005).
2. K. Schugerl, T. Burmaster, and M. Gudorf, “Selective Extractive Recovery of Metals from Heavy-Metal-Hydroxy Sludges of a Pickling Plant and Galvanic Processing,” ISEC 1996, Vol. 2, D. Shallcross, R. Paimin and L. Prvcic, Eds., University of Melbourne Publisher, Parkville, Australia; pp. 1549-1552.
3. A. Agrawal, K. K. Sahu, and B. D. S. Pandey, “Removal of Zinc from Aqueous Solutions using Sea Nodules Residue,” *Colloids Surf. A,* **237**, 133-140 (2004).
4. M. B. Mansur, S. D. F. Rocha, F. S. Magalhães, and J. S. Benedetto, “Selective Extraction of Zinc(II) over Iron(II) from Spent Hydrochloric Acid Pickling Effluents by Liquid–Liquid Extraction,” *J. Hazard. Mater.,* doi:10.1016/j.jhazmat.2007.05.019.
5. D. S. Flett, “Solvent Extraction in Hydrometallurgy: the Role of Organophosphorus Extractants,” *J. Organomet. Chem.*, **690**, 2426–2438 (2005).

SEPARATION OF ZINC AND COPPER FROM SULFURIC ACID LIQUOR OBTAINED IN THE LEACHING OF ZINC-INDUSTRY RESIDUES BY LIQUID-LIQUID EXTRACTION

Ligiane R. Gouvea and Carlos A. Morais

Centro de Desenvolvimento da Tecnologia Nuclear, CDTN/CNEN,
Av. Presidente Antônio Carlos, 6627 - Campus da UFMG – Pampulha, CEP 31270-901,
Belo Horizonte, MG, Brazil. Corresponding author email address: cmorais@cdtn.br

ABSTRACT

This paper describes a study of zinc and copper separation by liquid-liquid extraction from leach liquor generated in the treatment of zinc residue. The influence of extractant type and concentration, aqueous phase acidity, contact time, and stripping-agent concentration were investigated. Organophosphorus extractants (D2EHPA and CYANEX 272) and chelating extractants (LIX 63 and LIX 984N) were investigated. The organophosphorus reagents extracts preferably zinc, while the chelating extractants are selective for copper. D2EHPA was selected as the best extractant. The stripping study was carried out with sulfuric acid solution.

INTRODUCTION

Metallurgical extraction is employed to obtain pure metal from ores or by-products. Metallic zinc production from sulfide zinc concentrate comprises of roast–leach–electrowinning stages. In the calcine leaching step, minor metals such as cadmium, nickel and cobalt are leached with the zinc. The liquor purification, typically carried out by cementation, produces a residue containing high levels of zinc, cadmium, and copper. Generally, the treatment of this residue to recover zinc produces other residues that are stockpiled, generating an environmental liability. Recovering metals from such secondary source reduces environmental impact and could bring an economic return to metal producers [1].

The solid residue containing 26.9% Zn, 36.9% Cu, 1.9% Cd, 0.18% Co, and 0.21% Ni was obtained from a hydrometallurgical zinc facility. The residue was leached with a sulfuric acid solution. The resulting sulfuric liquor contained 29.6 g/L Zn, 37.4 g/L Cu, 1.94 g/L Cd, 0.127 g/L Co, and 0.100 g/L Ni.

Zinc and copper can be separated from sulfuric liquor by cementation or liquid-liquid extraction. In the former process, the high copper content of the solution consumes much reagent [2]. The metals separation is therefore more appropriate by solvent extraction. The solvent-extraction technique has become essential to the hydrometallurgical industry due to a growing market demand for high-purity metals,

rigid environmental regulations, the need for lower production costs, and the diminishing supply of high-grade ores reserves, requiring the treatment of ores of lower grade and greater complexity [2–3].

Flett [4] proposed di(2-ethylhexyl)phosphoric acid (D2EHPA) and CYANEX® 272 (acid extractants) for cobalt/nickel separation, as well as for zinc and rare earth extraction. LIX reagents (acid chelating extractants) are proposed for copper and nickel extraction. According to Zhang and collaborators [5], LIX® 63 was the first extractant to be commercialized specifically for copper extraction.

In the present study, the organophosphorus extractants (D2EHPA and CYANEX 272) and the chelating extractants (LIX 63 and LIX 984N) were investigated for Zn/Cu separation. The following process variables were tested using D2EHPA as extractant: aqueous phase acidity, D2EHPA concentration, contact time, and stripping agent concentration (sulfuric acid).

EXPERIMENTAL

Reagents and Solutions

D2EHPA, 97 wt %, was manufactured by Albright and Wilson Americas and supplied by Pecos Brasil Ltda. Bis(2,4,4-trimethylpentyl)phosphinic acid (CYANEX 272), 99 wt %, was manufactured by Cytec Canada Inc, and supplied by Cytec do Brasil Ltda. Both LIX 63 and LIX 984N are manufactured by Cognis and were supplied by Cognis do Brasil Ltda. LIX 63 is 5,8-diethyl-7-hydroxydodecane-6-oxime (2.27 mol/L oxime). LIX 984N is a mixture of oximes: 5-nonylsalicylaldoxime and 2-hydroxy-5-nonylacetophenone oxime (1.66 mol/L oxime). Exxsol® D-100 (purified kerosene), used as diluent, was supplied by Exxon Química.

The sulfuric acid (H_2SO_4) used in the stripping experiments and the ammonium hydroxide (NH_4OH) used for pH control were analytical grade. Solutions were prepared with distilled water.

The acidic sulfate liquor containing 29.6 g/L Zn, 37.4 g/L Cu, 1.94 g/L Co, and 0.100 g/L Ni was obtained from leaching residue of zinc and copper generated by a zinc producer.

Experimental Procedure

Extraction and stripping experiments were carried out in an agitated reactor (150 mL beaker with 5.3 cm diameter) at 500 rpm agitation and room temperature (~25 ^{o}C), using equal volumes (20 mL) of aqueous and organic phases. During extraction experiments, the pH of the aqueous phase was controlled with ammonium hydroxide solution (1-3 mol/L). After contact, the aqueous/organic mixture was transferred to a separation funnel, and the phases were collected separately. The metal content of each phase was determined by atomic absorption spectrometry. Unless specified otherwise, the O/A phase ratio was 1 and the equilibrium pH was 2.

RESULTS AND DISCUSSION

Extraction Step

Four cationic extraction agents were investigated: two organophosphorus acids (D2EHPA and CYANEX 272) and two chelating acids with oxime functional groups (LIX 63 and LIX 984N). The concentration of the organophosphorus extractants was 1 mol/L. The concentration of the LIX extractants was 1 mol/L oxime. The equilibrium pH was 3, and the agitation time was 15 min. The results of these experiments are shown in Table 2.

Table 2. Impact of extractant on zinc and copper extraction

Extractant	pH_{eq}	Separation factor		% Extraction	
		Zn/Cu	Cu/Zn	Zn	Cu
LIX 63	3.0	—	60	4.2	72.4
LIX 984N	3.1	—	37	9.4	79.3
D2EHPA	3.0	296	—	95.0	5.5
CYANEX 272	3.0	361	—	70.9	0.7

D2EHPA and CYANEX 272 are selective for zinc, while LIX 63 and LIX 984N are selective for copper. In metals separation, the separation factor is more important than the extraction coefficient. Experiments showed that the coalescence time for organophosphorus extractants was lower than the coalescence time for chelating extractants (<30 s and 8 min., respectively). This may be due the high LIX concentration used in the experiments. A good separation factor was obtained with all extractants tested. As D2EHPA is cheaper than the other extractants investigated, this reagent was selected to continue the study.

Contact Time

The aqueous and organic contact time adopted was between 10 and 15 min. With efficient pH control, 5 min. is sufficient to attain the extraction equilibrium.

Equilibrium pH

After choosing the extractant, the influence of the aqueous-phase acidity on metals separation was investigated. The effect of the equilibrium pH was investigated between 0.70 (without NH_4OH addition) and pH 3.5. The optimum contact time varied from 5 min. (without correction of pH) to 15 min. (pH 3.5). Results obtained are shown in Figure 1. The equilibrium pH is an important variable in the metals separation. Above pH 2, copper extraction increases and the Zn/Cu separation factor decreases. At low pH, the zinc extraction is not efficient.

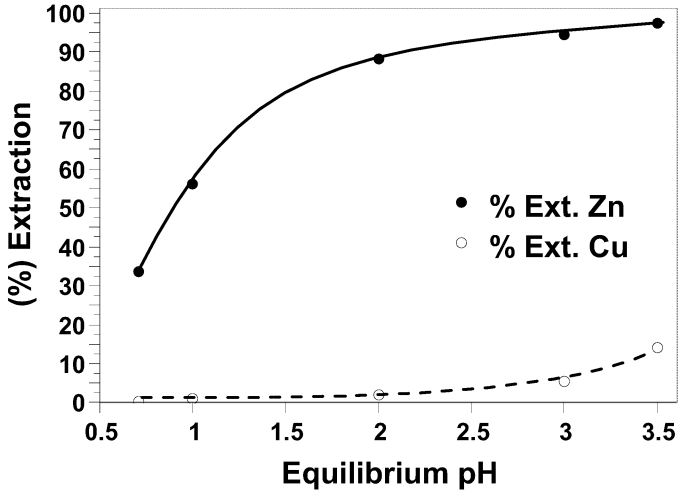

Figure 1. Influence of equilibrium pH in extraction of Zn and Cu with 1 mol/L D2EHPA.

Concentration of Extractant

The effect of extractant concentration in Zn/Cu separation was investigated between 0.25 mol/L and 1.0 mol/L D2EHPA. The equilibrium pH was maintained at 2 and the contact time varied from 10 to 15 min. The experiments indicated that zinc extraction increases with D2EHPA concentration, from 30% (0.25 mol/L D2EHPA) to 88% (1.0 mol/L D2EHPA). In the range of D2EHPA concentration investigated, copper extraction varied from 0.3% to 2.1%. The concentration of D2EHPA selected for the remainder of the study was 1.0 mol/L.

Stripping Step

The strip experiments were carried out with sulfuric acid solution. The influence of the sulfuric acid concentration was investigated from 0.01 mol/L to 3.0 mol/L using a volumetric phase ratio (O/A) of 1. The contact time was 5 min and the separation time was less than 30 s. The loaded solvent used in the stripping experiments contained 33 g/L Zn, 0.14 g/L Cu, 0.003 g/L Cd, and less than 0.001 g/L of Co and Ni. This loaded solvent was obtained by two successive discontinuous contacts with the liquor while maintaining an equilibrium pH of 2.

As shown in Figure 2, copper is more easily stripped than zinc. For 0.05 mol/L H_2SO_4, the percentages of metals stripped were 81% Cu and 12% Zn. This indicates that co-extracted copper can be scrubbed in a countercurrent mixer-settler system using a low H_2SO_4 concentration. Zinc will subsequently be stripped at a higher H_2SO_4 concentration.

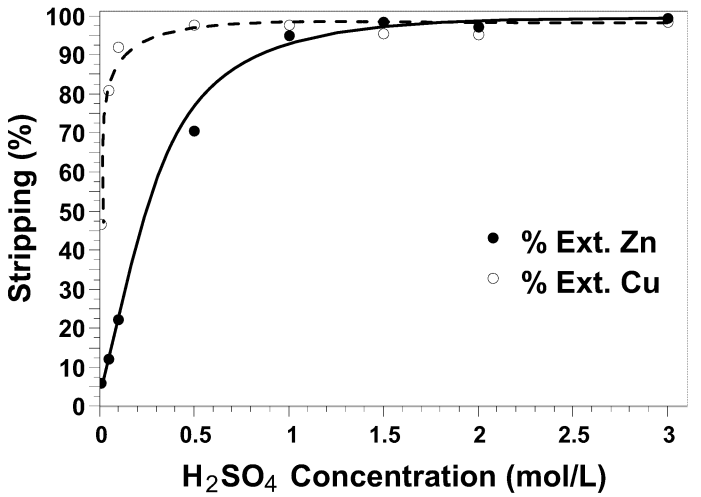

Figure 2. Influence of H_2SO_4 concentration in stripping of Zn and Cu from 1 mol/L D2EHPA.

McCabe-Thiele Diagrams

Using the laboratory test results, extraction and stripping isotherms (equilibrium curves) were constructed and McCabe-Thiele diagrams were drawn to determine the theoretical number of stages and the volumetric feed ratio of the liquor and solvent for the continuous experiments. The equilibrium curves were constructed according to the successive contacts technique using phase ratios of 1. The McCabe-Thiele diagrams are shown in Figures 3a and 3b.

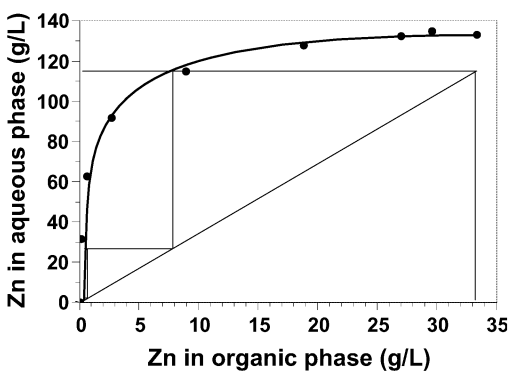

Figure 3a. Isotherm/McCabe-Thiele of Zn extraction from the sulfuric liquor with 1 mol/L D2EHPA.

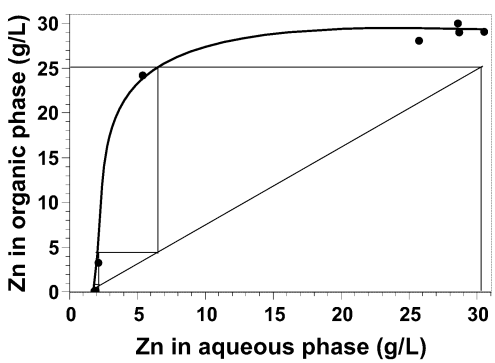

Figure 3b. Isotherm/McCabe-Thiele of Zn stripping from the loaded 1mol/L D2EHPA with 2 mol/L H_2SO_4.

Figure 3a indicates that three extraction stages at a phase ratio of 0.8 A/O will quantitatively extract zinc from the aqueous phase. For a loaded solvent containing 33 g/L Zn, a phase ratio of 3.5 (O/A) and three stripping stages are required (Figure 3b).

CONCLUSIONS

Organophosphorus extractants (D2EHPA and CYANEX 272) presented higher Zn/Cu separation factors compared to the chelating extractants investigated. The extractants of the LIX group (LIX 63 and LIX 984N) preferentially extract copper, while organophosphorus extractants are selective for zinc.

For D2EHPA and CYANEX 272, Zn/Cu separation factors about 296 and 361, respectively, were obtained. For the chelating extractants, the separation factor was about 60 for LIX 63 and 30 for LIX 984N. Further investigations carried out with D2EHPA indicated an ideal equilibrium pH of about 2.

Sulfuric acid stripping of loaded D2EHPA was very efficient. Copper was preferentially stripped, indicating that co-extracted copper could be removed from the organic phase in a scrubbing step using dilute sulfuric acid. Zinc can stripped with a more concentrated sulfuric acid solution.

ACKNOWLEDGMENTS

Sincere thanks to CNPq and FAPEMIG for financial support. The authors are also thankful to the CDTN's technicians who were involved with this work, mainly Luiz C. da Silva, Liliane P. Tavares, Marcos A. Evangelista, and Eugênio M. Oliveria.

REFERENCES

1. M. K. Jha, V. Kumar, and R. J. Singh, "Review of Hydrometallurgical Recovery of Zinc from Industrial Wastes," *Resources, Conservation and Recycling*, **33**, 1–22 (2001).
2. E. K. Alamdari, "Synergistic Effect of MEHPA on Co-extraction of Zinc and Cadmium with DEHPA," *Minerals Engineering*, **17**, 89–92 (2004).
3. G. Owusu, "Selective Extractions of Zn and Cd from Zn-Cd-Co-Ni Sulphate Solution using Di(2-ethylhexyl)phosphoric Acid Extractant," *Hydrometallurgy*, **47**, 205–215 (1998).
4. D. S. Flett, "Solvent Extraction in Hydrometallurgy: The Role of Organophosphorus Extractants," *Journal of Organometallic Chemistry*, **690**, 2426–2438 (2005).
5. P. Zhang, K. Inoune, K. Yoshizuka, and H. Tsuyana, "Extraction and Selective Stripping of Molybdenum(VI) and Vanadium(IV) from Sulfuric Acid Solution Containing Aluminum(III), Cobalt(II), Nickel(II) and Iron(III) by LIX 63 in Exxsol D80," *Hydrometallurgy*, **41**, 45–53 (1996).

SELECTIVE EXTRACTION AND RECOVERY OF COPPER FROM ZINC LEACHING LIQUOR

A. Deep, S.M.C. Santos, R.M. Machado, and J.M.R. Carvalho

Centre of Chemical Processes, Department of Chemical Engineering
Instituto Superior Técnico, Av. Rovisco Pais, 1049-001, Lisbon, Portugal
Corresponding author email address: jcarv@ist.utl.pt

ABSTRACT

The present paper describes solvent-extraction and separation studies of Cu from a leaching liquor obtained by the direct atmospheric leaching of a Zn concentrate with an oxidative mixture of $Fe_2(SO_4)_3$ (0.4 M) and H_2SO_4 (0.5 M) in the presence of O_2 at 353 K. The obtained leaching solution, containing 34 g L^{-1} Zn^{2+}, 1.1 g L^{-1} Cu^{2+}, 5 mg L^{-1} In^{3+}, and 41 g L^{-1} Fe (20% Fe^{3+}, 80% Fe^{2+}) was subjected to the extraction with a solution of 25% v/v ACORGA M5640 modified with 12.5% v/v isodecanol in ESCAID 110. Quantitative (>98%) and selective transfer of Cu^{2+} in to the organic phase was achieved in the equilibrium pH range of 1.3–1.5 (A/O = 1). The presence of isodecanol in the extractant solution helped in obtaining complete stripping of Cu^{2+} using a synthetic spent electrolyte solution. Cu^{2+} was distributed in the organic phase by forming the complex CuR_2 (R = anionic moiety of the extractant molecule). Three stages of extraction at an A/O ratio of 5 were applied to preconcentrate the metal content ($Cu^{2+}_{\text{initial-aqueous}}$ = 1.1 g L^{-1}) in the organic phase ($Cu^{2+}_{\text{after extraction, in LO}}$ = 5.4 g L^{-1}). This step selectively and quantitatively extracted Cu^{2+} leaving Zn^{2+}, Fe^{3+}, Fe^{2+}, and In^{3+} in the raffinate. The loaded organic phase was scrubbed with dilute acid solution (20 g L^{-1} H_2SO_4) followed by the stripping of Cu^{2+} with a solution of 25 g L^{-1} of Cu^{2+} in 180 g L^{-1} of H_2SO_4 (A/O = 1, two stages).

INTRODUCTION

Leaching–solvent extraction–electrowinning is a popular technology for the recovery of copper. Efforts are devoted to the development of more environmentally friendly and economical ways of oxidative pressure leaching or direct atmospheric leaching of sulfide concentrates, coupled with solvent extraction. The present study incorporated the treatment of a zinc sulfide (S ≈ 36%) concentrate, which is composed of values of Zn (40–45%), Cu (2.5–4.0%), and In (0.016–0.020%). Its direct atmospheric leaching with ferric sulfate as an oxidant produces a leaching liquor with a typical composition of 35 g L^{-1} Zn^{2+}, 1.2 g L^{-1} Cu^{2+}, 6 mg L^{-1} In^{3+}, and 42 g L^{-1} Fe^{3+} + Fe^{2+}. Generally, leaching solutions in the Zn industry are processed through a number of purification steps,for example the oxidation of Fe^{2+}, precipitation of the resulting Fe^{3+} to jarosite/goethite/hematite slurry, cementation of Cu^{2+}, and the solvent extraction of Zn^{2+}. The precipitation and to some extent the cementation parts of the purification process

pose two significant problems. Metal contents of value are lost, and the solid wastes generated require special landfills for their disposal.

The work presented in this paper is a part of an ongoing project in collaboration with Somincor, Portugal, to develop a hydrometallurgical flow sheet for the production of Cu, In, Fe, and Zn in some saleable form. The four metals, in this order, are planned to be extracted in separate extraction circuits using different extractants. Copper extractant market is dominated by LIX (Cognis) and ACORGA (Cytec) brands of oximes [1]. ACORGA M5640 has been picked up in the present work to be used in the copper extraction circuit. This reagent is known for its copper selective nature, more specifically with respect to iron [2,3], and it seems suitable *vis-à-vis* the objectives undertaken herein. Several parameters including the effect of equilibrium pH, extractant concentration, and modifier are investigated to find out the most suitable conditions for the quantitative and selective recovery of copper from the leaching liquor. Extraction and stripping isotherms have been drawn to identify experimental conditions for the upgrading of a synthetic spent cell electrolyte.

MATERIALS AND PROCEDURE

ACORGA M5640 and Escaid 110 (200-248 °C fraction hydrocarbon fluid with 99.5% aliphatic content) were received from Cytec Netherlands and ExxonMobil Spain, respectively. The active substance of ACORGA M5640 was 5-nonylsalicylaldoxime. A fatty ester, 2,4,4-trimethyl-1,3-pentanediol di-isobutyrate, was present as a modifier. Isodecanol, a 99% pure product from Riedel-de Haën, Germany, was used as a second modifier. All other chemicals were of Analytical Reagent grade from Merck UK. Working solutions of the metal ions were prepared by dissolving their suitable salts, namely, $CuSO_4.5H_2O$, $ZnSO_4.7H_2O$, $In_2(SO_4)_3$, and $Fe_2(SO_4)_3$, in dilute sulfuric acid, and making up the required volume with deionized water. The pH values were measured with a Metrohm 827 pH lab pH meter using a Metrohm 6.0228.010 glass electrode.

For the solvent-extraction experiments, the aqueous and the organic phases, contained in 250 mL separating funnels (A/O = 1, unless otherwise reported), were contacted (150 rpm) in an orbital shaker (Aralab Agitorb 160 E) at ambient temperature (298 ± 1 K) for 10 min to ensure maximum mass transfer. Longer contact time (15, 20, 25, 30 min) of the two phases did not change the results. Wherever necessary, the pH of the aqueous phase was adjusted by adding suitable volumes of NaOH or H_2SO_4 solution. After the separation of the equilibrated phases, the metal concentration in the aqueous phase was determined by atomic absorption spectrophotometry (AAnalyst 200, Perkin Elmer). The metal concentrations in the organic phase were calculated by mass balance given that the volumes of aqueous and organic phases did not change during the equilibration. The stripping of the loaded organic phase was carried out (t = 10 min) at 298 ± 1 K by using 25 g L^{-1} of Cu^{2+} in 180 g L^{-1} H_2SO_4 (A/O = 1) as the reagent.

Oxidative leaching of a sample of zinc concentrate mined from the Neves-Corvo Mine, Portugal, was carried out with 0.40 M $Fe_2(SO_4)_3$ and 0.50 M H_2SO_4 (S/L ratio = 100 g in 1 L) in a five-necked round bottom reactor (1 L, 13 cm diameter) fitted with an agitating (450 rpm) single round paddle impeller. The reaction temperature was maintained at 353 ± 3 K. Throughout the course of the experiment, oxygen gas was

sparged into the reaction vessel (60 L/h) to maintain the ferric form of the oxidant. Under these conditions, the dissolution of zinc took place according to the following equation

$$ZnS + Fe_2(SO_4)_3 \Rightarrow ZnSO_4 + 2FeSO_4 + S^0 \quad (1)$$

Twelve hours of leaching reaction yielded 85 and 50% recovery of Zn^{2+} and Cu^{2+}, respectively. Final total concentrations of Fe (total) and In^{3+} were 42 g L^{-1} (80% Fe^{2+}, 20% Fe^{3+}) and 6 mg L^{-1}, respectively. The pH of the leaching solution was observed to be 0.5. It was raised to 1.4 by slow addition of 5 M NaOH solution. Finally the leaching solution had the following composition: 1.1 g L^{-1} Cu^{2+}, 34 g L^{-1} Zn^{2+}, 5 mg L^{-1} In^{3+}, and 41 g L^{-1} Fe (total).

RESULTS AND DISCUSSION

Cu^{2+} Extraction as a Function of Equilibrium pH

Figure 1 shows the extraction behavior of Cu^{2+} with 25% extractant solution (A/O = 1). Apparently, a cation-exchange mechanism was involved. Quantitative extraction (~96%) was achieved at pH values higher than 1.3. An unchanged pattern of Cu^{2+} extraction with respect to the equilibrium pH was observed in the metal ion concentration range of 0.50 – 2.0 g L^{-1}. Figure 1 also shows the extraction behaviors of Zn^{2+} (15–40 g L^{-1}), In^{3+} (1–50 mg L^{-1}), Fe^{3+} (1–40 g L^{-1}), and Fe^{2+} (1–40 g L^{-1}). These associated metal ions were negligibly extracted over the entire range of aqueous phase acidity investigated.

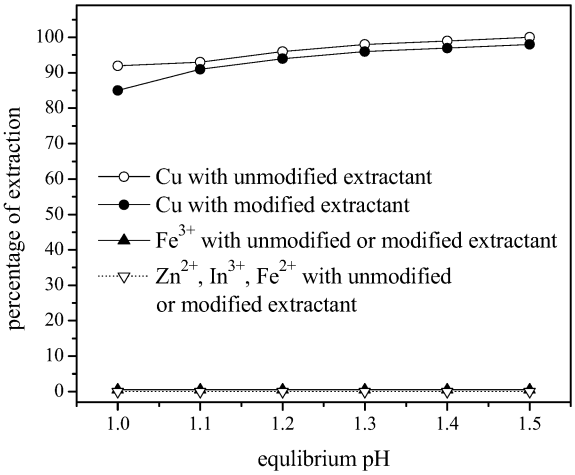

Figure 1. Extraction of Cu^{2+}, Zn^{2+}, In^{3+}, Fe^{3+}, and Fe^{2+} in unmodified and modified (with isodecanol) 25% v/v ACORGA M5640.

Since the solvent extraction of copper is frequently coupled with electrowinning, industrial utility of the copper-extraction process would depend upon the successful stripping of the loaded metal with spent electrolyte from the cell house. Investigations on

the stripping of Cu^{2+} from the loaded organic phase (25% ACORGA M5640, $Cu^{2+}_{organic}$ = 1.0 – 5.0 g L^{-1}, A/O = 1) with a synthetic spent electrolyte (25 g L^{-1} Cu^{2+} solution in 180 g L^{-1} H_2SO_4) indicated only 45 ± 10% recovery of the metal ion from the organic phase in a single stage operation. Increasing the time of equilibration to 45 min did not change the results. This difficulty in the stripping can be attributed to a strong interaction between ACORGA M5640 and Cu^{2+}. Using a higher A/O phase ratio (5) improved the stripping efficiency (up to 90%), but it did not usefully upgrade the spent electrolyte.

The mixing of isodecanol with ACORGA M5640 improved the stripping of Cu^{2+} to around 90% in a single stage experiment (A/O = 1). The use of the modified extractant solution, however, tended to decrease the extraction of Cu^{2+}. Table 1 gives the data on the effect of isodecanol addition on the extraction and stripping characteristics of the presented system. For further studies, an extractant solution of 25% v/v M5640 + 12.5% isodecanol was chosen. Figure 1 also shows the extraction of Cu^{2+} and other associated metals as function of equilibrium pH. Clearly, there was a decrease in the extraction percentage of Cu^{2+}, but the extractant's selectivity remained unaffected.

Table 1. Effect of isodecanol (second modifier) addition on the extraction and stripping of Cu^{2+} ($Cu^{2+}_{initial}$ = 1.1 g L^{-1}, T = 298 K, t = 10 min, shaking speed = 150 rpm, stripping reagent = 25 g L^{-1} Cu^{2+} in 180 g L^{-1} H_2SO_4)

M5640 conc. % v/v	Modifier conc. % v/v	Equil. pH in extraction	A/O in extraction	% extraction	A/O in stripping	% stripping
25	0	1.4	1	99	1	50
25	12.5	1.4	1	96	1	90
25	20	1.4	1	89	1	93
25	25	1.4	1	78	1	97

Cu Extraction as a Function of Extractant Concentration

The extraction of Cu^{2+} has been studied against extractant solutions of various concentrations (5–25% v/v; or 0.18 – 0.91 M), both in absence and in presence of modifier (2:1 v/v M5640 isodecanol). Figure 2 shows the results. The slope of around 1 between the extractant concentration and the distribution ratio highlighted the involvement of one molecule of M5640 in the formation of extracted species. This observation also indicated about the dimerization of the extractant molecule in the given experimental conditions. The extraction reaction can be proposed as

$$Cu^{2+} + (HR)_2 \rightarrow CuR_2 + 2H^+ \qquad (2)$$

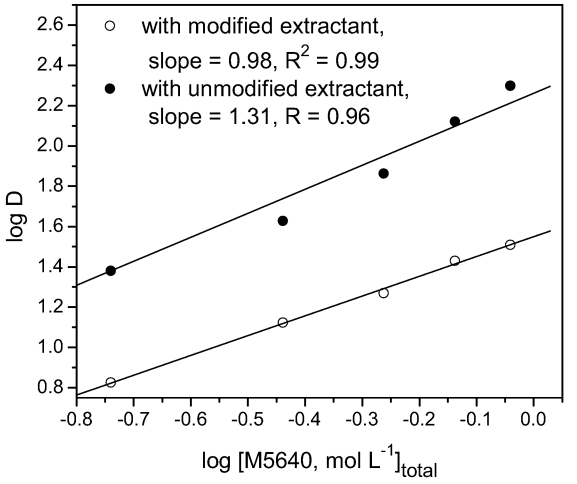

Figure 2. Extraction of Cu^{2+} as a function of extractant concentration.

Extraction Isotherm

Figure 3 shows the loading of the organic phase with increasing amounts of copper (A/O = 1, 2, 5, 7.5, 10) in the aqueous phase. Higher loading of the organic phase is required to upgrade the spent electrolyte from the electrowinning cell. Further studies were focused on using A/O ratio of 5 during the extraction, which provided an upgrading of around 5 g L^{-1} of spent electrolyte after the stripping. As shown in Figure 3, three stages of the extraction completely (>98%) extracted Cu^{2+} ($Cu^{2+}_{initial}$ = 1.1 g L^{-1}) from the aqueous phase. The A/O ratio and number of stages can be maneuvered depending upon the composition of the leaching solution and equipment inventory available.

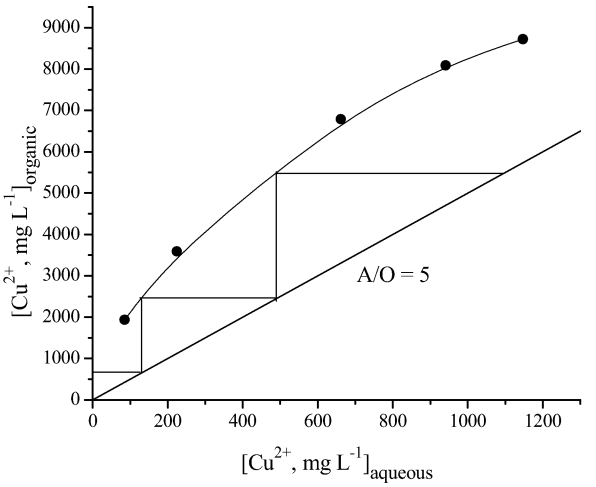

Figure 3. Extraction isotherm for Cu^{2+} - M5640 (equilibrium pH = 1.4) system.

Quantitative stripping of the extracted metal was achieved in two stages (A/O = 1) using a synthetic spent electrolyte solution of 25 g L^{-1} Cu^{2+} in 180 g L^{-1} of H_2SO_4. The final concentration of the stripping liquor was 30 g L^{-1} Cu^{2+}.

Separation and Recovery of Copper from the Zinc Concentrate Leaching Liquor

Leaching liquor, containing 1.1 g L^{-1} Cu^{2+}, 34 g L^{-1} Zn^{2+}, 41 g L^{-1} Fe (total), and 5 mg L^{-1} In^{3+}, was subjected to solvent extraction with 25% v/v M5640 (+ 12.5% v/v isodecanol) in three stages (A/O = 5) (T = 298 K, t = 10 min in each stage, shaking speed = 150 rpm). The initial pH of the leaching solution was 1.4; and this pH was maintained during the extraction step. After the extraction step, the composition of the raffinate was found to be 20 mg L^{-1} Cu^{2+}, 34 g L^{-1} Zn^{2+}, 41 g L^{-1} Fe (total), and 5 mg L^{-1} In^{3+}. The organic phase was then scrubbed (A/O = 0.2) with 20 g L^{-1} H_2SO_4 solution. Finally, the loaded amount of Cu^{2+} was recovered by stripping in two stages (A/O = 1) with 25 g L^{-1} Cu^{2+} in 180 g L^{-1} of H_2SO_4 (T = 298 K, t = 10 min, shaking speed = 150 rpm). Pure copper electrolyte (30 g L^{-1} Cu) was obtained, while the treated leaching solution can further be treated for the separation and recovery of In^{3+}, Fe^{3+}, and Zn^{2+}.

CONCLUSIONS

ACROGA M5640 has been successfully used for the separation and recovery of pure copper from a zinc concentrate leaching solution. The extractant solution needs to be modified with isodecanol in order to improve the stripping characteristics. Negligible co-extraction of associated metals, such as In, Fe, and Zn, is observed.

ACKNOWLEDGMENTS

Authors are thankful to Cytec, Netherlands, for the sample of extractant. Thanks are due to ExxonMobil, Spain, for the sample of diluent. AD acknowledges the postdoctoral fellowship (SFRH/BPD/20321/2004) from the FCT, Portugal. We thank the Portuguese innovation agency (ADI; PRIME-IDEIA, Project no. 70/00191), Somincor, and the Center of Chemical Processes, IST, for providing use of the research facilities.

REFERENCES

1. G. A. Kordosky, “Copper Solvent Extraction Reagents Past Present and Future,” Paper presented at the International Conference on Clean Technologies for the Mining Industry, May 9–13, 2000, Santiago, Chile, 2000. http://www.cognis.com/mining/mid/services/pdfs/Expomin_2000.pdf (accessed on 29th October 2007).
2. J. L. Vander and R. F. I. De Ketelaere, “Selective Recuperation of Copper by Supported Liquid Membrane (SLM) Extraction,” *J. Membrane Science*, **139**(1), 125–135 (1998).
3. J. R. Spence and M. D. Soderstrom, “Practical Aspects of Copper Solvent Extraction from Acidic Leach Liquors,” CYTEC report, http://www.cytec.com/specialty-chemicals/pdf/practical.pdf (accessed on 29th October 2007).

SOLVENT-EXTRACTION SEPARATION OF ZINC, MANGANESE, AND COBALT IN SULFATE SOLUTIONS BY D2EHPA

A.R. Eivazi Hollagh,[1,2] D. Moradkhani,[2,3] E. Keshavarz Alamdari,[4,5] and D. Darvishi [4,5]

[1]Young Research Club Azad University South Tehran Branch, Iran
[2]R&D Center, Iranian Zinc Mines Development Company, Zanjan, Iran
[3]Faculty of Engineering, Zanjan University, Zanjan, Iran. [4]Mining & Metallurgical Engineering, Amirkabir University of Technology, Tehran, Iran
[5]Materials and Energy Research Center, P.O. Box 14155-4777, Tehran, Iran
Corresponding author E-mail address: alireza.eivazi@gmail.com

ABSTRACT

The effect of pH on the extraction of zinc, manganese, and cobalt at different temperatures has been investigated. Different percentages of tributylphosphate (TBP) as modifier were used with di(2-ethylhexyl)phosphoric acid (D2EHPA) as extractant. Increasing the ratio of TBP to D2EHPA at ambient temperature shifts the extraction curves of cobalt and manganese to higher pH, and there was no effect observed on the extraction of zinc. The most suitable extractant for separation of zinc over manganese is 20% v/v D2EHPA with 2.5 to 5% v/v TBP, and for manganese over cobalt, 20% v/v D2EHPA with 2.5 or 5% v/v TBP was selected. The experiments were carried out at temperatures of 10, 23, 40, and 60 °C. The best temperature for separation of manganese from cobalt was 23 ºC. Cobalt extraction is endothermic, while manganese extraction is exothermic. The values of the enthalpy change for cobalt and manganese extrantion were determined to be 24.3 and -7.2 kJ/mol, respectively.

INTRODUCTION

Hydrometallurgical methods can be used for the production zinc, manganese, and cobalt. Solvent extraction (SX) can be applied to separate and recover the metals of interest from a leach liquor because of its low energy consumption, small volume of waste for disposal, and lower levels of toxic emissions, compared say, to a smelter [1]. The leach liquor used for this study contained cobalt, manganese, and zinc. The manganese and other impurities such as zinc could be separated by SX. This process could be much simpler, and there may be significant savings in capital and operating costs [2].

A survey of published literature indicates that many studies have been carried out to examine the separation of cobalt from impurities such as Mn, Ca, Mg, Cu, and Zn. Dhadke and Ajgaonkar [3] have quantitatively extracted manganese and cobalt from sulfate solutions using CYANEX® 302 (Cytec) in toluene. Co(II) was extracted in the pH

range 7.0–7.5, whereas Mn(II) was extracted in the range 8.5–9.5 [3]. Also, Devi et al. [4] examined D2EHPA, PC-88A (Daihachi), and CYANEX 272 (Cytec) in order to separate cobalt from manganese in sulfate solutions. Their study proposed the use of 0.05 M NaD2EHPA to extract Mn(II) from Co(II) at pH 4.45. Cheng (2000) [2] studied the separation of manganese from cobalt by D2EHPA in kerosene. At pH 3.5, separation of manganese from cobalt was achieved at ambient temperature. The separation of manganese from cobalt in sulfate solution using D2EHPA in kerosene was also reported by Hoh et al. [1]. Cheng (2006) [5] reported on the ease of separation of nickel and cobalt from manganese, calcium, and magnesium with the synergistic mixture of 0.5 M Versatic 10 acid (Shell)/0.35 M LIX® 63 (Cognis) in Shellsol® 2046 (Shell) diluent. Moreover, this study reported a complete separation of nickel, cobalt, zinc, and copper from manganese, magnesium, and calcium with Versatic 10/decyl-4-pyridinecarboxylate [5]. Ocana and Alguacil [6] studied the extraction of cobalt by CYANEX 301 (Cytec) in Iberfluid® (CS) diluent from manganese sulfate solutions. Maximum extraction of Co(II) occurred at pH 1.0, while Mn(II) remained in the raffinate. Simultaneous solvent extraction of cobalt and nickel in the presence of manganese and magnesium from sulfate solutions was carried out using CYANEX 301 in Exxsol® D-80 (Exxon) by Tsakiridis and Agatzini [7]. Darvishi et al. [8] found that 0.6 M D2EHPA was more effective for separating manganese from cobalt than a mixture of 0.3 M D2EHPA and 0.3 M Cyanex 302. Keshavarz et al. [9] mentioned that addition of tri-*n*-butylphosphate (TBP) to D2EHPA could be useful to counterbalance the effect of M2EHPA (mono(2-ethylhexyl)phosphoric acid), which is present as an impurity in D2EHPA, and TBP improves the selectivity for zinc over cadmium.

The purpose of this work was to study the effect of adding TBP to D2EHPA on cobalt separation from zinc and manganese and to assess the effect of temperature on the separation of cobalt and manganese. A second goal in this project was to ascertain cobalt and manganese extraction enthalpy changevalues for mixtures of D2EHPA and TBP.

EXPERIMENTAL PROCEDURES

Materials and Reagents

All extractants, metal (zinc, manganese, and cobalt) sulfates, and sodium sulfate were laboratory grade materials. D2EHPA was purchased from Bayer, Germany, and the TBP was manufactured by Merck, Germany. Tehran Refinery Company supplied kerosene used as the diluent.

Experimental Method

Experiments were carried out in a 2 L glass beaker placed in a water bath and equipped with a mechanical stirrer. The bath temperature was digitally controlled within ±0.5 °C. Extractant concentration in all cases was 20% v/v D2EHPA. Equal volumes of aqueous and organic solutions were agitated. The pH of the mixed solutions was measured using a WTW portable pH meter. The electrode of the pH meter that was used for the mixed solution was calibrated with a suitable electrode for aqueous solution with

automatic temperature compensation, and then the pH values were reported. Sulfuric acid and ammonia solution were used to adjust the solution pH as required. The test was continued until each of the solution equilibrium pH values had been obtained. The aqueous samples were analyzed by atomic absorption spectrophotometry.

RESULTS AND DISCUSSION

Effect of TBP Addition on Extraction

Experiments were carried out to investigate the effect of TBP on the extraction of zinc, manganese, and cobalt at ambient temperature. Figure 1 shows the pH isotherm extraction curves for zinc, manganese, and cobalt, using D2EHPA and varying amounts of TBP as modifier. As can be seen, adding TBP affected the cobalt and manganese extraction curves, shifting them to higher pH values. There was no effect on the zinc extraction. Table 1 shows $pH_{0.5}$ (pH at 50% metal extraction) and $\Delta pH_{0.5}$ (the $pH_{0.5}$ differences of two metals) values for the three metals.

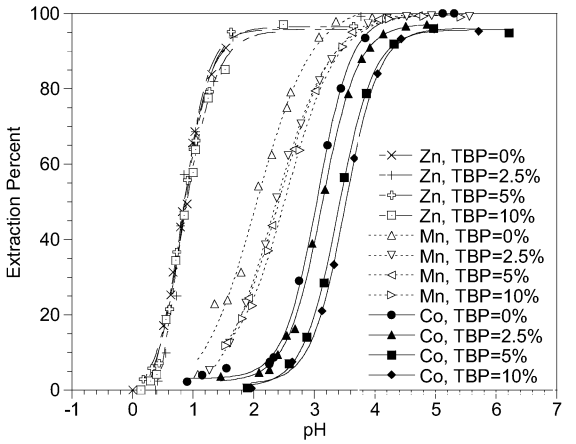

Figure 1. Effect of TBP on extraction of zinc, manganese, and cobalt by 20% D2EHPA at 23 ºC.

Table 1. Variation in $pH_{0.5}$ values due to TBP additions to 20% D2EHPA (23 °C)

TBP (% v/v)	$pH_{0.5}$			$\Delta pH_{0.5}$	
	Zn	Mn	Co	Mn-Zn	Co-Mn
0	0.86	2.05	3.03	1.2	1.0
2.5	0.86	2.37	3.14	1.5	0.8
5	0.90	2.41	3.43	1.5	1.0
10	0.89	2.51	3.52	1.6	1.0

Separation of Zinc and Manganese

As can be seen in Figure 1, adding TBP as modifier to D2EHPA as extractant increases the Zn-Mn $\Delta pH_{0.5}$ values. The differences between $pH_{0.5}$ values of zinc and manganese can be attributed to the selectivity of zinc and manganese extraction. The

results from Table 1 may indicate that the mixture of 20% v/v D2EHPA and 2.5-5% v/v TBP increases the separation.

Separation of Manganese and Cobalt

Based on the results of Table 1, it can also be seen that $\Delta pH_{0.5}$ values between cobalt and manganese were not affected significantly by additions of TBP to the D2EHPA. However, using the same percent TBP here as was found best for Mn-Zn separation, that is, 2.5% or 5% TBP, seems to have significant benefit.

Effect of TBP Concentration on Separation Factors

Variation of $\beta_{Mn/Co}$ and $\beta_{Zn/Mn}$ with pH is illustrated in Figure 2. As can be seen in Figure 2a, the separation factor for manganese over cobalt decreases by adding 2.5% v/v TBP to 20% v/v D2EHPA, but the separation factor is improved by adding 5% v/v TBP to D2EHPA. Figure 2b shows that the separation of zinc over manganese was improved by adding the first 2.5% TBP, but further additions had no significant effect.

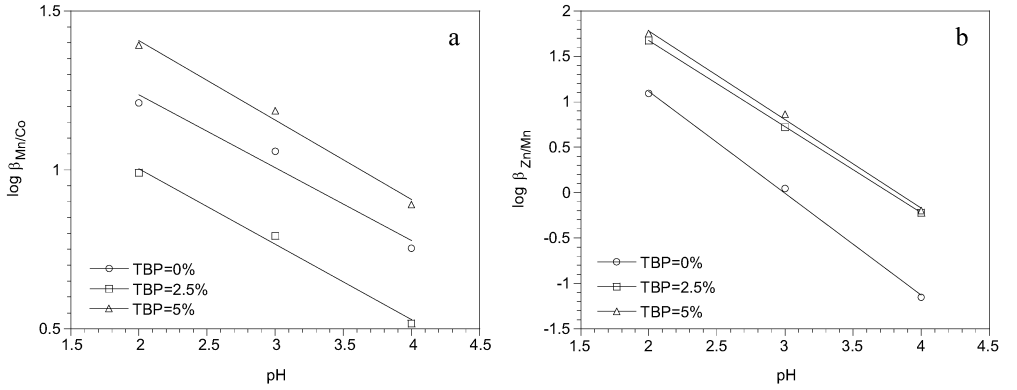

Figure 2. Variation of log β with pH for different amounts of TBP at 23 °C. (a) Mn over Co; (b) Zn over Mn.

Effect of Temperature on Manganese and Cobalt Extraction

Manganese-Cobalt Separation

In order to achieve the best separation between cobalt and manganese, the effect of temperature on percent extracted was also carefully examined at four different temperatures, 10, 23, 40, and 60 °C. As shown in Figure 3, the cobalt extraction curve shifted slightly to lower pH at the higher temperatures in the range studied. No change was observed in manganese extraction. Considering $\Delta pH_{0.5}$ values for manganese over cobalt, the best separation is observed at temperatures of 23 °C or lower (Figure 4).

Reaction Thermochemistry

The equilibrium constants were calculated from the equilibrium aqueous and organic concentrations for the metal and extractant using the assumed extraction

stoichiometry and further assuming ideal behavior (activity coefficients = 1). Plotting the logarithm of these values against the temperature yielded straight lines as seen in Figure 5, and the slope of the lines is the reaction enthalpy. The equilibrium constants, however, were calculated by applying the method of Darvishi et al. [8,10]. Figure 5 shows that the cobalt extraction is endothermic, while the manganese extraction is exothermic, with reaction enthalpy change values for cobalt and manganese estimated at 24.3 and -7.2 kJ/mol, respectively. The relatively smaller reaction enthalpy for Mn, compared to Co, supports the observation that temperature has comparatively less effect on manganese than on cobalt extraction.

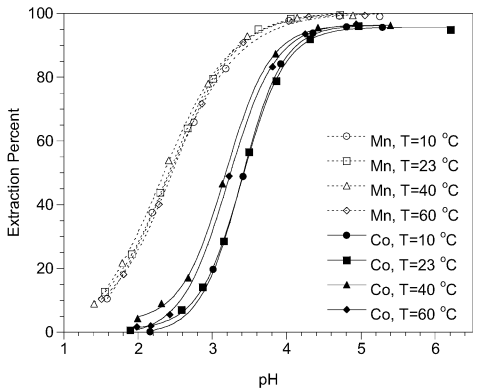

Figure 3. Effect of temperature on Mn and Co extraction (20% v/v D2EHPA + 5% v/v TBP).

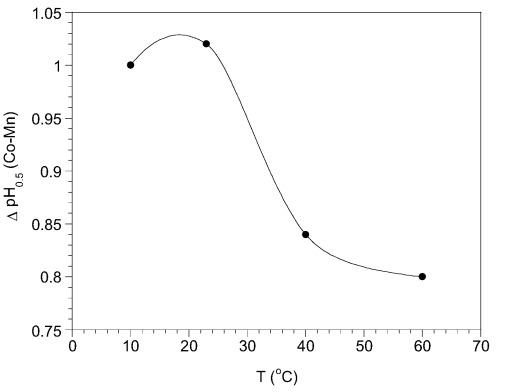

Figure 4. Effect of temperature on $\Delta pH_{0.5(Co\text{-}Mn)}$ (20% v/v D2EHPA + 5% v/v TBP).

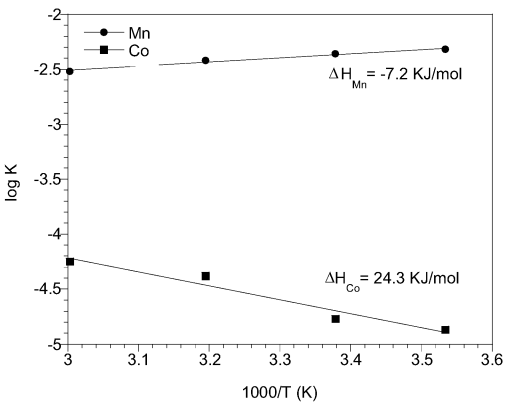

Figure 5. Temperature dependence of the equilibrium constant (20% D2EHPA + 5% TBP).

CONCLUSIONS

Experiments were carried out to investigate the effect of pH on the extraction of zinc, manganese, and cobalt at ambient temperature. The most suitable extractant for

separation of zinc and manganese was 20% v/v D2EHPA with 2.5-5% v/v TBP. Examination of $\Delta pH_{0.5}$ values for cobalt and manganese showed that adding TBP had little effect. However, due to the obtained $\Delta pH_{0.5}$ values, using the same percent TBP as was found best for Mn-Zn separation could be selected for the separation of manganese and cobalt. Examination of the effect of TBP addition on the separation factor supports conclusions from the ΔpH data. The extraction of cobalt shifted to lower pH with increasing temperature, whereas the extraction curve of manganese was unaffected. According to these results, the best separation of cobalt and manganese is at ambient temperature. The relative reaction enthalpies for Co and Mn extraction predict that Mn extraction should be less sensitive to temperature compared to cobalt extraction, as was observed.

ACKNOWLEDGMENTS

The authors would like to acknowledge the Iranian Zinc Mines Development Company, Zanjan, Iran, for financial support and the permission to publish this paper.

REFERENCES

1. Y.-C. Hoh, W.-S. Chuang, B.-D. Lee, and C.-C. Chang, "The Separation of Manganese from Cobalt by D2EHPA," *Hydrometallurgy*, **12**, 375–386 (1984).
2. C. Y. Cheng, "Purification of Synthetic Laterite Leach Solution by Solvent Extraction using D2EHPA," *Hydrometallurgy*, **56**, 369–386 (2000).
3. P. M. Dhadke and H. S. Ajgaonkar, "Liquid-Liquid Extraction of Cobalt(II) and Manganese(II) with Bis(2,4,4-trimethylpentyl)monothiophosphinic Acid (Cyanex 302)," *Indian J. Chem. Technol.*, **3**(6), 358–362 (1996).
4. N. B. Devi, K. C. Nathsarma, and V. Chakravortty, "Separation of Divalent Manganese and Cobalt Ions from Sulfate Solutions using Sodium Salts of D2EHPA, PC 88A and Cyanex 272," *Hydrometallurgy*, **54**, 117–131 (2000).
5. C. Y. Cheng, "Solvent Extraction of Nickel and Cobalt with Synergistic Systems consisting of Carboxylic Acid and Aliphatic Hydroxyoxime," *Hydrometallurgy*, **84**, 109–117 (2006).
6. N. Ocana and F. J. Alguacil, "Cobalt-Manganese Separation: the Extraction of Cobalt(II) from Manganese Sulfate Solutions by Cyanex 301," *J. Chem. Technol. Biotechnol.*, **73**, 211–216 (1998).
7. P. E. Tsakiridis and S. L. Agatzini, "Simultaneous Solvent Extraction of Cobalt and Nickel in the Presence of Manganese and Magnesium from Sulfate Solutions by Cyanex 301," *Hydrometallurgy*, **72**, 269–278 (2004).
8. D. Darvishi, E. Keshavarz Alamdari, M. Teimori, S. K. Sadrnezhaad, and D. F. Haghshenas, "Extraction of Manganese from Solutions containing Zinc and Cobalt by D2EHPA and of D2EHPA-Cyanex 272 or D2EHPA-Cyanex 302 Mixtures," Proceedings of the International Solvent Extraction Conference, Beijing, China, 2005.
9. E. Keshavarz Alamdari, D. Darvishi, S. K. Sadrnezhaad, and D. F. Haghshenas, "Synergistic effect of TBP on separation of zinc and cadmium with D2EHPA," Proceedings International Solvent Extraction Conference, Beijing, China, 2005.
10. D. Darvishi, D. F. Haghshenas, E. Keshavarz Alamdari, S. K. Sadrnezhaad, and M. Halali, "Synergistic Effect of Cyanex 272 and Cyanex 302 on Separation of Cobalt and Nickel by D2EHPA," *Hydrometallurgy*, **77**, 227–238 (2005).

EFFECT OF TBP ON THE THERMODYNAMICS OF Zn, Cd, Co AND Mn EXTRACTION WITH D2EHPA

D. Darvishi,[1,2] D. Haghshenas Fatmehsari,[1] S. Etemadi,[1] and E. Keshavarz Alamdari[1,2]

[1]Department of Mining and Metallurgical Engineering, Amirkabir University of Technology P.O. Box. 15875-4413, Tehran, Iran. [2]Materials and Energy Research Center, P.O. Box 14155-4777, Tehran, Iran. Corresponding author email address: alamdari@aut.ac.ir

ABSTRACT

This paper investigates the synergistic effect of TBP and the thermodynamic effects of TBP on the extraction of divalent zinc, cadmium, cobalt, and manganese by di(2-ethylhexyl)phosphoric acid (D2EHPA) in kerosene to establish an accurate extraction equation. Empirical results show that extraction curves shift to higher pH due to addition of TBP and counterbalance the effect of mono(2-ethylhexyl)phosphoric acid (M2EHPA) as an impurity in D2EHPA. It seems that the equivalent concentration of D2EHPA decreases as a function of TBP because of formation of new bonds (hydrogen bonds) between TBP and D2EHPA. The effect of TBP on the reduction of D2EHPA concentration was estimated by applying a curve-fitting method. Equations for the equivalent concentration of D2EHPA at different concentration of TBP during extraction of zinc, cadmium, manganese, and cobalt were calculated.

INTRODUCTION

Di(2-ethylhexyl)phosphoric acid (D2EHPA), as a common and practical extractant, is widely used in solvent extraction of several metals [1-3]. A large amount of this extractant is lost each year because of phase-separation difficulties, which is a common problem in many solvent-extraction circuits. Another of the issues of using D2EHPA is its decomposition to the analogous mono-acid (M2EHPA) [4-5].

The presence of M2EHPA as an impurity in D2EHPA yields an undesirable synergistic effect, for instance on co-extraction of zinc and cadmium. For the extraction of zinc, the presence of M2EHPA in D2EHPA causes the extraction isotherms of Zn and Cd to move closer together [6]. The separation efficiency of these two metals depends on their $\Delta pH_{0.5}$ value (difference in the equilibrium pH values at which 50% extraction of each metal occurs), and the presence of M2EHPA in D2EHPA causes the $\Delta pH_{0.5}$, or the selectivity factor, to decrease [4-6]. To deal with this problem, addition of tri-*n*-butyl phosphate (TBP) to the organic phase can improve the separation efficiency [6]. In other words, TBP can influence the extraction mechanism and shift the extraction curves [6-7].

The addition of TBP as a phase modifier to D2EHPA not only improves the separation efficiency and phase separation, but fewer stages could be used to achieve the required zinc recovery and separation from mainly cadmium [6-9]. Keshavarz et al.

(2005) showed that with the addition of, for example 5% v/v TBP, the influence of M2EHPA on co-extraction of zinc and cadmium can be countered [6].

Although the effects of TBP as phase modifier and synergist have been published widely, information on the thermodynamics of the synergistic effects of TBP is limited and requires more detailed studies. The results obtained from studies of the thermodynamics of the synergistic effects of TBP on the extraction of some metals in MSO_4/TBP/D2EHPA–kerosene systems, where M is a divalent metal ion such as zinc, cadmium, cobalt, and manganese are reported in this paper. The number of TBP molecules taking part in the extraction is estimated by a curve-fitting analysis.

EXPERIMENTAL PROCEDURE

Materials and Reagents

All chemical reagents, except kerosene, were analytical grade. D2EHPA was purchased from Sandong Chemical Company, Chengdu, China. TBP was provided by Fluka. Kerosene was provided by Tehran Refinery Company, Iran. Organic phases, containing D2EHPA as extractant plus 0%, 2.5%, 5%, and 10% TBP as modifier, were prepared by dissolving the required volumes of the respective solvents into pure kerosene. The aqueous solution, containing 5 g/L each of zinc, cadmium, manganese, and cobalt, was prepared by dissolving sulfate salts of the respective metals in distilled water. These salts were obtained from Panreac, Barcelona, Spain. Sulfuric acid and ammonium hydroxide solution were employed for pH adjustment during extraction and were obtained from Baran Chemical Company, Iran.

Experimental Method

Batch experiments were carried out in flasks containing equal volumes (20 mL) of both aqueous and organic phases. The mixture was agitated at a constant temperature with a mechanical shaker. The experiments were allowed to run for 1 h to reach equilibrium. The samples were allowed to stand for 3 h, and the two phases were then separated by passing through a separation funnel. The initial concentration of zinc, cadmium, manganese, and cobalt in the aqueous phase in all experiments was 5 g/L. The metal content of the aqueous phase was analyzed by titration against a standard solution of EDTA. The metal concentrations on the organic phase were determined through mass-balance calculations.

RESULTS AND DISCUSSION

Effect of Addition of TBP on Metals Extraction

The extraction curves obtained for Zn, Cd, Mn, and Co using D2EHPA, containing various TBP concentrations, are shown in Figure 1. TBP caused the extraction of cadmium, manganese, and cobalt to shift to higher pH, while that of zinc remained similar, hence an increase in the $\Delta pH_{0.5}$ between Zn and the other metals. The addition of

TBP to D2EHPA improved the selectivity factor for Zn over Cd, Mn, and Co. The $pH_{0.5}$ values for these metals at the various TBP concentrations are listed in Table 1. The $pH_{0.5}$ of Cd was 0.4 pH units higher, and those of Mn and Co were about 0.5 pH units higher at 10% TBP when compared to D2EHPA alone.

Based on these results, it can be concluded that TBP is involved in the metal extraction process by forming different bonds to D2EHPA alone. The extraction mechanism of these metals in the D2EHPA–TBP–kerosene system is therefore important.

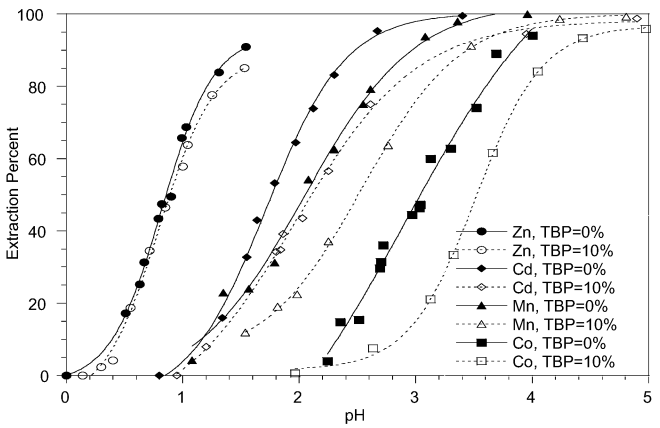

Figure 1. Zinc, cadmium, manganese, and cobalt extraction by 20% v/v D2EHPA and various concentrations of TBP in kerosene at 25 °C.

Table 1. $pH_{0.5}$ values for zinc, cadmium, manganese and cobalt at various TBP contents

TBP (vol %)	$pH_{0.5}$			
	Zn	Cd	Mn	Co
0	0.86	1.76	2.03	3.03
2.5	0.86	1.94	2.35	3.13
5	0.87	2.04	2.41	3.41
10	0.89	2.11	2.50	3.52

D2EHPA-TBP-Kerosene/Aqueous Metal Sulfate System

Keshavarz et al. (2002) claimed that some extractant molecules are chained together through hydrogen bonds and, therefore, the reason for synergistic shifts is the formation of new bonds in the organic media between D2EHPA and TBP [7]. If the reaction between TBP and D2EHPA is assumed to be as presented in Equation 1, an equivalent organic molar concentration of the 'bonded' reagent can thus be defined, and the molar concentration of the extractant can be considered as a function of TBP:

$$\alpha(RH) + TBP = [RH_{\alpha} \,.\, TBP] \quad (1)$$

where RH represents D2EHPA. The molar concentration of 'free' D2EHPA can then be calculated from Equation 2:

$$[RH]_{equivalent} = [RH]_{o} - \alpha[TBP] \quad (2)$$

the extraction reaction of a divalent metal by D2EHPA can be rewritten as Equation 3:

$$n(\mathrm{RH})_{\mathrm{equivalent}} + \mathrm{M}^2 = [\mathrm{R_2M}] \,.\, (\mathrm{RH})_{n\text{-}2}] + 2\mathrm{H}^+ \quad (3)$$

the equilibrium concentration of D2EHPA is considered as:

$$[\mathrm{RH}]_{\mathrm{equilibrium}} = [\mathrm{RH}]_{\mathrm{equivalent}} - n[\mathrm{M}]_{\mathrm{org}} = [\mathrm{RH}]_{\mathrm{o}} - \alpha[\mathrm{TBP}] - n[\mathrm{M}]_{\mathrm{org}} \quad (4)$$

by taking the logarithm of the equilibrium reaction (Equation 3), Equation 5 is obtained:

$$\log D_{\mathrm{M}} - \mathrm{nlog}\,([\mathrm{RH}]_{\mathrm{o}} - \alpha[\mathrm{TBP}] - n[\mathrm{M}]_{\mathrm{org}}) = \log K + 2\mathrm{pH} \quad (5)$$

in which the distribution ratio D is defined as $D = [\mathrm{M_{org}}]/[\mathrm{M_{aq}}]$.

It has been reported that the value of n is equal to 3, 6, 4, and 4 for zinc, cadmium, cobalt, and manganese, respectively [6,10-11]. These values of n are obtained when the pH coefficient in Equation 5 is 2. However, when TBP is added to the organic phase, the exact value of the pH coefficient in Equation 5 is estimated to be less than 2. By applying the effect of the [TBP] term in Equation 5, one can modify the pH coefficient. Cobalt and manganese were used as two examples to demonstrate the accuracy of Equation 5.

Figure 2 shows the plots of ($\log D_{\mathrm{M}} - \mathrm{nlog}\,([\mathrm{RH}]_{\mathrm{o}} - \alpha[\mathrm{TBP}] - n[\mathrm{M}]_{\mathrm{org}})$) against pH plotted for various concentrations of TBP. The stoichiometric coefficient of RH in Equation 1, α, can be calculated by a trial and error method. Plotting ($\log D_{\mathrm{M}} - \mathrm{nlog}([\mathrm{RH}]_{\mathrm{o}} - \alpha[\mathrm{TBP}] - n[\mathrm{M}]_{\mathrm{org}})$) against pH at different values of α and n, gives straight lines with different slopes and intercepts. The applicable one for the divalent metal extraction equation is the line with a slope of 2, because of the stoichiometry of the hydrogen ion (H^+) in the extraction as outlined in Equation 3. Likewise, similar results were obtained for manganese with only changing the value of α (Figure 3).

For comparison, the value of α for cadmium was also calculated. Since no change was observed in the $\mathrm{pH}_{0.5}$ for zinc, the value of α_{Zn} for different concentrations of TBP was considered to be zero. The calculated values of α are listed in Table 2.

Due to obtained values of α, the equivalent concentration of D2EHPA is predictable. As an illustration, if 2.5 vol % (0.09 M) of TBP is added to 20 vol % D2EHPA in kerosene, the equivalent concentration of D2EHPA could be estimated as equal to 0.56 M or 18.7 vol %. Hence, it can be predicted that cobalt extraction by 18.7 vol % D2EHPA should be similar to that by a mixture of 20 vol % D2EHPA and 2.5 vol % TBP%. Because of this effect, TBP can counteract the effect of the presence of a limited amount of M2EHPA on extraction.

The results listed in Table 2 show that by increasing the concentration of TBP in D2EHPA, the values of α decrease. As a result, by applying a curve-fitting method and values of α, one can estimate the equivalent concentration of D2EHPA when TBP is added to the organic phase to improve extraction conditions. It should be noticed that α is a modifying factor by which the equivalent concentration of D2EHPA in presence of TBP can be calculated. The value of this factor depends on nature of extracted metal. Considering the results of our previous work [6], it seems that the more M2EHPA, as an impurity, is present in D2EHPA, the more TBP is needed in order to counter the undesirable effect of M2EHPA on the separation efficiency. Due to the presence of TBP in D2EHPA and formation new bonds (hydrogen bonds) between them, the equivalent concentration of extractant changes. In order to estimate the real extractant concentration, considering the α factor is essential.

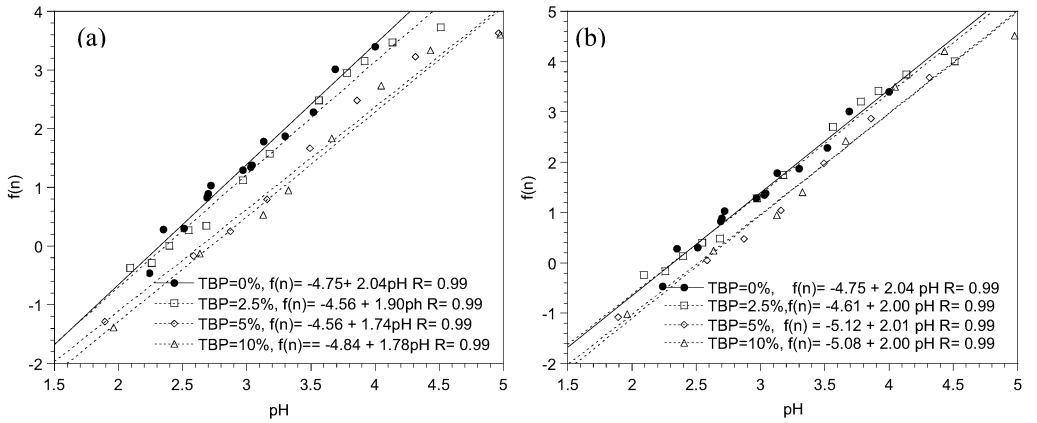

Figure 2. Plots of (log D_{Co} – nlog ($[RH]_o$ – α$[TBP]$ – $n[M]_{org}$)) vs. pH for Co; D2EHPA = 20% v/v, T = 25 °C. (a) without considering the effect of TBP (α = 0); (b) considering the effect of TBP.

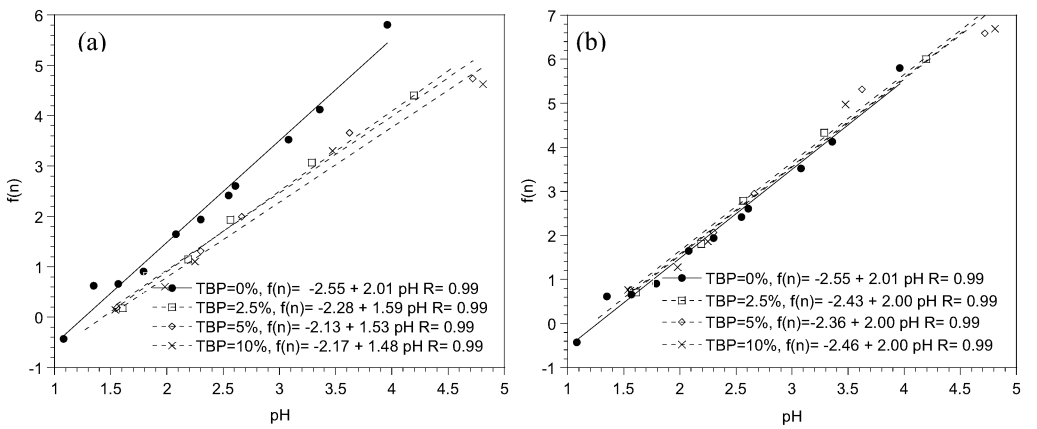

Figure 3. Plots of (log D_{Mn} – nlog ($[RH]_o$ – α$[TBP]$ – $n[M]_{org}$)) vs. pH for Mn; D2EHPA = 20% v/v, T = 25 °C. (a) without considering the effect of TBP (α = 0); (b) considering the effect of TBP.

Table 2. Calculated values of α for zinc, cadmium, manganese, and cobalt with respect to variation of TBP

TBP (vol %)	$\alpha_{Zn,(n=3)}$	$\alpha_{Cd,(n=6)}$	$\alpha_{Mn,(n=4)}$	$\alpha_{Co,(n=4)}$
0.0	0.0	0.0	0.0	0.0
2.5	0.0	0.44	1.61	0.45
5	0.0	1.19	0.87	0.37
10	0.0	0.69	0.46	0.31

CONCLUSIONS

It was found that the addition of TBP to D2EHPA leads to improved selectivity factors for zinc over cadmium, cobalt, and manganese in sulfate systems. The $pH_{0.5}$

values for these metals at TBP concentrations varying from 0-10% were calculated. The shifts in the $pH_{0.5}$ values for mainly Cd, Mn, and Co indicate that TBP is involved in the metal extraction process by forming bonds with D2EHPA in order to decrease the equivalent or real concentration of D2EHPA for these metal ions. Considering the equivalent D2EHPA concentration and defining it as a linear function of TBP, the value of the pH coefficient is estimated at 2. For all the concentrations of TBP, an equation for equivalent concentration of D2EHPA and the variation of the distribution ratio (*D*) against D2EHPA concentration were calculated. The equivalent concentration of 20 vol % of D2EHPA plus 2.5 vol % of TBP, for example during extraction of cobalt, could be estimated as equal to 18.7 vol % D2EHPA organic phase. Therefore, the results of cobalt extraction by 18.7 vol % by D2EHPA are predicted to be similar to those by 20 vol.% D2EHPA plus 2.5 vol % of TBP.

REFERENCES

1. G. Owusu, "Selective Extractions of Zn and Cd from Zn-Cd-Co-Ni Sulfate Solution using Di-2-ethylhexyl Phosphoric Acid Extractant," *Hydrometallurgy*, **47**(2-3), 205–215 (1998).
2. J. Aparicio and M. Muhammed, "Extraction Kinetics of Zinc from Aqueous Perchlorate Solution by D2EHPA Dissolved in Isopar-H," *Hydrometallurgy*, **21**(3), 385–399 (1989).
3. A. M. Sastre and M. Muhammed, "The Extraction of Zinc from Sulfate and Perchlorate Solutions by Di(2-ethylhexyl)phosphoric Acid Dissolved in Isopar-H," *Hydrometallurgy*, **12**(2), 177–193 (1984).
4. E. Keshavarz Alamdari, D. Moradkhani, D. Darvishi, M. Askari, and D. Behnian, "Synergistic Effect of MEHPA on Co-extraction of Zinc and Cadmium with DEHPA," *J. Miner. Eng.*, **17**, 89–92 (2004).
5. Y. R. Rao and S. Acharya, "A Rapid Titrimetric Determination of D2EHPA and M2EHPA," *Hydrometallurgy*, **32**(1), 129–135 (1993).
6. E. Keshavarz Alamdari, D. Darvishi, S. K. Sadrnezhaad, and D. F. Haghshenas, "Synergistic Effect of TBP on Separation of Zinc and Cadmium with D2EHPA," Proc. International Solvent Extraction Conference, Beijing, China, 2005.
7. E. Keshavarz Alamdari, D. Darvishi, S. K. Sadrnezhaad, Z. Mos'hefi Shabestari, A. O'hadizadeh, and M. Akbari, "Effect of TBP as a Modifier for Extraction of Zinc and Cadmium with a Mixture of DEHPA and MEHPA," Proc. International Solvent Extraction Conference, Cape Town, South Africa, 2002; pp. 1052–1057.
8. K. L. Nash and G. R. Choppin, "The Thermodynamics of Synergistic Solvent Extraction of Zinc(II)," *J. Inorg. Nucl. Chem.*, **39**(1), 131–135 (1977).
9. V. M. P. Forrest, D. Scargill, and D. R. Spickernell, "The Extraction of Zinc and Cadmium by Tri-n-butyl Phosphate from Aqueous Chloride Solutions," *J. Inorg. Nucl. Chem.*, **31**(1), 187–197 (1969).
10. D. Darvishi, D. F. Haghshenas, E. Keshavarz Alamdari, S. K. Sadrnezhaad, and M. Halali, "Synergistic Effect of Cyanex 272 and Cyanex 302 on Separation of Cobalt and Nickel by D2EHPA," *Hydrometallurgy*, **77**, 227–238 (2005).
11. D. Darvishi, "Thermodynamic of Solvent Extraction of Cobalt by Organo-Phosphorus Extractant," M.Sc. Thesis, Sharif University of Technology, Iran, 2003.

USE OF SOLVENT EXTRACTION TECHNIQUE IN BRAZILLIAN URANIUM MILLS – AN OVERVIEW

Luiz A. Gomiero[1] and Carlos A. Morais[2]

[1]Indústrias Nucleares do Brasil S/A–INB, Unidade de Caetité, P.O. Box 7,46400 – 000 Caetité, BA, Brazil. [2]Centro de Desenvolvimento da Tecnologia Nuclear CDTN/CNEN Rua Mário Werneck, s/n, Campus da UFMG, Pampulha,30123-970 Belo Horizonte, MG, Brazil
Corresponding author email address: gomiero@inb.gov.br; cmorais@cdtn.br

ABSTRACT

Solvent extraction has been applied to uranium-concentrate production in Brazil. At the first plant, uranium minerals associated with Zr and Mo were acid leached. Extraction was carried out by a mixture of Alamine 336 and Alamine 304, followed by selective Zr, U, and Mo stripping. At the currently operating facilities, a single U mineral is processed by acid heap leaching. Uranium is extracted with Alamine 336 and stripped with NaCl solution. As all water is recycled, chloride contents in the liquor have increased, causing detrimental effects to the extraction process. The current plant operating conditions and the improvements arisen from the research developed to solve these problems are presented.

INTRODUCTION

The first Brazilian mining and milling facility for uranium-concentrate production started operating in 1982, in the Municipality of Caldas, Minas Gerais State. Uranium ore containing zirconium and molybdenum minerals was crushed, ground, and leached in agitated tanks with high sulfuric acid consumption. A pregnant leach solution (PLS) containing these both contaminants, among others of lower significance, was produced. To solve some operating and product specification trouble due to the Zr and Mo presence in the PLS, some changes to the previous extraction and stripping process were introduced. It will be shown that, after introducing such improvements the facilities were operated with good results till 1995, when the shut-down process started.

A new mining and milling facility started operating at the beginning of 2000, processing a single uranium mineral containing ore by the sulfuric acid heap leaching technique as shown by Matos and Gomiero [1]. It is located in the Municipality of Caetité, Bahia State. Uranium is separated from the other species present in the PLS by solvent extraction. In this plant, all aqueous effluent generated in the process is reused after treatment with lime and solid/liquid separation. As a consequence of using sodium chlorate as an oxidizing agent during leaching and an acidified sodium chloride (NaCl)

solution for U stripping in a process where chloride ions are not removed in the lime treatment, the chloride content increased in the PLS, causing a detrimental effect on the U extraction and stripping processes. The current plant operating conditions and the results of research developed and introduced to solve this problem are discussed.

CALDAS SOLVENT-EXTRACTION PROCESS EXPERIENCE

Caldas mine is formed by three main ore bodies named A, B, and E. All of them have Mo and Zr associated with the U mineral but A and B ore bodies have higher Mo and Zr contents than E ore body. E ore body has higher U content than the others.

Mine exploitation was started by leaching of the E ore body, giving a PLS with the typical analysis shown in Table 1.

Table 1. U, Mo and Zr content in a typical PLS from E ore body

Chemical species	Content (g/L)
U_3O_8	0.475
MoO_3	0.062
ZrO_2	0.044

Extraction

Uranium recovery from the PLS was done by solvent extraction in a five-stage mixer-settler arrangement with a C_8-C_{10} tertiary amine. At the beginning of the plant operation, the solvent composition was 5 vol % Alamine® 336 (Alamine® is a trade mark of Cognis Corporation), 3 vol % tridecanol and commercial kerosene. Under these conditions, U and Mo are fully extracted from the PLS, and Zr is only partially extracted. Raffinate was treated with lime up to pH 10 and disposed of in a tailing dam. The liquid phase was released to the environment after barium chloride treatment and monitoring. Caldas plant did not face water shortage problems, but the following undesirable results were observed along the first operating year:

- Reduction in U loading on the solvent when $MoO_3/U_3O_8 > 0.5$, leading to a lower U production,
- High Zr extraction, causing a high Zr/U ratio in the final uranium precipitate.

Stripping

U and Mo were stripped separately. U was stripped from the loaded solvent in five-stage mixer-settlers by a 1.75 mol/L NaCl aqueous solution acidified to pH 1.2–1.5 with sulfuric acid. Zr and Mo were also partially stripped, causing contamination of the final U precipitate. Mo was stripped in a one-stage mixer-settler after U stripping using a 0.75 mol/L sodium carbonate (Na_2CO_3) aqueous solution. It was observed that the formation of an organic-insoluble Mo-amine complex caused emulsion formation and solvent losses.

Solving the Problems

Research was carried out to overcome the above-mentioned chemical and operational problems. The process flowsheet presented in Figure 1 shows the previous and the final operating solvent extraction process at Caldas facilities.

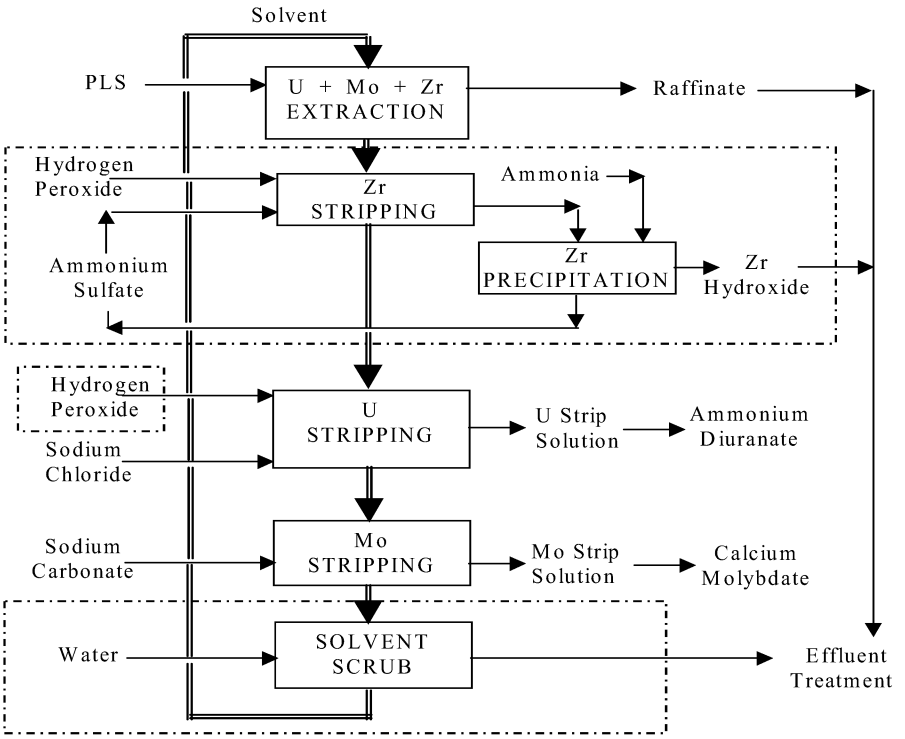

Figure 1. Caldas extraction flowsheet. Unit operations surrounded by broken lines were introduced after plant start-up.

The following improvements were introduced to the process:

- Solvent flow rate was increased in the extraction step to overcome the reduction of the U loading on the solvent when $MoO_3/U_3O_8 > 0.5$.
- Use of a mixture of decyl and dodecyl tertiary amines to increase Mo solubility on the loaded solvent and to overcome the organic-insoluble Mo-amine complex forming in the Mo stripping circuit. A mixture of 70 vol % Alamine 304, 30 vol % Alamine 336, and 3.5 vol % tridecanol in commercial kerosene was adopted.
- Addition of a proper amount of phosphate ore concentrate (raw apatite) to the grinding step of the U ore from E ore body to precipitate the soluble zirconium as a Zr-phosphate complex during the leaching step to avoid Zr contamination of the final U precipitate. After introducing this

improvement, Zr analysis in the PLS was reduced from 0.044 g/L ZrO_2, as shown in Table 1, to 0.002 g/L.

- Introduction of Zr stripping from the loaded solvent before U and Mo stripping to operate with the processing of A and B uranium ore bodies. Bench and pilot assays with such ore gave a loaded solvent containing 2.55 g/L U_3O_8, 5.60 g/L MoO_3, and 0.40 g/L ZrO_2. After Zr stripping as indicated in Figure 1, the analysis of these species on the loaded solvent were 2.54 g/L U_3O_8, 5.60 g/L MoO_3, and 0.008 g/L ZrO_2. Zr was stripped by 1 mol/L ammonium sulfate solution containing 3 g/L H_2O_2 100 wt % in three stages at pH 4.5. This unit was constructed but it was not operated, because ore bodies A and B were not exploited.
- Addition of 50 wt % H_2O_2 solution at a rate of 0.1 kg 100 wt % H_2O_2/kg U_3O_8 to the mixer of the first U stripping stage in order to oxidize Mo to reduce its solubility on the U stripping solution, thus overcoming Mo contamination of the U concentrate.

CAETITÉ SOLVENT EXTRACTION PROCESS EXPERIENCE

Mining and milling facilities constituted of an open-pit mine and a physical and chemical processing plant. Uranium is acid leached by heap leaching and purified by solvent extraction.

U Extraction/Stripping

U extraction is carried out in a circuit configuration consisting of a series of mixer-settlers arranged as a four-stage extraction, four-stage U strip, and a single stage solvent scrub or regeneration. The solvent consists of a mixture of 5 vol % Alamine 336 and 3 vol % tridecanol, both supplied by Cognis do Brasil Ltda, in a paraffin-type diluent SOLBRAX ECO 175/235 supplied by Petrobras Distribuidora S/A. Aqueous raffinate from the extraction step is treated with lime up to pH 10 and disposed of in lined settling ponds equipped with a bottom water drainage system named sub-aerial drains. As Caetité's facilities are located in a region with low water availability, all the used plant water must be recovered, treated, and recycled to the leach process.

U stripping is carried out by an aqueous NaCl solution acidified to pH 1.2-1.5 with sulfuric acid. At the start-up, the stripped solvent was recycled to the extraction circuit without any prior treatment. At such operating conditions, the tertiary amine on the recycled solvent was in the chloride form, and the U extraction and stripping process may be represented by Equations 1 and 2:

$$4\,[(R_3NH^+\,Cl^-)]_{org} + UO_2(SO_4)_3^{4-} \rightarrow [(R_3NH^+)_4UO_2(SO_4)_3^{4-}]_{org} + 4\,Cl^- \quad (1)$$

$$[(R_3NH^+)_4UO_2(SO_4)_3^{4-}]_{org} + 4\,Na^+Cl^- \rightarrow 4\,[(R_3NH^+\,Cl^-)]_{org} + UO_2(SO_4)_3^{4-} + 4\,Na^+ \quad (2)$$

Equation 1 shows that the chloride ion from the amine is released to the aqueous raffinate. Uranium is precipitated from the aqueous chloride strip solution as ammonium diuranate (ADU) by ammonium hydroxide solution addition according to Equation 3:

$$2\ UO_2(SO_4)_3^{4-} + 6\ NH_4^+OH^- \rightarrow (NH_4)_2U_2O_{7(s)} + 6\ SO_4^{2-} + 4\ NH_4^+ + 3\ H_2O \quad (3)$$

Some 70 vol % of the ADU filtrate is recycled to the preparation of a new NaCl stripping solution. At the plant start-up, the excess ADU filtrate was added to the raffinate before lime treatment. As the chloride ion is not removed by the lime treatment, its content in liquor has increased, causing a strong reduction of U-loading capacity of the solvent and effectively reducing plant throughput.

To overcome this problem, a new one-stage mixer-settler was introduced to scrub the stripped solvent with a 1 mol/L Na_2CO_3 solution. The resulting aqueous strip solution is added to the excess ADU filtrate and is disposed of in a specific lined pond for future reuse.

Some alternative U-stripping systems were also investigated [2,3]. The ammonium sulfate/ammonia system was also shown to be highly sensitive to the presence of chloride ions in the liquor, since chloride competes with uranyl sulfate anions being partially extracted by the amine [4]. U stripping with a concentrated sulfuric acid solution is not affected by the presence of chloride ion in the liquor and is a good alternative to be considered for a future change in the Caetité's process.

Stable Emulsion

Another undesirable experience faced by Caetité's plant operating staff was a strong emulsion formation in the extraction circuit. The phenomenon was evaluated, showing that the main causes were the high sulfate, chlorides, and suspended solids contents in the liquor [5]. From that experience, these variables were carefully controlled to avoid another emulsion formation.

Caetité's current process flowsheet is shown in Figure 2.

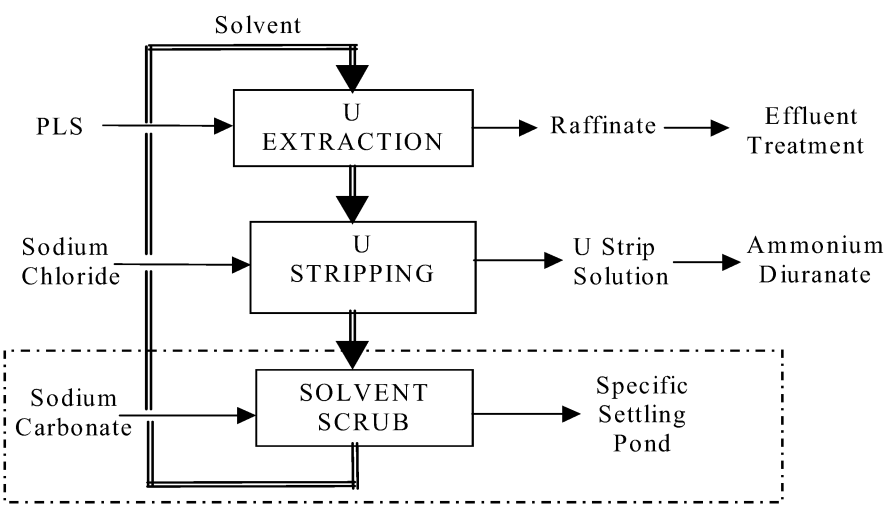

Figure 2. Caetité extraction flowsheet. Unit operations surrounded by broken lines were introduced after plant start-up.

FINAL CONSIDERATIONS

Solvent extraction has proven to be a good choice for uranium recovery and purification in the processing of Brazilian uranium ores. In the first operating milling facility, simultaneous U and Mo extraction were conducted with good operating conditions by using a suitable mixture of Alamine 304 and Alamine 336. Good separation of U, Mo, and Zr was achieved by selective stripping of each metal from the loaded solvent.

In the second circuit, the use of NaCl solution for stripping of U, combined with the recycle of circuit water, means that the stripped solvent must be regenerated to remove chloride ions before the solvent is recycled to U extraction. Also, all excess filtrate from the U precipitation and the aqueous phase from the solvent regeneration step must be segregated.

Care must be taken in the control of chloride, sulfate, and suspended solids contents in the PLS to avoid emulsion formation and to maintain the solvent loading capacity.

ACKNOWLEDGMENTS

This work is published with the permission of Indústrias Nucleares do Brasil S/A–INB. The authors would like to acknowledge Mr. Renato Rosa Pinto for important help with this report.

REFERENCES

1. E. C. Matos and L. A Gomiero, “Uranium Ore Concentrate Production in Caetité – BA, Brazil,” VI International Conference on Clean Technologies for the Mining Industry, Concepción, Chile, 2004.
2. C. A Morais and L. A Gomiero, “Uranium Stripping From Tertiary Amine Loaded Solution by Ammonium Sulfate,” *Minerals Engineering*, **18**, 1277−1281 (2005).
3. C. A Morais, L. A Gomiero, W. Scassiotti Filho, and H. Rangel Jr., “Uranium Stripping From Tertiary Amine by Sulfuric Acid Solution and its Precipitation as Uranium Peroxide,” *Minerals Engineering*, **18**, 1331−1333 (2005).
4. K. Soldenhoff, D. Wilkins, M. Shamieh, and R. Ring, “Solvent Extraction of Uranium in the Presence of Chloride,” International Symposium on the Process Metallurgy of Uranium, E. Özberk and A J. Oliver, Eds., Saskatoon, Saskatchewan, Canada, 2000; pp. 339−351.
5. C. A Morais, J. S. Benedetto, and L. A Gomiero, “Emulsion in Uranium Solvent Extraction Plant. Case Study,” Proceedings of the International Solvent Extraction Conference, Beijing, People’s Republic of China, 2005.

EXPANSION CAPACITY OF AN SX UNIT IN URANIUM PROCESS PILOT TESTS

B. Courtaud,[1] F. Auger,[1] P. Morel,[1] and M. Sanoussi[2]

[1]AREVA-NC/SEPA, Bessines sur Gartempe, France. [2]SOMAÏR, Arlit, Niger
Corresponding author email address: Bruno.courtaud@areva.com

ABSTRACT

The rising price of uranium has led uranium producers to increase their plant capacity. The new project proposed to increase capacity is based on processing low-grade uranium by heap leaching. It is necessary to modify the plant, particularly the solvent extraction unit, to handle the increased flow. The goal of our study is to determine the minimal changes necessary to process the whole flow. Several stages have been carried out (i) thermodynamic modelling of the solvent extraction process to determine the capacities of the SX plant and the impact of the modification and (ii) pilot tests at the plant of the different configurations proposed by modelling. This paper presents results of the pilot tests performed at the plant.

INTRODUCTION

The rising price of uranium is compelling suppliers to produce more and as a result to increase the capacity of their plants. Solvent extraction (SX) units are often at the heart of uranium-ore processing and as a result are the first units to be affected by this increase in capacity.

A study was initiated to examine how to increase the capacities of solvent-extraction units in a plant in Niger, while keeping the modifications to be made to the existing installation to a minimum. This project was broken down into three parts: (i) technical assessment of the unit, (ii) modelling of the SX unit, and (iii) pilot tests in the plant. The aim of this document is to present the results of the pilot tests, as the two other points are already covered in separate publications.

TARGETS

Purpose of the Study

The study presented in this document concerns the increase in capacity of a plant consequent upon the development of new uranium-ore processing projects. The rising price of uranium is now making the processing of low-grade uranium-ores economically viable.

Currently, the plant processes ores from its own open-cast mine. Two SX units are sufficient, although the plant actually has three. The new projects, especially ore processing using heap leaching, will increase the flow of uranium-bearing solution into the solvent units (Table 1). This study should enable us to define the modifications required to handle this increased flow.

Table 1. Increased flow rate due to the new heap-leach project

		Plant Solution	Leach Solution
At present	3 SX plants*	2 x 80 $m^3.h^{-1}$	/
In future	3 SX plants*	220 $m^3.h^{-1}$	250 $m^3.h^{-1}$
	U content	1.5 g L^{-1}	0.4 g L^{-1}

*SX capacity per stage: 273 m^3 h^{-1} (including aqueous, organic and recycled organic flow rates).

The maximum flow rate in the aqueous phase is 120 m^3 h^{-1}, with an organic phase flow of 30 m^3 h^{-1}, and recycling of the organic phase at 123 m^3 h^{-1} (O/A, 1.27). From the separation stage the maximum solvent flow is 30 m^3 h^{-1}.

Resources

The study was carried out as shown in the following logic diagram:

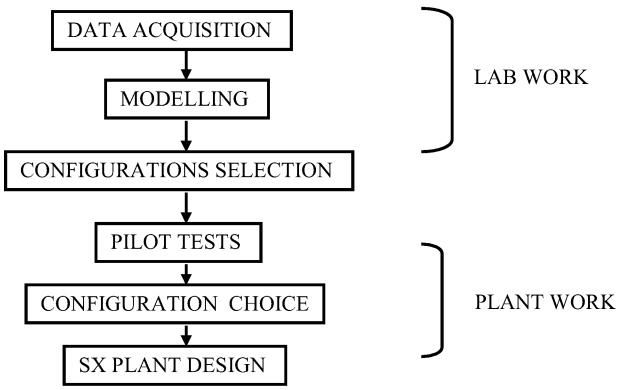

PILOT TESTS

Base Data

The pilot-scale factor was determined from the plant size as shown in Table 2.

Table 2. Pilot-scale factors

		Plant	Pilot
PLS flow rate		90 m^3 h^{-1}	1.05 Lh^{-1}
U concentration		1.60 g L^{-1}	1.56 g L^{-1}
Extraction	Mixer volume	14 m^3	0.12 L
	Residence time	3 min	2 min
Stripping	Mixer volume	3.6 m^3	0.06 L
	Residence time	6 min	9 min
U pregnant strip solution		35 g L^{-1}	40 g L^{-1} (objective)
U raffinate		<2 mg L^{-1}	<2 mg L^{-1} (objective)

Results

Reference Test

The purpose of this reference test (Figure 1) is to reproduce the plant's operating conditions in the pilot unit. The results obtained in the pilot unit are identical to those from the plant, that is loss of uranium in the raffinate of less than 2 mg L^{-1} and a uranium concentration of 40 g L^{-1} in the pregnant strip solution.

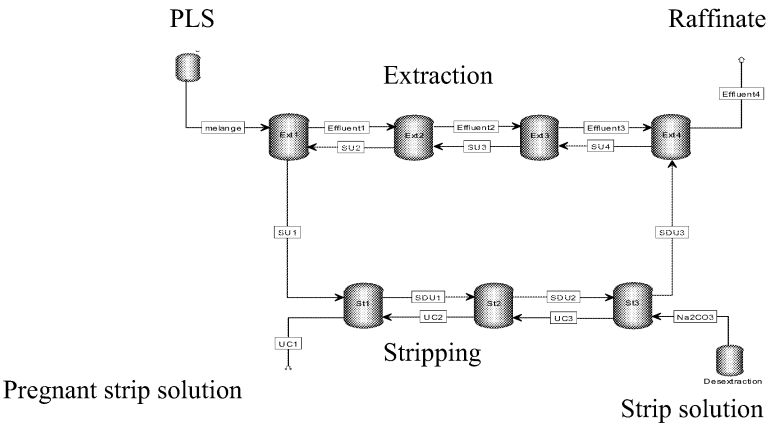

Figure 1. Reference diagram.

Processing Heap Leach Solutions in a Series-Parallel Configuration

This test corresponds to the use of a single solvent unit to process all the leach solutions. The total flow rate to be processed is 250 m^3 h^{-1}, with a maximum capacity of 120 m^3 h^{-1} per stage. The series-parallel configuration is the only configuration that would enable such a flux to be processed. The results of the tests are shown in Table 3.

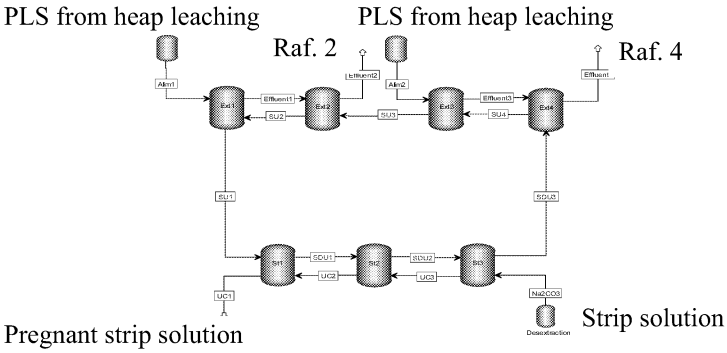

Figure 2. Series-parallel configuration.

Table 3. Results of trial

	Pilot flow rates	Equivalent plant flow rates
Flow rate, feed 1	1.35 L h^{-1}	121.5 m^3 h^{-1}
Flow rate, feed 2	1.40 L h^{-1}	126 m^3 h^{-1}
Total flow rate	2.75 L h^{-1}	247.5 m^3 h^{-1}
Loss of U in raffinate 2	4 mg L^{-1}	
Loss of U in raffinate 4	2 mg L^{-1}	
U content in pregnant strip solution	30 g L^{-1}	

The loss of uranium in the raffinates is still low, especially as the latter are recycled through the leach heap. These results were obtained without increasing the amine (extractant) concentration of the solvent relative to that in normal plant operation, which is 0.14 M. Furthermore, the saturation factor of the solvent for the reference test is 74%, whereas it is no more than 46% for this test. The flow rate is greater, but as the solutions are carrying less uranium, the incoming uranium flux in the leach solutions is also lower.

The uranium losses are still very low, leaving this configuration as a possibility. The most significant losses are unfortunately in the raffinate from the plant effluent, which is not recycled to the leach heap.

Processing All the Plant Effluent in a Single Unit in a Series-Parallel Configuration

Here the objective is to devote a solvent unit solely to the main plant effluents. The disadvantage of a standard series-parallel configuration is that the solvent reaching the second extraction stage is already partly loaded by the first loop in stages 3 and 4. Its efficiency is reduced and major losses in the raffinates may be anticipated.

We tested a so-called “improved series-parallel” configuration, which operates by dividing the organic flow into two identical fluxes. We then recombine these fluxes after they have passed through the extraction loops. In effect, this means that we have two distinct extraction units with shared stripping.

The disadvantage of this assembly is the low flow of organic effluent generated, which is offset by a higher solvent recycling factor.

The incoming quantity of uranium is greater than the capacity of the solvent with an amine concentration of 0.14 M. We increased this concentration to 0.28 M, which corresponds to a theoretical solvent saturation of 65%.

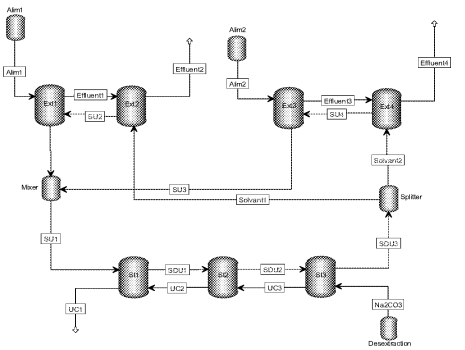

Figure 3. Improved series-parallel configuration.

In Table 4, the performances for the standard and the improved series-parallel assemblies are compared for an identical extractant concentration of 0.28 M.

Table 4. Comparison of circuit configurations

	Standard configuration	Improved configuration
Total feed flow rate (plant equiv.)	223.2 $m^3 h^{-1}$	223.2 $m^3 h^{-1}$
Loss of U in raffinate 2	20 mg L^{-1}	4 mg L^{-1}
Loss of U in raffinate 4	4 mg L^{-1}	4 mg L^{-1}
U content of pregnant strip solution	55 g L^{-1}	50 g L^{-1}

The improved series-parallel configuration led to a reduction in the uranium lost in the raffinate relative to the standard configuration. These losses remain high, as the target concentration of 2 mg L^{-1} is not attained, and this raffinate cannot be recycled to the leach heaps.

Summary of Results and Definitions of Configurations per Unit

Table 5 provides a summary of the results. Apart from the effectiveness of some configurations relative to others, the choice must also take account of the investment costs needed to restore Unit 3 to good working order, as well as the cost of the modifications required to transform a unit from counter-current to series-parallel configuration. The quantity of uranium lost in the raffinates is also a decisive criterion in the selection process.

Availability of installations during maintenance and shutdowns is yet another factor that must be considered when choosing the configuration. The only way of stopping the supply of effluent from the plant is to shut down the plant, whereas the heap leach process generates a continuous flow of effluent, which must be stored if the solvent unit is not taking the feed. This situation makes it difficult to manage a unit processing

effluent from the plant and the heap-leaching process simultaneously; managing shutdowns can become very complicated, and this may interfere with the running of the solvent unit. Taking all these constraints into account, Option A is the most attractive configuration.

Table 5. Summary of results

Option	SX Unit	Effluent	Total flow ($m^3\ h^{-1}$)	Configuration
A	1	Plant	110	Counter-current
	2	Plant	110	Counter-current
	3	Heap leach	250	Series-parallel
B	1	Plant + heap leach	110+125	Series-parallel
	2	Plant + heap leach	110+125	Series-parallel
	3	/	/	/
C	1	Plant	220	Improved series-parallel
	2	Heap leach	250	Series-parallel
	3	/	/	/

CONCLUSION

The whole project, including laboratory work, modelling and pilot tests took place over a period of eight months. It was possible to complete the project so quickly by performing these phases in succession.

Modelling enabled us to select the most promising configurations for pilot testing and also set the optimum operating conditions such as the supply flow rates from the various phases (aqueous and organic), the best O/A ratio to produce a pregnant strip solution containing around 40 g L^{-1} of uranium and to minimize the amount of uranium lost in the raffinates.

For their part, the pilot tests confirmed the results from modelling using real solutions, made it possible to estimate the amount of solvent lost through entrainment (not mentioned in this document) and allowed a visual check on whether or not interface crud appeared during certain tests.

The project is currently in the engineering phase, which means that modifications to the units will be initiated over the coming months.

REFERENCES

1. T. Lo, M. Baird, and C. Hanson, Handbook of Solvent Extraction, John Wiley & Sons, New York, 1983.
2. M. Bogacki, G. Cote, and J. Szymanowski, “Modelling of Nickel Extraction with Decanal Oxime,” *Sep. Sci. Tech.*, **28**(9), 1783-1788 (1993).
3. M. Bogacki, G. Cote, J. Szymanowski, and D. Bauer, “Modelling of Extraction Equilibrium and Computer Simulation of Extraction-Stripping Systems for Nickel Extraction by Di-n-Butylphosphorodithioate,” *Ind. Eng. Chem. Res.*, **31**, 1768-1780 (1992).
4. E. D. Galvez, C. A. Vega, R. E. Swaney, and L. A. Cisternas, Design of Solvent Extraction Circuit Schemes, *Hydrometallurgy*, **74**, 19-38 (2004).

EXTRACTION OF URANIUM: COMPARISON OF STRIPPING WITH AMMONIA VS. STRONG ACID

B. Moldovan,[1] B. Grinbaum,[2] and A. Efraim[2]

[1]Cameco Corporation, Canada. [2]Bateman Solvent Extraction, Israel.
Corresponding author email address: Brett_Moldovan@cameco.com

ABSTRACT

Following extraction of uranium in the first stage of solvent extraction using a tertiary amine, typically Alamine 336, the stripping of the extracted uranium is accomplished either by use of an aqueous solution of $(NH_4)_2SO_4$ /NH_4OH or by strong-acid stripping using 400-500 g/L H_2SO_4. Both processes have their merits and determine the downstream processing. The classical stripping with ammonia is followed by addition of strong base, to precipitate ammonium uranyl sulfate $(NH_4)_2UO_2(SO_4)_2$, which yields finally the yellow cake. Conversely, stripping with H_2SO_4, followed by oxidation with hydrogen peroxide yields uranyl oxide as product. At the Cameco Key Lake operation, both processes were tested on a pilot scale, using a Bateman Pulsed Column (BPC). The BPC proved to be applicable to both processes. It met the process criteria both for extraction and stripping, leaving less than 1 mg/L of U_3O_8 in the raffinate, and product solution had the required concentration of U_3O_8 at high flux and reasonable height of transfer unit. In the Key Lake mill, each operation can be carried out in a single column. The main advantages of the strong-acid stripping over ammonia stripping are: (1) 60% higher flux in the extraction, (2) tenfold higher concentration of the uranium in the product solution, and (3) far more robust process, with no need of pH control in the stripping and no need to add acid to the extraction in order to keep the pH above the point of precipitation of iron compounds. The advantages of the ammoniacal process are easier stripping, that is, less stages needed to reach equilibrium and lower concentration of modifier needed to prevent the creation of a third phase.

INTRODUCTION

The process for solvent extraction (SX) of uranium by Cameco is described in detail by Ritcey [1]. The extraction is done using Alamine® 336 in kerosene diluent and isodecanol as modifier. Extraction occurs according to the reactions:

$$2\ R_3N_{(org)} + H_2SO_4 \rightarrow 2\ (R_3NH^+)HSO_4^-{}_{(org)} \quad (1)$$

$$2\ (R_3NH^+)HSO_4^-{}_{(org)} + UO_2(SO_4)^{2-} \rightarrow (R_3NH^+)_2UO_2(SO_4)_{(org)}^{2-} + 2\ HSO_4^- \quad (2)$$

For the stripping operation, two different processes are described. In the Key Lake mill, the stripping is done in four mixer-settlers using $(NH_4)_2SO_4$ as the stripping reagent (Reaction 3). The pH in the stripping process is controlled by the addition of ammonia:

$$(R_3NH^+)_4UO_2(SO4)_3^{4-}{}_{(org)} + 4\ NH_4OH \rightarrow 4\ R_3N_{(org)} + (NH_4)_2UO_2(SO_4)_2 + (NH_4)_2SO_4 + 4\ H_2O \quad (3)$$

In the Cameco Rabbit Lake mill, the stripping is done in five mixer-settlers using strong-acid stripping (SAS), with a solution containing ~400 g/L H_2SO_4. In this process, Reaction 2 occurs in the reverse direction, yielding $UO_2(SO_4)_3^{4-}$ in the aqueous phase and the regenerated Alamine hydrogensulfate $R_3NH^+HSO_4^-$ in the organic phase (barren organic (BO)) is then prepared for use in the extraction stage of the SX process.

Cameco decided to test the applicability of columns for both processes and chose the disk-and-doughnut Bateman Pulsed Columns (BPC) for the test. The test was completed in two campaigns at the Key Lake mill, using the pregnant leach solution (PLS) and the solvent from the current SX process. The PLS contained about 10 g/L uranium. The solvent contained 10 vol % Alamine 336 and 4 vol % isodecanol. For the application of the SAS, the concentration of the modifier was increased from 4% to 7.5% to prevent the creation of a third phase under the strongly acidic conditions. In the extraction, the organic-to-aqueous (O:A) phase ratio was about 1.1:1. The column was run based on an organic-continuous configuration, similar to the mixer-settlers (MS).

In the SAS circuit, the phase ratio O:A phase ratio was about 20. This is almost the maximum phase ratio applicable to any type of columns, due to increased axial mixing at extreme phase ratios. The dispersion in the column must be aqueous-continuous to ensure good mass transfer. As columns were not considered for the ammoniacal stripping in Key Lake, this process was not tested.

The PLS in the process has above 10 g/L H_2SO_4, and relatively high acidity must be kept along the column, as above pH 3 iron oxides precipitate, resulting in a dramatic increase in the amount of crud. Using the SAS process, the solvent arrives from the stripping at maximum acidity, so that, all the extractant is in the form of $(R_3NH^+)HSO_4^-$.

The testwork was carried out using the standard Bateman process development procedure of laboratory tests followed by piloting, as previously described in detail [2].

EQUIPMENT

The BPC is described in detail by Coleman et al. [3]. In the pilot plant, two columns were used: a 100 mm diameter BPC for extraction and an 80 mm BPC for stripping. Their heights were 8 m and 7 m, respectively. PVDF disc-and-doughnut internals were used. Sampling points were provided along the active section of each column. Two glass settlers were located at either end of the active section. Pulsation was provided by a mechanical pulsator.

The SX solvent was fed to the upper part of the lower settler, and the PLS was pumped to the lower part of the upper settler. The solvent flows out the column by overflow from the top of the column. The aqueous flows out by gravity and is regulated by a manual valve. Intermediate tanks for PLS, BO, and the raffinate were used. The

solutions were pumped from storage tanks to the column through rotameters. All solution temperatures were maintained at 45-50 °C prior to introduction to the column.

RESULTS

Extraction

The extraction was tested in the BPC using both barren organic (BO) that was obtained directly from the ammoniacal process in the plant and after the SAS in the pilot.

Hydraulic Test

The hydraulic test proved that the maximum flux using BO after stripping with ammonia was 30 $m^3/m^2/h$. Further, this flux was obtained with no pulsation on the column. The aqueous phase did not disperse to the preferred drops but created "lumps" or "curtains" that moved through the organic continuum. Occasionally, the aqueous phase changed to be large "normal" aqueous drops, with diameter above 5 mm. In addition, at flux of 35 $m^3/m^2/h$ or greater, phase inversion occurred. With low pulsation, the results were similar, and medium pulsation (PI > 600 mm/min.) caused phase inversion at any flux.

In the extraction with BO stripped with strong acid, the flux increased substantially, and it did improve significantly with pulsation. Without pulsation the maximum steady flux was about 40 $m^3/m^2/h$, and the dispersion consisted of large lumps. Pulsation enabled an increase in the flux up to 53 $m^3/m^2/h$. Under these conditions, the dispersion was better, with drops of 2-5 mm in diameter. In comparison, the flux without pulsation was higher by 30% than in the ammoniacal extraction process and was 65% higher with pulsation.

Mass Transfer

The daily average results of the mass-transfer tests using BO from both stripping procedures appear in Table 1. In all tests, the O:A ratio was 1.1:1.

The mass balances on the experiments, calculated as the difference between the amounts of U_3O_8 in the inlet and the outlet streams relative to its amount in the inlet streams, closed with average deviation below 10% (i.e., within the experimental accuracy).

Visual Observations

In the extraction, thick crud was observed after a few hours of work, regardless of the type of stripping. This did not come as a surprise as crud is a well-known problem in the current Key Lake SX process. Still, it is important to note that, in spite of the crud, the entrainment of organic in the aqueous phase was below 50 mg/L. Taking into consideration that the decanters were deliberately designed small (to decrease the residence time and speed up the testwork), it is quite satisfactory. The amount of crud with solvent from SAS was less than that from the ammoniacal stripping.

Table 1. Extraction of U_3O_8 in BPC

Date	PLS (g/L)	BO (g/L)	Raff (g/L)	LO (g/L)	Flux ($m^3/m^2/h$)	Length (m)
BO from stripping with ammonia						
Day 1	14.3	0.154	0.002	11.0	25	8
Day 2	14.5	0.09	0.002	12.7	25	8
Day 3	14.4	0.206	0.002	11.7	29	8
Day 4	14.7	0.24	0.001	10.6	29	8
Day 5	14.7	0.24	0.065	12.2	31	6
Day 6	14.3	0.205	0.030	11.9	30	6
Day 7	14.3	0.205	0.003	11.7	30	8
Day 1	14.3	0.205	0.004	10.8	30	8
BO from Strong Acid Stripping						
Day 1	13.69	0.59	0.019	12.68	50	8
Day 2	12.18	0.39	0.001	11.70	50	8
Day 3	12.26	0.43	0.095	12.42	50	6
Day 4	13.1	0.42	0.003-0.005	12.2	50	7

Comment: The high U tenor on BO from ammonia stripping is surprising.

Stripping

The tests were carried out for the SAS process only. The strip solution contained 500 g/L H_2SO_4.

Hydraulic Test

In the stripping with strong acid, the hydraulic test proved that, without pulsation, a flux of 60 $m^3/m^2/h$ could be obtained. With pulsation, the maximum flux decreased to 50 $m^3/m^2/h$. Visually, the dispersion with pulsation was better; namely, the drops were about 2-3 mm in size, compared with lumps or large drops above 5 mm without pulsation. Accordingly, it is reasonable to expect that the mass transfer with pulsation will be better than without it. As a flux of 50 $m^3/m^2/h$ is more than reasonable, the mass-transfer tests were done with pulsation.

Mass Transfer

The results are provided in Table 2. The results are not satisfactory, as the process demands are that the concentration of U_3O_8 in the BO should not exceed 100 mg/L. Apparently, the column was not high enough to provide the necessary five transfer units. The BO was stripped again with 500 g/L H_2SO_4 in a 3 m high column. The resulting BO was between 60-80 mg/L U_3O_8. This indicated that an experimental 10 m high column was needed to carry out the stripping process to meet process constraints on both BO and product. The scale-up to the industrial column was carried out accordingly.

Table 2. Stripping of U_3O_8 in BPC

Date	LO (g/L)	BO (g/L)	Prod. (g/L)	O:A	Flux ($m^3/m^2/h$)
Day 1	12.5	0.50	267	20	47
Day 2	12.6	0.38	282	20	47
Day 3	12.0	0.58	288	20	47
Day 4	12.1	0.39	244	20	60
Day 5	11.6	0.30	261	18	55
Day 6	11.9	0.47	282	18	55

ANALYSIS OF RESULTS AND DISCUSSION

Extraction

The testwork proved that BPC technology is suitable for extraction of uranium from the Key Lake PLS using both the ammoniacal and SAS stripping routes. The process can be carried out successfully in an 8 m high BPC, reaching the required recovery. The concentration of U_3O_8 in the raffinate does not exceed a few mg/L, regardless of the stripping process, comparable with the results obtained in four mixer-settlers in the current SX process. However, there is an advantage in the strong-acid stripped-solvent route. Although the residual U_3O_8 in the BO was double that in the ammoniacal process (see next section), the concentration of U_3O_8 in the raffinate was similar or even slightly lower when using SAS. As the flux with the SAS stripped solvent was higher by 60%, the advantage of the SAS process is obvious. A simple example may demonstrate it: to process 100 m^3/h of PLS at phase ratio 1:1, a column of diameter 2.3 m is needed (flux of 50 $m^3/m^2/h$) in the SAS process vs. a 3.0 m diameter column in the ammoniacal process (flux of 30 $m^3/m^2/h$) or four MS with area of 30 m^2 each (assuming flux of 7 $m^3/m^2/h$).

Attempts to carry out the process in shorter column failed, and the concentration of U_3O_8 in the raffinate climbed from 1 mg/L in an 8 m column to 3-5 mg/L in a 7 m and near to 100 mg/L in a 6 m column. This showed that in the 100 mm diameter BPC the average height of transfer unit (HTU) is 2 m, regardless of the type of the strip process.

It should be noted that the efficiency of Alamine 336 in the Cameco process is very high. The phase ratio was set to O:A= 1.1:1, similar to the MS plant, loading more than 90% of the extractant with uranium.

Stripping

Operating the 7 m high by 80 mm diameter BPC, the concentration of the U_3O_8 in the product (loaded strip solution) was satisfactory, above 240 g/L, but the BO failed to get below 300 mg/L U_3O_8, compared with the required <100 mg/L U_3O_8. It was hardly a surprise, as assuming height of transfer unit (HTU) of 2 m, as per the extraction stage, a column 10 m high by 80 mm diameter could have been used to replicate the performance of the five mixer settlers currently in use at Key Lake (a higher column was not used due to technical limitations on site). The problem was solved by re-running the BO against the SAS in a short 3 m column. The results were satisfactory, and a BO of 60-80 mg/L

U_3O_8 was obtained during an 8 h run. The bottom line is that 10 m of an 80 mm diameter column is needed to strip the LO below 100 mg/L U_3O_8; that is, the HTU is ~2 m, similar to the extraction.

CONCLUSIONS

The comparison between the ammoniacal and SAS stripping processes relates mainly to downstream considerations and is beyond the scope of this paper. Both processes can be carried out efficiently in a BPC column. A single column is sufficient to replace the four MS in the extraction circuit or the five stripping MS.

The ammoniacal stripping requires fewer stages of MS. However, the operation is far more difficult, as it involves strict pH control, and the product is about 10 times more diluted.

As the SAS stripped solvent is fully loaded with H_2SO_4, there is no need to add acid to the extraction in order to keep the pH above the point of precipitation of iron compounds. The SAS enables far higher flux in the extraction.

REFERENCES

1. G. M. Ritcey and A. W. Ashbrook, Solvent Extraction, Vol. 2, Elsevier, New York, 1985; pp. 526-528.
2. B. Grinbaum, “Integrative Method for Development of Solvent Extraction Processes,” Ion Exchange and Solvent Extraction, Vol. 15, Y. Marcus and A. SenGupta, Eds., Dekker, New York, 2001; pp. 1-106.
3. E. Colman, I. Ilan, B. Grinbaum, and G. Stevens, “Comparison of Disk & Doughnut vs. Sieve Tray Internals,” Proceedings International Solvent Extraction Conference 2005, Beijing, China, 2005.

SOLVENT-EXTRACTION AND PURIFICATION OF URANIUM(VI) AND MOLYBDENUM(VI) BY TERTIARY AMINES FROM ACID LEACH SOLUTIONS

Ana M. G. La Gamma, Elena T. Becquart, and Mauricio Chocron

Gerencia Química, Comisión Nacional de Energía Atómica, Av. del Libertador 8250 (1429), Buenos Aires, Argentina. Corresponding author email address: lagamma@cnea.gov.ar

ABSTRACT

Considering international interest in the yellow-cake price, Argentina is seeking to exploit new uranium ore bodies and processing plants. A study of similar plants would suggest that solvent-extraction with Alamine 336 is considered the best method for the purification and concentration of uranium present in leaching solutions. In order to study the purification of these leach liquors, solvent-extraction tests under different conditions were performed with simulated solutions which containing molybdenum and molybdenum-uranium mixtures. Preliminary extraction tests carried out on mill acid-leaching liquors are also presented.

INTRODUCTION

Considering the current increase in the uranium price, the República Argentina is studying the exploitation of new mines. One of them, founded a few years ago, contains uranium associated with molybdenum in different ratios. The treatment of these minerals, which facilitates the production of ammonium diuranate (yellow cake), is based on the fundamental steps of comminution, leaching, solid-liquid separation, clarification, purification, and precipitation. When the mineral leaching is carried out in sulfuric acid, the resulting leach solution from this operation contains various ions in different concentrations and must be purified in order to obtain yellow cake that meets market specifications.

The possible purification processes for these acid pulps are the use of ion-exchange resins and solvent-extraction. A leach solution that contains Mo must be purified by means of solvent-extraction, due to the fact that Mo poisons and pollutes the resins [1].

One of the factors used to define the solvent-extraction process is the selectivity of the uranium-molybdenum separation. A bibliographical study of U and Mo separation in sulfuric acid media by solvent-extraction and the methodologies used in the world mining industry, suggested the use of tertiary amines [2]. The bibliography and technical information [3-4] suggest that Alamine 336 (Cognis, tri-octyl/decyl amine) is a good

extractant to purify these solutions, because in spite of the fact that the U and the Mo are co-extracted, the former can be stripped with sodium chloride [1], and molybdenum is later recovered by means of a sodium carbonate strip [1-2]. Besides U, the acid leach solutions can contain molybdenum, silica, and phosphate. In extraction with tertiary amines, crud can appear, depending on the relative concentration of these elements [2-5].

The Somair plant in Niger [6] and Pozos de Caldas plant in Brazil [7] purify acid leach solutions of U/Mo by means of solvent-extraction with Alamine 336, but the Mo/U concentration ratios are less than 0.1.

In order to understand the purification of this type of leach solution and because extraction of these solutions by means of solvent-extraction with Alamine 336 is a possible method for the leach treatment of U ores that contain Mo, and taking into account the lack of recorded data on the presence of Mo, experiments with simulated solutions of Mo and U blends were carried out. In these experiments, the phase separation time, extraction isotherms at different pH values, phase ratios, and organic-phase composition were studied. The influence of Mo on the U extraction was determined. Preliminary tests with mineral acid leach solutions were also carried out.

EXPERIMENTS PERFORMED WITH SYNTHETIC SOLUTIONS

Experiments with Molybdenum Solutions

The aim of these tests was to obtain a fundamental understanding of the extraction of Mo with tertiary amines. The choice of concentrations studied was based on the typical Mo concentrations in uranium acid leach solutions. The aqueous phase was a synthetic solution of sodium molybdate dissolved in sulfuric acid at typical pH values. The solvent composition (selected according to the bibliographical information) was 0.1 M Alamine 336 (extractant), 5 vol % isodecanol (modifier) in kerosene (diluent). The amine must be protonated before being used. To do so, it must be contacted with acid (sulfuric acid in this case), and the contacts were carried out until the final pH of the aqueous solution was the same as that of the sulfuric acid solution used for protonation.

The technique employed to establish the extraction isotherms was the following: for each experimental condition, solvent contacts with successive aqueous portions loaded in the initial concentration were performed. Different volume ratios of aqueous solution to solvent (R) were used. The molybdenum concentration was determined for each aqueous phase and by difference, the concentration in the organic. From the concentration values in the aqueous solution and solvent, the extraction isotherm was determined. The experimental conditions and the results of the different tests are given in Table 1.

Determination of Basic Parameters

The choice of the basic parameters values was based on the need to establish the required experimental conditions to carry out a purification plant design for uranium leaching in the presence of Mo.

Following the techniques described previously and under the conditions of experiments 1, 2, and 4 (Table 1), the experimental isotherms were obtained. These

experiments led to the conclusion that stirring for 2 min is not convenient, as crud was obtained when the concentration of Mo ([Mo]) in the solvent was 2.5 g/L (experiment 1) and when the [Mo] in the solvent was 8.5 g/L (experiment 2). No crud was obtained in experiment 4. Therefore 1.5 min time stirring was suggested as adequate.

The diluents JP1 (Repsol YPF, aromatics 25%) and SS 2046 (ShellSol 2046, Shell Chemical Co, aromatics 16%) were used for experiments 3 and 6 in Table 1. The isotherms obtained show that with SS 2046 the Mo loading was maximized in fewer contacts.

Table 1. Operational conditions for solvent-extraction of Mo by 0.1 M Alamine 336, 5% isodecanol in kerosene

No.	pH	*R*	Stirring time (min)	[Mo] (mg/L)	No. of contacts	Diluent	Results
1	1.8	3	2	1000	6	JP1	Crud in solvent, [Mo] 2.5 g/L
2	1.8	1	2	1000	13	JP1	Crud in solvent, [Mo] 8 g/L
3	1.8	1	1.5	1000	19	SS 2046	[Mo] 18.44 g/L. No crud in solvent after 2 months
4	1.8	1	1.5	1000	21	SS 2046	[Mo] 19.87 g/L. No crud in solvent after 2 months
5	1.3	1	1.5	500	27	SS 2046	[Mo] 12.51 g/L. No crud in solvent after 2 months
6	1.8	1	1.5	1000	21	JP1	[Mo] 15.74 g/L. Crud in solvent after 2 months
7	1.3	1	1.5	200	19	SS 2046	[Mo] 4.89 g/L. No crud in solvent after 2 months
8	1.3	1	1.5	1000	21	SS 2046	[Mo] 20.6 g/L. No crud in solvent after 2 months
9	1.3	1	1.5	2000	11	SS 2046	Crud in solvent, [Mo] 18 g/L
10	1.3	1	1.5	4000	10	SS 2046	Crud in solvent, [Mo] 19 g/L

Influence of pH

Tests on the influence of pH on the loading of Mo were performed on acid leach solutions from the uranium minerals. The tests results (corresponding to experiments 3 and 8 of Table 1) show that at lower pH, higher Mo loading of the solvent occurs.

Influence of the Molybdenum Concentration

One of the variables that influences the formation of Mo cruds in extraction by tertiary amines is the Mo concentration of the feed. With the aim of determining the values of [Mo] at which the crud appears, experiments were performed using different [Mo] concentrations in the feed solution (experiments 5, 7, 8, 9, and 10 in Table 1). Equilibrium was reached when the solvent loaded to 20 g/L on average, with a 1 g/L Mo feed solution. Lower concentrations (0.2 and 0.5 g/L Mo) did not reach equilibrium. At 2 and 4 g/L Mo concentrations, Mo crud appeared before equilibrium was reached.

Uranium Extraction Isotherm

The U extraction isotherm (Figure 1) was obtained from a uranium sulfate solution (1.13 g/L U), pH 1.3, using 1.5 min stirring time, and the solvent composition same as in the previous experiments. The solvent loading capacity coincided with the expected values that are given in the bibliography [8].

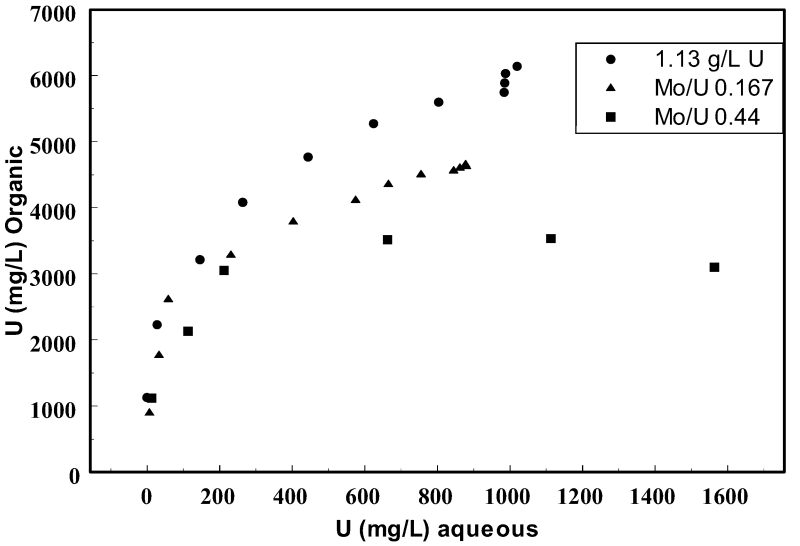

Figure 1. Influence of molybdenum concentration on uranium loading.

Experiences with Solutions Containing Uranium and Molybdenum

The presence of both ions in the leach liquor was studied using a solvent containing 0.1 M Alamine 336 and 5% isodecanol in kerosene at pH 1.3. The stirring time was 1.5 min. The aqueous feed solution contained uranium sulfate and sodium molybdate in different [Mo]/[U] ratios. The extraction isotherms obtained for uranium are shown in Figure 1. It can be concluded that U concentration ([U]) in the solvent varies according to the different [Mo]/[U] ratios in the feed. The higher the Mo/U ratio became, the lower the [U] loading was obtained in the solvent. At a [Mo]/[U] ratio of 0.44 and [U] in the solvent of 3.9 g/L, the U was re-extracted by the aqueous phase. Mo loading in the solvent is the same as when the feed contains only Mo. This indicates that this solvent system is selective for Mo over U.

EXPERIMENTS WITH LEACH SOLUTIONS

The mineral leach solutions were provided by Mendoza Laboratories, Comisión Nacional de Energía Atómica, Argentina. Their compositions are presented in Table 2. Leach solutions 1, 2, and 3 correspond to sucessive leaches of the same mineral. Purification of these leach solutions (tests 1, 2, 3, and 4) by solvent-extraction with 0.1 M

Alamine 336 and 5% isodecanol in SS 2046 at pH 1.3 was performed. The stirring time was 1.5 min. The solvent was contacted with successive portions of aqueous solution and the [U] of each aqueous solution was determined. The concentration in the solvent was calculated by difference. The extraction isotherms obtained are shown in Figure 2. In tests 1, 2, and 4, an emulsion was formed in the solvent, which was destroyed on filtering. Leach solution 3 did not show any operational problems.

Table 2. Leach composition and uranium solvent loading

Leach	U (mg/L)	Mo (mg/L)	Fe (mg/L)	[Mo]/[U]	pH	[U] solvent (mg/L)
1	6650	100	540	0.015	1.2	5797
2	1110	90	40	0.081	1.3	5006
3	3190	170	210	0.053	1.2	5624
4	800	—	—	—	1.0	5570

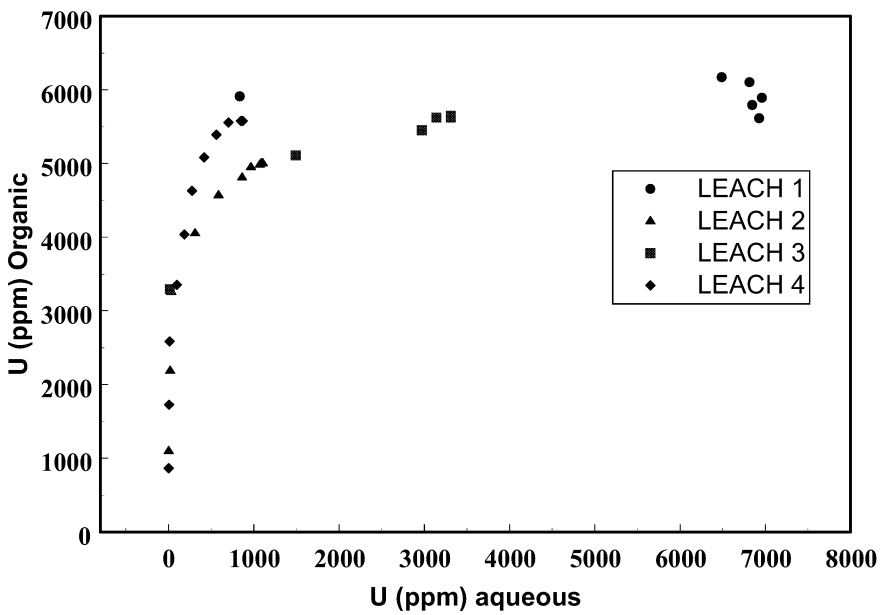

Figure 2. Uranium extraction isotherms obtained for leach solutions.

CONCLUSIONS

The laboratory solvent-extraction of synthetic aqueous solutions containing Mo, U, and Mo and U mixtures, and of actual leach solutions, using 0.1 M Alamine 336 and 5% isodecanol in kerosene allowed the following conclusions:

(i) The solvent is capable of loading up to 20 g/L Mo. In order to avoid the formation of Mo crud, the aqueous-phase concentration of Mo must be <1 g/L.

(ii) In the absence of Mo, the solvent loading is 6.1 g/L U.

(iii) The presence of Mo in the aqueous solution lowers the U loading in the solvent. This behavior was corroborated by the leaching tests. The solvent loading capacity of Mo is not affected by the presence of U. In tests containing [Mo]/[U] 0.44 or above, the U is re-extracted to the aqueous phase, indicating the selectivity of this solvent system for Mo over U.

ACKNOWLEDGEMENTS

Cognis (USA), Shell, and Repsol YPF representatives in Argentina are gratefully acknowledged for providing chemicals samples and information, as are Lic.G. Tomellini, Comisión Nacional de Energía Atómica, Mendoza, Argentina for providing leach liquros, and Ms. Valeria Díaz and Mr. Matías Lucas, students at Facultad de Ingeniería, Universidad de Buenos Aires, for their assistance.

REFERENCES

1. Uranium Extraction Technology, Technical Reports Series Nº 359, International Atomic Energy Agency, Vienna, Austria, 1993; pp. 252.
2. R. C. Merrit, The Extractive Metallurgy of Uranium, Colorado School of Mines, USA (1971); pp. 199−200.
3. B. Floh, A. Abrao, and E. Calmon Costa, “Amine Extraction of Uranium, Molybdenum and Vandium from Acid Leach Liquors,” Recovery of Uranium, IAEA-SM-135/18, Vienna, Austria, 1971; pp. 267−285.
4. G. M. Ritcey and A. W. Ashbrook, Solvent-extraction Principles and Applications to Process Metallurgy (Part II), Elsevier Scientific Publishing Co., 1979; pp. 463−464.
5. B. A. Moyer and W. J. McDowell, “Characterization of Molybdenum Interfacial Crud in a Uranium Mill that Employs Tertiary Amine Solvent-extraction,” 3rd International Symposium Hydrometallurgy, Atlanta, USA, March 1983.
6. L. Gabillat, P. Mouret, G. Boutonnet, J. Grenier, and J. Poitte, “Du Laboratoire a la Marche Industrielle: l'Úsine Chimique de la Somair au Niger,” Industrie Minerale-Mineralurgie, Saint Etienne, France FR, 1974; pp. 98−124.
7. E. Calmon Costa, H. F. Batista, L. O. Castro, and A. G. De Olliveira, “Processing of a olybdenum-Uranium Ore from the Pocos de Caldas Plateau,” Recovery of Uranium, IAEA-SM-135/18, Vienna, Austria, 1971; pp. 67−78.
8. J. M. W. Mackenzie, “Uranium Solvent-extraction using Tertary Amines,” Uranium Ore Yellow Cake Seminar, Melbourne, Australia, February 1977.

DEGRADATION PROBLEMS WITH THE SOLVENT EXTRACTION ORGANIC AT RÖSSING URANIUM

Brodrick Munyungano,[1] Angus Feather,[2] and Michael Virnig[3]

[1]*Rössing Uranium Ltd, Private Bag 5005, Swakopmund, Namibia*
[2]*Cognis, P. O. Box 361, Honeydew, 2040, South Africa*
[3]*Cognis Corporation, 2430 N. Huachuca Dr, Tucson, Az, USA*
Corresponding author email address: angus.feather@cognis.com

ABSTRACT

Rössing Uranium Ltd recovers uranium from a low-grade ore in Namibia. Uranium is recovered and purified from an ion-exchange eluate in a solvent-extraction plant. The solvent-extraction plant uses Alamine 336 as the extractant for uranium, with isodecanol used as a phase modifier in Sasol SSX 210, an aliphatic hydrocarbon diluent. Since the plant started in the mid 1970s, there have been a few episodes where the tertiary amine has been quickly and severely degraded when the plant was operated outside certain operating parameters. The Rössing experience is discussed in more detail in this paper.

INTRODUCTION

At Rössing Uranium mine, the uranium-bearing alaskite ore undergoes the sequential processes of crushing, grinding, leaching, solid-liquid separation, uranium recovery, precipitation, and calcination, to produce a saleable uranium oxide product. The crushed and milled ore is leached with sulfuric acid under oxidizing conditions to dissolve the uranium.

After solid-liquid separation, clear leach solution contains 0.18 g/L U_3O_8 that is fed to the ion-exchange (IX) plant. The IX circuit is a Porter system, where a countercurrent flow arrangement is used in a series of six fluidized-bed contactors. The main reason for using this plant design was the belief that it would cope with large volumes of leach solution with a high concentration of suspended solids.

Loaded resin is advanced countercurrently to the leach solution from one contactor to another by means of air-lift pumps. The loaded resin is then transferred to conventional columns for elution. Barren solution returns to the washing circuit. Elution is carried out using raffinate from the solvent-extraction (SX) plant containing 100 g/L sulfuric acid. Eluted resin, typically containing 1 g/L uranium or less, is returned to the sixth contactor in the Porter system.

The SX plant follows conventional uranium plant design. The concentrated eluate from IX is contacted countercurrently in five mixer-settler stages with stripped organic

phase at a O:A ratio of 0.7-1:1. The plant organic comprises 7 vol. % Alamine® 336 and 3 vol. % isodecanol in an aliphatic diluent (Sasol SSX 210). The raffinate from SX contains <100 mg/L uranium and is returned for elution of resin in IX. Loaded solvent passes through two stages of water scrub to displace acid and then into four stages of stripping using aqueous ammonia in ammonium sulphate solution. The loaded strip liquor (OK liquor) leaving the stripping section typically contains 12 g/L U_3O_8.

The OK liquor is contacted with ammonia in a precipitation tank at pH of 7.3, and ammonium diuranate (ADU) is precipitated. This is thickened and washed on two stages of rotary drum filters. The final filter cake is fed to two six-hearth roasters where it is calcined to uranium oxide and then sold.

During pilot-plant trials of the Eluex process for Rössing in the early 1970s, a sudden loss of tertiary amine content from the organic phase was noted. At the time, it was concluded that the sodium chlorate used as an oxidant in the leach was responsible for the loss of amine by oxidation [1].

The problem experienced during the piloting re-occurred at the Rössing SX plant during 1985-7, some nine years after plant start-up. Analysis of the circuit organic phase by Warren Springs laboratory using infrared spectroscopy and gas chromatography-mass spectrometry (GC-MS) showed high levels of N-nitrosoamines and secondary amines [2]. On the recommendation of their consultant, Rössing added iron wire to the aqueous overflow weirs in the SX extraction stages to control redox potential in the IX eluate [3]. The oxidation of amine was prevented by maintaining redox potential in the aqueous phase below 510 mV *vs*. Ag/AgCl.

The problem re-occurred during 1993, 2000, and 2005 [4-6], the latter two occasions resulting in loss of the entire inventory of amine in the circuit within periods of less than a week. From analyses carried out at Rössing over the last 30 years, it is known that rapid loss of amine from the SX circuit is strongly linked to high concentrations of nitrate and ferric ion in the IX eluate. Significant amounts of nitrate are found in the circuit, due to the use of water-based explosives containing ammonium nitrate in the mining of the uranium ore. At the same time, Rössing Uranium analyzed plant solvent samples for bacterial activity. While this was considered a remote possibility, it needed to be ruled out. No evidence of bacterial activity was found.

CHEMISTRY OF AMINE DEGRADATION

Analysis of a typical Rössing circuit organic (USX organic) by gas chromatography (GC) is summarized in Table 1. The determination was carried out with a 30 meter x 0.32 mm ID DB-5 column with a 0.25 micron film thickness. Helium gas was used as the carrier. The oven program started at 100 °C with a 1 min hold followed by a 10 °C/min. ramp up to 300 °C with a final hold of 5 min. For comparison purposes, a fresh solution of Alamine 336 was also analyzed. The diluent and alcohol modifier come off the column very early in the chromatogram and are not included in the GC area % values.

Table 1. Summary of GC Analytical Results

Component	Retention Time (min.)	Fresh Organic (GC Area %)	USX Org (GC Area %)
C8,C8 amine	9.82	0.09	0.26
C8,C10 amine	11.78	0.14	0.48
C8,C8 nitrosoamine	12.68	0	3.47
C10,C10 amine	13.58	0.04	0.20
C8,C10 nitrosoamine	14.45	0	5.36
C8,C8,C8 amine	14.82	26.6	23.6
C10,C10 nitrosoamine	16.07	0	1.54
C8,C8,C10 amine	16.31	42.0	38.5
C8,C10,C10 amine	17.69	22.1	20.4
C10,C10,C10 amine	18.97	4.0	3.8

The identification of the peaks for the individual components (the three secondary amines (C8,C8; C8,C10; and C10,C10), the three nitrosoamines, and the four tertiary amines that make up Alamine 336) has been confirmed by either comparison with known substances or a combination of Gas Chromatagraph-Fourier Transform Infrared Spectroscopy (GC-FTIR) and GC-MS. While the nitrosoamines are clearly present in this sample of USX organic, they are present at a relatively low level.

Under severe degradation conditions, the level of the nitrosoamines has been observed to be present at levels 3 to 4 times that of the tertiary amines. The GC data also indicate that there is an increase in the level of secondary amines relative to the tertiary amines. Fresh reagent contains trace levels of the secondary amines as by-products from manufacture. After a short period of operation, one typically sees a small increase in the level of secondary amines in all uranium circuit organics. The fact that there has been a slight increase in the secondary amine level in the Rössing USX organic may or may not be related to the attack of the nitrate on the organic.

In heavily degraded samples of the Rössing USX plant organic, low levels of alkyl aldehydes and their acid-catalyzed aldol condensation products, higher molecular weight α,β-unsaturated aldehydes, are also observed. This suggests that the degradation chemistry leading to the nitrosoamines also involves cleavage of an alkyl group from the tertiary amines as an alkyl aldehyde. Since the C8 and C10 aldehydes would be expected to be somewhat water soluble, the fact that they are only present in low levels is probably due to the fact that they tend to wash out of the organic phase.

The proposed chemical pathway for the degradation is summarized in Equations 1 through 5. The chemistry is very similar to that proposed by Smith and co-workers to explain the degradation of tertiary amines by nitrous acid [7]. The major difference is that there should not be any substantial amount of nitrous acid present in the incoming feed stream due to the high redox potential. To account for the chemistry, it is necessary to start with the nitrate that is in the feed solution. In the presence of acid, nitric acid will form a nitronium ion. It reacts with the tertiary amines to generate an imine which is rapidly hydrolyzed in the presence of water and acid to the corresponding aldehyde and the secondary amine.

$$H^+ + HONO_2 \rightleftharpoons NO_2^+ + H_2O \quad (1)$$
Nitronium Ion

$$R_3N + NO_2^+ \rightarrow R_2N{=}CHR' + HONO \quad (2)$$
Imine Nitrous Acid

$$R_2N{=}CHR' + H_2O \rightleftharpoons R_2NH + R'CHO \quad (3)$$
Aldehyde

$$HONO + H^+ \rightleftharpoons NO^+ + H_2O \quad (4)$$
Nitrosyl Cation

$$R_2NH + NO^+ \rightarrow R_2N\text{-}NO + H^+ \quad (5)$$
Nitrosoamine

At the same time, the nitronium ion is converted to nitrous acid. Nitrous acid behaves very similarly to nitric acid under these conditions and forms a nitrosyl cation which then reacts with the secondary amine to form the nitrosoamine. Both the nitronium ion and the nitrosyl cation are very reactive, highly oxidized species. If there is a high enough concentration of species present in the aqueous phase that can reduce these cations to neutral species, their lifetime in the aqueous phase will not be long enough to allow them to attack the organic phase. This is consistent with the observation that reducing the redox potential of the aqueous by passing it over iron wire stops attack on the solvent.

DEGRADATION CONTROL

A typical analysis of the eluate from IX is shown in Table 2. The IX process is not particularly selective for uranium over other anionic species such as nitrate and chloride. The operation of the Porter IX system will always be a compromise between maximizing uranium extraction efficiency and minimizing the transfer of impurities.

Table 2. Typical composition of feed solution to SX (g/L)

U_3O_8	H_2SO_4	NO_3	Cl^-	Fe^{2+}	Fe^{3+}
4	90	0.4	2	2.25	2.1

The IX eluate which feeds to the SX plant contains a significant concentration of nitrate. At high solution potential, this plays some role in oxidation of the amine. Once nitrate finds its way into the SX circuit, and through into the OK liquor, it is recycled in the ammonium sulfate solution from ADU precipitation back into the strip section of SX. In the strip, nitrate can be re-extracted, only to be displaced from the organic phase in the extraction section by the high uranium concentration in the eluate. In this manner, nitrate levels in and around SX can quickly build up to significant concentrations.

In the past, Rössing has controlled the redox potential of the aqueous phase in SX by adding rolls of iron wire to the aqueous launders of the extraction stages. The wire is leached by the ferric species in solution, thus reducing the ferric to ferrous. This drops the redox potential of the solution to a level where the amine is not oxidized. Besides the cost of the iron wire, the wire addition adds significant amounts of Fe to the circuit.

From time to time, both SX raffinate and the ammonium sulfate solution from ADU precipitation are bled out of the circuit to control iron and nitrate concentrations. This requires the use of fresh water to make up the lost volume.

DEGRADATION CONTROL IN THE FUTURE

As Rössing Uranium is currently involved in an expansion phase, maximizing the availability of the SX circuit is becoming more important. The loss of revenue during SX downtime, at current uranium prices, can be significant. This loss of revenue can far outweigh any potential replacement costs for degraded organic. Rössing has recently carried out an in-depth study of their plant and process to identify areas where production could be compromised. In each of these areas, steps have been taken to minimize any risk to production.

The first step of controlling the extractant degradation problem on the plant is to understand it fully. While the exact mechanism of the amine degradation is not completely understood, enough information exists to develop a strategy to prevent catastrophic oxidation of Rössing's amine inventory. A number of factors need to be considered when developing this strategy.

- Water-balance restrictions. Rössing Uranium is located in a desert, with limited access to clean fresh water. While bleeding of the SX raffinate, ammonium sulfate solution and the aqueous from the organic regeneration stage is the best method of controlling nitrate build-up, this has to be done with a view to minimizing the fresh water usage that would result. Rössing is currently evaluating the provision of more fresh water to the mine. While this would certainly help, it will always be costly due to the plant locality.
- Extractant quality. The tertiary amine used in the circuit should contain as little secondary and primary amines as possible. Cognis has recently made extensive improvements to the manufacturing process for Alamine 336. These have resulted in a significant increase in tertiary amine content and decrease in secondary amines and other impurities.
- Nitrate removal. Rössing is considering methods of selectively removing nitrates from the SX-precipitation circuit. Both SX and IX are being investigated. The eventual disposal of the concentrated nitrate solution may pose some problems, depending on the concentration factor achievable.
- Control of solution potential. The oxidation of tertiary amine in the SX circuit can occur very quickly. The entire inventory can be lost within a few days. Rössing Uranium is considering methods to quickly reduce the solution potential using a reducing agent as an emergency measure.

Various reducing agents are being considered. It is hoped that an automatic addition system could be used to control solution potential at a particular point in the circuit, thus reducing the reaction time if left to manual operator intervention. A butylhydroxytoluene, Merisol®, will be evaluated in SX to determine its effectiveness as an anti-oxidant in the organic phase. However, it is unlikely that even a relatively high concentration of anti-oxidant in the organic phase would offer significant protection.

CONCLUSIONS

The effect of various plant operating parameters on SX plant extractant degradation have been identified. Rössing has established upper and lower limits for most parameters that are known to have a contributing role in amine degradation. While an understanding of the chemistry of the degradation has been gained over the last 20 years, more work in this area remains to be done.

Rössing Uranium and Cognis are undertaking further research into the degradation of amines in uranium SX plants using the Eluex process. Work is being done to analyze all impurity and breakdown products in the plant organic phase to improve understanding of the chemistry of the degradation.

Significant work has been done to overcome the reagent-degradation problem at Rössing Uranium. Solutions being implemented have to be practically possible in a plant environment and also cost effective. In current market conditions, it is imperative to maximize plant availability and minimize downtime.

REFERENCES

1. J. B. Scuffham and G. A. Rowden, "An Investigation into Solvent Degradation," Divisional Report, Research and Development Division, Power-Gas Ltd., Stockton-on-Tees, 1971.
2. D. W. West and J. C. Baily, "Loss of Amine from Solvent Extraction Plant," Warren Springs Laboratory, Stevenage, Hertfordshire SG1 2BX, 1986.
3. R. Pascoe, "Modification of the Conc Eluate Redox to Reduce Alamine Loss," Rössing Uranium Mine Report, Swakopmund, Namibia, 1986.
4. J. Coetzee, "Operational Problems Experienced in SX from September to October 1993," Rössing Uranium Report, Swakopmund, Namibia, 1993.
5. J. M. W. Mackenzie, "Rössing Uranium–Alamine Loss Summary Report," Henkel South Africa Trochem Division Report 92/86, Johannesburg, South Africa, 1986.
6. B. M. Munyungano, "Solvent Degradation–Rössing Uranium Mine," *J. S. Afr. Inst. Min. Metall.*, **107**(7), 415-417, 2007.
7. P. A. S. Smith and R. N. Loeppky, "Nitrosative Cleavage of Tertiary Amines," *J. Am. Chem. Soc.*, **89**(5), 1147-1157 (1967).

ROLE OF VANADIUM(V) IN THE AGING OF THE ORGANIC PHASE IN THE EXTRACTION OF URANIUM(VI) BY ALAMINE 336 FROM ACIDIC SULFATE LEACH LIQUORS

A. Chagnes,[1] G. Cote,[1] B. Courtaud,[2] and J. Thiry[2]

[1]Ecole Nationale Supérieure de Chimie de Paris - ENSCP Université Pierre et Marie Curie – Paris6 - Laboratoire d'Electrochimie et de Chimie Analytique - UMR7575 CNRS-ENSCP-Paris6 ENSCP, 11 Rue Pierre et Marie Curie, 75231 Paris Cedex 05 France. [2]AREVA-NC, Service d'Etudes de Procédés et d'Analyses (SEPA), B.P. N°71 – 87250 Bessines sur Gartempe (France).
Corresponding author email address: alexandre-chagnes@enscp.fr

ABSTRACT

The present work is focussed on the chemical degradation of Alamine 336-tridecanol-*n*-dodecane solvent which used in the recovery of uranium by solvent extraction. Degradation occurs due to the presence of vanadium(V), an oxidant, in the feed solution. After a brief overview of the chemistry of vanadium, the kinetics of degradation of the solvent when contacted with acidic sulfate leach liquor was investigated and interpreted by the Michelis-Menten mechanism. GC-MS analyses evidenced the presence of tridecanoic acid and dioctylamine as degradation products. A mechanism of degradation is discussed.

INTRODUCTION

Solvent extraction (SX) processes are used worldwide for the production of base and strategic metals and in the nuclear industry for the reprocessing of spent nuclear fuels [1]. Nevertheless, hydrometallurgists may still encounter technical problems in SX plants. These problems include progressive degradation of the extractants with an associated loss of extraction capacity, etc. [2]. All of these problems increase the production, cost as there is a need for regular additions of fresh solvent and implementation of processes for effluent treatment to cope with increasingly stringent environmental regulations.

The present work is focussed on the aging of the organic phases in the extraction of uranium(VI) from acidic sulfate leach liquors containing vanadium(V). Here, the fresh organic phases typically contain Alamine® 336 as uranium extractant, *n*-dodecane as a diluent, and 1-tridecanol as a modifier used to prevent third-phase formation.

Acidic sulfate leach liquors of uranium ores usually contain a wide range of metal species as shown in Table 1. Some of these species, including Mn(VI), Cr(VI), V(V), etc., are known to be capable of reacting with organic compounds such as alcohols, α-

hydroxyacids, aldehydes, or ketones [3] and probably contribute to the chemical degradation of the extractants used in the hydrometallurgy of uranium.

Table 1. Typical composition of acidic sulfate leach liquors of uranium

Species	Concentration (mg/L)	Species	Concentration (mg/L)
U	3765	Ti	220
Mo	885	Si	101
Zr	82	K	206
V	235	Mg	2.5
Fe	8520	Na	2120
Ni	16.2	P	540
Cr	19.7	SO_4^{2-}	98000
Mn	198	NO_3^-	154
Pb	15.2		

In this study, attention is paid to the role of vanadium(V) in the degradation of Alamine 336-tridecanol-*n*-dodecane organic phase in contact with acidic sulfate solution. After a brief description of the vanadium chemistry, this paper will focus on the kinetics of oxidation of the organic phase containing Alamine 336 extractant, tridecanol modifier, and *n*-dodecane diluent. Gas chromatography coupled with mass spectrometry (GC-MS) was used to identify the degradation products. All of these data are useful in proposing parades to limit the chemical degradation of the solvent. This would minimize the solvent loss in uranium SX plants and increase extraction efficiency.

EXPERIMENTAL

Reagents

n-Dodecane (purity, >99%), 1-tridecanol (purity, >98%), trioctylamine (purity, >99%), hexane (analytical grade), and acetyl acetate (analytical grade) from Aldrich were used as delivered. Sulfuric acid (purity, 98%), sodium metavanadate (purity, >99.9%) from Aldrich and water (resistivity > 18 MΩ. cm) purified with a Milli-Q Gradient system from Millipore Corporation were used for preparing the aqueous solutions. Alamine 336 was provided by Cognis and used without further purification.

Methods and Equipment

The chemical degradation of the organic phase in contact with sulfuric acid leach liquors containing V(V) occurs via a redox reaction that leads to the formation of V(IV). The oxidation of the solvent was investigated by following the formation of V(IV) concentration in the aqueous phase by UV-visible spectrophotometry with a Varian Carry 100 Scan spectrophotometer.

For each experiment, a sample of organic phase (5 mL) was mixed with an aqueous phase (5 mL) containing sulfuric acid and sodium metavanadate. During kinetic measurements, the two phases were stirred at 25 °C or 50 °C with a mechanical stirring

apparatus (Gherardt Laboshake) thermostated with a Gherard Thermoshake. All samples were protected from light in order to avoid photo-induced degradation of the organic compounds in the presence of vanadium(V). Degradation of organic phases was only observed in the presence of vanadium(V) in the aqueous phases.

Each sample of the aqueous phase was periodically removed with an Eppendorf pipette. The sample was then analyzed by UV-Vis spectrophotometry at 760 nm, and the sample was then returned to the experimental flask.

At the end of the kinetics degradation experiment, aqueous and organic phases were analyzed by GC-MS. Before GC-MS analyses, each sample was treated as follows: aqueous phases were contacted with hexane after neutralization and with sodium hydroxide and acetyl acetate in order to extract polar and nonpolar degradation products, respectively. All samples were dried with magnesium sulfate before GC-MS analyses. Hexane and acetyl acetate phases were analysed without chemical treatment such as derivatization.

GC-MS analyses were performed with a Varian 3300 gas chromatograph coupled with a Ribermag R1010 C (Bermag S.A.) mass spectrometer. The chromatographic separations were carried out using a fused silica capillary column (30 m x 0.2 mm x 0.2 μm) with cross-linked octadecanyl silicone of CP Sil 5 CB Low Bleed type (Chrompack). The other conditions were as follows: detector temperature 250 °C, injection 1 μL in split mode, carrier gas helium, and ionizing energy 70 eV.

RESULTS AND DISCUSSION

Vanadium may exist in solution as V(V), V(IV), V(III), and V(II), but only V(V) is considered in this paper as an oxidation of the feed solution by chlorate is carried out during the leaching process.

In slightly acidic solution ($3 \leq pH \leq 6$), neutral and alkaline media, the main vanadium species in solution are [4,5] (i) hexavanadate anions ($H_2V_6O_{17}^{2-}$, $HV_6O_{17}^{3-}$); (ii) metavanadate anions (VO_3^-, $V_3O_9^{3-}$); pyro- and orthovanadic anions such as $V_2O_7^{4-}$ and VO_4^{3-}, respectively. VO_2^+ ion exists in solution when $pH \leq 1$ [4,5]. It is a very strong oxidant of organic compounds, and its oxidation activity depends strongly on the pH of the medium.

Based on general literature data, one of the products of degradation of the Alamine 336-tridecanol-*n*-dodecane arising from the presence of V(V) should be tridecanoic acid. The presence of tridecanoic acid as degradation product of tridecanol has been confirmed by gas-chromatography coupled with GC-MS analyses after prolonged contact of the solvent with 1 M sulfuric acid containing 0.05 M V(V) at 50 °C. Nevertheless, the presence of secondary amines has also been identified in the solvent. On the other hand, analysis of amines in the solvent during extraction in a uranium plant (composition of the feed solution in Table 1) shows a slow drop of the concentration of tertiary amines and an increase of secondary amines (Figure 1). The slight decrease of the total concentration of amines in the solvent of extraction is most likely due to soluble losses of the secondary amine to the aqueous phase.

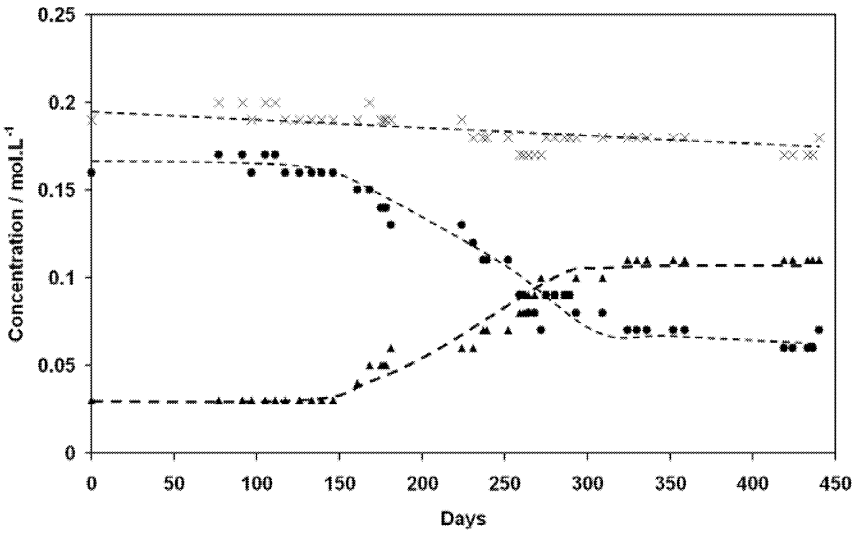

Figure 1. Formation of secondary amines by degradation of Alamine 336 during the uranium solvent extraction in a solvent-extraction plant. ● Tertiary amine; ▲ secondary amine; × total concentration of amines. (t = 0 corresponds to a solvent reloaded with tertiary amine but not to a fresh solvent, which explains the presence of secondary amine at that time).

Therefore, during the SX process, it is necessary to periodically add Alamine 336 in order to compensate the degradation losses

The kinetics of degradation were investigated by following the change of concentration of V(IV) in the aqueous phase by UV-Vis spectroscopy. Any V(IV), formed by the reduction of V(V) during the oxidation of the solvent, is spontaneously stripped from the organic phase to the aqueous phase (Figure 2).

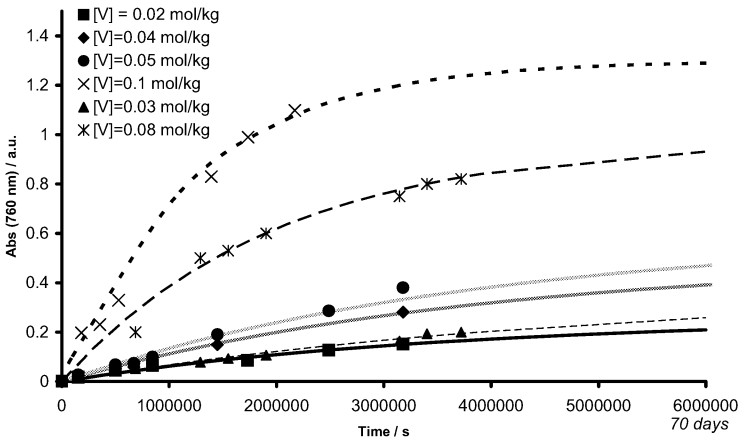

Figure 2. Variation of the absorbance of vanadium(IV) at 760 nm in the aqueous phase during the degradation of the organic phase (0.2 mol/kg Alamine 336 and tridecanol at 5% wt/wt dissolved in *n*-dodecane) at different concentration of vanadium(V) in 1 mol/kg sulfuric acid (t = 50 °C).

Results have been interpreted by using the Michelis-Menten mechanism, which is usually used to describe oxidation reactions of organic compounds by metal ions [8]:

$$V(V)_{org} + S_{org} \underset{k_1}{\overset{k_{-1}}{\rightleftharpoons}} C^*_{org} \xrightarrow{k_2} V(IV)_{aq} + P_{org} \quad (1)$$

where P is the product of the oxidation, C* is a transition complex, and the subscripts "aq" and "org" refer to aqueous and organic phases, respectively.

The change of the absorbance at 760 nm, corresponding to the absorbance band of V(IV) [6-7], gives useful information to describe the kinetics of degradation. The degradation rate constant can be easily derived from Equation 2 to describe the variation of the absorbance of V(IV) during the degradation:

$$Ln\left(\frac{A_{\infty}^{V(IV)} - A^{V(IV)}}{A_{\infty}^{V(IV)}}\right) = -k_{obs}t \quad (2)$$

where $A_{\infty}^{V(IV)}$ is the absorbance of V(IV) in the aqueous phase at infinite time (at the end of the oxidation, when the absorbance remains constant), and $A^{V(IV)}$ is the absorbance of V(IV) in the aqueous phase at the time *t*.

The variation of absorbance of the aqueous phase against time of contact at various concentrations of vanadium(V) and at a constant sulfuric acid concentration (1 mol kg^{-1}) shows a low kinetic rate of degradation as the degradation is not fully completed after 500 h (i.e., absorbance at 760 nm does not still reach a constant value). The kinetic rate constants (k_{obs}) have been calculated by using Equation 7 with UV-Vis experimental data (Figure 2).

The kinetic rate remains constant when vanadium concentration is lower than 0.05 mol/kg ($k_{obs} \approx 2.3 \times 10^{-7}$ s^{-1}). For higher concentration, the kinetic rate constant increases ($k_{obs} = 5 \times 10^{-7}$ s^{-1} for [V(V)] = 0.08 mol/kg and $k_{obs} = 8.1 \times 10^{-7}$ s^{-1} for [V(V)] = 0.1 mol/kg). According to Equation 2, the order of reaction toward V(V) is equal to 1 when vanadium concentration is lower than 0.05 mol/kg as k_{obs} remains constant whereas the order of reaction is different from unity at higher vanadium concentration. The results may be explained by two routes of degradation of the extraction solvent depending on the vanadium concentration.

Therefore, the concentration of V(V) is a critical parameter as the degradation of the solvent extraction increases when the concentration of V(V) in the feed solution is higher than 0.05 mol/L. Consequently, the presence of V(V) in uranium ores may result in a significant degradation of the solvent of extraction and a significant loss of extraction efficiency.

CONCLUSIONS

The presence of highly-oxidizing metal ion species may degrade components of a typical uranium SX organic phase. The degradation of Alamine 336-tridecanol-*n*-dodecane occurs in presence of V(V) in sulfuric media. This results in the formation of tridecanoic acid, from the oxidation of tridecanol, and of dioctylamine, from the

degradation of Alamine 336. The degradation rate is strongly dependent on the vanadium concentration in the feed solution. To avoid or at least to delay the degradation of the organic phase, it may be possible to use a solvent without tridecanol but containing an aromatic diluent instead of *n*-dodecane, since aromatic diluents are better solvents, and a solvation modifier such as isotridecanol may not be required. Work is in progress to assess the influence of the composition of the organic and aqueous phases, that is, Alamine 336, tridecanol, and sulphuric acid concentrations, on the degradation rate.

REFERENCES

1. G. Cote, "Hydrometallurgy of Strategic Metals," *Solvent Extraction and Ion Exchange*, **18**, 703–727 (2000).
2. J. Rydberg, M. Cox, C. Musikas, and G. R. Choppin, Eds., Solvent Extraction Principles and Practice, 2nd Edition, Marcel Dekker, New York, 2004.
3. K. B. Wiberg, Oxidation in Organic Chemistry, Part A, Academic Press, New York, 1965.
4. P. Pascal, Nouveau Traité de Chimie Minérale (tome XII), Masson et Cie editors, Paris, 1960.
5. M. Takaya and K. Samatari, "Speciation of Vanadium(IV) and Vanadium(V) using Ion-Exchange Chromatography and ICP-AES," *Industrial Health*, **32**, 165-178 (1994).
6. A. Zhang, K. Li, and J. Hu, "Hydroxylamine Derivative in Purex Process. Part VIII. The Kinetic and Mechanism of the Redox Reaction of N-methylhydroxalamine and Vanadium(V)," *Journal of Radioanalytical and Nuclear Chemistry*, **261**(2), 301-307 (2004).
7. C. M. Zigli and K. Takashima, "Oxidation of Malic Acid by Vanadium(V) in Sulfuric Acid Medium: A Kinetic and Mechanistic Investigation," *International Journal of Chemical Kinetics*, **27**, 1055-1064 (1995).
8. M. Fatima, C. Guedes da Silva, J. Armando L. Da Silva, J. J. R. Fausto da Silva, Armando J. L. Pombeiro, C. Amatore, and J.-N. Verpeaux, "Evidence for a Michaelis-Menten Type Mechanism in the Electrocatalytic Oxidation of Mercaptopropionic Acid by an Amavadine Model," *Journal of the American Chemical Society*, **118**, 7568-7573 (1996).

THE DEGRADATION OF THE KETOXIME LIX84-I AND ITS IMPACT ON THE SOLVENT EXTRACTION OF PALLADIUM

Stephen F. Woollam[1] and Richard A. Grant[2]

[1]*Anglo Research, 4 Barbara Road, Primrose East, Germiston 1410, South Africa*
[2]*Johnson Matthey Technology Centre, Sonning Common, Reading, UK, RG4 9NH*
Corresponding author email address: swoollam@angloresearch.com

ABSTRACT

Laboratory investigations to increase palladium output at the Precious Metals Refiners (PMR) showed that a 100% increase in capacity could be achieved by doubling the LIX 84-I concentration and modifying the operating conditions. However, problems were encountered during the PMR plant trials with high levels of acid entrainment in the solvent exiting the strip section due to slow phase disengagement. The cause was rapidly identified as the acid-catalyzed degradation of the ketoxime by hydrolysis to the ketone. The doubling of the extractant concentration decreased the predicted life span of the solvent from over a year to less than two months.

INTRODUCTION

Anglo Platinum is the world's leading producer of platinum (40% of primary production in 2006). The other Platinum-Group Metals, including palladium, are found naturally with the ores exploited by Anglo Platinum and consequently need to be separated from each other and from base metals in the refining processes. Anglo Platinum has stated its intention to increase production of platinum by approximately 5% per annum over several years, to meet the forecasted increase in demand [1]. Demand for platinum has increased steadily over the period 1987 to 2006 at a rate of over 5% per annum to the most recent value of 7.9 million ounces per annum [2].

The vast majority of Anglo Platinum's mining output, and that of its joint-venture partners, is treated through its concentrators, smelters, base metal refinery, and single precious metals refinery. The plans to continue increasing production through more intensive mining has necessitated a major expansion of Anglo Platinum's Precious Metals Refiners (PMR) near Rustenburg, South Africa. Where possible, increasing the capacity of the individual process units for this plant would be achieved through modification of the process parameters within the framework of the existing plant, rather than multiplication of existing units.

The PMR flowsheet is chloride-based and incorporates four solvent-extraction stages for the separation of Au, Pd, Pt, and Ir [3-5]. Palladium is present as the stable

square-planar anion $[PdCl_4]^{2-}$, which can readily form a chelated complex with hydroxyoximes, with bonding to the metal through a nitrogen and oxygen-donor functionality. The extractant employed at PMR is the ketoxime, LIX® 84-I, a reagent that is part of the family of well-known extractants for copper, and in this instance using Solvesso 150 as the diluent. Extraction is strongly favored under low-chloride concentrations, albeit kinetically controlled. Stripping is effected by increasing the chloride concentration, by using strong hydrochloric acid, and under these conditions, the process is primarily equilibrium-controlled [6]. The overall extraction and stripping of palladium in this system are represented by the following equation, where RH represents the protonated ketoxime:

$$[PdCl_4]^{2-}_{(m)} + 2RH_{(org)} \rightleftharpoons [PdR_2]_{(org)} + 4Cl^-_{(aq)} + 2H^+_{(aq)} \quad (1)$$

The solvent-extraction circuit for palladium contains extraction, scrub, strip, and wash stages, using mixer settlers operated in counter current fashion throughout. Increasing the capacity of the existing palladium solvent-extraction circuit could be achieved through either increasing all flow rates or by increasing the concentration of feed and proportionally increasing the extractant concentration. Options for the former were limited due to the extraction stages being kinetically-controlled [7]; focus was therefore aimed at the latter.

Batch extraction tests confirmed the required higher loading of palladium in the organic was feasible, while stripping tests confirmed that the number of stages required was within the scope of the existing plant. A series of pilot-plant trials were successfully conducted to verify the batch data. The modified concentrations were then tested in a full-scale plant trial. LIX 84-I was added to the solvent in one of the twin-stream solvent-extraction circuits. It was discovered, however, that phase separation in the strip section was extremely poor. As a result, a significant amount of acid was being carried over in the solvent to the wash. Due to this diversion of acid, the stripping of palladium from the solvent was incomplete. This palladium remaining in the solvent impacted the extraction section to the extent that the plant could not be operated.

The phase separation time for the plant solvent and hydrochloric acid mixture was found to be significantly longer than for the same system where freshly prepared LIX 84-I in Solvesso 150 was used. Investigation of the plant solvent, which had been approaching the end of its normal life, showed significant levels of degradation of the ketoxime. It was known that the ketoxime slowly hydrolyzes to the parent ketone [8]. The reaction for this process is illustrated in Figure 1.

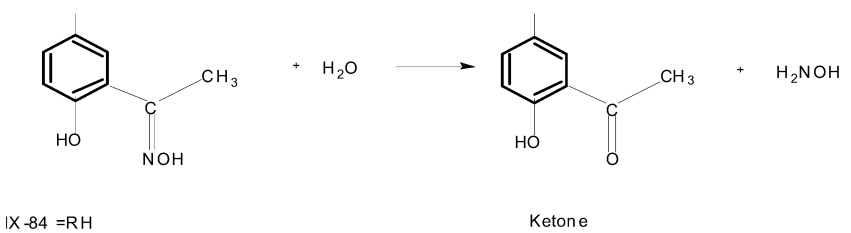

Figure 1. Acid-catalyzed hydrolysis of ketoxime to ketone.

This reaction is catalyzed by strong acid, and the wash section was introduced to remove entrained acid to avoid degradation continuing in the organic reservoir. Under normal operating conditions on the plant, the steady reduction in ketoxime concentration was accommodated by a regular top-up of LIX 84-I. This resulted in a steady build-up of the ketone degradation product in the organic phase but had been shown not to have any adverse effects on performance. The batch and pilot-plant tests confirming the feasibility of increasing the feed and extractant concentrations to achieve higher throughputs had been of relatively short duration. However, these conditions were not viable with the exiting inventory of solvent in the plant due to the high levels of degradation.

It was therefore evident that the ability to increase the capacity of the palladium solvent-extraction plant would be dependent on fundamentally understanding the rate of degradation of the ketoxime under various conditions as well as the effect of the ketoxime and ketone concentrations on the phase separation during stripping with strong acid.

RESULTS AND DISCUSSION

Effect of Ketoxime Concentration on Phase-Separation Time

Investigations showed that increasing the ketoxime concentration resulted in an exponential increase in the time for the phases to separate, where the aqueous phase is a high concentration of hydrochloric acid (6 M). This is illustrated in Figure 2. The consequence of this relationship would imply a limitation on the degree to which the capacity of the circuit can be expanded by increasing the active extractant concentration (at about 150 g/L ketoxime), due to the limitation of residence time in the settler compartment of the mixer settler boxes (*ca*. 20 min).

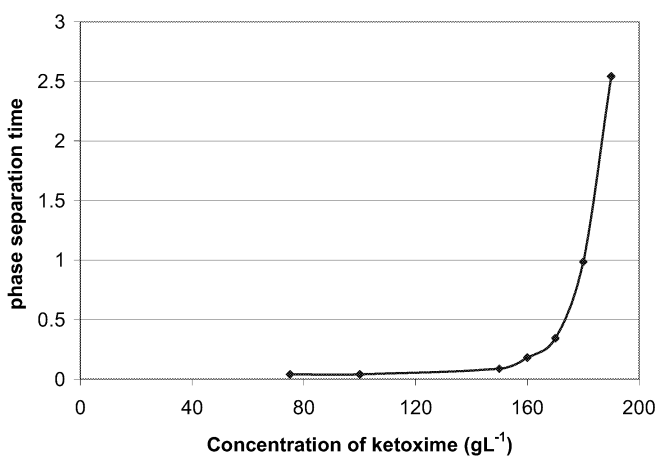

Figure 2. Effect of the ketoxime concentration (in Solvesso 150) on the phase-separation time following contacting with 6 M HCl.

Effect of Ketone Concentration on Phase Separation Time

It was established that increasing the concentration of the ketone degradation product had a similar effect on phase-separation time, as shown in Figure 3. Therefore, the phase-separation time (where the aqueous is 6 M HCl) is dependent on the sum of ketoxime and ketone concentrations. The rate at which the ketoxime degrades will therefore dictate the life-time of the organic phase before replacement is required.

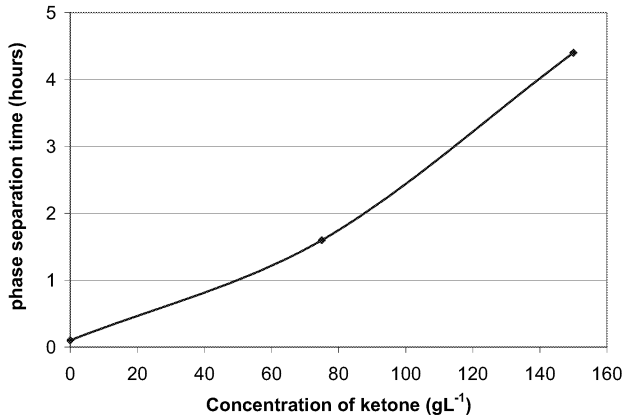

Figure 3. Effect of the ketone concentration on the phase separation time, of 150 g/L ketoxime in Solvesso 150 mixed with 6 M HCl.

Effect of Ketoxime Concentration on Rate of Degradation to the Ketone Derivative

Increasing ketoxime concentrations leads to significantly higher rates of degradation to the ketone derivative (Figure 4). Calculations show a doubling of the ketoxime concentration would result in a solvent life-time of less than 2 months, an untenable situation for the plant.

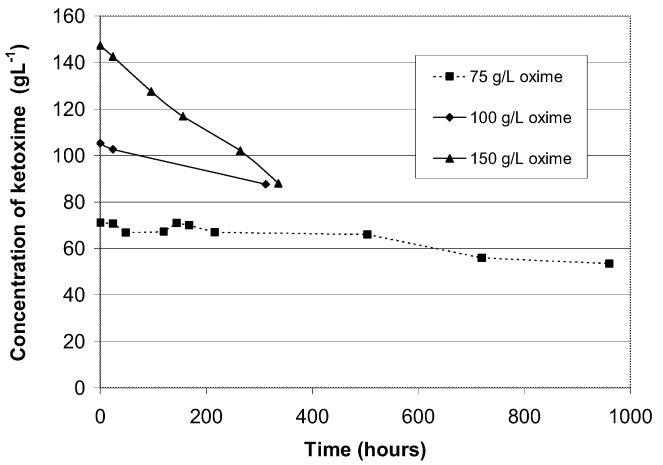

Figure 4. Effect of ketoxime concentration on the rate of degradation to ketone.

Effect of Acid Concentration on Rate of Degradation of Ketoxime to its Ketone Derivative and on Phase-Separation Time

It was found that reduction in acidity of the aqueous phase significantly slows the rate of degradation of ketoxime to ketone (Figure 5). Moreover, the effect of reducing the aqueous acidity was to significantly shorten the time required for the phases to separate (Figure 6).

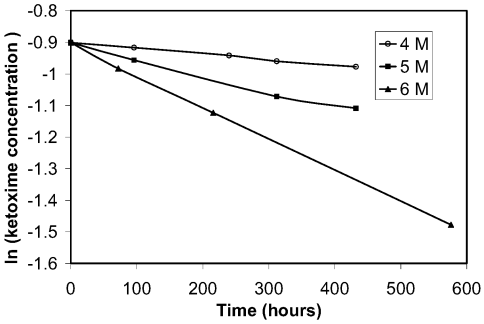

Figure 5. Effect of acid strength on the separation time.

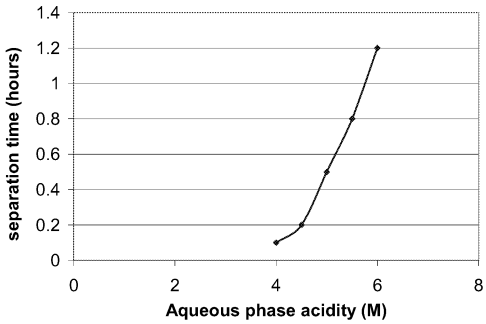

Figure 6. Effect of acid strength on the phase rate of degradation of ketoxime to ketone.

This effect is believed to be due to the phenolic hydroxyl groups of the organic-phase ketoxime and ketone (RH) extracting acid by the "solvation" protons. This extraction of protons increases exponentially above 4 M HCl. The resulting "ion-pair" formed with chloride is very viscous, and it is the formation of this which appears to be responsible for the deterioration in phase separation.

$$n\mathrm{RH} + \mathrm{H^+} + \mathrm{Cl^-} \rightleftharpoons (\mathrm{RH})_n\mathrm{H^+Cl^-} \quad (2)$$

The "solvated" protons also re-extract palladium that has been stripped from the ketoxime as $[PdCl_4]^{2-}$:

$$[\mathrm{PdR_2}] + 4\mathrm{Cl^-} + 2\mathrm{H^+} \rightleftharpoons [\mathrm{PdCl_4}]^{2-} + 2\mathrm{RH} \quad (3)$$

$$(\mathrm{RH})_n\mathrm{H^+Cl^-} + [\mathrm{PdCl_4}]^{2-} \rightleftharpoons (\mathrm{RH})_n\mathrm{H^+}[\mathrm{PdCl_4}]^{2-} + 2\mathrm{Cl^-} \quad (4)$$

As a result, there was a much smaller difference than would have been expected in the amount of palladium stripped using 5 M HCl instead of 6 M HCl. Mini-pilot plant tests confirmed that an acceptable stripping efficiency could be achieved with 5 M HCl, and this was confirmed in plant-scale trials at PMR.

CONCLUSIONS

An increase in capacity of the Pd solvent extraction circuit at Anglo Platinum PMR could be achieved by increasing the concentrations of feed and active organic extractant. However, this would result in an unacceptably short life-time of the solvent, due to the build-up of the ketone degradation product and consequent problems with phase separation in the strip section. This problem was resolved by a reduction in the strip acidity, from 6 to 5 M HCl, giving rise to much slower rates of degradation and improved rates of phase separation. The effect of this reduction in strip acidity on the overall efficiency of the strip circuit was quantified and found to be acceptable.

ACKNOWLEDGMENT

The authors would like to thank Anglo Platinum Limited for permission to publish this paper and Cognis for helpful discussions.

REFERENCES

1. Anglo Platinum Annual Report 2000, www.angloplatinum.com.
2. Annual PGM Market Reviews, Johnson Matthey PLC, www.platinum.matthey.com.
3. F. L. Bernardis, R. A. Grant, and D. C. Sherrington, "A Review of Methods of Separation of the Platinum-Group Metals through their Chloro-Complexes," *React. Funct. Polymers*, **65**, 205−217 (2005).
4. M. J. Cleare, R. A. Grant, and P. Charlesworth, "Separation of the Platinum-Group Metals by Use of Selective Solvent Extraction Techniques," Extraction Metallurgy '81, IMM, London, UK, 1981; pp. 34−41.
5. M. J. Cleare, P. Charlesworth, and D. J. Bryson, "Solvent Extraction in Platinum Group Metal Processing," *J. Chem. Technol. Biotechnol.*, **29,** 210−214 (1979).
6. J. H. Brits and D. A. Deglon, "Palladium Stripping Rates in PGM Refining," *Hydrometallurgy*, **89**, 253−259 (2007).
7. K. Inoue and T. Maruuchi, "Solvent Extraction of Palladium with SME529: Equilibrium and Kinetics," *Hydrometallurgy*, **16,** 93−104 (1986).
8. G. Kordosky, M. Virnig, A. Tello, and G. Vera, "Copper Solvent Extraction as Applied to Copper Concentrate Leach Liquors: Reagent Properties and Reagent Choice," Mining Chemicals Technology, Cognis Corporation, USA.

LIQUID-LIQUID EXTRACTION OF GOLD(III) BY 2-ETHYLHEXANOL AND ITS APPLICATION TO EMULSION PERTRACTION TECHNOLOGY

C. Vargas,[1] F. J. Alguacil,[2] E. G. Palacios,[1] I. Corona,[1] F. Chavez,[1] M. Alonso,[2] F. Lopez,[2] and A. Lopez-Delgado[2]

[1]Departamento de Ingenieria Metalurgica, ESIQIE, Instituto Politecnico Nacional. A.P. 118-616, 07738 D.F., Mexico City, Mexico. [2]Centro Nacional de Investigaciones Metalurgicas (CSIC), Avda. Gregorio del Amo 8, Ciudad Universitaria, 28040 Madrid Spain. Corresponding author email address: fjalgua@cenim.csic.es

ABSTRACT

The extraction of gold(III) by 2-ethylhexanol from hydrochloric acid solution has been investigated under various experimental conditions: equilibration time, and extractant and gold concentrations. The numerical analysis of metal-distribution data suggests the formation of $HAuCl_4 \cdot L$ (L = extractant) in the organic phase. The results obtained for gold(III) distribution have been implemented in emulsion pertraction technology. The influence of feed-phase stirring speed (600-1400 rpm), organic-phase composition (25-75% v/v carrier concentration and diluent), and metal concentration (5-20 mg/L) on gold transport have been investigated together with the selectivity of the system against the presence of base metals and platinum group metals in the feed solution.

INTRODUCTION

The extensive use of gold in a number of industrial applications has led to a growing interest in the need for gold recycling. Among the separation technologies, liquid-liquid extraction is often suggested for the separation-purification-concentration of this precious metal from chloride media.

Recently, several reagents such as monoamide compounds [1], ω-thiocaprolactam [2], ketoxime derivatives [3], and amiloride mono hydrochloride [4] have been proposed as extractants for gold(III) in HCl solutions.

These extraction systems can also be used in liquid-membrane configurations, where the separation performance is enhanced by the combination of extraction and stripping processes in one step. Moreover, some of the problems encountered in liquid-membrane configurations are greatly diminished by the use of the emulsion pertraction in a hollow-fiber contactor. This arrangement combines the advantages of the liquid membrane separation and dispersion-free liquid-liquid extraction. The characteristics of the emulsion pertraction technology are described elsewhere [5].

Few recent data are available in the literature about the use of 2-ethylhexanol in the role of extractant and carrier for gold(III) from hydrochloric acid media; thus, the present investigation was undertaken to obtain data about the extraction of this precious metal by this extractant and to investigate the performance of such system in emulsion pertraction technology.

EXPERIMENTAL

A stock solution of gold(III) was obtained by dissolving $HAuCl_4$ (Fluka) in HCl (Fluka), and working aqueous solutions were prepared by dilution of the above. HCl concentration was kept constant at 6 M in all the experiments, since this concentration should be representative of solutions used in the treatment of jewellery scrap and printed circuit boards.

The extractant 2-ethylhexanol (Merck) was used without further purification, but was presaturated with water in order to avoid the risk of change of the organic-aqueous volume phases under the various experimental conditions. Other chemicals were of AR grade.

Liquid-liquid extraction experiments were performed at 20 ºC by shaking equal volumes of the organic and aqueous phases in separating funnels for the required time. After phase separation, the metal remaining in the aqueous solution was analyzed by atomic absorption spectrophotometry (AAS) using a Perkin Elmer 1100B spectrophotometer.

The emulsion pertraction experiments were performed at 20 ºC in a permeation cell as described elsewhere [6]. The feed and the organic/stripping phases emulsion were mechanically stirred at 1200 and 700 rpm, respectively. Once the membrane support was placed in the cell, the feed solution (200 mL) and the organic (100 mL) and stripping (100 mL) phases were placed in their corresponding chambers and the operation begun. From the initial moment of mixing, an organic-stripping phases emulsion was formed, and providing adequate stirring speeds in the feed phase and in the emulsion phase, the membrane stabilized similarly to conventional flat-sheet supported-liquid-membrane operation; that is, the organic phase wets, and it is retained into the micropores of the hydrophobic support by capillarity. The support was a Millipore GVHP4700 film with a thickness of 125 μm, 75% porosity, and 0.22 μm average pore size. Membrane permeabilities were determined by monitoring metal concentration by AAS in the feed phase as a function of time. The permeation coefficient (P) was computed using:

$$\ln \frac{[C]_t}{[C]_0} = -\frac{A}{V_{feed}} Pt \qquad (1)$$

where A is the effective membrane area (11.3 cm^2), V_{feed} is the volume of the feed phase, and $[C]_t$ and $[C]_0$ are the metal concentration in the feed phase at elapsed time t and time zero, respectively.

RESULTS AND DISCUSSION

Liquid-Liquid Extraction System

A preliminary test was carried out to determine the time needed to achieve equilibrium. From the results shown in Table 1, at 35 g/L Au(III) and 6 M HCl and 75% v/v 2-ethylhexanol in kerosene, equilibrium is nearly reached after 2 min of contact. All subsequent experiments were carried out using 5 min contact time.

Table 1. Extraction of gold(III) with 2-ethylhexanol at various times

Time (min)	Gold extraction (%)
1	70.0
2	97.5
5	98.5
10	98.0
15	98.3
30	98.4

The influence of the composition of the organic phase on gold extraction was investigated for 2-ethylhexanol in the 25-100% v/v concentration range in kerosene. The aqueous phase contained 35 g/L Au(III) in 6 M HCl. Table 2 shows that, on increasing the extractant concentration up to 70% v/v in the organic phase, the percentage of gold extraction increases and then levels off.

Table 2. Influence of extractant concentration on gold (III) extraction

Extractant (% v/v)	Gold extraction (%)
25	57.5
40	78.3
50	88.1
70	96.6
80	98.8
90	97.9
100	98.3

On the other hand, the variation of the initial 5-100 g/L gold(III) concentration in the aqueous phase had a negligible effect on metal extraction, though for higher initial gold concentrations the metal extraction decreased. These results are shown in Table 3 for experiments carried out for aqueous solutions containing gold(III) in 6 M HCl and organic phases of 75% v/v 2-ethylhexanol in kerosene.

To determine the composition of the extracted species and their extraction equilibrium constants, extraction data were numerically treated by using the LETAGROP-DISTR program. The data were found to be consistent with the existence of the $HAuCl_4 \cdot L$ (L = 2-ethylhexanol) species in the organic phase, and the value of log K_{ext} was calculated to be -6.7 ± 0.09 with $U = 0.27$ ($\sigma = 0.13$).

Table 3. Influence of initial metal concentration on gold(III) extraction

[Au(III)] (g/L)	Gold extraction (% v/v)
5	98.3
10	98.5
25	98.4
50	98.5
75	96.5
100	95.7
150	93.5
200	88.0

Emulsion Pertraction System

The extraction of gold(III) by 2-ethylhexanol has been implemented in a liquid membrane, where the transport of gold species across the membrane depends not only on the equilibrium distribution ratios but also on the kinetics of the extraction and stripping processes. However, previous tests had shown that gold is strippable from loaded organic solutions using water; thus, this variable was not investigated in the present study.

To achieve effective permeation of gold(III) in a liquid-membrane system, it is necessary to explore the effect of stirring speed on the permeability coefficient. Diffusional resistances encountered during the transport of a metal species across a liquid membrane are of two types: (i) the resistance due to the liquid boundary layer, and (ii) that due to the membrane.

Sometimes, the magnitude of the boundary-layer resistance is comparable to or even greater than the membrane resistance. In the present investigation, the stirring of the feed phase was varied from 600 to 1400 rpm (Table 4). The permeability coefficient increased from 600 to 1000 rpm, and beyond that no appreciable increase in gold(III) permeability was observed. Consequently, the thickness of the aqueous diffusion layer and the aqueous resistance to mass transfer were minimized, and the diffusion contribution of the aqueous species to the mass transfer process is assumed to be constant.

Table 4. Influence of stirring speed on permeability of gold(III)

Stirring speed (rpm)	$P \times 10^3$ (cm/s)
600	0.95
800	2.6
1000	5.7
1200	5.7
1400	5.5

Feed phase: 0.01 g/L Au(III) and 6 M HCl.
Organic phase: 50% v/v 2-ethylhexanol in toluene. Stripping phase: water.

A study of the effect of the initial concentration of gold(III) (0.005-0.02 g/L) in the feed solution revealed that the metal flux, defined as $J = P_{Au}[Au(III)]_0$, increased with the increase of the initial gold concentration. The results of gold permeation coefficient

and permeability flux through the membrane as a function of gold(III) concentration are shown Table 5.

Table 5. Variation in the metal permeation and in the metal flux with the initial gold concentration

[Au(III)] (g/L)	P x 10^3 (cm/s)	J x 10^{10} (mol/cm^2 s)
0.005	2.7	0.7
0.01	5.7	2.9
0.02	4.5	4.5

Feed phase: gold (III) in 6 M HCl. Organic phase: 50% v/v 2-ethylhexanol in toluene. Stripping phase: water.

The effect of carrier concentration on gold permeation was also studied. Table 6 shows permeability values for the transport of gold through the membrane impregnated with various solutions of 2-ethylhexanol in toluene. It can be seen that the permeability increased up to 50% v/v of carrier concentration and then decreased. The maximum in the permeability value, P_{lim}, known as limiting permeability, can be explained by assuming that diffusion in the membrane is negligible compared with that for aqueous diffusion, and the permeation process is controlled by the diffusion in the stagnant film of the aqueous feed phase. Thus, $P_{lim} = D_{aq}/d_{aq}$, where D_{aq} is the average aqueous diffusion coefficient of the metal-containing species and d_{aq} is the thickness of the aqueous feed boundary layer; assuming a value of D_{aq} 1x10^{-5} cm/s [6], and P_{lim} equal to 5.7 x 10^{-3} cm/s, the value of d_{aq} is 1.8 x 10^{-3} cm, this value being the minimum thickness of the stagnant aqueous diffusion layer within the present experimental conditions.

Table 6. Gold(III) permeability as a function of carrier concentration

Carrier concentration (% v/v)	P x 10^3 (cm/s)
25	2.7
50	5.7
75	3.0

Feed phase: 0.01 g/L Au(III) and 6 M HCl.
Organic phase: 2-ethylhexanol in toluene. Stripping phase: water.

The effect of carrier diluent on the permeability of gold(III) was also studied. The diluent employed as a membrane should retain the carrier to the maximum extent and yet at the same time retain a relatively high concentration of water to aid in the transfer of hydrated species without loss of carrier to the aqueous solution. Membrane performance is mostly dependent on intrinsic membrane diluent properties such as viscosity, volatility, surface tension, *etc*. The transport behaviour of gold using various diluents is presented in Table 7. Best gold(III) permeation was achieved using toluene as the diluent for 2-ethylhexanol.

Table 7. Effect of diluents on permeability of gold(III)

Diluent	P x 10^3 (cm/s)
n-decane	2.6
xylene	3.1
toluene	5.7

Feed phase: 0.01 g/L Au(III) and 6 M HCl.
Organic phase: 50% v/v 2-ethylhexanol in each diluent.
Stripping phase: water.

Since base metals and platinum group metals are normally found in gold-HCl bearing solutions, the selectivity of the present transport system against the presence of various metals in the feed phase was investigated. From the results obtained of this study, it is inferred that gold was preferably transported over these metals. The selectivity with respect to gold seems enough to separate this precious metal selectively from the base metals (Fe, Ni, Cu) and especially from the platinum group metals, which do not permeate. However, it should be noted that the presence of these metals in the feed phase decreased the value of the gold permeation coefficient from 5.7 x 10^{-3} to 2.3 x 10^{-3} cm/s, this probably being due to a multi-ion competition or crowding effect [7].

CONCLUSIONS

2-Ethylhexanol is effective for the separation of gold(III) from high HCl concentration media using liquid-liquid extraction and emulsion pertraction technologies.

REFERENCES

1. H. Narita, M. Tanaka, K. Morisaku, and T. Abe, "Extraction of Gold(III) in Hydrochloric Acid Solution using Monoamide Compounds," *Hydrometallurgy*, **81**, 153-158 (2006).
2. M. E. Nuñez, E. Rodriguez de San Miguel, F. Mercader-Trejo, J. C. Aguilar, and J. de Gyves, "Selective ω-Thiocaprolactam-Based recovery of Au(III) from Chloride Media in Solvent Extraction and Polymer Inclusion Membranes," *Separation and Purification Technology*, **51**, 57-63 (2006).
3. Y. F. Shen and W. Y. Xue, "Recovery of Palladium, Gold and Platinum from Hydrochloric Acid Solution using 2-Hydroxy-4-*sec*-octanoyl Diphenyl-Ketoxime," *Separation and Purification Technology*, **56**, 278-283 (2007).
4. M. S. El-Shahawi, A. S. Bashammakh, and S. O. Bahaffi, "Chemical Speciation and Recovery of Gold(I, III) from Wastewater and Silver by Liquid-Liquid Extraction with the Ion-Pair Reagent Amiloride Mono Hydrochloride and AAS Determination," *Talanta*, **72**, 1494-1499 (2007).
5. W. S. W. Ho, "Removal and Recovery of Metals and Other Materials by Supported Liquid Membranes with Strip Dispersion," *Annals of the New York Academy of Science*, **984**, 97-122 (2003).
6. F. J. Alguacil, M. Alonso, and A. M. Sastre, "Facilitated Supported Liquid Membrane Transport of Gold(I) and Gold(III) using Cyanex® 921," *J. Membrane Science,* **252**, 2005, 237-244.
7. J. de Gyves and E. Rodriguez de San Miguel, "Metal Ion Separations by Supported Liquid Membranes," *Industrial and Engineering Chemical Res.*, **38**, 2182-2202 (1999).

RECOVERY OF SILVER AND GOLD FROM THIOUREA LEACH LIQUORS BY DI(2-ETHYLHEXYL)DITHIOPHOSPHORIC ACID

Z. Gamino Arroyo,[1,2] M. Stambouli,[1] A. Buch,[1] D. Pareau,[1]
J. El Bekri,[1] and M. Avila Rodriguez[2]

[1]Ecole Centrale Paris, LGPM, Chatenay-Malabry 92295, France
[2]Facultad de Química, Universidad de Guanajuato, México
Corresponding email address: arnaud.buch@ecp.fr

ABSTRACT

This study deals with solvent extraction of gold and silver from thiourea media as an alternative to the traditional leach process involving cyanide. The extraction mechanism of gold and silver from acidic thiourea solution had not been clearly established to date. The extraction behavior of silver and gold using di(2-ethylhexyl)dithiophosphoric acid was studied. The effect of various parameters such as concentrations of mineral acid, thiourea, and extractant has been investigated. The extracted complexes have been identified through slope analysis as AgX and AuX for silver and gold extraction, where HX denotes the extractant. Moreover, complete stripping was ensured with either $(NH_4)_2S_2O_3$ or a mixture of NH_4SCN and H_2SO_4.

INTRODUCTION

The use of thiourea (TU) for the recovery of gold and silver from ores as an alternative to the traditional process involving cyanide has been suggested by several authors. The thiourea leaching of gold and silver presents some advantages over the common cyanide process such as faster kinetics and lower toxicity, but the costs due to high thiourea consumption, caused by its fast degradation, limit its industrial application. In the presence of a suitable oxidizing agent, such as, H_2O_2 or Fe(III), thiourea solubilizes Ag(I) and Au(I).

Various processes were considered for gold and silver recovery from thiourea or cyanide solutions, but solvent extraction is the most convenient process when Ag(I) and Au(I) come from thiourea leaching solution. Different extractants have been tested in different acid and basic media. Di(2,4,4-trimethylpentyl)thiophosphinic acid (CYANEX® 302) and di(2-ethylhexyl)dithiophosphoric acid (D2EHDTPA) [1] were reported as the most efficient extractants for the silver(I) and gold(I) extraction.

Di(*n*-butyl)dithiophosphoric acid is reported as an extractant for the separation of different metals from sulfuric and hydrochloric acid [2]. Dialkylphosphorodithioic acids exhibit high chemical stability at room temperature. Thus, they could be quite suitable for selective extraction of silver and gold. For example, the extraction of Ag(I) from

nitrate media has been studied by D2EHDTPA. The complex was identified as a 1:1 complex with Ag(I) [3]. However, relatively little research on silver and gold solvent extraction from acidic thiourea solutions has been carried out.

EXPERIMENTAL

Reagents and Materials

The extractants CYANEX 272, CYANEX 302, and CYANEX 471X were supplied by CYTEC Canada Inc. Tributylphosphate (TBP) and trioctylamine (TOA) were supplied by Acros Organics and di(2-ethylhexyl)phosphoric acid (D2EHPA) by Alfa-Aesar. D2EHDTPA was obtained by stripping from a commercial zinc salt (Rhein Chemie). The purity of D2EHDTPA was determined to be 95%. The extractants were diluted in pure dodecane (Acros Organic) or eventually mixed with 10% v/v of *n*-octanol (Acros Organic). All other chemical products were of analytical reagent grade. After dilution, the metals were analyzed by atomic adsorption spectrophotometry. The thiourea concentration was determined by titration with potassium iodate using starch as indicator and UV-visible spectrophotometry.

Experimental Procedure

Equal volumes (10-20 mL) of the aqueous and the organic phases were contacted for 30 min. at 20 ± 1 °C. The concentration of Ag(I) and Au(I) in the loaded organic phase was determined after complete stripping with a mixture of NH_4SCN/H_2SO_4 and with $(NH_4)_2S_2O_3$, respectively. Determination of the distribution ratio *D* and extraction rate was accomplished by measurement of the equilibrium concentration in the aqueous phase and in the organic phase by using atomic adsorption. Mass balance was always verified.

RESULTS AND DISCUSSION

Extraction Kinetics

For both gold(I) and silver(I) extraction, at constant pH and thiourea concentration, equilibrium was reached in less than 10 min. with all extractants. According to the results, equilibrium has been considered as reached after 30 min.

Effect of the Nature of the Extractants

Table 1 presents the equilibrium extraction concentrations of Ag(I), Au(I), and Fe(III) with various extractants at different concentrations. Experiments were carried out with or without thiourea (0.1 mol L^{-1}). When a third phase occurred, octanol was added in order to prevent its formation.

Due to the formation of metal-thiourea complexes in the presence of thiourea, the extraction of Fe(III), Ag(I), and Au(I) is lower for all investigated extractants. In absence of thiourea, CYANEX 471X showed good selective extraction of Ag(I) and Au(I) over

Fe(III). However, in the procedure used, the silver solubilization was always performed by thiourea leaching. Furthermore, a low level of concentration (4.4%) of Fe(III) was extracted by CYANEX 471X. The presence of Fe(III) could be also a problem for the purification processing of silver, which is why CYANEX 471X was ruled out. In thiourea media, the extraction was nearly complete for Fe(III) with CYANEX 272 or D2EHPA. With CYANEX 302 and D2EHDTPA, extraction reveals a good efficiency for Ag(I) and Au(I). A new process could be proposed based on a primary selective extraction of Fe(III) using CYANEX 272 or D2EHPA, followed by an extraction of Ag(I) and Au(I) with D2EHDTPA.

Table 1. Extraction of silver(I), gold(I), and iron with various extractants.
[Au(I)] = 0.44 mmol L^{-1}, [Fe(III)] = 2.7 mmol L^{-1}, [TU] = 0.1 mol L^{-1}, pH = 2,
Phase ratio O/A= 1:1, T = 20 °C

Extractant	Conc. extract. (mol L^{-1})	Octanol (% v/v)	Ag(I) extraction (%)		Au(I) extraction (%)		Fe(III) extraction (%)	
			without TU	with TU	without TU	with TU	without TU	with TU
TBP	0.1	0	3.2	1.6	8.7	4.7	4.5	1.1
D2EHPA	0.1	0	9.7	4.7	3.8	6.2	100	92.9
TOA	0.1	0	5.7	2.3	99.8	2.0	19.2	0
CYANEX 302	0.1	10	100	73.7	99.9	93.4	96.6	81
CYANEX 471X	0.1	10	100	0	98.8	2.1	4.4	0.5
CYANEX 272	0.1	10	4.5	0.9	8.4	2.0	99.2	94.7
D2EHDTPA	$1x10^{-3}$	0	100	99.9	99.8	67.5	41.8	32.8

Effect of Thiourea Concentration

The effect of thiourea concentration on the extraction of Ag(I) and Au(I) was investigated using D2EHDTPA (2 mmol L^{-1}). A plot of log D versus log [TU] was traced. The slopes of the straight lines were equal to −2 for Au(I) and ranging from −3 to −4 for Ag(I). Thiourea then acts as an inhibitor of Ag(I) and Au(I) extraction in relation to the predominance of the complexes $Au(TU)_2^+$, $Ag(TU)_3^+$, and $Ag(TU)_4^+$ in the aqueous phase. In addition, ultraviolet-spectroscopy analysis showed that the extracted metallic complexes of Au(I) and Ag(I) did not include any thiourea molecule.

Extraction Equilibrium of Ag(I)

Taking into account the low level of metal ion concentrations, it has been assumed with D2EHDTPA and CYANEX 302 extraction that only mononuclear species are extracted into the organic phase. The extraction of Ag(I) and Au(I) with D2EHDTPA could be represented by the following general equation:

$$M^{n+} + \frac{m+n}{p}\overline{(HX)}_p \rightleftharpoons \overline{MX_n(HX)}_m + nH^+ \quad (1)$$

where M^+ denotes Ag^+ or Au^+ and overbars denote species in the organic phase, HX is the dithioorganophosphorus acid, and p is the degree of aggregation of the extractant.

From the expression of equilibrium constant K and the distribution ratio D, the following expression is obtained:

$$\log D = n\,\mathrm{pH} + \left((n+m)/p\right)\log\left[\overline{\mathrm{HX}}\right]_p - \log\alpha_{\mathrm{M}\,f([\mathrm{TU}])} + \log K_{ext} \qquad (2)$$

where $\alpha_{Mf([TU])}$ is the complexation constant for the thiourea.

Aggregation Study

For D2EHDTPA, vapor pressure osmometry (VPO) measurements were conducted using TOA as the reference material and pentane as the solvent at 29 °C according to the procedure presented by Buch et al. [4]. This study proved that D2EHDTPA is mainly in monomeric form in the investigated range of concentration (<100 mmol L^{-1}).

Effect of pH

Figure 1 shows the effect of the pH on the log of the extracted Ag(I) and Au(I) concentrations according to the slope method. The concentration of all the other reagents was kept constant. Extractant concentrations of D2EHDTPA was 1.0 mmol L^{-1} for Ag(I) extraction and 2 mmol L^{-1} for Au(I) extraction. The experimental values of n are 0.91 and 1.00 for Ag(I) and Au(I), respectively; thus, only one proton is exchanged through silver and gold extraction. This result is compatible with the electroneutrality principle.

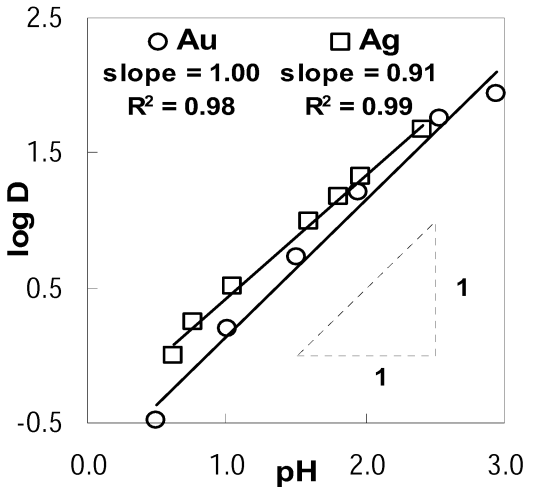

Figure 1. Influence of the pH. [TU] = 0.1 mol L^{-1}, [HX] = 1 for Ag(I) and 2 mmol L^{-1} for Au(I).

Effect of Extractant Concentration

The effect of concentration of D2EHDTPA (0.2 to 1 mmol L^{-1}) on silver and gold extraction from acidic thiourea (0.1 mol L^{-1}) solutions was studied. Initial concentrations of metal ions, acid, and thiourea were kept constant.

According to the slope-analysis method (Figure 2), the experimental values of $(m+n)/p$ are nearly 1 for D2EHDTPA. In order to confirm the results obtained with D2EHDTPA, the organic-saturation method was applied. Organic phases containing different concentrations of D2EHDTPA were loaded up to saturation in constant aqueous conditions. After saturation, organic phases were stripped and analyzed. The experimental value of the ratio $[Ag]_{org}/[D2EHDTPA]$ equal to 1.05 confirms the previous 1:1 stoichiometry.

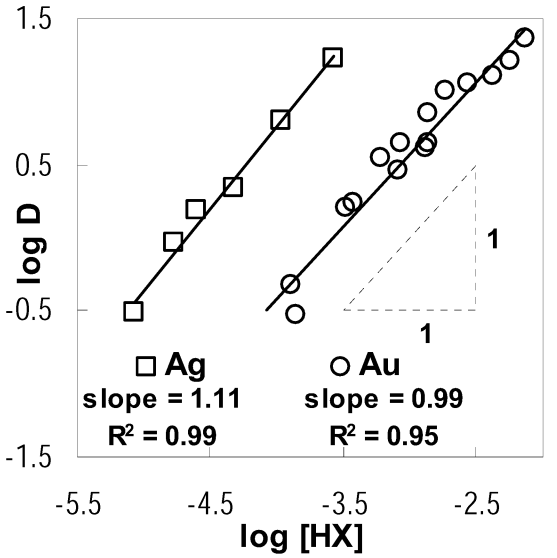

Figure 2. Influence of HX concentration. pH = 2, [TU] = 0.1 mol L^{-1}.

Complex Stoichiometry

Experimental results related to the extracted complex stoichiometry and the mean value of the apparent extraction constant were determined and summarized in Table 2.

Table 2. Experimental results the extracted complex stoichiometry

Extractant (HX)	Metal	*p*	*n*	*m*	Extracted complex	log K_{ext}
D2EHDTPA	Ag	1	1	0	AgX	12.64 ± 0.19
	Au	1	1	0	AuX	21.64 ± 0.13

Effect of Stripping Agents

Different stripping agents were tested alone or mixed with others. Stripping performance is reported in Table 3. $(NH_4)SCN$ (1 mol L^{-1}) would be preferred for the selective stripping of Au(I) from Ag(I) and a second step of striping with the mixture $(NH_4)SCN$ (1 mol L^{-1}) + H_2SO_4 (0.5 mol L^{-1}) would be preferred for the selective stripping of Ag(I).

Table 3. Efficiency of different stripping agents
$[Ag(I)]_{org}$ = 0.4 mmol L^{-1}, $[Au(I)]_{org}$ = 0.3 mmol L^{-1}. [D2EHDTPA] = 1 mmol L^{-1}, Phase ratio O/A = 1:3, T = 20 °C

Metal	Stripping efficiency (%)		
	$(NH_4)_2S_2O_3$ (1 mol L^{-1})	$(NH_4)SCN$ (1 mol L^{-1})	$(NH_4)SCN$ (1 mol L^{-1}) + H_2SO_4 (0.5 mol L^{-1})
Ag(I)	42.2	4.5	89.6
Au(I)	>99.0	>99.0	12.9

CONCLUSIONS

This study clearly demonstrates the performance of D2EHDTPA for the extraction of Ag(I) and Au(I) from acidic thiourea solutions. Equilibrium studies were carried out. Apparent equilibrium constants were determined, and the stoichiometries of the extracted metal complexes were identified as AgX and AuX for silver and gold extraction, respectively, by D2EHDTPA. Different stripping reagents were tested and the best stripping was achieved with a mixture of NH_4SCN and H_2SO_4 for Ag(I) followed by $(NH_4)_2S_2O_3$ for Au(I). The separation of Ag(I) from Au(I) could be achieved by selective stripping.

In the frame of the development of a new process for silver recovery from a silver leach solution containing Fe(III), either D2EHPA or CYANEX 272 could suitably be used for the selective elimination of Fe(III) prior to Ag(I) and Au(I) recovery using D2EHDTPA.

REFERENCES

1. I. S. Levin, V. V. Sergeeva, V. A. Tarasova, V. I. Varentsova, T. F. Rodina, I. A. Vorsina, N. E. Kozlova, and B. I. Kogan, "Extraction of Metals by Alkylphosphorodithioic Acids," *Zh. Neorg. Khim.*, **18**(6), 1643-1649 (1973).
2. T. H. Handley, "Di-n-Butyl Phosphorothioc Acid as an Extractant for Metal Ions," *Anal. Chem.*, **35**(8), 991-995 (1963).
3. K. Shong, Y. Shong, and H. Li, "The study of Ag with Di-2-Ethylhexylphosphoric Acid (D2EHPA) and Di-2-Ethylhexyldithiphosphoric Acid (D2EHDTPA)," *Gaodeng Xuexiao Huebao (Chem. J. Chinese Universities)*, **7**, 1-6 (1986).
4. A. Buch, D. Pareau, M. Stambouli, and G. Durand, "Solvent Extraction of Nickel(II) by 2-Ethylhexylhexanal Oxime from Various Aqueous Solutions," *Solvent. Extr. Ion Exch.*, **19**(2), 277-299 (2001).

THERMODYNAMIC MODELS FOR GOLD AND SILVER EXTRACTION FROM COPPER-AMMONIA-THIOSULFATE SOLUTIONS

P. Mendoza-Muñoz,[1] G.T. Lapidus,[1] and M. Ávila-Rodríguez[2]

[1]Depto. de IPH, Universidad Autónoma Metropolitana – Iztapalapa, Av. San Rafael Atlixco 186, Col. Vicentina, México, D.F. 09340. [2]Instituto de Investigaciones Científicas, Universidad de Guanajuato, Guanajuato
Corresponding author e-mail address: gtll@xanum.uam.mx

ABSTRACT

Thermodynamic models that implicitly contain the reaction stoichiometries are developed for gold and silver extraction from ammonium copper thiosulfate solutions with CYANEX 302. The extracted complexes have the following stoichiometry: $AuNaT(HL)_2$ and $AgNa_2TL(HL)_3$. Since these contain sodium ions, a method to account for its variation as a function of the thiosulfate concentration was employed. Equilibrium constants for gold and silver extraction in this system were estimated. Since the extracted complex was shown to be very stable, stripping from the organic phase was only partially accomplished using a highly concentrated solution of a non-sodium thiosulfate salt.

INTRODUCTION

In order to replace cyanide ions in gold and silver leaching, several alternative systems have been proposed. One of the most promising substitutes is ammoniacal copper thiosulfate, which has shown high gold and silver recoveries from minerals and concentrates [1]. For this system, liquid-liquid extraction has been considered an interesting option to concentrate and purify the precious metals before electrolytic refining. For this application, the organophosphinic compounds have received much attention as extractants in the past three decades, and their properties have been extensively investigated [2]. CYANEX 302 (Cytec) is an organophosporus extractant, which contains approximately 80% (by weight) bis(2,4,4 trimethylpentyl)thiophosphinic acid, as the active ingredient. Investigations by Alonso et al. [3] show high extraction recoveries (>98%) for gold and silver ions from thiosulfate leaching solution. In the present work, a thermodynamic study for gold and silver extraction is developed in order to determine the nature of the extracted species. The slope method was employed to determine the stoichiometry of the reactions from the distribution curves of both metals as a function of pH, extractant, and complexing agent concentrations.

EXPERIMENTAL METHODS

The acid extractant used in this study was bis(2,4,4-trimethylpentyl)thiophosphinic acid (CYANEX 302), provided by Cytec (Canada). The organic phase consisted of the extractant, diluted in kerosene with 10% v/v *n*-decanol, while the aqueous phase contained the Ag(I), Au(I), Cu(II), and Na(I) ions, in addition to the ammoniacal thiosulfate solution.

Equal volumes of the organic and aqueous phases (V_{org} = V_{aq} = 5 mL) were contacted using a multi-wrist shaker at a temperature of 25 °C, for 90 minutes (sufficient time to reach equilibrium). The aqueous solution pH measurement and adjustment was performed employing a potentiometer (Conductronics 120). Once the required time was completed, the phases were separated with Whatman 1 P/S filter paper. The metal ion concentrations were determined in the aqueous phase with atomic absorption spectrometry (Varian, SpectrAA20). The corresponding organic-phase metal concentrations were calculated by mass balance.

THERMODYNAMIC EXTRACTION MODEL

Au(I) and Ag(I) extraction from ammoniacal thiosulfate solutions by CYANEX 302 may possibly include thiosulfate in the organic-phase extracted complex. If gold and silver are considered to be extracted into the organic as single complexes, the general reaction may be written in the following manner:

$$M^{+} + pT^{-2} + (n+m)\overline{HL}_m + oNa^{+} \rightleftharpoons \overline{Na_oML_n(HL)_mT_p} + nH^{+} \quad (1)$$

where T is the thiosulfate ion, HL represents the active component of CYANEX 302, bis(2,4,4-trimethylpentyl)thiophosphinic acid, and the overbar indicates that the species are present in the organic phase.

The objective of the present study is to determine the stoichiometric coefficients *m*, *n*, *o* and *p* for each metal complex extracted into the organic phase. For Reaction 1, the apparent equilibrium constant may be represented as follows:

$$K_{extM}^{app} = \frac{[\overline{Na_oML_n(HL)_mT_p}][H^{+}]^n}{[M^{+}][T^{-2}]^p[\overline{HL}]^{(n+m)}[Na^{+}]^o} \quad (2)$$

The extraction efficiency of both metallic ions may be represented using the distribution ratio (D_M), which is defined in the following manner:

$$D_M = \left[\overline{M(I)}\right] \Big/ [M(I)] \quad (3)$$

where $[\overline{M(I)}]$ corresponds to the organic phase total metal concentration, while [M(I)] is the corresponding total concentration in the aqueous phase.

It is important to consider the influence of aqueous phase complexation on the extraction process. In the present case, the metallic ions are found in the aqueous phase mainly as the AgT_2^{3-} and AuT_2^{3-} complexes. Despite the high ammonia concentration, ammoniacal complexes are less stable than those of thiosulfate [2]. Thus, a complexation coefficient $\alpha_{M(I)}$ can be calculated:

$$\alpha_{M(I)} = \left[M(I)\right] \Big/ \left[M^+\right] = 1 + \beta\left[T\right]^2 \tag{4}$$

The components in the organic phase must comply with the principle of electroneutrality; consequently, the stoichiometric coefficients of Na^+, H^+, and T^{2-} are related by $o = n - 1 + 2p$.

Introducing the definitions for D_M, $\alpha_{M(I)}$, and the value for o into Equation (2), the equilibrium constant takes on the following form:

$$K_{extM}^{app} = \frac{D_{M(I)}\left[H^+\right]^n \alpha_{M(I)}}{\left[T^{2-}\right]^p \left[\overline{HL}\right]^{(n+m)} \left[Na^+\right]^o} \tag{5}$$

Taking the base-10 logarithm of the above expressions, substituting the definition of pH ($-\log_{10}[H^+]$) and solving for D_M:

$$\log D_M + \log \alpha_{M(I)} = \log K_{extM}^{app} + p\log\left[T^{2-}\right] + (n+m)\log\left[\overline{HL}\right] + (n-1+2p)\log\left[Na^+\right] + n\,pH \tag{6}$$

Since the thiosulfate is added as its sodium salt, the sodium concentration automatically varies with that of the thiosulfate. In this case, the thiosulfate and sodium concentration terms cannot be varied independently and should be grouped together; therefore, Equation 6 will take on the following form:

$$\log D_M + \log \alpha_{M(I)} - (n-1)\log\left[Na^+\right] = \log K_{extM}^{app} + (n+m)\log\left[\overline{HL}\right] + n\,pH + p\log\left[T^{2-}\right]\left[Na^+\right]^2 \tag{7}$$

With the above equation, the stoichiometric coefficients of $[H^+]$, $[Na^+]$, $[T^{-2}]$, and [HL], involved in the extraction process, may be determined by the slope method.

RESULTS AND DISCUSSION

Ag(I) and Au(I) Distribution Curves

The extraction of gold and silver from leaching solutions is very complex, since these contain large quantities of other components, including ammonia, copper, and ethylenediamminetetraacetate (EDTA). However, in studies not reported here, the concentrations of these components do not influence the extraction efficiency of either

precious metal. Therefore, in the subsequent figures, the log D_M for each metal is plotted only against the log [concentration] of H^+, CYANEX 302, or thiosulfate x sodium[2].

In general, the distribution ratio is an order of magnitude larger for silver than for gold at the same solution conditions, increasing with higher pH values. Figure 1 shows the plots of log D_{Ag} and log D_{Au} versus pH, where the slopes are 0.16 and 0.63, respectively. Fractional slopes usually are an indication of two or more different complexes. In the case of gold, it may be observed that H^+ is not appreciably involved in the extraction process, while with silver, the slope is nearer to one.

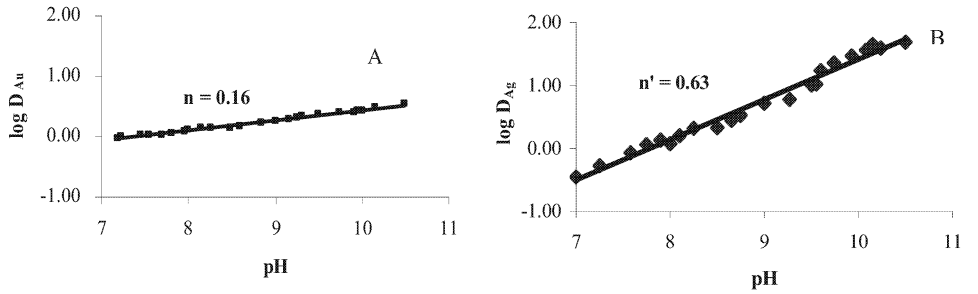

Figure 1. Variation of log D_{Au} and log D_{Ag} as a function of pH for (A) at $[Au]^o$ = 10 ppm and for (B) at $[Ag]^o$ = 10 ppm. Aqueous phase: ammoniacal medium with [thiosulfate] = 0.2 M and $[Cu^{2+}]$ = 0.05 M. Organic phase: [CYANEX 302] = 0.02 M in kerosene with 10% decanol.

The results of the CYANEX 302 variation are shown in Figure 2, as log D_{Au} and log D_{Ag} versus log[CYANEX 302], where it may be observed that both silver and gold extractions are enhanced dramatically as the CYANEX 302 concentration increases. For gold (Figure 2A), there are two distinct regions where the slopes (n + m) are 1 and 2. Considering that n = 0, then the organic complex has one or two CYANEX 302 molecules. In the case of silver, over the entire concentration range investigated, the slope of (n' + m') is 4.5; after considering the value of n', it is safe to assume that the organic complex contains four CYANEX 302 molecules.

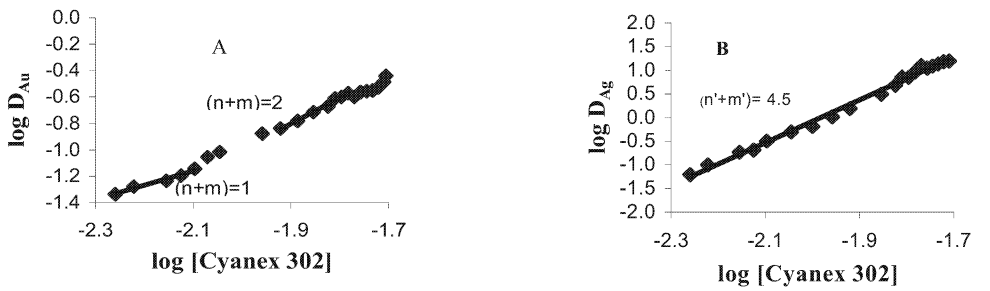

Figure 2. Variation of log D_{Au} and log D_{Ag} as a function of log [CYANEX] for (A) at $[Au]^o$ = 10 ppm and for (B) at $[Ag]^o$ = 10 ppm. Aqueous phase: ammoniacal medium at pH = 10 with [thiosulfate] = 0.2 M and $[Cu^{2+}]$ = 0.05 M. Organic phase: [CYANEX 302] in kerosene with 10% decanol.

In Figures 3A and B, the variation of log D_M + log$\alpha_{M(I)}$ - (n-1)log[Na^+] is shown as a function of log[T^{2-}][Na^+]^2, according to Equation 8 for the case of Au (n = 0, Figure 3A) and for Ag (n = 1, Figure 3B). Using the calculated slopes, it is possible to determine the value of p for each metal complex (Au and Ag) extracted into the organic phase. In both cases, the slopes are near unity, which implies that for both metals one thiosulfate molecule is incorporated into the complex extracted by the organic phase.

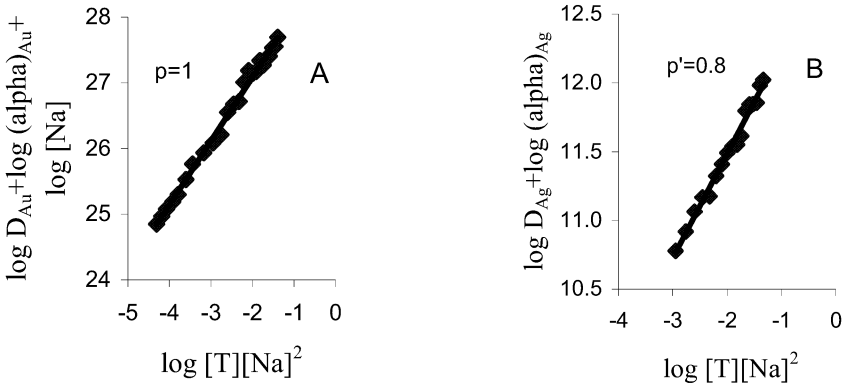

Figure 3. Variation of log $D_{Au(I)}$ + logα_{Au} + log[Na] and log $D_{Ag(I)}$ + logα_{Ag} as a function of log log[T][Na]^2 for (A) gold and (B) silver. Aqueous phase: ammoniacal medium with at pH = 10 and [Cu^{2+}] = 0.05 M. Organic phase: [CYANEX 302] = 0.02 M in kerosene with 10% decanol.

From the results obtained by employing the slope method, the extraction reaction for each metal ion is represented as follows: $Au^+ + Na^+ + T^{-2} + 2\overline{HL} \rightleftharpoons \overline{(AuT(HL)2)Na}$ and $Ag^+ + 2Na^+ + T^{2-} + 4\overline{HL} \rightleftharpoons \overline{(AgTL(HL)_3)Na_2} + H^+$.

The apparent extraction constant (K_{ext}^{app}) was calculated for both metal ions by minimization of the function $U = \Sigma(D_{teo} - D_{exp})^2$ through the use of the Excel™ macro Solver. The calculated value of $D_{teo,}$, the value predicted by the model, was obtained for the stoichiometries developed above. For Ag, the value for K_{ext}^{app} determined with the experimental data varying [CYANEX 302], was $10^{11.85}$ with U = 2.56; while varying [thiosulfate], a value of $10^{11.87}$ was calculated with U = 1.67. These calculations confirm that the proposed model is representative of the extraction process (see Figure 4). For Au, the K_{ext}^{app} was estimated at $10^{32.3}$.

Stripping of Ag(I) and Au(I) from the Organic Phase

Because gold and silver have a great affinity with CYANEX 302, as shown by the large extraction constants, the stripping process represents a complex problem. At first, a stripping solution containing a high concentration of a strongly complexing compound was tried (2 M EDTA). The stripping values were very low for both metal ions (1% for Ag(I) and practically 0% for Au(I)). Later, a solution with a higher concentration of $Na_2S_2O_3$ (1 M) was employed, in order to shift the equilibrium towards the aqueous phase ions; however, the stripping was less than 3% in both cases. This last

result is logical considering that sodium ions participate in the extraction processes and that the mass-action effect towards the reactants is unfavorable due to the increase in the $Na_2S_2O_3$ concentration. On the other hand, the opposite should occur if thiosulfate were added, but with a different counterion, such as the ammonium ion. When the stripping solution containing 1 M $(NH_4)_2S_2O_3$ was employed, 23% of the Ag(I) and 18% of the Au(I) were stripped. It may be possible to increase these values by raising the concentration of ammonium thiosulfate.

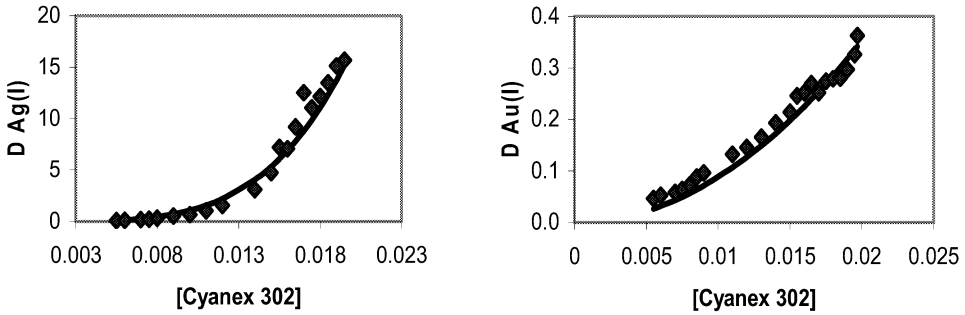

Figure 4. Variation of $D_{Ag(I)}$ and $D_{Au(I)}$ as a function of [CYANEX 302]. Points indicate experimental data; (—) model prediction. Extraction conditions: ammoniacal medium; [thiosulfate] = 0.2 M at pH = 10. Organic phase: CYANEX 302 diluted in kerosene with 10% decanol.

CONCLUSIONS

Ag(I) and Au(I) extraction from ammoniacal thiosulfate media is possible using CYANEX 302. The proposed extraction models permitted the determination of the stoichiometries of the complex extracted into the organic phase ($\overline{(AuT(HL)_2)Na}$ and $\overline{(AgTL(HL)_3)Na_2}$), as well as the values of their respective apparent extraction constants ($K^{app}_{extAg} = 10^{11.86}$ y $K^{app}_{extAu} = 10^{32.3}$). Incomplete stripping of both metal ions was possible employing a solution of ammonium thiosulfate.

REFERENCES

1. M. G. Aylmore and D. M. Muir, "Thiosulfate Leaching of Gold–A Review," *Minerals Engineering*, **14**(2), 135-174 (2001).
2. G. M. Ritcey, "Solvent Extraction in Hydrometallurgy: Present and Future," *Tsinghua Science & Technology*, **11**(2), 137-152 (2006).
3. A. Alonso, J. A. Cervantes, P. Mendoza, and M. Ortiz, "Diseño de una Planta para la Extracción de Oro y Plata por Lixiviación con Tiosulfato, Extracción por Solventes y Electrodepositación," Chemical Engineering undergraduate thesis, Universidad Autónoma Metropolitana-Iztapalapa, Mexico City, Mexico, 2000.
4. R. M. Smith and A. E. Martell, Critical Stability Constants, Plenum, New York, 1982.

EXTRACTION, SEPARATION, AND RECOVERY OF Pt(IV) AND Rh(III) USING CYANEX EXTRACTANTS

Bina Gupta and Indu Singh

Department of Chemistry, Indian Institute of Technology Roorkee, Roorkee Uttarakhand, India
Corresponding author email address: dr.binagupta@gmail.com

ABSTRACT

Platinum metals are extensively used in automobile catalysts, electronic devices, jewellery, space materials, and cancer therapy. Since the resources of these metals are limited, their worth has increased in recent years. Thus, the recovery and recycling of these metals from secondary sector have assumed paramount significance. The extraction behavior of Pt(IV) and Rh(III) was studied from hydrochloric and sulfuric acid media (0.1–6 mol L^{-1} acid) using toluene solution of two CYANEX extractants. Effect of different parameters such as concentration of acid and extractant, nature of diluent, temperature, and equilibration time on the distribution of Pt(IV) has been investigated and probable stoichiometry of the extracted complexes suggested. It is possible to strip Pt(IV) and Rh(III) from the organic phase using selective stripping agents. Conditions for their binary separation have been optimized.

INTRODUCTION

The platinum-group metals, because of their specific physical and chemical properties, are being used in diversified fields such as jewellery making, as catalyst in automobiles and petroleum refining, and in industries as corrosion-resistant materials. Therefore, it has become imperative to develop effective methods for their recovery and purification. Solvent extraction is being implemented widely for purification and separation of precious metals. Though a number of papers are reported every year on platinum metals, there is still scarce literature available about the purification and separation of platinum metals with solvent extraction [1].

Rhodium is the most expensive of all the platinum metals, hence should be given preference in the extraction flowsheet. The separation and purification of rhodium is a difficult process because of its chemical behavior in chloride medium [2]. Literature on the separation of rhodium from other platinum group metals [3] is meager.

The studies presented here are focused on the extraction and separation of Pt(IV) and Rh(III) from HCl and H_2SO_4 media with commercially available organophosphorus extractants. Two such extractants—CYANEX® 923, a mixture of four trialkylphosphine

oxides and CYANEX 301, bis(2,4,4-trimethylpentyl)dithiophosphinic acid—have been explored for the separation and recovery of platinum and rhodium from their mixtures.

EXPERIMENTAL

Apparatus and Reagents

The CYANEX extractants were provided by Cytec Canada Industries Inc. and were used without further purification. The standard solutions of Pt(IV) and Rh(III), were obtained from Sigma-Aldrich and were diluted as required. All other chemicals used were of analytical-reagent grade. Atomic absorption spectrophotometry (AAS) (Perkin Elmer AAnalyst 800) was used for the determination of Pt(IV) and Rh(III) concentration in the aqueous phases before and after extraction.

Extraction Procedure

An aliquot of solution containing Pt(IV) or Rh(III) in HCl/H_2SO_4 was equilibrated with an equal volume of organic phase (extractant solution in an organic diluent) in a separatory funnel. The two phases were allowed to separate. The Pt(IV) and Rh(III) concentrations in the aqueous phase were determined before and after extraction by AAS. All experiments were carried out at room temperature except when the effect of temperature was studied.

RESULTS AND DISCUSSION

Influence of Equilibration Time

The aqueous phase containing Pt(IV)/Rh(III) was equilibrated for 30 s to 30 min. with both the extractants (0.1 mol L^{-1} in toluene) at 1 mol L^{-1} HCl. An equilibration period of 3 min. was required for Pt(IV) and Rh(III) with CYANEX 923, whereas in the case of CYANEX 301, a minimum of 1 min. equilibration time was sufficient for both the metal ions. Increasing the shaking period up to 30 min. had no adverse effect on extraction, so a shaking time of 5 min. was used for both metal ions for further studies.

Influence of Acid Concentration

The partition studies for Pt(IV) and Rh(III) were carried out from either HCl or H_2SO_4 media (0.1 to 6 mol L^{-1}) using 0.1 mol L^{-1} solution of either CYANEX 301 or CYANEX 923 in toluene (Figures 1 and 2). In the case of HCl, Pt(IV) showed high extraction in the investigated acid molarity, whereas Rh(III) showed poor (≤15%) extraction with both the extractants. Rh(III) was negligibly extracted from H_2SO_4 medium in both extractants, except a slight increase was observed below 1 mol L^{-1} H_2SO_4. Extraction of Pt(IV) increased with increasing acidity in the case of CYANEX 923, whereas the trend was reversed for CYANEX 301.

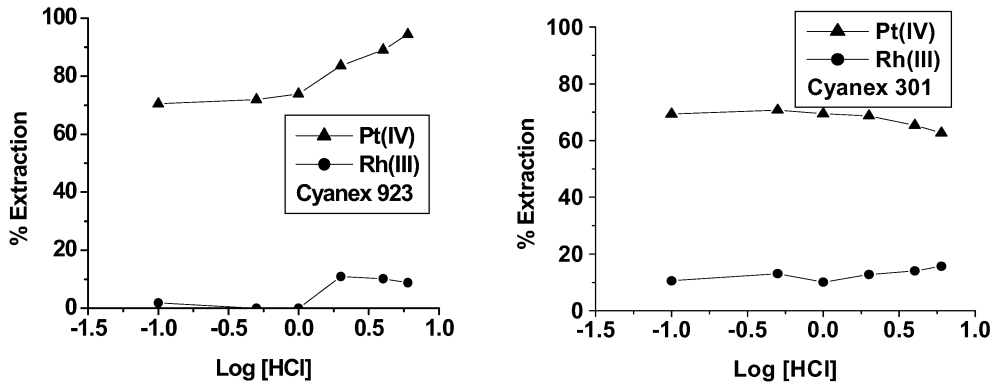

Figure 1. Effect of HCl concentration on the extraction of Pt(IV) and Rh(III) using CYANEX 923/301.

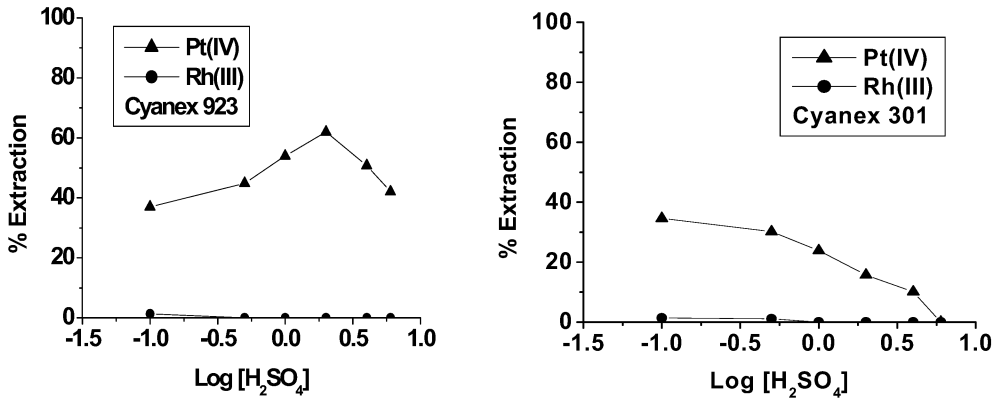

Figure 2. Effect of H_2SO_4 concentration on the extraction of Pt(IV) and Rh(III) using CYANEX 923/301.

As Rh(III) showed poor extraction at the investigated HCl molarity, detailed studies were carried out for Pt(IV) only.

Effect of Various Diluents

Various aromatic and aliphatic diluents, such as toluene, nitrobenzene, xylene, cyclohexanone, chloroform, *n*-hexane, and carbon tetrachloride, were employed. With all the diluents, almost the same percent extraction of Pt(IV) was obtained, indicating that the nature of diluents does not affect the distribution of Pt(IV). Toluene was preferred as the diluent for the extraction of Pt(IV), since it provided better phase separation.

Influence of Temperature

Distribution studies for Pt(IV) using 0.1 mol L^{-1} CYANEX 923 or CYANEX 301 at 1 mol L^{-1} were performed at different temperatures ranging from 283 K to 333 K. The

extraction of Pt(IV) with CYANEX 301 increased with increasing in temperature, indicating the extraction to be endothermic. In the case of CYANEX 923, the extraction of Pt(IV) decreased with increasing temperature, indicating the extraction to be exothermic.

The plots of log D against $1/T$(K) x 1000 are shown in Figure 3. ΔH values, as calculated using $-\ln D = \Delta H/RT + C$, are 15 kJ mol^{-1} and -7.0 kJ mol^{-1} with CYANEX 301 and CYANEX 923, respectively.

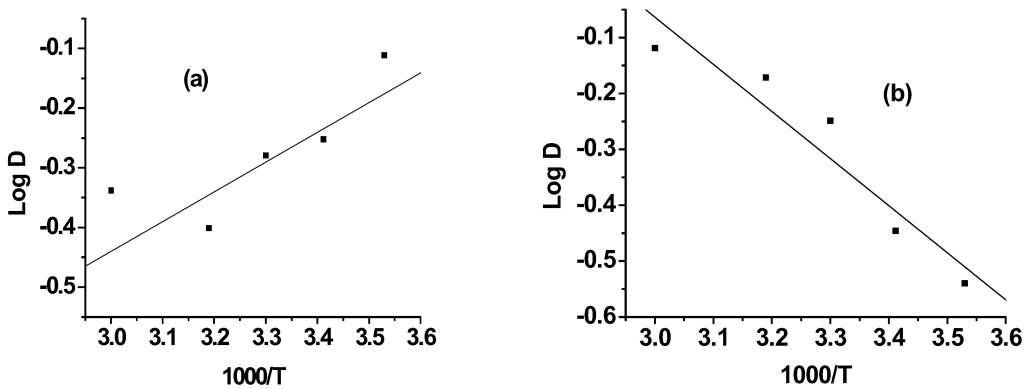

Figure 3. Effect of temperature on the extraction of Pt(IV) with (a) CYANEX 923 and (b) CYANEX 301.

Effect of Extractant Concentration

To investigate the effect of extractant concentration on the partition of Pt(IV), CYANEX 923 (0.05 to 0.5 mol L^{-1}) and CYANEX 301 (0.01 to 0.5 mol L^{-1}) concentrations were varied, keeping HCl concentration constant at 1 mol L^{-1}. Log-log plots (Figure 4) drawn between extractant concentration and distribution ratio gave straight lines with a slope value around 2 for CYANEX 923 and 1 for CYANEX 301. This indicates the metal:ligand ratio of the extracted species to be 1:2 for CYANEX 923 and 1:1 for CYANEX 301.

Stripping Studies

Studies reveal that Pt(IV) and Rh(III) can be stripped quantitatively from the loaded CYANEX 923 phase using 5 mol L^{-1} $HClO_4$ and 3 mol L^{-1} H_2SO_4, respectively, but it is difficult to recover the extracted Pt(IV) and Rh(III) from the loaded CYANEX 301 phase. A flowsheet has therefore been designed using CYANEX 923.

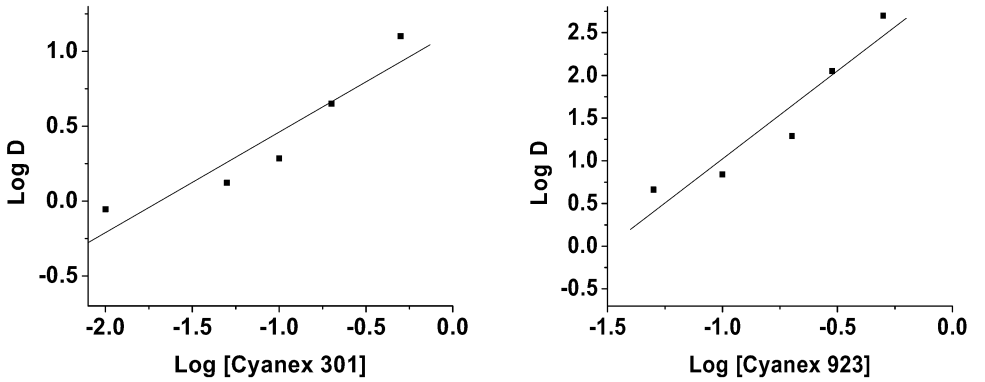

Figure 4. Effect of extractant concentration on the extraction of Pt(IV) using CYANEX 301 and CYANEX 923.

IR Spectra of Extractants and Complexes

The IR spectra of CYANEX 301, CYANEX 923, and their extracted complex species were recorded in dry KBr on a Thermo Nicolet IR instrument. Comparing the spectrum of CYANEX 301 with that of its complex, it can be seen that in the spectrum of the complex, the peak at 2577 cm^{-1} corresponding to S-H is almost eliminated. The intensity of the peak at 733 cm^{-1} corresponding to P=S decreases notably; this is due to the coordination of Pt(IV) with the P=S group in the CYANEX 301 molecule.

Comparing the spectrum of CYANEX 923 with that of its Pt complex, it can be seen that in the spectrum of the complex, the peak at 972 cm^{-1}, corresponding to P-O, is almost eliminated, and the intensity of the peak at 1151 cm^{-1} due to the stretching frequency of P=O bond decreases and shifts to 1148 cm^{-1}. This is due to the coordination of Pt(IV) with the P=O group in the CYANEX 923 molecule.

Separation of Pt(IV) and Rh(III)

The separation of Pt(IV) and Rh(III) from their mixtures was carried out by taking advantage of the difference in their extraction and stripping behavior using CYANEX 923 (Figure 5). The proposed scheme can also be applied to real samples.

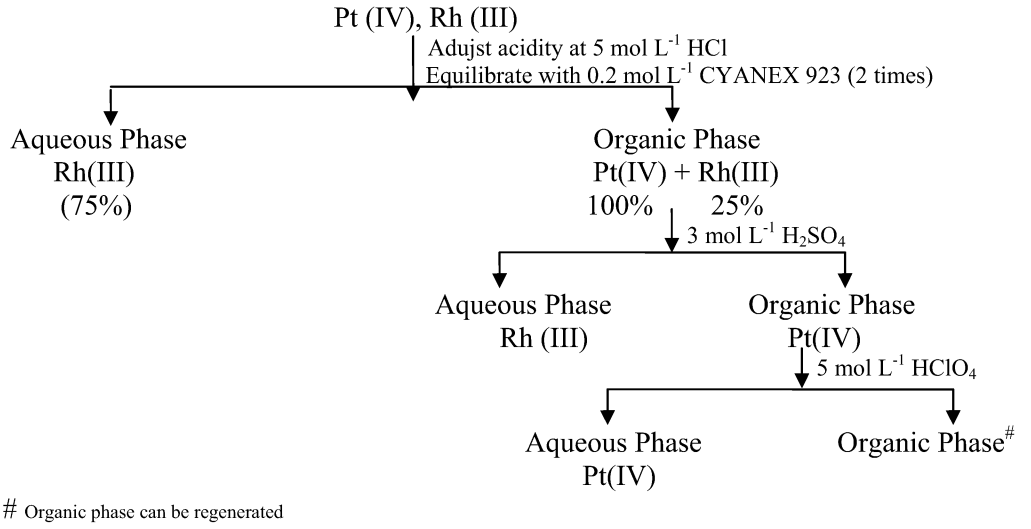

Figure 5. Separation of Pt(IV) from Rh(III).

CONCLUSION

The results obtained show that CYANEX 923 in toluene can be effectively used for the quantitative extraction of Pt(IV) and its separation from Rh(III) with the recovery of Pt(IV) more than 98%. The proposed method is simple. A major fraction of Rh(III) remaining in the aqueous phase can also be separated and purified by equilibrating the raffinate with 0.5 mol L^{-1} CYANEX 923 three times followed by its stripping with 5 mol L^{-1} H_2SO_4. These studies are in progress. Besides, palladium recovery is envisaged to be practiced following Pt-Rh separation, because most of the matrices contain Pt, Pd, and Rh together. In addition to this, the behavior of Ag and Au are also important as Pt, Pd, and Rh are being used in jewellery making.

ACKNOWLEDGMENTS

The support of Council of Scientific and Industrial Research, India, for funding the project and Cytec Canada for gifting CYANEX samples is gratefully acknowledged.

REFERENCES

1. Z. Ping, G. O. Guobang, Q. U. Zhiping, H. Yanfei, and Y. Wenxue, “The Pilot Test of Pt-Pd and Pt-Rh Feeds Extracted and Separated with a New Sulfoxide Extractant,” *Rare Metals,* **25**(2), 99-105 (2006).
2. E. Benguerel, G. P. Demopoulos, and G. B. Harris, “Speciation and Separation of Rh from Chloride Solutions. A Critical Review,” *Hydrometallurgy,* **40**, 135-152 (1996).
3. G. P. Demopoulos, “Solvent Extraction of Precious Metal Refining,” *J. Metals*, **38**(6), 13-17 (1986).

INFLUENCE OF GOLD AND ZINC ON FREE CYANIDE EXTRACTION FROM ALKALINE SOLUTIONS USING TRIOCTYLPHOSPHINE OXIDE

G.C. Guimarães, M.B. Mansur, and A.H. Martins

Universidade Federal de Minas Gerais, Departamento de Engenharia Metalúrgica e de Materiais Rua Espírito Santo 35 sala 206AG, Centro,Belo Horizonte(MG) CEP 30160-030, Brazil
Corresponding author email address: ahmartin@demet.ufmg.br

ABSTRACT

This technical note presents the preliminary experimental results at laboratory scale for a study involving the influence of gold and zinc in the aqueous phase on free cyanide extraction using CYANEX 921 (trioctylphosphine oxide) diluted in Exxsol in a single contact. Zinc and gold present in the aqueous phase of the solvent-extraction system did not contribute to increasing the free cyanide extraction. The system containing only cyanide reached 22.0% extraction, while the system containing zinc (CN-Zn) reached 17.0%. The systems containing gold (CN-Au) and zinc/gold (CN-Zn-Au) resulted in 5.0% and 9.0% free cyanide extraction, respectively.

INTRODUCTION

Cyanide is used in the leaching for gold extraction from ores. Most of the cyanide for gold leaching is consumed by its oxidation or due to metal cyanocomplex formation in the leach liquor. Cyanide recovery procedures assume an important role for industrial mineral plants for gold recovery from an economic point of view. Besides, cyanide is a highly toxic compound, for which its emission to the environment is limited to 0.2 g/L by the legislation of some countries [1].

Several cyanide-recovery techniques from industrial cyanidation liquors have been studied [2,3]. Among these, some with potential application can be mentioned: for instance, oxidation using SO_2, natural degradation, the AVR (acidification, volatilization, regeneration) process, chemical oxidation, and biological treatment. However, little attention has been paid to the application of solvent extraction as an alternative process for cyanide recovery [4-9].

This work presents the experimental results on the influence of zinc and gold on free cyanide extraction from an alkaline synthetic aqueous solution with a cyanide concentration similar to typical leach liquor for gold extraction by using CYANEX® 921 (trioctylphosphine oxide) diluted in Exxsol®. The zinc and gold influence on the free cyanide extraction by solvent extraction was evaluated by comparison of the

experimental results between aqueous phases containing metals (CN-Zn, CN-Au, and CN-Zn-Au systems) and aqueous phases containing only cyanide ions (CN^-).

EXPERIMENTAL

Tests were performed by contacting an aqueous phase containing cyanide and organic phase formed by CYANEX 921 (Cytec Industries, USA) diluted in Exxsol (Exxon Mobil, USA). The two phases were put into physical contact for different times and submitted to different experimental conditions taking into consideration parameters such as initial cyanide concentration in the aqueous phase, CYANEX 921 concentration in the organic phase, and time of contact between phases. The potential influence of zinc and gold in the aqueous phase of the solvent-extraction system on the percent of free cyanide extraction was measured by comparison between the aqueous phase containing only cyanide and zinc and gold cyanocomplexes.

Tests were carried out at room temperature in Erlenmeyer glass flasks of 500 mL capacity, where the organic and aqueous phases were kept mixed under intense magnetic stirring for different times. After contact between organic and aqueous phases, they were fed to a glass separation funnel for separation/decantation. After separation, a sample of aqueous phase was collected for determination of free cyanide by chemical analysis.

Synthetic aqueous solutions were prepared by dissolving 40 g NaOH and 25 g NaCN in 1000 mL of distilled water. The initial pH values of all aqueous solutions used in the experiments of this work were adjusted to pH 10.5 by addition of sulfuric acid. Aqueous solutions containing zinc and gold were prepared by dissolution of 0.5 g of each metal in 1000 mL of 40 g NaOH and 25 g NaCN aqueous solution at 60 ± 2 ºC and intense stirring for 24 h.

Different concentrations of CYANEX 921 diluted in Exxsol were used to prepare organic phases for each test. The maximum solubility of CYANEX 921 in Exxsol used in the experiments was 450 g/L.

Free cyanide in the aqueous-phase samples collected during the experiments was determined by titration using $AgNO_3$ (0.0192 N) solution and 5-(p-dimethylamino-benzylidene rhodanine as indicator [10,11]. The percentage of free cyanide extraction was determined by the difference between the initial free cyanide concentration in the aqueous solution and the free cyanide concentration in the aqueous phase after contacting with the organic phase.

RESULTS AND DISCUSSION

Previous research work [11] has determined some parameters used in the experiments of this work, for instance, aqueous-organic phase ratio and organic phase volume used for contacting the aqueous phase. Figures 1 to 3 present the experimental results for aqueous phases containing only cyanide ions, that is, without any zinc and gold in the aqueous solution.

Figure 1 shows the experimental results for free cyanide extraction versus mass of CYANEX 921 in the organic phase. The maximum extraction of free cyanide (22.0%) was obtained for 4.0 g CYANEX 921 in 20 mL of organic phase (200 g/L CYANEX

921). This result was expected because higher extractant concentration means that more organic functional groups are in contact with free cyanide ions from the aqueous solutions resulting in higher percent of free cyanide extraction.

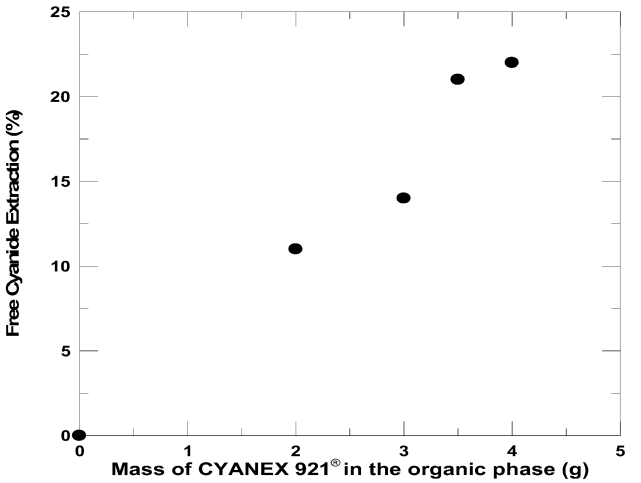

Figure 1. Percent free cyanide extraction versus mass of CYANEX 921 in the organic phase. Experimental conditions: 10 min contact time between phases, 20 mL aqueous phase containing 4.0 g/L CN^-, 20 mL organic phase and 60 min for phase separation.

Figure 2 shows the results for free cyanide extraction versus time of phase contact. These experiments were performed for aqueous solutions containing just cyanide. The results showed that 10 min phase contact extracted 22.0% free CN^-. A longer contact time resulted in lower percent of free cyanide extraction.

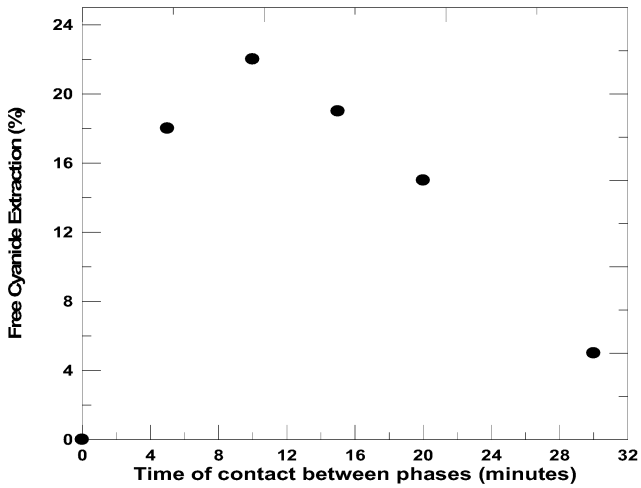

Figure 2. Percent free cyanide extraction versus time of contact between phases. Experimental conditions: 20 mL aqueous phase containing 4.0 g/L CN^-, 60 min for phase separation and 200 g/L CYANEX 921 in Exxsol as organic phase.

Figure 3 presents the experimental results for the free cyanide extraction versus initial concentration of cyanide in the aqueous solution. The percent of free cyanide extraction became greater when the initial cyanide concentration in the aqueous solution increased. Higher free CN^- ions available in the aqueous solution resulted in a significant increase in the free cyanide extraction from 9% at 2 g/L cyanide to 15% at 8 g/L cyanide.

After evaluating the influence of initial mass of CYANEX 921 in the organic phase, time of contact between phases and initial concentration of cyanide in the aqueous solution on the percent of free cyanide extraction using aqueous phases containing only cyanide ions, experiments were carried out with the presence of zinc and gold in the aqueous phase. The highest free cyanide extraction was 22.0%, obtained for 20 mL of aqueous phase containing 4.0 g/L CN^-, 10 min contact time, 20 mL of organic phase containing 200 g/L CYANEX 921 diluted in Exxsol, and 60 min for phase separation.

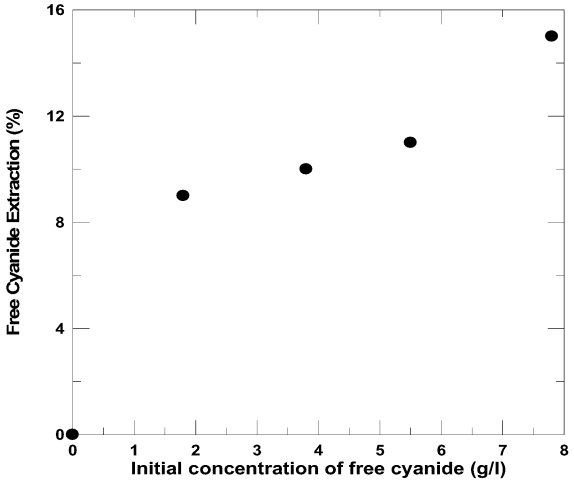

Figure 3. Percent free cyanide extraction versus initial concentration of cyanide in the aqueous phase. Experimental conditions: 200 g/L CYANEX 921 in 20 mL of Exxsol as organic phase, 20 ml aqueous solution, and 60 min for phase separation.

Figure 4 presents the free cyanide extraction versus contact time for three systems: CN-Zn, CN-Au and CN-Zn-Au. The initial concentration of zinc and gold in the aqueous solutions was 0.5 g/L for each metal. The highest free cyanide extraction (17.0%) was reached for 15 min contact time for the CN-Zn system. For the gold-containing systems, the maximum free cyanide extraction was obtained at 30 min contact for CN-Au (5.0%) and CN-Zn-Au (9.0%).

The influence of the initial free cyanide concentration in the aqueous phase containing zinc and gold on the percent of free cyanide extraction was also studied. Figure 5 shows the experimental results for free cyanide extraction versus initial free cyanide concentration in systems containing zinc and/or gold. The maximum free cyanide extraction was obtained for the CN-Zn system (17.0%). The highest values found for CN-Au and CN-Zn-Au systems were just 5.0% and 9.0% of free cyanide extraction, respectively.

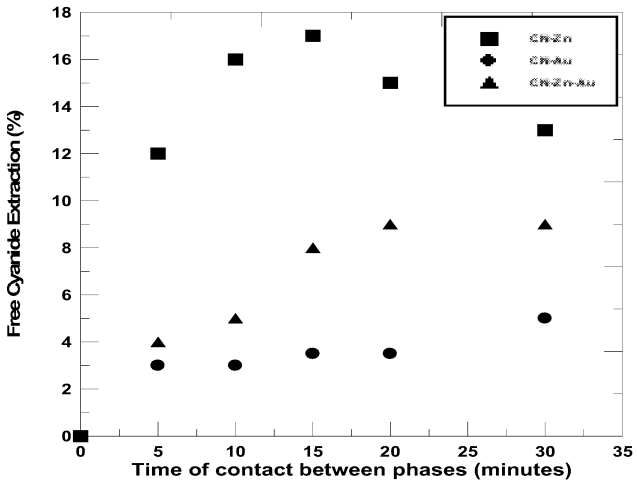

Figure 4. Percent free cyanide extraction versus contact time between phases for CN-Zn, CN-Au, and CN-Zn-Au systems. Experimental conditions: 20 mL aqueous phase containing 4.0 g/L CN^-, 20 mL organic phase of 200 g/L CYANEX 921 in Exxsol, 60 min phase separation.

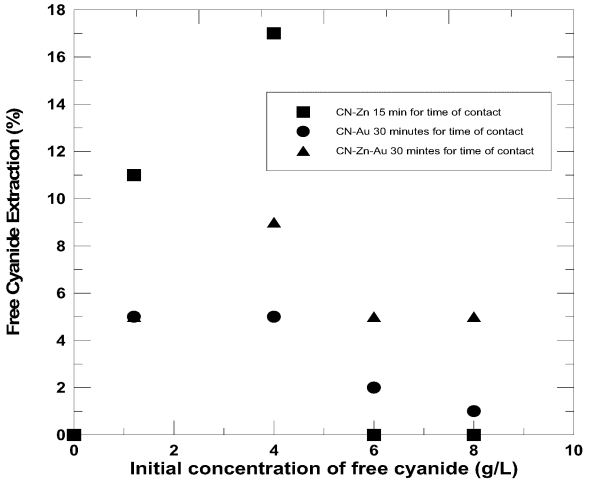

Figure 5. Percent free cyanide extraction versus initial concentration of cyanide (g/L) in the aqueous phase for the CN-Zn, CN-Au, and CN-Zn-Au systems and times of contact between phases for maximum CN^- recovery. Experimental conditions: 20 mL aqueous phase, 20 mL organic phase containing 200 g/L CYANEX 921 in Exxsol, 60 min for phase separation.

According to the experimental results of this technical note, there was no positive contribution of the initial zinc and gold concentrations in the aqueous phase on the free cyanide extraction by solvent extraction with CYANEX 921 diluted in Exxsol. On the contrary, there was 22.0% of free cyanide extraction in the system without zinc and gold (Figure 1), while just 17.0% (Figure 4) was extracted in the presence of zinc in the aqueous phase. Gold also had a high negative effect on the free cyanide extraction when

compared with zinc because the percent of extraction was much lower (5.0%) than the value obtained when only zinc was present in the aqueous solution.

CONCLUSIONS

Zinc and gold present in the aqueous phase of the solvent extraction system CYANEX 921 diluted in Exxsol did not increase the free cyanide extraction. On the contrary, the free cyanide extraction from the system containing only cyanide in the aqueous phase reached 22.0%, while the system containing zinc (CN-Zn) reached 17.0%. The systems containing gold (CN-Au) and zinc/gold (CN-Zn-Au) resulted in 5.0% and 9.0% free cyanide extraction, respectively.

ACKNOWLEDGMENTS

The authors thank Foundation for Supporting Scientific Research Minas Gerais State (FAPEMIG)/Brazil and Brazilian Science Foundation-CNPq for financial support.

REFERENCES

1. Unites States Environmental Protection Agency (USEPA), http://www.epa.gov/safewater/dwh/c-ioc/cyanide.html (accessed 11/26/2007).
2. J. S. Scott, "An Overview of Cyanide Treatment Methods for Gold Mill Effluents," Proc. Cyanide and the Environment Conference, Vol. 2, D. van Zyl, Ed., Tucson, Arizona, 1984; pp. 307–327.
3. M. M. Botz, "Overview of Cyanide Treatment Methods," The Gold Institute, 1999, http://www.infomine.com/publications/docs/Botz1999.pdf (accessed 11/26/2007).
4. F. J. Alguacil, C. Caravaca, A. Cobo, and S. Martinez, "The Extraction of Gold(I) from Cyanide Solutions by the Phosphine Oxide CYANEX 921," *Hydrometallurgy*, **35**, 41–52 (1994).
5. F. J. Alguacil and C. Caravaca, "Synergistic Extraction of Gold(I) Cyanide with the Primary Amine Primene JMT and the Phosphine Oxide CYANEX 921," *Hydrometallurgy*, **42**, 197–208 (1996).
6. C. Caravaca, F. J. Alguacil, and A. Sastre, "The Use of Primary Amines in Gold(I) Extraction from Cyanide Solutions," *Hydrometallurgy*, **40**, 263–275 (1996).
7. F. J. Alguacil, C. Caravaca, J. Mochon, and A. Sastre, "Solvent Extraction of $Au(CN)^-_2$ with Mixtures of the Amine Primene JMT and the Phosphine Oxide CYANEX 923," *Hydrometallurgy*, **44**, 359–369 (1997).
8. M. I. Martin and F. J. Alguacil, "Synergism in Gold-Cyanide Extraction with Primene JMT-CYANEX 925 Mixed Extractant System," *Hydrometallurgy*, **49**, 309–322 (1998).
9. J. H. Bright, "A Feasibility Study for the Extraction of Cyanide from Aqueous Solution by Solvent Extraction with Tri-n-Octylphosphine Oxide (TOPO)," Progress Report No. 83-17, American Cyanamid Company, USA, 1983.
10. N. H. Furman and F. J. Welcher, Standard Methods of Chemical Analysis. R. E. Krieger, Ed., 6th edition, Florida, USA, 1975.
11. R. C. Andrade, "Solvent Extraction Applied to the Cyanide Recovery," Scientific Initiation Program/FAPEMIG/PROBIC, Final Report, Belo Horizonte, Minas Gerais, Brazil, 2004. (In Portuguese).

RECOVERY OF INDIUM FROM SPENT FLAT-PANEL DISPLAY WITH SOLVENT-IMPREGNATED RESINS

K. Inoue, M. Nishiura, H. Kawakita, K.Ohto, and H. Harada

Department of Applied Chemistry, Saga University, Honjo 1, Saga 840-8502, Japan
Corresponding author email address: inoue@elechem.chem.saga-u.ac.jp

ABSTRACT

An effective recovery process for indium(III) from waste liquid-crystal display panels was developed using porous resins impregnated with each of CYANEX 923 and Aliquat 336. Total dissolution of the powdered sample of the waste in aqua regia suggests the metal contents (mg/L) as follows: Al, 230; In, 205; Ba, 175; Si, 105; Ca, 95; Fe, 60; Zn, 39.5; Cr, 29; Sn, 24; and Mg, 10. The powdered sample was leached with 3 M HCl, and extracted metals can be mutually separated and recovered by passing through the column packed with the resin impregnated with Aliquat 336 followed by that with CYANEX 923. The former column recovered Sn, Fe, and Zn, while the latter column only In. The metal ions trapped in these columns were eluted with 0.1 M H_2SO_4 concentrated more than 10 times.

INTRODUCTION

Due to the rapid spread of liquid-crystal television (TV) and plasma TV in recent years, the demand for indium is now increasing as the feed material for indium tin oxide (ITO) transparent electrode, produced by means of sputtering. Since indium is contained in sphalerite in small amounts, it is produced as a byproduct in the smelting of zinc. The resources of indium are limited on the earth and the countries or areas which can provide indium are also limited, which has resulted in a rapid increase in the price of indium in recent years.

Although large efforts have been devoted to the development of new technologies for substituting indium with common metals such as zinc, these are expected to take a long time to commercialize. Consequently, only one choice to avoid the shortage of indium is its effective recovery from various indium-containing wastes and its recycle. Although spent target generated in the production of ITO transparent electrode by sputtering is now fully recycled, indium contained in flat-panel display (FPD) of liquid-crystal TV and plasma TV has not yet been attempted to be recovered for recycling. In the present work, we conducted a fundamental investigation of a hydrometallurgical recovery process of indium from waste FPD.

EXPERIMENTAL

Materials and Reagents

The actual waste sample of FPD produced by Samsung Electronics Co. Ltd. was supplied from Shimada Shokai Co. Ltd. The sample of the solvent-extraction reagent, CYANEX® 923, which is a mixture of four kinds of trialkylphosphine oxides with different alkyl radicals, produced and marketed by CYTEC Industries Inc., Canada, was kindly donated by Fujitec Co., Japan. Aliquat® 336, the main component of which is trioctylmethylammonium chloride, was purchased from Cognis Corp.

In the solvent-extraction experiments using these reagents, reagent-grade toluene was employed as a diluent. The sample of Amberlite® XAD-7, the porous spherical beads of acrylic ester resin, was purchased from ORGANO Corp.

Preparation of Solvent-Impregnated Resins (SIR)

Two types of SIR were prepared, that impregnated with CYANEX 923 and that with Aliquat 336. In both cases, 2.0 g XAD-7 beads were put in 20 mL acetone containing 2.0 g reagent to be shaken for 12 h, after which the beads were taken by filtration and vacuum dried to remove acetone. The contents of the impregnated reagent in the beads were 1.29 and 1.23 mol/kg for the former and latter resins, respectively.

Leaching of Indium from Spent FPD

Actual sample of spent FPD was crushed by hammer into small particles. One g of particles was mixed with 10 mL of aqua regia, 3 M hydrochloric acid, sulfuric acid, and nitric acid to be shaken for a required time, after which the sample acid solution was taken for the analysis of metal concentration using a Shimadzu ICPS-8100 ICP/AES spectrometer.

Solvent-extraction and Adsorption Tests

In order to examine the solvent-extraction behaviors of some extraction reagents for In(III), 10 mL of toluene solution containing 80 mM of the reagent was shaken together with 10 mL of varying concentration of hydrochloric acid containing 4 mM In(III) at 303 K for 3 h.

Batchwise adsorption tests were carried out using the resin impregnated with CYANEX 923 to examine the adsorption isotherm of In(III) at first by shaking 30 mg resin together with 15 mL of 3 M hydrochloric acid containing varying concentrations of In(III) at 303 K for 12 h. Similar batchwise adsorption tests were carried out using the two types of impregnated resins by shaking 30 mg resin together with 15 mL of varying concentrations of hydrochloric acid containing 0.2 mM of all metal ions mentioned above to examine the adsorption behaviors of these impregnated resins.

On the basis of the results of these tests, continuous adsorption tests using two columns packed with 0.60 g of each of two types of impregnated resins connected in

series as shown in Figure 1 was carried out. In this test, synthetic test solution of 3 M hydrochloric acid containing the same concentration of each metal ion measured in the leaching test was fed to the columns at the feed rate of 5.0 mL/h with a peristaltic pump.

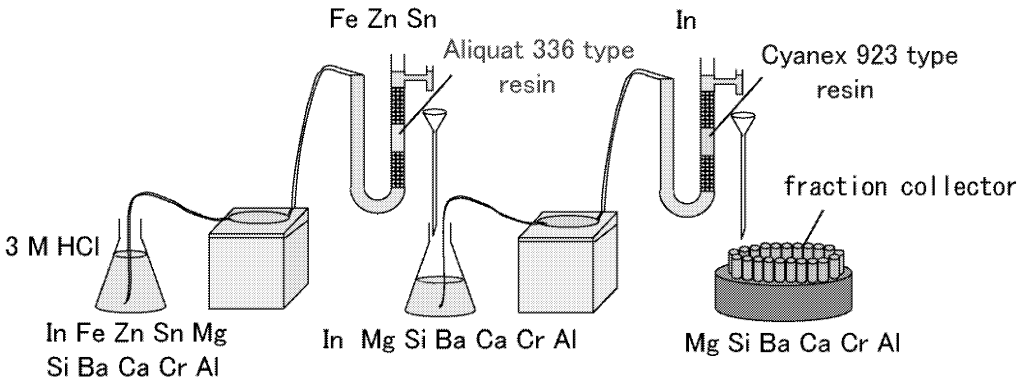

Figure 1. Experimental setup for the continuous adsorption test for selective recovery of indium.

RESULTS AND DISCUSSION

Leaching of Spent FPD

Figure 2 shows the relationship between the concentration of In(III) in the various leach liquors and leaching time. In(III) is most effectively leached with aqua regia; however, nearly the same leaching behavior was observed with 3 M hydrochloric acid, while effective leaching was not observed with 3 M nitric acid and sulfuric acid. On the other hand, total dissolution of the powdered sample in aqua regia suggested the metal contents (mg/L) as follows: Al, 230; In, 205; Ba, 175; Si, 105; Ca, 95; Fe, 60; Zn, 39.5; Cr, 29; Sn, 24; and Mg, 10.

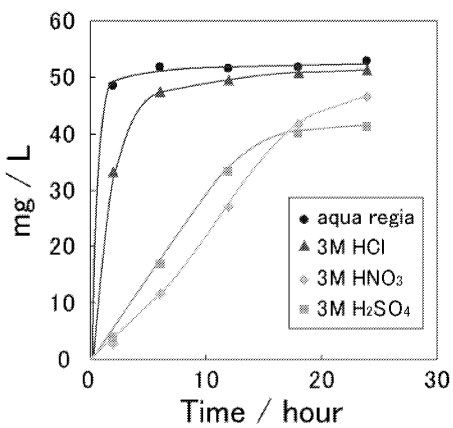

Figure 2. Leaching of indium from powder of crushed spent FPD with various acids.

Solvent-extraction of Indium

Figure 3 shows the plot of percent extraction of In(III) from varying concentrations of hydrochloric acid with some solvent-extraction reagents in toluene. It is seen that CYANEX 923 exhibits the highest extraction, though TOPO (trioctylphosphine oxide) also exhibits similar extraction behavior. On the other hand, TBP (tributylphosphate) exhibited no extraction of In(III) over the whole hydrochloric acid concentration range.

Figure 4 shows the percent extraction of In(III) with CYANEX 923 in toluene from varying concentrations of hydrochloric acid and sulfuric acid as well as that containing 0.2 M ammonium chloride. It is seen that, although In(III) is not extracted from sulfuric acid the addition of some amount of chloride improves the extraction similar to hydrochloric acid, suggesting that chloride ion plays an important role in this extraction system and that sulfuric acid can be employed as stripping agent for In(III).

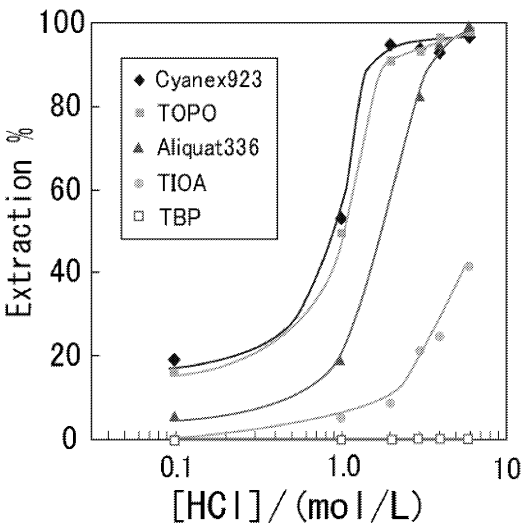

Figure 3. Percent extraction of In(III) with some sovent extraction reagents in toluene from varying concentration of hydrochloric acid.

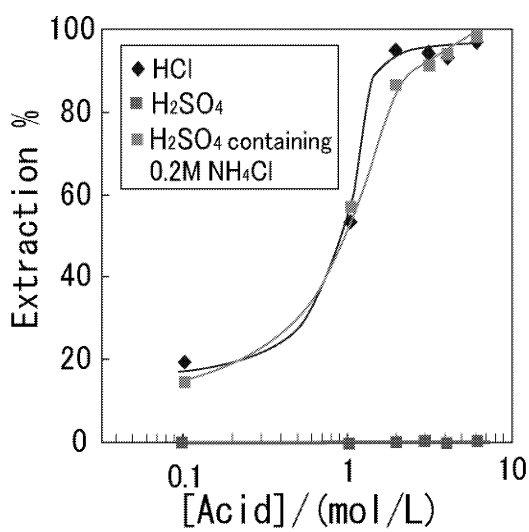

Figure 4. Percent extraction of In(III) with CYANEX 923 in toluene from hydrochloric acid and sulfuric acid.

Adsorption of Metal Ions on Solvent-Impregnated Resins

From the test of adsorption isotherm of In(III) from 3 M hydrochloric acid on the resin impregnated with CYANEX 923, it was found that adsorption takes place according to the Langmuir adsorption mechanism, and the maximum adsorption capacity for In(III) was evaluated as 0.45 mol/kg-resin.

Batchwise Adsorption of Various Metal Ions on the Solvent-Impregnated Resins

Figures 5 and 6 show the percent adsorption of all metal ions existing in the leach liquor from varying concentration of hydrochloric acid on the resins impregnated with CYANEX 923 and Aliquat 336, respectively. From Figure 5, it is seen that, although In(III) is effectively adsorbed on the CYANEX 923 impregnated resin at 3 M hydrochloric acid, Sn(IV), Zn(II), and Fe(III) are more selectively adsorbed over In(III), suggesting these impurity metal ions should be removed prior to the recovery of In(III). Figure 6 indicates that although percent adsorption of these three impurity metal ions is higher than 90%, that of In(III) is less than 20% at 3 M hydrochloric acid in the case of Aliquat 336 impregnated resin, suggesting that this resin is suitable for selectively removing these impurity metal ions from In(III). On the other hand, adsorption of other metal ions, Al(III), Mg(II), Si(IV), Ca(II), and Ba(II), are only negligible on both of these resins.

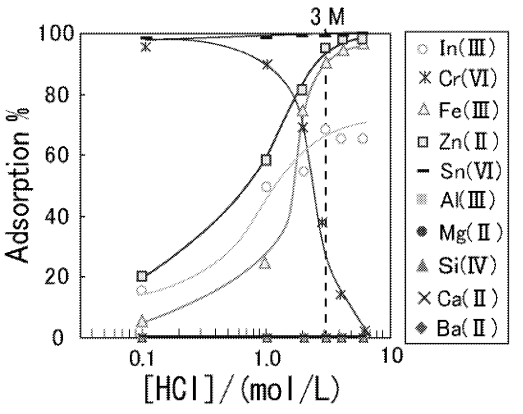

Figure 5. Percent adsorption of all metal ions existing in the leach liquor of the spent FPD from varying concentration of hydrochloric acid on the CYANEX 923 impregnated resin.

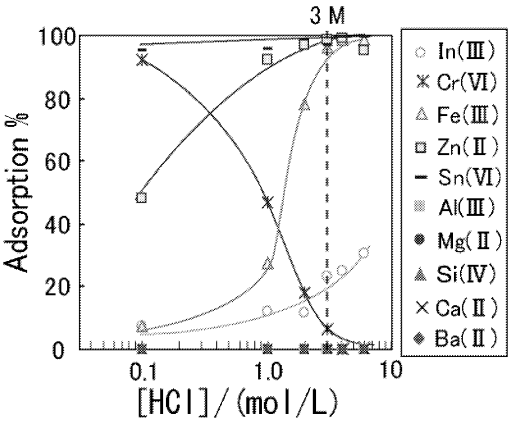

Figure 6. Percent adsorption of all metal ions existing in the leach liquor of the spent FPD from varying concentration of hydrochloric acid on the Aliquat 336 impregnated resin.

Adsorptive Recovery and Purification of Indium from Model Leach Liquor by Means of Continuous Operation Using Columns Packed with Two Types of Impregnated Resins

Figure 7 shows the breakthrough profiles of all metal ions tested from the first column shown in Figure 1 packed with the resin impregnated with Aliquat 336. Although Fe(III), Zn(II), and Sn(IV) were not detected in the effluent from the column even after 100 bed volumes (B.V.), Al(III), Mg(II), Si(IV), Ca(II), Ba(II), and Cr(VI) immediately broke through just after the initiation of the feed. On the other hand, In(III) gradually broke through until 50 B.V., suggesting that some amount of In(III) is retained in this column.

Figure 8 shows the breakthrough profiles from the second column packed with CYANEX 923 impregnated resin together with the elution profile of In(III) (after 50 B.V.) from the same column. All Al(III), Mg(II), Si(IV), Ca(II), Ba(II), and Cr(VI), which had passed through the first column without being adsorbed, also immediately broke through just after the initiation of the feed in the second column. On the other hand, In(III) was not detected at all in the effluent from the second column up to 50 B.V., suggesting that In(III) is successfully purified free from the contamination of other metal ions. As mentioned earlier, after 50 B.V., the second column was washed by water and, subsequently, with 0.1 M sulfuric acid. As seen from the elution profile of In(III) in Figure 8, all In(III) adsorbed in the second column is eluted enriched more than 10 times compared to the feed solution.

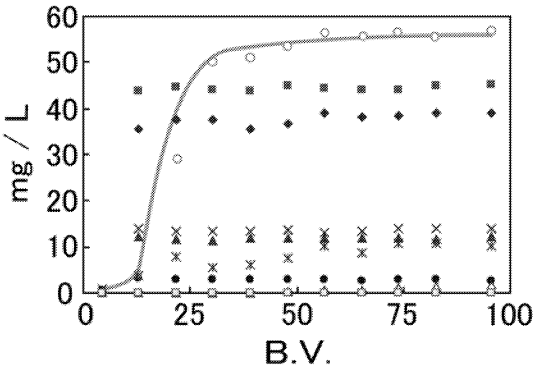

Figure 7. Breakthrough profiles of all metal ions tested from the first column packed with Aliquat 336 impregnated resin. Symbols: ○ In (III), * Cr(VI), △ Fe(III), □ Zn(II), —Sn(VI), ▩ Al(III), ● Mg(II), ▲ Si(IV), ×Ca(II), ◆ Ba(II).

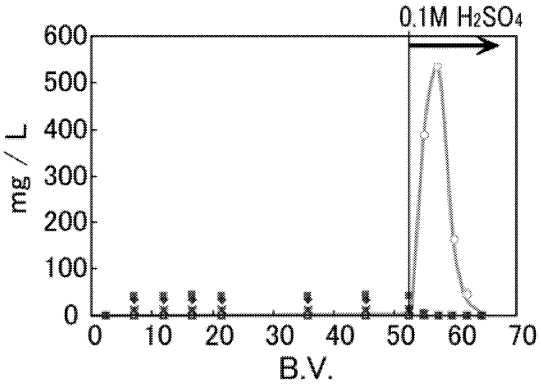

Figure 8. Breakthrough profiles (up to 50 B.V.) from the second column packed with CYANEX 923 impregnated resin and the elution profile of In(III) (after 50 B.V.) from the same column.

CONCLUSIONS

From the present work, it can be concluded that small amounts of indium can be effectively extracted with 3 M hydrochloric acid from crushed spent FPD and can be purified and enriched by passing through the columns packed with porous resins impregnated with Aliquat 336 and CYANEX 923.

ACKNOWLEDGMENTS

The present work was financially supported in part by the 2007 research project of Kyushu Recycle and Environmental Industry Plaza (K-RIP). The authors are also deeply indebted to Fujitec Co. for the kind supply of the samples of CYANEX 923 and TOPO.

LIQUID-LIQUID EXTRACTION OF Hg(II) FROM HYDROCHLORIC ACID SOLUTIONS BY CYANEX 923

Francine de M. Fábrega and Marcelo B. Mansur

Department of Metallurgical and Materials Engineering, UFMG
R. Espírito Santo, 35, 2° andar, Centro, 30160-030, Belo Horizonte, MG, Brazil
Corresponding author email address: marcelo.mansur@demet.ufmg.br

ABSTRACT

The extraction of Hg(II) from HCl solutions containing 200 to 600 mg/L of mercury using CYANEX 923 as extractant was investigated (A/O ratio = 1 and T = 25 °C). The reaction was found to be rapid, and mercury was quantitatively extracted at pH ≥ 1 within 1 minute. The slope analysis method was used to evaluate the effects of chloride ions and extractant concentrations on the mercury extraction with CYANEX 923. An equilibrium model was proposed and equilibrium constant valid for the operational conditions investigated was determined by data fitting. Mercury was stripped using thiourea as stripping agent.

INTRODUCTION

Mercury is present in a variety of waste products including contaminated soil, medical waste, fluorescent lamps, and contaminated water streams. Industrial processes that may result in Hg-containing effluents include chlorine and caustic soda production, mining and ore processing, metallurgy and electroplating, paper milling, chemical and ink manufacturing, leather tanning, textile manufacturing and pharmaceutical production. The control and removal of mercury from polluted effluents and waste streams are therefore important issues for reducing the total amount of discharged metal to the environment, because mercury can be highly toxic for living bodies depending on its chemical form.

The concentration of mercury in effluents may vary depending on the volume of water involved, which differs for different processes and plants. In the case of the Hg cell chloralkali process, which utilizes elemental Hg as the cathode in an electrolytic process producing chlorine and caustic soda from saturated salt solutions (brine), wastewaters generated by this process contaminated with mercury typically range between 10 to 70 mg/L total mercury [1]. Conventional precipitation, ion-exchange, and absorption methods for metals removal often have difficulty in consistently treating certain compounds to the low levels being enforced by state and federal regulators. In the state of Minas Gerais, Brazil, the maximum concentration of mercury allowed in effluents to be discharged is 0.01 mg/L [2]. Therefore, environmental and water-resource managers constantly look for better, more cost-effective alternatives to conventional water

treatment for metals and also for other inorganic species in solution. Biological wastewater treatment methods seem to be a reasonable alternative for dilute effluents. However, in the case of effluents containing higher concentrations of mercury, from 100 to 600 mg/L of Hg, biological methods may fail because microorganisms more resistant to Hg are required, so liquid-liquid extraction can be an effective method to treat them. In this study, CYANEX® 923 (which is a mixture of four trialkylphosphine oxides produced by Cytec Co.) was chosen as reagent for Hg(II) removal.

The choice of CYANEX 923 was based on a previous investigation where 98.8% of Hg(II) was extracted from HCl media with no formation of precipitates (C_{Hg}^0 = 400 mg/L (or 2 mM), pH = 1, C_{923}^0 = 0.4 M dissolved in Exxsol® D-80, A/O = 1, T = 25 °C, where subscripts Hg and 923 denote mercury and extractant species, respectively, and superscript 0 denotes the initial condition) [3]. CYANEX 923 behaves as a neutral reagent in dilute conditions at excess extractant, and the following reaction has been proposed to describe the extraction of Hg(II) with CYANEX 923 (C_{Hg}^0 = 20 mg/L (or 0.1 mM), C_{923}^0 = 0.1 M dissolved in xylene, A/O = 1, [HCl] = 1 M, T = 30 °C) [4]:

$$HgCl_2 + 3\ TRPO_{(org)} \leftrightarrows HgCl_2.3TRPO_{(org)} \qquad \log K = 5.51 \qquad (1)$$

where TRPO denotes the molecule of CYANEX 923 and K is the equilibrium constant. With regard to the stripping of Hg(II), it was observed that 0.01 M $Na_2S_2O_3$ (99.4%), 5% thiourea in HCl 1% (99.0%), and 0.01 M NH_4Cl (95.8%) are potential stripping solutions for this reactive system (figures in parenthesis indicate the percentage of mercury stripping) [4].

In this paper, the extraction of Hg(II) from HCl solutions containing higher levels of mercury (from 200 to 600 mg/L of mercury) was studied. The effluent obtained after treatment by solvent extraction could be polished by a biological method, for instance, to meet environmental regulations and finally be sent for final discharge.

EXPERIMENTAL

An aqueous stock solution 1 M Hg(II) was prepared by dissolving $HgCl_2$ (Vetec, 99% purity) and HCl (Vetec, 35-37% purity) in deionized water. The organic solutions were prepared by dissolving CYANEX 923 (purity of 90% and used without purification) in Exxsol D-80 (Exxon Chem., 100% aliphatic), which was chosen based on a previous study [3]. No modifier agent was necessary. Thiourea (Vetec, purity of 99%) was used as stripping agent. All other chemicals used in this study were of analytical grade.

The extraction experiments were carried out by contacting specific volumes of both solutions in a beaker (for a given A/O volumetric ratio), at room temperature, which were brought together by mechanical stirring using a marine-type glass impeller. The initial concentration of Hg(II) in the aqueous phase varied from 1 to 3 mM and that of CYANEX 923 in the organic phase from $0.5 < C_{923}^0/C_{Hg}^0 < 5.0$ (high mercury extractions over 96% were obtained at $C_{923}^0/C_{Hg}^0 \geq 4.5$). In the stripping tests, the concentration of thiourea varied from 1 to 8 mM dissolved in 0.5 M HCl. The total concentration of mercury in the aqueous phase was determined by atomic absorption

spectrophotometry (GBC 932 plus Spectrometer at a wavelength of 253.7 nm) while that in the organic phase was calculated by mass-balance difference. No third-phase formation was noted.

RESULTS AND DISCUSSION

Firstly, preliminary tests were carried out in order to establish the time of contact and equilibrium pH for the equilibrium experiments. To determine the time of contact, equal volumes of the aqueous (C_{Hg}^0 = 2 mM, pH = 1, [Cl^-] = 0.1 M) and the organic (C_{923}^0 = 9 mM) phases were contacted and samples were withdrawn at different times until 20 minutes. The extraction reaction of Hg(II) with CYANEX 923 was found to be very rapid, corroborating a previous study [4], reaching equilibrium in the first minute (around 98%), so it was decided to use a 10 minute contact time. No effect of pH was observed after a range of aqueous solutions with similar metal concentration but pH values of 0 to 2 were contacted with an organic phase with the same amount of CYANEX 923. In every case, 98% extraction of mercury was seen. All subsequent tests were done at pH = 1.0. In addition, no change in volume was observed.

The effect of chloride ions on the extraction of Hg(II) with CYANEX 923 was investigated at pH = 1 and C_{923}^0/C_{Hg}^0 ratio of 4.5 by changing NaCl concentration from 0 to 1 M. According to results shown in Figure 1, an increase of chloride ions in the aqueous phase negatively affects Hg(II) extraction. A significant drop in the extraction of Hg(II) from 98.7% to 74.8% was noted when the concentration of chloride ions increased from 0.1 M to 1.1 M.

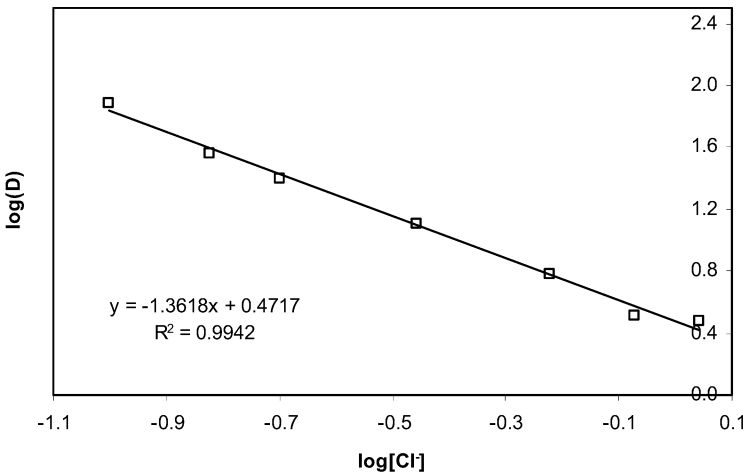

Figure 1. Effect of chloride ions on the extraction of Hg(II) with CYANEX 923
Aqueous phase: C_{Hg}^0 = 2 mM, pH = 1. Organic phase: C_{923}^0 = 9 mM; A/O = 1.

In fact, the increase of the concentration of chloride ions in the aqueous phase favors the formation of mercury anionic aquo-complexes according to Equations 2 and 3. Assuming that CYANEX 923 reacts solely with neutral species $HgCl_2$ as pointed out by

Equation 1, the higher the concentration of chloride ions becomes, the lower is the extraction of mercury by CYANEX 923 due to competition of $HgCl_2$ species to react with both extractant and chloride ions.

$$HgCl_2 + Cl^- \leftrightarrows HgCl_3^- \qquad K_a = 9.117 \tag{2}$$

$$HgCl_3^- + Cl^- \leftrightarrows HgCl_4^{-2} \qquad K_b = 1.123 \tag{3}$$

where K_a and K_b are the stepwise formation constants of Equations 2 and 3, respectively. At this condition, the theoretical aquo-complexes of mercury predominant in the aqueous phase are neutral $HgCl_2$ (35.2%) and anionic $HgCl_3^-$ (31.0%) and $HgCl_4^{2-}$ (33.8%) species.

The distribution data for the extraction of Hg(II) from 0.1 M HCl solutions by CYANEX 923 at various concentration levels are shown in Figure 2 as log D versus log [C_{923}]. It is shown that an increase in the concentration of CYANEX 923 favors the metal extraction as expected. Practically all mercury was extracted at C_{923}^0/C_{Hg}^0 ratio near to 4.5.

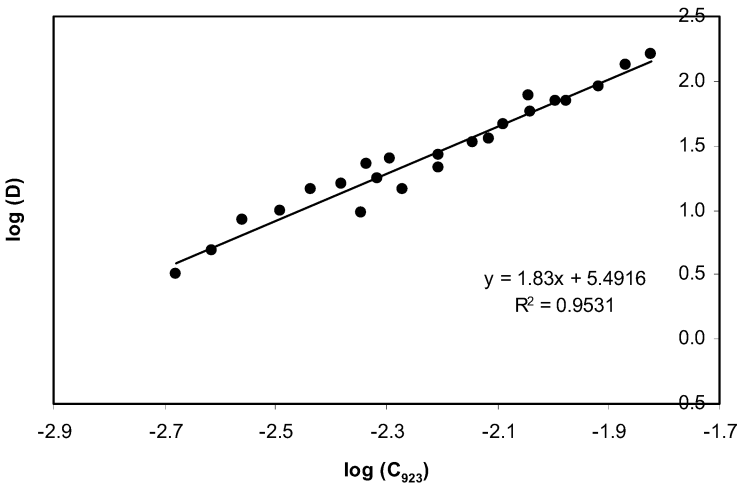

Figure 2. Effect of CYANEX 923 concentration on the extraction of Hg(II). pH = 1, [Cl^-] = 0.1 M, A/O = 1.

In order to investigate the reaction scheme for the Hg(II)-CYANEX 923 system, the following equation was derived, assuming that CYANEX 923 reacts only with neutral $HgCl_2$ species and that neutral and anionic complex species are in equilibrium according to Equations 2 and 3 [4]:

$$\log D = \log K + n \log [C_{923}] - \log (1 + K_a[Cl^-] + K_aK_b[Cl^-]^2) \tag{4}$$

Based on the result of Figure 2, the fitted stoichiometric coefficient n shows that 2 molecules of CYANEX 923 react with one molecule of $HgCl_2$ (9.3% deviation). In addition, as [Cl^-] = 0.1 M, so log K = 5.80, which value is relatively close to that from the

literature [4] despite the difference in the number of molecules of CYANEX 923 involved in the reaction with Hg(II). Such differences in the stoichiometry of reaction can be possibly due to the concentration range for mercury and CYANEX 923 used in this study. In addition, no excess extractant was used in the present study. Therefore, in order to confirm our estimates, a new fitting incorporating the effect of chloride ions as given by Equation 4 is shown in Figure 3.

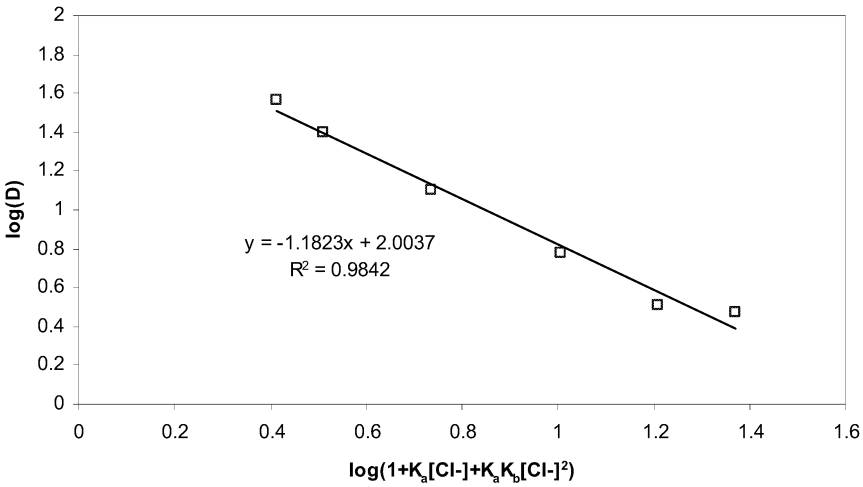

Figure 3. Effect of chloride ions on the extraction of Hg(II) with CYANEX 923. Aqueous phase: C_{Hg}^{0} = 2 mM, pH = 1. Organic phase: C_{923}^{0} = 9 mM; A/O = 1

According to the fitting shown in Figure 3, the slope is near unity (±18.2% deviation). In addition, as C_{923}^{0} = 0.009 M, so log K = 6.09, confirming previous calculations (±5.1% deviation), and the following reaction scheme is proposed for the Hg(II)-CYANEX 923 system. It must be emphasized that differences on the estimates may arise from assuming constant concentrations of CYANEX 923 and chloride ions in the fitting of the Figures 2 and 3, respectively.

$$HgCl_2 + 2\ TRPO_{(org)} \leftrightarrows HgCl_2.2TRPO_{(org)} \qquad \log K = 5.9 \pm 0.4 \qquad (5)$$

The stripping of mercury from the loaded organic phase was done with thiourea. As shown in Figure 4, an increase in the concentration of thiourea favor the stripping of mercury from the extract phase, stabilizing at around 100% of mercury stripping after 6 mM of thiourea, thus corroborating previous studies [4].

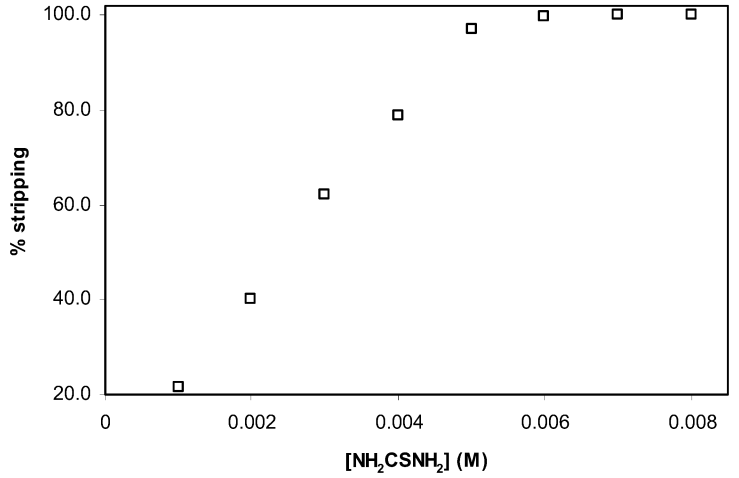

Figure 4. Mercury stripping with thiourea ($C_{Hg^0 org,total} \approx 2$ mM, A/O = 1).

CONCLUSIONS

It has been demonstrated that the removal of mercury from concentrated effluents is feasible by liquid-liquid extraction using CYANEX 923 as extractant. The method must be used prior to polishing methods in order to meet environmental regulations. Mercury was easily and quantitatively extracted at room temperature and stripped from the loaded organic phase using dilute solutions of thiourea. An equilibrium reaction valid for the operational conditions studied was proposed. It has been found that a lower number of molecules of CYANEX 923 is required at higher loading conditions.

ACKNOWLEDGMENTS

Sincere thanks to CNPq, CAPES, and FAPEMIG for financial support and to Eng. Ricardo Capanema from Cytec (Brazil) for the supply of CYANEX 923.

REFERENCES

1. D. R. T. Tonini, D. A. Gauvin, R. W. Soffel, and W. P. Freeman, "Achieving Low Mercury Concentrations in Chlor-alkali Wastewaters," *Environmental Progress*, **22**(3), 167–173 (2003).
2. COPAM, Minas Gerais State Regulation no. 10, 16/12/1986, Brazil.
3. F. M. Fábrega, F. S. Magalhães, and M. B. Mansur, "A Comparative Study of Various Reactive Systems to Extract Mercury from Chloride Medium," Proceedings ISEC 2005, Beijing, China, 2005; pp. 466–472.
4. R. Meera, T. Francis, and M. L. P. Reddy, "Studies on the Liquid-Liquid Extraction of Mercury(II) from Acid Chloride Solutions using CYANEX 923," *Hydrometallurgy*, **61**, 97–103 (2001).

PRODUCTION OF HIGH-PURITY AMMONIUM METAVANADATE BY SOLVENT EXTRACTION: PILOT-PLANT EVALUATION

K.C. Sole,[1] K. Field,[1] R. Maluleke,[1] J. Schulze-Messing,[1] K. Viljoen,[1] and D.F. Dutton[2]

[1]Anglo Research, a division of Anglo Operations Limited, Johannesburg, South Africa
[2]Highveld Steel and Vanadium Corporation, Witbank, South Africa. Corresponding author email address: ksole@angloresearch.com

ABSTRACT

The purification of a vanadium-containing liquor produced in the roast-leach flowsheet of a titaniferous magnetite from the Bushveld Complex of South Africa is reported. Solvent extraction using a tertiary amine produces an ammonium decavanadate liquor which can be converted to ammonium metavanadate and then calcined to produce V_2O_5. The applicability of the process to meet the specifications for vanadium battery electrolyte and high-purity vanadium chemicals was evaluated with respect to chemistry, operability, and control in a pilot-plant trial.

INTRODUCTION

Having several oxidation states and narrow regions of species stability, vanadium has eluded a robust refining process for many years. With the premium for high-purity ammonium metavanadate (AMV) and vanadium pentoxide products approaching 100% (targeting specifications for vanadium battery electrolyte and other vanadium chemicals), vanadium producers have a strong incentive for improving current processes.

A tertiary amine solvent-extraction (SX) process was selected to purify the so-called desilicated liquor produced by Highveld Steel and Vanadium Corp. (Vanchem), Witbank, South Africa. The loaded strip liquor (LSL), a high-purity ammonium decavanadate solution, was precipitated with ammonia to yield AMV which was calcined to V_2O_5. A four-week continuous trial assessed the flowsheet with respect to chemistry, operability, and control, with the aims of producing high-purity AMV and maximizing vanadium recovery.

CHEMISTRY OF VANADIUM SX BY TERTIARY AMINES

Vanadium in the feed liquor (pH 8) exists as the metavanadate species in a sodium sulfate matrix (VO_3^- and polymeric forms thereof) (Figure 1). Since tertiary amines only extract under acidic conditions, pH adjustment of the feed is required,

converting the metavanadate to the decavanadate species. A region of solid-phase stability exists at ~pH 2; in the Vanchem system, this is an insoluble sodium vanadium oxide, commonly referred to as “red cake”, the formation of which is essentially irreversible.

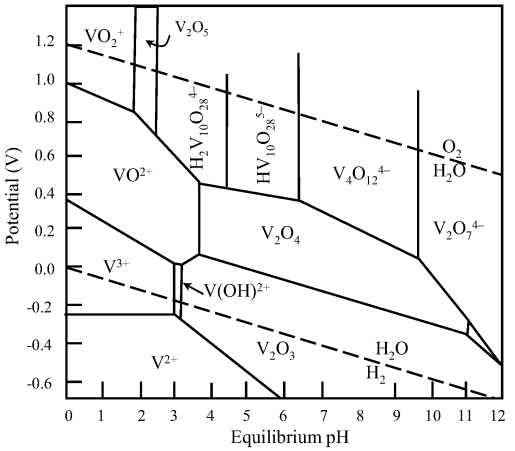

Figure 1. Pourbaix diagram of the vanadium-water system at 25 °C and $a(V) = 0.01$ mol/L [1].

The extractant, a trialkylamine commercially available as Alamine® 336, must be protonated to function as an anion exchanger. This was achieved by addition of H_2SO_4:

$$R_3N_{(org)} + 2H^+_{(aq)} + SO_4^{2-}{}_{(aq)} \leftrightarrow (R_3NH^+)_2\,SO_4^{2-}{}_{(org)} \quad (1)$$

where R represents the alkyl chain (C_8 to C_{10}). Acidification of the desilicated liquor (conversion to the decavanadate), is followed by extraction:

$$10\ VO_3^- + 5\ H^+ \rightarrow HV_{10}O_{28}^{5-} + 2\ H_2O \quad (2)$$

$$^5/_2(R_3NH^+)_2SO_4^{2-}{}_{(org)} + HV_{10}O_{28}^{5-}{}_{(aq)} \rightarrow (R_3NH)_5HV_{10}O_{28\,(org)} + {}^5/_2SO_4^{2-}{}_{(aq)} \quad (3)$$

The amine is stripped on deprotonation, thereby releasing the extracted species from the organic phase. Conventional stripping agents, such as Na_2CO_3 or $(NH_4)_2SO_4$, would introduce contaminant elements into the product, so ammonia was used:

$$(R_3NH)_5HV_{10}O_{28\,(org)} + 5\ NH_4OH_{(aq)} \rightarrow 5\ R_3N_{(org)} + (NH_4)_5HV_{10}O_{28\,(aq)} + 5\ H_2O \quad (4)$$

The ammonia decavanadate product is converted to ammonium metavanadate:

$$(NH_4)_5HV_{10}O_{28\,(aq)} + 5\ NH_4OH_{(aq)} \rightarrow 10\ NH_4VO_{3\,(s)} + 3\ H_2O \quad (5)$$

If excess ammonia is added to the strip circuit, reactions (4) and (5) will both occur, causing the formation of an insoluble ammonia metavanadate precipitate.

PILOT-PLANT EQUIPMENT, REAGENTS, AND PROCEDURES

The optimized flowsheet (Figure 2) processed ~1.5 m^3/day of feed (~27 g/L V, pH 8). This was acidified to pH 3 prior to entering the extraction circuit. The vanadium-loaded organic (LO) phase was washed with acidified water (pH 2.7) to reduce entrainment of aqueous feed and associated contaminants to the strip circuit. After passing the washed organic (WO) phase through an after-settler (AS1), vanadium was stripped at controlled pH with NH_4OH to generate a LSL containing 50−60 g/L V. The high-purity solution was returned to Vanchem for precipitation and calcination.

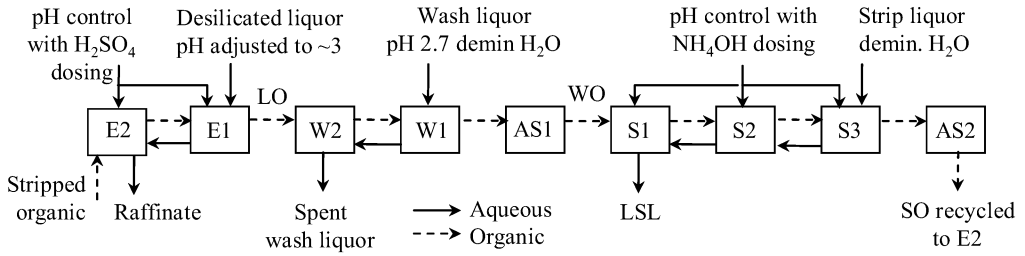

Figure 2. SX circuit configuration.

Conventional polyvinylchloride mixer settlers, configured for counter-current flow, were used. Each mixer, of 32 L active volume, was equipped with a flat-vaned pumping impeller (190 mm diam.). Settlers, of settling area 0.091 m^2, were fitted with picket fences. Solutions were introduced to the circuit by peristaltic pumps. Mixers were run aqueous continuous to facilitate pH control. The prescribed pH profiles were maintained by adding concentrated H_2SO_4 and NH_4OH to the extraction and strip circuits respectively *via* dosing pumps linked to pH controllers. The use of pressurized pH probes (Hamilton) avoided contamination by the organic phase and any precipitated solids.

Fresh desilicated liquor was supplied daily from Vanchem. The organic phase comprised 10 vol.% Alamine 336 (Cognis) in the aromatic diluent ShellSol A150 (Shell Chemicals). Commercial-grade H_2SO_4 (98%) and NH_4OH (25%) were employed. The wash and strip liquors were made up using deionized water. All streams were analyzed 8-hourly for Al, Ca, Cr, Fe, K, Mg, Na, Si, and V by inductively coupled plasma optical emission spectroscopy (ICP). The extractant concentration was monitored by potentiometric titration with standard NaOH solution. Crud and precipitate samples were analysed by fusion-ICP and x-ray diffraction.

METALLURGICAL RESULTS AND PERFORMANCE EVALUATION

Operating Philosophy

The feed had variable composition, and thus, a fixed V transfer was maintained by varying the feed flowrate to achieve a constant V organic-phase loading, that is, variation of the advance O:A in the extraction circuit. The strip O:A ratio was adjusted to

give the highest possible LSL concentration without exceeding the solubility of $(NH_4)_5HV_{10}O_{28}$.

Extraction Circuit

Extraction was controlled at pH 2.5−4. Above pH 4, amine protonation is reduced, and the extractant exists predominantly in its neutral form, while below pH 2, HSO_4^- competes with $HV_{10}O_{28}^{5-}$ for complexation, and red-cake formation occurs. Vanadium extraction exceeded 99.9% throughout this pH range. Extraction was optimized at pH 2.8−3.0 to minimize acid consumption while maintaining high extraction efficiency. Crud formation increased markedly above pH 3.4. An advance O:A = 2 gave an organic-phase loading of 14−15 g/L V. Stage-wise profiling showed that extraction was essentially quantitative within one stage, leaving the second extraction stage as a scavenging unit.

Most impurities exist as cationic species and were rejected, but some co-extraction of anionic Cr and Cl occurred (Table 1). Cr was particularly problematic to control, as the feed concentration varied widely (1 to 35 mg/L). The order of extraction of anions was determined in laboratory studies to follow the trend V > Cr > Cl, and therefore it should be possible to 'crowd off' less strongly complexed species from the organic phase by operating close to maximum loading capacity. Upgrading of the V:Cr mass ratio from ~3000 to 6000 was achieved by minimizing availability of the amine to Cr.

Washing Circuit

The wash stage was intended to remove entrained impurities, particularly Na and K. Table 1 shows generally disappointing rejection of aqueous-phase contaminants at a wash liquor acidity of pH 2.7 (selected to maintain V and amine speciation). The volume of the spent wash liquor (a waste stream in this flowsheet) was minimized by increasing the advance O:A ratio to an optimum of ~11:1. The good settling characteristics of the extraction circuit gave very low entrainments that did not compromise the quality of the product. The after-settler between the extraction-wash and strip circuits served to avoid the carryover of solids from a crud run and separated the acidic and alkaline circuits.

Stripping Circuit

The optimized configuration used demineralized water as the strip liquor and individual control of the pH in each strip mixer (pH 6.0 in S1, pH 7.0 in S2, pH 7.8 in S3) to minimize reagent consumption while allowing quantitative stripping of the decavanadate species without the formation of AMV. Stripping efficiency was excellent (Table 1), provided accurate control of pH was maintained. Below pH 5, inadequate deprotonation of the amine occurred. However, if excess NH_4OH was added, a yellow solid (analyaed as $(NH_4)_4Na_2V_{10}O_{28}.10H_2O$) precipitated. The strip O:A was gradually decreased to establish the maximum achievable LSL concentration (the solubility limit of ammonium decavanadate) and was optimized at O:A ~ 3.3. An orange precipitate,

identified as $(NH_4)_4Na_2V_{10}O_{28}.10H_2O$, formed above 55 g/L V.

The product specifications were dictated by the AMV purity requirements. Excellent selectivity over cations was achieved, but some transfer of Cr to the LSL remained, even under optimized conditions (Table 1).

Product Quality

An advantage of SX is that NH_4OH can be used for AMV precipitation (Eqn. (5)), rather than $(NH_4)_2SO_4$ (used in the current process and which can introduce further impurities to the system). Several batches of ammonium decavanadate solution were precipitated with ammonia. Further selectivity was introduced by this precipitation step, and the purity targets for all specified elements in the AMV were attained (Table 1).

Table 1. Average composition of process streams under optimized conditions

Element	PLS	LO	WO	SO	LSL (mg/L)		AMV (%)	
	(mg/L)	(mg/L)	(mg/L)	(mg/L)	Target	Actual	Target	Actual
V	27 100	15 700	15 600	23	50 000	50 000	44.0	43.4
Al	13	2.6	2.5	2.0	50	0.6	0.08	0.003
Ca	97	11.6	12	13	50	11	0.08	0.008
Cr	13	15	15	6	5	19	0.005	0.003
Fe	4	42	38	25	10	2	0.010	0.002
K	520	6	6	6	5	3	0.008	0.002
Na	48 200	17	17	17	5	21	0.008	0.002
Si	81	5	6	3	5	0.5	0.005	0.005

Extractant Concentration

The amine concentration was gradually increased from 10 to 15 vol. %, to determine whether a smaller plant footprint could be used to treat a fixed feed flowrate. This decreased selectivity, increased viscosity and crud formation, and phase separation deteriorated. Prior studies [2, 3] similarly indicated that 10 vol. % Alamine 336 performed without physical problems, but that 15 vol. % gave rise to crud problems. It is recommended that the extractant concentration should be maintained at $\leq$ 12 vol. % Alamine 336 in an aromatic diluent.

Reagent Consumptions

The consumptions of H_2SO_4 (for protonation of the amine and extraction of vanadium) and NH_4OH (stripping of the vanadium) are summarized in Table 2. Reagent usage was very close to stoichiometric, validating the assumed reactions.

Table 2. Reagent consumptions

Reagent	H_2SO_4 (98%)	NH_4OH (25%)
Stoichiometric consumption (mol/mol V)	1.00	0.50
Measured consumption (mol/mol V)	1.00	0.48

DISCUSSION AND CONCLUSIONS

The applicability of SX to purify Vanchem desilicated liquor to enable processing to high-purity vanadium chemicals was assessed. The process was robust with respect to the feed composition (20−35 g/L V, 1−35 mg/L Cr) and range of impurities that were removed. The LSL was upgraded to 55−60 g/L V (the solubility limit of $(NH_4)_5HV_{10}O_{28}$). Vanadium recovery exceeded 99.9%. The strip circuit functioned well with accurate pH control. The quality of the LSL was extremely high with respect to cationic impurities, but some transfer of anionic species (Cl, Cr, and S) occurred. Of these, only Cr is significant to the product specifications (due to the colour that it imparts to the chemicals). Precipitation of ammonium decavanadate from the LSL introduced further selectivity, producing AMV that met the target purities for all elements.

The Cr content of the feed was highly variable. To achieve further selectivity, the organic phase could be loaded to saturation with V, such that less strongly complexed species are "squeezed off". It may be preferable to lower the extraction efficiency (increase the raffinate [V]) to maximise V organic-phase loading and consequent rejection of the competing anions. Conversion of the wash to pH-controlled scrub stages using a high V-containing solution as the scrub liquor (a bleed of the LSL, for example) and feeding the spent scrub liquor back to the extraction circuit to avoid vanadium losses, may improve Cr rejection further. The Vanchem process also allows minimization of incoming Cr by appropriate control of the upstream roasting operation, so opportunities exist to meet the Cr target by better control of the desilicated feed liquor composition.

Reliable, accurate, and integrated pH control is essential to maintain appropriate aqueous and organic speciation and avoid precipitation. Inadequate pH control can cause irreversible precipitation of either red cake in the extraction circuit or yellow or orange cake in the strip circuit, severely compromising operation.

ACKNOWLEDGMENTS

Vanchem management and seconded technical staff B. Buthelezi, T. Digaoto, N. Maqubela, E. Masombuka, R. Mokone, R. Motseki, and C. Seroke are thanked for their contributions to this project. ShellSol A150 was donated by Shell Chemicals. This paper is published by permission of Highveld Steel and Vanadium Corp. and Anglo Research.

REFERENCES

1. C. K. Gupta and N. Krishnamurthy, Extractive Metallurgy of Vanadium, Elsevier, Amsterdam, 1992.
2. R. Sadanandam, M. F. Fonseca, S. S. Gharat, N. K. Menon, S. K. Tangri, and T. K. Mukherjee, "Recovery of Pure Vanadium Pentoxide from Spent Catalyst by Solvent Extraction," *Trans. Ind. Inst. Met.*, **49**(6), 795−801 (1996).
3. S. K. Tangri, A. K. Suri, and C. K. Gupta, "Development of Solvent Extraction Processes for Production of High Purity Oxides of Molybdenum, Tungsten and Vanadium," *Trans. Ind. Inst. Met.*, **51**(1), 27−39 (1998).

SOLVENT EXTRACTION OF TANTALUM FROM SYNTHETIC CONCENTRATES

Raj P. Singh Gaur

Chemicals & Powders R&D, Precision Material & Components Division
OSRAM SYLVANIA, Towanda, PA 18848, USA
Corresponding author email address: raj.singh@sylvania.com

ABSTRACT

This paper pertains to the optimization of solvent extraction of tantalum values from solutions obtained from the dissolution of synthetic tantalum concentrates. These concentrates are generated from tungsten carbide scrap after the recovery of tungsten and cobalt. In this work, dissolution of synthetic concentrates was carried out in acidic media of hydrofluoric and sulfuric acids. The dissolved concentrate contained different concentrations of tantalum and other impurities such as niobium, titanium, tungsten, and cobalt as well as sulfuric and hydrofluoric acids. A design-of-experiment approach was used for the optimization of dissolution and the solvent extraction of tantalum. The following parameters were studied: 1) amount of synthetic concentrate, 2) volume of sulfuric acid, and 3) volume of nitric acid. Solvent extraction of tantalum was performed in 2-octanol, and the results were analyzed for tantalum extraction efficiency. Tributylphosphate was tested as an alternative solvent.

INTRODUCTION

Tantalum, present in tungsten carbide scrap, is potentially a valuable source for higher value-added tantalum products, such as electronic-grade Ta_2O_5 and K_2TaF_7 [1]. After the recovery of tungsten and cobalt from oxidized tungsten carbide scrap, tantalum is concentrated in the sludge. These sludges contain 15-20% tantalum and are typically known as tantalum synthetic concentrates (SC). A typical composition of tantalum synthetic concentrates together with the typical compositions of tantalum ore concentrates is presented in Table 1.

Prior to 1957, niobium and transition metals were separated from tantalum by a fractional crystallization process known as the Marignac process [2], which exploits the difference in solubility between K_2TaF_7 and $K_2NbOF_5 \bullet H_2O$ and other fluorometallates. However, tantalum pentoxide obtained by this process contains high levels of impurities such as Nb (1000-3000 ppm), Si (up to 3000 ppm), Ti (up to 100 ppm), and Fe (up to 2000 ppm). These exceed the total allowable transition metal impurity level (less than 1000 ppm) in the tantalum wire used in the manufacture of capacitors.

Table 1. Approximate compositions of tantalum synthetic and ore concentrates

Components (%)	Synthetic Concentrates	Tantalite	Niobite	Pyrochlore /Microlite	Loparite	Tin slags
Ta_2O_5	30	53-60	12-18	0-70	8-10	9
Nb_2O_5	7	12-30	50-58	0-63	8-10	10
TiO_2	31	0.3-6	7-12	2-4	39-40	3
ThO_2	-	-	-	0-5	0.2-1	-
UO_2	-	-	-	0-11	-	-
UO_3	-	-	-	0-16	-	-
Na_2O	15	-	-	1-6	8-9	-
K_2O	-	-	-	0-1	0.2-1	-
CaO	<1	-	-	4-18	4-5	15
SrO	-	-	-	-	2-4	-
MnO	<1	3-17	2.5-8	0-8	-	3
CoO	5	-	-	-	-	-
Fe_2O_3	1	2-16	11-19	0-10	-	11
Ln_2O_3	-	-	-	2-13	32-34	-
Y_2O_3	-	-	-	0-5	-	-
SnO_2	-	0.1-1-	0.1-3	0-4	-	2
ZrO_2	-	-	-	0-6	-	-
WO_3	6	-	-	0-<1	-	-
H_2O	-	-	-	0-6	-	-

In the late 1950s, modern solvent-extraction (SX) and ion-exchange processes supplanted [3-7] the use of the Marignac process. In a SX process, ore concentrates containing at least 25 m/m % tantalum and niobium pentoxide are decomposed chemically in HF media, and the dissolved Ta and Nb species are separated from the residue by filtration. The filtrate containing tantalum (as TaF_7^{2-}) and niobium (as $NbOF_5^{2-}$) in an HF/H_2SO_4 medium is brought into contact with an organic phase, usually methyl *iso*-butyl ketone (MIBK), which selectively extracts Ta and Nb species leaving impurities such as Ti, Fe, and Si in the aqueous phase. Niobium is separated from tantalum by back extraction with sulfuric acid. Finally, tantalum (TaF_7^{2-}) is eluted from the MIBK by an ammonium fluoride solution and converted into K_2TaF_7 by precipitation with KCl.

Although MIBK is the most commonly used extractant for the SX of tantalum [8], its solubility in water and other properties makes it less appropriate than other possible solvents as suggested in Table 2. The purpose of this work was, therefore, to develop a SX method, which can be used for the conversion of a tantalum synthetic concentrate into high-purity tantalum oxide using 2-octanol. The work reported in this paper pertains to the investigation of dissolution of synthetic Ta concentrates in HF-H_2SO_4 media and optimization of its solvent extraction in 2-octanol. The following factors were included in the design-of-experiment (DOE) study: amount of SC (g), volume of H_2SO_4 (mL), and volume of HF (mL).

Table 2. Physical properties of 2-octanol, tributylphosphate (TBP), and methyl isobutyl ketone (MIBK)

Parameters	Properties		
	2-Octanol	TBP	MIBK
Chemical formula	$CH_3(CH_2)_5CHOHCH_3$	$(C_4H_9O)_3PO$	$CH_3COC_4H_9$
Formula mass	130.23	266	86.0
Boiling point (°C)	175	289	116
Density (g/cm^3)	0.82	0.97	0.80
Flash point (°C)	73	145	23
Viscosity (cP)	0.075	3.45	0.554
Solubility in H_2O (%)	0.08	0.6	1.7-2.2

EXPERIMENTAL

Design Summary

A 2^3 design with 4 center points was used. Data was processed by *Design-Expert* version 5.09 software. The range for design parameters/factors is presented in Table 3. Table 4 presents the design layout and the resulting data.

Table 3. Design parameters / factors and their chosen values

Factor	Unit	Chosen Values		
		Low	Mid	High
SC (A)	g	200	250	300
H_2SO_4 (B)	mL	0	125	250
HF (C)	mL	175	225	275

Table 4. Design layout and results*

Run Order	SC (g)	SA (mL)	HA (mL)	Ta in AP (g/L)	Ta in R (g/L)	Ta in WS (g/L)	Ta SX (%)	Ta_2O_5 (g)
1	300	0	175	18	20	0.27	0	0
2	300	0	275	51	34	9.3	33.3	0.38
3	300	250	175	38	2.2	18	94.2	1.01
4	250	125	225	41	1.8	21	95.6	1.1
5	200	250	275	30	0.7	10	97.7	1.01
6	200	0	175	31	25	4.1	19.4	0
7	300	250	275	56	0.9	20	98.4	1.78
8	250	125	225	43	2.2	19	94.8	1.1
9	250	125	225	45	0.9	18	98.1	1.47
10	200	250	175	33	0.9	12	97.3	1.65
11	250	125	225	38	2.1	17	94.5	1.08
12	200	0	275	39	29	-	25.6	0.17

*SA = Sulfuric acid; HA = hydrofluoric acid; AP = Aqueous phase; R = Raffinate
WS = Wash solution (1 M sulfuric acid)

Solvent-Extraction Procedure

Amounts of 25 mL organic solvent (2-octanol) and 50 mL of aqueous (Ta/Nb) solution were placed in a plastic 100-mL separatory funnel. The funnel was shaken on a laboratory shaker for 10 min. After 10-min shaking, the funnel was removed from the shaker and allowed to stand for about two minutes for phase separation. Aqueous phase (raffinate) was drained off and collected in a polyethylene vial and submitted for ICP analysis. To the organic phase (remaining in the funnel), 50 mL of 1 M H_2SO_4 was added and mixed for 2 min on the shaker for washing. The funnel was then removed from the shaker and was allowed to stand for about two minutes for phase separation. Aqueous phase was removed (washes) and was submitted for ICP analysis.

For stripping Ta, 50 mL water was added to the organic phase and mixed for 2 min on shaker. Tantalum solution was separated, and tantalum values were precipitated with an equal volume of 7.5 M ammonium hydroxide. White precipitate containing Ta was separated by filtration. Filtrate was submitted for ICP analysis.

Solids were washed with 400 mL DI water followed by 400 mL 2.0 M ammonium hydroxide. Wash solution was submitted for ICP analysis. Ammonium tantalate solids were dried overnight at 110 °C, weighed and were submitted for quantitative X-ray fluorescence (XRF), qualitative spectroscopic, and glow-discharge mass-spectrometric (GDMS) analyses.

Percent solvent extraction (SX) values for Ta and Nb were calculated by Equation 1.

$$\% \text{ Solvent Extraction} = [(Ta\text{-}in\text{-}AP - Ta\text{-}in\ R) / (Ta\text{-}in\text{-}AP)] \times 100 \quad (1)$$

RESULTS AND DISCUSSION

Design Analysis

Tantalum extraction efficiency data, from designed experiments, are presented in Table 4. Experimental conditions leading to optimum conditions for the dissolution of tantalum from synthetic concentrate as well as selective SX of tantalum by 2-octanol are the desirable results. The *Design-Expert*™ software was utilized to calculate the factor effects from the data presented in Table 4.

The normal probability plot for the analysis of tantalum extraction with 2-octanol indicated that factor B (H_2SO_4) is a significant effect. Analysis of variance (ANOVA) of this data indicated that the probability of a zero difference between pure error and the selected effects was <0.01%. The effect plot for factor B (H_2SO_4) suggested that SX of tantalum was higher when high factor-value (250 mL, Table 4) of sulfuric acid was used for the dissolution of tantalum from synthetic concentrates. The optimum conditions for %Ta-extraction and %Ta-dissolution were in fact the same: 200 g SC, 250 mL H_2SO_4, 175 mL HF and/or 300 g SC, 250 mL H_2SO_4, 275 mL HF.

Product Evaluation

Amounts of tantalum oxide obtained by SX of tantalum are reported in the last column of Table 4. Run #7 (Table 4) gave the maximum product with 55% efficiency and 93.7% accountability. The main reason for low efficiency was the loss of tantalum during washing of loaded 2-octanol with 1 M H_2SO_4 to separate Nb. About 48% Ta was lost in this step from the loaded 2-octanol. This problem can be overcome by either optimizing concentration of sulfuric acid in washing solution or recycling tantalum-containing washes in the process.

Purity of the Ta_2O_5 sample obtained from Run #7 (Table 5) was acceptable except Mo, Ca, and W were present in slight excess than desired.

Table 5. Analytical results of tantalum oxide obtained from SX with 2-octanol in Run #7 of Table 4 (element concentrations in ppm)

Elements	Ta_2O_5 from Run #7	Specification
Na	0.6	50
Mg	2	50
Al	50	100
Si	110	200
Ca	91	50
Ti	25	50
Cr	1	50
Mn	0.4	50
Fe	2.5	200
Co	4.6	100
Ni	<0.1	50
Zn	3.6	50
Nb	1000	1500
Mo	580	50
Sn	<0.5	50
W	1000	500

Extraction with TBP

The efficiency of tantalum extraction with TBP using the solutions from Run #7 and #10 in Table 4 was greater than 99% including the washing step. However, phase separation in the case of TBP was poorer than 2-octanol, and stripping of loaded tantalum required 5 M ammonium fluoride rather than just water, which was needed for 2-octanol. Scale-up of the SX method reported here in is planned using laboratory LIX cells.

CONCLUSIONS

The optimum conditions for the dissolution of tantalum synthetic concentrate in H_2SO_4/HF media and SX of Ta with 2-octanol were the same: 200 g SC, 250 mL H_2SO_4, 175 mL HF and/or 300 g SC, 250 mL H_2SO_4, 275 mL HF. SX of tantalum using TBP as an alternative solvent also provided promising results.

ACKNOWLEDGMENT

Bob Mendenhall performed the experimental work; his efforts and cooperation are thankfully acknowledged. The author is thankful to Dr. Thomas Wolfe for useful suggestions. Thanks are also due to Kathy Hammerly for manuscript preparation.

REFERENCES

1. R. P. Singh Gaur and R. G. Mendenhall, "Tantalum Concentrates Dissolution and Purification Method," United States Patent No. 7,182,925, Feb. 27 (2007).
2. L. V. Belyaevskaya, "Chapter II, Tantalum and Niobium," Jerusalem, 1966, Available from the US Department of Commerce, Clearinghouse for Federal Scientific and Technical Information, Springfield, Va. 22151.
3. J. R. Werning, K. B. Higbie, J. T. Grace, B. F. Speece, and H. L. Gilbert, "Separation of Tantalum and Niobium by Liquid-Liquid Extraction," *Industrial and Engineering Chemistry*, **46,** 644−652 (1954).
4. R. E. Droegkamp, M. Schussler, J. B. Lambert, and D. F. Taylor, "Tantalum and Tantalum Compounds," In: Kirk-Othmer Encyclopedia of Chemical Technology, Third Edition, Vol. 22, John Wiley & Sons, New York, 1983; pp. 541−564.
5. J. A. Pierret, "Process of Purifying and Separating Columbium and Tantalum Values From Each Other," US Patent No. 3117833, 16 Jan. 1964.
6. C. W. Carlson and R. H. Nielsen, "Pure Columbium and Tantalum Oxides by Liquid-Liquid Extraction," *Journal of Metals*, (June), 472−475 (1960).
7. H. Endo, N. Hirate, and M. Tezuka, "Method of Recovering Tantalum from Silicon-Containing Tantalum Scrap," US Patent No. 4446115, 1 May 1984.
8. R. P. Singh, "Processing of Ta_2O_5 Powders for Electronic Applications," *Journal of Electronic Materials*, **30**, 1584−1594 (2001).

THE RECOVERY OF SULFURIC ACID FROM NICKEL ELECTROLYTE BY SOLVENT EXTRACTION: PILOT-PLANT EVALUATION

Karen Viljoen,[1] Kathryn C. Sole,[1] Bronwynne K. Ferreira,[1] and Lesley J. Bryson[2]

[1]*Anglo Research, a division of Anglo Operations Ltd, Johannesburg, South Africa*
[2]*Anglo Platinum, Johannesburg, South Africa*
Corresponding author email address: karenv@angloresearch.com

ABSTRACT

The pilot-plant evaluation of a solvent-extraction process for the recovery of sulfuric acid from Anglo Platinum's Base Metal Refinery nickel spent electrolyte using a tertiary amine extractant is reported. Stripping with ammonia yields a saleable ammonium sulfate product which meets the specifications of the agricultural industry.

INTRODUCTION

Anglo Platinum is currently undertaking an expansion program at its Base Metal Refinery (BMR) (Rustenburg, South Africa), which will increase production from 21,000 to 33,000 t/a nickel and 12,000 to 19,000 t/a copper by 2010. The flowsheet involves sulfuric acid leaching of sulfide smelter products followed by solution purification and electrowinning (EW) of nickel and copper [1,2]. At present, the only outlet for sulfur is via the production of Na_2SO_4, which is crystallized following neutralization of nickel spent electrolyte (SE) with NaOH to precipitate $Ni(OH)_2$. The cost of producing sodium sulfate far exceeds its resale value. Of the various alternative processes to remove sulfur considered for this flowsheet, the most viable was the use of solvent extraction (SX) [3].

Tertiary amines have been employed for acid removal from other electrolytes. Tumilty patented H_2SO_4 extraction from cobalt electrolytes using 10 vol % Alamine 336 to improve cobalt EW efficiency [4]. Gottliebsen et al. investigated the recovery of H_2SO_4 from copper tankhouse electrolyte bleeds with 40 vol % tris(2-ethylhexyl)amine, which would allow acid to be returned to the circuit without the accompanying impurities that accumulate in the closed SX-EW loop [5,6].

Although reasonable extraction of H_2SO_4 from the nickel electrolyte can be achieved with various extractant functionalities (including amines, alcohols, and phosphine oxides), the recovered acid is considerably more dilute than the initial acid content of the feed and cannot be substantially upgraded by distillation or evaporation due to azeotrope formation. A promising alternative is removal of H_2SO_4 from the nickel SE using a tertiary amine extractant (Equation 1) and its recovery as ammonium sulfate (Equation 2)—a product saleable as fertilizer in the agricultural industry.

$$R_3N_{(org)} + H_2SO_{4\,(aq)} \leftrightarrow R_3NH^+HSO_4^- + R_3N \leftrightarrow (R_3NH^+)_2SO_4^{2-}{}_{(org)} \quad (1)$$

$$(R_3NH^+)_2SO_4^{2-}{}_{(org)} + 2\ NH_4OH_{(aq)} \leftrightarrow 2\ R_3N_{(org)} + (NH_4)_2SO_{4\,(aq)} + 2\ H_2O_{(aq)} \quad (2)$$

The results of a 15-day pilot-plant trial, treating ~60 L/h of nickel SE containing 40 g/L H_2SO_4, 60 g/L Ni, and 1.2 g/L B, are reported. The main objectives were to maximize acid extraction and $(NH_4)_2SO_4$ concentration of the loaded strip liquor (LSL) while minimizing transfer of nickel and boron (added as boric acid to the electrolyte to maintain cathode quality in EW). The deportment of nickel to the product is important because of possible limitations on that element in fertilizer specifications, whereas the recovery of H_3BO_3 to electrowinning could have cost savings implications for the plant.

PILOT-PLANT EQUIPMENT AND EXPERIMENTAL METHODS

The circuit configuration for the pilot plant is shown in Figure 1. Mixer-settlers (7 L mixing volume and 0.032 m^2 settling area) were configured for counter-current flow of the aqueous and organic phases. Solutions were pumped into the plant via peristaltic pumps; interstage solution transfer was by means of pumping impellers. The pH of each stage was monitored using pressurized pH electrodes (Hamilton), and the pH of the strip circuit was controlled by pH controllers linked to aqueous ammonia dosing pumps. Laboratory tests had shown that aqueous continuity in both the extraction and strip stages was essential to allow reasonable rates of phase disengagement (ca. 60 s): organic continuity resulted in settling times of >10 min. To ensure aqueous continuity, aqueous recycles were employed.

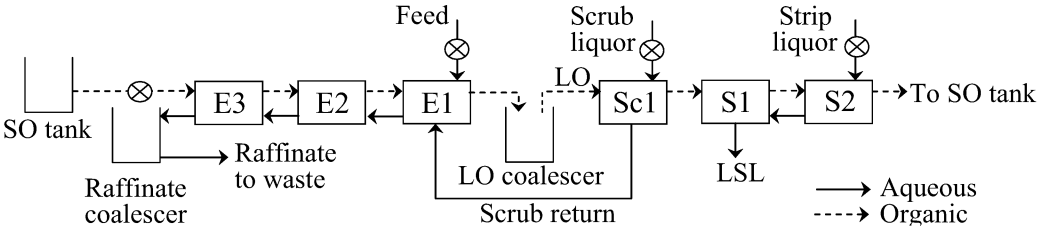

Figure 1. Pilot-plant circuit configuration.

The nickel SE (feed to SX) was supplied by Anglo Platinum BMR. The organic phase comprised 20 vol % Alamine® 336 (Cognis) in the aromatic diluent ShellSol® A150 (Shell Chemicals). Demineralized water was used as the scrub and strip liquor, with 25% NH_4OH solution added directly into the strip mixers to maintain the required strip pH profile. Flowrates, pH, and other relevant operational variables were measured hourly. All streams were assayed 4-hourly for acid concentration (by titrimetric analysis) and 8-hourly for nickel and boron (by inductively coupled plasma optical emission spectroscopy).

RESULTS AND DISCUSSION

Effect of O:A on the Extraction Efficiency and Deportment of Impurities

From extraction isotherms, the maximum loading capacity was 1.3−1.4 g/L H_2SO_4 per vol % Alamine 336 for this system. Assuming a stoichiometry of 2 moles of Alamine 336 per mole of H_2SO_4 (Equation 1), the maximum theoretical loading capacity should be 0.98-1.01 g/L. The higher loading measured suggests that some extraction as the bisulfate ion occurs. As maximum loading is approached, more acid is apparently complexed as the bisulfate [5]. This is probably due to fact that increasing the concentration of the amine-acid complex in the organic phase increases the polarity of the organic phase, which allows the extraction of bisulfate.

To achieve quantitative extraction, an organic:aqueous volumetric flowrate ratio (O:A) of 2.2 was initially targeted. Under these conditions, acid extraction was 100%, but the residual available extractant capacity allowed co-extraction of H_3BO_3. Changing the operating strategy to decrease acid extraction efficiency to ~95% (by lowering the O:A) improved boron rejection from the loaded organic (LO) phase (Table 1). Unexpectedly, nickel followed the boron trend. Since organic samples were filtered through phase-separating paper before analysis to remove aqueous entrainment, it was postulated that trace amounts of nickel may be extracted by the diluent via a solvation mechanism. Further speciation work is necessary to confirm this.

Table 1. Limitation of impurity deportment by crowding of organic phase

Extraction O:A	Extraction stages	Acid extraction efficiency (%)	Average concentration on LO (g/L)		
			H_2SO_4	B	Ni
2.2	2	100.0	20.0	0.046	0.006
1.1	2	95.3	31.8	0.012	0.004
1.1	3	95.6	34.6	0.007	0.003

Figure 2(a) shows the increase in H_2SO_4 loading associated with the decrease in O:A. The corresponding effect on the boron content of organic phases exiting stages E1 and E2 is shown in Figure 2(b). At the higher O:A ratio (Days 4 to 6), the LO ($E1_{org}$) contained more boron than $E2_{org}$ due to available capacity. On lowering the O:A, the boron loading on $E2_{org}$ increased in contact with the stripped organic (SO), but this was crowded off by the stronger complexation of the extractant with H_2SO_4 and contact with feed in E1, resulting in lower boron co-extraction (Days 6 to 13). On decreasing the extractant concentration to 10 vol % on Day 13, the O:A was again increased but boron rejection from the LO was maintained.

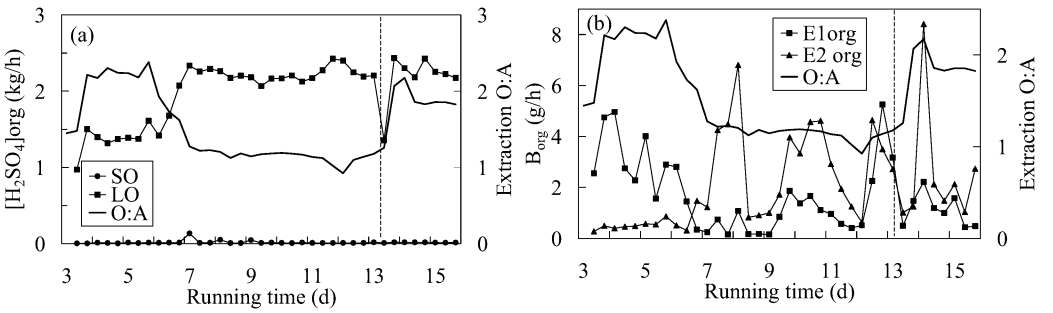

Figure 2. Effect of advance O:A on the loading of (a) H_2SO_4 and (b) B in the extraction circuit.

Limiting Impurity Deportment by Increasing the Extraction Stages

Since H_2SO_4 is more strongly complexed than H_3BO_3, the positive effect of lowering the acid extraction efficiency on the transfer of boron was enhanced by the addition of a third extraction stage on Day 11. Figure 3 shows the organic-phase concentration profiles of H_2SO_4 and boron before and after stage E3 was brought on line, while the average values are given in Table 1. With the third stage, the LO was reduced to <10 mg/L B, a significant improvement compared to two extraction stages. The addition of an extra extraction stage resulted in better crowding, thereby improving boron rejection and increasing H_2SO_4 loading.

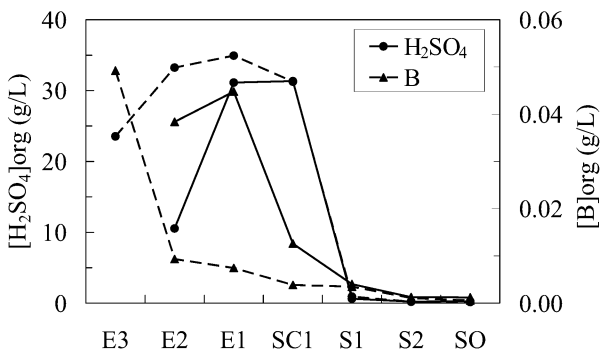

Figure 3. Acid and boron organic-phase profiles, showing the impurity-crowding effects of two (solid lines) or three (dotted lines) extraction stages (extraction advance O:A = 1.1).

Influence of Extractant Concentration and Phase Modifier Addition

A significant adverse aspect of this system noted during the trial was high levels of both aqueous and organic entrainment in the extraction and scrub circuits. Attempts to limit these physical losses, including the use of polypropylene and stainless steel picket fences in settlers, an organic coalescer (polypropylene beads) installed on the raffinate line, and an aqueous coalescer (stainless steel shavings) installed on the LO line, introduced only marginal improvements. The extractant concentration was then reduced from 20 to 10 vol %. This reduced the organic-phase H_2SO_4 loading from ~35 to 19 g/L,

and the organic flowrate was increased to compensate for the reduction in extractant concentration (Figure 2(a), Day 13). The $(NH_4)_2SO_4$ concentration in the LSL therefore remained constant. Under these conditions, entrainments remained disappointingly high and there was no associated improvement in rejection of the impurities by crowding. Addition of isodecanol to the organic phase as a potential phase modifier also yielded negligible improvement.

Influence of the Scrub Circuit

A single scrub stage, operating with demineralized water as scrub liquor and advance flowrate ratio O:A ~30, was brought on line on Day 8. Since H_3BO_3 (as an anion) is chemically extracted, while the nickel (present mainly as a cation) is transferred by physical entrainment, this stage provided both scrubbing and washing functions. As shown in Figure 4, the scrub was effective in reducing the boron and nickel entering the strip circuit at both extractant concentrations. Some stripping of H_2SO_4 did occur in the scrub stage, and this was returned to the extraction circuit via the spent scrub liquor.

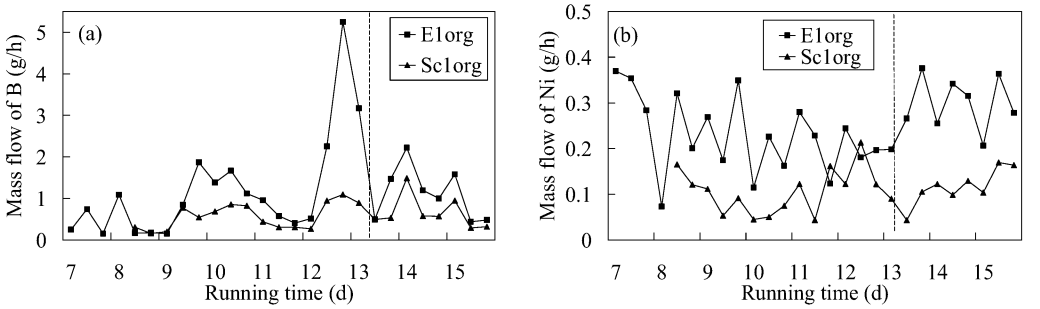

Figure 4. Effect of the scrub circuit on the mass flow of (a) B and (b) Ni in the organic phase.

Stripping Efficiency

Investigating the influence of pH on stripping, it was found that a pH of greater than 7 was required to ensure quantitative stripping. The strip O:A was steadily increased throughout the campaign to maximize the LSL concentration. This was optimized at an advance O:A = 15 (relative to the aqueous flowrate of the strip liquor itself or O:A ~7, taking into account the NH_4OH addition and water generated in the strip process (Equation 2)), giving 280–300 g/L $(NH_4)_2SO_4$ in the product liquor. Although the solubility of $(NH_4)_2SO_4$ is ~700 g/L, the O:A could not be increased further, given the constraint of aqueous-continuous mixing. Using more concentrated NH_4OH or gaseous NH_3 for pH control or a column contactor should allow greater product upgrading, thereby reducing downstream crystallization requirements.

Product Purity

Table 2 presents typical analyses of the various process streams under optimized conditions, indicating the product purity achieved in this trial.

Table 2. Compositions of process streams under optimised conditions*

Component	Feed	Raffinate	LO	ScO	SO	LSL
H_2SO_4 (g/L)	40.1	2.8	34.6	31.3	0.160	218.0†
B (g/L)	1.2	1.2	0.007	0.004	0.001	< 0.03
Ni (g/L)	58.9	58.9	0.003	0.001	0.000	< 0.01

*20 Vol % Alamine 336 in ShellSol AB, 3E-1Sc-2S circuit, extraction O:A = 1.1, strip O:A = 15.
† Equivalent to 293 g/L $(NH_4)_2SO_4$.

CONCLUSIONS

Sulfuric acid can be recovered from a nickel electrolyte with >99% extraction efficiency and stripped with ammonia to yield a product liquor containing ~300 g/L $(NH_4)_2SO_4$. Impurity deportment to the LSL was limited by operating close to the loading capacity of the organic phase (and thereby reducing extraction efficiency to ~95%), by including an additional extraction stage, and by introducing a scrub stage. The inclusion of a fourth extraction stage and additional scrub/wash stages, possibly with pH adjustment, could further improve rejection of boron and nickel.

High aqueous and organic entrainments were measured in the acidic extraction and scrub stages, which undoubtedly contributed to the impurity deportment to the LSL and organic losses to the raffinate. Further chemical and engineering measures are under consideration to mitigate these effects so that process viability is not impacted.

ACKNOWLEDGMENTS

Betty Songo, Mellow Mohoase, Ntumi Molefe (Anglo Research), and Jan de Bruyn (De Bruyn Spectroscopic Solutions) are thanked for their contributions to the success of this project. ShellSol A150 was kindly donated by Shell Chemicals. This paper is published by permission of Anglo Platinum and Anglo Research.

REFERENCES

1. Z. Hofirek and D. G. E. Kerfoot, “The Chemistry of the Nickel-Copper Matte Leach and its Application to Process Control and Optimisation,” *Hydrometallurgy*, **29**, 357−381 (1992).
2. Z. Hofirek and P. Halton, “Production of High Quality Electrowon Nickel at Rustenburg Base Metals Refiners,” Electrometallurgical Plant Practice, P. L. Claessens and G. B. Harris, Eds., Pergamon, New York, 1990; pp. 233−251.
3. Z. Hofirek, “Alternative Methods of Sulphur Removal Applicable to Rustenburg Base Metals Refining Process,” Rustenburg Base Metals Refinery Report No. 11360, 2002.
4. J. A. Tumilty, “The Electrowinning of Metals,” S. Afr. Patent, No. 73/1535, 1973.
5. K. Gottliebsen, B. Grinbaum, D. Chen, and G. W. Stevens, “Recovery of Sulfuric Acid from Copper Tank House Electrolyte Bleeds,” *Hydrometallurgy*, **56**, 293-307 (2000).
6. K. Gottliebsen, B. Grinbaum, D. Chen, and G. W. Stevens, “The Use of Pulsed Perforated Plate Extraction Column for Recovery of Sulfuric Acid from Copper Tank House Electrolyte Bleeds,” *Hydrometallurgy*, **58**, 203-213 (2000).

EXTRACTION OF MINERAL ACIDS AND METAL SALTS WITH BINARY EXTRACTANT BASED ON DINONYLNAPHTHALENESULFONIC ACID

S.A. Kulichenkov,[1] V.V. Belova,[1] A.I. Kholkin,[1] A.A. Voshkin[1], and T.I. Zhidkova[2]

[1]Institute of General and Inorganic Chemistry of Russian Academy of Sciences 31 Leninskii pr., Moscow, 119991, Russia. [2]Institute of Chemistry and Chemical Technology of SB RAS, 42 K. Marksa, Krasnoyarsk, 660049, Russia
Corresponding author email address: belova@igic.ras.ru

ABSTRACT

Extraction isotherm data for trioctylmethylammonium dinonylnaphthalenesulphonate in toluene showed that extractability of the hydrogen halide acids decreases in the order HI > HBr > HCl > HF, which corresponds to the expected anion-exchange order for salts of quaternary ammonium bases (QAB). Among oxygen-containing acids, $HClO_4$ extractability is higher than that of H_2SO_4. The concentration constants of mineral acid extraction were calculated. The dependence of the extraction of the chlorides of Cu(II), Ni(II), Co(II), Zn(II), and Fe(III) with trioctylmethylammonium dinonylnaphthalenesulphonate in toluene on aqueous acidity was studied. In the 1-3 M HCl region distribution ratios of metals increased with increasing concentration of hydrogen ions in the aqueous phase in accordance with the order of binary extraction of chlorocomplex metal-containing acids. With decreasing aqueous acidity, distribution ratios of metals increased owing to changing extraction mechanism and increasing portion of the extracted species in the form of dinonylnaphthalenesulphonates of metals.

INTRODUCTION

Binary extractants have been widely studied for the recovery and separation of several metals in acidic media [1,2]. These binary extractants were, as a rule, based on relatively weak oxygen-containing organic acids. A study of binary extractants based on dinonylnaphthalenesulfonic acid appears to be of special interest because of the potential for simplifying the stripping process. Dinonylnaphthalenesulfonic acid can be characterized as belonging to a group of organic acids having the highest known acidity constants. In this paper, the results of an investigation of the extraction behavior of mineral acids and metal salts in the system involving trioctylmethylammonium dinonylnaphthalenesulphonate are given.

EXPERIMENTAL METHODS

Aqueous solutions of mineral acids were prepared by dilution of concentrated H_2SO_4, $HClO_4$, HF, HCl, HBr, or HI into water. Aqueous solutions of metal salts were prepared by dissolution of metal chlorides into water. A solution of trioctylmethylammonium dinonylnaphthalenesulphonate in toluene was used as the extractant. The binary extractant, R_4NA, was prepared by mixing equimolar amounts of trioctylmethylammonium chloride (R_4NCl) and dinonylnaphthalenesulfonic acid (HA) in toluene with subsequent washing of the organic solution with 1 M NaOH for 10 min. The extraction of mineral acids and metal salts with aqueous-to-organic phase ratios of 1 was carried out at 20 ^{o}C. Samples in glass-stoppered bottles were mechanically shaken for 15 min.

Concentrations of mineral acids in aqueous solutions were determined by acid-base titration. Concentrations of mineral anions in the aqueous and organic phases were determined by argentometric titration. Concentrations of metals in aqueous solutions were determined by EDTA titration and spectrophotometric methods. The differences in metal concentration between the initial and final aqueous solutions were used to calculate the concentrations of metals in the organic phase. All chemicals were of reagent grade.

RESULTS AND DISCUSSION

Extraction of Mineral Acids

The isotherms for the extraction of mineral acids with 0.1 M solution of trioctylmethylammonium dinonylnaphthalenesulphonate in toluene are given in Figures 1 and 2.

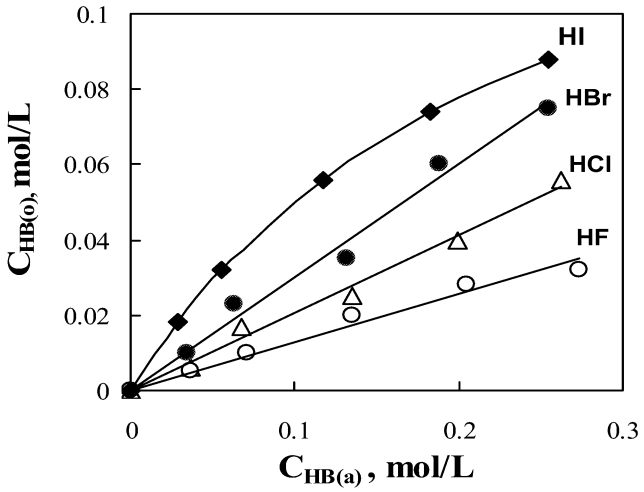

Figure 1. Isotherms for the extraction of halogen hydride acids with 0.1 M solution of trioctylmethylammonium dinonylnaphthalenesulphonate in toluene.

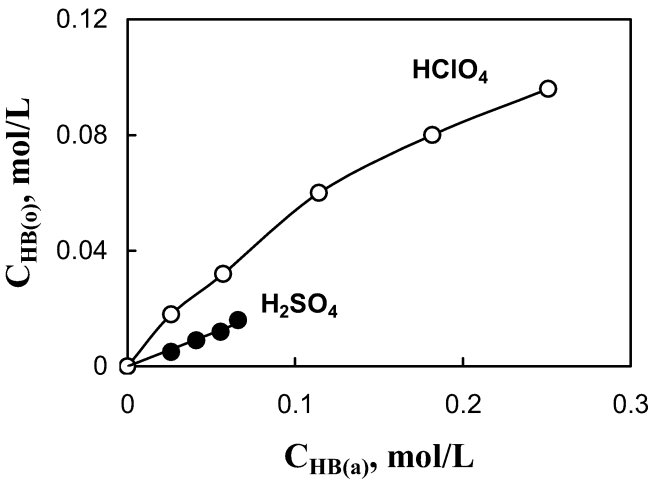

Figure 2. Isotherms for the extraction of oxygen-containing acids with 0.1 M solution of trioctylmethylammonium dinonylnaphthalenesulphonate in toluene.

The distribution of H_mB acid in binary extractant systems such as salts of QAB with organic acids is described as follows [1]:

$$m\ H^{+}_{(a)} + B^{m-}_{(a)} + m\ R_4NA_{(o)} \Leftrightarrow (R_4N)_mB_{(o)} + m\ HA_{(o)} \qquad (1)$$

With stoichiometric amounts of protons and anions of mineral acids in the aqueous (salting-out reagent absence) and organic phases and constant activity coefficients of components in the organic phase, extraction isotherms in binary extractant systems are described by the following equation [1]:

$$C_{H_mB_{(o)}} = \overline{K}^{1/(m+1)}_{H_mB} \cdot C^{m/(m+1)}_{R_4NA_{(o)}} \cdot C_{H_mB_{(\phi)}} \cdot \gamma \pm \qquad (2)$$

As follows from the experimental data, the extractability of hydrogen halide acids (Figure 1) decreased in the order HI > HBr > HCl > HF, which corresponds to the anion-exchange order for salts of QAB [1]. Among oxygen-containing acids, $HClO_4$ extractability is higher than that of H_2SO_4, because of essential differences in the hydration energy of ClO_4^- and SO_4^{2-} anions in the aqueous phase (Figure 2).

The data showed that the binary extraction isotherms have a linear character independent of the nature of the extracted acids. Accordingly, distribution ratios of mineral acids do not depend on H_mB concentration in the aqueous phase, in contrast to neutral extractant systems. The effective extraction constants ($\overline{K}_{H_mB}$) can be calculated taking into account the Equation 2 as follows:

$$\log\ \overline{K}_{H_mB} = (m+1)\log\ D_{H_mB} - m\log(C_{R_4NA_{(init.)}} - mC_{H_mB_{(o)}}) - (m+1)\log\gamma \pm \qquad (3)$$

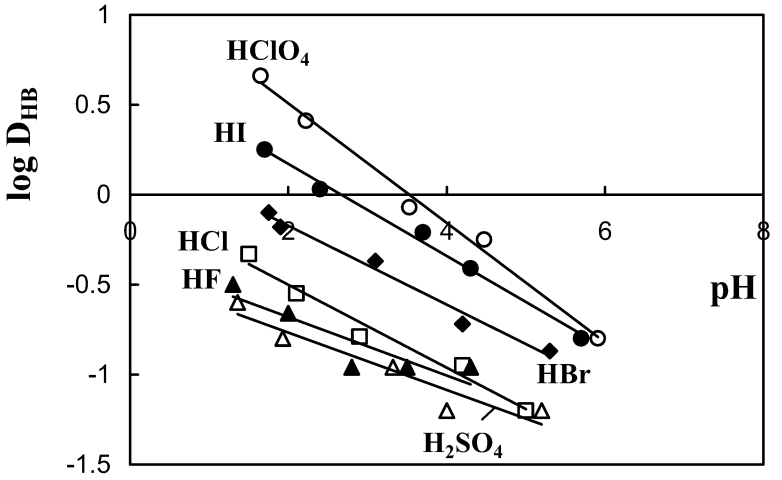

Figure 3. Extraction of mineral acids depending on aqueous acidity with 0.05 M solution of trioctylmethylammonium dinonylnaphthalenesulphonate in toluene.

where $C_{R_4NA(init.)}$ is the initial concentration of binary extractant in the organic phase. According to Equation 3, the effective extraction constants were calculated:

1. $\log \overline{K}_{HCl} = -0.123 \pm 0.200$
2. $\log \overline{K}_{HBr} = 0.310 \pm 0.300$
3. $\log \overline{K}_{HI} = 0.760 \pm 0.055$
4. $\log \overline{K}_{H_2SO_4} = 0.820 \pm 0.310$
5. $\log \overline{K}_{HClO_4} = 0.806 \pm 0.055$.

Experimental data for distribution of mineral acids depending on acidity of the aqueous phase are given in Figure 3. One can see that distribution ratios of mineral acids decrease with increasing pH of the aqueous phase in accordance with regularities of binary extraction.

Extraction of Metal Salts

The extraction of chlorides of Cu(II), Ni(II), Co(II), and Fe(III) with dinonylnaphthalenesulfonic acid in toluene depending on aqueous acidity was studied. In the range of low values of distribution ratios of Cu, Ni, and Co, that is, in the presence of considerable amount of dinonylnaphthalenesulfonic acid in the organic phase, the dependencies $\log D_M = f(\text{pH})$ were found to be linear with the slopes equal to 2, indicating that species such as MA_2 were extracted into the organic phase.

The dependence of the extraction of chlorides of Cu(II), Ni(II), Co(II), Zn(II), and Fe(III) with 0.05 M solution of trioctylmethylammonium dinonylnaphthalenesulphonate in toluene on aqueous acidity was studied (Figure 4). All aqueous solutions had a constant

ionic strength and chloride concentration with NaCl as supporting electrolyte (C_{HCl} + C_{NaCl} = 3 M). In the 1-3 M HCl region distribution ratios of metals increased with increasing concentration of hydrogen ions in the aqueous phase in accordance with the order of binary extraction of chlorocomplex metal-containing acids. With decreasing aqueous acidity, distribution ratios of metals increased owing to changing extraction mechanism and increasing portion of the extracted species in form of dinonylnaphthalenesulphonates of metals.

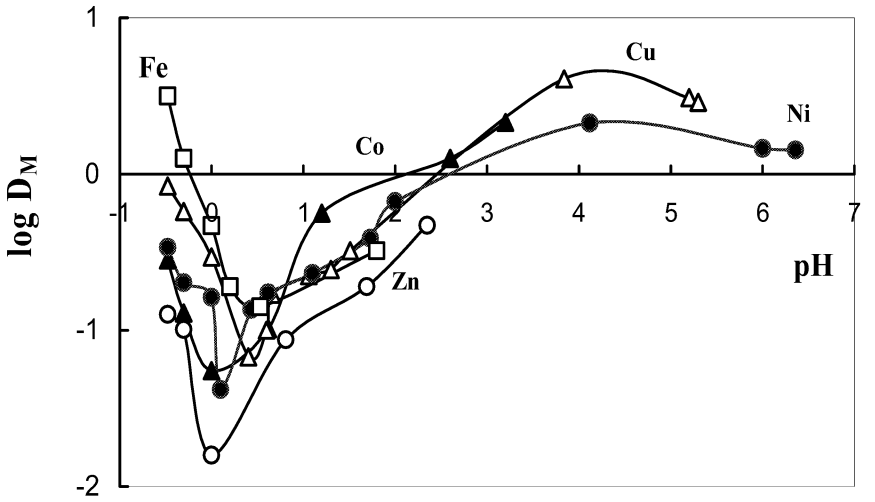

Figure 4. Extraction of metals depending on aqueous acidity with 0.05 M solution of trioctylmethylammonium dinonylnaphthalenesulphonate in toluene.
C_M = 0.025 mol/L; C_{HCl} + C_{NaCl} = 3 mol/L.

In the acidic range, extractability of metals is basically determined by stability of the complex metal-containing anions and corresponds to the order Fe(III) > Cu(II) > Co(II) > Ni(II). When metals are mainly extracted as dinonylnaphthalenesulphonates, their separation appears not to be effective, as in the initial systems involving dinonylnaphthalenesulfonic acid. Under these conditions, an effective extraction of all metals may be possible. Thus, distribution of metals from chloride solutions occurs with the formation of extracted species of different composition depending on acidity of the aqueous phase, which allows control of extraction processes in systems involving binary extractants based on dinonylnaphthalenesulfonic acid.

CONCLUSIONS

It was shown that binary extractants based on dinonylnaphthalenesulfonic acid can be effectively used for recovery of mineral as well as complex metal-containing acids from acidic solutions.

ACKNOWLEDGMENTS

Financial support of Russian Foundation for Basic Research (grant N 06-03-81020) and the Russian President (grant N NSN-7079.2006.3) are gratefully acknowledged.

REFERENCES

1. A. I. Kholkin, V. V. Belova, G. L. Pashkov, I. Yu. Fleitlikh, and V. V. Sergeev, "Solvent Binary Extraction," *J. Molec. Liq.*, **82**, 131-146 (1999).
2. A. I. Kholkin, G. L. Pashkov, I. Yu. Fleitlich, V. V. Belova, K. S. Luboshnikova, V. V. Sergeev, A. M. Kopanev, and O. K. Kulmuhamedov, "Application of Binary Extraction in Hydrometallurgy," *Hydrometallurgy*, **36**, 109-125 (1994).

RECOVERY OF HEAVY METALS FROM WPA PHOSPHORIC ACID

M. P. Elizalde, A. Ocio, A. Almela, and B. Menoyo

Department of Analytical Chemistry, Faculty of Science and Technology, University of the Basque Country, P.O. Box 644, 48080 Bilbao, Spain. Corresponding author email address: maria.elizalde@ehu.es

ABSTRACT

The feasibility of using CYANEX 301, CYANEX 302, and LIX 622 for the recovery of heavy metals from WPA phosphoric acid was investigated. CYANEX 301 allows the extraction of copper, cadmium, and zinc, whereas iron can be extracted from the diluted acid. CYANEX 302 is able to recover copper and cadmium. The efficiency of LIX 622 is lower but allows the extraction of copper. Separation factors between coextracted cations were calculated as a function of the experimental conditions. Finally, the results were compared with those obtained in synthetic phosphoric acid.

INTRODUCTION

Industrial wet-process phosphoric acid (WPA) is obtained by leaching the phosphate ores with sulfuric acid. Heavy metals from the original rock are common impurities in the phosphoric acid, and their elimination can be of interest depending upon the final use of the acid. Liquid-liquid extraction, among other techniques, has been applied for this purpose.

Due to their strategic value, some works concerning the extraction of uranium and lanthanides from WPA have been published. On the other hand, the toxicity of cadmium has led to several extraction studies on its removal from WPA by different types of extractants.

Regarding the use of alkylthiophosphinic acids, Tijoe *et al*. reported that dicyclohexyldithiophosphinic and diphenyldithiophosphinic acids allow cadmium and copper extraction from industrial phosphoric acid [1,2]. CYANEX 302 was able to recover copper and cadmium from WPA phosphoric acid, but the best selectivity for cadmium was obtained with Aliquat 336 [3]. Extractants based on alkylsalicylaldoximes could partially extract copper from the industrial acid [3].

On the other hand, several works are focused on metal recovery from WPA by non conventional liquid-liquid processes using CYANEX reagents. Techniques based on supported liquid membranes, hollow fibers, liquid emulsion membranes, impregnated resins, and mixed alginate gels were used.

In general, most works are focused on applied purposes. In this work the extraction of several metal ions from industrial phosphoric acid is presented and compared with those obtained in synthetic phosphoric acid.

EXPERIMENTAL

Reagents and Solutions

Samples of WPA were kindly supplied by Fertiberia S.A. (Huelva, Spain). After filtering the industrial acid through a 0.45 μm membrane (Millipore) the sample was analyzed by ICP–AES (ARL 3410), yielding the concentrations of Cd, Cu, Zn, Ni, and Fe as 32, 72, 632, 88, and 4243 mg/L, respectively. The sample was 10.8 M H_3PO_4. Diluted solutions of WPA of concentrations 1.1, 2.7, 5.4, and 8.1 M H_3PO_4 were also prepared.

CYANEX 301 and CYANEX 302 were kindly donated by Cytec Co. (Ontario, Canada) and LIX 622 by Cognis (Cork, Ireland). All extractants were used without further purification. CYANEX 301 and CYANEX 302 were considered to contain 77.2% bis(2,4,4-trimethylpentyl)dithiophosphinic acid (HR) and 85% bis(2,4,4-trimethylpentyl)thiophosphinic acid (HA), respectively [4]. LIX 622 contains 67.7% 5-dodecylsalicylaldoxime (HL) [5] and 15.9% isotridecanol [6]. Organic solutions of the extractants in concentration ranges 0.03 mM to 0.24 M HR, 1.0–60.0 mM HA, and 0.02–0.18 M HL in toluene (Fluka p.a.), were used.

Solutions of 2 M HCl (Merck, p.a.) and 5 M HNO_3 (Merck p.a.) were used as stripping reagents (Merck, p.a.) for CYANEX reagents and LIX 622, respectively.

Liquid–Liquid Extraction Procedures

The extraction experiments were carried out by shaking equal volumes of organic and aqueous solutions in special stoppered tubes for 30 min without taking into consideration the time needed to attain equilibrium state for all the elements. After phase separation with a high speed centrifuge (Eppendorf 5804), the metal concentration was measured by atomic absorption spectroscopy (Perkin Elmer Aanalyst 100). The metal content in the organic phase was determined after stripping organic extracts into equal volumes of 5 M HNO_3 or 2 M HCl solutions. The mass balance was always fulfilled with %RSD < 10%.

RESULTS AND DISCUSSION

Extraction with CYANEX 301

Figure 1 illustrates the experimental results on metal extraction from the industrial phosphoric acid and their diluted solutions as a function of CYANEX 301 concentration. It can be appreciated that concentrations of about 10 mM bis(2,4,4–trimethylpentyl)dithiophosphinic acid are enough to extract copper and cadmium quantitatively. It is to be noticed that copper extraction from WPA is higher than that

obtained at more diluted conditions, which can probably be attributed to the effect of other components present in the industrial acid as well as to the change of all concentrations derived from the dilution of WPA.

Higher concentrations (0.02–0.25 M) of CYANEX 301 allow the recovery of zinc from crude WPA. CYANEX 301 is also able to extract iron from diluted solutions. Although iron extraction is relatively low, the amount of metal extracted can be superior to that of copper and cadmium due to the high concentration of iron in the industrial sample. Finally, 50% nickel extraction can be achieved only in the case of the diluted 1.1 M phosphoric acid.

Literature data reveal that in the extraction of Cd(II) and Zn(II) from synthetic phosphoric acid media by CYANEX 301 the complexes CdR_2 and ZnR_2 are formed and their extraction constants at different phosphoric acid concentrations are available [7, 8]. The same information is available for Fe(III) although in this case the extraction process leading to FeR_3 has been shown to be kinetically slow (20 h shaking to reach equilibrium conditions) [9]. Finally, copper extraction has been modelled assuming the formation of CuR_2 [9].

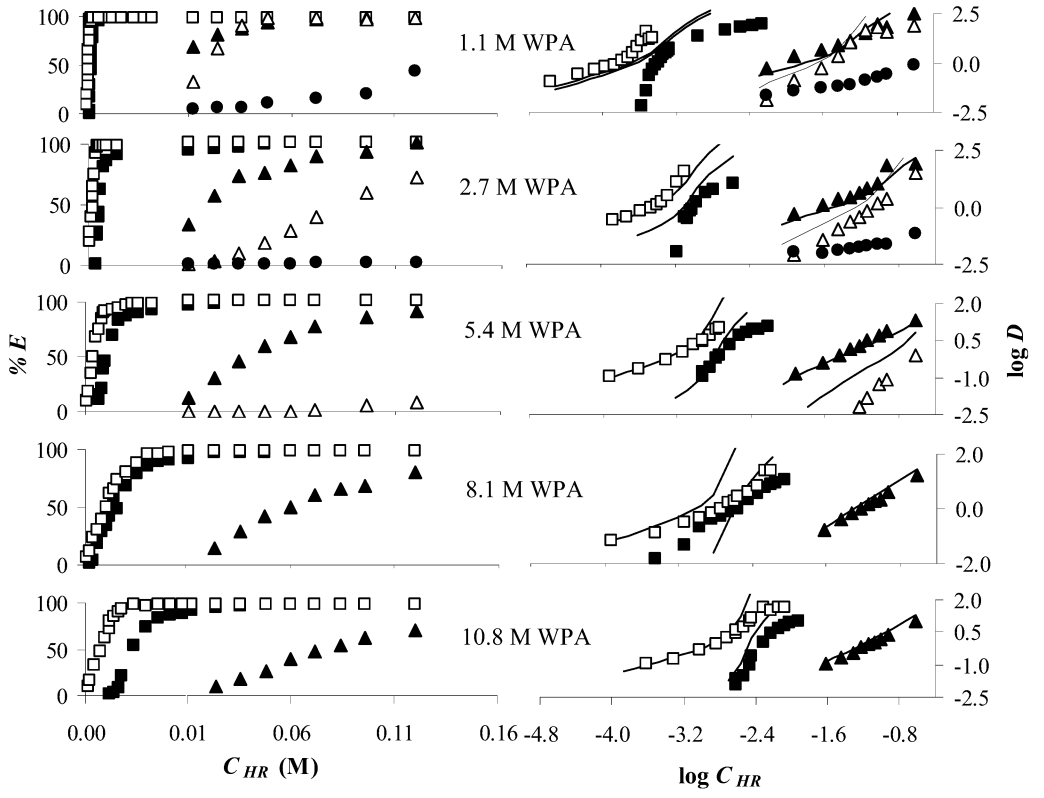

Figure 1. Heavy-metal uptake from WPA and their diluted solutions with CYANEX 301. Continuous lines have been drawn taking into account extraction constant values from synthetic media. □: Cu, ■: Cd, ▲: Zn, ●: Ni, △: Fe.

Taking into account equilibrium constant values in synthetic solutions and by extrapolation to the phosphoric acid concentrations in the present work, the theoretical behavior has been deduced and represented in Figure 1 as continuous lines. It can be seen that there is a good agreement in the case of zinc extraction, whereas the theoretical models do not reproduce the experimental behavior obtained in the case of iron, copper, or cadmium. The observed differences can be due, apart from kinetic aspects that can be important in the case of iron, to the formation of mixed complexes in the organic phase and to interactions of the metal ions with chloride, fluoride, organic matter, or other ligands in the aqueous solutions.

In a complex sample such as WPA, it is useful to know the best conditions to separate the different metal ions. As can be appreciated from Figure 2, total separation of cadmium and copper from zinc, iron, and nickel is possible, but the separation between copper and cadmium is not possible. Similarly, in the second stage, the separation of zinc, iron and a little of nickel from unextracted cations is also possible but not the separation between them. In Figure 2 the separation factors $\alpha_{Cu/Cd}$, $\alpha_{Zn/Fe}$, and $\alpha_{Fe/Ni}$ as a function of the extractant concentration are represented.

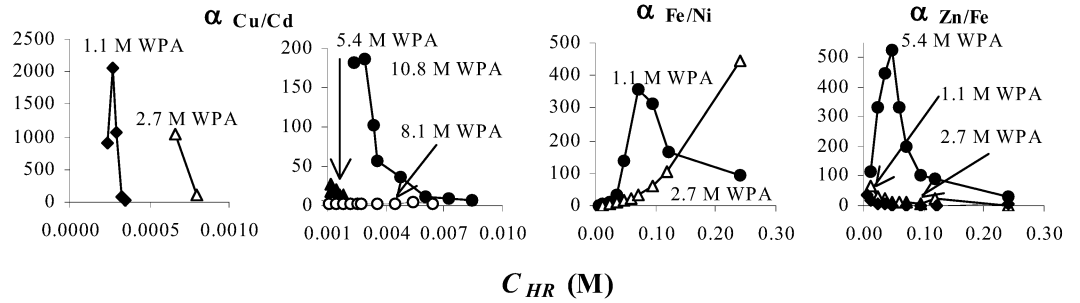

Figure 2. Separation factors from different dilutions of WPA with CYANEX 301.

Extraction with CYANEX 302

CYANEX 302 only allows the recovery of copper and cadmium, as seen in Figure 3. Moreover, their separation is not possible, since similar extraction percentages are obtained for both metal ions. Surprisingly, the extraction from crude WPA is again more effective than that obtained from the diluted acid.

Equilibrium extraction-constant values are available only for cadmium extraction from synthetic phosphoric acid solutions by CYANEX 302 [10], but the theoretical behavior in synthetic solutions does not explain satisfactorily the results observed in the industrial acid.

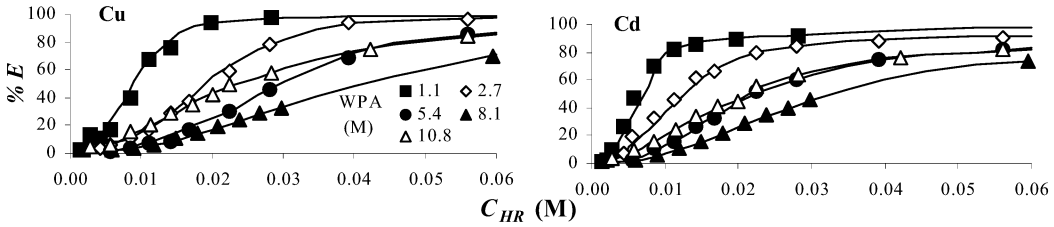

Figure 3. Copper and cadmium uptake from WPA and their diluted solutions with CYANEX 302.

Extraction by LIX 622

High concentrations of LIX 622 allow the removal of copper only from the diluted acid solutions, as seen in Figure 4. The theoretical extraction behavior based on the formation of CuL_2, being L 5-dodecylsalicylaldoxime [11] is also included in Figure 4. It can be appreciated that the experimental results obtained with the industrial solutions are in good agreement with the theoretical model.

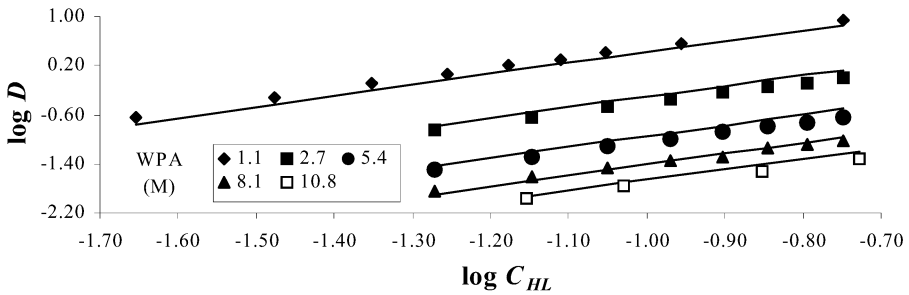

Figure 4. Copper extraction from WPA and their diluted solutions with LIX 622. Continuous lines correspond to the theoretical extraction model in synthetic solutions.

CONCLUSIONS

CYANEX 301 is able to extract Cu(II), Cd(II), and Zn(II) from crude WPA. Fe(III) is also extracted from diluted solutions. Step-by-step separation of heavy metals is difficult, but they can be partially separated by fitting the extractant concentration. The theoretical models proposed in synthetic media can predict accurately the extraction of Zn(II), but deviations are observed with the other cations.

CYANEX 302 eliminates Cu(II) and Cd(II) from WPA phosphoric acid, although with less efficiency than CYANEX 301. The separation of Cu(II) and Cd(II) using these reagents was not found possible. Moreover, their extractions from crude acid are higher than from more diluted WPA samples.

LIX 622 is only able to extract Cu(II); it is a less effective copper extractant but more selective. In this case, the simulation of the liquid-liquid extraction process considering the equilibrium extraction constant values for CuL_2 obtained in synthetic phosphoric acid predicts accurately the experimental results.

ACKNOWLEDGMENTS

Authors thank the Basque Government for the project PI-1999-107.

REFERENCES

1. T. T. Tijoe, P. F. M. Durville, and G. M. van Rosmalen, "Extraction of Cadmium from Phosphoric Acid with Diorganyldithiophosphinic Acids. Part I: Equilibrium Data," *Solvent Extr. Ion Exch.*, **7**(3), 435–459 (1989).
2. T. T. Tijoe, P. F. M. Durville, and G. M. van Rosmalen, "Extraction of Cadmium from Phosphoric Acid with Diorganyldithiophosphinic Acids. Part II: Rate of Extraction and Decomposition," *Solvent Extr. Ion Exch.,* **7**(3), 461–487 (1989).
3. I. Ortiz, S. Zamacona, and A. M. Urtiaga, "Selection of Extractants for the Removal of Cadmium from Industrial Grade Phosphoric Acid," M. Cox, M. Hidalgo, and M. Valiente, Eds., Society of Chemical Industry, London, UK, 2002; pp. 1487–1491.
4. Cyanamid & Co. CYANEX 302 and CYANEX 301 Technical Bulletin, American Cyanamid, Wayne, N. J., 1990.
5. A. Ocio, M. Elizalde, and J. A. Prieto, "Determination of 5-Dodecylsalicylaldoxime and 5-Nonylsalicylaldoxime in Commercial Extractants by HPLC with Photometric Detection," *J. Chromatography A*, **1032**, 129–132 (2004).
6. A. Ocio, B. Menoyo, and M. P. Elizalde, "Identification and Quantification of Alkylsalicylaldoximes and Alcoholic Modifiers in Commercial Extractants by Gas Chromatography–Mass Spectrometry," *Book of Abstracts Euroanalysis XIII PS2-231, Salamanca (Spain) 2004.*
7. A. Ocio and M. P. Elizalde, "Zinc(II) Extraction from Phosphoric Media by Bis(2,4,4-trimethylpentyl)dithiophosphinic Acid (CYANEX 301)," *Solvent Extr. Ion Exch.*, **21**(2), 259–271 (2003).
8. A. Ocio, A. Almela, and M. P. Elizalde, "Cadmium(II) Extraction from Phosphoric Media by Bis(2, 4, 4-trimethylpentyl)dithiophosphinic Acid (CYANEX 301)," *Solvent Extr. Ion Exch.,* **22**(6), 961–977 (2004).
9. A. Ocio, "Eliminación de Metales de Disoluciones de Ácido Fosfórico con Extractantes Quelatantes Comerciales," Ph.D. Thesis, University of the Basque Country, Bilbao, Spain 2007.
10. A. Almela, M. P. Elizalde, and J. M. Gómez "Cadmium(II) Extraction from Phosphoric Media by Bis(2,4,4-trimethylpentyl)thiophosphinic Acid (CYANEX 302)," *Fluid Phase Equilibr.,* **145**, 301–310 (1998).
11. A. Ocio and M. P. Elizalde, "Copper(II) Extraction from Phosphoric Acid Media by 5-Dodecylsalicylaldoxime (LIX 622)," *Solvent Extr. Ion Exch.*, 24, 861–875 (2006).

Process Chemistry & Engineering

SUCCESSFUL DESIGN OF AGITATED LIQUID-LIQUID EXTRACTION COLUMNS VIA PILOT PLANT TESTING

D.J. Glatz and W.L. Parker

Koch Modular Process Systems, LLC., 45 Eisenhower Drive, Suite 350, Paramus, NJ, USA. Corresponding author email address: donald.glatz@modularprocess.com

ABSTRACT

A well-designed and conducted pilot-plant test followed by empirical scale-up to a production column is the most accurate and efficient method used to design liquid-liquid extraction (LLE) columns. Three (3) unique cases are studied, where testing was used for successful design and implementation of agitated LLE columns. Each case involved a new process for which the authors knew of no previous operation. The processes and requirements for these applications were significantly different, demonstrating the versatility of this design method.

INTRODUCTION

Accurate design of the LLE column is critical to the technical and economic feasibility of a LLE process. However, selecting and designing an extraction column from basic principles alone has not proven to be an effective method. This is due to numerous difficult-to-predict aspects of system behavior. Some of these aspects are physical property changes, flow-rate changes for each phase, coalescing effects, interfacial and drop-turbulence effects, wetting characteristics, presence of solids, tendency to form emulsions, axial mixing, and the effect of density gradients [1].

Engineers require a fast and accurate method for the design of LLE columns. Since design from basic principles is not reliable, another method is required to determine the type and size extraction column that will provide accurate and robust designs.

EXPERIMENTAL

LLE processes are tested in glass columns for observation of the phase behavior (droplet formation, dispersed phase holdup, coalescence, interface behavior, etc.). Observation allows the experienced engineer to assess the column performance and systematically “tweak” the process conditions to obtain optimal performance. Variable-speed pumps with manual adjustment are used for the feed and solvent streams, and heat

exchangers control the inlet temperatures. The interface is manually controlled using a bottoms pump, and the light phase leaves by overflow. The test procedure follows:

- For start-up each day, the column is filled with the continuous phase. Once full, the agitator is turned on at a low speed, and the dispersed phase is also added.
- Inlet flows are adjusted to the desired rates and the interface level controlled by adjusting the bottoms take-off pump as required.
- The agitator speed is adjusted to the specified rate.
- The test supervisor specifies the conditions for each run. Feed and solvent rates are confirmed on a regular basis. The temperature is adjusted as required using the heat exchangers for the feed and solvent streams. At the completion of the run, raffinate and extract flow rates are measured and samples of each phase taken for analyses.
- During start-up each day, a total of five turnovers are performed before the initial samples are taken. A turnover is defined as the total column volume divided by the combined flow of feed and solvents. After the first run, and following adjustments of the variables, a total of three turnovers are performed before additional sampling.

The authors use step-by-step optimization during pilot-plant testing. This method requires experience and immediate access to analytical equipment. Initial conditions are set based upon an understanding of the physical and chemical properties, equilibrium data, observation of the phase behavior, and experience. During the initial runs, the agitation speed is incrementally increased until flooding is achieved. Flooding is recognized as the formation of a second interface within the agitated zone caused by disperse-phase holdup. Based upon the results from the initial series of runs, variables are adjusted and evaluated at several levels including the height, capacity, and solvent to feed ratio (S/F). Results are continuously used to determine the operating conditions for the next set of runs. Testing continues until the desired results are achieved. Data from the runs producing optimal performance are used for empirical scale-up to the production column using proven design correlations.

RESULTS AND DISCUSSION

Application #1—Extraction of Organic Impurities from Waste Caustic Solution

A refinery operation generated effluent caustic solution that was contaminated with unreacted monomers, making the solution environmentally hazardous as a waste stream. In addition, the organic contaminants polymerized upon heating, causing fouling of the downstream distillation tower. Thus, removal of the organic contaminants prior to heat treatment was essential in order to generate useful caustic solution.

Toluene was selected as the solvent for this application and laboratory “shake tests” [2] were performed with the waste caustic stream and the plant toluene. The distribution ratio (m) for the most difficult organic impurity (Impurity A) was determined to be relatively constant at a value of 1.5 in the concentration range required for this application. The Kremser equation [1] was used to calculate that greater than 99% removal of all impurities (process requirement) can be achieved with 5 theoretical stages

at a solvent to feed ratio (S/F) of 1.5, mass basis. The key was to reduce Impurity A to less than 10 ppm. The Kremser equation follows:

$$N = \log([(x_f - y_s/m)/(x_n - y_s/m)] \text{ x } [1\text{-}1/E] + 1/E)/\log E \quad (1)$$

Where N is the number of theoretical stages, x_f is the concentration of solute in the feed, x_n is the concentration of solute in the raffinate (with the feed and raffinate each on a solute-free basis), y_s is the concentration of solute in the solvent, m is the distribution ratio, and E is the extraction factor.

During the shake tests, it was observed that this system had a high tendency to emulsify. Thus, the KARR® Column was selected as the best extraction device for this application [3]. The set-up for the test using a 25 mm diameter x 3 m plate stack height column is shown in Figure 1. The plates and spacers were 316SS.

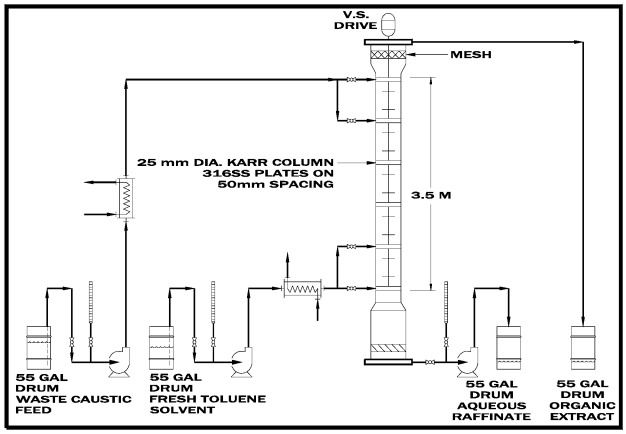

Figure 1. Pilot-plant set-up for inorganic impurity extraction from waste caustic solution.

Table 1. Pilot-plant data for extraction of Impurity A.

Capacity (m^3/m^2 hr)	Agitation (SPM)	Impurity A (Raff. ppm)
28.5	180	32
28.5	220	13
28.5	250	5
28.5	270	Flood
35.4	180	68
35.4	220	15
35.4	230	5
35.4	250	Flood

Plate Stack Height = 2.4 m
S/F = 1.5 wt. basis for all runs

A portion of the data generated in the pilot column is shown in Table 1. The results from the pilot testing indicated the following:

- The column gave acceptable results when operating with either the aqueous or organic as the continuous phase. Aqueous-continuous was susceptible to emulsification and, the data reported in Table 1 are only for organic-continuous.
- Acceptable extraction efficiency was achieved at a solvent-to-feed ratio of 1.5 (weight basis) with 2.4 m plate stack height.
- Capacities of 28.5 and 35.4 m^3/m^2 hr were tested successfully. However, scale-up based upon 28.5 m^3/m^2 hr was specified in order to provide spare capacity.

The standard scale-up procedure suggested by Karr [4] was used to design the production column for a caustic feed rate of 4,745 kg/hr. The resulting column was 762 mm diameter x 9.14 m plate stack height (Figure 2). This column was built in 1999, started up smoothly and has consistently produced acceptable caustic solution quality. This has allowed the plant to sell the effluent caustic to a local plant to be used for neutralization purposes.

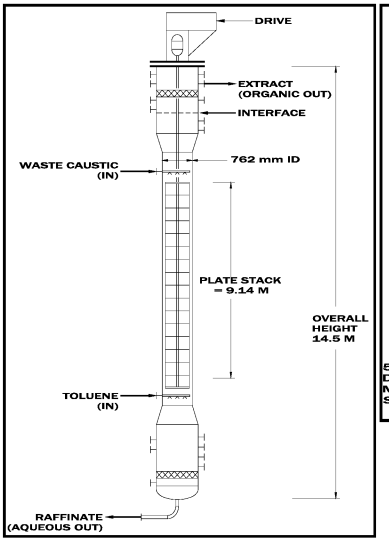

Figure 2. Production KARR® column for waste caustic treatment process

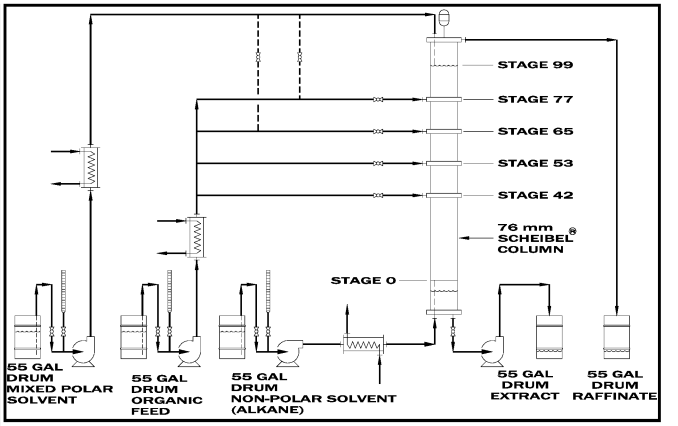

Figure 3. Pilot-plant set-up for aromatic purification by fractional extraction.

Application #2—Aromatic Purification by Fractional Liquid-Liquid Extraction

This application involves a light "tar" feed stream from a refinery operation that included aromatic compounds and many organic impurities. A minimum 90% aromatic recovery with <1% impurities was required. Lab work indicated that a polar solvent was effective for removing the aromatic compounds from the feed mixture. However significant co-extraction of impurities occurred. Thus, an alkane was selected to counter-extract the impurities using a fractional extraction technique [1].

Preliminary screening tests in a pilot RDC column indicated that >10 extraction stages were required as well as high solvent usage. Also, it was determined that the feed location should be near the top of the column. Due to the large number of theoretical stages, the SCHEIBEL® Column was selected as the best extraction device for scale-up because this column has high stage efficiency [5].

The set-up for the pilot-plant test is shown in Figure 3 and included a 76 mm diameter SCHEIBEL Column with up to 99 agitated stages. Variables tested were:

- The total number of agitated stages was varied in the range 65-99. The stages above the feed were varied in the range 12–34, and the stages below the feed in the range 42–65.
- The capacity (specific throughput) was varied between 21 and 25.5 m^3/m^2 hr.
- Many variations of the S/F ratios were tested. The range for polar solvent to feed was 0.5:1 and 1.4:1. The range for nonpolar solvent-to-feed was 1.1:1 and 3:1.
- The agitation speed range was 400–850 RPM.

At the completion of the test program, it was determined that the optimal operating conditions were as follows:

Capacity	24.8 m^3/m^2 hr
Number of stages	65 agitated stages
Feed location	Stage #13 from top
Polar solvent:feed	0.7:1.0
Nonpolar solvent:feed	1.8:1.0

For these conditions, the aromatic recovery was 92% with <1.0% impurities.

Using the data generated in the 76 mm diameter column, the standard scale-up procedure suggested by Scheibel and reported by Cusack [3] was used to design the production column for a light tar feed rate of 13,439 kg/hr. The resulting SCHEIBEL column was 1778 mm diameter x 65 agitated stages as shown in Figure 4. This column was fabricated and installed in 2004. It started up smoothly and has consistently achieved excellent performance.

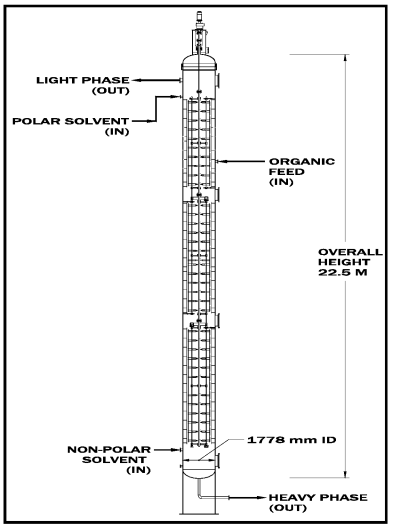

Figure 4. SCHEIBEL® Column for aromatic recovery and purification.

Application #3—Neutralization and Washing Process

In a specialty chemical plant, a nitrated organic was produced with unreacted nitric acid contamination. Purification required removal of the nitric acid to <10 ppm. An extraction column was considered for neutralization and washing in a single unit.

Due to the hazardous nature of the nitrated organic feed, this material could not be shipped to a pilot-plant facility for testing. Instead, the pilot plant equipment was shipped to and set up in the operating plant. The set-up is shown in Figure 5 utilizing a 25 mm diameter x 3 m plate stack height KARR Column. This column was selected due to an observation of emulsion formation for this system. Since the organic phase was the continuous phase, PTFE plates and spacers were used to ensure the proper wetting characteristics [1]. During a five-day test program the following results were achieved:

- The design capacity was selected as 36.7 m^3/m^2 hr, although higher capacities were successfully tested. It was determined that this column would be built with spare capacity.
- The amount of ammonia solution and water were minimized to the following volumetric ratios: organic feed:ammonia:fresh water = 1.0:0.087:0.26.
- The full 3 m plate stack height was required in order to achieve the acceptable results at the low phase ratios. Also, it was determined that the best location for the organic feed was in the middle of the column, with 1.5 m plate stack above and below.

The standard scale-up procedure [4] was employed to design the production column for a nitrated organic feed rate of 12.2 m^3/hr. The resulting KARR Column was

763 mm diameter x 12.2 m plate stack height. This column was fabricated and installed and has been operating successfully since 2000.

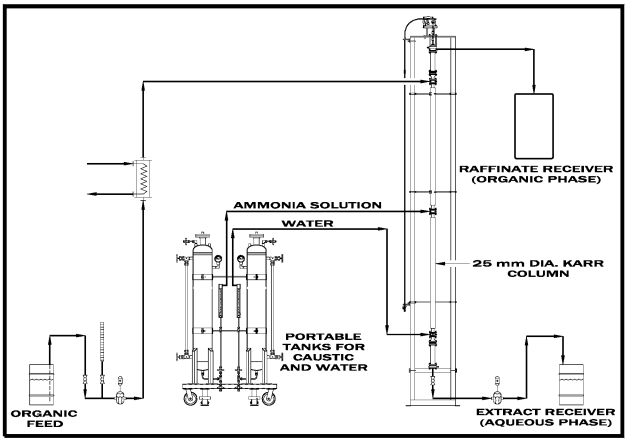

Figure 5. Portable liquid-liquid extraction equipment for on-site testing of a neutralization and washing process.

CONCLUSION

Pilot-plant testing followed by proven empirical scale-up techniques is the most reliable and effective method for the design of liquid-liquid extraction columns. The pilot-plant test can be performed quickly and economically to provide the data for scale-up to a production column design that is both accurate and robust. Production columns that have been design based upon pilot-plant test work have proven to start up smoothly and meet or exceed process expectations.

REFERENCES

1. R. Cusack and A. Karr, "A Fresh Look at Liquid-Liquid Extraction, Extractor Design and Specification," *Chem. Eng.*, April 1991.
2. D. Glatz and W. Parker, "Extraction Enhancement, One Step at a Time," *Chem. Eng.*, November 2004
3. R. Cusack and P. Fremeaux, "A Fresh Look at Liquid-Liquid Extraction, Inside the Extractor," *Chem. Eng.*, March 1991.
4. A. Karr and S. Rananujam, "Scaleup and Performance of 5 ft. (1.52 m) Diameter Reciprocating Plate Extraction Column," *Solvent Ext. Ion Exch.*, **6**(2), 221-231 (1988).
5. T. Holmes, A. Karr, and R. Cusack, "Performance Characteristics of Packed and Agitated Extraction Columns," AIChE Summer National Meeting, August 17, 1987.

KARR® and SCHEIBEL® are registered trademarks of Koch-Glitsch, L.P.

MODELLING OF COPPER EXTRACTION IN A PULSED SIEVE-PLATE COLUMN

M. Lurdes F. Gameiro, Shiva Agarwal, M. Rosinda C. Ismael, and Jorge M.R. Carvalho

Department of Chemical and Biological Engineering, Instituto Superior Técnico
Av. Rovisco Pais, 1049-001 Lisboa, Portugal
Corresponding author email address: pcjcarv@mail.ist.utl.pt

ABSTRACT

This work aims to study the extraction of copper in a pulsed sieve-plate column, using purified Acorga M 5640 (5-*t*-nonylsalicylaldoxime) in Escaid 100. Axial mixing coefficients for continuous and dispersed phases were determined using the dispersion model. Correlations for these data were proposed. Drop-size distribution and hold-up were determined along the height of the column. Measured concentrations profiles were compared with ones predicted by numerical simulation using the axial dispersion model. The mathematical-model resolution was performed by the gPROMS modelling system. The overall mass-transfer coefficient was evaluated from the experimental data by the least-squares method and compared with the one obtained from the resistances-in-series model.

INTRODUCTION

The recovery of copper from sulphuric acid solutions can be efficiently carried out by using oxime extractants [1], particularly the Acorga reagent M 5640 (5-*t*-nonylsalicylaldoxime). The extraction of copper with M 5640 (HR) can be described by the following reaction [2]:

$$Cu^{2+} + 2HR_{(org)} \leftrightarrow CuR_{2(org)} + 2H^{+} \quad (1)$$

In the present work, a pulsed sieve-plate column was used for continuous extraction of copper from an acidic aqueous solution in sulphate medium. The main advantages of this type of column are its high efficiency, capacity for high throughput while maintaining high dispersed flow rates, and reduced inventory of solvent [3]. The hydrodynamic features, such as axial mixing, influenced the column performance adversely. These deviations from the ideal plug flow can be taken into account by the axia- dispersion model. The model equations for continuous and dispersed phases are as follows:

$$(1-\phi)E_c \frac{d^2 c_{Cu,c}}{dz^2} - V_c \frac{dc_{Cu,c}}{dz} - aK_{oc}(c_{Cu,c} - c_{Cu,c,eq}) = 0 \quad (2)$$

$$\phi E_d \frac{d^2 c_{Cu,d}}{dz^2} + V_d \frac{dc_{Cu,d}}{dz} + aK_{oc}(c_{Cu,c} - c_{Cu,c,eq}) = 0 \quad (3)$$

where ϕ represents the hold-up, E the axial mixing coefficient, c the solute concentration, z the height, V the superficial phase velocity, a the specific interfacial area, and K_{oc} the continuous phase based overall mass transfer coefficient of extraction. The subscripts c and d denote, respectively, the continuous and the dispersed phases, while *eq* stands for the equilibrium. The boundary conditions at the bottom and top of the column [4] are expressed by:

$$z = 0 \qquad -(1-\phi)E_c \frac{dc_{Cu,c}}{dz} + V_c c_{Cu,c} = V_c c_{Cu,c,0} \; ; \qquad \frac{dc_{Cu,d}}{dz} = 0 \quad (4)$$

$$z = L \qquad \frac{dc_{Cu,c}}{dz} = 0 \; ; \qquad -\phi E_d \frac{dc_{Cu,d}}{dz} + V_d c_{Cu,d} = V_d c_{Cu,d,0} \quad (5)$$

where the subscript 0 denotes the initial condition.

The system of differential equations presented before (Equations.2 and 3) can be solved by the simulator gPROMS® (Process Systems Enterprise Ltd., UK). The optimal value for the overall mass-transfer coefficient of extraction was achieved from experimental data by the least-squares method.

As stated before, the present study was therefore focused on the extraction of copper from a sulphuric solution using the extractant M 5640 in a pulsed sieve-plate column. It was intended to carry out some studies on axial mixing and to analyze the influence of the pulse frequency and amplitude on the mass-transfer data. The interest of this work is justified by the lack of data in the literature for copper extraction in pulsed sieve-plate columns.

EXPERIMENTAL

Reagents

The aqueous solutions were prepared using $CuSO_4$ and H_2SO_4, commercial-grade reagents. The organic phase consisted of 200 g L^{-1} M 5640 (5-*t*-nonylsalicylaldoxime) (Acorga) diluted in Escaid 100 (ExxonMobil).

Equipment and Procedure

The experiments were performed at room temperature in a pulsed sieve-plate column. The effective height of the column was 4.70 m. The main column section comprised a long glass tube of 25 mm internal diameter, enclosing 86 perforated stainless steel plates, spaced 50 mm apart, supported on a 3.2 mm diameter central rod. Holes diameter was 3 mm, giving a nominal free-area fraction of 0.23. Pulsation was applied using compressed air and a solenoid valve. The pulse amplitude and frequency were adjusted to the desired values, 2.5 or 4.0 cm and 54.0 min^{-1}, respectively.

After filling the column with the aqueous phase (continuous), the organic phase (dispersed) was introduced. When the steady-state conditions were reached, nine samples of each phase (aqueous and organic) were collected from taps distributed along the column. The dispersed-phase hold-up was determined by withdrawing five samples of the dispersion. The drop diameters were also measured at five different points inside the column using a photographic method.

The axial mixing studies for continuous and dispersed phases were performed under transient-state and steady-state conditions using a tracer technique [5]. The aqueous tracer, a nickel aqueous solution, was introduced at the middle of the column. Under transient conditions the aqueous samples were taken, at different time intervals, 161 cm below the tracer injection. When the steady-state conditions were attained, the aqueous phase was sampled at five different points above the tracer injection. The organic tracer, nickel in a M 5640 organic solution, was injected 25 cm below the aqueous tracer, and the transient response was analyzed 178 cm above it. The backmixing samples were collected at five different points below the tracer injection. The experiments were carried out at 20 ºC.

The concentration of copper, in both phases (organic and aqueous) was measured with an atomic absorption spectrophotometer (Perkin Elmer, AAnalyst200) at 324.75 nm.

RESULTS AND DISCUSSION

Axial Mixing Coefficients

For the aqueous phase, the experimental results (not shown) revealed that the relative deviation between the coefficients obtained under transient and steady-state conditions was in the range of 4-20%. Thus, it was decided to use the mean arithmetic value of these data for E_c in the subsequent work. Figure 1 shows the dependence of E_c on ψ, which is expressed as follows:

$$\psi = \frac{d_0 L_0}{m_h D^{2/3}} A^n f^m \left(1 + \frac{V_c}{2A^n f^m \gamma}\right)\gamma = 2.09 A^{1.5} f^{1.1} \left(1 + \frac{V_c}{2A^{1.5} f^{1.1} \gamma}\right)\gamma \qquad (6)$$

where d_0 is the diameter of sieve-plate holes, m_h the fraction of free total holes area at plate, L_0 the plate spacing, D the column diameter, A the pulse amplitude, and f the frequency. In Equation 6, γ is equal to 1 $cm^{-0.5}$ $s^{0.1}$. It is worth noting that ψ is a parameter similar to the one previously used by Miyauchi [6] for correlating axial dispersion data in pulsed sieve-plate columns. The difference is in the powers, n and m, of the pulse amplitude and frequency. While Miyauchi used $n = m = 1$, in the present study, the values $n = 1.5$ and $m = 1.1$ were adjusted by using the E_c experimental results.

The experimental results of the dispersed-phase axial-mixing coefficients are also shown in Figure 1. As one can conclude, there is a reasonable correlation between E_d and the product of the pulse amplitude by the frequency.

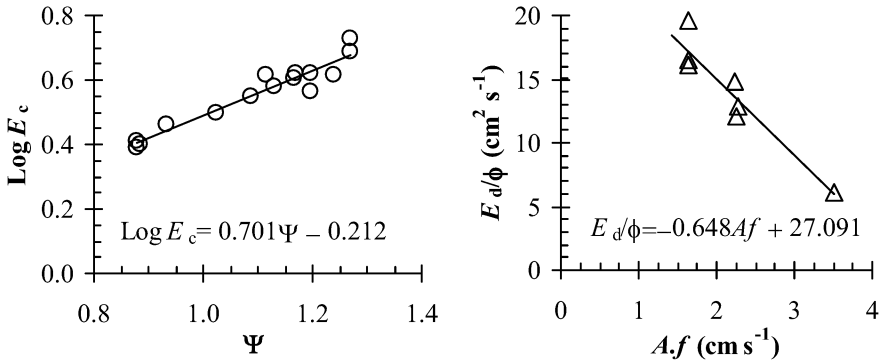

Figure 1. Axial-mixing coefficients for continuous and dispersed phases. Aqueous phase: (○) – Cu = 16 g L^{-1}, H_2SO_4 = 10 g L^{-1}; (△) – tap water. Organic phase: (○,△) Cu_{org} = 2-14 g L^{-1}; M 5640 = 200 g L^{-1}.

Mass-Transfer Data

Figure 2 illustrates the comparison between the simulated concentration profiles (lines) and the experimental data (marks). These profiles are obtained by solving the set of Equations 2 and 3 with the parameters listed in Table 1. The optimal value of the overall mass-transfer coefficient K_{oc} was achieved by minimizing the error-square sum U:

$$U = \sum (c_{Cu,c,calc} - c_{Cu,c,\exp})^2 \tag{7}$$

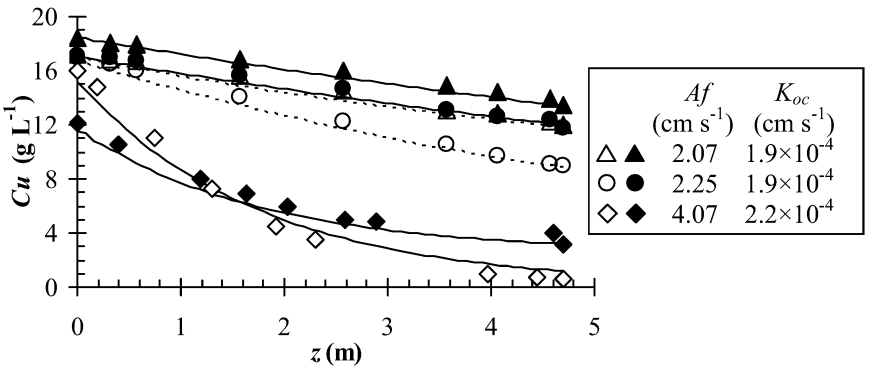

Figure 2. Simulated and experimental concentration profiles. Aqueous phase: Cu = 16.3-17.2 g L^{-1}, H_2SO_4 = 10 g L^{-1}. Organic phase: Cu = 3.2-11.4 g L^{-1}, M 5640 = 200 g L^{-1}. Open marks: continuous phase. Full marks: dispersed phase.

Table 1. Parameters used in the copper extraction simulation in the pulsed sieve-plate column

Af (cm s^{-1})	$R=Q_c/Q_d$	Q_c (mL s^{-1})	$c_{Cu,c,0}$ (g L^{-1})	$c_{Cu,d,0}$ (g L^{-1})	ϕ	d_{32} (cm)	E_c (cm^2 s^{-1})	E_d (cm^2 s^{-1})
2.07	0.99	1.35	17.2	13.4	0.07	0.35	4.1	1.0
2.25	0.63	1.33	17.0	11.8	0.10	0.27	4.5	2.7
4.07	0.56	1.24	16.3	3.2	0.17	0.14	3.9	1.4

As observed in Figure 2, there is a reasonable agreement between experimental and calculated concentration profiles. From Figure 2 it is also possible to conclude that, under the experimental conditions tested, the K_{oc} parameter remained nearly constant. Having as the main objective to identify the limiting step on the extraction process, it was decided to compare the experimental K_{oc} with the one calculated by the conventional resistance in series model. This model assumes that the process is only diffusion controlled. Thus K_{oc} can be calculated by the expression:

$$\frac{1}{K_{oc}} = \frac{1}{k_c} + \frac{1}{mk_d} \tag{8}$$

k_c and k_d denote, respectively, the mass-transfer coefficient for the continuous and the dispersed phase, while m represents the slope of the equilibrium curve ($c_{Cu,d} = m\, c_{Cu,c}$). k_c was determined by the Steiner correlation [7] and k_d by the Handlos and Baron equation [8]. The densities and viscosities of the continuous and the dispersed phases, necessary for these calculations, were measured at 25 ºC, and the values were, respectively, ρ_c = 1.046 g cm^{-3}, ρ_d = 0.851-0.861 g cm^{-3}, μ_c = 0.012 g cm^{-1} s^{-1}, and μ_d = 0.043-0.045 g cm^{-1} s^{-1}. The diffusivity of Cu^{2+} in the continuous phase is also required for the Steiner correlation and was estimated to be 8.56 × 10^{-6} cm^2 s^{-1} by the Nernst-Haskell equation [9].

The experimental and calculated K_{oc} values are listed in Table 2. From these results, it is inferred that the experimental overall resistance to mass transfer ($R = 1/K_{oc,exp}$) is higher than the one calculated by Equation 8. This difference was calculated and attributed to an additional contribution of a chemical-reaction resistance ($R_r = 1/k_r$) to the mass transfer overall resistance. Then, the relative contribution of each resistance (Δ_i) to the mass transfer overall resistance was calculated. The results presented in Table 2 show that the extraction of copper from an acidic solution by M 5640 in a pulsed sieve-plate column is mainly controlled by the chemical reaction (90-93%). This is consistent with the kinetic data obtained in a stirred tank (data not shown).

Table 2. Overall mass-transfer coefficient of copper extraction, K_{oc}: experimental and calculated (resistances in series model) values

	Exp.	Aq. phase	Org. phase	Calc.*	Kinetic	Resistances**		
Af (cm s^{-1})	$K_{oc}\times10^4$ (cm s^{-1})	$k_c\times10^3$ (cm s^{-1})	$k_d\times10^3$ (cm s^{-1})	$K_{oc}\times10^3$ (cm s^{-1})	$k_r\times10^4$ (cm s^{-1})	Δ_c (%)	Δ_d (%)	Δ_r (%)
2.07	1.90	2.32	11.3	2.29	1.97	7.8	0.1	92.1
2.25	1.90	2.63	12.0	2.60	1.96	6.9	0.1	93.0
4.07	2.20	2.66	8.9	2.62	2.90	9.8	0.2	90.0

* Slope of the equilibrium curve m = 16.67, ** $\Delta_i = R_i/(R_c+R_d+R_r)$

CONCLUSIONS

The extraction of copper from sulphuric acid solutions with M 5640 was studied by using a pulsed sieve-plate column. The axial mixing studies for the continuous and dispersed phases were carried out in the presence of mass transfer and a correlation for

each phase was proposed. The axial-dispersion model predicted reasonably well the experimental mass-transfer data in the column. The experimental values of the overall mass-transfer coefficients are lower (K_{oc} = 1.90-2.20 × 10^{-4} cm s^{-1}) than the ones obtained by using the conventional resistance in series model (K_{oc} = 2.29-2.62 × 10^{-3} cm s^{-1}). Thus, under the experimental conditions tested, the extraction process is mainly controlled by chemical reaction. The relative contribution of chemical reaction resistance to the overall extraction was evaluated to be 90-93 %, while the resistances due to the transport in the aqueous and organic phases were found to be 6.9-9.8 % and 0.1-0.2 %, respectively.

ACKNOWLEDGMENTS

Financial support for this study by Fundação para a Ciência e a Tecnologia (FCT) through the Ph.D. (M. Lurdes F. Gameiro, SFRH/BD/18329/2004) and post Ph.D. (Shiva Agarwal, SFRH/BPD/32429/2006) grants and the project PDCT/EQU/61733/04 is gratefully acknowledged. Many thanks to the Portuguese innovation agency (ADI, PRIME-IDEIA, Project 70/00191), Somincor, and CPQ (IST) for the research facilities.

REFERENCES

1. M. R. C. Ismael and J. M. R. Carvalho, "Copper Recovery from Spent Ammoniacal Etching Solutions", Proceedings of International Solvent Extraction Conference (ISEC´2002), K. C. Sole, P. M. Cole, J. S. Preston, and D. J. Robison, Eds., Chris van Rensburg Publications Ltd, South Africa, 2002; pp. 781–786.
2. J. M. R. Carvalho, "Solvent Extraction of Copper in Pulsed Sieve-Plate Columns," Ph.D. Thesis, University of Bradford, Bradford, England, 1982.
3. K. Gottliebsen, B. Grinbaum, D. Chen, and G. W. Stevens, "The Use of Pulsed Perforated Plate Extraction Column for Recovery of Sulphuric Acid from Copper Tank House Electrolyte Bleeds," *Hydrometallurgy*, **58**(3), 203–213 (2000).
4. T. C. Lo, M. H. I. Baird, and C. Hanson, Handbook of Solvent Extraction, John Wiley & Sons, New York, 1983.
5. A. Kreft and A. Zuber, "On the physical meaning of the dispersion equation and its solutions for different initial and boundary conditions," *Chem Eng. Sci*., **33**, 1471-1480 (1978).
6. T. Miyauchi and H. Oya, "Longitudinal Dispersion in Pulsed Perforated-Plate Columns," *AIChE J.*, **11**(3), 395–402 (1965).
7. L. Steiner, "Mass-Transfer Rates from Single Drops and Drop Swarms," *Chem. Eng. Sci.*, **41**(8), 1979–1986 (1986).
8. A. E. Handlos and T. Baron, "Mass and Heat Transfer from Drops in Liquid-Liquid Extraction," *AIChE J.*, **3**(1), 127–136 (1957).
9. D. R. Lide, CRC Handbook of chemistry and physics: a ready-reference book of chemical and physical data, 85th ed., Boca Raton, 2004-2005, pp. 5-95/96.

COMPARISON OF DISK & DOUGHNUT AND SIEVE-PLATE INTERNALS IN PULSED COLUMNS AT EXTREME PHASE RATIOS

Baruch Grinbaum[1] and Geoff Stevens[2]

[1]Bateman Solvent Extraction, 5 Hamada St., Yokneam 20692, Israel; [2]Chemical and Biomolecular Engineering, University of Melbourne, Victoria, Australia 3010
Corresponding author email address: baruchgr@bateman.co.il

ABSTRACT

The purpose of this work was to compare the dispersion created in pulsed columns with Sieve-Plate (SP) and Disc-and-Doughnut (DD) internals and their combination at high phase ratios. The tested system was DEHPA in kerosene and an aqueous solution of $ZnSO_4$. At phase ratio 1:1, both types of internals created regular drops even at low energy input. At extreme phase ratios in the SP regular drops were obtained, while in the DD, lumps were created. An attempt to use sieve plates as a distributor in a DD column in order to improve the dispersion did not help. The sieve plates, with the right wetting properties, were installed near the entrance of the dispersed phase, before the DD internals. They created the required small drops, but after a few compartments of DD, the effect faded, and the characteristic lumps were obtained.

INTRODUCTION

Both Disk & Doughnut (DD) and Sieve Plate (SP) internals are well known and utilized in pulsed extraction columns. Previous studies [1,2] showed that there is little difference in the performance of both types of internals, as far as the HTU and flux are concerned. These comparisons were done on standard systems: physical extraction of acetone from water to toluene [1], and chemical extraction of H_2SO_4 by Alamine 336 [1], and Zn^{++} by DEHPA [2]. All three are relatively "easy" processes, with quick kinetics and moderate phase ratio (O:A between 1:4 and 4:1).

It is difficult to deduce from these investigations what happens in the more difficult cases, when the phase ratio exceeds 10:1 or the dispersed phase clearly does not create well-defined drops. Unfortunately, many processes in hydrometallurgy follow this description. It happens either when extracting small concentration of the metal from feed with a small volume of solvent e.g., extraction of uranium or in stripping and scrubbing batteries, where small amount of aqueous solution has to scrub/strip a huge volume of solvent.

For SP internals, data about scrubbing of uranium in TBP based solvent at O:W phase ratio of 17:1 and stripping at O:W = 25:1 were published by Ritcey [3]. The highest reported phase ratio for DD was O:A = 1:7, in extraction of uranium [4], with the major phase dispersed. In DD columns, a few processes at phase ratio of 20 were carried

out (e.g., stripping of nickel in O:A of 20 and extraction of uranium at A:O of 20), but they have not yet been published (proprietary data). In all of those situations, the major phase was dispersed in order to provide reasonable mass transfer.

The importance of drop size is common knowledge and is analyzed in many reference books [5,6,7]. The drop size, combined with the holdup, determines the mass-transfer area. As the rate of mass-transfer is proportional to the mass transfer area, small drop size usually improves the mass transfer. For different column types (SP vs. DD), there may be a huge difference in the drop size that may lead to significant difference in the mass-transfer characteristics.

The purpose of this work was to compare qualitatively the drop size, while operating a pulsed column with both SP and DD internals and their combination, at high phase ratio.

EXPERIMENTAL

The Process

The experiments were done in the standard system of extraction and stripping of Zn^{2+} using DEHPA in Kerosene. The column was operated both in the extraction and the stripping steps at ambient temperature. The solvent contained 10% DEHPA in kerosene, the aqueous feed 60 g/L Zn^{2+} and the stripping solution 175 g/L H_2SO_4. At these compositions, mass transfer above 50% was expected both in extraction and stripping. As the main goal of the experiments was to compare visually the drop size and shape, no mass-transfer tests were carried out. In order to view clearly the dispersion, the aqueous phase was colored by traces of Tartrazine (acid yellow 23), and the organic phase by Waxolin blue.

For each type of internals, both aqueous- and organic-continuous dispersions were tested. In the extraction, the dispersion was organic continuous and the aqueous phase was the major one. In stripping, the dispersion was aqueous-continuous, and the organic was the major phase.

Pilot Equipment

The pulsed column had a 72.5 mm internal diameter, and its active section was 1 m high. The column had two small decanters, above and below the active section. Both inlets flowed through a 0.5" pipe, without any distributor. Four sets of internals were used:

1. Stainless steel (SS) sieve plates (SP), 1.5 mm thick, with 50 mm spacing between them. The internal diameter of the holes was 2.64 mm, and the free-flow area was 23%.
2. Plastic (PVC) sieve plates, with thickness, spacing, open area, and diameter of holes similar to set 1.
3. Stainless steel (SS) disk & doughnut (DD) plates, 1 mm thick, 12 mm spacing between each disk and doughnut (26 mm compartment height, i.e., disk to disk). The free-flow area was 23%.

4. Plastic (Teflon) DD plates, with spacing and dimensions similar to set 3. The internals were thicker (3 mm each), and the freeflow area was 26%.

RESULTS AND DISCUSSION

Uniform Internals

For each type of internals, both aqueous- and organic-continuous dispersion were tested at phase ratio of 10:1 and above. For organic-continuous, the aqueous phase was the major phase and vice versa for aqueous-continuous. For some configurations, 1:1 phase ratio was also tested. The amplitude was always 10 mm in the column, while the frequency was varied. The pulsation is expressed as pulse intensity (PI = amplitude x frequency), [cm/s].

Tables 1 and 2 summarize the results.

Table 1. Hydraulic test for stripping with uniform internals-aqueous-continuous

Type of internals	R (O:A)	Flux ($m^3/m^2/h$)	PI (cm/s)	Holdup (%)	Flow Regime*	Appearance
SP ss	10	21	1.0	28	MS	Drops
SP ss	10	27	1.0	43	Dispersion	Fine Drops
SP $_{PVC}$	1	21	2.0	37	Dispersion	Drops
SP $_{PVC}$	1	37	1.0	25	Dispersion	Clusters of drops
SP $_{PVC}$	20	31	1.67	30	MS	Hazy bulks
DD ss	1	24	1.2		Dispersion	Drops
DD ss	10	33	1.0	35	Dispersion	Lumps
DD ss	10	24	1.0	30	MS	Lumps/Big drops
DD ss	10	10	1.67	30	MS	Drops
DD $_{Teflon}$	1	20	1.0	20	MS	Lumps
DD $_{Teflon}$	13	34	1.0	40	MS	Lumps
DD $_{Teflon}$	15	15	1.35	20	MS	Lumps
DD $_{Teflon}$	10	24	1.05	25	MS	Lumps
DD $_{Teflon}$	7.5	16	1.67	37	Dispersion	Drops

*MS means mixer-settler flow regime; that is, the separated layer may be observed in the compartment.

Table 2. Hydraulic test for extraction with uniform internals-organic-continuous

Type of internals	R (A:O)	Flux $m^3/m^2/h$	PI (cm/min)	Holdup (%)	Flow Regime	Appearance
SP ss	10	21	1.25	36	MS	Lumps /Big Drops
SP ss	10	21	1.6	45	Emulsion	Drops
SP $_{PVC}$	1	21	1.67	22	Dispersion	Drops
SP $_{PVC}$	20	15	1.25	18	Dispersion	Fine drops
DD ss	10	22	1.2	30	Dispersion	Lumps
DD $_{Teflon}$	1	25	1.0	13	Dispersion	Drops
DD $_{Teflon}$	10	15	1.5	28	Dispersion	Lumps

Visual Observations:

a. At O:W=10 and low energy, the organic phase dispersed to drops in the SP, but remained in lumps in the DD. With high energy, drops were obtained along the entire column with both types of internals
b. The drops (if present) appear to be at their final size already after the first plate in both types of columns. As the column was below one meter, it is difficult to predict what would happen in a longer column.
c. The drops are smaller approaching the sieve plate and larger after passing it. The size of the drops was always larger than the diameter of the holes in the plate.

The results show that SP internals from the appropriate material increased the chance of obtaining small drops at high phase ratio, without the risk of flooding or phase inversion. With aqueous continuity, metal SP resulted in fine drops, while for organic-continuous, the plastic SP produced a haze that seemed to have good mass-transfer characteristics. The disk & doughnut internals did not produce reasonable drops at high phase ratio in MS or even dispersion regime. As DD internals have their obvious merits, an attempt was made to test a combined column.

Combined Column

All possible options, namely both metal and plastic SP at the bottom of the column with plastic DD internals and plastic SP at top of column with metal DD internals, were tested. They were installed (sequentially of course) in the same column, to make the comparison as exact as possible.

SP at bottom of a Teflon DD column

The results with plastic (PVC) SP are summarized in Table 3, and with metal (SS) SP – in Table 4.

Table 3. Two Plastic SP at Top of Plastic DD Internals—Organic Phase Continuous

Flux ($m^3/m^2/h$)	Phase ratio (A:O)	PI (cm/s)	Flow Regime	Holdup (%)	Flood	Remarks
24	1	1.0	Dispersion		N	Drops in SP, big drops + lumps in DD
24	1	1.25	Dispersion		N	Drops in SP & DD
20	10	1.0	MS	20	N	Drops in SP, lumps in DD
20	10	1.25	Dispersion	30	N	Drops in SP, lumps in DD
23	10	1.25	Dispersion	35	N	Drops in all parts
23	10	1.67	Dispersion		Y	Flooding in SP

Table 4. Metal (SS) SP at top of plastic DD—Organic phase continuous

Flux ($m^3/m^2/h$)	Phase ratio (A:O)	PI (cm/s)	Flow Regime	Holdup (%)	Flood	Remarks
24	1	1.0	Dispersion		N	Drops in SP, big drops in DD
24	1	1.25	Dispersion		N	Drops in SP & DD
20	10	1.0	MS	20	N	Drops in SP, lumps in DD
20	10	1.25	Dispersion	30	N	Drops in SP, lumps in DD
23	10	1.25	Dispersion	35	N	Drops in all parts
23	10	1.67	Dispersion		Y	Flood in SP

Plastic (PVC) SP at Bottom of Metal (SS) DD Internals—Aqueous Phase Continuous

The experiment was carried out with two plastic (PVC) sieve plates installed 50 mm below the last disk. The phenomenon was very similar to the previous test: at O:A=10 at low energy, the organic phase dispersed as well-defined small drops in the SP, but within one compartment height, they had coalesced and got the bulky shape that they had without the SP. With high pulsation intensities, drops were obtained along the entire column. At phase ratio 1:1, drops were obtained along the entire column even at low energy.

Flooding

When flooding happened, it always developed in the SP section, both in aqueous-continuous and organic-continuous dispersions. Apparently at the tested conditions, the DD internals may work at higher flux than the SP.

DISCUSSION

As one may see from the results, at high phase ratio (either organic- or aqueous-continuous), the dispersed phase tends to agglomerate and creates lumps, especially when internals with the wrong wetting properties are used. It could have been expected, as at high phase ratio, the holdup of the dispersed phase increases (as noticed by Gayler & Pratt [8] 50 years ago) and it occupies a larger part of the column, causing, in some cases, coalescence of the drops to big lumps.

Sieve plates create a better dispersion, that is, more regular and smaller drops than disk & doughnuts at high phase ratio, in both dispersions. However, at a phase ratio about 1:1, the dispersion is similar, at phase ratio of 10 and above it, the difference is huge. This result suggests that at high phase ratio there may be an advantage to SP over DD internals. Still, the drops that go though the holes in the plates are larger than the holes themselves.

An attempt was made to create a combined column, that is, to use sieve plates with the right wetting properties, as a distributor for a DD internals. The results were poor; during the passage through the SP, the phase was dispersed to regular small drops, as any good distributor would do, but within a few compartments of DD, their influence

had faded. After flow through less than 50 cm in the column, the distribution was exactly as it was without any SP, and the characteristic lumps were obtained.

CONCLUSIONS

While at standard phase ratios there is no obvious difference neither between the dispersion created by both types of internals nor the available flux and HTU, at high phase ratio the DD pulsed column tends to create *huge lumps* instead of drops, potentially harming the mass transfer (although it was not proven experimentally). The phenomenon is more pronounced when using internals that are not wetted by the continuous phase. The SP internals create reasonable drops even at high phase ratio.

Addition of a sieve plate with the right wetting properties on top of the DD internals to serve as a distributor, does not help. The SP creates the required small drops, but within few compartments of DD, their influence fades and the characteristic lumps are regenerated. Unfortunately, it means that *combined SP+DD internals do not help to improve dispersion in the column*. Accordingly there was no point to make any mass-transfer tests to further investigate this point.

REFERENCES

1. A. Jahya, H. R, C, Pratt, and G. W.Stevens, "Comparison of the Performance of a Pulsed Disc and Doughnut Column with a Pulsed Sieve Plate Liquid Extraction Column," *Solvent Extr. Ion Exch.*, **23(**3), 307-317 (2005).
2. E. Kolman, I. Ilan, B. Grinbaum, and G. Stevens, "Comparison of Disk & Doughnut vs. Sieve Tray internals," ISEC 2005 proceedings, Beijing, 2005.
3. G. M. Ritcey, Solvent Extraction, vol. 2, Gordon M. Ritcey, Canada, 2006; pp. 547-548.
4. R. L. Movsowitz, R. Kleinberger, E. M. Buchalter, and B. Grinbaum, "Comparison of the Performance of Full Scale Pulsed Columns vs. Mixer-Settlers for Uranium SX," Solvent Extraction for the 21st Century, M. Cox, Hidalgo, and M. Valiente, Eds., SCI, London, UK, 2001; **2** pp. 1455-1460.
5. T. C. Lo, M. H. I. Baird, and C. Hanson, Handbook of Solvent Extraction, Wiley, New York, 1983.
6. H. J. Bart, Reactive Extraction. Springer, Berlin, 2001.
7. H. J. Bart and G. W Stevens, "Reactive solvent extraction," Ion Exchange and Solvent Extraction, Y. Marcus and A..K. Sengupt,a (Eds), Marcel Dekker, 2004; 17, pp. 37-83.
8. R. Gayler and H. R. C.Pratt, "Holdup and pressure Drop in Packed Columns", *Trans. Instn. Chem. Engr.,* **35**, 273 (1957).

DESIGN OF PASSIVE DECANTERS FOR SX COLUMNS

B. Grinbaum

Bateman Solvent Extraction, 5 Hamada St., Yokneam 20692, Israel
Corresponding author email address: baruchgr@bateman.co.il

ABSTRACT

This paper analyzes the functioning of the passive decanter in solvent-extraction columns and offers both a theoretical and experimental procedure for the design of the decanter. The calculation of the flux in the passive decanter as a function of the drop size of the entrainment, physical properties, and phase ratio are described. Once a reliable correlation between the drop size and the entrainment is available, it may be directly applied to the design of decanters. As of now, there is no such model available, just as there is no reliable model for settlers. An experimental procedure to evaluate the separation velocity is recommended. It involves the measurement of the entrainment leaving the passive decanter when the column is operated at the design conditions (temperature, flux, phase ratio, and energy input if applicable) with the smallest reasonable decanter. If the entrainment is within the process constraints, the measured velocity is used as the separation velocity in the design of the decanter. Otherwise, a larger decanter should be utilized and the measurement repeated until the required level of entrainment is obtained. The procedure is simple and may be easily incorporated into the standard piloting of the column.

INTRODUCTION

In any solvent-extraction (SX) device, there is an element in which the mixed phases separate after mass transfer has taken place. In mixer-settlers (MS), this element is the *settler*. To ensure efficient phase separation, SX columns have two settling chambers. Usually they reside at the bottom and top of the column, but may otherwise be detached from the column. In the literature, these settling chambers are often referred to as *settlers*. In this paper, to avoid confusion, the separating chambers of columns are named *decanters*, while the term *settler* refers to the separating chamber of mixer-settlers.

Much has been published on the development of improved procedures for the scale up of SX columns. A few papers have been published on the design and scale-up of settlers, and they are summarized in books [1,2]. On the other hand, very little has been reported on the design of the column decanters, and no model is available to calculate the permissible flux through them. This article analyzes the functioning of decanters and offers rules for the improved design of the passive decanter. The analysis is valid for all types of columns, as the separation mechanism is similar in all columns.

DECANTER VS. SETTLER

The settler is fed with the dispersion created in the mixer. In most cases, the major phase is continuous. The flux through the settler, J, is calculated as the total volumetric flow of the dispersion from the mixer divided by its cross-sectional area.

In the settler three zones are distinguished:

- Continuous phase with some entrainment of the dispersed phase.
- Dispersion zone that consists of sedimentation and coalescence subzones.
- Separated dispersed phase (with some entrainment of the continuous phase).

In decanters, there is a major functional difference between the *active* and the *passive* decanter. The active decanter is located near the entrance of the continuous phase, while the passive decanter is near the entrance of the dispersed phase.

In the *active* decanter, the dispersed phase separates from the continuous phase. Part of the decanter is occupied by the continuous phase and the rest with the dispersion and separated dispersed phase. The action of the *active* decanter is similar to zones 2 and 3 in the settler. The active decanter is not dealt with here.

The passive decanter is filled with the continuous phase, which contains a small amount of entrained dispersed phase. Its function is similar to zone 1 in the settler.

THE FLUX THROUGH THE PASSIVE DECANTER

The function of the passive decanter is twofold, namely:

- to separate the entrained droplets of the dispersed phase from the continuous phase, and
- to serve as a buffer in case of flooding.

Separation of the Dispersed-Phase Drops

While the total amount of the entrained dispersed phase varies as a function of the system and the operating conditions, it is usually small enough to neglect in the calculation of the flux in the passive decanter. Thus, the flux through the passive decanter J_p and the velocity of the continuous phase in the decanter V_c have the same value:

$$V_c = J_p = Q_c/A \tag{1}$$

where Q_c is the volumetric flow rate of the continuous phase [m^3/h] and A is the cross sectional area of the decanter [m^2]. Note that in a one-phase flow, both the flux and the velocity have the same dimension, m/h. From dimensional-analysis considerations, the unit of flux, $m^3/m^2/h$, can be reduced to m/h.

Settling Velocity

The settling velocity V_s of dispersed phase droplets is defined as the velocity of the drops through a static continuous phase. This definition is almost identical to the

characteristic velocity V_o defined by Gayler and Pratt [3] in their work on packed columns.

For creeping flow, as expected in a decanter, the settling velocity may be calculated using Stokes law:

$$Vs = g\, d^2\, \Delta\rho / 18\, \mu_c \tag{2}$$

where d - the diameter of the drop [m], Vs – the separation velocity of the drop [m/s], $\Delta\rho$ – the difference in density between the phases [kg/m^3] and μ_c – the viscosity of the continuous phase [Pa×s].

Stokes Law may be applied for low Reynolds number ($Re < 2$), where

$$Re = d \times Vs \times \rho_c / \mu_c \tag{3}$$

For $Re>2$, modifications to Stokes Law are required.

From Equation 2 the separation velocity in the Stokes range is inversely proportional to the viscosity. As the viscosity usually doubles with a 10°C decrease in the temperature, it is clear why higher temperatures sharply decrease the entrainment of especially tiny droplets.

In the passive decanter, after a briefly slowing down, the continuous phase flows with a constant velocity Vc. In order to prevent all the drops above a given diameter, d, from being entrained out of the decanter, *Vc must be smaller than Vs.*

This implies that the minimum diameter of the decanter D_{dec} [m] required to separate drops above a given diameter, (*i.e.* to have flow rate of Vs), is:

$$D_{dec} = 2[Q_c/(\pi Vs)]^{0.5} \tag{4}$$

where Q_c is the flow rate of the continuous phase. This means that, unlike with conventional settlers, *additional height does not decrease the entrainment.*

While no explicit data on the flux in decanters were found in the open literature, it is known that the flux in industrial columns is between 15 to 50 m^3/m^2/h and the ratio of the diameter of the decanter to the diameter of the column D_{dec}/D_{col} is usually 1.5 to 2 [2] and may go down to 1. This implies that the maximum flow velocity in the decanters is usually below 25 m/h.

Table 1. Separation velocity in the passive decanter vs. entrained drop size

Drop diameter (mm)	0.05	0.1	0.15	0.2	0.3	0.5	1.0	1.5
Aqueous continuous								
Vs (m/h)	1.2	4.9	11.0	19.6	44.0	64.5	142	227
Re	0.02	0.14	0.48	1.14	3.9	9.4	42	99
Organic continuous								
Vs (m/h)	0.4	1.6	3.7	6.5	14.7	40.8	96	153
Re	0.01	0.05	0.16	0.38	1.3	2.12	9.4	22.2

Table 1 shows the calculated Reynolds numbers and settling velocity in a passive decanter, as a function of the maximum entrained drop size. The following parameters

were assumed: μ_a = 1000 Pa×s; μ_o = 3000 Pa×s**;** ρ_a = 1050 kg/m^3; ρ_o = 800 kg/m^3. These conditions are typical for many SX processes.

The main conclusions from the table are:

- In the range of interest, up to a separation velocity of 25 m/h, *Re* is really below 2 and Stokes Law may be safely applied. Higher velocities in decanters are not of practical interest.
- The smallest droplets that may be retained in the passive decanter are in the range of 0.1-0.3 mm, depending on the physical properties of both liquids, phase ratio, continuity and the size of the decanter.

It is important to remember that *knowledge of the critical drop size alone is of no practical value,* as long as the drop size distribution in the decanter is unknown. At present, it is difficult to measure or to predict drop size, and only the experimental measurement of the entrainment delivers the true information.

The superficial velocity of the continuous phase in the column is equal to:

$$Vc_{col} = J/(1+R) = J/[1+ Vd/(Vc + Vd)] \quad (6)$$

where R is the phase ratio *d:c.* The velocity is shown, as function of R, in Figure 1.

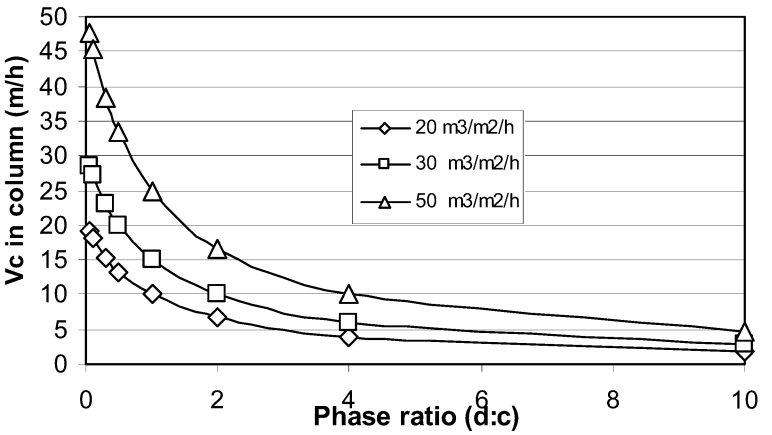

Figure 1. Velocity of the continuous phase in the column vs. phase ratio.

The velocity of the continuous phase in the passive decanter is equal to:

$$Vc_{dec} = Vc_{col} \times (D_{col}/D_{dec})^2 \quad (7)$$

with Vc_{col} given by Equation 6. Knowing (or assuming) the required velocity in the passive decanter V_{dec}, the diameter of the decanter is given by:

$$D_{dec} = D_{col} \times (Vc_{col}/V_{dec})^{0.5} = D_{col} \times [J/(1+R)\ /V_{dec})]^{0.5} \quad (8)$$

For $D_{dec} = D_{col}$ the flux in the decanter is given by Figure 1. It can be seen that for phase ratio *d:c>4* the flow rate is low enough (10 m/h at high flux in the column and ~4 $m^3/m^2/h$ for a low flux) that there is no need to make a decanter larger than the column diameter, regardless of the flow characteristics.

Figure 2 shows the ratio D_{dec}/D_{col} as a function of the flux in the column *J* and the phase ratio *R*, assuming that the permitted velocity in the decanter V_{dec} is 10 m/h.

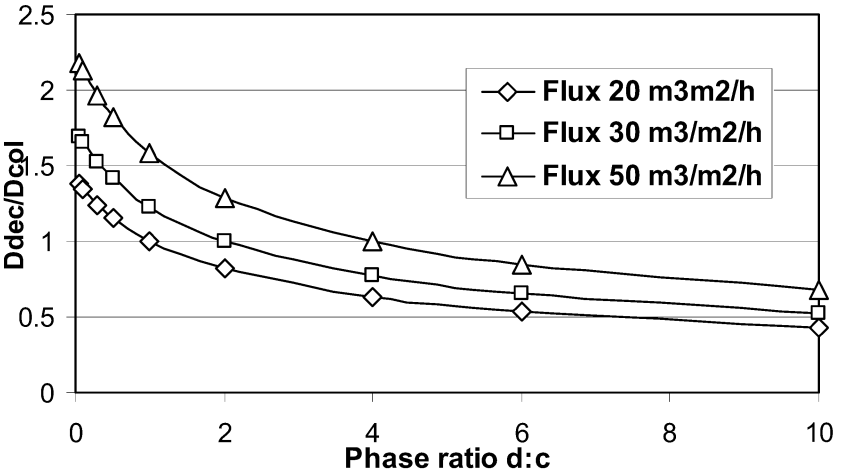

Figure 2. D_{dec}/D_{col} vs. the flux in the column and the phase ratio for V_{dec} =10 m/h.

From Figure 2 it is clear that the phase ratio is of paramount importance in calculating the size of the passive decanter. For low *c:d* ratios (i.e. the major phase is dispersed) given entrainment may be separated with rather small decanter, while at high *c:d* ratios (major phase is continuous) the decanter must be far larger.

EXPERIMENTAL PROCEDURE FOR DESIGN OF INDUSTRIAL DECANTERS

As there is no valid model to calculate the drop size distribution, an experimental procedure to find the separation velocity in the passive decanter is required. The procedure is based on the assumption that the drop size distribution leaving a pilot scale column is similar to that of an industrial column. It is valid only for diameter above 50 mm, as at smaller vessels the wall effects become large and predictions and scale up are poor.

The diameter of the passive decanter in the pilot plant should be set according to the expected phase ratio and flux in the tested column, using Equations 6 - 8. During the experiments the entrainment in the outlet should be measured. If the entrainment is within the design criteria, the velocity in the decanter is the separation velocity *Vs* or below, and the diameter of the industrial unit may be calculated directly using Equation. 8. If the entrainment is too high, a larger passive decanter should be installed and tested in the pilot plant *after* the basic piloting has been finished, and the recommended design

conditions, (e.g. dispersion, flux, pulsation intensity, phase ratio etc.) have been determined. During testing of the decanter, the experimental column should be run at these conditions. This means additional experimental work that is labor intensive, especially with an aqueous continuous dispersion, where the lower decanter has to be replaced with a wider one. The shortcut procedure of decreasing the flux in the column instead of replacing the decanter is risky, as it may result in the variation of the drop size distribution near the outlet of the continuous phase.

The scale up of this procedure is simple: Calculate the diameter of the industrial decanter keeping the same linear velocity that delivered satisfactory results in the pilot, with an increased height as a safety factor to allow for possible flooding.

CONCLUSIONS

The calculation of the flux in the passive decanter as a function of the drop size of the entrainment, physical properties and phase ratio is described. Once a reliable correlation between the drop size and the entrainment is available, it may be directly applied to the design of decanters. As of now, there is no such model available, just as there is no reliable model for settlers.

An experimental procedure to find the separation velocity is recommended as an alternative. It involves the measurement of the entrainment leaving the passive decanter when the column is operated at the design conditions (flux, phase ratio and energy input if applicable) with the smallest reasonable diameter of the decanter. If the entrainment is within the process constraints the measured velocity will constitute the separation velocity and the decanter is designed using Equation 8. Otherwise a bigger decanter should be installed and the measurement repeated until the required level of entrainment is obtained. The procedure may be incorporated into the standard piloting of the column.

REFERENCES

1. T. C. Lo, M. H. Baird, and C. Hanson, Handbook of Solvent Extraction, John Wiley & Sons, New York, 1983.
2. G. M. Ritcey, Solvent Extraction, vol. 1, Gordon M. Ritcey, Eds., Canada, 2006.
3. R. Gayler and H. R. C. Pratt, Hold-up and Pressure Drop in Packed Columns. *Trans. IChemE.,* **29**, 110-125 (1951).
4. G. M. Ritcey, Solvent Extraction, vol. 2, Gordon M. Ritcey, Eds., Canada, 2006; pp. 526-528.

SX PURIFICATION OF FERTILIZER-GRADE PHOSPHORIC ACID USING BPC: LABORATORY SCALE TO INDUSTRIAL PLANT

A. Efraim and R. Movsowitz

Bateman Advanced Technologies Ltd, 5 Hamada St., Industrial Zone, Yokneam 20692 Israel. Corresponding author email address: alone@bateman.co.il

ABSTRACT

The use of solvent extraction has become common practice in the purification of phosphoric acid, replacing the traditional P4 process that is being phased out due to environmental issues and high energy costs. To produce purified phosphoric acid for industrial applications, laboratory test work should first be performed to verify the process. The testwork starts with the screening of a suitable solvent for the particular application and the preparation of the relevant equilibrium curves. The results are interpreted using proprietary simulators. Pilot tests follow to determine operating and scale-up parameters based on Bateman Pulsed Column technology. Based on parameters obtained in laboratory and pilot tests on a client's fertilizer-grade phosphoric acid, an industrial plant was built and commissioned. The commissioning was successfully concluded during the first quarter of 2007 and confirmed all the design parameters without any modifications.

INTRODUCTION

The paper deals with the scale up of the Purified Phosphoric Acid (PPA) process from laboratory, through pilot to industrial scale. An experimental program carried out at the Bateman Advanced Technologies Laboratories in Israel, determined the feasibility of producing food-grade phosphoric acid (FGA) from wet-phosphoric acid (WPA) obtained from a client and provided the scale-up parameters for an industrial PPA plant.

The solvent-extraction (SX) section in the PPA process includes the following four main operations:

- Extraction using a Bateman Pulsed Column (BPC)
- Sulfate Removal using a Mixer-Settler
- Purification using BPC
- Washing using BPC

In addition, several side streams are treated to adjust product concentration or to remove impurities. Theses stages are not addressed in this paper.

PROCESS DESCRIPTION

In the extraction step, pre-treated WPA and recycled return acid (RA) from the purification column, together termed Feed Acid (FA), enter the extraction column, where the FA is contacted with barren organic solvent. A large portion of the phosphoric acid passes into the organic phase, leaving most of the impurities in the aqueous raffinate stream. The "overall split" is such that ~53% of the phosphoric acid is extracted and about 47% remains in the raffinate.

In the sulfate removal step, sulfate and arsenic ions in the loaded solvent (LS) are reduced prior to purification, to satisfy the FGA specification. A mixer-settler is used for this step.

In the purification step, the scrubbed solvent after sulfate reduction is contacted in the purification column with a reflux stream of purified phosphoric acid (PA), from the washing column. The PA must be in equilibrium with the scrubbed solvent, and thus only impurities are transferred to the RA, while the phosphate concentration in the scrubbed solvent remains unchanged.

The purified loaded solvent is then contacted with treated water or steam condensate in the washing column. Here, the phosphoric acid is washed from the organic phase using de-ionized (conductivity below 10 μS) water to yield the PPA stream.

LABORATORY SX TEST WORK

The solvent applied in this process was chosen based on Bateman's previous experience. The laboratory experiments generated equilibrium data between the selected solvent and the aqueous solutions in the process for phosphate (expressed as P_2O_5), metal contaminants, and H_2O. A number of methods for sulfate removal were tested at different SO_4 concentrations in the FA in order to reach the target concentration of sulfate in the PA.

These equilibria were studied in systems simulating the various stages of the SX section of the process using the methodology described by Grinbaum [1]. The results show that the ability of the solvent to extract H_3PO_4 from the relevant aqueous phases follows the order: Purification/Washing>FA>Pre-treated WPA. This order is the result of two main factors: the amount of H_3PO_4 that is neutralized in the pretreatment process and is present in the aqueous solution as a $H_2PO_4^-$ salt and the concentration of impurity salts. The greater the available free acidis, the isbetter the extraction yield. Phosphate that is present in the salt form ($H_2PO_4^-$) is not extractable by the solvent; only phosphoric acid (H_3PO_4) is extracted. The presence of impurity salts in the aqueous phase decreases the distribution constants of phosphoric acid between the two phases so that the equilibrium curve is shifted to the right. The concentration of water in the solvent, is strongly dependent on the H_3PO_4 concentration in the solvent and it was found to be higher in Extraction than in Purification/Washing.

On the basis of past experience, the three impurity metals, Fe, Mg, and Al, were selected to produce metal equilibrium curves for the purification step. Since the Al was significantly lower in the present case, the study was based on the equilibrium curves of Mg and Fe.

The laboratory results were used to prepare liquid-liquid equilibrium correlations for all three steps, and these were incorporated into a solvent-extraction simulation program. Using the simulator, initial phase ratios and NTU for each column are determined. There is always a trade-off between phase ratio and NTU. Optimization is done by the simulator and is confirmed during the pilot tests.

PILOT RESULTS AND THE IMPLICATION ON INDUSTRIAL PLANT

Pilot test work is divided into two sections: hydraulic tests and mass-transfer tests. The PPA pilot plant comprises three 40 mm diameter BPCs: the extraction column (7m active height), the purification column (7m active height), and the washing column (5m active height). The columns are insulated to minimize heat losses.

Hydraulic Tests

Hydraulic tests (HT) are performed to determine the optimum conditions in terms of flux and pulsation intensity (PI) for each process step. The flooding curve is the HT output. The standard Bateman procedure for HTs described in detail elsewhere [1] was used. Since the BPC pilot units have PVDF internals and stainless steel is being considered as material of construction for the industrial units, the effect of column internals on the flux in the BPCs was compared in tests with both PVDF and stainless internals. Similar results were obtained, and this meant that there was no need to make any changes to the proposed operating conditions for the pilot and full-scale units.

Based on previous experience, tests were carried out in organic-continuous mode for all three steps.

The HTs are started in closed circuit with both phases recirculated in a closed loop for each of the pilot columns. It was however known, based on the laboratory tests, that in the PPA process the large inter-phase mass transfer of both H_3PO_4 and H_2O can significantly affect phase density, viscosity, and surface tension, and hence results should be used only as a preliminary indication of operating conditions. The operating parameters (flux, PI, etc.) were checked during the pilot-plant operation and altered, as required, in order to optimize process constraints.

All three process steps were designed to operate at 40-45 ^{o}C, and thus some feed streams were preheated. The maximum fluxes attained without flooding were:

- Extraction: ~45 $m^3/m^2/h$ at a PI of 700 mm/min and O:A flow ratio of 5:1;
- Purification: ~25 $m^3/m^2/h$ at a PI of 600 mm/min and O:A flow ratio of 10:1;
- Washing: >60 $m^3/m^2/h$ at a PI of ~2000 mm/min and O:A flow ratio of 7:1.

Column hold-up varied but was typically low, between 3 and 8%, as expected when the quantity of dispersed phase is relatively small. Typical drop size observed was <1 mm in both extraction and purification steps. In the washing column, the droplets were larger at 2-5 mm and tended to decrease as the PI increased.

Based on the pilot results and including certain safety factors, the optimum fluxes chosen for the design and scale-up to industrial-scale units were:

- 40 $m^3/m^2/h$ for extraction,
- 22.5 $m^3/m^2/h$ for purification,

- 42 $m^3/m^2/h$ for washing.

The flux determines the diameter of the industrial column.

Mass-Transfer Tests

The intention of the mass-transfer tests (MT) is to optimize operating parameters such as flux and PI, determined in the HT phase, and to develop data for the design and scale-up of the pilot columns to full scale. As all the available BPCs had identical diameters, the operating parameters were chosen to give maximum nonflooding flux in the limiting step (i.e. the purification column). In addition, each column was operated at its optimum conditions, with the others used only to service the column being tested for long test runs.

This section deals with only the extraction column. The purification and washing columns use the same methodology. While always operating organic-continuous, the O:A ratio was varied over a narrow range of 4.5-5:1 and operating temperatures were 40-45 ^oC. In most tests, the flux was 20 $m^3/m^2/h$ and PI maintained at 2,700 mm/min. As mentioned previously, these are not the optimal parameters found during the HTs but rather the extraction conditions required to operate the entire SX system. The selected PI, while adequate, is considered high. The required flux, 50% from the nominal value, required the dramatic increase in PI. This PI is neither applicable, nor required, in industrial application. Thereafter, the tests were carried out at steady-state conditions, and the data was reproducible and consistent with prior experience. The variation in physical properties was found to be minimal. It was also found that the interfacial tension was very low at 0.08-0.17 mN/m.

The control, stability and consistency of the BPC operation is assessed by means of overall and P_2O_5 mass balances carried out on cumulative samples in each run. The design factors inherent in the scale-up of the BPC depend on the concentration profiles measured along the height of the column. The design procedure itself is a function of the nature of the process under consideration (whether mass transfer or kinetically controlled), and the parameters of flux, PI, hold-up, and extraction efficiency are determined in the pilot study. The columns are equipped with special valves for collecting samples of one phase at a given location. In this way a concentration profile of any element along the column can be obtained to assist with deciding the height of the industrial column.

SCALE-UP CONSIDERATIONS

The industrial plant design is based on laboratory and pilot test work, using proprietary simulators and in-house data base. Scale-up considerations for the primary design parameters are discussed in this section.

Dispersion: Generally, both dispersion modes are checked during the HT phase, and the dispersion yielding the higher fluxes is selected. Hold-up and droplet size, although sometimes misleading, are other factors used to evaluate performance for each continuity mode. In the case of both dispersions exhibiting similar performance, mass-transfer tests are done using both organic and aqueous dispersions, and the preferred

continuity mode is selected according to the analytical results. If both continuities yield similar performance, aqueous-continuous mode is always preferred for economic and safety reasons. The laboratory results and pilot operation proved, however, that all of the process steps should be carried out in the organic-continuous mode, as it enabled higher fluxes and better mass transfer.

Phase ratio: Initial phase ratio is determined using the simulator. Efficient use of the simulator requires input of the H_3PO_4 equilibrium curve or, in the case of the purification step, the limiting impurity equilibrium curve. In the specific application discussed here, the limiting impurity is Fe. Thus, Fe was the representative impurity for determination of the purification-step operating parameters, such as phase ratio and column height. The simulation is iterative, and once acceptable convergence is achieved, the pilot plant is operated using the representative results in order to confirm the results. Any fine adjustments are made on-line during the pilot test.

Flux: The flux can be directly scaled up from pilot unit to industrial application. The nominal flux of the industrial BPC was based on the flux obtained during the pilot MT and includes some safety factors.

Column diameter: Column diameter is based on the nominal flux determined as described above. The column diameter (D_{col}) is calculated using the equation:

$$D_{col} = ((4 \text{ x } (Q_{aq} + Q_{org}))/(\Pi \text{ x } J))^{0.5} \quad (1)$$

Where Q represents volumetric flow rate (m^3/h), J nominal flux ($m^3/m^2/h$), and the subscripts aq and org denote conditions in the aqueous or organic phase, respectively. The decanter diameter is generally 1 to 1.5 times the D_{col} and depends on separation times and is a function of entrainment considerations. The column leg diameter is generally 25% of D_{col}.

Height of active section: Scale-up of height of a BPC is calculated using the equation:

$$H_i = H_p \text{ x } (D_i / D_p)^a \quad (2)$$

Where a is a constant, H is column height (m), D is column diameter (m), and the subscripts i and p denote industrial or pilot scale, respectively.

Pulsation system: The PI needed at the optimal flux is determined from hydraulic tests and confirmed and/or adjusted in mass-transfer tests to optimize column operation. In the pilot BPC, either a mechanical pulsator or pulsation leg is used, as they have the same effect in terms of stroke amplitude and frequency for the same column operating conditions. The PI is defined as the product of the stroke amplitude in an active section and the frequency of the stroke. For a mechanical pulsator, the two parameters are independent, while for a pulsation leg at a given pressure, the higher is the frequency, the lower is the amplitude and vice versa. The maximum frequency applicable in industrial applications, due to mechanical and kinetic considerations, is 30 spm, while for a pilot unit, frequency can reach values of 150 spm. A dedicated simulator calculated the PI and the air requirements for the industrial columns, based on geometrical and physical properties of the experimental columns and the solutions.

PILOT VS. THE INDUSTRIAL PLANT

Operating parameters and inlet and outlet profile analyses for pilot- and industrial-scale plant extraction-column operation are compared in Tables 1 and 2, respectively. The plant results fit those of the pilot plant within experimental error (referring mainly to instrumentation inaccuracy).

Table 1. Comparison of pilot- and industrial-plant extraction-column operating parameters

Pilot/ Plant	Ratio	Flux	Temp. Top	Temp. Bot.	Hold-up Ave.	Ent.* W/O	Amp.	Freq.	PI
		$m^3/m^2/h$	°C	°C	%	ppm	mm	spm	mm/min
Pilot	4.9	40.3	46.1	49.6	4	<100	9.3	75	698
Plant	5.0	43.6	45.0	41.0	2	<100	138	10	1380

* Ent. W/O denotes water in organic phase entrainment

Table 2. Comparison of pilot and industrial plant Extraction col. P_2O_5 inlets and outlets

	P_2O_5 Concentration (%)			
	Aqueous		Organic	
	in	out	in	out
Pilot	54.57	42.38	0.02	12.18
Plant	53.5	34	0.2	12

CONCLUSIONS

An intensive laboratory study was carried out at the Bateman laboratories in Israel to evaluate the necessary physico chemical data and define suitable operating conditions for the pilot study. The proprietary simulators together with pilot study confirmed the process and determined the necessary design and scale-up conditions. The commissioning of the industrial plant was successfully concluded during the first quarter of 2007and has confirmed all of the design parameters.

REFERENCE

1. B. Grinbaum, “Integrative Method for Development of Solvent Extraction Processes,” Ion Exchange and Solvent Extraction, Vol. 15, Y. Marcus and A. Sengupta, Eds., Marcel Dekker, New York, 2001; pp. 1-106.

PILOT-SCALE STUDIES OF AN ELECTROSTATICALLY AGITATED SOLVENT-EXTRACTION COLUMN

M.J. Steffens and D.C. Ibana

Western Australian School of Mines, Curtin University of Technology
PMB 22 Kalgoorlie, W.A. 6433, Australia
Corresponding author email address: M.Steffens@curtin.edu.au

ABSTRACT

Bench-scale studies have shown that the use of contactors utilizing electrostatic agitation in solvent extraction has numerous advantages over conventional mechanically agitated contactors, including vigorous low-shear mixing, significantly higher mass-transfer rates, higher energy efficiency and vigorous low-shear mixing, but the low fluxes previously achieved appear to hinder commercialization of the technique. As part of an effort to develop a commercial application of an electrostatically agitated solvent-extraction (ESX) contactor, a pilot-scale ESX column was constructed, and its application in the extraction of nickel from an acidic pregnant liquor stream generated by pressure acid leaching was investigated. It was found that an applied voltage of 6.0 kV/cm at a frequency of 40 Hz yielded fluxes up to 55 $m^3/h/m^2$, which is comparable to that typically achieved in mechanically agitated (pulsed) columns but allowed high mass-transfer rates over a wider range of fluxes. This is a significant step towards commercialization of the technique.

INTRODUCTION

Electrostatic agitation involves the use of an electrostatic field to disperse the aqueous feed in the solvent and facilitate the motion of the dispersed droplets in a way that favors mass transfer. Several bench-scale studies, including those from our laboratory show that electrostatically assisted solvent extraction (ESX) provides a more uniform dispersion [1], higher mass-transfer rates [2] and energy efficiencies [3], as well as a vigorous low-shear mixing [4]. The main limitation of the technique appears to be the apparently lower fluxes that have been achieved previously [3,5-8] compared to those values typical [9] in conventional pulse columns used commercially (Table 1).

The aqueous flux is the volumetric flow rate of aqueous feed solution per cross-sectional area of the column, typically expressed in the units of $m^3/h/m^2$. The flux that can be achieved within a column is a basic consideration for any new contactor to progress beyond pilot scale, because if the throughput of current contactors cannot be met or, preferentially, exceeded, then there is little incentive for commercialization. In addition to fluxes, the mass-transfer performance of the column must also be considered,

as a sufficient flux without adequate mass transfer will, again, provide no significant advantage over current contactors.

To address this issue, a pilot-scale ESX column was designed and constructed, the electrostatic field conditions were optimized, and the fluxes at various phase ratios and nickel extraction capacities were explored. This paper reports the results.

Table 1. Aqueous fluxes for various ESX and pulse columns

Source	Column Type	Highest Aqueous Flux ($m^3/h/m^2$)
Martin et al. (1983) [5]	ESX Column	3.77
Suyama et al. (1993) [6]	ESX Column	0.48
Usami et al. (1993) [7]	ESX Column	2.95
Scott et al. (1994) [3]	ESX Column	9.15×10^{-4}
Briggs et al. (2000) [8]	ESX Column	2.41
Ritcey (2006) [9]	Bateman Pulse Column	15-70
	Sieve-Plate Column (Typical Ni-Co system)	~37
	Sieve-Plate Column (with solids, gels)	~20

EXPERIMENTAL

Reagents

The following reagents were used in this experimental work: Shellsol® 2046 (Industrial, Shell), Versatic 10 (Industrial, Resolution), Murrin-Murrin nickel feed solution to the electrowinning circuit (~95 g/L Ni, Murrin-Murrin Nickel Operations), sodium chloride (Industrial, Pool Supply), sodium sulfate (Industrial, Sigma), sulfuric acid (AR, Sigma), sodium hydroxide (LR, Sigma), and ammonia gas (99.4%, BOC Gasses Australia). All reagents were used as supplied.

The solvent was prepared by mixing the appropriate amount of Versatic 10 with Shellsol 2046 to make a 10 % v/v solution. Prior to experiments that involved mass transfer, ammonia gas was sparged into the solvent to preneutralize the extractant. The nickel feed solution was prepared by diluting the Murrin-Murrin nickel feed solution with tap water so that it simulated the nickel feed solution in the direct solvent extraction of nickel, similar to that at the former Bulong Nickel Operations, which had the following composition: 3 g/L Ni^{2+}, 15 g/L Mg^{2+}, 80 g/L Cl^-, and 45 g/L SO_4^{2-}, except that it contained residual ammonium. The pH was adjusted to 5.5 for mass-transfer experiments and to 3.0 for maximum-flux tests using either sodium hydroxide or sulfuric acid.

The Pilot-Scale Column and Experimental Set-up

The ESX column used for this work was constructed of Perspex™, with a 3.6 m active column length and cross-sectional area of 5 × 4 cm (20 cm^2). The upper settler had

the dimensions 7.5 × 7.5 × 80 cm (4.5 L) and that of lower settler was 14 × 14 × 35 cm (6.9 L). The electrodes were Teflon™-coated stainless steel. The electrostatic field was generated by a variable voltage-variable frequency power supply (California Instruments, 801RP). The loaded solvent was stripped with sulfuric acid (1 M) using a mixer-settler.

Test Procedures

Mass-Transfer Tests

The column was first completely filled with the solvent, and the pumps were calibrated to the desired flow rate. The power supply for the electrostatic field was then turned on with the appropriate frequency and voltage selected, after which the pumps were turned on. The stripping mixer-settler and acid pump were turned on concurrently. The column operation was allowed to stabilize for approximately 1.5 h, after which the feed, raffinate, and loaded-organic samples were collected for analysis of nickel by inductively coupled plasma-atomic emission spectroscopy (ICP-AES0 (Varian Liberty 200).

Maximum Flux Tests

The column was first filled with the solvent, and the electrostatic field was applied. For the given phase ratio being tested, a specific flow rate was selected and the solvent and then the aqueous pumps turned on. The column was allowed to reach steady state for 20 min. and, if flooding had not occurred, the flow rates were increased accordingly and the procedure repeated.

RESULTS AND DISCUSSION

Optimization of the Electrostatic Field Strength

The effect of the electrostatic field strength on column performance was determined by measuring the nickel extraction achieved over a range of applied field strengths. The flow rates of both the PLS and solvent phase were maintained at 20 L/h, and the electrostatic field frequency was maintained at 20 Hz, as this value had previously been shown as optimal for mass transfer [10]. The effect of applied field strength on nickel extraction is shown in Figure 1.

The overall trend in nickel extraction obtained was comparable to those obtained in bench-scale studies [5, 8]. The initial decreases in nickel extraction with increases in applied voltage (0-2.5 kV/cm) indicated that the column was running in the droplet coalescence regime. The small increases in nickel extraction with further increases in applied voltage signified the start of the dispersion regime, although the field strengths were clearly insufficient to effect significant dispersion. Only when the field strength reached 5.7 kV/cm did the nickel extraction exceed that obtained when no field was applied, signifying the start of a significant dispersion regime. The main difference between these results and those obtained in bench-scale studies was the significantly higher applied field required to achieve optimum nickel extraction. Owing to

confidentiality issues, further explanation of these observations is not possible at this stage.

Optimisation of the Frequency of the Electrostatic Field

The frequency of the electrostatic field influences droplet oscillation and lateral motion and thus mass transfer [10-12], that is,high droplet oscillation and lateral motion lead to high mass transfer. The influence of frequency on mass transfer, however, is also affected by, among other factors, the natural frequency of the droplet, which in turn, is affected by the droplet size [12]. Since droplet size is also influenced by several factors including configuration and size of the specific contactor, optimization of the frequency should always be a part of any study on the application of electrostatic dispersion.

To determine the optimum frequency of the applied field in the column used in this study, the frequency was systematically varied from 20 to 50 Hz, while the applied voltage was maintained at 6 kV/cm. The results, summarised in Figure 2, were consistent with those obtained in bench-scale studies [10], except that the extractions achieved at lower frequencies in this study were lower. This may be attributed to different physico chemical properties of the extraction system in this study. The optimal frequency of 40 Hz indicated that this provided optimal oscillation and lateral motion of the droplets at the applied field used in this particular column.

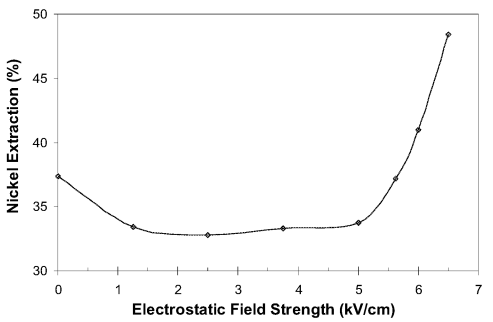

Figure 1. The effect of the electrostatic field strength on nickel extraction.

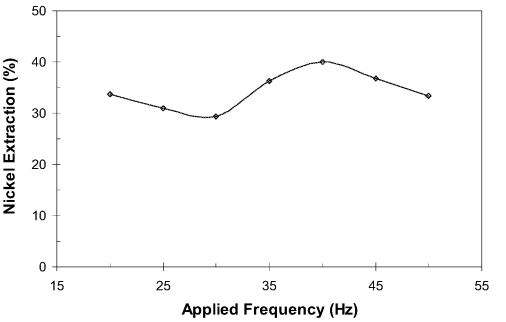

Figure 2. The effect of the frequency of the electrostatic field on nickel extraction.

Determination of Maximum Flux

The maximum fluxes achievable within the ESX column used in this study at various phase ratios were determined by increasing the aqueous and organic flow rates stepwise until flooding occurred. All tests were carried out at an electrostatic field strength and frequency of 6 kV/cm and 40 Hz, respectively. The flooding curve obtained is shown in Figure 3.

The increases in the flux required to effect flooding with decreases in the phase ratio from 4:1 to 2:1 and thus, the proportion of A:O, may be attributed to the lessening tendency for phase inversion. The substantial decreases in the maximum aqueous flux achievable with further decreases in the phase ratio appeared to be due to greater upward

flow of solvent within the column hindering the downward flow of the dispersed aqueous droplets, leading to flooding. Nonetheless, the maximum fluxes achievable within this column (35 to 55 $m^3/h/m^2$) were much higher than those achieved by previous investigators on ESX columns (9.15×10^{-4} to 3.77 $m^3/h/m^2$) and comparable to that typically used in conventional sieve-plate pulse column treating a comparable chemical system (~37 $m^3/h/m^2$).

The Effect of Flux on Nickel Extraction

A good flux without adequate mass transfer would provide no advantage over conventional contactors. Thus, the effect of the flux on the nickel extraction at a 2:1 phase ratio, which provided maximum throughput in the column used in this study, was investigated. The results, summarized in Figure 4, showed increases in nickel extraction with increases in fluxes from 15 to 25 $m^3/h/m^2$, after which further increases in the flux to 40 $m^3/h/m^2$ yielded only slight decreases in nickel extraction. This trend is comparable to that observed in conventional pulse columns, where the initial increase in extraction is attributed to corresponding increases in dispersed phase hold-up and thus contact time, and the ensuing slight decreases are attributed to increase in droplet coalescence. An attempt, however, to run a conventional sieve-plate pulse column with comparable dimensions at the same flux, failed due to flooding. This indicated that the ESX column developed in this study has a higher tolerance to flooding than a conventional sieve-plate pulse column.

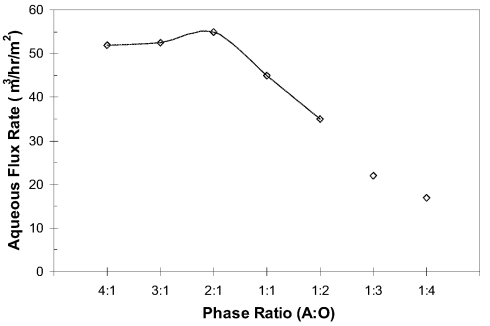

Figure 3. Maximum flux achievable prior to flooding for a range of phase ratios. (Free points indicate flooding was not reached owing to pump capacity.)

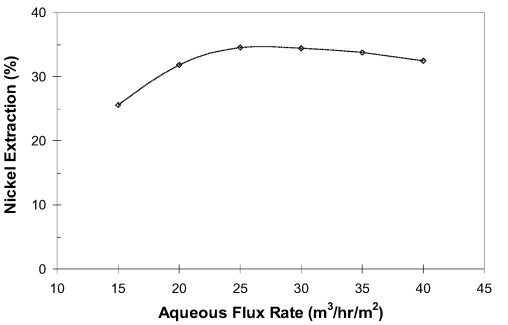

Figure 4. The effect of feed rate on nickel extraction (A:O = 2:1).

CONCLUSIONS

This study revealed that at an applied electrostatic field strength of 6 kV/cm at a frequency of 40 Hz, an ESX column can be operated at fluxes comparable to a conventional sieve-plate pulse column but has the advantage of maintaining high mas-transfer rates over a wider range of fluxes. These equate to a more versatile solvent-extraction contactor. Research and development work on this column is continuing.

ACKNOWLEDGMENTS

The authors thank Shell Chemicals for supplying the Shellsol 2046 and Versatic 10 and Minara Resources for supplying the nickel solution used in this work.

REFERENCES

1. M. Steffens, D. Ibana, and E. Paatero, "Factors that Affect Phase Dispersion in ESX," 11th International Conference on Environment and Mineral Processing, Vol. 2, P. Fečko and V. Čablík, Eds., VSB-TU Ostrava, Czech Republic, 2007; pp. 7-13.
2. T. Scott and R. Wham, "An Electrically Driven Multistage Counter-current SX Device: The Emulsion Phase Contactor," *Ind. Eng. Chem. Res.*, **28**, 94-97 (1989).
3. T. Scott, D. DePaoli, and G. Sisson, "Further Development of the Electrically Driven Emulsion-Phase Contactor," *Ind. Eng. Chem. Res.*, **33**, 1237-1244 (1994).
4. G. Taylor, "Studies in Electrohydrodynamics I: The Circulation Produced in a Drop by an Electric Field," *Proc. Roy. Soc. London*, **A291**(1425), 159-166 (1966).
5. L. Martin, P. Vignet, C. Fombarlet, and F. Lancelot, "Electrical Field Contactor for Solvent Extraction," *Sep. Sci. Technol.*, **18**(14&15), 1455-1471 (1983).
6. T. Suyama, Y. Awakura, T. Hirato, M. Konto, and H. Majima, "Extraction and Stripping of Ni(II) with D2EHPA under High Electrostatic Field," *Mat. Trans. JIM,* **34**(1), 37-42 (1993).
7. T. Usami, Y. Enokida, and A. Suzuki, "Application of Electrically driven Liquid-Liquid Dispersion to SX using TBP," *J. Nucl. Sci. Technol.,* **30**(10), 1017-1023 (1993).
8. M. Briggs, C. Cheng, and D. Ibana, "An Electrostatic SX Contactor for Ni-Co Recovery," *Miner. Eng.*, **13**(12), 1281-1288 (2000).
9. G. M. Ritcey, Solvent Extraction: Principles and Applications to Process Metallurgy, Vol. 1 & 2, G. M. Ritcey and Associates Inc., Ottawa, 2006.
10. J. Collard and D. Ibana, "Extraction of Cobalt by the ESPLIM Technique," 11th International Conference on Environment and Mineral Processing, P. Fečko and V. Čablík, Eds., VSB-TU Ostrava, Czech Republic, 2007; pp. 273-278.
11. T. Scott, O. Basaran, and C. Byers, "Characteristics of Electric-field Induced Oscillations of Translating Liquid Droplets," *Ind. Eng. Chem. Res.*, **29**, 901-909 (1990).
12. T. Scott, "Surface Area Generation and Droplet Size Control Using Pulsed Electric Fields," *AIChE J.*, **33**(9), 1557-1559 (1987).

TRANSIENT DROP BEHAVIOR OF SINGLE DROPS IN REACTIVE EXTRACTION

M. Kalem and A. Pfennig

AVT – Thermal Process Engineering, RWTH Aachen University
Wüllnerstr. 5, D-52062 Aachen, Germany
Corresponding author email address: andreas.pfennig@avt.rwth-aachen.de

ABSTRACT

The single-drop behavior of the reactive standard test system zinc and D2EHPA has been investigated. Results measuring the velocity of single droplets indicate that the drops change velocity depending on residence time in the continuous phase. The drop behavior for reactive extraction differs significantly compared to physical systems. Also mass-transfer experiments with sieve trays do not show an improvement in mass transfer as reported for physical extraction.

INTRODUCTION

To better simulate the behavior of extraction columns, the focus must be on the smallest units encountered in a column, single drops [1-4]. When droplets move in the column, they are undergoing mass transfer, coalescence, and splitting. The sedimentation of single droplets and the influence of column internals have been investigated in detail for the case of physical extraction [3,5]. For reactive systems, data on sedimentation are scarce. Also the influence of internals on the reactive mass transfer is not determined. Therefore, experiments in single-drop laboratory cells have been carried out with the reactive standard test system, zinc and D2EHPA [6]. The aqueous phase of this system consists of zinc sulfate and sulfuric acid dissolved in water, and the organic phase is D2EHPA dissolved in isododecane. Zinc and D2EHPA react at the interface between the phases:

$$\mathrm{Zn} + 1.5\ \overline{\mathrm{R_2H_2}} \rightleftharpoons \overline{\mathrm{ZnR_2RH}} + 2\,\mathrm{H} \qquad (1)$$

where the over-bar indicates components in the organic phase. The zinc-D2EHPA complex is only soluble in the organic phase, and for this reason zinc is extracted from the aqueous to the organic phase. Using this system, sedimentation experiments were first carried out. Then a single-drop levitation cell was used to investigate mass transfer for the zinc-D2EHPA system, particularly with regard to the influence of an inserted sieve tray.

EXPERIMENTAL

Materials and Analytical Techniques

Zinc sulfate monohydrate (99%) and sulfuric acid (98%) were purchased from Merck. D2EHPA (analytical grade) and isododecane were kindly donated by Bayer AG and EC Erdölchemie, respectively. Zinc sulfate monohydrate and sulfuric acid were dissolved in deionized water. D2EHPA was dissolved in isododecane to the desired weight percent. Before using, isododecane and deionized water were equilibrated with each other. The zinc concentration in the continuous phase was determined by titration with EDTA (ethylendiaminetetraacetate, Merck) [7]. The pH was measured with the pH meter E520 of Metrohm Herisau.

Single Drop Cells

A sketch of the sedimentation cell used is shown in Figure 1.

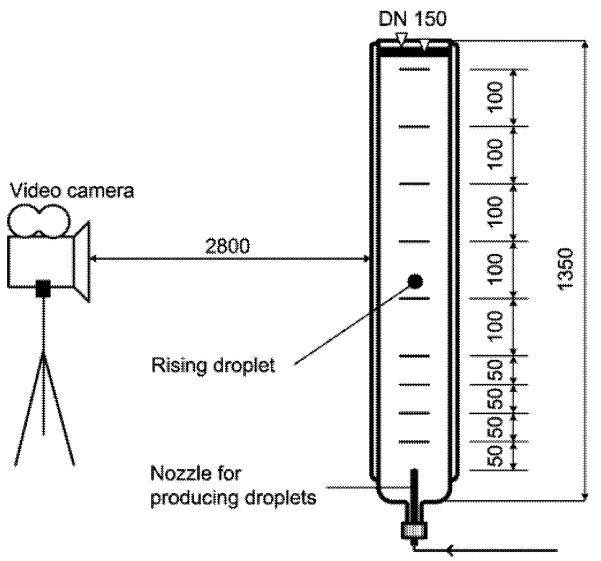

Figure 1. Sketch of the sedimentation cell.

A droplet with a known volume was produced with a computer-driven syringe. Due to the density difference, the droplet rises in the stagnant continuous phase. A video camera was used to record the rise of the droplet. Analyzing the video recording enabled the sedimentation velocity of a droplet in each section of the cell to be determined. For each section of the cell, at least 10 droplets were analyzed. To minimize the distortion in the position of the droplet, the camera was positioned at three different vertical positions. The cell is equipped with a water jacket to control the temperature to 20 °C.

A detailed description of the mass-transfer cell is given elsewhere [1,2,8,9]. A schematic drawing of the mass-transfer cell used is shown in Figure 2.

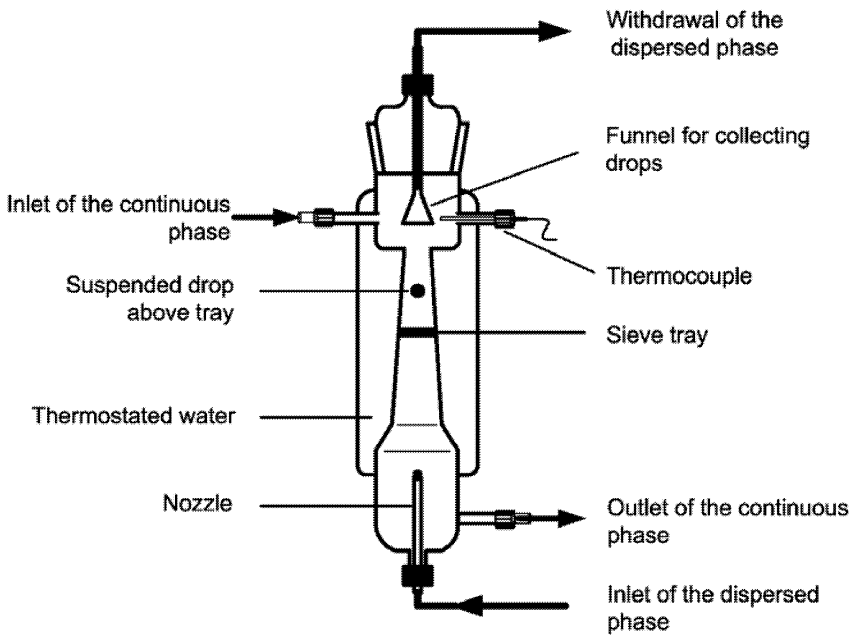

Figure 2. Mass-transfer cell with an inserted sieve-tray.

When a droplet detaches from the glass nozzle the countercurrent flow of the continuous phase is started. The droplet then rises in the conical part of the cell until the continuous flow matches its sedimentation velocity. The flow rate of the continuous phase is adjusted so that the droplet remains below the sieve tray. After a period, the pump is switched off and the droplet passes the sieve tray. Again, the pump for the continuous phase is turned on to levitate the drop above the sieve tray. Finally, the pump is switched off, and the drops are collected by a funnel and analyzed with regard to the transfer component. With this cell, the diameter of the drop, the total residence time, the residence time underneath the sieve tray, and the compositions of both phases can be varied. Using a thermostated water jacket, the temperature was controlled at 20 °C.

EXPERIMENTAL RESULTS

Sedimentation experiments with and without mass transfer were conducted. It was observed that mass transfer accelerates single drops. Figure 3 shows the average sedimentation velocity of the droplets averaged over the entire cell. The open symbols represent droplets that always collide with the wall. Since drops not undergoing mass transfer rise in a straight path, mass transfer has to be responsible for this effect. For larger droplets, mass transfer does not change the sedimentation behavior of drops. An influence of mass transfer was also seen for physical systems. However, mass transfer slowed down the droplets, so a reverse effect is obviously induced.

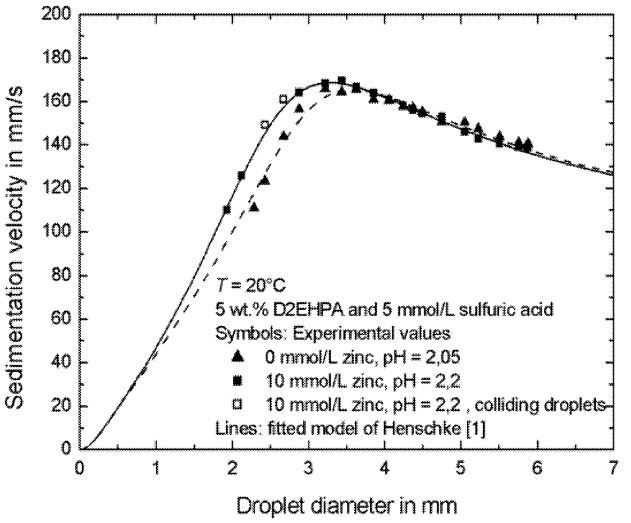

Figure 3. Influence of reactive mass transfer on single-drop sedimentation.

The fact that reactive mass transfer increases the sedimentation velocity of droplets is confirmed when measuring the transient velocity of the drops shown in Figure 4. The height in the cell is defined as the intermediate height of the cell sections as shown in Figure 1.

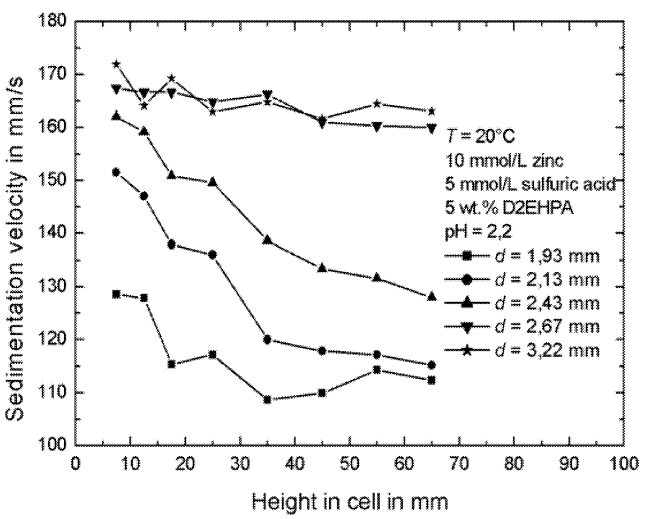

Figure 4. Transient sedimentation behavior.

In the first seconds when the mass-transfer rate is high, the droplets rise faster. As time proceeds, the mass-transfer rate decreases. A similar decrease is seen for the sedimentation velocity.

Mass-transfer experiments with internals showed that a sieve-tray does not improve the mass transfer for the case of reactive extraction. Earlier experiments with the physical systems toluene + water + acetone showed that a sieve-tray intensifies the convective mixing inside the droplet and therefore improves the mass-transfer rate [1,9]. Figure 5 shows the different influence of a sieve tray on physical and reactive mass transfer. For these experiments, the total residence time of the droplet t_{total} was kept constant, while the time below the sieve tray was varied. The dimensionless driving force c^* states the relative distance between the measured concentration $c(t)$ and the equilibrium concentration c^{Eq}. C^0 is the initial concentration of the transfer component in the droplet. The experimental data for the physical system are taken from Henschke [1]. Acetone was extracted from water (continuous phase) to toluene (dispersed phase). The sieve tray used for both systems was the same. It has a hole diameter of 6 mm and a ratio of the hole area to the total area of 49%.

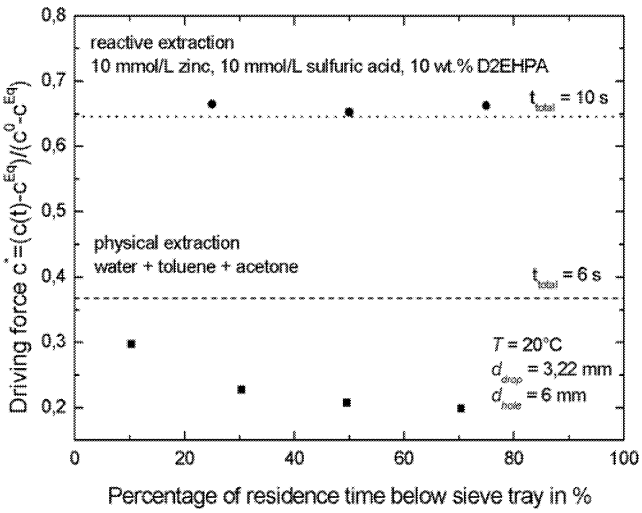

Figure 5. Influence of a sieve tray on single-drop mass transfer.

For the physical system, mass transfer increases with increasing residence time under the sieve tray. For the reactive system, no effect of the sieve tray on mass transfer can be seen.

DISCUSSION

Different phenomena have to be induced at the interface and in the droplet due to different behavior of droplets in physical and reactive extraction. In physical systems, mass-transfer induced Marangoni convections reduce the internal circulation of the droplets. This makes the droplets slower. In the reactive system zinc + D2EHPA, the

interface of the droplet is occupied with the surface-active D2EHPA. Mass transfer reduces the concentration of D2EHPA at the interface, and the emerging free surface area is used to transfer momentum to the droplet. So the droplet will become faster. Experiments with a sieve-tray showed no improvement in mass transfer. Therefore, the resistance to inner mixing can be neglected for reactive systems. In combination with the sedimentation results, the main resistance to mass transfer is assumed to be at the interface.

CONCLUSION

The drop behavior of reactive systems is different than that is physical systems. In the reactive system, mass transfer increases the sedimentation velocity of droplets, while in the physical system the velocity decreases. For reactive extraction, a sieve tray has no effect on mass transfer, whereas a marked effect is observed for physical systems.

REFERENCES

1. M. Henschke, Auslegung pulsierter Siebboden-Extraktionskolonnen, Shaker Verlag, Aachen, 2003.
2. M. Henschke and A. Pfennig, "Auslegung von Siebbodenkolonnen für die Flüssig/Flüssig Extraktion auf der Basis von einfachen Laborversuchen," *Chem. Eng. Tech.*, **72**(9), 964-965 (2000).
3. M. Altunok, T. Grömping, and A. Pfennig, "Prediction of extraction-column behaviour based on lab-scale experiments," International Solvent Extraction Conference (ISEC) Beijing, China, 19-23 September, 2003.
4. M. Kalem and A. Pfennig, "ReDrop – A general method for solving drop-population balances with an arbitrary number of property variables," 17th European symposium on computer aided process Engineering (ESCAPE), Bucharest, Romania, 27-30 May, 2007.
5. D. Garthe, Fluid dynamics and Mass Transfer of Single Particles and Swarms in Extraction Columns, Dr. Hut, München, 2006.
6. H.-J. Bart, Reactive Extraction, Springer, Heidelberg, 2001.
7. H. Klocker, Multikomponentenstoffaustausch bei der Reaktivextraktion im System Zinksulfat / Di(2-ethylhexyl)phosphorsäure.
8. M. Henschke and A. Pfennig, "Mass-Transfer Enhancement in Single-Drop Extraction Experiments," *AIChE J.*, **45**, 2079 (1999).
9. M. Henschke and A. Pfennig, "Influence of Sieve Trays on the Mass Transfer of Single Drops," *AIChE J.*, **48**, 227 (2002).

CFD-SUPPORTED DESIGN IN LIQUID-LIQUID EXTRACTION

T. Gurker,[1] T. Haderer,[2] and R. Marr[1]

[1]*Department of Chemical Engineering and Environmental Technology, Graz University of Technology, Austria.* [2]*VTU-Engineering GmbH, Grambach/Graz, Austria*
Corresponding author email address: Thomas.Gurker@TUGraz.at

ABSTRACT

A Computational Fluid Dynamics (CFD) simulation of a laboratory-scale Rotating Disc Contactor (RDC) column, investigating the axial dispersion coefficient for the continuous phase, has been applied with notable success. The influence of different optimization parameters was developed and it was found that the realizable k-ε turbulence model applied on a discrete phase model simulation shows acceptable results. The attained data were compared with a 100 mm RDC test system implementing Laser Doppler Anemometry (LDA) measurements. Significant improvements in CFD simulation of two-phase flow in RDC reactors are expected from the further development of this experimental approach.

INTRODUCTION

From CFD, progress is expected in the design and scale-up of equipment in liquid-liquid extraction in the near future. Among a variety of established designs, the Rotating Disk Contactor (RDC) is capable of combining compact design with sufficient extraction efficiency. Basically, the design of a RDC can be subdivided in a) the hydrodynamic layout, which results in the determination of the column diameter, and b) the mass transfer between the phases which determines the height of the column. Presently the layout of an extractor is mainly based on experience and existing empirical and semi-empirical models shown by several researchers (e.g. [1-3]).

Unfortunately, the inherent flow non-idealities of actual reactors, which can be summed up as “axial dispersion effects”, have great influence on the hydrodynamic flow regime in the apparatus, and consequently, on the mass transfer. A good overview on nonidealities flow can be found in Levenspiel [4] and (emphasis on RDC design) in Kumar and Hartland [5].

However, in most cases, the specific hydrodynamics of an apparatus cannot be calculated with sufficient accuracy, and the traditional method to scale-up from laboratory stage is advisable. The drawback of this approach is that the method is only valid for the investigated geometry and is therefore system specific. Consequently, it can be designated as extraordinarily time-consuming and expensive.

At this point, CFD can play a major role in an improved layout process for large-scale reactors. It offers the possibility to simulate the specific hydrodynamic situation in a reactor, taking also the nonideal conditions into consideration. The predominating aim of this study is to develop the appropriate models for the simulation of flow patterns of an RDC by determining the axial dispersion coefficient of the continuous phase $E_{ax,c}$ as a characteristic scale-up parameter.

However, simulation of flow patterns using FLUENT® needs careful consideration, regarding the accuracy and scope of the results. To verify the simulation results the obtained data needs to be validated with classical experiments determining holdup, droplet-size distribution, and residence-time distribution. Hence, experiments on the basis of a laboratory-scale RDC using a Toluene/Water standard test system is an essential measure.

The matching between simulative and experimental data can be realized comparably fast, which makes a determination of the crucial parameters for the layout of a large-scale RDC possible in near future.

EXPERIMENTAL

With a test system of toluene/water, the Residence Time Distribution (RTD), holdup and drop-size distribution were investigated in previous studies using LDA measurements [6]. A 100 mm diameter RDC unit was set up as a laboratory test system with a total height of approximately 3.2 m. The active part of the column consisted of 33 compartments with an overall height of 1188 mm. The outer vessel was made of silica-glass whereby the internals, consisting of the rotor and the stator plates, were crafted from austenitic steel due to corrosion stability. The rotation speed could be adjusted from 50 to 900 rpm. A detailed sketch of a single compartment is presented in Figure1.

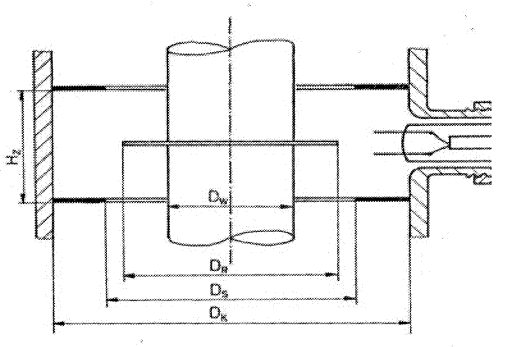

Figure 1. Construction scheme of one-compartment geometry of the investigated RDC. D_{Rotor} = 60 mm; D_{Stator} = 70 mm; D_{Shaft} = 35 mm; H_{Comp} = 36 mm [6]

CFD Simulation of Flow Field and Calculation of RTD

In previous research activities [7], the influence of technically sophisticated turbulence models on the results of the calculated flow pattern in RDC extraction columns was discussed, and the realizable k-ε-model and the Reynolds stress model were

ascertained as models for use. In the continuative work the axial dispersion coefficient $E_{ax,c}$ should be computed with the aid of CFD. For the determination of this parameter, the calculation of the RTD had to be realized using the Discrete Phase Model (Euler Lagrange Model).

The Discrete Phase Model (DPM)

The DPM provides modeling of spherical particles, bubbles or droplets that are dispersed in the continuous phase. The fluid phase (water) is treated as continuous by solving the time-averaged Navier-Stokes equations, while the dispersed phase is solved by tracking a large number of particles through the previously calculated flow field. In this study, the DPM was used to simulate a "pseudo-two-phase" flow field to determine $E_{ax,c}$. For the designation of the RTD, the computation of the continuous-phase interaction between dispersed particles and the continuous phase can be neglected. Essential for this approach is that the particles follow strictly the flow field. Therefore, the generated particles must have the same physical properties as the continuous phase and must be of a very small diameter of 1×10^{-6} m [8,9].

Determination of Residence Time Distribution

For determination of the RTD of the continuous phase with the DPM approach, seven injection locations are generated at which the droplets were released. The injection locations were placed in a plane at the height of a stator-ring. The boundary conditions for the calculation of the particle trajectory at the column shell and the internal equipment were set to "reflect," whereby at the inlet plane and the outlet plane, it was set to "escape," enabling the particles to leave the observation space. The transition time was recorded by passing a distinct counting line created at the height of a stator ring. A residence time curve was plotted and fitted by the RTD-solution of Levenspiel [4] for the open-open systems. With the computed Peclet number and mean residence time τ, the dispersion coefficient $E_{ax,c}$ and the mean flow velocity v_c could be calculated.

The results generated through CFD simulation were compared with experimental data and empirically determined correlations (Bauer [10], Kumar and Hartland [11]) to finally establish a simulation set-up that showed a correlation between the simulated and the real flow field.

Simulation Set-up in FLUENT

Based on the results of several test computations [8], it was decided to carry out the computations by creating a two-dimensional, axis-symmetric case file for the simulation. The boundaries of the intake and the outflow face were set periodically, which means that the velocity profile at the inlet is equal to that at the outlet [7]. In all simulations, the enhanced wall-treatment method was used. For the proper implementation of this method the original 0.2 x 0.2 mm grid was adapted by computation of the y^+-values in wall adjacent cells. At the face side of the rotor disk, values between 1.9 and 2.1 could be obtained, which is well within the proposed boundaries between 1 and 5 [12].

RESULTS AND DISCUSSION

The flow field of four compartments was calculated for different operating conditions without disperse-phase flow. The flow rate of the continuous phase was varied from 28.3 L/h to 160 L/h and the rate of rotation from 50 rpm to 900 rpm. The flow pattern was calculated considering turbulence with the realizable k-ε model [7]. The RTD of the continuous phase is calculated for compartments 2 and 3 in the center of the 4 compartment geometry. Compartments 1 and 4 were reserved for a sufficient development of the inlet and outlet flow pattern. In Figure 2, a comparison of the calculated RTD data (CFD,4C) with data records from experiments by Sommeregger [6] is shown. The generated results clearly show a significant discrepancy between CFD simulation and experiments at higher rate of rotation. A possible reason for this poor agreement is that the simulated mean velocity is higher than the experimentally obtained values, which is discussed later.

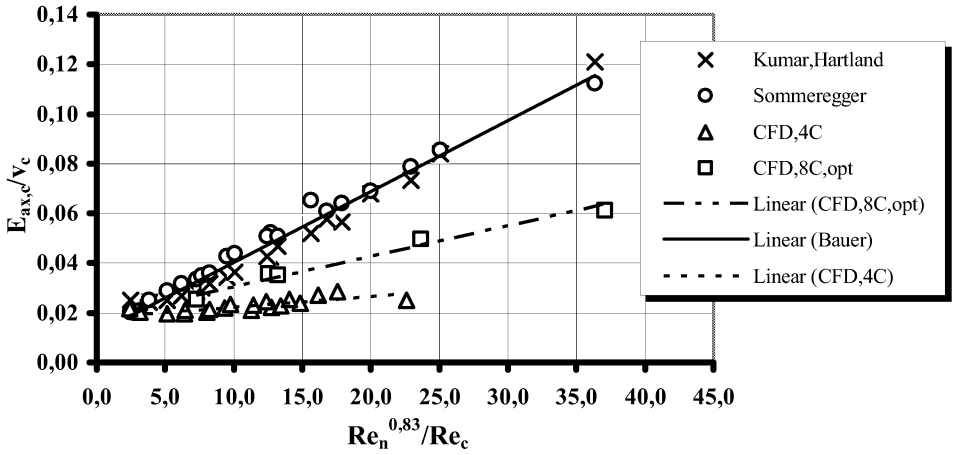

Figure 2. Comparison of optimized CFD data with empirical correlations and experiments.

Optimization of the Simulation Parameters

Strategy of improvement of CFD-results was generally focused on extension of the simulation area. A greater number of compartments were expected to improve the attained results. Also the simulated mean velocity, which deviates slightly from experiments, was adjusted to obtain conformity of the x-axis data and consequently better comparability of simulated axial dispersion coefficient.

To analyze the influence of the geometry size, a simulation series was worked out with a simulation area of eight compartments. The RTD calculations of the continuous phase were extended to compartments 3, 4, 5, and 6. Compartments 1 and 2, below the passing line, and compartment 7 and 8, above the injection plane, were again left for consideration of recirculation zones. Additionally, it was found that limiting the simulation area to the inlet causes an irrecoverable loss of particles for RTD simulation. These "late" particles will pass the counting line retarded to injection and affect the RTD graph by a significant tailing in comparison to the experimentally determined RTD. The

contemporary loss of particles creates a smaller mean residence time τ compared with experiments. To avoid the significant effect of tailing on the axial dispersion coefficient $E_{ax,c}$, the boundary condition for the disperse phase was set on "reflect," and good agreement with experiments could be obtained. The new computed data is referred to as "CFD,8C,opt" in Figure 2.

At first sight, the enlargement of the simulated geometry improves the results at higher energy input and lower throughput but still does not result in satisfying agreement of experiments and simulation. Following RTD simulation was carried out for a cascade of 16 and 32 compartments, but the expected improvement of the simulated dispersion coefficient through enlarging the simulation area could not be observed. It can be stated that the optimization of simulation parameters had a stronger effect on the results compared with the extension of the simulation area.

Further Development of the Simulation Strategy

Due to better computational resources (Intel® Xeon Dual Processor, 2 x 3.0GHz, 16 gigabyte RAM, 1 terabyte drive), also a simulation of a fully meshed 3-D compartment cascade is feasible and currently investigated. The maximum cell number during earlier studies was limited to a number of approximately 1 x 10^6 cells, expecting calculation times up to one week and more. With the new computer system, it is possible to simulate a theoretical number up to 16 x 10^6 cells within a maintainable calculation time of one day, depending on the complexity of the chosen model.

The promising idea behind this strategy is that a better resolution of macroscopic turbulence within the compartments is expected. This would lead to a greater mean residence time τ and to a better fitting with the experimentally attained data.

In the first step of the 3-D simulation, a similar simulation environment was used for a comparison of the results from new simulation data with earlier studies. A cascade of three compartments was chosen and a "Tet/Hybrid" mesh applied with approximately 4 x 10^6 cells. The selected "TGrid" option specifies that the mesh is primarily composed of tetrahedral mesh elements but may include hexahedral, pyramidal, and wedge elements where appropriate. The advantage of a "Tet/Hybrid" mesh is its applicability for a comparably fast mesh construction for preliminary studies. It was possible to maintain a mesh skewness of 0.9, which is the limit for a reliable mesh quality [12]. Resolution of the mesh was refined to a $y+$ value between 2.1 and 3.2 at the face side of the rotor disk, which is again well within the boundaries of the proposed value between 1 and 5 [12].

Unfortunately, at this early stage of the 3-D studies it was not possible to produce results that were clearly independent of the mesh resolution, which is essential for good CFD results. Additionally, recently attained results from application of the Reynolds Stress Model showed great potential in comparison with the 2-D plots for velocity vectors but showed the same dependency on the mesh resolution. However, a clear trend to a better fitting with experimental data is expected within the near future.

CONCLUSIONS

Target of investigations was to establish simulation of axial dispersion coefficients of the continuous phase in RDC extraction columns. After optimization of

the parameter settings, the computed results are in acceptable accordance with experimental data and empirical correlations. The influence of the size of computation area on RTD was worked out, but no clear trend could be found. It can be stated that the optimization of simulation parameters had a stronger effect on the results than the extension of the simulation area.

The results of recent realizable k-ε simulations lead to the assumption that RTD investigation should be executed in 3-D geometries, for a better resolution of macroscopic turbulence in the compartments. Although no results can be presented in this early stage of development, contribution to the simulation of RDC two-phase flow is expected in the near future.

REFERENCES

1. T. Misek, "Rotating Disk Contactors and their Calculation," State Publishing House of Technical Literature, Prague, 1964.
2. R. Marr, "Konzepte für die Auslegung von Extraktionsapparaten," Habilliatationsschrift, Graz University of Technology, Graz, Austria, 1976.
3. W. C. G. Kosters, "Rotating-Disk Contactor," in T. C.Lo, H. M. I. Baird, and C. Hanson, Handbook of Solvent Extraction, John Wiley & Sons, New York, 1983.
4. O. Levenspiel, "Chemical Reaction Engineering," John Wiley & Sons, New York, 1972.
5. A. Kumar, S. Hartland, "Prediction of Axial Mixing Coefficients in Rotating Disk Extraction Columns," *Can. Journal of Chem. Eng*., **70**, (1992).
6. E. Sommeregger, "Hydrodynamik in Drehscheibenextraktoren," Ph.D. Thesis; Graz University of Technology, Graz, Austria, 1980.
7 T. Haderer, C. Huber, R. Marr, and S. Martens, "Numeric flow simulation of a RDC extraction column," Proceeding of 15th International Congress of Chemical and Process Engineering, CHISA 2002, Praha, CZE, 2002 (CD-ROM 1295.pdf).
8. T. Haderer, "CFD-Simulation der Hydridynamik einer gerührten Extraktionskolonne und Vergleich mit experimentell ermittelten hydrodynamischen Kenngrößen," PhD Thesis, Graz University of Technology, Graz, Austria, 2004.
9. P. Kolb, H.-J. Bart, and L. Fischer, "Entwicklung einer Miniplant-Extraktionskolonne," *Chemie Ingenieur Technik*, **74**(3), 243-247 (2002).
10. R. Bauer, "Die Längsvermischung beider Phasen in einer gerührten Extraktionskolonne," Ph.D. Thesis, ETH Zürich, 1976.
11. A. Kumar and S. Hartland, "Prediction of Axial Mixing Coefficients in Rotating Disc and Asymmetric Disc Extraction Columns," *Can. J. Chem. Eng.*, 77-89 (1992).
12. Fluent User's Guide, 2006.

DYNAMIC MODEL FOR A MIXER-SETTLER SYSTEM

E.F. Gomes,[1,2] G.A. Pinto,[1,2] M.M.L. Guimarães,[2] and L.M. Ribeiro[3]

[1]Instituto Superior de Engenharia do Porto, Rua Dr. António Benardino de Almeida 431, Porto, Portugal. [2]CIGAR – Centro de Investigação Geo-Ambiental e Recursos
[3]Faculdade de Engenharia da Universidade do Porto, Portugal
Corresponding author email address: efg@isep.ipp.pt

ABSTRACT

This paper describes a dynamic model for the shallow-layer settler unit of a mixer-settler system that is able to simulate the transient state, including hydrodynamic phenomena of drop-drop and drop-interface coalescence. This dynamical model uses a new kinetic formulation in which the movement of the dispersion is caused by gravity. The modelling of the longitudinal transport of the drops is set up by taking into account the gravitational instability caused in the dispersion band by the nonuniform thickness of the band. The viscous character of the draining of the continuous phase is also taken into account in this model.

INTRODUCTION

Gravity settlers are noticeably lacking of mathematical models apt to simulate their transient states resulting from variation of the feed or operating conditions, a sorry situation which results in poor design and control of this important type of equipment.

As a part of a continuing effort to understand and simulate the behavior of the shallow-layer settler unit [1-8], a new model is described here that enables the simulation of the hydrodynamic phenomena in the transient state of the liquid-liquid system. A direct numerical resolution technique adapted from the one already used by the authors for the simulation of other liquid-liquid systems [1-4] is used for the implementation of the mathematical model and is also described in this work. Preliminary computational results indicate that the model provides satisfactory qualitative predictions of the settler dynamic behavior and in particular that the length of the band changes adequately when input parameters are affected by step changes and the system later converges to steady state. In this new mathematical model we have introduced new parameters with unknown values. In order to fit them to experimental results, we have linked the mixer-settler simulation algorithm to an optimization algorithm.

THE MATHEMATICAL MODEL

Our mathematical approach models the phenomena that occur in each volume element ($H \times w \times \Delta x$), or vertical slice, of the dispersion band, in the settler, where x is its longitudinal position in the dispersion band, H is the thickness of the dispersion band, and w is the width of the settler. The modelling of the longitudinal transport of the drops is set up by taking into account the gravitational instability caused in the dispersion band by the nonuniform thickness of the band. The viscous character of the draining of the continuous phase is also taken into account in this model.

This model for the shallow-layer gravity settler assumes there is a large enough horizontal area, such that, given the inflow at one end and the outflow at the other, a dispersion wedge is formed by settling (buoyancy) effect. This wedge does not cover the entire phase boundary between the two liquids. In this wedge, we assume the following: a) binary drop-drop coalescence; b) negligible drop breakage, due to low turbulence; c) drop-interface coalescence; d) gravitational drainage of the continuous phase to the passive interface; e) essentially plug flow movement of the drops away from the entrance; e) negligible mass transfer between phases; f) continuous distribution of drop volumes at any position at the slice; g) uniform longitudinal velocity of drops in each slice; and finally, h) negligible changes of the physical properties of the dispersion band in the vertical direction.

The calculation of the drop volume variation in time is performed for each volume element. For each time step, the events that occur in each volume element of the dispersion band are computed. They are:

(*i*) the dispersion (from the mixer unit into the settler);

(*ii*) the coalescence between drops of the dispersed phase;

(*iii*) the coalescence of drops with the active interface;

(*iv*) the draining of the continuous phase to the passive interface and

(*v*) the transport of the dispersion between consecutive volume elements in the dispersion band (Equation 1). The dispersion flows between consecutive slices from the thicker to the thinner slice.

The following differential equation describes these phenomena, the volume variation of the dispersion for each slice at the position x, over time being given by:

$$\frac{\partial V(x,t)}{\partial t} = F(x,t).w.\Delta x + \alpha.w.\Delta x\left\{\left[\frac{H(x-\Delta x,t)-H(x,t)}{\Delta x}\right]-\left[\frac{H(x,t)-H(x+\Delta x,t)}{\Delta x}\right]\right\}-\frac{\partial C(x,t)}{\partial t}-\frac{\partial D(x,t)}{\partial t} \qquad (1)$$

where w is the width of the settler, α is a parameter describing the effects of inner friction on the longitudinal movement of the dispersion, and F is the velocity of the dispersion entering into the settler from the mixer at position x and time t.

$\partial C(x,t)/\partial t$ represents the volume rate of the drops coalescing to the active interface, which, in the pioneer work of Ruiz [5] is expressed as

$$\frac{\partial C(x,t)}{\partial t} = \frac{w.\eta^*(x).\lambda^*(v).n(v,x).dv}{A_p(x).N(x)}\Delta x.dv \equiv \frac{w.\Delta x.\eta^*.(x)\lambda^*(v).n(v,x).dv}{\frac{\pi}{4}.\left(\frac{6}{\pi}\right)^{\frac{2}{3}}.\int_0^{\infty} v^{\frac{2}{3}}.n(v,x).dv} \tag{2}$$

$\partial D(x,t)/\partial t$ represents the volume variation of the dispersion due to the draining to the passive interface. To describe this variation, we use the expression:

$$\frac{\partial D(x,t)}{\partial t} = k.V(x,t).\left[\left(1-\eta(x,t)\right)-\left(1-\eta_M\right)\right] \tag{3}$$

where k is a constant describing the effects of the friction between the continuous and the dispersed phases, V is the volume of the dispersion, η is the present local holdup, and η_M is the maximum holdup.

In the above expressions, $n(v,x)dv$ is the number of drops of size from v to $v + dv$ (volume class v) per unit volume of the dispersion band at position x, $\eta^*(x)$ is the fraction of dispersion phase projected onto the surface, $\lambda^*(v)$ is the drop-interface coalescence frequency, $A_p(x)$ is the average projected area of drops and $N(x)$ is the total number of drops per unit volume at position x.

For the calculation of the volume at position x, we have by definition

$$V(x,t) = H(x,t).w.\Delta x \tag{4}$$

From this, the thickness of the dispersion band, H, along the settler may be obtained. The calculation of the holdup, η, is calculated directly as the ratio of the volume of dispersed phase to the total volume of the dispersion. Thus, besides the volume of the dispersed phase, we need to know the volume of the continuous phase. We break up the expression of the volume variation into two terms, one describing the volume variation of dispersion phase (Equation 5), and the other describing the variation of the continuous phase (Equation 6).

$$\frac{\partial V_d(x,t)}{\partial t} = F_d(x,t).w.\Delta x + \alpha.w.\Delta x.\eta(x,t).\left\{\left[\frac{H(x-\Delta x,t)-H(x,t)}{\Delta x}\right]-\left[\frac{H(x,t)-H(x+\Delta x,t)}{\Delta x}\right]\right\}-\frac{\partial C(x,t)}{\partial t} \tag{5}$$

$$\frac{\partial V_c(x,t)}{\partial t} = F_c(x,t).w.\Delta x + \alpha.w.\Delta x.(1-\eta(x,t)).\left\{\left[\frac{H(x-\Delta x,t)-H(x,t)}{\Delta x}\right]-\left[\frac{H(x,t)-H(x+\Delta x,t)}{\Delta x}\right]\right\}-\frac{\partial D(x,t)}{\partial t} \tag{6}$$

Notice that, at present, for simplicity, we consider the dispersion in each slice of the dispersion band as being vertically homogeneous and thus feel free to ignore any eventual vertical transport effects.

As to the drop-interaction (hydrodynamic) phenomena that may occur within the dispersion band, given the reigning low turbulence, we assume that breakage is negligible. However, we consider two types of coalescence, drop-drop coalescence and drop-interface coalescence.

To represent the volume of drops coalescing to the active interface per unit time we use Equation 2. To represent the volume rate of the drops disappearing and appearing

by drop-drop coalescence within the element of dispersion volume, we use Equations 7 and 8, respectively.

$$\frac{wH(x)\Delta x}{N(x)}\left[\int_0^{\infty}\lambda(v,v')n(v,x)n(v',x)dv'\right]dv \equiv \frac{wH(x)\Delta x}{\int_0^{\infty}n(v,x)dv}\left[\int_0^{\infty}\lambda(v,v')n(v,x)n(v',x)dv'\right]dv \tag{7}$$

$$\frac{wH(x)\Delta x}{2N(x)}\left[\int_0^{v}\lambda(v-v',v')n(v-v',x)n(v',x)dv'\right]dv \equiv \frac{wH(x)\Delta x}{2\int_0^{\infty}n(v,x)dv}\left[\int_0^{v}\lambda(v-v',v')n(v-v',x)n(v',x)dv'\right]dv \tag{8}$$

In Equations 7 and 8

$$\lambda(v,v') = \lambda_0\left(v^{-1/3} + v'^{-1/3}\right)^2 \tag{9}$$

represents the drop-drop coalescence frequency according to Ruiz [5], where λ_0 is a parameter which depends on the physicochemical properties of the system.

THE NUMERICAL MODEL

In previous works, the present authors have used a direct numerical approach by means of the discretization of space and time into adequate grids. The phase-space coordinates are the position of the slice in the dispersion band and the size (volume) of the drops. For each time step, we compute the dispersion changes in each volume element (slice) of the dispersion band, taking into account the variations of the volume of the continuous phase and of the properties of the dispersed phase due to the acting discrete phenomena. In this algorithm, the variation of the volume of the dispersed phase and the volume of the continuous phase are calculated separately. The continuous phase in each slice of the dispersion band is analyzed from the point of view of volume variation alone and is calculated from the balance of the volume of the continuous phase. The dispersed phase in each slice is analyzed from both the volume variation and drop-size composition points of view. Drops move from cell to cell in the discretized phase-space at each time step.

From the volume variation of the two phases, we know the total variation of the volume at the position x of the dispersion band into the settler, and we may calculate the holdup and the thickness of the dispersion band at position x. Knowing the volume variation of the dispersed and continuous phases, we may obtain the total volume by using a numerical method of ordinary differential equations.

ALGORITHM IMPLEMENTATION AND STRATEGIES FOR PARAMETER OPTIMIZATION

Since a direct numerical method of resolution of ordinary differential equations is used, the choice of the space (length) and time integration step, as well as of the convergence criterion, is very important for the successful implementation of the algorithm. At each time integration step, a convergence criterion is used for the space discretization of the ordinary differential equation to evaluate each solution.

Given the complexity of the model, its specification is still under development. In particular, the values for the newly introduced parameters of the drop-transport process need careful study. For this study, experimental results for the transient state are needed for parameter tuning. These experiments are currently being planned and tried in our laboratory. In order to identify and interpret the parameter values of the mixer-settler model that best fit the experimental results, we use our simulation algorithm for the mixer-settler unit as a subroutine in an optimization algorithm.

RESULTS AND CONCLUSIONS

Present preliminary computational results were found to be meaningful and indicate that the model and the simulation strategy provide adequate qualitative predictions of the settler dynamic behavior (Figure 1). In particular, the length of the band changes in a plausible fashion (as against comprehensive experimental data) when input parameters (incoming holdup, volume flow, and agitation speed at the mixer) are given appropriate step changes, and the system converges to the predicted steady state (previously simulated by the steady-state algorithm [6]) if the process variables are kept unchanged. However, the behavior of the thickness and shape of the dispersion band need further analysis and validation. At the same time, experimental work is being carried out in our laboratory using a pilot-scale model of the mixer-settler. We hope to obtain the presently lacking experimental data necessary for a more accurate validation of the mathematical model and for parameter tuning.

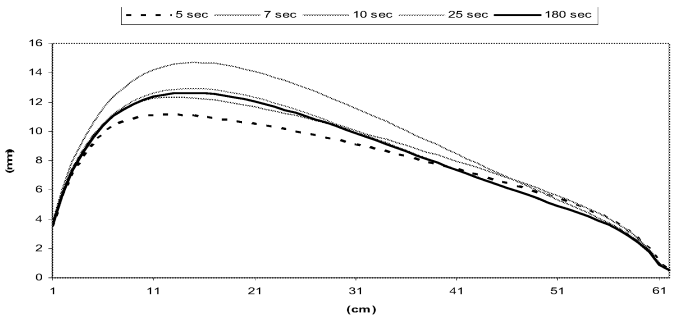

Figure 1. Band Thickness for the transient simulation of start-up of the settler

REFERENCES

1. E. F. Gomes, M. M. L. Guimarães, and L. M. Ribeiro, "Numerical modelling of a gravity settler in dynamic conditions," *J. Adv. Eng. Software*, **38**, 810–817 (2007).
2. E. F. Gomes, M. M. L. Guimarães, G. A Pinto, and L. M. Ribeiro, "Dynamical model for a settler unit using kinetic formulation," in Proceedings of The Fifth International Conference on Engineering Computational Technology, B. H. V. Topping, G. Montero, and R. Montenegro, Eds., Civil-Comp Press, Stirlingshire, United Kingdom, 2006, paper 176.
3. E. F. Gomes, C. M. N. Madureira, M. M. L. Guimarães, and L. M. Ribeiro, "Numerical modelling of a gravity settler in dynamic conditions," Proceedings of the Fourth

International Conference on Engineering Computational Technology, B. H. V. Topping and C. A. Mota Soares, Eds., Civil-Comp Press, Stirling, United Kingdom, 2004, paper 59.

4. M. M. M. Ribeiro, M. M. L. Guimarães, C. M. N. Madureira, and J. J. C. Cruz-Pinto, *Chem. Eng. J.*, **97**, 173-182 (2004).
5. M. C. Ruiz, "Mathematical Modelling of a Gravity Settler," Ph.D. Thesis, University of Utah, 1985.
6. G. A Pinto, F. O. Durão, A. M. A Fiuza, M. L. Guimarães, and C. M. N. Madureira, *Hydrometallurgy*, 131-147 (2004).
7. G. A. Pinto, "Optimização Multicritério da Exracção Líquido-Líquido em Misturadores-Decantadores," Dissertação para Doutoramento, Faculdade de Engenharia da Universidade do Porto, 2004.
8. G. A. Pinto, M. Baptista, A. Guedes, A. Fiúza, M. M. L. Guimarães, C. M. N. Madureira, and J. J. C. Cruz – Pinto, "Model Validation for Mixer-Settler Units," 6th World Congress of Chemical Engineering, Melbourne, Austrália, 2001.

NOMENCLATURE

$A_p(x)$	Average projected area of drops at the active interface	(L^2)
$C(x,t)$	Volume of dispersion coalescing with the active interface	(L^3)
$D(x,t)$	Volume of dispersion draining with the passive interface	(L^3)
dv	Volume increment	(L^3)
$F(x,t)$	Velocity of the inlet dispersion	$(L.T^{-1})$
$F_c(x,t)$	Velocity of the inlet continuous phase	$(L.T^{-1})$
$F_d(x,t)$	Velocity of the inlet dispersed phase	$(L.T^{-1})$
$H(x,t)$	Thickness of the dispersion band	(L)
K	Constant defined by equation (5)	(T^{-1})
$n(v,x)dv$	Number of drops v to $v+dv$ per unit volume of dispersion at position x	(L^{-3})
$N(x)$	Total number of drops per unit volume at position x	(L^{-3})
$Q(x)$	Volumetric flow rate of dispersion	$(L^3.T^{-1})$
$Q_c(x,t)$	Volumetric flow rate of continuous phase and time t	$(L^3.T^{-1})$
T	Time	(T)
$V(x,t)$	Volume of the dispersion band at position x	(L^3)
v, v'	Drop volume	(L^3)
$V_c(x,t)$	Volume of the continuous phase at position x and time t	(L^3)
$V_d(x,t)$	Volume of the dispersed phase at position x and time t	(L^3)
w	Settler width	(L)
x	Length coordenate of the settler	(L)

Greek Letters

A	Constant of equation (1)	$(L.T^{-1})$
Δx	Small increment in the dispersion band	(L)
$\eta(x)$	Volume fraction of dispersed phase (hold-up)	*dimensionless*
$\eta^*(x)$	Surface fraction of dispersed phase	*dimensionless*
η_M	Maximum volume-packing efficiency	*dimensionless*
$\lambda(v,v')$	Drop-drop coalescence frequency	(T^{-1})
λ^*	Drop-interface coalescence frequency	(T^{-1})
λ_0	Constant of equation (9)	$(L^2.T^{-1})$

DEVELOPMENT OF A COMPUTER SIMULATION OF THE PLATINUM SOLVENT EXTRACTION AT PRECIOUS METALS REFINERS (PMR)

Richard A. Grant[1] and Stephen F. Woollam[2]

[1]*Johnson Matthey Technology Centre, Sonning Common, Reading, UK, RG4 9NH*
[2]*Anglo Research, 4 Barbara Road, Primrose East 1410, South Africa*
Corresponding author email address: grantra@matthey.com

ABSTRACT

Precious Metals Refiners employ a secondary amine Amberlite LA2 for the solvent extraction of platinum. A significant expansion of the Solvex sections was required to support Anglo Platinum's expansion program. The platinum solvent-extraction process is highly complex and therefore a computer simulation has been developed. This comprises a pseudo-equilibrium constant based model of the extraction chemistry coupled to a dynamic simulation of the mixer-settler operation. The computer simulation was used to evaluate options for decreasing the requirements for concentrated hydrochloric acid for stripping. The predictions obtained were then successfully verified in mini-pilot plant trials.

INTRODUCTION

The production of the Platinum-Group Metals (PGM) is significantly lower than the other precious metals. This is due both to their low natural abundance and the very complex processes required for their extraction and refining. However, they are of major technological importance due to their unique properties. Platinum is the most important of the PGM, and annual demand over the period 1987-2006 has risen steadily from 2.9 to 7.9 x 10^6ozT (1 ounce Troy (ozT) = 31.1g) [1]. The majority of the platinum (ca. 54%) is consumed in automotive exhaust catalysts. A wide range of other industrial applications account for a further ca. 24%, with jewellery (ca. 21%) being the other major area of consumption. Anglo Platinum is the world's leading platinum producer (40% in 2006) and is increasing production by 5% per annum to satisfy the rising demand [2]. This has necessitated a major expansion of Anglo Platinum's Precious Metals Refiners (PMR) near Rustenburg, South Africa.

DISCUSSION

The PMR flowsheet is chloride based and incorporates four solvent-extraction stages for the separation of Au, Pd, Pt, and Ir [3]. Platinum is present as the kinetically inert $[PtCl_6]^{2-}$ anion, which can be extracted by a wide range of strong and weak-base

anion exchangers [4]. The extractant employed at PMR is the secondary amine Amberlite LA2

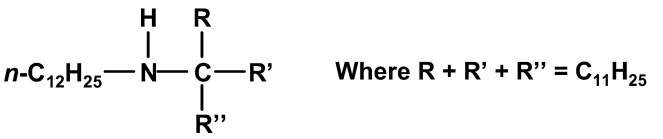

which gives a reasonable balance between extraction at low acidity and an acceptable distribution ratio for stripping with concentrated HCl (Figure 1).

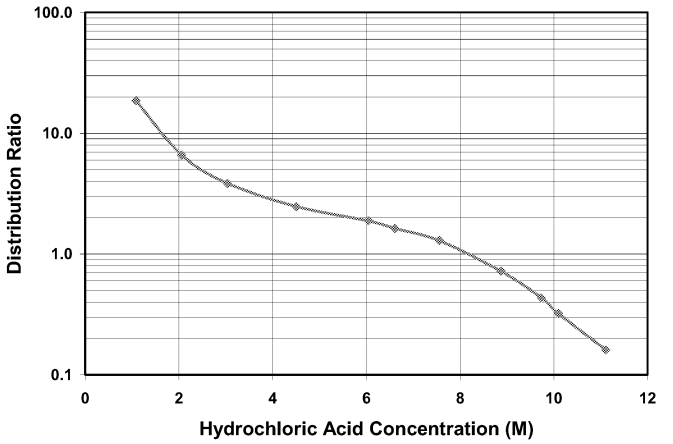

Figure 1. Effect of HCl concentration on the extraction of $[PtCl_6]^{2-}$ by 0.3 M Amberlite LA2 in Solvesso® 150.

The solvent-extraction (Solvex) sections at PMR are dual-streamed in open-air bays sited away from the main process building in order to minimize the risk to PGM supply in the very unlikely event of a fire. As a result of Anglo Platinum's expansion of Pt Production, these Solvex sections were expected to reach their design capacities in 2006. Increasing the capacity by constructing additional Solvex sections would be extremely capital intensive. Consequently, modifying the operation of the existing sections to increase capacity was investigated.

Data on the current operation of the Pt Solvex were largely limited to routine "process control" analyses of the aqueous streams. A comprehensive program of benchmarking exercises was therefore carried out by Anglo Research and Johnson Matthey Technology Centre. These confirmed that the mixer-settlers had been conservatively designed. As a result, the depths of the dispersion bands in the settlers were limited, and entrainment levels were negligible. It was established experimentally that the kinetics of extraction/stripping with LA2 were extremely fast (3-5 seconds). Consequently the mixer-settlers could be operated at up to double the design flowrate before hydraulic constraints occurred.

In practice, however, only a limited increase in flowrates could be achieved due to constraints in the supply of strip acid. For optimal stripping, an acidity of >11 M is required. "Commercial" concentrated HCl supplied from Johannesburg (altitude 1690 m)

only has an acidity of around 10 M. The Pt strip acid must therefore be generated at PMR (altitude 1120 m) by evaporating hydrogen chloride from concentrated HCl and then absorbing it into 10 M HCl to increase the concentration to the >11 M required. This acid plant was already operating at close to capacity. Consequently, the capacity of the Pt Solvex could only be increased if the requirement for strip acid could be reduced.

The PMR Pt Solvex consists of 10 extraction, 5 scrub, and 10 strip mixer-settlers. The large number of stages is due to the necessary compromise between the distribution ratios for extraction and stripping required with LA2. Concentration profiles were determined by sampling every mixer-settler. The Pt profile showed (Figure 2) that over 99.5% of the platinum was extracted in the first 3 of the 10 extraction boxes.

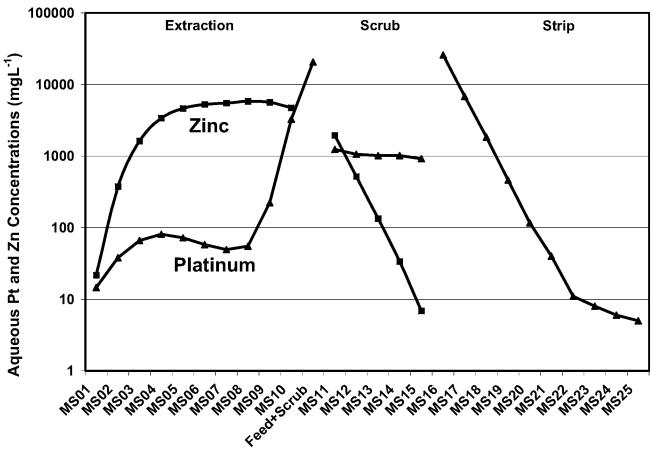

Figure 2. Aqueous Pt and Zn concentration profiles across a PMR Pt Solvex section.

This is as a result of changes upstream to the Pd Feed Preparation stage that has decreased the chloride concentration. The profile showed a small build-up of Pt occurring in MS01-MS08. The profiling exercise also indicated a much larger build-up of zinc. Zinc is extracted by Amberlite LA2 as the $[ZnCl_4]^{2-}$ anion. Calculations using the stability constants [5] for the zinc chloro-complexes indicate that concentration of this anion is low at the chloride concentration in the extraction section (0.8-1.2 M). As a result, the distribution ratio for zinc is significantly lower than that of $[PtCl_6]^{2-}$. Consequently, when the latter loads into the organic MS08 onwards it "crowds" the zinc out into the aqueous phase, causing reflux to build-up. The same mechanism is responsible for the build-up of weakly extracted platinum species in MS01-MS08. The concentration of Zn in the Pt Feed is only 40-50 mg L^{-1}, and the build-up of zinc would have taken an estimated 3 months to accumulate.

The Pt profile also shows that >99.9% of the platinum is stripped in the first six strip boxes. Consequently both the extraction and strip sections are over-sized. The possibility of exploiting this to decrease the requirement for >11 M HCl was therefore investigated. The standard approach for investigating modification of solvent-extraction flowsheets is to employ McCabe-Thiele constructions. However, this was not possible for the Pt Solvex, as the profiles indicated that Amberlite LA2 extracts a number of other Pt species in addition to $[PtCl_6]^{2-}$. It also extracts chloride as well as a number of other

metals including zinc, bismuth, and selenium. All these entities compete for extraction, and therefore multidimensional distribution isotherms would be required. Furthermore, McCabe-Thiele constructions are not ideally suited to situations where there is a build-up of metals occurring within a solvent-extraction process. The decision was therefore taken instead to establish a dynamic computer simulation of the Pt Solvex.

The computer simulation was developed in-house. It is written in PowerBasic (www.powerbasic.com) which is an extremely efficient native code compiler for 32-bit Windows®. The program comprises a model of the Amberlite LA2 extraction chemistry coupled to a dynamic simulation of the mixer-settler operation. In contact with HCl Amberlite LA2 protonates forming the hydrochloride. Extraction of $[PtCl_6]^{2-}$ and other anions then occurs by anion-exchange, for example,

$$2RR'NH_2Cl_{(org)} + [PtCl_6]^{2-} \rightleftharpoons (RR'NH_2)_2[PtCl_6]_{(org)} + 2Cl^- \quad (1)$$

The extraction equilibria for the different entities are modelled by employing a series of pseudo-equilibrium constants K_{eq}, for example,

$$K_{eq} = \frac{\left[(RR'NH_2)_2[PtCl_6]\right] \times \left[Cl^-\right]^2}{\left[[PtCl_6]^{2-}\right] \times \left[RR'NH_2Cl\right]^2} \quad (2)$$

The K_{eq} are calculated using the concentrations instead of activities as these are not known. The K_{eq} are not constant (Figure 3) but vary with the chloride concentration, due not least to significant changes in the activity of chloride with ionic strength. The K_{eq} for zinc also changes with chloride concentration due to the effect on formation of $[ZnCl_4]^{2-}$.

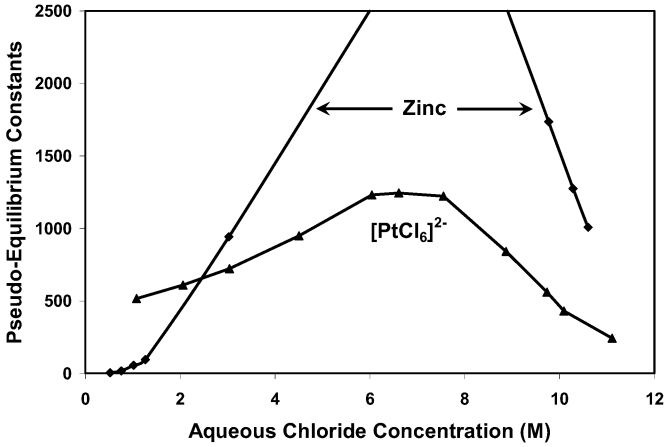

Figure 3. Effect of the chloride concentration on K_{eq} for $[PtCl_6]^{2-}$ and zinc.

The simulation of the mixer-settlers models the mixer as a continuously stirred tank and the settler as "plug flow". The program functions by repeatedly moving the small volumes of organic and aqueous that flow during a short time period (1 to 10 seconds) through the countercurrent mixer-settlers and then recalculating the equilibria in the mixers. The settlers are divided into a series of small segments each the size of the

small volume flowing during that short time period. The concentrations of all of the species in the two phases in both the mixer and the segments of the settler of each of the mixer-settlers are stored in the elements of a series of multidimensional arrays. At the start of the cycle, the concentrations in the end segments of the settler are moved countercurrent to the next mixer-settler. The concentrations in the segments are then all moved along the array and a small volume is transferred out of the mixer into the first segment. The small volume moved from the neighboring mixer-settlers is then added to the mixer and the new equilibrium concentrations in the mixer calculated. This cycle is then repeated.

The equilibrium concentrations in the mixer are calculated by an iterative routine. The program estimates a concentration of chloride in the aqueous **[**Cl^-**]** and then calculates the concentration in the organic phase **[**$RR'NH_2Cl$**]** by mass balance. Equation 2 can be re-written as a function of the distribution ratio *D*, for example,

$$\mathbf{D} = \frac{\mathbf{[}(RR'NH_2)_2[PtCl_6]\mathbf{]}}{\mathbf{[}[PtCl_6]^{2-}\mathbf{]}} = K_{eq} \times \frac{\mathbf{[}RR'NH_2Cl\mathbf{]}^2}{\mathbf{[}Cl^-\mathbf{]}^2} \qquad (3)$$

Consequently *D* can be calculated for each entity using the estimated values of **[**$RR'NH_2Cl$**]** and **[**Cl^-**]**. The concentrations of each entity in the organic phase can then be computed. These can then be used to calculate a second value for **[**$RR'NH_2Cl$**]** by mass balance.

$$[RR'NH_2Cl]_{calc.} = [LA2] - ([RR'NH_2)_2[PtCl_6]] \times 2 + ([RR'NH_2)_2[ZnCl_4]] \times 2 + [\text{anion A}] \times \text{charge} + [\text{anion B}] \times \text{charge etc.}) \qquad (4)$$

The value of the initial estimated $[Cl^-]$ is then adjusted iteratively until $[RR'NH_2Cl]_{est'd}$ and $[RR'NH_2Cl]_{calc.}$ converge to $\pm 1 \times 10^{-8}$M. This equates to an accuracy for $[PtCl_6]^{2-}$ of 0.01 mg L^{-1}. Simulation of six months operation requires 2-3 hours using a medium specification PC. The simulation creates data files containing the concentrations in every box at regular intervals to enable the build-up of entities such as zinc to be monitored. These data files can be used to restart the computer simulation to allow changes in the operating conditions to be investigated.

A number of different flowsheet options were investigated using the computer simulation. The simulations predicted that halving the flowrate of strip acid would only increase the concentration of platinum in the final strip mixer-settler (MS25) to approximately 140 mg L^{-1} (Figure 4). This would leave ca 20 mg L^{-1} Pt as $[PtCl_6]^{2-}$ in the stripped organic whilst all the other platinum species would still be completely stripped. The acidity of the raffinate in MS01 is ca. 1 M, and therefore the distribution ratio is ca. 10. Consequently the raffinate would contain an additional 2 mg L^{-1} Pt which represents a negligible increase.

A series of mini-pilot plant trials were then carried out at Anglo Research to confirm these predictions. The mixer-settlers employed were MSU-05 PVDF units supplied by MEAB, Göteborg, Sweden. The platinum chloro-complexes are potent sensitizers, and the mixer-settlers were therefore operated inside glove-boxes. Problems were encountered with corrosion due to the acid fumes from the 11 M HCl, resulting in

regular failures of the low-voltage stirrer motors, but otherwise the MEAB units functioned well.

The results from the mini-pilot plant trials showed very good agreement with the predictions of the computer simulation (Figure 4). Subsequent trials at PMR on the Pt Solvex plant successfully confirmed these results. As a result the requirement for 11 M HCl has been decreased by 50%, and consequently the capacity of the PMR Pt Solvex section can potentially be doubled with minimal capital expenditure by operating at double the feed flowrate.

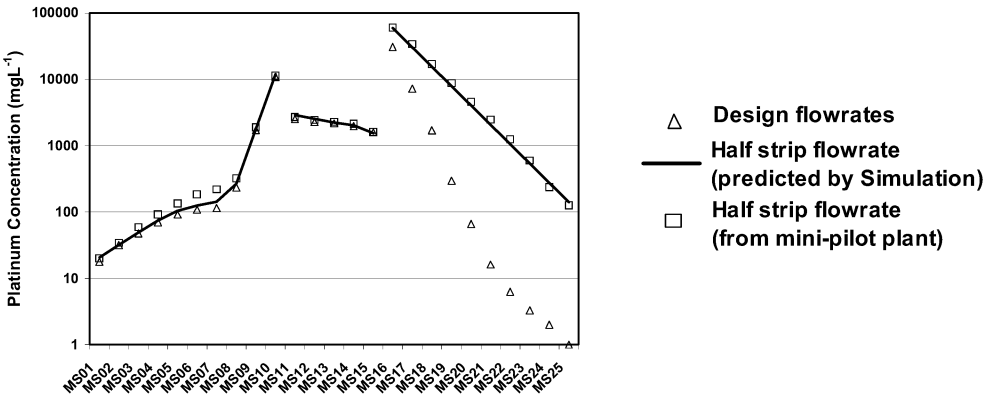

Figure 4. Effect of halving the flowrate of Pt strip. Comparison of computer simulation with result from mini-pilot plant trials.

ACKNOWLEDGMENTS

The authors would like to thank Anglo Platinum Limited for permission to publish this paper.

REFERENCES

1. Annual PGM Market Reviews, Johnson Matthey PLC, www.platinum.matthey.com.
2. Anglo Platinum Annual Report 2006, www.angloplatinum.com.
3. F. L. Bernardis, R. A. Grant, and D. C. Sherrington, "A review of methods of separation of the platinum-group metals through their chloro-complexes," *React. Funct. Polymers*, **65**, 205-217 (2005).
4. M. J. Cleare, R. A. Grant, and P. Charlesworth, "Separation of the platinum-group metals by use of selective solvent extraction techniques," Extraction Metallurgy 1981, IMM, London, UK; pp. 34-41
5. IUPAC Stability Constant Database, Academic Software, www.acadsoft.co.uk.

STABILITY OF THE DISPERSED BAND IN A SHALLOW-LAYER SETTLER

M.M.M. Ribeiro,[1,2] E.V. Soares,[2,3] M.M.L. Guimarães,[1] and A.M.A. Fiúza[4]

[1]SIPROM-Modelação e Simulação de Processos Multifásicos do Instituto Superior de Engenharia do Instituto Politécnico do Porto, R. Dr. António Bernardino de Almeida, 431, 4200-072 Porto, Portugal. [2]Chemical Engineering Department, Superior Institute of Engineering from Porto Polytechnic Institute, Rua Dr António Bernardino de Almeida, 431, 4200-072 Porto, Portugal. [3]IBB-Institute for Biotechnology and Bioengineering, Centre for Biological Engineering, Universidade do Minho, Campus de Gualtar 4710-057, Braga, Portugal. [4]CIGAR - Centro de Investigação Geo-Ambiental e Recursos, Faculdade de Engenharia, Universidade do Porto, R. Roberto Frias, Porto, Portugal. Corresponding author email address: mgr@isep.ipp.pt

ABSTRACT

The present study is aimed at shallow-layer settlers, involving pilot-plant data collection about the thickness of the dispersion band at different points along its length and its use in simulation work. At steady state, after step inputs in the agitation power, the length of the dispersed band varied in time and didn't return to its initial condition. Although clean, pure fluids were used, crud formation was observed and acquired relevance especially for long-period experiments. This behavior brought out the fact that crud formed during the experimentation disturbed the stability of the dispersed band. Crud analysis, performed by fluorescence microscopy, suggested the presence of bacteria. This bacterial nature of the crud was confirmed, and biocide utilization seemed to be adequate for its minimization.

INTRODUCTION

The analysis of the dynamic behavior of rectangular gravity settlers, where the dispersion flow is primarily horizontal, is complicated because the horizontal drop velocity, the dispersion-band thickness, and the drop-size distributions vary along the length of the settler [1]. Mathematically, this implies a formulation in terms of partial differential equations (distributed parameters model), contrasting with the simpler, concentrated parameters models used for the simulation of agitated vessels and/or compartmented extraction columns.

Simulation of the hydrodynamics of mixer-settler units requires a mathematical representation of the dispersion behavior in the mixing and settling chambers and has great relevance for proper design and performance analysis. While mixing models and algorithms are well established, scarce work has been published regarding settler

modeling [2-4], since application to particular physical-chemical systems requires accurate knowledge, obtainable only through detailed adequate experimentation and determination of the relevant parameters.

Also, gravity settlers are usually designed for steady-state operation using experimental data obtained from small-scale batch tests, often without pilot-scale tests. However, transient conditions frequently occur in industrial continuous-flow systems, due to uncontrolled variations in feed-rate and/or agitation speed. Such transient regimes may imply variations in the thickness and length of the dispersion band, which, in turn, may have damaging consequences such as flooding and ensuing solvent loss. Thus, it is important for the designer to understand the effects of such variations in order to achieve safe design and trouble-free operation.

The main initial objective of the present long-term research program was to measure settler parameters, such as length and thickness of the dispersion band as well as drop-diameter distribution, drop velocity along the settler, and the response of these variables to disturbances in the operating conditions, in order to acquire parameter values for accurate modeling. Given this limited, theoretically oriented objective, pure water and kerosene (which is a light oil fraction mainly composed of aliphatic hydrocarbons from C_9 to C_{16}, eventually with small amounts of aromatics) were used, without addition of metals, salts, or extractant reagents, since our primary objective is the study of the hydrodynamics. Therefore, the formation, during our experiments, of great amounts of crud, compelled us to a previous study of its occurrence and growth prevention.

Previously reported observations focused on the study of crud influence in the performance of industrial equipment have shown that crud formation often occurs and that its presence may modify some dispersion characteristics, such as the coalescence rate, that affect phase-separation efficiency [5-6]. Also, oscillations in the dispersion bands typical in settlers have been justified by formation of crud at the aqueous organic interfaces in some industrial installations [5-7], and this fact modifies the drop coalescence. This crud layer may affect phase continuity and promote emulsion stability. Ultimately, it may initiate phase inversion, making correct work impossible [5]. So, crud presence increases organic-phase losses and increases operation costs. This crud layer composition, which is quite site specific, is not well known and—in an industrial environment—may be due to solid particles and chemical and/or biological impurities.

However, in our pilot plant installation, where pure products are used, similar layers were also present [8], which have now been shown to be of organic character. In our work, various problems were found in experimentation, one of the more relevant being crud formation that was observed and acquired great importance especially for long-period experiments. This behavior brought out the fact that crud formed during the experimentation disturbs the stability of the dispersed band. Thus, in order to make for reliable and reproducible experimental data, the effects of the formation and accumulation of crud at the water-organic interface must be taken into consideration, controlled, and minimized by using appropriate biocides.

EXPERIMENTAL PROCEDURE

For our stated objectives, an acrylic pilot-scale mixer-settler was specially designed and built, as reported in Baptista [8]. The installation works in closed circuit (Figure 1) with the liquid-liquid system water-kerosene, which flows from two separate drums being pumped to a well-agitated mixer, where the kerosene is dispersed in the water. The dispersion flows together to the settler, where the two phases are separated, then returning to the drums.

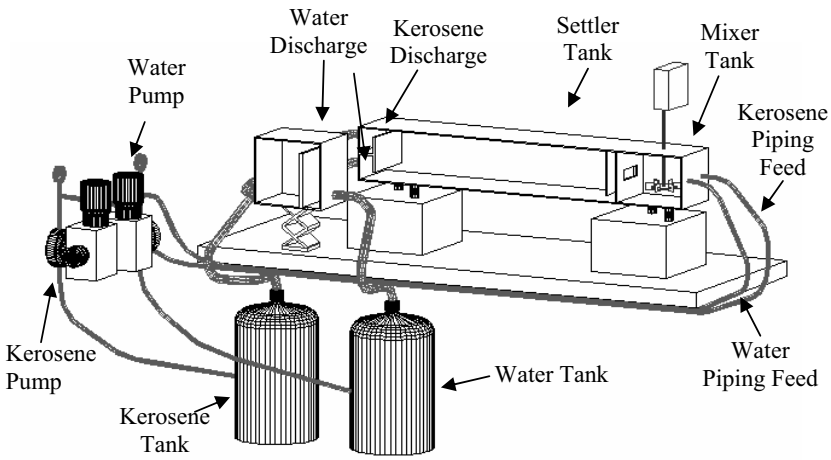

Figure 1. Experimental setup.

To determine the settler parameters, a standard procedure was followed. The installation was in operation for several days (sometimes weeks) and during this process, a sizeable amount of crud was formed in the kerosene-water interface at the end of the dispersion band, towards the discharge end, which acted as a mechanical barrier to the longitudinal expansion of the dispersion layer (Figures 2A and 2B). It was observed that the crud formation had as effect the reduction of the length of the dispersion band. When that crud was removed, the band grew up again, but it became quite impossible to stabilize it. Thus, the main objective was postponed and the experimentation focus was changed to understanding the crud nature and to try its elimination, if possible, which is the specific object of the present paper.

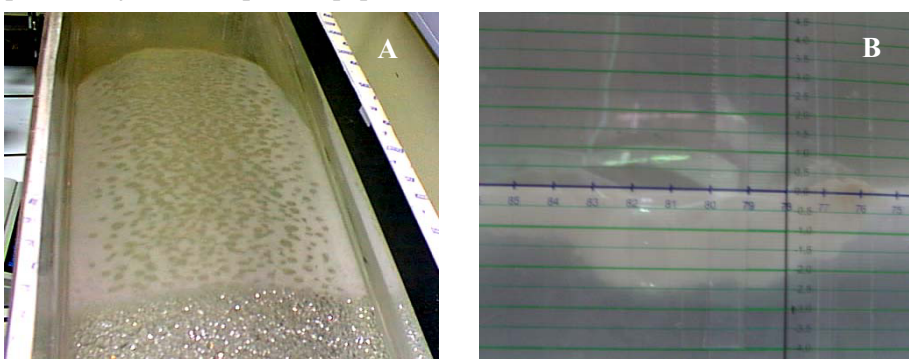

Figure 2. (A) Top view of the settler showing the accumulated crud, and (B) side view of the settler showing phase turbidity and crud accumulation.

As stated above, the products used were clean (without solid particles) and pure (deionized water and kerosene). However, at long operating time in closed circuit, a colorless and gelatinous-like crud layer was formed, as described above. In order to investigate the possible presence of microorganisms, crud was heated at 65,ºC, during one hour, and then 4.5 μmol L^{-1} propidium iodide (PI) was added. PI binds to DNA by intermixing with the bases, exhibiting an orange-red fluorescence [9] (Figures 3A and 3B).

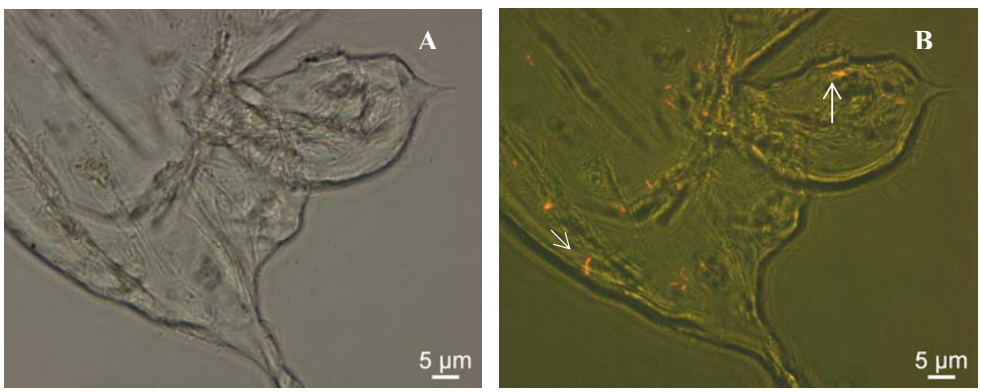

Figure 3. Photomicrographs of crud, treated with Propidium Iodide. Phase-contrast (A) and fluorescence plus phase-contrast (B) observations. Arrows: visualization of rod-like structures (bacteria) in the crud.

After the biological nature of the crud has been confirmed as bacterial, the next step was a first attempt to use a biocide in order to minimize its formation. Consequently, starting from extremely unfavorable system conditions (large amount of accumulated crud), the crud was mechanically removed, and 4 drops of biocide were added. The biocide used was aqueous-soluble EQ B91 (Enkrott Química). After this procedure, the crud accumulation rate markedly diminished, and the dispersion band significantly extended towards the discharge end of the settler. After 260 more hours (11 days), 12 additional drops of biocide were added. The experiment was carried on for 8 more days. This result is shown in Figure 4.

RESULTS AND DISCUSSION

The observed crud is definitely not a simple water-kerosene-air emulsion nor particulate solid accumulation. Its analysis by fluorescence microscopy, after treatment with PI, revealed the presence of orange, rod-like structures, strongly suggesting the presence of bacteria (Figures 3A and 3B). This observation is in agreement with the description of growing of bacteria, yeasts, and filamentous fungi in different fuels, namely in aviation kerosene [10]. Microorganisms might have entered in the system via the air, contaminated settler and storage-tank walls, or being already present in the kerosene (which may occur in the supplier's storage tanks, according to information by the refinery's technical personnel) used in the experiment. The growth of bacteria in the

interface water-kerosene was most likely due to the presence of water, oxygen (introduced in the mixer, which provides enough oxygen dissolved in both phases), and a carbon source (kerosene); nitrogen and phosphorous, could also be present as minor contaminants, promoting microorganism growth and development of the gelatinous-like material (crud*)*.

Given the impossibility of totally avoiding crud formation, the only experimental strategy that may be used is to control and prevent its growth. Figure 4 shows the results of biocide utilization on crud development and its effect on the dispersion band length and stabilization under steady state conditions.

As stated above, the experiment was achieved using dirty phases with abundant crud. Without crud removal, the dispersion-band length was not stabilized, and its length was less than 76 cm. By removing the crud and adding biocide, the length rapidly increased, the crud-development rate was seen to diminish, and the dispersion-band length attained values between 85 and 88 cm, even though it was not completely stabilized. A second addition of biocide, without crud removal, led to a short instability followed by the complete stabilization of the dispersion band length at 84 cm. No significant further crud formation was observed. The shorter length after this second biocide addition may be justified by use of excess biocide and/or by an interfacial tension variation. However, many more systematic and well-planned experiments are necessary to better understand this process.

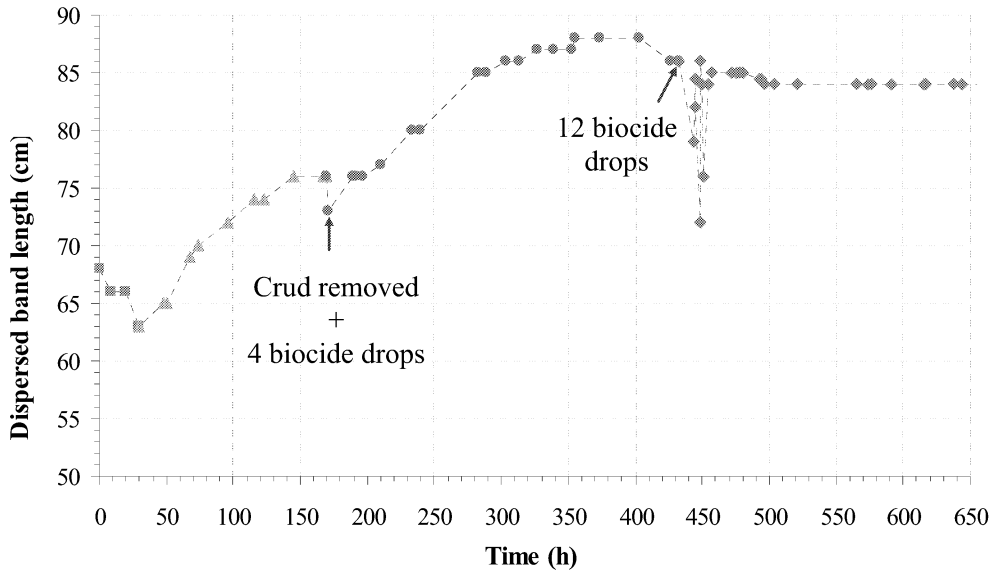

Figure 4. Behavior of the settler dispersion-band length as a function of time.

CONCLUSIONS

(1) Pilot-plant experiments using pure water and kerosene phases in closed circuit and under permanent operating conditions have shown that dispersion-band length

stabilization was not attained, even at long experimentation times. Crud formation at the interface was observed. (2) The crud formation did not allow the normal progression of dispersion-band and its removal, by means of invasive methods, leads to a permanent instability in the length of the dispersion band. (3) Fluorescence microscopy analysis suggests the presence of bacteria in the gelatinous-like material (crud). (4) Preliminary experiments using a biocide revealed a dramatic decrease in crud formation and allowed the dispersion-band stabilization. (5). Future work must be focused on the utilization of an adequate biocide, so that detailed experiments using different biocides must be carried out and its influence on dispersion properties (namely interfacial tension) analyzed.

ACKNOWLEDGMENTS

Thanks are due to ENKROTT QUÍMICA Company and GALP ENERGIA S.A. Company for their precious help in furnishing us some samples of biocide and kerosene respectively. Also, thanks are due to MSc. student Rui Silva and undergraduate students Ana Pimenta, Bruno Pinto e Maria João Marques for their patient help in experimental work, over and above their duty in normal research work.

REFERENCES

1. M. C. F. Baptista, R. P. M. Silva, M. M. M. Ribeiro, M. M. L. Guimarães, and A. M. A. Fiúza, "Measuring Dispersion Band Quantities in Shallow-Layer Settlers," 9th Int. Chemical Engineering Conf., Coimbra, Portugal, 2005; EFS28.
2. M.C. Ruiz, "Mathematical Modeling of a Gravity Settler," Ph.D. Thesis, University of Utah, USA, 1985.
3. G. A. Pinto, F. O. Durão, A. M. A. Fiúza, M. M. L. Guimarães, and C. M. N. Madureira, "Design Optimisation Study of Solvent Extraction: Chemical Reaction, Mass Transfer and Mixer-Settler Hydrodynamics," *Hydrometallurgy*, **74**, 131-147 (2004).
4. E. F. Gomes, M. M. L. Guimarães, and L. M. Ribeiro, "Numerical Modelling of a Gravity Settler in Dynamic Conditions," *Advances in Eng. Software*, Elsevier, **38**, 810–817 (2007).
5. Wang Chengyan, "Crud Formation and its Control in Solvent Extraction," Int. Solvent Extraction Conf., Beijing, China, 2005, 1066-1071.
6. R. F. Dalton, C. J. Maes, and K. J. Severs, "Aspects of Crud Formation in Solvent Wxtraction Plants," Annual Meeting of the Arizona Conf. AIME, Tucson, 1983.
7. G. M. Ritcey, "Enhancement of Plant Performance by Control of Organic Surfactants and Poisons," Int. Solvent Extraction Conf., Beijing, China, 2005; pp. 1205-1210.
8. M. C. F. Baptista, "Determinação experimental de parâmetros condicionantes da coalescência num decantador de fluxo horizontal," Msc. Thesis, University of Porto, Portugal, 2004.
9. R. P Haugland, Assays for cell viability, proliferation and function, The Handbook – A guide to fluorescent probes and labeling technologies, 10th ed., Invitrogen, USA, 2005; pp. 699-776.
10. C. C. Gaylarde, F. M. Bento, and J. Kelley, "Microbial contamination of stored hydrocarbon fuels and its control," *Revista de Microbiologia*, **30**, 1-10 (1999).

OPTIMIZATION OF THE DESIGN OF MIXER-SETTLERS IN Zn SOLVENT EXTRACTION

D. Martín, F. Sánchez, M. Frades, and A. B. Mejías

Técnicas Reunidas. Hydrometallurgy and Electrochemistry
28830 San Fernando de Henares, Madrid, Spain.
Corresponding author email address: dmartin@trsa.es

ABSTRACT

After many years of successful industrial application, the Modified ZINCEX™ Process has demonstrated to be a robust and efficient process for zinc production. This process consists of the integration of three stages: leaching, solvent extraction, and electrowinning, ensuring production of SHG zinc quality. Because zinc electrowinning is very sensitive to the impurities, this process guaranties the highest purity of the advanced electrolyte feeding the cellhouse. The key points for ZINCEX™ technology are the process flexibility, the appropriate combination of each unit process conditions, and its adaptability to treat any kind of raw materials. One reason for the success of the process is the high efficiency and performance of the mixers-settlers (MS), producing ultra-pure zinc electrolyte. The proper design of a MS is achieved by means of a suitable combination of pump-and-mixing conditions, linked with the optimized design of the settler. Hydrodynamics models for mixing and settling, as well as experimental works made on a MS prototype (1:1 scale in critical dimensions), are used by Técnicas Reunidas (TR) for proprietary equipment design. Computational fluid dynamics simulation and prototype test results obtained by TR for solvent-extraction design are presented in this paper.

INTRODUCTION

One of the main concerns about Solvent Extraction (SX) industrial plants is equipment design. Chemical behavior, mostly referred to metal transfer from one phase to the other, can be easily scaled up from bench-scale or pilot plant, but this is not the only aspect of SX. There are significant physical aspects like phase dispersion in mixing, type of droplet formation, and rate and completeness of coalescence [1]. Scaling-up of these physical parameters from pilot-plant data and low-scale models results in uncertainties and doubts.

The experience with copper solvent extraction plants, which are the biggest in operation, reinforces the necessity of design optimization when the equipment requires a large scale in order to minimize problems related to physical behavior of the system, like crud formation, second-phase entrainment, and others that are difficult to detect in a pilot plant [2].

TR's experience in massive zinc SX [3-6] has confirmed similar difficulties with zinc electrowinning, in which it is more restrictive than copper electrowinning and requires finer control of the SX unit [7].

The critical equipment in the design of a SX plant are mixing and settling units, which provide for the intimate contact of both liquid phases, mass transfer, and subsequently, their separation into an organic and an aqueous phase [8]. Scaling-up procedures for this equipment are not fully understood yet, and issues like phase inversion, residence time distribution, entrainment, and drop size are not yet defined to establish a firm theoretical design basis. This is the reason why research and innovation in MS design is still essential to optimize their size and performance [9].

Ideally the design of this equipment should be made from basic principles that estimate coalescence velocities and mass transfer. However, in practice, this is rather difficult and the scaling-up must be made from the experimental results provided by pilot plants at the proper scale and full-size prototypes [10-12] combined with modelling using Computational Fluid Dynamics (CFD) techniques.

TR EXPERIMENTAL TOOLS FOR MIXER-SETTLERS DESIGN

Although the knowledge of extraction operations has increased in the last years, there are two main limitations for designers: (1) the process must be carefully studied in the laboratory and pilot plant; and (2) the process operation must be guaranteed in a stable system. Operations must be designed with a high confidence level, taking into account all the possible effects that may influence the process performance, and in consequence on the equipment design and scale-up from data obtained in small scale. Small-scale pilot-plant operations show physical and hydrodynamic effects that can influence the final results. Equipment design from this basis is very risky and may result in incorrect conclusions.

To solve these difficulties, it is also necessary to perform experiments at a relatively large scale; otherwise, the scaling-up of equipment to full-scale equipment requires safety factors that may result in an uneconomical situation.

Equipment and Facilities Description

The Hydrometallurgy & Electrochemistry Division of Técnicas Reunidas uses a MS prototype and a semi-industrial mixer model with the purpose of equipment design and optimization. This equipment provides reliable information about design parameters, thus reducing the uncertainty in scaling-up. Its last application was applied to the Modified Zincex^{TM} Process in the Skorpion Plant (Namibia) that is showing excellent results [5,6].

Mixer-Settler Prototype

The MS prototype includes two cascade mixers of 1 m^3 each and made in fiber-glass reinforced polyester (FGRP), connected to a transparent methacrylate settler 25 m long, 0.25 m wide and 1 m high. To operate this prototype, there is some auxiliary equipment, including holding tanks, recirculation pumps, heat exchangers, etc. which can

simulate the operation of a complete SX unit. Operation length and height of the settler can be easily changed to maintain full-size values, so that there is only one dimension, width, for further scaling-up. This equipment has the additional feature of being transparent, which allows the observation of the liquid-liquid separation (dispersion band and "visual" quality of the settling) along the settler. This is very helpful for tracking the evolution and the effect of internals on the dispersion band.

This facility has been designed to modify and control the following variables:

- Temperature of the process can be increased from room temperature to 45 ºC.
- The length of the settler can be changed up to a maximum of 22 m of effective settling distance.
- The level of the interface can be changed, viewed and measured along the settler.
- Agitation power in the mixers can be varied by means of the respective frequency inverter, determining the residence time, homogeneity of the mix, and mass transfer.
- Phase continuity can be varied, giving to continuous-aqueous or continuous-organic media.
- Phase composition can be adjusted depending on the SX stage to be simulated.
- Organic/aqueous ratio can be adjusted according to requirements.
- Flow rates can be controlled up to a maximum of 60 m^3/h (aqueous plus organic).
- Different internals can be inserted and studied anywhere in the settler.
- Aqueous phase can be recycled and mixed with fresh feed to the mixer, thus making it possible to increase the aqueous flow rate in the system.

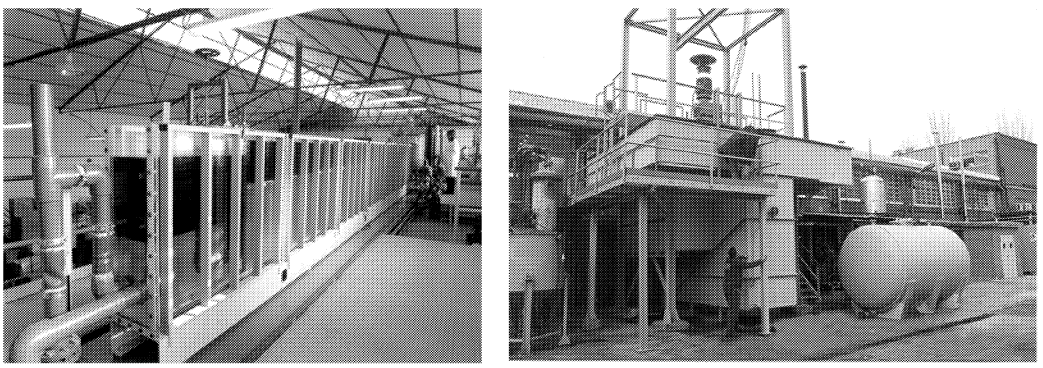

Figure 1. Left: Mixer-settler prototype. Right: Industrial mixer model.

Industrial Mixer Model

The industrial model of mixer is made of carbon steel and has a capacity of 34 m^3. It contains an agitator with exchangeable blades and a 45 kW motor with an inverter that allows selecting the rotor speed. This combination allows testing the agitation power over a wide range of values. Figure 1 shows a general view of this facility.

This facility makes it possible to:

- Measure unit power requirements, which confirms power consumption.
- Determine pumping capacity under the different operating conditions.
- Check the grade, homogeneity and type of agitation in the mixer.
- Analyze the effect of main hydrodynamic parameters and variables.
- Study the agitation turbine design and geometry, using different types of agitators and multiple configurations.

HYDRODYNAMIC EXPERIMENTAL STUDIES

TR test program using the above facilities for a specific applications leads to define the optimized design for the SX MS. The following properties and parameters for the system can be analyzed:

- Homogeneity of mixing, intensity, and agitation, which are essential for a good mass transfer between both liquids.
- Influence of the type of agitation on the separation of both liquid phases.
- Power required for agitation (which affects the power consumption of the system).
- Influence of the temperature on the general behavior of the system.
- Pumping capacity of the mixer, required for an appropriate operation.
- Specific settling flow rate and the relative speed of both liquid phases.
- Width of the dispersion band, which determines the total length of the settler.
- Organic and aqueous entrainment of phases.
- Influence of the internals within the settler.
- Optimization of other operational conditions: interface layer, recirculation system, etc.

A conscientious study of the outputs from the experimental test work, for each different SX stage, must be accomplished due to the complexity of the hydrodynamics for an SX process. The obtained data will then be used in the design. Figure 2 shows a comparative plot of the maximum total specific flow rate in the settler as a function of the organic-to-aqueous ratio obtained during the test work for determined conditions. This type of curve is used to determine the total settling surface and, once the coalescence behavior is known, to design the size and dimensions of the settler.

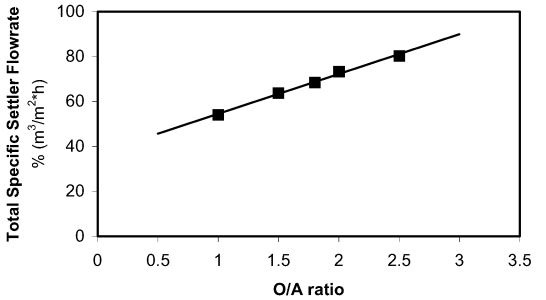

Figure 2. Maximum specific flow rate in the settler as a function of organic/aqueous (O/A) ratio for zinc extraction with D_2EHPA.

Additional examples are presented in Figure 3. The pump head of a particular turbine for a mixer is plotted as a function of the feed flow rate for different agitation conditions. Additionally the figure shows the power consumed by the agitator as a function of the pumped water flow rate obtained under different agitation speeds. These two graphs are the characteristic curves of the agitator that can be used in a similar way as the characteristic curve of a centrifugal pump.

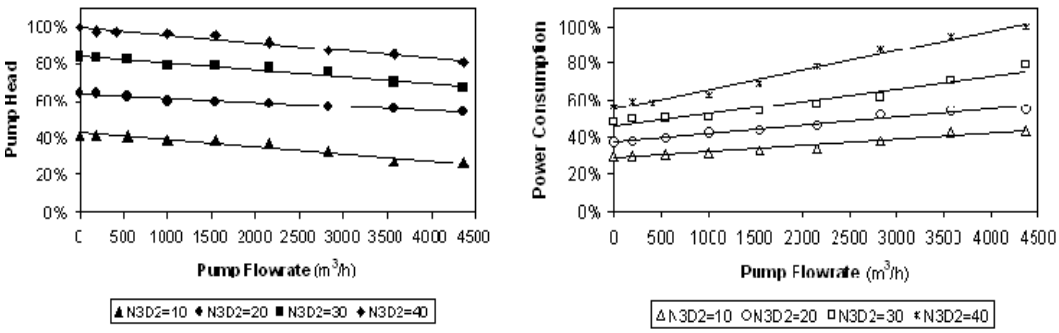

Figure 3. Pump head and power versus pumping flow rates at different agitation power N^3D^2 ($rps^3\ ft^2$).

COMPUTATIONAL FLUID DYNAMIC SIMULATION

As standard procedure for TR mixer settler design, the precalculated settlers are simulated with commercial Computation Fluid Dynamic software (CFD). The objective is to check and complete the optimized design obtained after the experimental testwork by means of the calculation of the fluid-dynamic behavior of the industrial-size settler. The use of the computer-aided tool allows the study of different settler configurations pertaining to any internal design.

The final aim of the simulation is to ensure the optimized conditions for an effective liquid-liquid separation into the previous selected settler configuration. Different parameters are analyzed using the CFD software, for example:

- Distribution of flow into the settler, checking that disturbances are not present in the flow (dead zones, backflows, etc. have to be avoided) within the model.
- Velocity and pressure of the fluid along the settler can be determined, aiming to produce a smooth flow within the equipment, and defining the internals to avoid preferential channelling.
- Determination of fundamental parameters such as pressure drops, temperature, profile, etc., that are necessary for the complete design of the mixer-settler unit.

Following are shown two examples of how the CFD software is used to optimize the design of particular internals inside the settler.

Flow Distributor

Based on the best configuration obtained in the prototype test-work, a model of the industrial-plant-size settler is developed. The first step for the study is to simulate the predesigned flow distributor. The results are shown in Figure 4A. The wide range in the colors indicates dead zones as well as turbulences areas. These disturbances will decrease the effective settling surface of the equipment and have to be avoided. The optimization of the process is achieved using different geometric parameters for the design of the flow distributor.

Finally, in Figure 4B the final optimized design is simulated, showing no disturbances in the flow distribution within the settler. Thus the minimum settler size for a specific application may be calculated.

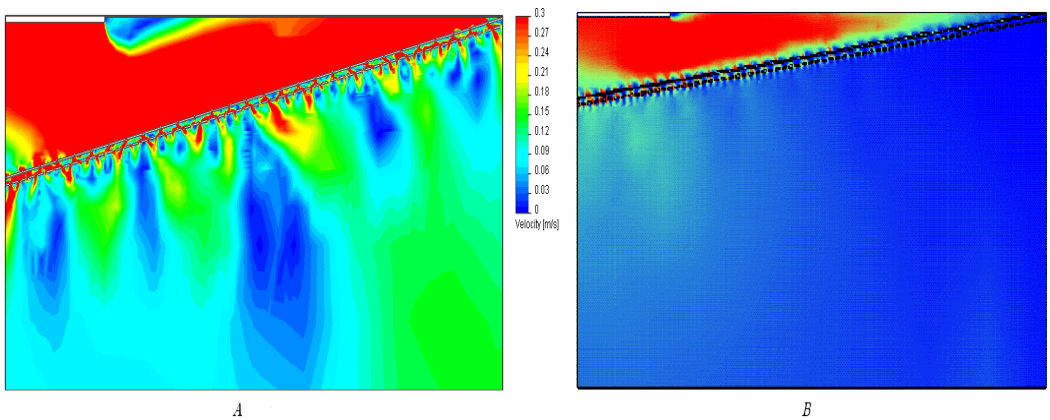

Figure 4. Simulation A, the flow shows dead zones and disturbances.
In Simulation B, the Flow was homogeneously distributed in the settler.

Recirculation Manifold

The study of the flow through the aqueous recirculation manifold within a settler is another important example of CFD support to optimize the equipment design. As in the previous case, different designs have to be simulated in order to achieve the best hydrodynamic conditions. An inefficient design of the aqueous recirculation system will promote flow disturbances inside the settler, and consequently settling performance per square meter will decrease. In addition, mentioned flow disturbances will produce higher entrainments than expected.

Figure 5 shows the difference between an inefficient design (A) and an optimized design (B). In the first case, flow lines show backflows and high disturbances produced by the recirculation manifold. In case B, the disturbances have been attenuated by a redefinition of the geometry for the recirculation system.

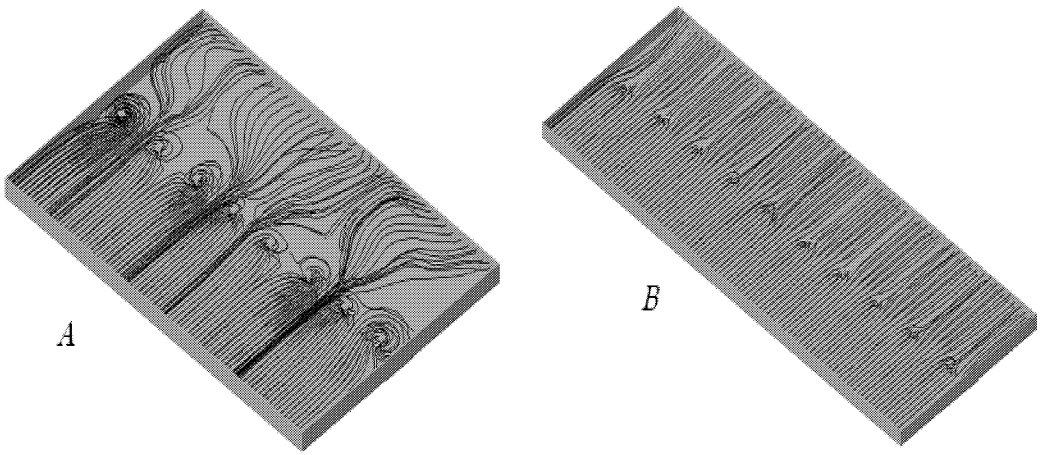

Figure 5. Case A: Inefficient aqueous recirculation design. Case B: Optimized design.

CONCLUSIONS

Chemical behavior of SX units can be easily scaled up from bench-scale or small-scale pilot tests; however, physical behavior cannot be inferred with full guaranties from such small scales. If available, design criteria are obtained from data on industrial equipment, but when no sufficient data are available, scale-up from pilot to industrial size is necessary.

For this reason, TR uses the combination of test work and computational modelling for the mixer-settler design of a specific solvent-extraction application. TR testing facilities are specifically focused to provide reliable data for scaling up to some of the largest mixer-settlers operating currently in the world. Such test units provide reliable information for optimization of equipment design with the purpose of improving performance at the smallest possible size and at the lowest investment cost.

Experimental results obtained are type of mixing, settling conditions for every solvent extraction stages, pumping capacity, and organic- and aqueous-phase entrainments. Using this information, the preliminary design of the mixer-settler system is performed, which is finally refined by the use of CFD modelling producing the final optimized design.

TR has been applying this methodology for industrial Zinc SX units design. The information obtained from experimental works and CFD modelling, together with the accumulated know-how result in good engineering practices that facilitate the construction of highly efficient and reliable industrial SX plants. These techniques are available not only for the study of zinc solvent extraction, but also for other metals such as copper, nickel, etc., producing the same degree of design optimization. Depending on the solvent-extraction application, it is possible to save up to 30% on equipment design by the application of this methodology.

The most recent industrial application of the TR design of mixer-settlers units was for the zinc SX Skorpion project. The design permitted the optimization of the mixer-settler units by determination of the proper specific flow rate in the settler

(minimizing the dispersion band and phase entrainments) and by the mixing parameters based on mass transfer combined with pumping requirements, taking into account the coalescence behavior. As a consequence, reagent consumption and equipment size were reduced due to the final optimized design, producing important savings for the industrial project.

REFERENCES

1. G. M. Ritcey, "Development of Industrial Solvent Extraction Processes", in J. Rydberg, C. Musikas, G. R. Choppin, Eds., Principles and Practices of Solvent Extraction: Industrial Solvent Extraction Development, Marcel Dekker, New York, 1992.
2. H. H. Bieber and R. Kern, "Engineering Design Considerations for an Extraction Plant." Handbook of Solvent Extraction, Canada-USA, 1983.
3. E. D. Nogueira, J. M Regife, D. Martín, and G. Díaz, "Using zinc secondaries to feed an Electrowinning Plant," Zinc' 85. International Symposium on Extractive Metallurgy of Zinc, K. Tozawa, Tokyo, Japan, 1985; pp. 763-781.
4. E. D. Nogueira, J. M Regife, and M. P. Viegas, "Design features and operating experience of the Quimigal Zincex Plant," Chloride Electrometallurgy, Peter D. Parker, Dallas, USA, 1982; pp. 59-76.
5. G. Díaz and M. A. García, "The saluctary tale of Skorpion: A breakthrough in SHG zinc production by using ZINCEX TM solvent extraction." Metal Bulletin 9th Zinc and its Markets Seminar, Spain, Madrid, 2007.
6. M. A. García, F. S. Ruiz, A. B. Mejias, M. Frades, and C. Frías, "The Skorpion zinc plant: ZINCEX^{TM} solvent extraction-The best expectations confirmed after commissioning," Lead-Zinc 2005 Symposium, Tokyo (Japan), 2007; pp. 1327-1336.
7. TR internal report "Optimización de variables de diseño hidrodinámico en el mezclador-sedimentador", ITR/I-5895/004/2001, 2001.
8. A. K. Biswas and W. G. Davenport, "Solvent Extraction Transfer of Copper from Leach Solution to Electrolyte," Extractive Metallurgy of Copper, 3rd Edition, UK, 1994.
9. J. C. Godfrey and M. J. Slater, "Principles of Mixer-Settler design." Handbook of Solvent Extraction, Canada-USA, 1983.
10. H. R C. Pratt and C. Hanson, "Selection, Pilot Testing and Scale-up of Commercial Extractors," Handbook of Solvent Extraction, Canada-USA, 1983.
11. R. E. Johnstone and M. W. Thring, "Mixing Equipment," Pilot Plants, Models, and Scale-up Methods in Chemical Engineering, McGraw-Hill, USA, 1957; pp. 173-181.
12. J. R. Orjans, C. W. Notebaart, J. C. Godfrey, C. Hanson, and M. J. Slater, "The design of mixer-settlers for the Zambian Copper Industry," ISEC '77, Canada, 1979; pp. 340-346.

COPPER SOLVENT EXTRACTION—2007 WORLD OPERATING DATA

T. Robinson,[1] M. Moats,[2] W. Davenport,[3] G. Karcas,[4] S. Demetrio,[5] and E. Domic[6]

[1]Freeport McMoran, Phoenix, AZ, USA . [2]University of Utah, Salt Lake City, UT, USA [3]University of Arizona, Tucson, AZ, USA. [4]Outokumpu Technology, Metals processing Athens, Greece. [5]Smeltec S.A. Las Condes, Santiago, Chile. [6]Domic S.A, Providencia Santiago,Chile. Corresponding author email address: tim_robinson@fmi.com

ABSTRACT

World copper solvent-extraction plant practices have been surveyed. This survey is a supplement to previous surveys carried out in 1997 and 1999. On a world basis, process technology trends include higher process flows, new mixer-settler materials of construction, reverse-flow mixer-settlers, and advanced mixer technology and designs. These changes have resulted in reduced capital and operating costs. Most of the greenfield copper SX projects are in South America and Central Africa.

INTRODUCTION

This manuscript is an update of previous world copper solvent-extraction (SX) surveys performed in 1997 and 1999 [1-3]. This paper presents operating data and plant practices from 24 copper SX operations from around the world. The present survey includes respondents from Australia (1), Chile (6), Laos (1), Myanmar (1), Peru (1), USA (13), and Zambia (1). Many of the Chilean plants are not included in the survey. Several recent African projects such as Kansanshi are also not included. The detailed survey results are presented "as received" in the CD-ROM version of the ISEC 2008 proceedings. This paper summarizes the results of the survey and discusses process-technology trends and greenfield developments.

SURVEY SUMMARY AND ANALYSIS

The survey data was analyzed to determine most common practices and ranges of values. In the analysis of numerical values, if a range was given, then the average of the two values was used. If a response was questionable in the authors' opinion, it was excluded from the analysis.

Plant Design

Plant design summaries are given in Tables 1 to 3. All plants either operate two or three extraction stages per train with about an equal percentage for each. Of the plants

operating three extraction stages, 75% operate in series-parallel mode. Both of the plants that operate in parallel mode use three extraction stages. Most plants, 75%, use one stripping stage per train. The use of an organic wash is evenly split with slightly more plants using it than not.

Settlers are specifically designed for each plant's flow rate. Most settlers are 15 to 30 m in length and width with a length-to-width ratio around 1. Settler depth is typically 1 m. Settling velocities range from 2 to 8 $m^3/m^2/h$ with a median value of 4.4. All plants surveyed use picket fences with most employing two per settler.

There is a wide range in the style of impellers used. They range in size from 1.3 to 2.9 m in diameter. The mixers operate at 37 to 69 RPM, with most using 10 to 40 kW of power.

Table 1. Summary of extraction train designs

Category	Data Summary
Extraction Stages Per Train	2 (52%), 3 (48%)
Extraction Operation	Series (46%), Parallel (8%), Series-Parallel (46%)
Stripping Stages Per Train	1 (75%), 2 (25%)
Organic Wash	Yes (55%), No (45%)

Table 2. Summary of settler designs

Category	Data Summary
Settler Length:Width Ratio	Min. – 0.6, Median – 1.0, Max. – 2.6
Settler Depth (m)	Min. – 0.8, Median – 1.0, Max. – 9.9
Settling Velocity ($m^3/m^2/h$)	Min. – 1.95, Median – 4.4, Max. – 8
# of Picket Fences per Settler	1 (29%), 2 (57%), 3 (10%), 4 (5%)

Table 3. Summary of mixer designs

Category	Data Summary
Extraction Mixers	
Impeller Dia. (m)	Min. – 1.27, Median – 1.9, Max. – 2.9
RPM	Min. – 36.4, Median – 48, Max. – 69
Power (kW)	Min. – 10, Median – 19, Max. – 134
Stripping Mixers	
Impeller Dia. (m)	Min. – 1.22, Median – 1.8, Max. – 2.9
RPM	Min. – 36.4, Median – 49, Max. – 69
Power (kW)	Min. – 10, Median – 19, Max. – 134

Flow Rates and Phase Continuity

A summary of flow rates is presented in Table 4. Pregnant leach solution (PLS) flow rates range from 266 m^3/h for small plants, to 10,000 m^3/h for very large plants, with most treating less than 2000 m^3/h. The ratio of PLS to organic flow rates range from 0.2 to 4.2, with 70% of the plants between 0.75 and 3. The ratio of organic to electrolyte flow rates is between 0.6 and 47, with two thirds of the plants between 2 and 10. The percentage of electrolyte flowing to SX is typically between 20 and 40%.

Table 4. Summary of flow rates

Category	Data Summary
PLS per train (m^3/h)	Min. – 266, Median – 1200, Max. – 10000
Electrolyte per train (m^3/h)	Min. – 7.5, Median – 327, Max. – 1249
% of electrolyte flow to SX	Min. – 1, Median – 25, Max. – 100
Organic from ext. to strip (m^3/h)	Min. – 64, Median – 1055, Max. – 4000

The use of aqueous-and organic-phase continuity for each stage appears to be very plant specific. A summary of phase continuity by stage is given in Table 5. The highest proportion of plants operate aqueous-continuous in the first extraction stage especially for trains in series, and organic-continuous in the first stripping stage. The plants are otherwise evenly split on phase continuity in second and third extraction stages, washing and second stripping stage.

Table 5. Summary of phase continuity by stage

Stage	Data Summary
E1 (all)	Aqueous (76%), Organic (24%)
E1 (series)	Aqueous (87%), Organic (13%)
E1P (parallel)	Aqueous (50%), Organic (50%)
E2	Aqueous (52%), Organic (48%)
E3	Aqueous (50%), Organic (50%)
W	Aqueous (55%), Organic (45%)
S1	Aqueous (16%), Organic (84%)
S2	Aqueous (60%), Organic (40%)

Solution Compositions

Summaries of PLS, raffinate, organic, and electrolyte compositions are presented in Tables 6 to 9. The median PLS composition is 2.75 g/L Cu, 2.6 g/L Fe (2.0 g/L Fe^{3+}), 2.5 g/L H_2SO_4, and 0.65 g/L Mn at a pH of 2.0, with 20 ppm of suspended solids. There is a considerable range of values for every PLS variable except pH, which only ranged from 1.3 to 2.15. The median raffinate composition is 0.2 g/L Cu and 7.2 g/L H_2SO_4 at a pH of 1.66, with an organic loss of 40 ppm. The median copper concentrations of the loaded and barren organic are 6.45 g/L and 2.1 g/L, respectively. While the specific extractant is highly variable, all of the plants report using either LIX (Cognis) or Acorga (Cytec) extractants, with more in this survey using LIX. Eight different suppliers of diluent are listed, with the most common being Penerco and Shellsol. The median spent electrolyte (sent to SX) composition is 34 g/L Cu, 184 g/L H_2SO_4, and 151 ppm Co. The median rich electrolyte (returned to electrowinning) composition is 48 g/L Cu, 165 g/L H_2SO_4, and traces of organic phase (many plants report $\leq$ 10 ppm).

Table 6. Summary of PLS composition

Component (unit)	Data Summary
Cu^{2+} (g/L)	Min. – 0.24, Median – 2.75, Max. – 41
pH	Min. – 1.3, Median – 2.0, Max. – 2.15
Total Fe (g/L)	Min. – 0.06, Median – 2.6, Max. – 32.4
Fe^{3+} (g/L)	Min. – 0.12, Median – 2.0, Max. – 25.3
H_2SO_4 (g/L)	Min. – 0.69, Median – 2.5, Max. – 20
Mn (g/L)	Min. – 0.09, Median – 0.65, Max. – 3.4
Solids (ppm)	Min. – 1.5, Median – 20, Max. – 60

Table 7. Summary of raffinate composition

Component (unit)	Data Summary
Cu^{2+} (g/L)	Min. – 0.015, Median – 0.2, Max. – 11
pH	Min. – 0.7, Median – 1.66, Max. – 1.9
H_2SO_4 (g/L)	Min. – 1.75, Median – 7.2, Max. – 65
Organic loss to raffinate (ppm)	Min. – 20, Median – 40, Max. – 89

Table 8. Summary of organic composition

Component (unit)	Data Summary
Cu^{2+} (g/L) in Loaded Organic	Min. – 1.05, Median – 6.45, Max. – 20
Cu^{2+} (g/L) in Barren Organic	Min. – 0.25, Median – 2.1, Max. – 6.5
Extractant Family (% of Data)	LIX (74%), Acorga (26%)
Diluent Supplier (% of Data)	Penreco (30%), Shellsol (30%), 6 others (40%)

Table 9. Summary of electrolyte composition

Component (unit)	Data Summary
Spent Electrolyte	
Cu^{2+} (g/L)	Min. – 28, Median – 34, Max. – 43
H_2SO_4 (g/L)	Min. – 165, Median – 184, Max. – 195
Co (ppm)	Min. – 50, Median – 151, Max. – 200
Rich Electrolyte	
Cu^{2+} (g/L)	Min. – 37, Median – 48, Max. – 55
H_2SO_4 (g/L)	Min. – 140, Median – 165, Max. – 186
Organic Loss in Electrolyte	43% of plants ≤10 ppm

Operational Variables and Methods

Table 10 gives summaries of process variables and operating methods. Most process variables reported in the survey indicate a wide range of operating conditions utilized by the various plants. The median values indicate perhaps what a “typical” plant would be, if one actually existed.

The most common operation methods are the use of interfacial pumping to remove crud and dual-media filters for electrolyte treatment. The majority of plants do not operate organic coalescers or organic filters. Some plants use both dual-media filters and Jameson cells for aqueous streams.

Table 10. Summary of operational variables and methods

Component (unit)	Data Summary
Extraction Efficiency (%)	Min. – 85.0, Median – 92.5, Max. – 95.6
Extraction Mixer Residence Time (min)	Min. – 1.6, Median – 2.5, Max. – 3.0
Organic Depth in Settler (mm)	Min. – 12, Median – 268, Max. – 500
Aqueous Depth in Settler (mm)	Min. – 24, Median – 498, Max. – 2140
Extractant in Organic Vol%	Min. – 3, Median – 15.4, Max. – 34
Net Cu Transference (Cu g/L per % Extractant)	Min. – 0.15, Median – 0.25, Max. – 0.36
Stripping Efficiency (%)	Min. – 34, Median – 69, Max. – 97.5
Stripping Mixer Residence Time (min)	Min. – 0.13, Median – 3, Max. – 4.8
Phase Disengagement Time	92% between 40-120 seconds
Organic Coalescers	Yes (32%), No (68%)
Organic Filters	Yes (40%), No (60%)
Crud Removal	Pump from Interface (74%)
Crud Treatment	Clay and Filter (41%)
Electrolyte Coalescer	Yes (44%), No (56%)
Electrolyte Treatment	Dual Media Filter (91%), Jameson Cell (28%)

Materials of Construction

Table 11 shows that materials used for construction of SX plants are becoming more standardized. A majority of plants use stainless steel for settlers, mixers (each as a liner or complete vessel), piping, and tanks. High-density polyethylene (HDPE) is also used extensively in piping. Gratings are typically fiber-reinforced plastic (FRP) or fiberglass.

Table 11. Summary of materials construction

Component (unit)	Most Common Material
Settlers	Stainless Steel (60%)
Mixers	Stainless Steel or Stainless Steel Liner (70%)
Piping	Stainless Steel (79%), HDPE (67%)
Tanks	Stainless Steel (71%)
Grating	FRP (50%), Fiberglass (32%)

PROCESS TECHNOLOGY AND DESIGN TRENDS

Copper SX plant practices and design where last reviewed in 2003 [4]. Recent process technology improvements and design trends are:

- New and improved copper SX extractant reagents that do not transfer iron and in some cases are modified mixtures of aldoxime and ketoximes.
- New and improved SX diluents that have higher flash points.
- Conventional SX mixer settler design trends include:
  - SX circuits that are now designed up front with pipe work for multiple configurations between series and series parallel and other combinations. The purpose of this is for operations flexibility.
  - Reverse-flow mixer settlers.
  - Deeper settlers.
  - Advanced conventional mixer designs that reduce shear and small droplet generation.

  - Advanced and multiple picket-fence designs for enhanced settling.
  - Advanced in-settler coalescer designs and installation for enhanced settling.
  - Utilization of more stainless steel materials of construction due to fire-safety reasons.
  - Separating SX trains for fire-retardation purposes.
  - Higher specific flows.
  - CFD modelling of SX mixer and settling technology for further enhancement.
- As yet, no copper SX circuit has installed a multi-stage settler column (as used in uranium SX).
- No copper SX circuit has installed an in-line plug-flow mixer-settler such as proposed by Koch, but Zinc SX is investigating this technology.

GREENFIELD DEVELOPMENTS AND POSSIBLE FUTURE SX PROJECTS

Future copper SX projects are centered in Central Africa and are associated with cobalt (from tailings and ore), gold and concentrate (through pressure leaching) production. The major copper SX projects include Tenke Fungurume, Kolwesi Tailings, Kinsevre, Nikanor in the DRC, and Chambishi in Zambia.

CONCLUSIONS

It is clear from the latest 2007 copper SX survey that recent copper SX projects and expansions are implementing the world's latest and best-practice process technologies. These technologies include the latest mixer and settler designs and copper SX circuits are being designed for enhanced operational flexibility.

ACKNOWLEDGMENTS

The authors would like to thank the plant personnel who kindly provided the data for the surveys. Without them, this paper would have been impossible.

REFERENCES

1. J. Jenkins, W. G. Davenport, B. Kennedy, and T. Robinson, "Electroytic Copper - Leach, Solvent Extraction and Electrowinning World Operating Data," Copper 99-Cobre 99, Vol. 4, Hydrometallurgy of Copper, S. K. Young, D. B. Dreisinger, R. P. Hackl, and D. G.Dixon, Eds., The Minerals, Metals & Materials Society, Warrendale, PA, 1999; pp. 493-566.
2. T. Robinson, W. G. Davenport, and J. Jenkins, "Electrolytic Copper Electrowinning and Solvent Extraction World Operating Data," ALTA 1997 Copper Hydrometallurgy Forum, Brisbane, Australia, 1997.
3. T. Robinson, W. G. Davenport, and J. Jenkins, "Electrolytic Copper Electrowinning and Solvent Extraction World Operating Data," Randol Copper Hydromet. Roundtable, Vancouver, BC Canada, 1997.
4. T. Robinson, S. Sandoval, and P. Cook, "World Copper Solvent Extraction Plants: Practices and Design," *JOM*, **55**(7), 24-26 (2003).

A SIMPLE MODEL FOR PREDICTING ZINC-DEHPA EXTRACTION ISOTHERMS

J.R. Harlamovs

Box 2000, Applied Research and Technology, Teck Cominco Metals Ltd., Trail, BC Canada, V1R 4S4
Corresponding author email address: juris.harlamovs@teckcominco.com

ABSTRACT

A simple model was developed to predict zinc extraction isotherms with di-(2-ethylhexyl) phosphoric acid (DEHPA). The model takes into account temperature, and initial zinc, acid, and extractant concentrations. The model can calculate isotherms, which can be used to construct McCabe-Thiele diagrams for extraction, scrubbing, and stripping. Data for the model can be obtained from a few experimental extraction isotherms. Extraction isotherm data can be linearized to provide values for pseudo-equilibrium constants, which can be used to extrapolate to a wide range of starting conditions. This paper describes derivation of the equation for the isotherms, a method to linearize isotherm data and calculate the equilibrium constants. McCabe-Thiele predictions are compared with actual HydroZinc™ pilot plant data. Some limitations and opportunities are briefly discussed.

INTRODUCTION

The origin of this paper started with the question, "why is the zinc extraction isotherm with DEHPA 's' shaped?" A couple of possible explanations are given by Ritcey [1], but they do not appear to explain what could be causing the 's' shape. Grimm and Kolarik [2,3] described the extraction of zinc as four DEHPA complexes changing with increasing loading, $ZnA_2.2HA$, $ZnA_2.HA$, ZnA_2, and the aggregate $(ZnA_2)_n$, where A is the di-(2-ethylhexyl)phosphate anion.

Academic slope analysis tends to be based on pH; other than the initial pH, metallurgists rarely measure pH, unless pH control is required. Consequently, slope analysis has not routinely been used to predict extraction isotherm shapes.

Derivation of the Model

The simplest of the extracted species was assumed for this model, as relatively high loadings are used in practice, but very high loadings are avoided, because the solvent becomes viscous. This extracted zinc complex also provides a simple solution to potential isotherm shapes.

The equation for the extraction of zinc by DEHPA is given in Equation 1 and its equilibrium constant *K* in Equation 2.

$$Zn^{2+} + (HA)_2 \rightleftharpoons ZnA_2 + 2H^+ \quad (1)$$

$$K = [ZnA_2]\,[H^+]^2/([Zn^{2+}]\,[(HA)_2]) \quad (2)$$

where $(HA)_2$ is the dimerized organophoshoric acid in the solvent phase and ZnA_2 is extracted zinc complex in the solvent phase. The free extractant concentration and acidity can be calculated from Equations 3 and 4. The subscript "in" denotes initial concentration.

$$[(HA)_2] = [(HA)_2]_{in} - [ZnA_2] \quad (3)$$

$$[H^+] = [H^+]_{in} + 2([Zn^{2+}]_{in} - [Zn^{2+}]) \quad (4)$$

The free extractant concentration in Equation 3 is the difference between the initial extractant concentration and the extracted zinc concentration. The free acidity is the sum of the initial acidity and sum of the protons released by the zinc extraction, Equation 4.

Combining Equations 2, 3, and 4 and rearranging for the solvent zinc concentration yields a simple equation for the zinc extraction isotherm.

$$[ZnA_2] = \frac{K\,[Zn^{2+}]\,([(HA)_2]_{in} - [ZnA_2])}{([H^+]_{in} + 2\,([Zn^{2+}]_{in} - [Zn^{2+}]))^2} \quad (5)$$

Figure 1 shows predicted extraction isotherms for six extraction equilibrium constants covering five orders of magnitude. The initial concentrations assumed are 0.05 g/L H_2SO_4, 20% DEHPA on a volume basis, and 20 g/L zinc.

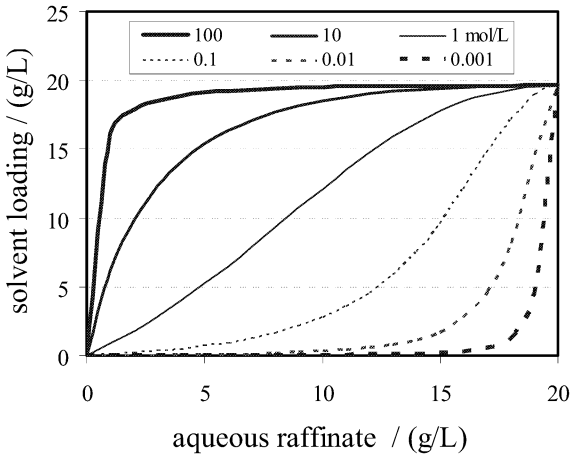

Figure 1. Effect of the equilibrium-constant magnitude on the predicted isotherm shape.

The shape of the first three lines (left to right) would be similar to the extraction of copper by an improbably strong reagent, an aldoxime and a ketoxime respectively. The line for the 0.1 mol/L equilibrium constant resembles the "s" shaped isotherm obtained with zinc and DEHPA. The remaining two lines would likely be similar to isotherms that would be obtained with cobalt and nickel extractions with DEHPA without the neutralization.

Essentially the 's' shape of the zinc-DEHPA isotherm can be explained by a classical treatment of the mass-action equation for extraction when using a moderately weak equilibrium constant.

There, of course, could be concerns with this model, regarding the simplification of various parameters such as activities, the effect of thebisulphate equilibrium, and complexation of zinc in the aqueous phase. This would complicate the model dramatically, but this will be discussed briefly later.

Linearization of the Isotherm

The equilibrium constant could be determined by fitting curves for different equilibrium constants to equilibrium isotherm points by trial and error; a more elegant method would be linearizing Equation 5 so that the equilibrium constant could be determined by regression. Taking the inverse of Equation 5 and rearranging gives Equation 6: a linear form of Equation 5.

$$\frac{1}{[ZnA_2]} = \frac{1}{K\,[(HA)_2]_{in}} \cdot \frac{([H^+]_{in} + 2\,([Zn^{2+}]_{in} - [Zn^{2+}]))^2}{[Zn^{2+}]} + \frac{1}{[(HA)_2]_{in}} \qquad (6)$$

The intercept of plotting the reciprocal of the solvent zinc concentration versus the square of the calculated acid concentration divided by the aqueous zinc concentration (*f(aqueous)*) gives the reciprocal extractant concentration. The inverse of the slope gives the product of the equilibrium constant and extractant concentration.

Small errors in determining the slope gave poorly reproducible estimates of the extractant concentration. If the initial extractant concentration is known then an estimate of the equilibrium constant can be obtained from equation 7. The left hand of equation 7 is essentially the ratio of free extractant and solvent zinc concentrations, (*f(solvent)*).

$$\frac{[(HA)_2]_{in}}{[ZnA_2]} - 1 = \frac{1}{K} \cdot \frac{([H^+]_{in} + 2\,([Zn^{2+}]_{in} - [Zn^{2+}]))^2}{[Zn^{2+}]} \qquad (7)$$

Plotting *f(solvent)* versus *f(aqueous)* gave relatively consistent estimates of the equilibrium constant K and is described below in more detail.

Curve Fitting

Figure 2 shows example extraction data for zinc with three DEHPA concentrations at 40 °C, 32 g/L zinc, and 0.05 g/L sulphuric acid. The extraction data were plotted as described by Equation 7. All three extraction curves fell on a line

equivalent to an equilibrium constant of 0.24 mol/L (Figure 3). The predicted isotherms are plotted together with the extraction data in Figure 2.

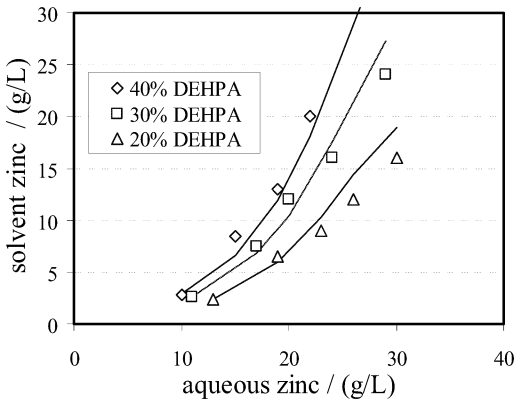

Figure 2. Zinc extraction isotherms and model fit 40 °C, 32 g/L Zn, are 0.05 g/L H_2SO_4.

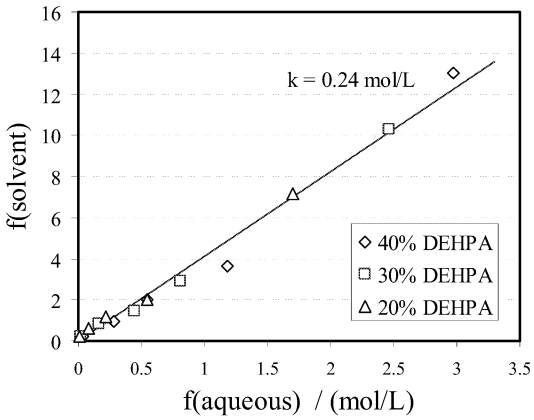

Figure 3. Equation 7 fit to Figure 2 data at 40 °C, 32 g/L Zn, and 0.05 g/L H_2SO_4.

The predicted equilibrium constant is particularly sensitive to the isotherm points at low loadings. Thus, particular care should be taken when measuring low concentrations. Varying the magnesium sulphate concentration (0 to 80 g/L $MgSO_4$) showed a minimal effect on the shape of the isotherm and predicted zinc recovery. A possible explanation could be that, although the bisulfate equilibrium should increase extraction, the complexation of the hydrated zinc complex by the sulphate anion hinders extraction.

Extraction isotherms at various temperatures between 2 °C and 50 °C for both extraction and stripping were evaluated in a similar fashion. The data is presented as a van't Hoff plot in Figure 4.

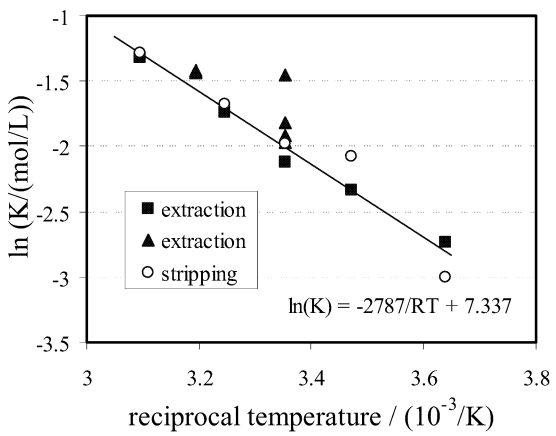

Figure 4. van't Hoff plot for extraction and stripping of zinc with DEHPA.

Figure 4 shows that the extraction of zinc with DEHPA is endothermic with a heat of reaction of about 23 kJ/mol. The equation given by van't Hoff plot can be used to calculate the extraction equilibrium constant within the temperature range 0 °C to 50 °C.

Comparison of McCabe-Thiele Predictions and Pilot-Plant Data

The van't Hoff equation and Equation 7 can be used to define the isotherm for a given set of initial conditions from which the McCabe-Thiele construction can be calculated iteratively to predict zinc concentrations in each stage. Table 1 compares data predicted from the model and batch experiments using synthetic solutions with pilot plant data. Lizama et al. [4] describe the pilot plant operation in more detail.

Table 1. Comparison of predicted and pilot plant zinc concentrations

	zinc concentration / (g/L)							
	E2	E1	feed	Sc1	Sc2	Sc3	S1	S2
aqueous								
plant	13.4	18.5	24	27	38	68	115	80
prediction	13.6	17.8		29	40	61	110	78
solvent								
plant	4.7	9.4		9.4	9.6	8.7	2.5	0.5
prediction	4.5	10.1		10.2	10.2	9.1	3.0	0.7

Table 1 shows that the predicted zinc concentrations and the actual plant concentrations are very similar, considering the assay errors and the fact that pilot plants are rarely at steady state.

Limitations and Opportunities

Zinc can be a difficult element to analyze when at high concentrations; consequently, some of the subtleties that may occur in the zinc-DEHPA system are no doubt lost, and are not highlighted in the model.

The model for copper would be essentially the same as those derived for zinc. Early evaluations of copper data have showed that using a similar technique may allow a simple copper model to be developed.

Some early testwork with zinc and DEHPA that used decanol as a modifier could not be made to fit the model. Further work to identify how the model could be made to fit modified DEHPA systems is required. Consequently, care must be taken when using modifiers. This may apply to copper systems using modified aldoximes.

CONCLUSIONS

A simple model to predict the zinc DEHPA system is proposed. The resulting isotherms have allowed satisfactory prediction of the HydroZinc pilot plant operation when used in conjunction with McCabe-Thiel constructions.

ACKNOWLEDGMENTS

Permission to publish this paper by Teck Cominco Metals Ltd. is gratefully acknowledged. The contributions from Donna Backus, Vic Steiner and Scott Varley who did the bulk of the testwork are also gratefully acknowledged.

REFERENCES

1. G. M. Ritcey, "Solvent Extraction, Principles and Applications to Process Metallurgy," Revised 2nd Edition 2006, Published by G. M. Ritcey and Associates Inc., Volume 1; pp. 57–62.
2. R. Grimm and Z. Kolarik, "Acidic Organophosphorus Extractants. XIX. Extraction of Copper(II), Cobalt(II), Nickel(II), Zinc(II), and Cadmium(II) by Bis(2-ethylhexyl) Phosphoric Acid," *Journal of Inorganic and Nuclear Chemistry*, **36**, 189–192, (1974).
3. R. Grimm and Z. Kolarik, "Acidic Organophosphorus Extractants. XXII. Complexes of Some Bivalent Transition Metals with Bis(2-ethylhexyl) Phosphoric Acid in Highly Loaded Organic Phases," Proceedings of the International Solvent Extraction Conference, Lyon, Edited by G. V. Jeffreys, Society of Chemistry and Industry, London 1974; pp. 767–778.
4. H. M. Lizama, J. R. Harlamovs, S. Belanger, and S. H. Brienne, "The Teck Cominco HydroZinc™ Process," Hydrometallurgy 2003 Fifth International Conference in Honor of Professor Ian Ritchie, Vol. 2, C. A. Young, A. M. Alfantazi, C. G. Anderson, D. B. Dreisinger, and A. James, Eds., The Minerals, Metals and Materials Society, 2003; pp. 1503–1516.

OPERATIONAL PRACTICES FOR CYANEX® 272 EXTRACTANT CIRCUITS

Cyril Bourget and Boban Jakovljevic

CYTEC CANADA INC., 9061 Garner Road, Niagara Falls, Ontario, Canada L2E 6S5
Corresponding author email address: cyril.bourget@cytec.com

ABSTRACT

Various technical issues unique to the CYANEX® 272 circuits have been encountered over the years. Examples of such common problems include chromium poisoning of the organic solution, pH control, and subsequent high pH localization, which leads to precipitation and crud formation, degree of preneutralization, diluent oxidation, extractant cross-contamination, high organic viscosity due to either excess cobalt loading or extractant concentration, and extractant losses through aqueous solubility. Over the last twenty years, much experience has been gained by working with operators, and various recommendations for operating practices have been developed that can lead to efficient operation of a profitable solvent-extraction process.

INTRODUCTION

CYANEX® 272, bis(2,4,4-trimethylpentyl)phosphinic acid, was developed in the early 1980's specifically for the separation of cobalt from nickel by solvent extraction from weakly acidic sulfate liquors [1-3]. Following market introduction in 1982, the first commercial plant to use this reagent came on-stream in 1985. There are currently over 15 commercial plants using CYANEX 272 for the purification and recovery of cobalt from such solutions. Over the last twenty years, much experience has been gained by operating circuits that use CYANEX 272 extractant, and various technical issues unique to these circuits have been encountered. Examples of such common problems are discussed in this paper.

EXPERIMENTAL

The experimental conditions for the diluent oxidation tests are described elsewhere [4]. For the preneutralization tests, the organic solution was prepared by diluting CYANEX 272 to approximately 0.26 mol/L phosphinic acid with ISOPAR M diluent. The desired preneutralization levels ranged from 20 to 80% (% molar ratio of $R_2P(O)ONa$ and $R_2P(O)OH$) using a 5 mol/L NaOH solution.

For the viscosity tests, the viscosity of CYANEX 272 solutions (0.26 mol/L extractant in ISOPAR M) was measured as a function of cobalt loading (0 to 95%).

Cobalt loading was carried out at different A/O phase ratios with a 10.9 g/L cobalt sulfate solution at 50 ^{o}C and a constant pH of 6.40 ± 0.10 for 15 minutes.

RESULTS AND DISCUSSION

Diluent Oxidation

The ability of metals such as cobalt to catalyze the oxidation of aliphatic and aromatic hydrocarbons to carboxylic acids is well known in the petroleum industry, where the property is used, for example, for the production of aromatic carboxylic acids from toluene [5]. The oxidation of the diluent in a cobalt/nickel solvent-extraction plant was first reported at the Rustenburg Base Metal refinery in South Africa where problems such as smell, slow phase disengagement, and loss of cobalt-over-nickel selectivity were encountered. Rickelton [4] suggested the mechanism to be a succession of radical reactions in which the alkanes present in the aliphatic diluents could be catalyzed by oxygen carriers such as divalent cobalt to produce successively hydroperoxides (RCH_2OOH), alcohols (RCH_2OH), aldehydes (RCHO), and finally carboxylic acids (RCO_2H). One direct consequence of the accumulation of carboxylic acids is the serious loss of cobalt-over-nickel selectivity due to the inherent property of these carboxylic acids as active nickel extractants. Accelerated oxidation tests (See Figure 1) performed at Cytec [4] showed a decrease in cobalt-over-nickel selectivity from 830 to 2 in 8 days, while the carboxylic acid concentration increased to 50 g/L.

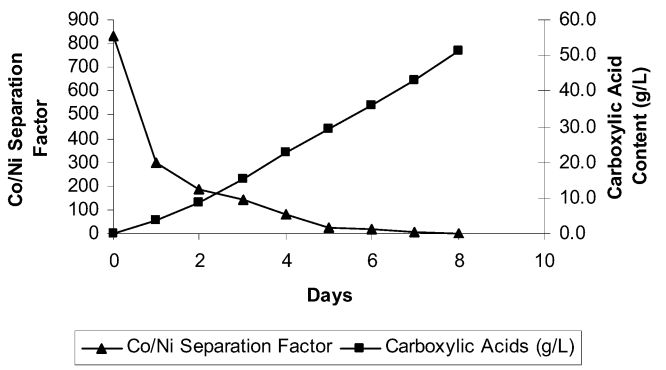

Figure 1. Effect of carboxylic acid formation on cobalt-over-nickel selectivity.

The formation of the hydroperoxide radicals cannot be prevented, but the completion of the reaction (carboxylic acid formation) can be prevented by reacting the hydroperoxide radicals with an antioxidant such as BHT (**B**utylated **H**ydroxy **T**oluene or 2,6-di-*tert*-butyl-4-methylphenol). As an example, a CYANEX 272 commercial plant using BHT has shown that the carboxylic acid levels had been maintained to 0-0.2 g/L for over 6 years [2]. Common practice in CYANEX 272 commercial plants for the BHT dosage is 1.0-1.5 g/L with make-up required when the BHT levels are close to 0.2-0.5 g/L.

Inter-stage pH Control and/or Salt Formation

Since the extraction of cobalt with CYANEX 272 is pH dependent [2], the generation of protons, requires addition of a base to maintain a constant pH of 5.5-6.0. For inter-stage pH control (i.e. direct addition of a base into the mixers) [2], the most common base used in CYANEX 272 commercial plants is a sodium hydroxide solution. Care must be taken to avoid using concentrated sodium hydroxide solutions, as they are highly viscous and can lead to "hot spots" or regions of high pH that result in the formation of cobalt and nickel hydroxide precipitates and can then result in crud generation. The maximum recommended concentration of sodium hydroxide for inter-stage pH control is 100 g/L. In some cases, ammonium hydroxide is used as the base and being less viscous than sodium hydroxide, higher ammonium hydroxide concentrations (i.e. 28% w/w) can be used. The use of ammonium hydroxide can be problematic with the precipitation of metal ammonium sulfate double salts ($NiSO_4(NH_4)_2SO_4.6H_2O$) [6]. Regardless of the base used, inter-stage pH control is commonly used when the metal concentration (cobalt plus impurity metals extracted) in the aqueous solution is less than 2-3 g/L, for which the base requirements will be moderate.

If metal concentration significantly exceeds the 2-3 g/L level, direct base addition to the mixers becomes difficult, and it is sensible to partially preneutralize CYANEX 272 ahead of the extraction mixers, thereby minimizing direct addition to the mixers. Preneutralization or salt formation with either ammonium or sodium hydroxide is a stoichiometric reaction between the sodium/ammonium and hydrogen ions and means that the complexation of cobalt does not involve proton generation during extraction [2].

The preneutralization of CYANEX 272 is limited to a specific degree of conversion to the sodium or ammonium salt and the concentration of the base is adjusted to avoid problems such as third-phase formation, CYANEX 272 losses, and increased organic viscosity. For example, Figure 2 clearly indicates that the CYANEX 272 losses become significant above 70% neutralization. Current practice in the commercial CYANEX 272 plants using preneutralization is to aim for 50-55% conversion of the CYANEX 272 to its salt using maximum base solution concentrations of 28% w/w ammonium hydroxide or 400 g/L sodium hydroxide. Under these conditions, a single phase system prevails.

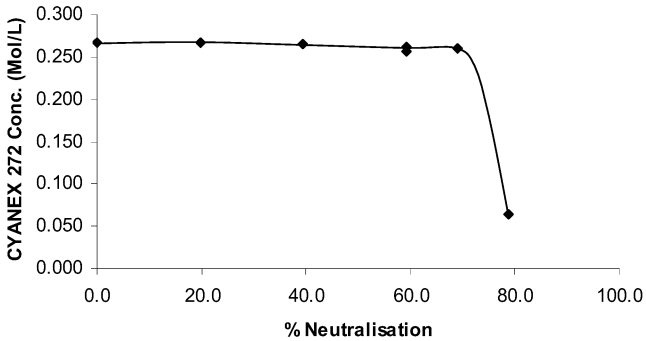

Figure 2. CYANEX 272 content in organic phase as a function of extent of preneutralization.

Organic Phase Viscosity

A parameter that is reported to affect the viscosity of a CYANEX 272 organic solution is cobalt loading [7]. Figure 3 shows little change in the viscosity of the organic phase below cobalt loading of 70-75% and an exponential increase for higher loadings.

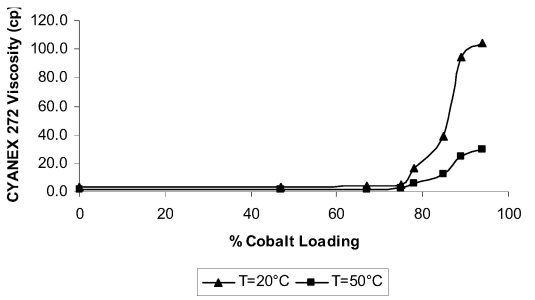

Figure 3. Organic-phase viscosity as a function of cobalt loading of CYANEX 272.

The increase in viscosity is due to a rapid change in the stoichiometry of the CYANEX 272/cobalt complex, where the extractant-to-cobalt molar ratio changes from 4 (tetrahedral cobalt complex) to 2 (polymer formation) as the cobalt loading increases and less extractant molecules are available for metal complexation [7]. To avoid high organic entrainment losses due to high viscosity, a compromise between maximum cobalt loading and the extractant concentration is required. The compromise is in the range of 70-75% cobalt loading, where the extractant-to-cobalt molar ratio is 3. Typically, CYANEX 272 plants use a maximum cobalt loading of 60-65%.

Chromium Poisoning of the Organic Phase

Chromium(III) is generally removed by hydrolytic precipitation along with iron and aluminium ahead of a cobalt solvent-extraction circuit. Nevertheless, since chromium(III) extracts onto CYANEX 272 close to cobalt, any chromium(III) remaining after precipitation will be co-extracted along with the cobalt in a CYANEX 272 solvent-extraction plant. A study by others [8] showed that the stripping of chromium(III) with sulfuric, hydrochloric, or nitric acids became increasingly difficult if the chromium-loaded organic solution was allowed to age before stripping. This suggested a possible change in the chromium extracted species that with time become more resistant to stripping. The color of the organic phase was observed to become darker green with time. If chromium poisoning in CYANEX 272 plants is observed, attempts must be made to remove as much chromium as possible during precipitation and also to prevent the organic phase from aging by quickly transferring to the stripping section. An alternative solution to the chromium poisoning problem is to allow a bleed of the organic phase and makeup with fresh CYANEX 272. This has obvious economic implications.

CYANEX 272 Losses through Aqueous Solubility

Losses of CYANEX 272 are primarily caused by entrainment due to factors such as formation of small organic droplets, high organic viscosity, and high settling rates. Equipment commonly used in commercial CYANEX 272 plants to recover entrained organic phase includes, but is not exclusive to, Spintek dual media filters, air column flotation Jameson cells, after-settlers, diluent wash circuit, and activated carbon absorption columns. Typically, the final CYANEX 272 entrained organic losses are maintained to a level of less than 1-2 ppm in either the raffinate or the cobalt advance electrolyte streams.

Although representing a minor proportion of overall CYANEX 272 loss, losses encountered via aqueous solubility cannot be recovered using the methods described, and alternatives need to be found. Aqueous-solubility losses will depend largely on two major factors: ionic strength and pH of the aqueous solution [3]. CYANEX 272 solubility losses increase with increase in pH and decrease with increase in the ionic strength of the aqueous solution ranging between 0.5 and 25 ppm depending on these conditions. While the equilibrium pH is often set for all plants at 5.5-6.0 for complete cobalt extraction, most plants operate in high ionic-strength regimes and therefore do not exhibit high CYANEX 272 aqueous-solubility losses. Some plants [9], however, have low ionic-strength solutions, which can result in CYANEX 272 soluble losses of 20 to 30 ppm in the raffinate. Since it is the sodium salt of the phosphinic acid ($R_2P(O)ONa$) that is primarily dissolved in the aqueous solution, a method to recover the CYANEX 272 is to acidify the solution and to add fresh diluent to extract the CYANEX 272 back into an organic solution.

Extractant Cross-contamination

An extractant commonly used ahead of CYANEX 272 solvent extraction is D2EHPA (di-2-ethylhexylphosphoric acid) primarily for removal of impurity metals like iron, zinc, manganese and calcium [9]. In some circumstances, cross-contamination between the two solvent-extraction circuits is unavoidable. The consequences of getting D2EHPA into a CYANEX 272 circuit are serious loss in cobalt-over-nickel selectivity, gypsum formation in the strip circuit due to the calcium co-extraction, and iron poisoning of the organic solution. In the case of a hydroxyoxime reagent being used for copper solvent extraction ahead of cobalt solvent extraction [9], cross-contamination with the CYANEX 272 can result in a loss in cobalt-over-nickel selectivity. Operating pH ranges for a CYANEX 272 solvent-extraction plant are 4.0-4.5 and 2.0-2.5, respectively, for the nickel scrubbing and cobalt stripping sections. If nickel is extracted by the hydroxyoxime reagent, nickel scrubbing at pH 4.0-4.5 will also be difficult, since the hydroxyoxime extracts nickel in a lower pH range than 4.0-4.5. Cobalt stripping may also be problematic if cobalt has been extracted by the hydroxyoxime and has been oxidized to the trivalent state.

The inclusion of devices such as dual-media filters, air column flotation cell, activated carbon, and diluent wash is required to minimize or prevent cross-over extractant contamination. A note should also be made with regards to the inclusion of an

impurity-removal precipitation step between two solvent-extraction circuits where the precipitate would act efficiently as an organic absorption barrier for the PLS.

CONCLUSIONS

Similar to other solvent-extraction refineries, technical operating issues in the CYANEX 272 commercial plants are to be expected. However, the operating experience that has been gained from some of these CYANEX 272 plants that have been running for as long as 20 years has proven invaluable in avoiding or eliminating most of these common issues.

REFERENCES

1. W. A. Rickelton, A. J. Robertson, and D. R. Burley, "Selective Extraction of Cobalt(II) from Aqueous Solutions with Phosphinic Acid Extractants," US Patent, No 4,353,883, 12 October 1982.
2. W. A. Rickelton and D. Nucciarone, "The Treatment of Cobalt/Nickel Solutions Using CYANEX® Extractants," Hydrometallurgy and Refining of Nickel and Cobalt, W.C. Cooper and I. Mihaylov, Eds., Canadian Institute of Mining, Metallurgy and Petroleum, Sudbury, Ontario, Canada, 1997; 1, pp. 275-292.
3. CYTEC, "CYANEX® 272 Extractant", CYTEC Technical Brochure, 2003, 34 pages.
4. W. A. Rickelton, A. J. Robertson, and J. H. Hillhouse, "The Significance of Diluent Oxidation in Cobalt-Nickel Separation," *Solvent Extraction and Ion Exchange*, **9**(1), 73-84 (1991).
5. K. J. Abrams, D. W. Marsh, and B. B. Doll, "Catalyst Recovery Method," US Patent, No 4,769,489, 6 September 1988.
6. B. G. Nyman and S. E. Hultholm, "Method for Preventing the Formation of Jarosite and Ammonium and Alkali Based Double Salts in Solvent Extraction Circuits Connected to Acidic Leaching Processes," US Patent, No 5,779,997, 14 July 1998.
7. Fu Xun and J. A. Golding, "Solvent Extraction of Cobalt and Nickel in Bis(2,4,4-trimethylpentyl) Phosphinic Acid, CYANEX®-272," *Solvent Extraction and Ion Exchange*, **5**(2), 205-226 (1987).
8. M. D. Lanagan and D. C. Ibana, "The Solvent Extraction and Stripping of Chromium with CYANEX® 272," *Minerals Engineering*, **16**, 237-245 (2003).
9. O. Tinkler, D. S. Flett, and C. Bourget, "Flowsheet Considerations for Copper-Cobalt Projects in the DRC," ALTA Nickel/Cobalt 2007, ALTA Metallurgical Services, Melbourne, Australia, 2007; 17 pages.

ASPECTS OF THE DESIGN OF SX PLANTS FOR THE MODERN HYDROMETALLURGICAL REFINERY

E. Robles,[1] I. Cronje,[1] S. Poulter,[2] and R. Haywood[2]

[1]*Hatch, Private Bag X20, Gallo Manor, 2052, South Africa.* [2]*Hatch, 152 Wharf Street Brisbane, Australia. Corresponding author email address: erobles@hatch.cl*

ABSTRACT

Developments in hydrometallurgy in the last decades are likely to shift the process of extraction of base metals from ores and concentrates using smelting towards processes that potentially provide economically viable metal production for smaller plant throughput capacity at lower capital and operating costs. This paper provides an overview of many of the relevant aspects to be considered in the design of robust and efficient solvent-extraction plants for the modern hydrometallurgical plant environment.

INTRODUCTION

Pressure Acid Leach and Pressure Oxidation are core processes included in modern hydrometallurgical refineries [1]. Often the downstream processing of the metal-rich liquor produced by these processes includes solvent-extraction (SX) step(s) to separate and refine the metals.

This paper addresses key elements of the design of modern SX plants like the use of computational fluid dynamics (CFD) used as a tool to simulate multiphase flow for the selection of the most suitable mixer-settler configuration and the criteria for the selection and integration of ancillary systems to prevent organic cross-contamination between different SX circuits and high entrainment in metal-loaded liquors.

USING COMPUTATIONAL FLUID DYNAMICS

The optimal design of the main phase-separation equipment in SX plants is critically important, since excessive turbulence and insufficient coalescence and phase separation results in increased entrainment. Until recently, limited tools have been available to predict fluid behavior. The advent of commercially available software for CFD modelling has dramatically changed this. CFD allows the designer to visualize and test innovative design concepts quickly and economically.

The multiphase nature of flows in settlers in conjunction with the intricate geometry associated with picket fences and other internal flow-control devices makes the modelling of SX settler vessels a significant challenge when using CFD codes. Until

recently, there has been only limited application of CFD to settler design. Early efforts [2] employed single-phase treatments and/or simplified geometries to make the problems more tractable. More recent work has seen CFD models developed to include better descriptions of the fluid behavior and greater levels of geometric detail [3,4,5].

Hatch has employed CFD modelling for over 5 years as an aid in the troubleshooting and design of SX settlers with strict emphasis on the appropriate level of detail for the problem being analyzed. In most cases, the use of CAD geometry, automated mesh generation, and significant advances in computational power have made it possible to represent the detail of settler internals with a high degree of accuracy. Improved computing algorithms (specifically the coupled multiphase flow solver currently available in ANSYS-CFX), have made it possible to achieve robust convergence in Eulerian-Eulerian multiphase models. Increasing levels of complexity are, however, not always required, and in many cases, important design alternatives can be evaluated using a simpler "equivalent single-phase" approach.

Figure 1 shows the preliminary design of a cross-over duct from mixer to settler in a recent nickel project. Here the flow issuing from the mixer has not had sufficient time for significant phase separation and a single-phase model has been utilized. The CFD model showed significant flow separation, and recirculation along the sloping floor of the diffuser and regions of local-flow acceleration at both lateral walls and along the free surface. Using the CFD model as a design tool, the cross-over duct and guide vanes were modified to provide an optimum low-speed transition into the settler vessel which is critical to its overall performance.

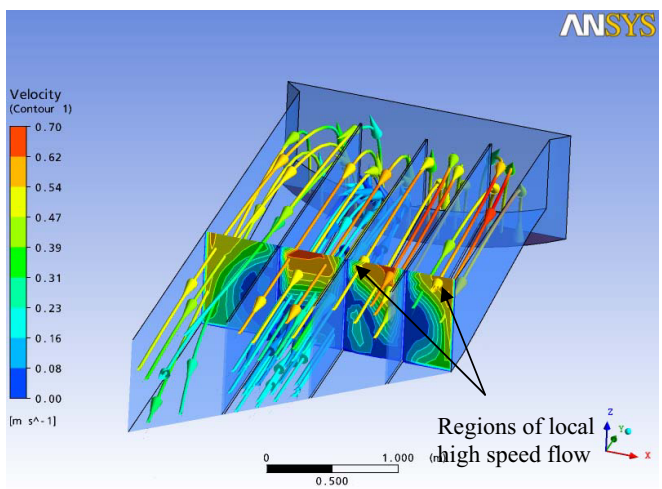

Figure 1. Cross-over duct from mixer to settler showing flow streamlines and velocity contour.

Single and multi-phase CFD models have been used to predict the flow behavior and flow distribution in the entrance and early-flow development regions of settler vessels. In reality, all settlers deviate from an ideal "plug-flow" distribution, and results from visual inspection or physical modelling can be difficult to interpret and are therefore of limited use in design.

CFD post-processing provides an ideal tool for a quantitative evaluation of design alternatives. Computation of the integrated mass-flow distributions across the width of the settler, as shown in Figure 2, has been recently used to evaluate and rank a number of feasible designs. The optimal design is such that the mass flow is uniformly distributed across the width of the settler.

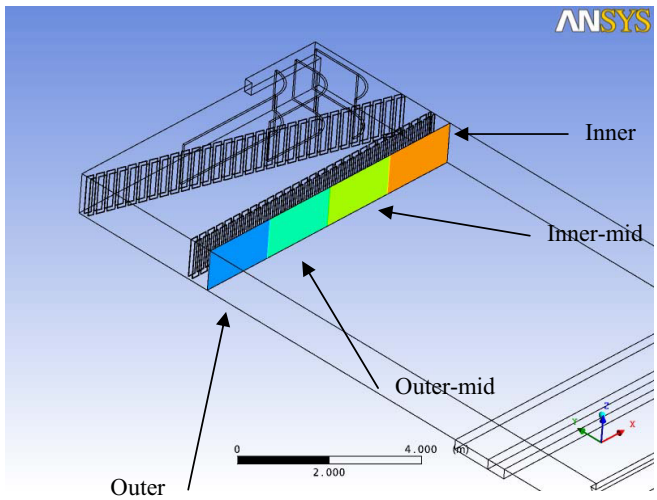

Figure 2. Postprocessing is used to evaluate the mass flow across each 1/4 of the setter width.

The computed mass flow rates through each of the lateral quarters of the settler for the original design and after using CFD analysis are listed in Table 1. The optimized design provided a significantly more uniform flow distribution with a lower overall pressure drop.

Table 1. Distribution of mass flow across width of settler for original design and after using CFD analysis

	Integrated mass flow through lateral quarters of the settler cross-section (kg/s)			
	Inner	Inner-mid	Outer-mid	Outer
Original Design	106	46	66	105
Optimized Design	91	92	90	87

Multiphase modelling has also provided significant guidance in the design of picket fences and launders.

The application of CFD modelling to organic and aqueous-phase separation as a tool to improve and enhance process design of SX mixer-settlers is now a reality. In combination with a strong understanding of the process, this minimizes the risk of implementing new or modified settler configurations [5]. Other examples where the authors have applied CFD as a design tool in SX trains include

- Agitation optimization in mixing tanks,
- Comparison of different types of settlers,

- Improvement of feed distribution in the settler,
- Modification and improvement of picket fences, organic launder, and aqueous launder.

In addition to the use of CFD, intelligent Process/Piping & Instrumentation Diagrams (P&IDs) form the basis for development of the piping design in an SX circuit. The use of 3D models based on these P&IDs allow the generation of isometrics for piping fabrication, thus improving accuracy and saving construction time. Integration of all design information including mechanical components, structures, piping, and fire-suppression systems within the 3D model ensures smooth and efficient construction. Integration of the hazardous area classification into the same model also allows optimization of instrument and electrical drive placements so that costs are minimized and a safe design is ensured.

INTEGRATION OF ANCILLARY EQUIPMENT

SX plant ancillary equipment typically falls into four major categories: organic-phase recovery from aqueous-product streams, organic-phase regeneration, crud removal, and fluid management. Each of these facilities must be custom designed, specified for the required duty and integrated into the overall SX plant detailed design.

Organic recovery and removal requirements are dependant on the downstream process for each product stream. A common trend in the design of modern hydrometallurgical refineries is that more than one metal could need to be extracted from the leach liquor that advances to the metals recovery steps. As the extractants are relatively metal-specific, this fact may lead to the use of more than one type of reagent in the same plant. Entrained organics in product streams impact negatively on downstream processes, like further solvent-extraction circuits (organic cross-contamination) and electrowinning. The replacement cost of lost reagent may also drive the level of organic recovery specified [6].

Organic-Removal Equipment

Various strategies and equipment exist for the removal of organic phase from aqueous streams. These may include physical or chemical processes depending on the state of the organic for recovery (dissolved and/or entrained). Organic-recovery processes fall into four process levels:

- **Primary**—reducing organic entrainment from ≥200 ppm down to <50 ppm and recovering the organic phase.
- **Secondary**—reducing organic entrainment from 100 ppm to <2 ppm and recovering the organic phase.
- **Dissolved Organic Recovery**—reducing the soluble organic content from >200 ppm to <10 ppm.
- **Tertiary**—reducing the total organic content, both entrained and soluble, from 10 ppm to <1 ppm.

Primary: Three primary recovery systems have been considered and discussed. Nonmechanically agitated flotation cells can recover 70 to 75% of the entrained organic from streams containing 100 to 300 ppm organic. Particularly at higher temperatures, the induction of high volumes of air (at air-to-solution volumetric ratios of about 0.8:1) results in the evaporative loss of significant proportions of the valuable organic phase. Introduction of air may also cause other process problems including oxidation of the organic phase.

An after-settler can provide a large area for additional phase separation of the entrained organic from the aqueous stream.

Coalescers are used extensively for the separation of oil and water industrially. Such devices can be applied to the separation of entrained organic from aqueous streams in SX processes. The coalescer generates large organic droplets from small entrained droplets by creating random collision opportunities. Larger droplets are separated more readily. The coalescers operate under pressure or atmospheric conditions, depending on the equipment selected and the downstream requirements.

Secondary: The two commonly used secondary organic-removal systems are flotation and pressure filtration. Secondary flotation is barely capable of achieving the target level of <10 ppm organic entrainment.

Pressure filtration using a combination of anthracite and garnet media can reduce entrained organic level to <2 ppm. These filters are also referred to as dual-media filters. Feed liquors containing up to 100 ppm organic are accepted. The frequency of filter back-washing increases with the organic entrainment levels.

Combined coalescer/filtration systems are also available [6]. These systems provide both primary and secondary organic recovery in a single unit with a capacity five times that of conventional media filters. This is achieved by including a coalescence matrix surface in the same vessel ahead of the filtration medium. These units can achieve product stream organic levels of <2 ppm from feed levels up to 800 ppm organics. Back-washing is less frequent than for the conventional dual-media filter.

Dissolved: Highly soluble extractants need to be recovered through chemical means as opposed to simple physical removal. The primary method for bulk removal of soluble organic from the aqueous phase is to wash with diluent in a single stage in which the pH may be adjusted to reduce organic solubility in the aqueous phase [7].

Tertiary: Tertiary organic recovery equipment is employed as an insurance to ensure the achievement of <5 ppm organic in product. Single- and two-stage carbon adsorption columns are typically used. In the single-column adsorption system, the carbon is not fully loaded at breakthrough. Partially loaded carbon is replaced prior to returning the unit to service. The two-stage column system operates in series. When breakthrough occurs in the first column, the solution continues to flow through the second column, thereby allowing the carbon in the first column to fully load prior to replacement. When the fully loaded carbon is replaced, the flow through the units is reversed to allow the second column to become fully loaded.

MATERIALS OF CONSTRUCTION

Materials of construction directly influence project costs, and therefore, great care needs to be exercised when selecting the appropriate materials. Many of the leach liquors produced in modern processes contain sulphuric acid, ferric ion, and halides. These conditions preclude the use of the lower grades of stainless steels like 316 SS. The use of Fibre Reinforced Plastic (FRP) has became an industry standard for highly corrosive applications at temperatures above ambient. Vessels and piping that contain solvent should be made conductive to prevent sparking. Graphite is added to the FRP to ensure conductivity. Duplex stainless steels, such as SAF 2205, can be used when metallic parts are required, provided that enough corrosion testwork data supports its use.

CONCLUSIONS

A simplified overview of some of the relevant aspects that need to be taken into consideration in the design of robust and efficient solvent-extraction plants in a modern hydrometallurgical environment has been presented. In this environment, the engineer needs to integrate the use of new tools, such as CFD modelling, with extensive knowledge of the process fundamentals, plant operation, and risk management to address the new challenges that will arise in the design of a SX plants in the future.

REFERENCES

1. J. Peacey, X. J. Guo, and E. Robles, "Copper Hydrometallurgy—Current Status, Preliminary Economics, Future Direction and Positioning versus Smelting," COPPER 2003—COBRE 2003, Vol. VI, Santiago, Chile, 2003; pp. 205–222.
2. C. Ta, J. Beckley, and A. Eades, "A Multiphase CFD Model of DAF Process," *Water Sci. Technol.*, **43**(8), 153-157 (2001).
3. M. P. Schwarz, G. Lane, J. Nikolov, W. Yang, J. M. Bujalski, C. B. Solnordal, and M. Houchin, "Development of a Design Capability for SX Contactors Using Multi-Phase CFD and Experimental Modelling," ALTA Copper 2007, ALTA Metallurgical Services, Melbourne, Australia, 2007.
4. M. Giralico, B. Gigas, and M. Preston, "Advanced Mixer Settler Designs that will Optimize Tomorrow's Large Flow Production Requirements," Hydrometallurgy 2003, Vol. 1, Leaching and Solution Purification, TMS, 2003.
5. L. H. Gunnewiek, L. Oshinowo, T. Plikas, and R. Haywood, "Using CFD in the Design and Scale-up of Hydrometallurgical Processes," 3rd International Conference on CFD in the Minerals and Process Industries, CSIRO, Melbourne, Australia, 2003
6. K. C. Sole, R. J. Steward, R. F. Maluleka, A. Rampersad, and A.E. Mavhungu, "Removal of Entrained Organic Phase from Zinc Electrolyte: Pilot plant Comparison of Comatrix and Carbon Filtration ," *Hydrometallurgy,* **89**, 11–20 (2007).
7. G. Bacon and I. Mihaylov, "Solvent Extraction as an Enabling Technology in the Nickel Industry," International Solvent Extraction Conference ISEC 2002, K. C. Sole, P. M. Cole, J. S. Preston, and D. J. Robinson, Eds., South African Institute of Mining and Metallurgy, Johannesburg, 2002; pp. 853–863.

MODELLING COBALT EXTRACTION WITH CYANEX 272

H.A. Evans,[1] P.A. Bahri,[1] J.A. Rumball,[2] and K.R. Barnard[3]

[1]Murdoch University, South St, Murdoch, Western Australia 6150. [2]Barrick Gold Corporation, Vancouver, Canada. [3]The Parker Centre (CSIRO Minerals),Waterford Western Australia

Corresponding author email address: Heather.Evans@murdoch.edu.au

ABSTRACT

A model has been developed to calculate the equilibrium constant *K* for cobalt extraction using Cyanex 272. This involved defining the pH extraction isotherm in terms of the extractant concentration, pH, and percent extraction. Using the calculated *K* values, it is possible to generate pH extraction isotherms for various conditions and calculate change in enthalpy (ΔH^0) for the extraction. Although relationships between temperature, ionic strength, and organic concentrations have been expressed mathematically and incorporated in the model, the present paper focuses solely on the effects of temperature.

INTRODUCTION

The development of a solvent-extraction (SX) flowsheet for cobalt extraction requires a detailed understanding of the chemistry of the system. Most new nickel-cobalt SX projects go through initial laboratory screening tests and extensive piloting [1-5] before the final flowsheet is established. The information generated in these testwork programs is then used to design the commercial plant. This is an essential but time consuming and costly requirement for developing projects.

The ultimate aim of this project is to produce an integrated solvent-extraction model of a cobalt-nickel circuit that can adjust the overall extraction extent for each stage based on the pH, temperature, ionic strength of the aqueous phase and the extractant concentration and loading capacity of the organic phase, thereby reducing test-program requirements. The first phase of this work is to develop a model based on the cobalt-Cyanex 272 system. Cyanex 272 (bis (2,4,4-trimethylpentyl) phosphinic acid) is the extractant of choice for cobalt–nickel separation due to its higher selectivity for cobalt over nickel in both sulfate and chloride media [6-8]. The chemical structure of Cyanex 272 is shown in Figure 1.

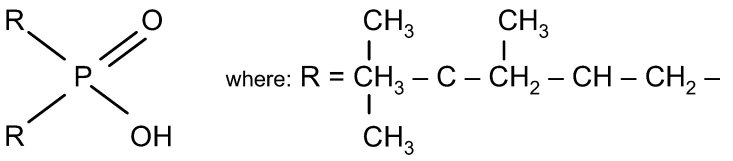

Figure 1. Chemical Structure of Cyanex 272.

Process Equilibria

The metal loading of the phosphinic extractant, Cyanex 272 has been described by a number of researchers [9-15] and can be expressed by Equation 1 [14]:

$$M^{n+} + \frac{n+x}{y} \cdot \overline{(RH)_y} \Leftrightarrow \overline{MR_n(RH)_x} + n \cdot H^+ \tag{1}$$

where RH is Cyanex 272, the superscript bar represents the organic phase, *n* represents the valence of the metal (M), *x* is the number of additional Cyanex 272 molecules required due to the co-ordination number of the complex formed, and *y* usually represents either a dimer in aliphatic or a monomer in aromatic diluents [14].

The equilibrium constant (*K*) for a single metal loading onto Cyanex 272 can be expressed by Equation 2, where γ represents the activity coefficient of each species:

$$K = \frac{\left[\overline{MR_n(RH)_x}\right] \cdot \left[H^+\right]^n}{\left[M^{n+}\right] \cdot \left[\overline{(RH)_y}\right]^{\frac{n+x}{y}}} \cdot \frac{\gamma_{MR_n(RH)_x} \cdot \gamma_{H^+}^n}{\gamma_{(RH)_\gamma}^{\frac{n+x}{y}} \cdot \gamma_{M^{n+}}} \tag{2}$$

At low concentrations, we can assume ideal conditions whereby the activity coefficients can be assumed to be equal to 1, thereby simplifying Equation 2 to Equation 3:

$$K = \frac{\left[\overline{MR_n(RH)_x}\right] \cdot \left[H^+\right]^n}{\left[M^{n+}\right] \cdot \left[\overline{(RH)_y}\right]^{\frac{n+x}{y}}} \tag{3}$$

The nature of the extracted metal species with respect to coordination stoichiometry and geometry affects the values of *x* and *y*. At low metal loadings, the structure of the metal-Cyanex complex is different for Co and Ni. Cobalt is tetrahedrally coordinated in Cyanex 272 as $Co(R_2H)_2$, and nickel forms the hydrated octahedral complex $Ni(R_2H)_2(RH)_2$ [10] as shown in Equations 4 and 5, respectively. These have been written assuming the Cyanex 272 is present as a dimer (*y* = 2) in the diluent, although they can also be expressed as $CoR_2(RH)_2$ and $NiR_2(RH)_4$, respectively [13].

$$Co^{2+} + 2\overline{(RH)_2} \Leftrightarrow \overline{Co(R_2H)_2} + 2H^+ \tag{4}$$

$$Ni^{2+} + 3\overline{(RH)_2} \Leftrightarrow \overline{Ni(R_2H)_2(RH)_2} + 2H^+ \tag{5}$$

To control the pH for maximum extraction requires the addition of a base to neutralize the acid generated. To avoid excessive dilution of the aqueous phase with base

during the reaction, a pre-equilibriation step of the organic is performed using ammonia or sodium hydroxide to convert the extractant into its salt [16-17]. However, when more than 50 to 70% of the Cyanex 272 is converted to its salt, there is a tendency for third-phase formation to occur [12,17-18]. Therefore, when comparing equilibrium constants quoted by different authors, it is important to note the exact experimental conditions used.

Calculating pH-Extraction Isotherms

An equation was derived for calculating the percentage extraction versus pH isotherm for the Co-Cyanex 272 system. This was used as the basis to recreate mathematically the pH-extraction isotherms for the experimental data. This was achieved by rearranging the equilibrium constant (Equation 6) for the cobalt-Cyanex 272 system given in Equation 4:

$$K = \frac{\overline{[Co(R_2H)_2]} \cdot [H^+]^2}{[Co^{2+}] \cdot [\overline{(RH)}_2]^2} \tag{6}$$

from which the following equation can be derived:

$$\frac{\overline{[Co(R_2H)_2]}}{\overline{[Co(R_2H)_2]} + [Co^{2+}]} = \frac{K[\overline{(RH)}_2]^2}{K[\overline{(RH)}_2]^2 + [H^+]^2} \tag{7}$$

Using the assumptions that the initial cobalt loading on the extractant prior to contact with the aqueous phase was zero, the O:A ratio was 1, and the change in volume of the two phases during the reaction is negligible, it follows that at equilibrium the final molar concentration of the cobalt Cyanex 272 complex is equal to the molar amount of cobalt extracted and the total molar amount of cobalt initially present is equal to the concentration of the cobalt Cyanex 272 complex plus the concentration of the cobalt remaining in the aqueous phase (Equation 8):

$$Extraction\ fraction = \frac{\overline{[Co(R_2H)_2]}}{\overline{[Co(R_2H)_2]} + [Co^{2+}]} \tag{8}$$

Therefore, Equations 7 and 8 can be combined to express the extraction fraction for cobalt by Cyanex 272 by using Equation 9:

$$Extraction\ fraction = \frac{K[\overline{(RH)}_2]^2}{K[\overline{(RH)}_2]^2 + [H^+]^2} \tag{9}$$

EXPERIMENTAL

The aqueous phases consisted of 0.5 g/L of cobalt added as $CoSO_4.7H_2O$, dissolved in deionized water. Sodium sulfate (0.2 M) was added to the aqueous phase to increase the ionic strength and enhance phase separation. An 12.5% NH_3 solution was used for pH adjustment. Sulfuric acid was diluted to 100 g/L with deionized water and

used for stripping the organic samples. The organic phase was prepared by diluting as-received Cyanex 272 with Shellsol 2046 to make 20 % v/v Cyanex 272. Assuming a purity of 88%, density of 0.92 g/L, and molecular weight of 290, the molar concentration of RH = 0.558 M.

Each experiment involved placing a predetermined volume of aqueous solution in a stainless steel square mixing box with a pH probe and overhead stirrer in a water bath set to the desired temperature. The starting pH of the aqueous phase was adjusted to between 3.0 and 4.0. A Metrohm 776 Dosimat auto titrator and D50 datataker logger were set up to accurately control and record the amount of alkali (NH_4OH) added. A set volume of organic phase to meet the desired organic-to-aqueous ratio (O:A of 1:1) was allowed to reach temperature before being added to the mixing box. After 5 minutes of aqueous-continuous mixing at constant pH, it was assumed that equilibrium had been reached, and a sample was taken. The pH of the mixture was increased to the next set point by the addition of a small volume of ammonia solution via the auto titrator. Once the pH had stabilized, a further 5 minutes mixing was allowed before the next sample was taken. This process was repeated until the final pH setpoint.

The organic samples were stripped (100 g/L sulphuric acid, A:O 2:1) prior to assay. The aqueous raffinate and aqueous strip solutions were submitted for assay by ICP-OES.

RESULTS AND DISCUSSION

The baseline temperature for the experiments was 35 °C, and this test was repeated in triplicate to verify the reproducibility of the pH isotherms and calculated K values produced. Keeping all other factors constant, increasing the temperature from 25 °C to 55 °C caused the extraction isotherms to shift to lower pH values (Figure 2).

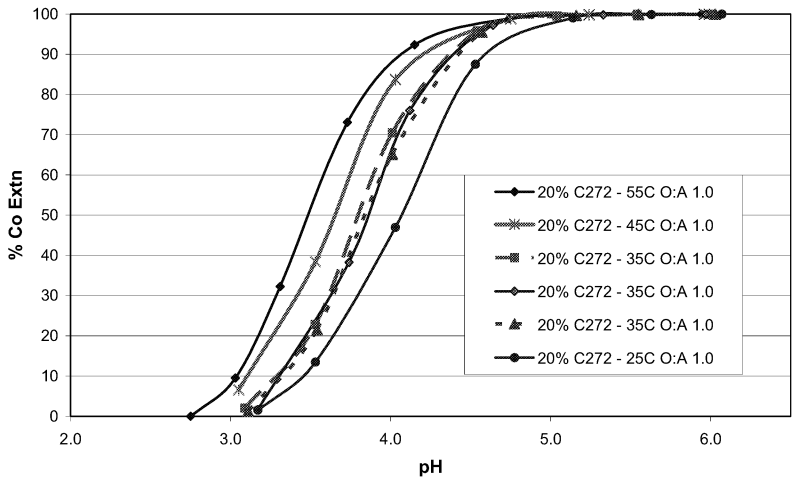

Figure 2. Effect of temperature on cobalt extraction using Cyanex 272.

Using the extractant concentration (RH), pH, and calculated percentage extraction (extraction fraction) for each data set and a least-squares approximation of the

equilibrium constant (K) for this system, it was possible to recreate the pH isotherms and calculate the equilibrium constant for each system using Equation 9. An example of the close fit between the experimentally determined pH isotherm and the calculated pH isotherm for the baseline conditions is shown in Figure 3. The variation of K and ln K with temperature results are shown in Table 1.

Table 1. Calculated K and ln K values for Co extraction at increasing temperatures.

Temperature (°C)	K (x 10^{-8})	ln K
25	2.54	-17.49
35	6.23, 6.14, 7.60	-16.59, -16.60, -16.39
45	16.7	-15.60
55	32.3	-14.95

The change in enthalpy (ΔH^0) for cobalt extraction with Cyanex 272 was then determined by substituting the Gibbs relationship $\Delta G^0 = -RT\ln K$ into $\Delta G^0 = \Delta H^0 - T\,\Delta S^0$ and differentiating with respect to temperature at constant pressure (p) (Equation 10) to get a plot of ln K versus $1/T$, a straight line with a gradient equal to $-\Delta H^0/R$ [19]. A plot of the current data (Figure 4) gave a ΔH^0 value of 69.3 kJ/M. Previous work at 8-32% v/v Cyanex 272 reported a ΔH^0 of 51.18 kJ/M [20].

$$\left(\frac{\partial LnK}{\partial\left(\frac{1}{T}\right)}\right)_p = -T^2\left(\frac{\partial LnK}{\partial T}\right)_p = -T^2\frac{\Delta H^\theta}{RT^2} = -\frac{\Delta H^\theta}{R} \qquad (10)$$

K = Equilibrium constant at constant temperature T = Temperature in Kelvin
ΔH^θ = Change in Enthalpy R = Ideal Gas Constant (8.314 J.K^{-1}. Mol)

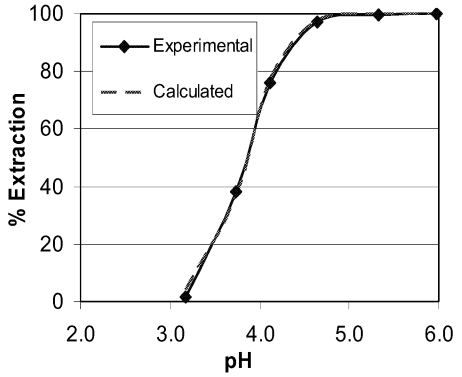

Figure 3. Comparison between experimental and calculated pH isotherm.

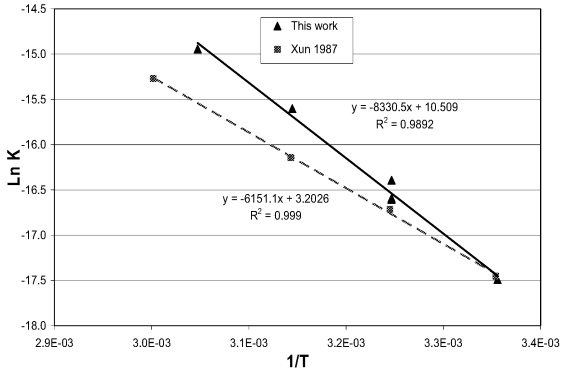

Figure 4. Arrhenius plot for Co-Cyanex 272 extraction.

Further work has been conducted to determine the effect of nickel and magnesium, ionic strength, organic concentration, and O:A ratio on the equilibrium constant *K* for Co-Cyanex 272 extraction and will be reported separately.

CONCLUSIONS

The first step in building versatile functionality into a commercial flowsheeting package was to define the pH extraction isotherm mathematically. The resulting equation defines an S-shaped curve characteristic of pH extraction isotherms and allows determination of *K*, the equilibrium constant. Operation at several different temperatures allowed the ΔH^0 of the system to be determined.

Future work will aim to incorporate the effect of multiple metals and activity coefficients into the model. This will lead to a better understanding of the system. The model will then be incorporated into a commercially available flowsheeting package to give improved modelling capabilities for SX circuits.

ACKNOWLEDGMENTS

This project was funded as part of the Parker Centre's Technology Transfer program. Jean-Pierre Veder is thanked for his assistance with the laboratory work.

REFERENCES

1. A. Feather, W. Bouwer, A. Swarts, and V. Nagel, "Pilot-Plant Solvent Extraction of Cobalt and Nickel for Avmin's Nkomati Project," ISEC'02, Cape Town, South Africa, 2002; pp. 946-951.
2. J. H. Kyle and D. Furfaro, "The Cawse Nickel/Cobalt Laterite Project Metallurgical Process Development," Nickel - Cobalt 97, CIM, Sudbury, Ontario, 1997; pp. 379-389.
3. K. H. Soldenhoff and D. Wilkins, "Direct Solvent Extraction of Cobalt and Nickel from Laterite-acid Pressure Leach Liquors," EPD Congress, TMS, 1998; pp. 153-165.
4. A. M. M. Daudinot and E. G. Liranza "Cobalt-nickel separation by solvent extraction in Cuba," ISEC'02, Cape Town, South Africa, 2002; pp. 964-969.
5. G. M. Ritcey, "Process options using solvent extraction for the processing of laterites," *Nickel'96,* AusIMM, Kalgoorlie, Western Australia, 1996; pp. 251-257.
6. W. A. Rickelton, D. S. Flett, and D. W. West, "Cobalt-Nickel Separation by solvent extraction with bis (2,4,4 trimethylpentyl)phosphinic acid," *Solvent Extr. Ion Exch.*, **2**(6), 815-838 (1984).
7. Technical Brochure: Cyanex 272 Extractant. (1996) *Cytec Industries Inc,* West Paterson, NJ.
8. G. Bacon and I. Mihaylov, "Solvent extraction as an enabling technology in the nickel industry," ISEC'02, Cape Town, South Africa, 2002; pp. 1-13.
9. J. S. Preston, "Solvent extraction of Co and Ni by organophosphorus acids I. Comparison of phosphoric, phosphonic and phosphonic acid systems," *Hydrometallurgy*, **9**(2), 115-133 (1982).
10. K. C. Sole and J. B. Hiskey, "Solvent extraction characteristics of thiosubstituted organophosphinic acid extractants," *Hydrometallurgy*, **30** (1-3), 345-365 (1992).
11. M. Martinez, N. Miralles, A. M. Sastre, and C. Herranz, "Comparative study of mono(n-

octyl)phosphinic and di(n-octyl)phosphinic acids as metal extractants," *Hydrometallurgy*, **33**(1-2), 95-106 (1993).

12. W. A. Rickelton and D. Nucciarone, "The treatment of cobalt/nickel solutions using Cyanex extractants," Nickel - Cobalt 97, CIM, Sudbury, Ontario, Canada, 1997; pp. 275-292.
13. R. B. Manski, H.-J. Bart, A. Gorge, M. Traving, J. Strube, and W. Backer, "Equilibria based on G exp E -models in a Co/Ni/phosphinic acid system," ISEC'02*,* Cape Town, South Africa, 2002; pp. 161-166.
14. J. Leistner, A. Gorge, W. Backer, A. Gorak, and J. Strube, "Modelling Methodology for the simulation of SX processes - Co/Ni," ISEC'02, Cape Town, South Africa, 2002; pp. 958-963.
15. B. K. Tait, "Cobalt-nickel separation: the extraction of cobalt(II) and nickel(II) by Cyanex 301, Cyanex 302 and Cyanex 272," *Hydrometallurgy,* **32**(3), 365-372 (1993).
16. Y. Zhuang, A. Siemon, N. Ireland, and G. Johnson, "pH measurement and control in solvent extraction using column contractors," *Minerals Engineering*, **14**(1), 13-23 (2001).
17. N. B. Devi, K. C. Nathsarma, and V. Chakravortty, "Na salts of D2EHPA, PC-88A and Cyanex-272 and their mixtures as extractants for Co(II)," *Hydrometallurgy*, **34**(3), 331-342 (1994).
18. X. Fu and J. A. Golding, "Equilibrium and Mass Transfer for the Extraction of Cobalt and Nickel From Sulfate Solutions Into Bis(2,4,4-Trimethylpentyl) Phosphinic Acid--Cyanex 272," *Solvent Extr. Ion Exch.*, **6**(5), 889-917 (1988).
19. M. R. Wright, An Introduction to Aqueous Electrolyte Solutions, John Wiley & Sons, Chichester, England, 2007
20. F. Xun, and J. A. Golding, "Solvent Extraction of Co and Ni in Bis(2,4,4-Tri-Methylpentyl) Phosphinic Acid, Cyanex-272," *Solvent Extr. Ion Exch.*, **5**(2), 205-226 (1987*).*

SOLVENT STABILITY TESTING IN DEVELOPMENT OF LIQUID-LIQUID EXTRACTION PROCESSES

Z. Gross and O. Lerner

Bateman Solvent Extraction, 5 Hamada St., Yokneam 20692, Israel
Corresponding author email address: odedlerner@bateman.co.il

ABSTRACT

Screening of a suitable solvent for a solvent-extraction process includes consideration of solvent stability. This issue has, however, been only scarcely discussed in the literature. The economic consequences of solvent stability are obvious: deterioration of the solvent will result in poor extraction, reducing the specificity and selectivity of the solvent, and will interfere with phase separation. BATEMAN Solvent Extraction Division of BATEMAN Litwin have devised a Solvent Stability Testing System that simulates loading of the solvent followed by stripping of the loaded solvent using parameters (temperature, phase ratio, etc.) similar to those of the process. Under these intensified solvent-degradation conditions, an idea of the expected stability of the solvent in terms of percentage deterioration per loading-stripping cycles or per time is gained. Preferably the aqueous feed solution is authentic, as obtained from the operating process-testing facility. Meaningful solvent-stability information may require running the Solvent Stability Testing System for as long as a few months. The paper describes the testing system and discusses a few specific test examples.

INTRODUCTION

Solvent extraction (SX) has been used for over a century as an industrial unit operation, and engineers know what issues to address when considering an SX process. Screening for the suitable solvent is the first step to be addressed. Solvent stability should be part of that early stage screening [1-3].

The economic consequences of solvent stability are obvious: deterioration of the solvent will result in poor extraction, while degradation products can alter the specificity and selectivity of the mixture. With that in mind, Bateman Solvent Extraction (BSX) division of BATEMAN Litwin have devised a Solvent Stability Testing System (SSTS) that simulates loading of the tested solvent (under the proper conditions), then stripping the loaded solvent with the appropriate stripping solution. Under these repeatedly cycling conditions, one can get an idea of the stability parameters of the solvent and thus obtain a crucial economic parameter needed for process evaluation.

SOLVENT-STABILITY TESTING SYSTEM

The SSTS is composed of a 1 liter agitated, jacketed vessel, that can be blanketed with inert gas atmosphere (e.g. nitrogen) and kept at a constant temperature by circulating water from a hot-water bath. The vessel is charged by means of metering pumps and actuated valves. An optical sensor determines the interface level. The solutions are contacted for a desired time, the agitator turned off, and the phases are allowed to settle. The first aqueous phase is drained to the raffinate storage tank. The loaded solvent is then contacted for a desired time with the stripping solution, phases are allowed to settle, and the aqueous phase is drained to the strip solution storage tank. The work is conducted with desired predetermined extraction and stripping conditions, for example, pH (which is maintained by the addition of aqueous alkaline solution) and A:O ratio.

The aqueous feed solution to be extracted (PLS) could be an authentic solution obtained from a client or a synthetic solution. The organic phase is prepared according to the client's instructions when available. Active extractant and diluent components of the organic phase are supplied by their manufacturers. In many cases, an equivalent of these components may be sourced from local suppliers. *n*-Hexadecane may be added to the organic phase, to serve as an internal standard for gas chromatographic analysis.

The outlet of the inert gas blanket is directed to an oxygen analyzer. Sampling of each phase is performed according to a predetermined sampling schedule. The cycling is controlled by means of a Programmable Logic Controller (PLC). Metals analyses are performed by use of an Inductively Coupled Plasma Atomic Emission Spectrometer (ICP-AES) or an Atomic Absorption Spectrometer. Organic-phase samples are analyzed by a Gas Chromatograph (GC), equipped with a Flame Ionization Detector (FID).

For operation of the system, the organic phase is placed in the reactor, and the extraction and stripping cycle sequence is as follows:

1. PLS feed (with volume determined by O:A pre-determined ratio ~10 min.).
2. pH adjustment (10-20% Na_2CO_3, by pH controller ~10 min.)
3. Stirring (for predetermined time 15-30 min.)
4. Phase separation (15-20 min.)
5. Raffinate draining (1-2 min.)
6. Strip solution feed (volume determined by desired phase ratio ~10 min.)
7. Stirring (for predetermined time 15-30 min.)
8. Phase separation (15-30 min.)
9. Strip solution draining (1-2 min.)

If so desired, more steps can be added (such as "scrubbing") or altered to suit various processes with different components.

In some tested cases the pretreating of the PLS (e.g., by reductive agent) or the pretreating of the solvent (e.g., by removing extractant production by-products) may enhance solvent stability. The scheme of the Solvent Stability Testing System is shown in Figure 1.

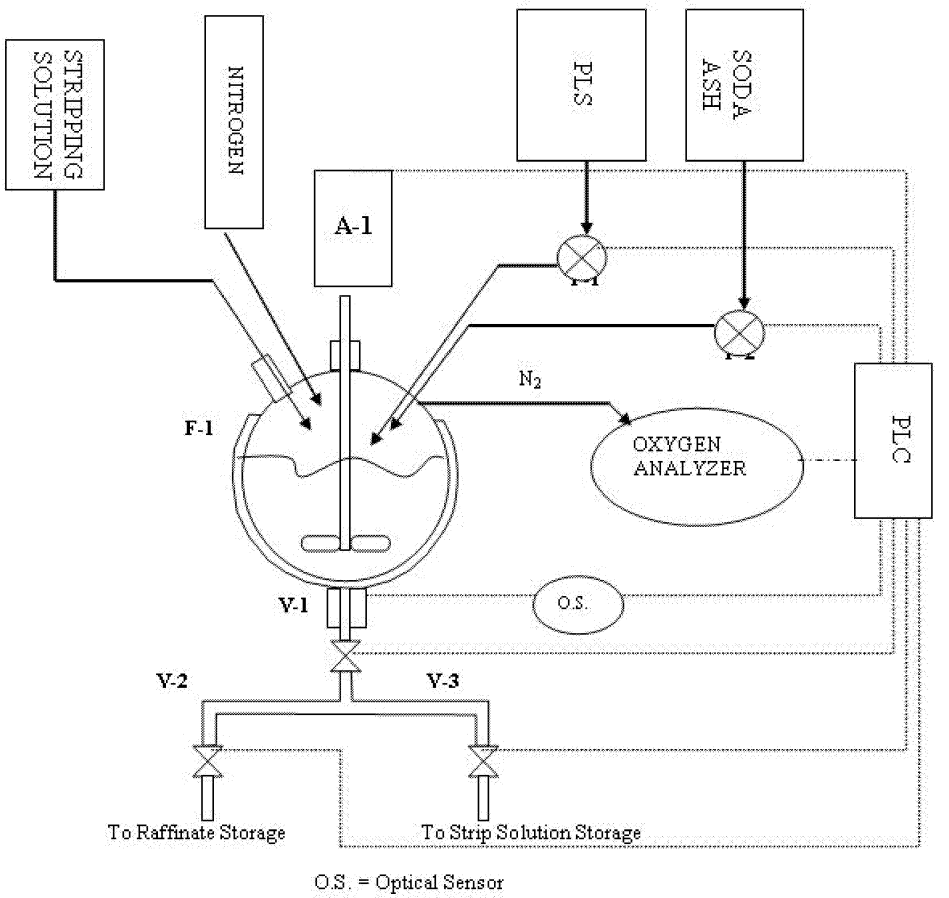

Figure 1. Conceptual schematic of the Solvent Stability Testing System.

REPRESENTATIVE RESULTS

Numerous organic compounds are used in SX systems. Some common examples are the octyl derivatives of phosphinic and thiophosphinic acids, long chained aliphatic (and aromatic) oximes and tertiary amines. Thio (and dithio) phosphinic acids tend to lose the sulphur, mainly under oxidative conditions [1,2], while oximes can undergo either hydrolytic or oxidative degradation [3]. Analysis of the major related compounds, the active extracting agent (oxime, thiophosphinic acid, or tertiary amine) and their degradation products or related contaminants is performed by Gas Chromatography.

Studies by the authors revealed that long-chained aliphatic oximes (LIX® 63) are sensitive to oxidative degradation. When oxygen is replaced with an inert gas, the oxime is degraded via a hydrolytic route as is shown in Figure 2.

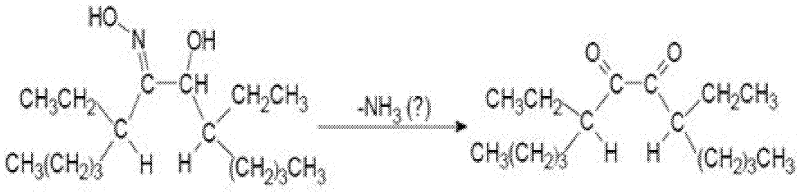

Figure 2. 5,8-diethyl-6,7-dodecanedione (diketone) formed via hydrolytic degradation of LIX 63 oxime.

Degradation data of a number of extractants determined in various studies are presented here.

Figure 3 shows oxime degradation (via a hydrolytic route) in process for the synergistic extraction of copper is fast and gives an indication that the hydrolytic degradation is catalyzed by one (or more) of the components of the PLS. Further study has revealed that the removal of Mn from the PLS results in a substantial decrease in degradation rate as shown in Figure 4.

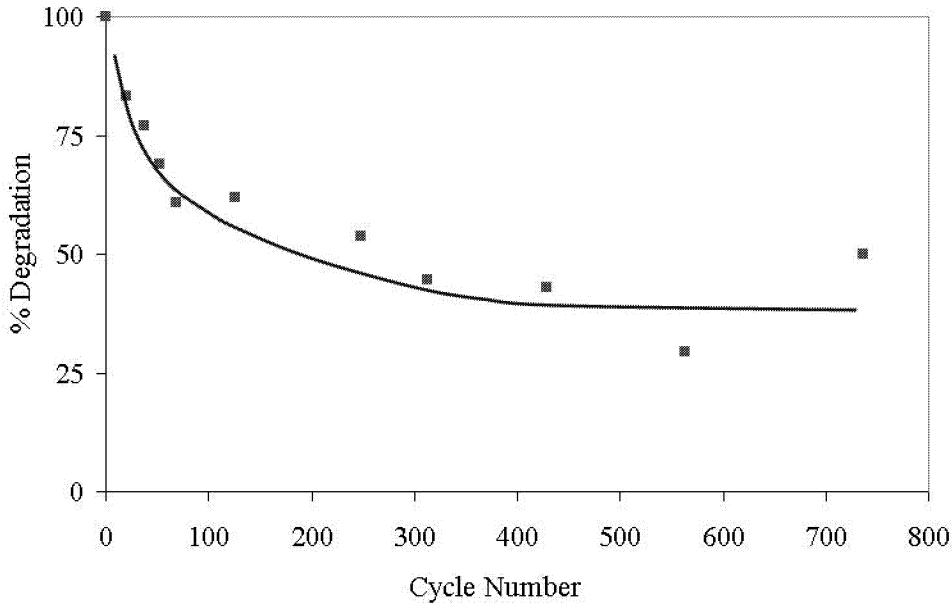

Figure 3. Degradation of oxime based LIX 63 in the absence of oxygen.

In another study, shown in Figure 5, a CYANEX extractant which was used to extract and separate cobalt from nickel was degraded relatively fast. Reductive pretreatment of the PLS substantially reduced the degradation rate as shown in Figure 6.

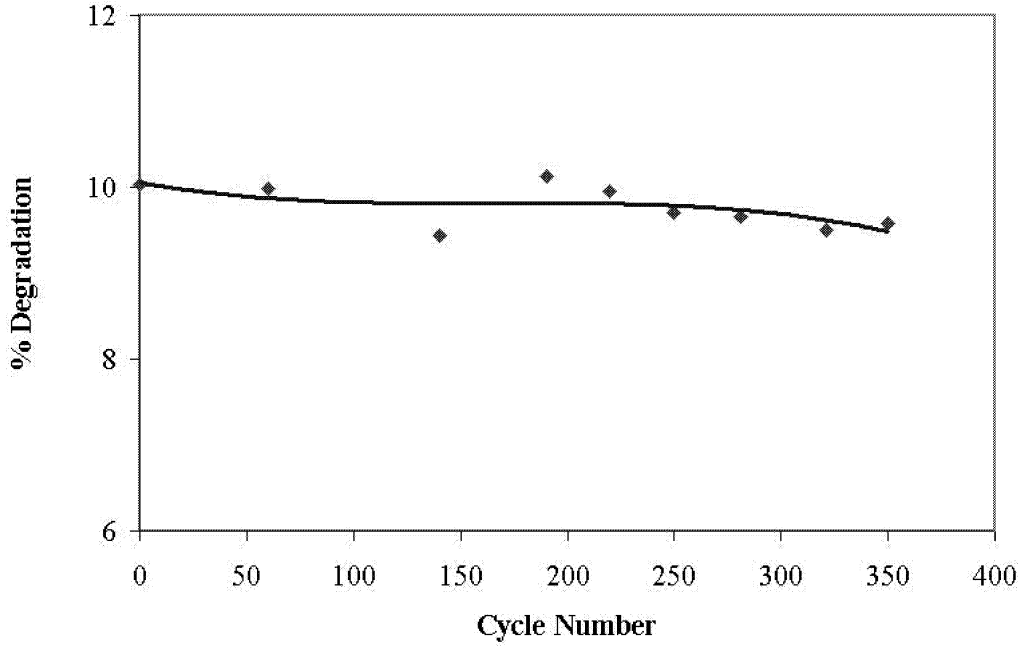

Figure 4. Degradation of oxime-based LIX 63 after removal of Mn.

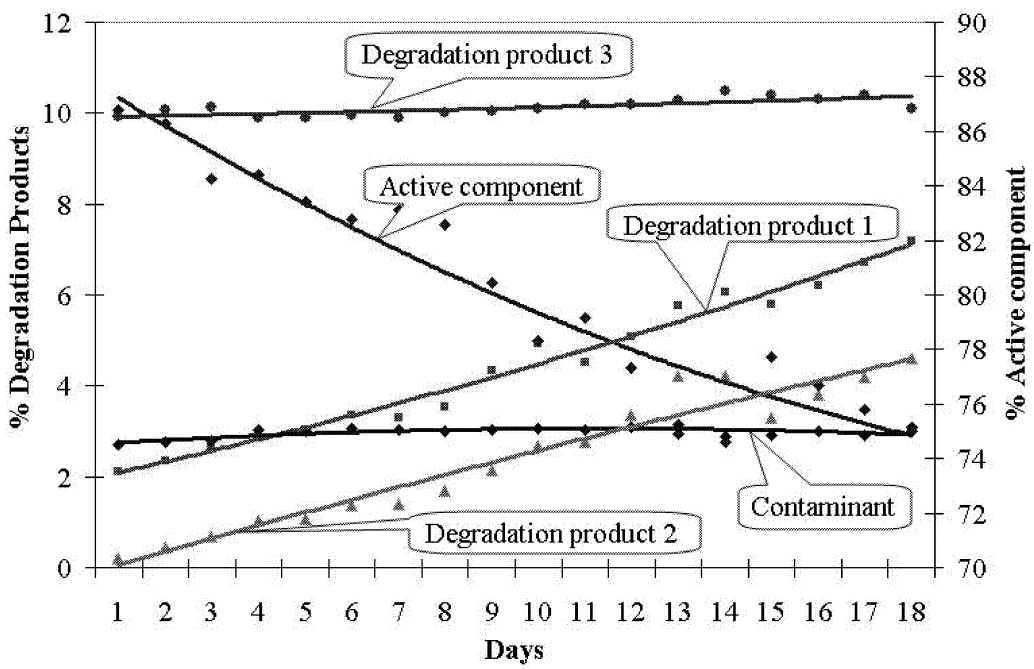

Figure 5. Degradation of a CYANEX extractant.

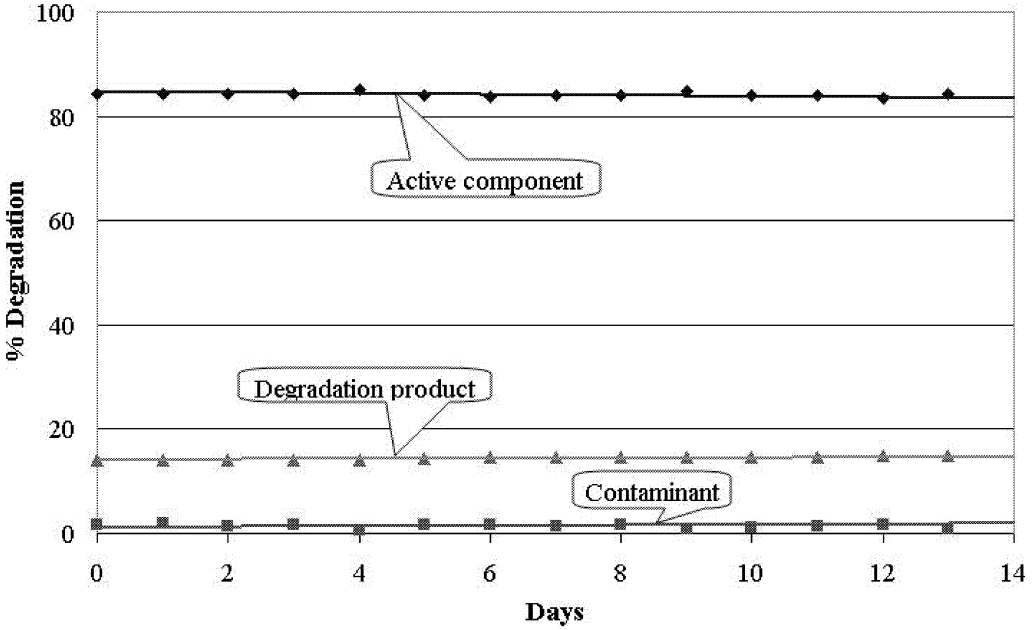

Figure 6. Degradation of the a CYANEX extractant after reductive pretreatment of the PLS.

CONCLUSIONS

As can be seen from the two examples studied, one can assess the necessary measures needed to improve a solvent-extraction process in terms of extending the life-time of the active component of the solvent or avoiding an extractant that is unstable under the specified process conditions.

The study usually includes a follow-up of the metals—extracted and stripped—as additional information needed to confirm the solvent stability or degradation. Metal analysis can shed light on the quality of the extraction/stripping process.

A typical solvent-stability test, unless the solvent is immediately degraded, is in the range of 40-60 days.

REFERENCES

1. Hydrolytic Stability – CYTEC Industries Inc, CYANEX®302 Extractant.
2. K. C. Sole, J. B. Hiskey, and T. L. Ferguson, "An Assessment of the Long-Term Stabilities of CYANEX 302 and CYANEX 301 in Sulfuric and Nitric Acids," *Solvent Extraction and Ion Exchange*, **11**(5), 783-796 (1993).
3. G. Kordosky and M. Virnig, "Degradation of Copper Solvent Extraction Reagents in the Presence of Nitrate-Contributing Factors," The John E. Dutrizac International Symposium on Copper Hydrometallurgy, Cu2007, Vol. **IV**, 25-34 (2007).

SOME PRACTICAL ASPECTS FOR IMPURITY AND CRUD CONTROL IN SOLVENT-EXTRACTION PROCESSES

H. Laitala, E. Ekman, and G. Karcas

Outotec Oyj, Riihitontuntie 7 C, P.O. Box 86, FI-02201 Espoo, Finland
Corresponding author email address: hannu.laitala@outotec.com

ABSTRACT

Solids or precipitating compounds can greatly disturb a solvent-extraction process. For some solvent-extraction plants, crud and impurity entrainments are one of the main reasons for serious process disturbances, production losses, and increased operating costs. Lost revenue due to loss of production or decreased production quality may be several million dollars per annum. This paper presents a short list of activities which can be tried, or have been tried, by several plants when crud or precipitating solids have been a major problem to a solvent-extraction process.

INTRODUCTION

In solvent-extraction (SX) processes, the problems associated with crud and impurity deportment can cause significant process disturbances resulting in economic losses. In this paper the authors draw on extensive interaction with operations around the world to compile a list of solutions applied to the problems encountered. Operations include Finnish nickel (Harjavalta), cobalt (Kokkola) and zinc (Kokkola) plants, the Bulong nickel and cobalt plant in Australia, and the Skorpion zinc plant in Namibia. Each SX process is unique and no universal solutions for the problem of crud and impurity control can be given.

IMPURITY AND CRUD CONTROL BEFORE SX PROCESSES

The simplest way to reduce impurity and crud problems in an SX process is to ensure that solids and impurities are removed before the pregnant leach solution (PLS) enters the SX process. It is sensible to carefully examine the process during the design phase to identify potential problems and allow space in the plant layout for additional equipment to be installed at a later date. In this way, it is easy to install the equipment in the right location when required.

Ore Treatment and Leaching

Milling and Ore Pretreatment

Effective grind control and ore feed blending stabilizes leaching conditions, maintaining stable downstream process conditions like control of PLS concentrations and solids removal.

Leaching Temperature and Agitation

High process temperature maximizes leach recoveries but can increase the leaching of impurities. Control of leach temperature is an optimization balance between recovery of the valuable metal and impurities transfer to the PLS. Reactor agitation with variable-speed drives assists in optimizing and stabilizing the process conditions in the leaching reactors. Effective agitation speed and gas-flow control have been applied at the Harjavalta nickel and Kokkola zinc plants in Finland. These operational principles will be applied at Cobre Las Cruces in Spain in 2008.

When the agitation level is high enough, leaching recovery is acceptable, solids are suspended, and gas dispersion in the reactor is effective. In this way, local concentration variations are avoided [1,2].

Leach pH and pH Profile

Mechanically agitated leaching processes usually contain several reactors in series. How the leach liquid and solids are fed to the reactors is an important consideration. If all the liquid and solids are fed to the first reactor, the pH of that reactor may drop significantly. A low pH with high or moderate leaching temperature accelerates the leaching of impurities. Dividing leach liquid between the first two or three reactors can help to make the leaching pH low enough for the main leaching reaction, but without promoting the leaching of impurities. Illustrated in Figure 1, this type of leaching pH control has been used at Harjavalta nickel plant and Kokkola zinc plant.

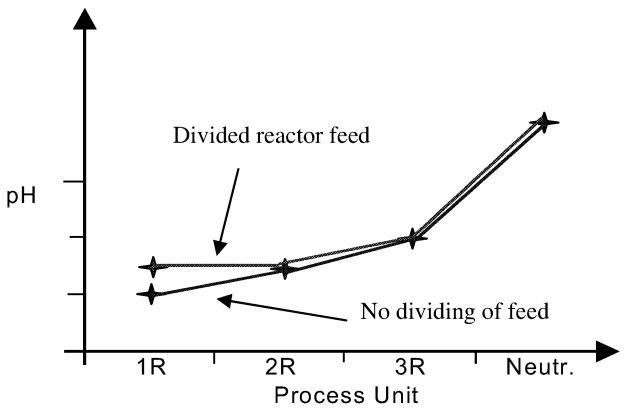

Figure 1. Stabilizing the pH profile in a reactor cascade by staging reactor feed.

Solids and Impurity Removal From PLS

Thickener and Clarifiers

Thickeners and clarifiers are effective separation equipment for solids, being quite inexpensive and simple to use. Downsides are that a large footprint and heavy foundations are required, and the overflow from a thickener is never totally free of solids. Since the particle size of these solids tends to be small, they cause significant problems in SX processes. Problems include phase-separation difficulties, crud formation, and impurity transfer from the extraction to the stripping stages through the loaded organic tank and washing stage. Clarifiers are usually not good with precipitating solids, because they contain small internal-flow channels that can be easily blocked with precipitants like gypsum. Thickeners are robust against precipitating solids but produce a 'dirtier' overflow than clarifiers.

Filtration

Filters are effective for removing solids from the PLS. Filtration is not usually used alone, since filtration capacity is expensive and operating and maintenance costs are higher than for thickeners or clarifiers. Filters are more automated, and filter cloths and belts need to be changed regularly. Any type of solids in the PLS can be removed with the right type of thickener and filter combination.

PLS Temperature Control

If a PLS stream contains a significant quantity of precipitants, changes to the PLS temperature prior to the SX process can be used to either accelerate or slow down precipitation reactions. Cooling the stream before it enters a cooling tower will promote precipitation in the cooling tower and subsequent thickener. If thickener overflow is used for the cooling duty, the PLS flow entering the SX process will be heated and the precipitation reaction in the SX will be minimized, as concentrations are below saturation limits. The process scheme described has several advantages:

- PLS from leaching or neutralization is cooled and compounds like gypsum start to precipitate.
- PLS leaving the cooling tower thickener as overflow will be heated. Heating will increase the solubility of the precipitating compounds and stop or minimize the precipitation in the SX equipment.
- Precipitated matter from cooling tower thickener underflow can be sent to the preceding process step to be used as seeds in a neutralization process.
- A cooling tower will have a positive effect on plant water balance and PLS metal concentrations.

Since precipitation can start quickly in the PLS heat exchanger, the unit must be specially designed for this kind of service. The process scheme will be applied at the Cobre Las Cruces copper plant. If solids precipitation from the PLS is intermittent, the PLS line can be equipped with a solids collector trap. When precipitation is continuous, a solids trap in the PLS line is not effective, because the area needed for the trap is large

and the trap would need to be equipped with a constantly operating crud-removing device.

CRUD AND IMPURITY CONTROL IN SX PROCESSES

Solids and Impurity-Washing SX Stage

Usually the first SX stage is the most affected with the incoming solids, causing crud in an SX process. In some SX plants, the first stage is designed to circulate diluent in a closed loop with incoming PLS. This diluent loop is separate from the main organic circulation in the SX process [3].

With this design, most of the crud formed in the SX process is formed in the first diluent-wash step before solids can enter the extraction circuit. Therefore, organic phase lost in the crud formed will be cheap diluent, and crud formation will not interfere with the primary SX process. A crud-removal system can be specially designed to deal with crud from this SX stage, and cleaning of the diluent wash stage will not interfere with the main production process. This type of process has been used since 1990 at Kokkola and Harjavalta nickel and cobalt plants in Finland. The Bulong nickel plant in Australia also used a diluent wash stage [4]. Diluent wash stages to recover reagents like Versatic 10, D2EHPA, and CYANEX® 272 have been used in the Harjavalta and Kokkola plants and at Bulong.

Impurity SX

A separate impurity SX can be installed prior to the main SX circuit. This is commonly practiced when producing cobalt and nickel but is not common in copper SX processes. Removal of Fe^{3+} from a copper SX PLS could in some cases be an interesting solution to associated problems encountered. There are copper SX processes in North and South America where iron content in the incoming PLS is 30 to 60 g/L. These plants usually experience low current efficiencies in EW (75 to 85%) and have significant crud problems in SX. Ferric iron control in the incoming PLS streams are vital for these plants.

SX Equipment

Important design considerations that affect crud formation, entrainment, and impurity transfer in SX equipment are mixing, air intake, and materials of construction. Controlled and gentle mixing increases the SX process solids handling capability. To minimize the organic phase degradation and crud formation, air intakes to the SX equipment can be minimized using covers and air locks. All SX plants delivered by Outotec have covered pumps, mixers, and settlers.

With different construction materials or liners like FRP, HDPE, or Teflon, solids build-up on the settler and pipe walls can be controlled or minimized. If precipitation occurs in an SX plant, the use of stainless steel can be problematic because scaling can be severe on these surfaces.

A water spray in the settlers can effectively compact loose crud in the organic phase. Compacted crud is more easily removed from the settler. A water spray combined with controlled mixing produces compact crud. Bulong reported very fluffy crud formed in the diluent wash stages, and it can only be assumed that no crud-compacting method was used [4]. Water spray can also be used to remove dissolved impurities like chloride (Na_2SO_4 solution/Cl^-). These methods have been used in Finnish and in South American plants.

Extractants, Diluents, and Modifiers

Crud and impurity transfer in an SX process can be controlled with proper extractant, diluent, and phase-modifier selection. High flashpoint nonaromatic diluents will be favoured in the future, because of environmental, process, and work-safety issues. In some cases in copper SX, if crud is present, ester-based modifiers are preferred over alcohol-based ones. In practice, reagent selection has grown to satisfy changes in copper SX processes. Different extractant and extractant/modifier mixtures like M5640, M5774, M5910, LIX973, and LIX984 are readily available from suppliers.

Active Process Control

On-line analyzers like Outotec's Courier® have been used in nickel and cobalt SX processes. The Courier analyzes the SX process streams on a constant basis, and results are used directly in the process-control system to change the controlled parameters (PLS and organic flows, pH, and phase continuity) automatically without human intervention. This automated process principle has been applied at Outotec's nickel and cobalt SX processes for over 20 years with very good results. Increased capacity, higher production quality, and less operating staff are needed to run the process. Capacity increase in these cases has varied from 3% to 20%. Impact on production quality has been usually greater, especially for Ni and Co SX processes.

With the use of an on-line analyser, loading of the organic phase and rich electrolyte metal concentrations can be controlled. The on-line analyzer can be used to control the feed to the EW circulation tank. Poor-quality electrolyte can be automatically rejected from the EW circuit. The authors predict that these automatic control principles including on-line analyzers and high-level process-production models will see applications in large copper, zinc, and uranium SX processes (PLS > 500 m^3/h) during the next few years. This automated control differs significantly from the more simple PID control and represents a substantial improvement to the process.

Some General Solutions

In a number of processes, anti-scalents have worked well to control and reduce precipitation problems. Since anti-scalents are usually organic compounds, they could potentially have a negative influence on the overall performance of an SX process, and careful consideration is needed before their use. The Bulong operation used anti-scalents very successfully to resolve a gypsum precipitation problem [4].

For economic reasons, the use of a three-phase centrifuge for treating crud and returning associated organic and aqueous solutions to the plant is becoming a popular choice in copper SX operations [5]. Some plants in North and South America have used cyclones to remove organic and crud from the aqueous streams with variable degrees of success.

Electrolyte filters positioned prior to the electrolyte circulation tank should not be used for crud removal. Solids entering the electrolyte filter decrease the time to breakthrough of organics impacting negatively on EW production quantity and quality.

CONCLUSIONS

There are a number of techniques that can be used to solve the problems caused by crud and impurity transfer in an SX process. Treating the symptom can be easy but can also be very expensive for an operating plant.

It is recommended to try find out as much as possible about the main process operating conditions, to then isolate the reasons for the main process disturbances, and then work towards eliminating these. Fast, easy solutions should be avoided, as they either don't help or have been attempted previously.

REFERENCES

1. R. W. Hicks and L. E. Gates, "How to Select Agitators for Dispersing Gas into Liquids," *Chem. Eng.*, 141–148 (1976).
2. L. E. Gates, J. R. Morton, and P. L. Fondy, "Selecting Agitator Systems to Suspend Solids in Liquids," *Chem. Eng.*, 144–150 (1976).
3. K. Knuutila, S-E Hultholm, B. Saxen, and L. Rosenback, "New Nickel Process Increasing Production at Outokumpu Harjavalta Metals Oy, Finland," ALTA Nickel/Cobalt Pressure Leaching & Hydrometallurgy Forum 1997, ALTA Metallurgical Services, Melbourne, 1997.
4. S. Donegan, "Direct Solvent Extraction of Nickel at Bulong Operations," *Min. Eng.,* **19**(12), 1234–1245 (2006).
5. S. A. Mukutumo, N. Schwarz, G. Chisakuto, B. Mbao, and A. Feather, "A Case Study on the Operation of a Flottweg Tricanter® Centrifuge for Solvent-Extraction Crud Treatment at Bwana Mkubwa, Ndola, Zambia," Fourth Southern African Conference on Base Metals, South African Institute for Mining and Metallurgy, Johannesburg, 2007; pp. 393–403.

A NEW TECHNOLOGY FOR TREATING WASTEWATER PRODUCED IN THE OIL INDUSTRY: A SEMI-INDUSTRIAL SCALE OPERATION

W.E. Fernandes Jr., J.B.A. Paulo, N.A. Moraes, and G.S. Medeiros

Universidade Federal do Rio Grande do Norte (UFRN) - Centro de Tecnologia - Programa de Pós-graduação em Engenharia Química – Campus Universitário, s/n - Lagoa Nova - Natal-RN-Brazil. Corresponding author email address: jbosco@eq.ufrn.br

ABSTRACT

This work presents a new device, originally conceived on a laboratory scale, for treating wastewater in the petroleum industry. Up-stream water must be treated according to the specifications of the environmental legislation in force, which, in Brazil, establishes maximum total oil and grease (TOG) of 20 mg/L. The functioning principle of the equipment is based on the combination of liquid-liquid extraction and the innovative phase-inversion method®. With the field prototype (scale factor = 100), we intend to continue studies on oily water treatment aimed at recycling part of this water in the petroleum industry itself.

INTRODUCTION

The prototype of a semi-industrial device developed by the Postgraduate Program in Chemical Engineering of the Universidade Federal do Rio Grande do Norte (UFRN) was installed in an effluent treatment plant (ETP) belonging to the Petrobras oil company. The equipment, designated MDIF® (Phase Inversion Mixer-Settler), uses liquid-liquid extraction (without chemical reaction) to treat part of the water flowing into the ETP, where the process currently being used has proven to be costly. The operation transfers the oil dispersed in the produced water to an organic solvent by mechanical agitation. After the transfer, the next stage in the process is phase separation of the treated water/solvent impregnated with oil. This separation is done using a sufficiently compact vertical settler. The functioning principle of the phase-inversion mixer-settler is shown in Figure 1 by Paulo [1] and Hadjiev [2]. According to this design, the first O/W dispersion, generated by mechanical agitation in the mixing chamber (1), causes the transfer of oil from the aqueous phase to the organic phase. This dispersion is forced through a perforated plate disperser (2) that separates the settler from the mixer. The original continuous phase becomes a dispersed phase inside the decanter in the form of dispersed drops (6), which contain droplets from the preliminarily disperse phase. During the movement of the carrier drops towards the interface (4), the transported droplets, consisting of solvent and oil, move upwards and coalesce in the organic bed. The drops not released by the organic band during the trajectory can still be recovered near the

interface (4). The organic phase impregnated with oil exits the top of the decanter (ORG), while the aqueous phase, represented by the treated water, is removed from the base of the decanter (5). Using this method, we intend to increase the coalescence rate by decreasing the distance between the dispersed drops and the interface, since each carrier drop acts as a microdecanter (Chiavenato [3], Fernandes Jr.[4]).

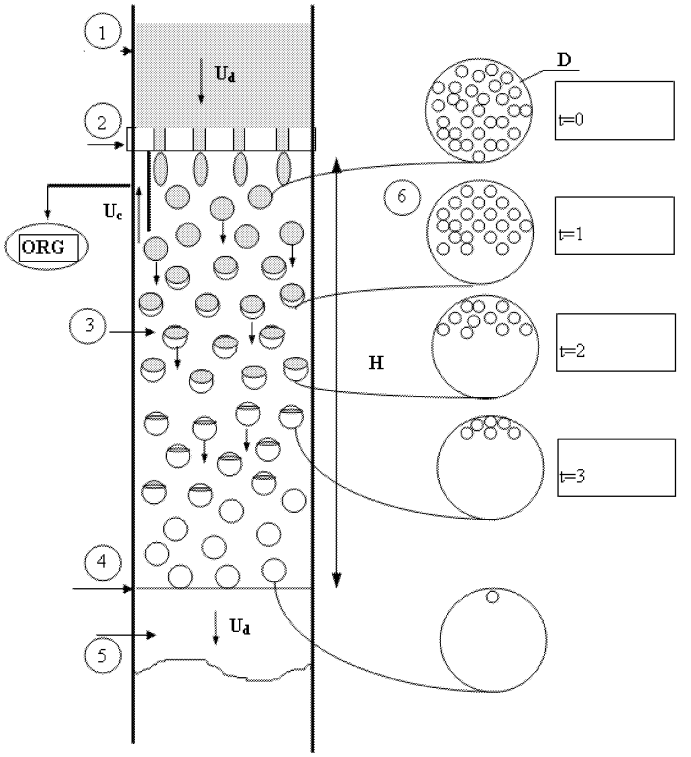

Figure 1. Functioning principle of the MDIF, Paulo [1].

The efficiency of oil/water separation can be calculated according to Equation 1.

$$E = \frac{Ce - Cs}{Ce} \tag{1}$$

In this equation, C_e is the oil/water inlet concentration, and C_s is the oil/treated water outlet concentration; both concentrations are expressed in mg/L.

The design of the field equipment considered a scale factor 100 times greater than the laboratory prototype, which represents a mean flow of 10 m^3/h. All the scale extrapolation calculations considered the treatment of oily water with oil concentrations between 50 and 150 mg/L. The data during the operation of the semi-industrial MDIF underwent surface-plot analysis using a statistics experimental design. Owing to supply problems, we used aviation kerosene supplied by Petrobras. The preliminary results are promising, since under the most favorable experimental design conditions and at

oil/water inlet concentrations varying between 30 and 50 mg/L, we obtained water quality that met the specifications of current environmental legislation.

MATERIALS AND METHODS

The aqueous phase was water contaminated with petroleum termed "formation water or produced water" originating at the ETP inlet. The organic phase was a complex mixture of hydrocarbons called aviation kerosene obtained from Petrobras. The physical-chemical properties of both phases are shown in Table 1.

Table 1. Physical-chemical properties of the phases studied.

Product	Density (ρ) 10^3 kg/m^3	Viscosity (μ) 10^{-3} Pa.s	Surface tension (γ) 10^{-3} N/m	Interfacial tension (γ) 10^{-3} N/m
Formation water	1.0022	0.851	70.48	26.50
Aviation kerosene	0.7841	0.910	27.14	32.67

The concentrations used in Equation 1 are obtained using the standard infrared absorbance method for determining oil and grease content (TOG). The device used for these measurements was the InfraCal® TOG/TPH Model HATR-T2 (Wilks Enterprise, Inc.). It should be emphasized that this method has been adopted by the national petroleum industry.

We used a Statistics Experimental Design software to study the separation efficiency of the new equipment. The aim is to plan activities so that appropriate data can be collected with a minimum of time and expense. The analysis of these data by statistical techniques is useful for obtaining the variable response, that is, separation efficiency. The statistical methodology selected was Experimental Design. This optimization technique is based on the use of factorial design. In this study, we used a composite central design with type 2 complete factorial and six repetitions at the central point with star-type amplification, [5]. By means of the experimental design, we analyzed three independent variables that influence the separation efficiency of MDIF: effective flow, organic/aqueous (O/A) volumetric ratio, and agitation velocity in the mixing chamber. The height of the settler chamber was constant, and the oil concentration fed into the machine varied between 30 and 50 mg/L. Experimental Design statistical software, version 5.5, was used to analyze the results.

RESULTS AND DISCUSSION

The separation-efficiency results of the valid tests are shown in Table 2. Test 8 showed the greatest separation efficiency with 80.95%, while Test 9 had the lowest performance with 19.92%. Post-treatment TOG results met the legal standards ($\leq$20 mg/L) in 80% of the experiments. This fact is important, given that it was possible to specify the water produced for waste in a single separation stage. The rise in total effective flow and in the volume of the organic solvent is a determinant factor for the increased separation efficiency. The higher effective flow generates carrier drops from the perforated plate with smaller diameters, thus creating a distance between the disperse

droplets and the interface separation, which favors the coalescence rate and the separation efficiency.

Table 2. Results of the valid tests obtained for MDIF composite central planning

Test Number *	Effective Flow (m^3/h)	Volumetric Ratio O/A	Agitation Velocity (rpm)	Separation Efficiency (%)
1	8,0	1/5	83	28,43
2	12,0	1/5	83	68,21
3	8,0	2/5	83	46,96
4	12,0	2/5	83	71,25
5	8,0	1/5	97	28,03
6	12,0	1/5	97	66,87
7	8,0	2/5	97	46,71
8	**12,0**	**2/5**	**97**	**80,95**
9	**6,6**	**1/3**	**90**	**19,92**
10	13,4	1/3	90	74,53
11	10,0	1/6	90	63,32
12	10,0	½	90	59,69
13	10,0	1/3	78	49,90
14	10,0	1/3	102	54,72
15	10,0	1/3	90	56,06
16	10,0	1/3	90	61,84
17	10,0	1/3	90	67,29
18	10,0	1/3	90	58,49
19	10,0	1/3	90	68,78
20	10,0	1/3	90	68,90

*All the experiments with MDIF were performed in duplicate to confirm the results.

Figure 2 shows the surface plot for the separation efficiency applied to an effective flow of 13.4 m^3/h. This was the best performance obtained, since high separation efficiency was found in all the O/A volumetric ratio range studied, even at low O/A ratios. In this condition, agitation velocity remains near the central point (90 rpm), which represents lower energy costs.

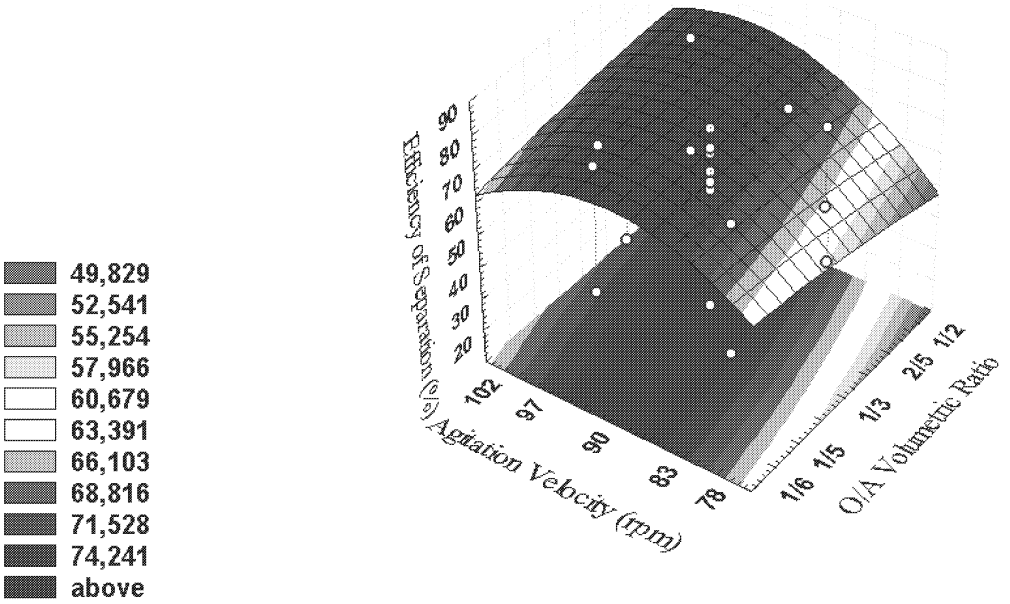

Figure 2. Surface plot for separation efficiency of UT-MDIF. Agitation velocity vs. O/A volumetric ratio. Total flow, 13.4 m^3/h; height 2.0 m; oil/water inlet concentration, 30 to 50 ppm.

CONCLUSIONS

The vertical design of the device economizes space in the plant layout. The MDIF maintains the general characteristics of conventional mixers-settlers, such as strong operational loads, facility of operation and maintenance, and simple operational start-ups. The best performance, represented by a separation efficiency greater than 74%, occurred for operations with high effective flows of around 13.4 m^3/h or greater (>47.4 $m^3\ m^{-2}\ h^{-1}$). For the system studied, this separation efficiency meets the water-quality standards stipulated by the environmental legislation (<20 mg/L). These results corroborate those of previous laboratory experiments.

We conclude that it is possible to operate at low O/A ratios and high effective flows. This operational condition is highly favorable from the industrial point of view, because, in addition to representing a saving in the amount of solvent used, it enables the treatment of larger volumes of water, with consequent higher equipment output.

The MDIF may be a real alternative for treating water contaminated with oil at low concentrations (30 to 50 mg/L) and might also be able to treat waste water to a low residual (20 mg/L) or for recycling, using one or two of the operation stages.

ACKNOWLEDGMENTS

The authors would like to thank the Petrobras/Cenpes/UN-RNCE for its financial support in the accomplishment of this research work.

REFERENCES

1. J. B. A. Paulo, D. Hadjiev, and G. Casamatta “Desempenho de um novo tipo de mixer-settler na extração de cobre,” Congresso Ítalo-brasiliano d’ingegneria Mineraria, Verona, Italia, 1994; pp. 156-160.
2. D. Hadjiev and Y. Aurelle, “Phase inversion: a method for separation of fine liquid-liquid dispersions,” *Chem. Eng. J.,* **58**, 45-51 (1995).
3. M. C. Chiavenato, “Utilização de um novo design de mixer-settler à inversão de fases para tratamento de dispersões e/ou emulsões do tipo óleo bruto/água de formação,” Dissertação de Mestrado, PPGEQ/UFRN, Natal-RN, Brasil, 1999; pp. 1-146.
4. W. E. Fernandes, Jr., “Planejamento experimental aplicado a um novo separador líquido-líquido utilizado no tratamento de águas residuais contaminadas com petróleo,” Dissertação de Mestrado, PPGEQ/UFRN, Natal-RN, Braisl, 2002; pp. 1-125.
5. B. de Barros Neto, I. S. Scarmínio, and R. E. Bruns, Como Fazer Experimentos: pesquisa e desenvolvimento na ciência e na indústria, Ed. da Unicamp, Campinas, 2001.

INNOVATIONS IN THE CONFIGURATION OF A PINNED-BED CLARIFIER FOR CLARIFICATION OF A ZINC LEACH LIQUOR

M. Langton,[1] H.F. Fuls,[2] K.C. Sole,[3] A. Rampersad,[3] C. Blaauw,[2] and B. Martinson[1]

[1]Roymec Technologies, Sandton, South Africa. [2]Skorpion Zinc, Rosh Pinah, Namibia
[3]Anglo Research, a division of Anglo Operations Ltd, Johannesburg, South Africa
Corresponding author email address: ksole@angloresearch.com

ABSTRACT

One of the physical factors that can have a significant impact on the operation of a solvent-extraction process is clarity of the feed liquor. When the leach liquor results from the leaching of an ore, the presence of high levels of suspended solids is common. In solvent-extraction plants where the specification for suspended solids in the feed is <10 mg/L, the use of a pinned-bed clarifier consistently achieves this target and offers significant advantages. Optimization of a pinned-bed clarifier for solids removal from the zinc leach liquor at Skorpion Zinc is reported.

INTRODUCTION

One of the critical factors influencing the operability of a commercial solvent-extraction (SX) circuit is the clarity of the feed liquor. The presence of suspended solids in solutions entering the circuit causes a variety of difficulties, including crud formation, phase separation retardation, and transfer of impurities through the circuit.

Skorpion Zinc, located in southern Namibia, is the world's first operation producing cathode zinc from primary ore using SX [1,2]. The ore contains significant silicates, so the propensity for crud formation in the SX circuit, promoted by suspended solids in the PLS, is severe. In addition to the operational problems posed by crud, its carryover has been linked to contamination of the zinc electrolyte by impurities such as Ni, which have deleterious effects on the downstream electrowinning operation [3].

The specification for total suspended solids (TSS) entering the Skorpion Zinc SX circuit in the pregnant leach solution (PLS) is <10 mg/L. In the original process design, sand filters were intended to provide clarification duty. Calcium saturation of the PLS, however, caused frequent blockage of the sand filters by gypsum precipitation, and consequent by-passing of the units resulted in TSS levels sometimes rising to >200 mg/L. PLS ponds were subsequently installed to increase buffer capacity to allow for planned maintenance in the leach plant, and which provided an additional 6 to 20 h residence time for settling of solids. Although this improved the quality of the PLS, clarification remained inadequate. In 2006, an Ishigaki-Fiber Washikimizu filter was tested as a clarification unit to treat the PLS [4]. Although the results from this

equipment were good, the anticipated operating costs due to routine replacement of the filtration media were prohibitive. More recently, a Waterex pinned-bed clarifier (PBC) [5] was tested for this application and, under optimized conditions, was found to permit close to quantitative solids removal from the PLS when operating above the target solution rise rate of 10 m/h, using novel reagent addition and operating configurations.

PILOT-PLANT EQUIPMENT AND PROCEDURES

An 8-week trial was carried out on-site using a PBC pilot unit of 0.5 m diameter and 6 m height (Figure 1). The PLS (typical composition (g/L): 35 Zn, 2.0 Mn, 1.1 Mg, 0.6 Ca, 0.5 Cu, 0.2 Cd, 0.2 Ni, 0.1 Al, 0.1 Si, and 1.7 Cl), taken on-line from the Skorpion circuit, was mixed with flocculant and coagulant before entering the feedwell. Flocculation was improved by adding recycled sludge to the feed ahead of flocculant addition. The bulk of the solids proved amenable to flocculation and/or coagulation, settling by gravity to the base of the unit. Excess accumulated sludge was intermittently removed to control the underflow sludge level. Unsettled solids were removed from the PLS by filtration through a bed of filtered solids beneath an inert media pinned against a perforated plate at the top of the PBC unit during forward flow. The media comprised epoxy-coated polystyrene beads (3 mm diam.) and uncoated expanded polystyrene (1 and 2.5 mm diam.). Clarified liquor exited from the overflow at the top of the column.

The media bed was periodically backwashed to remove accumulated solids, triggered by a predetermined pressure build up in the bed. In backwash mode, the PLS flow was stopped, and a backwash valve below the media bed opened. Filtered PLS flowed downward through the bed, expanding the media and flushing accumulated solids out of the backwash outlet. Total backwash time was 30 s.

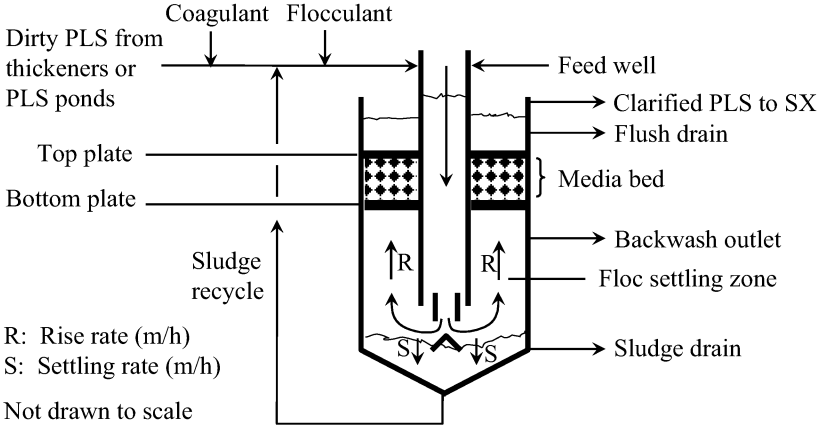

Figure 1. Schematic of Waterex pinned-bed clarifier pilot-plant unit.

Flowrates and other relevant operational parameters were measured on an hourly basis. Samples, taken 4-hourly from the PLS, PBC midbed, and PBC outlet, were analyzed for TSS and turbidity (measured in nephelometric turbidity units, NTU). Inlet

and outlet metal concentrations in the PLS were assayed 12-hourly.

The effects of several PBC operating parameters and circuit configurations were evaluated, including the use of flocculant and coagulant, sludge recycle, varying rise rate, and alternative bed-media sizes. The initial trials employed thickener overflow as the feed (with TSS values typically in the range 50 to 250 mg/L), while the later trial used PLS taken from the holding ponds downstream of the thickeners (30 to 100 mg/L TSS).

RESULTS AND DISCUSSION

PBC Operation without Flocculant and Sludge Recycle

The first phase of testwork aimed to optimize operating conditions without recycle of the sludge bed to assist in seeding for flocculation. This would give a baseline to identify the natural settling characteristics of the solids in this system. Table 1 compares the TSS and turbidity results for different rise rates. Under these conditions, a vertical rise rate of 5 m/h gave the best performance. Good agreement between the TSS and turbidity data was achieved at the lower flowrates, but the turbidity data at 15 m/h showed better removal of ultrafines. Since the turbidity measurement provides a better indication of deportment of colloids and ultrafine particles, this may indicate that at the higher rise velocity, filtration is improved by compression of the solids trapped in the finer media in the PBC bed.

Table 1. Effect of flocculant addition and sludge recycle on performance of PBC

		No flocculant or sludge recycle			With flocculant and sludge recycle		
PLS flowrate (m^3/h)		1	2	3	1	1.5	2
Rise rate (m/h)		5	10	15	5	7.5	10
Flocculant flowrate (L/h)		—	—	—	16	35	32
Sludge recycle (L/h)		—	—	—	190	190	580
TSS	PBC inlet (mg/L)	59	56	56	79	58	82
	PBC outlet (mg/L)	20	38	38	40	51	87
	Solids removal efficiency (%)	62	31	32	56	22	~0
Turbidity	PBC inlet (NTU)	28	28	20	29	33	36
	PBC outlet (NTU)	9	16	8	8	33	39
	Solids removal efficiency (%)	64	33	55	72	4	~0

PBC Operation with Flocculant and Sludge Recycle

During the second trial, the bulk of the sludge was recycled from the base of the PBC, mixed with the incoming feed and flocculant. The sludge acted as seed material for flocculation, and any residual flocculant was recycled. The flocculant selected, SNF Floerger 920VHM, was that employed in the thickening process at Skorpion Zinc. It was made up daily at a concentration of 0.036% and aged for 5 h. From the results of this trial (Table 1), it is evident that, even at the lowest rise rate tested, solids removal was poor.

The discrepancy between the TSS and turbidity data indicated that the presence of ultrafine material was contributing to this poor performance. This fine material was also observed to cause blinding of the bed.

Characterisation of Flocculation and Coagulation Behaviour of Solids

To understand the relatively poor performance of the PBC even at the low rise rates tested, flocculation behavior of the solids was re-evaluated. Particle-size distribution analysis of the solids in the thickener overflow (feed to the PBC test unit) indicated that 14% could be classified as ultrafines (<10 μm) and 53% as fines (<45 μm). Inefficient flocculation in the PBC would therefore allow a high percentage of fines and ultrafines through to the clarified outlet solution. Bench-scale flocculation tests showed that under controlled and optimized conditions, the larger particles formed flocs of ~300 μm, but that, the fines and ultrafines were not flocculated. The particle-size distribution of the suspended solids in the flocculated PLS was bimodal (Figure 2), with the finer material apparently nonresponsive to flocculation.

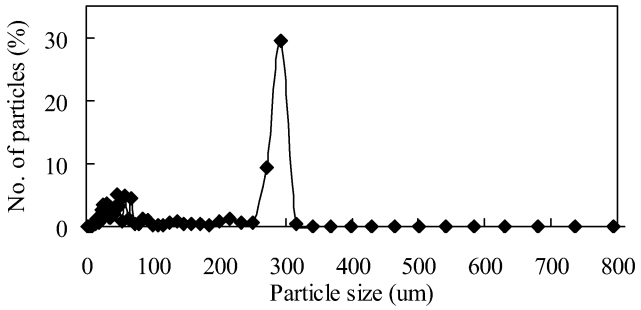

Figure 2. Particle-size distribution of solids in PLS after optimized flocculation.

A wide range of commercial flocculants and coagulants was evaluated, but these had negligible effects on the settling rate of the fine solids in the PLS. Coagulants are positively charged, and operate by neutralizing any negative surface charge on suspended particles, eliminating the Coulombic repulsion between them and allowing a flocculant to work successfully. The lack of any influence of conventional coagulants indicated that the solids are not negatively charged. Only one coagulant was found that gave extremely good coagulation and excellent supernatant clarity. This coagulant was employed in the third phase of the trial.

PBC Operation with Flocculant, Coagulant, and Sludge Recycle

The coagulant was made up daily, at a concentration of 1%, and dosed directly into the PLS line. Recycled sludge was added and the seeded feed introduced to a high-energy mixing chamber where 50% of the flocculant was added. The overflow from the high-energy mixing chamber was directed to a low-energy flocculation chamber, where the balance of the flocculant was added before the feed overflowed into the PBC

feedwell. The high-energy mixing (10 kW/m^3) ensured good dispersion of flocculant into the sludge (with the resultant partial break-up of the polymer chains), while the low-energy mixing (1 kW/m^3) served to gently mix the flocculant into the preflocculated sludge, thereby agglomerating the solids.

Figure 3 compares the feed and outlet turbidity measurements obtained at rise rates of 10 to 15 m/h during the third trial. The corresponding TSS data are summarized in Table 2. It is evident that excellent clarification of the PLS was achieved under optimized conditions. The target specification for the performance of the PBC (reducing solids in the feed to the SX circuit to <10 mg/L TSS) was consistently achieved, irrespective of the incoming solids concentrations. No gypsum build up was detected in the unit or on the media. An unexpected further advantage of this operating configuration was that ~5% Si and ~10% Al soluble in the PLS were also removed with the solids—adding further benefit to the downstream SX operation.

Table 2. Optimized average performance of PBC (29 days running time)

PLS flowrate (m^3/h)	3	Flocculant concentration (mg/L)	2.0
Rise rate (m/h)	15	Coagulant concentration (mg/L)	11.5
Sludge recycle (L/h)	24	Flocculant consumption (g/kg Zn)	0.05
Sludge density (kg/L)	1.1	Coagulant consumption (g/kg Zn)	0.29
PBC inlet (mg/L TSS)	63.3	PBC inlet (NTU)	15.6
PBC outlet (mg/L TSS)	6.1	PBC outlet (NTU)	0.5

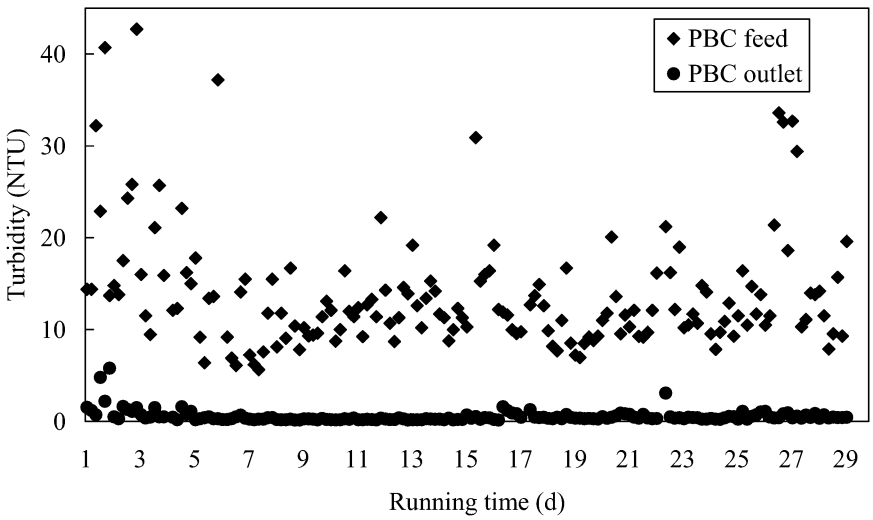

Figure 3. Comparison of the feed and outlet turbidity concentrations on passing the PLS through a PBC operating optimally with flocculant, coagulant, and sludge recycle.

CONCLUSIONS

The presence of suspended solids in the feed to an SX circuit can be responsible for considerable operational difficulties and increased operating costs. At Skorpion Zinc, the specification for the SX feed is <10 mg/L TSS. It was conclusively demonstrated on a pilot scale (2 m^3/h PLS, corresponding to a vertical rise rate of 10 m/h) that this can be achieved using a Waterex pinned-bed clarifier, optimized for rise rate, media size, flocculant and coagulant addition, and with recycle of settled sludge to minimize reagent consumption. Incoming solids concentrations of up to 200 mg/L (average ~80 mg/L) were consistently reduced to <10 mg/L TSS (average 6.1 mg/L) (<1 NTU) in the clarified PLS (Figure 4).

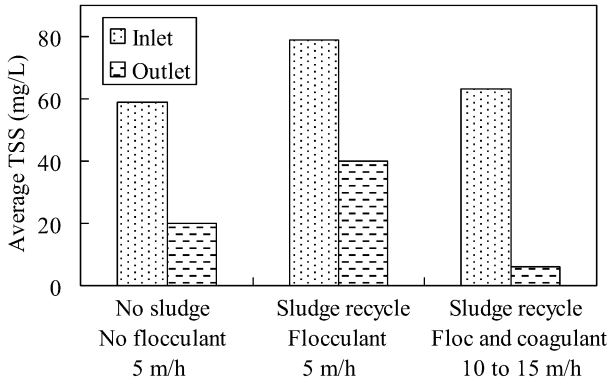

Figure 4. Optimization of pinned-bed clarifier for processing of Skorpion Zinc PLS.

ACKNOWLEDGMENTS

Appreciation is extended to the management of Skorpion Zinc for support of this project. We also thank R. Crosbie for technical advice, and H. Alcock, M. Anderson, W. Dent, M. Gurirab, K. Ledwaba, C. Ngcanga, M. Pather, P. Segoai, L. Sibiya, L. Tjatindi, A. van Staden, and D. Wohler for excellent analytical and operational assistance. This paper is published by permission of Skorpion Zinc and Anglo Research.

REFERENCES

1. H. Fuls, K. C. Sole, and T. Bachmann, "Solvent Extraction in the Primary Processing of Zinc: the Skorpion Zinc Experience," Proceedings ISEC 2005, Beijing, China, 2005.
2. P. M. Cole and K. C. Sole, "Zinc Solvent Extraction in the Process Industries," *Miner. Proc. Extr. Met. Rev.*, **24**, 91-137 (2003).
3. J. Gnoinski, T. Bachmann, and S. Holtzhausen, "Skorpion Zinc: Defining the Cutting Edge of Zinc Refining," Proceedings Lead-Zinc 2005, Kyoto, Japan, 2005; pp. 1315-1325.
4. H. F. Fuls and K. Nong, "Piloting of the Ishigaki Fibre-Wakishimizu (Fibre Media Rapid Filtration Equipment) at Skorpion Zinc," Africa's Base Metals Resurgence, Southern African Institute for Mining and Metallurgy, Johannesburg, 2007; pp. 223-240.
5. "Waterex Clarifiers," http://members.iinet.net.au/~waterex/clarifiers.htm.

IMPROVED ORGANIC RECOVERY WITH HYDROCYCLONES AT FREEPORT-McMORAN COPPER AND GOLD MORENCI OPERATIONS

M.A. Thumberg and E.P. Kramer

Freeport-McMoRan Copper and Gold Morenci Operations, 4521 US Hwy 191
Morenci, Arizona 85540
Corresponding author email address: melissa_thumberg@fmi.com

ABSTRACT

Due to high extractant concentration in the Stargo solution-extractant plant at Morenci Operations, a method was needed to decrease the amount of entrained solvent from the raffinate stream. Liquid-liquid separation hydrocyclone units were purchased in 2006 from KREBS Engineering in Tucson, Arizona to remove the entrained organic phase via centrifugation. This unit was designed to recover entrained organic phase and return it to the SX circuit, thereby reducing the make-up of extractant and diluent added to the plant. Analysis of the recovery stream for a two-month period after completion of the full-scale hydrocyclone unit gave an average recovery in the overflow stream of 21%.

INTRODUCTION

The Freeport-McMoRan Copper and Gold Morenci Operations is home to one of the largest integrated solvent-extraction (SX) and electrowinning (EW) facilities in the world. Copper cathode production began in 1987 and is currently achieved in a facility composed of six SX circuits and three EW tankhouses. Total pregnant leach solution (PLS) flow across all of the circuits is approximately 116,000 gallons per minute (gpm), and the three electrowinning tankhouses can produce in excess of 900 million pounds of copper cathode per year.

Stargo SX is the newest SX circuit, commissioned in 1998 as a series circuit. A parallel mixer/settler was added in 2000 as part of the Mine-for-Leach (MFL) Expansion Project. Stargo SX is currently configured as a series-parallel extraction, single-strip circuit with a loaded organic wash stage as shown in Figure 1. The circuit extracts approximately 800,000 pounds of copper into the electrolyte per day, which is sent to the tankhouse for plating. Due to the higher grade of pregnant leach solution to the circuit (3 grams per liter), Stargo SX operates with a higher volume-percent extractant than the other SX circuits, thereby increasing the operating costs associated with organic entrainment.

Starting in April 2005, Morenci began an organic loss-reduction project with a goal of reducing organic losses, property wide, by 15%. This project included installation

of picket fences to help distribute flow across the settlers, belt mops to pick up organic phase off of the raffinate ponds, and increasing organic inventories in the organic tanks to reduce air entrainment and achieved a 35% reduction in organic losses [1]. The next phase of organic-loss reduction focused on improved separation though centrifugation with hydrocyclones. Due to its high volume-percent extractant, Stargo SX was identified as the plant with the most viable economic drivers for the installation and commissioning of the hydrocyclones.

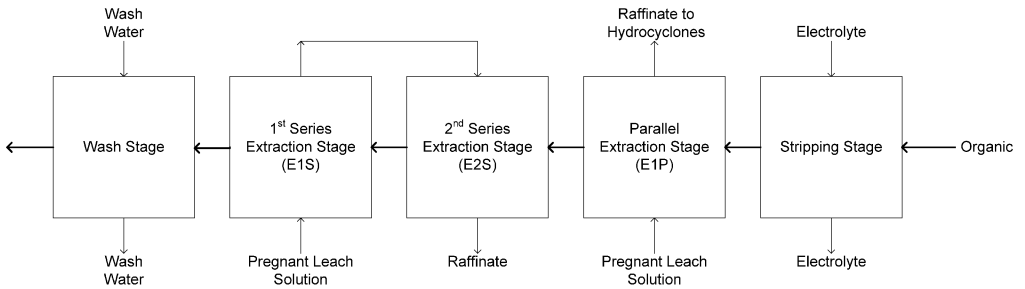

Figure 1. Flowsheet for Stargo SX.

EQUIPMENT INSTALLATION

The selected hydrocyclone vendor was KREBS Engineering in Tucson, Arizona. For the project, four 48-inch diameter CycloClean vessels were purchased, each containing 376 L40-gMAX hydrocyclones. The hydrocyclones and their pumps are designed for a maximum of 13,500 gallons per minute raffinate distributed evenly through all four units. Design pressure drop is approximately 45 pounds per square inch (psi) from inlet to discharge of the units [2]. The inlet pressure is typically 90 psi, while the discharge pressure is approximately 45 psi. The recovered overflow back to the settler is between 300 and 400 gpm.

The hydrocyclone units were delivered in April 2006, and installation was complete in May 2006. The units were installed on the parallel raffinate advance line with an overflow recovery line discharging across the back of the settler; primarily over the uptake channel of the mix box to the settler. The units and pumps were placed below ground and were aligned with pre-existing piping from the raffinate weir to the raffinate tank.

A setback in the equipment commissioning came not from the hydrocyclones but from the pipe feeding to, and discharging from, the hydrocyclones. The hydrocyclones were initially commissioned at the end of May 2006. During this process, the 30-inch diameter raffinate advance line from the E1P flexed due to back pressure in the line related to opening and closing of the bypass valves during startup, weakening the integrity of the line and causing the project to be put on hold until the line could be replaced with a higher-schedule pipe. In August 2006, 100 feet of the 30-inch Schedule 10 pipe was replaced with Schedule 40 pipe. The unit was restarted in September but was not fully operational until November, because a 60-foot section of the 24-inch discharge

line also needed to be replaced with Schedule 40 pipe and a 30 inch x 24 inch eccentric reducer added.

At the same time that the discharge pipe was being upgraded, a 4-inch diameter distribution manifold was installed over the inlet to the E1P. The manifold was added in order to reduce the amount of turbulence introduced to the system and allow for phase separation throughout the settler. The manifold consisted of numerous holes along the bottom of the pipe allowing for even distribution of flow over the mix box uptake channel. All installation and repair efforts were performed without any safety events occurring.

In February 2007, a technical representative from KREBS Engineering came to observe the installation and check that it was running at optimal performance levels. It was determined that the unit was successfully running according to the design specifications.

Best Practices and Safe Operating Procedures

All components of the hydrocyclones are set up remotely and can be controlled in the SX control room. A Safe Operating Procedure (SOP) for start-up of the unit was developed and included parameters for the unit itself as well as weir and flow levels. Best practices identified during the commissioning and initial operating include back-flushing the units daily to ensure that recovered organic phase does not build up in the pipe and cause blockages and continual monitoring via the planned maintenance function in the Ellipse software package to ensure the hydrocyclones maintain their efficiency.

Since commissioning, the hydrocyclone vessels have been opened and the hydrocyclones removed and cleaned. This process showed that, due to the collection of gunk and other debris through the raffinate line, regular downtime for cleaning needs to be scheduled. However, standard planned maintenance schedules for opening and cleaning the hydrocyclones have not yet been established. Figure 2 gives both inlet and discharge views of the KREBS Hydrocylone units.

Other safeguards to the system include weir level indication, hydrocyclone inlet and discharge pressure readings, and fail open bypass automatic (REXA) valves. The hydrocyclones shut down when the raffinate weir level is above or below standard operating levels. Since weir levels do not normally change a significant amount during normal operating conditions, a high or low weir level alarm indicates abnormal plant activities like no flow or a backed-up settler caused by poor organic advancement to the next settler. Hydrocyclone inlet and discharge pressures are important because a strong pressure delta, preferably 45 psi, is required for a good liquid-liquid separation. If pressure deltas are too great or too small, adjustments can be made to the manual valves at the discharge of each hydrocyclone pair (see Figure 2b). One of the most important safeguards to the system is the bypass line and REXA valve. If there were a failure with the hydrocyclone pumps, for example, the system would shut down automatically, and the autovalve would open, bypassing the raffinate flow directly from the 30-inch raffinate discharge line to the 24-inch raffinate line leading to the raffinate tank. The same would occur during a power loss or if the hydrocyclones were taken down intentionally for service or due to plant instabilities.

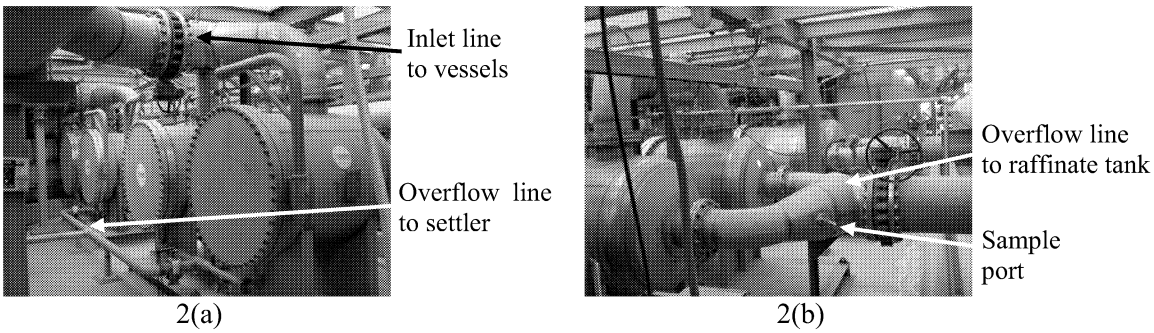

Figure 2. Inlet and outlet views of KREBS CycloClean units.

EXPERIMENTAL

A test hydrocyclone unit was run prior to purchasing to gauge its effectiveness at recovering organic phase from the raffinate stream. Data collection on the full-scale units began at the beginning of November and continued almost daily until the beginning of February. Samples were collected on a nearly daily basis from each of the vessel underflow streams as well as the inlet stream and the overflow stream returning to the settler (see Figure 2). Analytical sampling was performed by collecting samples at six different sample ports and centrifuging 50 mL samples in 0.5% glass graduated bottles for 10 minutes. The organic content was then read off of the bottles and recorded. Since the commissioning period, samples were taken on a biweekly basis with the same procedure to track and ensure unit efficiency.

RESULTS

Calculations based on the test units prior to purchasing gave 70% organic recovery across the hydrocyclones. Analysis of the recovery stream for a two-month period after completion of the full-scale hydrocyclone unit installation gave an average recovery in the overflow stream of 21%. The data in Figure 3 shows not only that the hydrocyclones are recovering product, but that as organic-in-aqueous entrainment increases in the raffinate stream, organic recovery increases in the return stream to the E1HP. Figure 4 is a mass balance based on average performance of the hydrocyclones during the three-month data-collection period.

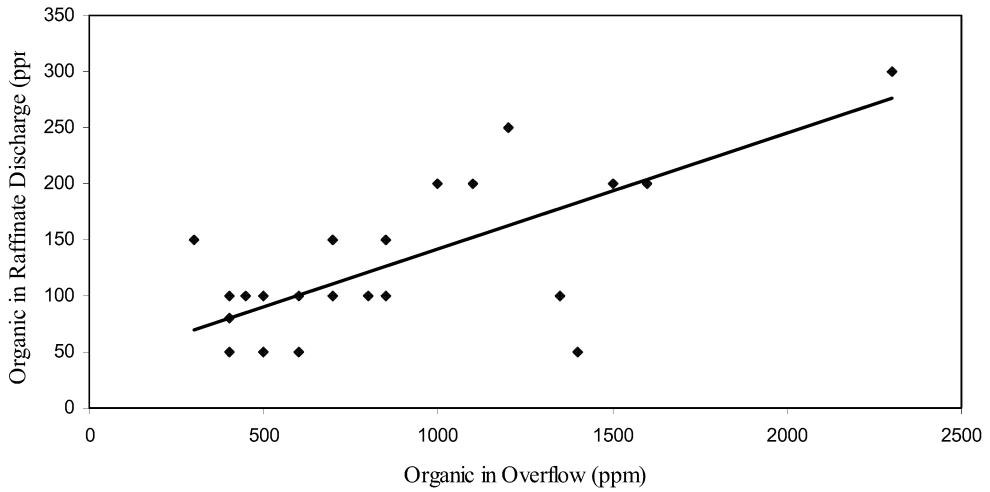

Figure 3. Results for full-scale hydrocyclone operation.

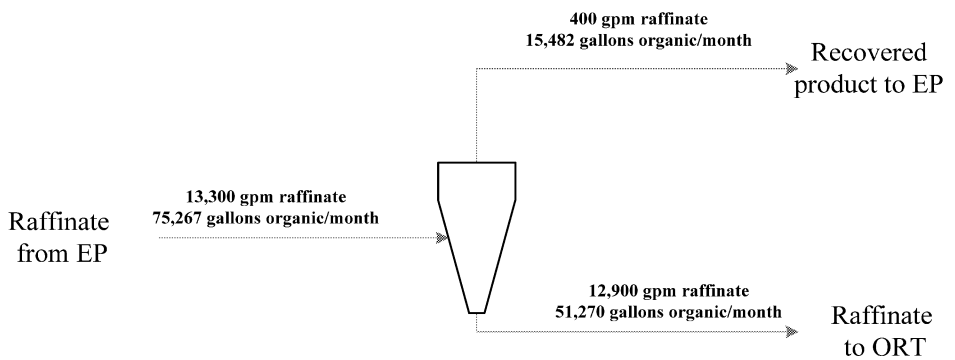

Figure 4. Current mass balance across hydrocyclones.

DISCUSSION

Throughout the installation and commissioning process, several recommendations for future installations developed. The location of the hydrocyclone unit is difficult to access. In order to replace parts such as pumps or motors, the grating must be moved and fall protection put in place prior to work being done on the unit. It is recommended that in future installations, the unit be installed above ground and ideally closer to the organic-recovery tank. At Stargo SX, for example, if a second unit was installed in the tank farm near the organic-recovery tank, the unit would not only be more readily accessible for repairs, but the piping and pumping would be minimal compared to the current configuration.

Another factor to consider in future installations is the type and number of flowmeters around the unit. Slide-in Magmeters are not suitable for the overflow line due to the higher organic concentration in the line. Instead, an Endress-Hauser (E&H) slide-

in flowmeter was installed in the overflow line, because it is better designed to handle organic content in solutions. Also, the number of flowmeters could be reduced to simplify the inlet line to the hydrocyclones and the overflow line back to the settler. This will provide enough information to ensure that the unit is working within design specifications.

CONCLUSION

Installation of hydrocyclones at Stargo SX reduced organic-in-aqueous losses by 21% in the raffinate stream, thus reducing monthly organic expenses. The percent recovery remained constant as organic entrainment in the feed fluctuated. The project coincided with other organic-loss-reduction projects presently operating at Freeport-McMoRan Copper and Gold Morenci Operations that were in place both upstream and downstream from the hydrocyclones. Together, all organic-loss-reduction projects contributed to the overall reduction of organic cost and losses at Stargo SX. Future installations will be considered at other Freeport-McMoRan locations where economic indicators such as high volume-percent extractant or high organic losses are present.

REFERENCES

1. R. Blosser and W. Sircy, “Morenci Hydrometallurgical Process Improvement: Application of Six Sigma in Process Improvement,” Hydrometallurgy Symposium of Copper 2007, Toronto, Canada, 2007; pp. 3-19.
2. “Installation, Operation and Maintenance Manual for KREBS Cycloclean® Hydrocyclone Vessels,” KREBS Engineers, Tucson, Arizona, 2005.

OPERATION OF A FLOTTWEG TRICANTER® CENTRIFUGE FOR CRUD TREATMENT AT BWANA MKUBWA SOLVENT-EXTRACTION PLANT

Anthony Mukutuma,[1] Nils Schwarz,[2] and Angus Feather [3]

[1]Bwana Mkubwa Mining Ltd., Ndola, Zambia. [2]Schwarz Global Consulting, 1230 Muurbal Ave, Weltevreden Park, Gauteng, R.S.A. [3]Cognis Corporation. Corner Bosworth & Potgieter Streets Alrode, Johannesburg
Corresponding author email address: nils@sgconsulting.co.za

ABSTRACT

Bwana Mkubwa is a 50,000 tons per annum copper cathode producer, owned by First Quantum Minerals and located in Ndola, on the Zambian Copperbelt. The Bwana Mkubwa solvent-extraction circuit was started up in 1997. In 2002, the plant began treating ore from First Quantum's Lonshi mine located in the Democratic Republic of Congo. Lonshi ore is exceptionally fine, and the amount of solids in the feed solution reporting to the solvent-extraction circuit increased dramatically. Initially, crud was filtered in a filter press, but this rapidly blinded and seldom produced anything better than a wet sludge containing large quantities of solvent. In December 2003, the decision was made to install a Flottweg Z4E-3/441 Tricanter® centrifuge to recover solvent from the crud. The installation was completed in June 2004 and has since led to significant improvements in plant operability and savings in solvent consumption. A case study of a three-year operational period of the Tricanter is presented.

INTRODUCTION

Bwana Mkubwa Mine Site (BMMS) is an agitation leach plant that treats ore from the Lonshi mine in the Democratic Republic of Congo (DRC). The ore is trucked to the plant site outside Ndola, where it is crushed, milled, and leached to solubilize the copper. Liquid/solid separation takes place in a countercurrent decantation (CCD) system. Pregnant leach solution (PLS) is clarified using two Bateman pinned-bed clarifiers, after which it is pumped to solvent extraction (SX), where copper is recovered using LIX® 984N in a hydrocarbon diluent. Figure 1 shows a schematic diagram of the flow arrangement at Bwana Mkubwa.

Lonshi ore, with a d_{50} of around 23 μm, contains large amounts of fine solids making solid/liquid separation difficult. Even with the pinned-bed clarifiers, the exiting PLS contains some fine solids. The solids enhance crud formation in the SX settlers and reduce phase separation capacity.

As production levels increased, crud treatment became an important process in BMMS SX operations. Continuous removal of crud and its treatment was required to

ensure undisturbed SX operations. The former mitigates incidences of crud movement; the latter ensures quick return of solvent to the circuit and minimizes organic losses associated with crud disposal following treatment.

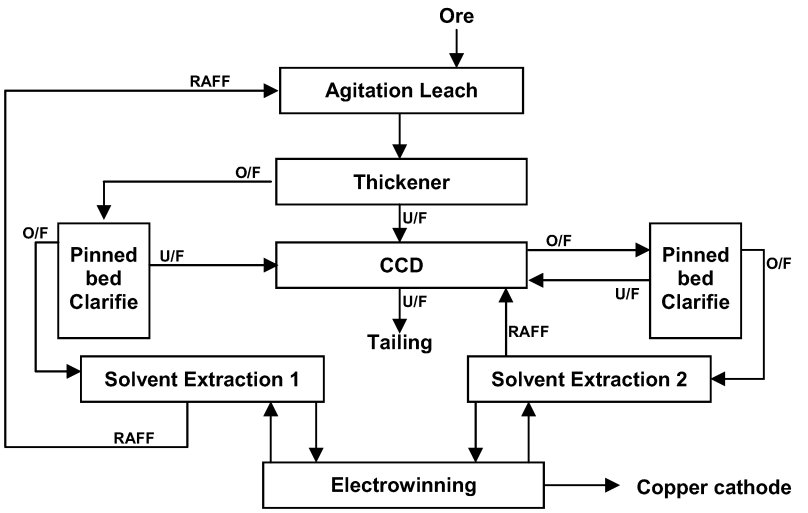

Figure 1. Bwana Mkubwa process flowsheet.

Crud treatment using a filter press at BMMS has significant disadvantages, detailed below.

- **Slow Treatment Rate:** Poor filterability of crud resulted in extremely slow filtration rates compounded by high cycle rates presenting a bottleneck to crud removal and resulted in frequent crud movements. Periodic emptying of settlers to clean out crud reduced SX plant utilization.
- **High Treatment Costs:** Filter cloth cost US$ 12,000 per month. Washing of the filter and cake disposal required between required 20 to 30 man hours per day. Precoating with filter aid was necessary to get any form of performance out of the filter press, which added to the labor requirement, operating costs, and waste-disposal problems.
- **High Organic Losses:** Table 1 shows an analysis of solvent losses in the filter press 'cake'. The loss of organic was calculated on the basis of a filter press solids catchment tray volume of 1.8 m^3, 24% LIX 984N, and disposal rate of 1.5 trays per day.

Table 1. Analysis and cost evaluation of solvent lost in crud disposal

Composition	Organic	Crud	Aqueous
Proportion vol.%	27.3	57.6	15.6
Proportion t/tray	0.4	1.4	0.3
US$/tray	1,100	-	-
US$/day	1,650	-	-

INSTALLATION OF A FLOTTWEG TRICANTER CENTRIFUGE

Based on the successful use of the Flottweg Tricanter® for crud treatment at various copper SX plants in Chile, as well as at KCM in Chingola, Zambia, it was proposed that this technique be used at BMMS. The unit was installed in June 2004.

Mode of Operation

The Tricanter is a horizontal, solid bowl, decanter centrifuge. The feed is separated into a light liquid phase (organic), a heavy liquid phase (aqueous), and a solid phase (crud). The discharge of the separated organic phase is done by gravity, while the separated aqueous phase is discharged by an impeller under pressure.

The separated solids are conveyed by the scroll to the conical end of the bowl and are discharged. A variable-speed drive permits changes in the rate at which the crud is removed, maximizing the removal of organic solution from the crud.

A movable weir ensures accurate control over the phase separation, allowing operators to adjust for process fluctuations while the machine is in operation. This is a critical aspect in the use of centrifuges for crud treatment, as the composition of crud is highly variable.

Typically the crud discharged from the Tricanter is a slightly damp granular solid, with in excess of 95% of the organic phase having been recovered. A feedback control loop ensures that the machine is never overloaded with solids. The torque on the scroll is monitored, and when it rises above a set point, the control loop speeds up the scroll to discharge the solids faster, and at the same time slows down the feed pump to reduce the solids load. This allows the machine to absorb significant variances in feed consistency. The organic recovered proved to be free of residual solids.

The Presence of a Fourth Phase in the Crud

At the time of commissioning it became evident that the aqueous discharge contained significant amounts of solids, giving it the appearance of mud. It was then noted that the Tricanter experienced intermittent blockages in the heavy-phase discharge port and occasional breakthrough of solids to the organic phase. During investigation of the problem by Flottweg's service agent, Centrifuge Technology Services, it became evident that the crud did not consist of three phases but that, even after centrifugation, a fourth phase existed between the aqueous and organic phases. The phase is made up of ultra-fine solid particles, and is very stable. Minor adjustments to the operation of the centrifuge resolved the problem of discharge port blockages.

The fourth phase does, however, present a peculiar problem, as three-phase separating centrifuges are simply not designed to separate four phases. It is essential that the fourth phase be discharged, as it would otherwise lead to rapid blocking of the entire machine. It is also not desirable to have this phase discharged with the organic phase, as the significant amounts of ultra fine-solids would cause further crud problems in the SX system.

The only option remaining is for the solids to be discharged with the aqueous phase. To achieve this, it is not only essential that the centrifuge be equipped with an adjustable weir to give precise control over the pond depth of the aqueous and organic phases within the machine, but this weir also has to be in contact with both the aqueous phase and the fourth phase.

The significance of the fourth phase to crud treatment cannot be overemphasized. Flottweg has tested numerous crud samples from all around the world and has found that virtually all of these contain a fourth phase. While little is known about the composition of the fourth phase, other than that it has been associated with clay-containing ores, the fourth phase becomes more prevalent with increased flocculant additions in the CCD circuit. When planning a crud treatment system utilizing centrifuges—in particular where no pilot studies have been carried out on the crud—engineers will have to design for crud with four phases. They will need to be certain to choose not just a three-phase separating centrifuge, but one designed to deal with a fourth phase.

ECONOMIC ANALYSIS OF CENTRIFUGE INSTALLATION

Organic-Phase Consumption—Before and After the Tricanter Centrifuge Installation

Before the treatment of the Lonshi ore began, extractant consumption was typically less than 2 kg/t of copper at Bwana Mkubwa. With the start of Lonshi ore treatment, extract consumption was variable, but increased to above 3.5 kg/t before the centrifuge installation in June 2004, and it now averages below 3.0 kg/t (Figure 2). This has resulted in savings of over US$ 50,000 per month.

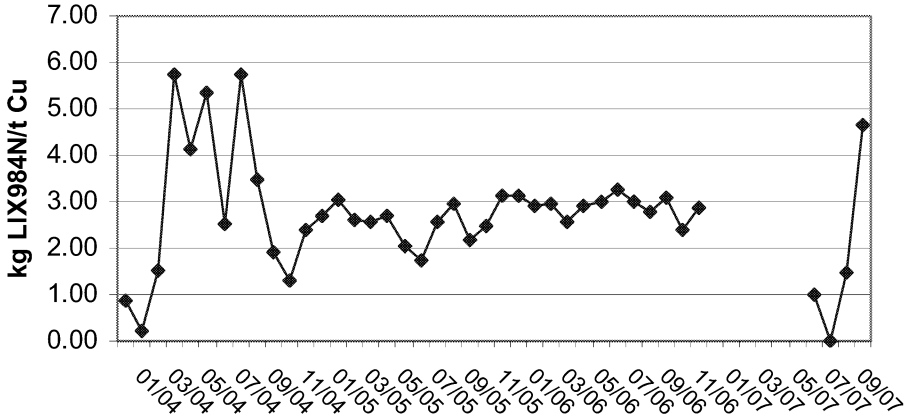

Figure 2. Extractant consumption at BMMS 2004 – 2006.

At the same time that extractant consumption was reduced, changes were made to the configuration of the SX circuit. The low-grade SX wash stage was converted to a parallel extraction stage. From time to time, the high-grade wash stage also used a parallel stage for the recovery of copper from dam return solution. These changes would

usually be expected to double the extractant consumption, but consumption was significantly reduced by use of the centrifuge.

SX Plant Downtime—Before and After the Tricanter Centrifuge Installation

Before installation of the centrifuge, settlers were emptied every eight months on a rotational basis for cleaning, because there was a build-up of crud that the press filter could not cope with. Since the installation of the centrifuge, removal of crud is done online, and this has resulted in increased SX plant utilization (Figure 3).

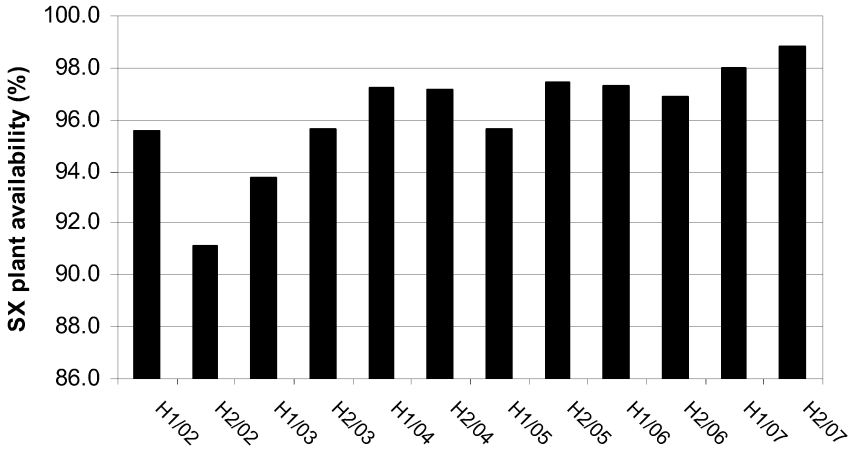

Figure 3. BMMS SX plant availability.

The bulk of ore mined at Lonshi produces fine material, which causes such severe crud generation that it was generally not possible to operate the SX plant when the PLS was derived from this material alone. A proportion of the more rocky ore would have to be fed to the leach circuit at the same time. Failure to do this would at times result in severe crud runs, one of which brought the SX plant operation to a standstill for six days. As the rocky material was not always available, the logistics of feeding the leach section were quite complicated. Since the installation of the Tricanter, no crud runs have occurred, and it has been feasible to operate the plant on a feed of only Lonshi ore for periods in excess of nine months. This has significantly simplified the control of feed to the leach section

Maintenance Costs on the Tricanter

To ensure extended life and optimum performance of the machine, about US$ 20,000 has been spent per annum on annual planned maintenance. It also includes regular site visits from Centrifuge Technology Services, the appointed service agent for Flottweg centrifuges. The training and technical support from CTS has been key to the success of this machine. The cost of maintenance has proved insignificant on the basis of US$/kg of copper produced.

Labor Requirement—Before and After the Tricanter Centrifuge Installation

Unlike a filter-based crud treatment system which required 20 to 30 man hours per day, the centrifuge only required 1 to 2 man hours per day. The centrifuge is set up according to the nature of the feed, and then occasional checks are made to make sure that no major change in the feed consistency has occurred. After treating a batch of crud, the machine is flushed with water.

Clay Treatment

At the time the centrifuge installation was planned, it was not considered for use in clay treatment of recovered organic phase. Subsequent test work to use the centrifuge to remove clay from the organic phase after clay treatment proved successful. The weir is simply adjusted to ensure that all of the liquid is discharged from the light phase port. In this manner two-phase separation is made possible. Flow rates during clay treatment are about 25% higher than during crud treatment

CONCLUSIONS

a) Use of a Flottweg Tricanter centrifuge at Bwana Mkubwa has significantly reduced organic losses by approximately US$ 50,000 per month.
b) More efficient operation of SX plants has been achieved due to ability to continuously remove crud.
c) Crud treatment is now fast and allows quick return of organic to the SX circuit.
d) Instances of crud movement have been eliminated.
e) These improvements to the SX operation have had significant financial and process advantages.
f) The presence of a fourth phase in SX crud needs to be considered when selecting a centrifuge for crud treatment applications.

ACKNOWLEDGMENTS

The authors thank FQM and Bwana Mkubwa for allowing the operational data to be used in this paper, and Bravo Mbao of Bwana Mkubwa and Gift Chisakuta for compiling the data.

REFERENCES

1. A. Mukutuma, B. Mbao, N. Schwarz, G. Chisakuta, and A. Feather, “A case study on the operation of a Flottweg Tricanter® centrifuge for solvent-extraction crud treatment at Bwana Mkubwa, Ndola, Zambia,” Fourth Southern African Conference on Base Metals, South African Institute of Mining & Metallurgy, Johannesburg, 2007; pp. 393–404.

CRUD TREATMENT AND CLAY TREATMENT WITH ONE MULTIPURPOSE SOLID BOWL CENTRIFUGE

Tore Hartmann

Westfalia Separator Industry GmbH, Werner Habig Strasse 1, D-59302 Oelde, Germany
Corresponding author email address: hartmann.tore@gea-westfalia.de

ABSTRACT

The presence of crud represents a permanent challenge for solvent extraction in the hydrometallurgical industry. The crud is a stable emulsion that slowly spreads along the phase boundary between the aqueous and the organic phases. The crud can significantly impair the efficiency of metal extraction, because the phase boundary between the aqueous and the organic phases assumes substantial proportions, and the settlers cannot react flexibly. In a chain reaction, all settlers connected in series become infected with crud. The transfer of organic phase to the electrowining (EW) cell can cause "cathode burn." Continuous treatment of the crud is extremely effective and reliable with a three-phase separating solid bowl centrifuge. All three phases, the organic phase, the aqueous phase, and the solid phase, are separated distinctly from one another. All associated process steps exhibit a steady uniform efficiency. First and foremost, they ensure a reliable, continuous extraction process and, secondly, they recover valuable re-usable organics from the crud. It has become standard practice in industry to clay-treat solvent that has extended phase break times, has been contaminated by surfactant, or has been recovered from the raffinate pond. The clay serves to remove contaminants and restores the phase-disengagement times back to similar levels shown by fresh solvent.

INTRODUCTION

The method involving solvent extraction of metals has become established throughout the world. During this process, large quantities of crud form, which consists of an emulsion of a fluid organic, an aqueous phase, and insoluble solids like mica or clay. On account of its relatively strong bonding forces, this stable emulsion can substantially reduce the separation properties between the different phases. While a thin layer of crud at the aqueous/organic interface can aid coalescence of fine droplets, excess crud can interfere with phase separation and severely reduce the efficiency of the settlers.

The use of a three-phase solid bowl centrifuge from Westfalia Separator is ideal here to continuously separate the phases. Firstly, the stable crud emulsion is broken up, and secondly, the phase separation rate is increased. The organic phase is to be cleaned by way of clay treatment. In addition, the organic phase and the extraction agents used are recovered and can be recycled back into the extraction process.

THE THREE-PHASE AND TWO-PHASE SOLID-BOWL CENTRIFUGE

A three-phase solid-bowl centrifuge is shown in Figure 1. Feed crud, after having been accelerated in the rotating feed compartment or accelerator, is introduced to the annular pool. Under high centrifugal force, only the heavier insoluble solids migrate radially outward, towards the bowl wall, to form a cake whilst displacing the lighter liquid towards the center. Solids are accumulated against the bowl wall under centrifugal force and conveyed for discharge to the small diameter of the conical beach by the screw conveyor, rotating at differential speed relative to the bowl. As the cake is lifted above the annular pool in the dry beach, liquid continues to drain back to the pool, leaving a drier cake for discharge. The gear unit and backdrive control the differential speed between the bowl and conveyor, changing the solids-retention time as needed. The clarified liquids, the organic phase, and the aqueous phase flow over different weirs located at the opposite end of the machine. A significant density difference between the liquids ensures a continuous flow via different weir diameters. The pool depth is controlled by the discharge diameter of the liquid weirs. The performance of the centrifuge depends on the various operating variables, such as feed rate, pool depth, G-force, and differential speed, and should be optimized for a given process.

Feed Rate

The retention time of the suspension in the bowl can directly affect the obtainable centrate clarity. Decreasing the feed rate will increase the liquid-retention time and permit more efficient settling of suspended solids.

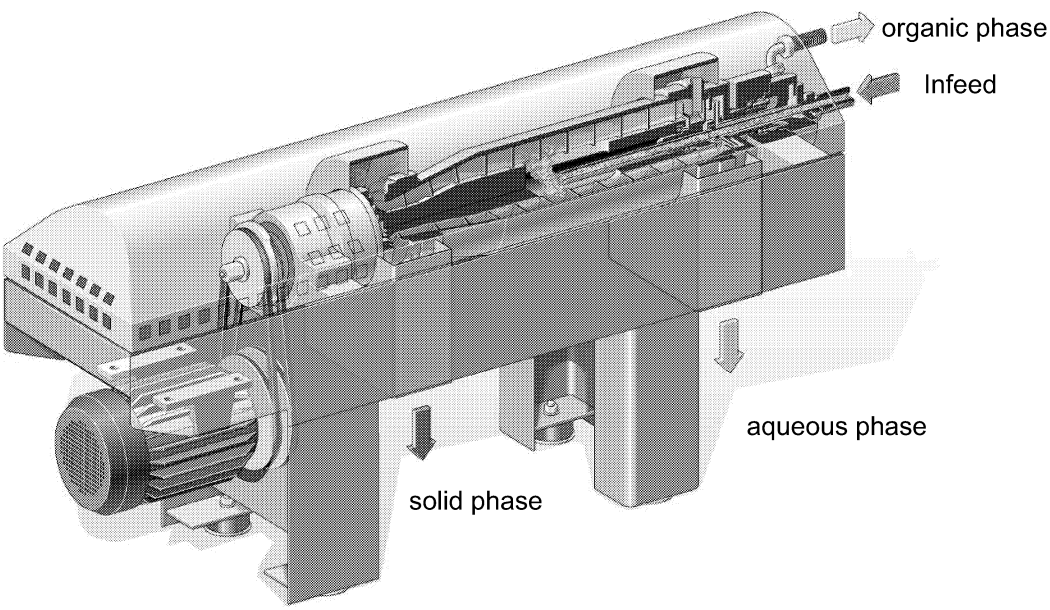

Figure 1. Schematic of a 3-phase centrifuge with solid-wall bowl

G-Force

Higher rotation speeds produce higher centrifugal forces acting on the solids in the cake and an improved settling rate. The consequence is lower cake moisture and/or a clear centrate. However, this does not necessarily occur in every case. Some solids, especially the finer-size fraction, have densities very close to that of the suspension (i.e., somewhat neutrally buoyant) due to adhesion of contaminants or bubbles to the solid surfaces. They do not settle regardless of the magnitude of the centrifugal force. Also, different solids tend to pack tightly (i.e., compactable cake) under high centrifugal force, and some drain more readily under lower speeds, where larger voids exist with higher cake permeability. For compactable cake, a G-value increasing beyond a certain point does not absolutely ensure an increase in cake dryness, due to increasing cake resistance to solidification. In general, for maximum clarity, cake dryness, and minimum power consumption, the equipment must operate at the "lowest possible" speed compatible with the material characteristics and performance requirements. It is always good practice to compare cake dryness and centrate clarity at different rotational speeds and Gs during the initial start-up period. This allows the determination of the optimum centrifugal forces for the specific application.

Differential Speed

By lowering the speed differential between the conveyor and the bowl, the solids-retention time is increased. In most cases, this causes an increase in cake depth against the bowl wall with greater compacting stress and higher cake dryness. This cake depth is often accompanied by an increasing conveyance torque. Lower conveyor speed differential provides less turbulence and less resuspension of solids. However, low conveyor speed differential may have the opposite effect if the solids load in the incoming feed is higher than the ability of the conveyor to remove them; in such cases, solids that could not be conveyed build up in the cylinder and finally flow over at the liquid discharge ports. In the course of time, the latter often occurs along with an increasing conveyance torque. There must be a balance between solids input and solids removal in order to prevent plugging of the machine and loss of centrate clarity.

THREE-PHASE SOLID-BOWL CENTRIFUGE FOR CRUD TREATMENT

The solid-wall bowl has both a cylindrical part for efficient separation and clarification of two liquids with different densities and a flat-angle or steep-angle conical part for solids dehydration. The feed product is sent into the solid-bowl centrifuge via the feed tube and led into the separation chamber past the distributor. The scroll conveys the solids towards the solids discharge port.

The level of the liquid pond can be adjusted by inserting regulating rings or plates having the appropriate inner diameter. In the separating zone, the two liquid phases are separated from each other; whereas the light phase is displaced towards the bowl axis, the heavy phase is sent towards the bowl wall. This is illustrated in detail in Figure 2.

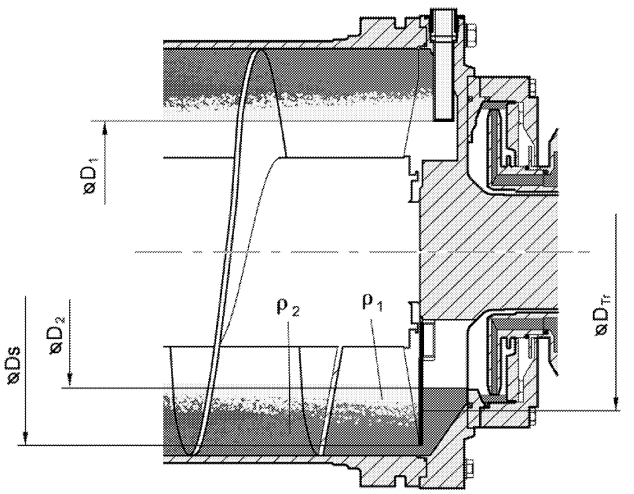

Figure 2. Three-phase solid bowl centrifuge defining the separating zone on the liquid side.

The light-liquid component leaves the separating chamber via an exchangeable regulating ring and is pressure discharged by means of paring disk. Simultaneously, the heavy-liquid component is gravity discharged via exchangeable regulating tubes.

TWO-PHASE SOLID-BOWL CENTRIFUGE FOR CLAY TREATMENT

For the two-phase solid-bowl centrifuge, the operating principle is similar to that of the three-phase solid-bowl centrifuge, however processing one less liquid phase. Hence, the entire processing space of the centrifuge is available for separating one liquid from an insoluble solid matter. The difference in densities between liquid and solids, as well as the dynamic viscosity and the solid-particle size, determine the degree of clarification.

PROCESS DESCRIPTION

In practice, for crud treatment, the product is separated into its components in the centrifugal field under high G-forces. Figure 3 shows the results of laboratory test runs performed as an example.

The valuable organic phase undergoes subsequent processing. In the so-called clay-treatment phase, the clay binds contaminants contained in the organic phase so that the chemical load on the organic phase is reconverted into its original state. Consequently, the recycled clean organic phase can be re-used in the solvent-extraction process. The organic consumption will vary from operation to operation. The use of a centrifuge can reduce organic consumption by as much as 30%.

The installation now established allows crud treatment and clay treatment to be performed with one machine, as illustrated in Figure 4. Typically, the crud discharged in this manner is a slightly damp granular solid, with more than 95% of the organic phase having been recovered. After centrifugation, the valuable organic phase contains only traces of insoluble solids and 0.1% v/v aqueous phase.

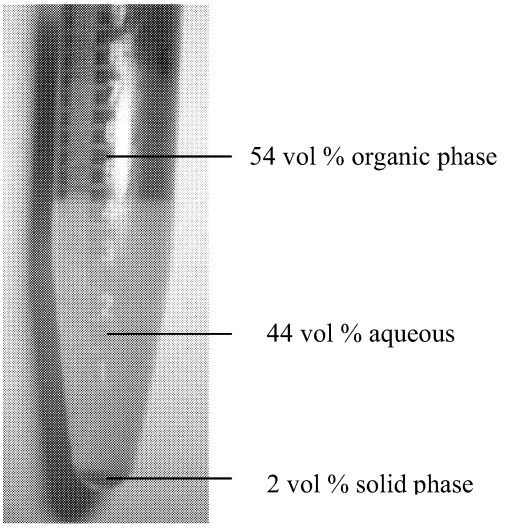

Figure 3. Centrifugal spin test to determine crud composition

For clay treatment, the aqueous-phase discharge line behind the centrifuge is closed completely, thus ensuring that this machine can be continuously used as a two-phase centrifuge for clay treatment. The filling capacity of the centrifuge can be used more efficiently in the two-phase clay-treatment mode, which allows 25% higher throughput rates compared with crud treatment.

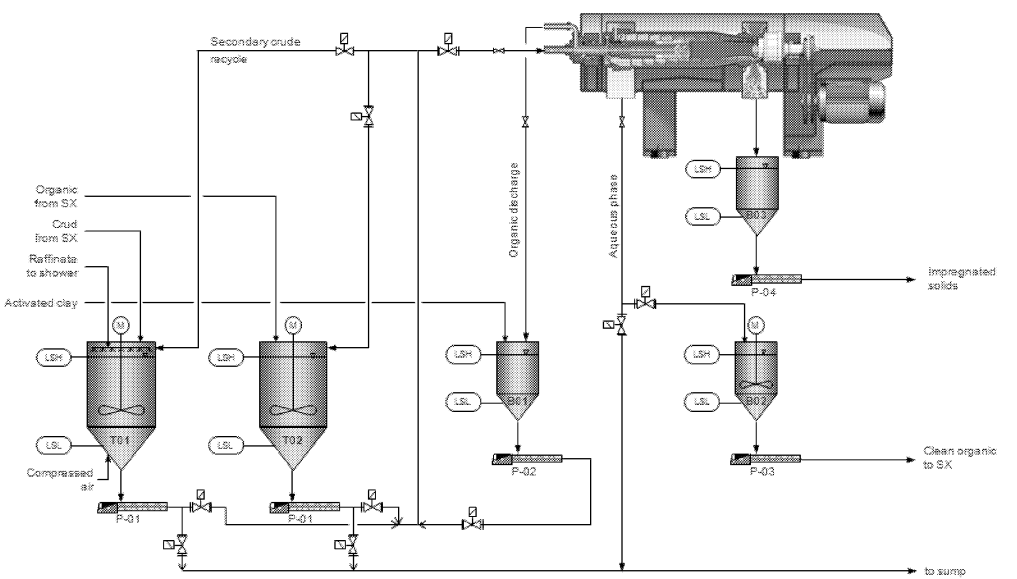

Figure 4. Double-purpose installation for crud treatment and clay treatment.

CONCLUSION

The intelligent combination of crud treatment and clay treatment with one centrifuge allows the organic phase to be definitely recycled in thesolvent extraction of metals. Flexible adaptation of the centrifuge to current operating conditions ensures maximum availability of the process equipment, together with full automation of the plant stage. In addition, because the equipment is enclosed, organic vapors are prevented from escaping into the atmosphere.

Nuclear Fuel Reprocessing

KEY FEATURES OF THE TALSPEAK AND SIMILAR TRIVALENT ACTINIDE-LANTHANIDE PARTITIONING PROCESSES

Kenneth L. Nash

Washington State University, Chemistry Department, P.O. Box 644630, Pullman, WA 99164-4630. Corresponding author email address: knash@wsu.edu

ABSTRACT

As closing of the nuclear-fuel cycle via the suite of UREX processes under development in the U.S. progresses, the Trivalent Actinide-Lanthanide Separation by Phosphorus Extractants and Aqueous Komplexants (TALSPEAK) process has been selected as the baseline process for partition of trivalent actinides away from fission-product lanthanides. In this report, selected features of the chemistry of the TALSPEAK process and the limited parallel information on other TALSPEAK-like processes are discussed.

INTRODUCTION

Among the methods currently considered to be ready for technological deployment for separation of transplutonium actinides from fission-product lanthanides is the TALSPEAK (Trivalent Actinide - Lanthanide Separation by Phosphorus reagent Extraction from Aqueous Komplexes) Process. TALSPEAK was developed in the late 1960s at Oak Ridge National Laboratory in the U.S. to support the production of the tran-americium elements for research purposes. [1] Group separation by this method relies on the differences in the partitioning of lanthanides and actinides between an acidic organophosphorus extractant ($(RO)_2PO_2H$) solution and an aqueous phase containing a high concentration of a carboxylic acid buffer and a polyaminopolycarboxylate complexant. Both the organophosphorus extractant (usually bis(2-ethylhexyl)phosphoric acid, HDEHP) and the polyaminopolycarboxylic acid (typically diethylene-triamine-N,N,N',N",N"-pentaacetic acid, DTPA) are powerful complexants, whose effects must be balanced one against the other to achieve the group separation. The balance, pH control, and other positive features are achieved by modifying the aqueous medium using high concentrations (1 M or greater) of lactic acid. Trans-lanthanide extraction trends indicate declining extraction from La to Nd but increased extraction strength for the heavier lanthanides. The most important separations for spent-fuel applications are for the light lanthandes (La-Gd) from Am and Cm [2]. The lowest separation factor for lanthanides from actinides occurs near Nd and averages around 100 in most reports.

Several combinations of different extractants and aqueous complexants have been investigated, as have the effect of diluent, temperature, and $p[H^+]$, on separation

efficiency, as summarized in a recent review [3]. At the process scale, the basic operational philosophy of TALSPEAK has been employed in the development of the CTH process [4-9], the DIDPA process [10-12], and adapted to another separation platform in the SETFICS process [13-16]. In this report, selected aspects of the chemistry of TALSPEAK are discussed.

Baseline Chemical Equilibria of TALSPEAK

In the previous review [3], the basic thermodynamic features of TALSPEAK were discussed in some detail. The extraction reaction for all metal ions under the pH conditions of this system can be described as an ion-exchange reaction:

$$M^{3+} + 3\ (HA)_{2,o} \rightleftharpoons M(AHA)_{3,o} + 3\ H^{+}, \quad K_{ex} = [M(AHA)_{3,o}][H^{+}]^3/[M^{3+}][(HA)_{2,o}]^3 \qquad (1)$$

The aqueous-phase complexation of metal ions by protonated forms of DTPA (L) under TALSPEAK conditions can be described using:

$$M^{3+} + H_nL^{n-5} \rightleftharpoons M(L)^{2-} + n\ H^{+}, \quad K_D = \beta_1/\Pi(K_h) = [M(L)^{2-}][H^{+}]^n/[M^{3+}][H_nL^{n-5}] \qquad (2)$$

where K_D is the ratio of the equilibrium constant and the appropriate product of protonation equilibria for DTPA. Finally, lactate is known to form 1:1, 1:2, and 1:3 complexes with lanthanides and actinides:

$$M^{3+} + n'\ X^{-} \rightleftharpoons M(X)_n^{3-n'}, \quad \beta_L = [M(X)_{n'}]/[M^{3+}][X^{-}]^{n'} \qquad (3)$$

where the free lactate is represented by X^-. A correction is necessary for the protonation equilibrium of lactate. Appropriate equilibrium constants are available in the literature at several ionic strengths. The database is inadequate to allow correction for the changes in activity coefficients that would be needed to model the system from concentrated lactate solutions. The effect of lactate on water activity cannot be predicted from first principles. Prior calculations reveal a general agreement with observations in the biphasic system, but there is little doubt that more complex processes occur in the biphasic system than simplified model predictions can incorporate, as will be discussed in the following.

The Effect of pH

The lactate-based TALSPEAK process is designed to operate near the pK_a of lactic acid (3.6, I = 1 M, T = 25 °C); therefore, under most conditions the species HX and X^- represent 50% (each) of the free lactate species. The predominant species of DTPA is H_3L^{2-}. It is assumed that the HDEHP remains the dimer of the free acid $(HA)_2$. As pH rises, the phase-transfer equilibrium shifts toward greater extraction, but is compensated by increased ionization of the aqueous ligands and thus an increase in complex strength in the aqueous medium. The simplest model based on the above-described equilibria predicts no change in distribution ratios for most of the lanthanides between pH 3 and 4, based on the competition between HDEHP and DTPA for the metal ion:

$$M(AHA)_{3,o} + H_3L^{2-} \rightleftharpoons ML^{2-} + 3(HA)_{2,o} \qquad (4)$$

Thus, distribution is pH-independent. Various authors have reported that the distribution ratios of lanthanides decline with pH dependencies between –0.5 and –2 as pH increases [3]. This result suggests the presence of mixed ligand complexes (An/Ln-DTPA-lactate).

The Effect of DTPA Concentration

The limited solubility of DTPA in acidic solutions reduces the range of concentrations that can be considered. Studies that have been done indicate that increasing concentration of DTPA at constant pH produces a predictable decline in distribution ratios with an approximate 1:1 stoichiometry. Several authors have reported similar observations on related systems in the range of pH 3.0 to pH 3.3 and for several different organic solvent compositions. This result would appear to confirm the action of DTPA as a simple holdback reagent forming 1:1 complexes with the metal ions in the system. These results allow no conclusions regarding the role of mixed lanthanide-lactate-DTPA complexes, as all observations were made at constant lactate concentration.

The Effect of Lactate Concentration

Besides its obvious value as a buffer, lactate at concentrations above 1 M in typical TALSPEAK conditions likely substantially alters (probably lowers) the activity coefficient of water, hence modifying the equilibrium position of all aqueous reactions. The hydrophobic backbone of lactic acid will exhibit some tendency to partition into the organic phase, a phenomenon that might be expected to increase at higher concentrations due to the natural tendency of carboxylic acids to dimerize in non-polar media. The high concentrations of lactate present in the aqueous phase, its position as the smallest of the three complexants in the system and the ease with which trivalent lanthanide/actinide ions expand their coordination spheres combine to make postulation of mixed complexes of the type $M(L)X_n^{3-5-n}$ or $MX_n(AHA)_{3-n,\,o}$ reasonable.

There are in fact reports attributing additional roles to lactate in TALSPEAK-type extraction systems. Svantesson et al. [4] report that lactic acid appears to increase the solubility of DTPA in the aqueous phase. Kolarik [17] indicates that lactic acid impacts the kinetics of the complexation reaction between DTPA and metal ions in the aqueous phase, possibly forming an intermediate mixed complex. It also appears to increase phase-transfer kinetics and phase-disengagement rate [4]. There are indications that lactic acid may participate in the metal-ion phase-transfer reaction. [18-20]. Molecular-level explanations for most of these effects have not been established. Interpretations must be offered with caution, as typical equilibrium calculations involve assumptions regarding constancy of activity coefficients that might not apply in these complex systems.

Kosyakov and Yerin [18,19] systematically investigated the effect of varying the lactate concentration on the distribution ratio of curium. Based on slope analysis, they postulated the existence of a mixed lactate-curium-HDEHP complex in the organic phase. They postulate the existence of a mixed extracted complex, $M(AHA)_2L$. This species should exhibit reduced affinity for the organic phase, hence have lower extractability than the standard $M(AHA)_3$ complex. Their results at high lactate

concentration also indicated the formation of a non-extractable Cm-lactate complex. It has been reported that lactate partitioning into the organic phase only occurs in the presence of extractable lanthanide cations [1]; that is, HL is not extracted significantly by association with HDEHP or its inherent solubility in organic diluents.

The Effect of Temperature

Kinetically, the effect of temperature is predictable; rates of reactions increase as temperature rises. Thermodynamically, the effect of changing the temperature on the final equilibrium position of the reaction is less predictable. For a system as complex as TALSPEAK, the thermodynamic features of several reactions occurring in the aqueous phase and in the biphasic system contribute to the net effect. Fidelis has reported that the distribution ratios of Ln3+ into HDEHP from mineral acid solutions decrease with increasing temperature [21], indicating a net exothermic process. Kosyakov et al. [19] reported that extraction of lanthanides from DTPA and lactic acid into HDEHP is favored at low temperature. Thermodynamic parameters are available for most of the individual reactions contributing to TALSPEAK. The data are not adequate to allow accurate predictions to be made of the effect of temperature on TALSPEAK performance.

Diluent Effects, Different Complexants, and Different Buffers

Two principal advantages of solvent-extraction systems are the almost unlimited potential for making minor adjustments to improve separation efficiency, and the small energy differences that are needed to improve marginal separations. Weaver and Kappelmann [1] noted that in TALSPEAK, aliphatic diluents increased distribution ratios but lowered separation factors of europium from americium. They also investigated the effect of different carboxylic acids on the extraction and separation of americium, lanthanum, cerium, and europium with DTPA present and the $p[H^+]$ corrected to 3.0. All of the carboxylic acids used gave higher distribution ratios for the lanthanides than americium, but lactic acid gave the best overall separation factor between americium and the lanthanides. Del Cul et al. [22] evaluated the feasibility of using citric acid rather than lactic acid in extraction and process application for the TALSPEAK system, noting that a high concentration of carboxylic acid results in a loss of organic phase due to increased solubility of the organic phase in the aqueous phase. Neither citric acid nor glycolic acid partitioned significantly into the organic phase. Finally, Weaver and Kappelmann [1] investigated the extraction and separation of americium from europium and cerium using 0.005 or 0.05 M of nitrilotriacetic acid (NTA), N-hydroxyethylethylenediamine-N,N',N'-triacetic acid (HEDTA), ethylenediamine-N,N,N',N'-tetraacetic acid (EDTA), trans-1,2-diaminocyclohexane-N,N,N',N'-tetraacetic acid (DCTA), and DTPA. They showed that with 1 M lactic acid at $p[H^+]$ 3.0, DTPA was clearly superior to all the other complexants for separating americium from europium or cerium.

Kinetics of Phase-Transfer Reactions

Kolarik and Kuhn [17] reported the results of a thorough investigation of the kinetics of TALSPEAK-relevant systems in stirred reactions, the rates characterized by partitioning of Eu^{3+} from DTPA-lactate phases into HDEHP solutions. They observed that the rate of extraction of Eu(III) into HDEHP + TBP from a DTPA-lactic acid solution slowed as p[H^+] increased, slowed with increased [DTPA], and became faster as the concentration of protonated lactic acid increased. Addition of moderate concentrations of TBP increased the rate but lowered distribution ratios. Low concentrations of mono(2-ethylhexyl)phosphoric acid, H_2MEHP, a degradation product of HDEHP, increase the rate, but the distribution ratios remain nearly constant. The rate of phase transfer was not impacted in a predictable manner by changing the diluent among *n*-dodecane, benzene, and carbon tetrachloride, though the distribution ratios did vary with diluent. The dependence of the rate on [HDEHP] was complex. The authors concluded that mixed complexes (Eu-DTPA-lactate) are important in controlling the rate of the net phase-transfer reaction. There is also a significant contribution from acid-catalyzed processes. When examined in more conventional kinetic terms, these data reveal that the mechanism of phase-transfer reactions is complex, often indicating high-order reagent dependences. It does not appear likely that a single reaction mechanism can describe the kinetics of this system [3].

The Effect of Radiolysis

In the processing of dissolved spent-fuel raffinates, it is inevitable that radiation damage of the reagents and solvents will occur. At best, the effects will have to be addressed with the addition of process cleanup steps; at worst, the application of the process will fail if materials exhibit excessive susceptibility to radiation damage. The effect of irradiation on HDEHP has been studied by a couple of research groups [23,24]. The major degradation product is the monosubstituted phosphoric acid, H_2MEHP. In moderate amounts as an impurity in HDEHP, H_2MEHP has been reported to increase the distribution ratios of trivalent metals, to decrease separation factors between actinides and lanthanides, and to make stripping more problematic. A high concentration of H_2MEHP however, will lead to a decrease in distribution ratios [23,25]. Schultz [23] attributed the decrease in extraction capacity to polymerization by hydrogen bonding between H_2MEHP and HDEHP, rendering the HDEHP useless for extraction. An antagonistic effect results at moderate-to-high H_2MEHP concentrations. Tachimori and Nakamura [25] investigated the effect of gamma radiation on the entire TALSPEAK system. They found that the concentration of DTPA decreased with increasing dose to the aqueous phase, which yielded increasing distribution ratios and decreasing separation factor between americium and neodymium. However, when lactic acid was present in the system, the degradation rate of DTPA was slower.

TALSPEAK Chemistry Demonstrations to Process Scale

Though the TALSPEAK process has not yet been put into practice at the industrial scale, there are at least three examples of significant pilot-scale demonstrations of the essential features of having been completed:

CTH process

Basic TALSPEAK chemistry can be applied to the selective removal of trivalent actinides from a loaded organic phase. Such separations systems are known as Reverse TALSPEAK. A Reverse TALSPEAK separation was most extensively tested and used as a part of a process for treating high-level liquid waste from spent nuclear fuel in the CTH-process (Chalmers Tekniska Högskola) [4-9]. The CTH-process treats HLLW in three stages: U, Pu, and Np are removed from 6 M HNO_3 in the first HDEHP extraction stage; In the second stage, the concentration of HNO_3 is reduced to 0.1 M by contact with TBP to extract the nitric acid, leaving the metal ions in the aqueous phase. Americium, curium, and the lanthanides are co-extracted away from the other fission products in a second HDEHP extraction stage; the loaded organic phase is then contacted with an aqueous phase containing DTPA and lactic acid to selectively strip the actinides. The actinides are then extracted from this aqueous solution with 1 M HDEHP using a high organic-to-aqueous phase-volume ratio. The stripping solution can therefore be recycled, reducing the amount of secondary waste. It was found that one of the crucial aspects of controlling TALSPEAK separations was the control of $p[H^+]$.

DIDPA process

One of the smallest steps from TALSPEAK that resulted in a discrete process is the "DIDPA process" [10-12]. Tachimori et al. [10] investigated the possibility of replacing HDEHP with di-isodecyl phosphoric acid, DIDPA, shown to extract americium and neodymium at a higher acidity than HDEHP. However, the separation factor between americium and the least extracted lanthanide is lower in the DIDPA system. The proposed process [10], with DIDPA as an alternative to HDEHP, is to first co-extract the An(III) and Ln(III) with DIDPA from nitric acid media to remove the trivalent metals from other fission products. Both groups are stripped with 2 M HNO_3. The strip solution is subsequently denitrated; then DTPA and lactic acid are added. Finally, the lanthanides are separated from the trivalent actinides by extraction with DIDPA at $p[H^+]$ 3.

SETFICS process

The TRUEX process utilizes a neutral bidentate organophosphorus ligand, *n*-octyl(phenyl)-N,N-diisobutylcarbamoylmethylphosphine oxide, CMPO, to co-extract trivalent actinides and lanthanides from other fission products. Since CMPO is a neutral solvating extractant, this extraction must be conducted from a medium of moderate-to-high salt or acid concentration. The SETFICS process (Solvent Extraction for Trivalent f-elements Intra-group separation in CMPO-complexant System) [13], takes advantage of the opportunity to co-extract the two groups of metals and introduces selective stripping of the trivalent actinides using DTPA (analogous to Reverse TALSPEAK) [14,15]. The CMPO (often used in conjunction with TBP), also extracts nitric acid, so the organic

phase must be deacidified before the selective stripping, since DTPA would otherwise precipitate. The SETFICS process can be divided into four steps: co-extraction of An(III) and Ln(III) with CPMO + TBP; acid stripping using diluted sodium nitrate; selective stripping of An(III) using DTPA; and finally stripping of the lanthanides using dilute nitric acid. The SETFICS process is a part of the advanced aqueous reprocessing system NEXT (New EXtraction system for TRU recovery) developed in Japan [16].

CONCLUSIONS

Though it has not yet been deployed at the process scale, the TALSPEAK process must be considered as a proven approach to the partitioning of trivalent actinides from fission-product lanthanides. It has been demonstrated at the pilot scale using actual spent fuel and process simulants. The research that has been done on the system provides a mix of useful insights, but with some lingering mysteries. For most purposes, it would appear that the combination of HDEHP, lactic acid, and DTPA are mutually compatible and well-suited to this particular application. Our earlier examination of the separations data in comparison with available thermodynamic data describing the individual system components [3] suggest that the primary roles of the components (lactate = buffer, DTPA = actinide holdback reagent, HDEHP = lanthanide extractant) do not describe the complete function of each species. The complexity of the overall system should remain a source of concern for process-scale deployment, particularly in view of the gaps in understanding the fundamental chemical processes that allow the process to function. It would seem also to be prudent to invest effort in developing the means to understand the thermodynamic features of the ternary complexes that are almost certain to play a role in TALSPEAK. Such data on mixed ligand complexes are virtually non-existent. This potentially powerful actinide-partitioning technique could have far more impact on spent-fuel partitioning efficiency if additional studies of its basic features were conducted.

REFERENCES

1. B. Weaver and F. A. Kappelmann, "Preferential extraction of lanthanides over trivalent actinides by monoacidic organophosphates from carboxylic acids and from mixtures of carboxylic and aminopolyacetic acids," *J. Inorg. Nucl. Chem.*, **30**, 263-272 (1968).
2. G. R. Choppin and J. Rydberg, "Treatment of spent nuclear fuel," Radiochemistry and Nuclear Chemistry, 1st ed. Pergamon Press Ltd.: Oxford, England, 1980; pp. 502–559.
3. M. Nilsson and K. L. Nash, "A Review of the Development and Operational Characteristics of the TALSPEAK Process," *Solvent Extr. Ion Exch.*, **25**, 665–701 (2007).
4. I. Svantesson, I. Hagström, G. Persson, and J. O. Liljenzin, "Separation of americium and neodymium by selective stripping and subsequent extraction with HDEHP using DTPA-lactic acid solution in a closed loop," *Radiochem. Radioanal. Lett.*, **37**(4-5), 251-222 (1979).
5. G. Persson, S. Wingefors, J. O. Liljenzin, and I. Svantesson, "The CTH-process for HLLW treatment, Part II. Hot test," *Radiochim. Acta*, **35**, 163-172 (1984).
6. I. Svantesson, G. Persson, I. Hagström, and J. O. Liljenzin, "Distribution ratios and empirical equations for the extraction of elements in PUREX high level waste solution – II: HDPHP," *J. Inorg. Nucl. Chem.*, **42**, 1037-1043 (1980).

7. J. O. Liljenzin, G. Persson, I. Svantesson, and S. Wingefors, "Experience from cold tests of the CTH actinide separation process," ACS symposium series 161, Las Vegas, Nevada, 1980; pp. 203-221.
8. J. O. Liljenzin, G. Persson, I. Svantesson, and S. Wingefors, "The CTH-process for HLLW treatment, Part I. General description and process design," *Radiochim. Acta*, **35**, 155-162 (1984).
9. G. Persson, I. Svantesson, S. Wingefors, and J. O. Liljenzin, "The CTH-process for HLLW treatment, Part II. Hot test," *Solvent Extr. Ion Exch.*, **2**(1), 89-113 (1984).
10. S. Tachimori, A. Sato, and H. Nakamura, "Separation of transplutonium and rare-earth elements by extraction with di-isodecyl phosphoric acid from DTPA solution," *J. Nucl. Sci. Technol.*, **16**(6), 434-440 (1979).
11. S. Tachimori and H. Nakamura, "Extraction of some elements by mixture of DIDPA-TBP and its application to actinoid partitioning process," *J. Nucl. Sci. Technol.*, **19**(4), 326-333 (1982).
12. T. Ishimori, "Studies on actinides separation in JAERI," ACS symposium series 117, Honolulu, Hawaii, 1979; pp. 333-350.
13. Y. Koma, M. Watanabe, S. Nemoto, and Y. Tanaka, "Trivalent lanthanide and actinide intra-group separation by solvent extraction with CMPO-complexant system," *J. Nucl. Sci. Technol.*, **35**(2), 130-136 (1998).
14. Y. Koma, M. Watanabe, S. Nemoto, and Y. Tanaka, "A counter current experiment for the separation of trivalent actinides and lanthanides by the SETFICS process," *Solvent Extr. Ion Exch.*, **16**(6), 1357-1367 (1998).
15. M. Ozawa, Y. Koma, K. Nomura, and Y. Tanaka, "Separation of actinides and fission products in high-level liquid wastes by the improved TRUEX process," *J. Alloys Comp.*, **271-273**, 538-543 (1998).
16. T. Takata, Y. Koma, K. Sato, M. Kamiya, A. Shibata, K. Nomura, H. Ogino, T. Koyama, and S. Aose, "Conceptual design study on advanced aqueous reprocessing system for fast reactor fuel cycle," *J. Nucl. Sci. Technol.*, **41**(3), 307-314 (2004).
17. Z. Kolarik and W. Kuhn, "Acidic organophosphorus extractants – XXI. Kinetics and equilibria of extraction of Eu(III) by di(2-ethylhexyl) phosphoric acid from complexing media," Proc. Int. Solvent Extr. Conf., ISEC 74, Lyon; 8-14th September, 1974, 3; pp. 2593-2606.
18. V. N. Kosyakov and E. A. Yerin, "Separation of transplutonium and rare-earth elements by extraction with HDEHP from DTPA solutions," *J. Radioanal. Chem.*, **43**, 37-51 (1978).
19. V. N. Kosyakov and E. A. Yerin, "On the mechanism of trivalent actinide extraction in the system HDEHP – lactic acid with DTPA," *J. Radioanal. Chem.*, **56**, 93-104 (1980).
20. M. I. Mel'nik, V. T. Filimonov, and E. A. Karelin, "Mechanism of extraction of weighable amounts of lanthanides(III) with HDEHP from nitric and acetic acid solutions," *Radiokhimiya*, **41**(1), 67-70 (1999).
21. I. Fidelis, "Influence on the temperature on the extraction of lanthanides in the HDEHP [di(2-ethylhexyl) phosphoric acid]-nitric acid system," Proc. Int. Solvent Extr. Conf. ISEC 71, The Hague, 1971, 2; pp. 1004-1007.
22. G. D. Del Cul, L. M. Toth, W. D. Bond, G. D. Davis, and S. Dai, "Citrate-based "TALSPEAK" actinide-lanthanide separation process," *Sep. Sci. Technol.*, **32**(1-4), 431-446 (1997).
23. W. W. Schulz, "Radiolysis of Hanford B plant HDEHP extractant," *Nucl. Technol.*, **13**(2), 159-167 (1972).

24. S. Tachimori, B. Krooss, and H. Nakamura, "Effect of radiolysis products of di-(2-ethylhexyl)phosphoric acid upon the extraction of lanthanides," *J. Radioanal. Chem.*, **43**, 53-63 (1978).
25. S. Tachimori and H. Nakamura, "Radiation effects of the separation of lanthanides and transplutonides by the TALSPEAK-type extraction," *J. Radioanal. Chem.*, **52**(2), 343-354 (1979).

PARTITIONING OF TRIVALENT ACTINIDES FROM A PUREX RAFFINATE USING A TODGA-BASED SOLVENT-EXTRACTION PROCESS

G. Modolo,[1] H. Vijgen,[1] R. Malmbeck,[2] D. Magnusson,[2] and C. Sorel[3]

[1]Forschungszentrum Jülich GmbH (FZJ), Institute for Energy Research, 52425 Jülich Germany. [2]European Commission, JRC, Institute for Transuranium Elements (ITU) 76125 Karlsruhe, Germany. [3]Commissariat à l 'Énergie Atomique Valrho (CEA) DRCP/SCPS, BP17171, 30207 Bagnols –sur-Cèze, France
Corresponding author e-mail address: g.modolo@fz-juelich.de

ABSTRACT

A TODGA/TBP process has been developed to separate trivalent actinides from a PUREX raffinate using a mixture of tetraoctyldiglycolamide (TODGA) and tributylphosphate (TBP). Batch extraction experiments allowed us to choose and optimize the composition of the organic extractant and the aqueous feed solutions. With the aid of computer-code calculations, a countercurrent process has been developed, and an optimized flowsheet has been tested with a spiked feed solution and finally with a genuine PUREX raffinate. The results of the two tests were very promising, demonstrating that more than 99.9% of the trivalent actinides are extracted, and very high decontamination factors are obtained to the non-lanthanide fission products. Co-extracted ruthenium (10% during spiked test, 18% during hot test) is less efficiently back-extracted and therefore requires further process development.

INTRODUCTION

Reducing the radiotoxicity of spent nuclear fuel is an important objective to ensure the sustainability of nuclear energy. This objective can be obtained by separation of the long-lived minor actinides (MA) from the fuel constituents and their conversion into short-lived radionuclides by nuclear reactions, the so-called partitioning and transmutation strategy.

Several processes have been developed for the co-extraction of americium and curium from a raffinate solution containing lanthanides and other fission products. The first was the TRUEX process, which employs as extractant CMPO (*n*-octyl(phenyl)-N,N-diisobutyl carbomoylmethylphosphine oxide) [1]. CMPO is a powerful extractant with high affinity for +3 actinides (An(III)) at high acidities, but it does not discriminate between An(III) and Ln(III). Other processes that feature co-extraction of actinides and lanthanides are the so-called TRPO and DIDPA processes [1].

The European research over the last decade, that is, in the NEWPART, PARTNEW, and the recent EUROPART programs, has resulted in the development of

the combination of DIAMEX and the SANEX processes [2-4]. These are based on the co-separation of trivalent actinides and lanthanides (DIAMEX) by a diamide followed by the subsequent selective separation of MA in the SANEX process.

The DIAMEX process use malonamide extractants such as DMDOHEMA (N,N`-dimethyl-N,N`-dioctyl-hexylethoxy-malonamide) dissolved in an aliphatic diluent (e.g., kerosene) [5]. The DIAMEX extractant follows the CHON principle; that is, the molecule is built from constituents that can be easily incinerated, thus minimizing generation of secondary waste. Recent research has shown that the tridentate TODGA extractant [6] exhibits even higher affinity for trivalent actinides and lanthanides than the reference diamide and could therefore be an interesting alternative to the DIAMEX process. Extensive batch extraction studies have been carried out for the development of a new continuous countercurrent process [7]. These investigations have led to the proposal to use a mixture of TODGA and TBP dissolved in an industrial aliphatic solvent (TPH) for the effective co-separation of actinides(III) and lanthanides(III) from a PUREX raffinate [8]. This paper reports the results from tests run with the optimized flowsheet of the TODGA/TBP process using a simulated feed solution and finally a genuine PUREX raffinate. In order to optimize the extraction processes, these experiments were accompanied by computer-code calculations.

EXPERIMENTAL

Centrifugal Contactors

The TODGA/TBP tests with spiked and genuine PUREX raffinates were carried out using miniature centrifugal extractors in a counter-current mode. The contactor setup at Research Centre Jülich that was used for the spiked test consisted of four batteries with four stages each. The contactors with a rotor diameter of 10 mm were designed and fabricated at INET, Tsinghua University, Beijing, China. The centrifugal contactors installed in the hot cells of ITU are of the BXP012 type (12 mm rotor diameter) manufactured by Rousselet-Robatel (France). The installation includes 16 stages with full flexibility concerning the distribution of stages in the different sections of the setup.

Solvent

TODGA was synthesized in Jülich according to a known synthesis route based on diglycolyl chloride and dioctylamine as starting materials [7]. TBP from Aldrich Chemical company, purity 99%, was used without further purification. The organic phase consisted of a mixture of 0.2 mol/L TODGA and 0.5 mol/L TBP diluted in the industrial diluent TPH (hydrogenated tetrapropylene) used in AREVA's reprocessing plants.

Feeds Used for the Spiked and Hot Test

The genuine PUREX raffinate was produced by reprocessing a dissolved commercial UO_2 fuel (60-70 GWd/tM) in a 32-stage centrifugal-contactor PUREX process. The PUREX process removed more than 99.99% of the U and Pu (<2 and 0.04

ppm in the raffinate, respectively). Also Tc was almost completely extracted (99.7%). The acidity was adjusted to ~4.4 M with concentrated HNO_3, after which oxalic acid and HEDTA were added [9]. The feed solution used for the batch extraction studies as well for the spiked test was a simulated raffinate. Concentrations of stable fission products were similar to the genuine feed. The complexing agents oxalic acid and HEDTA and trace amounts (2-6 MBq/L) of ^{241}Am, ^{244}Cm, ^{252}Cf, ^{152}Eu, and ^{134}Cs were also added to the feed [8].

RESULTS AND DISCUSSION

Batch Extraction Studies

The distribution data for nitric acid, oxalic acid, actinide nitrates, lanthanide nitrates, and fission products (e.g., Zr, Mo, Pd, Ru, and Sr) were measured at ambient temperature and are reported elsewhere [7]. The lanthanide(III) loading and the effect of TBP as a modifier were also studied to determine the limits of the third-phase formation. Further batch extraction experiments were carried out in this study on simulated feed solutions to adjust experimental conditions at each step of the process (extraction, scrubbing, and stripping).

The experimental conditions of the extraction, scrubbing, and stripping experiments are reported in Table 1. No third-phase formation was observed, and the phase separation was good for both extraction and scrubbing. Subsequent stripping of the loaded organic phase with 0.01 mol/L HNO_3 proved to be problematic. As oxalic acid is to some extent carried over in the organic phase from the scrub to the strip step, the probable reason is the formation of lanthanide oxalates at lower acidities. Two changes were introduced in order to wash out oxalic acid before reaching the stripping section, that is, a reduction of the oxalic acid concentration in the scrub step and addition of an extra oxalic acid scrub step with pure nitric acid (cf. columns 3 and 4 in Table 1). It was shown that a second scrubbing step with 1 mol/L HNO_3, added before the stripping section, solved this problem.

From the distribution ratios (Table 1), it is seen that lanthanides and MA (i.e., Am) are very well extracted. The oxalic acid and HEDTA manage to keep the *D* values low for Zr, Mo, and Pd in the extraction section, but in both scrub and strip steps, the *D* values tend to rise. This is not a problem, as the distribution ratios are low in the extraction, and consequently almost no Zr, Mo, and Pd will reach the scrub and strip sections. Stripping of actinides and lanthanides is also possible and will be even more efficient in a multistage strip section due to a lower acidity.

Flowsheet Design

Based on previous batch tests and a first-spiked countercurrent test using 16 stages for extraction, scrubbing, and stripping [7], an optimized TODGA/TBP flowsheet was designed (Figure 1) using the CEA PAREX code. The main goals of the flowsheet design were to achieve a recovery yield of actinides greater than 99.9% and to obtain decontamination factors for fission products (FP) as high as possible. The constraints

taken into account for the calculations were the number of stages involved. Thanks to the large distribution ratios for the actinides and lanthanides, the extraction section consisted of only four stages. Oxalic acid and HEDTA were added to the feed and the scrub solutions in order to decrease the extraction and make the scrubbing more efficient for some of the fission products.

Table 1. Extraction of Am(III) and fission-product elements by 0.2 mol/L TODGA and 0.5 mol/L TBP in TPH from a synthetic PUREX Feed[a]

D	Extraction	1st Scrub	2nd Scrub	1st Back-extraction	2nd Back-extraction
Conditions	sim. Feed + 0.3 M $H_2C_2O_4$ + 0.05 M HEDTA	1.0 M HNO_3 + 0.1 M $H_2C_2O_4$ + 0.1 M HEDTA	1.0 M HNO_3	0.01 M HNO_3	0.01 M HNO_3
Am-241	864	103	60	0.32	0.016
Eu-152	1162	461	387	1.4	0.070
La	70	13	8.3	0.11	n.m
Ce	183	20	13	0.16	n.m
Pr	389	33	21	0.18	n.m
Nd	704	69	43	0.26	n.m
Sm	767	203	209	0.90	n.m
Eu	262	240	350	1.7	n.m
Gd	771	128	98	1.1	n.m
Y	867	325	770	4.0	n.m
Sr	1.1	0.35	0.08		n.m
Ru	0.16	9.7	23	10	n.m
Pd	0.016	1.8	53	31	n.m
Ba	0.012	0.011			n.m
Cs	0.000	1.4			n.m
Mo	0.092	1.0	0.61	2.8	n.m
Rh	0.003	1.5			n.m
Zr	0.11	0.49	0.58	1.0	n.m

[a]Organic phase: 0.2 mol/L TODGA + 0. 5 mol/L TBP in TPH (not equilibrated with nitric acid). Aqueous phase: synthetic feed containing 0.3 mol/L $H_2C_2O_4$, 0.05 mol/L HEDTA, and 3.3 mol/L HNO_3. The back-extraction of the loaded organic phase was conducted as listed above in column 3–6. n.m = not measured

Considering that only 16 centrifugal-contactor stages were available at both laboratories, the An/Ln stripping step had to be performed separately. By taking into account the slow back-extraction kinetics, the strip section involved 12 stages (spiked test). For convenience reasons, the hot test was carried out with 16 stages, since cleaning and dismantling of the apparatus in the hot cells is complicated.

Full Spiked and Hot TODGA/TBP Demonstration

A spiked test using the flowsheet shown in Figure 1 was carried out at FZJ in June 2006, and the main results were reported recently [8]. The final hot demonstration of the TODGA/TBP flowsheet was performed in November 2006 at ITU [9]. The results

obtained in both tests were similar and can be summarized as following: Thanks to the huge distribution ratios obtained with the solvent, both actinides and lanthanides are extremely well extracted, and no An(III) and Ln(III) were found in the raffinate (below detection limit). The results of back-extraction during the spiked test show that 12 stages are sufficient for An(III) and Ln(III) stripping. No trivalent actinides and less than 0.01% of the lanthanides (III) were found in the spent solvent after stripping. The back-extraction during the hot test was also very efficient, and after only 8 stages, the concentrations reached the detection limit. The troublesome fission products Sr, Zr, Mo, and Pd were efficiently scrubbed in both tests, thanks to complexation with oxalic acid and HEDTA and due to acidity adjustment during scrubbing. Ruthenium shows a strange behavior, and during the spiked test 10% (18% in the hot test) was co-extracted, and still 8% (17% in the hot test) remained in the spent solvent. The "An(III)/Ln(III)" product contained in both tests less than 0.1% Sr, Zr, and Pd and 1.5% (1% in the hot test) of back-extracted Ru.

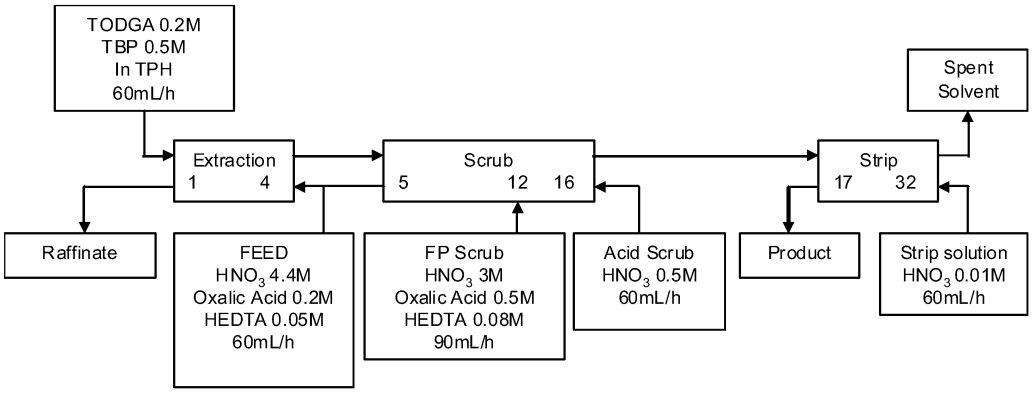

Figure 1. Flowsheet proposed for the spiked and hot TODGA/TBP demonstration experiments. For the spiked test, only 12 stages were used for stripping.

CONCLUSIONS

The results of the spiked and hot countercurrent centrifugal contactor tests showed that the mixture of TODGA and TBP dissolved in an aliphatic organic diluent is a promising solvent for the partitioning of trivalent actinides from a feed containing many fission products. This was demonstrated in an optimized flowsheet involving 28 stages using a simulated PUREX raffinate and 32 stages using a genuine feed. The main goals of the process, namely high recovery yields for the trivalent actinides (>99.9%) and excellent decontamination of non-lanthanide fission products, were all realized. The results obtained within the TODGA+TBP process are comparable with earlier DIAMEX tests [5]. However, TODGA has higher distribution ratios for An(III) and Ln(III) than the diamide DMDOHEMA (used in the DIAMEX), which results in an extremely efficient extraction but at the cost of a more complicated scrubbing/stripping. It is also important to note that the TODGA/TBP process produces more raffinate-waste solution (3.5 times dilution of the feed) compared to the diamide (2 times dilution of the feed). The acidity

of the collected product containing actinides(III) and lanthanides(III) (0.07 mol/L H^+) after stripping was found to be considerably lower here than in the DIAMEX process (>0.3 mol/L H^+). This solution can be used in a subsequent process for the separation of actinides(III) from lanthanides (e.g., SANEX process). Depending on the extractant that will be used, the acidity must be moderately adjusted. In the process presented in this paper, almost all objectives were realized. Ruthenium proved to be the only exception and remained to a large extent in the spent solvent after the actinides/lanthanides co-stripping step. The behavior of Ru in the solvent clean-up operation step should therefore be studied in the future.

ACKNOWLEDGMENTS

Financial support for this research was provided by the European Commission (project EUROPART, contract FI6W-CT-2003-508854).

REFERENCES

1. J. N. Mathur, M. S. Murali, and K. L. Nash, "Actinide Partitioning—A Review", *Solvent Extr. Ion Exch.*, **19**(3), 357-390 (2001).
2. C. Madic, M. J. Hudson, J. O. Liljenzin, J. P. Glatz, R. Nannicini, A. Facchini, Z. Kolarik, and R. Odoj, "New partitioning techniques for minor actinides," EU-report 19149, 2000.
3. C. Madic, F. Testard, M. J. Hudson, J. O. Liljenzin, B. Christiansen, M. Ferrando, A. Facchini, G. Geist, G. Modolo, A. Gonzales-Espartero, and J. De Mendoza, "PARTNEW—New Solvent Extraction Processes for Minor Actinides," Final Report, CEA-report 6066, 2004.
4. European EUROPART project (2004-2007), contract FI6W-CT-2003-508854.
5. D. Serrano-Purroy, P. Baron, B. Christiansen, R. Malmbeck, C. Sorel, and J. P. Glatz, "Recovery of minor actinides from HLLW using the DIAMEX process," *Radiochim. Acta*, **93**(3), 351-355 (2005).
6. Y. Sasaki, Y. Sugo, S. Suzuki, and S. Tachimori, "The novel extractants, diglycolamides, for the extraction of lanthanides and actinides in HNO_3-n-dodecane system," *Solvent Extr. Ion Exch.*, **19**, 91–103 (2001).
7. G. Modolo, H. Asp, C. Schreinemachers, and H. Vijgen, "Development of a TODGA based Process for partitioning of Actinides from a PUREX Raffinate Part I: Batch Extraction Optimization Studies and Stability Tests," *Solvent Extr. Ion Exch.*, **25**, 703-721 (2007).
8. G. Modolo, H. Asp, H. Vijgen, R. Malmbeck, D. Magnusson, and C. Sorel, "Demonstration of a TODGA/TBP Process for recovery of trivalent actinides and lanthanides from a PUREX Raffinate," Proceedings of GLOBAL 2007, Boise, Idaho, USA, September 9-13, 2007; pp. 1111-1116.
9. D. Magnusson, B. Christiansen, J. P.Glatz, R. Malmbeck, G. Modolo, D. Serrano Purroy, and C. Sorel, "Partitioning of Minor Actinides from PUREX raffinate by the TODGA process," Proceedings of GLOBAL 2007, Boise, Idaho, USA, September 9-13, 2007; pp-713-718.

COMPLEXATION OF LANTHANIDES AND ACTINIDES BY ACETOHYDROXAMIC ACID

R.J. Taylor,[1] S.I. Sinkov,[2] and G.R. Choppin[3]

[1]British Technology Centre, Nexia Solutions, Sellafield, Seascale, CA20 1PG, U.K. [2]Pacific Northwest National Laboratory, Richland, WA 99352, U.S.A. [3]Department of Chemistry and Biochemistry, Florida State University, Tallahassee, FL., U.S.A. Corresponding author email address: robin.j.taylor@nexiasolutions.com

ABSTRACT

Acetohydroxamic acid (AHA) has been proposed as a suitable reagent for the complexant-based, as opposed to reductive, stripping of plutonium and neptunium ions from the tributylphosphate solvent phase in advanced PUREX or UREX processes designed for future nuclear-fuel reprocessing. Stripping is achieved by the formation of strong hydrophilic complexes with the tetravalent actinides in nitric acid solutions. To underpin such applications, knowledge of the complexation constants of AHA with all relevant actinide (5f) and lanthanide (4f) ions is therefore important. This paper reports the determination of stability constants of AHA with the heavier lanthanide ions (Dy-Yb) and also U(IV) and Th(IV) ions. Comparisons with our previously published AHA stability-constant data for 4f and 5f ions are made.

INTRODUCTION

We have previously reported the stability-constant determinations for AHA complexes with the lighter lanthanide (Ln) ions Ce-Tb and the analogous trivalent actinide (An) ions Pu, Am, and Cm [1-2]. We have also determined stability constants for key tetravalent actinides, Np^{4+} and Pu^{4+}, and compared these to the actinyl ions NpO_2^+ and UO_2^{2+} [3-4]. The latter studies, coupled with solvent-extraction experiments to measure distribution ratios between HNO_3 and tributylphosphate (TBP), indicate a high selectivity of AHA for An(IV) over An(V,VI) ions that can be used as the basis for complexant-based actinide separations processes [5]. Notably, we have developed advanced PUREX-type flowsheets where AHA can be used to co-strip Np and Pu from a U-loaded TBP phase [6]. Additional proliferation resistance can be incorporated by configuring the flowsheet to leak a few percent of the U into the Np-Pu aqueous product, thus avoiding pure separated Pu at all stages of the process (i.e., co-processing). An alternative approach to a future fuel-cycle plant is proposed with the UREX+1a process in which AHA is used in the primary separation contactor to hold back Np and Pu with the highly active raffinate [7]. In this instance, fission-product lanthanides are present, and so the interactions between AHA and trivalent lanthanide ions must be quantified.

Here, we report stability-constant determinations for the remaining heavier lanthanide ions Dy-Yb (except Pm) and examine trends across the series. Additionally, we extend the trends in the actinide(IV) series by the determinations of AHA stability constants for the earlier tetravalent actinide ions U(IV) and Th(IV). These data can now be used to predict lanthanide and actinide ion speciation in advanced solvent-extraction processes where AHA is proposed as the separating agent.

EXPERIMENTAL

The reagents and experimental methods have been described in detail elsewhere [1-4]. Briefly, alkaline titrations (carbonate-free NaOH) in the presence of a metal ion and AHA ligand were monitored spectrophotometrically over a wide pH range. A micro pH electrode in combination with a pH/ion meter (equipped with an automatic temperature-control function) was used to control acidity of solutions. $NaClO_4$ was used as an inert electrolyte to maintain a constant ionic strength (I = 2.0 M). Ln(III) stock solutions were prepared by dissolution of the corresponding oxides (better than 99.9% purity in an appropriate amount of perchloric acid followed by a number of evaporation-redissolution cycles to reduce excessive acidity. Standardization of stock solutions was performed by complexometric titration with EDTA using xylenol orange as an indicator. Thorium stock solution was prepared by dissolution of hydrated $Th(NO_3)_4$ salt in water with subsequent fuming with concentrated $HClO_4$ to remove nitrate. The U(IV) stock solution was prepared by electrochemical reduction of U(VI) solution in the presence of hydrazine. U(IV) concentrations were determined spectrophotometrically (λ_{max} = 646 nm; ε = 56.1 M^{-1} cm^{-1}). Data processing used Singular Value Decomposition (SVD) and a modified version of the SQUAD code to refine stability constants.

RESULTS AND DISCUSSION

Trivalent lanthanides

Alkaline titrations for these lanthanide ions proceeded smoothly, and data processing ultimately led to the stability-constant values given in Table 1 for 1:1–1:4 complexes. An example of the electronic absorption spectra (EAS) accumulated during one of these titrations is included in Figure 1.

Thorium(IV)

Th(IV) is the only colorless An(IV) ion in aqueous solution, without suitable metal ion absorption bands for spectrophotometric-based stability-constant measurements. However, a steep UV absorbance (250-280 nm), due to the deprotonated AHA ligands surrounding the Th(IV) center was shown to be present in the EAS. The titration of AHA-containing Th(IV) solution with NaOH is shown in Figure 2. In the pH range 7–8.5, the absorbance increased dramatically as the solution pH approached the

Table 1. Derived stability constants of trivalent lanthanides Dy–Yb with AHA (T = 22 °C, I = 2.0 M). Associated errors in brackets.

	log β_1	log β_2	log β_3	log β_4
Dy	6.66 (0.08)	12.39 (0.08)	15.70 (0.20)	17.92 (0.15)
Ho	6.64 (0.03)	12.42 (0.10)	16.72 (0.26)	19.13 (0.31)
Er	6.59 (0.07)	12.52 (0.13)	16.63 (0.20)	18.44 (0.21)
Tm	6.70 (0.05)	12.82 (0.17)	17.08 (0.02)	18.78 (0.04)
Yb	7.25 (0.06)	14.00 (0.23)	18.06 (0.23)	19.79 (0.37)

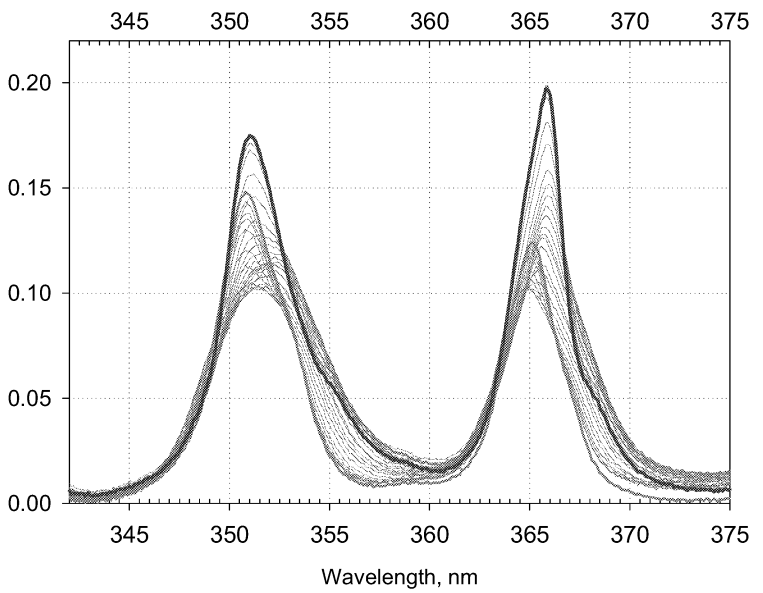

Figure 1. Example EAS recorded during an alkaline (NaOH) titration of a lanthanide ion, Dy(III), in the presence of AHA. Initial Dy concentration = 5.8 mM; AHA was added in a single addition to give a concentration of 365 mM; L:M = 64.7:1; pH range = 1.49–8.97; T = 22 °C; I = 2.0 M $NaClO_4$; y-axis = optical absorbance.

pK_a of AHA, and substantial concentrations of L^- were formed in solution. These spectra were therefore not used in the data analysis. Over the reduced pH range, three complexed species were suggested and their respective stability constants calculated (Table 2).

Uranium (IV)

The freshly electrolyzed U(IV) solution comprised 97% U(IV) and 3% U(VI). EAS between 600 and 700 nm were used to monitor changes in the most intense peak of U(IV) upon complexation without interference from U(VI). The titration was carried out under nitrogen scrubbing with preliminary degassing of the starting solution to minimize

U(IV) oxidation. Twenty five spectra were collected throughout the titration experiment (data not shown), although above pH 7.80 there was an indication of yellow coloration attributed to some U(VI)-AHA species. Therefore, the spectra taken in the pH range from 7.80 to 8.39 were excluded from data analysis. The calculated stability constants are given in Table 2.

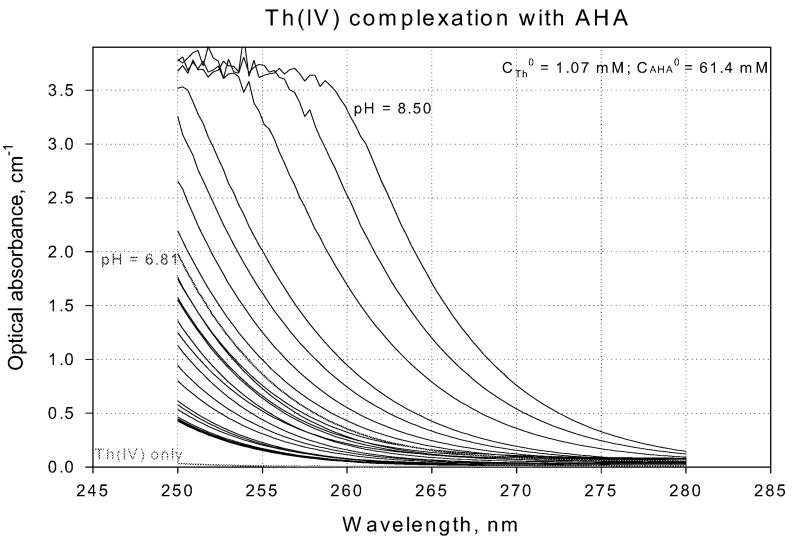

Figure 2. Spectrophotometrically monitored pH titration of Th(IV) solution by NaOH in the presence of AHA. L:M ratio was increased in one step from 0 to 57; total pH range, 0.19–8.50; the pH range used for data processing was limited to pH 6.81.

Table 2. Derived stability constants of tetravalent actinides Th(IV) and U(IV) with AHA (T = 22 °C, I = 2.0 M)

	Th(IV)	U(IV)
log β_1	10.53 (0.05)	12.26 (0.04)
log β_2	19.06 (0.10)	22.08 (0.11)
log β_3	25.92 (0.14)	29.54 (0.13)

Discussion

The later Ln-AHA stability-constant values presented herein are consistent with the earlier Ln-AHA complexes, as can be seen from plotting log β_1 *vs*. (1/ionic radius) across the series (Figure 3). While there is a general increase across the series due to increasing ligand attraction as metal charge densities increase due to the lanthanide contraction, the 'gadolinium break' is evident in these data. This has been attributed to either the stability of the $4f^7$ electronic configuration or a change in coordination geometry between the lighter and heavier lanthanide ions [8]. For comparison, the An(III) stability constants are also included in Figure 3. A decrease in the equilibrium

constant for the 1:4 Ln(III)-AHA complex formation (i.e., log K_4, where $K_4 = \beta_4/\beta_3$) from Ho(III) onwards is also evident from these data, presumably due to increased steric difficulties in accommodating the fourth ligand around the metal ion center. The values of log β_1 for AHA actinide complexes follow the usual trend for actinide ion complexes, AnO_2^+ < An(III) < AnO_2^{2+} < An(IV), reflecting the effective charges on the actinide center [8], although our data with the actinyl ions are limited to Np(V) and U(VI). The high selectivity of AHA for An(IV) over An(III) and Ln(III) ions is evident from Figure 3.

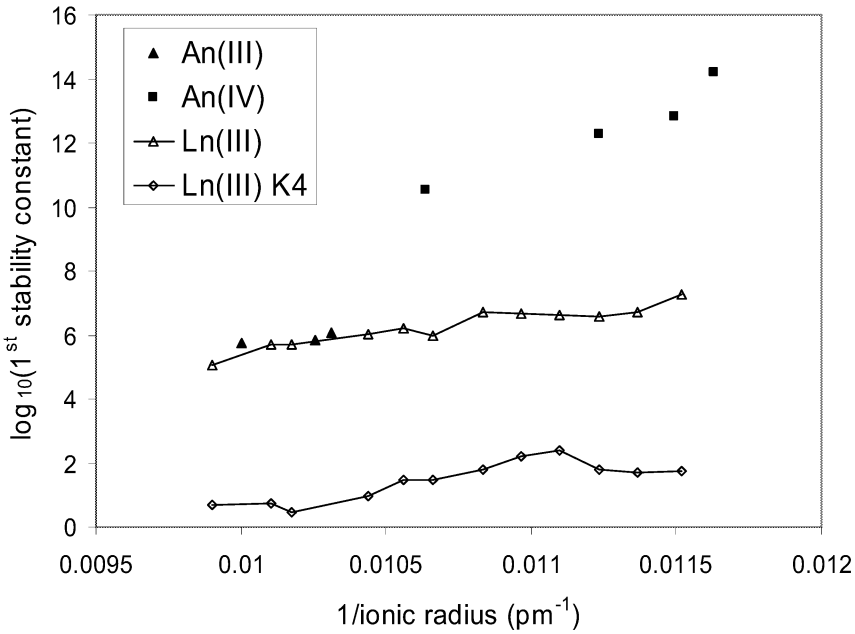

Figure 3. 1:1 metal:ligand complex stability constants for lanthanide(III) and actinide(III,IV) AHA complexes (log β_1) at 22 °C (I = 2.0 M $NaClO_4$) as a function of the reciprocal of the ionic radius (CN = 6 [9]). Also shown are the equilibrium constants for the 4th complexation step (log K_4) for the 1:4 Ln(III)-AHA complexes.

CONCLUSIONS

A comprehensive range of stability constants for complexes between the ligand AHA and 4f and 5f ions in $HClO_4$ at a constant ionic strength (I = 2.0 M) have now been determined. These include ions in the III, IV, V, and VI oxidation states and follow established trends for f-elements. The values of the stability constants confirm the high selectivity of AHA for An(IV) ions seen in other investigations, including batch distribution-ratio measurements made between aqueous HNO_3 and 30% TBP diluted in odorless kerosene (OK) [3-4]. For a fuller understanding of Ln/An AHA equilibria, some refinements to the values reported are advisable, particularly with Pu(III) and Pu(IV)

ions, where redox changes and nitrate complexes complicated the analysis, and also further experiments at variable metal concentrations to check for multinuclear species. Associated complexation temperature dependencies and solution-phase structural studies would also be most interesting.

ACKNOWLEDGMENTS

We wish to thank BNFL and the Nuclear Decommissioning Authority for funding.

REFERENCES

1. S. I. Sinkov and G. R. Choppin, "Acetohydroxamic Acid Complexes with Trivalent f-Block Metal Cations," *J. Nucl. Sci. Tech.*, **Supp. 3**, 359-362 (2002).
2. S. I. Sinkov, G. R. Choppin, and R. J. Taylor, "Spectrophotometry and luminescence spectroscopy of acetohydroxamate complexes of trivalent lanthanide and actinide ions," *J. Solution Chem.*, **36**, 815-830 (2007).
3. R. J. Taylor, S. I. Sinkov, G. R. Choppin, and I. May, "Solvent extraction behaviour of neptunium (IV) ions in the presence of simple hydroxamic acids," *Solvent Extr. Ion Exch.*, **26,** forthcoming (2008).
4. M. J. Carrott, O. D. Fox, C. J. Maher, C. Mason, R. J. Taylor, S. I. Sinkov, and G. R. Choppin, "Solvent extraction behaviour of plutonium (IV) ions in the presence of simple hydroxamic acids," *Solvent Extr. Ion Exch.*, **25**, 723-745 (2007).
5. J. E. Birkett, M. J. Carrott, O. D. Fox, C. J. Jones, C. J. Maher, C. V. Roube, R. J. Taylor, and D. A. Woodhead, "Recent Developments in the PUREX Process for Nuclear Fuel Reprocessing: Complexant Based Stripping for Uranium - Plutonium Separation," *Chimia*, **59**, 898-904 (2005).
6. J. E. Birkett, M. J. Carrott, O. D. Fox, C. J. Jones, C. J. Maher, C. V. Roube, R. J. Taylor, and D. A. Woodhead, "Controlling Neptunium and Plutonium within Single Cycle Solvent Extraction Flowsheets for Advanced Fuel Cycles," *J. Nucl. Sci. Tech.*, **44**, 337-343 (2007).
7. T. A. Todd, and R. A. Wigelund, "Advanced Separation Technologies for Processing Spent Nuclear Fuel and the Potential Benefits to a Geologic Repository," Separations for the Nuclear Fuel Cycle in the 21st Century, G. J. Lumetta, K. L. Nash, S. B. Clark, and J. I. Friese, Eds., ACS Symposium Series 933, American Chemical Society, Washington DC., 2006; pp. 41-56.
8. N. Kaltsoyannis, and P. Scott, The f elements, Oxford University Press, Oxford, 1999.
9. N. M. Edelstein, J. Fuger, J. J. Katz, and L. R. Morss, "Summary and comparison of properties of the actinide and transactinide elements," The chemistry of the actinide and transactinide elements, third edition, L. R. Morss, N. M. Edelstein, and J. Fuger, Eds., Springer, Dordrecht, 2006; pp. 1753-1835.

AMERICIUM/EUROPIUM SEPARATION BY SYNERGISTIC EXTRACTION MIXTURES OF BIS-TETRAZOLYL PYRIDINES WITH CHLORINATED COBALT DICARBOLLIDE

I.V. Smirnov, V.A. Babain, and A.V. Chirkov

V.G. Khlopin Radium Institute, St.-Petersburg, 2nd Murinskiy Ave, 28, Russia, 194021
Corresponding author email address: igor_smirnov@atom.nw.ru

ABSTRACT

Americium and europium extraction by synergistic mixtures of 2,6-bis(1-aryl-1H-tetrazol-5-yl)pyridines (ATP) with chlorinated cobalt dicarbollide (CCD) in polar diluents from acidic media was studied. The effect of diluent, composition of aqueous phase, and substituent nature in the aryl ring of ATPs on the extraction efficiency and selectivity of americium and europium separation was investigated. The Am-Eu separation factor was close to 100 at the optimal ratio of ATPs:CCD ~ 1:1 in the synergistic mixture. High resistance of 2,6-bis-aryltetrazolyl pyridines to the action of acids and radiolysis was demonstrated.

INTRODUCTION

Transplutonium elements (TPE) have very high radiotoxicity and prolonged half-lives. Preliminary recovery of TPE allows one to simplify the process of HLW vitrification and final disposal. Dialkyl-substituted bistriazinylpyridines (BTPs) effectively separate americium and europium in moderately acidic media (up 1 M HNO_3) [1] but have low stability to acid. During the tests on stability of nPrBTP (0.01 M nPrBTP in *n*-octanol) to 1 M HNO_3, it was revealed that the Am distribution ratio decreases by a factor of 31 after 9 days [2]. In 2001, countercurrent tests were carried out with the mixture of 0.01 M iPrBTP and 0.5 M solubilizer, dimethyldioctyl hexylethoxy malonamide as extractant. To prevent BTP degradation, hydrazinium nitrate was added into the wash solution [2]. But after two cycles, the extraction efficiency decreased by 40%. BTPs and bistriazinyl bipyridines (BTBPs) [3] exhibit better stability to hydrolysis. We have found that 2,6-bis(1-aryl-1H-tetrazol-5-yl)pyridines (ATPs) have very high stability to hydrolysis and γ-radiolysis [4]. The main goal of our work was to investigate properties of the synergistic extraction mixture of 2,6-bis(1-aryl-1H-tetrazol-5-yl)pyridines with chlorinated cobalt dicarbollide.

EXPERIMENTAL PROCEDURE

Synthesis of Extractants

The substituted 2,6-bis(1-aryl-1H-tetrazol-5-yl) pyridines (ATP's, Figure 1) used in this work were synthesized at St.-Petersburg State Technological Institute (Russia) by the reaction of imidoyl chlorides with sodium azide in two-phase system with catalysts for interphase transfer [5].

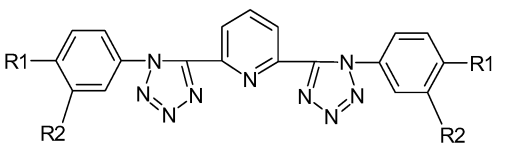

Substituents	Designation	Substituents	Designation
$R_1 = R_2 = H$	PhATP	$R_1 = CH_3$; $R_2 = H$	MePhATP
$R_1 = C_4H_9$; $R_2 = H$	BuPhATP	$R_1 = R_2 = CH_3$	Me2PhATP
$R_1 = OC_2H_5$; $R_2 = H$	EtOPhATP	$R_1 = R_2 = Cl$	Cl2PhATP

Figure 1. Substituted 2,6-bis-aryltetrazolyl pyridines (ATPs).

The obtained products were purified by liquid chromatography and recrystallized. All synthesized ATPs are crystalline, water-insoluble, colorless or light yellow substances. Most of 2,6-bis-aryltetrazolyl pyridines are moderately soluble (up to 0.1 M) in chloroform, DCE, DMF, and nitrobenzene. Only 2,6-bis(1-(4-nitrophenyl)-1H-tetrazol-5-yl)pyridine cannot be dissolved and was not investigated.

Reagents and Methods Used

Metanitrobenzotrifluoride (F-3), phenyltrifluoromethyl sulfone (FS-13), and 1,2-dichloroethane (DCE) were used as diluents for the ATPs. The cesium salt of chlorinated cobalt dicarbollide (CCD) was produced by "KatChem" Co (Czech Republic). Process solutions were prepared by exact weighing. When studying the extraction of radionuclides, 1×10^{-6} M of stable metal salt was added into the aqueous phases, and for extraction of americium, 1×10^{-6} M of europium salt.

To study the hydrolytic stability of the ATPs, the organic and aqueous phases (6 M HNO_3) were placed into polyethylene test tubes and kept at 100 °C and stirred periodically for 32 hours. To study the stability of PhATP *vs* γ-radiolysis, 10 mL of the solvent (0.02 M PhATP–0.02 M CCD in F-3) and 5 mL of the 3 M HNO_3 were placed into a glass test tube. Irradiation was conducted on gamma-setup with Co^{60} at 22 °C. Integral dose was 2.4 MGy (667 W h/L).

To determine the distribution ratios of the radionuclides, organic and aqueous phases were poured into polyethylene test tubes and stirred at 20 ± 2 °C for 5 min. As follows from the preliminary test data, this duration was sufficient to establish equilibrium. The phases were separated by centrifugation; then samples of each phase

were taken into polyethylene tubes. Radiometric measurements were conducted on a scintillation gamma-spectrometer using a 51 × 51 mm NaI well detector (Canberra).

RESULTS AND DISCUSSION

Factors Affecting Extraction Efficiency and Selectivity

ATP/CCD Ratios.

The efficiency of radionuclide recovery by a synergistic extraction mixture depends on the ratio between the extractants. The method of isomolar series was used to determine the best composition (Figure 2).

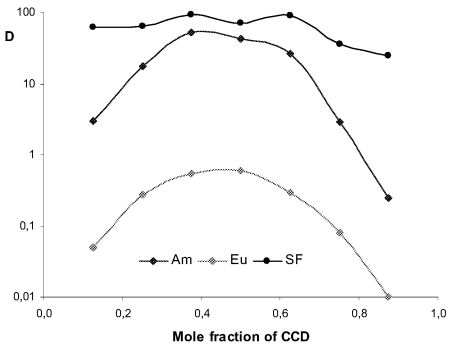

Total concentration of PhATP and CCD: 0.08 M in F-3. Aqueous phase: 1 M HNO_3.

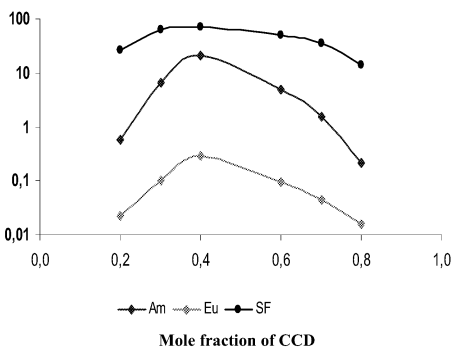

Total concentration of MePhATP and CCD: 0.02 M in F-3. Aqueous phase: 0.4 M HNO_3.

Figure 2. Extraction of Am and Eu from HNO_3 as a function of [ATPs]/[CCD] ratio.

It is evident that the americium distribution ratios are rather high over a wide range of ATP:CCD ratios from 1:5 to 5:1. The highest recovery of radionuclides is attained for the ratio of ATP:CCD ≈ 1:1. The separation of Am and Eu does not practically depend on PhATP:CCD ratio.

Acidity of Aqueous Phases.

The distribution ratios of Am and Eu decrease with increasing the acid concentration in the aqueous phase. The dependence character of the distribution ratios on the aqueous phase acidity is typical for an ion-exchange mechanism of extraction (Figure 3).

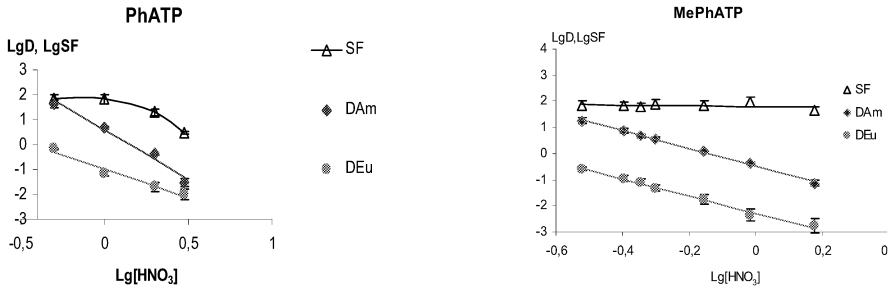

Figure 3. Dependence of Am and Eu distribution ratios on HNO_3 concentration in the aqueous phase. Organic phase: 0.02 M PhATP–0.02 M CCD or 0.01 M MePhATP–0.01 M CCD in F-3.

The slopes of straight-line trends of the plots of log D versus log[HNO_3] for BuPhATP, EtOPhATP, and MeATP are in the range 2.8–3.4. There are no differences in slopes for americium and europium, and the separation factor only slightly depends on HNO_3 concentration. The slope for PhATP is equal to 3.9 in the case of americium and only 2.3 for europium. As a consequence, the separation ratio of americium and europium decreases with increasing acid concentration. This difference may be caused by a different composition of the extracted complexes.

The nature of the acid in the aqueous phase has an influence on the efficiency and selectivity of americium and europium recovery. Radionuclides are likely not extracted from H_2SO_4 solutions due to formation of strong sulfate complexes. On extraction from nitric and perchloric acids, the increase of acidity results in a decrease of distribution ratios. The slope of straight lines on the plot of log D_{Am} versus log[H^+] is 3.5 for HNO_3 and 2.5 for $HClO_4$. As for europium, the slopes for perchloric and nitric acids are the same and equal to 2.5. This confirms our assumptions about the different composition of extracted americium and europium complexes.

Substituent Nature in Aryl Ring of ATPs

The distribution ratios of americium and europium decrease in the series EtOPhATP > MePhATP > PhATP >> Cl2PhATP (Figure 4). This means that the rise of electrodonating ability of substituent in aryl ring results in increasing the distribution coefficient. The component BuPhATP is outside this dependence; this may be explained by steric hindrance.

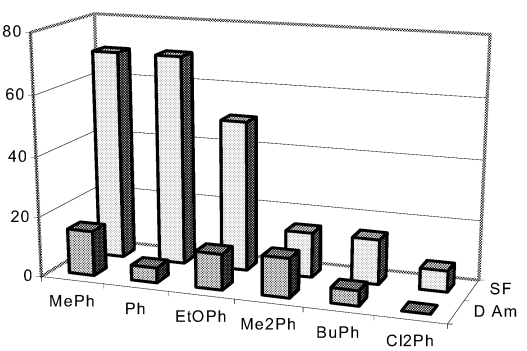

Figure 4. Dependence of Am distribution ratio and Am/Eu separation factor on ATP's structure. 1 M HNO_3 aqueous phase; 0.02 M ATPs + 0.02 M CCD in F-3 as organic phase.

Influence of Diluent on Extraction

The data on the diluent effect on the efficiency and selectivity of radionuclide extraction are presented in Figure 5. The distribution ratios of Am and Eu are maximal in F-3 and DCE, and when transferring to FS-13, they decrease a hundred-fold. As can be seen from the data of Figure 5, the diluent has no effect on PhATP selectivity, and the separation factors of americium and europium remain constant. The solubility of PhATP decreases in the following sequence: DCE ≈ F-3 > FS-13, and F-3 can dissolve up to 0.1 M of nonsubstituted ATP.

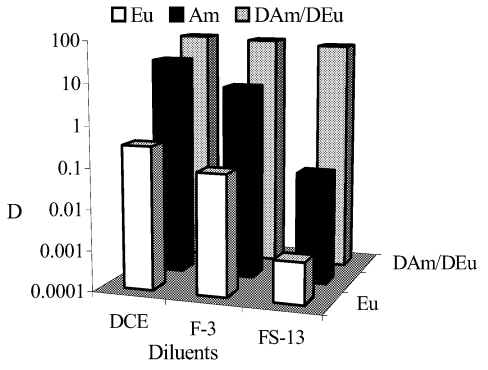

Figure 5. Extraction of Am and Eu from 0.3 M HNO_3 by solutions of 0.01 M PhATP–0.01 M CCD in three diluents.

Radionuclide Extraction

In addition to americium and europium, the extractions of ^{85}Sr, ^{137}Cs, and ^{133}Ba were studied. The mixture of 0.02 M of PhATP and 0.02 M CCD extracts cesium and strontium from 1 M HNO_3 with the distribution ratios 33 and 1.7, respectively. By this is meant that strontium is recovered in the same manner as americium (D_{Am} = 2.9). Barium is extracted to a much lesser degree than cesium and strontium, and the separation factor of Sr-Ba pair is 35. The previously described extraction mixtures based on CCD recovered barium much better than strontium [6].

Chemical and Radiolytical Stabilities of ATP

The stability of the ATPs was evaluated by changes in efficiency and selectivity of Am and Eu extraction after prolonged contact of extractant with 6 M HNO_3 at 100 °C. By comparison, a similar test was performed with CMPO, which is a hydrolytically stable extractant used for HLW treatment. After 30 hours treatment of CMPO-based extractant, the distribution ratios of radionuclides decreased 10-fold, but the properties of the PhATP-based extractant were almost unaffected. The distribution ratios and separation factors of radionuclides are invariant after contacting the extractant with 6 M HNO_3 at 100 °C for 24 hours. Thus, PhATP possesses high hydrolytic stability and can be used under conditions of prolonged contact with HNO_3 media.

The distribution ratio of americium decreased by a factor of 4 after irradiation (2.4 MGy) of MePhATP–CCD solvent in the presence of 3 M HNO_3; Am/Eu separation factor decreased 2-fold. Such a decrease of the distribution ratio agrees with

approximately 25% of MePhATP destruction. Thus, MePhATP–CCD solvent has a high radiation stability and can be used for processing of HLW.

CONCLUSIONS

The conducted investigations have shown that the 2,6-bis-aryltetrazolyl pyridines offer advantages over the known N-polydentate extractants, owing to their ability to recover americium effectively and selectively from HNO_3 medium and the high stability to acid attack.

The synergistic mixture of ATPs–CCD in polar diluents extracts Am and Eu from HNO_3 and $HClO_4$ media by a cation-exchange mechanism. The americium distribution ratios and the selectivity of Am–Eu separation are constant over a wide range of ATP:CCD ratios from 1:5 to 5:1. The diluent nature has no influence on the separation of Am and Eu. The synergistic mixture of ATP–CCD effectively separates the Sr/Ba pair.

Extraction and physicochemical properties of 2,6-bis-aryltetrazolyl pyridines permit one to use the synergistic mixture of ATP–CCD for selective recovery of americium from acidic HLW.

ACKNOWLEDGMENTS

The work was partly carried out under financial support of ISTC Project 3405.

REFERENCES

1. Z. Kolarik, U. Müllich, and F. Gassne, *Solvent Extr. Ion Exch.*, **17**, 23 (1999); et *ibid* p. 1155.
2. C. Hill, D. Guillaneux, L. Berthon, C. Madic, “Sanex-BTP process development studies,” *J. Nucl. Sci. Technol.*, Nov., sup. **3**, 309-312 (2002).
3. M. J. Hudson, C. E. Bouucher, D. Braekers, and J. F. Desreux, et al., “New bis(triazinyl)pyridines for selective extraction of americium (III),” *New J. Chem.*, **30**, 1171-1183 (2006).
4. I. V. Smirnov, V. A. Babain, and A. V. Chirkov, "New hydrolytically stable solvent for am/eu separation in acidic media," proceedings of GLOBAL 2007, Boise, USA, Sep. 9-13, 2007, published in cd-rom.
5. T. V. Artamonova, A. B. Zhivich, M. Yu. Dubinskii, and G. I. Koldobskii, “Preparation of 1,5-disubstituted tetrazoles under phase-transfer conditions,” *Synthesis*, **12**, 1428-1430 (1996).
6. J. Rais and B. Grüner, “Extraction with metal bis(dicarbollide) anions: metal bis(dicarbollide) extractants and their applications in separation chemistry,” in Ion Exchange and Solvent Extraction, Vol. 17, Y. Marcus and A. K. Sengupta, Eds., Dekker, New York, 243-334, 2004.

LANTHANIDE AND ACTINIDE EXTRACTIONS USING FUNCTIONALIZED COBALT BIS(DICARBOLLIDE) ION DERIVATIVES SUBSTITUTED WITH METAL LIGATING FUNCTIONS

M. Lučaníková,[1] P. Selucký,[1] J. Rais,[1] B. Grüner,[2] and M. Kvíčalová[2]

[1]Nuclear Research Institute plc., 250 68 Řež near Prague, Czech Republic. [2]Institute of Inorganic Chemistry, Academy of Sciences of the Czech Republic, v.v.i. 250 68 Řež near Prague, Czech Republic. Corresponding author email address: luc@ujv.cz

ABSTRACT

Several extractants based on cobalt bis(dicarbollide) ion of formula $[(1,2\text{-}C_2B_9H_{10})(1',2'\text{-}C_2B_9H_{11})\text{-}3,3'\text{-}Co(III)]^-$ with covalently bonded CMPO group of general formulation $[(Ph)_2P(O)(CH_2)C(O)N(H)_{n=0,1}]$ were prepared and tested for extraction of trivalent radionuclides. The compounds studied differ in mode of attachment of CMPO group to COSAN moiety. Compound **1** with diethylene glycol connector between the COSAN cage and CMPO group provided better extraction properties than compounds with direct attachment (**2**) and *N*-bridge connection of COSAN moiety to nitrogen of CMPO group (**3a** or **3b**). The compounds allowed the use of a less-polar solvent mixture of hexylmethylketone and *n*-dodecane, which could replace the polar and less environmentally friendly solvent nitrobenzene.

INTRODUCTION

Nuclear wastes, produced by the reprocessing of spent nuclear fuel, contain long-lived radionuclides (LLR), essentially belonging to the family of the actinide elements (An). These induce important long-term radiotoxicity. Therefore, the elimination via partitioning of these LLR, mainly minor actinides (MAn), will reduce the radiotoxicity of waste for final disposal and minimize their possible impact to the biosphere. Several different hydrometallurgical processes are currently under development in order to extract Ln and An from the fission-product mixture after PUREX processing. The most studied methods for extraction of trivalent radionuclides are based on the use of substituted malonamides (DIAMEX process [1]), (*N,N*-dialkylcarbamoylmethyl)-dialkylphosphine oxides (CMPO) (TRUEX process [2]), and *N,N,N′,N′*-tetraoctyl diglycolamide (TODGA) (ARTIST process [3]).

Cobalt bis(dicarbollide)(1-) ion $[(1,2\text{-}C_2B_9H_{10})(1',2'\text{-}C_2B_9H_{11})\text{-}3,3'\text{-}Co(III)]$ (COSAN) is a singly-charged (1-) anion and belongs to the class of electron-deficient 26-electron 12-vertex icosahedral *closo* borane cluster ions of extraordinary high chemical and thermal stability, hydrophobicity, and inorganic super-acid behavior [4, 5]. Synthetic combination of favorable properties of COSAN with CMPO group in one single

molecule proved efficient for extraction of trivalent radionuclides from nuclear waste solutions [6]. Therefore, several new types of extractants of this series were prepared, and the influence of structural modifications of COSAN compounds functionalized with structural analogues of CMPO (e.g., substituents on phosphine oxide and amidic groups) on the extraction properties was evaluated [7,8]. Recently, new type of extractants based on calixarenes substituted with CMPO and COSAN groups have been also prepared and proposed for Ln and An separation [9].

In this work, the extraction properties of several selected COSAN derivatives differing in mode of attachment of CMPO group to the COSAN moiety are studied in detail. Comparison is given on CMPO having no *N*-alkyl substituent in this particular case. The influence of structural modification of COSAN derivatives on their efficiency and selectivity for trivalent Ln/An extraction are evaluated.

EXPERIMENTAL

Chemicals

The bis(1,2-dicarbollide)-cobalt(III) (1-)ate (COSAN) was supplied by Katchem Ltd., Prague, Czech Republic. COSAN's substituted with a CMPO group (with diphenylphosphine terminal end of the CMPO functionality and hydrogen on the amidic nitrogen atom) used in this work were synthesized; (*N*-isobutylcarbamoylmethyl)-diphenylphosphine oxide was introduced using reactions of the respective ammonium-COSAN derivatives with nitophenyl ester of diphenyl phosphoryl acetic following the reliable procedure [6,7,9] developed originally for substitutions on calixarene platforms [10]. These include compounds (see Figure 1) with opened dioxane ring (diethyleneglycol) connector between COSAN cage and CMPO group (**1**), with direct attachment of COSAN moiety to nitrogen of CMPO group (**2**), and with bridge connection of COSAN moiety to nitrogen of CMPO group (**3**). The latter compound was prepared and studied in the respective anionic keto-form (**3a**) and neutral enol-form (**3b**). The (*N*-isobutylcarbamoylmethyl)-diphenylphosphine oxide $(Ph)_2$CMPO was prepared by the modified procedure described above (without using COSAN compound). All other chemicals used were of analytical reagent grade. Radioactive isotopes of ^{152,154}Eu and ^{241}Am used (in trace amounts) were of radiochemical purity.

Extraction Tests

The extraction experiments were performed in stoppered test-tubes with a shaking time of 1 hour in a thermostated box at 25 ± 0.1 °C. Aliquots of the phases were measured using single-channel γ analyzer with NaI (Tl) well-type detector.

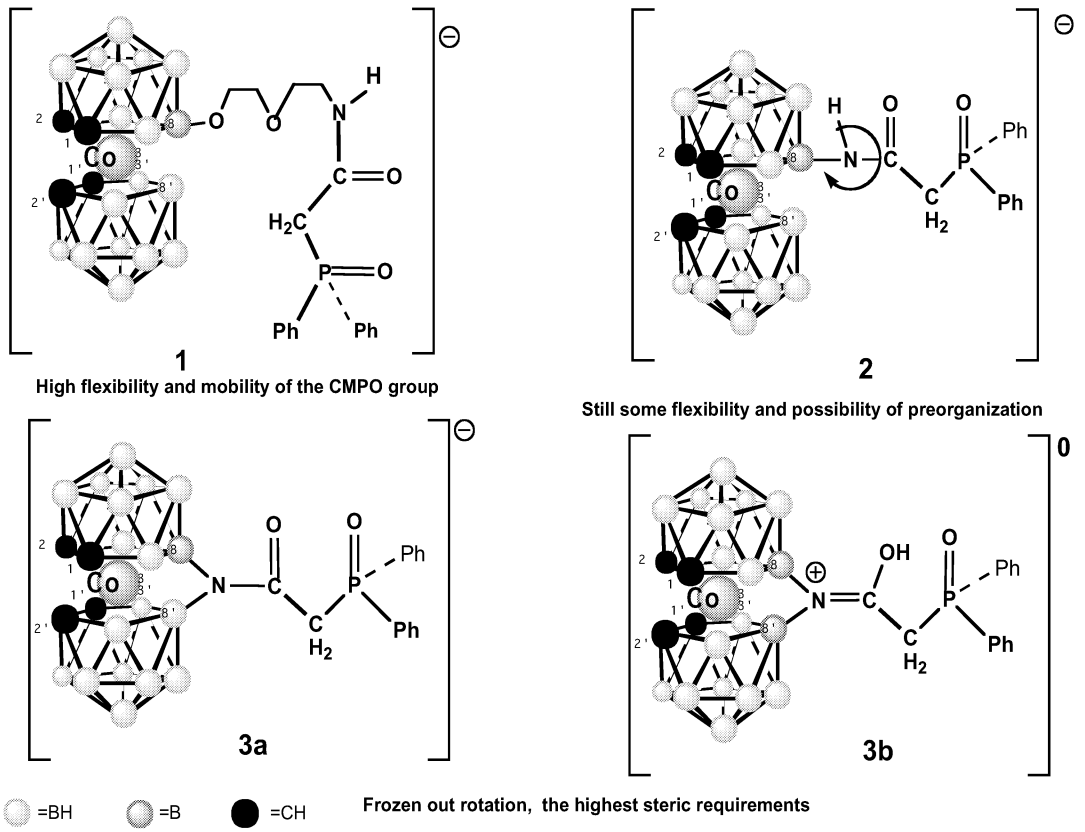

Figure 1. Schematic drawing of the structures of extractants **1-3**. The structure of **3b** is only tentative; some possibility for protonation on the P(O) group cannot be fully excluded.

RESULTS AND DISCUSSION

The extraction of trace amounts of Eu by derivates of COSAN with CMPO group into different solvents, namely nitrobenzene and a mixture of hexylmethylketone (2-octanone) and *n*-dodecane (HMK/D) (as representatives of polar and less-polar solvent series) respectively, was investigated. As Figure 2 shows, all compounds extracted europium well down to pH 1 (D_{Eu} close to, or higher than, 100). With further increase of acidity, the Eu distribution ratios decrease steeply. Comparing extraction results in different solvents (see Figure 2), no significant effect of solvent polarity was observed for **1** and **2**. The significant preference for less-polar mixture HMK/D was observed for compound **3a** and **3b**. In general, the COSAN based derivatives require polar solvents, preferably aromatic nitrosolvents. However, for technological use, ecological and nonpolar solvents are preferred. From the extraction results, it is obvious that HMK/D is a reasonable alternative to polar solvents.

Results plotted in Figure 2 show an evident effect of attachment of the CMPO group to COSAN skeleton on extraction properties. Extraction ability at higher nitric acid

concentration (>1 M) decreases in the following order: **1** > **2** > **3a** ~ **3b**. The highest extraction efficiency was observed for compound **1** with a longer diethyleneglycol connector between the COSAN cage and CMPO group. Distribution ratios for **1** are about one order of magnitude higher than those of compound **2** with direct attachment via nitrogen of CMPO complexant to COSAN skeleton and approximately two orders of magnitude higher than those of compounds with *N*-bridge attachment of CMPO group to the COSAN moiety (**3a** and **3b**). The high extraction efficiency of **1** indicates that diethyleneglycol connector probably enables better flexibility of CMPO moiety in order to adopt favorable geometric orientation around the Eu^{3+} cation. Reduced complexing ability of compounds with direct attachment is probably caused by steric hindrance, which limits ability of CMPO group to tightly complex the Ln cation. Influence of structural effects is even more pronounced for rigid arrangement around *N*-bridge in compound **3a** and **3b**. This type of COSAN derivative is the least effective from the series, which is ascribed to high structural rigidity. This type of ionic ligand is also most prone to protonation by strong acids. Nevertheless, as can be seen from results, extraction efficiency for the two different forms of the *N*-bridged compound (keto **3a** and enol **3b**) is almost the same. It can be assumed the free ligand exists in the *enol* form in strongly acidic conditions and reverts to the anionic *keto* form upon M^{3+} complexation. Presence of the anionic form of the ligand (L^-) **3** in the solid-state complex EuL_3 was confirmed by X-ray crystallography. The ligands **1** and **2** are usually found in their anionic form in solution, although some keto-enol equilibrium of the free ligands cannot be excluded at high acidic concentrations.

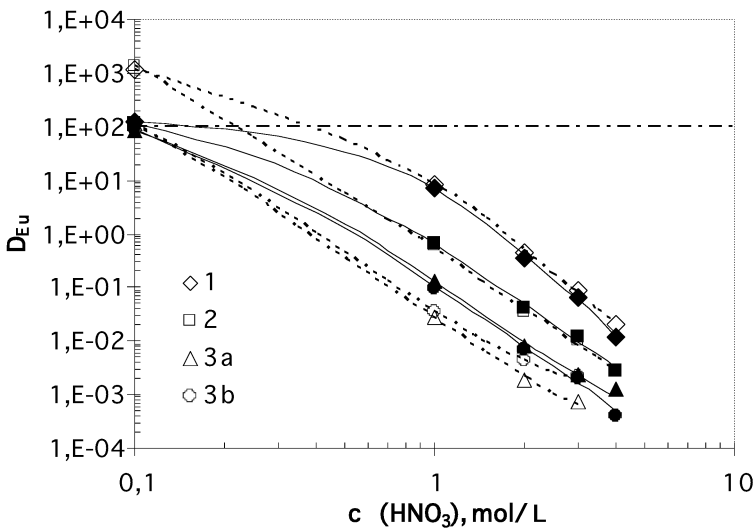

Figure 2. Extraction of Eu microquantities by 10^{-3} M solutions of compounds **1**, **2**, **3a**, and **3b** in nitrobenzene (dashed line) and hexylmethylketone/*n*-dodecane (full line) at variable nitric acid concentration.

Extraction properties of COSAN's with covalently bonded CMPO groups and the structurally comparable organic ligand (*N*-isobutylcarbamoylmethyl)-diphenylphosphine

oxides, $(Ph)_2CMPO$, and its synergic mixtures with COSAN anion at 1 M HNO_3 in nitrobenzene (because of negligible solubility $(Ph)_2CMPO$ in mixture of HMK/*n*-dodecane) were investigated. It was found that the efficiency of Eu^{3+} extraction for **1** is approximately four orders of magnitude better than for classical organic ligand $(Ph)_2CMPO$ compound and about two orders of magnitude better than that of its synergic mixtures with COSAN. The results are in accordance with the observation reported previously [6].

To investigate the composition of extracted species with COSAN functionalized CMPO derivates, Eu^{3+} extraction was studied as a function of extractant concentration. In all cases, the log-log dependences of D_{Eu} yielded straight lines with the slopes close to 3 (the slopes were 3.06, 2.76, and 2.65 for **1**, **2**, and **3** in nitrobenzene, respectively; the slopes were 2.62, 2.89, and 2.77 for **1**, **2**, and **3** in HMK/*n*-dodecane mixture, respectively; correlation factors were close to $R^2 = 0.99$). The observed results indicate that the composition of the extracted species is 1:3. This composition corresponds to charge compensation of Eu^{3+} ion by three single-charged extractant anions. Similar results were obtained for other COSAN derivates of this series and the assumed extraction mechanism was proposed as [7]:

$$Eu^{3+}_{aq} + 3HL_{org} \leftrightarrow (Eu^{3+}, 3L^{-})_{org.} + 3H^{+}_{aq}$$

where HL is acidic form of the extractant. The increase of distribution ratios with approximate third-power dependency confirms that suitable distribution ratios could be achieved by increasing extractant concentration even at high acidity.

For the studied COSAN derivates, no effective Ln/An separation could be achieved (separation factors close to 1). A similar effect was observed also for other COSANs functionalized by CMPO groups [6-8]. Therefore, the possible use of such compounds for the treatment of PUREX solution is the envisaged extraction of the joint Ln/An groups before the pertinent second step, that is, the Ln/An separation by another process (e.g. “SANEX“).

CONCLUSIONS

All extractants studied proved to be very effective for extraction of trivalent radionuclides for acidity up to pH 1. The steep decrease of distribution ratios at higher acidities (≥1 M) can be compensated by an increase of extractant concentration. It was found that polarity of the diluents used does not have any significant influence on extraction efficiency for **1** or **2.** Partial preference of **3** was observed with the less-polar solvent mixture, which is preferable from a technological view. The mode of attachment of CMPO groups to the COSAN moiety had a marked effect on the extraction ability. The compound **1** with a diethyleneglycol connector between COSAN cage and CMPO group is the most effective extractant from all studied compounds. Additionally, the extraction of Eu^{3+} by **1** is approximately four orders of magnitude higher than for comparable CMPO compound and two orders of magnitude higher than for its synergic mixtures with cobalt bis(dicarbollide) anion. None of the compounds from this series

showed any Ln/An selectivity. Therefore, the possible use of such compounds should consist in the removal of the M^{3+} class of cations as the whole from highly acidic waste.

ACKNOWLEDGMENTS

We acknowledge support from EU Project EUROPART and the Ministry of Education of the Czech Republic (Project LC 523 and Research Plan AV0Z40320502). Support by Grant Agency of the Czech Republic (Project No. 104/05/2667 to J. R.) is appreciated.

REFERENCES

1. See for example: G. Modolo, H. Vijgen, D. Serrano-Purroy, B. Christiansen, R. Malmbeck, C. Sorel, and P. Baron, "DIAMEX counter-current extraction process for recovery of trivalent actinides from simulated high active concentrate," *Sep. Sci. Technol*, **42**, 439-452 (2007) and references therein.
2. See for example: T. Fujii, K. Aoki, and H. Yamana, "Effect of nitric acid distribution on extraction behavior of trivalent F-elements in a TRUEX system," *Solvent Extr. Ion Exch.*, **24**, 347-357 (2006) and references therein.
3. See for example: S. A. Ansari, P. N. Pathak, M. Husain, A. K. Prasad, V. S. Parmar, and V. K. Manchanda, "Extraction of actinides using N,N,N'',N'-tetraoctyl diglycolamide (TODGA): a thermodynamic study," *Radiochim. Acta*, **94**, 307-312 (2006) and references therein.
4. I. B. Sivaev and V. I. Bregadze, "Chemistry of cobalt bis(dicarbollides). A review," *Collect. Czech. Chem. Commun.*, **64**, 783-805 (1999).
5. J. Plešek, "Potential Applications of the Boron Cluster Compounds," *Chem. Rev.*, **92**, 269-278 (1992).
6. B. Grűner, J. Plešek, J. Báča, I. Císařová, J.-F. Dozol, H. Rouquette, C. Viňas, P. Selucký, and J. Rais, "Cobalt bis(dicarbollide) ions with covalently bonded CMPO groups as selective extraction agents for lanthanide and actinide cations from highly acidic nuclear waste solutions," *New J. Chem.*, **26**, 1519-1527 (2002).
7. P. Selucký, J. Rais, M. Lučaníková, B. Grűner, M. Kvíčalová, K. Fejfarová, and I. Císařová, "Lanthanide and actinide extractions with anionic ligands based on cobalt bis(dicarbollide) ions with covalently bonded CMPO functions," *Radiochim. Acta*, in press.
8. B. Grűner, M. Kvíčalová, I. Císařová, P. Selucký, and M. Lučaníková, manuscript in preparation.
9. L. Mikulášek, B. Grűner, C. Dordea, V. Rudzevich, V. Böhmer, J. Haddaoui, V. Hubscher, F. A. Neu, J. Čáslavský, and P. Selucký, "*Tert*-Butyl-calix[4]arenes Substituted at the Narrow Rim with Cobalt Bis(dicarbollide)(1–) and CMPO Groups – New and Efficient Extractants for Lanthanides and Actinides," *Eur. J. Org. Chem.*, 4772-4783 (2007).
10. F. Arnaud Neu, V. Bohmer, J.-F. Dozol, C. Gruttner, R. A. Jakobi, D. Kraft, O. Mauprivez, H. Rouquette, M. J. Schwing Weill, N. Simon, and W. Vogt, "Calixarenes with diphenylphosphoryl acetamide functions at the upper rim. A new class of highly efficient extractants for lanthanides and actinides," *J. Chem. Soc.-Perkin Trans.*, **2**(6), 1175-1182 (1996).

A COMPARATIVE STUDY OF SOME BTP AND BTBP CLASS LIGANDS

T. Retegan,[1] C. Ekberg,[2] A. Fermvik,[1] M.R. StJ. Foreman,[1,2] and G. Skarnemark[1]

[1]Nuclear Chemistry, [2]Industrial Materials Recycling Department of Chemical and Biological Engineering, Chalmers University of Technology, 412 96 Gothenburg Sweden. Corresponding author email address: tretegan@chalmers.se

ABSTRACT

Partitioning and transmutation (P&T) of the long lived nuclides in spent nuclear fuel into short-lived ones is an important step in decreasing the radiotoxicity, volume, and time necessary for storage in a repository. A proper separation of the metals used in the transmutation process is necessary and solvent extraction with different ligands is one of the possibilities. This separation has been extensively tested in Europe using the BTP and BTBP class ligands. In this paper a comparative study of the extraction capabilities of $CyMe_4$-BTP and $CyMe_4$-BTBP as function of different diluents and kinetics has been made.

INTRODUCTION

Partitioning and transmutation (P&T) of the long-lived nuclides in spent nuclear fuel into short lived ones is important for shortening storage time of nuclear waste and to make nuclear power more sustainable due to higher energy efficiency. Efficient extraction molecules for partitioning of the actinides(III) from lanthanides(III) exist [1], but now also the environmental aspect is considered. Ligands consisting only of carbon, oxygen, hydrogen, and nitrogen (known as CHON principle) [2] are currently known and are being further developed [3]. This allows the incineration of the organic phase reducing the amount of secondary waste. Several CHON molecules were designed, under consecutive European Union projects, for example, NEWPART, PARTNEW, and EUROPART, aiming at improving the earlier models with the respect to, for example, radiolysis and acidic degradation [4-6]. When trying to design a large scale separation system based on solvent extraction, using novel extraction agents, a clear procedure for selection of, for example, organic diluent and appropriate extracting ligand must be made [7,8]. Typically a simple dissolution test screens out the totally unsuitable combinations of molecules and diluents. Then extraction and extraction kinetic experiments are performed to find the optimal combination [9].

It has been long known that by changing the diluent highly affects the D (distribution ratios) and SF (separation factors) for the selected metals with different extraction mechanisms [10,11]. However, whether or not SF between metals extracted by the same mechanism will change with the diluent is not as well known.

Experiments were carried out with 2,6-bis(5,5,8,8-tetramethyl-5,6,7,8-tetrahydrobenzo[1,2,4]triazin-3-yl)pyridine ($CyMe_4$-BTP) and 6,6'-bis(5,5,8,8-tetramethyl-5,6,7,8-tetrahydro-benzo[1,2,4]triazin-3-yl)-[2,2']bipyridine ($CyMe_4$-BTBP), dissolved in two different diluents, cyclohexanone and nitrobenzene. The aim of these experiments was to compare the extraction kinetics of these ligands in different diluents but also to show that, by changing the diluent, the SF achievable with these systems can be significantly influenced.

EXPERIMENTAL

The organic phases consisted of 0.01 M $CyMe_4$-BTBP or $CyMe_4$-BTP dissolved in either cyclohexanone or nitrobenzene. The aqueous phase consisted of 0.01 M HNO_3 keeping 1 M total nitrate with $NaNO_3$ and spiking with trace amounts of ^{241}Am and $^{152,154}Eu$. Due to mutual solubility in water (2.3 wt % in water and 8.0 wt % of water for cyclohexanone; 0.19 wt % in water and 0.24 wt % of water for nitrobenzene), the cyclohexanone and the nitrobenzene were pre-equilibrated with pure aqueous phase, and the aqueous phase was also pre-equilibrated with pure diluents before contact.

Volumes of 500 µL of organic phase and 500 µL of aqueous phase were contacted by vigorous manual shaking for various periods of time (5 to 25 or 40 min) in 3.5 mL glass vials in a plastic device designed to protect the samples from the heat of the hand. After contact, the samples were centrifuged at 1000 g for ten min to allow phase separation. Aliquots of 200 µL were taken from each phase and measured in HPGe detectors (Canberra, Ortec Gamma Analyst GEM 23195). The experiments were performed in triplicate and the uncertainties reported are based on the standard deviation calculated from these samples. The temperature during the experiments was 19 ± 1 °C. The experimental conditions remained the same throughout the test.

MATERIALS

The $CyMe_4$-BTP and $CyMe_4$-BTBP molecules were synthesized according to literature procedures [12,13]. All other reagents used in the experiments were of laboratory grade (except for ^{241}Am and $^{152,154}Eu$, which were laboratory stock solutions [19]) and purchased from Fisher Reagent Chemical: cyclohexanone (p.a.), nitrobenzene (p.a.); from Merck: HNO_3 (63%) suprapure; and from Acros: $NaNO_3$ (p.a.). MQ water was produced by "Milli-Q gradient" provided by Millipore®.

RESULTS AND DISCUSSION

The extraction kinetics was very fast for both ligands dissolved in cyclohexanone, and the extraction equilibrium was reached within 5 min for both Am and Eu. In nitrobenzene, the kinetics was slightly slower, the equilibrium being reached after 15 min for $CyMe_4$-BTBP for both Am and Eu, and after 10 min for $CyMe_4$-BTP for Am. In the case of $CyMe_4$-BTP, Eu did not reach equilibrium, even after 25 min contact time.

It has already been reported that Am(III) forms a 1:3 complex, $Am(NO_3)_3.3(BTP)$, with BTP type ligands [12,14,15], while Eu(III) can form 1:1; 1:2,

and 1:3 $Eu(NO_3)_y.n$(BTP) complexes [14-16], which can coexist in the solution. In the BTBP ligand type case, both Am(III) and Eu(III) complexes with a 1:2 metal:ligand ratio were reported: $Am(NO_3)_3.2$(BTBP) and $Eu(NO_3)_3.2$(BTBP) [17-19].

The observed *D* values and SF varied significantly from system to system, and an attempt to clarify the phenomena was made with the help of a 2 x 2 experimental matrix (see Figure 1). The matrix will be discussed in the following order: vertical, for the same ligand and horizontal, for the two ligands.

	Ligands	
Diluents	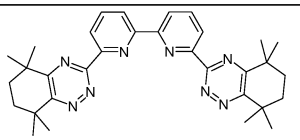 **$CyMe_4$-BTBP**	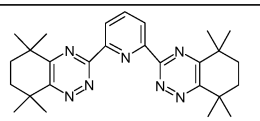 **$CyMe_4$-BTP**
Cyclohexanone	*D* Am: 12.8 ± 0.18 *D* Eu: 0.093 ± 0.01 $SF_{Am/Eu}$: 136 ± 3.00 Kinetics: fast Equilibrium: 5 min for Am 5 min for Eu	*D* Am: 212 ± 19.00 *D* Eu: 0.84 ± 0.10 $SF_{Am/Eu}$: 253 ± 23.00 Kinetics: fast Equilibrium: 5 min for Am 5 min for Eu
Nitrobenzene	*D* Am: 728 ± 69.00 *D* Eu: 9.2 ± 0.10 $SF_{Am/Eu}$: 79.4 ± 8.00 Kinetics: slow Equilibrium: 15 min for Am 15 min for Eu	*D* Am: 322 ± 32.00 *D* Eu: 22.5 ± 0.40* $SF_{Am/Eu}$: 14.20* Kinetics: slow Equilibrium: 10 min for Am * after 25 min, not at equilibrium.

Figure 1. Experimental matrix showing the main results of the kinetic extraction using 0.01 M $CyMe_4$-BTBP and $CyMe_4$-BTP dissolved in cyclohexanone and nitrobenzene in contact with 0.01 M HNO_3 (where nitrate concentration was kept equal to 1 M by adding $NaNO_3$) spiked with trace amounts of ^{241}Am and ^{152,154}Eu.

$CyMe_4$-BTBP in Nitrobenzene or Cyclohexanone

The dissolution of $CyMe_4$-BTBP is faster in nitrobenzene than in cyclohexanone, which can probably be attributed to the polarity of the diluents (Є = 34.8 for nitrobenzene and 18.2 for cyclohexanone) or due to the fact that nitrobenzene has an aromatic π system, similar with that of the BTPs or BTBPs. Cyclohexanone has a very small π system, associated with the carbonyl group. Thus, the dissolution should work by the rule "like dissolve like".

As mentioned above, the complex stoichiometry specific to BTBP molecules is 1:2 with the respect to metal:ligand ratio and three nitrates. The higher *D* value of Am and Eu in nitrobenzene systems can probably be explained by the fact that an oxygen

atom from the more polar nitrobenzene molecule can coordinate to the metal, thus increasing lipophilicity of the complex and easing the extraction.

As for the difference in SF between the two systems, this can also be explained by the fact that the coordinated oxygen from nitrobenzene is less selective than nitrogen towards actinides and lanthanides; therefore as nitrobenzene coordinates, it is expected that *D* for Eu should increase towards that of Am.

Another explanation can be that the nitrates are in outer sphere complexes in the organic phase. A reason for better extraction could then be that the transfer energy of nitrate from the aqueous phase to the organic phase is less for nitrobenzene than for cyclohexanone. At present we can not say which explanation is the correct one.

$CyMe_4$-BTP in Nitrobenzene or Cyclohexanone

The solubility and polarity previously discussed can be applied without any amendments in this case, too.

The differences in *D* for Am are not as significant as in the previous systems, and this can be explained by the different complexes formed for Am 1:3 with respect to metal:ligand ratio. Thus, 9 coordination sites are already taken, and the coordination of one or more oxygen from nitrobenzenes will not be easily done.

The *D* for Eu shows a different trend: in cyclohexanone, Eu reaches equilibrium in the same time as Am. It is assumed that Eu also forms only a 1:3 complex in this diluent.

In nitrobenzene, the extraction of Eu is still increased even after 25 min; thus, the SF in this case will decrease even further and will certainly be different than in the cyclohexanone-containing system. This can probably be attributed to the fact that nitrobenzene can contribute to the extraction as described before but here it is also assumed that two different complexes between Eu and BTP can exist, 1:2 and 1:3.

$CyMe_4$-BTBP and $CyMe_4$-BTP in Cyclohexanone

The *D* values for Am are higher in the BTP case due to the fact that there are 9 coordination sites occupied by the ligand, since the complex is 1:3 with the respect to metal:ligand ratio, and three nitrate groups per molecule coordinate. This way, the complex is more lipophilic than one formed by $CyMe_4$-BTBP, which only uses 8 coordination sites.

$CyMe_4$-BTBP and $CyMe_4$-BTP in Nitrobenzene

In this case, the *D* values for Am decrease in the $CyMe_4$-BTP containing system whereas the *D* for Eu increases without reaching equilibrium, even after 25 min.

The longer equilibrium time can probably be explained as before with more Eu:BTP species, but the decrease in the Am extraction can not yet be explained. That the selectivity goes down in nitrobenzene is, as said before, probably due to the coordination of the nonselective oxygens from the nitro group in the diluent.

CONCLUSIONS

The SF can be significantly modified by changing the diluent for an extraction system utilizing the same extraction mechanism.

A 2 x 2 experimental matrix was used to show the main results of the kinetic extraction using 0.01 M $CyMe_4$-BTBP and $CyMe_4$-BTP dissolved in cyclohexanone and nitrobenzene in contact with 0.01 M HNO_3 (where nitrate concentration was kept to equal 1 by adding $NaNO_3$) spiked with trace amounts of ^{241}Am and $^{152,154}Eu$.

A possible explanation was presented, where the classical extraction mechanisms for the two ligands described in previous literature are combined with the contribution of the diluent as phase-transfer booster.

Further experiments and quantum-mechanical calculation for better understanding are planned.

ACKNOWLEDGMENTS

The authors wish to thank Swedish Nuclear Fuel and Waste Management Co. (SKB) and the European Union (EUROPART Project FI6W-CT-2003-508854).

REFERENCES

1. M. Nilsson and K. L. Nash, "Review Article: A review of the Development and Operational Characteristics of the TALSPEAK Process," *Solvent Extr. Ion Exch.*, **25**(6), 665-701 (2007).
2. C. Madic and M. J Hudson, "High Level Liquid Waste Partitioning by means of Completely Incinerable Extractants, Final Report," European Commission Contract No. FI2W-CT91-0112, EUR 18038, 1998.
3. C. Ekberg, A. Fermvik, T. Retegan, G. Skarnemark, M. R. S. Foreman, M. J. Hudson, S. Englund, and M. Nilsson, "An Overview and Historic Look Back at the Solvent Extraction Using Nitrogen Donor Ligands to Extract and Separate An(III) from Ln(III)," Submitted to *Radiochim. Acta* (2007).
4. M. Nilsson, S. Andersson, C. Ekberg, M. R. S. Foreman, M. J. Hudson, and G. Skarnemark, "Inhibiting Radiolysis of BTP molecules by Addition of Nitrobenzene," *Radiochim. Acta*, **94**, 103-106 (2006).
5. T. Retegan, C. Ekberg, S. Englund, A. Fermvik, M. R. S. Foreman, and G. Skarnemark, "The Behaviour of Organic Solvents containing C5-BTBP and CyMe4-BTBP at Low Irradiation Doses," *Radiochim. Acta*, **95**, 637-642 (2007).
6. A. Fermvik, C. Ekberg, T. Retegan, and G. Skarnemark, "Radiolysis and Ageing of C2-BTP in Cinnamaldehyde/Hexanol mixtures," Scientific Basis for Nuclear Waste Management XXX, D. S. Dunn, C. Poinssot, and B. Begg, Eds., Mater. Res. Soc. Symp. Proc. 985, Warrendale, PA, 0985-NN03-20, 2007.
7. S. Andersson, "Extraction Properties of Some Nitrogen-Containing Extractants and Determination of Nitrate Complex Formation for Lanthanides and Selected Actinides using Solvent Extraction," Ph.D. Thesis, Chalmers University of Technology, Gothenburg, Sweden, ISBN 91-7291-582-X, 15 (2005).
8. T. Retegan, "The Influence of Diluents and Side Groups of the Ligands on Liquid-Liquid Extraction of Actinides and Lanthanides," Ph.D. Thesis, Chalmers University of Technology, Gothenburg, Sweden, Technical report No. 2007:2, 2007.

9. T. Retegan, C. Ekberg, A. Fermvik, and G. Skarnemark, "The Effect of Diluents on Extraction of Actinides and Lanthanides," Scientific Basis for Nuclear Waste Management XXX, D. S. Dunn, C. Poinssot, and B. Begg, Eds., Mater. Res. Soc. Symp. Proc. 985, Warrendale, PA, 0985-NN14-05, 2007.
10. G. W. Mason, A. F. Bollmeier, and D. F. Peppard, "Diluent Effects in the Extraction of Selected Metallic Cations by Bis(Hexoxy-Ethyl)Phosporic Acid," *J. Inorg. Nucl. Chem.*, **29**, 1103-1112 (1967).
11. D. F. Peppard, G. W. Mason, A. F. Bollmeier, and S. Lewey, "Extraction of Selected Metallic Cations by a Highly Hindered $(GO)_2PO(OH)$ Extractant in Two Different Diluents From an Aqueous Chloride Phase," *J. Inorg. Nucl. Chem.*, **33**, 845-856 (1971).
12. M. J. Hudson, C. E. Boucher, D. Braekers, J. F. Desreux, M. G. B. Drew, M. R. S. Foreman, L. M. Harwood, C. Hill, C. Madic, F. Marken, and T. G. A. Youngs, "New Bis(Triazinyl)Pyridine for Selective Extraction of Americium(III)," *New J. Chem.*, **30**, 1171-1183 (2006).
13. M. R. S. Foreman, M. J. Hudson, M. G. B. Drew, C. Hill, C. Madic, "Complexes Formed Between the Quadridentate, Heterocyclic Molecules 6,6'-Bis(5,5,8,8-tetramethyl-5,6,7,8-tetrahydro-benzo[1,2,4]triazin-3-yl)[2,2']bipyridine (BTBP) and Lanthanides(III): Implications for the Partitioning of Actinides(III) and Lanthanides(III)," *Dalton Trans.*, 1645-1653 (2006).
14. M. Weigl, A. Geist, U. Mullich, and K. Gompper, "Kinetics of Americium(III) Extraction and Backextraction with BTP," *Solvent Extr. Ion Exch.*, **24**(6), (2006).
15. M. A. Denecke, A. Rossberg, P. J. Panak, M. Weigl, B. Schimmelpfennig, and A. Geist, "Characterization and Comparison of Cm(III) and Eu(III) Complexes with 2,6-Di(5,6-dipropyl-1,2,4-triazin-3-yl)pyridine Using EXAFS,TRFLS and Quantum-Chemical Methods," *Inorg. Chem.*, **44**, 8418-8425 (2005).
16. L. Petit, C. Adamo, and P. Maldivi, "Toward a Clear-Cut on the Origin of 2,6-Di(1,2,4-triazin-3-yl)pyridine Selectivity for Trivalent Actinides: Insights from Theory," *Inorg. Chem.*, **45**, 8517-8522 (2006).
17. M. Nilsson, S. Andersson, F. Drouet, C. Ekberg, M.Foreman, M. Hudson, J.-O. Liljenzin, D. Magnusson, and G. Skarnemark, "Extraction Properties of 6,6'-bis-(5,6-dipentyl-[1,2,4] triazin-3-yl)-[2,2']bipyridinyl (C5-BTBP)," *Solvent Extr. Ion Exch.*, **24**(3), 299-318 (2006).
18. A. Geist, C. Hill, G. Modolo, M. R. S. Foreman, M. Weigl, K. Gompper, and M. J. Hudson, "6,6'-Bis(5,5,8,8-tetramethyl-5,6,7,8-tetrahydro-benzo[1,2,4]triazin-3-yl)[2,2'] bipyridine, an Effective Extracting Agent for the Separation of Am(III) and Curium(III) from the Lanthanides," *Solvent Extr. Ion Exch.*, **24**, 463-483 (2006).
19. T. Retegan, C. Ekberg, I. Dubois, A. Fermvik, T. J. Wass, and G. Skarnemark, "Extraction of Actinides with Different 6,6'-Bis(5,6-Dialkyl-[1,2,4]-Triazin-3-yl)-[2,2']Bipyridines (BTBP's)," *Solvent Extr. Ion Exch.*, **25,** 1-15 (2007).

THE EFFECT OF IRRADIATION ON EXTRACTION OF VARIOUS METALS BY C5-BTBP

A. Fermvik,[1] C. Ekberg,[2] M.R.S. Foreman,[1,2] T. Retegan,[1] and G. Skarnemark[1]

[1]Nuclear Chemistry, [2]Industrial Materials Recycling, Department of Chemical and Biological Engineering, Chalmers University of Technology, 412 96 Göteborg, Sweden
Corresponding author email address: anna.fermvik@chalmers.se

ABSTRACT

Different polycyclic molecules containing nitrogen have been developed to be used as extractants in the separation of actinides(III) from lanthanides(III) in the spent nuclear-fuel treatment. During a potential industrial process involving nuclear waste, the extractant will be exposed to high doses of ionizing radiation; hence, the extractant should be resistant towards irradiation. This study explores the capacity of an irradiated solution of C5-BTBP in cyclohexanone to extract Eu and Am but also the fission and corrosion products Pd, Ag, and Cd.

INTRODUCTION

The power production in nuclear-power reactors generates large amounts of waste, which have to be safely stored for long periods of time (e.g., 100,000 years) [1]. This is due to the long half-lives of some of the elements present in the spent fuel, such as neptunium and americium. To shorten the required storage time and minimize the volume of the waste the concept of partitioning and transmutation (P&T) has been developed. It is based on the separation of certain fractions of the spent fuel, followed by various treatments to finally only have nuclides with shorter half-lives or even stable ones. Such separation is traditionally performed with solvent extraction (the PUREX process) [1]. The high-level liquid waste (HLLW) stream resulting from the PUREX process can then undergo further treatment (e.g. DIAMEX and SANEX) [2], to reach the final goal. Since the HLLW contains elements emitting ionizing radiation, the extracting systems must be stable towards radiolytic degradation. An estimated prospective annual dose to the organic system in the SANEX process is 100 kGy to 1 MGy [3]. Accumulation of various radiolysis products has among other things been shown to deteriorate the selectivity of extracting agents [4].

THEORY

One of the most difficult parts of the separation processes for spent nuclear fuel is the separation of trivalent actinides (An) and lanthanides (Ln). Several polydentate N-

donor ligands have been proposed as extractants for such a process [5]. Nilsson et al. [6] showed that the extraction of europium (Eu) and americium (Am) by 6,6'-bis-(5,6-dipentyl-[1,2,4]triazin-3-yl)-[2,2']bipyridinyl (C5-BTBP) decreased when a solution with cyclohexanone as diluent was irradiated. Similar behaviour has been reported for a number of polydentate N-donor ligands [7], but the interesting observation regarding this specific system was that the extraction of Am decreased much more than the extraction of Eu. Thus, the separation factor between the metals ($SF_{Am/Eu}$) decreased from around 150 to almost 30. In this study, the experiments by Nilsson et al. were repeated, but with a slightly lower dose rate and the addition of pre-equilibration of the phases before contact. This was done to establish whether or not pre-equilibration affected the results.

When an organic system is being irradiated it can undergo either primary processes, energy transfer from the radiation to the original components, or secondary processes, chemical reactions involving free radicals and other species formed in the primary processes. Due to the resonance stabilization of the benzene ring, aromatic compounds are generally relatively stable towards radiolysis [8], but the carbonyl group in cyclohexanone increases the radiolytic reactions taking place in the diluent [9]. The BTBP molecules (6,6'-bis(5,6-dialkyl-[1,2,4-]triazin-3-yl)-2,2'-bipyridines) were designed to be more resistant towards irradiation than its precursor BTP (2,6-*bis*-(1,2,4-triazine-3-yl)pyridines), but still the molecule is susceptible to radiolysis [6,7].

Many of the polydentate N-donor ligands also show high affinity for various transition metals [10], most of which are present in the HLLW solution resulting from the PUREX process [11]. C5-BTBP in particular has proven to enable separation between metals that are generally regarded as difficult to separate, such as the separation of palladium(II) from rhodium(III) and ruthenium(II) nitrosyl [12]. In addition to Eu and Am experiments, this study also investigated the effect on extraction behaviour towards palladium (Pd), silver (Ag), and cadmium (Cd) of an irradiated organic system containing 0.005 M C5-BTBP in cyclohexanone. Pd, Ag, and Cd are present in the HLLW in typical concentrations of approximately 4.15, 0.20, and 0.21 mM, respectively [11]. Distribution ratios for Pd have been shown to be independent of the C5-BTBP concentration in an octanol/kerosene mixture at high nitric acid concentrations, probably due to a change in extraction mechanism [12]. Thus the acid concentration in this study was kept low, 0.01 M.

EXPERIMENTAL

The following chemicals were used for the experiments: C5-BTBP (synthesized according to [13]), cyclohexanone (>99.5%, Sigma Aldrich), $NaNO_3$ (>99% pro analysi, Merck), HNO_3 (FIXANAL, Sigma-Aldrich), $Pd(NO_3)_2.2H_2O$ (purum ≥97%, Fluka AG), $AgNO_3$ (pro analysi >99.9% May&Baker Ltd), $Cd(NO_3)_2.4H_2O$ (Fisher Scientific Comp.), and MQ water (Milli-Q gradient, Millipore®). The spike solution of $^{152,154}Eu$ and ^{241}Am was prepared from laboratory stock solutions [14]. The internal standards used for ICP-MS measurements were In and Pt (High-Purity Standards (HPS)). During the experiments the temperature was 19 ± 1 ˚C.

Pd, Ag, and Cd Experiments

A 50 mL 0.005 M C5-BTBP solution was made by dissolution in cyclohexanone. A 25 mL sample of this solution was placed in a glass bottle in a gamma-irradiating cobalt source (Gamma cell 220, Atomic Energy of Canada ltd) with an estimated dose rate to water of ~13 Gy/h. The rest of the solution was placed outside the gamma source, at a remote distance, to act as a reference. Triple samples were taken from each flask at different times during a total period of 1341 hours, corresponding to a total dose for the irradiated samples of 17.4 kGy. The aqueous phase consisted of 0.99 M $NaNO_3$, 0.01 M HNO_3, and 50 μM each of Pd, Ag, and Cd.

Before conducting the extraction experiments, the organic phases were pre-equilibrated with a solution of 0.99 M $NaNO_3$ and 0.01 M HNO_3, and the aqueous phase was pre-equilibrated with fresh cyclohexanone. A 500 μL aliquot of each phase was contacted for six hours in a shaking device, sufficient time to reach chemical equilibrium. After contact, the samples were centrifuged at 800 g for five minutes, and aliquots of 300 μL were taken from each phase. Samples were also taken from the pre-equilibrated aqueous phase before contact with the organic phase. All aqueous samples were measured by ICP-MS (Elan 6100 DRC, Perkin Elmer Sciex), and the distribution ratios for Pd, Ag, and Cd were calculated.

During the experiments with Pd, Ag, and Cd, a dark precipitate at the interface between the phases was observed when a metal-containing aqueous phase was left in contact with the organic phase. A contact experiment with Pd as the only metal present in the aqueous phase showed the same type of precipitation, confirming that Pd is reacting with the cyclohexanone. This behavior, often referred to as palladium black, has been reported for solutions of ketones in diluents such as 1,2-dichloroethane, 1-octanol, *n*-dodecane, benzene, and toluene, but it was not observed when the diluent was nitrobenzene [15].

Eu and Am Experiments

The radiolysis experiment performed by Nilsson et al. [6] was repeated, with the addition of a pre-equilibration of the phases before contact similar to the procedure described above. All other experimental details were kept the same, except that the samples were measured in an HPGe detector (EG&G Ortec) instead of a NaI(Tl) well-type detector. The same gamma-emitting cobalt source as above was used, but at the time of this experiment, the estimated dose rate to water was ~15 kGy/h. Initially, only single samples were taken from the reference solutions, since no degradation was expected, but this was changed to double samples at higher doses.

RESULTS AND DISCUSSION

No change in color of the irradiated solutions compared to the reference solutions was visible during the time of the experiments. A fading of color has previously been reported for some irradiated organic solutions containing BTBP (bis-triazine-bipyridine) and BTP (bis-triazine-pyridine) type molecules [7].

Figure 1 shows the change in $SF_{Am/Eu}$ for the study by Nilsson et al. and the new corresponding study that included pre-equilibration of the phases before contact. The uncertainty bars in the figure are based on the calculated standard deviations in the triplicates. Similar to the old study, the new one showed an evident decrease in $SF_{Am/Eu}$, going from around 160 to 35 at a received dose of just over 20 kGy. This change in selectivity is very interesting and may be due to a number of reasons, one being that one or more of the degradation products lost their original affinity for Am. The experiment including pre-equilibration generally gave slightly higher values of $SF_{Am/Eu}$, but the trend is the same for both curves.

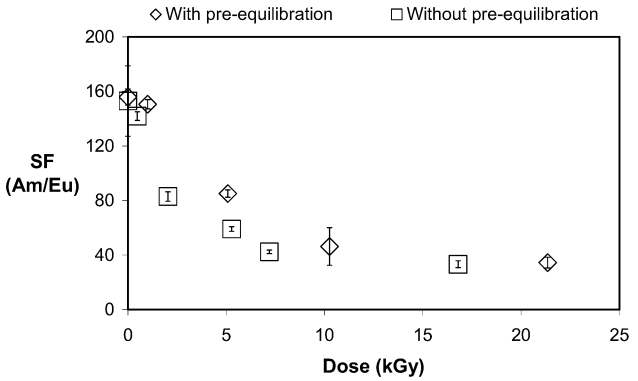

Figure 1. Separation factor (Am/Eu) as a function of received dose for two different sets of experiments, one with pre-equilibration of the phases and one without pre-equilibration. Organic phase: 0.005 M C5-BTBP in cyclohexanone. Aqueous phase: 0.99 M $NaNO_3$, 0.01 M HNO_3, and traces of $^{152,154}Eu$ and ^{241}Am.

To determine whether or not any degradation due to aging took place, the reference solutions were studied in terms of change in *D*. The extraction of Pd, Ag, and Cd seemed to be relatively stable when comparing the *D* at various times, while for Eu and Am, a small decrease could be observed as the solution aged.

The effect of radiolysis upon extraction is illustrated in Figure 2 as the ratio (in %) between *D* for the irradiated solution and *D* for the reference solution as a function of the dose received by the irradiated solution. Uncertainty bars are based on the calculated standard deviations of the samples. The metal extraction decreases as the organic phase is being irradiated with the exception of Ag, which requires further studies. Most of the decrease occurs at low doses; hence the solution starts to degrade just as the irradiation starts. For Am, the *D* for the irradiated solution goes down to ca. 25% of the *D* for the reference solution, while for Pd it decreases to ca. 50% and for Eu to around 80%.

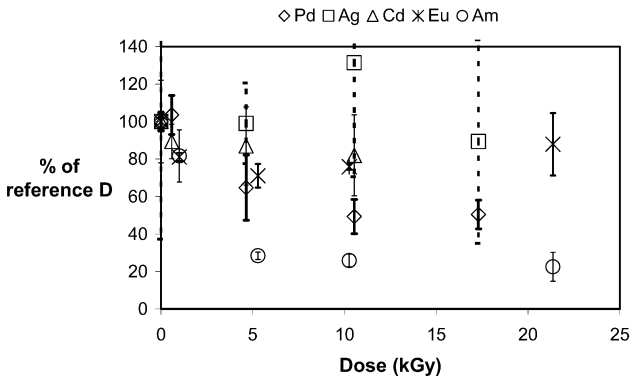

Figure 2. Extraction of Pd, Ag, Cd, Eu, and Am by irradiated solutions, expressed as the percentage of distribution ratio for the reference solution as a function of the received dose. Three data points were removed (two for Ag and one for Cd) due to problems with the measurements. The value for Eu at ~5 kGy is taken from the experiments by Nilsson et al. [6].

An experiment was made with pure cyclohexanone as the organic phase, in order to establish to what extent the metals are extracted by cyclohexanone alone. The distribution ratios obtained were approximately 0.3 for Pd, 0.04 for Ag, and 0.02 for Cd, compared to corresponding values for the reference solution at $t = 0$ of approximately 200, 500, and 600. For Eu and Am, the distribution ratio for pure cyclohexanone was 0.001 for both metals. The reference solution at $t = 0$ gave distribution ratios of about 0.2 for Eu and 30 for Am.

CONCLUSION

The extraction behaviour of irradiated C5-BTBP in cyclohexanone of Pd, Ag, Cd, Eu, and Am was tested. The extraction of Am is the one that decreases the most, followed by Pd and then Eu. The extraction of Cd is not affected by the irradiation, while Ag probably is affected similarly to Eu and Pd, but needs to be further studied. The degradation of the organic system starts already at low doses.

The $SF_{Am/Eu}$ is substantially decreased for the irradiated solution, and therefore the system should be studied in more detail, since structural information about the degradation products may be very useful for the future synthetic design of new extracting molecules for the An/Ln separation. The organic solution is still being irradiated, which enables more results in the near future.

ACKNOWLEDGMENTS

This work was supported by the Swedish Nuclear Fuel and Waste Management Co., SKB, and the European Union (EUROPART F16W-CT-2003-508854). The authors would like to express their appreciation to MSc Kristian Larsson and LicEng. Arvid Ødegaard-Jensen for their valuable work with ICP-MS measurements.

REFERENCES

1 G. Choppin, J-O. Liljenzin, and J. Rydberg, Radiochemistry and Nuclear Chemistry, 3rd ed., Butterworth-Heinemann, Woburn, USA, 2002; p. 627.

2 C. Madic, M. J. Hudson, J-O. Liljenzin, J.-P. Glatz, R. Nannicini, A. Facchini, Z, Kolarik, and R. Odoj, "Recent Achievements in the Development of Partitioning Processes of Minor Actinides from Nuclear Wastes Obtained in the Frame of the Newpart European Programme (1996-1999)," *Prog. Nucl. Energy,* **40**(3-4), 523-526 (2002).

3 M. Nilsson, S. Andersson, C. Ekberg, M. R. S. Foreman, M. J. Hudson, J-O. Liljenzin, D. Magnusson, and G. Skarnemark, "Inhibiting Radiolysis of BTP Molecules by Addition of Nitrobenzene," *Radiochim. Acta*, **94** (1), 1-4 (2006).

4 G. F. Egorov and O. P. Afanas'ev, "Radiation Chemistry of Hydrocarbon Diluents in Solvent-Extraction Processes," Translated fr. *Atomnaya Energiya* **54**(5), 347-50 (1983).

5 C. Ekberg, A. Fermvik, T. Retegan, G. Skarnemark, M. R. S. Foreman, M. J. Hudson, S. Englund, and M. Nilsson, "An Overview and Historic Look Back at the Solvent Extraction Using Nitrogen Donor Ligands to Extract and Separate An(III) from Ln(III)," Accepted for publication in *Radiochim. Acta* (2007).

6 M. Nilsson, S. Andersson, F. Drouet, C. Ekberg, M. Foreman, M. Hudson, J-O. Liljenzin, D. Magnusson, and G. Skarnemark, "Extraction Properties of 6,6'-bis-(5,6-dipentyl-[1,2,4]triazin-3-yl)-[2,2']bipyridinyl (C5-BTBP)," *Solvent Extr. Ion Exch.*, **24**(3), 299-318 (2006).

7 I. Dubois, C. Ekberg, S. Englund, A. Fermvik, J-O. Liljenzin, D. Neumayer, T. Retegan, and G. Skarnemark, "Partitioning and Transmutation Annual Report 2006," SKB Report R-07-09, Swedish Nuclear Fuel and Waste Management Co., Stockholm, Sweden, 2007.

8 I. György and L. Wojnarovits, in *Radiation Chemistry of Hydrocarbons*, G. Földiak, Ed., Elsevier Scientific Publishing Company, Budapest, 1981; pp. 17-53.

9 A. Singh and G. Freeman, "Radiolysis of Cyclohexanone I. Pure Liquid," *Can. J. Chem.*, **42,** 1869-1889 (1964).

10 Z. Kolarik, "Extraction of Selected Mono- to Tetravalent Metal Ions by 2,6-Di-(5,6-dialkyl-1,2,4-triazin-3-yl)pyridines," *Solvent Extr. Ion Exch.*, **21**(3), 381-397 (2003).

11 I. Svantesson, G. Persson, I. Hagström, and J-O. Liljenzin, "Distribution Ratios and Empirical Equations for the Extraction of Elements in PUREX High Level Liquid Waste Solution – II: HDEHP," *J. Inorg. Nucl. Chem.,* **42,** 1037-1043 (1980).

12 M. Foreman, M. Hudson, A. Geist, C. Madic, and M. Weigl, "An Investigation into the Extraction of Americium(III), Lanthanides and D-Block Metals by 6,6'-Bis-(5,6-dipentyl-[1,2,4]triazin-3-yl)-[2,2']bipyridinyl (C5-BTBP)," *Solvent Extr. Ion Exch.,* **23**(5), 645-662 (2005).

13 M. R. S. Foreman, M. J. Hudson, M. G. B. Drew, C. Hill, and C. Madic, "Complexes Formed Between the Quadridentate, Heterocyclic Molecules 6,6'-Bis-(5,6-dialkyl-1,2,4-triazine-3-yl)-2,2'-bipyridine (BTBP) and Lanthanides(III): Implications for the Partitioning of Actinides(III) and Lanthanides(III)," *Dalton Trans.,* **13**, 1645-1653 (2006).

14 T. Retegan, C. Ekberg, I. Dubois, A. Fermvik, G. Skarnemark, and T. J. Wass, "Extraction of Actinides with Different 6,6'-Bis(5,6-Dialkyl-[1,2,4]-Triazin-3-yl)-[2,2']-Bipyridines (BTBPs)," *Solvent Extr. Ion Exch.,* **25**(4), 417-431 (2007).

15 N. T. Hung, M. Watanabe, and T. Kimura, "Solvent Extraction of Palladium(II) with various Ketones from Nitric Acid Medium," *Solvent Extr. Ion Exch.,* **25**(3), 407-416 (2007).

IMPROVED SEPARATION OF Am(III) FROM THE LIGHT LANTHANIDES USING A SOFT-DONOR SYNERGIST

Dale D. Ensor and Matthew H. Zimmerman

Chemistry Department, Tennessee Technological University, Cookeville, TN 38505
Corresponding author email address: densor@tntech.edu

ABSTRACT

The separation of minor actinides from fission products, especially the trivalent lanthanides, remains a difficult problem. Current research has focused on the use of soft-donor groups that have a greater affinity for the trivalent actinides than for the lanthanides. The extractant bis(chlorophenyl)dithiophosphinic acid was used in combination with a synergist, 4,7-diphenyl-1,10-phenanthroline, to extract Am(III) and Eu(III) from aqueous nitrate media. The extraction efficiencies of Am(III) and Eu(III) were measured by varying the total ionic strength and concentrations of the extractant, synergist, and nitric acid. Results suggest that this synergistic system may be useful for group separation of the minor actinides from the lanthanides.

INTRODUCTION

The anticipated resurgence of nuclear power and its acceptance as a CO_2 emission-free energy source will require improved waste-management techniques. The development of a closed fuel cycle which supports the recycling of fissile U and Pu as fuel for thermal reactors for power generation requires the partitioning of fission products and minor actinides for better waste management [1]. Further separation of the minor actinides (Am and Cm) from the trivalent lanthanide elements is an important part of the Advanced Fuel Cycle Initiative, which would allow the minor actinides to be fabricated into fuel and burned in advanced reactors [2]. The long-lived isotopes, ^{241}Am and ^{243}Am, as well as other minor actinides (Cm and Np), are the major contributors to the long-term radiotoxicity of spent nuclear fuel [3]. These elements, if successfully removed from other fission products, could eventually be burned in fast reactors. In order for this to be feasible, the actinides must be separated from the lanthanides, since several of the lanthanides are neutron poisons. Application of better partitioning techniques to spent nuclear fuel would reduce the amount of waste and the time that this waste would need to be isolated from the environment.

The minor actinides and trivalent lanthanides possess very similar physical and chemical characteristics in aqueous solutions, making their separation a challenging problem. A number of group separation methods have been developed over the past 60 years with the largest separation factors being observed in systems that utilize soft-donor

atoms, such as N or S [4]. The reasons for the stronger binding of the minor actinides over the lanthanides with these soft-donor atoms is not clear but are most likely a summation of small differences in their interactions that produce effective group-separation schemes. A number of studies have shown that Cyanex 301, a dithiophosphinic acid, can successfully separate the minor actinides from the lanthanides [5,6], but these systems must operate in a pH range of 3.5–5.0 to be efficient. Unfortunately, Cyanex 301 is not stable in high radiation fields and is oxidized by nitric acid, conditions found in current methods for reprocessing of spent nuclear fuel.

A series of dithiophosphinic acid extractants with phenyl substituents have been reported to yield separation factors, D_{Am}/D_{Eu}, of up to several thousand, based on a single contact. Improvements in the thermal and radiation stability, as well as the acidity of these molecules have been reported [7]. Combinations of diorganyldithiophosphinic acids and neutral organophosphorus compounds showed mixed results, with only moderately enhanced separation factors being reported [7]. Recently, bis(chlorophenyl)dithio-phosphinic acid (BCDT) was combined with a synergist, tris(2-ethylhexyl)phosphate, which yielded separation factors of >2000 for Am over Eu at 0.1 M HNO_3 and 0.9 M $NaNO_3$ [8]. These results were obtained using a soft-donor extractant and a hard-donor synergist. This research reports the results of the combination of a soft-donor extractant, bis(chlorophenyl)dithiophosphinic acid (BCDT), with a soft-donor synergist, 4,7-diphenyl-1,10-phenanthroline (DIPHEN). The use of DIPHEN as an effective synergist has been previously reported [9].

EXPERIMENTAL

Materials

Reagent Chemicals

All chemicals used were ACS analytical grade or better and used as received. Water purified by reverse osmosis, then deionized using a Barnstead purification system (resistivity >18MΩ) was used to prepare all aqueous solutions. Sodium hydroxide solution (50% w/w), nitric acid (A.C.S. plus), and sodium nitrate (A.C.S. certified) were obtained from Fisher Scientific.

Stock solutions of HNO_3, $NaNO_3$, and NaOH were prepared, and working concentrations of these solutions were made by volumetric dilutions of the appropriate stock solutions. Solutions of NaOH (0.1 M, 1.0 M, and 5.0 M) were standardized by titration using the primary standard, potassium hydrogen phthalate (KHP), to the phenolphthalein endpoint. The nitric acid stock was standardized by titration using standardized NaOH to a phenolphthalein endpoint. A cation-exchange resin procedure [10] was used to standardize the sodium nitrate stock solution.

The bis(chlorophenyl)dithiophosphinic acid (BCDT), Figure 1, was used as received from Oak Ridge National Laboratory. 4,7-Diphenyl-1,10-phenanthroline (DIPHEN), Figure 1, was purchased from GFS Chemicals and used as received. The diluent, 1,2-dichloroethane (ACS reagent), was obtained from Fisher Scientific. Organic-phase stock solutions were prepared by dissolving the weighed masses of extractant and

synergist volumetrically in 1,2-dichloroethane. More dilute concentrations of the required organic phases were prepared by volumetric dilution of the stock.

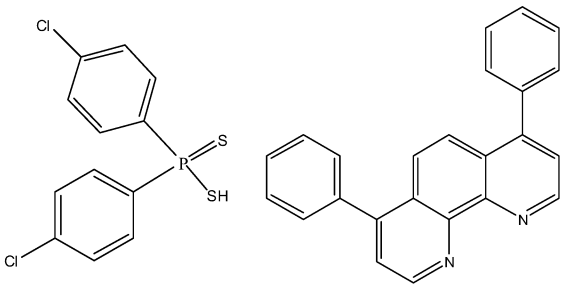

BCDT DIPHEN

Figure 1. Structures of bis(chlorophenyl)dithiophosphinic acid (BCDT) and 4,7-diphenyl-1,10-phenanthroline (DIPHEN).

Radiotracers

The radiotracers, ^{241}Am and $^{152\text{-}54}$Eu, were obtained from Nuclear Materials Processing Group, REDC, Oak Ridge National Laboratory. A known volume of the desired aqueous phase was spiked with either or both tracers so that the concentration of activity was 50,000 cpm/mL. The activity of the analytical samples was determined by measuring the gamma activity using a Packard Cobra II Auto-Gamma counter equipped with a three inch NaI crystal. Counting times were adjusted to reduce the statistical error in the count rate to 1% or better.

Contacting Procedures

All extractions were performed in duplicate using a batch equilibrium method. Equal volumes, 400 µL, of aqueous and organic phases were placed in 2.5 mL polypropylene microcentrifuge tubes (Fisher Scientific). The mixtures were vortexed for 30 s using a touch mixer and allowed to equilibrate for 15 minute in a controlled-temperature water bath at 25 ± 0.05 °C. Each sample was vortexed three times to ensure complete phase equilibrium. Samples were centrifuged for 5 minutes and the phases separated. Two counting samples containing 150µL each were prepared from both phases. The distribution ratios (D_{Am} or D_{Eu}) were determined from the background-corrected count rate of the organic phase divided by that of the background-corrected rate of the aqueous phase.

RESULTS AND DISCUSSION

Previous work [7] with BCDT dissolved in toluene showed that it was not an effective extractant for either Am(III) or Eu(III) at [HNO_3] > 0.001 M. The extraction of these metals by BCDT using dichloroethane as the solvent yielded similar results with D_{Eu} < 0.002 and D_{Am} < 0.005, with [HNO_3] varying in the range 0.010–0.001 M. The

addition of DIPHEN to the extraction mixture greatly enhanced the extraction of Am(III) with $D_{Am} < 20$, while the extraction of Eu(III) was only slightly enhanced, $D_{Eu} < 0.004$. The enhancement was evident in the separation factors $D_{Am}/D_{Eu,}$ shown in Table 1. Large separation factors were evident as a result of the addition of DIPHEN to the extraction mixture, with the highest separation factor observed for the extraction at 0.001 M HNO_3.

TABLE 1. Separation Factors with and without DIPHEN at various acid concentrations

$[HNO_3]$ + 0.50 M $NaNO_3$	0.050 M BCDT			0.050 M BCDT + 0.015 M DIPHEN		
	D_{Am}	D_{Eu}	D_{am}/D_{Eu}	D_{Am}	D_{Eu}	D_{am}/D_{Eu}
0.010	1.4×10^2	1.4×10^3	10	3.85	1.0×10^2	385
0.050	2.8×10^2	1.6×10^3	18	8.78	3.0×10^2	292
0.0010	5.1×10^2	2.1×10^3	24	17.7	3.7×10^2	478

The effectiveness of the addition of DIPHEN to the extraction mixture was evaluated by holding the [BCPT] constant and measuring the distribution of Eu(III) and Am(III) as a function of the [DIPHEN]. The aqueous phase contained 0.50 M $NaNO_3$, 1.0×10^{-3} M HNO_3, and 0.01 M sulfanilic acid buffer to control the pH; the results are shown in Figure 3. The distribution of Am (III) is enhanced by the addition of DIPHEN and increases with increasing DIPHEN. The distribution of Eu(III) is enhanced only slightly by the DIPHEN.

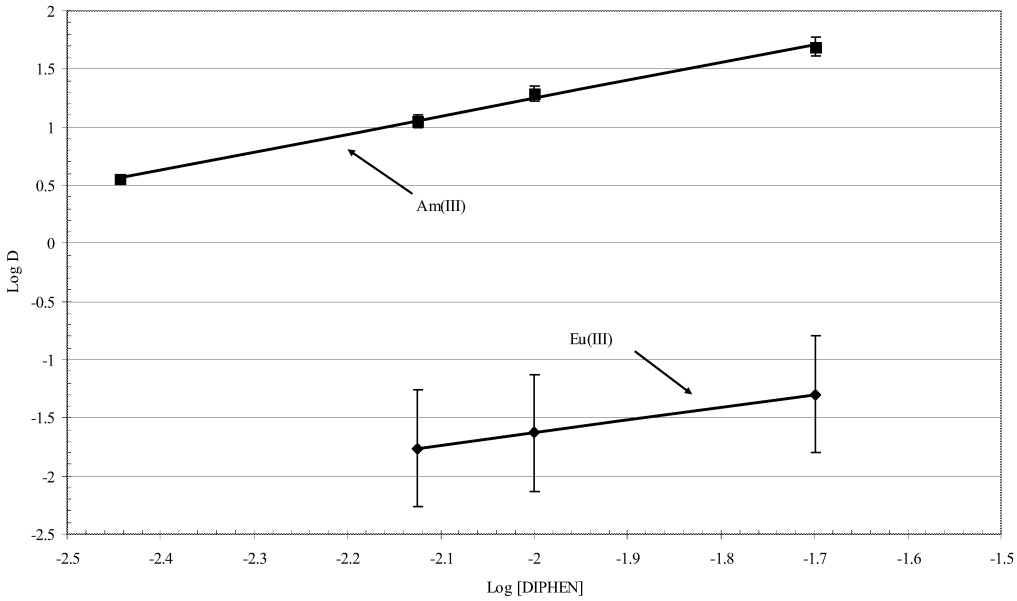

Figure 2. Plot of log D versus log[DIPHEN]. Experimental conditions: (aqueous phase) $[HNO_3]$ = 0.0010 M, 0.50 M $NaNO_3$; (organic phase) [BCPT] = 0.050 M in dichloroethane.

The overall reaction for the extraction of the two metal ions can be inferred from slope analysis of the distribution data. Based on this data, the predominant extraction equilibrium equation is:

$$M^{3+} + 2[BCPTH]_{2(org)} + x\,Syn_{(org)} \rightleftharpoons [M(BCPT)_3BCPTH(Syn)_x]_{(org)} + 3H^+ \quad (1)$$

The BCPT behaves as a dimer, and the pH dependency implies that three deprotonated molecules of BCPT and a fourth protonated molecule are participating in the coordination sphere of the metal ion. The slope of 1 in Figure 2 for the Eu(III) indicates that one DIPHEN molecule is in the extracted Eu(III) complex. For Am(III), the slope in Figure 2 is 1.5, indicating that mixed complexes with different stoichiometries are extracted. Modolo and Nabet [8] report a similar slope for the extraction of Am(III) with BCPT and TEHP. The incorporation of more DIPHEN molecules in the extraction complex for Am(III) is one possible explanation for the high selectivity over Eu(III), as well as the greater affinity that soft-donor molecules have for the actinide elements. Further investigations of the distribution behavior of these two metals under varying conditions are necessary to describe a detailed extraction mechanism.

CONCLUSIONS

The combination of a soft-donor extractant and a soft-donor synergist enhanced the extraction of Am(III) over Eu(III) with separation factors approaching 400. These results provide confirmation that use of a soft-donor synergist will yield larger separation factors at lower pH than using oxygen-donor molecules, such as tributylphosphate and tris(2-ethylhexyl)phosphate. Further investigation of these types of synergistic systems could provide a better understanding of how these soft-donor systems can enhance the group separations of the trivalent lanthanides and actinides.

ACKNOWLEDGMENT

Partial support for this research was provided by the Nuclear Materials Processing Group, Oak Ridge National Laboratory.

REFERENCES

1. J. J. Laidler, “GNEP and the International Fuel Cycle,” Abstract NUCL-065, 233rd ACS National Meeting, March 25–29, 2007, Chicago, IL.
2. G. F. Vandegrift, M. C. Regalbuto, S. Aase, A. Bakel, T. J. Battisti, B. Delbert, J. P. Byrnes, M. A. Clark, D. G. Cummings, J. W. Emery, J. R. Falkenberg, A. V. Gelis, C. Pereira, L. Hafenrichter, Y. Tsai, K. J. Quigley, and M. H. Vander Pol, “Designing and Demonstration of the UREX+ Process Using Spent Nuclear Fuel,” in Atalante 2004, Nimes, France, Commissariat Energie Atomique.
3. G. R. Choppin and J. Rydberg, Nuclear Chemistry, Theory, and Applications, Pergammon, Oxford, England, 1980; Appendix H, Fission Products and Actinides in LWR Waste, pp. 593-599.

4. K. L. Nash, C. Madic, J. N. Mathur, and J. Lacquemont, in The Chemistry of the Actinide and Transactinide Elements, L. R. Morss, N. M. Edelstein, and J. Fuger, Eds., Springer, Dordrecht, The Netherlands, 2006; Vol. 4, pp. 2622-2798.
5. X. Wang, Y. Zhu, and R. Jiao, "Separation of Am from lanthanides by a synergistic mixture of purified Cyanex 301 and TBP," *J. Radioanal. Nucl. Chem.,* **251**(3), 487-492 (2000).
6. J. Chen, G. Tian, R. Jiao, and Y. Zhu, "A hot test for separating americium from fission product lanthanides by purified Cyanex 301 extraction in centrifugal contactors," *J. Nucl. Sci. Tech.*, (Suppl. 3), 325-327 (2002).
7. G. Modolo and R. Odoj, "Synergistic Selective Extraction of Actinides(III) over Lanthanides from Nitric Acid Using New Aromatic Diorganyldithiophosphinic Acids and Neutral Organophosphorus Compounds," *Solvent Extr. Ion. Exch.*, **17**(10), 33-53 (1999).
8. G. Modolo and S. Nabet, "Thermodynamic Study on the Synergistic Mixture of Bis(chlorophenyl)dithiophosphinic Acid and Tris(2-ethylhexyl)phosphate for Separation of Actinides(III) from Lanthanides(III)," *Solvent Extr. Ion. Exch.*, **23**, 359–373 (2005).
9. D. D. Ensor, G. D. Jarvinen, and B. F. Smith, "The Use of Soft Donor Ligands, 4-Benzoyl-2,4-Dihydro-5-Methyl-2-Phenyl-3H-Pyrazol-3-Thione and 4, 7-Diphenyl-1,10-Phenanthroline, for Improved Separation of Trivalent Americium and Europium," *Solvent Extr. Ion. Exch.*, **6**(3), 439-445 (1988).
10. J. S. Fritz and G. H. Schenk, Jr., Quantitative Analytical Chemistry, 2nd ed**.,** Allyn and Bacon, Inc., Boston, 1969; pp. 597-599.

THE BEHAVIOR AND IMPORTANCE OF LACTIC ACID COMPLEXATION IN TALSPEAK EXTRACTION SYSTEMS

Travis S. Grimes, Mikael Nilsson, and Kenneth L. Nash

Chemistry Department, Washington State University, P.O. Box 644630 Pullman, WA 99164-4630. Corresponding author email address: tsgrimes@wsu.edu

ABSTRACT

Advanced partitioning of spent nuclear fuel in the UREX +1a process relies on the TALSPEAK process for separation of fission-product lanthanides from trivalent actinides. The classic TALSPEAK utilizes an aqueous medium of both lactic acid and diethylenetriaminepentaacetic acid and the extraction reagent di(2-ethylhexyl)phosphoric acid in an aromatic diluent. In this study, the specific role of lactic acid and the complexes involved in the extraction of the trivalent actinides and lanthanides have been investigated using ^{14}C-labeled lactic acid. Our results show that lactic acid partitions between the phases in a complex fashion.

INTRODUCTION

As momentum towards increased nuclear-power production in the U.S. continues to grow, research into reprocessing of the spent nuclear fuel has increased. The U.S. currently practices a once-through policy for its nuclear fuel cycle, that is, direct geologic disposal following a period of monitored cooling above ground. The creation of programs like the Advanced Fuel Cycle Initiative (AFCI) and Global Nuclear Energy Partnership (GNEP) demonstrates the need for spent-fuel solutions if the expansion of the nuclear-power program is to be realized. These programs are currently considering the UREX processes, which avoid creating a pure Pu stream at any time during reprocessing [1]. The UREX processes are a combination of solvent-extraction processes that separate the spent fuel into manageable components. Fission-product lanthanides and transuranic (TRU) elements are isolated from UREX raffinate using the TRUEX process. The subsequent separation of lanthanides from TRUs, needed for transmutation of the latter, is challenging. The current baseline process for this separation is TALSPEAK.

TALSPEAK is an acronym for Trivalent Actinide-Lanthanide Separations by Phosphorus reagent Extraction from Aqueous Komplexes. TALSPEAK is a proven separation process developed in the 1960s by B. Weaver and F. A. Kappelmann [2], the separation is based on the extraction of the trivalent lanthanides using di(2-ethylhexyl) phosphoric acid (HDEHP) from an aqueous medium that selectively retains the trivalent actinides. This selective retention is achieved with the addition of two different complexing agents, lactic acid (HL) and diethylenetriaminepentaacidic acid (DTPA).

This separation scheme takes advantage of the slightly greater spatial extension of the actinide's 5f electron shell [3]; Am and Cm both contain a softer character than the lanthanides and bind more strongly to the nitrogen donor atoms of the DTPA. The binding of the Am and Cm with the DTPA suppresses their extractability, thus, making the selective partitioning of lanthanide ions to the extractant phase possible. Though TALSPEAK is a proven process, significant portions of the fundamental chemistry are not known. In particular, the role of HL is more complex than simply serving as a means of pH control. Literature reports indicate a role for HL in enhancing phase compatibility and improving phase-transfer kinetics, while possibly partitioning between the phases. In this report, some preliminary results describing the partitioning of lactate between typical TALSPEAK phases in the presence of La^{3+} are presented.

THEORY

Under the pH range of TALSPEAK operation, extraction of trivalent lanthanides and/or trivalent actinides occurs predominantly as a result of cation exchange/chelate formation [1]. Under most conditions, three hydrogen-bonded HDEHP dimers surround one metal ion, as defined by the following reaction [4-7]:

$$M^{3+} + \overline{3(HA)_2} \rightleftharpoons \overline{M(AHA)_3} + 3H^+ \quad (1)$$

where HA represents the monomeric HDEHP and the line above the species indicates its presence in the organic phase. Because three hydrogen ions are released to the aqueous phase for every cation extracted, TALSPEAK is sensitive to pH changes and requires buffering. HL concentrations are kept high to achieve the desired buffering effect, as well as other more subtle effects. The concentration of lactate in TALSPEAK ranges from 0.5 to 2 M. At these concentrations, lactate's affinity for the trivalent lanthanides and actinides is high enough to enable the possibility of mixed complexes (e.g., Am-DTPA-lactate or $ML(AHA)_{2,org}$). The presence of the $ML(AHA)_{2,org}$ has been inferred in previous TALSPEAK studies, although it has never been observed directly. Kosyakov and Yerin [7] systematically investigated the effect of varying the lactate concentration on the distribution ratio of curium. They modeled the complexation of the curium lactate complex in the aqueous phase. They hypothesized the presence of a mixed $CmL(AHA)_{2,org}$ complex in the organic phase. If the HL is co-extracted with the metal, additional biphasic equilibrium constants would be needed to describe the overall phase-transfer reaction. One proposed equilibrium for the mixed complex is shown [7,8]:

$$M^{3+} + \overline{2(HA)_2} + HL \rightleftharpoons \overline{M(AHA)_2L} + 3H^+ \quad (2)$$

Other routes of extraction for mixed complexes may exist. However, since no concrete evidence establishes the stoichiometry of the mixed complex, the simplest solution is used as a first approximation. The definition of an equilibrium constant for the mixed complex (K_{ex}) along with the development of a model is the main focus of this research.

EXPERIMENTAL

The extractant di(2-ethylhexyl)phosphoric acid (97%) was purchased from Aldrich and purified by the salt precipitation purification method [9]. The purified HDEHP was then titrated and determined to be 99.8% pure. The organic diluent 1,4-diisopropylbenzene (99%) supplied by Alfa Aesar was used without further purification. The organic phases were prepared by dissolving weighed amounts of HDEHP into the 1,4-diisopropylbenzene to achieve the desired concentration. The aqueous phases were prepared using lanthanide nitrate stocks from lab supplies (prepared from 99.999% lanthanide oxides or carbonates from Arris International Co.). The solutions were standardized to determine metal concentration, nitrate concentration, and H^+ concentration. The 85% (w/w) lactic acid (Baker) was used to prepare a 3 M lactic acid solution with a pH of 3.5. The prepared solutions were then combined together with 18 MΩ water to create the aqueous phases.

Experiments were carried out as a function of lactic acid and of metal concentration. The nitrate concentrations in the aqueous phases were maintained constant at 1 M by addition of $NaNO_3$, and the phases were pre-equilibrated with the organic diluent 1,4-diisopropylbenzene. The organic phases contained 0.2 M HDEHP for all extractions and were pre-equilibrated with 1 M $NaNO_3$. The pre-equilibrations consisted of 30 min. of vortex mixing followed by 15 min. of centrifugation.

The [HL] dependencies were investigated in the concentration range 0-2 M at constant metal concentration of 1 mM. The acidity was adjusted for all extractions to a pH of around 3.9. The experiments were carried out in triplicate and in two parallel sets, with and without a 10 µL spike of ^{14}C labeled HL added to each aqueous phase. The experiments evaluating the effect of $[M^{3+}]$ were carried out by varying the concentration of metal used from 0-20 mM while holding the HL concentration constant at 1 M.

The extraction procedure was identical for all experiments. However, the extraction volumes differed for the two different types of extractions. The nonradioactive extractions contained 700 µL organic phases and 700 µL aqueous phases, while the radiotracer experiments utilized 500 µL phases. The extractions were carried out by vigorous shaking on the vortex mixer for 30 min., followed by 15 min. centrifugation. For the nonradioactive extractions, the organic phase was removed and a 300 µL sample of the aqueous phase was taken and diluted to 3 mL with 2% HNO_3 for analysis by Inductively Coupled Plasma Optical Emission Spectra (ICP-OES). For the radiotracer experiments a 150 µL sample was taken from both phases and analyzed by liquid scintillation. Hydrogen ion concentration was measured at equilibrium using a glass electrode. The p[H] of the solution was determined directly, based on a strong acid-strong base titration used as a calibration curve.

RESULTS AND DISCUSSION

The observed partitioning of both La^{3+} and lactate between the aqueous solutions at pH 3.5-3.9 and variable concentrations of each species in 0.2 M HDEHP in 1,4-diisopropylbenzene are shown in Figure 1. The distribution ratio of lactate remains at or below 0.005, the distribution of La^{3+} above 600 on average from 0.01 to 0.7 M total

lactate. At higher concentrations, the distribution ratio of lactate increases with a first-order dependence on $[Lac]_{tot}$, while D_{La} decreases at a surprisingly high –4.5 dependency. Setting aside the contribution of changing activity coefficients, this result suggests the existence of a previously unreported $La(L)_4^-$ complex in the aqueous phase at high concentrations of lactate.

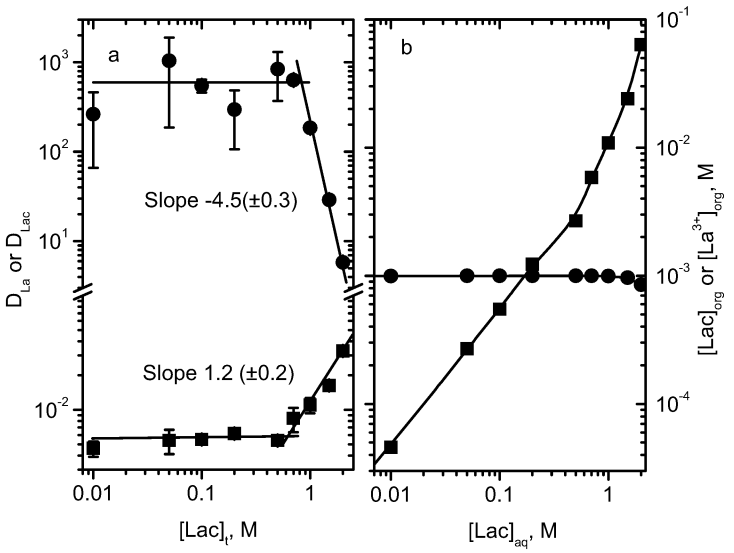

Figure 1. Distribution of HL and La^{3+} between an organic phase of 0.2 M HDEHP in 1,4-diisopropylbenzene and an aqueous phase of 0-2 M HL, 1 mM La^{3+}, 1 M $NaNO_3$, andpH ~3.9. a) Distribution ratios for La^{3+} (●) and HL (■). b) Organic-phase concentration of La^{3+} and HL.

In Figure 1b, the concentration of lactate in the organic phase increases steadily with increasing total lactate. At the highest concentration of total lactic acid, the ratio $[Lac]_{org}/[La^{3+}]_{org}$ is about 75. To establish a K_d value for the distribution of HL into the organic phase (absent metal ion or HDEHP), a separate set of experiments was run in which HL concentrations ranged from 0 to 1 M and aqueous solutions were contacted with the organic diluent 1,4-diisopropylbenzene. The value for $K_{d,HL}$ remained constant over this range at 0.0042 (as compared with the 0.033 value of the distribution ratio of HL observed at 2 M HL). Further investigation will be needed to establish the identity of the extracted lactate species in the presence of metal and extractant.

In Figure 2, the relationship between the experimentally observed values for the extraction of La^{3+} are compared with calculations based on a simplified model in which HL is presumed to remain in the aqueous phase under all conditions and that metal complexation equilibrium/extraction equilibrium constants remain constant over the range of concentrations of HL. Experimentally, it was observed that the $p[H^+]$ value was not constant; hence, it was necessary in the calculations to take this effect into account.

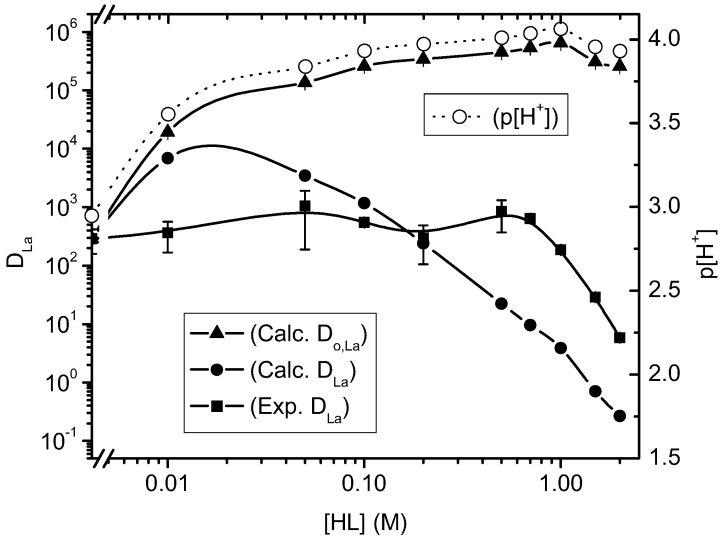

Figure 2. Distribution of La^{3+} as a function of [HL].
Experimental results (■) refer to an organic phase of 0.2 M HDEHP in 1,4-diisopropylbenzene and an aqueous phase with 0-2 M HL, 1 mM La^{3+}, 1.0 M $NaNO_3$, and p[H^+] at equilibrium. The calculated values of $D_{o,La}$ (▲) are based on the value of the distribution ratio of lanthanum with no added lactic acid and adjusted for the change in [H^+]. The calculated D_{La} (◆) are based on the $D_{o,La}$ values adjusted for lactate complexation of the lanthanum in the aqueous phase, using the stability constants found in [1]. No organic-phase lactate interaction is considered.

The experimental p[H^+] values are shown in the figure. In the simplified model, increases in p[H^+] should both increase partitioning of La^{3+} to the organic phase and increase the strength of lactate complexing in the aqueous phase, suppressing extraction. Increasing concentration of HL should lower extraction (at constant p[H^+]). The pattern for the experimental data shown in Figure 1 is reproduced in Figure 2 to facilitate the comparison.

The calculated values for $D_{o,La}$ are based on the reaction shown in Equation 1 and using constants from the previous report [1]. Changes in $D_{o,La}$ show the direct parallel between increasing p[H] and D_o. The second calculated line (D_{La}) corrects $D_{o,La}$ for the presence of $La(L)_n^{3-n}$ using stability constants from [1] (I = 0.1 M, T = 25.0 °C). The D_{La} calculated line shows the suppression of metal distribution (as the lactate concentration is increased) at a lower concentration than is seen experimentally. The mismatch between calculated and experimental observations in this system could indicate the inadequacies of the simplified thermodynamic calculations (that do not take into account activities of ions), or they could indicate the operation of a more complex set of equilibria than the simplified model employs. The pattern of unexplained increases in partitioning of lactate into the organic phase (Figure 1b) suggests that the simplified model is inadequate. Additional work is being done on these systems to improve the accuracy of the modeling.

CONCLUSION

The investigations of the TALSPEAK process have led to some answers regarding the fundamental chemistry. The specific role of HL remains a question. Experimental evidence supports the proposal of one or more mixed complexes being present in the TALSPEAK process. However, medium effects in the aqueous phase at high lactate concentrations cannot be disregarded. Future work includes performing extractions for the entire lanthanide series, and some actinide work as well. The immediate goal is to create a model for the extraction system. Once the model is completed, construction of a speciation diagram will answer questions regarding the principal reactions and determination of the specific role of HL.

ACKNOWLEDGMENTS

This work was supported by the U.S. Department of Energy Office of Nuclear Energy Science and Technology under the University-Nuclear Energy Research Initiative (U-NERI) program.

REFERENCES

1. M. Nilsson and K. L. Nash, "A Review of the Development and Operational Characteristics of the TALSPEAK Process," *Solvent Extr. Ion Exch.,* **25**(6), 665-701 (2007).
2. B. Weaver and F. A. Kappelmann, "TALSPEAK, A New Method of Separating Americium and Curium from the Lanthanides by Extraction from an Aqueous Solution of an Aminopolyacetic acid complex with a Monoacetic Organophosphate or Phosphonate," Report ORNL-3559, Oak Ridge National Laboratory, August 1964.
3. G. T. Seaborg and W. D. Loveland, The Elements Beyond Uranium, John Wiley and Sons, New York, 1990
4. D. F. Peppard, G. W. Mason, J. L. Maier, and W. J. Driscoll, "Fractional Extraction of the Lanthanides as their di-alkyl Orthophosphates," *J. Inorg. Nucl. Chem.,* **4,** 334-343 (1957).
5. I. Svantesson, G. Hagström, and J. O. Liljenzin, "Distribution Ratio and Empirical Equations for the Extraction of Elements in PUREX High Level Waste Solution—II: HDPHP," *J. Inorg. Nucl. Chem.,* **42**, 1037-1043 (1980).
6. V. N. Kosyakov and E. A. Yerin, "Separation of transplutonium and Rare-Earth Elements by Extraction with HDEHP from DTPA Solutions," *J. Radioanal. Chem.,* **43**, 37-51 (1978)
7. V. N. Kosyakov and E. A. Yerin, "On the Mechanism of Trivalent Actinide Extraction in the System HDEHP-Lactic Acid with DTPA," *J. Radioanal. Chem.,* **56**, 93-104 (1980).
8. M. I. Mel'nik, V. T. Filimonov, and E. A. Karelin, "Mechanism of Extraction of Weighable Amounts of Lanthanides(III) with HDEHP from Nitric and Acetic Acid Solutions," *Radiokhimiya,* **41**(1), 67-70 (1999).
9. J. A. Partridge and R. C. Jensen, "Purification of di(2-ethylhexyl) Phosphoric Acid by Precipitation of Copper (III) di(2-ethylhexyl) Phosphate," *J. Inorg. Nucl. Chem.,* **31**, 2587-2589 (1969).

SEPARATION OF LANTHANIDES FROM TRIVALENT ACTINIDES, THE ROLE OF AQUEOUS-PHASE SOFT-DONOR COMPLEXING AGENTS

Mikael Nilsson, Cortney Hoch, G. Patrick Meier, and Kenneth L. Nash

Chemistry Department, Washington State University, P.O. Box 644630, Pullman, WA 99164-4630. Corresponding author email address: mikaeln@wsu.edu

ABSTRACT

Closing the nuclear fuel cycle to reduce storage volumes and times requires advanced separation processes, among which is the separation of trivalent actinides from lanthanides that are present in the waste. A proven system is TALSPEAK, utilizing polyaminocarboxylates for this group separation. However, the narrow pH range these molecules require complicates their use. Soft-donor molecules that may complex actinides at low pH have been investigated. Results indicate that, although DTPA gives the best selectivity, all molecules tested showed preference for americium. The solubility of some reagents at low pH suggests the need for further development.

INTRODUCTION

With the current atomic energy usage and waste policy, the storage facilities for spent nuclear fuel may be virtually overfilled even before they are constructed. There are two viable solutions to this problem: increase the capacity of the storage facilities, or decrease the amount of waste. For Yucca Mountain, the limit is the amount of heat that the waste generates rather than the actual volume; hence, separation of the isotopes responsible for this heat will be necessary. In the U.S., the processes under consideration for treating spent nuclear fuel are collectively described as the UREX+ suite. At some point in this process, it may be necessary to separate trivalent actinides (An(III) (e.g., americium and curium) from lanthanides (Ln). One proven separation process for this separation is the TALSPEAK process, developed in Oak Ridge National Laboratory in the 60s [1]. This process utilizes soft-donor atoms, in this case nitrogen, to separate the two groups of elements on the basis that the 5f-elements (actinides) have a slightly softer character than the 4f-elements (lanthanides). The soft donor is in the form of diethylenetriamine pentaacetic acid (DTPA). It is maintained in the aqueous phase and complexes the actinides, while the lanthanides are extracted into an organic phase using bis-2-ethylhexyl phosphoric acid (HDEHP). Moderate to high concentrations of lactic acid are present to buffer the pH of the system and improve kinetics, among other things. The reprocessing of the spent fuel is done, with few exceptions, in nitric acid, and it would be beneficial to operate a TALSPEAK type process at a pH lower than 3, the classical condition. An operating pH of 1 to 2 would greatly simplify the need for careful

pH control and possibly reduce the need for the large amount of lactic acid used. The molecule responsible for the group separation is the polyaminocarboxylate DTPA, which is also the most pH-sensitive reagent in the process. It has been reported to begin to precipitate at a pH around 2.7 [2]. To make this process less pH-sensitive a number of different polyaminocarboxylates have been tested as well as some other aqueous complexing agents containing soft donors. Using these different aqueous reagents the extraction behaviors of the lanthanide series and americium have been studied.

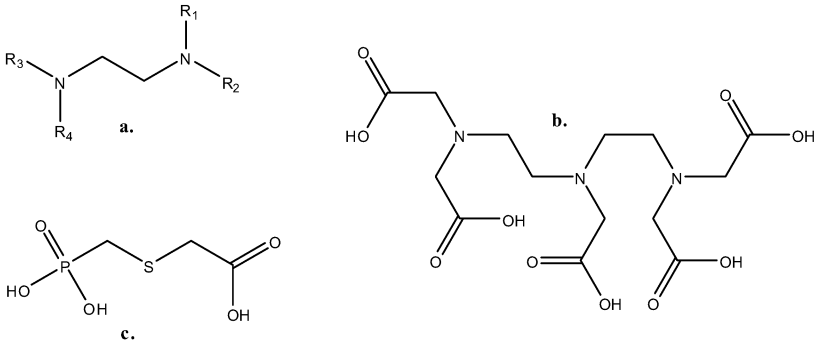

Figure 1. Aqueous complexing reagents used in this work. a: $R_{1\text{-}4}$ =CH_2COOH is ethylenediamine tetraacetic acid (EDTA); $R_{1\text{-}3}$ = CH_2COOH, R_4 = CH_2CH_2OH is N-(2-hydroxyethyl)ethylenediamine-N,N′,N′-triacetic acid (HEDTA), and $R_{1\text{-}4}$ = $CH_2PO(OH)_2$ is ethylenediamine tetramethylene phosphonic acid (EDTMP). b: DTPA. c: 2-(phosphonomethylthio)acetic acid (PMTAA).

EXPERIMENTAL

The HDEHP used was obtained 97% pure from Sigma-Aldrich and was purified before use by the copper precipitation method [3]; the product of purification was above 99% pure. The *n*-dodecane was obtained from Alfa Aesar with a purity of 98% and was used as received. The lanthanides and yttrium used were obtained from Arris International Co. as the metal oxides (carbonate in the case of cerium) and had a purity of 99.999%. These were dissolved in nitric acid and standardized as regards to metal concentration (ICP-OES), acidity, and nitrate concentration (ion exchange and potentiometric titration). The concentrated nitric acid (69.9% w/v) and an 85% (w/v) aqueous solution of lactic acid was obtained from J.T. Baker and used as supplied. EDTMP was obtained from Sigma-Aldrich and purified by repeated recrystallization from ethanol. HEDTA was obtained from Sigma-Aldrich with a purity of 98% and used as received. EDTA (puriss) and DTPA (puriss) were both obtained from Fluka and used as received. Sodium hydroxide was obtained from Sigma-Aldrich in the form of 50% (w/w) solution. Sodium nitrate used was obtained from Ricca Chemical Company; a saturated solution was filtered and recrystallized to remove all impurities prior to use. The analytical grade KHP used to standardize the base in the potentiometric titrations was obtained from Sigma-Aldrich and stored in an oven at 80 °C to keep it dry. PMTAA was synthesized according to Kazikowski's procedure [4] and hydrolyzed with Maier's process [5] to give the product in 95% purity (^{1}H-NMR). The ^{241}Am tracer in 0.1 M HNO_3 solution was obtained from Pacific Northwest National Laboratory.

Aqueous solutions were prepared by weighing suitable amounts of the different reagents into graduated glassware and diluting to the required volume. All aqueous solutions were prepared in a similar way; 1.0 M lactic acid, 1.0 mM total metal concentration with equal amounts of each lanthanide and yttrium, 0.05 M aqueous complexant (e.g. DTPA) pH-adjusted to desired value by addition of NaOH or HNO_3, and the final concentration of Na^+ adjusted to 1.0 M by adding $NaNO_3$ after final pH adjustments. The organic phase consisted of 0.3 M HDEHP in *n*-dodecane. Before extraction, the aqueous and organic phases were pre-equilibrated. All experiments were carried out in triplicate. Similar experiments were carried out in parallel where one set of triplicates were spiked with trace amounts of ^{241}Am. Gamma analysis of samples containing americium were performed on a NaI(Tl) solid scintillation counter (Packard Cobra 5003). For the samples containing only nonradioactive metals, the organic phase was removed, and only the aqueous phase was analyzed by ICP-MS. The aqueous phase was sampled prior to contact to observe any change in aqueous concentration due to extraction of the metal. All aqueous phases were finally checked for pCH by measuring the potential with a combination glass electrode calibrated for $[H^+]$ vs. mV.

RESULTS AND DISCUSSION

Extractions were carried out at pH ~3.7 with each of the different aqueous complexant to set a reference point. Some of the systems resulted in quantitative extraction of the lanthanides, and pH was adjusted to see if any trans-lanthanide trend could be observed. In general, the ICS-MS measurements give large uncertainties when distribution ratios fell outside the bounds 10^3 and 10^{-3}. The extraction trend for the lanthanides normalized to the distribution ratio of americium in the classical TALSPEAK system using DTPA is shown in Figures 2 and 3 and is useful for comparison to the other aqueous complexants. The results with DTPA are in good agreement to previous observations using this system [1] and resulted in a complete group separation with a separation factor (SF) for the least extracted lanthanide, neodymium, and americium of around 30. The trend for DTPA shows yttrium (~0.98 $Å^{-1}$) somewhat deviating from its expected position near holmium, not an uncommon phenomenon in yttrium chemistry. DTPA still gives the overall best separation performance, even though separation factors above 1 are obtained for all the lanthanides using other aqueous complexants. A comparison of the distribution ratios is shown in Table 1, where it is clear that americium is most effectively complexed by DTPA. The phosphorous-containing reagents are not very efficient hold-back reagents for An(III) under the conditions investigated here. The theoretical value for Am using HDEHP alone is calculated as in [6], where theoretical values for americium distribution using 1 M lactic acid alone are also reported. For the polyaminopolycarboxylic acid reagents, the trend for the lightest lanthanides are fairly similar, resulting in the lowest distribution ratios for neodymium. The heaviest lanthanides show somewhat different behavior with a decrease in distribution using EDTA and HEDTA, while with DTPA there is an increasing trend.

EDTMP yielded a steadily increasing trend in extraction efficiency for the lanthanides, although the high distribution ratios result in large uncertainties in the ICP-MS measurements. The novel reagent PMTAA also gives complete group separation at

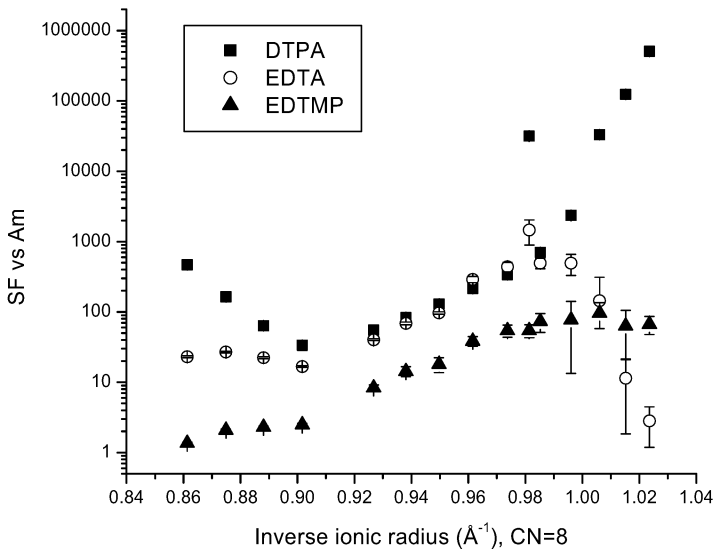

Figure 2. SF for Ln + Y vs. americium (D_{Ln}/D_{Am}) using different aqueous complexants. Organic phase: 0.3 M HDEHP in *n*-dodecane. Aqueous phase: 1.0 M lactic acid, 1.0 mM total metal conc., 1.0 M Na+, and [DTPA] and pH as follows: (■) 0.05 M DTPA, pH 3.74 ± 0.04; (○) 0.05 M EDTA, pH 3.71 ± 0.05; (▲) 0.05 M EDTMP, pH 2.75 ± 0.05.

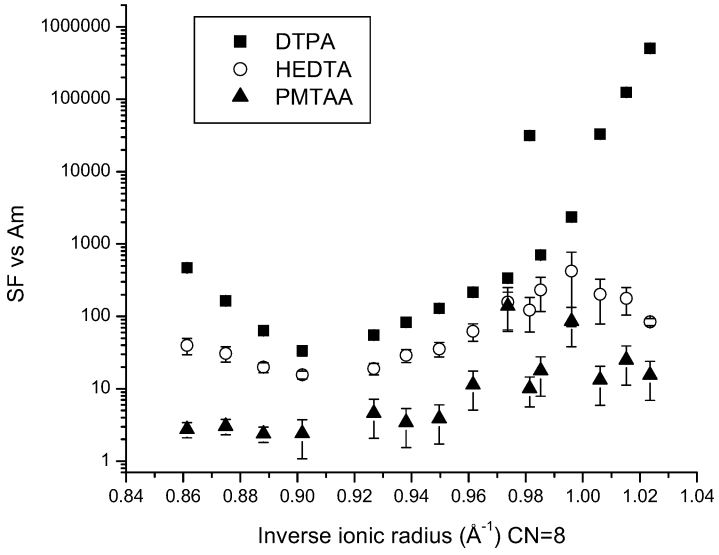

Figure 3. SF for Ln + Y vs. americium (D_{Ln}/D_{Am}) using different aqueous complexants. Organic phase: 0.3 M HDEHP in *n*-dodecane. Aqueous phase: 1.0 M lactic acid, 1.0 mM total metal conc., 1.0 M Na+, and [DTPA] and pH as follows: (■) 0.05 M DTPA, pH 3.74 ± 0.04; (○) 0.05 M HEDTA, pH 3.24 ± 0.01; (▲) 0.05 M PMTAA, pH 3.66 ± 0.01.

pH 2.5 and above; however, the distribution ratios for the lanthanides using PMTAA are very high and for americium results in a distribution ratio of several hundred. At pH 1,

the distribution ratios decrease and show a trend similar to what is expected using HDEHP without the presence of aqueous complexants. It is likely that at this acidity (0.1 M HNO_3) the PMTAA ligand forms a weak americium complex, depressing the distribution ratio of americium slightly (it would be expected to be between neodymium and samarium).

Table 1. Comparison of the extraction efficiency for americium using different aqueous complexants at pH ~3.7, 1.0 M lactic acid, and 1.0 M Na^+. *

Ligand	DTPA	EDTA	HEDTA	EDTMP	PMTAA	HDEHP
D_{Am}	0.07 ± 0.004	1.44 ± 0.015	11.0 ± 0.28	149 ± 15	555 ± 130	8×10^6

*SD is based on triplicate assays. For comparison, a theoretical value for Am extraction using HDEHP alone in toluene is given. The extraction constant is taken from [7], log $K_{ex,Am}$ = -1.70; comparative values are reported in [6].

Table 2. Comparison of SF between americium lanthanides using different aqueous complexants with the experimental conditions identical to those in Figures 2 and 3.*

M^{3+}	log K DTPA	log K EDTA	log K HEDTA	SF Ln/Am DTPA	SF Ln/Am EDTA	SF Ln/Am HEDTA	log K_{ex}
La	19.49	15.36	13.48	470 ± 21	23 ± 0.7	39 ± 10	-2.22
Nd	21.26	16.51	14.88	34 ± 5.3	17 ± 0.5	15 ± 2.0	-1.35
Eu	22.39	17.25	15.34	83 ± 11	69 ± 2.9	29 ± 6.0	-0.22
Dy	22.83	18.30	15.26	340 ± 21	440 ± 68	160 ± 93	+0.90
Er	22.75	18.89	15.38	2300 ± 68	490 ± 160	420 ± 350	+1.52
Lu	22.46	19.74	15.93	*500000*	2.8 ± 1.6	84 ± 9.5	+2.76

*Stability constants for the 1:1 (metal:ligand) complex, log K, are taken from the Martell and Smith database [8] for an ionic strength of 0.1 M; the extraction constants log K_{ex} are taken from [7] and represent HDEHP extracting into toluene. Errors are given as SD and are based on triplicate assays. No error is reported for extraction of lutetium with DTPA, since only one value was obtained by ICP-MS.

The extraction constant K_{ex} and the stability constant of aqueous complex and metal in Table 2 can be used to some degree to explain the shape of the extraction curve. Though the constants were determined in media different from that used in this work, comparing differences between the individual lanthanide ions may still be done. The extraction constants gradually increase, resulting in an approximately linear trend of the distribution ratios over the series for HDEHP extraction from mineral acid. Considering the constants across the lanthanide series, the aqueous complexants show a large increase in complex strength going from La to Nd; that is, distribution ratios may decrease. Then a small gradual increase up to dysprosium means that distribution ratios may increase somewhat, due to relatively stronger complexation with HDEHP. For DTPA, the aqueous complexes after dysprosium become weaker, resulting in a sharp increase in extraction. For EDTA and HEDTA, the aqueous complexes continue to grow in strength, and from erbium the distribution ratios start to decrease. Of course, these values only provide a partial answer, as the complete system will be very complicated to describe theoretically.

CONCLUSIONS

Based on these results, it is clear that, for a complete group separation at pH 3.5, DTPA remains the best alternative of the reagents investigated. The trans-lanthanide extraction trends show interesting behavior using different aqueous complexants. This system represents a good opportunity for computer-modeling insights, as it is only the metal ion that changes. The phosphorous reagents result in an approximately quantitative extraction of the lanthanides; however, the distribution ratios for americium are still too high to be useful in a process. The benefit of further pursuing these reagents is the possibility of working at lower pH and without lactic acid. Lanthanide complexes with EDTMP have been reported to precipitate at low pH [9], making EDTMP unsuitable for extractions; however, the phosphoric analog of DTPA may prove more useful, and this investigation is currently underway. The novel ligand PMTAA is worth pursuing, since it is soluble even at low pH, avoiding unwanted precipitation. Current work is focused on adding functional groups to PMTAA to increase the acidity of this ligand, so that a complete group separation may be possible at a pH of 1 or less.

ACKNOWLEDGMENTS

The authors wish to thank the US DOE, U-NERI program for financial support.

REFERENCES

1. B. Weaver and F. A. Kappelmann, "Preferential Extraction of Lanthanides Over Trivalent Actinides by Monoacidic Organophosphates from Carboxylic Acids and from Mixtures of Carboxylic and Aminopolyacetic Acids," *J. Inorg. Nucl. Chem.*, **30**, 263-272 (1968).
2. G. Persson, S. Wingefors, J. O. Liljenzin, and I. Svantesson, "The CHT-Process for HLLW Treatment, Part II. Hot test," *Radiochim. Acta*, **35**, 163-172 (1984).
3. J. A. Partridge and R. C. Jensen, "Purification of Bis(2-ethylhexyl) Hydrogen Phosphate by Precipitation of Copper(II) Bis(2-ethylhexyl) Phosphate," *J. Inorg. Nucl. Chem.*, **31**(8), 2587-2589 (1969).
4. J. L. Musachio, J. Hong, M. Ichise, N. Seneca, A. K. Brown, J.-S. Liow, C. Halldin, R. B. Innis, V. W. Pike, R. He, J. Zhou, and A. P. Kozikowski, "Development of new brain imaging agents based upon nocaine-modafinil hybrid monoamine transporter inhibitors," *Bioorg. Med. Chem. Lett.*, **16**, 3101-3104 (2006).
5. L. Maier and M.M. Crutchfield, "Organic phosphorus compounds 70: Preparation and properties of new phosphorus containing chelating agents for calcium and magnesium ions," *Phosph. Sulf.*, **5**, 45-51 (1978).
6. M. Nilsson and K. L. Nash, "Review article: A review of the development and operational characteristics of the TALSPEAK process," *Solvent Extr. Ion Exch.* **25**(6), 665-701 (2007).
7. J. Stary "Separation of Transplutonium Elements," *Talanta*, **13**(3), 421-437 (1966).
8. A. E. Martell and R. M. Smith, "NIST Critically Selected Stability Constants of Metal Complexes Database," Version 8.0, 2004.
9. E. Princz, I. Szilágyi, K. Mogyorósi, and I. Labádi "Lanthanide Complexes of Ethylenediaminotetramethylenephosphonic Acid," *J. Therm. Anal. Calorim.*, **69**, 427-439 (2002).

BIS-DIGLYCOLAMIDES (BIS-DGA) AS NEW EXTRACTANTS FOR An(III) AND Ln(III) FROM AQUEOUS HIGH-LEVEL WASTES ISSUED FROM THE PUREX PROCESS

A. G. Espartero,[a] M. T. Murillo,[b] M. Almaraz,[b] J. Sánchez-Quesada,[b] M. Segura,[b,c] J. C. Iglesias-Sánchez,[b] P. Prados,[b] and J. de Mendoza[b,c]

[a]Centro de Investigaciones Energéticas, Medioambientales y Tecnológicas (CIEMAT), Avda. Complutense 22, 28040-Madrid, Spain. [b]Departamento de Química Orgánica, Facultad de Ciencias, Universidad Autónoma de Madrid, carretera de Colmenar Viejo km 15.3, 28049-Madrid, Spain. [c]Current Address: Institut Catalá d'Investigació Química (ICIQ) Av. Països Catalans 16, 43007-Tarragona. Spain.
Corresponding author email address: amparo.espartero@ciemat.es

ABSTRACT

A new family of compounds with two diglycolamide moieties in their molecule have been synthesized and studied as suitable extractants for trivalent actinides (An(III)) and trivalent lanthanides (Ln(III)) present in high-level wastes (HLW) issued from the PUREX process. Although the obtained distribution ratios are comparable with those from TODGA under similar experimental conditions, the bis-DGA compounds showed higher selectivity towards Ln(III). The number of bis-DGA molecules involved in the formation of the dominant complex is two, and it is possible to recover more than 99% of the extracted An and Ln with 0.01 M nitric acid in order to recycle the solvent in subsequent extraction cycles.

INTRODUCTION

The so-called minor actinides (MA, Am-Cf), present in the high-level waste (HLW) issued from the PUREX process, are mainly responsible for the long-term radiotoxicity of this HLW stream [1]. Partitioning and transmutation as a means to reduce the need of a geological repository require MA elements to be first removed from the HLW (partitioning) and then fragmented by fission (transmutation), which allow reduction of the radiotoxicity inventory of the remaining waste by a factor of 100. A first step consists of An(III)/Ln(III) co-extraction, thus eliminating most of the fission products and the nitric acid. For this purpose, a number of partitioning processes (e.g., TRUEX, TRPO, DIDPA, or DIAMEX, based on diamide-like ligands) has been developed in recent years [2-5]. We have recently demonstrated that the use of two malonamide moieties attached to a suitable linker in a more preorganized chemical structure improves the extraction properties [6]. A similar strategy could be developed for the highly efficient extractant TODGA, based on the diglycolamide function [7]. We describe herein the synthesis of the bis-diglycolamide compounds shown in Figure 1 and the assessment of their extraction properties, including thermodynamics and kinetics, towards An(III) and Ln(III).

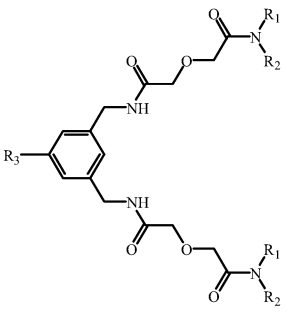

1a $R_1 = R_3 = H$, $R_2 = C_4H_9$
1b $R_1 = CH_3$, $R_2 = C_4H_9$, $R_3 = H$
1c $R_1 = R_2 = C_4H_9$, $R_3 = H$
1d $R_1 = CH_3$, $R_2 = C_8H_{17}$, $R_3 = H$
1e $R_1 = R_2 = C_8H_{17}$, $R_3 = H$
1f $R_1 = R_2 = i\text{-}C_5H_{11}$, $R_3 = H$
2a $R_1 = R_2 = C_4H_9$, $R_3 = OC_6H_{13}$
2b $R_1 = R_2 = C_4H_9$, $R_3 = OC_{12}H_{25}$
2c $R_1 = R_2 = C_4H_9$, R = O*sec*-C_7H_{15}

Figure 1. Compounds **1** and **2**.

EXPERIMENTAL SECTION

Procedure to Obtain Diglycolic Acids

A solution of the corresponding amine (butyl amine, *N*-methylbutylamine, dibutylamine, *N*-methyloctylamine, dioctylamine, or isopentylamine) in tetrahydrofurane (THF) was added to a solution of 0.8 M diglycolic anhydride in dry THF. The mixture was stirred at room temperature for 48 h. A solution of 1 M HCl was added to the mixture, and the resulting solution was stirred until a precipitate appeared. The solid was filtered, washed with water, and dried.

Procedure to Obtain Diglycolamides

Under argon atmosphere, the corresponding diamine (compounds **3** and **11**) and *N*-(3-dimethylaminopropyl)-*N*-ethylcarbodiimide hydrochloride (EDC·HCl) were added to a 0.4 M of the corresponding carboxylic acid in CH_2Cl_2. The mixture was stirred at room temperature for 48 h. A solution of 1 M HCl was added; the aqueous phase was extracted with diethyl ether; and the organic phases were combined and washed with brine and dried ($MgSO_4$). RMN (^1H and ^{13}C), elemental analysis, and mass spectrometry were used to identify and characterize the obtained compounds.

Procedure for Extraction Studies

Stock solutions were prepared by dissolving the extractant in 800 μL of the diluent at known concentrations. The solvent solution was pre-equilibrated with the corresponding nitric acid solution. The extraction process was carried out by mixing 600 μL of both, the pre-equilibrated solvent and the corresponding aqueous solution for 10 minutes in an oscillating mixer at 900 rpm at room temperature (22 ± 2 ºC). Phases were separated by centrifugation at 5000 rpm and 400 μL of each were used for metal concentration determination. An(III) and Ln(III) were simulated, respectively, by ^{241}Am and ^{152}Eu tracers from Amersham. Solutions of 4000 Bq/mL of each radionuclide were

prepared in nitric acid solutions. The concentration of each radionuclide was determined by high-energy gamma ray-spectrometry using a HP-Ge detector, suitable electronics, and Genie-2000 software from Canberra. Aqueous and solvent solutions were potentiometrically titrated after the extraction (automatic titrator Metrohm 798 MPT titrino). HPT (Hydrogenated Polypropylene Tetramer) kindly supplied by CEA (France), 1-octanol, 1,1,2,2-tetrachloroethane, and nitric acid were of analytical grade.

RESULTS AND DISCUSSION

Synthesis

Compounds 1 **were synthesized by activation of the carboxylic acids** 4-9 **with EDC·HCl followed by the addition of the corresponding commercially available diamine** 3 **(** Scheme 1).

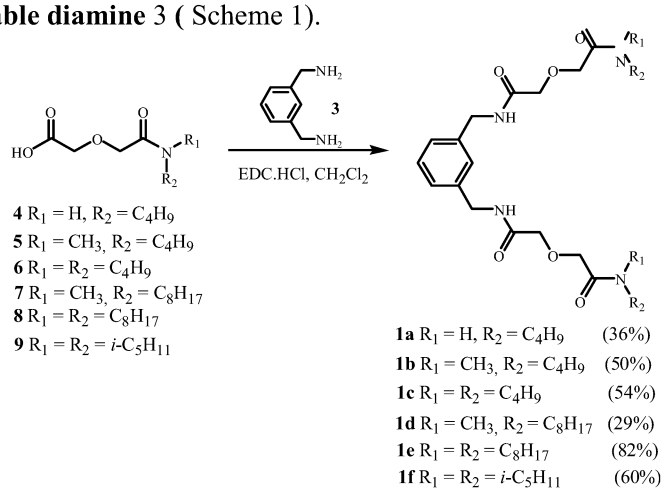

Scheme 1. Synthesis of compounds **1a**–**1f**.

In order to obtain compounds with high solubility in apolar diluents, the possibility to introduce additional alkyl chains was taken into account. The diamine derivative 11 (Scheme 2) was chosen as starting material, since this precursor allows the introduction, by O-alkylation, of different lengths lineal and branched chains.

Compounds **2** were synthesized from dimethyl 5-hydroxyisophthalate as starting material. First, the phenol was protected as benzyl ether and after six synthetic steps the intermediate **12** was obtained. Finally, compounds **2** were obtained, with moderated yields, by *O*-alkylation of **12** with the corresponding alkyl bromide, using K_2CO_3 (

Scheme **2**).

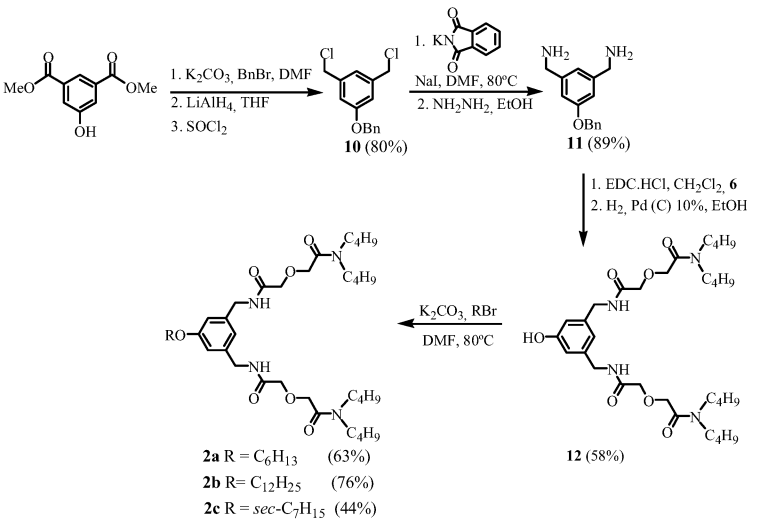

Scheme 2. Synthesis of compounds **2a-2c**.

Metal(III) Extraction

First extraction tests were carried out with compounds **1a**–**1b** in 1,1,2,2-tetrachloroethane, since they were not soluble in nonchlorinated diluents. Compounds **1c**–**1f** and **2a**–**2c** were soluble in 50:50 vol % HPT/1-octanol mixtures, and the distribution ratios for Am(III) and Eu(III) are shown in Table 1, and are compared to those for TODGA [7] and two other diglycolamides (TBDGA and DMDODGA) under the same experimental conditions.

Table 1. Am(III) and Eu(III) extraction by bis-DGA and mono diglycolamides*

Compound	D_{Am}	D_{Eu}	$\alpha_{Eu/Am}$
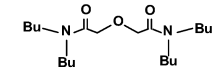 **TBDGA**	476	680	1.4
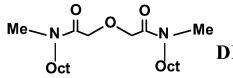 **DMDODGA**	477	789	1.7
TODGA	170	330	1.9
1c	99	183	1.8
1d	83	310	3.7
1e	43	165	3.8
1f	82	251	3.0
2a	104	330	3.2
2b	41	276	6.7
2c	88	335	3.8

*Solvent: [extractant] = 0.1 M in 50:50 vol % HPT/1-octanol mixtures. Aqueous Phase: ^{241}Am and ^{152}Eu in 3 M $[HNO_3]_{aq}$. Mixing for 10 min at room temperature (22 ± 2 ºC).

For compounds shown in Table 1, the extraction kinetics are very fast, and the equilibrium is reached within five minutes of mixing time. The preliminary values of the distribution ratios for Am(III) and Eu(III) obtained with compound **1c** in 1,1,2,2-tetrachloroethane were one order of magnitude lower than those obtained in 50:50 vol % HPT/1-octanol mixtures, in accordance with studies performed with TODGA by Sasaki et al [7]. Although the $D_{M(III)}$ values showed by the pre-organized molecules (**1c**–**2c**) are lower than those obtained with the diglycolamides TBDGA and DODMDGA, they are high enough for quantitative M(III) extraction, allowing easy M(III) back-extraction.

Avoiding the use of chlorinated diluents, Figure 2 shows the systematic study of the $D_{M(III)}$ variation at different HPT/1-octanol ratios with compound **1e**. Values of $D_{M(III)}$ increase when the volume content of 1-octanol in the diluent decreases and when the $[HNO_3]_{aq}$ increases. Having high nitric acid concentration is important, since it is closer to the PUREX process conditions where the high-active nitric acid concentration of the raffinate is equal or higher than 3 M. The $D_{M(III)}$ values at 0.06 M $[HNO_3]_{aq}$ are low enough, indicating that the M(III) back-extraction is thermodynamically favored.

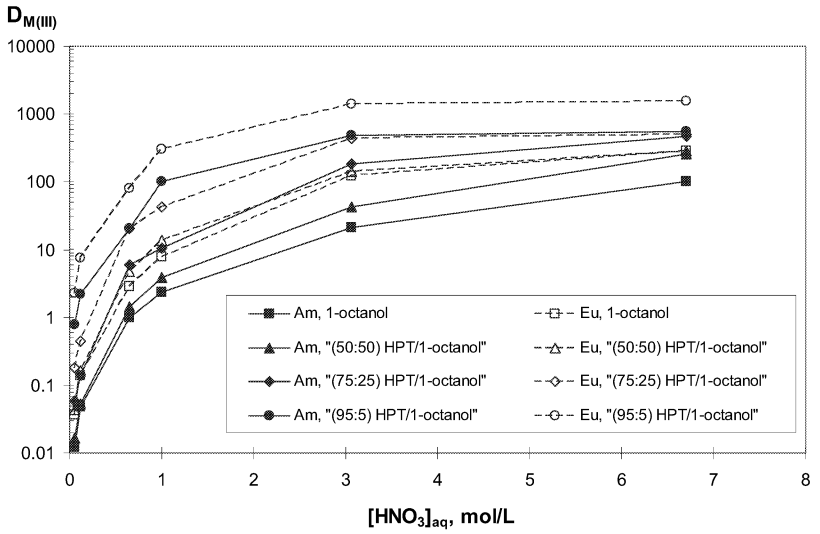

Figure 2. Influence of the diluent and the aqueous nitric acid concentration on the Am(III) and Eu(III) extraction by compound **1e**. Solvent: 0.1 M of **1e** extractant in HPT/1-octanol mixtures from 0:100 to 95:5 vol %. Aqueous phase: ^{241}Am and ^{152}Eu tracers from 0.06 M to 7 M $[HNO_3]_{aq}$. Mixing for 10 min at room temperature (22 ± 2 ºC).

For industrial An(III) extraction process development, it is crucial to recover them from the loaded solvent to regenerate it both for subsequent extraction cycles and for the next selective actinide separation from lanthanides process. In order to study that, Am(III) and Eu(III) extractions were performed with solutions of **1e** in 50:50 vol % HPT/1-octanol mixture from two different 3 M nitric acid aqueous solutions: solution-1 of ^{241}Am and ^{152}Eu tracers and solution-2 containing ^{241}Am and ^{152}Eu tracers besides 0.016 M Eu(III), that is the total lanthanide concentration present in the PUREX raffinate.

The Am(III) and Eu(III) back-extraction were carried out using 0.01 M nitric acid solutions, simulating a countercurrent process. The results obtained with solution-1 and solution-2 showed that, after four times of contact with fresh 0.01 M nitric acid, over 99% of the initially extracted Am(III) and Eu(III) were recovered from the loaded solvent.

When the **1e** extractant concentration was increased, higher $D_{M(III)}$ were obtained. Assuming that the extraction mechanism is similar to that proposed for single diglycolamides, and taking into account the calculated M(III)[TODGA]$_4$ stoichiometry [8], the stoichiometry of the dominant complex M(III):[**1e**]$_x$ was determined by slope analysis. For low concentrations of **1e**, the value of the slope for Am(III) and Eu(III) is two, indicating that this is the number of molecules of **1e** in 95:5 vol % HPT/1-octanol mixture involved in the composition of the dominant complex. At higher concentrations, the slope deviates from this value, probably due to some aggregation effects.

CONCLUSIONS

Previously, the benefits of the pre-organization of two malonamide moieties in a suitable linker to improve Am(III) and Eu(III) extraction were shown [6]. In this work, we have shown the Am(III) and Eu(III) extraction properties of a new family of bis-diglycolamides with an aromatic ring as linker. These extractants are soluble in suitable industrial diluents, and it is easy to recover the extracted Am(III) and Eu(III) from the loaded solvent. Studies in progress have shown some benefits of this pre-organized structure over the diglycolamide TODGA, allowing us to register a joint European Patent [9]. The radiolytic and hydrolytic stability of these new compounds is also under study.

ACKNOWLEDGMENTS

This work was financially supported by grants from EUROPART Project (FI6W-CT-2003-508854) and ENRESA.

REFERENCES

1. V. K. Manchanda and P. N. Pathak, *Sep. Sci. Technol.,* **35**, 85 (2004).
2. W. W. Schulz and E. P. Horwitz, *I Chem E Symposium Series, No 103*, 1987.
3. Y. Zhu and R. Jiao, *Nucl. Technol.*, **108**, 361 (1994).
4. Y. Koma, M. Watanabe, S. Nemoto, and Y. Tanaka, *J. Nucl. Sci Technol.*, **35**, 130 (1998).
5. J. N. Mathur, M. S. Murali, and K. L. Nash, *Solvent Extr. Ion Exch.*, **19**, 357 (2001).
6. M. T. Murillo, A. G. Espartero, M. Almaraz, J. Sánchez-Quesada, M. Segura, J.-C. Iglesias-Sánchez, P. Prados, and J. de Mendoza, *Radiochim. Acta* (in press) (2007).
7. Y. Sasaki, Y. Sugo, S. Suzuki, and S. Tachimori, *Solvent Extr. Ion Exch.*, **19**, 91 (2001).
8. Y. Sasaki, Z.-X. Zhu, Y. Sugo, and T. Kimura, *J. Nucl. Sci. Technol.*, **44**, 405 (2007).
9. P. Prados, M. T. Murillo, A. G. Espartero, J. Sánchez-Quesada, M. Almaraz, G. Modolo, J. de Mendoza, European Patent Application No. 06380268.0, 2006.

MODIFIED PUREX FIRST-CYCLE EXTRACTION FOR NEPTUNIUM RECOVERY

Binh Dinh, Philippe Moisy, Pascal Baron, Jean-Noël Calor,
Denis Espinoux, Brigitte Lorrain, and Magali Benchikouhne-Ranchoux

Département de radiochimie et procédés, Commissariat à l'énergie atomique
Centre de VALRHO BP 17171 30207, Bagnols-sur-Cèze CEDEX
Corresponding author email address :binh.dinh@cea.fr

ABSTRACT

A new PUREX first-cycle flowsheet was devised to enhance the extraction yield of neptunium at the extraction step of this cycle. Simulation results (using a qualified process-simulation tool), led to raising the nitric acid concentration of the feed from 3 M to 4.5 M to allow extraction of more than 99% of the neptunium. This flowsheet was operated in the shielded process cell of ATALANTE facility using pulsed columns and mixer-settlers banks. A 15 kg quantity of genuine oxide fuel of average burn up of 52 GWd/t with cooling time of nearly five years was treated, and the neptunium extraction yield obtained was greater than 99.6%.

INTRODUCTION

The French radioactive waste management act of December 1991, aims to reduce the radiotoxicity of the ultimate wasteforms produced by the nuclear industry, by removing the minor actinides from the wastes produced. The path chosen to reach this goal was to extract neptunium in the PUREX process, and eliminate the other minor actinides from the PUREX raffinate by the DIAMEX-SANEX processes. For this purpose, simple modification of operating conditions was sought to enhance the extraction yield of neptunium.

BACKGROUND

Neptunium Behavior in PUREX Process

In the dissolution solution, neptunium is mainly in the +V and +VI oxidation state, 80% to 90% of it being in the +V oxidation state. This results from the following equilibrium between this two oxidation states

$$NpO_2^+ + \tfrac{3}{2} H^+ + \tfrac{1}{2} NO_3^- \Leftrightarrow NpO_2^{2+} + \tfrac{1}{2} HNO_2 + \tfrac{1}{2} H_2O \qquad (1)$$

In an extraction operation, this equilibrium is shifted towards the formation of neptunium(VI), because its products, neptunium(VI) and nitrous acid, are extracted into the solvent phase. Thus, the neptunium extraction yield in such an operation depends on neptunium(V) oxidation kinetics. Results reported from industrial plants of La Hague show that about 25% of the neptunium contained in the feed dissolution remains in the first purification-cycle raffinate. Published kinetics studies of these redox reactions of the Np(V)/Np(VI) system [1-2] show that the oxidation kinetics of neptunium(V) can be enhanced by raising the acidity or nitrate concentration of the aqueous phase. So it was decided to raise the nitric acid concentration of the feed solution of the first purification cycle to increase the neptunium extraction yield.

Validation of the Flowsheet Evolution

Preliminary tests performed in a pilot unit equipped with pulsed columns (4 m high and 27 mm in diameter) using surrogate feed solutions of uranium, plutonium, and neptunium have validated this path. With the flowsheet tested for the extraction and scrubbing functions, in which the parameters are similar to that run in industrial plants in La Hague, it has been verified that the increase in the nitric acid concentration of the feed does increase the extraction yield of neptunium. More than 90% of the neptunium was extracted with a nitric acid concentration of the feed raised from 3 M to 4 M, with a residence time of the phases in the extraction column roughly half that of the industrial column which is 8 m high. Nevertheless, because of the use of an inactive feed solution, an introduction of nitrous acid was necessary at the bottom of the extraction column to catalyze the oxidation of neptunium(V).

Goals of the Active Test in Process Shielded Cell

It was decided to demonstrate the technical feasibility of minor-actinide separation from the waste that is to be disposed of by the treatment of a quite significant amount of genuine oxide fuel. The processes developed for this purpose will be operated using pilot apparatus that could be easily scaled up to an industrial level. A 15 kg quantity of genuine oxide fuel with an average burn-up of 52 GWd/t and a cooling time of nearly five years had to be treated. We had to design and perform the PUREX first purification-cycle flowsheet, to achieve the first step of this demonstration, which means leaving less than 1% of the neptunium content of the fuel in the raffinate of this cycle.

FLOWSHEET DESIGN

Kinetics Study of Np(V) Oxidation Reaction

In order to determine the nitric acid concentration of the feed solution needed to achieve the targeted neptunium extraction yield, a set of kinetics laws for both oxidation of neptunium(V) and reduction of neptunium(VI) were developed and implemented in the PAREX code, our process-simulation tool, formerly used to design the flowsheets of the purification cycles of the La Hague site. Because of the poor distribution ratio of

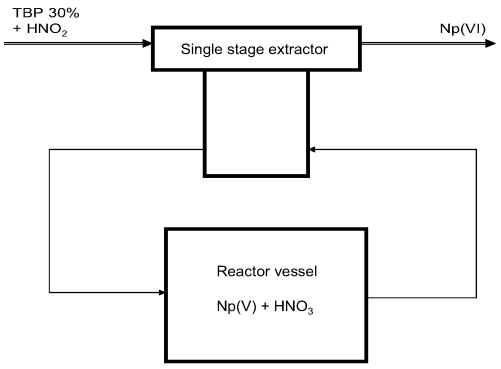

Figure 1. Specific apparatus for neptunium(V) oxidation-kinetics measurements.

neptunium(V) between the nitric aqueous phase and dilute TBP (30%), only the kinetics of the reactions in the aqueous phase were considered.

This set of kinetics laws is based on the work published by several authors [1-2]. But the kinetics of neptunium oxidation derived from these studies are not fast enough to simulate the neptunium extraction yield obtained from laboratory flowsheet experiments and from industrial feed back reported above with the PAREX code. Higher kinetics constants were needed to correctly simulate the extraction yield measured. The slow kinetics from published studies could be due to operating conditions which are not really representative of what happens in a liquid-liquid extractor. Most of the kinetics studies have been done either in aqueous phase alone or with both organic and aqueous phases but in batch mode. The neptunium(VI) formed is not removed from the aqueous phase, and the kinetics measured could include the effect of neptunium(VI) reduction, which could lower the global kinetics of neptunium(V). In a liquid-liquid contactor, neptunium(VI) is extracted into the solvent phase as it is formed and thus eliminates the effect of neptunium(VI) reduction. Or it could be a solvent effect that leads somehow to an increase in the neptunium(V) oxidation kinetics. For instance, Wehrey [3] studied neptunium(V) oxidation kinetics in the TBP organic phase and found it faster than the kinetics measured in the aqueous phase, and this could accelerate the overall neptunium(V) oxidation kinetics, even though its partition ratios between the aqueous and solvent phase under the applicable operating conditions are quite low (~10^{-2}).

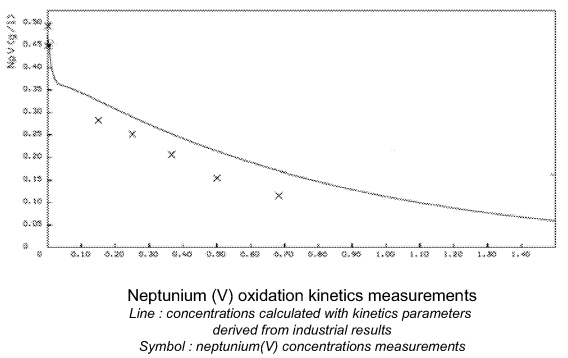

Figure 2. Neptunium(V) oxidation kinetics.

Kinetics measurements of neptunium(V) oxidation reaction were then done in the specific apparatus shown below, which was thought to ensure the removal of neptunium(VI) as it is formed. The aqueous phase in the reactor vessel, which initially contained neptunium(V) in nitric acid solution, is recycled through a centrifugal contactor fed with 30% TBP. The solvent was pre-equilibrated in nitric acid to avoid the extraction of nitric acid and contained nitrous acid. The nitrous acid brought by the solvent phase to the aqueous phase started the oxidation reaction of neptunium(V), and the neptunium(V) concentration decrease in the vessel was monitored. The experimental results show that neptunium(V) oxidation kinetics is even faster than the one used to simulate the neptunium extraction yield measured in the industrial plant. Thus, we chose to use this set of kinetics laws to develop the flowsheet, as it appeared to be conservative.

Main Characteristics of the Modified Flowsheet

The chart below sums up the main characteristics of the modified flowsheet to increase the neptunium extraction yield.

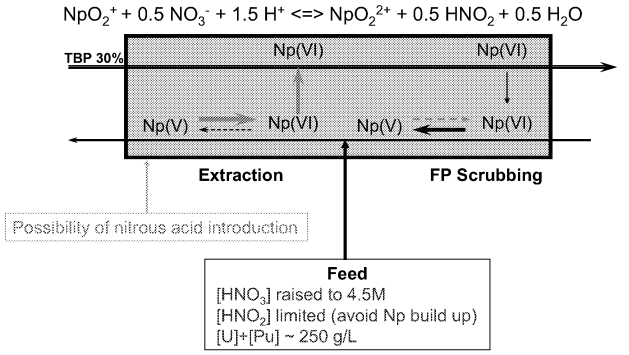

Figure 3. Main characteristics of the modified flowsheet for neptunium extraction.

Simulations using the PAREX code simulation with the chosen kinetics parameters for neptunium, as described above, show that the concentration of nitric acid of the feed solution has to be raised to 4.5 M to achieve the targeted neptunium extraction yield. To maintain favorable conditions for neptunium(VI) extraction, the concentrations of both uranium and plutonium have to remain as in the former flowsheet. We lowered the concentration of nitrous acid in the feed solution in order to limit neptunium accumulation in the contactors and thus the time needed for the process to reach steady state. We also managed to introduce nitrous acid in the bottom of the extraction section (near the solvent feed point) to increase the neptunium(V) oxidation reaction if needed.

TEST OPERATION AND MAIN RESULTS

Test Operation

The process shielded cell of Atalante is equipped with pulsed columns 4 meters high and with a diameter of 15 mm, equipped with truncated plates, and mixer-settler banks. The flowsheet tested used two pulse columns for the extraction functions, one for scrubbing. The technetium scrubbing, and complementary extraction functions were performed in mixer-settler banks.

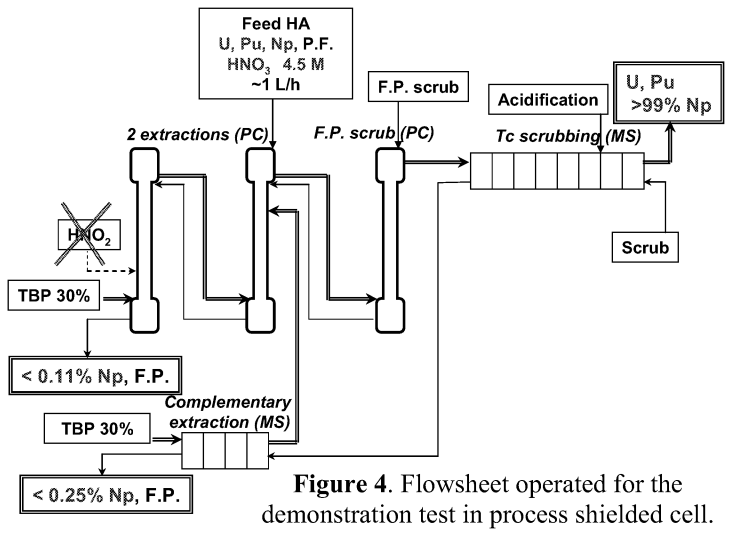

Figure 4. Flowsheet operated for the demonstration test in process shielded cell.

The dissolution solution of the fuel oxide, once adjusted, had a volume of 50 liters. The feed flowrate was about 1 L/h.

Main Results

The mass balance performed after the test is presented in the chart below. The neptunium concentrations in the raffinates of the cycle were below the detection limit and represent less than 0.11% and 0.25% for the raffinates of principal and complementary extraction functions, respectively. More than 99% of neptunium was extracted in the loaded solvent. In addition, no complementary introduction of nitrous acid was needed.

An overloading in uranium of the solvent phase occurred during the test, and there was a delay before it was corrected, because a malfunction of an on-line monitored measure. Thus, an accumulation of matter was observed during the test, as revealed by the evolution during the test of uranium, plutonium, and neptunium concentrations in the aqueous outlet of the fission product scrubbing column, reported in the Figures 5-6. The accumulation of neptunium observed is another proof of neptunium(V) oxidation.

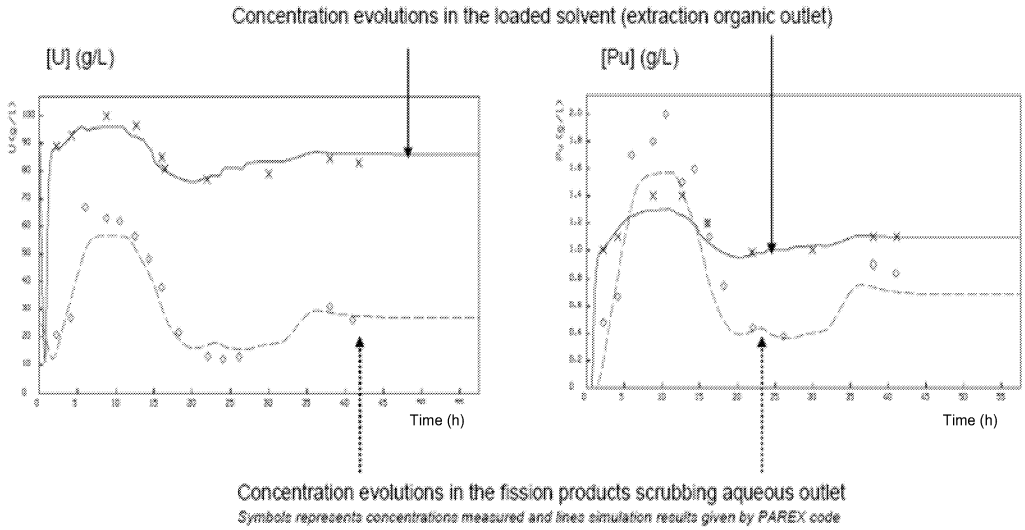

Figure 5. Uranium and plutonium concentration evolutions during the overloaded solvent period.

The evolutions of uranium and plutonium concentrations at these points of the process were quite well simulated by the PAREX code as shown in the same figures. This means that the solvent load with the main component, uranium, is quite well simulated. The simulated neptunium accumulation was lower than the experimental. This confirms that the global kinetics of neptunium(V) oxidation is finally faster than that given by the set of kinetics laws chosen for the flowsheet design, which was known from the kinetics studies. The kinetics parameters were modified to better fit the neptunium concentration evolution reported during the test, and we found out that those identified parameters led to a better representation of the kinetics results as well, making all these calculations and measurements consistent. However, complementary development is still needed to have a more complete kinetic model to describe neptunium behavior.

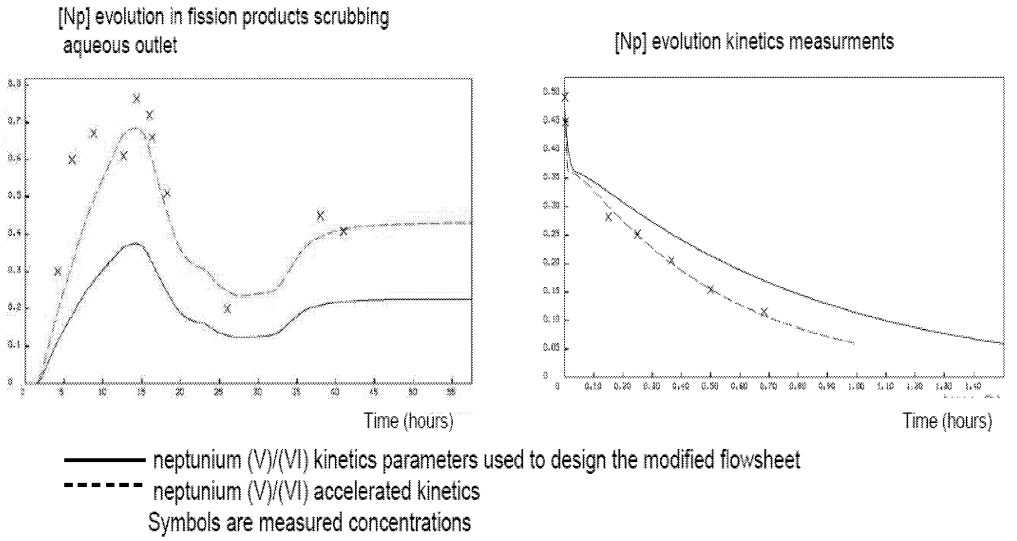

Figure 6. Neptunium behavior in the flowsheet experiment and kinetics study.

CONCLUSIONS

The modelling approach based on the available knowledge of neptunium behavior from laboratory results and industrial feed back as well, combined with appropriate complementary experimental support, was a success in the development of the modified flowsheet of the PUREX first purification cycle for neptunium extraction. The final neptunium extraction yield obtained was greater the 99.6% without the need of a complementary introduction of nitrous acid.

ACKNOWLEDGMENTS

Our sincere thanks to AREVA NC for their financial support.

REFERENCES

1. J. P. Moulin, “Kinetics of redox reactions of neptunium in aqueous nitric solutions: neptunium(IV) oxidation in neptunium(V), neptunium(V) oxidation in neptunium(VI) by nitric acid, catalysed by nitrous acid,” CEA-R-4912 (1977).
2. I. Gaquer, “Redox behavior of Np(V)/Np(VI) system with nitrous acid in concentrated nitric acid aqueous solution,” Ph.D. Thesis, University Paris XI, Orsay, December, 1996.
3. F. Wehrey, “Redox reactions of neptunium in TBP-dodecane mixtures,” CEA-R-5478 (1989).

PLUTONIUM PURIFICATION CYCLE IN CENTRIFUGAL EXTRACTORS: FROM FLOWSHEET DESIGN TO INDUSTRIAL OPERATION

P. Baron,[1] B. Dinh,[1] J. Duhamet,[1] F. Drain, F. Meze,[2] and A. Lavenu[3]

[1]CEA VALRHO, BP 17171, 30207 Bagnols sur Cèze Cedex, France
[2]SGN, 1, rue des Hérons 78182 St-Quentin-en-Yvelines Cedex, France
[3]AREVA NC, Ets La Hague, 50444 Beaumont-Hague Cedex, France
Corresponding author email address: baron.pascal@cea.fr

ABSTRACT

The extension of the UP2 plant at La Hague includes a new plutonium purification cycle using multistage centrifugal extractors to replace the previous cycle that used mixer/settler banks. This type of extractor is suitable for the treatment of fuel containing a high proportion of plutonium-238, as its short residence time limits solvent degradation. This paper deals with the research done to devise its flowsheet, the centrifugal extractors in which it is operated, as well as the feedback of six years of industrial operation.

INTRODUCTION

For the plutonium purification cycle of the UP2-800 plant at La Hague, multistage centrifugal extractors were chosen to replace the mixer/settler banks of the preceding cycle. From the chemical process standpoint, the short residence time is an advantage for the treatment of fuel containing a high proportion of plutonium 238 as it limits the solvent degradation. In addition, the compactness of this type of equipment helps to optimize the actual size and thus the cost of the plant.

FLOWSHEET DESIGN

Two types of reducing agents have been considered for the plutonium stripping operation, uranous nitrate and hydroxylamine nitrate (HAN). Uranous nitrate displays very fast reduction kinetics, ideal for the very short residence time of the phases in the centrifugal extractors. However, its extractability exacerbates the undesirable re-oxidation of plutonium, which is present in high concentration in this stage of the process. The short residence time of the centrifugal extractors is an advantage in as much as it could conceivably be adequate to obtain sufficient reduction efficiency, while minimizing undesirable re-oxidation mechanisms. HAN helps to minimize undesirable re-oxidation and is the normal choice for this type of operation, as in the Pu purification cycles of UP3 plant, in pulsed columns [1]. However, the Pu(IV) reduction kinetics are

slower than with uranous nitrate, making it necessary to check whether its use is compatible with the very short residence times of centrifugal extractors. A large amount of research has been done to devise the flowsheets for both reducing agents [2].

An Approach Based on Modelling

Preliminary flowsheets were elaborated using the PAREX code [3], which has been used to devise the flowsheets of the previous purification cycles of La Hague industrial site [1-4]. Series of tests were then conducted in single-stage centrifugal extractors to measure the plutonium stripping performance at different points of interest. The exploitation of the results of these tests led to the modification the preliminary flowsheets. The feasibility study of the two flowsheets was continued with test campaigns in an active pilot plant designed to simulate a complete plutonium purification cycle. The centrifugal extractors used were of the same type as those used in the previous studies, assembled in benches of four stages as shown in Figure 1.

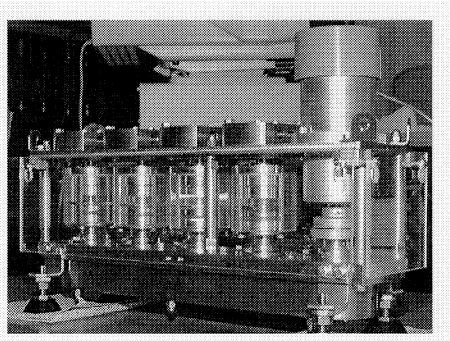

Figure 1. Four-stage testing bench of laboratory centrifugal extractors.

Flowsheet Using Uranous Nitrate

Single-stage experiments confirmed the plutonium stripping efficiency obtained with this reducing agent. High plutonium decontamination factors are obtained for very short contact times (Pu DF 4 for phase contact time of 1 s), with a relatively high acid concentration (~1 M in the outgoing aqueous phase). High consumption of reducing agent was observed, especially at high plutonium concentration. It was accordingly decided, for the plutonium stripping operation, to subdivide the introduction of reducing agent over several stages in order to prevent all the excess reducing agent from being consumed in the first stages, where the plutonium concentration is the highest.

Owing to lower transfer efficiency (Murphree efficiency 0.85) of the extractors, Pu re-oxidation turned out to be more substantial than anticipated, preventing the achievement of the required Pu stripping during the first flowsheet run. A second flowsheet, in which the U(IV)/Pu ratio was raised to 2.5 by two additional introductions of reducing agents (stages 5 and 7) helped to achieve highly efficient Pu stripping. While all the excess reducing agent was consumed, very significant hold-up of U(IV) was

observed in the Pu stripping stages, explaining the good performance obtained. It was decided to lower the O/A flow ratio in the Pu stripping operation to reduce Pu re-oxidation, primarily by obtaining weaker acid profiles. The U(IV)/Pu ratio was thus restored to the value of 1.75 initially set, without any loss in Pu stripping performance.

The flowsheet for the final test is shown in Figure 2. Plutonium stripping performance was excellent. Plutonium leakage in the outgoing solvent of Pu stripping was 0.2 mg/L, giving decontamination factor of 10^5. The feasibility of Pu stripping with uranous nitrate applied in centrifugal-extractors benches is thus demonstrated.

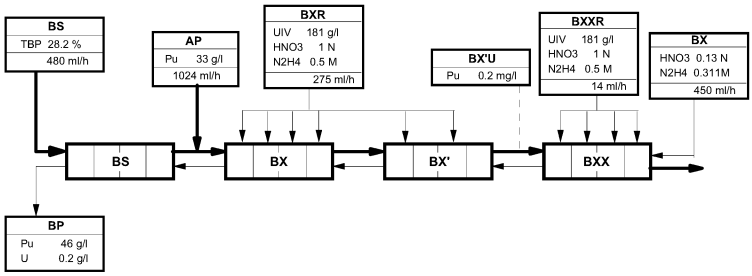

Figure 2. Flowsheet of plutonium stripping using U(IV).

Flowsheet Using Hydroxylamine Nitrate

In single-stage contactor experiments, significantly lower stripping performance was observed in comparison with uranous nitrate and very high sensitivity to the acidity of the aqueous phase. The best performance was obtained at low acidity (0.1 to 0.5 M), with virtually zero performance for acid concentrations close to 1 M. This high sensitivity of stripping performance to aqueous phase acidity entails a limitation of the concentration factor of the plutonium stripping operation.

Since HAN is much less effective than uranous nitrate for reducing plutonium(IV), the integration tests were conducted in the most favorable conditions. The reduction of the O/A flow ratio in the Pu stripping operation adopted for the uranous nitrate flowsheet was reinforced by discarding the uranium scrubbing function, which was unnecessary due to the low uranium content entering a Pu cycle.

A test conducted without uranium scrubbing, and with an O/A ratio of 1.4, a temperature of 54 °C, and an average residence time in the mixers of 1.7 s, for the Pu stripping operation, helped obtain excellent performance, very slightly under that obtained with a uranous nitrate flowsheet. The residual Pu concentration in the effluent solvent was 0.5 mg/L, corresponding to a Pu decontamination factor of 7 x 10^4. A test performed under identical conditions but at a temperature of 45 °C revealed the sensitivity of the operation to a drop in temperature. Plutonium leakage in the solvent rose significantly but remained moderate (up to 5 mg/L, corresponding to a Pu decontamination factor of 7 x 10^3). The test flowsheet is shown in Figure 3. A similar flowsheet, but including uranium scrubbing (O/A 0.2 in uranium scrubbing), confirmed the unfavorable effect of increasing the O/A flow ratio for the Pu stripping operation. Plutonium leakage in the outgoing solvent from Pu stripping was 2 g/L.

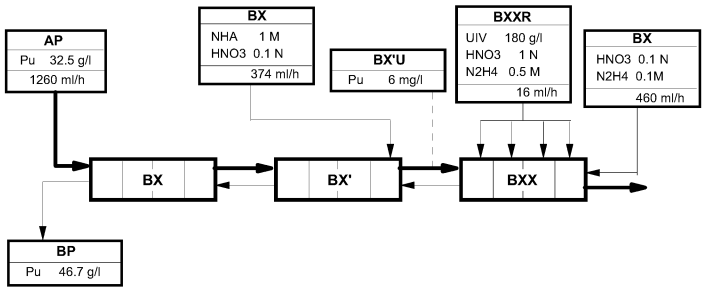

Figure 3. Flowsheet of plutonium stripping using HAN.

CENTRIFUGAL-CONTACTOR DESIGN

Development and deployment of this type of equipment, in particular for a Pu cycle, required broad-ranging studies covering the hydraulic and thermal behavior of the equipment and the equipment's ability to perform extraction operations comprising a limiting stage related to the kinetics of a chemical reaction [5].

Hydraulic and thermal R&D was carried out mainly on full-scale industrial equipment (Figure 4) or models representing components. The work enabled us to define and optimize the equipment internal components, ensuring that the either-phase carryover at the extractor outlet were compatible with the required chemical performance. The thermal behavior of multistage centrifugal extractors was closely examined from a safety standpoint. The temperature of the solutions flowing through the equipment must not exceed the flash point of the solvent used in the extraction operations.

Nonradioactive tests, followed by full-scale uranium tests, were carried out to determine mass-transfer efficiency of the contactors and quantify the heating of the phases that results from the dissipation of the mechanical energy in the mixing chambers. Terms such as thermal bridges between stages and losses to the surrounding environment were identified as well. The experiments showed that industrial equipment was more efficient than lab equipment when comparable tests were performed without radiation and with uranium transfer. All these experimental results served to set the PAREX code parameters related to heat and mass transfer inside the industrial contactor. The PAREX code was then used to determine the appropriate measurements to be taken (phase cooling at the inlet) to meet safety requirements and to analyze the consequences of any disruption to the process.

INDUSTRIAL PLANT AND FEED BACK

For the industrial plant, the flowsheet using HAN as a reducing agent has been chosen, because it led to simpler process implementation. The first-cycle Pu product doesn't need further uranium scrubbing in the second Pu purification cycle. In addition, only one reducing agent introduction is required instead of three or four in the case of uranous nitrate.

Figure 5 gives an overview of the R4 plant. Three centrifugal extractors of 8 stages each were used for the extraction zone: 4 stages for diluent washing of the raffinate, 12 stages for extraction function, and 8 stages for the fission-product scrubbing. Plutonium stripping was performed in two identical centrifugal extractors. The Pu barrier was operated in a 6-stage mixer-settler bank and diluent washing of the Pu product in a 4-stage mixer-settler bank.

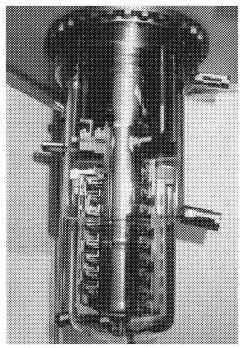

Figure 4. Cut-away view of centrifugal extractor.

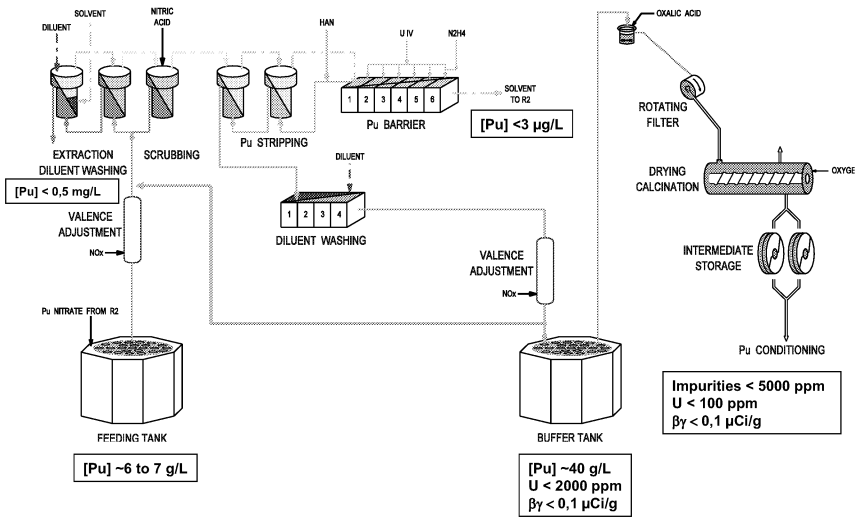

Figure 5. R4 plant overview.

The conversion process is shown also in Figure 5. After Pu oxidation by nitrous fumes, the 40 g Pu/L solution discharged from the extraction cycle is mixed with oxalic acid. A rotary filter under vacuum separates plutonium oxalate from oxalic mother liquors. Plutonium oxalate is then dried and calcinated to oxide in a rotary kiln before conditioning in stainless-steel cans. The oxalic mother liquors are concentrated in a

zirconium evaporator, which also destroys the excess oxalate ions. The concentrated nitric solution Pu is recycled to the extraction cycle.

The R4 plant was started in 2001 [6] and has produced up to now more than 40 tons of Pu oxide, with a great reliability of the contactors. In six years of operation, there has been no intervention in the active area, thanks to the pendular conception of the extractor. The main results are represented in Figure 5. The Pu feed coming from the first purification cycle (R2) had 6–7 g/L Pu. To obtain a Pu product concentrated to 40 g/L, part of the aqueous outlet is recycled at the feed input of the plant. The targeted purity of the Pu product has been easily reached; its specific gamma activity is one order of magnitude below the targeted value of 1 μCi/gPu. The total concentration of impurities in the Pu oxide is less than 5000 ppm (U is less than 100 ppm). Plutonium leaks in both raffinate and discharged solvent are very low (less than 0.02% of Pu plant feed).

CONCLUSIONS

The excellent performance of the UP2-800/R4 Pu purification cycle and the remarkable reliability of the centrifugal extractors confirm that technology chosen for this plant is a new proven solution to perform Pu finishing using solvent extraction. So AREVA has gained much experience in the industrial use of the two types of extractors for this Pu purification cycle: pulsed columns at UP3 or centrifugal extractors at UP2-800. Depending on the fuel to be treated and the specific context of the future project plant, one technology would be preferred. The approach based on process modelling used for design of the core process results in the capitalization of the knowledge gained from this research. Thus, the code appears to be an outstanding tool to design future fuel-reprocessing plants using either pulsed columns or centrifugal extractors.

REFERENCES

1. P. Baron, B. Boullis, M. Germain, J. P. Gué, P. Miquel, F. J. Poncelet, J. M. Dormant, and F. Dutertre, “Extraction cycle design for La Hague plants,” GLOBAL’93, Seattle (US), 12-17 Sept 1993.
2. P. Baron, B. Dinh, F. Drain, B. Gillet, and B. Mauborgne, “Plutonium Purification Cycle in Centrifugal Extractors: Comparative Study of Flowsheets using Uranous Nitrate and Hydroxylamine Nitrate,” RECOD ’98, 401-408, Nice, France.
3. B. Dinh, B. Mauborgne, and P. Baron, “Dynamic simulation of extraction operations. Application in nuclear fuel reprocessing,” European Symposium on Computer-Aided Process Engineering-2 (ESCAPE-2), Toulouse (France), 5-7 Oct. 1992.
4. F. Drain, P. Miquel, J. P. Moulin, D. Alexandre, B. Kniebihli, B. Boullis, and P. Baron, “Uranium Plutonium Separation in Annular Pulsed Column,” GLOBAL '97, 250-254, Yokohama, Japan.
5. F. Drain, R. Vinoche, and J. Duhamet, “40 years of experience with Liquid-Liquid Extraction Equipment in the Nuclear Industry,” Waste Management ‘03 Conference, February 23-27, 2003, Tucson, AZ.
6. F. Drain and R. Vinoche, “A step towards a new generation of reprocessing plant: Plutonium finishing facility,” R4 start-up, ENC’02, October 7-9, 2002, Lille, France.

PARTITIONING OF Eu(III) BETWEEN ACIDIC AQUEOUS $Al(NO_3)_3$ AND TRI-*n*-OCTYL PHOSPHINE OXIDE

J.C. Shafer, R.C. Harrington, K.L. Nash

Chemistry Department, Washington State University, Pullman, WA USA
Corresponding author email address: jenifer_shafer@wsu.edu

ABSTRACT

As the Hanford site undergoes remediation, significant economies could be realized if aluminum is kept from High-Level Waste glass. An acidic scrub of the Hanford sludge could enhance Al removal; however, a caveat is the potential mobilization of transuranic elements, which would require a secondary cleanup of the Al/Cr waste stream. Previous solvent extraction (SX) studies have shown that >99% of the Eu and U can be extracted from simulated acidic Al/Cr waste. This study examines the use of extraction chromatographic methods. Results indicate the systems behave comparably and either method could be considered for Hanford clean-up purposes.

INTRODUCTION

The Hanford Site, in south central Washington State, was the first facility to mass-produce plutonium for nuclear weapons. Both the volume and composition of waste resulting from Pu production are major remediation concerns [1]. The most problematic waste component is the sludge created by the caustic environment of the tanks. Research and remediation efforts have focused on caustic leaching to remove problematic nonradioactive elements, aluminum and chromium. Removal of these species would decrease volume and improve the glass matrix of the vitrified high-level waste (HLW). While some significant successes have been experienced, the most stubborn Al phase, boehmite (γ-AlO(OH)) has been resistant to caustic leaching.

An alternative, acidic leaching, has been shown to perform complete removal of Al [2]. A caveat of acidic leaching is the potential to mobilize radioactive species into the Al/Cr waste stream. If acidic leaching were to be performed, knowledge of how to remove radioactive species, predominantly actinides, from conditions of variable [HNO_3], [$Al(NO_3)_3$], and [CrO_4^{2-}] would be required. Previous studies have shown solvent extraction (SX) with 0.1 M TOPO/*n*-dodecane to be an effective means of handling the secondary cleanup [3]. An alternative to SX, extraction chromatography (EXC), provides different potential benefits, such as preconcentration, avoidance of a liquid organic diluent, and the ease of handling of ion-exchange resins.

Extraction chromatography is a type of liquid-liquid chromatography that couples the selectivity of solvent extraction with the multistage character of a chromatographic

process [4]. Solvent-impregnated resins allow the benefits of a functionalized polymeric resin without the difficulties associated with synthesis. Omission of functionalized resin synthesis, however, can lead to extractant bleed off from the polymeric support, and this must be considered when examining separation goals.

As a means of further understanding EXC, comparison is frequently made to similar SX systems [5]. As the organic diluent will affect SX results, pore size, bead size, and hydrophilic/phobic characteristics of the resin can affect EXC results. Other variables can affect results, especially when attempting comparison with SX; however, the organic phase, solid or liquid, is usually not physically inert and must be considered carefully.

In this work, the hypothetical problem of how to remove the radioactive components of the leachate solutions that could emerge if one were to attempt Al leaching with HNO_3 solutions is addressed. The decontamination method investigated examines the efficiency of an EXC approach employing a 60% $m_{TOPO}/m_{(TOPO+XAD7)}$ resin extractant phase to selectively separate radioactive Eu(III) from aqueous solutions of HNO_3 and $Al(NO_3)_3$ in the presence of low concentrations of Cr.

EXPERIMENTAL

Materials and Instrumentation

All aqueous solutions were prepared from analytical-grade reagents and ultra-pure (18 MΩ) H_2O. A density determination was performed on all solutions. Solutions of HNO_3 were prepared by mass using Fischer Scientific concentrated (15.8 M) HNO_3 solution. Solutions of K_2CrO_4 and $Al(NO_3)_3$ were prepared by mass using analytical grade J.T. Baker solids. The L-ascorbic acid solutions were prepared by mass from Fisher Scientific ACS certified reagent. Experiments done using $^{152/154}Eu(NO_3)_3$ solutions were prepared by dilution of standardized stocks from the Washington State University (WSU) inventory. Radioactive $^{152/154}Eu$ was created by neutron activation of 99.999% Eu_2O_3 (Arris International) at the Nuclear Radiation Center at WSU. The tri-*n*-octyl phosphine oxide (TOPO) organic solutions (TOPO p.a., Acros Organics) were diluted volumetrically using methanol (>99%, Sigma-Aldrich). Amberlite XAD-7 (Rohm & Hass) was treated as described in the following section. Radiotracer experiments using $^{152/154}Eu$(III) were analyzed on a NaI(Tl) solid scintillation counter, a Packard Cobra-II auto gamma, for gross gamma counting.

Resin Impregnation

Removal of acidic impurities in XAD7 beads was performed with a deionized water rinse. Drying of the resin was expedited by methanol (MeOH) addition and removal, followed by placement in an oven at 80 °C. The dried resin was removed from the oven, allowed to cool in a vacuum dessicator, weighed, and contacted for 15 minutes by vigorous shaking with 0.1 M TOPO in MeOH with excess impregnation solution. Excess impregnation solution after contact was removed, and the impregnated beads were oven dried at 80 °C overnight. The amount of impregnation can be defined as the

ratio of mass of organic extractant present to the total final mass of the impregnated resin. The impregnation provided 0.60 ± 0.01 $m_{TOPO}/m_{(TOPO+XAD7)}$.

Batch Extractions

For both the acid-partitioning and Eu^{3+} extraction studies, 1 mL of appropriate aqueous solution and 100 mg of TOPO-XAD7 resin were used. Phases were contacted for 15 minutes by vigorous shaking, and the aqueous phase was removed and analyzed as described below.

The weight distribution ratio, D_w (mL g^{-1}), was calculated according to the following equation:

$$D_w = [(A_o - A_s)/w]/(A_s/V) \quad (1)$$

where A_0 and A_s are the aqueous-phase activity (counts per minute) before and after equilibration, w the weight of resin (g), and V the volume of the aqueous phase (mL). Triplicate experiments showed that the reproducibility of the distribution measurements was generally within 10%, although the uncertainty interval was somewhat higher for the highest distribution values ($D \geq 10^3$).

The amount of HNO_3 in the aqueous phase after contact was determined by titration with standardized NaOH using a phenolthalien indicator. All extractions and titrations were performed in triplicate. The TOPO-XAD7 system included a dependency study of $[Al(NO_3)_3]$ at 0.1 and 1 M HNO_3. Possible binding of Al with phenophthalien required a strip of the organic phase to accurately determine $[HNO_3]$ after contact. TOPO-XAD7 beads were therefore centrifuged using 2 mL Durapore filters for 5 min. to ensure complete removal of unbound acid. TOPO-XAD7 was washed multiple times with deionized water to wash off any bound HNO_3, and this water was titrated.

The aqueous phase for the Eu extraction experiments contained various amounts of HNO_3, $Al(NO_3)_3$, Cr(III/VI), Eu(III), and ascorbic acid. This study was designed to encompass a wider variety of aqueous-phase conditions than could be encountered during HNO_3 leaching of Hanford tank sludges. Investigations of the extraction behavior of Eu(III) with varying $[HNO_3]$ in the presence of constant $[Al(NO_3)_3]$ or constant $[HNO_3]$ with varying $[Al(NO_3)_3]$ were completed. All aqueous solutions used in the study initially contained 1 mM K_2CrO_4. The Eu(III) extraction experiments had a 2:1 ratio of ascorbic acid to K_2CrO_4. The chromate anion is extractable by TBP [3], and a similar extraction is expected by TOPO. Reduction of Cr(VI) to Cr(III) by the addition of ascorbic acid prevents CrO_4^{2-} extraction and possible competition with Eu(III).

Eu(III) distribution experiments were done by using $^{152/154}$Eu(III) radiotracer. Aliquots of 800 µL were obtained of the aqueous phase and counted. Counting times were adjusted to minimize counting error for each sample.

RESULTS AND DISCUSSION

HNO_3 Partitioning

Literature has shown the possibility of a TOPO·2HNO_3 adduct in the solvent extraction system [6], and it is unclear whether this complex forms in the EXC system. For this paper, only the presence of the 1:1 TOPO:HNO_3 adduct was assumed. The difference between the total amount of TOPO and the amount of HNO_3 in the organic phase allowed the determination of the amount of uncomplexed TOPO (free TOPO). These results were used to calculate the percentage of free TOPO under specific HNO_3/$Al(NO_3)_3$ conditions available for Eu(III) extraction

Europium Distribution

Figures 2 and 3 present Eu(III) distribution data as a function of aqueous $[NO_3^-]_{tot}$. Extraction was determined as a function of increasing $[Al(NO_3)_3]$ (0.010 M–0.50 M) at three constant $[HNO_3]$ (Figure 1) and also for increasing $[HNO_3]$ (0.01 M–1.50 M) at two constant $[Al(NO_3)_3]$ (Figure 2). Corrections for the formation of inextractable $Eu(NO_3)^{2+}$ and the TOPO:HNO_3 adduct have been previously derived [3]. The partitioning of Eu(III) into the TOPO-XAD7 resin from solutions of constant $[HNO_3]$ increased significantly with increasing $[Al(NO_3)_3]$ (Figure 1) over the $[Al(NO_3)_3]$ range of 0.10–1.50 M. The highest value observed for corrected $D_{w,Eu}$ was ~10,000. The partitioning of Eu(III) between the TOPO-XAD7 phase from solutions of constant $[Al(NO_3)_3]$ with increasing $[HNO_3]$ (Figure 2) increased slightly over the $[HNO_3]$ range 0.10–1.50 M with a maximum corrected $D_{w,Eu}$ of ~1000. Not unexpectedly, $Al(NO_3)_3$ and HNO_3 affect the partitioning of Eu and the performance of the proposed decontamination system differently.

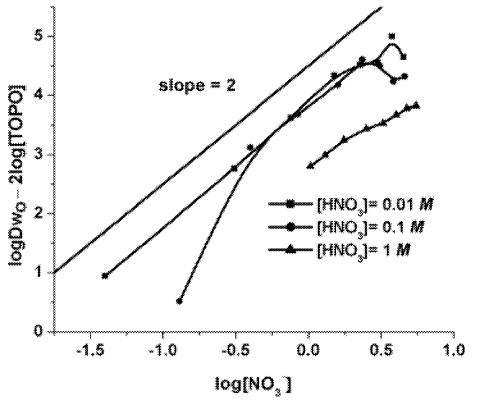

Figure 1. Partitioning of Eu^{3+} into TOPO-XAD7 from solutions of variable $[Al(NO_3)_3]$ and constant $[HNO_3]$ at 0.01 M HNO_3 (■), 0.1 M HNO_3 (●), and 1 M HNO_3 (▲).

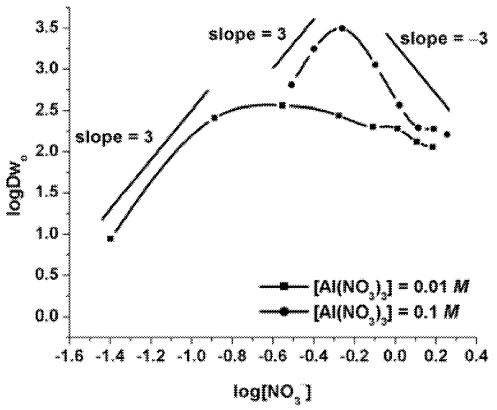

Figure 2. Partitioning of Eu^{3+} into TOPO-XAD7 resin from solutions containing variable $[HNO_3]$ and constant $[Al(NO_3)_3]$ at 0.01 M $Al(NO_3)_3$ (■) and 0.1 M $Al(NO_3)_3$ (●).

The extraction increase observed as $Al(NO_3)_3$ increases is assumed to be related to the decline in the activity of water, which allows more effective release of the Eu^{3+} to the organic phase; that is, Eu^{3+} is salted out of the aqueous phase. Corrected $D_{w,Eu}$ values shown in Figure 1 decrease as $[HNO_3]_{aq}$ increases in large part because of the increased association of TOPO with HNO_3 in the organic phase. The loss of free extractant molecules to a 1:1 HNO_3:TOPO complex in the organic phase does not completely account for the decreased extraction in the 1M HNO_3, and this may be due to the TOPO:HNO_3 adduct sterically preventing extraction on the TOPO-dense beads. This also illustrates the substantial weakness of the thermodynamic driving force for TOPO extraction of $Eu(NO_3)_3$ relative to that for HNO_3. The variations in the corrected D_{wo} values seen at $[Al(NO_3)_3] > 1.0$ M is probably not attributable to a change in the NO_3^- dependency of the extracted species, but rather several other possible effects such as the formation of the $Eu(NO_3)^{2+}$ species, change in nitrate ion activity at high $[Al(NO_3)_3]$, or possibly Al extraction. An approximate slope of 3 would be expected on the basis of charge neutrality required for extraction; however, a suppression is present for the SX [3] and EXC systems. The reason for this is unresolved.

The slope suppression observed in the $Al(NO_3)_3$ analysis was not an issue for the HNO_3 system. Figure 2 reveals an increasing slope of 3 log-log plot for the variable $[HNO_3]$ data for the lower $[HNO_3]$ conditions. The inversion of the slope at high acid concentrations is most likely attributable to the TOPO:HNO_3 adduct. The steeper decrease observed in the 0.1 M $Al(NO_3)_3$ would then be due to increased adduct formation from salting effects observed in the HNO_3 partitioning studies. The exact origin of these effects assumed to be derived from decreased activity of the water.

CONCLUSIONS

This investigation has addressed the concept of applying extraction chromatography methods to the task of decontaminating radioactive sludge leachate solutions that could result if acidic leaching procedures were adopted for the cleanup of

recalcitrant, aluminum-containing tank waste sludge residues at the Hanford Site. The results presented indicate TOPO-XAD7 can remove >90% of Eu(III) in HNO_3 solutions containing $Al(NO_3)_3$ when $[NO_3^-]_{total}$ is greater than ~0.25 M. The results for Eu(III) may be taken as generally characteristic of the behavior of the light lanthanides and trivalent actinide cations in a system of this type. Also potentially interesting could be the behavior of readily redox-active actinides (i.e., Np and Pu) in the mixed electrolyte system; however, great care would be required to differentiate salting effects from redox effects. Further studies will also be required to focus the adaptation of this approach to the development of decontamination strategies applicable to alkaline solutions that are relevant to more conventional sludge-leaching procedures.

ACKNOWLEDGMENTS

The authors would like to thank the Department of Energy Environmental Management Science Program for funding this work. Much appreciation is felt towards all the members of the Dr. Kenneth L. Nash radiochemistry laboratory at Washington State University. A final acknowledgement is due to the Nuclear Radiation Center (NRC) at WSU for the production of the Eu radioisotopes used in this study.

REFERENCES

1. S. F. DeMuth and G. R. Thayer, "An Updated Cost Study for Enhanced Sludge Washing of Radioactive Waste," Remediation Spring, 2002; pp. 87–97.
2. A. H. Bond, K. L. Nash, A. V. Gelis, J. C. Sullivan, M. P. Jensen, and L. Rao, "Plutonium mobilization and matrix dissolution during experimental sludge washing of bismuth phosphate, Redox, and PUREX waste simulants," *Sep. Sci. Technol.,* **36**(5 & 6), 1241-1256 (2001).
3. R. C. Harrington, "Separation of Hanford Tank Wastes by Liquid-Liquid Extraction Employing Organophosphorus Extractants," M.S. Thesis, Washington State University, Pullman, Washington State University, 2006.
4. M. L. Dietz, E. P. Horwitz, and A. H. Bond, "Extraction Chromatography: Progress and Opportunities," Metal in Separation and Preconcentration: Progress and Opportunities, A. H. Bond, M. L. Dietz, and R. D. Rogers, Eds., ACS Symposium Series 716, American Chemical Society, Washington, DC, 1999; pp. 234-250.
5. E. P. Horwitz, D. R. McAlister, and M. L. Dietz, "Extraction chromatography versus solvent extraction: how similar are they?" *Sep. Sci. Technol.*, **41**(10), 2163-2182 (2006).
6. V. T. Orekhov, V. A. Minaev, and V. D. Federov, "Extraction of nitric acid by various organophosphorus compounds in the presence of salting-out agents," *Zh. Neorg. Khim.*, **13**(8), 2230-2233 (1968).

MODELING OF DISTRIBUTION AND SPECIATION OF PLUTONIUM IN THE UREX EXTRACTION SYSTEM

A. Paulenova,[1] P. Tkac,[1] G.F. Vandegrift,[2] and J.F. Krebs[2]

[1]*Radiation Center, Oregon State University, Corvallis, OR 97331-5903.*
[2]*Argonne National Laboratory, Chemical Sciences and Engineering Division Argonne, IL 60439-4837*
Corresponding author email address: alena.paulenova@oregonstate.edu

ABSTRACT

The PUREX extraction process is used worldwide to recover uranium and plutonium from dissolved spent nuclear fuel using the tributylphosphate-nitric acid extraction system. In the recent decade, significant research progress was achieved with the aim to modify this system by addition of a salt-free agent to optimize stripping of plutonium from the tributylphosphate (TBP) extraction product (UREX). Experimental results on the extraction of Pu(IV) with and without acetohydroxamic acid in the HNO_3/TBP (30 vol %) were used for the development of a thermodynamic model of distribution and speciation of Pu(IV) in this separation process. Extraction constants for several sets of nitric acid, nitrate, and acetohydroxamic acid concentrations were used to model the obtained data. The extraction model AMUSE (Argonne Model for Universal Solvent Extraction) was employed in our calculations.

INTRODUCTION

The UREX+3a process is a cascade of four separate solvent-extraction processes [1]:

- UREX for recovery of technetium and uranium;
- CCD-PEG for recovery of cesium and strontium;
- TRUEX process separates the rare earth and transuranic actinides from the other components in the CCD-PEG raffinate;
- TALSPEAK for separation of lanthanide fission products from transuranic elements.

Acetohydroxamic acid (AHA) was proposed as a scrubbing agent for UREX process with the aim to reduce the hexavalent Np(VI) to Np(V) and complex tetravalent Np and Pu into nonextractable species. We used our experimental results on the extraction of Pu(IV) with 30% TBP in *n*-dodecane from nitric acid solutions with and without AHA for the development of a thermodynamic model on distribution and speciation of tetravalent plutonium in this separation process.

Simulation of metal extraction requires an ability to predict distribution of all extractable metal species present in the initial aqueous solution [2,3]. The effect of

aqueous matrix on speciation of Pu in both the aqueous and organic phases was included in the speciation model. Several plutonium species were identified in the investigated system. The model predicted also the presence of mixed complexes of Pu(IV) with AHA and nitrate in the organic extraction phase. In this paper, identification of Pu-species, formed in both extraction phases, and their distribution between phases will be discussed.

EXPERIMENTAL

Materials and Methods

Plutonium was obtained from Argonne National Laboratory as oxide. After dissolution in nitric acid, a mixture of hexavalent and tetravalent oxidation states in the stock solution was found by Vis-NIR spectroscopy. Therefore, the tetravalent oxidation state of Pu was adjusted by cautious addition of acidified hydrogen peroxide and a few crystals of solid $NaNO_2$. Impurities of Am-241 were removed by anion-exchange chromatography. Purity of the tetravalent oxidation state was confirmed by extraction with thenoyl trifluoroacetone (TTA) in xylene from 1 M nitric acid and Vis-NIR spectroscopy.

A solution of 1.1 M tri-*n*-butyl phosphate (30 vol %) in *n*-dodecane was used as a solvent for all extraction experiments. Before the use, TBP was pre-equilibrated with the aqueous phase containing various concentrations of HNO_3 and $LiNO_3$ as used in the extraction experiment. Distribution ratios of Pu(IV) were measured in batch experiments. Samples with the 1:1 organic/aqueous volume phase ratio were placed in plastic extraction vials, spiked with tetravalent Pu-239 (10^{-7} M) and rigorously agitated by vortex for 4 minutes at ambient conditions, which ranged from 20 to 24 °C. Aqueous and organic phases were split by centrifugation, and aliquots were taken for analyses. Relative equilibrium concentrations of plutonium in the organic and aqueous phase were determined with liquid scintillation counting using 200 µL of sample and 6 mL of Ultima Gold scintillation cocktail. The reported experimental distribution ratios are an average from at least two extraction experiments. When desired, AHA was added to extraction vials immediately prior to contacting with the solvent; thus, the effect of hydrolysis of AHA was negligible.

RESULTS AND DISCUSSION

Effect of Nitrate on Extraction of Pu(IV)

In general, upon addition of a nonextractable nitrate salt ($LiNO_3$), a strong salting-out effect is observed, and increased extraction yields of extractable species such as nitric acid and neutral metal-nitrate complexes (e.g., with tetra- and hexavalent actinides) into the organic phase by TBP are measured [4-6]. The mechanism of this increase is the conversion of other complexes to the neutral species, as the neutral species in the aqueous phase are extracted by TBP [5]. Figure 1A displays the results of extraction experiment with tetravalent plutonium for several concentration combinations

of HNO_3 and $LiNO_3$. Distribution ratios are plotted versus the chemical activity [7] of total nitrate in the initial extraction aqueous phase (Figure 1A).

As predicted, higher concentrations of nitric acid and nitrate in the aqueous phase resulted in larger distribution ratios of plutonium with a maximum at 7-8 M of total nitrate concentration. Due to the formation of anionic Pu species and the saturation of TBP with nitric acid, extraction of Pu(IV) under high HNO_3 conditions decreases. The increase of total nitrate concentration leads to formation of higher Pu-nitrate complexes in the aqueous phase that can be: $Pu(NO_3)^{3+}$, $Pu(NO_3)_2^{2+}$, $Pu(NO_3)_4$, and $Pu(NO_3)_6^{2-}$. $Pu(NO_3)_3^{+}$ and $Pu(NO_3)_5^{-}$ are not likely to be formed in considerable amounts [8]. If β_i is the stability constant for the particular Pu-nitrate complex, the total concentration of metal in the $Pu/HNO_3/LiNO_3$ aqueous matrix can be described as:

$$[Pu]_{(aq)} = [Pu^{4+}]_{free} + [Pu(NO_3)]^{3+} + [Pu(NO_3)_2]^{2+} + \ldots \quad (1)$$

$$[Pu]_{(aq)} = [Pu^{4+}]_{free}\ (1 + \sum_{i=1}^{n} \beta_i [NO_3]^i) \quad (2)$$

To identify the extracted species, that is, to determine the solvate number for nitrate, the measured data are plotted as a ratio of $D/([Pu]_{free} \cdot TBP_{free}^2)$ vs. activity of nitrate $\{NO_3^-\}$ (Figure 1B). "Free" means the fraction of metal that is not bound in the nitrate complex, and free TBP is not bound in solvate adduct with metal or HNO_3.

Increase of the total nitrate concentration favors formation of multiple Pu-nitrate complexes that force the extraction of Pu into TBP. If only extractable species are believed to be $Pu(NO_3)_4$, the logarithmic plot of experimental values of $D_{Pu(IV)}$ vs. $\{NO_3^-\}$ should give a slope of 4:

$$Pu(H_2O)_n^{4+} + 4NO_3^- + 2TBP_{(org)} \rightleftharpoons Pu(NO_3)_4.2TBP_{(org)} + nH_2O \quad (3)$$

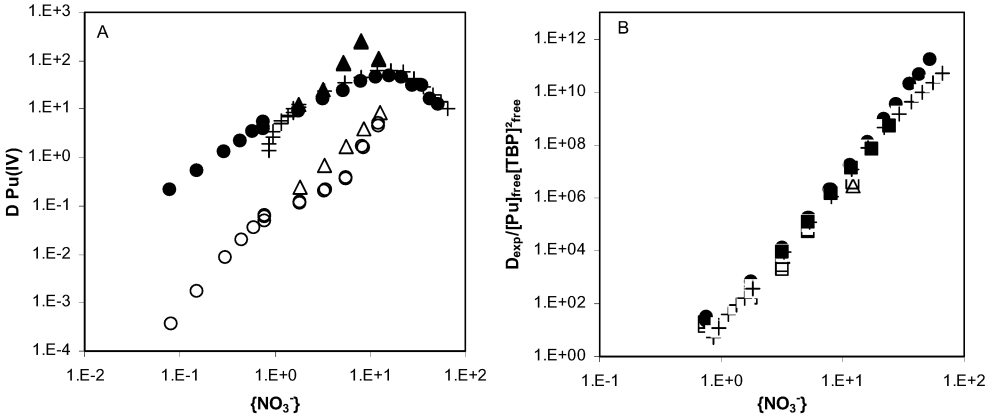

Figure 1. Experimental data of the distribution ratio of Pu(IV) as a function of nitrate: (●) 0.1-12 M HNO_3; (▲) 1 M HNO_3 + 0.98-4.87 M $LiNO_3$; (+) 1 M $LiNO_3$ + 0.1-12 M HNO_3; (○) 0.1-6 M HNO_3 + 0.4M AHA; (△) 1 M HNO_3 + 0.98-4.87 M $LiNO_3$ + 0.4M AHA; (■) 2 M HNO_3 + 0.96-5.84 M $LiNO_3$; (□) 0.5 M HNO_3 + 0.48-5.36 M $LiNO_3$.

However, we have found that the average slope of the log-log plots of all measured $D_{Pu(IV)}$ vs. activity of total nitrate $\{HNO_3 + LiNO_3\}$ is about 5 (Figure 5),

which can be explained by extraction of at least three different neutral solvate species (Equations 3–5). A simple plutonium tetranitrate disolvate is coextracted with trinitrohydroxide at lower nitric acid concentration (<1 M) when also hydrolyzed species of metal must be considered (Equation 4), while at high concentrations of HNO_3, a co-extraction of another nitric acid molecule occurs (Equation 5):

$$Pu(OH)(H_2O)_q^{3+} + 3NO_3^- + 2TBP_{(org)} \rightleftharpoons Pu(OH)(NO_3)_4.2TBP.HNO_{3(org)} + qH_2O \quad (4)$$

$$Pu(H_2O)_n^{4+} + 4NO_3^- + TBP_{(org)} + TBP.HNO_{3(org)} \rightleftharpoons Pu(NO_3)_4.2TBP.HNO_{3(org)} + nH_2O \quad (5)$$

Effect of AHA on Extraction of Pu(IV)

Upon addition of AHA to the aqueous solution containing Pu(IV) in nitric acid, a significant decrease of distribution ratio of plutonium (Figure 1A) was observed [9-12], due to various Pu-acetohydroxamate complexes formed in the aqueous phase. A much lower extraction of Pu(IV) was observed when the same amount of AHA was added to lower than to higher nitric acid concentration; ternary mono- and di-acetohydroxamate nitrate species of plutonium were predominant. A higher concentration of nitric acid leads to protonation and hydrolysis of AHA, followed by an increase of distribution ratio of Pu, because the fraction of plutonium not complexed with AHA increases. Our recent spectroscopic investigation [11,12] confirmed that, in the presence of AHA and investigated range of HNO_3 concentrations, co-extraction of acetohydroxamate complexes of plutonium to the organic phase must be also taken into account. Therefore, the co-extraction of Pu-hydroxamate species formed in the aqueous phase was also included in the model with formation of species presented in Equations 6-8:

$$Pu(AHA)(H_2O)_n^{3+} + 3NO_3^- + 2TBP_{(org)} \rightleftharpoons Pu(AHA)(NO_3)_3.2TBP_{(org)} + nH_2O \quad (6)$$

$$Pu(AHA)_2(H_2O)_n^{2+} + 2NO_3^- + 2TBP_{(org)} \rightleftharpoons Pu(AHA)_2(NO_3)_2.2TBP_{(org)} + nH_2O \quad (7)$$

$$Pu(OH)(H_2O)_q^{2+} + HAHA + 3NO_3^- + 2TBP_{(org)} \rightleftharpoons Pu(AHA)(NO_3)_3.2TBP_{(org)} + (q+1)H_2O \quad (8)$$

Modeling of Pu(IV) Extraction with TBP

We used our experimental data to develop a Pu(IV) extraction model for the AMUSE (Argonne Model for Universal Solvent Extraction) code, which was developed for highly accurate predictions of chemical behavior in a solvent-extraction process by calculating component distribution ratios using chemically correct equilibria and thermodynamic activities for major components (hydrogen ion, nitrate, and water) [13]. Activity coefficients for nitrate, hydrogen ion, and water were calculated using the AMUSE code, which is considered commercially sensitive information and Applied Technology. The effects of other extractable species (e.g., HNO_3, U(VI), and Zr(IV)) are handled by this model also, and the concentrations of TBP species with nitric acid are calculated as are the effects of solvent loading by extractable species. The aqueous-phase speciation used to fit the experimental data is included in the AMUSE data base, which successfully predicts extraction of Pu(IV) in the TRUEX process. AHA complexation constants were added to the speciation model based on fitting of these experimental data.

The correlation plots of D_{exp} vs D_{calc} for extraction of tetravalent plutonium from nitric acid/nitrate matrices without (Figure 2A) and with AHA (Figure 2B) show a very

good fit, especially for higher concentrations of $HNO_3/LiNO_3$ and AHA, and confirm that AMUSE is well suited for modeling of real extraction processes such as UREX.

The only concentrations set when the experimental and calculated D values for no-AHA system) differ are the sets with low nitric acid concentration, where hydrolysis of Pu is possible. Interestingly, while $D_{exp} > D_{calc}$ for low nitric acid with no $LiNO_3$ added (open squares in Figure 2A), this relation is contrary when nitrate is added: $D_{exp} < D_{calc}$ for the set of 0.5 M HNO_3 with added $LiNO_3$ (solid triangles in Figure 2A).

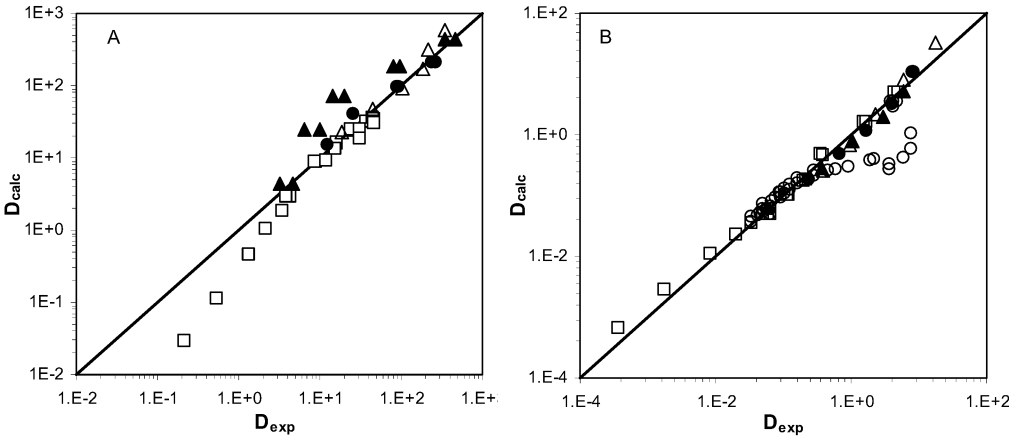

Figure 2. Comparison of calculated and experimental data for distribution ratio of Pu(IV):
A: (□) 0.1-12 M HNO_3; (▲) 0.5 M HNO_3 + 0.48-5.36 M $LiNO_3$;
(●) 1 M HNO_3 + 0.98-4.87 M $LiNO_3$; (△) 2 M HNO_3 + 0.96-5.84 M $LiNO_3$.
B: (□) 0.1-6 M HNO_3 + 0.4 M AHA; (▲) 0.5 M HNO_3 + 0.48-4.39 M $LiNO_3$ + 0.4 M AHA;
(●) 1 M HNO_3 + 0.98-4.87 M $LiNO_3$ + 0.4 M AHA; (△) 2 M HNO_3 + 0.96-5.84 M $LiNO_3$ +
0.4 M AHA; (○) 1 M HNO_3 + 0.0001-0.83 M AHA.

The correlation plot 2B was built for the case when AHA was added to the $HNO_3/LiNO_3$ system. All calculated data fit the experimental results very well, except for conditions at very low concentration of acetohydroxamic acid. Calculated $D_{Pu(IV)}$ for small concentrations of AHA (1 x 10^{-4} to 1 x 10^{-2} M) were significantly lower than the experimental one (open circles), because the calculation model doesn't include the effect of hydrolysis yet, and such low concentrations of AHA are more affected by hydrolysis of AHA in HNO_3 than larger ones. However, with the short contact time (2-3 seconds/stage) in a centrifugal contactor, hydrolysis of AHA will be negligible in a multistage operating UREX process.

CONCLUSIONS

Experimental extraction data for tetravalent Pu measured for the $HNO_3/LiNO_3$/AHA/30% TBP system were successfully modeled by the AMUSE extraction modeling code. In the absence of AHA, the $Pu(OH)_x(NO_3)_y \cdot 2TBP \cdot (HNO_3)_z$ species with x = 0-1, y = 3-4, and z = 0-1 can be extracted to TBP. In the presence of AHA, also a co-extraction of Pu-AHA species $Pu(OH)_x(AHA)_w(NO_3)_y \cdot 2TBP$ with x = 0-1, y = 2-3 and w = 0-2 was included in the model. These data and the improved $D_{Pu(IV)}$

model derived from them were used at Argonne National Laboratory to design a successful UREX flowsheet that cut the concentration of AHA used in the scrub section to less than 1/3 of the concentration originally used in earlier flowsheets. The decontamination factor for Pu in the uranium product was $>10^7$, providing a non-TRU uranium waste form.

ACKNOWLEDGMENTS

This work was funded by the U.S. DOE University Program U-NERI 05-062.

REFERENCES

1. C. Pereira, G. F. Vandegrift, M. C. Regalbuto, A. J. Bakel, D. L. Bowers, A. V. Gelis, A. S. Hebden, L. E. Maggos, D. Stepinski, Y. Tsai, and J. J. Laidler, "Lab-scale demonstration of the UREX+1a process using spent fuel," Waste Management, WM'07 Conference, Tucson, AZ, 2007; #526e.
2. P. J. Ly, "Contribution a la modelisation des systemes d'extraction liquide-liquide," *Rev. Gen. Nucl.,* **3**, 211 (1985).
3. D. J. Chaiko and G. F Vandegrift, "A thermodynamic model of nitric acid extraction by tri-n-butyl phosphate," *Nuclear Technol.*, **82**, 52 (1988).
4. E. Hesford and H. A. C. McKay, "The extraction of nitrates by Tri-n-Butyl Phosphate (TBP). III," *Trans. Faraday Soc.*, **54**, 573 (1958).
5. E. A. Kyser, "Extraction of plutonium into 30% tributyl phosphate from nitric acid solutions containing fluoride, aluminum, and boron," *Sep. Sci. Technol.*, **36**(5&6), 729–741 (2001).
6. W. W. Schulz and J. D. Navratil, Science and Technology of Tributyl Phosphate, Vol. I-IV, CRC Press, Boca Raton, FL, 1984.
7. L. A. Bromley, "Thermodynamic Properties of Strong Electrolytes in Aqueous Solutions," *AIChE J.*, **19**, 313 (1973).
8. K. Veirs, C. A. Smith, J. M. Berg, B. D. Zwick, S. F. Marsh, P. Allen, and S. D. Conradson, "Characterization of the nitrate complexes of Pu(IV) using absorption spectroscopy, 15N NMR, and EXAFS," *J. All. Comp.*, **213/214**, 328 (1994).
9. G. Karraker, T. S. Rudisill, and M. C. Thompson, "Studies of the effect of acetohydroxamic acid on distribution of plutonium and neptunium by 30 vol % tributyl phosphate," Westinghouse Savannah River Company, WSRC-TR-2001-00509, 2001.
10. M. J. Carrott, C. J. Maher, R. J. Taylor, et al., "Solvent Extraction Behavior of Plutonium(IV) Ions in the Presence of Simple Hydroxamic Acids," *Solvent Extr. Ion Exch.*, **25**(6), 723-745, 2007
11. A. Paulenova, P. Tkac, and B. Matteson, "Speciation of plutonium and other metals under UREX process conditions," GLOBAL 2007, Advanced Nuclear Fuel Cycles and Systems, Boise, ID, September 9-13, 2007; pp. 723-727.
12. P. Tkac and A. Paulenova, "The effect of acetohydroxamic acid on extraction and speciation of plutonium," *Sep. Sci. Technol.*, 2008, submitted for publication.
13. G. F. Vandegrift, M. C. Regalbuto, S. Aase, A. Bakel, T. J. Battisti, D. Bowers, J. P. Byrnes, M. A. Clark, J. W. Emery, J. R. Falkenberg, A. V. Gelis, C. Pereira, L. Hafenrichter, Y. Tsai, K. J. Quigley, and M. H. Vander Pol, "Designing and Demonstration of the UREX+ Process Using Spent Nuclear Fuel," Atalante, Nimes, France, 2004; O12-01.

INVESTIGATING THE USE OF BISMUTH(V) FOR THE OXIDATION AND SUBSEQUENT SOLVENT EXTRACTION OF AMERICIUM(VI)

L.R. Martin, B.J. Mincher, and N.C. Schmitt

Idaho National Laboratory, P.O. Box 1625, Idaho Falls, ID, 83415-2208, USA
Corresponding author email address: leigh.martin@inl.gov

ABSTRACT

The separation of Am from Cm and the lanthanides is still one of the most complex separations facing analytical chemistry, as well as any proposed advanced fuel cycle. Current research is focused on the oxidation of americium for its selective separation from the trivalent lanthanides and curium. We have already successfully demonstrated that Am oxidized to the hexavalent state using sodium bismuthate at room temperature can be extracted into 30% TBP/dodecane. Its behavior has been demonstrated to be analogous to that of hexavalent uranyl, neptunyl, and plutonyl ions. Using UV-visible spectrophotometry, the mechanism of the oxidation with sodium bismuthate has been probed to identify if it is a suitable reagent for deployment in solvent extraction systems. It has been identified that 97% of the Am is oxidized within the first 5 minutes. Significantly longer periods of time are required to obtain a solution containing greater than 50% Am(VI) limiting the use of Bi(V) for process applications.

INTRODUCTION

The separation of the transplutonium elements from lanthanide fission products has been receiving increased attention in recent years in support of the development of advanced fuel cycles [1]. The majority of current research in this area is driven by repository issues such as the need to minimize waste volumes and the management of heat-generating isotopes [2]. Commercially around the world, the PUREX process is employed for the separation of U and Pu from spent nuclear fuel. However, there is no current precedent for commercial-scale separation of the minor actinides from the lanthanides. It is expected that any large-scale separation of this nature will be performed on a PUREX type raffinate.

In these raffinates, americium and curium almost exclusively exist in the +3 oxidation state, thus complicating the separation from the trivalent lanthanides because of their nearly identical chemistries. However, the use of extractants with donor atoms softer than O or F such as N, S, and Cl [3] have been essential in producing effective separations for An^{3+} and Ln^{3+}.

Although Am primarily exists as the +3 oxidation state, it has other oxidation states available in acidic solution Am(V and VI). The preparation of Am(VI), which should be extractable in PUREX type conditions, was first reported by Asprey et al., in

1950 [4] using ammonium persulfate and hot nitric acid. As with the other actinide elements, each americium oxidation state has a distinct electronic absorption spectra consisting primarily of sharp *f-f* transitions [5]. Although both the +5 and +6 oxidation states are available, with reduction potentials of E°(III/V) = +1.73V and E°(III/VI) = +1.68V in 1.0 M $HClO_4$, oxidized Am species are powerful oxidants themselves, and hence, long term stability is problematic [6]. Due to these high potentials, only certain reagents can perform these oxidations. The classical methods to produce these oxidation states oxidation with ozone and persulfate. Unfortunately both come with drawbacks: ozone will not directly oxidize Am(III) to Am(VI), and persulfate will not completely oxidize Am(III) above 0.5 M H^+, due to the hydrolysis of the $S_2O_8^{2+}$ ion. The only other reagent in the literature that has been demonstrated to perform this oxidation is sodium bismuthate [7,8]. Although this reagent is known to oxidize americium in acidic solution, the mechanism of oxidation and the chemistry of the oxidized americium has not been adequately studied.

Using UV-vis-nIR spectroscopy, the use of sodium bismuthate as an oxidant for americium in acidic solution has been studied. The results presented here will be used to discuss the oxidation mechanism.

EXPERIMENTAL

The oxidation of americium was performed by the addition of 30-40 mg of sodium bismuthate ($NaBiO_3$) powder to 2 mL of 0.5 M nitric acid spiked with 20 μL ^{243}Am from stock on-hand at the Idaho National Laboratory (INL). In separate experiments, this mixture was agitated for 5, 10, 20, 40, and 120 minutes at room temperature. Bismuth(V) is sparingly soluble in nitric acid, leaving visible amounts of undissolved solid remaining.

The absorbance spectra measurements were made using a Liquid Waveguide Capillary Cell (LWCC - World Precision Instruments) with a 1 meter pathlength coupled to a Cary 50 Bio spectrophotometer. The initial concentration of americium solutions used for spectroscopy was 1.6×10^{-5} M. Oxidized americium solutions were filtered with a 0.45 μm PTFE filter to remove any undissolved bismuth solids prior to introducing the americium solution into the waveguide. There was found to be no significant loss of radioactivity to these filters. All spectra were referenced to a blank solution containing the background electrolyte. Data collection is restricted to 450-750 nm due to the absorption of water and nitrate in the 1-m pathlength cell.

RESULTS AND DISCUSSION

Oxidized Am species are known to form soluble fluoride complexes in aqueous solution, in contrast to Am(III), which only forms the insoluble species AmF_3. By the introduction of F^- into aqueous solution, the oxidized and reduced forms of Am can be separated [9]. Experimental results have shown that solutions of americium oxidized using sodium bismuthate do not co-precipitate when contacted with lanthanum fluoride [7,10]. These solutions have since been interrogated by UV-vis spectroscopy and found not to be pure AmO_2^{2+} as initially thought. It appears that when solutions of Am at ca.

1 x 10^{-5} M are oxidized with sodium bismuthate at room temperature, a mixture of oxidation states are observed at contact times of 2 hours [10]. Intriguingly, using this method of oxidation allows for the preparation of Am in higher oxidation states up to 6 M HNO_3. This has permitted TBP extractions to be conducted on these systems. Distribution ratios of 1.6 have been obtained at 3-6 M nitric acid idicating that AmO_2^{2+} has been extracted, since the other oxidation states present (III and V) are considered inextractable (Figure 1).

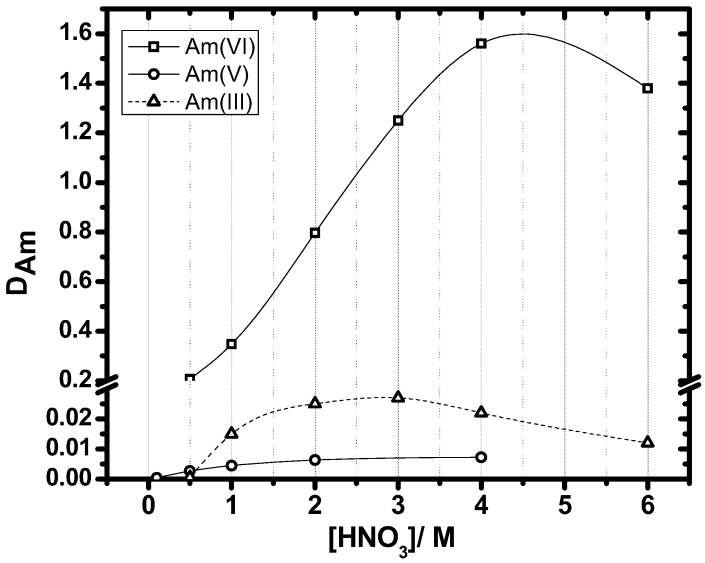

Figure 1. Distribution ratios obtained for Am(III, V, and VI) extraction into 30% TBP/dodecane as a function of nitric acid concentration. Figure adapted from Mincher et al. [10].

It has been assumed that the oxidation takes place by Bi(V) being dissolved into solution, which then reacts with the Am(III); however, there is currently no discussion of the oxidation mechanism in the open literature. As already indicated, after 2 hours of oxidation with sodium bismuthate, solutions containing AmO_2^{2+}, AmO_2^{+}, and Am^{3+} are obtained. In addition, an absorbance due to Bi(V) was also observed in solution that masks the absorption bands of Am(III) and Am(V) at 503 and 513 nm, respectively (Figure 2). As Bi(V) is only slightly soluble in aqueous acidic solution, it was expected that shorter contact times would lead to different ratios of the Am oxidation states. This should yield information about the oxidation mechanism and some of the kinetics involved in the oxidation. The UV-visible spectra obtained after contacting separate Am solutions with 30-40 mg of sodium bismuthate for 5, 10, and 40 minutes are also shown in Figure 2.

The results obtained were to some extent unexpected, as each solution contained appeared to have almost identical distributions of Am^{3+}, AmO_2^{+}, and AmO_2^{2+} and very little evidence of Bi(V) in solution, apart from the contact at 2 hours. Closer analysis of the spectra found some variation in the distribution of Am between each oxidation state with increasing contact time. Table 1 shows the distribution of Am between the three

oxidation states after each contact; in all cases, over 97% of the americium was in an oxidized form.

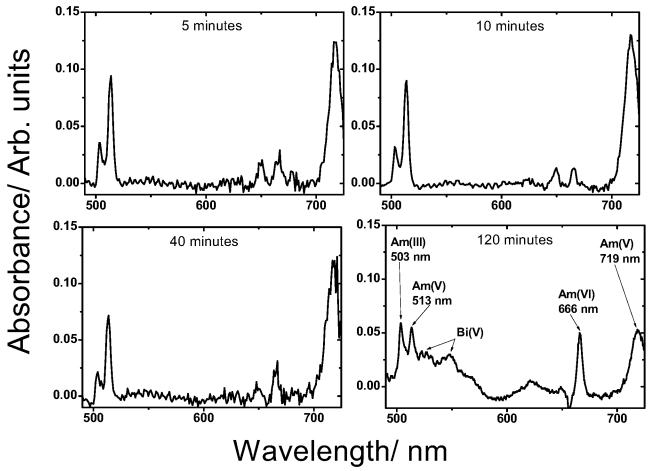

Figure 2. Electronic absorbance spectra recorded after mixing a 1.65 x 10^{-5} M Am solution in 0.5 M HNO_3 with 30-40 mg sodium bismuthate for 5, 10, 20, and 40 minutes at room temperature.

Table 1. Distribution of Am between each oxidation state after various contact times with sodium bismuthate in 0.5 M HNO_3.

Contact time/ minutes	% Am^{3+} in solution	% AmO_2^{+} in solution	% AmO_2^{2+} in solution
5	3.04	78.07	18.88
10	2.89	74.58	22.53
20	2.02	66.14	31.68
30	2.66	64.40	32.94
40	1.76	57.07	44.53
120	4.08	34.67	61.25

The majority of the oxidized Am after five minutes is in the AmO_2^{+} form. Longer contacts with the bismuthate leads to increased AmO_2^{2+} production primarily at the expense of AmO_2^{+}, although Am^{3+} concentration is also seen to decrease between 5 and 40 minutes. The distribution of oxidation states at 120 minutes suggests that the reaction has significantly slowed by this point and may be approaching the end point.

These results are somewhat interesting when comparing the conditions required for oxidation of americium using persulfate in acidic solution. This reagent has a standard electrode potential of +2.12 [11], which is higher than that of Bi(V) at +1.7 V [12].

Equation 1 describes the oxidation of Am^{3+} with persulfate, a reaction that is known to require significantly longer periods of time and elevated temperatures than is

required with sodium bismuthate. However, this is probably due to the mechanism proceeding via thermal-decomposition products of the $S_2O_8^{2-}$ ion and not a direct reaction with the $S_2O_8^{2-}$ ion, as is expected with the Bi(V).

$$3/2\ S_2O_8^{2-} + Am^{3+} + 2H_2O \rightarrow 3SO_4^{2-} + AmO_2^{2+} + 4H^+ \quad (1)$$

The absence of the Bi(V) absorption in the experiments run at 5, 10, 20, and 40 minutes, indicates that Bi(V) is slowly dissolved and constantly being consumed at shorter contact times. Only when the contact time is extended to 2 hours do we see significant Bi(V) accumulation in solution. This observation in addition to those noted above seems to suggest that there are probably two stages to the oxidation, an initial fast oxidation of Am^{3+} probably to AmO_2^+, then a slower conversion of AmO_2^+ to AmO_2^{2+}. Due to the relative insolubility of dissolved bismuthate, it seems that the initial oxidation may result from the reaction of Am^{3+} at the surface of the bismuthate solid, rather than relying on the dissolution of Bi(V), which seems more important for the second oxidation step.

It has become clear from the results obtained that further experimentation is required to determine the mechanism by which americium is oxidized in this system. The use of sodium bismuthate works well as a reagent for the oxidation of Am to AmO_2^+ and AmO_2^{2+} for fundamental solution-chemistry studies. However, before Bi(V) can be considered in the development of a solvent-extraction system to separate AmO_2^{2+}, the mechanism by which the oxidation takes place has to be determined. The addition of any solid to such a process may be highly undesirable. However, it also may have some practical application in chromatographic/analytical-scale separations.

CONCLUSIONS

Sodium bismuthate has been shown to be a suitable reagent for the oxidation of Am^{3+} to AmO_2^+ and AmO_2^2 in nitric acid solutions. Oxidation at room temperature produced a mixture of the higher oxidation states after an unexpectedly short five-minute contact in 0.5 M HNO_3 solution. Spectroscopic interrogation of the solutions resulting from varying oxidation times indicates that oxidation occurs within minutes at room temperature but does not go to completion even at long contact times of two hours. Due to the initial rapid conversion of the americium to the oxidized form and then slow appearance of increased concentrations of AmO_2^{2+}, primarily at the expense of AmO_2^+, it appears that the oxidation is a more complicated process than originally thought. These initial results suggest that Am^{3+} is oxidized at the Bi(V) surface; this is then followed by a solution-phase oxidation of AmO_2^+ to AmO_2^{2+}. However, it is clear more work is required to identify the oxidation mechanism.

ACKNOWLEDGMENT

This research was funded by the INL-LDRD program, sponsored by the US Department of Energy, Office of Nuclear Energy, Science, and Technology under DOE Idaho Operations Office contract DE-AC07-99ID13727.

REFERENCES

1. K. L. Nash, "Actinide Solution Chemistry and Chemical Separations: Structure-Function Relationships in the Grand Scheme of Actinide Separation Science," Recent Advances in Actinide Science, R. Alvarez, N. D. Bryan, and I. May, Eds., The Royal Society of Chemistry, Cambridge, England, 2006; pp. 465-472.
2. T. A. Todd and R. A. Wigeland, "Advanced Separation Technologies for Processing Spent Nuclear Fuel and the Potential Benefits to a Geologic Repository," Separations for the Nuclear Fuel Cycle in the 21st Century, G. J. Lumetta and K. L. Nash, Eds., Oxford University Press, 2006; pp. 41-55.
3. K. L. Nash, "Twenty-First Century Approaches to Actinide Partitioning," Separations for the Nuclear Fuel Cycle in the 21st Century, ACS Symposium Series 933, G. J. Lumetta, and K. L. Nash, Eds., Oxford University Press, 2006; pp. 21-40.
4. L. B. Asprey, S. E. Stephanou, and R. A. Penneman, "A New Valence State of Americium, Am(VI)," *J. Am. Chem. Soc.*, **72**, 1425-1426 (1950).
5. L. B. Asprey, S. E. Stephanou, and R. A. Penneman, "Hexavalent Americium," *J. Am. Chem. Soc.*, **73**, 5715-5717 (1951).
6. L. R. Morss, N. M. Edelstein, and J. Fuger, The Chemistry of the Actinide and Transactinide Elements, Third Edition, Springer, Dordrecht, 2006.
7. M. Hara and S. Suzuki, "Oxidation of Americium(III) with Sodium Bismuthate," *J. Radioanal. Chem.*, **36**, 95-104 (1977).
8. M. Hara and S. Suzuki, "The Chemistry of Americium. IV. The Stability of Am(V) and Am(VI) in Nitric Acid Solutions and in Solutions Containing Ozone Gas, Fluoride, or Phosphate Ions," *Bull. Chem. Soc. Jpn.*, **52**, 1041-1045 (1979).
9. F. L. Moore, "Separation of Americium from Other Elements: Application to the Purification and Radiochemical Determination of Americium," *Anal. Chem.*, **35**, 715-719 (1963).
10. a) B. J. Mincher, L. R. Martin, and N. C. Schmitt, "Tributylphosphate Extraction Behavior of Bismuthate-oxidized Americium," Manuscript submitted to Inorganic Chemistry, 2007. b) B. J. Mincher, L. R. Martin, and N. C. Schmitt, "Co-Extraction of Am(VI) and the Major Actinides with Tributyl Phosphate," Global 2007 Advanced Nuclear Fuel Cyvles and Systems, Boise ID, USA, 2007; pp. 1500-1502. c) L. R. Martin, B. J. Mincher, and N. C. Schmitt , "Understanding the Chemistry of Uncommon Americium Oxidation States for Application to Actinide/Lanthanide Separations," Global 2007 Advanced Nuclear Fuel Cyvles and Systems, Boise ID, USA, 2007; pp. 719-722.
11. A. J. Bard, R. Parsons, and J. Jordan, Standard Potentials in Aqueous Solutions, Marcel Dekker, New York, 1985.
12. M. Oku, J. Kimura, M. Omori, and K. Hirokawa, "Determination of the oxidation states of bismuth and copper in superconductor Bi-Ca-Sr-Cu-O by oxidation-reduction titration," *Fress. Z Anal. Chem.*, **335**, 382-385 (1989).

STUDIES ON THE STRIPPING OF TRANSURANIC ELEMENTS FROM LOADED TRPO BY N,N-DIMETHYL-3-OXA-GLUTARAMIC ACID

Jing Chen, Jianchen Wang, and Wuhua Duan

Institute of Nuclear and New Energy Technology, Tsinghua University,
P.O. Box 1021, Beijing 102201, China
Corresponding author email address: jingxia@tsinghua.edu.cn

ABSTRACT

The partitioning and transmutation of long-lived nuclides such as minor actinides from HLW is a method to reduce the long-term radiotoxicity of high-level waste (HLW). The TRPO partitioning process to remove actinides from HLW was developed in China. In the original TRPO process, Am and lanthanides, Pu, and Np are stripped by 5.5 M HNO_3 and 0.6 M oxalic acid from the loaded solvent, respectively. In order to simplify the stripping of transuranic elements, a new compound N,N-dimethyl-3-oxa-glutaramic acid (DOGA) was synthesized. Two pilot tests were carried out in the centrifugal-contactor facility. Nd and Zr were used to simulate Am and Pu, respectively. Stripping of >99.9% Zr and >99.9% Nd was achieved using DOGA from the loaded 30% TRPO-kerosene.

INTRODUCTION

Partitioning-transmutation is a promising method to reduce the volume of high-level waste (HLW). The first step is to realize the effective partitioning of transuranic elements from HLW. Solvent-extraction technology has been employed to partition the actinides from HLW, for example, using the TRPO [1] and TRUEX processes [2]. The effective stripping of actinides from the loaded solvent is a key problem. Some water-soluble oxa-amides have been found to be strong complexants for the actinides in the aqueous phase and suitable for actinide stripping from the loaded organic phase [3]. Compared with the phosphorus-containing compounds, they have the advantage of complete decomposition or incineration without secondary wastes, because they are composed of only C, H, O, and N atoms. They are promising stripping agents in the treatment of HLW.

N,N-dimethyl-3-oxa-glutaramic acid (DOGA) is a typical water-soluble oxa-amide with a solubility of about 0.5 mol/L at 25 °C. The stripping behaviors of Am(III), Nd(III), Pu(IV), Zr(IV), Np(IV), Np(VI), and U(VI) by DOGA from 30% TRPO-kerosene were studied. Am(III) and Nd(III) as well as Pu(IV), Np(IV), and Zr(IV)

have similar stripping behavior. DOGA is a suitable stripping agent for transuranic elements from loaded TRPO. In the original TRPO process, Am and Pu (Np) are stripped separately [4]. It is possible to simplify the TRPO process by stripping Am, Pu, and Np together using DOGA. In order to demonstrate the feasibility of the simplified process, a pilot test was carried out in the centrifugal-contactor facility.

EXPERIMENTAL

Reagents

Based on reference [5], DOGA was synthesized by the synthetic route described in Figure 1. The product was purified by recrystallization in water. The purity was determined to be >99% by NaOH titration. The pure product was found to be colorless quadrangular crystal [6]. DOGA aqueous solutions were adjusted to different pH values with ammonia.

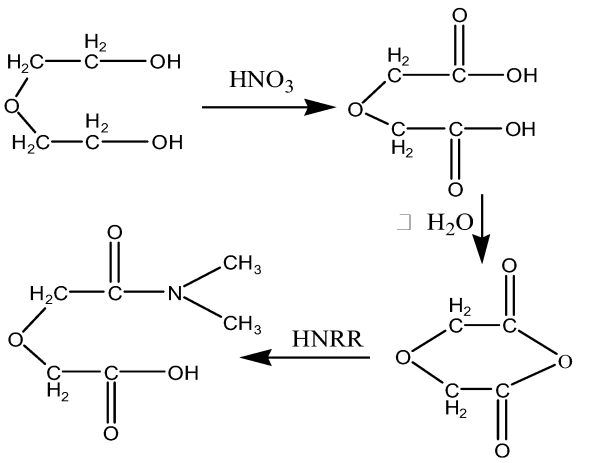

Figure 1. The synthetic route of DOGA.

The simulated high-level waste was prepared according to reference [7] and contacted with 30% TRPO-kerosene. The separated organic phase was the loaded 30% TRPO-kerosene. The main nuclides in the loaded TRPO were Nd, Zr, Fe, and Mo. Nd and Zr were used to simulate Am(Cm) and Pu(Np), respectively, because of their similar distribution behaviors between TRPO and DOGA solution.

Pilot Test

The pilot test was carried out in the centrifugal-contactor facility. After equilibrium was achieved, the aqueous and organic phases were sampled and measured by ICP-AES. The objective of the test was to achieve a Nd and Zr stripping percentage of 99.9%.

Two tests were arranged according to different processes (see Figures 2 and 3 and corresponding Tables 1 and 2). Figure 2 gives the flowsheet of the first test with the stage numbering from right to left, and Table 1 lists the corresponding process parameters. In Section B, 0.05 M HNO_3 was used to scrub the nitric acid from the load TRPO. A 0.35 M DOGA solution with pH 5.3 was used to strip Nd and Zr in Section C1. In Section C2, 0.35 M DOGA solution with pH 3.8 was used to remove the raffinate Fe from the solvent in order to avoid the precipitation during Section D, where uranium was stripped by 5% ammonium carbonate. TRPO was washed by 0.05 M HNO_3 before recycle.

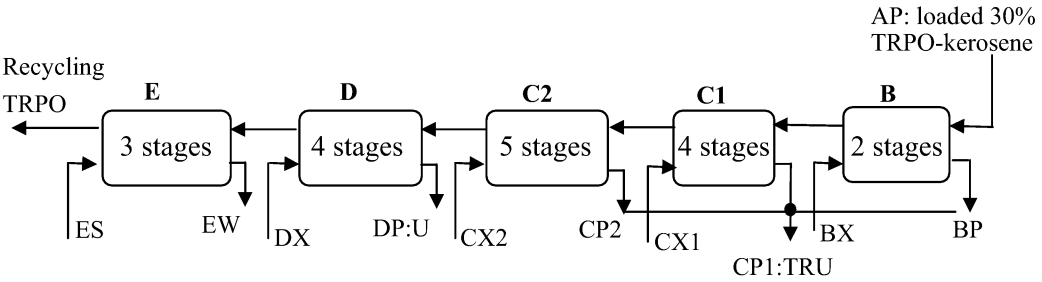

Figure 2. The flowsheet of the first pilot test.

Table 1. The process parameters for the first test

No.	Name	Code	Flow rate (L/h)
1	Loaded TRPO	AP	54
2	0.05 M HNO_3	BX	27
3	0.35 M DOGA (pH 5.3)	CX1	57
4	0.35 M DOGA (pH 3.8)	CX2	57
5	5% ammonium carbonate	DX	54
6	0.05 M HNO_3	ES	54

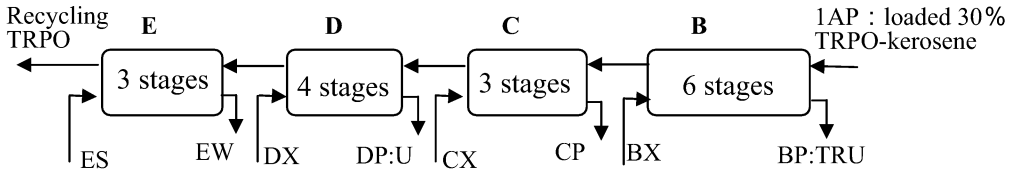

Figure 3. The flowsheet of the second pilot test.

Figure 3 gives the flowsheet of the second test with stage numbering from right to left, and Table 2 lists the corresponding process parameters. A 0.4 DOGA solution with pH 5.7 was used to strip Nd and Zr in Section B. Ammonium oxalate at 0.3 M was used to remove the raffinate Fe from the solvent. Compared with the first test, the DOGA process was simplified, but Fe removal by ammonium oxalate was added.

Table 2. The process parameters for the second test

No.	Name	Code	Flow rate (L/h)
1	Loaded TRPO	AP	55
2	0.4 M DOGA (pH 5.7)	BX	65
3	0.3 M ammonium oxalate	CX	54
4	5% ammonium carbonate	DX	54
5	0.05 M HNO_3	ES	54

RESULTS AND DISCUSSION

First Test

In the DOGA process, pH is a key factor affecting the stripping efficiency. Figure 4 gives the profile of aqueous pH in Section C1 and C2 in the first test. The initial concentration of nitric acid in the loaded 30% TRPO-kerosene was 0.59 M. About 0.3 M HNO_3 remained in the organic phase after Section B. The pH increased sharply in Section C1 and kept constant in Section C2.

Figures 5 and 6 give the distribution of Nd and Zr in Section B, C1, and C2, respectively. In Section B, 3.7% Nd was stripped. 99.98% Nd and 99.6% Zr were stripped after Section C1. Stripping of >99.99% Nd and >99.9% Zr was obtained after Section C2. Most Nd and Zr entered Stream CP1. However, these results imply that just Section C1 is not enough to strip transuranic elements. Stream BP, CP1, and CP2 were discharged into the same group, because Stream BP and CP2 contained a little amount of Nd (simulating Am) or Zr (simulating Pu).

Most Fe in the organic phase needs to be removed before Section D in order to avoid the precipitation of ferric carbonate. Fe was easily stripped by DOGA solution with a high pH. Only 39% Fe was stripped from the organic phase after Section C1. 61% Fe was stripped after Section C2. About 35% Fe was stripped in Section D without observable precipitation.

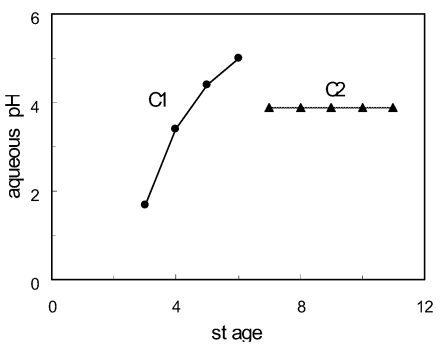

Figure 4. The aqueous pH distribution in Sections C1 and C2.

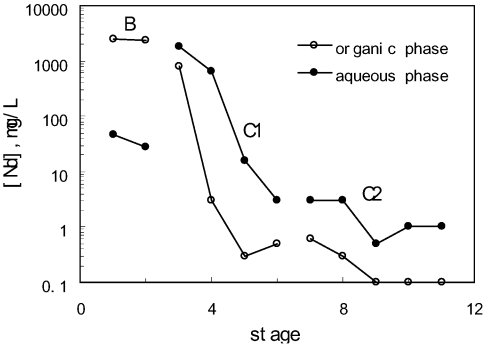

Figure 5. The distribution of Nd in Sections B, C1, and C2.

Second Test

Figure 7 gives the profile of aqueous pH in Section B. The initial concentration of nitric acid in the loaded 30% TRPO-kerosene was 0.59 M. From Figure 7, the aqueous pH increased sharply from stage 1 to 4 and then held constant at ~5 after stage 4.

Figure 8 and 9 give the distributions of Nd and Zr in Section B, respectively. 99.98% Nd and >99.9% Zr were stripped after Section B. This implies that Section B is enough to strip transuranic elements from the organic phase. Stream CP was separated from Stream BP.

In Section B, 53% Fe was stripped. 91% Fe was stripped after Section C. This ensured the absence of precipitation during Section D.

Compared with the first test, a simpler DOGA process achieved a satisfactory stripping percentage. This mainly results from a higher concentration of DOGA, a higher flow ratio of stripping solution to the solvent and higher initial pH of the stripping solution in the second test.

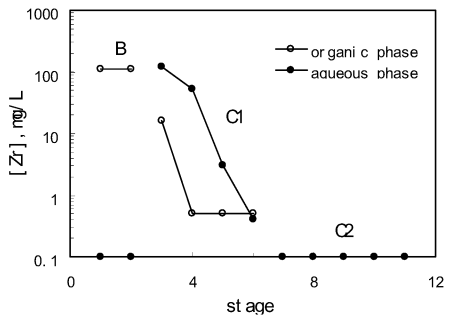

Figure 6. The distribution of Zr in Sections B, C1, and C2.

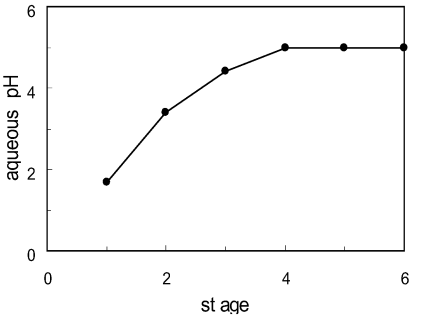

Figure 7. The aqueous pH distribution in Section B.

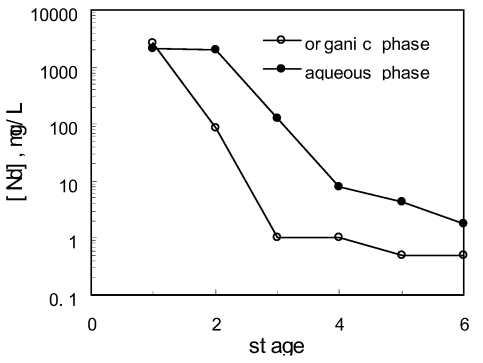

Figure 8. The distribution of Nd in Section B.

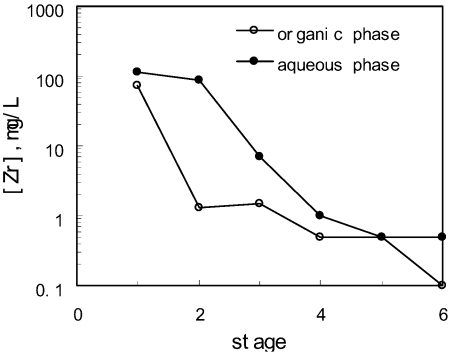

Figure 9. The distribution of Zr in Section B.

CONCLUSIONS

In the original TRPO process, actinides are extracted by 30% TRPO-kerosene from HLW. Am with lanthanides and Pu with Np are stripped from the loaded solvent by 5.5 M HNO_3 and 0.6 M oxalic acid, respectively. So, an objective is to simplify TRPO process by stripping transuranic elements Am, Pu, and Np together and cancel the stripping solution of concentrated nitric acid. The results of present work indicate that DOGA can effectively strip Nd (simulating Am) and Zr (simulating Pu) together from the loaded 30% TRPO-kerosene, and the raffinate Fe will not affect the subsequent step. It implies that DOGA process can be used to simplify the TRPO process. The DOGA process of the second test is preferable based on the experimental results.

REFERENCES

1. Y. J. Zhu and C. L. Song, "Recovery of Neptunium, Plutonium and Americium from Highly Active Waste, Trialkyl Phosphine Oxide Extraction, In: Transuranium Element, A Half Century," Washington D.C., USA: American Chemical Society, 1992.
2. E. P. Horwitz, D. G. Kalina, H. Diamond, et al., "The TRUEX process - a process for the extraction of the transuranic elements from nitric acid wastes utilizing modified PUREX solvent," *Solvent Extr. Ion Exch.*, **3**(1-2), 75-109 (1985).
3. P. Zhang, J. Chen, G. X. Tian, and J. C. Wang, "Methods for the Stripping and Separation of Radioactive Nuclides from the Organic Phase by the Water-soluble Oxa-amides," Chinese Patent No. 03146394.0, 2003.
4. C. L. Song, G. Y.Jin, J. C.Wang, and Y. J. Zhu, "Treatment of Chinese HLLW by partitioning," *Tsinghua Science and Technology*, **1**(1), 81-85 (1996).
5. P. Zhang, J. Chen, C. Y. Li, et al., "Synthesis of N,N,N',N'-tetra- butyl-3–oxa - pentanediamide and its analogous compounds," *Chemical Journal on Internet*, **5**(7), 52-55 (2003).
6. N. Huang, J. C. Wang, P. Zhang, et al., "Investigation of the Structure of the Complexes of Lanthanides with N,N'-Dimethyl-3-Oxa-Glutaramic Acid," *J. Rare Earths*, **23**(1), 12-16 (2005).
7. J. Chen, J. C. Wang, and S. Jing. "A Pilot Test of Partitioning for the Simulated Highly Saline High-level Waste." Global 2007, Boise, Idaho, USA Sept. 9-13, 2007; pp. 1831-1835.

SOLVENT-EXTRACTION PURIFICATION OF NEPTUNIUM

E.A. Kyser[1] and S.L. Hudlow[2]

[1]Savannah River National Laboratory, Actinide and Chemical Technology Section, 773-A Aiken, SC 29808. [2]H-Canyon Engineering, 221-H, Aiken, SC 29808
Corresponding author email address: eddie.kyser@srnl.doe.gov

ABSTRACT

The Savannah River Site (SRS) has recovered ^{237}Np from reactor fuel that is currently being processed into NpO_2 for future production of ^{238}Pu. Several purification flowsheets have been utilized. An oxidizing solvent-extraction (SX) flowsheet was used to remove Fe, sulfate ion, and Th while simultaneously ^{237}Np, ^{238}Pu, U, and nonradioactive Ce(IV) was extracted into the tributyl phosphate (TBP) based organic solvent. A reducing SX flowsheet (second pass) removed the Ce and Pu and recovered both Np and U. The oxidizing flowsheet was necessary for solutions that contained excessive amounts of sulfate ion. Anion exchange was used to perform final purification of Np from Pu, U, and various non-actinide impurities. The Np(IV) in the purified solution was then oxalate-precipitated and calcined to an oxide for shipment to other facilities for storage and future target fabrication. Performance details of the SX purification and process difficulties are discussed.

INTRODUCTION

SRS has historically recovered ^{237}Np via SX as a by-product from the recycling of heavy-water reactor fuel. SX flowsheets that used 30 vol % TBP were developed to recover either Np(IV) or Np(VI) depending on the impurities that required separation from the Np [1]. A reducing flowsheet that used ferrous sulfamate to maintain Np(IV) and separate Pu(III) was typically utilized. When required, an oxidizing flowsheet was used to separate Th and produce Np(VI).

Over the last several years, SRS has been processing an inventory of relatively pure Np solution through anion exchange and oxalate precipitation to convert the Np to an oxide product that can be stored and shipped offsite. The relatively impure Np solutions from various purification operations were temporarily stored in multiple tanks in shielded canyon facilities. These solutions were evaporated to reduce the solution volume and have common characteristics, such as high concentrations of impurities (especially Fe, sulfate ion, and Na) and relatively low Np concentrations (~1.5 g Np/L). Consideration was given to discarding these solutions to the SRS tank farm, but the solubility of Np in highly alkaline liquid waste would result in significant Np discarded with the supernate salt solution. These solutions had excessive amounts of sulfate ion, which limited the opportunity to directly convert them into a vitrified waste form. As a

result, the decision was made to recover the Np by SX processing in order to separate the Np from the sulfate ions. Once purified and concentrated, the purified Np will be converted into pure NpO_2 by the existing anion exchange-oxalate precipitation process for future production of ^{238}Pu.

Flowsheet Development

Preparations were made to recover and purify up to 60 kg of impure Np by SX using 7.5 vol % TBP prior to converting the Np into oxide with the existing anion exchange-oxalate precipitation process. The 30 vol % TBP process equipment was not available during this campaign, and the high concentrations of sulfate ion were found to lower the distribution ratio ($D_{o/a}$) of Np(IV) into 7.5 vol % TBP sufficiently to make the recovery of Np(IV) impractical. High sulfate ion concentration lowers the $D_{o/a}$ of the +4 actinides (Th(IV), Np(IV), and Pu(IV)) due to complexation. Karraker [2] and Pickett performed an initial experimental investigation and recommended that an oxidizing flowsheet in 7.5 vol % TBP be utilized to recover Np(VI) from the sulfuric-nitric acid matrix.

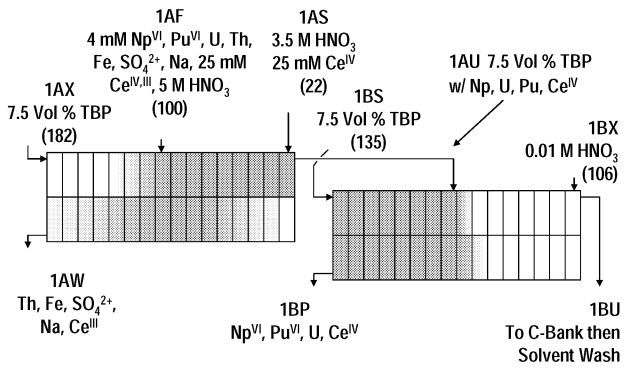

Figure 1. Oxidizing flowsheet for the recovery of Np(VI) from nitric acid solutions with high concentrations of sulfates.

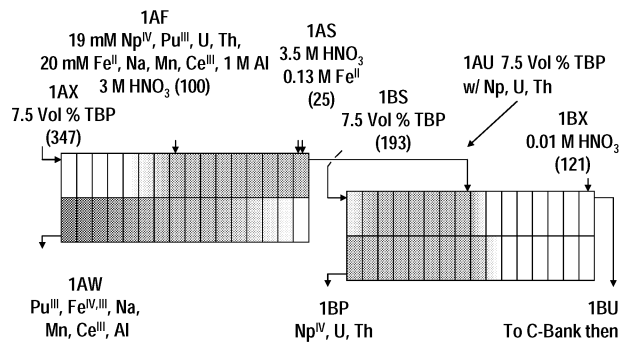

Figure 2. Reducing flowsheet for the recovery of Np(IV) and the rejection of Pu(III).

Utilizing literature and internal SRS data for $D_{o/a}$ values, Laurinat [3,4] modeled the proposed flowsheet using a spreadsheet-based model developed by Argonne National Laboratory [5]. Flowrate ratios were modified based on equipment constraints and need to reduce the risk of high Np losses. Limited batch extraction tests with process solutions showed the $D_{o/a}$ for Np(VI) to be between 1 and 2. A Np $D_{o/a}$ of >1 was anticipated to produce acceptable Np losses in the production process. The modeling work showed that a large fraction of the Ce(IV) would be recovered along with the Np(IV). Since the total mass of Ce oxidant used in the flowsheet was much greater than the total

mass of Np, a second SX pass (reducing flowsheet) was added to the program to remove the Ce and Pu contamination. The composition of the streams and relative flow rates for both processes are shown in Figures 1 and 2.

Major impurities in the original solutions (e.g., Fe, Na, Mn, sulfate ion, and Ce) were expected to be removed by the combined oxidizing and reducing SX flowsheets. Pu and U are the primary remaining impurities of interest after that point in the process. The expected purity of the Np solution after two cycles of SX purification was expected to rival that of the original pure Np solution with the exception of U. U was expected to be present at ~5 wt % on a Np basis, but it should be easily removed by extended washing in the anion-exchange polishing process. Pu was expected to be readily removed in the SX processing, but it was still a concern due to its significant impact on the oxide product and the ample opportunity for its re-introduction into the process equipment.

RESULTS

Material Balance

A 30,000 L nitric acid solution containing 45 kg of Np and up to 1 M sulfate ion was processed through production-scale mixer-settler banks using an oxidizing flowsheet. Recovery of Np was greater than 99%. The material balance for the combined oxidizing process runs is shown in Table 1. Rejection of most impurities was high with the exception of U and Pu. Limited recovery of Ce was observed, and a significant amount of the Pu was rejected.

Table 1. Oxidizing Flowsheet Material Balance

	1AF kg	1BP kg	1AW kg	*
Np	45	45	0.3	0.6%
Pu	0.7	0.4	0.3	44.4%
Th	0.5		0.5	
U	2.5	2.5	0.05	2.0%
Fe	2310	24	>2000	99.0%
Sulfate	5760	41	>5000	99.3%
Ce	>200	6	>130	>97%
Na	450		>400	

Additional Np solution (15 kg Np) that contained significant quantities of Na and Mn but virtually no sulfate ion were combined with the 1BP product from the oxidizing flowsheet (45 kg Np) for feedstock to the reducing flowsheet. After concentration by evaporation, the combined solutions were valence-adjusted and salted with ferrous sulfamate and aluminum nitrate before being processed through the same equipment with the reducing flowsheet. After processing with the reducing flowsheet and subsequent concentration by evaporation, the ~60

Table 2. Reducing Flowsheet Material Balance

	1AF kg	1BP kg	1AW kg	Product kg	*
Np	56	67	0.9	61	1.3%
				0.00	
Pu	0.20	0.001	0.19	2	99.6%
U	3.0	3.1	0	2.9	0.2%
Ce	12		18	0.03	99.8%
Fe		2.8		11	
Na				3.6	
Cr				2.5	
Ni				1.3	
Th				0.1	
Sulfate				10	

kg of Np was concentrated into only ~3000 L of relatively pure nitric acid solution. After transfer to the anion-exchange process, the Pu, at 40 ppm on a Np basis, was well within limits. A material balance for the combined reducing flowsheet process is shown in Table 2. This table includes both 1BP data and product data. The product data reflect the more complete characterization of this solution after concentration by evaporation and transfer to the anion-exchange process equipment. The reducing flowsheet campaign had somewhat higher losses of Np than the oxidizing flowsheet campaign at 1.3 %.

DISCUSSION

The primary concern during the development of the flowsheet was to limit the losses of Np to the waste streams. The long-term issues with the presence of Np in the waste systems made complete recovery of Np as a product attractive. The project schedule and resources limited the process development mostly to past process experience and computer modeling. As such, the experimental development work consisted of mL-scale batch extractions with both simulated and actual process samples. During the production campaign, several difficulties were encountered that had to be overcome.

Ce(IV) Reduction

Etchant-grade ceric ammonium nitrate (CAN) was used as the oxidant for the oxidizing flowsheet. Potassium permanganate was not used due to the handling issues with large amounts of MnO_2 solids that would be produced. Ceric sulfate had previously been used, but the limited solubility of that reagent during cold make-up was a known disadvantage. CAN was chosen for use, due to its ease of dissolution. It does introduce additional ammonium ion into the process streams that complicates waste handling, but that issue was thought to be under control. Plans were to prepare the 1AS stream with Ce(IV) to ensure that sufficient oxidizing potential was present to prevent loss of Np due to reduction to Np(IV) or Np(V). The use of Ce(IV) in the 1AS stream was probably not necessary, and it increased the quantity of Ce introduced to the process streams. If it was not reduced quickly, it would have been extracted and transferred to the B bank. Analysis of both the 1AF and 1AS streams was planned to assure that the planned levels of oxidant were added to both of these streams. The effectiveness of the oxidation was also checked by a laboratory test that utilized extractive chromatographic resins to determine Np oxidation states [6].

Analyses performed on the 1AS for oxidizing normality found that the prepared solution was reduced by the surfaces of the stainless steel tank in which it was prepared. Although Ce(IV) instability was observed in the laboratory tests, the reduction was far more pronounced in the stainless-steel production equipment. This phenomenon delayed the start of the campaign while it was investigated in the field and resulted in additional CAN reagent usage in the process. As a result, the process solutions had higher concentrations of both ammonium and Ce species than originally planned.

Ammonia Waste Handling Issues

The canyon facility has controls in place to limit the accumulation of ammonium nitrate solids in the ventilation system due to the combination of ammonia fumes that are evolved after neutralization of ammonium bearing solutions with nitric acid fumes. There are also flammability issues in the ventilation system of the caustic liquid waste handling systems that limit the amount of ammonia that can be discarded.

The introduction of ammonium by the use of CAN was anticipated, but significant ammonium was not recognized to already be present in the initial impure Np solutions. Issues related to ammonium levels interrupted the second of three SX process runs while an investigation was performed. In itself, this delay amounted to a relatively minor process interruption; however, it appears to have contributed to an additional problem.

Sodium Cerous Sulfate Solubility

The feed solution for this process initially contained 0.5 to 1 M concentrations each of Fe, Na, and sulfate ion. The use of additional CAN resulted in a higher total Ce concentration than was tested in the laboratory tests. During the process interruption caused by issues with the high ammonium levels, process solution remained in the mixer settler bank for ~ten days. Shortly after processing was resumed, the 1AW weir box (which allows only the aqueous phase to gravity flow to the 1AW decanter) became plugged with sodium cerous sulfate hydrate solids. As the Ce(IV) was reduced to Ce(III) in the relatively high concentrations of Na and sulfate ion that were present in the solution, these solids formed within the equipment. After considerable effort, the blockage was removed, and the process equipment was cleaned out. Significant quantities of these solids (estimated at several hundred kilograms of solids) were flushed from the equipment, and processing was resumed. The campaign was completed without further incident by limiting the amount of CAN in the process to that specified in the flowsheet.

This serious problem was not recognized in the few mL-scale batch extractions performed during process development. These tests focused on the minimum amount of Ce(IV) required to recover the Np, rather than the possible effect of higher levels of Ce(IV). Larger-scale mixer-settler experiments were not performed, due to the short duration of the campaign and the limited time and resources available to perform the development work. Ce solubility was not a problem until the Ce(IV) was reduced to Ce(III). The additional CAN that was added to the process to compensate for unexpectedly high Ce(IV) compounded the solubility difficulties. The process delays provided sufficient time for the solids formed to settle out of solution and plug the equipment.

CONCLUSIONS

A 60 kg inventory of impure Np solutions that were problematic to dispose of were purified by the use of a combination of oxidizing and reducing SX flowsheet conditions. The Np can now be converted to an oxide product for future use, and the waste solutions can be discarded. A solubility issue with sodium cerous sulfate was recognized that apparently limits the concentration of Ce that can be used when high concentrations of both Na and sulfate ions are present. The value of realistic-scale experimental studies to avoid serious processing issues was once again shown.

ACKNOWLEDGMENTS

This work was performed by Washington Savannah River Co. under contract number DE-AC09-96SR18500 for the U.S. Department of Energy. The authors would like to acknowledge the significant contributions of Dr. Dave Karraker (SRNL, retired) and Carlisle Pickett (H-Canyon Engineering, deceased) to the initial proposal for the oxidizing flowsheet. James Laurinat (SRNL) for performing the process modeling. F. R. Weitz (H-Canyon Engineering, retired) dealt with much of the process implementation details. Wanda Matthews (SRNL) performed the laboratory work. Major Thompson (SRNL, retired) provided invaluable advice during the course of this program.

REFERENCES

1. M. L. Hyder, W. C. Perkins, M. C. Thompson, G. A. Burney, E. R. Russell, H. P. Hocomb, and L. F. Landon, "Processing of Irradiated Enriched Uranium Fuels at the Savanah River Plant," DP-1500, E. I. Du Pont de Nemours & Co, Savannah River Laboratory, Aiken, SC, April, 1979.
2. D. G. Karraker, "Neptunium Recovery from Sulfuric Acid-Nitric Acid Mixture," WSRC-TR-2004-00542, Rev. 0, Westinghouse Savannah River Co, Aiken SC, November, 2004.
3. J. E. Laurinat, "SASSE Modeling of First Cycle Neptunium(VI) Recovery Flowsheet," WSRC-TR-2006-00104, Washington Savannah River Co, Aiken SC, April, 2006.
4. J. E. Laurinat, "SASSE Modeling of First Cycle Neptunium(IV) Flowsheet," WSRC-TR-2006-00187, Washington Savannah River Co, Aiken SC, June, 2006.
5. R. A. Leonard and M. C. Regalbuto, "A Spreadsheet Algorithm for Stagewise Solvent Extraction," *Solvent Extr. Ion Exch.*, **12**(5), 909-930 (1994).
6. D. P DiPrete, "Development of a Method to Measure Neptunium Oxidation States," WSRC-TR-2006-00254, Washington Savannah River Co, Aiken SC, July, 2006.

SIMULTANEOUS RECOVERY OF ALL ACTINIDES FROM SPENT NUCLEAR FUEL BY CARBAMOYLMETHYLPHOSPHINE OXIDE IN FLUORINATED DILUENTS

M. Ozawa,[1] T. Iwai,[1] V. Babain,[2] and A. Shadrin[2]

[1]*Japan Atomic Energy Agency, 4002 Narita-cho, Oarai-machi, Ibaraki-ken, 311-1393 Japan.* [2]*V.G. Khlopin Radium Institute, Murinskiy Ave. 28, 194021 St.-Petersburg Russia. Corresponding author email: Ozawa.masaki@jaea.go.jp*

ABSTRACT

Bifunctional organophosphorus extractants dissolved in polar fluorinated diluents were studied, aiming at directly recovering all *f*-elements from the dissolver solution of spent nuclear fuel. Octyl(phenyl)-N,N-diisobutylcarbamoylmethylphosphine oxide (OØD[iB] CMPO, 0.2–0.8 M) with 30% TBP dissolved in metanitrobenzotrifluoride (Fluoropole-732) dramatically expanded its extraction region without splitting out a heterogeneous third phase. Distribution ratios of U, Np, and Pu were sufficiently high for 0.4–0.8 M CMPO in this solvent system. Combination of *salt-free*, methylamine carbonate (MAC), citric acid, and hydrazine reagents were evaluated to obtain fractional stripping of *f*-elements such as TRU group and U. Static multistage extraction using artificial FBR dissolver solution supported the process feasibility. When all *f*-elements are extracted simultaneously, and TRU and U recovered separately with a single extraction cycle, the new extraction process, named ORGA-process, can be expected to be highly proliferation-resistant and systematically and economically advantageous.

INTRODUCTION

Bifunctional neutral organophosphorus compounds (BNOPC) have been investigated as extractants for recovery of actinides and lanthanides (*f*-elements, as a generic term) from highly acidic high-level liquid wastes (HLW). Such processes like TRUEX and SETFICS for HLW treatment were developed using these extractants. However, the low solubility of actinide complexes with BNOPC results in formation of a third phase at high concentration of actinides in the organic phase [1], which limits the use of BNOPC in SNF reprocessing. All existing separation processes for minor actinides (MA: Am, Cm, and Np) by solvent extraction must follow the PUREX and related processes for this reason. At present, there are two variants of extraction schemes for HLW treatment on the basis of BNOPC:

- carbamoylphosphonate or carbamoylphosphine oxide with TBP in kerosene
- carbamoylphosphine oxide in polar fluorine-containing diluent

It was previously suggested that the use of polar diluents allowed the abandonment of the introduction of TBP as phase modifier into the system by increasing the solubility of BNOPC complexes with actinides in the organic phase. Namely, despite the extremely low solubility (< 5 g/L) of uranium complexes with BNOPC in the mixture of 30 vol % TBP and 70 vol % kerosene [1], the solubility became more than 20 g/L in the mixture of BNOPC in fluorine-containing polar diluent [2].

The objective of the present work is to study the feasibility of using BNOPC for SNF reprocessing, including the preliminary investigations on extraction of *f*-elements and some other FP elements by carbamoylphosphonates and carbamoylphosphine oxides in organofluoric polar diluents [3].

EXPERIMENTAL

The HNO_3 solutions of stable elements, Eu, U, Fe, Zr, and Mo, were prepared with the content of 1×10^{-3} M for each element in solution. The tracer ^{152}Eu was introduced into the Eu-containing solutions. For investigation of Pu, Np, Am extraction, the radioactive isotopes ^{239}Pu, ^{237}Np, and ^{241}Am were added into HNO_3 solutions containing 1×10^{-3} M Eu. Extractants and diluents formulas are given in Figure 1. All extractants were used without any additional purification. "Metanitrobenzotrifluoride" (Fluoropole-732) was washed by NaOH solution before use. Di(tetrafluoropropyl) ether of diethylene glycol (Fluoropole-1083) was synthesized by the procedure described in [4]. All diluents exceeded 99% in purity by gas-liquid chromatography.

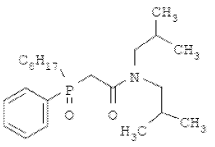	OØD[iB]CMPO Octylphenyl-N,N-diisobutylcarbamoyl-methylenephosphine oxide
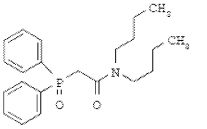	Ph2Bu2CMPO Diphenyl-N,N-dibutyl carbamoylmethylene oxide
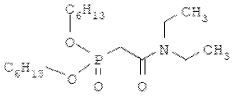	(HexO)2/Et2CMPO Dihexyl-N,N-diethylcarbamoylmethylene phosphonate
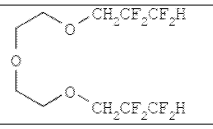	Ditetrafluoropropyl ether of diethylene glycol (fluoropole-1083, F-8)
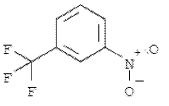	Metanitrobenzo-trifluoride (fluoropole-732, F-3)

Figure 1. Formulas of extractants and diluents.

Several physicochemical properties of investigated diluents are given in Table 1. Diluents were polar enough, as the dielectric constants ε compare with those of ethanol (ε

= 32.6) and supercritical water (ε = 2–30); hence, they were capable of dissolving polar metal-ligand complexes. Similarly, Fluoropole diluents seemed to be radiologically more stable than the usual kerosene and TBP. The yields of fluoride ion, a major product of fluorinated-diluent radiolysis, were 2.4 atoms/100eV for Fluoropole 732 and 2.6 atoms/100eV for Fluoropole-1083, respectively. Note that about 5.5 of non TBP molecules/100eV for TBP radiolysis, and more than 7 of molecules (ΣRNO_2, RCOR', etc) /100eV for Kerosene-TBP mixture radiolysis.

Table 1. Main physicochemical properties of investigated diluents

Diluent	Density, ρ, g/cm^3	Viscosity, η, mPa*s	n_D^{20}	ε	Bp, °C (mm Hg)	Solubility in 3M HNO_3, g/l
Ditetrafluoropropyl ether of diethylene glycol (fluoropole-1083)	1.374	8.9	1.3610	24	79 –80 (0.6)	0.60
Metanitrobenzo-trifluoride (fluoropole-732)	1.436	3.02	1.4730	22.3	203 (760)	1.23
Dioctylether of diethylene glycol	0.881	16.0	1.4398	---	160 –165 (0.05)	---

Static extraction was carried out as follows: A solution of elements at the required acidity with, if necessary, a radionuclide "tracer" was introduced into test tubes with ground-glass stoppers (centrifugal test tubes). Then the mixture was contacted on stirring with an equal volume of CMPO or CMP, centrifuged, and sampled for analysis. The content of stable elements was determined by X-ray fluorescence, and radioactive elements were determined by α- and γ-spectrometry. Basing on these data, the distribution ratios (*D*) and percent recovery were determined. Three parallel experiments were performed.

RESULTS AND DISCUSSION

In the preliminary stage of the study, OØD[iB]CMPO with 30% TBP in Fluoropole-732 system was chosen for the candidate solvent in the point of preventing the third-phase formation [5,6]. It was indicated that this solvent had the highest uranium capacity of ca. 110-130 g U_{org}/L for 0.2–0.8 M CMPO in the studied systems

Extraction of Elements Depending on HNO_3 Concentration

The basic distribution of elements ($Me_{aq} = 10^{-3}$ M) is shown in Figure 2 in the system HNO_3/0.2 M OØD[iB]CMPO with 30% TBP in Fluoropole-732, with reference to the other solvent systems.

The solvent 0.2 M OØD[iB]CMPO with 30% TBP in Fluoropole-732 (data indicated by No. 1) showed sufficient extractability for U(VI), and 0. 2 M Ph2Bu2CMPO with 30% TBP in Fluoropole-732 (No. 3) also was sufficient for U(VI) but rather poor

for Eu(III) extraction. 30% (HexO)2Et2CMP in Fluoropole-732 system (No. 4) showed the lowest extractability, although its loading capacity was the same as that of 0. 2 M OØD[iB]CMPO with 30% TBP in Fluoropole-732. Addition of 30% TBP significantly increased U(VI) extraction for 0. 2 M OØD[iB]CMPO in Fluoropole-732 at around 1 M HNO_3 (Nos. 1 and 2, left). The most effective extraction of U and Eu was attained above 0.5 M HNO_3 less extraction of Fe in 0. 2 M OØD[iB]CMPO with 30% TBP in Fluoropole-732 (right figure):

$$U(VI) > Zr\ (IV) > Mo(VI) \cong Eu\ (III) >> Fe(II)$$

At 0.1 M HNO_3, however, *D* values for U, Zr, and Mo were still high. Thus, some complexant to inhibit the extraction of Zr and Mo, as well as to cause effective stripping of U, must be required.

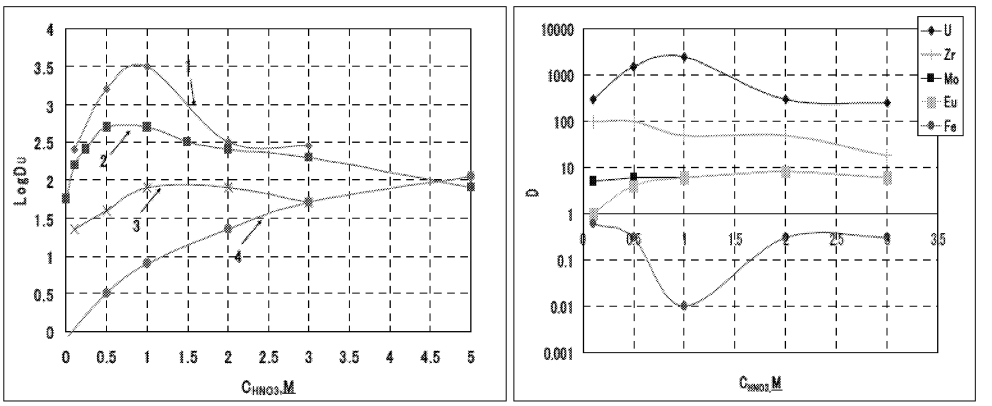

Figure 2. Dependence of distribution ratios of uranium [$U_{aq} = 10^{-3}$ M] on HNO_3 concentration in different extraction systems (left). 1: 0.2 M OØ D[iB]CMPO with 30% TBP in Fluoropole-732. 2: 0.2 M OØD[iB]CMPO in Fluoropole-732. 3: 0. 2 M Ph2Bu2CMPO with 30% TBP in Fluoropole-732. 4: 30% (HexO)2Et2CMP in Fluoropole-1083. Dependence of distribution ratios of elements [$Me_{aq} = 10^{-3}$ M] on acidity of initial solution in the system HNO_3/0.2 M OØD[iB]CMPO with 30% TBP in Fluoropole-732 (right figure).

Effect of Extractant Concentration on the Distribution Ratios Under the High U Loading

The effect of CMPO concentration on the *D* values of *f*-elements under the high U(VI) loading for OØD[iB]CMPO with 30% TBP in Fluoropole-732 system is shown in Figure 3. The U(VI) loading ratio was represented as Pu100, for instance, where aqueous initial U concentration was 100 $gU_{aq.}/L$ in 3 M HNO_3. In this figure, higher loading led *D* values of all *f*-elements to decrease. However, *D* values of Np and Pu could still be kept at their high values for 0.4-0.8 M CMPO even at 100 g U_{org}/L. For the extraction of trivalent Eu (simulator of MA) on the other hand, lower loading (*e.g.*, <50 g U_{org}/L) with higher concentration of CMPO (*e.g.*, >0.4 M) would be necessary.

Selective Stripping of Actinides by *Salt-free* Complexant

The stripping scheme should meet the requirements of nonproliferation of Pu and recycling of MA at the same time. Namely, recovery of pure Pu should be ruled out. Tentatively, fractionation to two actinide product groups, Pu with MA (Am, Cm, and Np) and U (permit containing Np), was considered. As MA/Ln separation is indispensable for MA recycling, it can be done in the next step by using, for instance, soft pyridine-containing compounds under development [7].

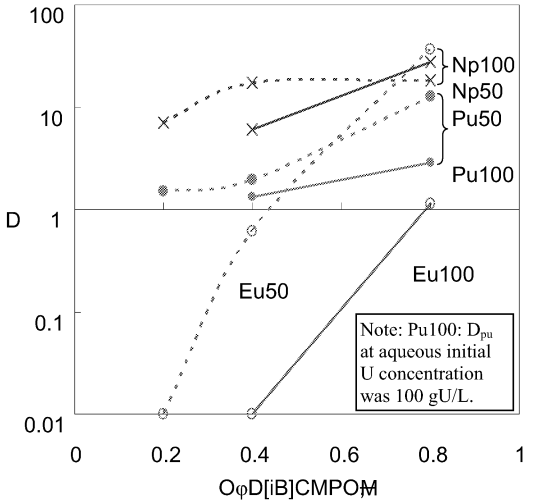

Figure 3. Distribution ratios of *f*-elements vs. CMPO concentration under the U loading condition.

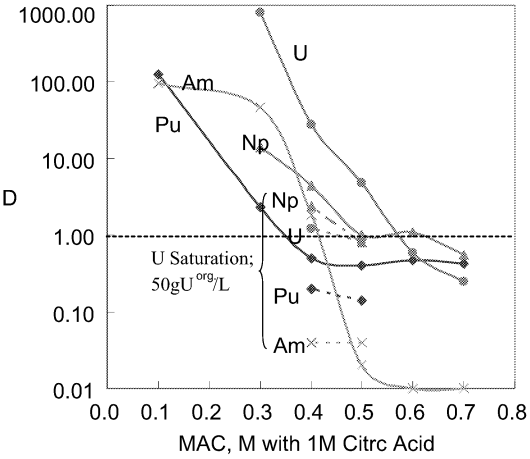

Figure 4. Distribution ratios of actinides vs. conc. of MAC with 1 M citric acid in the system 0.4 M OØD[iB]CMPO with 30% TBP in Fluoropole-732.

Figure 4 shows D values of actinides vs. MAC (methylamine carbonate; $(CH_3NH_3)_2CO_3$) with 1 M citric acid for 0.4 M OØD[iB]CMPO with 30% TBP in Fluoropole-732. By the co-presence of citric acid ($C_3H_4(OH)(COOH)_3$) with the MAC, any precipitation by U, Pu, and metals would be avoided. The tendency was clear that increasing MAC concentration decreased their D values. At the loading of 50 g U_{org}/L, ≤0.4 M MAC with 1 M citric acid (pH 3.5-3.8) suggested the target group stripping with providing D_{Pu} 0.20, D_{Am} 0.04, D_{Np} 2.4, and D_U 1.2 (for "HB" part). After the simultaneous stripping of Pu and Am, complete stripping of U and Np with trace of TPU from the loaded solvent was possible by >0.5 M MAC or 1 M citric acid at pH = 6 (neutralized by hydrazine hydrate) with D_{Pu} 0.04, D_{Am} < 0.0001, D_{Np} 0.04, and D_U < 0.001 (for "HC" part).

CONCLUSIONS

A new solvent system with bifunctional extractant dissolved in highly polar diluent was current strategy for the ORGA process (abbreviation of **Or**ganophosphoryl-

fluoropole solvent for **R**ecovery of **G**roup **A**ctinides) [6]. The 0.4 M OØD[iB]CMPO with 30% TBP dissolved in metanitrobenzotrifluoride (Fluoropole-732) was primarily chosen to satisfy simultaneous extraction of all of actinides without splitting out third phases. The *salt-free* complexants combined by MAC (methylamine carbonate) and citric acid suggested the promising group recovery of Pu with MA and U (with Np) groups. Static multistage extraction using artificial FBR dissolver solution supported this reprocessing system. Hot counter-current extraction tests are planned in the FY2007.

REFERENCES

1. Ozawa M., Koma Y., et al., "Separation of actinides and fission products in high level liquid wastes by improved TRUEX process," *J. Alloys Compd.*, **271-273**, 538 (1998).
2. Shadrin, A., Babain, V., et al., "Fluoropole-732 as diluent for SETFICS-process," Proc. of Global 2003; pp.728-731.
3. M. Ozawa, V. Babain, Yu. Fedorov, V. Romanovskiy, et al., "Potential of Bifunctional Neutral Phosphororganic Compounds For Reprocessing of Spent Fuel," Int. Conf. Global 2001, Abstracts, 2001; Vol. 2, pp. 178.
4. V. A., Babain, L. N. Lazarev, A. Yu. Shadrin, et al., *Radiochemistry*, **2**, 81-85 (In Russian) (1993).
5. M. Ozawa, et al., "Extraction Mixture for Recovery of Actinide Elements from Acidic Solutions," RF Patent 2 273 507, *Bulletin of Invention*, **10**,10. Apr. 2006.
6. M. Ozawa, V. Babain, A. Shadrin, S. Strelkov, et al.,"Joint Recovery of *f*-Elements Using Solvent based on Carbamoylphosphine Oxide Heading Toward ORGA-Process," CD-ROM, Global 2007 Advanced Nuclear Fuels Cycles and Systems, September 9-13, Boise, Idaho, USA, 2007.
7. T. Suzuki, Y.Fujii, et al., "Concept of Advanced Spent Fuel Reprocessing Based on Ion Exchange," CD-ROM, Global 2007 Advanced Nuclear Fuels Cycles and Systems, September 9-13, Boise, Idaho, USA, 2007.

STUDIES ON THE STRIPPING OF CERIUM FROM THE LOADED TBP-KEROSENE SOLUTION

S.E. Rizk, N. Abdel Rahman, J.A. Daoud, and H.F. Aly

Hot Laboratories Centre, Atomic Energy Authority, Cairo, Egypt
Corresponding author email address: jadaoud@yahoo.com

ABSTRACT

The reductive stripping of Ce(IV) from the loaded organic phase (30% TBP in kerosene) was investigated, using two stripping agents, EDTA and H_2O_2, in nitric acid. The results are compared to determine the optimum conditions for the reduction of Ce(IV) in the organic phase to Ce(III) in the aqueous phase. For each of the two stripping agents, the effect of different parameters affecting the reduction process was investigated: stripping-agent concentration, nitric acid concentration, phase ratio, shaking time, and temperature. The results are compared and discussed in terms of the conditions required for maximum reductive stripping of Ce(IV).

INTRODUCTION

Reductive stripping of metal ions from loaded organic extractants is a practical approach for selective separation of metal ions. In this respect, Malek et al. [1] proposed a method for obtaining the cerium concentrate and the remaining concentrate of rare earth element oxides. In this method, the rare-earth concentrate is exposed to a high stoichiometric excess of an alkali metal hydroxide at high temperature. The obtained rare-earth hydroxides are filtered, dissolved in concentrated HNO_3, and Ce(IV) is separated by single- or multi-stage extraction using TBP, while the residual Ce(III) in the solution is oxidized by oxidizing agents between the individual extractions. The stripping of cerium(IV) is carried out by a dilute HNO_3 solution with an addition of H_2O_2. $Ce(OH)_3$ is precipitated from the obtained solution by an ammonia solution.

Miyake et al. [2] studied the extraction system Ce–TBP–HNO_3 from the viewpoint of complexation and photo-reduction behavior. Ce(IV) was rapidly extracted by TBP in proportion to the concentration of TBP and nitric acid; however, the extracted cerium was back-extracted into the aqueous phase with increasing stirring time. The stripped cerium was found to be trivalent; this reduction was induced by light. The chemical formulas of Ce complexes in the Ce–TBP–HNO_3 system were found to be $Ce(NO_3)_3 \cdot 3TBP \cdot H_2O$ for Ce(III) and $Ce(NO_3)_3(OH) \cdot 3TBP$ for Ce(IV). Mathur et al. [3] studied the uptake of cerium at tracer level to millimolar concentration range encountered in high-level radioactive waste (HLW) solutions and from the simulated HLW solutions containing $K_2Cr_2O_7$ by 30% TBP and showed that its extraction takes place only at

tracer-level concentrations and not at millimolar levels. The stripping of the metal ions from the loaded organic phase was done with a mixture of 0.01 M ascorbic acid and 0.1 M H_2O_2 in 2 M HNO_3 at organic-to-aqueous phase ratios of 1:1, 2:1, and 4:1. Saha et al. [4] reported that Ce(IV) can be selectively and quantitatively separated from Ru by employing the extraction-chromatography technique that was developed employing HDEHP with Amberlite XAD-7 as an inert support; cerium could be selectively stripped from the HDEHP phase by reduction to Ce(III) using H_2O_2.

The extraction of Ce(IV) from nitric acid solution by TBP in kerosene and the stability towards reduction of the extracted Ce(IV) using sulphamic acid and sodium bromate was previously investigated [5]. The present work addresses the reductive stripping of cerium(IV) from the loaded organic phase (30% TBP in kerosene) using either EDTA or H_2O_2 as stripping agents in nitric acid media. The results are compared to determine the optimum conditions for reduction of Ce(IV) in the organic phase and subsequent partitioning of Ce(III) to the aqueous phase.

EXPERIMENTAL

Chemicals and Reagents

All the chemicals, materials, and reagents used were of analytical grade. Cerric ammonium nitrate is a product of May and Baker, and nitric acid a BDH product. Tri-*n*-butyl phosphate was obtained from Merck and purified from di-*n*-butyl phosphate using the Alcock Method [6]. Both hydrogen peroxide and EDTA disodium salt were ADWIC products. Sodium bromate is a product of Colnbrook Berks.

Procedure

The stripping experiments were carried out by vigorously shaking, in stoppered glass tubes, equal volumes of the TBP/kerosene solution loaded with Ce(IV) and nitric acid solution containing EDTA or H_2O_2 using a thermostated water bath shaker adjusted at 25 ± 1 °C. After equilibration and phase separation, the tetravalent and trivalent cerium concentrations were determined spectrophotometrically using a Shimadzu UV-160A UV-visible recording spectrophotometer. The determination of Ce(IV) was based on its absorbance at 340 nm, while Ce(III) was based on the absorbance of its complex with Arsenazo (III) at 650 nm.

RESULTS AND DISCUSSION

When EDTA is used for the reductive stripping of cerium, the reported kinetic study of the oxidation in the EDTA-Ce(IV) system indicates the formation of free radicals, which react rapidly with Ce(IV) to give the final products [7]. On the other hand, hydrogen peroxide (30% H_2O_2) is used as a reductive stripping agent for stripping Ce(IV) from the loaded organic phase (30% TBP in kerosene) to the aqueous phase as Ce(III) according to the following reactions:

$$H_2O_2 - 2\ e^- \leftrightarrows O_2 + 2\ H^+ \quad (1)$$

$$Ce^{4+} + e^- \leftrightarrows Ce^{3+} \quad (2)$$

$$2\ Ce^{4+} + H_2O_2 \leftrightarrows 2\ Ce^{3+} + O_2 + 2H^+ \quad (3)$$

The effect of initial EDTA concentration on the reductive stripping of Ce(IV) from the loaded organic phase, 30% TBP in kerosene, was studied over the range 1 x 10^{-4} to 0.05 M. The relationship between the EDTA concentration and the percent of Ce(IV) reduced and stripped as Ce(III) is illustrated in Figure 1. An increase in the EDTA concentration was found to decrease the percentage of Ce(IV) stripped as Ce(III). The EDTA concentration used in stripping of Ce(IV) is therefore preferred to be 0.001 M.

On the other hand, the effect of hydrogen peroxide concentration on the reductive stripping of cerium(IV) from the loaded organic phase was investigated over the range 0.001–0.2 M. The relation between the H_2O_2 concentration and the percent of Ce(IV) reduced and stripped as Ce(III) illustrated in the same figure indicates that increasing the hydrogen peroxide concentration decreases the stripping of the reduced Ce(IV). Therefore, the H_2O_2 concentration used in stripping Ce(IV) was fixed at 2 x 10^{-3} M.

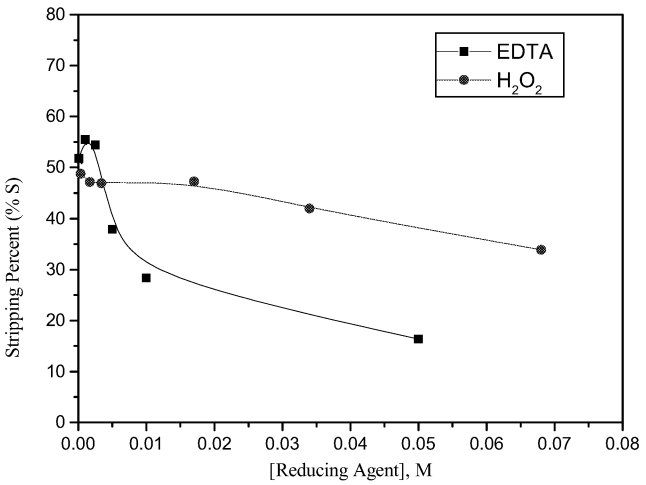

Figure 1. Effect of reducing agent concentration in 3 M HNO_3 on the reductive stripping of the loaded 5.4 x 10^{-}4 M Ce(IV) from 30% TBP (at T = 25 ± 1 °C).

The effect of shaking time on the reductive stripping of cerium(IV) from the loaded organic phase 30% TBP in kerosene, using 0.001 M EDTA or 2 x 10^{-3} M H_2O_2 in 3 M HNO_3, investigated in the range 2-120 minutes at 25 °C, showed that the best shaking time for both systems is 10 minutes. Increasing the nitric acid concentration gradually decreased the reductive stripping of Ce(IV) while using 0.001 M EDTA or 2 x 10^{-3} M H_2O_2, represented by the percent of the amount of Ce(IV) reduced to Ce(III) (see

Figure 2). Hence, the 3 M nitric acid was chosen for the reductive stripping of Ce(IV) from the loaded organic phase when using either EDTA or H_2O_2.

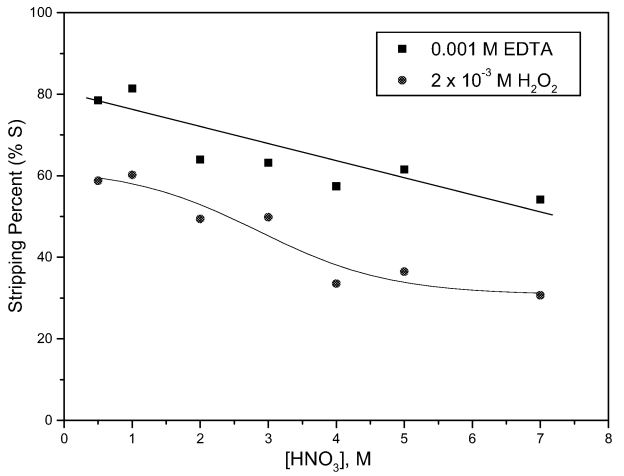

Figure 2. Effect of $[HNO_3]$ on the reductive stripping of the loaded 5.4 x 10^{-}4 M Ce(IV) from 30% TBP using reducing agents in nitric acid as stripping agent (at $T = 25 \pm 1$ °C).

The data plotted in Figure 3 show that increasing the phase ratio increases the stripping percent of Ce(IV) as Ce(III) in the aqueous phase, either by EDTA or hydrogen peroxide, until it reaches a maximum at an aqueous/organic ratio of 3:1, then remains constant with further increase in the phase ratio. Thus, the preferred phase ratio is when the aqueous/organic ratio equals 3:1.

The data plotted in Figure 4 show that the increase in temperature has a negligible effect on the stripping of Ce(IV) from the loaded organic phase either by EDTA or hydrogen peroxide.

The above results of the reductive stripping of Ce(IV) using EDTA or H_2O_2 indicate that the percentage of cerium stripped with EDTA is slightly higher than with H_2O_2. However, the use of hydrogen peroxide does not add species to the aqueous medium as is the case with EDTA.

In this context, the effect of the number of reductive-stripping stages necessary when using hydrogen peroxide as stripping agent was studied by repeating the reductive-stripping step for the same organic phase with fresh aqueous reductive-stripping solution at fixed aqueous/organic phase ratio of 1:1. For this test, five mL of the Ce(IV) loaded organic phase was shaken with the same volume of the reductive stripping solution containing 2 x 10^{-3} M H_2O_2 in 3 M nitric acid medium; the phases were separated, Ce(III) concentration was determined, and the same organic phase was used again for the reductive stripping with fresh H_2O_2 solution. The procedure was repeated until there was no cerium (III) in the aqueous phase. The obtained results indicate that a maximum concentration of 4.28 x 10^{-4} M Ce(III), equivalent to a reductive stripping percent of 80%, could be reached after five reductive stripping stages with H_2O_2.

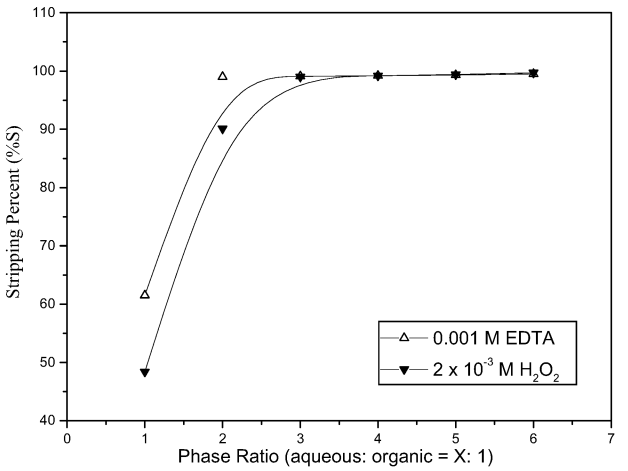

Figure 3. Effect of phase ratio on the reductive stripping of the loaded 5.4 x 10^{-4} M Ce(IV) from 30% TBP using reducing agents in 3 M HNO_3 as stripping agent (at $T = 25 \pm 1$ °C).

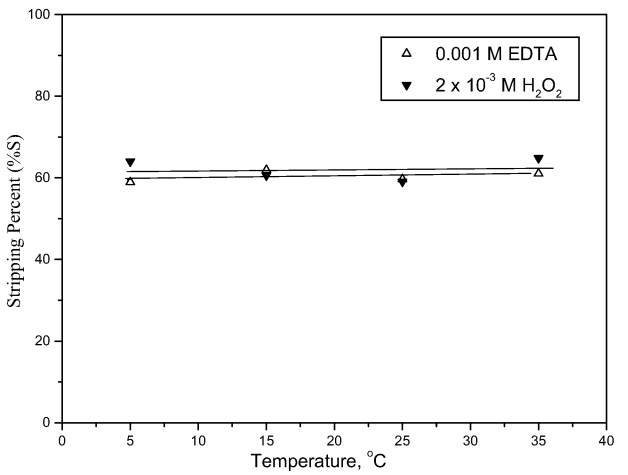

Figure 4. Effect of temperature on the reductive stripping of the loaded 5.6 x 10^{-4} M Ce(IV) from 30% TBP using reducing agents in 3 M HNO_3 as stripping agent.

CONCLUSION

EDTA or H_2O_2 could be used for the reductive stripping of Ce(IV) from loaded TBP solution. H_2O_2 is preferred, as it dissociates into water, while EDTA adds species to the nitric acid. The percent reductive stripping of Ce(IV) with 2 x 10^{-3} M H_2O_2 in 3 M nitric acid solution reaches 80% after five stripping stages at an aqueous/organic phase

ratio of 1:1. As the stripping percent increases with the phase ratio, higher stripping is expected by increasing the aqueous/organic ratio to 3:1.

REFERENCES

1. Z. Malek, M. Novak, and M. Mrnka, "Method of Obtaining the Cerium Concentrate and the Cerium-free concentrate of rare earth element oxides," CS patent document 175625/B, 1978.
2. M. Chie, I. Nobuyasu, and S. Jun, "Complexation and photo-reduction of Ce–TBP–HNO_3 extraction system," 3rd International Conference on Nuclear Fuel Reprocessing and Waste Management, Osaka Univ., Suita, Japan, Faculty of Engineering, RECOD 91, Sendai, Japan, 1991.
3. J. N. Mathur, M. S. Murali, M. V. B. Krishna, and R. H. Iyer, "Recovery of Neptunium from Highly Radioactive Waste Solutions of Purex Origin using Tributyl phosphate," *Sep. Sci. Technol.*, **31**(15), 2045 (1996).
4. B. Saha, K. Swaminathan, C. R. Venkata–Subramani, and P. R. Vasudeva Rao, "Quantitative Separation of Carrier-free Cerium from Fission Products," *J. Radioanal. Nucl. Chem. Lett.*, **214**(1), 17 (1996).
5. S. E. Rizk, N. Abdel-Rahman, J. A. Daoud, and H. F. Aly, "Studies on the Stability of Ce(IV) in Nitric Acid Medium," *Arab J. Nucl. Sci. Applic.*, **36**(2), 23-33 (2003).
6. H. A. C. McKay, K. Alcock, F. C. Bodford, W. H. Hardwick, D. Scargill, J. M. Fletcher, G. F. Best, and P. R. Woodgate, "Tri-*n*-butyl phosphate as an Extracting Solvent for Inorganic Nitrates—I : Zirconium nitrate," *J. Inorg. Nucl. Chem.*, **4**, 100 (1957).
7. G. N. Rao, "A Kinetic Study of the Oxidation of Ethylenediaminetetraacetic Acid & Its Analogues by Cerium (IV) in Sulphuric Acid Medium," *Indian J. Chem.*, **8,** 328 (1970).

NEXT-GENERATION PUREX FLOWSHEETS WITH ACETOHYDROXAMIC ACID AS COMPLEXANT FOR FBR AND THERMAL-FUEL REPROCESSING

Shekhar Kumar and S.B. Koganti

Reprocessing R&D Division, Reprocessing Group
Indira Gandhi Centre for Atomic Research, Kalpakkam 603102 India
Corresponding author email address: shekhar@igcar.gov.in

ABSTRACT

Acetohydroxamic acid (AHA) is a novel complexant for recycle of nuclear-fuel materials. It can be used in ordinary centrifugal extractors, eliminating the need for electro-redox equipment or complex maintenance requirements in a remotely maintained hot cell. In this work, the effect of AHA on Pu(IV) distribution ratios in 30% TBP system was quantified, modeled, and integrated in SIMPSEX code. Two sets of batch experiments involving macro Pu concentrations (conducted at IGCAR) and one high-Pu flowsheet (literature) were simulated for AHA based U-Pu separation. Based on the simulation and validation results, AHA based next-generation reprocessing flowsheets are proposed for co-processing based FBR and thermal-fuel reprocessing as well as evaporator-less macro-level Pu concentration process required for MOX fuel fabrication. Utilization of AHA results in significant simplification in plant design and simpler technology implementations with significant cost savings.

INTRODUCTION

Aceto-hydroxamic acid (AHA) is a novel reductant and complexant for Pu(IV). For a comprehensive review, readers are referred to Taylor et al. [1-2] and Nunez and Vandegrift [3]. In contrast to the usual reductants, hydroxylamine nitrate (HAN) or U(IV), AHA complexes Pu(IV) first and then reduces it to Pu(III) as effected by its hydrolysis product HAN.

In the nitric acid-TBP system, Karraker et al. [4] reported that the presence of AHA reduced significantly distribution ratios of Pu(IV) and Np(IV). Pathak et al. [5-6] discussed experimental data for Pu(IV) in the presence of AHA. Birkett et al. [7] presented results of few experimental runs for high-Pu flowsheets. Recently Govindan et al. [8] reported distribution ratios of Pu(IV) for macro-level aqueous concentrations (~1-18 g/L). Results of Govindan et al. indicated a clear suitability of AHA as a partitioning agent for U-Pu separation.

Recently Kumar and Koganti [9] and Kumar et al. [10] reported apparent molar volume, densities, and osmotic and activity coefficients of aqueous AHA solutions. In this report, computer simulation of AHA based U-Pu separation and conceptual next-generation AHA based flowsheets for FBR and thermal-fuel reprocessing are discussed.

DISCUSSION

Decomposition of AHA in Nitric Acid Solutions of Different Ionic Strengths

The decomposition data of AHA, as reported by Karraker et al. [4] was fitted to following form of equation

$$t_{1/2} = \exp^{\left(2.8617 \pm 1.3095 \times 10^{-2}\right)} \mathrm{H}_{aq}^{\left(-1.4194 \times 10^{-1} \pm 1.7284 \times 10^{-2}\right)} \; I_{\mathrm{M}}^{\left(-1.0839 \pm 1.7105 \times 10^{-2}\right)} \quad (1)$$

For 95% confidence interval, R^2 statistic for Equation 1 was 0.938 against 0.91 reported by Karraker et al. [4] for the linear model. Data listed by Nunez and Vandegrift [3] was not used. Equation 1 is useful in predicting the standing-time of AHA-bearing nitric solutions for acid-induced decomposition of AHA. The molar ionic strength used to obtain Equation 1 was obtained using Equation 2 where C and z are the charge and molar concentration of solution species, respectively.

$$I_{\mathrm{M}} = \frac{1}{2} \sum_{i=1}^{N} C_i z_i^2 \quad (2)$$

The reported decomposition kinetics of AHA in nitric solutions by Taylor et al. [1] was compared with the recent experimental data reported by Pathak et al. [5] and verified.

Computer Simulation of AHA Based Flowsheets

Lowering of Pu(IV) Distribution Ratios in the Presence of AHA

Karraker et al. [4] reported the lowering of Pu(IV) distribution ratios (k_{D}) in the presence of AHA in the 30% TBP/nitric acid system. Authors analyzed their data and found that the data could be well correlated in the form of a correction factor applied to the Pu(IV) k_{d} data in absence of AHA

$$k_{d_{Pu(IV)}}\Big|_{\mathrm{AHA}} = k_{d_{Pu(IV)}}\Big|_{\mathrm{AHA}=0} * f\left(\mathrm{C}_{\mathrm{AHA}}, \mathrm{C}_{\mathrm{H}_{aq}}\right) \quad (3)$$

where the correction factor is modeled in this work as an empirical function of aqueous acidity and AHA concentration:

$$f\left(\mathrm{C}_{\mathrm{AHA}}, \mathrm{C}_{\mathrm{H}_{aq}}\right) = \begin{pmatrix} 1.0 + 0.0036\,\mathrm{C}_{\mathrm{H}_{aq}} - 11.2353\,\mathrm{C}_{\mathrm{AHA}} \\ -0.0010\,\mathrm{C}_{\mathrm{H}_{aq}}{}^{2} + 26.9159\,\mathrm{C}_{\mathrm{AHA}}{}^{2} \\ -0.0107\,\mathrm{C}_{\mathrm{H}_{aq}}\mathrm{C}_{\mathrm{AHA}} \end{pmatrix} \quad (4)$$

Back-calculated distribution ratios of Pu(IV) had a mean deviation of -1.06% and standard deviation of 11.86% when compared to the literature values. Figures 1 and 2 show variation of Pu(IV) k_{d} with aqueous acidity and AHA concentration, the

comparison was excellent. Equations 3 and 4 are the first literature models of lowering of distribution ratios of Pu(IV) in the presence of AHA for the 30% TBP system.

Simulation of BNFL Run Reported at Global-2005

Birkett et al. [7] reported a flowsheet trial demonstrating U/Pu separation using AHA with a high Pu content in the HAF (40 wt %, C_{Pu} = 99.7 g/L). In this experimental run, 28 stages of miniature (10 mm rotor Φ) centrifugal contactors were used at ambient temperatures. The experimental run demonstrated sufficiently good U/Pu mass balances and very high recoveries for U (>99.999%) and Pu (>99.97% to >99.995%). Decontamination factors (DFs) obtained in this experimental run were 1.45 x 10^6 (Pu DF) and ~360 (U DF). The high Pu DF enabled use of U product in recycle as thermal MOX fuel, FBR blanket fuel, or even as LLW for disposal. Low U DFs were in tune with the current paradigm of incomplete U-Pu separation needed for product Pu recycle as either thermal MOX fuel or FBR fuel.

Some of the flowrate values were not listed in Birkett et al. [7]. The above flowsheet could be easily reduced to a system of linear equations, but exact solution is not guaranteed due to assumptions of volume swelling (or contacting) factors and inexactness of chemical analyses. In this case, volume swelling/contacting factors of the various streams were taken from information on the flowsheets published in the literature.

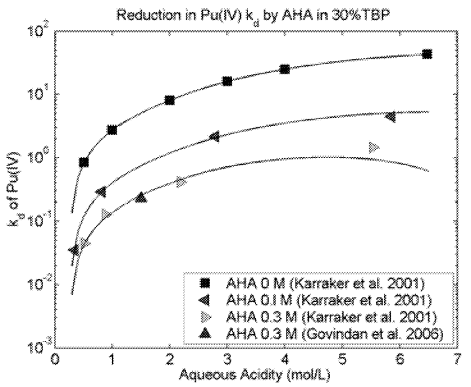

Figure 1. Reduction in Pu(IV) k_d. Karraker et al. [4] were for tracer level. Expt. data [8] were for macro Pu (~10 g/L).

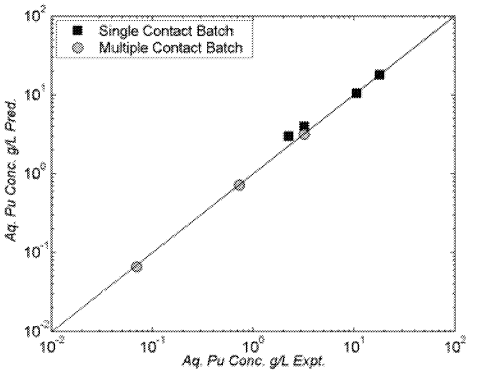

Figure 2. Parity plot for aqueous Pu(IV) concentrations. Experimental points are from Govindan et al. [8].

The resultant system of equations was solved by a constrained optimization method, and rounded-up results were used in the flowsheet simulation. This flowsheet was simulated by in-house developed code SIMPSEX (SIMulation Program for Solvent EXtraction) of Kumar and Koganti [11-13]. Table 1 shows a comparison between the reported end results and SIMPSEX simulated end results. The agreement was good.

Application of AHA in Reprocessing Flowsheets

The use of AHA in the FBR fuel reprocessing would be an important step towards the cost reduction due to simplification in plant design, technology

implementation and ease of operation. Based on the computer simulations reported in this paper, a conceptual flowsheet step using AHA can be visualized either in the first (after HA) Cycle itself or in the second cycle (after 1A). The separation of Pu from FPs after the HA cycle is better than either the prereduction step based on U(IV) where generated Pu(III) is prone to re-oxidation and subsequent extraction leading to poor DF_{Pu} or AHA based UREX process, where Pu is diverted to HAW and later it is to be recovered in NPEX process (a variant of PUREX process using 30% TBP as solvent).

Table 1. Computer simulation of flowsheet run of Birkett et al. [7]

Parameter	Exp. Birkett et al. [7]	Pred. SIMPSEX, this work
HAF Composition		
U(VI) g/L	150	
Pu(IV) g/L	99.7	
HNO_3 mol/L	3.0	
HAP Composition*		
U(VI) g/L	40.3	39.894
Pu(IV) g/L	26.8	26.524
HNO_3 mol/L	0.32	0.36
HAW Composition		
U(VI) g/L	Not listed	$<1 \times 10^{-8}$
Pu(IV) g/L	Not listed	$<1 \times 10^{-8}$
HNO_3 mol/L	2.58	2.50
U Product Stream Composition*		
U(VI) g/L	27.4	27.32
Pu(IV) g/L	Trace	$<1 \times 10^{-8}$
HNO_3 mol/L	Not listed	0.02
Pu Product stream Composition*		
U(VI) g/L	Trace	$<1 \times 10^{-4}$
Pu(IV) g/L	27.1	27.24
HNO_3 mol/L	0.52	0.49
Overall agreement:		Good

*In computer simulation, the efficiency of centrifugal extractors was taken as 100%.

Figure 3 shows a conceptual step for AHA based U-Pu separation for typical FBR feed compositions. For thermal-reactor fuel reprocessing, plutonium levels are significantly lower than that in FBR fuel reprocessing; thus, AHA concentration in the strip can be marginally reduced. By suitably increasing AHA concentration in the strip feed, a similar flowsheet can be used for evaporator-less concentration of Pu solution to the levels of 70 g/L and more for MOX fuel preparation. Figure 4 shows a co-processing step using reducing strip for co-stripping U and Pu as well for solvent-extraction based concentration.

In the case of flowsheets for reprocessing of Pu-topped Th/U-233 reactor fuels (e.g., AHWR fuels), AHA can be used to partition unspent Pu from Th/U-233 in a 5% TBP system in a salt-free way without employing any energetic chemicals like HAN or hydrazine nitrate. In addition, use of AHA makes it possible to concentrate the lean Pu

solutions via a solvent-extraction route, paving the way for elimination of evaporators in the Pu streams. This would result in immense simplification of the technology, resulting in significant cost reduction for thermal-reactor fuel reprocessing.

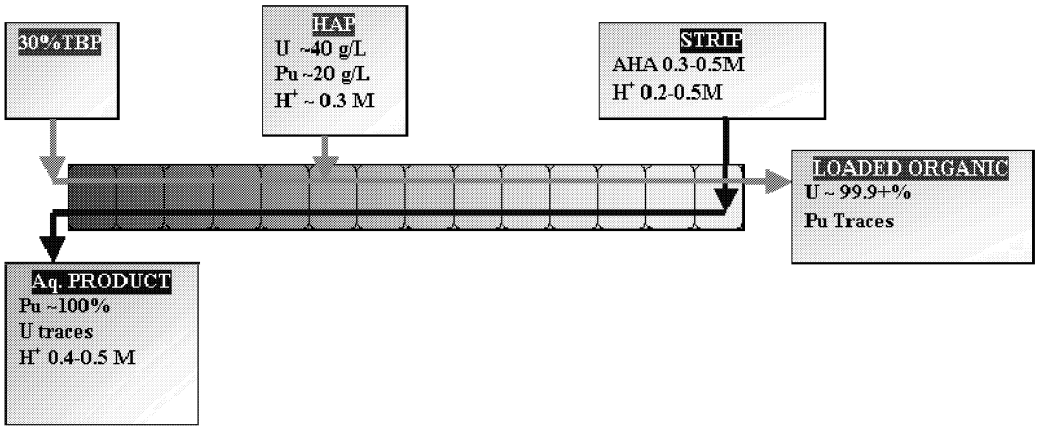

Figure 3. Schematic flowsheet for U-Pu separation for FBR feed compositions. A similar flowsheet was simulated by SIMPSEX for evaporator-less concentration of Pu solution to the levels of 70 g/L and more.

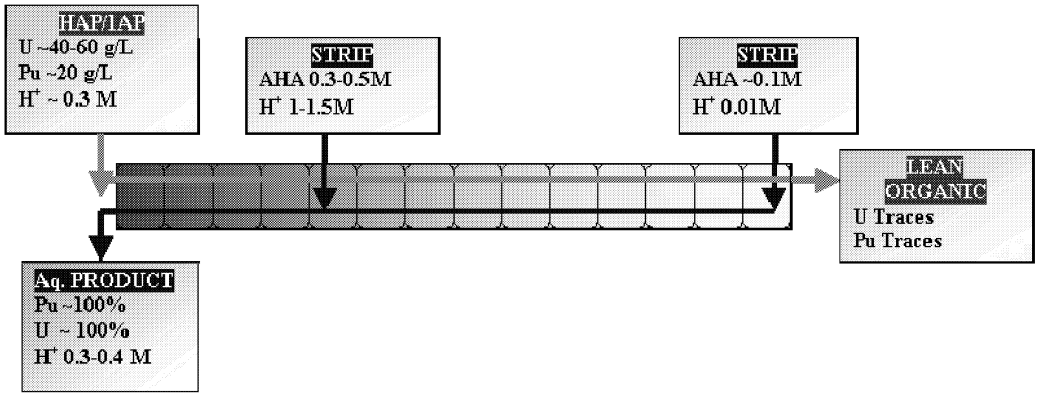

Figure 4. Schematic flowsheet for co-processing of U-Pu for FBR feed compositions.

CONCLUSIONS

The reported kinetics of AHA decomposition in nitric solutions was verified. The effect of AHA on Pu(IV) distribution ratios in 30% TBP system was quantified and modeled. Two sets of batch experiments and one high-Pu flowsheet were simulated for AHA based U-Pu separation. The agreement between the predicted and literature-reported Pu(IV) concentrations was good. Based on the results obtained, two conceptual flowsheets for FBR feed compositions were proposed for AHA based U-Pu separation as well as co-processing options. Possible application of AHA in thermal fuel (PHWR) reprocessing is also mentioned.

ACKNOWLEDGMENTS

The authors sincerely acknowledge the encouragement and kind support by Dr. Baldev Raj, Distinguished Scientist and Director IGCAR.

REFERENCES

1. R. J. Taylor, I. S Deniss, and I. May, "Hydroxamic Acids-Novel Reagents for Advanced Purex Process," ATALANTE-2000, France, 2000; Paper No. P2-15.
2. R. J. Taylor, I. May, A. L. Wallwork, I. S. Deniss, N. J. Hill, B. Galkin, B. Zilberman, and Yu. S. Fedorov, "The Applications of Formo- and Aceto-Hydroxamic Acids in Nuclear Fuel Reprocessing," *J. Alloys & Compounds*., **271-273**, 534-573 (1998).
3. L. Nunez and G. F. Vandegrift, "Evaluation of Hydroxamic Acid in Uranium Extraction Process: Literature Review," Technical Report ANL-00/35, Argonne National Laboratory, Argonne, Illinois 60439, 2000.
4. D. G. Karraker, T. S. Rudisill, and M. C. Thomson, "Studies on the Effect of Acetohydroxamic Acid on Distribution of Plutonium and Neptunium by 30% Vol.% Tributyl Phosphate," Technical Report WSRC-TR-2001-00509, Westinghouse Savannah River Company, Aiken, SC 29808, 2001.
5. P. N. Pathak, D. R. Prabhu, A. S. Kanekar, and V. K. Manchanda, "Evaluation of Acetohyroxamic Acid (AHA) as Complexant/Reductant in Nitric Acid Media," Proceeding NUCAR-2005, Amritsar, 2005; pp. 277-278.
6. P. N. Pathak, D. R. Prabhu, A. S. Kanekar, and V. K. Manchanda, "Evaluation of Alternate Reductants for Plutonium Partitioning during the Reprocessing of Advanced Heavy Water Reactor (AHWR) Spent Fuel," Proceeding NUCAR-2005, Amritsar, 2005; pp. 279-280.
7. J. E. Birkett, M. J. Carrott, O. D. Fox, C. J. Jones, C. J. Maher, C. V. Roube, R. J. Taylor, and D. A. Woodhead, "The Control of Neptunium and Plutonium in Single Cycle Solvent Extraction Flowsheets for Advanced Fuel Cycles," Proceedings of GLOBAL 2005, Tsukuba, Japan, Oct. 9-13, 2005; Paper No. 161.
8. P. Govindan, S. Sukumar, and R. V. Subba Rao, "Partitioning of Uranium and Plutonium by Acetohydroxamic Acid," Proceeding SESTEC-2006, Mumbai, 2006; Paper No. H6.
9. S. Kumar and S. B. Koganti, "Aqueous Density and Apparent Molar Volume of Aceto-Hydroxamic Acid Solutions," Technical Report IGC-267, IGCAR, 2005.
10. S. Kumar, R. Kumar, and S. B. Koganti, "Osmotic and Activity Coefficients of Aqueous Aceto-Hydroxamic Solutions at 298.15 K and 0.1 MPa," Technical Report IGC-291, IGCAR, 2007.
11. S. Kumar and S. B. Koganti, "Development and Application of a Computer Code SIMPSEX for Simulation of FBR Fuel Reprocessing Flowsheets," Technical Report IGC-234, IGCAR, 2002.
12. S. Kumar and S. B. Koganti, "Development of a Computer Code SIMPSEX for Simulation of FBR Fuel Reprocessing Flowsheets. II Additional Benchmarking Results," Technical Report IGC-251, IGCAR, 2003.
13. S. Kumar and S. B. Koganti, "Development and Application of Computer Code SIMPSEX for Simulation of FBR Fuel Reprocessing Flowsheets. III. Additional Benchmarking Results for HAN and U(IV) Based U-Pu Partitioning and a HAN Based Alternate Partitioning Step for FBTR Fuel Reprocessing," Technical Report IGC-257, IGCAR, 2004.

STUDY ON THE PROPERTIES OF SALINE HLLW IN CHINA

J.F. Liang,[1] X.G. Liu,[1] C.L. Song,[1] and R.Z. Jiao[1]

[1]*Institute of Nuclear and New Energy Technology, Tsinghua University, Beijing, China*
Corresponding author email address: liu-xg@mail.tsinghua.edu.cn

ABSTRACT

The properties and the components of HLLW (High-level Liquid Waste) were studied. The genuine saline HLLW is a blue-green liquid with 1.399 g/mL density. The activities of ^{137}Cs, ^{90}Sr, ^{99}Tc, ^{237}Np, ^{239}Pu, ^{241}Am, and total $\alpha/\beta/\gamma$ were determined. The extractive properties of actinides in the HLLW were examined in a five-stage cross-extraction test. More than 98% of the Pu in HLLW is Pu^{4+}, and more than 70% of the Np is Np^{4+}. It was shown that >99.97% of the α-nuclides were extracted by 30% TRPO-kerosene from the HLLW. The separation performance of actinides is excellent.

INTRODUCTION

Reprocessing can recover fissile materials from spent nuclear fuel, but it produces large amounts of high-level liquid waste (HLLW). Due to the high activity, radiotoxicity, and long half-lives of actinides, HLLW is seen as a problematic aspect of nuclear energy. An extractive process, named the TRPO process, was developed to partition long-lived nuclides with from Chinese HLLW [1]. However, during the long-term storage of HLLW, the composition has changed. The key problem we are concerned with is the extractive properties of radionuclides in Chinese saline HLLW.

In this paper, the properties and composition of HLLW were studied, and results of the TRPO process for removal of actinides from Chinese genuine HLLW are presented.

EXPERIMENTAL

Analysis of the Density and the Acidity of the HLLW

Samples of HLLW were sampled quantitatively with an electronic pipettor (1 ch, 0.020-0.500 mL, Biohit Finland) and balanced at 23 ± 1 °C. The density is an average value of six samples.

The quantitative samples were added to 30 mL 8% potassium oxalate solution (adjusting to pH 7.0 with 1% oxalic acid and 0.1 mol/L KOH). The solution was titrated with standard basic solution to pH 7.0. The acidity of the HLLW was calculated from the consumption of the standard basic solution.

Determining the Radionuclides in the HLLW

Uranium

Uranium was extracted by 30% TRPO-kerosense (TRPO, trialkylphosphine oxide, Jinan Phosphorous Fertilizer Factory, China; kerosene, 240#, Jinzhou Refinery Factory, China) in 1.0 mol/L HNO_3 from the HLLW twice, and was stripped with 5% Na_2CO_3 from the organic phase. The stripping solution was diluted and adjusted to pH 7.0; the concentration of uranium was determined with a laser fluorometric analyzer.

α-Nuclides

The activity of total α-nuclides was determined with Au-Si surface-barrier detector (FH445,Φ20mm, Beijing Nuclear Instrument Factory, China). The activities of ^{237}Np, ^{239}Pu, and ^{241}Am were determined after Np, Pu, and Am were separated from the HLLW with HDEHP extraction [2].

Technetium

^{99}Tc was extracted by cyclohexenone from 1 mol/L H_2SO_4 and is the detected with a liquid scintillation counting method. The activity is obtained by the efficiency tracing DPM method.

Strontium-90

After the separation of rare earth and transuranium elements by 30% TRPO-kerosene extraction twice in 0.5 mol/L HNO_3 solution, the aqueous phase is stored for >30 days. When ^{90}Y gets to equilibrium with ^{90}Sr, ^{90}Y is extracted with 30% TRPO-kerosene again and detected by a liquid scintillation analyzer (TRL-CARB 2200-CA, Packard, USA).

Other Radionuclides

The activity of total β in HLLW was detected with a liquid scintillation analyzer. The activity of total γ in HLLW was determined with a Ge-Li detector (EG&G, USA). A multichannel γ analyzer was scaled with standard solutions of the γ nuclides ^{137}Cs, $^{152+154}Eu$, and ^{60}Co.

Crosscurrent Extraction of TRU Elements by 30% TRPO-Kerosene

30% TRPO-kerosene was washed with 5% Na_2CO_3, 1 mol/L HNO_3, and deionized water in sequence. Before extraction, the 30% TRPO-kerosene solution was pre-equilibrated with 1 mol/L HNO_3. The genuine HLLW was diluted 3 times and adjusted to 1 mol/L HNO_3 acidity. The flowsheet of the extractive experiments is shown in Figure 1. The extractive experiments were tested with equal volumes of aqueous and organic solutions in a stoppered tube for 5 min. at 23 ± 1 °C. The two phases were separated after centrifugation. After separation, the organic phase was collected, and the aqueous phase was contacted with fresh organic phase. The cross-extraction process was repeated several times. The activities of the actinide elements in the final aqueous samples were analyzed by α-spectrometry.

RESULTS AND DISCUSSION

The Density and the Acidity of the HLLW

The density was 1.39 g/mL, which is consistent with previous results [3]. The acidity was 2.1 mol/L HNO_3, which is lower than the previously reported 2.6 mol/L HNO_3 [3], because some HNO_3 in the HLLW was decomposed by irradiation during the ten years of storage.

The Radionuclides in the HLLW

The radionuclides in the HLLW are given in Table 1. It shows that the major α-nuclide in HLLW is ^{241}Am, with >66% of total α-activity. ^{237}Np and $^{235+238}U$ activities are respectively <1% and <0.5%. The β activities of $^{90}Sr/^{90}Y$, ^{137}Cs, ^{147}Pm, ^{99}Tc, and ^{155}Eu are respectively 57%, 41%, 1%, <1%, and <1% of the total β activity. The activities of ^{137}Cs, ^{134}Cs, ^{125}Sb, ^{155}Eu are respectively 98%, <1%, <1%, and <1% of the total γ activity. Taking into the consideration of storage time and half-life, the composition of the radionuclide activities in the HLLW we measured are consistent with previous reports [4-6]. The results show that the analytical methods are suitable for the HLLW.

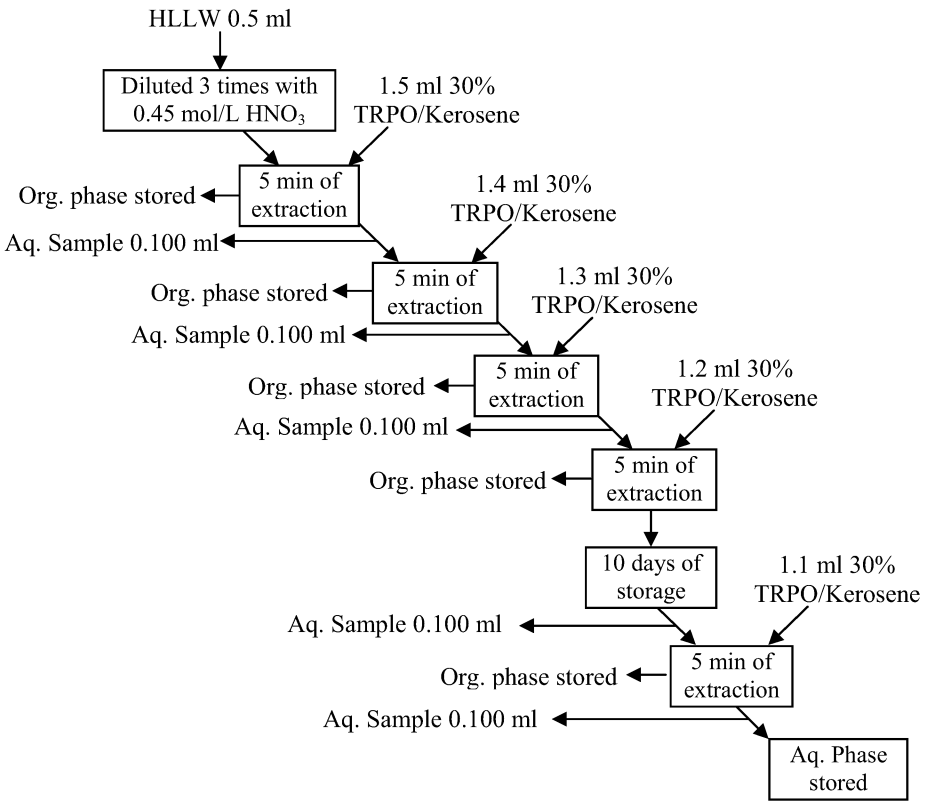

Figure 1. Flowsheet of the cross-current extraction.

Table 1. The activities of the radionuclides in the HLLW

Nuclides	U g L^{-1}	Tc g L^{-1}	^{90}Sr Bq mL^{-1}	^{137}Cs Bq mL^{-1}	^{237}Np Bq mL^{-1}
Activity or concentration	5.54	0.26	7.71×10^8	1.13×10^9	7.74×10^2

Nuclides	$^{238\text{-}240}Pu$ Bq mL^{-1}	^{241}Am Bq mL^{-1}	$\sum\alpha$ Bq mL^{-1}	$\sum\beta$ Bq mL^{-1}	$\sum\gamma$ Bq mL^{-1}
Activity or concentration	--	2.90×10^5	3.74×10^5	2.71×10^9	1.14×10^9

The Extractability of the α-Nuclides in the HLLW

In the extractive test, the distribution ratios of americium varied in different cross-extraction stages (see Table 2). In the first three stages of cross-extractions, the distribution ratios of americium increased with stage number, resulting from the decrease of the total concentration of extractable elements, such as rare earth elements and Fe^{3+}. After four stages of the cross-extraction, the concentration of Am in aqueous solution was very low. In the fifth stage, the americium activity was very close to the detection limit, and a high decontamination factor for Am was obtained.

Table 2. The distribution ratios for Np, Pu, and Am

Stage	^{237}Np		$^{239+240}Pu$		^{241}Am		Total α
	D	Activity Bq mL^{-1}	*D*	Activity Bq mL^{-1}	*D*	Activity Bq mL^{-1}	Activity Bq mL^{-1}
Feed	--	258	--	1	--	9.59×10^4	1.25×10^5
1	3.78	54	387	2.6×10^{-3}	4.2	1.85×10^4	1.85×10^4
2	0.59	34	3.7	5.5×10^{-4}	9.8	1.71×10^4	1.76×10^3
3	0.55	22	<0.01	7.6×10^{-4}	11.0	1.43×10^2	1.87×10^2
4	0.57	14	<0.01	4.8×10^{-4}	12.0	11	39
5*	3.7	3	2.9	1.4×10^{-4}	1.8	4	11

*The fifth stage of cross-extraction was carried out after 10 days.

Table 2 also shows that TRPO has good extractive ability for plutonium. After the first two stages, the plutonium was almost completely extracted. From the third stage, the contents of plutonium in the aqueous phases did not change. This fact means that about 0.05% of Pu in HLLW feed solution might be in the form of polymerized or hydrolyzed species, which are not extractable by TRPO. In the experiment, the aqueous phase had been laid aside for 10 days after the fourth stage extraction. During this period,

some polymerized or hydrolyzed plutonium depolymerized and became extractable. So, at the fifth stage, some plutonium was further extracted to the organic phase.

The extraction behaviour of Np was also interesting. Although 30% TRPO has good extractive ability for tri-, tetra- and hexavalent actinides, its extractive distribution ratio for Np(V) was very poor from 1 mol/L HNO_3. $D_{Np(IV)}$, $D_{Np(V)}$, and $D_{Np(VI)}$ between 30% TRPO-kerosene and 1 mol/L HNO_3 are given in Table 3. In the experiment, D_{Np} in the first stage is 3.78. It is much lower than that for Np(IV) and Np(VI), but higher than that for Np(V). From the second to the fourth stage, the D_{Np} is about 0.5~0.6. It is higher than that for Np(V). These results show that more than 70% of the Np in the HLLW is in the Np(IV) valence state, while other Np species were in the form of Np(V) probably. In the first stage, all Np(IV) and a few parts of Np(V) were extracted into the organic phase. From the second to fourth stage, not only NpO_2^+ but also some tetra- and hexavalent Np species were extracted. This fact indicates that some Np(V) was converted to Np^{4+} or NpO_2^{2+} in the experimental conditions.

Table 3. The distribution ratio of Np between 30% TRPO and 1 mol/L HNO_3

Np valance	Np^{4+}	NpO_2^+	NpO_2^{2+}
D	1000	0.25	100

The valence state of Pu in genuine HLLW was studied by the extraction method with 0.2 mol/L HDEHP/kerosene and 0.5 mol/L TTA-Xylene [7]. The results indicate that in the genuine HLLW more than 98% of Pu is Pu^{4+}, about 0.86% is Pu^{3+}, and only a very small amount of Pu is in the form of PuO_2^{2+}. It proves that Pu^{3+}, Pu^{4+}, and PuO_2^{2+} are in equilibrium in the genuine HLLW based on the following reaction equation:

$$3Pu^{4+} + 2H_2O \rightarrow 2Pu^{3+} + PuO_2^{2+} + 4H^+$$

Removal Experiments of Np and Pu in Genuine HLLW

Hot experiments of the TRPO process were carried out in our hot cell to remove actinide elements (U, Np, Pu, and Am/Cm) from Chinese concentrated HLLW released from a military-reactor [7]. The experimental process is shown in Figure 2.

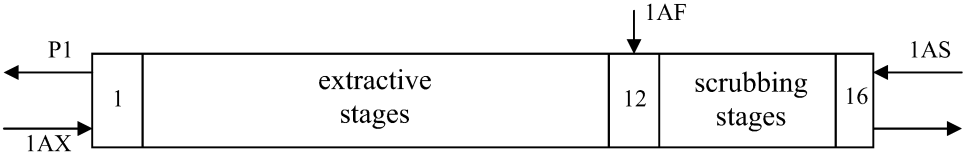

Figure 2. The TRPO process for removal of actinide elements from HLLW.

Hot experimental results demonstrate that extractive percentages of U, Np, Pu, and Am are higher than 99.99%, 92%, 99.8%, and 99.8%, respectively. The TRPO process can treat such high-saline HLLW without pre-adjustment of the Np and Pu valence states.

CONCLUSIONS

The density of the HLLW was 1.399 g/mL. The acidity of the HLLW was 2.11 mol/L HNO_3 and was decomposed by the irradiation. The results of determining the activities of the radionuclides show that the analytical methods are suitable for the HLLW.

Cross-extraction using the TRPO process with genuine HLLW proves that TRPO has good extraction ability for actinide elements. The TRU elements, except ^{237}Np, were completely removed by 30% TRPO-kerosene with four stages of cross-extraction from 1 mol/L HNO_3 solution, and the HLLW became a non-α-waste solution. The decontamination factors are as high as 3200, 18, 2100, and 8700 for total α, ^{237}Np, ^{239}Pu, and ^{241}Am, respectively. The results prove that the parameters selected for the TRPO process in the cross-extraction experiment worked quite well. Hot experimental results demonstrated that 30% TRPO-kerosene has good extractability of Np, U, Pu, and Am.

ACKNOWLEDGMENT

Some work was finished by Wang Nan-Jie, Xia Gang-Jian, and Dai Shu-Zhen at Atomic Energy United Company of Jiuquan, China.

REFERENCES

1. Zhu Youg-Jun, Song Chong-Li, Xu Jing-Ming, et al., "The Removal of Actinides from High level Radioactive Waste by TRPO Extraction," *Chin. J. Nucl. Sci. Eng.,* **9**(2), 141-150 (1989).
2. Tian Guo-Xing and Liang Jun-Fu, "The Solvent Separation for Analysing α-nuclides in HLLW," *Chin. J. Nucl. Radiochem.*, **18**(2), 122-128 (1996).
3. Jin Li-Yun, Zhang Huai-Li, and Chen Liau-Zhong, "Chemical Composition Analysis of High-level Liquid Waste (HLLW)," *Chin. At. Energ. Sci. Technol.,* **26**(5), 1-5 (1992).
4. Qiao Sheng-Zhong, Liu Heng-Jun, Tang Boting, et al., "Determination of Pu, Am and Total α-Activity for HLLW," *Chin. At. Energ. Sci. Technol.,* **26**(5), 61-65 (1992).
5. Lu Feng, Lin Can-Sheng, and Zhang Xian-Zi, "Measurement of Gross beta Radioactivity in HLLW," *Chin. At. Energ. Sci. Technol.,* **26**(5), 86-89 (1992).
6. Yang Liu-Cheng, Huang Hao-Xing, Jia Jin-Cai, et al., "Analysis and Determination of Radioactive Nuclides Emitting γ-rays in HLLW," *Chin. At. Energ. Sci. Technol.,* **26**(5), 90-92 (1990).
7. Liang Junfu and Liu Xuegang, "The Analysis of Valence State of Np and Pu in Chinese High-Level Liquild Waste," *Solvent Extr. Ion Exch.*, **24**(4), 485-498 (2006).

ACTINIDE EXTRACTION FROM SIMULATED AND IRRADIATED SPENT NUCLEAR FUEL USING TBP SOLUTIONS IN HFC-134a

A. Shadrin, V. Babain, V. Kamachev, A. Murzin, D. Shafikov, and A. Dormidonova

Khlopin Radium Institute, RPA, 28, 2-nd Murinskii av., St-Petersburg, Russia
Corresponding author email address: shadrin@atom.nw.ru

ABSTRACT

It was demonstrated that solutions of TBP-nitric acid adduct in liquid Freon HFC-134a (1.2 MPa, 25 °C) allowed for recovery of uranium with nearly the same effectiveness as supercritical CO_2 at 30 MPa. At nearly quantitative recovery of U and Pu, a DF of ca. 10 can be attained on dissolution and extraction of simulated SNF samples. The possibility of recovery of actinides contained in cakes produced by oxide conversion of simulated and irradiated SNF with solutions of TBP and DBE in Freon HFC-134a was shown.

INTRODUCTION

At present, the search for alternative energy sources has become more urgent, owing to the increase in electrical power consumption along with increasing organic fuel costs. An alternative energy source is nuclear power. However, development of nuclear power engineering and moreover, its reorganization for nuclear-fuel reproduction, requires the development of large-scale, environmentally safe, and profitable treatment processes for spent nuclear fuel (SNF). At present, only the hydrometallurgical methods of SNF treatment based on the PUREX process are the most developed and industrially tested. Unfortunately, hydrometallurgical SNF treatment methods often lead to large volumes of liquid radioactive wastes. The task of decreasing radioactive waste volume can be solved by recently developed low-temperature, low-water SNF treatment processes such as Super-DIREX (**Super**critical fluid **DIR**ect **EX**traction, Mitsubishi, Japan [1,2]) and RELICT (**RELICT** - **RE**processing by **LI**quid **C**arbon dioxide **T**reatment, Khlopin Radium Institute and Mining Chemical Combine, Russia [3,4]).

Experimental data showed that low-temperature and low-water treatment of SNF oxides provided a sharp decrease in the secondary radioactive waste volume. However, this process also has certain disadvantages, principly high pressure (20-30 and 7 MPa in the case of supercritical (SC) and liquid CO_2, respectively) and difficult recovery of radioactive ^{14}C from CO_2. If CO_2 is proposed as a possible medium for SNF treatment, then the problem of ^{14}C treatment makes it reasonable to either design a plant with a capacity smaller than 200 t/y (in this case the total exhaust of ^{14}C would exceed maximal permissible level), or to develop an additional high-temperature stage for SNF oxidation

(UO_2 conversion into U_3O_8 or UO_3), during which ^{14}C will be removed as well as radioactive tritium and iodine. Both these disadvantages can be eliminated using freons instead of carbon dioxide. Ozone-friendly freons contain no chlorine atoms and thus are safe for the ozone layer. Freon-125 (1,1,1,2,2-pentafluoroethane) was used earlier as a fluid for the extraction of metal complexes [5]. The aim of this work was to demonstrate the possibility of using freons instead of CO_2 as a medium for SNF treatment. Freon HFC-134a (1,1,1,2-tetrafluoroethane) was chosen because it is readily available and is typical of an ozone-friendly freon (ODP = 0, atmospheric half-life = 14 y).

EXPERIMENTAL

A schematic of the extraction device is found in Figure 1. To study dissolution of simulated WWR-1000 SNF and actinide extraction, a weighed sample was placed into cell 5, neat TBP was placed in bubbler 3, and concentrated nitric acid was placed in bubbler 4. Freon HFC-134a was then pumped through bubbler 3, where it solubilized TBP to saturation. That phase flowed through bubbler 4, where TBP.nHNO$_3$ adducts were formed in the Freon HFC-134a solvent. The adduct-modified solvent was then pumped into cell 5, where the sample resided.

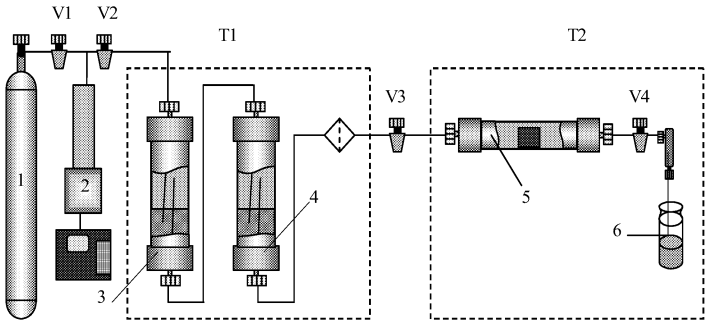

Figure 1. Setup for actinide extraction into Freon. 1, Freon cylinder; 2, syringe pump; 3, bubbler with TBP; 4, bubbler with HNO_3; 5, cell; 6, fraction collector; V1-V4, valves; T1,T2, thermally-controlled areas.

To study the extraction of actinide nitrates and products arising from conversion of irradiated or simulated SNF, the sample was placed into cell 5, and TBP was poured in bubbler 3. In this experiment, the mixture of TBP in Freon HFC-134a that exits bubbler 3 was directly diverted to the sample in cell 5. The setup for dissolution, conversion, and extraction using irradiated SNF was placed in a “heavy glove” box.

The solutions of TBP-actinide complexes in Freon HFC-134a formed in cell 5 were transferred into a fraction collector 6 filled with methanol. The fraction collector was changed when 10 mL of Freon HFC-134a passed through the cell. In each fraction, we determined the content of nitric acid by titration with alkali, the content of uranium by spectrophotometric analysis (with Arsenaso III) and by the volumetric method with vanadate [6], and the content of isotopes added into the simulated SNF by radiometric methods. Fraction collection during the course of actinide extraction from converted irradiated SNF was impossible due to high radiation fields.

The studies used irradiated WWER-1000 SNF (53 GWt day/t U cooled for 13 years) and simulated WWR-1000 SNF, whose composition is presented in Table 1 [7]. The simulated WWER SNF was prepared from actinide and fission product nitrate

solutions spiked with ^{152}Eu and ^{241}Am by precipitation with hydrazine hydrate. The resulting precipitate was dried, and Ba and Cs nitrates and Cs molybdates spiked with ^{137}Cs were added. The precipitate was mixed well and annealed in a H_2 flow at 1000 °C. The simulated and irradiated SNF oxides were converted in the presence of N_2O_4 and H_2O at 75 °C in an autoclave. The conversion conditions were described previously [8].

Table 1. Composition of simulated WWR-1000 SNF [7].

Element	Content of element (%) in the simulator, recalculated to metal	Element	Content of element (%) in the simulator, recalculated to metal
U	95.52	La	0.16
Th or Pu	1.47	Ce	0.03
Cs	0.58	Pr	0.14
Sr	0.15	Nd	0.56
Zr	0.53	Sm	0.11
Mo	0.48	Eu	0.02
Ba	0.25	Sum total	100

RESULTS AND DISCUSSION

We previously showed the dissolution of uranium dioxide by formation of TBP-nitric acid adducts in liquid Freon HFC-134a [9]. As seen from Figure 2, the effectiveness of uranium dioxide dissolution in Freon HFC-134a at 1.2 MPa is close to that of SC CO_2 at 30 MPa. Simulated WWER-1000 SNF is also effectively dissolved in Freon HFC-134a solutions containing TBP-nitric acid adducts. Comparison of the data in Figures 3 and 4 shows that the dissolution of simulated WWER-1000 SNF in Freon HFC-134a at higher temperature (80 °C) is faster than at room temperature, other conditions being equal. However, in both cases, almost equal extraction times and amounts of TBP-nitric acid adduct are required for quantitative recovery of U and Pu.

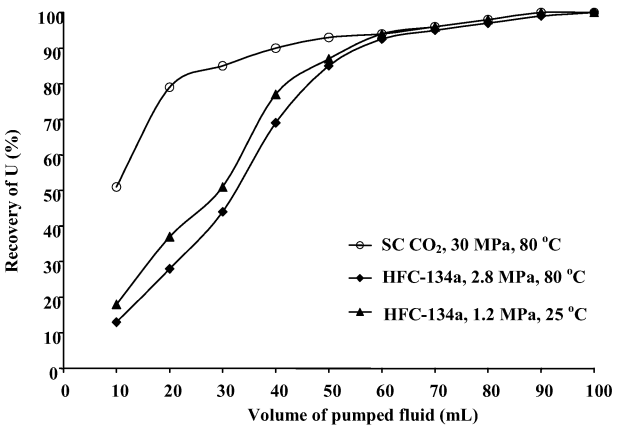

Figure 2. Uranium recovery from its dioxide by dissolution with TBP.nHNO$_3$ adducts in SC fluid or liquid gas as influence by the volume of pumped fluid.

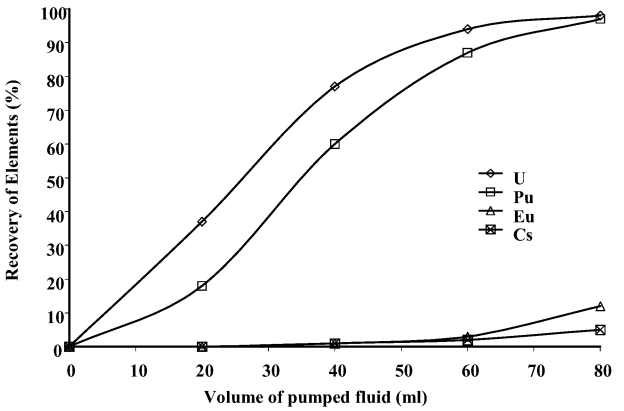

Figure 3. Recovery of the elements from simulated WWER-1000 SNF by TBP-HNO_3 solution in Freon HFC-134a (1.2 MPa, 25 °C) as influenced by the volume of pumped fluid.

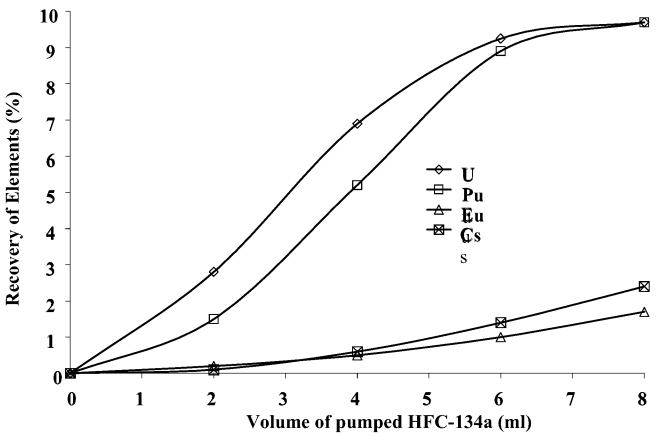

Figure 4. Recovery of the elements from simulated WWER-1000 SNF by TBP-HNO_3 solution in Freon HFC-134a (2.8 MPa, 80 °C) as influenced by the volume of pumped fluid.

It was found that U and Pu are recovered simultaneously and much more effectively than the other elements but only in the first two fractions. The total recovery of the other elements (primarily RE) begins to increase in the third fraction. Based on experimental results, the factors of U decontamination (K_F) from the other elements were calculated (Table 2). It should be noted, that at nearly quantitative recovery of U and Pu the decontamination factor ~10 can be attained even at dissolution and extraction stages, which along with sorption treatment of the saturated solvent on silica gel [10] will increase decontamination factors up to 300-3000. The data agree well with results for dissolution of simulated SNF in compressed CO_2 obtained by both Japanese and Russian researchers [2,8,11,12]. The other area of freon application can be the recovery of actinide, uranyl nitrate, and fission products from the cakes obtained by conversion of SNF oxides in CO_2 media [13]. Studies conducted with simulated SNF showed the availability of this approach [8]. It was found that TBP solutions in liquid Freon HFC-134a allow for simultaneous recovery of U and Pu (Figure 5), whereas solutions of dibutyl ether (DBE) in the same solvent provides recovery of only U (Figure 6).

Table 2. Uranium decontamination factor at simultaneous U and Pu recovery from simulated SNF using a solution of TBP-HNO_3 adducts in HFC-134a.

Element	Uranium decontamination factor
Freon HFC-134a (1.2 MPa, 25 °C)	
Pu	1.0
Eu	5.7
Cs	4.0
Freon HFC-134a (2.8 MPa, 80 °C)	
Pu	1.0
Eu	6.3
Cs	17

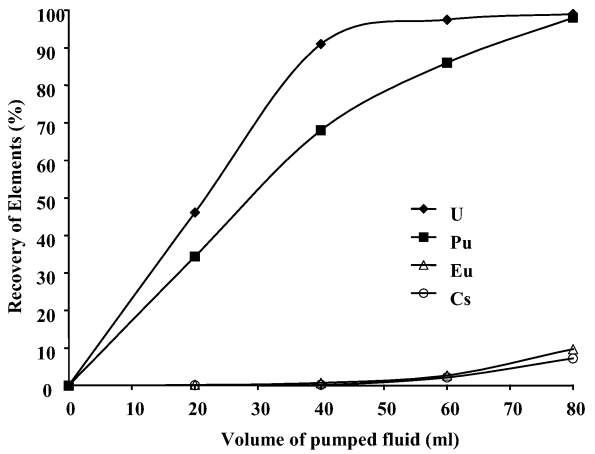

Figure 5. Uranium and FP extraction by 18 vol % TBP solution in Freon HFC-134a from simulated SNF conversion product (80 °C, 2.8 MPa).

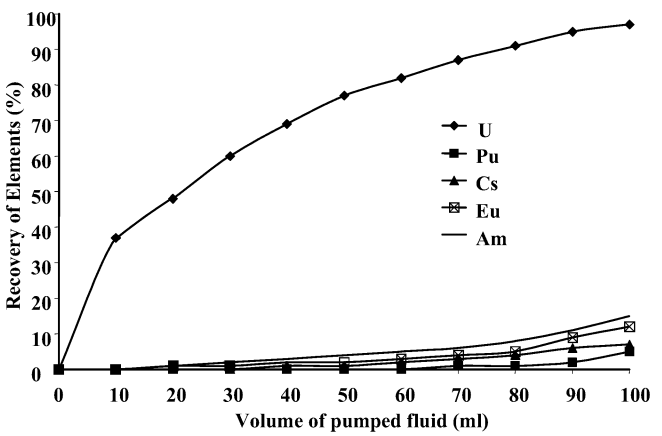

Figure 6. FP and actinide extraction by DBE solutions in Freon HFC-134a saturated with 6 M HNO_3 from simulated SNF conversion product (1% Pu, 18 vol % DBE, 2.8 MPa, 80 °C).

Using the conversion product of irradiated WWER-1000 SNF, it was shown that U and Pu were nearly completely recovered from the sample (1.5 g) after pumping of 18 vol % TBP solution (100 mL) in liquid Freon HFC-134a (80 °C, 2.8 MPa).

CONCLUSIONS

It was demonstrated that solutions of TBP.HNO_3 adducts in liquid Freon HFC-134a (1.2 MPa, 25 °C) allow for recovery of U with nearly the same effectiveness as SC CO_2 at 30 MPa. At nearly quantitative recovery of U and Pu, a decontamination factor of about 10 can be attained in the course of dissolution and extraction of the SNF. The variant of actinide recovery with TBP in liquid freons from SNF converted to oxides of the actinides and fission products was also studied. As shown, nitrate cake (conversion product) allows either simultaneous extraction of U and Pu using TBP solutions in liquid Freon HFC-134a or extraction of only U using DBE solutions in this freon. Using the conversion product of irradiated WWER-1000 SNF it was shown that U and Pu were nearly completely recovered from the sample (1.5 g) after pumping of 18 vol % TBP solution (100 mL) in liquid Freon HFC-134a (80 °C, 2.8 MPa). Hence, using Freon HFC-134a, the possibility of using freons for SNF treatment was demonstrated. The use of Freon HFC-134a instead of CO_2 would allow one to overcome the problems related to high operating pressure of SNF treatment in liquid gases and the problems concerning ^{14}C processing while still retaining process effectiveness.

REFERENCES

1. Y. Enokida, Proceedings International Conference SuperGreen 2002, Kyung Hee University, Korea, 2002; p. 35.
2. T. Shimada, S. Ogumo, N. Ishihara, et al., *J. Nucl. Sci. Technol.,* **3**, 757 (2002).
3. A. Shadrin, A. Murzin, V. Babain, et al., 7th Italian Conf. and 9th Meeting on Supercritical Fluids, Trieste, Italy, Abstracts, 2004; p. 52.
4. A. Shadrin, A. Murzin, V. Romanovsky, et al., Proceedings of GLOBAL 2005, Tsukuba, Japan, 2005; Paper No. 12.
5. V. Babain, V. Kamachev, R. Kiseleva, et al., *Radiochemistry*, **45**, 602-605 (2003).
6. V. K. Makarov, A. V. Vinokurov, S. V. Elison, et al., Uranium and Methods of its Analysis, Gosatomizdat, Moscow, 1960; p. 163.
7. M. Kolabashkin, P. M. Rubstov, P. A. Ruzhanskii, and I. D. Sidorenko, Radiation Characteristics of Irradiated Nuclear Fuel, Handbook, Energoatomizdat, Moscow, 1983.
8. A. Shadrin, A. Murzin, V. Romanovsky, et al., Proceedings of GLOBAL 2005, Tsukuba, Japan, 2005; Paper No. 128.
9. A. Shadrin, V. Kamachev, A. Murzin, and D. Shafikov*, J. Supercritical Fluids,* **42**, 347-350 (2007).
10. D. Shafikov, V. Kamachev, A. Murzin, et al., *Radiochim. Acta,* **94**, 87-90 (2006).
11. T. Shimada, S. Oguma, K. Sawada, et al., *Anal. Sci.*, **22**, 1387-1391 (2006).
12 Yu. Kulyako, A. Shadrin, and B. Myasoedov, *Russ. Khim. Zh.,* **49**, 97 (2005).
13. Y. A. Revenko, E. G. Kudravtzev, A. Y. Shadrin, et al., "Conversion of Actinide Oxides into nitrates," RF Patent no. 2005131461/06, 10.10.2005, BI 8, 2007.

DEVELOPMENT OF A PROCESS FOR THE EXTRACTION OF ^{137}Cs FROM ACIDIC HLLW BASED ON CROWNCALIX EXTRACTANT—USE OF DIALKYLAMIDE MODIFIER

J. Alexová,[1] M. Šírová,[1] J. Rais,[1] S. Suzuki,[2] M. Hirata,[2] T. Kimura,[2] and S. Tachimori[3]

[1]*Nuclear Research Institute Řež plc, 25068 Řež, Czech Republic*
[2]*Japan Atomic Energy Agency, Tokai-mura, Ibaraki, Japan*
[3]*Secretariat of the Nuclear Safety Commission of Japan, Tokyo, Japan*
Corresponding author email address: rai@ujv.cz

ABSTRACT

Within the framework of the ARTIST project of total fuel retreatment with ecological mixtures of solvents and extractants containing only C, H, O, and N atoms, a process segment of extraction of ^{137}Cs from acidic stream was developed. The process with 25,27-Bis(1-octyloxy)calix[4]arene-crown-6, DOC[4]C6, dissolved at its 0.01 M concentration in a mixture of 90 vol % 1-octanol and 10% dihexyl octanamide, DHOA was proposed as a viable variant due to its good multicycle performance, even with irradiated solvent, and due to the good chemical stability of the chosen combination of solvent mixture.

INTRODUCTION

In the complex process of nuclear-fuel retreatment ARTIST proposed by JAEA, Japan, we studied the ^{137}Cs separation segment to be included after the extractive separation of U, Pu, trivalent lanthanides and actinides, and ^{90}Sr. The process ARTIST is conceived as a total process of retreatment using only ecological solvents, diluents, and extractants of CHON (molecules containing only C, H, O, and N atoms) type and primarily based on the use of amide extractants [1].

The separation of strong heat-output isotopes ^{137}Cs and ^{90}Sr is currently considered important for the increase of the capacity of high-level repository sites if these two isotopes are to be stored separately [2].

Modern methods of ^{137}Cs (also ^{135}Cs) extraction use calixcrown compounds for the purpose, since these add to Cs^+ binding by both crown and calixarene rings. The most popular calixcrowns are shown in Figure 1 together with their full chemical names and technical abbreviations.

The use of these compounds was first described by Dozol from the CEA [3]. Whereas in France attention was paid to mono-crown calixarenes, in USA bis-crown calixarenes were studied by the group of Moyer from ORNL to a large extent (e.g.[4]). The aqueous feed also differed in these two groups; whereas the ORNL group was

interested mainly in the treatment of strongly alkaline solutions, in CEA the primary goal was to separate ^{135}Cs from acidic PUREX wastes.

Since in the ARTIST project we were interested in acidic HLLW, we collected in the Table 1 the extant newly studied and developed processes only for acidic wastes using calixcrown compounds. For a comparison also our previous dicarbollide process is shown in Table 1.

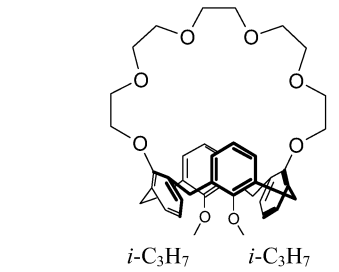

25,27-bis(2-propyloxy)calix[4]-26,28-crown-6
diisopropyloxy calix[4]crown-6
DiPC[4]C6

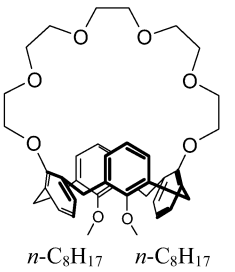

25,27-bis(1-octyloxy)calix[4]-26,28-crown-6
dioctyloxy calix[4]crown-6
DOC[4]C6

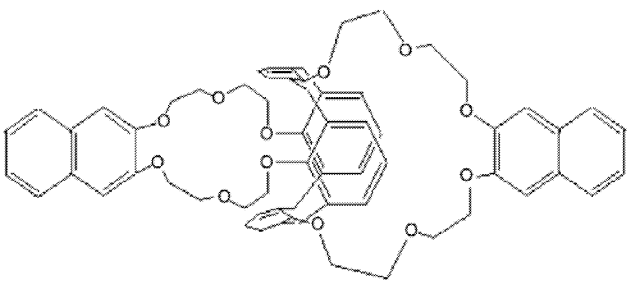

calix[4]arene-bis-(naphtocrown – 6)
CC-C

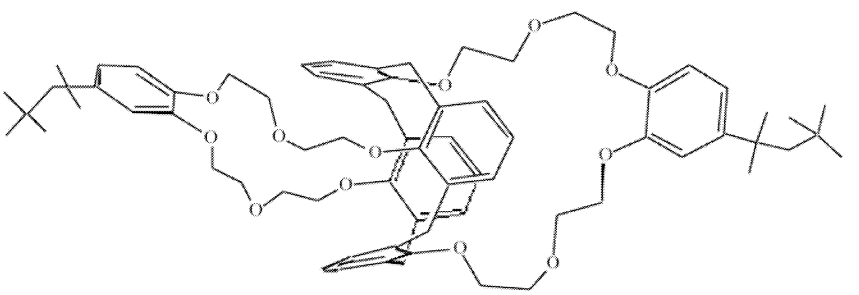

calix[4]arene-bis-(*t*-octylbenzo-crown-6)
BoBCalixC6

Figure 1. Calixcrowns used for extraction of ^{137}Cs.

In the present paper, we describe an optimized process—as concerns chemical and radiation stability of extraction mixture as well as an expedient choice of the ^{137}Cs extraction suppressor needed for a complete strip of Cs from the organic phase—for extraction of ^{137}Cs from acidic HLLW based on the use of DOC[4]C6. Fortunately, we have also found that an effective modifier and suppressor can be used from the amide family, dihexyl octanamide; hence, its use is fully compatible with the overall ARTIST process.

Table 1. Radiochemical extraction processes for isolation of ^{137}Cs from acidic HLLW.[a]

Process	Nuclide	Extractant	Extraction Strip	Year, country, [reference]
Dicarbollide CDC + PEG	^{137}Cs, ^{90}Sr	0.06 M Chloroprotected bis(dicarbollyl) cobaltate + 1% Triton X100, in nitrosolvent, phenyl trifluoro methyl sulphone	3 M HNO_3 ~10 M HNO_3, Cs 0.5 M hydrazine + 2 M HNO_3, Sr	1985 CR, NRI; 1996 Russia plant [5]; 2004 USA, INL [6]
Calix-mono-crown A	^{135}Cs	0.062 M DOC[4]C6 in 1.5 M TBP in TPH	4 M HNO_3 + 0.2 M oxalic acid 0.05 M HNO_3	2004 France CEA [7]
Calix-mono-crown B	^{135}Cs	0.1 M R14 in 1 M methyloctyl -2-dimethylbutanamide in TPH	4 M HNO_3 + 0.2 M oxalic acid 0.05 M HNO_3	2004 France CEA [7]
Calix-mono-crown	^{137}Cs	0.025 M DiPC[4]C6 in 1-octanol	1 M HNO_3 0.005 M HNO_3	2005 China INET [8]
FPEX	^{137}Cs, ^{90}Sr	0.007 M BOBCalixC6 (Cs) 0.15 M DtBuCH18C6 (Sr) 0.75 M Cs-7SB in Isopar®L	0.5–2.5 M HNO_3 0.01 M HNO_3	2005, USA INL [9]
CC-C	^{137}Cs	$4.8.10^{-3}$ M CC-C in nitrobenzene	3 M HNO_3 6–8 M HNO_3 or 0.1-1 % Alamine 336 in dist. water	2006, India, BARC [10]

[a]In the left column, the shortened name of the process is given, and isotopes extracted are given in the second column. Extractant and solvent (third column) are either defined in Figure 1 or are as follows: *Chloroprotected bis(dicarbollyl) cobaltate* is H^+ polychlorinated bis(dicarbollyl)cobaltate with mean composition H^+ $[(C_2B_9H_8Cl_3)_2Co]^-$; *Triton X100* is substituted polyethylene glycol with n_{EOU} (mean) = 9, but sometimes an

older product Slovafol 909 was used; *TBP* is tri-*n*-butylphosphate; *TPH* hydrogenated propylene, branched alkane used in the PUREX cycle in France, *R14* is the French variant mono-crown calixarene 1,3[(2,4-diethyl-heptylethoxy)oxy]-2,4-crown-6-calix[4]arene. In the FPEX process, the following chemicals are used: *DtBuCH18C6* is 4,4',(5')-di-(*t*-butyldicyclohexano)-18-crown-6; *Cs-7SB* is 1-(2,2,3,3-tetrafluoropropoxy)-3-(4-*sec*-butylphenoxy)-2-propanol; and *Isopar® L* is a branched aliphatic kerosene. In the fourth column of the table, the composition of the aqueous phase during the extraction and underlined compositions during strip are given. In the last column, the abbreviations of the institutes are given; these are as follows: *NRI* is Nuclear Research Institute, Řež; *CEA* is Comissariat à l'Énergie Atomique; *INET* is Institute of Nuclear and New Energy Technology; *INL* is Idaho National Laboratory; and *BARC* is Bhabha Atomic Research Centre. There are many references for the extraction with dicarbollides; for shortness, only a review paper and recent testing from INL are given here.

EXPERIMENTAL

All current chemicals of p.a. grade were used without further purification. Radioactive isotopes were of standard radiochemical purity. Dihexyl octanamide DHOA, $(C_6H_{13})_2NCOC_7H_{15}$, was supplied by Katchem, Ltd. Praha with claimed purity 97%. 25,27-Bis(1-octyloxy)calix[4]arene-crown-6, abbreviated as DOC[4]C6 was purchased from the Institute of Organic Chemistry National Academy of Sciences of Ukraine with purity 97%. Special attention on our request was paid to remove from the prepared DOC[4]C6 any small quantities of cesium, since these led to unexpected results.

The extraction experiments were done in stoppered test-tubes with a shaking time of 60 minutes in a thermostated box at 25 ± 0.1 °C. Aliquots of the phases were measured with a standard γ (NaI) well detector. A special procedure of repeated batch cycles consisted of equilibrating always fresh aqueous phase with extraction solvent to simulate a countercurrent extractor. No preliminary saturation of the phases was done.

RESULTS AND DISCUSSION

On the basis of previous screening tests, we have found that DHOA modifier is also an especially effective Cs suppressor for the region of planned strip by dilute acid, whereas for high acidities (extraction segment) its effect in the system is practically negligible (see Figure 2). TBP is not a suitable suppressor. Extraction into 1-octanol is also particularly suitable, since we can use a concentration of relatively expensive calixcrown in the region of 0.01 mol/L, almost 10-fold lower than in the French process.

Studies of the kinetics of the process have shown that more than 95% of the ^{137}Cs is extracted already after 30 s of shaking. The selectivity of the process towards other isotopes is excellent; among alkaline cations, only Rb and K are extracted to some extent. Practically no extraction was confirmed by radioactive measurements for Eu, Na, and Sr, and by ICP-MS for Cr, Ni, Y, Zr, Ru, Rh, Pd, Ag, Cd, Ba, La, Ce, Pr, Nd, Sm, Eu, and Gd. Small amount of Cu seems to be extracted into the organic phase.

We studied the chemical and radiation stability of the extractant phase. The results of chemical stability testing were quite unexpected. At first, we tried to use (i) pure 1-octanol or (ii) a mixture of 30 vol % 1-octanol + 70% *n*-dodecane. Both systems

were chemically stable over two months of contact with 3 M HNO_3. But if contacted with 10 M HNO_3, the system with pure 1-octanol proved to be much more stable, and the system with addition of *n*-dodecane totally decomposed during some two weeks.

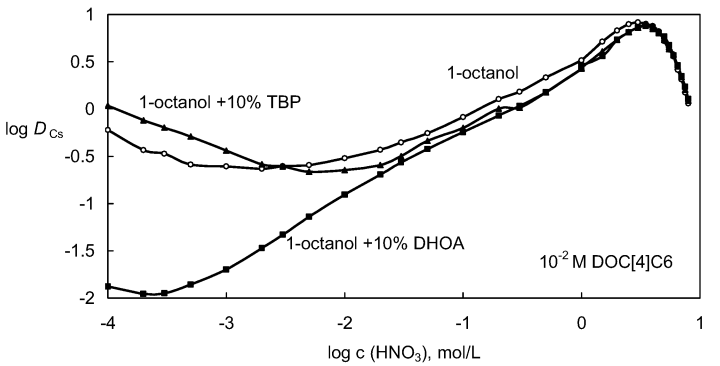

Figure 2. Extraction of microamounts of ^{137}Cs into 1-octanol.

Thus, as an optimal solvent mixture 0.01 M DOC[4]C6 in a mixture of 10 vol % of DHOA in 1-octanol was chosen. This choice is further supported by the results of multicycle batch experiments as shown in Figure 3. Practically the same results as in Figure 3 were also obtained with γ-irradiated solvent up to the dose of 400 kGy.

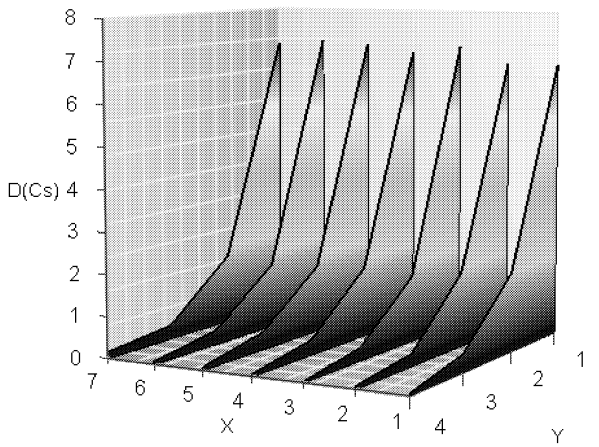

Figure 3. Repeated extractions from 3 M HNO_3 ($Y = 1$), washing off the acid from the organic phase ($Y = 2$ and 3) and strip of ^{137}Cs ($Y = 4$), all steps $Y = 2$–4 with 0.001 M HNO_3; for successively continued cycles ($X = 1$–7).

CONCLUSIONS

A viable process for the extraction of ^{137}Cs from acidic HLLW using 0.01 M DOC[4]C6 in a mixture of 10 vol % DHOA in 1-octanol was proposed, which satisfies the criteria of effectivity, low losses of reagents, economy of calixcrown, chemical and

radiation stability, high selectivity, as well as repeatability of the process with no change of extraction parameters. The process compares well with the previous dicarbollide process, with the added advantage of an easy strip of ^{137}Cs.

ACKNOWLEDGMENT

The NRI authors thank for financial support for this program by the Japanese MEXT in the frame of ARTIST project, and for financing from GAČR, Czech Republic, Project No. 104/05/2667. Authors thank Dr. F. Sus, PhD from NRI, Řež and Dr. L. Strnad, PhD from The Charles University Praha, Geochemical Laboratory for ICP-MS measurements.

REFERENCES

1. S. Tachimori, S. Suzuki, and Y. Sasaki, "A Process of Spent Nuclear Fuel Treatment with the Interim Storage of TRU by Use of Amidic Extractants," Japanese Nuclear Energy Association, **43,** 1235 (2001**)** (in Japanese).
2. T. E. Radel, P. P. H. Wilson, T. H. Bauer, and R. M. Grady, "Effect of Separation Efficiency on Repository Loading Values in Fuel Cycle Scenario Analysis Codes" in Global 2007, Boise, Idaho, September 9-13, 2007.
3. J.-F. Dozol, N. Simon, V. Lamare, H. Rouquette, S. Eymard, B. Tournois, D. De Marc, and R. M. Macias, "A Solution for Cesium Removal from High-Salinity Acidic or Alkaline Liquid Waste: The Crown Calix[4]arenes," *Sep. Sci. Technol.*, **34**, 877 (1999).
4. P. V. Bonnesen, L. H. Delmau, B. A. Moyer, and R. A. Leonard, "A Robust Alkaline-Side CSEX Solvent Suitable for Removing Cesium from Savannah River High Level Waste," *Solvent Extr. Ion Exch.*, **18**, 1079 (2000).
5. J. Rais and B. Grüner, "Extraction with Metal Bis(dicarbollide) Anions. Metal Bis(dicarbollide Extractants and Their Application" in Separation Chemistry, in Ion Exchange and Solvent Extraction, Series of Advances, Vol. 17 (Y. Marcus and A. K. SenGupta, Eds,), Marcel Dekker, New York, 2004; pp. 243-334.
6. R. S. Herbst, J. D. Law, T. A. Todd, V. N. Romanovskiy, I. V. Smirnov, V. A. Babain, V. N. Esimantovskiy, and B. N. Zaitsev, "Development of the Universal Extraction (UNEX) Process for the Simultaneous Recovery of Cs, Sr, and Actinides from Acidic Radioactive Wastes," *Sep Sci. and Technol.*, **38**, 2685 (2003).
7. N. Simon, N. Eymard, B. Tournois, and J.-F. Dozol, "Caesium Extraction from Acidic High Level Liquid Wastes with Functionalized Calixarenes," in Atalante 2000 Scientific Conference, October 20-26, 2000, Avignon, France; poster no. 02-06.
8. J. Wang, X. Zhu, and Ch. Song, "Extracting Performance of Cesium by 25,27-Bis(2-Propyloxy) Calix[4]-26,28-Crown-6 (iPr-C[4]C-6) in *n*-Octanol," *Sep. Sci. Technol.*, **40**, 3381 (2005).
9. C. L. Riddle, J. D. Baker, J. D. Law, C. A. McGrath, D. H. Meikrantz, B. J. Mincher, D. R. Peterman, and T. A. Todd, "Fission Product Extraction FPEX: Development of a Novel Solvent for the Simultaneous Separation of Strontium and Cesium from Acidic Solutions," *Solvent Extr. Ion Exch.*, **23,** 449 (2005).
10. P. K. Mohapatra, S. A. Ansari, A. Sarkar, A. Bhattacharyya, and V. K. Manchanda, "Evaluation of Calix-Crown Ionophores for Selective Separation of Radio-Cesium from Acidic Nuclear Waste Solution," *Anal. Chim. Acta.,* **571**, 308 (2006).

SIMULTANEOUS SEPARATION OF CESIUM AND STRONTIUM FROM SPENT NUCLEAR FUEL USING THE FISSION-PRODUCT EXTRACTION PROCESS

J.D. Law, D.R. Peterman, C.L. Riddle, D.A. Meikrantz, and T.A. Todd

Idaho National Laboratory, P.O. Box 1625, Idaho Falls, Idaho 83415-3870
Corresponding author email address: jack.law@inl.gov

ABSTRACT

The Fission-Product Extraction (FPEX) Process is being developed as part of the United States Department of Energy Global Nuclear Energy Partnership (GNEP) for the simultaneous separation of cesium and strontium from spent LWR fuel. Separation of the Cs and Sr will reduce the short-term heat load in a geological repository and, when combined with the separation of Am and Cm, could increase the capacity of the geological repository by a factor of approximately 100. The FPEX process is based on two highly-specific extractants: 4,4′,(5′)-di-(*t*-butyldicyclo-hexano)-18-crown-6 (DtBuCH18C6) and calix[4]arene-bis-(*t*-octylbenzo-crown-6) (BOBCalixC6). The DtBuCH18C6 extractant is selective for strontium, and the BOBCalixC6 extractant is selective for cesium. Results of flowsheet testing of the FPEX process with simulated and actual spent-nuclear-fuel feed solution in centrifugal contactors are detailed. Removal efficiencies, coextraction of metals, and process hydrodynamic performance are discussed along with recommendations for future flowsheet testing with actual spent nuclear fuel. Recent advances in the evaluation of alternative calixarenes with increased solubility and stability are also detailed.

INTRODUCTION

As part of the Advanced Fuel Cycle Initiative (AFCI), the reduction in volume and heat generation of spent nuclear fuel requiring geologic disposal is currently being addressed. The goal is to optimize utilization of the nation's first repository and potentially reduce or eliminate the need for additional repositories. This will be achieved through separating long-lived, highly toxic elements, reducing high-level waste volumes and the toxicity of spent nuclear fuel, and reducing the heat generation of spent nuclear fuel. The Idaho National Laboratory (INL) is working closely with a team of national laboratories to support development of these separations processes.

Key to the reduction of short-term heat load in a geological repository is the separation of ^{137}Cs and ^{90}Sr. Removal of these highly radioactive fission products reduces the short-term (~100 yr) heat-generation source of the spent nuclear fuel. Once separated, the Cs and Sr would be placed in decay storage.

To support development of this separations process, technologies for the simultaneous separation of Cs and Sr from dissolved spent nuclear fuel are being developed. In previous work, cesium and strontium have been removed from acidic nuclear-waste solutions and related alkaline wastes using separate solvent-extraction processes designed specifically for these elements. In general, crown ethers have been selected for the removal of strontium [1–3], and calixarenes [4–9] have been selected for separation of cesium. A novel process is being developed at the INL, combining these two types of extractants to create a solvent that will extract both cesium and strontium from acidic media, simultaneously. This technology, the Fission Product Extraction (FPEX) Process, utilizes 4,4',(5')-di-(*t*-butyldicyclohexano)-18-crown-6 (DtBuCH18C6) for the extraction of Sr, calix[4]arene-bis-(*t*-octylbenzo-crown-6) (BOBCalixC6) for the extraction of Cs, 1-(2,2,3,3-tetrafluoropropoxy)-3-(4-*sec*-butylphenoxy)-2-propanol (Cs-7SB) as a modifier, TOA (trioctylamine), and an Isopar® L diluent. The extractants and modifiers are presented in Figure 1. Initial development of the FPEX process at the INL began in FY-03 [10]. Results from this initial testing were promising, and further testing was performed in FY-2005 and FY-2006.

Process goals for the separation of Cs and Sr from the spent LWR fuel require ≥99.9% removal. Additionally, the TRU content of the Cs/Sr product must be less than 100 nCi/g so that this waste stream will be classified as a non-TRU LLW once the ^{137}Cs and ^{90}Sr decay. This requires a decontamination factor of approximately 1 x 10^8 for the TRU from the Cs/Sr product.

Laboratory testing indicates that the FPEX process can effectively separate Cs and Sr from acidic solutions containing large quantities of actinides and lanthanides, such as spent LWR fuel [10]. It should be noted that there are issues relative to the stability of the BOBCalixC6. An effort is in progress to develop an alternative calixarene for the extraction of Cs that exhibits increased stability. However, the scope of the flowsheet testing was to evaluate the performance of the FPEX process with the BOBCalixC6 Cs extractant.

EXPERIMENTAL

Deionized water was used to prepare all aqueous acid solutions. The nitric acid was reagent grade from Aldrich Chemical Co. (Milwaukee, WI). Isopar® L isoparaffinic diluent was obtained from Exxon Chemical Company (Houston, TX). The ^{85}Sr and ^{137}Cs radiotracers used for spiking the simulants were obtained as $^{85}SrCl_2$ in 1 M HCl and $^{137}CsCl$ in 1 M HCl from Isotope Products (Burbank, CA). The DtBuCH18C6 crown ether was purchased from Eichrom Industries, Inc. (Darien, IL). The BOBCalixC6 calixarene crown ether was received from Marshallton Research Laboratories (King, NC). The FPEX solvent used in these studies consisted of 0.075 M DtBuCH18C6, 0.007 M BOBCalixC6, 0.75 M Cs-7SB modifier, and 0.003 M TOA in Isopar® L.

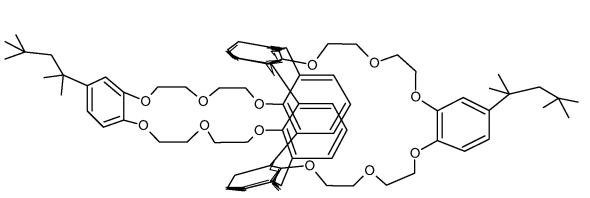

BOBCalixC6
Calix[4]arene-bis-(*t*-octylbenzo-crown-6)

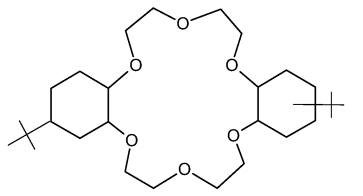

DtBuCH18C6
4,4′,(5′)-Di-(*t*-butyldicyclohexano)-18-crown-6

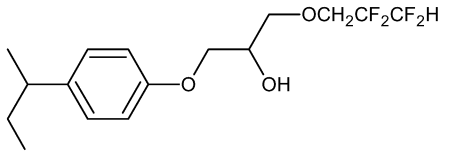

Cs-7SB modifier
1-(2,2,3,3-tetrafluoropropoxy)-3-(4-*sec*-butylphenoxy)-2-propanol

Figure 1. Molecular structures of the cesium and strontium extractants and the Cs-7SB modifier.

The simulant compositions used in this testing are based on a typical composition expected for leaching of spent LWR fuel with nitric acid. It was also assumed that the UREX process for the separation of U and Tc from the spent LWR would precede this process; therefore, the simulant used did not contain U.

Concentrations of stable metals were determined by ICP-MS. Stable metals in the organic phase were digested in 10% HNO_3 with gentle heating, diluted with 1% HNO_3, and analyzed by ICP-MS analysis.

RESULTS AND DISCUSSION

Flowsheet Testing with Simulant

Flowsheet testing of the FPEX process for the separation of Cs and Sr from dissolved LWR fuel was performed using 24 stages of 3.3-cm diameter centrifugal contactors and simulated feed solution. The flowsheet shown in Figure 2 was used for testing.

The percentages of Cs, Sr, Ba, Rb, and the lanthanides in the effluent streams at the time of shutdown are shown in Table 1. The removal efficiencies were >99.99% for Cs, Sr, and Ba and 99.88% for Rb. Concentrations of Cs and Sr in the solvent effluent were below detection limits.

To get an idea of how much TRU would be extracted with this flowsheet, ^{241}Am and ^{154}Eu were spiked into the stage samples, re-equilibrated, sampled and analyzed. Extraction distribution ratios for Am ranged from <0.009 to <0.04 and for Eu ranged

from <0.001 to <0.004. In all cases, activities in the organic phase were below analytical detection limits, and so actual distribution ratios are not known.

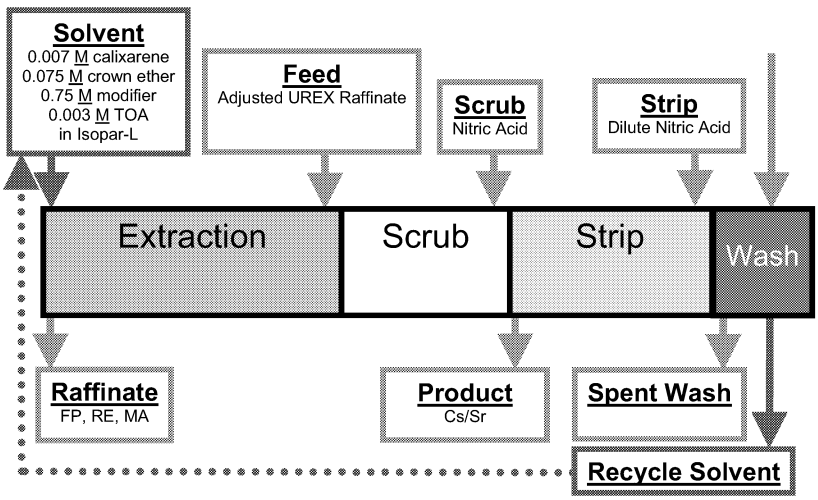

Figure 2. Flowsheet for testing of the FPEX process.

Table 1. Percentage of each component in each of the effluent streams

Effluent Stream	Cs	Sr	Ba	La	Ce	Nd	Sm	Zr	Rb
Raffinate	<2E-04%	<3E-04%	<3E-04%	89.7%	90.6%	96.6%	96.4 %	96.1%	0.12%
Strip Product	98.9%	101%	101%	0.03%	9E-4%	1E-03%	2E-3%	<1.4E-3%	101%
Wash Effluent	2E-04%	<3E-04%	<1E-4%	3E-4%	3E-4%	2E-4%	2E-49%	2E-3%	<2E-4%

Flowsheet Testing With Actual Fuel

Flowsheet Testing of the FPEX Process with actual spent fuel was performed at Argonne National Laboratory in 2007 using 2-cm centrifugal contactors. The flowsheet tested was very similar to the flowsheet presented in Figure 2. Feed to the process was the raffinate from a UREX demonstration in which the uranium and technetium were separated from the spent fuel. Preliminary results of this testing indicates >99.99% of the Cs and 99.9% of the Sr were separated from the spent fuel [11]. Preliminary results for TRU contamination indicate that the TRU activity in the Cs/Sr product exceed the 100 nCi/g limit by approximately one order of magnitude. It is anticipated that greater TRU decontamination can be achieved by increasing the number of scrub stages. The number of scrub stages in the ANL test was limited due to the total number of centrifugal contactors available for testing.

Development of Alternative Calixarenes for the FPEX Process

The flowsheet testing to date indicates that the FPEX solvent can effectively separate Cs and Sr from acidic solutions containing large quantities of actinides and lanthanides, such as spent LWR fuel. However, there are issues relative to the solubility of the BOBCalixC6 in the Isopar® L diluent and with the stability of the BOBCalixC6 extractant in acidic media. The maximum BOBCalixC6 concentration in the FPEX solvent is solubility-limited to 0.007 M. As a result, loading of the BOBCalixC6 with Cs reduces distribution ratios for Cs. Due to the alkyl substituent on benzyl moiety of the BOBCalixC6, the benzyl ring is activated towards nitration. While nitration of the BOBCalixC6 does not severely impact the measured Cs distribution ratios, the products of the nitration of BOBCalixC6 are less soluble in the organic solvent. This further exacerbates the limited BOBCalixC6 solubility in the process solvent. The goal of ongoing research at the INL is the identification of alternative calixarenes which exhibit higher solubility in isoparaffinic solvents and increased resistance to acidic degradation processes. It should be noted that radiolysis of the FPEX solvent is being investigated, and results to date indicate that the solvent is very resistant to radiolysis [12].

Six alternative calixarenes have been synthesized and their performance as an alternative cesium extractant in the FPEX process evaluated. In general, all of the alternative calixarenes have increased solubility and stability in the FPEX solvent, as compared to the calixarene (BOBCalixC6) used in the baseline FPEX solvent. The performance of the FPEX solvent containing the alternative calixarenes, relative to Cs and Sr extraction is acceptable, but increased calixarene concentrations will likely be necessary. Further testing led to the selection of a single compound, coded as AC4, as the alternative calixarene for the FPEX II process. The data indicate that AC4 exhibits the characteristics (synthetic, extraction behavior, and stability) necessary to improve the overall performance of the FPEX solvent extraction process. Continued testing of the alternative calixarene-crown extractant is recommended so that a flowsheet can be developed and tested as a replacement to the baseline FPEX process.

CONCLUSIONS

An FPEX flowsheet has been successfully demonstrated with spent LWR fuel simulant. Hydraulic performance of the process was excellent. Removal efficiencies of >99.99 and >99.98% were obtained for Cs and Sr, respectively. These results exceeded the process goals of 99.9% separation. Additionally, distribution ratios for Am and Eu were very low, indicating little of the TRU should be extracted with this flowsheet. Preliminary results from flowsheet testing with actual spent fuel supports these results. Development of alternative calixarenes for the extraction of Cs is in progress in order to increase the solubility and stability of the calixarene during long-term operation.

REFERENCES

1. E. P. Horwitz, M. L. Dietz, and D. E. Fisher, "SREX: a new process for the extraction and recovery of strontium from acidic nuclear waste streams," *Solvent Extr. Ion Exch.*, **9**(1), 1–25 (1991).
2. D. J. Wood, T. J. Tranter, and T. A. Todd, "Effect of the interference of alkali and earth metal ions on the extraction of ^{90}Sr from acidic nuclear waste solutions by 18-crown-6 derivative," *Solvent Extr. Ion Exch.,* **13**(5), 829–844 (1995).
3. W. J. McDowell, "Crown ethers as solvent extraction reagents: where do we stand?" *Sep. Sci. and Technol.*, **23**, 1251–1268 (1998).
4. J. F. Dozol, N. Simon, V. Lamare, H. Roquette, S. Eymard, B. Tournois, D. DeMarc, and R. M. Macias, "Solution for Cs removal from high-salinity acidic or alkaline liquid waste: the crown calix[4]arenes," *Sep. Sci. and Technol.*, **34**(6&7), 877–909 (1999).
5. P. V. Bonnesen, L. H. Delmau, T. J. Haverlock, and B. A. Moyer, "Alkaline-Side Extraction of Cesium from Savannah River Tank Waste Using a Calixarene Crown Ether Extractant," Oak Ridge National Laboratory, Report ORNL/TM-13704, 1998.
6. J. F. Dozol, Z. Asfari, C. Hill, and J. Vicens, "Bis-crown calix[4]arenas, their preparation process and their use for the selective extraction of cesium and actinides," French Patent n892 14245 B11385.3/MDT, 26 Nov 1992.
7. A. Casnati, A. Pochini, R. Ungaro, F. Ugozzoli, F. Arnaud, S. Fanni, M. J. Schwing, R. J. M. Egberink, F. DeJong, and D. N. Rienhoudt, "Synthesis, complexation and membrane transport studies of 1,3-alternate calix[4]arene crown-6 conformers: a new class of cesium selective ionophores," *J. Am. Chem. Soc.*, **117**, 2767–2777 (1995).
8. R. A. Sachleben, P. V. Bonnesen, T. Descazeaud, T. J. Haverlock, A. Urvoas, and B. A. Moyer, "Surveying the extraction of cesium nitrate by 1,3-alternate calix[4]- arene crown-6 ethers in 1,2-dichloroethane," *Solvent Extr. Ion Exch.*, **17**(6), 1445–1459 (1999).
9. P. V. Bonnesen, T. J. Haverlock, N. L. Engle, R. A. Sachleben, and B. A Moyer, "Development of Process Chemistry for the Removal of Cesium from Acidic Nuclear Waste by Calix[4]arene-crown-6 Ethers," ACS Symposium Series 757 (Calixarenes for Separations), American Chemical Society, Washington, D.C., 2000; pp. 26–44.
10. C. L. Riddle, J. D. Baker, J. D. Law, C. A. McGrath, D. H. Meikrantz, B. J. Mincher, D. R. Peterman, and T. A. Todd, "Fission Product Extraction (FPEX): Development of a Novel Solvent for the Simultaneous Separation of Strontium and Cesium from Acidic Solutions," *Solvent Extr. Ion Exch.*, **23**(3), 449-461 (2005).
11. C. Perreira, Argonne National Laboratory, personal communication, October 2007.
12. B. J. Mincher, S. P. Mezyk, W. F. Bauer, G. Elias, C. R. Riddle, and D. R. Peterman, "FPEX – Radiolysis in the Presence of Nitric Acid," *Solvent Extr. Ion Exch.*, **25**(5), 593-601 (2007).

RADIONUCLIDE PARTITIONING IN THE MODIFIED UNEX PROCESS

V. Babain,[1] I. Smirnov,[1] M. Alyapyshev,[1,3] T.A. Todd,[2] J.D. Law,[2] R.S. Herbst,[2] and A. Paulenova[3]

[1] *Khlopin Radium Institute, St-Petersburg, Russia.* [2]*Idaho National Laboratory, Idaho Falls, ID, USA.* [3]*Oregon State University, Corvallis, OR, USA*
Corresponding author email address: babain@atom.nw.ru

ABSTRACT

The Universal Extraction (UNEX) process has been developed for simultaneous extraction of long-lived radionuclides (cesium, strontium, actinides, and lanthanides) from acidic solutions in one extraction cycle. Modification of this organic solvent through the use of diamides of dipicolinic acid instead of CMPO increases the extraction capacity of UNEX solvent toward lanthanides and actinide metals, allowing for the processing of spent nuclear fuel. The possibility of radionuclide group separation using the modified UNEX solvent [HCCD (chlorinated cobalt dicarbollide), TBDPA (tetrabutyldiamide of dipicolinic acid), PEG in FS-13 (phenyltrifluoromethylsulfone)] is being investigated. Individual strip products, including a) actinides and lanthanides, b) strontium, and c) cesium, can be obtained by selective stripping from UNEX solvent. Such partitioning will make it possible to transform the Cs/Sr product into the most stable matrices for long-term storage and to further process the actinide/lanthanide product for recycling to a nuclear reactor.

INTRODUCTION

The Universal Extraction (UNEX) process has been developed for simultaneous extraction of cesium, strontium, actinides (An) and lanthanides (Ln) from acidic solutions [1]. This process utilizes an extractant consisting of 0.08 M HCCD (chlorinated cobalt dicarbollide), 0.007-0.02 M PEG-400 (polyethylenglycol), and 0.02 M CMPO (diphenyl-*N,N*-di-*n*-butylcarbamoylmethyl phosphine oxide) in the diluent FS-13 (phenyltrifluoromethyl sulfone, $C_6H_5SO_2CF_3$). Numerous tests with simulated and actual high-level waste show that it is possible to effectively and simultaneously extract all these metals from aqueous nitric acid solutions up to ~2 M HNO_3 and ~4 M total nitrates [2,3].

The process was initially developed for the treatment of acidic aqueous radioactive wastes, which contain relatively low concentrations of the radionuclides, to minimize the volume of material requiring long-term geological disposal. The UNEX process is of limited utility for processing aqueous, acidic solutions containing large quantities of lanthanides and/or actinides, such as present in dissolved spent nuclear fuel

solutions. These constraints are primarily attributed to the limited solubility of CMPO (a maximum of 0.02 M) and the CMPO-metal complexes in the organic phase.

Various diamides have been investigated as synergistic extractants with HCCD for the extraction of actinide and lanthanide ions from acidic media [4-7]. It was found that diamides of 2,6-pyridinedicarboxylic (dipicolinic) acid (DPA) in polar fluorinated diluents are promising extractants for uranium, lanthanide, and transplutonium elements [8], and their synergistic mixtures with chlorinated cobalt dicarbollide extract cesium and trivalent metals from nitric acid [4-7]. Modification of UNEX solvent through the use of DPA instead of CMPO increases the extraction capacity of UNEX solvent toward lanthanide and actinide metals, allowing for the processing of spent nuclear fuel [4,6].

The N,N'N,N'-tetrabutyl-diamide of dipicolinic acid (TBDPA), of the numerous diamides tested to date, possesses the most promising features for an alternative actinide/lanthanide extractant in the modified UNEX process. The structure of the TBDPA is presented on the Figure 1. The solvent (0.1 M HCCD, 0.05 M TBDPA, and 0.025 M PEG in FS-13) extracts cesium, strontium, lanthanides, and actinides from nitric acid solutions [6].

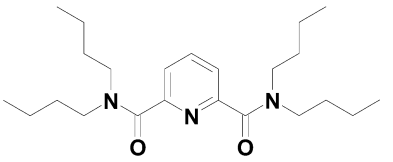

Figure 1. Structure of the N,N'N,N'-tetrabutyl-diamide of dipicolinic acid.

With an appropriate stripping protocol, the diamide-UNEX process can be used for extraction of Cs, Sr, An, and Ln followed by selective separation of these metals to individual products: a) An and Ln, b) Sr, and c) Cs. Such partitioning will make it possible to transform the Cs and Sr into the most stable matrices for long-term storage and further process the actinide-lanthanide product for recycling in reactors.

In the present work, the separation scheme developed for simultaneous extraction of Cs, Sr, An, and Ln with modified UNEX solvent and selective group stripping to individual fractions is discussed and compared with traditional UNEX solvent.

EXPERIMENTAL

Chlorinated cobalt dicarbollide was obtained from Katchem Co. (Czech Republic) as the Cs salt (CsCCD) and used without additional purification. The stock solution of CsCCD in FS-13 was converted to the acid form, HCCD, by repeated contacts with dilute $HClO_4$. Two 5-minutes agitations were applied, and the concentration of HCCD solution in FS-13 was determined by titration with 0.1 M NaOH in the presence of indicator bromocresol green.

The N,N'N,N'-tetrabutyl-diamide of dipicolinic acid (TBDPA) was synthesized as described earlier [4]. The extraction organic solvent was a 0.1 M solution of HCCD, 0.05 M TBDPA, and 0.025 M PEG in FS-13.

The chelating complexants tested as stripping compounds are listed in Tables 1 and 2. Aqueous stripping solutions were prepared by dissolving the required amounts of appropriate chemicals in distilled water. Concentrations of stable metal nitrates of Eu, Sr, and Cs were of 1×10^{-5} M with trace quantities of ^{152}Eu, ^{85}Sr, and ^{137}Cs radioisotopes added. Americium was extracted in the same manner using a 1×10^{-5} M $Eu(NO_3)_3$ carrier solution spiked with ^{241}Am tracer.

Stripping distribution experiments were carried out in 2 mL plastic vials at room temperature (21 ± 1 °C). Equal volumes (0.5 mL) of the organic and aqueous phases were agitated for 3 minutes, split by centrifugation, and 0.4 mL aliquots of each phase were counted using a 3" well-NaI(Tl) detector (Cobra Packard auto-gamma).

RESULTS AND DISCUSSION

During development of the UNEX Process, a single strip solution was desirable for the flowsheet, since the fractionating the radionuclides and actinides was not of interest at that time [3]. A guanidine carbonate/diethylene triamine pentaacetic acid (DTPA) solution and later a regenerable methylamine carbonate (MAC)/DTPA strip solution have been proposed for the simultaneous removal Cs, Sr, actinides, and lanthanides from saturated solvent [9]. As a result of numerous experiments with various aqueous complexants, the experimental conditions which provide common separation of Cs, Sr, An, and Ln using a regenerable strip reagent were found [10].

In recent years, the effort toward a closed nuclear fuel cycle has grown in importance and interest because chemically similar radionuclides (e.g., Cs and Sr) can be vitrified in the most stable matrix for long time storage, and the actinides and lanthanides can be further processed for recycle to a reactor.

Separate stripping of different nuclides was studied for the CCD–phosphorylated polyetheleneglycol solvent [11]. As a result of numerous experiments with various aqueous complexants, the experimental conditions which provide selective separation of Cs, Sr, An, and Ln using a regenerable strip reagent were found [10]. The lanthanide and actinide elements can be stripped only with a mixture of complexant solution and buffer, which provide pH > 3, while the same mixture with pH = 6 allows stripping of plutonium and neptunium. The uranium stripping can be carried out only by using a solution containing carbonate [11].

The data on selective stripping of metals from both organic solvents are presented in Tables 1 and 2. It can be seen that in the case of saturated UNEX solvent (0.08 M CCD, 0.015 M PEG-400, and 0.013 M CMPO in FS-13), actinides and lanthanides can be stripped with solution (A) of ammonium carbonate and acetohydroxamic acid (AHA) first; then Sr can be separately stripped from Cs with solution of $(NH_4)_2CO_3$ with AHA and DTPA (B). Cesium is stripped on the last stage using 2 M methylamine carbonate solution [10].

Table 1. Selective stripping of metals from UNEX-solvent (0.08 M CCD, 0.015 M PEG-400, and 0.013 M CMPO in FS-13).

Stripping solution		*D*					
		Cs	Sr	Eu	Pu	Np	U
A	1 M $(NH_4)_2CO_3$ + 0.1 M AHA	4.4	2.3	0.005	0.02	0.005	0.02
B	1 M $(NH_4)_2CO_3$ + 0.1 M AHA + 0.05 M DTPA	4.1	0.002	0.002	0.01	0.001	0.06

The same stripping solutions were examined for the recovery of metals of interest from the modified UNEX-solvent (0.1 M CCD, 0.05 M TBDPA, and 0.025 M PEG in FS-13). Contrary to previous case, the use of the solution 1 M $(NH_4)_2CO_3$ and 0.013 M AHA does not provide stripping of the Ln and An elements; therefore, different complexants, such as citric acid, nitrilotriacetic acid (NTA), hydroxyethylene-diphosphonic acid (HEDPA), and diethylene triamine pentaacetic acid (DTPA), mixed with ammonium carbonate were examined. The most promising data were obtained with aminoacetic acid (glycine) used as a buffer compound (solutions H and I). Taking into account the data presented in Table 2, the principal scheme for selective stripping is indicated in Figure 2. In the first stage, the selective stripping of Sr with solution H (1 M $(NH_4)_2CO_3$, 0.02 M glycine, and 0.013 M DTPA) will be applied. In the second stage, solution G (1 M $(NH_4)_2CO_3$ and 0.039 M DTPA) provides the selective separation of An and Ln. Cesium can be stripped on the last stage using 2 M methylamine carbonate solution [10].

Table 2. Stripping of metals from *modified* UNEX-solvent (0.1 M CCD, 0.025 M PEG-400, and 0.05 M TBDPA in FS-13)

	Aqueous Phase	*D*			
		Cs	Sr	Am	Eu
A	1 M $(NH_4)_2CO_3$ + 0.13 M AHA	1.9	2.7	21	561
C	1 M $(NH_4)_2CO_3$ + 0.078 M Citric Acid	1.7	0.45	11	-
D	1 M $(NH_4)_2CO_3$ + 0.052 M NTA	2.0	0.46	1.2	-
E	1 M $(NH_4)_2CO_3$ + 0.024 M HEDPA	2.1	1.1	2.9	-
F	1 M $(NH_4)_2CO_3$ + 0.013 M DTPA	1.8	0.009	0.04	0.02
G	1 M $(NH_4)_2CO_3$ + 0.039 M DTPA	2.0	0.008	0.04	0.0001
H	1 M $(NH_4)_2CO_3$ + 0. 2 M Glycine + 0.013 M DTPA	1.8	0.031	1.6	-
I	1 M $(NH_4)_2CO_3$ + 0. 2 M Glycine + 0.026 M DTPA	2.1	0.030	1.4	-

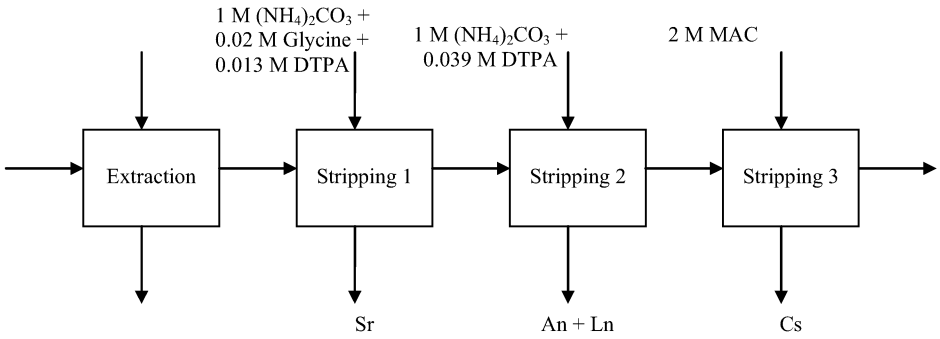

Figure 2. Scheme of selective metal stripping from the modified UNEX-solvent.

CONCLUSIONS

The possibility of obtaining individual strip products a) actinides + lanthanides, b) strontium, and c) cesium are shown. Such partitioning will make it possible to transform the Cs/Sr products into the most stable matrix for long-term storage and further process the actinide + REE product for recycle to a reactor.

REFERENCES

1. V. N. Romanovskiy, I. V. Smirnov, V. A. Babain, T. A. Todd, R. S. Herbst, J. D. Law, and K. N. Brewer, "The Universal Solvent Extraction (UNEX) Process. I. Development of the UNEX Process Solvent for the Separation of Cesium, Strontium, and the Actinides from Acidic Radioactive Waste," *Solvent Extr. Ion Exch.*, **19**(1), 1–21 (2001).
2. R. S. Herbst, J. D. Law, T. A. Todd, V. N. Romanovskiy, V. A. Babain, V. M. Esimantovskiy, I. V. Smirnov, and B. N. Zaitsev, "Universal Solvent Extraction (UNEX) Flowsheet Testing for The Removal of Cesium, Strontium, and Actinide Elements from Radioactive, Acidic Dissolved Calcine Waste," *Solvent Extr. Ion Exch.*, **20**(4&5), 429–445 (2002).
3. R. S. Herbst, J. D. Law, T. A. Todd, V. N. Romanovskiy, I. V. Smirnov, V. A. Babain, V. N. Esimantovskiy, and B. N. Zaitsev, "Development of the universal extraction (UNEX) process for the simultaneous recovery of Cs, Sr, and actinides from acidic radioactive wastes," *Sep. Sci. Technol.,* **38**(12-13), 2685-2708 (2003).
4. V. N. Romanovskiy, V. A. Babain, M. Yu. Alyapyshev, I. V. Smirnov, R. S. Herbst, J. D. Law, and T. A. Todd, "Radionuclide Extraction by 2,6-Pyridinedicarboxylamide Derivatives and Chlorinated Cobalt Dicarbollide," *Sep. Sci. Technol.*, **41**(10), 2111–2127 (2006).
5. M. Yu. Alyapyshev, V. A. Babain, and I. V. Smirnov, "Extractive properties of synergistic mixtures of dipicolinic acid diamides and chlorinated cobalt dicarbollide," *Radiochem.*, **46**(3), 270-271 (2004).
6. D. R. Peterman, R. S. Herbst, J. D. Law, R. D. Tillotson, T. G. Garn, T. A. Todd, V. N. Romanovskiy, V. A. Babain, M. Yu. Alyapyshev, and I. V. Smirnov, "Diamide Derivatives of Dipicolinic Acid as Actinide and Lanthanide Extractants in a Variation of the Unex Process," Global 2007, Boise, Idaho, 2007; pp. 1106–1110.

7. V. A. Babain, I. V. Smirnov, M. V. Logunov, M. Yu. Alyapyshev, et al., "UNEX process for processing of HLW with high concentration of rare-earth metals.II," *Voprosi radiatsionnoy bezopasnosti* (in Russian), **44**(4), 3-12 (2006).
8. V. A. Babain, M. Yu. Alyapyshev, and R. N. Kiseleva, "Metal Extraction by N,N'-Dialkyl-N,N'-Diaryl-Dipicolinamides from Nitric Acid Solutions," *Radiochim. Acta*, **95**(4), 217–223 (2007).
9. J. D. Law, R. S. Herbst, T. A. Todd, V. N. Romanovskiy, V. A. Babain, V. M. Esimantovskiy, I. V. Smirnov, and B. N. Zaitsev, "The Universal Solvent Extraction (UNEX) Process. II. Flowsheet Development and Demonstration of the UNEX Process for the Separation of Cesium, Strontium, and Actinides from Actual Acidic Radioactive Waste," *Solvent Extr. Ion Exch.*, **19**(1), 23–36 (2001).
10. J. D. Law, R. S. Herbst, D. R. Peterman, T. A. Todd, V. N. Romanovskiy, V. A. Babain, and I. V. Smirnov, "Development of Regenerable Strip Reagent for Treatment of Acidic, Radioactive Waste with Cobalt Dicarbollide-based Solvent Extraction Process," *Solvent Extr. Ion Exch.*, **23**(1), 59–83 (2005).
11. I. V. Smirnov, A. Yu. Shadrin, and V. A. Babain, "Combined reprocessing of HLW by Universal Solvent on the Base of Cobalt Dicarbollyde and Phosphorylated Polyethylehe Glycol," Spectrum'98, Denver, Colorado, USA, American Nuclear Society Inc, USA, 1998; pp. 606-609.

THE RADIATION CHEMISTRY OF Cs-7SB, A SOLVENT MODIFIER USED IN Cs AND Sr EXTRACTION

B. J. Mincher,[1] S.P. Mezyk,[2] L.R. Martin,[1] and G. Elias[1]

[1]Idaho National Laboratory, P.O. Box 1625, Idaho Falls, ID, 83415, USA, [2]California State University- Long Beach, Long Beach, CA, 90820, USA
Corresponding author email address: bruce.mincher@inl.gov

ABSTRACT

The solvent modifier 1-(2,2,3,3-tetrafluoropropoxy)-3-(4-*sec*-butylphenoxy)-2-propanol, (Cs-7SB) is used in conjunction with calixarenes and crown ethers dissolved in alkane diluents for the extraction of Cs and Sr from highly radioactive solutions. Its purpose is to solvate the ligands and the resulting ligand-metal complexes in the organic phase. Given this role, and its relatively high concentration in the formulations used for solvent extraction, radiolytic degradation of Cs-7SB might decrease the extraction efficiency of these elements as the solvent accumulates absorbed radiation dose. This work presents the results of studies of Cs-7SB using post-radiolysis gas chromatography with electron-capture detection and solvent-extraction distribution-ratio measurements. Also presented is the kinetic analysis of the bimolecular rate constant for the modifier's reaction with nitrogen trioxide and nitrogen dioxide radicals, major radiolytically-produced radical species in irradiated aqueous nitric acid. Although Cs-7SB was found to undergo reactions with nitrogen-centered radicals, little decrease in extraction efficiency was found. It is concluded the modifier, always present at concentrations much higher than the ligands, acts as a radical scavenger, protecting ligands from radiolytic attack.

INTRODUCTION

Current concepts for the solvent extraction of Cs and Sr from dissolved nuclear fuel rely on the presence of an organic solvent modifier. Alkylphenoxy alcohols were originally developed for use in alkaline solution [1], where the modifier enhances Cs and Sr extraction by solvation of the extractant and the ligand-metal complex. Following research on a number of derivatives, the modifier Cs-7SB (1-(2,2,3,3,-tetrafluoropropoxy)-3-(4-*sec*-butylphenoxy)-2-propanol), shown in Figure 1, was selected at ORNL for optimized Cs extraction from alkaline solution [3], and it has been proposed for Cs and Sr extraction from acidic solution by INL [2]. It has been shown that the efficiency of the solvent extraction of both metals is very sensitive to modifier concentration [2,3].

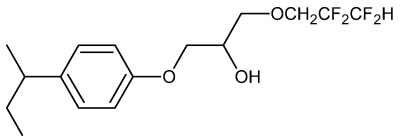

Figure 1. The structure of Cs-7SB (1-(2,2,3,3,-tetrafluoropropoxy)-3-(4-*sec*-butylphenoxy)-2-propanol).

The acidic-side solvent formulation called FPEX (**F**ission **P**roduct **Ex**traction) consists of the macrocyclic compound calix[4]arene-bis-(*t*-octylbenzo-crown-6) (BOBCalixC6) at 0.007 M for Cs extraction, the crown ether 4,4',(5')-di-(*t*-butyldicyclo-hexano)-18-crown-6 (DtBuCH18C6) at 0.15 M for Sr extraction, and 0.75 M Cs-7SB in Isopar L, a branched-chain, alkane diluent [2]. While the solvent-extraction performance of FPEX for Cs and Sr extraction from 1-1.5 M HNO_3 is favorable, the radiation stability of this solvent has received only limited investigation and needs to be evaluated prior to implementation of a large-scale process [4].

The radiolytic decomposition of any solute is primarily due to reaction with reactive species created by radiolysis of the diluent. In an organic diluent such as Isopar L, the reactive species electrons, hydrogen atoms, and various alkane radicals ($\bullet C_xH_y$), produced result in a reducing environment. However, in aerated aqueous nitric acid, the electrons are scavenged by nitrate, dissolved oxygen, and acid (H^+) (Equations 1-3) [5]:

$$e^-_{solv} + NO_3^- \rightarrow NO_3^{-2}\bullet \qquad k = 9.7 \times 10^9 \text{ L mol}^{-1} \text{ s}^{-1} \qquad (1)$$

$$e^-_{solv} + O_2 \rightarrow \bullet O_2^- \qquad k = 1.9 \times 10^{10} \text{ L mol}^{-1} \text{ s}^{-1} \qquad (2)$$

$$e^-_{solv} + H^+ \rightarrow H\bullet \qquad k = 2.3 \times 10^{10} \text{ L mol}^{-1} \text{ s}^{-1} \qquad (3)$$

The bimolecular rate constants *k* for these reactions indicate that these are fast, diffusion-controlled processes. Similarly, hydrogen atoms (Equation 4) [5] and carbon-centered radicals (Equation 5) [6] are scavenged by dissolved oxygen:

$$H\bullet + O_2 \rightarrow HO_2\bullet \qquad k = 2.1 \times 10^{10} \text{ L mol}^{-1} \text{ s}^{-1} \qquad (4)$$

$$\bullet C_xH_y + O_2 \rightarrow \bullet OOC_xH_y \qquad k \sim 10^9 \text{ L mol}^{-1} \text{ s}^{-1} \qquad (5)$$

Therefore, oxidizing species will dominate system chemistry. Oxidizing hydroxyl (•OH) radicals are also directly produced by water radiolysis (Equation 6) [5], and nitrogen dioxide radicals ($\bullet NO_2$) result from the hydrolysis of $NO_3^{-2}\bullet$ (Equation 7) [7]:

$$H_2O \text{ -}\backslash\!/\!\backslash\!/\!\backslash\!/\!\backslash\rightarrow \bullet OH + e^-_{aq} + H\bullet + H_2O_2 + H_3O^+ + H_2 \qquad (6)$$

$$NO_3^{-2}\bullet + H^+ \rightarrow \bullet NO_2 + OH^- \qquad k = 2 \times 10^{10} \text{ L mol}^{-1} \text{ s}^{-1} \qquad (7)$$

Finally, the nitrogen trioxide radical is produced from direct radiolysis of the nitrate anion product of nitric acid dissociation, as shown in Equation 8, and by the reaction of nitric acid with hydroxyl radical, as shown in Equation 9 [8]:

$$NO_3^- \text{-}\wwvy\rightarrow e^-_{sol} + \bullet NO_3 \quad (8)$$

$$\bullet OH + HNO_3 \rightarrow \bullet NO_3 + H_2O \qquad k = 5.3 \times 10^7 \text{ L mol}^{-1} \text{ s}^{-1} \quad (9)$$

Since the rate of the reaction in Equation 1 is fast, the reaction in Equation 8 relies on direct radiolysis, and the reaction in Equation 9 is slow and relies on undissociated nitric acid, it may be assumed that nitrogen dioxide radical ($\bullet NO_2$) reactions will be somewhat more important than nitrogen trioxide radical ($\bullet NO_3$) reactions in the low nitric acid concentrations envisioned for FPEX applications.

Here, we present the results of studies of Cs-7SB irradiated in the presence of nitric acid under FPEX process conditions. The effects of nitrogen oxide radical reactions on Cs and Sr solvent extraction distribution ratios are of special interest.

EXPERIMENTAL SECTION

The steady-state ^{60}Co γ-ray irradiation and solvent-extraction distribution-ratio techniques have been previously described [4]. Absolute rate-constant measurements were conducted by pulse radiolysis at the Notre Dame Radiation Laboratory (NDRL) linear accelerator (LINAC). The radicals of interest were produced using 2-3 ns electron beam pulses depositing 3-5 Gy per pulse. Nitrogen trioxide radical ($\bullet NO_3$) was produced in 6 M HNO_3 with kinetics determined from its absorbance measured at 633 nm, while nitrogen dioxide radical ($\bullet NO_2$) was produced in 0.1 M $NaNO_2$ and measured at 450 nm.

RESULTS AND DISCUSSION

When the FPEX solvent was irradiated with ^{60}Co γ-rays while in contact with 1.5 M HNO_3, there was very little change in solvent-extraction distribution-ratios for either Cs or Sr to the maximum absorbed dose investigated of 200 kGy at a dose rate of 20 kGy/h [4]. The plot of the distribution ratios versus absorbed dose is shown in Figure 2. Visual inspection of irradiated mixed-phase samples showed that the organic phase turned yellow at absorbed doses as low as 3.5 kGy, and that this color deepened to yellow-orange with increasing absorbed dose. Color did not develop in samples irradiated in the presence of only 0.01 M HNO_3. This color is similar to that observed with the longer-term thermal reaction with nitric acid in the absence of radiation. This implies that nitration reactions are occurring, as has previously been reported for the thermal reaction of nitric acid with alkylphenoxy alcohol modifiers after several weeks of contact [3]. Irradiation may accelerate these reactions.

Samples of the FPEX formulation and 0.75 M Cs-7SB in Isopar L were irradiated in contact with 1.5 M HNO_3 to an absorbed dose of 400 kGy (t = 1200 minutes duration) to generate products for gas chromatography-electron capture detection (GC-ECD) analysis [4]. It can be seen in Figure 3 that unirradiated Cs-7SB in Isopar L (t = 0

minutes) has three main peaks, with retention times of 25.2, 25.4, and 25.7 minutes. When the Cs-7SB in Isopar L solution is irradiated in the absence of the aqueous phase, the peak at 25.4 minutes, which was barely discernable at this scale in the pre-irradiation sample, increased in height, while the 25.2 and 25.7 minute peaks decreased. When irradiated in the presence of the acidic aqueous phase, a new peak appeared at 25.5 minutes retention time, presumably due to nitrated Cs-7SB. Similar results were obtained when the FPEX solvent formulation was irradiated under the same conditions. These results are also shown in Figure 3.

Since nitration reactions may play a major role in Cs-7SB radiation chemistry, a pulse-radiolytic investigation of the reaction of nitrogen-centered radicals with this modifier was conducted. A range of modifier concentrations up to a maximum of 150 μM in 6 M HNO_3 was used to evaluate the reaction of $\bullet NO_3$ radical. Nitrogen trioxide radical is produced to the quantitative exclusion of $\bullet NO_2$ under these strongly acidic conditions. The resulting decay kinetic profiles are shown in Figure 4a. Figure 5 shows the second order rate constant determination, resulting in a value of (2.90 ± 0.08) x 10^9 L mol^{-1} s^{-1}.

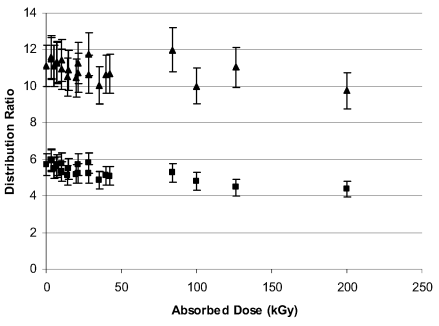

Figure 2. Solvent-extraction distribution ratios for Sr (diamonds) and Cs (squares) versus absorbed dose for FPEX solvent irradiated in the presence of 1.5 M HNO_3.

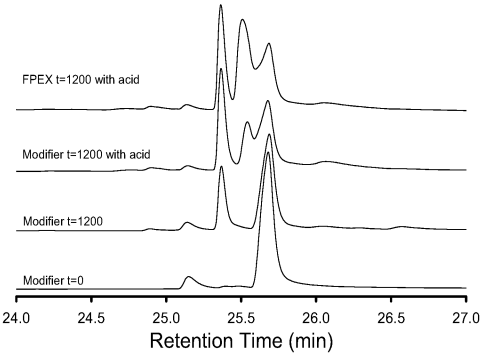

Figure 3. Gas chromatography-electron capture detection chromatogram of unirradiated Cs-7SB modifier in Isopar L diluent (bottom), modifer in Isopar L irradiated to 400 kGy (second from bottom), modifier in Isopar L irradiated to 400 kGy in the presence of 1.5 M HNO_3 (second from top), and FPEX solvent irradiated to 400 kGy in the presence of 1.5 M HNO_3 (top).

Although no comparison data exists for $\bullet NO_3$ radical reactions in water, literature values for this radical reaction in acetonitrile for the Cs-7SB analogues toluene [9] (Equation 10), p-xylene [10] (Equation 11), and dimethoxybenzene [9] (1,4-$CH_3C_6H_4OCH_3$, Equation 12) occurs by hydrogen-atom abstraction and electron abstraction:

$$\bullet NO_3 + C_6H_5\text{-}CH_3 \rightarrow HNO_3 + \bullet CH_2C_6H_5 \qquad k = 1.3 \times 10^8 \text{ L mol}^{-1} \text{ s}^{-1} \qquad (10)$$

$$\bullet NO_3 + 1,4\text{-}C_6H_4(CH_3)_2 \rightarrow NO_3^- + [1,4\text{-}C_6H_4(CH_3)_2]^{\bullet+} \quad k = 6.2 \times 10^9 \text{ L mol}^{-1} \text{ s}^{-1} \quad (11)$$

$$\bullet NO_3 + 1,4\text{-}C_6H_4(OCH_3)_2 \rightarrow NO_3^- + [1,4\text{-}C_6H_4(OCH_3)_2]^{\bullet+} \; k = 1.3 \times 10^{10} \text{ L mol}^{-1} \text{ s}^{-1} \quad (12)$$

This suggests that the $\bullet NO_3$ radical reaction with the modifier could produce significant amounts of the radical cation (Cs-7SB$^{\bullet+}$). This cation could then recombine with nitrite radicals present to give the final nitrated product (Equation 13):

$$\text{Cs-7SB}^{\bullet+} + \bullet NO_2 \rightarrow H^+ + \text{Cs-7SB-NO}_2 \quad (13)$$

A similar kinetic analysis was attempted in 0.1 M $NaNO_2$, where $\bullet NO_2$ radical is produced to the exclusion of $\bullet NO_3$ radical. However, the limited solubility of Cs-7SB in neutral aqueous solution precluded making this measurement. However, based on our previous work with other aromatic compounds it is believed that this rate will be slow.

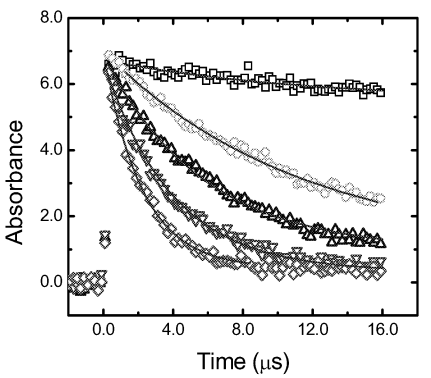

Figure 4. Decay kinetics of $^{\bullet}NO_3$ radical in aqueous 6.0 M HNO_3 for modifier concentrations of zero (□), 22.0 (O), 53.2 (Δ), 95.0 (∇), and 151.5 (◊) μM. Solid lines correspond to pseudo-first-order fits with rate constants of 4.4 x 10^2 s^{-1}, 7.43 x 10^4 s^{-1}, 1.51 x 10^5 s^{-1}, 2.69 x 10^5 s^{-1}, and 4.45 x 10^5 s^{-1}, respectively.

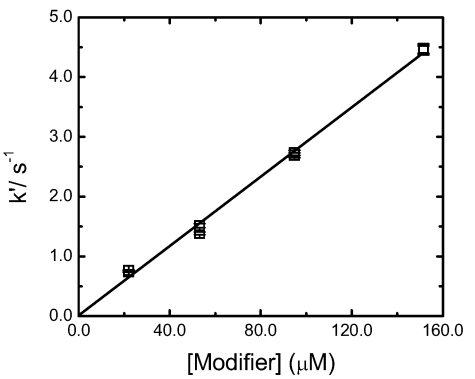

Figure 5. Reaction of $^{\bullet}NO_3$ radicals with modifier in aqueous 6 M HNO_3 solution. Slope corresponds to a linear fit, with reaction rate constant of (2.90 ± 0.08) x 10^9 L mol^{-1} s^{-1}.

CONCLUSION

The Cs-7SB modifier reacts with the $\bullet NO_3$ radical product of nitric acid radiolysis with a rate constants of (2.90 ± 0.08) x 10^9 L mol^{-1} s^{-1}. This initiates a series of reactions that lead in part to nitrated modifier derivatives, detectable as at least one new peak in GC-ECD chromatography. However, these reactions appear to have only minor effect on the solvent-extraction efficiency of FPEX for Cs and Sr, even at absorbed doses as high as 200 kGy, a dose equivalent to approximately 10 years of solvent recycle. In addition to its roles in solvating the ligands and their metal complexes, the modifier acts as a scavenger of radiolytically-produced radicals, protecting the ligands from radiolytic degradation.

ACKNOWLEDGMENTS

This research was sponsored by the US Department of Energy, Office of Nuclear Energy, Science, and Technology under DOE Idaho Operations Office contract DE-AC07-99ID13727. Pulse radiolysis was conducted at the Notre Dame Radiation Laboratory, University of Notre Dame, IN, USA.

REFERENCES

1. P. V. Bonnesen, D. J. Presley, T. J. Haverlock, R. A. Sachleben, G. Das, and B. A. Moyer, "Development of an Alkaline-Side Solvent Extraction Process for the Removal of Cesium from Tank Waste," ORNL/TM-13704, Oak Ridge National Laboratory, Oak Ridge, TN, USA, 1998.
2. C. L. Riddle, J. D. Baker, J. D. Law, C. A. McGrath, D. H. Meikrantz, B. J. Mincher, D. R. Peterman, and T. A. Todd, "Fission Product Extraction (FPEX): Development of a Novel Solvent for the Simultaneous Separation of Strontium and Cesium from Acidic Solutions," *Solvent Extr. Ion Exch.*, **23**, 449-461 (2005).
3. P. V. Bonnesen, L. H. Delmau, and B. A. Moyer, "Review of Solvent Modifier Data for Implementation in the FPEX Process," unpublished report, Oak Ridge National Laboratory, Oak Ridge, TN, USA, 2006.
4. B. J. Mincher, S. P. Mezyk, W. F. Bauer, G. Elias, C. L. Riddle, D. R. Peterman, "FPEX γ-Radiolysis in the Presence of Nitric Acid," *Solvent Extr. Ion Exch.*, **25**, 593-601 (2007).
5. G. V. Buxton, C. L. Greenstock, W. P. Helman, and A. B. Ross, "Critical Review of Rate Constants for Reactions of Hydrated Electrons, Hydrogen Atoms and Hydroxyl Radicals (•OH/•O-) in Aqueous Solution," *J. Phys. Chem. Ref. Data*, **17**, 513-886 (1988).
6. Z. B. Alfassi, Ed., Peroxyl Radicals, John Wiley and Sons, New York, 1997.
7. V. A. Benderskii, A. G. Krivenko, E. A. Ponomarev, and N. V. Fridovich, "Protonation Rate Constants of the NO_3^{-2} Radical-Ion," *Sov. Electrochem.*, **23**, 1343-1348 (1987).
8. Y. Katsumura, P. Y. Jiang, R. Nagaishi, T. Oishi, K. Ishigure, and Y. Yoshida, "Pulse-Radiolysis Study of Aqueous Nitric-Acid Solutions – Formation Mechanism, Yield, and Reactivity of NO_3 Radical," *J. Phys. Chem.*, **95**, 4435-4439 (1991).
9. E. Baciocchi, T. DelGiacco, S. M. Murgia, and G. V. Sebastiani, "Rate and mechanism for the reaction of the nitrate radical with aromatic and alkylaromatic compounds in acetonitrile," *J. Chem. Soc. Chem. Commun.*, 1246-1248 (1987).
10. T. Del Giacco, E. Baciocchi, and S. Steenken, "One-electron oxidation of alkylbenzenes in acetonitrile by photochemically produced NO_3: Evidence for an inner-sphere mechanism," *J. Phys. Chem.*, **97**, 5451-5456 (1993).

THE RADIATION CHEMISTRY OF CCD-PEG, A SOLVENT-EXTRACTION PROCESS FOR Cs AND Sr FROM DISSOLVED NUCLEAR FUEL

B.J. Mincher,[1] R.S. Herbst,[1] R.D. Tillotson,[1] and S.P. Mezyk[2]

[1]*Idaho National Laboratory, PO Box 1625, Idaho Falls, ID, 83415, USA*
[2]*California State University- Long Beach, Long Beach, CA, 90820, USA*
Corresponding author email address: bruce.mincher@inl.gov

ABSTRACT

Cobalt dicarbollide and polyethylene glycol in phenyltrifluoromethyl sulfone (HCCD/PEG in FS-13) is currently under consideration for use in the process-scale selective extraction of fission-product cesium and strontium from dissolved nuclear fuel. This solvent will be exposed to high radiation doses during use and has not been adequately investigated for radiation stability. Here, HCCD/PEG was γ-irradiated to various absorbed doses, to a maximum of 432 kGy, using ^{60}Co. Irradiations were performed for the neat organic phase and also for the organic phase in contact with 1 M-nitric acid mixed by air sparging. Post-irradiation solvent-extraction measurements showed that Cs distribution ratios were unaffected; however, Sr extraction efficiency decreased with absorbed dose under both conditions and was greater when in contact with the aqueous phase. Stripping performance was not affected. A mechanism, initiated by direct radiolysis of the sulfone diluent, is proposed.

INTRODUCTION

Acidic, chloro-protected cobalt bis(dicarbollide) (HCCD) and polyethylene glycol with an average molecular weight of 400 (PEG-400), in an appropriate organic diluent have been investigated for three decades for use in recovering Cs and Sr from acidic radioactive solutions. Pioneering efforts on dicarbollide chemistry were initially performed by the Nuclear Research Institute and the Institute of Inorganic Chemistry located at Řež, Czech Republic. Later, collaborative efforts further enhanced the understanding and development of HCCD with synergistic additives for the simultaneous efficient recovery of Cs and Sr for nuclear applications. For over a decade, the Khlopin Radium Institute (KRI, St. Petersburg, Russia) and the Idaho National Laboratory (INL, Idaho Falls, Idaho, USA) collaborated on expanding the use of HCCD in the presence of appropriate synergists for the recovery of major radionuclides from acidic radioactive waste streams [1]. Most of these development efforts were described and reviewed in the recent literature [2] and have culminated in the use of the diluent phenyltrifluoromethyl sulfone ($C_6H_5SO_2CF_3$), designated FS-13.

However, there has been very little work on the effects of radiolysis of the HCCD-PEG solvent-extraction formulation. The radiolytic decomposition of any solute is primarily due to reaction with reactive species created by radiolysis of the diluent. When the FS-13 diluent was irradiated in previous work, the main products identified were hexafluoroethane and benzenesulfonic acid for pure FS-13 and also for FS-13 in the presence of nitric acid [3,4]. In the presence of nitric acid, trifluoronitromethane, nitrobenzene, sulfate, and fluoride ions were also reported, in decreasing order of abundance [4]. Here we report the effects of γ-irradiation of HCCD/PEG as a single organic phase and when in contact with aqueous nitric acid. The post-irradiation distribution ratios of Cs and Sr extraction were used as metrics. We also propose a mechanism for the radiolysis of the sulfone diluent, and its effects on solvent-extraction efficiency for Sr and Cs.

EXPERIMENTAL SECTION

The steady-state ^{60}Co γ-ray irradiation and solvent-extraction distribution ratio techniques have been previously described [5]. Briefly, the CCD-PEG sulfone solution was irradiated for durations to achieve selected absorbed doses, at a dose rate of 20 kGy/h. Samples were irradiated in septum-sealed glass vials, either as the neat single phase or in contact with an equal volume of 1.0 M HNO_3 with air sparging to mix the phases. The irradiated organic solutions were then separated from the aqueous phase by centrifugation and used for solvent-extraction experiments. The aqueous phase was a light-water-reactor-fuel dissolution stimulant consisting of 1 M HNO_3 and appropriate concentrations of rare earths, Zr, Ba, and carrier Cs and Sr, spiked with radio-Cs and Sr [5]. The distribution ratios (D_{Sr}, D_{Cs}, where $D_x = [X]_{org}/[X]_{aq}$) were determined as the ratio of the appropriate specific activities in the organic and aqueous phases as determined by γ-ray counting. Stripping was performed with an equal volume of 100 g L^{-1} guanidinium carbonate/20 g L^{-1} DTPA.

RESULTS AND DISCUSSION

Irradiation had no effect on Cs extraction for single-phase HCCD/PEG in FS-13 or when irradiated while mixing with 1 M HNO_3 by air sparging to the highest absorbed dose investigated of 432 kGy. In contrast, the Sr forward extraction distribution ratios decreased with absorbed dose under both irradiation conditions. These data are shown in Figure 1. There was no decrease in D_{Sr} over time for samples that were mixed with 1 M HNO_3 and air-sparged at irradiator temperature in the absence of radiation. Exponential functions provide a reasonable fit to the decreasing D_{Sr} values (R = 0.87 for D_{Sr} with aerated acid; R = 0.92 for D_{Sr} with the neat organic phase). This suggests that the Cs ligand (HCCD) is more stable to degradation, while the Sr ligand (PEG-400) is susceptible to radiolytically-induced damage. Exponential solute concentration decreases are common in irradiated solutions [6]. This is due to the reaction of solutes with constant concentrations of radiolytically-produced reactive species, resulting in pseudo-first-order kinetics. Based on the exponential fit, the pseudo-first order rate constant for

the loss in Sr extraction efficiency was about 5-fold higher in the presence of aerated acid ($7 \pm 2 \times 10^{-3}$ kGy^{-1}) than for the single-phase irradiation ($1.4 \pm 0.4 \times 10^{-3}$ kGy^{-1}).

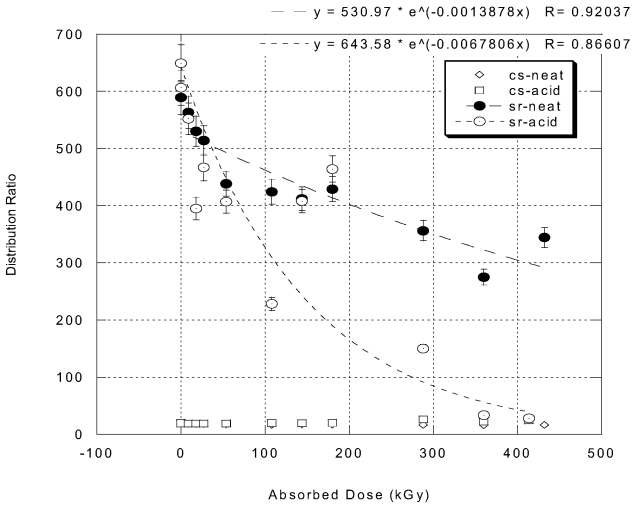

Figure 1. Extraction distribution ratios for Sr and Cs versus absorbed γ-dose in single-phase HCCD/PEG and in HCCD/PEG irradiated in the presence of 1M-HNO_3 with air-sparging. Individual error bars are ± 5%.

Cesium stripping was not affected by irradiation, as shown in Figure 2. There may be an increase in stripping distribution ratios for Sr at higher absorbed doses, also shown in Figure 2, which accompanied the decrease in Sr forward extraction distribution ratios at these doses. However, the magnitude of the Sr stripping distribution ratio remained low, at approximately 6.8×10^{-4}.

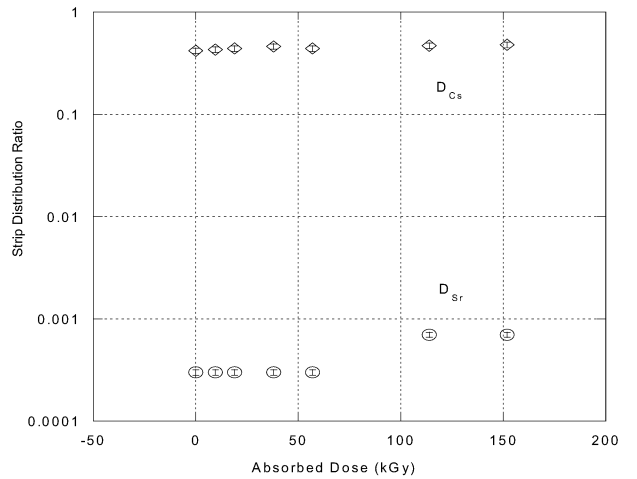

Figure 2. (Guanidine carbonate/ DTPA strip (back-extraction) distribution ratios for Sr and Cs versus absorbed γ-dose, from HCCD/PEG samples irradiated in contact with the acidic aqueous phase and air-sparging. Individual error bars are ± 5%.

The radiolytic decomposition of PEG-400 in irradiated HCCD/PEG is expected to be the result of reaction with a product of the direct radiolysis of the diluent. The reported production of benzenesulfonic acid and hexafluoroethane in irradiated FS-13 [3,4] suggests a sequence of reactions initiated by direct radiolysis of the sulfone diluent as shown in Equation 1:

$$C_6H_5SO_2CF_3 \text{ -\VVV\} \rightarrow } C_6H_5S^{\bullet+}O_2CF_3 + e^- \quad (1)$$

This would be followed by decay of the radical cation to a sulfur-centered cation and the trifluoromethane radical, shown in Equation 2:

$$C_6H_5S^{\bullet+}O_2CF_3 \rightarrow C_6H_5S^{+}O_2 + {}^{\bullet}CF_3 \quad (2)$$

Radical-radical combination, shown in Equation 3, would result in the production of the measured product hexafluoroethane [4]:

$$2({}^{\bullet}CF_3) \rightarrow CF_3CF_3 \quad (3)$$

The solvent also contains up to 0.2 M H_2O, and thus, hydrolysis of the sulfur-centered cation of Equation 2 would result in the measured benzenesulfonic acid product [4], as shown in Equation 4:

$$C_6H_5S^{+}O_2 + H_2O \rightarrow C_6H_5SO_2OH + H^+ \quad (4)$$

The sulfur-centered cation product of Equation 2 could also react with PEG, again producing benzenesulfonic acid and the carbocation shown in Equation 5:

$$C_6H_5S^{+}O_2 + \text{-(-CH(OH)CH}_2\text{CH(OH)-)-} \rightarrow C_6H_5SO_2OH + \text{-(-CH(OH)CH}_2\text{CH}^{+}\text{-)-} \quad (5)$$

The carbocation product of Equation 5 would undergo dehydration, as shown in Equation 6, resulting in a product with less complexing ability than PEG. This would account for the resulting decrease in Sr distribution ratios:

$$\text{-(-CH(OH)CH}_2\text{CH}^{+}\text{-)-} \rightarrow \text{-(-CH(OH)C=C-)-} + H^+ \quad (6)$$

According to Figure 1, the decrease in Sr extraction efficiency with irradiation was faster in the presence of 1 M HNO_3. The hydroxyl radical (${}^{\bullet}OH$) product of water radiolysis and the nitrogen trioxide radical (${}^{\bullet}NO_3$) product of nitric acid radiolysis are the two main oxidizing species that might be expected to react with PEG in irradiated aqueous solution.

The rate constants for the reactions of these radicals with ethylene glycol have been measured (Equation 7 [7] and Equation 8 [8]):

$$HOCH_2CH_2OH + {}^{\bullet}NO_3 \rightarrow HNO_3 + \bullet CHOHCH_2OH \qquad k = 1.6 \times 10^6 \text{ L mol}^{-1} \text{ s}^{-1} \quad (7)$$

$$HOCH_2CH_2OH + {}^{\bullet}OH \rightarrow H_2O + {}^{\bullet}CHOHCH_2OH \qquad k = 2.4 \times 10^9 \text{ L mol}^{-1} \text{ s}^{-1} \qquad (8)$$

In general, the rate of hydroxyl radical reaction with alkanes increases with chain length. By analogy, the rates for polyethylene glycol may be higher than those shown here for ethylene glycol, although the relative rates for these two reactions should be similar. In terms of both concentration and rate, Equation 8 is expected to dominate; however, the resulting carbon-centered radical is the same for both reactions. In the presence of dissolved oxygen, which is continually replenished by the air sparging, the carbon-centered radical would react with O_2 to produce a peroxyl radical [9]:

$$^{\bullet}CHOHCH_2OH + O_2 \rightarrow {}^{\bullet}OOCHOHCH_2OH \qquad (9)$$

Peroxyl radicals combine to produce tetroxides, shown in Equation 10, followed by decomposition via four possible pathways into aldehydes, ketones, or alcohols as shown in Equation 11 [9]:

$$2(^{\bullet}OOCHOHCH_2OH) \rightarrow OHCH_2OHCHOOOOCHOHCH_2OH \qquad (10)$$

$$OHCH_2OHCHOOOOCHOHCH_2OH \rightarrow \text{aldehydes, ketones, and alcohol products} \qquad (11)$$

These product species would have less complexing ability for Sr.

CONCLUSIONS

The ^{60}Co γ-irradiation of the HCCD/PEG in FS-13 diluent as a single phase, or during mixing with 1 M HNO_3 by air sparging, had no effect on D_{Cs} to an absorbed dose of 432 kGy. Cesium stripping was also not affected. The Sr extraction efficiency decreased with absorbed dose in an exponential fashion, with the rate of D_{Sr} decrease in the presence of the acidic aqueous phase and air sparging being ~5-fold faster than that for irradiation of the single organic-phase solution. Strontium extraction efficiency losses may be due to decreases in the PEG-400 concentration, and mechanisms for the decomposition of PEG-400 based on direct radiolysis of the FS-13 diluent, and on reaction with hydroxyl radical due to direct water radiolysis are proposed. The distribution ratio for Sr was still greater than that for Cs, even at the highest absorbed doses examined. Strontium stripping was essentially unaffected.

ACKNOWLEDGMENTS

This research was sponsored by the US Department of Energy, Office of Nuclear Energy, Science, and Technology under DOE Idaho Operations Office contract DE-AC07-99ID13727.

REFERENCES

1. R. S. Herbst, J. D. Law, T. A. Todd, V. N. Romanovskii, V. A. Babain, V. M. Esimantovski, B. N. Zaitsev, and I. V. Smirnov, "Development and testing of a cobalt dicarbollide based solvent extraction process for the separation of cesium and strontium from acidic tank waste," *Sep. Sci. Technol.*, **37**, 1807-1831 (2002).
2. J. Rais and B. Gruner, "Extraction with metal bis(dicarbollide) anions," in Y. Marcus and A. K. SenGupta, Eds, Ion Exchange and Solvent Extraction, Volume 17, Marcel Dekker, New York, 2004.
3. R. S. Herbst, J. D. Law, T. A. Todd, V. N. Romanovskiy, I. V. Smirnov, V. A. Babain, V. M. Esimantovskiy, and B. N. Zaitsev, "Development of the Universal Extraction (UNEX) Process for the Simultaneous Recovery of Cs, Sr and Actinides from Acidic, Radioactive Waste," *Sep. Sci. Technol.*, **38**, 2685-2708 (2003).
4. Khlopin Radium Institute, "Applicability of the Russian Separation technology to Processing of US Radioactive Waste, Final Report," unpublished report, Khlopin Radium Institute, St. Petersburg, Russia, 1999.
5. B. J. Mincher, R. S. Herbst, R. D. Tillotson, and S. P. Mezyk, "γ-Radiation Effects on the Performance of HCCD-PEG for Cs and Sr Extraction," *Solvent Extr. Ion Exch.*, **25**, 747-755 (2007).
6. B. J. Mincher and R. C. Curry, "Considerations for Choice of a Kinetic Fig. of Merit in Process Radiation Chemistry for Waste Treatment," *Appl. Radiat. Isot.*, **52**, 189-193 (2000).
7. A. K. Pikaev, G. K. Sibirskaya, E. M. Shirshov, P. Ya. Glazunov, and V. I. Spitsyn, "Pulse-Radiolysis of Concentrated Aqueous-Solutions of Nitric-Acid," *Dokl. Phys. Chem., Proc. Acad. Sci. USSR*, **215**, 328-331 (1974).
8. M. S. Matheson, A. Mamau, J. Silverman, and J. Rabani, "Reaction of Hydroxyl Radical with Polyethylene Oxide in Aqueous Solution," *J. Phys. Chem.*, **77**, 2420-2424 (1973).
9. Z. B. Alfassi, Ed., Peroxyl Radicals, John Wiley and Sons, New York, 1997.

A STUDY OF RADIOLYTIC STABILITY OF 25,27-BIS(2-PROPYLOXY) CALIX[4]-26,28-CROWN-6 (IPR-C[4]C-6)

Wang Jianchen and Song Chongli

Institute of Nuclear and New Energy Technology (INET), Tsinghua University, Beijing 102201, P.O. Box: 1021, China
Corresponding author email address: Wangjianchen@mail.tsinghua.edu.cn

ABSTRACT

The radiolytic stability of 25,27-bis(2-propyloxy)calix[4] arene -26,28-crown-6 (iPr-C[4]C-6) was studied. ^{60}Co was used as a radiation source. Its dose rate was 437Gy/min., and the total absorbed dose of the iPr-C[4]C-6 was from 10^4 to 10^6 Gy. The iPr-C[4]C-6 solid and 0.025 mol/L iPr-C[4]C-6/*n*-octanol which were pre-equilibrated with 0.01 mol/L and 3 mol/L nitric acid, respectively, were given different doses, and their extraction performance was researched. Their degradation mechanism was investigated by mass spectrometry (MS) and infrared spectroscopy (IR). The results show that radiolytic stability of the iPr-C[4]C-6 solid and 0.025 mol/L iPr-C[4]C-6/*n*-octanol are good when their absorbed dose is less than 10^6 Gy. The extracting system of iPr-C[4]C-6/*n*-octanol is promising for separating cesium from high-level liquid waste(HLLW).

INTRODUCTION

Calixcrowns have been studied widely in the recent two decades for their stronger selectivity and complexing ability to alkali and alkaline-earth metals [1-6]. The research results of IR, MS, NMR, and other techniques indicated that the main structure of calixcrown was not changed when the radiation absorbed dose was less than 10^6 Gy [7]. The radiolytic stability of calixcrowns is quite good; therefore, it is a good extractant type for separating cesium from HLLW. Solvents containing iPr-C[4]C-6 were investigated, and *n*-octanol was selected in INET [8]. The extracting system iPr-C[4]C-6/*n*-octanol shows higher extracting ability for cesium in HLLW. This paper is to research the radiolytic stability of the iPr-C[4]C-6 and iPr-C[4]C-6/*n*-octanol and to investigate the mechanism of radiolytic degradation.

EXPERIMENTAL

Reagent and Apparatus

iPr-C[4]C-6 as a white-colored powder was synthesized by INET. All other regents were of analytical grade.

Measurements were performed using the following: EKCON700A NaI γ counter; IRIS Advantage ICP-AES; Nicolet 470 IR spectrum; Perkin Elmer SCIEX API 3000: Electro-spray ionization mass spectrometry (ESI-MS).

Procedure

The following samples were irradiated with a ^{60}Co radiation source in air in 25 ± 2 °C. The dose rate was 437Gy/min.

A: iPr-C[4]C-6 solid

B: 0.025 mol/L iPr-C[4]C-6/*n*-octanol pre-equilibrated with 0.01 mol/L HNO_3.

C: 0.025 mol/L iPr-C[4]C-6/*n*-octanol pre-equilibrated with 3.0 mol/L HNO_3.

Prior to measuring the distribution ratio (*D*), the above irradiated samples were pre-equilibrated again with 0.01 mol/L or 3.0 mol/L HNO_3 respectively. The pre-equilibrated organic phase was mixed with an equal volume of nitric acid solution containing trace ^{137}Cs at 25 ± 0.1 °C for 10 min. The two phases were separated by centrifugation and analyzed using a EKCON 700A NaI(TI) γ counter, and then the D_{Cs} values were calculated.

RESULTS AND DISCUSSION

The Properties of Irradiated Extractant

The Color Changes

The color changes of samples A, B, and C for different irradiated dose are listed in the table 1.

Table 1. The color changes of irradiated samples

Irradiated dose (x10^4 Gy)	0	1	5	10	50	100
A	white	white	white	white	buff	buff
B	colorless	colorless	colorless	colorless	colorless	buff
C	colorless	yellowish	yellowish	buff	buff	yellow

Table 1 shows that the color of iPr-C[4]C-6 solid was not changed when the irradiated dose was less than 10^5 Gy, but its color changed to buff when the irradiated dose was larger than 10^5 Gy. The color of sample B changed to buff when the irradiated dose was larger than 10^6 Gy. But for sample C, its color gradually changed from yellowish to buff and then to yellow when the irradiated dose was increased from 10^4 Gy to 10^6 Gy. Comparing to these three samples, the color changes of sample B is the least one, and that of the sample C is the largest one. The reasons may be following: The one reason is that the *n*-octanol solvent may have absorbed some irradiated dose and resulted in the decreasing of the absorbed irradiated dose to iPr-C[4]C-6 for sample A. The authors are comparing two different processes in samples A and B; A is direct radiolysis of the calixarene, where in B the calixarene is attacked by solvent radicals, so in this regard it's true that the octanol is absorbing some radiation that may have been absorbed by neat calixarene. However it's also true that this results in a whole new mechanism of

radiolysis, and possibly different products, which also may account for differences in color. Another reason is that some of nitric acid is decomposed' and it may enhance the degradation of iPr-C[4]C-6 for its higher nitric acid concentration in sample C.

The Effect of Irradiation on the Extraction Ability to Cesium

Samples B and C were mixed with the equal volume aqueous phase with 0.01 mol/L and 3 mol/L HNO_3 containing tracer ^{137}Cs, respectively. The D_{Cs} values were measured and are listed in Table 2.

Table 2. The effect of irradiated extraction system on D_{Cs}.

Irradiated dose (x10^4 Gy):	0	1	5	10	50	100
B	1.71	2.31	2.04	1.31	0.31	0.28
C	25.43	27.86	27.36	24.44	17.19	13.66

Table 2 shows that D_{Cs} increases with an increase of the irradiated dose from 10^4 to 10^5 Gy, and then D_{Cs} decreases markedly with further increase of the irradiated dose when it was above 10^5 Gy for sample B and C. The reason is that iPr-C[4]C-6 may be decomposed, producing some new and synergistic components to make the D_{Cs} increase at lower irradiated dose. But iPr-C[4]C-6 was decomposed much to make D_{Cs} decrease at higher irradiated dose, and the synergistic components do not play as important roles. The results indicated that the iPr-C[4]C-6 in *n*-octanol was decomposed obviously when the irradiated dose was higher 10^5 Gy.

The Changes of Structure For iPr-C[4]C-6 After Irradiation

The samples A, B, and C were irradiated to 10^4 Gy and 10^6 Gy, respectively. They were analyzed by electro-spray ionization mass spectrometry (ESI-MS).

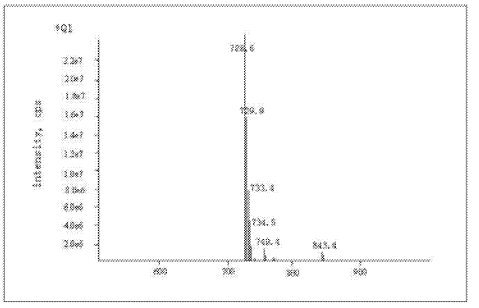

Figure 1. The mass spectrum (MS) of iPr-C[4]C-6 (sample A) for irradiated dose 10^4 Gy.

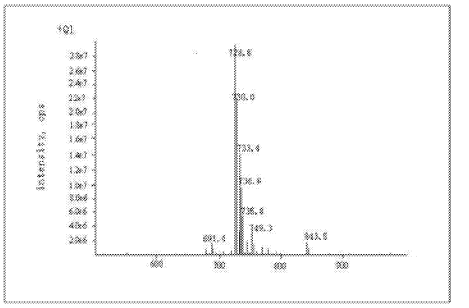

Figure 2. The MS of iPr-C[4]C-6 (sample A) for irradiated dose 10^6 Gy.

The MS results of the irradiated iPr-C[4]C-6 are showed in Figure 1. Some peaks with molecular weight 729, 734, 749, and 844 were found when the absorbed irradiation dose was 10^4 Gy for iPr-C[4]C-6. They may correspond to 711+18(NH_4^+), 711+23(Na^+), 711+39(K^+), and 711+133(Cs^+), respectively, because the molecular weight of

iPr-C[4]C-6 is 711. The $Na^+/K^+/Cs^+$ containing the iPr-C[4]C-6 samples came from the synthesis process. There were not any other peaks on the MS spectrum. The results showed that the iPr-C[4]C-6 was not decomposed remarkably at the absorbed irradiation dose 10^4 Gy. Some other molecular peaks occurred in Figure 2 for the irradiation dose of 10^6 Gy. The noticeable peak of them was 691. It means that some iPr-C[4]C-6 molecules were decomposed. This degradation product might be the molecule produced when the iPr-C[4]C-6 lost a 2-propyl radical:

$$M(C_{44}H_{54}O_8) - M(-C_3H_7) + M(Na^+) = 711-43+23 = 691$$

The broken bond position in the iPr-C[4]C-6 molecule was between –O- and $-CH(CH_3)_2$ and was not between phenyl and $-OCH(CH_3)_2$, because the bond between phenyl and $-OCH(CH_3)_2$ is stronger than that between–O- and $-CH(CH_3)_2$ for the reason of the stronger p-π conjugated bond.

The ESI-MS results of the irradiated sample B are shown in Figures 3 and 4 for irradiation doses of 10^4 Gy and 10^6 Gy, respectively. Besides the main peaks 729, 734, 749, and 844, there were some very small peaks for which the molecular weights were between 690 and 770 in Figure 3 for irradiation dose of 10^4 Gy. Comparing irradiated sample A and B, the sample B containing nitric acid decomposed more readily than that of sample A.

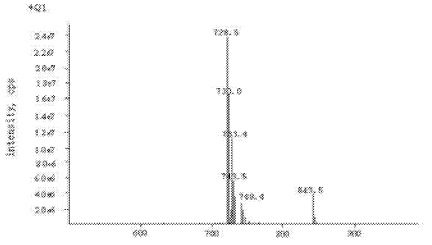

Figure 3. The MS of the sample B for irradiated dose 10^4 Gy.

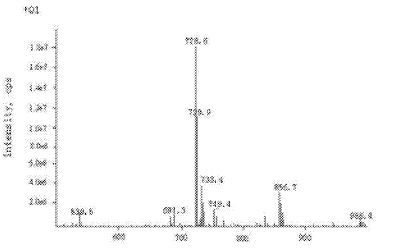

Figure 4. The MS of the sample B for irradiated dose 10^6 Gy.

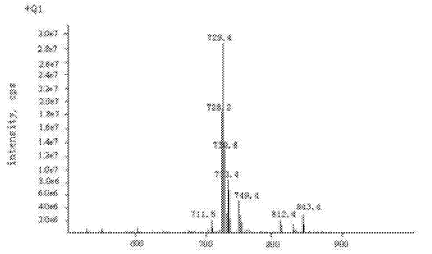

Figure 5. The MS of sample C for irradiated dose 10^4 Gy.

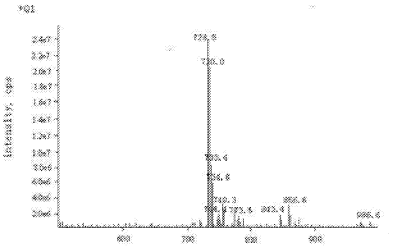

Figure 6. The MS of sample C for irradiated dose 10^6 Gy.

The ESI-MS results of the irradiated sample C are given in Figures 5 and 6 for irradiation doses of 10^4 Gy and 10^6 Gy, respectively. Besides the main peaks 729, 734, 749, and 844, more small peaks were found than that of sample B in Figure 5 for the irradiated dose 10^4 Gy. Much more minor peaks occurred besides the peak 812. The ESI-MS results of the sample C with irradiated dose of 10^6 Gy were shown in Figure 6.

Many more peaks occurred in Figure 6 than that in Figure 5 of sample B with the same irradiated dose of 10^6 Gy. Comparing the irradiated sample B and C, the sample C containing higher nitric acid was more readily decomposed than that of sample B. The above results indicated that the higher nitric acid concentration in the samples and the higher irradiated dose lead to higher radiolysis of the iPr-C[4]C-6 samples.

Information on organic functional groups is attained from IR spectra. The IR spectra of iPr-C[4]C-6 (sample A) with different irradiated doses are presented in Figure 7. The weaker absorbed peak occurred at 1582.80 cm^{-1} for the sample with irradiated dose of 10^5 Gy, and other weaker peaks occurred both at 654.24 and 1729.66 cm^{-1} when the irradiated dose was increased to 5 x 10^5 and 10^6 Gy. In addition, the intensity of these peaks increased with an increase of the irradiated dose. The IR spectra of the irradiated samples pre-equilibrated with 0.01 mol/L HNO_3 were not changed markedly until the irradiated dose of 10^6 Gy. The results are presented in Figure 8. But the IR spectrum for the irradiated samples pre-equilibrated by 3 mol/L HNO_3 was quite different; the peak at 1724 cm^{-1} appeared when the irradiated dose was above 10^4 Gy, and furthermore, the peaks were higher with the increasing irradiated dose. The new weaker peak at 1554 cm^{-1} appeared when the irradiated dose was higher than 10^5 Gy. The results are showed in Figure 9. These results agreed with the color changes in the above test.

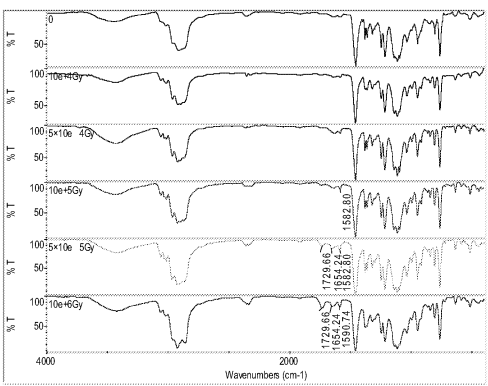

Figure 7. IR spectra of iPr-C[4]C-6 with different irradiated dose**.**

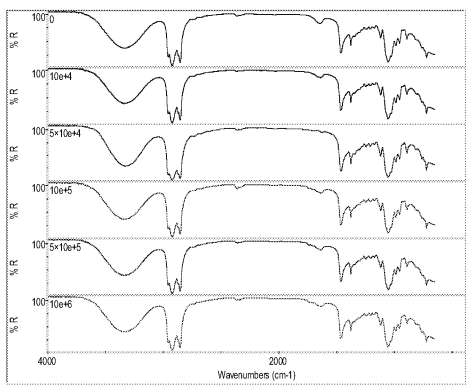

Figure 8. IR spectra of sample B with different irradiated dose.

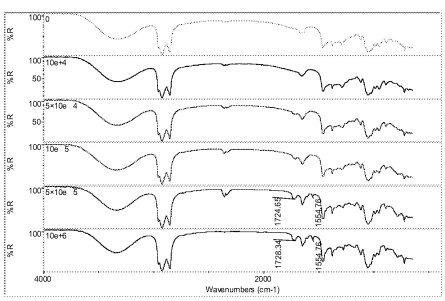

Figure 9. IR spectra of the sample C for different irradiated dose.

The 1870-1650 cm^{-1} peaks correspond to the stretching vibration zone of the C=O group and 1500~1690cm^{-1} to the stretching vibration zone of the group C=C according to the IR spectral data. According to the changes in the IR spectra and analysis from MS spectra above, the degradation route of iPr-C[4]C-6 might be deduced, and it is shown in Figure 10. The phenol was formed firstly after iPr-C[4]C-6 lost its propyl (-$CH(CH_3)_2$); then the phenol was turned into quinine at higher irradiated dose.

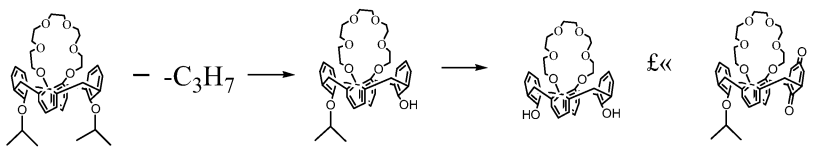

Figure 10. The degradation route of iPr-C[4]C-6 in the irradiated process.

CONCLUSIONS

Extraction of Cs decreased remarkably for iPr-C[4]C-6/*n*-octanol extractant when the irradiated dose was higher than 10^5 Gy. The ESI-MS spectrum showed that the molecular of iPr-C[4]C-6 lost easily one propyloxy (-$CH(CH_3)_2$) when irradiated dose was higher than 10^5 Gy. The IR analysis of iPr-C[4]C-6 showed that the C=O group peak occurred for higher irradiated dose. A conclusion could be deduced from the results that the iPr-C[4]C-6 first loses a propyl group (-$CH(CH_3)_2$) and then combines with a proton to form a phenol; at last, a quinone forms. But the extractant iPr-C[4]C-6 and iPr-C[4]C-6/*n*-octanol have good radiolytic stabilities when the irradiated dose is lower than 10^5 Gy. The extraction system of iPr-C[4]C-6/*n*-octanol is promising to use in separating cesium from high-level liquid waste.

REFERENCES

1. Z. Xiaowen, G. Jianxun, and W. Jianchen, "The Progress of Researching the Extraction of Cesium by Calixcrown from High Level Liquid Waste," *Chinese Atomic Energy Science and Technology*, **36**(3), 238-245(2002).
2. G. Jiancun, Z. Xiaowen, and W. Jianchen, "The Complexing Ability of Calixcrown to Cesium and its Application in Treating Waste Solution Containing Radioactive Cesium," *Chinese Organic Chemistry*, **22**(2), 115-122 (2002).
3. P. Thuery, M. Nierlich, and E. Lamare, "A Review of Structural Information from Crystallographic and Modeling Studies," *J. Inclusion Phenom. Marcrocyclic Chem.*, **36**(4), 375-408 (2000).
4. N. Simon, S. Eymard, and B. Tokurnois, "Cesium Extraction from Acidic High Level Liquid Waste with Functionalized Calixarenes," ATALANTE 2000, Avinon France, 2000; pp. 02-06, 24-26.
5. B. A. Moyer, P. V. Bonnesen, and L. H. Delmau, "Solvent Extraction of Tc and Cs from Alkaline Nitrate Wastes," ISEC'99, Barcelona, Spain, 1999; pp.1365-1370
6. P. V. Bonnesen, L. H. Delmau, and B. A. Moyer, "A Robust Alkaline-side CSEX Solvent Suitable for Removing Cesium from Savannah River High Level Waste," *Solvent Extr. Ion Exch.*, **18**(6), 1079-1107 (2000).
7. W. Feng, L. H. Yuan, and S. Y. Zheng, "The Effect of p-tert-butylcalix[n]arene on γ-radiation Degradation of Polypropylene," *Radiat. Phys. Chem.*, **57**, 425-429 (2000).
8. Z. Xiaowen, W. Jianchen, and S. Chongli, "Novel Extractant Calixcrown Used in High-level Liquid Waste (II). Extractive Capability of Bis(2-propyloxy)calix[4]crown-6 in Different Solvents," *Chinese Atomic Energy Science and Technology*, **38**(1), 21-24 (2004).

DRAMATIC IMPROVEMENTS IN CAUSTIC-SIDE SOLVENT EXTRACTION OF CESIUM THROUGH MORE EFFICIENT STRIPPING

Lætitia H. Delmau,[1] Eve Bazelaire,[1] Peter V. Bonnesen,[1] Nancy L. Engle,[1] Maryna G. Gorbunova,[1] Tamara J. Haverlock,[1] Bruce A. Moyer,[1] Dale D. Ensor,[2] Viola M. Meadors,[2] Benjamin W. Harmon,[2] Richard A. Bartsch,[3] Malgorzata A. Surowiec,[3] and Hui Zhou[3]

[1]Chemical Sciences Division, Oak Ridge National Laboratory, P. O. Box 2008, Oak Ridge, TN 37831, USA. [2]Department of Chemistry, Tennessee Technological University P.O. Box 5055, Cookeville, TN, 38505. [3]Department of Chemistry and Biochemistry Texas Tech University, Box 41061, Lubbock, TX 79409
Corresponding author email addresses: delmaulh@ornl.gov and moyerba@ornl.gov

ABSTRACT

Dramatic potential improvements to the chemistry of the Caustic-Side Solvent Extraction (CSSX) process are presented as related to enhancement of cesium stripping. The current process for removing cesium from the alkaline high-level waste (HLW) at the USDOE Savannah River Site employs acidic scrub and strip stages and shows remarkable extraction and selectivity properties for cesium. It was determined that cesium stripping can be greatly improved with caustic or near-neutral stages using sodium hydroxide and boric acid as scrub and strip solutions, respectively. Improvements can also be achieved by appending pH-sensitive functional groups to the calix[4]arene-crown-6 extractant. Addition of a proton-ionizable group to the calixarene frame leads to a dramatic "pH swing" of up to 6 orders of magnitude change in cesium distribution ratio.

INTRODUCTION

Oftentimes the key to improving the overall performance in a solvent-extraction process lies in finding improved stripping chemistry. Clearly, a better performing stripping section can be highly desirable in terms of obtaining a more concentrated, cleaner product in fewer stages, for example. Further motivation may be better compatibility with downstream processing and waste disposal, with obvious consequences to overall plant economics. A third category of benefits includes potential positive impacts on extraction. For example, more efficient stripping means that higher distribution ratios can be accommodated on extraction, alleviating the classical trade-off between achieving high distribution ratios on extraction and low distribution ratios on stripping. Thus, chemistry that permits lower stripping distribution ratios may allow the use of conditions permitting better performance on extraction.

The advent of calix[4]arene-crown-6 compounds [1] represents a breakthrough in cesium recovery from nuclear-reprocessing streams, either acidic or alkaline [2,3]. Our

work initially focused on recovery of Cs from reprocessing wastes made alkaline and stored for decades in underground storage tanks [3]. As a result of this research, the processing of so-called tank wastes by the Caustic-Side Solvent Extraction (CSSX) Process will begin in 2008 at the U.S. Department of Energy Savannah River Site. The key ingredients of the CSSX solvent include the cesium-selective extractant BOBCalixC6 at 7 mM and the modifier Cs-7SB at 0.75 M (Figure 1). In addition, the solvent includes the suppressor (see below) tri-*n*-octylamine (TOA) at 3 mM and the isoparaffinic diluent Isopar® L. The development of this solvent system, optimized for highly alkaline sodium nitrate media, has been summarized previously [3]. The full process flowsheet, designed for a Cs decontamination factor of >40,000 and a concentration factor of 15, employs a "nitrate swing" principle. The flowsheet entails 15 stages of extraction (O/A = 0.33), 2 stages of scrubbing with 50 mM HNO_3 (O/A = 5) to acid-condition the solvent and remove smaller alkali metals (Na and K), and 15 stages of stripping with 1 mM HNO_3 (O/A = 5). The suppressor, which is protonated on the acid side, is key to efficient stripping, suppressing the effects of trace lipophilic anions and ion-pair dissociation at exceedingly low organic-phase $CsNO_3$ concentrations [4].

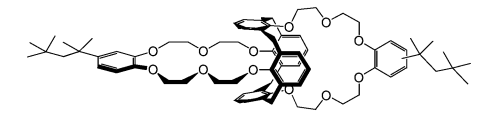

Calix[4]arene-bis(4-*tert*-octylbenzo-crown-6)
BOBCalixC6

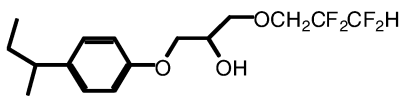

1-(2,2,3,3-Tetrafluoropropoxy)-3-(4-*sec*-butylphenoxy)-2-propanol
Cs-7SB

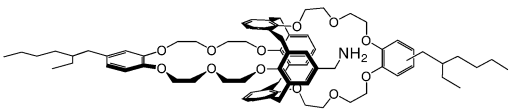

5-Aminomethylcalix[4]arene-bis[4-(2-ethylhexyl)benzo-crown-6]

AMBEHB

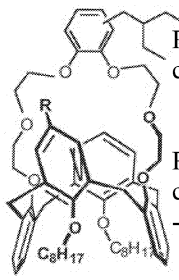

Proton-ionizable calix-crowns.
PICalix

R = anisole-N-sulfonyl carboxamide
-C(O)$NHSO_2$-$C_6H_4OCH_3$
PICalix-PhOMe

Figure 1. Calix-crowns and Cs-7SB modifier used in this study.

In this work, two general approaches were explored to improve Cs stripping, both based on avoiding nitrate swing, which is inherently limited by a first-power nitrate dependence. The first approach involves replacing nitrate with a more hydrophilic anion on stripping, aiming for use of boric acid as the stripping agent for compatibility with downstream borosilicate vitrification. The second approach involves pH swing, exploiting the huge pH variation between alkaline extraction at >1 M hydroxide and acid stripping at pH 1–2. Although excellent stripping improvement using the unchanged CSSX solvent was obtained, most dramatic results involved use of an alternative suppressor or novel pH-responsive calix-crown extractants (Figure 1). Whereas amino calix-crowns extract $CsNO_3$ ion pairs [5–7], the proton-ionizable calix-crowns function by cation exchange [8]. In both cases, contact with acidic strip solutions results in proton transfer from the aqueous phase to the calix-crown with release of extracted Cs^+ ion.

EXPERIMENTAL SECTION

All diluents were reagent grade and used as received. Deionized water was used to prepare all aqueous solutions. Boric acid was 99.5% from Sigma Ultra. All other salts were obtained as reagent grade and used as received. Isopar L diluent is a product of ExxonMobil Chemical Company, distributed by Chem Central. BOBCalixC6 was obtained from IBC Advanced Technologies, Inc. (97% purity), and the Cs-7SB modifier was obtained from Boulder Scientific Company (≥96% purity). LIX 79 was obtained from Cognis Corporation Mining Chemicals as a dilute solution in a kerosene-type diluent and precipitated as the chloride salt. pH-responsive calix-crowns were synthesized by methods reported elsewhere [5–8]. The ^{137}Cs tracer (Isotope Products Laboratories) activities in the samples were determined by standard gamma counting (Packard Cobra Quantum Model 5003 with a 3" NaI (Tl) crystal through-hole detector).

RESULTS AND DISCUSSION

Stripping Improvement Using Boric Acid as Strip Solution

It was found that boric acid performs as an excellent stripping agent, but the nitrate must first be scrubbed out of the solvent. The first column of Table 1 shows the typical performance of the CSSX solvent on sequential contacts of the same solvent with a simple alkaline HLW simulant and process scrub and strip solutions. Helpful, but modest, decrease of the Cs distribution ratio (D_{Cs}) on stripping occurs when 10 mM boric acid is substituted for the 1 mM HNO_3 CSSX process strip solution (column 3), keeping the same 50 mM HNO_3 scrub solution. When a scrub with 0.1 M NaOH is used (column 4), however, stripping improves over an order of magnitude. A further order-of-magnitude improvement may be obtained with a change of suppressor, whose importance to stripping is evident in column 5. As shown in column 6, the active guanidine extractant in LIX 79, a stronger base than TOA, is highly effective.

Stripping Improvement Using pH-Responsive Calix-Crown Extractants

Extraction experiments have demonstrated that the proton-ionizable calix-crowns [8] PICalix (where R is a sulfonyl carboxamide group) are not only strong extractants for cesium under alkaline conditions but also possess a striking switching-off effect under acidic conditions. A large variety of substituents on the sulfonyl carboxamide group was examined (Figure 1, R = -CH_3, -CF_3, -Ph, -C_6H_4-NO_2, -C_6H_4-OCH_3, -C_6H_4-^{t}Bu). The results reported here for the anisole group were characteristic of the overall behavior encountered in the family. Tests have involved measuring the cesium distribution ratios for each calixarene at different pH values under constant aqueous nitrate conditions. Extraction competition tests (Figure 2) were conducted with aqueous phases containing sodium at 1.5 M, potassium at 15 mM, and cesium at 0.15 mM, corresponding to a 1:100:10,000 ratio. A typical sigmoidal pH dependence of D_{Cs} is observed, where PICalix is predominantly in the form of the Na (60%) and K (5%) salts at pH 13. Thus, at high pH, the effective extraction reaction is effectively an exchange of sodium for more

Table 1. Effect of scrub solution composition and suppressor on stripping efficiency[a]

Step			D_{Cs}		
Scrub:	50 mM HNO_3	50 mM HNO_3	0.1 M NaOH	0.1 M NaOH	0.1 M NaOH
Strip:	1 mM HNO_3	10 mM H_3BO_3	10 mM H_3BO_3	10 mM H_3BO_3	10 mM H_3BO_3
Suppressor:	TOA 3 mM	TOA 3 mM	TOA 3 mM	No TOA	LIX 79 3 mM
Extraction	6.24	6.56	7.04	7.13	6.93
Scrub #1	1.02	1.09	1.12	1.78	1.32
Scrub #2	1.35	1.39	1.33	1.90	1.33
Strip #1	0.054	0.034	2.3×10^{-3}	0.055	$<2 \times 10^{-4}$ [c]
Strip #2	0.043	0.022	$<2 \times 10^{-3}$	0.213	$<2 \times 10^{-4}$ [c]
Strip #3	0.039	0.016	1.1×10^{-3} [b]	0.485[b]	NP[d]
Strip #4	0.044	0.012	NP[d]	NP[d]	NP[d]

[a]Aqueous phases: simple alkaline HLW simulant for the extraction step (3 M $NaNO_3$, 2 M NaOH, 50 mM KOH, 0.5 mM $CsNO_3$, and 0.5 µCi/mL $^{137}CsNO_3$). Organic phase: 7 mM BOBCalixC6 and 0.75 M Cs-7SB with or without LIX 79 or TOA in Isopar L. O/A = 1; T = 25 °C. [b]Spiked with ^{137}CsCl. [c]Limit of detection in this experiment. [d]NP denotes "Not Performed."

strongly favored cesium. Decreasing pH results in sharply dropping D_{Cs} and eventual levelling at low pH. It is hypothesized that the extraction reaction effectively becomes ion-pair extraction of cesium nitrate by the non-ionized calix-crown at sufficiently low pH. The selectivity of cesium over sodium at low pH could not be detected with precision, as the extraction of sodium was negligible. Results were more accurate at high pH, where all calixarenes exhibited a separation factor of 10,000 (Cs/Na) and of 200-1,000 (Cs/K). Under noncompetitive conditions (not shown), D_{Cs} swings as much as six orders of magnitude between alkaline and acidic conditions, and D_{Cs} values >200 are reached for all N-sulfonylcarboxamide derivatives.

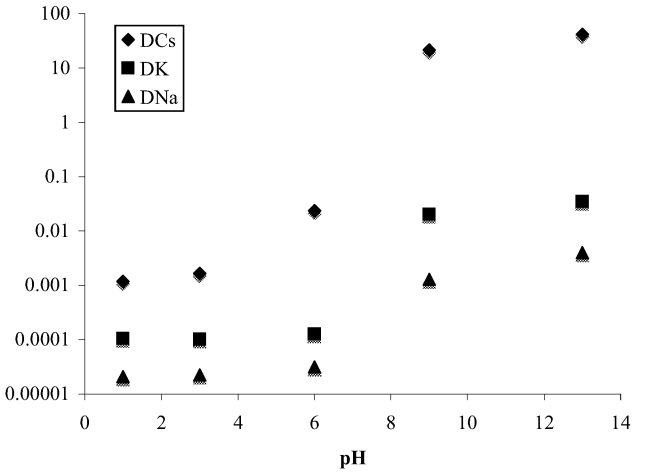

Figure 2. Cs, K, and Na distribution ratios as a function of pH. Aqueous phase: buffered pH solutions containing 0.15 mM $CsNO_3$, 15 mM KNO_3, and 1.5 M $NaNO_3$. Organic phase: 10 mM PICalix-PhOMe in toluene. O/A = 1; T = 25 °C.

As an alternative to calix-crowns bearing an acidic group, those bearing basic groups were hypothesized to extract the $CsNO_3$ ion pair in the same way as BOBCalixC6 but "switch off" upon protonation owing to Cs^+–H^+ charge-charge repulsion [5–7]. This idea proved valid in effect, though it was not nearly as impressive a switching vehicle as found for the acidic calix-crowns PICalix. As shown in Table 2, under alkaline conditions, the presence of the neutral amino group in AMBEHB does not change D_{Cs} significantly (Caustic extr.). However, under acidic aqueous conditions (constant 1 M NO_3^-), AMBEHB exhibits over a 100-fold decrease in D_{Cs}, in either forward (Acidic extr.) or reverse (1st strip) direction. The D_{Cs} value drops still further on a 2nd strip with 10 mM HNO_3, as does the BOBCalixC6 + TOA control, D_{Cs} for AMBEHB remaining a factor of 71 below the control. The BOBCalixC6 system without TOA does not strip.

When the diluent is changed to the more process-relevant *iso*-octane, the stripping enhancement of the amino group, while still present, is strongly diminished. Cesium distribution ratios were measured as a function of pH using 2.5 mM AMBEHB and 0.75 M Cs-7SB modifier in *iso*-octane. Aqueous phases were buffered solutions containing 10^{-4} M $CsNO_3$ and 1 M $NaNO_3$. The D_{Cs} values were 1.1 for pH > 10 and decreased to only 0.35 for pH 1–6. The weak switching factor (3.1) is interpreted as implying that the expected Cs^+–H^+ charge-charge repulsion is sharply attenuated owing to the effect of nitrate ion pairing in the organic phase and to strong solvation by the Cs-7SB modifier.

Table 2. Cesium distribution ratios for aminocalixarene and controls in nitrobenzene[a]

Calixarenes	D_{Cs} Caustic extr.	D_{Cs} Acidic extr.	D_{Cs} 1st Strip	D_{Cs} 2nd Strip	Switching factor[b]
BOBCalixC6	36.8	31.9	26.0	14.3	2.6
BOBCalixC6 + TOA	39.2	16.0	17.5	0.787	49.8
AMBEHB	27.2	0.229	0.246	0.011	2500

[a]Organic phases: 2.5 mM BOBCalixC6 or AMBEHB in nitrobenzene; when present, TOA added at 2.5 mM. Aqueous phases: (caustic extraction) 1 M $NaNO_3$, 0.05 M NaOH, 10^{-4} M $CsNO_3$; (acidic extraction) 0.95 M $NaNO_3$, 0.05 M HNO_3, 10^{-4} M $CsNO_3$; (1st strip) 0.95 M $NaNO_3$, 0.05 M HNO_3; (2nd strip) 0.01 M HNO_3. O/A = 1; T = 25 °C. [b] $D_{Cs,caustic\ extr}/D_{Cs,2nd\ strip}$.

CONCLUSIONS

These studies have demonstrated that dramatically improved cesium stripping may be obtained either by use of an inextractable anion, borate, on stripping or by use of pH-responsive calix-crown extractants. The option most ready for scale-up and deployment entails a caustic scrub and boric acid stripping, keeping the CSSX solvent unchanged. Boric acid offers the potential added advantage of excellent compatibility with downstream production of the borosilicate waste form. Replacing the TOA suppressor by the guanidine active component in LIX 79 further allows removal of detectable ^{137}Cs activity from the solvent in a single step, which could afford a reduction in the number of strip stages. In the longer term, adding pH-responsive functional groups to the calix-crown extractant introduces a pH-switching effect, where the use of proton ionizable calixarenes in particular appears especially promising. Introducing this class of calixarenes in solvents suitable for process conditions is our next challenge.

ACKNOWLEDGMENTS

This research was sponsored by the Environmental Management Science Program, Office of Science, U. S. Department of Energy, under contract number DE-AC05-00OR22725 with Oak Ridge National Laboratory, managed and operated by UT-Battelle, LLC.

REFERENCES

1. R. Ungaro, A. Casnati, F. Ugozzoli, A. Pochini, J.-F. Dozol, C. Hill, and H. Rouquette, "1,3-Dialkoxycalix[4]arenecrowns-6 in 1,3-Alternate Conformation: Cesium-Selective Ligands that Exploit Cation-Arene Interactions," *Angew. Chem., Int. Ed. Engl.*, **33**, 1506–1509 (1994).
2. J.-F. Dozol, N. Simon, V. Lamare, H. Rouquette, S. Eymard, B. Tournois, D. De Marc, and R. M. Macias, "A Solution for Cesium Removal from High Salinity Acidic or Alkaline Liquid Waste: The Crown Calix[4]arenes," *Sep. Sci. Technol.* **34**, 877–909 (1999).
3. B. A. Moyer, J. F. Birdwell, Jr., P. V. Bonnesen, and L. H. Delmau, "Use of Macrocycles in Nuclear-Waste Cleanup: A Real-World Application of a Calixcrown in Technology for the Separation of Cesium," In Macrocyclic Chemistry—Current Trends and Future, K. Gloe, Ed., Springer, Dordrecht, 2005; pp 383–405).
4. L. H. Delmau, P. V. Bonnesen, and B. A. Moyer, "A Solution to Stripping Problems Caused by Organophilic Anion Impurities in Crown-Ether Based Solvent Extraction Systems: A Case Study of Cesium Removal from Radioactive Wastes," *Hydrometallurgy*, **72**(1,2), 9–19 (2004).
5. M. G. Gorbunova, P. V. Bonnesen, N. L. Engle, E. Bazelaire, L. H. Delmau, and B. A. Moyer, "New Amino-Functionalized 1,3-Alternate Calix[4]arene Bis- and Mono-(benzo-crown-6 ethers) for pH-Switched Cesium Nitrate Extraction," *Tetrahedron Lett.*, **44**, 5397-5401 (2003).
6. E. Bazelaire, M. G. Gorbunova, P. V. Bonnesen, B. A. Moyer, and L. H. Delmau, "pH-Switchable Cesium nitrate Extraction with Calix[4]arene Mono and Bis(benzo-crown-6) Ethers Bearing Amino Functionalities," *Solvent Extr. Ion Exch.*, **22**, 637-661 (2004).
7. B. W. Harmon, D. D. Ensor, L. H. Delmau, and B. A. Moyer, "Extraction of Cesium by a Calix[4]arene-crown-6 Ether Bearing a Pendant Amine Group," *Solvent Extr. Ion Exch.*, **25**(3), 373–388 (2007).
8. V. S. Talanov, G. G. Talanova, M. G. Gorbunova. and R. A. Bartsch, "Novel Caesium-Selective, 1,3-Alternate Calix[4]arene-bis(crown- 6-ethers) with Proton-Ionizable Groups for Enhanced Extraction Efficiency," *J. Chem. Soc.-Perkin Trans. 2*, 209-215 (2002).

AN OVERVIEW OF SPENT-FUEL PROCESSING IN THE GLOBAL NUCLEAR-ENERGY PARTNERSHIP

James J. Laidler

Applied Science and Technology Directorate, Argonne National Laboratory
9700 South Cass Avenue, Argonne, Illinois 60439
Corresponding author email address: laidler@anl.gov

ABSTRACT

Spent nuclear fuel is being generated at a prodigious rate in the U.S. and in other countries with robust nuclear-power-generation infrastructures, and the annual rate of production is likely to triple by 2050. The U.S. is engaged in the development of commercial light-water-reactor spent-fuel-treatment processes that are intended to meet certain rigorous criteria for separations efficiency, waste management benefits, and economy of industrial-scale operations. Aqueous solvent-extraction processes are the technology of choice, and a variety of process options have been designed and tested for technical feasibility. In general, the processes involve substantial partitioning of the constituents of spent nuclear fuel, so that effective use can be made of the recovered unburned uranium and other fissile isotopes that can be recycled as fuel for contemporary or advanced reactors. Those constituents that are destined for disposal as waste are also separated in order that they can be placed into durable waste forms that are expressly tailored for a particular disposition pathway. The U.S. is also working with international partners as part of the Global Nuclear Energy Partnership (GNEP) to develop a consistent worldwide approach to the treatment of spent fuel and the disposition of wastes arising from such processing.

INTRODUCTION

The Global Nuclear Energy Partnership (GNEP) was unveiled by the President of the United States in March 2006 as a major initiative to deal with the issue of worldwide proliferation of nuclear-weapons technology. A principal precept of this partnership is that countries without an extensive nuclear-energy and nuclear-fuel-cycle infrastructure can enjoy the societal benefits of nuclear-generated electricity, provided that they agree to forego the enrichment of uranium and the reprocessing of spent nuclear fuel. In turn, these "user" countries would be guaranteed a supply of fresh nuclear fuel at competitive cost under a leasing arrangement in which they would return spent nuclear fuel to the group of "supplier" countries having extensive nuclear systems in place (presently, the United States, Russia, France, the United Kingdom, China, and Japan). The supplier countries would process the spent fuel, recover the actinide elements for internal recycle,

and dispose of the processing wastes so that the user nations are spared the additional costs of high-level waste repositories. In the case of GNEP supplier countries that have restrictions against disposal of foreign high-level wastes, other member countries may accept the waste for disposal; this makes it imperative that the wastes to be disposed are of small volume and low hazardous-materials content, to minimize the impact on the accepting country. The GNEP initiative has the further objective of facilitating the development of a sustainable nuclear power system for the U.S. and other countries, enabling them to achieve the level of growth in electricity generation projected for the balance of the 21st century without significant generation of greenhouse gases.

With the increase in nuclear-electricity generation comes an increase in worldwide production of spent nuclear fuel. In 2008, the U.S. generates about 2,100 metric tons of spent fuel annually from commercial nuclear-power plants. If the commercial nuclear fleet grows to 300 GWe by 2050 as predicted, that number will increase to over 6,000 metric tons of spent fuel per year. Total world production of spent nuclear fuel could reach 15,000 metric tons per year by 2050. Clearly, such quantities of spent fuel would severely stress national capabilities for direct disposal of the material. The legislated capacity of the U.S. Yucca Mountain geologic repository is 63,000 metric tons, and the U.S. spent fuel inventory will exceed this limit before 2015. Furthermore, disposal of spent nuclear fuel is considered by many to be a waste of a valuable energy resource, particularly when there are questions whether the uranium supply will be able to meet world energy needs throughout the balance of the 21st century. These considerations have led to renewed interest in nuclear-fuel recycling and the development of advanced technologies for application at industrial scale in the future. A typical light-water-reactor fuel assembly is shown in Figure 1. Indicated on this figure are the compositions of the fuel before and after service in a reactor.

THE ADVANCED FUEL CYCLE INITIATIVE

Technology development in the U.S. program is carried out under the scope of the Advanced Fuel Cycle Initiative (AFCI). A major element of the AFCI is the development of spent-fuel processing and waste-management technologies, collectively known as the Separations Campaign. At an early stage of program development, it was decided to emphasize aqueous solvent-extraction processing for the treatment of light-water-reactor (LWR) spent fuel. Two basic requirements were placed on the design of processing methods: (1) no production of a separated plutonium stream, to reduce the risk of the widespread availability of fissile materials and the proliferation of nuclear weapons; and (2) tangible benefits to repository disposal of high-level wastes, in the form of increased repository capacity, so that a single high-level waste repository would suffice for the U.S. until the end of the 21st century, even with significant increases in the generation of electric power by nuclear plants. The first requirement imposed the need to develop a co-extraction process, either of uranium with selected transuranics or a group extraction of all transuranic elements.

Aqueous solvent-extraction processing has been selected as the reference means for treatment of spent fuel discharged from light-water reactors. This choice was based in part on the technological maturity of these processes, but also in view of the ability to

tailor a process to meet special needs. The GNEP program has a number of constraints that are placed on the system for fuel cycle closure that will be deployed in the future. These include the following.

Emphasis on Recycle

Fissionable elements should be recovered from LWR spent fuel at a high level of efficiency, so that these materials can be recycled for future power generation; the recovered materials should also be free of contaminants that would impact recycle-fuel performance.

Proliferation Risk Reduction

There shall be no separation of a stream of pure plutonium in any spent fuel treatment process to be deployed in the United States. Eventually, this constraint may be accepted in other GNEP fuel-cycle countries.

Resource Preservation

Excess uranium not required in the near term for use in recycle fuel must be recovered at high efficiency to minimize the volume and mass of material that is sent as waste to a geologic repository. Recovery of uranium must be accomplished at a high level of purity as well, so that it can be conveniently stored for future use in advanced reactors.

Repository Benefits

Radionuclides with high rates of decay-heat generation, both short-lived and long-lived, must be recovered and kept out of the mainstream high-level waste destined for repository disposal, in order to deal with heat-management issues that presently restrict the capacity of the Yucca Mountain geologic repository. By doing so, the effective capacity of the repository can be greatly increased. This requires the removal of at least 99% of the cesium, strontium, plutonium, americium, and curium present in the spent fuel.

Dose Reduction

Certain radionuclides are likely to be primary contributors to the long-term radiation dose received by future inhabitants of the area near the Yucca Mountain repository site, and it is our obligation to minimize the potential for such exposure. The labile and mobile long-lived fission products ^{99}Tc and ^{129}I are the main dose contributors in the first 50,000 years of repository storage of spent fuel or its constituents, while ^{237}Np dominates in the longer term. The source term for these radionuclides can be reduced significantly by designing processes for their efficient removal and sequestration or destruction. Of course, it must be recognized that a 20-fold increase in effective

repository capacity is negated unless the long-term retention of the important radionuclides is increased to well more than 20-fold. For this reason, target recovery efficiencies for technetium, iodine, and neptunium have been set at between 99 and 99.5%. In the case of ^{237}Np, that means the removal also of its precursor isotopes, including ^{241}Am.

Planning for the Future

Because it is currently unknown what the characteristics of the U.S. nuclear energy system will be in the future, it is necessary to provide contingency planning for events in which the level of spent-nuclear-fuel generation (as well as the receipt of take-back spent fuel from client countries) will increase significantly. Therefore, one of the programmatic goals is a substantial reduction (perhaps 10-fold or more) in the volume of high-level waste produced. This has the added benefit of a reduction in the number of complex and costly repository containers that are required.

Economics

Finally, it is important to recognize that the deployment of LWR spent-fuel reprocessing plants in the U.S. will be industry-driven, and thus it is imperative that the system be designed to minimize the impact of reprocessing on the busbar cost of electricity. While increasing profit margins will be the purview of industry, it is necessary to design the basic system so that it meets the general goals of reducing added costs to less than 10% of the current once-through fuel-cycle busbar costs (on the order of $0.04 per kilowatt-hour).

STAGE OF DEVELOPMENT

The development of aqueous solvent-extraction processes for GNEP applications benefits greatly from past experience in defense programs, where the PUREX process was extraordinarily successful (after many years of optimization) in producing very pure plutonium in great quantities. Since the introduction of PUREX in the early 1950s, much has been learned about aqueous solvent-extraction process design and operation. Much of that knowledge is transferable to modern process design. Unfortunately, much of the U.S. facility infrastructure for pilot-scale hot testing of solvent-extraction processes has decayed over the past twenty years or so, and the U.S. GNEP program has been reduced to laboratory-scale testing. Even so, process design and laboratory-scale tests over the past six years have instilled a high level of confidence in the separations chemistry of the somewhat more complex processes that are envisioned for future use (see Figure 2 and Table 1).

The future characteristics of the U.S. nuclear-energy system are relatively indeterminate at this time. Because current-generation LWRs are performing so well, it is likely that they will continue to be ordered, perhaps in the Generation III manifestation, as replacement or incremental power sources for many years to come. Eventually, uranium resource availability will mandate the introduction of fast breeder reactors,

Typical PWR Fuel Assembly:
Length: 4.1 meters
Weight: 636 kilograms
No. of fuel rods: 264
Active fuel length: 3.9 meters
Heavy metal content: 425 kilograms
Fuel composition: UO_2 (482 kilograms)
Hardware: 154 kilograms

Composition after Irradiation:
Uranium: 398 kilograms (93.6%)
Plutonium: 3.9 kilograms (0.9%)
Neptunium: 0.5 kilogram (0.1%)
Americium: 0.5 kilogram (0.1%)
Curium: 0.07 kilogram (0.016%)
Fission Products: 22.5 kilograms (5.3%)
[50,000 MWd/t burnup]
Hardware: 154 kilograms

Figure 1. Typical makeup of a pressurized water reactor fuel assembly before service and after discharge from the reactor. Nominal ^{235}U content before reactor insertion is between 3.5 and 4%. The fuel is discharged when its nuclear reactivity is degraded by the buildup of fission products that act as neutron absorbers. Upon discharge, the ^{235}U content has decreased to less than 1% as a result of fissioning of this isotope. Photos courtesy of AREVA.

which will be able to support a sustainable nuclear-energy system for centuries. This transition to fast-spectrum reactors will occur over a long period, and development program planning must provide for the smooth and unremarkable evolution from one system to the next. To facilitate this evolution, the development program in the U.S. has been based on a suite of solvent-extraction processes that can be deployed when needed and as national policies dictate. An example of the possible variations in process design, all given the generic designation "UREX+", is shown in Table 1. It will be noted that all of the process variants have in common the removal of the bulk of the LWR spent-fuel uranium content, followed by the removal of the long-lived fission products and the short-lived heat-generating fission products. Because the licensing and regulatory regime for U.S. reprocessing plants is not yet established, measures are being developed for the removal and sequestration of tritium, krypton, and ^{14}C as CO_2, in the event that such requirements are imposed in the future.

The potential applications of these process variants can be easily visualized. For example, the UREX+1a process, with its group extraction of transuranic elements, is intended for the production of fast-reactor recycle fuel; the fast-spectrum reactor is more tolerant of minor actinides with low fission cross-sections. Because the TRU-bearing fuel would require remote fabrication technologies not available today at competitive costs, the UREX+3a and UREX+3b variants were designed to preclude the need for remote fabrication by limiting the fast-reactor recycle fuel to the comparatively benign and glovebox-fabricable plutonium and neptunium, with UREX+3b adding the co-extraction of uranium with plutonium and neptunium to reduce proliferation concerns. These

processes separately extract the minor actinides for production of transmutation targets or for separate repository disposal in waste forms with high durability. The UREX+3c process, as illustrated in Figure 2, is intended for thermal-reactor recycle of a mixed-oxide fuel that is currently fabricated in gloveboxes at industrial scale. The UREX+4 variants go a step further, with the separation of curium from the other minor actinides (in a process yet to be demonstrated experimentally).

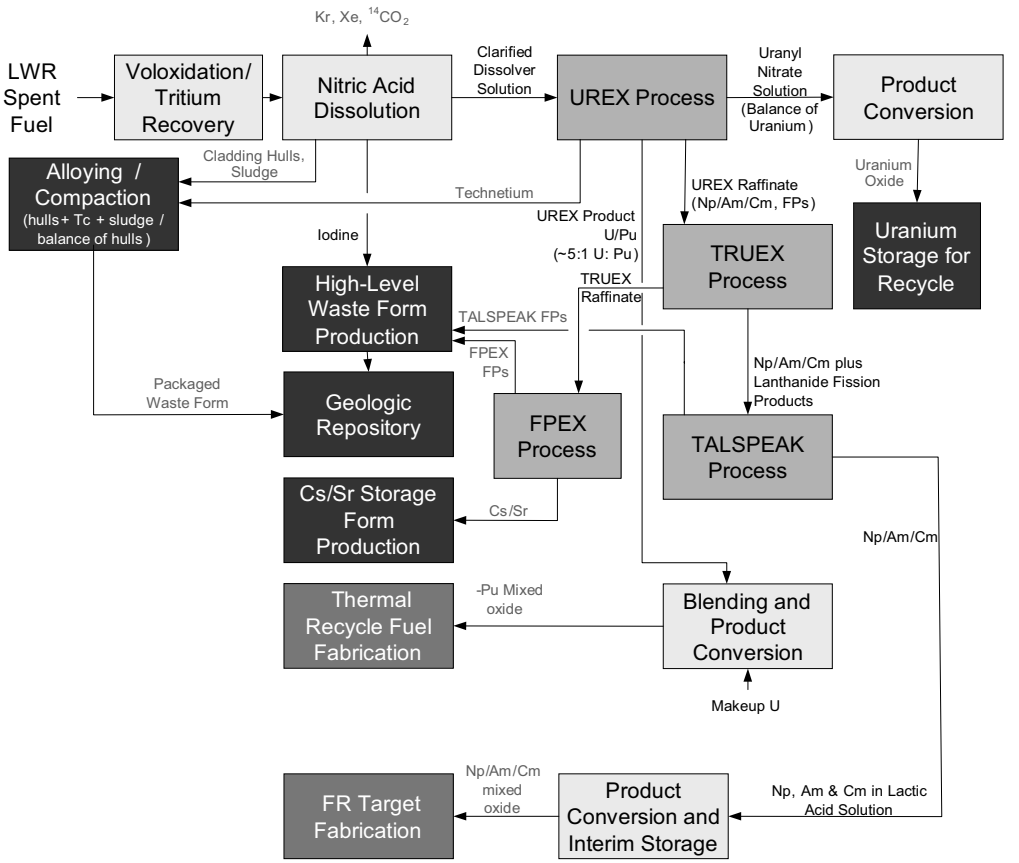

Figure 2. The UREX+3c process. It is designed for thermal recycle of mixed U-Pu oxide fuel. Uranium and plutonium are co-extracted at a composition that is considered to be of little use as a weapons material (20% Pu or less). Shown in red are the various product and waste streams for this process. The minor actinide elements can be directed to fast-reactor (FR) target fabrication for subsequent transmutation or stored indefinitely in an appropriate facility.

Table 1. Partial listing of the UREX+ process variations, illustrating the potential applications of each variant.

Process	1st Product	2nd Product	3rd Product	4th Product	5th Product	6th Product	7th Product
UREX+1a	U (highly purified)	Tc, I (LLFPs, dose issue)	Cs,Sr (short-term heat mgmt.)	FPs (including lanthanides)	TRU (group extraction)		
UREX+2	U (highly purified)	Tc, I (LLFPs, dose issue)	Cs,Sr (short-term heat mgmt.)	Other FPs	Pu+Np (for FR recycle fuel)	Am+Cm+Ln (temp. storage)	
UREX+3a	U (highly purified)	Tc, I (LLFPs, dose issue)	Cs,Sr (short-term heat mgmt.)	FPs (including lanthanides)	Pu+Np (for FR recycle fuel)	Am+Cm (heterogeneous targets)	
UREX+3b	U (highly purified)	Tc, I (LLFPs, dose issue)	Cs,Sr (short-term heat mgmt.)	FPs (including lanthanides)	U+Pu+Np (for FR recycle fuel)	Am+Cm (heterogeneous targets)	
UREX+3c	U (highly purified)	Tc, I (LLFPs, dose issue)	Cs,Sr (short-term heat mgmt.)	FPs (including lanthanides)	U+Pu (for thermal recycle fuel)	Am+Np+Cm (heterogeneous targets)	
UREX+4a	U (highly purified)	Tc, I (LLFPs, dose issue)	Cs,Sr (short-term heat mgmt.)	FPs (including lanthanides)	U+Pu+Np (for FR recycle fuel)	Am (heterogeneous targets)	Cm (storage)
UREX+4b	U (highly purified)	Tc, I (LLFPs, dose issue)	Cs,Sr (short-term heat mgmt.)	FPs (including lanthanides)	U+Pu (for thermal recycle fuel)	Am+Np (heterogeneous targets)	Cm (storage)

CONCLUSIONS

Laboratory-scale tests of these processes, through the UREX+3 variants, have been successfully completed with actual LWR spent fuel. Design criteria have been met and exceeded, and the technologists await a decision on process selection and future larger-scale hot testing or commercial-scale deployment. If a conservative near-term decision is made to select commercially-proven processes in the first third-generation U.S. spent-fuel processing plant, the development program will persist because it is highly probable that several more industrial plants will be built in the U.S. throughout this century, in order to keep pace with the expected growth in nuclear-power generation of electricity. These follow-on plants will of necessity involve the introduction of innovative, but proven, solvent-extraction process technologies.

DEVELOPMENT AND APPLICATION OF CENTRIFUGAL CONTACTORS IN CHINA

Pijia Cao and Wuhua Duan

Institute of Nuclear and New Energy Technology, Tsinghua University, Beijing 102201, China. Corresponding author email address: dwh203@mail.tsinghua.edu.cn

ABSTRACT

Compared with mixer-settlers and extraction columns, centrifugal contactors have some advantages. Since the late 1970s, a series of centrifugal contactors with rotor diameters of 10 to 550 mm have been developed and applied in some industrial fields in China. In this paper, both new improvements and applications of centrifugal contactors in China are reviewed.

INTRODUCTION

Compared with mixer-settlers and extraction columns, centrifugal contactors (CCs) have some advantages such as low hold-up volume, short residence time, good mixing, good phase separation, high mass-transfer efficiency, compact size, rapid to reach steady-state, and rapid start-up and shut-down. Especially, they can contribute to economic advantages, produce less solvent degradation, and are easy to manage with regard to criticality safety. Therefore, they are favored for reprocessing of the spent nuclear fuel and partitioning of high-level waste [1,2].

The primary CC, which was the paddle type, was successfully developed and operated for many years at Savannah River Plant (SRL). In the late 1960s, the paddle-type CC was modified to the annular type at Argonne National Laboratory (ANL). The ANL CC was reliable and easy to operate and maintain [3]. In particular, it was applied in the hot tests of the TRUEX process at ANL [1]. Recently, USA, Russia, France, Germany, U.K, India, and Japan achieved new progress on developments and applications of CCs in the nuclear industry [4-9].

Since the late 1970s, a series of CCs with rotor diameters of 10 to 550 mm that range in throughput from 0.5 to 40000 L/h have been successfully developed and applied in some industrial fields in China [10-18]. In this paper, new developments of CCs in China are introduced, and new applications of CCs in some fields including hydrometallurgy, wastewater treatment, biotechnology, and the pharmaceutical industry, especially partitioning of high-level waste in China, are reviewed.

DEVELOPMENT OF CENTRIFUGAL CONTACTORS IN CHINA

Specifications of CCs developed in China at the normal conditions are presented in Table 1 [10-20]. The main material of these CCs is stainless steel (ST) or titanium (Ti) or glass fibre-reinforced plastic (GFRP). The GFRP CCs have high corrosion resistance to HCl and H_2SO_4, high strength- and stiffness-to-weight ratios, and low cost, and therefore they have a good applied prospect in the hydrometallurgical field [20].

Table 1. Specifications of centrifugal contactors in China

Type	ϕ 10 mm	ϕ 20 mm	ϕ 50 mm	ϕ 70 mm	ϕ 120 mm	ϕ 200 mm	ϕ 230 mm	ϕ 550 mm
Rotor Diameter (mm)	10	20	50	70	120	200	230	550
Nominal Throughput (L/h)	0.5	5	30	300	1500	2000	6000	40000
Main Material	ST or Ti	ST or Ti	ST	ST or GFRP	GFRP	GFRP	ST or Ti	ST

In particular, some types of CCs, including ϕ 10, ϕ 20, ϕ 50, and ϕ 70 mm, have been developed since the early 1980s for reprocessing spent nuclear fuel and partitioning high-level waste at the Institute of Nuclear and New Energy Technology (INET), Tsinghua University, China. Structures of both ϕ 10 mm and ϕ 20 mm CCs are similar, except that diameter of their rotors is different, thereby leading to differences in their performance [16,19]. Structures of both ϕ 50 mm and ϕ 70 mm CCs are also similar [17,18].

16-Stage ϕ10 mm CCs are shown in Figure 1. In order to meet the requirements of the TRPO process tests for laboratory scale, some advanced designs have been achieved [19]. The ϕ10 mm CC was divided into a housing part and a rotor part in order to operate it easily in hot cells. The two parts were mounted separately and joined by a cylindrical joint with clearance fit. Every part was inserted on the other one without screws and nuts. To further reduce the liquid holdup, a multi-stage group housing was developed, containing multiple stages in a set with no interstage line between any two stages. A remote-sampling system was built in order to easily get samples from many contactors by a manipulator in the hot TRPO process tests, and a rotor-speed acquisition and monitoring system was developed so that CCs could be remotely controlled.

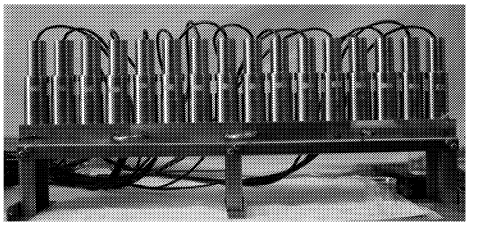

Figure 1. 16-Stage ϕ10 mm centrifugal contactors.

The ϕ70 mm centrifugal contactor was developed for semi-industry scale tests of the TRPO process in 1996. It is shown in Figure 2 [18] and consists of three modules: the

motor module, the rotor module, and the housing module. Modules were installed by simply inserting each other on the other one and were fitted by mating cone without screws and nuts or pins. The contactor could be assembled and disassembled fast by simply moving modules up and down. The magnetic coupling was also used in the contactor to provide the torque to rotate the rotor without losing any speed. All these designs made remote maintenance easy and reliable. In addition, two kinds of overflow line were designed in the housing module; therefore, if a contactor ceased to work due to a motor failure or due to other abnormal accidents, the heavy phase and the light phase could separate by gravity in the housing of the stopped contactor and overflow in the opposite direction through their own overflow line into adjacent stages respectively. In other words, when a multi-stage cascade was operated, even though one stage or non-adjacent stages ceased to work, the cascade could continue to operate.

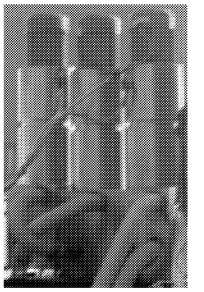

Figure 2. Three-stage ϕ70 mm centrifugal contactors.

APPLICATION OF CENTRIFUGAL CONTACTORS IN CHINA

Hydrometallurgy

Separation and purification of Y by solvent extraction from RE mixture is widely known to be difficult due to their similar chemical properties. Zhou et al. developed an extraction flowsheet for producing high-purity Y with HA (naphthenic acid) and HEHEHP (2-ethylhexhyl phosphonic acid mono-2-ethylhexyl ester) as extractants [14]. The bench-scale test and the pilot-plant test of the flowsheet were performed with ϕ20 mm ST and ϕ120 mm GFRP CCs, respectively. In these tests, Y_2O_3 with 99.99% of purity was obtained, and the total recovery of Y was about 95%.

Zhou et al. also developed a non-equilibrium extraction process for separation of In and Fe with HDEHP (di(2-ethylhexyl) phosphoric acid) as extractant and CCs, exploiting the extraction kinetics difference between the metals [10]. Two-stage ϕ230 mm Ti CCs were applied in the industry-scale test, and In can be well separated from Fe. Bao et al. studied separation of Ni and Co with N235 tertiary amine-isooctanol-kerosene as solvent and carried out a semi-industry-scale test with 30-stage ϕ70 mm GFRP CCs [21]. In the test, recoveries of both Ni and Co were higher than 99.9% and 97%, respectively, and Co/Ni mass ratio was higher than 5000. Chen et al. studied extraction of germanium from zinc sulphate solution with 15-stage ϕ200 mm GFRP CCs. In the extraction process, 7815 (hydroxamic acid)-additive-kerosene was used as the organic phase, and NaOH was used as the back-extracting agent. The recovery of Ge was about 80% [22].

Wastewater Treatment

Solvent extraction is an effective way to treat and recover the phenolic compounds from the high content phenolic wastewater at present. Xu et al. studied

extraction of phenol from wastewater with ϕ20 mm CCs and QH-1 extractant (a mixed amine extractant containing R_3N and $(R_3NH)_2SO_4$) [13]. The experimental results showed the mass-transfer efficiency of the single-stage CC was more than 95%, and the extraction rate of the three-stage cascade was more than 99% under experimental conditions. When 15% NaOH was used for stripping of phenol in QH-1, the stripping efficiency of the three-stage cascade was also more than 99% under the experimental conditions.

Gong et al. developed a process for treating poor gold-bearing liquor from a gold-metallurgy plant to recover copper and zinc with ϕ70 mm GFRP CCs [23]. A 20% N_{235} (tertiary amine, R_3N)/20% ethylhexanol/60% kerosene system was used to extract copper cyanide and zinc cyanide, and alkaline solution was used to strip the loaded organic phase in this process. Results showed higher than 99.0% of copper, zinc, and cyanide was extracted from the poor gold-bearing liquor respectively.

Biotechnology and Pharmaceutical Industry

Caffeine in industrial mother liquor was extracted with a static mixer by chloroform for routine recovery in the production of caffeine. High loss of chloroform and only about 90% caffeine extraction are the chief drawbacks of the process. Duan et al. developed an extraction process for caffeine with 4-stage ϕ230 mm CCs [11]. Moreover, this technique has been applied to the industrial production of caffeine. When the rotor speed was 1800 rpm, the mother-liquor flow was 2000 L/h, and the chloroform flow was 1000 L/h, and the extraction of caffeine was more than 99%.

Hydrocortisone is an important hormone drug. In the pharmaceutical industry, a microbiological fermentation process is used to produce hydrocortisone, and then the solvent-extraction method is used to extract hydrocortisone from the fermentation liquor with butyl acetate. At present, the crosscurrent extraction process is used to extract hydrocortisone from the fermentation liquor in many pharmaceutical plants of China. High consumption of the butyl acetate extractant (the total phase ratio V_O/V_A is 0.7) and low recovery of hydrocortisone (<90%) are the main drawbacks. Zhou et al. developed a continuous countercurrent extraction process for the recovery of hydrocortisone from the fermentation liquor with 8-stage ϕ230 mm CCs [12]. In the plant tests, the rotor speed was 2000 rpm, the fermentation liquor flow was 2000 L/h, the butyl acetate flow was 1000 L/h, and the percent recovery of hydrocortisone was about 96.5~98%.

Partitioning of High-Level Waste

A cold test of the TRPO (a mixed trialkylphosphine oxide, alkyl is C_6-C_8) process for actinides removal from simulated high-level waste was performed with 34-stage ϕ10 mm CCs at INET [15]. Results of the cold test showed that 99.9% of Am, RE, Pu, and U were removed from the simulated high-level waste with 12 extraction stages and 4 scrub stages, and the cross contamination between them was small. A hot test of the TRPO process was completed with 50-stage ϕ10 mm CCs in a hot cell. The flowsheet of the hot test included two parts. One was to remove ^{90}Sr and ^{137}Cs with crown ether, which included 10 extraction stages, 2 scrubbing stages, and 4 stripping stages. The other

was to remove α nuclides (including U, Np, Pu, and Am) with TRPO, which was similar to the cold test. The whole hot test was operated for 6 h. It was shown that 99.85% of Am, 93.4% of Np, 99.86% of Pu, 99.99% of U, and 99.2% of ^{99}Tc were removed with TRPO from the genuine high-level waste, namely 99.83% of the total α nuclide was removed, and 99.96% of ^{90}Sr was removed with crown ether from the genuine high-level waste. Moreover, the cross contamination between them was also small. Meanwhile, the whole system ran smoothly during the hot test, and the advanced designs were helpful for the hot test. Currently, ϕ70 mm CCs are being applied in cold industrial-scale testing of the TRPO process.

Ye et al. also studied the partitioning of actinides from simulated high-level waste using DHDECMP (a mixture of dihexyl-N,N-diethylcarbamoylmethyl-phosphonate) and TBP in kerosene and 14-stage ϕ10 mm CCs (6 stages for extraction, 2 stages for scrubbing, and 6 stages for stripping) [24]. The results showed that the removal efficiency of actinides is greater than 99.9%. Based on this study, a conceptual flowsheet for the removal of actinides from high-level waste was proposed.

CONCLUSION

Centrifugal contactors are efficient solvent-extraction contactors. Since the late 1970s, a series of centrifugal contactors have been successfully developed and applied in some industrial fields in China, and satisfactory results have been obtained.

REFERENCES

1. R. A. Leonard, D. B. Chamberlain, and C. Conner, "Centrifugal Contactors for Laboratory-scale Solvent Extraction Tests," *Sep. Sci. Technol.,* **32**(1-4), 193-210 (1997).
2. R. J. Taylor, I. May, and I. S. Denniss, "The Development of Chemical Separation Technology for an Advanced PUREX Process," RECOD'98, Nice Acroplic, France, Oct. 25-28, 1998; pp. 417-424.
3. R. A. Leonard, G. J. Bernstein, A. A. Ziegler, and R. H. Pelto, "Annular Centrifugal Contactor for Solvent Extraction," *Sep. Sci. Technol.,* **15**(4), 925-943 (1980).
4. R. S. Herbst, J. D. Law, T. A. Todd, V. N. Romanovskiy, I. V. Smirnov, V. A. Babain, V. N. Esimantovskiy, and B. N. Zaitsev, "Development of the Universal Extraction (UNEX) Process for the Simultaneous Recovery of Cs, Sr, and Actinides from Acidic Radioactive Wastes," *Sep. Sci. Technol.,* **38**(12&13), 2685-2708 (2003).
5. G. I. Kuznetsov, A. A. Pushkov, and A. V. Kosogorov, "Industrial Application of Centrek Centrifugal Extractors," Proceedings of ISEC 2002, Cape Town, South African, Mar. 17-21, 2002; pp. 1174-1179.
6. G. Modolo, H. Vijgen, D. Serrano-Purroy, B. Christiansen, R. Maimbeck, C. Sorel, and P. Baron, "DIAMEX Counter-current Extraction Process for Recovery of Trivalent Actinides from Simulated High Active Concentrate," *Sep. Sci. Technol.,* **42**(3), 439-452 (2007).
7. R. J. Taylor and I. May, "Advances in Actinide and Technetium Kinetics for Applications in Process Flowsheet Modeling," *Sep. Sci. Technol.,* **36**(5&6), 1225-1240 (2001).
8. S. B. Koganti, K. Periasamy, C. V. Rajagopalan, V. Sreedharan, and Balasubramanian, "Experience with Centrifugal Extractors," RECOD'94, London, UK, 1994; V1, 3B-4.

9. T. Washiya, M. Takeuchii, H. Ogino, and S. Aose, "Development of Centrifugal Contactor System in JNC," Proceedings of GLOBAL 2005, Tsukuba, Japan, Oct. 9-13, 2005; Paper No. 305.
10. X. Z. Zhou, J. Z. Zhou, C. Q. Zhang, and W. D. Yu, "Application of Annular Centrifugal Contactor on Separating Indium from Iron," *Sep. Sci. Technol.,* **32**(16), 2705-2713 (1997).
11. W. H. Duan, X. Z. Zhou, and J. Z. Zhou, "Extraction of Caffeine with Annular Centrifugal Contactors," *Sep. Sci.Technol.,* **41**(3), 573-581 (2006).
12. J. Z. Zhou, W. H. Duan, X. Z. Zhou, and C. Q. Zhang, "Extraction of Hydrocortisone from the Fermentation Liquor with Annular Centrifugal Contactors," *Solvent Extr. Ion Exch.,* **24**(2), 251-259 (2006).
13. J. Q. Xu, W. H. Duan, X. Z. Zhou, and J. Z. Zhou, "Extraction of Phenol in Wastewater with Annular Centrifugal Contactors," *J. Hazard. Mater.*, **131**(1-3), 98-102 (2006).
14. J. Z. Zhou, W. H. Duan, X. Z. Zhou, and C. Q. Zhang, "Application of Annular Centrifugal Contactors in the Extraction Flowsheet for Producing High Purity Yttrium," *Hydrometallurgy*, **85**(2-4), 154-163 (2007).
15. J. C. Wang, G. X. Tian, J. Chen, and C. L. Song, "Application of Miniature Centrifugal Contactors for Treating High-level Liquid Waste," *Sep. Sci. Technol.,* **36**(13), 2983-2996 (2001).
16. J. Z. Zhou, "Study on Performance of 10-mm Miniature Annular Centrifugal Extractor," *Chinese Chem. Eng.,* **12**(6), 25-29 (1984) (in Chinese).
17. W. H. Duan, C. X. Zhang, X. Z. Zhou, J. Chen, and J. Z. Zhou, "Development and Hydraulic Performance of ϕ50 mm Centrifugal Extractor Used in Nuclear Industry," *Chinese J. Nucl. Sci. Eng.,* **26**(2), 97-102 (2006) (in Chinese).
18. W. H. Duan, C. L. Song, Q. L. Wu, X. Z. Zhou, and J. Z. Zhou, "Development and Performance of a New Annular Centrifugal Contactor for Semi-industry Scale," *Sep. Sci. Technol.,* **40**(9),1871-1883 (2005).
19. X. M. He, Y. S. Yan, Q. R. Zhang, and B. R. Liu, "Recent Advances of Annular Centrifugal Extractor for Hot Test of Nuclear Waste Partitioning Process," *Nucl. Sci. Technol.,* **9**(3),157-162 (1998).
20. J. Z. Zhou, W. H. Duan, and X. Z. Zhou, "Development and Performance of a Glass Fiber Reinforced Plastic Centrifugal Contactor," *Sep. Sci. Technol.,* **41**(9), 1942-1951 (2006).
21. F. Y. Bao, M. D. Yang, J. Fang, Z. G. Zhang, P. J. He, and D. H. Zhu, "A Process for Purification of the Nickel Leacheate from Chlorination Leaching in Centrifugal Contactors," Mining Metallurgical Eng., 15(1), 42-47 (1995) (in Chinese).
22. S. M. Chen, X. Q. Li, H. T. Huang, T. Liu, X. F. Zhang, D. X. Yang, K. Wang, Y. F. Huang, F. Y. Bao, J. Fang, and D. H. Zhu, "Extraction of Germanium from Zinc Sulphate Solution," *Yunnan Metallurgy*, **31**(3), 101-105 (2002) (in Chinese).
23. X. T. Gong, J. Dang, J. F. Wang, M. D. Yang, X. C. Wang, S. R. Song, A. K. Zhang, F. Z. Jiao, X. W. Qin, and R. Q. Liu, "Treatment of Poor Gold Bearing Liquor from Gold Metallurgy Plant by Solvent Extraction with N_{235} (II) Piolt Plant Tests," *Nonferrous Metals*, **50**(1), 55-59 (1998) (in Chinese).
24. Y. X. Ye, J. X. Hu, Z. L. Huang, W. Q. Shi, G. M. Wu, H. B. Tang, W. B. Zhu, X. R. Wang, H. G. Zhao, Y. Dong, D. Sheng, F. X. Luo, and Y. J. Zhao, "Extraction of Actinides from Simulated HLLW by DHDECMP-TBP/OK," *J. Radioanal. Nucl. Chem.*, **261**(2), 365-374 (2004).

INDUSTRIAL APPLICATION OF GNEP SOLVENT-EXTRACTION PROCESSES

S. T. Arm, C. Phillips, and A. Dobson

EnergySolutions, 2345 Stevens Drive, Richland, Washington 99352, USA
Corresponding author email address: starm@energysolutions.com

ABSTRACT

EnergySolutions is currently studying the feasibility of commercially recycling spent nuclear fuel in the USA as part of the Global Nuclear Energy Partnership. Uranium, plutonium, and neptunium recycling are accomplished by employing well-established solvent-extraction technology based on the tributylphosphate extractant and acetohydroxamic complexant stripping in a commercially demonstrated configuration. Americium and curium recycling is best achieved by employing the TRUEX and TALSPEAK solvent-extraction processes or a simplified variant of them. Facility design is not predicated on performing any research and development a priori. Process development and demonstration will proceed in parallel with design by proven design-management techniques.

INTRODUCTION

As part of President Bush's Advanced Energy Initiative, the Global Nuclear Energy Partnership (GNEP) seeks to develop worldwide consensus on enabling expanded use of economical, carbon-free nuclear energy to meet growing electricity demand. This will use a nuclear fuel cycle that enhances energy security, while promoting nonproliferation. It would achieve its goal by having nations with secure, advanced nuclear capabilities provide fresh fuel and recovery of used fuel to other nations that agree to employ nuclear energy for only power generation. The closed fuel cycle envisioned by GNEP requires deployment of technologies that enable recycling and consumption of long-lived radioactive waste. The benefits of GNEP include:

- Provision of abundant energy without generating carbon emissions or greenhouse gases.
- Waste minimization and reduction in proliferation concerns by recycling spent nuclear fuel (SNF).
- Safe and secure deployment of nuclear power by developing nations to meet their energy needs.
- Assurance of maximum energy recovery from still-valuable SNF to limit the number of required U.S. geologic waste repositories to one for the remainder of this century.

The U.S. Department of Energy (DOE) selected the team led by EnergySolutions to prepare a Technology Roadmap, Conceptual Design Study, Communications Plan, and Business Plan for a Consolidated Fuel Recycle Center (CFRC) and Advanced Recycle Reactor. DOE will use the information and recommendations provided by EnergySolutions as well as other data and analyses to evaluate the development and deployment of GNEP activities and to inform decision making on the path forward for GNEP. This paper focuses on the down-selection and demonstration requirements for the CFRC solvent-extraction processes.

SOLVENT-EXTRACTION TECHNOLOGY DOWN-SELECTION

Drivers for Radionuclide Management

The purpose of the CFRC is to produce actinide products that can be recycled for energy production and transmutation while generating an immobilized high-level waste (IHLW) that optimizes the disposal capacity in the National Geologic Repository, Yucca Mountain (YM). Given the purpose of GNEP, the following radionuclides need to be optimally managed within the CFRC:

- Volatile fission products (C-14, I-129, and Kr-85) need to be separated from the off-gas before aerial discharge in compliance with 40CFR190.10.
- Tritium, in the form of tritiated water, needs to be managed to meet our objective of no contaminated liquid discharges to the environment.
- Uranium should be recovered and made available for recycling as fuel and because it is the greatest contributor (>90%) to the volume of IHLW.
- Heat-generating fission products (Cs-137 and Sr-90) and actinides (Pu-238, Am-241, and Cm) because they otherwise limit the quantity of IHLW that can be emplaced in YM.
- Long-lived radionuclides contributing most to the radiation dose to future populations from IHLW (Tc-99, I-129, and Np-237).
- Plutonium should be recovered, because it is a valuable resource for energy production. However, the desire to minimize proliferation risks means that no pure plutonium must be separated.

EnergySolutions' approach is to separate the volatile radionuclides from the dissolver off-gas by established methods, while tritium is managed by recycling the process water with a purge for solidification. The remainder of this paper now considers those radionuclides applicable to solvent-extraction processing.

Desirable Industrial Attributes of SNF Solvent-Extraction Processes

One approach to managing the radionuclides discussed above is to separate and manage them as groups or individually. Solvent extraction is a chemical separations technology well established for recycling SNF with over 50 years of industrial deployment. There are numerous solvent-extraction processes one could consider to achieve the separations desired in the CFRC. To assist in the down-selection of management approaches and solvent-extraction processes, EnergySolutions considered the following desirable attributes:

- Minimize the number of extractants in the CFRC to minimize the risk of cross-contamination and process upsets.
- Standardization of equipment.
- Utilize established, industrially proven technology to facilitate immediate commencement of design.
- Maximize the operating envelope to minimize the impact of operational fluctuations and process upsets and the production of off-specification products.

Actinide Separation

Uranium, Plutonium, and Neptunium

U and Pu separation from SNF solution has been industrially practiced for several decades using processes based on tributylphosphate (TBP) extractant in a hydrocarbon diluent. The NUEX process was developed by EnergySolutions for GNEP application from these industrially proven processes by modifying the plutonium and neptunium separation systems. In current plants, some Np inevitably co-extracts [1] because of its complex redox chemistry. EnergySolutions is leveraging its considerable expertise in Np valency manipulation to achieve bulk Np co-extraction.

Current industrial methods use U(IV) stabilized with hydrazine to reductively strip Pu and separate it from U [2]. However, hydrazine introduces requirements to ensure azide safety, adding to process complexity. Instead, EnergySolutions will use an aqueous-soluble complexant, acetohydroxamic acid (AHA), which complexes Pu and reduces Np to the V state, in which form it is stripped [3,4]. NexiaSolutions is the originator of the AHA technology, and it has been well demonstrated in actual SNF testing such that it is ready for deployment. Routing the Np with Pu introduces proliferation resistance, which is enhanced by allowing the co-stripping of some U with the transuranics.

The flowsheet modifications described above are significant in tailoring currently proven flowsheets to GNEP. However, they are sufficiently minor that they have no impact on the equipment configuration already proven in commercial SNF recycling plants.

Americium and Curium

Am and Cm extraction with TBP is impractical because it requires oxidation of these metals, which is hard to achieve and maintain. One option would be to recycle SNF very quickly after reactor discharge to minimize Am content and so eliminate the need for Am/Cm separation on economic or technical grounds. However, there is already a large back-log of long-cooled SNF, and TBP-based recycling of future high-burn-up SNF with <5 years decay will be challenging given the higher fission-product content (particularly moderately extractable ruthenium-106 and high-dose radionuclides). Therefore, EnergySolutions selected separation as the most effective means of managing Am/Cm if it remains a GNEP requirement.

The TRUEX process is well established in the US and has received much international attention for separating Am and Cm from waste and SNF, although it has

never been industrially deployed [5]. Lanthanide fission products inevitably co-extract with the Am and Cm in the TRUEX process, and so they must be subsequently separated from the Am and Cm. TALSPEAK is the only solvent-extraction process available for effecting lanthanide–Am/Cm separation with a developmental pedigree over 40 years [6]. There are processes under development that employ selective stripping of the Am/Cm from the TRUEX solvent, which would eliminate the need for TALSPEAK [7]. These processes have not been shown to provide a sufficiently good separation of the lanthanides to date but are nonetheless attractive, because their adoption would avoid employing a third solvent in TALSPEAK.

Fission-Product Separation

Cesium-137 and Strontium-90

One potential process utilizes chlorinated cobalt dicarbollide (CCD) and polyethylene glycol (PEG) in a phenyltrifluoromethyl sulfone diluent and has been suggested for UREX [8]. However, the organic phase is heavier than the aqueous phase, contrary to the situation with TBP. Therefore, solvent-extraction ancillary equipment (e.g., solvent float-off tanks and pipe lutes) for a CCD-PEG process would be necessarily nonstandard and require redesign and demonstration under industrial conditions. The fission-product extraction (FPEX) process [8] is based on the Strontium Extraction process developed at Argonne National Laboratory and the Caustic Side Solvent Extraction process developed at Oak Ridge National Laboratory for alkaline waste. However, this technology is immature for SNF recycling applications. Therefore, EnergySolutions chooses not to separate Cs-137 and Sr-90 but to decay-store the IHLW in vitrified form for ~100 years in a proven passively-cooled store prior to emplacement in YM. This approach also avoids creation of an orphan Cs/Sr waste-form that would still require storage.

Technetium-99

In current commercial SNF recycling plants utilizing the TBP-based solvent-extraction process, Tc-99 is co-extracted with the U and Pu and then separated in the subsequent Pu purification process [1]. The use of AHA means that the Tc-99 is routed instead to the uranium stream where it is stripped by a standard high-acidity feed. EnergySolutions' current approach is to combine and vitrify the Tc-99 with the HLW, given that an alternate waste form is not yet defined. However, the Tc-99 can easily be routed for alternative immobilization if desired.

The NUEX Flowsheet

EnergySolutions has integrated the processes and approaches described above into its NUEX flowsheet. The primary separation portion of NUEX is illustrated in Figure 1. This shows how the U and transuranics are routed in a process identical in configuration to that successfully deployed in the Thermal Oxide Reprocessing Plant (THORP) at Sellafield, UK. In the NUEX flowsheet, Tc follows U and is separated by employing the well-established high-acid scrub. EnergySolutions has tailored commercially deployed flowsheets to derive the NUEX flowsheet, but the modifications

are sufficiently minor that they have no configurational impact, so that the processing equipment is identical to that already industrially proven in THORP. Therefore, facility design can immediately commence and is not predicated on performing research and development (R&D) a priori.

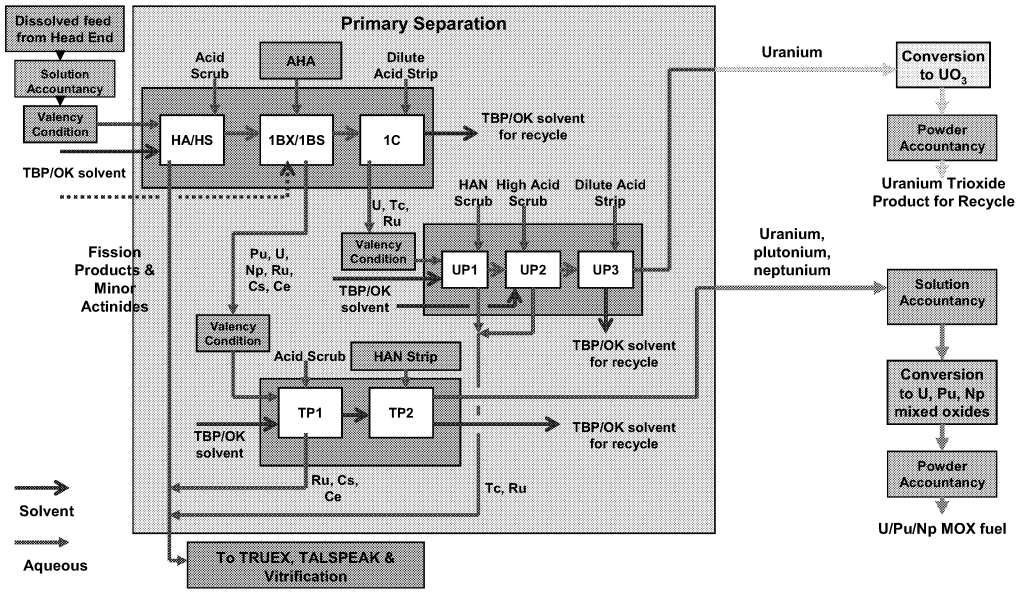

Figure 1. NUEX Primary Separation.

TECHNOLOGY ROADMAPPING FOR PLANNING, DEVELOPMENT, AND DEMONSTRATION ACTIVITIES

Technology road-mapping is a needs-driven technology-planning process to help identify, select, and develop technology alternatives to satisfy a set of system needs. It first involves identifying the technology gaps that need to be filled for confident deployment of the subject technology.

The predominantly more mature NUEX technologies (e.g., primary separation) have gaps largely in the flowsheet area, reflecting the incremental evolutions of currently deployed technology but with chemistry adjustments to improve them for GNEP application. These gaps are characterized by a desire for the technology suite to be demonstrated over broad operational and feed envelopes in coupled end-to-end demonstrations. Less mature NUEX technologies (e.g., TALSPEAK) have gaps largely in the process and equipment areas. All SNF recycling processes are envisioned as being performed in proven equipment and configurations. EnergySolutions has selected a technology suite requiring no inventions so that design can be immediately implemented.

Technology needs are identified based on the gap analysis. These needs are largely for flowsheet demonstration for the mature technologies and equipment or process demonstration and optimization for those less mature. Most technology needs are satisfied with small-scale prototypic tests using simulated feeds and modeling.

Ultimately, EnergySolutions will conduct a coupled end-to-end demonstration of the whole flowsheet at small scale and under hot conditions with actual irradiated fuel feed.

TECHNOLOGY DEVELOPMENT APPROACH

EnergySolutions integrates their project technology development and design functions to focus development activities on design needs and avoid protracted research programs. Technology development proceeds in parallel with design on this basis. Technical uncertainties are managed by maintaining a risk register that documents uncertainties and the means by which they are resolved. Contingencies in the design allow for uncertainties and are then affirmed as technical uncertainties and resolved by technology demonstration. This approach was successfully implemented by EnergySolutions staff in many nuclear-processing projects, including THORP.

CONCLUSIONS

EnergySolutions has demonstrated that the GNEP SNF recycling objectives can be achieved in a facility configurationally identical to those operating in Europe and Japan but using a flowsheet tailored for this application. As such, facility design can immediately commence and is not predicated on performing a R&D a priori.

REFERENCES

1. I. S. Denniss and C. Phillips, "The Development of a Three-Cycle Chemical Flowsheet to Reprocess Oxide Nuclear Fuels," ISEC, Kyoto, Japan, July 1990.
2. C. Phillips, "Development and Design of the Thermal Oxide Reprocessing Plant at Sellafield," *Trans. IChemE*, **71**, Part A, 134-142 (1993).
3. O. D. Fox, C. J. Jones, J. E. Birkett, M. J. Carrott, C. J. Maher, C. V. Roube, and R. J. Taylor, "Advanced PUREX Flowsheets for Future Np and Pu Fuel Cycle Demands," Separations for the Nuclear Fuel Cycle in the 21st Century, ACS Symposium Series 933, G. J. Lumetta, K. L. Nash, S. B. Clark, and J. I. Friese, Eds., ACS, Washington DC, 2006.
4. D. Y. Chung and E. H. Lee, "The Reduction of Np(VI) by Acetohydroxamic Acid in Nitric Acid Solution," Recent Advances in Actinide Science, R. Alvarez, N. D. Bryan, and I. May Eds., Royal Society of Chemistry, Cambridge, 2006.
5. K. Nomura, Y. Koma, S. Nemoto, M. Ozawa, and T. Kawata, "Japanese Experience in Application of the TRUEX Process to High Level Waste from Reprocessing," GLOBAL '93, Seattle, WA, USA.
6. M. Nilsson and K. L. Nash, "Review Article: A Review of the Development and Operational Characteristics of the TALSPEAK Process," *Solvent Extr. Ion Exch.*, **25**, 665-701 (2007).
7. M. Nakahara, Y. Sano, Y. Koma, M. Kamiya, A. Shibata, T. Koizumi, and T. Koyama, "Separation of Actinide Elements by Solvent Extraction Using Centrifugal Contactors in the NEXT Process," *J. Nucl. Sci. Technol.*, **44**(3), 373-381 (2007).
8. J. L. Swanson, C. Pereira, and G. F. Vandegrift, "Preliminary Evaluation of Solvent-Extraction and/or Ion-Exchange Process for Meeting AAA Program Multi-Tier Systems Recovery and Purification Goals," ANL-02/29, Argonne National Laboratory, 2002.

TECHNICAL FEASIBILITY OF THE DIAMEX PROCESS

C. Sorel, M. Montuir, D. Espinoux, B. Lorrain, and P. Baron

CEA Valrhô, DEN/DRCP, BP 17171, Bagnols-sur-Cèze, 30207, France
Corresponding author email address: christian.sorel@cea.fr

ABSTRACT

The DIAMEX process was developed at the CEA as the first of the two-step strategy to separate trivalent actinides from trivalent lanthanides. It consists of coextracting trivalent actinides and lanthanides using a diamide extractant, dimethyldioctylhexylethoxymalonamide (DMDOHEMA). To demonstrate the technical feasibility of this process, a test has been successfully carried out with a PUREX raffinate solution in pulsed columns and mixer settlers, which are representative of the solvent-extraction contactors that could be used at the industrial scale. At the end of the trial, the americium and curium recovery yield exceeded 99.9% with high decontamination factors.

INTRODUCTION

The DIAMEX process was developed at the CEA [1] to perform the coextraction of trivalent actinides and lanthanides from a PUREX raffinate by using the diamide extractant. Since the early 1990s, the malonamide extractant structure has been optimized with regards to its solubility in the industrial diluent HTP, its degradation behavior, and of course its affinity towards the extractible constituents. Thus, early studies were conducted with DiMethylDiButylTetraDecylMaloamide (DMDBTDMA), and the reference molecule DiMethylDiOctylHexylEthoxyMalonamide (DMDOHEMA) depicted in Figure 1 was finally adopted in 1999.

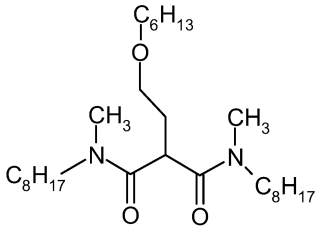

Figure 1. Structure of DMDOHEMA.

This process was successfully tested at the laboratory scale, in mixer-settlers [1-4], and subsequently in centrifugal extractors [5-9] from 1999 to 2003, on surrogate solutions

and on active solutions issued from the dissolution of actual spent-fuel samples. Actinide recovery factors greater than 99.9% were obtained with high purification factors for spurious fission products.

The main objectives of the final "technical feasibility" demonstration test at the end of 2005 with a PUREX raffinate solution were to test the continuous solvent recycling (not addressed during former tests) and to carry out essential operations in continuous contactors, representative of the pulsed columns that could be used at the industrial scale. We therefore decided to carry out the demonstration tests in the shielded process line (CBP) with some of the devices already used for a former PUREX test [10].

EXPERIMENTAL

Reagents

Twelve kilograms of DMDOHEMA was purchased from Pharmasynthèse company (F) with a purity greater than 98%. The test was performed with DMDOHEMA 0.65 mol L^{-1} diluted in HTP furnished by Novasep SAS. The feed solution was a fraction of a PUREX raffinate collected during a previous test conducted in the CBP facility [10]. Prolabo 68% nitric acid was used to prepare both scrub and strip solutions. Oxalic and N-(hydroxyethyl)-ethylenediaminetriacetic (HEDTA) acid solutions were prepared from high-purity commercial reagents from Merk.

Flowsheet Design

The flowsheet comprises four main sections. The first section consists of a coextraction step of trivalent actinides and lanthanides from high-acidity solution by the diamide. The second section is a scrubbing section to get rid of some fission products (Zr, Mo, Fe, and Pd) by a mixture of oxalic acid and HEDTA, followed by an acid stripping to prepare the stripping section of the actinides and lanthanides at low acidity. Finally, a solvent treatment prior to recycling is performed.

To perform the flowsheet design, a physicochemical model describing the extraction behavior of both nitric and oxalic acids, actinides, lanthanides, and the other extractible FPs (Fe, Mo, Zr, and Pd) has been developed and integrated in the process-simulating software PAREX [11]. The model is based on the application of the mass-action law on each extraction equilibrium taken into account. The complexation of the fission (Mo, Zr, and Pd) or corrosion (Fe) products by both oxalate ions or HEDTA were explicitly integrated in the model to quantify the scrubbing of these elements. A predictive model estimating the solubility of lanthanide oxalates was also included in the calculation code to optimize the operating conditions with regards oxalic precipitation limitations.

Finally, the flowsheet design, that is, the determination of the optimal flowrates and the compositions of the scrubbing solutions, was done to achieve a recovery yield of both actinides and lanthanides exceeding 99.9% with the highest decontamination factors towards the other FPs.

Implementation of the Flowsheet

As shown in Figure 2, the first two steps of the flowsheet were carried out in pulsed columns, 4 meters high. Two pulsed columns were devoted to the extraction section and one pulsed column was dedicated to the scrubbing section. The stripping of both actinides and lanthanides was performed in mixer-settlers and the solvent treatment in annular centrifugal contactors with immersed stirring rotors (ECRAN).

Liquid flows were delivered by rotative piston pumps: flow rates were measured and controlled by Coriolis effect flow meters. All the process parameters (flow rates, temperatures, interface levels, and pulsation rates of the pulsed columns and stirring speed of the mixer-settler motors) were controlled with instrumentation and control system and were recorded online.

The steady state was checked with the help of an online spectrophotometric monitor supplemented by laboratory analyses. Americium and neodymium concentrations were monitored in three different relevant flows: the aqueous phase coming back from the scrubbing section ①, the organic loaded solvent ② and the aqueous product ③.

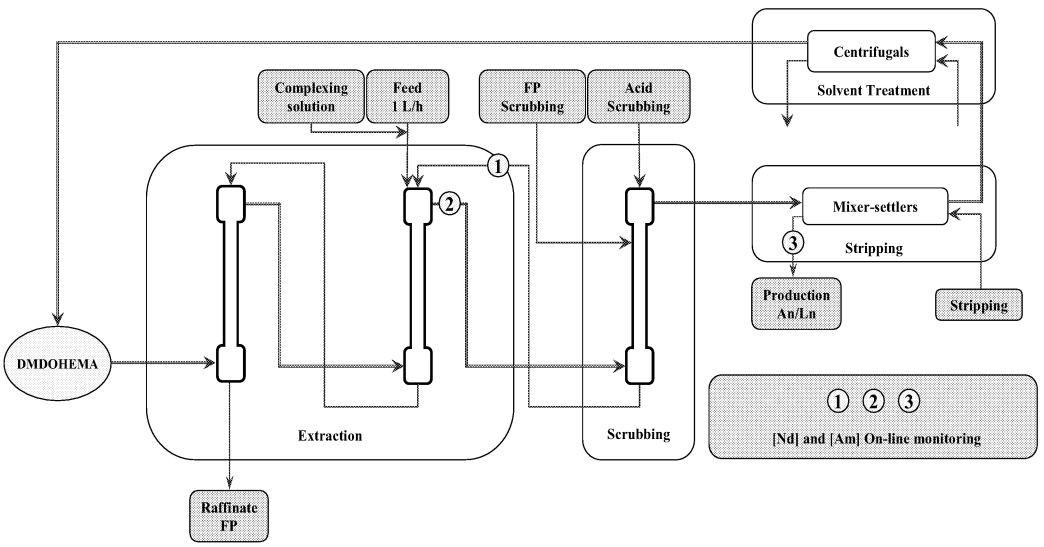

Figure 2. DIAMEX "technical feasibility" demonstration test flowsheet.

RESULTS AND DISCUSSION

The test carried out in November 2005 lasted 33 hours. The main results reported in Table 1 demonstrate that the objectives in terms of actinide-recovery yields and fission-product decontamination factors were totally reached. The loss of actinides in the raffinate and in the solvent were maintained at a value lower than 0.1%. The decontamination factors obtained with respect to the major fission products, Zr, Mo, and Fe, reached expected values.

Table 1. Recovery and decontamination factors (*vs* FP) obtained during the CBP test

Element	% in Raffinate	% in Solvent	DF
Am	< 0.03%	0.05%	-
Cm	< 0.008%	0.002%	-
Zr	-	-	889
Mo	-	-	108
Fe	-	-	10

The comparison between online, laboratory analysis, and predicted values of americium and neodymium concentrations are reported in Figure 3 and in Figure 4. The simulated concentrations are in very close agreement with the experimental determinations.

During this hot test, the solvent was recycled more than three times in addition to the ten recycles operated during previous hydrodynamic and spiked tests. The solvent treatment was elaborated with the help of continuous degradation and regeneration operations performed in the MARCEL γ irradiation facility [12].

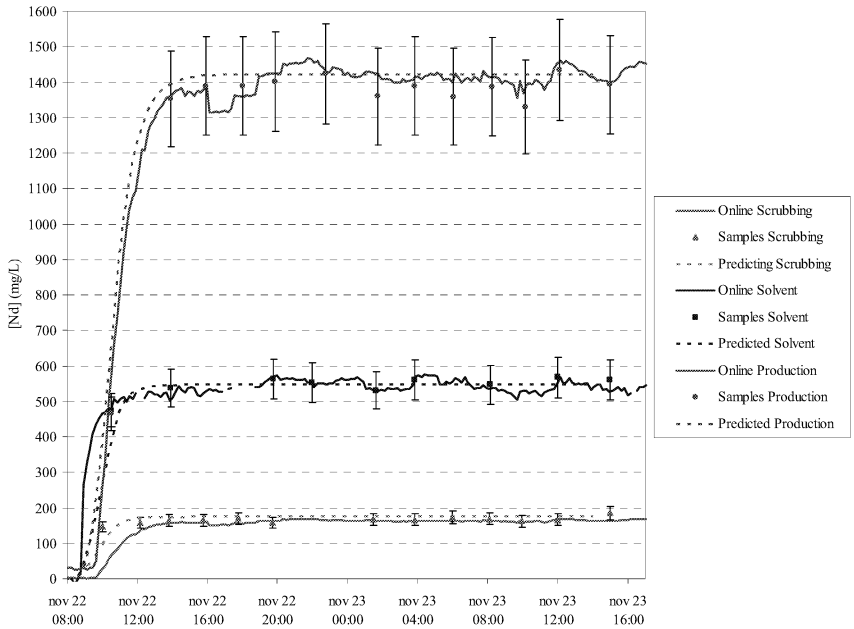

Figure 3. Comparison between online, laboratory analysis, and predicted neodymium concentration.

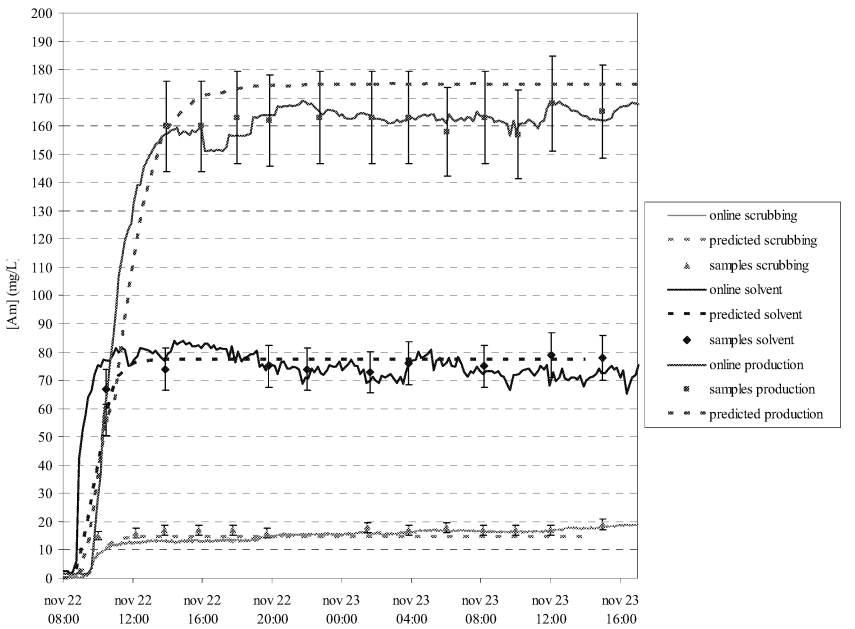

Figure 4. Comparison between online, laboratory analysis, and predicted americium concentration.

CONCLUSIONS

The technical feasibility of the DIAMEX process was demonstrated in contactors representative of those used at the industrial scale. The americium and curium recovery yields exceeded 99.9% with good decontamination factors with respect to fission (Zr and Mo) and corrosion (Fe) products. The physicochemical model developed to describe the extraction behaviors of actinides(III), lanthanides(III), and other fission products has helped us to optimize the chemical and operational conditions of the flowsheet. In addition, the close agreement obtained between predicted and experimental data has validated the model.

REFERENCES

1. C. Madic, P. Blanc, N. Condamines, P. Baron, L. Berthon, C. Nicol, C. Pozo, M. Lecomte, M. Philippe, M. Masson, and C. Hequet, "Actinide partitioning from high level liquid waste using the DIAMEX process," RECOD '94, London, England, 1994.
2. I. Bisel, C. Nicol, M. C. Charbonnel, P. Blanc, P. Baron, and F. Belnet, "Inactive DIAMEX test with the optimized extraction agent DMDOHEMA," Fifth International Information Meeting on Actinide and Fission Products Partitioning and Transmutation, Mol, Belgium, November 25-27, 1998, pp 153-159.
3. M. C. Charbonnel, C. Nicol, L. Berthon, and P. Baron, "State of Progress of DIAMEX Process," GLOBAL '97, Yokohama, Japan, October 5-10, 1997, pp 366-370.
4. A. Facchini, L. Amato, G. Modolo, R. Nannicini, C. Madic, and P. Baron, "Transient and steady-state concentration profiles in a DIAMEX-like countercurrent process for An(III)+Ln(III) separation," *Sep. Sci. Technol.*, **35**(7), 1055-1068 (2000).

5. P. Baron, X. Hérès, M. Lecomte, and M. Masson, "Separation of the minor actinides: The DIAMEX-SANEX concept," GLOBAL 2001, Paris, France, September 9-13, 2001.
6. R. Malmbeck, O. Courson, G. Pagliosa, B. Sätmark, J. P. Glatz, and P. Baron, "Partioning of minor actinides from HLLW using the DIAMEX process. Part 2 - "Hot" continuous counter-current experiment," *Radiochim. Acta*, **88**, 865-871 (2000).
7. G. Modolo, H. Vijgen, D. Serrano-Purroy, B. Christiansen, R. Malmbeck, C. Sorel, and P. Baron, "DIAMEX counter-current extraction process for recovery of trivalent actinides from simulated high active concentrate," *Sep. Sci. Technol.*, **42**, 439-452 (2007).
8. D. Serrano-Purroy, P. Baron, B. Christiansen, J. P. Glatz, C. Madic, R. Malmbeck, and G. Modolo, "First demonstration of a centrifugal solvent extraction process for minor actinides from a concentrated spent fuel solution," *Sep. Purif. Technol.*, **45**, 157-162 (2005).
9. D. Serrano-Purroy, P. Baron, B. Christiansen, R. Malmbeck, C. Sorel, and J. P. Glatz, "Recovery of minor actinides from HLLW using the DIAMEX process," *Radiochimica Acta*, **93**, 351-355 (2005).
10. P. Blanc, D. Ode, M. Ranchoux, and C. Viallesoubranne, "CEA ATALANTE Facility: Initial Experiments in High-Level Process (CBP), and Analysis (CBA) Shielded Lines," GLOBAL 2005, Tsukuba, Japan, 9-13 October, 2005, Paper N°225.
11. B. Dinh, B. Mauborgne, and P. Baron, "Dynamic simulation of extraction operations. Applications in nuclear fuel reprocessing," European Symposium on Computer Aided Process Engineering-2, ESCAPE2, Toulouse (France), Octobre 5-7, 1992.
12. I. Bisel, B. Cames, M. Faucon, F. D. Rudlof, and B. Saucerotte, "DIAMEX-SANEX Solvent Behavior under Continuous Degradation and Regeneration Operation," Global 2007, Boise (USA), September 9-13 2007, pp 1857-1860.

EXTRACTION OF URANIUM(VI) BY N,N-DI-(2-ETHYLHEXYL)ISOBUTYRAMIDE (DEHIBA): FROM THE BATCH EXPERIMENTAL DATA TO THE COUNTERCURRENT PROCESS

M. Miguirditchian, C. Sorel, B. Camès, I. Bisel, and P. Baron

CEA Valrhô, DEN/DRCP/SCPS, BP 17171, Bagnols-sur-Cèze, 30207, France
Corresponding Author Email Address: manuel.miguirditchian@cea.fr

ABSTRACT

The selective separation of uranium(VI) in the first cycle of the GANEX process is operated by a hydrometallurgical process using a monoamide extractant DEHiBA (N,N-di-(2-ethylhexyl)isobutyramide). Distribution ratios of uranium(VI) and nitric acid in 1 M DEHiBA/HTP were determined with macroconcentrations of uranium, and the experimental data were modelled by taking into account the activity coefficients of the constituents in aqueous phases. A flowsheet was designed and tested in a countercurrent process in laboratory-scale mixer-settlers on a surrogate U(VI)/HNO_3 feed. More than 99.999% of the uranium was recovered.

INTRODUCTION

The GANEX process (Group ActiNide EXtraction), developed by the CEA for the hydrometallurgical reprocessing of Generation IV spent nuclear fuels and the homogenous recycling of actinides, is composed of two extraction cycles following the dissolution of the spent fuel in nitric acid [1]. Uranium(VI) is selectively extracted from the dissolution solution before the group separation of transuranic elements (Np, Pu, Am, and Cm), which occurs in the second cycle prior to the co-conversion step [2]. The preliminary separation of uranium in the first cycle is required in order to recover it at a high purity, to adjust the ratio U/TRU before the co-conversion of the actinides, and to handle the excess of uranium due to the reprocessing of fuels unloaded both from light water and fast reactors in the future. Besides, the separation of the major constituent of the spent fuels is helpful for the hydrodynamics of the second extraction cycle.

The selective separation of uranium is achieved by solvent extraction using N,N-dialkylamide extractants. These molecules strongly extract U(VI) from high nitric acid medium. They have been studied as alternative extractants to tributylphosphate (TBP) for the co-extraction of uranium and plutonium and for the selective separation of uranium [3-6]. Indeed, by tuning the monoamide structure, it is possible to significantly increase the U(VI)/Pu(IV) selectivity. The branched-alkyl monoamides can selectively extract U(VI) without addition of any reducing or complexing agents for Pu(IV) to avoid its co-

extraction in the process [4,5]. Furthermore, these molecules are good candidates for the development of a hydrometallurgical process, because they show interesting properties, such as high solubility in the aliphatic diluents preferred in reprocessing (hydrogenated tetrapropylene HTP, dodecane, hyfrane), high decontamination factors versus fission products, low solubility in aqueous phases, low synthesis cost, and (most of the time) formation of water-soluble degradation products via hydrolysis and radiolysis.

DEHiBA (N,N-di-(2-ethylhexyl)isobutyramide), depicted in Figure 1, was selected among different N,N-dialkylamides as the extracting molecule for the GANEX 1st cycle, because it shows a good compromise between a quantitative extraction of uranium and a high U(VI)/Pu(IV) selectivity ($SF_{U(VI)/Pu(IV)}$ ~80 at 3 M HNO_3) [5] and a high loading capacity for uranium [6], in addition to the criteria described above.

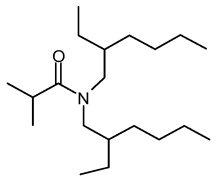

Figure 1. Structure of DEHiBA.

Most of the published distribution ratios of U(VI) and nitric acid with DEHiBA were measured at low concentrations of U(VI) (<10 g L^{-1}) [3-5,7-9], while very few distribution data are available at higher concentrations [5,10]. It is, however, important to acquire the distribution ratios of U(VI) and nitric acid for higher uranium concentrations to simulate their extraction by a uranium-loaded solvent in the process. Batch experiments were therefore carried out in this work to determine these distribution ratios from 0.01 to 6 M HNO_3 and for initial uranium concentrations ranging from 2 to 120 g L^{-1}. Based on these experimental data, extraction equilibria involved in the U(VI)/HNO_3/DEHiBA system were modelled, and equilibrium constants were adjusted for the extraction of uranium and nitric acid. After developing the model, a flowsheet was designed and tested on a uranium solution in mixer-settler contactors in order to check the extraction performance of this extracting system in a countercurrent process.

EXPERIMENTAL

Reagents

DEHiBA was purchased from Pharmasynthese with a purity of 99.3%. The purity was confirmed by GC-MS. The characterization of the extractant was also carried out by ElectroSpray-Ionization Mass Spectrometry, nonaqueous potentiometry and GC-FID. HTP diluent was furnished by Novasep SAS. Depleted uranyl nitrate from Prolabo®, purity 99.9%, was used without further purification.

Distribution Studies

Distribution ratios of nitric acid and uranium(VI) were measured with DEHiBA 1.05 mol L^{-1} diluted in HTP for initial concentrations of uranium ranging from 2 to 120 g L^{-1} and nitric acid concentration from 0.01 to 6 mol L^{-1}. The pre-equilibrated organic phase was shaken mechanically with the same volume of aqueous phase containing U(VI) in nitric acid for 10 min. at 25 °C. The uranium concentration in each phase was measured by X-ray fluorescence (Metorex International, ^{241}Am source) after dilution in either 1 mol L^{-1} HNO_3 or 1 mol L^{-1} DEHiBA /HTP.

Modelling Calculations

A physicochemical model has been developed to describe experimental distribution ratios obtained for nitric acid and uranyl nitrate. The model is based on the application of the mass-action law on each extraction equilibrium taken into account. Due to the high nitric acid and uranium(VI) concentrations, the assumption of ideal behavior for the aqueous phase is not valid. Thus, deviations from ideal behavior were estimated by calculating the activity coefficient of each component in the aqueous phase according to the "simple solutions" concept. This concept exploits the experimental behavior of isopiestic solutions first observed by Zdanovskii [11] and confirmed later by Stokes and Robinson [12]. The use of this concept dramatically simplifies the McKay-Perring integral thermodynamic relation [13] to finally obtain the Mikulin relation [14].

The equilibrium constants optimized to represent the extraction of both nitric acid and uranium(VI) were integrated into the process simulation software PAREX developed by CEA [15] to design a flowsheet for a demonstration test.

Mixer-Settler Test Procedure

The uranium separation was performed in three sections of laboratory-scale mixer-settlers corresponding to the extraction, the scrub, and the strip steps. The contactor set-up consisted of three batteries of mixer-settlers of eight stages each, three centrifugal contactors for the solvent clean-up step, reagent feed, receiving vessels, and pumps with associated controllers. The experimental flowsheet is shown in Figure 2. Once the surrogate uranium(VI)/HNO_3 feed (200 g L^{-1} at 4 M HNO_3) was added, ten hours of running were sufficient to reach equilibrium for nitric acid and uranium; the test was performed for 28 hours at the steady state. At the end of the experiment, the profiles of the experimental concentrations of uranium and nitric acid were measured by collecting an aliquot of the emulsion from each stage of the process flowsheet. After separation of organic and aqueous phases by centrifugation, the uranium concentration was measured in each phase by potentiometry and ICP-AES (after mineralization of the organic samples). The uranium concentration remaining in the solvent and in the raffinate were determined by time-resolved laser-induced spectrofluorimetry (TRLIF). The nitric acid concentration in the aqueous and organic phases was measured by potentiometry (in ethanol/water for the organic samples).

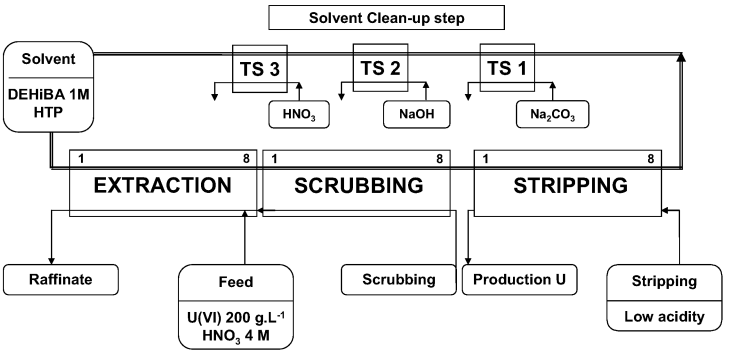

Figure 2. Flowsheet for the uranium extraction process.

RESULTS AND DISCUSSION

Batch Experiments

Batch distribution ratios of uranium versus nitric acid concentration show that $D_{U(VI)}$ increases with the nitric acid concentration, which seems to confirm that uranium is extracted by DEHiBA with a solvation mechanism. This increase is steep for a small quantity of uranium in the solvent and becomes flat when the solvent is loaded with uranium as a classical saturation phenomena. Beyond 5 M HNO_3, the extraction of uranium slightly decreases due to the competition with the proton extraction.

Modelling Calculations

Nitric acid extraction is well represented by taking into account the formation of three different solvates in organic phases: $(HNO_3)(DEHiBA)$, $(HNO_3)(DEHiBA)_2$, and $(HNO_3)_2(DEHiBA)$. The solvate $(HNO_3)(DEHiBA)$ is predominant on the whole acidity range, and the equilibrium constant associated with its extraction was estimated to be $K_H = 0.112 \pm 0.04$. These results confirm the values with traces of uranium [3,7].

Regarding uranium, uranyl nitrate extraction is well modeled by taking into account the formation of a unique complex, the disolvate $UO_2(NO_3)_2(DEHiBA)_2$. This speciation is consistent with previous experimental studies using slope analysis [4,8], saturation technique [8], and IR spectroscopy [3,8], which lead to the same stoichiometry of the uranyl extracted complex between 1 and 4 M HNO_3. The extraction equilibrium constant of U(VI) for 1 M DEHiBA/HTP was calculated as $K_U = 1.42 \pm 0.13$. At 2 M HNO_3 and for trace ^{233}U, Pathak et al. [4] determined by the slope-analysis method an equilibrium constant of 0.87 ± 0.08 for the extraction of U(VI) by 1 M DEHiBA/HTP, but without taking into account the activity coefficients of the constituents in aqueous phase.

Countercurrent Test

A flowsheet, calculated with the PAREX [15] simulation software was designed to recover more than 99.9% of uranium from the feed solution. This flowsheet, illustrated in Figure 2, was tested in a countercurrent process in laboratory-scale mixer-settlers to

validate the extraction performance of DEHiBA in liquid-liquid centrifugal contactors. The uranium concentration remaining in the raffinate and in the solvent was too low to be measured by classical techniques (ICP-AES, potentiometry), TRLIF was used to determine the yield of extraction and recovery of uranium at the end of this test. 1.2 mg/L of uranium was measured in the raffinate, which represents an extraction yield of 99.9992%, while 0.103 mg/L of uranium remained in the solvent, which corresponds to a recovery yield of 99.9997%. The uranium was quantitatively extracted and well stripped from the solvent, which confirms that DEHiBA is suitable for the selective separation of uranium. At the end of the test, the experimental profiles of uranium and nitric acid concentration in organic and aqueous phases were measured and compared to the calculated concentrations (Figure 3). The good agreement between experimental and calculated profiles confirms the validity of the model. Regarding the profiles of the nitric acid concentration, the model predicts the trends; however, the deviation of the calculated organic concentration from the experimental data reaches 20% (while it is only about 5% in aqueous phase). This difference could be explained by flooding or other problem during the sampling or by larger analytical errors in the organic phase. Overall, the model seems valid, and the values of the distribution ratios of nitric acid calculated from the aqueous composition are consistent with the experimental results.

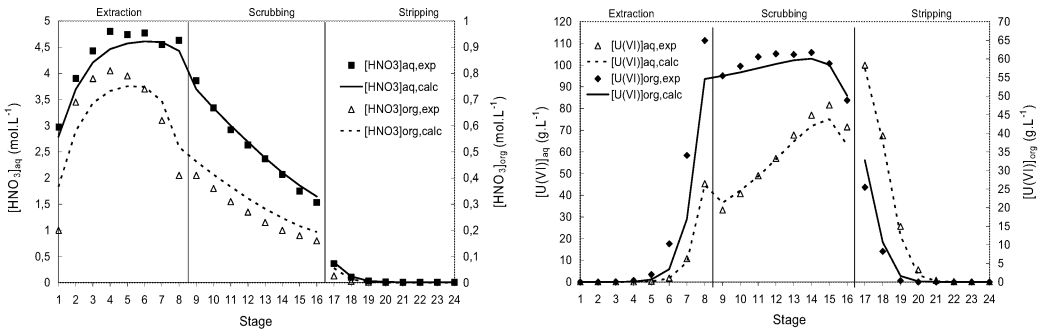

Figure 3. Aqueous and organic concentration profiles of nitric acid and uranium.

CONCLUSION

The countercurrent test reached the objective of the GANEX 1st cycle after recovering more than 99.99% of the total amount of uranium. This test confirmed the good performance of DEHiBA for the extraction of uranium from nitric acid and was a pertinent simulation of the hot test planned in the future. The model based on the acquisition of experimental distribution data with corrections for the activity coefficients of the components in the aqueous phase was verified by the good agreement between the experimental and calculated profiles. Optimization of the flowsheet is ongoing with implemention of Pu(IV), Np(V, VI) and Tc(VII) extraction data in the code. The scrub stage will be sized to recover sufficiently pure uranium to avoid further decontamination cycle. The process will be tested on a genuine highly active dissolution solution in 2008 in the Atalante facility to confirm the selectivity of DEHiBA for uranium versus transuranic elements and fission products under representative conditions.

ACKNOWLEDGMENTS

The authors would like to thank L. Pasqualini for the distribution studies, T. Rossetti, D. Rudloff, B. Saucerotte for the countercurrent test, L. Berthon for the DEHiBA characterization and L. Couston for the TRLIF measurements.

REFERENCES

1. J.-M. Adnet, M. Miguirditchian, C. Hill, X. Heres, M. Lecomte, M. Masson, P. Brossard, and P. Baron, "Development of New Hydrometallurgical Processes for Actinide Recovery: GANEX concept," GLOBAL'05, Tsukuba, Japan, October 9-13, 2005; n°119.
2. M. Miguirditchian, L. Chareyre, X. Heres, P. Baron, and M. Masson, "GANEX: Adaptation of the DIAMEX-SANEX Process for the Group Actinide Separation," GLOBAL '07, Boise, Idaho, USA, September 10-14, 2007; pp. 550-552.
3. N. Condamines, "*Contribution à l'étude de l'extraction d'acides minéraux et de cations actinides aux degrés d'oxydation (IV) et (VI) par des N,N-Dialkylamides*, Ph.D. Thesis, Université Paris VI, 1990.
4. P. N. Pathak, R. Veeraraghavan, D. R. Prabhu, G. R. Mahajan, and V. K. Manchanda, "Separation Studies of Uranium and Thorium Using Di-2-ethylhexyl Isobutyramide (D2EHIBA) ," *Separ. Sci. Technol.*, **34**(13), 2601-2614 (1999).
5. S. Suzuki, Y. Sasaki, T. Yaita, and T. Kimura, "Study on selective separation of uranium by N,N-dialkylamide in ARTIST process," Atalante 2004, Nimes, France, June 21-25.
6. P. N. Pathak, D. R. Prabhu, P. B. Ruikar, and V. K. Manchanda, "Evaluation of di(2-ethylhexyl)isobutyramide (D2EHiBA) as a process extractant for the recovery of ^{233}U from irradiated Th," *Solv. Ext. and Ion Exch.*, **20**(3), 293-311 (2002).
7. N. Condamines and C. Musikas, "The extraction by N,N-dialkylamides. I. Extraction of nitric acid," *Solv. Ext. and Ion Exch.*, **6**, 1007 (1988).
8. N. Condamines and C. Musikas, "The extraction by N,N-dialkylamides. II. Extraction of actinide cations," *Solv. Ext. and Ion Exch.*, **10**(1), 69-100 (1992).
9. D. R. Prabhu, G. R. Mahajan, and G. M. Nair, "Di(2-ethyl hexyl) butyramide and di(2-ethyl hexyl)isobutyramide as extractants for uranium(VI) and plutonium(IV)", *J. Radioanal. Nucl. Chem.*, **224(1-2)**, 113-117 (1997).
10. P. N. Pathak, R. Veeraraghavan, P. B. Ruikar, and V. K. Manchanda, "Solvent Extraction Studies on Th(IV), Pa(V) and U(VI) from Nitric Acid Medium using Di-2-Ethyl Hexyl Isobutyramide (D2EHIBA) ," *Radiochimica Acta*, **86**, 129-134 (1999).
11. A. B. Zdanovskii, *Trudy Solyanoï Lab. Akad. Nauk. SSSR*, **6** (1936).
12. R. H. Stockes and R. A. Robinson, "Interactions in Aqueous Nonelectrolyte Solutions. I. Solute-Solvent Equilibria," *J. Phys. Chem.*, **70**, 2126-2130 (1966).
13. H. A. C. Mc Kay and J. K. Perring, "Calculation of the Activity Coefficients of Mixed Aqueous Electrolytes from Vapour Pressures," *Trans. Faraday Soc.*, **49**, 163-165 (1953).
14. G. I. Mikulin, "Voprosy Fizicheskoî Khimii Rastvorov Electrolitov", Izdatelstvo "Khimiya," Lenigrad Otdelenie, 1968.
15. B. Dinh, B. Mauborgne, and P. Baron, "Dynamic simulation of extraction operations. Applications in nuclear fuel reprocessing," European Symposium on Computer Aided Process Engineering-2, ESCAPE2, Toulouse (France), October 5-7, 1992.

MASS-TRANSFER TESTING OF A 12.5 cm ROTOR CENTRIFUGAL CONTACTOR

D.H. Meikrantz, T.G. Garn, J.D. Law, N.R. Mann, and T.A. Todd

Idaho National Laboratory, 2525 North Fremont Avenue, Idaho Falls, ID 83415
Corresponding author email address: david.meikrantz@inl.gov

ABSTRACT

TRUEX mass-transfer tests were performed using a single-stage commercially available 12.5 cm centrifugal contactor and stable cerium (Ce) and europium (Eu). Test conditions included throughputs ranging from 2.5 to 15 LPM and rotor speeds of 1750 and 2250 rpm. Ce and Eu extraction forward distribution ratios ranged from 13 to 19. The first- and second-stage strip back distributions were 0.1 to 1.4 and 0.001 to 0.004, respectively, throughout the dynamic test conditions studied. Visual carryover of aqueous entrainment in all organic phase samples was estimated at <0.1% and organic carryover into all aqueous phase samples was about ten times less. Mass-transfer efficiencies of essentially 100% for both Ce and Eu in the extraction section were obtained over the entire range of test conditions. The first-strip-stage mass-transfer efficiencies ranged from 75 to 93%, trending higher with increasing throughput. Second-stage mass transfer was greater than 99% in all cases. Increasing the rotor speed from 1750 to 2250 rpm had no significant effect on efficiency for all throughputs tested.

INTRODUCTION

Centrifugal contactors are being evaluated for the selective partitioning of actinide, lanthanide, and fission products from dissolved Light Water Reactor nuclear fuel solutions. Solvent-extraction processes utilizing centrifugal contactors realize three important advantages over historically used equipment. First, the units are capable of processing plant-scale throughputs with less in-process volume compared to pulse columns or mixer settlers. Secondly, the short residence times associated with contactor processing minimizes negative solvent degradation such as hydrolysis and radiolysis when processing nuclear-fuel solutions. Lastly, the shorter time to reach process equilibrium and the ability to tolerate in-process upsets and changes in flowrates and phase ratios makes centrifugal contactors quite attractive for more complex flowsheets. However, shorter residence times and differences in mixing dynamics can impact mass-transfer rates. Therefore, the performance and efficiency of various sized contactors is being measured and their operating ranges are being defined for engineering-scale applications.

Commercialization of annular centrifugal-contactor technology in the U.S. began about 15 years ago with the technology transfer of a patent from the Department of Energy's Idaho National Engineering Laboratory [1]. Since that time, a number of design enhancements have been made and patented, leading to a device better suited for a wide range of liquid-liquid processes. Multiple sizes were designed to provide total throughput ranging from 0.4 to 800 liters per minute (LPM) and interchangeable heavy-phase weir rings were incorporated into the rotor to allow separation of a wide range of density pairs [2,3]. A low-mix sleeve option was added to aid in the separation of viscous or shear-sensitive liquid mixtures [4]. Clean-in-Place (CIP) capability was achieved by adding a hollow central shaft with spray nozzles to the rotor design to enhance use as a clarifier and to improve utility in both hands-on and remote applications [5].

In the past, various centrifugal-contactor designs have been used at the Idaho National Laboratory (INL) to demonstrate novel solvent technologies for the selective partitioning of radioactive material from acidic media. The most recently designed, commercially available units have been evaluated at the INL for the past five years. Hydraulic and mass-transfer test results for the CINC V-02 (5 cm) model were reported in September 2005 [6]. The Clean-in-Place test results for a CINC V-05 (12.5 cm) model unit were reported in June 2006 [7], followed by the hydraulic and reliability test results for the 12.5 cm unit reported in September 2006 [8]. Most recently the mass-transfer testing of a single stage V-05 (12.5 cm) unit for the TRUEX process was completed.

EXPERIMENTAL

The experimental assembly consisted of a commercially available model V-05 CINC annular centrifugal contactor with a 12.5 cm (5 inch) diameter rotor fitted with a 2.600 inch heavy phase weir [9]. A variable-frequency drive was used to adjust rotor speed during testing. The V-05 contactor is designed with a rotor shaft that runs the entire length of the unit, which provides CIP capability and serves to stabilize the rotor. This added stability enhances reliability via minimized vibration and reduced bearing and seal wear when compared to top-shaft-only rotor designs. A detailed listing of the test equipment used for the mass-transfer testing is found in Table 1.

Mass-transfer testing of the contactor was limited to a nonradioactive area. Therefore, the Transuranic Extraction (TRUEX) process solvent was chosen for the extraction of stable cerium and europium. The TRUEX solvent was prepared by combining octyl(phenyl)-N,N-diisobutyl-carbamoylmethylphosphine oxide (CMPO) and tributylphosphate (TBP) to a final concentration of 0.2 M CMPO + 1.4 M TBP in *n*-dodecane. CMPO was acquired from Eichrom Technologies, Inc. (Darien, IL). The reagent grade TBP and *n*-dodecane were received from Aldrich Chemical Co. (Milwaukee, WI). Following the adjustment, the solvent was washed three times with 0.25 M Na_2CO_3 at an O/A of 4 using fresh wash solution each time. The washed solvent was then reacidified with 0.1 M HNO_3 at an O/A of 3. The solvent was then pre-equilibrated twice with 3.2 M HNO_3 at an O/A of 1.

Table 1. Detailed description of the mass-transfer test equipment

Contactor: model CINC V-05TA CIP 12.5 cm rotor (O.D.) fitted with 2.600 inch weir	
Material of construction	316L stainless steel
Inlet and outlet ports	Male 1" NPT, tangential
Motor	Baldor, inverter duty, 2 hp, 3450 rpm, 230/460 V XP Class 1 Group D
Speed controller	Allen Bradley Powerflex 4, cat. # 22A-V1P5N104
Rotor speed	Fully adjustable 0-5400 rpm
Configuration	Single-stage units, interconnectable
Size	Footprint 16" X 16", height 42" with motor
Weight	140 lbs (63.6 kg) with motor
Rated Capacity	0-19 LPM, (5 gpm)
Feed pumps (2)	Micropump series 5000/56C model GL H25 FFSE
Capacity	Variable 2-27 LPM
Material of construction	316 Stainless steel
Drive motors (2)	LEESON Elec. Co. model C6T34F41D 1 hp 208-230 V 3 phase
Speed controllers (2)	LEESON Speed Master micro series model 174915
Tubing 1 "supply 1.25" discharge	Gates Mustang 45 HW type K polyethylene

The feed for the extraction section was 3.2 HNO_3 with stable cerium and europium added at 1.0 and 0.25 g/L, respectively. The extraction section tests were then performed by pumping the TRUEX solvent and aqueous feed into the contactor at an O/A ratio of 0.5 using the test parameters listed in Table 2. The system was allowed to reach equilibrium before both aqueous and organic samples were collected and all extraction, scrub and strip tests were run at ambient temperature (19-21 °C). Samples were visually examined for phase carryover at each test condition. No noticeable phase carryover was observed in the samples obtained for all test parameters for the extraction-section testing.

Table 2. Mass-transfer testing parameters for the extraction section

Total throughput (LPM)	Rotor speed (rpm)	Aqueous flowrate (LPM)	Organic flowrate (LPM)
3	1750	2	1
3	2250	2	1
5	1750	3.4	1.7
5	2250	3.4	1.7
10	1750	6.6	3.4
10	2250	6.6	3.4
15	1750	10	5
15	2250	10	5

The scrub-section testing consisted solely of a single pass of the loaded organic solvent contacted with 0.1 M HNO_3 acid at an O/A of 1, processing a total throughput of 10 LPM at a rotor speed of 2250 rpm. The scrub reduces the acid in the solvent so the lanthanides can be stripped. During the scrub testing, collected samples were not submitted for analysis but were used only to observe phase carryover of either phase during processing. No evidence of other-phase carryover was observed in the scrub section.

The strip section consisted of contacting the scrubbed organic with a strip solution at an O/A of 1.3. The strip solution consisted of a 1.5 M lactic acid and 0.05 M

diethylenetriaminepentaacetic acid (DTPA) in H_2O solution with a measured pH of 3. The strip section test conditions are shown in Table 3. Again, samples were examined for other-phase carryover observations at each test condition. No measurable phase carryover was observed in any samples taken during the first-strip-section testing.

Table 3. Mass-transfer testing parameters for the strip sections

Total throughput (LPM)	Rotor speed (rpm)	Aqueous flowrate (LPM)	Organic flowrate (LPM)
2.5	1750	1.1	1.4
2.5	2250	1.1	1.4
5.7	1750	2.5	3.2
5.7	2250	2.5	3.2
8.5	1750	3.7	4.8
8.5	2250	3.7	4.8
13	1750	5.7	7.3
13	2250	5.7	7.3

RESULTS AND DISCUSSION

ICP-MS sample results were used to calculate distribution ratios of Ce and Eu for single-stage contacts for each test condition in the extraction and strip sections. Forward distribution ratios for Ce and Eu in the extraction stage ranged from 13 to 19 at all process flow rates and rotor speeds tested. The higher rotor speeds combined with higher throughput levels tested had somewhat higher distribution ratios. First-strip-stage distribution values differed when comparing Ce to Eu. Distributions for Ce ranged from 1.4 to 0.5, while those for Eu were measured at 0.8 to 0.1. In every set, Eu stripping was at least twice the magnitude of that for Ce. Overall, the strip distributions indicated better stripping with higher rotor speed and throughput. In addition, higher-efficiency stripping was expected in the first strip stage based on modeling. However, measured acid concentrations of the scrubbed organic entering the strip section were slightly higher than those predicted. The single scrub employed in this test may have been insufficient for efficient stripping in the first stage. For this reason, a second-stage-strip study was conducted.

The TRUEX solvent was washed with Na_2CO_3 solution after the first-strip study and recycled for another bulk extraction, scrub, and first-strip process to prepare it for the second-stage-strip study. Fresh Ce and Eu feed was prepared for the second TRUEX solvent loading and fresh scrub and strip solutions were used. The extraction, scrub, and first-strip processes were repeated, but with only several process verification samples, and the once-stripped organic was collected for the second-strip-stage testing. This first strip, done to just provide organic feed for the second strip, was all processed at 8.5 LPM and 2250 rpm. In the second-strip-stage test, the same test parameters as used for the original first-stage strip were repeated and each set sampled.

Distribution ratios for the second-strip stage were measured from 0.003 to 0.001 for Ce and 0.004 to 0.002 for Eu for all test parameters. No trends were observed due to flow rate or rotor speed, as very efficient second stage stripping occurred.

Mass-transfer efficiencies for extraction- and strip-section test parameters were calculated using the ICP-MS sample results taken from each test parameter and re-equilibrated samples. The mass-transfer equation used is of the form:

$$\eta = \frac{(X - X_{in})}{(X_{eq} - X_{in})} * 100$$

where X is the metal concentration of the effluent, X_{in} is the inlet metal concentration, and X_{eq} is the metal concentration of the effluent following re-equilibration. Efficiency can be calculated based on aqueous- or organic-phase concentrations. Aqueous-phase concentrations were used for all extraction calculations and organic-phase concentrations for strip calculations, since these phases contained the Ce and Eu.

The mass-transfer efficiencies for the V-05 were calculated for the extraction, first strip stage and second strip stage. For all parameters studied, the forward extraction efficiency was essentially 100%. The first-strip-stage efficiencies ranged from 75 to 93% with the least effective stripping at the lowest flow rate of 2.5 LPM. However, the second-stage-strip mass-transfer efficiency was also essentially 100%, even for the lowest flow rate studied.

CONCLUSIONS

Two mass-transfer tests were performed using a single-stage commercially available 12.5 cm centrifugal contactor. The TRUEX portion of the uranium extraction (UREX)+1a flowsheet format was processed to measure the distribution ratio and mass-transfer efficiencies of stable Ce and Eu. Mass-transfer efficiency measurements of essentially 100% for both Ce and Eu in the extraction section indicated the 12.5 cm contactor is very capable of efficiently extracting Ce and Eu from a simulated dissolved fuel solution with the TRUEX solvent at tested throughputs and rotor speeds. The first-strip-contact mass-transfer efficiencies were lower than those determined for the extraction section. Efficiencies determined for Ce ranged from 75 to 91% while the Eu efficiencies ranged from 76 to 93%, each increasing with increasing throughput. The rotor speeds studied had no measurable impact on efficiency for all throughputs.

As a result of the lower-than-expected efficiency measurements in the first strip contact, a second mass-transfer test incorporating a second strip contact was performed. The mass-transfer efficiencies for all second stage strip test conditions were >99 % for both Ce and Eu. The higher-than-expected acidity of the scrubbed organic significantly impacted the strip efficiency in the first stage.

Overall, visual and measurable carryover levels of aqueous entrainment in all organic phase samples were less than or equal to 0.1%. However, organic carryover into all aqueous-phase samples was estimated to be at least an order of magnitude lower.

The high single-stage mass-transfer efficiencies indicate the 12.5 cm centrifugal contactor is a viable equipment option for the TRUEX portion of the UREX+1A solvent-extraction flowsheet. In addition, very good phase disengagement using centrifugal contactors is common and should lead to process savings via reduced extractant loss in plant applications.

ACKNOWLEDGMENTS

This work was carried out under the auspices and financial support of the U. S. Department of Energy, Office of Nuclear Energy, Science and Technology through contract DE-AC07-99ID13727.

REFERENCES

1. D. H. Meikrantz, “Method for Separating Disparate Components in a Fluid Stream”, U. S. Patent 4,959,158, 1990.
2. D. H. Meikrantz, L. L. Macaluso, H. W. Sams, C. H. Schardin, and A. G. Federici, “Centrifugal Separator,” U. S. Patent 5,591,340, 1997.

3. D. H. Meikrantz, L. L. Macaluso, H. W. Sams, C. H. Schardin, and A. G. Federici, “Centrifugal Separator,” U. S. Patent 5,762,800, 1998.
4. D. H. Meikrantz, A. G. Federici, L. L. Macaluso, and H. W. Sams, “ Rotor Sleeve for a Centrifugal Separator,” U. S. Patent 5,571,070, 1996.
5. L. L. Macaluso and D. H. Meikrantz, “Self Cleaning Rotor for a Centrifugal Separator,” U. S. Patent 5,908,376, 1999.
6. D. H. Meikrantz, J. D. Law, R. S. Herbst, T. G. Garn, N. R. Mann, T. A. Todd, “Hydraulic and Mass Transfer Testing of Commercial 5 cm Centrifugal Contactors at INL,” INL/EXT-05-00793, September 2005.
7. N. R. Mann, T. G. Garn, D. H. Meikrantz, J. D. Law, T. A. Todd, “Clean in Place Testing of a Commercial 12.5 cm Annular Centrifugal Contactor at the INL,” INL/EXT-06-11533, June 2006.
8. T. G. Garn, N. R. Mann, D. H. Meikrantz, J. D. Law, T. A. Todd, “Hydraulic and Reliability Tests of the CINC V-05TA-CIP 12.5 cm Annular Centrifugal Contactor,” INL/EXT-06-11958, September 2006.
9. CINC Manufacturing, 5224 US Hwy 50 East, Carson City, NV 89701, (775) 887-0787.

HYDRAULIC AND CLEAN-IN-PLACE EVALUATIONS FOR A 12.5 CM ANNULAR CENTRIFUGAL CONTACTOR AT THE INL

Troy G. Garn, Dave H. Meikrantz, Nick R. Mann, Jack D. Law, and Terry A. Todd

Idaho National Laboratory, 2525 N. Fremont Ave. Idaho Falls, ID 83415 USA
Corresponding author email address: Troy.Garn@inl.gov

ABSTRACT

Commercially available, Annular Centrifugal Contactors (ACC) are currently being evaluated for processing dissolved nuclear-fuel solutions to selectively partition integrated elements using solvent-extraction technologies. These evaluations include hydraulic and clean-in-place (CIP) testing of a commercially available 12.5 cm unit. Data from these evaluations is used to support design of future nuclear-fuel reprocessing facilities. Hydraulic testing provides contactor throughput performance data on two-phase systems for a wide range of operating conditions. Hydraulic testing results for a simple two-phase stable kerosene (oil)/water system followed by a 30% tributylphosphate, *n*-dodecane (UREX)/nitric acid system are reported. Maximum total throughputs for this size contactor ranged from 18 to 32 L/min without significant other-phase carryover. A relatively new contactor design enhancement providing CIP capability for ACCs was also investigated. Spray nozzles installed into the hollow central rotor shaft enable the rotor internals to be cleaned, offline. Testing of the solids capture of a diatomaceous earth/water slurry feed followed by CIP testing was performed. Solids-capture efficiencies of >95% were observed for all tests, and short cold-water cleaning pulses proved successful at removing solids from the rotor.

INTRODUCTION

The United States Department of Energy's Global Nuclear Energy Partnership (GNEP) was formed to expand economical, carbon-free nuclear energy to meet growing electricity consumption demands. The development of advanced separation technologies to close the fuel cycle by processing dissolved nuclear-fuel solutions while promoting nuclear nonproliferation is an integral part of this partnership.

Advanced separation technologies include the selective partitioning by solvent extraction (SX) of bulk uranium for reuse in nuclear-fuel fabrication and minimizing heat-generating fission products sent to a repository. Annular centrifugal contactors (ACC) have important advantages over historically used equipment. First, the units are capable of processing plant-scale throughputs with a smaller in-process volume compared to pulse columns or mixer settlers. Secondly, the short resonance times using ACCs minimizes solvent effects such as hydrolysis and radiolysis. In addition, ACCs will tolerate wide ranges of organic/aqueous (O/A) ratios and can maintain separation equilibrium during flow interruptions. However, shorter resonance times and differences

in mixing dynamics can impact mass-transfer rates; hence, the hydraulics and total throughputs of these contactors must be experimentally measured to define operating conditions. One potential disadvantage is the inherent ability of contactors to efficiently separate entrained particulates from process feed streams. These particulates can be captured in the separation zone and, over time, form cake-like layers, which can significantly impede phase separation and ultimately reduce process performance. Clean-in-place (CIP) capability was added by using a hollow central rotor shaft fitted with spray nozzles to wash solids from rotor internals offline. A second disadvantage is the complexity of the units, each constructed with numerous moving components, which may require additional maintenance in a radioactive operating environment.

This paper discusses hydraulic testing results for two independent two-phase systems: kerosene (Oil)/ water, and 30% tributylphosphate in *n*-dodecane (UREX)/nitric acid. The paper also includes results from a CIP test reporting solids capture and cleanout using a 0.1 wt % diatomaceous earth-in-water slurry feedstock.

EXPERIMENTAL

Equipment Description for Hydraulic and CIP Evaluations

The experimental setup for both tests consisted of a commercially available model V-05 CINC annular centrifugal contactor with a 12.5 cm (5 inch) diameter rotor fitted with a 2.500 inch heavy phase weir. Additional heavy-phase weirs are available from 2.300 to 3.000 inches in 0.050 in. increments. It was also fitted with an optional clear-polymer lower housing to view two-phase mixing and measure mixing-annulus height during operation.

A Seepex® progressive cavity pump (BN#2) was used to pump the diatomaceous earth slurry to the contactor inlet for CIP testing. A Gould G&L series centrifugal pump was installed to pump cleaning solution at 40 psig and flow rates of 25 L/min to the spray nozzles.

Stable Kerosene (oil)/water Hydraulic Testing

The initial testing focus was to examine two-phase mixing and determine the maximum throughput by running total flow rates of 2 L/min to 24 L/min at an O/A of 1 and a rotor speed of 2000 rpm. The point at which other-phase carryover is observed to be measurably present gives good indication of the maximum amount of solution that can be processed with the V-05 unit equipped with any chosen heavy phase weir. Three weir sizes were tested to help define the best fit for the overall testing objective. The 2.600 inch weir was chosen based on final rotor volumes measured at selected test conditions.

To further examine the operating range for the V-05, total flow rates of 10, 12, and 16 L/min, O/A ratios ranging from 0.2 to 5.0, and rotor speeds of 1500, 2000, 2500, and 3000 rpm were tested. Samples were visually inspected for phase carryover at each set of parameters.

30% Tributylphosphate in *n*-Dodecane/Nitric Acid Hydraulic Testing

The maximum throughput for the TBP solvent/nitric acid pair was experimentally determined following the oil/water test scheme. Flowrates of 14-26 L/min at an O/A of 1 at 2000 rpm were tested. Stated flowrates were within 5%, based on previous measurements at pump-controller settings.

Following the initial throughput testing, two equipment modifications were made to the contactor. Vents (1 in. I.D. × 12 in. Ht.) were installed on both phase outlets to prevent vapor lock that leads to excessive other-phase carryover at high throughput. Sample taps were also installed on both discharge lines to facilitate safe and convenient performance monitoring.

A simplified flowsheet was then employed consisting of an extraction, scrub, and strip section. The extraction section was performed at O/A ratios of 1, 2, and 3 at an initial rotor speed of 2000 rpm. Beginning at a total flowrate of 16 L/min, the flowrate was increased by 2 L/min intervals until measurable either-phase carryover was observed in the samples. At that point, the rpm was increased to 2250 and finally to 2500 rpm to determine the impact on carryover. The scrub section was performed at O/A ratios of 4, 6, and 8 each beginning with a rotor speed of 2000 rpm and an initial total flowrate of 16 L/min. Again, the rotor speed was increased once measurable carryover was observed in phase samples. The strip section was performed at O/A ratios of 0.5, 0.7, and 1.0 following the same test scheme as done for the extraction and scrub sections.

Clean-in-Place (CIP) Evaluation

The initial phase of the CIP testing was to determine percent capture of solids in the contactor rotor by processing a 0.1 wt % diatomaceous earth feed slurry at flowrates ranging from 1.9 L/min to 11.4 L/min at rotor speeds of 1750 to 3500 rpm. The 0.1 wt % feed slurry was prepared by adding diatomaceous earth (mean particle size 80 micron and a density of approximately 2.4 g/mL) to normal tap water under agitation. Diatomaceous earth was not selected as a surrogate for fines normally encountered in nuclear-fuel reprocessing but rather as a nonhazardous material for a first-time CIP scoping evaluation. Before testing began, a feed slurry sample was analyzed for solids concentration. During testing, four-liter samples were collected at each test condition, then vacuum filtered through Nalgene 0.2 micron (CN) disposable filters. Percent capture was calculated from the following equation:

$$\text{Percent Capture} = [1 - (\text{solid conc. in sample} / \text{solid conc. in feed slurry})] * 100\ \%$$

The CIP evaluation was initiated by pumping the feed slurry to the contactor at a flowrate of 7.5 L/min; the rotor speed was set to 2300 rpm. After the feed slurry (~110 L) had been pumped through the contactor, the pump was turned off, and the contactor rotor was shut down. The drain valve was opened slowly to minimize solids loss during draining. The contactor was then carefully disassembled to observe collected solids. Photographs of the solids captured in the rotor and vane package are shown in Figures 1 and 2.

Figure 1. Caked solids on rotor interior.

Figure 2. Solids collected in vane package.

After cleaning the rotor and reassembly, loading tests were repeated for two CIP tests using water as the cleaning solution. The rotor was stopped, slowly drained, then with the drain valve open, water was pumped through the spray nozzles at 25 L/min and 40 psig for 10 and 15 s, three times, while visually monitoring the discharged fluids. After each third-wash pulse, the effluent appeared free of solids. The contactor was again disassembled and inspected.

RESULTS

Hydraulic Evaluations

The maximum V-05 throughput for all solvent pairs was noted as the final total flowrate tested, where either-phase carryover was not measurable and defined to be <0.1% aqueous in organic (A in O) or organic in aqueous (O in A). Table 1 includes the maximum throughput obtained for (oil)/water and 30% TBP/1 M nitric acid pairs and is denoted with an asterisk.

Table 1. Maximum throughput without vents at O/A of 1 and rotor speed of 2000 rpm

(Oil)/water		**30% TBP/1 M nitric acid**	
Flowrate (L/min)	Carryover	Flowrate (L/min)	Carryover
2-16	Not measurable	14-20	Not measurable
18*	Not measurable	22*	Not measurable
20	0.3 % A in O, A is ok	24	0.2 % A in O, 4 % O in A
22	0.5 % A in O, A is ok	26	3 % A in O, 12 % O in A

Maximum throughputs for both solvent pairs agree favorably with the manufacturers rating of 20 L/min. The throughputs listed in Table 1 were measured before the vents were installed on discharge lines. Carryover determinations were then continued at changing flowrates, rotor speeds, and O/A ratios again with (Oil)/ water. Flowrates of 10, 12, and 16 L/min were tested with rotor speeds of 1500, 2000, 2500, and 3000 rpm and at O/A ratios of 0.2, 0.5, 1.0, 2.0, and 6.0. Overall, phase samples from this

entire test matrix revealed <0.1% phase carryover, excluding one test condition at 16 L/min with a rotor speed of 3000 rpm at an O/A ratio of 0.2.

A 30% TBP flowsheet testing provided maximum-throughput carryover results for changing flowrates, rotor speeds, and O/A ratios for three different solvent/nitric acid pairings. The test matrices started at 16 L/min at 2000 rpm and increasing flowrate at 2 L/min intervals. Rotor speed was increased when carryover was measured to examine rotor speed increase impact on carryover. Tables 2, 3, and 4 include the carryover measurements for the three solvent pairs at respective O/A ratios tested.

Table 2. 30% TBP extraction section tests

O/A = 1		**O/A = 2**		**O/A = 3**	
Flowrate (L/min)	Carryover	Flowrate (L/min)	Carryover	Flowrate (L/min)	Carryover
16-30	Not measurable	16-34	Not measurable	16-28	Not measurable
32	Not measurable	36	Not measurable	30-34	0.5 % A in O, A is OK

Table 3. 30% TBP scrub section tests

O/A = 4		**O/A = 6**		**O/A = 8**	
Flowrate (L/min)	Carryover	Flowrate (L/min)	Carryover	Flowrate (L/min)	Carryover
16-30	Not measurable	16-28	Not measurable	16-26	Not measurable
32	Not measurable	30	Not measurable	28	Not measurable
34	0.3 % A in O, A is OK	32	0.7 % A in O, A is OK	30	0.1 % A in O, A is OK

Table 4. 30% TBP strip section tests

O/A = 0.5		**O/A = 0.7**		**O/A = 1**	
Flowrate (L/min)	Carryover	Flowrate (L/min)	Carryover	Flowrate (L/min)	Carryover
16-20	Not measurable	16-24	Not measurable	16-30	Not measurable
22	Not measurable	26	Not measurable	32	Not measurable
24	0.1 % A in O, 0.3 % O in A	28	O is ok, 0.5 % O in A	34	1.3 % A in O, 0.6 % O in A

It is clear that the addition of the vents on the discharge lines resulted in a dramatic increase of throughput for the 30% TBP solvent/nitric acid pair in comparing carryover at an O/A ratio of 1. In all cases, increased rotor speed reduced overall carryover at maximum throughput. However, over mixing associated with increased rotor speeds can occur, so care must be used when applying this technique.

Percent Capture and CIP Capability

Percent capture results are shown in Figure 3. The percent capture at 1.9 L/min with a rotor speed of 3500 is omitted due to pump failure during testing but is expected to be >99% as related to those reported at the three lower rotor speeds.

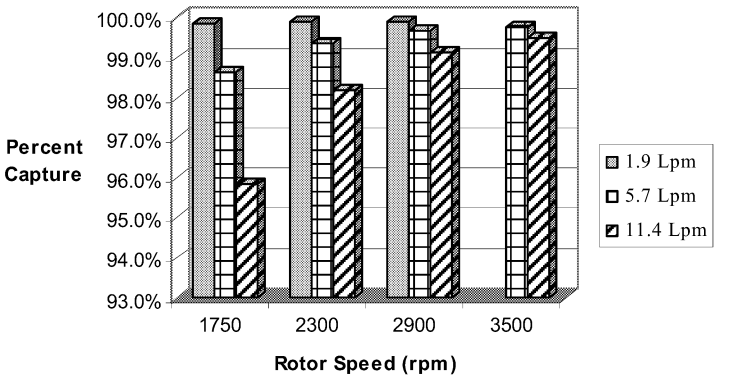

Figure 3. Percent capture as a function of flowrate and rotor speed.

The graph in Figure 3 illustrates that the percent capture is dependent on both flowrate and rotor speed. As expected, as rotor speed is increased, the percent capture increases and conversely, if flowrate is decreased, percent capture increases. Centrifugal contactors equipped with cleaning nozzles are effective at removing captured solids with small wash volumes. Three 10 s or three 15 s pulses performed at 25 L/min and 40 psig effectively cleaned the contactor internals.

CONCLUSIONS

Maximum hydraulic throughputs were confirmed using kerosene/water and 30% tributylphosphate in *n*-dodecane/nitric acid. Test results indicate that maximum throughputs of 18–32 L/min can be processed with the V-05 contactor without measurable phase carryover. The addition of vents on the discharge lines dramatically increased throughput compared to initial testing without vents. Annular centrifugal contactors are very effective at capturing solids. Greater than 95% of solids were captured in the rotor at all conditions tested. The CIP testing indicated captured solids can be effectively removed from the rotor interior using either three 10 s or three 15 s pulses. A future CIP evaluation with more representative solids is recommended.

CATALOG SOLVENT EXTRACTION: ANTICIPATE PROCESS ADJUSTMENTS

S.G. Campbell, E.A. Brass, S.J. Brown, and M.W. Geeting

Washington Savannah River Company, Savannah River Site, Aiken, SC
Corresponding author email address: seth.campbell@srs.gov

ABSTRACT

The Modular Caustic-Side Solvent Extraction Unit (MCU) utilizes commercially available centrifugal contactors to facilitate removal of radioactive cesium from highly alkaline salt solutions. During the fabrication of the contactor assembly, demonstrations revealed a higher propensity for foaming than was initially expected. A task team performed a series of single-phase experiments that revealed that the shape of the bottom vanes and the outer diameter of those vanes are key to the successful deployment of commercial contactors in the Caustic-Side Solvent Extraction Process.

BACKGROUND

In 2004, the Department of Energy (DOE) directed Washington Savannah River Company to deploy a Caustic-Side Solvent Extraction (CSSX) process at the Savannah River Site to provide interim processing of cesium-containing alkaline salt solution until the Salt Waste Processing Facility (SWPF) is operational. The CSSX process was developed in the DOE complex by multiple researchers [1-3]. In the process, cesium is extracted from the waste, concentrated, and stripped out of the solvent resulting in a low-level waste salt solution and a concentrated cesium nitrate stream. The concentrated cesium stream can be vitrified into borosilicate, and the salt solution can be dispositioned as a low-level grout.

The heart of the MCU process is 18 centrifugal contactors purchased from a vendor whose product is based on a DOE patent. There are 7 extraction contactors with 10-inch rotors (rotor diameter), due to the higher total flow rate in the extraction bank. The remainder of the contactors have 5-inch rotors. There are two scrub contactors, 7 strip contactors, and 2 wash contactors. A generic contactor cut-away diagram is shown in Figure 1. The contactors, support frame, temperature control, and interstage piping were assembled by a subcontractor as a modular piece of the MCU construction.

PROBLEM DESCRIPTION

During individual contactor testing at the subcontractor's facility, the goal was to determine an acceptable range of rotor speeds and aqueous (upper) weir sizes to minimize organic carryover in the aqueous phase. Copious amounts of foam were generated in many of those tests, and a surprising amount of air was expelled from some of the vents. The large air flow was suspected to be a primary cause of the foam. The CSSX process had been successfully demonstrated on several occasions, although on a smaller scale, with no comparable foam issues. This undesired operating condition prompted formation of a task team to resolve the excessive foam generation issue [4].

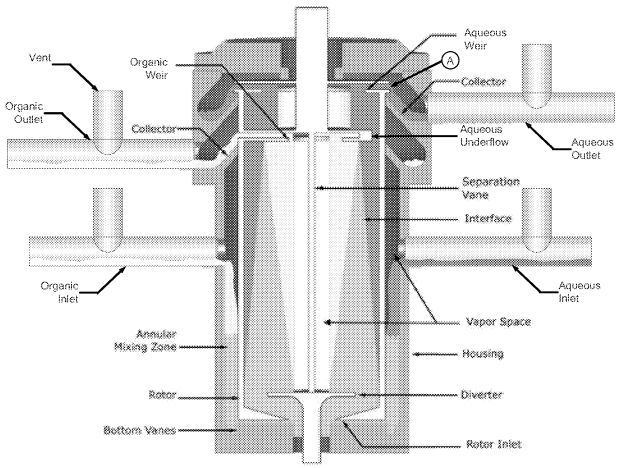

Figure 1. Centrifugal contactor cut-away.

The first objective of the task team was to determine the differences, other than scale, in the previous testing and the individual contactor testing. Most of the previous testing had been performed with contactors designed and fabricated at Argonne National Laboratory (ANL). Only a few tests had been performed with different designs and sizes. The Department of Energy (DOE) owns the patent on the ANL design. The vendor had purchased the right to use the DOE patent, and so their contactors were originally based on the same design. This was one reason the vendor's product was selected for the MCU.

Over the years, the vendor had made changes to simplify the design for manufacturing and to target the oil-water separation market. One change that had been previously investigated was the vendor's use of curved vanes in the contactor housing. Other changes, such as vane diameter and gap between the rotor and vanes, were not identified until the task-team investigation. Additionally, the vendor was requested to modify their design to expand the cleaning function. The original design directed spray to the rotor internals, but not the collector rings. The requested modification included adding spray nozzles in the collector rings to reduce contamination prior to maintenance.

The spray nozzles protruded into the collector rings tangentially by about in. at the time the foaming was identified as an issue. The hypothesis was that the solvent

exiting the rotor at high velocity was impacting the spray nozzle, which disrupted the flow path of the solvent and resulted in foam generation. It was also thought that the air flow was exacerbating the foaming issue. Due to schedule constraints, redesign and testing of the spray nozzles was pursued separately from the task team. The final collector ring nozzle design was flush with the contactor wall and therefore resulted in almost no change in the wall contour.

The task team agreed that the large amount of air flow was an indication that the amount of liquid in the mixing zone was not sufficient to "seal" the rotor. With an open air path through the annulus, the contactor was functioning like a fan, drawing air in through the inlet vents and blowing it out the exit vents. A series of tests were developed to attempt to increase the height of liquid in the mixing zone, thereby sealing the rotor. The test variables selected were the parameters that differed between the ANL and the vendor design that were likely to have an effect on the mixing zone liquid level: vane shape, vane outer diameter (major-vane diameter), rotor inlet diameter, and vane-to-rotor gap height.

EXPERIMENTAL

In order to determine the liquid level in the mixing zone (i.e., mixing zone height), 5-inch and 10-inch contactor housings, which had a glass window to view the annulus, were procured from the vendor. The windowed housings also had changeable bottom vane plates and the ability to add spacers to increase the vane-to-rotor gap. Straight-vane and curved-vane bottom plates were manufactured with several different major-vane diameters for use in the testing as well as the spacers for use in varying the vane-to-rotor gap. Five and 10-inch rotors were also procured and modified to facilitate changing the diameter of the rotor inlet by changing a plate on the bottom. Since testing was performed at subcontractor facilities, only water was used to minimize chemical hazards, except for a final two-phase demonstration with the recommended configuration to validate the results.

RESULTS AND DISCUSSION

In general, reducing the major-vane diameter increased the mixing-zone height. As the major-vane diameter approaches the rotor diameter, however, a point is reached where the contactor loses its ability to pump material into the rotor. The 5-inch contactor's mixing zone floods with a major-vane diameter of 5.1 in. and less, as seen in Figure 2A. A major-vane diameter of 5.17 in. provided the greatest increase in mixing-zone liquid height for the 5-inch contactor. When comparing straight vanes to curved vanes, the straight vanes maintain a slightly higher level in the mixing zone; however, the curved vanes facilitate a liquid seal of the rotor at lower mixing-zone heights. A comparison of air flows for both vane shapes in the 5-inch contactor is shown in Figure 2B. A dramatic drop in air flow is a sign that the liquid has sealed the rotor. The curved vanes seal the rotor with less liquid in the mixing zone, as seen in Figure 2B, specifically with a 5.17 in. major-vane diameter.

The 10-inch contactor demonstrated the same general behavior as the smaller unit with changes in major-vane diameter and vane shape. A major-vane diameter of 10.2 in. resulted in a flooded mixing zone as seen in Figure 3A. The larger contactor differed, however, in that no change in vane shape or size stopped the air flow (Figure 3B).

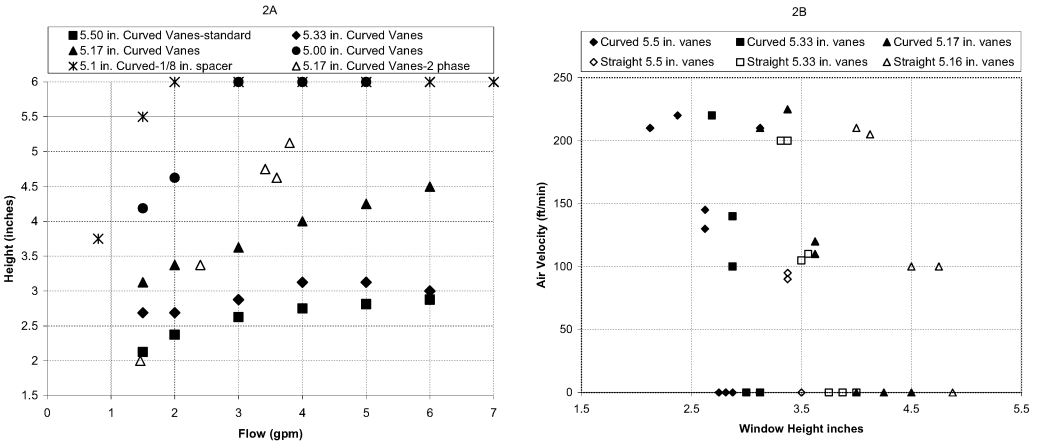

Figure 2. Curved-vane diameter effect on 5-inch contactor annulus height (2A) and air flow (2B).

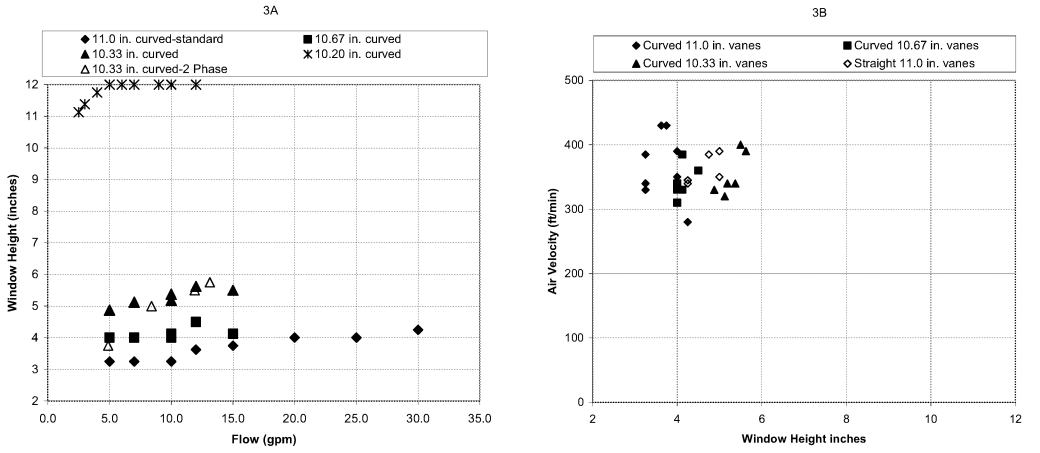

Figure 3. Curved-vane diameter effect on 10-Inch contactor annulus height (3A) and air flow (3B).

The testing also revealed that the vane-to-rotor gap height did not have a strong effect on the mixing-zone height until the gap is increased to the point that the contactor can no longer pump. Similarly, the rotor inlet size did not have a strong effect on the mixing-zone height, either. Like the gap height, once the rotor inlet increases beyond a certain point, the contactor loses its ability to pump, but up to that point, changing the size did not affect the mixing zone height.

Since the air flow was considered to be a primary contributor to excessive foaming and the collector ring spray nozzles had been successfully redesigned, no changes were proposed for the 10-inch contactors. It was recommended that the major-vane diameter of the 5-inch contactor be reduced to 5.17 in., since that modification resulted in both an increased mixing-zone height and reduced air flow through the contactor. While the vane shape did have an effect, in favor of straight radial vanes, the effect was relatively small. In addition, modifications to change the vane shape would be extremely difficult and time consuming.

Centrifugally-Induced Siphon

During the task team testing, the one-phase zero-point flow rate was established according to Leonard [1]. The one-phase zero-point flow rate is defined as the point where, as the flow is increased, liquid starts to come out the less-dense-phase (organic) exit. For these tests, water is used for the liquid phase, and flow rates are measured both above and below the zero point.

Tests showed that when using the vendor's contactor design, there was not only a zero-point but also a point where a siphon was created between the aqueous underflow and the aqueous weir, which drew both phases out the aqueous exit. This phenomenon, dubbed "centrifugally-induced siphon" by R. A. Leonard, can be seen in Figure 4 as a drop in the flow exiting the organic outlet as total flow increases.

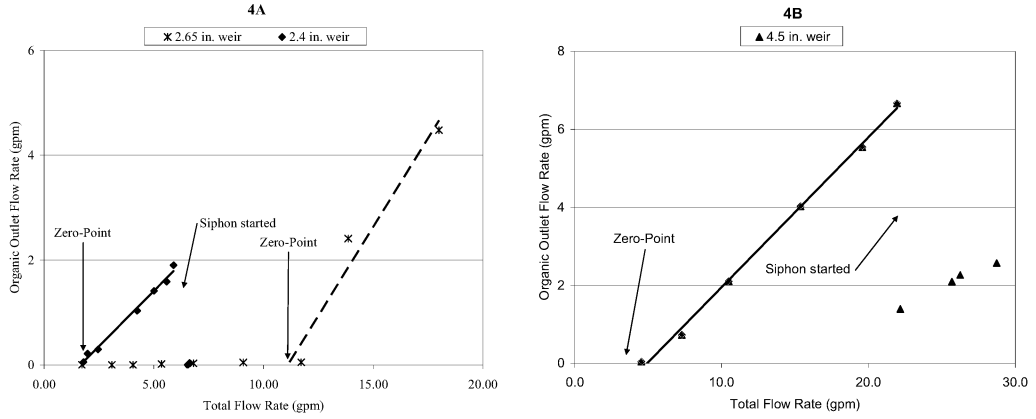

Figure 4. One-phase zero-point test data showing the actual zero-point and the point when siphoning started for a 5-inch rotor contactor (4A) and a 10-inch rotor contactor (4B).

A centrifugally-induced siphon occurs when the flow through the contactor is sufficient to flood the exit channel (A on Figure 1). The ANL contactor design prevented this phenomenon, because the exit channel is much larger, and it is vented. The vendor's design has a removable aqueous weir plate that is held in place by the rotor cover. The cover creates the aqueous exit channel, but does not have a dedicated vent. This design is exceptionally flexible when determining the optimum weir for processing, but it had the unintended effect of eliminating the vent path for the exiting aqueous stream.

The siphon was not considered an operational issue, since it occurred at flows much higher than the MCU operating range. During start-up, however, the siphon recurred at much lower flows. One significant difference was that this event occurred with two-phase flow. Still, the siphon would not have occurred, but the salt-solution flow had been surging during startup. As the salt solution surged into the contactor at the same time the solvent flow was starting, the flow through the aqueous outlet channel was sufficient to initiate the siphon.

CONCLUSIONS

Understanding the effects of collector-ring smoothness and vane diameter facilitated modifications that created a hydraulically stable process for MCU. Based on the single-phase testing, the task team recommended a reduction in the 5-inch contactor's bottom-vane major diameter from 5.5 in. (standard) to 5.17 in. The curved vanes resulted in a liquid seal of the rotor at lower annulus liquid heights versus straight vanes, so the standard curved vanes were maintained in the design, even though this departed from the DOE patented design. No changes were recommended for the 10-inch contactors. Redesign of the collector-ring spray nozzles, in combination with the recommended changes, resulted in a robust contactor for the CSSX process.

The same series of single-phase tests identified a phenomenon dubbed "centrifugally-induced siphon." The siphon occurs when the aqueous flow exiting the contactor rotor floods the exit channel. The knowledge gained about the centrifugally-induced siphon phenomenon has allowed MCU to develop operating procedures to prevent future occurrences and successfully complete cold runs.

ACKNOWLEDGMENTS

The authors thank the other members of the Contactor Issues Resolution Team for their contribution and support: R. A. Leonard, J. T. Carter, and W. E. Narrows.

REFERENCES

1. R. A. Leonard, M. C. Regalbuto, S. B. Aase, H. A. Arafat, and J. R. Falkenberg, "Hydraulic Performance of a 5-cm CINC Contactor for Caustic-Side Solvent Extraction," Argonne National Laboratory Report ANL-02/18, Argonne, IL, Dec. 21, 2001.
2. P. V. Bonnesen, L. H. Delmau, T. J. Haverlock, and B. A. Moyer, "Alkaline-Side Extraction of Cesium from Savannah River Tank Waste Using a Calixarene-Crown Ether Extractant," Oak Ridge National Laboratory Report ORNL/TM-13704, Oak Ridge, TN, Dec., 1998.
3. R. A. Leonard et al., "Multi-Day Test of the Caustic-Side Solvent Extraction Flowsheet for Cesium Removal from a Simulated SRS Tank Waste," Argonne National Laboratory Report ANL-02/11, Argonne, IL, Jan. 15, 2002.
4. S. Campbell, J. Carter, E. Brass, and S. Brown, "Hydraulic Test Report for the MCU Contactors," Washington Savannah River Company Letter Report CBU-SPT-2006-00110, Aiken, SC, July 25, 2006.

EXTRACTION OF ACTINIDES BY MULTIDENTATE DIAMIDES AND THEIR EVALUATION WITH COMPUTATIONAL MOLECULAR MODELING

Y. Sasaki,[1] Y. Kitatsuji,[1] M. Hirata,[1] T. Kimura,[1] and K. Yoshizuka[2]

[1]Japan Atomic Energy Agency, Tokai-mura, Ibaraki 319-1195, Japan. [2]The University of Kitakyushu, Wakamatsu, Kitakyushu, Fukuoka 808-0135, Japan
Corresponding author email address: sasaki.yuji@jaea.go.jp

ABSTRACT

Multidentate diamides have been synthesized and examined for actinide (An) extractions. Bi- and tridentate extractants are the focus in this work. The extraction of actinides was performed from 0.1-6 M HNO_3 to organic solvents. It was obvious that *N,N,N',N'*-tetraalkyl-diglycolamide (DGA) derivatives, 2,2'-(methylimino)bis(*N,N*-dioctylacetamide) (MIDOA), and *N,N'*-dimethyl-*N,N'*-dioctyl-2-(3-oxapentadecane)-malonamide (DMDOOPDMA) have relatively high *D* values (*D*(Pu) > 70). The following notable results using DGA extractants were obtained: (1) DGAs with short alkyl chains give higher *D* values than those with long alkyl chain, (2) DGAs with long alkyl chain have high solubility in *n*-dodecane. Computational molecular modeling was also used to elucidate the effects of structural and electronic properties of the reagents on their different extractabilities.

INTRODUCTION

The development of the novel extractants for the actinide (An) ions has been widely studied for the chemical treatment of the high-level radioactive liquid waste (HLW) [1-4]. Diamide extractants can extract the metal ions directly from HLW of 3 M HNO_3, because an ion-pair extraction by the neutral donor gives high distribution ratios of metals from solutions of high ionic concentration. One of the significant advantages of the diamide extractants is incinerability; these ligands can be combusted and therefore produce no radioactive solid waste. The amide and diamide derivatives are synthesized easily from appropriate carboxylic acids and amines [2,5-6]; a wide variety of diamide structures through the organic reactions using the different initial materials can be expected. A structural study on solvent extraction and computational molecular modeling can be correlated and discussed.

In the present investigation, nine diamide type extractants having bi- and tri-dentation were employed for actinide extraction: 2,2'-(methylimimno)-bis(*N,N*-dioctylacetamide) (MIDOA), *N,N,N',N'*-tetraoctyl-3-thiadiglycolamide (TOTDGA), *N,N,N',N'*-tetraoctyl-3-oxopentanediamide (TOOXPDA), trioxaheptacosane (TOHCO), *N,N'*-dimethyl-*N,N'*-dioctyl-2-(3-oxapentadecane)-malonamide (DMDOOPDMA),

N,N,N',N'-tetradecyl-3-diglycolamide (TDDGA), *N,N,N',N'*-tetradodecyl-3-diglycolamide (TDdDGA), *N,N,N',N'*-tetraoctylmalonamide (TOMA), and *N,N,N',N'*-tetraoctyl-3-diglycolamide (TODGA). The structures of the examined diamides are illustrated in Figure 1. We have studied the effect of the diamide structures on an extraction.

EXPERIMENTAL

Chemicals

All the reagents used for organic synthesis were commercially available. The radioactive tracers of ^{99}Tc, ^{233}U, ^{230}Th, ^{237}Np, and ^{241}Am were obtained from Isotope Products Laboratories. All the other reagents were of analytical reagent grade.

Organic Synthesis

MIDOA, TOTDGA, TOMA, and DGA derivatives were synthesized from the carboxylic chloride and the secondary amines [7-8]. The carboxylic chlorides were prepared by the corresponding acids by the reaction with thionyl chloride. The products were mixed slowly in chloroform with triethylamine under the freezing point (0-5 °C) and stirred overnight. The mixture was washed with distilled water, 1 M HCl, and 1 M NaOH, and the final products were purified by distillation and column chromatography with silica gel. All diamides synthesized were identified by NMR (UNITY plus 400, Varian) and GC-MS (TurboMass, Perkin Elmer Inc.). Other diamides, TOOXPDA, TOHCO, and DMDOOPDMA were purchased from Wako-Pure Chemical Ind. Ltd.

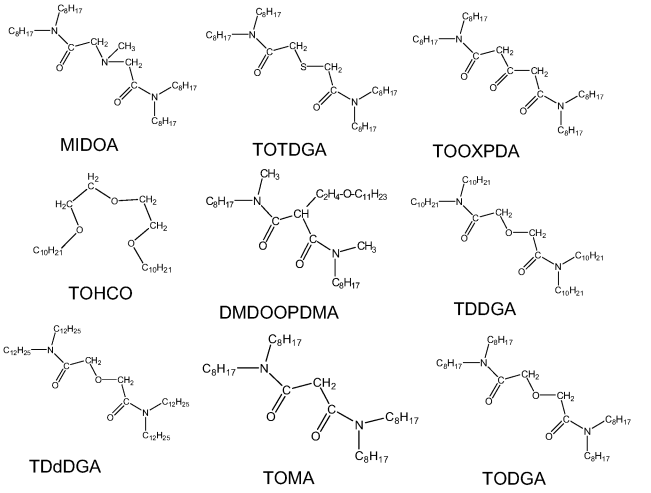

Figure 1. Structures of extractants used in this work.

Extraction Procedure

Three mL of the organic solution containing diamide of the concentration from 5 x 10^{-6} to 0.2 M was shaken with an equal volume of nitric acid solution. After centrifugation, 2 mL of the pre-equilibrated organic phase was taken and mixed with 2 cm^3 of the aqueous phase of the same concentration as in pre-equilibration, spiked with 10^{-2} mL of the radioactive tracer solution. The mixture was shaken mechanically for 2 h controlled at 25 ± 0.1 °C. After phase separation through centrifugation, duplicate 0.50

mL aliquots were measured with a NaI scintillation counter (COBRA 5003, Packard Instrument Company) for the gamma activities of ^{241}Am and a liquid-scintillation counter (Tri-Carb 1600 TR, Packard Instrument Company) for the alpha activities of ^{230}Th, ^{233}U, and ^{238}Pu in 5 mL of ULTIMA-FLO (Packard Instrument Company) cocktail.

Molecular Modeling

The quantum-chemical calculations of the reagents shown in Figure 1 were carried out by Gaussian03 software. The calculation method was density functional theory with 6-31G* basis set. All the molecules were optimized in vacuo. Input coordinates of the reagents were produced with the graphics package HyperChem™ [9]. The quantum-chemical calculations of all the reagents converged smoothly to obtain the optimal structures and the electron-density distributions.

RESULTS AND DISCUSSION

Solubility in *n*-Dodecane and Melting and Boiling Points for Diamide Compounds

The solubility in *n*-dodecane and melting and boiling points for newly-synthesized reagents were measured, and the results are shown in Table 1. All reagents show high solubility in *n*-dodecane, allowing for the preparation of diamide solutions with concentrations of 1 M or higher. With the exception of TDDGA and TDdDGA, the reagents are liquids at room temperature.

Table 1. Solubility of the new reagents in *n*-dodecane and melting and boiling points

	Solubility in *n*-dodecane/ g/mL	melting point °C	boiling point* °C
1 MIDOA	> 1.66	liquid at room temperature	270
2 TOTDGA	> 1.66	liquid at room temperature	337
3 TOOXPDA	> 1.00	liquid at room temperature	290
4 TOHCO	> 1.66	liquid at room temperature	270
5 DMDOOPDMA	> 1.00	liquid at room temperature	330
6 TDDGA	> 1.00	28	400
7 TDdDGA	> 1.04	32	500
8 TOMA	> 1.00	liquid at room temperature	350
9 TODGA	> 1.38	liquid at room temperature	380

*gasified with heat-decomposition

Extraction of Actinides by Different Diamides

The distribution ratios, *D*(Am), *D*(Pu), and *D*(U), are expressed by the ratio of An concentration in the organic phase to that in the aqueous phase. These values were obtained at 0.1 and 3 M HNO_3 and are shown in Table 2. Since diamide extractants are

neutral donors, the extraction reactions are ion-pair in nature and accompanied by co-extracted counteranions. The trivalent Ans have very low affinities with most of the diamides used here; only DGA-based ligands have a high *D*(Am). Since tetravalent An(Pu) is, in general, the most extractable of An metals [10], *D*(Pu) for respective ligands are higher than those for Am and U. *D*(U) values of more than unity are obtained by DMDOOPDMA and DGA ligands. From the results obtained in this work, Am(III) can be extracted quantitatively by one batch experiment using DGA ligands, Pu(IV) can be extracted by one batch experiment using MIDOA (**1**), DMDOOPDMA (**5**), TOMA (**8**), and DGA series (**6**, **7**, and **9**), and U(VI) can be extracted by multistep extraction using extractants described above. The order of *D* values for these ligands is Pu(IV) > U(VI) > Am(III) for (**1**-**3**), (**5**), and (**8**), and Pu(IV) > Am(III) > U(VI) for (**6**, **7**, and **9**). The extractability trend of the extractants determined for *D*(Pu) is **6**, **7**, **9** > **5** > **1** > **8** > **2** > **3** > **4**. It is clear that DGAs have high *D* values for all actinide species studied at 3 M HNO_3.

Table 2. Distribution ratios of actinides for new reagents

	0.1 M HNO_3			3 M HNO_3		
	Am(III)	Pu(IV)	U(VI)	Am(III)	Pu(IV)	U(VI)
1 MIDOA	<0.001	2.68	0.42	<0.001	79.6	0.26
2 TOTDGA	<0.001	0.093	<0.001	<0.006	5.8	0.46
3 TOOXPDA	<0.001	0.188	<0.001	<0.001	0.37	0.019
4 TOHCO	<0.001	<0.001	<0.001	<0.001	<0.001	<0.001
5 DMDOOPDMA	<0.005	0.176	<0.008	0.058	87.1	7.93
6 TDDGA	0.038	3.08	0.015	>1000	>100	7.91
7 TDdDGA	0.030	0.845	0.001	>1000	>1000	4.02
8 TOMA	<0.006	<0.006	<0.009	<0.01	59	0.296
9 TODGA	0.037	2.71	0.0105	>1000	>1000	5.4

Extractant concentration: 0.1M in *n*-dodecane.

Molecular Modeling of the Reagents

Table 3 shows the electron density of donor atoms of the new reagents. In DGA derivatives, the electron densities of carbonyl oxygen and nitrogen atoms are almost the same regardless of the alkyl chain length. This suggests that the extractability is mainly controlled by the lipophilicity of the reagents.

In **1** and **2**, which substitute *N* or *S* atoms for ether *O* atom, the electron density of the *N* or *S* atoms as a centre atom is lower than that in DGA derivatives such as **9**, and especially, the electron density of the *S* atom is positive. This suggests that the coordination abilities of these reagents decrease slightly, while the affinities of the soft metals having lower electron density are preferable. The electron densities of centre atoms in **4** are comparably low, which means a low coordination ability with metals. The electric density of the center *O* atom in **3,** in which a carbonyl moiety substitutes for the ether moiety, is slightly low compared with DGA derivatives.

In malonamide derivatives such as **5** and **8**, the electron density of the *O* atom is increased by introducing an ether moiety or phenyl moiety between the two carbonyl

moieties. However, extractabilities of An by **5** and **8** are lower than these of DGA derivatives, as mentioned later. This suggests that the ether *O* atom in DGA may contribute to the coordination with metal.

Table 3. Electron density of donor atom of the new reagents

Extractants	Carbonyl (amide)	Carbonyl (center)	Ether (ROR)	Sulfur (RSR)	Nitrogen (center)	Nitrogen (amide)
1 MIDOA	-0.529	-	-	-	-0.403	-0.453
2 TOTDGA	-0.517	-	-	0.138	-	-0.441
3 TOOXPDA	-0.527	-0.439	-	-	-	-0.439
4 TOHCO	-	-	-0.510	-	-	-
5 DMDOOPDMA	-0.545	-	-0.510	-	-	-0.449
6 TDDGA	-0.523	-	-0.483	-	-	-0.446
7 TDdDGA	-0.524	-	-0.492	-	-	-0.440
8 TOMA	-0.524	-	-	-	-	-0.443
9 TODGA	-0.524	-	-0.492	-	-	-0.440

Effect of the Alkyl Groups Attached to *N* atoms of DGA on Extraction

The dissolution of synthesized DGA was tested using water and *n*-dodecane. The structures of DGA derivatives used here are: $(O\text{-}(CH_2CON(C_nH_{2n+1})_2)_2$ (n = 1, 2, 3, 4, 5, 6, 8, and 10). The solubilities of 8 kinds of DGA derivatives into water are shown in Table 4. These values also support the fact that DGAs with shorter alkyl chains exhibit

Table 4. Solubility of DGA* in water and *n*-dodecane and distribution ratios (*D*) for Am(III)

	n	solubility in water/ mM	dissolution in *n*-dodecane	*D*(Am)**	
				chloroform	*n*-dodecane
TMDGA	1	> 1000	suspension	-	-
TEDGA	2	> 1000	suspension	-	-
TPDGA	3	57	suspension	0.41	-
TBDGA	4	2.3	soluble	0.24	-
TADGA	5	0.25	soluble	0.11	-
THDGA	6	0.11	soluble	0.089	40
TODGA	8	0.042	unlimited	0.071	30
TDDGA	10	0.042	unlimited	0.042	18

* General structure of DGA: $O\text{-}(CH_2CON(C_nH_{2n+1})_2)_2$ (n = 1, 2, 3, 4, 5, 6, 8, 10).
** Determined by using 0.1 M DGA/solvent and 1 M HNO_3.

higher hydrophilicity; TMDGA and TEDGA can be used in the aqueous phase. TPDGA, TBDGA, TADGA, and THDGA are slightly soluble in water and *n*-dodecane; besides, these have the high solubility in polar solvents. TODGA and TDDGA, which show low solubility in water, can be dissolved in *n*-dodecane satisfactorily. The distribution ratios for Am(III) in the system of 1 M HNO_3 and 0.1 M DGA in organic diluent decreases with increase in alkyl chain length.

ACKNOWLEDGMENTS

The authors gratefully acknowledge Professor Emeritus G. R. Choppin of Florida State University and Drs. Y. Morita and Y. Sugo of Japan Atomic Energy Agency for useful discussions and experimental support. Staff of Wako-Pure Chemical Ind. Ltd. are thanked for the organic synthesis.

Present study includes the result of "Development of separation technology of transuranium elements and fission products by using new extractants and adsorbents" entrusted to "Japan Atomic Energy Agency" by the Ministry of Education, Culture, Sports, Science, and Technology of Japan (MEXT).

REFERENCES

1. E. P. Horwitz, D. G. Kalina, L. Kaplan, G. W. Mason, and H. Diamond, "Selected Alkyl(phenyl)-N,N- Dialkylcarbamoylmethylphosphine Oxide as Extractants for Am(III) from Nitric Acid Media," *Sep. Sci. Technol.*, **17**, 1261-1279 (1982).
2. C. Cuillerdier, C. Musicas, P. Hoel, L. Nigond, and X. Vitart, "Malonamide as New Extrcatants for Nuclear Waste Solutions," *Sep. Sci. Technol.*, **26**, 1229-1244 (1991).
3. Z. Kolarik, U. Müllich, and F. Gassner, "Selective Extraction of Am(III) over Eu(III) by 2,6-Ditriazolyl- and 2,6-Ditriazinylpyridine," *Solvent Extr. Ion Exch.*, **17**, 23-32 (1999).
4. A. N. Turanov, V. K. Karandashev, and V. E. Baulin, "Extraction of Rare-Earth Elements from Nitric Solutions by Phosphoryl-Containing Podands," *Solvent Extr. Ion Exch.*, **17**, 1423-1444 (1999).
5. G. M. Gasparini and G. Grossi, "Long Chain Distributed Aliphatic Amides as Extracting Agents in Industrial Applications of Solvent Extraction," *Solvent Extr. Ion Exch.*, **4**, 1233-1271 (1986).
6. Y. Sasaki and S. Tachimori, "Extraction of Actinides(III), (IV), (V), and (VI) and Lanthanides(III) by Structurally Tailored Diamides," *Solvent Extr. Ion Exch.*, **20**, 21-34 (2002).
7. T. H. Siddall III and M. L. Good, "Proton Magnetic Resonance Studies and Extraction Properties of Some Simple Daimides," *J. Inorg. Nucl. Chem.*, **29**, 149-158 (1967).
8. Y. Sasaki and G. R. Choppin, "Solvent extraction of Eu, Th, U, Np, and Am with *N,N'*-Dimethyl-*N,N'*-dihexyl-3-oxapentanediamide and its Analogous Compounds," *Anal. Sci.*, **12**, 225-230 (1996).
9. HyperChem™ Release 7, Hypercube, Inc., Canada, 2006.
10. G. R. Choppin, "Separation Processes for Actinide Elements," *Sep. Sci. Technol.*, **19**, 911-925 (1984-1985).

CHEMICAL INTERACTION MATRIX BETWEEN REAGENTS IN A PUREX BASED PROCESS

R. K. Brahman,[1] W.P. Hennessy,[1] and P. Paviet-Hartmann[2]

[1]*Shaw AREVA MOX Services, LLC.* [2]*Idaho State University/Idaho National Laboratory*
Corresponding author email address: rbrahman@moxproject.com

ABSTRACT

The United States Department of Energy (DOE) is the responsible entity for the disposal of the United States excess weapons grade plutonium. DOE selected a PUREX-based process to convert plutonium to low-enriched mixed oxide fuel for use in commercial nuclear power plants. To initiate this process in the United States, a Mixed Oxide (MOX) Fuel Fabrication Facility (MFFF) is under construction and will be operated by Shaw AREVA MOX Services at the Savannah River Site. This facility will be licensed and regulated by the U.S. Nuclear Regulatory Commission (NRC). A PUREX process, similar to the one used at La Hague, France, will purify plutonium feedstock through solvent extraction. MFFF employs two major process operations to manufacture MOX fuel assemblies: (1) the Aqueous Polishing (AP) process to remove gallium and other impurities from plutonium feedstock and (2) the MOX fuel fabrication process (MP), which processes the oxides into pellets and manufactures the MOX fuel assemblies. The AP process consists of three major steps, dissolution, purification, and conversion, and is the center of the primary chemical processing. A study of process hazards controls has been initiated that will provide knowledge and protection against the chemical risks associated from mixing of reagents over the life time of the process. This paper presents a comprehensive chemical interaction matrix evaluation for the reagents used in the PUREX-based process. Chemical interaction matrix supplements the process conditions by providing a checklist of any potential inadvertent chemical reactions that may take place. It also identifies the chemical compatibility/incompatibility of the reagents if mixed by failure of operations or equipment within the process itself or mixed inadvertently by a technician in the laboratories.

INTRODUCTION

The US Mixed Oxide (MOX) Fuel Fabrication Facility (MFFF) is being designed to produce MOX fuel assemblies for use in domestic commercial nuclear power reactors. This facility will be a major component in the United States program to dispose of surplus weapon-grade plutonium. The facility will take surplus weapon-grade plutonium, remove impurities by aqueous process, and fabricate plutonium dioxide, which will be mixed with uranium dioxide to form MOX fuel pellets for reactor fuel assemblies. These assemblies will be irradiated in commercial nuclear power reactors. The design of the facility is based on AREVA's MELOX and La Hague facilities in France. The facility is

under construction at the Savannah River Site (SRS) and will be regulated and licensed by the Nuclear Regulatory Commission (NRC). The facility consists of the two major sections (1) Aqueous Polishing process (AP) and (2) MOX process (MP), as shown in Figure 1. Before surplus weapon grade plutonium can be used to make MOX, the plutonium oxide must be purified. The purification process is applied to purify weapon-grade material through solvent extraction; it is accomplished in three basic steps and uses chemical reagents to remove impurities such as gallium, americium, and uranium. This process is conducted prior to the mechanical process of combining uranium and plutonium oxides to produce MOX fuel rods. This paper presents a comprehensive chemical interaction matrix of reagents and process fluids used in the AP process to supplement the AP process conditions by providing a checklist of any potential inadvertent chemical reactions that may accidentally take place and could create a safety hazard for the process. The chemical interaction matrix identifies chemical-reaction hazards among the reagents used in the AP process.

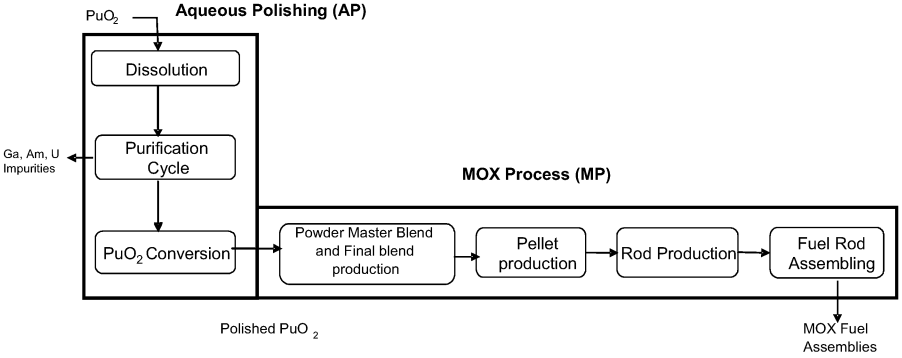

Figure 1: Mixed oxide (MOX) fuel fabrication

CHEMICAL INTERACTION MATRIX

One of the safety concerns is that if an unsafe amount of compound A is added to the process by an operation failure, or if compound A is mixed inadvertently with non-compatible compound B, a hazard such as fire or explosion due to a chemical reaction might occur. To investigate this concern, all potential adverse reactions between the reagents used in the AP process are examined. The chemical interaction matrix is a particularly useful tool that is used early in the development of safety demonstration of process plant operations. To create this matrix, the reagents used in the AP process have been listed (Table 1). Reagents in the following table are used at various stages of the purification process for liquid-liquid extraction and scrubbing, solvent washing, or as catalyzer. The process involves mixing several of them under controlled conditions. In addition, because solutions are transferred from one equipment to another, there is the potential for inadvertent mixing of those same reagents. The interaction matrix is an important tool in understanding intended/unintended interactions among various chemical species used in the process at any stage in the process. The interaction matrix is particularly valuable in the development of a new chemical process to identify possible/known chemical reactions and early application of the matrix. To create this

matrix, chemical interactions between each of the reagents used in the AP process were evaluated and researched. There is no single/consolidated resource that integrates this entire binary interaction of reagents. The interaction potential of each reagent is identified in Table 1. This matrix goes beyond a simple Yes/No answer by providing notes that give detailed information on the nature of the interaction. This is supported by referencing to a publication or a Material Safety Data Sheet (MSDS). Three classes of chemical compatibility have been identified as follows: (1) "NO" means mixing may form gases, generate heat, and produce vigorous exothermic reactions. It has to be noted that "NO" does not mean mixing those reagents would necessarily lead to an accident. In fact, the normal process involves mixing, on a routine basis, several reagents falling in that category; this is done in defined, safe conditions. However, inadvertent mixing of the same reagents, in uncontrolled conditions, has to be prevented or mitigated. (2) "C" means caution, mild reaction possible or unknown reaction. (3) "YES" means the two chemicals can be mixed without adverse reactions. Table 1 and the following notes provide information on the chemical compatibility/incompatibility while mixing the reagents within the AP process or during their preparation in the laboratory. For MFFF, it is essential to note that no chemical incompatibilities between the reagents have been observed at the reference plant La Hague under this PUREX-based process

Table 1: Chemical interaction matrix between reagents used in the AP process

CHEM. NAME	HNO_3	HAN	TBP	DODECANE	H_2O_2	$AgNO_3$	Na_2CO_3	NaOH	Na_2SO_3	$H_2C_2O_4$	$Zr(NO_3)_4.5H_2O$	N_2O_4	$Mn(NO_3)_2$	$Al(NO_3)_3.9H_2O$	$NaNO_3$
HNO_3		NO[1]	NO[2]	NO[3]	C[4,44]	NO[28]	C[7,49]	NO[7]	**C[26,35]**	NO[34]	YES[34]	YES[34]	YES[34]	NO[36]	YES[39]
HAN	NO[1]		YES[32]	YES[32]	**C**[5]	YES[6]	YES[32]	NO[31]	YES[9]	C[33]	NO[31]	NO[11]	C[13, 31]	C[18]	NO[39]
TBP	NO[2]	YES[32]		YES[46]	NO[45]	YES[29]	YES[48]	NO[47]	YES[37]	YES[48]	NO[25]	**C**[23]	YES[14]	C[40]	YES[39]
Dodecane	NO[3]	YES[32]	YES[46]		NO[45]	YES[29]	YES[50]	YES[51]	YES[37]	NO[34]	YES[42]	NO[12]	YES[15]	C[40]	YES[39]
H_2O_2	C[4,44]	**C**[5]	NO[45]	NO[45]		NO[28]	YES[8]	C[8,44]	NO[35]	C[22,44]	YES[42]	NO[43]	YES[16]	**C**[19]	NO[39]
$AgNO_3$	NO[28]	YES[6]	YES[29]	YES[29]	NO[28]		YES[29]	NO[28]	C[35]	NO[10]	C[30]	C[30]	C[17]	C[30]	YES[39]
Na_2CO_3	**C**[7,49]	YES[32]	YES[48]	YES[50]	YES[8]	YES[29]		YES[50]	YES[37]	C[49]	YES[42]	YES[50]	YES[38]	YES[41]	YES[39]
NaOH	NO[7]	NO[31]	NO[47]	YES[51]	C[8,44]	NO[28]	YES[50]		YES[37]	NO[52]	YES[42]	YES[27]	YES[38]	YES[41]	YES[39]
Na_2SO_3	**C[26,35]**	YES[9]	YES[37]	YES[37]	NO[35]	C[35]	YES[37]	YES[37]		C[26,35]	C[35]	C[35]	YES[38]	C[35]	YES[37]
$H_2C_2O_4$	NO[34]	C[33]	YES[48]	NO[34]	C[22,44]	NO[10]	C[49]	NO[52]	C[26,35]		YES[42]	YES[53]	YES[34]	YES[20]	YES[39]
$Zr(NO_3)_4.5H_2O$	YES[34]	NO[31]	NO[25]	YES[42]	YES[42]	C[30]	YES[42]	YES[42]	C[35]	YES[42]		YES[42]	YES[34]	C[54]	YES[39]
N_2O_4	YES[34]	NO[11]	**C**[23]	NO[12]	NO[43]	C[30]	YES[50]	YES[27]	C[35]	YES[53]	YES[42]		YES[38]	YES[21]	YES[39]
$Mn(NO_3)_2$	YES[34]	C[13,31]	YES[14]	YES[15]	YES[16]	C[17]	YES[38]	YES[38]	YES[38]	YES[34]	YES[34]	YES[38]		YES[38]	YES[39]
$Al(NO_3)_3.9H_2O$	NO[36]	**C**[18]	C[40]	C[40]	**C**[19]	C[30]	YES[41]	YES[41]	C[45]	YES[20]	C[54]	YES[21]	YES[38]		YES[39]
$NaNO_3$	YES[39]	NO[39]	YES[39]	YES[39]	NO[39]	YES[39]	YES[39]	YES[39]	YES[39]	YES[39]	YES[39]	YES[39]	YES[24]	YES[39]	

NO - Mixing may form gases, generates heat and produces a vigorous exothermic reaction. These potential chemical incompatibilities are mitigated or prevented through the control of process parameters (temperature, concentration, etc...) or alternate controls within the MFFF Process.
C - Caution, mild reactions possible.
YES - Chemicals can be mixed without reaction.

Notes

[1]Nitrous acid (HNO_2) resulting from the decomposition of nitric acid under standard storage and use conditions reacts with HAN to produce more nitric acid to initiate autocatalysis [1].

[2]Concentrated nitric acid (HNO_3) can cause decomposition of TBP to 'red oil' at temperatures approximately of ~130 °C, leading to explosion and fire hazards [2]. [3]HNO_2, resulting from the decomposition of nitric acid under standard storage and use conditions, can degrade in nitrate hydrocarbons and are a potential fire hazard [3]. [4]High concentrations (i.e., 90%) of H_2O_2 can form the explosive compound pernitric acid (HO_2NO_2) In addition, the reaction with highly concentrated nitric acid and oxalate ions ($C_2O_4^{2-}$) can be vigorous [4]. [5]Hydroxylamine react with hydrogen peroxide, although these reactions may be slow without the presence of a catalyst [5,6]. [6]Hydroxylamine can reduce silver nitrate to metallic nitrate along with some release of heat [7,8]. [7]Reactions of strong acids and strong bases can be highly exothermic, evolve gases, and proceed rapidly, leading to explosion and/or spill hazards. [9]; [8]H_2O_2 is slowly decomposed by alkaline solution [10]. [9]Sodium sulfite can react with hydroxylamine, though the parameters for this reaction are not well known [11]. [10]Reaction of silver nitrate and oxalic acid can produce silver oxalate ($Ag_2C_2O_4$), a thermally unstable compound [12]. [11]Dinitrogen tetroxide (N_2O_4) is in equilibrium with $2NO_2$, which generates more nitrous acid in the HAN/HNO_3 reaction, which accounts for autocatalysis [1]. [12]N_2O_4 is in equilibrium with $2NO_2$, the active species for the reaction of HNO_2 with hydrocarbons, resulting in short-chain nitrated hydrocarbons that present a fire hazard [3]. [13]Under high pH conditions with unique supporting ligands, Mn(II) can catalyze the reduction of O_2 to H_2O_2 [13]. Also, hydroxylamine may be used as the electron source in reduction of O_2 to H_2O_2 with special ligands at high pH [14]. [14]Mn(II) can form complexes with TBP, though no further reaction is expected [15]. [15]Aromatic compounds can be oxidized by Mn(II) complexes with a special ligand set in the presence of H_2O_2 [16]. Since, there are no aromatic compounds in dodecane, there is no chemical incompatibility between manganese nitrate and dodecane. [16]See note 15. Under some conditions, Mn(II) complexes with the appropriate ligands can activate H_2O_2 to oxidize various substrates [17]. [17]An inert solid can precipitate from Mn(II) and $AgNO_3$ with supporting ligands [18]. Manganese nitrate is an oxidizer and, according to [19], it may be incompatible with silver nitrate under specific conditions. [18]Aluminum nitrate is not combustible but is a strong oxidizer, and its heat of reaction with reducing agents such as hydroxylamine may cause ignition [20]. [19]Decomposition of H_2O_2 by contact with Al is inhibited by dissolving in the H_2O_2 2-25 ppm Al as an inorganic salt, (e.g., $Al(NO_3)_3.9H_2O$) [21]. [20]At low solution pH, a neutral salt of the composition of $Al_2(C_2O_4)_3$ forms, while in a neutral or weakly alkaline solution, the compound $NaAl(C_2O_4)_2$ is stable [22]. [21]No chemical incompatibility has been found between N_2O_4 and $Al(NO_3)_3$ [23,24]. [22]No chemical incompatibility has been found when H_2O_2 is added to heated oxalic acid solution [25]. [23]The excess ratio of N_2O_4 in TBP indicates possible formation of charge-transfer complexes with molecular or ionic structure [26]. [24]The reactivity of Mn nitrate was studied in four media, $NaNO_3$, $NaNO_2$, KNO_3, and KNO_2. The Mn salts give a variety of compounds, mainly oxides and also oxychloride and Na manganate [27]. [25]The TBP-Zirconium reaction has been investigated in [28]. Extracted zirconium $Zr(NO_3)_4.2TBP$, has been found to react with TBP to produce a relatively insoluble, crystalline zirconium organic phosphate. [26] Contact with acids will release SO_2 [29]. [27]Models of the absorption of NO_x by NaOH solutions are presented, with consideration of the diffusion rate of NaOH, finding no incompatibility [30]. [28-42]Refer MSDS of chemical reagents. [43,44,48,50]Hydrogen peroxide is incompatible with acid and base [31]. It is recommended to be cautious if there is a potential mixing with sodium hydroxide, nitric acid, and oxalic acid. [45,51]Mixtures of hydrogen peroxide and organic materials such as TBP are known for their hazard potential. There exists a range of concentrations where they have explosive properties [32]. [46,53]TBP is compatible with alkane-type diluents such as dodecane [33], and water. [47]TBP is incompatible with base such as sodium hydroxide [34]. It may degrade to oxides of carbon and phosphorus. [49]Sodium carbonate is incompatible with strong acid and aluminum

[35]. [52]Sodium hydroxide is incompatible with acid [36]. [54]There is a potential exothermic reaction when aluminum nitrate and zirconium nitrate are dissolved in water [37].

CONCLUSION

This paper is the basis for identifying chemicals that cannot be mixed or if mixed could create a safety hazard. This is used as an input to the MFFF process hazard analysis. The interaction matrix supplements the process safety analysis by providing a tool to identify potential inadvertent chemical reactions. It also establishes chemical compatibility/incompatibility of reagents if mixed by operator error or equipment within the process itself or mixed inadvertently by a technician in the laboratories.

REFERENCES

1. G. S. Barney, Technical Report on Hydroxylamine Nitrate, DOE/EH-0555 (1998). W. W. Schulz, J. D. Navratil, Eds., Science and Technology of Tributyl Phosphate, CRC Press, 1987.
2. A. Tahraoui and J. Morris, "Decomposition of solvent extraction media during nuclear reprocessing: literature review," *Sep. Sci. Technol.*, **30**, 2603-2630 (1995).
3. E. Kim, D. Chung, J. Park, and J. Yoo, "Dissolution of oxalate precipitate and destruction of oxalate ion by hydrogen peroxide in nitric acid solution," *J. Nucl. Sci. Technol.*, **37**, 601-607 (2000).
4. L. Bargallo, F. Borrull, V. Cerda, and J. Guasch, "Copper(II) trace determination by means of a catalytic thermometric method based on the hydroxylamine-hydrogen peroxide reaction," *Thermochim. Acta*, **117**, 283-289 (1987).
5. D. P. Graham, "Promoter action in reactions of oxidation concomitant with the catalytic decomposition of hydrogen peroxide I- The oxidation of hydrazine," *J. Am. Chem. Soc.*, **52**, 3035-3045 (1930).
6. N. Leopold and B. Lendl, "A new method for fast preparation of highly surface-enhanced Raman scattering (SERS) active silver colloids at room temperature by reduction of silver nitrate with hydroxylamine hydrochloride," *J. Phys. Chem., B*, **107**, 5723-5727 (2003).
7. H. Weber, "Photographic filter layers of colloidal silver," DE 1184211 19641223, 1964 p. 3.
8. J. E. Brady and J. R. Holum, Chemistry: The Study of Matter and Its Changes; John Wiley & Sons Inc., New York, 1993.
9. H. Lee, A. Park, and C. Oloman, **"**Stability of hydrogen peroxide in sodium carbonate solutions," *Tappi Journal*, **83**(8), 94 (2000).
10. D. S. Brackman and W. C. E. Higginson, "The reaction between hydroxylamine and sodium sulfite in solution in dilute acid," *J. Chem. Soc. Abs.*, 3896-3898 (1953).
11. D. Dollimore and T. A. Evans, "Thermal decomposition of oxalates," *Thermochim. Acta*, **179**, 49-59 (1991).
12. D. F. Evans and T. S. Sheriff, "The production of hydrogen peroxide from dioxygen and hydroxylamine catalyzed by manganese complexes," *J. Chem. Soc., Chem. Commun.*, **20**, 1407-1408 (1985).
13. T. S. Sheriff, "Production of hydrogen peroxide from dioxygen and hydroxylamine or hydrazine catalyzed by manganese complexes," *J. Chem. Soc., Dalton Trans.,* **6**, 1051-1058 (1992).

14. T. Sato, "Solvent extraction of manganese(II) from aqueous thiocyanate solutions by Tributyl phosphate," *Solvent Extr. Res. Dev., Jpn.*, **5**, 70-82 (1998).
15. J.-F. Pan and K. Chen, "A facile catalytic oxidation of activated hydrocarbons to the carbonyl functionality mediated by Mn(II) complexes," *J. Mol. Catal. A: Chem.*, **176**(1-2), 19-22 (2001).
16. T. Wieprecht, J. Xia, U. Heinz, J. Dannacher, and G. Schlingloff, "Novel terpyridine-manganese(II) complexes and their potential to activate hydrogen peroxide," *J. Mol. Catal. A: Chem.*, **203**(1-2), 113-128 (2003).
17. N. Stock and T. Bein "High – throughput investigation in the synthesis of the alluaudite type manganese arsenate: $AgMn_3(AsO_4)(HAsO_4)_2$," *Solid State Sci.*, **5**(9), 1207-1210 (2003).
18. http://avogadro.chem.iastate.edu/MSDS/AgNO3.htm
19. NFPA No. 491M, Manual of Hazardous Chemical Reactions, Fourth Edition, National Fire Protection Association, Boston, Massachusetts, 1971.
20. R. S. Treseder,"Hydrogen peroxide stabilization," US Patent 3037622/19620605, 1962.
21. G. S. Savchenko, "Investigation of the reactions of aluminum nitrate with oxalic acid and its sodium salts," LNL report, LA-TR-79-5, 1979.
22. V. M. Kaut, N. S. Tsareva, and N. E. Vorob'eva, "Aluminum nitrate solubility in concentrated nitric acid containing nitrogen oxides," *Ukrainskii Khimicheskii Zhurnal*, **33**(5), 515-517 (1967).
23. N. K. Levashova, G. L. Antipenko, and V. Poznyak, "A Solubility of some metal nitrates in liquid nitrogen tetroxide," *Zhurnal Neorganicheskoi Khimii*, **14**(7),1989-1990 (1969).
24. Yomo Nobuo; Higuchi Shigeo, and Akimoto Hidetoshi, "Chemical removal of radioactivity," *Jpn. Kokai Tokkyo Koho*, 1987; pp. 5.
25. V. G. Tsvetkov, A. V. Ivanov, V. V. Sokolov, Aleksandrov, and A. Yu., "Calorimetric study of coordination capability and reactivity of nitrogen tetroxide in solutions," *Z. Prikladnoi Khimii*, **56**(3), 501-504 (1983).
26. R. Lyonnet, C. Ciaravino, P. Marote, J. P. Scharff, B. Durand, and J. P. Deloume, "Reactivity in molten oxonitrates of lanthanum and manganese salts. Synthesis of $La_{1-x}MnO_3$," *High Temp. Material Processes*, **3**(2 & 3), 269-278 (1999).
27. A. J. Moffat and R. D. Thompson "Basic studies of chemical stability in extraction systems I- The effect of zirconium nitrate and nitric acid upon the chemical stability of tributyl phosphate," Report IDO-14543, 1961.
28. http://www.jtbaker.com/msds/englishhtml/S5066.htm
29. K. Ninomiya, A. Kuribayashi, and H. Kono, "Absorption of nitric oxide and nitrogen dioxide mixture gas by aqueous sodium hydroxide solutions," *Kagaku Kogaku Ronbunshu*, **8**(5), 590-597 (1982).
30. http://www.bu.edu/es/labsafety/ESMSDSs/MSHydPeroxide.html#anchor890962
31. A. Schreck, A. Knorr, K. D. Wehrstedt, P. A. Wandrey, T. Gmeinwieser, and J. Steinbach, "Investigation of the explosive hazard of mixtures containing hydrogen peroxides & different alcohols," *J. Hazard. Mater.*, **108(**1-2), 1-7 (2004).
32. W. Schulz and J. Navratil, Eds., Science and Technology of Tributyl Phosphate, Vol. 1, 1984.
33. http://www.sciencestuff.com/msds/C2920.html
34. http://www.physchem.ox.ac.uk/MSDS/SO/sodium_carbonate_monohydrate.html
35. http://www.physchem.ox.ac.uk/MSDS/SO/sodium_hydroxide.html
36. Kim Weon-Ju, Park Ji Yeon, Oh Seok Jin, Kim Young Suk, and Kuk Il Hiun, "Microstructure of Al_2O_3-ZrO_2 nanocomposites prepared by combustion process," *J. Mater. Sci. Lett.*, **16**(9), 719-721(1997).

STUDIES ON REACTION RUNAWAYS FOR UREX/PUREX SOLVENT-NITRIC ACID AND RED-OIL SYNTHESIS

Shekhar Kumar, Rajnish Kumar, and S.B. Koganti

Reprocessing R&D Division, Reprocessing Group
Indira Gandhi Centre for Atomic Research, Kalpakkam 603102 India
Corresponding author email address: shekhar@igcar.gov.in

ABSTRACT

In PUREX/UREX processes for recycling of spent nuclear fuels, 30% TBP solvent is used. This solvent has a small solubility in the aqueous phase. During concentration of the process solutions by an evaporation route, a runaway reaction between TBP and nitric acid is initiated at above 130 ^{o}C, leading to rapid pressurization and finally containment failure if proper venting is not provided. Red oil was synthesized for the first time in India, and its physical properties as well as thermodynamic parameters for the reaction were determined. It was experimentally established that the presence of metallic nitrates was not essential for red-oil formation as thought earlier. Various experiments have been completed for single-phase as well as two-phase runs**.** The most important finding of this work was lowering of the limiting acid concentration from the conventional values. In fact, in these experiments, red oil could be formed even at 2 N aqueous acidity. Thus, safety guidelines based on the classical literature are obsolete. New guidelines for the red-oil–safety are required.

INTRODUCTION

Liquid-liquid extraction, also known as solvent extraction, is a cost effective industrial process to recover, purify, or separate metals. Although several solvents can effectively extract uranium, plutonium, or thorium from acid solutions, the commercially chosen solvent is only tri-*n*-butyl phosphate (TBP). Most solvent-extraction operations in the PUREX process, used to recover valuable material from spent nuclear fuel with TBP have been performed safely for decades. The 30% TBP solvent has a small solubility in the aqueous phase. During concentration of the process solutions by an evaporation route, if these trace level organics are present, above 130 °C, a runaway reaction between TBP and nitric acid is initiated, leading to rapid pressurization [1-4] and finally to containment failure if proper venting is not provided. The intermediate product of this runaway reaction is nitrated organic solvent, which is red in color. Hence, this event is termed as red-oil formation. Red oil, having nitration product of solvent as a major constituent, is prone to rapid oxidation, leading to rapid pressurization, resulting in containment failure. The gaseous products includes N_2, CO, CO_2, NO, and N_2O. Liquid products include di-butyl phosphoric acid, butyl nitrate, and water. Gaseous products are the reason for the

violent explosion. Runaway reactions of nitric acid-industrial solvent mixtures are potentially damaging in nature, as evident from the explosion occurred in B-204 facility of BNFL in the early seventies, which caused closure of the plant as well as the end of the BUTEX (diBUTyl carbitol EXtraction) process for nuclear-fuel reprocessing.

In fact, there have been several instances of explosive-type reactions with TBP/nitric acid systems in industrial processes [5-9]. The latest occurrence was at the Tomsk-7 facility in Russia, at which faulty operations are believed to have resulted in the runaway reaction of a solution of considerable volume of TBP inadvertently saturated with strong nitric acid and self-heated, resulting in explosive failure of the storage vessel and subsequently blowing out a wall of the reprocessing building. The damage to the civil structures is believed to have been a result of the deflagration of flammable gases, most likely butene and CO, released from the initiation explosion [10].

EXPERIMENTAL WORK

Description of the Experimental Setup

The study of the runaway reaction between TBP and HNO_3 was conducted in a high-pressure high-temperature chemical reactor, which was fabricated from Stainless Steel-316 and has a capacity of 1 L. Figure1 shows a schematic of the experimental setup. A rupture disk, provided as a passive safety system, was rated at a nominal opening pressure of 3158 psi. For controlling speed of the impeller and temperatures (as well as readout of pressure), there was a control tower employing digital electronics.

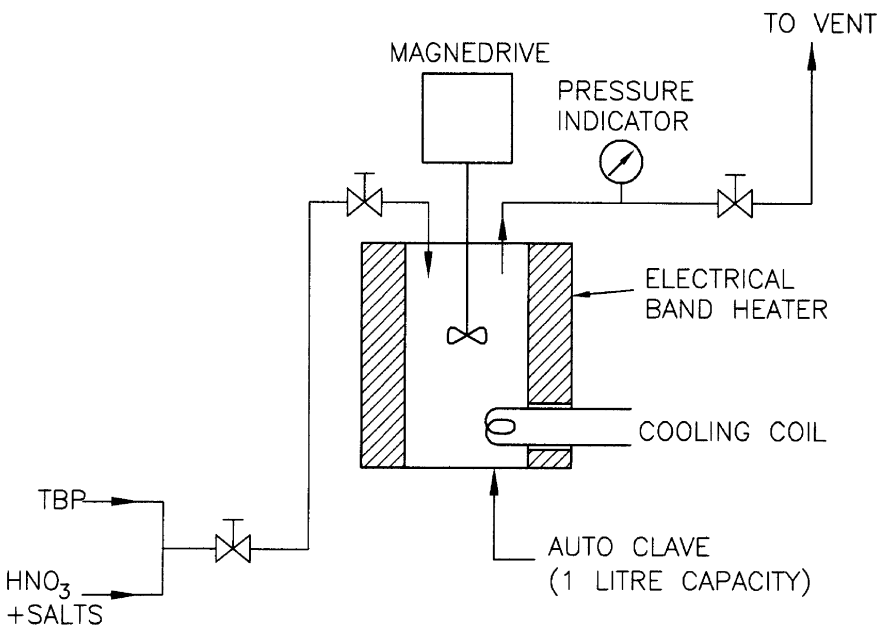

Figure 1. Schematic of the experimental setup for study of runaway reactions.

General Experimental Procedures

Aqueous solutions of several concentrations of nitric acid were prepared by diluting 70% nitric acid with ASTM-Grade-1 water from a Millipore purifier. AR grade nitric acid (~70% w/w, Rankem), AR grade anhydrous sodium carbonate (SRL), AR grade tri-*n*-butyl phosphate (Merck®), and AR Grade *n*-dodecane (Sigma-Aldrich®) were used as received. Density was measured by an automatic vibrating-tube densitometer (Anton-Paar® DMA-5000). Acidities of aqueous and organic solutions were analyzed by means of an automatic titroprocessor METROHM®-809 with Titrino-800 coupled with a 10 mL burette and controlled by Tiamo® running on a IBM® Thinkpad. The uncertainty in the dosing is estimated to be ±0.5 μL. A 0.05 N sodium carbonate solution was used as titrant. Typically 25 μL sample were weighed in SBC-21 balance (80/220 g, ±0.01 mg) and with determined density values, the precise volume of the sample was estimated.

Red-oil Synthesis/Reaction Runaway Experiments

The runaway-reaction experiments between TBP and HNO_3 can be conducted in two different conditions, closed system and open system (not performed in this study).

Closed System

The apparatus used for closed-system experiments is shown schematically in Figure 1. Single-phase experiment and two-phase experiment were performed in a closed system. In single-phase experiment, TBP equilibrated with nitric acid alone was fed in to the reactor in which nitric acid was used as a limiting reactant. In two-phase experiment, equilibrated organic TBP, mixed with fresh nitric acid of indicated concentration was fed into the reactor where TBP was the limiting reactant. A sample of known volume was charged through the charging port of the reactor. All the inlet and outlet lines were closed. Skin temperature of the reactor was kept at 275 °C. The temperature inside the reactor was set at 225 °C. The agitation speed was set at 600 rpm. The stopwatch was started as soon as the reactor was switched on. The temperature inside the reactor and reactor pressure were noted for every one minute. The pressure and temperature were increased until a particular time due to the exothermic reaction taking place inside the reactor, then reduced to a particular value and again started to increase as an effect of some other side reaction. At that time, the experiment was terminated by turning off the electrical band heater. The inside temperature of the reactor vessel was set to 20 °C, and cooling water supply was started. After reaching ~30 °C, the vent was kept open to vent the gases formed by the runaway reaction between TBP and HNO_3. The reactor was purged using compressed air. Liquid product was taken out through the sample line and kept for analysis. The closed-system experiment was performed using nitric acid concentrations including 16 N, 8 N, 4 N, and 2 N (two phases); 6 N, 10 N, 12 N, and 14 N (single phase); 8N (with 30% TBP, single phase). Selected results are shown in Figure 2. The initiation temperature of the decomposition of nitrated TBP was estimated from the plots of temperature vs. time.

The density of the synthesized red oil was measured at 25.001 °C (298.151 K) as 0.985425 g/mL.

Simulation of an Industrial Red-oil Event

A 10 mL solution of TBP was heated with 200 mL of 15.6 N nitric acid in closed conditions. It resulted in a rapid pressure increase (~1000 psi/min) after the initiation of the reaction, and the rupture disk opened at the rated pressure (~3158 psi) (Figure 3).

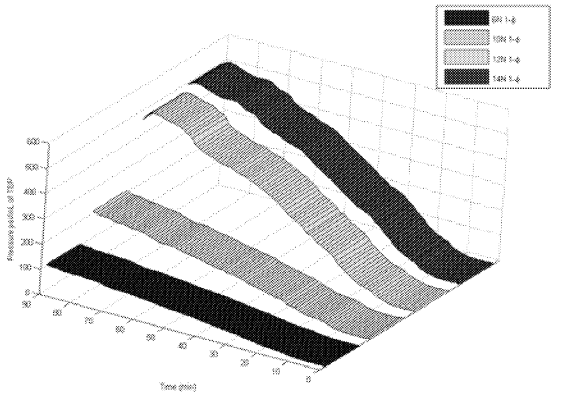

Figure 2. Comparison of single-phase experiments.

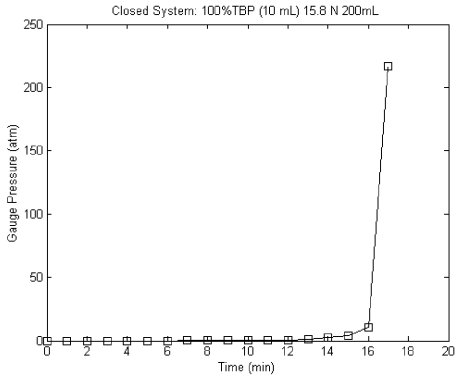

Figure 3. Simulation of an industrial red-oil event.

RESULTS AND DISCUSSION

Based on the above experimental work, the activation energy ΔE for red-oil formation was estimated as 24.4 ± 3.6 kcal/mol. This value compares well with the values reported earlier by Nichols [11] and Agnew et al. [12] as 26.8 kcal/mol and 24 ± 6 kcal/mol, respectively. Based on the above data, the pre-exponential factor was estimated as 6.1561×10^{11} s^{-1}. It was reported as 3.3×10^{11} s^{-1} by Agnew et al. [12] and 4.3×10^{10} s^{-1} by Nichols [11]. This comparison is satisfactory considering the possible sources of errors in the measurements in these "early" experiments. The value of k for esterification was found to be 1.42×10^{-2} at 180 °C as against 1.33×10^{-3} reported by Nichols.

The TBP-Nitric acid runaway reaction starts only at the temperatures at or greater than 130 °C. This was found valid for all the runs, either single- or two-phase system. Once the runaway reaction starts, the heating rate increases due to autocatalytic reactions involved and the pressure starts to shoot up. This feature can be used to detect the onset of runaway reactions and for setting of process interlocks to prevent energetic reaction.

The pressure generated per g or per mL of the Feed TBP is a function of several variables like acidity of the equilibration, amount of acid present in the system during reaction, and the temperatures prevailing during reactions.

From Figure 2, the amount of pressure generated per mL of TBP exceeds even 500 psi /mL of TBP. It illustrates the absolute necessity of removal of dissolved as well as entrained organics from the aqueous salt solutions before they are concentrated by means of evaporation. A single mL or its part of the present solvent would be enough for an explosion in the case of a red-oil event.

The most important finding is that for prevention of red-oil formation, the 10 M limit as earlier proposed in the literature is strictly not valid, as found from the recent experiments conducted by authors. A red-oil event was observed in the experiments with nitric acid as low as 2 N nitric acid concentration. Thus, safety guidelines based on the classical literature are obsolete. New guidelines for the red-oil–safety are required.

Table 1. Estimated activation energies and comparison with literature values.

***ΔE* Measurement**	**Value (kcal/mol)**
Nichols [10]	26.8
Agnew et al. [11]	24 ± 6
This work, $[H^+]$ = 2 N, 2-ϕ	18.98
This work, $[H^+]$ = 4 N, 2-ϕ	26.62
This work, $[H^+]$ = 6 N, 1-ϕ	29.93
This work, $[H^+]$ = 8 N, 2-ϕ	21.70
This work, $[H^+]$ = 10 N, 1-ϕ	24.40
This work, $[H^+]$ = 12 N, 1-ϕ	23.43
This work, $[H^+]$ = 14 N, 1-ϕ	27.94
This work, $[H^+]$ = 16 N, 2-ϕ	22.59
This work, $[H^+]$ = 16 N, 1-ϕ	23.07
This work, Mean *ΔE* (100% TBP)	24.3 ± 3.4
This work, $[H^+]$ = 8 N, 1-ϕ (30% TBP)	16.52

Notes:

- 1-ϕ experiment denotes run in which TBP alone (1 volume of TBP equilibrated with 5 volumes of nitric acid of indicated normality) was fed to reactor.
- 2-ϕ experiment denotes run in which TBP (1 volume of TBP equilibrated with 5 volumes of nitric acid of indicated normality) along with fresh nitric acid of the indicated normality was fed to reactor.
- Value for 30% TBP not accounted in this calculation.

CONCLUSIONS

Red oil was synthesized for the first time in India, and its physical properties were determined. It was established experimentally that the presence of metallic nitrates was not essential for red-oil formation as thought earlier. The limit on acid concentration was also found to be considerably less than the conventional values. In fact, in these experiments, red-oil could be formed even at 2 N aqueous acidity. Various single- as well as two-phase experiments have been completed, and further studies are in progress.

ACKNOWLEDGMENTS

Authors sincerely acknowledge the encouragement and kind support by Dr. Baldev Raj, Distinguished Scientist and Director IGCAR.

NOMENCLATURE

k	Pseudo-equilibrium rate constant (s^{-1})
n-DD	*n*-Dodecane
NPH	Normal Paraffin Hydrocarbon.
PUREX	Plutonium Uranium Extraction
TBP	Tri-*n*-Butyl phosphate
UREX	Uranium Extraction.
ΔE	Energy of activation (kcal/mol)

REFERENCES

1. T. S. Rudisill and W. J. Crooks III, "Initiation Temperature for Runaway Tri-n-Butyl Phosphate/Nitric Acid Reaction," Technical Report WSRC-TR-2000-00427, Westinghouse Savannah River Company, Aiken SC, 2000.
2. Y. Hou, E. K. Barefield, D. W. Tedder, and S. I. Abdel-Khalik, "Thermal Decomposition of Nitrated Tri butyl Phosphate," Technical Report WSRC-RP-95-259, Westinghouse Savannah River Company, Aiken SC, 1995.
3. G. S. Barney, "The Chemistry of Tributyl Phosphate at Elevated Temperatures in the Plutonium Finishing Plant Process Vessels," Technical Report WHC-EP-0737, Westinghouse Hanford Company, Richland, 1994.
4. "Control of Red Oil Explosions in Defense Nuclear Facilities 2003," Technical Report DNFSB/TECH-33, Defense Nuclear Facilities Safety Board, 2003.
5. W. S. Durant, "Red Oil Explosions at the Savannah River Plant," Technical Report DP-MS-83-142, E.I. du Pont De Nemours & Co., Savannah River Laboratory, Aiken SC, 1983.
6. V. N. Usachev and G. S. Markov, "Incidents Caused by Red Oil Phenomena at Semi-Scale and Industrial Radiochemical Units," *Radiochemistry*, **45**(1) 1-8 (2004).
7. R. E. Vandercook, "Summary of Red Oil Issues at Hanford," Technical Report WHC-WM-TI-466, Westinghouse Hanford Company, Richland, 1991. Fauske and Associates, Inc., "Tributyl Phosphate-Nitric Acid Reaction and Vent Requirements," Technical Report FAI/94-68, 1994.
8. D. F. Paddleford and H. K. Fauske, "Safe Venting of "Red-Oil" Runaway Reactions," Technical Report WSRC-MS-94-0649, Westinghouse Savannah River Company, Aiken SC, 1994.
9. M. L. Hyder, "Safe Conditions for Contacting Nitric Acid or Nitrates with Tri-*n*-Butyl Phosphate (TBP)," Technical Report WSRC-TR-94-059, Westinghouse Savannah River Company, Aiken SC, 1994.
10. S. F. Agnew, "Investigation Report on the Tomsk Reprocessing Plant Nuclear Accident in Russia," LA-UR-95-372 (1994)
11. G. S. Nichols, "Decomposition of the Tributyl Phosphate-Nitrate Complexes," Technical Report DP-526, E.I. du Pont De Nemours & Co., Savannah River Laboratory, Aiken SC, 1960.
12. S. F. Agnew, T. Constantopolos, D. Pinnick, C. Johnson, and J. Morris, "Reactions of Tributyl Phosphate with Nitric Acid under Containment," Accessed from Internet, March 2007 (1994)

DEVELOPMENT OF NOVEL CONTACTOR FOR NUCLEAR SOLVENT EXTRACTION

Shekhar Kumar, Rajnish Kumar, D. Sivakumar, M. Balamurugan, and S.B. Koganti

Reprocessing R&D Division, Reprocessing Group
Indira Gandhi Centre for Atomic Research, Kalpakkam 603102 India
Corresponding author email address: shekhar@igcar.gov.in

ABSTRACT

For current designs of radiochemical plants, solvent-extraction contactors with no periodic maintenance like pulse column are the first choice. In addition, as costs of specialty solvents for nuclear extraction are quite high, there is a demand for operation at extreme phase ratios. Recently a novel mixer-settler was visualized and developed for this kind of service. The mixer of the novel contactor is based on rotated helical tubes and does not involve any mechanical moving part. Mass-transfer runs were carried out with aqueous nitric acid and 30% TBP solvent at A/O of 0.25-200 (in extraction) and A/O of 0.25-10 (in back-extraction mode). The developed contactor exhibited nearly 100% efficiency for all the cases.

INTRODUCTION

Helical coils have been used the chemical industry for intensive mixing of fluids and blending of solids in liquids. Commercial applications of helical-coiled mixer include mixing of two part epoxies at the point of application. Sakra et. al. [1] reported that, contrary to the case of straight pipe for laminar flow through helical pipe, the dispersion number decreases with an increase in Reynolds number. Recently Nigam and co-workers [2] proposed use of rotated helical-coiled unit as in-line mixer. Still, application of helical coiled mixer as an in-line mixer for solvent-extraction applications has not been established in the literature.

For better mass transfer, good mixing is required. However for easier settling of the resultant two-phase mixture, low shearing of the fluid streams is also important. Rotated helical–coil based mixer-settler would be a possible candidate for this kind of high-mixing, low-shearing contactor. As a part of developmental effort, a prototype miniature single-stage mixer-settler with rotated coils and a settler fabricated out of glass was realized and tested experimentally for a wide range of A/O ratios in extraction as well as stripping. Based on the obtained encouraging results, a multi-stage miniature mixer-settler bank is being designed, and inter-stage pumping is proposed based on miniature fluidic pumps consisting of pulsed vortex diodes.

EXPERIMENTAL WORK

Description of the Setup

The experimental setup consisted of a mixer-settler and two feed pumps along with the product and feed tanks. The mixer consisted of 5 helical coils made of glass of 6 mm internal diameter. The coils were connected at right angles to each other. The aqueous and the organic solutions were fed from two ground-level HDPE cans into the mixer through two precision metering pumps (ISMATEC® MFP Process drives (ISM-909) + FMI® Q series Pumpheads). The power supply was regulated through an uninterrupted power supply (APC® SU-2200). The settler consisted of a vertical cylindrical vessel made of glass of 10 cm diameter and 32 cm height. The mixed phase from the mixer was fed to the settler through soft-tubes. The settler consisted of two sampler points at the top and the bottom for organic and aqueous output, respectively. The settler was provided with an overflow tube and a drain tube for continuous operation of the mixer-settler. The aqueous outlet was connected to a movable pot named interface controller; by changing its height, one could control the interface in the settler. The product solutions were collected in the two HDPE cans with periodic sampling for further analysis and processing (only in the mass-transfer runs). The schematic diagram of the entire experimental setup is as shown in Figure 1 and a view of the unit in operation is shown in Figure 2.

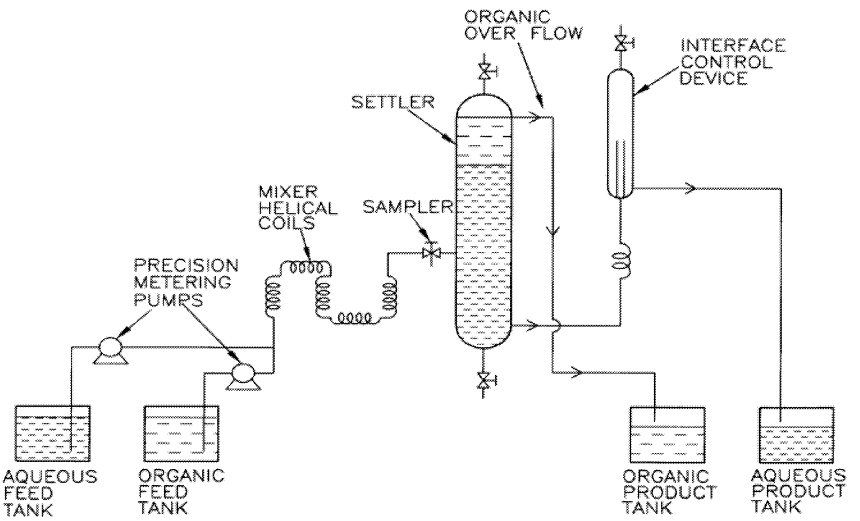

Figure 1. A schematic of the experimental setup.

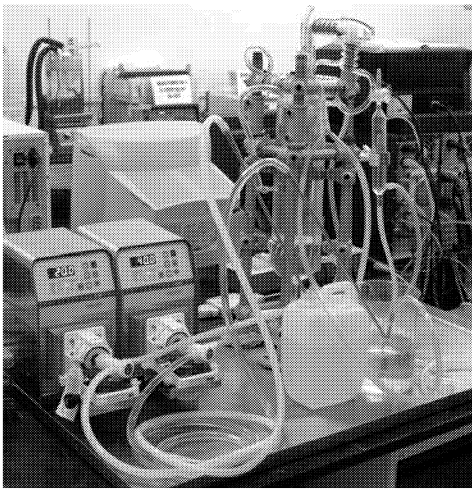

Figure 2. A view of novel mixer-settler in operation.

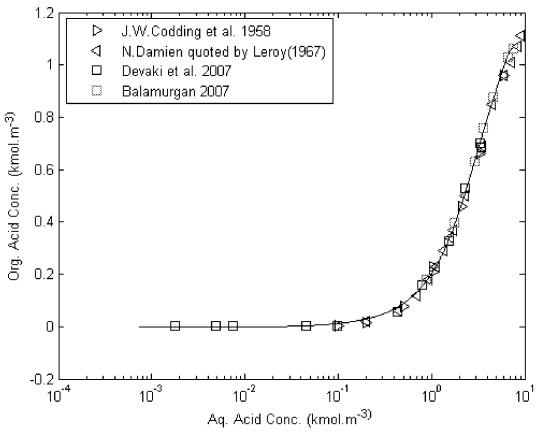

Figure 3. Distribution of nitric acid between water and 30% TBP solvent at 298.15 K.

General Procedure

The experimental work consists of the following four types of experiments to be made: generation of equilibrium data for nitric acid-TBP/*n*-dodecane system, hydrodynamic studies (non-mass-transfer region) for drop-size measurements and holdup estimation, mass-transfer runs with ~4 N HNO_3 as aqueous feed (Extraction Runs), and mass-transfer runs with 0.01 N HNO_3 as aqueous feed (Stripping Run).

Generation of Equilibrium Data

Organic solution of 30% TBP was prepared by diluting 100% TBP (MERCK) with 99+% *n*-dodecane (Lancaster). Different solutions of nitric acid concentrations were prepared by adding ~70 wt % AR grade HNO_3 (RANCHEM) in ASTM Grade-1 water from a Millipore treatment unit in the required proportion. After thorough mixing, solutions were allowed to settle and phases were separated in a separating funnel. Aqueous as well as organic samples were analyzed for acidity. Results shown in Figure 3 were in excellent agreement with literature values [3-6].

Chemical Analysis

Densities of the samples were determined with Anton Paar® densitometer (DMA 5000). The actual acidities of the samples were determined by Metrohm® 809 TITRANDO (Automatic Titrator system), by titrating it with 0.05 N Na_2CO_3 solution. The sample volumes were determined by weighing the samples in a Shimadzu® BX-220 balance and dividing by their respective density.

Hydrodynamic Studies (Non-Mass-Transfer Region)

The hydrodynamic studies in the non-mass-transfer region conducted include drop-size distribution and holdup estimation. A 30% TBP/NPH solution was used as the

organic phase. Acidified distilled water (0.01 N) was used as the aqueous phase. Different runs were carried on at different phase ratios.

Variation of the Drop Size

In solvent extraction, the interfacial area, required for mass transfer is given by the following relation-

$$a = \frac{6\Phi}{d_{32}} \tag{1}$$

Where, d_{32} is the sauter mean diameter and Φ, the volume fraction of the dispersed phase. Sauter mean diameter is defined as the diameter of the sphere that has the same volume/surface area ratio as a particle of interest. As Φ increases, the number of droplets increases, which results in the increase of mass-transfer rates due to rapid coalescence and redistribution of drops. Thus, it is advantageous to use dispersion with increased Φ.

Experimental Drop-size Measurement

In the non-mass-transfer run with different O/A ratios, the dispersed phase was checked first. If the dispersed phase was found to be organic, then the sample was collected in a beaker, containing a small amount of surfactant (3% sodium dodecyl sulphate, SDS). SDS was added to minimize the coalescence. The samples were analyzed in a laser-based drop-size analyzer (CIS-100, Galai Instruments, Israel). Figure 4 shows one such analysis.

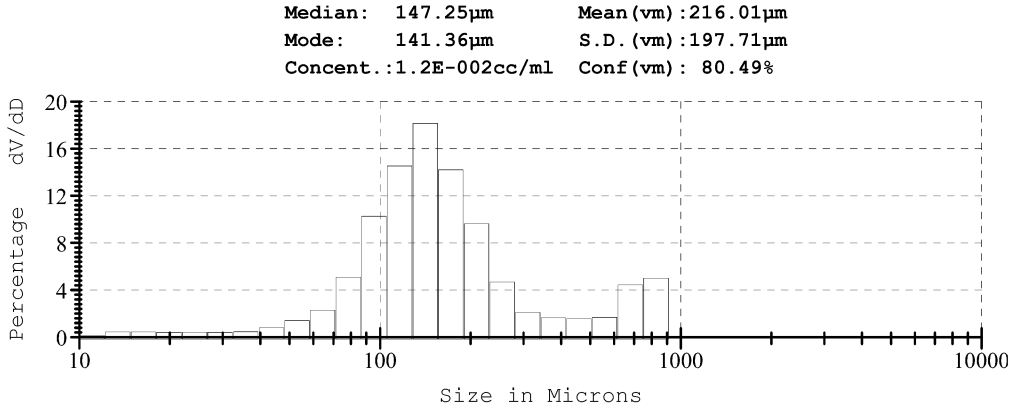

Figure 4. A typical drop-size measurement during non-mass-transfer run at A/O = 4 and 3% surfactant (SDS) concentration. (Please note: 1 mm = 1000 microns.)

Mass-Transfer Experiments with 4 N HNO_3 as Aqueous Feed (Extraction Run)

The extraction efficiency mainly depends upon the mass-transfer coefficients. In nuclear-fuel reprocessing, typical feed acidity is 4 N. Thus, ~4 N HNO_3 was used as the aqueous phase. Samples were collected for every 15 minutes time interval from the organic and aqueous sampler points and analyzed for acidity.

Mass-Transfer Experiments with 0.01 N HNO_3 as Aqueous Feed (Stripping Run)

The loaded organic is to be freed from the loaded solute (nitric acid in this case). Thus, loaded organic with ~0.36 M acidity was stripped with 0.01 N aqueous feed. This concentration was also chosen on the basis of PUREX process application. Stripping operation is also called back extraction. This operation can also be used for solvent-extraction based concentration, an essential feature of nuclear-fuel reprocessing flowsheets.

RESULTS AND DISCUSSION

In non-mass-transfer runs, d_{32} could be correlated with the throughput for 3% SDS solution as

$$\ln d_{32} = -9.7201 + 5.4876x - 0.4894x^2; \quad x = \ln(\textit{throughput}, \text{ mL/min}) \tag{2}$$

Holdup was correlated with the throughput as well as the phase ratio prevailing as

$$\phi = 0.7156 - 0.0139x + 0.0004x^2; \quad x = \textit{throughput}, \text{ L/h} \tag{3}$$

and

$$\phi = 0.5635 + 0.0310x + 0.0607x^2; \quad x = {}^{O}\!/_{A} \tag{4}$$

It may be noted that a high value of holdup of dispersed phase was observed, indicating high mass transfer and consequently high mass-transfer efficiency.

Table 1. Estimated Efficiency of Novel Mixer-Settler

Run	Aq. Flow, mL/min	Org. Flow, mL/min	Phase ratio *R* = A/O	$\eta_{Extraction}$	$\eta_{Stripping}$
1	100	400	0.25	84.51	
2	250	25	10	88.80	
3	400	20	20	90.10	
4	500	10	50	97.51	
5	600	6	100	100.92	
6	600	3	200	101.31	
7	100	400	0.25		97.46
8	100	20	5		96.50
9	150	20	7.5		97.63
10	200	20	10		97.62

The developed static-mixer settler performed well in extraction as well as stripping runs with 30% TBP/nitric acid system with nearly 100% efficiency. Temporal acidity profiles for extraction and stripping runs could not be shown due to lack of space.

CONCLUSIONS

A novel mixer-settler based on the rotated helical coils as mixer was developed at RR&DD. This mixer-settler was used in extraction and stripping runs with 30% TBP, NPH/Nitric acid, water system with a wide range of phase flow ratios. Several non-mass-transfer runs were conducted with 30% TBP solvent and 0.01 N aqueous nitric acid solutions for drop-size estimation and holdup measurements. A/O ratios of 0.25-200 for extraction runs and 0.25-10 for stripping runs were employed. Nearly 100% mass-transfer efficiency in almost all the cases was observed. Therefore, the developed static-mixer settler performed well in extraction as well as stripping runs with 30% TBP/nitric acid system and a single stage was realized for single pair of mixer and settler.

ACKNOWLEDGMENTS

Authors sincerely acknowledge the encouragement and kind support by Dr. Baldev Raj, Distinguished Scientist and Director IGCAR.

NOMENCLATURE

a	Interfacial area (m^2)
A/O	Aqueous-to-organic ratio.
D_{32}	Sauter mean diameter (μm)
HDPE	High density polyethylene polymer
NPH	Normal paraffinic hydrocarbon.
O/A	Organic-to-aqueous ratio.
SDS	Sodium dodecyl sulphate.
TBP	Tri-*n*-butyl phosphate
Greek	
Φ	Volume fraction of dispersed phase
η	Mass-transfer efficiency

REFERENCES

1. T. Sakra, F. Lesek, H. Cermankova, *Chem. Commun.* **36**, 3543-3548 (1971).
2. M. Mridha and K. D. P. Nigam, Chemical Engineering Science (2007), doi: 10.1016/ j.ces.2007.10.028.
3. J. W. Codding, W. O. Haas Jr., F. K. Heumann, *Ind. Engg. Chem.* **50**, 145 (1958).
4. N. Damien, Quoted by P. Leroy, Technical Report CEA-R-3207 (Trans. ORNL-Tr-4344, US-DOE), 1967.
5. S. Devaki, M.Tech Project, IGCAR, Kalpakkam, India, 2007.
6. M. Balamurugan, IGCAR Training School Project IGCAR, Kalpakkam, India, 2007.

EXTRACTION OF PROTACTINIUM-233 AND SEPARATION FROM THERMAL NEUTRON-IRRADIATED THORIUM-232 USING CROWN ETHERS

Moayyed G. Jalhoom,[1,2] Dawood A. Mohammed,[1] and Jumah S. Khalaf[1]

[1]*Chemistry Department, NRC, IAEC, Tuwaitha, Baghdad, Iraq.*
[2]*Ibn Sina State Company, Baghdad, Iraq.*
Corresponding author e-mail address: Jalhoom2007@yahoo.com

ABSTRACT

A new method was developed for the extraction and separation of ^{233}Pa from thermal neutron-irradiated ^{232}Th. Solutions of Pa^{233} were prepared in LiCl-HCl solutions from which appreciable extraction was obtained using dibenzo-18-crown-6 in 1,2-dichloroethane. The effects of cavity size, substitutions on the crown ring, type of the organic solvent, and temperature on extraction are discussed. Very high separation factors were obtained for the pairs ^{233}Pa/^{232}Th (>105), ^{233}Pa/^{233}U (>1000), and ^{232}U/^{232}Th (>60).

INTRODUCTION

The complexation of actinide ions by macrocyclic compounds, represented mainly by crown ethers and cryptands, has paved the way for several extraction studies where a liquid-liquid extraction technique was mainly the method of choice [1-17,18]. The equilibria of the extraction of actinides as cationic and anionic species can be represented by the following equilibria:

$$M^{m+} + 1L_{org.} + aA^{n-} \overset{K_1}{\rightleftharpoons} (ML_1{}^{m+}A^{n-}{}_a)_{org} \quad (1)$$

$$\log D_M{}^{m+} = \log K_1 + 1 \log [L]_{org} + a \log [A^{n-}] \quad (2)$$

$$cC^{z+} + 1L_{org} + mM^{n-} \overset{K_2}{\rightleftharpoons} (C_cL^{z+}{}_1M^{n-}{}_m)_{org} \quad (3)$$

$$\log D_M{}^{n-} = \log K_2 + c \log [C^{z+}] + 1 \log [L]_{org} \quad (4)$$

where M^{m+}, M^{n-} are actinide cationic and anionic species, L = crown ether or cryptand, A^{n-} is the counteranion, C^{z+} is H^+ or alkali or alkaline earth metal ions, and K_1 and K_2 are conditional extraction constants specific for the aqueous matrix employed.

From chloride media, complexes such as $HLUO_2Cl_3$ and H_2LUCl_6 were identified to be extracted into nitrobenzene [1]. From nitric acid, thorium could be extracted as

$Th(NO_3)_4.2L$ (L = DCH18C6 or DCH24C8) [2]. Uranium, on the other hand, was extracted as a 1:2 complex (metal:crown) by 4MB15C5 or DB18C6 and a 2:3 complex with 18C6 dissolved in 1,2-dichloroethane [2]. It was shown that the order of U(VI) extraction by various crowns changes with the type of the organic solvents. For example, in benzene, the sequence is 4MB15C5 > DCh18C6 > 18C6, while in 1,2-dichloroethane it is 18C6 > DCH18C6 > 4MB15C5 [2]. This effect reflects the important role of the solvent in the formation and structure of the extracted ion-pairs. The complex extracted for U(VI) was reported to be as $UO_2Cl_2.2$DCH18C6 from HCl acid solutions. X-ray crystallography revealed the structures of the solid complexes as [(DCH18C6-isomer A)(H_3O^+)]$_2[UCl_6]$ [6] and [(DCH18C6-isomer A)(H_3O^+)]$_2[UO_2Cl_4^{2-}]$ [7] to involve a role of the crown ether as hydronium ion receptor. The slope-analysis method for U(VI) extraction data revealed a 1:2 (metal:crown) stoichiometry for isomer A and 2:3 for isomer B [8-10]. The separation factor at 6 M HCl for U(VI)/Th(IV) exceeds 1000. Carboxylic and amido carboxylic acid crown ethers were used for the extraction of UO_2^{2+} ions [18]. As thiocyanates, U(VI), Np(IV), and Am(III) could also be extracted into MIBK [5]. The complexes extracted were $UO_2(SCN)_2.3$(15C5) and UO_2(TTA)2.L (L = 15C5 or DCH18C6C) from perchloric acid solutions and as $Np(NO_3)_4.3$(DCH18C6) from nitric acid solutions. On the other hand, from picrate media americium is extracted as $Am(Pi)_3.2$(15C5) [5]. Synergism by cyclic and linear polyethers has also been reported [3,4]. Enhancement was obtained for the extraction of Am(III), Cm(III), and Eu(III) by mixtures of HTTA and linear polyethers from aqueous acetate buffer solutions [3]. The 15C5-HTTA mixture in chloroform showed also synergism for the lanthanides as $Ln(TTA)_3(15C5)_2$ and Am(III) but not for Pu(IV) [4]. Some complexes of protactinium with polydentate ligands was reported also [11]. According to our knowledge, articles dealing with the extraction of protactinium by crown compounds have not been published. This work aimed at the extraction of Pa and separation from thermal neutron-irradiated ^{232}Th and the daughter product ^{233}U.

EXPERIMENTAL

The crown compounds 12-crown-4 (12C4), 15-crown-5 (15C5), 18-crown-6 (18C6), dibenzo-18-crown-6 (DB18C6), dicyclohexano-18-crown-6 (DCH18C6), dicyclohexano-24-crown-8 (DCH24C8), and dibenzo-24-crown-8 (DB24C8) were obtained from Merck. The organic solvents benzene, chlorobenzene, nitrobenzene, *o*-dichlorobenzene, 1,2-dichloroethane, hexanol, and hexone were analar BDH products. Radioisotopes were prepared according to the reaction:

$$^{232}\text{Th} + {}^{1}\text{n} \longrightarrow {}^{233}\text{Th} \xrightarrow[22.2\ \text{min.}]{} {}^{233}\text{Pa} + e^- \xrightarrow[27\ \text{days}]{} {}^{233}\text{U} + e^-$$

Protactinium-233 was prepared by irradiating 13 mg of the ThO_2 in the Iraqi reactor IRT-5000 for 1 h at a neutron flux of 2×10^{13} cm^{-2} sec^{-1}. The sample was dissolved in a mixture of 0.1 M HF and concentrated HCl solution. Protactinium-233 was separated from the ^{232}Th using a strong-acid cation-exchange resin [12]. Samples of resulting ^{233}Pa solution were evaporated, treated at least two times with concentrated HCl solutions, evaporated, and finally dissolved in the medium of extraction.

Distribution ratios (D_{Pa}) for ^{233}Pa were determined by mixing equal volumes of the organic and aqueous phases. After 15 min. (which was found to be adequate for equilibration) of mechanical shaking, equivalent aliquots were counted, using either a NaI(Tl) crystal detector with a single-channel analyzer or a Ge crystal detector with a minicomputer/multichannel analyzer [14-16].

RESULTS AND DISCUSSIONS

In spite of the existence of complexes such as K_2PaF_3 and Na_3PaF_8 [13], negligible extraction was obtained from various HF concentrations and alkali fluoride mixtures. Hydrochloric acid solutions showed also negligible extraction up to 6 M, above which a very slight increase in the D values was noticed ($D \sim 0.055$ at 10 M HCl) in the system 0.1 M 15C5 in 1,2-dichloroethane. At 1 M HCl, weak extraction was noticed after the addition of 0.5-6 M LiCl. However, 8 M LiCl gave $D \sim 0.34$, and very strong extraction was obtained from 8 M HCl and 6 M LiCl. Slope analysis of the data in the extraction system extraction of Pa from 6 M LiCl-1 M HCl by 15C5, 18C6, and DB24C8 in 1,2-dichloroethane revealed the presence of one crown molecule in the extracted complex. It should be mentioned that the presence of Pa(V)-macrocylic complex, after separation from irradiated ^{232}Th, was investigated using various techniques; however, definite structure could not be finally realized [1]. Extraction data for various crown compounds is shown in Figure 1. In agreement with our previous data, the value of D_{Pa} increases sharply with number of donor atoms and basicity of the crown cavity [14-16]; however, charge density, electronic structure, compromise of sizes, and conformations may play also role in the extraction. Cyclohexano groups enhance the electron density inside the cavity almost equivalent to adding two oxygen-donor atoms. The decrease of extraction by DB24C8 and DB18C6 may be ascribed to the larger cavity size and the presence of the phenyl groups, which have electron-withdrawing properties. Similar behavior was noticed on the extraction of $\{H_3O^+LTcO_4^-.nH_2SO_4\}$ and $\{H_3O^+LI_2Cl^-\}$ ion-pairs [14-17,22]. At this point, a preliminary suggestion for the structure of the extracted complex is $(H_3O^+)_2LPaCl_7^{2-}$ or $(H_3O^+)LHPaCl^-_7$ species [21]. The increase in the basicity of the cavity, good matching between the cation, and cavity size in addition to the better conformation and configuration may give enhanced electrostatic, dipole-dipole, and ion-dipole interactions. The data of Figure 2 most probably suggest the presence of H_3O^+ ions bonded through hydrogen with the crown cavity because of the incompatibility of the ion size with the larger cavities applied. On the other hand, Table 1 shows that the extraction of ^{233}Pa increases steadily with the dielectric constant (ε) of the organic solvents. Almost linear relations were obtained between Log D and Log (ε) [14-17]; however, solvents which have high donor number do not follow the linear relation. Both solvents hexone and hexanol can extract ^{233}Pa efficiently in the absence of crown compounds under the studied conditions.

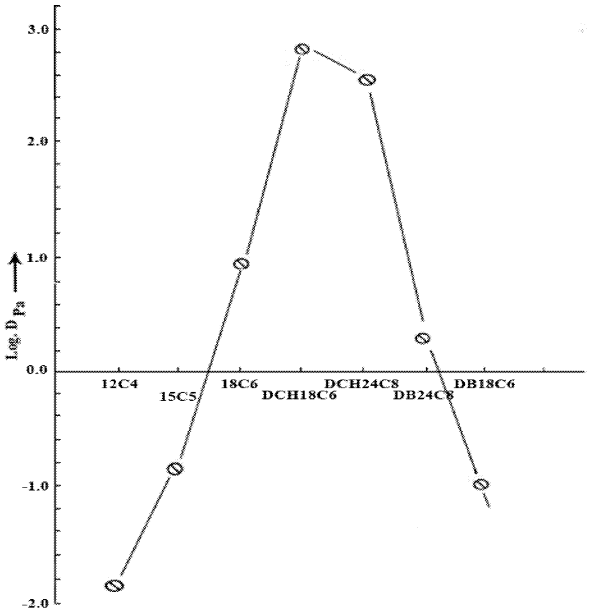

Figure 1. Effect of structure of crown compounds on the extraction of protactinium from 8 M LiCl-1 M HCl with 0.1 M crown compound in 1,2 dichloroethane.

Table 1. Effect of organic diluents on the extraction of protactinium-233 from 8 M LiCl-1 M HCl with 15-crown-5

Organic Solvent	Dielectric Constant	D_{Pa}
Benzene	2.284	0.0020
Chlorobenzene	5.708	0.0034
o-Dichlorobenzene	9.90	0.104
1.2-Dichloroethane	10.4	0.140
Nitrobenzene	35.74	24.90
Hexanol[b]	13.3	226
Hexone[b]	13.1	C.E.[a]

[a]Complete extraction (practically all activity is in the aqueous phase).
[b]Extractions have almost the same level in the absence of the crown compound.

Interesting data were achieved upon the study of the effect of temperature on the distribution ratio of ^{233}Pa in the presence of various crown compounds (Figure 2). The first observation is the nonlinearity of the relations for 15C5, 18C6, and DB24C8. This might be attributed to either the change of the heat capacity of the system or to the presence of more than one species in the system. As mentioned before [1], it was proved that Pa exists as Pa(V) macrocyclic complex. Another possibility is the presence of two types of ion pairs, solvent-separated and contact ion pairs. Good size matching for the cation-crown moiety is reflected in the higher negative extraction enthalpy change ($\triangle H_{ex}$); such relation was realized from a study of the extraction of $[M^{n+}L_1](ReO_4^-)_n$ ion pairs when $M^{n+} = H^+$, NH_4^+, alkali, and earth metal ions [22]. The second observation is

that the reaction is exothermic for DB24C8 and endothermic for 15C5. The first reflects stronger interaction in comparison with 15C5 and 18C6. 18C6 shows a very slow variation between 10 and 40 °C. Similar behavior by the large cavities was noticed on the extraction of lanthanides from picrate media [17]. It is known that the larger cavities have the ability of wrapping around the cations. Finally, it is also interesting to mention that crown compounds can be used for the selective separation of ^{233}Pa from thermal neutron-irradiated ^{232}Th.

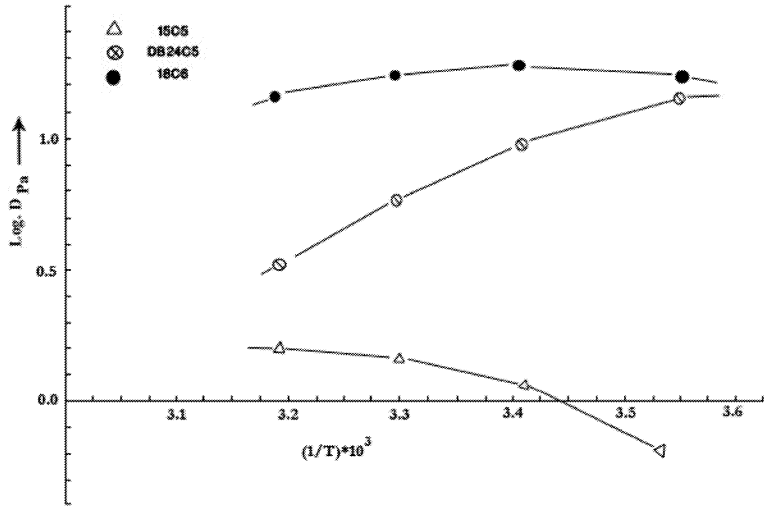

Figure 2. Effect of temperature on the extraction of protactinium in the system 0.1 M crown ether-1,2 dichloroethane/8 M LiCl–1 M HCl.

After the decay of ^{233}Pa to ^{233}U, the later can also be easily separated from ^{232}Th as can be seen from the Table 2. Using DCH24C8, separation factors of 36, 14,000, and 140 were respectively obtained for the pairs Pa/Th, U/Th, and Pa/U; DCH18C6 gave 58, 57,000, and 1000 for the same pairs.

Table 2. Extraction of Protactinium-233[a]

Crown Compound	Distribution Ratio (*D*)			Separation Factor		
	Th	U	Pa	Pa/Th	U/Th	Pa/U
15C5	N.E.[b]	0.28	0.141	V.H.[c]	V.H.[c]	0.504
18C6	0.025	1.67	9.19	368	67	5.503
DB24C8	N.E.[b]	0.62	0.099	V.H.[c]	V.H.[c]	0.160
DCH24C8	0.025	0.900	369	14,760	36	410
DCH18C6	0.012	0.69	691	57,583	58	1000

[a]Crown ether 0.1 mol/L in 1,2-dichloroethane (organic phase); 8 mol/L LiCl, 1 mol/L HCl (aqueous phase). [b]Practically all activity is in the aqueous phase. [c]Very high (D > 1000).

CONCLUSIONS

An efficient extraction-based separation method was developed for protactinium obtained from thermal neutron-irradiated thorium. Protactinium was extracted from aqueous HCl-LiCl using crown ethers in 1,2-dichloroethene (or nitrobenzene). A very high separation factor was also obtained from uranium-233.

ACKNOWLEDGMENT

A research contract (No. 5650/RB) with the International Atomic Energy Agency on the Development of the Radiochemical Separation for Environmental Research is gratefully acknowledged.

REFERENCES

1. Z. Lin, C. Shao-Jin, F. Yijuin, L. Zongquin, and C. Wenjun, Proc. Int. Solvent Extr. Conf., Denver, USA, 1983; pp. 453.
2. W. Wenji, C. Bozhon, J. Zhong-Kao, and W. Ailing, *J. Radioanal. Chem*., **76**, 49 (1983).
3. D. D. Ensor and A. H. Shah, *Solvent Extr. Ion Exch*., **1**, 241 (1983).
4. H. F. Aly, S. M. Khalifa, J .D. Navratil, and M. T. Saba, *Solvent Extr. Ion Exch*., **3**, 623 (1985).
5. A. G. Godbole, N. V. Thakur, R. Swarup, and S. K. Patil, *J. Radioanal. Nucl. Chem. Lett.*, **108**, 89 (1986).
6. W. J. Wang, J. Jie-Lin, and S. Hong, *Radiochim. Acta*, **40**, 199 (1986).
7. W. J. Wang and B. Chen, *Inorg. Chim. Acta*, **117**, 81 (1986).
8. W. J. Wang, Q. Sun, and B. Chem, *J. Radioanal. Nucl. Chem. Art.*, **98**, 11 (1986).
9. W. J. Wang, Q. Sun, and B. Chem, *J. Radioanal. Nucl. Chem. Art.*, **110**, 227 (1987).
10. C. Allen-Change, V. K. Manchanda, and Peng, *J., Inorg. Chim. Acta*, **130**, 117 (1987).
11. M. Solache-Rios and A. G. Maddock, *J. Less Common Met.*, **122**, 347 (1986).
12. R. Kuroda, *J. Chromatogr*. **18**, 438 (1965).
13. C. Keiler, The Chemistry of The Transranium Elements, Verlag Chemie , GmbH, 1971; pp. 169.
14. M. G Jalhoom, *Radiochim. Acta*, **40**, 203 (1986).
15. M. G Jalhoom, *Radiochim. Acta*, 39, 195(1986).
16. M. G Jalhoom, *J. Radioanal. Nucl. Chem. Lett.*, 104, 131(1986).
17. M. G Jalhoom, D. A. Mohammed, J .S. Khalaf, NRC, IAEC-CH-85.
18. Z. Lin, C. Show-Jin, L. Zhong-Qun, and C. Wen-Jun, ISEC-90 , Japan 1990; pp. 273.
19. P. Th. Gerontopolus, L. Rigali, and P. G. Babano, *Radiochim. Acta*, **4**, 244 (1965).
20. K. Venkate Swarles and V. Subramanian, *Radiochim. Acta*, **5**, 175 (1966).
21. D. Brown, "Actinides in Perspectivs," Proc. Actinides, Conf. Pacific Grove, California, N. M. Edelstein, ed 1981; pp. 343-359.
22. S. K. Jewad, S. R. Al-Murab, and M. G. Jalhoom, Proc. Int. Solvent Extr. Conf., ISEC-90, Kyoto, Japan, 1990; pp. 165.

Analytical and Preparative Applications

CHIRAL RECOGNITION BY MOLECULAR AGGREGATION AT LIQUID-LIQUID INTERFACE

H. Watarai

Department of Chemistry, Graduate School of Science, Osaka University, Toyonaka, Osaka 560-0043 Japan
Corresponding author email address: watarai@chem.sci.osaka-u.ac.jp

ABSTRACT

New methods to measure the optical chirality of liquid-liquid interfaces have been developed, which include a centrifugal liquid membrane–circular dichroism (CLM-CD) method, a second harmonic generation–circular dichroism (SHG-CD) method, and their microscopic versions. Using these methods, generation of optical chirality due to the chiral aggregation at the liquid-liquid interface has been observed in two-phase systems including of porphyrin, phthalocyanine, or bilirubin, which could be applied for interfacial chiral molecular-recognition analysis.

INTRODUCTION

Optical chirality is an important issue not only in analytical chemistry but also in other various fields, including organic chemistry, biochemistry, coordination chemistry. and supramolecular chemistry. The separation and detection of optically active compounds has usually been achieved by HPLC and CE using chiral stationary phases or chiral surfactants. Solvent extraction has also been applied for the enantioseparation of organic compounds with ion-pair formation using chiral ions [1] and chelate formation using chiral ligand [2], although the enantioselectivity is not enough. The use of chiral biological molecules for chiral separation of proteins has been demonstrated recently [3].

On the other hand, the determination of chirality of molecular compounds has usually been attained by the measurement of optical rotatory dispersion or circular dichroism (CD) spectra using a circular dichroism spectropolarimeter. The difference in UV/vis absorbance between enantiomers is very small in almost all compounds. Therefore, for the accurate measurement of CD spectra, a sensitive and stable spectropolarimeter is necessary.

The liquid-liquid interface has a unique ability to concentrate a dilute solute into the two-dimensional region, provided that the solute is somewhat surface active. Therefore, the interface shows characteristic functions such as a catalytic effect in solvent-extraction kinetics and nanoparticle formation of molecular aggregates. Optical measurements of interfacial species have been developed by some innovative methods, including a centrifugal liquid membrane (CLM) method, a total internal-reflection

method, and a microscopic spectroscopy method in our laboratory [4]. However, the measurement of optical chirality of the interface has rarely been studied, because of the difficulty to discriminate the interfacial chiro-optical signal from that of bulk-phase signal. Recently, we have succeeded to measure the optical chirality at liquid/liquid interfaces, which included a centrifugal liquid membrane (CLM)-circular dichroism (CD) method [5] and a second harmonic generation (SHG)-circular dichroism (CD) method [6]. The CLM method was fit to measure the CD spectra of the interfacial species generated at the interface between two thin liquid phases. Figure 1 shows the schematic drawing of the CLM-CD method.

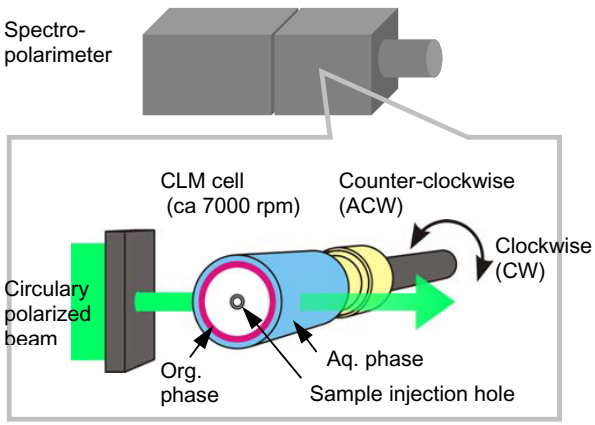

Figure 1. Schematic drawing of the centrifugal-liquid-membrane method combined with a spectropolarimeter to measure the circular dichroism spectra of the liquid-liquid interface.

Furthermore, these methods were combined with an optical-microscope device to measure a microscopic area of the transferred "interface" from the liquid interface to a cover glass or a single microparticle on a glass. As for the SHG method, a microscope SHG-CD spectrometer has been newly constructed in the present study. By these new methods, the chiral recognition of small amount of adsorbed molecules such as ions and alcohols has been attained by the formation of interfacial molecular aggregate for the first time. In the present study, the interfacial aggregate of phthalocyanine derivatives, bilirubin, and porphyrin, which have rather strong absorptivity in the visible light wavelength region, have been used to detect the interfacial chirality.

EXPERIMENTAL

Enantiomeric thioether-substituted phthalocyanine derivatives ((2,3,9,10,16,17,23,24-octakis-1-phenylethylthiophthalocyaninato)magnesium(II) [MgPc(SEtPh)$_8$]) were synthesized in our laboratory as shown in Figure 2. After purification by silica gel chromatography (eluent: $CHCl_3$:MeOH = 9:1), they were identified by NMR, FT-IR, and elemental analysis. Almost all measurements in this

study were carried out under the condition that the ionic strength and pH were fixed at 0.1 M (1 M = 1 mol dm^{-3}) and 2.0 with sodium chloride and sulfuric acid, respectively, in a thermostated room at 25 ± 2 °C. Under these conditions, Pd(II) exists as $PdCl_4^{2-}$ in the aqueous phase

The reagents bilirubin (BR) and fatty acid free bovine serum albumin (BSA) were purchased from Sigma Chemical Co. and used as received. A stock solution of BR was prepared by dissolving it in chloroform, and then an aliquot of BR in chloroform was diluted in heptane at the concentration of 5.83×10^{-5} M in the centrifugal liquid membrane (CLM) experiments. In these experiments, the volume ratio of $CHCl_3$ to heptane was always kept at 1/5. In any cases, BSA was dissolved in water, which was deionized and purified by a Milli-Q system. The pH value of BSA solution was 6.04 without any buffer in all experiments.

The interfacial formation of the optically active aggregate of $MgPc(SEtPh)_8$-Pd(II) complexes in the toluene/water system was directly observed using the centrifugal liquid membrane-absorption and circular dichroism spectroscopy (CLM-Abs and CLM-CD)[7]. A UV-vis spectrophotometer (8453, Agilent, USA) and a spectropolarimeter (J-810E, JASCO, Japan) combined with the CLM device were used to measure UV-vis absorption and CD spectra, respectively, of the interfacial species. In the CLM-CD measurement, a cylindrical cell, whose height and outer diameter were 3.3 and 2.1 cm, respectively, was placed horizontally in the sample chamber and rotated at 10,000 rpm by a speed-controlled electric motor (NE-22E, Nakanishi Inc., Japan). The toluene solution of $MgPc(SEtPh)_8$ and the aqueous solution of Pd(II) (each 0.500 mL) were introduced into the cylindrical cell using a microsyringe. The sum of UV-vis absorption or CD spectra of the both bulk phases and the interface was measured in the range 330-850 nm. The values of thickness of the toluene and aqueous phase were 293 and 289 μm, respectively. The interfacial area (S_i) between two phases was calculated as 17.3 cm^2. The aqueous phase with Pd(II) and toluene phase without $MgPc(SEtPh)_8$, which were introduced into a CLM cell, was used for a baseline measurement.

The microscopic SHG-CD instrument has been built in our laboratory. The SHG apparatus included a Ti:sapphire laser (Spectra-physics Maitai; 80MHz, 100fs, tuning range of 780-920nm) and a microscope system optimized for the detection of SHG light from the surface of a flat sample under an objective.

UV-vis and CD spectra in toluene solution were obtained on a V-570 spectrometer (JASCO, Japan) and J-810 spectropolarimeter (JASCO, Japan), respectively. pH values of the aqueous phase were measured using a F-14 pH meter (HORIBA, Japan) equipped with a 6366-10D glass electrode.

RESULTS AND DISCUSSION

Optical Chirality of Thioether-Substituted Phthalocyanine Interfacial Aggregates

The interfacial adsorptivity of chiral and racemic $MgPc(SEtPh)_8$ in the toluene/water system was investigated by the high-speed stirring (HSS) spectrometry [8] at various $MgPc(SEtPh)_8$ concentrations. The interfacial-adsorption constant of $MgPc(SEtPh)_8$ compound was defined by,

$$K' = \frac{[\mathrm{MgPc(SEtPh)_8}]_i}{[\mathrm{MgPc(SEtPh)_8}]_o}$$

where $[\mathrm{MgPc(SEtPh)_8}]_o$ and $[\mathrm{MgPc(SEtPh)_8}]_i$ are the concentrations of $\mathrm{MgPc(SEtPh)_8}$ in the toluene and at the toluene/water interface, respectively. The interfacial adsorption constants of (*R*)-, (*S*)-, and (*rac*)-$\mathrm{MgPc(SEtPh)_8}$ were determined as 9.84×10^{-6}, 9.31×10^{-6}, and 10.2×10^{-6} dm, respectively (Table 1), which are thought to be in agreement with each other within experimental error.

Table 1. Summary of composition ratio and various constants of $\mathrm{MgPc(SEtPh)_8}$ compounds observed from spectral changes.

Compounds	Molar ratio *n* (Pd(II)/$\mathrm{MgPc(SEtPh)_8}$)	Agg. Number *m*	$\log(K_d$ / $\mathrm{mol^1dm^3})^a$	$\log(K'$ / $\mathrm{dm})^b$	$\log(K'_{cpx}{}^5K'_{agg}$ / $\mathrm{mol^{-6}dm^{14}})^c$
(*R*)-$\mathrm{MgPc(SEtPh)_8}$	2	5	3.45	-5.01	104.9
(*S*)-$\mathrm{MgPc(SEtPh)_8}$	2	5	3.48	-5.03	103.2
(*rac*)-$\mathrm{MgPc(SEtPh)_8}$	2	5	3.44	-4.99	101.2

(a) K_d, dimerization constant in toluene; (b) K', interfacial adsorption constant;
(c) K'_{cpx}, interfacial complexation constant; K'_{agg}, interfacial aggregation constant.

The interfacial aggregation of $\mathrm{MgPc(SEtPh)_8}$-Pd(II) complexes in the toluene/water system was directly measured using the centrifugal liquid membrane-absorption spectrometry (CLM-Abs) and the centrifugal liquid membrane-circular dichroism spectroscopy (CLM-CD). From a preliminary experiment, it was confirmed that Pd(II) ions were not extracted with $\mathrm{MgPc(SEtPh)_8}$ from the aqueous phase to the toluene phase. Figure 2(c) shows the CLM absorption spectral change occurring upon the titration of Pd(II) aqueous solution. We have previously reported the interfacial aggregation behaviour of some thioether-substituted phthalocyanine ($\mathrm{MgPc(SR)_8}$) with Pd(II) in the toluene/water system [9]. The most notable feature of the interfacial aggregation of $\mathrm{MgPc(SR)_8}$-Pd(II) complexes was that the Q band was observed as blue-shifted (*H*-aggregate) or red-shifted (*J*-aggregate), depending on whether the length of the hydrophobic substituent (L_{sub}) is shorter or longer than 3.5 Å, which is a typical van der Waals distance between Pc planes in its *H*-aggregate. In the present result, the absorption maximum was red-shifted to 741 nm from the absorption maximum of $\mathrm{MgPc(SEtPh)_8}$ monomer (710 nm), indicating that the (*R*)-$\mathrm{MgPc(SEtPh)_8}$-Pd(II) complex formed a *J*-aggregate at the toluene/water interface. (*S*)- and (*rac*)-$\mathrm{MgPc(SEtPh)_8}$ also showed similar spectral change upon Pd(II) titration (not shown). The formation of the *J*-aggregate is supported by the calculation that the L_{sub} value of $\mathrm{MgPc(SEtPh)_8}$ compound is estimated to be 5.25 Å from a CPK model and is longer than the critical value of 3.5 Å. No CD spectra were observed for the toluene solution or its toluene/water systems including $\mathrm{MgPc(SEtPh)_8}$ in the absence of metal ions, indicating no chiral electron delocalization in the skeleton ring of phthalocyanine. According to the scheme for the interfacial adsorption, complexation, and aggregation shown in Figure 3, the corresponding constants were obtained as listed in Table 1.

CD spectra in Figure 2(a) and (b) clearly show the generation of optical chirality due to the addition of Pd(II) aqueous solution. The two-phase CD spectrum in (*R*)-

MgPc(SEtPh)$_8$-Pd(II) system showed negative chirality with a positive Cotton effect at 677 nm and negative Cotton effect at 720 nm. Inversely, in (*S*)-MgPc(SEtPh)$_8$-Pd(II) system, it showed just the positive chirality with a positive Cotton effect at 719 nm and negative Cotton effect at 680 nm. Up to the saturation at the molar ratio of [Pd(II)]/[MgPc(SEtPh)$_8$] ≈ 5, the intensity of the CD signal increased upon the titration, while its shape remained nearly unaltered. In the case of Langmuir-Schaefer (LS) film of optically active dye aggregate, it is known that the CD signal can be affected by linear dichroism (LD). To check the LD effect in this system, we also measured the LD spectra under the same sample conditions with the CD measurement. However, there showed no LD spectra in this case, then it was concluded that the CD spectra of the aggregate of MgPc(SEtPh)$_8$-Pd(II) complexes at the toluene/water interface did not include any LD contribution. These absorption and CD spectral results in (*R*)-MgPc(SEtPh)$_8$-Pd(II) and (*S*)-MgPc(SEtPh)$_8$-Pd(II) systems certainly suggested that the phthalocyanine skeletons are arranged in left-handed and right-handed helical *J*-aggregates, respectively. The *J*-aggregate formation of MgPc(SEtPh)$_8$-Pd(II) at the interface is recognized as a specific interfacial phenomena, when we compare it with the H-dimer formation observed in the bulk toluene solution in rather high concentrations of MgPc(SEtPh)$_8$-Pd(II).

The aggregate of MgPc(SEtPh)$_8$-Pd(II) complexes formed at the toluene/water interface was deposited onto MALDI-TOF/MS sample plate with 2,5-dihydroxybenzoic acid (DHB) as a matrix and MS spectra were measured, which gave several peaks at *m/z* = 4317 (J-dimer), 6298 (J-trimer), 8279 (J-tetramer), and 10260 (J-pentamer) for the aggregate of MgPc(SEtPh)$_8$-Pd(II) complexes. There was no signal due to *H*- dimer of MgPc(SEtPh)$_8$ with four $PdCl_2$ (*m/z* = 3962), which was observed in the dry toluene solution, in all observed mass spectra of the interfacial aggregate. This result indicated that the toluene/water interface preferred the linear *J*-dimer than the co-facial *H*-dimer, probably because of the hydration of the magnesium at the interface.

Moreover, to obtain visual insights into the aggregate structure at the interface, we prepared dry samples for scanning electron microscope (SEM) observation [9]. In the SEM images thus obtained, well-grown fibrous structures with the width of ca. 80-120 nm were abundantly observed. The fibers were long (>500 nm), suggesting that the aggregate of MgPc(SEtPh)$_8$-Pd(II) complexes tends to grow into a bundle of one-dimensional molecular wire. Since CD measurements confirmed the formation of optically chiral aggregate on the molecular level, it can be expected that the optical chirality should generate chiral morphology of the aggregate fibers. However, an observation of a particular chiral structure in the fibers was found to be difficult because of the low degree of twisting. Nevertheless, we fortunately found that the aggregate of (*S*)-MgPc(SEtPh)$_8$-Pd(II) complexes with positive chirality have right-handed helical structure. It should be emphasized that this result allows us, for the first time, to correlate the handedness of the supramolecular morphology of the interfacial aggregate to the sign of the optical CD spectra [10].

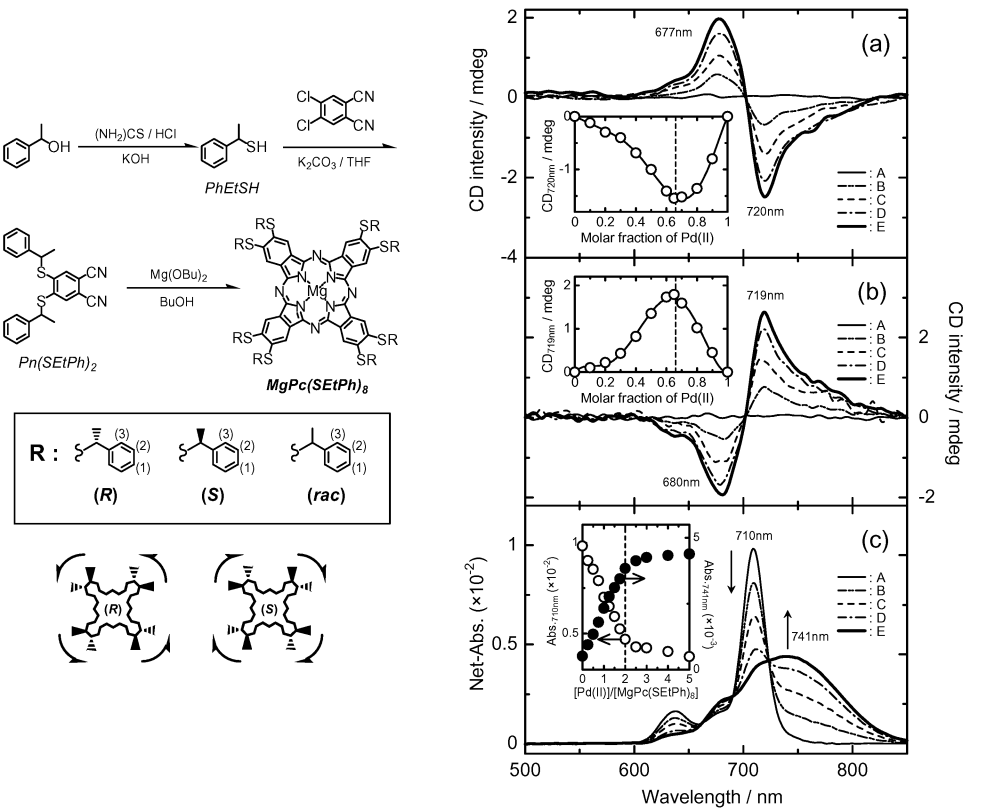

Figure 2. Change of circular dichroism (CD) spectra of (a) (*R*)-MgPc(SEtPh)$_8$ and (b) (*S*)-MgPc(SEtPh)$_8$ in the toluene/water system as a function of added $PdCl_2$ into the aqueous phase. The concentration of MgPc(SEtPh)$_8$ compound in the toluene phase is constant at 1.0×10^{-6} M. Molar ratios ([Pd(II)]/[MgPc(SEtPh)$_8$]$_o$) as follows: (A) 0, (B) 0.5, (C) 1.0, (D) 2.0, (E) 5.0. (c) Corresponding set of UV-vis absorption spectra of (*R*)-MgPc(SEtPh)$_8$.

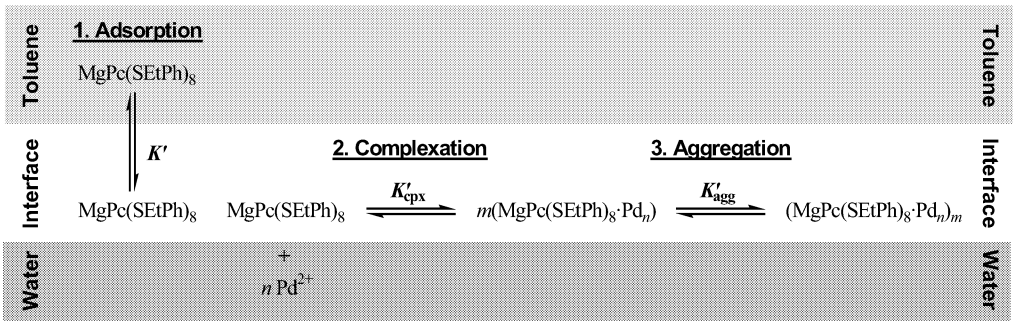

Figure 3. Schematic representation of the interfacial adsorption and aggregation mechanisms of MgPc(SEtPh)$_8$-Pd(II) complexes in the toluene/water system.

Interfacial Aggregation of Bilirubin (BR)–Bovine Serum Albumin (BSA)

Chiral complexation of bilirubin (BR) with bovine serum albumin (BSA) and aggregation of the complexes at liquid-liquid interface have been studied by using UV/vis absorption, circular dichroism (CD) and resonance Raman spectroscopy. Centrifugal liquid membrane (CLM) method was applied to measure the interfacial absorption and CD spectra. The interfacial complexation of BR with BSA was detected by the spectral shift of BR around 452 nm and the broadening in its bandwidth. The formation of aggregates of the BR-BSA complex at the interface was observed as the decrease of the absorbance at 452 nm and its shift, and the generation of bisignate Cotton effects. The toluene solution of BR gave no CD signals, since it existed as the equi-molar mixture of M and P conformers (see Figure 4). Upon addition of BSA to the aqueous phase, however, a CD signal appeared. Figure 4 shows the CLM-CD spectra of the interfacial complex of BR-BSA as a function of reaction time at a 1:1 molar ratio of BSA to BR. Here, the CD signals appear after 410 seconds, after those observed at a 3:1 molar ratio, which appear at 190 seconds. On the other hand, the absorbance of the complex at [BSA]/[BR] = MR = 1 reaches a maximum fastest in the mole ratio range considered, indicating that the 1:1 complex of BR and BSA is the most stable.

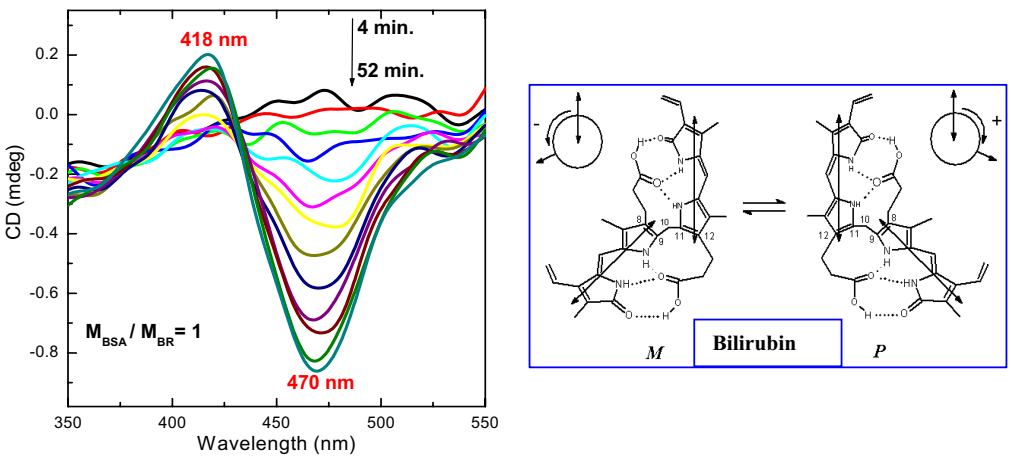

Figure 4. M conformer increased by the formation of a 1:1 bilirubin-BSA complex at the heptane/water interface, measured by CLM-CD.

Macroscopic and Microscopic SHG-CD Measurements of Porphyrin Aggregates

Porphyrins showed characteristic CD signals in the visible wavelength region by forming interfacial aggregates with chiral ions or chiral surfactant. In the micro-CD measurements, we used a newly constructed microscopic SHG-CD apparatus after transferring the interfacial aggregate to a cover glass plate. SHG signal was much more sensitive for the chiral compounds than the ordinary CD signals. The SHG-CD spectra of 5,10,15,20-tetraphenyl-21H,23H-porphinetetrasulfonic acid (TPPS) aggregate, including an enantiomeric tartaric acid, reflected the chirality of the tartaric ion.

CONCLUSIONS

Methods for the measurement of optical chiral signals of the aggregate formed at the liquid/liquid interface have been developed, which include CLM-CD and SHG-CD. The interfacial aggregates of phthalocyanine and porphyrin are found to be sensitive candidates for the interfacial chiral recognition of ions or surface-active molecules.

ACKNOWLEDGMENTS

These studies have been supported by the Grant-in-Aid for Scientific Research (S) (No. 16105002) of the Ministry of Education, Culture, Sports, Science and Technology of Japan. The cooperation of Dr. Kenta Adachi, Mr. Tokunaga and Dr. J-H. Yin in these research works is deeply appreciated.

REFERENCES

1. S. Tsurubou, "Solvent Extraction of a Chiral Ion-Pair between Some Cinchona Alkaloids and Acid Derivatives of Camphor," *Anal. Sci.*, **7**, 45-48 (1991).
2. S. Tsurubou and T. Sakai, "Stereoselective Adduct Formation of α-Acylcamphorato-copper(II) Chelates with Some Chiral Lewis Bases," *Anal. Chim. Acta*, **244**, 289-292 (1991).
3. M. Goto, "Recent Advances in Protein Extraction and Chiral Separation of Biomolecules," *Tsinghua Science and Technology*, **11**, 194-201 (2006).
4. H. Watarai, N. Teramae, and T. Sawada, Interfacial Nanochemiatry: Molecular Science and Engineering at Liquid-Liquid Interfaces, Kluwer Academic/Plenum Publishers, New York, 2005.
5. S. Wada, K. Fujiwara, H. Monjushiro, and H. Watarai, "Measurement of Circular Dichroism Spectra of Liquid/Liquid Interface by Centrifugal Liquid Membrane Method," *Anal. Sci.*, **20**, 1489-1491 (2004).
6. K. Fujiwara, H. Monjushiro, and H. Watarai, "Non-linear Optical Activity of Porphyrin Aggregate at the Liquid/Liquid Interface," *Chem. Phys. Lett.*, **394**, 349-353 (2004).
7. H. Nagatani, and H. Watarai, "Direct Spectrophotometric Measurement of Demetallation Kinetics of Tetraphenylporphyrinato Zinc(II) at the Liquid-Liquid Interface by a Centrifugal Liquid Membrane Method," *Anal. Chem.*, **70**, 2860-2865 (1998).
8. H. Watarai, K. Sasaki, K. Takahashi, and J. Murakami, "Interfacial Reaction in the Synergistic Extraction Rate of Ni(II) with Dithizone and 1,10-Phenanthroline," *Talanta*, **42**, 1691-1700 (1995).
9. K. Adachi, and H. Watarai, "Interfacial Aggregation of Thioether-Substituted Phthalocyaninatomagnesium(II)-Palladium(II) Complexes in the Toluene/Water System." *J. Mater. Chem.*, **15**, 4701-4710 (2005).
10. K. Adachi, K. Chayama, and H. Watarai, "Control of Optically Active Structure of Thioether-Phthalocyanine Aggregates by Chiral Pd(II)-BINAP Complexes in Toluene and at the Toluene/Water Interface," *Chirality*, **18**, 599-608 (2006).

PARTITION BEHAVIOR OF SEVERAL EXTRACTANTS AND THEIR IRON(III) COMPLEXES IN SOME MICELLAR SYSTEMS

Kazuho Inaba,[1] Taeko Doi,[1] Junji Noro,[2] and Hirochika Naganawa[3]

[1]National Institute for Environmental Studies, Tsukuba, Ibaraki 305-8506 Japan.
[2]Nissan ARC Ltd., Yokosuka, Kanagawa 237-0061 Japan,
[3]Nuclear Science and Engineering Directorate, Japan Atomic Energy Agency, Tokai, Ibaraki 319-1195 Japan. Corresponding author email address: inabakz@nies.go.jp

ABSTRACT

To determine the factors that affect the efficiency of extraction of solutes in micellar systems, we investigated the partitioning behavior of several β-diketones and their tris-iron(III) complexes between $C_{12}POE_8$, Brij 35, or Triton X-100 micelles and the bulk aqueous phase. The trend of the partition constants for the extractants and their tris-complexes differed from those observed in typical liquid-liquid systems. We discuss the effects of the substituent groups on the extractants and of the innersphere chemistry of the micelles. The locus of the solutes in the micelles seemed to play an important role in the extraction efficiency.

INTRODUCTION

Micellar systems behave as two-phase systems without the use of toxic or flammable organic solvents. From this “environmentally benign” character, they have been used instead of liquid-liquid systems as extraction media for separation and concentration of several metals or toxic chemicals [1]. Thorough consideration of the equilibrium and kinetic factors that control the efficiency of micellar extraction, is important to develop effective extraction systems [2]; however, systematic information on there factors is still limited. We have studied the extraction of several β-diketones and their tris-iron(III) complexes in a Triton X-100 (polyethyleneglycol *tert*-octylphenylether) micellar system to clarify the factors that affect the efficiency of extraction of metal chelates into the micellar pseudophase [3-8]. On the basis of results from our previous studies, we concluded that the ability of solutes to interact with the micellar mantle, which is formed by the polyoxyethylene group, is a key determinant of the extractability of the extractants and their complexes [4]. In the present study, we investigated the extraction behavior of five β-diketones and their iron(III) complexes in several micelles formed from nonionic surfactants. The skeletons of all the surfactants have an alkyl chain and an oxyethylene chain, but the chain lengths, and thus the micellar sizes, differ. By comparing the partitioning data obtained with micelles of different sizes, we determined the locus of the solutes in the micelles.

EXPERIMENTAL

Materials and Methods

All reagents were of analytical grade and were used without purification. The β-diketones (HAs) used were as follows: acetylacetone (2,4-pentanedione, AA), benzoylacetone (1-phenyl-1,3-butanedione, BZA), trifluoroacetylacetone (1,1,1-trifluoro-2,4-pentanedione, TFA), benzoyltrifluoroacetone (1-phenyl-4,4,4-trifluoro-1,3-butanedione, BFA), and 2-thenoyltrifluoroacetone (1-(2-thienyl)-4,4,4-trifluoro-1,3-butanedione, TTA). Three nonionic surfactants, $C_{12}POE_8$ (octaethyleneglycol *n*-dodecylether), Brij 35 (polyoxyethylene(23) laurylether), and Triton X-100, were used as the micelle-forming reagents. The critical micellar concentration (CMC), the molar volume of micelle (ϕ), the aggregation number of micelle (N), the whole volume of one micelle (V_t), and the volume of the core region of one micelle (V_c) are listed in Table 1.

Table 1. Physical and chemical parameters of micelles examined.

Surfactant	Structural formula	CMC (M)	ϕ (M^{-1})	N (-)	V_t (nm^3)	V_c (nm^3)
$C_{12}POE_8$ [a]	$CH_3(CH_2)_{11}(OCH_2CH_2)_8OH$	1.0×10^{-4}	0.97	120	125 [c]	19 [c]
Brij 35 [a]	$CH_3(CH_2)_{11}(OCH_2CH_2)_{23}OH$	1.0×10^{-4}	3.94	40	230 [c]	9.4 [c]
Triton X-100 [b]	$(CH_3)_3CC(CH_3)_2CH_2(C_6H_4)(OCH_2CH_2)_{9.5}OH$	2.4×10^{-4}	1.29	140	160 [d]	15 [d]

[a] From [9]. [b] From [10]. [c] Calculated as ellipsoid using the semiaxes data in [9].
[d] Calculated as ellipsoid using the semiaxes data in [10].

Experiments were carried out in a thermostated room at 298 K. The partition constants for the HAs were measured by three methods: the UV method uses the difference between UV absorbances of the HAs in the micellar and the bulk aqueous phases [7]; the EQ method uses differences in the distribution of iron(III) [3,4]; and the KIN method uses differences in the formation rates of a mono-iron(III) complex [8]. The partition constants for tris(β-diketonato)iron(III) complexes (FeA_3) were obtained simultaneously with partition constants of the HAs by means of the EQ method [3,4]. Measurements were made as described previously [3,4,7,8].

Data Treatment

The chemical species and their concentrations in the micellar pseudophase are denoted by a subscript m, and those in the bulk aqueous phase bear no subscript. The concentrations based on the total volume of the micellar solution are denoted by a subscript t. The volume fractions of the micellar and bulk aqueous phases (F_m and F, respectively) are defined by using CMC and ϕ as $F_m = \phi([\text{surfactant}] - \text{CMC})$ and $F = 1 - F_m$. The partition constant for the HAs between whole micelle and the bulk aqueous

phase are given by K_d = $[HA]_m/[HA]$, and the partition constants for tris-iron(III) complexes are given by $K_{dm} = [FeA_3]_m/[FeA_3]$.

The mass balance for each HA can be expressed as,

$$[HA]_t = [HA]_m F_m + [HA]F + [A^-]F = \{(K_d F_m + F)[H^+] + K_a F\}[A^-]/K_a \quad (1)$$

In the present study, no additional salt was dissolved in the solution; only the uncharged FeA_3 complex was extractable. Thus, the distribution ratio of iron(III), D, between the micellar and bulk aqueous phases is given by

$$D = [FeA_3]_m/\{[Fe^{3+}] + \sum[FeA_n^{(3-n)+}]\} = \beta_3 K_{dm}[A^-]^3/\{1 + \sum\beta_n[A^-]^n\} \quad (2)$$

Here, β_I is the stability constant of the n-th complex ($FeA_n^{(3-n)+}$). The partition constants, K_{dm}, were calculated from plots of D as a function of $[A^-]$.

RESULTS AND DISCUSSION

The partition constants for the five β-diketones obtained in the three micellar systems are summarized in Table 2, along with the values in hexane-H_2O and diethylether-H_2O systems.

Table 2. Log K_d values in several micellar and liquid-liquid systems

HA	$C_{12}POE_8$			Brij 35			Triton X-100			HX [d]	DE [e]
	UV	EQ	KIN	UV	EQ	KIN	UV [a]	EQ [b]	KIN [c]		
AA	- [f]	- [f]	0.41	- [f]	- [f]	0.18	0.37	0.42	0.36	-0.05	0.50
BZA	2.08	2.18	1.91	1.38	1.79	1.43	1.84	1.93	1.76	2.01	2.70
TFA	0.46	- [f]	0.58	0.14	- [f]	0.15	0.45	0.63	0.63	-0.54	1.19
BFA	1.85	1.86	1.78	1.36	1.59	1.30	1.54	1.76	1.52	1.87	3.71
TTA	1.57	1.65	1.13	0.90	1.40	0.94	1.33	1.59	1.39	0.69	2.91
DBM [g]	ND [h]	ND [h]	ND [h]	ND [h]	ND [h]	ND [h]	ND [h]	4.0	ND [h]	3.92	4.70

[a] From [7]. [b] From [4]. [c] From [8]. [d] Hexane-H_2O system [4]. [e] Diethylether-H_2O system [4].
[f] The error was too large. [g] Dibenzoylmethane (1,3-diphenyl-1,3-propanedione) [4].
[h] Not determined in the present study.

The relationships between the K_d values for the hexane-H_2O system and the values for the diethylether-H_2O, $C_{12}POE_8$, Brij 35, and Triton X-100 systems are shown in Figure 1(a). The correlation between the K_d values for AA, BZA, and DBM, which have no trifluoromethyl group, in hexane-H_2O and the values in diethylether-H_2O was good (line i). The correlation between the values for the other three HAs, all of which have a trifluoromethyl group, in these two systems was also good, but the K_d values in diethylether-H_2O were much higher than the values in hexane-H_2O (line ii). This difference can be explained in terms of solute-solvent interactions involving the acidic proton in the extractants and the oxygen atom in the diethylether: the stronger acids were extracted more efficiently into the solvating-type solvent. The linear relationship between the values for the two liquid-liquid systems suggests that the change in bulkiness of the solutes had no obvious effect in these systems.

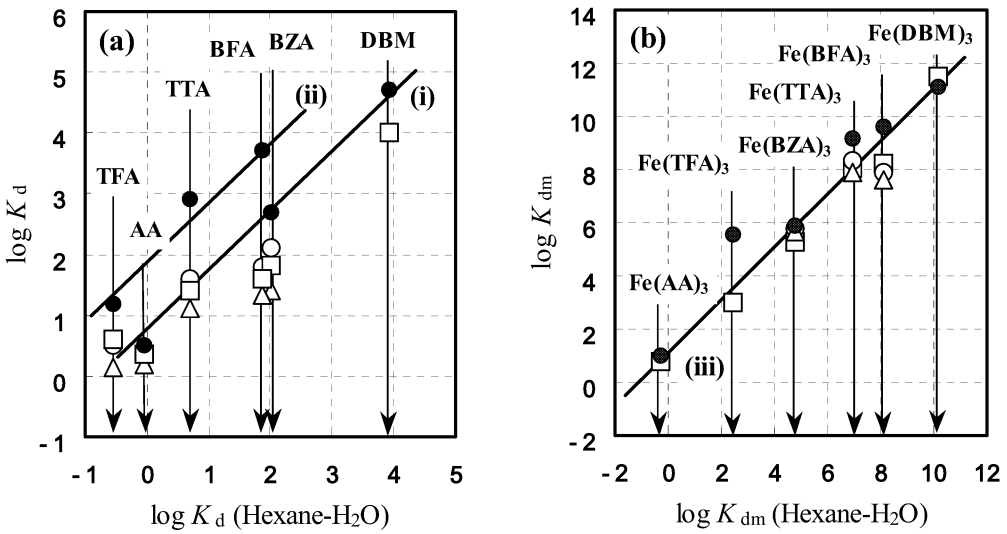

Figure 1. Plots of log K_d (a) and log K_{dm} (b) in the diethylether-H_2O (closed circles), $C_{12}POE_8$ (open circles), Brij 35 (open triangles), and Triton X-100 (open squares) systems versus the values in the hexane-H_2O system.

The relationships between the K_d values for the hexane-H_2O system and for the three micellar systems differed from the relationship between the values for the two liquid-liquid systems (Figure 1(a)). The effect of the trifluoromethyl group seems to have been small; only a small enhancement was observed for TFA and TTA in all three micellar systems. These results may indicate that the interaction between the examined extractants and the surfactant molecules in the micelles was weak, except in the case of TFA and TTA. Previously, we concluded that the enhancement of K_d for these extractants in Triton X-100 is due to the greater ability of these extractants to penetrate the mantle region of the micelles [4]. The linear shape of the molecule without the bulky substituent group (TFA) and the presence of the S atom in the thienyl group, which can interact with water molecules dissolved in the mantle region (TTA), may also explain the enhancement in the present study.

The relationships between the K_d values for the hexane-H_2O system and the micellar systems showed similar trends for the three micellar systems, although the K_d values for each extractant differed somewhat (by 0.8 log unit). The ratio of the volume of the core region to the whole micellar volume varied for the three micellar systems (0.15 for $C_{12}POE_8$, 0.04 for Brij 35, and 0.09 for Triton X-100; calculated from the V_t and V_c values in Table 1). If we can assume that all the HA was extracted into the core region, the partition constant between the micellar core and bulk aqueous phase ($K_{d(core)}$) is given by $K_{d(core)} = K_d \times V_t/V_c$. The calculated log $K_{d(core)}$ values for $C_{12}POE_8$, Brij 35, and TritonX-100 are 1.2, 1.6, and 1.4 for AA; 2.9, 3.0, and 2.8 for BZA; 1.3, 1.6, and 1.6 for TFA; 2.6, 2.8, and 2.6 for BFA; and 2.4, 2.3, and 2.4 for TTA, respectively. The three values are similar for each extractant, which may also indicate that the interaction between the extractants and the mantle region is small and that the extractants existed mainly in the core region of the micelles.

The partition constants for the FeA_3 complexes obtained in the three micellar systems are summarized in Table 3, along with the values in the hexane-H_2O and diethylether-H_2O systems [4]. The relationships between the K_{dm} values for the hexane-H_2O system and the values for the diethylether-H_2O, $C_{12}POE_8$, Brij 35, and Triton X-100 systems are shown in Figure 1(b). The K_{dm} values for $Fe(AA)_3$, $Fe(BZA)_3$, and $Fe(DBM)_3$ in diethylether-H_2O were proportional to those obtained in hexane-H_2O (line iii). These three extractants are weaker acids (the acid-dissociation constant, K_a, is about 10^{-10} [4]) than the other three extractants, and thus, the tris-complexes of the former are much stable (the stability constant, β_3, for these iron(III) complexes is reported to be $10^{26.3}$ [4]). The other three extractants are stronger acids, and thus the stability of their tris-complexes is lower ($\beta_3 = 10^{16.3}$ [4]). The low degree of saturation may enhance the K_{dm} values by an interaction like a synergistic effect.

Table 3. Log K_{dm} values in the several micellar and liquid-liquid systems

	$C_{12}POE_8$		Brij 35		Triton X-100 [a]		HX [b]	DE [c]
	Whole [d]	Core [e]	Whole [d]	Core [e]	Whole [d]	Core [e]		
$Fe(AA)_3$	- [f]	- [f]	- [f]	- [f]	0.8	1.8	-0.3	1.0
$Fe(BZA)_3$	5.8	6.6	5.7	7.1	5.3	6.3	4.8	5.9
$Fe(TFA)_3$	- [f]	- [f]	- [f]	- [f]	3.0	4.0	2.5	5.6
$Fe(BFA)_3$	7.9	8.7	7.6	9.0	8.2	9.2	8.1	9.6
$Fe(TTA)_3$	8.3	9.1	7.9	9.3	8.1	9.1	7.0	9.2
$Fe(DBM)_3$ [g]	ND [h]	ND [h]	ND [h]	ND [h]	11.5	12.5	10.2	11.1

[a] From [4]. [b] Hexane-H_2O system [4]. [c] Diethylether-H_2O system [4]. [d] Based on the whole micellar volume. [e] Based on the micellar core volume. [f] The error was too large.
[g] Dibenzoylmethane (1,3-diphenyl-1,3-propanedione) [4]. [h] Not determined in the present study.

The relationship between the values for the hexane-H_2O system and the three micellar systems differed from the relationship between the values for the hexane-H_2O and diethylether-H_2O systems. No enhancement of K_{dm} was found in the complexes containing trifluoromethyl-substituted extractants; the K_{dm} values were proportional to those obtained in the hexane-H_2O system. The differences between the K_{dm} values for the three micellar systems were small, 0.4–0.6 log units. These differences may indicate that the interaction between the complexes and the mantle region of the micelles was smaller than that observed in the diethylether-H_2O system. If we assume that the entire tris-complex was extracted into the core region, the partition constant between the micellar core and the bulk aqueous phase ($K_{dm(core)}$) can be calculated as $K_{dm(core)} = K_{dm} \times V_t/V_c$., as summarized in Table 3. The $K_{dm(core)}$ values for each complex were quite similar for the three micellar systems, which suggests that the tris-complexes penetrated into the core region of the micelles and existed mainly in the core region.

The K_{dm} values for $Fe(BFA)_3$ were somewhat lower than expected from the proportional relationship in Figure 1(b). This decrease in $Fe(BFA)_3$ may be due to the bulkiness and the hydrophobic character of the complex and may reflect a difference between the chemistry of the micellar innersphere and the typical organic solvents.

CONCLUSIONS

By comparing the partition constants obtained in three micellar systems, we concluded that the β-diketones and their tris-iron(III) complexes existed mainly in the core region of the micelles. Studies of surfactant micelles with different inner-sphere chemistry may be an important key to further clarifying the extraction behavior.

ACKNOWLEDGMENTS

The authors are grateful to Emeritus Professor Henry Freiser of the University of Arizona and Professor Subramaniam Muralidharan of Western Michigan University for their helpful comments throughout the study. We thank the late Professor Tatsuya Sekine of Tokyo University of Science for his guidance to the life of scholarship.

REFERENCES

1. W. L. Hinze and E. Pramauro, "A Critical Review of Surfactant-Mediated Phase Separations (Cloud-Point Extractions): Theory and Applications," *Crit. Rev. Anal. Chem.*, **24**, 133-177 (1993).
2. C. Tondre, "Surfactant-Based Colloidal Particles as the Extracting Phase for the Removal of Metal Ions from Aqueous Environments: Kinetic and Applied Aspects," ACS Symposium Series, Vol. 740, J. F. Scamehorn and H. Harwell, Eds., American Chemical Society, Washington DC, USA, 2000; pp. 139-157.
3. K. Inaba, "Extraction of Iron(III) with Some β-Diketones into a Triton X-100 Micellar Phase: Is a Micellar System Similar to a Liquid-Liquid System?," Value Adding Through Solvent Extraction, Vol. I, D. C. Shallcross, R. Paimin, and L. M. Prvcic, Eds., University of Melbourne, Melbourne, Australia, 1996; pp. 57-62.
4. K. Inaba, "Extractability and Solubulization Locus of Six β-Diketones and Their Iron(III) Complexes in Triton X-100 Micellar Solutions," *Langmuir*, **13**, 1501-1509 (1997).
5. K. Inaba, "Unusually Slow Extraction Rate and Mechanism of Iron(III) with Trifluoroacetylacetone in Triton X-100 Micellar System. Part I. Extraction Routes," *Anal. Sci.*, **16**, 811-817 (2000).
6. K. Inaba, "Unusually Slow Extraction Rate and Mechanism of Iron(III) with Trifluoroacetylacetone in Triton X-100 Micellar System. Part II. Interfacial Transport," *Anal. Sci.*, **16**, 819-824 (2000).
7. K. Inaba, "Spectrophotometric Determination of Partition Constants for Five β-Diketones in Triton X-100 Micellar solutions," *Anal. Sci.*, **17**, 349-352 (2001).
8. K. Inaba, "Transfer Rate of Several Tris(β-diketonato)iron(III) Complexes at the Bulk Aqueous-Triton X-100 Micellar Interface: Effects of Substituent Groups in the Extractants," *J. Colloid Interface Sci.*, **262**, 243-252 (2003).
9. C. Tanford, Y. Nozaki, and M. F. Rohde, "Size and Shape of Globular Micelles Formed in Aqueous Solution by *n*-Alkyl Polyoxyethylene Ethers," *J. Phys. Chem.*, **81**, 1555-1560 (1977).
10. R. J. Robson and E. A. Dennis, "The Size, Shape, and Hydration of Nonionic Surfactant Micelles. Triton X-100," *J. Phys. Chem.*, **81**, 1075-1078 (1977).

ANALYSIS OF BINDING REACTIONS OF IONIC SUBSTANCES TO NONIONIC SURFACTANT MICELLES

Toshio Takayanagi,[1,2] Yu Takimoto,[2] Ayumi Ikuta,[2] and Shoji Motomizu[1,2]

[1]Graduate School of Natural Science and Technology, Okayama University, 3-1-1 Tsushimanaka, Okayama, 700-8530, Japan. [2]Department of Chemistry, Faculty of Science, Okayama University, 3-1-1 Tsushimanaka, Okayama 700-8530 Japan. Corresponding author email address: takayana@cc.okayama-u.ac.jp

ABSTRACT

Binding reactions of ionic substances to nonionic surfactant micelles were investigated. Brij 35, Brij 58, Brij 78, and Triton X-100 were used as the nonionic surfactants to form micelles. The electrophoretic mobility of analyte ions was measured by capillary zone electrophoresis in the presence of the nonionic surfactant micelle as a separation modifier. When some alkylbenzene sulfonate ions were used as model analytes, their mobility changes were analyzed to determine the binding constants, and the contribution of alkyl moiety to the binding equilibrium was quantitatively understood. Property of the micelles as binding matrix was also investigated with dansyl amino acids as model substrates: the binding constants were compared with the distribution ratio of the amino acids between water and 1-octanol. In the case of alkylpyridinium ions, the binding constants were significantly smaller than the alkylbenzene sulfonate ions, which indicated the affinity of the nonionic surfactant micelle toward the cations and the anions.

INTRODUCTION

Hydrophobic substances in aqueous solution can be extracted and separated into water-immiscible organic solvents. The technique for estimating the extraction constants has been established, and plenty of extraction data are available for various types of the solvent extraction systems. The toxicity and environmental burden of the organic solvents have promoted a trend toward less harmful extraction matrices such as membrane filters and solid cartridges. They are alternative extraction media to the organic solvents, and the separation technique is so-called solid-phase extraction (SPE) [1].

Surfactant micelles provide the hydrophobic partition media in a pseudo-homogeneous aqueous solution, in which hydrophobic substances can be extracted. However, no phase separation accompanies micelle extraction, and therefore, a chromatographic separation is necessary to utilize the micelle extraction. Capillary zone electrophoresis (CZE) is frequently used for the separation of ionic substances, and surfactant micelles are often used as separation modifier [2]. In addition to the anionic

surfactants such as sodium dodecyl sulfate, nonionic surfactants can develop the resolution among ionic substances. Advantages using the nonionic surfactants in CZE are low critical micelle concentration, less Joule heating, and partition based on hydrophobicity. Since the nonionic surfactant micelles are electrically neutral, they are considered to be equivalent to water-immiscible organic solvents.

In this study, nonionic surfactant micelles as binding matrix of ionic substances have been investigated through the changes in electrophoretic mobility of analytes. Change in electrophoretic mobility of analyte ions with the binding reaction to the micelle is schematically illustrated in Figure 1, where A^- represents anionic analyte.

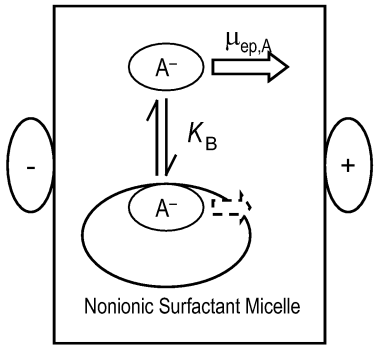

Figure 1. Schematic illustration for the binding reaction of ionic species to a nonionic surfactant micelle.

EXPERIMENTAL

Apparatus

A Hewlett-Packard ^{3D}CE system equipped with a photodiode array detector (Waldbronn, Germany) was used as a capillary electrophoresis system and for the measurement of the electrophoretic mobility. A fused silica capillary (Agilent Technologies, Waldbronn, Germany) with its total length of 64.5 cm, effective length from the injection end to the detection point of 56 cm, and its inner diameter of 50 μm was held in a capillary cassette and attached on the system. The temperature of the capillary cassette was controlled at 25.0 ± 0.1 ^{o}C. The migrating solution and the sample solutions were put in 1 mL vials, and the vials were set in the system tray. A Hewlett-Packard ChemStation (ver. 5.01) was used for the control of the system, data acquisition, and the analysis of the electropherograms.

Reagents

Two series of anions of alkylbenzene sulfonates and dansyl amino acids were used as model analytes. Cationic alkylpyridinium ions were also used. The nonionic surfactants polyoxyethylene (23) lauryl ether (Brij 35), polyoxyethylene (20) cetyl ether (Brij 58), polyoxyethylene (20) stearyl ether (Brij 78), and polyoxyethylene (9.6)

octylphenyl ether (Triton X-100) were used as nonionic surfactants to form micelles. The surfactant was added to the migrating solution in the concentration ranges from 0 to 3.0% w/v. Appropriate pH buffer was chosen to control the pH of the migrating solution.

Standard Procedure

A migrating solution was prepared from the pH buffer and a known amount of the nonionic surfactant. After the capillary was conditioned and equilibrated in an ordinary manner, a sample solution containing the analyte ions was injected into the capillary from the anodic end for 5 s hydrodynamically by applying pressure (50 mbar). A voltage of 20 kV was then applied, and electrophoresis was started. The analyte ions were photometrically detected. Ethanol at the concentration of 1-3% v/v was added in the sample solution to detect it and to monitor the electroosmotic flow (EOF). The electrophoretic mobility of the analyte ions, $\mu_{ep,A}'$, was calculated in an ordinary manner using Equation 1:

$$\mu_{ep,A}' = (L_T \times L)/(V \times t) - (L_T \times L)/(V \times t_{EOF}) \quad (1)$$

where L_T, L, V, t, and t_{EOF} are the total capillary length, the effective capillary length from the injection end to the detection point, the applied DC voltage, the migration time of the analyte anion, and the migration time of the EOF, respectively.

RESULTS AND DISCUSSION

Binding Reaction of Alkylbenzene Sulfonate Ions

The binding reaction of ionic substance (A) to nonionic surfactant micelle, as well as its equilibrium, are expressed as in Equations 2 and 3.

$$A + (NIS)_m \rightleftharpoons A\text{-}(NIS)_m \quad (2)$$

$$K_B = [A\text{-}(NIS)_m]/[A][(NIS)_m] \quad (3)$$

where $(NIS)_m$ is the nonionic surfactant micelle, and K_B is the binding constant of the analytes to the nonionic surfactant micelle. The concentration of the nonionic surfactant micelle was calculated from the concentration of the nonionic surfactant, its critical micelle concentration, and its aggregation number (n) [3]. Aggregation numbers used are 40 for Brij 35 and 70 for Brij 58. Apparent electrophoretic mobility of the analyte, $\mu_{ep,A}'$, is expressed as in Equation 4.

$$\mu_{ep,A}' = \mu_{ep,A}/(1 + K_B[(NIS)_m]) \quad (4)$$

where $\mu_{ep,A}$ is the electrophoretic mobility of the free analyte ions. A series of the pairs of $[(NIS)_m]$ and $\mu_{ep,A}'$ were input in Equation 4, and K_B and $\mu_{ep,A}$ were optimized to minimize the difference between the experimental data and the simulated curve [4].

The alkylbenzene sulfonate ions possess a hydrophobic character, and they can be bound to the nonionic surfactant micelle as an anionic form. The K_B values increased with increasing size of the anions. The hydrophobicity of the sulfonate ions plays an important role in the binding reaction as expected. However, the decreases in $\mu_{ep,A}'$ were too large with octylbenzenesulfonate and dodecylbenzene sulfonate ions to determine the K_B values. The nonlinearity of the mobility decrease should be attributed to the formation of mixed micelle with the nonionic surfactant; the reaction is different from the simple binding reaction of the anions.

Binding Reaction of Dansyl Amino Acids

Eight kinds of dansyl amino acids (DAAs) were adopted as model analytes of binding probes, since the partition equilibrium of the amino acids between water and 1-octanol is well known [5-6]. The DAAs used are monovalent anions at pH around 9, and the binding constants were also determined through the changes in electrophoretic mobility of the DAAs. The molar concentration of the surfactant was used in the analysis, because the critical micelle concentration is negligibly smaller than the concentration ranges of the nonionic surfactant, and the aggregation number of the surfactant (n) is different among the surfactants [3]. Therefore, the binding constants determined are the values divided by the aggregation number of the surfactant (n), K_B/n.

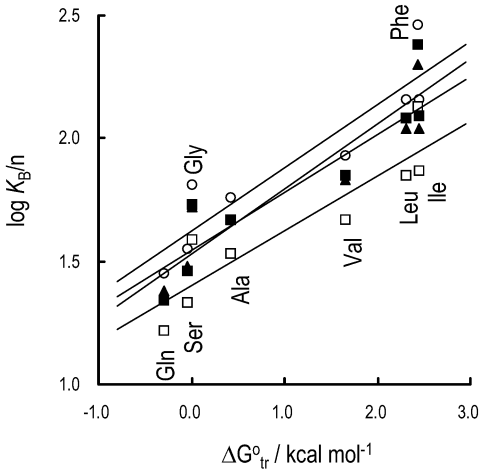

Figure 2. Linear free energy relationship between ΔG^o_{tr} and log K_B/n. Surfactants: ▲, Brij 35; ■, Brij 58; ○, Brij 78; □, Triton X-100. DAAs are represented with the amino acid.

The micelle binding reaction is based on the partition between the aqueous and the micelle phases, and thus, the micelle binding system would be equivalent to the liquid-liquid partition system. A linear free energy relationship was examined on the two partition systems. We adopted transfer energy of amino acid from water to 1-octanol, ΔG^o_{tr}, for the amino acids proposed by Fauchere and Plisca [5]. We used anionic species of DAAs on evaluating the partition phenomena. The dansyl group, however, will give a

common perturbation from the viewpoint of the increase in the molecular volume of the amino acids. The binding constants of DAAs to the nonionic surfactants are plotted against ΔG^{o}_{tr} values, as is shown in Figure 2. A clear relationship was observed with some exceptions that amino acid possessing larger ΔG^{o}_{tr} showed large K_B/n values with all the surfactant micelles examined.

The binding constants were compared among the nonionic surfactant micelles (Figure 3). Conventionally, Brij 58 was used as a standard surfactant. It can be noticed from Figure 3 that such DAA showing a larger K_B/n value with Brij 58 micelle also gave a larger K_B/n value with other nonionic surfactant micelles. By comparing the absolute value of the K_B/n, a good correlation can be seen among the surfactants: Triton X-100 < Brij 35 and Brij 58 < Brij 78. The order agreed with the hydrophile-lipophile balance (HLB) of the surfactant [3]; the HLB values calculated are 17.2, 16.0, and 15.6 for Brij 35, Brij 58, and Brij 78, respectively. More hydrophobic surfactant micelles can bind the hydrophobic DAA strongly.

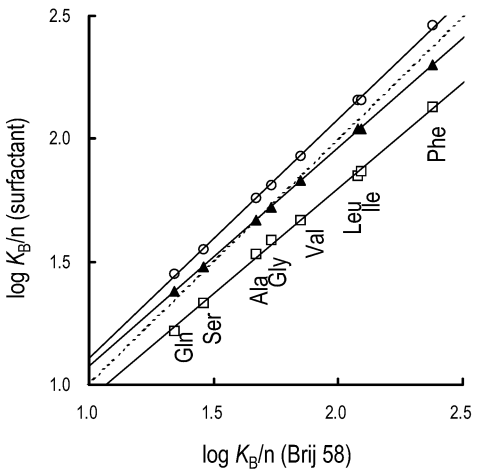

Figure 3. Comparison of the binding constants among the nonionic surfactant micelles. Brij 58 was used as a standard surfactant. Surfactants: ▲, Brij 35; ○, Brij 78; □, Triton X-100. DAAs are represented with the amino acids.

Binding Reaction of Alkylpyridinium Ions

The binding analysis using the electrophoretic mobility has been applied to the cationic alkylpyridinium ions. The binding constants determined are plotted against the molecular volume of the substrates (Figure 4). The van der Waals volume of the substrates has been estimated by MOPAC 2007 with AM1 Hamiltonian. An obvious relationship was observed for the alkylpyridinium ions in that more bulky ones showed larger binding constants (Figure 4a). However, the values, as well as the slope, are smaller than the alkylbenzene sulfonate ions (Figure 4b). The results reflect the binding affinity of the nonionic surfactant micelle toward cationic and anionic substrates.

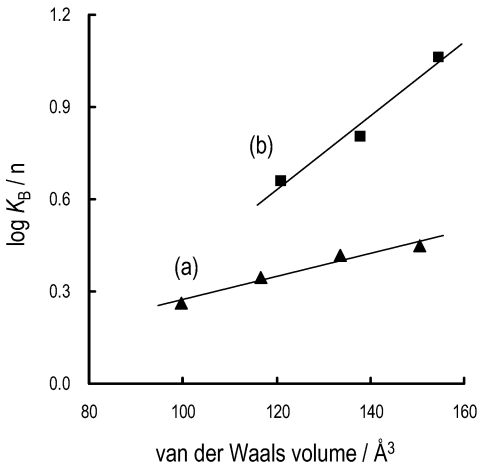

Figure 4. Relationship between binding constant and van der Waals volume of the analyte using: Brij 58 surfactant. (a), Alkylpyridinium ions; (b), alkylbenzene sulfonate ions.

CONCLUSIONS

Binding reactions of alkylbenzene sulfonate ions, dansyl amino acids, and alkylpyridinium ions to nonionic surfactant micelles have been analyzed through the mobility change in CZE. Hydrophobic character of the substrates, as well as the nonionic surfactant micelles as partition matrix, have been elucidated.

ACKNOWLEDGMENT

This study has been supported in part by a Grant-in-Aid for Scientific Research (C) No. 19550090 from Japan Society for the Promotion of Sciences (JSPS).

REFERENCES

1. H. Kataoka, "New trends in sample preparation for clinical and pharmaceutical analysis," *Trends Anal. Chem.*, **22(4)**, 232-244 (2003).
2. P. G. Muijselaar, K. Otsuka, and S. Terabe, "Micelles as pseudo-stationary phases in micellar electrokinetic chromatography," *J. Chromatogr. A*, **780**(1+2), 41-61 (1997).
3. M. J. Rosen, Surfactants and Interfacial Phenomena, Wiley, New York, 2nd ed., 1989.
4. T. Takayanagi and S. Motomizu, "Equilibrium analysis of reactions between aromatic anions and nonionic surfactant micelles by capillary zone electrophoresis," *J. Chromatogr. A*, **853**(1+2), 55-61 (1999).
5. J-L. Fauchere and V. Pliska, "Hydrophobic parameters π of amino acid side chains from the partitioning of N-acetyl-amino-acid amides," *Eur. J. Med. Chem.*, **18**(4), 369-375 (1983).
6. P. A. Karplus, "Hydrophobicity regained," *Protein Sci.*, **6**(6), 1302-1307 (1997).

TETRAALKYLPHOSPHONIUM POLYOXOMETALATES AS NOVEL IONIC LIQUIDS

Mark L. Dietz,[1] Paul G. Rickert,[1] Mark R. Antonio,[1] Millicent A. Firestone,[2] James F. Wishart,[3] and Tomasz Szreder[3]

[1]Chemical Sciences and Engineering and [2]Materials Science Divisions, Argonne National Laboratory, Argonne, IL 60439. [3]Chemistry Department, Brookhaven National Laboratory, Upton, NY 11973. Corresponding author email address: mdietz@anl.gov

ABSTRACT

The pairing of a Lindqvist or Keggin polyoxometalate (POM) anion with an appropriate tetraalkylphosphonium cation, $[R_3R'P]^+$, yields an original family of ionic liquids (POM-ILs), among them liquid salts at or near ambient temperature. The physicochemical properties of several such "inorganic liquids", in particular their thermal properties, suggests the possible application of these compounds as robust, thermally-stable solvents for liquid-liquid extraction. A preliminary evaluation of POM-ILs in this application is presented.

INTRODUCTION

Growing recognition of the need to devise more environmentally friendly chemical processes and to extend the principles and practices of "green chemistry" to chemical separations has recently led to substantial interest in ionic liquids (ILs), particularly those that are liquids at ambient temperature (designated "room temperature ionic liquids" or RTILs), as alternatives to conventional organic diluents in various solvent-extraction processes [1]. Many ionic liquids exhibit a variety of unique properties that make them promising in such applications, including low flammability, good thermal stability, and a near-absence of vapor pressure. In contrast to ordinary organic diluents, ionic liquids are also extraordinarily tunable solvents, with even the slightest changes in the structure of the anionic or cationic components frequently leading to substantial alterations in physicochemical properties [2]. Despite recent studies indicating that the use of various common ionic liquids (*e.g.*, N, N'-dialkylimidazolium salts) in combination with certain well-known neutral extractants (*e.g.*, crown ethers) may prove problematic [3], other work suggests that the unique solvation environment afforded by these liquids may offer new opportunities for novel separations [4].

With this in mind, we have been exploring the properties and potential applications of an as yet small, but potentially significant sub-class of ILs, "inorganic liquids" [5], in which one component of the IL consists of a metal oxide cluster [6], a silica nanoparticle [7], or other similar inorganic moiety. Recent work in This Laboratory

has concerned the possibilities afforded by inorganic liquids comprising combinations of a polyoxometalate anion (*e.g.*, Keggin, Lindqvist) and tetraalkylphosphonium cations [8,9]. In this report, we summarize the characteristics of these materials relevant to their potential application as solvents in liquid-liquid extraction and present preliminary data concerning the application of one of them as an extraction solvent.

EXPERIMENTAL

Preparation of ILs

Trihexyl(tetradecyl)phosphonium bromide was obtained as a generous gift from Cytec Canada, Inc. (Niagra Falls, Ontario) and used without further purification. All other materials were reagent grade and unless noted otherwise, were used as received. Lindqvist-based ($W_6O_{19}^{2-}$) ILs were prepared from sodium tungstate by the method of Klemperer [10], modified by substitution of a tetraalkylphosphonium bromide for the corresponding tetraalkylammonium salt. The analogous Keggin heteropolytungstate ($[PW_{12}O_{40}]^{3-}$) salts were prepared by reaction of $H_3PW_{12}O_{40}$ with a tetraalkylphosphonium bromide under the same conditions. Addition of absolute methanol to the reaction mixture led to precipitation of the product, which, following methanol and diethyl ether washes, was dried at 80 ºC for 24 hours. Product purity was confirmed by NMR, elemental analysis, and high-resolution FAB-MS.

Characterization of ILs

A Cambridge Applied Systems ViscoLab400 reciprocating piston viscometer equipped with a flow-through jacket for temperature control was used for all viscosity measurements. Temperature control was achieved using a Lauda Proline RP-845 circulating bath. Placement of the viscometer head in an N_2-purged acrylic box eliminated absorption of atmospheric moisture by the samples.

For differential scanning calorimetry (DSC), 5-10 mg aliquots of the IL of interest were sealed in Al pans and equilibrated at -75 ºC for 5 minutes before the start of the heating cycle. Data were collected using a scan rate of 2 ºC/min. Calibration of the instrument, a TA Instruments model Q100 equipped with a refrigerated cooling system, was performed using an indium standard. For thermogravimetric analyses (TGA), a TA Instruments Q50 was employed. In a typical run, a weighed portion (2-5 mg) of sample was heated in a Pt pan from 25-600 ºC at a rate of 10 ºC/min under nitrogen flow.

All distribution ratios were determined radiometrically. Specifically, aliquots (500 μL) of the organic phase were pre-equilibrated *via* two contacts with twice their volume of an appropriate nitric acid solution. A portion of each pre-conditioned organic phase was then combined with an equal volume of an appropriate uranium (^{233}U)-spiked aqueous phase. Following a period (30-60 min.) of intermittent of vortex mixing, the mixture was centrifuged until phase separation was complete. Two 50 μL aliquots of each phase were then withdrawn for analysis by liquid scintillation counting on a Packard Model 2200CA Liquid Scintillation Analyzer.

RESULTS AND DISCUSSION

Among the most important of the parameters that determine the suitability of a particular solvent for liquid-liquid extraction are its physical/chemical stability and viscosity, along with the efficiency of extraction of the metal ion(s) of interest. Prior work in a number of laboratories indicates that ionic liquids, while often more viscous than conventional organic solvents, offer the advantages of higher extraction efficiency [4] and excellent physical, thermal, and radiolytic stability [11-14]. Our efforts to evaluate the utility of inorganic liquids as extraction solvents began with an examination of the extraction of uranium by tri-*n*-butyl phosphate (TBP) into *bis*[trihexyl(tetradecyl)phosphonium][W_6O_{19}]. Figure 1 shows the nitric acid dependency of D_U obtained for a "PUREX-like" process solvent comprising a 1.2 M solution of TBP in this Lindqvist IL. Also shown for purposes of comparison are the results obtained for the same concentration of the extractant in dodecane and in a "traditional" ionic liquid, 1-pentyl-3-methylimidazolium *bis*[(trifluoromethyl)sulfonyl] imide ($C_5mim^+Tf_2N^-$).

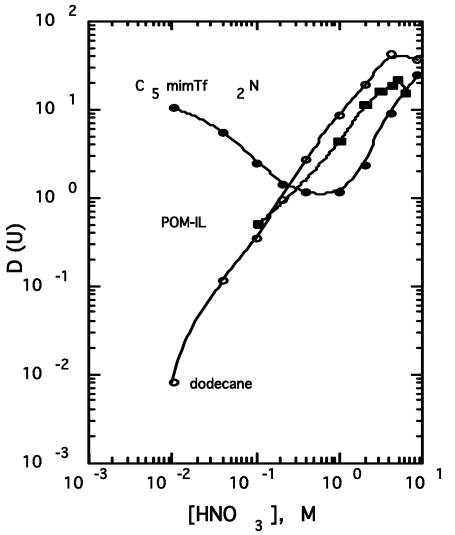

Figure 1. Nitric acid dependency of D_U for dodecane and two ionic liquids (T = 22 ºC).

As can be seen, in contrast to the relatively hydrophilic, imidazolium-based IL, which exhibits a complex dependency of D_U upon nitric acid concentration (the result of the gradual replacement of partitioning *via* an ion-exchange process by extraction of a neutral uranyl nitrato-TBP complex), the nitric acid dependency of D_U for the POM-IL closely resembles that observed for dodecane. As has been noted previously in studies of the partitioning of various metal ions into $C_nmim^+Tf_2N^-$ ILs in the presence of neutral extractants, as the hydrophobicity of the cation comprising an IL is increased, the acid dependency of D_M observed increasingly resembles that observed for conventional organic solvents (in which D_M rises with increasing acidity) [15]. Thus, it is not unexpected that the Lindqvist IL, with its comparatively hydrophobic phosphonium cation, would exhibit an acid dependency of D_U similar to that of the hydrocarbon

solvent. It is important to note, however, that at any given acidity, the D_U value observed for the POM-IL is actually ~2-fold lower than that observed for dodecane, a result which calls into question the superiority of ILs over conventional diluents in extraction [4]. Nonetheless, the values of D_U observed are more than adequate for purposes of devising a workable POM-IL-based extraction system.

In the course of efforts to measure uranium extraction into the Lindqvist IL, it became apparent that this solvent is inconveniently viscous, despite the presence of nearly 40% (v/v) TBP. For this reason, we next examined the temperature-dependence of the viscosity of the Lindqvist IL and, for purposes of comparison, the analogous bromide salt. Figure 2 shows the results obtained, presented as plots of the dependence of the viscosity on reciprocal temperature.

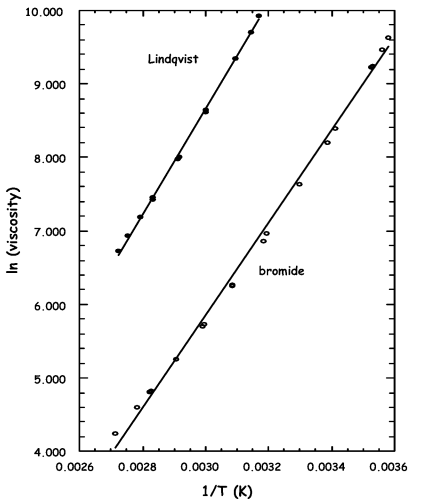

Figure 2. Temperature dependence of viscosity for two tetraalkylphosphonium ILs.

Although the Arrhenius-like behavior of the temperature dependence is interesting from a fundamental point of view, of more importance from a practical perspective are the IL viscosities over the range of temperatures that might be encountered in an extraction process (*ca.* 20-90 ºC). It is readily evident that over much of this range, the viscosities are quite high; at temperatures less than 40 ºC, in fact, the viscosity of the Lindqvist IL exceeds the working range of the viscometer employed (20,000 mPa•s) and is estimated to approach 75,000 mPa•s at room-temperature, although the steep temperature-dependence means that by 90 ºC, the viscosity falls to less than 1000 mPa•s. (While the viscosities of related ILs incorporating smaller cations or anions, such as the analogous bromide salt (shown), are typically much lower, the not insignificant water solubility of many of them precludes their use as extraction solvents.) If these results prove to be representative of typical inorganic liquids, their application at near-ambient temperatures in a conventional liquid-liquid mode is likely to be problematic.

Given the steep decline in the viscosity of the Lindqvist IL that accompanies rising temperature, it seems reasonable to expect that if inorganic liquids do find application in extraction processes, it will be at elevated temperatures. For this reason, some consideration of the thermal properties (in particular, the stability) of these compounds is important. Differential scanning calorimetry on the Lindqvist IL revealed no primary transitions over the range of temperatures studied (up to 100 ºC), only a glass transition at -48 ºC. Results for the analogous Keggin-based IL were similarly straightforward, revealing only the presence of a melting point at 65 ºC (thus indicating that the substitution of a Keggin anion for the Lindqvist ion would do nothing to improve the viscosity results shown in Figure 2). In neither case was any evidence of decomposition noted. Because prior studies concerning the relationship between IL structure and physicochemical properties have noted that for a given cation, there exists an approximately inverse relationship between anion nucleophilicity and the IL decomposition temperature [16], ILs comprising phosphonium cations and bulky, charge-diffuse anions such as POMs should exhibit excellent high-temperature stability. In fact, thermogravimetric analyses indicate that the onset of decomposition of the *tris*[trihexyl(tetradecyl)phosphonium] Keggin and the corresponding Lindqvist ILs does not occur until 456 ºC and 482 ºC, respectively, more than 100 ºC above the decomposition of the analogous bromide IL. Isothermal gravimetric measurements, in which the Lindqvist IL showed no decomposition while held at 360 ºC for several hours, lead to the same conclusion: that POM-based ILs exhibit excellent thermal stability.

CONCLUSIONS

The preliminary results presented here provide a mixed picture concerning the potential utility of POM-based ionic liquids as extraction solvents. Despite exhibiting excellent thermal stability and yielding uranium extraction efficiencies approaching those observed for a conventional organic solvent in the presence of TBP, the "inorganic liquids" considered are highly viscous at ambient temperature. Systematic studies of the influence of co-solvents and extractants on POM-IL viscosity and of alternative configurations (*e.g.*, supported liquid membranes) for employing these solvents are clearly needed if the possibilities afforded by these unique materials as extraction solvents are to be realized. Work addressing these opportunities is now underway in This Laboratory.

ACKNOWLEDGMENTS

This work was supported by the U.S. Department of Energy, Office of Basic Energy Sciences, Divisions of Materials Sciences and Chemical Sciences, Geosciences, and Biosciences, under contract numbers DE-AC02-06CH11357 (ANL) and DE-AC02-98CH10886 (BNL).

REFERENCES

1. M. L. Dietz, "Ionic Liquids as Extraction Solvents: Where do we Stand? ," *Sep. Sci. Technol.,* **41**, 2047-2063 (2006).
2. H. Olivier-Bourbigou and L. Magna, "Ionic Liquids: Perspectives for Organic and Catalytic Reactions," *J. Mol. Catal. A*, **182**, 419-437 (2002).
3. P. G. Rickert, D. C. Stepinski, D. J. Rausch, R. M. Bergeron, S. Jakab, and M. L. Dietz, "Solute-Induced Dissolution of Hydrophobic Ionic Liquids in Water," *Talanta* **72**, 315-320 (2007).
4. S. Dai, Y. H. Ju, and C. E. Barnes, "Solvent Extraction of Strontium Nitrate by a Crown Ether Using Room-Temperature Ionic Liquids," *J. Chem. Soc., Dalton Trans*., 1201–1202 (1999).
5. B. Smarsly and H. Kaper, "Liquid Inorganic-Organic Nanocomposites: Novel Electrolytes and Ferrofluids," *Angew. Chem. Int. Ed.,* **44**, 3809-3811 (2005).
6. A. B. Bourlinos, K. Raman, R. Herrera, Q. Zhang, L. A. Archer, and E. P. Giannelis, "A Liquid Derivative of 12-Tungstophosphoric Acid with Unusually High Conductivity," *J. Am. Chem. Soc.,* **126**, 15358-15359 (2004).
7. H. Sawada, S. Kodama, K. Tsunashima, M. Sugiya, "Preparation and Properties of Novel Phosphonium-Type Ionic Liquids/Silica Gel Nanocomposites," *J. Mater. Sci*., **42**, 2532-2535 (2007).
8. P. G. Rickert, M. R. Antonio, M. A. Firestone, K. -A. Kubatko, T. Szreder, J. F. Wishart, and M. L. Dietz, "Tetraalkylphosphonium Polyoxometalates: Electroactive, 'Task-Specific' Ionic Liquids," *Dalton Trans*., 529-531 (2007).
9. P. G. Rickert, M. R. Antonio, M. A. Firestone, K. –A. Kubatko, T. Szreder, J. F. Wishart, and M. L. Dietz, "Tetraalkylphosphonium Polyoxometalate Ionic Liquids: Novel, Organic-Inorganic Hybrid Materials," *J. Phys. Chem. B.,* **111**, 4685-4692 (2007).
10. W. G. Klemperer, "Early Transition-Metal Polyoxoanions," *Inorg. Synth*., **27**, 71-135 (1990).
11. C. J. Bradaric, A. Downard, C. Kennedy, A. J. Robertson, and Y. Zhou, "Industrial Preparation of Phosphonium Ionic Liquids," *Green Chem*., **5**, 143-152 (2003).
12. D. Allen, G. Baston, A. E. Bradley, T. Gorman, A. Haile, I. Hamblett, J. E. Hatter, M. J. F. Healey, B. Hodgson, R. Lewin, K. V. Lovell, B. Newton, W. R. Pitner, D. W. Rooney, D. Sanders, K. R. Seddon, H. E. Sims, and R. C. Thied, "An Investigation of the Radiochemical Stability of Ionic Liquids," *Green Chem*., **4**, 152-158 (2002).
13. I. A. Skrob, S. D. Chermerisov, and J. F. Wishart, "The Initial Stages of Radiation Damage in Ionic Liquids and Ionic Liquid-based Extraction Systems," *J. Phys. Chem. B.,* **111**, 11786-11793 (2007).
14. L. Berthon, S. I. Nikitenko, I. Bisel, C. Berthon, M. Faucon, B. Saucerotte, N. Zorz, and P. Moisy, "Influence of Gamma Irradiation on Hydrophobic Room-Temperature Ionic Liquids [BuMeIm]PF_6 and [BuMeIm]$(CF_3SO_2)_2N$," *Dalton Trans,*. 2526-2534 (2006).
15. M. L. Dietz, J. A. Dzielawa, I. Laszak, B. A. Young, and M. P. Jensen, "Influence of Solvent Structural Variations on the Mechanism of Facilitated Ion Transfer into Room-Temperature Ionic Liquids," *Green Chem*., **5**, 682-685 (2003).
16. J. L. Anthony, J. F. Brennecke, J. D. Holbrey, E. J. Maginn, R. A. Mantz, R. D. Rogers, P. C. Trulove, and A. E. Visser, "Physicochemical Properties of Ionic Liquids," Ionic Liquids in Synthesis, P. Wasserscheid and T. Welton, Eds., Wiley-VCH, Weinheim, Germany, 2006; p.41.

EFFECT OF SOLVENT ON THE EXTRACTION OF CHROMIUM(VI)¬ WITH QUATERNARY AMMONIUM IONS

Junji Noro[1] and Yu Komatsu[2]

[1]Research Department, NISSAN ARC LTD., 1 Natsushima-cho, Yokosuka, 2370061 Japan. [2]Department of Environmental Chemistry, College of Environmental Engineering and Architecture, Kanazawa Institute of Technology, 7-1 Ohgigaoka, Nonoichi, Ishikawa 9218501, Japan. Corresponding author email address: noro@nissan-arc.co.jp

ABSTRACT

The solvent extraction of chromium(VI) in 0.1 mol dm^{-3} sodium nitrate solutions with tetrabutylammonium ions (tba^+) into 1-octanol or chloroform was studied. From the dependence of extraction on the concentrations of hydrogen ion, tba^+, and chromium(VI), it was concluded that chromium(VI) was extracted into both solvents in the form $tba^+HCrO_4^-$. The first and second acid dissociation constants for chromic acid and the extraction constant for the ion pairs were determined. Although there was not much difference in the extraction of NO_3^- with tba^+ into 1-octanol and into chloroform, the extraction of $HCrO_4^-$ with tba^+ into 1-octanol was much improved compared with chloroform.

INTRODUCTION

The solvent extraction of chromium(VI) in the form of H_2CrO_4 with 4-methyl-2-pentanone (MIBK) [1-4], tributyl phosphate (TBP) [5,6], and trioctylphosphine oxide (TOPO) [7,8] has been studied. The extraction of chromium(VI) in the form of $HCrO_4^-$ with tetrabutylammonium ions (tba^+) [9] into chloroform was also studied. It was reported [9] that the extraction of chromium(VI) with tba^+ into chloroform was not effective. On the other hand, it was also reported in [10] that 1-octanol is effective for solvent extraction of ion-pairs [10]. In the present work, the solvent extraction of chromium(VI) with tba^+ into 1-octanol was studied in order to find a more effective solvent-extraction method for chromium(VI).

EXPERIMENTAL

All of the reagents and experimental procedures were similar to those in the previous study [9] except that 1-octanol was used as the solvent. All of the solvent-extraction experiments were carried out at 298 K. The concentration of tba^+ in the aqueous phase at equilibrium was measured by the method previously described [11].

RESULTS AND DISCUSSION

In the present paper, chemical species in the organic phase are denoted by the subscript "org", and those in the aqueous phase are shown without any subscript. The volume of the two liquid phases is the same. The data are treated in the same manner as described earlier [9] on the basis of the following equations.

The equilibrium constants can be written as follows

$$H_2CrO_4 \rightleftarrows H^+ + HCrO_4^- \; ; \; K_{a1} = [H^+]\,[HCrO_4^-] / [H_2CrO_4] \quad (1)$$

$$HCrO_4^- \rightleftarrows H^+ + CrO_4^{2-} \; ; \; K_{a2} = [H^+]\,[CrO_4^{2-}] / [HCrO_4^-] \quad (2)$$

$$tba^+ + HCrO_4^- \rightleftarrows tba^+HCrO_4^-{}_{(org)} \; ; \; K_{ex1} = [tba^+HCrO_4^-]_{org} / [tba^+]\,[HCrO_4^-] \quad (3)$$

$$2tba^+ + CrO_4^{2} \rightleftarrows (tba^+)_2CrO_4^{2-}{}_{(org)} \; ; \; K_{ex2} = [(tba^+)_2CrO_4^{2-}]_{org} / [tba^+]^2\,[CrO_4^{2-}] \quad (4)$$

$$2tba^+HCrO_4^-{}_{(org)} \rightleftarrows (tba^+)_2Cr_2O_7^{2-}{}_{(org)} + H_2O \; ;$$

$$K_{dim} = [(tba^+)_2Cr_2O_7^{2-}]_{org} / [tba^+HCrO_4^-]_{org}^2 \quad (5)$$

The distribution ratio of chromium(VI) extracted with tba^+ can be written as:

$$D = ([tba^+HCrO_4^-]_{org} + [(tba^+)_2CrO_4^{2-}]_{org} + 2[(tba^+)_2Cr_2O_7^{2-}]_{org}) / ([H_2CrO_4] + [HCrO_4^-] + [CrO_4^{2-}]) \quad (6)$$

$$= (K_{ex1}[tba^+] + K_{ex2}K_{a2}[tba^+]^2 / [H^+] + 2K_{dim}K_{ex1}[tba^+]^2[HCrO_4^-]) / ([H^+] / K_{a1} + 1 + K_{a2} / [H^+]) \quad (7)$$

When the extracted ion pairs undergo dissociation, the extraction equilibrium of tba^+ with the anion of the background salt, NO_3^-, can be written as:

$$tba^+ + NO_3^- \rightleftarrows tba^+\,NO_3^-{}_{(org)} \; ; \; K_{exAB} = [tba^+\,NO_3^-]_{org} / [tba^+][NO_3^-] \quad (8)$$

$$tba^+\,NO_3^-{}_{(org)} \rightleftarrows tba^+{}_{(org)} + NO_3^-{}_{(org)} \; ; \; K_{diss} = [tba^+]_{org}\,[NO_3^-]_{org} / [tba^+\,NO_3^-]_{org} \quad (9)$$

The chemical form of tba^+ in the organic phase should be $tba^+NO_3^-{}_{(org)}$ or $tba^+{}_{(org)}$. Since NO_3^- could not be extracted except with tba^+, the concentrations of $tba^+{}_{(org)}$ and $NO_3^-{}_{(org)}$ should be identical. Thus, the distribution ratio of tba^+, $D_{tba} = [tba^+]_{org,total} / [tba^+]_{aq,total}$, can be written as:

$$D_{tba} = ([tba^+NO_3^-]_{org} + [tba^+]_{org}) / [tba^+] = K_{exAB}\,[NO_3^-] + (K_{exAB}K_{diss}\,[NO_3^-])^{0.5} / [tba^+]^{0.5} \quad (10)$$

The extraction of tba^+ with NO_3^- from aqueous 0.1 mol dm^{-3} sodium nitrate solution into 1-octanol is given in Figure 1. Literature data on the extraction of this ion pairs into chloroform [12] are also given in Figure 1.

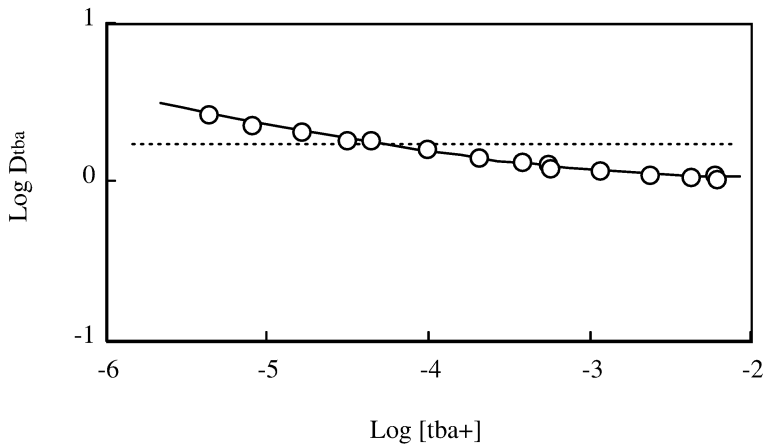

Figure 1. Distribution ratio of tba^+ as a function of tba^+ concentration in the aqueous phase. The aqueous phase is 0.1 mol dm^{-3} sodium nitrate solutions. (The solid line is calculated by Equation 8 using the values given in Table 1. The dotted line is the plots when solvent is chloroform taken from reference 12.)

As can be seen from Figure 1, more than 50% of the tba^+ in the initial aqueous phase is transferred as the ion pair, $tba^+NO_3^-$, into 1-octanol. It can also be seen from Figure 1 that the degree of extraction of the tba^+ ion pair differs little between these two solvents. The decrease in the extraction of tba^+ into 1-octanol with increasing tba^+ concentration is explained in terms of a partial dissociation of the ion pair in 1-octanol, while the lack of dependence of the distribution ratio on the tba^+ concentration when the solvent is chloroform should indicate negligible dissociation of the ion pair. From these data, the extraction constant K_{exAB} in Equation 8 and the dissociation constant K_{diss} in Equation 9 of the ion pair are calculated on the basis of Equation 10. The values obtained are listed in Table 1. The solid line in Figure 1 was calculated by introducing the values of K_{exAB} and K_{diss} in Table 1 into Equation 10.

Table 1. Summary of equilibrium constants

	Log K_{a1}	Log K_{a2}	Log K_{ex1}	Log K_{diss}	Log K_{exAB}	Log K_{dim}
1-octanol	-1.3	-6.1	-2.4	-4.4	1.0	-
chloroform	-0.8[a]	-	1.0[a]	-	1.32[b]	4.7[a]

[a] Taken from reference [9]. [b] taken from reference [12]

Figure 2 gives the distribution ratio of chromium(VI) as a function of the hydrogen-ion concentration when the initial concentration of tba^+ is 2.5×10^{-3} mol dm^{-3} and that of chromium(VI) is 10^{-4} mol dm^{-3}. As can be seen, the extraction is nearly independent of $-\log[H^+]$ except when it is lower than 2 and higher than 5. Thus chromium(VI) should be present in the $HCrO_4^-$ form in the aqueous phase in this $-\log[H^+]$ range. The acid dissociation constants were calculated from these data on the basis of Equation 7 by a successive-approximation approach using a least-squares computer program. The values of K_{a1} and K_{a2} obtained are listed in Table 1.

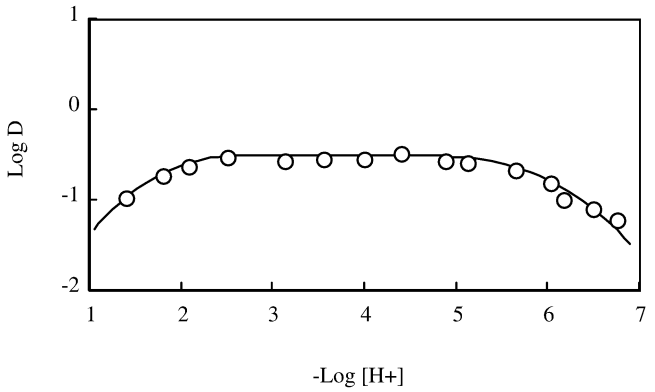

Figure 2. Distribution ratio of chromium(VI) as a function of the hydrogen-ion concentration. The solid line is calculated by Equation 7 using the values given in Table 1.

Figure 3 gives the extraction curves of chromium(VI) with tba^+ when -log[H^+] is 3.0 and about 6. As can be seen from Figure 3, the distribution ratio when -log[H^+] is 3.0 is proportional to the tba^+ concentration. It is also found that the distribution ratio is not much affected by the change in -log[H^+] in this range, as can be seen from Figure 2. On the other hand, when -log[H^+] is about 6, the slope of the plot gradually increases, and this slope reaches an asymptote with a slope of +2. However, this is only an apparent effect. The extraction from the aqueous solutions when -log[H^+] is around 6 is much affected by the concentration, as can also be seen from Figure 2. In this -log[H^+] range, the formation of H_2CrO_4 in the aqueous phase should be negligible. Thus, the data when -log[H^+] is in this range are normalized to the change in the hydrogen-ion concentration on the basis of the following equation which is derived from Equation 7.

$$D(1 + K_{a2} / [H^+]) / [tba^+] = K_{ex1} + K_{ex2}K_{a2}[tba^+] / [H^+] \quad (11)$$

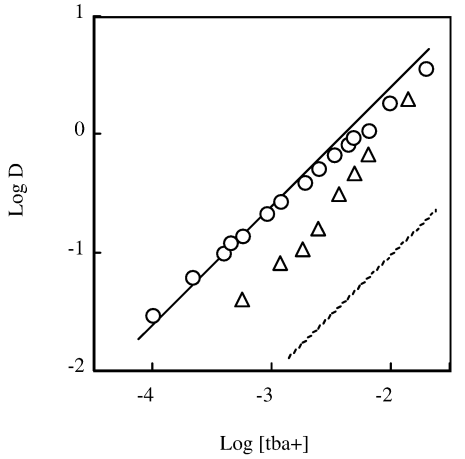

Figure 3. Distribution ratio of chromium(VI) as a function of the tba^+ concentration at equilibrium. The hydrogen-ion concentration is 10^{-3} (circles) and about 10^{-6} (triangles) mol dm^{-3}. (The solid line is calculated by Equation 7 using the values given in Table 1. The dotted line, representing the plot when the solvent is chloroform, is taken from reference [9].)

When $X = [tba^+]/[H^+]$, $Y = D(1 + K_{a2} / [H^+])/[tba^+]$, $K_1 = K_{ex1}$, and $K_2 = K_{ex2}K_{a2}$ (K_1 and K_2 are the constant), Equation 11 can be written as $Y = K_1 + K_2X$. Figure 4 gives the plot of log X vs. log Y. If the reaction in Equation 4, that is, the extraction of the $(tba^+)_2CrO_4^{2-}$ species is taking place, the slope of this plot should reach an asymptote with a slope of +1. However, as can be seen from Figure 4, the slope of the plot is 0. From this, it can be concluded that the data, when $-\log[H^+]$ is about 6, where nearly half of the chromium(VI) is in the CrO_4^{2-} form, are well explained by the extraction of the $tba^+HCrO_4^-$ species only.

From these data, the extraction constant of hydrochromate ions with tba^+, K_{ex1} in Equation 3, is calculated on the basis of Equation 7, as is listed in Table 1. The solid lines in Figures 2 and 3 are calculated by introducing the values of K_{a1}, K_{a2}, and K_{ex1} in Table 1 into Equation 7. Each of the lines fits well with the experimental data.

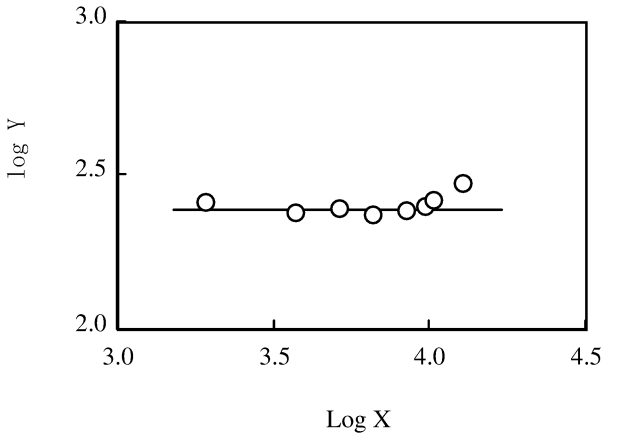

Figure 4. Relation between the log X vs. log Y when $-\log [H^+]$ (cf. Equation 11). where $X = [tba^+] / [H^+]$ and $Y = D(1 + K_{a2} / [H^+]) / [tba^+]$.

CONCLUSION

The extraction of chromium(VI) with tba^+ at the same concentration into 1-octanol is about one order of magnitude higher than that into chloroform. Moreover, 1-octanol is much less harmful to the environment than is chloroform. Taken together, these results indicate that 1-octanol is much more effective than chloroform for the solvent extraction of chromium(VI).

REFERENCES

1. H. A. Bryan and J. A. Dean, *Anal. Chem.*, **29,** 1289 (1957).
2. P. D. Blundy, *Analyst*, **83**, 555 (1958).
3. S. A. Katz, W. M. McNabb, and J. F. Hazel, *Anal. Chim. Acta.*, **25**, 193 (1961).
4. G. B. Marshall and T. S. West, *Analyst*, **95**, 343 (1970).
5. K. H. Arend and H. Specher, *Z. Anorg, Allg. Chem.*, **333**, 18 (1964).
6. A. A. Yadav and S. M. Khopkar, *Indian J. Chem.*, **8**, 290 (1670).
7. C. K. Mann and J. C. White, *Anal. Chem.*, **30**, 989 (1958).

8. M. Niitsu and T. Sekine, *J. Inorg. Nucl. Chem.*, **38**, 1057 (1976).
9. M. Yamada and T. Sekine, *Solvent Extr. Res. Dev. Jpn.*, **3**, 99 (1996).
10. T. Naito, Y. Tsuiki, and H. Yamada, *Anal. Sci.*, **17**, 291 (2001).
11. J. Noro and T. Sekine, *Bull. Chem. Soc. Jpn.*, **65**, 1910 (1992).
12. J. Noro and T. Sekine, *Bull. Chem. Soc. Jpn.*, **66**, 450 (1993).

EXTRACTION EQUILIBRIUM OF LANTHANIDES(III) WITH 2-THENOYLTRIFLUOROACETONE IN THE WATER-1-PROPANOL-CHLOROFORM TERNARY SOLVENT SYSTEM

A. Ohashi,[1] T. Hashimoto[1], H. Imura[1], T. Hori,[2] and K. Ohashi[1]

[1]*Faculty of Science, Ibaraki University, 2-1-1 Bunkyo, Mito, Ibaraki, Japan 310-8512.*
[2]*Graduate School of Human and Environmental Studies, Kyoto University, Yoshida-nihonmatsu-cho, Sakyo-ku, Kyoto, Japan 606-8501.*
Corresponding author email address: oakira@mx.ibaraki.ac.jp

ABSTRACT

Extraction equilibrium of lanthanides(III) (Ln(III) = La(III), Eu(III), and Lu(III)) with 2-thenoyltrifluoroacetone (Htta) was investigated in the water-1-propanol-chloroform ternary solvent system. Quantitative extraction of Ln(III) with Htta was accomplished in this system. The extractability increased in the order La(III) < Eu(III) < Lu(III). From the equilibrium analysis, it was clarified that Ln(III) was extracted as Ln(tta)3 into the organic phase. The extraction constants of Ln(III) with Htta were also obtained in the ternary solvent system.

INTRODUCTION

Rare earth metals have been used in various industrial products such as strong magnets, magnetic embrocation, solid metal hydrides, the fluorescent materials, and high-temperature superconducting compounds, because they have useful and specific physical properties [1]. In our country, most of the supply of rare earth metals must be imported from foreign countries. Therefore, the development of the separation and preconcentration methods for recycle of rare earth metals is desired for their availability of for industrial products. Solvent extraction is widely used as a method for rare earth metals [2-5].

In conventional solvent extraction, hydrophilic organic solvents such as methanol, acetonitrile, and acetone cannot be used, because they can be mixed with water without limitation. However, they may become particularly useful for extraction of polar compounds due to their high dielectric constants and donor number, if they can be used in solvent extraction. From such a reason, various examinations to use the polar organic solvents in solvent extraction have been performed. For example, the phase separation depended on the temperature of the water-propylene system [6] or the salt effect in the water-acetonitrile system [7] have been reported. A water-pyridine-ethyl chloroacetate

ternary solvent system based on pH-dependent phase separation has also been developed [8].

In this study, a water-1-propanol-chloroform ternary solvent system is applied to the extraction of lanthanides(III) (Ln(III)) with 2-thenoyltrifluoroacetone (Htta). From the equilibrium analysis, the extraction constants of Ln(III) with Htta were also obtained in the ternary solvent system.

EXPERIMENTAL

Reagents and Apparatus

Ln(III) stock solutions were prepared by dissolving high-purity Ln(III) oxide, La_2O_3 (Spectrographically Standardized, Johnson Matthey Chemicals Ltd.), Eu_2O_3 (99.999%, Aldrich), and Lu_2O_3 (99.99%, Nippon Yttrium Co. Ltd.), in nitric acid, evaporating to dryness, and redissolving in perchloric acid. Htta (99.0%, Aldrich) was purified by vacuum sublimation at 25 °C. Chloroform (GR, Kanto Chem.) and 1-propanol (HPLC grade, Kishida Chem.) were used as obtained. Water was doubly distilled and further purified with Milli-Q (Millipore) equipment. All other chemicals were of analytical reagent grade.

The metal concentration in an aqueous phase was determined using an inductively coupled plasma atomic-emission spectrophotometer (ICP-AES, Nippon Jarrell-Ash ICAP-575). A capillary gas chromatography (GC, Hewlett-Packard HP-6890) equipped with a fused silica capillary column (J&W Scientific DB-1ms, 530 μm i.d. x 15 m, 1.5 μm film-thickness, 100% dimethylpolysiloxane, and non-polar), and an FID detector was used to determine the equilibrium concentration of Htta in the organic phase. The GC conditions were as follows: injector, column, and detector temperatures were 270, 180, and 250 °C, respectively; flow rates of H_2, air, and He gases were 40, 450, and 50 mL min^{-1}, respectively. The pH measurements were performed by HORIBA pH METER F-22 equipped with a combination glass electrode.

Extraction Procedure

A Ln(III) aqueous solution (9 mL), 1-propanol (0.5 mL), and chloroform (0.5 mL) were placed in an extraction vial with a screw cap, and then vigorously shaken for 5 min. After phase separation by centrifugation, the pH in the aqueous phase was measured. The aqueous phase (6 mL) was taken out and diluted with 0.5 mol L^{-1} perchloric acid aqueous solution to 10 mL. The resulting solution was utilized to determine the concentration of Ln(III) by ICP-AES. The distribution ratio of Ln(III) between the organic and aqueous phases was calculated from the difference of the Ln(III) concentration in the aqueous phase before and after the extraction and the volumes of both phases after the phase separation (V_o = 0.4 mL and V_a = 9.6 mL). The initial concentration of Ln(III) was 3.5 x 10^{-5} mol L^{-1}. Total Htta concentration was varied from 5.0 x 10^{-3} to 8.0 x 10^{-3} mol L^{-1}. The pH value was changed from 1.6 to 5.2. The pH was controlled with 0.01 mol L^{-1} acetate buffer. The ionic strength was constant at 0.2 mol L^{-1} with $NaClO_4$.

Determination of the Distribution Constant of Htta between Organic and Aqueous Phases in Ternary Solvent System

A mixture containing Htta of 1-propanol (0.5 mL), chloroform (0.5 mL), and water (9.0 mL) was placed in an extraction vial with a screw cap and then vigorously shaken for 5 min. After phase separation, 300 μL of the organic phase was taken out, and 3 μL of toluene as an inner standard was added. Then, 1 μL of this organic solution was injected into the GC port in the split mode. From the area ratio of the chromatogram peaks of Htta and toluene, the equilibrium concentration of Htta in the organic phase was determined. Total Htta concentration and pH were 5.0 x 10^{-3} mol L^{-1} and 4.0, respectively.

RESULTS AND DISCUSSION

Extraction Behavior

Figure 1 shows the extraction behavior of Ln(III) with Htta in the ternary solvent system. The extractability increases in the order La(III) < Eu(III) < Lu(III). Quantitative extraction was accomplished for all Ln(III). The broken curve in Figure 1 was the calculated-extraction behavior of La(III) with 5.0 x 10^{-3} mol L^{-1} Htta in chloroform/water system by using the extraction constant (K_{ex} = $10^{-11.06}$ [9]), the distribution constant (K_D = $10^{1.73}$ [10]) of Htta between chloroform and water, and the acidic dissociation constant (K_a = $10^{-6.18}$ [11]) of Htta. (Here, the volumes of the chloroform and aqueous phases were set to 0.5 mL and 9.5 mL, respectively, and the Htta concentration in chloroform was 5.0 x 10^{-3} mol L^{-1}.) The extractability of La(III) in ternary solvent extraction was much better than that in conventional solvent extraction. The result indicates that the ternary solvent extraction is useful method to the separation and the preconcentration of Ln(III) from the aqueous solution.

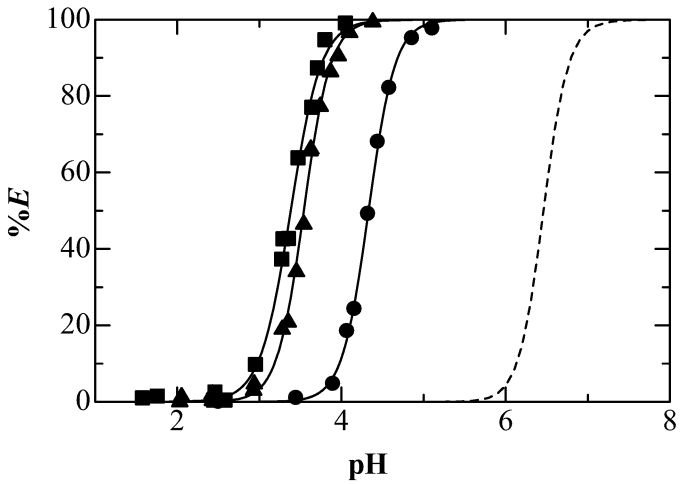

Figure 1. Extraction behavior of Ln(III) with Htta in ternary and conventional solvent-extraction systems. Ternary solvent-extraction system (water-1-propanol-chloroform): (●) La(III), (▲) Eu(III), and (■) Lu(III). Conventional solvent-extraction system (chloroform (0.5 mL)-water (9.5 mL)): (----) La(III). Ln(III), 3.5 x 10-5 mol L-; Htta, 5.0 x 10-3 mol L-1 [9].

Extraction Equilibrium

The extraction equilibrium of Ln(III) with Htta into the organic phase is assumed to be

$$\mathrm{Ln(III)} + 3\mathrm{Htta}_o \rightleftharpoons \mathrm{Ln(tta)}_{3,o} + 3\mathrm{H}^+ \quad (1)$$

where the subscript o denotes the organic phase. The extraction constant (K_{ex}) is expressed by

$$K_{ex} = \frac{[\mathrm{Ln(tta)_3}]_o[\mathrm{H}]^3}{[\mathrm{Ln(III)}][\mathrm{Htta}]_o^3} . \quad (2)$$

If the existence of the Ln(III)-Htta complexes in the aqueous phase can be ignored, the distribution ratio (D) of Ln(III) is given by

$$\mathrm{Log}\ D = \log K_{ex} + 3\ \log[\mathrm{Htta}]_o + 3\ \mathrm{pH} \quad (3)$$

The equilibrium concentration of Htta in the organic phase can be calculated by

$$[\mathrm{Htta}]_o = \frac{C_{\mathrm{Htta}}(V_o + V_a)}{V_o + \frac{V_a}{K_D} + \frac{K_a V_a}{K_D[\mathrm{H}^+]}} \quad (4)$$

where C_{Htta} is the total concentration of Htta. The K_D value in this ternary solvent system was obtained as $10^{0.06}$ from the GC measurement. The composition of Ln(III)-Htta complex extracted and the extraction constant can be determined by a slope analysis. Figure 2 shows the effect of pH on the distribution ratio of Ln(III) with 5.0 x 10^{-3} mol L^{-1} Htta in ternary solvent system. Plots of log D vs. pH gave straight lines with the slopes of 2.9 for La(III), 2.7 for Eu(III), and 2.9 for Lun(III). This result indicates that the extracted species is $Ln(tta)_3$. From the intercept values of the straight lines, the K_{ex} values were obtained as $10^{-4.97}$ for La(III), $10^{-2.61}$ for Eu(III), and $10^{-2.23}$ for Lu(III).

CONCLUSIONS

A detailed study on the extraction of La(III),Eu(III),and Lu(III) with HTTA in the water-1-propanol-chloroform ternary solvent system was carried out. Quantitative extraction for all Ln(III) was accomplished in this system. The extractability of La(III) in theternary solvent system was much better than that in chloroform-water system. From the equilibrium analysis, it was clarified that Ln(III) was extracted as $Ln(tta)_3$ into the organic phase. The extraction constants of La(III), Eu(III), and Lu(III) with Htta in the ternary solvent system were determined as $10^{-4.97}$, $10^{-2.61}$ and $10^{-2.23}$, respectively.

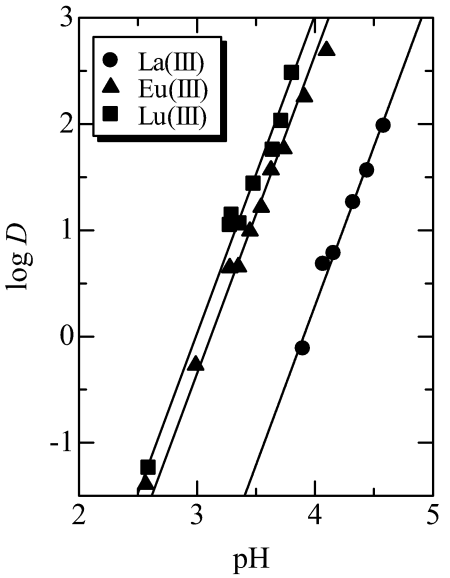

Figure 2. Effect of pH on the distribution ratio of Ln(III) with Htta in the water-1-propanol -chloroform ternary solvent system. Ln(III), 3.5 x 10^{-5} mol L^{-1}; Htta, 5.0 x 10^{-5} mol L^{-1}. Solid lines are the ones of slope of 3.

REFERENCES

1. V. S. Sastri, J.-C. Bünzli, V. R. Rao, G. V. S. Rayudu, and J. R. Perumareddi, Modern Aspects of Rare Earths and their Complexes, Elsevier, Amsterdam, 2003.
2. G. W. Mason, D. N. Metta, and D. F. Peppard, "The Extraction of Selected M(III) Metals by Bis 2-Ethylhexyl Phosphoric Acid in *n*-Heptane," *J. Inorg. Nucl. Chem.*, **38**, 2077–2079 (1976).
3. K. Ohto, K. Inoue, M. Goto, F. Nakashio, and T. Nagasaki, "Solvent Extraction of Trivalent Yttrium, Holmium, and Erbium by Novel Types of Acidic Organophosphonates," *Bull. Chem. Soc. Jpn.*, **66**(9), 2528–2535 (1993).
4. S. Nakamura, S. Takei, and K. Akiba, "Synergistic Enhancement in the Extraction of Lanthanides by LIX 51 and Bidentate Amines," *Solvent Extr. Res. Develop. Japan*, **10**, 103–111 (2003).
5. A. Shimada, T. Yaita, H. Narita, S. Tachimori, T. Kimura, K. Okuno, and Y. Nakano, "Extraction of Am(III) and Lanthanide(III) Ions from HNO_3 Solutions using *N,N'*-Dimethyl-*N,N'*-diphenylpyridine-2,6-dicarboxyamide," *Solvent Extr. Res. Develop. Japan*, **11**, 1–10 (2004).
6. K. Murata, Y. Yokoyama, and S. Ikeda, "Homogeneous Liquid-Liquid Extraction Method: Extraction of Iron(III) Thenoyltrifluoroacetonate by Propylene Carbonate," *Anal. Chem., Bunseki Kagaku*, **44**(4), 805–810 (1972).

7. C. E. Matkovich and G. D. Christian, "Salting-Out of Acetone from Water-Basis of a New Solvent Extraction System," *Anal. Chem.*, **45**(11), 1915–1921 (1973).
8. S. Igarashi, N. Ide, K. Takahata, and Y. Takagaki, "HPLC Spectrophotometric Determination of Metal-Porphyrin Complexes Following a Preconcentration Method by Homogeneous Liquid-Liquid Extraction in a Water/Pyridine/Ethyl Chloroacetate Ternary Component System," *Bunseki Kagaku*, **48**(12), 1115–1121 (1999).
9. T. Sekine, Y. Koike, and Y. Hasegawa, "Studies of Actinium(III) in Various Solutions. II. Distribution Behavior of Lanthanum(III) and Actinium(III) in Some Chelate Extraction Systems," *Bull. Chem. Soc. Jpn.*, **42**(2), 432–436 (1969).
10. T. Wakahayashi, S. Oki, T. Omori, and N. Suzuki, "Some Applications of the Regular Solution Theory to Solvent Extraction–I, Distribution of β-Diketones," *J. Inorg. Nucl. Chem.*, **26**, 2255–2264 (1964).
11. K. L. Cheng, K. Ueno, and T. Imamura, CRC Handbook of Organic Analytical Reagent, CRC Press, Inc., Boca Raton, Fla., 1982.

QUANTITATIVE SEPARATION OF ALKALINE EARTH METAL IONS COMBINING TWO KINDS OF SOLVENT EXTRACTION

Syunichi Oshima,[1] Junji Noro,[2] Kaoru Fujinaga,[1] Hisao Kokusen,[3] Shigekazu Tsurubou,[4] and Yu Komatsu[1]

[1] Department of Environmental Chemistry, College of Environmental Engineering and Architecture, Kanazawa Institute of Technology, 7-1 Ohgigaoka, Nonoichi, Ishikawa 921-8501, Japan. [2]Nissan Arc. Ltd., 1 Natsushima, Yokosuka, Kanagawa 237-0061, Japan. [3]Department of Essential Education, School of Pharmacy, Hokkaido Pharmaceutical University, 7-1 Katsuraoka-cho, Otaru, Hokkaido 047-0264, Japan. [4]Department of Chemistry, School of Dentistry, Asahi University, 1851 Hozumi, Mizuho, Gifu 501-0296, Japan.

Corresponding author email address: s.oshima@neptune.kanazawa-it.ac.jp

ABSTRACT

In an effort to achieve the mutual separation of the alkaline earth metal ions magnesium, calcium, strontium and barium, two kinds of solvent extraction methods have been applied. In the first, a multistage solvent extraction method called centrifugal partition chromatography (CPC) was applied for the separation of calcium and strontium ions, and of strontium and barium ions. In the second, a normal solvent extraction method using BFA and TBP in cyclohexane with cryptand[2.2.1] as the ion-size selective masking reagent was applied for the separation of magnesium and calcium ions. Using these two solvent extraction methods, mutual separation has been achieved among the four alkaline earth metal ions.

INTRODUCTION

Centrifugal partition chromatography (CPC) is a multistage solvent-extraction method that has been developed to enhance the separation of natural organic compounds [1]. The CPC method has been applied in the separation of organic compounds [2], alkaline earth metal ions [3], transition metal ions [4], and lanthanide and actinide ions [5]. Earlier, we studied the separation of alkaline earth metal ions by this method and reported that only Ba^{2+} could be separated from the other alkaline earth metal ions [6]. The separation of Mg^{2+} and Ca^{2+} is difficult due to their similar extraction behavior. The separation of Mg^{2+} and Ca^{2+} is also limited in normal extraction methods. Therefore, it is desirable to use an extractant having higher selectivity for Mg^{2+} or Ca^{2+} in order to enhance the efficiency of their separation.

The extraction selectivity and the separation ability can also be enhanced by using various extractants in combination with appropriate masking reagents [7,8]. Among the

masking reagents, it is known that cryptands (diazapolyoxabicyclic ligands) exhibit high stability in complexation of alkaline earth metals [9]. Because their selectivity for metal ions depends largely on the ring size, one can choose an appropriate cryptand according to the purpose.

In the present paper, the mutual separation of neighboring alkaline earth metal ions (Mg^{2+}-Ca^{2+}, Ca^{2+}-Sr^{2+}, and Sr^{2+}-Ba^{2+}) was studied by the combination of two kinds of solvent-extraction methods. In the first step, the separations for Ca^{2+}-Sr^{2+} and Sr^{2+}-Ba^{2+} were studied by the multistage solvent-extraction method using CPC. In the second step, the separation of Ca^{2+}-Mg^{2+} was studied by the normal extraction method into cyclohexane using cryptand [2.2.1] as the ion-size selective masking reagent.

EXPERIMENTAL

Reagents

All chemicals were reagent-grade materials, and distilled deionized water was used throughout. Thenoyltrifluoroacetone (TTA), tri-*n*-octylphosphine oxide (TOPO) and 4,4,4-trifluoro-1-phenylbutane-1,3-dione (BFA) were purchased commercially from Dojindo, tri-*n*-butylphosphate (TBP) from Nacalai Tesque, 4,7,13,16,21-pentaoxa-1,10-diazabicyclo[8.8.5]tricosane (cryptand [2.2.1]) from Merck, and they were used without further purification.

First Step: Multistage Solvent Extraction Method by Using CPC Device

The outline figure in the rotor of CPC device (Senshu Scientific co., ltd.) is shown in Figure 1. By applying centrifugal force within the CPC device, very small drops of mobile aqueous phase were moved into the stationary organic phase containing TTA and TOPO. In this process, the metal ion complexes with TTA-TOPO are extracted into the stationary phase. The condition of CPC device was as follows: (i) In the packing stationary phase, the flow rate of organic solvent was 25 cm^3 min^{-1}, and the rotor speed was controlled to 200 rpm. (ii) In making the steady state of device and flowing mobile phase, the flow rate of mobile phase was 5.0 cm^3 min^{-1}, and the rotor speed was 600 rpm. (iii) In sampling stage, the flow rate of the mobile phase was 1.0 cm^3 min^{-1} and the rotor speed was 600 rpm. The solutions containing the required amount of two alkaline metal ions (Ca^{2+}-Sr^{2+} and Sr^{2+}-Ba^{2+}) were prepared by dissolving the corresponding metal chlorides. The stationary phase containing 1×10^{-1} mol dm^{-3} of TTA and TOPO, respectively, was prepared by dissolving TTA and TOPO into cyclohexane. The mobile phase was prepared by 2×10^{-1} mol dm^{-3} of 2-(*N*-morpholino)ethanesulfonic acid (MES) and controlled to pH 5.5 by 1×10^{-1} mol dm^{-3} sodium hydroxide. The elution of the metal ion from the stationary phase was effected by an acidic mobile phase whose pH was adjusted by nitric acid addition to 3.2 and 3.7 for the Ca^{2+}-Sr^{2+} and Sr^{2+}-Ba^{2+} systems, respectively. The recovery of the other metal ions was made by changing the pH to 1.0. Every 5 min, a 5 cm^3 fraction of effluent was collected in sampling tube and the concentration of metal ion in the fraction was determined by ICP-OES. From these results, the recovery rate (%) was calculated.

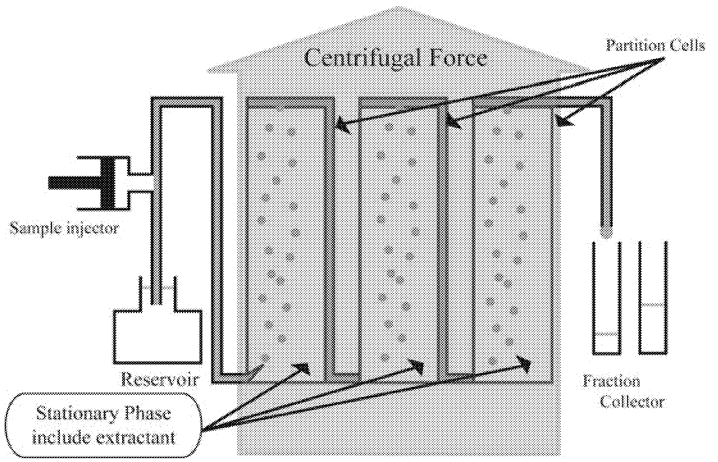

Figure 1. The outline in rotor of CPC device.

Second Step: Normal Solvent Extraction Method Using Cryptand [2.2.1]

The extraction of alkaline earth metal ions using cryptand [2.2.1] as the ion-size selective masking reagent was studied as follows: A 10 cm^3 portion of an aqueous phase containing the required amount of metal ions (Mg^{2+} or Ca^{2+}), cryptand [2.2.1], and 0.02 mol dm^{-3} Good's buffer such as tris(hydroxymethyl)aminomethane was adjusted to the desired pH with hydrochloric acid and tetramethylammonium hydroxide. The aqueous phase was shaken with an equal volume of an organic phase (cyclohexane) containing the required amount of BFA and TBP for 3 hours until the reaction reached equilibrium at 25 ± 1 C. After centrifugation of the mixture, the pH of the aqueous phase was measured. The metal concentration in the aqueous phase was determined by AAS. After back-extraction into a hydrochloric acid solution, the metal concentration in the organic phase was determined by AAS.

RESULTS AND DISCUSSION

First Step: Multistage Solvent Extraction Method Using CPC Device

In this method, the stationary phase of cyclohexane contained TTA and TOPO, and then aqueous solution containing two metal ions (Ca^{2+}-Sr^{2+} or Sr^{2+}-Ba^{2+}) for the mobile phase at pH 5.5 was flowed into the CPC device. In this process, both metal ions in the mobile phase were extracted into stationary phase as a metal addition complex with TTA and TOPO. Subsequently, the back-extraction of the metal ion having larger ionic radius into the mobile phase was done by flowing the mobile phase adjusted to pH 3.2 and 3.7 in the Ca^{2+}-Sr^{2+} and the Sr^{2+}-Ba^{2+} systems. These pH values of the eluent were determined on the basis of the $pH_{1/2}$ values in normal solvent-extraction system. The other metal ion was recovered by changing pH of the mobile phase to 1.0. The recovery rate (%) was calculated as follows:

$$\text{Recovery rate}\,(\%) = \frac{\text{the amount of metal ion in the } 5\,\text{cm}^3 \text{ fraction}}{\text{the total amount of metal ion injected in CPC device}}$$

The recovery rate versus the effluent volume from the CPC device in the Ca^{2+}-Sr^{2+} and the Sr^{2+}-Ba^{2+} systems are shown in Figure 2 and 3, respectively. As can be seen from Figs. 2 and 3, Sr^{2+} and Ba^{2+} could be separated efficiently from Ca^{2+} and Sr^{2+}, respectively, by using the multistage solvent-extraction method.

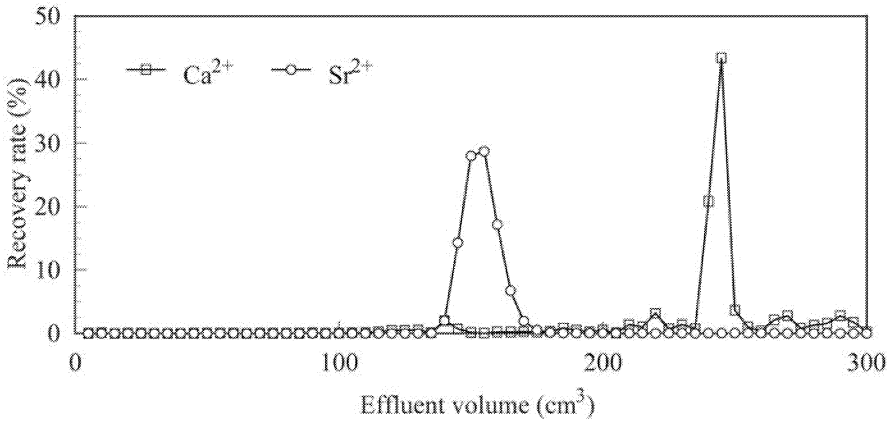

Figure 2. The measured recovery rate (%) of Ca^{2+} and Sr^{2+} versus effluent volume (cm^3).

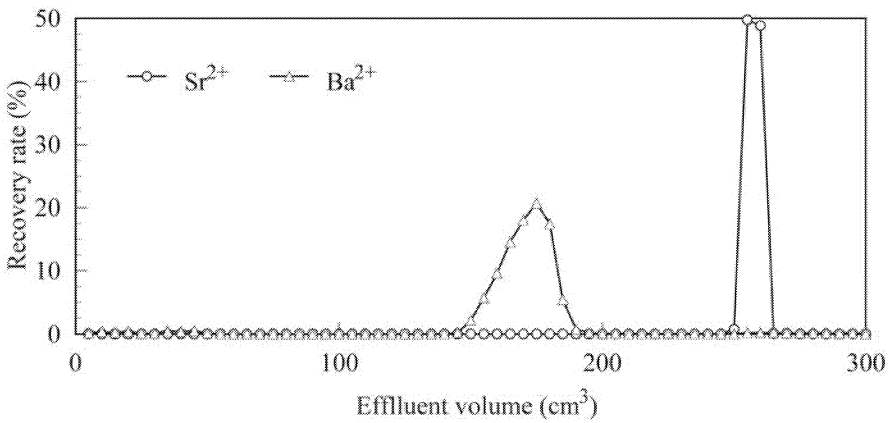

Figure 3. The measured recovery rate (%) of Sr^{2+} and Ba^{2+} versus effluent volume (cm^3).

Second Step: Solvent Extraction Method Using Cryptand [2.2.1]

The stability constants of cryptand [2.2.1] for alkaline earth metal ions have been reported by Lehn et al. [10] as shown in Table 1. From this table, the stability constants between Mg^{2+} and Ca^{2+} show considerable difference as may be seen from the values <2

for Mg^{2+} and 6.95 for Ca^{2+}. In this study, the quantitative separation between Mg^{2+} and Ca^{2+} has been examined using cryptand [2.2.1] as the ion-size selective masking reagent in the aqueous phase.

Table 1. Stability constants (log K_s) of cryptand [2.2.1] for alkaline earth metal ions [10]

	Mg^{2+}	Ca^{2+}	Sr^{2+}	Ba^{2+}
log K_s	<2.0	6.95	7.35	6.30

The distribution ratio (D) for Ca^{2+} and Mg^{2+} into cyclohexane in the presence of cryptand [2.2.1] was plotted as a function of equilibrated pH in Figure 4. The slope of the straight portion of the plots in the extraction of Mg^{2+} is 2.0, indicating that two protons are released through the extraction reaction. As shown in Figure 4, the distribution ratio of Ca^{2+} decreases rapidly above pH 7.5, while the Mg^{2+} is extracted quantitatively above pH 8.3 (log D > 1.5). This fact shows that above the pH 8.3, more than 98% of Mg^{2+} is extracted into cyclohexane as a metal addition complex with BFA and TBP, while more than 98% of Ca^{2+} (log D < –1.8) remains in the aqueous phase. As a result, Ca^{2+} can be separated from Mg^{2+} quantitatively.

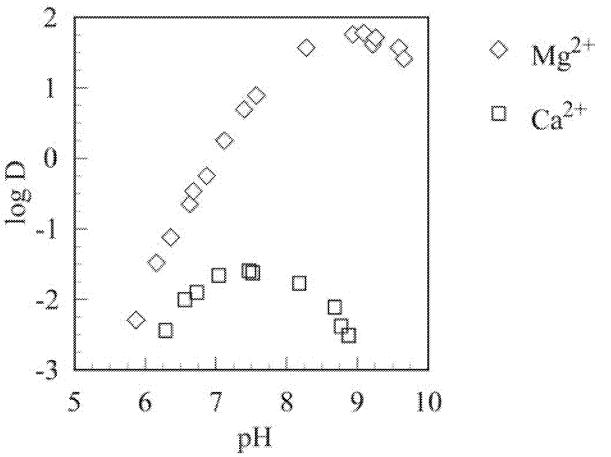

Figure 4. Plots of the logarithmic distribution ratios (log D) for Mg^{2+} and Ca^{2+} into cyclohexane in the presence of cryptand [2.2.1] as a function of equilibrated pH value.

CONCLUSION

It was found that the multistage solvent-extraction method using CPC device and step elution technique make it possible to separate efficiently the Ca^{2+}-Sr^{2+} and the Sr^{2+}-Ba^{2+} systems, and may provide an automatic ion separation technique. In addition, the masking effect of cryptand [2.2.1] will give efficient separation between Mg^{2+} and Ca^{2+}, which was difficult for the CPC method, by the normal solvent-extraction method with BFA and TBP into cyclohexane. The present study shows that the mutual separation

efficiency can be enhanced remarkably among all alkaline metal ions studied (Mg^{2+}, Ca^{2+}, Sr^{2+}, and Ba^{2+}) by combining the CPC multistage solvent-extraction method and the normal solvent-extraction method using cryptand [2.2.1] as an ion-size selective masking reagent.

REFERENCES

1. J. Cazes, Encyclopedia of Chromatography, Marcel Dekker, New York, 2001.
2. K. Ingkaninan, A. Hazekamo, A. C. Hoek, S. Balconi, and R. Verpoorte, "Application of Centrifugal Partition Chromatography in a General Separation and Dereplication Procedure for Plant Extracts," *Journal of Liquid Chromatography & Related Technologies*, **23**, 2195-2208 (2000).
3. T. Wang and Y. Nagaosa, "Separation of Calcium (II), Magnesium (II), Strontium (II), and Barium (II) by High Performance Centrifugal Partition Chromatography with Some Organophosphorus Compounds," *Journal of Liquid Chromatography & Related Technologies*, **26**, 629-640 (2003).
4. T. Wang and Y. Nagaosa, "High Performance Centrifugal Partition Chromatographic Separation of Cu (II), Mn (II), Co (II), and Ni (II) Using Di-2-Methylnonylphosphoric Acid," *Analytical Letters*, **36**, 441-450 (2002).
5. H. Hoshi, S. Nakamura, and K. Akiba, "Separation of Lanthanoids and Actinoids by Centrifugal Partition Chromatography," *Journal of Liquid Chromatography & Related Technologies*, **22**, 1319-1330 (1999).
6. S. Oshima, H. Kokusen, T. Tanemoto, J. Noro, S. Tsurubou, M. Sekita, H. Yamada, and Y. Komatsu, "Separation of Alkaline Earth Metal ions by the Multistage Solvent Extraction Method," Proceedings of ISEC'05, 2005; pp. 911-915.
7. G. H. Morrison and H. Freiser, Solvent Extraction on Analytical Chemistry, Wiley, New York, 1957.
8. J. Stary, The Solvent Extraction of Metal Chelates, Pergamon Press, London, 1964.
9. S. Tsurubou, S. Umetani, and Y. Komatsu, "Quantitative extraction separation systems of alkali and alkaline earth metal ions using cryptands as ion-size selective masking reagents," *Analytica Chimica Acta*, **394**, 317-324, (1999).
10. J. M. Lehn and J. Sauvage, "[2]-Cryptates: Stability and Selectivity of Alkali and Alkaline-Earth Macrobicyclic Complexes," *Journal of the American Chemical Society*, **97**, 6700-6707 (1975).

THE IN SITU EXTRACTANT FORMATION METHOD AS A USEFUL TOOL FOR DEVELOPING A NEW FUNCTIONAL CHELATE REAGENT: PIPERIDINEDITHIOCARBAMIC ACID FORMING SYSTEM

Kaoru Fujinaga,[1] Aya Yamauchi,[2] Yasushi Seike,[2] Yu Komatsu,[1] and Minoru Okumura[2]

[1]College of Environment and Architecture, Kanazawa Institute of Technology, 7-1 Ohgigaoka, Nonoichi, Ishikawa 921-8501 Japan. [2]Faculty of Science and Engineering, Shimane University 1060 Nishikawatsu, Matsue 690-8504 Japan.
Corresponding author e-mail address: fujinaga@neptune.kanazawa-it.ac.jp

ABSTRACT

A mixture of carbon disulfide (CS_2), piperidine, and chloroform ($CHCl_3$) produced piperidinedithiocarbamic acid in the aqueous phase by equilibrating with aqueous phase and could extract Cu^{2+}, Co^{2+}, Ni^{2+}, and Cd^{2+} successfully. As piperidine derivative, dimethylpiperidine (DMP) and tetramethylpiperidine (TMP) were used as a component of mixed solvents. The mixtures containing 0.5% v/v piperidine extracted four metal ions quantitatively in almost all the examined pH range, and that containing 1.0% DMP gave similar results. While, the extractabilities of Co^{2+} and Ni^{2+} with the mixture containing 5.0% v/v TMP did not reach to 100%. Metals were extracted in the form of dithiocarbamate complexes.

INTRODUCTION

The present in situ extractant-formation method is originated by one of the authors and is characterized by forming a chelate extractant during the course of extraction, so that metal ions can be extracted into the organic phase without adding any chelate extractants. The following extraction systems have proposed; isoamylxanthate ion forming system [1,2], diethyldithiocarbamate ion forming system [3,4], pyrrolidinedithiocarbamate ion forming system [5,6], and salicylaldoxime forming system [7], and so on. By analogy to the previous extraction systems, for example, in which the mixture of pyrrolidine, CS_2, and *p*-xylene yielded pyrrolidinedithiocarbamate ion, it was expected that a mixture of CS_2, $CHCl_3$, and piperidine would form piperidinedithiocarbamate ion (P_iDC^-) and could extract metals into the organic phase. As piperidine derivative, DMP and TMP were also used as a component of mixed solvent, in expectation of the formation of dimethylpiperidinedithiocarbamate ion (DMP_iDC^-) and tetramethylpiperidine- dithiocarbamate ion (TMP_iDC^-), respectively. The formation of P_iDC^-, DMP_iDC^-, and TMP_iDC^- were proved experimentally by the spectrophotometric method, and their yields in the aqueous phase equilibrated with

mixed solvents were determined spectrophometrically to decrease in the order piperidine > DMP > TMP. The extractabilities of these mixed solvents were evaluated by using divalent transition metals, such as Cu^{2+}, Co^{2+}, Ni^{2+}, and Cd^{2+}.

EXPERIMENTAL

Reagents and Apparatus

A Hitachi CF7D cooling centrifuge was used for phase separation, and a Hitachi model Z-5000 atomic absorption spectrophotometer was used to measure the metal concentration with a flame atomizer, and a Nihonbunko V-560 double-beam spectrophotometer was used to obtain absorption spectra with 1.0 cm pathlength quartz cells. The metal solutions were stored in polyethylene bottles and were mixed in a volumetric flask so that the concentration of each metal was 2.0×10^{-4} M (mol dm^{-3}), prior to use. Piperidine, DMP, and TMP used in this research were obtained from Tokyo Chemical Industry Co., LTD. and were used as received without further purification. The other reagents were of analytical grade. $CHCl_3$ was washed with pure water twice before use.

Extraction Procedure

As for the *in situ* extractant-formation method, an aqueous solution was prepared by mixing metal ions, diammonium hydrogen citrate-citric acid masking solution, and potassium nitrate to be 0.20 M, 0.050 M, and 0.10 M, respectively, and was adjusted pH appropriately by adding 2.0 M KOH and/or 2.0 M HNO_3 aqueous solution. A 10 cm^{-3} volume of the aqueous phase was equilibrated with an equal volume of the P_iDC-forming mixed solvent in a 50 mL extraction vial by shaking vigorously for 1 h. Then, the aqueous phase was separated from the organic phase by a centrifuge at 20° at 3000 rpm for 20 min and was subjected to the measurement of an equilibrated pH. The metal ion concentration in the aqueous phase was determined by flame atomic absorption spectrophotometry.

In the case of metal extraction with the synthesized chelating reagent, potassium dithiocarbamates usually don't dissolve in $CHCl_3$ and are decomposed by the acid although the rate of decomposition varies with the acidity. Therefore, it was dissolved in 0.10 M NaOH solution to a concentration of 0.50 M, and 1.0 cm^{-3} of this solution was added to the aqueous phase after the pH was adjusted. The constituents of the aqueous phase were same as to the in situ extractant-formation method except for the total volume was 11 cm^{-3}. 10 cm^{-3} of $CHCl_3$ was added to the aqueous phase, and both phases were equilibrated by vigorously shaking for 1 h. The procedure was same as to that of the in situ extractant formation method hereafter.

Syntheses of Potassium Dithiocarbamates

Potassium piperidinedithiocarbamate (KP_iDC) and potassium dimethylpiperidine-dithiocarbamate ($KDMP_iDC$) were synthesized according to reference [8]. A 0.10 mol quantity of piperidine or DMP and 0.10 mol of CS_2 were dissolved in 10 cm^{-3} of ethanol, and then 20 cm^{-3} of 1:1 ethanol aqueous solution containing 0.10 mol of KOH was added to it. The mixture was stirred for 2 h (in the case of DMP, 4 h) at room temperature, open to the air. After that, the mixture was poured into diethylether to precipitate the product, which was purified by recrystallization from THF-hexane mixture repeatedly. Unfortunately, tetramethyl- piperidinedithiocarbamate salt ($KTMP_iDC$) could not be successfully synthesized by this method.

RESULTS AND DISCUSSION

The Formation of Dithiocarbamate Ion

In order to explain the mechanism in this extraction system, the UV spectra of aqueous solutions of KP_iDC and $KDMP_iDC$ were compared to those of 0.1 M KNO_3 aqueous solutions equilibrated with the mixed solvents separately (Figures 1a and 1b). For both cases, the shape and absorption maxima (λ_{max}) of the spectrum for these aqueous solutions coincide fairly well each other. Thus, it was proved that P_iDC^- or DMP_iDC^- was formed in the aqueous phase by shaking with the mixed solvent, respectively, and therefore, it can be inferred that metals were extracted into the organic phase in the form of dithiocarbamate complex. However, the formation of TMP_iDC^- was not fully confirmed yet, since the standard sample of TMP_iDC^- salt could not be synthesized successfully. In this case, the aqueous phase was shaken with the mixed solvent composed of 5.0:5.0:90 vol % CS_2-TMP- $CHCl_3$ gave the spectrum having the

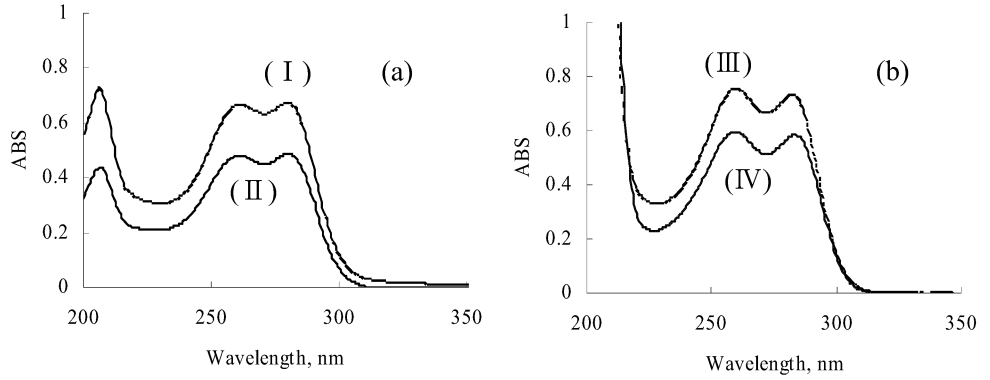

Figure 1. Absorption spectra of the aqueous solutions equilibrated with P_iDC-forming mixed solvents and KP_iDC and $KDMP_iDC$ aqueous solutions. (a) (I): the aqueous phase shaken with a mixed solvent composed of 0.5:0.5:99 vol % CS_2-piperidine-$CHCl_3$. (II): KP_iDC aqueous solution. (b) (III): the aqueous phase shaken with a mixed solvent composed of 1.0:1.0:98 vol % CS_2-DMP-$CHCl_3$. (IV): $KDMP_iDC$ aqueous solution. All solutions were adjusted at pH 9.0 with 0.10 M NH_4Cl-NH_3 aqueous buffer solution.

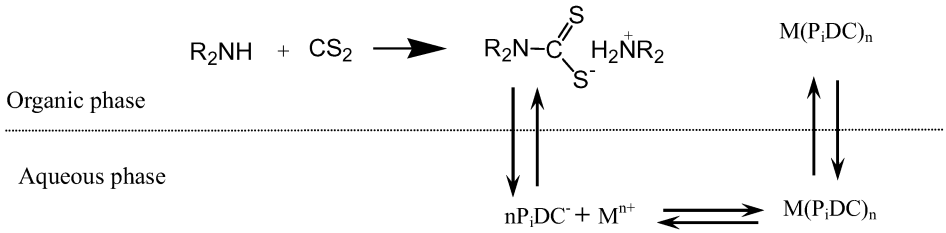

Figure 2. Extraction mechanism of ternary mixed solvents system.

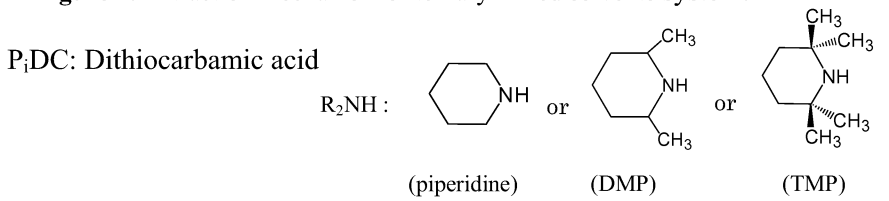

twin peaks characteristic of the dithiocarbamate group at λ_{max1} 247 nm and λ_{max2} 287 nm, although they are a little different from those of P_iDC^- or DMP_iDC^-, namely, λ_{max1} 260 nm and λ_{max2} 280 nm, respectively. Then, by analogy to the mixed solvents containing piperidine and DMP, it was thought reasonable that TMP and CS_2 reacted to form TMP_iDC^- in the aqueous phase and extracted metals into the mixed solvent in the form of metal-TMP_iDC^- complexes. Based on the results, the overall process of the metal extraction in this system is proposed in Figure 2.

Effect of pH on the Metal Extraction with PDTC Forming Solvent

The yield of dithiocarbamate ion in the aqueous phase adjusted to pH 9.0 was determined spectrophometrically by using the absorbance at 280 nm as follows: [P_iDC^-] = 58 mM, [DMP_iDC^-] = 0.26 mM, and [TMP_iDC^-] = 0.023 mM. That is, the reactivity between piperidine derivatives and CS_2 decreases in the order of piperidine > DMP > TMP. Then, in order to make the concentration of the formed dithiocarbamate ion in the aqueous phase the same as much as possible, the following volume ratios (vol %) of the mixed solvents were employed in this study: piperidine:CS_2:$CHCl_3$ = 0.5:0.5:99; DMP:CS_2:$CHCl_3$ = 1.0:1.0:98; and TMP:CS_2:$CHCl_3$ = 5.0:5.0:90. The extractabilities of these three mixed solvents were shown as a function of pH in Figures. 3a, 3b, and 3c. The mixtures containing 0.5 vol % piperidine extracted Cu^{2+}, Co^{2+}, Ni^{2+}, and Cd^{2+} in quantitatively in the pH range 4.21-9.35, and that containing 1.0% DMP extracted all the metals only in the pH range of 8.87-9.85. However, the mixture containing 5.0 vol % TMP extracted Co^{2+} and Ni^{2+} incompletely in the examined pH range. Incidentally, in the TMP-CS_2-$CHCl_3$ system, since the concentration of TMP in the mixed solvent was fairly high, the pH of the aqueous phase converges to the alkaline region irrespective of the adjusted pH values, and therefore the metal extraction in the acidic region could not be

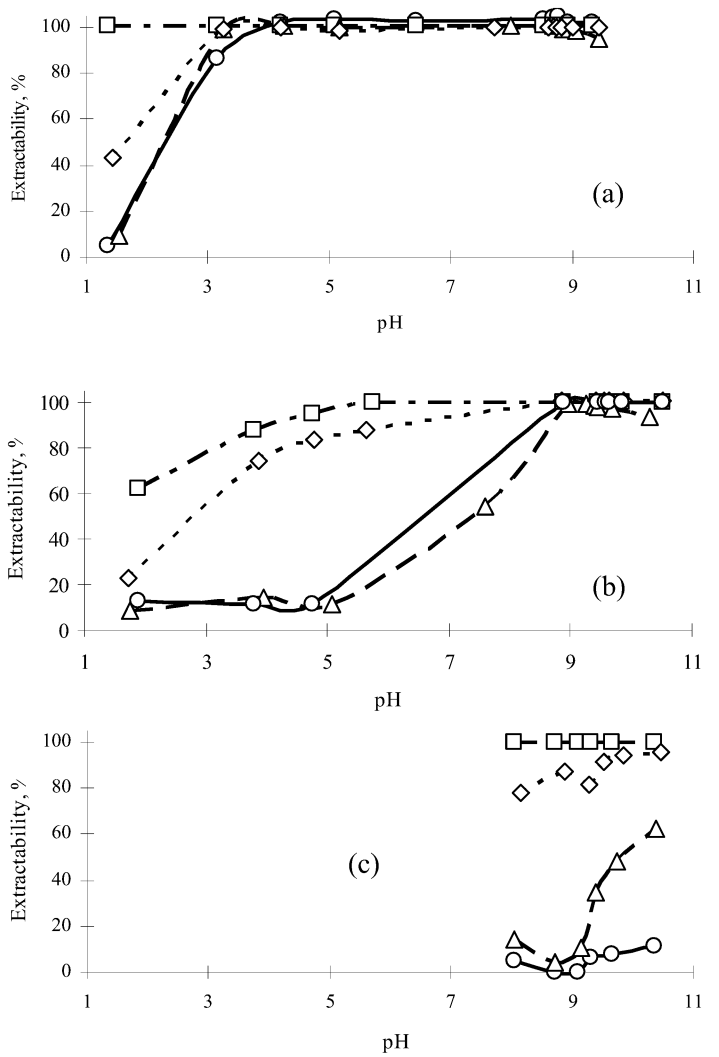

Figure 3. Effect of pH on the metal extraction with the mixed solvent.
(a) The organic phase was the mixture of piperidine:CS_2:$CHCl_3$ = 0.5:0.5:99.
(b) The organic phase was the mixture of DMP:CS_2:$CHCl_3$ = 1.0:1.0:98. (c) The organic phase was the mixture of TMP:CS_2: $CHCl_3$ = 5.0:5.0:90. ○:Ni^{2+}, ◊:Cd^{2+}, Δ:Co^{2+}, □:Cu^{2+}.

examined. The extractabilities of Co^{2+} and Ni^{2+} with the mixed solvents decreased in the order piperidine > DMP > TMP. Two hypotheses were considered to explain this phenomenon: (1) the extractabilities of P_iDC^-, DMP_iDC^-, and $TMPDC^-$ against metal ions were different, and (2) the decrease in the concentrations of formed dithiocarbamate ion as described above affected the extraction. When Cu^{2+}, Cd^{2+}, and Ni^{2+} were extracted by the reagent $KDMP_iDC$, all metal ions were extracted with quantitatively in the pH range 3.03-9.96. It means that the extractability of Ni^{2+} with $KDMP_iDC$ extraction

method was better than that with the DMP_iDC^- forming method. And moreover, the explicit hierarchy of $Cd^{2+} > Ni^{2+} \geq Co^{2+} > Zn^{2+}$ was observed in the extractability in the pyrrolidinedithiocarbamic acid-forming system [5]. These facts support the second hypothesis. That is, Cu^{2+} and Cd^{2+} have superior extractability for dithiocarbamate ion over Co^{2+} and Ni^{2+} and preferentially consume the produced dithiocarbamate ion, so that Cd^{2+} and Ni^{2+} were forced to be extracted under the very low concentration of dithiocarbamate ion in the mixed solvent containing DMP and TMP. However, when the reagent $KDMP_iDC$ was used, the concentration of DMP_iDC^- was sufficiently high and the difference in the extractabilities between Cu^{2+}, Co^{2+}, Ni^{2+}, and Cd^{2+} did not appear.

CONCLUSIONS

In the conventional solvent-extraction method, in order to evaluate the extractability of unknown extractant, laborious work is necessitated to synthesize a sufficient amount of it. However, according to the in situ P_iDC^- forming method, the extractability of P_iDC^- for Cu^{2+}, Co^{2+}, Ni^{2+}, and Cd^{2+} could be simply demonstrated, without synthesizing KP_iDC. And by changing the component of the organic phase, the separation of Cu^{2+} and Cd^{2+} from Co^{2+} and Ni^{2+} could be achieved conveniently.

REFERENCES

1. K. Fujinaga, "The Solvent Extraction of Some Divalent Transition Metals with Mixed Solvent," *Anal Sci.,* **7**, Supplement 29 (1991).
2. K. Fujinaga, "Liquid-Liquid Extraction of Some Transition Metals with a Mixed Solvent System," *Anal. Chem. Acta,* **264**, 71-77 (1992).
3. K. Fujinaga, Y. Seike, and M. Okumura, "A new role of solvent - Solvent Extraction of Some Transition Metals with a Mixed Solvent," 1996, *Proc. ISEC'96*, edited by D. C. Shallcross, et al., The University of Melbourne; pp. 93-98.
4. K. Fujinaga, Y. Seike, and M. Okumura, "Solvent Extraction of Transition Metal Ions by an in situ Extractant Formation Method: Diethyldithiocarbamate-forming System," *Anal. Sci.*, **13**, 225-230 (1997).
5. K. Fujinaga, M. Fukai, Y. Seike, and M. Okumura, "Solvent Extraction of Transition Metals by an in situ Extractant Formation Method. Utilization of an Easily-solidifying Solvent," *Anal Sci.,* **15,** 333-337 (1999).
6. K. Fujinaga, Y. Seike, and M. Okumura, "Solvent Extraction of Transition Metals by an in situ Extractant Formation Method. II. Utilization of an easily-Solidifying Solvent," 2001, *Proc. ISEC'99*, Volume 1, M. Cox, *et al.,* Eds., Society of Chemical Industry; pp. 341-345.
7. K. Fujinaga, Y. Sakaguchi, T. Tsuruhara, Y. Seike, and M. Okumura, "Solvent Extraction of Transition Metal Ions by an in situ Extractant Formation Method: Salicylaldoxime-forming System," *Solvent Extr. Res. Dev. Jpn.,* **8,** 144-158 (2001).
8. R. D. Bereman and D. Nalewajek, *Inorg. Chem.,* **17**, 1085-1087 (1978).

DESCRIPTION OF SMART-LEVEL SOLVEX

The unit comprises a water-jacketed reactor with integrated water bath, variable speed stirrer, sensing probe, computer-based display and control software, and dedicated control panel or computer interface (Figure 1). The unique feature is the chemically resistant resistivity probe (150 mm length), with 128 sensors enabling a reading every 100 ms at 1.2 mm vertical resolution. Experimental parameters are fully programmable. A real-time phase disengagement profile is generated, and data are recorded graphically or transformed to *Excel* spreadsheet format. The measurement principle relies on differences in conductivity between the phases; in addition to detection of aqueous and organic phases, this allows identification of emulsions, crud, and third-phase formation.

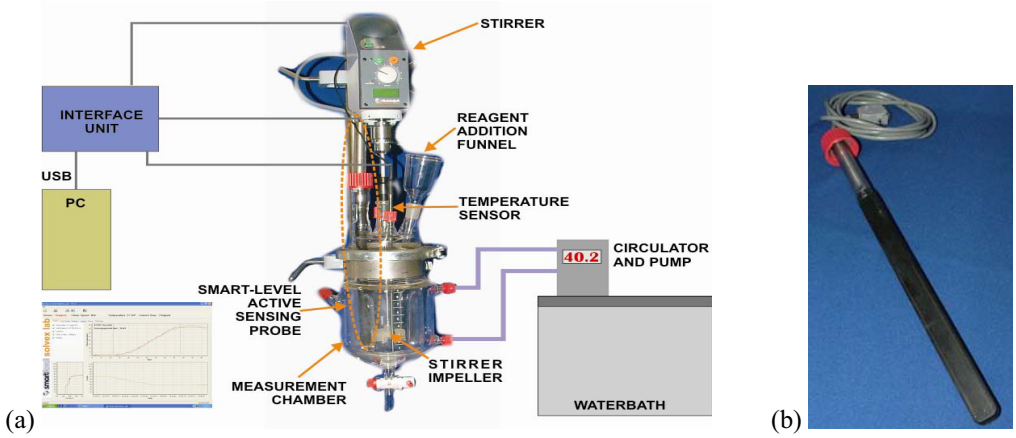

Figure 1. (a) Schematic of Smart-Level Solvex equipment. (b) Close-up of the detection probe.

EXPERIMENTAL

Solvent-Extraction Systems

For copper-oxime systems, the aqueous phase contained 6 g/L Cu, 2 g/L Fe (as sulfate salts) at pH 2, while the organic phase comprised 10 vol. % LIX® 984N or ACORGA® M5640 in the diluents SSX 210, ShellSol® 2325, or ShellSol A150. The zinc system used an aqueous phase containing (g/L) 31.5 Zn, 0.5 Ca, 0.5 Cu, 0.2 g/L Cd, and 0.2 g/L Ni (as sulfates) at pH 4 and organic phase of 40 vol. % di(2-ethylhexyl)phosphoric acid (D2EHPA) in Escaid® 100. The uranium system employed a 4 g/L U plant solution and organic phase of 10 vol. % Alamine® 336, 5 vol. % isodecanol in ShellSol A150.

Standard Methods for Determination of Phase Separation Times

The standard methods of Cognis [1], Cytec [2], and Técnicas Reunidas (TR) [3] were employed. Cognis employs a baffled glass beaker, TR uses an open polyvinylchloride reactor with a tapered base and tap, while Cytec has a graduated water-

jacketed glass vessel with a tapered base and tap to facilitate removal of the phases. The latter is also used for the Smart-Level Solvex. In all methods, prescribed volumes of each phase are stirred under preset conditions, then allowed to separate and the time required for phase separation measured. In the Cytec and TR methods, the position of the interface is additionally recorded at regular intervals to obtain information regarding the rate of separation. The main differences between the methods are summarized in Table 1.

Table 1. Comparison of differences between the four experimental methods

Parameter	Cognis	Cytec	TR	SL Solvex
Volume of phases (mL)	350	400	1000	400
Temperature control	No	Yes	No	Yes
Mixing time (min.)	5	3	3	3
Stirring speed (rpm)	1750	600	580	variable
PST measurement	stopwatch	stopwatch	stopwatch, ruler	electronic
Time profile data	No	Yes	Yes	Yes

Experimental Procedures

Clean, dry glassware is essential for reproducible results. Each reactor was washed with laboratory detergent and water and then sequentially rinsed with deionized water, ethanol, acetone, and deionized water again before each experiment. The four methods were compared for each SX system, under aqueous- and organic-continuous mixing conditions. In the first evaluation, the same aqueous and organic phases were recycled ten times under identical conditions and the PSTs recorded. In the second evaluation, fresh phases were employed each time and the experiment repeated six times. Statistical analysis of the results (using standard *Excel* functions) was undertaken to calculate the precision and reproducibility of each method.

RESULTS AND DISCUSSION

Copper-Oxime Systems

Figure 2 shows the average PST results and variances (square of the standard deviation) of (a) six replicates on fresh phases and (b) ten replicates on recycled phases measured for copper-oxime systems following aqueous-continuous mixing. Significant differences in PST were measured for the same systems using the different techniques, confirming the inherent problems with accurate measurement of this parameter. For copper-oxime systems, a PST of ~60 s would typically be expected. PST is expected to increase with decreasing aromaticity of the diluent, that is, Shellsol A150 (fully aromatic) < Shellsol 2325 (~ 20% aromatic) < SSX 210 (aliphatic). This was not observed in the system studied. There was also little difference in PST between LIX 984N (ketoxime-aldoxime blend) and ACORGA M5640 (ester-modified aldoxime). Based on the PST values and calculated variances, it is evident that the Smart-Level Solvex and Cognis methods gave best reproducibility for PST measurement in these systems.

jacketed glass vessel with a tapered base and tap to facilitate removal of the phases. The latter is also used for the Smart-Level Solvex. In all methods, prescribed volumes of each phase are stirred under preset conditions, then allowed to separate and the time required for phase separation measured. In the Cytec and TR methods, the position of the interface is additionally recorded at regular intervals to obtain information regarding the rate of separation. The main differences between the methods are summarized in Table 1.

Table 1. Comparison of differences between the four experimental methods

Parameter	Cognis	Cytec	TR	SL Solvex
Volume of phases (mL)	350	400	1000	400
Temperature control	No	Yes	No	Yes
Mixing time (min.)	5	3	3	3
Stirring speed (rpm)	1750	600	580	variable
PST measurement	stopwatch	stopwatch	stopwatch, ruler	electronic
Time profile data	No	Yes	Yes	Yes

Experimental Procedures

Clean, dry glassware is essential for reproducible results. Each reactor was washed with laboratory detergent and water and then sequentially rinsed with deionized water, ethanol, acetone, and deionized water again before each experiment. The four methods were compared for each SX system, under aqueous- and organic-continuous mixing conditions. In the first evaluation, the same aqueous and organic phases were recycled ten times under identical conditions and the PSTs recorded. In the second evaluation, fresh phases were employed each time and the experiment repeated six times. Statistical analysis of the results (using standard *Excel* functions) was undertaken to calculate the precision and reproducibility of each method.

RESULTS AND DISCUSSION

Copper-Oxime Systems

Figure 2 shows the average PST results and variances (square of the standard deviation) of (a) six replicates on fresh phases and (b) ten replicates on recycled phases measured for copper-oxime systems following aqueous-continuous mixing. Significant differences in PST were measured for the same systems using the different techniques, confirming the inherent problems with accurate measurement of this parameter. For copper-oxime systems, a PST of ~60 s would typically be expected. PST is expected to increase with decreasing aromaticity of the diluent, that is, Shellsol A150 (fully aromatic) < Shellsol 2325 (~ 20% aromatic) < SSX 210 (aliphatic). This was not observed in the system studied. There was also little difference in PST between LIX 984N (ketoxime-aldoxime blend) and ACORGA M5640 (ester-modified aldoxime). Based on the PST values and calculated variances, it is evident that the Smart-Level Solvex and Cognis methods gave best reproducibility for PST measurement in these systems.

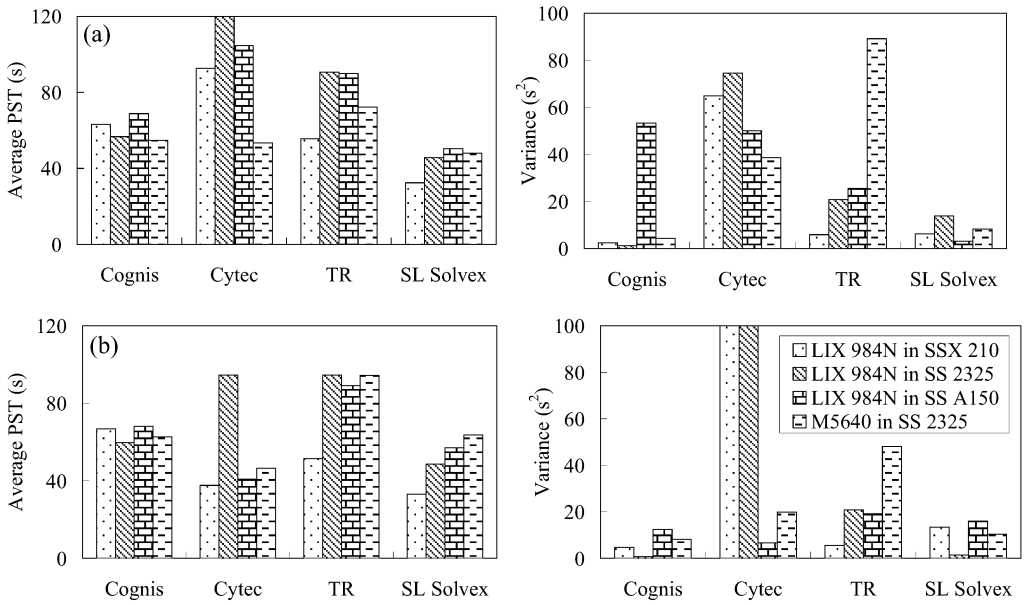

Figure 2. Average PST and calculated variances on the copper-oxime systems for (a) fresh phases and (b) recycled phases following aqueous-continuous mixing.

Zinc-D2EHPA System

The TR method was specifically established for the Zn-D2EHPA system, while the Cognis and Cytec methods are generally used for copper systems. Figure 3 shows PSTs and standard deviations measured for recycled phases in the Zn-D2EHPA (10 replicates) system following aqueous- and organic-continuous mixing for all four methodologies. As with the copper system, there is lack of agreement between the three methods with respect to PSTs measured. Reproducibility was slightly better using the Smart-Level Solvex compared to the Cytec and TR methods, while the Cognis method was poor for this application.

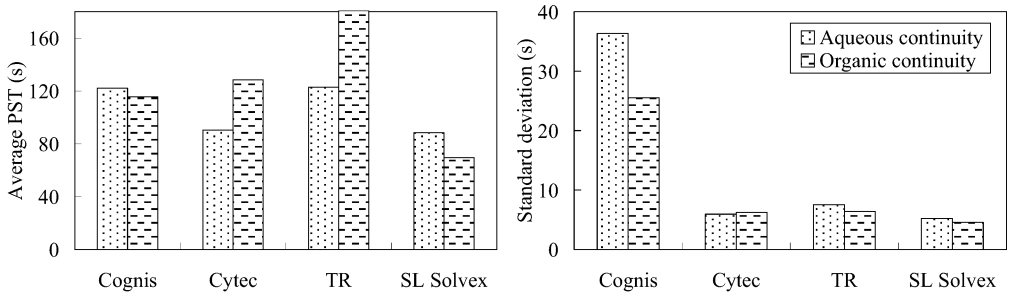

Figure 3. Effect of measurement technique on average PST and standard deviation for the Zn-D2EHPA recycled system following aqueous and organic-continuous mixing.

Uranium-Amine System

Figure 4 shows results obtained under aqueous-and organic-continuous mixing conditions for the uranium system. The Smart-Level Solvex demonstrated the best reproducibility of PST of the four methods and the closest correlation between results for the fresh and recycled phases. The TR method showed the opposite trend for phase continuity compared to the other three methods and poorest reproducibility. This may be attributed to the difficulties of adequately cleaning the plastic reaction vessel, and possible interfacial activity of the organic phase with the reactor walls.

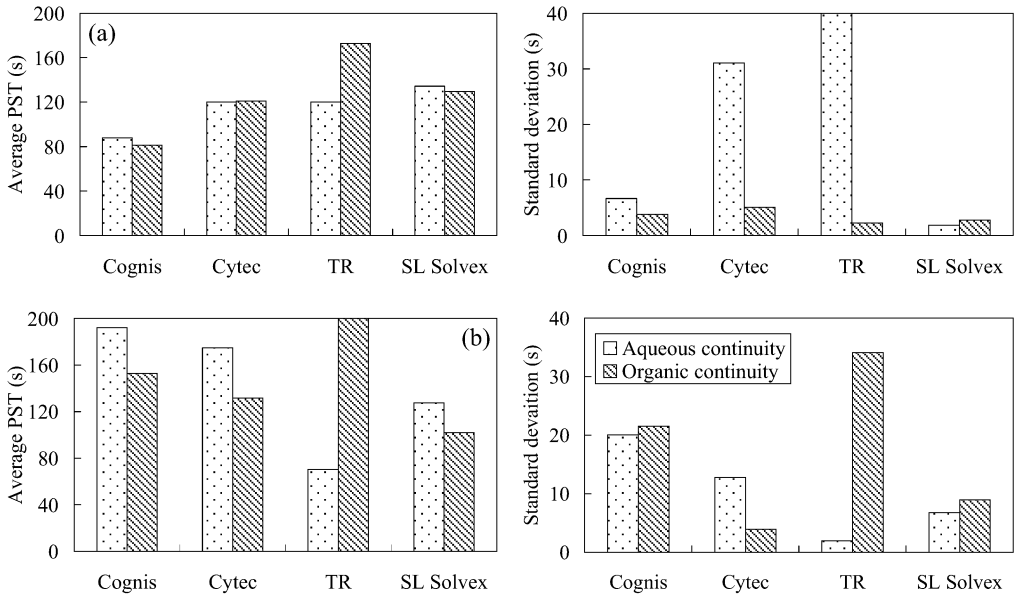

Figure 4. Average PST and calculated standard deviations for PST measurements on the uranium-amine system for (a) fresh phases (6 repeats) and (b) recycled phases (10 repeats).

Phase-Separation Characteristics

One advantage of the electronic detection technique is that more detailed information regarding the phase-separation process can be obtained. In Figure 5(a) (aqueous-continuous phase separation in uranium system), three distinct processes can be identified: an initial phase break (A), primary separation (B), and secondary separation (C). The profiles under organic-continuous conditions are different (Figure 5(b)), showing an initial increase in the emulsion-band thickness (A) and "bounce" (B) before the main separation (C) occurs. Speculation on the reasons for these reproducible effects is beyond the scope of this paper.

The influence of the presence of a phase modifier, crud, or alternative diluents on the rate of phase disengagement can be similarly evaluated and better understood.

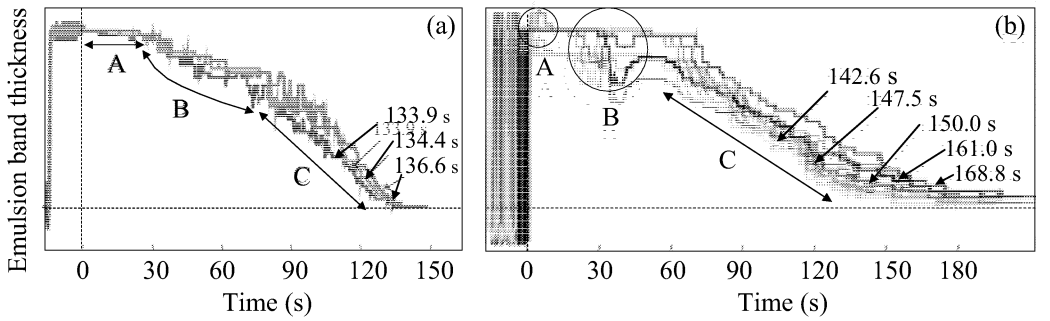

Figure 5. Overlaid replicate profiles of phase separation in the uranium-amine system following (a) aqueous- and (b) organic-continuous mixing conditions, showing comparison of final phase-separation times and different processes detected during phase separation.

CONCLUSIONS

A general lack of conformity in the measurement of phase separation exists. The methods in most widespread use rely heavily on operator experience and objectivity. Even for identical systems, considerable variation in results is measured using different techniques. The introduction of the Smart-Level Solvex, an instrument with electronic detection of phase disengagement and tight control of environmental and operating variables, allows better reproducibility of measurement to be achieved. Furthermore, information on the phase-disengagement profile with time and the behavior of emulsions, third phases, crud, and other interfacially active phenomena can be obtained.

ACKNOWLEDGMENTS

Appreciation is extended to the Anglo American Innovation Fund for financial support for this project, and to Cognis, Cytec, ExxonMobil, Rhodia, Sasol, Shell Chemicals, and AngloGold Ashanti's Vaal River South uranium plant for supply of reagents. Features of this work are the subject of a Danntech cc patent application.

REFERENCES

1. Cognis, "Standard Cognis Quality Control Test for LIX® Oxime Reagents," Blue Line Technical Bulletin, 1996.
2. Cytec, "ACORGA Extraction Reagents Standard Test Methods," Technical Note MCT-1019, 2005.
3. Técnicas Reunidas, "Protocols for DEHPA and Solvent Characterisation and Verification for their Use in the Modified Zincex Process," Report ITR/I-5862/049/2001 Rev. 1.3, 2002.

ANALYTICAL APPLICATIONS OF ION-TRANSFER AT A LIQUID|LIQUID INTERFACE ILLUMINATED WITH AN ULTRAVIOLET LASER BEAM

Teruo Hinoue[1] and Takashi Kimoto[2]

[1]*Department of Chemistry, Faculty of Science, Shinshu University, 3-1-1 Asahi, Matsumoto, Nagano 390-8621,* JAPAN.
[2]*Kimoto Electric Co., LTD., 3-1 Funahashi-cho, Tennouiji-ku, Osaka 543-0024,* JAPAN.
Corresponding author email address: thinoue@gipac.shinshu-u.ac.jp

ABSTRACT

Two different kinds of alternative current voltammetric measurements were attempted at aqueous|nitrobenzene (NB) solution and aqueous|1,2-dichloroethane (DCE) solution interfaces intermittently illuminated with at a 325-nm beam from a He-Cd laser. One is thermal-modulation voltammetry (TMV), and the other is photomodulation voltammetry (PMV). In the former, we used a light-to-heat conversion process to generate a thermal modulation field at an aqueous|NB solution interface. With TMV, we determined values of the standard entropy change of ion-transfer for four tetraalkylammonium ions, that is, TMA^+, TEA^+, $TPrA^+$, and TBA^+. In the latter, we used a photodecomposition reaction at an aqueous|DCE solution interface caused by an ultraviolet laser beam for the determination of organic compounds. Even if the compounds are electrically neutral, and hence soluble only in organic media, the determination is possible by detecting ionic species produced through the photodecomposition with a voltammetric technique. The PM voltammograms for *p*-aminodiphenylamine (*p*-ADPA) showed peaked waves, and the peak heights were proportional to their concentration, respectively.

INTRODUCTION

For the last several decades, electrochemical methods have been developed for examining ion-transfer at an interface between two immiscible electrolyte solutions (ITIES).[1] Among them, ion-transfer voltammetry has been available for analyzing ions and understanding several phenomena related to ion-transfer at an ITIES, such as ion-selective electrode and solvent extraction. In order to expand the ion-transfer voltammetry, we tried illuminating an ITIES with a laser beam, expecting selective heating of the ITIES and photodecomposition of solutes contained in either phase forming the ITIES. As the result, we could propose thermal-modulation voltammetry (TMV)[2] and photomodulation voltammetry (PMV)[3,4] based on the selective heating and the photodecomposition, respectively. In this paper, we summarize both of the voltammetric methods and discuss their possibilities.

EXPERIMENTAL SECTION

The same experimental setup was used for TMV and PMV. Figure 1 shows the experimental arrangement. The He-Cd laser (Kimmon, IK545IR-E, KR1801C) was used as a source for the heating and the photodecomposition. The wavelength of the laser beam was 325 nm and its power was 13.0 mW. The laser beam was chopped with a mechanical chopper at 10 Hz and then introduced into the electrolytic cell from the optically non-absorbing aqueous solution. The electrolytic cell, which was machined from poly(chlorotrifluoroethylene) resin blocks, consisted of two compartments for the aqueous solution and the nitrobenzene (NB) or 1,2-dichloroethane (DCE) solution. The two compartments were separated by a thin polyester film 16 μm thick with a microhole 30 μm in diameter, serving as the aqueous|NB (or DCE) solution interface. As soon as the laser beam impinges upon the interface, it is rapidly absorbed by the NB (or DCE) solution. As the result of the absorption, heat is generated through a non-radiative process in the NB solution, and thereby the interface and the interfacial region are warmed through a thermal-diffusion process, or solutes contained in the DCE solution are photochemically decomposed. When the laser beam is chopped at a certain frequency, a current for ion-transfer is expected to be modulated at the same frequency. The four-electrode type potentiostat (Hokuto Denko, HA1010mM1A) and the potential sweep unit (Fuso, 1104) were used for the potential control and the current detection, and the potential sweep. The current signals from the potentiostat were amplified with the lock-in amplifier (PAR, 5101), and the signal intensity was recorded as a function of the potential on the *X-Y* recorder (recorder 2). Simultaneously with recording the thermal modulation (or photomodulation) voltammogram, the linear sweep (LS) voltammogram was also recorded on the *X-Y* recorder (recorder 1).

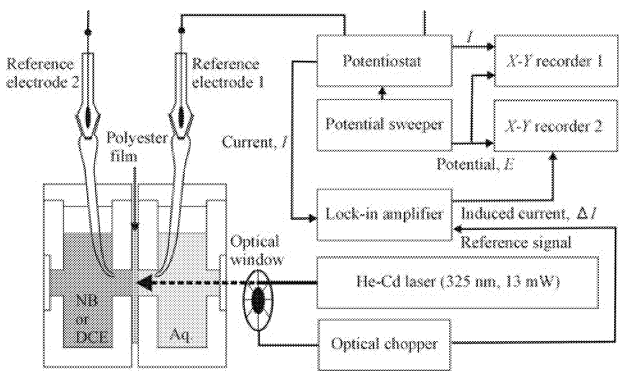

Figure 1. Experimental arrangement for TMV and PMV

RESULTS AND DISCUSSION

Thermal Modulation Voltammetry

The electrochemical system examined was as follows:

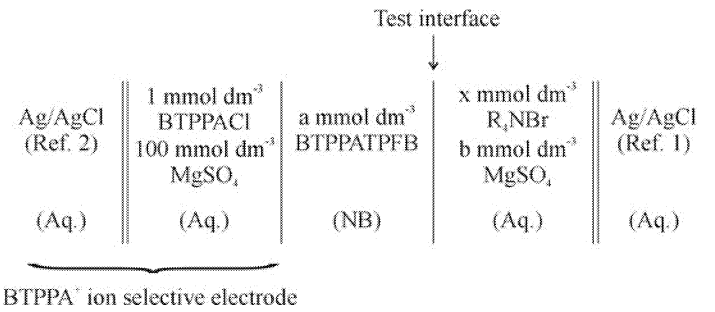

Here BTPPATPFB denotes bis(triphenylphosphoranylidene)ammonium tetrakis(penta-fluorophenyl)borate. In this study, ion-transfer from the aqueous solution to the NB solution was examined forfour tetraalkylammonium ions, such as tetramethylammonium ion (TMA^+), tetraethylammonium ion (TEA^+), tetrapropyl- ammonium ion ($TPrA^+$), and tetrabutylammonium ion (TBA^+). Figure 2 shows the LS voltammograms and the TM voltammograms for the alkyl-ammonium ions. The positive currents indicate ion-transfer of a cation from the aqueous solution to the NB solution, or that of an anion from the NB solution to the aqueous solution. As can be seen in this figure (a), all of the LS voltammograms showed S-shaped waves with steady-state currents, I_{ss}. On the other hand, the half-wave potential, $E_{1/2}$ was shifted to more positive potentials with decreasing alkyl chain length of the alkylammonium ion. The shift is obviously attributable to increasing hydrophilicity of the ion with decreasing length of the alkyl chain. The final discharge is due to ion-transfer of $BTPPA^+$ from the NB solution to the aqueous solution at the negative potential limit and that of $TPFB^-$ from the NB solution to the aqueous solution at the positive potential limit. On the other hand, as can be seen in Fig. 2(b), the TM voltammogram was characteristic to each ion in shape, in contrast to that of the LS voltammogram. However, the sign of the standard entropy change for ion-transfer, $\Delta S°$(tr. O to W), could be estimated from the shape of the TM voltammogram. That is, the curves indicate that $\Delta S°$(tr. O to W) is positive for TMA^+, nearly zero for TEA^+ and $TPrA^+$, and negative for TBA^+. This

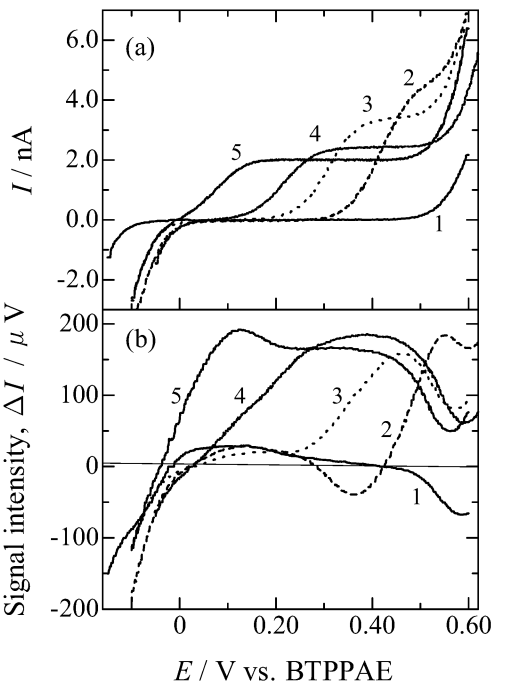

Figure 2. LS voltammograms (a) and TM voltammograms (b). 1, blank solution (1.00 mM $MgSO_4$ in the aqueous solution and 0.05 mM BTPPATPFB in the NB solution); 2, TMA^+; 3, TEA^+; 4, $TPrA^+$; 5, TBA^+. The concentrations of the tetraalkyl- ammonium ions are all 0.5 mM.

suggests that more hydrophilic ions tend to operate more destructively on the structure of bulk water. From the expression,

$$\Delta S°(\text{tr. O to W}) = (2RT/D_W)\times(dD_W/dT) \times(\Delta T_{diff}/\Delta T_{int}) \times\{(1\text{-}2(\Delta I_{E1/2}/\Delta I_{ss}))\} \quad (1)$$

the values of $\Delta S°$(tr. O to W) were determined. Here, D and T are the diffusion coefficient and the temperature, respectively. ΔT_{diff} and ΔT_{int} are the temperatures in the diffusion layer and at the interface. Since ΔT_{diff} and ΔT_{int} were difficult to directly measure, the ratio of ΔT_{diff} to ΔT_{int} was theoretically estimated to be 0.633 by solving a one-dimensional thermal-diffusion equation at the interface. $\Delta I_{E1/2}$ and ΔI_{ss} are the signal intensity at the half-wave potential, $E_{1/2}$, and a certain potential in the steady-state current region. Table 1 lists the values together with the literature values. The values determined by TMV agreed fairly well with the literature values by the electromotive force measurement.[5] On the other hand, we tried TMV by using a visible laser beam at 442 nm with a power of 57 mW, which is another beam from the He-Cd laser, and the aqueous solution containing Chinese ink as light absorber. In this case, the laser beam was introduced from the 1,2-dichloroethane (DCE) solution to the aqueous solution. The Chinese ink consisted of 15.5% carbon black, 6.5% polyvinylalcohol (PVA), and 76.0% water. In the concentration range to 0.50%, the signal intensity increased with increasing concentration, which indicates that the magnitude of thermal modulation, ΔT, increased due to the increasing optical absorption. The value of $S°$(tr. O to W) determined from this TMV was much larger than that in TMV described previously. The reason is under investigation.

Table 1. Standard entropy changes of ion-transfer, $\Delta S°$(tr. O to W), for tetra-alkyl ammonium ions

Ion	$\Delta S°$(tr. O to W) / J K^{-1} mol^{-1}		
	This work (TMV)	Electromotive force measurement[5]	Voltammetric measurement[6]
TMA^+	+85.2	+71.7	+27.4, +42.6[7]
TEA^+	+10.0	+16.8	-8.3
$TPrA^+$	-47.0	-49.3	-
TBA^+	-78.5	-83.3	-92.6

Photomodulation Voltammetry

In PMV, solutes contained in the organic solution is photochemically decomposed to form ionic species. We tried detecting ion-transfer of the ionic species across the aqueous and DCE solution interface. The electrochemical system examined was as follows:

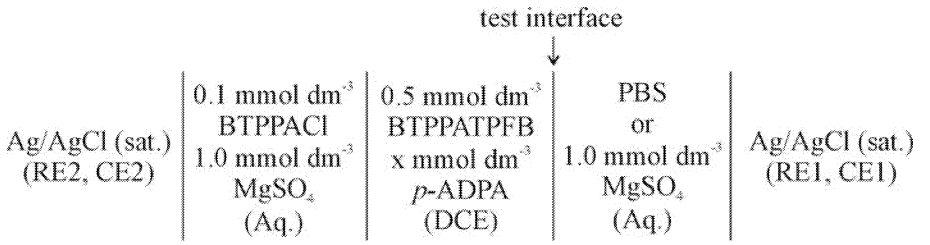

Here *p*-ADPA and PBS denote *p*-aminodiphenylamine and a phosphate buffer solution, respectively. *p*-ADPA, known as a head-to-tail coupling dimer of aniline, is readily photodecomposed. UV-vis spectra of *p*-ADPA (Ph-NH-Ph-NH_2) in DCE and in phosphate buffer (pH 2.35) measured after 30-min irradiation at 325 nm suggested that a dimer dication was formed. Figure 3 shows PM voltammograms at the concentration of *p*-ADPA to 0.10 mM, where the aqueous solution contained 1.0 mM $MgSO_4$ (pH *ca.* 5). As can be seen in this figure, each PM voltammogram clearly exhibited a peaked wave at 0.61 V, and the signal intensity at the peak potential was proportional to the concentration of *p*-ADPA. These facts indicate not only that the peaked wave arises from *p*-ADPA, but also that PMV could be used as a sensitive analytical technique. On the other hand, taking into account that the pK_a value of *p*-ADPA is 4.4 for Ph-NH-Ph-NH_3^+ · H^+ + Ph-NH-Ph-NH_2, the pH dependence of the LS and PM voltammogram was examined, as shown in Figure 4. While the LS voltammograms at pH 2.03 (a) and 4.01 (b) under non-irradiation exhibited the waves at *ca.* 0.60 and 0.67 V, those under irradiation exhibited no waves, except for a slight increase in the current in the potential ranges between 0.17 and 0.54 V at pH 2.03 and between 0.17 and 0.62 V at pH 4.01. Since a large amount of *p*-ADPA is distributed to the aqueous solution as the cation (Ph-NH-Ph-NH_3^+) in the pH region lower than the pK_a value, the waves in the LS voltammograms at pH 2.03 and 4.01 are clearly assigned to ion-transfer of the cation from the aqueous solution to the DCE solution. However, no exhibition of the waves in the LS voltammograms under irradiation suggests that the cation is photochemically decomposed. On the other hand, the slight increase in the current in the LS voltammograms implies that some cation is transferred across the interface. Assuming that an ion resulted from the photodecomposion is a dimer dication of *p*-ADPA, the slight increase is probably due to ion-transfer of the dimer dication from the aqueous solution to the DCE solution. The PM voltammogram can emphasize such a slight difference

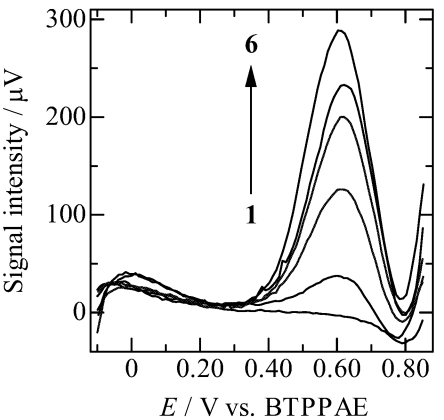

Figure 3. PM voltammograms of *p*-ADPA. 1, blank; 2, 0.02; 3, 0.04; 4, 0.06; 5, 0.08; 6, 0.10 mM. The aqueous solution contained 1.0 mM $MgSO_4$. The scan rate and the chopping frequency were 5 mVs^{-1} and 10 Hz, respectively.

between the LS voltammograms measured under irradiation and non-irradiation. In fact, the PM voltammograms at pH 2.03 and 4.01 clearly exhibited peaked waves at 0.43 and 0.56 V, respectively. At pH 8.01 (c), the LS voltammogram exhibited no wave. This is obvious, because most of *p*-ADPA exists in the DCE solution as Ph-NH-Ph-NH_2. However, a slight increase in the current was also seen in the potential region above 0.3 V. Consequently, the peaked wave in the PM voltammogram is probably due to the slight increase. The mechanism for the slight increase in the LS voltammogram or the peaked wave in the PM voltammogram is assumed to be explained as follows: First, *p*-ADPA is photochemically decomposed in the DCE solution under irradiation at 325 nm. As the result, the dimer dication is formed, and it is distributed to the aqueous solution. After that, the dimer dication is transferred from the aqueous solution to the DCE solution.

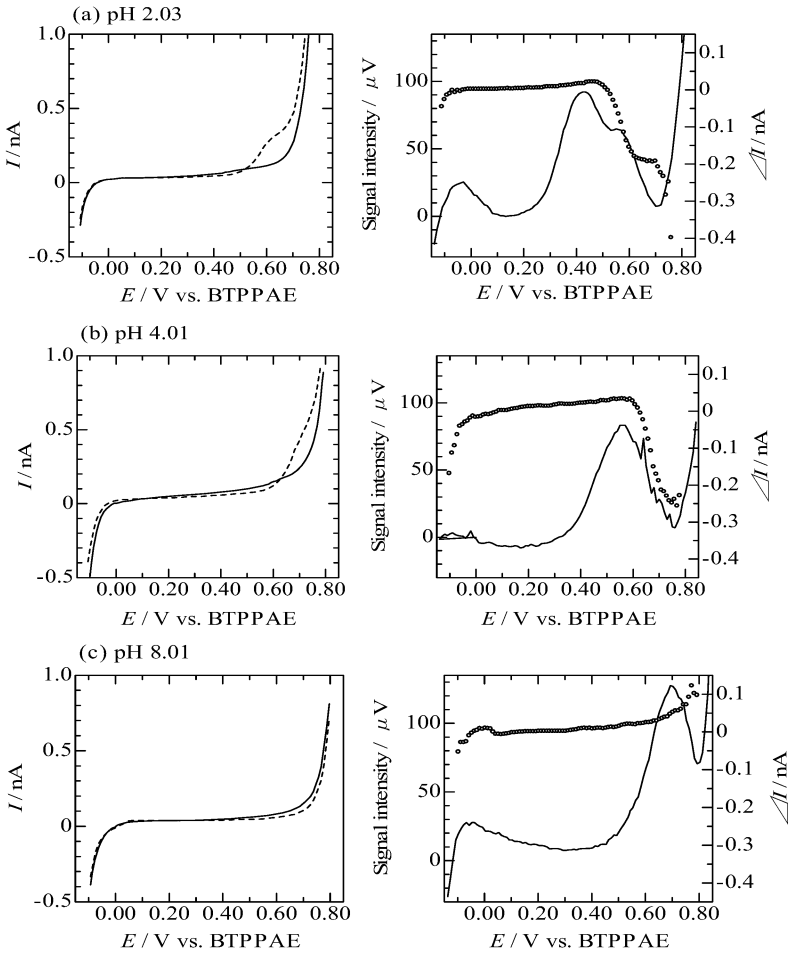

Figure 4. pH dependence of the LS and PM voltammogram of *p*-ADPA. The left figures show LS voltammograms measured under irradiation at 325 nm (solid lines) and nonirradiation (broken lines). The right figures show PM voltammograms and difference voltammograms of the LS voltammograms (dotted lines). The aqueous solutions were 0.10 M PBS. The concentration of *p*-ADPA was 0.10 mM.

CONCLUSION

Illuminating an interface between two immiscible electrolyte solutions (ITIES) with light allows us to heat only the interfacial region and to form ionic species through a photochemical process. Based on the heating and the photodecomposition, two voltammetric methods, thermal-modulation voltammetry (TMV) and photomodulation voltammetry (PMV) have been developed. In addition, illuminating the interface with light will have new possibilities in separation chemistry.

REFERENCES

1. M. Senda, T. Kakiuchi, and T. Osakai, *Electrochim. Acta*, **36**, 253-262 (1991). F. Reymond, D. Fermín, H. J. Lee, and H. H. Girault, *Electrochim. Acta*, **45**, 2647-2662 (2000). T. Osakai and H. Katano, *Bunseki Kagaku*, **54**(4), 251-266 (2005).
2. T. Hinoue, E. Ikeda, S. Watariguchi, and Y. Kibune, *Anal. Chem.*, **79**, 291-298 (2007).
3. S. Watariguchi, E. Ikeda, and T. Hinoue, *Anal. Sci.*, **21**, 1233-1236 (2005).
4. S. Watariguchi, Y. Kibune, and T. Hinoue, *Anal. Sci.*, **23**, 1143-1146 (2007).
5. T. Osakai, H. Ogawa, T. Ozeki, and H. H. Girault, *J. Phys. Chem. B.*, **107**, 9829-9836 (2003).
6. T. Wandlowski, Z. Marcěk, Z. Samec, and R. J. Fuoco, *J. Electroanal. Chem*., **331**, 765-782 (1992).
7. H. Makrík, and Le Q. Hung, *J. Electroanal. Chem.*, **158**, 269-276 (1983).

SOLVENT EXTRACTION AS A TOOL FOR DESIGN OF SULFONAMIDE-DERIVED Pb(II) SENSORS

Konstantinos Kavallieratos, Robert J. Alvarado, and Jay M. Rosenberg

Department of Chemistry and Biochemistry, Florida International University
11200 SW 8th St., CP 326, University Park, Miami, FL 33199-0001.
Corresponding author email address: kavallie@fiu.edu

ABSTRACT

The selective extraction and sensing of toxic metals and Pb(II) in particular remains a challenging problem, with the presence of legacy Pb in the environment still posing a serious health risk. Our research group has undertaken an effort to utilize solvent extraction as a tool for the design of selective sensors for Pb and other toxic metals. Disulfonamides derived from *o*-phenylenediamine provide an easily available and versatile framework, which is capable of extracting Pb(II) from water into 1,2-dichloroethane via ion exchange in the presence of a base and—in some cases—of additional co-ligands, such as 2,2'-bipyridine (2,2'-bipy). The latter influence Pb(II) coordination properties and extraction selectivity. The simple dansylamide analog 1,2-$C_6H_4(NHSO_2C_{10}H_6$-5-$N(CH_3)_2)_2$ (**3**) was found to be capable of selective fluorescent sensing via ion-exchange extraction of Pb(II) into 1,2-dichloroethane (DCE). NMR, ESI-MS, X-ray crystallography, and competitive distribution experiments with various ligand analogs reveal unique coordination properties for the Pb(II) complexes, which have a "hemidirected" geometry with a stereochemically expressed lone pair. The selective sensing is attributed to selective extraction of Pb(II), which is highly favored over other divalent metals, presumably because of its unique coordination chemistry and extractability in less polar organic solvents.

INTRODUCTION

Despite the environmental significance of Pb and its legacy contamination problems, due to widespread past use in paint and gasoline [1], there is relatively little attention to extraction applications in relation to Pb(II) sensor design. In designing selective extractants [2] and sensors [3] for Pb(II), which is the most mobile form of lead in the environment, the physicochemical and coordination-chemistry parameters that play an important role in transport phenomena [4] should be taken into account.

Pb(II) has some unique coordination properties that distinguish it from transition metals and other divalent post-transition metals [5]. Unlike other metals that often prefer to adopt in their complexes well-defined geometries for specific coordination patterns, such as tetrahedral for CN = 4, and octahedral for CN = 6, Pb(II) presents a wide variety of different geometries, with coordination numbers usually varying between 4 and 8. Many of these geometries show a peculiar apparent vacancy in the coordination sphere of

Pb, due to the presence of a stereochemically active $6s^2$ lone pair, and thus are defined as "*hemidirected*". Other geometries, more often encountered for higher coordination numbers, do not show this apparent vacancy and are defined as "*holodirected*" [6]. Another characteristic of Pb(II), which should be taken into account in separation and extraction-based sensing applications is its relative "softness" and modest charge density, as underscored by its low (in absolute terms) $\Delta G°$ of hydration of -1434 kJ/mol [7]. Higher background concentrations of Zn(II), Cu(II), and Ca(II) are often an obstacle in designing efficient and practical Pb(II) sensors. Thus, building selectivity against these metals is of importance for biochemically relevant applications.

In this paper, we summarize our recent investigations of ion-exchange extraction of Pb(II) by simple sulfonamides derived from *o*-phenylenediamine, which coordinate and extract Pb(II) by forming distinct complexes with hemidirected geometries. We investigate the influence of additional co-ligands, such as 2,2'-bipy, on extraction and their role in altering selectivity. Furthermore, we summarize the properties of the bis-dansylated analog of *o*-phenylenediamine **3** as a nonratiometric extraction-based Pb(II) sensor. Solutions of **3** and $(i\text{-Pr})_2$NH in DCE show selective fluorescence quenching upon contact with $PbNO_3$ solutions, even in the presence of higher concentrations of other metals. The observed selectivity is attributed to the formation of a low-coordinate 1:1 complex.

EXPERIMENTAL SECTION

Materials and Methods

Ligands **1-3** and their Pb(II) binary and ternary complexes with 2,2'-bipy were synthesized and characterized as previously reported [8-10]. All chemicals (purchased from Aldrich or ACROS) were reagent grade and used without further purification, with the exception of DCE, which was distilled from CaH_2 before use. NMR spectra were recorded on a 400 MHz Bruker NMR spectrometer and were referenced to the residual solvent resonances. ICP-MS measurements were carried out on a Perkin-Elmer Elan-II. Negative-mode Electrospray Ionization Mass Spectra (ESI-MS) were obtained on a Finnigan ThermoQuest LC-MS instrument using 0.01 mg/mL solutions directly infused to ESI-MS at 0.01 mL/min. (cone voltage, -10 V; capillary, 2.71 kV; probe heater, 100 °C; acquisition time, 4 s; mass range, 500 to 1400). Fluorescence spectra were collected on a Jobin Yvon Horiba Fluoromax-3 fluorometer.

Distribution Experiments

Typical ICP-MS distribution experiments were performed as follows: Glassware was contacted with 8 M HNO_3 overnight and washed with twice-distilled, deionized water. A stock solution was prepared containing ligand (at 0.5–3 mM) and 2.2 eq. of $(i\text{-Pr})_2$NH and diluted with water-equilibrated DCE. An appropriate amount of stock solution and DCE was used in preparing 800 μL organic phases, which were placed in 2 mL plastic centrifuge tubes. Stock solutions of 3 μM to 3 mM $M(NO_3)_2$ and 800 μL aqueous phases using appropriate amounts of the metal stock solution were prepared.

The phases were contacted for 12 h on a rotating wheel and then separated. For stripping, 500 μL aliquots of the organic phases and a 0.1 M HNO_3 solution were contacted for 3 h. The source and stripped aqueous phases for each sample were diluted twice to a final concentration not higher than 125 ppb before ICP-MS. A 2% HNO_3 Tl internal standard solution was used for Pb in the dilution of the source and aqueous phases as well as for the determination of an external calibration curve. Internal standards solutions for Co, Ni, Cu, and Zn were prepared using Sc or In (for Cd). Calibration curves with metal standards and a minimum of 7 points ranging for 0 to 150 ppb were used. For Pb the total isotopic counts for m/z of 206, 207, and 208 were measured. The measurements were corrected and referenced to a metal/DCE blank sample, before determining distribution ratios. All experiments were performed in independent triplicate samples. For the fluorescence experiments, the samples were prepared in a similar fashion as for ICP-MS. The organic phases were diluted twice to a maximum concentration of 1.20×10^{-6} M. Emission spectra were collected at $\lambda_{exc} = 340$ nm. The dansyl emission was monitored at $\lambda = 516$ nm. For the NMR distribution experiments, DCE-d_4 or CD_2Cl_2 were used. The recovery of the sulfonamide ligand after stripping was followed by comparing the integrals with 4,4'-di-(*t*-Bu)-biphenyl, used as an internal standard.

RESULTS AND DISCUSSION

The *o*-phenylenediamine sulfonamide framework was selected because of its synthetic versatility, tunability, and ability to incorporate the dansyl fluorophore, which has been successfully employed previously in Pb(II) sensing applications [11]. Sulfonamides have a potential for straightforward synthetic modification. Moreover sulfonamides are weak acids, which can be deprotonated by Et_3N and $(i\text{-Pr})_2NH$ under extraction conditions and stripped with 0.1 M HNO_3. Sulfonamides **1** and **2** (Scheme 1) were initially used. The presence of a bipy co-ligand was deemed necessary, due to precipitation of the Pb-ligand binary complex, which for **1** was an unusual Pb(II) coordination polymer with 1-D chains and a stereochemically active Pb lone pair [8]. The binary complex Pb·**2**·$(DMSO)_2$ was isolated and characterized by X-ray crystallography, showing a hemidirected structure [9]. The ternary Pb(II)-sulfonamide-bipy complexes for ligands **1** and **2** (Scheme 1) were characterized by NMR and ESI-MS as protonated adducts (cation-detection mode) [12] or anionic nitrate adducts (anion-detection mode) [13]. The X-ray structure of Pb·**1**·(bipy) [9] also showed a hemidirected geometry. It is noteworthy that Zn(II) and Cd(II) showed completely different coordination patterns, with soluble, presumably tetrahedral, anionic complexes of the ZnL_2^{2-} and CdL_2^{2-} type [14]. In the presence of bipy, Cd forms the octahedral complex Cd.**1**.$(bipy)_2$ [14]. These results illustrate the differences in coordination chemistry of Pb(II) vs. other metals with these sulfonamide ligands. The extraction by **1** and **2** and 2.2 eq. of bipy showed similar efficiencies. Slightly more efficient extraction was observed for the more bulky ligand **2**. Specifically, when $[Pb]_t = 6.30$ mM and in the presence of 1.0 eq. of bipy, 2.2 eq. of $(i\text{-Pr})_2NH$ and 1:1 Pb/ligand ratio, as much as 97.5% for **2** and 95.0% for **1** of Pb was extracted. When $[L]_t = 3.30$ mM, $[2,2'\text{-bipy}]_t = 3.30$ mM, $[NH(i\text{-Pr})_2]_t = 7.26$ mM, $[Pb(II)]_t$ was between 3 μM and 300 μM, and $([L]_t/[Pb(II)]_t)$ was between 8.9 and 970, ligand **1** extracted between 98.4 and 98.8%, while **2** extracted between 99.5 and 100%.

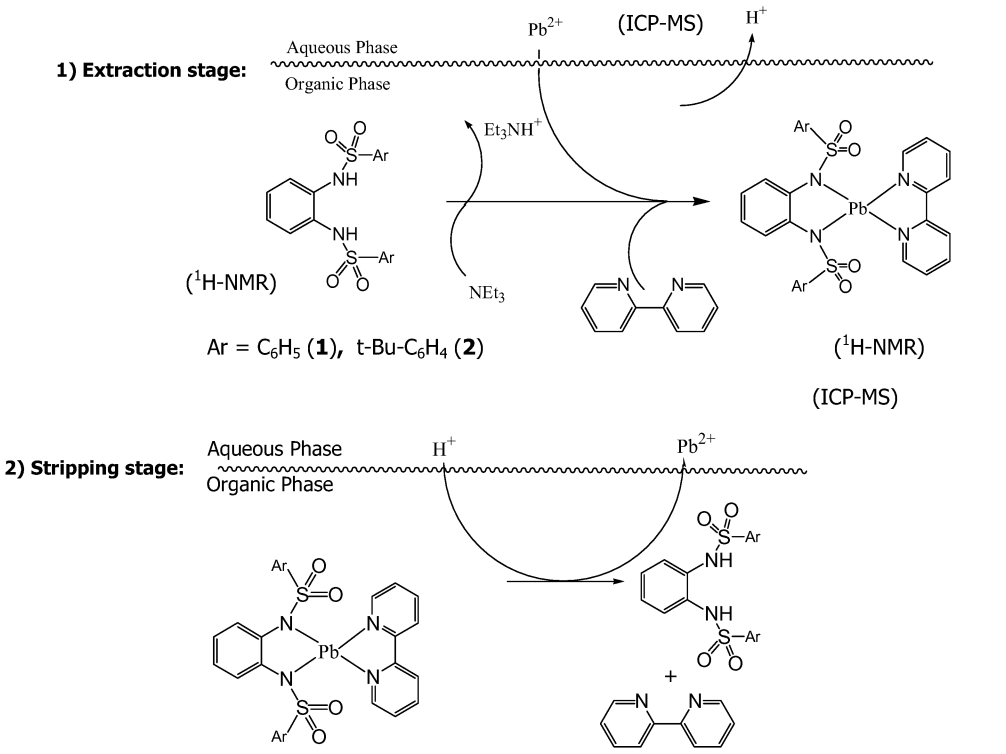

Scheme 1. Pb(II) extraction-stripping sequence for ligands **1** and **2**, which proceeds via formation of ternary Pb-sulfonamide-bipy complexes.

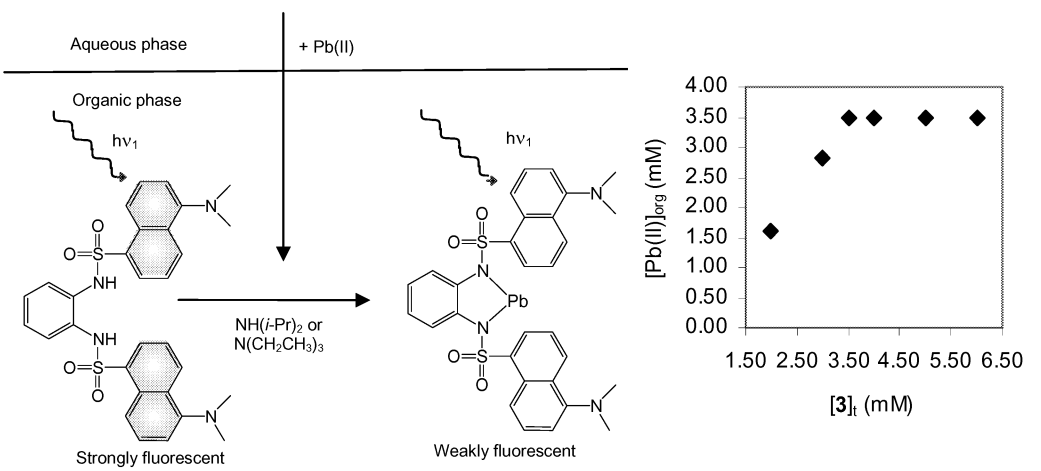

Scheme 2. Pb(II) extraction-based sensing by bis-dansylamide **3**, which proceeds via formation of a 1:1 Pb-sulfonamide complex, as also indicated by the graph on the right. The initial Pb concentration is $[Pb]_t = 3.49$ mM.

Ligand **3** (Scheme 2) showed stronger extraction than **1** and **2**, even in the absence of bipy co-ligand. Specifically, when **1** (3.5 mM) was used together with 2.2 eq. of $NH(i\text{-}Pr)_2$, 99.5% of Pb was extracted from a 3.5 mM $Pb(NO_3)_2$ solution. Unlike **1**, there were no precipitation problems, presumably because the steric bulk of the dansyl ligand prevents additional coordination. The 1:1 complex was identified as the $[Pb\cdot\mathbf{3}\cdot NO_3]^-$ adduct in negative-ion mode ESI-MS [13], and distribution experiments (Scheme 2) confirmed this stoichiometry. The 1:1 complex was isolated as $Pb\cdot\mathbf{3}\cdot(DMSO)_2$ and characterized by NMR and X-ray crystallography [14], showing hemidirected geometry. Fluorescence quenching was observed upon Pb(II) binding, which by comparison of the ICP-MS and fluorescence studies, was directly correlated with the amount of extracted Pb. The monosufonamide control $(CH_3)_2NC_{10}H_6SO_2NHC_6H_5$ showed no quenching and no metal extraction. The response was found to be selective in the presence of 10 to 40-fold higher concentrations of competing metals, such as Ca(II), Zn(II), Cu(II), and Cd(II).

A comparison of the observed extraction selectivities for the binary vs. the ternary complex facilitated extractions for **1**-**3**, shows surprising difference in selectivity trends when bipy is present. While high extraction selectivity for the extraction of Pb(II) vs. all other metals was observed when **3** was used alone with base, and without a bipy co-ligand (Figure 1), both Cu(II) and Zn(II) were extracted to a much greater extent than Pb(II), when bipy was present. We attribute this difference to strong Cu-bipy and Zn-bipy complexation, which is favored over Pb-sulfonamide-bipy complexation. On the other hand, in the absence of bipy, **3** overwhelmingly complexes Pb(II), even in a competitive experiment with 10- to 40-fold excess of competing metals, suggesting that sulfonamide **3** strongly favors the formation of the low-coordinate PbL 1:1 complex.

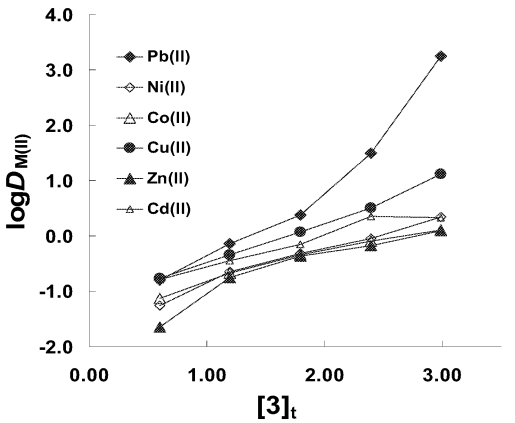

Figure 1. Plot of log $[M(II)]_t$ *vs.* $[\mathbf{3}]_t$ with 2.2 eq. of diidoproplylamine. $[Pb]_t$ = 2.72 mM, $[Ni]_t$ = 2.72 mM, $[Co]_t$ = 2.67 mM, $[Cu]_t$ = 2.80 mM, $[Zn]_t$ = 2.53 mM, amd $[Cd]_t$ = 2.59 mM. Errors in concentrations are estimated to be <5%.

CONCLUSIONS

Recent advances in Pb(II) selective extraction and sensing based on coordination by disulfonamides derived from *o*-phenylenediamine were presented. The presence of a

bipy co-ligand was shown to adversely affect selectivity against Cu(II) and Zn(II), presumably because of strong affinity of bipy for these metals. The bis-dansylated analog **3** showed sensing via fluorescence quenching in a 1,2-DCE solution of the ligand and diisopropylamine upon contact with aqueous $PbNO_3$. ESI-MS and distribution studies show the formation of 1:1 Pb-sulfonamide complexes, which have also been isolated and characterized. The X-ray structures of the complexes had previously shown hemidirected geometries with a stereochemically active lone pair. We are currently investigating other modified frameworks with potential for ratiometric sensing, and we are studying the coordination properties of these sulfonamides with other metals, as well as the potential of co-ligand influence in altering selectivity for extraction of Pb(II) vs. other metals.

ACKNOWLEDGMENTS

We thank Dr. Mahesh Pattabiraman, Dr. Weihua Zhang, and Mr. Michael T. Lago, for experimental help with synthesis and the ESI-MS characterization. This project was supported by NIH-NIEHS/SCORe (506GM008205-205L), NIH-MBRS/RISE (R25 GM061347, as support for JMR), and Florida International University.

REFERENCES

1. J. S. Lin-Fu, "Lead Poisoning, a Century of Discovery and Rediscovery," Human Lead Exposure, H. L. Needleman, Ed., Lewis Publishing, Boca Raton, FL 1992.
2. (a) R. D. Hancock, H. Maumela, and A. S. De Sousa, *Coord. Chem. Rev.*, **148**, 315-347, (1996). (b) A. T. Yordanov, and D. M. Roundhill, *Coord. Chem. Rev.,* **170**, 93-124, (1998), (c) G. G. Talanova, H.-S. Hwang, V. S. Talanov, and R. A. Bartsch, *Chem. Commun.,* 419-420, (1998).
3. (a) R. Métivier, I. Leray, and B. Valeur, *Chem. Eur. J.,* **10**, 4480-4490 (2004). (b) A. P. de Silva, D. B. Fox, A. J. M. Huxley, and T. S. Moody, *Coord. Chem. Rev.,* **205**, 41-57 (2000). (c) J. Liu and Y. Lu, *J. Am. Chem. Soc.,* **126,** 12298-12305 (2004). (d) M. Crego-Calama and D. N. Reinhoudt, *Adv. Materials,* **13,** 1171-1174 (2001).
4. B. A. Moyer, "Complexation and transport" Comprehensive Supramolecular Chemistry, Vol. 1, G. W. Gokel, Ed., Pergamon, Oxford, 1996; pp. 401-405.
5. E. S. Claudio, H. A Godwin, and J. S. Magyar, *Prog. Inorg. Chem.*, **51**, 1-144 (2003).
6. L. Shimoni-Livny, J. P. Glusker, and C. W. Bock, *Inorg. Chem.*, **37**, 1853-1867 (1998).
7. Y. Marcus, Ion properties, Marcel Dekker, New York, 1997.
8. K. Kavallieratos, J. M. Rosenberg, and J. C. Bryan, *Inorg. Chem.*, **44**, 2573-2575 (2005).
9. R. J. Alvarado, J. M. Rosenberg, A. Andreu, J. C. Bryan, W.-Z. Chen, T. Ren, and K. Kavallieratos, *Inorg. Chem.*, **44**, 7951-7959 (2005).
10. K. Kavallieratos, J. M. Rosenberg, W.-Z. Chen, and T. Ren, *J. Am. Chem. Soc.*, **127**, 6514-6515 (2005).
11. S. Deo and H. Godwin, *J. Am. Chem. Soc,* **122**, 174-175 (2000).
12. W. Zhang, Y. Cai, and K. Kavallieratos, *Rapid Commun. Mass Spectrom.*, **20**, 303-306 (2006).
13. W. Zhang, R. J. Alvarado, Y. Cai, and K. Kavallieratos, *Rapid Commun. Mass Spectrom.*, Submitted for publication.
14. R. J. Alvarado, J. M. Rosenberg, M. Pattabiraman, R. A. Middleton, M. J. Zaworotko, and K. Kavallieratos, Manuscript in preparation.

CELLULOSE TRIACETATE BASED NOVEL OPTICAL SENSOR FOR URANIUM ESTIMATION

J. M. Joshi,[1] P. N. Pathak,[2] A. K. Pandey,[2] and V. K. Manchanda[2]

[1]Chemical Engineering Division, [2]Radiochemistry Division, Bhabha Atomic Research Centre, Trombay, Mumbai - 400 085, India.
Corresponding author email address: vkm@barc.gov.in

ABSTRACT

A cellulose triacetate (CTA) based optode has been developed by immobilizing tricaprylmethyl ammonium chloride (Aliquat 336) as the extractant and 2-(5-bromo-2-pyridylazo)-5-diethylaminophenol (Br-PADAP) as the chromophore. The optode changes color (from yellow to magenta) due to uranium uptake in bicarbonate medium (~10^{-4} M) at pH 7-8 in the presence of triethanolamine (TEA) buffer. The detection limit of the optode film (dimension: 3 cm x 1 cm) was determined to be ~0.3 µg/mL for a 15 mL pure uranium sample at pH 7-8 (in TEA buffer). The effects of experimental parameters have been evaluated in terms of maximum uptake of U(VI), minimum response time, and reproducibility and stability of the Br-PADAP-U(VI) complex formed in the optode matrix. The applicability of the optimized optode has been examined in the effluent samples obtained during magnesium diuranate precipitation step following the TBP purification cycle.

INTRODUCTION

Various activities at the front end and back end of fuel cycle, for example, mining of uranium ore, purification, fuel fabrication, spent fuel reprocessing, and nuclear-waste management, generate environmental concerns with regard to possible water contamination by radionuclides, including uranium. Uranium is known to be nephrotoxic as a heavy metal and radiologically harmful as a radionuclide. The World Health Organization has assigned a tolerable limit of daily intake of uranium as 0.6 µg/kg of body weight/day [1]. Although radiological impact is determined by the total concentration of the decay products of ^{235,238}U, the chemical toxicity of uranium is dependent on the chemical form of its species that interacts with biomolecules [2]. Therefore, it is desirable to have an analytical method that can determine a specific U(VI) species present in the aqueous medium at trace level. In recent years, portable chemical sensors have been employed for monitoring the concentration of toxic metal ions. The chemical sensors respond to a particular analyte through a chemical recognition and can be used for the qualitative/quantitative determination of the analyte. These sensors offer good detection limits with wide range of linearity. Preconcentration is a key

step for sensitivity enhancement of the sensors. Membrane-based preconcentration methods can be tailor-made for a specific analytical application. By immobilizing a suitable chromophore, the analyte selective membrane can be converted to an optical chemical sensor (optode) that responds to an analyte in a concentration-dependent manner [3]. These optodes are based on the preconcentration of the analyte as a chromophoric species on a solid substrate and subsequent direct measurement of the absorbance/reflectance of the solid phase. The presence of an extractant in the membrane increases the selectivity and sensitivity of an optode as compared with the corresponding solution spectrophotometry using same chromophore [4-6]. The color-changeable optode for uranium and thorium have been reported using nonspecific Alizarin Red S and 4-(p-nitrophenylazo)-pyroctachol (NAP) [7,8], respectively. These optodes usually suffer from a drawback of possible interferences from other metal ions in actual applications.

This paper deals with the development of a cellulose triacetate based uranium selective sensor by physical inclusion of 2-(5-bromo-2-pyridylazo)-5-diethylaminophenol (Br-PADAP) as chromophore into cellulose triacetate (CTA) matrix plasticized by tris(2-ethylhexyl)phosphate (TEHP). The choice for Br-PADAP was based on its high sensitivity and selectivity for uranium estimation by spectrophotometry [9]. Tricaprylylmethyl ammonium chloride (Aliquat 336) was used as the carrier for transferring U(VI) anions from aqueous carbonate medium to the membrane matrix as an ion pair. The carrier in the optode is necessary, as immobilized Br-PADAP cannot interact with U(VI) present in the aqueous medium. The effects of experimental parameters such as pH, uranium concentration, interference of cations and anions on the determination of uranium are investigated. The stability of the optode has been investigated. The optode developed was tested on an alkaline waste sample generated during magnesium diuranate precipitation after TBP purification cycle.

EXPERIMENTAL

Br-PADAP, Aliquat-336, triethanolamine, cellulose triacetate (Sigma-Aldrich), TEHP (Koch-Light Laboratories, England), uranyl nitrate, and dichloromethane (Merck) were used as received. A standard stock solution of uranium (10^{-2} M) was prepared by dissolving suitable quantities of $UO_2(NO_3)_2 \cdot 6H_2O$ in distilled water. Working standard stock solutions of uranium were prepared by suitable dilution in the desired medium. Triethanolamine (TEA) buffer was prepared by dissolving a required amount in distilled water and neutralizing with perchloric acid (pH 7.8). The solution pH and absorbance measurements (of the membrane) were done using a microprocessor-based pH meter model PHAN (Lab India, Mumbai, India) and UV-vis spectrophotometer model V 53 from JASCO (Tokyo, Japan), respectively. The absorbance measurements were done by mounting the optode samples (3 cm x 1 cm) inside a quartz cuvette. Blank corrections were also done during these measurements. The membrane films were prepared by physical immobilization of Br-PADAP, TEHP, and Aliquat 336 in cellulose triacetate (CTA) matrix. After complete dissolution, the casting solution was prepared by mixing the components and homogenization by ultrasonication for 5-10 min. The casting solution was poured in a Petri dish to allow the slow evaporation of dichloromethane and the formation of the homogeneous transparent membrane (thickness: ~50 μm).

Uranium-uptake experiments were done by equilibrating the membrane strips (dimension: 3 cm x 1 cm) in sample solutions under desired experimental conditions containing 1 x 10^{-4} M CO_3^{2-} ions. The membrane strips were taken out of the sample solutions and washed with a jet of distilled water. The color of the optode strips changed from yellow to magenta depending on the uranium concentration in the sample solution. The change in absorbance of U(VI)-Br-PADAP complex was monitored at λ_{max} = 578 nm under different experimental conditions. The calibration plots for uranium uptake were obtained by the spectrophotometric analysis of sample solutions before and after equilibration with the optode.

RESULTS AND DISCUSSION

The membrane response used in the present work is dependent on the efficiency of the transfer of anionic uranyl-carbonato species, for example, $UO_2(CO_3)(HCO_3)^-$, $UO_2(CO_3)_2^{2-}$ or $UO_2(CO_3)_3^{4-}$, Aliquat 336 from the bulk solution to the de matrix followed by the interaction of Br-PADAP leading to color change (from yellow to magenta) of the film (Figure 1). The change in the absorbance is correlated with the uranium uptake by the membrane.

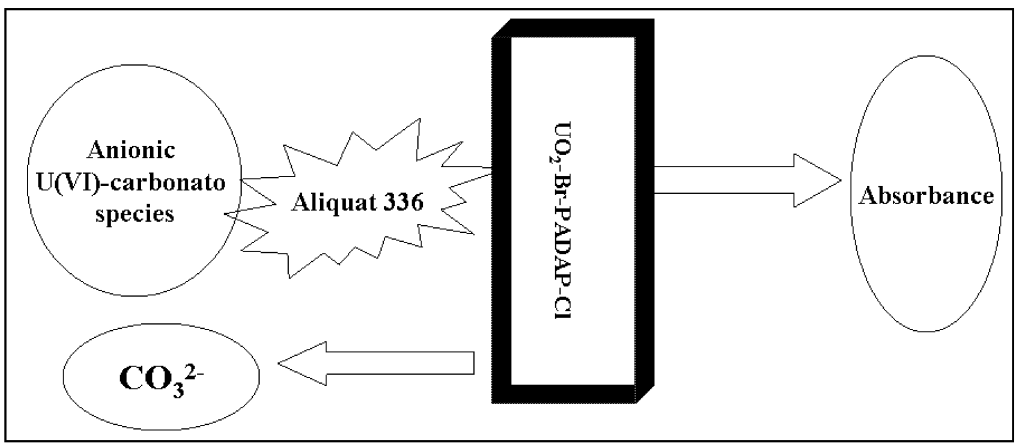

Figure 1: Probable mechanism for the uptake of uranium from carbonate medium to the optode film.

Extensive studies on the effects of the concentrations of different components led to the optimized membrane optode composition as 23 wt % CTA + 30 wt % Aliquat 336 + 46 wt % TEHP + 0.09 wt % Br-PADAP for uranium uptake studies with an equilibration time of 2-3 h in pH 7-8 (TEA buffer) containing 1 x 10^{-4} M bicarbonate/carbonate. The optode samples were found to be unstable in the sample solution containing uranium without buffer. Use of TEHP as plasticizer helps in relatively faster transfer of anionic U(VI) from the solution phase to the optode matrix. Under these conditions, ≥50% of uranium uptake was observed from the sample containing uranium in the concentration range of 5-30 ug in 15 mL solutions. Figure 2

shows the calibration plots for absorbance vs uranium concentration in the 15 mL equilibrating solutions with and without 2 M nitrate ion. The uptake experiments using membranes of varying area showed that the sensitivity of the membrane can further be improved by taking a smaller membrane size, wherein uranium can be concentrated on a smaller volume for absorbance measurements.

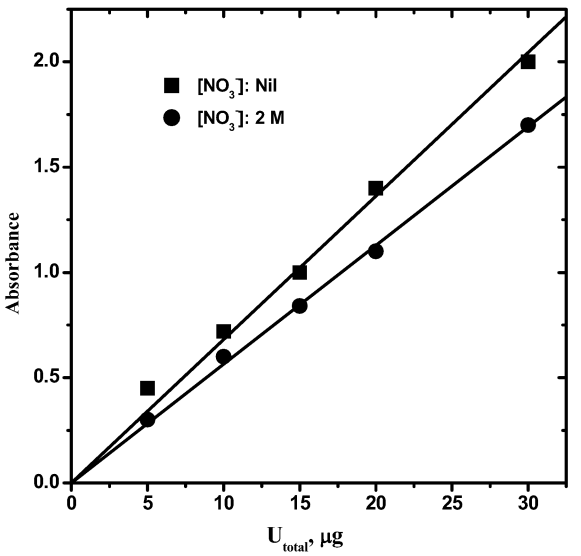

Figure 2: Calibration plot for the uptake of uranium.
$[CO3^{2-}] = 1 \times 10^{-4}$ M; pH = 7.8 (TEA buffer); 3 hrs duration.

The absorbance at 578 nm for the estimation of U(VI) ions in TEA medium recorded over a period of 24 h did not show any evidence of leakage of Br-PADAP in the sample solution. There was no drift in the absorbance signal when the film used for uranium uptake was exposed to light. No appreciable change in the optode absorbance value was observed when the film was dipped in deionized distilled water overnight. These observations suggest that the optode film was quite stable under the conditions of present studies. Excellent precision in the absorbance values (1.8 ± 0.1) of the membrane film (3 cm x 1 cm) equilibrated with six different sample solutions, each containing 8.7 µM U(VI) at pH = 7-8 (TEA buffer) in 15 mL solution for 3 h suggested the reproducibility of the membrane response under the conditions of the present study. It was interesting to note that a uranium-loaded optode sample could be regenerated after dipping the used membrane strip in 0.01 M HNO_3 for 10-15 minutes.

The selectivity of the optode was tested by equilibrating optode samples with solutions containing 8.7 µM U(VI) and 1 µM concentrations of different cations such as. Fe^{3+}, Nd^{3+}, and Th^{4+}, and anions such as. NO_3^-, F^-, Cl^-, and $C_2O_4^{2-}$, separately at pH 7-8 in TEA buffer along with 1 x 10^{-4} M bicarbonate/carbonate. In all cases except $C_2O_4^{2-}$, the absorbance variations in the optode due to the uptake of uranium were within ±10%, suggesting that these cations andanions in the micromolar concentrations can be tolerated

in the uranium sample solutions. In case of $C_2O_4^{2-}$, the absorbance was reduced significantly indicating that $C_2O_4^{2-}$ ions interfere in the sorption of U(VI) in the optode. This method offers sensitivity over the conventional spectrophotometric determination of uranium by Br-PADAP (optode, 0.3 μg/mL; spectrophotometry, 0.8 μg/mL), and regeneration of the optode helps in economy of chromophoric reagent.

This optode was used for uranium estimation in alkaline effluent sample in the presence of ~2 M nitrate concentration. A calibration plot was obtained under the sample conditions (Figure 2). To calculate the uptake of uranium, its concentration in the sample was determined by conventional Br-PADAP based spectrophotometric method. The uptake experiment was done under specified experimental conditions such as pH 7-8 (with TEA buffer) and 15 mL volume, using 0.5 mL of the effluent sample containing ~33 μg U. The optode film (3 cm x 1 cm) was taken out for the absorbance measurements after exposure for 3 h. The mean absorbance values (from five samples) were found to be 1.23 ± 0.1. The uranium uptake was only 40% by the optode in the presence of 2 M nitrate concentration. However, the response of the optode with the sample solution was highly reproducible, suggesting its possible application in process samples.

CONCLUSIONS

A CTA based optode has been developed for uranium preconcentration and its determination. The intensity of color in the optode sample was found to be dependent on the uranium uptake from the sample solution as well as the composition of the membrane. The composition of the optode was optimized as 23 wt % CTA + 30 wt % Aliquat-336 + 46 wt % TEHP + 0.1 wt % Br-PADAP, with an equilibration time of 3 h. The detection limit of the optode film (dimension: 3 cm x 1 cm) was determined to be ~0.3 μg/mL U(VI) for a 15 mL sample at pH 7-8 (in TEA buffer). The presence of micromolar concentrations of cations such as Fe^{3+}, Nd^{3+}, and Th^{4+}, and of anions such as NO_3^-, F^-, and Cl^- can be tolerated. The optode film is quite stable, regenerable, and reproducible under the conditions of the present studies. The membrane has been used for the estimation of uranium of alkaline waste solutions containing ~2 M nitrate ion.

REFERENCES

1. World Health Organization, WHO, Guidelines for Drinking Water Quality, 3rd ed., 2003.
2. D. C. Kocher, *Health Phys.,* **57**, 9 (1989).
3. E. Bakker, P. Bühlmann, and E. Pretsch, *Chem. Rev.,* **97,** 3083 (1997).
4. P. T. Varineau, R. Duesing, and L. E. Wangen, *Appl. Spectrosc.,* **45,** 165 (1991).
5. G. E. Collins, Q. Lu, S. Abubeker, and E. Vajs, *Appl. Spectrosc.*, **56,** 464 (2002).
6. G. E. Collins and Q. Lu, *Anal. Chim. Acta*, **436,** 181 (2001).
7. A. Safavi and M. Bagheri, *Anal. Chim. Acta*, **530** 55 (2005).
8. A. Safavi and M. Sadeghi, *Anal. Chim. Acta*, **567** 184 (2006).

LIQUID PHASE HEADSPACE MICROEXTRACTION INTO A SINGLE DROP OF WATER

A.Y. Nazarenko

Chemistry Department, SUNY College at Buffalo, 1300 Elmwood Ave, Buffalo, NY, 14222, USA. Corresponding author email address: nazareay@buffalostate.edu

ABSTRACT

The continuous search for better sample-preparation procedures has led to new methods, the main advantages of which are short processing time and negligible quantity of solvents used. Single-drop microextraction was employed to transfer hydrophobic analytes into a drop of organic solvent with further GC or HPLC determination. This paper suggests the use of ultrapure water as a solvent for headspace microextraction of various hydrophilic analytes. The surface area of a liquid drop is visibly larger than that of an SPME fiber, resulting in a relatively fast extraction process. Because a new drop is employed for each consecutive extraction, no memory effects are observed. This approach was first tested with GC-FID determination of volatile analytes: FID is a natural choice for detector showing zero blank signals for a pure solvent. Headspace liquid-phase microextraction provides a simple, low-cost alternative method for the analysis of volatile compounds. It is amenable to future developments with various other detection methods. The use of water, a 100% "green" solvent, is an attractive approach for the extraction of hydrophilic analytes.

INTRODUCTION

Sample preparation is a necessary part of most analytical procedures. The continuous search for better sample preparation procedures has led to new methods whose main advantages are short processing time and negligible volume of solvents used. Indeed, in many common analytical methods the quantity of the sample is very small. In gas chromatography (GC), this volume is around 1-3 μL while in HPLC and graphite furnace AAS it is usually around 5-20 μL. Therefore, the traditional sample-preparation procedures resulting in volumes of several milliliters may lead to unnecessary dilution of the analyte and waste of time and reagents.

Among the microextraction procedures developed in recent years, the most known and efficient is solid-phase microextraction (SPME) [1]. The liquid-phase analogue (liquid-phase microextraction, LPME) has been also developed. Most of LPME designs included liquid-liquid extraction from the bulk aqueous phase into a small volume of organic solvent immiscible with water [2,3]. SDME (single-drop

microextraction) was employed to transfer hydrophobic analytes into an organic solvent drop with further GC, CE, or HPLC determination [4].

For many complex samples, headspace extraction is the fastest and cleanest method for analyzing volatile components in dirty matrixes [5,6]. The possibility of applying headspace microextraction into a single drop of ethylene glycol was demonstrated [7]. Another design, in which extraction occurs inside the syringe, was suggested for chlorobenzenes [8]. Recent developments in headspace extraction are reviewed in [9].

The FID detector is insensitive to nonhydrocarbons such as water and carbon disulfide. Therefore, they are attractive solvents for microextraction (no blank signal!). In this publication, we suggest the use of ultra-pure water as a solvent for headspace microextraction of hydrophilic volatiles. A long-standing tradition [10] of using small volumes of water as a medium for analytical separation of volatile analytes serves as an encouragement.

EXPERIMENTAL

An HP5890 gas chromatograph (Agilent Technologies Inc.) with FID detectors and nitrogen as a carrier gas was used throughout this work. Various types of capillary and packed columns were tested.

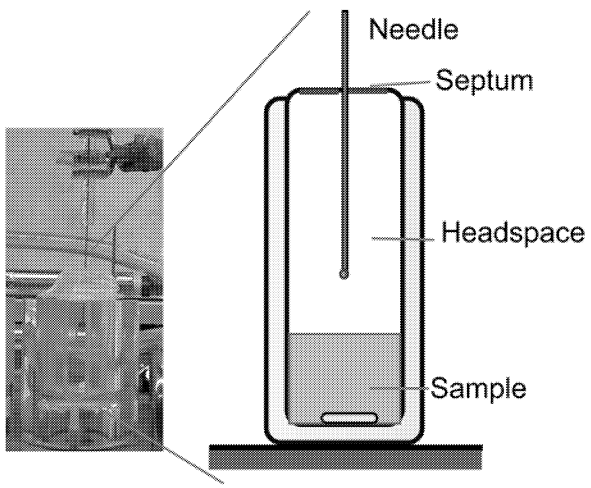

Figure 1. A simple device for headspace LPME. Stirring and thermostating are optional.

A sample (usually 5-10 mL) was placed into a 25 mL vial covered with a membrane (Figure 1). A needle of GC syringe containing water was introduced into the vial; the plunger was gently pushed to create a 1 μL drop (Figure 2). Volatile compounds evaporate from the sample into headspace and are extracted from the headspace into a drop of water. After 2-3 min, the drop is retracted back into the needle and then injected into the GC instrument for further separation and determination. Adjusting the temperature and mixing improve the transfer of volatile analytes from the sample into the

headspace of the vial. For volatile amines, addition of NaOH or Na_2CO_3 to the source phase can be helpful. An analogous approach will be necessary for extraction of volatile acids. Same volume is enough to record an FTIR spectrum using Golden Gate Diamond ATR Unit (Specac Inc.) or to record an UV-visible spectrum using a SpectroPipetter for microliter-volume samples (OceanOptics Inc.).

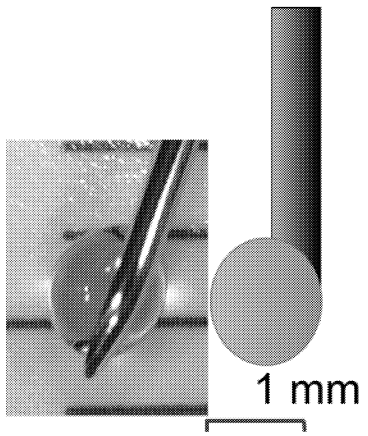

Figure 2. A 1 μL water drop at the end of a syringe needle.

RESULTS AND DISCUSSION

The natural limitation of headspace LPME is the quick evaporation of small amounts of volatile liquids. Simple tests show that even in open air the 1 μL water drop is stable for more than 7 min at 25 °C. Inside the vial with an aqueous sample, no change in drop volume was visible after 20 min. Therefore, 2-3 min extraction does not affect the water drop. Because of faster evaporation of volatile solvents, larger drop volumes and strict time control may be suggested for non-aqueous extraction. Presaturation of headspace volume with a small calculated amount of extractant solvent is another possible solution. The necessary amount for water is around 10-30 μg/mL at usual laboratory temperatures. Because of short extraction times, the experimental conditions in our case never reached equilibrium.

The surface area of a liquid drop is visibly larger than that of SPME fiber (Table 1), resulting in a relatively fast extraction process. Because a new drop is employed for each consecutive extraction, no memory effects are observed. Extraction properties of water in air/water extraction system were systematically studied [6]. While partition coefficients of ethanol and dioxane are above 1000, hydrocarbons like hexane and cyclohexane show low values (around 0.1) resulting in significant separation of hydrophobic and hydrophilic analytes.

Table 1. Surface area of liquid drops in mm^2 and SPME fiber (diameter 0.1 mm)

1 μL liquid drop	3 μL liquid drop	1 cm long SPME fiber
5	10	3

As an example, results of alcohol determination in an aqueous sample are presented in Figure 3 (0.08% of each alcohol in water). Propanol or *tert*-butanol was employed as an internal standard. Separate peaks for all propanols, butanols, and pentanols were easily achieved. Determination of 0.16 mg/mL ethanol showed relative standard deviation of 10%, which is similar to most SPME procedures. Little extraction of hydrophobic hydrocarbons was detected in appropriate tests; this observation allows suggesting extraction by water drop as a possible GC method for determination of alcohol admixture in hydrocarbon matrix.

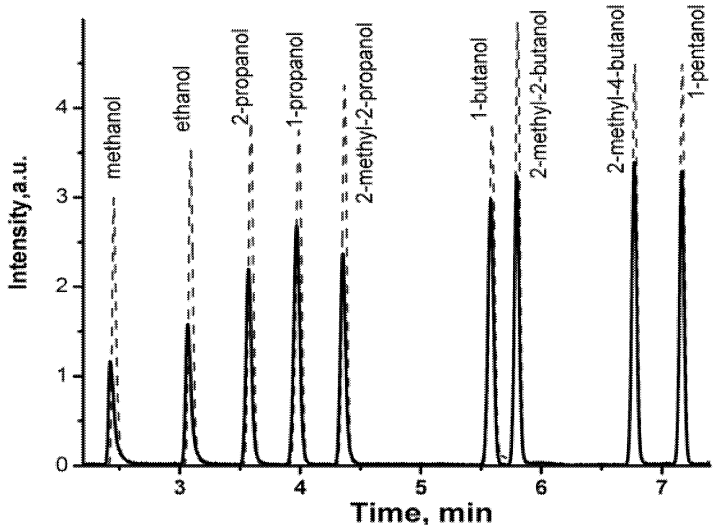

Figure 3. Chromatograms of alcohols: source (dash) and receiving (solid line) aqueous samples. Because of short extraction time (1 min), equilibrium is not reached, and concentrations in a drop are visibly smaller. Nevertheless, it does not affect the results if an internal standard is used.

It was demonstrated [11] that injecting water would not harm the stationary phase of most capillary columns. Many of the problems often associated with water injections are caused by other phenomena, such as backflash. Of the commonly used solvents, water has by far the largest vapor expansion volume. To minimize these problems, it is important to use liners with large volumes, lower the injector temperature, and maintain a high column head pressure and carrier-gas flow rate.

Possible applications of microextraction into a water droplet are not limited to gas chromatography. Acidic aqueous solutions are natural sorbents for volatile bases that can be identified by their spectra (as an example, see Figure 4). Appropriate spectrophotometric procedures are available for UV-vis determination of primary amines in a microvolume. Various aqueous solutions which were sucssesfully employed for

selective sorption of volatile organic compounds in macroscale [5] are also suitable for selective microextraction.

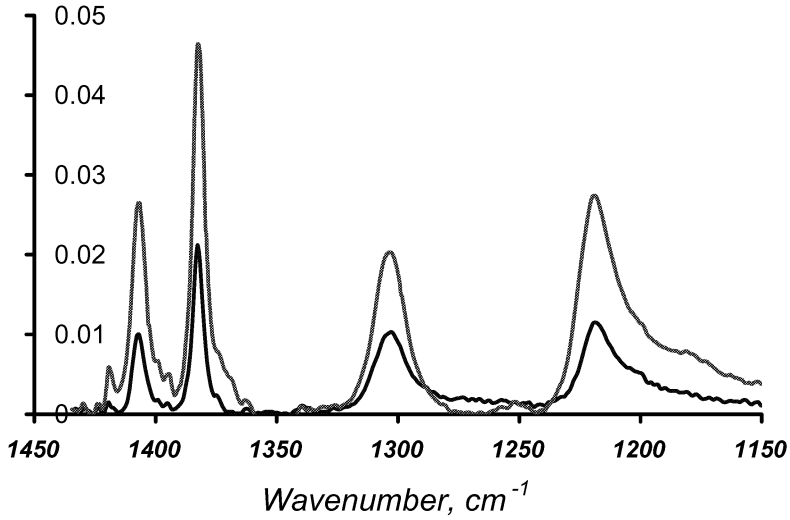

Figure 4. Identification of *tert*-butylamine after preconcentration from a 20 mL aqueous sample into a droplet of 0.5 M HCl. FTIR-ATR (Thermo-Nicolet Nexus 470) spectra using diamond as an ATR crystal. Spectrum of higher intensity belongs to the standard solution.

CONCLUSIONS

Headspace liquid phase microextraction provides a simple, low-cost alternative method for analysis of volatile compounds. We envision it as a great field for future developments with methods other than GC/FID. The use of water, a 100% "green" solvent, is an attractive approach for the extraction of hydrophilic volatiles.

REFERENCES

1. J. Pawliszyn, Sample and sample preparation in field and laboratory, Elsevier, New York, 2002.
2. E. Psillakis, and N. Kalogerakis, "Developments in a single-drop microextraction," *Tr. Anal. Chem.,* **21**(1), 53-63 (2002).
3. M. A. Jeannot, and F. F. Cantwell, "Solvent Microextraction into a Single Drop," *Anal. Chem.,* **68**(13), 2236-2240 (1996).
4. M. C. Lopez-Blanco, S. Blanco-Cid, B. Cancho-Grande, and J. Simal-Gandara, "Application of single-drop microextraction and comparison with solid-phase microextraction and solid-phase extraction for the determination of α– and β- endosulfan in water samples," *J. Chromatography A*, **984**, 245-252 (2003).
5. B. V. Joffe and A. G. Vitenberg, Head-Space Analysis and Related Methods in Gas Chromatography, Wiley, New York, 1986.

6. B. Kolb and L. S. Ettre, Static Headspace-Gas Chromatography, Wiley, New York, 1997.
7. A. Tankevichuite, R. Kazlauskas, and V. Vickakaite, "Headspace extraction of alcohols into a single drop," *Analyst*, **126**, 1674-1677 (2001).
8. G. Chen and H. K. Lee, "Headspace Liquid-Phase Microextraction of Chlorobenzenes in Soil with Gas Chromatography – Electron Capture Detection," *Anal. Chem.,* **75**(1), 98-103 (2003).
9. D. A. Lambropoulou and T. A. Albanis, "Recent developments in headspace microextraction techniques for the analysis of environmental contaminants in different matrices," *J.Chromatography A,* **1152**(1-2), 70-96 (2007).
10. E. J. Conway, Microdiffusion Analysis and Volumetric Error, 5th Ed., Crosby Lockwood, London, 1958.
11. E. Kuhn, "Water Injection in Gas Chromatography. A Guide to Better Results when Analyzing Aqueous Samples," *Separation Times,* **14**(1),10-11(2001) and **14**(2), 5-7 (2001) (http://www.agilent.com/chem).

INTENSIFICATION OF LIQUID-LIQUID REACTION AND SEPARATION PROCESSES WITH MINIATURIZATION

G. S. Luo, J. H. Xu, S. W. Li, K. Wang, and J. Tan

The State Key Lab of Chemical Engineering, Department of Chemical Engineering, Tsinghua University, Beijing 100084, China
Corresponding author email address: gsluo@tsinghua.edu.cn

ABSTRACT

The microstructured chemical system has been identified as one of the main tools for the development of advanced sustainable chemical technologies. The use of microfluidics offers a number of advantages over conventional flow-control technology. Recently, attention has been paid to immiscible liquid–liquid systems at the microscale with a focus on intensification of mass transfer and reactions by dispersing one phase into the other as micrometers sized droplets or slugs. Novel micromixers have been developed using the microchannel or microfiltration membrane dispersion method in our research group. The results showed that, in microscale dispersion extraction processes, the mass-transfer efficiency could be as much as 100% and the residence time less than 0.5 s. Droplet-based microfluidic systems have been also applied for liquid-liquid micro-extraction, nanoparticle synthesis, and rapid reaction processes. Some critical developments and new applications will be reviewed in the present work. In addition, the interfacial mass-transfer and reaction performance of liquid–liquid dispersed systems by using droplet flow in microfluidic devices will be briefly described.

INTRODUCTION

It is well known that how successful chemists and engineers are in bringing starting materials and products to the right place at the right time, and controlling the heat and mass transfer is becoming the key point for the development of sustainable chemical industry. The microstructured chemical system has been identified as one of the main tools for the development of advanced sustainable chemical technologies, because it provides a lot of advantages over conventional chemical-engineering processing, such as high volumetric surface area, short diffusion distance, fast mixing and transfer properties, easy control, short and uniform residence time, and inherent safety [1-3]. The development of microchannel devices for heat-exchange applications began in the late 1960s. Microreactor applications in chemical processing emerged in the early 1990s [1]. Since then, many research groups began their work in this highly promising field. We may say that the microstructured chemical system is still in its infancy stage, but its development is very fast. The development of the microstructured system has been well

explained by several reviews [1-3]. Our group began to develop microstructured devices in the 1990s. We focused on the study of their transfer and reaction properties. Their applications in separation, chemical reaction, and nanoparticle preparation have been paid great attention. This paper will review the development of our research work in the field of microstructured chemical systems. New microdevices, multiphase microflow patterns, and properties of mass transfer and chemical reaction will be introduced. Especially the new applications in liquid-liquid extraction and reaction, as well as the controllable preparation of nanoparticles will be presented [4-12].

MICRODEVICES AND TWO-PHASE MICROFLOW PATTERNS

The microstructured chemical system is defined as the system that has microstructures for separation and chemical reaction. It is not required its total size be on the micrometer scale. The essential feature is the microstructures, which are implemented in separators and reactors. Typical dimensions of microstructures are in the range of 10-1000 μm. The microstructures can be microchannel, microsieve, or microfiltration membrane. With these microstrucutres we have developed several microdevices for reaction and separation, such as membrane dispersion extractor [4,6], membrane dispersion mini-reactor [5], capillary embedded microchannel device [7-10], and other microchannel devices with special structures. The membrane dispersion devices usually apply microfiltration membranes as the dispersion medium. The characteristic scale is around several micrometers. The characteristic scale of microchannel devices is normally in several hundred micrometers. With these microdevices, we can easily control the two-phase flow patterns and the dispersed-phase size.

With the microchannel devices, we can control the two-phase flow patterns in a simple way. As shown in Figure 1, the flow patterns can be distinguished by capillary number, *Ca*, and two-phase flow rates [7-9].

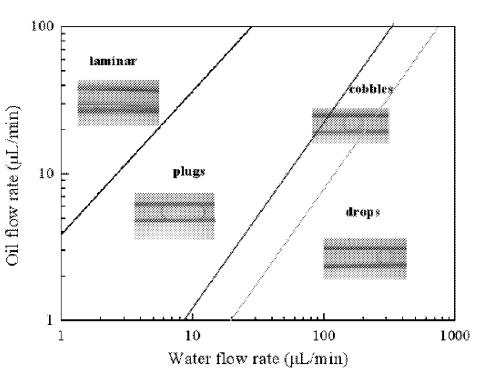

(a) Liquid-liquid systems [7].

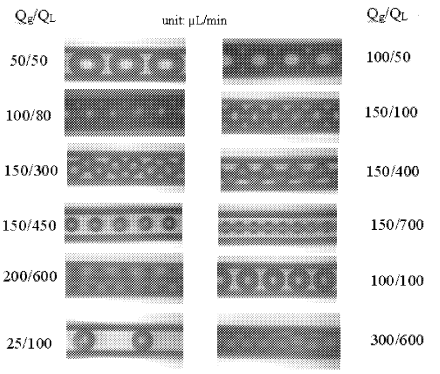

(b) Gas-liquid systems [8].

Figure 1. Two-phase microflow patterns.

We have developed a dynamic surface-modification method to change the wetting ability of the channel surface with different surfactants. In the same

microchannel devices, we prepared O/W or W/O emulsions successfully [10]. By changing the two-phase flow conditions and microchannel structures, we could realize the control of dispersed-phase size (droplet or slug size). The forces acting on the two-phase microflow systems were analyzed, and a general model has been developed to predict the size of the dispersed phase. The model is in the form of $l/w - \varepsilon = k(Q_d/Q_c)^{\alpha}(1/Ca)^{\beta}$; herein α, β, ε, and k are parameters, l is the size of dispersed phase, w is the channel size, Q_c and Q_d represent the flow rate of the two phases, and Ca is capillary number. With this model, the drop size or slug size can be well predicted.

We have studied the microflow conditions in the membrane dispersion devices, and it was found that in this kind of mcirostructured device only drops flow occurs. The droplet size was greatly influenced by the shear force of the continuous phase, and a mathematical model has been developed, too. Figure 2 shows the mixing conditions for liquid-liquid systems; the droplet size is around 10 times larger than the membrane pore size [5].

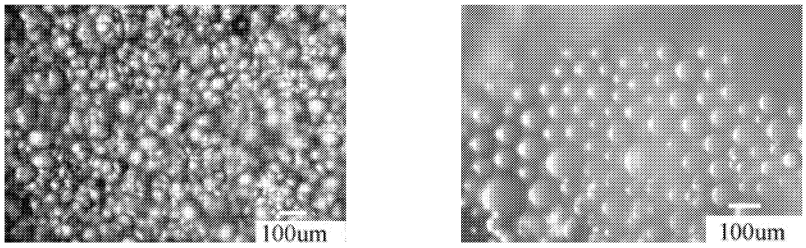

(a) With water as the continuous phase and *n*-butanol as the dispersed phase;
(b) With water as the continuous phase and *n*-hexyl alcohol as the dispersed phase.

Figure 2. Droplet photos in the microstructured reactor [5].

TRANSFER AND REACTION PERFORMANCES OF MICRODEVICES

We have investigated the interfacial mass-transfer and reaction performance of liquid–liquid dispersed systems by using droplet flow in microfluidic devices, as shown in Figure 3. The effects of two-phase flow rates and two-phase concentrations on droplet size and mass transfer have been studied. The mass-transfer rate was compared with that of conventional extraction processes, and the mass-transfer mechanisms were discussed. A simple acid-base reaction was used as the basis of this study because, being extremely rapid, its progress is controlled by the diffusion of the reactants within the two phases. The comparison of results is listed in Table 1. It can be found that the mass-transfer coefficients are much greater than the values in conventional columns, because the formation time of the droplet is relatively longer and the slip velocity is high at this stage, which results in internal circular flow and high mass-transfer coefficients. The mass transfer during the droplet formation stage contributed at least 30% of the total mass transfer.

We have studied the performance of membrane dispersion devices. The results showed that the membrane dispersion extractor has the advantages of easy fabrication,

high efficiency, low energy cost, and fast phase separation [6]. The mass-transfer performance of the new extractor was evaluated with six working systems. Figure 4 shows the effect of the total volume flow rate (u) on extraction efficiency (E) with a phase ratio of 1:1. The efficiency increased rapidly with an increase in the flow rate. The efficiency was close to 1 at flow rates about 300 mL/min. The residence times were less than 0.2 s. Despite the extremely short resident time, nearly 100% extraction efficiency was reached. Our experimental results proved that the novel mini-extractor has the advantages of high mass-transfer performance, fast phase-separation rate, and large capacity.

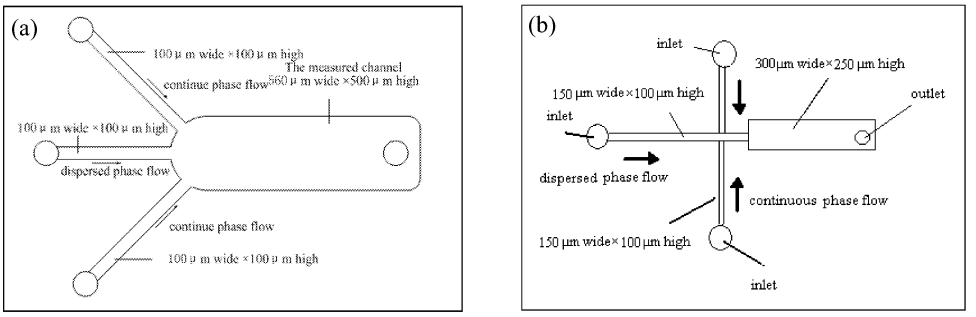

(a) Co-flowing device (b) Flow focusing device

Figure 3. The microfluidic devices.

Table 1. Comparison of $K_c \cdot (a)$ and average droplet diameter between droplet flow in micro-scale and conventional extraction processes

Mass-transfer process	d_{av} (mm)	$K_c(a)$(s^{-1})
Droplet flow in co-flowing microchannels	0.35 — 0.55	0.02 — 0.1
Droplet flow in flow-focusing microchannels	0.13 — 0.25	0.23 — 0.5
Conventional extraction columns	2.0 — 3.0	10^{-4} — 10^{-3}

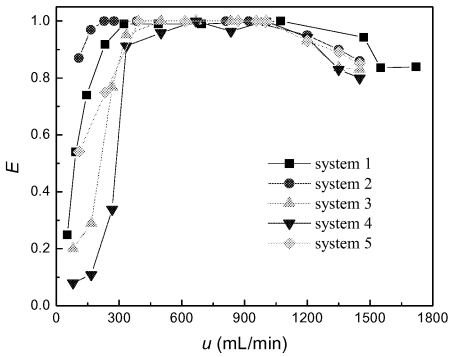

Figure 4. Effect of flow rate on efficiency [6].

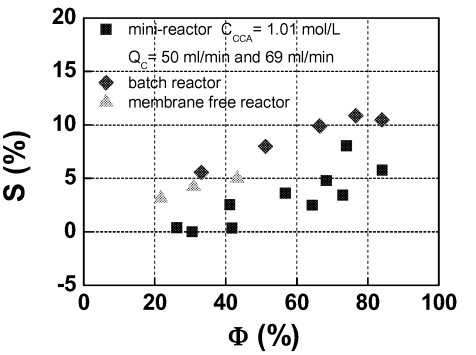

Figure 5. Selectivity in different reactors [11].

Fast mass-transfer rate and short reaction time are required to reduce side-product formation in the premixing reaction, SNIA Viscosa process, as a liquid-liquid competitive consecutive system. In order to obtain high selectivity, the microstructure device of the membrane dispersion mini-reactor was designed and tested at several operating conditions. The mass-transfer rate of cyclohexanecarboxylic acid (CCA) was significantly increased by membrane dispersion in this mini-reactor compared with a traditional batch reactor and a membrane-free one, just with a residence time less than 80 ms. The results showed that the nominal yield of side products was lower than 10 percent and about 5 percent lower than the traditional stirring method. Figure 5 shows the comparison of the microreactor with the conventional batch reactor.

NANOPARTICLE PREPARATION WITH THE MICRODEVICES

In our research work, a T-junction microchannel device was used to produce liquid-liquid drop flow and plug flow with different sizes. $BaSO_4$ nanoparticles were produced by the interphase reaction. The influence of mass transfer and chemical reaction on two-phase flow patterns in the T-junction microchannel device was investigated. Well-controlled two-liquid phase flows in a T-junction microchannel device have been realized, and $BaSO_4$ nanoparticles with narrow size and good dispersibility were produced through drop or plug flows in the microdevice. It was found that an increase of the amount of mass transfer and chemical reaction could change the flow patterns from plugs flow to drops flow. The drop diameter or plug length could be changed in a wide range. The prepared nanoparticles ranged from 10 nm to 40 nm.

In our group, the microstructured device of a membrane dispersion reactor has been successfully applied in controllable preparation of $BaSO_4$, anatase-TiO_2, and $CaHPO_4$ nanoparticles [5]. In this reactor, a microfiltration membrane with pore size of several micrometers was taken as the dispersed medium. One phase was divided into numerous substreams of micrometer size to mix with the main stream when it passed through the microfiltration membrane. It was found that the mixing scale could be easily controlled by varying the membrane pore size and flow rate of the reagent solutions in the microstructured reactor [12]. The particle size and its distribution are greatly influenced by the mixing scale. And the particle size can be controlled in the range from 20 nm to 150 nm.

Not only for the liquid/liquid systems but also for the gas/liquid systems, the membrane dispersion reactor has been applied in the preparation of $CaCO_3$ nanoparticles. A plant microreactor that has a throughput of 10,000 ton per year has been successfully built up. $CaCO_3$ nanoparticles with average diameters from 35 nm to 110 nm were controllably produced in the industrial reactor, and the whole research process from beginning of the lab experiments to the end of the industrial experiment took only 8 months.

CONCLUSIONS

Our results have clearly shown that mass transfer and chemical reaction can be greatly enhanced with the miniaturization of separators or reactors. Because of the high

efficiency and very good mixing conditions, the microstructured system can be applied to the controllable preparation of nanoparticles. Just as we mentioned above, the development of microstructured systems is still in its infancy stage, and it requires multidisciplinary interaction. To develop new microdevices, to disclose the fundamental knowledge, to simulate and model the new processes, as well as to find new applications will attract more researchers to this highly promising field.

ACKNOWLEDGMENT

We gratefully acknowledge the supports of the National Natural Science Foundation of China (20476050, 20490200, 20525622) and National Basic Research Program of China (2007CB714302) on this work.

REFERENCES

1. W. Ehrfeld, V. Hessel, and H. Lowe, Microreactors, Wiley-VCH, Weinheim, 2000.
2. O. Geschke, H. Klank, and P. Tellemann, Microsystem Engineering of Lab-on-a-Chip Devices, Wiley-VCH, Weinheim, 2004.
3. A. Gunther and K. F. Jensen, "Multiphase microfluidics: from flow characteristics to chemical and materials synthesis," *Lab on a Chip,* **6**, 1487-1503 (2006).
4. G. G. Chen, G. S. Luo, Y. Sun, et al., "A Ceramic Microfiltration Tube Membrane Dispersion Extractor," *AIChE J.*, **50**(2), 382-387 (2004).
5. G. G. Chen, G. S. Luo, J. H. Xu, and J. D. Wang, "Membrane dispersion precipitation method to prepare nanopartials," *Powder Technol.,* **139**, 180–185(2004).
6. J. H. Xu, G. S. Luo, G. G. Chen, et al., "Mass transfer performance and two-phase flow characteristic in membrane dispersion mini-extractor," *J. Membr. Sci.*, **249**(1-2), 75-81 (2005).
7. J. H. Xu, G. S. Luo, S. W. Li, et al., "Shear force induced monodisperse droplet formation in a microfluidic device by controlling wetting properties," *Lab Chip,* **6**(1), 131-136 (2006).
8. J. H. Xu, S. W. Li, Y. J. Wang, and G. S. Luo, "Controllable gas-liquid phase flow patterns and monodisperse microbubbles in a microfluidic T-junction device," *Appl. Phys. Lett.*, **88**(13), No. 133506 (2006).
9. J. H. Xu, S. W. Li, G. G. Chen, and G. S. Luo, "Formation of monodisperse microbubbles in a microfluidic device," *AICHE J.*, **52**(6), 2254-2259 (2006).
10. J. H. Xu, S. W. Li, J. Tan, et al., "Controllable preparation of monodisperse O/W and W/O emulsions in the same microfluidic device," *Langmuir*, **22**, 7943-7946 (2006).
11. K. Wang, Y. C. Lu, J. H. Xu, et al., "Reducing side product by enhancing mass transfer rate," *AIChE J.*, **52**(12), 4207-4213 (2006).
12. S. W. Li, J .H. Xu, Y. J. Wang, and G. S. Luo, "Mesomixing scale controlling and its effect on micromixing performance," *Chem. Eng. Sci.,* **62**(13), 3620-3626 (2007).

THE INTENSIFICATION OF MASS TRANSFER PERFORMANCE OF LIQUID-LIQUID DISPERSED SYSTEM IN MICROCHANNELS

J. H. Xu, J. Tan, S. W. Li, and G. S. Luo

The State Key Lab of Chemical Engineering, Department of Chemical Engineering, Tsinghua University, Beijing 100084, China.
Corresponding author email address: gsluo@tsinghua.edu.cn

ABSTRACT

Two multiphase flow microfluidic devices based on the use of droplet flow to enhance the mass-transfer performance have been specially developed. Mass-transfer performance data has been obtained by monitoring the extraction of succinic acid from *n*-butanol to aqueous drops containing NaOH. Monodisperse aqueous droplets with average diameters of 130–550 μm were generated, and the mass-transfer time was 0.4 - 4.0 s accordingly. The mass-transfer rate was 10–1000 times higher comparing to the traditional liquid-liquid systems. Vortex flow patterns within the droplet were generated during droplet-forming stage, which enhanced the mass-transfer rate greatly. The mass transfer during droplet formation stage contributed at least 30% of the total mass transfer quantities from the theoretical analysis.

INTRODUCTION

The use of microfluidics offers a number of advantages over conventional flow-control technology [1-3]. High surface-to-volume ratio and small volume expedite the chemical reaction in microfluidic devices and improve the product yield. A high-efficiency way for two-phase immiscible systems micromixing is by segmentation of the fluids in microchannels or capillaries. Vortex flow patterns generated by the shearing motion within fluid segments enhances mixing within segments and improves mass transfer across the interface [4-6]. Micro-segments can be applied in modular synthetic chemistry, quantitative chemical analyses, and synthesis of colloidal nanoparticles.

Recently, attention has been paid to immiscible liquid–liquid systems at microscale with a focus on intensification of mass transfer and reactions by dispersing one phase into the other as micrometer-sized droplets. Dispersed flow in which droplets are smaller than the channel diameter offers potentially further improvement in mass transfer. The time to equilibrium scales with the diffusive path length squared. Therefore, if a droplet of radius 300 μm is created, the time to equilibrium would be expected to decrease about 100-fold compared to a 3 mm droplet. Novel micromixers have been developed using the microchannel dispersion method by Benz and Pennemann et al. [7-8]. They found that as much as 95% efficiency could be reached in a short time with the droplet diameters from 20 to 150 μm in a liquid-liquid extraction process. In the same

period, our research group developed another kind of microstructured mixer based on membrane emulsification technology [9-11]. The results showed that in microscale dispersion extraction processes the mass-transfer efficiency could be as much as 100%, and the resident time was less than 0.5 s. Droplet-based microfluidic systems hava been also applied for liquid-liquid micro-extraction, nanoparticle synthesis, rapid reaction processes, and so on.

In the present work, we attempt to investigate the interfacial mass transfer and reaction performance of liquid–liquid dispersed system by using droplet flow in microfluidic devices. The effects of two phase flow rates on droplet size and the mass-transfer process have been studied. And the mass-transfer rate was compared with that of conventional extraction processes. Finally, the mass-transfer mechanisms were discussed.

EXPERIMENTAL SECTION

The experiments were performed in two types of microfluidic devices fabricated on 100 mm × 20 mm × 5 mm polymethyl methacrylate (PMMA) plates using an end mill. The dimensions of the channels are showed in Figure 1. Two microsyringe pumps and three gastight microsyringes were used to pump the two phases into the microfluidic devices respectively.

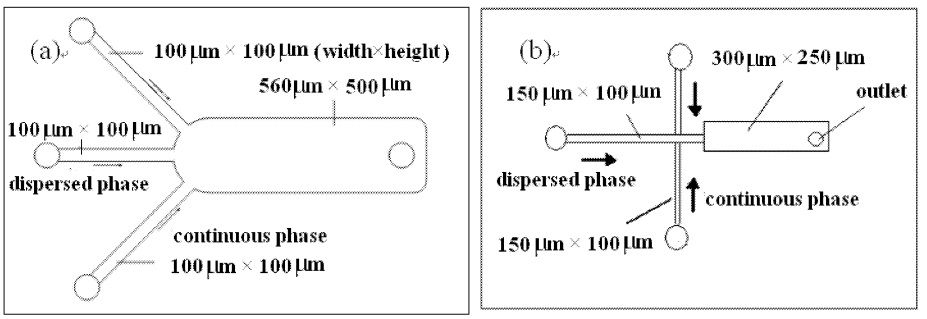

Figure 1. The microfluidic devices. (a) Co-flowing device (b) Flow-focusing device.

A simple acid-base reaction was used as the basis of this study. Methyl phenol red pH indicator was added to distilled water to create a saturated system, which was filtered and then diluted to by a factor of two with more distilled water. This was then used to produce aqueous solutions of NaOH in the range from 0.1 to 0.3 mol L^{-1}. *n*-Butanol was used as the organic phase. Succinic acid was added into *n*-butanol to produce organic solutions of 0.138 and 0.23 mol L^{-1}. The reaction is assumed to take place solely in the aqueous phase as succinic acid diffuses across the interface. The reaction involved in this work is given in the following equation. This requires a half mole of succinic acid per mole NaOH.

$$HOOC(CH_2)_2COOH + 2\ NaOH \rightarrow NaOOC(CH_2)_2COONa + 2H_2O \quad (1)$$

Experiments were carried out with a microscope at the magnification of 100×. A high-speed CCD video camera was connected to the microscope, and the images were recorded with a frequency of 200 images per second. The diameter of aqueous drops generated was measured from microscope images. The droplet sizes and distances

required to achieve a complete color change within the aqueous droplet for all the experiments were recorded and analyzed. Then the average droplets diameters (d_{av}), time requirements for droplet formation (t_F), and time requirements for acid transfer during moving stage (t_m) could be obtained in different experimental conditions. And the color change time could be calculated as the sum of t_F and t_m.

RESULTS AND DISCUSSION

Typical Micrographs During Mass-Transfer Processes

Figure 2 shows the typical micrographs of color change within the droplet during droplet forming stage at the cross-junction and moving in the measured channel separately. Vortex flow patterns within the aqueous droplet could be observed during droplet forming stage from Figure 2a. The vortex was mainly generated by the shearing motion of the continuous phase, and it enhanced mixing within the droplet. While during droplet moving stage, there was no relative-moving between two phases because of the co-flowing of continuous organic phase and aqueous phase. And the mass transfer process could be treated as the mass transfer of succinic acid at the interface of stagnant droplet in the quiescent continuous phase.

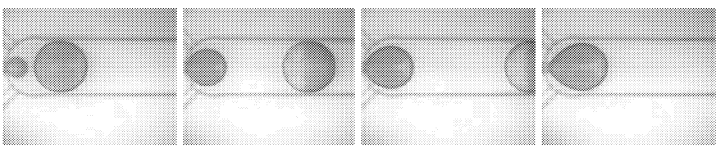

(a) droplet forming stage

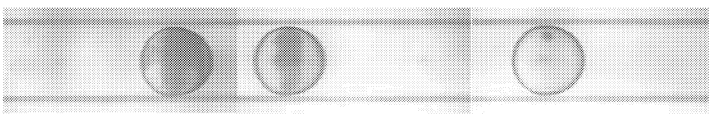

(b) droplet moving stage

Figure 2. Typical micrographs of color change within the droplet during mass-transfer processes.

Effects of Two-Phase Flow Rates on Droplet Size and Time Required for Acid Transfer

We investigated the influences of two-phase flow velocities on the droplet size and mass-transfer time. Figure 3 shows the effects of total flow velocity on the calculated average droplet diameter and color change time at three fixed flow ratios of the two phases in the co-flowing device. The average droplet diameter was observed to decrease with the increase of total flow velocity, while it increased with the increase of the phase ratio (Q_w/Q_o). These results were similar to that of without mass transfer. On the other hand, the color-change time decreased as total flow velocity was increased, while it increased with the increase of the phase ratio (Q_w/Q_o). The results can be explained by the differences in droplet size, which affected the mass-transfer rate. It also can be seen

that the color-change time decreased from 3.0 s to 2.0 s with the average droplet diameter from 550 μm to 380 μm.

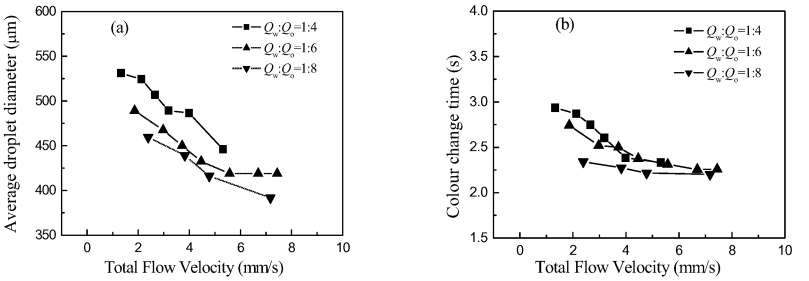

Figure 3. Effects of two-phase flow velocities on the average droplet diameter and color-change time in the co-flowing device. C_{NaOH} = 0.1 mol/L, C_{acid} = 0.138 mol/L.

Figure 4 shows the effects of total flow velocity on the average droplet diameter and color change time in the flow-focusing device. It can be seen that color change time decreased from 0.8 s to 0.4 s with the average droplet diameter from 200 μm to 130 μm. And the mass-transfer rate increased about 10 times by reducing the droplet size from 550μm to 130 μm.

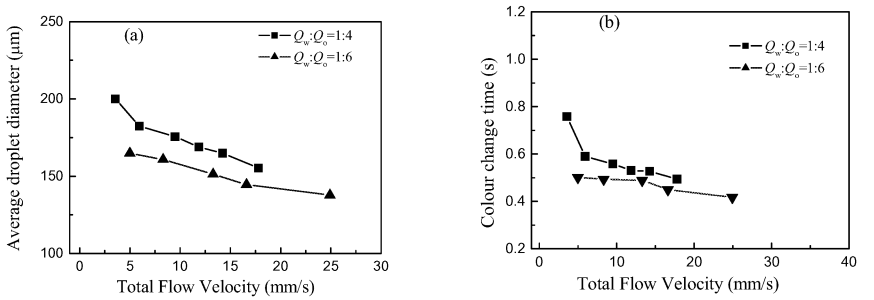

Figure 4. Effects of two-phase flow velocities on the average droplet diameter and color-change time in the flow-focusing device. C_{NaOH} = 0.1 mol/L, C_{acid} = 0.138 mol/L.

Enhancement of Mass Transfer Process

A more formal comparison of the mass transfer performance of the droplet flow in microscale with other systems may be achieved through an estimation of the volumetric mass transfer coefficient. From the mass transfer equation, the time required for the proportion α of succinic acid to be consumed in the titration could be given by

$$t = -\frac{1}{K_c a}\ln(1-\alpha) \tag{2}$$

So the estimation of the product of mass-transfer coefficient and interfacial area per unit volume, which means the volumetric mass-transfer coefficient $K_c{\cdot}a$, could be provided from the following equation:

$$K_c a = -\frac{1}{t}\ln(1-\alpha) \tag{3}$$

Values of $K_c{\cdot}a$ were obtained from the experimental data using Equation 3. Table 1 shows the comparison of volumetric mass-transfer coefficient between the droplet flow

in microchannels and that in the conventional extraction columns. It is found that the mass-transfer rate was increased with the decrease of formed droplet diameter. In the co-flowing microchannels, the value of $K_c \cdot a$ was about 0.1 s^{-1} when the droplet diameter was 0.35 mm, which was around 100 times higher to that in the extraction columns with the droplet diameter 3.0 mm. In the flow-focusing microchannels, the volumetric mass-transfer coefficient could be increased to 0.5 s^{-1} with the droplet diameter decreased to 0.13 mm. The increase of mass-transfer rate was mainly caused by the enhancement of mass transfer during droplet forming and moving stages at the microscale. So we should consider the contribution of mass-transfer enhancement at both stages.

Table 1. Comparison of $K_c \cdot a$ and average droplet diameter d_{av} between droplet flow in microscale and conventional extraction processes

Mass-transfer process	d_{av} (mm)	$K_c \cdot a$ (s^{-1})
Droplet flow in co-flowing microchannels	0.35–0.55	0.02–0.1
Droplet flow in flow-focusing microchannels	0.13–0.25	0.23–0.5
Conventional extraction columns	2.0–3.0	10^{-4}–10^{-3}

Discussion of Mass Transfer Contributions During Droplet Forming and Moving Stages

During droplet moving stage, there was no relative-moving velocity between two phases because of the co-flowing of continuous organic phase and aqueous drops. So we could assume the mass transfer during droplet moving stage as the mass transfer of succinic acid at the interface of stagnant droplet in the quiescent continuous phase. Then we can quantitatively confirm the mass-transfer contribution during droplet moving stage.

The mass-transfer coefficients inside and outside a stagnant droplet in the quiescent continuous phase could be calculated from the tranditional model. Based on the full traditional two-phase resistance model, the total mass-transfer coefficient K_c could be calculated. From the mass-transfer equation and mass-conservation equation, the initial concentration of the acid during droplet moving stage can be calculated from Equation 4. We define a parameter y, which means the mass-transfer contribution fraction of droplet-forming stage, as the Equation 5.

$$\ln\left(\frac{c_0^{'}}{c_t}\right) = \frac{6tK_c}{rd_d} \tag{4}$$

$$y = \frac{c_0 - c_0^{'}}{c_0 - c_t} \tag{5}$$

Then, the contribution of mass transfer during droplet-forming stage to the total mass-transfer process could be obtained. The results show that the mass transfer during the droplet-forming stage contributed at least 30% of the total mass transfer quantities in our experiments. So the contribution of mass transfer during the droplet-forming stage can't be neglected at droplet flow in microchannels. While in the conventional extraction process, the contribution of mass-transfer during the droplet-forming stage is usually less than 10%. The mass-transfer mechanism during the droplet forming stage on the microscale should be investigated fundamentally in the further work.

CONCLUSIONS

In this work, we investigated the enhancement of mass transfer performance of liquid–liquid dispersed system in micro-scale by droplet flow in two types of microchannels. Color change time decreased from 4.0 s to 0.4 s with the average droplet diameter from 550 μm to 130 μm. Mass transfer rates were 10~1000 times higher compared with that of the conventional extraction processes. Based on the qualitative analysis, mass transfer occurred both at droplet forming and moving stages. During droplet forming stage, vortex flow patterns within the droplet could enhance mass transfer process. The mass transfer during droplet formation stage contributed at least 30% of the total mass transfer quantities from the theoretical analyzing. Our results indicate that droplet flow within a microscale environment offers a viable alternative for two-phase reaction or mass transfer systems.

ACKNOWLEDGMENT

We gratefully acknowledge the supports of the National Natural Science Foundation of China (20476050, 20490200, 20525622) and National Basic Research Program of China (2007CB714302) on this work.

REFERENCES

1. P. A. Auroux, D. Iossifidis, D. R. Reyes, and A. Manz, "Micro Total Analysis Systems. 2. Analytical Standard Operations and Applications," *Anal. Chem.,* **74**, 2637-2652 (2002).
2. K. Jensen and A. P. Lee, "The Science & Applications of Droplets in Microfluidic Devices," *Lab Chip*, **4**, 31N-32N (2004).
3. M. Tokeshi, T. Minagawa, and T. Kitamori, "Integration of a Microextraction System on a Glass Chip: Ion-Pair Solvent Extraction of Fe(II) with 4,7-Diphenyl-1,10-phenanthrolinedisulfonic Acid and Tri-n-octylmethylammonium Chloride," *Anal. Chem.,* **72**, 1711-1714 (2000).
4. J. R. Burns and C. Ramshaw, "The intensification of rapid reactions in multiphase systems using slug flow in capillaries," *Lab Chip*, **1**, 10-15 (2001).
5. M. Ueno, H. Hisamoto, T. Kitamori, and S. Kobayashi, "Phase-transfer alkylation reactions using microreactors," *Chem. Commun.,* **7**, 936-937 (2003).
6. N. Harries, J. R. Burns, D. A. Barrow, and C. Ramshaw, "A numerical model for segmented flow in a microreactor," *Int. J. Heat Mass Transf.,* **46**, 3313–3322 (2003).
7. K. Benz, K. P. Jäckel, K. J. Regenauer, J. Schiewe, K. Drese, W. Ehrfeld, V. Hessel, and H. Lowe, "Utilization of micromixers for extraction processes," *Chem. Eng. Technol.,* **24**, 11-17 (2001).
8. H. Pennemann, S. Hardt, V. Hessel, P. Lob, and F. Weise, "Micromixer based liquid/liquid dispersion," *Chem. Eng. Technol.,* **28**, 501-508 (2005).
9. G. G. Chen, G. S. Luo, Y. Sun, et al., "A Ceramic Microfiltration Tube Membrane Dispersion Extractor," *AICHE J.*, **50**(2), 382-387 (2004).
10. J. H. Xu, G. S. Luo, G. G. Chen, et al., "Mass transfer performance and two-phase flow characteristic in membrane dispersion mini-extractor," *J. Membr. Sci.*, **249**(1-2), 75-81 (2005).
11. G. G. Chen, G. S. Luo, S. W. Li, and J. H. Xu, "Experimental approaches to understanding of a micro-structure device," *AIChE J.,* **51**, 2923-2929 (2005).

PROTEIN EXTRACTION TO IONIC LIQUIDS AND ITS CHANGE OF BIOLOGICAL FUNCTION

Masahiro Goto,[1] Kojiro Shimojo,[2] and Fukiko Kubota[1]

[1]*Kyushu University, 744 Moto-oka, Fukuoka, 819-0395, Japan.*
[2]*Japan Atomic Energy Agency, To-kaimura, Ibaraki, Japan.*
Corresponding author email address: mgototcm@mbox.nc.kyushu-u.ac.jp

ABSTRACT

We report on the extraction of cytochrome *c* (Cyt-*c*) from an aqueous phase into ionic liquids (ILs) with dicyclohexano-18-crown-6 (DCH18C6). We have found that DCH18C6 enables transfer of Lys-rich proteins into ILs via supramolecular complex formation. The hydrophobicity and functional groups of ILs have a great influence on protein partitioning, while protein transfer using conventional organic solvents is negligibly small. Spectroscopic characterization indicates that the sixth ligand, Met 80, in the heme group of the Cyt-*c*–DCH18C6 complex in an IL is replaced by other amino acid residues of the peptide chain. Solubilization of Cyt-*c* in an IL causes an environmental change of the heme vicinity of Cyt-*c*, which triggers the functional conversion of Cyt-*c* from an electron-transfer protein to peroxidase.

INTRODUCTION

Ionic liquids (ILs) have been widely investigated as alternatives to conventional organic solvents in liquid-liquid extraction, and they show remarkably high extraction performance and separation ability for metal ions in comparison with conventional organic solvents when using certain neutral ligands [1]. Recently, several research groups have focused on the application of ILs to the liquid-liquid extraction of amino acids. In a preliminary communication, in order to expand the potential of ILs as extracting media for biomolecules, we clarified that dicyclohexano-18-crown-6 (DCH18C6) can form a supramolecular complex with cytochrome *c* from horse heart (Cyt-*c*) and is capable of quantitative partitioning of Cyt-*c* into a hydroxyl group–containing IL [2]. Cyt-*c* is a representative heme protein and mediates an electron transfer in the mitochondrial respiratory chain. Cyt-*c* represents an excellent model protein with which to investigate bio-applications in ILs, since it is one of the most thoroughly physicochemically characterized metalloproteins and has a covalently protein-bound heme group and a stable protein backbone. The heme active site in Cyt-*c* consists of a six-coordinate low-spin heme-binding His 18 and Met 80 in the axial ligands.

In this study, we provide novel data on the partitioning of Cyt-*c* from an aqueous phase into ILs with DCH18C6, and we discuss the extraction mechanism of Cyt-*c* by

comparing it with the extraction behaviors of other heme proteins. Furthermore, the structure–function relationship of Cyt-*c* dissolved in ILs by complexation with DCH18C6 is probed through various spectroscopic methods, the catalytic oxidation reaction analysis, and its kinetics. The structure of the heme vicinity of Cyt-*c* dissolved in IL is fully characterized by UV-Vis, CD, and resonance Raman spectroscopic methods. Cyt-*c* displays minor peroxidase activity in aqueous solution; however, we demonstrate that the solubilization of Cyt-*c* in IL causes a structural transformation of Cyt-*c* and is able to convert a catalytically inactive biological form to an active form.

EXPERIMENTAL

Materials

Cytochrome *c* from horse heart (Cyt-*c*) and myoglobin from horse heart (Mb) were purchased from Sigma Co. (St. Louis, MO, US). Dicyclohexano-18-crown-6 (DCH18C6) was purchased from Aldrich Chemical Co., Inc. A substrate, 2,6-dimethoxyphenol (2,6-DMP) was obtained from Tokyo Kasei Kogyo Co., Inc. (Tokyo, Japan). All other reagents were of commercially available analytical grade and used as received.

IL Syntheses

A typical alkyl methylimidazolium bis(trifluoromethanesulfonyl)imide IL and ILs incorporating hydroxyl, ether, or urea groups were synthesized as described elsewhere [1,3], with minor variations. Details of the synthetic procedures were summarized in the Supporting Information of reference [3]. All ILs were colorless, and the halide content of the ILs was undetectable by the $AgNO_3$ test.

Liquid-Liquid Extraction of Heme Proteins into ILs

Extracting phases were prepared by dissolving DCH18C6 (20 mM) in ILs with ultrasonic agitation. Aqueous phases were prepared by dissolving the respective heme proteins (10 μM) in deionized water without buffer, as buffers containing alkali metal ions or amines may form complexes with DCH18C6. Equal volumes of the IL and aqueous solutions were mixed and gently shaken at 30 °C for 6 h to attain equilibrium. After phase separation, the concentrations of protein in both phases were determined by the absorbance of the Soret band peak using a UV–vis spectrophotometer (JASCO U-best 570), which then allowed calculation of the extractability (E = $[\text{protein}]_{IL}/[\text{proteins}]_{aq.ini.}$; aq. and ini. denote the aqueous phase and initial condition, respectively).

Catalytic Performance of Cyt-*c*

The $[C_2OHmim][Tf_2N]$ solution containing Cyt-*c* was prepared according to the same extraction procedure as described above. The IL solution containing the Cyt-*c*–

DCH18C6 complex and a dry IL solution containing 2,6-DMP as a substrate were added to a quartz cell. The oxidative reaction was initiated by the addition of hydrogen peroxide methanol solution. The reaction was followed spectroscopically by monitoring the absorbance of the product dimer at 469 nm. Catalytic oxidation of 2,6-DMP by peroxidases proceeds as shown in Figure 1. Catalytic oxidation of 2,6-DMP by native Cyt-*c* in aqueous solution was also compared with that in IL.

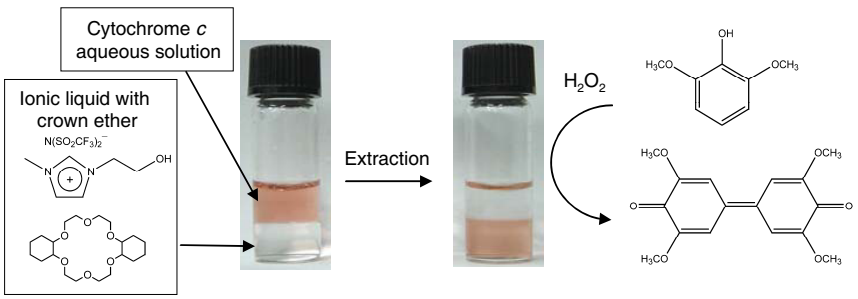

Figure 1. Extraction of Cyt-c with crown ether and its catalytic oxidation.

RESULTS AND DISCUSSION

Extraction of Cyt-*c* into ILs with Crown Ether

In a preliminary experiment, we examined the direct solubilization of Cyt-*c* powder into nonaqueous hydrophobic ILs containing 18-crown-6 by means of the solid (Cyt-*c*)-liquid (crown/ILs) extraction. However, Cyt-*c* was not solubilized in the ILs tested in the present study, in spite of the fact that the high solubility in methanol containing 18-crown-6 was attained by means of the solid (Cyt-*c*)-liquid (crown/methanol) extraction. Therefore, we first dissolved Cyt-*c* into deionized water and then investigated the extractive solubilization of Cyt-*c* from the aqueous phase into [C_2OHmim][Tf_2N], which provides the highest hydrophilicity among the ILs tested in the present study. The substituted crown ether DCH18C6 was employed as the extractant because of its high hydrophobicity compared to 18-crown-6. Figure 2 shows the extraction behavior of Cyt-*c* with increasing DCH18C6 concentration in [C_2OHmim][Tf_2N]. In the absence of DCH18C6, the partitioning of Cyt-*c* into [C_2OHmim][Tf_2N] is negligible, although it is expected to interact with proteins through hydrogen bonding. The transfer of Cyt-*c* into [C_2OHmim][Tf_2N] is promoted with increasing DCH18C6 concentration. Quantitative extraction is achieved when the DCH18C6 concentration is around 1000-fold higher than that of Cyt-*c*. If converted to the molar ratio of the lysine residues, the DCH18C6 concentration is around 50 equiv. and is a modest concentration as an extractant. Quantitative extraction of Cyt-*c* is also apparent to the naked eye, since the red color of Cyt-*c* visually indicates its distribution between the phases.

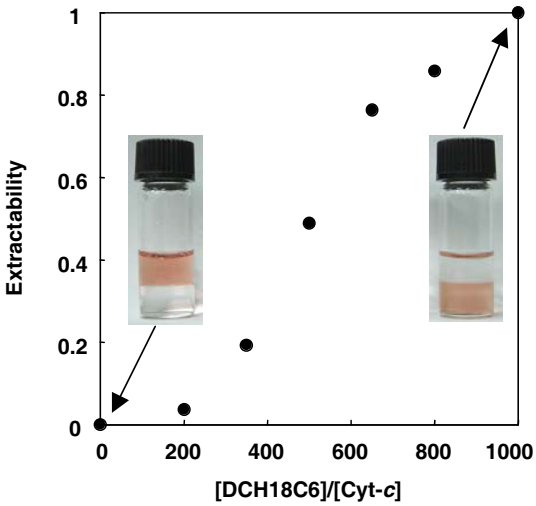

Figure 2. Effect of crown ether concentration on protein extraction.

Extraction Behavior of Heme Proteins into ILs with Crown Ether

The main driving force of Cyt-*c* extraction into ILs is considered to be the interaction between DCH18C6 and the amino group in the lysine residues on the protein surface. To elucidate the participation of the amino group in the Cyt-*c* extraction, four heme proteins (Cyt-*c*, G-Cyt-*c*, Mb, and HRP) were employed as guest biomolecules. All proteins tested in the present study have a heme molecule; however, their characteristics are greatly different. As shown in Table 1, Cyt-*c* and Mb, which are "Lys-rich proteins," have 19 lysine residues as well as 2 arginine residues. On the other hand, HRP, which is an "Arg-rich protein," has 6 lysine residues as well as 21 arginine residues. G-Cyt-*c* is a chemically-modified protein, in which 9.7 lysine residues of Cyt-*c* are transformed into homoarginine moieties. The extractability of these proteins into $[C_2OHmim][Tf_2N]$ with DCH18C6 is compared in Table 1. Lys-rich proteins, Cyt-*c* is quantitatively transferred into $[C_2OHmim][Tf_2N]$, and Mb is moderately extracted. However the degrees of G-Cyt-*c* and HRP extraction are extremely low. The results demonstrate that DCH18C6 recognizes the $-NH_3^+$ group in the lysine residues on the protein surface. Multiple DCH18C6 molecules can strongly coordinate with the lysine residues and can form a supramolecular complex with Lys-rich proteins. The complex formation can enhance the solubility of Lys-rich proteins in $[C_2OHmim][Tf_2N]$.

Electroneutrality must be maintained in the extraction of cationic species from an aqueous phase into ILs. However, the cationic protein Cyt-*c* is quantitatively extracted into the IL phase, in spite of the absence of counteranions in the aqueous phase. That is, the protein transfer into IL does not involve anion co-extraction. The result in the present study also implies that the transfer of Cyt-*c* into ILs proceeds through a cation-exchange process, not an ion-pair extraction. The structural change in Cyt-*c* dissolved in an IL by complexation with DCH18C6 were probed using UV-vis, CD, and resonance Raman spectroscopic methods. These spectroscopic data suggest that the sixth ligand Met 80 in

the heme group of the Cyt-*c*–DCH18C6 complex in [C_2OHmim][Tf_2N] is replaced by other amino acid residues of the peptide chain, which causes an environmental change of the heme vicinity of Cyt-*c*, retaining a six-coordinate low-spin heme.

Table 1. Properties and extractability of proteins tested in the present study with DCH18C6 into [C_2OHmim][Tf_2N]

Protein	Molecular weight	Isoelectric point	Number of Lys	Number of Arg	Extractability (%)[a]
Cyt-*c*	12300	10.6	19	2	99.8 ± 0.3
G-Cyt-*c*	–	–	9.3 (19-9.7)	11.7 (2+9.7)	4.1 ± 1.4
Mb	17000	7.0	19	2	63.4 ± 1.3
HRP	44000	7.2	6	21	15.2 ± 8.5

[a] The number of measurements is four. [protein] = 10 μM, [DCH18C6] = 20 mM.

Catalytic Performance of 2,6-DMP by Cyt-*c*–DCH18C6 Complex in IL

The catalytic oxidation reaction of 2,6-DMP with H_2O_2 was carried out to evaluate the peroxidase activity of the Cyt-*c*–DCH18C6 complex in ILs. The substrate 2,6-DMP, which is soluble in both water and ILs, was used to monitor its oxidation reaction. Figure 3 shows the time course of the oxidation reaction of 2,6-DMP catalyzed by the Cyt-*c* complex. In the absence of Cyt-*c* as a control experiment, very little 2,6-DMP is oxidized (υ = 0.1 μM/min). Native Cyt-*c* displays minor peroxidase activity (υ = 0.5 μM/min). On the other hand, the Cyt-*c*–DCH18C6 complex in [C_2OHmim][Tf_2N] offers high peroxidase activity (υ = 2.6 μM/min), and accelerates the initial reaction rate by 5.5-fold relative to that of native Cyt-*c*. The kinetic parameters in the Michaelis-

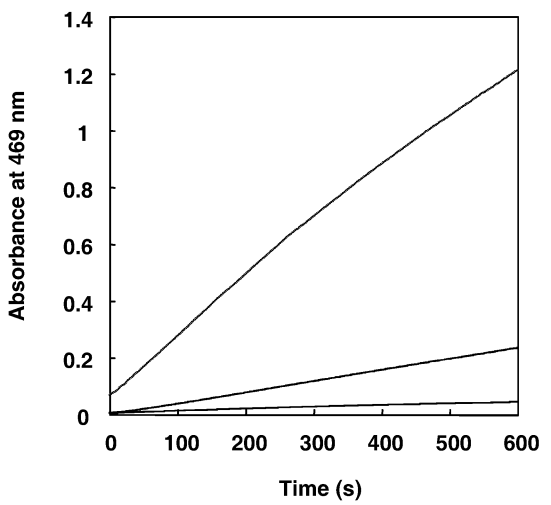

Figure 3. Time course of catalytic oxidation of 2,6-DMP with Cyt-*c*. [Cyt-*c*] = 1 μM; [2,6-DMP] = 10 mM. Absence of Cyt-*c* in water (a); Cyt-*c* in water (b); Cyt-*c* in [C_2OHmim][Tf_2N] (c).

Menten scheme were obtained as follows: k_{cat} = 34 min^{-1}, K_m = 11 mM, and k_{cat}/K_m = 3.1 min^{-1} mM^{-1} for the Cyt-*c*–DCH18C6 complex in [C_2OHmim][Tf_2N], k_{cat} = 109 min^{-1}, K_m = 166 mM, and k_{cat}/K_m = 0.6 min^{-1} mM^{-1} for native Cyt-*c* in aqueous solution. The k_{cat} and K_m for the Cyt-*c*–DCH18C6 complex in [C_2OHmim][Tf_2N] is around 3-fold and 15-fold lower than the value for native Cyt-*c*. These results indicate that dissolution of Cyt-*c* in the IL facilitates peroxidase activity by the greatly increased affinity for H_2O_2 (K_m), in spite of the decreased catalytic efficiency (k_{cat}). The increased affinity for H_2O_2 is probably caused by the structural change of the heme vicinity of Cyt-*c*, which results from the replacement of the axial ligand Met 80 in the heme group.

CONCLUSIONS

Dicyclohexano-18-crown-6 (DCH18C6) enables solubilization of Lys-rich proteins into ILs by formation and extraction of a noncovalent supramolecular complex. The hydrophobicity and functional groups of ILs greatly influence protein partitioning, and quantitative partitioning of Cyt-*c* into a hydroxyl group–containing IL is possible in the presence of DCH18C6. Solubilization of Cyt-*c* in an IL causes replacement of the axial ligand Met 80 in the heme group, yielding a non-natural six-coordinate low-spin ferric heme structure. The environmental change of the heme vicinity of Cyt-*c* solubilized in IL converts a catalytically inactive biological form to an active form. The Cyt-*c*–DCH18C6 complex acts as a homogeneous biocatalyst in ILs and provides remarkably high peroxidase activity compared with native Cyt-*c*, because of yjr enhancement of the affinity for H_2O_2.

REFERENCES

1. K. Nakashima, F. Kubota, T. Maruyama, and M. Goto, “Feasibility of ionic liquids as alternative separation media for industrial solvent extraction processes,” *Ind. Eng. Chem. Res.*, **44**, 4368–4372 (2005).
2. K. Shimojo, K. Nakashima, N. Kamiya, and M. Goto, “Crown Ether-Mediated Extraction and Functional Conversion of Cytochrome c in Ionic Liquids,” *Biomacromolecules*, **7**, 2–5 (2006).
3. K. Shimojo and M. Goto, “Solvent extraction and stripping of silver ions in room-temperature ionic liquids containing calixarenes,” *Anal. Chem*., **76**, 5039–5044 (2004).

EXTRACTION OF AMINO ACIDS AND DIPEPTIDES BY CALIXARENE CARBOXYLIC ACID DERIVATIVES

T. Oshima,[1] A. Irie,[2] K. Ohto,[2] K. Inoue,[2] H. Kodama,[2] T. Ishii,[1] and Y. Baba[1]

[1]Department of Applied Chemistry, Faculty of Engineering, University of Miyazaki, 1-1, Gakuen Kibanadai Nishi, Miyazaki, Japan 889-2192. [2]Department of Applied Chemistry, Faculty of Science and Engineering, Saga University, 1-Honjo, Saga, Japan 840-8502. Corresponding author email address: oshimat@cc.miyazaki-u.ac.jp

ABSTRACT

A calix[6]arene carboxylic acid derivative (^{t}Oct[6]CH_2COOH) functions as a powerful extractant for various biomolecules bearing an amino group. In the present paper, the extraction of amino acid derivatives and dipeptides bearing two amino groups using a series of the calixarene carboxylic acid derivatives is examined, in order to understand the extraction mechanism of amino acids and proteins. *L*-Lysine β–naphthyl amide and a dipeptide derivative Fmoc-Lys-Lys-OMe, which have two amino groups, were extracted with ^{t}Oct[6]CH_2COOH and the stoichiometry was studied by slope analysis. The diamine compounds were extracted with the calix[6]arene by forming an unexpected 1:1 complex.

INTRODUCTION

Macrocyclic compounds such as calixarenes have been used as a platform for preparing novel extractants [1]. Various calixarene derivatives have been developed as extractants for not only metal ions but also biomolecules such as amino acids and bioactive amines [2,3]. A calix[6]arene carboxylic acid derivative (^{t}Oct[6]CH_2COOH), for example, has been found to function as a powerful extractant for various biomolecules bearing an amino group. The structure is preferable for the encapsulation of an amino compound (RNH_3^+): the large cavity to include an organic molecule, the preorganized carboxylic acid groups for electrostatic interaction with a protonated amino group, and the complementary C_3 symmetry. The macrocyclic compound quantitatively extracts amino acids, catecolamines, and nucleobases into an organic phase through a proton exchange reaction [4-9]. Furthermore, the calix[6]arene exhibits extractability for a cationic protein cytochrome *c* [10,11]. The protein extraction by ^{t}Oct[6]CH_2COOH is considered to proceed by the recognition of several ε-amino groups of lysine residues on the protein surface.

The present study examines the extraction of a diamine compound with ^{t}Oct[6]CH_2COOH in order to investigate the recognition mechanism of biomolecules. Figure 1 displays the schematic illustration of this study. The macrocyclic molecule

^{t}Oct[6]CH_2COOH encapsulates a monoamino compound to form a 1:1 complex (Figure 1(a)). On the other hand, the cationic protein cytochrome *c* is likely to form the complex with multiple ^{t}Oct[6]CH_2COOH molecules (Figure 1(c)). However, the exact stoichiometry between the protein and the calixarene is not known. If the calix[6]arene molecules form a 2:1 complex with the diamine compound (Figure 1(b)), complexation between multiple calixarene molecules and a protein molecule is indirectly suggested.

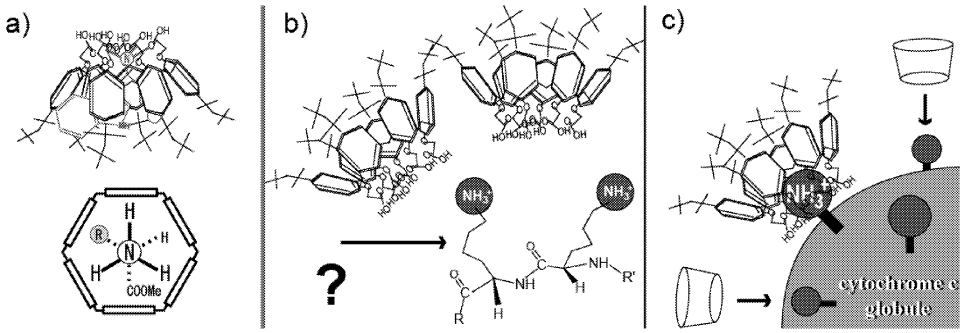

Figure 1. Schematic illustrations of the complexation between the calix[6]arene and biomolecules: (a) for amino acid [4-5], (b) for dipeptides, and (c) for protein [9,10].

EXPERIMENTAL

Reagents

Figure 2 exhibits molecular structures of calix[*n*]arene derivatives used in this study. The calix[4]arene tetracarboxylic acid derivative in the cone conformation (^{t}Oct[4]CH_2COOH), the calix[6]arene hexacarboxylic acid derivative (^{t}Oct[6]CH_2COOH), and the calix[8]arene octacarboxylic acid derivative (^{t}Oct[8]CH_2COOH), were synthesized according to previously described procedures [4,12]. The final products were purified by recrystallization and identified by means of FT-IR, ^{1}H-NMR, and elemental analysis.

Figure 3 shows the structures of the amino acid β–naphthyl amide derivatives used as guest molecules for the liquid-liquid extraction experiments (i.e., *L*-arginine β–naphthyl amide (Arg-βNA), *L*-lysine β–naphthyl amide (Lys-βNA), *L*-serine β–naphthyl amide (Ser-βNA), and *L*-glutamic acid β–naphthyl amide (Glu-βNA)). They were purchased from Bachem AG and employed without further purification. The other reagents were of reagent grade and were used as received.

Synthesis of a Dipeptide Derivative (Fmoc-Lys-Lys-OMe)

A dipeptide derivative Fmoc-Lys-Lys-OMe as a model compound bearing two amino groups was prepared according to the Scheme 1 [13,14]. As the first step, Fmoc-Lys(Boc)-OH and H-Lys(Boc)-OMe are coupled using carbodiimide reagent EDC (1-(3-dimethylaminopropyl)-3-ethylcarbodiimide hydrochloride) in the presence of HOBt (hydroxy-benzotriazole). Later the *t*-butoxycarbonyl (Boc) groups of Fmoc-Lys(Boc)-Lys(Boc)-OMe were deprotected using 4 mol/dm^3 HCl/dioxane. The following properties of the resulting dipeptide Fmoc-Lys-Lys-OMe were observed. White powder, 90% yield. ^{1}H-NMR (300 MHz, MSO): 1.35 (4H, m, CH_2), 1.54 (8H, m, CH_2), 2.73 (4H, m,

$NH_2C\underline{H}_2$), 3.61 (3H, s, $OC\underline{H}_3$), 4.23 (5H, m, CH, CH_2O), 7.32 (2H, t, ArH), 7.41 (2H, t, ArH), 7.70 (2H, d, ArH), 7.82 (2H, s, NH), 7.90 (2H, d, ArH).

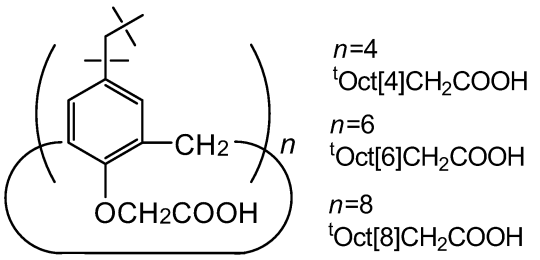

Figure 2. Molecular structures of calix[*n*]arene derivatives used in this study.

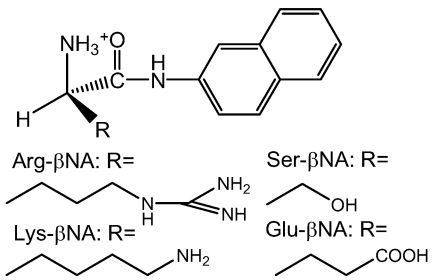

Figure 3. Molecular structures of amino acid derivatives used in this study.

Scheme 1.

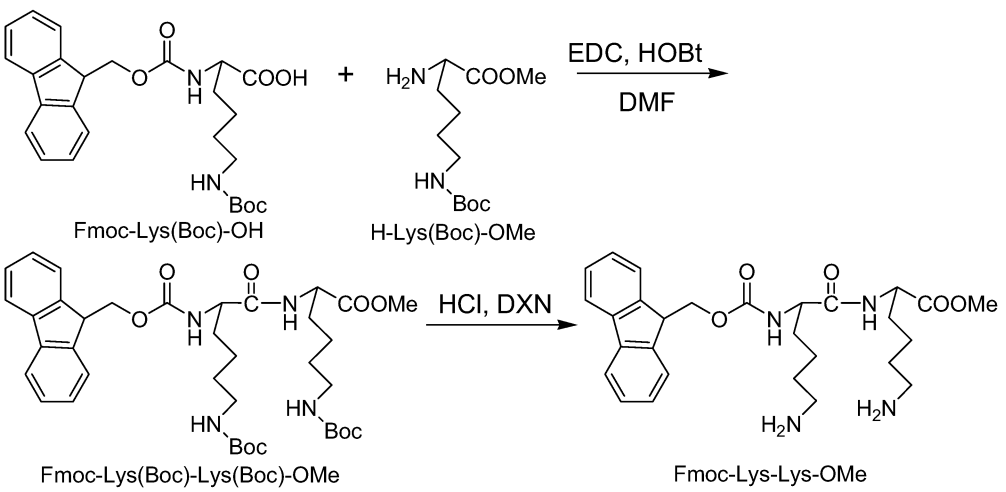

Extraction Equilibrium of Amino Acid Derivatives in Liquid-liquid Extraction

An aqueous solution was prepared by dissolving 0.20 mmol/dm^3 of an amino acid derivative. The pH in the aqueous solution was adjusted using 20 mmol/dm^3 glycine and small amount of HCl. An organic solution was prepared by dissolving 2.0 mmol/dm^3 of an extractant into chloroform. Equal volumes (5 dm^3) of the aqueous and organic solutions were mixed in a stoppered grass tube and gently shaken in a thermostatted water bath at 30 ºC. After 20 hours, when the extraction attained equilibrium, each phase was separated. The concentration of amino acids in the aqueous solution was determined by a UV-VIS spectrometer (PerkinElmer LAMBDA 190) to evaluate the degree of extraction ($E = 1\text{-}C_{aq,\,eq}/C_{aq,\,ini}$ [-]) and the degree of distribution ($D = C_{org,\,eq}/C_{aq,\,eq}$).

RESULTS AND DISCUSSION

Figure 4 shows the extraction behaviour of Lys-βNA using calix[*n*]arene carboxylic acid derivatives. The guest molecule has two amino groups and should exist as dicationic species under acidic condition. As shown in Figure 4, the extraction increases with increase of the aqueous pH, because the extraction proceeds proton-exchange reaction. The order of extractabilities with the calix[n]arenes is as follows:^{t}Oct[6]CH_2COOH > ^{t}Oct[8]CH_2COOH > ^{t}Oct[4]CH_2COOH. This order agrees with the extractabilities for various primary monoamino compounds such as amino acid esters and catecholamine in the previous studies [4-9]. The result suggests that the diamine compound Lys-βNA is extracted with the calix[*n*]arenes in a manner similar to that of monoamino compounds.

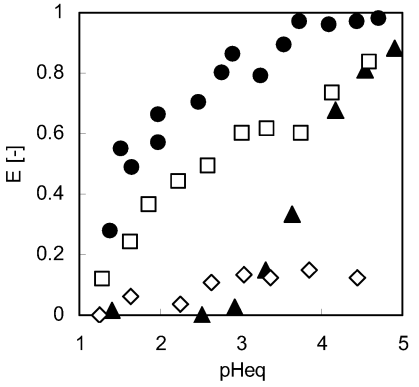

Figure 4. Extraction profiles of Lys-βNA with ^{t}Oct[*n*]CH_2COOH (*n* = 4,6,8): extractant free (diamond), *n* = 4 (triangle), *n* = 6 (circle), *n* = 8 (square).

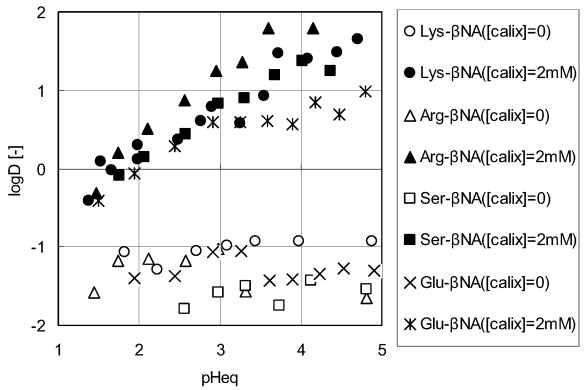

Figure 5. Extraction profiles of amino acid β–naphthyl amide derivatives with ^{t}Oct[6]CH_2COOH. Conditions: $[\text{amino acid}]_{aq}$ = 0.2 mmol/dm^3, $[^{t}\text{Oct[6]CH}_2\text{COOH}]_{org}$. = 0 (open keys) or 2.0 mmol/dm^3 (filled keys).

Figure 5 shows the extraction behaviour of amino acid β–naphthyl amide derivatives with ^{t}Oct[6]CH_2COOH. As Arg and Lys are basic amino acids, Arg-βNA and Lys- βNA have two cationic functional groups. Ser-βNA is a monocationic species. Glu-βNA is a zwitterionic species, which has a carboxylic acid group in the side chain. The extraction selectivity for amino acid derivatives is small; however, the extraction of basic amino acid derivative Arg-βNA is the highest. The extraction of Glu-βNA does not increase under weakly acidic condition due to the deprotonation of carboxyl group.

The slope of the relationship between the logarithmic distribution ratio of dicationic species Arg-βNA and Lys- βNA and the equilibrium pH is unexpectedly unity. It suggests that only one hydrogen ion is released from the extractant for the extraction. On the other hand, the relationship between the logarithmic distribution ratio of Lys-βNA and the logarithmic ^{t}Oct[6]CH_2COOH concentration is about 1.3 (data not shown). The result suggests that one or two ^{t}Oct[6]CH_2COOH molecules participates in the complex formation with Lys-βNA. It is likely that one ^{t}Oct[6]CH_2COOH molecule is sufficient for the extraction of the relatively hydrophobic amino acid β–naphthyl amide.

Figure 6 shows the extraction behavior of Fmoc-Lys-Lys-OMe with ^{t}Oct[6]CH$_2$COOH. The dipeptide has two amino groups, which can interact with ^{t}Oct[6]CH$_2$COOH molecules individually. The extraction of the dipeptides increases with increase of the aqueous pH. As the slope of the relationship between the logarithmic distribution ratio and the equilibrium pH is unity, only one hydrogen ion is released from the extractant.

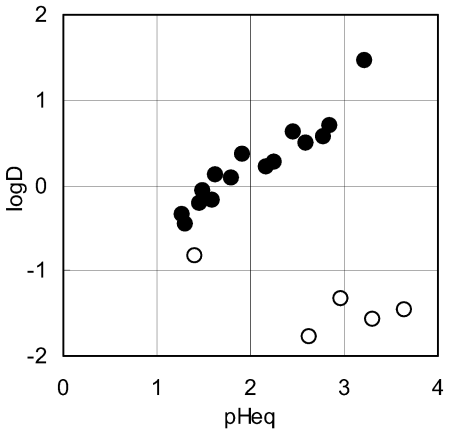

Figure 6. Extraction profile of Fmoc-Lys-Lys-OMe with ^{t}Oct[6]CH$_2$COOH. Conditions: extractant free (open circle), [^{t}Oct[6]CH$_2$COOH]$_{org.}$ = 2.0 mmol/dm^3 (filled circle). [dipeptide]$_{aq}$ = 0.05 mmol/dm^3.

From the results, a possible equation for the extraction of diamine compound with ^{t}Oct[6]CH$_2$COOH is expressed as follows (Equation (1)):

$$H_6R + (NH_3^+)R'(NH_3^+) + X^- \rightleftharpoons \{H_5R(NH_3^+)\}R'(NH_3^+)X^- + H^+ \qquad (1)$$

where H_6R denotes a ^{t}Oct[6]CH$_2$COOH molecule, $(NH_3^+)R'(NH_3^+)$ denotes a diamine molecule such as Lys-βNA and Fmoc-Lys-Lys-OMe, and X^- denotes an anion. Namely, only one ^{t}Oct[6]CH$_2$COOH molecule is necessary for the extraction of the diamine molecule. The hydrophobicity of complex is one of the dominating factors for the extraction of amino compound using calixarene. In the diamine compound, there are two amino groups that are available for the complexation with ^{t}Oct[6]CH$_2$COOH molecules. However, only one ^{t}Oct[6]CH$_2$COOH molecule can afford enough hydrophobicity for extraction of the guest molecule. Therefore, it is likely that two ^{t}Oct[6]CH$_2$COOH molecules are not necessary for the extraction of diamine compound under the experimental conditions.

CONCLUSIONS

A calix[6]arene derivative ^{t}Oct[6]CH$_2$COOH exhibited the highest extractability for amino acid derivatives in the series of calix[*n*]arenes. However, the stoichiometry between the calix[6]arene and diamine compound is not clarified completely in this study.

Additional study is necessary in order to clarify both this and the recognition mechanism of cationic protein by the calix[6]arene derivative.

ACKNOWLEDGMENTS

The authors gratefully acknowledge the financial support of a Grant-in-Aid for Scientific Research (No. 14350419) from the Ministry of Education, Science, Sports and Culture of Japan.

REFERENCES

1. R. Ludwig, "Calixarenes in Analytical and Separation Chemistry," *Fresenius J. Anal. Chem.*, **367**, 103-128 (2000).
2. H.-J. Buschmann, L. Mutihac, and K. Jansen, "Complexation of Some Amine Compounds by Macrocyclic Receptors," *J. Incl. Phenom* , **39**, 1-11 (2001).
3. R. Ludwig "Calixarenes for Biochemical Recognition and Separation," *Microchim. Acta,* **152**, 1-19 (2005).
4. T. Oshima, M. Goto, and S. Furusaki, "Extraction Behavior of Amino Acids by Calix[6]arene Carboxylic Acid Derivative," *J. Incl. Phenom.*, **43**, 77-86 (2002).
5. T. Oshima, K. Inoue, S. Furusaki, and M. Goto, "Liquid Membrane Transport of Amino Acids by a Calix[6]arene Carboxylic Acid Derivative," *J. Membr. Sci.*, **217**, 87-97 (2003).
6. T. Oshima, K. Inoue, K. Uezu, and M. Goto, "Dominant Factors Affecting Extraction Behavior of Amino Compounds by a Calix[6]arene Carboxylic Acid Derivative," *Anal. Chim. Acta*, **509**, 137-144 (2004).
7. T. Oshima, K. Oishi, K. Ohto, and K. Inoue, "Extraction Behavior of Catecholamines by Calixarene Carboxylic Acid Derivatives," *J. Incl. Phenom.*, **55**, 79-85 (2006).
8. K. Shimojo, T. Oshima, and M. Goto, "Calix[6]arene Acetic Acid Extraction Behavior and Specificity with Respect to Nucleobases," *Anal. Chim. Acta*, **521**, 163-171 (2004).
9. T. Oshima, R. Saisho, K. Ohe, Y. Baba, and K. Ohto, "Adsorption Behavior of Catecholamines on Calixarene Carboxylic Acid Impregnated Resin," *Solvent Extr. Res. Dev. Jpn.*, **13**, 123-129 (2006).
10. T. Oshima, M. Goto, and S. Furusaki, "Complex Formation of Cytochrome *c* with a Calixarene Carboxylic Acid Derivative: As a Novel Solubilization Method for Biomolecules in Organic Media," *Biomacromolecules*, **3**, 438-444 (2002).
11. T. Oshima, H. Higuchi, K. Ohto, K. Inoue, and M. Goto, "Selective Extraction and Recovery of Cytochrome *c* by Liquid-Liquid Extraction Using a Calix[6]arene Carboxylic Acid Derivative," *Langmuir*, **21**, 7280-7284 (2005).
12. K. Ohto, M. Yano, K. Inoue, T. Yamamoto, M. Goto, F. Nakashio, S. Shinkai, and T. Nagasaki, "Solvent extraction of trivalent rare earth metal ions with carboxylate derivatives of calixarenes," *Anal. Sci.* **11**, 893-902 (1995).
13. S.-Y. Han and Y.-A. Kim, "Recent Development of Peptide Coupling Reagents in Organic Synthesis," *Tetrahedron*, **60**, 2447-2467 (2004).
14. D. L. Boger, S. Miyazaki, S. H. Kim, J. H. Wu, S. L. Castle, O. Loiseleur, and Q. Jin, "Total Synthesis of the Vancomycin Aglycon," *J. Am. Chem. Soc*, **121**, 10004-10011 (1999).

SPECTROPHOTOMETRIC DETERMINATION OF ULTRA-TRACE BERYLLIUM AFTER SEPARATION AND PRECONCENTRATION USING QUINALIZARINE-MODIFIED MAGNETIC MICROPARTICLES

P. Ashtari,[1,2] K. Wang,[2] X. H. Yang,[2] K. Ashtari,[1] A. Khanchi[1]

[1]Chemistry Department, Nuclear Science School, Nuclear Science and Technology Research Institute, Tehran, Iran, 14395-836. [2]State Key Laboratory of Chemo/ Biosensing & Chemometrics, Biomedical Engineering Center, College of Chemistry & Chemical Engineering, Key Laboratory for Bio-Nanotechnology and Molecular Engineering of Hunan Province, Hunan University, Changsha, P. R. China, 410082. Corresponding author email address:ashtaricn@yahoo.com

ABSTRACT

In this report, quinalizarine was used as a selective beryllium extractant for modifying the magnetic microparticles. The major achieved advantages are the elimination of organic-solvents consumption and the applicability of the method for samples containing suspended particles. The influence of different parameters such as pH, equilibrium time, ionic strength, and type of stripping solution were investigated. Also, the interfering effects of various cationic and anionic interferences on the percent recovery of beryllium were studied. Beryllium ions were extracted from solution at pH 7.4 and were stripped from microparticles using 0.5 M HNO_3. The method was applied to certified reference water sample.

INTRODUCTION

Beryllium metal, alloys, and salts have attracted much attention in various industrial applications [1-3]. Pure beryllium and its metal alloys with copper, aluminum, magnesium, nickel, zinc, and iron have been widely used for electrical equipment, electronic instrumentation, and structural components of aircrafts, missiles, satellites, rockets materials, nuclear reactors, missiles fuels, and detector (^{7}Be) [1,4-7]. Whereas the abundant of beryllium in earth crust is so little (~2.8–5.0 μg/g) [1,8], the entry into water supplies could be the result of such industries discharges. Although there is no available data to evaluate its carcinogenicity in humans, it is clear that beryllium in high concentration causes death [4-5]. It is preferred to develop the simple, effective, and reliable methods for recovery and analysis of the environmental and biological samples.

Current separation and preconcentration techniques of Be suffer from major drawbacks such as large secondary wastes, significant chemical additives, solvent losses, and can be time consuming [8,9]. It is of great importance to develop the new methods, for solving mentioned problems. This method uses magnetic microparticles for the

separation and preconcentration. In this study, Magnetically Assisted Chemical Separation (MACS) principles were used to perform the separation and preconcentration of Be in aqueous solution. The magnetic microparticles were modified with extractant, quinalizarine, and the Be is determined by spectrophotometeric method using Chrome Azurol S as photometric reagent.

Different experimental conditions were investigated and the method was used for the separation of nano-gram amounts of Be from real and certified reference water.

EXPERIMENTAL

Chemicals

All the chemicals were of analytical-reagent grade and were used without any further purification. Reagent-grade quinalizarine (1, 2, 5, 8-tetrahydroxy anthraquinone), dibenzo-18-crown-6, 2-thenoyl-trifluoroacetone, Chrome Azurol S, cetyl pyridinium chloride, and Hexamethylene-tetramine, from Merck, were used as received. The magnetic particles were from Cortex Biochem, Inc. (San Leandro, CA, USA).

Apparatus

All UV-Visible absorbance measurements were performed by DU-800 Spectrophotometer (Beckman, England). An 868 digital Orion pH meter equipped with a combined glass-Calomel electrodes was used for pH adjustment. A Lab-lines shaker was used to shake the samples. An ED53 Binder oven was used to heat the microparticles.

Procedure

The microparticles were made ready for extraction according to the following procedure: after washing of the microparticles, the appropriate amount of microparticles was poured into a Teflon beaker, and quinalizarine solution was added. The mixture was stirred gently by a Teflon rod, and the solvent was evaporated slowly. Finally, the modified microparticles were heated at 100 ^{o}C for 24 hours to stabilize the modified layer.

The extraction experiments were performed in the test tube containing 200.0 ng Be ions in 10.0 mL solution of ammonium acetate 0.05 M. The pH of the solution was adjusted to 7.4-7.5. Then the solution was added to 5.0 mg modified and conditioned microparticles, and then was shaken for an appropriate time to complete the extraction. Finally, the test tubes were placed in a magnetic concentrator, where a permanent magnet in the wall causes the particles to aggregate on one side of the test tube. The back extraction was performed by using appropriate amounts of 0.5 M nitric acid solution. The Be determination was carried out on using an UV-Visible spectrometer at the wavelength of 605.0 nm.

RESULTS AND DISCUSSION

Effect of Modification on Extraction Efficiency

The 2% quinalizarine modified microparticles, the 5% modified microparticles using 2-thenoyltrifluoroacetone, the dibenzo-18-crown-6, and also nonmodified microparticles were investigated for determining the selectivity and selecting the appropriate ligand. The extraction was found to be quantitative at optimum pH, when microparticles were loaded with 2% quinalizarine.

Effect of Microparticles Amount

Figure 1 shows the effect of amount of extractant modified microparticles for quantitative extraction of beryllium. The extraction was found to be quantitative when 3.0 mg and/or more microparticles were used. Hence, subsequent experiments were carried out with the 5.0 mg modified microparticles.

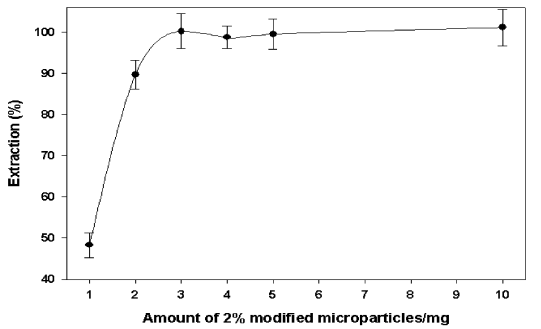

Figure 1. Effect of amount of modified microparticles (2%) on extraction efficiency of Be.

Effect of pH

The effect of pH on the extraction of beryllium ions from water samples was investigated in the pH range of 2.0-9.5, and the results are shown in Figure 2. The results have shown that the percent extraction was nearly constant and quantitative in the pH range of 6.8-7.8. Hence, a pH of 7.4 was chosen as the optimum pH.

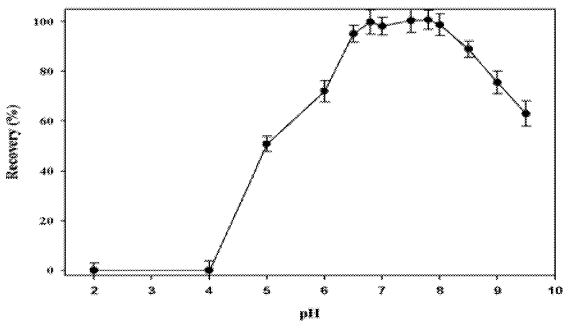

Figure 2. Effect of pH on the recovery of Be.

Equilibrium Time

The experiments were carried out at 1.0, 3.0, 5.0, 10.0, 20.0, 40.0, and 60.0 minutes time intervals, and the recovered amounts of beryllium were detected, respectively. The obtained results showed that the extraction is quantitative and complete in 10.0 minutes and more. Thus, for more confidence, the extraction reactions have been done in shaking time of 20.0 minutes in the subsequent experiments.

Selectivity

Selective separation and determination of beryllium from its binary mixtures with diverse metal ions was investigated by using the aqueous solutions containing 200.0 ng of beryllium and milligram amounts of interfering ions. The results are summarized in Table 1. The results revealed that the beryllium recovery was almost quantitative in the presence of milligram amounts of the diverse ions and interfering reagents.

Table 1. Effect of foreign ions on the recovery of 200ng Be from binary mixtures

Ions	Add as	Amount (mg)	Recovery of Be[a] (%)
Mg^{2+}	$MgSO_4.7H_2O$	2	101.9 (2.8)
Zn^{2+}	$Zn(CH_3COO)_2.2H_2O$	2	94.9 (3.3)
Co^{2+}	$CoCl_2.6H_2O$	2	102.4 (3.6)
Ni^{2+}	$NiSO_4.6H_2O$	0.8	99.3 (3.9)
Pb^{2+}	$Pb(NO_3)_2$	0.4	98.0 (4.0)
Ca^{2+}	$CaCl_2$	1.6	96.4 (2.8)
Cd^{2+}	$CdSO_4.8/3H_2O$	0.2	100.4 (3.2)
Cu^{2+}	$Cu(NO_3)_2.3H_2O$	0.05	97.5 (3.5)
Fe^{3+}	$FeCl_3.6H_2O$	1.6	99.3 (3.7)
Cr^{3+}	$CrCl_3.6H_2O$	0.2	104.8 (4.1)
MoO_4^{2-}	Na_2MoO_4	0.4	97.7 (2.6)
Na^{+}	NaCl	2	100 (2.0)
Ba^{2+}	$BaCl_2.2H_2O$	2	103.1 (2.7)
Li^{+}	$LiClO_4.3H_2O$	2	102.6 (4.1)
$EDTA^{2-}$	Na_2EDTA	10^{-4} M	102.2 (2.5)
Zr^{4+}	$Zr(SO_4)_2.4H_2O$	0.8	cannot detect
Mn^{2+}	$MnSO_4.H_2O$	0.2	96.5 (2.7)

[a] Mean of triplicates with %R.S.D.

Effect of Ionic Strength and Maximum Capacity of the Microparticles

The influence of ionic strength on the beryllium extraction was investigated in the presence of various concentrations of the potassium nitrate solution (0.02-2.0 M). Quantitative separation of beryllium was obtained in the presence of 0.02-1.0 M KNO_3. The extraction efficiency was 85.8% even in 2.0 M KNO_3 solution.

Portions of the microparticles (5.0 mg) were contacted with appropriate solutions containing 1.0 μg (1000.0 ng) beryllium, and the recovery of the extracted beryllium was determined. The maximum capacity of microparticles was found to be about 661.0 ± 8.9 ng/5.0 mg of modified magnetic microparticles.

Stripping of Beryllium and Stability of Modified Microparticles

Because the high extraction efficiency was achieved by using the magnetic microparticles, an efficient recovery stage for stripping of the microparticles is required. Several stripping solution were tested. The 0.5 M nitric acid was chosen as the best eluent. Also, the stability of the modified microparticles under experimental conditions was tested by using of the 5.0 mg microparticles for several extraction and back-extraction (stripping) processes. It was observed that after four cycles, some darkness appeared in the solution that could not be separated from solution even using centrifugation, and then the recovery efficiency decreased.

Real Sample Analysis and Analytical Performance

To assess the applicability of the method to real samples with different matrices containing varying amounts of diverse ions, the method was applied to the separation, extraction, and determination of beryllium from 100.0 ml of two different water samples, tap water and spring water without any filtration. The water samples were collected from Hunan University area located in west of Changsha City (Yuelu Shan) in Hunan Province of P.R. of China.

Table 2 shows the results of the extraction and recovery of the added 200.0 ng beryllium into 100.0 ml of the water samples using 15.0 mg of modified microparticles. The obtained detection limit (LOD) of the mentioned method under optimal experimental conditions was 12 ng/L.

Table 2. Recovery of beryllium ions from 100 mL spiked water samples

Sample	Added Be (ng)	Found Be (ng)*	Recovery %
Tap Water	200.0	189.6 (3.4)	94.8
Spring Water	200.0	194.2 (3.3)	97.1

* Mean of triplicates with percent R.S.D.

Certified Reference Material Analysis

A mixture of two environmental Certified Reference Materials (GSBZ 50009-88 and GSB 07-1178-2000) from the National Certified Reference Materials of P.R. of China was prepared and analyzed by the mentioned procedure. It contains 20.0 ppb Be and Cu and Pb, Zn, Cd, Ni, Cr, K, Na, Ca, and Mg at 1.13, 1.56, 0.390, 0.129, 0.648, 0.791, 4.60, 10.0, 20.0, and 5.1 ppm, respectively. It was analyzed five times. The achieved percent recovery of beryllium was 100 ± 5 %. Hence, the method's precision and accuracy has found in good agreement in comparison to other procedures.

CONCLUSION

In summary, the introduced method, which uses the quinalizarine-modified magnetic microparticles as extractant, has shown good capability for the selective separation and preconcentration of beryllium from the water samples. The most important advantage of the method is that the separation and determination of beryllium can be done by a simple and fast process. Based on these principles, which had been introduced for selective separation of copper previously [9], it is going to open and develop a general, simple, and novel recovery procedure for metal ions and other compounds. A great decrease in the usage of organic and inorganic chemicals is promising for the introduction of this environmentally-friend method.

ACKNOWLEDGMENT

This work was supported in part by the National Key Basic Research Program of China (2002CB513110), Key Project of Natural Science Foundation of China (90606003), Natural Science Foundation of China (20475015), and China National Key Projects (2005EP090026).

REFERENCES

1. M. B. Robert and O. Mark, "Beryllium and Beryllium Compounds," Concise International Chemical Assessment Document 32, World Health Organization, Geneva; 2001; pp. 1-11.
2. Reference library at web site: www.espi-metals.com (2007-10-25).
3. D. R. McAlister and E. P.Horwitz, "A method for the separation of beryllium from spectral interfering elements in inductively coupled plasma-atomic emission spectroscopic analysis," *Talanta*, **67**(5), 873-879 (2005).
4. T. Okutani, Y. Tsuruta, and A. Sakuragawa, "Determination of a Trace Amount of Beryllium in Water Samples by Graphite Furnace Atomic Absorption Spectrometry after Preconcentration and Separation as a Beryllium-Acetylacetonate Complex on Activated Carbon," *Anal. Chem.*, **65**(9), 1273-1276 (1993).
5. A. E. Greenberg, L. S. Clesceri, and A. D. Eaton, APHA, Standard Methods for the Examination of Water and Wastewater 18th ed., Washington, D.C., 1992; pp. 3-53.
6. U. S. EPA, "Beryllium and Compounds," Office of Air Quality Planning & Standards, Research Triangle Park, North Carolina, Technology Transfer Network, 107-02-8, 1998.
7. T. Ohtsuki, H. Yuki, M. Muto, et al., "Enhanced Electron-Capture Decay Rate of ^{7}Be Encapsulated in C60 Cages," *Phys. Rev. Lett.*, **93**(11), 112501-1112501-4 (2004).
8. M. D. Kaminski and L. Nunez, "Extractant-coated Magnetic Particles for Cobalt and Nickel Recovery from Acidic Solution," *J. Magn. Magn. Mater.*, **194**(1-3), 31-36 (1999).
9. P. Ashtari, K. Wang, X. Yang, S. Huang, and Y. Yamini, "Novel separation and preconcentration of trace amounts of copper(II) in water samples based on neocuproine modified magnetic microparticles," *Anal. Chim. Acta*, **550**, 18-23 (2005).

PREPARATION OF BINUCLEAR COMPLEXES BY SOLVENT EXTRACTION AND THEIR PHOTOPHYSICAL PROPERTIES

Y. Hasegawa, S. Tamaki, M. Inoue, and H. Yajima

Department of Chemistry, Faculty of Science, Science University of Tokyo, Kagurazaka, Shinjuku-ku, Tokyo, 162-8601, Japan.
Corresponding author email address: yhasegaw@rs.kagu.tus.ac.jp

ABSTRACT

To prepare a useful binuclear complex as a functional material by solvent extraction, europium(III) was extracted with pivaloyltrifluoroacetone (Hpta: 1,1,1-trifluoro-5,5-dimethyl-2, 4-hexanedione) and bis(salicylidene)cyclohexyl diamine complex with zinc(II) (Zn(salchn)). The extracted species was found to be Eu(pta)3Zn(salchn), which shows stronger luminescence at 613 nm than that of Eu(pta)3 itself and that of Eu(pta)3H2(salchn), at an excitation wavelength of 394 nm. Further, when Eu ion was extracted with Hpta and H2(salchn) in the presence of Zn2+ in the aqueous phase at pCH < 5, the binuclear complex represented by Eu(pta)3Zn(salchn) was easily and readily prepared, and it gave strong luminescence. Accordingly, the proposed method should be a promising method to prepare effective phosphor.

INTRODUCTION

Recently binuclear complexes incorporating d- and f-electrons have been the subject of increasing interest, particularly by inorganic chemists. In addition to properties such as luminescence and magnetism arising from their electronic properties, these complexes would be expected to exhibit new properties arising from the interaction of the two metals. Among the binuclear complexes reported [1], we found a binary complex consisting of tris(hexafluoroacetonato)gadolinium(III) and Cu(II) complex with bis(salicylidene)ethylenediamine, [Gd(hfa)$_3$Cu(salen)][2]. When lanthanides(III) are extracted with β-diketone and a Lewis base, the ternary complex consisting of tris(β-diketonato)Ln(III) and Lewis base has been well-known to be formed. Thus, we tried to measure the extraction of Eu(III) with Htta (2-thenoyltrifluoroacetone) and Cu(saltn). It was reported that the use of the complex, Cu(saltn), formed between Cu(II) and H_2saltn (bis(salicylidene)propylenediamine) gave a large synergistic effect for the extraction of Eu(III) with Htta [3]. The extraction enhancement was equivalent to that of Eu(III) with Htta and trioctylphosphine oxide, which is known as one of the strongest Lewis bases [4]. In the present study, we measured the luminescence spectra of the ternary complexes as well as the extraction of Eu(III) with Hpta and Zn(salchn), and also the effect of Zn(II) in the aqueous phase on the extractability. Further, we compared the spectra of the $CHCl_3$

solution of extracted ternary complex with those of the mixed solution between $Eu(pta)_3$ solution and Zn(sal*c*hn), and confirmed the spectra are similar to each other.

EXPERIMENTAL

Reagents

All reagents were analytical grade. Chloroform was washed three times with deionized water. Pivaloyltrifluoroacetone (1,1,1-trifluoro-5,5-dimethyl-2,4-hexanedion, Hpta) was purchased from Aldrich. Tris(β-diketonato)Eu(III) was prepared in a similar way as described elsewhere [5]. Bis(salicylidene)cyclohexyldiamine (H_2sal*c*hn) and the Zn(II) complex were prepared with Shimada Chemical Research, Tokyo. The Eu(III) aqueous solution was prepared by dissolving the oxide, Eu_2O_3 (99.99%), into perchloric acid whose concentration was in a little excess of the stoichiometric amount of Eu(III).

Procedures

The luminescence spectra were measured for the mixed solutions consisting of $Eu(pta)_3$ and one of the ligands at several molar ratios and were recorded in a Hitachi F4500 fluorescence spectrophotometer.

The solvent extraction procedures were performed usual manner [5]. One tenth molar (0.1 M) $NaClO_4$ containing 10^{-4} M Eu(III) was shaken with an identical volume of $CHCl_3$ containing a constant concentration of Hpta and various amounts of one of the ligands. After attaining the distribution equilibrium, both the phases were separated. The pC_H (pC_H = -log[H^+]) was measured potentiometrically using 1.00×10^{-2} M $HClO_4$ of which total ionic concentration was adjusted to 0.1 M as a standard of pC_H 2.00. The concentration of Eu(III) and Zn(II) in both phases was determined by ICP/AES (Horiba JY70C).

RESULTS AND DISCUSSION

Luminescence Spectra and Stability Constants of the Ternary Complexes

Figure 1 shows the luminescence spectra of the mixed solutions between $Eu(pta)_3$ and bis(salicylidene)propylenediamine complexes with Cu(II) or Pd(II) as well as that of $Eu(pta)_3$ at the excited wavelength of 394 nm. All luminescence spectra show the peak at 613 nm. However, each luminescence is weaker than that of $Eu(pta)_3$, itself. The luminescence was largely sensitized by using Zn(II) instead of Cu(II) or Pd(II). It seems that Zn(saltn) is a promising ligand; however, the solubility of Zn(saltn) is too low to measure the solvent extraction behavior. We tried to use several Schiff bases and found that Zn(sal*c*hn) has enough solubility in $CHCl_3$. Figure 2 shows the luminescence spectra of the solutions containing 1.0×10^{-4} M of $Eu(pta)_3$ and/or different amounts of Zn(sal*c*hn). Figure 2a shows the spectra of Zn(sal*c*hn) without $Eu(pta)_3$. With increasing ligand concentration, the luminescence intensity increased. The spectra show a broad band at around 450 nm. Figure 2b shows the spectra of the mixed solution containing

Eu(pta)$_3$ and Zn(sal*c*hn). Compared to Figure 2-a, the luminescence at 450 nm based on Zn(II) is much weaker, while the intensity at 613 nm based on the Eu(III) increased. The spectra were analyzed on the basis of mass balance of Zn(II) and Eu(III), and the stability constant ($\overline{\beta}_1 = [EuA_3B]_o[EuA_3]_o^{-1}[B]_o^{-1}$) was obtained to be 5.50 ± 0.1.

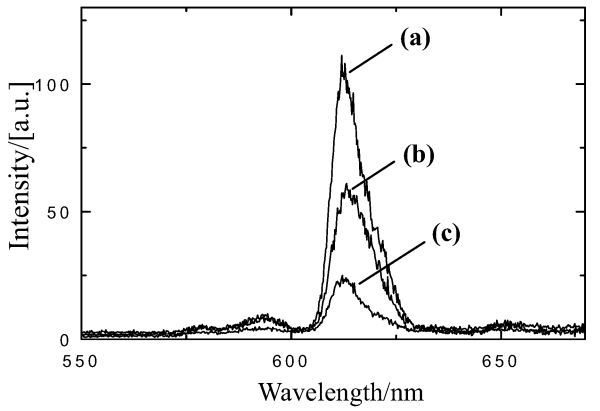

Figure 1. The effect Pd(saltn) (b) and Cu(saltn) (c) on the luminescence spectra of Eu(pta)$_3$ (a). 1 x 10^{-4}M Eu(pta)$_3$(a) 1 x 10^{-4}M Eu(pta)$_3$ +7.5 x 10^{-5}M Pd(saltn)(b) or +7 .5x 10^{-5}M Cu(saltn)(c)

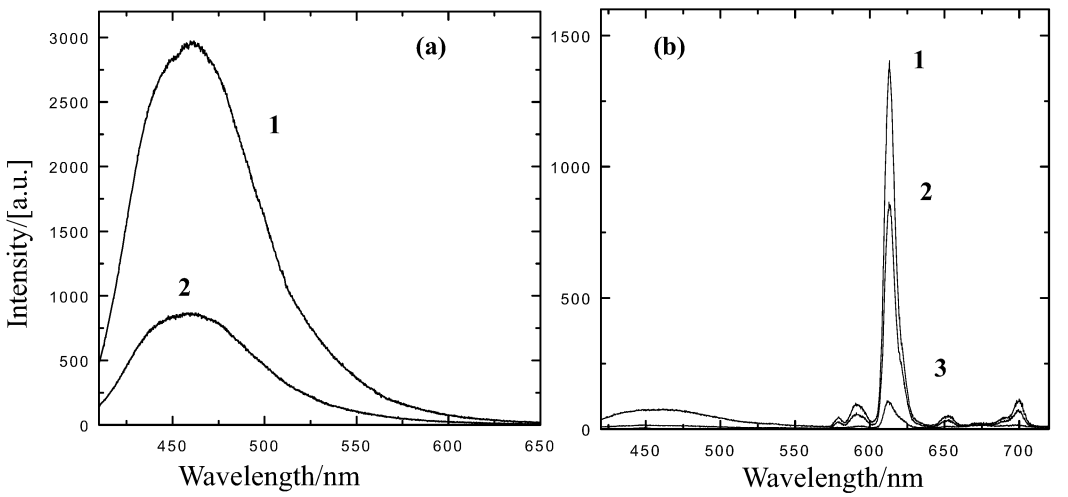

Figure 2. Luminescence spectra of Zn(sal*c*hn) (a) and of the mixed $CHCl_3$ solution containing Eu(pta)$_3$ and Zn(sal*c*hn) (b). (a) $[Zn(salchn)]_T$: 1, 1.1 x 10^{-4} M; 2, 3.8 x 10^{-5} M. (b) $[Eu(pta)_3]_T$ = 1 x 10^{-4} M + $[Zn(salchn)]_T$ (1.1 x 10^{-4} M (1), 3.8 x 10^{-5} M (2), 0 M (3))

Solvent Extraction and Stability Constants of the Ternary Complexes

When Eu(III) was extracted with Hpta and Zn(sal*c*hn), the distribution ratio, *D*, defined by the total Eu(III) concentration ratio between the organic and aqueous phases, was enhanced with increasing Zn(sal*c*hn) concentration as shown in Figure 3a. When the concentration of Zn(II) in both phases was measured, it was found that most of the Zn(II) was in the aqueous phase. The Zn(II) complex seems to interact with H^+ as follows;

$$Zn(salchn)(o) + 2H^+ \rightleftharpoons H_2(salchn)(o) + Zn^{2+} \quad (1)$$

Figure 3b shows the extraction enhancement of Eu(III) as a function of Zn(II) concentration in the organic phase. Each point that refers to a given extraction (the value of Y-axis) in Figure 3a corresponds to that in Figure 3b. The enhancement smoothly changes with increasing Zn(II) concentration. The extraction data can be generally represented with the following equation:

$$D = \frac{[EuA_3]_o + [EuA_3B]_o + \ldots}{[Eu^{3+}]} = K_{ex}[H^+]^{-3}[HA]_o^3(1 + \Sigma\overline{\beta}_n[B]_o^n) \quad (2)$$

where HA and B represent Hpta and the Schiff base, respectively, and K_{ex} is the extraction constant of EuA_3 ($K_{ex} = [EuA_3]_o[H^+]^3[Eu^{3+}]^{-1}[HA]_o^{-3}$). The data were analyzed by a successive approximation method according to Equation 2 to be 5.56 ± 0.05 as $\log\overline{\beta}_1$. The value agrees with that from luminescence data within experimental accuracy. The species, H_2(salchn), produced on the contact of Zn(sal*c*hn) with water, and $Zn(pta)_2$ produced on the extraction of Zn(II) with Hpta, may influence the extractability of Eu(III). Then, the extraction of Eu(III) with Hpta and H_2sal*c*hn was also measured and showed in Figure 3a (●) as a function of the initial H_2(sal*c*hn) concentration. The enhancement is much smaller than that with Zn(sal*c*hn) over the concentration range studied. It suggests that H_2sal*c*hn does not influence the extraction enhancement with Zn(sal*c*hn). To examine the influence of $Zn(pta)_2$ on the extractability of Eu(III), the extraction of Zn(II) with Hpta was checked, giving -9.60 ± 0.05 as log $K_{ex(ZnA_2)}$. Accordingly even at pC_H 5.0, the proportion of $Zn(pta)_2$ is only ca. 0.6% for all Zn(II) in the organic phase, because in the present study, 0.05 M Hpta was used. When Zn ion was added into aqueous phase, the extractability with Hpta and H_2(salchn)(●), as well as with Hpta and Zn(sal*c*hn)(Δ), was improved because of increasing effective Zn(sal*c*hn) as shown in Figure 3b. Special difference between Zn(sal*c*hn) and H_2(sal*c*hn) was not observed. The extraction enhancement seems only to depend on the Zn(II) concentration in the organic phase. Even if H_2(sal*c*hn) is used as the ligand, it may form the complex with Zn ion in the aqueous phase, and the complex Zn(sal*c*hn) will function as an effective synergist. In other words, the binuclear complex $Eu(pta)_3$Zn(sal*c*hn) can be easily formed by the simultaneous extraction of Eu(III) and Zn(II) with Hpta and H_2(sal*c*hn).

Luminescence of the Extracted Species

The pattern and the intensity at peak of the luminescence spectra of the $CHCl_3$ containing 1 x 10^{-4}M Eu(III) and 1 x 10^{-4}M Zn(II) extracted when Eu(III) was extracted with Hpta and Zn(sal*c*hn) at pC_H 4.7 was similar to that of the mixed solution between $Eu(pta)_3$ and Zn(sal*c*hn) (See Figure 2). Then it was concluded that using synergistic extraction of Eu(III) with Hpta and Zn(sal*c*hn), the binuclear complex can be prepared. However, it was found that the presence of $Zn(pta)_2$ gives serious quenching to the

luminescence of $Eu(pta)_3$. Then the extraction should be performed at $pC_H < 5$ to avoid the extraction of $Zn(pta)_2$.

To use as phosphor, it is required for the particle to be fine and uniform. The concentration of the ternary complex obtained as the extracted species can be controlled, and the distribution of the binuclear complex in solution is uniform differing from that in the solid. When the solution is spread over any carrier such as alumina or zeolite and dried, uniform and fine particles should be obtained.

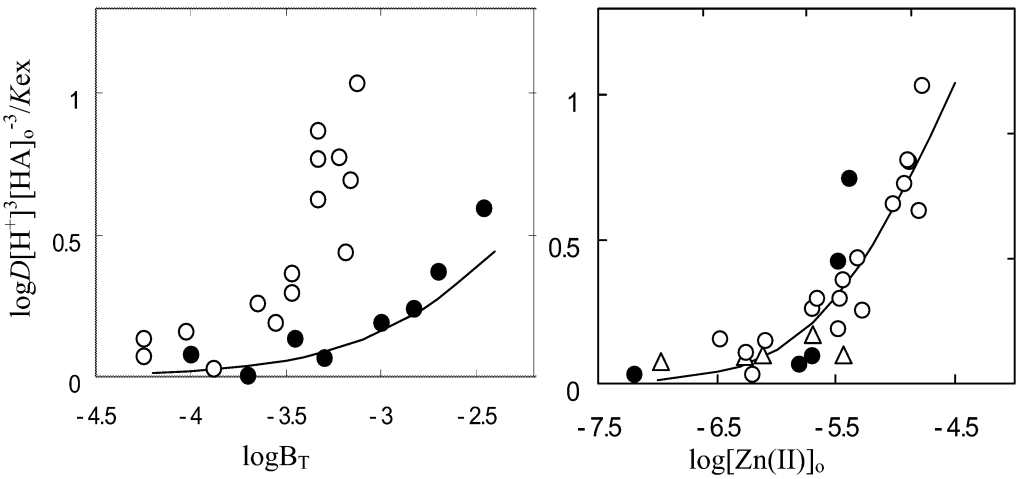

Figure 3. Extraction enhancement of Eu(III) when it was extracted with 0.05M Hpta and Zn(salchn) (○) or with 0.05M Hpta and H_2(salchn)(●). (a) The extraction enhancement as a function of the initial ligand concentration.The solid curve was calculated from $Y = (1 + 10^{2.65}X)$. (b) The extraction enhancement as a function of Zn(II) concentration in the $CHCl_3$.The solid curve was calculated from $Y = (1 + 10^{5.6}X)$. The symbol of Δ and ● represents the extraction of Eu(III) with Hpta and H_2(salchn) (●) or with Hpta and Zn(sal*c*hn) (Δ) in the presence of Zn(II) in the aqueous phase.

CONCLUSION

Binuclear complex, $Eu(pta)_3Zn$(sal*c*hn), was easily and rapidly prepared by shaking aqueous solutions containing Eu(III) and Zn(II) with $CHCl_3$ containing Hpta and Zn(sal*c*hn) or H_2(sal*c*hn). The binuclear complex showed much stronger luminescence than $Eu(pta)_3H_2$(sal*c*hn) as well as $Eu(pta)_3$ itself. Since fine and uniform particles are required as effective phosphor, the preparation by solvent extraction has an advantage, because the distribution of the binuclear complex in solution is uniform, differing from that in the solid. Accordingly, the use of the offered synergistic extraction should be a promising method for preparation of binuclear complexes, which can be applied as phosphor.

ACKNOWLEDGMENTS

This research is partly supported by a Grant-in-Aid for Scientific Research(C), No. 19550096 from the Ministry of Education, Science, Sports, and Culture, Japan.

REFERENCES

1. "D-f Heteronuclear Complexes: Synthesis, Structures and Physicochemical Aspects", *Coord. Chem. Rev.*, **219-221**, 379-3414 (2001).
2. I. Ramade, O. Kahn, Y. Jeannin, and F. Robert, "Design and magnetic properties of a magnetically isolated $Gd^{III}Cu^{II}$ pair. Crystal structures of $[Gd(hfa)_3Cu(salen)]$, $[Y(hfa)_3Cu(salen)$, $[Gd(hfa)_3Cu(salen)(Meim)]$, and $[La(hfa)_3(H_2O)Cu(salen)]$," *Inorg. Chem.,* **36**, 930-936 (1997).
3. Y. Hasegawa, S. Kumaki, and K. Tanaka, "Synergistic Extraction of Lanthanoids(III) with β-Diketone and Lewis Bases and the Application to Preparation of Binuclear Complexes," Proceedings of ISEC 05, Beijing, 2005; pp. 252-258.
4. T. Sekine and Y. Hasegawa, Solvent Extraction Chemistry, Marcel Dekker, New York, 1974
5. T. Ito and Y. Hasegawa, "Some observations on the synergistic extraction behavior of rare earths(III) with pivaloyltrifluoroacetone and neutral bidentate ligands," *Solvent Extr. Res. Develop., Jpn.*, **8**, 47-62 (2001).

NEPTUNIUM ESTIMATION IN DISSOLVER AND HIGH-LEVEL-WASTE SOLUTIONS

P. N. Pathak, D. R. Prabhu, A. S. Kanekar, and V.K. Manchanda*

Radiochemistry Division, Bhabha Atomic Research Centre, Trombay, Mumbai - 400 085, India. Corresponding author email address: vkm@barc.gov.in

ABSTRACT

This papers deals with the optimization of the experimental conditions for the estimation of ^{237}Np in spent-fuel dissolver/high-level waste solutions using thenoyltrifluoroacetone as the extractant.

INTRODUCTION

Due to the relatively long half-life and pentavalent oxidation state of ^{237}Np, there is a concern over its environmental behavior in natural waters. This radionuclide is expected to be formed during the irradiation of uranium in thermal reactors. The estimation of exact quantities of minor actinides (viz., Np, Am, and Cm) is essential prior to their separation from dissolver/high-level waste (HLW) solutions. During spent-fuel reprocessing, the emphasis is mainly on plutonium and uranium. ^{237}Np ($t_{1/2} = 2.16 \times 10^6$ years) is one of the longest-lived minor actinides present in the dissolver/HLW solutions, however. ORIGEN-2 computer code has been employed to calculate the production of minor actinides in the discharged fuel [1-3].

^{237}Np is produced in uranium fuelled reactors (in kg quantities) by the successive neutron capture of ^{235}U followed by beta decay. It can also be formed as an alpha-decay product of ^{241}Am ($t_{1/2} = 432.7$ y) [4,5]. There is interest in the recovery of ^{237}Np, as it can be used as a target for the production of ^{238}Pu, which has potential applications in compact power sources. Neptunium can exist in three oxidation states, viz. Np^{4+}, NpO_2^+, and NpO_2^{2+} in aqueous solutions. However, it exists primarily as the pentavalent $Np(V)O_2^+$ ion in natural oxic waters [6,7]. The solubility of NpO_2^+ is relatively high (4.4×10^{-4} M, pH 7.00±0.10) as the cation has a low affinity for many geological minerals, resulting in relatively short retention times in various matrices and high mobility [8]. Neptunium ions in different oxidation states exhibit different extraction behavior with tri-*n*-butyl phosphate (TBP) under PUREX process conditions [5,6,9]. These oxidation states are interconvertible depending on the nitric acid/nitrous acid concentrations. Accordingly, the knowledge of the exact quantities of Np in dissolver/HLW solutions is important prior to the reprocessing and actinide partitioning steps to account for its distribution/losses in various streams.

The separation and determination of neptunium from uranium, plutonium, americium, fission products, activation products, structural materials, and process chemicals, has been attempted using an HTTA (2-thenoyltrifluoroacetone)-based extraction method [10]. This method is based on the different extractabilities of Pu(III), Np(IV), U(VI) etc., from acidic media. However, due to the higher extraction of Pu(IV), the major difficulty in the radiometric analysis of ^{237}Np is expected from the interference due to Pu, and from the dissolved degradation products of TBP, viz. monobutylphosphoric acid (MBP). The separation of Pu(IV) and Np(IV) is very difficult, and therefore Pu has to be reduced to Pu(III) by using suitable reductants. Moore demonstrated that the HTTA extraction method was efficient for the selective extraction of Np(IV) from 1 M HCl/HNO_3 medium over U, Pu, and Am under tracer concentrations [10]. However, it becomes important to evaluate this process under process conditions wherein large amounts of U, Pu, Am, and the degraded products of TBP are present in HLW solutions.

This paper evaluates the effects of different experimental conditions, viz. aqueous phase acidity, nature of acid, time of equilibration, and the degradation products of TBP on the extraction behavior of Np(IV) using HTTA as the extractant.

EXPERIMENTAL

^{239}Np ($t_{1/2}$ = 2.3 d) was used as the tracer, and gamma spectrometry was employed to quantify the yield of the Np extraction experiments. It was prepared by irradiating uranium (U_3O_8) in the APSARA reactor at a flux of ~10^{12} n/cm^2/s for 6 hr. The irradiated target was dissolved in nitric acid, and ^{239}Np was obtained by HTTA (Aldrich) extraction at 1 M HNO_3 after reduction to Np(IV) using reductants. A solution of 0.5 M HTTA in xylene was used as the extractant, and hydroxylamine hydrochloride ($NH_2OH{\cdot}HCl$, Aldrich) and Fe(II)Cl_2 salt (Loba Chemicals) were used for reduction of Np to Np(IV). The stock solutions of reductants were prepared by dissolving the desired quantities for 5 M $NH_2OH{\cdot}HCl$ and 2 M Fe(II) solutions, respectively [10]. of Fe powder (20 mg) was also added to ensure quantitative reduction of Np to Np(IV).

Table 1. Composition of simulated PHWR-HLW solution; 6500 MWD/te burn up; cooling period, 10 years

Element	g/L	Element	g/L
Fe	0.49	Ba	0.06
Cr	0.12	La	0.13
Ni	0.10	Ce	0.06
Na	5.5	Pr	0.09
K	0.22	Nd	0.12
Mn	0.22	Sm	0.086
U	6.0	Y	0.06
Sr	0.02	Zr	0.004
Cs	0.32	Mo	0.14

A stock solution of uranium (300 g/L) was used for Np(IV) extraction experiments under the dissolver solution conditions. Generally, a mixture of 1 M $NH_2OH{\cdot}HCl$ + 0.25 M Fe(II) was used as reductant, and 10 minutes waiting period was used for the reduction process. 10 M HNO_3 was used as the stripping solution. Table 1 lists the constituent metal ions present in simulated HLW solution for Pressurised Heavy Water Reactor (PHWR) spent fuel. Alpha spectrometry or liquid scintillation counting was done for ^{233}U, ^{237}Np, ^{239}Pu, and ^{241}Am., while gamma spectrometry was carried out for ^{239}Np. The distribution ratio (D_M) was defined as ratio of concentration (expressed in terms of activity) of metal ions in the organic phase to that in the aqueous phase. The deviations in experimental measurements are within error limits (±5%).

RESULTS AND DISCUSSION

Pure Tracer Experiments

Table 2 compares the distribution data of U, ^{239}Np, ^{239}Pu, and ^{241}Am under tracer conditions in the presence of 1 M $NH_2OH{\cdot}HCl$ + 0.25M Fe(II) as reductants at 1 M HCl and using 0.5 M HTTA/xylene as the extractant. The data clearly suggested that metal ions like U, Pu, and Am are extracted poorly under the experimental conditions. Quantitative stripping (>99.9%) of extracted Np was achieved in a single contact with 10 M HNO_3.

Table 2. Extraction of metal ions from HCl medium under tracer conditions Reductant, 1 M $NH_2OH{\cdot}HCl$ + 0.25M Fe(II) at 1 M HCl; O/A = 1, T = 25 °C

Metal ion	D_M
Np	280
U	2.5×10^{-3}
Pu	6.1×10^{-3}
Am	1.5×10^{-3}

Np Estimation in SHLW

To test the feasibility of ^{237}Np alpha counting in the simulated HLW solution, two solvent-extraction experiments were carried out independently using ^{239}Np (gamma spectrometry) and ^{237}Np (alpha spectrometry) tracers. Quantitative extraction (>99.9%) was observed in both the cases. Even though direct planchetting of the Np/HTTA extract is proposed for alpha spectrometry, it was observed that alpha counting would be better after stripping with 10 M HNO_3 [10]. Table 3 shows that the extraction of metal ions follows the order Np(IV) > Pu > U > Am. Even though the extraction of U, Pu, and Am appears to be lower under the conditions of present study, it may be of interest to scrub out the extracted metal ions in view of their relatively higher concentrations and specific activities to get an alpha spectrum of ^{237}Np free from Pu and Am. Extraction of Fe(III) was also observed along with that of Np. 1 M acid (HNO_3/HCl) solution containing the reducing mixture was proposed for use as the scrub solution. Alternatively, repeated extraction cycles for stripped ^{237}Np from the HTTA/xylene phase are desired.

Table 3. Extraction of metal ions from simulated HLW conditions. Reductant,: 1 M $NH_2OH{\cdot}HCl$ + 0.25M Fe(II); O/A = 1, T = 25 °C

Metal ion	D_M	
	1 M HNO_3	1 M HCl
Np	~100	~100
U	4.2×10^{-3}	--
Pu	6.1×10^{-3}	4.5×10^{-3}
Am	2.3×10^{-3}	1.4×10^{-3}

Extraction Kinetics

The extraction kinetics of Np(IV) by HTTA/xylene were also investigated under simulated HLW conditions at 1 M acidity (HCl/HNO_3). The sample solution was prepared by evaporating to dryness the simulated HLW solution with ^{239}Np and dissolving in 1 M HCl/HNO_3 containing the reducing mixture 1 M $NH_2OH{\cdot}HCl$ + 0.25M Fe(II). The waiting period before extraction was maintained as 10 minutes to allow complete reduction of Np to Np(IV). Table 4 shows the variation of percent extraction with time of equilibration. It is evident that even 10 minutes equilibration time is sufficient for quantitative extraction of Np from the aqueous phase under HLW conditions [10]. However, for the sake of convenience, the reduction and extraction periods (for Np and Pu) were maintained as ~15 and 30 minutes, respectively. Even though both 1 M HNO_3 and 1 M HCl showed quantitative extraction of Np from the simulated HLW solutions, the latter was preferred in view of the oxidizing nature of HNO_2 present in HNO_3.

Table 4. Extraction kinetics of Np under from 1 M HCl under simulated HLW conditions. Reductant, 1 M $NH_2OH{\cdot}HCl$ + 0.25M Fe(II); O/A = 1, T = 25 °C

Time, min.	% Extraction
5	99.3
10	99.6
20	99.7
30	99.7

Effect of Degradation Products of TBP

TBP undergoes radiolytic degradation during spent-fuel reprocessing. Therefore, Np(IV) extraction behavior was investigated in the presence of the radiolytic degradation products of TBP. Synthetic solutions containing dissolved degradation products of TBP in simulated HLW were prepared by irradiating TBP in a gamma-irradiation chamber in contact with nitric acid. This acid was used for the sample preparation of simulated HLW solution. Typically, under simulated HLW conditions, the D_{Np} value decreased from ~100 (without degradation product) to 10 (for TBP/HNO_3 irradiated for a dose of 50 MR). Under this condition, the presence of Fe powder in the aqueous phase suppressed the Np extraction significantly (D_{Np} = 0.26), due to loading of HTTA phase by Fe(III).

The optimized conditions for Np estimation are (i) extraction and scrub, 1 M $NH_2OH{\cdot}HCl$ + 0.25 M $FeCl_2{\cdot}4H_2O$ in 1 M HCl; (ii) stripping, 10 M HNO_3. An excess of Fe(III) in the stripped aqueous phase can be removed with 0.5 M TTA/xylene.

Np Estimation in Dissolver Solution

^{237}Np estimation in dissolver solution is free from the interferences of degradation products of TBP. However, the presence of large concentration of plutonium can interfere in the estimation process of Np. Extraction experiments were done in the presence of 300 g/L U at 1 M HNO_3 containing the reducing mixture 1 M $NH_2OH{\cdot}HCl$ + 0.25M Fe(II). Table 5 clearly shows that the extraction of metal ions like U, Pu, and Am is negligible under the conditions of the experiments. However, the feed solution containing Np, Pu, and Am in 300 g/L U at 1 M HNO_3, showed interference in alpha spectrum due to Pu (4.8 MeV) and Am (5.4 MeV) and planchett was of poor quality due to deposition of Fe and U. Therefore, prior scrubbing of U, Pu, Am, and Fe is desirable for alpha spectrometry. It is also proposed to irradiate the stripped ^{237}Np in reactor to produce ^{238}Np and assay by gamma counting.

Table 5. Extraction of metal ions from 1 M HNO_3 in presence of 300 g/L U. Reductant, 1 M $NH_2OH{\cdot}HCl$ + 0.25M Fe(II); O/A = 1, T = 25 °C

Radionuclide	D_M
^{233}U	$\sim 10^{-3}$
^{239}Pu	$\sim 10^{-3}$
^{241}Am	$<10^{-3}$
^{237}Np / ^{239}Np	~100

CONCLUSIONS

The concentration of ^{237}Np in the simulated HLW and in dissolver solutions can be determined using 0.5 M HTTA/xylene as the extractant at 1 M HNO_3 containing 1 M $NH_2OH{\cdot}HCl$ + 0.25 M Fe(II) as the reductants. Quantitative extraction (>99.9%) of Np(IV) was achieved in single contact for tracer as well as for the simulated HLW solution. The extraction of metal ions follows the order Np(IV) > Pu > U > Am. Extraction of Fe(III) was also observed along with that of Np. In view of the higher concentrations of Fe, Pu, and Am, and the specific activities of Pu and Am, a scrub step is required for alpha spectrometry of ^{237}Np. Extracted Np(IV) was quantitatively stripped by 10 M HNO_3 in a single contact. Both 1 M HNO_3 and 1 M HCl showed quantitative extraction of Np from the simulated HLW solutions, the latter was preferred due to the oxidizing nature of HNO_2 present in HNO_3. The degradation products of TBP in simulated HLW suppressed the extraction of Np. However, there was no problem during the assay of ^{237}Np in dissolver solution. The optimized conditions for Np estimation are (i) extraction and scrub 1 M $NH_2OH{\cdot}HCl$ + 0.25 M $FeCl_2{\cdot}4H_2O$ in 1 M HCl; (ii) stripping 10 M HNO_3. Excess of Fe(III) in the stripped aqueous phase can be scrubbed with 0.5 M TTA/xylene.

REFERENCES

1. A. G. Croff, "ORIGEN-2.1, Isotope generation and depletion code, matrix exponential method," Report ORNL-5621, 1980.
2. A. G. Croff, "ORIGEN-2: Versatile Computer Code for calculating the nuclide composition and characteristics of the nuclear materials," *Nucl. Tech.*, **62**, 335 (1983).
3. S. Mukerji, P.D. Krishnani, and R. Srivenkatesan, Radio-toxicities of the minor actinides in the discharged PWR, PHWR, and AHWR fuel, Nuclear Fuel Cycle Technologies: Closing the Fuel Cycle, B. Raj, P.R. Vasudeva Rao (Eds.), p.395, 2006.
4. R. C. Thomson, *Radiation Research,* **90**, 1 (1982).
5. M. V. Ramaniah, S. K. Patil, V. V. Ramakrishna, R. Swarup, and A. Chadha, "Process chemistry of neptunium, Part – I," Report BARC-428, 1969.
6. N. Srnivasan, M. V. Ramaniah, S. K. Patil, V. V. Ramakrishna, R. Swarup, A. Chadha, and G.V.N. Avadhany, "Process chemistry of neptunium, Part – II," Report BARC-736, 1974.
7. B. Allard, Actinides in Perspective, N. M. Edelstein (Ed.), Pergamon Press, Oxford, 1982.
8. H. Nitsche, N. M. Edelstein, *Radiochim. Acta*, **39**, 23 (1985).
9. V. A. Drake, "Extraction Chemistry of Neptunium," Science and Technology of Tributyl Phosphate, W. W. Schulz, L. L. Burger, J. D. Navratil, and K. P. Bender, Eds., Vol. 3, Chapter 3, p. 123, CRC Press, Inc., Boca Raton, Florida, 1990.
10. F. L. Moore, *Anal. Chem.*, **29**, 941 (1957).

THE USE OF VOLTAMPEROMETRY IN THE DETERMINATION OF THE ACTIVE COMPONENTS OF COMMERCIAL EXTRACTANTS

M. P. Elizalde, M. S. Rúa, A. Almela, and M. Huebra

Department of Analytical Chemistry, Faculty of Science and Technology, University of the Basque Country, P. O. Box 644, 48080 Bilbao, Spain.
Corresponding author email address: maria.elizalde@ehu.es

ABSTRACT

The use of voltamperometric techniques for the determination of the active components in commercial extractants containing 5-nonylsalicylaldoxime and 2-hydroxy-5-nonylacetophenoneoxime is presented. Among the different components in the commercial extractants, only the active ones are electroactive, giving rise in hydroalcoholic medium to reduction or oxidation peaks that allow their determination. Calibration and statistical parameters are reported. As an application, percentages of 5-nonylsalicylaldoxime in several commercial extractants have been determined. The presence of small amounts of 2-hydroxy-5-nonylacetophenoneoxime in some of the samples has also been detected.

INTRODUCTION

Commercial extractants based on alkylsalicylaldoxime or alkylacetophenoneoxime have been used for copper removal from industrial acidic effluents. It is well known that, in order to carry out fundamental metal extraction studies, the composition of the extractants must be known; and therefore the development of methods of quantification methods of their active components becomes necessary. Apart from the information given by the suppliers; little is known about the composition of these reagents. Gas chromatography-mass spectrometry and high performance liquid chromatography have been widely applied both to the characterization and to the analysis of the commercial extractants [1].

Voltamperometric techniques are widely used for trace determination of metal ions and other compounds in different fields such as pharmacology, medicine, agriculture, food analysis, organic synthesis, etc. However, these techniques are not very usual in the solvent-extraction field, and few works are found on the quantification of chelating extractants [2-5], despite the fact that voltamperometric methods usually provide low detection limits that could be used to quantify traces of the extractants in the aqueous phases during the liquid-liquid extraction processes.

Taking into account that the extractants usually are complex mixtures of isomeric compounds, chromatographic techniques are able to identify these different compounds

present in the commercial reagents, whereas voltamperometric techniques can provide simple methods of determination of the active components in the case that these are electroactive species. The sensitivity of the voltamperometric methods can be also useful for determination of the extractants in aqueous solutions at very small concentrations such as those currently obtained in solvent-extraction systems.

In the present work, the determination of the active components of commercial extractants based on 5-nonylsalicylaldoxime and 2-hydroxy-5-nonylacetophenone-oxime, LIX 622N, LIX 860N-I, LIX 860N-IC, Acorga P5100, Acorga PT5050 and LIX 84 has been carried out by differential pulse voltamperometry. For this purpose, pure 5-nonyl-salicylaldoxime and 2-hydroxy-5-nonylacetophenoneoxime have been previously obtained from commercial Acorga P5100 and SME 529 extractants.

EXPERIMENTAL

Reagents and Solutions

The commercial extractants LIX 622N (two different lots), LIX 860N-I, and LIX 860N-IC were kindly supplied by Cognis (Little Island, Co., Cork, Ireland), LIX 84 by Henkel Corporation (now Cognis). Acorga P5100 and Acorga PT5050 were donated by Avecia (Phoenix, AZ, USA) and SME 529 by Shell Chemical Co.

Stock solutions of the extractants in methanol (Carlo Erba, p.a.) were prepared. Isotridecanol-N (Basf) and *p*-nonylphenol (Acros) were also used.

Britton–Robinson buffer solution was prepared from H_3PO_4 (Carlo Erba, p.a.), HAc (Carlo Erba, p.a), and H_3BO_3 (Fluka, p.a.) (0.04 M each). HCl or NaOH at 5 M were used to adjust different pH values. KCl (Panreac, p.a.) was used as the ionic medium.Pure 5-nonylsalicylaldoxime (99.0% purity) and 2-hydroxy-5-nonylacetopheno-neoxime (98.8% purity) were obtained from Acorga P5100 and SME 529 industrial extractants, respectively, according to the method proposed by Preston and Whewell [6].

Apparatus

Voltamperometric measurements were performed with an μAutolab/GPES (General Purpose Electrochemical System) Package. μAutolab is equipped with a potentiostat model III and was connected to a Metrohm 647 VA stand. A conventional electroanalytical cell (50 mL) was used. The working electrode was a hanging mercury drop electrode (HDME) (Metrohm) in the reduction studies, whereas a platinum electrode was used for oxidation studies. Ag/AgCl (3 M KCl) as reference electrode and platinum wire as auxiliary counter electrode were used. pH measurements were carried out with a Radiometer-Copenhagen pHM-93 pHmeter.

Procedure

Differencial Pulse Voltamperometry (DPV) mode was applied for the study of the reduction and oxidation of the active components. All the experiments were performed at 298 ± 0.5 K. Dissolved air was removed from the solution by bubbling oxygen-free

nitrogen through the cell for 4 minutes, and after 5 seconds a scan was initiated. It was proved that the measured solutions remained stable at least for one hour.

The following parameters were optimized in reduction studies at the mercury electrode: 0.012 s modulation time, 0.2 s time interval, 0.01 V potential step, and 0.075 V modulation amplitude. Oxidation scans with the platinum electrode were carried out using the same parameter values except 0.15 s (time interval) and 0.002 V (potential step).

RESULTS

In order to look for the best experimental conditions for the voltamperometric study of the extractants, chemical and instrumental variables were optimized. First, a hydroalcoholic medium was selected in order to obtain the high peak intensity and avoid solubility problems: 40% methanol and 0.1 M KCl to adjust the ionic strength. On the other hand, the maximum intensity was found at acidic pH values and pH = 2 (reduction) or 0.5 (oxidation) were selected. Instrumental values were also optimized for the measurements in differential pulse and square-wave modes.

Under these conditions, the extractants LIX 622N, LIX 860N-I, LIX 860N-IC, Acorga P5100, and Acorga PT5050 show a common reduction peak at around -0.78 V. Only two of them, LIX 860N-I and LIX 622N (lot 2), present another small peak at -0.95 V together with the main one at -0.78 V. LIX 84 originates a reduction peak at -0.95 V. On the other hand, all the extractants give rise to oxidation peaks at the platinum electrode near the solvent barrier (0.93 V), as seen in Figure 1b for Acorga P5100 and SME 529.

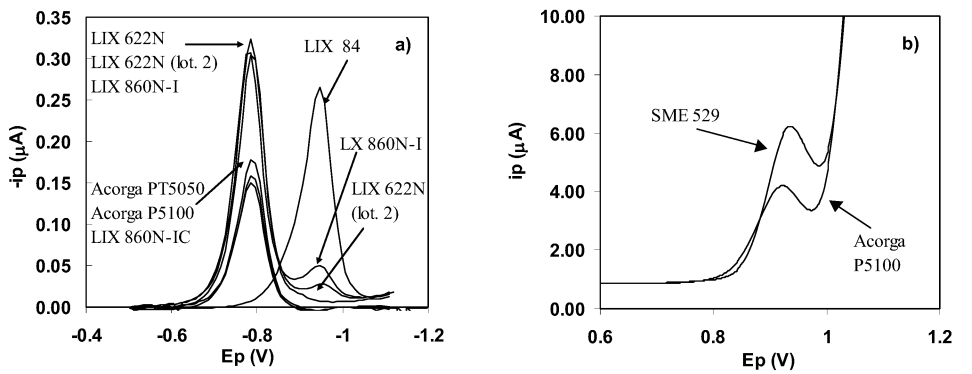

Figure 1: Differencial pulse voltammograms of the commercial extractants in hydroalcoholic medium (40 % methanol, 0.1 M KCl) a: Reduction peaks at pH = 2. b: Oxidation peaks of Acorga P5100 (pH = 0.7) and SME 529 (pH = 0.5)

Moreover, the extractants also contain modifiers such as *p*-nonylphenol (in all cases except Acorga PT5050) or isotridecanol (LIX 622N and Acorga PT5050). No reduction peak was obtained for the reagents *p*-nonylphenol and isotridecanol-N under the same conditions. Moreover, the addition of *p*-nonylphenol and isotridecanol-N to LIX 622N and *p*-nonylphenol to LIX 84 did not modify the peak potentials and intensity. It

can be concluded that 5-nonylsalicylaldoxime and 2-hydroxy-5-nonylacetophenone-oxime are the only electroactive species, their reduction peaks not being affected by the presence of other components in the commercial extractants.

Determination Methods of 5-Nonylsalicylaldoxime and 2-Hydroxy-5-nonylacetophenone- oxime. Analysis of Commercial Extractants

Calibration of 5-nonylsalicylaldoxime (40% methanol, 0.1 M KCl at pH = 2.0) using the pure compound was carried out by measuring the reduction peak intensity obtained by differential pulse voltamperometry at a mercury electrode (Figure 2a). On the other hand, and by measuring the intensity of the oxidation peak obtained at the platinum electrode for pure 2-hydroxy-5-nonylacetophenoneoxime (40 % methanol at pH = 0.5), the calibration curve shown in Figure 2b was obtained. Statistical parameters are collected in Table 1.

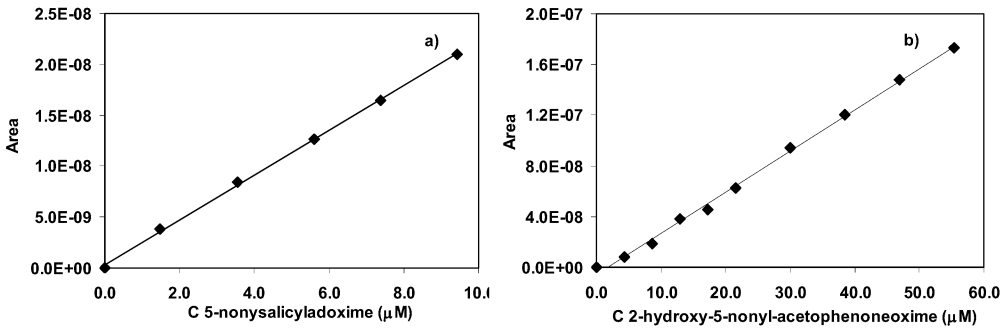

Figure 2: Calibration of the reduction peak of 5-nonylsalicylaldoxime (a) and the oxidation peak of 2-hydroxy-5-nonylacetophenoneoxime (b) by differencial pulse voltamperometry.

Table 1. Statistical parameters of the voltammetric calibration methods

	5-Nonylsalicylaldoxime	2-Hydroxy-5-nonylacetophenoneoxime
Linear range (M)	1.47×10^{-6} - 9.44×10^{-6}	4.32×10^{-6} – 5.53×10^{-5}
Slope ± σ	$(2.20x \pm 0.031) \times 10^{-3}$	$(3.24 \pm 0.058) \times 10^{-3}$
Intercept ± σ	$(3.4 \pm 1.7) \times 10^{-10}$	$(-5.3 \pm 1.7) \times 10^{-9}$
r^2	0.9992	0.997
Detection limit (M)	0.3×10^{-6}	3.0×10^{-6}
Quantification limit (M)	1.1×10^{-6}	1.0×10^{-5}
Intra-day repeatability %R.S.D. (n = 5) at (5.61×10^{-6} M)	1.63	
Inter-day repeatability %R.S.D. (n = 3) at (5.61×10^{-6} M)	2.20	

The next step consisted of the determination of the percentage of 5-nonylsalicyl-aldoxime present in the different commercial extractants. For this purpose, solutions of the extractants LIX 622N (two lots), LIX 860N-I, LIX 860N-IC, Acorga P5100 and

Acorga PT5050 in methanol were prepared and measured in the polarographic cell at the above experimental conditions.

Table 2 collects the percentage of the active component, 5-nonylsalicylaldoxime, present in the industrial extractants LIX 622N, LIX 860N-I, LIX 860N-IC, Acorga P5100, and Acorga PT5050 as well as the percentage of 2-hydroxy-5-nonylacetophenoneoxime in LIX 84 determined through the above calibration curves. Percentages of 5-nonylsalicylaldoxime deduced by this technique are in agreement with those obtained by HPLC [7].

As it has been mentioned, the extractants LIX 860N-I and the newest lot of LIX 622N give rise to a small second reduction peak at -0.95 V (Figure 1a) that can be attributed to the presence in these two extractants of 2-hydroxy-5-nonylacetophenoneoxime. This hypothesis was verified through the application of the standard-addition method to samples of the extractants. Thus, Figure 3a shows the results obtained with the addition of LIX 84 to a sample of LIX 860N-I. It can be appreciated that the peak corresponding to 5-nonylsalicylaldoxime remains invariable, whereas the intensity of the reduction peak of 2-hydroxy-5-nonylacetophenoneoxime increases gradually with the addition of LIX 84, thus indicating that its active component is present in LIX 860N-I. In a similar way LIX 622N-I (lot 2) was analyzed. The results obtained are illustrated in Figure 3b, where the variation of the reduction-peak intensities for both extractants with the addition of LIX 84 is shown. From this plot, and taking into account the purity of LIX 84, percentages of 2-hydroxy-5-nonylacetophenoneoxime present in these two extractants have been obtained and are collected in Table 2.

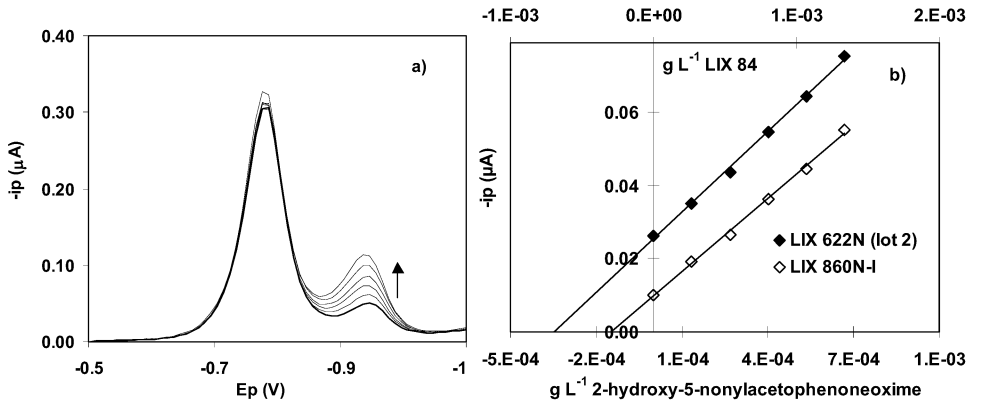

Figure 3. a: Differential pulse voltamperograms of a hydroalcoholic solution (pH=2) of LIX 860N-I with the addition of LIX 84. b: Addition standard method applied to LIX 860N-I and LIX 622N (lot 2).

CONCLUSIONS

Voltamperometric techniques have shown to be useful for the determination of the active components in commercial extractants, since among their components, only these species behave as electroactive. The reduction peak of 5-nonylsalicylaldoxime at a mercury electrode and the oxidation peak of 2-hydroxy-5-nonylacetophenoneoxime at a

platinum electrode obtained in hydroalcoholic media by differential pulse voltamperometry have been used to develop two determination methods of these components.

Percentages of 5-nonylsalicylaldoxime in the commercial extractants LIX 622N, LIX 860N-IC, LIX 860N-I, Acorga P5100, Acorga PT5050, and 2-hydroxy-5-nonylacetophenoneoxime in LIX 84 are reported. Finally, the presence of 2-hydroxy-5-nonylacetophenoneoxime has been detected in two of the extractants, LIX 860N-I and a new lot of LIX 622N. Percentages of 2-hydroxy-5-nonylacetophenoneoxime in the extractants using the method of standard additions have been also deduced.

Table 2. Percentages (w/w) of 5-nonylsalicylalodoxime and 2-hydroxy-5-nonylaceto phenoneoxime in commercial extractants

Extractant	% 5-Nonylsalicylaldoxime	% 2-Hydroxy-5-nonyl-acetophenoneoxime
LIX 622N (lot 1)	54.2 ± 3.1	-
LIX 622N (lot 2)	48.6 ± 2.2	3.35 ± 0.83
LIX 860N-I	47.7 ± 2.3	7.6 ± 1.0
LIX 860N-IC	70.6 ± 3.7	-
Acorga P5100	50.8 ± 2.8	-
Acorga PT5050	56.0 ± 3.5	-
LIX 84	-	49.8 ± 3.4

ACKNOWLEDGMENTS

The authors thank the University of The Basque Country for the financial support (Project Nº 00171.310-E-15418/2003).

REFERENCES

1. J. Szymanowski, Hydroxyoximes and Copper Hydrometallurgy, CRC Press, Boca Ratón, Florida, 1993.
2. M. J. Citores, R. M. Alonso, and L. A. Fernández, "Voltammetric study of the oxine-based extractant Kelex 100," *Electroanalysis*, **4**(7), 733-736 (1992).
3. M. M. Huebra, M. P. Elizalde, and M. Castresana, "Electrochemical study of chelating extractants: LIX 34," *J. Electroanalysis*, **6**, 785-790 (1994).
4. A. Abelairas. M. J. Puertollano, R. M. Alonso, M. P. Elizalde, R. M. Jiménezy, and M. M. Huebra, "Voltammetric Study of the Extractant 4-methyl-N-8-quinolinylbenzene-sulfonamide at a Carbon Paste," *Analyst*, **119**, 323-326 1994.
5. I. Alava, M. P. Elizalde, and M. M. Huebra, "Electrochemical study of the industrial extractant LIX 54," *Analyst*, **120**, 1069-1072 (1995).
6. J. S. Preston and R. J. Whewell, "Purification and acid-base properties of hydroxyoxime extractants for copper," *J. Inorg. Nucl. Chem.*, **39**, 1675-1678 (1977).
7. A. Ocio, M. Elizalde, and J. A. Prieto, "Determination of 5-dodecylsalicylaldoxime and 5-nonylsalicylaldoxime in Commercial Extractants by HPLC with Photometric Detection," *J. Chromatography A*, **1032**, 129–132 (2004).

AQUEOUS IN ORGANIC ENTRAINMENT ANALYSIS

K. R. Barnard

The Parker Centre (CSIRO Minerals), P. O. Box 7229 Karawara, WA 6152, Australia.
Corresponding author email address: Keith.Barnard@csiro.au

ABSTRACT

Karl Fischer (KF) titration was found to be a useful technique for measuring the aqueous content in solvent-extraction organic phases down to low ppm levels with good reproducibility. It was found to be independent of aqueous-phase pH. KF analysis before and after centrifugation enables determination of dissolved and entrained water levels. Addition of isopropanol as a cosolvent to water-containing organic solutions dissolves the aqueous content of the organic phase, thereby overcoming issues associated with ongoing disentrainment subsequent to sampling. Application of this cosolvent procedure would enable site-based investigations of sampling protocol to be undertaken in an effort to develop a more consistent sampling procedure.

INTRODUCTION

Hydrometallurgical solvent-extraction (SX) processes inevitably result in some dissolution and entrainment of aqueous phase in the organic phase (A-in-O), and organic phase in the aqueous phase (O-in-A). A-in-O entrainment/dissolution can result in cross-contamination of aqueous streams, sometimes with severe consequences [1]. O-in-A entrainment/dissolution can result in the loss of valuable organic reagents and organic contamination of downstream processes [2]. The extent of entrainment occurring can be a function of a range of factors including the physical hydrodynamics of the mixing vessel, operating continuity, and the chemistry of the system [3,4]. Some methods to minimize entrainment in operating systems and some ramifications of O-in-A entrainment in particular have been listed previously [5].

Entrainment levels are regularly analyzed at operating sites, although feedback from several operations in 2003 indicated a general dissatisfaction with the accuracy of the O-in-A sampling methods and analysis procedures used. Although generally less important, similar issues apply to A-in-O entrainment/dissolution.

There are a number of techniques available for measuring aqueous contents in oil or other organic phases [6], two of which are centrifugation and Karl Fischer (KF) analysis. Centrifugation using specialized tubes fitted with a capillary has been used at several sites to monitor entrained aqueous, but it does not measure chemically dissolved water and suffers from poor reproducibility.

KF titration is the most widespread technique for the determination of total water contents in organic solvents [7] and permits the determination of total aqueous content in an organic solution. KF analysis of an organic solution before and after centrifugation can permit the total, dissolved, and therefore entrained aqueous volumes to be determined.

Accurate assessment of entrainment levels is complicated by ongoing disentrainment of immiscible phases with time. Central to any entrainment analysis technique is the need to develop and maintain consistent sampling and subsampling protocols that provide a sample representative of the bulk at the time of sampling. Of these, a subsampling procedure that overcomes the effect of ongoing disentrainment subsequent to sampling is required before any attempt can be made to assess a sampling protocol for consistency.

The present work aimed to assess the applicability of the KF procedure to analyze both acidic and alkaline water content in SX organics and assess the merits of three subsampling protocols (manual agitation, surfactant addition, and cosolvent addition) in an effort to develop a consistent and reliable A-in-O subsampling procedure.

EXPERIMENTAL

All aqueous determinations were carried out by the KF method using a Mettler DL70 titrator fitted with KF accessories. Organic samples were titrated with Hydranal® composite KF Reagents 1 and 5 in dried methanol or KF solvent medium to a potential of -5 mV, detected with a platinum electrode connected to a polarization source and set to achieve a starting potential more negative than – 150 mV. (Reagent 5 is the same as Reagent 1, just five times more concentrated). The composite KF reagents were initially calibrated using sodium tartrate dihydrate, then subsequently using known volumes of deionized water.

Using a water-spiked organic solution (Cyanex 272 in Escaid 110), the three subsampling procedures tested included: sampling after vigorous manual shaking in a sealed container [8], sampling after addition of an emulsifying agent and vigorous manual shaking, and sampling after dissolution of aqueous entrainment in the organic phase by addition of isopropanol as a cosolvent. The procedure is summarized in Figure 1.

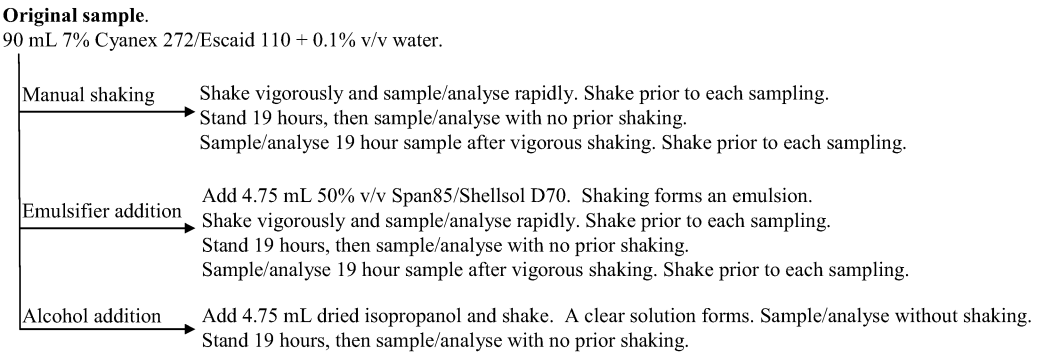

Figure 1. Outline of the three different analysis procedures.

RESULTS AND DISCUSSION

Aqueous Analysis Using Karl Fischer Titration

Organic-free Aqueous Analysis

Titration of eight 0.50 μL replicate injections of deionized water using Hydranal composite 1 resulted in a value of 0.52 mg water, close to the expected 0.50 mg, and with a relative standard deviation of 3%. The precision of the technique was found to increase with the amount of water present, achieved by injection of larger volumes.

As strongly acidic or alkaline conditions can affect the titration time and/or the end point of the KF titration [9], analysis (typically eight 5 μL replicates) of a series of aqueous samples of differing pH using composite 5K (Table 1) was performed. The results afforded values close to those expected within acceptable time limits (<5 min/sample), indicating detection of water in both alkaline (up to 0.27 M NaOH and 12.5% NH_3) and acidic (160 g/L H_2SO_4) solutions did not appear to be problematic. A relative standard deviation of about 1% was noted for the water, ammonia, and sulfuric acid solutions. A larger relative standard deviation (up to 5%) was noted in the presence of NaOH.

Aqueous Analysis in the Presence of SX Organics

KF titration of 10 mL aliquots of both Shellsol 2046 and Acorga M5640 before and after spiking with 0.01% v/v water using composite 1 in methanol solvent yielded the expected results (Table 1), suggesting the presence of these organic SX reagents does not affect the KF titration procedure. Similarly, analysis of other unspiked and water-spiked samples using composite 5K and solvent medium K all afforded expected results.

Table 1. KF-determined water content of selected organic solutions

Sample	Sample volume (mL)	No. of analyses	Water Content (mg/L) Expected Value	Mean Value	SD*	RSD* (%)
Hydranal Composite 1, methanol						
Shellsol 2046	10.0	5		29	1	2
Shellsol 2046 + 1 uL (0.01% v/v) water	10.0	6	129	127	2	2
10% Acorga M5640 in Shellsol 2046	10.0	3		112	9	8
Above + 1 uL (0.01%) water	10.0	4	212	212	7	3
Hydranal Composite 5K, solvent medium K						
Shellsol 2046	3.5	11		23	4	19
Shellsol 2046 + 3 uL (0.1% v/v) water	3.0	6	1023	1038	14	1
7% Cyanex 272 in Escaid 110 centrifuged	3.0	6		243	11	5
7% Cyanex 272 in Escaid 110	3.0	6		263	17	7
Above + 4 uL (0.1%) water	4.0	6	1263	1280	14	1
10% LIX84-I in Shellsol D70	3.0	6		210	10	5
9% LIX84-I + 9% tridecanol in Shellsol D70	3.0	5		717	15	2
Above + 3 uL (0.1%) $(NH_4)_2CO_3$ + NH_3**	3.0	5	1683	1683	27	2

* SD is standard deviation, RSD is relative standard deviation.

** Analysis of 80 g/L $(NH_4)_2CO_3$ + 2 g/L NH_3 found 4.83 mg water in 5.0 uL solution.

Entrained and Dissolved Aqueous Analysis

Determination of total and dissolved water in any given organic sample can be achieved by analysis of samples before and after centrifugation, respectively. Entrainment levels are calculated by subtraction of the dissolved water level from the total water level. Centrifugation at 3000 rpm for 10 minutes was found to be sufficient to remove entrained aqueous phase from both a laboratory-prepared solution of Acorga M5640/Shellsol 2046 and a different sample from a commercial operating plant.

Comparison of Subsampling Procedures

Results from the three subsampling procedures (manual shaking, surfactant addition, and isopropanol addition) of water-spiked Cyanex 272 organic as detailed in Figure 1 are summarized in Table 2 and discussed in turn below.

Table 2. KF-determined water content (after correction for any added isopropanol and surfactant) in water-spiked Cyanex 272/Escaid 110 organic solution after different sample pre-treatments.

Sample	Sample volume (mL)	No. of analyses	Water Content (mg/L)			
			Expected Value*	Mean Value	SD	RSD (%)
50% v/v Span 85 in Shellsol D70	3.0	4		302	17	6
Dried isopropanol	3.0	5		1136	23	2
Manual shaking	3.0	6	1263	1185	12	1
Manual shaking after standing 19 hours	3.0	5	1263	1071	40	4
Manual shaking, then stand 19 hours	3.0	4	1263	324	15	5
Surfactant & shaking	3.0	6	1263	1249	32	3
Surfactant, stand 19 hours, then shake	3.0	5	1263	1127	43	4
Surfactant & shaking, then stand 19 hours	3.0	3	1263	979	23	2
Isopropanol and shaking	3.0	5	1263	1302	19	1
Isopropanol and stand, 16 hours	3.0	6	1263	1299	29	2
Second isopropanol solution	4.0	5	1263	1275	23	2

* From Table 1.

Subsampling after Vigorous Manual Shaking

KF analysis of the 0.1% v/v water-spiked Cyanex 272/Escaid 110 organic samples taken immediately after vigorous manual shaking afforded a reproducible but slightly (6%) lower than expected result (Table 2). Reanalysis of the sample after standing for 19 hours and subsequent vigorous manual shaking gave a result 15% below the expected value, suggesting time between sampling and subsampling/analysis may affect the results obtained using this procedure. This effect may be due to adherence of disentrained aqueous droplets on the glass surface of the jar acting against complete resuspension of the aqueous phase with shaking. Analysis of the sample after standing for 19 hours, but without subsequent vigorous manual shaking, gave a much lower water content, indicative of ongoing disentrainment occurring in the sample upon standing. It is concluded that results obtained from manual shaking of samples are both mixing- and sample storage time-dependent.

Subsampling after Addition of an Emulsifying Agent

Stabilization of entrained aqueous droplets using Span 85 surfactant was attempted. A solution of 50% v/v Span 85 surfactant in Shellsol D70 was found to have a water content of 302 ppm (Table 2). Addition of 4.75 mL to 90 mL organic solution accounted for 15 ppm water in the sample.

Surfactant-spiked samples analyzed immediately after vigorous manual shaking reproducibly yielded the expected result. Reanalysis of the sample after standing for 19 hours gave lower than expected results both before (22% lower) and after (10% lower) vigorous manual shaking. Relative to the manually agitated sample, these results were closer to the expected value, particularly for the non-agitated sample. However, the results remained mixing- and sample storage time-dependent.

Subsampling after Addition of Isopropanol

Addition of isopropanol to 5% v/v in the organic solution enabled dissolution of 0.1% v/v water in the organic phase, thereby avoiding disentrainment issues. The isopropanol used, which was briefly dried over sodium sulfate, was found to have a water content of 1136 ppm (Table 2). Addition of 4.75 mL to 90 mL organic solution therefore accounted for 57 ppm water in the sample. If desired, use of more thoroughly-dried isopropanol would reduce the amount of water added by this procedure.

Results from KF analysis of water-spiked organic samples containing 5% v/v isopropanol (after accounting for associated water addition and sample dilution by its addition) taken after manual shaking afforded a reproducible value within 3% of the expected result (Table 2). Reanalysis of the sample after standing for 16 hours without subsequent shaking afforded an identical result, confirming the sample storage time- and mixing-independent nature of this procedure. Preparation and analysis of a second solution also gave the expected result.

General Applicability of Isopropanol to Dissolve Entrained Aqueous

It was found that addition of isopropanol to approximately 4% v/v in the aliphatic diluent Shellsol D70 enabled the dissolution of 0.1% v/v water. As other organic components such as extractants and modifiers are as, or more polar than, Shellsol D70, the presence of these species should make the organic phasemore amenable to dissolution of water. This implies water dissolution by cosolvent addition should be possible for all SX systems. The typical amount of cosolvent required to be added to ensure complete dissolution of entrained aqueous in the organic sample would be circuit-specific but could be readily determined during any initial scoping study.

This procedure may not be universally applicable. Consideration should be given to the possibility of isopropanol reacting with aldehydes or ketones which may be present in some organic SX samples as a major component (e.g., di-isobutylketone) or potentially even as trace degradation products to give acetals or ketals and water [9]. Aldehydes can also undergo bisulfite addition which consumes water [9]. Where such a reaction(s) is found to occur and believed to materially affect the results, use of alternate cosolvents (e.g., an organic-soluble analog of 2-chloroethanol which is used in the composite K solvent) could be pursued.

Relevance to a Site Operation

As this cosolvent procedure circumvents the effect of subsampling and disentrainment subsequent to sampling, it would permit site-based investigations into sampling protocol such as sampling site, sampling procedure, and sample reproducibility (inter- and intra-operator) to be undertaken in an effort to develop a more consistent and reliable site sampling procedure.

SUMMARY AND CONCLUSIONS

KF titration was found to be a useful technique for measuring the aqueous content of SX organic phases down to low ppm levels. Reproducibility in the order of 2% RSD could readily be achieved down to concentrations of 30 ppm water. The technique was found to be independent of aqueous phase pH. By carrying out KF determinations before and after centrifugation for 10 minutes at 3000 rpm, values for dissolved and physically entrained water can be determined.

Addition of isopropanol as a cosolvent to water-containing organic solutions results in the dissolution and hence stabilization of entrained aqueous in the organic phase. Cosolvent addition circumvents ongoing disentrainment subsequent to sampling, allowing total water content in organic subsamples to be readily and reproducibly determined.

REFERENCES

1. J. N. West and J. W. Connor, "Nifty-Hydrometallurgy in the Sand Dunes," Proc. 1996 AusIMM Annual Conference, AUSIMM, Victoria, Australia, 1996; pp.181-183.
2. L. Farias, A. Reghezza, and G. Slanzi, "Technological Innovations in the Chuquicamata Division SX Plant," Proc. Copper 95-Cobre 95 Vol. III, Electrorefining and Hydrometallurgy of Copper, W. C. Cooper, D. B. Dreisinger, J. E. Dutrizac, H. Hem, & G. Ugarte, Eds. CIMM&P, Canada, 1995; pp. 691-709.
3. I. E. Lewis, "Design of Mixer-Settlers to Achieve Low Entrainment Losses and Reduce Capital Costs," Proc. Int. Solvent Extr. Conf., 1977, CIM Spec. Vol. 21, B. H. Lucas, G. M. Ritcey, and H. W. Smith, Eds., Can. Inst. Min. & Metall., Montreal, 1979; pp. 325-333.
4. J. N. Greenshields and P. E. Tetlow, "Solvent Extraction Process," U.S. Patent 5,024,821, 1990.
5. G. Miller and D. Readett, "Solvent Extraction Entrainment Control-Needs and Strategies," ALTA 2003 SX/IX World Summit, ALTA, Melbourne, Australia, 2003.
6. R. Pal, "Techniques for Measuring the Composition (Oil and Water Content) of Emulsions – A State of the Art Review," *Colloids and Surfaces*, **84**, 141-193 (1994).
7. D. A. Skoog, D. M. West, and F. J. Holler, "Fundamentals of Analytical Chemistry," Saunders College Publishing, Fort Worth, USA, 1992; p. 393.
8. K. Dudley and D. Readett, "Impurity Transfer in Copper Solvent Extraction Plants-Understanding and Managing the Problem," ALTA SX/IX-1, ALTA, Melbourne, Australia, 2000.
9. Reidle-de-Haen, "Hydranal Manual – Eugon Scholz Reagents for Karl Fischer Titration," Riedel-deHaen, Seelze, Germany, 1995.

DETERMINATION OF INDIUM BY SOLVENT EXTRACTION SPECTROPHOTOMETRICALLY

D. D. Malkhede,[1] Y. S. Thakare,[1] and S. M. Khopkar[2]

[1,]*Department of Chemistry, Sant Gadge Baba Amravati University, (M.S.), India,*
[2]*Indian Institute of Technology, Mumbai, India.*
Corresponding author email address: malkhededd@yahoo.com

ABSTRACT

Indium is present in trace amounts in zinc and lead ores and has therefore been recovered as a byproduct. The present work investigates a simple, rapid, and selective extractive method for the determination of In(III) using the acetyl derivative of calix[6]arene. Specifically, In(III) is extracted at pH 6.0 into toluene and stripped quantitatively with 5 M hydrochloric acid. Indium(III) is then determined photometrically following complexation with PAR. Studies using a variety of binary mixtures indicate that the method is selective, and thus, it is applicable to the analysis of real samples. The results obtained are both reproducible and accurate.

INTRODUCTION

Solvent extraction is the most versatile technique for the recovery of metals from various sources. Indium, a valuable metal widely used in the field of electronics, is found in low concentrations in some sulfide ores of zinc, copper, and lead, from which it is obtained as a byproduct [1-2]. Indium is used for semiconductor devices, optical devices, IR LEDs, indium solar batteries, and as control rods in reactors. Demand for indium has increased rapidly in recent years.

Many methods have been developed for the extraction and separation of In(III), among them methods using Cyanex 923 [3], acidic organophosphorus compounds [4] and LIX 973N [5]. It has been observed, however, that high concentrations of these reagents are required for the quantitative extraction of Indium(III). Similarly, processes for extracting In(III) with D2EHPA [6] and Cyanex 272 [7] are time consuming. Extraction with bis(2-ethylhexyl)phosphinic acid [8] and mixtures of P204 and Cyanex 923 [9] require longer equilibration periods for complete extraction of In(III). High temperatures are required when extraction of In(III) is carried out with H2PMBPP [10].

In analytical chemistry, calix[n]arenes [11] are used in solvent-extraction processes because of the variety of possible structures, distinct coordination properties, variable cavity size, and increased receptor power arising from substitution of a donor group to the lower rim of these compounds. Although solvent extraction of transition metal ions has been carried out by calixarene-based cyclic ligands [12], there has been no

systematic study of the extraction of In(III) with the acetyl derivative of calix[6]arene [hexaacetato calix[6]arene]. Therefore, in this paper, the possibility of utilizing this compound for the solvent extraction and separation of In(III) at sub-microgram concentrations is explored. The advantages of the proposed method over the reported ones for the extraction of In(III) include the need for only very low reagent concentrations, the possibility of extraction of In(III) from real samples at both micro and macro levels, and the eco-friendly nature of the method due to the relatively low toxicity [13] of extractant.

EXPERIMENTAL

Apparatus and Reagents

The hexaacetato calix[6]arene was synthesized in our laboratory according to a published method [14]. The purity of the ligand was checked by its melting point, elemental analysis, and spectral characterization. A solution of the extractant (1×10^{-4} M) was prepared in toluene. A stock solution of In(III) was prepared using anhydrous indium trichloride. A 0.1% solution of PAR [4-(2-pyridylazo)resorcinol] was prepared for determination of extracted In(III).

General Procedure

An aliquot of 20 ppm of In(III) was taken and its pH was adjusted to 6.00 with dilute HCl or NaOH. The total volume was made up to 10 mL with distilled water and it was transferred to separatory funnel. Then 10 mL of reagent, hexaacetato calix(6)arene, was added and shaken vigorously for 10 minutes. Indium(III) was stripped with 10 mL of 5 M HCl from the organic phase and determined spectrophotometrically at 520nm as its complex with PAR [15].

RESULTS AND DISUSSION

Extraction as a Function of pH

Indium(III) was extracted with 1×10^{-4} M of reagent in toluene, varying the pH from 2.0 to 9.0. The extraction was found to be quantitative at pH 6.0. Both above pH 8.0 and below pH 4.0, the extraction was incomplete, since no complexation takes place under these conditions. Therefore, pH 6.0 was selected for further work (Figure 1).

Effect of Period of Equilibration

The extraction of In(III) was carried out using various shaking periods between 1 and 15 minutes. The percentage of extraction increased with increasing shaking time up to 10 minutes, then decreased beyond it. Prolonged equilibrium period may adversely affect extraction due to dissociation of complex. Hence, a period of equilibration of 10 minutes was chosen.

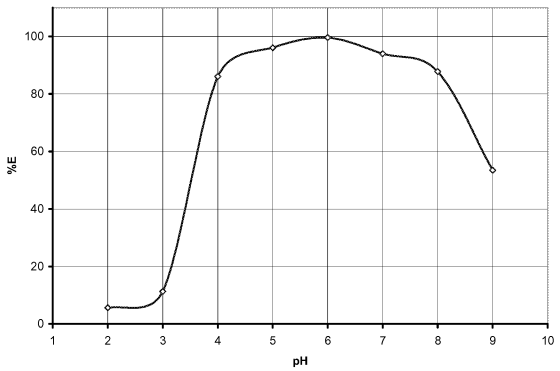

Figure 1. Extraction as a function of pH.

Table 1 Effect of period of equilibration on extraction of In(III)

Sr. No.	Shaking period (minutes)	% E	Distribution Ratio
1	1	63.91	1.77
2	2	75.2	3.032
3	4	91.3	10.49
4	6	93.47	17.47
5	8	95.65	21.98
6	10	99.56	226.27
7	12	99.5	199.0
8	15	94.78	18.15

Effect of Diluents

During the extraction of In(III), various polar and nonpolar solvents with different dielectric constants were used. The extraction of In(III) using cyclohexane, xylene, and toluene was found to be quantitative. With kerosene, carbon tetrachloride, and chloroform, extraction was more than 90%. It may be noted that not only the dielectric constant but also spatial configuration of diluents affect the extraction. Toluene was chosen for further extractions, as it was relatively less toxic diluent and easy to handle.

Table 2 Effect of various diluents on extraction of In(III)

Sr.No	Diluent	Dielectric constant	% *E*	Distribution Ratio
1	Cyclohexane	2.00	99.1	110.11
2	Kerosene	2.00	93.04	13.36
3	Toluene	2.30	99.6	249.0
4	Xylene	2.38	99.6	249.0
5	Carbon tetrachloride	2.24	90.1	9.10
6	Chloroform	4.80	92.17	11.77
7	Dichloromethane	8.08	89.13	8.90
8	1,2 Dichloroethane	10.50	86.95	6.66

Effect of Reagent Concentration

Indium(III) was extracted at pH 6.0 into toluene containing different concentrations of reagent. The extraction was found to increase with increasing reagent concentrations. Hence, 0.0001 M of reagent concentration was used for further studies.

Nature of Extracted Species

The plot of log *D* versus log of reagent concentration (Figure 2) shows a slope of 2.7. Therefore, the probable composition of extracted species is a 1:3 complex, $In(Reagent)_3$.

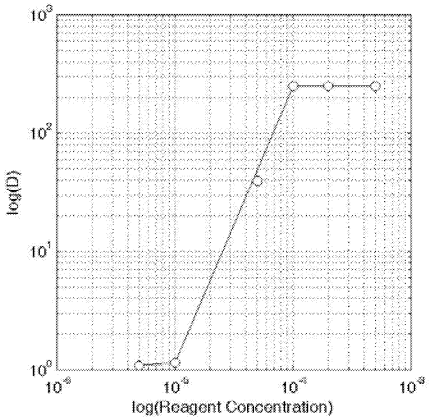

Figure 2. Effect of reagent concentration on extraction of In(III)

Metal-Loading Effect

Indium(III) was extracted with 1 x 10^{-4} M hexaacetato calix[6]arene into toluene from solutions containing increasing concentrations of the ion (Table 3). Extraction was quantitative up to 150 ppm.

Table 3. Metal loading capacity of 1 x 10^{-4} M of Hexaacetato Calix[6]arene

Sr. No	Concentration of In(III)(ppm)	% E	Distribution Ratio
1	20	99.6	249.0
2	40	99.6	249.0
3	60	99.6	249.0
4	80	99.6	249.0
5	100	99.6	249.0
6	150	99.6	249.0
7	200	90.29	9.29

Effect of Stripping Agents for In(III)

Extracted In(III) was stripped using several mineral acids in varying concentrations from 0.05 N to 5 N (Table 4). For 5 N HCl and HNO_3, the stripping was

quantitative. For 5 N acetic acid, stripping was only 89.13%. Because 5 N HCl also facilitates colorimetric determination of In(III), it was selected as the stripping agent.

Table 4. Effect of stripping agents

Acid/N	0.05 N	0.1 N	0.5 N	1 N	2 N	3 N	4 N	5 N
				% E				
HNO_3	-	76.08	-	84.34	90.43	97.39	98.26	99.6
HCl	-	44.34	-	83.47	87.82	91.30	94.34	99.6
CH_3COOH	-	62.17	-	74.78	80.86	83.47	86.0	89.13
$HClO_4$	57.39	68.26	82.17	89.13	-	-	-	-
H_2SO_4	60.86	70.43	86.08	94.34	-	-	-	-

Effect of Diverse Ions

Indium(III) was quantitatively extracted in the presence of other metal ions. Of the ions tested, only Cr^{3+}, Fe^{2+}, Co^{2+}, Cu^{2+}, Pb^{2+}, and Bi^{2+} strongly interfere in the extraction of In (III). It is observed that some of the interfering ions may exist in association with indium in real samples. For example, spallerite contains iron and copper, whereas galena contains lead, iron and copper. The tolerance limit was set at the amount of the foreign ion that could be present to give an error less than ± 1% in the recovery of In(III).

Table 5. Effect of diverse ions on extraction of In(III)

Sr. No.	Tolerance limit	Metal ions
1	1:20	Na^{+}, K^{+}, Ca^{2+}, Sr^{2+}, Mn^{2+}, Hg^{2+}, La^{3+}, As^{3+}
2	1:15	Fe^{3+}
3	1:10	Li^{+}, Zr^{4+}, NO_2^{-}, NO_3^{-}, CO_3^{2-}, SO_3^{2-}, F^{-}, tartarate
4	1:5	Mg^{2+}
5	1:2.25	Ni^{2+}, Zn^{2+}, SO_4^{2-}, PO_4^{3-}
6	1:1	Al^{3+}, Sn^{2+}, V^{5+}, Mo^{6+}, Cd^{2+}, Sm^{3+}, Th^{4+},Cl^{-}, Br^{-},I^{-}, oxalate
7	Interfering ions	Cr^{3+}, Fe^{2+}, Co^{2+}, Cu^{2+}, Pb^{2+}, Bi^{2+}

APPLICATION

The proposed method was used to separate and extract In(III) from IR light-emitting diode (LED) waste materials. This sample (0.1g) was dissolved in aqua regia and evaporated to dryness. The residue was dissolved in water and filtered. The Fe(III) and Al(III) present in the sample were precipitated out using a mixture of NH_4Cl and NH_4OH. Finally, the sample was diluted to 100 mL for analysis by the proposed method.

Table 6 Application of In(III)

Sr. No.	Sample	Amount taken (gm)	Amount of In(III) in the aliquot	Standard value	% E
1	IR LEDs	0.1	14.9 ppm	15 ppm	99.3

CONCLUSIONS

The proposed method is simple, rapid, and selective. It permits a quantitative extraction of In(III) with very low reagent concentration and with a short equilibration period. The method is suitable for extracting low concentrations of In(III) from real samples.

ACKNOWLEDGMENT

The authors are grateful to the University Grants Commission, New Delhi-India for the partial financial support.

REFERENCES

1. M. C. B. Foretes, and Bendetto, "Separation of Indium and Iron by Solvent Extraction," *Minerals Engineering*, **11**(5), 447-451 (1998).
2. J. Lee, Concise Inorganic Chemistry, Fifth edition, Chapman and Hall, London, 1996; pp. 360.
3. B. Gupta, A. Deep, and P. Malik, "Liquid-Liquid Extraction and Recovery of Indium using Cyanex 923," *Anal. Chim. Acta*, **513**, 463-471 (2004).
4. K. Inou, Y. Baba, and K. Yoshizuka, "Equilibria in Solvent Extraction of In(III) from Nitric acid with acidic organophosphorus compounds," *Hydrometallurgy*, **19**, 393-399 (1988).
5. F. J. Alguacil, "Solvent Extraction of Indium(III) by LIX 973N," *Hydrometallurgy*, **51**, 97-102 (1999).
6. M. S. Lee, J. G. Ahn, and E. C. Lee, "Solvent Extraction of Indium and Gallium from sulphate solutions using D2EHPA," *Hydrometallurgy*, **63**, 269-276 (2002).
7. Bina Gupta, Niti Mudhar, and Indu Singh, "Separation and recovery of Indium and Gallium using bis (2,4,4-trimethylpentyl) phosphinic acid (Cyanex 272)," *Separation and Purification Technology*, **57**, 292-301 (2007).
8. M. T. Naik and P. M. Dhadke, "Solvent Extraction of Indium(III) with bis (2-ethyl hexyl) phosphinic acid in toluene," *J. Chem. Eng. Jpn.*, **32**, 366-369 (1999).
9. J. Zhang, "Extraction of Indium with mixture of P_{204} and Cyanex 923," *Yingyong Hauxue*, **17**, 401-404 (2000).
10. GAO Jinzhang, DENG Qiliang, PENG Bo, and GUO Xiaojun, "Paraffin wax as a diluent for extraction and separation of trivalent Gallium, Indium and Thallium with 2,6-bis-(1'-phenyl-3'-methyl-5'-oxopyrazole-4') pyridineacyl," *Rare Metals*, **22**(2), 86 (2003).
11. C. D. Gutsche, Calixarenes Revisted, Royal Society of Chemistry, Cambridge, UK, 1998.
12. Takeshi Nagasaki and Seiji Shinkai, "Solvent extraction of transition metal cations by Calixarene-Based cyclic ligands," *Bull Chem. Soc. Jpn*, **65**, 471-475 (1992).
13. S. M. Khopkar, Analytical Chemistry of Macrocyclic and Supramolecular Compounds, Springer Verlag, 2001.
14. D. D. Malkhede, P. M. Dhadke, and S. M. Khopkar, "Solvent-Extraction Separation of Manganese (II) with Calixarene Substituted with an Acetyl Group at the Lower Rim," *Analytical Sciences*, **15**, 781-784 (1999).
15. Foster Dee Snell, Photometric and Fluorometric methods of Analysis, Part 1, Wiley Interscience Publication, 1978; 480-481.

Biotechnology, Pharmaceuticals, Life-Science Products, and Organic Products

CONTINUOUS PRODUCTION OF BIODIESEL VIA AN INTENSIFIED REACTIVE/EXTRACTIVE PROCESS

C. Tsouris, J. McFarlane, J. F. Birdwell Jr., and H. L. Jennings

Nuclear Science and Technology Division, Oak Ridge National Laboratory,
P. O. Box 2008, Oak Ridge, Tennessee 37831-6181
Corresponding author email address: tsourisc@ornl.gov

ABSTRACT

Biodiesel is considered as a means to diversify our supply of transportation fuel, addressing the goal of reducing our dependence on oil. For a number of reasons ranging from production issues to end use, biodiesel represents only a small fraction of the transportation fuel used worldwide. This work addresses the aspect of biodiesel production that limits it to a slow batch process. Conventional production methods are batch in nature, based on the assumption that the rates of the key chemical reactions are slow. The hypothesis motivating this work is that the reaction kinetics for the transesterification of the reagent triglyceride is sufficiently fast, particularly with an excess of catalyst, and that interfacial mass transfer and phase separation control the process. If this is the case, an intensified two-phase reactor adapted from solvent-extraction equipment may be utilized to greatly increase biodiesel production rates by increasing interphase transport and phase separation. To prove this idea, we are investigating two aspects: (a) determining the rate-limiting step in biodiesel production by evaluating the reaction kinetics, and (b) enhancing biodiesel production rates by using an intensified reactor. A centrifugal contactor combining interphase mass transfer, chemical reaction, and phase separation is employed for process intensification.

INTRODUCTION

The synthesis chemistry of biodiesel, or alkyl esters, is well known [1]. There are basically three routes to the ester production from oils and fats:

- Base-catalyzed transesterification of the oil with an alcohol,
- Direct acid-catalyzed esterification of the oil with an alcohol,
- Conversion of the oil to fatty acids, and then to alkyl esters with acid catalysis.

The majority of the alkyl esters are produced with the base-catalyzed reaction, because it is the most economic for several reasons, including:

- Processing at low temperature (65 °C) and pressure (20 psi),
- High conversion (98%) with minimal side reactions and reaction time,
- Direct conversion to methyl ester with no intermediate steps,
- Exotic materials of construction are not necessary.

The general process is depicted below. A fat or oil reacts with an alcohol, like methanol, in the presence of a catalyst to produce glycerol and methyl esters or biodiesel. The methanol is added in excess to promote rapid conversion to the ester. The catalyst is usually sodium or potassium hydroxide that has already been mixed with the methanol. Nonreacted methanol is recovered for reuse:

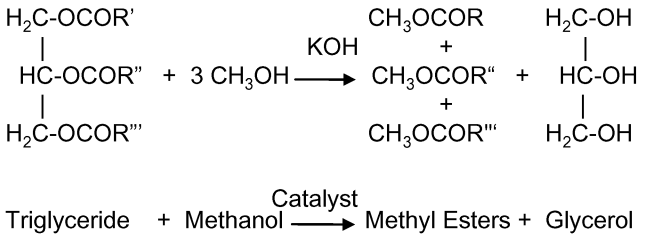

Issues still remain in the production of biodiesel that limit its adoption and viability. Some of these are listed below. It is evident that these concerns are not independent, and so progress in one area will generate improvements in the other areas:

1. Even though the synthesis is simple, the production of biodiesel is energy intensive because of the required post-processing of products, by-products, and waste.
2. Feedstocks are variable, complicating quality control of the products. Even for a given feedstock, such as soy biodiesel, there can be considerable variation in composition [2].
3. Production is done in batch mode, rather than continuously, because of the slow separation of byproduct glycerol from the methyl esters. Removal of the glycerol is critical to the quality of the fuel product, as it will contribute to clogging of fuel filters and engine failure [3]. Improvements in phase separation could vastly improve production costs and product quality.
4. The volatility and flammability of the methanol reagent is a safety concern in biodiesel production. Improved reactor design would allow use of minimal amounts of solvents, reducing safety risks in production.
5. In homogeneous base catalysis, the ester is often purified using an aqueous rinse to separate it from the glycerol. However, the wastewater is highly alkaline and must be treated before discharge. Neutralization produces waste salt. In addition, saponification can occur from reaction of the base with free fatty acids creating additional separation problems. To be effective, the separation device must be able to skim off the aqueous phase from the reactor while minimizing saponification and emulsion formation.

These issues could be addressed by applying principles of process intensification, matching the chemical processing steps to an optimized reactor design. Current methods for producing biodiesel are slow and cumbersome. Producers and investigators elsewhere have focused on the chemical kinetics but are not directly addressing the primary reason

for long residence times in production. A kinetics study on the transesterification of pongamia oil has suggested that, at approximately 60 °C, the forward reaction is fast with high yields [4] but slows down upon further reaction [5]. Many of the problems outlined above could potentially be ameliorated by the use of a continuous rather than batch process, with energy savings generated by combined reaction and separation. The development of an intensified continuous process could directly address the problem of long residence times required in biodiesel production processes.

There is recognition elsewhere that biodiesel production must move towards a more technologically sophisticated approach if biodiesel is to become a mainstay of domestic transportation fuels. Technologies to improve mass transfer and separation currently under consideration include reactive distillation, with solid acid catalyst being located in the distillation column [6]. The most promising results for this technology came from the reaction of dodecanoic acid on sulfonated zirconia; however, this process needs further investigation. A primary difficulty with catalysts immobilized on resins is the affinity of glycerol for the catalyst and subsequent poisoning of the catalyst in the column [7].

Enzymatic hydrolysis has been carried out using immobilized Candida lipase in a flow-through reactor, but care has to be taken to prolong the life of the enzyme, as it is subject to deactivation [8]. Furthermore, those reactors require such a long residence time that they are hardly continuous [9]. The glycerolysis of soybean oil to form mono- and di-glycerides for chemical synthesis has been studied in a continuous-flow tubular reactor, but the synthesis relies on a batch distillation process for the separation of products, and so the advantages of process intensification are not fully realized [10]. A continuous, stirred reactor has been used for the transesterification of palm oil, but higher yields were found to come at the expense of longer residence time, up to 1 h, and decreased production rate [11]. Another means tested to improve mass transfer was ultrasonification, but this leads to formation of an emulsion that takes a long time to separate [12]. These efforts are all worthwhile; however, the application of process intensification concepts to biodiesel production has promise to overcome limitations that are problematic in other approaches.

The present work is focused on the application of process-intensification principles to facilitate the production of biodiesel in two ways: first, to allow rapid reaction permitting the biodiesel to be produced by a continuous process rather than in batch mode and, second, to continuously separate the products, allowing efficient recovery of catalyst and reduction in environmental impact. The hypothesis is that the reaction kinetics, in the absence of mass-transfer limitations, is sufficiently fast to allow substantial improvements through innovative process concepts, including combined reaction and phase separation in a continuous-flow centrifugal contactor. If the hypothesis is correct, batch processes that take hours can be replaced by continuous processes that take seconds to produce purified biodiesel.

MATERIALS AND METHODS

Centrifugal contactors were initially developed as solvent-extraction devices for use in actinide recovery from spent nuclear reactor fuel as an evolution of mixer-settlers [13].

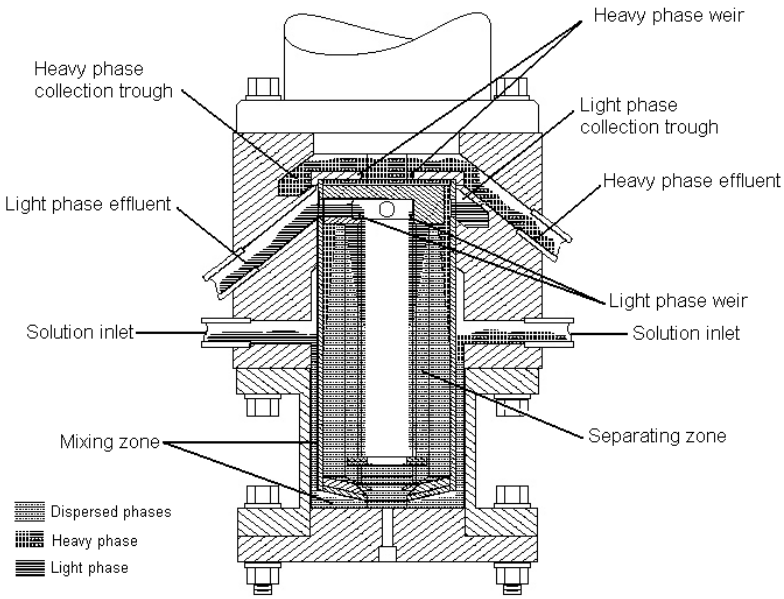

Figure 1. Schematic of centrifugal contactor flows.

The distinctive feature of the centrifugal-contactor apparatus is the use of rotor within a stationary cylinder (the housing) to accomplish both the intimate mixing of two immiscible solutions to produce a dispersion and to generate centrifugal force used to separate the dispersion. In conventional applications, the generation of finely divided dispersion promotes the selective transfer of one or more solutes from one liquid phase into another. This transfer is accomplished by means of Couette mixing; the creation of shear forces in solutions contained within the annulus between a stationary outer cylinder and a rotating inner cylinder (Figure 1).

This contactor minimizes mass-transfer limitations and effectively separates the phases in a continuous-flow operation. It allows high throughput and can be used for intensified processing by combining reaction and phase separation, providing intensive mixing, allowing a short residence time and requiring a small footprint. A picture of the experimental setup is shown in Figure 2, where a water bath is used to control the reaction temperature. The centrifugal contactor, Costner Industries Texas #V-2, 5-cm-diameter stainless-steel, is normally operated above 3000 rpm.

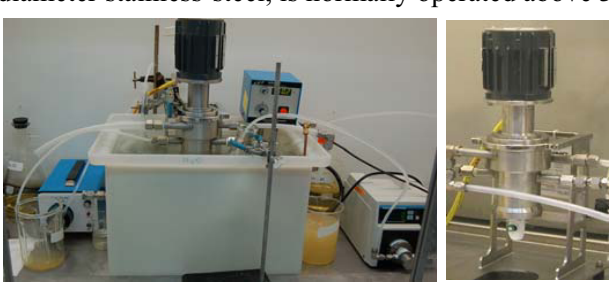

Figure 2. The experimental setup for biodiesel synthesis (left) using a centrifugal contactor (right).

The raw materials used in the esterification reaction were food-grade vegetable and corn oils and methoxide produced by reaction of potassium hydroxide with methyl alcohol, the standard base catalysis [1], at a volumetric phase ratio of 5:1 oil:methoxide. The oils, methanol (EM Science 99.8%), NaOH, and KOH (EM Science) reagents were used without further purification. There are slight differences in triglyceride content in the two vegetable oils tested, as shown in Table 1, with data taken from Knothe et al. [11], but these were not expected to change the kinetics of the reaction significantly. The reaction was carried out at 55-60 °C by preheating reagents and the contactor.

Table 1. Triglyceride content in vegetable oils (Weight %)

	16:0	18:0	18:1	18:2	18:3
Corn	7.0-13.0	2.5-3.0	30.5-43.0	39.0-52.0	1.0
Soybean	2.3-11.0	2.4-6.0	22.0-30.8	49.0-53.0	2.0-10.5

Fatty Acid Component (chain length:degree of unsaturation)

Reactants and products were analyzed by gas-chromatography flame-ionization detection GC-FID following ASTM Method D6854 [12]. Samples of 2-5 mL were immediately contacted with 1 mL of 0.1 N HCl to arrest the transesterification reaction, as recommended by studies done elsewhere [10,13]. The samples were centrifuged to separate aqueous from organic phases. The organic phase was dried with anhydrous Na_2SO_4 (EM Science) and diluted with a 1:1 volume mixture of petroleum ether and *n*-hexane (EM Science). Analysis of organics dissolved or entrained in the aqueous phase was accomplished by solvent extraction with a 1:1 volumetric mixture of petroleum ether and *n*-hexane. The samples were filtered through 0.2-μm Gelman nylon filters, and derivatized with bis(trimethylsilyl)trifluoroacetamide BSTFA (Supelco) before injection into an Agilent HP 5890 GC running Chemstation Plus™ software. Separation was achieved with a temperature ramp to 380 °C on an HP-5 30m x 0.53mm x 0.88μm capillary column. Calibration standards included glycerol (EM Science), glyceryl tridecanoate, glyceryl trioleate, and 1,3-diolein, all purchased from Sigma.

RESULTS AND DISCUSSION

The first test was to demonstrate the utility of the contactor for the separation of well-mixed presynthesized glycerol and methyl ester phases. A batch mixture prepared through a base-catalyzed synthesis was immediately introduced into the contactor and was separated in one pass, with a residence time of less than one minute. Samples were taken from “light” and “heavy” phases separated by the contactor. A similarly prepared control batch that was not passed through the contactor took several hours to achieve separation between the glycerol and methyl ester phases. This experiment demonstrated that continuous centrifugation can successfully separate product and byproduct streams. Figure 3 shows the superposition of two labeled gas chromatograms, the green line from the contactor-separated methyl ester product, and the red from the oil starting material. It is apparent from the chromatograms that the synthesis was essentially complete, with greater than 99% conversion, and the amount of entrained glycerol was negligible after separation.

The premise of using an intensified process relies on the reaction kinetics being much faster than mass transfer. This hypothesis was tested by following the progression of a reaction of potassium methoxide and vegetable oil in a well mixed batch reactor, and measuring residence-time requirements. A high-speed homogenizer (IKA Labortechnik model T25) was used to stir vigorously 120 mL of the reaction mixture, held at 56 ± 4 °C in a 300 mL beaker to minimize mass-transfer limitations. Samples were taken online during the transesterification reaction at 15, 30, 60, 120, and 240 s after the reagents were mixed in the homogenizer. Peak areas from GC-FID analysis attributed to the methyl esters were ratioed to that of the oil, and results are given in Figure 4 in terms of mole % biodiesel and molar ratio of biodiesel-to-oil. In the graph, the ratio of the peak attributed to the oil and the peaks attributed to the methyl esters are plotted as a function of time. Little intermediate monoglyceride and byproduct glycerol were observed in the methyl ester mixture. It is apparent the reaction nears completion at about 1 min., giving a lower bound to the desired residence time in a continuous reactor.

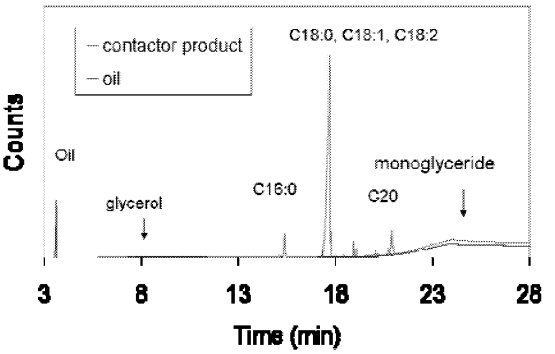

Figure 3. Superposition of two gas chromatograms showing peaks arising from the vegetable oil starting material, as well as the derivatized methyl ester product.

The reaction to produce methyl ester from vegetable oil was carried out in continuous mode in a centrifugal contactor. Potassium methoxide and corn oil were introduced separately into the mixing zone of the contactor at flow rates of 10 and 50 mL/min., respectively. Reagents and the contactor were heated to 60 °C prior to being mixed. Samples were collected from the outlets of the contactor at 1 min., 3 min., 6 min., and 10 min. after the beginning of the experiment and were neutralized immediately. A sample was also taken from the reactor at the end of the test and represents the "equilibrium" sample on the graph. Results from GC-FID analysis of the product streams are shown in Figure 5. It took some time for the contactor to reach steady state. The methyl ester product was the less dense phase and, as shown in Figure 5a, flowed consistently from the beginning of the test. The ratio of biodiesel to oil in the equilibrium sample was 69. However, the composition of the heavy phase flow was more complex and varied considerably from the beginning to the end of the test, Figure 5b. The heavy

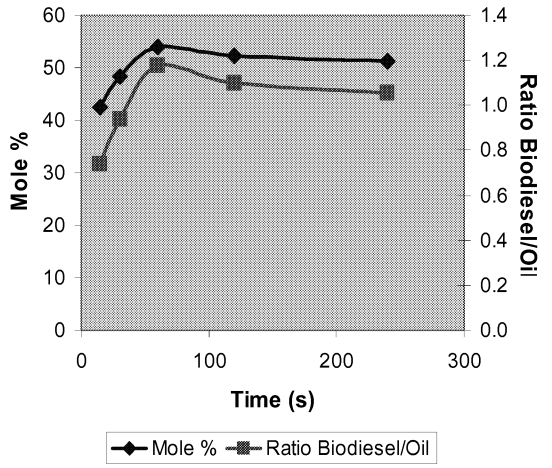

Figure 4. Graph showing production of methyl esters as a function of time.

phase flow was initially primarily similar in composition to the light-phase flow, suggesting that separation was not very good until about 3 minutes into the test. The heavy-phase flow then switched and became water soluble, mainly consisting of the byproduct glycerol with trace amounts of entrained unreacted oil and methyl ester. At this point, the flow rate from the heavy side became greatly reduced, reflecting the substantially lower amount of glycerol than biodiesel expected from the reaction stoichiometry, as presented earlier in the paper.

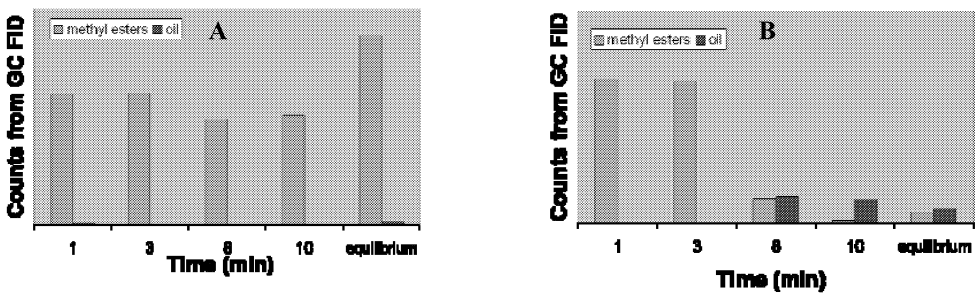

Figure 5. Samples of methyl ester product and reagent oil sampled from output streams of the intensified process: from the less dense flow (A), from the more dense flow (B).

The results of this experiment show the complexity of the reaction/separation device, as the "organic phase", the oil reagent, is initially the high-density phase, but the "organic phase" product, the methyl ester, is of lower density than the byproduct glycerol. The densities are given in Table 2. In spite of the time-dependent changes in composition and density, this test successfully demonstrated a continuous one-step biodiesel synthesis and separation.

Table 2. Densities of reagents and products in biodiesel manufacture

Material	Density ($g \cdot cm^{-3}$)	Material	Density ($g \cdot cm^{-3}$)
Vegetable oil	0.91-0.93 (15-25 °C) [14]	Biodiesel	0.8843 (20 °C) [15]
Methanol	0.7914 (20 °C) [14]	Glycerol	1.2613 (20 °C) [14]

CONCLUSIONS

The main conclusion of this work is that the esterification reaction in biodiesel synthesis processes is relatively rapid, and it is primarily the phase-separation step that delays the process. Process-intensification principles can be applied to substantially improve the process, leading to compact, efficient, high-throughput units that can also be made mobile.

ACKNOWLEDGMENTS

Research sponsored by the Laboratory Directed Research and Development Program of Oak Ridge National Laboratory (ORNL), managed by UT-Battelle, LLC. for the U. S. Department of Energy under Contract No. DE AC05-00OR22725. The authors are thankful to Ms. Denise Schuh for assisting in the experiments.

REFERENCES

1. B. Freedman, E. H. Pryde, and T. L. Mounts, "Variables Affecting the Yields of Fatty Esters from Transesterified Vegetable Oils," *J. Amer. Oil Chem. Soc.*, **61**(10), 1638-1643 (1984).
2. Biodiesel Fuel Quality Study, Brabmij, Inc., http://www.biodiesel.org/resources/reports database/reports/gen/19951229_gen-227.pdf.
3. G. Kenreck, "Improving Biodiesel Stability with Fuel Additives," *Biodiesel Magazine*, Feb. (2007).
4. K. Karmee, P. Mahesh, R. Ravi, and A. Chadha, "Kinetic Study of the Base-Catalyzed Transesterification of Monoglycerides from Pongamia Oil," *J. Amer. Oil Chem. Soc.*, **81**(5), 425-429 (2004).
5. D. Darnoko and M. Cheryan, "Kinetics of Palm Oil Transesterification in a Batch Reactor," *J. Amer. Oil Chem. Soc.*, **77**(12), 1263-1267 (2000).
6. A. A. Kiss, F. Omota, A. C. Dimian, and G. Rothenberg, "The Heterogeneous Advantage: Biodiesel by Catalytic Reactive Distillation," *Topics in Catalysis*, **40**(1), 141-150 (2006).
7. P. Bondioli, "The Preparation of Fatty Acid Esters by Means of Catalytic Reactions," *Topics in Catalysis*, **27**(1), 77-82 (2004).
8. Y. Watanabe, Y. Shimada, A. Sugihara, H. Noda, H. Fukuda, and Y. Tominaga, "Continuous Production of Biodiesel Fuel from Vegetable Oil Using Immobilized *Candida Antarctica* Lipase," *J. Amer. Oil Chem. Soc.*, **77**(4), 355-359 (2000).
9. A.-F. Hsu, K. C. Jones, T. A. Foglia, and W. N. Marmer, "Continuous Production of Ethylesters of Grease Using an Immobilized Lipase," *J. Amer. Oil Chem. Soc.*, **81**(8), 749-752 (2004).
10. H. Noureddini, D. W. Harkey, and M. R. Gutsman, "A Continuous Process for the Glycerolysis of Soybean Oil," *J. Amer. Oil Chem. Soc.*, **81**(2), 203-207 (2004).
11. D. Darnoko and M. Cheryan, "Continuous Production of Palm Methyl Esters," *J. Amer. Oil Chem. Soc.*, **77**(12), 1269-1272 (2000).
12. J. A. Colucci, E. E. Borrero, and F. Alape, "Biodiesel from an Alkaline Transesterification Reaction of Soybean Oil Using Ultrasonic Mixing," *J. Amer. Oil Chem. Soc.*, **82**(7), 525-530 (2005).
13. R. A. Leonard, G. J. Bernstein, A. A. Ziegler, and R. H. Relto, "Annular Centrifugal Contractors for Solvent-Extraction," *Sep. Sci. Technol.,* **15**(4), 925-943 (1980).
14. G. Knothe, R. O. Dunn, and M. O. Bagley, "Biodiesel: The Use of Vegetable Oils and Their Derivatives as Alternative Fuels," Oil Chemical Research, National Center for Agricultural Utilization Research, Agricultural Research Service, U.S. Department of Agriculture, Peoria, IL 61604, 1996.
15. ASTM Method D6854 "Standard Test Method for the Determination of Free and Total Glycerin in B-100 Biodiesel Methyl Esters by Gas Chromatography," ASTM International, 2007.
16. M. Mittelbach, G. Roth, and A. Bergmann, "Simultaneous Gas Chromatographic Determination of Methanol and Free glygercol in biodiesel," *Chromatographia*, **42**, 431-434 (1996).
17. D. R. Lide, Editor-in-Chief, "CRC Handbook of Chemistry and Physics. Boca Raton: CRC Press, 88th Ed., 2007-2008.
18. M. E. Tat and J. H. Van Gerpen, "The Specific Gravity of Biodiesel and its Blends with Diesel," *JAOCS*, **77**, 115-119 (2000).

PURIFICATION OF BIOFUELS USING IONIC LIQUIDS

F. Santangelo,[1] A. E. Wentink,[1] A. Górak,[1] W. Pitner,[2] and M. Schulte[2]

[1]*Department of Biochemical and Chemical Engineering, Universität Dortmund, Emil-Figge-Str. 70, 44227 Dortmund, Germany.*
[2]*Merck KGaA, Frankfurter Str. 250, 64293 Darmstadt, Germany.*
Corresponding author email address: Francesca.Santangelo@bci.uni-dortmund.de

ABSTRACT

Butanol for biofuel is expected to become an important topic in white biotechnology. An interesting option for the purification of butanol is its *in-situ* extraction with ionic liquids (ILs). Suitable ILs were identified by measuring the butanol distribution ratio and selectivity. Common ionic liquids yield a selectivity of 100 or higher, but the distribution ratios are around unity. Ionic liquids with functional groups (for example, hydroxyl) increase the distribution ratio of butanol, but the selectivity remains approximately 100.

INTRODUCTION

Biofuels are increasingly important in white biotechnology. While bioethanol has received most of the attention, butanol also has potential as a biofuel, but its purification from fermentation broths is very challenging [1]. Distillation is not feasible because the boiling point of butanol is higher than that of water. Extraction circumvents this disadvantage but relies on solvents that are flammable, hazardous, or toxic [2]. Ionic Liquids (ILs) can be suitable substitutes for these conventional solvents [1]. Furthermore, some ILs are nontoxic towards micro-organisms, which enables the in-situ extraction of the butanol from fermentation broth [3]. This improves fermentation productivity by avoiding inhibition of the micro-organisms by butanol.

The goal of this paper is to identify ILs with a high distribution ratio and selectivity for butanol. In laboratory-scale extraction experiments, butanol was extracted from aqueous solutions at a concentration similar to that in a fermentation broth. Effects of the butanol concentration on the distribution ratio were examined. The solubility of water in ILs was measured to determine the selectivity of the extraction process.

PURIFICATION PROCESS

Acetone-Butanol-Ethanol (ABE) fermentation is one of the oldest industrially applied fermentation processes and was in the first half 20th century the second most important industrially applied fermentation after ethanol production. With the

development of petrochemical-based production routes for butanol, interest in this process decreased [4]. Today, the ABE-fermentation process is again attracting attention as an alternative for producing butanol from biomass. One of the major issues of this process is its limited productivity, due to the toxicity of butanol towards the micro-organisms [4]. New micro-organisms, which produce only butanol, have been developed, but these are still only tolerant of up to 2 wt % butanol [3,5].

The flowsheet for a process using ILs as in-situ extractants is presented in Figure 1. The fermentation broth is contacted with an IL phase, which selectively extracts butanol. After phase separation the butanol is recovered from the IL by distillation or flash at reduced pressure. The IL, now free of butanol, can be recycled.

In literature reports, the solvents reported to have the highest distribution ratios for butanol are mainly aliphatic alcohols [6]. One of the most investigated solvents for the extraction of butanol from fermentation broths is oleyl alcohol (OA), a C_{18}-fatty alcohol; this alcohol was selected as the benchmark for the ILs tested for this report. OA has the disadvantage that it acts as emulsifier [7].

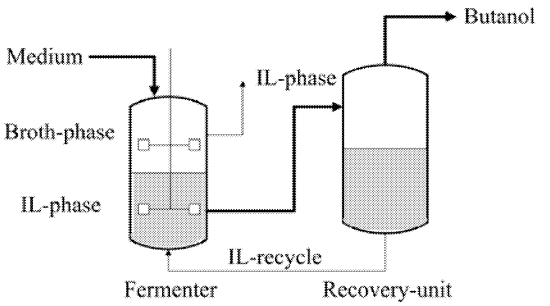

Figure 1. Process flowsheet of butanol recovery from fermentation broth.

EXPERIMENTS AND PROCEDURES

Equal masses (ca. 10 g) of each phase were contacted in double-wall glass vessels with a maximum volume of 40 mL. The initial aqueous concentration of the butanol was 1 wt %, except in Figure 2b, where it varied between 0.5 wt % and 2 wt %. A magnetic stirrer (Variomag telesystem 06.07) was used to ensure intensive contact between both phases. The temperature was kept constant at 25 ± 0.1 °C by a thermostatic circulating water bath (Julabo F25 ME). The difference in concentration of butanol after 6 and 20 hours is negligible, but in any case, the phases were stirred for 20 hours. After 10 min. settling time, samples were taken from the clear phases by an automated pipette (VWR).

The butanol concentration in the aqueous phase was analyzed with an HPLC (Merck-Hitachi) equipped with an RI detector (K-2300, Knauer) in a Supersphere RP60-select b column (Merck) using as eluent acetonitrile/water (30:70). The water content in the IL phase was analyzed with a Karl-Fischer titrator (DL31, Mettler-Toledo) using methanol as basis and Hydranal Composite 5 (Sigma-Aldrich) as titrant.

The concentration of butanol in the IL-phase ($w_{\text{butanol}}^{\text{IL}}$ in g/g) was calculated from the difference between the initial and equilibrium concentrations of butanol in the aqueous phase ($w_{\text{butanol}}^{\text{aq}}$ in g/g) using a mass balance. It is assumed that the mutual

solubility of IL and water is small or negligible. With these data, the distribution ratios for butanol ($D_{butanol}$) and water (D_{water}) and the selectivity (S) were defined as:

$$D_{component} = \frac{w^{IL}_{component}}{w^{aq}_{component}}, \quad S = \frac{D_{butanol}}{D_{water}} \tag{1}$$

Butanol (99.8%) and acetonitrile (for analysis, 99.5%) were purchased from Merck. In all experiments and analysis Milli-Q water was used (Milli-Q Synthesis). Table 1 presents the tested ILs, which were provided by Merck and used as received. Selected ILs should fulfil the following criteria: stable against hydrolysis, nontoxic, water-insoluble, and high capacity/selectivity for butanol.

Table 1. List of investigated ILs

Cation \ Anion	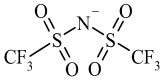 **(NTF)**	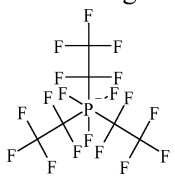 **(FAP)**	**(BF_4)**	**(PF_6)**
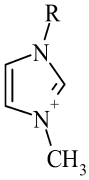 **(MIM)**	**HMIM** R: hexyl **OMIM** R: octyl **EOHMIM** R: hydroxyethyl **EOEMIM** R:ethoxyethyl	**HMIM** R: hexyl **EOHMIM** R: hydroxyethyl	**OMIM** R: octyl	**OMIM** R: octyl
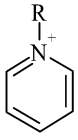 **(PYR)**	**POHPYR** R: hydroxypropyl **HPYR** R: hexyl	**pOHPYR** R: hydroxypropyl		
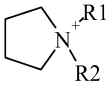 **(PL)**	**MOPL** R1: methyl R2: octyl			
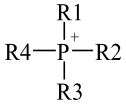 **(P)**		**PH_3T** R1, R2, R3: hexyl R4: tetradecyl		

RESULTS AND DISCUSSION

Conventional Ionic Liquids

Figure 2a presents the selectivity for butanol of different conventional ILs as function of the distribution ratio of butanol. The bench mark OA has a butanol distribution ratio of 3.36 and a selectivity of 208, which should be exceeded by the ionic liquids. Previous work with the common ILs, OMIM (PF_6) and OMIM (BF_4) did not yield satisfactory results [2]. The capacity was too low (OMIM (PF_6)) or the water solubility too high (OMIM (BF_4)). Furthermore, these anions are not stable against hydrolysis, making recycling and long-term operation very problematic due to generation of HF.

The results for two anions which are stable against hydrolysis (FAP and NTF) are mixed. The highly hydrophobic FAP anion (black symbols in Figure 2a) yielded a very high selectivity, while the water solubility was very low, but the distribution ratio of butanol is below unity and insufficient for practical purposes. Altering the cation HMIM to PH_3T reduced the selectivity, while the distribution ratio of butanol remained constant. Changing the anion from FAP to NTF increases the distribution ratio of butanol but only to slightly above unity; at the same time, the water solubility of the IL is also increased. Therefore, the selectivity is reduced to around 100, well below the bench mark. With NTF, changes in the cation had little influence on the distribution ratio and selectivity for butanol.

The distribution ratio and selectivity for butanol are influenced only slightly by the butanol concentration in the aqueous phase, as presented in Figure 2b. Furthermore, in all cases, the distribution ratio is below or around unity.

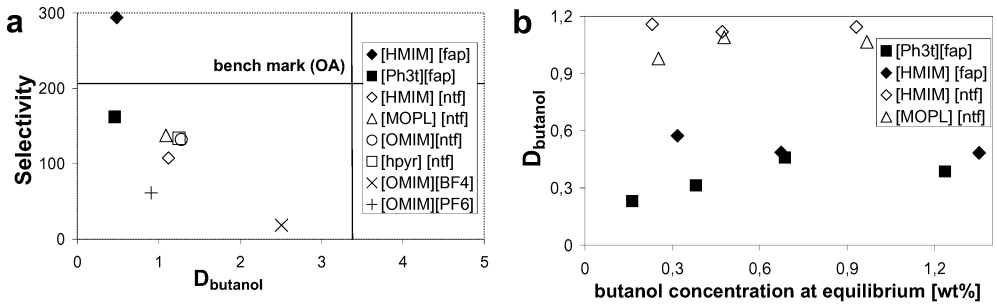

Figure 2. a Selectivity and distribution ratio of different ILs and bench mark (OA).
b Distribution ratio as function of butanol concentration in aqueous phase.

Functionalized Ionic Liquids

To improve upon the results observed with conventional ILs, functionalized ionic liquids were selected. The selection criterion was that the cation should be capable of hydrogen bonding. The experimental results are presented in Figure 3; it shows clearly that overall the results of selectivity vs. distribution ratio have shifted from a very high selectivity and low capacity to a high selectivity and much higher distribution ratios.

The introduction of an ethereal functional group (EOEMIM NTF) did not significantly increase the butanol distribution, while this reduced the selectivity, because of the higher water solubility in the IL. Appending a hydroxyl group onto the imidazolium cation (EOHMIM NTF) resulted in a slight change of the distribution ratio (from 1.12 to 1.48), but the selectivity was reduced to 62. EOHMIM FAP had a reduced selectivity with respect to HMIM FAP (from almost 300 to 90), but at the same time, the distribution ratio increased threefold from around 0.5 to above 1.5 With both the FAP and NTF anions, introduction of the hydroxyl-functionalized POHPYR cation led to a reduction in selectivity with respect to the EOHMIM-based ILs. In all cases, FAP-based ILs have consistently higher selectivity values than comparable NTF-based ILs, demonstrating the importance of hydrophobicity in choosing the right IL.

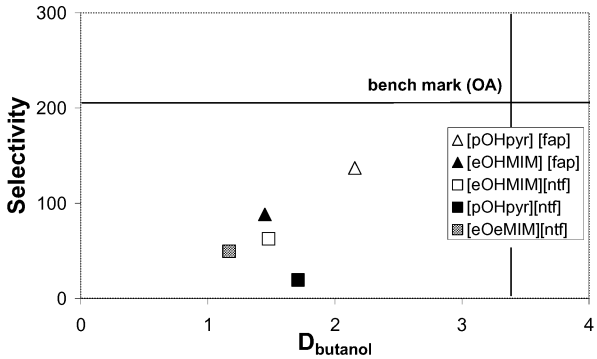

Figure 3. Selectivity as function of distribution ratio for butanol for functionalised ILs.

Solubility of Water in Ionic Liquids

Vital for the application of ILs to butanol extraction is a low mutual solubility of the IL and water. In Figure 4, the water solubility in different tested ILs is presented.

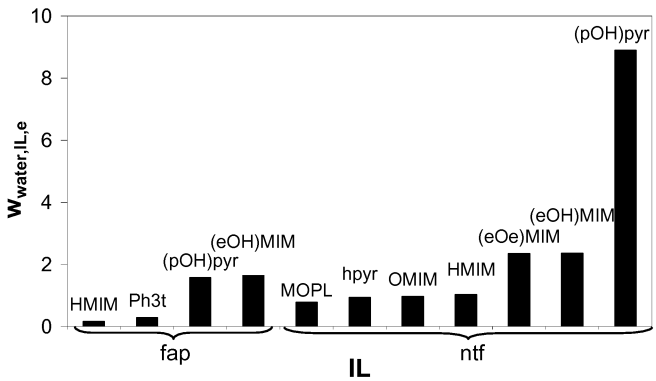

Figure 4. Water solubility in IL for aqueous solutions initially containing 1 wt % butanol.

FAP-based ILs dissolve less water than NTF-based ILs, independent of the cation used. Therefore, the FAP-based ILs have very high selectivity but also low distribution

ratios. Introduction of hydroxyl groups on the cation increases the water solubility, even if combined with the highly hydrophobic FAP anion. Thus, functional groups can be used to modulate hydrophobicity of ILs.

ILs with a high water capacity, such as POHPYR NTF (8.9 wt %), should not be considered for any process, such as this one, involving extraction from an aqueous phase. The co-extracted water needs to be removed from the product (butanol), and the high water solubility in the IL can be indicative of a high IL solubility in water, which would be lost and create waste disposal/treatment problems.

CONCLUSIONS

Conventional (that is, unfunctionalized) ILs lack the capacity to act as solvents for butanol extraction from aqueous solutions. The selectivity, however, is in many cases more than sufficient. The introduction of an ethereal functionality does not increase the butanol distribution ratio but does reduce the selectivity, because of increased water solubility. ILs functionalized with hydroxyl groups have a dramatically increased capacity for butanol but reduced selectivity. Future work will focus on improving the capacity and selectivity of the ionic liquids.

ACKNOWLEDGMENTS

This work was made possible by financial and material support by Merck KGaA.

REFERENCES

1. J. G. Huddleston, H. D. Willauer, R. P. Swatloski, A. E. Visser, and R. D. Rogers, “Room temperature ionic liquids as novel media for 'clean' liquid-liquid extraction,” *Chem. Commun.*, **16**, 1765–1766 (1998).
2. A. G. Fadeev, Y. A Selinskaya, S. S. Kelley, M. M. Meagher, E. G. Litvinova, V. S. Khotimsky, and V. V. Volkov, “Extraction of butanol from aqueous solutions by pervaporation through poly(1-trimethylsilyl-1-propyne),” *J. Membr. Sci.*, **186**(2), 205–217 (2001).
3. S. Minteer, Alcoholic fuels, CRC Press, Boca Raton, 2006.
4. I. S. Maddox, “New Technologies for the Acetone-Butanol-Ethanol Fermentation,” *Aust. J. Biotechnol.*, **4**(1), 63–66 (1988).
5. J. Huang, and M. M. Meagher, “Pervaporative recovery of n-butanol from aqueous solutions and ABE fermentation broth using thin-film silicalite-filled silicone composite membranes,” *J. Membr. Sci.*, **192**(1-2), 231–242 (2001).
6. Z. Shi, C. Zhang, J. Chen, and Z. Mao, “Performance evaluation of acetone–butanol continuous flash extractive fermentation process,” *Bioprocess Biosys, Eng,,* **27**(3), 175–183 (2005).
7. Ullmann’s Encyclopedia of Industrial Chemistry, Fatty Alcohols, 2006.

EXTRACTIVE CATALYST RECOVERY IN AN IONIC-LIQUID PROCESS FOR THE PRODUCTION OF 2,5-DIHYDROFURAN

J. S. Kanel,[1] S. N. Falling,[1] J. R. Monnier,[2] G. W. Phillips,[1] and S. A. Godleski[3]

[1]Eastman Chemical Company, Kingsport, TN, 37662., [2]University of South Carolina, Columbia, SC. [3]Eastman Kodak Company, Rochester, NY, 14650.
Corresponding author email address: jskanel@eastman.com

ABSTRACT

2,5-Dihydrofuran (2,5-DHF) is an intermediate with utility in the production of commodity, specialty, and fine chemicals. The homogeneous, Lewis acid/iodide anion-catalyzed rearrangement of 3,4-epoxy-1-butene (EPB, **1**) to 2,5-DHF has been known since 1976. Typically, these rearrangement processes use a metal halide Lewis acid with an inorganic or quaternary onium iodide catalyst system in a high-boiling solvent. Commercial processes utilizing this chemistry have been unattractive due to the high cost of **1** and side reactions in the rearrangement step. Among these side reactions is the polymerization of **1** to a polyether oligomer. In continuous operation, the nonvolatile oligomer accumulates, dilutes the catalysts, and fills the reaction vessel. Recovery of the expensive catalysts and solvent from the reaction mixture is expensive at the commercial scale. Following the discovery of an inexpensive, continuous, vapor-phase oxidation of 1,3-butadiene to produce **1** in 1986, the production of 2,5-DHF from **1** was once again of industrial interest. A continuous, liquid-phase process was developed utilizing a trialkyltin iodide Lewis acid/tetraalkylphosphonium iodide co-catalyst system which gave high selectivity for 2,5-DHF. Here we will focus on separation of the catalyst from the oligomer via extraction. This process was scaled up to a semiworks facility that successfully used extraction to separate the catalyst and oligomer.

INTRODUCTION

EPB is a versatile intermediate for producing chemicals [1]. An important derivative of **1** is 2,5-DHF. This heterocycle is useful in the production of THF [2], 2,3-DHF [3], 1,4-BDO [4], and fine chemicals (e.g., cyclopropanes [6]). The homogeneous, Lewis acid and iodide salt-catalyzed rearrangement 2,5-DHF has been known since 1976 [7] and is the only practical method for 2,5-DHF synthesis.

Typically, this rearrangement process is catalyzed by an inorganic Lewis acid and inorganic or quaternary onium iodide in a polar, aprotic solvent (e.g., ZnI_2, KI, and NMP) [7,8]. For years, commercial processes utilizing this chemistry were unattractive due to the high cost of **1** and poor reaction selectivity. In 1986, a process to produce **1** by vapor-phase oxidation of 1,3-butadiene over a silver-on-alumina catalyst was discovered by Monnier [9]. The process was refined and commercialized by Eastman [10].

Following this discovery of a viable process for **1**, the production of 2,5-DHF was once again of commercial interest.

RESULTS AND DISCUSSION

Unfortunately, the product (2,5-DHF) and starting material **1** are both liquids with identical boiling points (66 ºC) and with no practical method to separate the isomers. This fact requires the catalytic process be performed at high conversion for acceptable economics. Furthermore, the major side products in this homogeneous catalysis process are crotonaldehyde (also isomeric with **1**) and the polyether oligomer of **1**. Crotonaldehyde is a volatile liquid with a boiling point of 104 ºC so it is separable from the reaction mixture and product. However, the oligomeric material is nonvolatile and accumulates in the reaction mixture causing catalyst dilution. Because Lewis acid and iodide catalysts are normally too expensive to discard, a rearrangement process was needed with high selectivity for product and a means for catalyst recovery (or oligomer removal). For the rearrangement process to be economically and environmentally acceptable, the recovery/reuse of the catalyst components is imperative.

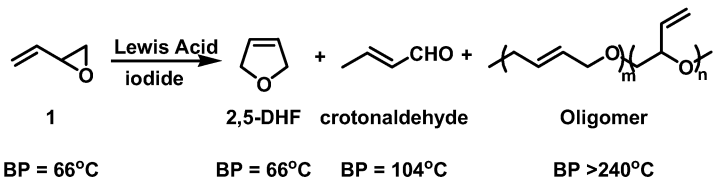

Due to **1**'s conjugated vinyl and epoxide functional groups, it can polymerize (oligomerize) with repeat units that are linear 1,4-substituted [*m*-units above] or branched 1,2-substituted (*n*-units). The *m*/*n* repeat unit ratio depends on the catalyst and conditions, but it is usually about 15/85 [11]. The oligomer produced as a side product in the 2,5-DHF process is typically a viscous liquid with a broad molecular weight distribution averaging about 1100 and SG > 1. An important property of this byproduct is the poor solubility of the higher molecular-weight oligomers in nonpolar alkane solvents. This property facilitated the separation of catalysts from oligomers using an alkane solvent in liquid extraction.

With these process factors in mind, a continuous, homogeneous reaction process concept was developed in which the starting epoxide **1** is fed as a liquid to the reactor containing the soluble Lewis acid and iodide salt while continuously removing the 2,5-DHF and crotonaldehyde by distillation. Continuously, or as needed, the catalysts are recovered from the oligomer by extraction with an alkane and the undissolved oligomer is discarded.

The rearrangement reaction of **1** requires a two-component catalyst system consisting of a Lewis acid and a soluble source of iodide anion. The process concept had a number of requirements for the catalysts in order to achieve commercial operation:the four Ss, as well as low cost and toxicity. The four Ss are Speed or catalytic activity, Selectivity for low oligomerization, Stability (both chemical and thermal) for catalyst lifetime, and Separation.

For adequate reaction rates, a high concentration of iodide anion is necessary. The cation portion of the salt appears to have little or no effect on catalytic activity or reaction selectivity. Inorganic iodides (e.g., KI) are the obvious first choice based on availability and cost, but they need added solubilizers. Quaternary ammonium iodides are attractive choices because they generally have good activity, low cost, and solubility in the reaction and recovery processes, but they have poor thermal stability due to breakdown by dealkylation.

Quaternary phosphonium iodides are also good choices for the iodide salt catalyst component because they are highly active and, in some cases, soluble in the reaction and recovery processes. Although the number of available tri(alkyl/aryl)phosphine starting materials may be somewhat lower than with the tri(*n*-alkyl)amines, the large number of commercially available *n*-alkyl iodides allows for the synthesis of many phosphonium iodide catalyst candidates. Triphenylphosphine is an attractive starting material due to its industrial availability and low cost. However it was found that the resulting (*n*-alkyl) (triphenyl)phosphonium iodides had poor solubility in alkane solvents (see Table 1). They also tended to have high melting points, which are a disadvantage in process operation. Fortunately, a number of trialkylphosphines are also produced in bulk industrially. Of particular interest is tri(*n*-octyl)phosphine, which is manufactured in large volume for production of tri(*n*-octyl)phosphine oxide (TOPO, a mining extraction reagent). The critical advantage of the quaternary phosphonium iodides is their excellent temperature stability.

Table 1. Tetra(*n*-alkyl)phosphonium iodides tested.

Tetra(n-alkyl) phosphonium iodide	Carbon count	M.W.	M.P. (°C)	Solubility in octane
$(n\text{-}Oct)_3(n\text{-}Bu)P^+I^-$	28	554.63	55-57	insol.
$(n\text{-}Oct)_3(n\text{-}Hexyl)P^+I^-$	30	582.68	semisolid	insol.
$(n\text{-}Oct)_3(n\text{-}Heptyl)P^+I^-$	31	596.71	77-79	insol.
$(n\text{-}Oct)_4P^+I^-$	32	610.73	86-88	sol. hot
$(n\text{-}Oct)_3(n\text{-}Nonyl)P^+I^-$	33	624.76	79-81	sol. hot
$(n\text{-}Oct)_3(n\text{-}Decyl)P^+I^-$	34	635.79	64-65	sol. hot
$(n\text{-}Oct)_3(n\text{-}Dodecyl)P^+I^-$	36	666.84	50-52	sol. warm
$(n\text{-}Oct)_3(n\text{-}Hexadecyl)P^+I^-$	40	722.94	56-58	sol. warm
$(n\text{-}Oct)_3(n\text{-}Octadecyl)P^+I^-$, **TOP18**	42	750.99	62-65	sol. warm
$(n\text{-}Dodecyl)_4P^+I^-$	48	835.15	77-79	sol. hot
$(n\text{-}Hexadecyl)_4P^+I^-$	64	1059.57	87-88	sol. hot

Thus, the selected iodide catalyst, **TOP18**, has good speed, selectivity, and stability. It is readily soluble in 2,5-DHF and in warm alkane solvents. As a salt, **TOP18** has virtually no vapor pressure, and it is reasonably low melting. It is easily synthesized by reaction of tri(*n*-octyl)phosphine with *n*-octadecyl iodide at a reasonable cost. Toxicity studies on **TOP18** showed low toxicity: Oral LD-50 (rat), >2000mg/kg; Dermal LD-50 (rat), >2000 mg/kg.

As in the case of the iodide salt component, a high concentration of Lewis acid is necessary for adequate reaction rate. Inorganic Lewis acids (e.g., ZnI) are the obvious first choice based on availability and cost. However, these catalysts also have very poor

solubility in the reaction mixture without the use of a polar, aprotic solvent. Fortunately, a family of Lewis acids was found with improved reaction selectivity and good solubility—tri(organo)tin iodides. These Lewis acids were investigated due to their known activity in the formation of cyclic carbonates from epoxides and carbon dioxide. Tri(organo)tin iodides were found to be considerably better than di(organo)tin diiodides and mono(organo)tin triiodides for the desired rearrangement. Tri(organo)tin bromides and chlorides [in conjunction with an onium bromide or chloride] were less active and less selective than the all-iodide systems.

Organotin compounds are produced commercially for use in PVC stabilization and as agricultural chemicals [12]. Tri(organo)tin iodides are appropriate candidates for consideration due to their excellent catalytic activity, high selectivity, availability of starting materials and ease of preparation. The loss of catalyst and contamination of product with benzene when using triphenyltin iodide caused us to select the more stable tri(*n*-alkyl)tin iodides. These catalysts are not as active as the triaryltin iodides but exhibit very good stability under normal reaction conditions. They are also readily prepared from industrially-available bulk starting materials. Tri(*n*-octyl)tin iodide ((*n*-Oct)$_3$SnI, referred to as "**TOT**") can be prepared from three different starting materials, although the iodide displacement is preferred. Tri(*n*-butyl)tin iodide is also an effective catalyst, but **TOT** was selected due to its lower volatility. The octyltin compounds are also generally less toxic than their butyltin counterparts.

Thus, the selected Lewis acid catalyst, **TOT**, has good catalytic activity, selectivity and stability. It is a nonviscous liquid that is compatible with **TOP18** and is miscible with 2,5-DHF and non-polar alkane solvents. It has a very low vapor pressure, so it is not lost during product distillation and catalyst recovery operations. **TOT** is easily synthesized at low cost, and it has low toxicity (Oral LD-50 [rat], >2000 mg/kg; Dermal LD-50 [rat], >2000 mg/kg).

The optimized catalyst system consisted of a 1:1 mole ratio of **TOP18** and **TOT** [13]. No additional solvents are used in the reaction stage of the 2,5-DHF process. The reaction mixture therefore consists of only reactant **1**, 2,5-DHF product, catalysts, and side-products [oligomer crotonaldehyde]. Indeed, because of the high loading of catalysts, the reaction mixture may be considered as an ionic liquid. Analysis of the reaction mixture is performed using X-ray fluorescence spectrometry (XFS, for %P, Sn, I, and Cl) and by quantitative carbon-13 NMR (for % catalysts and oligomer). C-13 NMR is especially useful for observing the condition of the organotin catalyst.

The catalyst system of **TOP18** and **TOT** is remarkably stable and long-lived if the reaction system is kept free of water and air. Contamination of the reaction mixture with water will lead to **TOT** decomposition [14]. This reaction produces hydrogen iodide, which reacts with **1**. Air is deleterious to both catalyst components. Introduction of air into the process can cause oxidation of iodide anion to iodine, which will dealkylate **TOT**. Another mode for loss of catalyst is in the oligomer. Low levels of Sn, I, and P were found in the oligomer waste. Presumably some of this lost catalyst value is via covalent attachment (end groups) as well as unextracted active catalyst.

Laboratory studies of the rearrangement process began with semi-continuous operation in a single, 200-mL, glass reactor, feeding **1** as a liquid and simultaneous distillation of 2,5-DHF, crotonaldehyde, and unreacted **1**. Catalyst recovery was

performed as needed in a separatory funnel with *n*-octane as the extraction solvent. Further laboratory development was performed with one or more 1000-mL continuous reactors in series, and catalyst recovery used a continuous Karr extractor. Final scale up was to a semiworks plant (capacity ca. 4500 kg/day) using three CSTRs.

The process is typically operated at 100-110 ºC and close to atmospheric pressure. When the oligomer level has built up sufficiently, a small purge stream is removed and sent to the Oligomer Removal Unit [ORU] for catalyst recovery. The ORU employs a 6-inch by 24-ft Karr extractor operating with mixed heptanes as the solvent (B.P. 118 ºC, SG 0.76). The solvent is fed as the continuous phase at the bottom of the extractor and the catalyst/oligomer concentrate at the top. The oligomer (raffinate) is collected as the underflow from the extractor for incineration. The Karr column was optimized by varying the flux, reciprocation rate, plate spacing, continuous phase, and thermal profile.

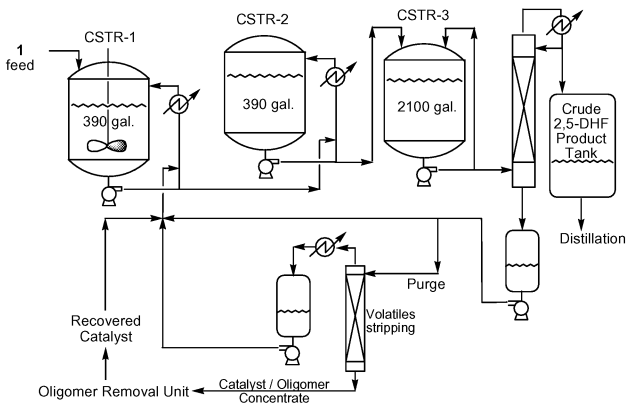

Figure 1. Semiworks-scale continuous process for 2,5-dihydrofuran.

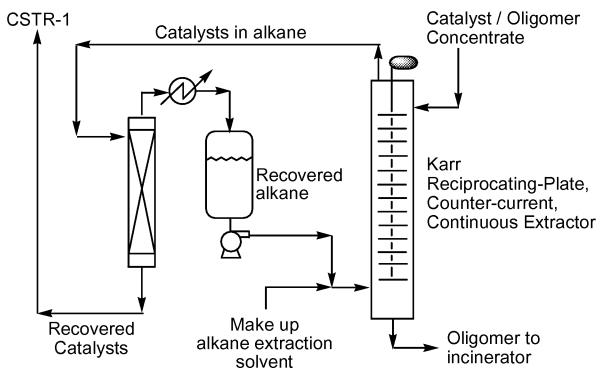

Figure 2. Oligomer Removal Unit [catalyst recovery].

Because the low-molecular-weight oligomers are soluble in the alkane extraction solvent, an unavoidably high concentration of oligomers is returned with recovered catalyst. Therefore, during steady-state operation, the reaction mixture is about one-third oligomer. Normal operation gives about 99% conversion of **1** with selectivities of

approximately 94% 2,5-DHF, 1% crotonaldehyde, and 4.5% oligomer. Typically, the catalyst level in oligomer is 3.5% **TOP18** and 0.5% **TOT**. In view of the high value of the product 2,5-DHF, this level of catalyst loss is fully acceptable. Optimized laboratory extraction conditions show 99.5% recovery of **TOP18** and 99.9% recovery of **TOT** from the oligomer.

CONCLUSION

A novel homogeneous process for the catalytic rearrangement of EPB to 2,5-DHF has been successfully developed and scaled up to production scale. A tri(*n*-alkyl)tin iodide and tetra-(*n*-alkyl)phosphonium iodide co-catalyst system was developed that met the many process requirements. The production of a minor, nonvolatile side-product (oligomer) was the dominating factor in the design of catalysts. Extraction provided the needed catalyst-oligomer separation process.

REFERENCES

1. D. Denton, S. Falling, J. Monnier, J. Stavinoha, Jr., and W. Watkins, *Chimica Oggi*, **14**, 17 (1996).
2. S. N. Falling and B. L. Gustafson, US. 4,962,210 to Eastman Kodak Co. (1990).
3. J. R. Monnier, US 5,536,851 to Eastman Chemical Co. (1996); J. R. Monnier and C. S. Moorehouse, US 5,670,672 to Eastman Chemical Co. (1997); T. R. Nolen, S. N. Falling, D. M. Hitch, J. L. Miller and D. L. Terrill, US 5,681,969 to Eastman Chemical Co. (1997); J. R. Monnier, J. W. Medlin, Y.-J. Kuo, *Appl. Catal. A*, **194-195**, 463 (2000).
4. S. N. Falling and G. W. Phillips, US 5,254,701 to Eastman Kodak Co. (1993).
5. W. A. Beavers, US 5,945,549 to Eastman Chemical Co. (1999).
6. S. Liang, T. Price, T. R. Nolen, D. B. Compton, and D. Attride, US 5,502,257 to Eastman (1996); S. Liang and T. Price, US 5,504,245 to Eastman Chemical Co. (1996).
7. V. P. Kurkov, US 3,932,468 to Chevron Research Co. (1976); R. G. Wall and V. P. Kurkov, US 3,996,248 to Chevron Research Co. (1976).
8. M. Fischer and D. E. Offen. 3926147 to BASF AG (1989); J. R. Monnier, S. A. Godleski, H. M. Low, L. G. McCullough, L. W. McGarry, G. W. Phillips, and S. N. Falling, US 5,082,956 to Eastman Kodak Co. (1992).
9. J. R. Monnier and P. J. Muelbauer, US 4,897,498 and 4,950,773 to Eastman Kodak Co. (1990); J. R. Monnier, J. W. Medlin, and M. A. Barteau, *J. Catal*., **203**, 362 (2001).
10. J. L. Stavinoha, Jr. and J. D. Tolleson, US 5,117,012 to Eastman Kodak Co. (1992); J. L. Stavinoha, Jr., J. R. Monnier, D. M. Hitch, T. R. Nolen, and G. L. Oltean, US. 5,362,890 to Eastman Chemical Co. (1994).
11. J. C. Matayabas, Jr. and S. N. Falling, US 5,434,314 to Eastman Chemical Co. (1995); S. N. Falling, S. A. Godleski, P. Lopez-Maldonado, P. B. MacKenzie, L. G. McCullough, and J. C. Matayabas, Jr., US 5,608,034 to Eastman Chemical Co. (1997); T. Kuo, E. E. McEntire, S. N. Falling, Y.-C. Liu, and W. A. Slegeir, US 6,451,926 to Eastman Chemical Co (2002).
12. P. J. Smith, "Chemistry of Tin," P. J. Smith, Ed., Blackie Academic & Professional, Thomson Science, London, Second Edition, 1998; pp. 431-435.
13. G. W. Phillips, S. N. Falling, S. A. Godleski, and J. R. Monnier, US 5,315,019 to Eastman Chemical Co. (1994).
14. S. N. Falling and P. Lopez, US 5,693,833 to Eastman Chemical Co. (1997).

STUDY OF VANILLIN EXTRACTION FROM SOLUTIONS OF LIGNIN OXIDATION

V. E. Tarabanko, Yu. V. Chelbina, K. L. Kaygorodov, N. V. Tarabanko, and N. V. Koropachinskaya

Institute of Chemistry and Chemical Technology, Siberian Branch of Russian Academy of Sciences, K. Marksa Street, 42, Krasnoyarsk, 660049, Russia. Corresponding author email address: veta@icct.ru

ABSTRACT

This paper deals with vanillin extraction for its isolation and purification. Extraction with water-insoluble alcohols, tributylphosphate, and their solutions was studied and discussed. The distribution ratios were found to attain values up to 100 for extraction with tributylphosphate and 20 – 30 for extraction with alcohols. Stripping vanillin from the alcohol solutions with alkali permits vanillin to be concentrated in the water phase. The equilibrium constant of the vanillin-hydrogen sulfite derivative formation was estimated (K = 350).

INTRODUCTION

Vanillin is one of the most valuable products obtained from waste materials of chemical processing of wood. A very important stage in vanillin production is the product extraction from the reaction solutions that contain about 10 g/L of vanillin and an order of magnitude greater amount of organic byproducts. Thus, extraction pursues two goals: vanillin concentration and its separation from admixtures.

In laboratory practice, a sequence of extraction–distillation of solvent is commonly used for recovering organic compounds, but in industry a technology of extraction–stripping is more desirable. An overview of possible methods of vanillin extraction and of corresponding extractants has been published [1-2]. Table 1 summarizes the data on different methods of vanillin extraction.

Despite the large number of works devoted to the problem of vanillin extraction, all of them have serious disadvantages: low selectivity or efficiency of extraction (high content of tar and low distribution ratio, respectively) by simple and affordable extractants like esters or paraffin hydrocarbons; complicated or even impossible vanillin stripping or extractant recovery (alkylamines); extractant toxicity (benzene); and solubility of extractants in water (butanol, butyl acetate, and benzene). A serious obstacle to the choice of an extractant can be its price, as vanillin is not a very expensive product (about 10 USD/kg).

Two principal ways of vanillin stripping are known: by sodium hydrogen sulfite or by alkaline solutions. The former method yields high selectivity, as extractant reacts with vanillin's carbonyl group. The formation constant of the sodium hydrogen sulfite derivative of benzaldehyde is quite high (K = 6.4 x 10^3 at 21 °C and pH 3.5–6.8 [7]). However, according to reported data [8] for vanillin stripping in the form of hydrogen sulfite derivative from industrial extracts, a triple treatment with sodium hydrogen sulfite solution is used; thus, the hydrogen sulfite derivative of vanillin is not sufficiently stable to carry out one-stage stripping.

Table 1. Characteristics of methods of vanillin extraction

Extractant	D	Advantages	Disadvantages	Ref.
Benzene	6.3	Industrially used	Toxicity of extractant, phase-separation difficulties	[3]
Toluene	4.1	Moderate toxicity	Low D value	[3]
Hexane	0.20	High extraction selectivity	Very low D value	[3]
Chloroform	26.5	High D value, quick phase separation	Low extraction selectivity	[3]
Butyl acetate	28.2	High D value	Low extraction selectivity, stripping difficulties	[4]
Butanol	27	High D value	Solubility of extractant in water	[5]
Octanol	20.5	High D value	Low extraction selectivity, stripping difficulties	[3]
Octylamine	Up to 600	High extraction selectivity and D value	Stripping difficulties	[2]
Tetraalkyl-ammonium chloride	50-100	Possibility of extraction from alkaline media	Difficulties with extractant recovery	[6]

For most solvents used for extraction, stripping with alkaline solutions allows very high distribution into the water phase, thus concentrating vanillin on stripping. This is due to the fact that, except for alcohols and alkylamines, hydrophilic vanillate ion only slightly distributes into the organic phase. Esters are unstable in aqueous alkaline media, and so they are unsuitable for such stripping processes. Thus, for creating an effective extraction–stripping process, aliphatic alcohols as extractant and aqueous alkaline solutions for stripping is a prospective combination. Possibilities for vanillin stripping from aliphatic alcohol solutions are practically unresearched and, in the case of butanol, are ineffective, as the sodium vanillate distribution ratio in the system butanol–water is close to unity (D = 0.7–0.8) [5].

Tributylphosphate is a useful industrial extractant, and the distribution ratio of phenol in the water–tributylphosphate system is equal to 400 [3]. This indicates the possibility of efficient extraction and stripping of vanillin with tributylphosphate and sodium hydrogen sulfite, correspondingly.

The goal of the present work is to study vanillin extraction with the aliphatic C_5–C_8 alcohols and tributylphosphate and stripping with alkali and sodium hydrogen sulfite solutions towards finding conditions for a conceptual vanillin separation process.

EXPERIMENTAL

Extractants were purified according to commonly used methods [9].

The batch of vanillin was dissolved in water in a 100 mL volumetric flask, and the calculated amounts of sodium sulfate, hydrochloric acid, or sodium hydroxide were added to provide the required pH and ionic strength.

Aqueous phase (2 mL) and extractant were put into a glass tube, which was then shaken for 300-450 seconds. Phases were separated by centrifugation. The total time of phase contact was 1200-1500 s. Preliminary experiments had shown that extraction equilibrium is attained after 250–300 s. Then from each phase a sample of 1.0 mL was removed and diluted to 10.0 mL by solution of a neutralizing agent in aqueous ethanol. The concentration of vanillin in the resulting solution was determined by the spectrophotometric method.

RESULTS AND DISCUSSION

Vanillin Extraction with Alcohols and Tributylphosphate (TBP)

Figure 1 shows the dependency of observed vanillin distribution ratio versus the pH of the aqueous phase in the water–alcohol systems. Distribution ratios obtained at pH < 7 (30.5 for hexan-1-ol, 24.6 for heptan-1-ol, and 20.3 for octan-1-ol) coincide with known data [3,10].

Distribution ratios in the pH range 11-14 (0.21 ± 0.02 for hexan-1-ol, 0.18 ± 0.02 for heptan-1-ol, and 0.15 ± 0.03 for octan-1-ol) characterize the efficiency of vanillate-anion extraction. Residual concentrations of molecular vanillin in the aqueous phase at pH 11 and above are less than 10^{-5} mol/L in correspondence with the acid dissociation constant of vanillin (pK_a = 8.2 [11]); thus, they can't explain the observed vanillin concentration in the organic phase in alkaline media.

In an extraction–stripping process, the possibility of concentrating the product is determined by the change of distribution ratios in going from acid to alkaline media (Table 2). Except for hydrophilic butanol, for higher alcohols, these values are close to each other and range from 135 to 145. An order-of-magnitude greater values of this ratio are obtained for octane-1-ol solutions in heptane (Table 2). These data indicate high efficiency of vanillin extraction (from acid media) and stripping (into alkaline media) with higher alcohols and their solutions.

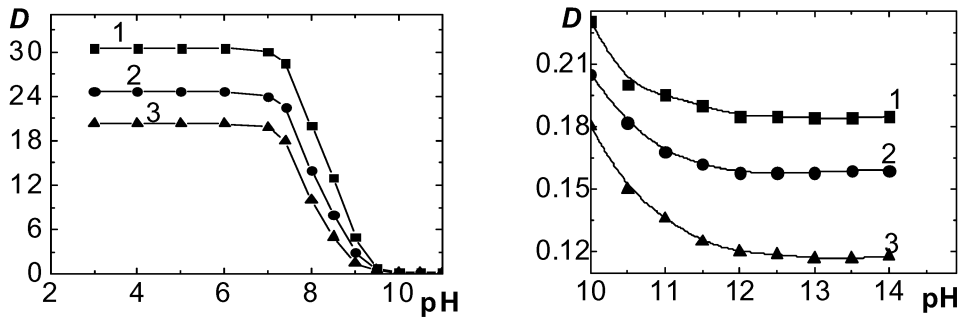

Figure 1. Dependency of vanillin distribution ratio *D* versus pH. Extractant: 1 – hexan-1-ol, 2 – heptan-1-ol, 3 – octan-1-ol (initial vanillin concentration in the aqueous phase 0.01 mol/L, ionic strength 0.1 mol/L).

Table 2. Influence of the alcohol's nature and concentration on vanillin distribution ratios from acid and alkaline media

Extractant	C_4	C_6	C_7	C_8	C_8, 65 %*	C_8, 40 %*
D (pH 1-4)	27	30.5	24.6	20.3	7.3	2.0
D (pH 11-14)	0.75	0.21	0.18	0.15	0.0046	5.7×10^{-4}
D (pH 1-4)/*D* (pH 11-14)	36	145	136	135	1590	3510

* Octane-1-ol solution in heptane.

In the pH range close to the pK_a of vanillin, the observed distribution ratio decreases with increasing pH, from values equal to the distribution ratio of molecular vanillin to the distribution ratio of vanillate ion. Reaction solutions of vanillin production have a pH of about 9, at which the apparent vanillin distribution ratio values are 5, 3, and 1.5 for hexan-1-ol, heptan-1-ol and octan-1-ol, respectively. These values are close to the vanillin distribution ratio in the water–benzene system in acid media (D = 6.3 [3]). That is, C_6–C_8 alcohols can be used to extract vanillin from reaction solutions without acidification with expenses similar to that in the technology of vanillin extraction by benzene from acidified liquors.

The results obtained indicate that C_6–C_8 aliphatic alcohols have substantial advantages over benzene, butanol, and many other vanillin extractants. Unlike benzene, these alcohols can be used to extract vanillin from weakly alkaline media, that is, from industrial reaction solutions of lignin oxidation without their acidification. This eliminates the serious technological problems related to lignoacids precipitation that follows the solution acidification (emulsifying the extraction system and vanillin sorption by the solid phase). In comparison to butanol, the studied alcohols are practically insoluble in water and are characterized by a 4–5 times weaker distribution ratio of vanillate ion, which allows effective stripping of vanillin from alcohol extracts into aqueous alkaline solutions.

The results on the vanillin extraction with tributylphosphate solutions at different pH values are shown in Figure 2. The pH dependency is of extreme character with a maximum at pH 6. The decreasing distribution ratio at pH > 6 is probably due to acid dissociation of vanillin ($pK_a = 7.2$). In acidic media (pH < 6), the acetate ion of the buffer solution produces acetic acid, and its concurrent extraction may suppress the vanillin distribution. The vanillin distribution ratio at pH 6 increases with increase of TBP concentration up to the large values $D = 100–110$.

Vanillin Stripping with Sodium Hydrogen Sulfite Solutions

To strip vanillin from TBP, solutions of sodium hydrogen sulfite can be applied. Figure 3 demonstrates the results on the influence of the sodium hydrogen sulfite concentration on the observed vanillin distribution ratio in the water–octanol system. The observed vanillin distribution ratio is related to the equilibrium constant of the vanillin-hydrogen sulfite derivative formation by the equation:

$$\frac{1}{D_{obs}} = \frac{K \times \left[HSO_3^-\right]}{D} + \frac{1}{D}, \qquad (1)$$

where D_{obs} is the observed vanillin distribution ratio, K is the equilibrium constant of the vanillin-hydrogen sulfite derivative formation, D is the vanillin distribution ratio in the pure water-octanol extraction system, and $[HSO_3^-]$ is the hydrogen sulfite ion concentration. The linear dependence with slope of $tg\varphi = K/D = 17.3 \pm 0.8$ gives $K = 350$, which is about 18 times less in comparison to the constant for benzaldehyde hydrogen sulfite derivative formation. Nevertheless, this value is great enough to strip vanillin from TBP and alcohol solutions.

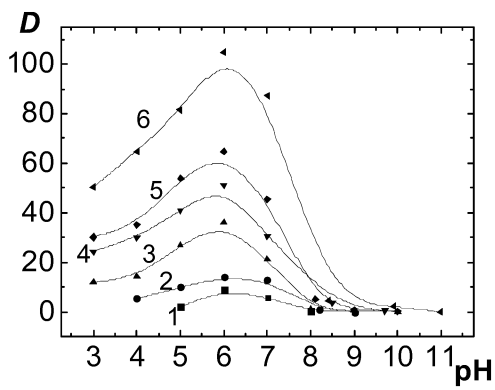

Figure 2. The dependence of the vanillin distribution ratio on pH in TBP solutions in heptane. TBP concentration, mol/L: 1 – 0.54; 2 – 0.99; 3 – 1.50; 4 – 2.26; 5 – 2.92; 6 – 3.65. Vanillin concentration 0.07 mol/L.

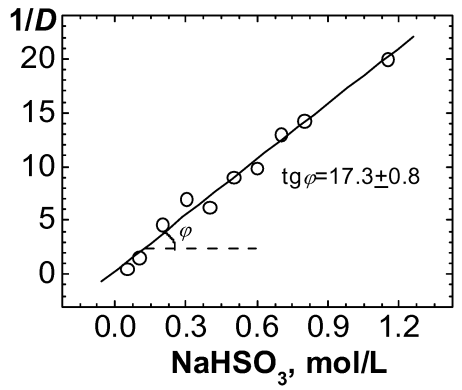

Figure 3. The influence of aqueous sodium hydrogen sulfite concentration on the observed vanillin distribution ratio in the water–octanol system. Vanillin concentration, 0.07 mol/L.

CONCLUSION

The industrial process of lignosulfonate oxidation into vanillin is carried out in strong alkaline media. However, due to the acidity increase during the process, the reaction mass can have pH 9-10, which is suitable for extraction by alcohol or tributylphosphate followed by vanillin stripping with alkali or sodium hydrogen sulfite solutions.

REFERENCES

1. V. E. Tarabanko and N. V. Koropachinskaya, "Catalytic methods for producing the aromatic aldehydes from lignins," *Chemistry of plant raw materials* (Russia), **1**, 5-25 (2003).
2. V. E. Tarabanko, Yu. V. Chelbina, V. A. Sokolenko, and N.V.Tarabanko, "The study of vanillin extraction by octylamine," *Solvent Ext. Ion Exch.*, **25**, 99–107 (2006).
3. Ya. I. Korenman, Distribution Ratios of Organic Compounds, Voronej University, Voronej (Russia), 1992.
4. V. E. Tarabanko, N. M. Ivanchenko, A. V. Kudryashev, G. R. Gulbis, and B. N. Kuznetsov, "Method for extraction of vanillin," Russian Patent, No 2065434, 20 August 1996.
5. V. E. Tarabanko, N. M. Ivanchenko, A. V. Kudryashev, and G. R. Gulbis, "Vanillin extraction from alkaline solutions," *Russ. J. Appl. Chem.*, **69**, 580-582 (1996).
6. V. E. Tarabanko, A. V. Kudryashev, G. R. Gulbis, and B. N. Kuznetsov, "Method for recovering vanillin and syringaldehyde," Russian Patent. No 2055831, 10 March 1993.
7. F. C. Kokesh and E. R. Hall, "A reexamination of the equilibrium addition of hydrogen sulfite and sulfite ions to benzaldehyde," *J. Org. Chem.*, **40**, 1632–1636 (1975).
8. O. D. Kamaldina and Ya. A. Massov, "Production of vanillin from lignosulfonates," TsBTI TsINIS, Moscow, USSR, 1959.
9. H. Rayhard, Solvents in Organic Chemistry, Moscow, USSR, 1973.
10. Ya. I. Korenman and N. G. Sotnikova, "Vanillin extraction from water solutions," *Rus. J. App. Chem.*, **48**, 195-198 (1975).
11. V. A. Palm, Tables of Rate and Equilibrium Constants of Heterolytic Organic Reactions, Moscow, USSR, 1975.

EXTRACTION CHARACTERISTICS OF PHTHALIC AND TRIMELLITIC ACID WITH 1-OCTANOL AND 10 % TRPO/KEROSENE

Zhiyong Zhou, Wei Qin, and Youyuan Dai

State Key Laboratory of Chemical Engineering, Department of Chemical Engineering, Tsinghua University, Beijing 100084, China.
Corresponding author email address: qinwei@tsinghua.edu.cn

ABSTRACT

To explore the added value of coal tar, the feasibility of extracting aromatic acid products from oxidizing coal tar was studied. Two aromatic acids, phthalic acid and trimellitic acid, were selected as the solutes, and the extraction equilibrium of both acids was studied using 1-octanol and 10% trialkylphosphine oxides (TRPO) in kerosene as the extractants. The results showed that the degree of extraction for phthalic and trimellitic acid with 10% TRPO was larger than that with 1-octanol. The recovery of trimellitic acid with 10% TRPO was higher than that of phthalic acid. Moreover, the recovery was dependent on both the concentrations of the solutes and the pH of the solutions.

INTRODUCTION

The oxidation of coal in alkaline solutions at elevated temperatures is an important process to produce coal chemicals, which are difficult to obtain from petroleum [1-3]. In the middle of the 20th century, pilot operations of coal oxidation to produce aromatic acid had already succeeded in sodium hydroxide solutions at high temperatures [4,5]. A large extent of water-soluble aromatic polycarboxylic acids can be obtained in the coal oxidation products, where the total yields of aromatic acids sometimes reach 50 wt % of the oxidation products [6]. Additionally, the efficient and practical separation and analysis of these aromatic acids have not been developed, since the coal oxidation products involve a fairly complicated mixture of aromatic acid isomers [7-9]. Separation of aromatic acids using quaternary ammonium salts on reversed-phase HPLC has been studied by Kawamura and Okuwaki [10].

In this study, the feasibility of extracting aromatic acid products from oxidizing coal tar was studied. Two acids, phthalic acid and trimellitic acid, were selected as the solutes and two solvents, 1-octanol and 10% TRPO/kerosene, as the extractants.

EXPERIMENTAL SECTION

Chemicals

Phthalic acid, from Sinopharm Chemical Reagent Co. Ltd, is an analytical reagent with purity greater than 99.8%, and trimellitic acid, from Tokyo Kasei Kocyo Co. Ltd, is an analytical reagent with purity greater than 97%. 1-Octanol, from Beijing Chemical Reagent Plant, is an analytical reagents with purity greater than 99%. TRPO is kindly supplied by CYTEC Canada Incorporation free of charge. Physical properties of the chemicals obtained from the manufacturers are listed in Tables 1 and 2, respectively.

Table 1. Physical properties of aromatic acids

Chemical	Formula	Avg MW	pK_a	Hydrophobicity*, log P
Phthalic acid	$C_6H_4(COOH)_2$	166.13	2.95	0.73
Trimellitic acid	$C_6H_3(COOH)_3$	210.14	2.52	0.94

* $\log P$ is the partition coefficient with 1-octanol in log form suggested by Hansch.

Table 2. Physical properties of extractants and diluents

Chemical	Formula	Avg, MW	ρ/g·cm^{-3}
1-Octanol	$CH_3(CH_2)_7OH$	130.23	0.83
TRPO	$R_3P(O)R_2R'P(O)R'R_2P(O)R_3'P(O)$*	348.00	0.88
Kerosene	$CH_3(CH_2)_{8\text{-}16}CH_3$	142.17-254.30	0.80

*R = $CH_3(CH_2)_7$, R' = $CH_3(CH_2)_5$

Extraction Experiments

All extraction experiments were conducted in 50 mL flasks at 25 ± 2 °C. Solvent (10 mL) and 10 mL of the aromatic acid aqueous solution were added to each flask, and the solution pH was adjusted to 1.1 and 1.6 with H_2SO_4 solution. The flask containing the mixture was shaken for about 10 minutes by hand, and then it was left to equilibrate for 10 minutes, followed by separation of the two phases. An aqueous-phase sample was taken from the bottom layer using a syringe with a long needle for pH and solute concentration analyses at 25 ± 2 °C.

Sample Analysis

The aqueous samples were analyzed for acid concentration by using a high-pressure liquid chromatography (HPLC) system with a C_{18} analysis column (ZORBAX SB-C18) and a UV spectrophotometer (Waters 2487 at 276 nm wavelength). The eluent was 50% methanol, run at a flow rate of 0.6 mL min^{-1}. The concentration of aromatic acid in the organic phase was calculated by material balance. The preliminary experiment on the stripping of the organic phase indicated that the deviation of calculated values of the acid concentrations was within ±3%. The pH value of the

aqueous phase was determined with a pH meter (Hanna pH 201 model) with a precision of ±0.02.

RESULTS AND DISCUSSION

1-Octanol as Extractant

As shown in Figure 1, the degree of extraction for both acids was similar at pH = 1.6. The distribution ratios (*D*) for phthalic and trimellitic acid were obtained by regression of the curves to get 4.7 and 6.1, respectively. On the basis of Table 1, where the log*P* values of phthalic and trimellitic acid are given as 0.73 and 0.94, respectively, then, the experimental data are in accordance with the published results.

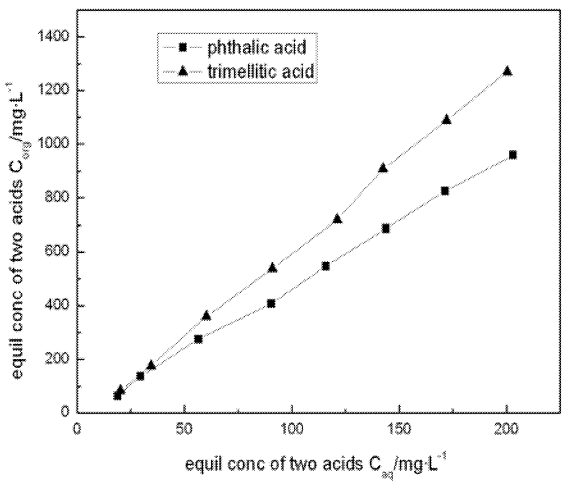

Figure 1. Equilibrium data of aromatic acidsextracted with 1-octanol.

10% TRPO/Kerosene as the Extractant

As shown in Figure 2, the degree of extraction for trimellitic acid is higher than that of phthalic acid with TRPO. As TRPO associates with aromatic acids by H-bonding in extraction processes, the degree of extraction is more sensitive to the acidities of the solutes than to their hydrophobicities. The pK_a of trimellitic acid (2.52) is less than that of phthalic acid (2.95); the higher the acidity of the acid, becomes the greater will be the degree of extraction.

Effect of pH Value

As shown in Figure 3, the *D* value decreases with an increase in the pH value for 1-octanol as the extractant, and it approaches zero when the pH value is 4; that is, 1-octanol cannot extract H_2SO_4. However, for 10% TRPO/kerosene, the *D* value increases with an increase in pH and then decreases, as shown in Figure 4. There is a

maximum in *D* at around pH = 2.4. The reason for the difference in behavior between 1-octanol and 10% TRPO/kerosene is that TRPO could extract H_2SO_4, and H_2SO_4 competes with phthalic acid for the TRPO. As the pH decreases with increasing concentration of H_2SO_4, *D* increases with the pH value at pH < pK_a.

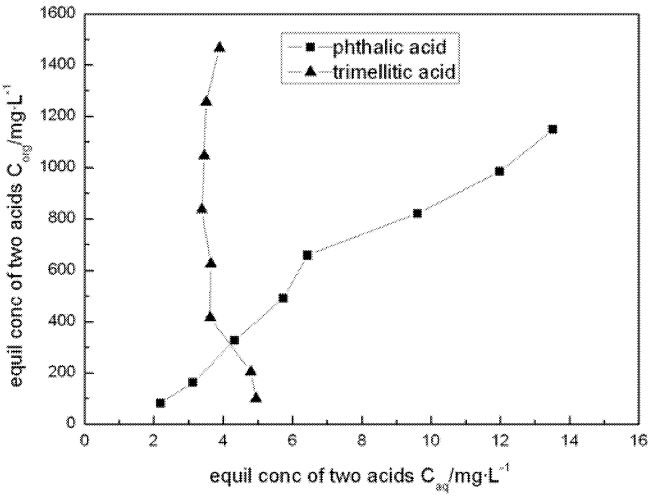

Figure 2. Equilibrium data for aromatic acids with 10% TRPO/kerosene.

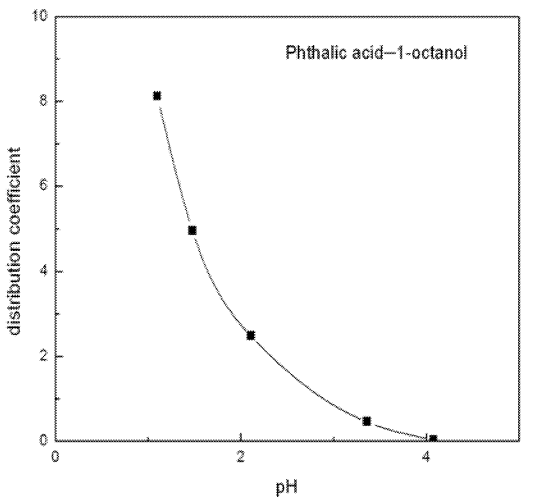

Figure 3. Effect of pH on the distribution ratio of phthalic acid with 1-octanol.

Equilibrium Behavior for a Mixture of Both Acids

The effect of the concentration ratio of trimellitic acid to phthalic acid on the equilibrium behavior was investigated. As shown in Table 3, the separation factor of trimellitic acid relative to phthalic acid increases with an increase in the concentration

of the two acids. Then, for fixed initial concentration of trimellitic acid and with increasing initial concentration of phthalic acid, the separation factor is steady as presented in Table 4.

It should be noted that the separation factor for the mixture of both acids is much larger than that estimated using the single-acid results.

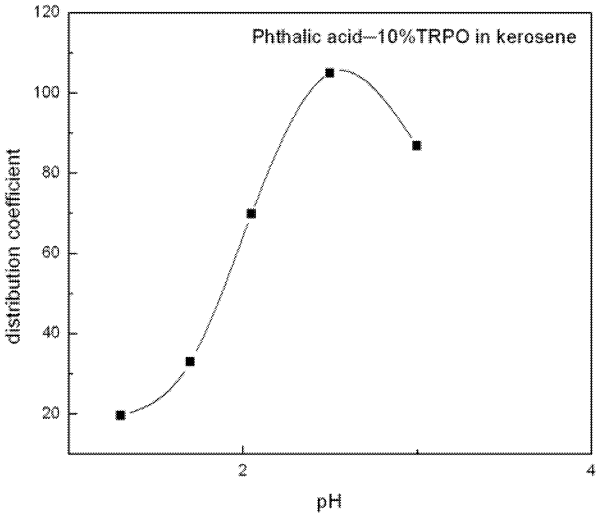

Figure 4. Effect of pH on the *D* value of phthalic acid with 10% TRPO/kerosene.

Table 3. Effect of the acid concentration on the equilibrium data for mixtures of acids*

Init conc of phthalic acid / mgL^{-1}	Init conc of trimellitic acid / mgL^{-1}	D_P	D_T	separation factor (T/P)
83	105	24.9	134	5.39
166	210	27.0	263	9.77
249	315	29.1	230	7.88
332	420	30.0	277	9.22
415	525	30.7	233	7.60
498	630	32.2	278	8.62
581	735	30.2	314	10.39
664	840	30.9	673	21.76

* Concentration proportion (T/P) was 1.25.

CONCLUSIONS

In this work, the extraction of phthalic acid and trimellitic acid by 1-octanol and 10% TRPO/kerosene was investigated. The degree of extraction for trimellitic acid is higher than that of phthalic acid with 10% TRPO/kerosene as the extractant. Extraction experiments with mixed solutions of phthalic acid and trimellitic acid showed that 10% TRPO/kerosene could be used to remove trimellitic acid from such mixtures.

Table 4. Effect of acid concentration ratio on the equilibrium data for mixtures of acids*

Init conc ofphthalic acid /mg·L^{-1}	Concentration proportion (T/P)	D_P	D_T	separation factor (T/P)
83	0.20	20.2	226	11.21
166	0.40	27.0	258	9.57
249	0.59	28.1	263	9.35
332	0.79	28.6	277	9.69
415	0.99	28.2	246	8.75
498	1.19	29.4	221	7.53
581	1.38	27.7	237	8.57
664	1.58	26.0	238	9.16

*Initial concentration of trimellitic acid was 420 mg L^{-1}.

REFERENCES

1. R. C. Smith, R. C. Tomarelli, and H. C. Howard, "Oxidation of Carbonaceous materials to organic acids by oxygen at elevated pressure," *J. Am. Chem. Soc.*, **61**, 2398–2402 (1939).
2. T. Oshika and A. Okuwaki, "Formation of aromatic carboxylic-acids from coal-tar pitch by 2-step oxidation with oxygen in water and in alkaline-solution," *Fuel*, **73**, 77–81 (1994).
3. K. Mae, H. Shindo, and K. Miura, "A new two-step oxidative degradation method for producing valuable chemicals from low rank coals under mild conditions," *Energy & Fuels*, **15**, 611–617 (2001).
4. N. W. Franke, M. W. Klebler, C. H. Rouf, J. R. Savich, and H. C. Howard, "Water-soluble polycarboxylic acids by oxidation of coal," *Ind. Eng. Chem.*, **44**, 2784–2792 (1952).
5. F. G. Parkin, I. P. Fugassi, and H. C. Howard, "Conversion of coal to simple compounds," *Ind. End. Chem.*, **47**, 1586–1592 (1955).
6. A. Okuwaki, N. Sutoh, H. Furuya, A. Amano, and T. Okabe, "Production of Oxalate by the Oxidation of Coal with Oxygen in a Concentrated Sodium Hydroxide Solution," *Ind. Eng. Chem. Prod. Res. Dev.*, **23**, 648–651 (1984).
7. K. Ohta, M. Ohashi, J. Y. Jin, T. Takeuchi, C. Fujimoto, S. H. Choi, J. J. Ryoo, and K. P. Lee, "Separation of Aliphatic Carboxylic Acids and Benzenecarboxylic Acids by Ion-Exclusion Chromatography with Various Cation-Exchange Resin Columns and Sulfuric Acid as Eluent," *J. Chromatogr., A*, **997**, 117–125 (2003).
8. M. Waksmundzka-Hajnos, "Chromatographic Separations of Aromatic Carboxylic Acids," *J. Chromatogra. B Anal. Tech. Biomed. Life Sci.*, **717**, 93–118 (1998).
9. F. Pucciarelli, P. Passamonti, and T. Cecchi, "Separation of all isomers of pyridinedicarboxylic acids by ion-pairing chromatography," *J. Liq. Chromatogr. Rel. Tech.*, **20**, 2233–2240 (1997).
10. K. Kawamura and A. Okuwaki, "Separation of aromatic carboxylic acids using quaternary ammonium salts on reversed-phase HPLC. 2. application for the analysis of Loy Yang coal oxidation products," *Sep. Sci.Technol.*, **41**, 723-732 (2006).

EXTRACTION OF *Linum usitatissimum* L. USING SUPERCRITICAL CO_2 AND ORGANIC SOLVENT

E. L. Galvão,[1] H. N. M.Oliveira,[1] L. A. G. Gonçalves,[2] A. V. B. Moreira,[3] and E. M. B. D. Sousa[1]

[1]Departamento de Engenharia Química, Universidade Federal do Rio Grande do Norte, Campus Universitário s/n, CT/DEQ/PPGEQ, Lagoa Nova-59072970, Natal-RN, Brazil. [2]Laboratório de Óleos e Gorduras-FEA-UNICAMP, CP 6091-Campinas, CEP 13081-970-Campinas-SP. [3]Departamento de Nutrição, Universidade Federal do Rio Grande do Norte, Av. Gen. Cordeiro de Farias, s/n. Petrópolis-59010-180-Natal-RN, Brazil. Corresponding author email address: elisa@eq.ufrn.br

ABSTRACT

In this study, experimental results of brown linseed extraction are presented. Comparative analysis was performed between supercritical CO_2 extraction (SC-CO_2) and organic solvent extraction (OS). The experiments were conducted in an SFE unit containing a fixed-bed cell. Oil extraction was carried out at 30 MPa and 343.15 K. OS extraction consists of sample incubation, vacuum filtration, and solvent evaporation. Extraction yields using OS were higher than those obtained with the SC-CO_2 technique. Characterization of the extracts was performed using the GC system. The results showed the presence of linoleic and linolenic acids as the main components in both techniques.

INTRODUCTION

The extraction of essential oils and vegetables using supercritical fluids as solvent is a technique that has been gaining worldwide prominence. The success of the technique is due to the characteristics that the fluids exhibit under supercritical conditions, that is, physicochemical properties between those of a liquid and a gas, which increases their solvent action. Their relatively high density also contributes to their high-solvency power, while their high diffusivity values along with low viscosity give them a considerable power of penetration into the solute matrix [1]. The most widely used solvent has been carbon dioxide (isolated or with the addition of co-solvents), because of its favorable properties, such as ease of separation, nontoxicity, nonflammability, inertness, etc. The advantage of using this technique over conventional extraction methods is the purity of the product at the end of the process, given the absence of residues. Another advantage is that this technique is considered clean and environmentally correct, since CO_2 can be recovered at the end of the process. The literature is replete with studies that used this technique to obtain vegetables and essential oils [2].

Linseed is highly oleaginous (around 40%) and rich in alpha-linolenic acid [3]. It is widely used in the production of paint, resin, and varnish [4]. In this study, experimental results of brown linseed oil extraction are presented. A comparative analysis was performed between supercritical extraction (SC-CO_2) and extraction with organic solvents (OS) in order to observe the influence of the extraction technique on the process yield and the composition of the final product, mainly in terms of linoleic and alpha-linolenic acid content.

MATERIALS AND METHODS

Two extraction techniques were used to obtain the linseed oil: a) extraction with supercritical CO_2 (SC-CO_2) at 300 bar and 70 ºC, with and without the addition of 5% ethanol as co-solvent; and b) extraction with organic solvent (OS), where two solvents were tested, ethanol and ethyl ether. The experiments were carried out to determine which of the techniques used would result in the highest recovery of linoleic and alpha-linolenic acids.

Raw-Material Preparation

The samples of brown linseed (*Linum usitatissimum* L.) used in the experiments were obtained from 3 supermarkets in Natal (Brazil), homogenized, stored in vials, and maintained below -20 ºC until use. The seeds were ground in a domestic multiprocessor (ARNO, model PRO, Brazil) for 10 s. Moisture content was determined by the AOCS 2-54 method [5]. To obtain the extracts using the OS technique, the ground seeds were separated on a 24-mesh Tyler sieve. For the SC-CO_2 technique, samples of approximately 140 g (capacity of the extractor column) were prepared at predetermined granulometry (30% of 24-, 30% of 28-, 20% of 32-, and 20% of 48-mesh). The experiments were performed in duplicate for each experimental condition tested.

SC-CO_2 Extraction

For this extraction technique, the linseed sample is placed in an extractor column, forming a fixed bed of particles through which the supercritical CO_2 drains. Thus, the desired components (linseed oil) are transported from the solid phase (seed) to the supercritical fluid phase. A pilot extraction unit built in the Laboratory of Supercritical Technology of UFRN (Brazil) was used in the experiments.

The extraction conditions were:

- Condition 1: P = 300 bar, T = 70 ºC, mean flow rate of 1.5 g CO_2/min., without the addition of co-solvent.
- Condition 2: P = 300 bar, T = 70 ºC, mean flow rate of 1.5 g CO_2/min., with the addition of co-solvent (5% ethanol).

Extraction time was fixed at 4 h for each experiment.

Organic Solvent Extraction (OS)

The methodology used for extraction by organic solvents was developed by Povh [6]. It consists of three stages: sample incubation, vacuum filtration and solvent evaporation. The samples (30 g of brown linseed oil at a granulometry of 24 mesh + 180 mL of solvent – ethanol or ethyl ether) were incubated at 15 ºC and agitated at 190 rpm for 8h. This was followed by vacuum filtration, where the extracts were separated from the solid matrix, weighed and placed in Petri plates to evaporate the solvent at a temperature of 20 ºC. After the solvent was completely evaporated, the plates were weighed and extraction yield was calculated from the ratio between the total mass of the extract present in the filtrate and the initial mass of linseed used. The product of each extraction was conditioned and stored below -20 ºC for subsequent analyses.

Extract Analysis

The extracts produced by both techniques (OS, SC-CO_2) were sterified, and the samples were prepared to obtain fatty acid methyl esters and subsequent chromatographic analyses.

Obtaining Fatty Acid Methyl Esters

Hartman and Lago's [7] method was used to prepare the fatty acid methyl esters. The methyl esters obtained were resuspended in 1 mL of hexane. This solution was injected into the chromatograph.

Gas Chromatography

The analyses were performed by capillary gas chromatography–CGC AGILENT 6850 SERIES GC SYSTEM. An AGILENT DB-23 capillary column (50% cyanopropyl-methylpolysiloxane, 60m x 0.25 mm x 0.25 μm) was used. The chromatographic conditions were the following: 1) temperature gradient—initial temperature was 110 °C for 5 min., and heat was increased by 5 °C/min. up to 215 °C, remaining at this temperature for 24 min.; 2) vaporizer temperature—250 °C; 3) detector temperature—280 °C; and 4) carrier gas—He (1.0 μL) with flow rate of 1 mL/min. The identification of fatty acids in the samples was made by comparison with fatty acid patterns determined under the same conditions.

RESULTS AND DISCUSSION

Process Yield

The yield of each extraction process used to obtain linseed oil is shown in Table 1. The yield values were calculated from the ratio between the mass of oil obtained and the mass of the sample used.

According to Table 1, the highest yields were obtained for extraction with ethyl ether organic solvent (SO), with percentages of 25.9%. The same technique, using ethanol as solvent resulted in much lower yields of around 6.1%. These results were expected, since ethyl ether is an extraction solvent with wider applications than those of

ethanol. In addition to oil, it is capable of extracting phospholipids, pigments, and unsaponifiable substances, resulting in higher yields [8].

Table 1. Linseed oil extraction: yield for two extraction techniques

Legend[a]	Extraction technique	Solvent	Yield (%)
LOSET	OS[b]	Ethanol	6.1 ± 1. 8
LOSER		Ethyl ether	25.9 ± 1.3
LSC	SC-CO_2[c]	CO_2	10.3 ± 0.7
LSCE		CO_2 + co-solvent (5% ethanol)	15.4 ± 2.6

[a]See nomenclature. [b]Organic solvent extraction. [c]Supercritical CO_2 extraction

Supercritical extraction with CO_2 (SC-CO_2) had a mean yield of 10.3% for the extractions performed without the addition of co-solvent and mean yield of 15.4% when 5% v/v ethanol was used as co-solvent. An increase of around 50% was obtained with the addition of ethanol as co-solvent. This result may be attributed to the fact that CO_2 is an apolar substance, which would compromise the solubilization of some of the oil components. In these cases, the use of polar co-solvents is indicated to increase recovery of the most polar components.

FA Composition

The main fatty acids found in the brown linseed extracts were palmitic (C16:0), stearic (C18:0), oleic (C18:1), linoleic (C18:2), and α-linolenic (C18:3). The mean FA concentration values as a function of the extraction technique used are shown in Table 2.

The table shows that the percentage of the main fatty acids found in linseed did not change significantly with the extraction technique. The saturated (palmitic and stearic) and monounsaturated (oleic) fatty acids were found in higher concentrations for the LOSET (linseed extraction by the OS technique with ethanol as solvent) experimental condition, with percentages of 8.4% for palmitic acid, 6.8% for stearic, and 23.7% for oleic. As for α-linolenic acid content, the LOSET sample suffered a statistically significant loss ($p < 0.05$) when compared to the other samples, which had mean C18:3 preservation of around 51.5%. No statistically significant differences were found for the remaining fatty acids.

Table 2. Fatty acid composition (% w/w) of linseed oil obtained by different extraction techniques

Fatty acid	LOSET[a]	LOSER[a]	LSC[a]	LSCE[a]
Palmitic (C16:0)	8.4	6.6	7.1	6.5
Stearic (C18:0)	6.8	4.7	5.2	5.2
Oleic (C18:1)	23.7	20.0	22.7	22.2
Linoleic (C18:2*n*-6)	15.2	15.1	14.0	13.6
Linolenic (C18:3*n*-3)	45.4	53.2	50.1	51.4
ni[b]	0.4	0.5	0.8	1.1

[a]See nomenclature. [b]Unidentified

Figure 1 shows the profile of linoleic fatty (C18:2*n*-6) and α-linolenic acids (C18:3*n*-3) in brown linseed oil for all the experimental conditions tested.

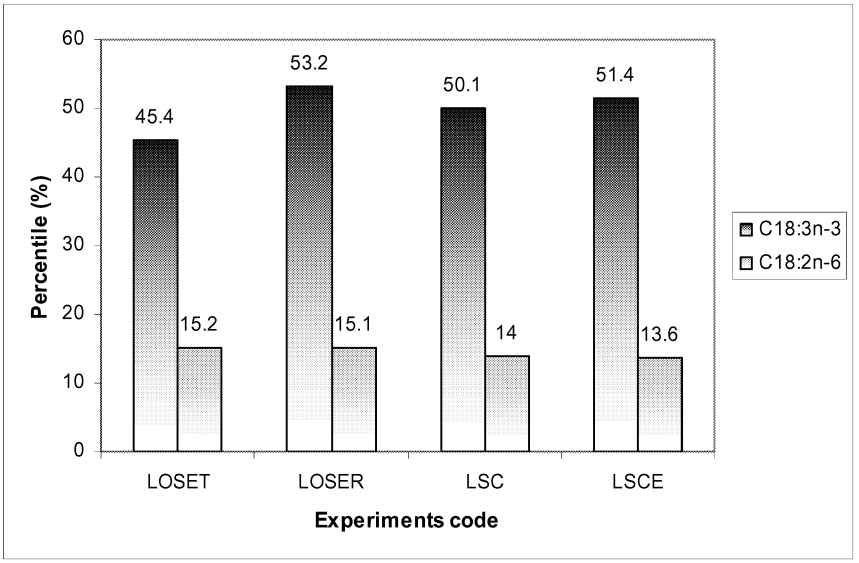

Figure 1. Profile of linoleic and α-linolenic fatty acids in the different extraction techniques.

The higher recovery of α-linolenic acid (53.2%) was obtained by the OS extraction, with ethyl ether as solvent. For linoleic acid, the highest percentage (15.2%) was also obtained with the use of organic solvents. There was no significant difference between the solvent type used (ethanol or ethyl ether). Considering only the supercritical technique (SC-CO_2), the highest percentage of α-linolenic acid (51.4%) was obtained for trials that used 5% (v/v) ethanol as co-solvent (LSCE).

CONCLUSIONS

The different extraction techniques tested (OS and SC-CO_2) for obtaining brown linseed oil resulted in satisfactory yields, the highest value (25.9%) being reached with the OS technique and ethyl ether as solvent (LOSER trial). This experimental condition also yielded the highest α-linolenic fatty acid recovery (53.2%). As to the percentage of the remaining fatty acids for the experimental conditions tested, no significant differences were found with the use of different extraction techniques.

ACKNOWLEDGMENTS

We wish to express our gratitude to the collaborators of the Oils and Fats Laboratory- FEA/UNICAMP (Brazil) and to the National Council for Scientific and Technological Development (CNPQ) for financial support.

NOMENCLATURE

LOSET—linseed extracted by the OS technique with ethanol as solvent.
LOSER—linseed extracted by the OS technique with ethyl ether as solvent.
LSC—linseed extracted by the SC-CO_2 technique without co-solvent.
LSCE—linseed extracted by the SC- CO_2 technique with ethanol as co-solvent.

REFERENCES

1. G. Brunner, Gas Extraction: An introduction to fundamentals of supercritical fluids and the application to separation processes, Springer, New York, 1994.
2. E. L. Galvão, "Extração do óleo essencial de *Cymbopogon winterianus* J. com CO_2 pressurizado," Ph.D. Thesis, UFRN, Natal, Brazil, 2004; pp. 33-35.
3. W. M. N. Ratnayake, W. A. Behrens, P. W. F. Fisher, M. R. L'Abbé, R. Mongeau, and J. L. Beare-Rogers, "Chemical and nutritional studies of flaxseed (variety Linott) in rats," *J. Nutr. Biochem,* **3**, 232–240 **(**1992).
4. C. Bickert, W. Lühs, and W. Friedt, "Variation for fatty acid content and triacylglycerol composition in different *Linum* species," **2**, 229-237 (1994).
5. Official Methods and Recommended Practices of the American Oil Chemistis' Society, 4th ed., AOCS Press, Champaign, **1**, 1993.
6. N. P. POVH, "Obtenção do óleo essencial de camomila (Matricaria recutita L. Rauschert) por diferentes métodos: destilação por arraste a vapor, extração com solventes orgânicos e extração com CO_2 supercrítico," Ph.D. Thesis, FEA, Universidade Estadual de Campinas, Campinas, Brazil, 2000; pp. 40-45.
7. L. Hartman and R. C. A. Lago, "Rapid preparation of fatty acids methyl esters," *Lab. Pract*., London, **22**, 475-476 (1973).
8. H. M. CECCHI, Fundamentos teóricos e práticos em análise de alimentos, Campinas, SP Editora da Unicamp, 1999; p. 212.

EXTRACTION OF TRITERPENES – OLEANOLIC AND URSOLIC ACID FROM SAGE

M. Schmidt and H.-J. Bart

Lehrstuhl f. Thermische Verfahrenstechnik, TU Kaiserslautern, Postfach 3049, 67653 Kaiserslautern, Germany. Corresponding author email address: bart@mv.uni-kl.de

ABSTRACT

Natural extracts from plant material are increasingly used to produce pharmaceuticals, nutraceuticals, and cosmetic products. The annual growth rate for phytopharmaceuticals, especially for triterpenes, is at about 10%. The production of a highly concentrated triterpene extract from sage is carried out with several solid-liquid extraction methods. The extraction with sc-CO_2 in the presence of different solid and/or liquid modifiers leads to good results for the extraction of oleanolic and ursolic acid. Nevertheless, the extraction with common organic solvents (e.g., ethanol or methanol) shows higher yields, and improvement in extraction yield can be gained by pretreating the plant material.

INTRODUCTION

Like other herbs, sage is known as a very effective source of traditional medicine and food enhancer. It consists of many antioxidants and other secondary plant ingredients and has manifold medicinal effects [1].

One group of pharmaceutically active substances found in sage is triterpenes and their acids. They occur not only in sage, but in a large variety of plants like seaweeds, the wax-like coatings of fruits and many medicinal herbs [2-5]. Some representatives of this group are oleanolic (1), ursolic (2), maslinic, pomolic, morolic, and betulinic (3) acids and betulin and lupeol (Figure 1). Oleanolic acid is described to be effective in restraining inflammation, protecting the liver, relieving pain, and strengthening the heart [6]. Furthermore, it is reported to have antitumor, antiulcer, antifungal, anti-HIV, diuretic, hypoglycaemic, and antihyperlipidaemic properties and shows protective effects against LDL oxidation [5,7-10]. The selective inhibition of the multidrug resistance protein ABCC1(MDR1) gives a hint towards a possible use in cancer chemotherapy [5]. Ursolic acid is characterized as anti-angiogenetic, apoptosis-inducing in different cancer cell lines, inhibiting invasion and metastasis in HT 1080 cells, and stimulating collagen production in cultured fibroblasts [2,8]. Both isomers show effects in α-amylase inhibition, which make them work as a biological antidiabetic [4]. Another field of interest is the activity of oleanolic, ursolic, and betulinic acids against the larvae of

different insects [7,11]. The aim of much recent work has been the extraction of triterpenes from different herbal sources [7,11,12].

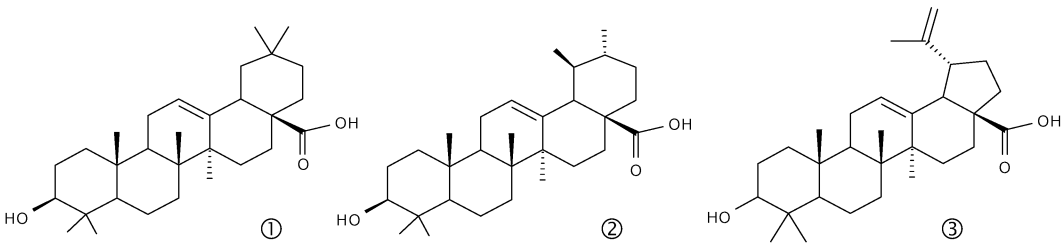

Figure 1. Structures of oleanolic ①, ursolic ②, and betulinic ③ acids.

EXPERIMENTAL

Pretreatment

Conditioning the plant material before extraction was realized in a pretreatment step in which 2g of sage were soaked in 100 mL of water or pH buffer at changing values. The duration varied in order to find the best time-range of pretreatment. After removing the water, the plant material was macerated with ethanol for 15 h under ambient temperature conditions.

Maceration and Soxhlet Extraction

Maceration was performed with 4 g of sage and 100 mL of organic solvent at ambient temperature for 15h. For Soxhlet extraction 4 g of plant material was placed in a cellulose thimble and transferred to the Soxhlet apparatus, which was filled with 100 mL of the appropriate solvent and extraction at the boiling point was allowed to proceed for 15 h. To eliminate the effects of light, all apparatus was kept in the dark during extraction. The solvents were removed from the extract with a vacuum evaporator (Büchi, Switzerland) at 323 K and 15 kPa for 1 h.

Supercritical Fluid Extraction (SFE)

SFE was carried out in a lab-scale extraction apparatus from Sigmar Mothes Hochdrucktechnik (Berlin, Germany). Ground herbs were placed in the extraction tube and fixed by two grids at the top and bottom of the extractor. In separate experiments, mixtures of pure oleanolic and ursolic acids were used. The extraction was undertaken at pressures between 10 and 28 MPa in a temperature range 323 to 363 K. Liquid modifiers was supplied via HPLC-pump in variable amounts. Solid modifiers were added directly carried to the extraction tube. Ethanol and methanol were tested as liquid modifiers, and menthol and camphor as solid modifiers. Preliminary results of using ethanol as a liquid modifier have been reported previously [13].

HPLC Analysis

Extracts were analyzed using the Gilson HPLC system (Gilson, Germany), equipped with a Hitachi 655A model UV detector, two HPLC pumps, and a mixing and a degassing unit. The Gilson application software UniPoint (Version 3.2) is used to automate the measurement and also for data evaluation. The triterpenoic acids were separated on a 250 mm x 4.6 mm Luna C18(2) column (Phenomenex, Germany), connected in series with a Luna C18(2) pre-column (particle size: 5 µm). The injection loop size was 20 µL, and the flow rate of eluent was 0.5 mL/min. The separations were carried out with an isocratic mixture of methanol/water (92:8). The extracts were diluted in eluent and passed through a 0.2 µm filter before injection. The peaks were monitored at a wavelength of 210 nm, using a linear calibration curve from appropriate standards.

RESULTS

Pretreatment

The effects of pretreatment to improve higher extraction yields of oleanolic and ursolic acids from sage were tested. It can be seen from Figure 2 that the amount of triterpenoic acids increases with pretreatment for a period up to 4 h. After this, a slight decrease is observed, but after 24 h the amount is still higher than for the short contact time of 1 h. Changing the pH with a buffering system to pH 3 or 12 leads to higher yields.

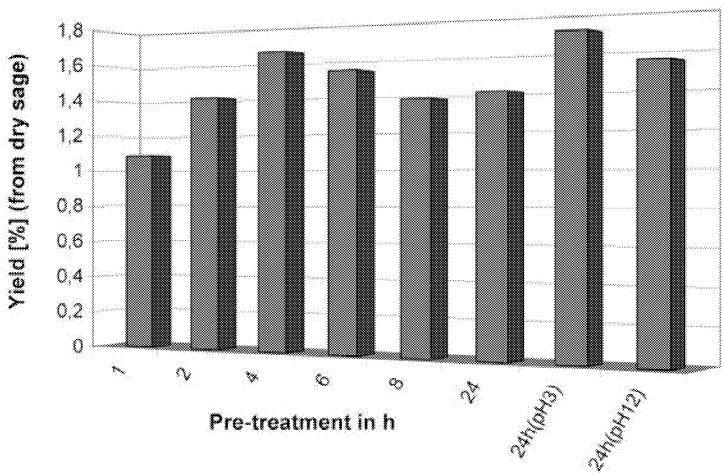

Figure 2. Effect of pretreatment and pH.

The swelling of sage can be estimated by comparing leaves before and after 24 h immersion in water (Figure 3), and it is a possible cause of the improved extraction. The length of the leaf increases 30% from the dry to the swollen state. It is not yet known which effect leads to the decrease of extraction yield with longer pretreatment times. It is possible that intracellular enzyme systems destroy the triterpenoic acids after the time

interval needed for the enzymes to become active. It is also possible that such enzymes will be deactivated by nonphysiological environment at very high or low pH values.

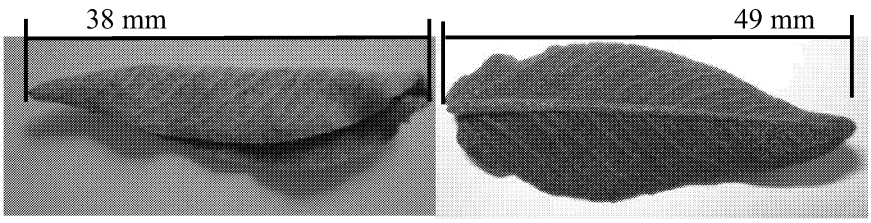

Figure 3. Dry and swollen leaves of sage after 24 h in water.

Maceration and Soxhlet Extraction

Soxhlet extraction with a pure solvent leads to better recovery than maceration at an ambient temperature (Figure 4). The increased extractability of oleanolic and ursolic acids by acetonitrile from maceration to Soxhlet are caused by little solubility and an earlier achievement of equilibrium concentrations. The tests also showed that the presence of an aqueous buffer at both high and low pH values during the extraction resulted in higher recovery of triterpenoic acids.

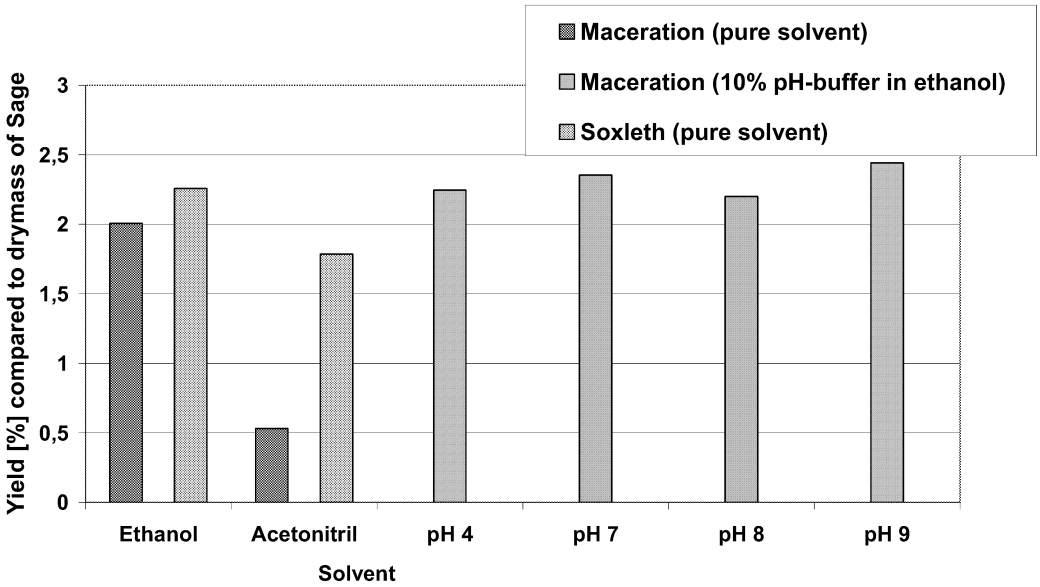

Figure 4. A comparison of results after 15 h extraction in different systems.

Supercritical Fluid Extraction

The extractability of oleanolic and ursolic acid in pure supercritical carbon dioxide ($scCO_2$) is very low. Liquid modifiers such as ethanol or methanol have been used to improve the extraction into $scCO_2$. In this work, menthol and camphor, two

monoterpenes structurally related to the triterpenoic acids, also were used as modifiers. Results are shown in Figure 5. The extraction of oleanolic and ursolic acid increases from less then 0.5% without modifiers 2% with menthol and 8% with ethanol. A mixture of ethanol and menthol is the most effective, giving a yield of 12.5%. Ethanol and camphor are slightly less effective, giving a 10% recovery of the triterpenoids.

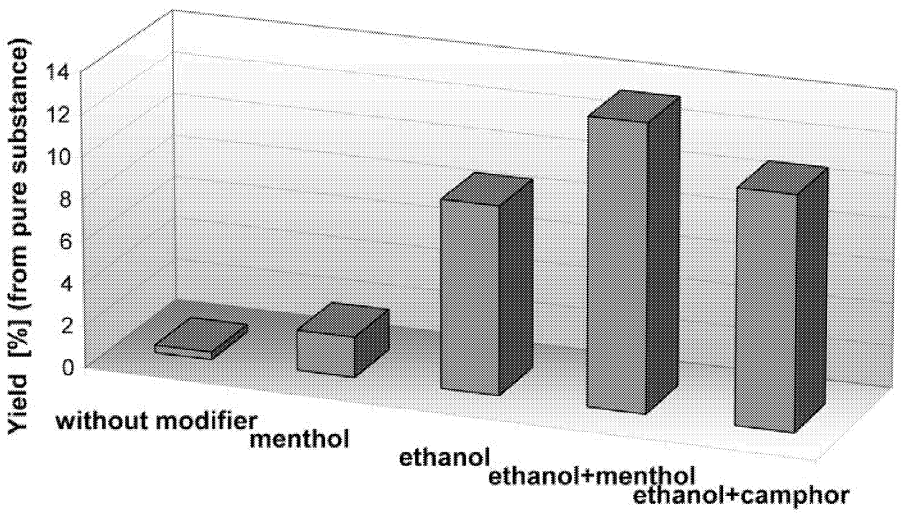

Figure 5. Extraction with $scCO_2$ at 20 MPa and 353 K.

CONCLUSIONS

It is shown that different extraction methods and media can be used to recover triterpenoic acids from sage. The highest yields are obtained by common organic solvents after pretreating the plant material. Separation of the position isomers, oleanolic and ursolic acid, is not realizable with these methods. Based on the structural similarity of these acids, it is assumed that methods similar to those involved in chiral separations will be required, and further work using chiral compounds to induce chiral information to the solvent will be carried out to attempt the separation of these two triterpenoids. To improve the practicality, it is essential to combine efficient extraction and separation steps. With this in mind, the extraction media have to be chosen carefully, and improvements to supercritical extraction by the use of appropriate modifiers might prove to be a useful approach.

ACKNOWLEDGMENTS

We wish to thank Boehringer Ingelheim Pharma GmbH & Co. KG for providing the Greek sage and a triterpenoic acid mixture and Stiftung Rheinland-Pfalz for supporting this work.

REFERENCES

1. C. F. Lima, F. Carvalho, E. Fernandes, M. L. Bastos, P. C. Santos-Gomes, M. Fernandes-Ferreira, and C. Pereira-Wilson, "Evaluation of toxic/protective effects of the essential oil of Salvia officinalis on freshly isolated rat hepatocytes," *Toxicol. In Vitro,* **18**(4), 457-465 (2004).
2. P.-O. Harmand, R. Duval, B. Liagre, C. Jayat-Vignoles, J.-L. Beneytout, C. Delage, and A. Simon, "Ursolic acid induces apoptosis through caspase-3 activation and cell cycle arrest in HaCat cells," *Int. J. Oncol.,* **23**, 105-112 (2003).
3. J. Liu, "Oleanolic acid and ursolic acid: Research perspectives," *J. Ethnopharmacol*, **100**, 92-94 (2005).
4. H. Ali, P. J. Houghton, and A. Soumyanath, "α-Amylase inhibitory activity of some Malaysian plants used to treat diabetes; with particular reference to Phyllanthus amarus," *J. Ethnopharmacol*, **107**(3), 449–455 (2006).
5. Z. Ovesna, A. Vachalkova, K. Horvathova, and D. Tothova, "Pentacylic triterpenoic acids: new chemoprotective compounds," *Neoplasma*, **51**(5), 327–333 (2004).
6. H. Liu, Y. Shi, D. Wang, G. Yang, A. Yu, and H. Zhang, "MECC determination of oleanolic acid and ursolic acid isomers in Ligustrum lucidum Ait.," *J. Pharm. Biomed. Anal.*, **32**(3), 479-485 (2003).
7. Y. N. Shukla, A. K. Tripathi, and V. K. Mehta, "Feeding-deterency of Oleanolic acid isolated from Panax quinquefolium against Lepidopterans," *Phytother. Res.*, **11**, 591-593 (1997).
8. A. Kim, J. Lee, H. Park, J. Kim, C. Kim, I. Shim, N. Kim, S. Han, and S. Lim, "Inhibition of cytochrome P450 activities by oleanolic acid and ursolic acid in human liver microsomes," *Life Sci.*, **74**, 2769-2779 (2004).
9. L. I. Somova, F. O. Shode, and M. Mipando, "Cardiotonic and antidysrhytmic effects of oleanolic ans ursolic acids, methyl maslinate and uvaol," *Phytomedicine*, **11**, 121-129 (2004).
10. R. Rodriguez-Rodriguez, J. S. Perona, M. D. Herrera, and V. Ruiz-Gutierrez, "Triterpenic Compounds from 'Orujo' Olive Oil Elicit Vasorelaxation in Aorta from Spontaneously Hypertensive Rats," *J. Agric. Food Chem.*, **54**, 2096–2102 (2006).
11. C. Chandramu, R. D. Manohar, D. G. Krupadanam, and R. V. Dashavantha, "Isolation, characterization and biological activity of betulinic acid and ursolic acid from Vitex negundo L.," *Phytother. Res.*, **17**(2), 129-134 (2003).
12. S. Zhu, K. Zou, S. Cai, M. Meselhy, and K. Komatsu, "Simultaneous determination of triterpene saponins in ginseng drugs by high-performance liquid chromatography," *Chem. Pharm. Bull.* , **52**(8), 995-998 (2004).
13. M. Schmidt and H.-J. Bart, "Extraction of Triterpenoic Acids from Greek Sage," 3rd Meeting on High Pressure Chemical Engineering, Erlangen, Germany, 2006.

EXTRACTION OF LEVULINIC ACID TO INCREASE THE SELECTIVITY AND EFFICIENCY OF THE CARBOHYDRATE ACID-CATALYZED CONVERSION

V. E. Tarabanko, M. A. Smirnova, and M. Yu. Chernyak

Institute of Chemistry and Chemical Technology, Siberian Branch of Russian Academy of Sciences, K. Marksa street, 42, Krasnoyarsk, 660049, Russia.
Corresponding author e-mail address: veta@icct.ru

ABSTRACT

This paper is devoted to the application of extraction methods for increasing the selectivity and efficiency of the carbohydrate acid-catalyzed conversion to levulinic acid, 5-hydroxymethyl-2-furaldehyde and their derivatives. The carbohydrate conversion has been studied in a two-phase system (water–butanol and $NaHSO_4$ as the regenerable catalyst and stabilizer of the heterogeneous system) and in homogeneous water or butanol media. The main products of carbohydrate conversion in the presence of butanol are butyl levulinate and 5-butoxymethyl-2-furaldehyde. The selectivity of these processes and the product distribution ratios were estimated. The best selectivity of the catalytic conversion in the two-phase system (83–90 mol %) exceeds the selectivity in the homogeneous systems by a factor of 5–8. The mechanism to explain the influence of the extraction on the selectivity of the process has been suggested. The extraction method to regenerate HCl as the catalyst of the carbohydrate conversion was developed.

INTRODUCTION

Hexose carbohydrates, like cellulose, sucrose, and fructose, are known to produce levulinic acid (4-ketopentanoic acid, LA) and 5-hydroxymethylfurfural (5-hydroxymethyl-2-furaldehyde, 5-HMF) in acidic media. Levulinic acid is applied in polymer production and in other fields of chemical industry. 5-Hydroxymethylfurfural is used as the food flavor and can be applied for different organic syntheses [1-2].

The most important problem of improving the efficiency of the acid-catalyzed conversion of carbohydrates to LA and 5-HMF is to maintain high selectivity with increasing the substrate concentration. The most convincing data on the selectivity of fructose conversion is published by Kuster [3-6]. The total selectivity of obtaining 5-hydroxymethylfurfural and levulinic acid from fructose does not exceed 85 mol %. The

main side process that decreases the selectivity is humic-substance formation. Recently, this process was shown to take place as a result of the reaction between levulinic acid and carbohydrate [7]. The highest selectivity is attained at low temperatures (90–120 ^{o}C) and requires high acid concentrations. Under these conditions, regeneration of the catalysts becomes the main problem. The products of the hexose conversion have too-low vapor pressures and can not be removed from the reaction mass by distillation. Hence, the catalyst should be separated from the products by extraction, and the efficient catalytic process should combine the highest possible distribution ratio for levulinic acid and the least possible one for the catalyst.

However, levulinic acid is a rather hydrophilic compound, and its distribution ratios are not high (D = 0.28 for diethyl ether, and D = 1.2 for furfural). One of the most efficient and readily available extractants for levulinic acid is butanol (D = 4) [8-9]. Lengthening the carbon chain of the alcohols leads to a decrease of the distribution ratio (D = 0.28 for pentanol) [8]. Butanol forms a stable two-phase system with water, but concentrated sulfuric (above 5.1 M) and hydrochloric acids are known to give homogeneous solutions with the alcohol [10].

To prevent homogenization, the mixture of sodium sulfate and sulfuric acid as the catalyst (sodium hydrosulfate with or without addition of sulfuric acid) can be used. This approach allows one to create a stable two-phase water–butanol system with good catalytic activity. Comparison of sulfuric and hydrochloric acids from this viewpoint demonstrates the advantages of the former catalyst: HCl distribution ratio in the water–isopentanol system is 5–10 times greater than that of sulfuric acid, and hydrochloric acid is distributed into the organic phase when adding calcium chloride to the water phase [10]. The possibility to use sodium hydrosulfate solution to catalyze the process is described only in a patent [11], and data on the HCl regeneration are absent.

In this paper, the application of extraction methods for increasing the selectivity and efficiency of the carbohydrate acid-catalyzed conversion with $NaHSO_4$ and HCl as the catalyst is studied. The conversion of fructose and sucrose is studied and compared in the homogeneous water-butanol solutions and in two-phase water–alcohol systems.

EXPERIMENTAL

Fructose, glucose, and sucrose of food quality were used in the experiments. Carbohydrate conversion in water solutions and in the presence of aliphatic alcohols was carried out in a 250 mL thermostated magnetically stirred glass flask. Solutions of sodium hydrosulfate with or without additives of sulfuric acid were used as the catalyst. Heated water solutions of the catalyst and carbohydrates were mixed with necessary volumes of butanol heated to the same temperature. Aqueous-phase aliquots (1 mL) were sampled and analyzed by GLC. The byproducts and intermediates were analyzed by GC-MS with a Hewlett–Packard GCD Plus spectrometer. 5-HMF and α- and β-angelicalactones were registered as intermediates or byproducts of fructose degradation.

The potassium chloride was used to regenerate the HCl catalyst. Levulinic conversion was carried out in a thermostated magnetically stirred glass flask. The hydrochloric acid was used as catalyst, and 100–200 g/L potassium chloride was added. Then the salt concentration was increased to 300–450 g/L, and butanol extraction of LA

as butyl levulinate was carried out. The reaction mixture was then cooled to 10 ^{o}C, and crystallized potassium chloride was separated. The aqueous solution containing HCl and KCl was used for new carbohydrate conversion. The catalyst wastes were estimated by the potentiometric titration of butanol and water phases.

RESULTS AND DISCUSSION

Comparing the Efficiency of Carbohydrate Conversion in Homogeneous and Two-Phase Systems with Sodium Hydrosulfate as Catalyst

The main products of the acid-catalyzed sucrose and fructose conversion in the presence of butanol are butyl levulinate and 5-butoxymethylfurfural. Their structures were confirmed by GC-MS, ^{13}C, and ^{1}H NMR spectra [7].

Table 1 shows the influence of phase volume ratio on the product yield (butyl levulinate, levulinic acid, 5-butoxymethylfurfural, and 5-hydroxymethylfurfural) of carbohydrate conversion.

Table 1. Influence of water–butanol volume ratio on the product yield*

Water : Butanol ratio	Water	1:1	1:1.5	1:2	1:3	1:4	Butanol**
Butyl levulinate yield, mol%	17	37	38	48	32	22	18
5-Butoxymethyl-furfural yield, mol%	4	13	23	32	22	20	16

*4.2 M $NaHSO_4$ and 0.5 M fructose in water phase, 95 ^{o}C, 3 h stirring.
**1.8 M H_2SO_4 and 0.5 M fructose, 92 ^{o}C, 2.5 h stirring.

The maximum product yield is attained at the water–butanol volume ratio 1:2, and it exceeds the result in homogeneous water system by a factor 4. Increase of the yield with increase of the volume ratio up to 1:2 is caused by separation of the products from the carbohydrate that prevents their interaction and humic acid formation [7]. The decrease of the product yields at the volume ratio above 1:2 may be associated with the fructose extraction into the butanol phase.

Figure 1 shows the dependencies of maximum total yields of the products of fructose conversion (the sum of LA, 5-HMF, and their ester and ether) versus the substrate concentration in the different media: homogeneous water solution, homogeneous butanol medium, and two-phase water–butanol system.

These results are obtained under rather close conditions (the same temperature, nature, and activity of the catalysts), and therefore, they convincingly demonstrate the influence of the phases present in the reaction system on the product yields of the catalytic conversion.

Moderate and high product yields (40–90 mol %) in the homogeneous water and butanol solutions are observed only at the fructose concentration less than 0.2 M. With increase of the substrate concentration up to 0.8 M, the yields of the products decrease by a factor of 4–7. In contrast to homogeneous solutions, decrease of the yields below 80%

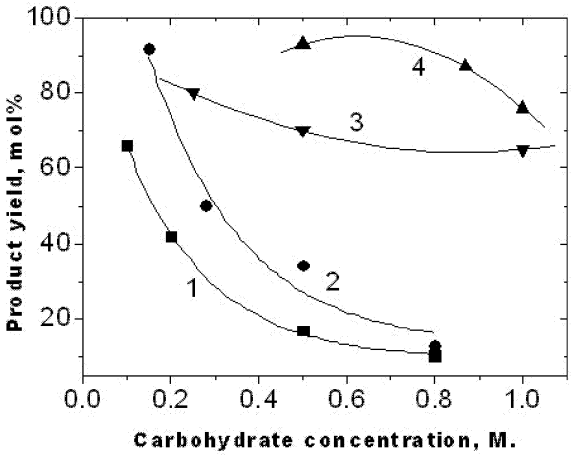

Figure 1. Influence of carbohydrate concentration on the product yield. (1—water, 4.2 M $NaHSO_4$; 2—butanol, 1.8 M H_2SO_4; 3—water, 1 M HCl; 4—water, 4.2 M $NaHSO_4$, butanol)

in the two-phase system takes place at fructose concentrations over 0.8 M. Thus, the yield of the products in the two-phase system is 6–8 times greater than in the homogeneous media at high fructose concentrations. These are the greatest known results on the selectivity of the acid-catalyzed conversion of concentrated solutions of carbohydrates, and they were attained due to separation of the products from the substrates and the catalyst by the extraction. The process can be described by the scheme:

Product yields up to 83-90 mol%	Organic phase (butanol) Products: Butyl levulinate 5-butoxymethylfurfural	Distribution ratios of the alkylated products $D \geq 70$
	↑ Extraction and alkylation	
Distribution ratios of the catalyst $D \leq 0.05$	Water solution of fructose and catalyst ($NaHSO_4$). Products: 5-hydroxymethylfurfural, levulinic acid.	Distribution ratios of the products $D = 2\text{-}4$

Scheme 1

In constant to sulfuric acid, sodium hydrogen sulfate stabilizes the two-phase water–butanol system, and the distribution ratio for the catalyst does not exceed 0.03–0.05 even for its concentrated solutions in water. The distribution ratios of levulinic acid and 5-hydroxymethylfurfural produced in water solution are equal to 2–4 [9], but as a result of the product alkylation with butanol, their distribution ratios increase up to the values of 70–100 (see Scheme 1). Such distribution ratios for the catalyst and products provide for their efficient separation, and these effects prevent side reactions of the products with the catalyst and substrate.

In such manner, removing the reaction products from the reactive water phase by combining the processes of alkylation and extraction allows increasing the product yields at high fructose concentration, and this is the most efficient approach among described processes.

Extraction Method for Recycling Hydrochloric Acid as the Catalyst

The two-phase water–butanol system permits one to separate the $NaHSO_4$ catalyst from target product and regenerate it correspondingly. The hydrochloric acid is a more active catalyst than sulfuric acid and sodium hydrosulfate, but it does not promote a stable two-phase water-butanol system. The potassium chloride addition into the system can lead to the phase separation, but salt additives decreases the yield of levulinic acid in the process [7].

To overcome this contradiction, we carried out the catalytic conversion in the solution with a low salt concentration, and the extraction of levulinic acid in a form of butyl ester was carried out at high KCl content (see Scheme 2). Cooling the water phase after extraction precipitates KCl and recycles the catalyst solution. The optimal conditions of LA extraction from the reaction mixture were found.

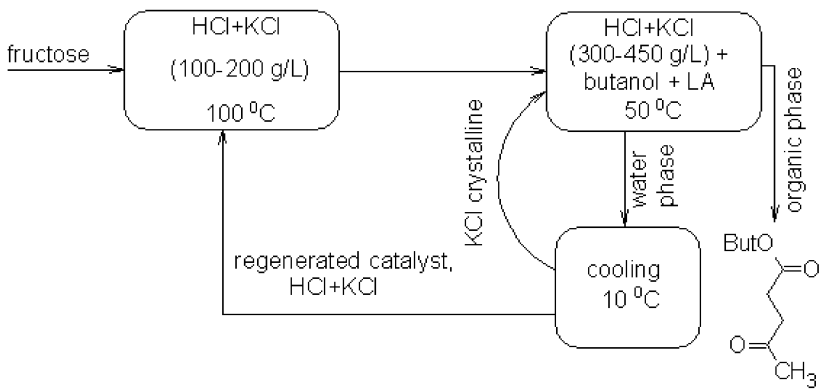

Scheme 2

The conversion selectivity slightly decreases (27 mol %) in comparison with HCl-catalyzed conversion without salt additions (30 mol %) [4]. The LA maximum extraction degree (94%) is attained at the chloride 200 g/L addition at the conversion stage and 450 g/L at the extraction and 2:1water–butanol ratio. HCl wastes in all experiments are 5–7%. This approach allows reducing the catalyst consumption by a factor of 10–20 in comparison to the usual LA extraction after acid neutralization [12]. Moreover, in this case, the product distribution ratio (D = 34) is 10 times greater than for LA extraction from water solutions [9].

CONCLUSION

The sodium hydrogen sulfate catalyst allows one to create a stable two-phase catalytic system for carbohydrate conversion: water solution of carbohydrate and sodium hydrosulfate–butanol. The main products of the acid-catalyzed carbohydrate conversion under these conditions are 5-butoxymethylfurfural and butyl levulinate, and their total yield attains 83–90 mol % at fructose concentration as great as 1 M. This selectivity exceeds the results in homogeneous water and butanol solutions by a factor of 6–8. Moreover, such a great selectivity of the acid-catalyzed conversion of carbohydrates at high substrate concentration has not been described before. Similar approach permits to successfully regenerate the HCl catalyst of the carbohydrate conversion. In this way, removing the target products from the active water phase by extraction and alkylation allows one to substantially increase the selectivity of the process.

REFERENCES

1. F. W. Lichtenthaler, "Towards improving the utility of ketoses as organic raw materials," *Carbohydr. Res.*, **313,** 69-89 (1998).
2. B. M. Levitin, Levulinic Acid. Properties, Production and Applications, Moscow, 1978.
3. B. F. M. Kuster and H. M. G. Temmink, "The influence of pH and weak–acid anions on the dehydration of D-fructose," *Carbohydr. Res.*, **54,** 185–191 (1977).
4. B. F. M. Kuster and H. S. van der Baan, "The influence of the initial and catalyst concentration on the dehydration of D-fructose," *Carbohydr. Res.*, **54**, 165–176 (1977).
5. B. F. M Kuster, "Manufacture of 5-Hydroxymethylfurfural," *Starch/Starke*, **43,** 312–314 (1990).
6. B. F. M Kuster, "The influence of water concentration on the dehydration of D-fructose," *Carbohydr. Res.*, **54**, 177–183 (1977).
7. V. E. Tarabanko, M. A. Smirnova, and M. Yu. Chernyak, "5-Hydroxymethylfurfural, levulinic acid and their derivatives from carbohydrates. Catalysis by the sodium hydrosulfate," *Chem. Industry Today (Russia)*, **10**, 13-23 (2007).
8. Ya. I. Korenman, The Distribution Coefficients of Organic Compounds, Voronej (Russia), 1992.
9. A. A. Efremov and A. P. Konstantinov, "Extraction of levulinic acid and levoglucosenon from water solutions by several organic solvents," *J. Anal. Chem. (Russia)*, **49**, 822–824 (1994).
10. F. G. Jarovskii and V. F. Melnik, "The distribution ratios of several organic substances," *J. Inorg. Chem*. (USSR), **6,** 1466–1470 (1961).
11. A. P. Dunlop, "Method of obtaining of levulinic acid and its derivatives", U.S. Patent, No. 2813900, 25 May 1957.
12. V. E. Tarabanko, M. Yu. Chernyak, and B. N. Kuznetsov, "Method of levulinic acid preparation," Russian Patent, No. 2174509, 24 April 2000.

PURIFICATION OF CYCLITOLS USING BIOEXTRACTION

A. E. Wentink, J. Micović, K. Gerlach, and M. Raventos

Department of Biochemical and Chemical Engineering, Universität Dortmund, Emil-Figge-Str. 70, 44227 Dortmund, Germany.
Corresponding author email address: Annebart.Wentink@bci.uni-dortmund.de

ABSTRACT

The investigation of reactive extraction of cyclitols (shikimic acid) shows that tertiary amines in aliphatic alcohols are the most suited among different diluents and extractants. An anti-solvent process is shown to be very efficient in recovering shikimic acid. A simple model, based on an interfacial reaction, is able to describe the phase equilibrium.

INTRODUCTION

Cyclitols or polyhydroxyl cyclic carboxylic acids are a versatile feedstock for the production of pharmaceuticals. The most prominent cyclitol is shikimic acid which is used to make Tamiflu, the most promising agent active against Bird flu [1]. Cyclitols occur naturally in, and are currently produced from, Chinese star anice (a plant), but a fermentation process is under development to overcome supply problems (both the amount and seasonal limitations) [1,2]. Bioextraction could be a viable purification process, requiring few process steps and having low production costs with high recovery. Bioextraction uses affinity extractants in benign diluents to extract the solute, while producing no waste, minimizing energy consumption, and being economically attractive.

In carboxylic acid purification by extraction in general the most critical step is the recovery of the acid from the solvent phase. In this work a volatile anti-solvent is employed. This is an aliphatic hydrocarbon, liquid at standard conditions yet easy to evaporate and with a low heat of evaporation. The anti-solvent facilitates the recovery by reducing the stability of the extractant-carboxylic acid complex.

The feasibility of the proposed concept is demonstrated in this paper for the extraction of shikimic acid. Different combinations of diluent and affinity extractant are tested experimentally to find the best combination. The effects of concentration of shikimic acid and extractant on the distribution of shikimic acid are determined. Three different anti-solvents are tested, *n*-hexane, *n*-heptane and *n*-octane, at different ratios with the solvent. This should show if the process efficiency depends on the molecular weight and volatility of the anti-solvent. A model is developed that can describe the experimental results and is used to compare the different anti-solvents.

PURIFICATION PROCESS

Figure 1 presents the process based on a volatile anti-solvent for the purification of cyclitols from fermentation broths (or plant extracts). An aqueous solution containing the acid ('broth') is contacted with an organic phase ('solvent', extractant in a diluent). The extractant selectively reacts with the cyclitol, forming a complex and solubilizing the acid in the organic phase. Tertiary amines or phosphine oxides are typically used as the extractants, which react with cyclitols via an acid-base interaction [3]. The diluent improves the physical properties of the solvent and enhances the extraction of the cyclitol. Aliphatic alcohols and ketones, especially, are known to have a stabilizing effect on the extractant-carboxylic acid complex [3,5]. Once equilibrium is attained, the phases are separated, and the solvent is contacted with a fresh aqueous phase to recover the cyclitol. Different recovery methods are possible, but these have various disadvantages, like waste production (pH swing), energy (temperature swing), or recycling (an acidic displacer) [4]. A volatile anti-solvent employed in the process does not have these disadvantages. It destabilizes the complex between the cyclitol and extractant, enhancing the recovery [3-5]. Aliphatic hydrocarbons, in particular, are suitable, as they are easily removed from the solvent by distillation or flash.

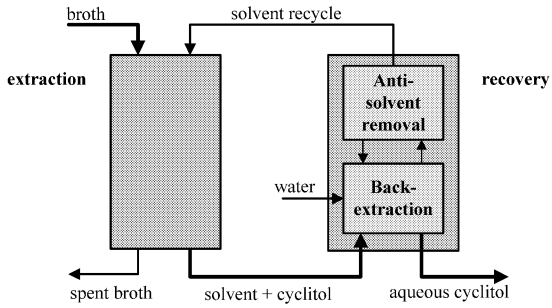

Figure 1. Purification process for cyclitols from fermentation broth or plant extract.

State of the Art in Cyclitol Purification

The current purification of shikimic acid is based on chromatography and requires five distinctive steps: removal of cells, adsorption on an anion exchanger, elution with acetic acid, adsorption on a cation exchanger, concentration by evaporation, and finally acetic acid-induced crystallization [2,6]. It demonstrates that shikimic acid recovery is complex, mainly because of the broth complexity containing other carboxylic acids (e.g., quinic acid), cell debris, salts, or unconverted feedstock (glucose).

Reactive extraction of carboxylic acids is an intensely researched topic, and sources detailing chemistry and process considerations are available [3-5]. The reactive extraction of shikimic acid was studied where in tridodecyl amine in butanol or heptanol gave the best results, with a distribution ratio for shikimic acid of up to 5 [5,7]. The recovery, was achieved by displacement back-extraction using oleic acid ('displacer') combined with a temperature swing. Oleic acid reduces the energy required in the recovery, but creates the problem that it must be removed before the solvent is recycled.

Modelling

Figure 2 shows a simplified representation of the equilibrium distribution of shikimic acid (SAH) between the aqueous (aq) and organic phase (org) containing a tertiary amine (R_3N). The physical solubility of shikimic acid in the solvent system employed (octanol/TOA) is low and assumed equal to zero (see Figure 4). Therefore, it is assumed that the amine and shikimic acid only react at the interface. A mass-action law approach is applied, and in the range of experiments performed, the findings could be described by the formation of a 1:1 complex, as is depicted in Figure 2.

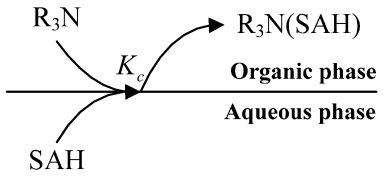

$$K_c = \frac{\left[R_3N(SAH)\right]_{org}}{\left[R_3N\right]_{org}\left[SAH\right]_{aq}}$$

Figure 2: Distribution of cyclitol between an aqueous and organic phase.

It is assumed that the tertiary amine and complex remain in the organic phase, and pH effects are not taken into account at this stage. The distribution ratio of shikimic acid (D_{SAH}), based on the molalities (M_{SAH}, in mol SAH/kg water or kg solvent) is then described by Equation 1. $(M_{R_3N})^T$ is the total amine molality in the organic phase. The equilibrium constant (K_c) is determined for each amine molality separately by minimizing the sum of squared errors between model predictions and experiments.

$$D_{SAH} = \frac{\left(M_{SAH}\right)_{org}}{\left(M_{SAH}\right)_{aq}} = \frac{K_c\left(M_{R_3N}\right)^T}{1 + K_c\left(M_{SAH}\right)_{aq}} \qquad (1)$$

EXPERIMENTS AND PROCEDURES

Equal masses of organic and aqueous solutions were contacted in double-jacket glass extraction cells and mixed using a magnetic stirrer (Variomag telesystem 06.07). The masses were determined on an analytical balance (Mettler-Toledo XS105). The change in the shikimic acid concentration was negligible after two hours; the reported experiments were all stirred for at least three hours. A constant temperature of 25 ± 0.1 °C was maintained by a thermostatic circulating water bath (Julabo F25 ME) with an external pt-100. Once equilibrium had been attained and the phases allowed to separate for 15 min, samples were withdrawn by an automated pipette (VWR). To fully separate both phases, samples were centrifuged (Eppendorf miniSpin), organic phase for 3 minutes at 13400 rpm and the aqueous phase twice, using the same settings but with intermediate removal of the clear organic phase.

The (equilibrium) concentrations were determined by titration (Mettler-Toledo DL58 Titrator with ST20A autosampler) employing a pH-sensor (MT DG115-SC). Samples, both organic and aqueous phase, were weighed and made up to a volume of around 40 mL using demineralized water and subsequently titrated with 0.01 mol/L

NaOH. A mass balance for shikimic acid was used to calculate the organic phase molality; in the results a difference around 3% and most often less than 2% was observed.

Octanol (99.5%), heptanol (99.0%), trioctylamine (TOA, >99.0%), and *n*-heptane (99.5%) were acquired from Fluka; *n*-octane (>99%), *n*-hexane (>99.0%), and NaOH (Titrisol 0.01 M) from Merck; trioctylphosphine oxide (TOPO, 99.0%) and tributylphosphine oxide (TBPO, 95%) from Aldrich; and MIBK (99%) and shikimic acid (SAH, >99.0%) from Sigma. To set the titre of NaOH, potassium phthalate (99.989% Fluka) was used. All solutions were prepared with Millipore water.

RESULTS AND DISCUSSION

Screening of Extractants and Diluents

Figure 3 presents the distribution ratio of shikimic acid for different diluent and extractant combinations. The diluents and extractants selected are common in the extraction of carboxylic acids; the diluents are oxygenated hydrocarbons that should stabilize the formed complex, whereas the extractants are different organic bases. The results show clearly that aliphatic alcohols are much better diluents than are ketones (MIBK). MIBK yields distribution ratios that are very low (practically not feasible) and show little dependence on the extractant or its concentration.

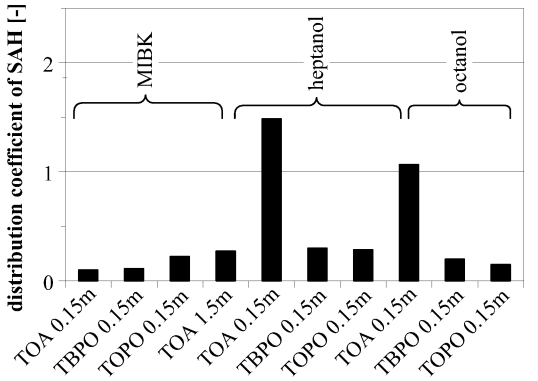

Figure 3. Distribution ratio of SAH for different extractants and diluents. Initial shikimic acid molality $(M_{SAH})_{aq,ini}$ 0.05 mol/kg water.

Aliphatic alcohols yield higher distribution ratios as they are better stabilizers for the complex, because of the hydrogen bonding of the hydroxyl group [3]. The distribution ratio of shikimic acid in heptanol/TOA is higher than it is in octanol/TOA, because of higher water solubility, but heptanol is also more soluble in the aqueous phase and might thus create waste problems. The distribution ratio of shikimic acid in heptanol and octanol can be increased to above unity, depending on the extractant type and concentration. Trioctylamine shows higher distribution ratios than do the phosphine oxides of trioctylphosphine and tributylphosphine and is thus the better extractant.

Influence of Shikimic Acid and Amine Concentration on Organic-Phase Concentration

Figure 4 (left) presents the influence of the amine molality in octanol or heptanol on the distribution ratio of shikimic acid. Pure heptanol/octanol yields a distribution ratio close to zero, as shikimic acid is highly polar (3 hydroxyl groups) and thus virtually insolulable in the aliphatic alcohol. Adding amine dramatically increases the distribution ratio, but it reaches a maximum, as is common for carboxylic acid extraction [3].

Figure 4 (right) presents the influence of the shikimic acid molality on the distribution ratio of shikimic acid for three different amine molalities. A higher aqueous shikimic acid molality decreases the distribution ratio, which directly follows from Equation 1. Equation 1 can describe the experimental distribution ratio accurately, but only if the equilibrium constant is made dependent on the amine molality as a result of using concentrations instead of activities. The calculated K_c (7.83(0.15)/6.33(0.3)/ 4.43(0.5)) show a linear trend, decreasing with increasing amine concentration.

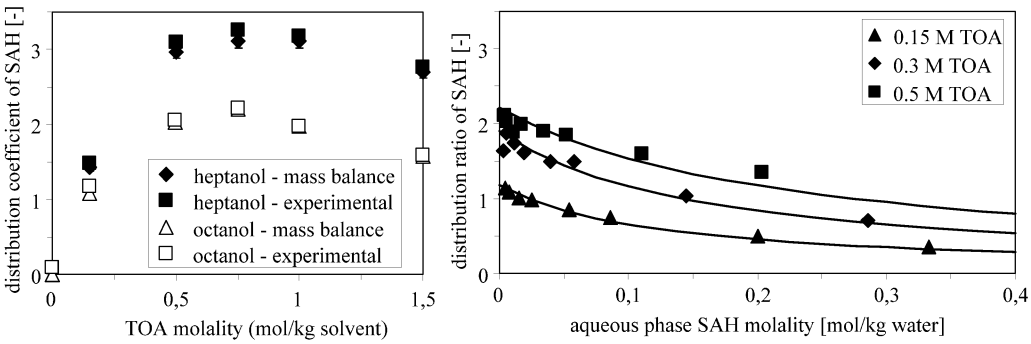

Figure 4. Effect of the TOA and SAH concentration on the distribution of SAH.

Comparison of Anti-solvent

Figure 5 presents the distribution ratio of shikimic acid as function of the anti-solvent/solvent ratio for three different anti-solvents: *n*-hexane, *n*-heptane, and *n*-octane. It is presented in two ways: as if the anti-solvent is not present ('anti-solvent free basis') and including the anti-solvent. The first is directly comparable to the results in Figure 4.

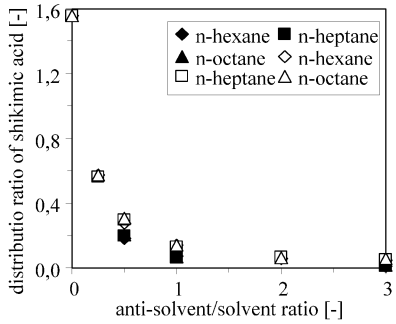

Figure 5. Effect of the anti-solvents NH, NHe, and NO on the distribution of SAH in TOA/OCT.

The addition of the anti-solvent has a rather dramatic effect: at an anti-solvent/solvent ratio of only unity already 90% of the shikimic acid can be recovered. For all three anti-solvents, an increasing amount of anti-solvent reduces the distribution ratio of shikimic acid. This clearly illustrates the effectiveness of the anti-solvent process in the recovery of shikimic acid. The differences between the three tested anti-solvents (*n*-hexane, *n*-heptane, and *n*-octane) are negligible, although at ratios below unity, *n*-octane is more efficient, but as the anti-solvent/solvent ratio increases the differences diminish. In increasing order, the expected expenses to remove the anti-solvent are *n*-hexane > *n*-heptane > *n*-octane as a consequence of the decreasing vapor pressure.

CONCLUSIONS

Trioctylamine in octanol is an effective solvent for shikimic acid. The distribution ratio of shikimic acid obtained is sufficient for practical applications. The tested anti-solvents are all very effective at reducing the distribution ratio of shikimic acid. *n*-Hexane is considered optimal, as it easiest to remove. Future work will look at the influence of impurities (other acids and remaining feedstock) and effect of temperature on the distribution ratio of shikimic acid.

ACKNOWLEDGMENTS

This work was made possible through funding from DAAD and the Marie Curie Research Training Network 'Towards Knowledge-Based Processing Systems' (PRISM) part of the Framework 6 programme from the EC (MRTN-CT-2004-512233).

REFERENCES

1. A. Yarnell, "Complexity of Tamiflu manufacturing may hamper on demand production," *Chem. Eng. News*, **83**(35), 22-23 (2005).
2. J. W. Frost, K. M. Frost, and D. R. Knop, "Biocatalytic synthesis of shikimic acid," US patent 6,613,552, 2 Sept 2003.
3. J. A. Tamada and C. J. King, "Extraction of carboxylic acids with amine extractants. 2. Chemical interactions and interpretation of data," *Ind. Eng. Chem. Res.*, **29**(7), 1327–1333 (1990).
4. J. A. Tamada and C. J. King, "Extraction of carboxylic acids with amine extractants. 3. Effect of temperature, water coextraction and process considerations," *Ind. Eng. Chem. Res.*, **29**(7), 1333–1338 (1990).
5. D. Miles, A. A. García, M. Sadaka, and G. Whited, "Recovery of shikimic acid using temperature-swing complexation extraction and displacement back extraction," *Isolation & Purification*, **2**, 75-82 (1994).
6. M. Malmberg and B. Westrup, "Process for the isolation of polyhydroxyl cyclic carboxylic acids," US patent 6,794,164 B2, 24 July 2004.
7. M. G. Sadaka and A. A. García, "The effect of temperature on forward/back extraction using an amine extractant for the recovery of cyclic hydroxyl carboxylic acids," *Sep. Sci. Technol.*, **33**(11), 1667-1680 (1998).

CONTINUOUS ENANTIOSELECTIVE EXTRACTION OF AMINO ACIDS IN A HIGHLY INTENSIFIED CENTRIFUGAL EXTRACTOR

B. Schuur, J. G. M. Winkelman, and H. J. Heeres

University of Groningen, Department of Chemical Engineering, Nijenborgh 4, 9747 AG, Groningen, The Netherlands. Corresponding author email address: b.schuur@rug.nl

ABSTRACT

Chiral amino acids are important building blocks in the pharmaceutical industry. We report our experimental studies on the resolution of the racemic amino acid 3,5-dinitrobenzoyl-d,l-leucine (DNB-d,l-leu) using reactive extraction with a chiral cinchona alkaloid extractant (CA) in a centrifugal extractor (CINC V02). The CINC V02 performed very well with yields up to 80% and enantiomeric excesses (EEs) up to 52%. Experiments at different residence times gave comparable results, implying that the extraction unit acts as an equilibrium stage. This is also supported by the observation that the experimental yields are in line with those predicted by a previously developed equilibrium stage extraction model for the system.

INTRODUCTION

The chiral business is growing strongly, especially in the fragrances and pharmaceutical industries [1]. The synthetic strategy to obtain enantiopure compounds often involves racemic synthesis followed by enantioseparation. An enantioseparation technique with great potential is liquid-liquid extraction. Over the past few decades, a number of studies have shown the potential of this technique [2–5]. However, to the best of our knowledge, processes making use of enantioselective liquid-liquid extraction have not yet been commercialized.

In the pharmaceutical and fragrances industries, the typical production scales range from kilograms to tons per annum. On this scale, multipurpose reactors and flexibility of process design are required. A very suitable device for enantioselective liquid-liquid extraction could be a CINC. The CINC is a centrifugal separator for liquid-liquid contacting and separation that was originally invented for oil-water separation. The CINC basically consists of a rotating hollow centrifuge in a static housing (Figure 1). After entering the reactor in the annular zone, the liquid(s) are mixed intensely. Next, they are transferred into the hollow centrifuge, where separation occurs by the action of centrifugal forces. The CINC V02 used in this study is a table-top scaled version with a maximum total throughput of 2 L min^{-1}. Due to large centrifugal forces (up to 900 g) applied for phase separation, the design of the apparatus can be very compact and still

capable of separating two immiscible liquids efficiently, even when their densities differ by only 10 kg m^{-3}.

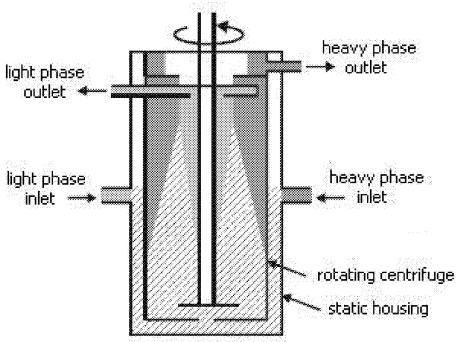

Figure 1. Sketch of the CINC.
Hatched, dispersion; darker gray, heavy phase; lighter gray, light phase.

To demonstrate the suitability of the CINC device for enantioselective liquid-liquid extraction, we report here the extraction of aqueous 3,5-dinitrobenzoyl-d,l-leucine (DNB-d,l-leu, Figure 2, left) using O-(1-t-butylcarbamoyl)-11-octadecylsulfinyl-10,11-dihydro-quinine (CA, Figure 2, right) dissolved in 1,2-dichloroethane. The effect of the operating variables on the extraction performance was studied, and the performance of the continuous extraction experiments in the CINC was compared with a previously developed equilibrium extraction model for this system [6].

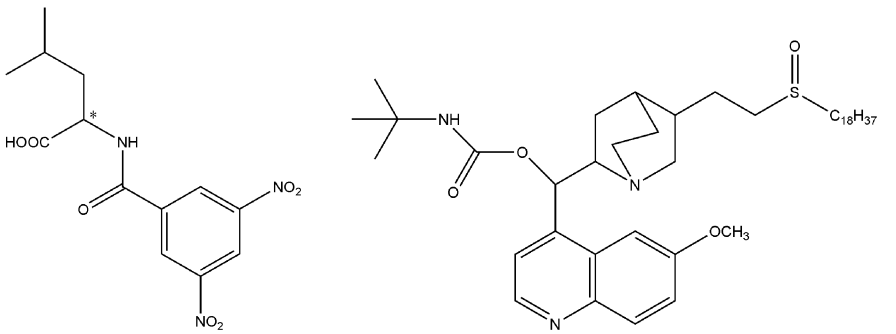

Figure 2. Structures of the solute DNB-d,l-leu (left) and the extractant CA (right).

EXPERIMENTAL

Chemicals

Purified water was obtained by reverse osmosis followed by deionization using an apparatus from Labconco; 1,2-dichloroethane (99%) from Sigma-Aldrich; potassium dihydrogen phosphate (*pa*), di-sodium hydrogen phosphate dodecahydrate (*pa*), and triethylamine (99%) from Merck; glacial acetic acid from Acros, methanol (AR); and

acetonitrille from Labscan. O-(1-*t*-butylcarbamoyl)-11-octadecylsulfinyl-10,11-dihydro-quinine, 3,5-dinitrobenzoyl-d,l-leucine, 3,5-dinitrobenzoyl-d-leucine, and 3,5-dinitrobenzoyl-l-leucine were kindly provided by DSM Research.

Experimental Setup

All experiments were carried out in CINC V02 devices (a version with a maximum total throughput of 2 L min^{-1} ($3.3 \cdot 10^{-5}$ m^3 s^{-1}) and a maximum rotational frequency of 100 Hz). Both liquids were transferred to the reactor using Verder VL1000 Control peristaltic tube pumps equipped with double pump heads (1.6 x 1.6 x 8R). Isothermal operation (typically 294 – 299 K) could be achieved by cooling the reactor jacket with tap water (288 K), enabling comparison with the previously determined equilibrium extraction model [6] for extraction at room temperature (294 K). The aqueous and organic outlet streams were equipped with temperature sensors (CMA, Amsterdam) connected to a PC via a CoachLab II interface (CMA, Amsterdam), and aqueous and organic phase inlet flows were monitored by placing the storage vessels on Mettler PM4000 balances connected to a PC using Labview 7.1 software (National Instruments).

Procedures

Extraction experiments were started by feeding the CINC with 1,2-dichloroethane. When the first liquid exited the heavy phase outlet of the CINC, the pump for the aqueous DNB-d,l-leu solution (the light phase) was started. After achieving steady-state operation, the heavy phase feed was switched from pure 1,2-dichloroethane to a CA solution in 1,2-dichloroethane, All feeds were at 294 K. When cooling was applied, this was done by flowing tap water of about 288 K through the jacket. After achieving steady-state, the experiments were continued for about 15 minutes. Samples were taken from the aqueous phase at regular time intervals, starting directly after the first liquid exited the reactor outlet.

The samples were analyzed with HPLC using an Agilent LC 1100 series apparatus equipped with an Astec Chirobiotic T column (now Supelco, Sigma-Aldrich). Detection was by 270 nm UV light absorption.

RESULTS AND DISCUSSION

Proof of Suitability of the CINC V02 for Enantioselective Extraction

An experiment, operated at equal flowrates of both phases (30 mL min^{-1}) and a rotational frequency of 50 Hz, was initiated with pure 1,2-dichloroethane as the organic solvent and aqueous DNB-d,l-leu. After operating several minutes in steady-state, the organic feed was switched to a CA solution in 1,2-dichloroethane. This moment is regarded as $t = 0$. In Figure 3, the yield of both enantiomers is depicted in time for an experiment in which the aqueous DNB-d,l-leu solution with intial concentration of 1×10^{-3} M was buffered at pH 5.12. The yields are defined as the fraction of the feed that

ends up in the organic (extract) phase (e.g., $Y_d = (c_{DNB\text{-}d\text{-}leu,aq,0} - c_{DNB\text{-}d\text{-}leu,aq,eq})/ c_{DNB\text{-}d\text{-}leu,aq,0}$).

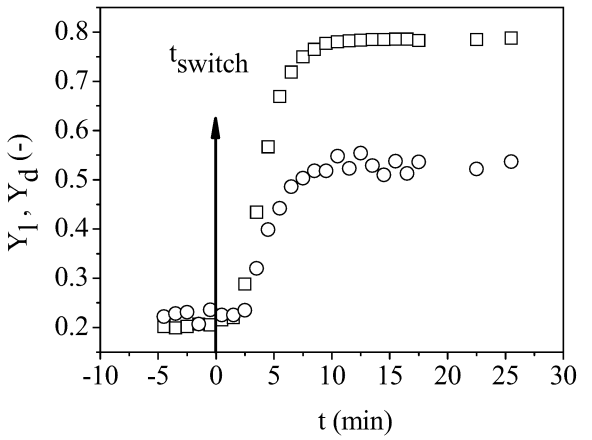

Figure 3. Yields (□ = Y_l, ○ = Y_d) versus time ($F_{aq} = F_{org} = 30$ mL min^{-1}, $N = 50$ Hz, $pH = 5.12$, $c_{DNB\text{-}d,l\text{-}leu,aq,0} = 1 \times 10^{-3}$ M, $c_{CA,org,0} = 0.5 \times 10^{-3}$ M).

Figure 3 clearly shows that when pure 1,2-dichloroethane without extractant is applied, the yields of the d- and l-enantiomer are very close, indicating a negligible EE of the product stream. Furthermore, the yields are less than 25%. After switching the organic feed from pure 1,2-dichloroethane to a 0.5×10^{-3} M CA solution in 1,2-dichloroethane, the yields of both enantiomers increase dramatically. The steady-state yield of the l-enantiomer is about 0.80, whereas the steady-state yield of d-enantiomer is about 0.52. The data also indicate that steady-state operation is achieved within 10 minutes.

On the basis of this experiment, it can be concluded that the CINC device is well suited for enantioselective liquid-liquid extraction.

Extraction Yields at Varying Residence Times

To gain insights into the effect of the flow rates on the extraction performance, three experiments were performed with varying total flowrate (58.4, 90.2, and 188 mL min^{-1}). The results are given in Figure 4. It is clear that the extraction yields are independent of the total flowrate, at least at the studied flowrates of up to 188 mL min^{-1}. Thus, under these conditions, the CINC operates as a single equilibrium extraction stage.

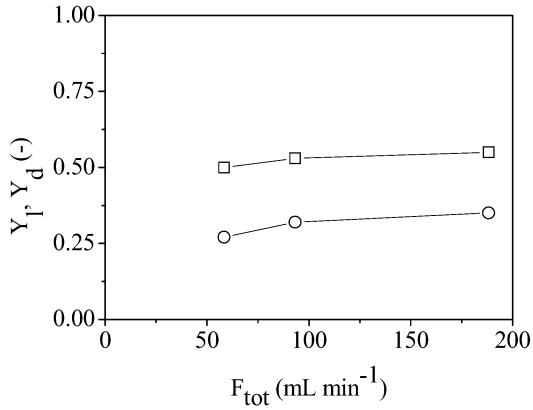

Figure 4. Extraction yields (-□- = Y_l, -○- = Y_d) at varying total flowrates. Ratio $R = F_{org}/F_{aq}$ of the flows is 1.25, 1.28, and 1.30, respectively, with increasing total flow.

Equilibrium Stage Extraction of DNB-d,l-leu

In a previous study, we developed an equilibrium extraction model for the system (294 K) and determined important chemical and physical parameters [6]. The parameters are the aqueous-phase dissociation constant of DNB-d,l-leu (K_a = 1.92·10^{-4} mol L^{-1}), the distribution of nondissociated DNB-d,l-leu over the phases (m = 8.04) and the homogeneous complexation constants of DNB-d,l-leu with CA in the organic phase ($K_{eq,L}$ = 9.31 × 10^4 L mol^{-1} and $K_{eq,D}$ = 2.71 × 10^4 L mol^{-1}). The experimental yields of the CINC V02 experiments were compared with those predicted by the equilibrium model. The correlation between the continuous experiments and the equilibrium model prediction is very good (R^2 = 0.974), as illustrated in Figure 5. This supports also the statement that the CINC device operates as a single equilibrium extraction stage.

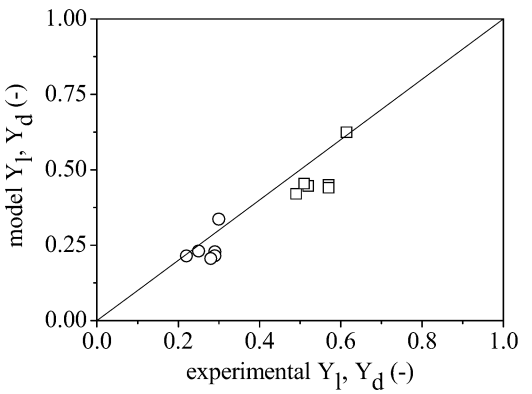

Figure 5. Parity plot for CINC experiments and model predictions. R^2 = 0.974. □ = Y_l, ○ = Y_d.

CONCLUSIONS

The enantioselective extraction of an amino acid derivative (DNB-d,l-leu) by a cinchona alkaloid extractant has been demonstrated in a CINC V02 centrifugal extractor. Under the operating conditions applied here, the extractor was shown to behave as a single equilibrium extraction stage. The correlation between the previously developed equilibrium stage model [6] and the experimental results was very good (R^2 = 0.974), indicating that the model may also be used for prediction and optimization of a multistage countercurrent process for realization of high enantiomeric excess and yield. The design and optimization of such a countercurrently operated cascade of CINCs is currently under investigation.

REFERENCES

1. R. A. Sheldon, Chirotechnology; Industrial Synthesis of Optically Active Compounds, Marcel Dekker, Inc., New York, 1993.
2. Y. Abe, T. Shoji, S. Fukui, M. Sasamoto, and H. Nishizawa, "Enantioseparation by Dual-Flow Countercurrent Extraction: Its Application to the Enantioseparation of (+/-)-Propranolol," *Chem. Pharm. Bull.,* **44**(8), 1521–1524 (1996).
3. J. Lacour, C. Goujon-Ginglinger, S. Torche-Haldimann, and J. Jodry, "Efficient Enantioselective Extraction of Tris(Diimine)Ruthenium(II) Complexes by Chiral, Lipophilic TRISPHAT Anions," *Angew. Chem. Int. Ed.,* **39**(20), 3695–3697 (2000).
4. V. Prelog, Z. Stojanac, and K. Kovacevic, "Separation of Enantiomers by Partition Between Liquid-Phases," *Helv. Chim. Acta,* **65**(1), 377–384 (1982).
5. H. Tsukube, S. Shinoda, J. Uenishi, T. Kanatani, H. Itoh, M. Shiode, T. Iwachido, and O. Yonemitsu, "Molecular Recognition With Lanthanide(III) Tris(Beta-Diketonate) Complexes: Extraction, Transport, and Chiral Recognition of Unprotected Amino Acids," *Inorg. Chem.,* **37**(7), 1585–1591 (1998).
6. B. Schuur, J. G. M. Winkelman, and H. J. Heeres, "Equilibrium Studies on the Enantioselective Liquid-Liquid Extraction of 3,5-Dinitrobenzoyl-d,l-Leucine using a Cinchona Alkaloid Extractant," submitted.

CENTREK® CENTRIFUGAL EXTRACTORS IN BIOTECHNOLOGY AND PHARMACEUTICS

G. I. Kuznetsov,[1] A. V. Kosogorov,[1] A. A. Pushkov,[1] Z. I. Kuvaeva,[2] and A. V. Mikulich[2]

[1]Research and Design Institute of Construction Technology - NIKIMT, 43 Altufievskoe Chosse, Moscow, Russia 127410. [2]The State Scientific Institute Institute of Physical Organic Chemistry of National Academy of Science of Belarus, 13 Surganov Street, Minsk, Belarus 220072. Corresponding author email address: centrek@online.ru

ABSTRACT

The paper is devoted to the extraction of amino acids, antibiotics, and drugs from vegetable raw materials with CENTREK centrifugal extractors. The extractors' design and their technical characteristics are presented.

INTRODUCTION

Problems arising in the extraction of amino acids, antibiotics, and drugs from vegetable raw materials are known: formation of stable emulsions, rapid destruction of products, and use of large volumes of volatile, inflammable, toxic, and expensive reagents. The utilization of fast, compact, and highly-efficient centrifugal extractors allows to successfully solve these problems [1].

CENTREK extractors in which it is possible to widely change the hydrodynamic and mass-transfer characteristics of working operations have been developed. In particular, depending on conditions of the technological process, it is possible to change the intensity of mixing by changing the rotor speed or stirrer diameter, separation ability by changing the rotation speed, liquids contact time by changing the volume of the mixing chamber and flowrate. It is also possible to change the overflow radii of the aqueous and organic solutions for proper extractor operations. In such a manner, the CENTREK extractors possess bright possibilities for process optimization.

The extractor (Figure 1) works as follows: aqueous and organic solutions enter the mixing chamber 2 and are stirred by mixer 1; the emulsion thus formed is fed by means of screw conveyer 8 to rotor 7, where it is separated under the effect of centrifugal force; from the rotor, separated liquids flow to ring collectors 3 (the inner ring collector is for organic phase) in static body 6 and then gravitate out the extractor. The conical form of the rotor and the special design of hydrolock 4 of heavy phases together with the activator 5 facilitate the continuous removal of solid admixtures from the rotor together

with a heavy phase. The extractors are made of stainless steel and titanium. Their technical characteristics are given in Table 1.

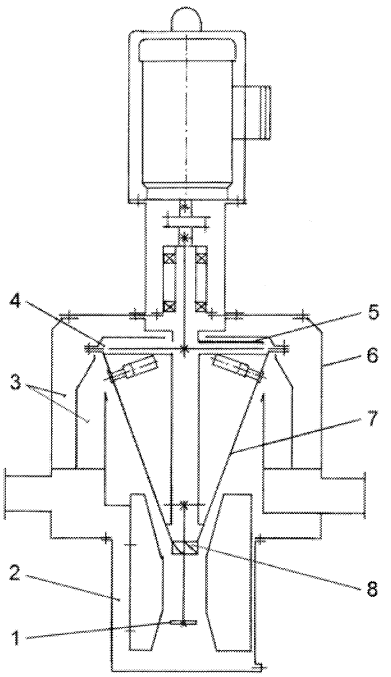

Figure 1. Schematic view of the CENTREK centrifugal extractor.

AMINO ACIDS

Development of extraction technology for the production of amino acids from microbiological synthesis media has been started using the CENTREK laboratory centrifugal extractor model EC33F made from fluoroplastic. The original product "Sulfex," representing a mixture of alkylnaphthalenesulphonic acids (ANSA) in an organic solvent, was used in the process.

Features of extraction technologies using CENTREK centrifugal extractors compared with currently used sorption processes on solid ion-exchange resin are following:

- High rate of extraction and stripping processes (Figure 2). Equilibrium achieved in not more than 1 minute at different *R (R* is the quantitative ratio of amino acid to extractant in moles in the extraction system);
- Small size of the equipment;
- Practical absence of washing waters;
- Significant reduction of the quantity of liquid waste;
- Reduction (at approximately 30 times) of reagent inventory;
- High concentration and purity of amino acids;
- Reduction of processing time.

Fast processing is often necessary for the avoidance of the decomposition of unstable substances, and is also important if reagents are unstable or if there is radiation damage to the solvent (nuclear applications).

Table 1. Technical characteristics the CENTREK centrifugal extractors

Parameter*	Extractor's model									
	EC33	ECK100	ECK125	ECK140	ECK160	ECK200	EC250	ECK280	ECK320	EC400
D_r, mm	33	100	125	140	160	200	250	280	320	400
N, s^{-1}	50	25	25	25	25	25	25	25	25	25
Q, m^3/h	0.02	0.3	0.6	0.8	1.2	2.5	5	7	10	20
V_r, L	0.021	0.35	0.9	1.2	2.1	3.5	8.4	7	11	36
V_m, L	0.015	0.4	0.7	1.2	2.2	2.3	5	6	18	20
P, kW	0.04	0.12	0.37	0.37	0.75	1.5	2.2	3	3	5.5
L, mm	135	300	260	294	333	420	490	513	620	880
W, mm	103	240	265	240	280	365	490	500	675	880
H, mm	300	590	590	617	782	900	1100	1350	1648	1900
M, kg	4.5	18	20	24	45	37	260	260	340	1100

*D_r – rotor diameter; N – rotating speed; Q – capacity for the solutions 1 mol/L TBP in kerosene and 2 mol/L HNO_3 when the ratio of flows of organic-to-aqueous phases equals 1, emulsion type "oil-in-aqueous," and phase entrainment up to 0.05% (volumetric); V_r – holdup volume of the separating chamber; V_m – holdup volume of the mixing chamber; P – electrodrive power; L, W, H – length, width, height of the apparatus; M – mass of the apparatus.

The developed technology has laid down the basis for the production of high-purity amino acids at the Grodno medicinal plant (Belarus). A countercurrent flowsheet of the continuous action (Figure 3) with model ECK320 CENTREK centrifugal extractors was proposed. It includes the following operations: extraction (number 1 extractor made from titanium), stripping with 15% ammonia (number 2 and 3 extractors made from stainless steel), and clarification of the stripped solution from the entrained organic phase (number 0 extractor used without mixing device). The need to use titanium for extractor 1 is connected with the presence of chloride ions in the native solution.

Experimental results are presented in Table 2. By now, the extraction processes for some of the amino acids listed in Table 2 have been tested on an industrial scale. As follows from Table 2, the yield of amino acids at an extraction stage is 89.5-95.5%, and at a stripping stage, practically full extraction is achieved. It should be noted that, due to the complex conditions of the emulsion separation, it is necessary to decrease flows of all amino acids compared with the data of Table 1, as well as to decrease the mixing intensity and to clarify the stripped solutions from entrained organics.

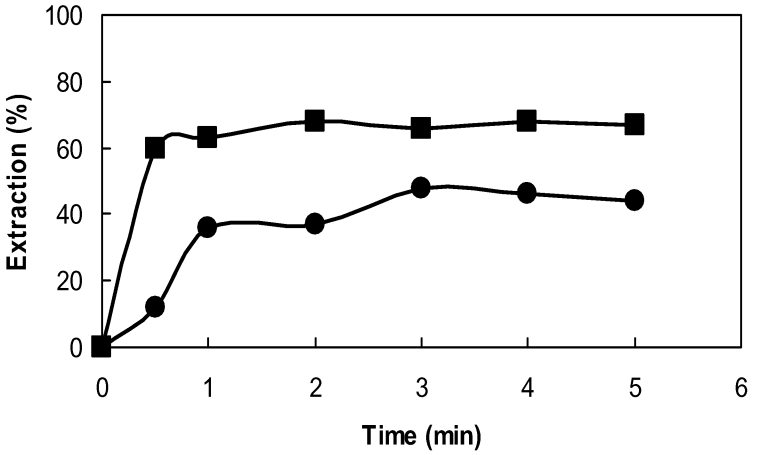

Figure 2. The kinetics of a tryptophan extraction at different *R*.
(■) *R* = 0.39; (●) *R* = 0.77.

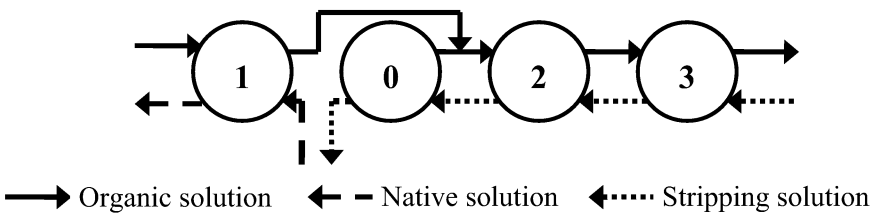

Figure 3. The scheme of the extraction installation at Grodno medicinal plant.

The production of the amino acid tryptophan (local name avitran) has been started in 2006 at the "Biovet" plant (Bulgaria). Two ECK320 extractors are used (one for extraction, one for stripping). A large R&D effort has been carried out on the optimization of the apparatus design and their operations. In particular, factors considered include the overflow radii of the aqueous and organic phases in the extractor and stripping apparatus, the dependence of admissible entrainments of organic phase in aqueous at rotating speed, and others. Under these conditions, tryptophan extraction equals 94-94.5%. Native solution flow was up to 1200 L/h. This installation is being now in operation.

ANTIBIOTICS

In the process of antibiotics production, an installation of six stages of EC250 centrifugal extractors is used in continuous countercurrent mode of operations in the Moscow pharmaceutical association "Ferein". Due to difficulties in emulsion separation, the capacity is much lower then indicated in Table 1. For example, in a lincomycinum production process, it was only 2140 L/h (1900 L/h aqueous solution, 240 L/h butanol solvent).

Table 2. Experimental data on the extraction of amino acids (AA)*

Name of amino acid	C_{AA} in native solution (g/L)	Q_{NF} (L/h)	Q_{OF} (L/h)	Q_{SF} (L/h)	C_{AA} in stripped solution (g/L)	Yield of extraction (%)
L-Leu	26.4	250	275	90	37.6	91.0
L-Val	17.0	340	400	80	38.1	91.5
L-Ile	20.6	230	400	70	40.0	89.5
L-Arg·HCl	17.7	260	400	60	40.0	91.9
L-Trp	6.0	300	300	50	31.3	95.5

* C_{AA} – amino acid concentration; Q_{NF} – native solution flow; Q_{OF} – organic solution flow; Q_{SF} – stripping solution flow.

The lincomycinum extraction process is characterized by use of partially miscible liquids: butanol and lincomycinum in water. Butanol solubility in water is 9.1% and water in butanol is 17.2%, which led to considerable change of flows in the stages of the cascade. Due to the mutual solubility, the organic-to-aqueous flow ratio is considerably (5-fold) changed from one stage to another: from 0.146 in the first to 0.033 in the sixth stage when the ratio of initial flows equal 0.126.

The use of a countercurrent process instead of the previously used process with crossed flow allowed the decrease of the consumption of extractant 2-fold and to increase lincomycinum concentration in the extract (as well as for partial mutual solubility) by 6-fold. All this allows to exclude the operation of extract vaporization. The product yield was increased by 5%, product quality is improved, and the technological time of lincomycinum production is decreased [2].

A specific feature of the process of lincomycinum production is the presence of solid contaminants in the processing solutions, which negatively affects centrifugal-extractor operation. For example, feed solutions after filtration contain up to 0.1 g/L solids (mainly albumin), and up to 0.4 g/L are formed in working solutions under their contact. The measurement of the quantity of suspended matter in solutions and their distribution in input and output solutions shows that the basic mass of solids is removed from the cascade in the raffinate. In this way, the installations have been operated for a long time without notable clogging of the separating chambers. This allows considerably longer operating time of installations without cleaning.

Also were successively tested (with use of various models of CENTREK centrifugal extractors) the production other antibiotics, for example, carminomycinum, olivomycinum, and ampicillini trihydrate [3].

MEDICAL PRODUCTS FROM VEGETABLE RAW MATERIALS

For extraction of flaminum by an ethyl acetatealcohol mixture from a water concentrate of flowers, in the Kharkov pharmaceutical association “Health” (Ukraine) [4] and Joint-Stock Company “VIFITECH” (Moscow) uses a six-stage installation of ECK100 and ECK140 centrifugal extractors. Application of centrifugal extractors has

allowed to reduce by 10-fold the volume of the necessary extractant, to increase the yield of flaminum, and considerably (from 12 to 4 hours) to lower the time of carrying out the process in comparison with processes where gravitational devices are used.

In the "Health" association, the installation of 10 centrifugal extractors having a 1500 L/h capacity for caleflonum production is used [4]. They replace the bulky equipment from tanks with mixers in which separation of phases is carried out under gravitational conditions. The use of centrifugal extractors has allowed:

- Increased output of caleflonum from 60 up to 90%;
- Reduction of the volume of the solvent directed on regeneration by 20%;
- Avoidance of vaporization of feed solutions after washing by dichlorethane;
- Decreased extraction time from 12 to 4 hours.

CONCLUSIONS

Extraction processes of biologically active substances (amino acids, antibiotics, and medicinal from vegetable sources) are characterized by relatively fast mass transfer and separations form emulsions, which are the basis for using fast CENTREK centrifugal extractors. These extractors have been successively tested on a semi-industrial level and later passed on to industrial operation.

REFERENCES

1. G. I. Kuznetsov, A. A. Pushkov, and A. V. Kosogorov, CENTREK Centrifugal Extractors, D. Mendeleyev University of Chemical Technology of Russia, Moscow, 2000 (in Russian).
2. G. I. Kuznetsov, A. A. Pushkov, A. V. Kosogorov, and M. I. Semenov, “Lincomycin Processing with Centrifugal Extractors CENTREK,” Separations for Biotechnology 3, D. L. Pyle, Ed., London, UK, 1994; pp. 255-259.
3. G. I. Kuznetsov, A. A. Pushkov, A. V. Kosogorov, M. I. Semenov, and Yu.V. Reshetov, “Intensification of Antibiotics Processing on the Base of Centrifugal Extractors CENTREK,” International Organic Substances Solvent Extraction Conference, Conference Papers, Voronezh, Russia, 1992; pp. 313-315.
4. L. I. Shklyar, G. I. Kuznetsov, A. A. Pushkov, V. I. Emeljanov, and I. S. Chernishov, “Flaminum and Caleflonum Extraction in Centrifugal Extractors CENTREK,” International Organic Substances Solvent Extraction Conference, Conference Papers, Voronezh, Russia, 1992; pp. 413-414.

REVERSED-MICELLE SIZE-DRIVEN SOLUBILIZATION AND STRIPPING OF α-AMYLASE WITH WEAK NET CHARGE

K. Tonova[1] and Z. Lazarova[2]

[1]Institute of Chemical Engineering—Bulgarian Academy of Sciences, Acad. G. Bontchev Str., Bl. 103, 1113 Sofia, Bulgaria. [2]Austrian Research Centers GmbH-ARC, Biogenetics-Natural Resources-Water, 2444 Seibersdorf, Austria.
Corresponding author email address: Zdravka.Lazarova@arcs.ac.at

ABSTRACT

Solubilization of industrial α–amylase (crude, *Aspergillus oryzae*) from an aqueous source of neutral pH and low ionic strength was performed using a cationic (CTAB) reversed-micelle (RM) solvent. The RM size was tailor-made through the co-surfactant (1-hexanol) or by the surfactant concentration. Subsequent stripping of the weakly negative α-amylase from the low surfactant-loaded solvent was possible at pH values below or above that of solubilization, and in both cases, the same purification factor of 1.4 was reached. Protein expulsion occurred along with water deflation out of micelles caused by the higher ionic strength of the bulk stripping solution.

INTRODUCTION

Surfactant-based reversed-micelle (RM) solvents, which allow a nano-sized aqueous environment to be stabilized inside a hydrophobic solvent, have been found to perform liquid-liquid extraction of hydrophilic biomolecules. Their potential has been directed towards protein separation from fermentation media, as shown for some extracellular enzymes [1,2]. α-Amylase is an enzyme widely employed in industries. Production of both bacterial and fungal growth-associated α-amylases is performed at a pH value of 7 [2,3]. However, most studies on α-amylase RM extraction have been devoted to sources with higher pHs, and RM solvent with high surfactant content thus provides a strong electrostatic driving force at the interface [2,4-6].

In this work, RM-solubilization and subsequent stripping of the α-amylase were achieved under less intense electrostatic field, that is, at lower pH and ionic strength of the source (as in the real fermentation medium) and less surfactant in the RM solvent (as it is economically profitable).

EXPERIMENTAL

Materials

The crude enzyme, industrial α-amylase (fungal from *Aspergillus oryzae*), was a domestic product (Razgrad, Bulgaria) with the following characteristics: total protein (modified micro-Lowry Method, SIGMA Diagnostics) of 56% w/w, α-amylase activity (assayed according to Pantschev et al. [7]) of 717 units mg^{-1} crude enzyme, and α-amylase molecular weight (SDS-gel electrophoresis, 6% gel) of 57 kDa. The aqueous source was a buffer of 0.012 mol dm^{-3} ethylenediamine (Merck) containing 0.046 mol dm^{-3} NaCl, and the pH was adjusted by HCl. The initial concentration of the crude enzyme was 0.656 g dm^{-3} unless otherwise stated. The stripping medium was a buffering acetate or phosphate solution (0.142 mol dm^{-3}) containing 0.075 mol dm^{-3} KBr (Fluka). In all the aqueous solutions (except for phosphates), ca. 0.006 mol dm^{-3} $CaCl_2 \cdot 2H_2O$ (Merck) was added to stabilize the α-amylase structure. The RM solvent was composed of CTAB, 15% v/v *i*-butanol, 1-hexanol, and *i*-octane. All the organic compounds (Merck or Sigma-Aldrich) were of analytical reagent grade.

Analytical Methods and Calculations

The enzyme concentration (as total protein) in the aqueous solutions was determined by measuring the solution absorbance at 280 nm. The protein absorbance inside the equilibrated RM-solvent (after solubilization) was also detected, and the mass balance was fulfilled within 10%. The following expressions were used for the calculations:

$$\%\ \text{protein yield} = (\text{protein inside RMs}) \times (\text{protein stripped from RMs}) \times 100 \tag{1}$$

$$\underset{\text{(SOLUBILIZATION)}}{\%\ \text{protein inside RMs}} = \frac{C^*_{\text{RM}} V^*_{\text{RM}}}{C^0_{\text{AQ}} V^0_{\text{AQ}}} \times 100 \tag{2}$$

$$\underset{\text{(STRIPPING)}}{\%\ \text{protein stripped from RMs}} = \frac{C^*_{\text{STR}} V^*_{\text{STR}}}{C^*_{\text{RM}} V^*_{\text{RM}}} \times 100 \tag{3}$$

where C and V respectively indicate the protein concentration and the phase volume; superscripts ^{0} and *respectively indicate initials or equilibrium; and subscripts AQ, RM, and STR respectively indicate the source, the RM solvent and the stripping solution.

The volume-specific activity of the α-amylase (U) in the aqueous solutions was assayed according to the method described by Pantschev et al. [7] and used in [4-6]. The approach of the phase mass balance was applied to evaluate the activity transferred:

$$U^*_{\text{RM}} = \frac{U^0_{\text{AQ}} V^0_{\text{AQ}} - U^*_{\text{AQ}} V^*_{\text{AQ}}}{V^*_{\text{RM}}} \tag{4}$$

For the activity yield, the same approach as in the case of protein yield (Equation 1) was followed. The purification factor was evaluated by the ratio of the specific enzyme activity (in U[α-amylase activity] mg^{-1}[total protein]) in the stripping solution versus that one in the initial source. The water content was analyzed on an automatic Karl-Fischer

titrator. The values of *W*o were then calculated as a molar ratio of the water to the initial CTAB.

The radius of the aqueous core of the RMs (R_{RM}) was given as shown by Regalado et al. [8]. In the latter calculations, the CTAB surfactant headgroup area was 0.65 nm^2 [2]. The electrostatic potential set up by the charged RM interface reduces to 5% of its initial power at the distance of $r = 3/\kappa$ inwards the electrolyte aqueous core [2] ($1/\kappa$ is Debye length and is proportional to $I_{AQ}^{-1/2}$; I_{AQ} is the ionic strength of the aqueous source). The full formula used for Debye length calculation was according to IUPAC [9].

Equilibrium Procedure

Both steps, solubilization and stripping, were performed using the phase-transfer method. Equal volumes (20 cm^3) of aqueous and organic phases were stirred (5.5 rps) in 100-cm^3 flasks at room temperature (22 ± 1°C). To reach equilibrium, solubilization was performed for 15 min., and stripping for 20 min., as shown for similar systems [2].

RESULTS AND DISCUSSION

Solubilization of α-Amylase inside RM solvent with CTAB

Effect of pH and Ionic Strength of the Aqueous Source

It is seen in Figure 1 that solubilization of α-amylase can be executed at lower pH values and using lower CTAB content if the source has lower ionic strength (see system 1). When an ionic surfactant is applied, it is considered that protein solubilization is governed by the electrokinetics at the interface.

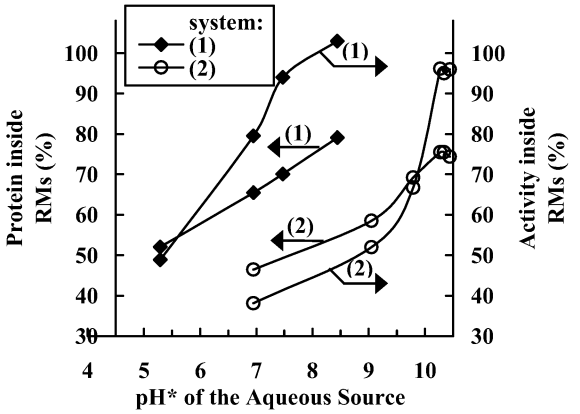

Figure 1. Effect of pH and buffer capacity of the aqueous source on the α-amylase solubilization. Both systems consisted of RM solvent with CTAB/1-hexanol (1.02 mol dm^{-3})/i-butanol/*i*-octane; and aqueous source with enzyme (0.6 g dm^{-3})/ buffer/ NaCl (0.046-0.058 mol dm^{-3}). CTAB ratio system (1):system (2) = 1:10 (0.015 mol dm^{-3} CTAB for system (1)); buffer capacity ratio system (1):system (2) = 1:10 (0.012 mol dm^{-3} EDA/HCl for system (1)); system (1) contained studied crude enzyme; system (2) contained α-amylase (from *B. licheniformis*, SIGMA) [4].

Whilst the surfactant headgroup charge is predetermined (CTAB is a cationic surfactant), the electronegative net charge on the α-amylase surface is a progressive function of the source pH above pI of 5.2. At lower ionic strength of the source, because larger RMs tend to form, and the electrostatic interactions are not shielded, less enzyme-surfactant attraction is needed in order to gain solubilization.

Effect of *W*o of the Reversed Micelle Solvent

Despite the permanent fluidity, RMs remain as ordered structures and can be described by definite radius (size) and weight (aggregation number). The RM size is linearly proportional to the parameter *W*o. Hydrophilic enzymes which solubilize in the RM pool can be changed in structure in the low *W*o range when the RM size becomes comparable to the protein's dimensions [10]. When the micelle fits the size of the biomolecule, the solubilized enzyme can refold or be recovered with superior activity by an appropriate stripping procedure [11]. As shown in Figure 2, the best α-amylase transfer (as activity) was achieved at *W*o ~ 26 (*W*o was increased by varying the CTAB-concentration). This value corresponds to a R_{RM} of 3.59 nm. Within this radius, the electrostatic potential drives the solubilisation, as the electrostatic attraction decreases at the distance of r = 3.34-3.17 nm. Thus, the electrical double layer exists almost all over inside the micelle core.

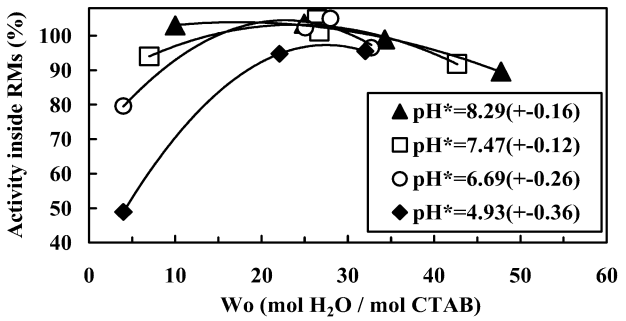

Figure 2. Effect of *W*o on the α-amylase solubilization. RM-solvent: CTAB (0.015, 0.0375, 0.075, 0.15 mol dm^{-3})/1-hexanol (1.02 mol dm^{-3})/*i*-butanol/*i*-octane. Aqueous source: crude enzyme/buffer/NaCl, I_{AQ} 0.075-0.083 mol dm^{-3}.

On the other hand, the radius of gyration of the α-amylase macromolecule of 57 kDa could be calculated to be 1.98 nm [12]. Thus, the enzyme molecule entrapped into a reversed micelle of the same or smaller size would be squeezed out and damaged due to the close and strong electrostatic interactions with the charged RM interface.

In Figure 3, *W*o (R_{RM}, respectively) was varied through the co-surfactant (1-hexanol) concentration, and a drop in activity was seen when the micelle size approached the enzyme dimension. When the co-surfactant concentration exceeded a critical value of ca. 0.383 mol dm^{-3} (4.8% v/v), the RMs were formed spontaneously. The critical value was probably not related to the surfactant concentration but to the nature of the system as it was found using 4-fold higher CTAB-concentration [2,4]. Below the critical value, the surfactant aggregation number was too large to pack and hold stable

RMs; the enzyme was deactivated upon the contact with the surfactant molecules. RMs of smaller size (0.97 nm at 1.71 mol dm^{-3} 1-hexanol) than the target enzyme solubilized the impurities, and the α-amylase source was purified by a factor of 1.4.

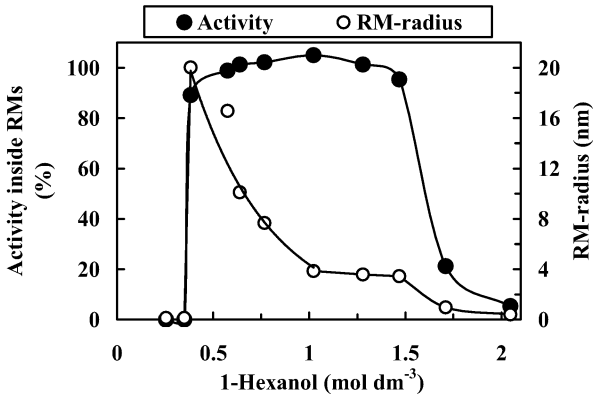

Figure 3. Effect of co-surfactant (1-hexanol) on RM size and α-amylase solubilization. RM solvent: CTAB (0.0375 mol dm^{-3})/1-hexanol/*i*-butanol/*i*-octane. Aqueous source: crude enzyme/buffer/NaCl, pH 7.37, I_{AQ} 0.0785 mol dm^{-3}.

Desolubilization of the α-Amylase from RM Solvent with CTAB

The enzyme was stripped from the loaded RM solvent at pHs below and above that of the solubilization (see Table 1). The expulsion occurred under deflation of water out of the RM core due to the higher ionic strength of the bulk stripping solution (osmotic pressure difference between the RM core and the bulk stripping solution). The recovery yields were further increased through a second stripping step with distilled water.

Table 1. Desolubilization of the α-amylase from RM solvent with CTAB into stripping solutions of various pH and composition*

No.	pH*	Activity Yield (Equation 1) (%)	Protein Yield (Equation 1) (%)	Purification Factor (-)
1	5.39	27.82	22.65	1.45
2	5.76	45.75	32.47	1.40
2[a]	5.35	46.62	48.47	0.98
3	7.93	37.55	26.5	1.40
3[a]	6.09	46.85	50.35	0.51

*Stripping solution: 1, 2, and 3 described in Materials; for 2[a] and 3[a] second strippings performed with distilled water. Solubilization: CTAB (0.0375 mol dm^{-3})/1-hexanol (1.02 mol dm^{-3})/ *i*-butanol/*i*-octane. Aqueous source: crude enzyme/buffer/NaCl, pH 7.35, I_{AQ} 0.0785 mol dm^{-3}.

Stripping in 2 and 2[a] (Table 1) recovered 92% of the initial activity with an average purification factor of 1.2. In stripping 3[a], a water swelling inside the solvent was registered, which destabilized the RM interface, and the core content was "washed-out"

of the micelle. A concentrated solution of α-amylase was obtained but it was of poor purity.

CONCLUSIONS

Under low ionic strength of the aqueous source, the solvent consisting of CTAB (0.0375 mol dm^{-3})/1-hexanol (1.02 mol dm^{-3})/*i*-butanol/*i*-octane formed RMs of an optimal size ($Wo \sim 26$, $R_{RM} \sim 3.59$ nm) for solubilization of α-amylase molecules (57 kDa, radius of gyration 1.98 nm). Much wider RMs (at higher CTAB concentration or less 1-hexanol) showed worse selectivity. They solubilized also the impurities, as the selective electrostatic enzyme-surfactant attraction became weaker with the distance. The smaller micelles squeezed out the biomolecule.

At the desolubilization step, the RM size was controlled by the ionic strength of the bulk stripping solution. The enzyme molecule was ejected or washed out under water deflation or water swelling of the RM solvent. A purer stripping solution of α-amylase (1.4 times over the initial one) can be obtained in a large pH range (5.4-8).

REFERENCES

1. A. Pessoa, Jr. and M. Vitolo, "Separation of Inulinase from *Kluyveromyces marxianus* using Reversed Micellar Extraction," *Biotechnol. Tech.*, **11**(6), 421-422 (1997).
2. G. A. Krei, "Flüssig-Flüssig Extraction von Enzymen mittels inverser Mizellen," Ph.D. Thesis, Technical University Carolo-Wilhelmina, Braunschweig, Germany, 1993.
3. M. Carlsen, A. B. Spohr, J. Nielsen, and J. Villadsen, "Morphology and Physiology of an α-Amylase Producing Strain of *Aspergillus oryzae* during Batch Cultivations," *Biotechnol. Bioeng.*, **49**(3), 266-276 (1996).
4. Z. Lazarova and K. Tonova, "Integrated Reversed Micellar Extraction and Stripping of α-Amylase," *Biotechnol. Bioeng.*, **63**(5), 583-592 (1999).
5. Z. Lazarova and K. Tonova, "Reversed Micellar as Mobile Carriers for separations in Bioprocess Systems," *Hung. J. Ind. Chem.*, **28**, 85-88 (2000).
6. K. Tonova and Z. Lazarova, "Influence of Enzyme Aqueous Source on RME-based Purification of α-Amylase," *Sep. Purif. Technol.*, **47**(1-2), 43-51 (2005).
7. C. Pantschev, G. Klenz, and B. Häfner, "Vergleichende Charakterisierung von Alpha-Amylasepräparaten," *Lebensmittelindustrie, Getränke*, **28**(2), 71-74 (1981).
8. C. Regalado, J. Asenjo, and D. L. Pyle, "Protein Extraction by Reverse Micelles: Studies on the Recovery of Horseradish Peroxidase," *Biotechnol. Bioeng.*, **44**(6), 674-681 (1994).
9. PAC, Manuel of Symbols and Terminology for Physicochemical Quantities and Units. Appendix II. Part I: Definitions, Terminology and Symbols in Colloid and Surface Chemistry, **31**, 619 (1972) on http://goldbook.iupac.org (28th Sept. 2007).
10. K. Naoe, K. Noda, M. Kawagoe, and M. Imai, "Higher Order Structure of Proteins Solubilized in AOT Reverse Micelles," *Colloids Surf., B*, **38**(3-4), 179-185 (2004).
11. X. Y. Wu, Y. Liu, X. Y. Dong, and Y. Sun, "Protein Refolding Mediated by Reverse Micelles of Cibacron Blue F-3GA Modified Nonionic Surfactant," *Biotechnol. Progr.*, **22**(2), 499-504 (2006).
12. C. Tanford, Physical Chemistry of Macromolecules, John Wiley & Sons, New York, fourth printing 1966.

DEVELOPMENT OF INORGANIC MICROCAPSULES FOR THE ORAL DELIVERY OF A HYDROPHILIC DRUG

Eiichi Toorisaka, Makoto Hirata, and Tadashi Hano

Department of Applied Chemistry, Oita University, Oita 870-1192, Japan.
Corresponding author email address: torisaka@cc.oita-u.ac.jp

ABSTRACT

Porous microcapsules with a hollow structure are useful for releasing drugs in the gastrointestinal fluid over a long period of time because the microcapsule floats in aqueous solution due to its low density. In this study, a hollow microcapsule was prepared by an inorganic precipitation reaction based on an ion exchange reaction between the internal and external aqueous phases of a Water-in-Oil-in-Water (W/O/W) emulsion. The molecular structure of surfactants used for the preparation of the W/O/W emulsions affected the formation of the hollow capsule. It was found that the ion transport resulting from the thin lamella membrane formed between the internal and external aqueous phases yielded an insoluble shell along the interface.

INTRODUCTION

Oral administration is a major route for the delivery of drugs to the body. However, many kinds of drugs administered orally need a delivery tool that will help to slow the degradation of the drug in the gastrointestinal tract, promote the absorption of the drug from the intestinal mucosa, and maintain the effect for a long time [1]. Microcapsules are generally employed as a form of drug delivery and can offer several of these benefits [2].

In a previous study, a liquid surfactant membrane method was used to prepare inorganic capsules [3-4]. This method needs neither special techniques nor apparatus and allows for the preparation of particles by a simple operation. In addition, this method has the advantage that spherical solid particles can be prepared at ordinary temperatures. Moreover, it is possible to control the particle size by changing the size of the water drops in the W/O emulsion. Thus, this procedure can be considered as a new method for the development of drug capsules that enables the preparation of particles by using a single metal silicate or a mixture of various metal silicates. The resulting porous microcapsules with a hollow structure are able to release the drug into the gastrointestinal fluid over a long period, because these microcapsules remain suspended in aqueous solution due to their low density.

In this study, the effect of metal transport on capsule formation by the liquid-surfactant-membrane method is discussed, and the encapsulation of the hydrophilic drug theophyline into the capsule is estimated.

EXPERIMENTAL

Preparation of Hollow Microcapsules

An aqueous sodium silicate solution (25 mL) and a toluene solution (50 mL) containing sorbitan monoolate (Span80) or tetraglycerin-condensed ricinolate (TGCR) as a surfactant and di-2-ethylhexyl phosphoric acid (D2EHPA) as a cation carrier were mixed with a homogenizer at 2500 rpm for 10 min. to produce the W/O emulsion. The emulsion obtained was poured into an aqueous metal chloride solution (150 mL) and spun at 200 rpm for 2 h. For the preparation of microcapsules, equal salt concentrations in both aqueous solutions ensured that the emulsion did not collapse. Solid products formed in the solution were filtered off, washed, and dried. The preparation was performed at room temperature. When theophyline was employed as a hydrophilic drug, it was added to the internal aqueous sodium silicate solution prior to the capsule preparation.

Analysis

Surface and cross-sectional views of the microparticles were observed with a scanning electron microscope (SEM, JOEL, JSM-6060, Japan). Particle size and shell thickness were determined by a comparison with the scale shown in the SEM photographs. Sodium and calcium cation concentrations in the external aqueous solution were measured by inductively coupled plasma spectrometry (ICP, Shimadzu, ICPS-7000, Japan).

RESULTS AND DISCUSSION

Effect of Cation Carrier on Metal Transport

In this study, metal silicate microcapsules were prepared by ion-exchange reactions mediated by the liquid surfactant membrane. A cation carrier, D2EHPA, was employed in the oil phase to accelerate metal transport between the internal and external aqueous phases. Figure 1 shows the time course of the external phase metal cation concentration measured with different D2EHPA concentrations. This figure clearly reveals that the addition of D2EHPA into the oil phase promoted the ion-exchange reaction. When D2EHPA was not added, the transport of metal cations was minimal. Furthermore, the higher the concentration of D2EHPA is, the higher is the rate of metal cation transport. At steady state, the amount of metal transported was a constant and was not related to D2EHPA concentration. Figure 2 shows SEM photographs of particles prepared with 0.4 wt % and 0.2 wt % D2EHPA. When 0.4 wt % D2EHPA was used, most of particles formed hollow structures. It can be seen that since D2EHPA at higher

concentrations made metal cation transport occur more rapidly, inorganic precipitation reactions at the vicinity of the interface between the oil and internal aqueous phases progressed instantly and hollow spheres were formed. On the other hand, the preparation made with D2EHPA at a low concentration (0.2 wt %) caused the inner particles to fill. This likely occurred because in this case, the transport of metal cations was slow, and thus, the precipitation reaction took place entirely in the inner aqueous phase.

From these results, it was found that the acceleration of cation transport plays an important role in the formation of calcium silicate microcapsules.

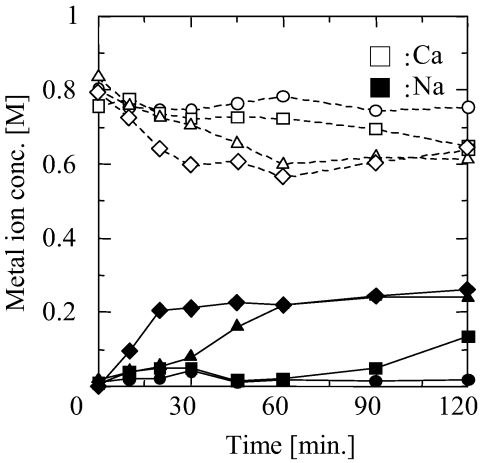

Figure. 1. Time course of metal cation concentrations in the external aqueous phase with varying D2EHPA concentrations: (○) 0.1 wt %, (□) 0.2 wt %, (△) 0.4 wt %, and (◊) 0.6 wt %.

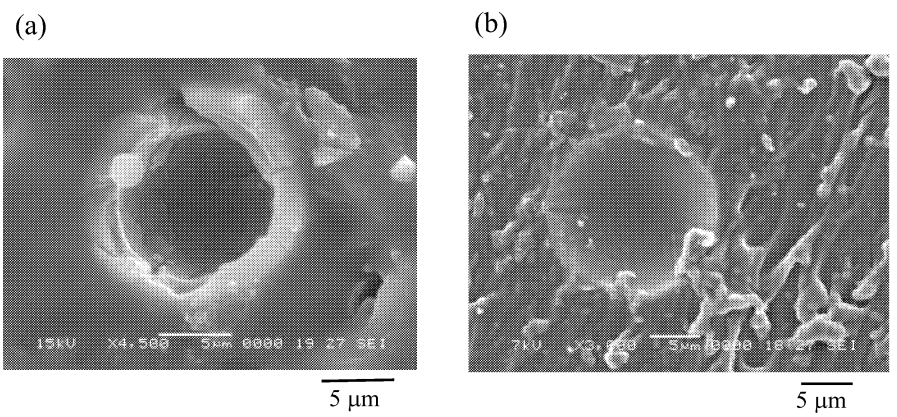

Figure 2. SEM photographs of cross sections of microparticles formulated with different D2EHPA concentrations: (a) 0.4 wt %, (b) 0.2 wt %.

Effect of Lipophilic Surfactant on Metal Transport

It was confirmed that the metal transport with a cation carrier allows the formation of fine capsules. However, since a cation carrier can be toxic, another method for capsule formation

is preferred. Thus, we focused on the alkyl chain length of the lipophilic surfactants and the dispersibility of the W/O water droplets and how they would affect the transport of small molecules [5].

Either SPAN80 or TGCR was employed as a lipophilic surfactant to prepare calcium silicate capsules. Figure 3 shows the transport of the metal cation from the external to the internal phase of the W/O/W emulsion. W/O/W emulsions prepared with TGCR rapidly transported both calcium and sodium. On the other hand, the transport rate within a W/O/W emulsion prepared with SPAN80 was low. The formation of W/O/W emulsions was observed under an optical microscope. As shown in Figure 4, the inner water droplets of a W/O/W emulsion prepared by TGCR were dispersed well throughout the oil droplets, while droplets prepared with SPAN80 aggregated. From this result, it was concluded that the dispersibility of the inner water droplets depended on the alkyl chain structure. The alkyl chain of TGCR is far longer than that of SPAN80 and has greater flexibility, permiting better dispersibility of the inner water droplets. These results suggested that the transport of metal cations was controlled by the lamella membrane formed between the internal and external aqueous phases. That is, a surfactant with a flexible alkyl chain disperses aqueous droplets effectively throughout the globule, and the metal cation is transported rapidly through the lamella membrane. The SEM photographs of the surface and the cross-section of particles prepared with TGCR are shown in Figure 5. It was also determined that this method is useful for preparing the fine hollow capsules. Moreover, it was confirmed that in the experiment containing theophyline in the internal aqueous phase of W/O/W, it was encapsulated in hollow space (Figure 6).

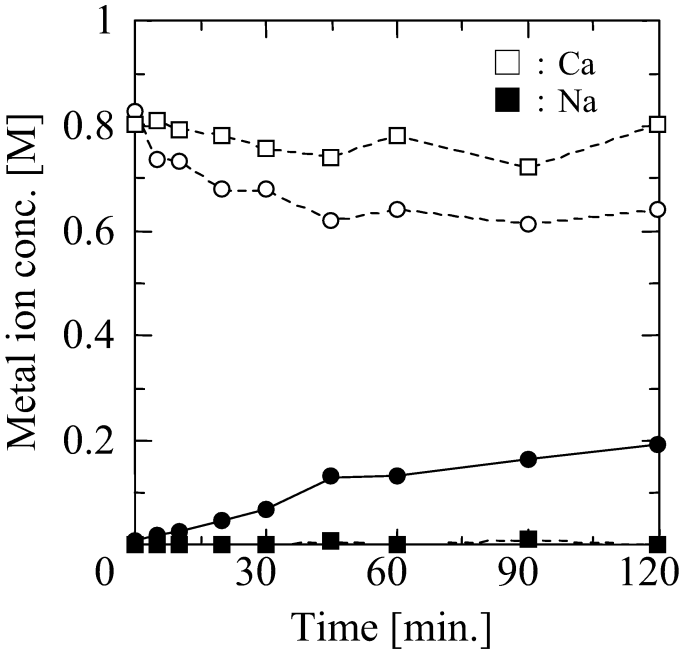

Figure 3. Time course of metal cation concentration in the external aqueous phase with different surfactants (□) SPAN80 and (○) TGCR.

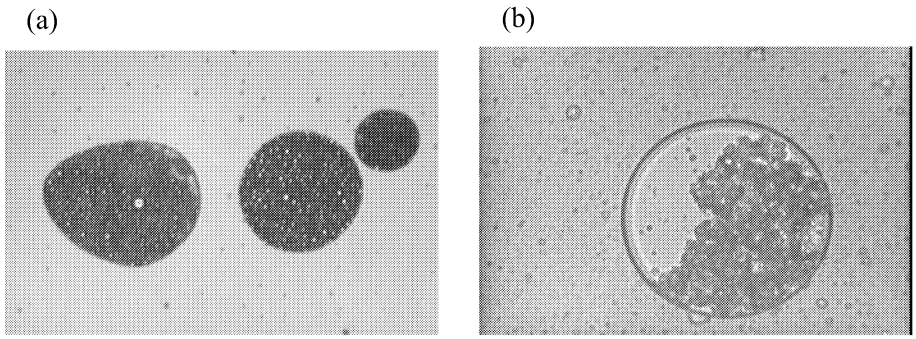

Figure 4. Photomicrographs of W/O/W emulsions prepared with the lipophilic surfactants (a) TGCR and (b) SPAN80

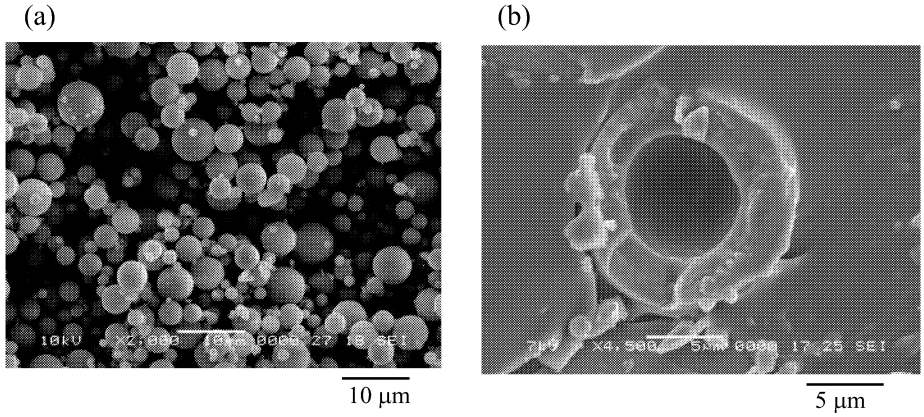

Figure 5. SEM photographs of surface and cross sections of microcapsules prepared with TGCR: (a) surface, (b) cross section

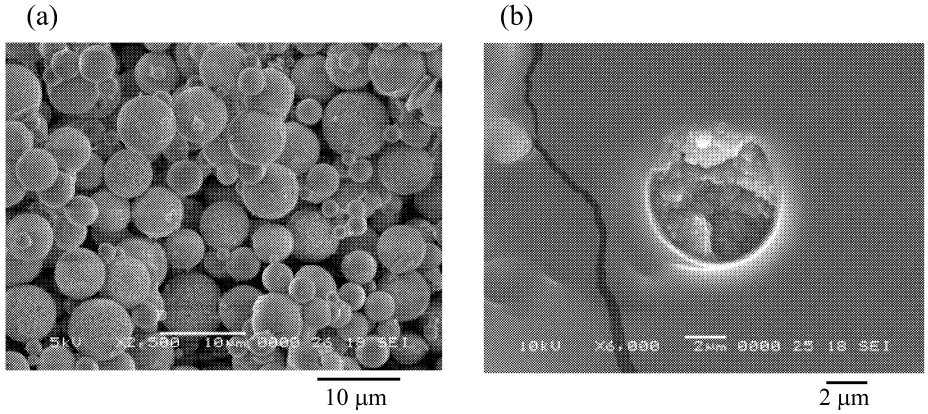

Figure 6. SEM photographs of surface and cross sections of microcapsules with encapsulated theophyline: (a) surface and (b) cross section.

CONCLUSION

Hollow inorganic microcapsules for oral delivery of a hydrophilic drug were prepared by an inorganic precipitation reaction in a Water-in-Oil-in-Water (W/O/W) emulsion. The molecular structure of surfactants used for the preparation of the W/O/W emulsions affected the formation of the hollow capsules. The surfactant with the more flexible alkyl chain was the most effective for the formation of hollow capsules. This was because the surfactant extensively dispersed the internal aqueous droplets and that the metal cation was transported rapidly through the emulsion lamellae to the internal phase droplets. It was also found that the ion transport from the thin lamella membrane formed between the internal and external aqueous phases yielded an insoluble shell along the interface.

REFERENCES

1. R. Langer and N. A. Peppas, "Advances in biomaterials, drug delivery, and bionanotechnology," *AIChE J.*, **49**(12), 2990-3006 (2003).
2. S. Freitas, H. P. Merkle, and B. Grander, "Microencapsulation by solvent extraction/evaporation: reviewing the state of the art of microsphere preparation process technology," *J. Controlled Release,* **102**, 313-332 (2005).
3. I. Morishige, M. Hirata, and T. Hano, "Preparation of Metal-Silicate Microballoons Based on Ion Exchange through Liquid Surfactant Membrane," *J. Ion Exch.*, **14**, 365-368 (2003).
4. I. Morishige, E. Toorisaka, M. Hirata, T. Ohtake, and T. Hano, "Preparation of various metal-silicate micro-balloons using W/O/W emulsion," *J. Microencapsulation*, **22**(3), 291-301 (2005).
5. E. Toorisaka, N. Kamiya, M. Goto, M. Hirata, and T. Hano, "Release Mechanism of an Anticancer Drug from W/O/W Emulsions," Solvent Extraction for Sustainable Development (ISEC'05), 2005; pp. 817-821.

RATIONALIZATION OF THE EMULSIFICATION PROCESS OF EMULSIONS USED FOR DETOXIFICATION OF CHLOROQUINE

Michèle Grosber-Manon,[1] Dominique Pareau,[1] Monique Seiller,[2] Arnaud Buch,[1] Jamila el Bekri,[1] Jean-Louis Grossiord,[2] and Moncef Stambouli[1]

[1]Laboratoire de Génie des Procédés et Matériaux, Ecole Centrale Paris, 92295 Châtenay-Malabry, France. [2]Université de Paris-Sud, Centre d'Etudes Pharmaceutiques. Laboratoire de Physique Pharmaceutique, UMR CNRS 8612, 92296 Châtenay-Malabry, France.
Corresponding author email address: moncef.stambouli@ecp.fr

ABSTRACT

Emergency treatments in case of drug intoxification (stomach washing, activated charcoal, etc.) are very limited and not very efficient. This work presents an alternative solution based on the use of detoxifying water/oil emulsions. The organic phase includes a specific extractant able to form a lipophilic complex with the toxic compound that then diffuses to the internal aqueous phase where a trapping agent captures the toxic compound and releases the extractant. The stability and the extractive performance of the detoxifying emulsions depend on the physicochemical parameters. The optimal composition of an emulsion able to trap chloroquine has been determined, and extraction has been proved.

INTRODUCTION

The methods generally used for the treatment of drug intoxication are stomach washing and administration of activated charcoal. The efficiency of these emergency treatments is quite limited, and the procedure is very painful for the patient. An alternative approach is the use of water/oil emulsions composed of aqueous drops dispersed in an organic phase containing an extractant that is able to trap the drug. The extractant forms a lipophilic complex with the drug that is able to diffuse to the aqueous internal phase of the emulsion, where it is captured and trapped by a stripping agent. The extractant is regenerated during this step [1-3].

An example of a drug that can be captured in this way is chloroquine, a 4-aminoquinoline drug used in the treatment or prevention of malaria (Figure 1). Intoxication by this drug can lead to death by cardiac arrest, and just doubling the normal dose of chloroquine can be fatal. In this study, we present the results on the thermodynamics of solvent extraction of chloroquine by di-(2-ethylhexyl) phosphoric acid (D2EHPA). These results are used to determine the composition of an emulsion for the effective trapping of chloroquine. Extractions have been made with these emulsions. Moreover, viscosity and drop sizes have been measured to determine the properties of the detoxifying emulsions. The influence of emulsification parameters and of the internal-phase volume fraction on the trapping efficiency of this drug has been studied.

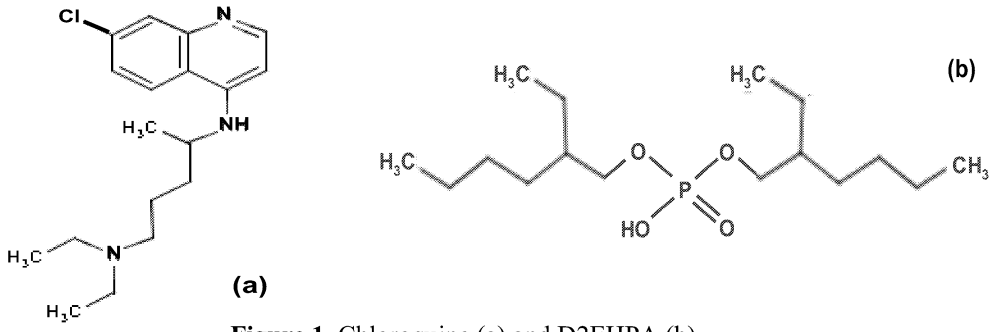

Figure 1. Chloroquine (a) and D2EHPA (b).

EXPERIMENTAL APPARATUS AND PROCEDURE

Solvent Extraction

To identify the extraction mechanism of chloroquine by D2EHPA, some solvent extraction experiments have been made. The organic phase was contacted with the aqueous phase of equal volume during 15 minutes under agitation. The organic phase contained an extractant (D2EHPA, >95%) diluted in dodecane or hydrogenated polyisobutene. The aqueous phase contained chloroquine sulfate or chloroquine diphosphate (concentration of chloroquine 300 mg L^{-1}). In separate experiments, we varied the aqueous phase pH and the extractant concentration in the organic phase.

Emulsion Formulation

The organic phase was composed of 4% by weight of a lipophilic surfactant, cetyl dimethicone copolyol (Abil EM 90) and 1% by weight of D2EHPA in hydrogenated polyisobutene. The aqueous internal phase was composed of hydrochloric acid (0.05 mol L^{-1}) and of an electrolyte, magnesium sulfate $MgSO_4.7H_2O$ (1.6% by weight). Emulsions were obtained by stirring the aqueous and organic phases with a rotor-stator agitator. The temperature of emulsification was controlled by a using a double-envelope reactor. For each experiment, 60 mL of emulsion was prepared. Emulsions of various volume fractions were prepared at different temperatures, speeds, and duration of emulsification. Extraction of the drug was achieved by stirring 80 mL of chloroquine solution and 40 mL of emulsion in a beaker. The extraction rate was monitored over time.

Analysis Methods

The chloroquine concentration was determined in the aqueous phase by UV-Vis spectrophotometry (Varian) before and after the extraction procedure (400 to 200 nm). Acidities were measured with a pH meter (PHM210 Radiometer). Viscosities of emulsions were determined with a rheometer at 25.3 °C (RotoVisco1, ThermoHaake). Drop sizes were determined with a particle-size analyzer (Malvern Mastersizer).

RESULTS AND DISCUSSION

Study of the Extraction Mechanism of Chloroquine by D2EHPA

Chloroquine (CQ) is extracted by D2EHPA by a cation-exchange mechanism [4]:

$$CQH_n^{n+} + (n+p)\overline{AH} \rightarrow \overline{CQH_nA_n(AH)_p} + nH^+ \quad (1)$$

where CQH_n^{n+} is the protonated form of chloroquine, $\overline{AH}$ is the extractant monomer in the organic phase (whose concentration is calculated from previously determined aggregations constants [5]), and $\overline{CQH_nA_n(AH)_p}$ is the extracted lipophilic complex. The apparent equilibrium constant is:

$$K_{eq} = \frac{[H^+]^n[\overline{CQH_nA_n(AH)_p}]}{[\overline{AH}]^{n+p}[CQH_n^{n+}]} \quad (2)$$

The distribution ratio of chloroquine can be defined by:

$$D = \frac{[CQ]_{org}}{[CQ]_{aq}} = \frac{[\overline{CQH_nA_n(AH)_p}]}{[CQH_n^{n+}]} \quad (3)$$

from which we can write:

$$\log D = \log K + (n+p)\log[\overline{\mathrm{AH}}] + n\,\mathrm{pH} \quad (4)$$

Effects of pH

We consider that the concentration of extractant remains constant because the concentration of complexed extractant is very low in comparaison with the initial concentration of extractant. So Equation 4 leads to

$$\log D = n\,\mathrm{pH} + \text{constant} \quad (5)$$

The variation of log D with pH is is shown to be a straight line with slope n = 2 (Figure 2). Chloroquine has three protonation sites, and so this molecule can exist in an aqueous phase as different species. This result suggests that the diprotonated species CQH_2^{2+} is involved in the extraction mechanism.

Effects of the Extractant Concentration

For constant pH, Equation 4 leads to

$$\log D = (n+p)\log[\overline{\mathrm{AH}}] + \text{constant}$$

When log D is plotted as a function of $\log[\overline{\mathrm{AH}}]$ with constant pH, a straight line with slope (n + p) = 7 is obtained, which suggests that one molecule of chloroquine reacts with 7 monomers of D2EHPA (Figure 3) [5].

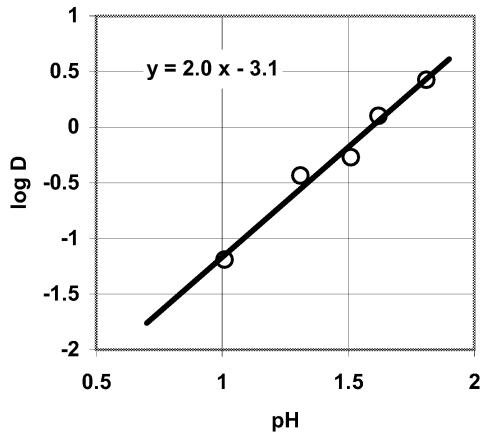

Figure 2. Effect of pH on the distribution ratio ($[D2EHPA]_{initial}$ = 0.124 mol L^{-1}).

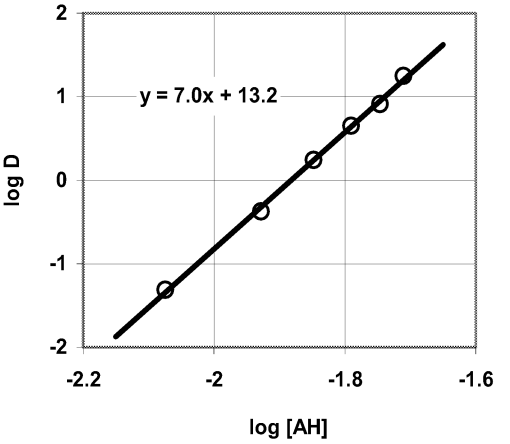

Figure 3. Effect of extractant concentration on the distribution ratio (pH = 2).

Chloroquine can be stripped from an organic phase by hydrochloric acid (Figure 4). Concentrations of hydrochloric acid greater than 0.5 mol L^{-1} lead to a complete stripping of chloroquine.

Thus D2EHPA is able to extract chloroquine in its diprotonated state to form the lipophilic complex $\overline{CQ_2A_2(AH)_5}$. Complete stripping can be achieved using hydrochloric acid. This knowledge of the extraction mechanism allows selection of the optimal composition of the detoxifying emulsions.

Extraction of Chloroquine by a Reactive Emulsion

In vitro extraction of chloroquine by a reactive emulsion is quick and complete (volume fraction 45%, T = 45° C, speed = 13,500 rpm, duration = 3 min.). More than 85% of chloroquine is extracted in 5 minutes (Figure 5). Moreover, the emulsion remains stable during the extraction.

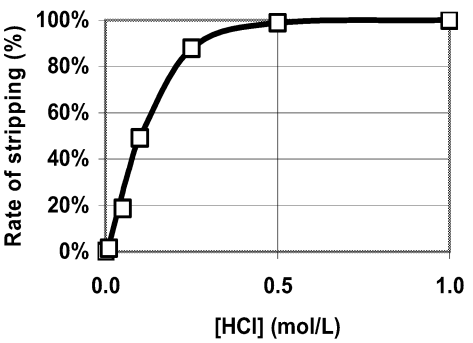

Figure 4. Rate of chloroquine stripping versus HCl concentration.

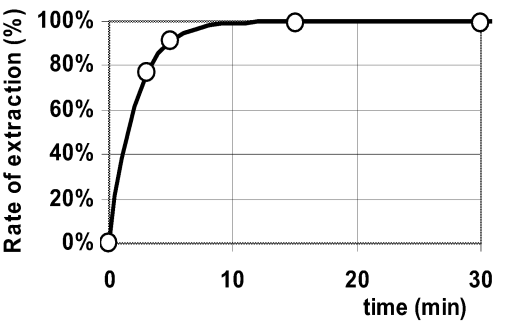

Figure 5. In vitro extraction kinetics of chloroquine by a detoxifying emulsion.

Effect of the Emulsion Composition

The emulsions used must be stable before and during the extraction. However, the concentrations of extractant and hydrochloric acid might impact the stability. The stability of detoxifying emulsions depends on their viscosity and their drop sizes [6]. An experimental design was started to determine optimal compositions (Table 1). A compromise has to be found to obtain a stable emulsion with a good extraction rate.

Table 1. Effects of hydrochloric acid concentration, D2EHPA and Abil concentrations, and volume fraction on drop sizes and viscosities (cP = 10^{-2} Poise)

No.	[HCl] (mol L^{-1})	% D2EHPA	% Abil	Vol. fraction	Drop size (µm)	Viscosity (cP)
1	0.1	1	4	0.17	1.42	7.4
2	0.5	1	4	0.17	1.43	7.4
3	0.1	5	4	0.17	1.22	8.6
4	0.5	5	4	0.17	1.01	6.9
5	0.1	1	12	0.17	0.91	13.1
6	0.5	1	12	0.17	0.94	14
7	0.1	5	12	0.17	0.84	12.2
8	0.5	5	12	0.17	0.82	11.2
9	0.1	1	4	0.5	1.83	34.9
10	0.5	1	4	0.5	1.94	35.4
11	0.1	5	4	0.5	1.52	41.8
12	0.5	5	4	0.5	1.51	39.4
13	0.1	1	12	0.5	1.49	65.5
14	0.5	1	12	0.5	1.46	67.8
15	0.1	5	12	0.5	0.92	65.4
16	0.5	5	12	0.5	0.96	52

The results of this experimental design showed that the concentrations of extractant and surfactant and the volume fraction have the most important effects on drop sizes. The concentration of hydrochloric acid has a low effect on the drop sizes. High concentrations of extractant and surfactant and a small volume fraction lead to the smallest drops.

The surfactant concentration and volume fraction have the greatest effects on viscosity. Increases in the concentration of surfactant and of the volume fraction lead to increases in the viscosity. The extractant and hydrochloric acid concentrations have a low effect on viscosity. These results show that the extractant and the hydrochloric acid don't modify the stability of the emulsions in the investigated conditions.

CONCLUSIONS

D2EHPA is able to extract chloroquine in its diprotonated state, leading to the formation of the lipophilic complex $\overline{CQ_2A_2(AH)_5}$. A complete stripping is obtained with hydrochloric acid. These results are very important, because they help to understand how the drug is trapped inside the emulsions. In vitro extraction of chloroquine by a detoxifying emulsion showed that more than 85% of the chloroquine

is extracted in 5 minutes. The emulsions stay stable during the extraction. One important result of the experimental design is that the addition of an extractant and of hydrochloric acid doesn't significantly modify the stability of the emulsions. So the emulsions used are stable before and during extraction and are very efficient.

REFERENCES

1. E. Assouly, J.-L. Grossiord, M. Seiller, D. Pareau, and M. Stambouli, "Émulsions simples et multiples destinées à la détoxication de l'organisme ou des surfaces," *Patent* No. FR 02 06849, (2002).
2. M. Hamoudeh, M. Seiller, C. Chauvierre, D. Auchère, B. Lacour, D. Pareau, M. Stambouli, and J.-L. Grossiord, *J. Drug Del. Sci. Technol.*, **16**(3), (2006).
3. Y. Marcus and A. S. Kertes, "Ion Exchange and Solvent Extraction of Metal Complexes," Wiley-Interscience, (1969).
4. P. M. O'Neill, P. G. Bray, S. R. Hawley, S. A. Ward, and B. K. Park, "4-Aminoquinolines : Past, present and future: A chemical perspective," *Pharmacology & Therapeutics*, **77**(1), 29-58 (1998).
5. A. Buch, "Etude thermodynamique et cinétique de l'extraction liquide-liquide du nickel(II) par la 2-éthylhexanal oxime et un mélange de 2-éthylhexanal oxime et d'acide di-2-(éthylhexyl)-phosphorique," Ph.D. Thesis, Université Pierre et Marie Curie - Paris VI, (2001).
6. P. Brochette, "Émulsification : élaboration et étude des émulsions," [J 2 150], *Techniques de l'Ingénieur*, Traité Génie des Procédés, (1999).

Fundamentals

TOWARD THE COMPUTER-AIDED DESIGN OF ION SEQUESTERING AGENTS

B. P. Hay

Oak Ridge National Laboratory, P.O. Box 2008, Oak Ridge, Tennessee 37831-6119.
Author email address: haybp@ornl.gov

ABSTRACT

A major impediment to introduction of new extractants to practical use is the large cost and long lead times for synthesis and testing of candidate molecules. Toward the goal of reducing this experimental burden, this talk describes a computational approach to the design of molecular receptors that are structurally organized for optimal coordination with ions. With a molecular-level understanding of how host architecture influences ion-binding affinity, it is possible to identify promising potential extractants before they are prepared and tested. Exploiting powerful concepts embodied in structure-based drug design to bear on host design, we have devised novel algorithms for building potential host structures from molecular fragments and rapid methods for comparing the binding-site organization of the resulting candidates. The result is a computer software program, called HostDesigner, which can generate and evaluate millions of new molecular structures per minute on a desktop personal computer. The utility of this software has been illustrated in the structural design of cation receptors such as crown ethers and anion receptors bearing urea groups.

INTRODUCTION

Host-guest chemistry plays an important role in the development of a wide variety of separation methods and analytical techniques. Organic sequestering agents (hosts) with a high degree of recognition for specific ions (guests) provide the basis for many solvent-extraction processes. Consequently, there has been large effort expended to design effective and selective hosts for targeted ionic species. Simple extractants bearing one or two donor groups exhibit relatively weak binding and selectivities limited by intrinsic binding affinities [1,2]. As demonstrated by research on Cs^+/Na^+ separation [3], truly remarkable recognition for specific ions can be achieved using hosts that contain multiple binding sites arranged in a constrained configuration. The design of such hosts involves selecting the set of binding sites and then choosing the connecting geometric structure that ties them together, in other words, the molecular architecture. To achieve strong complexation with a specific guest, the host architecture must satisfy two conditions [1,2,4]. First, the host must be able to adopt a conformation in which all binding sites are positioned to structurally complement the guest. Second, the host should exhibit a limited

number of stable conformations, the binding conformation being low in energy relative to other possible forms.

Molecular architecture strongly impacts binding affinity, and even simple modifications can result in dramatic enhancements. An example is provided by diamide extractants for trivalent f-block cations [5]. Structural evaluation of conventional malonamide extractants developed for use in the DIAMEX process revealed the O-donor atoms in these architectures to be poorly organized for complexation (see Figure 1). Using structural design criteria obtained from theoretical and experimental data regarding the conformations of amides and metal-amide complexes, an alternative bicyclic architecture was designed and tested. Liquid-liquid extraction measurements with hydrophobic analogs revealed the designed extractant gave a spectacular performance enhancement, exhibiting Eu(III) and Am(III) distribution ratios 10 million times larger than obtained using the best engineered malonamide extractant under identical experimental conditions [5,6]. Aqueous formation-constant measurements confirm that the performance enhancement is due to an increase in metal binding affinity [7].

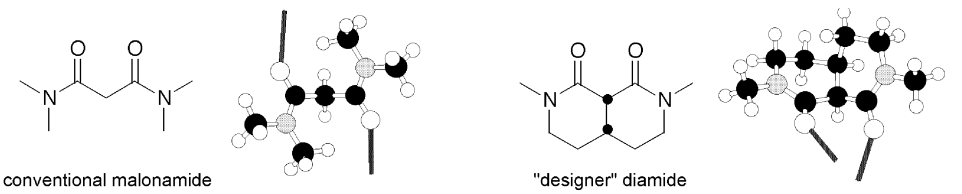

Figure 1. Conventional malonamide architecture (left) and designed bicyclic diamide architecture (right). Geometries for the minimum energy conformations have vectors attached to each oxygen atom illustrating the optimal direction of approach for the metal ion. These vectors are divergent in the poorly organized malonamide scaffold, but locked in a more convergent orientation with the "designer" diamide.

Whereas criteria for selecting the number and type of binding sites are well established [1,2,4], the identification of optimal host architecture remains a challenge. The deliberate design of host structures by assembling sets of disconnected binding sites in three dimensions is not a trivial task. Until recently, we could only generate trial structures by hand with a graphical user interface, an extremely time-consuming process. Often, it is not readily obvious which linkage structures might be best used to connect the binding sites to obtain a host cavity that is organized for guest coordination. To address the problem of how to identify new host molecules that recognize and bind strongly to specific guests, we have adopted a computational approach pioneered by the pharmaceutical industry.

Drug designers have developed methods to address the inverse of this problem, in other words, how to identify molecular structures (guests) that complement the binding site of a protein (host) [8]. These approaches include de novo structure-based design strategies that couple molecule-building algorithms with scoring functions used to prioritize the candidate structures. The building algorithms assemble guest-molecule structures that can physically interact with a known protein structure from pieces that are either atoms or larger, chemically reasonable fragments. The ability to generate large numbers of potential guest structures necessitates the use of simple scoring functions to

prioritize the output. To this end, methods have been developed to estimate the binding free energy by summing free energy increments for hydrogen-bond interactions, ionic interactions, lipophilic interactions, number of rotatable bonds in the guest molecule, etc.

The computer programs that have been developed to perform de novo structure-based drug design are, in general, not applicable to the design of host molecules. These programs require input of the atomic coordinates of a protein binding site, are highly specialized to address protein-organic interactions, and do not contain scoring functions to address the interactions that occur in other types of host-guest systems. To apply the powerful concepts embodied in de novo structure-based drug design to the design of ion-sequestering agents, it is necessary to develop methods for (i) the generation of candidate structures and (ii) evaluating and prioritizing these structures with respect to their binding affinity for the guest. This article summarizes progress that we have made in these areas. Our approach, which involves consideration of 3D host structure, is distinct from alternative methods based on 2D host structure, that is, molecular connectivity [9].

STRUCTURE GENERATION

We have developed de novo structure-based design software, HostDesigner (HD), specifically created to identify host architectures that are organized for the complexation of small ions and molecules [10,11]. HD generates and evaluates millions of candidate structures in minutes on a desktop computer and rapidly identifies 3D architectures that position binding sites for optimal interaction with the guest. As implied by the term de novo, molecules are assembled from molecular fragments. The building algorithms combine user-input host-guest fragments with linking fragments taken from a database. The host-guest fragments define the optimal geometry for one or more binding sites interacting with the guest. The linking fragments are taken from a database that contains over 10,000 structures composed of Csp^3, Csp^2, and H atoms. The fragments consist of all connectivities and low-energy (≤12 kJ/mol) conformers that can be made from 0–6 carbons, excluding 3- and 4-membered rings. The fragments also include all dimethylated 5- and 6-membered rings and selected bicyclic structures. During the building process, all possible connectivities, stereochemistries, and conformations are constructed, which generates large numbers of structures. After evaluation and ranking (vide infra), Cartesian coordinates for the top candidates are output to a file.

STRUCTURE EVALUATION

Deliberate host design requires the ability to distinguish a good architecture from a poor architecture. Various scoring approaches can be used to evaluate the degree of binding-site organization offered by a host structure. Because of the number of structures being generated, HD uses very fast methods for accomplishing these evaluations. This is achieved by using geometric factors to rank structures on the basis of how well their binding sites correspond to those of the guest [10,11]. In addition, conformational energy increments, based on potential surfaces for simple hydrocarbon analogs, are used to estimate the conformational stability of the host structures, allowing them to be ranked on the basis of their degree of preorganization [11]. Although approximate in nature, these

methods provide a rapid means of selecting a list of the best candidates from a large group of potential structures. This list can subsequently be reprioritized using more accurate evaluation methods.

In our recent design work [12,13], subsequent ranking of candidate structures was accomplished in a two-step process using molecular mechanics (MM) models. Such models provide an ideal, computationally efficient tool to evaluate the degree to which a host is structurally organized for guest complexation. MM models partition the steric energy into stretching, bending, torsion, and nonbonded (van der Waals, electrostatics, hydrogen bonding) interactions. Examination of the steric energy components in the calculation output provides a way to identify problem areas in the structure and quantify the effect of cavity size mismatch and poor donor-group orientation [4].

The first step of the MM scoring process is a determination of how strongly the binding conformation of the host binds the guest. This is measured by the binding energy or, alternatively, by the induced strain in the host [14]. In either case, the calculations involve optimization of the host-guest complex followed by the optimization of the host and guest after they have been separated. This step is relatively inexpensive and can be applied to thousands of structures within a few hours time, resulting in a list that is reprioritized with respect to how strongly the host can bind the guest. The second step of the MM scoring process is the determination of the conformational stability of the host binding conformation, in other words, the degree of preorganization. Calculations involve analysis of the host molecule to locate all low-lying conformations and determining the stability of the binding conformation relative to the global minimum conformation. This step is much more expensive and, depending on the size of the molecules under consideration, can take hours per structure. In practice, we have limited conformational analysis to ≤500 of the top candidates from the first step. The final output is a list of structures ranked with respect to the degree of binding site organization.

APPLICATIONS

The utility of the computer-aided molecular design methods described above, structure generation and evaluation by HD followed by subsequent scoring using MM calculations, has been demonstrated in two studies summarized below. The first study focused on the design of optimal linkages for diether chelate rings [12]. The common–CH_2CH_2– linkage, ubiquitous in crown ether macrocycles, yields oxygen orientations that are poorly organized for cation binding, and as a result, common crown ethers suffer from a low degree of binding-site organization. With the idea that better-organized chelate rings would lead to better-organized macrocycles [4,14], we set out to design such structures. The basis for the design process derived from electronic structure calculations and crystal structure analysis to define host-guest fragments as well as to extend the MM3 force field used for scoring. When the best chelating structures were used as building blocks for novel crown ethers, significant enhancements in alkali cation binding affinities are predicted compared to crown ethers that contain the poorly organized ethylene-bridged building blocks (Figure 2).

In the second study, computational methods were deployed to design of bisurea "tweezers" structurally organized for binding tetrahedral oxoanions [13]. The basis for

the design process derived from electronic-structure calculations, which provided information needed both to define host-guest fragments as well as to validate the force field used in the MM scoring steps. In this exhaustive analysis, over 1.8 billion candidate geometries were built and evaluated, 12,000 binding energies were calculated, and 3000 conformational analyses were performed to yield a short list of 30 best candidate architectures. Although some of these architectures were already known to complex with tetrahedral oxoanions, a number of novel architectures were identified (Figure 3).

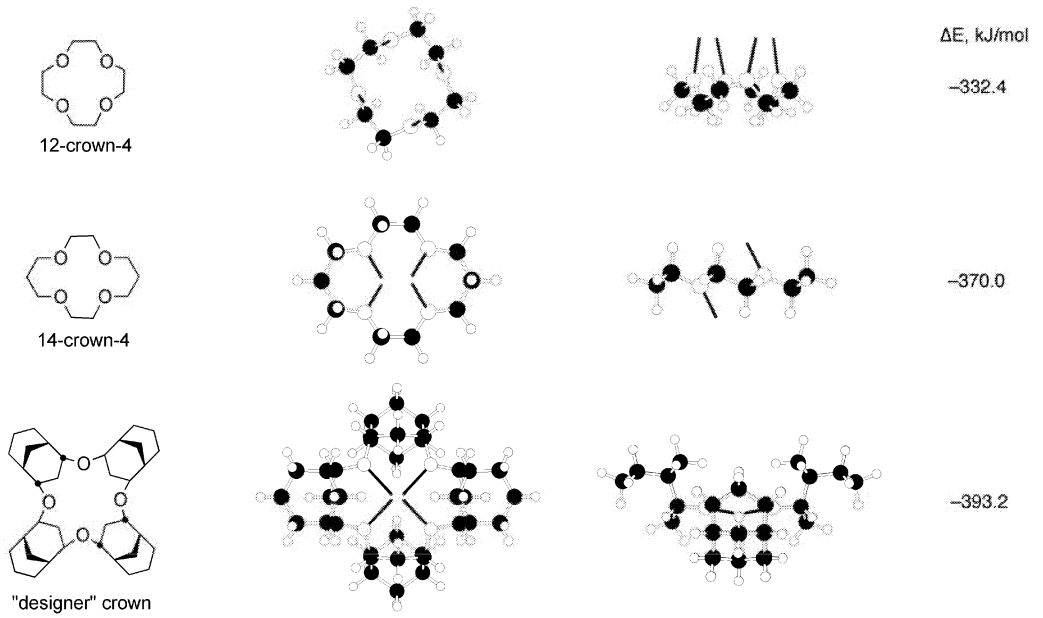

Figure 2. Comparison of conventional crown ethers, 12-crown-4 and 14-crown-4, with a crown ether built from designed linkages [12]. Geometries the binding conformations have vectors attached to each oxygen atom illustrating the optimal direction of approach for an alkali cation. These vectors, which illustrate the degree to which the oxygen atoms are properly oriented with respect to the cavity, are divergent in conventional crowns, but convergent in the "designer" crown. Binding-site orientation is reflected in interaction energies for binding Li^+, ΔE values.

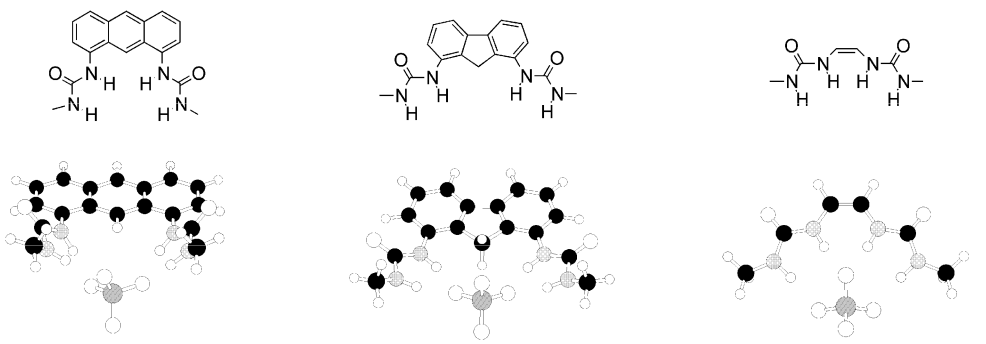

Figure 3. Representative architectures for bisurea "tweezer" molecules that were obtained by molecular design [13]. Geometries for sulfate complexes, shown below each connectivity, show how the urea groups are oriented to engage in hydrogen bonding with the anion.

ACKNOWLEDGMENTS

Funding for this overview was provided by the Division of Chemical Sciences, Geosciences, and Biosciences, Office of Basic Energy Sciences, U.S. Department of Energy, under contract number DE-AC05-00OR22725 with Oak Ridge National Laboratory (managed by UT-Battelle, LLC).

REFERENCES

1. J. W. Steed and J. L. Atwood, Supramolecular Chemistry, Wiley, New York, 2000.
2. H.–J. Schneider and A. Yatsimirsky, Principles and Methods in Supramolecular Chemistry, Wiley, New York, 2000.
3. N. L. Engle, P. V. Bonnesen, B. A. Tomkins, T. J. Haverlock, and B. A. Moyer, "Synthesis and Properties of Calix[4]arene-bis[4-(2-ethylhexyl)benzo-crown-6], a Cesium Extractant with Improved Solubility," *Solvent Extr. Ion. Exch.*, **22**(4), 611–636 (2004).
4. B. P. Hay and R. D. Hancock, "The Role of Donor Group Orientation as a Factor in Metal Ion Recognition by Ligands," *Coord. Chem. Rev.*, **212**, 61–78 (2001).
5. G. J. Lumetta, B. M. Rapko, P. A. Garza, B. P. Hay, R. D. Gilbertson, T. J. R. Weakley, and J. E. Hutchison, "Deliberate Design of Ligand Architecture Yields Dramatic Enhancement of Metal Ion Affinity," *J. Am. Chem. Soc.*, **124**(20), 5644–5645 (2002).
6. G. J. Lumetta, B. M. Rapko, B. P. Hay, P. A. Garza, J. E. Hutchison, and R. D. Gilbertson, "A Novel Bicyclic Diamide with High Binding Affinity for Trivalent f-Block Elements," *Solvent Extr. Ion Exch.*, **21**(1), 29–39 (2003).
7. S. I. Sinkov, B. M. Rapko, G. J. Lumetta, B. P. Hay, J. E. Hutchison, and B. W. Parks, "Bicyclic and Acyclic Diamides: Comparison of Their Aqueous Phase Binding Constants with Am(III), Pu(IV), Np(V) and U(VI)," *Inorg. Chem.*, **43**(26), 8404–8413 (2004).
8. P. Krogsgaard-Larsen, T. Liljefors, and U. Madsen, Textbook of Drug Design and Discovery, Taylor and Francis, New York, 2002.
9. A. Varnek, D. Fourches, V. Solov'ev, O. Kimchuk, A. Quadi, and I. Billard, "Successful 'in Silico' Design of New Efficient Uranyl Binders," *Solvent Extr. Ion Exch.*, **25**(4), 433-462 (2007).
10. B. P. Hay and T. K. Firman, "HostDesigner: A Program for the de Novo Structure-Based Design of Molecular Receptors with Binding Sites that Complement Metal Ion Guests," *Inorg. Chem.*, **41**(21), 5502–5512 (2002).
11. B. P. Hay and T. K. Firman, "HostDesigner, Version 2.0, User's Manual," PNNL-13850, Richland, Washington, USA, 2003. Both this manual and HostDesigner software are available free of charge by contacting the author.
12. B. P. Hay, A. A. Oliferenko, J. Uddin, C. Zhang, and T. K. Firman, "Search for Improved Host Architectures: Application of De Novo Structure-Based Design and High Throughput Screening Methods to Identify Optimal Building Blocks for Multidentate Ethers," *J. Am. Chem. Soc.*, **127**(48), 17043–17053 (2005).
13. V. S. Bryantsev and B. P. Hay, "De Novo Structure-Based Design of Bisurea Architectures for Anion Recognition," *J. Am. Chem. Soc.*, **128**(6), 2035–2042 (2006).
14. B. P. Hay, D. L. Zhang, and J. R. Rustad, "Structural Criteria for the Rational Design of Selective Ligands. 2. The Effect of Alkyl Substituents on Metal Ion Complex Stability with Ligands Bearing Ethylene Bridged Ether Donors," *Inorg. Chem.*, **35**(9), 2650–2658 (1996).

AGGREGATION OF ORGANIC EXTRACTANT PHASES: CONSEQUENCES ON EXTRACTION PROPERTIES

L. Berthon,[1] Y. Meridiano,[1] S. Lagrave,[1] X. Crozes,[1] C. Sorel,[1] N. Zorz,[1] F. Testard,[2] and T. Zemb[3]

[1]CEA Valrhô, DEN/DRCP/SCPS/LCSE, B.P. 17171, 30207 Bagnols sur Cèze cedex. [2]CEA Saclay, DSM/DRECAM/SCM/LIONS, 91191 Gif sur Yvette. [3]ICSM, UMR5257, 30207 Bagnols sur Cèze cedex. Corresponding author: laurence.berthon@cea.fr

ABSTRACT

The self-association properties of *N,N'*-dimethyl-*N,N'*-dioctylhexylethoxymalonamide (DMDOHEMA) were investigated for the DIAMEX process to establish a link between the structures of the extractant molecules in the organic phase and their lanthanide(III) extraction properties. Their aggregation depends on the experimental conditions, such as the compositions of the organic and aqueous phases. This study reports on the effect of the extractant concentration and the solute concentration on the aggregation behavior and the extraction properties.

INTRODUCTION

Studies carried out for the DIAMEX process have demonstrated that the malonamide organic phase is not a molecular solution [1-4]. Due to their surface-active properties, malonamide extractants can be organized into reverse micelles composed of a polar core (extracted solute, co-extracted water, and malonamide polar heads) surrounded by the hydrophobic chain of the extractant molecule. Recently, concentrated *N,N'*-dimethyl *N,N'*-dibutyl tetradecylmalonamide (DMDBTDMA)/dodecane solutions have been investigated [2,5,6] and it has been shown that, for concentrations exceeding 1 mol L^{-1}, the shape of the extractant aggregates changes.

In order to establish a link between the structure of the organic phase containing the extractant molecules and their extraction properties, a parametric study was performed with *N,N'*-dimethyl-*N,N'*-dioctylhexylethoxymalonamide (DMDOHEMA). Bosland [7] and Gannaz [8] have shown the existence of aggregates in DMDOHEMA solutions.

The effect of the composition of the extracting system was investigated (concentrations of extractant, solute, acidity, nature of diluent, etc.) by varying each parameter individually. This paper deals with the effect of the extractant concentration (DMDOHEMA diluted in *n*-heptane) and the effect of the europium nitrate concentration (for a given extractant concentration) from a $LiNO_3$ aqueous phase. Our objective is to identify the impact of these parameters on the aggregation and extraction behavior of DMDOHEMA solutions.

EXPERIMENTAL

Materials and Procedure

Malonamides were supplied by Pharmasynthèse (Lisses, France). The purity was better than 99%. Equal volumes of the organic phase containing DMDOHEMA in *n*-heptane were contacted at 25 °C with an appropriate aqueous solution for several minutes. After centrifugation and phase separation, the organic phases were analyzed. The diamide concentration in organic solution was determined by potentiometric titration with $HClO_4$ in acetic anhydride. The water content of the organic phases was determined by Karl Fischer titration. The europium nitrate concentration in each phase was determined by ICP-AES.

VPO Measurements

The osmometry measurements were carried out at 25 °C using a Knauer Model K7000 vapor pressure osmometer. The osmometer was calibrated using bromotetradecane and trioctylamine diluted in *n*-heptane, which are known to form only monomers in alkane diluents. The aggregation number, the constant of aggregate formation, and activity coefficient of aggregate were determined by the procedure described in [3], completed by the calculation of activity coefficient for monomer species estimated from the ideality deviation of the calibration curve.

ESI-MS Measurements

The mass spectrometry measurements were recorded in the positive ionization mode using a Bruker Esquire-LC quadrupole ion trap equipped with an electrospray interface. The experimental conditions are described in [8].

RESULTS AND DISCUSSION

Effect of DMDOHEMA Concentration

VPO measurements on DMDOHEMA solutions in *n*-heptane at 25 °C indicated that the diamide is monomeric up to ~0.12 mol L^{-1} and forms larger aggregates at higher concentrations (Figure 1a). The aggregation equilibrium of the malonamide can be described by Equation 1 (*L* stands for the malonamide), which is characterized by an aggregate formation constant ψ_N (Equation 2), where $\overline{X}$ is the species *X* in the organic phase, *N* the aggregation number, $[\overline{L}]$ the monomer concentration, $[\overline{L_N}]$ the aggregate concentration, and a_X: activity of species *X*.

$$N\overline{L} \longleftrightarrow \overline{L_N} \quad (1)$$

$$\psi_N = \frac{a_{B_N}}{a_{B_1}^N} = \frac{\gamma_N * [\overline{L_N}]}{\gamma_1^N * [\overline{L}]^N} \quad (2)$$

In a neutral medium ($LiNO_3$) and in free lanthanide/actinide solutions, the calculated aggregation number was $N = 4.4$ with an aggregation constant $\psi_N = 7.5$. From the

aggregation constant and the mass-balance equation, the supramolecular speciation diagram was established and is indicated in Figure 1b.

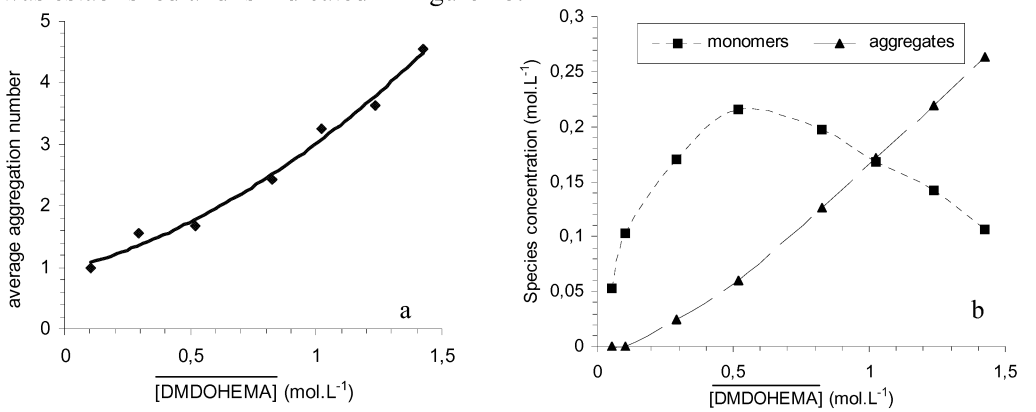

Figure 1. Aggregation properties of DMDOHEMA diluted in *n*-heptane in contact with a 3 mol L^{-1} $LiNO_3$ aqueous phase. a: Average aggregation number. b: Speciation diagram of species (monomers, $[\overline{L}]$; and aggregates, $[\overline{L_{4,4}}]$).

Water analyses on the DMDOHEMA-*n*-heptane' system at 25 °C after equilibration with $LiNO_3$ aqueous phase showed that the water concentration in the organic phase increases with the extractant concentration. The Sergievskii-Dannus theory [9] was used to determine the role of the aggregate in water extraction and to distinguish hydration from solubilization. This theory considers both specific interactions (hydrated species) and nonspecific ("physical") interactions between water and species in organic phases. The water concentration can be expressed by Equation 3, where $[\overline{X}]$ is the concentration of species *X* in the organic phase, *h* the number of water molecules in the hydrated solvate, $S^{\oplus}_{L_N(H_2O)_h}$ the quantity of water solubilized by the hydrated aggregate for $a_{H2O} = 1$, $[\overline{Dil}]$ the diluent concentration, and $S^{\oplus}_{Dil}$ the quantity of water solubilized by the diluent (*n*-heptane) for $a_{H2O} = 1$.

$$\overline{[H_2O]} = (h + \sum_{n=1}^{N} S^{\oplus}_{L_n(H_2O)h}.a_{H_2O}).\overline{[L_n(H_2O)_h]} + S^{\oplus}_{Dil}.a_{H_2O}.[\overline{Dil}] \quad (3)$$

The quantity of water solubilized by *n*-heptane can be disregarded; assuming that only one type of aggregate is formed ($L_{4,4}$), that monomers are not hydrated, and that no hydrated aggregates are formed (based on Bosland's experimental data [7]), Equation 3 becomes:

$$\overline{[H_2O]} = S^{\oplus}_{L}.a_{H_2O}.[\overline{L}] + S^{\oplus}_{L_N}.a_{H_2O}.\overline{[L_N]} \quad (4)$$

where $S^{\oplus}_{L}$ and $S^{\oplus}_{L_N}$ are the quantity of water solubilized, respectively, by the monomers and aggregate of DMDOHEMA for $a_{H2O} = 1$. The variation in water activity was induced with variable $LiNO_3$ concentrations. Three sets of experiments were carried out with DMDOHEMA concentrations of 0.05 mol L^{-1} (taken as a monomer system); 0.5 mol L^{-1} and 1.2 mol L^{-1}. $[\overline{L}]$ and $[\overline{L_N}]$ were determined from VPO measurements; $S^{\oplus}_{L}$ was determined by slope analysis of the $\overline{[H_2O]} = f(a_{H2O})$ curve for DMDOHEMA 0.05 mol L^{-1} (the

aggregate concentration was negligible); and $S^{\oplus}_{L_N}$ was calculated by taking into account the contribution of the monomers. The results of the modeling are the following: $S^{\oplus}_{L} = 0.19$; $S^{\oplus}_{L_N} = 1.7$ for $\overline{[DMDOHEMA]} = 0.5$ mol L^{-1}, and $S^{\oplus}_{L_N} = 2.4$ for $\overline{[DMDOHEMA]} = 1.2$ mol L^{-1}. The variation of $S^{\oplus}_{L_N}$ with the malonamide concentration could be attributed to a change in the organization of aggregates, as observed for DMDBTDMA in dodecane [2,5,].

Effect of the Europium Concentration

VPO measurements on 0.5 mol L^{-1} DMDOHEMA solutions in *n*-heptane at 25 °C after extraction of europium nitrate showed that the average aggregation number increased with the europium concentration in the organic phase (Figure 2a). At a high organic europium concentration (0.17 mol L^{-1}), the average aggregation number increased to 7 indicating a modification of the aggregation as a function of the organic solute concentration.

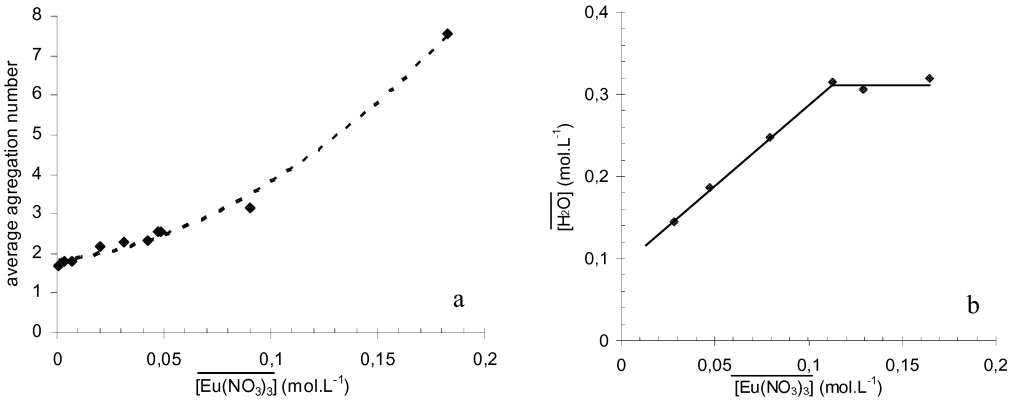

Figure 2. Average aggregation number (a) and water concentration in organic phase (b) vs organic europium concentration for 0.5 mol L^{-1} DMDOHEMA in *n*-heptane.
a: Aqueous phase was europium nitrate in 3 mol L^{-1} $LiNO_3$ ($0.83 < a_{H20} < 0.87$).
b:Water activity in aqueous phase was $a_{H20} = 0.86$.

The water concentration in the organic phase depends on the water activity in the aqueous phase. Europium extraction by 0.5 mol L^{-1} DMDOHEMA in *n*-heptane was therefore investigated with increasing europium concentrations in the aqueous phase at constant water activity ≈ 0.86 (Table 1).

For organic concentrations of europium below 0.11 mol L^{-1}, the water concentration in the organic phase increases with the europium organic concentration (2 molecules of water for one of europium nitrate). The organic water concentration then remains constant, although the europium concentration continues to increase. The break point corresponds to a [diamide]/[Europium] ratio of about 4.5−5 (Figure 2b). A likely interpretation would be that, without europium, malonamide is organized as spherical aggregates (N = 4-5): each aggregate, can extract one europium and two water molecules until [diamide]/[Europium] ~ 4.5−5. Further europium extraction modifies the DMDOHEMA aggregation leading to a change in the water extraction.

Table 1. Composition of the aqueous and organic phases after extraction of europium nitrate by 0.5 mol L^{-1} DMDOHEMA in *n*-heptane for a constant water activity.

Aqueous Phase			Organic Phase	
$[LiNO_3]$ (mol L^{-1})	$[Eu(NO_3)_3]$ (mol L^{-1})	a_{eau}	$\overline{[Eu(NO_3)_3]}$ (mol L^{-1})	$\overline{[H_2O]}$ (mol L^{-1})
3.075	0.023	0.859	0.028	0.145
2.945	0.039	0.865	0.047	0.187
3.114	0.086	0.850	0.080	0.248
2.652	0.209	0.864	0.113	0.315
2.852	0.199	0.852	0.129	0.307
2.562	0.276	0.861	0.165	0.319

To gain information about the complexes formed in the organic phase, experiments were performed in which a 0.5 mol L^{-1} DMDOHEMA solution in *n*-heptane was contacted with a 0.1 mol L^{-1} $Eu(NO_3)_3$, 3 mol L^{-1} $LiNO_3$ aqueous solution and a 0.4 mol L^{-1} $Eu(NO_3)_3$, 3 mol L^{-1} $LiNO_3$ aqueous solution. The ESI-MS data exhibited peaks corresponding to several Eu-diamide species, with 2 to 7 diamide molecules for each metal center (Figure 3, where *L* stands for DMDOHEMA). The influence of the cone voltage was determined, and the intensity of ions such as $[EuL_x]^{3+}$ where $x \geq 5$, strongly decreases as the cone voltage increases, showing that these species are not very stable and are probably formed during the ionization process as already observed for Nd extraction [8]. The spectra show that the stoichiometry of complexes in organic phase depends on the [diamide]/[Europium] ratio. When [diamide]/[Europium] > 4.5−5, europium appears to be surrounded by 4 malonamides, but when [diamide]/[Europium] < 4.5−5, the most abundant species contains only 2 malonamides around europium. Several complexes are probably formed with the stoichiometry $Eu(NO_3)_3L_x$ (where x = 2, 3, and 4), and their abundance depends on the experimental conditions.

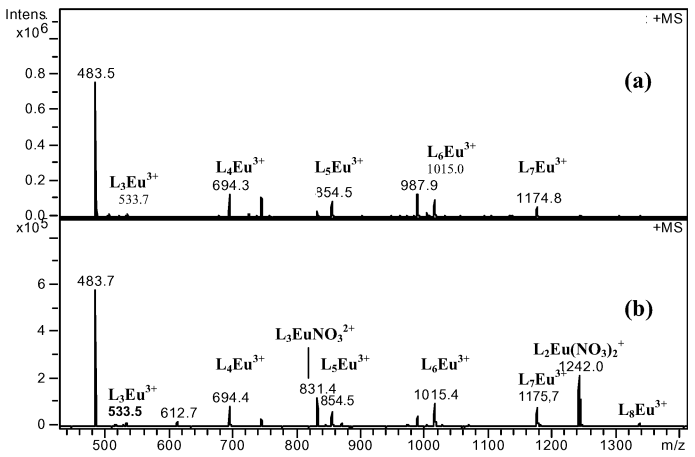

Figure 3. Positive ESI mass spectrum for 0.5 mol L^{-1} DMDOHEMA in *n*-dodecane after equilibration with (a) 0.1 mol L^{-1} $Eu(NO_3)_3$ in 3 mol L^{-1} $LiNO_3$ or (b) 0.4 mol L^{-1} $Eu(NO_3)_3$ in 3 mol L^{-1} $LiNO_3$ (*L* stands for DMDOHEMA).

CONCLUSION

This study shows that small aggregates can be formed when the DMDOHEMA concentration in *n*-heptane exceeds 0.12 mol L^{-1}. An increase of the malonamide concentration leads to an increase of the aggregate proportion and an increase of the quantity of water solubilized by the aggregates. An increase of europium(III) nitrate concentration in the organic phase leads to a modification of the stoichiometry of the complex and a change in the aggregation (for DMDOHEMA 0.5 mol L^{-1} solution, average aggregation number is about 2 without europium and increases to 7 for europium concentration ~0.17 mol L^{-1}). Consequently, the extracting properties and the aggregation seem correlated. These results will be checked by Small Angle neutron and X-ray scattering, which give information about the organisation of malonamides.

REFERENCES

1. C. Erlinger, L. Belloni, T. Zemb, and C. Madic, "Attractive Interactions Between Reverse Aggregates and Phase Separation in Concentrated Malonamide Extractant Solutions," *Langmuir*, **15**, 2290-2300 (1999).
2. L. Martinet, "Organisation supramoléculaire des phases organiques de malonamides du procédé d'extraction DIAMEX," CEA Report R-6105, 2006.
3. L. Berthon, L. Martinet, F. Testard, C. Madic, and T. Zemb, "Solvent Penetration and Sterical Stabilization of Reverse Aggregates Based on DIAMEX Process Extracting Molecules: Consequences on Third Phase Formation," *Solvent Extr. Ion Exch.*, **25**, 545-576 (2007).
4. F. Testard, P. Bauduin, L. Martinet, B. Abécassis, L. Berthon, C. Madic, and Th. Zemb, "Self-assembling properties of malonamide extractants used in separation processes," (submitted to *Radiochimica Acta*).
5. P. Bauduin, F. Testard, L. Berthon, and Th. Zemb, "Relation between the hydrophile/hydrophobe ratio of malonamide extractants and the stability of the organic phase: investigation at high extractant concentrations," *Phys. Chem. Chem. Phys.*, **9**, 3776–3785 (2007).
6. H. Dozol and C. Berthon, "Characterization of the supramolecular structure of malonamides by application of pulsed field gradients in NMR spectroscopy," *Phys. Chem. Chem. Phys.*, **9**, 5162-5170 (2007).
7. L. Bosland, "Étude thermodynamique et cinétique de l'extraction des nitrates de lanthanides par un malonamide (N,N' diméthyl-N,N' dioctyl hexyléthoxy malonamide ou DMDOHEMA)," CEA Report R-6099, 2006.
8. M. R. Antonio, R. Chiarizia, B. Gannaz, L. Berthon, N. Zorz, C. Hill, and G. Cote "Aggregation in Solvent Extraction Systems Containing a Malonamide, a Dialkylphosphoric Acid and Their Mixtures" (submitted to *Sep. Sci. Technol.*).
9. C. Sorel, "Modélisation de l'extraction du nitrate de césium par un calixarène. Application à la modélisation du transport à travers des membranes liquides supportées," Ph.D. Thesis Université de Paris VI, 1996.

FROM DATABASES TO *IN SILICO* DESIGN OF NOVEL METAL BINDERS

Alexandre Varnek

Laboratoire d'Infochimie, UMR 7177 CNRS, Université Louis Pasteur, 4, rue B. Pascal, Strasbourg, 67000, France. URL:http://infochim.u-strasbg.fr
Corresponding author e-mail address: varnek@chimie.u-strasbg.fr

ABSTRACT

Chemoinformatics approaches open new opportunities for computer-aided design of new efficient metal binders. Generally, such an *in silico* design can be performed in three steps: (*i*) acquisition, storage, and organization of experimental data; (*ii*) extraction of the knowledge hidden in those data; and (*iii*) exploitation of this knowledge. To store and organize available experimental data, we've developed Solvent eXtraction Database tools that allow users to supply, to search and to share experimental information using any internet browser. In order to predict new compounds, we employ homemade ISIDA (**I**n **SI**lico design and **D**ata **A**nalysis) software, which builds quantitative structure-property relationships, generates combinatorial libraries, and performs virtual screening of large collections of molecules. Using ISIDA tools, quantitative models linking molecular structure with various thermodynamics extraction properties (extraction constants, distribution ratio, and separation factors) have been obtained for different classes of ligands. Some new uranyl binders based on monoamides and on phosphoryl-containing podands were designed theoretically with ISIDA, then synthesized and tested experimentally. Remarkable agreement between experimental uranyl distribution ratios and predicted values was observed.

INTRODUCTION

Development of new extractants for selective binding and separation of metal represents a real challenge because of complexity of the extraction systems involving various chemical and physical interactions of molecular species (extractant, co-extractant, and counterions) situated in two immiscible liquid phases. Even in the simplest case, an extraction process involves a formation of metal-ligand complex in one of the phases or at the liquid-liquid interface followed by its diffusion into the organic phase. This could be accompanied by formation of more complex species like inverse micelles, vesicle, etc.

Chemoinformatics approaches [1] open new opportunities for computer-aided design of new efficient metal binders. Generally, such an *in silico* design can be performed in three steps: (*i*) acquisition, storage, and organization of experimental data, (*ii*) extraction of the knowledge hidden in those data; and (*iii*) exploitation of this knowledge. Here, we demonstrate the efficiency of theoretical calculations to predict

structures of two classes of new uranyl extractants, monoamides and phosphoryl-containing podands. Our challenge was to enrich the list of the most efficient metal binders, and even to suggest extractants which are more efficient than the previously studied ones. In most of calculations, we used the homemade ISIDA program package [2]. The commercial CODESSA PRO program [3] was used in some cases for the purpose of comparison.

This study involves four main steps: (*i*) compilation of available experimental data; (*ii*) structure—property modelling of the logarithm of the distribution ratio (log *D*) of UO_2^{2+}, which quantitatively measures extraction efficiency of ligands; (*iii*) generation, enumeration, and screening of a virtual combinatorial library; and (*iv*) synthesis of theoretically predicted compounds and their experimental extraction studies.

It should be emphasized that a synthesis of suggested molecules and corresponding extraction experiments has been performed when calculations have been completed.

ISIDA PROGRAM

ISIDA (**I**n **SI**lico design and **D**ata **A**nalysis) program package [2] has been developed at the Laboratory of Chemoinformatics at the University of Strasbourg for computer-aided design of new compounds. ISIDA involves three main elements: (1) a database management system; (2) an expert system that builds quantitative structure-property relationships (QSPR); (3) a generator of combinatorial libraries; and (4) a knowledge base, to store, and to apply the developed QSPR models. Figure 1 illustrates links between these modules, where experimental data collected in the database are treated by the expert system, which establishes relationships between structure of compounds and their extraction properties. Then, structure-property models stored in the knowledge base are applied to screen a virtual combinatorial library, leading to potential actives which then can be experimentally tested, in turn providing the database with new information.

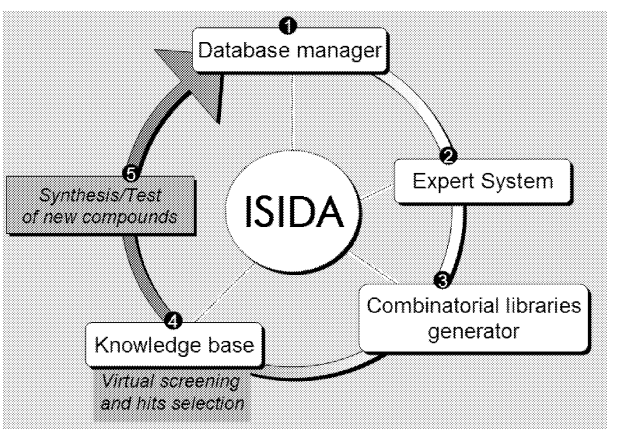

Figure 1. In Silico molecular design using the ISIDA program.

To store and organize available experimental data, we've developed Solvent eXtraction Database [4] which allows users to supply, to search, and to share experimental information using any internet browser. Actual version of SXD contains about 3500 extraction equilibria. To establish structure-extraction property relationships, the ISIDA

expert system uses several machine learning techniques: multi-linear regression analysis (MLR), k Nearest Neighbours (*k*NN), Radial Basis Functions Neural Networks (RBFNN), Associative Neural Networks (ASNN), and Support Vector Machine (SVM). The combinatorial module of ISIDA generates virtual combinatorial libraries using Markush structures. It uses its own editor of 2D structures *EdChemS,* allowing the user to prepare the molecular core, to define the type of the attachment "reaction," to select the attachment positions (atoms, bonds), and to prepare collections of substituents. The screening of the prepared library is performed using available structure-property models. ISIDA builds structure-property models based on two sub-classes of fragment descriptors: "sequences" and "augmented atoms." The sequences may contain connected atoms and bonds, atoms only, or bonds only. An "augmented atom" represents a particular atom with its environment, including either neighboring atoms and bonds, or atoms only, or bonds only. Any molecular descriptors generated by other programs could be also used in calculations together with fragment descriptors.

Earlier, ISIDA has been successfully applied to develop predictive QSPR models linking the structure of ligands with some thermodynamic extraction properties: extraction constants, distribution ratios, and separation factors [4-8].

COMPUTER-AIDED DESIGN OF NEW EXTRACTANTS

Alkyl-substituted monoamides are known as extractants for the uranyl cation, and potentially they could be considered as alternatives to organophosphorous compounds in nuclear-fuel reprocessing. In the toluene phase, the uranyl cation forms complexes with two monoamide molecules. These relatively simple molecules were selected [6] for computer-aided design, taking into account a lot of synthetic and experimental work to be done to prove modeling predictions.

Structure-property models were trained on a set of 19 alkyl-substituted monoamides for which the distribution ratio of uranyl nitrate extracted from water to toluene (D) were reported by Siddall [9] and by Rabbe et al. [10]. In the modelling with the ISIDA program, fragment descriptors (atom/bond sequences or augmented atoms) were used together with several different machine-learning techniques: MLR, *k*NN, RBFNN, ASNN, and SVM. Some models involving physico chemical descriptors were obtained with the CODESSA PRO program. The virtual combinatorial library containing about 10500 alkyl-substituted monoamides was generated with ISIDA by systematically attaching different alkyl substituents to the C and N atoms of the monoamide's scaffold.

A screening of the virtual combinatorial library was performed in several steps. Since potential extractants must be insoluble in the water phase, the ISIDA-Log S module incorporating QSPR models for aqueous solubility (log S) [11] has been used for the filtering of the library. Thus, the compounds for which log $S \leq -3$ were considered insoluble in water; other compounds were excluded. A subset containing 9306 potentially insoluble molecules has been screened using the "structure – log D" models. The main goal of screening was selection of potentially efficient extractants. However, in order to assess the performance of theoretical approach to reproduce the whole range of log D variation, both strong and weak uranyl binders were selected as hits. The screening and

hits selection was performed using the ISIDA consensus model involving more than 200 individual linear models. More time-consuming calculations involving ASNN, RBFNN, SVM, and CODESSA PRO models were applied only for those selected hits. The compounds with problematic synthetic feasibility were excluded from the hits list. Remaining compounds were recommended to experimentalists.

A distribution of experimental values of log D for the data sets of initial and novel compounds is given on Figure 2. One can see that population of efficient extractants is much higher among novel compounds than that for previously studied molecules. Thus, the number of molecules with log $D > 0.9$ is 4 for the initial set and 9 for the new set of monoamides. One of the novel molecules displays slightly larger affinity for uranyl than previously known extractants. Figure 3 demonstrates a prediction performance of structure property models for novel 21 novel extractants: a reasonable linear correlation log D_{pred} vs log D_{exp} has been observed ($R^2_{rel} = 0.675$, $R^2_{abs} = 0.573$, $RMSE_{abs} = 0.16$).

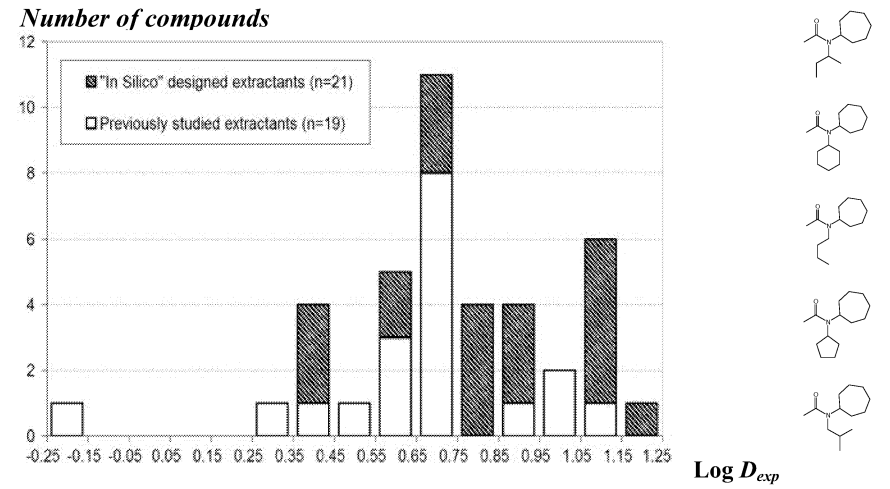

Figure 2. Experimental distribution ratio of UO_2^{2+} for the initial set of 19 amides (blank bars) and for 21 newly designed amides (filled bars). Structures on the right correspond to the most efficient new extractant (log $D > 1$).

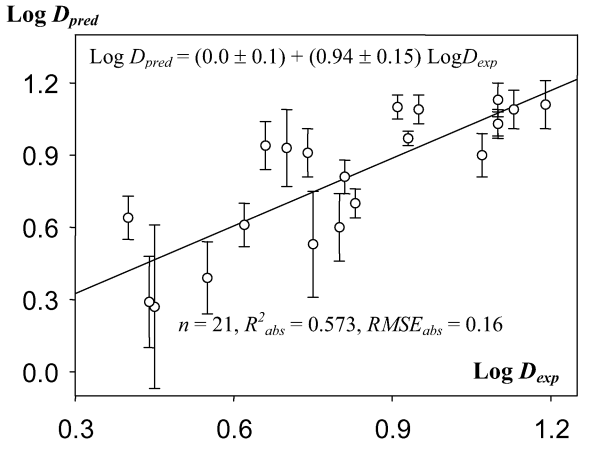

Figure 3. Experimental vs predicted log D values for 21 designed monoamides.

Phosphoryl-containing podands are acyclic molecules with polyether spacer(s) linking two (in monopodands), three (in dipodands and tripodands), or four (in tripodands) terminal phosphine oxide groups. Variation of the length of the spacers, of molecular topology and of the substituents at the phosphorous atoms may lead to desirable complexation or extraction properties of podands for selected metal cations. In particular, these molecules extract the uranyl cation, forming 1:1 complexes [12] whose structures were not studied so far. Analysis of the data from the Solvent eXtraction Database shows that the set of distribution ratios (log *D*) for uranyl extraction in 1,2-dichloroethane for 32 podands [12] is one of the largest available in the literature data sets where extraction properties of the compounds were studied strictly at the same conditions.

Two different approaches were used in [5] for a QSPR modeling of log *D*: one based on classical structural and physicochemical descriptors (implemented in the CODESSA PRO program) and another one based on fragmental descriptors (implemented in the ISIDA program). Three statistically significant models obtained with ISIDA involved as descriptors either sequences of atoms and bonds or atoms with their close environment (augmented atoms). The best models of CODESSA PRO included its own molecular descriptors as well as fragmental descriptors obtained with ISIDA. At the second step, a virtual combinatorial library of 2024 podands was generated for the Markush structure $R_1R_2R_3P{=}O$ for which a set of "optimal" substituents R_1, R_2, and R_3 was prepared using fragment contributions a_i calculated by ISIDA for the three best models obtained at the training stage. The activity of each compound in the combinatorial library was evaluated by ISIDA consensus model. Eight hits were selected among many potential candidates in order to span the range of log *D* variation for experimentally studied molecules (log *D* = -0.05–3.05). Their extraction ability has been also assessed using the best models of CODESSA PRO. Then, these 8 podands were prepared and experimentally studied as uranyl extractants using the same protocol as for the compounds from the parent set [12]. Comparison of experimental log *D* values with those predicted by ISIDA and CODESSA PRO (Figure 4) shows that the both QSPR approaches reasonably estimate log *D* for 7 from 8 compounds from the “blind” test set.

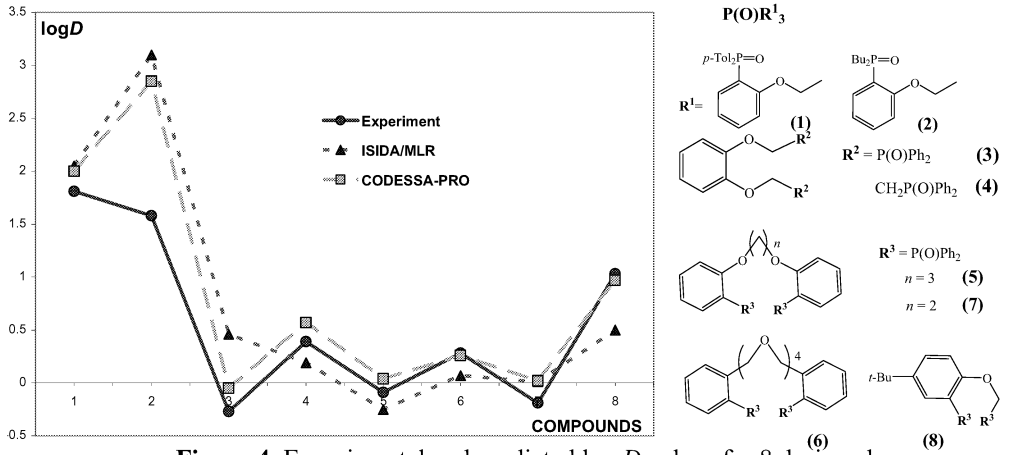

Figure 4. Experimental and predicted log *D* values for 8 designed phosphoryl-containing podands.

ACKNOWLEDGMENTS

I thank Drs V. Solov'ev, G. Marcou, D. Fourches, and O. Klimchuk for the fruitful collaboration and GDR PARIS, GDRE SupraChem, and the ARCUS project for the support.

CONCLUSIONS

Here, we demonstrate the performance of the chemoinformatics approach to generate "*in silico*" novel uranyl extractants belonging to two families, monoamides and phosphoryl-containing podands. We believe that the developed structure-property tools could be rather efficient to design theoretically complex extraction systems, thus providing experimentalists with structure of new potential extractants and, in such a way, decreasing costs of synthesis and experimental tests.

REFERENCES

1. J. Gasteiger, "Chemoinformatics: a new field with a long tradition," *Anal. Bioanal. Chem.,* **384***,* 57-64 (2006).
2. http://infochim.u-strasbg.fr/recherche/isida/index.php
3. http://www.codessa-pro.com/manual/manual.htm
4. A. Varnek, G. Wipff, and V. P. Solov'ev, "Towards an information system on solvent extraction," *Solv. Extr. Ion Exch*., **19,** 791-837 (2001).
5. A. Varnek, D. Fourches, V. P. Solov'ev, V. E. Baulin, A. N. Turanov, V. K. Karandashev, D. Fara, and A. R.Katritzky, "'In Silico' design of new uranyl extractants based on phosphoryl-containing podands: QSPR studies, generation and screening of virtual combinatorial library and experimental tests," *J. Chem. Inf. Comput. Sci*, **44**, 1365-1382 (2004).
6. A. Varnek, D. Fourches, V. Solov'ev, O. Klimchuk, A. Ouadi, and I. Billard, "Successful "In Silico" Design of New Efficient Uranyl Binders", *Solv. Extr. Ion Exch.*, **25**(3), 433–462 (2007).
7. I. V. Tetko, V. P. Solov'ev, A. V. Antonov, X. J. Yao, B. T. Fan, F.Hoonakker, D. Fourches, N. Lachiche, and A.Varnek, "Benchmarking of Linear and Nonlinear Approaches for Quantitative Structure-Property Relationship Studies of Metal Complexation with Ionophores," *J. Chem. Inf. Model.*, **46**, 808-819 (2006).
8. V. P. Solov'ev and A. A. Varnek, "Structure – property modeling of metal binders using molecular fragments," *Rus. Chem. Bull*., **53**, 1434-1445 (2004).
9. T. H. Siddall III, "Effects of Structure of N,N-Disubstituted Amides on Their Extraction of Actinide and Zirconium Nitrates and of Nitric Acid," *J. Phys. Chem.,* **64**, 1863-1866 (1960).
10. C. Rabbe, C.Sella, C. Madic, and A. Godard, "Molecular Modeling Study of Uranyl Nitrate Extraction with Monoamides. II. Molecular Mechanics and Lipophilicity Calculations. Structure-Activity Relationships," *Solv. Extr. Ion Exch.*, ***17***, 87-112 (1999).
11. A. Varnek, D. Fourches, F. Hoonakker, and V. P. Solov'ev, "Substructural Fragments: an Universal Language to Encode Reactions, Molecular and Supramolecular Structures," *J. Comp.-Aided Mol. Design*, **19**, 693-703 (2006).
12. A. N. Turanov, V. K. Karandashev, and V. E. Baulin, "Extraction of Uranium and Thorium with Neutral Phosphoryl Containing Podands from Nitric Acid Solutions," *Radiokhimiya (Rus.)*, **40**, 36-43 (1998).

EXTRACTANT AGGREGATION AS A MECHANISM OF METAL ION SELECTIVITY

Mark P. Jensen,[1*] Tsuyoshi Yaita,[2] and Renato Chiarizia[1]

[1]Chemical Sciences and Engineering Division, Argonne National Laboratory, 9700 South Cass Avenue, Argonne, IL 60439, USA. [2]Actinide Coordination Chemistry Group, Synchrotron Radiation Research Center, Japan Atomic Energy Agency, Hyogo 679-5148, Japan. Corresponding author email address: mjensen@anl.gov

ABSTRACT

The formation of supramolecular extractant aggregates can create new extracting species with specific affinity for particular metal ions, as is the case for the extraction of trivalent lanthanide and actinide species by tetra-*n*-octyldiglycolamide (TODGA) in alkane diluents. TODGA monomers and dimers are present at the lowest aqueous acidities. The speciation of these solutions transitions to a polydisperse mixture containing TODGA monomers, dimers, and small reverse-micelles of $(TODGA)_4$ at aqueous HNO_3 acidities of 0.7 M or higher. These tetrameric TODGA species persist and come to dominate the TODGA speciation when Nd is extracted. The peculiar selectivity of TODGA for the trivalent lanthanide and actinide nitrates appears to arise from the unique affinity of these metal cations for the supramolecular TODGA tetramers.

INTRODUCTION

The aggregation of extractants in nonpolar diluents is a common occurrence in solvent extraction, which can have important kinetic and thermodynamic impacts on the partitioning of metal ions [1]. If the active extractant species aggregates to form higher oligomers, the result can be a reduction in the extractability of metal ions brought about by a lower available concentration of the active extractant. However, extractant aggregation also can increase the extractability of metal ions by increasing the solubility of the extractant and extracted species in the organic phase, or by creating a new supramolecular species that is a more active extractant, e.g. hexamers of P,P'-di(2-ethyl-hexyl)ethane diphosphonic acid or reverse micelles of DNNS [2, 3].

Diamide extractants (Figure 1), such as *N*,*N*'-dimethyl-*N*,*N*'-dibutyltetradecyl-malonamide (DMDBTDMA), or *N*,*N*,*N*',*N*'-tetra-*n*-octyldiglycolamide (TODGA), are of current interest for nuclear separations [4]. TODGA is particularly interesting for separations involving the lanthanide (Ln) and trivalent actinide (An) elements, as it is an unusually effective extractant for these metals relative to *f*-elements in other oxidation states, such as Pu(IV) or U(VI) [5]. This aspect of TODGA extractions cannot be understood through simple electrostatic bonding models, which are usually sufficient to

explain the selectivity of most extractants for one type of *f*-ion ion over another. Such models predict the order of extraction for Ln or An cations An(IV) > An(VI)/An(III)/Ln(III) >> An(V). Instead with TODGA, the observed order is An(III)/Ln(III)/An(IV) > An(VI) >> An(V) [5]. The chemical origins of the enhanced extractability of the Ln(III) and An(III) species by TODGA are not understood.

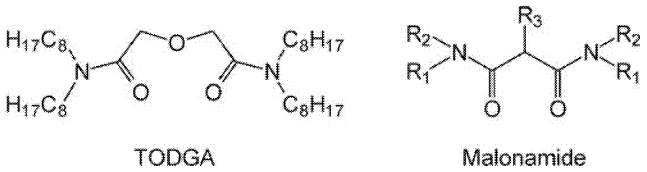

Figure 1. Structures of example diamide extractants, *N*,*N*,*N*',*N*'-tetra-*n*-octyldigylcolamide (TODGA) and the malonamides where, for example, *N*,*N*'-dimethyl-*N*,*N*'-dibutyltetradecyl-malonamide (DMDBTDMA) has $R_1 = CH_3$, $R_2 = C_4H_9$, and $R_3 = C_{14}H_{29}$.

As with other amphiphilic extractants, both the malonamides and the diglycolamides aggregate in aliphatic diluents, and the metal-free aggregates have been studied in alkane diluents by various researchers [6-9] at extractant concentrations and acidities relevant to proposed extraction processes. The consensus of these studies is that the aggregates formed by the diamide extractants in alkane diluents are best represented as small, reverse micelle-like particles containing 3-9 malonamide monomers [6,10] or 4 TODGA monomers [8,11] as well as extracted water and acid. We hypothesize that the selectivity of TODGA for An(III)/Ln(III) arises from the formation of these preorganized supramolecular tetrameric aggregates, which we refer to as $(TODGA)_4$ without reference to any associated water and acid, and the unique interaction of An(III)/Ln(III) cations with $(TODGA)_4$.

EXPERIMENTAL

Solutions of 0.10 M TODGA were prepared from 99% TODGA (Kanto Chemical Co.) by dilution with *n*-heptane (Aldrich, 99+%), *n*-octane (Alfa-AESAR, 99.7%), or *n*-octane-d_{18} (Aldrich, 98 atom% D) as appropriate. Neutron scattering measurements were made at 25 °C, while all other operations were conducted at 23 ± 1 °C. TODGA solutions pre-equilibrated twice with appropriate metal-free aqueous phases at an organic to aqueous phase ratio of 1:2. The pre-equilibrated organic phases were then vortexed for 2 min. with an equal volume of aqueous phase containing nitric or hydrochloric acid and, when appropriate, Nd or Am. This time was sufficient to attain equilibrium. The techniques used to study these solutions have been previously reported [9,11].

RESULTS AND DISCUSSION

When 0.10 M TODGA in *n*-alkane diluents is contacted with aqueous HNO_3 in the absence of metal cations, we find that the mixture of TODGA monomers and dimers in the low-acidity systems begins to transition to a solution containing tetrameric aggregates of TODGA, water, and nitric acid as the acidity of the aqueous phase

increases. The data in Table 1 show the aggregation number of the largest aggregate in solution, n_{max}, when an equilibrium between TODGA monomers and *n*-mers is assumed. More detailed analysis [11], allowing for a mixture of TODGA monomers, dimers, and *n*-mers using the aggregation numbers from small-angle neutron scattering (SANS) and vapor pressure osmometry data of metal-free systems is summarized in Figure 2A. The data demonstrate that appreciable amounts of $(TODGA)_4$ begin to form in the organic phase when the equilibrium aqueous phase contains ca. 0.7 M HNO_3. At constant total TODGA concentration, $[H_2O]_{org}$ and $[HNO_3]_{org}$ (Figure 2B) are linearly related to the experimentally derived $[(TODGA)_4]$. This suggests that the metal-free $(TODGA)_4$ species are reverse micelles, as first argued by Nave et al. [8]. While there is a linear relationship between $[HNO_3]_{org}$ and $[(TODGA)_4]$, the relationship between the equilibrium *aqueous* $[HNO_3]$ and $[(TODGA)_4]$ is not linear (log $[(TODGA)_4]$ vs. log $[HNO_3]_{aq}$ gives slope = 1.5 ± 0.3, Figure 2C). This discrepancy makes it difficult to understand the interactions between nitric acid and $(TODGA)_4$. Nevertheless, the *apparent* $[HNO_3]_{aq}$ dependency of 1.5 must be accounted for in the analysis of the acid dependence of metal extraction by $(TODGA)_4$.

Table 1. Maximum aggregation number of 0.1 M TODGA in solutions modeled as containing TODGA monomers and $(TODGA)_{n_{max}}$

	n_{max}	
Aqueous Acid	$[Nd]_{org}$ = 0 mM	$[Nd]_{org}$ = 10 mM
0.48 M HNO_3	2.4 ± 0.5	3.7 ± 0.4
1.0 M HNO_3	3.4 ± 0.5	4.0 ± 0.4
2.0 M HNO_3	4.0 ± 0.5	3.7 ± 0.4
4.0 M HCl	2 [a]	4.4 ± 0.4

[a] Estimated from weight-average aggregation number only.

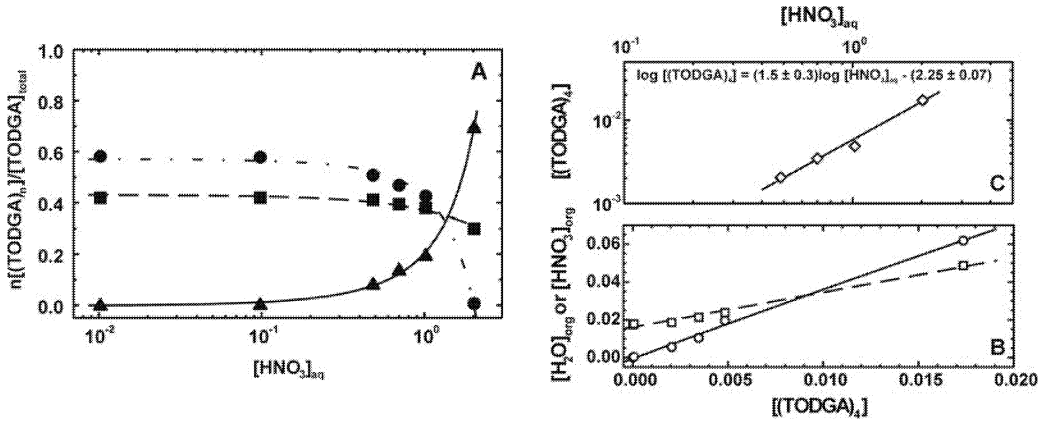

Figure 2. (A) Experimentally derived speciation diagram for 0.10 M TODGA/*n*-octane solutions equilibrated with metal-free solutions of HNO_3 (■) TODGA, (●) $(TODGA)_2$, and (▲) $(TODGA)_4$. (B) The concentrations of organic phase (□) H_2O and (○) HNO_3 are proportional to the concentration of $(TODGA)_4$. (C) Slope analysis of the dependence of the concentration of (◇) $(TODGA)_4$ on the aqueous-phase acidity. All concentrations are given in moles/liter.

Analysis of SANS measurements of 0.10 M TODGA/*n*-octane solutions loaded with varying amounts of Nd (5-15 mM) at various acidities (0.48-2.0 M HNO_3 or 4 M HCl), demonstrate that the Nd-TODGA complexes formed when Nd is extracted into the organic phase contain 1 Nd and 4 TODGA molecules in every case studied (Table 1 and ref. [11]). In addition, the shape and size of the Nd-loaded species in the organic phase (spheres with an average radius of 10.3 ± 0.2 Å) are indistinguishable from those of the metal-free reverse micelles of $(TODGA)_4$ (10.6 ± 0.4 Å) [11]. The 1:4 Nd:TODGA ratio found from SANS is in complete agreement with reports of the extractant dependencies of TODGA in aliphatic and aromatic diluents, which give extractant-dependency slopes near 4 for a variety of An(III)/Ln(III) cations in nitric acid [5].

Knowing the speciation of TODGA in both the metal-free and Nd-loaded extraction systems, one can now quantitatively examine the influence of $(TODGA)_4$ on An(III)/Ln(III) extraction. For 0.10 M TODGA/*n*-alkane solutions, both the extractant speciation (Figure 2A) and the distribution ratios of Am(III) [9] are known. This provides an opportunity to directly test the hypothesis of An(III)/Ln(III) extraction by $(TODGA)_4$. Based on a recent report [12] and the information in Figure 2C, we can write the average overall extraction equilibrium to be tested as

$$Am^{3+} + 3\ NO_3^- + 1.5HNO_3 + (TODGA)_{4,org} \rightleftharpoons Am(NO_3)_3(TODGA)_4 \bullet 1.5\ HNO_{3,org} \quad (1)$$

where the distribution ratio of Am, D_{Am}, is expected to have a 4.5 (from 3+1.5) power dependence on the aqueous nitrate/nitric acid concentration, as well as a first-power dependence on $(TODGA)_4$. However, varying the aqueous acidity at constant $[TODGA]_{total}$ in this system alters both $[NO_3^-]$ and, as demonstrated in Figure 2A, $[(TODGA)_4]$. Consequently, slope analysis of this system must consider the entire equilibrium expression, $K_{ex} = D_{Am}[NO_3^-]^{-3}[(TODGA)_4]^{-1}[HNO_3]^{-1.5}$. The results of direct slope analysis of the $[NO_3^-]$ dependence (and indirectly, the $[HNO_3]$ and $[(TODGA)_4]$ dependencies) using this approach is depicted in Figure 3. The deviation from linearity at low $[HNO_3]$ is likely caused by the very small concentration of $[(TODGA)_4]$ present in that solution and the lesser ability of TODGA monomers or dimers to extract the metal salt. Since both the $[HNO_3]$ and $[(TODGA)_4]$ span an order of magnitude in this experiment, the validity of each term presented in Equilibrium 1 is ensured over this concentration range, demonstrating the hypothesized extraction by $(TODGA)_4$.

In contrast to An(III)/Ln(III) extraction, other metals including the An(IV) and An(VI) nitrates do not appear to interact with $(TODGA)_4$. Only trivalent An and Ln species give extractant dependencies of 4 with TODGA [5]. All other elements display lower extractant dependencies. We conclude that only An(III)/Ln(III) cations can interact directly with $(TODGA)_4$ micelles as described above. This is made more clear by considering the malonamides such as DMDBTDMA, which show aggregation behavior similar to TODGA [6,10]. However, the malonamides give extractant dependencies of 2 for An(III)/Ln(III) extraction. Unlike the TODGA case, this metal:extractant ratio does not match the aggregation number of the DMDBTDMA aggregates [13], and there is no enhancement in the selectivity of the malonamides for An(III)/Ln(III) relative to other metals. The assembly of the supramolecular $(TODGA)_4$ species creates an extractant suited for the extraction of trivalent *f*-elements, while other metal species or other

extractants require other metal:extractant ratios. Thus, the formation of $(TODGA)_4$ and the unique interactions of An(III)/Ln(III) salts with this species are responsible for the enhanced selectivity of TODGA for these trivalent metals.

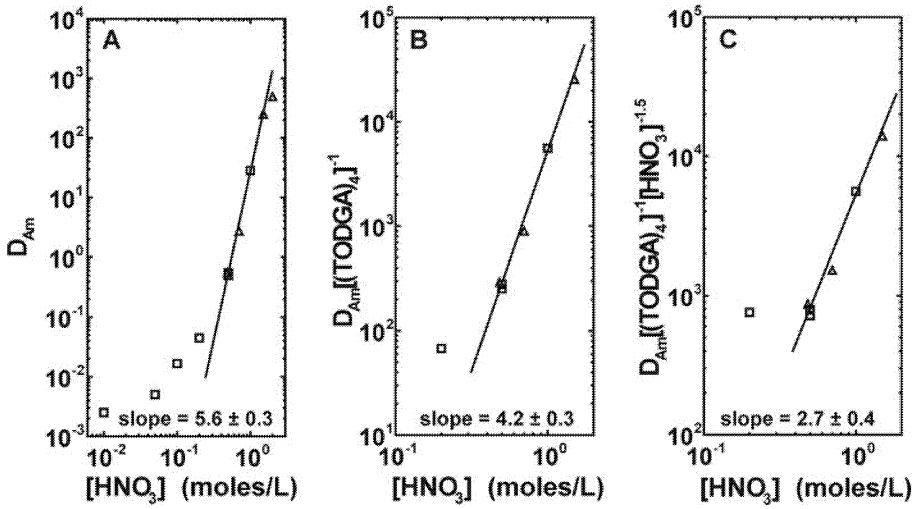

Figure 3. Correcting the (A) distribution ratios for Am extraction by 0.10 M TODGA in alkane diluents for (B) the change in concentration of $(TODGA)_4$ and (C) the dependence on the aqueous $[HNO_3]$ yields the expected NO_3^- dependence for Am extraction given in Equation 1, as shown in panel C. Am extraction data is for dodecane (□), adapted from [14], and octane (△).

CONCLUSIONS

The unusually high extractability of Ln(III) and An(III) nitrates by TODGA appears to arise from the stability of TODGA tetramers in the organic phases. The supramolecular $(TODGA)_4$ aggregates form whether An(III)/Ln(III) are extracted or not, and they appear to be specific for the extraction of trivalent *f*-element cations. Other species, for example An(IV) nitrates, do not form organic-phase complexes with $(TODGA)_4$, and the resulting free energy expended to reorganize TODGA to better suit $An(NO_3)_4$ salts will then result in lower distribution ratios, despite the stronger intrinsic bonding interactions expected to be present in an An(IV)-TODGA complex. Both the unique preference of An(III)/Ln(III) for TODGA tetramers and the ease of forming the $(TODGA)_4$ aggregates in metal-free systems appear to be foundational to the unusual selectivity of TODGA for these metals; however, the specific origin of this preference of An(III)/Ln(III) for $(TODGA)_4$ is not clear.

ACKNOWLEDGMENTS

This work was performed under the auspices of the U. S. DOE OBES, Divisions of Materials Science (for the SANS measurements at the IPNS) and of Chemical Sciences, Geosciences, and Biosciences under contract number DE-AC02-06CH11357.

REFERENCES

1. G. Cote, "The Supramolecular Speciation: A Key for Improved Understanding and Modeling of Chemical Reactivity in Complex Systems," *Radiochim. Acta*, **91**, 639-643 (2003).
2. A. W. Herlinger, R. Chiarizia, J. R. Ferraro, P. G. Rickert, and E. P. Horwitz, "Metal Extraction by Alkyl Substituted Diphosphonic Acids. Part 2. P,P'-Di(2-ethylhexyl)ethanediphosphonic Acid Aggregation and IR Study," *Solvent Extr. Ion Exch.*, **15**, 401-416 (1997).
3. G. Y. Markovits and G. R. Choppin, "Solvent Extraction with Sulfonic Acids," in Ion Exchange and Solvent Extraction, J. A. Marinsky and Y. Marcus, Eds., Marcel Dekker, New York, 1973; pp. 51-81.
4. K. L. Nash, C. Madic, J. N. Mathur, and J. Lacquement, "Actinide Separation Science and Technology," The Chemistry of the Actinide and Transactinide Elements, L. R. Morss, N. M. Edelstein, and J. Fuger, Eds., Springer, Dordrecht, Netherlands, 2006; pp. 2622-2798.
5. Z.-X. Zhu, Y. Sasaki, H. Suzuki, S. Suzuki, and T. Kimura, "Cumulative Study on Solvent Extraction of Elements by *N,N,N',N'*-Tetraoctyl-3-oxapantanediamide (TODGA) from Nitric Acid into *n*-Dodecane," *Anal. Chim. Acta*, **527**, 163-168 (2004).
6. C. Erlinger, L. Belloni, T. Zemb, and C. Madic, "Attractive Interactions between Reverse Aggregates and Phase Separation in Concentrated Malonamide Extractant Solutions," *Langmuir*, **15**, 2290-2300 (1999).
7. L. Lefrançois, J.-J. Delpuech, M. Hébrant, J. Chrisment, and C. Tondre, "Aggregation and Protonation Phenomena in Third Phase Formation: An NMR Study of the Quaternary Malonamide/Dodecane/Nitric Acid/Water System," *J. Phys. Chem. B*, **105**, 2551-2564 (2001).
8. S. Nave, G. Modolo, C. Madic, and F. Testard, "Aggregation Properties of *N,N,N',N'*-Tetraoctyl-3-oxapentanediaminde (TODGA) in *n*-Dodecane," *Solvent Extr. Ion Exch.*, **22**, 527-551 (2004).
9. T. Yaita, A. W. Herlinger, P. Thiyagarajan, and M. P. Jensen, "Influence of Extractant Aggregation on the Extraction of Trivalent f-Element Cations by a Tetraalkyldiglycolamide," *Solvent Extr. Ion Exch.*, **22**, 553-571 (2004).
10. H. Dozol and C. Berthon, "Characterization of the Supramolecular Structure of Malonamides by Application of Pulsed Field Gradients in NMR Spectroscopy," *Phys. Chem. Chem. Phys.*, **9**, 5162-5170 (2007).
11. M. P. Jensen, T. Yaita, and R. Chiarizia, "Reverse-Micelle Formation in the Partitioning of Trivalent f-Element Cations by Biphasic Systems Containing a Tetraalkyldiglycolamide," *Langmuir*, **23**(9), 4765-4774 (2007).
12. Y. Sasaki, P. Rapold, M. Arisaka, M. Hirata, T. Kimura, C. Hill, and G. Cote, "An Additional Insight into the Correlation between the Distribution Ratios and the Aqueous Acidity of the TODGA System," *Solvent Extr. Ion Exch.*, **25**, 187-204 (2007).
13. B. Gannaz, R. Chiarizia, M. R. Antonio, C. Hill, and G. Cote, "Extraction of Lanthanides(III) and Am(III) by Mixtures of Malonamide and Dialkylphosphoric Acid," *Solvent Extr. Ion Exch.*, **25**, 313-337 (2007).
14. Y. Sasaki, Y. Sugo, S. Suzuki, and S. Tachimori, "The Novel Extractants, Diglycolamides, for the Extraction of Lanthanides and Actinides in HNO_3-*n*-Dodecane System," *Solvent Extr. Ion Exch.*, **19**, 91-103 (2001).

EFFECTS OF HYDRATION AND SOLVATION OF METAL COMPLEXES ON SEPARATIONS OF METAL IONS BY SOLVENT EXTRACTION

Jerzy Narbutt

Department of Radiochemistry, Institute of Nuclear Chemistry and Technology, 03-195 Warsaw, Poland. Corresponding author email address: jnarbut@ichtj.waw.pl

ABSTRACT

Selectivity of solvent-extraction separations of metal ions depends not only on differences in stability constants but also on differences in partition constants of the extracted complexes. Both factors affect the distribution ratios and separation factors of the metal ions to a degree dependent on process conditions. Partition constants are strongly influenced by hydration and solvation phenomena, mainly in the inner sphere of the central metal ion but also by outer-sphere (ligands) interactions. The energy of hydration and solvation depends on the properties of both metal ion (charge, radius, and electronic structure) and ligands (basicity, donor atoms, and geometry).

INTRODUCTION

Solvent extraction is an efficient method for the separation of metal ions based on differences in the distribution of their complexes between two immiscible liquid phases. Numerous books and monographs (e.g., [1]) deal with the principles and practice of the method. Both stability constants and partition constants of the extracted metal complexes influence the distribution ratios and separation factors of the metal ions, depending on the conditions of the process. The role of complexation of metal ions has been well recognized [2]. In this paper, the effects of hydration and solvation of metal complexes (in both liquid phases) on partition equilibria have been discussed as well as their contributions to the efficiency of the separations of metal ions of similar properties.

SOLVENT-EXTRACTION EQUILIBRIA

According to the "complex formation–partition" model [3], the process of transferring a metal ion M^{n+} from an aqueous solution to a water-immiscible organic solvent by means of an acidic chelating extractant HL, represented by

$$M^{n+} + nHL_{org} \xleftrightarrow{K_{ex,M}} ML_{n,org} + nH^{+} \quad (1)$$

(subscript *org* denotes a species in the organic phase; no subscript denotes a species in the aqueous phase; hydrating water is neglected), may be divided into two main steps:

(1) **Formation**, in the aqueous phase, of a neutral complex ML_n, hydrated in the inner (if available) and outer coordination spheres of the central metal ion:

$$M^{n+}(H_2O)_k + nL^- \xleftrightarrow{\beta_n} ML_n(H_2O)_m + (k-m)H_2O \quad (2)$$

of the overall stability constant, $\beta_n = [ML_n]\,[M^{n+}]^{-1}[L^-]^{-n}$. The concentration of the ligand (anion) in the aqueous phase, $[L^-]$, depends on the partition constant of the extractant HL in the two-phase system, $P_{HL} = [HL]_{org}\,[HL]^{-1}$, and–at a certain pH range–on its dissociation constant, $K_a = [H^+]\,[L^-]\,[HL]^{-1}$. The extraction constant of the metal ion is:

$$K_{ex,M} = \beta_n P_{MLn} K_a^{\,n} P_{HL}^{\,-n} \quad (3)$$

(2) **Partition**, transfer of the neutral complex (only) from the aqueous to the organic phase, accompanied by full or partial dehydration of its molecules:

$$ML_n(H_2O)_m \xleftrightarrow{P_{MLn}} [ML_n \cdot rH_2O]_{org} + (m-r)H_2O \quad (4)$$

where the equilibrium constant of the reaction (partition constant of the complex) is equal to $P_{MLn} = [ML_n]_{org}\,[ML_n]^{-1}$. The partial dehydration relates to coordinatively unsaturated metal chelates, which retain several (r) water molecules in the inner sphere of the central ion after being extracted to organic solvents [4]. Therefore, the high energy change accompanying the transfer of such species (dehydration energy) [5] must be attributed to breaking mainly the water-water hydrogen bonds in the outer sphere of the ion.

The measure of selectivity of separation of two similar metal ions A^{n+} and Z^{n+} extracted from the same aqueous solution is the separation factor, $SF_{A/Z} = D_A\,D_Z^{-1}$, where the distribution ratio of a given metal ion, $D_M = [ML_n]_{org}/(\Sigma[M^{n+}])$, is the ratio of its total concentrations in both phases. If we assume that only one neutral complex ML_n is extracted and neglect adduct formation in the organic phase, we arrive at

$$SF_{A/Z} = \frac{\beta_{n,A} \cdot P_{ALn}(1 + \sum_{i=1}^{w} \beta_{i,Z}[L^-]^i)}{\beta_{n,Z} \cdot P_{ZLn}(1 + \sum_{i=1}^{w} \beta_{i,A}[L^-]^i)} \quad (5)$$

where $\beta_{i,M}$ denotes the stability constant of i-th complex ML_i^{n-i} (M = A or Z), and w is the number of various ML_i^{n-i} complexes, including anionic ones if $w \geq n$.

The often-used formulation of $SF_{A/Z}$ as the ratio of extraction constants (Equation 3) of the metal ions [6] is justified only under conditions when the sum of concentrations of ML_i^{n-i} complexes in the aqueous phase is negligible in comparison to that of M^{n+} (at low pH). Equation 5 simplifies then to the ratio of the respective $\beta_{n,M}$ and P_{MLn} values:

$$SF_{A/Z} = \frac{K_{ex,A}}{K_{ex,Z}} = \frac{\beta_{n,A} \cdot P_{ALn}}{\beta_{n,Z} \cdot P_{ZLn}} \quad (6)$$

Formula 6 shows that, in the acidic region, both $\beta_{n,M}$ and P_{MLn} values contribute to the selectivity of the metal ion separation. However, when (at a moderate acidity) practically the only form of the metal in the aqueous phase is the neutral chelate ML_n, the $\beta_{n,M}$ values no more influence D_M and $SF_{A/Z}$ values, and the latter becomes dependent only on the ratio of the respective partition constants [7]. Separation processes are rarely carried out under such conditions, but these are indispensable in fundamental studies on liquid-liquid partition of metal complexes [8].

The magnitude of P_{MLn} depends on the difference in the thermodynamic activities of ML_n solute in both immiscible liquid phases, water and organic solvent, namely on the energies of solute-solvent interactions. The interactions in the organic phase of inert solvent may be discussed in terms of nonspecific van der Waals forces [3], while non-inner solvents, both bases (electron-pair donors) and acids (proton donors), solvate the ML_n molecules either in the inner [9] or outer [10] sphere of metal ion in the solute, respectively. Also other lipophilic coordinating species that alone poorly extract metal ions, in particular Lewis bases, synergistically enhance extraction of metal chelates. The role of synergist can also be played by nondissociated HL molecules that form self-adducts, $ML_n{\cdot}p(HL)$, with the chelate. With the neutral synergist B in the extraction system, the third step of the partition process must be distinguished:

(3) **Adduct formation** in the organic phase:

$$ML_{n,org} + pB_{org} \xleftrightarrow{\beta_{as,p}} ML_n{\cdot}pB_{org} \tag{7}$$

where the equilibrium constant (stability constant of the adduct) is given by

$$\beta_{as,p} = \frac{[ML_nB_p]_{org}}{[ML_n]_{org} \cdot [B]_{org}^{p}} \tag{8}$$

The effect of solvation on the separation selectivity depends on numerous factors, as discussed elsewhere [11].

For the analysis of solute-solvent interactions in the aqueous phase, two different regions may be distinguished in each ML_n molecule: hydrophilic center and hydrophobic periphery (organic ligands). The interactions in each region can be examined separately, though their contributions to the ML_n properties are not additive [12]. The aqueous-phase interactions that affect partition of neutral metal complexes are (i) water structuring around nonpolar hydrocarbon regions of the solute (hydrophobic hydration); (ii) coordination of water molecule(s) to the central metal ion in coordinatively unsaturated chelates (inner-sphere hydration); and (iii) hydrogen bonding of water molecule(s) to ligands in the chelate molecule (outer-sphere hydration).

HYDROPHOBIC HYDRATION

Hydrophobicity of metal complexes with organic ligands promotes their transfer from the aqueous to the organic phase. Structuring of liquid water around hydrophobic solutes is accompanied by negative entropy and positive free energy changes, the magnitude of which depends on the volume or rather on the hydrophobic surface of the solute molecule [13,14]. Another approach compares the work in both liquid phases required to form cavities able to include the solute molecule [15]. Both approaches predict a negative free energy change for removing hydrophobic solutes from water, which means their spontaneous transfer to organic solvents (high P_{MLn} values). However, hydrophobic hydration alone is of little interest for the task of separation of similar metal ions of the same valency, because it generates similar changes in Gibbs free energy of partition of isostructural metal chelates, so it does not differentiate the ions.

Hydrophobic hydration increases the thermodynamic activity of solutes in liquid water, which promotes their transfer to the organic phase. In contrast, specific hydration

of metal complexes decreases their activity in the aqueous phase. The differences in partition constants of neutral chelates of metal ions of the same charge, with the same number of the same ligands, extracted into inert organic solvents, are almost entirely due to the differences in Gibbs free energy of their dehydration in the inner and outer spheres accompanying transfer of their molecules from the aqueous to the organic phase [5,7].

INNER-SPHERE HYDRATION (AND ADDUCT FORMATION)

Hydrophilicity of coordinatively unsaturated metal complexes stems mainly from coordination of water molecules to the central metal ion—the inner-sphere hydration of the complexes [9,16]. Hydration energy depends on properties of both ion and ligand. Let us consider, for example, neutral trisacetylacetonate chelates of Ln(III) ions, from La^{3+} to Lu^{3+}. The smaller the ion within the series is, the more stable is its $Ln(acac)_3$ complex and the higher is the $P_{Ln(acac)3}$ value [17]. This can be attributed to decreasing inner-sphere hydration of the complexes across the Ln series, that is, lower energy to dehydrate the complex upon transfer from water to the organic phase. This conclusion may appear surprising in the light of increasing hydration energy across the series of Ln^{3+} ions [18], but it may be understood in terms of (i) gradual decrease in the coordination number (CN) of Ln^{3+} ions due to lanthanide contraction (geometrical reason); (ii) the competition for the Ln^{3+} ion between acetylacetonate (strongly bonded) and water (less strongly bonded); and (iii) the influence of the bond strength of the chelating ligands on the bond strength of water molecules. The stronger the former is (which takes place across the Ln series), the weaker is the latter. The last relation has been confirmed on the example of zinc(II) β-diketonates (below). However, dehydration of coordinatively unsaturated metal complexes is incomplete. Each molecule of a Ln chelate extracted to the organic phase retains two or three water molecules in the inner sphere of the Ln(III) ion in the chelate [4]; thus, in spite of the name, the outer-sphere water molecules are released.

Albinsson reported formation of self-adducts (solvates) $Ln(acac)_3(Hacac)$ in benzene solution at higher Hacac concentrations. The smaller the Ln^{3+} ion becomes, the lower the solvation constant becomes, just as for inner-sphere hydration [17], but the inner-sphere solvation and inner-sphere hydration affect extraction of the complexes to the opposite directions. The parallelism between the degree of inner-sphere hydration and solvation of $Ln(acac)_3$ chelates, observed across the Ln series, makes the large effects exerted on the P_{LnL3} and SF values by decreasing inner-sphere hydration of LnL_3 molecules partly compensated by a similar decrease in their solvation. This compensation decreases the selectivity of Ln(III) separation, moreso with higher Hacac concentration [7]. In general, an increase in the concentration of a synergist decreases the selectivity of separation of metal ions extracted in the form of coordinatively unsaturated chelates by reducing their differentiation due to hydration. For example, in the system 10^{-2} M tropolone in toluene and water at pH 5, $SF_{Sc/Y} = P_{ScT3}/P_{YT3} = 190$ [19], while the values calculated for the same system containing TOPO in the concentrations of 10^{-4}, 10^{-3}, and 10^{-2} M drop to 50, 30, and 10.4, respectively [7].

The author's studies on liquid-liquid partition of Zn(II) chelates with ligands of the homologous series of acetylacetone illustrate the effect of strength of the metal-ligand bond on the inner-sphere hydration of coordinatively unsaturated metal complexes [20].

Minute differences in basicity of the ligands cause unusually high changes in partition constants of their chelates. The average difference of Gibbs free energy of partitioning of the homologous zinc alkanedionates, related to one CH_2 group in the ligand (–4.55 kJ/mol), is significantly greater than the value for the analogous beryllium chelates (–3.33 kJ/mol [8,21], typical for the effect of hydrophobic hydration). This difference has been explained in terms of increasing strength of Zn-O bonds and a gradual decrease in CN of Zn(II) ion in the chelates with increasing ligand basicity, accompanied by a decrease in the inner-sphere hydration of the chelates, and a decrease in the synergistic effect in their extraction with trioctylphosphine oxide (TOPO) across the ligand series [20]. Sekine and Ihara reported a similar correlation between the basicity of other β-diketones, stability of their zinc chelates and stability of the respective TOPO adducts [22].

Further dramatic decrease in the coordination number of the central metal ion was observed in some zinc chelates as a result of substitution of sulphur for oxygen donor atoms in the ligands. The sulphur-containing chelates exhibit practically no synergism in extraction, contrary to analogous coordinatively unsaturated zinc chelates with oxygen-containing ligands [20,23]. The monothioacetylacetonate complex, $Zn(Sacac)_2$, is almost coordinatively saturated (CN ≈ 4) as concluded from its very weak synergism in extraction with TOPO, much higher partition constant, much lower enthalpy and entropy of partition, and lower salting-out coefficient as compared to those for its analogue $Zn(acac)_2$ of CN ≈ 5–6 [20]. Apart from a greater radius of sulphur than oxygen anion, which hinders the access of TOPO molecules to the zinc ion in $Zn(Sacac)_2$, the very strong Zn–S bonds further restrict the access of TOPO to Zn(II) ion, in contrast to much weaker Zn–O bonds. Although the differences in the thermodynamic functions of partition of both chelates are also due to weaker outer-sphere hydration of $Zn(Sacac)_2$, the effect of its weaker inner-sphere hydration prevails.

Another important factor in adduct formation is the geometry of ligand molecules; not only the magnitude of donor atoms (X) radii, as mentioned above, but also the bite size of chelating ligands, which determines the magnitude of bite angle (X_1–M–X_2). Small bite angles in five-membered chelate rings facilitate attaining higher CNs by the metal ion in the chelates [24], so synergistic effects in their extraction are greater than those for chelates of similar strength of M–L bonds but with six-membered rings. Such a picture was observed in extraction of scandium(III) acetylacetonate and tropolonate with TOPO [25]. DFT calculations explain this difference as due to a greater contribution (into the energy of adduct formation) from the deformation energy of ligand molecule with larger bite angle [19]. The DFT calculations have also shown that the energy of adduct formation (M(III) tropolonate–TOPO) depends not only on the radius of the central metal ion but also on the electronic structure of the ion, that is, on the availability of its empty *d* orbitals to form bonding molecular orbitals in the adduct. The bonding MOs are easily formed with the participation of unoccupied $(n - 1)d$ orbitals of M(III) ions of Group 3. On the contrary, virtual *nd* orbitals of the Group 13 ions have too high energy to participate in the bonding. Therefore, *p*-block metal chelates form adducts (CN 7) that are hypervalent compounds of the bond order less than one [19]. This explains why the TOPO adducts with tropolonates of Sc and Y are much stronger than those of In and Tl, the differences in the ionic radii being less important [19].

OUTER-SPHERE HYDRATION (AND SOLVATION)

The inner coordination sphere of central metal ions in coordinatively unsaturated metal chelates is only a part of the hydrophilic center of the chelates. The other part (or the whole hydrophilic center in coordinatively saturated metal chelates) consists of donor oxygen atoms (sp^2) in coordinated ligands. That is because each of the atoms retains one lone electron pair not engaged in bonding, and the atom behaves as proton acceptor in hydrogen bonds with solvent water molecules. This conclusion was based on the analysis of standard thermodynamic functions of partitioning of coordinatively saturated BeL_2 chelates, where HL belonged to the homologous series of acetylacetone [21]. The hydrogen bonding of water to coordinated ligands, called "outer-sphere hydration" [21], has been evidenced by ^{1}H-NMR [26] of coordinatively saturated $Be(acac)_2$ and $Co(acac)_3$ chelates in water-saturated benzene solutions. Outer-sphere hydration makes the metal chelates much more hydrophilic than hydrocarbons of similar molar volume [5,21]. However, if an oxygen atom in the ligand is replaced by much less electronegative sulphur, the coordinatively saturated chelate becomes much less hydrated and more lipophilic, as found for the pair $Co(acac)_3$/$Co(Sacac)_3$ [27].

Outer-sphere hydration differentiates coordinatively saturated chelates with respect to partition. Water/heptane partition constants of trisacetylacetonates of 3*d* M(III) ions (from Sc to Co) [28] and of tetrakisacetylacetonates of 4*d*-6*f* M(IV) ions (from Th to Zr) [29] decrease in each series with decreasing radius of the M^{n+} ion by more than two orders of magnitude. This relationship makes it possible to explain the recently observed [30] inversion of hydrophilic properties of analogous anionic complexes of Sc(III) and Lu(III) with two pendant-arms macrocyclic ligands: hexadentate 1,4,7-triazacyclononane-1,4,7-triacetic acid (H_3NOTA) and octadentate 1,4,7,10-tetraazacyclododecane-1,4,7,10-tetraacetic acid (H_4DOTA). Coordinatively unsaturated $Lu(NOTA)^-$ complex (CN_{Lu} = 8) appeared more hydrophilic than its coordinatively saturated (CN_{Sc} = 6) $Sc(NOTA)^-$ analog. The reverse order found for the coordinatively saturated $Sc(DOTA)^-$ and $Lu(DOTA)^-$ species is in line with the stronger outer-sphere hydration of the former, expected [28] due to its smaller central metal ion (r_{Sc} = 74 pm and r_{Lu} = 86 pm).

Outer-sphere hydration of $Zr(acac)_4$ is so strong that this chelate crystallizes in the form of decahydrate with short distances, typical for hydrogen bonding, between the oxygen atoms in the ligands and those of hydrating water molecules in the solid structure [31]. DFT calculations confirm formation of hydrogen-bonded hydrates of $Sc(acac)_3$ and $Co(acac)_3$ and properly evaluate enthalpies of water-heptane transfer of the chelates [32].

Also, organic solvents of acidic character (e.g., chloroform and chlorophenols) form hydrogen bonds with metal complexes, which enhance their extraction [10,33]. The most strongly solvated acetylacetonates are $Zr(acac)_4$ and $Hf(acac)_4$ [34], as is the case of their outer-sphere hydration [29]. This shows that the effect of outer-sphere hydration of metal chelates (decrease in P_{MLn}), extracted to the proton-donor solvents, is cancelled to a large extent by the opposite effect of hydrogen bonding in the organic phase, which on the other hand further decreases selectivity of separation of metal ions in such systems.

ACKONWLEDGMENTS

The author thanks his collaborators, co-authors of common papers, whose contributions made most of this research possible. The present work is partly based on the author's lecture "Thermodynamics of solvent extraction of metal ions: Fundamentals," presented at Training Session of the Fifth Half-yearly Meeting, the FP6 Integrated Project "European Research Programme for the Partitioning of Actinides," (EUROPART), ENEA, Frascati/Rome, June 26-29, 2006.

REFERENCES

1. J. Rydberg, C. Musikas, G. R. Choppin, and M. Cox, Eds., Solvent Extraction, Principles and Practices, 2nd ed., Marcel Dekker, New York, 2004.
2. G. R. Choppin, "Complexation of metal ions," in Solvent Extraction, Principles and Practices, 2nd ed., J. Rydberg, C. Musikas, G. R. Choppin and M. Cox, Eds., Marcel Dekker, New York, 2004; pp. 81-107.
3. S. Siekierski, "The complex formation-partition and partition-association models of solvent extraction of ions," *J. Radioanal. Chem.*, **31**, 335-361 (1976).
4. I. Matsubayashi, E. Ishiwata, T. Shionoya, and Y. Hasegawa, "Synergistic extraction of lanthanoids with 2-thenoyltrifluoroacetone and benzoic acid," *Talanta*, **63**, 625-633 (2004).
5. J. Narbutt, "Acetylacetone and monothioacetylacetone as model extractants of metal ions. The influence of chelate hydration on partition equilibria," *J. Radioanal. Nucl. Chem.*, **163**, 59-67 (1992).
6. R. A. Sachleben and B. A. Moyer, "Ligand design for small cations: the Li^+/14-crown-4 system," in Metal Ion Separation and Preconcentration: Progress and Opportunities, A. H. Bond, M. L. Dietz, and R. D. Rogers, Eds., ACS Symposium Series 716, American Chemical Society, Washington DC, 1999; pp. 114-144.
7. J. Narbutt and M. Czerwiński, "Computational chemistry in modeling solvent extraction of metal ions," in Solvent Extraction, Principles and Practices, 2nd ed., J. Rydberg, C. Musikas, G. R. Choppin and M. Cox, Eds., Marcel Dekker, New York, 2004; pp. 679-714.
8. J. Narbutt, "Hydration of metal β-diketonates and its influence on partition equilibria in solvent extraction," (in Polish), Report INCT-2119/V, Warszawa, 1991.
9. I. P. Alimarin and Yu. A. Zolotov, "The influence of the nature of the organic solvent on the extraction of chelate compounds," *Talanta*, **9**, 891-899 (1962).
10. J. Hala, "Some aspects of synergic extractions with chelating extractants," *J. Radioanal. Chem.*, **51**, 15-25 (1979).
11. J. Narbutt, "Hydration and solvation of metal complexes in solvent extraction systems. Selectivity of metal ions separations," Proc. DAE-BRNS Symposium on Emerging Trends in Separation Science and Technology, SESTEC-2008, New Delhi, India, March 12-14, 2008, in press.
12. E. Gniazdowska and J. Narbutt, "Thermodynamics of liquid-liquid partition and hydration of aliphatic ethers," *Polish J. Chem.*, **76**, 111-116 (2002).
13. G. Nemethy and H. A. Scheraga, "Structure of water and hydrophobic bonding in proteins. II. A model for the thermodynamic properties of aqueous solutions of hydrocarbons," *J. Chem. Phys.*, **36**, 3401-3417 (1962).
14. B. Madan and K. Sharp, "Molecular origin of hydration heat capacity changes of hydrophobic solutes: perturbation of water structure around alkanes," J. *Phys. Chem. B*, **101**, 11237-11242 (1997).

15. H. Reiss, H. L. Frisch, and J. L. Lebowitz, "Statistical mechanics of rigid spheres," *J. Chem. Phys*., **31**, 369-380 (1959).
16. H. Irving and D. N. Edgington, "Synergistic effects in the solvent extraction of the actinides – I. Uranium(VI)," *J. Inorg. Nucl. Chem*., **15**, 158-170 (1960).
17. Y. Albinsson, "Solvent extraction studies of lanthanide acetylacetonates. Complexes formed by Tb, Ho, Tm and Lu," *Acta Chem. Scand*., **43**, 919 (1989).
18. Y. Marcus, Ion Properties, Marcel Dekker, New York, 1997.
19. J. Narbutt, M. Czerwiński, and J. Krejzler, "Seven-coordinate d^0 and d^{10} ions. Computational and experimental studies on tris(tropolonato)metal(III) - TOPO adducts," *Eur. J. Inorg. Chem*., 3187-3198 (2001).
20. J. Narbutt, "Liquid-liquid partition of zinc alkanedionates and zinc monothioacetylacetonate - the coordination number of zinc," *Polish J. Chem*., **67**, 293-303 (1993).
21. J. Narbutt, "Liquid-liquid partition and aqueous phase hydration of beryllium β-diketonates," *J. Inorg. Nucl. Chem*., **43**, 3343-3349 (1981).
22. T. Sekine and N. Ihara, "Studies of the liquid-liquid partition systems. VIII.Stabilities and extractabilities of copper(II) and zinc(II) complexes with acetylacetone, trifluoroacetylacetone and hexafluoroacetylacetone," *Bull. Chem. Soc. Jpn.*, **44**, 2942-2950 (1971).
23. Yu. A. Zolotov, O. M. Petrukhin, and L. G. Gavrilova, "Synergistic effects in the solvent extraction of chelate compounds," *J. Inorg. Nucl. Chem*., **32**, 1679-1688 (1970).
24. R. D. Hancock and A. E. Martell, "Ligand design for selective complexation of metal ions in aqueous solutions," *Chem. Rev*., **89**, 1875-1914 (1989).
25. J. Narbutt and J. Krejzler, "High coordination numbers of metal ions in chelate complexes. Molecular adducts of scandium tris-α-diketonates in solution," *Inorg. Chim. Acta*, **286**, 175-180 (1999).
26. P. Moore and J. Narbutt, "Proton nuclear magnetic resonance and infra-red studies of the outer sphere hydration of pentane-2,4-dionato metal complexes in benzene solution," *J. Solution Chem*., **20**, 1227-1235 (1991).
27. J. Narbutt, "Liquid-liquid partition and hydration of cobalt(III) acetylacetonate and cobalt(III) monothioacetylacetonate," *J. Phys. Chem*., **95**, 3432-3435 (1991).
28. J. Narbutt, B. Bartos, and S. Siekierski, "Effect of outer-sphere hydration on liquid-liquid partition of tris-β-diketonates of 3d metal ions," *Solvent Extr. Ion Exch*., **12**, 1001-1011 (1994).
29. J. Narbutt and L. Fuks, "Outer-sphere hydration - a factor differentiating tetrakis(acetylacetonato)actinides(IV) in liquid-liquid partition systems," *Radiochim. Acta*, **78**, 27-31 (1997).
30. A. Majkowska and A. Bilewicz, to be published.
31. J. Narbutt, J. Lipkowski, P. Staszewski, and L. Fuks, "Hydration pattern in tetrakis(pentane-2,4-dionato)zirconium(IV) decahydrate," to be published.
32. M. Czerwiński and J. Narbutt, "Outer-sphere hydration and liquid-liquid partition of metal-(III) chelates – Density Functional calculations," *Eur. J. Inorg. Chem*., 555-562 (2005).
33. S. Katsuta, H. Imura, and N. Suzuki, "Association of tris(acetylacetonato)chromium(III) with chlorinated phenols in the liquid-liquid partition system," *Bull. Chem. Soc. Jpn.*, **64**, 2470-2474 (1991).
34. S. Katsuta and H. Yanagihara, "Extraction of zirconium(IV) and hafnium(IV) with acetylacetone in the presence of 3,5-dichlorophenol," *Solvent Extr. Ion Exch*., **15**, 577-589 (1997).

THERMODYNAMIC AND STRUCTURAL DESCRIPTION OF EUROPIUM COMPLEXATION IN 1-OCTANOL SOLUTION

M-C. Charbonnel,[1] T-H. Vu,[1] N. Boubals,[1] L. Couston,[1] and F. Arnaud[2]

[1]CEA Valrhô Marcoule, DEN/DRCP/SCPS/LCAM, BP 17171, 30207 Bagnols-sur-Cèze, France. [2]Laboratoire de Chimie Physique, IPHC, 25 rue Becquerel, 67087 Strasbourg, France. Corresponding author email address: marie-christine.charbonnel@cea.fr

ABSTRACT

Polydendate N-bearing ligands such as bistriazinylpyridines (BTPs) are interesting extractants for actinide(III)/lanthanide(III) separation. A description of europium complexation in 1-octanol solutions was undertaken to enhance the knowledge of the extraction mechanisms. Time-Resolved Laser-Induced Fluorescence (TRLIF) spectroscopy allows determination of the first solvation shell for europium(III) nitrate, chloride, and perchlorate with different amounts of water. Europium nitrate complexation by *i*Pr-BTP was then studied by TRLIF and microcalorimetry; the stability constant related to the formation of $Eu(BTP)_3^{3+}$ is similar by both techniques ($\log \beta_3 = 11.3 \pm 0.5$). The difference of solvation of the cation seems to have an influence on the thermodynamic properties related to the complexation with organic ligands.

INTRODUCTION

The separation of minor actinides such as americium is one of the options investigated to manage high-level liquid nuclear waste. The trivalent actinides must be cleanly separated from the trivalent lanthanide fission products. Among numerous polynitrogen polycyclic ligands tested to extract actinides selectively from acidic solutions [1], BTP molecules (2,6-bis(5,6-dialkyl-1,2,4-triazin-3-yl)-pyridine) were found interesting because Am(III)/Ln(III) separation could be performed from a highly acidic medium (0.5–2 M nitric acid) through a solvating mechanism [2].

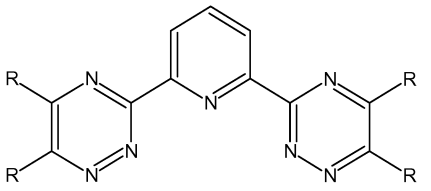

R = methyl — Ligand = Me-BTP
n-propyl — *n*Pr-BTP
iso-propyl — *i*Pr-BTP

Figure 1. 2,6-bis-(5,6-di-alkyl-1,2,4-triazin-3-yl)-pyridine.

In solution, different stoichiometries have been published for Ln(or An)-$(BTP)_x$ complexes depending on the experimental conditions; the major Eu(III) compounds have 1:1 (Me-BTP) or 1:1 and 1:2 (*n*Pr-BTP) stoichiometry in methanol-water mixtures [4,5]. With *i*Pr-BTP, the 1:3 complex has been identified in various media: methanol-water [4,5], octanol [6], and octanol-TPH [7], with some 1:2 in the last case.

The equilibria in the organic phase and the interactions at the molecular scale must be identified to enhance the knowledge of the extraction efficiency of such ligands. This study focuses on the complexation of Eu(III) nitrate by *i*Pr-BTP in *n*-octan-1-ol, a diluent selected for some process trials. After a spectroscopic investigation of Eu(III) salts (perchlorate, chloride, and nitrate) in (*n*-octan-1-ol)-water mixtures, complexation by iPr-BTP was investigated by TRLIF and microcalorimetry.

EXPERIMENTAL

Sample Preparation

Alcohol solutions were prepared by dissolving suitable salts in *n*-octan-1-ol (Merck Extrapur >99%); the simplified name 'octanol' will be used in the following discussion. The water content varied from 2×10^{-3} to 2 mol L^{-1}. Europium precursors based on three counterions were $Eu(NO_3)_3.6H_2O$ (Alfa Aesar, 99.99%), anhydrous $EuCl_3$ (Aldrich), and an aqueous solution of $Eu(ClO_4)_3$ (Aldrich 50 wt %). The water content was measured by Karl Fisher coulometry and Eu by ICP-AES.

The ligand *i*Pr-BTP was synthesized in our laboratory and dissolved in alcohol to obtain a 0.01 mol L^{-1} stock solution.

Time-Resolved Fluorescence Spectroscopy

All fluorescence measurements were performed at 298 K using a narrow-band Nd-Yag/OPO/Fx1 laser (Continuum, USA) as the excitation source. A wavelength of 526 nm ($^7F_0 \rightarrow {}^5D_1$ transition) was selected for excitation. Fluorescence was observed at right angles by an alignment of 9 Si/Si optical fibers illuminating the entrance slit of a flat field spectrometer (320i, Princeton Instruments, USA) equipped with a pulsed intensified CCD camera (Imax, 1024 × 256 pixels, Princeton Instruments, USA). The time delay and time gate for spectral fluorescence shape measurements were set to 100 µs and 40 µs, respectively. The lifetime measurement was performed from a sequence of 25 successive time-delayed spectra using suitable experimental parameters to scan as the fluorescence declined (normally the low-noise transition $^5D_0 \rightarrow {}^7F_2$ was selected).

Microcalorimetry

Microcalorimetric measurements were performed at 25 °C using an LKB-2277 Thermal Activity Monitor (TAM) microcalorimeter system from Thermometric. The cation in the octanol-water phase was introduced in the calorimeter using a 4 mL glass cell, and the ligand solution was added into the cell through fine gold tubing. The volume

of titrant was injected with a programmable motor-driven Thermometric Lund pump equipped with a 250 µL Hamilton syringe. The heat flows were detected by thermopiles. The results were presented as thermograms, which are plots of the measured power as a function of time. Related heat and stability constants were calculated with Digitam Software (Thermometric).

RESULTS AND DISCUSSION

Europium Perchlorate, Chloride, and Nitrate in Mixed Octanol-Water Solutions

The inner-sphere interactions, that is, the relative strength toward the cation by all the solutes in solution (mainly counter ions and water), must be identified to describe Eu(III) complexation in octanol phases. The macroscopic quantity of water in alcohol-based diluents is significant (for example $[H_2O]_{eq} = 3 \times 10^{-2}$ mol L^{-1} in commercial octanol and up to 2 mol L^{-1} after contact with an aqueous phase). Because of the strong interaction between lanthanides(III) and water, the presence of water molecules in the first shell must be considered, even for low macroscopic $[H_2O]$/[octanol] ratios. Counterions can also be considered as competitive ligands and to address shortcomings in existing data in octanol, a detailed spectroscopic investigation of europium salts in mixed water-octanol solutions was undertaken. This preliminary study gives the fluorescence spectra and related lifetimes of europium salts (nitrate, chloride, and perchlorate) in mixed water-octanol solutions without any organic ligand.

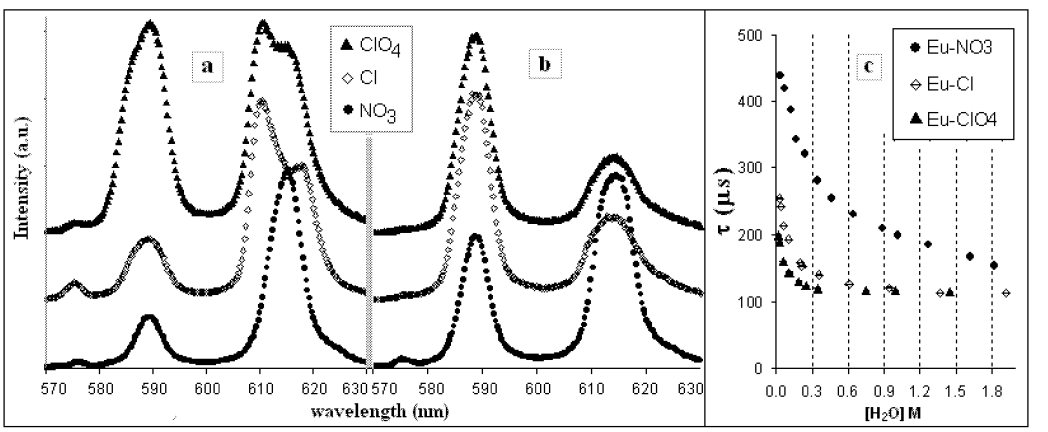

Figure 2. Fluorescence spectra of Eu(III) salts in mixed water-octanol solutions (water amount (a) 0.05 ± 0.01 mol L^{-1} and (b) 1.9 ± 0.01 mol L^{-1}) and lifetimes versus H_2O content (c).

Fluorescence spectra were recorded and the lifetimes of the related $^5D_0 \rightarrow {}^7F_2$ transition (616 nm) were measured for different europium concentrations ranging from 5×10^{-5} to 5×10^{-2} mol L^{-1}. The spectra of 10^{-3} mol L^{-1} europium are shown for two extreme water contents (0.05 mol L^{-1} and 1.9 mol L^{-1}).

Both spectral characteristics (mainly the I_{616}/I_{592} ratio, an indicator of changes in the ligand field due to the hypersensitive $^5D_0 \rightarrow {}^7F_2$ transition) and the lifetime

(measured from the luminescence decay curve and directly related to the number of water molecules in the inner sphere of europium) are useful to obtain information on the environment of the europium cation [7].

For a fixed Eu^{3+} concentration ($[X^-] = 3[Eu^{3+}]$, where X = ClO_4, Cl, or NO_3), we observe a significantly longer lifetime as the octanol/water molar ratio increases, as shown in Figure 2 for [Eu] = 10^{-3} mol L^{-1}. The ligands in the inner sphere are in rapid exchange, and the proposed stoichiometry (deduced from the ratio I_{616}/I_{592}, from the lifetime and the position of the transition at 597 nm) are averaged.

In europium perchlorate solutions, the counterion never enters the inner coordination sphere, as already described in aqueous or ethanol media [8]. In the range $[H_2O] > 0.3$ mol·L^{-1}, $\tau = 110 \pm 2$ µs, which is characteristic of aquo europium (cation surrounded by 8 or 9 water molecules). For lower water concentration, competition occurs in the inner sphere between alcohol and water molecules. The data related to the europium surrounded by 9 octanol molecules were estimated by extrapolating the k_{obs} (= $1/\tau$) = $f(H_2O)$ curve. For presumed $Eu(octanol)_9^{3+}$, $\tau = 215$ µs, and $I_{616}/I_{592} = 1.2$. The lifetime value is consistent with published values in ethanol and propan-1-ol [8]. The forbidden $^5D_0 \rightarrow {}^7F_0$ transition (579 nm) appears for the most alcohol-rich solutions, indicating a loss of symmetry around europium due to the presence of octanol molecules.

In europium chloride solutions, the lifetime is higher than in perchlorate solutions when the alcohol/water ratio > 30. The position of the $^5D_0 \rightarrow {}^7F_0$ transition (579,1nm) and EXAFS analysis indicate that one chloride ion is present in the inner sphere for low water concentrations (<1 mol L^{-1}); the competition between water and octanol is comparable to those described in perchlorate solutions when the water concentration is below 0.3 mol L^{-1}.

For the europium nitrate system, preliminary experiments with addition of large amount of nitrate ($[NO_3]/[Eu]$ up to 500) in a perchlorate solution lead to a decrease of k_{obs} and a shift of the $^5D_0 \rightarrow {}^7F_0$ transition towards 579 nm, related to $Eu(NO_3)_3$ [8,9]. Detailed analysis indicates the presence of nitrate ions in the inner sphere over the entire range of water content (from 10^{-3} to 2 mol L^{-1}), as mentioned for ethanol [8]. When the water content is below 0.3 mol L^{-1}, the europium is surrounded by three bidentate nitrate, octanol, and H_2O molecules. Then from 0.35 mol L^{-1} to 1.5 mol L^{-1}, octanol is absent, and nitrate is gradually replaced by water in the inner sphere, in accord with the position of the $^5D_0 \rightarrow {}^7F_0$ transition [9].

In conclusion, the fluorescence spectroscopic study in octanol-water phases indicates the average stoichiometry of complexes: $Eu(NO_3)_3(octanol)_2(H_2O)$ in 99% octanol (water content 2×10^{-3} mol·L^{-1}) and $Eu(NO_3)(H_2O)_7$ after equilibrium with aqueous phases, that is, for 2 mol L^{-1} water content.

Complexation with *i*Pr-BTP Molecule

Eu(III) nitrate complexation by *i*Pr-BTP in octanol was studied for [BTP]/[Eu(III)] ratios of 0 to 8 with a water concentration of 3×10^{-2} mol L^{-1}. The spectral evolution of the fluorescence spectra of Eu(III) resulting from $^5D_0 \rightarrow {}^7F_2$ and $^5D_0 \rightarrow {}^7F_1$ transitions in the presence of increasing BTP is shown in Figure 3a.

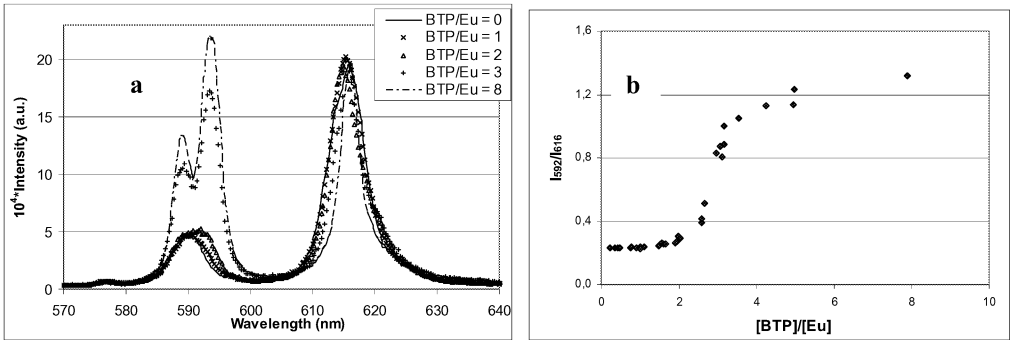

Figure 3. Fluorescence spectra of Eu(III) as a function of ligand-to-metal concentration ratios: (a) intensity between 570 and 640 nm; (b) $I_{^5D_0 \rightarrow {}^7F_1} / I_{^5D_0 \rightarrow {}^7F_2}$ ratio.

Some changes are observed: a small shift of the $^5D_0 \rightarrow {}^7F_2$ fluorescence peak (from 615 to 616.5 nm), a distinct splitting of the $^5D_0 \rightarrow {}^7F_1$ transition, similar to observations by Denecke in a TPH-*n*-octanol mixture [6], and also the disappearance of the $^5D_0 \rightarrow {}^7F_0$ transition for high [BTP]/[Eu] ratios, which is an indication of higher symmetry around europium. The fluorescence spectra for high BTP concentration are similar to Eu(*i*Pr-BTP)$_3$ obtained in methanol-water medium for [BTP]/[Eu] > 3 [4]. The high lifetime value (2500 µs) confirms the absence of water molecules in the inner sphere of europium. The analysis of both curves, I_{592}/I_{616} ratio and lifetime function of [BTP]/[Eu], allows the determination of the stability constant β_3 related to the equilibrium (1) found to be $\log \beta_3 = 11.3 \pm 0.5$.

$$Eu^{3+}_{solvated} + 3\ BTP \rightleftharpoons Eu(BTP)_3^{3+} \quad (1)$$

Complexation in octanol was also studied by microcalorimetry with a water content of 3×10^{-2} mol L^{-1}. Two models could account for the thermograms: the formation of a single EuL_3 or EuL_2 complex. However, the previous results obtained by TRLIF and ESI-MS analysis supported the formation of a EuL_3 complex. The stability constant ($\log \beta_{13}' = 11.2 \pm 0.3$) is consistent with the value calculated from the previous TRLIF study. This value is however lower than the published value obtained in methanol-water: $\log \beta_{13}' = 14.2 \pm 0.6$ [4]. In the same time, the enthalpy variation obtained for Eu(III) complexation by *i*Pr-BTP in octanol is significant ($\Delta H_{comp} = -90 \pm 3$ kJ mol^{-1}) compared with the data obtained in methanol-water ($\Delta H_{comp} = -29 \pm 3$ kJ·mol^{-1}) [4]. The important gap in thermodynamic properties could be due to the amount of water, which leads to a difference in the solvation of 'free' europium: $Eu(NO_3)_3(octanol)_x(H_2O)_y$ and $Eu(H_2O)_9$, respectively. This study points out the importance of solvation by water on complexation studies in diluents like octanol.

CONCLUSIONS

It was shown in this detailed study of the fluorescence properties of europium nitrate, chloride, and perchlorate in octanol-water solutions a strong dependency of europium solvation on the macroscopic water quantity. For Eu(III)/nitrate system and

$[H_2O] < 0.3$ mol L^{-1}, three nitrate and octanol molecules are present in the inner sphere of europium. The complexation of europium nitrate by *i*Pr-BTP was investigated by TRLIF and the microcalorimetry approach, and comparable stability constants related to the formation of $Eu(BTP)_3^{3+}$ were obtained. However, the significant differences obtained for thermodynamic data between octanol and methanol-water media seem to provide from the inner sphere composition of the cation. This study points out the importance of water amount in such polar diluents, and investigations are in progress in our laboratory to explore this area.

REFERENCES

1. C. Madic, M. J. Hudson, J. O. Liljenzin, J. P. Glatz, R. Nannicini, A. Facchini, Z. Kolarik, and R. Odoj, "New Partitioning Techniques for Minor Actinides," *European Report EUR.,* **19,** 149 (2000).
2. Z. Kolarik, U. Müllich, and F. Gassner, "Extraction of Am(III) and Eu(III) nitrates by 2,6-di-(5,6-dipropyl-1,2,4-triazin-3-yl)pyridines," *Solvent Extr. Ion Exch.*, **17**(5), 1155-1170 (1999).
3. S. Colette, B. Amekraz, C. Madic, L. Berthon, G. Cote, and C. Moulin, "Use of Electrospray Mass Spectrometry (ESI-MS) for the Study of Europium(III) Complexation with Bis(dialkyltriazinyl)pyridines and its Implications in the Design of New Extracting Agents," *Inorg. Chem.*, **41**(26), 7031-7041 (2002).
4. S. Colette, S. B. Amekraz, C. Madic, L. Berthon, G. Cote, and C. Moulin, "Europium(III) Interaction with a Polyaza-Aromatic Extractant Studied by Time-Resolved laser Induced Luminescence: A Thermodynamical Approach," *Inorg. Chem*, **43**(21), 6745-6751 (2004).
5. M-C. Charbonnel, N. Boubals, S. Giroux, and D. Guillaumont, "Thermodynamic properties accounting for differences in affinity and selectivity of BTPs toward Eu(III) and Am(III) extraction," Proceedings of ISEC'05 (International Solvent Extraction Conference), Beijing, The People's Republic of China, 19-23 September 2005; pp. 31-38.
6. M. A. Denecke, A. Rossberg, P. J. Panak, M. Weigl, B. Schimmelpfennig, and A. Geist, "Characterization and Comparison of Cm(III) and Eu(III) Complexes with 2,6-Di(5,6-dipropyl-1,2,4-triazin-3-yl)pyridine using EXAFS, TRFLS and Quantum-Chemical Methods," *Inorg. Chem.*, **44**(23), 8418-8425 (2005).
7. S. Lis, "Luminescence spectroscopy of lanthanides(III) ions in solution," *J. Alloys Compd.*, **341**, 45-50 (2002)
8. M. J. Lochhead, P. R. Wamsley, and K. L. Bray, "Luminescence spectroscopy of europium(III) Nitrate, Chloride, and Perchlorate in mixed Ethanol-water Solutions," *Inorg. Chem.*, **33**, 2000-2003 (1994).
9. M. Albin and W.D. Horrocks, "Europium(III) luminescence excitation spectroscopy. Quantitative correlation between the total charge on the ligands and the $^5D_0 \rightarrow {}^7F_0$ transition frequency in europium(III) complexes," *Inorg. Chem.*, **24**, 895-900 (1985).

POLYAMINES AS OXOANION AND CHLOROCOMPLEX RECEPTORS

M. G. Sánchez-Loredo,[1,2] M. Wenzel,[2] K. Gloe,[2] K. Gloe,[2] M. Grote,[3] H.-J. Holdt,[4] and A. Kelling[4]

[1]Institute of Metallurgy, Universidad Autónoma de San Luis Potosí, Sierra Leona 550, 78210 San Luis Potosí, Mexico. [2]Department of Chemistry, TU Dresden.
[3]Inorganic and Analytic Chemistry Department, University Paderborn.
[4]Institute of Chemistry, University Potsdam, Germany.
Corresponding author email address: msanchez@uaslp.mx

ABSTRACT

Polyamines based on the tris(2-aminoethyl)amine (Tren) platform are useful complexing agents for cations or anions depending on the pH of the solution. The binding and extraction behavior of the polyamines is a complex function of their structural features, protonation degree, and lipophilic properties. A series of different substituted Tren derivatives were synthesized, and their extractive properties towards several anions (oxoanions, chlorocomplexes) was investigated. Finally, the X-ray structure of an anionic Pd(II) complex with the protonated precursor Tren is presented.

INTRODUCTION

Anion binding is of considerable interest in several technical processes (platinum group metals separation and recovery from chloride media is a well-known example of the industrial application of anion hydrometallurgy), for environmental monitoring and clean up, as well as in health-related applications. Anions present some particular characteristics that have to be considered in order to synthesize adequate receptors [1]: they are large compared with metal ions; their geometries vary from spherical, triangular, tetrahedral, squared-planar, and octahedral to the more complex shapes of biologically relevant anions; they possess higher hydration energies in comparison with metal ions of similar charge density, and their distribution in two-phase systems normally follows the Hofmeister series. Finally, some of them have a limited pH range of existence.

The growing interest in the design of more selective and effective anion receptors has led to the synthesis and characterization of a number of extractants with open-chain, macrocyclic and three-dimensional scaffolds [2]. As anions are distinguished from other species by their negative charge, protonated polyamines and quaternary polyammonium salts are interesting receptors for them. Polyamine binding of cations takes place via coordinate bonds, but the interaction with anions occurs mainly through electrostatic and hydrogen bonding. The binding and structural behaviour of oxoanions and halide ions

with different types of polyamines was reported, showing the potential of these compounds for efficient and selective anion binding [3-6].

As part of our studies on synthesis of simple and easy-to-make tripodal, macrocyclic and macrobicyclic receptors for anion recognition, here we present some new results on the anion binding studies of receptors based on protonated derivatives of tris(2-aminoethyl)amine (Tren). Some of us undertook and already published the examination of the capabilities of tripodal, macrocyclic, and macrobicyclic polyamines as extractants for halides and oxoanions [7-9]. The phase transfer of iodide, perrhenate, and pertechnetate by amino cryptands and their open-chain counterparts, including structural aspects, were previously discussed. Solid-state structure of open-chain and macrocyclic polyammonium compounds with anions have shown such characteristic binding patterns based on multiple hydrogen bonds and edge to face C-H π interactions between aromatic substituents.

We report here some results of studies focused on both the extraction of oxoanions (chromate, vanadate) as well as chlorocomplexes of some platinum group metals (platinum, palladium, rhodium, and ruthenium) with a selected number of polyamines. Most of the attempts to prepare solid-state structures of the protonated polyammonium compounds with anions failed; only the mixed compound of Tren with tetrachloropalladate and chloride ions crystallized in X-ray quality, and the structure is presented. Some aspects of the complex formed are discussed.

EXPERIMENTAL

The chemicals used were A.R. grade. The metallic salts used were $PdCl_2$, K_2PtCl_4, $RuCl_3{\cdot}xH_2O$ (38.52% Ru(III)), $RhCl_3{\cdot}xH_2O$ (38.8% Rh(III)), NH_4VO_3, and Na_2CrO_4. The ligands were prepared as described elsewhere [8,10] using the Schiff base route *via* reaction of Tren with the appropriate aldehyde and subsequent borohydride reduction. We attempted to obtain X-ray quality crystals of the anion-polyamine complexes by slow diffusion of ether into a methanolic solution of the components according to the procedure reported by Antonioli et al. [7]. In one case, an X-ray quality crystal of the $PdCl_4^{2-}$ anion with Tren was obtained from MeOH/DMSO solutions of the components. A 0.05 mL volumeof concentrated HCl was added to the mixture in order to achieve the protonation of Tren. The X-ray crystal structure analysis was performed on an image-plate diffractometer (IPDS-2, STOE) using graphite-monochromated Mo-Kα radiation.

Extraction studies were performed at 25 ± 1 ºC in 2 mL microcentrifuge tubes with mechanical shaking. The ligands were dissolved in chloroform. The phase ratio $V_{(w)}$:$V_{(org)}$ was 1:1 (0.8 mL each); the shaking time was 30 min. (for the platinum group metals 24 h). All samples were centrifuged after extraction. The chromate concentration in both phases was determined radiometrically using γ-radiation of ^{51}Cr by means of a NaI(Tl) scintillation counter (Cobra II/Canberra-Packard). The pH of aqueous solution (except for the noble metal extraction experiments) was adjusted using MES/NaOH buffer solutions. The platinum group metals (PGM) and vanadium concentrations were determined by ICP spectrophotometry at the Forschungszentrum Rossendorf (ICP-MS ELAN 9000/Perkin Elmer spectrometer).

RESULTS AND DISCUSSION

Extraction of Chlorocomplexes of the PGMs

The results of the extraction of noble metal anions by tripodal Tren derivatives substituted with different aromatic moieties are shown in Figure 1. The extractabilities of the rhodium and ruthenium species are generally low for all ligands; in some cases, the formation of insoluble species was observed (experiments with ligand BPT). On the contrary, extraction rates of the palladium and platinum chlorocomplexes are significantly higher in most cases. The highest extractabilities are observed for the polyamine B7T: Pd(II) 98% (0.1 M NaCl) and 89% (0.1 M HCl) as well as Pt(II) 95% (0.1 M NaCl) and 92% (0.1 M HCl). As expected, metal extraction by the lipophilic quaternary ammonium compound B7T is both high and almost independent of acidity of the aqueous solution. B7T already has shown good extraction rates also for iodide (86% at pH 5.5) and some oxoanions [9,11]. The differences in the PGM extractabilities are clearly caused by the nature of the chlorometallate species. Palladium(II) and platinum(II) form pure chlorocomplexes, whereas the trivalent metals form mixtures of chloroaqua species depending on chloride concentration [12]. Under the experimental conditions used (0.1 M Cl^-), the predominant species in solution should be $[Rh(H_2O)Cl_5]^{2-}$, $[Ru(H_2O)Cl_5]^{2-}$, $PdCl_4^{2-}$ co-existing with $PdCl_3^-$, and $PtCl_4^{2-}$. Palladium(II) and platinum(II) chlorocomplexes are easily and quantitative extracted by tertiary and quaternary amines, whereas $[Rh(H_2O)Cl_5]^{2-}$ is extracted partially by such extractants [13].

There are two important factors influencing anion extraction behavior with polyamines: the lipophilicity and the protonation of the extractants [9]. Normally, the more lipophilic compounds extract anions better; this is also confirmed by comparable results obtained for the hydrophobic ligand B7T compared to B3T. B7T combines hydrophobicity and a positive charge over the whole pH range.

In order to obtain some information about the specific binding pattern and extraction behavior of the polyamines studied, it is useful to know their typical structural features in the crystalline state, although caution needs to be exercised when using solid-state structures as aid in the interpretation of the behaviour in solution. Crystal structures of anion complexes of protonated Tren with halides, sulfate, phosphate, perchlorate, molybdate and hexachlorocuprate have been reported [6,14-16]. In contrast, only a few structures of the tribenzylated derivative B3T have been described so far [15]. Attempts to obtain appropriated single crystals for X-ray diffraction of the related anionic-polyammonium complexes failed; only one X-ray quality crystal of the palladium(II) tetrachlorocomplex with the fully protonated Tren (present as impurity in ligand B7T) was obtained from MeOH/DMSO/chloride solutions of the components. As far as we know, this is the first time the crystal structure of such a polyamine anionic noble metal complex is reported. Its structural details are shown in Figure 2. The mixed tetrachloropalladate/chloride complex of the composition $[2(TrenH_4)^{4+}\cdot 2(PdCl_4)^{2-}\cdot 4(Cl)^-\cdot H_2O]$ forms a hydrogen-bonded network with moderate hydrogen bonds with N-H…O and N-H…Cl distances between 2.05 and 2.96 Å. The resulting spread orientation of the tripodal arms is caused by the electrostatic repulsion of the four positively charged amine

nitrogens and obviously does not allow chelation of the anions. Some structures of this type, with Tren and B3T, have been already reported [6,7,16]. A water molecule is also incorporated in the assembly. In a large number of anion complex structures with polyamines, water molecules play an important stabilizing role [6,9,14,17-19].

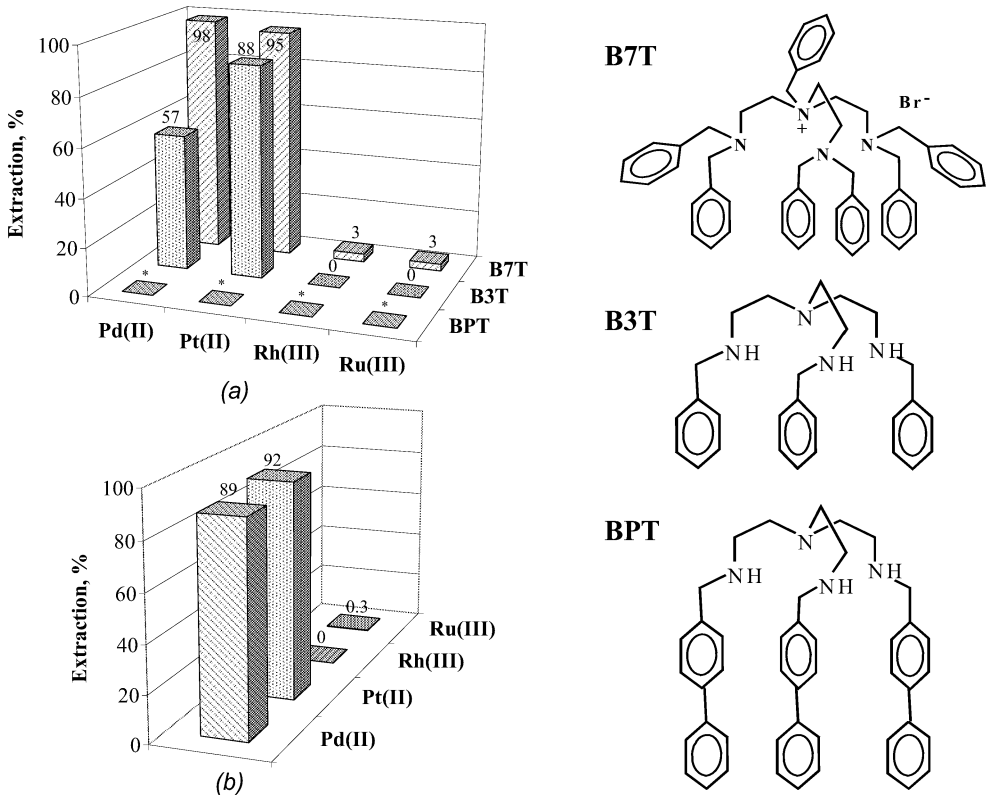

Figure 1. Noble metal extraction (%) by protonated Tren derivatives. (a) $[M^{n+}] = 1 \times 10^{-4}$ M in 0.1 M NaCl; [ligand] = 1×10^{-3} M in $CHCl_3$; O/A = 1:1, 24 h. (b) $[M^{n+}] = 1 \times 10^{-4}$ M in 0.1 M HCl; [B7T] = 1×10^{-3} M in $CHCl_3$; O/A= 1:1, 24 h. * Precipitate formed during extraction.

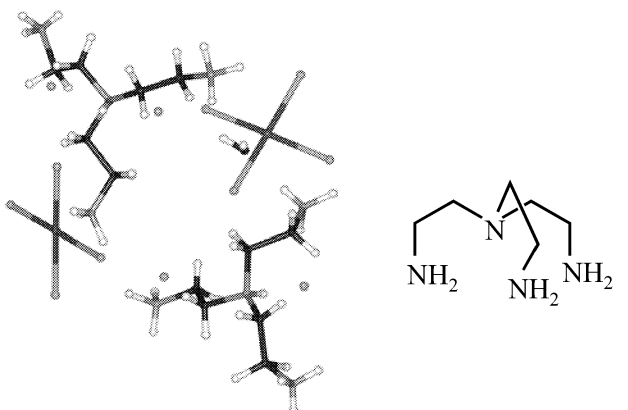

Figure 2. Molecular structure of the complex $[2(\mathbf{Tren}H_4)^{4+}\cdot 2(PdCl_4)^{2-}\cdot 4(Cl)^{-}\cdot H_2O]$.

Solvent Extraction Studies of Oxoanions with Polyamines

The tripodal substituted Tren derivatives have been investigated as extractants for chromate and vanadate ions, using the extraction system MX ($X^- = VO_3^-$ and CrO_4^{2-})-buffer (pH 5.5)-H_2O/polyamine-$CHCl_3$. The results are shown in Figure 3. In general, the extraction of vanadate was high, whereas the extraction of chromate was lower (except for the extraction with the quaternary ammonium compound B7T). The favored extraction of the first likely reflects the greater lipophilicity of the vanadium species comparing to the chromate ions, which are strongly hydrated.

The highest chromate extraction was obtained for the polyamines BPT (46%) and the quaternary ammonium extractant B7T (63%). In comparison with B3T and B6T, this fact clearly reflects again the influence of the two important factors in extraction with this kind of extractant: lipophilicity of the system and protonation behaviour of the extractants. The more lipophilic B7T and BPT show enhanced extraction over B3T. The extractant BPT, with secondary amine groups, shows better extraction as B6T, where protonation of the tertiary amine nitrogens is more difficult. The tribenzylated B3T gives only small extractabilities, which is obviously caused by the high hydrophilicity of the polyamine.

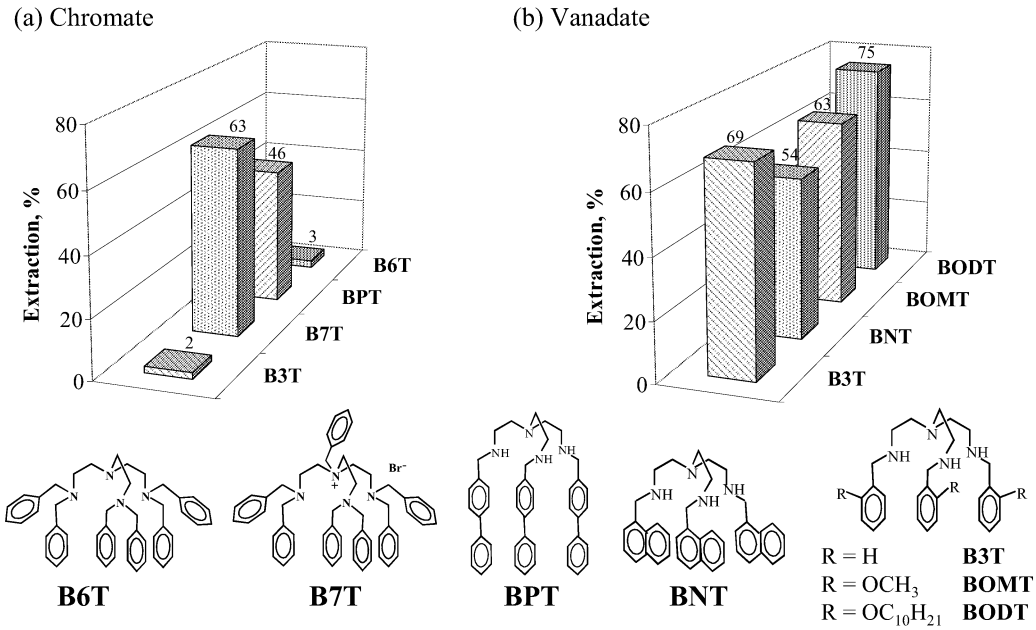

Figure 3. (a) Chromate and (b) vanadate extraction (%) by protonated tripodal polyamines. $[M^{n+}] = 1 \times 10^{-4}$ M; [ligand] = 1×10^{-3} M in $CHCl_3$; pH = 5.5 (MES/NaOH buffer), 30 min.

The role of lipophilicity is also evident when we compare the extractability of vanadate using the methoxy-substituted Tren derivative BOMT (64%) and the derivative BODT (75%) with a longer alkyl chain.

As already reported by the authors, from the structural studies could be assumed that water is an important structure-determining factor in this extraction systems. A

significant amount of water (particularly in the chromate extraction) has been detected by Karl Fischer titration of the organic phase after extraction [20].

CONCLUSIONS

Several tripodal protonated Tren derivatives substituted with aromatic moieties have been investigated as extractants for noble metal chlorocomplexes, as well as for two different oxoanions. As expected, the highest anion extraction has been achieved with the more lipophilic Tren derivatives. Although the preparation of X-ray quality crystals using these systems was not possible, the structure of the tetrachloropalladate ion with Tren helps to confirm results already reported about the important influence of the water content on the structure of this kind of complexes.

ACKNOWLEDGMENTS

We thank the Deutsche Forschungsgemeinschaft and the Deutscher Akademischer Austauschdienst for support of the research work and the collaboration. We acknowledge A. Heine, K. Schreppel, Dresden for synthesis of the ligands and U. Schäfer, Rossendorf for the metal content determination.

REFERENCES

1. E. García-España, P. Díaz, J. M. Llinares, and A. Bianchi, *Coord. Chem. Rev.,* **250**, 2952-2986 (2006).
2. a) K. Gloe, H. Stephan, and M. Grotjahn, *Chem. Eng. Technol.,* **26**, 1107-1117 (2003); b) K. Gloe, B. Antonioli, K. Gloe, L.,F. Lindoy, in Encyclopedia of Supramolecular Chemistry, J.,L. Atwood, J.,W. Steed, Eds., Marcel Dekker, New York, online-Version (2006).
3. A. Hossain, S. O. Kang, and K. Bowman-James, Macrocyclic Chemistry- Current Trends and Future Perspectives, K. Gloe, Ed., Springer, Heidelberg, 173-188 (2005).
4. J. Nelson, V. McKee, and R. M. Town in Ref. [3], 189-201.
5. C. A. Ilioudis, D. A. Tocher, and J. W. Steed, *J. Am. Chem. Soc.*, **126**, 12395-12402 (2004).
6. C. A. Ilioudis, K. S. B. Hancock, D. G. Georganopoulou, and J.W. Steed, *New J. Chem.,* **24**, 787-798 (2000).
7. B. Antonioli, K. Gloe, K. Gloe, G. Goretzki, M. Grotjahn, H. Hesske, M. Langer, L. F. Lindoy, A. M. Mills, and T. Soehnel, *Z. Anorg. Allg. Chem.,* **630**, 998-1006 (2004).
8. D. Farrell, K. Gloe, K. Gloe, G. Goretzki, V. McKee, J. Nelson, M. Nieuwenhuyzen, I. Pal, H. Stephan, R. M. Town, and K. Wichmann, *Dalton Trans.*, 1961-1968 (2003).
9. K. Wichmann, T. Soehnel, B. Antonioli, H. Hesske, M. Langer, M. Wenzel, K. Gloe, K. Gloe, J. R. Price, and L. F. Lindoy, International Solvent Extraction Conference 2005, China Academic Journal (CD) Electronic Publishing House, Beijing, China (2005).
10. A. A. Naiini, W. M. P. B. Menge, and J. G. Verkade, *Inorg. Chem.,* **30**, 5009-5012 (1991).
11. M. Wenzel and K. Gloe, unpublished results.
12. M. Ruiz-Planas, Development of techniques based on natural polymers for the recovery of precious metals, Ph.D. Thesis, Universidad Politécnica de Cataluña (2002).

13. G. Levitin and G. Schmuckler, *React. Funct. Polym.,* **54**, 149-154 (2003).
14. C. A. Ilioudis, D. G. Georganopoulou, and J. W. Steed, *Cryst. Eng. Comm.,* **4**, 26-36 (2002).
15. K. Wichmann, B. Antonioli, T. Söhnel, M. Wenzel, K. Gloe, K. Gloe, J. R. Price, L. F. Lindoy, A. J. Blake, and M. Schröder, *Coord. Chem. Rev.,* **250**, 2987-3003 (2006).
16. M. Wei, R. D. Willett, and K. W. Hipps, *Inorg. Chem.,* **35**, 5300-5303 (1996).
17. V. McKee, J. Nelson, and R. M. Town, *Chem. Soc. Rev.,* **32**, 309-325 (2003).
18. C. A. Ilioudis and J. W. Steed, *J. Supramol. Chem.,* **1**, 165-187 (2001).
19. J. M. Llindares, D. Powell, and K. Bowman-James, *Coord. Chem. Rev.,* **24**0, 57-75 (2003).
20. M. Wenzel, M. G. Sánchez-Loredo, K. Gloe, and K. Gloe, unpublished results.

COMPARISON OF CLOUD POINT AND SOLVENT EXTRACTION OF Gd(III) FROM AQUEOUS SOLUTIONS

Alain Favre-Réguillon,[1] Denis Murat,[2] Alexandre Chagnes,[3] Gérard Cote,[3] Jacques Foos,[2] and Micheline Draye[4*]

[1]Conservatoire National des Arts et Métiers, Laboratoire de Chimie Organique (UMR 7084), 2 rue Conté, 75003 Paris, France. [2]Conservatoire National des Arts et Métiers, Laboratoire des Sciences Nucléaires, 2 rue Conté, 75003 Paris, France. [3]Ecole Nationale Supérieure de Chimie de Paris - ENSCP Université Pierre et Marie Curie – Paris6 - Laboratoire d'Electrochimie et de Chimie Analytique - UMR7575 CNRS-ENSCP-Paris6 ENSCP, 11 Rue Pierre et Marie Curie, 75231 Paris Cedex 05, France. [4]Université de Savoie, Polytech'Savoie, Laboratoire de Chimie Moléculaire et Environnement, 73376 Le Bourget du Lac Cedex, France.
Corresponding authors email address: favrereg@cnam.fr and mdray@univ-savoie.fr

ABSTRACT

Gadolinium ion can be extracted from aqueous solution using Cloud Point Extraction (CPE) with 8-hydroxyquinoline (HQ) as chelating agent. The structure of the extracted gadolinium-HQ complex was determined in the micelle of Triton X-114 using log-log analysis. A ratio of HQ to Gd^{3+} of 3:1 was found. CPE was compared to classical liquid-liquid extraction with chloroform as solvent. It was stated that in both cases a $Gd(HQ)_3$ complex was extracted. The parameters of the extraction process in both media were determined and compared. A quantitative extraction of Gd^{3+} at pH 5.5 was obtained using a HQ/Gd^{3+} ratio of 10, although a HQ/Gd^{3+} ratio of 400 was necessary for liquid/liquid extraction using chloroform as solvent, illustrating then an increase of the mass action of extractants when using CPE instead of liquid/liquid extraction.

INTRODUCTION

The rare earth (RE) elements are widely utilized in metallurgy, glass, and ceramics and broadly used as high performance catalysts, as well as for high efficient production of permanent magnets and tri-color phosphors. The extraction behavior of rare earths has been studied since the 1950s, and the commercial production of these elements commonly employs solvent-extraction processes. There are several reports on the separation of RE elements with different extractants [1,2], such as organophosphorus extractants, carboxylic acid derivatives, quaternary ammoniums, and chelating agents, such as oximes. However, liquid/liquid extraction exhibits important restrictions and drawbacks related to the use of toxic and inflammable organic diluents. Thus, alternative

media based on innovative concepts are currently being developed such as ionic liquids [3] or aqueous two-phase systems.

The use of aqueous two-phase systems for the purpose of analytes extraction, isolation and/or preconcentration has become a field of increasing interest [4,5]. During the past few years, there has been a growing interest in the potentialities of particular aqueous two-phase system, i.e. micellar extraction or cloud point extraction [6,7]. Such systems have proved to be extremely promising in the field of metal preconcentration and separation [8]. Two different situations have been considered with either a simple extraction of the metal ion by the micelles or the formation of complex between metal ion and extractant solubilized in the micelles. The latter situation, which is more adapted for performing selective extraction, will be the one of interest in this work.

Metal extraction in micellar systems is in many respects analogous to solvent extraction if one considers the techniques or procedures used to separate the micelles from the continuous aqueous phase. Ultrafiltration (Micellar Enhanced UltraFiltration or MEUF) [9-13] and Cloud Point Extraction (CPE) [14-17] can be used to separate the two phases. The basis of the cloud point separation, technique initially reported by Watanabe [18] lies from the well-known phase phenomenon exhibited by some surfactant micellar solutions. Namely, upon appropriate increase of the temperature, the separation of an aqueous non ionic surfactant micellar solution into a concentrated phase containing most of the surfactant and a dilute aqueous phase containing low concentration of surfactant (cmc) is observed. Any components originally present that bind to the micelles in solution can thus be extracted from the original aqueous phase and concentrated in the small volume of the surfactant rich phase. However, controversy persists regarding the origin and microstructure in solutions of non ionic surfactants near the cloud point [19].

Compared to solvent extraction, metal extraction in micellar systems presents many advantages, because it's a purely aqueous process that does not require the presence of organic solvent. In addition, it leads to high values of concentration factors and then uses small volumes of sample for targeted component determination.

Figure 1 and its derivatives, alone or mixed with some synergistic ligands, were reported for the extraction of lanthanides [20-26]. In a previous study [14], we showed that 8-hydroxyquinoline (HQ) is more suitable for lanthanide extraction using the CPE process than hydrophobic substituted 8-hydroxyquinolines.

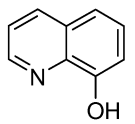

HQ

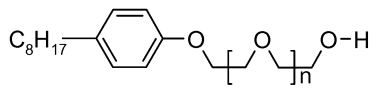

n = 7 : Triton X114

Figure 1. Structure of chelating agent and surfactant used.

The composition of HQ-lanthanides complexes extracted into organic phases has been studied [24,26-28] for liquid/liquid extraction systems, but HQ-lanthanide complexes extracted into surfactant-ich phases has not been studied for CPE systems. In our study, we thus investigate and compare the nature of the extracted species in both systems. We also determined the influence of solution acidity on the extraction efficiency

of CPE; we then compared this process with a classical solvent-extraction process using the same chelating agent. Cloud-point extraction was performed according to the procedure described in a previous paper133].

RESULTS AND DISCUSSIONS

Extraction of Gd^{3+} in 8-HQ/Triton X114 System

The overall reaction for the extraction of Gd^{3+} with HQ from awater phase can be described by Equation 1 where the subscripts "aq" and "org" denote "aqueous" and "organic" phases respectively:

$$Gd^{3+}_{aq} + nHQ_{org} \overset{Kex}{\rightleftharpoons} \left\{Gd^{3+} - nQ\right\}_{org} + nH^{+}_{aq} \quad (1)$$

The corresponding extraction equilibrium constant, K_{ex}, can be defined as in Equation 2.

$$K_{ex} = \frac{\left[Gd^{3+} - nQ\right]_{org}\left[H^{+}\right]^{n}_{aq}}{\left[Gd^{3+}\right]_{aq}\left[HQ\right]^{n}_{org}} \quad (2)$$

By introducing the distribution ratio

$$D = \frac{\left[Gd^{3+}\right]_{org}}{\left[Gd^{3+}\right]_{aq}} \quad (3)$$

the logarithmic expression of Equation 3 can be written

$$Log\ D = Log\ K_{ex} + nLog\left[HQ\right]_{org} + n\mathrm{pH} \quad (4)$$

A plot of Log *D* versus pH at constant ligand concentration this allows the evaluation of of *n* values. The data were analyzed using the linear-regression computer program Excel.

The experimental data for the extraction of gadolinium by CPE are given in Figure 2. Without HQ, almost no extraction of gadolinium was observed between pH 3.0 and 6.0. Using a HQ/Gd^{3+} ratio of 10, the extraction of gadolinium was strongly dependant on the pH, and the extraction was quantitative for a pH greater than 5.5. The $pH_{1/2}$ determined under those conditions was 4.8.

As the extraction of gadolinium with Triton-X114 alone is negligible, the value of the distribution ratio *D* Equation 3, obtained experimentally by using 10-fold more HQ than Gd^{3+}, can be used to determine the stoichiometry of the extracted complex according to Equation 4. A log-log plot of *D* versus the pH (Figure 2), keeping the Triton-X114 and HQ concentrations constant, indicates that gadolinium was extracted as a neutral complex in the micelle (i.e. $Gd(HQ)_3$). This observation is in accordance with the speciation models that could be calculated using stability constants [29].

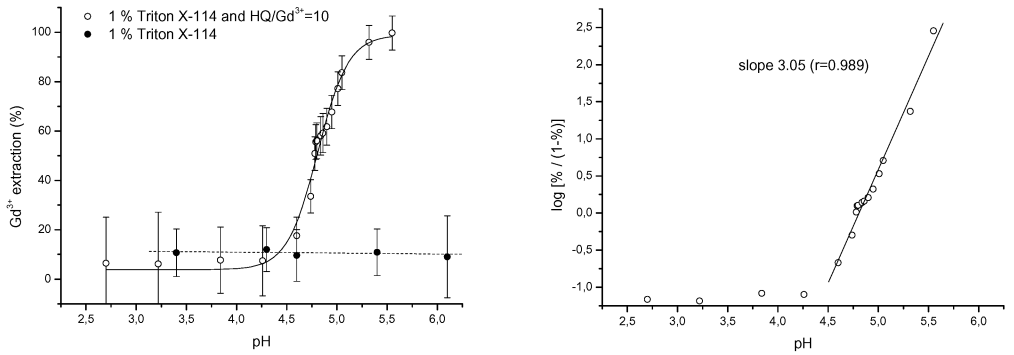

Figure 2. Extraction of gadolinium and log *D* as a function of pH.
Conditions: 0.7 wt % Triton X-114, [Gd^{3+}] = 0.1 mM, [HQ][Gd^{3+}] = 10, CPT = 40 °C.

Extraction of Gd^{3+} in HQ/$CHCl_3$ System

Different diluents were considered. But the solubility of the gadolinium complex with HQ in aliphatic and aromatic one was low, and precipitation occurred. The solubility of the gadolinium complex was higher in chloroform, but using the same experimental conditions (i.e. HQ/Gd^{3+} molar ratio of 10 and pH 5.5), a low gadolinium extraction efficiency of 25% was observed, compared to 98% with CPE. The molar ratio HQ/Gd^{3+} was thus increased and its influence on gadolinium extraction was studied at pH 5.4 (Figure 3).

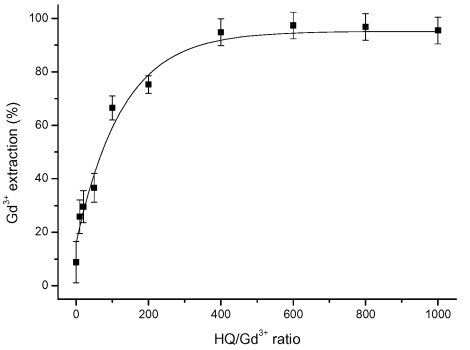

Figure 3. Extraction of Gd^{3+} as a function of [HQ]/[Gd^{3+}] ratio.
Conditions: $CHCl_3$ as diluent, [Gd^{3+}] = 0.1 mM, pH = 5.4, O/A phase ratio = 1, *T* = 22 °C).

An extraction of 95%, comparable to the 98% observed with CPE was obtained using a HQ/Gd^{3+} ratio of 400. A further increase of this ratio did not improve the extraction. The gadolinium extraction was then studied as a function of pH with a HQ/Gd^{3+} ratio of 1000 to make sure being at the maximum of extraction (Figure 4).

As the gadolinium extraction by neat chloroform is negligible (Figure 4), the stoichiometry of the extracted complex was determined from Figure 5 and found to be 3 with a HQ/Gd^{3+} molar ratio of 1000.

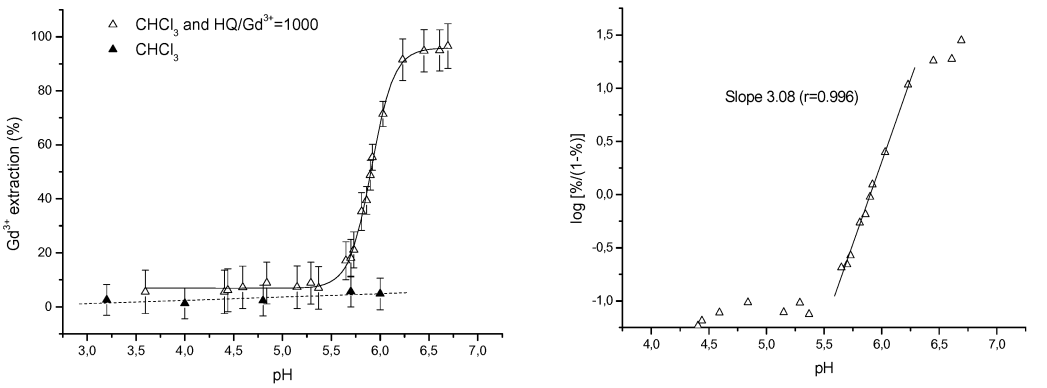

Figure 4. Extraction of Gd^{3+} and log D as a function of pH. Conditions: $CHCl_3$ as diluent, $[Gd^{3+}] = 0.1$ mM, $[HQ]/[Gd^{3+}] = 1000$, O/A phase ratio = 1, $T = 22$ °C).

Comparison of Liquid-Liquid Extraction and Cloud Point Extraction

Both liquid/liquid and cloud point processes allow an efficient extraction of gadolinium from acidic solutions to chloroform or micellar phase. Values of the pH for half-extraction ($pH_{1/2}$) in the extraction profiles are found to vary with the process used in the order: CPE (4.8) < L/L (5.9). HQ/Gd^{3+} is a hundred times lower for the cloud point extraction process than for the solvent-extraction one, making that process more interesting from an economic point of view.

CONCLUSIONS

Micellar extraction and solvent extraction show similar efficiencies without considering the phase-volume ratios. Nevertheless, the micellar process described herein avoids the use of organic solvent and proceeds in a 99% aqueous system without additional separating system. Moreover, micellar extraction is completely efficient with a $HQ\text{-}Gd^{3+}$ molar ratio of 10 compared to 1000 when using solvent extraction.

As a conclusion, this system is especially adapted for decontamination of aqueous effluents or preconcentration, but it can't be considered as an alternative to solvent extraction in hydrometallurgical processes [9].

REFERENCES

1. K. L. Nash, *Solvent Extr. Ion Exch.,* **11**(4), 729-768 (1993).
2. K. L. Nash, and M. P. Jensen, *Sep. Sci. Technol.*, **36**(5 & 6), 1257-1282 (2001).
3. K. Nakashima, F. Kubota, T. Maruyama, and M. Goto, *Anal. Sci.,* **19**(8), 1097-1098 (2003).
4. R. D. Rogers, and M. A. Eiteman, Aqueous Biphasic Separations: Biomolecules to Metal Ions. Plenum Press: New York, 1995; p. 191
5. J. G. Huddleston, H. D. Willauer, S. T. Griffin, and R. D. Rogers, *Ind. Eng. Chem. Res.,* **38**(7), 2523-2539 (1999).

6. W. L. Hinze and E. Pramauro, *Crit. Rev. Anal. Chem.*, **24**(2), 133-177 (1993).
7. F. H. Quina and W. L. Hinze, *Ind. Eng. Chem. Res.,* **38**(11), 4150-4168 (1999).
8. F. Merino, S. Rubio, and D. Perez-Bendito, *J. Sep. Sci.,* **28**(14), 1613-1627 (2005).
9. M. Hebrant, C. Provin, J. P. Brunette, and C. Tondre, *Colloids Surf.* A, **181**(1-3), 225-236 (2001).
10. C. Tondre, S. G. Son, M. Hebrant, P. Scrimin, and P. Tecilla, *Langmuir*, **9**(4), 950-955 (1993).
11. M. Hebrant, N. Francois, and C. Tondre, *Colloids Surf., A,* **143**(1), 77-88 (1998).
12. B. R. Fillipi, J. F. Scamehorn, S. D. Christian, and R. W. Taylor, *J. Membr. Sci.*, **145**(1), 27-44 (1998).
13. A. Favre-Reguillon, M. Draye, G. Lebuzit, S. Thomas, J. Foos, G. Cote, and A. Guy, *Talanta*, **63**(3), 803-806 (2004).
14. N. De Jong, M. Draye, A. Favre-Reguillon, G. LeBuzit, G. Cote, and J. Foos, *J. Colloid Interface Sci.,* **291**(1), 303-306 (2005).
15. M. Draye, S. Thomas, G. Cote, A. Favre-Reguillon, G. LeBuzit, A. Guy, and J. Foos, *Sep. Sci. Technol.*, **40**(1-3), 611-622 (2005).
16. A. Favre-Reguillon, D. Murat, G. Cote, J. Foos, and M. Draye, *J. Chem. Technol. Biotechnol.*, **81**(12), 1872-1876 (2006).
17. H. Watanabe and H. Tanaka, *Talanta*, **25**(10), 585-589 (1978).
18. A. Blom, G. G. Warr, and E. J. Wanless, *Langmuir*, **21**(25), 11850-11855 (2005).
19. D. Czakis-Sulikowska and N. Pustelnik, *Solvent Extr. Ion Exch.*, **21**(5), 751-762 (2003).
20. D. Czakis-Sulikowska, N. Pustelnik, B. Kuznik, and A. Malinowska, *J. Alloys Compd.*, **300-301**, 234-237 (2000).
21. F. A. Shehata, S. M. Khalifa, S. I. El-Dessouky, and H. F. Aly, *Solvent Extr. Ion Exch.*, **11**(5), 861-876 (1993).
22. M. Kawashima and H. Freiser, *Anal. Chem.*, **53**(2), 284-286 (1981).
23. T. Hori, M. Kawashima, and H. Freiser, *Sep. Sci. Technol.*, **15**(4), 861-875 (1980).
24. R. D. Gupta, G. S. Manku, A. N. Bhat, and B. D. Jain, *J. Less-Common Met.*, **20**(4), 345-352 (1970).
25. J. Stary, *Anal. Chim. Acta*, **28**, 132-149 (1963).
26. D. Czakis-Sulikowska and N. Pustelnik, *Chemia Analityczna (Warsaw, Poland)*, **37**(3), 265-272 (1992).
27. R. M. Smith and A. E. Martell, Critical Stability Constants, Vol. 2: Amines. Plenum Press: 1975.

SYNTHESIS AND EVALUATION OF STERICALLY FOCUSED TETRADENTATE NITROGEN LIGANDS CONTAINING THE 2-METHYLPYRIDYL MOIETY FOR THE SEPARATION OF An(III) FROM Ln(III)

Mark D. Ogden, G. Patrick Meier, and Kenneth L. Nash

Department of Chemistry, Washington State University, Pullman, WA, 99164-4630, USA.
Corresponding author email address: mogden@wsu.edu

ABSTRACT

The literature demonstrates that donor atoms softer than oxygen are effective for separating trivalent lanthanides (Ln) from trivalent actinides (An). It has also been shown that ligands which "focus" their donor groups in a favorable geometry have an increased binding affinity due to the reduction in energy required for preorientation when binding. A series of tetradentate nitrogen-containing ligands have been synthesized with increased steric "focus". The p*K*a values for these ligands were determined using potentiometric methods. Copper (II) chromophore formation has been investigated as a method to determine ligand distribution between the organic and aqueous phases.

INTRODUCTION

The separation of lanthanides from transplutonium actinides is critical to the efficient management of spent nuclear fuel. Transplutonium actinides do not have stable high oxidation states and are found predominantly in the +3 oxidation state. Therefore, the separation of these elements must exploit the small difference between the solution chemistry of lanthanides and transplutonium actinides in the trivalent oxidation state [1].

Actinides bind softer bases such as N, S, and Cl more strongly than the trivalent lanthanides and can be exploited for successful separations. The 2-methylpyridyl structural analogue of EDTA, N,N,N',N'-tetrakis(2-pyridylmethyl)-ethylenediamine (TPEN), shows a preference for An^{3+} over Ln^{3+}. The stability constant for the americium (Am) TPEN complex is 100 times greater than for the samarium (Sm) complex, resulting in an overall ΔG difference of 11.6 kJ mol^{-1} [2].

The effect of donor group preorganization is clearly seen in the chemistry of a novel optimized bicyclic diamide [3]. The difference between the formation constants for a 1:1 complex with Am(III) of N,N'-dimethyl bicyclic diamide (DMBCDA) and tetramethylmalonamide (TMMA) at 0.1 M HNO_3 and 0.9 M $NaNO_3$ is $\Delta\log\beta = 1.98$, which represents a difference in the Gibbs free energy of formation between TMMA and DMBCDA of -11.3 kJ mol^{-1} [3].

The energy difference required for a separation factor of 100 in a solvent extraction system is approximately 11.4 kJ mol^{-1}, which is comparable to the energy of a single hydrogen bond [1]. Even though "soft" donor containing ligands in general have an inherent selectivity for An(III) over Ln(III), the binding constants in general are low. To increase the binding constant of the complexant for metal ions the ligand can be structurally preorganized.

In Figure 1 the ligands are presented. It can be seen that by changing the steric hindrance of the bridging diamines, as in (B) N,N'bis(2-pyridylmethyl)-1,2-diaminoethane (BPMDAE), (C) N,N'bis(2-pyridylmethyl)piperazine (BPMPIP), and (D) N,N'bis(2-pyridylmethyl)-*trans*-1,2-diaminocyclohexane (BPMDAC), and by replacing the amine bonds with imine bonds as in (A) N,N'bis(2-pyridylmethylene)-1,2-diiminoethane (BPMDIE), and (E) N,N'bis(2-pyridylmethylene)-*trans*-1,2-diiminocyclohexane (BPMDIC), it is possible to preorganize the binding pyridyl nitrogens. In this paper, the acid dissociation constants for the ligands A, C, D, and E are reported for the first time. As an extension of this study, it is hoped that the necessary structural features required in a complexing ligand that will increase the binding affinity and selectivity for An(III) over Ln(III) can be identified.

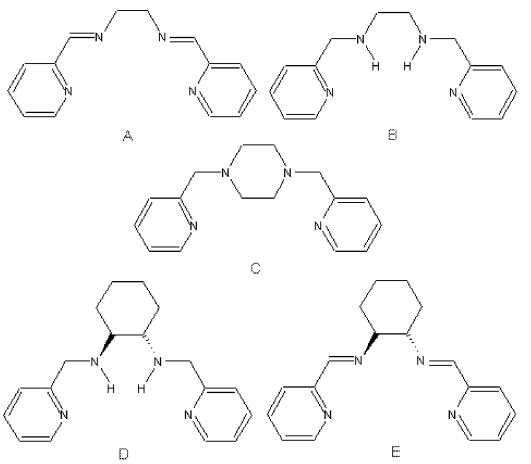

Figure 1. A to E represent the following ligands, BPMDIE, BPMDAE, BPMPIP, BPMDAC, and BPMDIC respectively

EXPERIMENTAL

Ligand Synthesis

The ligands in Figure 1 were synthesized using reported methods [4-7]. The synthesis of all ligands, except C, used a slight modification in the synthesis; the imine formation step was conducted over 3 Å molecular sieves in 99.8% anhydrous MeOH to remove water from the condensation reaction. The amines were precipitated as hydrochlorides from ethyl ether using 1 M HCl ethyl ether solution. All reagents used were of analytical grade. Ligand purity was verified by proton NMR.

Potentiometric Measurements of Acid Dissociation Constants

All measurements were made using a Mettler Toledo DL50 Autotitrator fitted with an Orion Ross ultra semi-micro glass electrode with 3 M NaCl as the filling solution. The experimental and titration solutions contained sufficient $NaClO_4$ to bring the ionic strength to 0.5 M; the temperature was maintained at 25 °C, and a slow stream of nitrogen was passed through the titration vessel in order to reduce the interference from CO_2. All the ligand solutions were titrated with standardized 0.01 M NaOH. Solutions of A, C, and E (1×10^{-3} M) were prepared by dissolving the crystalline material in 18 MΩ water with an excess of acid (10 equivalents 0.01 M $HClO_4$) to result in a solution of approximately pH 2. Solutions of B and D (1×10^{-3} M) were prepared from the weighed neutralized amine following a similar procedure to that described above. All potentiometric titrations were performed in triplicate, in both static and dynamic modes. The potentiometric curves were fitted using PSEQUAD and the first p*K*a fitted by minimization of the data.

Spectrophotometric Measurements

Ligand-metal complex solutions were made using $Cu(ClO_4)_2.6H_2O$ of 99.99% purity (0.001 M) and an excess of ligand (0.01 M). The solution was acidified using 0.5 M $HClO_4$ until the colored complex no longer formed. $NaClO_4$ was added to maintain the ionic strength at 0.5 M. The ligand-metal complex solution was then titrated with standardized 0.1 M NaOH. The absorption spectra of the copper complexes with A, B, and C were recorded as a function of pH at 23 °C (±2) in the range of 350-950 nm using a Varian Cary 50 Bio UV-Vis spectrophotometer.

RESULTS AND DISCUSSION

The potentiometric titration data of the ligands A-E are shown in Table 1. The acid dissociation constants for A, C, D, and E have not been determined until now, but the values for B are in good agreement with the literature, which are reported at 0.1 M ionic strength as 1.62, 1.81, 5.45, and 8.23, respectively [8]. The increase in pK_as for B is due to the increase in ionic strength (0.5 M) [9].

Table 1. Acid dissociation constants for 2-methylpyridyl based ligands

Compound:	A	B	C	D	E
Acronym:	BPMDIE	BPMDAE	BPMPIP	BPMDAC	BPMDIC
pK_1	3.75 (±0.09)	1.3 (±0.3)	1.5 (±0.6)	1.6 (±0.3)	3.88 (±0.08)
pK_2	4.47 (±0.06)	2.25 (±0.04)	2.62 (±0.04)	3.05 (±0.02)	4.44 (±0.05)
pK_3	7.17 (±0.03)	5.80 (±0.04)	5.11 (±0.03)	5.74 (±0.07)	6.42 (±0.04)
pK_4	9.07 (±0.02)	8.67 (±0.02)	7.27 (±0.02)	9.17 (±0.05)	9.40 (±0.03)

The higher values of the pK_as for A and E appear counterintuitive for the effect of conjugation on the overall pK_as of a ligand. The pK_1 for both A and E match that of 2-pyridine carboxaldehyde at 3.80 [10] and is a possible indication that both of these ligands undergo hydrolysis in aqueous solution. The remaining pK_as could possibly be assigned to a tridentate 2-pyridylmethylene amine or aminal species. The values of the pK_as for B, C, and D indicate the more acidic nature of the pyridyl moieties when

compared with the aliphatic analogue triethylenetetramine (trien) [8]. From previous studies, it has been shown for B (BPMDAE) that the relative affinity of the ligand for protons does not reflect its affinity for metal ions [8]. Also the pK_as of these ligands may not reflect their distribution between an organic and aqueous phase, as this is also a function of the lipophilicity of the amine backbone.

The complex formed between B (BPMDAE) and Cu^{2+} is very strong with a log K_{101} = 16.3 [8] and is present at pH 1, whereas the complexes of A (BPMDIE) and C (BPMPIP) begin to noticeably form at around pH 3.5 and 2.5, respectively. The absorption information for the ligands screened with copper is given in Table 2, and the spectrophotometric titration of C (BPMPIP) as a function of pH can be seen in Figure 2.

Table 2. Absorption data for the complexes of A, B and C with Cu^{2+}

Ligand	λ max (nm)	Molar absorptivity ε (mol^{-1} cm^{-1})	Lowest observable conc. of ligand (M)
A (BPMDIE)	606	156 (± 6)	1.28×10^{-5} (± 0.05)
B (BPMDAE	606	149 (± 6)	1.34×10^{-5} (± 0.06)
C (BPMPIP)	650	288 (± 8)	0.69×10^{-5} (± 0.02)

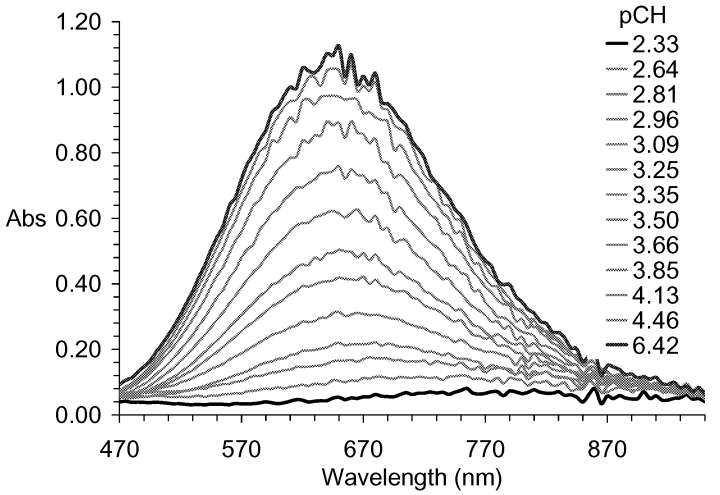

Figure 2. Spectrophotometric pH titration of BPMPIP (0.01 M) with Cu^{2+} (0.001 M). The black baseline represents pCH 2.33 and, each resulting spectra is after an incremental addition of 0.1 M NaOH.

In all the UV-Vis spectrophotometric pH titrations, the growth of a single peak is observed with pH increase (see Figure 2). The copper species stoichiometry was determined for all ligands A-C as 1:1 using Job plot analysis. Noticeably, the CuBPMPIP complex has a molar absorptivity nearly double the value of the other complexes. This is probably due to the distortion of the metal center from ideal symmetry when complexed to BPMPIP ligand [11]. It can also be seen that the ligand A (BPMDIE) even after hydrolysis can still complex copper and is most likely a tridentate 2-pyridylmethylene amine [12]. The quality of this data is adequate enough to fit stability constants, and this

work is currently in progress. The lowest observable amount of ligand is calculated from the observed spectra of the 1:1 complex greater than 3σ of the baseline at the λ max.

The equal values of λ max (606 nm) for both A and B could suggest that A coordinates to the copper metal as a tridentate chelate. This is not the case, as the energy of a transition is determined by the nature of the less strongly bonded axial ligands as well as the four donor atoms in the plane [13]. The crystal structure of the complex $[Cu(BPMPIP)(ClO_4)]ClO_4$ is a 5 coordinate square pyramidal complex with the ligand occupying the equatorial plane. A counter ion is held within the inner coordinating sphere in an axial position and the final counter anion is in the second coordination sphere with respect to the nitrate [14]. This is due to the steric interaction of the piperazine backbone with species coordinated in the axial positions. The tridentate hydrolysis product of A and the tetradentate ligand B both allow stronger axial ligand interaction due to reduced steric impact.

CONCLUSIONS AND FURTHER WORK

Even though these ligands are soluble in 1-octanol and more polar organic diluents, the aqueous solubility of these ligands make it clear that they may not extract on their own and will need to be used as a synergist or take the place of polyaminocarboxylates in the TALSPEAK process. The determination of the indiviual pK_as for ligands A-E shows that overall ligand C (BPMPIP) is the most acidic. The more acidic pK_1 and pK_2 of ligand B (BPMDAE) may allow for easier removal of the pyridyl protons upon complexation with a metal center and may result in stronger metal complex interactions. It is clear that, due to hydrolysis, ligands A and E are not suitable to be used for solvent extraction, although the tridentate chelate formed on degradation may extract or retain metal ions in the aqueous phase.

The formation of a Cu(II) chromophore may allow the direct measurement and detection of the ligand distribution ratio as a function of pH. The high extinction coefficients of the complexes formed with Cu^{2+} allow detection of ligand concentrations in the aqueous phase after distribution down to 1×10^{-5} M. The detection solution will consist of a pH 5 buffered solution at 0.5 M ionic strength containing 0.001 M Cu^{2+} as a perchlorate. It has been surmised that the λ max and molar absorptivity (ε) of the copper complexes of D (BPMDAC) and E (BPMDIC) will be similar to B (BPMDAE) and A (BPMDIC) respectively.

The work presented here is part of an on-going project to determine the necessary structural features required in a complexing ligand that will increase the binding affinity and selectivity for An(III) over Ln(III) can be identified. Consequently there are still a number of experiments to be performed. These include:

- Determination of the λ max and molar absorptivity (ε) of Cu^{2+} complexes of ligands D and E
- Determination of the ligand distribution ratios as a function of pH
- Determination of Am^{3+} and Eu^{3+} distribution coefficients as a function of pH, ligand and metal concentrations and ionic strength
- Determination of synergistic interaction and stoichiometry

ACKNOWLEDGMENTS

The authors would like to thank Dr. Mikael Nilsson and Dr. Sarah Pepper for their support and insight in this project. Funding of the project was made possible through the DOE UNERI program.

REFERENCES

1. K. L. Nash, Separation Chemistry for Lanthanides and Trivalent Actinides, Handbook on the Physics and Chemistry of Rare Earths Vol. 18 – Lanthanides/Actinides Chemistry, Elsevier Science, 1994; pp. 197-238.
2. M. P. Jensen, L. R. Morss, J. V. Beitz, and D. D. Ensor, "Aqueous complexation of trivalent lanthanide and actinide cations by N,N,N',N'-tetrakis(2-pyridylmethyl)ethylenediamine," *J. Alloys Comp*., **303-304**, 137-141 (2000).
3. S. I. Sinkov, B. M. Rapko, G. J. Lumetta, and B. P. Hay, "Bicyclic and Acyclic Diamides: Comparison of Their Aqueous Phase Binding Constants with Nd(III), Am(III), Pu(IV), Np(V), Pu(VI), and U(VI)," *Inorg. Chem.,* **43**(26), 8404-8413 (2004).
4. S. Oshima, N. Hirayama, K. Kubono, H. Kokusen, and T. Honjo, "Ion-pair extraction behavior of divalent transition metal cations as charged complexes with N,N'-bis(2-pyridylmethylidene)-1,2-diiminoethane and its analogues," *Anal. Chim. Acta,* **441**(1), 157-164 (2001).
5. I. Cukrowski, E. Cukrowska, R. D. Hancock, and G. Anderegg, "The effect of chelate ring size on metal ion size-based selectivity in polyamine ligands containing pyridyl and saturated nitrogen donor groups," *Anal. Chim. Acta,* **312**(3), 307-321 (1995).
6. H. Tsukube, K. Yamashita, T. Iwachido, and M. Zenki, "Sodium-selective macrocyclic polyamine carriers having pyridine-functionalized sidearms," *J. Chem. Soc. Perkin Trans. 1,* **7**, 1661-1665 (1991).
7. S. Schoumacker, O. Hamelin, J. Pecaut, and M. Fontecave, "Catalytic Asymmetric Sulfoxidation by Chiral Manganese Complexes: Acetylacetonate Anions as Chirality Switches," *Inorg. Chem*., **42**(24), 8110-8116 (2003).
8. R. G. Lacoste and A. E. Martell, "New multidentate ligands. I. Coordinating tendencies of polyamines containing a-pyridyl groups with bivalent metal ions," *Inorg. Chem*., **3**(6), 881-884 (1964).
9. A. E. Martell and R. M. Smith, "NIST Critically Selected Stability Constants of Metal Complexes Database," Version 8.0, 2004
10. D. D. Perrin B. Dempsey, and E. P. Serjeant, pKa Prediction for Organic Acids and Bases, Chapman & Hall, London, 1981
11. J. A. Halfen, J. M. Uhan, D. C. Fox, M. P. Mehn, and L. Que, Jr.," Copper(II) Complexes of Pyridyl-Appended Diazacycloalkanes: Synthesis, Characterization, and Application to Catalytic Olefin Aziridination," *Inorg. Chem*., **39**(21), 4913-4920 (2000).
12. C. M. Harris and E. D. McKenzie, "Five-coordinate copper(II) complexes of the quadridentate Schiff base ligand N,N'-bis(2-pyridylmethylene)ethane-1,2-diamine, and some related ligands," *J. Chem. Soc. (A)*, **5**, 745-753 (1969).
13. E. J. Billo, "Copper(II) chromophores and the rule of average environment," *Inorg. Nucl. Lett.,* **10**(8), 613-617 (1974).
14. J. Ratilainen, K. Airola, R. Frohlich, M. Nieger, and K. Rissanen, "Synthesis of a tetradentate piperazine ligand and a structural study of its coordination compounds," *Polyhedron,* **18**(17), 2265-2273 (1999).

ATOMISTIC SIMULATION OF WATER/TRIBUTYLPHOSPHATE-DODECANE INTERFACE

Shengting Cui,[1] Valmor de Almeida,[2] and Bamin Khomami[1]

[1]Department of Chemical and Biomolecular Engineering, University of Tennessee, Knoxville, TN 37996. [2]Nuclear Science and Technology Division, Oak Ridge National Laboratory, Oak Ridge, TN 37831. Corresponding author email address:cuis@ornl.gov

ABSTRACT

Molecular activities of interfacial extractant agents play an important role in the solvent-extraction process. In this study, we have conducted atomistic simulations to elucidate the interfacial behavior of an aqueous/organic interface in the presence of tributylphosphate, known for its effective complexation with metal ions. Specifically, we have conducted molecular dynamics simulations to determine the concentration and molecular orientation of tributylphosphate in *n*-dodecane as well as the organic/aqueous interfacial properties. Our simulations have clearly demonstrated the accumulation of tributylphosphate molecules with a preferred orientation that favors metal-complex formation at the interface. The specific orientation of tributylphosphate as well as the presence of an interface is also shown to cause polarization of the aqueous phase in the interfacial region. Evidently, interfacial polarization of the aqueous phase could significantly influence migration rates of ionic species from the aqueous phase.

INTRODUCTION

Current liquid-liquid extraction systems for reprocessing of spent nuclear fuel generally consist of an aqueous phase which contains the metal ions to be extracted and an organic phase consisting of a mixture of an extracting agent and a diluent. The extraction process involves many molecular-level events including binding of the extractant and the cations, chemical equilibrium, molecular migration, and interfacial processes. Aqueous reprocessing is the preferred separation and recovery process for various elements or element groups from spent nuclear fuel. The current models are highly empirical in nature, as they are based on limited experimental data. Hence, a fundamental understanding of interfacial transport phenomena is a necessary first step in developing high-fidelity models for solvent extraction in realistic systems.

In the liquid-liquid extraction process of interest to us, the basic extraction is based on a simple premise, namely, the extractant molecules bind to the metal cation and form a complex at the aqueous-organic interface. The complex then migrates into the organic phase due to its high solubility, effectively carrying the metal ion from the interface region into the bulk of the organic phase. This complex migration process

involves many molecular-level events heretofore unknown. In this initial study, we have focused our attention on characterizing the behavior of the extractant agent, tributylphosphate (TBP) at the aqueous/organic interface via molecular-dynamics simulations. Specifically, the interfacial details (i.e., molecular orientation and fluid structure) are computed to gain an insight into the complex formation process as well as the migration of charged species in the aqueous phase, particularly in the vicinity of the interface. In previous studies, Wipff's group has used chloroform [1] and CO_2 [2] as the model organic phase solvent to investigate the interfacial behavior. In this work, we are interested in n-dodecane as the organic phase solvent, which is being used at present for nuclear-fuel extraction.

Thus, as a first step, we investigate a 3-component system consisting of pure water as the aqueous phase and a TBP-dodecane mixture as the organic phase. Of particular interest is the determination of the interfacial TBP concentration distribution, the orientation and polarity of charged species, and their implication on complex formation and ionic species migration.

MOLECULAR MODEL AND METHODOLOGY

The molecular models used are as follows: For water we used a flexible SPC water model recently described in [3]. For the n-dodecane, we treated the methyl and methylene groups as united atoms, and the OPLS parameters were used in the simulation [4,5]. For TBP, we used the model developed by Wipff and coworkers [1,2]. The parameters for cross interactions between different molecular species (atomic groups) were derived using the Lorentz-Berthelot rules [5]. Molecular dynamics simulation at constant number of molecules, constant temperature at 25 °C, and constant volume are performed. A Verlet type multiple time step algorithm was used for the time evolution of the molecular dynamics [6,7]. In our simulations we have used 1728 water molecules, 350 *n*-dodecane molecules, and 230 TBP molecules which were uniformly dispersed in the organic phase initially. The system size and density of the organic subsystem was guided by the state condition of the *n*-dodecane/TBP mixture [8] and preliminary simulation of TBP accumulation at the interface. The aqueous and organic subsystems are created separately and briefly equilibrated. Then the two subsystems are combined into a single system with an aqueous system on one side and the organic subsystem on the other next to each other. The system size for the whole system is then 47.31 x 4 7.31 x 110.28 Å. Periodic boundary conditions are used in all three dimensions as customary in molecular-dynamics simulation. As a result, the system contains two interfaces. At the beginning, the interfaces between the two subsystems are sharp. The system is in turn relaxed via additional equilibration until a molecularly smooth interfacial region is observed. Specifically, we equilibrated the system for 1.38 ns, and data collection was performed from a subsequent 2.15 ns simulation.

RESULTS

In Figure 1, a snapshot of the final configuration of the system is depicted. In the snapshot, water molecules occupy the region about 0-25 Å; the organic phase occupies

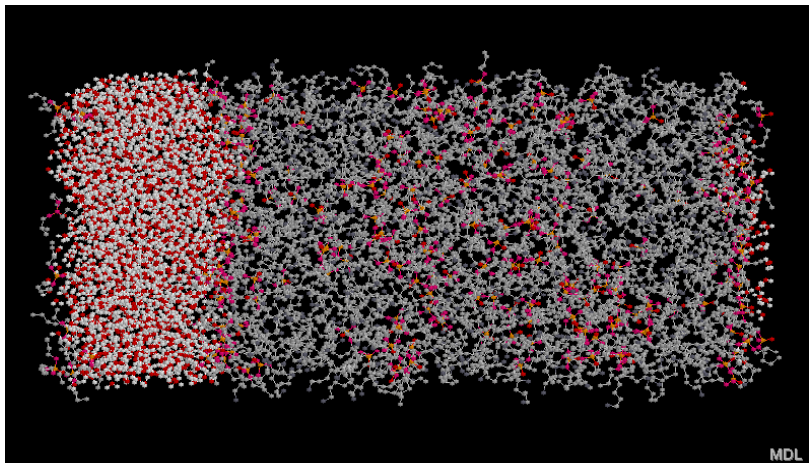

Figure 1. The snapshot at 3.53 ns showing the aqueous and organic phase and accumulation of TBP at the interface. TBP: P (yellow), phosphoryl oxygen (red), butyl oxygen (pink). Dodecane: CH_3 and CH_2 groups (gray). Water: oxygen (red), hydrogen (white).

the region about 25-110 Å. A close examination of the interfacial region reveals a high concentration of TBP molecules. A region in the organic phase near the interface that contains fewer TBP molecules is also observed. We attribute this to the polarity of the TBP molecule (surfactant like) and its relatively slow migration rate in the mixture than the *n*-dodecane molecules. As the TBP molecules migrate to the interface and adsorb to the interface, the *n*-dodecane quickly fills the void left by the TBP. Thus, the region near the interface in the organic phase has a lower concentration of TBP than the bulk organic phase.

The number-density profiles of water, CH_x (x = 2 or 3 groups) of the *n*-dodecane, and the phosphorous atoms of TBP are depicted in Figure 2. Clearly, away from the interface, the water-density profile reached its bulk density. On the organic-phase side, we see variation of the TBP and the *n*-dodecane density. In the region away from the interface, where *n*-dodecane density is low, the TBP density is high and vice versa. In the interfacial region, we see TBP peaks in the two interfacial regions centered at z = 25 Å and 108 Å. Figure 3 shows the cumulative number of TBP molecules across the entire

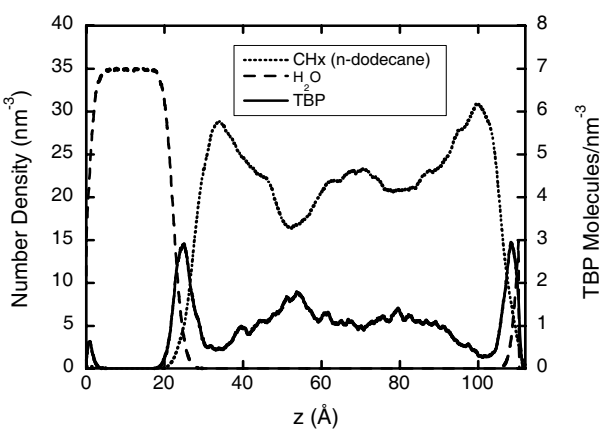

Figure 2. Density profile of the methyl and methylene groups of the *n*-dodecane, water molecules, and phosphorous atoms of TBP.

simulation box from z = 0 to 110.28 Å. This figure provides additional information regarding the TBP distribution. Clearly, the number of TBP molecules rises sharply at the interface. It should be noted that, as a consequence of the limited run time, the two interfaces possess slightly different numbers of TBP molecules. The interface centered at 25 Å has about 35 molecules, while the interface at z = 108 Å has about 25 TBP molecules. Thus, the average number of TBP molecules is approximately 1.34 molecules/nm^2, or 1.34 x 10^{18} molecules/m^2. This value is in reasonable agreement with reported experimental results [9].

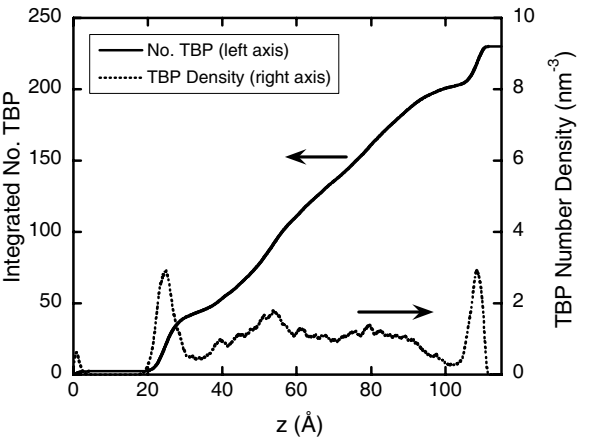

Figure 3. Integrated number of TBP molecules across the length of the simulation box.

Figure 4 shows the orientational order of the TBP molecules, which we define as the average cosine of the P=O bond of TBP molecules from P to O with respect to the normal of the interface. As expected, in the bulk region, the orientational order is zero however, in the interfacial region, the P=O bond of the TBP is preferentially pointed to the aqueous phase. This is expected, as TBP has a dipole moment of 3.1 Debyes [10], corresponding to the phosphate oxygen atom in the TBP carrying an equivalent negative charge. Also, its three hydrophobic tail branches prefer to be buried in the organic phase. In the interfacial region, the orientational order reaches essentially a plateau value, with a value about 0.7-0.8, corresponding to an average angle between the normal of the interface and the P = O bond of from about 37° to 45°. This preferential orientation has practical implication in the application of liquid-liquid extraction due to the fact that the chemical species being extracted comes from the aqueous side.

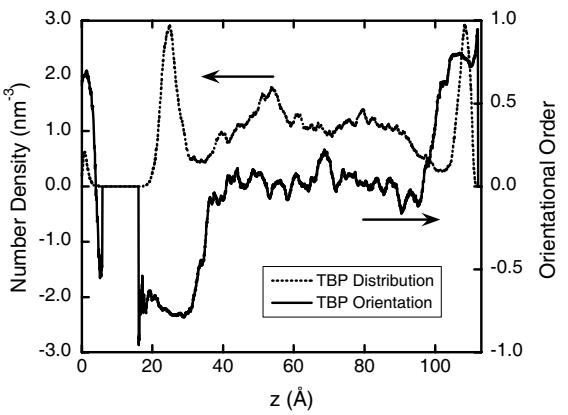

Figure 4. The orientational distribution of TBP molecules. Left axis is for TBP density distribution and right axis is for TBP orientational order. The orientational order is defined as the average cosine of the P = O bond of TBP molecules from P to O.

Therefore, the preferential orientation of the active group of the TBP molecules to the aqueous phase facilitates the combination of TBP with cationic species from aqueous phase to form complexes.

In Figure 5, we plot the orientational order of water molecules, defined as the average cosine of the dipole orientation with respect to the normal of the interface. As can be seen, the water dipole moments are oriented consistently with the orientation of TBP molecules. The positive orientation of water dipole at the interface around z = 25 Å and the negative orientation at the interface around *z* = 108 Å suggests that the water molecules are oriented with the oxygen buried in the aqueous phase and the hydrogen pointed to the organic phase. This is consistent with the stronger hydrogen-bonding capabilities of oxygen atom and its stronger electric interaction which lowers the interaction energy. The consistent dipole orientation of water molecules and the TBP molecules has the effect of enhancing the dipole field in the interfacial region.

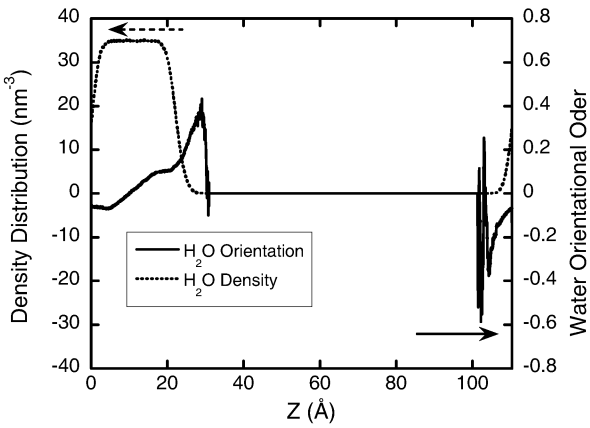

Figure 5. The density distribution of water molecules and the orientational order defined as the average cosine of the dipole of water molecules.

A result of the preferred orientation of polar molecules is that there is a net dipole electric field pointing to the organic phase. This field may affect the migration rate of the ions in the aqueous phase near the interface region. On the aqueous side, the electric field will tend to repel the negatively charged ions from the interface, while attract the positively charged ions to the interface. This should speed up the migration of the positively charged ions to the interface and slow down the migration of negatively charged ions. In practical terms, it may thus be preferable to increase the concentration of the negatively charged ions in the aqueous phase to increase the rate of flux to the organic phase. We have observed such an effect in other MD simulation [11].

SUMMARY

We have performed detailed atomistic simulations of a prototypical interface in liquid-liquid extraction processes in nuclear fuel reprocessing applications, namely that of the interface formed between water and a TBP-dodecane mixture. Through molecular-dynamics simulations, we have clearly demonstrated significant accumulation of tributylphosphatemolecules at the interface (i.,e., 2-3 times higher concentration than the bulk). In addition, it has been clearly demonstrated that the TBP molecules are preferentially orientated with the active head group pointing to the aqueous phase with an average angle about 37°-45°. These results are consistent with those observed by Wipff

et al. with their model system using chloroform, but quantitatively different since a different solvent is used here. Finally, it is shown that the aqueous phase is also polarized near the interface. It is suggested that the preferential orientation of TBP and the polarization of the interface should have important affects on molecular-complex formation and migration of ionic species to the interface.

ACKNOWLEDGMENT

The work is supported by a Joint Directed Research and Development program at University of Tennessee and a Laboratory Directed Research and Development project (ORNL), managed by UT-Battelle, LLC for the U. S. Department of Energy under contract No. DE AC05-00OR22725. The computations were performed on a cluster computer at ORNL.

REFERENCES

1. M. Baaden, M. Burgard, and G. Wipff, "TBP at the Water-Oil Interface: The Effect of TBP Concentration and Water Acidity Investigated by Molecular Dynamics Simulations," *J. Phys. Chem*. B, **105**, 11131-11141 (2001).
2. R. Schurhammer and G. Wipff, "Effect of the TBP and Water on the Complexation of Uranyl Nitrate and the Dissolution of Nitric Acid into Supercritical CO2. A Theoretical Study," *J. Phys. Chem. A,* **109***,* 5208-5216 (2005).
3. Y. Wu, H. L. Tepper, and G. A. Voth, "Flexible simple point-charge water model with improved liquid-state properties," *J. Chem. Phys*., **124**, 024503 (2006).
4. W. L. Jorgensen, J. D. Madura, and Carol J. Swenson, "Optimized Intermolecular Potential Functions for Liquid Hydrocarbons," *J. Am. Chem. Soc.,* **106**, 6638-6646 (1984).
5. M. G. Martin and J. I. Siepmann, "Transferable Potentials for Phase Equilibria. 1. United-Atom Description of *n*-Alkanes," *J. Phys. Chem.* B, **102**, 2569-2577 (1998).
6. M. Tuckerman, B. J. Berne, and G. J. Martyna, "Reversible multiple-time scale molecular dynamics," *J. Chem. Phys*., **97**, 1990-2001 (1992).
7. S. T. Cui, P. T. Cummings, and H. D. Cochran, "Multiple time step nonequilibrium molecular dynamics simulation of the rheological properties of liquid *n*-decane," *J. Chem. Phys.*, **104**, 255-262 (1996).
8. Q. Tian and H. Liu, "Densities and viscosities of binary mixtures of tributyl phosphate with hexane and dodecane from (298.15 to 328.15) K," *J. Chem. Eng. Data*, **52**, 892-897 (2007).
9. S. Haslam, S. G. Croucher, C. G. Hickman, and J. G. Frey, "Surface second harmonic generation studies of the dodecane/water interface: the equilibrium and kinetic behaviour of ***p***-nitrophenol and tri-*n*-butyl phosphate," *Phys. Chem. Chem. Phys.,* **2**, 3235-3245 (2000).
10. Wallace W. Schulz, James D. Navratil, ed., *The Science and Technology of Tributyl Phosphate*, vol. 1, Boca Raton, Fla. CRC Press, 1984.
11. Unpublished results.

EXPERIMENTAL DATA AND REGRESSIONS CONCERNING THE EVALUATION OF 1,2-PROPYLENE GLYCOL AS A NEW SOLVENT FOR AROMATIC HYDROCARBONS LIQUID-LIQUID EXTRACTION FROM CATALYTIC REFORMER PRODUCTS

F. Oprea[1] and O. A. Guțu[2]

[1]*Universitatea Petrol-Gaze din Ploieşti, Bd. Bucureşti 39, 100680, România.*
[2]*Snamprogetti Milano, Via A. de Gasperi, 16, 20097 San Donato Milanese, Milano, Italy. Corresponding author e-mail address: florin@oprea.org*

ABSTRACT

There are few data in literature concerning aromatic and paraffinic hydrocarbons with 1,2-propylene glycol. These data do not permit one to evaluate the liquid-liquid extraction ability of 1,2-propylene glycol as solvent for the recovery of aromatic hydrocarbons resulting from catalytic reformer products. This paper is focused on the determination of NTRL and UNIQUAC binary interaction parameters between 1,2-propylene glycol and various aromatic and paraffinic hydrocarbons, benzene, *n*-hexane, toluene, *n*-heptane, ethylbenzene, *m*-, *o*-, and *p*-xylene, and *n*-octane.

INTRODUCTION

Since 2003, a study regarding the possible use of 1,2-propylene glycol (1,2-propanediol) for the liquid-liquid extraction of aromatic and paraffinic hydrocarbons began in our department. The first researches showed interesting performance for extractive distillation of benzene from its mixture with *n*-hexane [1]. The experimental results for the liquid-vapor equilibrium showed an important increase of the relative *n*-hexane-benzene volatility (up to 2.3). The simulation of the process evidenced that elimination of benzene down to 50 ppm is possible at reasonable costs.

As it is commonly known, the processing of the liquid-vapor experimental data does not allow an appropriate estimation of liquid-liquid equilibrium. On the contrary, liquid-liquid equilibrium data permit a fair evaluation of the liquid-vapor equilibrium.

There are few data in the literature concerning aromatic and paraffinic hydrocarbons with 1,2-propylene glycol [2-4]. This paper is focused on the determination of NTRL and UNIQUAC binary interaction parameters between 1,2-propylene glycol (12PG) and various aromatic and paraffinic hydrocarbons such as benzene (B), *n*-hexane (NC6), toluene (T), *n*-heptane (NC7), ethylbenzene, *m*-, *o*-, and *p*-xylene (MX, OX, PX, repectively), and *n*-octane (NC8).

The PRO/II and ASPEN simulation softwares include binary interaction parameters for NRTL and UNIQUAC models [2,3]. In the NTRL model (Non-Random Two Liquids), activity coefficients are described by the following equation:

$$\ln \gamma_i = \frac{\sum_j \tau_{ji} G_{ji} x_j}{\sum_K G_{ki} x_k} + \sum_j \frac{x_j G_{ij}}{\sum_k G_{kj} x_k} \cdot \left(\tau_{ij} - \frac{\sum_k x_k \tau_{kj} G_{kj}}{\sum_k G_{kj} x_k} \right) \quad (1)$$

where parametrs are:

$$\tau_{ij} = a_{ij} + \frac{b_{ij}}{T} + \frac{c_{ij}}{T^2};\ G_{ji} = \exp\left(-\alpha_{ji}\tau_{ji}\right);\ \alpha_{ji} = \alpha'_{ji} + \beta'_{ji} \cdot T \text{, when unit of } T \text{ is K.}$$

This model is of great interest, as it permits the calculation of activity coefficients in liquid-liquid multicomponent systems from ternary or binary equilibrium data. Binary NRTL parameters are gathered in Table 1.

Table 1. The binary interaction NRTL parameters for the systems of C_6 and C_7 hydrocarbons with 1,2-propylene glycol that are present in the literature until 2007

i	j	a_{ij}	a_{ji}	b_{ij}	b_{ji}	$\alpha_{ij} = \alpha_{ji}$	UM (b_{ij})	Source
NC6	12PG	0	0	1282.9	668.09	0.2	K	[2]
NC6	12PG	0	0	1282.9004	668.0864	0.2	K	[3]
B	12PG	-4.6342	-2.518	2812.5000	822.617	0.2	K	[2]
B	12PG	-2.5834	-6.893	842.162	3536.4763	0.2	K	[3]
T	12PG	148.8289	-77.98	-3384.169	4019.3816	0.2	K	[3]
NC7	12PG	-6.4613	-1.911	3954.8	2055.9	0.2	K	[4]

EXPERIMENTAL

In this paper, liquid-liquid extraction data are obtained by determining the cloud point with a thermostated home-made cell (±0.05 ºC). The used substances were chromatographic etalons, dried in zeolites. The experimental data was then fitted in order to obtain the binary interaction parameters from the NRTL model.

RESULTS AND DISCUSSION

A fair agreement is obtained between experimental data and the litterature concerning the NC6-12PG system (Figure 1). In the other figures (Figures 1 to 9), x_1 and x_2 represent the molar fraction of the hydrocarbons in the two separated liquid phases.

On the other hand, experiment data are not in fair aggreement with litterature date (Figure 2), Figure 3 presents the experimental data ontained dor 12PG-B and 12PG-NC6 systems. Experimental and literature for the T-12PG system is displayed in Figure 4. Notable differences can be noticed between experimental and litterature data.

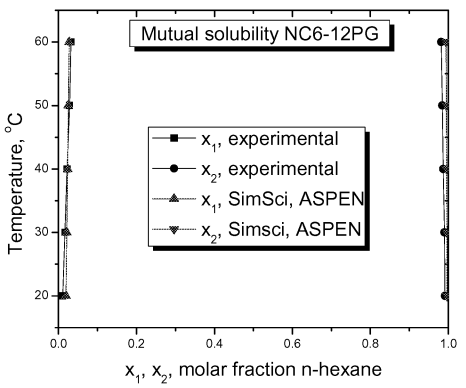

Figure 1. Experimental and literature data concerning system NC6 – 12PG.

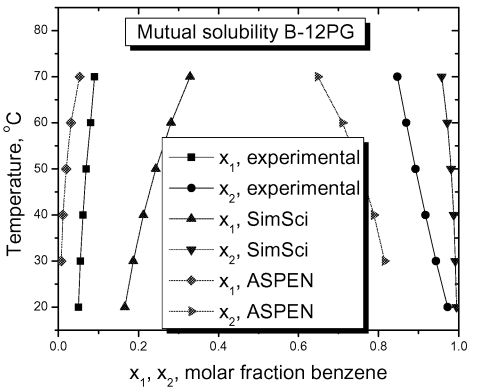

Figure 2. Experimental and literature data concerning system B – 12PG.

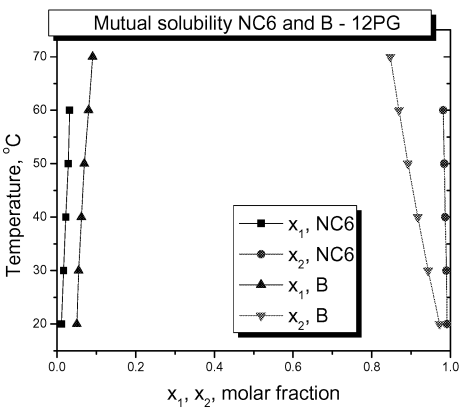

Figure 3. Comparative experimental LLE data for NC6 and B with 12PG.

No data are available concerning NC8. The following figures present the comparison of the experimental data for the system that consists of NC8 (alkane C_8) and EB, OX, MX, and PX (aromatics C_8).

The experimental data for each binary systems has been fitted by using the NRTL model in order to obtain the binary interaction parameters. Table 2 presents the binary interaction parameters of the NRTL model for these binary systems.

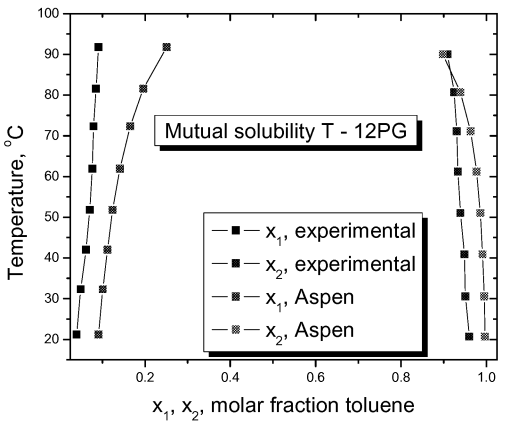

Figure 4. Experimental and literature data for T with 12PG.

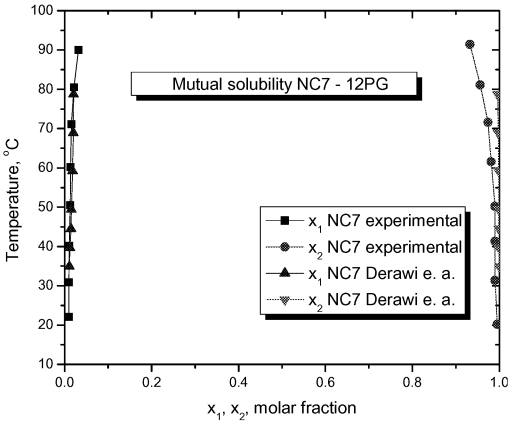

Figure 5. Experimental and literature data for NC7 with 12PG.

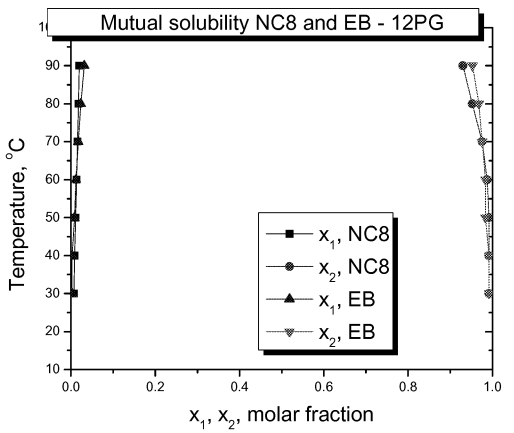

Figure 6. Comparative experimental ELL data for NC8 and EB with 12PG

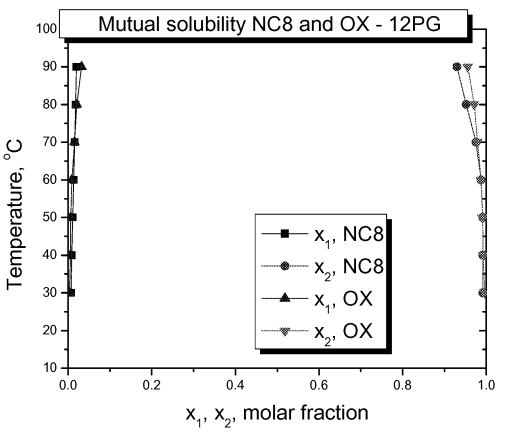

Figure 7. Comparative experimental ELL data for NC8 and OX with 12PG

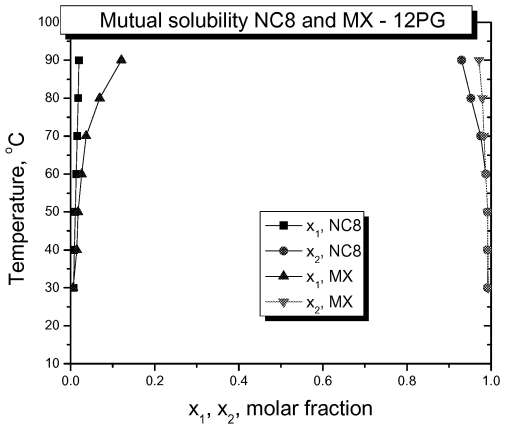

Figure 8. Comparative experimental LLE. data for NC8 and MX with 12PG.

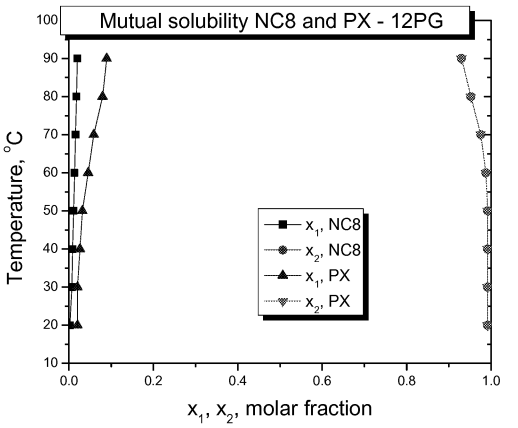

Figure 9. Comparative experimental LLE. data for NC8 and PX with 12PG.

Table 2. The binary NRTL interaction parameters for the C_6, C_7, and C_8 hydrocarbons with 12PG obtained after the regression of the experimental data

i	j	a_{ij} / a_{ji}	b_{ij} / b_{ji}	$\alpha_{ij} = \alpha_{ji}$	UM (b_{ij})	Temp. dev., avg. dev., %/max. dev. %
NC6	12PG	0 0	938.4172230 758.5992490	0.2	K	0.47311/3.06
B	12PG	-4.8583193 2.6337375	2026.186630 -198.186630	0.2	K	0.00018/0.05989
NC7	12PG	-7.2325292 -1.2177269	3389.541970 1471.671960	0.3	K	0.231695/3.937
T	12PG	158.386824 -78.199158	-7058.85444 4441.56325	0.2	K	0.03613/0.3807
NC8	12PG	0 0	1040.498860 1167.192790	0.3	K	0.53/2.72
EB	12PG	0 0	1030.229630 1214.556730	0.3	K	1.32207/6.117
OX	12PG	0 0	1141.603010 1230.777080	0.3	K	0.97/6.91
MX	12PG	0 0	1144.796980 982.0043530	0.3	K	0.799/5.57
PX	12PG	0 0	1052.456600 780.8529720	0.3	K	0.83524/3.04

CONCLUSIONS

This paper is focused on the determination of NRTL binary interaction parameters from liquid–liquid equilibrium data of binary systems containing paraffinic or aromatics hydrocarbons and 1,2-propanediol. These parameters can be used in order to elaborate an industrial process for the liquid-liquid extraction of aromatic hydrocarbon from petroleum fractions. Works are in progress for determining binary interaction parameters for iso-paraffinic and naphthenic hydrocarbons and 1,2-propanediol.

REFERENCES

1. F. Oprea and C. Strătulă, A New Solvent in Extractive Distillation for Benzene Removal, JICEC V, September 2005, Amman, Jordan.
2. PRO-II, Simsci Data Bank, Simulation Science, Vol. 8, 2007.
3. Aspen Plus 2004, Aspen Data Bank, Vol. 12, 2006.
4. S. Derawi, e. a., "Liquid-liquid equilibria for glycols+hydrocarbons: Data and correlation," *J. Chem. Eng. Data*, **47**(2), 169-173 (2002)
5. J. M. Prausnitz and J. M. Prausnitz, *AIChE J.*, **14**(1), 135-144 (1968).

ORIGINS OF *f*-ELEMENT SELECTIVITY IN SOLVENT EXTRACTION

Mark P. Jensen

Chemical Sciences and Engineering Division, Argonne National Laboratory, 9700 South Cass Avenue, Argonne, IL 60439, USA. Author email address: mjensen@anl.gov

ABSTRACT

Because of the great chemical similarity of the trivalent rare earth and trivalent actinide cations, all schemes proposed for the chemical separation of these elements exploit the modestly larger thermodynamic affinity of the actinide(III) cations for soft-donor ligands, those ligands which contain donor atoms that are softer than oxygen (e.g., nitrogen or sulfur). The thermodynamic effects driving the separation are believed to arise from the electronic differences between the 4*f* and 5*f* elements. Despite a large Am/Eu separation factor, structural studies of the complexes of model soft-donor ligands (dialkyldithiocarbamates) with trivalent lanthanide and actinide cations show no significant difference in the coordination environment (i.e., coordination numbers and average bond distances) across the series when the differences in cationic radii are considered.

INTRODUCTION

Chemical separation of the trivalent 4*f*, lanthanide (Ln), elements from the trivalent 5*f*, actinide (An), elements is among the most difficult separations in the periodic table, but it will be essential to the next generation of nuclear fuel cycles. As hard Lewis acids, Ln and An cations preferentially form complexes with hard Lewis bases. However, stable complexes with ligands containing donor atoms softer than oxygen, primarily those containing nitrogen, sulfur, or halide donors heavier than fluoride, will form under the proper conditions. When complexes form between *f*-element ions and these soft-donor ligands, An(III) cations form thermodynamically more stable complexes than the equivalent Ln(III) cations do, a fact that can be exploited to separate An(III) from Ln(III) [1]. This is usually attributed to a modestly greater degree of covalence in the An-soft-donor bonds as compared to the bonds in the Ln-soft-donor ligand complexes, but an understanding of the specific electronic origins of this enhanced covalence suggested by the thermodynamics is lacking. At various times, different investigators have proposed that the actinide 7*s*, 6*d*, or 5*f* orbitals may be primarily responsible for covalent bonding in different actinide complexes [2-6].

Physically, the stronger thermodynamic interaction between An(III) cations and soft-donor ligands brought about by the unidentified electronic differences in the Ln(III) and An(III) cations could be manifested in changes in the structures, coordination numbers, or stoichiometries of the complexes formed relative to the Ln(III) complexes.

For example, the thermodynamically stronger interactions could result in measurably shorter bonds for the An complexes or in complexes with more soft-donor atoms coordinated to the An than are observed for the equivalent Ln complex. The former case has been reported for U(III) complexes with soft-donor π-acceptor ligands [4,7,8], while the latter case is represented in certain concentration ranges by An(III)/Ln(III) chloro complexes [9] or the Cm(III) and Eu(III) complexes of bistriazinylpyridine (BTP) extractants [10].

One of the most selective An(III) solvent-extraction systems reported to date is dioctylammonium *N*,*N*-dioctyldithiocarbamate in nitrobenzene, with an Am/Eu separation factor of 3×10^4 [11]. Due to their instability in acidic solutions, dithiocarbamate extractants are unlikely to be used in practical An(III) recovery processes. Nevertheless, related dithiocarbamates such as *N*,*N*-diethyldithiocarbamate (Et_2dtc^- or $(C_2H_5)_2NCS_2^-$, Figure 1) provide an ideal opportunity to examine the structural chemistry, electronic structure, and separation thermodynamics of An(III) and Ln(III) cations with a highly selective soft-donor ligand that is also a well-known transition metal extractant. Dithiocarbamate complexes are easily synthesized and purified, and many Et_2dtc^- complexes are stable to oxidation and hydrolysis. This paper focuses on one specific aspect of our broader work. We hypothesize that the results of prior experiments on An(III)/Ln(III)-soft-donor complexes [10,12-14] are general—the An(III)/Ln(III) separation factor for transplutonium actinide cations caused by soft-donor ligands are not related to significantly shorter metal-ligand bonds as compared to the bonds in equivalent Ln(III) complexes when the slight differences in cationic radii are considered, and that this is true regardless of the type of donor ligand (e.g., σ-donor vs. π-acceptor ligands).

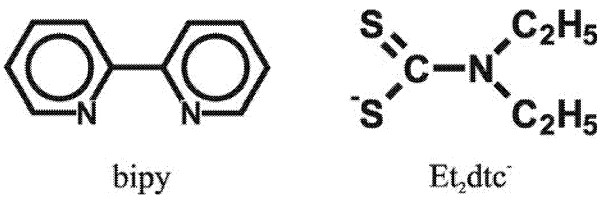

Figure 1. Ligands used in this study.

EXPERIMENTAL

Lanthanide dithiocarbamate-bipyridyl compounds were synthesized by the method of Su et al. [15]. In the case of the curium, Cm hydroxide was precipitated from an HCl solution of purified ^{248}Cm (96.77 atom % ^{248}Cm) and washed with water. The $Cm(OH)_3$ was dissolved with a minimal volume of 0.18 M $HClO_4$ in wet acetonitrile, and Cm-tris(dithiocarbamate)-bipyridyl crystals formed rapidly when $(Et_2NH_2)(Et_2dtc)$ and 2,2'-bipyridyl (bipy) in acetonitrile was added to this solution give a 1:3:1 Cm:Et_2dtc:bipy ratio. X-ray absorption measurements on the resulting solids were made and analyzed as described elsewhere [12,16]. Uncertainties are given at 95% confidence.

RESULTS AND DISCUSSION

To examine the interplay between separation factor, ligand type, and metal-ligand bond distances, we turned to a set of An(III)/Ln(III) ternary complexes containing two different soft-donor ligands that are selective for An(III) cations, the sulphur donor ligand Et_2dtc^- and the nitrogen donor ligand bipy. Both ligands form bidentate complexes with *f*-element cations, and together they form a homologous series of $M(Et_2dtc)_3(bipy)$ complexes across the entire lanthanide series [15,17]. In addition to being able to separate An(III) from Ln(III), these ligands are also interesting from an electronic perspective because they operate through different bonding modes. Dithiocarbamate ligands are strong σ-donors [18], while 2,2'-bipyridyl is a less selective ligand well-known as a π-acceptor, which is prone to allowing back-donation from metal-centered orbitals of the correct symmetry into empty ligand π orbitals. Such π-acceptor ligands have previously been shown to form unusually short metal-ligand bonds in uranium(III) complexes relative to those in similar Ln(III) complexes [4,7,8,19], but such behavior has been reported only for the light actinide, uranium. In those experiments, the contraction in the average U(III)-N bond length relative to the average Ce(III)-N bond length could be correlated with the U(III)/Ce(III) separation factor of the ligands [8]. However, measurable contractions in An-soft-donor ligand bond lengths have not been reported in Am(III) or Cm(III) complexes, regardless of the observed An/Ln separation factor, presumably due to differences in electronic structures between the light and heavier (transplutonium) 5*f* ions, which make light actinides, such as uranium, poor surrogates for the transplutonium actinides in studying the origins of the effectiveness of soft-donor complexes for An/Ln separations.

Typical results of EXAFS measurements on the $M(Et_2dtc)_3(bipy)$ complexes are summarized in Figure 2 and Table 1, which lists the average metal-sulfur bond distances found in the complexes. The results are consistent with crystallographic studies of the same compounds where available [20,23]. For all the Ln(III) and An(III) complexes studied, we find the same coordination geometry; that is, two nitrogen donors from one bidentate bipy ligand occur between ca. 2.5 and 2.7 Å from the metal center and six sulfur donors from three bidentate Et_2dtc^- ligands are observed at an average distance of ca. 2.8 to 2.95 Å, with the exact distance determined by the cationic radius of the Ln(III) or An(III) present. Since the cationic radii of the Ln(III) and An(III) cations vary across each series of elements, direct comparison of the bond distances must consider this variation. A simple way to do this is to subtract the cationic radius for the appropriate octacoordinate cation [22] from the metal-donor atom distance to obtain the effective average radius of the donor atom in that environment. For Et_2dtc^-, this value, $R_{M\text{-}S} - R_M$, is 1.78 ± 0.01 Å for the average of the Ln ions studied and 1.76 ± 0.02 Å for the actinide Cm (Table 1). Likewise, for the nitrogen donors of bipy, the average $R_{M\text{-}N} - R_M$ is 1.53 ± 0.01 Å for the Ln ions and 1.51 ± 0.02 Å for Cm. The Cm-ligand bonds appear to be 0.02 ± 0.02 Å shorter than the corresponding Ln-ligand bonds regardless of the type of ligand involved or its An/Ln separation factor. Given the uncertainties in the values, however, the difference cannot be considered indicative of anything without more precise measurements.

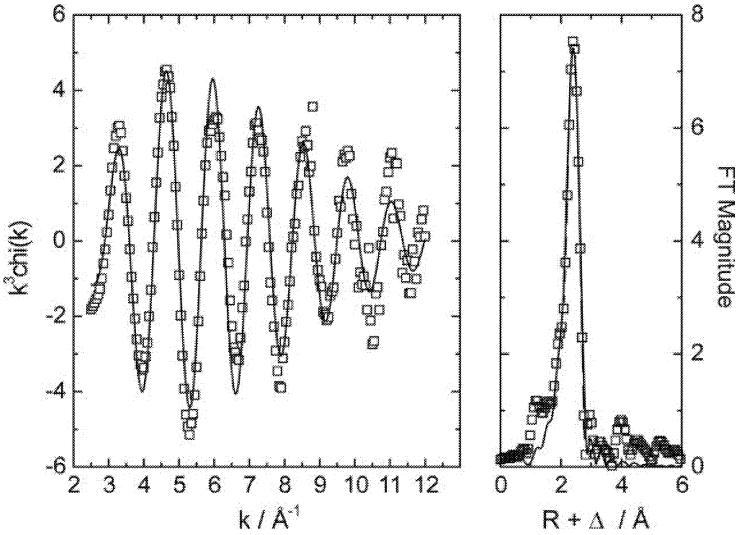

Figure 2. L_3-edge EXAFS of $Eu(Et_2dtc)_3(bipy)$ and its Fourier transformation. Every third data point (□) is shown, as is the best fit (—) of 2 N and 6 S atoms modeled from the $Eu(Et_2dtc)_3(bipy)$ crystal structure [20] with FEFF8 [21]. The data are not phase-shift corrected.

Table 1. Average metal-sulfur bond distances in Ln(III)- and An(III)-tris(*N*,*N*-diethyldithiocarbamato)(2,2'-bipyridyl) complexes as measured by EXAFS

	Ionic Radius / Å	EXAFS		Crystallography	
Element	CN=8 [22]	$R_{M\text{-}S}$ / Å	$R_{M\text{-}N}$ / Å	Avg. $R_{M\text{-}S}$ / Å	$R_{M\text{-}S} - R_M$ / Å
Nd	1.107	2.89 (2)	2.65 (4)		1.78
Sm	1.079	2.85 (4)	2.62 (4)	2.858 (30) [23]	1.77
Eu	1.065	2.84 (3)	2.60 (4)	2.850 (26) [20]	1.78
Gd	1.055	2.83 (2)	2.60 (4)		1.78
Cm	1.094	2.86 (2)	2.61 (4)		1.76

These measurements make it clear that neither the Cm-S bonds nor the Cm-N in $Cm(Et_2dtc)_3(bipy)$ are *much* shorter than the corresponding Ln-S or Ln-N bonds in $Ln(Et_2dtc)_3(bipy)$. It does not matter if the ligand is from the family of highly selective, σ-donor dithiocarbamate extractants, or from the less selective family of π-acceptor ligands like bipyridyl. This is in contrast to many X-ray diffraction measurements on uranium(III) soft-donor π-acceptor compounds, where the U-L bonds can be 0.04 Å to more than 0.1 Å shorter than the corresponding Ln-L bonds, even for ligands that show relatively low U(III)/Ln(III) separation factors (e.g., U/Ce = 3.3 [24]).

CONCLUSIONS

Extending the structural examination of An soft-donor complexes to additional classes of ligands, we find no evidence for differences in the stoichiometry or

coordination number of the complexes formed or significant (≥0.04 Å) bond-length contractions between the An(III) and Ln(III) complexes studied, despite the thermodynamic preference of Et_2dtc^- and bipy for An(III) cations. Since the thermodynamic preference of soft-donor ligands for An(III) cations has an electronic basis that is not being manifested in differing structural properties of these complexes, we have examined the electronic structure of the same An/Ln-Et_2dtc-bipy complexes using optical (e.g., [17,25]) and X-ray spectroscopies and are dissecting the free energies of separation into their enthalpic and entropic components to better understand these unique complexes and the specific origins of An(III) selectivity utilized in An/Ln separations.

ACKNOWLEDGMENTS

BESSRC-CAT and the Argonne Actinide Facility for Synchrotron Radiation Research provided the infrastructure for the EXAFS measurements. This work was performed under the auspices of the U. S. DOE OBES, Divisions of Materials Science (for the EXAFS measurements at the APS) and of Chemical Sciences, Geosciences, and Biosciences under contract number DE-AC02-06CH11357.

REFERENCES

1. K. L. Nash, "A Review of the Basic Chemistry and Recent Developments in Trivalent f-Elements Separations," *Solvent Extr. Ion Exch.*, **11**, 729-768 (1993).
2. R. J. Strittmatter and B. E. Bursten, "Bonding in Tris(η^5-cyclopentadienyl) Actinide Complexes. 5. A Comparison of the Bonding in Np, Pu, and Transplutonium Compounds with that in Lanthanide Compounds and a Transition Metal Analogue," *J. Am. Chem. Soc.*, **113**, 552-559 (1991).
3. G. R. Choppin, "Covalency in f-Element Bonds," *J. Alloys Compd.*, **344**, 55-59 (2002).
4. M. Mazzanti, R. Wietzke, J. Pécaut, J.-M. Latour, P. Maldivi, and M. Remy, "Structural and Density Functional Studies of Uranium(III) and Lanthanum(III) Complexes with a Neutral Tripodal N-Donor Ligand Suggesting the Presence of a U-N Back-Bonding Interaction," *Inorg. Chem.*, **41**, 2389-2399 (2002).
5. M. Miguirditchian, D. Guillaneux, D. Guillaumont, P. Moisy, C. Madic, M. P. Jensen, and K. L. Nash, "Thermodynamic Study of the Complexation of Trivalent Actinide and Lanthanide Cations by ADPTZ, a Tridentate N-Donor Ligand," *Inorg. Chem.*, **44**, 1404-1412 (2005).
6. D. Guillaumont, "Quantum Chemistry Study of Actinide(III) and Lanthanide(III) Complexes with Tridentate Nitrogen Ligands," *J. Phys. Chem,. A*, **108**, 6893-6900 (2004).
7. J. G. Brennan, S. D. Stults, R. A. Andersen, and A. Zalkin, "The Coordination Chemistry of Trivalent Uranium and Cerium," *Inorg. Chim. Acta*, **139**, 201-202 (1987).
8. J.-C. Berthet, C. Rivière, Y. Miquel, M. Nierlich, C. Madic, and M. Ephritikhine, "Selective Complexation of Uranium(III) over Cerium(III) and Neodymium(III) by 2,2',6',2"-Terpyridine. X-ray Crystallographic Evidence for Uranium-to-Ligand π Back-Bonding," *Eur. J. Inorg. Chem.*, 1439-1446 (2002).
9. R. M. Diamond, K. Street, and G. T. Seaborg, "An Ion-exchange Study of Possible Hybridized 5f Bonding in the Actinides," *J. Am. Chem. Soc.*, **76**(6), 1461-1469 (1954).

10. M. Denecke, A. Rossberg, P. J. Panak, M. Weigl, B. Schimmelpfennig, and A. Geist, "Characterization and Comparison of Cm(III) and Eu(III) Complexes with 2,6-Di(5,6-dipropyl-1,2,4-triazin-3-yl)pyridine Using EXAFS, TRFLS, and Quantum-Chemical Methods," *Inorg. Chem.*, **44**, 8418-8425 (2005).
11. S. Miyasita, M. Yanaga, I. Satoh, and H. Suganuma, "Separation of Americium(III) from Europium(III) by Dioctylammonium Dioctyldithiocarbamate/Nitrobenzene Extraction," *Chem. Lett.*, **35**, 236-237 (2006).
12. M. P. Jensen and A. H. Bond, "Comparison of Covalency in the Complexes of Trivalent Actinide and Lanthanide Cations," *J. Am. Chem. Soc.*, **124**, 9870-9877 (2002).
13. T. Yaita, S. Tachimori, N. M. Edelstein, J. J. Bucher, L. Rao, D. K. Shuh, and P. G. Allen, "EXAFS Studies of Americium(III)-Benzimidazole Complex in Ethanol," *J. Synchrotron Rad.*, **8**, 663-665 (2001).
14. G. Tian, Y. Zhu, J. Xu, T. Hu, and Y. Xie, "Characterization of Extraction Complexes of Am(III) with Dialkyldithiophosphinic Acids by Extended X-ray Absorption Fine Structure Spectroscopy," *J. Alloys Compd.*, **334**, 86-91 (2002).
15. C. Su, N. Tang, M. Tan, and K. Yu, "Synthesis, Properties and Structure of Lanthanide Complexes with N,N-Diethyldithiocarbamate and 2,2'-Bipyridyl," *Polyhedron*, **15**, 233-239 (1996).
16. M. P. Jensen, J. Neuefeind, J. V. Beitz, S. Skanthakumar, and L. Soderholm, "Mechanisms of Metal Ion Transfer into Room-Temperature Ionic Liquids: The Role of Anion Exchange," *J. Am. Chem. Soc.*, **125**(50), 15466-15473 (2003).
17. G. K. Liu, M. P. Jensen, and P. M. Almond, "Systematic Behavior of Charge-Transfer Transitions and Energy Level Variation in Soft Donor Complexes of the Trivalent Lanthanides," *J. Phys. Chem. A*, **110**, 2081-2088 (2006).
18. A. M. Bond and R. L. Martin, "Eletrochemistry and Redox Behavior of Transition Metal Dithiocarbamates," *Coord. Chem. Rev.*, **54**, 23-98 (1984).
19. C. Rivière, M. Nierlich, M. Ephritikhine, and C. Madic, "Complexation Studies of Iodides of Trivalent Uranium and Lanthanides (Ce and Nd) with 2,2'-Bipyridine Solutions," *Inorg. Chem.*, **40**, 4428-4435 (2001).
20. V. L. Varand, L. A. Glinskaya, R. F. Klevtsova, and S. V. Larionov, "Synthesis and Crystal and Molecular Structure of Mixed-Ligand Compounds $Eu(S_2CN(C_2H_5)_2)_3$(2,2'-Bipy) and $Eu(S_2CN(C_2H_5)_2)_3$(1,10-Phen)," *J. Struct. Chem.*, **39**(2), 244-252 (1998).
21. A. L. Ankudinov, B. Ravel, J. J. Rehr, and S. D. Conradson, "Real-space multiple-scattering calculation and interpretation of x-ray absorption near-edge structure," *Phys. Rev. B*, **58**, 7565-7576 (1998).
22. F. David, "Thermodynamic Properties of Lanthanide and Actinide Ions in Aqueous Solution," *J. Less-Common Met.*, **121**, 27-42 (1986).
23. V. L. Varand, L. A. Glinskaya, R. F. Klevtsova, and S. V. Larionov, "Synthesis and Crystal and Molecular Structure of Mixed-Ligand Compounds Sm(2,2'-Bipy)$(S_2CN(C_2H_5)_2)_3$ and SmPhen$(S_2CN(C_2H_5)_2)_3$: Crystal Structure of Sm(2,2'-Bipy)$(S_2CN(C_2H_5)_2)_3$," *J. Struct. Chem.*, **41**(3), 544-549 (2000).
24. L. Karmazin, M. Mazzanti, and J. Pécaut, "Unique Crown Thioether Complexes of f-elements: The Crystal Structure of U(III) and La(III) Complexes of 1,4,7-trithiacyclononane," *Chem. Commun.*, 654-655 (2002).
25. X. Y. Chen, M. P. Jensen, and G. K. Liu, "Analysis of Energy Level Structure and Excited-State Dynamics in a Sm^{3+} Complex with Soft-Donor Ligands: $Sm(Et_2Dtc)_3$(bipy)," *J. Phys. Chem. B*, **109**, 13991-13999 (2005).

PREDICTION AND OPTIMIZATION OF THE SEPARATION SELECTIVITY BETWEEN METALLIC ELEMENTS WITH SIMILAR CHEMICAL PROPERTIES

S.C. Belair[1] and P. Dannus [2]

[1]*Johnson Matthey Technology Centre, Sonning Common, Reading, RG4 9NH, UK.*
[2]*Commissariat à l'Energie Atomique, CEA-Saclay, INSTN, 91191 Gif-sur-Yvette Cedex, France. Corresponding author email address: belairsc@matthey.com*

ABSTRACT

Application of Mikulin's relationship to estimate the activity coefficients of two extracted elements shows that the selectivity factor is a combination of an intrinsic factor and a water-activity factor. The separation selectivity of a system can then be predicted and optimiZed by modifying the medium conditions. In the context of studies dealing with the recovery of the most radiotoxic elements from raffinate solutions of the PUREX process, the separation selectivity between lanthanides(III) and between americium(III) and europium(III) has been simulated using this approach for an extraction system using a CMPO-like calixarene extractant.

INTRODUCTION

Extractants that have several potential coordination sites can easily form a number of different complexes. A complete analytical model of these systems using the Mikulin-Sergievskii model [1] is therefore difficult. Studies on an extraction system involving a CMPO-like calixarene at 10^{-3} mol kg^{-1} in nitrophenylhexyl ether (NPHE) have shown this limitation [2]. Indeed, modelling of a system involving nitric acid, europium(III), and calixarene of this family revealed the formation of many complexes between these three components, but neither the complete stoichiometries nor the associated formation constants could be determined [2].

However, efficient predictions on the extraction selectivity can be achieved easily and rapidly in spite of the lack of thermodynamic data. This is particularly useful when the influence of the chemical conditions on the separation selectivity between two elements with similar chemical properties must be evaluated.

THEORY

The extraction Equilibrium 1 includes all of the organic complexes that can be formed between a metal(III) ion and a neutral solvating extractant in nitric acid media:

$$i\mathrm{M}^{3+} + (3i + j)\mathrm{NO}_3^- + j\mathrm{H}^+ + h\mathrm{H_2O} + q\overline{\mathrm{E}} \rightleftharpoons \overline{\mathrm{M}_i(\mathrm{E})_q(H)_{\mathrm{j}}(\mathrm{NO_3})_{3i+j}(\mathrm{H_2O})_h} \quad (1)$$

where the line above the species indicates they are in the organic phase.

The mass action law related to this equilibrium is:

$$K_{\mathrm{M}}^0 = \frac{\left[\overline{\mathrm{cpx}}\right]}{\left(a_{\mathrm{M(NO_3)_3}}\right)^i \times \left(a_{\mathrm{HNO_3}}\right)^j \times \left(a_{\mathrm{H_2}O}\right)^h \times \left[\overline{\mathrm{E}}\right]^q} \times \frac{\overline{y_{\mathrm{cpx}}}}{\left(\overline{y_{\mathrm{E}}}\right)^q} \quad (2)$$

where $\overline{\mathrm{cpx}} = \overline{\mathrm{M_i(E)_q(NO_3)_{3i+j}(H_2O)_h}}$, and $a_{\mathrm{M(NO_3)_3}}$, $a_{\mathrm{HNO_3}}$, and $a_{\mathrm{H_2}O}$ represent, respectively, the thermodynamic activities of the electrolyte $\mathrm{M(NO_3)_3}$, the nitric acid, and the water. $\left[\overline{\mathrm{E}}\right]$ is the free extractant concentration, $\overline{y_{\mathrm{cpx}}}$ and $\overline{y_{\mathrm{E}}}$ are the activity coefficients of the organic complex and the free extractant molecule. K_{M}^0 is the thermodynamic extraction constant of the metal M.

For a given set of chemical conditions, it can be assumed that two metallic elements with similar chemical properties will be extracted as complexes with the same stoichiometry. The distribution ratio expressions, D_{M}, for the metal A ($\mathrm{M_A}$) and the metal B ($\mathrm{M_B}$) will also take the same form. By assuming that each metal M is extracted as one major complex and that the activity coefficient ratio for the organic complexes $\mathrm{cpx_A}$ and $\mathrm{cpx_B}$ is close to 1, then the selectivity factor α between two metals $\mathrm{M_A}$ and $\mathrm{M_B}$, can be expressed as:

$$\alpha_{\mathrm{M_A/M_B}} = \frac{\mathrm{K_A^0}}{\mathrm{K_B^0}} \times \left[\frac{\mathrm{C_{M_A(NO_3)_3}}}{\mathrm{C_{M_B(NO_3)_3}}}\right]^{\mathrm{i\text{-}1}} \times \left[\frac{\mathrm{y_{st,M_A(NO_3)_3}}}{\mathrm{y_{st,M_B(NO_3)_3}}}\right]^{4\mathrm{i}} \quad (3)$$

where $C_{\mathrm{M(NO_3)_3}}$ is the concentration of the electrolyte $\mathrm{M(NO_3)_3}$ in the mixture and $y_{\mathrm{st,M(NO_3)_3}}$ is its stoichiometric activity coefficient.

Writing the stoichiometric activity coefficients of each metal using the Mikulin relationship [3], the selectivity factor becomes:

$$\alpha_{\mathrm{M_A/M_B}} = \frac{\mathrm{K_A^0}}{\mathrm{K_B^0}} \times \left[\frac{4 \times \mathrm{C_{M_A(NO_3)_3}^{bi}} \times \mathrm{y_{st,M_A(NO_3)_3}^{bi}}}{4 \times \mathrm{C_{M_B(NO_3)_3}^{bi}} \times \mathrm{y_{st,M_B(NO_3)_3}^{bi}}}\right]^{4\mathrm{i}} \times \left[\frac{\mathrm{C_{M_A(NO_3)_3}}}{\mathrm{C_{M_B(NO_3)_3}}}\right]^{\mathrm{i\text{-}1}} \quad (4)$$

where "bi" refers to the component in its binary solution with the same water activity ($a_{\mathrm{H_2O}}$) as in the mixture.

The selectivity factor is therefore a combination of an intrinsic factor, the thermodynamic constant ratio, and a water-activity factor. The latter is the ratio of the *water activity functions* ($F_{\mathrm{M(NO_3)_3}} = 4 \times C_{\mathrm{M(NO_3)_3}}^{\mathrm{bi}} \times y_{\mathrm{st,M(NO_3)_3}}^{\mathrm{bi}}$) of the extracted metals [4]. Moreover, if the major complex has the $i = 2$ stoichiometry (which is the case only if the

metals are in excess), the selectivity factor also depends on the ratio of the metal concentrations in the aqueous phase. The selectivity factor can then be expressed as:

$$\alpha_{A/B} = (\alpha_1) \times (\alpha_2)^{4i} \times (\alpha_3)^{i-1} \quad (5)$$

where $\alpha_1 = \frac{K_A^0}{K_B^0}$; $\alpha_2 = \frac{F_{M_A(NO_3)_3}}{F_{M_B(NO_3)_3}}$; $\alpha_3 = \frac{C_{M_A(NO_3)_3}}{C_{M_B(NO_3)_3}}$

The function F is an electrolyte feature that depends on the water activity of the mixture. It can be calculated easily for the lanthanide nitrates from binary data published in the literature as shown by Mokili et al. [4]. In infinitely dilute aqueous solution ($a_{H2O} \approx 1$), the F functions converge towards the same very low value ($\alpha_2 = 1$), whatever the electrolyte. For a_{H2O} values less than 1, the increase in the F value is greater when the atomic number of the lanthanide is higher. Moreover, the differences between F values become much greater as the water activity is lowered. Thus, in the case of a separation between two lanthanides Ln_A and Ln_B, with $Z_{LnA} > Z_{LnB}$, α_2 is always greater than 1 when a_{H2O} is less than 1.

No data are available in the literature to calculate the functions F_{Am} (a_{H2O}) and F_{Cm} (a_{H2O}) relative to the electrolytes americium and curium nitrates. However, as neodymium(III) is routinely chosen as a stable chemical analogue of americium(III) and curium(III) [5], it is legitimate to assume that the F_{Am} and F_{Cm} functions are close to that of $Nd(NO_3)_3$.

It can also be assumed that, when metal concentrations are low relative to the extractant concentration, the most likely stoichiometry is $i = 1$, in which case $\alpha_3 = 1$. The Expression 5 then becomes $\alpha_{A/B} = (\alpha_1) \times (\alpha_2)^4$. Due to the 1:3 stoichiometry of the lanthanide and actinide salts, the selectivity factor is very sensitive to variation in water activity (power of 4 for α_2).

EXPERIMENTAL

The CMPO-like calixarene used was the MN45 [6]. This extractant was diluted at 10^{-3} mol kg^{-1} in NPHE (1,2-nitrophenylhexylether). Extraction experiments were performed by contacting equal volumes of aqueous solutions and organic solvents for 1 hour at 25 ± 1 °C (equilibrium was reached in a few minutes). Samples were taken for analysis after centrifugation. Acidities were measured by titration with NaOH in aqueous media for aqueous and organic phases. In the experiments involving lanthanides only, the lanthanide concentrations in the aqueous phase were determined by ICP-OES while the lanthanide concentrations in the organic phase were determined by calculating the difference between the initial and the equilibrium concentration in the aqueous phase. In the experiment involving americium and europium, ^{241}Am and ^{152}Eu concentrations were analyzed by γ counting (γ spectrometry).

RESULTS AND DISCUSSION

Separation of Lanthanides(III)

Depending on the lanthanide pair involved, three possible situations can arise: firstly, $K_A^0 > K_B^0$ (i.e. $\alpha_1 > 1$) (case A); secondly $K_A^0 \approx K_B^0$ *i.e.* $\alpha_1 \approx 1$ (case B); and finally $K_A^0 < K_B^0$ (i.e. $\alpha_1 < 1$) (case C). In a dilute aqueous solution, the water activity is close to 1 (i.e. $\alpha_2 = 1$). When the acid concentration is increased, then a_{H2O} decreases (for example when $[HNO_3] = 3$ mol L^{-1}, $a_{H2O} \approx 0.88$), and consequently α_2 increases. A decrease in the water activity therefore leads to an increase in $\alpha_{A/B}$ value in all situations. Thus, for cases A and B, the extraction selectivity M_A/M_B increases. On the other hand, it decreases in case C and could even result in better extraction of M_A than M_B.

Figure 1a shows the experimental results obtained for solvent extractions of aqueous solutions containing two lanthanides (Eu/Pr, Eu/Nd, Eu/Sm) at 10^{-4} mol kg^{-1} with a nitric acid concentration ranging from 1 to 5.5 mol kg^{-1}. For a water activity close to 1, the selectivity factor is close to 1, whatever the couple. The extraction constants K_{Ln}^0 are therefore similar for the lighter lanthanides. This means that the CMPO-like calixarene has the same intrinsic affinity for praseodymium, neodymium, samarium, and europium (case B). When the water activity decreases, the selectivity factor increases, whatever the couple. The increase becomes greater as the difference between the atomic numbers of the two lanthanides increases. Thus, for solutions containing nitric acid at 3 mol kg^{-1} ($a_{H_2O} = 0.88$), the CMPO-like calixarene was shown to extract europium better than the lighter lanthanides. The previous qualitative predictions are therefore confirmed: when the extractant has a similar affinity for two lanthanides(III), a water activity decrease leads to a better separation in favor of the heavier element.

An extraction study has also been carried out with gadolinium and europium ($Z_{Gd} > Z_{Eu}$). The initial lanthanide concentrations were 10^{-4} mol kg^{-1} for the first experimental set and 5×10^{-3} mol kg^{-1} for the second set, with a nitric acid concentration ranging from 0.1 to 5.5 mol kg^{-1}. The results (Figure 1b) show that this system behaves as in case C, with the heavier element Gd(III) showing a lower affinity for the CMPO-like calixarene ($K_{Gd}^0 < K_{Eu}^0$) when the water activity is close to 1. When the water activity decreases, the $\alpha_{Gd/Eu}$ value increases and a drop in the separation selectivity between the two elements occurs. Experiments at high lanthanide concentrations enhance the formation of complexes involving two moles of lanthanide per mole of calixarene ($i = 2$). Under these conditions, the factor α_2 is increased from the power of 4 to the power of 8, which intensifies the effect of the variation of a_{H_2O} on $\alpha_{Gd/Eu}$.

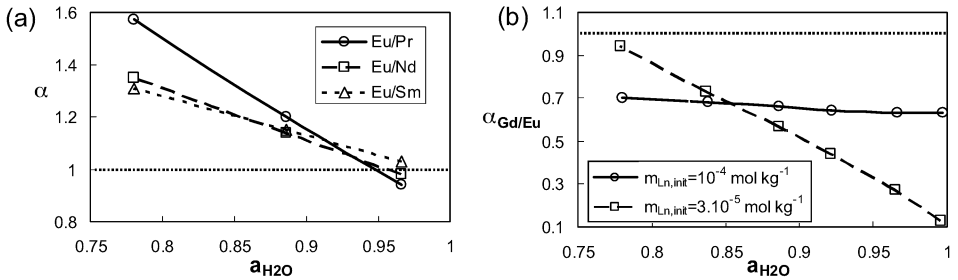

Figure 1. Influence of water activity on the separation between lanthanide(III) ions extracted by a CMPO-like calixarene at 10^{-3} mol kg^{-1} in NPHE, T = 25 °C. (a):Eu/Pr, Eu/Nd, Eu/Sm, (b):Gd/Eu.

Separation of Actinide(III) and lanthanide(III)

In the case of an actinide(III)/lanthanide(III) separation, K_{An} is always higher than K_{Ln} [7]. By assuming that the water activity functions for actinide(III) nitrates, F_{An}, are similar to that of the neodymium nitrate, F_{Nd}, two situations can arise. For lanthanides lighter than neodymium (case D), a decrease in the water activity should lead to an increase in the selectivity factor $\alpha_{An/Ln}$. The An/Ln separation would then be better. On the other hand, for lanthanides heavier than neodymium (case E), a decrease in the water activity should result in a decrease of the selectivity factor $\alpha_{An/Ln}$. The An/Ln separation would then be lower. For the lanthanides adjacent to neodymium, this trend could even give rise to better extraction of the lanthanides than the actinides ($\alpha_{An/Ln} < 1$).

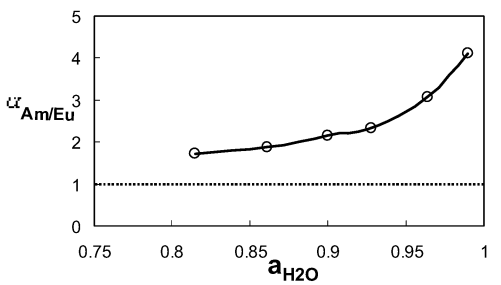

Figure 2. Influence of water activity on the separation of americium(III) and europium(III) at 10^{-8} mol kg^{-1} extracted by a CMPO-like calixarene at 10^{-3} mol kg^{-1} in NPHE, T = 25 °C.

The experimental results for the separation of americium/europium mixtures (10^{-8} mol kg^{-1}) with a nitric acid concentration ranging from 0.3 to 4.5 mol kg^{-1} are shown in Figure 2. The results are in accord with the predictions for case E. High acid concentrations result in a decrease of the selectivity factor $\alpha_{An/Ln}$ when the lanthanide is heavier than neodymium. Moreover, the extrapolation of $\alpha_{An/Ln}$ for $a_{H2O} = 1$ confirms that the extractant has a better affinity for An(III) than for Ln(III).

CONCLUSION

The results obtained in this study provide useful information on separation trends that can help optimize extraction processes, regardless of the extractant used. In the

particular case of an extractant that has a better affinity for actinides(III) than for lanthanides(III), a decrease in the water activity of the system will result in a decrease in the selectivity factor if the lanthanides are heavier than the neodymium, while the selectivity factor will increase if the lanthanides are lighter than the neodymium. For systems involving a neutral extractant, the water activity can be simply set by fitting the acid concentration in the media. The concentrations of the metals in the feed are also variables which can be changed in order to increase or decrease the water activity.

To classify unambiguously the intrinsic affinity of an extractant for two metals with similar chemical properties (K_A^0 vs K_B^0), it is recommended that the experimental values of α as a function of a_{H2O} be determined and then extrapolated to $a_{H2O} = 1$.

When the thermodynamic extraction constants are known, an efficient prediction on the evolution of the separation factor with a_{H2O} can be achieved easily by calculating the water activity functions of each element from binary data published in the literature. Therefore, the extraction selectivity can be determined for any chemical conditions. When the value of the thermodynamic extraction constants are not exactly known, but the relative intrinsic affinity of the extractant is, the evolution of the separation factor with a_{H2O} can be estimated by using the same approach.

ACKNOWLEDGMENTS

The authors thank Prof. V. Bohmer and his team from the University of Mainz, who synthesized the calixarene, and Dr. C. Mariet and M. Tabarant from CEA-Saclay for their assistance in the γ spectrometry and ICP-OES measurements.

REFERENCES

1. S. Belair, C. Lamouroux, M. Tabarant, A. Labet, C. Mariet, and P. Dannus, "Modeling of the Extraction of Lanthanide Nitrates from Aqueous Solutions over a Wide Range of Activities by CMPO," *Solvent Extraction And Ion Exchange*, **22**(5), 1-21 (2004).
2. S. Belair, "Thermodynamic modelling of the extraction of nitrates of lanthanides by CMPO and by CMPO-like calixarene in concentrated nitric acid medium," Ph.D. Thesis, Paris VI University, Paris, France, 2002; *CEA report No CEA-R-6017*; pp. 115-145.
3. V. M. Vdovenko and M. A. Rjazanov, "Activity Coefficients in Polycomponent Systems," *Soviet Radiochemistry*, **7**, 39-44 (1965).
4. B. Mokili and C. Poitrenaud, "Medium Effect on the Separation Factor in Liquid-Liquid Extraction. Application to the Separation of Trivalent Lanthanide Nitrates by Tri-N-Butylphosphate," *Solvent Extraction and Ion Exchange*, **15**(3), 455-481 (1997).
5. K. Nash, Handbook on the Physics and Chemistry of Rare Earth. Lanthanides/Actinides: Chemistry, Vol. 18, Gschneidner, K., Jr. et al., Amsterdam, 1994.
6. A. Garcia-Carrera, J. F. Dozol, P. Dannus, et al., "Modeling of Nitric Acid and Actinide/Lanthanide Extraction by CMPO-Like Calixarenes," ISEC 2002, K. C. Sole, P. M. Cole, *et al.*, Eds., Cape Town, South Africa, 2002; Vol. 2, pp. 1174-1179.
7. L. Delmau, N. Simon, M. J. Schwing-Weil, F. Arnaud-Neu, J. F. Dozol, *et al.*, "'CMPO-Substituted' Calix[4]arenes, Extractants with Selectivity among Trivalent Lanthanides and between Trivalent Actinides and Lanthanides," *Chemical Communications*, 1627-1628 (1998).

ANION-EXCHANGE EXTRACTION OF CARBOXYLATES

Alexander L. Gulevich,[1] Tatsiana N. Kiyko,[2] and Vadim A. Kovalevich[1]

[1]*Belarusian State University, 220050 Leningradskaya Street, Minsk, Belarus.*
[2]*Belarusian State Technological University, 220050 Sverdlova Street, Minsk, Belarus.*
Corresponding author email address: a.l.gulevich@mail.ru

ABSTRACT

The anion-exchange extraction of carboxylic acids, halogenacetic acids, and α-aminoacids anions by toluene solutions of higher quaternary ammonium salts has been investigated, and the concentration exchange constants and the nature of extracted anions have been interrelated. The influence of a series of trifluoroacetylderivatives with different structure on the anion-exchange extraction efficiency of carboxylates has been widely investigated; the average solvation numbers and the solvation constants have been calculated. It was established that the solvation efficiency of these compounds depends on the nature of substituents in the aromatic ring. New much more effective structures in comparison with known structures have been revealed.

INTRODUCTION

Higher quaternary ammonium salts (QAS) are effective extractants of anions of various nature and are widely used in extraction photometry as well as in the capacity of electrode-active substances for membranous ion-selective electrodes [1]. Unequivocal use of QAS in analytical chemistry is impossible without knowing corresponding exchange constants. While numerical values of exchange constants for simple nonorganic anions can be found in the reference literature [2], there are almost no such data for organic anions. This study, conducted in Belarus State University, contains experimental results of investigations of anion-exchange extraction of carboxylates by toluene solutions of trinonyloctadecylammonium in the 2,4-dinitrophenolate form, as well as in the presence of solvating additives, trifluoroacetophenone derivatives.

EXPERIMENTAL

Anion-exchange extraction of anions from awater phase by higher QAS toluene solution reaction, assumed to have the simple form

$$R_4N^+B^-_{org} + X^-_{aq} \rightleftharpoons R_4N^+X^-_{org} + B^-_{aq}, \quad (1)$$

can be described by a concentration exchange constant:

$$K_{B^-}^{X^-} = \frac{[R_4N^+X^-]_{org}[B^-]_{aq}}{[R_4N^+B^-]_{org}[X^-]_{aq}} \quad . \tag{2}$$

Calculation of the exchange constant by Formula (2) is easily done if acid dyes (Kp) are used as the B-anion, where [Kp] is determined by a spectrophotometric method:

$$K_{Kp^-}^{X^-} = \frac{[Kp^-]_{aq}^2}{(C_{0,R_4N^+Kp^-} - [Kp^-]_{aq})(C_{0,X^-} - [Kp^-]_{aq})}. \tag{3}$$

The QAS was trinonyloctadecylammonium $(C_9H_{19})_3C_{18}H_{37}N^+$ in the 2,4-dinitrophenolate (DNP) or picrate (Pic) form; starting concentration was maintained at 10^{-3} mol/L. The diluent of QAS was toluene. Water solutions of organic anions had concentrations within the range 10^{-1}–10^{-3} mol/L, in dependence on anion extractability. The extraction process was carried out at the 293 ± 0.5 K. Equilibrium concentrations of dye in water phase ([Kp]) were determined by a spectrophotometric method at λ = 410 nm in reference to a blank experiment.

RESULTS AND DISCUSSION

Table 1 lists the concentration exchange constants of carboxylates of different nature with respect to 2,4-dinitrophenolate- anions.

The analysis of experimental data demonstrates that logarithms of the monobasic fatty acid anion concentration exchange constants, except for formate, comply with the principle of free extraction energy additivity [3] and are described by the following equation:

$$\log K_{DNP^-}^{C_nH_{2n+1}COO^-} = I_{-COO^-/DNP^-}^{ex} + (n-1)I_{CH_2} + I_{CH_3}\ , \tag{4}$$

where the $I^{ex}_{-COO^-/DNP-}$ exchange increment is equal to the logarithms of the exchange constant of the hypothetical $-COO^-$-anion to DNP^--anion; and I_{CH_2} and I_{CH_3} are increment values for $-CH_2-$ and $-CH_3$ groups.

Substitution of one or several hydrogen atoms in acetate by halogen atoms, regardless of their nature, leads to an increase of exchange constants. Independent of the degree of halide-acetate substitution, extractability rises in the order fluoro-, chloro-, bromo-, and iodo-acetate. Within the range of one halide-acetate type, extractability rises with increasing substitution. This pattern of halogen atom influence on the extractability is determined by many factors, the main being the size of the halogen atom and its influence on the distribution of effective charges in extractable anion atoms.

Extractability of substituted benzoates also significantly depends on the substituent nature and its position with regard to the ionogenic group.

High extractability of o-oxybenzoate- and N-phenylanthranylate-anions, and the best extractability of ortho-aminobenzoate-anion among isomers can be explained by intraelectrostatic hydrogen-bond formation (ortho-effect). Introduction of nitrogen

groups, as well as halogen atoms, into the anion composition increases the anion extractability in all positions. An amino group in a *meta* and *para* position, incapable of forming a hydrogen bond with the carboxy group, is a second hydrophilic center and therefore reduces anion extractability. Large-sized substituents (in case of *ortho*-benzoylbenzoate- and *para*-hexyloxybenzoate-anions) increase anion extractability.

Table 1. Concentration exchange constants of carboxylates

Anion (X^-)	$\lg K^{X^-}_{DNP^-} \pm \delta$	Anion (X^-)	$\lg K^{X^-}_{DNP^-} \pm \delta$
$HCOO^-$	–7.00 ± 0.025	$C_6H_5COO^-$	–4.54 ± 0.07
CH_3COO^-	–7.36 ± 0.019	*o*-NO_2-$C_6H_4COO^-$	–3.84 ± 0.13
$CH_3CH_2COO^-$	–6.85 ± 0.045	*m*-NO_2-$C_6H_4COO^-$	–2.97 ± 0.13
$CH_3(CH_2)_2COO^-$	–6.37 ± 0.061	*p*-NO_2-$C_6H_4COO^-$	–3.21 ± 0.13
$(CH_3)_2CHCOO^-$	–6.35 ± 0.058	*o*-NH_2-$C_6H_4COO^-$	–4.15 ± 0.09
$CH_3(CH_2)_3COO^-$	–5.83 ± 0.022	*m*-NH_2-$C_6H_4COO^-$	–5.92 ± 0.15
$C(CH_3)_3COO^-$	–5.69 ± 0.080	*p*-NH_2-$C_6H_4COO^-$	–5.31 ± 0.11
$CH_3(CH_2)_5COO^-$	–4.03 ± 0.031	*o*-Cl-$C_6H_4COO^-$	–4.18 ± 0.06
$CH_3(CH_2)_6COO^-$	–3.42 ± 0.025	*o*-Br-$C_6H_4COO^-$	–4.01 ± 0.07
$CH_3(CH_2)_7COO^-$	–2.82 ± 0.028	*p*-Br-$C_6H_4COO^-$	–2.76 ± 0.06
$CH_3(CH_2)_8COO^-$	–2.24 ± 0.033	*o*-OH-$C_6H_4COO^-$	–1.57 ± 0.06
$CH_3(CH_2)_{10}COO^-$	–1.05 ± 0.035	2,4-$(OH)_2C_6H_3COO^-$	–3.34 ± 0.07
$CH_3(CH_2)_{12}COO^-$	0.12 ± 0.029	2,4-$(NO_2)_2C_6H_3COO^-$	–2.46 ± 0.06
$CH_3(CH_2)_{14}COO^-$	1.29 ± 0.038	2,3,5-$I_3C_6H_2COO^-$	–0.50 ± 0.13
$CH_3(CH_2)_{16}COO^-$	2.48 ± 0.036	$CH_2(NH_2)COO^-$	–8.05 ± 0.08
CH_2FCOO^-	–6.38 ± 0.015	$CH_3CH(NH_2)COO^-$	–8.08 ± 0.06
CH_2ClCOO^-	–5.56 ± 0.030	$CH_2(NH_2)CH_2COO^-$	–8.40 ± 0.05
CH_2BrCOO^-	–4.52 ± 0.026	$(CH_3)_2CHCH(NH_2)COO^-$	–6.93 ± 0.05
CH_2ICOO^-	–3.60 ± 0.024	$CH_3(CH_2)_2CH(NH_2)COO^-$	–6.90 ± 0.05
CHF_2COO^-	–5.03 ± 0.037	$(CH_3)_2CHCH_2CH(NH_2)COO^-$	–6.63 ± 0.04
$CHCl_2COO^-$	–3.75 ± 0.038	$CH_3(CH_2)_3CH(NH_2)COO^-$	–6.57 ± 0.05
$CHBr_2COO^-$	–2.75 ± 0.035	$C_6H_5CH_2CH(NH_2)COO^-$	–5.58 ± 0.06
CF_3COO^-	–3.25 ± 0.043	$CH_2(OH)CH(NH_2)COO^-$	–8.31 ± 0.06
CCl_3COO^-	–2.43 ± 0.021	$CH_3CH(OH)CH(NH_2)COO^-$	–7.80 ± 0.05
CBr_3COO^-	–1.73 ± 0.033	*p*-$(OH)C_6H_4CH(NH_2)COO^-$	–7.53 ± 0.05
Diclofenac	0.42 ± 0.032	Ketoprofen	–0.56 ± 0.015
Ibuprofen	–1.38 ± 0.018	Naproxen	–1.59 ± 0.030
Indomethacin	–1.73 ± 0.025		

To the effect of increasing the anion-exchange extraction of carboxylate-anions, solvating additives (trifluoroacetophenone derivatives, S) were added to the QAS toluene

solution. As can be seen from Table 2, trichloroacetates (TCA) exchange constants rise in proportion to the increase in electron-accepting properties of substituents.

Table 2. Concentration exchange constants of trichloroacetates, solvation constants (log K_s) and solvation numbers (p)

Solvating additive (S)	C_S, mol/L	$\lg K_{Pic}^{TCA}$	$\lg K_S \pm \delta$	$p \pm \delta$
without additive	–	–4.67 ± 0.01	–	–
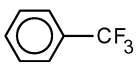	1×10^{-2}	–4.67 ± 0.02	–	–
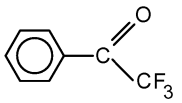	1×10^{-2}	–4.15 ± 0.01	2.35 ± 0.06	0.99 ± 0.04
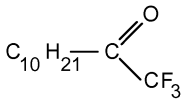	1×10^{-1}	–4.71 ± 0.01	–	–
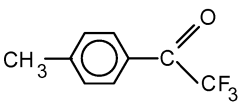	1×10^{-2}	–4.41 ± 0.01	1.61 ± 0.54	0.81 ± 0.35
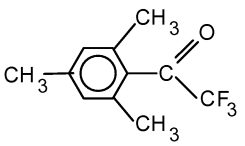	1×10^{-1}	–4.49 ± 0.01	–	–
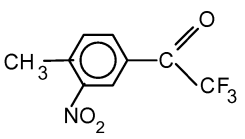	1×10^{-2}	–2.91 ± 0.12	3.46 ± 0.28	0.92 ± 0.10
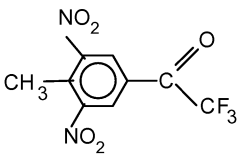	1×10^{-2}	–1.85 ± 0.03	4.79 ± 0.38	0.93 ± 0.10
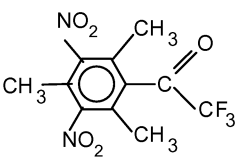	1×10^{-2}	–4.69 ± 0.04	–	–
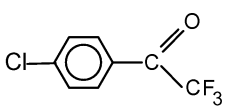	1×10^{-2}	–3.67 ± 0.02	2.73 ± 0.55	0.99 ± 0.25

Solvating additive (S)	C_S, mol/L	$\lg K_{Pic}^{TCA}$	$\lg K_S \pm \delta$	$p \pm \delta$
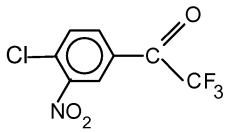	1×10^{-2}	–2.27 ± 0.04	4.61 ± 0.38	1.07 ± 0.12
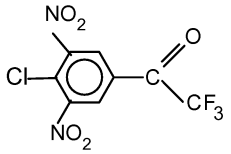	1×10^{-2}	–1.71 ± 0.04	4.99 ± 0.47	0.93 ± 0.12
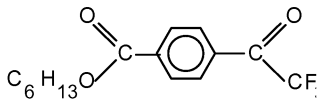	1×10^{-2}	–3.32 ± 0.02	3.20 ± 0.37	1.05 ± 0.14
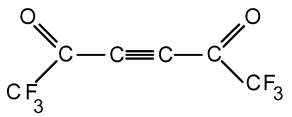	1×10^{-2}	–4.48 ± 0.11	1.55 ± 0.58	0.93 ± 0.27
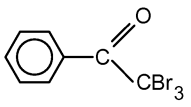	1×10^{-2}	–4.72 ± 0.05	–	–
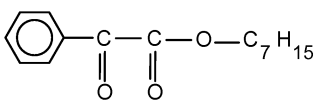	1×10^{-2}	–4.70 ± 0.03	–	–

For *meta* and *para* substituted trifluoroacetophenones, one can observe a good correlation between the exchange constants and Hammett σ-constants sum:

$$\log K_{Pic^-}^{TCA^-} = -4.1 + 1.65\,\Sigma\sigma, \quad (r = 0.978 \text{ when } n = 9). \tag{5}$$

Analyzing data from Table 2, it is possible to make certain conclusions concerning the solvating additive structure influence on its efficiency.

First, the structure requires the presence of the CF_3 group. Transition from trifluoroacetophenone to tribromoacetophenone leads to the complete fading of the effect. Second, the presence of the carbonyl group adjoining the trifluoromethyl group is required; that is the effect occurs only for those structures that contain the trifluoroacetyl group -CO-CF_3. It is proved by data obtained for trifluoromethylbenzene. The effect is not observed here. The presense of isolated carbonyl or ester groups does not lead to an increase of exchange constants. Third, the trifluoroacetyl group, being linked to a hydrocarbon radical or linked to a hydrocarbon radical via en ether oxygen, is ineffective.

Hence, the conducted studies demonstrated that solvating properties are appropriate to organic molecules that have a trifluoroacetyl group and benzene ring in their structure; that is the trifluoroacetophenone structure is the simplest having good solvating ability. This is, the initial structure that can be modified by different substituents to obtain more effective solvating additives.

Very important is the fact that complete substitution of hydrogen atoms in the benzene ring leads to a quantitative disappearance of the effect. This proves the participation of hydrogen atoms of the benzene ring in the formation of solvating particles.

Analysis of bilogarithmic dependences $\log K_{\text{Pic}}^{\text{TCA}} - \lg[\text{S}]$ allowed the calculation of solvation formation constants and stoichiometry of the nascent solvate complexes. As be seen from Table 2, the average solvation number is close to 1 for almost all solvating additives, and the solvation formation constants correlate with the exchange constants.

Thus, substituted trifluoroacetophenones have significant solvating properties and are capable of increasing the exchange constant by 3 orders of magnitude even with 10^{-2} mol/L concentration. Taking into account a proportional increase of the exchange constant with the increase of solvating additive concentration, it is possible to reach an even more significant effect (up to 5 orders of magnitude) using concentrated solutions of solvating additives.

CONCLUSIONS

A data base of 55 carboxylate concentration exchange constants with respect to 2,4-dinitrophenolate anions was created from exchange experiments. More than 15 trifluoroacetophenone derivatives were synthesized and their solvating properties analyzed. The corresponding solvation constants were calculated, and the stoichiometry of forming solvates was determined. A number of correlations suitable for the description of carboxylates anion-exchange extraction was also determined.

REFERENCES

1. E. M. Rakhman'ko, G. L. Starobinets, V. V. Yegorov, and A. L. Gulevich, "Analytical application of high molecular quaternary ammonium salts," *Frezenius J. Anal. Chem.*, **335**(1), 104-110 (1989).
2. G. N. Chichagova, I. M. Ivanov, and L. M. Gindin, "Anion-exchange extraction row. Thermodynamical characteristics of anion extraction by tetraalcylammonium salts," *Izvestia of USSR Academy of Science, Chem. Div.*, **7**(3), 48-53 (1974).
3. E. M. Rakhman'ko, G. L. Starobinets, and A. L. Gulevich, "The additivity principle as applied to characterization of anion-exchange extraction of organic anions," ISEC-88, Moscow, Russia, 1988; pp. 330–333.

SYNERGISTIC EXTRACTION OF TRIVALENT LANTHANIDES AND ACTINIDES FROM ACIDIC CHLORIDE MEDIA BY TETRA(*n*-OCTYL)DIGLYCOLAMIDE

D. R. McAlister and E. Philip Horwitz

PG Research Foundation, Inc., 8205 S Cass Ave., Suite 106, Darien IL 60561
Corresponding author email address: dmcalister@pgrf.com

ABSTRACT

Ferric chloride has been found to induce a significant synergistic enhancement of the extraction of trivalent lanthanides and actinides by tetra(*n*-octyl)diglycolamide (TODGA) from acidic chloride media. In this manuscript, results of a thorough investigation of the TODGA-HCl-Fe(III) system using solvent-extraction experiments designed to elucidate the stoichiometry of the synergistic species will be described. Results for Ac(III), Am(III), Eu(III), Pm(III), Y(III), Th(IV), Pu(IV), and U(VI) will be discussed.

INTRODUCTION

Recently, tetraalkyldiglycolamides (DGA) have been studied in solvent extraction (SX) [1-4] and extraction chromatographic (EXC) [5-8] systems for the separation and preconcentration of metal ions. DGA extractants have been shown to be particularly useful for the selective retention of lanthanide and actinide ions (III, IV, and VI) from acidic nitrate media [1-6].

During the development of a method to preconcentrate actinides from very large soil samples leached with HCl, the authors discovered a significant synergistic enhancement of the extraction of trivalent lanthanides and actinides by an extraction chromatographic (EXC) resin prepared from tetra(*n*-octyl)diglycolamide (TODGA) when Fe(III) was present in the leachate [7]. Further investigation of this system indicated that several other metal ions (Ga, In, Tl(III), Bi, Sn(IV), and Pd(II)) which form stable anionic chloride complexes also produced significant synergistic enhancement of the extraction of trivalent lanthanides and actinides by TODGA from HCl. Applications of this synergistic phenomenon were developed for the preconcentration of Am(III) and Pu(IV) from soil leachates and the isolation of Ac-227 from stainless steel and aluminum targets, ampoules, and neutron sources [8].

This manuscript will focus on results of solvent-extraction experiments designed to elucidate the stoichiometry of the extracted species in the TODGA-HCl-Fe(III) system. The extraction of selected trivalent lanthanides, actinides, and Y(III) will be

described. In addition, extraction data for selected non trivalent actinides, Pu(IV), Th(IV), and U(VI) will be presented.

EXPERIMENTAL

The tetra-*n*-octyldiglycolamide (TODGA) was obtained from Eichrom Technologies. Hydrochloric acid solutions were prepared from Trace Metal Grade acids (Fisher Scientific) using deionized water obtained from a Milli-Q2 water purification system. Iron(III) chloride hexahydrate and *o*-xylene were obtained from Fisher Scientific. Europium chloride hexahydrate was obtained from Strem Chemical. The radionuclides ^{241}Am, ^{239}Pu, ^{233}U, ^{230}Th, ^{152}Eu, ^{147}Pm, and ^{90}Sr were obtained from Isotope Products Laboratories. Actinium-225 was separated from ^{229}Th (Oak Ridge National Laboratory) and ^{90}Y was milked from ^{90}Sr as previously described [5,8].

The ^{239}Pu, ^{233}U, ^{230}Th, ^{147}Pm, and ^{90}Y were measured in 7 mL borosilicate glass tubes containing 5 mL of Ultima Gold scintillation cocktail using a Packard TriCarb 2550 TR/AB liquid scintillation counter. The radionuclides ^{152}Eu, ^{225}Ac(^{221}Fr), and ^{241}Am were measured in polypropylene tubes using a model E5003 Packard Cobra Autogamma counter. Aqueous Fe and Eu concentrations were measured using a Varian Liberty Series II inductively coupled plasma-atomic emission spectrometer. pH titrations were conducted using an Accumet AR25 pH meter with glass combination electrode.

Distribution ratios were measured by preconditioning an organic phase containing TODGA in *o*-xylene three times with an aqueous phase without any radioactivity. The aqueous phases were removed and discarded. The desired analyte (radionuclide) was then added to a fresh aliquot of the aqueous phase and contacted with the preconditioned organic phase for 10 minutes by vortex mixing. Phases were separated by centrifugation. Aliquots of each phase were transferred to ¼ dram glass shell vials and sub aliquots were transferred to the appropriate counting tube or vial using calibrated delivery pipettes.

RESULTS AND DISCUSSION

In Table 1, values for the distribution ratio for the extraction of selected metal ions from 3M HCl with and without 2000 mg/L (ppm) of Fe(III) by 0.1 M TODGA in *o*-xylene are listed. For all of the trivalent metal ions, a very significant enhancement is observed (10^3-10^5x) when Fe(III) is present, while very little enhancement is observed for U(VI), Th(IV), and Pu(IV). Several solvent-extraction experiments were performed to help elucidate the stoichiometry of the metal ion species extracted in this system and to help explain this large difference in behavior.

In Figure 1, data for the distribution ratio of selected metal ions vs. the organic phase concentration of TODGA is depicted. In Figure 1a, the data exhibits a positive slope of 3, suggesting coordination of the trivalent metal ions by 3 TODGA molecules from an aqueous phase of 8 M HCl. The data in Figure 1b also exhibits a positive slope of 3, suggesting coordination of these selected trivalent, tetravalent, and hexavalent metal ions by 3 molecules of TODGA from HCl media. Extractant dependency data for Am(III) and Th(IV) from 3 M HCl in the presence of 1000 ppm Fe is shown in Figure 1c. Both metal ions exhibit a positive slope of 3 suggesting that the number of

coordinating TODGA molecules doesn't change when 1000 mg/L of Fe(III) is added to the aqueous phase. However, for U(VI) (slope = 1.5) and Pu(IV) (slope = 1.1), the slope of data for *D* vs [TODGA] is reduced when 1000 ppm Fe(III) is present in the aqueous phase.

Table 1. Enhancement of D by 2000 ppm Fe(III) for 0.1 M TODGA in *o* -xylene

Metal Ion	D from 3 M HCl	D from 3 M HCl +2000 ppm Fe[a]	ratio[b]
U(VI)	4.1E-01	1.3E+01	3.2E+01
Th(IV)	4.5E-02	8.9E-01	2.0E+01
Pu(IV)	1.4E-01	1.0E+00	7.1E+00
Y(III)	5.0E-03	1.6E+03	3.2E+05
Eu(III)	9.7E-03	3.3E+02	3.4E+04
Pm(III)	2.6E-03	2.9E+02	1.1E+05
Am(III)	1.2E-03	1.2E+02	1.0E+05
Ac(III)	1.5E-04	9.6E-01	6.4E+03

[a]Initial Fe(III) concentration, no pre-equilibration of organic phase

[b]$D_{3M\ HCl\ +2000\ ppm\ Fe}/D_{3M\ HCl}$

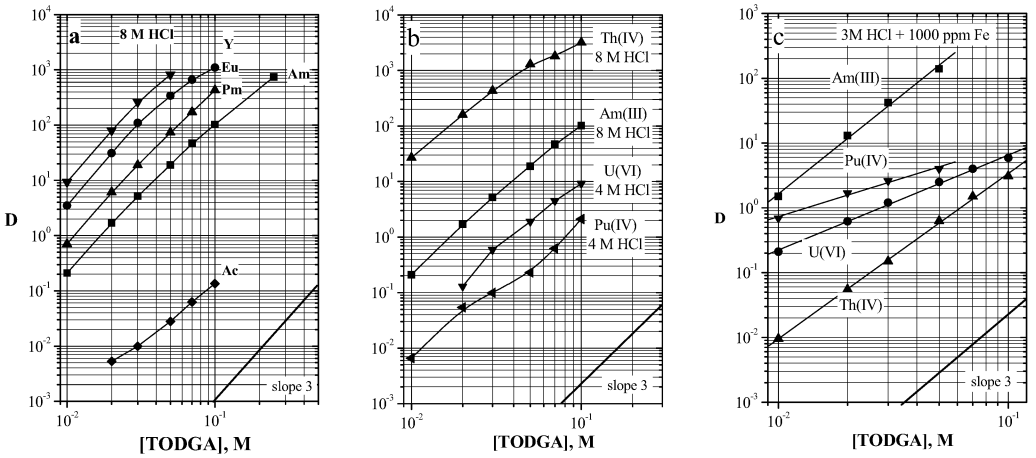

Figure 1. (a) *D* M(III) vs [TODGA] from 8 M HCl. (b) *D* Th(IV) and Am(III) from 8 M HCl and U(VI) and Pu(IV) from 4 M HCl vs [TODGA]. (c) *D* Am(III), Th(IV), Pu(IV) and U(VI) from 3 M HCl + 1000 ppm Fe vs [TODGA].

In Figures 2a and 2b, the HCl dependency of *D* for selected tri-, tetra-, and hexa-valent metal ions is shown. All of the metal ions show a high, positive dependence on the concentration of HCl in the aqueous phase. This is due, in part, to the steep increase in the activity of chloride ion as the HCl concentration in the aqueous phase increases [9] and the need of Cl^- to balance the positive charge of the metal ions extracted into the organic phase. In Figure 2c, data is depicted for D_{Am} as the concentration of H^+ in the aqueous phase is varied while keeping the concentration of TODGA (0.1 M), Cl^- (3 M (Li/H)Cl), and Fe(III) (500 ppm) constant. The D_{Am} value remains nearly constant over the entire range of H^+ concentrations, indicating that species extracted with Fe(III) in the aqueous phase do not include H^+. However, when Fe is not present in the aqueous phase,

the extraction of Am(III) by TODGA exhibits a positive slope of 2 from 1-3 M HCl, suggesting that 2 HCl are co-extracted with each Am. Similar results have been observed for the extraction of Eu and Am by TODGA in nonpolar diluents from nitric acid [11].

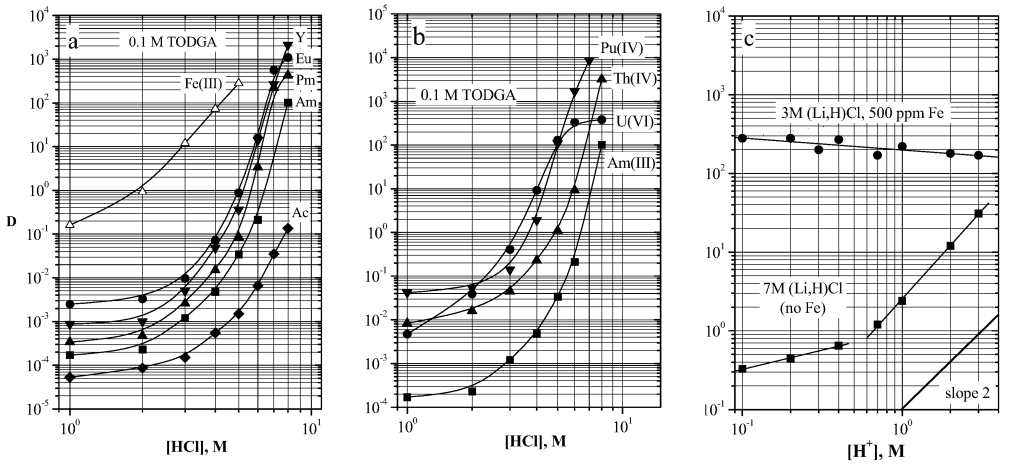

Figure 2. (a) *D* M(III) vs [HCl] for 0.1 M TODGA in *o*-xylene. (b) *D* Am(III), Th(IV), Pu(IV), and U(VI) vs [HCl] for 0.1 M TODGA in *o*-xylene. (c) *D* Am(III) vs [H^+] for 0.1 M TODGA, 500 ppm Fe(III) + 3 M (Li,H)Cl, and 7 M (H,Li)Cl.

In Figure 3, the data for the distribution ratio of selected metal ions vs the concentration of Fe(III) in the aqueous phase is depicted. In Figure 3a, *D* values for Y, Eu, Pm, Am, and Ac vs $Fe(III)_{aq}$ in 3 M HCl are plotted. The data exhibits slopes of 3, suggesting that 3 Fe(III) ions participate in the extraction of each tivalent metal ion by TODGA. Due to the need of 3 negative charges to balance the positive charge of M(III) and the tendency of Fe(III) to form anionic chloride complexes [10], it is likely that the Fe(III) in the extracted complex exists as $FeCl_4^-$.

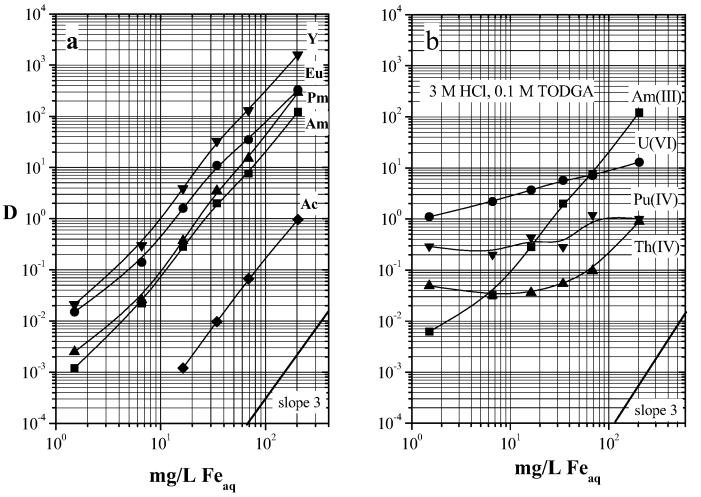

Figure 3. (a) *D* M(III) vs [$Fe(III)_{aq}$] for 0.1 M TODGA and 3 M HCl. (b) *D* Am(III), Th(IV), Pu(IV), and U(VI) vs [$Fe(III)_{aq}$] for 0.1 M TODGA and 3 M HCl.

The distribution ratios of U(VI), Pu(IV), and Th(IV) in Figure 3b exhibit very little dependence on the concentration of Fe(III) in the aqueous phase. This suggests that Fe(III) plays little role in the U(VI), Pu(IV), and Th(IV) complexes

extracted in this system and explains why little synergistic enhancement is observed for these metal ions. It is possible that steric hindrance, due to the uranyl oxygens or the four singly charge $FeCl_4^-$ counter ions needed to balance the positive charge of Pu(IV), and Th(IV), prevents formation of a complex involving the $FeCl_4^-$ and these metal ions. Small increases in k' observed for U(VI), Pu(IV) and Th(IV) with the addition of Fe(III) may be due to partial replacement of the chloride counter ions with $FeCl_4^-$.

Table 2. Extraction of Eu, Fe(III) and HCl by 0.1 M TODGA in *o* -xylene[1]

	aqueous phase[2]			organic phase[2,3]		
acid	**Eu (mM)**	**Fe (mM)**	**DGA (mM)**	**Eu (mM)**	**Fe (mM)**	**HCl (mM)**
3M HCl	33	90	100	29 ± 1	90 ± 1	0.1 ± 0.01
3M HCl	0	90	100		70 ± 2	87 + 3
3M HCl	0	0	100			3.1 ± 0.3
4 M HCl	33	90	100	28 ± 1	89 ± 1	25 ± 9
4 M HCl	0	90	100		91 ± 3	110 + 4
4 M HCl	0	0	100			4.4 ± 0.5
5 M HCl	33	90	100	26 ± 1	89 ± 1	29 ± 8
5 M HCl	0	90	100		92 ± 4	140 + 10
5 M HCl	0	0	100			6.4 ± 0.3
6 M HCl	33	90	100	25 ± 1	93 ± 3	26 ± 2
6 M HCl	0	90	100		92 ± 3	140 + 9
6 M HCl	0	0	100			31 ± 3
7 M HCl	33	90	100	22 ± 2	92 ± 3	33 ± 4
7 M HCl	0	90	100		91 ± 1	130 + 2
7 M HCl	0	0	100			110 ± 9
8 M HCl	33	90	100	21 ± 2	91 ± 2	60 ± 8
8 M HCl	0	90	100		88 ± 3	130 + 6
8 M HCl	0	0	100			170 ± 10

[1]Organic phase equilibrated twice with equal volume of aqueous phase. [2]Eu and Fe determined by ICP-OES from 100x diluted solution. [3]Eu, Fe and HCl back-extracted with deionized water. HCl determined by titration with 0.1 M NaOH, errors correspond to standard deviation of 3 replicates.

Analytical results for Eu, Fe and HCl extracted by 0.1 M TODGA in o-xylene are presented in Table 2. For solutions containing only HCl, extraction occurs via equation 1 (bars denote organic phase), and the amount of HCl extracted increases as the aqueous HCl concentration is increased. At an aqueous concentration of 8 M HCl, nearly two HCl are extracted for each TODGA in the organic phase. When Fe(III) and HCl are present in the aqueous phase, extraction occurs primarily via equation 2, with nearly 1 Fe(III) extracted per TODGA in the organic phase. When Eu, Fe(III) and HCl are present in the organic phase, extraction occurs via equations 1-3, with equation 3 being predominant from 3-6 M HCl. At 7-8 M HCl, equations 1 and 2 begin to compete with the mechanism in equation 3, decreasing the amount of Eu extracted and increasing the amount of HCl extracted by the organic phase. Data for the Eu, DGA, HCl system (no Fe) was not included due to the formation of a precipitate following equilibration when attempting to load the organic phase with large amounts Eu with no Fe(III) present.

$$\overline{\text{TODGA}} + x\text{HCl} \leftrightarrow \overline{\text{TODGA(HCl)}_x} \quad (1)$$

$$\overline{\text{TODGA}} + \text{H}^+ + \text{FeCl}_4^- \leftrightarrow \overline{\text{TODGA(HFeCl}_4\text{)}} \quad (2)$$

$$\overline{3TODGA} + Eu^{3+} + 3FeCl_4^- \leftrightarrow \overline{Eu(TODGA)_3(FeCl_4)_3} \quad (3)$$

CONCLUSIONS

A significant synergistic enhancement (10^3-10^5x) of the extraction of Am(III), Ac(III), Pm(III), Eu(III) and Y(III) by TODGA in o-xylene from HCl media in the presence of Fe(III) has been observed. Solvent extraction experiments suggest that the stoichiometry of the extracted complexes in this system is $M(DGA)_3(FeCl_4)_3$. Previous studies with an extraction chromatographic resin prepared from TODGA indicated a similar species was formed in the TODGA stationary phase [8]. Experiments with Th(IV), Pu(IV) and U(VI) did not produce a significant enhancement in extraction when Fe(III) was present in the aqueous phase.

REFERENCES

1. Y. Sasaki and G. R. Choppin, "Solvent Extraction of europium, thorium, uranium, neptunium and americium with N,N'-dimethyl-N,N'dihexyl-3-oxapentanediamide and its analogous compounds," *Anal. Sci.*, **12**, 225-230 (1996).
2. Y. Sasaki and G. R. Choppin, "Extraction behaviors of Eu, Th, U and Am with diamdes + thenoyltrifluoroacetone," *J. Radioanal. Nucl. Chem.*, **207**, 383-394 (1996).
3. Y. Sasaki and G. R. Choppin, "Extraction and mutual separation of actinide(III), (IV) and (VI) ions by N,N'-dimethyl-N,N'-dihexyl-3-oxapentanediamide and thenoyltrifluoroacetone," *J. Radioanal. Nucl. Chem.,* **246**, 267-273 (2000).
4. Y. Sasaki, Y. Sugo, S. Suzuki, and S. Tachiamori, "The novel extractants, diglycolamides, for the extraction of lanthanides and actinides in HNO_3-n-dodecane system," *Solvent Extr. Ion Exch.*, **19**, 91-103 (2001).
5. E. P. Horwitz, D. R. McAlister, A. H. Bond, and R. E. Barrans, Jr., "Novel extraction chromatographic resins based on tetraalkyldiglycolamides: characterization and potential applications," *Solvent Extr. Ion Exch.*, **23**, 319-344 (2005).
6. A. H. Bond, E. P. Horwitz, and D. R. McAlister, "Multicolumn selectivity inversion generator for production of high purity actinium for use in therapeutic nuclear medicine," U. S. Patent 7,087,206, 8 August 2006.
7. E. P. Horwitz, A. H. Thakkar, and D. R. McAlister, "A rapid method for the preconcentration of non-refractory Am and Pu from 100 gram soil samples," Proceedings of the 10th Annual Symposium on Environmental Radioactivity Analysis, Royal Society of Chemistry, 2007; pp. 77-85.
8. E. P. Horwitz, D. R. McAlister, and A. H. Thakkar, "Synergistic enhancement of the extraction of trivalent lanthanides and actinides by tetra(n-octyl)diglycolamide from chloride media," *Solvent Extr. Ion. Exch.*, in press (2008).
9. D. R. Lide, (Editor-in-chief), Handbook of Chemistry and Physics, CRC Press, New York, 2002, section 5, p. 100.
10. G. A. Gamlen and D. O. Jordan, "A spectrophotometric study of the Iron(III) Chloro-complexes," *J. Chem. Soc.*, 1435-1443 (1953).
11. Y. Sasaki, P. Rapold, M. Arisaka, M. Hirata, T. Kimura, C. Hill, and G. Cote, "An additional insight into the correlation between the distribution ratios and the aqueous acidity of the TODGA system," *Solvent Extr. Ion Exch.*, **25**(2), 187-204 (2007).

SYNERGISTIC EXTRACTION MECHANISM OF SAMARIUM WITH ALKYLPHOSPHORIC ACIDS AS MAIN EXTRACTANT

K. Kondo,[1] T. Watanabe,[1] E. Kamio,[2] and M. Matsumoto[1]

[1]Department of Chemical Engineering and Materials Science, Doshisha University, Kyotanabe, Kyoto, 610-0321, JAPAN. [2]Department of Environmental Chemistry and Materials, Okayama University, 3-1-1, Tsushima-naka, Okayama-shi, Okayama, 700-8530, JAPAN. Corresponding author email address: kkondo@mail.doshisha.ac.jp

ABSTRACT

The synergistic extraction of samarium with the two different organophosphoric acids as the main extractant and three organic phosphine oxides as the synergist was examined. A synergistic or antagonistic effect was observed in the investigated systems. The extraction of samarium from sodium thiocyanate solution with the synergists was also examined. The order of the extractability was explained by the order of the electron density of the oxygen atom in the synergists. The extraction mechanism of samarium could be reasonably interpreted by taking into account the reaction between extracted complex and the synergist.

INTRODUCTION

A synergistic extraction has been widely noticed as an effective extraction technique of rare-earth metals [1]. Significant increase in extractability is realized by using a commercially available extractant and a small quantity of synergist. A synergistic extraction system economizes the use of a main extractant and toxic organic solvent. However, the mechanism of synergistic extraction has not been fully clarified yet. Elucidation of the extraction mechanism gives a large choice of the combination of a main extractant and a synergist and helps the synergistic extraction system use in a practical process.

In this study, we investigated the synergistic extraction of Sm(III) in the presence of dibutylmonothiophosphoric acid (DBTPA) and dibutylphosphoric acid (DBPA) as extractants and tri-*n*-butylphosphine oxide (TBPO), bibutylphosphate (DBOBPO), and tri-*n*-butylphosphate (TBOPO) as synergists.

EXPERIMENTAL

Reagents

DBTPA was synthesized as described in the literature [2]. The obtained product (white needle crystals; yield, 52.8%) was characterized by FT-IR spectroscopy. DBPA, TBPO were purchased from Tokyo Kasei co. ltd. and DBOBPO, TBOPO were provided by Aldrich co. ltd. and Nacalai tesque co. ltd., respectively. They were used without further purification. Toluene as a diluent and other inorganic chemicals such as $SmCl_3$, HCl, aminoacetic acid, and sodium thiocyanate were purchased from Wako Pure Chemical Industry Co. Ltd.

The organic phase was prepared by dissolving the main extractant and/or the synergist in toluene. The aqueous phase was prepared by dissolving $SmCl_3$ in the HCl-aminoacetic acid buffer solution with or without sodium thiocyanate. The pH of the aqueous phase was adjusted by using HCl solution and a F-12 Horiba co. ltd pH meter.

Experimental Procedure

The distribution equilibrium of the mains extractants between aqueous and organics phases were determined as follows: Equal volumes (5 mL) of aqueous phase without sodium thiocyanate and organic phase containing DBTPA or DBPA were introduced into a stoppered flask. In some cases, the synergist was also dissolved in the organic phase. They were contacted for 24 hours at 303 K in a thermostatic shaking bath. After 24 hours, both phases were separated. The extractant concentration in the organic phase was determined by titration with NaOH solution.

The same procedure was used for determining the distribution equilibrium of Sm(III). The concentration of the metal in aqueous phase was measured by inductively coupled plasma spectrometry (ICPS-8000, Shimadzu co. ltd.). The amount of metal extracted was calculated from mass balance before and after equilibrium.

RESULTS AND DISCUSSION

Distribution Equilibrium of Main Extractant

The distribution ratio and acid dissociation constant of DBTPA were reported as $K_{D,DBTPA}$ = 19.1 and $K_{a,DBTPA}$ = 81.4 mol/m^3, respectively [2]. DBPA distributes between aqueous and organic phases and acid dissociates in the aqueous phase. Furthermore, DBPA exist in organic phase as dimers. The relationship between the concentrations of DBPA in aqueous and organic phases was derived from the above-mentioned three equilibrium relationships:

$$[HR]_{aq} + [R^-]_{aq} = \frac{1}{4K_{d,DBPA}K_{D,DBPA}}\left(1+\frac{K_{a,DBPA}}{[H^+]}\right)\left(-1+\sqrt{1+8K_{d,DBPA}[HR]_{org,total}}\right) \quad (1)$$

where HR and R^- denote monomeric DBPA and its anionic form, respectively. $K_{d,DBPA}$ is the dimerization constant of DBPA. Subscripts “aq” and “org” denote aqueous and

organic phases, respectively. $[HR]_{org,total} = [HR]_{org} + 2[(HR)_2]_{org}$, where $(HR)_2$ denotes the dimeric form of DBPA. From experimental data, the following parameters of Equation 1 were determined by the least-squares method: $K_{d,DBPA}$ = 311 mol/m^3, $K_{a,DBPA}$ = 0.34 m^3/mol, and $K_{D,DBPA}$ = 11.9.

Distribution and Association Equilibrium of Extractants for Mixed Extractant System

Distribution of the main extractant was investigated for the mixed extractant system under different pH conditions. The distribution ratios of the main extractant, D_{HA} and D_{HR}, are defined in Eqations 2 and 3, respectively,

$$D_{HA} = \frac{[HA]_{org,total}}{[HA]_{aq,total}} = \frac{[HA]_{org} + [HA \cdot S]_{org}}{[HA]_{aq} + [A^-]_{aq}} \quad (2)$$

$$D_{HR} = \frac{[HR]_{org,total}}{[HR]_{aq,total}} = \frac{[HR]_{org} 2[(HR)_2]_{org} + [HR \cdot S]_{org}}{[HR]_{aq} + [R^-]_{aq}} \quad (3)$$

where HA and A^- represent DBTPA monomers and its anionic form, respectively; S is the synergist; and HA·S and HR·S denote the associated complex of the main extractant with the synergist. As shown in Figure 1, D_{HA} and D_{HR} increase in presence of synergist.

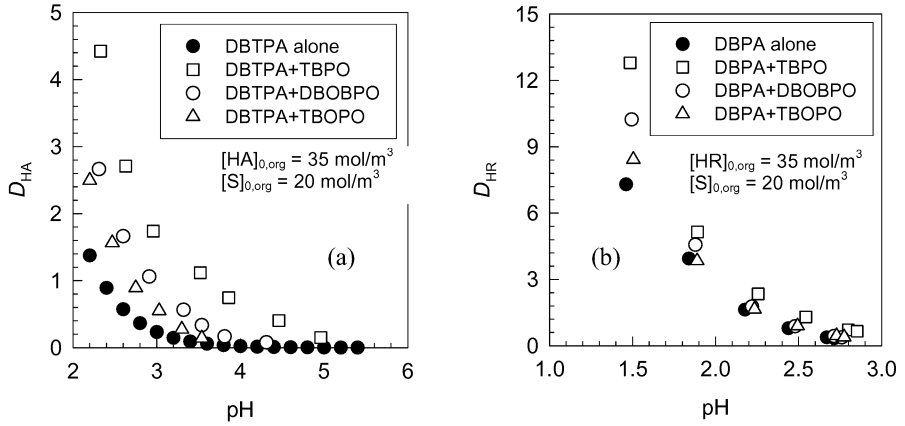

Figure 1. Effect of pH on distribution ratio of the main extractants.

We have to consider the association equilibrium between the main extractant and the synergist in order to estimate the concentration of "free" extractants. Considering the equilibria shown in Figures 2(a) and 2(b), the association constants of the main extractant and the synergist, K_s, were determined from experimental data displayed in Figures 1(a) and 1(b) (Table 1).

Table 1. Association constants of the extractants

	Synergist		
	TBPO	DBOBPO	TBOPO
$K_{s,HA}$ (m^3/mol)	3.77	2.59×10^{-1}	7.00×10^{-2}
$K_{s,HR}$ (m^3/mol)	1.37	5.27×10^{-1}	9.30×10^{-2}
$K_{s,HSCN}$ (m^3/mol)	4.10×10^{-2}	3.24×10^{-3}	1.96×10^{-3}

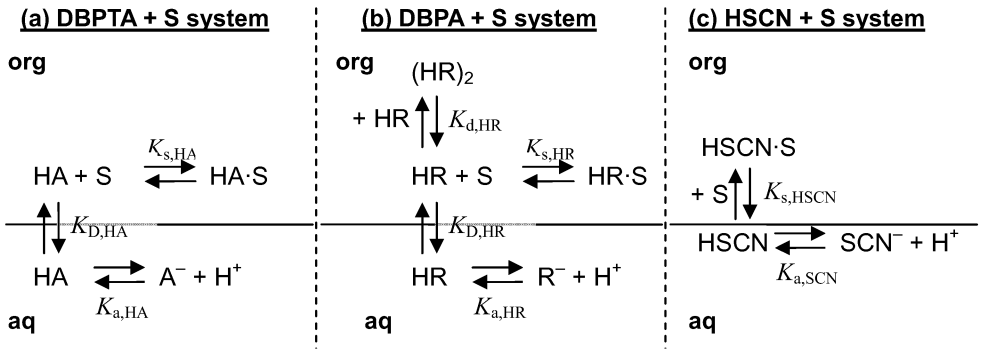

HA: DBTPA. HR: DBPA. S: synergist (TBPO, DBOBPO or TBOPO). SCN^-: thiocyanate anion.

Figure 2. Distribution and association equilibria of extractants.

Extraction Equilibrium of Sm(III) with the Main Extractant

The extraction equilibria of Sm(III) with DBTPA and DBPA were investigated. For both extractants, the extraction ratio increases when pH and extractant concentration increases. The experimental data were analyzed by the conventional slope analysis method, and the following extraction equilibria were deduced:

$$Sm^{3+} + (3+n)HA_{org} \rightleftarrows (SmA_3 nHA)_{org} + 3H^+ \quad ; \quad K_{ex,n}\ (n = 0,1,2,3) \tag{4}$$

where K_{ex} and n denote the extraction equilibrium constant and the number of DBTPA coordinated to the extracted complex, respectively. In this system, n = 0 under all conditions investigated in this study. This result indicates that the number of coordination bond of the Sm-DBTPA complex is 6 and independent of the DBTPA concentration.

$$Sm^{3+} + (3+n)HR_{org} \rightleftarrows (SmR_3 nHR)_{org} + 3H^+ \quad ; \quad K_{ex,n}\ (n = 0,1,2,) \tag{5}$$

In this system, n changes when DBPA concentration increases as n = 0 and n = 1 at $[HR]_{0,org}$ = 5–10 mol/m^3, n = 2 at $[HR]_{0,org}$ = 15–35 mol/m^3, and n = 3 at $[HR]_{0,org}$ = 50–100 mol/m^3. These results indicate that the number of coordination bonds of the Sm-DBPA complex ranges from 6 to 9 and depends on the DBTPA concentration. The extraction equilibrium constants are summarized in Table 2.

Table 2. Extraction equilibrium constant of Sm(III) with DBTPA and DBPA

	$K_{ex,0}$	$K_{ex,1}$	$K_{ex,2}$	$K_{ex,3}$
DBTPA	0.0121	–	–	–
DBPA	217	0.156	0.142	0.186

Recently, the structure of the lanthanide complex was estimated as tricapped trigonal prismatic geometry with 9 coordination bonds [3]. Therefore, if the synergist coexists with DBTPA, it additionally coordinates to the Sm-DBTPA complex. As a result, the extractability of Sm(III) would increase. On the other hand, even if the synergist coexists with DBPA under the condition of high concentration of DBPA, it cannot coordinate with the Sm-DBPA complex and, consequently, the extractability of Sm(III) would not increase.

Synergistic Extraction of Sm(III)

The influence of pH on the Sm(III) extraction was investigated (Figure 3). Synergistic effect was observed for the DBTPA + TBPO and DBTPA + DBOBPO systems (Figure 3a). On the other hand, an antagonistic effect was observed for the other system containing DBTPA + TBOPO. Such an antagonistic effect would occur because the formation of the associate complex between DBTPA and TBOPO is superior to the association of TBOPO to the Sm-DBTPA complex. Since TBOPO associated with DBTPA in an organic phase, the concentration of "free" DBTPA decreases, and the extractability is reduced. As for the extractability of the three synergists, the extraction ability of Sm(III) is as follows: TBPO > DBOBPO > TBOPO. The strength of the coordination bond between Sm-DBTPA complex and the synergist depends on the electron density of the oxygen atom of the synergists. For the synergistic extraction system containing DBPA, DBPA cannot be coordinated to the Sm-DBPA complex under high concentration of DBPA. Therefore, the extraction efficiency of all DBPA + synergist systems would be reduced.

Figure 3(b) displays the extraction efficiency of Sm(III) vs. pH in the DBPA + synergist system. The order of the extent of extractability decreases as follows: TBPO > DBOBPO > TBOPO. That is, the strength of the coordination bond between DBPA and the synergist depends on the electron density of the oxygen atom of the synergists.

The extraction of Sm(III) from an aqueous solution containing sodium thiocyanate was also investigated on the basis of the equilibrium relationship represented in Figure 2(c). The corresponding association constants are gathered in Table 1. Association constants for thiocyanate ion are much smaller than those for DBTPA and DBPA. This indicates that the association between thiocyanate ions and synergists can be ignored. Therefore, by comparing the extractabilities of Sm(III) with the synergists in the presence of aqueous solution containing sodium thiocyanate, we can compare the strength of the coordination bond between Sm-SCN complex and the synergist. The relationship between the extent of Sm(III) extracted and the concentration of synergist shows that the extractability of Sm(III) is enhanced as follows: TBPO > DBOBPO > TBOPO. This result also indicates that the strength of the coordination bond between

Sm-SCN complex and the synergist depends on the electron density of the oxygen atom of the synergists.

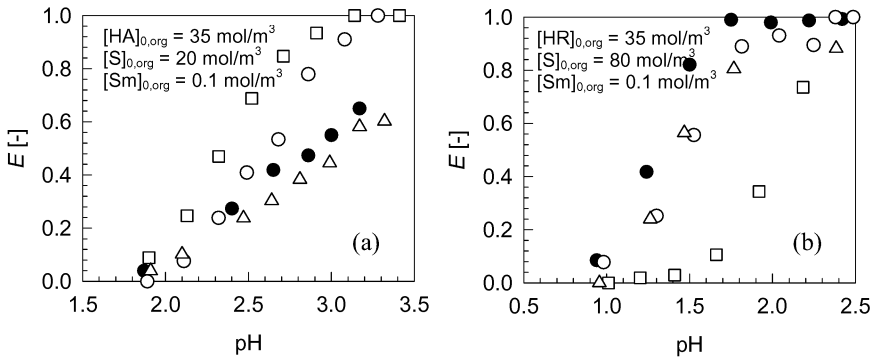

Figure 3. Effect of pH on extraction ratio of Sm(III). (a) DBTPA system and (b) DBPA system. Symbols: ●, main extractant alone; □, main extractant + TBPO; ○, main extractant + DBOBPO; and Δ, main extractant + TBOPO.

CONCLUSIONS

In order to estimate the mechanism of synergistic extraction, the extraction of Sm(III) with two different organophosphoric acids as main extractants and three organic phosphine oxides as synergists was investigated. As the result, the following information was deduced: (1) the extractability of Sm(III) decreases due to the decrease of the thermodynamic activity of the extractant when the associate complex between extractant and synergist is formed; (2) the extractability of Sm(III) increases when the Sm-extractant complexes and the synergist interact; (3) the extracted complex is more stable when the electron density of the oxygen atom of the synergists is larger.

REFERENCES

1. X. Sun, S. Meng, and D. Li, "Studies on the synergistic extraction of rare earths with a combination of 2-ethylhexylphosphonic acid mono-2-ethylhexyl ester and trialkylphosphine oxide," *J. Chem. Technol. Biotechnol.*, **81**, 755-760 (2006).
2. K. Kondo, H. Kawabata, K. Momota, N. Narikiyo, and F. Nakashio, "Synergistic Extraction of Lanthanide Ions with Dibutylmonothiophosphoric Acid and 1,10-Phenanthroline," *J. Chem. Eng. Jpn.*, **23**, 228-233 (1990).
3. I. L. Dukov and V. M. Jordanov, "Synergism and Separation Factors in Lanthanide Extraction with Mixtures of Chelating Extractant and Amine Salts in C_6H_6," *Sep. Sci. Technol.,* **32**, 2561-2568 (1997).

CALORIMETRIC INVESTIGATIONS OF METAL EXTRACTION FOR TWO-PHASE SYSTEMS

Peter R. Zalupski and Kenneth L. Nash

Chemistry Department, Washington State University, P. O. Box 644630, Pullman, WA 99163. Corresponding author email address: pzalupski@wsu.edu

ABSTRACT

Thermochemistry of metal ion extraction in liquid-liquid distribution systems has been predominantly investigated using a temperature dependence of the extraction constants—van't Hoff analysis. This rather laborious technique provides means of an indirect approximation of enthalpy of metal extraction, ΔH, revealing valuable knowledge of metal-ligand association in different liquid-liquid systems. With an objective of a systematic investigation of thermochemical properties of metal extraction, we have developed a new method for the direct calorimetric determination of heats of metal distribution in a two-phase system and compared them with those obtained using distribution studies.

INTRODUCTION

Liquid-liquid distribution of the metal ion is thermodynamically dominated by the opposing energies of its dehydration and complexation by a ligand. The resulting net energy difference—the enthalpy of metal extraction—may be influenced by several solvation effects occurring in both phases. Although quite simplified, such description of an enthalpy-level diagram allows one to identify a key advantage of a thermochemical assessment of a solvent-extraction reaction. It allows further partitioning of Gibbs free energy of reaction to its thermodynamic components, which offers a more descriptive account of the metal-ligand interactions in the investigated solvent-extraction system. Thermochemical characterization allows to identify a driving force of the extraction, journey into the realm of an electronic structure of the formed complex, and derive the details of the mechanism of its formation [1]. It clues into the structures of both aqueous and organic phases. Most of all, thermochemistry provides answers, following a traditional assessment of metal distribution, during the development of any separation process.

A tremendous potential of this analytical subset of solvent extraction has never been fully realized, however, mainly due to lack of convenient investigative routines. Thermodynamic parameters for the liquid-liquid metal distribution reactions have been almost exclusively obtained through the investigation of the temperature dependence of an equilibrium constant for the extraction reaction, according to the van't Hoff

relationship. When applied to two-phase systems, the analysis relies on several assumptions [2]. A truly thermodynamic definition of an extraction constant requires the use of activity coefficients. Our quantitative knowledge of nonidealities and their dependence on changes in temperature, especially in the organic solutions, is lacking, however, forcing a concentration-based approximation of the extraction constant. Furthermore, the van't Hoff analysis assumes no changes in the mechanism of the extraction over the studied temperature [2]. The effect of a changing heat capacity of the system on the enthalpy of the extraction is also omitted from the consideration. The main disadvantage of this work-intensive, indirect method of determining heats of extraction rests in its impractical lack of flexibility, which rules out any opportunity for a dynamic thermochemical investigation. The analysis relies on temperature as the sole variable, requiring a full set of studies, if thermodynamic dependency on a system component is sought.

Calorimetric measurements, when carefully designed, provide means for a direct determination of heats of solvent-extraction reactions. The measured temperature changes originate with the chemical processes taking place inside the calorimetric vessel, allowing a straightforward determination of thermodynamic parameters. Calorimetric investigations of solvent-extraction reactions, however, have been hindered by an inherent presence of a liquid-liquid interface. Efficient phase equilibration has been subject to elevated heats of mechanical mixing, demanding the use of high reagent concentrations and large volumes to produce appreciable heat signatures [2]. As a result, few limited thermochemical studies have used calorimetry for two-phase systems. Here, we report a new method for determining heats of extraction of metal ions using isothermal microcalorimetry. Several solvent-extraction reactions have been investigated in order to expand the analytical range of this method. Experimental design and the interpretation of the collected calorimetric traces will be discussed.

EXPERIMENTAL

Bis(2-ethylhexyl)phosphoric acid, HDEHP, (Aldrich) was purified by the method of copper salt precipitation. 2,6-Bis[(bis(2-ethylhexyl)phosphino)methyl] pyridine N,P,P'-trioxide, TEH(NOPOPO), was used without further purification. Thenoyltrifluoroacetate, HTTA Aldrich was purified by sublimation, protected from light, and stored in the refrigerator. Tributyl phosphate, TBP, (Aldrich), was distilled under reduced pressure. Barium chloride and lead nitrate were dried in an oven overnight prior to preparing standard calibration solutions. All aqueous solutions were prepared using previously recrystallized stock solutions of sodium nitrate and perchlorate, initially standardized by cation exchange, Dowex 50W-X8. Europium stock solutions were prepared by fuming Eu_2O_3 with a corresponding concentrated acid. The final pH of the stock solutions was 3.0 ± 0.2. Benzene (Aldrich) and *n*-dodecane (Alfa-Aesar) were reagent grade.

The isothermal titration microcalorimeter (CSC Model 4200, Calorimetry Sciences, UT) directly measures the heat flowing between the reaction vessel and a large heat sink maintained at a constant temperature. The instrument detects heat flow using semiconducting thermopiles (Peltier modules) situated between the reaction cell, the

reference cell and a heat sink. In a closed circuit of dissimilar metals, an electrical potential develops at the junctions of such a thermoelectric device, when the Hastelloy C cells and an aluminum block heat sink are at different temperatures. The detected voltage is amplified by a low-noise DC amplifier located in a temperature-controlled environment. The analog DC voltage is then converted to a digital signal using a built-in 24-bit digital voltmeter, consisting of an analog-to-digital converter, and read by the ITC microprocessor. The instrumental response is normalized through an electrical calibration, where precise power injections, supplied by a small 1000 ohm resistor heater, are used to position a thermoelectric response on a watt-per-volt scale. The power readouts are deconvoluted to improve the calorimeter's response time and shorten time between injections. The obtained power traces (μW/s) allow monitoring the heat flow throughout the course of an experiment, and each heat event may be quantified through integration. An electrical calibration, performed for a reaction vessel containing water, was followed by a series of identical power injections for a vessel containing equal volumes of organic solvent and water, as well as a two-phase system agitated by a stirrer. The resultant power readouts for all experiments, when integrated, returned the specified 500 μJ heat pulses within a 2σ uncertainty limit, where the highest coefficient of variation was ±1.6%. This agreement suggests minimal changes in the heat capacity of the investigated reaction vessel assemblies. Further chemical calibrations using aqueous solutions were performed to provide additional validity to the obtained calorimetric results. A standard complexometric titration of $BaCl_2$ and $Pb(NO_3)_2$ into an aqueous solution of 18-crown-6-ether was used to optimize the instrument's performance for a partially-filled cell mode. The determined heats of complexation for the reference reactions, when compared with the values reported in the NIST database, agreed within ±0.15 kJ/mol. Typical 2-phase calorimetric experiment involved sequential injection of a metal solution, spiked with $^{152,154}Eu$ (Washington State University, Nuclear Radiation Center, TRIGA reactor), into the calorimetric vessel, where an organic solution of a ligand and aqueous electrolyte solution were agitated with a stirring paddle at 400 rpm. All aqueous and organic solutions were pre-equilibrated and centrifuged prior to placement in the calorimetric vessel. The assembled two-phase system was thermally equilibrated prior to each titration. Ligand consumption was limited to 15%, and the final metal concentration in the organic phase did not exceed 5 mM to allow a reasonable assumption of a constant stoichiometry of the investigated metal extraction. Liquid-liquid metal distribution was measured radiometrically (NaI(Tl) solid scintillation counter, Packard Instrument Co., Meriden, CT) by sampling each phase at the end of the experiment. Quantitative extraction of europium by HDEHP was verified by the analysis of the aqueous phase collected after the calorimetric experiment using ICP-OES (Optima 3200 RL ICP-OES Spectrometer, Perkin Elmer, Norwalk, CT).

RESULTS AND DISCUSSION

Isothermal microcalorimetry was applied toward measuring the heats of liquid-liquid distribution reactions using several metal ion extraction mechanisms. Initial investigations focused on the well-characterized extraction of lanthanide nitrates by a liquid cation exchanger, bis(2-ethylhexyl)phosphoric acid, HDEHP. This fully dimerized

extractant chelates the metal ion, balancing its charge, before the complex partitions back into the organic phase, according to:

$$Ln^{3+} + 3\overline{H_2L_2} \Leftrightarrow \overline{Ln(LHL)_3} + 3H^+ \qquad L = HDEHP \qquad (1)$$

To obtain reproducible calorimetric heat signatures, the experimental conditions for this process targeted a quantitative transfer of the metal into an organic phase. A large excess of the ligand, the organic to phase ratio of 4, and the low acidity of the aqueous phase (pH = 3) ensured a complete metal extraction, verified by ICP-OES. Slope analyses showed no changes in the extraction stoichiometry for the extraction of macro amounts of the metal. The calorimetric heat traces for the injection of 10 μL of 0.051 M europium from 1.0 M nitrate media by 0.2 M HDEHP in *n*-dodecane is shown in Figure 1a. Several superimposed peaks from triplicate extraction experiments have been shown to illustrate the reproducibility of the method. Each peak corresponds with the injection of the titrant solution containing metal. The enthalpy of the extraction of europium by HDEHP was calculated using the $q = \Delta H \times \Delta m$ relationship, where q is the integrated energy corresponding with an injection and Δm is the molar quantity of the metal transferred into the organic phase.

Correct interpretation of any calorimetric data is contingent upon careful consideration of possible heat-contributing side reactions. The dilution of the titrant solution is the only blank experiment performed when studying aqueous equilibria using calorimetry. To extend this method to two-phase systems, several other blank experiments were studied to determine their heat-contributing influences. Heat of dilution of europium nitrate in the 1 M nitrate media (titrant dilution), heat of dilution of the dissociated protons, heat of dilution of HDEHP due to the ligand consumption, and heat of dilution due to the formation of a chelate complex were all investigated. It should be noted that such experiments address only dilution effects that occur during a particular extraction reaction. A purely thermodynamic assessment of the liquid-liquid distribution of the metal requires an extrapolation of the observed heats of extraction to infinite dilution [2]. The corrections that could be applied through the investigation of those naturally accompanying reactions may only lightly affect the enthalpy level diagram of a metal extraction; however, their influence on the overall enthalpy change, ΔH, could be significant and has to be examined. All dilution experiments mimicked changes, which take place during the metal extraction. For instance, a titration of 5 mM $Eu(LHL)_3$ in 0.17 M HDEHP in *n*-dodecane into 0.2 M HDEHP in *n*-dodecane allowed approximation of the heat contributions due to the dilution of the metal chelate. Similar titrations were performed for all other heat of dilution experiments [3]. None of the blank titrations were found to affect the observed heat signatures by more then ±1%. The heat trace for the titrant dilution is shown in Figure 1a. Similar assessment was performed for other solvent extraction reactions. In each case, the relevant changes in concentrations proved to be thermodynamically negligible. Furthermore, excellent linear correlations between the observed heats of extraction and the metal concentration in the titrant solution, r^2 = 0.9999, and the size of an injection, r^2 = 0.9999, were also obtained, suggesting a well-behaving direct correlation between the calorimetric measurements and the extraction of

the metal ion. Titrant dilution may thus be justified as the only blank experiment pertaining also to two-phase systems.

The distribution of europium into the organic phase forces the dissociation of the its aqueous nitrate complexes, $Eu(NO_3)^{2+}$ and $Eu(NO_3)_2^{+}$. At least the first complex is present in significant amounts in 1.0 M nitrate solution, $\beta_1 = 1.0$ [4]. The enthalpies of europium extraction from nitrate solutions were accordingly corrected for this endothermic heat contribution from the dissociation of the europium nitrate complex ($\Delta H_{dissoc} = 0.7$ kJ/mol) [4].

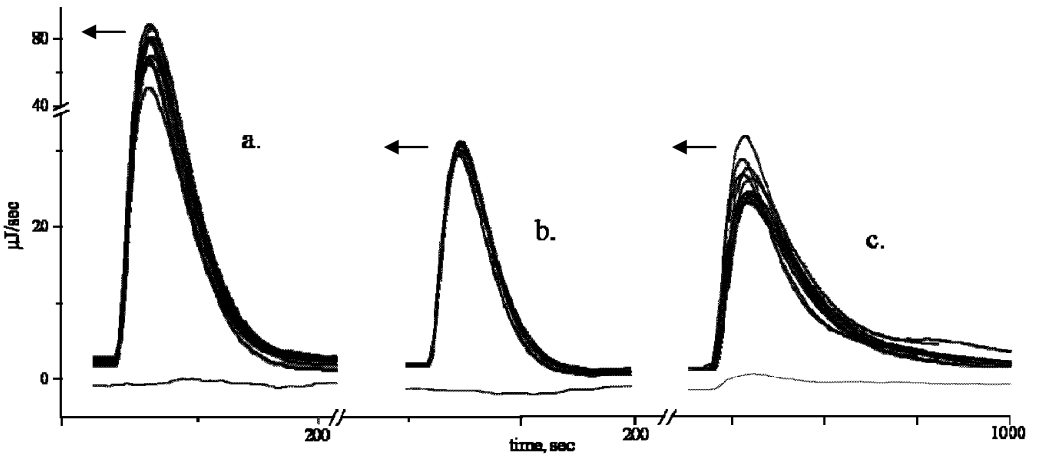

Figure 1. Superimposed heat signatures observed by two-phase calorimetric studies of a) chelating, b) solvating, and c) synergistic extraction of europium.

The calorimetric study of a representative liquid-liquid ion-exchanging extraction was followed by an ion-solvating mechanism, where a neutral ligand extracts a neutral adduct complex. A diphosphonate tetraester, 2,6-Bis[(bis(2-ethylhexyl)phosphino)-methyl]pyridine N,P,P'-trioxide, TEH(NOPOPO), was chosen for this study of the extraction of europium from the nitrate media.

$$Ln^{3+} + 3NO_3^- + 2\overline{L} \Leftrightarrow \overline{Ln(NO_3)_3 \cdot L_2} \qquad L = TEH(NOPOPO) \qquad (2)$$

Equal volumes of organic and aqueous phase were used in this study, to look at the mixing efficiency and the reproducibility of the europium distribution, D_{Eu}. The heat signatures for the equilibration of 5 µL aliquots of 0.0094 M $Eu(NO_3)_3$ in 0.5 M nitric acid with 0.05 M TEH(NOPOPO) in *n*-dodecane are pictured in Figure 1b, along with the blank titration for the heat of dilution of the titrant. For each injection of the titrant solution, the extraction has reached the equilibrium and the europium distribution, $D_{Eu} = 2.6 \pm 0.1$, was consistent for five titration experiments.

A classic synergistic extraction of europium by a mixed ligand complex of thenoyltrifluoroacetate, HTTA, and tributyl phosphate, TBP, was investigated next. The hydrophobicity of the $Eu(TTA)_3$ complex is enhanced by its adduct formation with TBP, substantially increasing the extraction of the metal:

$$Ln^{3+} + 3\overline{HL} + n\overline{S} \Leftrightarrow \overline{LnL_3 \cdot S_n} + 3H^+ \qquad L = HTTA \quad S = TBP \quad n = 2 \text{ for Eu} \qquad (3)$$

This solvent-extraction reaction was selected for the two-phase calorimetric analysis with intent to verify its capacity to handle an increased complexity of a system, where two independent reactions are necessary to transfer the metal into the organic phase. Figure 1c illustrates the equilibration of 10 μL injections of 0.010 M $Eu(ClO_4)_3$ in 0.115 m perchlorate media (pH = 4.1) with a mixture of 0.11 M HTTA and 0.11 M TBP in benzene. The calorimetric data mirrors the raised complexity of the extraction, where an endothermic formation of $Eu(TTA)_3$ complex is followed by an exothermic adduct formation [6]. The resultant calorimetric power traces represent the net heat transfer associated with the extraction of europium into the organic phase. The considerably longer equilibration time reflects an increased complexity of the extraction process, and significant peak tailing may imply that the metal extraction is hindered by the slow extraction kinetics. Although the observed difficulties may solely be due to intrinsic physical properties of this particular solvent-extraction system, the possibilities for improvements in sufficient phase agitation will need to be further investigated.

Table 1. Summary of the thermodynamic studies on the two-phase distribution of europium for the investigated extraction systems

	$Eu(LHL)_3$	$Eu(NO_3)_3 \cdot L_2$	$EuL_3 \cdot S_2$
$V_{injection.}$, μL	10	5	10
$[Eu^{3+}]$, mol/L	0.051	0.0094	0.010
q, μJ	-6429 ± 328	-2447 ± 30	-3176 ± 273
D_{Eu}	>100	2.6 ± 0.1	13.8 ± 3.5
ΔH(cal.)[a]	-14.1 ± 0.8[b]	-37.9 ± 1.4[b]	-34.1 ± 3.1
ΔH(temp.)[a]	-11.8 ± 1.0[c]	-35.0 ± 2.4[5]	-24.3 ± 3.6[6]

[a]kJ/mol. [b]corrected for ΔH of dissociation of $Eu(NO_3)^{2+}$. [c]this work

Table 1 summarizes key experimental parameters and compares the enthalpy of extraction of europium for all investigated solvent-extraction reactions. The enthalpy values obtained using two-phase calorimetry are also compared with those obtained from the linear regression of the temperature dependence of the extraction constants (i.e., van't Hoff analysis). The enthalpies of extraction of europium agree quite well for the initial two systems investigated, though, as mentioned, a full agreement should not be expected. The enthalpy values for the synergistic extraction of europium by HTTA and TBP significantly diverge, implying a future need for the analysis of individual reactions. The comparison with the solvent-extraction data is difficult, however, when facing large discrepancies for the reported thermodynamic parameters of the initial $Eu(TTA)_3$ chelate formation alone (ΔH = 65.7 kJ/mol[6], 40.4 kJ/mol[7]). This solvent-extraction system perhaps most clearly illustrates the advantageous position that calorimetry holds over its

indirect counterpart, where slope analysis may yield substantially different results without a universally followed procedure.

CONCLUSIONS

Despite the necessary improvements in the area of phase equilibration, two-phase calorimetry provides a tremendous opportunity for fundamental studies of solvent extraction. The method offers a convenient option for direct thermodynamic characterization of liquid-liquid distribution systems. The experimental flexibility of this type of a dynamic titration calorimetric analysis is particularly noteworthy, as the investigated system may be manipulated with each injection. This allows numerous thermodynamic dependency studies, where the effects of aqueous- or organic-phase composition on the thermochemistry of metal ion extraction can be identified. In addition, two-phase calorimetry may offer routine analyses for the structural features of metal–ligand interactions. Studies of synergistic systems, extraction mechanism changes, media effects, and competing reactions may all be evaluated.

ACKNOWLEDGMENTS

The authors wish to thank Dr. Robert T. Paine of University of New Mexico for preparation of TEH(NOPOPO). Work was supported under the subcontract to the Idaho National Laboratory, Laboratory Director's Research and Development program.

REFERENCES

1. G. R. Choppin and A. Morgenstern, "Thermodynamics of Solvent Extraction," *Solvent Extr. Ion Exch*, **18**(6), 1029-1049 (2000).
2. Y. Marcus and Z. Kolarik, "Thermodynamics of liquid-liquid distribution reactions. I. The dioxouranium(VI) nitrate-water-tri-*n*-butyl phosphate-*n*-dodecane system," *J. Chem. Eng. Data,* **18**(12), 155-163 (1973).
3. P. R. Zalupski and K. N. Nash, "Two-Phase Calorimetry. I. Studies on the Thermodynamics of Lanthanide Extraction by Bis(2-ethylhexyl)phosphoric Acid," *Solvent Extr. Ion Exch.,* manuscript in preparation.
4. C. Bonal, J.-P. Morel, and N. Morel-Desrosiers, "Interactions Between Lanthanide Cations and Nitrate Anions in Water. Part 2. Microcalorimetric Determination of the Gibbs Energies, Enthalpies and Entropies of Complexation of Y^{3+} and Trivalent Lanthanide Cations," *J. Chem. Soc. Faraday Trans.*, **94**(10), 1431-1436 (1998) and N. Morel-Desrosiers, Université Blaise Pascal, private communication, data at I = 1.0 mol kg^{-1}.
5. K. L. Nash, C. Lavallette, M. Borkowski, R. T. Paine, and X. Gan, "Features of the Thermodynamics of Two-Phase Distribution Reactions of Americium(III) and Europium(III) Nitrates into Solutions of 2,6-Bis[(bis(2-ethylhexyl)phosphino) methyl]pyridine N,P,P'-Trioxide," *Inorg. Chem.*, **41**(22), 5849-5858 (2002).
6. A. T. Kandil, H. F. Aly, M. Raieh, and G. R. Choppin, "Temperature Effects in Synergistic Solvent Extraction," *J. Inorg. Nucl. Chem.*, **37**, 229-232 (1975).

7. J. N. Mathur, S. A. Pai, P. K. Khopkar, and M. S. Subramanian, “Thermodynamics of synergistic extraction of europium(III) by mixtures of thenoyltrifluoroacetone and some neutral oxo-donors,” *J. Inorg. Nucl. Chem.*, **39**, 653-657 (1977).

THE EFFECT OF AQUEOUS-PHASE COMPOSITION ON THE SEPARATION OF HAFNIUM AND ZIRCONIUM FROM ACIDIC CHLORIDE-SULFATE MEDIA BY EXTRACTION WITH ALAMINE 336S IN BENZENE

Nevill M. Rice[1] and Robyn Lee[2]

[1]Retired, Formerly School of Process, Environmental and Materials Engineering, University of Leeds, Leeds, LS2 9JT, U.K. [2]Formerly Dept. of Mining and Mineral Engineering, University of Leeds, Leeds, LS2 9JT, U.K.
Corresponding Author e-mail address: nevjoy@hotmail.com

ABSTRACT

Extraction of Zr and Hf from acidic chloride-sulfate media by Alamine 336S in benzene diluent, pre-equilibrated with HCl, was investigated over a range of SO_4^{2-} and Cl^- concentrations up to 2 and 8 mol L^{-1} H_2SO_4 and HCl, respectively, at 298 ± 0.5 K, using radiotracers. Mixed-ligand chloro-sulphato-complexes of both Hf and Zr were identified by the slope analysis and 2nd derivative UV spectrophotometry. These species can explain the improved separation factors of Hf and Zr predicted for extraction by long–chain tertiary amines from acidic mixed Cl^-/ SO_4^{2-} solutions. The extraction equilibria can be written generally as:

$$n\mathrm{M(SO_4)}_j\mathrm{Cl}_i^{(4-i-2j)}{}_{\mathrm{aq}} + [(i+2j\text{-}4)\mathrm{R_3NHX})]_{n\,\mathrm{o}} \rightleftarrows n\mathrm{R_3NH}_{(i+2j-n)}\mathrm{M(SO_4)}_j\mathrm{Cl}_{i\mathrm{o}} + n(i+2j\text{-}4)\mathrm{X}^-{}_{\mathrm{aq}}$$

where X = Cl^- or HSO_4^- and n is the average organic-phase amine aggregation no. Hf forms a mixed-ligand complex, $Hf(SO_4)_2Cl^-$, less readily extracted than sulphato-complexes. Its stability constant β_{12} = (7.3 ± 1.5) x 10^8. In Zr solutions, sulphato-species predominate, even at high Cl^- concentration, giving improved separation factors >150 for solutions with >6 mol L^{-1} HCl.

INTRODUCTION

Zr and Hf are useful raw materials in nuclear-reactor engineering [1]. Naturally occurring ores contain up to ~2 % Hf, but use of Zr as a nuclear-construction material, for which it is ideally suited (thermal neutron capture c/s, 0.18 barn), requires separation of Hf to <100 ppm owing to the high c/s of Hf (110 barns) [1,2]. Traditional chemical methods for Zr/Hf separation are difficult and inconvenient because of their very similar chemical and physical properties. Many other techniques have been tried including solvent extraction with various extractants [2,3]. Commercial-scale separations have used extraction with MIBK from HCl/SCN^- [3,4] or TBP from HNO_3 [2,3,5]. In SO_4^{2-} media, extraction with amines, especially tertiary, can be used [3], but the minor element, Hf, is less strongly extracted. Baddelyite (ZrO_2) concentrates can be leached using H_2SO_4 [6].

LITERATURE REVIEW

Rice [7], Lee [8], and Yagodin and Sinegribova [3] have reviewed the solvent extraction of Zr and Hf by amines from SO_4^{2-} and Cl^- media. Both metals are prone to polynuclear hydrolysis and solution aging effects [9], but less so in sulfate media. Yagodin et al. [3,10] proposed the following reaction for the extraction of Zr by amines:

$$4\,(R_3NH)HSO_{4\ o} + Zr(SO_4)_3^{2-}{}_{aq} \rightleftarrows (R_3NH)_4Zr(SO_4)_{4\ o} + 2\,HSO_4^-{}_{aq} + H_2SO_{4\,aq} \qquad (1)$$

Extraction equilibrium constants for Zr and Hf were K_{ex} = 500 and 47 respectively [10]. Malek et al. [11] reported $((R_3NH)_4Zr(SO_4)_4.4H_2O)_2$ from SO_4^{2-} media with TOA in benzene. At >1.5 mol L^{-1} H_2SO_4, competition between H^+ and Zr^{4+} for SO_4^{2-} reduced extraction. Extraction from media with >8 mol L^{-1} HCl by amines was reported by Cerrai and Testa [12], but addition of up to 0.5 mol L^{-1} H_2SO_4 lowered extraction of both Zr and Hf. Omori and Suzuki [13] reported extraction of hydrolyzed species by amines from solutions <10 mol L^{-1} in HCl. Very few studies of Zr/Hf extraction from mixed acid media have been reported other than MIBK/HSCN/HCl [4]. Rice and Burkin [8,14] reported lowering of Hf extraction by tri-*n*-octylmine (TOA) in benzene (pre-equilibrated with 2 mol L^{-1} HCl) for HCl concentrations >0.5 mol L^{-1}. D_{Hf} values remained constant from tracer level (10^{-10}) up to 0.005 mol L^{-1} Hf (at 0.098 mol L^{-1} TOA, 0.5 mol L^{-1} HCl and 0.5 mol L^{-1} H_2SO_4), indicating no polynuclear complexes under these conditions. Limiting regression line slopes for plots of log D_{Hf} versus log $[TOA]_{org}$, log $[HSO_4^-]_{aq}$, log $[Cl^-]_{aq}$ and log $[H^+]_{aq}$ were 1.8, 0.91, -2.74, and -4.8, respectively, with correlation coefficients, $R^2 > 0.99$. The following extraction equilibrium was proposed [14]:

$$2\,R_3NHCl_{\ o} + HSO_4^-{}_{aq} + Hf(SO_4)_{2\ aq} \rightleftharpoons (R_3NH)_2Hf(SO_4)_{3\ o} + H^+{}_{aq} + 2\,Cl^-{}_{aq} \qquad (2)$$

with *K*ex' = 5.6±1.4. But at lower [HCl], log D_{Hf} vs. log $[HSO_4^-]_{aq}$ gave a parabolic plot, indicating another reaction might be involved. No Hf was extracted at <4 mol L^{-1} HCl in the absence of sulfate. The low values of D_{Hf} implied that addition of Cl^- ions might improve the separation factor, $S_{Zr/Hf}$, if Zr were not similarly affected. No other results appear to have been published on Zr/Hf extraction from mixed Cl^-/SO_4^{2-} media. A study [15] of the liquid ion exchange reaction between HSO_4^- and Cl^- with TOA(Equation 3) indicated that about <10% of the total sulfate was extracted, so R_3NHCl predominates.

$$R_3NHCl_{\ o} + HSO_4^-{}_{aq} \rightleftharpoons R_3NH_2SO_{4o} + Cl^-{}_{aq}, \text{ with } K_{ex}' = 0.2 \pm 0.15 \qquad (3)$$

Starik [16], Yagodin [17] and Sakelardis [18] have studied the UV spectra of Zr and Hf in Cl^- or SO_4^{2-} media. Ermakov et al. have reported the mixed-ligand species $HfCl(SO_4)^+$ with stability constant $\beta_{11} = (11 \pm 4) \times 10^2$ [19].

Extraction of Zr and Hf and separation from Hf in aq. Cl^-/ SO_4^{2-} are reported.

THEORY

Assuming the absence of polynuclear hydrolysis because of the high levels of the sulfate and acid concentrations and also the constancy of D_M for varying metal concentration and writing $M(SO_4)_jCl_i^{(4-i-2j)}$ as the predominant extractable aqueous

mixed-ligand species present (M = Zr or Hf), the extraction equilibrium may be written:

$$M(SO_4)_jCl_i^{(4-i-2j)}{}_{aq} + [(i+2j-4)R_3NHX)]_{n\,o} \rightleftarrows nR_3NH_{(i+2j-n)}M(SO_4)_jCl_{i\,o} + n(i+2j-4)X^-{}_{aq} \quad (4)$$

where $X^- = Cl^-$ or HSO_4^- and n is the average organic-phase amine aggregation number. The apparent extraction equilibrium constant (which subsumes all activity coefficients):

$$K_{ex}' = \frac{[R_3NH_{(i+2j-n)}M(SO_4)_jCl_i]_o^{\,n}\cdot[X^-]_{aq}^{\,n(i+2j-4)}}{[M(SO_4)_jCl_i^{(4-i-2j)}]_{aq}^{\,n}\cdot[R_3NHX]_o^{\,(i+2j}} \quad (5)$$

whence, if α_{ij} is the fraction of aqueous metal as the extractable species, $M(SO_4)_jCl_i^{(4-i+2j)}$ and $D_M = [M_{total}]_o/[M_{total}]_a$ is the distribution ratio of Zr or Hf,

$$n \log D_M = \log K_{ex}' + (i+2j-4)\log[R_3NX]_o - ((i+2j-4))\log[X^-]_{aq} + n\log\alpha_{ij} \quad (6)$$

Partial differentiation of equation (6) gives:

$$\frac{\partial \log D_M}{\partial \log[R_3NHX]_o} = (i+2j-4)/n \quad (7)$$

$$\frac{\partial \log D_M}{\partial \log[Cl^-]_{aq}} = i - i\alpha_{ij} = i - \overline{i_{aq}} \quad (8)$$

$$\frac{\partial \log D_M}{\partial \log[SO_4^{2-}]_{aq}} = j - j\alpha_{ij} = j - \overline{j_{aq}} \quad (9)$$

where $\overline{i_{aq}}$ and $\overline{j_{aq}}$ indicates the average aq. co-ordination numbers of the respective ligands [21].

Component peak wavelengths in UV spectra were identified from the minima of 2nd derivative plots and the spectra of individual components resolved by subtraction after reflection about the peak assuming a Gaussian shaped band [8,21,22] (see Figure 4).

EXPERIMENTAL

Alamine 336S (General Mills, now Cognis) [23], with >99% saturated C_8-C_{10} tertiary amine, diluted to with benzene (A.R.) was pre-equilibrated with HCl at the same concentration as the aqueous phase, washed with distilled water to remove entrained acid and filtered through phase separation paper (Whatman).

Recrystallized $ZrOCl_2.8H_2O$, (<2% Hf by XRF) and high-purity (i.e., negligible Zr) $HfOCl_2.8H_2O$ (Johnson Matthey) were made up to 0.5 mol L^{-1} stocks in 2 mol L^{-1} H_2SO_4 (to minimize polynuclear hydrolysis [9]), standardized gravimetrically with mandelic acid [9,24], and diluted to 2 x10^{-3} mol L^{-1} metal with standardized HCl or H_2SO_4. The concentration of the other anion was adjusted with either Na_2SO_4 or NaCl solution respectively. Zr or Hf tracer was added to give suitable count rates.

Equal volumes (10 mL) of each phase were shaken in polypropylene bottles placed in a thermostat bath at 298 ± 0.5 K for a total of 6 min. over 24 hours, sufficient to achieve equilibrium. Phases were separated by centrifuging in polypropylene tubes.

^{95}Zr or $^{175/181}Hf$ were measured by γ-scintillation counting (NaI detector) of both phases. Daughter ^{95}Nb was removed from ^{95}Zr immediately before addition by extracting

the ^{95}Nb with di-isobutyl carbinol [25]. Cl^- and SO_4^{2-} were determined by β-liquid scintillation co-incidence counting of ^{36}Cl or ^{35}S tracers, using ^{226}Ra as external standard for quenching correction. Both phases were sampled and counted (at least twice background) in triplicate and each experimental point determined in triplicate. Counts within 5% of the mean were accepted and mass balances were within 100 ± 2 %.

Were recorded using matching 10 mm quartz cells in a Pye-Unicam SP1800 spectrophotometer with a variable chart-speed linear recorder. Cyclohexane (A.R.) with isodecanol modifier was used as diluent for recording organic phase spectra because of the strong UV absorbance of benzene [7].

RESULTS AND DISCUSSION

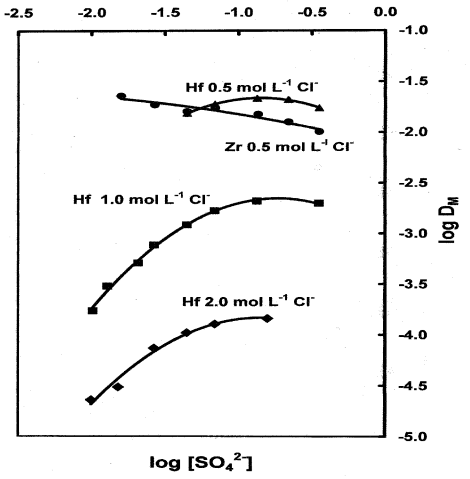

Figure 1: Variation of sulfate concentration.

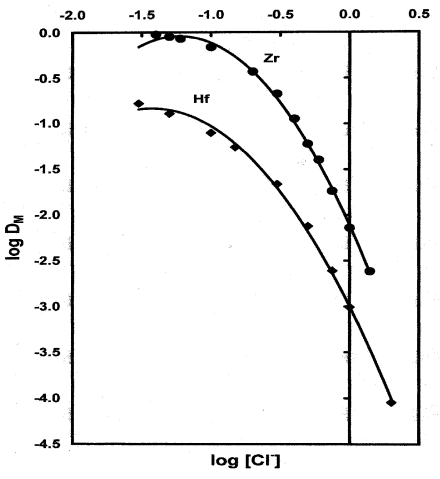

Figure 2: Variation of chloride concentration

Figures 1 and 2 show variation of log D_M with log $[SO_4^{2-}]_{aq}$ and log $[Cl^-]_{aq}$, respectively. Figure 1 shows various initial $[Cl^-]_{aq}$. In both figures, $[H^+]_{aq}$ = 2 mol L^{-1}. Figure 3 shows variation of log D_{Hf} and log D_{Zr} with log $[R_3NCl]_o$ for various $[Cl^-]_{aq}$ at $[SO_4^{2-}]_{aq}$ = 1 mol L^{-1} and $[H^+]$ = 2 or 5 mol L^{-1}. Most plots show parabolic variation of log D_M, with correlation coefficients, $R^2 > 0.98$, (except linear Zr at 4 mol L^{-1} Cl^-). In Figures 1 and 2, slopes agree with Equations 8 and 9, indicating constant organic coordination and steadily increasing aqueous coordination with rising concentration. In Figure 2, the slopes tend to –3. Curvature in Figure 3 may be due to increasing amine aggregation. The slopes of the linear portions of these plots are ~1.5, from the trend lines with $R^2 > 0.99$. In single acid media (not shown) slopes were close to 1 for both metals in both acids. Clearly, behavior is different in mixed media due to the differing parameters in Equations 4–9. The presence of 0.5 mol L^{-1} Cl^- in 1 mol L^{-1} H_2SO_4 decreases D_{Hf} by >100x compared to pure H_2SO_4. This could be due to simple competition with R_3NHCl (see Equation 3) but using ^{35}S and ^{36}Cl tracers to follow the uptake of the anions into the organic phase along with the metals, showed that while $[SO_4^{2-}]_o$ rose steadily with $[M]_o$ $[Cl^-]_o$ became constant indicating an equilibrium with possible mixed-ligand species.

Applying Equations 7-9 taking n = 2 as the predominant amine aggregation number [27,28] indicated possible aqueous species with i and j = 2 or 3 for both metals.

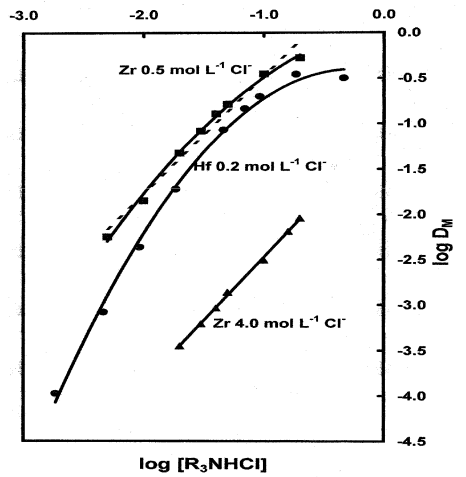

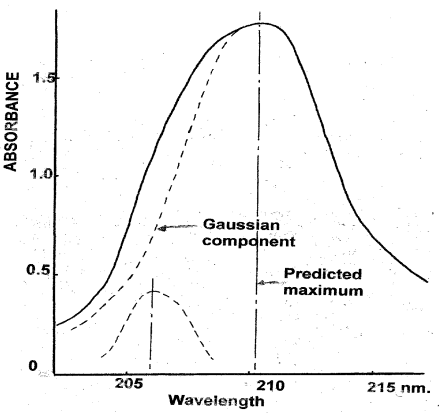

Figure 3: Variation of amine concentration. **Figure 4:** UV Spectrum of Hf in mixed Cl^-/ SO_4^{2-}.

Figure 4 shows the UV spectrum of Hf in a mixed solution with 1 mol L^{-1} Cl^- and 2 mol L^{-1} H_2SO_4. The peak at 210 nm is much stronger and broader than those obtained for $HfCl_i^{4-i}$ species in HCl alone (not shown). $Hf(SO_4^{2-})_j^{4-2j}$ complexes do not absorb in the range 200-220 nm [16], so this peak with a shoulder that can be resolved into several bands as $[Cl^-]$ decreases to 0.01 mol L^{-1} can be attributed to several aqueous $Hf(SO_4)_jCl_i^{(4-i-2j)}$ species with $j > i$ predominating at lower $[Cl^-]$. A peak at 268 nm in the organic phase was ascribed to a mixed-ligand species of Hf. The UV spectra for Zr were more complicated and difficult to interpret but probably also show mixed-ligand species.

The stability constants of $Hf(SO_4)_jCl_i^-$ species were estimated from the extraction data for varying $[Cl^-]_{aq}$ and $[SO_4^{2-}]_{aq}$, using Equations 7–9 and applying the graphical methods of either Rossotti [20,28,29] or Olerup [29,30]; details are given elsewhere [8]. Values of $\beta_{12} = (7.3 \pm 1.5) \times 10^8$ and $\beta_{11} = 3.5 \pm 0.4 \times 10^4$ were obtained in fair agreement with Ermakov's value $\beta_{11} = 1.7 \times 10^4$ [19]. A similar attempt to calculate β_{11} and β_{12} for Zr species led to inconsistent results.

Pure acid system plots (not shown) for varying amine concentration for a range of either $[H_2SO_4]_{aq}$ or $[HCl]_{aq}$ gave slopes tending to 1 ($R^2 > 0.99$) in agreement with Yagodin's proposed reaction (Equation 1) in H_2SO_4 [10]. In HCl, the Zr data agreed with Omori's results [13]. D_{Hf} is negligible in solutions containing less than ~ 6 mol L^{-1} HCl.

When HCl was added to individual Zr or Hf solutions in 2 mol L^{-1} H_2SO_4, the separation factor, $S_{Zr/Hf} = D_{Zr}/D_{Hf}$, increased from ~30 to 169 for <1 to 6 mol L^{-1} in HCl respectively. However, D_{Zr} was only 0.191 in the latter solution. The increase in $S_{Zr/Hf}$ is attributed to the presence of an increasing amount of the less extractable mixed-ligand $Hf(SO_4)_jCl_i^{(4-i-2j)}$ species, whereas for Zr, sulphato-species predominate. However, competition with the extraction of Cl^- decreases D_{Zr}.

CONCLUSIONS

The separation between Zr and Hf by extraction with Alamine 336S from sulfate media is increased by adding chloride ions up to 6 mol L^{-1} HCl, owing to the formation of a less extractable chloro-sulphatohafnate species, $Hf(SO_4)_jCl_i^{(4-i-2j)}$.

ACKNOWLEDGMENTS

The authors thank E.P.S.R.C., Rio Tinto plc. and Shell Chemicals plc. for funding.

REFERENCES

1. S. Glasstone, Principles of Nuclear Reactor Engineering, McMillan, London, 1956, 504-513.
2. M. Benedict and T. H. Pigford, Nuclear Chemical Engineering., McGraw-Hill, N.Y., 1957; pp. 162-179.
3. G. A. Yagodin and O A. Sinegrbova, Handbook of Solvent Extraction, T. H. Lo, M. H. I. Baird and C. Hanson, Eds., Wiley-Interscience, New York, 1983; pp. 805-812**.**
4. D. O. Voit, *Proc. Int. Solv. Extr. Conf 1980* Liège, Belgium, G. Duyckaerts *et al.* (Eds.), Université de Liège, 1980; Vol. 2, paper No. 80-59.
5 G. M. Ritcey and A. W. Ashbrook, Solvent Extraction: Principles and Applications to Process Metallurgy, Part II, Elsevier, Amsterdam, 1984; pp. 542-552.
6. T. H. Tunley & V. W. Nel, *Proc. Int. Solv. Extr. Conf. 1974*, Lyon, France, J. D. Thornton, A. Naylor, H. A. C. McKay & G. V. Jeffreys (Eds.), S. C. I., London, 1974, Vol. 2; pp. 1519-1533.
7. N. M. Rice, The Solvent Extraction of Iron, Zirconium and Hafnium with Tertiary Aliphatic Amines, PhD Thesis, Imperial College, University of London, U.K., 1966.
8. R. J. Lee, The Thermodynamics of Extraction of Ionic Complexes of Zirconium and Hafnium with Long-chain Amines, PhD Thesis, University of Leeds, U.K, 1973.
9. W. B. Blumenthal, Chemical Behaviour of Zirconium, van Nostrand, Princeton, N. J., 1958.
10. G. A. Yagodin and A. M. Chekmarev, *Proc. ISEC'80*, *loc. cit. 4*, Vol. 3 , paper No. 80-161.
11. Z. Malek *et al.*, *Proc. ISEC'74, loc. cit. 6*; Vol. 1, pp.477-486.
12. E. Cerrai and C. Testa, *Energia Nucleare*, **6**, 707-716, 768-780 (1959).
13. T. Omori and M. Suzuki, *Bull. Chem. Soc. Japan*, **36**, 850-854, (1963).
14. A. R. Burkin and N. M. Rice, *Proc. Int. Solv. Ext. Conf. 2005,* Beijing, P. R. China, Guangsheng Luo, Yundong Wang and Tun Zhu (Eds.), China Acad. J. Electronic Publ. House, Beijing 2005, **CD-ROM**, Paper No. B108, pp 446-453.
15. A. R. Burkin and N. M. Rice, *Ibid.,* Paper No. B137, pp 637-642.
16. I. E. Starik, *Doklady. Akad. Nauk USSR*, **137,** 356-358, (1961).
17. G. A. Yagodin et al., *Russ. J. Inorg. Chem.,* **11,** (1), 167-171, (1966).
18. P. Sakellaridis and M. Coromanzon, *Bull Soc. Chim. France,* pp. 289-291, (1963).
19. A. N. Ermakov *et al., Russ. J. Inorg. Chem.* **12**(12), 1784-1788 (1967).
20. F. J. C. Rossotti and H. Rossotti, The Determination of Stability Constants, McGraw-Hill, New York, 1961, 38-57, 108-114 and 203-239.
21. A. Savitzky and M. J. E. Golay, *Anal. Chem.,* **36,** 1627-1639 (1964).

22. H. E. Crabtree and N. M. Rice, *Proc. ISEC'74*, *loc cit. 6*, Vol. 1, 791-822.
23. J. House *et. al*., *Alamine 336*, General Mills Inc., Chem. Div. Tech. Bull., Minneapolis, Minn., *c.* 1970, 3 pp.
24. A. I. Vogel, A Textbook of Quantitative Inorganic Analysis, 3rd Edn., Longmans, London, 1964, 258-259, 476-8.
25. A. Jurriaanse and F. L. Moore, *Anal. Chem.,* **38,** 964-965 (1966).
26. E. Högfeldt, *Proc. Int. Conf. Solv. Extr. Chem., 1968,* Jerusalem, Israel, A.S. Kertes and Y. Marcus (Eds.), Wiley-Interscience, New York, 1969, 157-175.
27. P. R. Danesi and G. Scibona, *Ibid.* 237-248.
28. F. J. C. Rossotti, *Acta Chem. Scand*. **9,** 1166-1176 (1955).
29. M. T. Beck, The Chemistry of Complex Equilibria, van Nostrand-Reinhold, London, 1970; 55-61.
30. H. Olerup, *Svensk. Kem. Tidskr*. **55,** 324 (1943).

SOFTWARE "EXTREQ-2" FOR MATHEMATICAL MODELING OF MULTICOMPONENT EXTRACTION EQUILIBRIA

K. A. Slavinskiy, A. M. Chekmarev, and S. I. Stepanov

Department of Physics and Chemistry, D. I. Mendeleyev University of Chemical Technology of Russia. Miusskaya sq., 9, Moscow, Russian Federation.
Corresponding author email address: k.slavinskiy@mail.ru

ABSTRACT

There is an on-going demand for software suitable for analysis of experimental data obtained from investigation of equilibrium of extraction processes. We have developed a "user friendly" software "EXTREQ-2" in Borland Delphi environment for mathematical modeling of extraction isotherms in multicomponent systems. The results of the modeling of extraction isotherms of uranyl nitrate and thorium nitrate and lanthanides nitrates with mixtures of methyltriakyl-ammonium nitrate and neutral phosphorus-based organic compounds or di(2-ethylhexyl) phosphoric acid in toluene will be presented. The thermodynamic parameters and composition of organic phase for each system will be discussed.

INTRODUCTION

The “EXTREQ-2” software is designed for modeling of the extraction process and calculation of its parameters such as equilibrium constants (K_T), type and composition of the extractable species, and their hydration numbers (H_1) based on the data available from extraction isotherm.

The mass action law written in terms of components activities serves as a mathematical basis for the investigated models. We use the approach developed by Sergievskiy [1] to calculate the activity coefficients of the organic phase components. This method includes quantitative description of the hydration of the extractants and extractable compounds in the organic phase. It has been successfully applied in the work of Belair et al. [2], Mokili [3], and Poitrenaud [4]. Activities of the water components were calculated using electrolyte solution theory [5].

The formation of the synergistic complex in the organic phase according to general extraction equilibria can be written as

$$p\upsilon_+ Me^{z_+} + p\upsilon_- An^{z_-} + q_1\overline{S}_1 + q_2\overline{S}_2 \rightarrow \overline{pMe_{\upsilon_+}\left(An\right)_{\upsilon_-}\cdot q_1 S_1 \cdot q_2 S_2} \qquad (1)$$

with thermodynamical extraction constant:

$$K_{T_{\{q_1,q_2\}}} = \frac{\bar{a}_{Me}}{a_{Me}^{\ p} \cdot \bar{a}_{S1}^{\ q_1} \cdot \bar{a}_{S2}^{\ q_2}} = \frac{\bar{C}_{Me\{q_1,q_2\}} \cdot \bar{y}_{Me}}{a_{Me}^{\ p} \cdot \bar{C}_{S1}^{\ q_1} \cdot \bar{y}_{S1}^{\ q_1} \cdot \bar{C}_{S2}^{\ q_2} \cdot \bar{y}_{S2}^{\ q_2}} \tag{2}$$

where *a* and *a-bar* are activities in the aqueous and organic phases respectively; *y* and *y-bar* are activity coefficients in the aqueous and organic phases respectively; *p* is the number of distribution molecules; q_1, q_2 are the solvation numbers of the first and second extractants; indexes *Me*, *S1*, and *S2* means distributed component, extractant one, and extractant two.

According to Sergievskiy

$$y_c = y_c^* \cdot \exp\left[h_\infty \cdot (1 - a_W)\right] \tag{3}$$

where y^*_C is the activity coefficient of species *c* in the same organic phase (i.e., same diluent and same concentration), but in equilibrium with pure water ($a_{H20} = 1$); h_∞ is the number of water molecules solubilized by species *c*, for $a_{H20} = 1$; a_W is the water activity.

Hence, the thermodynamic-constant equation can be written as

$$K_{T_{\{q_1,q_2\}}} = \frac{\bar{C}_{Me\{q_1,q_2\}}}{a_{Me}^{\ p} \cdot \bar{C}_{S1}^{\ q_1} \cdot \bar{C}_{S2}^{\ q_2}} \cdot \frac{\bar{y}^*_{Me}}{\bar{y}^{*\ q_1}_{S1} \cdot \bar{y}^{*\ q_2}_{S2}} \cdot e^{\left[(h_{Me} - h_{S1} \cdot q_1 - h_{S2} \cdot q_2) \cdot (1 - a_W)\right]} \tag{4}$$

Let $H_1 = (h_{Me} - h_{S1} \cdot q_1 - h_{S2} \cdot q_2)$ and since

$$\frac{\bar{y}^{*\ q_1}_{S1} \cdot \bar{y}^{*\ q_2}_{S2}}{\bar{y}^*_{Me}} \approx 1$$

then the concentration of distributed component can be written as

$$\bar{C}_{Me\{q_1,q_2\}} = K_{T_{\{q_1,q_2\}}} \cdot a_{Me}^{\ p} \cdot \bar{C}_{S1}^{\ q_1} \cdot \bar{C}_{S2}^{\ q_2} \cdot e^{\left[H_{1\{q_1,q_2\}} \cdot (a_W - 1)\right]} \tag{5}$$

The material-balance equations in terms software “EXTREQ-2” are presented below.

$$\mathrm{Complex}_{i,j_{\{q1j-q2j-\upsilon j\}}} = \left(K_{T_j} \cdot a_{C_i}^{\ p_j} \cdot \bar{C}_{S1_i}^{\ q_{1j}} \cdot \bar{C}_{S2_i}^{\ q_{2j}} \cdot e^{\left[\upsilon_j \cdot H_{1j} \cdot (a_{W_i} - 1)\right]} \right)^{\frac{1}{\upsilon_j}} \tag{6}$$

$$Sa_i^{calc} = \sum_{j=1}^{m} p_j \cdot \mathrm{Complex}_{i,j_{\{q1j-q2j-\upsilon j\}}} \tag{7}$$

$$\left.\begin{aligned} \bar{C}_{S1_i} + \sum_{j=1}^{m} \left(q_{1_j} \cdot K_{T_j} \cdot a_{C_i}^{\ p_j} \cdot \bar{C}_{S1_i}^{\ q_{1j}} \cdot \bar{C}_{S2_i}^{\ q_{2j}} \cdot e^{\left[\upsilon_j \cdot H_{1j} \cdot (a_{W_i} - 1)\right]} \right)^{\frac{1}{\upsilon_j}} - \bar{C}^0_{S1} = 0 \\ \bar{C}_{S2_i} + \sum_{j=1}^{m} \left(q_{2_j} \cdot K_{T_j} \cdot a_{C_i}^{\ p_j} \cdot \bar{C}_{S1_i}^{\ q_{1j}} \cdot \bar{C}_{S2_i}^{\ q_{2j}} \cdot e^{\left[\upsilon_j \cdot H_{1j} \cdot (a_{W_i} - 1)\right]} \right)^{\frac{1}{\upsilon_j}} - \bar{C}^0_{S2} = 0 \end{aligned}\right\} \tag{8}$$

Where we have C_{S1i}, C_{S2i} equilibrium concentrations of the extractants; C^0_{S1i}, C^0_{S2i}— initial concentrations of the extractants; K_{Tj}—thermodynamic constant of extraction of j-compound; H_{1j}—parameter of hydration; p_j—number of distribution molecules; q_{1j}, q_{2j}— solvation numbers of the first and second extractants; v_j – degree of dissociation; Sa_i^{calc} and Sa_i^{exp}—calculated and experimental concentrations of the component in organic phase; a_{Ci}—activity of electrolyte in aqueous phase; *m*—number of estimated compounds.

Software "EXTREQ-2" is developed in Borland Delphi environment. The experimental data are stored in Microsoft Access database. The numbers of estimated compounds and initial values of optimization parameters are entered in the main program windows.

Software "EXTREQ-2" allows modeling both simple extraction systems, such as "one distributed component–one extractant" and more complex systems such as "one distributed component–two extractants," when up to six extractable species can be formed in the organic phase. Under these conditions, "EXTREQ-2" simulates the liquid-liquid extraction systems taking into account physical distribution either with or without dissociation of partitioned components in the organic phase or solvation either with or without dissociation of the formed species in the organic phase. Thus, it is possible to model the extraction using several mechanisms.

The criterion for the best model is the minimum squared error between calculated and experimental values of the concentrations of distributed component in the organic phase. The accuracy of the calculated model is estimated by three parameters:

Standard deviation
$$R = \frac{1}{n} \cdot \sum_{i=1}^{n} \left| \frac{y_i^{\exp} - y_i^{calc}}{y_i^{calc}} \right| \cdot 100 \qquad (9)$$

Mean square deviation
$$SSE = \sum_{i=1}^{n} \alpha_i \cdot \left(y_i^{calc} - y_i^{\exp} \right)^2 \qquad (10)$$

Residual dispersion
$$\delta_R{}^2 = \frac{\sum_{i=1}^{n} \left(y_i^{calc} - y_i^{\exp} \right)^2}{n - p} \qquad (11)$$

Where we have y^{calc}—calculated data; y^{exp}—experimental data; p – number of parameters; n—number of experimental points; and a—weighting coefficient.

Our computer program allows optimization of solvation numbers, degrees of dissociation of extractable compounds in the organic phase, and the composition of the stoichiometric hydrates that are formed with organic-phase components.

Computed thermodynamic parameters, the values of concentrations of all extractable compounds for every experimental point, and relative errors between experimental and calculated concentrations of the distributed component are exported into a Microsoft Excel file.

RESULTS AND DISCUSSION

Testing of the software was carried out for extraction isotherm of Th(IV) with 0.38 mol/L methyltrialkylammonium nitrate and 0.6 mol/L phosphorous organic reagents (PhOR) in toluene.

It was found earlier by the slope-analysis method that Th could be extracted into the organic phase as a synergistic complex $(R_4N)_2Th(NO_3)_6 \cdot 3PhOR$, anionic nitrate complex $(R_4N)_2Th(NO_3)_6$, and trisolvate $Th(NO_3)_4 \cdot 3PhOR$ [6].

Initial calculations showed that the deviation of the modeling curve from the experimental data is minimum under the assumption of formation of the above complexes.

Results of modeling of extraction of thorium nitrate and lanthanide nitrates and uranyl nitrate are presented in Table 1. Experimental data for the extraction systems presented in the figures below have been taken from Stepanov [6].

Table 1. Parameters of modeling of extraction isotherms of lanthanides nitrates with mixtures of methyltrialkylammonium nitrate and neutral phosphorus-based organic compounds

Composition of organic phase	$\ln(K_T)$	H_1	$R,\%$	SSE	δ_R^2
$Th(NO_3)_4$ with 0.38 mol/L methyltrialkylammonium nitrate and 0.6 mol/L PhOR in toluene *					
$(R_4N)_2Th(NO_3)_6 \cdot 3PhOR$	30.36	2.17			
$(R_4N)_2Th(NO_3)_6$	22.08	1.76	3.60	9.54×10^{-4}	1.19×10^{-4}
$Th(NO_3)_4 \cdot 3PhOR$	23.00	1.05			
$Dy(NO_3)_3$ with 0.4 mol/L methyltrialkylammonium nitrate and 0.6 mol/L tri-n-butyl phosphate (TBP) in toluene. *					
$(R_4N)_3[Dy(NO_3)_6 \cdot 3TBP]$	11.87	16.34			
$(R_4N)[Dy(NO_3)_4]$	1.49	-2.52	1.76	5.19×10^{-4}	7.42×10^{-5}
$Dy(NO_3)_3 \cdot TBP$	4.17	11.18			
$Dy(NO_3)_3$ with 0.25 mol/L methyltrialkylammonium nitrate and 0.25 mol/L di-*iso*-octylmethylphosphonate (DIOMP) in toluene					
$(R_4N)[Dy(NO_3)_4 \cdot 3DIOMP]$	10.41	0.99			
$(R_4N)[Dy(NO_3)_4]$	4.22	10.71	4.14	5.34×10^{-4}	8.89×10^{-5}
$Dy(NO_3)_3 \cdot DIOMP$	1.54	2.49			
$Dy(NO_3)_3$ with 0.20 mol/L methyltrialkylammonium nitrate and 0.3 mol/L PhOR in toluene					
$(R_4N)_2[Dy(NO_3)_5 \cdot 2PhOR]$	16.13	28.41			
$(R_4N)[Dy(NO_3)_4]$	4.37	8.26	3.22	1.14×10^{-3}	1.63×10^{-4}
$Dy(NO_3)_3 \cdot PhOR$	4.81	11.18			
$Tb(NO_3)_3$ with 0.3 mol/L methyltrialkylammonium nitrate and 0.7 mol/L tri-*n*-butyl phosphate (TBP) in toluene.					
$(R_4N)[Tb(NO_3)_4 \cdot 3\ TBP]$	8.27	63.06			
$(R_4N)[Tb(NO_3)_4]$	1.82	2.86	3.69	7.40×10^{-4}	9.25×10^{-5}
$Tb(NO_3)_3 \cdot 3\ TBP$	2.58	-13.91			
$Nd(NO_3)_3$ with 0.3 mol/L methyltrialkylammonium nitrate and 0.7 mol/L tri-*n*-butyl phosphate (TBP) in toluene.					
$(R_4N)[Nd(NO_3)_4 \cdot 3TBP]$	6.47	-10.28			
$(R_4N)[Nd(NO_3)_4]$	-4.91	-56.47	4.33	9.27×10^{-4}	1.16×10^{-4}
$Nd(NO_3)_3 \cdot 3\ TBP$	-8.31	-22.02			
$UO_2(NO_3)_2$ with 0.055 mol/L methyltrialkylammonium nitrate and 0.055 mol/L D2EHPA in toluene *					
$(R_4N)_{1.14}UO_2(NO_3)_{3.14} \cdot 1.77$ D2EHPA	28.39	1.07	2.36	2.22×10^{-5}	1.48×10^{-6}
$UO_2(NO_3)_2 \cdot D2EHPA$	8.23	3.36			

The curves for extraction isotherms marked (*) are shown below.

Modeling of extraction isotherm of $Th(NO_3)_4$ with 0.38 mol/L methyl-tri-alkyl-ammonium nitrate and 0.6 mol/L PhOR in toluene.

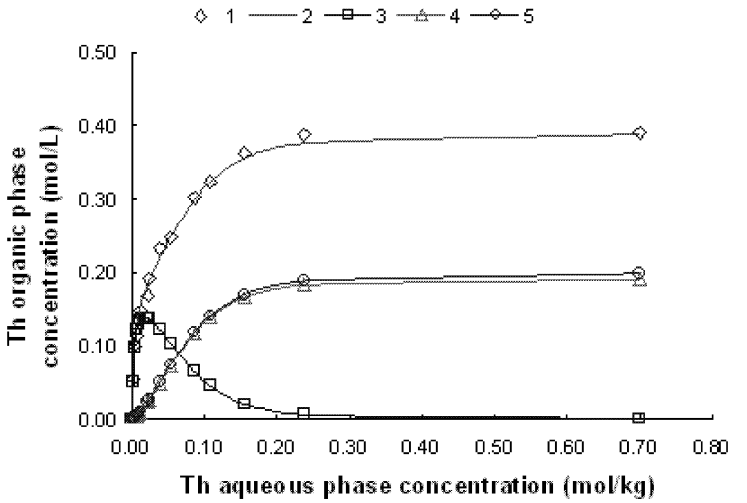

Figure 1. Experimental and calculated data of Th species distribution between aqueous and organic phases. 1 – Sa^{exp}; 2 – Sa^{calc}; 3 – $(R_4N)_2Th(NO_3)_6 \cdot 3PhOR$); 4 – $(R_4N)_2Th(NO_3)_6$; 5 – $Th(NO_3)_4 \cdot 3PhOR$. X-axis is in molality concentration.

Modeling of extraction isotherm of $Dy(NO_3)_3$ with 0.4 mol/L methyl-tri-alkyl-ammonium nitrate and 0.6 mol/L tri-*n*-butyl phosphate (TBP) in toluene.

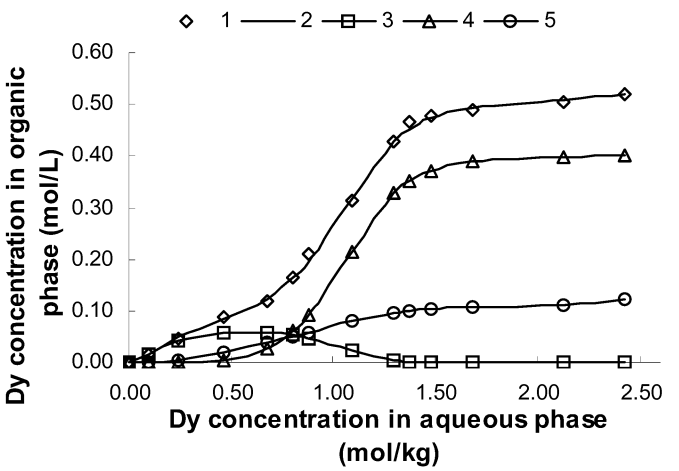

Figure 2. Experimental and calculated data of Dy species distribution between aqueous and organic phases. 1 – Sa^{exp}; 2 – Sa^{calc}; 3 – $(R_4N)_3[Dy(NO_3)_6 \cdot 3TBP]$; 4 – $(R_4N)[Dy(NO_3)_4]$; 5 – $Dy(NO_3)_3 \cdot TBP$. X-axis is in molality units.

Modeling of extraction isotherm of $UO_2(NO_3)_2$ with 0.055 mol/L methyl-tri-alkyl-ammonium nitrate and 0.055 mol/L D2EHPA in toluene.

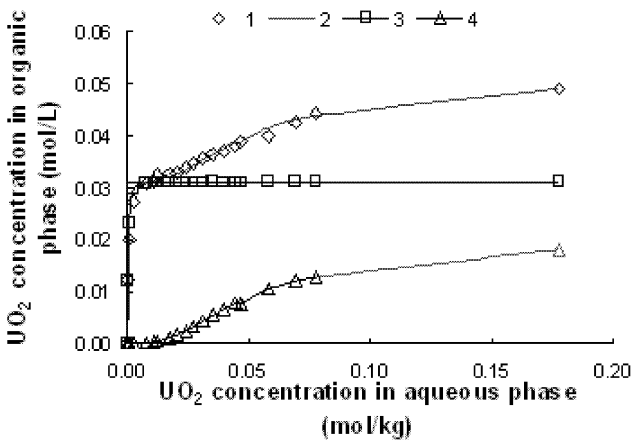

Figure 3. Experimental and calculated data of UO_2 species distribution between aqueous and organic phases. 1 – Sa^{exp}; 2 – Sa^{calc}; 3 – $(R_4N)_{1.14}UO_2(NO_3)_{3.14}\cdot 1.77$D2EHPA; 4 – $UO_2(NO_3)_2\cdot$D2EHPA. X-axis is in molality units.

CONCLUSIONS

Extraction equilibria of uranyl nitrate, thorium nitrate, and nitrates of some lanthanides with mixtures of methyltrialkylammonium nitrate and neutral phosphorus-based organic compounds or di-(2-ethylhexyl) phosphoric acid in toluene were modeled using software "EXTREQ-2". The thermodynamic parameters for each system were calculated and confirmed by independent analytical methods.

REFERENCES

1. V. V. Sergievskiy, "Influence of Components Hydratation of Organic Phase on Extraction Equilibrium," Inorganic. Chemistry Resume of the Science and Technique, Moscow, Russia, 1976; pp. 5–82.
2. S. Belair, C. Lamouroux; M. Tabarant, A. Labet, C. Mariet, and P. Dannus, "Modeling of the Extraction of Lanthanide Nitrates from Aqueous Solutions Over a Wide Range of Activities by CMPO," *Solvent Extr. Ion Exch.,* **22**(5), 791–811 (2004).
3. B. Mokili and C. Poitrenaud, "Modeling of the Extraction of Neodymium and Praseodymium Nitrates from Aqueous Solutions Containing a Salting-out Agent or Nitric Acid by Tri-n-butylphosphate," *Solvent Extr. Ion Exch.,* **14**(4), 617–634 (1996).
4. B. Mokili and C. Poitrenaud, "Modeling of Nitric Acid and Water Extraction from Aqueous Solutions Containing a Salting-out Agent by Tri-*n*-butylphosphate," *Solvent Extr. Ion Exch.,* **13**(4), 731–754 (1995).
5. G. I. Mikulin, Problems in Phisycal Chemistry of Electrolyte Solutions, Leningrad, 1968.
6. S. I. Stepanov and A. M. Chekmarev, Rare Metals Extraction with Quaternary Ammonium Salts, Moscow, 2004.

COMPLEXATION OF AMERICIUM WITH α-D-ISOSACCHARINATE

S. Allard,[1] C. Ekberg,[2] R. Jolsterå,[3] A. Knutsson,[1] and A. Ödegaard-Jensen[1]

Department of Chemical and Biological Engineering, [1]Nuclear Chemistry, [2]Industrial Materials Recycling, Chalmers University of Technology, 412 96 Gothenburg, Sweden.
[3]Department of Chemical Engineering and Geosciences, Division of Chemistry, Luleå University of Technology, 971 87 Luleå, Sweden.
Corresponding author email address: stefane@chalmers.se

ABSTRACT

Under alkaline conditions, cellulose will degrade, with isosaccharinate being the dominant end-product. One of the formed diastereomers, the α-D-isosaccharinate, is a strong complexing agent for tri- and tetravalent actinides and is the dominant conformation at pH > 5, rendering other conformations insignificant at neutral to alkaline conditions. The presence of α-D-isosaccharinate increases the amount of metal in solution and also affects the surface interactions. Understanding this complexation is of relevance for long-term repository assessments. This study has investigated the complexation of americium with α-D-isosaccharinate using solvent-extraction and radioanalytical techniques at 25 °C. The stability constants for the complexation reactions were determined by curve fitting of a distribution-ratio equation to experimental data.

INTRODUCTION

The diastereomers α- and β-D-isosaccharinate formed from the alkaline cellulose degradation are produced in approximately equal amounts with two corresponding enantiomeric lactone conformations each [1-4]. α-D-isosaccharinate forms strong complexes with tetravalent actinides, as well as with trivalent lanthanides [4,6-8], and at alkaline conditions, this form dominates [5]. In the presence of α-D-isosaccharinate, the amount metal in solutions of lanthanides and actinides increases several orders of magnitude due to the strong complexation while at the same time affecting their surface interactions [4]. To further increase the knowledge of the isosaccharinate system, the complexation of americium with α-D-isosaccharinate has been examined at pH 7, where it is the dominant species. The aim of this study has been to determine the metal-to-ligand ratio with americium as well as the stability constants of these complexation reactions. This has been accomplished by means of solvent extraction with ^{241}Am tracer.

THEORY

The α-isosaccharinic system consists of three species; the carboxylic α-isosaccharinic acid (HISA), α-D-isosaccharinate (ISA), and α-D-isosaccharino-1,4-

lactone (ISA_L). The conformations are pH-dependent, with the ISA form dominating at higher pH [5,9]. The extraction system was composed of a 1 M $NaClO_4$ aqueous phase with ^{241}Am and ISA in contact with concentrated tributylphoshate pre-equilibrated with 1 M $NaClO_4$. To ensure that all forms other than ISA are negligible, the pH of the aqueous phase was kept at approximately 7 [5,9]. The extraction reaction for this system may be written [10-12]

$$Am^{3+}_{aq} + rTBP_{org} + 3ClO^{-}_{4aq} \rightarrow Am\left(ClO_4\right)_3\left(TBP\right)_{r,org} \quad (1a)$$

The americium stripping from the organic phase is supposed to occur with ISA as observed with lactate [11]

$$Am\left(ClO_4\right)_3\left(TBP\right)_{r,org} + pISA^{-} \rightarrow Am\left(ISA^{-}\right)^{(3-p)+}_{p\ aq} + rTBP + 3ClO^{-}_4 \quad (1b)$$

The distribution ratio for americium is expressed as

$$D = \frac{\left[Am\right]^{tot}_{org}}{\left[Am\right]^{tot}_{aq}} \quad (2)$$

where the americium concentration is proportional to the radioactivity measured in each phase. The subscripts org and aq refer to organic and aqueous phases, respectively. The complexation of americium and a ligand L can be described by the following reaction

$$mAm^{3+} + nL^{-} \rightarrow Am_m L^{(3m-n)+}_n \quad (3)$$

Since the ionic strength is kept constant at 1.0 M, the activity coefficients for Reaction (3) have been included, resulting in a conditional stability constant expressed in Equation 4.

$$\beta_{mn} = \frac{\left[Am_m\left(L\right)^{(3m-n)+}_n\right]}{\left[Am^{3+}\right]^m \cdot \left[L\right]^n} \quad (4)$$

When several ligands are present in the solution, the stability constant can be expressed as β_{mnqp} where *m* refers to the number of Am^{3+}, and *n*, *q*, and *p* represent the ligands ClO_4^-, OH^-, and ISA^-, respectively.

Using Equation 4 and Equation 2 can be expressed as

$$D_{Am} = \frac{\left[ClO^{-}_4\right]^3 \cdot \left[TBP\right]^r_{org}}{1 + \sum_{n=1}^{3}\beta_{mn00} \cdot \left[ClO^{-}_4\right]^n + \sum_{q=1}^{3}\beta_{m0q0} \cdot \left[OH^{-}\right]^q + \sum_{p=1}^{3}\beta_{m00p} \cdot \left[ISA^{-}\right]^p} \quad (5)$$

The following expression can now be reached using Equation 5, where D_{Am} and $D_{Am,0}$ indicate the system with and without α-D-isosaccharinate.

$$\frac{D_{Am}}{D_{Am,0}} = \frac{1 + \sum_{n=1}^{3} \beta_{mn00} \cdot \left[ClO_4^-\right]_0^n + \sum_{q=1}^{3} \beta_{m0q0} \cdot \left[OH^-\right]_0^q}{1 + \sum_{n=1}^{3} \beta_{mn00} \cdot \left[ClO_4^-\right]^n + \sum_{q=1}^{3} \beta_{m0q0} \cdot \left[OH^-\right]^q + \sum_{p=1}^{3} \beta_{m00p} \cdot \left[ISA^-\right]^p} \quad (6)$$

The americium perchlorate complexation is weak and can consequently be neglected in Equation 6. The ionic strength of the aqueous phase is kept constant throughout the experiments and set to 1.0 M, and the relation between the measured pH and the proton concentration at this ionic strength and temperature is [13]

$$-\log\left(\left[H^+\right]\right) = pH_{measured} + 0.23 \quad (7)$$

β_{m00p} was determined by curve fitting of Equation 6 to experimental data employing a χ^2 method to estimate the standard deviation [14]. Since n and q = 0, β_{m00p} will hereafter be referred to as β_p.

EXPERIMENTAL

Concentrated TBP (tributyl phosphate, Sigma Aldrich) was shaken with aliquots of 1 M $NaClO_4$ for 12 minutes in order to saturate it. The solutions were stored in contact until they were used. A 4 mL 1 M $NaClO_4$ solution and 4 mL of the saturated TBP were shaken together in vials. To reduce sorption of americium on vial surfaces, 8 µL 50 mM $Nd(NO_3)_3$ (Fluka) solution was added as a hold-back carrier with a resulting concentration of about 1 x 10^{-4} M in the aqueous phase. Neodymium is stable in its trivalent state, it has a similar ionic radius to americium, and it does not precipitate significantly at the pH used in this study [15]. A 20 µL 360 MBq/mL ^{241}Am solution was added, resulting in an americium concentration of approximately 8.3 x 10^{-9} M. Small additions of 0.1 M NaOH (Riedel-de Haën, titrisol) were made to reach pH 7. ISA solutions of appropriate concentrations were prepared from 1 M $NaClO_4$, and a 0.55 M ISA stock solution was prepared as has previously been described [19]. The samples were shaken for 8 minutes, and the phases were allowed to separate. Samples of 1 mL from each phase and 10 mL liquid scintillation cocktail (Ultima Gold XR, Packard BioScience) were added to liquid-scintillation vials, and the activity in the samples was measured in a liquid-scintillation counter (LKB Wallac 1219 Rackbeta, channels 450-700). The pH was measured using a 1 M $NaClO_4$ combination electrode (InLab 423, Mettler Toledo) calibrated against pH 4.01, 7.00, and 9.21 standard buffers (Mettler Toledo).

RESULTS AND DISCUSSION

In the fitting of Equation 6 to the experimental data, the number of ISA ligands involved in this stripping can be determined, as well as the values of the respective stability constants. As can be seen in Equation 3, the complexation of Am^{3+} is independent of the proton concentration. It is probable that one or more hydrogen atoms of the hydroxyl-groups of ISA are involved in the complexation reaction [16];

nevertheless this aspect of the complexation cannot easily be examined in this specific system. The generalized coordination-ionization scheme for polyhydroxy carboxylic acids in water proposed by van Duin et al. [17], indicate that the ionized carboxylate group and the α-OH group of ISA are possibly both involved in the complexation with Am^{3+}. The fitting of Equation 6 to the experimental data could readily be done using the first and second stability constants (see Figure 1).

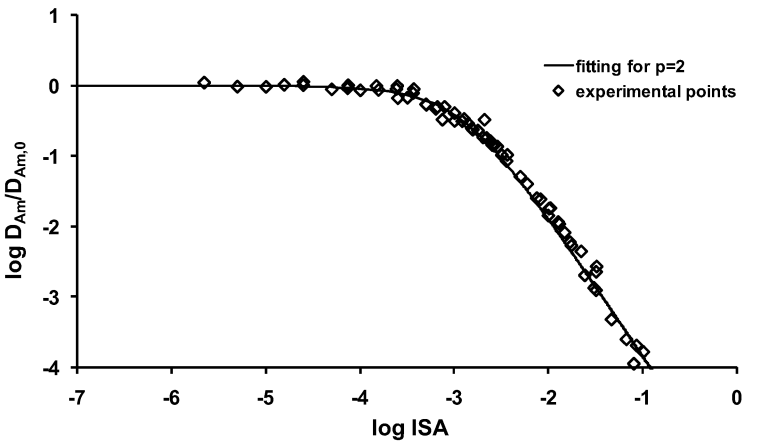

Figure 1. Influence of [ISA] on the $D_{am}/D_{am,0}$ ratio with fitting of the logarithm of Equation 6 for $p = 2$ to experimental points at 25 °C.

To examine the influence of hydrolysis, Equation 6 was fitted both with and without the hydroxide-containing term to the experimentally obtained values. The effect of hydroxide complexation was found to be negligible at this pH. The attained stability constants are presented in Table 1 along with values from literature.

Table 1. The logarithm of the stability constants attained in this study as well as values from the literature

T (°C)	pH	I (M)	log β_1	log β_2	Reference
25 ± 1	7.0	1.0	2.9 ± 0.4	5.8 ± 0.2	This study[(a)]
23 ± 3	Alkaline	0	-21.4 ± 1		Tits et al.[(b)] [18]

[a]Solvent extraction

[b]Sorption, log K^o = -21.4 ± 1 for the reaction $Am^{3+} + ISA^- \leftrightarrow Am(ISA_{-3H})^- + 3H^+$

The relative uncertainties in D_{Am} -values calculated from the measurements of the radioactive samples are less that 0.5%. However, the $D_{Am,0}$ is calculated as an average of four different shaking experiments, and the relative standard deviations of these experiments are 6.5%, which is the uncertainty in the method in this case. Data in the literature pertaining to Am-ISA^- complexation is scarce. The value presented by Tits et al. is difficult to compare, as no value for the reaction $ISA^- \longleftrightarrow ISA_{-3H}^{4-} + 3H^+$ is available. The deprotonation of ISA^- as described by this reaction would occur at very high pH regimes. It is interesting to note that their study indicates that only one ligand is involved in the complexation with americium.

CONCLUSION

Using a solvent-extraction technique, the stability constants for the complexation of americium with α-D-isosaccharinate at pH 7 and an ionic strength of I = 1.0 M have been investigated at 25 ^{o}C. Experimental data suggest that two ligands are involved in the complexation with americium, forming the complexes $Am(ISA)_1$ and $Am(ISA)_2$ of undetermined charge.

ACKNOWLEDGMENTS

This work was funded by SKB, the Swedish Nuclear Fuel and Waste Management Co.

REFERENCES

1. B. F. Greenfield, M. H. Hurdus, N. J. Pilkington, M. W. Spindler, and S. J. Williams, "The Degradation of Cellulose in the Near Field of a Radioactive Waste Repository," *Mat. Res. Soc. Symp. Proc.*, **333**, 705-710 (1994).
2. M. A. Glaus, L. R. Van Loon, S. Achatz, A. Chodura, and K. Fischer, "Degradation of Cellulose Materials under the Alkaline Conditions of a Cementitious Repository for Low and Intermediate-level Radioactive Waste. I. Identification of Degradation Products," *Analytica Chimica Acta*, **398,** 111-122 (1999).
3. R. L. Whistler and J. N. BeMiller, "Alkaline Degradation of Polysaccharides," *Advan. Carbohydr. Chem*., **13**, 289-329 (1958).
4. S. Holgersson, "Studies on the Effect of Concrete on the Chemistry in a Repository for Radioactive Waste," Ph.D. Thesis, Chalmers University of Technology, 2000.
5. S. Ekberg, C. Ekberg, and Y. Albinsson, "Characterization of α-Isosaccharinic Acid: Lactone and Carboxylic Conformations," *J. Soln. Chem.*, **33**(5), 465-477 (2004).
6. K. Vercammen, M. A. Glaus, and L. R. Van Loon, "Evidence for the Existence of Complexes Between Th(IV) and α-Isosaccharinic Acid under Alkaline Conditions," *Radiochim. Acta*, **84**(4), 221-224 (1999).
7. K. Vercammen, M. A. Glaus, and L. R. Van Loon, "Complexation of Th(IV) and Eu(III) by α-Isosaccharinic Acid under Alkaline Conditions," *Radiochim. Acta*, **89**, 393-401 (2001).
8. B. F. Greenfield, A. D. Moreton, M. W. Spindler, S. J. Williams, and D. R. Woodwark, "The Effects of the Degradation of Organic Materials in the Near-field of a Radioactive Waste Repository. In: Scientific Basis for Nuclear Waste Management," *Mat. Res. Soc. Symp. Proc.*, **465**, 299-306 (1992).
9. H. Cho, D. Rai, N. J. Hess, Y. Xia, and L. Rao, "Acidity and Structure of Isosaccharinate in Aqueous Solution: A Nuclear Magnetic Resonance Study," *J. Soln. Chem.*, **32**(8), 691-702, (2003).
10. R. Lundqvist, L. Jiu-Fang, and I. Svantesson, "Hydrophilic Complexes of the Actinides. II. Comparison of TBP, HTTA and HDEHP Liquid Distribution Systems," *Acta Chemica Scandinavica A*, **37,** 743-753(1983).
11. R. Lundqvist, L. Jiu-Fang, and I. Svantesson, "Hydrophilic Complexes of the Actinides. III. Lactates of Am^{3+}, Eu^{3+}, U^{4+} and UO_2^{2+}," *Acta Chemica Scandinavica A*, **38**, 501-512 (1984).

12. R. Lundqvist, "Hydrophilic Complexes of the Actinides. I. Carbonates of Trivalent Americium and Europium," *Acta Chemica Scandinavica A*, **36**, 741-750 (1982).
13. T. Fanghänel, V. Neck, and J. I. Kim, "The Ion Product of H_2O, Dissociation Constant of H_2CO_3 and Pitzer Parameters in the System $Na^+/H^+/HCO_3^-/CO_3^{2-}/ClO_4^-/H_2O$ at 25° C," *J. Sol. Chem.*, **25**(4), (1996).
14. G. Meinrath, C. Ekberg, A. Landgren, and J. O. Liljenzin, "Assessment of Uncertainty in Parameter Evaluation and Prediction," *Talanta*, **51**, 231-246 (2000).
15. G. T. Seaborg, "Overview of the Actinide and Lanthanide (the f) Elements," *Radiochim. Acta*, **61**, 115-122 (1993).
16. T. Gajda, B. Gyurcsik, T. Jakusch, K. Burger, B. Henry, and J.-J. Delpuech, "Coordination Chemistry of Polyhydroxy Acids: Role of the Hydroxy Groups," *Inorganica Chimica Acta*, **275-276,** 130-140 (1998).
17. M. van Duin, J. A. Peters, A. P. G. Kieboom, and H. van Bekkum, "A General Coordination-ionization Scheme for Polyhydroxy Carboxylic Acids in Water," *Recl. Trav. Chim. Pays-Bas*, **108**, 57-60 (1989).
18. J. Tits, E. Wieland, and M. H. Bradbury, "The Effect of Isosaccharinic Acid and Gluconic Acid on the Retention of Eu(III), Am(III) and Th(IV) by Calcite," *Applied Geochemistry*, **20**, 2082-2096 (2005).
19. S. Allard and C. Ekberg, "Complexing Properties of α-Isosaccharinate: Thorium," *Radiochim. Acta*, **94**, 537-540 (2006).

THE THERMODYNAMICS OF EXTRACTION OF BISMUTH BY P,P'-DI(2-ETHYLHEXYL)ETHYLENE- AND METHYLENE-DIPHOSPHONIC ACIDS

Chinedu G. Otu[1] and Emmanuel O. Otu[2]

[1]*Department of Biology, University of Kentucky, Lexington, KY 40506, U.S.A*
[2]*Department of Chemistry, Indiana University Southeast, New Albany, IN 47150, U.S.A.*
Corresponding author email address: eotu@ius.edu

ABSTRACT

The extraction of bismuth(III) from nitric acid by P,P'-di(2-ethylhexyl)ethylenediphosphonic acid (H_2DEH[EDP]) and P,P '-di(2-ethylhexyl) methylenediphosphonic acid (H_2DEH[MDP]) dissolved in *o*-xylene was studied in the temperature range 25-60 ^oC. The extractions were investigated as a function of the aqueous nitric acid concentration and organic phase extractant concentration. The slopes of the acid dependency approximated -3, and the slopes of the extractant dependencies were unity and 2.8, respectively, for H_2DEH[EDP] and H_2DEH[MDP]. These dependencies did not change with temperature. Thermodynamic parameters (enthalpy, entropy, and free energy changes) of the extraction were determined by the temperature coefficient of extractability in the temperature range 25-60^oC. The extraction by H_2DEH[EDP] is favored by entropy, whereas the process is enthalpy-controlled when the extractant is H_2DEH[MDP].

INTRODUCTION

The general formula for the P,P'-di(alkyl)alkylenediphosphonic acids is $RO(HO)OP(CH_2)_nPO(OH)OR$, where R is the 2-ethylhexyl group and n is one or two, for P,P'-di(2-ethylhexyl) methylene- (H_2DEH[MDP]) and ethylene- (H_2DEH[EDP]) diphosphonic acid, respectively. The length of the alkylene chain separating the two P atoms has been shown to influence the aggregation state of the extractant. In nonpolar solvents, H_2DEH[EDP] is hexameric, and H_2DEH[MDP] is dimeric [1-6]. It has been shown that the metal ion extraction processes and the type of metal-extractant complexes formed in the organic phase are different for H_2DEH[EDP] and H_2DEH[MDP] [6-9].

Extractant-dependency studies have reported unit slope for H_2DEH[EDP] and slopes of two for H_2DEH[MDP] for trivalent ions [4,8,10]. The H_2DEH[EDP] results arise from the hexameric aggregates and likened to extraction by a reverse micelle, with a hydrophilic internal cavity, which is available to accommodate metal ions. H_2DEH[MDP] involves the formation of chelate rings with two dimer moieties.

The chelate-ring formation by H_2DEH[MDP] is likely to require complete dehydration with concomitant formation of very strong bonding with the metal ion. In the

case of H_2DEH[EDP], where the extraction process is reminiscent of a micellar extraction, the metal cation can be transferred into the organic phase retaining at least some of its water of hydration.

Given the pronounced differences in extraction processes and type of metal species formed in the organic phase, it seems reasonable to expect that the extraction of metal ions by H_2DEH[MDP] and H_2DEH[EDP] should be accompanied by different enthalpic and entropic contributions to the overall stability of the species formed. The objective of this work was to gain information on the thermodynamics of the extraction of bismuth (III) by H_2DEH[EDP] and H_2DEH[MDP]. The temperature coefficient of the metal distribution ratio of Bi(III) was employed. The enthalpy and entropy changes upon metal complexation should shed further light on the metal extraction processes by the two extractants.

EXPERIMENTAL

Materials

The P,P'-di(2-ethylhexyl)alkyldiphosphonic acids (H_2DEH[EDP] and H_2DEH[MDP]) were received from Loyola University stock. These were purified to remove aqueous-soluble decomposition contaminants due to ester hydrolysis. The acids as received were dissolved in toluene and contacted three times with 0.1 M HCl. The toluene phase was washed with de-ionized water to get rid of any residual acid. Separation of the phases was aided by centrifugation and the toluene phase dried over anhydrous MgSO4. The toluene was removed by rotorary evaporation. The extractant solutions were prepared by dissolving weighed amounts in o-xylene (Baker), which was used without further purification.

The bismuth stock solution was prepared by dissolving a weighed amount of bismuth nitrate pentahydrate (Baker) in 5 M HNO_3 and diluting to a final volume that yielded 1 M HNO_3. The bismuth concentration was established by titration with ethylenediaminetetraacetic acid using xylenol orange as the indicator [11].

Procedures

The aqueous phase contained 10^{-5} to 10^{-4} M of bismuth and the organic phase contained 0.001–0.05 M of the extractant. Extractions were performed by mixing equal volumes (1 mL) of the organic and aqueous phases containing Bi(III) ions in a 13 x1 00mm Pyrex test tube with Teflon-lined screw caps and vortexing for one minute. The tubes were placed in a thermostated bath at selected temperatures in the range 25–60 °C for a minimum of 15 minutes, repeating vortexing several times during this time. The tubes were centrifuged and allowed to stay for 20 minutes in the bath (for temperature and chemical equilibrium to re-establish) before phase separation at each temperature. This was sufficient time for attainment of chemical equilibrium.

Triplicate extractions were performed at each temperature setting. The concentration of bismuth after each extraction was determined spectrophotometrically (Milton Roy Spectronic 20D+) as the tetraiodobismuth complex (BiI_4^-) at 460 nm [12]. Analyses of both the aqueous- and organic-phase fractions, the latter after wet ashing to destroy the extractant, gave mass recoveries of greater than 98%. Therefore, for much of the data, the concentration

of bismuth in the organic phase was calculated from the difference between the initial and final aqueous phase concentrations. Duplicate analyses were performed on the separated aqueous phases. The bismuth distribution ratio, *D*, was determined as customary as the ratio of the total metal concentrations in the organic and aqueous phases. The relative standard deviation of the distribution ratio measurements was approximately 5-10%. The measured molar *D* values were converted to molal values by multiplying them by the appropriate aqueous-to-organic phase density ratio. All uncertainties are given at the 95% confidence level.

RESULTS AND DISCUSSIONS

Extraction Stoichiometry and Equilibrium Constants

The extractant dependency (log *D* vs log [H_2Y]) plots for the extractants at 25 °C are shown in Figure 1a. The slopes of the best-fit linear regression approximated unity for H_2DEH[EDP] and 3 for H_2DEH[MDP] and showed no variation in the temperature range studied. The unity slope suggests that extraction of Bi(III) by H_2DEH[EDP] takes place through a micellar-type mechanism, as previously reported [6,13,14]. The micellar mechanism is similar to other highly aggregated extraction system such as dinonylnaphthalene- and didodecylnaphthalene-sulfonic acids [13-16] and quaternary alkylammonium salts [17]. The Bi(III) ion is extracted into the core of the H_2DEH[EDP] hexameric aggregate. The slope of 2 with H_2DEH[MDP] suggests that extraction of bismuth involves coordination to two extractant dimers.

The acid dependency (log *D* vs log [HNO_3]) plots for the extractants at 25 °C are shown in Figure 1b. The slopes of the best-fit linear regression approximated 3 for both H_2DEH[EDP] and H_2DEH[MDP] and remained the same in the temperature range 25 °C–60 °C. This indicates that three protons are lost from the extractants upon extraction of the Bi(III) ions. Also, the extraction stoichiometry did not change in the temperature range. This allowed us to use the temperature coefficient of extraction to estimate the heat effects involved in the extraction process.

The extraction equations can therefore be written as Equations 1a for H_2DEH[EDP] and 1b for H_2DEH[MDP], respectively:

$$Bi^{3+} + \overline{(H_2Y)_6} \rightleftharpoons \overline{Bi(H_9Y_6)} + 3H^+ \quad (1a)$$

$$Bi^{3+} + 3\overline{(H_2Y)_2} \rightleftharpoons \overline{Bi(HY)_3(H_2Y)_3} + 3H^+ \quad (1b)$$

where H_2Y is the diphosphonic acid, $(H_2Y)_6$ is the H_2DEH[EDP] hexamer, $(H_2Y)_2$ is the H_2DEH[MDP] dimer, species with overline exist in the organic phase, and charged species exist in the aqueous phase. For H_2DEH[EDP], the thermodynamic equilibrium constant can be written as:

$$K = 6\,\frac{[\overline{Bi(H_9Y_6)}]}{[Bi^{3+}]}\frac{[H^+]^3}{C_{H_2Y}}\frac{\gamma^6_{\pm,HN}}{\gamma^4_{\pm,BiN}} \quad (2)$$

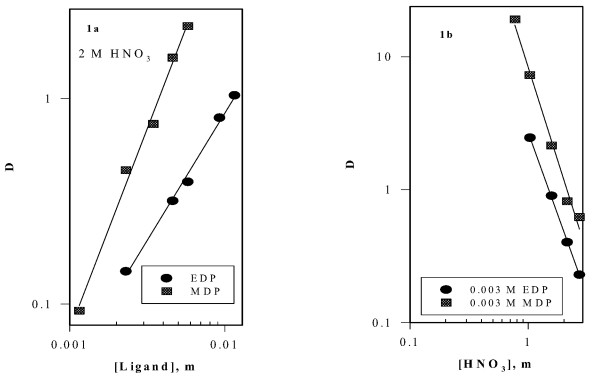

Figure 1. Extractant and acid dependencies for the extraction of Bi(III) from aqueous nitric acid solution with H_2DEH[EDP] and H_2DEH[EDP] in o-xylene.

where $\gamma_{\pm,HN}$ and $\gamma_{\pm,BiN}$ are the mean molal ionic activity coefficients of HNO_3 and $Bi(NO_3)_3$, respectively, and CH_2Y is the molal analytical concentration of H_2DEH[EDP]. At tracer metal ion concentration, if the extractant monomer concentration is negligible, the analytical concentration of H_2DEH[EDP] can be expressed as $C_{H_2Y} = 6[(H_2Y)_6]$.

Activity coefficients of bismuth nitrate are available and allowed nitrate complexing in the aqueous phase to be taken into account [18]. Recognizing that the distribution ratio, D, is the ratio of the concentration of metal in the organic phase and the total concentration of metal in the aqueous phase, the activity coefficient of neutral species is unity, and incorporating the mean molal activity coefficients of the Bi-nitrate species, $Bi(NO_3)^{2+}$, $Bi(NO_3)^{2+}$, and $Bi(NO_3)_3$, Equation 2 can be expressed as:

$$K = 6D\frac{[H^+]^3\gamma_{\pm,HN}^6}{C_{H_2Y}}\left\{\frac{1}{\gamma_{\pm,BN}^4}+\frac{\beta_1[NO_3^-]}{\gamma_{\pm,BN}^3}+\frac{\beta_2[NO_3^-]^2}{\gamma_{\pm,BN}^2}+\beta_3[NO_3^-]^3\right\} \quad (3)$$

where β is the formation constant for the nitrate complexes. The mean molal activity coefficients of the bismuth nitrates at the relevant ionic strengths were taken from [19]. The following β values were taken from [20]. The influence of temperature on activity coefficient was neglected in the calculations of equilibrium constants [21].

Free Energy, Enthalpy, and Entropy Changes

The extractant and acid dependencies indicate that the extraction stoichiometry and equilibria did not change in the temperature range of this study. Therefore, the temperature-coefficient method was used to determine thermodynamic parameters of the extraction. The thermodynamic parameters were calculated from the Gibbs-Helmholtz equation written in the form:

$$\log K = -\frac{\Delta G^o}{2.303RT} = -\frac{\Delta H^o}{2.303R}\frac{1}{T}+\frac{\Delta S^o}{2.303R} \quad (4)$$

where R (8.314 J/mol.K) is the gas constant. The enthalpy and entropy changes of the extraction processes were calculated from the slopes and intercepts of the plots of log K vs. $1/T$. The linear regression plots are shown in Figure 2, and each data point is the averaged value of log K for the different acid and extractant conditions employed in this study. The constancy of ΔH^o and aqueous-phase activity coefficients over the temperature range of this study had been discussed in a previous report [21].

The enthalpy and entropy changes of the extraction processes calculated from the slopes and intercepts of the plots, and free energy at 25 °C were calculated from $\Delta G° = -2303RT \log K$. The uncertainties reported for ΔH^0 and ΔS^0 are the standard errors of the slopes and intercepts, respectively. Those for ΔG° were obtained from propagation of the uncertainties in ΔH^0 and ΔS^0.

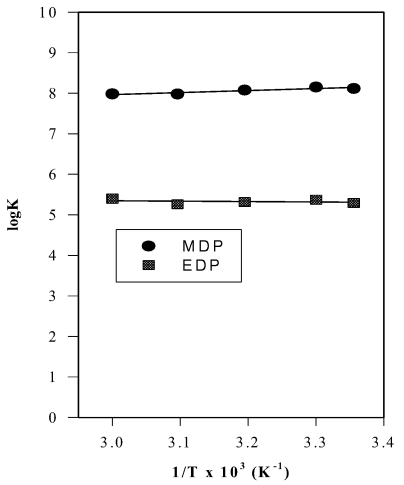

Figure 2. Variation of equilibrium constant with temperature.

Table 2. Thermodynamic parameters

Ligand	ΔH^o (kJ mol^{-1})	ΔS^o (J K^{-1} mol^{-1})	ΔG^o (kJmol^{-1})
H_2DEH[EDP]	1.79 ± 4.29	107.7 ± 13.7	-30.18 ± 4.29
H_2DEH[MDP]	-9.40 ± 2.32	124.4 ± 7.41	-46.30 ± 2.32

In the extraction of a metal cation by a liquid cation exchanger, the net enthalpy and entropy changes of the extraction are the result of several different processes. The dehydration of the metal cation generally involves a positive enthalpy change ($\Delta H > 0$) as a result of the breakage of ion-water bonds, and a positive entropy change ($\Delta S > 0$) as a result of an increase of disorder in the system by the release of coordinated water. The opposite will occur for the hydration of the proton(s) lost by the ligand. On the other hand, metal coordination by the organic ligand will result in a negative enthalpy change ($\Delta H < 0$), as a consequence of replacing relatively weak hydrogen bonds (typical of organophosphorus acids) with stronger metal coordination bonds, and in a negative entropy change ($\Delta S < 0$) due to the increase of order caused by the new bonds. The deprotonation of the extractant produces opposite effects.

CONCLUSIONS

Extraction of Bi(III) from nitric by the two extractants is favored by entropy changes. The favorable enthalpic contribution for H_2DEH[MDP] is indicative of strong chelate bonding mechanism. As well, the entropic contribution indicates a higher degree of dehydration of the bismuth ion by H_2DEH[MDP] compared to H_2DEH[EDP]. The

unfavorable enthalpic change for H_2DEH[EDP] is reminiscent of the micellar extraction mechanism [21-23].

ACKNOWLEDGMENT

Dr. Albert Herlinger of Loyola University provided the extractants used in this study.

REFERENCES

1. A. W. Herlinger, J. R. Ferraro, R. Chiarizia, and E. P. Horwitz, *Polyhedron,* **16**, 1843-1854 (1997).
2. A. W. Herlinger, R. Chiarizia, J. R. Ferraro, P. G. Rickert, and E. P. Horwitz, *Solvent Extr. Ion Exch.*, **15**, 401-416 (1997).
3. R. Chiarizia, V. Urban, P. Thiyagarajan, and A. W. Herlinger, *Solvent Extr. Ion Exch.*, **16**, 1257-1278 (1998).
4. R. Chiarizia, V. Urban, P. Thiyagarajan, and A. W. Herlinger, *Solvent Extr. Ion Exch.*, **17**, 113-132 (1999).
5. R. Chiarizia, V. Urban, P. Thiyagarajan, and A. W. Herlinger, *Solvent Extr. Ion Exch.*, **17**, 1171-1194 (1999).
6. R. Chiarizia, A. W. Herlinger, Y. D. Cheng, J. R. Ferraro, P. G. Rickert, and E. P. Horwitz, *Solvent Extr. Ion Exch.,* **16,** 505-526 (1998).
7. R. Chiarizia, A. W. Herlinger, and E. P. Horwitz, *Solvent Extr. Ion Exch.*, **15**, 417-432 (1997).
8. R. Chiarizia, E. P. Horwitz, P. G. Rickert, and A. W. Herlinger, *Solvent Extr. Ion Exch.*, **14**, 773-792 (1996).
9. R. Chiarizia, R. E. Barrans, J. R. Ferraro, A. W. Herlinger, and D. R. McAlister, *Sep. Sci. Technol.*, **36**, 687-708 (2001).
10. E. O. Otu and R. Chiarizia, *Solvent Extr. Ion Exch.*, **19**, 885-904 (2001)
11. H. A. Flaschka, EDTA Titrations: An Introduction to Theory and Practice, 2nd Edition, Pergamon Press, 1964; pp. 101-102.
12. E. O. Otu, *Thermochimica Acta,* **329**, 117-121 (1999).
13. E. Högfeldt, R. Chiarizia, P. R. Danesi, and V. S. Soldatov, *Chem. Scri.*, **18**, 13-44 (1981).
14. G. S. Rao, G. W. Mason, and D. F. Peppard, *J. Inorg. Nucl. Chem.*, **28**, 887-897 (1966).
15. G. J. Lumetta, B. A. Moyer, P. A. Johnson, and N. M. Wilson, *Solvent Extr. Ion Exch.*, **9**, 155-176 (1991).
16. B. A. Moyer, C. F. Baes, Jr., G. N. Case, G. J. Lumetta, and N. M. Wilson, *Sep. Sci. Technol.*, **28**, 81-113 (1993).
17. R. Chiarizia, R. C. Gatrone, and E. P. Horwitz, *Solvent Extr. Ion Exch.*, **13**, 615-645 (1995).
18. E. O. Otu, Proc. Inter. Solvent Extr. Conf., Beijing China, pp. 206-211, 2005.
19. Handbook of Chemistry and Physics, 77th Edition, 1996-1997; pp. **5**-102 – **5**-106.
20. S. Kotrly and L. Sucha, Handbook of Chemical Equilibria in Analytical Chemistry, Ellis Horwood Limited, Chichester, West Sussex, 1985; pp. 116-117.
21. E. O. Otu and A. D. Westland, *Solvent Extr. Ion Exch.*, **8**, 827-842 (1990).
22. P. R. Danesi, R. Chiarizia, M. A. Raieh, and G. Scibona, *J. Inorg. Nucl. Chem.*, **37**, 1489-1493 (1975).
23. M. A. Raieh, N. Zakareia, and H. F. Aly, *J. Radioanal. Chem.*, **52**, 285-293 (1979).

THERMODYNAMIC STUDY OF EXTRACTION OF Cr(III) FROM AQUEOUS SOLUTIONS BY BIS(2-ETHYLHEXYL) PHOSPHORIC ACID (DEHPA)

R. G. Turriza Cruz,[1] R. Navarro,[1] T. I. Saucedo,[1] P. Gonzalez, M. Stambouli,[2] D. Pareau,[2] and M. Avila-Rodriguez[1]

[1]Instituto de Investigaciones Científicas, Universidad de Guanajuato, Cerro de la Venada S/N. 36040 Guanajuato, Gto. Mexico. [2]Laboratoire de Génie des Procédés et Matériaux. Ecole Centrale Paris, Chateney-Malabry, France.
Corresponding author email address: avilam@quijote.ugto.mx

ABSTRACT

This paper presents the results of a thermodynamic study of Cr(III) extraction with DEHPA. The nature of the species extracted was determined from the reaction of the extractant and Cr(III), taking into consideration the complexes formed by Cr(III) and the OH^- ion, as well as the secondary reactions of the extractant. Through the application of a thermodynamic model, the existence of two species in the organic phase was determined: $\overline{CrL_3 \cdot (HL)_3}$ and $\overline{CrL_3 \cdot (HL)}$, with their respective extraction constants: $K_1 = 3.73 \times 10^{-4}$ and $K_2 = 1.45 \times 10^{-4}$. The extraction constants found enabled validation of the thermodynamic model through comparison of the theoretical extraction curves with respect to the experimental extraction curves.

INTRODUCTION

Different techniques have been used for the separation of chromium from tannery industry wastewaters, including the widely used technique of alkaline precipitation with $Ca(OH)_2$. However, this technique has the disadvantage of sludge accumulation. An interesting alternative for Cr(III) recovery is liquid-liquid extraction. Several authors have carried out studies on liquid-liquid extraction of Cr(III), such as Pandey [1], who studied Cr(III) extraction with mixtures of DEHPA, Cyanex, and isodecanol in kerosene. Islam and Biswas [2] studied the dependence of extraction equilibrium on acidity, extractant concentration, temperature, and nature of the diluent used. Mack and Hampe [3] studied the kinetics of Cr(III) extraction using DEHPA as extractant. Apostoluk and Bartecky [4] studied Cr(III) extraction using carboxylic acids and from sodium chloride solutions. Granzhan et al. [5] studied extraction of Cr(III) contained in natural waters. This paper describes the systematic study of Cr(III) extraction by DEHPA. From the data obtained, a physicochemical extraction model has been developed, which has enabled the determination of the stoichiometric relationship of the Cr-DEHPA complexes extracted in organic phase, as well as their respective extraction constants.

EXPERIMENTAL

All reagents used were analytical grade. Aqueous solutions of Cr(III) were prepared from a 1000 ppm $Cr(NO_3)_3$ solution and adjusted to the desired pH, with NaOH and HNO_3. The organic phase was composed of various concentrations of DEHPA extractant (SIGMA brand), diluted in kerosene (Aldrich US), boiling point 175-315 ºC with low aromatic content, and with 10% v/v decanol (Aldrich US). The volumes of the organic phase (V_{org}) and the aqueous phase (V_{aq}) for the extraction were 50 mL in all cases. The solutions (aqueous phase/organic phase) were placed in contact in a glass container with double wrapper for temperature control at 25 °C, stirred vigorously on a stirring plate for 2 hours, which is sufficient time to reach equilibrium. The temperature was kept constant at 25 °C (with a recirculating bath with temperature control). Once equilibrium was attained, the phases were separated and the metal ion concentration in the aqueous phase was determined with a (Perkin-Elmer 3110) atomic absorption spectrometer. The concentration of metal ions in the organic phase was calculated by mass balance. pH measurements were taken using a potentiometer (Methrom 716) with combined glass electrode (Ag/AgCl).

RESULTS AND DISCUSSION

Distribution Curves of Cr(III) as a Function of pH and [DEHPA]

Figure 1A shows the dependence of Cr(III) extraction yield on pH at various DEHPA concentrations (0.01 to 0.2 M).

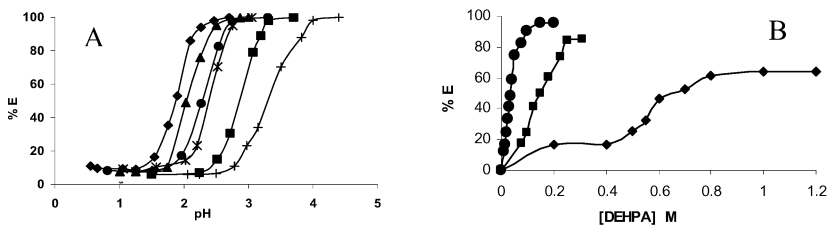

Figure 1. Variation of Cr(III) extraction percentage. A) As a function of pH at various [DEHPA]: (♦) 0.2 M; (▲) 0.15 M; (●) 0.075 M; (*) 0.05 M; (■) 0.025 M; (+) 0.01 M. B) As a function of [DEHPA] at various pH values: (♦) 1.5; (■) 2; (●) 2.5. [Cr(III)] = 100 ppm, [DEHPA] in kerosene/10% decanol, T = 25 °C.

It can be observed in this figure that, for each extractant concentration studied, extraction percentage increases when pH increases. Thus, at an extractant concentration of 0.2 M, it is observed that 50% extraction is attained at a pH value of 1.9, while for an extractant concentration of 0.025 M, 50% extraction is attained at a pH value of 2.8. At higher extractant concentrations, under the conditions studied, extraction percentages of 50% are attained at lower pH values.

Figure 1B shows variation in extraction percentage as a function of extractant concentration and pH. It can be seen that, in all cases, extraction percentage increases both with increased extractant concentration and increased pH. This figure also shows

that the curves with higher pH values reach maximum extraction percentages at lower extractant concentrations. Thus, in the curve corresponding to pH 1.5 (♦), it is observed that, although extractant concentration rises to 1.2 M, extraction percentage peaks at 63.9%, while for the pH 2 curve (■), the maximum percentage of 85% is achieved at an extractant concentration of 0.31 M. The foregoing can be explained by considering the influence of pH on the extraction process.

Determination of the Stoichiometry of Species Extracted in Organic Phase

The general reaction for the extraction of a metal ion by an ion exchanger with complexing properties can be written as follows:

$$M^{n+} + (n+m)\overline{HL} \Leftrightarrow \overline{ML_n \cdot (HL)_m} + nH^+$$

The species tested represent the species in organic phase.

The apparent extraction constant representing this equilibrium is:

$$K_{ext} = \frac{[\overline{ML_n(HL)_m}][H^+]^n}{[M^{n+}][\overline{HL}]^{(n+m)}} \quad (1)$$

Where: K_{ext} = apparent extraction constant.

The distribution ratio is defined as:

$$D = \frac{[\overline{M}]}{[M^{n+}]} \quad (2)$$

Relating K_{ext} and D and taking logarithms gives the expression:

$$LogD = \log K_{ext} + (n+m)\log[\overline{HL}] - n\log[H^+] \quad (3)$$

Figure 2A shows the variation of log *D* as a function of log [DEHPA] (at constant pH), and it is observed that for each pH value, the data are grouped around a straight line. Thus, for pH values of 1.5 and 2, straight lines were obtained with slopes near to 3 (3.29 for pH 1.5 and 2.80 for pH 2). At a pH value of 2.5 a straight line with slope near 2 was obtained. Thus, the results of the study of variation of log *D* as a function of log [DEHPA] suggest that, for the conditions studied, there are two complexes extracted into organic phase in the extraction of Cr(III) from aqueous solutions by DEHPA.

Figure 2B shows the variation of log *D* as a function of pH, keeping HL concentration constant. It can be seen that, for each extractant concentration, points are grouped around a straight line. The extractant concentrations studied were 0.2, 0.15, 0.075, 0.05, and 0.025 M, and the slopes obtained for each of the concentrations respectively are: 2.75, 2.80, 2.80, 2.92, and 2.78. From these results, it can be stated that, under the conditions studied, there are three protons exchanged in the reaction of Cr(III) extraction by DEHPA.

Thermodynamic Extraction Model. Calculation of Theoretical Distribution Ratio and Extraction Constant

The thermodynamic extraction model that has been developed considers the equilibria in the extraction reaction between DEHPA and Cr(III), the complexes formed by Cr(III) with OH^- ions, and the secondary reactions of the extractant (protonation,

dimerization, andsolubility in the aqueous phase), which can have an impact on the efficiency of the extraction system.

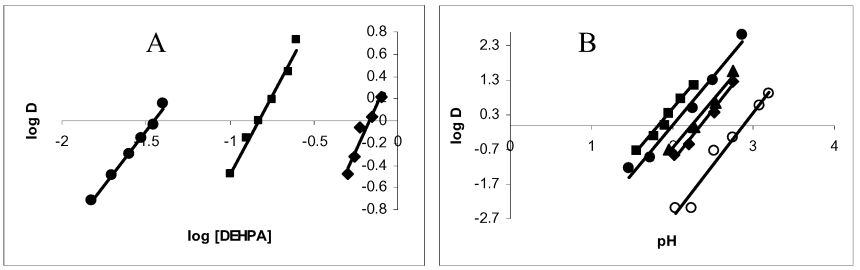

Figure 2. Variation of log *D* as a function of A) log [DEHPA] at pH values (♦) 1.5, (■) 2, (●) 2.5; B) pH at [DEHPA] (o) 0.025 M, (♦) 0.05 M, (▲) 0.075 M, (●) 0.15 M, and (■) 0.2 M. [Cr(III)] = 100 ppm. DEHPA extractant in kerosene/10% decanol.

The reaction for extraction of Cr(III) by DEHPA extractant is carried out by ion exchange with formation of complexes according to the following general extraction equation:

$$Cr^{3+} + \frac{(n+m)}{2}\overline{H_2L_2} \Leftrightarrow \overline{CrL_n \cdot (HL)_m} + nH^+ \quad (4)$$

This reaction considers, as a starting point, the Cr^{3+} species in the aqueous phase and the DEHPA dimmer in organic phase.

The apparent extraction constant for each complex formed is:

$$K_{extmn} = \frac{[\overline{CrL_n \cdot (HL)_m}] \cdot [H^+]^n}{[Cr^{3+}] \cdot [\overline{H_2L_2}]^{(n+m)/2}} \quad (5)$$

This extraction constant depends on conditions of the medium.

Moreover, Cr^{3+} forms mononuclear and polynuclear hydroxylated complexes with OH^- ions [6]. The formation of these species in aqueous phase is taken into account through the secondary reaction coefficient, which is defined as:

$$\alpha_{Cr(OH)} = \frac{[Cr(III)]}{[Cr^{3+}]} \quad (6)$$

$$[Cr(III)] = [Cr^{3+}] + [Cr(OH)^{2+}] + [Cr(OH)_2^+] + [Cr(OH)_3] + [Cr(OH)_4^-] + 2[Cr_2(OH)_2^{4+}] + 3[Cr_3OH_4^{5+}] \quad (7)$$

With regard to the extractant, the following secondary reactions were considered:

1) Solubility. While DEHPA is barely soluble in water, its partition co ratio has been reported as log P = 3.54 [7]. The equation representing P is:

$$P = \frac{[\overline{HL}]}{[HL]} \quad (8)$$

2) Dimerization. DEHPA exhibits a dimer formation equilibrium in the organic phase [6]. The expression of the dimerization constant is:

$$K_{Dm} = \frac{[\overline{H_2L_2}]}{[\overline{HL}]^2} = 4.42 \quad (9)$$

3) Acid-base reactions. DEHPA has acid-base properties in water, and its acidity constant K_a is expressed as:

$$K_a = \frac{[H^+][L^-]}{[HL]} = 10^{-1.27} \tag{10}$$

The secondary reactions of the extractant are taken into account by the secondary reaction coefficient:

$$\alpha_{H_2L_2} = \frac{[HL]_{Tot}}{2[\overline{H_2L_2}]} \tag{11}$$

$[\overline{HL}]_{Tot} = [\overline{HL}] + 2[\overline{H_2L_2}] + [L^-] + [HL]$ when $[\overline{HL}]_{Tot} >>> [\overline{CrL_n \cdot (HL)_m}]$ and $V_{aq}=V_{org}$

Relating $\alpha_{H_2L_2}$ to the extraction constants of the equilibriums involved gives:

$$\alpha_{H_2L_2} = \frac{1}{K_{Dm}[\overline{HL}]} + 1 + \frac{K_a}{PK_{Dm}[H^+][\overline{HL}]} + \frac{1}{PK_{Dm}[\overline{HL}]} \tag{12}$$

Introducing $\alpha_{Cr(OH)}$ and $\alpha_{H_2L_2}$ in the extraction constant equation gives the following expression:

$$K_{extmn} = \frac{[\overline{CrL_n \cdot (HL)_m}][H^+]^n \alpha_{Cr(OH)} \alpha_{H_2L_2}^{(n+m)/2}}{[Cr(III)][\overline{HL}]_{Tot}^{(n+m)/2}} \tag{13}$$

Applying a mass balance for *n* complexes:

$$[Cr(III)]_{Tot} = [Cr(III)] + \sum_n \sum_m [\overline{CrL_n \cdot (HL)_m}] \tag{14}$$

From this it is possible to obtain the Cr(III) concentration:

$$[Cr(III)] = \frac{[Cr(III)]_{Tot}}{1 + \sum_n \sum_m \frac{K_{ext}[\overline{HL}]_{Tot}^{(n+m)/2}}{[H^+]^n \alpha_{Cr(OH)} \alpha_{H_2L_2}^{(n+m)/2}}} \tag{15}$$

The extraction-constant values were determined using the program Excel Macro Solver, minimizing the function $U = \sum (D_{teo} - D_{exp})^2$. The model was run considering the formation of more than one complex in organic phase on the basis of the results obtained by the slope method. Based on this model, two complexes in organic phase were proposed, $\overline{CrL_3 \cdot (HL)_3}$ and $\overline{CrL_3 \cdot (HL)}$, with K_{ext33} = 3.73 x 10^{-4} and K_{ext13} = 1.45 x 10^{-4} mol/L respectively, with a minimum *U* value of 0.6937.

Validation of Thermodynamic Extraction Model

Using the extraction constants determined, theoretical extraction yields were calculated as a function of pH for a given ligand concentration. A comparison of the theoretical with the experimental curves is shown in Figure 3, from which it can be observed that, for extractant concentrations from 0.05 to 0.2 M, the correlation between theoretical and experimental curves is very good. At extractant concentrations of under 0.025 M, the difference between the theoretical and experimental distribution curves begins to become more evident. This is because the model considers that the system is buffered with respect to extractant concentration. It can be stated that the model is valid for an extractant concentration range high enough that its concentration remains constant and low enough to avoid deviations from the ideal in organic phase.

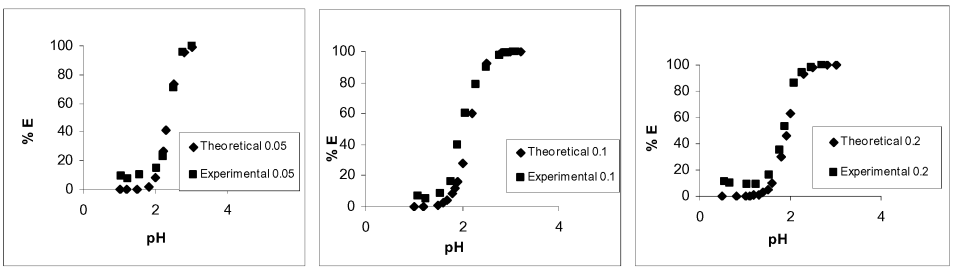

Figure 3. Variation of extraction percentage as a function of pH at various DEHPA concentrations. [Cr(III)] = 100 ppm; [DEHPA] in kerosene/10% decanol; (■) Theoretical, (♦) experimental. T = 25 °C.

CONCLUSIONS

A thermodynamic extraction model was developed for the Cr(III)/DEHPA kerosene and 10% decanol system, through which it was determined that there are two species extracted in the organic phase, $\overline{CrL_3 \cdot (HL)_3}$ and $\overline{CrL_3 \cdot (HL)}$, and with respective extraction constants K_{ext33} = 3.74 x 10^{-4} and K_{ext13} = 1.45 x 10^{-4} mol/L. The thermodynamic model was validated by comparing the theoretical and experimental curves of extraction percentage as a function of pH, finding it is accurate for extractant concentrations between 0.05 M and 0.2 M.

ACKNOWLEDGMENTS

The authors wish to thank CONACYT for its financial support (Project 44768-Q).

REFERENCES

1. B. D. Pandey, G. Cote, and D. Bauer, "Extraction of Chromium(III) from Spent Tanning Baths," *Hydrometallurgy*, **40**(3), 343-357 (1996).
2. M. F. Islam and R. K. Biswas, "The Solvent Extraction of Chromium(III) with Bis-(2-ethyl hexyl) Phosphoric Acid in Benzene and Other Solvents," *J. Inorg. Nucl. Chem.*, **41**(2), 229-233 (1979).
3. C. Mack and M. J. Hampe, "Synergetic Solvent Effects in the Kinetics of the Extraction of Chromium(III)," in Solvent Extraction for the 21st Century, M. Cox, M. Hidalgo, and M. Valiente, Eds., Society of Chemical Industry, Barcelona, Spain, 2001; pp. 329-333.
4. W. Apostoluk and A. Bartecki, "Extraction of Chromium(III) from Sodium Chloride Solutions by Means of Carboxylic Acids," *Hydrometallurgy*, **15**(2), 191-202 (1995).
5. A. V. Granzhan, G. M. Kuchuk, and A. K. Charykov, "Solvent Extraction and Atomic Absorption Determination of Bismuth(III) and Chromium(III) in Some Natural Materials," *J. Anal. Chem. USSR*, **46**(2), 585-587 (1991).
6. C. F. Baes, Jr. and R. E. Mesmer, The Hydrolysis of Cations. Wiley-Interscience, New York, 1976.
7. M. R. Ally, These de Doctorat de l'Universite Paris VI, Paris, France, (1995).

COMPARISON OF THE COORDINATION BEHAVIOR OF Cu(II) AND Fe(III) WITH ORGANOPHOSPHOROUS ACIDS AND HYDROXYOXIME-BASED LIGANDS IN AQUEOUS AND NONAQUEOUS MEDIA

I. Van de Voorde,[1] K. Latruwe,[1] L. Pinoy,[1] E. Courtijn,[1] and F. Verpoort[2]

[1]Department of Industrial Engineering, Chemistry Division, KaHo Sint-Lieven, Gebroeders Desmetstraat 1, B-9000 Gent, Belgium – associated with University of Leuven. [2]Department of Inorganic and Physical Chemistry, Ghent University, Krijgslaan 281 (S-3), B-9000 Gent, Belgium.
Corresponding author email address: ilse.vandevoorde@kahosl.be

ABSTRACT

Extraction equilibria of copper(II) and iron(III) from aqueous chloride media into an organic extractant phase and coordination behaviour in water-free circumstances was investigated. The applied ligands can be classified as organophoshoric acids (D2EHPA), organophosphinic acids (CYANEX 272, 302, 301), and hydroxyoxime-based ligands (Aloxime 800). The configuration of the metal complexes during liquid-liquid extraction has been determined by the method of continuous variation. Mostly, $[CuL_2]$ complexes were distinguished. In the case of CYANEX 301 and 302, the coordination type was less pronounced. Considering iron(III), a ligand:metal ratio of 1:1 was observed for D2EHPA and CYANEX 272. This implicates the participation of additional compounds in the coordination process. No chloride transport was observed during extraction, suggesting the formation of $[Fe(OH)_2L]$ complexes. Therefore, Job's method was compared to the coordination characteristics in anhydrous media. These studies showed that 1:1 ligand:metal complexes are formed in general, but depending upon the extractant:metal concentration ratio of the organic solution, higher ligand coordination is possible.

INTRODUCTION

Many industrial processes make use of metal ions. These metal ions, however, end up in several effluent streams. Due to very strict discharge values, companies are forced to optimize their wastewater treatment. Organophosphoric- and organophosphinic-acid extractants as well as hydroxyoximes have been studied widely in the past to recover heavy metals from solutions arising from the mining industry, metallurgical processes, and the galvanic industry [1-7]. A lot of research has been published on the determination of the ligand-to-metal ratio of various complexes. However, extraction circumstances and extraction chemistry are not always unequivocal [8-10]. Job's method or the method of continuous variation is a useful method for the determination of the ligand: metal ratio of a complex [11].

In the present work, Job's method is used for the identification of iron(III) and copper(II) complexes. The investigated ligands can be classified as organophoshoric acids (D2EHPA), organophosphinic acids (CYANEX 272 or bis(2,4,4-trimethylpentyl)phosphinic acid, CYANEX 302, and CYANEX 301, its monothio and dithioderivative, respectively), and hydroxyoxime-based ligands (Aloxime 800).

In order to prevent hydrolysis, the complexation characteristics were also examined under water-free circumstances. During this experimental procedure, no liquid-liquid extractions were performed, but the anhydrous metal salt was added directly to the organic phase [12]. By following the release of hydrogen chloride during complexation, formed by the acidic proton of the extractant and the chloride anion of the metal salt, a correlation can be obtained with the number of ligand molecules present in the iron(III) complexes.

EXPERIMENTAL

Materials and Methods

The CYANEX extractants were kindly supplied from Cytec Canada Inc., while Cognis Inc. kindly provided a sample of the pure component of LIX 860-I, called Aloxime 800. The extractants were used as received. D2EHPA is commercially available from VWR International. Hexane, previously purified by a fractional distillation, was chosen as organic diluent. All other chemicals were of analytical grade.

For the procedure of the experimental work in water-free circumstances, we refer to Van de Voorde et al. [12]. For Job's method, the same procedure was used as described in Van de Voorde et al. [11]. By varying the mole ratio of metal and ligand between 0 and 1 at a total concentration c, and by determining the absorbance of the solutions with varying composition, an absorbance-x_M plot can be made. The constant total concentration c is the sum of the analytical concentrations of both monomeric ligand and metal ion, while x_M denotes the mole fraction of metal ion and is given by the ratio of the metal ion concentration to the total concentration of metal and ligand. Separation funnels were placed into a shaker, IKA Labortechnik type H 5501, at 305 rpm for a whole night to assure equilibrium. The metal concentrations in the aqueous phases were measured with a Unicam 989 Atomic Absorption Spectrometer (AAS), and the pH measurements were performed with a Consort D714 pH meter with a calibrated glass combination electrode assembly. The absorbance of the organic phase was determined with a Cary 100 Bio UV-visible spectrophotometer from Varian. The total concentration of metal and ligand was kept constant at 0.05 mol L^{-1}. Metal solutions were prepared from a stock solution of 1 mol L^{-1} with the appropriate chloride salt ($FeCl_3.6H_2O$ or $CuCl_2.2H_2O$). pH adjustments were made with hydrochloric acid or sodium hydroxide. The pH was set at a value of 1.00 in the case of iron(III). For copper(II), the pH was kept at pH 2.00 by adding phosphoric acid/sodium dihydrogen phosphate buffer (0.5 mol L^{-1}). Extractant solutions were prepared from a stock solution of 0.05 mol L^{-1} and were diluted with hexane. In Table 1, an overview is given of some exceptions, especially for D2EHPA and CYANEX 272. Higher initial pH values or higher concentrations were used to reach sufficient absorbance.

Table 1. Overview of the exceptions on the general experimental circumstances

Metal ion (M^{n+})	Extractant (HL)	pH	Total concentration c (mol L^{-1})
Fe(III)	D2EHPA	1.80	0.05
	CYANEX 272	1.80	0.25
Cu(II)	D2EHPA	3.00	0.50
	CYANEX 272	2.00	0.50

RESULTS AND DISCUSSION

Job's Method

The results of Job's method for iron(III) and copper(II) are displayed in Figure 1. If only one complex is formed, the composition of the complex can be calculated from the abscissa of the maximum of the continuous variation plot obtained from the experimental data. The maximum of the continuous variation plot is calculated by fitting a third-order expression through the experimental points. In the case of iron(III), the maximum of the continuous variation plot for D2EHPA and CYANEX 272 is depicted at a mole fraction of metal ion of 0.50 and 0.51, respectively, indicating a ligand:metal ratio of 1:1. This maximum gradually shifts towards a lower mole fraction of metal ion in the case of the monothiophosphinic acid (x_M = 0.33, HL:M^{n+} = 2:1) and its dithio analogue (x_M = 0.20, HL:M^{n+} = 4:1). An octahedral coordination is mostly preferred by iron(III) [13]. Therefore, the ligand:metal ratio of 1:1 depicted for iron(III) with D2EHPA and CYANEX 272 implicates the co-transport of other anions towards the organic phase, although no change in chloride concentration was found during extraction. The ligand:metal ratio of 1:1 can be ascribed to the hydrolysis of iron [14]. The higher ligand participation in the case of the sulfur-substituted reagents can be explained either by the lower pH at which the experiments were performed, resulting in less hydrolysis, or by the possible reduction of iron(III) [10].

During the extraction of copper(II) with D2EHPA and CYANEX 272, minor differences in absorbance were found in the region of 0.20-0.40. A planar configuration is mostly preferred by copper(II) [10,13,15]. The formation of $[CuL_2]$ complexes is therefore more justified and is in accordance with the results based on slope analysis techniques [10]. In addition, the absorbance spectra of copper(II) ions obtained in previous work [3] indicated the formation of square-planar species in an inert diluent, such as hexane. A maximum of 0.20 was observed for copper(II) and CYANEX 301. The copper(II)-CYANEX 302 complex exhibited an extremely low absorption. Therefore, these results are not included. In fact, instability problems of the sulfur-substituted reagents may influence the results [10]. The extraction of copper(II) with the sulfur-substituted reagents can involve the reduction of the metal ion to copper(I) and the accompanying oxidation of the ligands to the disulfide $R_2P(S)$-S-S-$(S)PR_2$ [10].

In the case of Aloxime 800, the maximum is depicted at x_M = 0.21 for iron(III), and at x_M = 0.34 for copper(II). This implies the formation of planar $[CuL_2]$ complexes [16]. The formation of pseudo-macro cyclic units by intermolecular hydrogen bonding

between the oximic hydrogen and phenolic oxygen atoms in 2:1 complexes with copper(II) explains the high strength and selectivity of these reagents types when used in the solvent extraction of copper(II) [16].

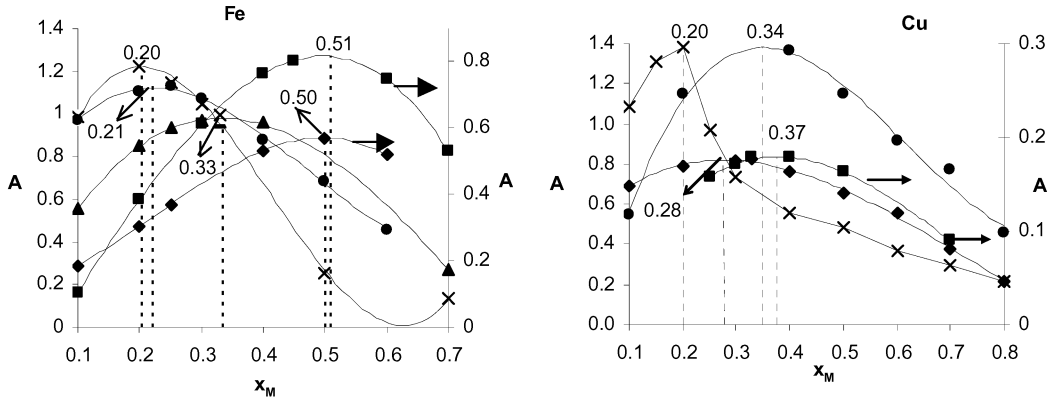

Figure 1. Continuous-variation plot of the iron(III) and copper(II) complexes with D2EHPA [◆, λ_{Fe} = 544 nm, λ_{Cu} = 866 nm], CYANEX 272 [■, λ_{Fe} = 500 nm, λ_{Cu} = 821 nm], CYANEX 302 [▲, λ_{Fe} = 500 nm], CYANEX 301 [✕, λ_{Fe} = 609 nm, λ_{Cu} = 438 nm], and Aloxime 800 [●, λ_{Fe} = 540 nm, λ_{Cu} = 677 nm].

In the case of iron(III), the experiment with x_M = 0.25 showed a distinctly higher absorbance compared to the calculated maximum at x_M = 0.21. If the electroneutrality of the iron(III) complex is taken into consideration, the simplest complex that might be proposed would be the octahedral [FeL_3], although in the literature, it was mentioned that no examples of mononuclear [FeL_3] complexes have been structurally identified [16].

The results with Job's method show that sometimes additional compounds are participating in the complexation process, viz. iron(III) with D2EHPA and CYANEX 272. No transport of the accompanying anion of the aqueous phase was determined, suggesting the formation of [$Fe(OH)_2L$] complexes [13]. Therefore, a comparative study was started in water-free circumstances.

Water-free Circumstances

The results of the experimental work in water-free circumstances are displayed in Figure 2. Two sets of experiments were performed for each metal ion, a stepwise and a direct procedure. During the stepwise procedure, the maximum extractant concentration was reached sequentially.

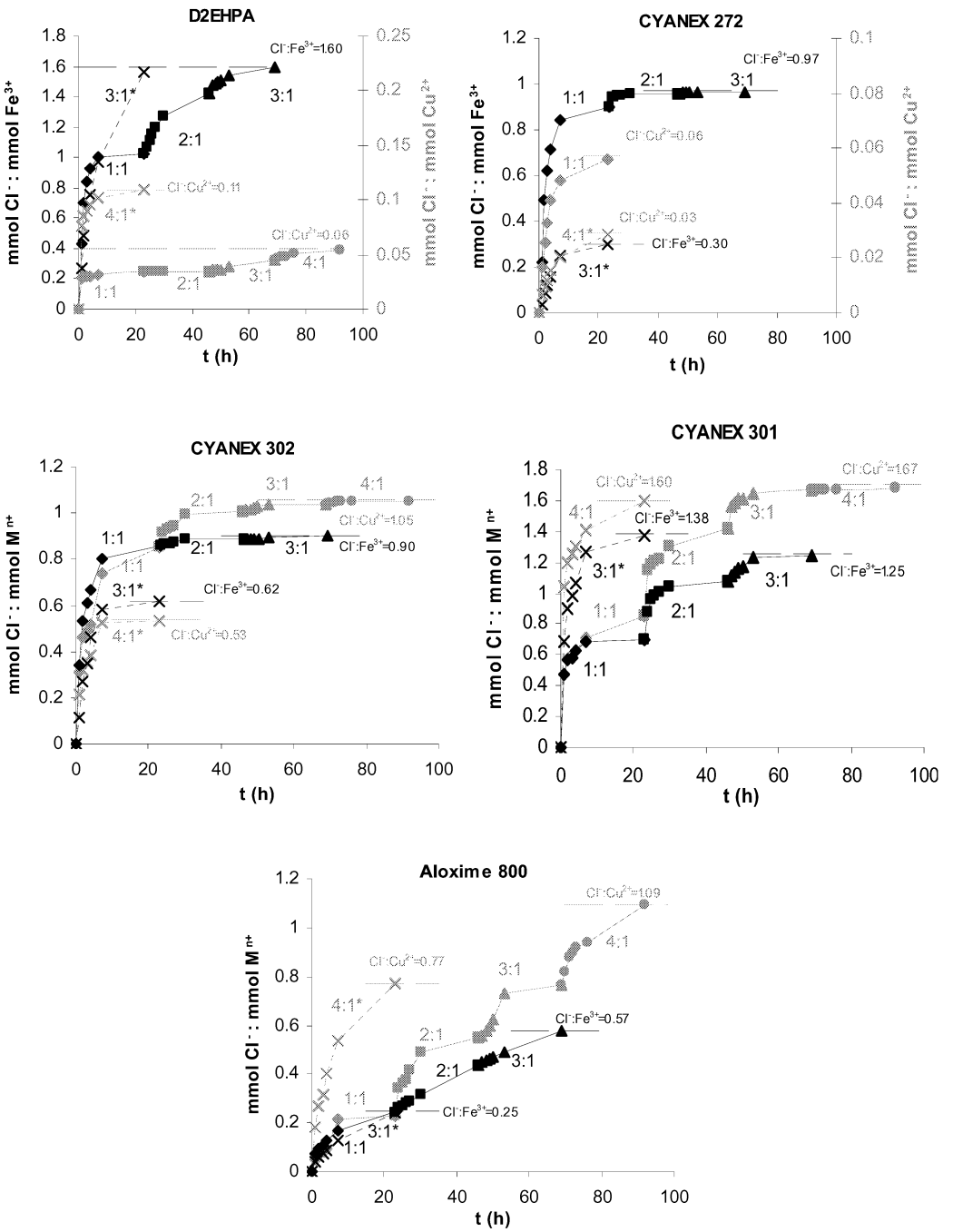

Figure 2. Release of chloride ions as a function of time during complexation of $FeCl_3$ (**black**) or $CuCl_2$ (grey) with D2EHPA, CYANEX 272, CYANEX 302, CYANEX 301, and Aloxime 800 in anhydrous media (◆, ■, ▲, ● stepwise procedure; ✕ direct procedure).

As far as D2EHPA is considered, a 1:1 ligand-Fe(III) ratio is easily achieved, in contrast to copper(II), that showed only a limited complexation. Higher ligand coordination is possible in the presence of more extractant, although a 3:1 ligand:metal ratio for iron(III) is not reached for any extractant investigated. In general, CYANEX 272 shows a similar behavior as D2EHPA for copper(II) and iron(III). The very good complexation characteristics of iron(III) with D2EHPA and CYANEX 272 are in accordance with the preference of iron(III) to coordinate with oxygen- donor ligands [13]. However, the direct procedures of CYANEX 272 showed only a limited release of hydrogen chloride compared to its stepwise procedures. The same difference between stepwise and direct procedure was also noticed for iron(III) and copper(II) with CYANEX 302, although the ratio difference between the stepwise and direct procedures was remarkably smaller in the case of CYANEX 302. In the case of CYANEX 301, this behavior disappeared. These changes can be justified by the lower electronegativity of sulfur. A slow release of hydrogen chloride—except for the direct procedure of copper(II)—was observed with Aloxime 800. In contrast to the other extractants, the $Cl^-:M^{n+}$ ratio may still be influenced by a longer reaction time.

During the progress of the experimental work, it was observed that the total metal amount was not always dissolved in the hexane phase. Therefore, 25 mL of the hexane phase was stripped at the end of step 1 (1:1) of the stepwise procedure and at the end of the direct procedure with 25 mL HCl (4 mol L^{-1}). Determination of the metal concentration in these acidic phases makes it possible to gain a better insight into the effective ligand-to-metal ratio. These results are shown in Table 2 and a comparison is made with the results of Job's method.

Table 2. Influence of the actual amount of metal ion dissolved in the hexane phase on the $Cl^-:M^{n+}$ ratio and comparison with the results of Job's method.

Extractant	Job's method	Water-free circumstances					
		$Cl^-:M^{n+}$		% metal dissolved		effective $Cl^-:M^{n+}$	
	$HL:M^{n+}$	1:1	D.P.*	1:1	D.P.*	1:1	D.P.*
Fe(III)[(1)]	1:1	1.02	1.60	100	100	1.02	1.60
Cu(II) [(1)]	2:1	0.04	0.11	-	6.4	-	-
Fe(III) [(2)]	1:1	0.90	0.30	87	93	1.04	0.32
Cu(II) [(2)]	2:1	0.06	0.03	13	37	0.46	0.08
Fe(III) [(3)]	2:1	0.86	0.62	61	86	1.41	0.72
Cu(II) [(3)]	-	0.85	0.53	7.9**	5.2**	-	-
Fe(III) [(4)]	4:1	0.70	1.38	42***	64***	1.67	2.16
Cu(II) [(4)]	4:1	0.85	1.60	31***	24***	-	-
Fe(III) [(5)]	3:1	0.24	0.25	58	67	0.43	0.37
Cu(II) [(5)]	2:1	0.23	0.77	40	98	0.58	0.79

* D.P.: result of direct procedure.
** Copper complexes too strong for stripping with 4 mol L^{-1} HCl.
*** Complexes too strong: destruction with 18 mol L^{-1} H_2SO_4. [(1)]D2EHPA; [(2)]CYANEX 272; [(3)]CYANEX 302; [(4)]CYANEX 301; [(5)]Aloxime 800.

Due to the high stability of the complexes with CYANEX 301, the hexane phases of comparable experiments were evaporated, followed by a destruction with concentrated sulfuric acid. However, no effective ligand:metal ratio is calculated, because of a still too-low recovery. In the case of copper(II) and CYANEX 302, the stripping results were also extremely low, indicating that a destruction is necessary to define a more justified ratio.

The dissolution of the metal ion depends upon the ease of metal extraction. Therefore, the lowest deviations on the $Cl^-:M^{n+}$ ratio were found for iron(III) with D2EHPA and CYANEX 272 and for copper(II) with Aloxime 800.

In general, the studies of Job's method and under water-free circumstances showed that depending upon the extractant:metal concentration ratio and type of extractant and metal ion, 1:1 complexes can be formed, although higher ligand coordination is also possible and depends on the extraction circumstances.

CONCLUSIONS

Using Job's method, complexes with a ligand:metal ratio of 1:1 were found for iron(III) with D2EHPA and CYANEX 272 instead of a ratio of 3:1, which would be expected it the electroneutrality of the complexes is considered. The absence of changes in chloride concentration in the aqueous phases during extraction infers the participation of hydroxyl ions in the extraction mechanism. In the case of copper(II), $[CuL_2]$ complexes have been distinguished. The complexation with CYANEX 301 deviated however, from these results. The higher ligand participation can be due to the possible instability of this reagent or the lower pH at which the experiments were performed.

To eliminate any hydrolysis, a comparative study was made under water-free circumstances. By following the release of hydrogen chloride during complexation, a correlation can be obtained with the number of ligand molecules present in the complexes. The results showed in general a ligand:metal ratio of 1:1, but depending upon the extractant:metal concentration ratio in the organic solution, higher ligand coordination is possible. One drawback of this procedure is that the dissolution of the metal depends upon the ease of extraction. Therefore, the $Cl^-:M^{n+}$ ratios were corrected with the real metal concentration dissolved in the hexane solution. An easy stripping is a prerequisite for calculating the effective ligand:metal ratio.

ACKNOWLEDGMENTS

The authors wish to thank Dr. W. Schwab from Cognis and Dr. D. Nucciarone from Cytec Canada Inc. for free samples respectively of LIX and CYANEX reagents. Appreciation for experimental assistance is extended to D. Van Beneden, E. C. Masachs and A. L. B. Ribeirinho.

REFERENCES

1. K. C. Sole and J. B. Hiskey, "Solvent extraction characteristics of thiosubstituted organophosphinic acid extractants," *Hydrometallurgy*, **30**, 345-365 (1992).

2. F. Xun and J. A. Golding, "Solvent extraction of cobalt and nickel in bis (2,4,4-trimethylpentyl)phosphinic acid, CYANEX-272," *Solvent Extr. Ion Exch.*, **5**(2), 205-226 (1987).
3. I. Van de Voorde, L. Pinoy, E. Courtijn, and F. Verpoort, "Influence of acetate ions and the role of the diluents on the extraction of copper(II), nickel (II), cobalt (II), magnesium (II) and iron (II, III) with different types of extractants," *Hydrometallurgy*, **78**, 92-106 (2005).
4. J. Vander Linden and R. F. De Ketelaere, "Selective recuperation of copper by supported liquid membrane (SLM) extraction," *J. Membr. Sci.*, **139**, 125-135 (1998).
5. P. E. Tsakiridis and S. Agatzini-Leonardou, "Process for the recovery of cobalt and nickel in the presence of magnesium from sulphate solutions by CYANEX 272 and CYANEX 302," *Minerals Engineering*, **17**, 913-923 (2004).
6. B. Zhang and G. Gozzelino, "Facilitated transport of Fe (III) and Cu (II) ions through supported liquid membranes," *Colloids Surf. A,* **215**, 67-73 (2003).
7. H. Matsuyama, Y. Miyake, Y. Izumo, and M. Teramoto, "Kinetics and mechanism of metal extraction with acidic organophosphorus extractants (II): extraction mechanism of Fe (III) with di(2-ethylhexyl)phosphoric acid," *Hydrometallurgy*, **24**, 37-51 (1990).
8. R. K. Biswas and D. A. Begum, "Solvent extraction of Fe^{3+} from chloride solution by D_2EHPA in kerosene," *Hydrometallurgy,* **50**, 153-168 (1998).
9. N. Miralles, A. M. Sastre, E. Figuerola, and M. Martinez, "Solvent extraction of iron(III) by bis(2,4,4-trimethylpentyl)phosphinic acid : experimental equilibrium study," *Hydrometallurgy*, **31**, 1-12, (1992).
10. K. C. Sole and J. B. Hiskey, "Solvent extraction of copper by CYANEX 272, CYANEX 302 and CYANEX 301," *Hydrometallurgy,* **37**, 129-147 (1995).
11. I. Van de Voorde, L. Pinoy, E. Courtijn, and F. Verpoort, "Equilibrium studies of nickel(II), copper(II), and cobalt(II) extraction with Aloxime 800, D2EHPA, and CYANEX reagents," *Solvent Extr. Ion Exch.,* **24**, 893-914 (2006).
12. I. Van de Voorde, K. Latruwe, L. Pinoy, E. Courtijn, and F. Verpoort, "Complexation behaviour or iron(III) with Aloxime 800, D2EHPA, CYANEX 272, CYANEX 302, and CYANEX 301," *Solvent Extr. Ion Exch.,* **25**, 1-21 (2007).
13. F. A. Cotton and G. Wilkinson, Advanced Inorganic Chemistry, John Wiley & Sons, Inc., 1988.
14. F. Islam, H. Rahman, and M. Ali, "Solvent extraction separation study of Ti(IV), Fe(III) and Fe(II) from aqueous solutions with di-2-ethylhexyl phosphoric acid in benzene," *J. Inorg. Nucl. Chem.*, **41**, 217-221 (1979).
15. T. Sato and T. Nakamura, "The complexes formed in the divalent transition metal-sulphuric acid di-(2-ethylhexyl)-phosphoric acid extraction systems – cobalt(II), nickel(II) and copper(II) complexes," *Inorg. Nucl. Chem.*, **34**, 3721-3730 (1971).
16. A. G. Smith, P. A. Tasker, and D. J. White, "The structure of phenolic oximes and their complexes," *Coord. Chem. Rev.*, **241**, 61-85 (2003).

SPECTROSCOPIC STUDY ON THE SOLVENT EXTRACTION OF CHROMIUM(VI) AND VANADIUM(V) BY PRIMARY AMINE

Xiao Lin, Hong-Bin Cao, Yu-Ping Li, and Yi Zhang

Institute of Process Engineering, Chinese Academy of Sciences, Beijing 100080, People's Republic of China.
Corresponding author email address: hbcao@home.ipe.ac.cn

ABSTRACT

The solvent extraction of Cr(VI) and V(V) by primary amine was experimentally studied and analyzed by FT-IR, Raman and ^{1}H NMR respectively. It was found that V(V) can be selectively extracted from nearly neutral Cr(VI) containing aqueous solutions, with the separation factor of V(V) to Cr(VI) being over 70. Spectroscopic analysis showed the extraction mechanism of V(V) and Cr(VI) extracted by primary amine in nearly neutral solution might be mainly attributable to molecular association not anion exchange. Finally, the oxidization of the primary amine by Cr(VI) in the presence of light is discussed.

INTRODUCTION

The solvent extraction separation of vanadium(V) and chromium(VI) has been studied by different kinds of extractants, such as quaternary ammonium salts or tertiary amines, mainly focusing on the extraction according to a mechanism of anion exchange [1-5]. Although primary amines were reported to separate these two ions [6,7], less attention have been paid compared with other amines and ammonium salts.

A novel process using a primary amine to selectively extract V(V) from Cr(VI) containing solution has been developed and optimized by our group and has gotten commercial use recently. Four stages mixer-settlers achieved over 95% extraction of V(V), only with less than 20% of Cr(VI) being extracted. The loaded organic phase was then stripped by sodium hydroxide to recover vanadium, and the purity of vanadium pentoxide produced by the process is over 99.3%. Up to the present, the commercial plant operation was capable of throughput of 200 tons per day of feed solution containing about 14 g/L of V(V) and 6 g/L of Cr(VI). During extraction studies, characteristics different from the reported amine extractions were found. The aim of this paper is to show the special characteristics in the novel extraction process by experiments and means of spectroscopic methods.

EXPERIMENTAL

Primene JM-T (Rohm & Hass) was used as delivered without further purification. All the other chemicals and reagents used were of analytical grade. All the aqueous solutions were prepared with Milli-Q water.

The simulated feed aqueous solution was prepared from sodium chromate and sodium metavanadate (Sigma-Aldrich) according to the practical one of the commercial plant. Concentration of V(V) and Cr(VI) was 14 g/L and 6 g/L, respectively. Primene JM-T was diluted to 15 volume percent in CCl_4. The primary amine salt was obtained by pre-equilibrated with 10% v/v H_2SO_4, then scrubbed by 50 g/L sulfate sodium solution until the aqueous phase was nearly neutral.

Equilibrium extractions were carried out by mechanically mixing the phases at 20 ± 1 ^oC for 15 minutes. The volumetric ratio of the phases was $\upsilon_{aq}:\upsilon_{org}$ = 1:1. The concentration of metals in the aqueous phase was determined by inductively coupled plasma-optical emission spectrometry (ICP-OES, PerkinElmer Optima 5300 DV), and the equilibrium pH was measured with Mettlor-Toledo Delta320 pH meter. The metal-loaded organic phases were analyzed by FT-IR (PerkinElmer, Spectrum GX), Raman (Thermo Nicolet, Almega XR) and ^1H NMR (Bruker, AV-400 spectrometer).

RESULTS AND DISCUSSION

Extraction of V(V) and Cr(VI)

Table 1 shows the effect of pH on the extraction separation efficiency of V(V) and Cr(VI). It is found that the extraction efficiency of both V(V) and Cr(VI) greatly depends on the pH value. Although the pH of the feed aqueous phase was 5, the equilibrium pH was 7.98; most of V(V) was selectively extracted, with the V/Cr separation factor being over 75. According to the results above, the equilibrium pH of the aqueous solution in the commercial operation was controlled in the range of 7.8-8.2.

Table 1. Effect of pH on V(V) and Cr(VI) separation

pH		Extraction efficiency, %		Separation factor (V/Cr)
Feed	Equil.	V	Cr	
2.0	7.13	97.02	47.93	35.37
3.0	7.68	92.74	28.74	31.67
4.0	7.86	91.87	24.79	34.28
5.0	7.98	89.12	9.73	75.99
6.0	8.14	71.34	8.13	28.12
6.5	8.26	49.47	4.14	22.69

Figure 1 shows the effect of pretreatment by H_2SO_4 on the extraction efficiency. The primary amine pre-equilibrated with acid needed a longer time to reach equilibrium and extracted less V(V) and more Cr(VI) than primary amine without acid pretreatment. These phenomena might be due to the fact that the primary amine pretreated by H_2SO_4

would be expected to form a primary amine salt, and the extraction would be occur by the mechanism of anion exchange (Equation 1) [5,8].

$$RNH_3X_{(0)} + A^- \rightleftharpoons RNH_3A_{(0)} + X^- \quad (1)$$

The extraction by primary amine without any pretreatment was performed at pH range of 7 to 8, where there is no such possibility of forming amine salts under the experimental conditions. Therefore, it seems not reasonable to assume V(V) is extracted according to an anion-exchange mechanism.

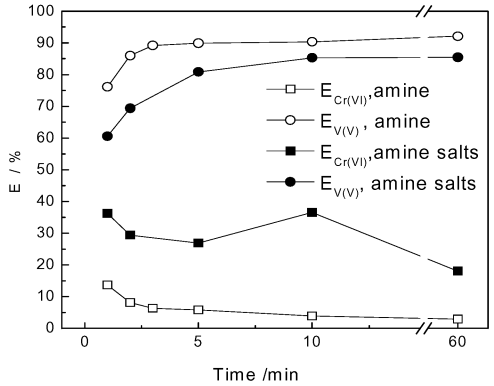

Figure 1. Effect of the pretreatment of primary amine with H_2SO_4 on the extraction of V(V) and Cr(VI).

Spectroscopic Analysis of the Organic Phases

The FT-IR spectra (Figure 2) indicate that V(V) and Cr(VI) extraction from a nearly neutral aqueous phase is obviously different from an anion-exchange mechanism. The broad band in the range of 3300-2700 cm^{-1} attributed to $-NH_3^+$ stretching vibration of amine salts can not be observed in the spectra of V(V) and Cr(VI) loaded organic phases. In addition, the characteristic bands of primary amine have no change after V(V) and Cr(VI) loading.

The newly appeared peaks of V-loaded organic phase at 955 and 904 cm^{-1} and Cr-loaded organic phase at 948 and 845 cm^{-1} were believed to be the characteristic bands of vanadate and chromate in the organic phases, because the strength of the peaks increases when the concentration of metal loaded in the organic phases increase. The bands at 955-904 cm^{-1} corresponding to the V=O stretching of the vanadate anion [4]. In addition, there is no new characteristic absorbance of the feed solution extraction besides the bands of Cr(VI) and V(V) extraction.

Therefore, FT-IR spectra indicate that the extraction process of V(V) and Cr(VI) by primary amine does not occur by the mechanism of anion exchange, but rather probably by molecular association without a structure change of the amine molecules (Equation 2).

$$m\mathrm{RNH}_{2(0)} + p\mathrm{MO}_x^{n-} + pn\mathrm{H}^+ \rightleftharpoons (\mathrm{RNH}_2)_m\mathrm{g}(\mathrm{H}_n\mathrm{MO}_x)_{p(0)} \quad (2)$$

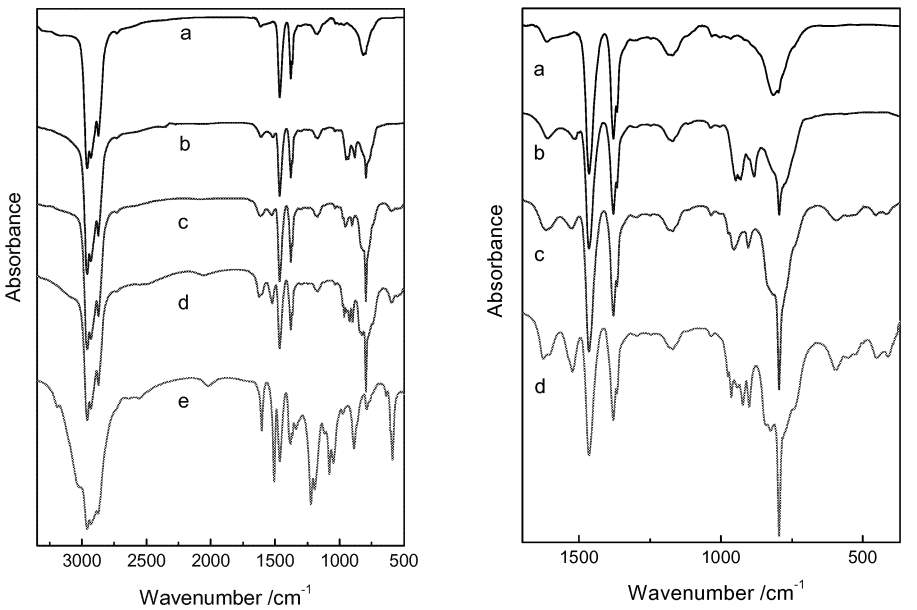

Figure 2. FT-IR spectra of organic phases.
a – blank primary amine; b – primary amine extracted Cr(VI); c – primary amine extracted V(V); d – primary amine contacted with feed solution; e – primary amine equilibrated with H_2SO_4.

To support the viewpoint above, Raman spectra of the V(V) and Cr(VI) loaded organic phase were studied (Figure 3). The spectrum of the primary amine has few changes after extracting V(V) and Cr(VI). In the V-loaded organic phase, the bands at 987, 963, and 925cm^{-1} are believed to be V=O Raman stretches [9]. In the Cr-loaded organic phase, the band at 890 cm^{-1} may be attributed to chromate, because the band at 884 cm^{-1} was reported to be due to chromate in aqueous solution [10]. Similar to the FT-IR results, the Raman spectrum of the feed solution extraction indicates that no new characteristic bands appeared besides the bands of Cr(VI) and V(V) extraction.

^{1}H NMR spectra of the organic phases were studied as shown in Figure 4. There are no similar -NH_3^+ resonance peaks in the spectra of V and Cr loaded organic phases after extraction from nearly neutral solution. After exchanging with D_2O, the signal at 1.31ppm disappeared due to the acidic proton of –NH_2. The value of the chemical shift of the acidic proton shifting from 1.31 ppm to 3.32 ppm indicates that hydrogen bonding formed in the process of Cr(VI) extraction.

It can be concluded from the IR, Raman, and ^{1}H NMR experimentsthat the extraction of vanadium and chromium by primary amine from nearly neutral solution does not occur according to an anion-exchange mechanism but rather occurs by a solvation mechanism with molecular association, such as H-bonds, between metals and primary amine.

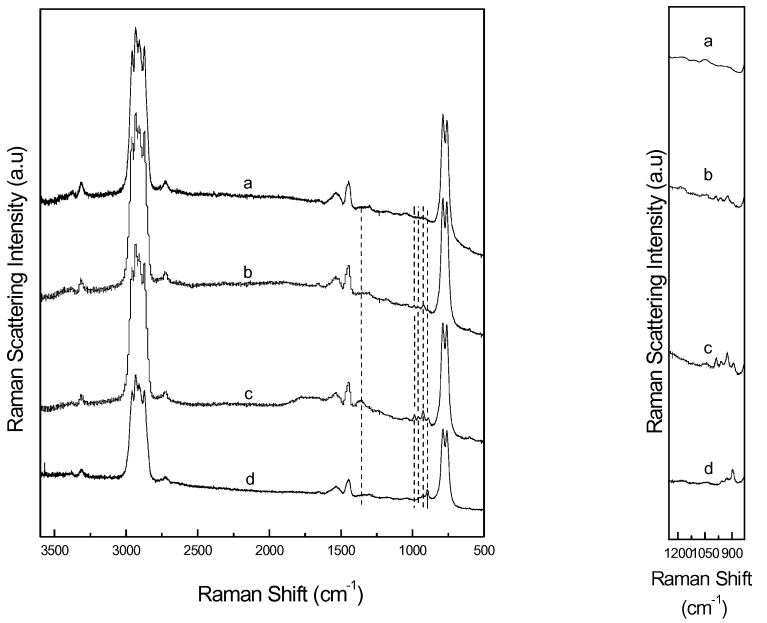

Figure 3. Raman spectrum of organic phases.
a – blank primary amine; b – primary amine extracted V(V);
c – primary amine contacted with feed solution; d – primary amine extracted Cr(VI).

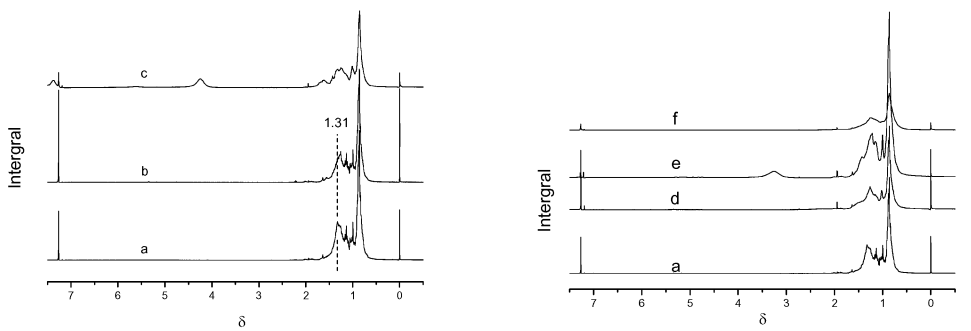

Figure 4. ^{1}H NMR spectra of organic phases.
a – blank primary amine; b – primary amine exchange with D_2O; c –primary amine equilibrated with H_2SO_4; d –primary amine extracted V(V); e – primary amine extracted Cr(VI);
f – oxidized Cr(VI)-loaded primary amine

Oxidization of the Primary Amine

During the experiments, we found that the color of Cr(VI)-loaded organic phase would change from yellow to brown and to nearly black finally in the presence of daylight. The same phenomenon was observed in the organic phase on extraction of the practical feed solution, but not in the V(V)-loaded organic phase. The ^{1}H NMR spectrum of the black Cr(VI)-loaded organic phase (Figure 4f) shows that the hydrogen bonding of the fresh Cr(VI)-loaded organic phase with the chemical shift 3.32 ppm disappeared after

the organic phase transferred to black. It is supposed that the hydrogen bonding between the Cr(VI) and the primary amine is unstable and easy to be oxidized in the presence of light.

Both in the process of extraction and stripping, the oxidized organic phase would exhibit crud formation. Experiments performed in the dark showed no crud even after the organic phase was recycled for extraction and stripping ten times.

CONCLUSIONS

Vanadium(V) and chromium(VI) in nearly neutral solution can be selectively extracted and separated by primary amine, with the separation factor of V(V) to Cr(VI) being over 70. By means of experiments and spectroscopic analysis, it is conducted that primary amine extracts the V(V) and Cr(VI) by molecular association, but not according to the mechanism of anion exchange.

ACKNOWLEDGMENTS

This work was financially supported by the hi-tech research and development program of China (NO. 2006AA06Z369) & Huihong Nonferrous Metal Co. Ltd.

REFERENCES

1. G. M. Ritcey and B. H. Lucas, "Recovery of Chromium and Vanadium from Alkaline Solutions Produced by an Alkaline Roast-Leach of Titaniferous Magnetite," Proc ISEC'77, B. H. Lucas, G. M. Ritcey, and H. W. Smith, Eds., Toronto, Canada, 1977; pp. 520-531.
2. S. Q. Yu, S. S. Meng, and C. Y. Chen, "Separation and Recovery of Vanadium and Chromium from Solutions by Solvent Extraction with Primary Amines as Solvent," Proc ISEC' 80, J. D. Navraltil, and E. Detilleux, Eds., Liege, Belgium, 1980; pp. 80-132.
3. A. E. Weinhardt and A. N. Hixson, "Separation of Chromium and Vanadium Salts by Liquid-Liquid Extraction," *Ind. Eng. Chem.*, **43**(7), 1676-1684 (1951).
4. Y. Bal, K-E. Bal, G. Cote, et al., "Characterization of the Solid Third Phases that Precipitate From the Organic Solutions of Aliquat 336 after Extraction of Molybdenum(VI) and Vanadium(V)," *Hydrometallurgy*, **75**(1-4), 123-134 (2001).
5. D. Schrötterová, P. Nekovár, and T. Dropa, "Extraction of Polyvanadates by Means of Amines," *J. Radioanal. Nucl. Chem.*, **183**(1), 73-84 (1994)
6. P. Nekovár, D. Schrötterová, and M. Mrnka, "Extraction of Metal Ions with A Primary Amine," *J. Radioanal. Nucl. Chem.*, **223**(1), 17-22 (1997).
7. S. Q. Yu, S. S. Meng, and C. Y. Chen, "Solvent Extraction of Vanadium(V) from Aqueous Solutions by Primary Amines (in Chinese)," *Scientia Sinica B*, **11**(1), 11-18 (1982).
8. H. H. Someda, E. A. El-Shazly, and R. R. Sheha, "The Role of Some Compounds on Extraction of Chromium(VI) by Amine Extractants," *J. Haz. Mater.*, **117**(2-3), 213-219 (2005).
9. W. P. Griffith and P. J. B. Lesniak, "Raman Studies on Species in Aqueous Solutions. Part III. Vanadates, Molybdates, and Tungstates," *J. Chem. Soc. A*, 1066-1071 (1969).
10. D. L. Kepert, "Isopolyanions and Heteropolyanions," in: D. L. Kepert Comprehensive Inorganic Chemistry, Pergamon, Oxford, 1973; pp. 607-672.

DISPERSED PHASE HOLDUP IN KARR RECIPROCATING COLUMNS

Ravi Arunachalam,[1] Tim Bowser[2], and Geoffrey W Stevens[1]

[1]*Particulate Fluids Processing Centre, Department of Chemical and Bimolecular Engineering, University of Melbourne, Victoria 3010, Australia.*
[2]*GlaxoSmithKline, Princes Highway, Port Fairy, Victoria 3284, Australia.*
Corresponding author email address: gstevens@unimelb.edu.au

ABSTRACT

Dispersed-phase holdup data has been obtained for a kerosene-phenol-aqueous system in a 50 mm diameter Karr column with stainless steel, Nylon, and Teflon plate materials. The plates were identical in geometry and only differed in their wetting characteristics with the phases in the column. Experimental data was obtained over a range of operating conditions and then compared with existing prediction models. The Kumar and Hartland [1] holdup model was found to be the most promising and was modified to incorporate the effect of wetting characteristics of the plate material. This modified model gave a good fit for all plate materials and dispersions used in this study.

INTRODUCTION

Van Dijck [2] originally proposed enhancing the mass transfer in liquid extraction columns by reciprocating the plates. This concept was further developed by Karr [3] by adding baffle plates for large-scale columns. Karr columns are known for their high volumetric efficiency, and their usage has increased considerably in the pharmaceutical industries in the last couple of decades. Studies have been conducted to understand the variables influencing the hydrodynamics of the columns. Variables such as phase flow rates, system physical properties, agitation intensity, geometry of the plates, and column diameter have been reported to influence the hydrodynamics of the column. Coalescence and drop break-up in the column predominantly occur as a result of the turbulence motion from the reciprocation of the plate. Little direct coalescence or drop break-up occurs on the plate; however, recent studies have shown that changes in the surface properties of the plates directly influence the performance both in terms of the separation efficiency and the throughput. Some work has been done on a pulsed perforated plate column to investigate the effect of the wetting characteristics of the plate material on the hydrodynamics of a column; however, this is not quantitative at this stage, and no work has been done on a Karr reciprocating plate column. This study aims to investigate the effect of the wetting characteristics of the plate material for a Karr reciprocating plate

column on the dispersed-phase holdup. A kerosene/10% TBP–phenol-aqueous system will be assessed with stainless steel, Nylon, and Teflon plate materials.

EXPERIMENTAL

A 50 mm diameter Karr reciprocating column was used in this study. There were 21 perforated plates in the plate stack, which were connected by three tie rods supported by an overhead central shaft. The plates were reciprocated using a motor with a crank at the top of the column. The speed of reciprocation was measured using a tachometer. The dispersed-phase holdup was measured by the drainage method given by Gayler, Roberts, and Pratt [4]. Further details on the column's specifications can be found in Table 1. Nylon, stainless steel, and Teflon plates were used in this column. The contact angles of the plates with aqueous droplets are listed in Table 2.

Table 1. Column specifications

Column Details	Symbol	Pilot Column
Column Diameter	Dc	50 mm
Effective Column Height	Hc	1.3 m
Effective Column Volume	vc	2725 cm^3
Number of Plates	N	25
Plate Thickness	e	3 mm
Perforation Diameter	dh	12.7 mm
Hole Pitch (Triangular)	P	17 mm
Plate Spacing	hc	50 mm
Plate Free Area	S	0.45

Table 2. Plate contact-angle details

Plate Material	Dispersed Phase	Continuous Phase	Advancing Contact Angle	Receding Contact Angle
Stainless Steel	Water	Kerosene/TBP	129	76.5
Nylon	Water	Kerosene/TBP	153	145
Teflon	Water	Kerosene/TBP	173	144
Stainless Steel	Kerosene/TBP	Water	162	148
Nylon	Kerosene/TBP	Water	87	60
Teflon	Kerosene/TBP	Water	33	18

RESULTS AND DISCUSSION

Slip-Velocity plots

Gayler, Roberts, and Pratt [4] have shown that the dispersed-phase holdup can be related to the superficial phase velocities by means of the slip velocity. This slip velocity was found to be dependent on the physical properties of the system and other variables but not the phase flow rates. In this study, different flow rates were used for the three

different plate materials (due to the difference in the wettability of the plates), and the slip velocity has been used to compare the effect of the plate material (refer to Table 3).

Table 3. Slip-velocity results for different plate materials with corresponding mass-transfer direction and agitation rate

Run No	Plate Type	Mass-Transfer Direction	Agitation rpm	Slip Velocity, m/s
SS	Stainless Steel	Continuous organic to dispersed aqueous	60	0.0584
			120	0.0554
			180	0.0441
SS Ex	Stainless Steel	Dispersed aqueous to continuous organic	60	0.0577
			120	0.0604
			180	0.0483
N	Nylon	Continuous organic to dispersed aqueous	60	0.0627
			120	0.047
			180	0.026
N Ex	Nylon	Dispersed aqueous to continuous organic	60	0.0659
			120	0.0501
			180	0.0315
T	Teflon	Continuous organic to dispersed aqueous	60	0.049
			120	0.0311
			180	0.0325
T Ex	Teflon	Dispersed aqueous to continuous organic	60	0.0575
			120	0.0444
			180	0.033
SS I Ex	Stainless Steel	Dispersed organic to continuous aqueous	60	0.0642
			120	0.0514
			180	0.0227
N I Ex	Nylon	Dispersed organic to Continuous aqueous	60	0.0562
			120	0.0605
			180	0.035
T I Ex	Teflon	Dispersed organic to Continuous aqueous	60	0.0623
			120	0.0521
			180	0.0441

Effect of Agitation

As reported in the literature (Baird and Lane [5]), increased agitation increases the holdup and reduces the slip velocity. It can be seen from Table 3 that the slip velocity decreased with an increase in agitation for all the plate materials. For this study, this effect was more prominent at low frequencies when the influence of the plate material is greater, due to the greater time for coalescence. The slip velocity for the Teflon plate was lower than the other plate types.

Effect of Mass-Transfer Direction

The slip velocity for the *D-C* mass-transfer direction was higher than the mass-transfer direction from the *C-D* for all the plate materials (Table 3). At 60 rpm, it can be seen that for the *D-C* mass-transfer direction, the difference in the slip velocities for the different plate materials was smaller when compared with the slip velocities for the *C-D* mass-transfer direction. Similar to the *C-D* mass-transfer direction, the Teflon plates had a lower slip velocity than the stainless steel and the Nylon plates due to the high contact angle with the dispersed aqueous phase.

Dispersed-Phase Holdup Prediction Models

Dispersed-phase holdup results obtained from this study have been compared to various models in the literature (refer to Table 4).

Table 4. Average absolute relative deviation for the holdup prediction models

Run No	Kumar & Hartland (1988)[6]	Kumar & Hartland (1995)[1]	Bensalem (1985) [7]	Prvcic et al. (1990) [8]	Ju et al. (1990) [9]	Ikeda & Suzuki (1995)[10]	Modified Model (this study)
SS	35%	50%	41%	41%	37%	50%	11%
SS Ex	49%	79%	104%	49%	48%		19%
N	38%	50%	32%	30%	31%		37%
N Ex	60%	83%	67%	28%	23%		29%
T	43%	55%	34%	21%	24%	118%	25%
T Ex	67%	87%	63%	16%	17%		14%
SS I Ex	59%	62%	83.5%	28%	30.5%		23%
N I Ex	46%	59%	97%	33%	39%		18%
T I Ex	40%	57%	103%	42%	42%		11%

Typically an error of ±10% would be expected in these measurements. The prediction accuracy for the different models has been shown in terms of the Average Absolute Relative Deviation (AARD) [1]:

$$AARD = \frac{1}{NDP}\sum_{i=1}^{NDP} \text{ABS}\,(\text{Predicted Value - Experimental Value})/\text{Experimental Value} \quad (1)$$

where NDP denoted the number of data points.

Modification of Existing Models

It is evident from the experimental data (Table 4) that the dispersed-phase holdup varies with the plate material and with the degree of wetting of the plate material. From the prediction models presented above, it was decided to modify the Kumar and Hartland [1] model to allow for the variation in plate material. The parameter C_Ψ in this model was

refitted to the experimental data and modified to incorporate the effect of the wetting characteristics of the plate material. The physical property term is shown in Equation 2:

$$\Psi = C_{\Psi}\left(\frac{\Delta\rho}{\rho_C}\right)^{n_4}\left(\frac{\mu_d}{\mu_w}\right)^{n_5} \tag{2}$$

where Ψ allows for the effect of the physical properties and C_{Ψ} allows for the effect of mass-transfer characteristics on dispersed-phase holdup. Holdup, ø, is then predicted from the Kumar and Hartland [1] model as shown in Equation 3:

$$\phi = \Pi\Phi\Psi\Gamma \tag{3}$$

where Π allows for the effect of the power input per unit mass; Φ includes the phase flow rates; Ψ includes the physical properties, and Γ allows for the geometrical characteristics of the column (refer to Kumar and Hartland [1] for equations). The values for the constants used in these equations are listed in Table 5.

Table 5. Constants used in the Kumar and Hartland [1] holdup model

Column Type	C_{Π}	C_{Ψ} c-d	C_{Ψ} c-d	C_{Γ}	N_1	n_2	n_3	n_4	n_5	n_6	n_7
Karr column	0.13	1	0.52	6.87	1	0.84	3.74	-0.92	0	0	-0.48

The parameter C_{Ψ} was modified for each run to fit the experimental data (refer to Figure 1). The modified parameter C_{Ψ} was plotted against the term (1 + Cosθ) which is related to the adhesion energy (Ikeda & Suzuki [10]). It can be seen from Figure 1 that a power series relationship between C_{Ψ} and (1 + Cosθ) was obtained.

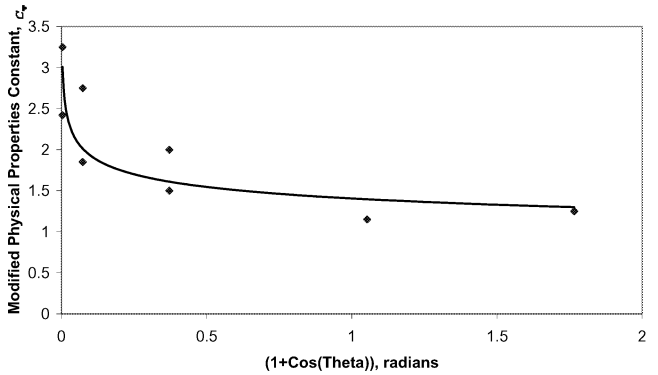

Figure 1. Correlation between the modified physical property parameter and the term (1 + Cosθ)

The physical property parameter C_{Ψ} was therefore modified using the term $1.406(1+\text{Cos}\theta)^{-0.1373}$. This was substituted into Equation 3 to predict the holdup for all experimental runs. Deviations between this modified model and experimental data have been presented in Table 4. The modified model clearly shows improved predictions.

CONCLUSIONS

The following conclusions were drawn from this study: (i) The dispersed phase holdup and flood point varied with the wetting characteristics of the plate material. (ii) None of the available models for predicting dispersed-phase holdup in Karr reciprocating plate liquid extraction columns predicted this variation. (iii) A new model has been proposed to allow for the influence of the variation of plate material wetting characteristics on the dispersed-phase holdup. This is particularly important, as dispersed-phase holdup is related to the maximum throughput and also the area available for mass transfer and so the mass-transfer efficiency of the column.

ACKNOWLEDGMENTS

The authors would like to acknowledge the funding provided by the Australian Postgraduate Award (APA) and GlaxoSmithKline, Port Fairy, for this project and would like to thank the Particulate Fluid Processing ARC Special Research Center (PFPC) for the resources provided for this project.

REFERENCES

1. A. Kumar and S. Hartland, "A Unified Correlation for the Prediction of Dispersed-Phase Hold-Up in Liquid-Liquid Extraction Columns," *Ind. Eng. Chem. Res.*, **34**(11), 3925-3940 (1995).
2. W. Van Dijck, US Patent, No. 2011186, 1935.
3. A. E. Karr, "Performance of a reciprocating plate column," *AIChE Journal*, **5**, 446-452 (1959).
4. R. Gayler, N. W. Roberts, and H. R. C. Pratt, "Liquid-liquid extraction. IV. Further study of hold-up in packed columns," *Trans. Insn. Chem. Eng*, **31**, 57-68 (1953).
5. M. H. I. Baird and S. J. Lane, "Drop size and holdup in a reciprocating plate extraction column," *Chem. Eng. Sci*, **28**(3), 947-957 (1973).
6. A. Kumar and S. Hartland, "Prediction of dispersed phase holdup & flooding velocities in Karr Reciprocating plate extraction columns," *Ind. Eng. Chem. Res.*, **27**, 131-138 (1988).
7. A. K. Bensalem, Ph.D. Thesis, Swiss Federal Institute Tech., Zurich, 1985.
8. L. M. Prvcic, H. R. C. Pratt, and G. W. Stevens, "Dispersed phase holdup in pulsed perforated plate columns," *Solvent Extr. Ion Exch.*, **8**, 695-712 (1990).
9. J. D. Ju, Y. H. Yu, and S. D. Kim, "Axial dispersion and phase holdup characteristics in reciprocating plate extraction columns," *Sep. Sci. Technol.*, **25** (7&8), 921-40 (1990).
10. H. Ikeda and A. Suzuki, "Wettability effects of plate materials on hydrodynamics in a pulsed perforated plate extraction column of pulser feeder type," *Ind. Eng. Chem. Res.*, **34**, 4110-4117 (1995).

CFD MODELING OF PUMP-MIXERS

K. K. Singh,[1,2] S. M. Mahajani,[1] K. T. Shenoy,[2] and S. K. Ghosh[2]

[1]Department of Chemical Engineering, Indian Institute of Technology, Powai, Mumbai, India-400076. [2]Chemical Engineering Division, Bhabha Atomic Research Centre, Trombay, Mumbai, India – 400085.
Corresponding author email address: sanjaym@che.iitb.ac.in

ABSTRACT

This work presents single-phase CFD simulations of pump-mixers employing top-shrouded turbines and draft tubes. Results from simulations have been used to predict the head developed and power consumed by the impellers. Results from simulations have been validated using the experimental data obtained on physical counterparts.

INTRODUCTION

A mixer-settler-based solvent-extraction cascade requires interstage and intrastage transport of the phases, which can be achieved by suitably designing the impeller itself. An impeller meant for dual duty of mixing and pumping is called a pump-mix impeller [1,2]. Pump-mix impellers help reduce turbo machinery in the plant, and capital and operating costs and leads to layout simplification. Quantitatively, the pumping and mixing requirement to be met by the impeller of the ith stage mixer of an N stage mixer-settler cascade, shown in Figure 1, can be written as:

$$\alpha < \hat{P} < \beta \text{ and } h > \frac{(\rho_m h_m - \rho_l h_l)}{\rho_l} \qquad (1)$$

where, $\hat{P}$ is the specific power input into the mixer, α is its lower limit corresponding to poor mixing, and β is its upper limit corresponding to formation of too fine a dispersion. These system-specific limits are determined from batch mixing and settling experiments. The variable h is the head of the light phase the pump-mix impeller should generate, and ρ_m and ρ_l are the densities of the mixed phase and light phase, respectively. To ensure whether a given impeller is able to meet the pump-mix requirement prescribed by Equation 1, its head and power characteristics, described by dimensionless head and power numbers, as defined below, should be known.

$$N_P = \frac{P}{\rho\, n^3 D^5} \text{ and } N_H = \frac{gh}{n^2 D^2} \tag{3}$$

where, N_P is the power number, P the power input, ρ the density, n the impeller speed, D the impeller diameter, g the acceleration due to gravity, N_H the head number, and h the head developed by the impeller.

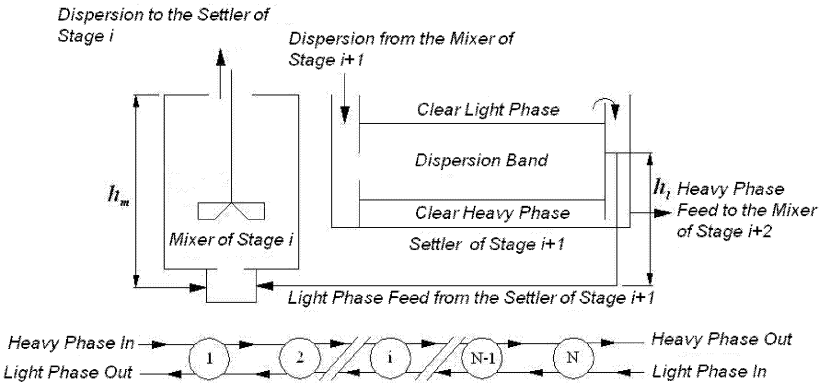

Figure 1. A cascade of N extraction stages, pump-mix mixer of ith stage, and settler of $i + 1^{th}$ stage.

Though CFD has been used extensively to study the batch mixers, its use for pump-mixers has been rare with only a few such CFD studies reported in the open literature [3-5]. Two of these studies [3,4] are focused on CFD simulations and validations of a pilot-scale and bench-scale pump-mixers. The third study [5] reports CFD-based comparison of different impellers for pump-mix action and suggests that the mixers with draft tubes can exhibit better pumping. The CFD simulations of the mixers with draft tubes are, however, not validated. The purpose of the present paper is to carry out a few CFD simulations and validation of mixers employing pump-mix impellers and draft tube.

EXPERIMENTAL

Shown in Figure 2, the experimental setup consists of a baffled mixer of 700 mm diameter and equal height with inlet from two side tanks through a suction box and outlet form a central opening at the top. The mixer is provided with a pump-mix impeller and a draft tube. At steady state, the water flows in a closed loop. For the set flow rate, levels in the feed tanks are measured both for still and rotating impeller. The difference of the two is recorded as the head developed by the impeller. Power is measured by using the voltmeter and ammeter in the DC power supply line to the motor after subtracting the armature losses and power in the dry runs. All the experiments are done at flow rate equal to 4 m^3/hr with four different mixer configurations employing either Type-1 or Type-2 impeller. The two impellers are shown in Figure 3. The impeller diameter is equal to 350 mm, blade width is equal to 70 mm, and the blade length is equal to 87.5

mm and 170 mm for Type-1 and Type-2 impellers, respectively. For the Type-2 impeller, which is rotated in retreat blade mode, the angle between the blade and radial line from center to the tip of blade is 10°. The details of the experiments are given in Table 1, where C is the impeller off-bottom clearance, T is the tank diameter, L_D is the draft tube length, Q is the flow rate, and n is the impeller speed.

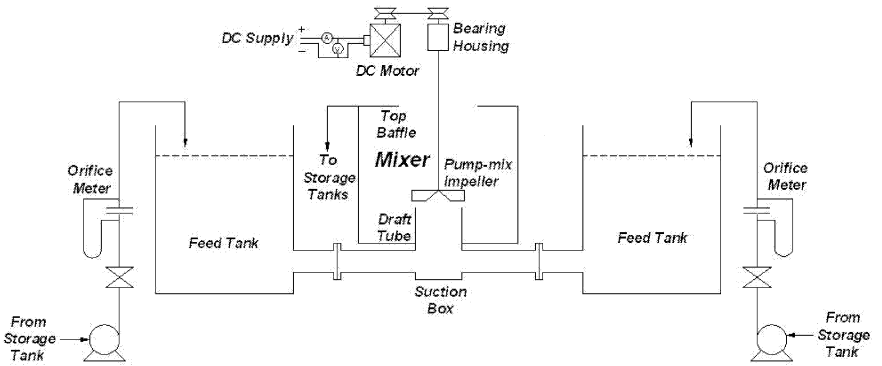

Figure 2. Schematic diagram of the experimental set-up.

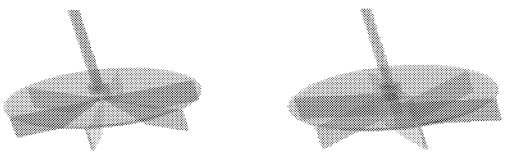

Figure 3. Impellers used in the experiments. Left: Type-1 with radial trapezoidal blades. Right: Type-2 with nonradial rectangular blades).

Table 1. Details of the experiments ($D/T = 0.5$, $Q = 4$ m^3/hr).

Configuration No.	Impeller	C/T	L_D (mm)	n (rpm)
1	Type-1	0.5	250	136.5, 150, 164, 177.5, 188
2	Type-1	0.5	115	136.5, 150, 164, 177.5, 188
3	Type-1	0.3	115	136.5, 150, 164, 177.5, 188
4	Type-2	0.3	115	136.5, 150, 164, 177.5, 188

CFD SIMULATIONS

CFD simulations involve solution of RANS (Reynolds Averaged Navier-Stokes) equations for incompressible fluid along with two equations of k-ε model of turbulence. The equations are omitted here for brevity. CFD software FLUENT is used for simulations. The computational domains of two of the four configurations are shown in Figure 4.

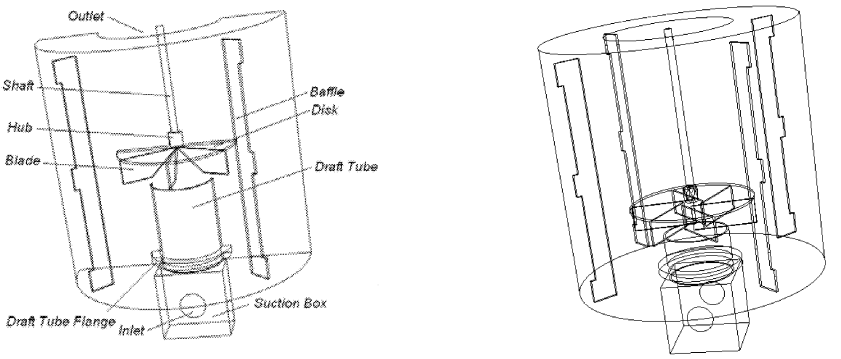

Figure 4. Computational domain for Configuration-1 and Configuration-4.

Unstructured tetrahedral grids are used with sizes based on grid-independence tests reported in a previous study [3]. Sliding mesh approach [6-9] is used for interaction between impeller and baffles. Second-order upwind and SIMPLE schemes are used for discretization and pressure-velocity coupling, respectively. Power is computed by calculating the torque acting on the impeller blades [10]. For each case, an initial run is carried out for the static impeller, and the difference between pressures at the outlet and the inlet are recorded. Head is computed by subtracting this difference from the difference of pressure at the outlet and the inlet obtained from a converged solution for rotating impeller. For Configurations 1-3, the symmetry of the geometry allows for simulation of only half of the mixers, which is not possible for Configuration–4, as any vertical central plane would cut through the impeller blades.

RESULTS

Figure 5 shows the validation of the CFD simulations for all four configurations with ±15% error bars around experimental points. A good agreement between experiments and simulated results can be observed. Results from CFD simulations were used to calculate the head and power numbers for different configurations, as reported in Table 2 and in graphical form in Figure 6. Figure 6 can be used to select as required to meet a specific combination of mixing and pumping requirement. A few simulations of the above configurations but without draft tubes were also carried out. Results of these simulations are also included in Figure 6.

Table 2. Head and power numbers of different configurations simulated in the study

Configuration No.	N_H	N_P
1	1.7393	4.7081
2	1.2835	5.0636
3	1.6890	3.9726
4	2.0723	3.6831

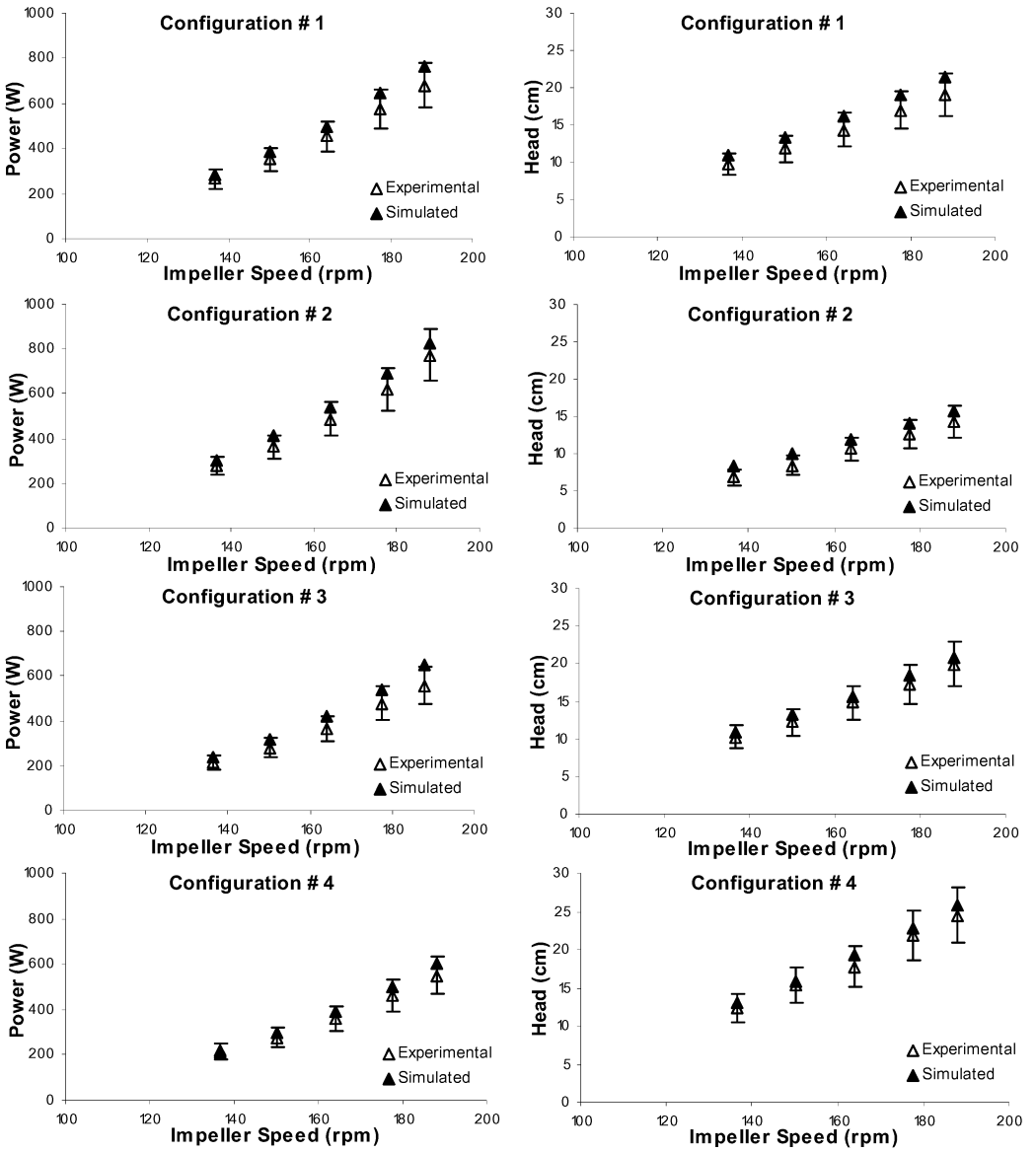

Figure 5. Comparison of experimental results and results from CFD simulations.

CONCLUSIONS

CFD simulations to predict head and power characteristics of different configurations of pump-mixers have been carried out. Comparison of experimental results and results from CFD simulations indicates that CFD techniques can be relied upon to predict head and power characteristics of different configurations of pump-mixers. Head and power numbers of different configurations have been used to draw a

pump-mix impeller design selection plot that can be used to find out the best configuration for a given mixing and pumping requirement.

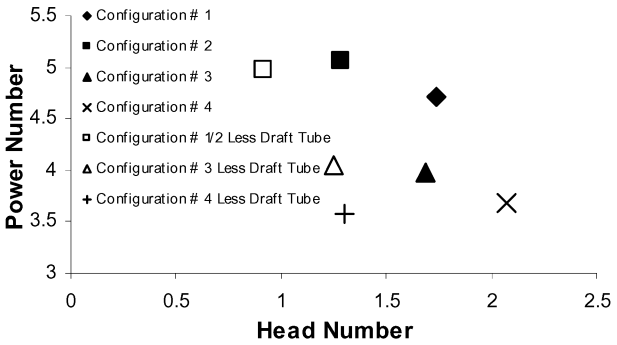

Figure 6. Pump-mix impeller-design selection plot ($H = T = 0.7$ m, $Q = 4$ m^3/h, $D/T = 0.5$).

REFERENCES

1. B. V. Coplan, J. K. Davidson, and E. L. Zebroski, "The Pump-mix Mixer Settler, a New Liquid-liquid Extractor," *Chem. Eng. Prog.*, **15**(8), 403 (1954).
2. J. G. Godfrey and M. J. Slater, Liquid-liquid Extraction Equipment, John Wiley & Sons Ltd., 1994.
3. K. K. Singh, S. M. Mahajani, K. T. Shenoy, A. W. Patwardhan, and S. K. Ghosh, "CFD Modeling of Pilot-scale Pump-mixer: Single Phase Head and Power Characteristics," *Chem. Eng. Sci.*, **62**, 1308 (2007).
4. K. K. Singh, S. M. Mahajani, K. T. Shenoy, and S. K. Ghosh, "Computational Fluid Dynamics Modeling of Bench-scale Pump-mixer: Head, Power and Residence Time Distribution," *Ind. Eng. Chem. Res.*, **46**, 2180 (2007).
5. K. K. Singh, S. M. Mahajani, K. T. Shenoy, and S. K. Ghosh, "CFD Modeling of Pump-mix Action in Continuous Flow Stirred Tank," *AIChE J.*, **54**(1), 42 (2008).
6. J. Aubin, D. F. Fletcher, and C. Xuereb, "Modeling of Turbulent Flow in Stirred Tanks with CFD: the Influence of Modeling Approach, Turbulence Model and Numerical Scheme," *Exper. Thermal Fluid Sci.*, **28**(5), 431 (2004).
7. S. L. Yeoh, G. Papadakis, and M. Yianneskis, "Numerical Simulation of Turbulent Flow Characteristics in a Stirred Vessel Using the LES and RANS Approaches with the Sliding / Deforming Mesh Methodology," *Trans. IChemE., Part A, Chem. Eng. Res. Des.*, **82**(A7), 834 (2004).
8. G. Montante, M. Mostek, M. Jahoda, and F. Magelli, "CFD Simulations and Experimental Validation of Homogenization Curves and Mixing Time in Stirred Newtonian and Pseudoplastic Liquids," *Chem. Eng. Sci.*, **60**(8-9), 2427 (2005).
9. M. Li, G. White, D. Wilkinson, and K. J. Roberts, "Scale Up Study of Retreat Curve Impeller Stirred Tanks Using LDA Measurements and CFD Simulations," *Chem. Eng. J.*, **108**(1-2), 81 (2005).
10. S. M. Shekhar and S. Jayanti, "CFD Study of Power and Mixing Time for Paddle Mixing in Unbaffled Vessels," *Trans. IChemE*, **80**(A), 482 (2002).

CFD-PBM COUPLED MODEL USING THE FINITE POINTSET METHOD AND THE SQMOM

C. Drumm,[1] S. Tiwari,[2] M. M. Attarakih,[3] J. Kuhnert,[2] and H.-J. Bart[1*]

[1]Lehrstuhl f. Thermische Verfahrenstechnik, TU Kaiserslautern, Postfach 3049, 67653 Kaiserslautern, Germany. [2]Fraunhofer Institut Techno- und Wirtschaftsmathematik, Fraunhofer-Platz 1, 67663 Kaiserslautern, Germany. [3]Faculty of Engineering Tech., Chem. Eng. Dept, Al-Balqa Applied University, P. O. Box 15008, 11134 Amman, Jordan.
**Corresponding author email address: bart@mv.uni-kl.de*

ABSTRACT

This contribution focuses on a combined Computational Fluid Dynamics (CFD) and Droplet Population Balance Model (DPBM), where the DPBM is solved as part of the CFD code. The coupling is done with the help of the Finite Pointset Method (FPM), which is a meshfree, Lagrangian, particle method. The droplet-population-balance equations are solved by the Sectional Quadrature Method of Moments (SQMOM). First simulations of the coupled algorithms are presented for an RDC extractor in which droplet coalescence and breakage (with constant kernels) are used.

INTRODUCTION

In the simulation and layout of liquid-liquid extraction columns, the dispersed phase is classically assumed as a pseudo-homogeneous phase. The state of the art for the design of extraction columns is to use the dispersion or back-mixing model, where one parameter accounts for all deviations from the ideal plug-flow behavior. Recent research focused on the droplet-population-balance models (DPBM) that take into account droplet transport (rise and backmixing) and interaction (breakage and coalescence) [1,2]. In typical DPBM codes, the dispersion model is still used for the description of the hydrodynamics and results from small-scale devices (single-droplet experiments) are needed to predict Sauter mean diameters and hold-up profiles [1,2]. The coupling of CFD with DPBM allows for a further improvement, since now the turbulent flow in an extraction column is fully resolved and described by CFD with much less simplifications. Neither pilot-plant experiments nor parameters are needed, since all required parameters in the DPBM equations (e.g., the turbulent energy dissipation, and velocities of the droplets) come from CFD, provided that the CFD predictions are accurate. Recent investigations show that CFD can predict the two-phase countercurrent flow field in a Rotating Disc Contactor (RDC) [3,4]. Only a few researchers investigated combined

CFD-DPBM models in the field of liquid-liquid extraction so far but achieved encouraging results for the combined models [5,6].

Hence, this contribution focuses on a combined CFD and DPBM to eliminate the classical simplifying assumptions imposed on this promising field of research. The coupling is done with the help of the Finite Pointset Method (FPM), which is a meshfree, Lagrangian, particle method. FPM is an in-house development of the Fraunhofer Institute. In comparison to a commercial code, the source code is fully modifiable, which eases the implementation of the DPBM. As a further benefit, the DPBM equations are solved by the Sectional Quadrature Method of Moments [7]. This method is found to track accurately any set of low-order moments with the ability to reconstruct the shape of the distribution. In this way, it combines the advantages of the classes methods (CM) [8] and the Quadrature Method of Moments (QMOM) [9], and at the same time, it minimizes their drawbacks. For the validation of the coupled algorithm, a five-compartment section of a Rotating Disc Contactor (RDC) was modelled in three dimensions. As a starting step, constant breakage and coalescence kernels were assumed, and simulations using the system butylacetate-water were carried out for the same operating conditions as in experiments of Simon [10].

THE POPULATION BALANCE EQUATION

The superstructure of the population balance equation and the general derivation based on the Reynold transport theorem is given in Ramkrishna [11]. The spatially-distributed population-balance equation could be written as:

$$\frac{\partial f(v,\xi,t)}{dt} + \nabla \cdot (uf(v,\xi,t)) = \rho\{f(v,\xi,t), v, \xi, t\}. \quad (1)$$

Since the particles are assumed to have in general a spectrum of sizes, this spectrum could be represented by a number-density function with particle size as an independent variable. So, let $f(v,\xi,t)\partial v$ be the average number of particles per unit volume of a fixed subspace at time t; then the above number-continuity equation is formally interpreted as follows: The first term on the left-hand side denotes the accumulated particles of size v, the second term is the convection of the particles along the physical space ξ, while the source term on the right-hand side represents the net number of particles produced due to breakage and coalescence per unit time and volume of physical space.

THE FINITE POINTSET METHOD

The FPM is a numerical method for solving fluid-dynamic equations. This is a meshfree, Lagrangian method. The basis of the computations is a point cloud which is referred to as particles or numerical grid points. Particles move with the fluid velocity, and they carry all relevant physical information. The point cloud represents the flow field, where they have to cover completely the whole flow domain; that is, the point cloud should fulfill certain adaptivity criteria (particles are not allowed to form “holes”, which means particles have to find sufficiently many neighbors; also, particles are not

allowed to cluster; etc.). The point cloud is a geometrical basis, which allows for a numerical formulation, making FPM a general finite difference idea applied to continuum mechanics. FPM is a strong formulation technique that models differential equations by direct approximation of the occurring differential operators. The method uses a moving least-squares idea which was especially developed for FPM. The primary (continuous) phase is modeled by the Navier-Stokes equations. The motion of the secondary (dispersed) phase is calculated by solving the equation of motion in which the inertia, drag, and buoyancy forces are taken into account. The coupling strategy within FPM framework is as follows: the separate point clouds are established for each phase. Primary and secondary phase equations are solved in their respective point clouds. These point clouds are decoupled from each other; however, the necessary information like velocities, volume fractions, etc. will be exchanged between these clouds. A complete two-way coupling is achieved in which the Sauter mean diameter of the droplets is calculated in every time step and substituted in the drag force, while the velocity of the droplets in the convective term of the DPBM is derived from the Navier-Stokes equations. This method is found to be appropriate for multiphase problems (e.g., a two-phase immiscible flow), and details about the numerical approach can be found elsewhere [4,12].

THE SECTIONAL QUADRATURE METHOD OF MOMENTS

In the finite-difference or sectional methods (e.g., [8]) the particle size is discretized into a finite number of sections, whereas the population in each section is considered to behave like a single particle. In the SQMOM framework of discretization, this single particle will be called the primary particle, and it will be responsible for the reconstruction of the distribution. Unfortunately, large number of primary particles in the classical sectional methods is required, not only to reconstruct the shape of the distribution, but also to estimate the desired integral quantities associated with the distribution. The interaction between primary particles in different sections, due to breakage and coalescence events, results in a new primary particle with no representative size due to the discrete approximation of the distribution. Because the newly-birthed particle could not conserve any of its low-order moments but one, the rest of the low-order moments are predicted with low accuracy and hence the associated integral quantities. To overcome this fundamental problem of the sectional methods, N_{sp} secondary particles in the SQMOM are generated in each section (i) with positions (abscissas: $d_j^{<i>}$) and weights ($w_j^{<i>}$) where $i = 1,2,...N_{pp}$, $j = 1,2,...N_{sp}$). The secondary particles are exactly equivalent to the number of quadrature points in Gauss-like quadratures or the QMOM [9]. Accordingly, each secondary particle could conserve or reproduce two low-order moments and in general $2N_{sp}$ moments in each section. The way in which the SQMOM works is started by dividing the particle size into contiguous sections (N_{pp} primary particles). Each section is then seeded by the desired number of secondary particles, which carry detailed information about the distribution. In this framework, the active particle mechanisms such as splitting and coalescence occur through interactions between the secondary particles. It is obvious now that N_{sp} x N_{pp}

particles are contributing in the splitting and aggregation events. Due to the increase of the number of interacting particles, more information is gathered about the distribution itself. This distribution could be reconstructed from the secondary particles by averaging the total weights of the secondary particles with respect to the section width (Δd_i) and locating them at the mean size of the secondary particles. In a purely mathematical sense, the above presentation is equivalent to applying the QMOM to each section of an arbitrary width, $[d_{i-1/2}, d_{i+1/2}]$: $i = 1,2,...N_{pp}$, resulting in a set of sectional moments that could be written as:

$$\mu_r^{<i>}(\xi,t) = \int_{d_{i-1/2}}^{d_{i+1/2}} d^r f(d,\xi,t)\partial d, \quad r = 0,2,...2N_{sp}-1 \tag{2}$$

More details about this approach can be found in the original paper of Attarakih et al. [7].

RESULTS

In this section, results of the simulations using the system butyl acetate-water are shown. Volume flow rates in the simulations are 100 L/h for both the aqueous and organic phases, while the stirrer speed is 150 rpm. As a starting point, constant kernels for breakage (1.0) and coalescence (1.0×10^{-10}), which were fitted to experimental data, are considered in the DPBM, and only one primary particle is chosen in the SQMOM. In this case the SQMOM corresponds exactly to the QMOM; however, with efficient numerical implementation. In Figure 1 the simulated Sauter mean diameters ($d_{32} = \mu_3/\mu_2$) in the five-compartment section are shown. The Sauter mean diameter is increasing from a value of 2.2 mm to around 2.7 mm and matches the experimental value of the Sauter mean diameter (around 2.6 mm [9]). In future simulations, real breakage and coalescence models will be considered to allow for a prediction of the drop-size distribution. Furthermore, more than one primary particles will be applied, whereas, each class will move with their own mean diameter by solving separate Navier-Stokes equations. A comparison of the SQMOM with analytical solutions showed that it is extremely accurate when an appropriate number of primary or secondary particles are used [7]. The results of the volume fraction in Figure 2 show that the droplets accumulate under stirrers and stators and rise mainly through the middle of the compartment without penetrating the outer regions. The same observations were also made in experiments [3]. Figure 3 shows the simulated 2D velocity vectors and 2D velocity magnitude in a *xz*-plane in the aqueous phase without considering the dominating swirl velocity in *y*-direction, since the developed two-phase flow field is better visible then. Although the aqueous phase flows from top to bottom, the vortices reverse at the positions between the stators and are directed to the top because the throughput of the ascending droplets is high enough to modify the flow pattern. In Figure 4 the contours of the velocity magnitude also consider the swirl velocity. The velocities near the stirrer correspond to the tip velocity (v_{tip} = 0.7 m/s) and decreases through the compartment to zero at the column wall. A detailed comparison of simulated and measured flow fields and velocities

in single- and two-phase flows using a constant diameter for the droplets in the same geometry showed that FPM is able to predict the flow fields and velocities [4].

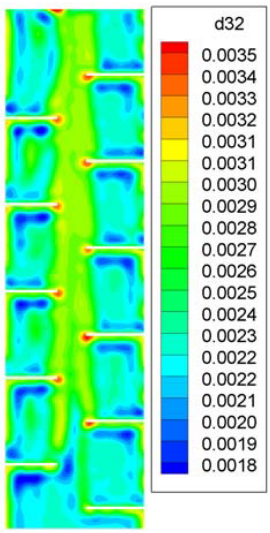

Figure 1. The simulated Sauter mean diameter (left).

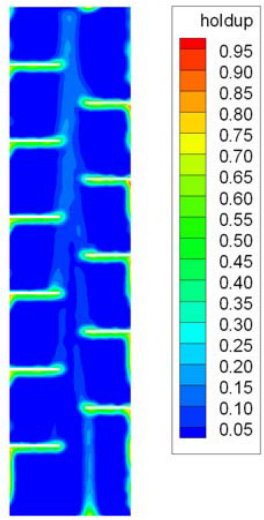

Figure 2. The simulated volume fraction of the dispersed phase (right).

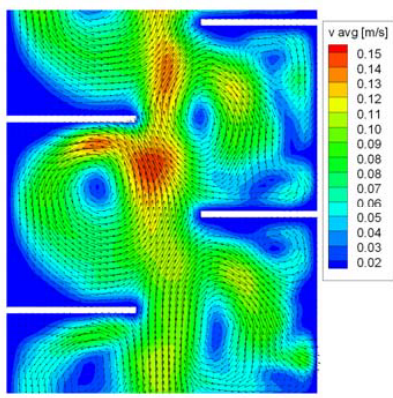

Figure 3. The simulated velocity vectors and magnitude (axial and radial velocity) in one compartment.

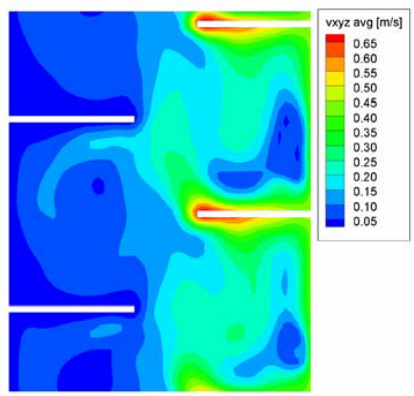

Figure 4. The simulated velocity magnitude (axial, radial and swirl velocity) in one compartment.

CONCLUSIONS

First results of the coupled CFD-PBM algorithm using the FPM and the SQMOM were presented. A complete two-way coupling is achieved, and the coupled model accounts for breakage and coalescence. FPM is able to predict the flow fields and velocities in an

RDC extractor. The SQMOM is found to be extremely accurate, and the flexibility of the method through its reduction to the standard QMOM when the number of primary particles equals one makes it very attractive from computational point of view. The constant kernels were fitted to experimental data and predict suitable results. Models for breakage and coalescence can be easily integrated and will allow for a prediction of the drop size distribution.

ACKNOWLEDGMENTS

This work was financially supported by the Deutsche Forschungsgemeinschaft (DFG).

REFERENCES

1. M. M Attarakih, H.-J. Bart, and N. M. Faqir, "Numerical solution of the bivariate population balance equation for the interacting hydrodynamics and mass transfer in liquid-liquid extraction columns," *Chem. Eng. Sci.*, **61**(1), 113-123 (2006).
2. S. A. Schmidt, M. Simon, M. M. Attarakih, L. Lagar, and H.-J. Bart, "Droplet population balance modelling - hydrodynamics and mass transfer," *Chem. Eng. Sci.*, **61**(1), 246-256 (2006).
3. C. Drumm and H.-J. Bart, "Hydrodynamics in a RDC extractor: single and two-phase PIV measurements and CFD simulations," *Chem. Eng. Techn.*, **29**(11), 1-8 (2006).
4. C. Drumm, S. Tiwari, J. Kuhnert, and H.-J. Bart, "Finite Pointset Method for Simulation of the Liquid-Liquid Flow Field in an Extractor," submitted to *Comp. Chem. Eng.*, (2007).
5. C. Drumm, M. M Attarakih, and H.-J. Bart, "Coupling of CFD with DPBM for a RDC extractor," submitted for publication in *Chem. Eng. Sci.*, special issue 3rd International Conference on Population Balance Modelling, Quebec, Canada, 19-21 Sep. 2007.
6. A. Vikhansky, M. Kraft, M. Simon, S. Schmidt, and H.-J. Bart, "Droplets population balance in a rotating disc contactor: an inverse problem approach," *AIChE J.*, **52**(4), 1441-1450 (2006).
7. M. M Attarakih, C. Drumm, and H.-J. Bart, "Solution of the Population Balance equation using the Sectional Quadrature Method of Moments", submitted for publication in *Chem. Eng. Sci.*, special issue 3rd International Conference on Population Balance Modelling, Quebec, Canada, 19-21 Sep. 2007.
8. M. J. Hounslow, R. L. Ryall, and V. R. Marshall, "A discretized population balance for nucleation, growth and aggregation," *AIChE J.*, **34**(11), 1821-1832 (1988).
9. R. McGraw, "Description of aerosol dynamics by the quadrature method of moments," *Aerosol Sci. & Tech.*, **27**(2), 255-265 (1997).
10. M. Simon, "Koaleszenz von Tropfen und Tropfenschwärmen," Dr.-Ing. Thesis, TU Kaiserslautern, Kaiserslautern, Germany, 2002.
11. D. Ramkrishna, Population Balances, Academic Press, San Diego, 2000.
12. S. Tiwari and J. Kuhnert, "Modeling of two-phase flows with surface tension by Finite Pointset Method (FPM) ," *J. Comp. Appl. Math.*, **203**(2), 376-386 (2007).

NUMERICAL APPROACH TO THE MARANGONI CONVECTION-ENHANCED MASS TRANSFER OF SINGLE MOVING DROPS

Jianfeng Wang,[1,2] Chao Yang,[1] and Zai-Sha Mao[1]

[1]*Instirute of Process Engineering, Chinese Academy of Sciences, Beijing 100080, China.*
[2]*Zhengzhou University, Zhengzhou 450052, China.*
Corresponding author email address: zsmao@home.ipe.ac.cn

ABSTRACT

A level-set approach was adopted to numerical simulation of interphase mass transfer from a deformable drop moving in a continuous immiscible liquid, and preliminary results on Marangoni effect are presented. In the MIBK-acetic acid-water system, three cases with different initial drop concentrations were simulated. Experiment shows that when the solute concentration is sufficiently high, the Marangoni effect would occur with the interphase mass transfer enhanced. Numerical results show that the mass-transfer coefficient with the Marangoni effect present is far larger than that without Marangoni effect. The predictions are qualitatively in accord with the experimental results. Numerical simulation depicts well the transient development of the Marangoni effect.

INTRODUCTION

The Marangoni convection can enhance or depress the rate of mass transfer or heat transfer in many industrial processes. The Marangoni convection induced by mass transfer and heat transfer has been studied extensively using different CFD methods. For example, a series of papers [1-3] reported the Marangoni flows in the binary mixtures where the surface tension varies with either temperature or solute concentration. The mixed buoyant-Marangoni convection due to dissolution of a droplet in a liquid-liquid system with miscibility gap was investigated by Lappa et al. [4]. The Marangoni convection in some different absorption processes was reported in [5,6].

To authors' knowledge, numerical simulation of the Marangoni effect induced by interphase mass transfer to or from drops was hardly reported, except for [7,8] (but not validated experimentally). In this work, the fluid flow and concentration field are solved simultaneously in a time-dependent way. The drop-surface evolution is modeled by the level set method. Numerical simulation of the Marangoni effect induced by interphase mass transfer to single drops in unsteady motion with finite deformation in liquid-liquid extraction systems is performed in a Eulerian axisymmetric reference frame. The

numerical results were compared with the experimental results in a MIBK-acetic acid-water system to validate the numerical simulation.

MATHEMATICAL MODELING

Basic Assumptions

The axisymmetric flow of a liquid drop moving under gravity through an immiscible continuous liquid phase with solute being transferred from drop to the continuous phase is considered with the following assumptions: (1) the two fluids are viscous, Newtonian, and incompressible, (2) the flow is isothermal, (3) the flow field is laminar even if locally disturbed by the Marangoni convection, and (4) mass transfer has no effect on the physical properties of the system, except the surface tension varies with the solute concentration at the surface.

Level-Set Method of Fluid Flow

The level-set method is a simple method for computing the fluid motion with interface Γ in a two- or three-dimensional domain. A smooth function, the level set function, $\phi(x,t)$ over the whole domain is defined as the normal distance from the interface and used to identify the drop surface as the zero set of $\phi(x,t)$.

The two-phase flow in a single Eulerian frame is governed by the continuity and Navier-Stokes equations:

$$\nabla \cdot \mathbf{u} = 0 \tag{1}$$

$$\rho\left(\frac{\partial \mathbf{u}}{\partial t} + \mathbf{u} \cdot \nabla \mathbf{u}\right) = -\nabla p + \rho \mathbf{g} + \nabla \cdot \boldsymbol{\tau} + \mathbf{F} \tag{2}$$

in which **u** is the fluid-velocity vector, ρ the density, p the pressure, **g** the gravity, and $\boldsymbol{\tau}$ the stress tensor. The source term **F** is the body force due to the variable surface tension leading to the Marangoni effect. The volume force is based on the well-known Continuum Surface Force (CSF) model [9], so that the surface-tension force given by

$$\mathbf{f}_s = \sigma\kappa\mathbf{n} + \nabla_s\sigma \tag{3}$$

can be incorporated into the term of **F**. Thus, the interfacial conditions at the unknown location of the interface are not required to be explicitly enforced. Here, σ is the surface tension, ∇_s the surface-gradient operator. **n** the outward unit vector normal to the interface, κ the mean curvature of the interface, and both are evaluated from $\phi(x,t)$.

The first term in Equation 3 is a force acting normal to the interface, and the second is tangential to the interface in the direction pointing to larger σ. In this work σ is dependent only on the solute concentration at the interface c_l^s. The experimental data on surface tension is fitted into the following nonlinear expression:

$$\sigma = \sigma_0\left(1 + ac_l^s + b(c_l^s)^2\right) \tag{4}$$

The detail of incorporating $\mathbf{f}_s$ into **F** may be referred to [8].

The level-set function $\phi(x,t)$ must be always maintained as the distance to the interface. A Hamilton-Jacobi type evolution equation is used to advance the interface in the computational domain. A re-initialization procedure is also necessary for $\phi(x,t)$ as described in [10].

Interphase Mass Transfer

The mass transfer of a solute from a drop to the continuous phase is described by

$$\rho\left(\frac{\partial c}{\partial t}+\mathbf{u}\cdot\nabla c\right)=D\nabla^2 c \tag{5}$$

The numerical solution of the above equation using the level set approach can be referred to Yang and Mao for procedure details [11].

Computational Domain and Boundary Conditions

A computational domain of $40R\times 15R$ is adopted for the numerical simulation of the transient motion of a single drop and the temporal interphase mass transfer. The coordinate system is fixed at the rising drop. The computational domain is found to be sufficient, and the velocity of the drop is not affected by the domain boundaries. The free slip boundary condition is imposed at the column wall. The boundary conditions of zero derivative are enforced at the top and bottom of the domain.

The concentration of solute in the continuous phase is assumed to be $c = 0$ at $t = 0$, and the initial concentration in the drop $c_{d,0}$ is uniform. The mass transfer direction is $d \rightarrow c$. The transient mass transfer from the MIBK drop to the continuous phase was simulated according to the experimental conditions.

EXPERIMENTAL

A single-drop experiment was performed in MIBK/acetic acid/water systems. Their physical properties are summarized in Table 1. The experiments on single-drop mass transfer were conducted following that suggested by Li et al. [12]. From the determined solute concentration in collected drops, the overall mass-transfer coefficient k_{od} is evaluated.

For Cases 1 and 2, the Marangoni effect is observed for the relatively high initial solute concentration in the drops $c_{d,0}$, which offers stronger driving force (larger variation of interfacial tension gradient along the surface) for the Marangoni convection at the interface. In Case 3, $c_{d,0}$ is quite low, and the Manrangoni effect is not observed. The evaluated values of k_{od} are correspondingly larger than that in Case 3.

RESULTS AND DISCUSSION

The streamline map in Figure 1 shows the occurrence of local interfacial circulation (interfacial turbulence or the Marangoni convection) of a single drop in Case

2. Both numerical simulation and experimental data indicate that the interphase mass transfer is enhanced. The Marangoni effect dies gradually as the solute is depleted from the drop. Similar behavior is also observed for Case 1 with high solute concentration. On the contrary, no such Marangoni effect is observed in Case 3, owing to its small $c_{d,0}$.

Table 1. Physical-property data and drop radius

Property	Case 1		Case 2		Case 3	
	Cont. phase (water)	Disp. Phase (MIBK)	Cont. phase (water)	Disp. Phase (MIBK)	Cont. phase (water)	Disp. phase (MIBK)
ρ (kg m^{-3})	995.71	827.40	995.71	864.60	995.71	806.14
$\mu \times 10^3$ (Pa s)	1.069	0.781	1.069	0.901	1.069	0.63
$D \times 10^9$ (m^2 s^{-1})	1.04	1.43	1.04	1.43	1.04	1.44
$\sigma_0 \times 10^3$ (N m^{-1})	9.66		9.66		9.66	
Distribution ratio	0.70		0.75		0.88	
Radius (mm)	0.93		0.90		0.95	
$c_{d,0}$ (wt %)	7.75		12.01		0.29	

Figures 2 and 3 show the overall mass-transfer coefficients with different initial concentration of solute (7.75% and 12.09%, respectively). The numerical simulation is observed in reasonable accord with the experimental measurements, particularly as the trend of variation with time is concerned. Numerical predictions are larger than the experimental data, for which the important reason is that the larger velocity predicted in the present numerical simulation would lead to higher convection intensity, especially in the initial stage of the rising drop.

Figure 4 shows the influence of Marangoni effect on the mass-transfer coefficient in the experiment and the simulation for drops with different initial concentrations. The mass-transfer coefficient for the case of 12.01% of the initial concentration is the largest in the numerical simulation as well as in the experiment. The trend in simulation is in accord with the experiment. The case of the initial concentration of 0.29% has no Marangoni effect, giving the lowest k_{od}. It can be inferred that the Maragnoni effect improves the mass-transfer coefficient in the MIBK-acetic acid-water system from Figure 4. It is noticeable that the Marangoni effect is more intense in the initial stage of the mass transfer, such as in first 0.1 s. However, it is difficult to measurement the mass transfer coefficient in that period due to the experimental technique. It is difficult to compare the experimental results with the simulation results.

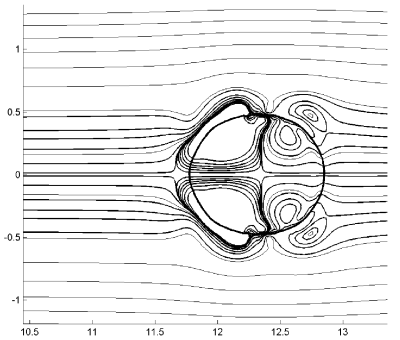

Figure 1. The streamline contours of the drop in Case 2 at t = 0.002 s showing the occurrence of the Marangoni effect.

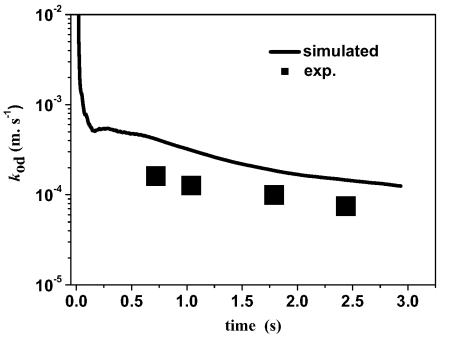

Figure 2. Overall mass-transfer coefficient k_{od} versus mass transfer time (Case 1).

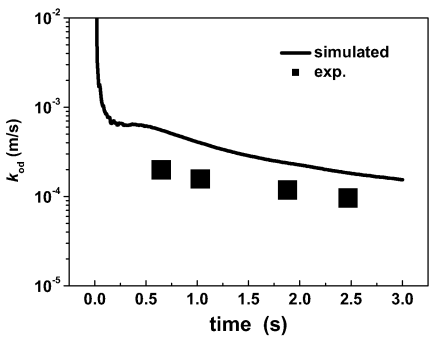

Figure 3. Overall mass-transfer coefficient k_{od} versus mass-transfer time (Case 2).

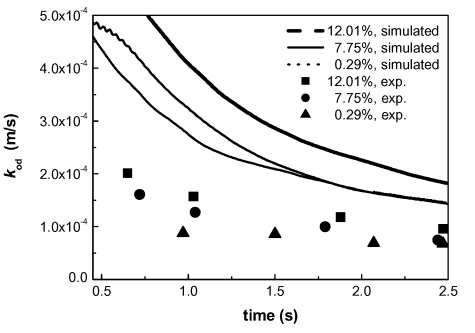

Figure 4. Influence of Marangoni effect on the mass-transfer coefficient k_{od}.

CONCLUSIONS

A level-set approach for numerical simulation of interphase mass transfer from a deformable drop moving in a continuous immiscible liquid in the laminar flow regime and companied with the Marangoni effect was presented. The Marangoni effect is for the first time successfully simulated in the real MIBK-acetic acid system, in which the relationship between the surface tension and solute concentration is nonlinear. The Marangoni effect is stronger when the solute concentration is higher, and the mass-transfer coefficient becomes larger accordingly.

Numerical results are qualitatively accord with the experimental results. Numerical simulation depicts well the development of the Marangoni effect. The present simulation overestimates the interphase mass transfer, possibly because the three-dimensionality of the real Marangoni effect and the error due to substantial mass transfer in the drop formation stage.

ACKNOWLEDGMENTS

Financial support from the National Natural Science Foundation of China (Nos. 20490206, 20576133, and 50404009), PetroChina and the National Basic Research Program of China (Nos. 2004CB619203 and 2004CB619203) is gratefully acknowledged.

REFERENCES

1. A. Bergeron, D. Henry, and H. Benhadid, "Marangoni-Bénard Instability in Microgravity Conditions with Soret Effect," *Int. J. Heat Mass Transfer*, **37**(11), 1545-1562 (1994).
2. R. Savino, C. Piccolo, M. Lappa, and L. Carotenuto, "Natural and Marangoni Convection in Partially Miscible Liquid Systems," *Acta Astronaut.*, **57**(2-8), 89-96 (2005).
3. A. Bahloul, R. Delahaye, P. Vasseur, and L. Robillard, "Effect of Surface Tension on Convection in a Binary Fluid Layer under a Zero Gravity Environment," *Int. J. Heat Mass Transfer*, **46**(10), 1759-1771 (2003).
4. M. Lappa, C. Piccolo, and L. Carotenuto, "Mixed buoyant-Marangoni convection due to dissolution of a droplet in liquid-liquid system with miscilbility gap," *Eur. J. Mech. B Fluids*, **23**, 781-794 (2004).
5. Y. T. Kang and T. Kashiwagi, "Heat Transfer Enhancement by Marangoni Convection in the NH_3–H_2O Absorption Process," *Int. J. Refrig.*, **25**(6), 780-788 (2002).
6. J. Kim, C. K. Choi, and Y. T. Kang, "Instability Analysis of Marangoni Convection for Absorption Process Accompanied by Heat Transfer," *Int. J. Heat Mass Transfer*, **47**(10-11), 2395-2402 (2004).
7. E. Bassano, "Numerical Simulation of Thermo-Solutal-Capillary Migration of a Dissolving Drop in a Cavity," *Int. J. Numer. Meth. Fluids*, **41**(7), 765-788 (2003).
8. Z.-S. Mao, and J. Y. Chen, "Numerical Simulation of the Marangoni Effect on Mass Transfer to Single Slowly Moving Drops in the Liquid–Liquid System," *Chem. Eng. Sci.*, **59**(8-9), 1815-1828 (2004).
9. J. F. Wang, C. Yang, and Z.-S. Mao, "Numerical Simulation of Marangoni Effects of Single Drops Induced by Interphase Mass Transfer in Liquid-Liquid Extraction Systems by the Level Set Method," *Sci. China*, (in press 2007).
10. J. U. Brackbill, D. B. Kothe, and C. Zemach, "A Continuum Method for Modeling Surface Tension," *J. Comput. Phys.*, **100**(2), 335-354 (1992).
11. C. Yang and Z.-S. Mao, "Numerical Simulation of Interphase Mass Transfer with the Level Set Approach," *Chem. Eng. Sci.*, **60**(10), 2643-2660 (2005).
12. T. W. Li, Z.-S. Mao, and J. Y. Chen, "Terminal Effect of Drop Coalescence on Single Drop Mass Transfer Measurements and its Minimization," *Chinese J. Chem. Eng.*, **9**(2), 204-207 (2001).

KINETICS OF SCANDIUM SOLVENT EXTRACTION BY N-(2-HYDROXY-5-NONYLBENZYL)-β, β-DIHYDROXYETHYLAMINE UNDER NON-STATIONARY PHASE CONTACT SURFACE

S. A. Semenov and A. M. Reznik

Lomonosov Moscow State Academy of Fine Chemical Technology, 86 Vernadskogo prospect, Moscow, Russia 119571. Corresponding author email address: sash@vmik.ru

ABSTRACT

The kinetics of scandium solvent extraction by N-(2-hydroxy-5-nonylbenzyl)-β,β-dihydroxyethylamine from chloride solutions has been investigated with purpose of intensification of scandium solvent extraction process. The research has been carried out using an original method of the study of solvent extraction kinetics under non-stationary liquid-liquid interface. The analysis of obtained data allows to recommend the conditions for carrying out the process of scandium solvent extraction.

INTRODUCTION

Scandium solvent extraction (SX) by N-(2-hydroxy-5-nonylbenzyl)-β,β-dihydroxyethylamine (NBEA) was reported recently [1]. Equilibrium in this system is reached during 30 minutes. To intensify the SX process from chloride solutions by NBEA the kinetics of scandium SX has been investigated. It is expedient to research the kinetics of this process in the conditions as much as possible close to industrial, at high values of liquid-liquid (L-L) interface, i.e. with reactor method in emulsive regime [2].

The research has been carried out using an original method of the SX kinetics study under non-stationary L-L interface that simplifies both the reactor device and the experiment compared to the known techniques [3,4]. Application of this method allows to carry out the process under conditions of high values of L-L interface and to control these values directly during the SX by the optical method [5,6]. Earlier we have tested the method of the SX kinetics study under non-stationary L-L interface at investigating the kinetics of copper, nickel and cobalt stripping from the organic phase containing para-tert.butylphenol disulphide [7,8] and gallium SX by phenol-formaldehyde oligomer «101 K» [9].

EXPERIMENTAL

General

All chemicals and solvents were of reagent grade purity. NBEA is the basic component of the technical product (80 % NBEA, 15 % diethanolamine (DEA), 3 % n-nonylphenol (NP), 2 % H_2O) which is used as the modifier in manufacture of synthetic rubbers. Refining of NBEA solutions from DEA was carried out by distilled water in the separating funnel during 15 minutes. The ratio of phases was 1:1. After 3 contacts NBEA was completely refined from DEA.

To separate from n-nonylphenol the benzene solution of NBEA was processed with gaseous chlorine hydride. Gaseous chlorine hydride was produced with apparatus described elsewhere [10]. The sediment formed at that – muriatic salt of this compound – was washed out with benzene, and then processed with the solution of sodium carbonate. The restored amino compound was extracted with n-octanol [11]. Purity of the obtained NBEA was verified by means of thin-layer chromatography.

Experiment was carried out at temperature 20±1°C. Volumes of water and organic phases in all cases was equal. Initial concentration of NBEA in n-octanol was 0.25 mol/L. Initial concentration of scandium in aqueous phase was 0.0231 mol/L. Aqueous solution contained 1 mol/L NaCl as salting-out agent. To have an opportunity to neglect of reversibility of SX process, maximal time of phases contact, according to [12], was chosen equal 1.5 minutes. Concentration of scandium was determined by means of chelatometry [13].

Experiment was hardware assisted with photometer-nephelometer LMF-69 that makes it possible to mix in the reactor with a magnetic stirrer and to study simultaneously the optical transmission of an SX system. Photocurrent alteration allowed to fix the L-L interface change according to the equation

$$\beta a_\tau = (\Phi_0 / \Phi - 1), \qquad (1)$$

where Φ_0 – photocurrent in system without mixing;

Φ – photocurrent in system with mixing;

a_τ – current value of L-L interface;

Factor β depends on parameters of refraction of the dispersed phase, the dispersion medium and the construction of a reactor [5, 6].

The reactor was a glass vessel with densely ground in conic cover supplied with a capillary for the air removal (fig.1).

Theoretical Methods

Rate of mass transfer which is defined by chemical reaction of the first or pseudo-first order, is described by the known equation:

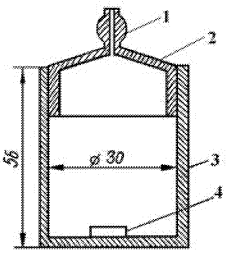

Figure 1. Reactor for the SX kinetics investigation.
1 – capillary, 2 – cover, 3 – glass vessel, 4 – magnetic stir bar.

$$\frac{dy_\tau}{d\tau} = \frac{K_0 \times (1+D)}{V_o} \times a_\tau \times \left(y^{eq} - y_\tau\right), \tag{2}$$

where:

y – current concentration of the extractive element in the organic phase;

y^{eq} – equilibrium concentration of the extractive element in the organic phase;

D – distribution ratio;

τ – time;

K_0 – mass transfer ratio;

V_o – volume of an organic phase.

Integration of the equation (2) within the limits of from zero up to τ at constant distribution ratio leads to an expression:

$$\ln(1 - I_\tau) = -\frac{K_0(1+D)}{V_o} \times \int_0^\tau a_\tau d\tau \ , \tag{3}$$

where $I = y_\tau / y_0$ – a current degree of SX.

Approximating dependence of the L-L interface on time by fractional-rational function

$$\beta a_\tau = lm\tau / (1 + l\tau), \tag{4}$$

where l and m – the parameters describing rate of L-L interface change and equilibrium value of L-L interface, respectively;

β – factor of proportionality,

and substituting values a_τ in an expression (3), we obtain expression:

$$\ln(1 - I_\tau) = -\frac{K_0(1+D)}{V_o\beta} \times m \times A \, , \tag{5}$$

where $A = \tau - (1/l) \ln (1 + l\tau)$.

From the analysis of dependences $\ln(1 - I_\tau)$ from A it is possible to draw a conclusion on the regime of SX process under the conditions of the non-stationary L-L interface, and also about the localization as well as the orders of the limiting stage of reaction [7-9].

RESULTS AND DISCUSSION

The question of the identification of the regime of SX process is one of the basic questions arising in the SX kinetics study. For this purpose the influence of mixing intensity on the rate of scandium SX has been studied. Values of intensity of mixing changed in a range from 680 up to 1265 min^{-1}. Dependences of L-L interface change on time contacting and intensity of phases mixing during scandium SX have been approximated by fractional-rational function:

$$\frac{\Phi_0}{\Phi} - 1 = \frac{l\tau}{1 + l\tau} \times m \qquad (6)$$

Values of the parameters of this function have been found with the least-squares method. Adequacy of the description of experimental data by the obtained equations has been checked up by the Fisher's criterion. Thus, to receive a reliable information about the regime of the process and to draw a correct conclusion on localization of the limiting stage of reaction, it is necessary to consider not only the equilibrium value of L-L interface at various intensity of mixing, but also the change of L-L interface in time during SX.

For the purpose of determination of mass transfer ratio the influence of phases contacting time and intensity of phases mixing on scandium SX from the aqueous phase into the organic one, taking into account the L-L interface change, has been studied. Linear character of the obtained dependences testifies to the first order of a limiting stage of SX reaction with respect to scandium. It is necessary to note, that for each series of experiments the values D, V_o and β in the equation (5) are constant. Therefore the slopes of the dependence

$$\ln(1 - I_\tau) = f[m (\tau - (1/l) \times \ln(1 + l\tau))] \qquad (7)$$

are identical to expression $K_0 (1+D) / V_o$. Hence, having considered the influence of mixing intensity on the slope of dependences (7), it is possible to draw a conclusion on influence of mixing intensity on mass transfer ratio. The analysis of the obtained data has shown that at increase of mixing intensity the mass transfer ratio in the studied range of the mixer speed is constant. That testifies that SX proceed in kinetic area, and the limiting stage of reaction is localized on L-L interface. The conclusion about localization of a limiting stage on L-L interface also proves to be true is direct-proportional dependence of rate of scandium SX from equilibrium value of the L-L interface.

The basic purpose of the majority of the kinetic researches concerning to various SX systems, is, as a rule, not only the determination of the limiting stage of reaction, but

also obtaining the information on the mechanism of this limiting stage. For the decision on this problem it is necessary to determine the values of orders of a reaction limiting stage with respect to the basic components of the reaction.

To determine the limiting stage orders of scandium SX reaction with respect to extractant and hydrogen ions the influence of extractant and acid concentrations on the rate of SX has been studied. The analysis of the obtained dependences has shown that the order of the reaction limiting stage with respect to extractant $n_{HR} = 1.28 \pm 0.28 \approx 1$, and with respect to the ion of hydrogen during the scandium SX is fractional ($n_{H^+} = 0.62 \pm 0.09$). It is possible to explain these orders by assuming the reaction to proceed by two pathways: with generation of a hydrogen ion (mechanism 1) and without generation of a hydrogen ion (mechanism 2).

Generally the process of scandium SX can be presented by the following equations of the first and zero order with respect to a hydrogen ion:

$$Sc(H_2O)_5(OH)^{2+}{}_{(w)} + Cl^-{}_{(w)} + HR_{(o)} \rightarrow ScCl(OH)R_{(o)} + 5H_2O_{(w)} + H^+{}_{(w)} \quad (8)$$

$$Sc(H_2O)_5(OH)^{2+}{}_{(w)} + 2Cl^-{}_{(w)} + HR_{(o)} \rightarrow ScCl_2R_{(o)} + 6H_2O_{(w)} \quad (9)$$

On the basis of the obtained data about the orders of the reaction limiting stage with respect to metal ($n_{Sc} = 1$), extractant ($n_{HR} = 1$) and a hydrogen ion and considering that the limiting stage of reaction is localized on the L-L interface, the mechanism of a limiting stage of scandium SX reaction is offered.

Scandium SX by NBEA proceeds by two pathways:

1) with generation of a hydrogen ion

$$[Sc(H_2O)_5(OH)]^{2+} + Cl^- \rightleftharpoons [Sc(H_2O)_5(OH)Cl]^+{}_s \quad (a)$$

$$\overline{HR} \rightleftharpoons HR_s \quad (b)$$

$$[Sc(H_2O)_5(OH)Cl]^+{}_s + HR_s \rightleftharpoons ScCl(OH)R_s + 5H_2O_s + H^+{}_s \quad (c)$$

$$ScCl(OH)R_s \rightleftharpoons \overline{ScCl(OH)R} \quad (d)$$

$$5H_2O_s \rightleftharpoons 5H_2O \quad (e)$$

$$H^+{}_s \rightleftharpoons H^+ \quad (f)$$

2) without generation of a hydrogen ion

$$[Sc(H_2O)_5(OH)]^{2+} + 2Cl^- \rightleftharpoons [Sc(H_2O)_5(OH)Cl_2]_s \quad (a)$$

$$\overline{HR} \rightleftharpoons HR_s \quad (b)$$

$$[Sc(H_2O)_5(OH)Cl_2]_s + HR_s \rightleftharpoons ScCl_2R_s + 6H_2O_s \quad (c)$$

$$ScCl2R_s \rightleftharpoons \overline{ScCl_2R} \quad (d)$$

$$6H_2O_s \rightleftharpoons 6H_2O \quad (e)$$

where the symbol below the line concerns to the organic phase, and index S denotes that the given compound is adsorbed on the L-L interface.

Limiting stage in the pathway 1 is the stage (c) – addition of the adsorbed on L-L interface molecule of extractant to the adsorbed scandium aquo-complex with obtaining

of scandium complex with extractant and generation of one hydrogen ion. In this case rate of SX process depends on pH.

Limiting stage in the pathway 2 is the stage (c) – addition of the adsorbed mole cule of extractant to the adsorbed scandium aquo-complex with obtaining of scandium complex with extractant without generation of a hydrogen ion.

CONCLUSIONS

The analysis of the obtained data allows us to recommend for performing the scandium SX by NBEA the following: 1) application of the extractors allowing to carry out process in conditions of a high L-L interface; 2) carrying out of SX process at high pH values, scandium and extractant concentrations.

REFERENCES

1. L. A. Gladikova, S. A. Semenov, and A. M. Reznik, "Complexation of Scandium upon Its Extraction with Solutions of N-(2-hydroxy-5-nonylbenzyl)-β,β-dihydroxyethylamine in Octanol", *Russian J. of Coord. Chem,* **28**(11), 798–800 (2002).
2. P. R. Danesi and R. Chiarizia, "The Kinetics of Metal Solvent Extraction", *Critical Reviews in Analytical Chemistry*, **10**(1), 1–126 (1980).
3. H. Rushton, S. Nagata, and T. B. Rooney, "Measurement of Mass Transfer Coefficients in Liquid-Liquid Mixing", *Amer.Inst. of Chem.Eng.J.*, **10**(3), 298–302 (1964).
4. G. A. Yagodin and V. V. Tarasov, "Method and Device for Investigation of the Solvent Extraction Kinetics in Electrolyte-Nonelectrolyte Systems", *Teoretich. Osnovi Khim. Technol.,* **4**(3), 426–429 (1970).
5. A. V. Yanishevsky and N. S. Pavlushenko, "Determination of the emulsion interface", *Zh. Prikl. Khim.,* **31**(8), 1215–1220 (1958).
6. G. E. Langlois, J. E. Gullberg, and T. Vermeulen, "Determination of Interfacial Area in Unstable Emulsion by Light Transmission", *Rev. Sci. Inst.*, **25**(4), 360–363 (1954).
7. S. A. Semenov, T. Z. Islanova, A. M. Reznik, and L. D. Yurchenko, "Kinetics Investigation of Nickel and Copper Stripping from para-tert.butylphenol Disulphide under Non-stationary Phase Contact Surface", *Trudi Mosk. Khimiko-tehnolog. Istituta im. D. I. Mendeleeva,* (143), 50–54 (1986).
8. S. A. Semenov, T. Z. Islanova, and A. M. Reznik, "Kinetics of Cobalt Stripping under Non-stationary Phase Contact Surface", *Zh. Physich. Khim.,* **64**(10), 2745–2748 (1990).
9. S. A. Semenov, T. Z. Islanova, A. M. Reznik, and L. D. Yurchenko, "Extraction Kinetics Investigation under Conditions of Non-Stationary Surface of Phase Contact", International Solvent Extraction Conference, Preprints, v.II, DECHEMA, Frankfurt am Main, Germany, 1986, pp. 377–384.
10. B. D. Stepin, Technics of Laboratory Experiment in Chemistry, Khimia, Moskva, 1999.
11. E. R. Alekperov and A. M. Reznik, Complexes of Boron: Synthesis, application, Publishing House MGU, Moskva, 2000.
12. J. B. Roddy, C. F. Coleman, and S. Arai, "Mechanism of the Slow Extraction of Iron (III) from the Acid Perchlorate Solutions of Di(2-ethylhexyl)phosphoric Acid in n-Octane", *J. of Inorg. Nucl. Chem.,* **33**(4), 1099–1118 (1971).
13. G. Schwarzenbach and H. Flaschka, Die komplexometrische Titration, Ferdinand Enke Verlag, Stuttgart, 1965.

EXTRACTION AND SEPARATION OF THORIUM(IV) FROM LANTHANIDES(III) WITH ROOM-TEMPERATURE IONIC LIQUIDS CONTAINING PRIMARY AMINE N_{1923}

Y. Zuo,[1,2] J. Chen,[1] Y. Bai,[1] and D. Q. Li[1]

[1]Changchun Institute of Applied Chemistry, Chinese Academy of Sciences, Changchun 130022, P. R. China. [2]Graduate School of Chinese Academy of Sciences, Beijing, P. R. China. Corresponding author email address: ldq@ciac.jl.cn

ABSTRACT

The extraction behavior of Th(IV) by primary amine N_{1923} in imidazolium-based ionic liquid namely 1-octyl-3-methylimidazolium hexafluorophosphate (N_{1923}/IL) was studied in this paper. Results showed that N_{1923}/IL had poorer extraction ability for Th(IV) than N_{1923} in *n*-heptane (N_{1923}/HEP). The separation coefficients between Th(IV) and lanthanides(III) ($\beta_{Th/Ln}$) were obtained and compared with those in the N_{1923}/HEP system. On this basis, we made a preliminary assessment for the possibility of using ionic liquids as solvents for the separation of Th(IV) from lanthanides(III) sulfate in a clean process.

INTRODUCTION

Ionic liquids (ILs) as potential replacements for noxious volatile organic compounds (VOCs) now have attracted much interest all over the world. As ILs consist of cations and anions, they possess many attractive properties such as negligible volatility, nonflammability, high thermal stability, wide electrical window, and tunable hydrophobicity [1]. These properties arouse wide attention for synthetic, catalytic, analytic, and electrochemical applications [2]. Considering the hydrophobicity and ionicity, which may favor the solvation of ionic species such as metal ion-ligand complexes, ionic liquids were investigated as extractants or diluents for the extraction of metal ions [3]. Recently, a study on the radiochemical stability of ILs indicated that ILs are more resistant to radiation than VOCs and thus may favor applications concerned with actinide separations [4]. In 1999, Dai et al. obtained unprecedentedly large distribution ratios for the separation of strontium ions (fission product) with crown ether in ionic liquids [5]. After that, plenty of work rushed into this area. However, later work suggests that the utility of ILs as extraction solvents may be limited by the solubilization loss of ILs and difficulty in stripping metal ions [6]. Recently, Mark L. Dietz made a summary about various efforts for overcoming these limitations [7]. As he pointed out in

his review, more work will be required before the potential of ILs employed as extraction solvents can be fully evaluated.

Thorium was borne from monazite, which is now coexisting with China's biggest rare-earth ore mineral, namely, bastnasite in Baiyunebo mine. A process for recovering Th(IV) from the sulfuric acid leaching of the roasted mineral was developed in our previous work [8,9]. Primary amine N_{1923} as extractant showed high efficiency for the separation of thorium(IV) from RE(III) sulfate solutions. However, as the process deals with volatile organic phase (i.e., kerosene) containing radioactive Th(IV), workers should be very careful. As the interest of our laboratory is seeking more efficient and environmental friendly process for rare earth metallurgy, one of the most commonly used imidazolium-based IL, $[C_8mim]PF_6$, was employed as solvent for the extraction of Th(IV) and lanthanides(III) (Ln(III)) from sulfuric acid medium in this study. On this basis, we made a preliminary assessment for the possibility of using ionic liquids as solvents for the separation of Th(IV) from Ln(III) sulfate solutions.

EXPERIMENTAL

The IL, $[C_8mim]PF_6$, was synthesized and characterized with the methods described in the literature [10]. Pre-experiment indicated that the solubility of $[C_8mim]PF_6$ in water was about 2.84 g/L. The primary amine N_{1923}, $(C_nH_{2n+1})_2CHNH_2$ (n = 9-11), was supplied by Tianjin Chemical Plant and was purified by vacuum distillation (175-205 °C, 667-1333 Pa) before use. The stock solution of thorium sulfate was prepared from $Th(NO_3)_4{\cdot}4H_2O$ via evaporating HNO_3 off with H_2SO_4. All stock solutions of Ln(III) sulfate were prepared directly by dissolving their 4N oxides in proper amount of sulfuric acid. All other chemicals were of A.R.

All the extraction experiments were performed by contacting 1 mL IL phase and 5 mL aqueous phase solutions for 1 hour at 25 ± 1 °C in a vibrating mixer. After that, the mixture was settled and centrifuged under 2000 rpm for 10 min. Then the metal ion concentration in the upper phase (aqueous phase) was determined by the following methods. Identical extraction experiments were conducted using *n*-heptane (HEP) as solvents in some of the investigations. For better phase separation, 5% v/v isooctanol was added to into all the diluents including the IL and molecular solvents that were used in this study. A notable observation that should be pointed out here is the decomposition of the IL ($[C_8mim]PF_6$) under high H_2SO_4 concentration condition. Our pre-experiment suggested that the decomposition became obvious when $[H_2SO_4]_{aq} \geq 5$ mol/L. However, most of our experiments were conducted with $[H_2SO_4]_{aq} < 1$ mol/L (acid dependence is an exception).

Thorium(IV) and Ln(III) ions were determined by spectrophotometric analysis with Arsenazo III at the wavelengths 660 nm and 653 nm, respectively. The concentrations of N_{1923} in IL and *n*-heptane were titrated by standard hydrochloric acid in ethanol medium using bromocresol green as indicator. The water content in the IL phase was determined by Karl-Fischer titration with a CA-02 Mitsubishi moisture meter.

RESULTS AND DISCUSSION

Extracting acid is a basic property of amine extractants. It is rather amine salts than amine itself that play an important role in the coordination with metal ions in extraction. For convenience, all the organic phases (N_{1923} in IL or HEP) were fully contacted with equal volumes of 0.2 mol/L H_2SO_4 solutions before the metal ion extraction was conducted in this study.

The acidity dependence of the extraction of Th(IV) by N_{1923} was investigated in Figure 1. Unlike N_{1923}/HEP, N_{1923}/IL showed poor extraction ability for $Th(SO_4)_2$ and had the maximum extraction percentage at about pH = 1. To improve the extraction percentage for Th(IV), Na_2SO_4 was added into the initial aqueous solutions. However, a sharp decrease of the extraction percentage occurred at about $[H_2SO_4]$ = 1.0 mol/L even when 0.4 mol/L Na_2SO_4 was added. The reason why sulfate played an important role for the extraction of Th(IV) by N_{1923}/IL is not clear, because this observation was not observed in the N_{1923}/HEP system (Figure 2). The different role of sulfate in the extraction of Th(IV) implied that different extraction mechanisms probably existed in the two systems.

Slope analysis of the dependence of D_{Th} on the concentration of N_{1923} in Figure 3 also suggests that the extraction behavior of Th(IV) by N_{1923} in IL is quite different from that in molecular-solvent systems. It is hard to explain the high slope (about 8) in N_{1923}/IL system from normal coordination chemistry perspective.

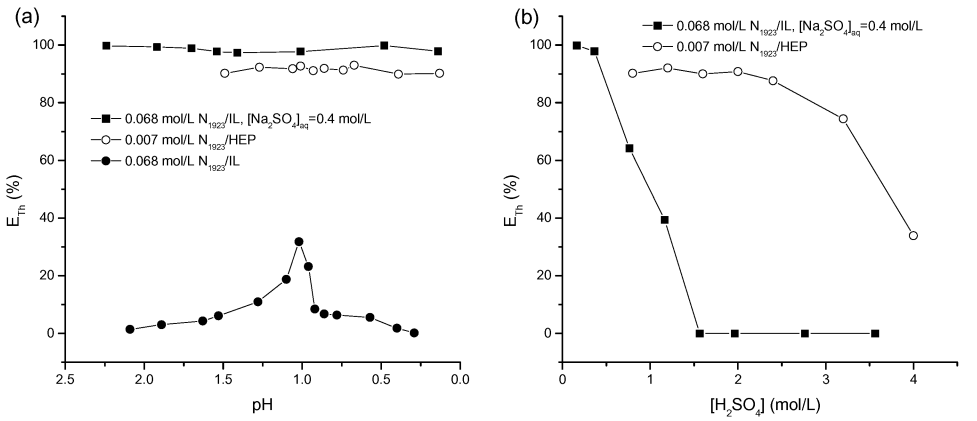

Figure 1. Dependence of extraction percentage of Th(IV) on the concentration of sulfuric acid. $[Th^{4+}]_{ini}$ = 44 μg/mL.

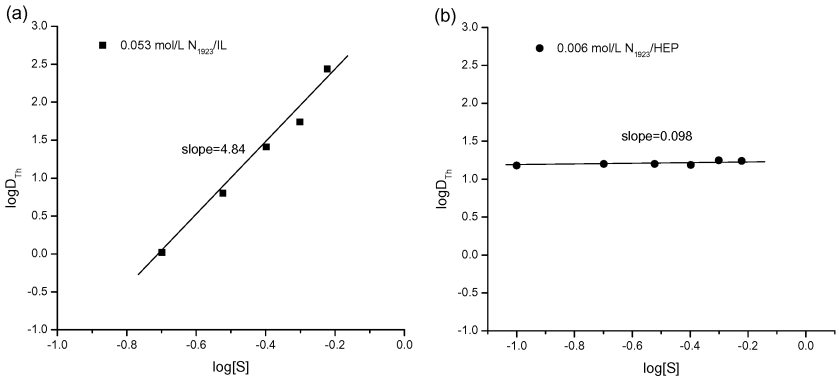

Figure 2. Dependence of D_{Th} on the concentration of total sulfate. $[Th^{4+}]_{ini}$ = 44 μg/mL, $[H_2SO_4]_{aq}$ = 0.1 mol/L, [S] = $[H_2SO_4]$ + $[HSO_4^-]$ + $[SO_4^{2-}]$.

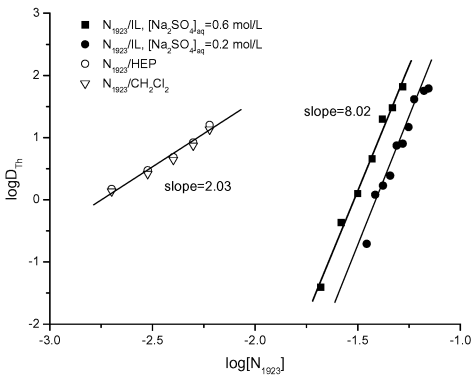

Figure 3. Dependence of D_{Th} on the concentration of N_{1923}. $[Th^{4+}]_{ini}$ = 44 μg/mL, $[H_2SO_4]_{aq}$ = 0.1 mol/L.

Several lanthanides were investigated as representatives in this study in order to evaluate the separation coefficients of Th(IV) vs. Ln(III). Figure 4 gives the *D* plots on the concentration of aqueous sulfuric acid; nearly all lanthanides(III) showed a negligible *D* value compared with D_{Th} when the $[H_2SO_4]$ < 1 mol/L. So, although N_{1923}/IL exhibited poor extraction ability for Th(IV) compared with N_{1923}/HEP, the separation coefficients of Th(IV) vs. Ln(III) in the N_{1923}/IL system is as high (>100) as those in VOC system [10] under proper conditions.

The back-extraction of Th(IV) from the loaded IL phase was conducted using some inorganic acids (HCl, HNO_3, and $HClO_4$) and some complexing agents (EDTA and critic acid) as stripping agents. The stripping results (see Table 1) indicated that complexing agents have no superiority in the back-extraction of Th(IV) over inorganic acids.

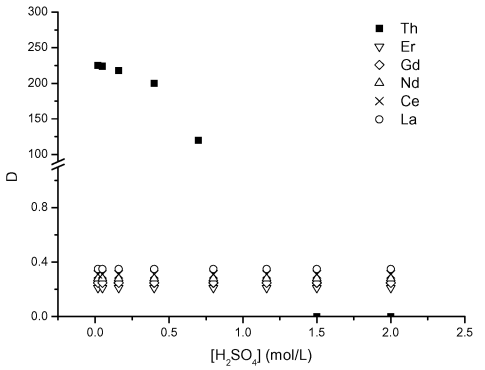

Figure 4. Dependence of on the concentration of H_2SO_4. $[N_{1923}]_{IL}$ = 0.068 mol/L, [Metal ion]$_{ini}$ = 2.0 × 10^{-4} mol/L, $[Na_2SO_4]_{aq}$ = 0.4 mol/L.

Table 1. Stripping of Th(IV) ($[Th(IV)]_{IL}$ = 237 μg/mL) using various strippants

Stripping phase	Stripping ratio	Stripping phase	Stripping ratio
0.5 mol/L HCl	61%	0.1 mol/L citric acid	33%
0.5 mol/L $HClO_4$	56%	0.1 mol/L EDTA	55%
0.5 mol/L HNO_3	46%	combined strippants*	71%

* 0.1 mol/L citric acid + 0.4 mol/L formic acid + 0.4 mol/L hydrazine hydrate.

CONCLUSION

Primary amine N_{1923} was proved to have poorer extraction ability for Th(IV) in $[C_8mim]PF_6$ than in conventional molecular solvents in this work. Slope analysis indicated that the extraction mechanism of Th(IV) by N_{1923} in IL was different from that in molecular solvents. More work needs to be done to learn the mechanism using IL as solvent. Although a high separation coefficient of Th(IV) vs. Ln(III) was obtained via adding Na_2SO_4 into the initial aqueous solutions, the employment of $N_{1923}/[C_8mim]PF_6$ as extracting phase for the separation of Th(IV) may not be suitable for practical application because of the relatively lower Th(IV) capacity and lower stripping ratio. The relative lower capacity for Th(IV) in $N_{1923}/[C_8mim]PF_6$ phase is probably caused by the poor solubility of N_{1923} and its complex with Th(IV) in the IL phase. Fortunately, we have 10^{18} kinds of ionic liquids accessible for utility. In seeking for the "golden partner" of ILs and extractants, the ILs with good solubility for N_{1923} and its complex with Th(IV) should be preferred.

ACKNOWLEDGMENTS

This project was supported by "Hundreds of Talents Program" from Chinese Academy of Science, Natural Science Foundation of China (50574080) and Distinguished Young Scholar Foundation of Jilin Province (20060114).

REFERENCES

1. S. V. Malhotra and Z. Hua, "Current Studies on Some Physical Properties of Ionic Liquids," *Phys. Chem. Liq.*, **42**(2), 215-215 (2004).
2. S. Pandey, "Analytical Applications of Room-Temperature Ionic Liquids: A Review of Recent Efforts," *Anal. Chim. Acta*, **556**(1), 38-45 (2006).
3. A. E. Visser and R. D. Rogers, "Room-Temperature Ionic Liquids: New Solvents for f-Element Separations and Associated Solution Chemistry," *J. Solid State Chem.*, **171**(1-2), 109-113(2003).
4. D. Allen, G. Baston, A. E. Bradley, T. Gorman, A. Haile, I. Hamblett, J. E. Hatter, M. J. F. Healey, B. Hodgson, R. Lewin, K. V. Lovell, B. Newton, W. R. Pitner, D. W. Rooney, D. Sanders, K. R. Seddon, H. E. Sims, and R. C. Thied, "An Investigation of the Radiochemical Stability of Ionic Liquids," *Green Chem.*, **4**(2), 152-158 (2002).
5. S. Dai, Y. H. Ju, and C. E. Barnes, "Solvent Extraction of Strontium Nitrate by a Crown Ether Using Room-Temperature Ionic Liquids," *J. Chem. Soc. Dalton Trans.*, (8), 1201-1202 (1999).
6. M. P. Jensen, J. Neuefeind, J. V. Beitz, S. Skanthakumar, and L. Soderholm, "Mechanisms of Metal Ion Transfer into Room-Temperature Ionic Liquids: The Role of Anion Exchange," *J. Am. Chem. Soc.*, **125**(50), 15466-15473 (2003).
7. M. L. Dietz, "Ionic Liquids as Extraction Solvents: Where Do We Stand?" *Sep. Sci. Technol.*, **41**(10), 2047-2063 (2006).
8. D. Q. Li, R. E. Ji, W. Xu, D. Y. Yu, G. F. Zeng, and J. Z. Ni, "Extraction Mechanism of Rare Earth Elements(III), Iron(III) and Thorium(IV) from Sulfuric Acid Solutions by Primary Amine N_{1923}," *Chin. J. Appl. Chem.*, **4**(2), 36-41 (1987).
9. D. Q. Li, Y. Zuo, and S. L. Meng, "Separation of Thorium(IV) and Extracting Rare Earths from Sulfuric and Phosphoric Acid Solutions by Solvent Extraction Method," *J. Alloys Compd.*, **374**(1-2), 431-433 (2004).
10. X. Q. Sun, D. B. Wu, J. Chen, and D. Q. Li, "Separation of Scandium(III) from Lanthanides(III) with Room-Temperature Ionic Liquid Based Extraction Containing Cyanex 925," *J. Chem. Technol. Biotechnol.*, **82**(3), 267-272 (2007).

THE KINETICS OF Cu(II) EXTRACTION BY 5-NONYL-2-HYDROXYBENZALDOXIME (P50) IN A MICELLE SYSTEM

Sarah Glasson, Geoff W. Stevens, and Jilska M. Perera

Particulate Fluids Processing Centre, Department of Chemical and Biomolecular Engineering, The University of Melbourne, Melbourne, Victoria, 3010, Australia.
Corresponding author email address: jilska@unimelb.edu.au

ABSTRACT

The rate of complexation between Cu(II) and P50 (5-nonyl-2-hydroxybenaldoxime, HL) in a neutral micelle system, Teric $G_{12}A_8$, (octa-ethyleneglycol mono-*n*-dodecyl ether) was monitored using a combination of stopped-flow and UV-visible spectrophotometry. A two-step mechanism was found to accurately describe the experimental data, and reaction rate constants for the forward and reverse reactions were obtained. The results of the modelling indicate that formation of the intermediate CuL^+ is the rate-determining step for the system.

INTRODUCTION

The transparency of micellar systems makes it advantageous to study the kinetics of complexation by conventional techniques such as stopped-flow and to use this data to develop models for the reactions occurring in the liquid-liquid extraction of metal ions [1]. Such studies contribute to the knowledge of mechanisms and sites of complexation reactions. They also allow the study of the effect of additives on the rate of complex formation [2], which is of value in many practical applications. The rate of complexation of metal ions by lipophilic extractants solubilized in microheterogeneous systems (micellar, mixed micellar, and microemulsions) is shown to be of major interest from both fundamental and applied points of view [3]. The aim of this study is to determine the extraction reaction mechanism for Cu(II) by the extractant P50 and to develop a model to predict the rate constants associated with the process.

EXPERIMENTAL SECTION

Chemicals

P50 (5-nonyl-2-hydroxybenaldoxime, Avecia Ltd.) was purified by the method of Preston and Whewell [4]. Teric $G_{12}A_8$, poly-dispersed octa-ethyleneglycol mono-*n*-dodecyl ether, MW (average) = 559 was supplied by the Huntsman Corporation Australia Pty. Ltd. All other reagents (AR grade) were used as supplied: copper sulfate

pentahydrate (Chem Supply Pty. Ltd.); sulfuric acid, sodium hydroxide, and anhydrous sodium sulfate, (BDH Laboratory Supplies). Distilled water was produced on site.

Extraction Equilibrium Constant

Equilibrium measurements for the micelle system were made as previously described [5]. The absorption data was converted to concentration using the previously determined extinction coefficient for Cu(II)/P50 complex (7040 M^{-1} cm^{-1}).

Kinetic Measurements

The micellar-kinetics work was conducted using the stopped-flow technique as previously reported [2]. Once the reference measurements were completed, solutions of known pH and containing known concentrations of Cu(II) and P50 at constant ionic strength were mixed in the reaction vessel and the absorbance spectra recorded at regular time intervals. This data was then processed using the extinction coefficient for the Cu(II)/P50 complex to provide the concentration of the complex as a function of time.

RESULTS AND DISCUSSION

Extraction Equilibrium Constant

In heterogeneous systems, Cu(II) reacts with P50 (HL) to form a colored 2:1 complex (CuL_2) that absorbs in the UV-visible region [6]. This is also the case in the $G_{12}A_8$ micellar system. The proposed overall reaction for the extraction of Cu(II) with P50 (HL) is:

$$Cu^{2+} + 2HL_{(org)} \underset{k_r}{\overset{k_f}{\Leftrightarrow}} CuL_{2(org)} + 2H^+ \quad (1)$$

Therefore, the extraction equilibrium constant, K_{ex}, for the system is defined as:

$$K_{ex} = \frac{[CuL_2][H^+]^2}{[Cu^{2+}][HL]^2} \quad (2)$$

Equation 2 can be rewritten as follows:

$$\log\left(\frac{[CuL_2]}{[Cu^{2+}]}\right) = -2\log\left(\frac{[H^+]}{[HL]}\right) + \log K_{ex} \quad (3)$$

From Equation 3, it can be seen that a plot of $\log\left(\frac{[CuL_2]}{[Cu^{2+}]}\right)$ versus $\log\left(\frac{[H^+]}{[HL]}\right)$ will be linear with a slope of –2 and intersect the y-axis at $\log K_{ex}$. As shown in Figure 1, the line of best fit was found to be in good agreement with Equation 3, having a slope of -2.00 and intersecting the y-axis at a value of -1.70. From this intercept, the extraction equilibrium constant was determined to be $10^{-1.70}$.

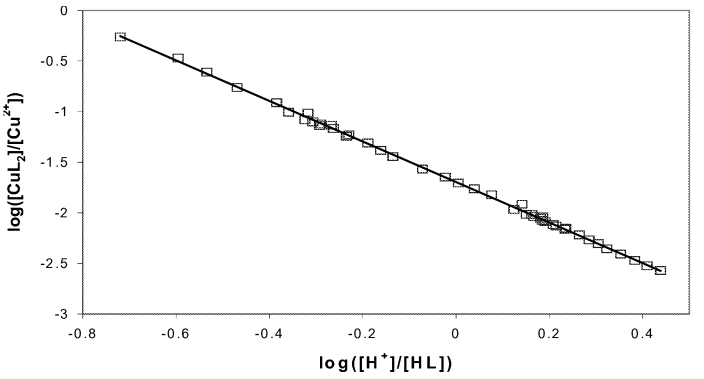

Figure 1. Equilibrium data for the extraction of Cu(II) with P50 in 0.1 M sodium sulfate/0.05 M $G_{12}A_8$ micellar solution. (–) line of best fit, slope = -2.0; $K_{ex} = 10^{-1.70}$.

Kinetics of Cu(II) Extraction by P50

The extraction of Cu(II) by P50 in micellar solution was monitored using the stopped-flow technique. In summary, this involved tracking the absorption at 355 nm, the wavelength of maximum absorbance for the Cu(II)/P50 complex at discrete time intervals, from an initial introduction of two solutions containing known concentrations of the reactants into the reaction vessel. The extinction coefficient (7040 M^{-1} cm^{-1}), determined previously, was then used to translate the absorbance into the concentration of the complex at a particular time. The experiment was repeated several times with varying initial concentrations of Cu(II), extractant, and hydrogen ions.

Reaction Mechanism, Rate Equations and Modelling

The proposed reaction mechanism for the extraction of Cu(II) with P50 (HL) in a micellar solution is given by Equations 4 and 5:

$$Cu^{2+}_{aq} + HL_m \underset{k_{-1}}{\overset{k_1}{\Leftrightarrow}} CuL^{+}_m + H^{+}_{aq} \tag{4}$$

$$CuL^{+}_m + HL_m \underset{k_{-2}}{\overset{k_2}{\Leftrightarrow}} CuL_{2,m} + H^{+}_{aq} \tag{5}$$

The rate of change in concentration of the intermediate complex CuL^+ can therefore be described by the following equation:

$$\frac{d[CuL^+]_m}{dt} = k_1[Cu^{2+}]_{aq}[HL]_m - k_{-1}[CuL^+]_m[H^+]_{aq} - k_2[CuL^+]_m[HL]_m + k_{-2}[CuL_2]_m[H^+]_{aq} \tag{6}$$

The rate of change of $[CuL_2]_m$, can be written as follows:

$$\frac{d[CuL_2]}{dt} m = k_2[CuL^+]_m[HL]_m - k_{-2}[CuL_2]_m[H^+]_{aq} \tag{7}$$

In the above equations, k_1 and k_2 represent the forward reaction rate constants, and k_{-1} and k_{-2} represent the back rate constants for the extraction reaction. The subscript *m* denotes the micellar phase and aq the bulk aqueous phase.

Through the use of NMR spectroscopy, it has been deduced that in micellar media, the extractants are present at the micelle/aqueous interface, and once reacted, the

complex moves to the more hydrophobic micelle core [5,7]. As all of the ligand resides at the micelle-water interface [1,5], $[HL]_m$ is equal to the total analytical concentration of P50 in the system, which during the course of the reaction, decreases proportionally with the formation of the complex. In addition, diffusion processes that can present difficulties in two-phase systems can be considered negligible in micellar solutions [8]. A program for the analysis of extraction reaction kinetic data was created using the Mathematica software package. In essence, the program numerically solves the differential equations (6 and 7) based on the kinetic data obtained through the stopped flow experiments with varying reagent concentrations.

Determination of Reaction Rate Constants

The results of the modelling of kinetic data using the Mathematica program are shown in Figures 2-4.

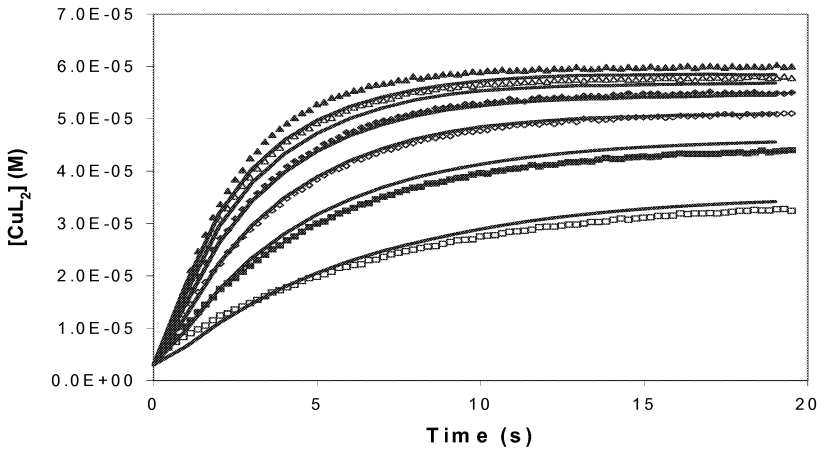

Figure 2. Effect of Cu(II) concentration on the kinetics in 0.1 M sodium sulfate/0.05 M $G_{12}A_8$ micellar solution. Initial concentrations: [P50] = 0.0002 M; pH = 4.2; (□) $[Cu^{2+}]$ = 0.0005 M, (■) $[Cu^{2+}]$ = 0.0010 M, (◇) $[Cu^{2+}]$ = 0.0015 M, (◆) $[Cu^{2+}]$ = 0.0020 M, (△) $[Cu^{2+}]$ = 0.0025 M, (▲) $[Cu^{2+}]$ = 0.0030 M. (–) Theoretical curve for k_1 = 2.5 x 10^2 M^{-1} s^{-1}, k_2 = 4.1 x 10^3 M^{-1} s^{-1}, k_{-1} = 3.6 x 10^4 M^{-1} s^{-1}, and k_{-2} = 1.4 x 10^4 M^{-1} s^{-1}.

It can be seen for the reaction rate constants (i.e., k_2 = 4.1 x 10^3 M^{-1} s^{-1}, k_{-1} = 3.6 x 10^4 M^{-1} s^{-1} and k_{-2} = 1.4 x 10^4 M^{-1} s^{-1}) determined by the Mathematica program, that the theoretical curves provide a close fit to the experimentally obtained data for a wide range of initial experimental conditions. It should be noted that, due to the experimental method whereby the reaction syringes were flushed with the reacting solutions prior to taking an experimental reading, a small amount of complex remained in the reaction vessel as the experiment was initiated, with the initial concentration of the complex being determined to be 3 x 10^{-6} M.

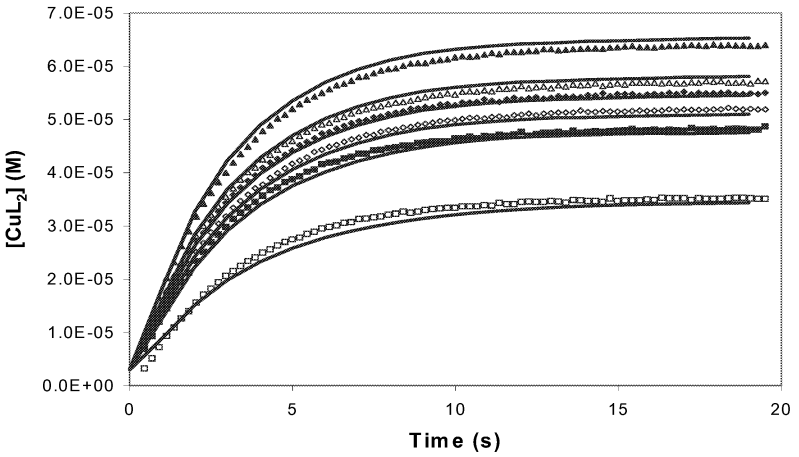

Figure 3. Effect of P50 concentration on the kinetics in 0.1 M sodium sulfate/0.05 M $G_{12}A_8$ micellar solution. Initial concentrations: $[Cu^{2+}]$ = 0.002 M; pH = 4.2; (□) [HL] = 0.00014 M, (■) [HL] = 0.00018 M, (◇) [HL] = 0.00019 M, (◆) [HL] = 0.00020 M, (△) [HL] = 0.00021 M, (▲) [HL] = 0.00023 M. (–) Theoretical curve for k_1 = 2.5 x 10^2 M^{-1} s^{-1}, k_2 = 4.1 x 10^3 M^{-1} s^{-1}, k_{-1} = 3.6 x 10^4 M^{-1} s^{-1}, and k_{-2} = 1.4 x 10^4 M^{-1} s^{-1}.

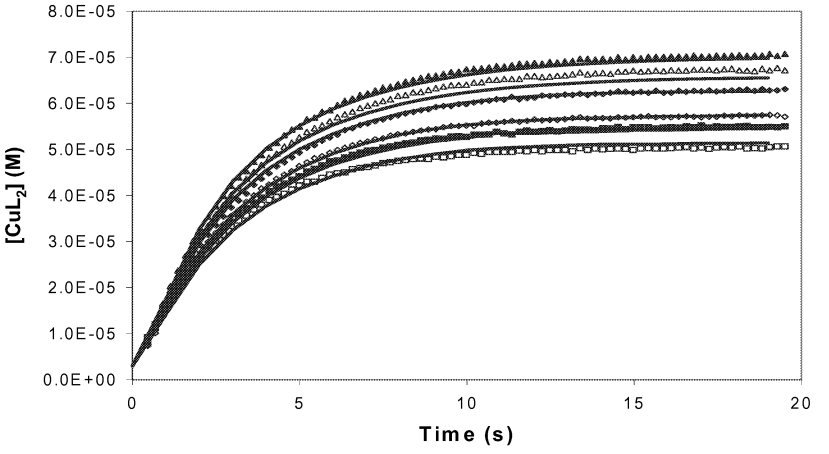

Figure 4. Effect of pH on the kinetics in 0.1 M sodium sulfate /0.05 M $G_{12}A_8$ micellar solution. Initial concentrations: [HL] = 0.0002 M; $[Cu^{2+}]$ = 0.002 M; (□) pH = 4.15, (■) pH = 4.20, (◇) pH = 4.25, (◆) pH = 4.35, (△) pH = 4.40, (▲) pH = 4.50. (–) Theoretical curve for k_1 = 2.5 x 10^2 M^{-1} s^{-1}, k_2 = 4.1 x 10^3 M^{-1} s^{-1}, k_{-1} = 3.6 x 10^4 M^{-1} s^{-1}, and k_{-2} = 1.4 x 10^4 M^{-1} s^{-1}.

CONCLUSIONS

The Cu(II)/P50 extraction reaction kinetics in a nonionic micellar phase were investigated. The proposed two-step mechanism was found to accurately describe the experimental data over a wide range of conditions. The forward and reverse reaction rate

constants were successfully determined with a program written using the Mathematica software package. The results of the modelling indicate that formation of the Cu(II)/P50 intermediate CuL^+ is the rate-determining step for the system. Future work will focus on the role of additives on the rate of extraction.

ACKNOWLEDGMENTS

Support from the Australian Research Council and the Particulate Fluids Processing Centre is gratefully acknowledged. We would also like to thank Huntsman Australia Pty Ltd. for the surfactant and Avecia Ltd. for the sample of P50.

REFERENCES

1. J. K. McCulloch, J. M. Perera, E. D. Kelly, L. R. White, G. W. Stevens, and F. Grieser, "A Kinetic Study of Copper Ion Extraction by Kelex 100 at the Heptane-Water Interface," *J. Coll. Interf. Sci.*, **184,** 406-413 (1996).
2 Dallas B. Warren, Franz Grieser, Jilska M. Perera, and Geoff W. Stevens, "Kinetics and the Effects of Electrostatic Surface Potential on Nickel (II) Extraction by 2-Hydroxy-5-Nonylacetophenone Oxime (LIX84) in a Micellar Phase," *Colloid & Surfaces A*, **243,** 127-132 (2004).
3. C. Tondre, M. Hebrant, M. Perdicakis, and J. Bessiere, "Removal of Copper Ions by Micelle-Based Separation Processes. Electrochemical Behavior of Copper Ions Trapped in Micellar Particles," *Langmuir,* **13,** 1446-1450 (1997).
4. J. S. Preston and R. J. Whewell, "Purification and Acid-Base Properties of Hydroxyoxime Extractants for Copper," *J. Inorg. Nucl. Chem.*, **39,** 1675-1678 (1977).
5. Dallas B. Warren, Gail Dyson, Franz Grieser, Jilska M. Perera, Geoff W. Stevens, and Mark A. Rizzacasa, "Characterisation of Nickel (II) Extraction by 2-Hydroxy-5-Nonylacetophenone Oxime (LIX84) in a Micellar Phase," *Colloid & Surfaces A*, **227,** 49-61 (2003).
6. R. Price and J. A. Tumilty, "An Interpretation of Some Aspects of Solvent Extraction as Related to the Extraction of Copper Using o-Hydroxyoximes," *Institute of Chemical Engineers Symposium Series*, **42**, 18-26 (1975).
7. J. K. McCulloch, D. Fornasiero, J. M. Perera, B. S. Murray, F. Grieser, and G. W. Stevens, "An NMR Study on the Adsorption of a Metal Chelating Agent at a Micelle/Water Interface," *J. Coll. Interf. Sci.*, **157,** 180-184 (1993).
8. J. Szymanowski and C. Tondre, "Kinetics and Interfacial Phenomena in Classical and Micellar Extraction Systems," *Solvent Extr. Ion Exch.*, **12,** 873-905 **(**1994).

MODELING OF MASS-TRANSFER INDUCED INSTABILITIES AT LIQUID-LIQUID INTERFACES

S. Miroshnichenko and A. Pfennig

AVT- Thermal Process Engineering, RWTH Aachen University, Wüllnerstr. 5, D-52062 Aachen, Germany. Corresponding author email address: andreas.pfennig@avt.rwth-aachen.de

ABSTRACT

Interfaces and especially mass transfer across interfaces are of great importance in many fields of chemical engineering. In the case of liquid-liquid extraction, mass transfer at the interface is dependent on various effects. Especially, interfacial instabilities may have a strong influence on mass transfer. Particularly unordered instabilities, (e.g. eruptions) enhance mass transfer noticeably [2]. The necessity for a description of these phenomena for apparatus design is obvious, but the presently available mass-transfer models are inefficient for this task. Results of Monte-Carlo simulations show that under certain conditions mass transfer across interfaces induces the formation of nanodroplets in the close vicinity of the interface. It has been shown in the past that these nanodroplets and their interactions with the main interface can be regarded as the cause for macroscopically observable interfacial instabilities. Based on these molecular simulations, a stability criterion for the occurrence of interfacial instabilities was derived and experimentally validated in single-droplet experiments. In order to investigate the interactions between nanodroplets and the main interface the more detailed Lattice-Boltzmann method is currently applied to the problem. The presentation will give a survey of the simulation methods developed in this project and compare the results obtained by the different approaches.

INTRODUCTION

Computer simulations at molecular and near-molecular levels allow the observation of phenomena that are not possible to be observed with the present experimental techniques. Pfennig [3] and Schott [5] showed that mass transfer at an interface in lattice systems can induce the formation of nanodroplets in the close vicinity of the interface. Figure 1 shows a possible mechanism of the onset of disordered interfacial instabilities caused by nanodroplet interaction in detail. After the formation of many nanodroplets that are layered over the major interface, one of these nanodroplets coalesces with the major interface, attracted by long-range forces. The time scale associated with nanodroplet formation, droplet motion towards the major interface, and coalescence is roughly some microseconds. Accordingly, a strong gradient of interfacial tension will be induced at the major interface, since $\sigma_d < \sigma_i$. This causes an abrupt

interfacial motion to compensate the strong gradient of interfacial tension. As a result, neighboring nanodroplets will fuse with the major interface causing a further increase of the interfacial motion. Under certain conditions, this mechanism may lead to macroscopically observable interfacial instabilities, for example, eruptions or turbulent movement at the interface, which are able to strongly increase mass transfer across the interface.

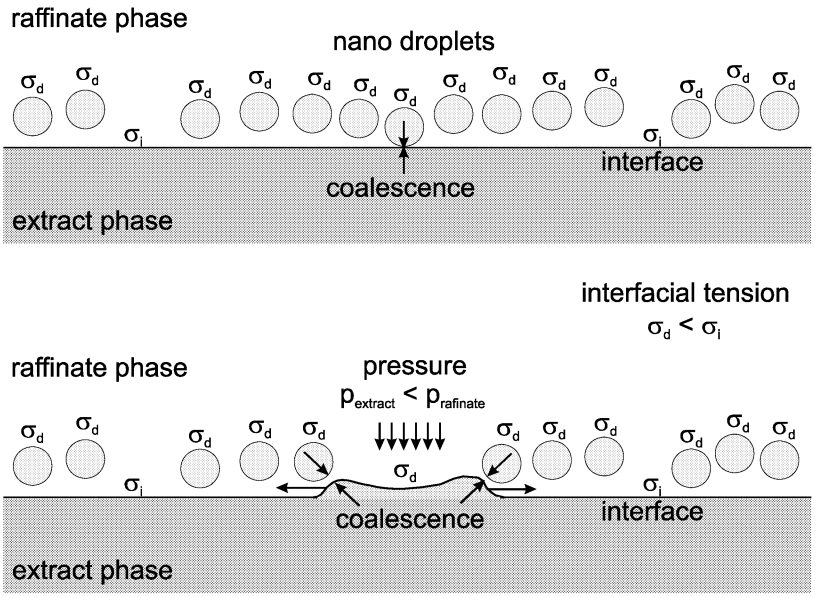

Figure 1. Possible effect of nanodroplets when they coalesce with the interface [4].

MONTE-CARLO RESULTS

In order to investigate the influence of mass transfer on liquid-liquid interfaces, molecular simulations have been performed. The benefit of molecular simulations compared to available experimental techniques is their extremely high resolution, where in with Monte-Carlo simulations some million particles can be simulated for a simulation time of some microseconds. The simulations were performed at a simple cubic lattice with a coordination number of six. To depict the diffusion in this lattice system, only exchanges between neighboring positions were allowed, where the exchanged particles were chosen at random. In order to depict the different molecular mobilities of the present components, a probability $p_{i,j}$ defining the exchange rate between particles of type i and j was introduced. Here the probabilities $p_{i,j}$ correspond to the activation energies that have to be overcome for particle exchange, which is also considered in some diffusion models [5].

Results of various Monte-Carlo simulations show that under certain conditions mass transfer across interfaces induced the formation of nanodroplets in the close vicinity

of the interface. Figure 2 explains the reason for nanodroplet formation regarding the quasi steady-state concentration profile orthogonal to the major interface in the diffusion tube after the formation of a nanodroplet. The initial composition of the liquid-liquid system at both ends of the diffusion tube is marked with black squares. It can be seen that the profile of the raffinate phase has a characteristic curvature leading to the intersection of the binodal. In order to come closer to the experimental data, continuum mechanics simulations were conducted, where the mass-transfer was considered differential. For the macroscopic modelling, the Maxwell-Stefan model was chosen. The properties of the system (i.e., activity or diffusion-coefficients) were treated locally. Thus, it was possible to conduct simulations for real test-systems. The results are in good agreement with the outcome of the Monte-Carlo simulations. The concentration profile also in this case is curved and intersects the miscibility gap with accordance to the initial concentrations, so that the imaging of nanodroplets is demonstrated. Thus it is diffusional cross effects that cause nanodroplet formation.

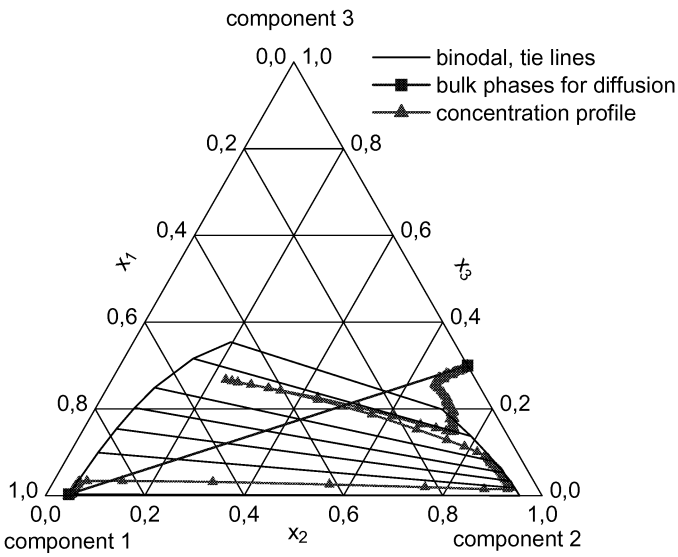

Figure 2. Concentration profile in a diffusion path of a two-phase system [4].

LATTICE-BOLTZMANN SIMULATION

In order to investigate the interactions between nanodroplets and the main interface, the more detailed Lattice-Boltzmann method is currently applied to the problem. The Lattice-Boltzmann method is a powerful technique for the computational modelling of a wide variety of complex fluid-flow problems including single- and multiphase flow in complex geometries. It is a discrete computational method based upon the Boltzmann equation. It considers a typical volume element of fluid to be composed of a collection of particles that are represented by a particle-velocity distribution function

for each fluid component at each grid point. The time proceeds in discrete time steps, and the fluid particles can collide with each other as they move due to applied forces.

A statistical description of a system can be made in terms of a distribution function $f_i(x,t)$ such that $f_i(x+e_i \cdot \delta t,t)$ describes the particle density between positions x and $x+\delta x$ at time t. The evolution of particle density during time δt is modelled by the Boltzmann equation. Neglecting external forces, the Boltzmann equation, discrete in both time and space, reads:

$$f_i(x+e_i \cdot \delta t,t+\delta t) - f_i(x,t) = \Omega_i(x,t) \tag{1}$$

The right hand side term $\Omega_i(x,t)$ represents the collisions between the particles, and it therefore referred to as the "collision term". The left-hand side represents the change in particle distribution function. Changes in the particle distribution function (also called single-particle distribution function) are only influenced by movement of particle distribution according to the particle velocity vector e_i or collision term Ω_i. The collision term is defined according to the so-called "single time relaxation approach" as:

$$\Omega_i(x,t) = -\frac{\delta t}{\tau}\left[f_i(x,t) - f_i(x,t)^{(0)}\right] \tag{2}$$

The single time relaxation approach was introduced by Bhatnagar, Gross and Krook [1]. In this approach, the collision of particles causes a convergence of the distribution function f_i toward the equilibrium distribution of particles $f_i(x,t)^{(0)}$ by the relaxation time τ during the time step δt. At the relaxation time τ, the distribution function is converged to the particle equilibrium distribution. The macroscopic quantities, such as the density ρ and the momentum ρv, can then be obtained by evaluating the first moments of the distribution function f:

$$\rho = \sum_{\sigma} f_i \quad \text{and} \quad \rho v = \sum_{\sigma} f_i \cdot e_i \tag{3}$$

For flow simulation of multi-phase, multi-component systems, four models are known: the Chromodynamic model, Pseudo Potential Model, Free Energy Model, and the Luo Model. All four models consider incompressible flows. Pseudo Potential and Free Energy Model are suited for flow simulations of thermal separation process. These models were applied to the simulations of central droplet collisions (Figure 3). Phenomena of central-drop collision, such as lentiform deformation, constriction and expansion in the direction normal to the deformation direction, are observed.

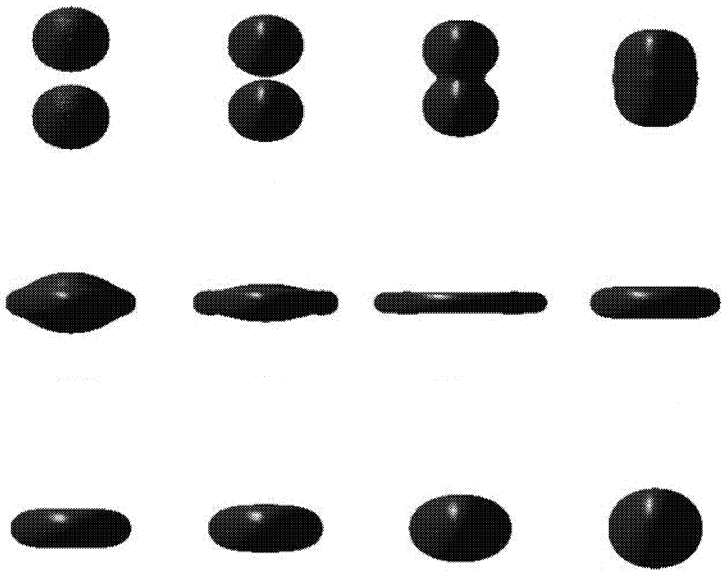

Figure 3. Simulation of the central-drop collision for two liquid droplets.

Currently we are implementing a Lattice-Boltzmann model based on the free energy, which allows us to simulate the dynamics of a multicomponent system with an arbitrary number of components. By using the Free-Energy-Model the thermodynamic properties, for example, the chemical potential of each component or the system pressure, can be considered. With this simulation tool, reliable simulations of liquid-liquid interfaces can be performed, and the behavior of nanodroplets with the main interface can be studied in detail.

CONCLUSIONS

With molecular simulations, disordered interfacial convections enhancing mass transfer (e.g. eruptions) are resolved. Monte-Carlo simulations of systems exhibiting such phenomena show the appearance of small clusters close to the interface referred to as nanodroplets. They are held to be responsible for disordered interfacial convection. Since the Lattice-Boltzmann method is classified as a mesoscopic approach to the simulation of fluid dynamics, the combination of Lattice-Boltzmann method and diffuse-interface methods is suitable for the simulation of two-phase fluid flows. The benefit of this method is that it is able to depict diffusive as well as convective flows, and attractive and repulsive forces between nanodroplet and main interface can be considered explicitly. Additionally, the size of the simulated system can be chosen to be almost any desired value. Thus, the method is able to bridge the gap between molecular simulation and experiment.

REFERENCES

1. P. Bhatnagar, E. P. Gross, and M. K. Krook, "A Model for Collision Processes in Gases. Small Amplitude Processes in Charged and Neutral One-Component Systems," *Phys. Rev.*, **94**(3), 511–525 (1954).
2. M. Henschke and A. Pfennig, "Mass-Transfer Enhancement in Single-Drop Extraction Experiments," *AIChE J.*, **45**(10), 2079-2086 (1999).
3. A. Pfennig, "Mass Transfer Across an Interface Induces Formation of Micro Droplets in Lattice Systems," *Chem. Eng. Sci.*, **55**(22), 5331-5337 (2000).
4. R. Schott and A. Pfennig, "Modelling of mass-transfer induced instabilities at liquid-liquid interfaces based on molecular simulations," *Mol. Phys.*, **102**(4), 331-339 (2004).
5. R. Schott, "Stofftransportinduzierte Nanotropfen und ihr Einfluss auf ungeordnete Instabilitäten an Flüssig-Flüssig-Phasengrenzen," Ph.D. Thesis, RWTH Aachen University, 2004.

NUMERICAL STUDY OF A RISING DROPLET USING COMMERCIAL CFD SOFTWARE

T. Atmakidis, and E. Y. Kenig

Department of Biochemical and Chemical Engineering, University of Dortmund, Emil-Figge-Str. 70, 44227 Dortmund, Germany.
Corresponding author email address: e.kenig@bci.uni-dortmund.de

ABSTRACT

A movement of a toluene droplet in a continuous aqueous phase is considered, and three different methods to describe interfacial phenomena are used, namely, the moving grid, the volume of fluid, and the level-set method. All methods are very popular and can be implemented into commercial solvers. Simulations are performed using different computational fluid dynamics software codes, namely CFX 4.3 and CFX 10.0 from ANSYS Inc. and COMSOL Multiphysics 3.3a. The advantages and limitations of these tools are highlighted.

INTRODUCTION

The phenomena occurring in liquid-liquid extraction units are very complex and not yet fully understood. Furthermore, the different length scale of the involved phenomena makes rigorous modelling of extraction units very difficult. As a first step towards better understanding of process behavior, smaller but representative flow elements can be used. For liquid-liquid extraction, a single droplet is often considered as the smallest representative element.

During the last 30 years, several numerical investigations by different methods have been performed to try to capture the phenomena at and around single droplets. Special attention has been paid to the movement and deformation of the droplet surface. There are two main strategies dealing with free moving interfaces. In the first one, a moving mesh is used to track the interface. As the interface topology changes, the mesh is transformed in accordance with this change. Methods falling under this strategy are called *front tracking methods* [1]. The second approach is based on a fixed (Eulerian) mesh, while the interface is tracked using different procedures, for example, special markers or functions. Such methods are called *front capturing methods* [1].

In the front tracking methods, the interface is resolved directly. It always lies between two neighborhood mesh elements. As the interface moves, the neighbourhood mesh elements transform in order to track the movement of the interface. For the description of the interface movement, additional explicit equations are necessary.

Usually, the latter can be derived from an overall consideration of the transport phenomena around the interface [2,3].

In the front capturing methods, the interface is described using special markers or functions in a fixed mesh. Depending on the function used to capture the interface, different methods have been developed, for example, the *marker particle method* [4], *the volume of fluid* (VoF) method [5], and *the level set* (LS) method [6]. For the functions mentioned, an additional implicit advection equation is used.

Some alternative methods can also be found in the literature. One of them is suggested by the group of Tryggvason [7]. They use a combination of both front tracking and front capturing methods, whereby a fixed grid is used to describe the motion of the fluid flow and another moving grid is used to track the interface. The latter has a lower dimension, that is, for example, when simulations are performed in a 2D fixed grid, the interface tracking is accomplished by a 1D moving grid.

Some of the methods presented above are implemented into commercial software. Examples are given by the moving grid (MG) in CFX 4.3, the VoF method in CFX 10.0 and the LS method in COMSOL Multiphysics 3.3a. In this work, we will focus on these examples. As a benchmark problem, the study of the hydrodynamics of a single toluene droplet in a continuous aqueous liquid phase is chosen.

SYSTEM DESCRIPTION AND GOVERNING EQUATIONS

The toluene droplet has a diameter of 2 mm. In all methods, the continuity and momentum equations are solved, whereas a 2D axial symmetric domain is used. The following general assumptions are made:

- Newtonian fluids,
- Incompressible flow,
- Isothermal system,
- Laminar flow of both phases,
- No mass transfer of the two carrier fluids across the interface,
- No chemical reaction in the system,
- Absence of surface active contaminants.

The main difference between the methods studied lies in the way they treat the movement of the interface. In the MG method, the toluene droplet remains stagnant, while the continuous phase moves around it. This problem formulation is chosen, because this method is not able to handle significant interface deformations. Furthermore, an additional assumption that the shape of the droplet remains spherical is made. Consequently, the change of the interface with time can be described as follows:

$$R(t+dt) = \sqrt[3]{R(t)^3 - \frac{3dt}{4\pi} \cdot \frac{M_A}{\rho_A} \int_A (J_A)\, dA} \qquad (1)$$

where R is droplet radius, J_A, M_A, and ρ_A is flux, molar mass, and density of transferred component, respectively, and t is time.

In the VoF and LS method, the droplet is not stagnant; it moves upwards in quiescence water. The initial toluene velocity is zero. To capture the interface, the VoF method uses the following volume-of-fluid function

$$f = \begin{cases} 1, & \text{if the mesh cell is occupied by phase 1} \\ 0, & \text{if the mesh cell is occupied by phase 2} \\ 0 < f < 1, & \text{if the two phases coexist in one cell} \end{cases} \quad (2)$$

and a corresponding advection equation

$$\frac{\partial f}{\partial t} + \nabla \cdot (f\,\mathbf{u}) = 0 \quad (3)$$

where $\mathbf{u}$ is velocity vector.

In the LS method, a function is used that takes positive values for one phase and negative for another phase. Directly at the interface, it takes zero values. A similar advection equation as Equation 3 is applied to determine this function.

MODEL IMPLEMENTATION

For all simulations, a two-dimensional axisymmetric computational domain is used in which the governing equations are solved (Figure 1). However, different methods require somewhat different problem formulations, because the MG method is unable to account for significant interface deformations. For this method, the continuous phase velocity is specified at the inlet in such a way that the toluene droplet remains suspended; at the outlet, a pressure value is preset. For the VoF and LS methods, periodic translating conditions are applied at both inlet and outlet (Figure 1). With the periodic boundary conditions, a direct translation of the upper mesh elements to the lower ones becomes possible, thus allowing the rising movement of the droplet to be modelled in a small computational domain. The other boundary conditions are the same for all methods.

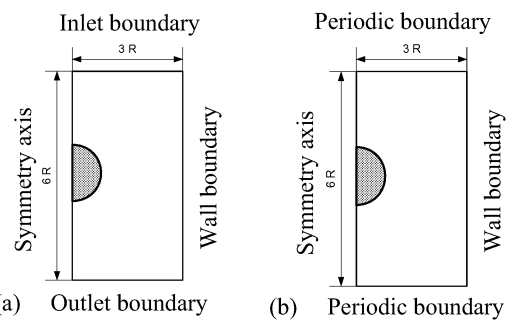

Figure 1. Boundary condition for the MG (a) and VOF and LS method (b).

For the MG method, a structured body fitted hexahedral mesh is used. Special attention has been paid near the interface, where a finer grid is used to track the interface movement [2].

On the other hand, for the VoF method, a uniform hexahedral structured grid is used. In this case, the droplet not only changes its volume (interface position change in the radial direction) but also moves in the vertical direction. Therefore, a fine uniform grid is needed for the whole domain. In order to further improve numerical results, a special grid refinement near the interface is also implemented. For the LS method, an unstructured grid containing triangles is used. For all cases, a grid independence study is performed.

To solve the set of equations for the MG, a commercial finite volume solver is used, namely CFX 4.3 from ANSYS. For the implementation of the MG method, the solver should provide full access to the grid elements. This access was available in the CFX 4.3, and therefore this tool was chosen. For the VoF method, CFX 10.0 from ANSYS is used. Unfortunately, in this solver, no access to grid elements is given. For the LS method, a solver based on the finite elements method from COMSOL Multiphysics 3.3a is used.

RESULTS AND DISCUSSION

Figure 2 shows the development of the velocity profiles inside and outside the droplet for Re = 100 using the MG method [2]. The initial velocities for both phases are zero, and it takes about 10 seconds until both velocity profiles are fully developed.

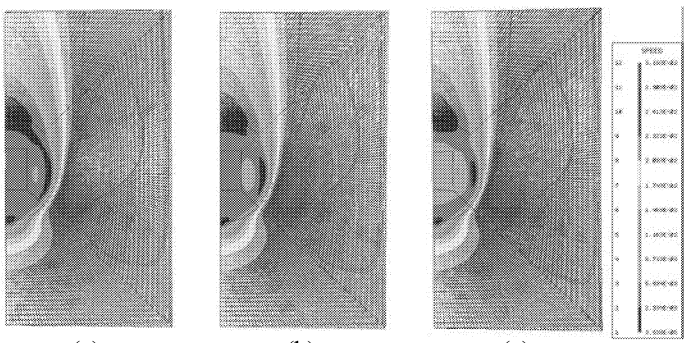

(a) (b) (c)

Figure 2. Development of velocity profiles using the MG method: t = 1s (a), t = 5s (b), t = 25s (c) [2].

A region directly behind the droplet with zero velocity is clearly visible. This region exists even after 25 seconds, when developed flow is established. The MG method was validated using the data on mass transfer, for example, concentration profiles and droplet radius change, with reasonable agreement between experimental and simulated results [2].

In Figure 3, the position and shape of a toluene droplet at a time of 0.09 s is depicted using the VoF method. In this figure, a large smearing of the interface is visible. As droplet moves upwards, a trace containing very small volume fractions of toluene remains, as if the droplet were partially dissolved.

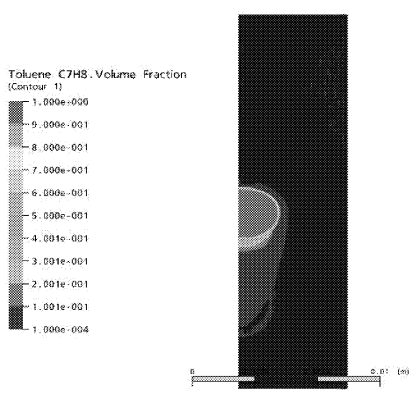

Figure 3. Toluene volume fraction at time 0.09 s.

Simulation results were substantially improved with the help of a transient mesh refinement. At each time step, the mesh is up to four times finer near the interface. Using this procedure, the large smearing disappeared, but a very small time step must be used in order to ensure that the Courant number (a stability criterion for transient moving boundary problems) is always smaller than one; this corresponds to a stable solution. For a rising droplet, a time step smaller than 10^{-6} s is necessary, and this gives no way to reach reasonable process times. The application of an interface reconstruction algorithm should be able to improve results, but this is not

possible within the CFX 10.0 solver, since it gives no access to the mesh nodes and corresponding variables.

In Figure 4, results obtained with the LS method are presented, which show the change of the droplet shape and velocity of the aqueous phase. Here, the droplet remains spherical during its upward movement, which is in accordance with the literature [2].

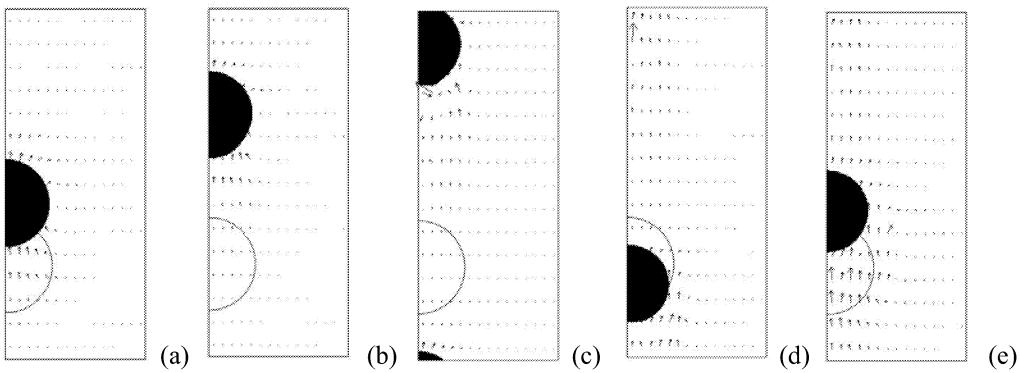

Figure 4. The toluene droplet movement and water velocity field at times 0.09 s (a), 0.15 s (b), 0.2 s (c), 0.25 s (d), and 0.3 s (e).

Table 1 gives a summary of all three methods applied in this work. The MG method, as it is implemented in the commercial CFD solver CFX 4.4, gives the most reliable results. Besides, it can be extended to account for the interfacial mass-transfer phenomena which are very important for extraction processes [2]. However, it is not able to handle large deformations of the interface.

Table 1. Properties of the investigated methods and tools

	MG (CFX 4.3)	VoF (CFX 10.0)	LS (COMSOL)
Advantages	• Accurate resolution of the interface • Mass conservation • Easy consideration of interfacial boundary conditions • Accurate calculation of interfacial mass-transfer phenomena	• Easy to implement • Mass conservation • Able to account large deformations of the interface • Straightforward extension to 3D	• Easy to implement • Exact position of the interface is known • Able to account for large deformations of the interface • Straightforward extension to 3D
Disadvantages	• Complex implementation • Unable to account for significant interface deformations • Extension to 3D is difficult	• Smearing of the interface • Reconstruction algorithm is not available (limited access to the nodes) • Accurate calculation of interfacial mass-transfer phenomena is not possible	• Mass conservation is not always met

The latter can be performed with the VoF method, but due to the smearing observed, simulations including mass transfer will have a substantially large error.

Numerical results could be improved by the implementation of an interface reconstruction algorithm. However, within CFX 10.0 this is not possible, because of the missing access to the mesh nodes.

A relatively new method is the LS method, which has a good potential due to its ablity to capture the movement of the interface accurately and within good computational times. Further investigations should be performed to identify the applicability of this method to problems including mass transfer.

CONCLUSIONS

In this work, the movement of a toluene droplet in a continuous aqueous phase is considered, and three different methods to describe interfacial phenomena are applied. All the simulations are carried out using commercial CFD codes in a 2D axial symmetric computational domain.

When the deformation is not significant, the MG method is best suited to capture phenomena in droplets. When the interface deformation is significant, the LS method, as it is implemented in COMSOL Multiphysics, appears advantageous compared with the VoF method in CFX 10.0, as it does not show significant interface smearing.

ACKNOWLEDGMENT

The support of the European Commission in the context of the 6th Framework Programme (PRISM, Contract No. MRTN-CT-2004-512233) is greatly acknowledged.

REFERENCES

1. A. Esmaeeli and G. Tryggvason, “Direct numerical simulations of bubbly flows. Part 1. Low Reynolds number arrays,” *J. Fluid Mech.*, **377**, 313-345 (1998).
2. S. Burghoff and E. Y. Kenig, “A CFD Model for Mass Transfer and Interfacial Phenomena on Single Droplets,” *AIChE Journal*, **52**, 4071-4078 (2006).
3. S. W. J., Welch, “Local Simulation of Two-Phase Flows Including Interface Tracking with Mass Transfer,” *J. Comput. Phys.*, **121**, 142–154 (1995).
4. S. Popinet and S. Zaleski, “Bubble collapse near a solid boundary: a numerical study of the influence of viscosity,” *J. Fluid Mech.*, **464**, 137-163 (2002).
5. C. W. Hirt and B. D. Nichols, “Volume of Fluid (VOF) Method for the Dynamics of Free Boundaries,” *J. Comput. Phys.*, **39**, 201–225 (1981).
6. S. Osher and R. Fedkiw, “Level Set Methods: An Overview and Some Recent Results,” *J. Comput. Phys.*, **169**, 463-502 (2001).
7. S. O. Unverdi and G. Tryggvason, “A Front-Tracking Method for Viscous, Incompressible, Multi-fluid Flows,” *J. Comput. Phys.*, **100**, 25-37 (1992).

NUMERICAL APPROACH TO THE THREE-DIMENSIONAL MARANGONI EFFECT IN A TWO LIQUID LAYER SYSTEM

Zai-Sha Mao, Ping Lu, Guangji Zhang, and Chao Yang

Institute of Process Engineering, Chinese Academy of Sciences, Beijing 100080, China.
Corresponding author email address: zsmao@home.ipe.ac.cn

ABSTRACT

The Marangoni effect induced by mass transfer at the phase interface between two immiscible liquids is an important issue for better understanding of industrial operation of solvent extraction. A preliminary numerical simulation of the three-dimensional Marangoni effect is conducted on the basis of the previous work on the 2-D simulation. As compared with the corresponding 2-D cases, 3-D Marangoni effect requires a higher threshold of the driving force than the hydrodynamic instability. Otherwise, it presents the similar qualitative features of hydrodynamic randomness as its 2-D counterpart.

INTRODUCTION

The phenomenon usually called the Marangoni effect is often encountered in mass transfer between two fluid phases in contact [1], and in solvent extraction systems it is manifested in diversified forms such as drop pulsation, localized eruption, kicking, and surface rippling in addition to enhanced rate of interphase mass transfer [2].

Many experimental investigations were reported with the focus on the conditions for the Marangoni effect to occur and its underlying mechanisms. It seems that the theoretical study of the Marangoni effect seems insufficient. The classical linear instability analysis on the criterion for the Marangoni effect to occur by Sternling and Scriven [1] remains to date the cornerstone in the theoretical research. Several later propositions on the criteria constitute improvements to the Sternling-Scriven criterion [3]. The nonlinear instability analysis to the Marangoni effect seems not available.

The Marangoni effect in solvent-extraction systems is scarcely approached numerically so far. The present authors simulated numerically the Marangoni effect in solvent-extraction systems by the finite-difference method on the boundary fitted coordinates [4] and the level set approach [5]. The mechanistic model needs further substantial experimental validation. Besides, numerical simulation extended to the three-dimensional Marangoni effect is of great importance to understand the nature of the Marangoni effect in solvent-extraction applications. In order to understand the mechanism of the Marangoni effect, simpler and more efficient simulation of liquid-layer systems is an easy route to pursue. As compared with the thermocapillary

instability, less research was focused on the mass transfer-induced Marangoni effect in two-liquid-layer systems [6,7]. The present authors presented the numerical simulation of interphase mass transfer between two planar layers of immiscible liquids and the accompanied Marangoni effect. In view of the previous results on 2-D simulation [8], the similarity and difference are elaborated to give suggestions on further study of the mechanisms underlying the Marangoni effect. The numerical simulation suggested that the 3-D Marangoni convection is typically random and dynamic in nature and fairly similar to the 2-D one reported previously. The 3-D Marangoni effect occurs less easily than the 2-D one for the same system. It seems very important to compromise between the simple 2-D simulation and more realistic 3-D one.

MATHEMATICAL MODELING

Basic Formulation

The following assumptions are made in formulating the viscous flow in both liquid phases in the two-liquid-layer system: (1) two fluids are incompressible, viscous, and Newtonian; (2) the flow is laminar and isothermal; (3) the physical properties of bulk liquids are constant irrespective of solute concentration; (4) the interface is always flat so that gravity becomes irrelevant in the momentum equations; and (5) the interfacial tension σ is a linear function of the solute concentration c:

$$\Delta\sigma = \frac{d\sigma}{dc}\Delta c \tag{1}$$

with $d\sigma/dc < 0$, which is thought the dominant factor to induce the Marangoni effect in liquid-liquid systems.

The transient fluid flow in both liquid layers is governed by the general Navier-Stokes equations for incompressible fluid in addition to the equation of continuity:

$$\nabla \cdot \mathbf{u}_i = 0 \tag{2}$$

$$\frac{\partial \rho_i \mathbf{u}_i}{\partial t} + \mathbf{u}_i \cdot \nabla \rho_i \mathbf{u}_i = -\nabla p_i + \mu_i \nabla^2 \mathbf{u}_i \tag{3}$$

in which $\mathbf{u}$ is the liquid velocity vector, μ the liquid viscosity, ρ the density, and p is the hydrodynamic pressure with the gravity incorporated.

The mass transfer in each liquid is governed by the convective diffusion equation:

$$\frac{\partial c_i}{\partial t} + \mathbf{u}_i \cdot \nabla c_i = D_i \nabla^2 c_i \tag{4}$$

in which D_i is the diffusion coefficient of the solute and i = t,b index the top and bottom fluid, respectively.

When the interfacial tension varies with the solute concentration at the interface, the interfacial-tension gradient contributes to the shear-stress balance at the interface:

$$\boldsymbol{\tau}_t - \boldsymbol{\tau}_b + \nabla_S \sigma = 0 \tag{5}$$

where $\boldsymbol{\tau}$ is the shear stress at the surface and the 3rd term in Equation 5 is the surface gradient of σ. The fluctuations of solute concentration at the interface gives rise to the tangential force exerted on the surface due to $\nabla_S \sigma$, which in turn induces the Marangoni convection at the interface.

Numerical solution of Equations 2 through 5 with solid box side wall and initial condition of quiescent layers is performed. The initial concentration field corresponds to the steady-state mass transfer through quiescent liquid layers with linear concentration profiles established in the vertical z direction. The instantaneous mass-transfer coefficient based on the top phase may be evaluated as

$$k_{\mathrm{ot}} = -\frac{D_{\mathrm{t}}}{L^2 \Delta c} \int_0^L \int_0^L \left. \frac{\partial c_{\mathrm{t}}}{\partial z} \right|_{z=0} dxdy \tag{6}$$

in which the total driving force for interphase mass transfer is

$$\Delta c = c_{\mathrm{t0}} - \frac{c_{\mathrm{b0}}}{m}$$

where L is the side length of the cross sectional square of the system box, c_{t0} and c_{b0} are the solute concentration at $z = H$ and $z = -H$, respectively (H being the thickness of a liquid layer), and the mass transfer is predominantly in the vertical z direction.

Computational Parameters

For a square box with the side length of L = 2 cm and the liquid depth is H = 0.5 cm, the grid used contains 32 × 32 × 16 cells (in x, y, and z directions, respectively) for each liquid. It may not pass a stringent grid-independency test, but is thought effective in giving some insight to the 3-D nature of the Marangoni effect distinguishing itself from the 2-D simulation.

The case studied is a typical system relevant to solvent extraction. Sternling and Scriven [1] chose the case with the kinematic viscosity ratio $\nu_{\mathrm{t}}/\nu_{\mathrm{b}} = 2$, dynamic viscosity ratio $\mu_{\mathrm{t}}/\mu_{\mathrm{b}} = 0.5$, and solute diffusivity ratio $D_{\mathrm{t}}/D_{\mathrm{b}} = 0.5$, distribution ratio m = 1, the sensitivity of interfacial tension to concentration $S_0 = \mathrm{d}\sigma/\mathrm{d}c = -10^{-4}$ N m^2/kg of solute, the specified solute gradient of $(\mathrm{d}c/\mathrm{d}z) = \pm 10^5$ kg/m^4. The dimensional physical properties used thus for simulation are listed in Table 1.

Table 1. Parameters of the case studied

Liquid	ρ (kg/m^3)	μ (Pa s)	D (m^2/s)
Top	0.5×10^3	0.001	2×10^{-9}
bottom	2×10^3	0.002	4×10^{-9}

RESULTS AND DISCUSSION

Preliminary numerical tests suggest that the Marangoni effect is difficult to be triggered as compared with the 2-D situation with the same parameters. When the surface sensitivity S is set at the original level of -10^{-4} N m^2/kg [1], no Marangoni effect occurs, no matter whether the solute is transferred from the bottom to top (term as Case A1) or vice versa (term as Case A2). The level of S is thus increased to 10 or 50 times the original S_0 to get the Marangoni convection into play. Figure 1 shows the contours of local w velocity component at the height of z = 1.25 mm above the interface. It indicates that at t = 6 s the local pattern of recirculation has been developed sufficiently. Correspondingly in Figure 2, the pattern of random variation of the interfacial solute concentration is presented. Both figures suggest the random and dynamic nature of the liquid flow and the mass transfer of solute when some infinitesimal disturbance evolves into discernible finite scale. The correspondence of patterns between two figures is apparent.

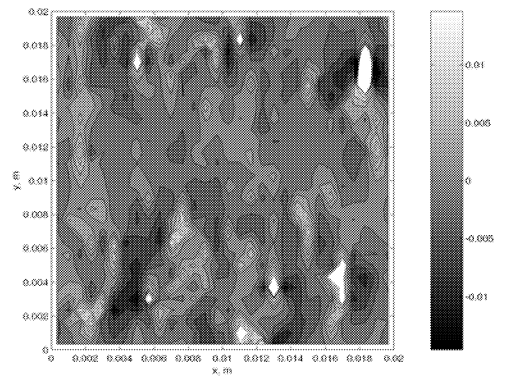

Figure 1. The contours of the vertical w velocity component in Case A2 with $S = 10S_0$ at t = 6 s with solute transfer into the bottom phase.

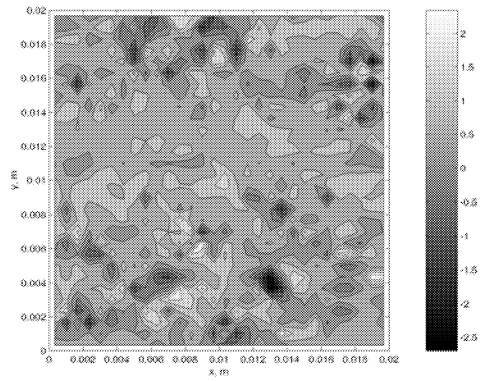

Figure 2. The contours of the solute concentration at the interface in Case A2 with $S = 10S_0$ at t = 6 s with solute transfer into the bottom phase.

When the system sensitivity is raised to $S = 50S_0$, the corresponding vertical velocity and interfacial concentration contour plots in Figures 3 and 4 keep the general features of dynamic randomness as that in Figures 1 and 2. Because the driving force to the Marangoni effect is stronger when $S = 50S_0$ in Figures 3 and 4, the induction time is a little shorter, the magnitude of the induced w velocity and range of variation of interfacial concentration is significantly larger (as evidenced by the corresponding legend bars in these figures). But the size of local circulation remains at the similar scale, suggesting the Marangoni convection pattern is near a stabilized stage. No evident hexagonal patterns are observed, in contrast to the well-known Benard patterns in temperature gradient-induced thermo-hydrodynamic instability in a one-liquid-layer system.

As compared with the 2-D cases in the same two-layer system [8], the 3-D Marangoni effect seems to evolve slower with a higher threshold of S.

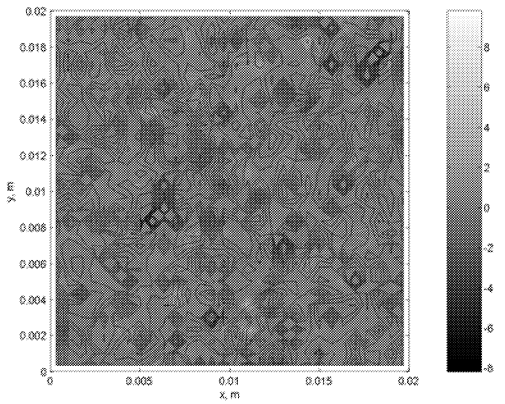

Figure 3. The contours of the vertical velocity component in Case A2 with $50S_0$ at $t = 6$ s with solute transfer into the bottom phase.

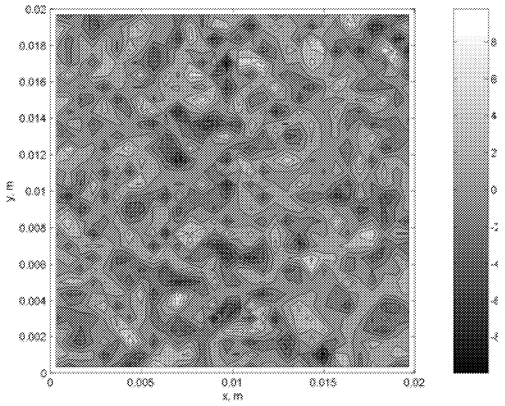

Figure 4. The contours of the solute concentration at the interface in Case A2 with $50S_0$ at $t = 6$ s with solute transfer into the bottom phase.

In Figure 5 the comparison is made in terms of the interphase mass-transfer coefficient k_{ot} based on the top-phase properties. In the 2-D case, a low-level surface tension sensitivity at S_0 is sufficient to allow the earlier induction of the Marangoni effect, while in the 3-D case the Marangoni effect develops quite slowly and the value of k_{ot} remains smaller, even at the high level of $50S_0$.

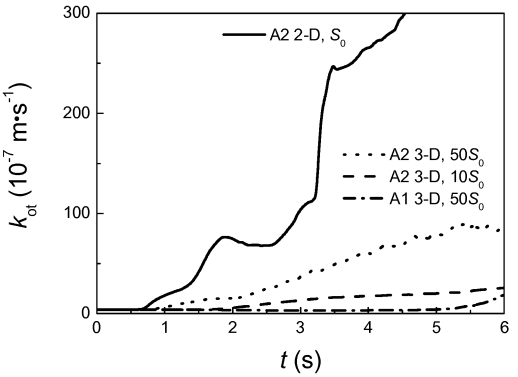

Figure 5. Evolution of the interphase mass-transfer coefficient kot in the 3-D case in comparison with 2-D Marangoni effect with S_0. A2 stands for transfer into the bottom phase and A1 for that from the bottom phase.

Intuitively, a potential embryo pattern in the 3-D surrounding has to be in coordination with its neighbor (probably 6 in number) before it grows to be sizable, while a 2-D one has only two neighboring rolls to deal with. Another interesting observation is that in the 2-D Case A1 (transfer to the top phase), no Marangoni effect is predicted either theoretically [1] or numerically [8] at S_0, but in the 3-D Case A1, the Marangoni effect is finally induced at the condition of $50S_0$, though it needs a much longer induction time as compared with Case A2 as shown in Figure 5.

CONCLUSIONS

Numerical simulation of the 3-dimensional Marangoni effect at the interface between two liquid layers is conducted for better understanding of the underlying mechanism so as to improve the efficiency of solvent extraction in the process industry. The simple linear model of the surface tension as a function of solute concentration only works for modeling the Marangoni effect in a two-liquid-layer system. The 3-D Marangoni effect shows similar features as the numerical counterpart in the 2-D case. It seems that 3-D Marangoni effect is more difficult to be induced, and the evolution is slower. The present investigation sheds some light on the mechanism of the Marangoni effect, but more cases need to be tested numerically so that some reliable and applicable criteria for the Marangoni effect may be established.

ACKNOWLEDGMENTS

Financial support from the National Natural Science Foundation of China (Nos. 20490206, 20576133, 50404009), PetroChina and the National Basic Research Program of China (No. 2004CB619203, 2004CB619203) are gratefully acknowledged.

REFERENCES

1. C. V. Sternling and L. E. Scriven, "Interfacial Turbulence: Hydrodynamic Instability and the Marangoni Effect," *AIChE J.*, **5**, 514-523 (1959).
2. H. Sawistowski, "Interfacial phenomena", Recent Advances in Liquid-Liquid Extraction, C. Hanson, Eds., Pergamon, Oxford, 1971; pp. 293-366.
3. D. Agble and M. A. Mendes-Tatsis, "The Prediction of Marangoni Convection in Binary Liquid-Liquid Systems with Added Surfactants," *Int. J. Heat Mass Transfer*, **44**, 1439-1449 (2001).
4. Z.-S. Mao and J. Y. Chen, "Numerical Simulation of The Marangoni Effect on Mass Transfer to Single Slowly Moving Drops in the Liquid-Liquid System," *Chem. Eng. Sci.*, **59**(8-9), 1815-1828 (2004).
5. J. F. Wang, C. Yang, and Z.-S. Mao, "Numerical Simulation of Marangoni Effects of Single Drops Induced by Interphase Mass Transfer in Liquid-Liquid Extraction Systems by the Level Set Method," *Sci. China*, (2008). (in press)
6. D. A. Bratsun, and A. de Wit, "On Marangoni Convective Patterns Driven by an Exothermic Chemical Reaction in Two-Layer Systems," *Phys. Fluids*, **16**(4), 1082-1096 (2004).
7. A. Grahn, "Two-Dimensional Numerical Simulations of Marangoni–Bénard Instabilities during Liquid–Liquid Mass Transfer in a Vertical Gap," *Chem. Eng. Sci.*, **61,** 3586-3592 (2006).
8. Z.-S. Mao, P. Lu, G. J. Zhang, and C. Yang, "Numerical Simulation of the Marangoni Effect with Interphase Mass Transfer between Two Planar Liquid Layers," *Chin. J. Chem. Eng.,* (2008). (in press).

SCALE-UP OF KARR RECIPROCATING-PLATE EXTRACTION COLUMNS

Kathryn H. Smith and Geoff W. Stevens

Particulate Fluids Processing Centre, Department of Chemical and Biomolecular Engineering, The University of Melbourne, Parkville, Victoria 3010, Australia.
Corresponding author email address: gstevens@unimelb.edu.au

ABSTRACT

The hydrodynamic and mass-transfer performance of Karr reciprocating-plate extraction columns with varying column diameters has been presented in order to examine how column performance changes with scale. Columns with diameters of 50, 100, and 300 mm have been studied using a phenolic alkaloid liquid system. Correlations have been developed to predict the dispersed-phase holdup and overall mass transfer coefficient. Results show that there were no significant changes in either dispersed phase holdup or mass-transfer coefficient with column diameter. It was therefore concluded that overall column performance was independent of column diameter, and the traditional scale-up equations were too conservative.

INTRODUCTION

The Karr column has been used effectively for numerous applications in a wide range of industries. However, there is still a need for a greater understanding into the design of the column, in particular the change in column performance with scale. Numerous studies have been performed to analyze both the hydrodynamic and mass-transfer performance of the Karr column. These studies have generally concentrated on developing correlations that can predict the dispersed-phase holdup, drop-size distribution, axial dispersion characteristics, and mass-transfer coefficients. However, these correlations tend to only be accurate for the systems and geometries for which they were developed. Mensforth [1] summarized the correlations available for predicting the hydrodynamic and mass-transfer characteristics in a Karr column. A summary of the correlations available for predicting the backmixing coefficient of the continuous phase in a Karr column has also been presented by Stella et al. [2].

This study aims to examine how the performance of a Karr reciprocating-plate extraction column changes with scale. This has been done by measuring the hydrodynamic and mass-transfer performance in columns of varying diameter over a range of operating conditions.

EXPERIMENTAL

Equipment and Liquid System

Three Karr columns with diameters of 50, 100, and 300 mm have been investigated in this study. The plate spacing and geometry, including hole size, plate thickness and free area, were kept constant in all columns regardless of diameter. Each column was made of glass and contained an upper T-section for the continuous-phase outlet and an expanded glass section at the bottom for the settling of the dispersed droplets before exiting from the column. All columns contained a stack of plastic perforated plates which were reciprocated using a variable speed motor at the top of the column. The amplitude of reciprocation was set via an adjustable yoke which was coupled to the reciprocating unit motor. The columns were operated with the dispersed aqueous phase entering from a distributor at the top of the column and the continuous organic phase entering through a distributor at the bottom of the column. The interface was maintained below the plate stack in all columns to ensure the continuous organic phase wet the plastic plates. Mass transfer of a phenolic alkaloid was studied from the dispersed aqueous phase to the continuous organic phase. Further details on each of the columns' specifications have been summarized in Table 1, and information on the physical properties of the liquid system have been provided in Table 2.

Table 1. Summary of column specifications

Column Specification	Column 1	Column 2	Column 3
Column Diameter, D_c	50 mm	100 mm	300 mm
Effective Column Height, H_c	1.95 m	5 m	5 m
Effective Column Volume, V_e	3,828 cm^3	39,270 cm^3	353,429 cm^3
Number of Plates, N	35	80	80
Plate Thickness, E	5 mm	5 mm	5 mm
Plate Material	PP	HDPE	HDPE
Perforation Diameter, d_h	12.5 mm	12.5 mm	12.5 mm
Hole Pitch (Triangular), P	17 mm	17 mm	17 mm
Plate Spacing, h_c	50 mm	50 mm	50 mm
Plate Free Area, S	0.469	0.531	0.531

Table 2. Test system and corresponding physical properties

Physical Property	Phase	Density, ρ (kg/m^3)	Viscosity, μ (Pas)	Interfacial Tension, γ (mN/m)
Continuous Phase	Organic solvent mixture	835	0.00119	6.35
Dispersed Phase	Alkaloid-rich extract	1017	0.00114	

Procedures

Dispersed-phase holdup was measured using the drainage technique developed by Gayler and Pratt [3]. Mass-transfer performance was determined by taking samples and measuring the solute concentration using high-performance liquid chromatography (HPLC). Equilibrium data was obtained via shake-up tests. A mass transfer performance program was developed based on the generalised design equations for backmixed liquid extraction columns with nonlinear equilibria to determine the overall mass transfer coefficient from the measured concentrations, physical properties and hydrodynamic data (Pratt & Stevens [4]). The range of operating parameters studied for each column is given in Table 3.

Table 3. Range of operating parameters studied for each column

Column Detail	Column 1	Column 2	Column 3
Column Diameter, D_c	50 mm	100 mm	300 mm
Frequency, f	0.75 – 2.4 Hz (45 – 144 rpm)	0.83 – 1.25 Hz (50 – 75 rpm)	0.92 – 1.08 Hz (55 – 65 rpm)
Amplitude, A	1.0 cm	1.0 cm	1.0 cm
Agitation Rate, Af	0.75 – 2.40 cm/s	0.83 – 1.25 cm/s	0.92 – 1.08 cm/s
Dispersed Phase Velocity, V_d	0.04 – 0.51 cm/s	0.21 – 0.44 cm/s	0.39 – 0.59 cm/s
Continuous Phase Velocity, V_c	0.17 – 0.66 cm/s	0.29 - 0.88 cm/s	0.20 - 0.28 cm/s
Phase Flow Ratio, $R=V_c/V_d$	0.8 – 6.0	0.8 – 3.1	1.5 – 2.5

RESULTS AND DISCUSSION

Dispersed-Phase Holdup

Dispersed-phase holdup was found to increase with increases in dispersed-phase velocity and agitation rate. Due to contamination of the plastic plates using industrial solutions, holdup was also found to be greatly influenced by the wettability of the plate surface. Higher holdup and lower flooding velocities were obtained when the dispersed aqueous phase wet the plates due to a change in the hydrophobicity of the plates as a result of contamination (Mensforth [1]). However, when plate wettability was not an issue, similar holdup was obtained in all three columns, indicating that there was no significant change in dispersed-phase holdup with column diameter.

A correlation has been developed for predicting dispersed-phase holdup in all three columns. Due to issues with wettability of the plastic plates and system physical properties, which were quite different than the ideal test systems, most correlations in the literature were not appropriate. The main parameters found to affect holdup in this study were the dispersed-phase velocity, agitation rate, mass-transfer direction, physical properties, and plate wettability. The most appropriate correlation in the literature that included these parameters was that developed by Kumar and Hartland [5]:

$$x_d = \Pi\Phi\Psi\Gamma \tag{1}$$

The constant which allowed for the variations in physical properties of the system, C_Ψ, was refitted to the current experimental data. The following constants were used with this equation:

$$C_\Pi = 0.13, \quad C_\Psi = 2.0, \quad C_\Gamma = 6.87,$$
$$n_1 = 1, \quad n_2 = 0.84, \quad n_3 = 3.74, \quad n_4 = -0.92, \quad n_5 = n_6 = 0, \quad n_7 = -0.48$$

This model with refitted constants was able to predict the experimental holdup data from this study to within 19% (see Figure 1). The same constants were used with all three columns, which indicated that dispersed-phase holdup did not change with scale, and it was concluded that holdup was independent of column diameter.

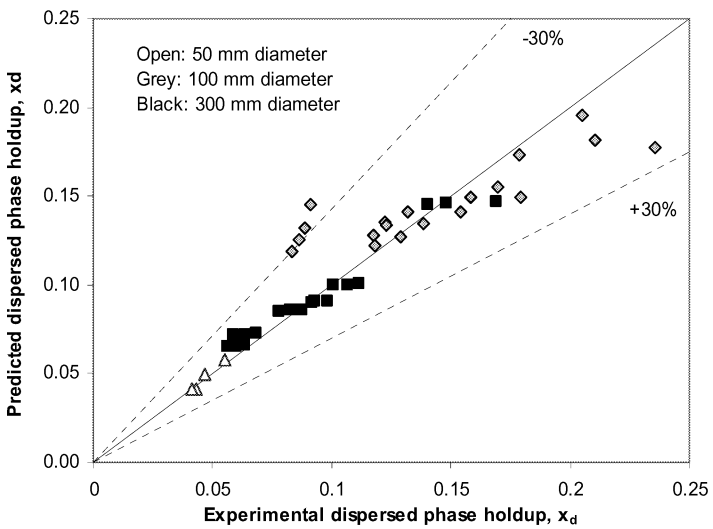

Figure 1. Comparison of experimental data with the correlation developed to predict holdup.

Mass-Transfer Performance

Mass-transfer performance was examined using the backflow model. This involved solving the material-balance equations using measured physical properties and

equilibrium data along with correlations developed for holdup, drop-size distribution, and backmixing (refer to Mensforth [1] and Stella et al. [2]). Higher overall mass-transfer coefficients were seen with an increase in the continuous-phase velocity and agitation rate. Poor mass-transfer performance was observed when the plates were wetted by the dispersed aqueous phase due to a change in the wettability of the plastic surface resulting in lower holdup and hence lower interfacial area for mass transfer.

A correlation has been developed for predicting the overall mass-transfer coefficient in all three columns. The most appropriate model from the literature was that presented by Stella [6]. This correlation incorporated the effects from phase flow rates, agitation rate, and physical properties as follows:

$$k_{0x}a = V_c^{\,n}\left(Af\right)\left[1+0.035\psi^{0.40}\left(\frac{V_c}{V_d}\right)^{0.1}\right] \qquad (2)$$

It was found that the same constant (n = 0.30) was applicable to both the 100 mm and 300 mm diameter columns. However, in the 50 mm diameter alkaloid column, the mass transfer performance was affected by the change in wettability of the plate surface, and hence a larger constant (n = 0.48) was required to fit the data. This mass-transfer model, represented by Equation (2) and the refitted values for the constant n, provided a good fit for the current data with an overall AARE of 24% (refer to Figure 2).

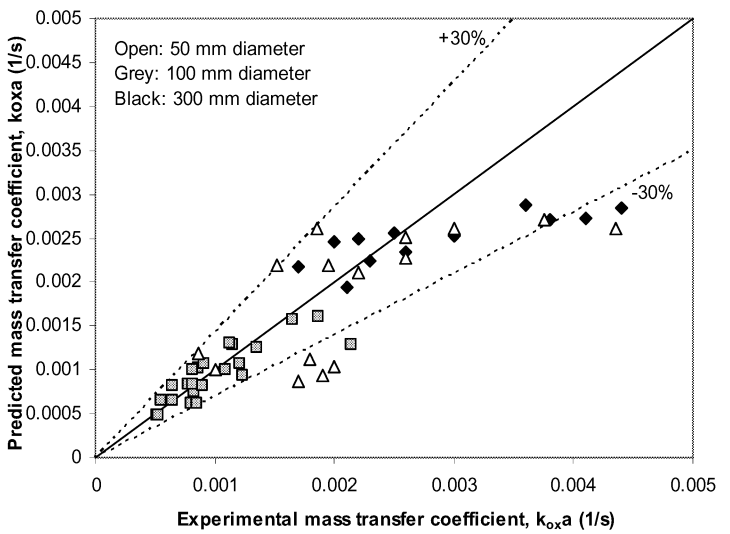

Figure 2. Comparison of experimental data with the correlation developed to predict mass-transfer coefficients in this study.

These results show that, as with the dispersed-phase holdup, there was no significant change in mass-transfer performance with column diameter. However, plate wettability does influence both holdup and mass-transfer performance and must be considered when examining column performance.

CONCLUSIONS

This study has examined the hydrodynamic and mass-transfer performance in columns of diameters 50, 100, and 300 mm. The dispersed-phase holdup, mass transfer coefficient, and specific interfacial area for mass transfer were found to be independent of column diameter. Therefore, the overall performance of the column was independent of column diameter, and the scale-up procedure presented by Karr and Lo [7] is too conservative.

ACKNOWLEDGMENTS

Thank you to GlaxoSmithKline (Opiates Division, Port Fairy) for support and access to plant resources that provided the basis for this study. Also thank you to the Particulate Fluids Processing Centre, a Special Research Centre of the Australian Research Council, for infrastructure support.

REFERENCES

1. K. H. Mensforth, "Performance and Scale-up of Karr Reciprocating Plate Extraction Columns," Ph.D. thesis, The University of Melbourne, Australia, 2006.
2. A. Stella, H. R. C. Pratt, K. H. Mensforth, G. W. Stevens, and T. Bowser, "Backmixing in Karr Reciprocating-Plate Extraction Columns," *Ind. Eng. Chem. Res.*, **45**(19), 6555-6562 (2006).
3. R. Gayler and H. R. C. Pratt, "Liquid-liquid extraction. V. Further studies of droplet behavior in packed columns," *Trans. Inst. Chem. Eng.*, **31**(1), 69-77 (1953).
4. H. R. C. Pratt and G. W. Stevens, "Generalized Design Equations for Backmixed Liquid Extraction Columns with Nonlinear Equilibria," *Ind. Eng. Chem. Res.*, **30**(4), 733-739 (1971).
5. A. Kumar and S. Hartland, "A Unified Correlation for the Prediction of Dispersed-Phase Hold-Up in Liquid-Liquid Extraction Columns," *Ind. Eng. Chem. Res.*, **34**(11), 3925-3940 (1995).
6. A. Stella, "Hydrodynamics and Mass Transfer Performance in Karr Reciprocating Plate Extraction Columns," Ph.D. thesis, The University of Melbourne, Australia, 2002.
7. A. E. Karr and T. C. Lo, "Scaleup of Large Diameter Reciprocating-Plate Extraction Columns," *Chem. Eng. Prog.,* **72**(11), 68-70 (1976).

EXPERIMENTAL INVESTIGATION OF DROPLET-DROPLET COALESCENCE IN LIQUID-LIQUID SYSTEMS

René T. Eiswirth and Hans-Jörg Bart

Lehrstuhl für Thermische Verfahrenstechnik, Technische Universität Kaiserslautern, Postfach 3049, 67653 Kaiserslautern, Germany.
Corresponding author email address: bart@mv.uni-kl.de

ABSTRACT

The coalescence process was investigated by means of coalescence experiments with the standard EFCE test systems toluene/acetone/water and butylacetate/acetone/water under defined conditions. A test stand for producing drops of equal size, contacting the drops, and observing the following processes (coalescence/repulsion) to identify different parameters influencing the droplet-droplet coalescence was developed. The coalescence process was investigated by modifying the chemical properties of the aqueous phase. The experimental unit consists of a high speed camera combined with the Schlieren technique. It is possible to investigate the coalescence process behavior with the combination of these two techniques.

INTRODUCTION

The process of droplet-droplet coalescence plays a crucial role in liquid-liquid extraction processes [1,2]. The coalescence process determining the efficiency and productivity of an extraction column is in the active zones during mass transfer and the phase separator is [3-5]. Generally, two coalescence mechanisms are distinguished, which is the coalescence at planar boundaries (e.g., settling zones) and the droplet-droplet coalescence. The latter is decisive for the hydrodynamics in extraction columns. Different models, describing the droplet-droplet coalescence in stirred liquid-liquid systems, have already been developed. These models are based on empirical [6,7] or semi-empirical [8,9] approaches. The coalescence rate is often calculated as a product of coalescence efficiency and collision rate. The parameters derived are only then valid for one chemical system or apparatus geometry. Furthermore, the general influence of the complex interaction of different phenomena, for example the influence of pH-value, salts, detergents, and mass-transfer direction is usually neglected in spite of the fact that the droplet-droplet coalescence is responding very sensitively to changes in local chemical composition [10]. Consequently, data of the chemical system, such as density, viscosity, and surface tension, are not sufficient to describe the properties of the chemical system. Electrostatic interactions induced by ions at the liquid interface influence the coalescence process, depending on the salt species and concentration. In spite of the importance of

these effects, they are usually not sufficiently considered [11-14]. Also the influence of detergents, especially with industrial systems, should not be neglected [15].

EXPERIMENTAL

Experimental Set-up

The experimental set-up (see Figure 1) consists of the measuring cell (5), in which the main connectors (B) for the capillaries (A) are implemented. The analytics are made with a Schlieren high-speed camera. The light of the nanoflashlight (1) is mapped on the Schlieren slit (3) with biconvex lens (2). The slit consist of two movable sharp edges. Therefore, it is possible to adjust the gap length of the slit. The outgoing light is widened to parallel light by the planar convex lens (4). The light passes the measuring cell (5) to the achromatic lens (6). The achromatic lens produces the picture in the focal point, caught by the sharp edge of the Schlieren aperture (7). The accruing Schlieren picture is captured by the high-speed camera (8) with an integrated memory of 512 Mb. If a resolution of 1024 x 512 pixel is used for one picture, it is possible to take nearly 1000 frames in one second.

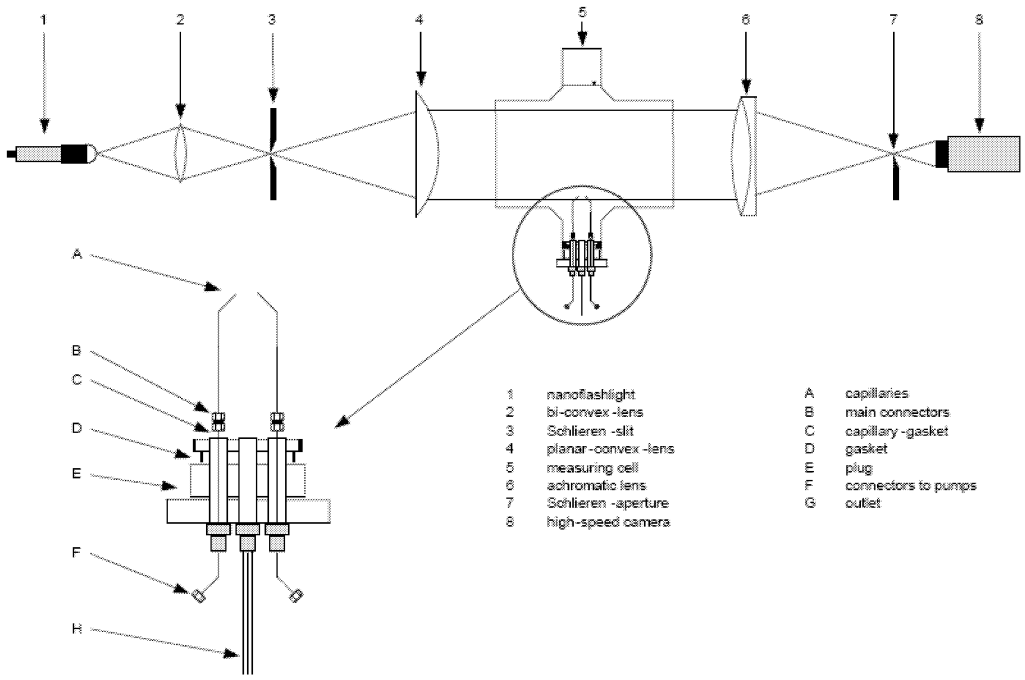

Figure 1. Experimental set-up consisting of measuring cell and Schlieren high-speed camera measuring section.

The drops can be produced continuously with different types of capillaries (A) directed towards each other feed from two pulsation-free metering pumps. The drops can collide during their way up through the cell. The drop formation and rising behavior of

the drops has been investigated with different types of capillaries. The capillaries differ in their inner and outer diameter and also in the construction of their tip (planar/angular/pointed).

Experimental Conditions

The coalescence process reacts very sensitively to changes in the chemical system. Impurities can also change the process and may hinder reproducibility. For this reason, the experiments have only been carried out with p.a. substances. As to this, analaR grade toluene was redistilled and bidistillated water with a conductivity of < 0.5 µS/cm was used. However, it is recommended to condition the water with 1 mmol/L sodium chloride prior to experiments to maintain conductivity and zeta potential at a constant value [17,18]. Prior to the experiments the aqueous phase was degassed in order to reduce the electrolyte influence of solute gasses, such as carbon dioxide. The pH value and the conductivity have been monitored during the experiments. The changes in the pH value have been induced with hydrochloric acid or a sodium hydroxide solution. Changes in the ionic strength have been adjusted with sodium chloride and toluene, and the aqueous phases have been saturated.

RESULTS

First experimental results show that it is possible to visualize the droplet-droplet coalescence process of two single rising droplets (see Figure 2). It is possible to measure different parameters, which can be used to characterize the process, for example, time for the film drainage or relative velocity of the drops. There is an indication for different coalescence affinities at different pH values. At pH values near the neutral point, the coalescence affinity seems to be much higher than at higher pH values. So the coalescence affinity at pH 8 and pH 5 is much higher than at pH 11. A coalescence event at pH 8 is shown in Figure 2.

In contrast to the high coalescence affinity at pH 8 or 5, when almost all droplets colliding with each other coalesce, they repel themselves at pH 11, even though there is enough time for a coalescence event compared to the events at pH 8 and pH 5. A typical behavior of two droplets at pH = 11 is shown in Figure 3. This behavior at high pH values may be explained with the adsorption of hydroxide anions at the liquid interface of the organic droplets, which causes a higher zeta potential of the interface and therefore higher repulsive forces. The increase of the zeta potential at higher pH values of a toluene/water emulsion can be seen in Figure 4. Consequently, the coalescence affinity in systems of high pH values is lower than in systems with lower pH value, as already reported in the literature [11,19]. It is well known, that this effect can be reduced by adding salts [13]. Furthermore, there is an indication for different mobility of the interface at different pH values. This is noteworthy because the mobility of the liquid interface is influencing the droplet-droplet coalescence. Systems with higher surface-tension difference have higher coalescence affinities than systems with lower surface-tension difference. Results on the influence on ionic strength, zeta potential, and interfacial mobility will be given in detail.

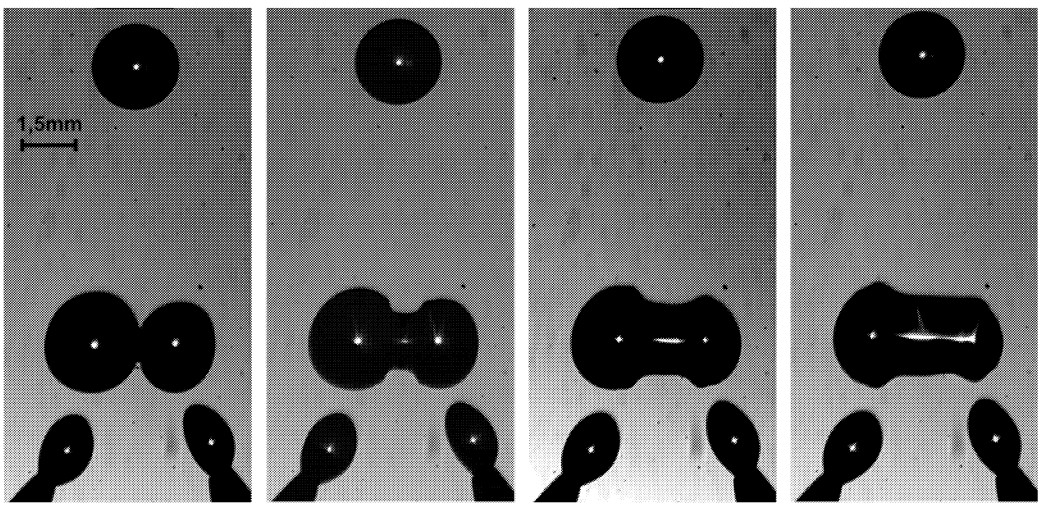

Figure 2. Droplet-droplet coalescence event of rising toluene droplets in 0.001 mol/L NaCl (pH = 8, captured with 922 fps).

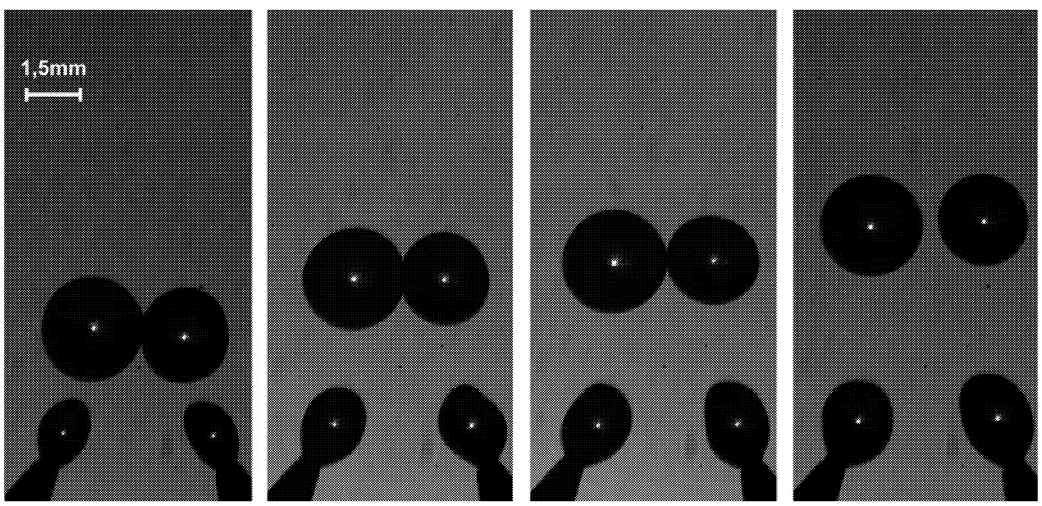

Figure 3. Droplet-droplet interaction of rising toluene droplets in 0.001 mol/L NaCl, (pH = 11, time between first and last picture, ca. 60 ms)

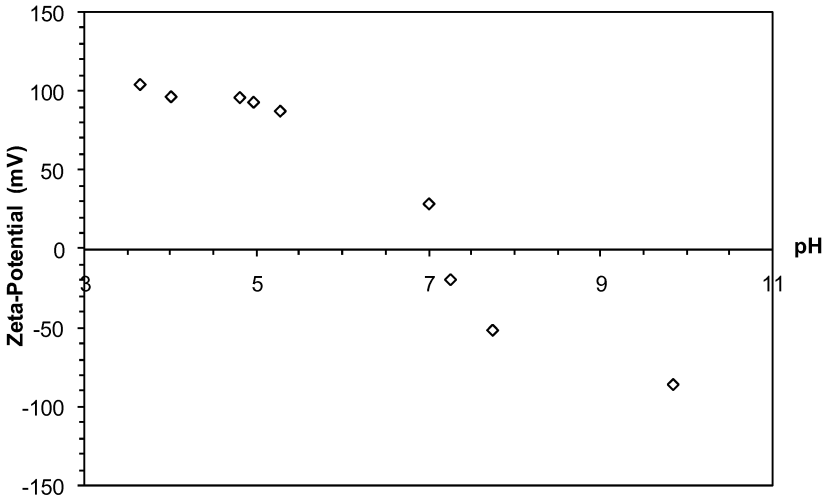

Figure 4. Zeta potential-pH curve for toluene/water emulsion

CONCLUSIONS

Coalescence phenomena are difficult to tackle, and there are only a few models in the literature which have a predictive character. This is also due to the fact that not all relevant system parameters (surface mobility, adsorption layers, interfacial tension, etc.) are decisive for coalescence efficiency being properly considered. It is known that small disturbances, resulting from mass transfer or impurities, can totally change the system behavior. A high-speed Schlieren optics allows to visualize the coalescence process of two single droplets at any experimental conditions. The experiments are performed with standard EFCE test systems and should be broadened to systems with equal densities to allow for longer contact and film drainage times.

ACKNOWLEDGMENTS

The authors wish to thank the DFG for financial support and Mr. L. Drumm and Mr. K. Steinhaus for their help with the experiments.

REFERENCES

1. L. Gomes, M. Guimaraes, J. Lopes, C. Madureira, J. Stichlmair, and J. Cruz-Pinto, "Reproducibility of the Hydrodynamic Performance and Measurements in a Liquid-Liquid Kühni Extraction Column-Relevance to Theoretical Model Evaluation," *Ind. Eng. Chem. Res.*, **43**, 1061-1070 (2004).
2. E. Blaß, "Bildung und Koaleszenz von Blasen und Tropfen," *Chem. Ing. Technol.*, **60**, 935-947 (1988).
3. E. Gross-Hardt, M. Henschke, S. Klinger, and A. Pfennig, "Design of pulsed extraction columns based on laboratory-scale experiments," Proceedings ISEC'02, Cape Town, 1358-1363 (2002)

4. S. Klinger, M. Henschke, and A. Pfennig, "Untersuchung von Spaltungs- und Koaleszenzvorgängen in einer Messzelle mit pulsierten Füllkörpern," *Chem. Ing. Technol.*, **74**, 256-261 (2002).
5. M. Kraume, A. Gäbler, and K. Schulze, "Influence of Physical Properties on Drop Size Distribution of Stirred Liquid-Liquid Dispersions," *Chem. Eng. Technol.*, **27**, 330-334 (2004).
6. S. Kentish, G. Stevens, and H. Pratt, "Estimation of Coalescence and Breakage Rate Constants within a Kühni Column," *Ind. Eng. Chem. Res.*, **37**, 1099-1106 (1998).
7. H. Wright and D. Ramkrishna, "Factors affecting coalescence frequency of droplets in a stirred liquid-liquid dispersion," *AIChE J.*, **40**, 767-776 (1994).
8. C. Coulaloglou and L. Tavlarides, "Description of Interaction Processes an agitated Liquid-Liquid Processes," *Chem. Eng. Sci.*, **32**, 1289-1297 (1977).
9. H. Sovova, "Breakage and Coalescence of Drops in a batch stirred Vessel - II. Comparison of Model and Experiments," *Chem. Eng. Sci.*, **36**, 1567-1573 (1981).
10. M. Simon and H.-J. Bart, "Experimental Studies of Coalescence in Liquid/Liquid Systems," *Chem. Eng. Technol.*, **25**, 481-484 (2002).
11. T. Tobin and D. Ramkrishna, "Coalescence of charged droplets in agitated liquid-liquid dispersions," *AIChE J.*, **38**, 1199-1205 (1992).
12. A. Pfennig and A. Schwerin, "Influence of Electrolytes on Liquid-Liquid Extraction," *Ind. Eng. Chem. Res.*, **37**, 3180-3188 (1998).
13. T. Tobin and D. Ramkrishna, "Modeling the Effect of Drop Charge on Coalescence in Turbulent Liquid-Liquid Dispersions," *Can. J. Chem. Eng.*, **77**, 1090-1104 (1999).
14. M. Henschke, L. H. Schlieper, and A. Pfennig, "Determination of a coalescence parameter from batch-settling experiments," *Chem. Eng. J.*, **85**, 369-378 (2002).
15. W. Rommel, W. Meon, and E. Blass, "Hydrodynamic Modeling of Droplet Coalescence at Liquid-Liquid Interfaces," *Sep. Sci. Technol.*, **27**, 129-159 (1992).
16. G. Gneist, "Untersuchung des Einflusses hochfrequenter elektrischer Felder auf die Hydrodynamik und den Stoffaustausch in der Extraktion," Technische Universität Kaiserslautern, Shaker Verlag GmbH, 2004
17. P. Kolb, "Hydrodynamik und Stoffaustausch in einem gerührten Miniplantextraktor der Bauart Kühni," Technische Universität Kaiserslautern, Kaiserslautern, Germany, 2004
18. M. Soika and A. Pfennig, "Extraktion - Eine Frage des Wassers?" *Chem. Ing. Technol.*, **77**, 905-911 (2005).
19. M. Simon, "Koaleszenz von Tropfen und Tropfenschwärmen," Technische Universität Kaiserslautern, Kaiserslautern, Germany, 2004

RELIABLE DESIGN OF PHYSICAL AND REACTIVE EXTRACTION BASED ON SIMPLE LAB-SCALE EXPERIMENTS

A. Pfennig

AVT – Thermal Process Engineering, RWTH Aachen University Wüllnerstr. 5, 52062 Aachen, Germany. Corresponding author email address: www.avt.rwth-aachen.de, and reas.pfennig@avt.rwth-aachen.de

ABSTRACT

Today, design methods based on single-drop measuring cells on lab-scale are available for extraction columns. For mixer-settler equipment, a comparably simple standardized lab cell is available as well. The lab cell for mass-transfer measurement is presented in some detail. Based on the measurements that require little time and substance, model parameters are determined that describe the drop behavior. These models are then used for column simulations. It turns out that column behavior can be accurately described over a wide range of operating conditions, and that even the flooding limit is detected. Thus, a powerful new tool is available for extraction-column design.

INTRODUCTION

For the proper design of (reactive) extraction equipment, experiments are required. The conventional design procedure relies on a series of experiments on pilot-plant scale with columns of typically 50 mm diameter or corresponding mixer-settler cascades. The reason for the necessity of such experiments is the strong influence that impurities and trace components may have on the sedimentation of drops, their mass-transfer rate, and their coalescence. Unluckily, these effects have a large influence, especially for that range of drop diameter which is relevant in technical extraction. The result of the effects can only be characterized by experiments with the original system.

Since such experiments on pilot-plant scale are time consuming, require a large amount of substance, and are only efficient if the type of column internals are selected early in the design process, an alternative design method has been sought that allows obtaining the necessary information in less time with a smaller amount of substance. For the design of extraction columns, lab cells have been designed to characterize the single-drop behavior with respect to sedimentation, mass transfer, and possibly splitting and coalescence. These single-drop experiments require only few liters of substance and roughly 1 to 2 weeks of experiments. The results of these experiments are then used to fit the parameters of appropriate models, These models are then linked together and combined with models describing swarm influence as well as the interaction between the

drops and the internals in the column. This solving of the population balances is achieved with the ReDrop model (representative drops) that traces a representative number of individual drops through the column [1,2]. This procedure can be regarded as a Monte-Carlo method to solve the drop-population balances. The schematic sketch of the algorithm is shown in Figure 1. The advantage of the algorithm as compared to other population-balance algorithms is that it has a very modular structure and that, with including additional drop descriptors, the complexity of the program scales linearly. Thus, each drop is currently characterized by its diameter, concentration of transfer component, age, and height in the column. Additional descriptors are currently included to describe all components relevant for reactive extraction.

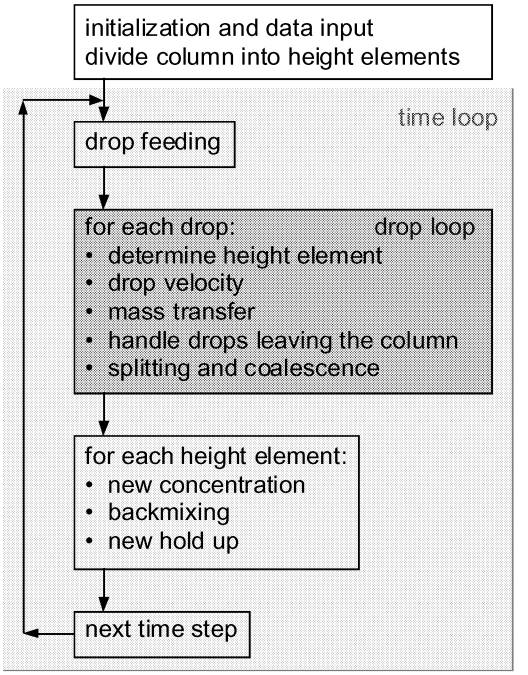

Figure 1. Sketch of ReDrop algorithm.

For the design of settlers, a small standardized settling cell has been designed for which it has been shown that it allows reliable design of technical settler equipment with and without internals.

LAB CELLS

A lab cell for determining mass-transfer rate of a drop is shown in Figure 2 [3,4]. The continuous phase is flowing downward in the glass cell. A single drop of known diameter is then generated with a computer-driven syringe. It rises until it reaches the position in the conical part where its sedimentation velocity matches the counterflow of

continuous phase, where it is levitated for an arbitrary time. By briefly switching off the continuous-phase flow the drop rises further and reaches the drop-collection funnel, where it is withdrawn, again with a computer-driven syringe. This procedure is repeated for some hundred drops, until sufficient sample has been collected as to analyze the concentration of the drops. The change in concentration is then a measure of mass-transfer rate as a function of drop diameter and contact time.

Inside the cell, a variety of internals can be mounted. Thus, also their influence is obtained. From experiments with the EFCE standard test systems it could , for example, be shown that the effect of a sieve tray is not only the mixing inside the drop as the drop passes through the holes. The major effect is rather that as the drop approaches the sieve tray, the jets of continuous phase being pressed through the holes, especially strongly with pulsation, hit the drop and increase mass transfer. A regular packing does, for example, not have an influence on the mass-transfer rate. The only effect of the packing is the increased residence time that improves the column performance. Also, a significant residence-time distribution is observed that needs to be accounted for in the simulation.

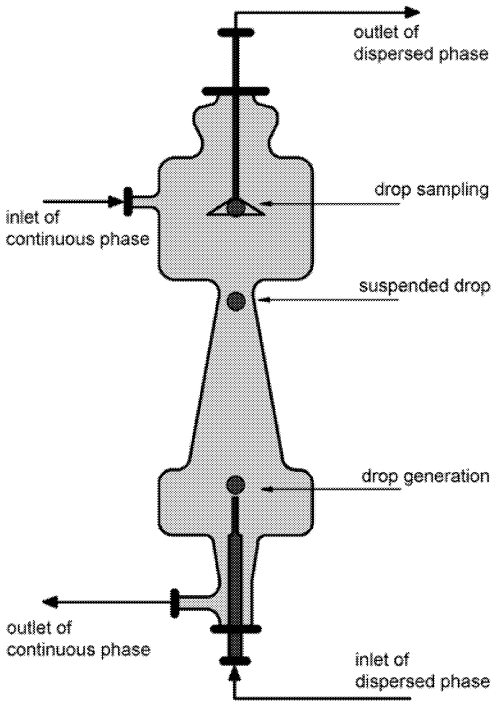

Figure 2. A lab-scale mass-transfer cell.

A variety of other lab cells is available, for example, for sedimentation and for drop splitting and coalescence. For investigating reactive extraction, this has been augmented by a so-called Nitsch cell, which allows measurement of mass-transfer rate at a plane and defined interface under variation of convective influence.

The conditions at which the experiments are performed are determined from a MEXA procedure (model-based experimental analysis). This method determines the conditions such that the information on the model parameters per experimental time is maximized. It has been shown in a variety of cases that MEXA suggests experimental conditions that are not directly obvious at first sight. If the problem posed is simple enough, the choice can usually be understood retrospectively. According to our experience the experimental effort could be reduced by MEXA in several cases by a factor between 3 and 10 with respect to random or evenly distributed choice of conditions while keeping the accuracy of the parameters determined unchanged. Thus, a factor of 3 to 10 less experimental time is required to obtain model parameters based on the data with identical accuracy if MEXA is applied as compared to evenly distributed experiments.

RESULTS

Once the model parameters have been determined in the lab cells, the models can be joined together in ReDrop. It should be noted that based on the lab-cell results, a variety of column types can be described. Thus, it is not necessary to make any early choice of column type. The decisions on the optimal column internals as well as the optimal operating conditions are result of the modeling.

In Figure 3 results obtained for a specified column are shown as an example. The column type and some of the operating conditions have been fixed, while the volume flow rates of both phases have been varied. The results show first that very detailed insight into the column behavior can be obtained, which can be understood, since every drop in a characteristic column is modeled. Here typically 1000 drops per 1 m of column height turn out to be sufficient to obtain reliable results.

Also, it can be seen in Figure 3 that the flooding limit is predicted with ReDrop. Thus, this method allows detecting the limits of operability consistently with all other results and does not require a separate flooding correlation.

This method has been applied to a variety of systems, and the results compared to pilot-plant scale results. It turns out that a characteristic accuracy of roughly 10% or better is achieved, even for technical systems [5]. Experience gained so far indicates that the detailed description of the drop and column behavior requires a correspondingly high accuracy in the experiments. This can be achieved in the standard lab cells, because significant experience in operating them is meanwhile available. But also the other experiments, like equilibrium measurement, have to be of sufficiently high accuracy. While, in the former design method based on pilot-plant scale, the equilibrium only needed to be determined to an accuracy that allows rough estimates of separation performance, since this was later checked and better quantified in the column experiment, now accurate data are substantial for drop-based design.

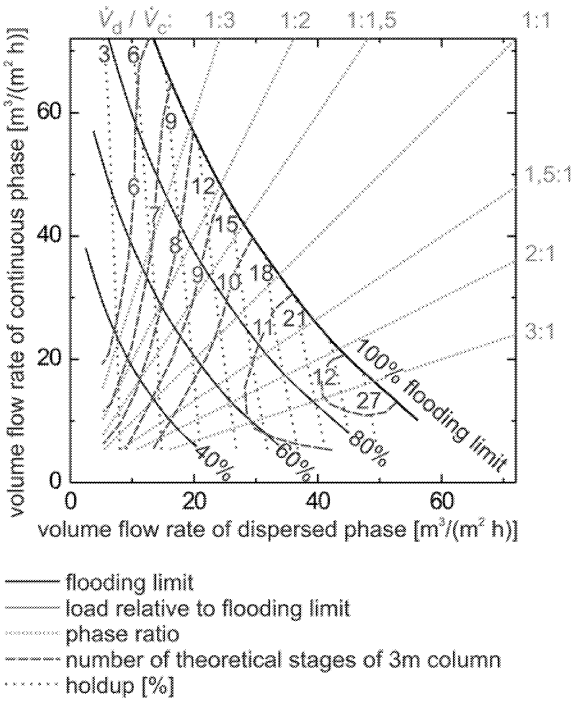

Figure 3. Results with ReDrop for a sieve-tray column with 3 m height, tray spacing of 0.1 m, 4 mm holes, hole area of 39%, *af* = 11.7 mm/s for the system water (c) + butyl acetate (d) + acetone.

CONCLUSIONS

Based on investigations of the single-drop behavior, it is possible to describe the performance of extraction equipment in a very detailed way. This allows simple optimization of operating conditions as well as column type and details of column internals. Thus, this method is a most flexible design tool that allows mimicking pilot-plant scale experiments on the computer in every detail and with high precision. Requirements for applying this method are accurate results obtained with lab cells, which can be obtained with only a few liters of substance and in roughly 2 weeks. Under certain conditions, even significantly less time is required. Thus, a new and reliable design method for solvent-extraction equipment has been developed.

REFERENCES

1. M. Henschke, Auslegung pulsierter Siebboden-Extraktionskolonnen, Shaker Verlag, Aachen, 2003.
2. M. Kalem and A. Pfennig, "ReDrop—A general method for solving drop-population balances with an arbitrary number of property variables," 17th European symposium on computer aided process Engineering (ESCAPE), Bucharest, Romania, 27-30 May, 2007.

3. M. Henschke and A. Pfennig, “Mass-Transfer Enhancement in Single-Drop Extraction Experiments,” *AIChE J.*, **45**, 2079 (1999).
4. M. Henschke and A. Pfennig, “Influence of Sieve Trays on the Mass Transfer of Single Drops,” *AIChE J.*, **48**, 227 (2002).
5. H.-J. Bart, D. Garthe, T. Grömping, A. Pfennig, S. Schmidt, and J. Stichlmair, “Vom Einzeltropfen zur Extraktionskolonne,” *Chem. Ing. Techn.*, **78**(5), 543-547 (2006).

MODELING OF UNIT OPERATIONS BY MOLECULAR SIMULATIONS

D. Babic and A. Pfennig

AVT - Thermal Process Engineering, RWTH Aachen University,
Wüllnerstr. 5, D-52062 Aachen, Germany.
Corresponding author email address: andreas.pfennig@avt.rwth-aachen.de

ABSTRACT

The behavior of separation columns can be simulated by molecular simulation, where the influence of all relevant elements of a separation stage is taken into account. In order to decrease the computational time, the column is divided into separation stages, where the simulation of each stage is carried out on an individual computer, and the number of stages can be set to any desired value. By performing a dimensional analysis, the residence time of the molecules in the molecular simulation can be adjusted such that the simulated mass transfer corresponds to a macroscopic stage; that is, the column simulation is also able to depict the influence of the residence time on the efficiency of separation stages.

INTRODUCTION

The properties and interactions of the molecules involved in chemical-engineering processes determine the behavior and thus the design of the used equipment. Nowadays, it is still considered impossible to bridge the length and time scales between molecules and technical equipment in only one or a few steps of model hierarchy. Nevertheless, it is generally accepted that the major effects in chemical engineering facilities can be modeled just with equilibrium and rate-based approaches. These effects have their origin at the molecular level, and corresponding data can be obtained by only taking the vicinity of the interface into account; that is, the simulation of a few hundred or thousand particles is sufficient.

The goal of this work is to develop a simulation tool that is able to predict the behavior of entire separation columns based on molecular simulations. The benefit of this approach is that the simulations are performed at the exact operating conditions, of composition, temperature, pressure, and their gradients corresponding to the real apparatus. Thus, it is not necessary to simulate data over the entire range of possible temperatures and compositions, where the data for the relevant conditions are then obtained afterwards by correlation or interpolation. Furthermore, molecular simulations are able to predict multicomponent effects in mass transfer as well as complex equilibrium data accurately and consistently.

MODELING

In principle, two alternatives are possible to realize the molecular approach. One method depicts the column by consecutive separation stages; that is, the simulation of one separation stage is performed for two flowing phases in contact. Thereby, the outflow of one stage is directly the inflow of the next stage with respect to material flow, composition, and temperature. The second concept is based on the HTU-NTU-method.

Separation Stages

In order to implement the first concept in a first step, the code of a molecular-simulation program has been modified as to allow different compartments and boundaries between them to be accounted for in a simulation. Thus, specific boundary properties can be applied to molecules that cross a border. By using different boundary properties, all relevant elements of a separation process can be depicted on a molecular level: partly penetrable walls simulate the behavior of sieve trays, heating and cooling regions by influencing the molecular velocities or feed and product flows by inserting and removing particles from the simulation. By introducing gravity, a counterflow is induced. It was already shown that with this setup the principle behavior of a distillation column can be simulated with less than a thousand particles [1]. The agreement with experimental data is excellent (Figure 1). This approach has been refined and applied to solvent extraction.

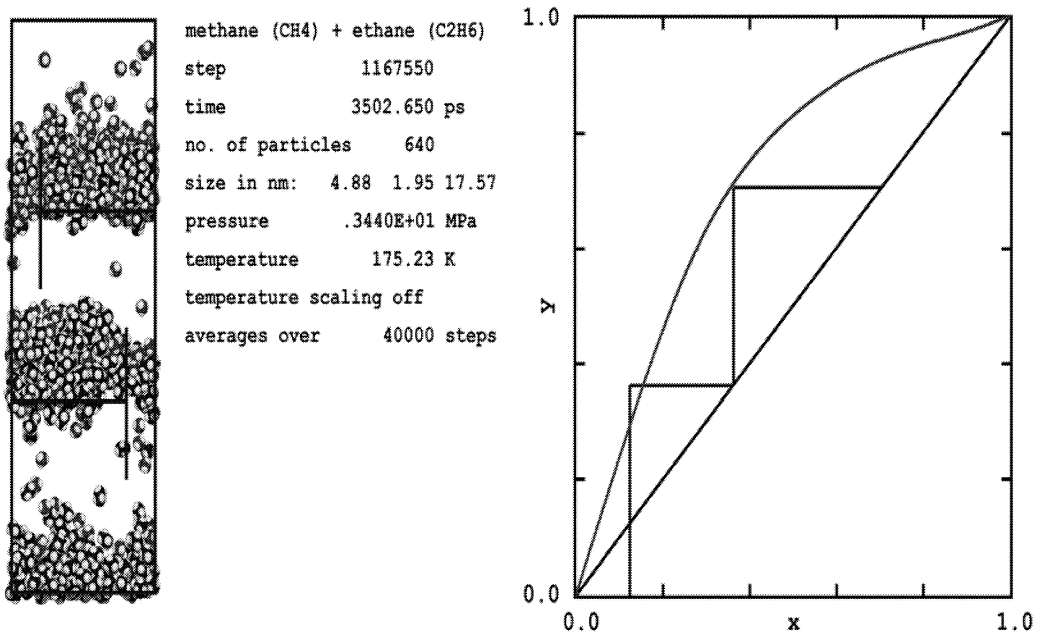

Figure 1. Snapshot of a distillation column simulated by molecular dynamics.

In order to make this method capable for liquid-liquid systems one has to be aware of the computational costs of the simulation presented in Figure 1, which took about one week on a PC. Thus neither more particles (two liquid phases) nor more stages can be simulated with this method in reasonable simulation times. Therefore, it is obvious that the method has to be parallelized. For that purpose, the simulation cell has been cut into individual separation stages, where each stage can be simulated on an individual PC. By connecting the individual stages with their entering and leaving streams, a separation column is depicted. The information that has to be exchanged between the stages (i.e., the PC) doesn't have to include data regarding every individual molecule that left one stage but only overall data like the amount of substance, the composition, or temperature of the flow rates. Additionally, after every simulation step the information does not have to be exchanged. It is sufficient to update the feed and product flows of every stage only after a few ten thousand steps. Thus the computational cost of the data exchange between the stages is negligible, and the number of separation stages can be set to any desired value.

In the McCabe-Thiele plot on the right hand side of Figure 1, one can see that the sieve trays of the column essentially behave as ideal separation stages, where in the products leaving one stage are in equilibrium. Due to the short length scales in the molecular simulation, the residence time of the particles on one stage is too high, which means that equilibrium will be achieved. In order to simulate also the non ideal character of separation stages on molecular level, a dimensional analysis has to be performed that provides the necessary residence time of the fluids in a molecular simulation that corresponds to a macroscopic separation stage.

In the triangular diagram in Figure 2 the compositions of the feed (open circles), the products in the case of high (solid line) and low residence times (dashed line), and the equilibrium data of a separation stage simulated on molecular level are shown. The equilibrium data were obtained in simulations where the feed- and product-flow rates were set to zero (i.e. for infinite residence times).

In both cases, short and long residence time, the A-rich product flow has a higher C concentration than the feed flow. Due to the finite residence time in both cases, the products are not in equilibrium; that is, their connecting line doesn't coincide with a tie line. Figure 2 also shows that increasing the flow rates (dashed line) leads to less C in the A-rich phase than in the case of low product flow rates (solid line), reflecting that the product compositions are less equilibrated. Hence, with these molecular simulations, it is possible to reproduce the influence of the residence time on the efficiency of a separation stage, and the molecular simulation doesn't depict adequately combined equilibrium stages like suggested by the McCabe-Thiele plot in Figure 1.

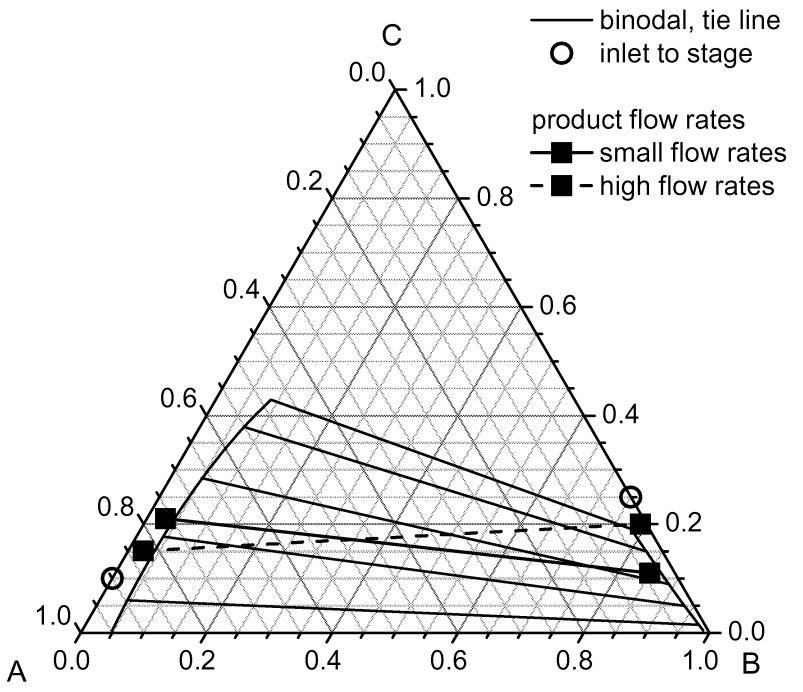

Figure 2. Compositions in the case of high (solid line) and low residence time (dashed line).

In order to simulate an extraction column, more than one separation stage has to be regarded. Therefore, individual simulations as shown in Figure 2 have to be connected, where in the outlet of one stage is the inlet of the consecutive stage and vice versa. In Figure 3 a snapshot of such a simulation is presented. On the left hand side a schematic sketch of the column is shown, where the blue particles indicate component A, the red ones component B, and green the transferred component C. The inlet and outlet streams are indicated by the arrows connecting the individual stages. On the right hand side, the process is represented in the triangular diagram. The compositions of the feeds (F) are indicated by circles, the compositions of the products (P) by squares, and the inlet and outlet streams connecting the individual stages by the dashed line.

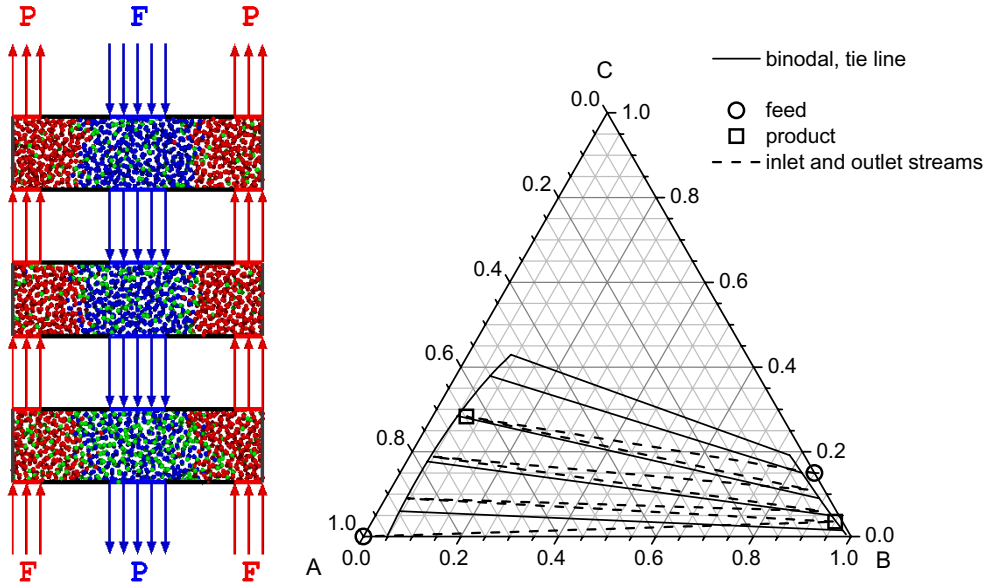

Figure 3. Simulation of an extraction column on themolecular level.

HTU-NTU Concept

The second concept combines the microscale molecular simulation with the HTU-NTU-method, which takes the macroscopic behavior into account, and provides, by numerical integration of the balance and kinetic equations, the concentration and temperature profiles within the column. The required material parameters in the equilibrium and transport models are determined by molecular simulations at some few selected positions in the vicinity of the interface at operating conditions. In this approach, the two-film theory is used for evaluation of the simulated conditions.

The multicomponent mass transfer is modeled by using the generalized Ficks law

$$J = -cD\nabla x, \tag{1}$$

where J is a vector of the molar fluxes, c the total concentration, ∇x the driving force and D the matrix of Fick diffusion coefficients which have to be fitted to the simulated data. For conditions where no diffusion coefficients are available (i.e., between the simulated points), the diffusion coefficients are determined by linear interpolations.

CONCLUSIONS

The results in Figures 1 and 3 demonstrate that a design of unit operations by molecular simulation is possible. Therefore, not all molecules in the column have to be regarded, but only the relevant conditions have to be taken into account. This means that

simulations that are performed in the vicinity of the interfacial region are sufficient to depict one separation stage. By connecting the inlet and outlet streams of the stages, all relevant conditions that the particles pass in the column are regarded. But the simulations don't just behave like adequately connected equilibrium calculations. They also include the non ideal character of a stage, which can be either caused by multicomponent effects of the mass transfer or by the finite residence time of the fluids in one stage. A dimensional analysis provides the necessary residence time of the fluids in the molecular simulation so that the mass transfer in the simulation corresponds to a macroscopic stage.

REFERENCES

1. A. Pfennig, "Distillation Simulated on Molecular Level," *Mol. Sim.*, **30**(6), 361-366 (2004).

PSEUDO-EQUILIBRIUM STATE OF THE SYSTEM Zr–HNO_3–TBP–diluent

Oksana A. Sinegribova, Olga V. Muraviova, and Kuaw Thu Win

D. Mendeleyev University of Chemical Technology of Russia,
Moscow, Russian Federation.
Corresponding author email address: oasinegr@rctu.ru

ABSTRACT

The attempt was made to find the cause of noncoincidence of the extraction and back-extraction of Zr isotherms after 30 min. contact of phases at the same acidity of the aqueous phases of the extraction system Zr–HNO_3–TBP – octane as described in [1]. The distribution of zirconium between the aqueous and organic phases has been investigated by simultaneous carrying out extraction and back-extraction at the same acidity (4 and 6 mole/L HNO_3) in an extractor with a liquid-membrane-contained extractant (40% and 70% TBP). The equilibrium state in the 3-phase system was obtained only for 6 mol/L HNO_3 in the aqueous phases and 40% TBP in the organic phase. It is supposed that, in the interval of aqueous phase acidity 4-6 mol/L, three types of zirconium extractable compounds can exist in the organic phase: $Zr(NO_3)_4$2TBP (I) and (or) $HZr(NO_3)_5$2TBP (II), which are formed in the reaction $Zr_{aq} \rightarrow Zr_{org}$ and are not in thermodynamic equilibrium, and $TBP(H_3O^+)Zr(NO_3)_5^-$ (III), which is the intermediate compound in the reaction $Zr_{org} \rightarrow Zr_{aq}$ and is formed as result of one TBP molecule loss by species (I) and (II). Predominance of species (I) or species (II) in the organic phase depends mainly on the concentrations of HNO_3 and TBP. The noncoincidence of the extraction and back-extraction isotherms may be caused by low rate of $Zr(NO_3)_4$2TBP transformation to an intermediate compound. Afer 30 min. of phase stirring, the extraction system with $Zr(NO_3)_4$2TBP in the organic phase achieves only a pseudo-equilibrium state. Therefore, use of Zr extraction isotherms obtained in laboratory experiments is not always acceptable for calculations of stage number for counterflow extraction process.

INTRODUCTION

It was found earlier [1], that the isotherms of Zr distribution during mass transfer to and from organic phase in the system Zr–HNO_3 (4-6 mol/L)–TBP (40-70% vol)–octane after 30 min. stirring were not coincident, although in both cases the kinetics curves reached a plateau after 30 min. phase contact. Subsequent investigation [2] showed that zirconium after extraction from 6 mol/L HNO_3 in 70% TBP is present in the organic phase as two different type of species: a part of Zr during multiple back-extraction (30 min. of every contact) by fresh aqueous solutions of similar acidity distributes between the aqueous and organic phases to complete removal into the aqueous

phase, but another part remains in the organic phase. It is known that the nature of Zr compounds that are extracted in TBP depends on acidity of the aqueous phase. At the concentration of $HNO_3 \geq 4$ mol/L, two species can be expected: a dissolvate of zirconium tetranitrate $Zr(NO_3)_4 2TBP$(I) at lower acidity and a complex acid $HZr(NO_3)_5 \cdot 2TBP$(II) at higher acidity [3,4]. It is reasonable to assume that behavior of these species during the contact of the organic phase with acidic aqueous solution will be different.

EXPERIMENTAL

In order to obtain in the organic phase the main part of zirconium as compound (I) or as compound (II), the following conditions of experiments were chosen: 4 mol/L HNO_3 and 6 mol/L HNO_3, 40% and 70% (vol) TBP .

The organic solutions before contact with aqueous solutions of zirconium nitrate were contacted with nitric acid solution of necessary acidity to equilibrium state. The concentration of Zr in the aqueous phases was determined by complexometric titration with EDTA or by the photometric method (for low concentrations); the concentration of Zr in the organic phases was calculated from material balances.

On Zr extraction, the change of HNO_3 distribution between phases can take place too, because activity of nitric acid in only nitric acid solution and in solutions which also contain zirconium at similar acidity is different.

In order to obtain equal activities of nitric acid in extraction and back-extraction aqueous phases, an apparatus with two separated aqueous phases that were in contact with the same organic phase was used (Figure 1). The volume of every phase was 400 mL. In this device, the organic phase works as a liquid membrane.

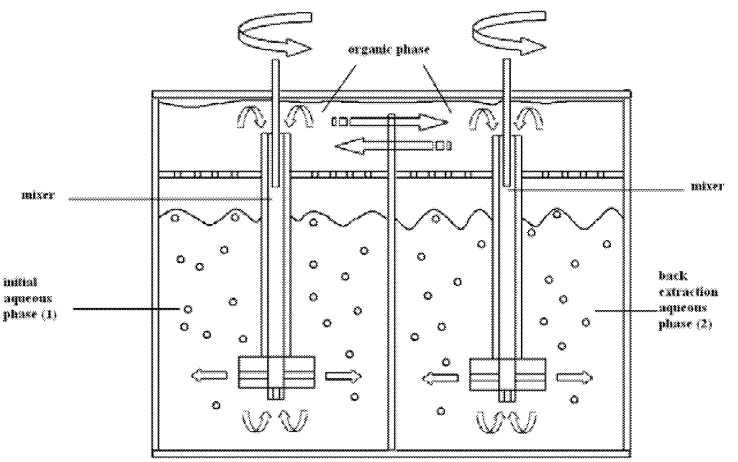

Figure 1. The scheme of the apparatus with two separated aqueous phases in contact with the same organic phase

RESULTS AND DISCUSSION

In the experiments, the initial concentration of zirconium in nitric acid solutions was 0.33–0.40 mol/L. The stirring of phases was stopped periodically, and the concentration of Zr in both aqueous phases was determined. The Zr concentration in the organic phase was calculated the from mass-balance equation. Experiments were finished when concentrations of zirconium in the phases ceased to change. The values of Δ[Zr] were calculated as difference between the final Zr concentrations in the aqueous phases 1 and 2. The results are presented in Table 1 and Table 2.

Table 1. Distribution of Zr between two aqueous phases (6 mol/L HNO_3) and organic phase

τ, min.	Aq. ph. 1 [Zr]	Aq. ph. 2 [Zr]	Org. ph. [Zr]	τ, min.	Aq. ph. 1 [Zr]	Aq. ph. 2 [Zr]	Org. ph. [Zr]
10	0.255	<0.001	0.084	5	0.271	0	0.121
20	0.204	<0.001	0.143	10	0.247	0	0.145
40	0.166	0.008	0.165	15	0.231	0.007	0.153
60	0.125	0.026	0.188	20	0.199	0.036	0.157
80	0.099	0.036	0.204	30	0.188	0.048	0.156
100	0.099	0.041	0.200	40	0.156	0.063	0.173
120	0.089	0.045	0.205	60	0.137	0.089	0.166
140	0.085	0.053	0.202	80	0.117	0.117	0.157
170	0.081	0.053	0.205	100	0.117	0.104	0.170
190	0.081	0.053	0.205	120	0.117	0.117	0.157
$[Zr]_{init}$ = 0.339 mol/L, 70% TBP Δ[Zr] = 0.028 mol/L				$[Zr]_{aq.init}$ = 0.392 mol/L, 40% TBP Δ[Zr] = 0			

Table 2. Distribution of Zr between two aqueous phases (4 mol/L HNO_3) and organic phase

τ, min.	Aq. ph. 1 [Zr]	Aq. ph. 2 [Zr]	Org. ph. [Zr]	τ, Min.	Aq. ph. 1 [Zr]	Aq. ph. 2 [Zr]	Org. ph. [Zr], g/L
5	0.337	0	0.067	5	0.327	0	0.005
10	0.312	0	0.092	20	0.287	0	0.045
15	0.271	0.007	0.126	30	0.279	0.003	0.050
20	0.214	0.032	0.158	40	0.272	0.013	0.047
30	0.197	0.048	0.159	60	0.259	0.020	0.053
40	0.180	0.048	0.176	90	0.248	0.028	0.054
60	0.178	0.064	0.162	120	0.226	0.032	0.074
80	0.148	0.069	0.186	150	0.223	0.041	0.068
100	0.149	0.072	0.182	180	0.220	0.045	0.066
120	0.146	0.079	0.179	210	0.219	0.043	0.070
$[Zr]_{init}$ = 0.404 mol/L , 70% TBP, Δ[Zr] = 0.067 mol/L				$[Zr]_{init}$ = 0.332 mol/L , 40% TBP, Δ[Zr] = 0.176 mol/L			

Comparison of Δ[Zr] values (Table 1 and Table 2) shows that this value is higher for the lower acidity of aqueous zirconium solution (4 mol/L HNO_3), and this fact indicates that the back-extraction rate of zirconium from $Zr(NO_3)_4$2TBP is slower than rate of Zr back extraction from the complex acid $HZr(NO_3)_5$2TBP, which is mainly extracted from 6 mol/L HNO_3.

The difference of $Zr(NO_3)_4$2TBP and $HZr(NO_3)_5$2TBP stability at the contact with nitric acid solutions of various concentration is confirmed by the extent of zirconium back-extraction from two extracts advance prepared at different acidities (Figure 2). Time of back-extraction was 30 min.

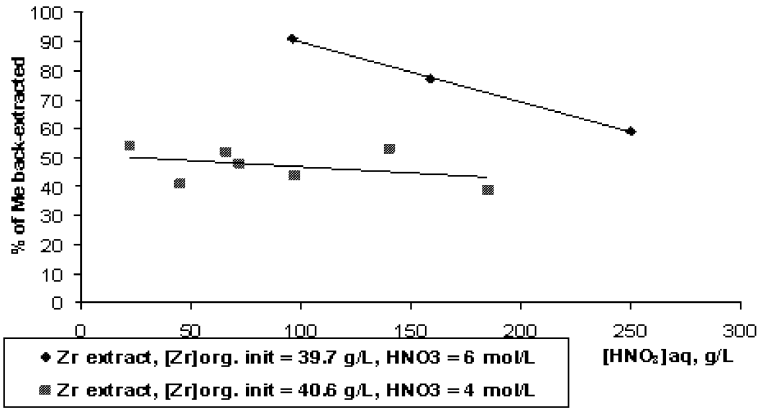

Figure 2. Effect of water solution acidity on extent of metal back-extraction from extracts prepared at different acidities.

Taking into account that after extraction from 4 mol/L HNO_3 the compound $Zr(NO_3)_4$2TBP predominates in the organic phase but after extraction from 6 mol/L HNO_3 the compound $HZr(NO_3)_5$2TBP predominates, the above presented data show that the higher the concentration of $Zr(NO_3)_4$2TBP in the organic phase goes, the farther the extraction system is from the equilibrium state. Only the presence of the complex acid $HZr(NO_3)_5$2TBP in the organic phase leads to fast achievement of the equilibrium state.

For mathematical simulation of the isotherm of zirconium extraction in TBP, the results of Zr distribution between 6 mol/L HNO_3 and 40% TBP solution were chosen. The data of Table 1 show that at these conditions it is possible to expect negligible concentration of non-equilibrium zirconium species in the organic phase; thus, only in this experiment zirconium concentration in the aqueous phases 1 and 2 became equal.

For modeling of this distribution curve, EXTREX-Q software was used. This software can be used to determine a number of extraction complexes with different solvate numbers that are formed in systems with one (or more) extractant and can be used for determination of degree of polymerization [5]. Because of the high concentration of nitric acid in the solutions the modeling was done by assuming that in the aqueous phase zirconium exists mainly as complex $Zr(NO_3)_2^{2+}$.

The optimal coincidence of calculated and experimental distribution curves (mean error < 5%) was obtained under the assumption that Zr was presented by three types of

species in the organic phase (Figure 3). We supposed that the first compound was $Zr(NO_3)_4 2TBP$ (I), the second compound was $HZr(NO_3)_5 2TBP$ (II), and the third compound was probably the complex acid $[TBPH_3O^+(H_2O)]Zr(NO_3)_5$ (III), which was described by Stoyanov at al [5]. The presence of these types of Zr compounds in TBP at various acidity was confirmed by IR spectroscopy. According to [5] the complex zirconium acid (III) is formed when the concentration of nitric acid increases but the concentration of zirconium decreases. It is possible to assume that compound of type III is formed during the contact of Zr extract with nitric acid aqueous solution and that species (III) is an intermediate compound in the equilibrium Zr_{org}–Zr_{aq} and it appears as a result of loss of one TBP molecule by compounds (I) and (II).

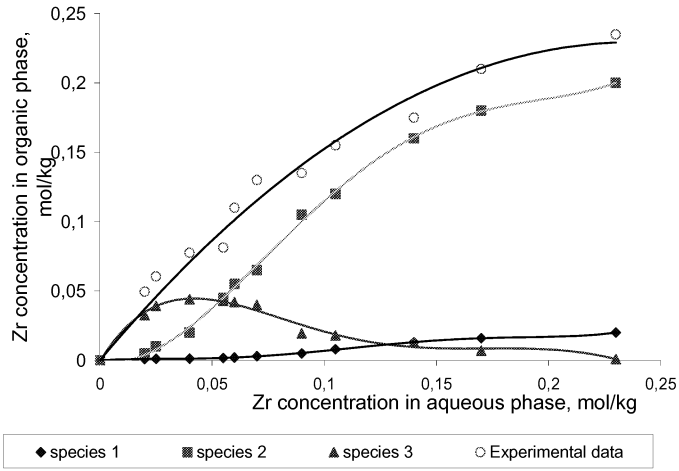

Figure 3. Experimental and calculated data of Zr species distribution between aqueous and organic phase.

The data of Table 1 and 2 may be explained if the complex acid $HZr(NO_3)_5 2TBP$ transforms easier to the intermediate compound $[TBP{\cdot}H_3O^+(H_2O)]Zr(NO_3)_5$, but the transformation of $Zr(NO_3)_4 2TBP$ to $[TBPH_3O^+(H_2O)]Zr(NO_3)_5$ takes more time. It should be noticed that earlier Tarasov at al. [6] investigated uranium back-extraction from organic solutions that contained $UO_2(NO_3)_2 2TBP$ into water solutions and found that the loss of the first TBP molecule (exchange for water molecule) was a considerably slower process than the loss of the second molecule.

Apparently, the slower stage of $Zr(NO_3)_4 2TBP$ desolvation in comparison with desolvatation of other compounds leads to non coincidence of extraction and back-extraction curves. Thus, the reason for non coincidence of isotherms is kinetics.

The attempt to get the coincidence of direct and back isotherms by means of carrying out experiments for much longer time failed because of very slow but gradual transfer of zirconium from the aqueous to the organic phase. After 30 min. of phase contact, a plateau on the kinetics curve was observed, but after 2-3 h of agitation, the increase of Zr extractability became noticeable. For example, from an aqueous solution containing 0.54 mol/L Zr in 6 mol/L HNO_3, after 30-60 min. of mixing with 70% TBP in octane, 0.27mol/L Zr was extracted; after 120 min., 0.29 mol/L; after 180 min., 0.3

mol/L; and after 210 min. of phase mixing, 0.31 mol/L Zr. Subsequently, after 3 days, 0.38 mol/L Zr transferred into the organic phase. The possible cause of this phenomenon is the association of extractable compounds in the organic phase. The availability of associated compounds containing zirconium in TBP solutions was earlier confirmed by laser light dispersion [7]. Mathematical simulation of the zirconium extraction isotherm (aqueous phase acidity was 6 mol/L HNO_3, 40% TBP, 30 min. of phase mixing) by EXTREX-Q software indicated the absence of polymerization in the organic phase but different solvate numbers of 3 types of zirconium compounds in the organic phase: the first compound with solvate number 2 (species 1, Figure 3), the second compound with solvate number approximately ~ 5 (species 2, Figure 3), and the third compound with solvate number ~ 15 (species 3, Figure 4). The high solvate numbers show the possibility of existence of zirconium compound associated with TBP or solvate HNO_3TBP in the organic phase, and even the possibility of micelle formation, as it was observed for the extraction of $HFeCl_4$ in TBP [8].

CONCLUSIONS

The presented results show that real attention should be paid to use of the extraction isotherms obtained in laboratory experiments for determination of the number of steps in counterflow extraction processes. It is necessary preliminarily to be convinced of the coincidence of the isotherms for metal transfer to and from organic phase, because this coincidence is the evidence of equilibrium state of extraction system.

REFERENCES

1. O. A Sinegribova, K. T. Win, L. V. Troegubova, O. V. Muraviova, G. V. Pokrovskaya, "Effect of non-equilibrium metal aggregation on parameters of metal extraction by TBP," ISEC' 2005, Beijing, China, 402-407 (2005).
2. O. A Sinegribova and K. T. Win, "Zirconium distribution between phases at mass transfer to and from organic phase," *Chemical Technology (Russ.)*, **3**, 129-133 (2007).
3. A. M. Reznik, A. M. Rozen, S. S. Korovin, "The extraction of zirconium and hafnium from solutions containing nitric acid," *Radiochemistry (Russ.)*, **1**(5), 49-53 (1963).
4. S. I. Stepanov and K. A. Slavinsky, "Program complex EXTREQ-2 for mathematic simulation of multicomponent extraction equilibriums," *Chemical Technology (Russ.)*, **10**, 40-43 (2006).
5. E. S. Stoyanov, S. V. Chizevskaya, A. M. Chekmarev, "Composition and structure of zirconium complexes in TBP extracts obtained from concentrate solutions of nitric acid," *J. Struct. Chem. (Russ.)*, **5**(34), 80-89 (1993).
6. V. V. Tarasov, G. A. Jagodin, A. A. Pichugin, "Extraction kinetics of inorganic substances." "*Inorganic Chemistry" (Results of science and technology VINITI AN SSSR*) (Russ.), **11**, 3-171 (1984).
7. O. A. Sinegribova and O. V. Muraviova, "Micellar mechanism peculiarities of metal extraction by organophosphorus extractants in the presence of surfactant," ISEC' 2002, Cape Town, South Africa, 186-192 (2002).
8. E. S. Stoyanov, "New type of nanoparticles, micelles formed in water-saturated organic solutions of $HFeCl_4$ and $HClO_4$: composition, structure and properties," *J. Chem. Soc., Faraday Trans.*, **94**, 2803-2812 (1998).

EXTRACTION OF SOME RARE EARTH ELEMENTS BY D2EHPA IN SYSTEMS WITH ARTIFICIAL MECHANICAL DISTURBANCE

N. F. Kizim and E. N. Golubina

Novomoskovsk Institute of Mendeleyev University of Chemical Technology, 301650, Street Druzhby, Novomoskovsk, Russia.
Corresponding author email address: nphk@mail.ru

ABSTRACT

The results of research on the influence of mechanical vibrations at the interfacial layer in the range 4–14 kHz in the extraction of Er(III) (Nd(III)) by solutions of D2EHPA in a diluent are presented. It is shown that the mechanical vibrations locally excited by the vibrator in a dynamic interfacial layer (DIL) influence the rate of extraction, especially at the end of the period of accumulation of Ln(III) in the DIL. At the resonant frequency, the rate of extraction is ca. 3–4 times above that in the absence of mechanical vibration. During the accumulation of Ln(III) in the DIL and structuring, the influence of a vibrational field on the rate of accumulation is observed. An increase in concentration of the extractant (0.01–0.05 M) leads to an increase of the factor of acceleration of extraction (the relation of amounts Ln(III) in an extract with oscillatory influence and in its absence). On extraction of Nd(III) (10^{-5}–0.03 M), the acceleration factor rises with concentration and pH (2–6.2). Distinction in the acceleration factor on individual extraction of Nd(III) and Er(III) is connected with the distinction of the structures formed in the DIL. The results are of interest in the development of new extraction equipment.

INTRODUCTION

One of the methods of allocation and division of rare earth elements (REE) is liquid extraction. The process of extraction of REE by solutions of D2EHPA is accompanied by the course of the chemical reactions leading to the formation of a structured interfacial layer, which creates an additional resistance to mass transfer and essentially reduces the rate of extraction of an element. Therefore, the search for ways of an intensification of the process is an actual problem.

Vibration has been in use for a long time in industrial extraction equipment [1] and in research on mass transfer in liquid/liquid systems [2]. Influence of vibration on a liquid/liquid system as a whole leads to dispersion, at the same time sharply increasing at the interface [1] or to the achievement of high intensity of turbulence in volumes of phases during the preservation of continuity of an interface [2].

Essentially another approach to influence mass transfer through an interface is offered by V. V. Tarasov [3,4]. In this case, a tape making alternating/reciprocal motion from one phase to another with a frequency less than 4 s^{-1} accelerates the extraction

process even in systems with strongly pronounced structuring in a dynamic interfacial layer as in the system of an aqueous solution of Ln(III) salt and organic solution of D2EHPA in a hydrocarbon diluent.

In our approach, local mechanical influence on the dynamic interfacial layer by means of a vibrating element placed at the interface prior to the beginning of experiment is carried out. Earlier it was shown [5] that stripping in systems of organic solvent and aqueous mineral acid is intensified by generating waves at the interface of the contacted liquids. In particular, in the system of toluene and aqueous HNO_3 at a frequency of 5.9 kHz, the factor of mass-transfer rate increases 5-8 times.

In this report, results on the influence of mechanical vibrations in the range 4–14 kHz at the interface in extraction of some REE by D2EHPA are presented.

EXPERIMENTAL

Experiments were carried out on a setup which includes a generator of low-frequency signals, a glass cell, and the vibrator.

In the experiments, a cell of cone-shaped form was used in which 8 mL of an aqueous solution of neodymium nitrate (chemically pure substance) or erbium chloride (chemically pure substance) had been placed, and 2 mL of 0.05 M D2EHPA in toluene (chemically pure substance) or heptane (chemically pure substance) was accurately poured on the cell wall. D2EHPA was purified by the usual technique [6]. The geometrical area of the interface was 6.07 cm^2. At set time intervals, the aqueous phase (to exclude possible influence of nonuniformity of distribution of a component) was separated from the organic phase and analyzed for Ln(III) content [7]. For this purpose, an aliquot was placed in a 25 mL volumetric flask to which was added 2 mL of a solution of the indicator Arsenazo I and 5 mL borate buffer and then water up to the mark.

The optical density of the solution was measured by means of a colorimeter with the use of a 590 nm optical filter. The REE concentration was found on a calibration curve obtained using solutions with known REE concentration. Measurements were made in the linear part of the calibration curve.

Determination of the organic-phase Ln(III) concentrations used the following method. After the experiment, the organic phase was separated from the aqueous phase and stripped with 0.5 M nitric acid (preliminary experiments has been shown that stripping proceeds quantitatively). Then the pH was raised to 6 with addition of an aqueous ammonia solution for colorimetric analysis.

The amount of Ln(III) accumulated in the interfacial layer was found from material balance.

Vibration influence on a dynamic interfacial layer was made by means of the vibrator [8], a high-frequency electrodynamic head with rigidly fixed in the center run-out a core from a stainless steel rod 0.05 cm and length 4.3 cm on the other end of which the vibrating element also is rigidly attached. The element was fabricated from Teflon in the form of a triangular prism having in section an appearance of an isosceles triangle with height of 0.5 cm and base of 1.1 × 0.3 cm, turned to the interface by the top of the triangle. Before the beginning of an experiment, an edge of the prism the vibrator established on the aqueous/air interface submitted on the cleats of the electromagnetic

head a voltage of the sine wave form of the set frequency. Then on the surface of the aqueous solution was poured (as it is specified above) the organic extractant solution.

For an estimation of the influence of the external parameters on the process used, the factor of acceleration (FA), which represented the relation of the concentration of REE in an organic phase when imposing mechanical vibrations of resonant frequency (C_f) to the concentration of REE in an organic phase at their absence (C). FA in all experiments was determined through 60 min. from the beginning of experiment.

RESULTS AND DISCUSSION

Extraction of Ln(III) solution by D2EHPA (HA) in the diluents proceeds as

$$Ln^{3+} + 3HA \Leftrightarrow LnA_3 + 3H^+,$$

and at high values of pH, when in a solution there are partially hydrolyzed forms of Ln(III), and reactions of a kind occur as

$$Ln(OH)_n^{(3-n)+} + (3-n)HA \Leftrightarrow Ln(OH)_n A_{3-n} + (3-n)H^+ \qquad (n = 1, 2)$$

These reactions are localized in a dynamic interfacial layer (DIL) if the initial concentration of Ln(III) in the aqueous phase and HA in the organic phase are commensurable. The formed salts LnA_3 and $Ln(OH)_nA_{3-n}$ are not soluble in water nor in organic phases accumulation in DIL. Their molecules with participation of HA quickly enough form particles of a new phase that grows together to form a spatial grid. In DIL the structuring is observable visually, identified by sharp increase of viscosity and the presence of a horizontal plateau in the dependence $-\ln(1-C/C^*) = f(t)$, where C and C^* are respectively the current and equilibrium concentrations of Ln(III) in the organic phase (Figure 1). At the same time, these salts cooperate further with HA to form a solvate of kind LnA_3HA, soluble in an organic phase, and this transition causes the extraction of Ln(III). At low initial aqueous concentration of Ln(III) and organic-phase concentration of HA 3-5 times exceeding the concentration of Ln(III), the reactionary region extends aside the aqueous phase, in view of penetration into these layers by HA. In this case, the significant part of arising particles of the new phase that are far from the interface is not kept and sediments. As such, the chemical aspect of extraction is represented. The real process is more difficult. As soon as the aqueous and organic phases are contacted, in the system develops a spontaneous interfacial convection (SIC) whose intensity depends on the conditions of the experiment and time elapsed from the beginning of the experiment. The SIC occurs more intensively in the first 5-10 min. of the experiment; thus, in the system not mixed compulsorily, noticeably spontaneous emulsification which is poorly expressed if the initial concentration of Ln(III) with the initial concentration of HA are expressed. Structuring leads to the suppression of SIC or to appreciable decrease in its intensity if the initial concentration Ln(III) is small.

The mechanical disturbance locally excited by the vibrator in a dynamic interfacial layer can influence different stages of the process (Figure 1). As revealed SIC the interfacial layer in liquid/liquid heterogeneous systems as shown by us earlier [11] has a resonant property; it is possible to expect that it will take place in systems containing an aqueous solution of Ln(III) salt and organic solution of D2EHPA in a

diluent. The dependence of the FA on frequency of the enclosed vibrations, presented on Figure 2, confirms our assumption.

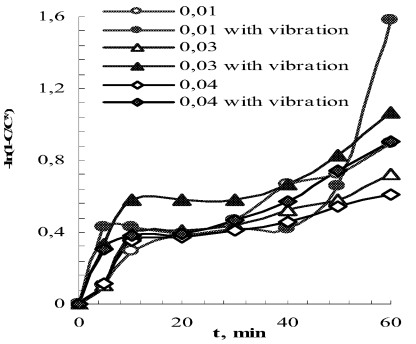

Figure 1. Dependence –ln(1–*C*/*C**) on the time of experiment during the extraction of Er(III). Aq: 0.05 M $ErCl_3$, pH = 5.2. Concentration (M) of D2EHPA in heptane is specified in the legend.

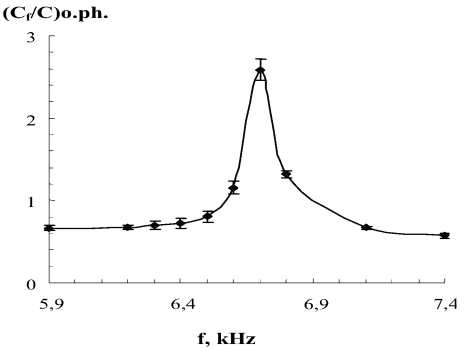

Figure 2. Effect of frequency on the enclosed vibrations on the FA during extraction of Er(III) by 0.05 M D2EHPA in heptane. Aq: [$ErCl_3$] = 0.05 M; pH = 5.2.

During the experiment, the resonant frequency slightly changes, which indicates a change of properties of the DIL. Resonant character is an important property of a DIL, and its application in practice for acceleration in the process of extraction can be found. Really, the pumping of energy in DIL is most effective on the resonant frequency, as it is possible to achieve the maximum FA with the least expenditure of energy.

The degree of influence on extraction from mechanical disturbance of DIL changes during the experiment (Figure 3). At elapsed times of 5–10 min., imposing of the mechanical vibrations leads to a 1.5–3.5-fold increase in the FA that grows out imposing the disturbances developing in the system of SIC and enclosed from the outside. The decrease in the FA at the increase in the concentration of HA is caused by the high rate of structuring in the DIL. At time of 10–40 min., SIC is suppressed by structuring in DIL; the FA is close to 1. After 40 min. from the beginning of experiments, the FA increases, which indicates a change of hydrodynamic conditions in DIL under the influence of the enclosed vibrations during dissolution of Ln(III) salts as a result of their further interaction with HA and restructuring of DIL. In particular, near the vibrator, an extensive transparent area is observed. Such character of dependence of the FA on time testifies the accumulation of Ln(III) in DIL.

The dependence of n_f/n, on time presented on Figure 4, indicates the influence of disturbance of the interfacial layer on the accumulation of Ln(III). At 10-30 min. from the beginning of the experiment and at the concentration of the extractant 0.01-0.03 M, external mechanical vibration influence on DIL lowers the rate of accumulation of Ln(III). It is connected with the increase of a share the sedimentating particles of the new phase, as the FA in this interval is close to 1. When the concentration of HA is more than 0.04 M, the external influence on DIL oppositely intensifies the accumulation of Ln(III). The accumulation of Ln(III) depends on the initial concentration D2EHPA (Figure 5) and the elapsed time. The influence of D2EHPA concentration is insignificant, and with increase in the concentration of D2EHPA in experiment without external mechanical disturbance, the accumulation of Ln(III) decreases. However, when imposing external

indignations on DIL, on the contrary, increases, especially noticeably when the elapsed time of experiment is more than 20 min. In DIL, accumulation can be up to 30% from the originally taken quantity of Ln(III). Similar dependences have been obtained for the process of the extraction of Nd(III) (Figure 6).

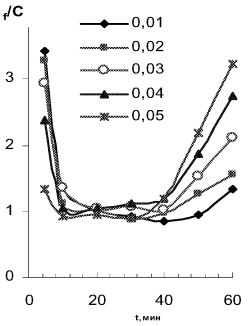

Figure 3. The dependence of the FA on the time of extraction of Er(III). The concentration (M) of D2EHPA in heptane is shown in the legend. Initial aqueous phase pH = 5.2.

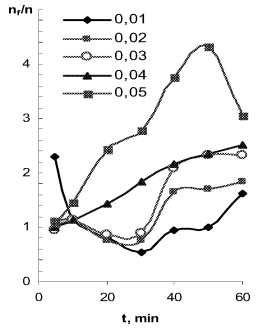

Figure 4. Time dependence of the amounts of Ln(III) accumulation in DIL when imposing vibrations and their absence when extracting Er(III) in a DIL. Org: D2EHPA in heptane. Aq: 0.05M $ErCl_3$, pH = 5.2.

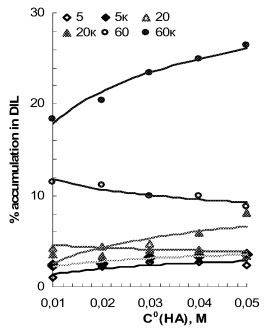

Figure 5. Influence of initial concentration extractant on the accumulation of Er(III) in a DIL. Org.: D2EHPA in heptane. Aq: 0.05 M $ErCl_3$; pH = 5.2.

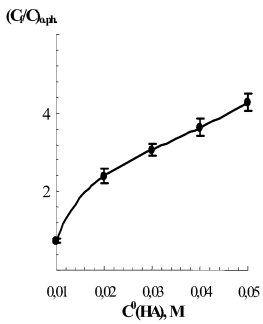

Figure 6. Influence of extractant concentration on the FA during the extraction of Nd(III) by D2EHPA in heptane. Aq: 0.05 M $Nd(NO_3)_3$; pH = 6.2.

It is necessary to note that the FA when imposing mechanical vibrations of resonant frequency in the system with Nd(III) is approximately 2 times above than that when extracting Er(III). This is connected with distinction of the structures formed in the interfacial layer. In the first case, the structure formed is a highly elastic gel. In the second case, there is a polymeric crystal gel. The distinction of structures in the interfacial layer proves to be true also in infrared-spectral data of samples taken from the dynamic interfacial layer and direct microscopic observation by a digital camera.

The increase in concentration of Nd(III) in the initial aqueous phase leads to an increase in FA (Figure 7). The change of pH of the initial aqueous solution, within the limits from 6.6 to 2, leads to a 5-fold change of the FA (Figure 8).

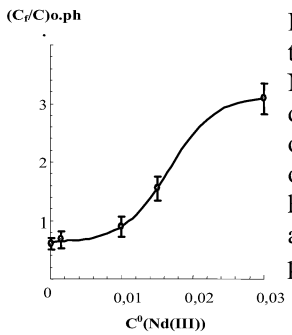

Figure 7. Effect of the concentration of Nd(III) on the FA during the extraction of a 0.05 M solution of D2EHPA in heptane. Initial aqueous phase pH = 6.2.

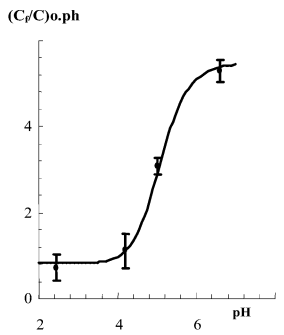

Figure 8. Effect of pH and initial aqueous solution on the FA during extraction of Nd(III) by D2EHPA in heptane.

CONCLUSIONS

It is experimentally established that the mechanical vibration disturbance of resonant frequency on a dynamic interfacial layer allows a 3–4-fold increase in the rate of extraction of Ln(III) by D2EHPA in a diluent. The mechanical disturbance influencing locally on a dynamic interfacial layer differently influences the rate of the process, which can be used as an additional opportunity (previously formulated in [9]) to increase the selectivity factor in solvent extraction. During the accumulation of Ln(III) in a dynamic interfacial layer, the influence of mechanical influences can promote it if the concentration of Ln(III) and extractant are commensurable and not too small, or, on the contrary, to reduce the rate of accumulation if the concentration of the extractant is great in relation to the concentration of Ln(III). The FA of extraction at vibration disturbance on a dynamic interfacial layer depends on the nature of Ln(III); in the case of Nd(III), it is two times more than the case of Er(III), which is connected with the distinction of the structures formed in the interfacial layer.

REFERENCES

1. Recent Advances in Liquid-Liquid Extraction, C. Hanson, Ed., Pergamon Press, 1971.
2. V. Hančil, V. Rod, and M. Řeháková, "Mass Transfer Cell with Vibrational Mixing," *Chem. Eng. J.,* **16**(1), 51-56 (1978).
3. V. V. Tarasov, "A dynamic interfacial layer in nonequilibrium systems a liquid/liquid," *Dokl. Russ. Acad. Sci.*, **350**(5), 647–649 (1996).
4. V. V. Tarasov and G. G. Larin, "Mass transfer at periodic disturbance of interface in system liquid/liquid," *Theor. Found. Chem. Eng., (in Russian)*, **34**(2), 188-194 (2000).
5. N. F. Kizim and E. N. Golubina, "Effect of Mechanical Vibrations on the Reextraction Kinetics in the Toluene-HNO_3-H_2O System," *Russ. J. Phys. Chem.*, **78**(3), 464-467 (2004).
6. W. J. McDowell, P. T. Perdue, and G. N. Case, "Purification of Di(2-ethylhexyl)phosphoric Acid," *J. Inorg. Nucl. Chem.*, **38**(11), 2127-2129 (1976).
7. A. I. Busev, V. G. Tiptsova, and V. M. Ivanov, "Manual in analytical chemistry of rare elements, Moscow," *Chemistry*, *(in Russian)*, 1978.
8. N. F. Kizim and E. N. Golubina, "The intensification of acid stripping upon generating waves at interface," International Solvent Extraction Conference, Beijing, The Peoples Republic of China, ISEC-2005, 2005; pp. 289-294.
9. G. Cote and D. Bauer, "The fundamental bases of selectivity in solvent extraction," Solvent Extraction. Proc. Int. Solv. Extr. Symposia, Moscow, 1998; pp. 20–32.

Novel Reagents, Materials, and Techniques

SEPARATIONS, COORDINATION, AND SOLVATION IN IONIC LIQUIDS; WHAT IS THERE THAT IS UNIQUE?

G. Gurau,[1] V. A. Cocalia,[2] and R. D. Rogers[1,2]

[1]QUILL, School of Chemistry and Chemical Engineering, The Queen's University of Belfast, Belfast, BT9 5AG, Northern Ireland (UK). [2]The University of Alabama, Department of Chemistry and Center for Green Manufacturing, Tuscaloosa, AL 35487 (USA). Corresponding author email address: R.Rogers@qub.ac.uk

ABSTRACT

Ionic liquids (ILs, salts that have a melting point less than 100 °C) have been investigated as potential replacement solvents for liquid/liquid separations, and the complex results have been highly dependent on the specific ILs, ligands, and systems studied. Nonetheless, ILs provide the opportunity to explore solvation in totally ionic media at relatively low temperatures, compared with the dissolution in high-temperature molten salts or in molecular solvents. In addition, because solutes are dissolved in ionic melts at lower temperatures, the effects of molecular solvents (including water) and organic or inorganic coordinating ligands can be studied. Such solvents or ligands would not survive the harsh conditions often used to generate high-temperature molten salts. Thus, we have begun to focus more on the fundamental interactions of solutes with and in IL solvents, and we are now gaining more insight into some of the unique aspects of IL solvation. Here we have briefly present some of our results investigating coordination and solvation of metal ions and ligands and put these results in context of previously published data.

INTRODUCTION

Ionic liquids (ILs) are, quite simply, liquids comprising only of ions [1]. (By common consensus, the term ILs is reserved for those salts with melting points below 100 °C.) Due to possible wide liquid ranges, favorable solvating properties for diverse compounds, high thermal stabilities, negligible vapor pressures, and tunable physical properties, ILs are much studied today as potential replacements for volatile organic compounds (VOCs) in liquid/liquid separations, hopefully reducing the use and generation of hazardous substances. Their unique composition (distinct cations and anions vs. molecular solvents), makes them interesting systems for studying the extraction mechanism, transport, and coordination chemistry of metal ions.

IL-based separations have been investigated via several techniques including liquid-liquid extraction [2], membrane separation [3], supported liquid membrane separation [4], liquid-phase microextraction [5], and salt-salt aqueous biphasic extraction

[6]. Aromatic and ionizable compounds have been found to be successfully separated, with the overall efficiency depending on a variety of factors, including the nature of both cation and anion, and pH. The solvation model of Abraham (a linear free energy relationship) was used as a tool to investigate IL solvent properties such as interactions with *n* and π electrons, their polarizability, hydrogen-bond basicity and acidity, dipolarity, and dispersion forces [7]. The results indicate that the most important interactions for ILs are polarity, hydrogen-bond basicity, and dispersion forces [8]. In general, ILs behave as moderately polar organic solvents, with their polarity being comparable to that of molecular dipolar non-hydrogen bond donors (acetone, DMF, DMSO) and dipolar hydrogen bond donor solvents (ethanol, cyclohexanol, phenol).

Gas-chromatography studies of ILs as stationary phases revealed that ILs show "dual-nature" properties, separating nonpolar compounds as if they were nonpolar stationary phases and polar compounds as if they were polar stationary phases [9]. Gas separation using different ILs, including functionalized ILs [10,11], which have one or more amino groups chemically attached, has been explored and shows much promise for CO_2 separation. Other separations using ILs include chromatographic electrophoresis [12], desulfurization of diesel fuels and gasoline [13], and breaking azeotropes [14], among others.

ILs have also been of high interest as substitutes for traditional solvents in separation of metal ions from aqueous media [15,16]. The most commonly reported metal-ion extraction mechanism is cation exchange [17,18]; however, the extraction of anionic complexes with the release of IL anions to the aqueous phase was also reported [19]. In both cases, the partitioning equilibria and the coordination environment differ from those observed in the traditional molecular solvents, and the loss of solvent ions to the aqueous phase is viewed as problematic for scale-up.

On careful selection of the IL solvent and the specific target separation process, it is possible to observe the same ligand coordination and extraction mechanism using an IL solvent as found for a molecular solvent, but judicious choices must be made. Studies on the coordination and extraction of Am^{3+} and UO_2^{2+} with Cyanex-272® and bis-(2-ethylhexyl)phosphoric acid (HDEHP) into 1-decyl-3-methylimidazolium bistrifylimide ($[C_{10}mim][Tf_2N]$) from acidic aqueous solutions were conducted, and the distribution ratios for both Am^{3+} and UO_2^{2+} vs. nitric acid concentration showed similar trends in the IL and dodecane, indicating that the same extraction mechanism takes place. Additional studies clearly showed that not only was the mechanism the same, but the ligand coordination to the metal was the same as well [20,21]. It is clear that a biphasic ionic liquid/aqueous system *can* behave identically to one using a molecular organic solvent with respect to both the partitioning equilibria and the coordination environment of metal ion complexes; however, in the current literature, this is not the usual case, and much care must be taken in selecting appropriate separations systems.

Overall, the studies published to date indicate that success or failure depends on how the ILs interact with the solutes and the second phase media. Thus, a good understanding of these interactions needs to be achieved in order to control and design IL-based applications. Here we present one such investigation into the coordination mode of N-N-diisobutyl-2-(octylphenylphosphinyl)-acetamide (CMPO, Figure 1) with the

uranyl ion in a hydrophobic IL, an example of isolation of an identical coordination complex of an f-element cation using an IL and a molecular solvent.

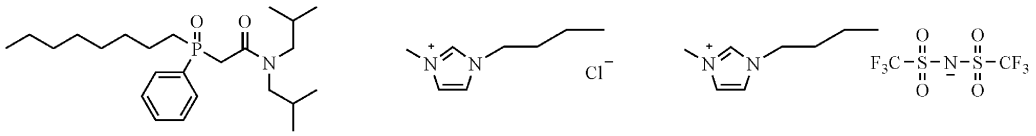

a) b) c)

Figure 1. a) N-N-Diisobutyl-2-(octylphenylphosphinyl)-acetamide; b) [C_4mim]Cl; c) [C_4mim][NTf_2].

EXPERIMENTAL

Uranyl nitrate hexahydrate was obtained from Alfa Aesar, Ward Hill, MA and used as received. Methylimidazole was purchased from Aldrich Chemicals, Milwaukee, WI and distilled prior to use. Cyanex-272® and lithium bis(trifluoromethanesulfonyl)-imide (Li[NTf_2]) were gifts from Cytec Industries Inc., Niagara Falls, Canada, and 3M, Minneapolis, MN, respectively, and were used as received. All other chemicals were of reagent grade, obtained from Aldrich, and used without further purification.

Synthesis of [C_4mim][NTf_2]. The IL, 1-butyl-3-methylimidazolium chloride ([C_4mim]Cl, Figure 1), was synthesized by following a previous literature procedure [22,23]. Equimolar amounts of 1-methylimidazole and 1-chlorobutane were refluxed for 48 h at 70 °C, with stirring. The resulting product was washed three times with ethyl acetate to remove any unreacted material. The resulting [C_4mim]Cl was dried in vacuo at 75 °C for 7 h to remove any traces of ethyl acetate. ^{1}H NMR (Bruker AM-360 MHz spectrometer; $CDCl_3$, 25 °C) δ 0.87 (t, 3H), 1.30 (quintet, 2H), 1.82 (q, 2H), 4.02 (t, 3H), 4.23 (t, 2H), 7.44 (s, 1H), 7.62 (s, 1H), 10.1 (s, 1H).

An excess equivalent molar ratio of 1:1.1 of [C_4mim]Cl and Li[NTf_2] were dissolved in 500 mL water. After overnight stirring, a two-phase system was observed, the top phase being aqueous LiCl and the bottom phase consisting of [C_4mim][NTf_2]. The top phase was decanted, and the remaining phase was washed 20 times with water to remove any remaining LiCl. The product was dried under reduced pressure for 3 h and in vacuo with heating (75 °C) for 7 h. The physical properties and purity of the IL were characterized and are comparable to data published in the literature.

Synthesis of $UO_2(NO_3)_2$(CMPO). In a 20 mL borosilicate vial, 0.023 g (0.006 mmol) of CMPO was dissolved in 0.691 g [C_4mim][NTf_2] at 60 °C. After complete dissolution of CMPO in the IL, 0.021 g (0.004 mmol) of $UO_2(NO_3)_2$•$6H_2O$ were added, and the mixture was heated at 60 °C with stirring for 10 min. The resulting yellow solution was left unsealed at ambient temperature. After one day, yellow single crystals (suitable for single crystal X-ray analysis diffraction) formed in the IL solution.

Single Crystal X-ray Diffraction. The data were collected on a Bruker SMART diffractometer with a CCD area detector using graphite monochromated Mo-Kα (λ = 0.71073 Å) radiation. A single crystal was mounted on a glass fiber and transferred to the goniometer for data collection. The crystal was cooled to -100 °C under a cold nitrogen gas stream. A matrix consisting of 30 frames at three positions around the reflection

sphere of the crystal was collected and used to determine the unit cell of the crystal. The unit-cell dimensions determined corresponded to the X-ray structure of $UO_2(NO_3)_2$(CMPO) crystallized from conventional solvents and reported in the literature [24].

RESULTS AND DISCUSSION

We have previously shown that using ILs instead of an organic diluent in some IL/aqueous separations does not necessarily induce any change in the separation mechanism or coordination environment of f-elements extracted into the IL phase when using organophosphorus ligands [20,21,25]. However, there have been numerous examples when separation of metal ions in IL/aqueous systems does proceed through different extraction mechanisms than reported for molecular solvents [18,19,26]. Also, in many cases, the coordination environment for the extracted metal species is significantly different than in conventional solvents [18,26]. Since the metal ion transfer in an IL/aqueous system cannot be predicted from the well-known behavior of molecular solvents, the challenge in deciding the future of ILs in this field lies in understanding how the ionic media influence the metal ion transfer and coordination behavior in ILs at a molecular level.

In IL/aqueous separation of metal ions, a strong binding ligand has to be involved in order to achieve the separation. The published studies of strong ligands coordinated to actinide ions in ILs are fairly limited [27]. An experimental EXAFS investigation of the CMPO/UO_2^{2+} complexation in IL/aqueous vs. dodecane/aqueous systems showed that the uranyl ion displays different coordination environments in the IL and dodecane ($(UO_2(NO_3)(CMPO)^+$ and $UO_2(NO_3)_2(CMPO)_2$, respectively) and different extraction mechanisms in the two systems:

$$UO_2^{2+}{}_{aq} + [C_nmim]^+{}_{IL} + NO_3^-{}_{aq} + CMPO_{IL} \rightleftharpoons [(UO_2)(NO_3)CMPO]^+{}_{IL} + [C_nmim]^+{}_{aq} \quad (1)$$

$$UO_2^{2+}{}_{aq} + 2NO_3^-{}_{aq} + 2CMPO_{org} \rightleftharpoons [(UO_2)(NO_3)_2(CMPO)_2]_{org} \quad (2)$$

A recent theoretical study of CMPO coordination to the uranyl ion in $[C_4mim][PF_6]$ has also been reported [28]. Molecular-dynamics results for the solvation of uranyl-CMPO complexes show that the most stable species in $[C_4mim][PF_6]$ is a neutral $UO_2(NO_3)_2(CMPO)_2$ complex, which is also found in conventional solvents. The authors attribute the formation of the reported $[(UO_2)NO_3]CMPO]^+$ cationic species found for the extracted uranyl complex in an IL/aqueous system to other factors such as the free energy of transfer of the ions from one phase to another.

The lack of structural evidence for the coordination modes of CMPO to the uranyl in ILs makes it difficult to conclude if these differences can be attributed to either the unique coordination environments in the ionic media or the other factors suggested. In order to further investigate these, we set out to crystallize uranyl/CMPO complexes directly from IL solvents for single-crystal X-ray diffraction analysis.

Both CMPO and $UO_2(NO_3)_2 \cdot 6H_2O$ are soluble in the IL $[C_4mim][NTf_2]$, a necessary first step for the attempted preparation of the coordination complex. (Despite their reputation as good solvents, it is actually not that easy to dissolve many metal salts

in ILs [29].) The CMPO was dissolved first at 60 °C, and then the uranyl salt was added and the mixture stirred at the same temperature for 10 min. until a yellow solution had formed. After cooling to room temperature, suitable single crystals for the X-ray analysis formed within one day.

The unit-cell dimensions obtained for the isolated complex matched those previously reported for the neutral $UO_2(NO_3)_2$(CMPO) complex isolated from an ethanol/chloroform solution [24]. Each uranyl ion is hexacoordinate with two nitrate ions and one bidentate CMPO molecule in the *cis* conformation (Figure 2). There are two independent formula units in the unit cell differing primarily in conformations of the octyl and isobutyl groups, but not in the coordination mode around each uranyl center.

Table 1. Crystal data for $UO_2(NO_3)_2$(CMPO) isolated from IL and conventional solvent

	$[UO_2(NO_3)_2(CMPO)]_{IL}$	$UO_2(NO_3)_2$(CMPO) [24]
Crystal System	Orthorhombic	Orthorhombic
Space group	*Pna*2$_1$	*Pna*2$_1$
Unit cell dimensions		
a/Å	19.93(2)	19.7821(3)
b/Å	10.4677(13)	10.6352(2)
c/Å	30.636(4)	31.4217(4)
Volume/Å^3	6382.7(13)	6610.7(2)
Radiation/wavelength/Å	MoKα (graphite monochromator)/0.71073	
Temperature/^{o}C	-100	30

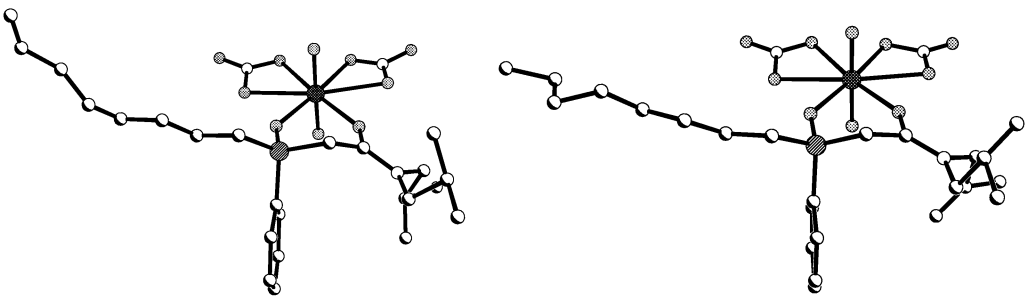

Figure 2. The two unique formula units in $UO_2(NO_3)_2$(CMPO). (Figure drawn from the cif file associated with the structure in reference [24].)

There are also no apparent relevant close contacts present in the structure. This suggests that the driving force in the formation of the crystalline packing lies in the segregation of hydrophobic octyl and isobutyl regions and hydrophilic $UO_2(NO_3)_2$ regions (Figure 3). The hydrophilic uranyl cores are separated by mixed aromatic-isobutyl regions.

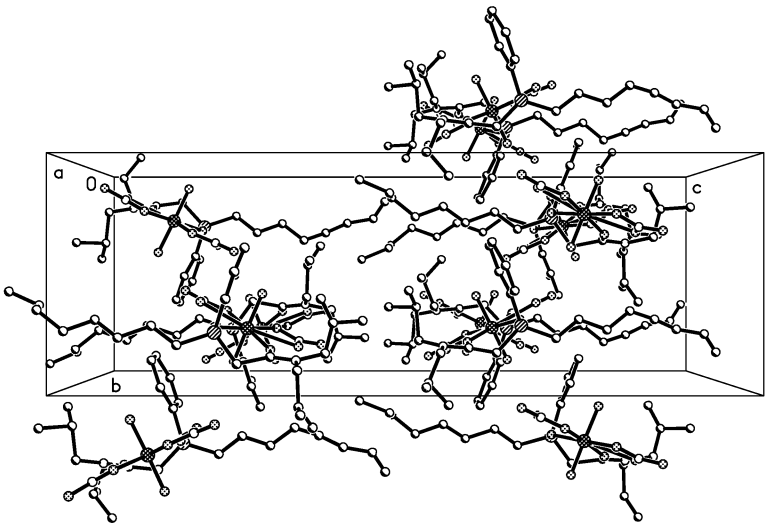

Figure 3. The segregation of hydrophobic and hydrophilic regions in $UO_2(NO_3)_2$(CMPO). (Figure drawn from the cif file associated with the structure in reference [24].)

While the structure is the same whether isolated from organic solvents or this IL, it is interesting to note that the water present from the starting salt and inherently present in many ILs, does not form part of the isolated complex. In addition, the crystal structure suggests that ILs can support regions of both hydrophilicity and hydrophobicity.

CONCLUSIONS

Single-crystal X-ray diffraction analysis of $UO_2(NO_3)_2$(CMPO) crystallized from $[C_4mim][NTf_2]$ revealed the same neutral complex commonly found for complexes isolated from traditional molecular solvents. Combined with Chaumont's theoretical results indicating this same neutral complex as the most stable in IL solution, this result suggests that the coordination mode of CMPO to uranyl is not responsible for the different extraction mechanisms. Thus, the cationic uranyl species extracted in the IL/aqueous systems are more likely the result of such factors as the free energy of ion transfer between the aqueous and ionic phases, where a competition exists between extraction of neutral ion pairs and an ion-exchange mechanism. This confirms the need to more fully understand the coordination behavior of common extractants to metal ions in ILs if they are to ever be used successfully in full-scale separations.

ACKNOWLEDGMENTS

This research was supported by the US Department of Energy Environmental Management Science Program (Grant DE-FG02-05ER63989) and by the Division of Chemical Sciences, Geoscience, and Bioscience, Office of Basic Energy Sciences, Office of Science, (Grant DE-FG02-96ER14673). The authors thank Cytec Industries Inc. and 3M for the gift of Cyanex-272® and $Li[NTf_2]$, respectively.

REFERENCES

1. See for example "Green Industrial Applications of Ionic Liquids," in NATO Science Series II. Mathematics, Physics and Chemistry,,Vol. 92, R. D. Rogers, K. R. Seddon, and S. Volkov, Eds., Kluwer: Dordrecht, 2003; pp. 553, and similar edited anthologies.
2. J. G. Huddleston, H. D. Willauer, R. P. Swatloski, A. E. Visser, and R. D. Rogers, "Room Temperature Ionic Liquids as Novel Media for 'Clean' Liquid–Liquid Extraction," *Chem. Commun*., 1765-1766 (1998).
3. J. Kröckel and U. Kragl, "Nanofiltration for the Separation of Nonvolatile Products from Solutions Containing Ionic Liquids," *Chem. Eng. Technol.*, **26**(11), 1166-1168 (2003).
4. L. C. Branco, J. G. Crespo, and C. A. M. Afonso, "Highly Selective Transport of Organic Compounds by Using Supported Liquid Membranes Based on Ionic Liquids," *Angew. Chem. Int. Ed.*, **41**(15), 2771-2773 (2002).
5. J.–F. Liu, Y.–G. Chi, G.–B. Jiang, C. Tai, J.–F. Peng, and J.–T. Hu, "Ionic Liquid-Based Liquid-Phase Microextraction, a New Sample Enrichment Procedure for Liquid Chromatography," *J. Chromatogr., A.*, **1026**, 143-147 (2004).
6. K. E. Gutowski, G. A. Broker, H. D. Willauer, J. G. Huddleston, R. P. Swatloski, J. D. Holbrey, and R. D. Rogers, "Controlling the Aqueous Miscibility of Ionic Liquids: Aqueous Biphasic Systems of Water-Miscible Ionic Liquids and Water-Structuring Salts for Recycle, Metathesis, and Separations," *J. Am. Chem. Soc.*, **125**(22), 6632-6633 (2003).
7. S. K. Poole and C. F. Poole, "Chemometric Evaluation of the Solvent Properties of Liquid Organic Salts," *Analyst*, **120**(2), 289-294 (1995).
8. J. L. Anderson, J. Ding, T. Welton, and D. W. Armstrong, "Characterizing Ionic Liquids On the Basis of Multiple Solvation Interactions," *J. Am. Chem. Soc.*, **124**(47), 14247-14254 (2002).
9. D. W. Armstrong, L. He, and Y. Liu, "Examination of Ionic Liquids and Their Interaction with Molecules, When Used as Stationary Phases in Gas Chromatography," *Anal. Chem*., **71**(17), 3873-3876 (1999).
10. P. Scovazzo, A. E. Visser, D. H. Davis Jr., R. D. Rogers, C. A. Koval, D. L. Dubois, and R. D. Noble, "Ionic Liquids Industrial Applications to Green Chemistry," R. D. Rogers, K. R. Seddon, Eds., ACS Symposium Series 818, American Chemical Society, Washington, DC, 2002; pp. 69-87.
11. E. D. Bates, R. D. Mayton, I. Ntai, and J. H. Davis, Jr., "CO_2 Capture by a Task-Specific Ionic Liquid," *J. Am. Chem Soc.*, **124**(6), 926-927 (2002).
12. E. G. Yanes, S. R. Gratz, and A. M. Stalcup, "Tetraethylammonium Tetrafluoroborate: a Novel Electrolyte with a Unique Role in the Capillary Electrophoretic Separation of Polyphenols Found in Grape Seed Extracts," *Analyst*, **125**, 1919-1923 (2000).
13. A. Bösmann, L. Datsevich, A. Less, A. Lauter, C. Schmitz, and P. Wasserscheid, "Deep Desulfurization of Diesel Fuel by Extraction with Ionic Liquids," *Chem. Comm.*, 2494-2495 (2001).
14. W. Arlt, M. Seiler, G. Sadowski, H. Frey, H. Kautz, and R. Mülhaupt, DE Patent, No 10160518.8, 2001.
15. R. D. Rogers, A. E. Visser, R. P. Swatloski, and D. H. Hartman, "Metal Separation Technologies Beyond 2000: Integrating Novel Chemistry with Processing," K. C. Liddell and D. J. Chaiko, Eds., The Minerals, Metals & Materials Society, Warrendale, PA, 1999; p. 139.

16 S. Dai, Y. H. Ju, and C. E. Barnes, "Solvent Extraction of Strontium Nitrate by a Crown Ether Using Room-Temperature Ionic Liquids," *J. Chem Soc., Dalton Trans*., 1201-1202 (1999).

17. M. L. Dietz and J. A. Dzielawa, "Ion-Exchange as a Mode of Cation Transfer into Room-Temperature Ionic Liquids Containing Crown Ethers: Implications for the Greenness of Ionic Liquids as Diluents in Liquid–Liquid Extraction," *Chem. Commun.*, 2124-2125 (2001).

18. A. E. Visser, M. P. Jensen, I. Laszak, K. L. Nash, G. R. Choppin, and R. D. Rogers, "Uranyl Coordination Environment in Hydrophobic Ionic Liquids: An in Situ Investigation," *Inorg. Chem*, **42**, 2197-2199 (2003).

19. M. P. Jensen, J. Neuefeind, J. V. Beitz, S. Skanthakumar, and L. Sodelholm, "Mechanisms of Metal Ion Transfer into Room-Temperature Ionic Liquids: The Role of Anion Exchange," *J. Am. Chem. Soc.*, **125**, 15466-15473 (2003).

20. V. A. Cocalia, M. P. Jensen, J. D. Holbrey, S. K. Spear, D. C. Stepinski, and R. D. Rogers, "Identical Extraction Behavior and Coordination of Trivalent or Hexavalent f-Element Cations Using Ionic Liquid and Molecular Solvents," *Dalton Trans.*, 1966-1971 (2005).

21. V. A. Cocalia, J. D. Holbrey, K. E. Gutowski, N. J. Bridges, and R. D. Rogers, "Separation of Metal Ions Using Liquids: The Challenge of Multiple Mechanism," *Tsinghua Science and Technology*, **11**(2), 188-193 (2006).

22. J. S. Wilkes, J. A. Levisky, R. A. Wilson, and C. L. Hussey, "Dialkylimidazolium Chloroaluminate Melts: a New Class of Room-Temperature Ionic Liquids for Electrochemistry, Spectroscopy and Synthesis," *Inorg. Chem.*, **21**, 1263-1264 (1982).

23. K. R. Seddon, A. Stark, and M. J. Torres, "Influence of Chloride, Water, and Organic Solvents on the Physical Properties of Ionic Solids," *Pure Appl. Chem.*, **72**, 2275-2287 (2000).

24. S. Cherfa, J. Pecaut, and M. Nierlich, "Crystal Structure of Octyl(phenyl)-N,N-diiso-butylcarbamoylmethylphosphine Dioxouranium Nitrate, $C_{48}H_{84}N_6O_{20}P_2U_2$," *Z. Kristallogr.- New Cryst. Struct.*, **214**(4), 523-525 (1999).

25. V. A. Cocalia, "Separations, Solvation, and Coordination of Actinides in Ionic Liquids," Ph.D. Thesis, The University of Alabama, Tuscaloosa, Alabama, 2006.

26. M. L. Dietz, J. A. Dzielawa, I. Laszak, B. A. Young, and M. P. Jensen, "Influence of Solvent Structural Variations on the Mechanism of Facilitated Ion Transfer into Room-Temperature Ionic Liquids," *Green Chem*., **5**(6), 682-685 (2003).

27. V. A. Cocalia, K. E. Gutowski, and R. D. Rogers, "The Coordination Chemistry of Actinides in Ionic Liquids: A Review of Experiment and Simulation," *Coord. Chem. Rev.*, **250**, 755-764 (2006).

28. A. Chaumont and G. Wipff, "Solvation of Uranyl–CMPO Complexes in Dry *vs*. Humid Forms of the [BMIM][PF_6] Ionic Liquid. A Molecular Dynamics Study," *Phys. Chem. Chem. Phys*, **8**, 494-501 (2006).

29. W. M. Reichert, J. D. Holbrey, K. B. Vigour, T. D. Morgan, G. A. Broker, and R. D. Rogers, "Approaches to Crystallization From Ionic Liquids: Complex Solvents-Complex Results, or, a Strategy for Controlled Formation of New Supramolecular Architectures?" *Chem Commun.*, 4767-4779 (2006).

COMPLEXATION STUDIES OF F-ELEMENTS IN IONIC LIQUIDS

A. V. Mudring

Anorganische Chemie I – Festkörperchemie, Ruhr-Universität Bochum, D-44780 Bochum, Germany. Corresponding author email address: anja.mudring@rub.de

ABSTRACT

Despite the great interest in using ionic liquids for liquid-liquid extraction for the separation and purification of f-elements the underlying fundamental solvation processes are still poorly understood. A combination of optical spectroscopy, single-crystal X-ray structure analysis, and electrochemistry can help to elucidate these. The aim of this work was to get a deeper understanding of the interaction of trivalent lanthanide cations with commonly used triflate- and bis(trifluoromethanesulfonyl)amide-based ionic liquids.

INTRODUCTION

Dissolution and solvation as well as ligand-exchange reactions of f-element cations in conventional inorganic solvents like water or liquid ammonia or classical organic solvents like tetrahydrofuran or acetonitrile are nowadays quite well understood, and extensive studies have appeared in the past. In contrast, little is known about lanthanide ions in ionic liquids. However, ILs (ionic liquids) are of interest with respect to liquid-liquid extraction for separation and purification of lanthanides as well as for the separation of fission materials from reusable fissile materials. Hydrophobic ILs have been discussed here as alternatives to the conventionally used VOCs (volatile organic compounds/solvents) [1-12]. The processing of nuclear fuel by high-temperature molten salt extraction has been extensively studied over the past and ionic liquids, especially room-temperature ionic liquids, RTILs, as molten salts with a particularly low melting point offer the unique opportunity of working at much lower temperatures.

In order to gain a basic understanding of the processes in the ligand shell of cationic lanthanide ions in hydrophobic ionic liquids that are of interest for the above-mentioned applications, we will focus in this work on triflate (OTf, trifluoromethanesulfonate) and bis(trifluoromethanesulfonyl)amide (Tf_2N) compounds.

EXPERIMENTAL

The compounds synthesized in this work as well as the educts are air and moisture sensitive. Therefore the materials were prepared and stored under inert-gas conditions. Reactions were carried out using either standard Schlenk-technique at a

vacuum/argon line or using glass ampoules in an argon dry box (MBraun, Garching). Reaction ampoules were sealed under dynamic vacuum conditions outside the dry box, connected to a vacuum-line. All reaction vessels were care fully dried several hours in a drying cupboard and evacuated in the chamber of the argon dry box prior to use. All educts were sublimed prior to use; the ionic liquids were synthesized according to common literature procedures and purified until they exhibited CV-grade purity and dried for at least 24 hours at 120 °C / 10^{-3} mbar.

To obtain structural information on lanthanide complex compounds, single crystals for X-ray analysis were grown out of the ionic liquid by supersaturating the ionic liquid with the respective salt with heat and carefully cooling until crystals of sufficient quality for structural analysis were obtained. Single-crystal data were obtained from an image-plate diffraction system with graphite monochromatic MoK_α radiation (IPDS, Stoe&Cie, Darmstadt, Germany). Crystal-structure solution was accomplished by direct methods using SHELXS-97 [13]. Subsequent difference Fourier analyses and least-squares refinements with SHELXL-97 [14] allowed the localization of the remaining atom positions. Data reduction was carried out with the program package X-Red [15], numerical absorption corrections with the program X-Shape [16]. For crystal-structure drawings, the program Diamond was employed [17].

DSC thermograms were measured on a DSC 204 F1 Phoenix (Netzsch, Selb, Germany*)* equipped with a τ-sensor and nitrogen cooling. All samples were measured in aluminum crucibles which were sealed under argon atmosphere. The reference was an empty aluminum crucible with a pierced lid. The measuring unit and the heating furnace were subjected to an argon stream during the measurement (20 mL/min, 70 mL/min, respectively). The heating rate was in all cases 5K/min, typical sample-masses are 10-20 mg. The temperature programs were all applied several times on each sample; all transitions were reversible and appeared at the same temperatures.

Cyclic voltammograms were measured on an Autolab PGStat-12 (Metrohm, Filderstadt, Germany). A platinum working electrode (12.57 mm^2), a glassy carbon counter electrode, and a silver-rod quasi reference electrode were used as a setup. All measurements were carried under an argon atmosphere with a scan rate of 100 mV/s. The electrodes were polished after each measurement with CeO_2, washed with acetone and deionized water, and dried in vacuum prior use.

RESULTS AND DISCUSSION

In order to elucidate the coordination of trivalent lanthanides in commonly used bis(trifluoromethanesulfonyl)amide-based ionic liquids, lanthanide bis(trifluoromethane-sulfonyl)amides $Ln(Tf_2N)_3$ (Ln = Pr, Nd, Sm, Eu, Tb, Dy, Tm, Yb, Lu) were dissolved in [bmpyr][Tf_2N] (bmpyr = N-butyl-N-methylpyrrolidinium, Tf_2N = bis(trifluoromethane-sulfonyl)amide). From such solutions, the compounds with a general composition of $[bmpyr]_2[Ln(Tf_2N)_5]$ for the larger lanthanides, Ln = Pr-Tb, and $[bmpyr][Ln(Tf_2N)_4]$ for the smaller lanthanides, Ln = Dy-Lu could be crystallized [20]. The larger lanthanides are ninefold coordinated by four bis(trifluoromethanesulfonyl)amide ligands binding in a chelating mode and one additional ligand anion coordinating monodentately to the metal

(see Figure 1). The smaller lanthanides prefer a coordination number of eight, which is realized by four anions binding in a chelating fashion.

The formed complexes $[bmpyr]_2[Ln(Tf_2N)_5]$ (Ln = Pr-Tb) are ionic liquids themselves, exhibiting melting points <100 °C (Scheme 1).

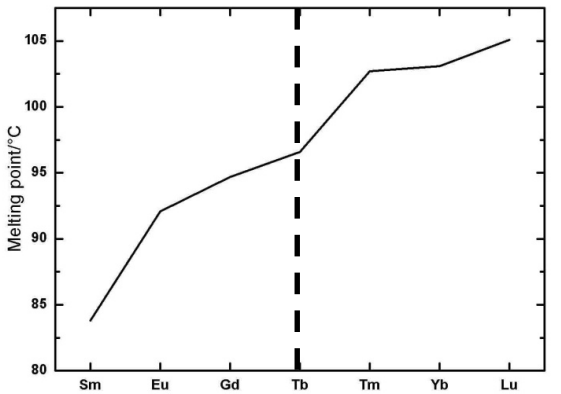

Scheme 1. Ion mass-dependence of the melting point of $[bmpyr]_n[Ln(Tf_2N)_{3+n}]$.

In order to obtain structural data on the coordination sphere of trivalent lanthanides in a second commonly used group of ionic liquids based on triflate anions, the solvation of $Yb(OTf)_3$ was investigated in [bmpyr][OTf] (OTf = trifluoromethanesulfonate). From a procedure similar to the bis(trifluoromethanesulfonyl)amides, single crystals of a compound with the formula $[bmpyr]_3[Yb(OTf)_6]$ were grown from solution. In this compound, all [OTf]-ligands coordinate monodentately in a nonbridging fashion, which yields isolated octahedra, embedded in a [bmpyr]-matrix. The triflate anions are all trans arranged, in a way that steric repulsion in minimized (see Figure 2). In the equatorial positions, the CF_3-groups are directed in opposite directions in a way that the trans-regiochemistry can also be realized with the axial CF_3-groups.

To finally investigate the ligand competition of trifluoromethanesulfonate (OTf^-) and bis(trifluoromethanesulfonyl)amide (Tf_2N^-) exchange reactions, $Yb(Tf_2N)_3$ was dissolved in the ionic liquid 1-butyl-1-methylpyrrolidinium-trifluoromethanesulfonate [bmpyr][OTf]. Indeed, ligand exchange could be evidenced by crystallization of a compound with the composition $[bmpyr]_4[Yb(OTf)_6][Tf_2N]$ (Figure 3), in which the $[Tf_2N]$-anions are incorporated only in a noncoordinating fashion in the crystal structure. The ytterbium cation is surrounded solely by the stronger coordinating (more Lewis basic) triflate anions in an octahedral fashion similar to that found in $[bmpyr]_4[Yb(OTf)_6]$.

Cyclic voltammetry turned out to be a well-suited tool to monitor ligand displacement reactions in solutions. Figure 4 shows the cyclic voltammograms of a 0.025 M solution of $Yb(Tf_2N)_3$ in $[bmpyr][Tf_2N]$(left), $Yb(Tf_2N)_3$ in [bmpyr][OTf] (middle), and $Yb(OTf)_3$ in [bmpyr][OTf](right). For $Yb(OTf)_3$ dissolved in [bmpyr][OTf], the reduction peak is found at a more negative value (-1.90 V) and the oxidation peak to more positive (-0.89 V) compared to $Yb(Tf_2N)_3$ in $[bmpyr][Tf_2N]$ (-1.21 and -0.95 V, respectively) with halfwave potentials of -1.39V found for $Yb(OTf)_3$ in [bmpyr][OTf] and -1.08 for $Yb(Tf_2N)_3$ in $[bmpyr][Tf_2N]$.

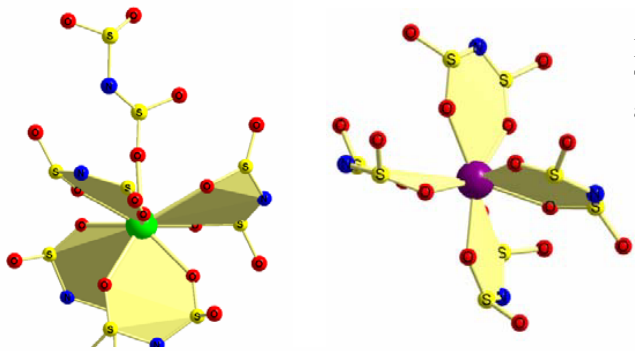

Figure 1. Coordination of Ln^{3+} by Tf_2N^- in $[bmpyr]_2[Ln(Tf_2N)_5]$ (left) and $[bmpyr][Ln(Tf_2N)_4]$ (right).

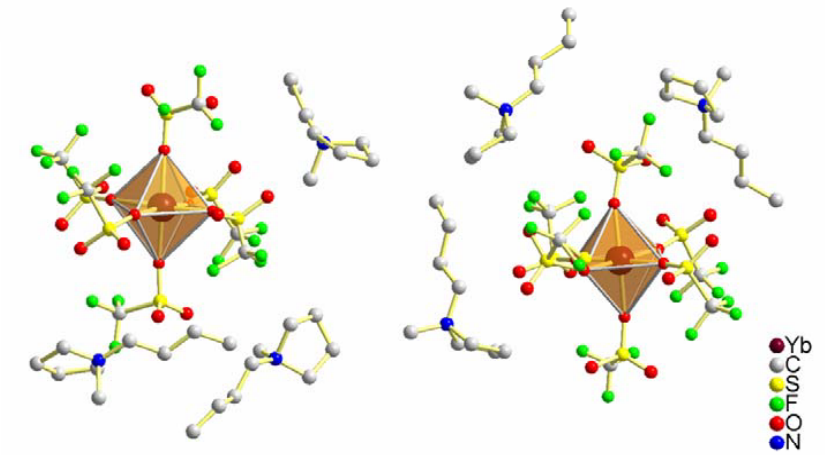

Figure 2. Asymmetric unit of the crystal structure of $[bmpyr]_3[Yb(OTf)_6]$.

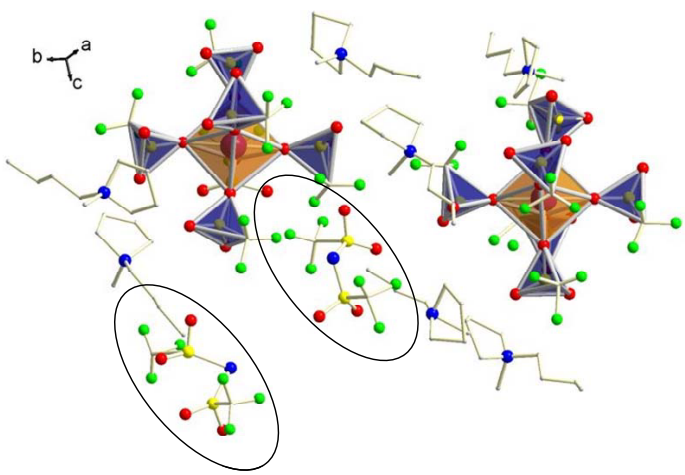

Figure 3. Part of the crystal structure of $[bmpyr]_4[Yb(OTf)_6][Tf_2N]$, noncoordinating Tf_2N encircled, coordinating SO_3R-groups shown as tetrahedra.

By comparing the cyclic voltammogram of $Yb(Tf_2N)_3$ in [bmpyr][OTf] (middle) with $Yb(OTf)_3$ in [bmpyr][OTf] (right), it strikes one that the reduction peaks of the trivalent species are both located at -1.89 V. Also, the halfwave potentials are very similar (-1.35 V and -1.39 V, respectively) and differ significantly from the observed one for the pure $[Tf_2N]$-sample (-1.08 V). The peak separation is increased (1.09 V), indicating poor reversibility. Thus, it can be anticipated that the local surrounding of Yb^{3+} in [bmpyr][OTf] is the same, regardless which salt, $Yb(OTf)_3$ or $Yb(Tf_2N)_3$, is used as the lanthanide source. Together with the information obtained from the crystal structure, it can be concluded that upon dissolving $Yb(Tf_2N)_3$ in the OTf-ionic liquid, the stronger Lewis base OTf^- replaces Tf_2N^- in the Yb^{3+} ligand sphere, and a $[Yb(OTf)_6]^{3-}$ complex forms.

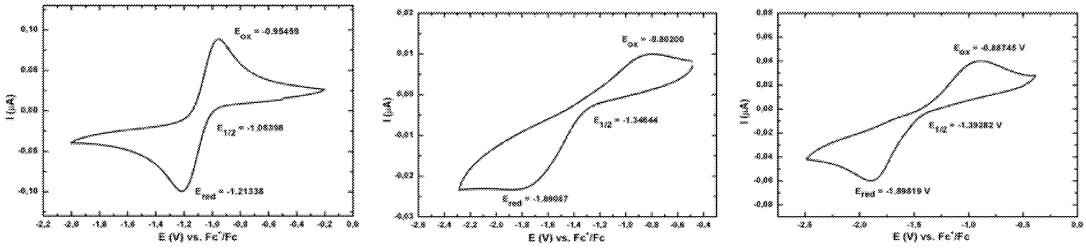

Figure 4. CV of $Yb(Tf_2N)_3$/[bmpyr][Tf_2N](left), $Yb(Tf_2N)_3$/[bmpyr][OTf] (middle), and $Yb(OTf)_3$/[bmpyr][OTf](right).

CONCLUSIONS

Putting all the gained information together, the following reaction paths can be concluded for dissolving rare-earth-compounds in $[Tf_2N]$ and [OTf]-based ionic liquids:

$$Ln(Tf_2N)_3 + 2\ [bmpyr][Tf_2N] \rightarrow [bmpyr]_2[Ln(Tf_2N)_5]\ (Ln = La\text{-}Tb) \quad (1)$$

$$Ln(Tf_2N)_3 + [bmpyr][Tf_2N] \rightarrow [bmpyr][Ln(Tf_2N)_4]\ (Ln = Dy\text{-}Lu) \quad (2)$$

$$Yb(Tf_2N)_3 + 6\ [bmpyr][OTf] \rightarrow [bmpyr]_4[Yb(OTf)_6][Tf_2N] + 2\ [bmpyr][Tf_2N] \quad (3)$$

$$Yb(OTf)_3 + 3\ [bmpyr][OTf] \rightarrow [bmpyr]_3[Yb(OTf)_6] \quad (4)$$

Lanthanide bis(trifluoromethanesulfonyl)amides $Ln(Tf_2N)_3$ dissolve upon complex formation in bis(trifluoromethanesulfonyl)amide ionic liquids. The smaller, later lanthanides (Dy-Lu) are surrounded by four Tf_2N ligands coordinating bidentately through their oxygen atoms. The earlier, larger lanthanides (La-Tb) prefer a higher coordination number; in order to achieve this, an additional Tf_2N ligand coordinates monodentately, and the overall coordination number is nine. $Yb(OTf)_3$ dissolves in the triflate ionic liquid [bmpyr][OTf] upon forming the $[YbOTf_6]^{3-}$ complex anion. Dissolution of $Yb(Tf_2N)_3$ in [bmpyr][OTf] yielded the compound $[bmpyr]_4[Yb(OTf)_6][Tf_2N]$, where the Tf_2N^- ligand has been replaced by the stronger Lewis basic OTf^- in the coordination sphere of Yb^{3+}. This ligand exchange cannot only be evidenced by X-ray structure analysis but also by cyclic voltammetry.

ACKNOWLEDGMENTS

AVM thanks the state of Northrhine-Westfalia, Germany, and the Universität Köln as well as the Ruhr-Universität Bochum for providing excellent research surroundings. The DFG is acknowledged for financial support within in the priority program "SPP 1166 – Lanthanoid Specific Functionalities". Thanks to Dr. Arash Babai, Dipl.-Chem. Anna Getsis, Dipl.-Chem. Slawomir Pitula and Dr. Sifu Tang for their outstanding work in the lab and Prof. Gerd Meyer and Prof. John Corbett for stimulating discussions in the field of lanthanide chemistry.

REFERENCES

1. J. G. Huddleston, H. D. Willauer, R. P. Swatlowski, A .E. Visser, and R. D. Rogers, *Chem. Commun.*, **1765** (1998).
2. F. Kubota and M. Goto, *Solvent Extr. Res. Dev., Jpn.*, **13**, 23 (2006).
3. K. Nakashima, F. Kubota, T. Maruyama, and M. Goto, *Ind. Eng. Chem. Res.*, **44**, 4368 (2005).
4. H. Zhao, S. Q. Xia, and P. S. Ma, *J. Chem. Technol. Biotechnol.*, **80**, 1089 (2005).
5. A. E. Visser and R. D. Rogers, *J. Solid State Chem.*, **171**, 109 (2003).
6. M. P. Jensen, J. V. Beitz, J. Neuefeind, S. Skanthakumar, and L. Soderholm, ACS Symp. Ser. 901, 19 (2005).
7. V. A. Cocalia, M. P. Jensen, J. D. Holbrey, S. K. Spear, D. C. Stepinski, and R. D. Rogers, *Dalton Trans.*, 1966 (2005).
8. P. Giridhar, K. A Vankatesan, T. G. Srinivasan, and R. P. Vasudeva Rao, *J. Radioanal. Nucl. Chem.*, **265**, 31 (2005).
9. K. Nakashima F. Kubota, T. Maruyama, and M. Goto, *Anal. Sci.*, **19**, 1097 (2003).
10. A. E. Visser, M. P. Jensen, I. Laszak, K. L. Nash, G. Choppin, and R. D. Rogers, *Inorg. Chem.*, **42**, 2197 (2003).
11. A. Ouzdi, B. Gadenne, P. Hesemann, J. J. J. Moreau, I. Billard, C. Gaillard, S. Mekki, and G. Moutiers, *Chem. – Eur. J.*, **12**, 3074 (2006).
12. K. Binnemans, *Chem. Rev.*, **107**, 2592 (2007).
13. SHELXS-97, W. S. Sheldrick, Universität Göttingen (1997).
14. SHELXL-97, W. S. Sheldrick, Universität Göttingen (1997).
15. X-RED, Stoe & Cie, Darmstadt (2002).
16. X-Shape, Stoe & Cie, Darmstadt (2002).
17. Diamond Version 2.1e, Crystal Impact GbR (1996-2001).
18. A. Babai and A.-V. Mudring, *Inorg. Chem.*, **25**, 4874 (2006).
19. A. Babai and A.-V. Mudring, *J. Alloys Compd.*, **418**, 122 (2006).
20. A. Babai and A.-V. Mudring, *Dalton Trans.*, 1828 (2006).

PRELIMINARY INVESTIGATION OF THE KINETICS OF THE SEPARATION OF YTTRIUM(III) USING CYANEX 923 IN IONIC LIQUIDS

H. L. Yang, J. Chen, and D. Q. Li

Key Laboratory of Rare Earth Chemistry and Physics, Changchun Institute of Applied Chemistry, Chinese Academy of Sciences, Changchun, 130022, China; *Graduate School of the Chinese Academy of Sciences, Beijing 100039,China.*
Corresponding author email address: jchen@ciac.jl.cn

ABSTRACT

The extraction thermodynamic mechanisms of metal ions using ionic liquids as the extracting phase have been investigated. Our laboratory has reported the separation of Y(III), Sc(III), from lanthanides(III) using Cyanex 923 as an extractant in $[C_8mim][PF_6]$. Unfortunately, there are still no reports about the extraction kinetics. In this paper, we made a preliminary investigation of the mass-transfer model in the process of extraction Y(III) from Cyanex 923/$[C_8mim][PF_6]$ by a constant interfacial area cell with laminar flow. In this research, the effect of different factors, such as stirring rate, temperature, and specific area, was discussed. Mass transfer of Y(III) was mainly controlled by diffusion and kinetics regime, and the extraction reaction occurred at the interface.

INTRODUCTION

Ionic liquids (ILs) are low-melting salts and composed of dissociated organic cations and anions. They possess fundamentally unique combinations of properties, such as being nonvolatile, nonflammable, and thermally stable, and have been considered as alternative solvents for a series of catalysis, synthesis, electrochemistry, and separation processes. At the same time, ILs still retain some properties of traditional organic solvents, such as immiscibility with water and other solvents.

Hydrophobic ILs have been investigated as one kind of potential solvents to separate metal ions [1-3]. In the presence of ligands capable of forming organophilic complexes, most metal ions were extracted into ILs phase from the aqueous phase. The complex structure or coordination environment of the metal ions has been observed by extended X-ray absorption fine structure (EXAFS) [4]. A cation-extraction [5] and anion-exchange [6] mechanism have already been demonstrated in the process of extracting metal ions in biphasic ILs systems.

The mass-transfer kinetics of metal ion extraction in IL-based systems is still at the beginning stage. In conventional organic solvent systems, Lewis cell, hollow-fiber membrane, and drop method were used to study the kinetics of mass transfer in biphasic

liquid/liquid extraction systems. But in the new system, ILs have more complex interaction with extractant and metal ions, and high viscosity will cause slow the mass-transfer process; thus, the conventional kinetics methods need to be modified to meet the new system. In our laboratory, we tried to use a constant interfacial-area cell with laminar flow [8], which was developed by Zheng and Li. During the experiment, this apparatus could keep the liquid interface steady and smooth and no flow towards the interface. So the constant interfacial cell with laminar flow was introduced into ILs/ aqueous systems.

EXPERIMENTAL SECTION

Mass transfer was investigated using a constant interfacial-area cell with laminar flow, which was described previously [7]. The apparatus has some special advantages on kinetics investigation. For instance, the interface between the two phases can keep not only stable, but also laminar, flow. In this report, we applied this instrument to study the extraction kinetics in high-viscosity [C_8mim][PF_6], and its synthesis and characterization has been reported in our early paper [8]. Compared with the "dried" [C_8mim][PF_6], 425.2 cp at 303K [9], the viscosities of water saturated-ILs are lower, even at 300 K (Table 1). In order to use the apparatus in the new special system, it is needed to redesign new parameters and optimize the device.

Table 1. Viscosity data* for [C_8mim][PF_6]) at different temperatures

Liquid phase	Temperature/K	Viscosity/cp (water equilibrated)
[C_8mim][PF_6]	300	320
	306	211
	314	155
	316	133

*Measured by NDJ-7 type of rotating viscometer.

Before starting the kinetics process, the extraction equilibrium experiments for Y(III) in aqueous nitric acidic solutions were carried out in hydrophobic [C_8mim][PF_6] with Cyanex 923 as the extractant. $Y(NO_3)_3$ was purchased from SCRC and used as received. Cyanex 923, a mixture of straight-chain alkylphosphine oxides, is a commercial extractant of Cytec Canada Inc. It has stronger extracting power in separating rare earth metals compared with Cyanex 925, a branched-chain mixture. The extraction mechanism of Sc(III) using Cyanex 925 as an extractant in [C_8mim][PF_6] has been proposed by our laboratory [8]. The equation of cation-exchange reaction has been deduced according to Dietz [10], basic cation-exchange equation of metal ions extraction in ILs:

$$Y^{3+} + 3Cyanex923_{org} + 3C_8mim^{+}_{org} \Leftrightarrow (Y \cdot Cyanex923_3)^{3+}_{org} + 3C_8mim^{+} \qquad [1]$$

In the extraction process, the transfer of $[Y(Cyanex\ 923)_3]^{3+}$ into [C_8mim][PF_6] was accompanied by the loss of [C_8mim^{+}] to the aqueous phase. An expression giving thermodynamic equilibrium constant is as follows:

$$K_{ex} = \frac{[Y \cdot Cyanex923_3]_o \cdot [C_8mim^+]_a^3}{[Y^{3+}]_a [Cyanex923]_o^3} = \frac{k_d [C_8mim^+]_a^3}{[Cyanex923]_o^3}$$

Theoretically supposing K_{ex} and [Cyanex 923] are constants, the distribution ratio (k_d) of the Y(III) was in inverse proportion to the concentration of [C_8mim^+] in the aqueous phase at equilibrium. C_8mim^+ in water was mainly supposed to result from two aspects in the extraction process: the solubility of [C_8mim][PF_6] in water, about 2.9×10^{-3} M for this experimental determination at room temperature, and the loss of C_8mim^+ to water, approaching 1.8×10^{-3} M when 100% Y(III) was extracted during the extraction process. But the result of no C_8mim^+ added (Table 2) clearly showed that [C_8mim^+] was 1.50×10^{-2} M, about 3.3 times of the sum of the theoretical result of [C_8mim] in the aqueous phase. The result was partly consistent with Dietz's work about TBPO-induced dissolution of IL in water [11]. It was also found that the addition of a small amount C_8mim^+ (4.93×10^{-2} M) into water can hardly affect the extraction rate of Y(III) (Table 2). Only when a high concentration of C_8mim^+ solution was added into water did the effect of [C_8mim^+] on extraction rate become very remarkable [8]. So, the extraction mechanism of metal ions in ILs system was very complex, especially the effect of ILs, extractant, and metal ions.

Table 2. Extraction efficiency (k_d) at different concentrations of C_8mim^+ in water*

	C ([C_8mim^+])(mol/L) in water			
	Before extraction	After extraction	E%	k_d
[C_8mim][NO_3]	4.93×10^{-2}	5.04×10^{-2}	97.61	40.9
[C_8mim][Cl]	4.93×10^{-2}	5.04×10^{-2}	98.33	58.9
No C_8mim^+ addition	0	1.50×10^{-2}	99.06	105.4

*[Y(III)] = 6.0×10^{-4} M, pH = 5.62.

Data Treatment

The changes of metal ion concentration with time have been detected during the experiment. Although the extraction process in ILs system is very complex, data can still be processed under some perfect assumption. The influence of reversible reaction and concentration decrease of the reaction rate can be neglected like the traditional organic solvent. The reaction rate (R_f) can be described as following:

$$M_{(a)} \rightleftharpoons M_{(o)}$$

$$R_f = \left(\frac{V}{A}\right) \cdot \frac{dC_{M_{(o)}}}{dt}$$

where, $M_{(a)}$ and $M_{(o)}$ stand for the concentrations of Y (III) in the aqueous and organic phases, respectively; V is the volume of the aqueous phase or organic phase; A is the interfacial area between two phases; Q ($Q = A/V$) refers to specific area; and C and t represent the concentration of metal ion and reaction time, respectively.

RESULTS AND DISCUSSION

Effect of Stirring Speed on Extraction Rate

In extraction kinetics experiments, there are always three types of extraction regimes such as diffusion, kinetics, and double-control regime during the extraction process. If R_f changes with the stirring speed of the two phases, it indicates diffusion-control regime. When R_f doesn't increase with the stirring rate after reaching a certain value, the mass transfer will become kinetics-control regime, and the fast diffusion process will no longer influence the extraction rate. In the new extraction system, viscosity differences between ionic liquids and water must be considered in the discussion of kinetics processes. At the same stirring speed, the two phases have different flow types, so it is necessary to adjust separately. When different stirring speeds were set in the two phases, the interfacial phenomena will become more complex. In general, when the stirring speed is more than 250 rpm, it will reduce the effect of diffusion, but at the same time the stirring speed could not be too high, or it will damage the stability of interface. The influence of the stirring rate of the IL-phase on R_f has been studied for Y(III) (shown in Figure 1). The relationship between R_f and stirring speed indicates that it is diffusion-control regime between 450 and 560 rpm, when stirring speed in the aqueous phase is maintained at 250 rpm. When the speed exceeds 550 rpm, the top water phase becomes turbid, and the interfacial stability will be influenced.

Effect of Temperature on Extraction Rate

Temperature is another important factor for the extraction rate. Generally speaking, if the reaction activation energy (Ea) is greater than 42 kJ mol^{-1}, the extraction process is kinetics-control regime. When Ea is between 20 and 42 kJ mol^{-1}, it indicates double-control regime. The Ea of the diffusion-control regime is less than 20 kJ mol^{-1}. Figure 2 shows the effect of temperature on extraction rate at 300-316 K. The extraction increases along with the increasing temperature. It is shown that the extractive reaction is an exothermic reaction. The relationship between temperature and reaction rate was in accordance with the Arrhenius equation:

$$\log R_f = -\frac{Ea}{2.303R} \cdot \frac{1}{T} + C$$

The experimental results show that the extraction apparent activation energy of Y(III) by Cyanex 923 in the IL-system is calculated to be 15.0 kJ mol^{-1} above 311 K and 81.2 kJ mol^{-1} below 311 K. It indicates that there are two stages for extracting Y(III) in ionic liquids at different temperatures: diffusion- and kinetics-control regime.

Effect of Specific Area on Extraction Rate

For diffusion- or double-control regime, the stirring speed and specific area have an important effect on the extraction rate. The experiments of changing specific area (Q

= *A/V*) from 0.06 to 0.21 cm show that the extraction rate increases with increasing specific area. The results prove that the extraction reactions occur at the interface and are in good agreement with above conclusion.

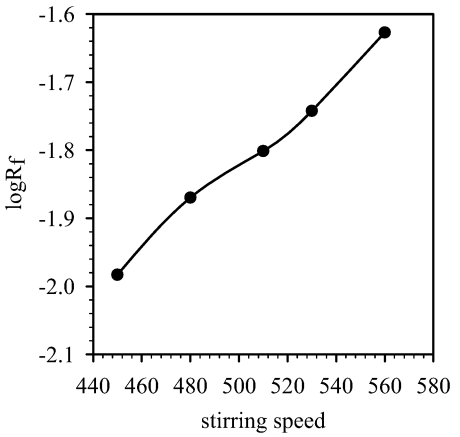

Figure 1. The effect of stirring speed on the extraction rate of Y(III) using Cyanex 923 in $[C_8mim][PF_6]$. pH = 5.62, T = 320 K, [Y(III)] = 6.0×10^{-4} M, [Cyanex 923] = 2.0×10^{-2} M.

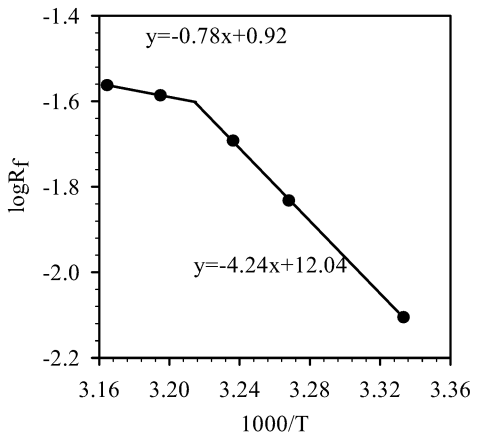

Figure 2. The effect of temperature on the extraction rate of Y(III) using Cyanex923 in $[C_8mim][PF_6]$. pH = 5.62, rpm = 450 rpm, [Y(III)] = 6.0×10^{-4} M, [Cyanex 923] = 2.0×10^{-2} M.

CONCLUSIONS

1. The reaction activation energy (*E*a) is shown that there are two stages at different temperature: the diffusion- and kinetics-controlled regime.
2. The extraction rate changed with the specific area in nitric acid medium. It is suggested that liquid-liquid extraction of Y(III) from aqueous solution occurred at interface but not in the fluid phase.

3. The thermodynamic equilibrium equation became more complex in the presence of C_8mim^+ in the IL system.
4. Different stirring speeds in the two phases might make idealized extraction reaction model no longer suitable for the IL system, so it is necessary to find a better model which can suit for the new system.

ACKNOWLEDGMENTS

This research is supported by 'Hundreds Talents Program' from Chinese Academy of Sciences, National Natural Science Foundation of China (50574080) and Distinguished Young Scholar Foundation of Jilin Province (20060114). The authors thank Cytec Inc. for gifts of Cyanex923.

REFERENCES

1. A. E. Visser, R. P. Swatloski, S. T. Griffin, D. H. Hartman, and R. D. Rogers, "Liquid/liquid Extraction of Metal Ions in Room Temperature Ionic Liquids," *Sep. Sci. Technol.*, **36**, 785-804 (2001**).**
2. Y. Liu, X. Sun, F. Luo, and J. Chen, "The Preparation of Sol-gel Material Doped with Ionic Liquids and Trialkyl Phosphine Oxides for Yttrium(III)," *Anal. Chim. Acta.*, **604**(2), 107-113 (2007).
3. X. Q. Sun, B. Peng, J. Chen, D. Q. Li, and F. Luo, "An Effective Method for Enhancing Metal-ions' Selectivity of Ionic Liquid-based Extraction System: Adding Water-Soluble Complexing Agent," *Talanta*, **74(4)**, 1071-1074 (2008).
4. M. P. Jensen, J. A. Dzielawa, P. Rickert, and M. L. Dietz, "EXAFS Investigations of the Mechanism of Facilitated Ion Transfer into a Room-Temperature Ionic Liquid," *J. Am. Chem. Soc.*, **124**(36), 10664-10665 (2002**).**
5. S. Dai, Y. H. Ju, and C. E. Barnes, "Solvent Extraction of Strontium Nitrate by A Crown Ether Using Room-temperature Ionic Liquids," *J. Chem. Soc., Dalton Trans.*, (8), 1201-1202 (1999**).**
6. M. P. Jensen, J. Neuefeind, J. V. Beitz, S. Skanthakumar, and L. Soderholm, "Mechanisms of Metal Ion Transfer into Room-temperature Ionic Liquids: the Role of Anion Exchange," *J. Am. Chem. Soc.*, **125**, 15466-15473 (2003**).**
7. Z. Zheng, J. Lu, D. Q. Li, and G. X. Ma, "The Kinetics Study in Liquid-liquid Systems with Constant Interfacial Area Cell with Laminar Flow," *Chem. Eng. Sci.*, **53** (13), 2327-2333 (1998**).**
8. X. Q. Sun, D. B. Wu, J. Chen, and D. Q. Li, "Separation of Scandium (III) from Lanthanides (III) with Room Temperature Ionic Liquid Based Extraction Containing Cyanex925," *J. Chem. Technol. Biotechnol.*, **82**, 267-272 (2006**).**
9. L. C. Branco, J. N. Rosa, J. J. M. Ramos, and C. A. M. Afonso, "Preparation and Characterization of New Room Temperature Ionic Liquids," *Chem. Eur. J.,* **8**(16), 3671-3677 (2002).
10. M. L. Dietz and J. A. Dzielawa, "Ion-exchange as A Mode of Cation Transfer into Room Temperature Ionic Liquids Containing Crown Ethers: Implications for The 'greenness' of Ionic Liquids as Diluents in Liquid-liquid Extraction," *Chem. Commun.*, **20**, 2124-2125 (2001).
11. P. G. Rickert, D. C. Stepinski, D. J. Rausch, R. M. Bergeron, S. Jakab, and M. L. Dietz, "Solute-induced Dissolution of Hydrophobic Ionic Liquids in Water," *Talanta*, **72**, 315-320 (2007).

ZINC AND IRON EXTRACTION WITH MIXTURES CONTAINING PHOSPHONIUM IONIC LIQUIDS

M. Regel-Rosocka and M. Wiśniewski

Poznan University of Technology, Institute of Chemical Technology and Engineering, pl. M. Skłodowskiej-Curie 2, 60-965 Poznan, Poland.
Corresponding author email address: Magdalena.Regel@put.poznan.pl

ABSTRACT

The use of Cyphos®IL101 as an extractant of Zn(II) and Fe(II) in mixtures with toluene and alkylene carbonates is investigated. Extraction kinetics and isotherms for Zn(II) and Fe(II) are determined. Mixtures of Cyphos IL101 with alkylene carbonates or toluene are effective in Zn(II) extraction from hydrochloric acid solution. Fe(II) extraction (up to 60%) is the main disadvantage of the mixtures because it makes impossible the selective separation of Zn(II) from Fe(II). Water transfer to the organic phase decreases with increasing concentration of Zn(II) in the feed solution. Water transfer to the mixture of Cyphos IL101 with toluene is twice as small as that for alkylene carbonates.

INTRODUCTION

Nonflammability, high thermal stability, and nonvolatility of ionic liquids (ILs) account for their application as solvents and catalysts for organic reactions, electrolytes in chemical sources of energy, plasticizers, and bactericides [1-3]. Studies on the application of imidazolium ILs as solvents in separation processes have been carried out for seven years. 1-Alkyl-3-methylimidazolium salts have been used the most frequently. Such reagents are considered to be potential solvents for "green chemistry." They can replace volatile organic compounds (VOCs), usually used as solvents in extraction. Ionic liquids are salts that exist in a liquid form at temperatures below 150 °C [4] and comprise a large, asymmetrical cation (e.g., 1-alkyl-3-methylimidazolium or N-alkylpyridinium) and organic or inorganic anion. Depending on the cation and anion used, the properties of ILs may be affected, changing their viscosity, cloud point, and solubility in water. It is the anion that influences the hydrophobicity of ILs. Most of ionic liquids containing a chloride anion are miscible with water, while those comprising PF_6^- or $N(CF_3SO_2)_2^-$ are highly hydrophobic. A great advantage of ILs is the ease in replacing the anion, making it possible to design compounds with properties suited to the particular systems [4-8].

Selective zinc recovery from spent pickling solutions (SPS) is an important issue in Poland, where there are more than 50 hot-dip galvanizing plants. One of the biggest Polish hot-dip galvanizing plants, Metalplast Oborniki, produces 360 m^3 of SPS

containing from 5 to 130 g/L of zinc and from 12.5 to 100 g/L of iron ions, mainly in the form of iron(II) [9]. According to the European Union Directive 2001/59/EC, concentrations in waste disposed of in sewage must not exceed 2 mg/L for Zn, 10 mg/L for Fe, and 1000 mg/L for Cl^-. Owing to environmental issues, efficient removal of metal ions from SPS is a crucial problem to solve in the hot-dip galvanizing industry [10]. In view of an ever growing demand for metals, particularly for zinc, recovery of metals from secondary sources, such as SPS, should be considered. Taking into account economic, environmental, and technical advantages and disadvantages of the various regeneration methods, solvent extraction seems to be a reasonable solution for hot-dip galvanizing plants [11].

As the result of an increasing number of literature records on ILs, their synthesis and applications [12], we propose studies on zinc and iron recovery from spent pickling solutions with phosphonium ionic liquids. Although no reports concerning phosphonium ILs in extraction systems have been available to date, they are considered to be prospective for substance separation [13]. Thus, it is the aim of our work to use trihexyltetradecylphosphonium chloride (Cyphos IL101) in mixtures with toluene or alkylene carbonates as novel reagents to extract zinc(II) and iron(II) from chloride media.

EXPERIMENTAL

A phosphonium ionic liquid, trihexyltetradecylphosphonium chloride (Cyphos IL101) supplied by Cytec Industry Inc. (Canada) is dissolved in toluene or the cyclic organic esters propylene carbonate (ICSO, Kedzierzyn Kozle, Poland) and 1,2-butylene carbonate JEFFSOL®BC (Huntsman, the Netherlands) and used as extractants (0.8 mol/L). JEFFSOL BC is reported to be an environmentally friendly solvent in many applications, for example, in lithium batteries (to decrease sulfur dioxide vapor pressure and to increase electrolyte solubility and ionic conductivity), in organic synthesis, in natural-gas purification, as a plasticizer, and accelerant in dyeing [14]. Toluene and alkylene carbonates are applied to overcome some drawbacks caused by the high viscosity of ILs. The structures of the IL and carbonates applied are presented in Table 1.

Table 1. Structures of extractants used

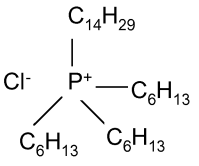	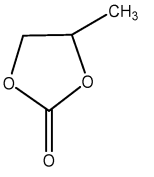	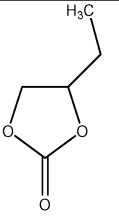
Cyphos IL 101	**PC**	**BC**
Trihexyltetradecylphosphonium chloride	Propylene carbonate	Butylene carbonate

The electrospray mass spectra of the aqueous phase after extraction with Cyphos IL101 do not indicate the presence of a phosphonium cation, which proves the insignificant solubility of IL in the studied aqueous phases.

Extraction has been carried out in a typical way: equimolar aqueous feeds containing 5 g/L of Zn(II) or Fe(II) added as chloride in 0.58 mol/L HCl or without HCl were mechanically shaken with the IL phase (w/o volume ratio = 1) for a period of time between 10 seconds and 50 minutes at 20 ºC in glass separatory funnels and then allowed to stand for phase separation. The chloride concentration adjusted with NaCl was equal to 5 mol/L in the initial aqueous feed containing HCl. Potentiometric titration was used for determination of Zn(II), hydrochloric acid, and chloride concentrations. The content of iron ions was determined by titration with $K_2Cr_2O_7$. The content of water in the organic phase was determined by Karl-Fischer titration. Each experiment was carried out twice, and the error did not exceed 5%.

RESULTS AND DISCUSSION

Kinetics of Extraction

Kinetics of Zn(II) and Fe(II) extraction from hydrochloric acid solutions with Cyphos IL101 mixtures with PC, BC, or toluene is shown in Figure 1. Percentage extraction differs hardly at all for the studied mixtures of IL applying alkylene carbonates or toluene. Zn(II) extraction exceeds 95% for all IL mixtures (Figure 1a), while Fe(II) extraction is lower and increases up to 60% after 5 minutes (Figure 1b). The kinetics is fast both for Zn(II) and Fe(II) transport; the maximum extraction is achieved after 5 minutes. No effect of the solvent type in mixture with Cyphos IL101 on Zn(II) extraction is observed.

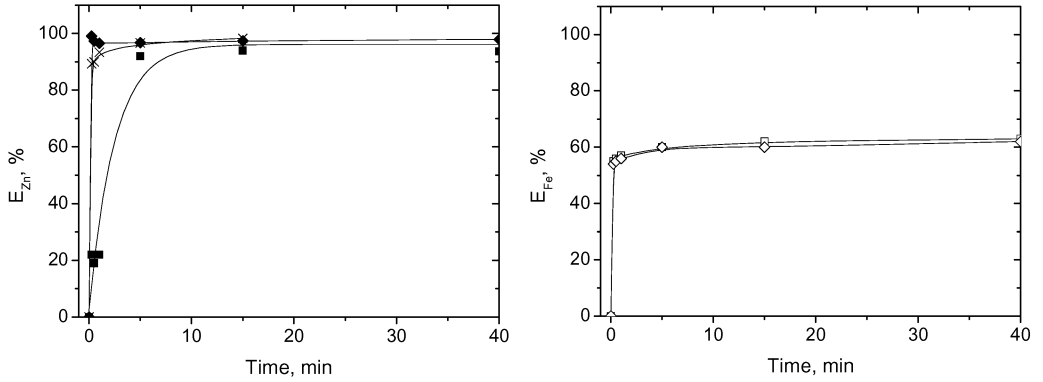

Figure 1. Extraction of a) Zn(II) and b) Fe(II) vs. time with Cyphos IL101 in PC (◆,◇), in BC (■, □), and in toluene (∗). Feed: 0.58 mol/L HCl, 5 mol/L Cl^-, [Zn(II)] or [Fe(II)] = 5 g/L. Organic phase: [Cyphos IL101] = 50 vol %.

Equilibrium of Zn(II) and Fe(II) Extraction

Extraction isotherms (Figure 2) indicate that 50 vol % Cyphos IL101 can be loaded with up to 37 g/L of Zn(II) and 20 g/L of Fe(II). No significant influence of the presence of PC and BC in the mixture is observed. Extraction of Fe(II) with Cyphos

IL101 is a drawback, because selective separation of Zn(II) from Fe(II) is not possible in the system. Although Zn(II) and Fe(II) form various chlorocomplexes in chloride systems, two different mechanisms of extraction are possible that make their separation ineffective. Depending on the concentration of chloride ions and, therefore, on the distribution of metal chlorocomplexes, extraction may be considered in terms of

a) addition of neutral chlorocomplex to the IL molecule

$$ZnCl_2 + 2\overline{[R_3R'P^+][Cl^-]} \Leftrightarrow \overline{[(R_3R'P^+)_2][ZnCl_4^{2-}]} \quad (1)$$

$$FeCl_2 + 2\overline{[R_3R'P^+][Cl^-]} \Leftrightarrow \overline{[(R_3R'P^+)_2][FeCl_4^{2-}]} \quad (2)$$

b) anion exchange of two chlorides for a negatively charged zinc tetrachlorocomplex

$$ZnCl_4^{2-} + 2H^+ + 2\overline{[R_3R'P^+][Cl^-]} \Leftrightarrow \overline{[(R_3R'P^+)_2][ZnCl_4^{2-}]} + 2H^+ + 2Cl^- \quad (3)$$

More detailed studies concerning the structure and composition of Zn(II) and Fe(II) species in the IL phase are necessary.

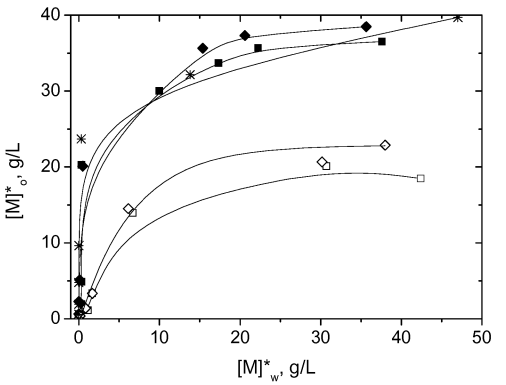

Figure 2. The isotherms of zinc(II) (◆, ■) and iron(II) (◇, □) extraction from 0.58 mol/L HCl with Cyphos IL101 in PC (◆,◇), in BC (■, □), and in toluene (∗). Feed: [M] = [Zn(II)] or [Fe(II)] = 0.5–65 g/L. Organic: [Cyphos IL] = 50 vol %.

Water Transfer to the Organic Phase

Replacement of toluene by alkylene carbonates seems to be reasonable due to their environmentally friendly characteristics. Moreover, they do not reduce the extraction ability of Cyphos IL101. However, as a disadvantage of alkylene carbonates, their hydrophilicity should be mentioned. As shown in Figure 3, after extraction the water content in the organic phase containing alkylene carbonates is higher than in Cyphos IL101 mixed with toluene. The water content decreases with increasing concentration of Zn(II) in the feed solution. The more Zn(II) is transported to the organic phase, the less water is extracted. For low (up to 10 g/L) concentrations of Zn(II), the water content equals 11 and 8% in the mixture of Cyphos IL101 with PC and BC, respectively. The water content reaches a constant value (near 4.5%) for the mixtures of Cyphos IL101 with alkylene carbonates after contact with the feed containing high (more than 50 g/L) concentrations of Zn(II). Water transfer to the mixture of Cyphos IL101

with toluene is twice as small as for alkylene carbonates and changes from almost 5 to near 1%, while Zn(II) concentration increases from 0.5 to 75 g/L in the feed. Unfortunately, water content in the organic phase after Fe(II) extraction could not be determined. Fe(II) extraction coincides with high water co-extraction, causing problems with obtaining the end point in Karl-Fischer titration.

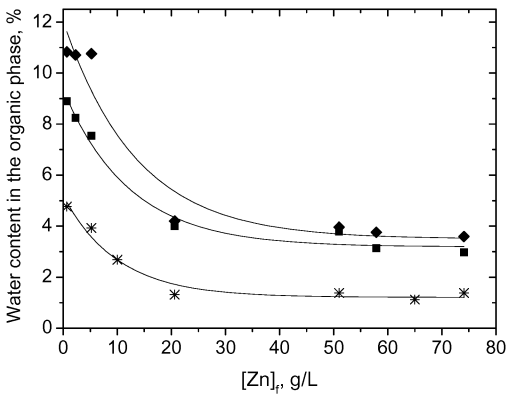

Figure 3. Water content in the organic phase after zinc(II) extraction from 0.58 mol/L HCl with Cyphos IL101 in PC (◆), in BC (■), and in toluene (✳). Feed: [Zn(II)] = 0.5–75 g/L. Organic: [Cyphos IL101] = 50 vol %.

CONCLUSIONS

1. Mixtures of Cyphos IL101 with alkylene carbonates or toluene are effective organic phases for Zn(II) extraction from hydrochloric acid solutions. Fe(II) extraction (up to 60%) is the main disadvantage of the mixtures, because it makes impossible selective separation of Zn(II) from Fe(II) .
2. The kinetics of both Zn(II) and Fe(II) extraction is very fast. More than 90% of Zn(II) and almost 60% of Fe(II) is transferred to the organic phase in less than 5 minutes.
3. There is no effect of toluene or alkylene carbonate type on percentage extraction of Zn(II) and Fe(II) with Cyphos IL101.
4. Water transfer to the organic phase decreases with increasing Zn(II) concentration in the feed solution. The more Zn(II) is extracted, the less water is transported to the organic phase. Water transfer to the mixture of Cyphos IL101 with toluene is twice as small as that for alkylene carbonates.

ACKNOWLEDGMENTS

We thank Cytec Industries Inc. for providing us with free samples of Cyphos IL101, and Huntsman for JEFFSOL BC. This work was supported by the Polish Ministry of Science and Higher Education with its grant No. 1T 09B 081 30.

REFERENCES

1. K. R. Seddon, A. Stark, and M. J. Torres, "Influence of Chloride, Water, and Organic Solvents on the Physical Properties of Ionic Liquids," *Pure Appl. Chem.*, **72**, 2275-2287 (2000).
2. C. J. Adams, "Neoteric Solvents: An Examination of Their Industrial Attractiveness," Ionic Liquids. Industrial Applications for Green Chemistry," R. D. Rogers and K. R. Seddon, Eds., Chapter 2, American Chemical Society, Washington, DC, ACS Symp. Ser. 818, 2002; pp. 15-29.
3. A. Cieniecka-Roslonkiewicz, J. Pernak, J. Kubis-Feder, A. Ramani, A. J. Robertson, and K. R. Seddon, "Synthesis, Anti-microbial Activities and Anti-electrostatic Properties of Phosphonium-based Ionic Liquids," *Green Chem.*, **7**, 855-862 (2005).
4. J. D. Holbrey and R. D. Rogers, "Green Chemistry and Ionic Liquids: Synergies and Ironies," Ionic Liquids. Industrial Applications for Green Chemistry, R. D. Rogers and K. R. Seddon, Eds., Chapter 1, American Chemical Society, Washington, DC, ACS Symp. Ser. 818, 2002; pp. 2-12.
5. K. Shimojo and M. Goto, "Solvent Extraction and Stripping of Silver Ions in Room-Temperature Ionic Liquids Containing Calixarenes," *Anal. Chem.*, **76**, 5039-5044 (2004).
6. K. Nakashima, F. Kubota, T. Maruyama, and M. Goto, "Ionic Liquids as a Novel Solvent for Lanthanide Extraction," *Anal. Sci.*, **19**, 1097-1098 (2003).
7. K. Nakashima, F. Kubota, T. Maruyama, and M. Goto, "Feasibility of Ionic Liquids as Alternative Separation Media for Industrial Solvent Extraction Processes," *Ind. Eng. Chem. Res.*, **44**, 4368-4372 (2005).
8. A. E. Visser, R. P. Swatloski, S. T. Griffin, D. H. Hartman, and R. D. Rogers, "Liquid/Liquid Extraction of Metal Ions in Room Temperature Ionic Liquids," *Sep. Sci. Technol.*, **36**, 785-804 (2001).
9. P. Maass and P. Peissker, Hot-dip Galvanizing, Agencja Wydawnicza Placet, Warsaw, 1998 (in Polish).
10. M. Regel-Rosocka and M. Wisniewski, "Ecological and Economical Aspects of Hot-Dip Galvanizing," Sustainable Mineral Supply for Europe—from Waste to Resources, J. Kudelko, J. Kulczycka, and H. Wirth, Eds., IGSMiE PAN, Krakow, 2007; pp. 46-53.
11. M. Regel-Rosocka, A. Cieszynska, and M. Wisniewski, "Methods of Regeneration of Spent Pickling Solutions from Steel Treatment Plants," *Pol. J. Chem. Technol.*, (2007), in press.
12. W. M. Nelson, "Are Ionic Liquids Green Solvents?" Ionic Liquids. Industrial Applications for Green Chemistry, R. D. Rogers and K. R. Seddon, Eds., Chapter 3, American Chemical Society, Washington, DC, ACS Symp. Ser. 818, 2002; pp. 30-41.
13. C. J. Bradaric, A. Downard, C. Kennedy, A. J. Robertson, and Y. Zhou, "Industrial Preparation of Phosphonium Ionic Liquids," *Green Chem.,* **5**, 143-152 (2003).
14. R. J. Lewis, Hawley's Condensed Chemical Dictionary, John Wiley & Sons, New York, 1997.

REACTIVE EXTRACTION IN ACIDIC IONIC LIQUID SYSTEMS

Deyan Naydenov and Hans-Jörg Bart

Lehrstuhl f. Thermische Verfahrenstechnik, TU Kaiserslautern, Postfach 3049, 67653 Kaiserslautern, Germany. Corresponding author email address: bart@mv.uni-kl.de

ABSTRACT

Ternary liquid-liquid equilibria for systems containing acidic ionic liquids (ILs) are measured at 40 °C. The ILs used are 1-methylimidazolium hydrogen sulphate [HMIM][HSO_4], 1-ethyl-3-methylimidazolium hydrogen sulphate [EMIM][HSO_4], and 1-butyl-3-methylimidazolium hydrogen sulphate [BMIM][HSO_4]. Kinetic data of the IL-catalyzed esterification of ethanol with acetic acid is presented, and the influence of parameters like temperature or catalyst mass on the reaction is discussed. Model-aided theoretical studies provide a means to evaluate new reactive extraction processes with the potential of cost reduction.

INTRODUCTION

Ionic liquids (ILs) are a class of new solvents attracting attention during the past years due to their remarkable properties, for example, as catalysts and solvents for chemical reactions or extraction [1,2]. Acidic ILs such as those containing hydrogen sulfate or hydrogen phosphate anions have been studied as catalysts for esterifications and seem to be promising solvents when used in high concentrations, since their catalytic effect can be combined with a liquid-liquid separation with the potential for conversion enhancements [3-5]. ILs suffer from the fact that the published data is still scarce; this is a major drawback when choosing an appropriate IL or developing processes with ILs.

The esterification of ethanol with acetic acid catalyzed by an acidic IL ([HMIM][HSO_4], [EMIM][HSO_4], [BMIM][HSO_4]) was chosen as a model reaction:

$$C_2H_5OH + CH_3COOH \rightleftharpoons CH_3COOC_2H_5 + H_2O \qquad (1)$$

This reaction is well studied; however, the conventional processes are known to be cost-intensive due to the formation of several azeotropes (one ternary and three binary for this system), and additional efforts are needed in order to separate products from reactants. Reactive distillation is the state of the art for esterification reactions, but problems may arise with thermally sensitive compounds or with high thermodynamic nonideality. By using ionic liquids as an alternative extractive reaction process, we expect to overcome or reduce problems with azeotropes, since here the liquid-liquid equilibria are determining, and separation is at ambient or slightly elevated temperatures.

To reveal the potential of these ILs for reactive separations and processing the reactive mixture, first the liquid-liquid phase equilibria (LLE) for these systems have to be known. Unfortunately, though there are some systematic studies [6-8], data on liquid-liquid equilibria for systems containing ionic liquids is still rare.

Data acquisition in the five-component systems ethanol + acetic acid + ethylacetate + water + IL can be done only when both phases are in chemical equilibrium. Data for the (nonreactive) ternary systems containing ester + alcohol or acetic acid + IL are needed in order to obtain the binary interaction parameters of a G^E-model like UNIQUAC. The ternary data should also give some information about the influence of chemical structure (e.g., alkyl chain length on the immidazolium cation) on the phase equilibria (size of the two-phase region, slope of the tie lines). This can be important for the estimation of LLE when considering other reactions or ionic liquids, since it is impossible to measure all combinations of IL + products/reactants of esterification reactions (or all combinations of, for example, cation + HSO_4^- anion).

In addition to the LLE data, other information like physicochemical properties or the kinetics of the IL-catalyzed reaction is needed for the estimation of residence times, reactor volumes, and thus the feasibility of an reactive extraction process.

The aim of this presentation is to propose a method for the evaluation of reactive extraction processes using the advantages of the ionic liquids. Using the experimentally obtained data, simulations shall show whether and how these ILs can be used as catalyst and reaction medium such as for an esterification reaction and as solvent for extracting a reaction product.

RESULTS AND DISCUSSION

Liquid-Liquid Equilibrium

The experimental liquid-liquid equilibria (LLE) of ternary systems containing ethylacetate + ethanol + an acidic IL or ethylacetate + acetic acid + acidic IL at 313.2 K have already been presented [9], and the influence of the alkyl chain length of the cation on the phase behavior will be reconsidered in brief, since they are the background for the further simulations.

At the conference, four experimental LLE diagrams will be presented. The studied systems are [EMIM HSO_4] + butylacetate + 1-butanol, [EMIM HSO_4] + butylacetate + acetic acid, [EMIM HSO_4] + propylacetate + 1-propanol, [EMIM HSO_4] + propylacetate + acetic acid. They are a continuation of our systematic study on ternary systems containing acidic ionic liquids and give the effect of the alkyl chain length on the ester and alcohol on the size of the binodal curve and the position of the tie lines. All systems are of type I at 40 °C (one immiscible pair: EMIM and ester); however, at room temperature, butanol and EMIM are immiscible, too. With increasing the alkyl chain length on the ester and alcohol, a slight increase of the two-phase region is observed. This is explained with the increase of hydrophobicity of the chemicals.

Kinetic Data

Kinetic data for the IL-catalyzed esterification of ethanol with acetic acid was measured only for the IL HMIM and EMIM. Samples containing ethanol + IL were put into a three-necked flask of 100 mL and placed in a water bath controlled at $T_{exp} \pm 0.1$ K. The acetic acid was preheated to experimental temperature and added to the alcohol and IL. The experiment duration was usually 4 h. If a second phase appeared, the experiments were stopped before that. Due to the low heat of the reaction and heat losses during the experiments, the uncertainty of the experimental temperature is estimated to be ± 0.5 K.

The effect of several parameters on the reaction ratio was studied: catalyst mass, temperature, and molar ratio of ethanol to acetic acid. A wide range, between 0.005 and 0.30 mass fraction of the IL was studied, since in order to obtain a phase separation, a higher quantity of IL is needed. As can be seen in Figure 1, the reaction is relatively slow even at higher IL contents. That means higher residence times are needed in order to achieve higher conversions. For these data, the experimental temperature was 60 °C, and the ratio of ethanol to acetic acid was 1:1. The temperature has a significant influence on the kinetics (see Figure 2); while the reaction can be frozen at room temperature, the conversion at 70 °C is quite acceptable. Through nonlinear regression, the coefficients of the following kinetic equation were obtained:

$$\frac{1}{m_k} \cdot \frac{1}{\nu_i} \cdot \frac{dn_i}{dt} = \cdot k_f \cdot (a_{ET} \cdot a_{HAc} - a_{EA} \cdot a_{H2O} / K) \qquad (2)$$

where n_i is the mole number, ν_i is the stoichiometric coefficient, a_i is the activity of the compound i, K is the equilibrium constant, k_f is the forward reaction constant, and m_k is the catalyst mass. A comparison of experimental data and calculations using Equation 2 are shown in Figure 3.

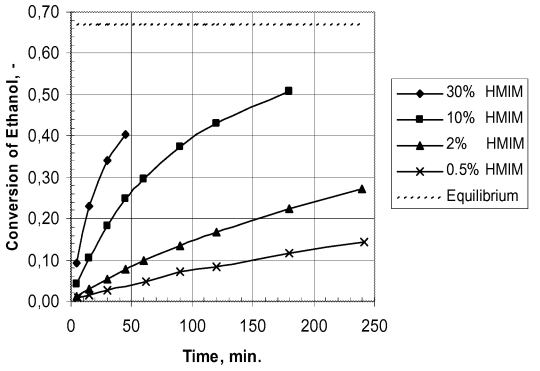

Figure 1. Effect of the catalyst mass on the reaction at 60 °C.

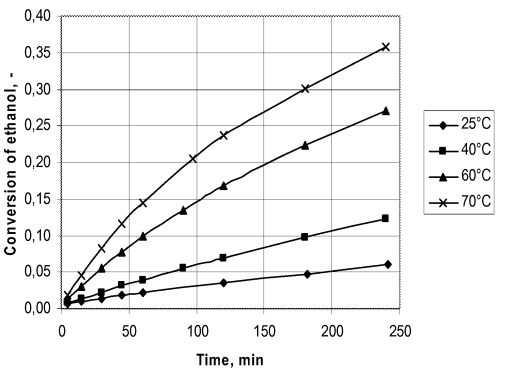

Figure 2. Effect of temperature. Molar ratio of ethanol to acetic acid, 1:1.

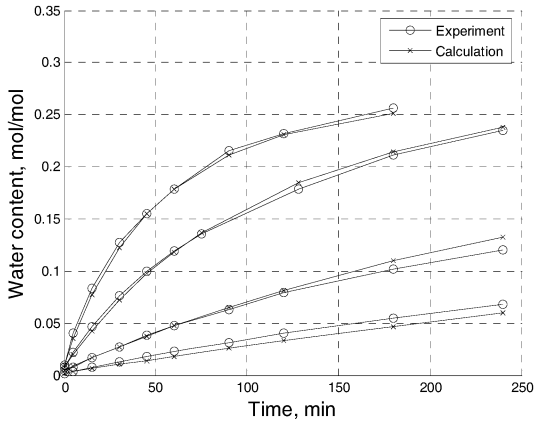

Figure 3. Comparison between experimental kinetic data and calculations for EMIM at 60 °C and 1:1 molar ratio of ethanol to acetic acid (effect of catalyst mass fraction).

Simulations

A theoretical stage model, assuming both liquid-liquid phase equilibrium and chemical equilibrium with the reaction in the ionic (catalytic) phase, was developed. The liquid-liquid equilibrium was approximated by constant distribution ratios and also by UNIQUAC to account for thermodynamic nonidealities. In a further step, kinetic data is taken into account, allowing a more realistic description of these systems. Using the one-stage module, a countercurrent multistage reactive extraction cascade was simulated. Depending on the distribution of the reactants between ester and IL, there are several theoretical configurations that can lead to higher reaction conversion and/or product purity.

When EMIM is used as catalyst/solvent (ethanol more soluble in ester, acetic acid more soluble in the IL), the process shown in Figure 4 is favorable.

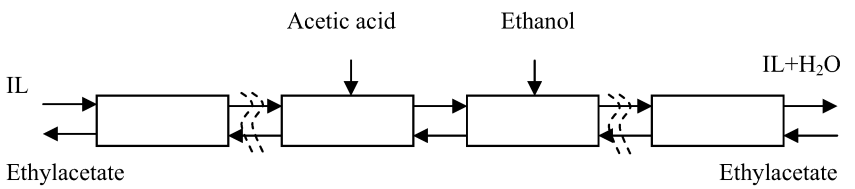

Figure 4. Simulated countercurrent reactive extraction process.

The compositions of the organic phase and the ionic phase for a simulation are shown in Figures 5 and 6, respectively. Since high conversions (>90 %) and relatively pure products are obtained, the proposed process has the potential for both low capital and energy costs.

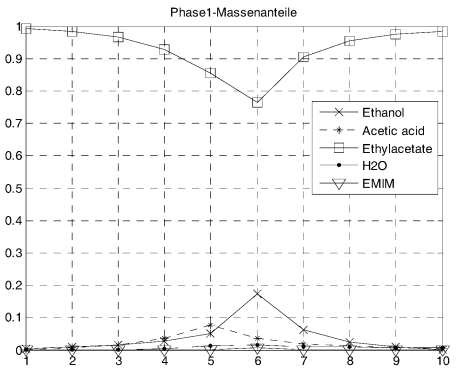

Figure 5. Composition of the organic phase along the cascade.

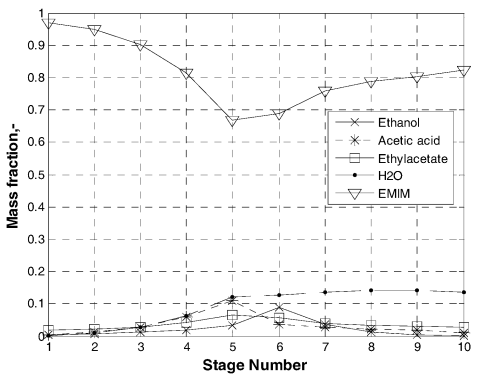

Figure 6. Composition of the ionic phase along the cascade.

When both reactants are more soluble either in the organic or in the ionic phase (HMIM-, BMIM-systems, respectively) one obtains a more unfavorable situation. In such cases, in comparison to the EMIM process, an additional separation (distillation) is required to separate product and reactants and the vapor-liquid equilibria of this system has also to be considered.

CONCLUSIONS

Ionic liquids are chemicals having some properties that can be advantageous for reactive extraction processes. However, due to the lack of experimental data, the development of such processes is hindered. We studied the esterification of ethanol with acetic acid in acidic ionic liquids with hydrogen sulphate anion.

Experimental data on the ternary liquid-liquid phase equilibrium for systems containing IL at 40 °C are presented. The effect of the alkyl chain length on the IL on the one side and on the ester and alcohol on the other side is obtained. As a general rule, with increasing the chain length on the ester and alcohol, the size of the two-phase region increases, and the solubility in the ionic liquid decreases. The opposite effect is observed when the chain length on the ionic liquid is increased.

Kinetic data for the IL-catalyzed esterification of ethanol with acetic acid is obtained, and the influence of several parameters (mass of the catalyst, temperature, ratio of ethanol to acetic acid) on the reaction ratio is discussed. We found a nonlinear relationship between the catalyst mass and the reaction ratio, probably due to the broad range studied (between 0.005 and 0.3 mass fractions of IL).

Using an equilibrium stage model, different possible reactive extraction processes were simulated. Due to the minimum additional separations needed and the high conversions obtained, simulations reveal that the process utilizing the ionic liquid [EMIM HSO_4] has the highest potential for cost savings when producing ethylacetate.

ACKNOWLEDGMENTS

We would like to thank BASF for providing the ionic liquids [EMIM][HSO_4] and [BMIM][HSO_4]. We are grateful for the financial support of "Bundesministerium für Wirtschaft und Technologie" (BMWI) and AIF.

REFERENCES

1. T. Welton, "Room-temperature ionic liquids. Solvents for Synthesis and Catalysis," *Chem. Rev.*, **99**, 2071-2083 (1999).
2. K. Marsh, A. Deev, A. C-T. Wu, E. Tran, and A. Klamt, "Room temperature ionic liquids as replacements for conventional solvents - a review," *Korean J. Chem. Eng.*, **19**, 357-362 (2002).
3. J. Fraga-Dubreuil, K. Bourahla, M. Rahmouni, J. P. Bazureau, and J. Hamelin, "Catalysed esterifications in room temperature ionic liquids with acidic counteranion as recyclable reaction media," *Catal. Commun.*, **3**, 185-190 (2002).
4. J. Gui, X. Cong, D. Liu, X. Zhang, Z. Hu, and Z. Sun, "Novel Brønsted acidic ionic liquid as efficient and reusable catalyst system for esterification," *Catal. Commun.*, **5**, 473-477 (2004).
5. H.-P. Zhu, F. Yang, J. Tang, and M.-Y. He, "Bronsted acidic ionic liquid 1-methylimiazolium tetrafluoroborate: a green catalyst and recyclable medium for esterification," *Green Chem.*, **5**, 38-39 (2003).
6. A. Heintz, "Recent developments in thermodynamics and thermophysics of non-aqueous mixtures containing ionic liquids. A review," *J. Chem. Thermodyn.*, **37**, 525-532 (2005).
7. J. M. Crosthwaite, S.N.V.K. Aki, E. J. Maginn, and J. F. Brennecke, "Liquid phase behaviour of imidazolium-based ionic liquids with alcohols," *J. Phys. Chem. B*, **108**, 5113-5119 (2004).
8. U. Domanska and A. Marciniak, "Solubility of ionic liquid [emim][PF6] in alcohols," *J. Phys. Chem. B*, **108**, 2376-2382 (2004).
9. D. Naydenov and H.-J. Bart, "Ternary Liquid-Liquid Equilibria for Six Systems Containing Ethylacetate + Ethanol or Acetic Acid + an Imidazolium-Based Ionic Liquid with a Hydrogen Sulfate Anion at 313.2 K," *J. Chem. Eng. Data*, Published on Web 10.10.2007, DOI: 10.1021/je700342k.

EXTRACTIVE REMOVAL OF PALLADIUM(II) FROM CHLORIDE MEDIA WITH PYRIDINECARBOXAMIDES AND PHOSPHONIUM IONIC LIQUIDS

A. Cieszyńska, M. Regel-Rosocka, and M. Wiśniewski

Poznan University of Technology, Institute of Chemical Technology and Engineering, pl. M. Skłodowskiej-Curie 2, 60-965 Poznan, Poland.
Corresponding author email address: Maciej.Wisniewski@put.poznan.pl

ABSTRACT

A comparison of the extraction abilities of the pyridinecarboxamides N-dodecylpyridine-3-carboxamide (3-C_{12}) and N-dodecylpyridine-4-carboxamide (4-C_{12}) and of the phosphonium ionic liquids trihexyltetradecylphosphonium chloride (Cyphos IL101) and trihexyltetradecylphosphonium bis(2,4,4-trimethylpentyl)phosphinate (Cyphos IL104) is made. They are used for the extraction of Pd(II) from hydrochloric acid solutions. Kinetics and equilibrium data indicate that phosphonium ionic liquids are very efficient extractants, and such extraction proceeds very fast. Pyridinecarboxamides are good extractants, too. However, there are more problems with phase separation and formation of precipitation in contact with concentrated HCl solutions. Extraction of Pd(II) depends upon the content of hydrochloridc acid and concentration of added sodium chloride. The increase in HCl concentration has a negative effect on the extraction of Pd(II).

INTRODUCTION

Noble metals, particularly platinum group metals (PGM), have a wide range of industrial applications, for example, as catalysts in organic processes, vehicle catalytic converters, and value-added components in metal alloys. They are used in the electronic, chemical, pharmaceutical, and petroleum industries and also in instrument and jewelry making. A demand for these metals has increased in recent years, whereas their natural sources are limited [1,2]. That is why an interest towards recycling spent materials containing these metals is observed. Among a variety of methods, solvent extraction is proposed as a suitable method for PGM recovery from low-concentration sources [3]. Several extractants have been studied and proposed, hydroxyoximes [4], dialkyl sulfides [5], alkyl derivatives of 8-hydroxyquinoline [6], and hydrophobic amines [7], among them. The pyridinecarboxamides have been synthesized and proposed as extractants of palladium(II) from hydrochloric acid solutions in our research group [8,9]. It has been found that the extraction of Pd(II) with monoalkylpyridinecarboxamides depends upon the number, length, and position of the alkylamide group.

As palladium(II) extraction is a very slow process due to both the nature of symmetrical palladium(II) chlorocomplex ($PdCl_4^{2-}$) and high hydrophobicity of the extractants, new organic reagents are sought after to improve the kinetics of the process. Some ionic liquids (ILs) seem to be prospective compounds for separation processes. Recently, imidazolium ILs have been applied as solvents in several separation processes, including extraction of Ag(I) [10], Ce(III), Eu(III), Y(III) [11], Hg(II) [12], alkali metals, and Sr(II) [13,14]. Replacement of traditional organic solvents with ILs resulted in a significant improvement in the extraction efficiency of the metal cations referred to above. Although no reports concerning phosphonium ILs in extraction systems have been available to-date, they are considered to be prospective for substance separation.

It is the aim of our work to examine the extractive properties of two phosphonium ILs (Cyphos IL101 and Cyphos IL104) towards Pd(II) in hydrochloric acid solutions and to compare their extraction efficiency with that of pyridinecarboxamides (3-C_{12} and 4-C_{12}).

EXPERIMENTAL SECTION

Two phosphonium ionic liquids: Cyphos IL101 and Cyphos IL104, supplied by Cytec Industry Inc. (Canada), are dissolved in toluene and used as extractants. Toluene is applied to overcome some drawbacks caused by the high viscosity of ILs. The electrospray mass spectra of the aqueous phase after extraction with both Cyphos ILs do not indicate the presence of a phosphonium cation, which proves the insignificant solubility of Cyphos ILs in the studied aqueous phases. Two pure individual monoalkylamides, 3-C_{12} and 4-C_{12}, are also used as extractants. The structures of the extractants used are presented in Table 1. The synthesis, purity, structures, and analytical data were described in previous papers [15]. The analytical and physicochemical data for the studied extractants were presented previously [8].

Table 1. Structures of extractants used

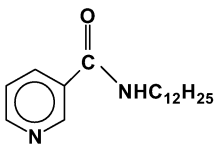 **3-C_{12}**	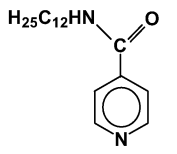 **4-C_{12}**
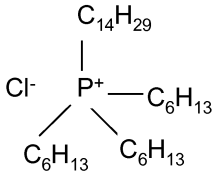 **Cyphos IL 101**	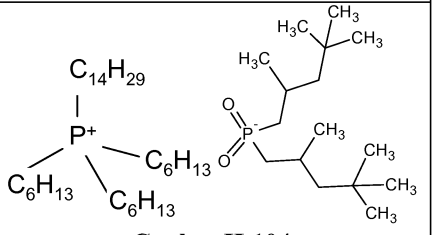 **Cyphos IL104**

Extraction was carried out in a typical way with five millimolar solutions of IL in toluene as an organic phase. Aqueous feeds containing 5×10^{-3} mol/L of palladium(II) chloride in 0.1–3 mol/L HCl and 0.1 mol/L HCl in the presence of 0.5 mol/L NaCl were used. Equal volumes (5 cm^3) of phases were mechanically shaken for a period of time between 30 s and 30 min. at 20 ºC and left to stand for phase separation. Inductively coupled plasma spectroscopy (ICP–Spectro, Analytical Instruments, Germany) was used for palladium(II) determination in the initial aqueous solutions and in the aqueous phases after the extraction (wavelength for Pd(II), 340.5 nm). Each experiment was carried out twice, and the error did not exceed ±5%.

RESULTS AND DISCUSSION

Phosphonium Ionic Liquids as Pd(II) Extractants

The kinetics of Pd(II) extraction from hydrochloric acid solutions with Cyphos IL101 and Cyphos IL104 is shown in Figure 1a and 1b, respectively. Extractions for both ILs differ hardly at all. In the presence of 0.1 mol/L HCl in the feed, about 95% Pd(II) is extracted. Addition of NaCl (0.5 mol/L) to 0.1 mol/L HCl results in a decrease in the extent of palladium(II) extraction to about 80%. Extraction decreases to 55% when HCl concentration is increased up to 3 mol/L. The differences in the extraction of Pd(II) from low- and high-concentration acid can be explained by the change of the distribution of Pd(II) chlorocomplexes with the increase in hydrochloric acid concentration. At 3 mol/L HCl solution, the following species are observed: $PdCl_6^{4-}$, $PdCl_4^{2-}$, and $PdCl_5^{3-}$, and at 0.1 mol/L HCl, only $PdCl_4^{2-}$ is present.

The kinetics is fast, and equilibrium is achieved after 5 minutes. As no effect of the anion type on the extraction of Pd(II) is observed, it suggests that the same extraction mechanism may be responsible for the transfer of Pd(II) to the organic phase.

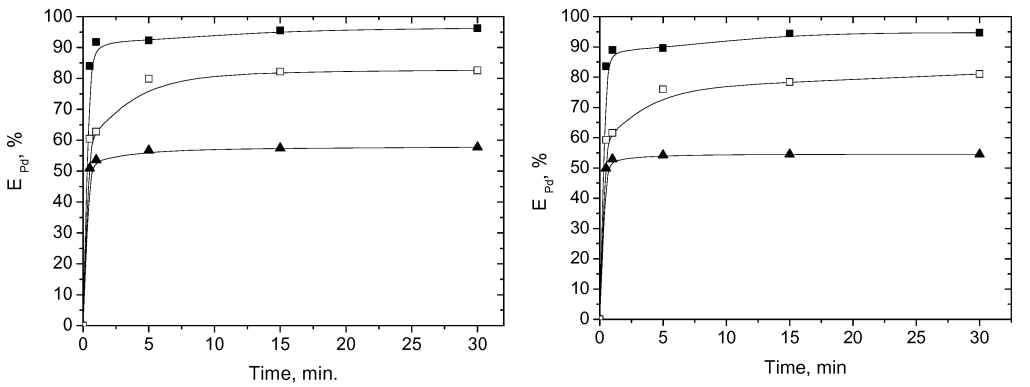

Figure 1. Extraction of Pd(II) vs. time of extraction with a) Cyphos IL101 and b) Cyphos IL104 from 0.1 mol/L HCl solution (■), 3 mol/L HCl solution (▲), and 0.1 mol/L HCl solution in the presence of 0.5 mol/L NaCl (□). [Pd(II)] = 5×10^{-3} mol/L, [Cyphos IL] = 5×10^{-3} mol/L.

Extraction isotherms (Figure 2) indicate that 5×10^{-3} mol/L Cyphos IL104 can be loaded with almost 4.8×10^{-3} mol/L Pd(II) and 5×10^{-3} mol/L Cyphos IL101 even up to 5.4×10^{-3} mol/L Pd(II). At such extractant and feed concentrations, we propose extraction of $PdCl_4^{2-}$ and H^+ to the organic phase at a molar ratio IL:Pd = 1 and formation of ionic pair [$HPdCl_4^-$] and [RR'_3P^+] in the IL phase. However, more detailed studies concerning the structure and composition of Pd(II) species in the IL phase will be carried out.

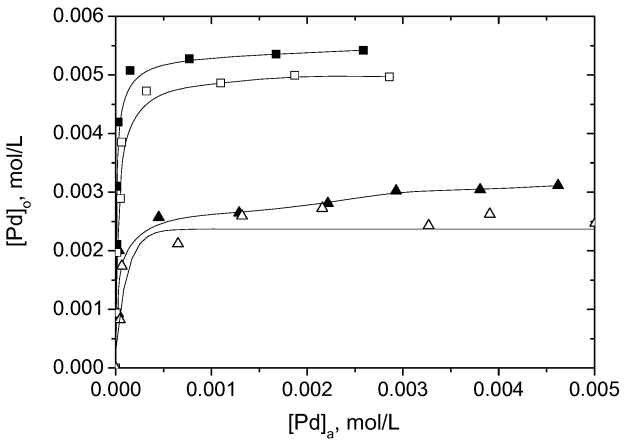

Figure 2. The isotherms of palladium(II) extraction from 0.1 mol/L HCl (■, □) and 3 mol/L HCl (▲, △) with Cyphos IL101 (■, ▲) and Cyphos IL104 (□, △). [Pd(II)] = 1×10^{-3} to 8×10^{-3} mol/L, [Cyphos IL] = 5×10^{-3} mol/L.

The differences in the extraction of Pd(II) from low- and high-concentration acid can be explained by the co-extraction of various species: at low proton concentrations, extractable anionic species ($PdCl_4^{2-}$) in the aqueous phase are effectively transferred by an anion-exchange extractant such as Cyphos IL101, whereas at high concentrations of HCl, the extraction of protons is likely to disturb the efficient extraction of Pd(II). Therefore, a significant decrease in the extraction of Pd(II) from 3 mol/L HCl is observed, both for Cyphos IL101 and Cyphos IL104 (Figure 2). However, further studies on the mechanism of Pd(II) extraction, particularly with Cyphos IL104, will be carried out.

Extraction with Pyridinecarboxamides and Phosphonium ILs

Protonated pyridinecarboxamides transport Pd(II) according to the addition mechanism, while ionic liquids at high Cl^- concentrations act rather by the anion-exchange mechanism. However, in all of the cases presented in Figure 3, both 3-C_{12} and 4-C_{12} exhibit q as high a percent extraction as do the ionic liquids. The basicity of pyridine nitrogen in monoalkylpyridinecarboxamides seems to enhance their extractive power. What is most important, extraction with 3-C_{12} and 4-C_{12} is efficient (E_{ex} = 100%) and rapid; the equilibrium is achieved in 30-60 s [9]. A significant difference in the extraction of Pd(II) is observed for the feed containing 3 mol/L HCl. Both ionic liquids

extract in one step about 55% of Pd(II), while 3-C_{12} and 4-C_{12} do more than 95%. Unfortunately, at high acid concentrations, precipitation at the phase interface is observed, which is the main drawback in applying the monoalkylpyridinecarboxamides at a large scale.

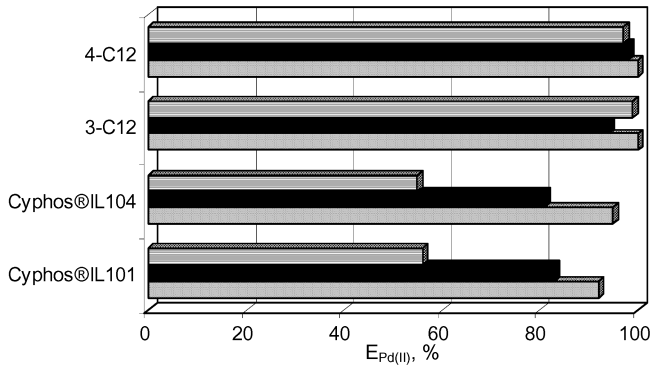

Figure 3. Extraction of Pd(II) from hydrochloric acid solutions. (□) 0.1 mol/L HCl; (■) 0.1 mol/L HCl in the presence of 0.5 mol/L NaCl; (▣) 3 mol/L HCl. [Pd(II)] = 5×10^{-3} mol/L; [Extractant] = 5×10^{-3} mol/L.

CONCLUSIONS

Phosphonium ILs (Cyphos IL101 and Cyphos IL104) and pyridinecarboxamides (3-C_{12} and 4-C_{12}) are very efficient and fast in the extraction of Pd(II) from hydrochloric acid solutions. The equilibrium of Pd(II) extraction from hydrochloric acid solutions with Cyphos IL101 and Cyphos IL104 is achieved after 5 minutes. No effect of the IL anion type on the extraction of Pd(II) is observed, suggesting that the same extraction mechanism can be responsible for Pd(II) transfer to the organic phase. Both phosphonium ILs exhibit very good extractive properties towards Pd(II) from low-concentration HCl solutions ($E_{Pd(II)} > 95\%$), and worse ($E_{Pd(II)} \sim 55\%$) from 3 mol/L HCl. No positive effect of NaCl addition to the feed on extraction of Pd(II) is noticed; however, a better phase separation after the extraction is observed. Compared with monoalkylpyridinecarboxamides, phosphonium ILs are less efficient extractants. However, they do not form precipitates over the studied HCl concentration range, which is very important in view of their application in separation processes.

ACKNOWLEDGMENTS

We thank Cytec Industries Inc. for providing us with free samples of Cyphos IL101 and Cyphos IL104. This work was supported by the Polish Ministry of Science and Higher Education with its grant No. 1T 09B 081 30.

REFERENCES

1. P. Yong, N. A. Rowson, J. P. G. Farr, I. R. Harris, and L. E., Macaskie, "A Novel Electrobiotechnology for the Recovery of Precious Metals from Spent Automotive Catalysts," *Environ. Technol.*, **24**, 289-297 (2003).
2. J. Matthey, "Platinum 2006 Interim Review," *Platinum Met. Rev.*, **51**, 45 (2007).
3. F. L. Bernardis, R. A. Grant, and D. C. Sherrington, "A Review of Methods of Separation of the Platinum-group Metals through Their Chloro-complexes," *React. Funct. Polym.*, **65**, 205–217 (2005).
4. M. J. Cleare, R. A. Grant, and P. Charlesworth, "Separation of Platinum Group Metals by Use of Selective Solvent Extraction Techniques," Extractive Metallurgy, IMM, London, 1981.
5. J. S. Preston and A. C. du Preez, "Solvent Extraction of Platinum-Group Metals from Hydrochloric Acid Solutions by Dialkyl Sulphoxides," *Solvent Extr. Ion Exch.*, **20**, 359-374 (2002).
6. B. Cote and G. P. Demopoulos, "New 8-Hydroxyquinoline Derivative Extractants for Platinum Group Metals Separation Part 2. Pd(II) Extraction Equilibria and Stripping," *Solvent Extr. Ion Exch.*, **12**, 393-421 (1994).
7. A. Zhang, G. Wanyan, and M. Kumagai, "Association Behavior of 4-Acylpyrazolone Derivative and Tertiary Amine of High Molecular Weight in Antagonistic Synergistic Extraction of Palladium," *J. Solution Chem.*, **33**, 1017-1028 (2004).
8. I. Szczepanska, A. Borowiak-Resterna, and M. Wisniewski, "New Pyridinecarboxamides for Rapid Extraction of Palladium from Acidic Chloride Media," *Hydrometallurgy*, **68**, 159-170 (2003).
9. M. Regel-Rosocka, M. Wisniewski, A. Borowiak-Resterna, A. Cieszynska, and A. M. Sastre, "Selective Extraction of Palladium(II) from Hydrochloric Acid Solutions with Pyridinecarboxamides and ACORGA®CLX50," *Sep. Purif. Technol.*, **53**, 337–341 (2007).
10. K. Shimojo and M. Goto, "Solvent Extraction and Stripping of Silver Ions in Room-temperature Ionic Liquids Containing Calixarenes," *Anal. Chem.*, **76**, 5039-5044 (2004).
11. K. Nakashima, F. Kubota, T. Maruyama, and M. Goto, "Feasibility of ionic liquids as alternative separation media for industrial solvent extraction processes," *Ind. Eng. Chem. Res.*, **44**, 4368-4372 (2005).
12. A. E. Visser, R. P. Swatloski, S. T. Griffin, D. H. Hartman, and R. D. Rogers, "Liquid/Liquid Extraction of Metal Ions in Room Temperature Ionic Liquids," *Sep. Sci. Technol.*, **36**, 785-804 (2001).
13. D. C. Stepinski, M. P. Jensen, J. A. Dzielawa, and M. L. Dietz, "Synergistic Effects in the Facilitated Transfer of Metal Ions into Room-temperature Ionic Liquids," *Green Chem.*, **7**, 151-158 (2005).
14. H. Luo, S. Dai, and P. V. Bonnesen, "Solvent Extraction of Sr^{2+} and Cs^{+} Based on Room-temperature Ionic Liquids Containing Monoaza-substituted Crown Ethers," *Anal. Chem.*, **76**, 2773-2779 (2004).
15. A. Borowiak-Resterna, "Extraction of Copper from Acid Chloride Solutions by N-Dodecyl- and N,N-Dihexylpyridinecarboxamides," *Solvent Extr. Ion Exch.*, **17**, 133-148 (1999).

GAS SORPTION USING IONIC LIQUIDS

Richard D. Noble, Douglas L. Gin, Jason E. Bara, B. Voss, A. Finotello, and T. Carlisle

University of Colorado, Chem. and Biol. Eng. Department, Boulder, CO 80309, USA.
Corresponding author email address: nobler@colorado.edu

ABSTRACT

The objective is to fabricate new sorbent structures based on ionic liquids and characterize their fundamental gas and vapor transport properties. Room temperature ionic liquids (RTILs) with polymerizable groups can be readily converted into solid-state poly(RTILs) for use as gas sorbents. The sorbents will be fabricated from ILs (which will act as the active component to provide high selectivity for the target agents) and polymerizable ILs (which can be formed directly into solid, mechanically stable and tunable polymeric solids). The use of polymerizable lyotropic liquid crystals (LLCs) as a blendable additive to these IL materials provides a means to obtain specific nanoporous morphologies that provide the potential for enhanced sorption capacity in the resulting films or particles. LLC systems have the ability to form ordered, phase-segregated nanoporous structures and incorporate the IL into the ordered hydrophilic regions to generate very high surface area materials. Separately, the addition of inorganic NPs to IL-based sorbent systems will allow formation of solid-state materials, and provide additional surface area and adsorption capacity for the target agents.

IONIC LIQUIDS

Room Temperature Ionic Liquids (RTILs) are solvents consisting entirely of ions (Figure 1) resembling the ionic melts of metallic salts; however, RTILs are liquids at much lower temperatures. RTILs have high thermal stability, high ionic conductivity, negligible vapor pressure and are nonflammable. Unlike traditional organic media, *RTIL's properties may be adjusted via chemical alteration of the cation or anion to produce application-specific compounds.* Many RTILs are liquids over a wide temperature range with some known melting points as low as -96 ^{o}C and some liquid ranges in excess of 300 ^{o}C. High coulombic forces constrain the RTIL constituents and thus, the RTILs exert practically no vapor pressure above the liquid surface. These features have led to current investigations of RTILs as alternative media for a variety of applications that use organic solvents.

The potential exists for a complexing agent to be one of the ions in an IL giving a maximum loading much greater than loadings typically observed in standard solvent systems. These so-called "task specific" ILs are capable of absorbing very high quantities of a specific gas. For example, Davis and co-workers reported the synthesis of an IL

containing an amine functionality that was capable of absorbing 0.5 mol of carbon dioxide per mole of IL (*approx. 6 mL/g IL*) [1]. Complexing agents can also be added or "doped" into ILs [2]. Recent studies on ILs have indicated that the combination of subtle (e.g., changing cation substitution patterns) and gross (e.g., changing anion type) modifications can permit very precise tuning of the IL solvent properties. Changes in solvation properties are possible in this way, thus enabling the rational design of application specific ILs.

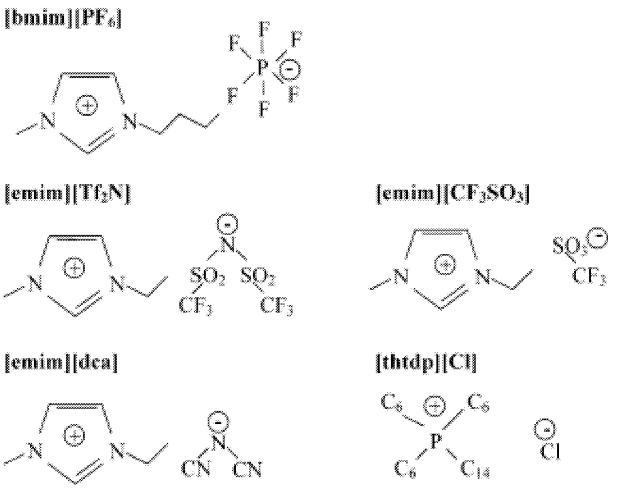

Figure 1. Room temperature ionic liquids.

REGULAR SOLUTION THEORY AND SOLUBILITY MEASUREMENTS

When using RTILs as a bulk fluid absorber, film or particle, it is necessary to understand the parameters that influence gas solubility. Previous work has been reported by our group on developing a solubility model for gases in Rmim-based RTILs (Figure 1) based on regular solution theory [3-7]. In this theory, the solubility is related to the difference of the solubility parameter for the solute and solvent squared. The solubility parameter for each component is an independent value. The solubility parameters of many gases and vapors have been tabulated. We have shown that the solubility parameter of the RTIL can be estimated from the lattice energy density of the RTIL using the Kapustinskii equation. This method was only applied to Rmim-based RTILs (Figure 1), because the main source of polarizability in Rmim-based RTILs is the imidazolium ring. Since the polarizability is dominated by the imidazolium ring, any error due to ignoring the polarizability by using the Kapustinskii equation would be applied to all the Rmim-based RTILs.

Using a simplified version of Regular Solution Theory (RST) and Equation 2, a simple relationship between the natural logarithm of the Henry's constant ($H_{2,1}$) (measure of solubility) and the molar volume can be shown in Equation 1 where α and β (or β^*) are constants that depend only on temperature and the gas being absorbed. V_1^L is the molar volume of the RTIL. It should be stated that very small molar volumes push the

limit of this assumption, but the solubility parameters would still stay within a 10% error for any reasonable molar volume of an RTIL.

Equation 1 was applied to CO_2, CH_4, and N_2 at 40 °C. Figure 2 shows that the solubility increases as the molar volume of Rmim-based RTILs increases.

$$\ln\left(H_{2,1}(atm)\right) = \alpha + \frac{\beta^*}{V_1^{L\,4/3}} \tag{1}$$

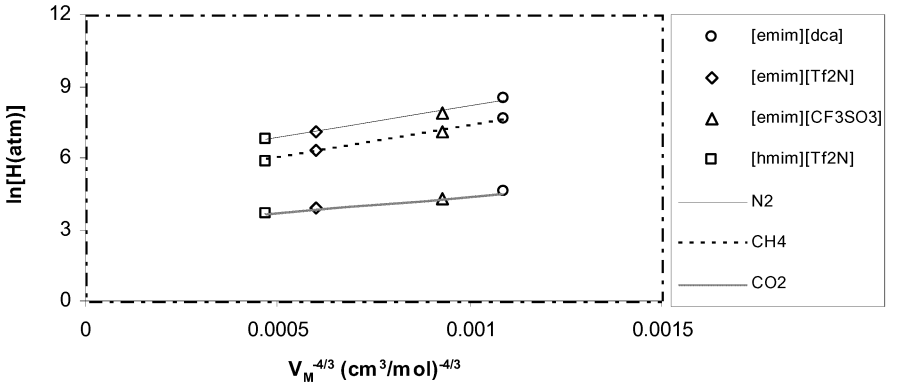

Figure 2. Plot of the natural log of the Henry's constant for CO_2, N_2, and CH_4 versus the molar volume of the RTIL to the negative 4/3 power at 40 °C.

In order to directly determine the bulk solubility of CO_2, Equation 1 was rearranged so that the solubility could be plotted using moles of gas per liter of RTIL (Equation 2) versus molar volume of the RTIL (Figure 3).

$$\frac{\text{Moles of Gas}}{\text{Liter of RTIL}} = \frac{1}{\left[\exp\left(\alpha + \beta^* \Big/ V_1^{L\,4/3}\right) - 1\right] V_1^L} \tag{2}$$

There is an inherent maximum amount of moles of gas per volume of RTIL that can be absorbed for Rmim-based RTILs, since the molar solubility increases with increasing molar volume of the RTIL. This can be shown mathematically by taking the derivative of Equation 2 with respect to the molar volume and setting the derivative equal to zero (Equation 3).

$$V_1^L = \left\{ \frac{\left(\frac{4}{3}\right)\beta^* \exp\left(\alpha + \beta^* \Big/ V_1^{L\,4/3}\right)}{\left[\exp\left(\alpha + \beta^* \Big/ V_1^{L\,4/3}\right) - 1\right]} \right\}^{3/4} = \left[\frac{\left(\frac{4}{3}\beta^*\right)}{(1 - x_2)} \right]^{3/4} \tag{3}$$

Equation 3 can then be simplified by letting $(1 - x_2)$ equal 1 (Equation 4), which is a good approximation at low pressures.

$$V_1^L = \left(\frac{4\beta^*}{3}\right)^{3/4} \quad (4)$$

Equation 4 provides a simple method to determine the molar volume of an Rmim-based RTIL that can absorb the maximum amount of moles of gas per volume of RTIL. The values of β*calculated for CO_2 are 1160, 1290, and 1280 $(cm^3/mol)^{4/3}$ for 25, 40 and 50 °C respectively.

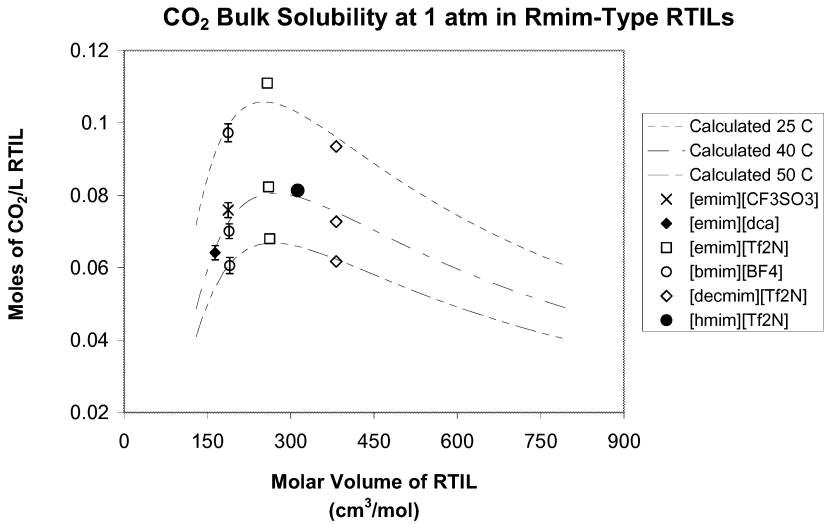

Figure 3. Plot of the moles of CO_2 per liter of RTIL at 1 atm versus the molar volume of the RTIL at various temperatures. The maximum loading corresponds to approximately 1 mL gas/g sorbent.

The molar volume where the maximum occurs for CO_2 is approximately the molar volume of [emim][Tf_2N] for all the temperatures shown in Figure 3. [decmim][Tf_2N] was synthesized in order to experimentally determine that the peak in Figure 3 does exist by showing a point on the right hand side of the curve maximum. The main difference of [decmim][Tf_2N] compared to the other Rmim-based RTILs used in this study is that the solubility is slightly lower than the predicted value due to its large alkyl chain length. This is due to a lower polarizability which decreases slightly with increasing alkyl chain length on Rmim-based RTILs.

Extension to IL Mixtures

This combined experimental/theoretical approach can be extended to mixtures of ILs to adjust the solubility properties [8].

$\overline{V_1}$, the molar volume of the mixture, can be defined as:

$$\overline{V}_1^{-4/3} = \overline{V}^{-4/3}{}_{1\_geometric-ave} = \left(\frac{(V_{1A}^L V_{1B}^L)^{-4/3}}{x_A (V_{1B}^{L\,-4/3} - V_{1A}^{L\,-4/3}) + V_{1A}^{L\,-4/3}} \right) \tag{5}$$

Equation 4 then becomes

$$\ln\left[H_{2,1}(atm)\right] = \alpha + \beta^* (\overline{V}_1^{-4/3}) \tag{6}$$

Experimental measurements were conducted with mixtures of [emim][Tf_2N] and [emim][BF_4]. The results are shown below and confirm that the theory can be extended to mixtures. Note that a smaller value of the Henry's constant corresponds to a higher solubility.

Ionic Liquid	H CO_2 (atm)	mL gas/g IL
[emim][Tf_2N]	42.5	0.41
25 mol % [emim][BF_4]	58.0	0.35
50 mol % [emim][BF_4]	64.7	0.43
75 mol % [emim][BF_4]	84.8	0.43
90 mol % [emim][BF_4]	90.3	0.46
95 mol % [emim][BF_4]	94.0	0.46
[emim][BF_4]	172.4	0.50

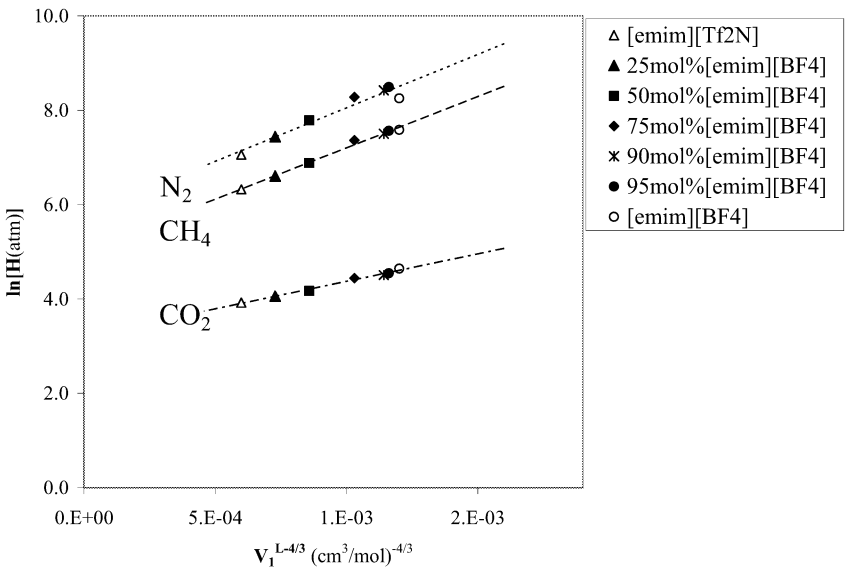

Figure 4. Plot of gas solubility (as ln *H*) as a function of the mixture molar volume.

Figure 4 demonstrates that RST is valid for RTIL mixtures. This linear relationship shows that RST can describe the behavior of gases in RTIL mixtures.

Extension to Polymers

Polymeric versions of ILs have been synthesized and gas solubility measured [9-10]. The addition of nitrile or ether groups enhanced the solubility and provided permeation and selectivity that was superior to conventional polymers for CO_2/N_2 separations.

REFERENCES

1. E. D. Bates, R. D. Mayton, I. Ntai, and J. H. Davis, Jr., "CO_2 Capture by a Task-Specific Ionic Liquid," *J. Am. Chem. Soc.*, **124**, 926-927 (2002).
2. P. Scovazzo, A. Visser, J. J. Davis, R. Rogers, C. A. Koval, D. DuBois, and R. D. Noble, "Supported Ionic Liquid Membranes (SILMs) and Facilitated Ionic Liquid Membranes (FILMs)," ACS Symp. Ser., **818**, 69-87 (2002).
3. D. Camper, P. Scovazzo, and R. D. Noble, "Gas Solubilities in Room Temperature Ionic Liquids," *Ind. Eng. Chem. Res.*, **43**(12), 3049-3054 (2004).
4. D. Camper, C. Becker, C. A. Koval, and R. D. Noble, "Low Pressure Hydrocarbon Solubility in Room Temperature Ionic Liquids Containing Imidazolium Rings Interpreted using Regular Solution Theory," *Ind. Eng. Chem. Res.*, **44**, 1928 (2005a).
5. D. Camper, C. Becker, C. A. Koval, and R. D. Noble, "Diffusion and Solubility in Room Temperature Ionic Liquids," *Ind. Eng. Chem. Res.*, **45**(1), 445-450 (2006).
6. P. Scovazzo, D. Camper, J. Kieft, and R. D. Noble, "Regular Solution Theory and CO_2-Gas Solubility in Room Temperature Ionic Liquids," *Ind. Eng. Chem. Res.*, **43**, 6855-6860 (2004).
7. D. Camper, J. E. Bara, C. A. Koval, and R. D. Noble, "Bulk Fluid Solubility and Membrane Feasibility of RMIM-based Room Temperature Ionic Liquids," *Ind. Eng. Chem. Res.*, **45**, 6279-6283 (2006).
8. A. Finotello, J. E. Bara, D. Camper, and R. D. Noble, "Ideal Gas Solubilities and Solubility Selectivities in a Binary Mixture of Ionic Liquids," *J. Phys. Chem.*, in press.
9. J. E. Bara, A. K. Kaminski, R. D. Noble, and D. L. Gin, "Influence of Nanostructure on Light Gas Separations in Cross-linked Lyotropic Liquid Crystal Membranes," *J. Membr. Sci.*, 2006, submitted.
10. J. E. Bara, E. S. Hatakeyama, C. J. Gabriel, S. Lessmann, D. L. Gin, and R. D. Noble, "Synthesis and Gas Separation Performance of Cross-linked Gemini Room Temperature Ionic Liquid Polymer Membranes," *J. Membr. Sci.*, 2007, in press.

NEW SORBENTS BASED ON THE IMMOBILIZATION OF CYPHOS IL-101 (TRIHEXYL(TETRADECYL)PHOSPHONIUM CHLORIDE) IN ALGINATE GEL BEADS FOR GOLD RECOVERY FROM HCL SOLUTIONS

K. Campos,[1] T. Vincent,[1] P. Bunio,[2] A. Trochimczuk,[2] and E.Guibal[1]

[1]*Ecole des Mines d'Alès. France, 6, avenue de Clavières, F-30319 Alès cedex, France.*
[2]*Wroclaw University of Technology, 50-370 Wrocław, Poland.*
Corresponding author email address: Eric.Guibal@ema.fr

ABSTRACT

New sorbents were synthesized by encapsulation of Cyphos IL-101 (an ionic liquid) in gelatin/alginate gel beads. They were tested for gold binding from HCl solutions. Maximum sorption capacities linearly increased with IL content and may exceed 200 mg Au g^{-1} in 1 M HCl solutions. Gold ions ($AuCl_4^-$) were removed by an ion-exchange mechanism. Kinetics were studied varying the metal concentration, the amount of sorbent, the IL content, and the size of the beads. Uptake kinetics were controlled by the resistance to intraparticle diffusion. Thiourea was used for metal desorption from loaded resins with desorption efficiency exceeding 90%.

INTRODUCTION

The increasing demand of industry for precious metals has driven the interest for the recycling of these metals from spent materials. The hydrometallurgical process generally produces very acidic leachates. Solvent extraction can be used for their recovery. The loss of extractant with dissolving in water induces environmental and economical drawbacks, which make the process poorly competitive for metal recovery from dilute effluents. Synthetic resins can be used [1], but an increasing interest has been paid in the last decades to the development of biosorbents (renewable resources) [2]; these biosorbents generally require weakly acidic media for optimum metal sorption. Impregnated resins have been proposed in order to combine the efficiency of solvent extraction and the stability of resins [3,4]. Ionic liquids (IL) represent a new class of extractants that can be efficiently used for metal recovery [5]. Cyphos IL 101 is part of the phosphonium IL compounds that are suitable for metal binding (ion-exchange properties). The present work focuses on the testing of Cyphos IL 101 immobilized into composite gelatin-alginate matrix and its testing for the binding of gold from HCl solutions [6]. The sorption isotherms, the uptake kinetics are carried out as a function of a series of experimental parameters. Gold desorption from loaded resin is finally investigated with the objective to verify the possibility to recycle the sorbent.

MATERIALS AND METHODS

Materials

The Cyphos® IL 101 (tetradecyl(trihexyl)phosphonium chloride) was kindly supplied by Cytec (Canada). Alginate and gelatin were supplied by Acros (France). Other reagents (metal salts, NaCl, $NaNO_3$, and mineral acids) were supplied as reagent-grade products by Fluka AG (Switzerland). The synthesis of the Cyphos-impregnated capsules was performed according the following procedure: (1) 25 g of Cyphos IL 101 (previously mixed with 5 g of a 10 M solution of NaOH) were mixed with 25 g of a 20% w/w aqueous solution of gelatin. (2) An amount of 445 g of alginate sodium solution (2% w/w) was then added to the gelatin-ionic liquid solution and mixed under ultrasonic treatment until a slightly viscous white solution was obtained. (3) The viscous solution was extruded through a nozzle (internal diam. 0.6 mm) into an ionotropic gelling solution ($CaCl_2$, 6% w/w in water), forming spherical particles. The beads were maintained in the coagulation bath overnight before being rinsed with 0.1 M HCl solution. Wet resins were stored in 0.1 M HCl to prevent the degradation of the resin (neutral media degrades alginate matrix). No loss of extractant was detected in acidic solutions (at storage or during sorption experiments). In most cases, resins were used in the dry state. Table 1 gives the main characteristics of the resins. Ionic liquid content was determined by phosphorus analysis by ICP-AES after resin mineralization.

Table 1. Characteristics of IL-immobilized resins

Resin	Diameter (wet, mm)	Diameter (dry, μm)	Cyphos content (%, d.w.)	Cyphos content (mmol/g d.w.)
C1S	1.00 ± 0.04	435 ± 80	35.9 ± 1.3	0.692
C1L	2.33 ± 0.02	988 ± 74	31.4 ± 0.6	0.604
C2S	0.85 ± 0.06	472 ± 75	50.3 ± 0.9	0.968
C2L	2.67 ± 0.03	1313 ± 48	44.6 ± 0.9	0.860
C3L	2.58 ± 0.02	1600 ± 51	57.3 ± 1.8	1.103

Sorption Experiments

Sorption experiments were performed in batch systems mixing for 96 hours a volume of acid solution (30 mL) containing the appropriate concentration of Au(III) with a known amount of resin (20 mg). Au concentration was measured by ICP-AES after filtration. Sorption capacity (q, mg Au g^{-1}) was determined by the mass-balance equation $q = V(C_o\text{-}C_{eq})/m$; C_o and C_{eq} are initial and equilibrium Au concentrations (mg Au L^{-1}), respectively; V is the volume of solution (L) and m the mass of resin (g). The influence of competitor ions was tested adding to the solution increasing amounts of NaCl, $NaNO_3$, $CuCl_2$, $NiCl_2$, and $ZnCl_2$ salts. Isotherms were obtained by mixing fixed amounts of resin (i.e., 20 mg, d.w.) with fixed volumes (i.e., 100 mL) of 1 M HCl solutions containing 20 to 200 mg Au L^{-1}. Uptake kinetics were investigated by mixing 80 mg (d.w.) with 400 mL of Au (C_o, 15-80 mg Au L^{-1}) solutions (in 1 M HCl). Samples were collected, filtered, and analyzed at fixed times.

RESULTS AND DISCUSSION

Influence of HCl and Chloride Concentration on Au sorption Capacity

Figure 1(a) shows that the concentration of HCl did not affect sorption capacity that remained close to 139.2 ± 3.4 mg Au g^{-1} for C1S and to 124.8 ± 3.4 mg Au g^{-1} for C2S in the range 0-4 M HCl. Similar experiments were performed with 0.1 M HCl solutions adding increasing amounts of NaCl (in the range 0-4 M): sorption capacities were not affected by Cl^- concentration, remaining close to 142.8 ± 2.8 mg Au g^{-1} for C1S and to 128.1 ± 2.9 mg Au g^{-1} for C2S. The sorbent is poorly affected by the acidity of the solution and by the total concentration of chloride ions. Gold is present in the form of $AuCl_4^-$, independently of HCl or Cl^- concentrations.

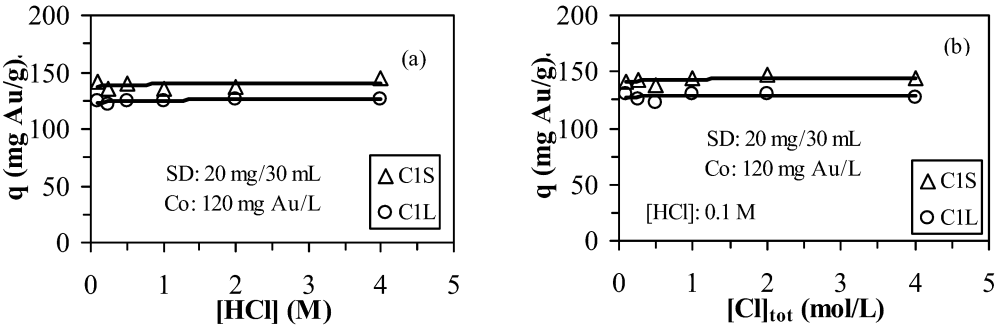

Figure 1. Influence of HCl concentration and Cl^- concentration on Au sorption capacity.

Sorption Isotherms

Sorption isotherms have been performed in 1 M HCl solutions for the different resins (Figure 2(a)).

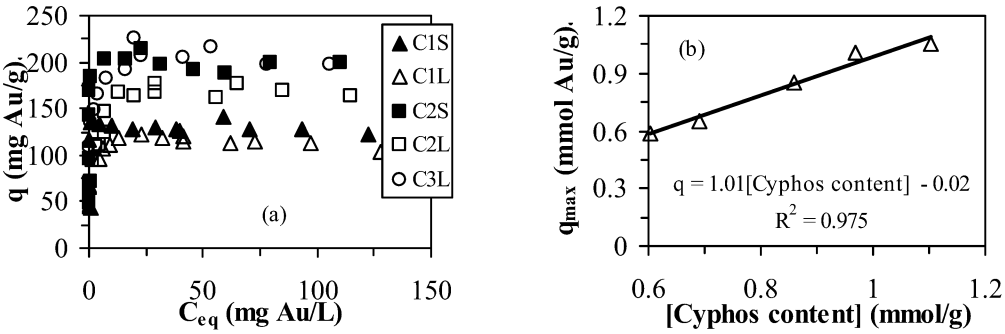

Figure 2. Sorption isotherms (a) and correlation between IL content and q_{max} (b).

The initial slope of the isotherms is very steep, indicating the strong affinity of the resins for gold. The isotherms are almost irreversible, being marked by a plateau reached

at low residual concentration (around 10 mg Au L^{-1}). The sorption capacity increased with the IL content in the resin. The maximum sorption capacity is linearly correlated to IL content Figure 2(b); the slope (close to 1) shows that the reaction may occur through the interaction of 1 molecule of $R_3R'P^+$ with 1 molecule of $AuCl_4^-$, ($R_3R'P^+ \cdot AuCl_4^-$).

Uptake Kinetics

Sorption kinetics were carried out varying a series of experimental parameters (Figure 3-5). The lines show the modeling of experimental data using the intraparticle diffusion model (D_e, intraparticle diffusion coefficient) [7]:

$$\frac{q(t)}{q_{eq}} = 1 - \sum_{n=1}^{\infty} \frac{6\alpha(\alpha+1)\exp\left(\frac{-D_e q_n^2 t}{r^2}\right)}{9 + 9\alpha + q_n^2 \alpha^2}$$

where $q(t)$ and q_{eq} are metal concentrations in the resin at time t and equilibrium, respectively, r being the radius of resin particles, and q_n are the non-zero roots of the equation

$$\tan q_n = \frac{3 q_n}{3 + \alpha q_n^2} \quad \text{with} \quad \frac{q_{eq}}{VC_o} = \frac{1}{1+\alpha}$$

Figure 3(a) shows the poor effect of agitation on the kinetic profile, implying film diffusion is probably not the controlling step. D_e increased from 1.7×10^{-11} to 3.6×10^{-11} m^2 min^{-1} when agitation speed increased from 300 rpm to 500 rpm. Increasing sorbent dosage increased sorption efficiency (Figure 3(b)), and D_e decreased from 3.4×10^{-11} to 1.2×10^{-11} m^2 min^{-1}. Figure 4 shows the influence of particle size and IL content. Increasing the size of the particles slightly increased D_e (from 1.9×10^{-11} to 4.1×10^{-11} m^2 min^{-1}) for low IL-content resins. For large particles, increasing IL content logically increased sorption efficiency, while D_e increased from 1.9×10^{-11} m^2 min^{-1} for C1L to 3.4×10^{-11} m^2 min^{-1} for C2L and 3.6×10^{-11} m^2 min^{-1} for C3L.

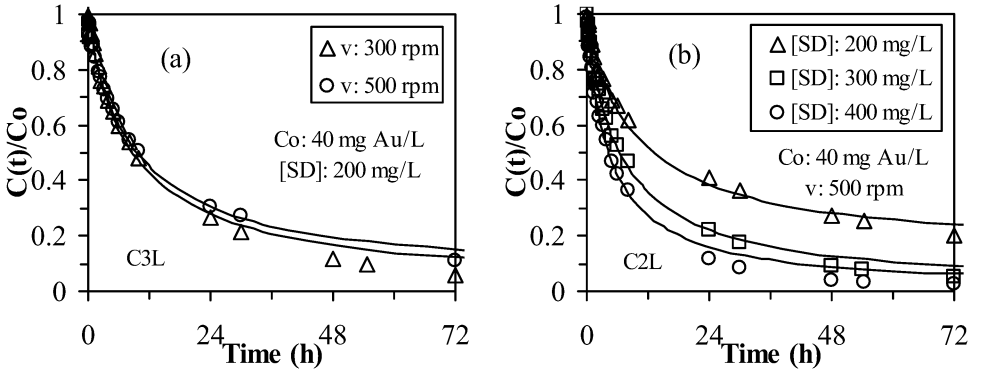

Figure 3. Influence of agitation speed (a) and sorbent dosage (b) on Au sorption kinetics.

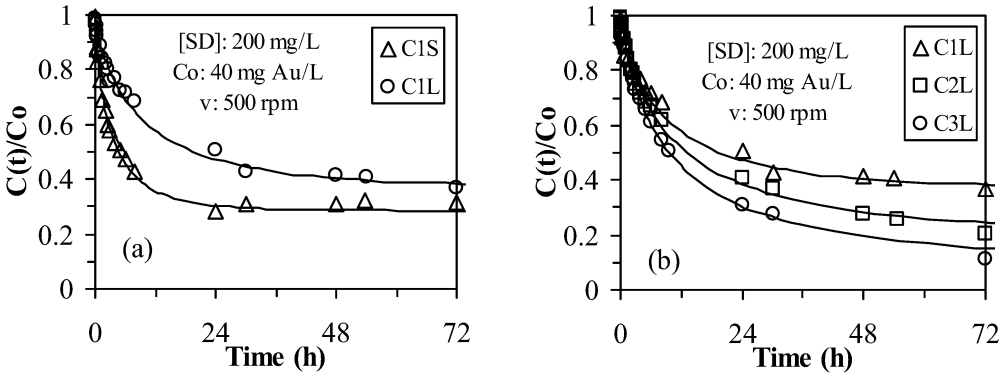

Figure 4. Influence of particle size (a) and IL content (b) on Au sorption kinetics.

Figure 5(a) shows the impact of increasing Au(III) concentration on kinetics. The equilibrium was reached at earlier contact time when using high concentrations due to favorable concentration gradient. D_e increased from 1.1×10^{-11} to 9.9×10^{-11} m^2 min^{-1} between 15 and 80 mg Au L^{-1}. Figure 5(b) shows that resin drying hardly influenced kinetics, contrary to results obtained with Hg(II), Pd(II), or Pt(II) (submitted for publication). D_e only varied from 3.6×10^{-11} to 3.1×10^{-11} m^2 min^{-1} after resin drying.

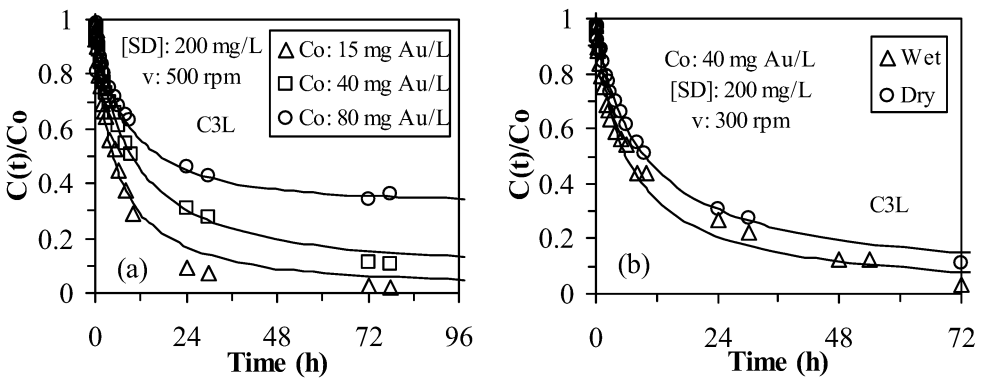

Figure 5. Influence of Au initial concentration (a) and resin drying (b) on Au sorption kinetics.

Competition Effects

The introduction of increasing amounts (0.1-1 g metal L^{-1}) of chloride salts of base metals (Zn(II), Ni(II), and Cu(II)) did not change the binding capacity (not shown); the variation of sorption capacity (compared to reference value obtained in absence of base metals) was generally lower than 9%. Gold sorption capacity remained close to 228.9 ± 9.4 mg Au g^{-1} in the case of 0.1 M HCl solutions containing 100 mg Au L^{-1} and 0 to 5 g NO_3^- L^{-1}. The resin is selective for Au(III) binding in the presence of base metals or conventional anions in 1 M HCl solutions. Previous investigations on Pd(II), Pt(IV),

and Hg(II) have shown a strong affinity of the resin for these metals forming stable chloro-anionic complexes. More competitive effect is thus expected from these metals.

Desorption and Recycling

Desorption was performed by 2 hours of contact of loaded sorbent (20 mg) with 100 mL of eluent (1 M thiourea in 1 M HCl). Best results where obtained with 1 M thiourea (in 1 M HCl), probably due to the strong complexation effect of thiourea for gold. Investigating desorption kinetics (that revealed faster than sorption), two hours of contact appeared sufficient to reach a 94% desorption yield (not shown). The sorbent was subjected to four sorption/desorption cycles; results (not shown) demonstrated a significant variation in the sorption performance after three cycles, while desorption revealed progressively less efficiency probably due to a partial reduction of gold (color change of the resins).

CONCLUSIONS

Cyphos IL 101 immobilized in gelatin/alginate composite matrix were very efficient for Au(III) sorption from HCl solutions. Au(III) binding involved and ion-exchange mechanism between phosphonium groups/Cl^- and $AuCl_4^-$. Uptake kinetics are controlled by intraparticle diffusion; D_e varied within the range 10^{-11}-10^{-10} m^2 min^{-1}. Sorption capacity is not significantly affected by the presence of base metals (0-1 g L^{-1}) or nitrate and chloride ions (0-5 M). Desorption can be performed using 1 M thiourea in 1 M HCl solutions, but the recycling of the resin requires complementary studies for optimization.

REFERENCES

1. M. Iglesias, E. Anticó, and V. Salvadó, "Recovery of palladium(II) and gold(III) from diluted liquors using the resin Duolite GT-73," *Anal. Chim. Acta*, **381**(1), 61-67 (1999).
2. M. Ly Arrascue, H. Maldonado Garcia, O. Horna, and E. Guibal, "Gold sorption on chitosan derivatives," *Hydrometallurgy*, **71**(1-2), 191-200 (2003).
3. R. M. Kautzmann, C. H. Sampaio, V. Korovin, Y. Shestak, M. Aguilar, and J. L. Cortina, "Evaluation of alkylguanidine based solvent impregnated resins for gold cyanide extraction." International Solvent Extraction Conference, K. C. Sole, P. M. Cole, J. S. Preston, and D. J. Robinson, Eds., Chris Van Rensburg Publications, Melville, RSA, 2002; pp. 506-511.
4. S. Nishihama, G. Nishimura, T. Hirai, and I. Komasawa, "Separation and recovery of Cr(VI) from simulated plating waste using microcapsules containing quaternary ammonium salt extractant and phosphoric acid extractant," *Ind. Eng. Chem. Res.*, **43**(3), 751-757 (2004).
5. M. Regel-Rosocka, A. Cieszynska, and M. Wisniewski, "Extraction of zinc(II) with selected phosphonium ionic liquids," *Przemysl Chemiczny*, **85**(8-9), 651-654 (2006).
6. E. Guibal and T. Vincent, "Palladium recovery from dilute effluents using biopolymer-encapsulated extractant," *Sep. Sci. Technol.*, **41**(11), 2533-2553 (2006).
7. J. Crank, The Mathematics of Diffusion, Oxford University Press, Oxford, U.K., 1975.

RECOVERY OF Cd(II) IONS FROM AQUEOUS HCl SOLUTIONS USING CYPHOS IL 101 (TRIHEXYL(TETRADECYL)PHOSPHONIUM CHLORIDE) IMMOBILIZED IN ALGINATE GEL BEADS

R. Navarro,[1] L. A. Arias,[1] I. Saucedo,[1] M. Avila,[1] and E. Guibal[2]

[1]*Instituto de Investigaciones Científicas, Universidad de Guanajuato, México. Cerro de la Venada s/n, Col. Pueblito de Rocha, Guanajuato, Gto., México, C.P. 36040.*
[2]*Ecole des Mines d'Alès, France.*
Corresponding author email address: navarrm@quijote.ugto.mx

ABSTRACT

An ionic liquid (Cyphos IL 101, trihexyl(tetradecyl)phosphonium chloride) was encapsulated in alginate gel beads. This new material efficiently removed Cd(II) from HCl solutions (0.01–8 M) in the form of chloro-anionic species ($CdCl_4^{2-}$) through an ion-exchange mechanism. Maximum sorption capacity was 86 mg Cd g^{-1}. Sorption kinetics were controlled by resistance to intraparticle diffusion (D_e = 2 × 10^{-11}–2.7 × 10^{-10} m^2 min^{-1}). Cd immobilized on the beads was successfully recovered through a desorption step using nitric or sulfuric acid solutions (0.5–2 M); desorption kinetics were markedly faster than sorption kinetics. Three sorption/desorption cycles were operated without significant loss of efficiency.

INTRODUCTION

Cadmium is widely used in industrial processes. Due to the high toxicity of Cd, regulations for the release of industrial effluents are becoming more and more strict [1]. This makes the development of alternative wastewater treatments necessary. Various processes have been developed, including chemical precipitation, liquid-liquid extraction, and impregnated resins [1–2]. Frequently these processes face technical limitations (concentration levels), economic constraints (investments and operating costs), or environmental drawbacks (sludge production, loss of extractant). To reduce the impact of extractant loss, a number of immobilization processes have been developed, including extractant encapsulation in alginate gel beads [3]. Ionic liquids (IL) such as Cyphos IL 101 (trihexyl(tetradecyl)phosphonium chloride) have been proposed for the recovery of metal ions. This IL has proved efficient for the extraction of metal ions (in the form of chloro-anionic complexes) in HCl solutions through an ion-exchange mechanism [4]. This work focuses on the recovery of Cd(II) from HCl solutions using Cyphos IL 101 immobilized in composite gelatin/alginate gel beads.

EXPERIMENTAL SECTION

Reagents

Sodium alginate was supplied by Acros (Switzerland) and Gelatin by VWR Prolabo (France). Cyphos IL 101 was kindly donated by Cytec (Canada). Other reagents were analytical grade, supplied by Industrial KEM (Mexico) or Fluka (France).

Preparation of Alginate Gel Beads Containing Cyphos IL 101

The alginate gel beads containing the encapsulated extractant were prepared as described by Guibal and Vincent [3]. A stable emulsion was made by agitation of a mixture of Cyphos IL 101 and solutions of sodium alginate and gelatin. Then, the emulsion was added dropwise into a $CaCl_2$ solution producing gel beads with the extractant immobilized into the alginate matrix. Water content was determined by mass loss, drying the beads for 24 h at 50 °C. IL content was also measured by weight variation after IL extraction using acetone.

Sorption Studies

The thermodynamic study of Cd(II) extraction was carried out in a batch system. A fixed amount of wet beads (0.25 g) was mixed for 24 h with 25 mL (m/V = 10 g L^{-1}) of metal-containing solution on a reciprocal shaker (Cole Palmer 51502), at 20 °C (in a thermostatic chamber, Terlab). Wet beads were mixed with Cd(II) solutions (20–200 mg L^{-1}) in HCl (0.01–8 M). Initial and equilibrium concentrations in solution (C_0 and C, respectively, mg L^{-1}) were measured using AAS (Perkin Elmer spectrometer, AAnalyst 200). The amount of Cd(II) immobilized on the beads q (mg g^{-1}) was obtained by the mass-balance equation: $q = (C_0 - C)\, V/m$, where V is the volume of the solution (L) and m is the amount of sorbent used (g, dry weight).

Kinetics were studied in batch using an helicoidal stirrer (Caframo, type RZR1) at a controlled speed (150 rpm) and at controlled temperature (i.e., 20 °C). A fixed amount of wet beads (i.e., 2.5 g) was mixed with 250 mL of Cd(II) solutions (100, 150, and 200 mg L^{-1}) in HCl (0.1, 1, and 5 M). Samples of 1 mL were regularly collected and analyzed. Kinetics were also compared for dried and rehydrated beads (rehydration operated in 0.1 M HCl solution for 24 h) with reference material (wet beads).

Cd(II) Recovery

Cd(II) desorption was operated by contact of loaded beads (0.25 g of wet beads mixed with 25 mL of 100 mg Cd(II) L^{-1} solution in 0.1 M HCl) with HNO_3 and H_2SO_4 solutions (concentration: 0.5, 1, and 2 M). Desorption kinetics were studied using 0.5 M HNO_3 solution at the same m/V ratio. Three sorption/desorption cycles were also performed using similar experimental procedures (sorption: 0.25 g of beads, 25 mL of 100 mg Cd(II) L^{-1} solution in 0.1 M HCl. desorption: 25 mL of 0.5 M HNO_3 solution).

RESULTS AND DISCUSSION

The alginate gel beads were characterized as white spherical particles having a diameter of 1.4 mm (in wet state) and 0.9 mm (in dry state). Water content was 87%, and IL content was 167 mg g^{-1} wet beads (759 mg g^{-1}, based on dry beads).

Influence of HCl Concentration on Cd(II) Extraction

A first series of experiments was performed using 100 mg Cd(II) L^{-1} solutions prepared in HCl solutions of different concentrations (0.01, 0.05, 1, 2, 3, 5, and 8 M). In most cases, Cd(II) was almost completely removed (extraction efficiency greater than 98%). With 8 M HCl solutions, the extraction was slightly less (95%). To evaluate the possible contribution of the matrix on metal binding, a series of experiments was carried out with beads from which the IL had been removed using 3 successive washing steps (acetone and 0.01 M HCl solutions). After IL elution, the testing of Cd(II) sorption with beads showed that metal recovery was systematically lower than 3%, indicating that the biopolymer matrix did not contribute significantly to metal binding, compared to IL.

Cyphos IL 101 can be represented as L^+Cl^-, where L^+ is the tetraalkylphosphonium cation. This extractant may react as an anionic exchanger, extracting metal ions in the form of anionic chlorocomplexes (MCl_x^{n-x}). Cd(II) has a great affinity for chloride anions, forming a large number of chlorocomplexes: cationic species ($CdCl^+$), neutral species ($CdCl_2$), and anionic species ($CdCl_3^-$ and $CdCl_4^{2-}$; these species predominate when chloride concentration exceeds 0.8 M) [2]. Cd(II) is probably extracted by IL in two forms: $L^+CdCl_3^-$ or $(L^+)_2CdCl_4^{2-}$. It is not possible at this stage of the study to precisely define which complex is bound to the beads. It would be necessary to determine the number of chloride ions and IL molecules involved in metal binding. However, the most probable reaction is described by Equation 1, since $CdCl_4^{2-}$ is characterized by the higher charge density, and thus the greater affinity for the extractant. Complementary experiments are currently being carried out to confirm this hypothesis.

$$CdCl_x^{2-x} + 2\ L^+Cl^- + y\ Cl^- \leftrightarrows (L^+)_2CdCl_4^{2-} \quad (1)$$

where $CdCl_x^{2-x}$ is the predominant species in solution, and y is the number of chloride ions exchanged during metal sorption. Other studies concerning Zn(II) recovery by Amberlite XAD-7 resins impregnated with Cyphos IL 101 showed that the metal was extracted in the form of the chlorocomplex $ZnCl_4^{2-}$ [4].

Cd(II) Extraction Isotherm

Figure 1 shows Cd(II) sorption isotherms for two concentrations of HCl (i.e., 0.01 and 5 M). The isotherms are very favorable, and they are characterized by a steep initial slope (showing the affinity of the beads for Cd(II)) and a plateau reached at low residual concentration. This is typical of the Langmuir-type isotherm described by the equation $q = q_m bC/(1 + bC)$, where b (L mg^{-1}) is the affinity constant related to sorption enthalpy, and q_m is the maximum sorption capacity (at saturation of the monolayer, mg g^{-1}). The

parameters of the Langmuir model were determined using the Mathcad Plus 6.0 software (nonlinear regression): q_m values reached 73.7 and 85.6 mg Cd(II) g^{-1}, and b values were 2.35 and 1.25 L mg^{-1} for the isotherms obtained with 0.1 and 5 M HCl solutions, respectively. The lines on Figure 1 show the modeling of experimental curves with the Langmuir equation.

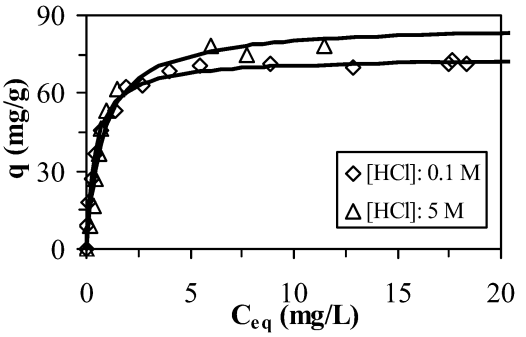

Figure 1. Influence of HCl concentration on Cd(II) sorption isotherms.

Maximum sorption capacities are much higher than those obtained for Zn(II) extraction using resins impregnated with Cyphos IL 101 (q_m = 21 mg g^{-1}) [4], or for the recovery of Cd(II) with Amberlite XAD-7 impregnated with Cyanex 921 (q_m = 17.5 mg g^{-1}) [2]. The maximum sorption capacities correspond to molar Cd/IL ratios of 0.52 and 0.45 (for 0.1 M and 5 M HCl solutions, respectively). This is close to the 0.5 molar ratio corresponding to the formation of the species $(L^+)_2CdCl_4^{2-}$, and this result confirms the hypothesis proposed above.

Cd(II) Extraction Kinetics

Uptake kinetics are controlled by several diffusion mechanisms; however, intraparticle diffusion is frequently cited as the controlling step in the sorption process. The intraparticle diffusion model described by Crank [5] was used for the determination of the intraparticle diffusion coefficient (D_e) [2,4]:

$$\frac{q(t)}{q_{eq}} = 1 - \sum_{n=1}^{\infty} \frac{6\alpha(\alpha+1)\exp\left(\frac{-D_e q_n^2 t}{r^2}\right)}{9 + 9\alpha + q_n^2\alpha^2} \qquad (2)$$

where $q(t)$ and q_{eq} are metal concentrations in the beads at time t and equilibrium, respectively, r is the particle radius, α is the effective volume ratio ($C/(C_0-C)$), and q_n are the non-zero roots of the equation: $\tan q_n = \frac{3\,q_n}{3 + \alpha\, q_n^2}$ with $\frac{q_{eq}}{VC_0} = \frac{1}{1+\alpha}$

Table 1. Intraparticle diffusion coefficients (D_e)

Beads	[HCl] (M)	$[Cd(II)]_0$ (mg L^{-1})	D_e (10^{-10} m^2 min^{-1})
Wet	0.1	100	0.17
	0.1	150	0.76
	0.1	200	2.7
	1.0	200	1.9
	5.0	200	2.6
Dry	0.1	200	0.59

Table 1 summarizes the different values obtained for D_e. The lines on Figure 2 show the modeling of experimental data using this model and the values reported in Table 1. Figure 2(a), graphing the kinetic profiles for variations of Cd(II) concentrations, shows that, under selected experimental conditions, the equilibrium was reached within 8 h of contact. The intraparticle diffusion coefficient increased with increasing initial metal concentration. The superimposition of the curves for varying HCl concentrations (not shown) demonstrated the limited impact of HCl concentration on kinetics; this was confirmed by the values of D_e, which did not vary significantly on changing the HCl concentration (Table 1). The values of D_e obtained with the present system (1.7×10^{-11} m^2 min^{-1}, for 0.1 M HCl and $[Cd(II)]_0$ = 100 mg g^{-1}) are lower than those obtained for Cd(II) extraction using Amberlite XAD-7 resin impregnated with Cyanex 921 (3.17×10^{-10} m^2 min^{-1}) [2], as well as in the case of Zn(II) extraction using XAD-7 impregnated with Cyphos IL 101 (0.58×10^{-10} m^2 min^{-1}) [4].

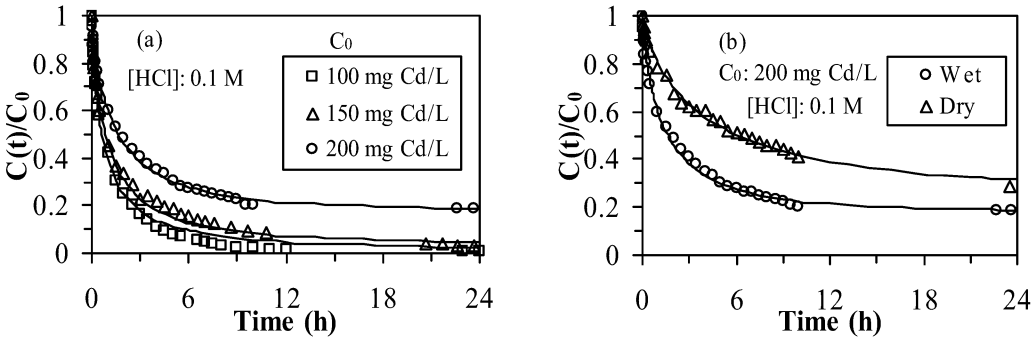

Figure 2. Influence of Cd(II) concentration (a) and bead drying (b) on Cd(II) uptake kinetics.

Bead drying caused irreversible shrinking of the beads, which in turn decreased the intraparticle diffusion coefficient below 0.6×10^{-10} m^2 min^{-1}; this is more than 4 times lower than the reference value (wet beads). The comparison of kinetic profiles for dry and wet beads shows the impact of the drying step on mass-transfer resistance (Figure 2(b)). The rehydration of dried beads did not improve the diffusion of cadmium (not shown).

Cd(II) Recovery and Reuse of Beads

Cadmium desorption from loaded beads was tested with 0.5, 1, and 2 M solutions of HNO_3 and H_2SO_4. Desorption was systematically higher than 98%. This high efficiency is due to the destabilization of the chlorocomplexes ($CdCl_4^{2-}$) in solutions free of chloride anions. The kinetics of desorption were quite fast (not shown): complete desorption was obtained within 20 minutes of contact. Three sorption/desorption cycles were operated maintaining high sorption yields (99, 95, and 96%, respectively) and desorption levels closed to 100%. This confirms that the beads can be used for at least three cycles without a very significant loss of activity.

CONCLUSIONS

Beads prepared by encapsulation of Cyphos IL 101 into a composite matrix made of gelatin and alginate show a great affinity for Cd(II) in a wide range of HCl concentrations (0.1–8 M). Sorption capacities as high as 85 mg Cd g^{-1} were obtained. The beads bind Cd(II) through an ion-exchange mechanism involving the anionic chlorocomplex $(L^+)_2CdCl_4^{2-}$. The intraparticle diffusion model fits the kinetic profile well with D_e in the range of 2×10^{-11}–2.7×10^{-10} m^2 min^{-1}. Cadmium can be easily and rapidly desorbed from loaded beads using nitric or sulfuric acid solutions (concentration range: 0.5–2 M). The beads were tested for three successive sorption/desorption cycles without significant decrease in sorption performance.

ACKNOWLEDGMENTS

The authors thank the Franco-Mexican PCP (Post-Graduate Cooperation Program, Ref. PCP 06/05) and CONACyT (Ref. 52961 and U44768-Q) for financial support.

REFERENCES

1. S. Satarug, J. R. Baker, M. Haswell-Elkins, D. J. Williams, and M. R. Moore, “A Global Perspective on Cadmium Pollution and Toxicity in Non-Occupationally Exposed Population,” *Toxicol. Lett.*, **137**, 65-83 (2003).
2. R. Navarro, T. I. Saucedo Medina, A. Nuñez, M. Ávila, and E. Guibal, “Cadmium Extraction from Hydrochloric Acid Solutions Using Amberlite XAD-7 Impregnated with Cyanex 921 (TriOctyl Phosphine Oxide),” in press *React. Funct. Polym*. (2007).
3. E. Guibal and T. Vincent, “Palladium Recovery from Dilute Effluents Using Biopolymer-Encapsulated Extractant,” *Sep. Sci. Technol.*, **41**(11), 2533-2553 (2006).
4. V. Gallardo, R. Navarro, I. Saucedo, M. Ávila, and E. Guibal, “Zinc(II) Extraction from Hydrochloric Acid Solutions Using Amberlite XAD-7 Impregnated with Cyphos IL 101 (Tetradecyl(trihexyl)phosphonium Chloride),” submitted for publication in *Sep. Sci. Technol.* (2007).
5. J. Crank, The Mathematics of Diffusion, Oxford University Press, Oxford, G.B., 1975.

EFFICIENT REMOVAL OF DICYCLOPENTADIENE IMPURITIES FROM CYCLOHEXANE USING IONIC LIQUIDS

P. Ruiz, A. Ruiz, D. Gorri, and I. Ortiz

Departamento de Ingeniería Química y Química Inorgánica, Universidad de Cantabria, Avenida de los Castros s/n, 39005 Santander, Spain.
Corresponding author email address: ortizi@unican.es

ABSTRACT

In the present work, the reversible reaction between dicyclopentadiene and Ag^+ in diluted solutions of $AgBF_4$ in $BMImBF_4$ was tested for the selective removal of dicyclopentadiene from cyclohexane. Experimental results were obtained working at different dicyclopentadiene concentrations (100-1000 ppm) in the organic phase and at a temperature range between 283 K and 323 K. Experimental results show that this process allows purification of cyclohexane, reducing also the content of dicyclopentadiene down to few ppm. Furthermore, the use of $BMImBF_4$ as extraction media involves important advantages due the regeneration capacity.

INTRODUCTION

Cyclohexane is used as a solvent and reaction medium in the manufacture of different types of synthetic rubbers. The catalyst for the hydrogenation reaction of styrene-based rubbers is very sensitive to impurities as cyclopentadiene (CP), and the preliminary treatment of raw materials is required. After reaction, cyclohexane is separated from the polymer by steam-stripping, recovered, and pumped to a distillation purification column for water removal. During the polymerization process, small quantities of cyclopentadiene are formed by degradation of the organometallic catalyst. Additionally, cyclopentadiene easily dimerizes at room temperature to form dicyclopentadiene (DCP) that must be also removed. In order to recycle cyclohexane to the reaction process, the cyclopentadiene and dicyclopentadiene contents must be reduced to less than several parts per million. Because of the low CP and DCP concentrations in the cyclohexane stream, separation based on conventional distillation is difficult and energy intensive [1].

The separation of condensed olefins from corresponding paraffins has been investigated widely in the literature [2-5]; the most promising alternative appears to be π-complexation with silver ions. Separation by π-complexation is a subgroup of chemical complexation reaction where the mixture is contacted with the second phase, which contains a complexing agent. The advantage of chemical complexation is that the bonds

formed are stronger than those formed by van der Waals forces alone, so it is possible to achieve high selectivity and high capacity for the component to be bounded. At the same time, the bonds are still weak enough to be broken by using simple engineering operations such as raising the temperature or decreasing the pressure.

Recently, considerable attention has been drawn to room-temperature ionic liquids (RTIL) as green alternative to common organic solvents. RTIL are organic salts with melting points at or below room temperature. They have substantial potential as diluents in separations and their application is an important step in the design of environmentally safe separation processes, because ionic liquids are considered to be nonflammable, nonvolatile, and thermally stable [6].

Reliable data on the solubility of the olefins in a compatible solvent are required for the proper design of extraction systems. In this work, $BMImBF_4$ has been selected for experiments, because it is essentially immiscible with cyclohexane and it is able to dissolve a suitable silver salt ($AgBF_4$), allowing absorption of dicyclopentadiene due to reversible complexation of silver ions with unsaturated olefinic double bonds. G. Foco et al. [7] reported activity coefficients at infinite dilution of alkanes in ILs. The value reported by these authors for cyclohexane in $BMImBF_4$ at 303 K is $\gamma_i^{\infty} = 45$.

In this work, experimental results were obtained working at different dicyclopentadiene concentrations (100-1000 ppm) in the organic phase, with a silver concentration of 0.02 mol/L in the extracting solution. The influence of temperature on the solubility of dicyclopentadiene in the RTIL-Ag^+ solution was assessed, and the enthalpy (ΔH^o) for the complex formation reaction was estimated.

Silver–Dicyclopentadiene Complexation

During complexation of unsaturated hydrocarbons by transition metals, the metal's d-orbitals can participate in bond formation with the π-electrons of the olefinic system [8].

Although in principle all transition metal ions can be used, copper(I) and silver(I) salts are mainly selected, because they exhibit a sufficiently strong complexation to achieve a good selectivity while complexation is still easily reversible [9].

Dicyclopentadiene dissolves from the organic phase into the aqueous or RTIL phase and subsequently reacts with the dissolved positively charged silver ions to form a silver-dicyclopentadiene complex.

EXPERIMENTAL

Dicyclopentadiene was purchased from Sigma Aldrich. Silver tetrafluoroborate (analytical grade) was supplied by Merck. Cyclohexane with a purity of 99.9% was also supplied by Sigma Aldrich and used without further purification. The ionic liquid $BMImBF_4$ (CAS number 174501-65-6) was supplied by Solvent Innovation (Germany).

A stirred mini-reactor with a volume of 50 mL was used to determine the extraction equilibrium of dicyclopentadiene in a 0.02 M RTIL solution of silver salt. The liquids in the mini-reactors were stirred with a flat-blade stirrer at 500 rpm. For

each experiment, the mini-reactor was filled with 10 mL of RTIL solution of silver salt like extractive phase and 10 mL of dicyclopentadiene (100-1000 ppm) in cyclohexane solution as organic phase. It has been verified that stirring the absorption vial for 3 hours is more than sufficient to establish the equilibrium. The organic phase was then removed from the ionic liquid phase for analysis.

The concentration of DCP in the IL phase was calculated from the DCP concentration in cyclohexane after extraction. Samples of organic phase were analyzed using a CE Instruments 8130 gas chromatograph equipped with a FID detector and with a semi-capillary column (length 30 m, nominal diameter 0.53 mm, model HP-1). The carrier gas was helium at a flow rate of 4 mL min^{-1}. The injector operated in the split mode (15/1) at 523 K. The oven temperature was set at 313 K for 7 min., then increased to 423 K at 40 K /min., and then it is increased up to 483 K at 10 K /min., and finally was held at 483 K for 1 min. For DCP solutions in the range 100-1000 ppm, the analytical error was less than 5%.

RESULTS

Experimental results were obtained working at different dicyclopentadiene concentrations (100-1000 ppm) in the organic phase, with a silver concentration of 0.02 mol/L in the extracting solution. In Figure 1, the results of partitioning of dicyclopentadiene between organic and RTIL phases are given.

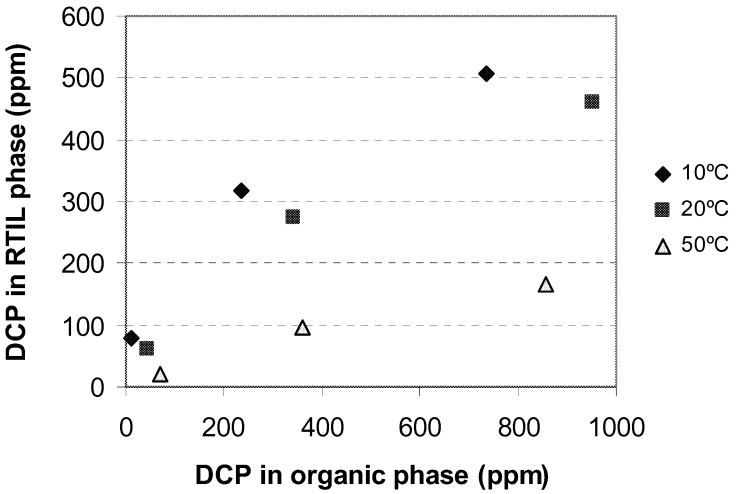

Figure 1. Partition of dicyclopentadiene between cyclohexane and $BMImBF_4$ phases. Cyclohexane–$BMImBF_4$ ratio = 1:1; $[AgBF_4]$ = 0.02 M.

The general reaction between dicyclopentadiene and Ag^+ in RTIL solution can be described as:

$$DCP + 2Ag^+ \Leftrightarrow DCPAg_2^{+2} \quad (1)$$

Dicyclopentadiene (DCP) dissolves from the organic phase into the RTIL phase and subsequently reacts with the dissolved positively charged silver ions to form a 2:1 silver-dicyclopentadiene complex species, that is, one silver ion per double bond. This is a reversible reaction described by the equilibrium constant *K*:

$$K = \frac{[DCP\,Ag_2^{+2}]}{[DCP][Ag^+]^2} \tag{2}$$

Working at a temperature of 293 K, a value of K = 2778 $(mol/L)^{-2}$ for the equilibrium constant was found. Factors influencing the reaction stoichiometry are the temperature, the silver concentration, and the concentration and structure of the olefin [5]. Here, equations are derived for the dicyclopentadiene solubility as a function of the silver tetrafluoroborate concentration in phase II and the dicyclopentadiene concentration in phase I. Kraus and Stern [10] report similar stoichiometric ratio for the complexation reaction of 1,3-butadiene with $AgNO_3$ in aqueous solutions. However, at high pressure of butadiene above the solution, they found a tendency for additional butadiene to be dissolved in accordance with a 1:1 stoichiometric ratio.

In this work, an increase in the solubility of dicyclopentadiene in the silver RTIL solutions with a decrease in temperature was observed. The influence of the temperature on equilibrium was evaluated by means of experiments carried out over a temperature range between 283 K and 323 K, as shown in Figure 2.

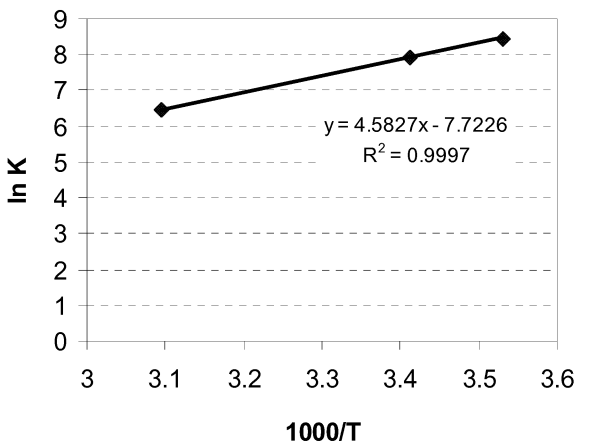

Figure 2. Temperature influence on the equilibrium constant.

Using the van't Hoff equation (Equation 3), from experimental data the enthalpy (ΔH^o) for the complex formation reaction was estimated, with a value of -38 kJ/mol. Complexation reactions are exothermic, and consequently the equilibrium constants will decrease with increasing temperature.

$$Ln\frac{K_{(T_2)}}{K_{(T_1)}} = \frac{\Delta H^o}{R}\left[\frac{1}{T_1} - \frac{1}{T_2}\right] \quad (3)$$

CONCLUSIONS

Two main conclusions have been obtained from this work: i) the recovery of the olefin (dicyclopentadiene) via silver complexation has been successfully carried out in ionic liquid media, and ii) the ionic liquid $BMImBF_4$ containing silver ions showed higher sorption capacity for dicyclopentadiene than the corresponding aqueous solution. It was found that after dissolution of the silver salt ($AgBF_4$) in a RTIL medium, the dissociation of silver ions is more efficient, leading to a percentage of extraction for the olefin higher than in aqueous media. The solubility of dicyclopentadiene in extractive mixtures decreases at higher temperatures due to a decreasing complexation constant as π-complexation reactions are exothermic. The equilibrium constant K was estimated, obtaining a value of K = 2778 $(mol/L)^{-2}$ at 293 K and an enthalpy (ΔH^o) for the complex formation reaction of -38 kJ/mol.

Furthermore, the use of $BMImBF_4$ as extraction media involves important advantages due its regeneration capacity. Negligible vapor pressure of the ionic liquid facilitates solvent and dicyclopentadiene recovery by flash distillation after the extraction process

ACKNOWLEDGMENTS

The Ministry of Education and Science (Spain) financially supported this research under projects CTQ2005-02583/PPQ and CTM2006-00317.

REFERENCES

1. R. B. Eldridge, "Olefin/paraffin separation technology: a review," *Ind. Eng. Chem. Res.*, **32,** 2208-2212 (1993).
2. R. D. Hughes, J. A. Mahoney, and E. F. Steigelman, in Recent Developments in Separation Science, N. N. Li and J. M. Calo, Eds., Vol. 9, CRC Press, Florida, 1986 (Chapter 9).
3. R. D. Noble and J. D. Way, "Description of facilitated transport and environmental applications," in Membrane Processes in Separation and Purification, J. G. Crespo and K. W. Böddeker, Eds., Kluwer Academic Publishers, 1994; pp. 317-342.
4. D. G. Bessarabov, J. P. Theron, R. D. Sanderson, H. -H. Schwarz, M. Schossig-Tiedeman, and D. Paul, "Separation of 1-hexene/n-hexane mixtures using a hybrid membrane/extraction system," *Sep. Purif. Technol.*, **16,** 167-174 (1999).
5. A. E. Wentink, D. Kockmann, N. J. M. Kuipers, A. B. de Haan, J. Schotz, and H. Mulder, "Effect of C6-olefin isomers on π-complexation for purification of 1-hexene by reactive extractive distillation," *Sep. Purif. Technol.*, **43**, 149-162 (2005).
6. P. Luis, I. Ortiz, R. Aldaco, and A. Irabien, "A novel group contribution method in the development of a QSAR for predicting the toxicity (Vibrio fischeri EC_{50}) of ionic liquids," *Ecotoxicol. Environ. Saf.*, **67**, 423-429 (2007).

7. G. M. Foco, S. B. Bottini, N. Quezada, J. C. de la Fuente, and C. J. Peters, "Activity coefficients at infinite dilution in 1-alkyl-3-methylimidazolium tetrafluoroborate ionic liquids," *J. Chem. Eng. Data*, **51**, 1088-1091 (2006).
8. C. M. D. Beverwijk, G. J. van der Kerk, A. J. Leusink, and J. G. Noltes, "Organosilver Chemistry," *Organomet. Chem. Rev. A*, **5,** 215-280 (1970).
9. J. S. Safarik and R. B. Eldridge, "Olefin/paraffin separations by reactive absorption: a review," *Ind. Eng. Chem. Res.*, **37**, 2571-2581 (1998).
10. J. W. Kraus and E. W. Stern, "Silver salt-olefin complexes. I. Silver nitrate butadiene," *J. Am. Chem. Soc.*, **84**, 2893-2895 (1962).

SELECTIVE REMOVAL OF NITROGEN-CONTAINING COMPOUNDS FROM STRAIGHT-RUN DIESEL FEED USING ILs

Li-Li Xie,[1,2] Alain Favre-Reguillon,[1,3] Marc Lemaire[1]

[1]ICBMS, Laboratoire de Catalyse et Synthèse Organique (UMR 5246), Université Lyon 1, 43 boulevard du 11 novembre 1918, Villeurbanne, F-69622, France. [2]Research Institute of Photocatalysis, Fuzhou University, 350002 Fuzhou, P. R. China. [3]CNAM, Laboratoire de Chimie Organique (UMR 7084), 2 rue Conté, 75003 Paris, France.
Corresponding author email address: favrereg@cnam.fr

ABSTRACT

To produce ultra low-sulfur gasoline and meet the new regulations, the improvement of the HDS reaction by the removal of inhibitors, like nitrogen-containing compounds (N-compounds) commonly found in middle distillates used for diesel feed, could be worth considering. The selective removal of neutral N-compounds from a straight run has been investigated by using a water-soluble ionic liquid BMImCl (1-butyl-3-methylimidazolinium chloride). The IL was first evaluated using a synthetic solution with dibenzothiophene and carbazole as model compounds, and a high selectivity for N-compounds was found. The extraction of heterocyclic aromatic compounds from a hydrocarbon mixture by BMImCl was found to be strongly dependent on the toluene/*n*-dodecane ratio. The extraction of sulfur-containing compounds and basic N-compounds decreased when the mass fraction of toluene increased, whereas the extraction of neutral N-compounds was found to be almost independent of the mass fraction of toluene. BMImCl was then evaluated using straight-run diesel feed containing 13400 ppm S and 105 ppm N. An extraction of up to 60% of the N-compounds was obtained in one step, whereas the sulfur concentration reduction was only 5%. Liquid-liquid extraction using ILs was therefore found to be a very promising approach for the removal of neutral N-compounds with high selectivity towards sulfur-containing compounds.

INTRODUCTION

The removal of sulfur from transportation fuels has been mandated by governments world-wide to meet the new regulations. For example, the U.S. Environmental Protection Agency requires the sulfur content in diesel fuels for on-board transportation to be 15 ppm. In Europe, the upper limit of sulfur content in diesel fuel will be 10 ppm, to be implemented by 2009. To produce ultra low-sulfur gasoline to meet the new regulations, two main routes can be considered: [1,2] on the one hand the improvement of the HDS catalysts and the HDS process, and on the other hand, alternative processes for the removal of refractory sulfur-containing compounds (S-compounds) such as adsorption, [3] liquid-liquid extraction, [4,5] oxidative desulfurization, [6] and bioprocesses [7].

In diesel fuels, the nitrogen-containing compounds (N-compounds) result from the blending of straight-run distillates and cracked products of heavier feedstocks having high nitrogen content. The N-compounds are present predominantly in heterocyclic aromatic compounds. These compounds (Figure 1) are classed as basic (**1**, **2**, and **3** derivatives) and nonbasic (**4** and **5** derivatives). Indeed, N-compounds have been identified [2] and observed [8-10] as strong inhibitors of the HDS reactions. This is due either to hydrogenation reactions occurring during this process that lead to the formation of basic species, or to a strong adsorption of the nonbasic N-compounds on the support surface.

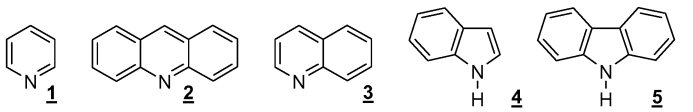

Figure 1. Nitrogen-containing compound in petroleum.

The removal of N-compounds by noncatalytic processes has been described in the literature.[11,12] All these methods are efficient for the removal of basic N-compounds, but none of them seem to be efficient or selective enough to remove the neutral N-compounds. We have proposed functionalized hydrophilic polymers for the selective adsorption of neutral N-compounds [8,10]. Our method is efficient, but the cost of the reagents and the polymer used limit the applicability of such a process.

Liquid extraction could be an interesting alternative to process hydrocarbon streams. This extraction process is a well-established process that can be carried out at around ambient temperature and pressure. However, the recovery of the solvent from the extract and the feed require additional distillation steps to separate the extraction solvent from both the extract and raffinate phases. In contrast to molecular solvents, ILs have several advantages: negligible vapor pressure and thermal stability over a wide range of temperature, even if their stability seems to be overestimated [13]. Several groups have already explored the application of ILs to replace conventional solvents. ILs have been used for the separation of aromatic from aliphatic hydrocarbon mixtures, [14,15] and for the extraction of refractory sulphur compounds [4,16-18] or basic N-compounds [18,19]. Although ILs were shown to be very effective in removing refractory sulphur compounds, their sensitivity to moisture, low stability of the anions (hexafluorophosphate), and their cost (fluorinated amides) make large-scale application difficult.

In view of these results, an effective removal of neutral nitrogen from diesel feed in conjunction with the deep removal of sulfur has become increasingly important. The primary objective of this study was to selectively remove neutral N-compounds, present in petroleum fractions, from sulfur and polyaromatic compounds. The selectivity of this first step is essential in order to obtain a high yield during subsequent refining.

RESULTS AND DISCUSSION

Chloride-based ILs are the precursors of most of the commercially available ILs via a metathesis reaction. The commercial availability of the starting materials, as well as their low price, makes water-miscible chloride-based ILs interesting compounds for the

replacement of molecular solvents in liquid-liquid extraction processes. Thus 1-butyl-3-methylimidazolinium chloride (BMImCl) was further evaluated.

Selective Extraction of Carbazole from a Model Fuel

The extraction of carbazole by the IL from toluene/*n*-dodecane containing dibenzothiophene is shown in Table 1. The selectivity of this extraction is essential in order to obtain a high yield during the subsequent refining process, as S-compounds will be transformed into valuable hydrocarbon compounds through the HDS process. Liquid-liquid equilibrium data were collected using a hydrocarbon feed with a high mass fraction of toluene. This was done to raise the solubility of carbazole, as it is weakly soluble in alkanes. The total concentration of N and S in the solvent was analyzed as a function of time by pyrolysis followed by chemiluminescence and UV fluorescence, respectively [10]. We could therefore determine the N and S concentration with high accuracy. Equilibrium was reached after 1 hour of contact at 60 °C in a batch reactor. BMImCl exhibited a high distribution ratio for carbazole as well as a high selectivity towards dibenzothiophene. It should be noted that the use of hydrophilic 1-alkyl-3-methylimidazolinium chloride results in a low solubility of ILs in the hydrocarbon feed (lower than 15 ppmw in pure toluene).

Table 1. Distribution ratio obtained with BMImCl using model fuel[a]

D N-compounds[b]	D S-compounds	Selectivity N/S[b]
46.2	0.36	128

[a]150 ppm N (carbazole) and 150 ppm S (dibenzothiophene) dissolved in toluene/*n*-dodecane (80/20 wt). Ratio RTIL/solvent, 1/10; 24 h @ 60°C. [b]The distribution ratio measured for carbazole could be slightly decreased due to the solubilization of the ILs in the model fuel and was not corrected.

Influence of the Toluene/*n*-Dodecane Ratio on the Extraction Efficiency

The high extraction of heterocyclic aromatic compounds by ILs has already been reported by several authors. However, most extractions of a pure compound from model diesel oil using ILs have been performed using *n*-heptane, [20] *n*-dodecane, [4,17,18] and *n*-tetradecane, [21] whereas diesel oil contained about 20 wt % of aromatic fraction. It has been suggested that the partitioning of S-compounds from diesel using water-insensitive ILs is more difficult than from gasoline due to the higher aromatic content.[18] In order to study this influence of the aromatic content on extraction efficiency, the extraction was carried out with single-component solutions containing 100 ppm of nitrogen in the form of neutral N-compounds (carbazole, indole), basic N-compounds (pyridine, acridine), or 100 ppm of sulfur in the form of S-compounds (benzothiophene or dibenzothiophene). The extraction of single components from a hydrocarbon mixture by BMImCl was strongly dependent on the toluene/*n*-dodecane ratio (Figure 2). Under those conditions, BMImCl was slightly soluble in the hydrocarbon mixture; thus, the extraction of N-compounds was corrected taking into account this solubility.

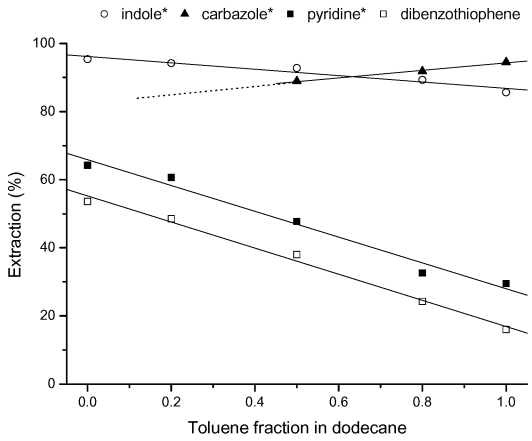

Figure 2. Extraction of pure compounds by BMImCl as the function of mass fraction of toluene (toluene/*n*-dodecane). Ratio BMImCl/hydrocarbon, 1/1; 100 ppm of pure compounds; 24 h at 60 °C. *Corrected value.

In pure *n*-dodecane, high extraction of heterocyclic aromatic compounds was observed. The order of extraction was S-compounds < basic N-compounds << neutral N-compounds. BMImCl showed a high affinity towards a neutral N-compound (indole). This high extraction of neutral indole using ILs has already been noticed [17]. However, using pure *n*-dodecane, no data could be determined for carbazole and acridine because of the low solubility of these compounds in alkanes. With an increase of the mass fraction of toluene, the extraction of S-compounds (benzothiophene and dibenzothiophene) as well as basic N-compounds (pyridine) decreased linearly. The interaction of the ILs with the aromatic compounds could be explained by the electron-pair acceptor properties of the imidazolium ring ($\pi - \pi$ interactions). Thus, we could suppose that in the presence of a high concentration of toluene, toluene would compete with the absorption of heterocyclic aromatic compounds. In other words, when the mass fraction of toluene in the hydrocarbon mixture was increased, the distribution ratio for heterocyclic aromatic compounds decreased. In pure toluene, within the uncertainity due to the solubilization of IL in the organic phase, BMImCl showed a very high affinity for the neutral nitrogen-containing compounds. The origin of this selectivity is unknown and is under investigation but may be due to hydrogen bound between the chloride anions (with nonbonding electrons) in combination with the imidazolium cation.

Extraction Efficiency of ILs for Straight-Run Feed

BMImCl was then evaluated at a mass ratio of 1/10 (BMImCl/feed) with a straight-run feed containing 13240 ppm of S and 105 ppm of neutral N-compounds. The total concentrations of N and S in the feed were analyzed as a function of time. Equilibrium was reached after 1 hour of contact at 60 °C in a batch reactor under continuous stirring. The results are presented in Figure 3. At 60 °C, more than 50% of the N-compound removal from the straight-run feed was achieved in a single contact with BMImCl with an IL/feed ratio of 1/10 by weight. Under those conditions, the sulfur level

was decreased by less than 2%, and a S/N selectivity higher than 60 can be calculated. Thus, the use of a hydrophilic IL allows the selective removal of neutral N-compounds.

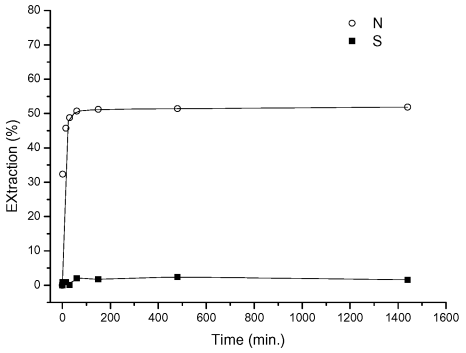

Figure 3. Sulfur and nitrogen extraction as the function of time and distribution ratio between BMImCl and straight-run feed containing 13240 ppm of N and 105 ppm of S. Ratio IL/feed, 1/10; 24 h @ 60 °C (uncorrected value).

CONCLUSIONS

Hydrophilic ILs can be considered as a novel medium for liquid/liquid extraction of neutral N-compounds from hydrocarbon feed with a high selectivity towards S-compounds. The extraction of heterocyclic aromatic compounds from a hydrocarbon mixture by BMImCl was found to be strongly dependent on the toluene/*n*-dodecane ratio. The distribution ratios for neutral N-compounds are an order of magnitude higher than the distribution ratios for the basic N- and S-compounds. The reasons for this have not yet been elucidated but may be due to hydrogen bounding between the chloride anion (with nonbonding electrons) in combination with the imidazolium cation.

This study demonstrates that neutral nitrogen-containing compounds could be selectively removed from diesel feed using hydrophilic IL as a solvent. The neutral nitrogen compounds were selectively extracted by a hydrophilic IL, BMImCl. The highly denitrogenated feed will be used to study the influence of the nitrogen compound concentration on HDS of diesel feed.

REFERENCES

1. M. Breysse, G. Djega-Mariadassou, S. Pessayre, C. Geantet, M. Vrinat, G. Perot, and M. Lemaire, "Deep desulfurization: reactions, catalysts and technological challenges," *Catal. Today,* **84**, 129-138 (2003).
2. C. Song, "An overview of new approaches to deep desulfurization for ultra-clean gasoline, diesel fuel and jet fuel," *Catal. Today,* **86**, 211-263 (2003).
3. M. Sevignon, M. Macaud, A. Favre-Reguillon, J. Schulz, M. Rocault, R. Faure, M. Vrinat, and M. Lemaire, "Ultra-deep desulfurization of transportation fuels via charge-transfer complexes under ambient conditions," *Green Chem.,* **7**, 413-420 (2005).
4. A. Böesmann, L. Datsevich, A. Jess, A. Lauter, C. Schmitz, and P. Wasserscheid, "Deep desulfurization of diesel fuel by extraction with ionic liquids," *Chem. Commun.,* 2494-2495 (2001).

5. Y. Shiraishi, K. Tachibana, T. Hirai, and I. Komasawa, "Desulfurization and Denitrogenation Process for Light Oils Based on Chemical Oxidation followed by Liquid-Liquid Extraction," *Ind. Eng. Chem. Res.,* **41**, 4362-4375 (2002).
6. M. F. Ali, A. Al-Malki, B. El-Ali, G. Martinie, and M. N. Siddiqui, "Deep desulphurization of gasoline and diesel fuels using non-hydrogen consuming techniques," *Fuel,* **85**, 1354-1363 (2006).
7. B. Yu, P. Xu, Q. Shi, and C. Ma, "Deep desulfurization of diesel oil and crude oils by a newly isolated Rhodococcus erythropolis strain," *Appl. Environ. Microbiol.,* **72**, 54-58 (2006).
8. M. Macaud, E. Schulz, M. Vrinat, and M. Lemaire, A new material for selective removal of nitrogen compounds from gas oils towards more efficient HDS processes," *Chem. Commun.,* 2340-2341 (2002).
9. G. Laredo, E. Altamirano, and A. De los Reyes, "Inhibition effects of nitrogen compounds on the hydrodesulfurization of dibenzothiophene: Part 2," *Appl. Catal. A,* **243**, 207-214 (2003).
10. M. Macaud, M. Sevignon, A. Favre-Reguillon, M. Lemaire, E. Schulz, and M. Vrinat, "Novel Methodology toward Deep Desulfurization of Diesel Feed Based on the Selective Elimination of Nitrogen Compounds," *Ind. Eng. Chem. Res.,* **43**, 7843-7849 (2004).
11. J. H. Kim, X. Ma, A. Zhou, and C. Song, "Ultra-deep desulfurization and denitrogenation of diesel fuel by selective adsorption over three different adsorbents: A study on adsorptive selectivity and mechanism," *Catal. Today,* **111**, 74-83 (2006).
12. A. J. Hernandez-Maldonado, and R. T. Yang, "Denitrogenation of transportation fuels by zeolites at ambient temperature and pressure," *Angew. Chem., Int. Ed.,* **43**, 1004-1006 (2004).
13. P. J. Scammells, J. L. Scott, and R. D. Singer, "Ionic Liquids: The Neglected Issues," *Aust. J. Chem.,* **58**, 155-169 (2005).
14. J. Zhang, C. Huang, B. Chen, P. Ren, and Z. Lei, "Extraction of Aromatic Hydrocarbons from Aromatic/Aliphatic Mixtures Using Chloroaluminate Room-Temperature Ionic Liquids as Extractants," *Energy Fuels,* **21**, 1724-1730 (2007).
15. A. Arce, M. J. Earle, H. Rodriguez, and K. R. Seddon, "Separation of aromatic hydrocarbons from alkanes using the ionic liquid 1-ethyl-3-methylimidazolium bis{(trifluoromethyl)sulfonyl}amide," *Green Chem.,* **9**, 70-74 (2007).
16. S. Zhang and Z. C. Zhang, "Novel properties of ionic liquids in selective sulfur removal from fuels at room temperature," *Green Chem.,* **4**, 376-379 (2002).
17. J. Eber, P. Wasserscheid, and A. Jess, "Deep desulfurization of oil refinery streams by extraction with ionic liquids," *Green Chem.,* **6**, 316-322 (2004).
18. S. Zhang, Q. Zhang, and Z. C. Zhang, "Extractive Desulfurization and Denitrogenation of Fuels Using Ionic Liquids," *Ind. Eng. Chem. Res.,* **43**, 614-622 (2004).
19. M. Matsumoto, M. Mikami, and K. Kondo, "Separation of organic nitrogen compounds by supported liquid membranes based on ionic liquids," *J. Jpn. Pet. Inst.,* **49**, 256-261 (2006).
20. C. Huang, B. Chen, J. Zhang, Z. Liu, and Y. Li, "Desulfurization of Gasoline by Extraction with New Ionic Liquids," *Energy Fuels,* **18**, 1862-1864 (2004).
21. W.-H. Lo, H.-Y. Yang, and G.-T. Wei, "One-pot desulfurization of light oils by chemical oxidation and solvent extraction with room temperature ionic liquids," *Green Chem.,* **5**, 639-642 (2003).

IMPROVED IONIC LIQUIDS FOR THE EXTRACTION OF AROMATIC HYDROCARBONS FROM NAPHTHA

A. R. Hansmeier, G. W. Meindersma, and A.B. de Haan

Group of Process System Engineering/Department of Chemical Engineering and Chemistry
Technical University of Eindhoven, P .O.Box 513, 5600MB Eindhoven, The Netherlands.
Corresponding author email address: a.hansmeier@tue.nl

ABSTRACT

For the separation of toluene/*n*-heptane, ionic liquids can outperform conventional solvents. The ionic liquid with the best performance so far is [EMIM][$AlCl_4$]. However, that ionic liquid is not water stable. Hence, the focus of this work is the development of an improved ionic liquid with comparable capacity but higher water stability. It was found that aromatic-type ionic liquids perform considerably better than conventional solvents, whereas ionic liquids with pyridinium type cations and linear anions are water stable and have higher capacities than imidazolium based ionic liquids. Moreover, the [3-Mebupy][DCA] ionic liquid is even 3 times more efficient than Sulfolane®.

INTRODUCTION

The separation of aromatic and aliphatic hydrocarbons is challenging due to close boiling points and azeotrope formation. Therefore, conventional processes for this type of separation are extraction or extractive distillation with polar, organic compounds, for example, Sulfolane (UOP/Shell Sulfolane Process) [1]. These separation processes are based on the polarity differences of aromatic and aliphatic hydrocarbons, whereas aromatic hydrocarbons have π-electrons and aliphatic hydrocarbons are nonpolar.

This work focuses on developing an improved ionic liquid for the separation of aromatic and aliphatic hydrocarbons. In the past, it was shown that ionic liquids can be good extraction solvents for this type of separation [3-5]. Up to now, [1-ethyl-3-methyl-imidazolium][tetrachloroaluminate] [EMIM][$AlCl_4$] is the ionic liquid that displayed the highest capacity and selectivity for the separation of toluene from n-heptane. However, most of these first and second generation ionic liquids are not water stable since they contain halogenic anions that dissociate in water and form acids like HCl and HF. For this reason, the objective of this work has been the design of an ionic liquid that can compete with [EMIM][$AlCl_4$] in terms of capacity in order to substitute the classical polar solvents by a water-stable ionic liquid.

Since it was observed that pyridinium- and imidazolium-containing ionic liquids tend to have good extraction properties for aromatic hydrocarbons, a systematic evaluation of ILs consisting of those cations and different anions was carried out [6].

EXPERIMENTAL SECTION

Liquid-liquid extraction experiments were carried out in jacketed glass vessels with a volume of about 70 mL and at constant temperature. Samples have been taken of raffinate and extract phase and were analyzed by means of a GC. The accuracy of this method is ±1%, whereas the reproducibility for the distribution ratio is ±2% and for the selectivity ±5%. A more detailed description is given by Meindersma [3].

RESULTS AND DISCUSSION

The distribution ratios D_i are directly calculated from the mole fractions in extract and raffinate phase at equilibrium. D_i is defined as the ratio of the mole fractions of the component in the extract phase (ionic liquid) and in the raffinate phase (organic phase):

$$D_{aromatic} = C_{arom}^{IL} / C_{arom}^{org} \quad \text{and} \quad D_{aliphatic} = C_{aliph}^{IL} / C_{aliph}^{org} \tag{1}$$

The selectivity α is derived from the ratio of the distribution ratios, according to:

$$\alpha = D_{arom} / D_{aliph} \tag{2}$$

Figure 1 illustrates the molar capacity (D_i) and selectivity (α) of several ionic liquids for the separation of toluene from *n*-heptane. The obtained values are compared with the distribution ratio and selectivity of Sulfolane, which is used as a benchmark. In order to replace Sulfolane, a suitable ionic liquid should combine a significantly higher capacity with an improved selectivity. However, process simulation studies showed that selectivity is less important than capacity; since capacity determines the solvent recycle rates, the sizes of the extraction column and other equipment as well as the energy consumption [3]. Thus, suitable ionic liquids will be in the right part of the graph. Figure 1 shows that the ionic liquid [EMIM][$AlCl_4$] is the ionic liquid with the best extraction properties, that is, high capacity and high selectivity for the binary feed toluene/*n*-heptane. All other tested ionic liquids have a lower molar capacity and/or selectivity. However, this ionic liquid is not water-stable. Therefore, [EMIM][$AlCl_4$] is not suitable as an extraction solvent, because in the presence of water HCl will be formed.

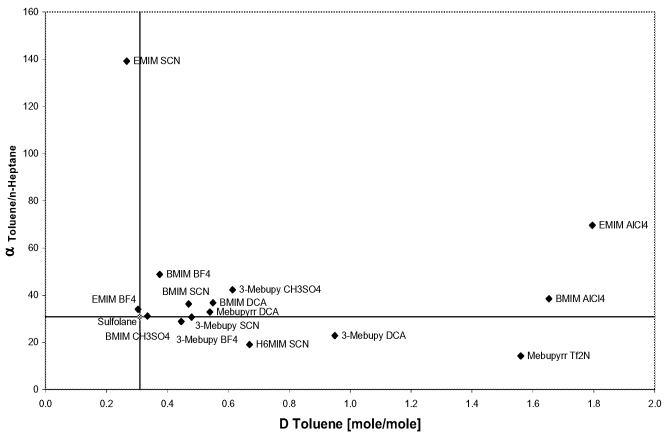

Figure 1. Comparison of selectivity and capacity of different ionic liquids for 10 mole % toluene/*n*-heptane mixture at T = 313 K.

It is important to note that not only the interaction between cation and aromatic solute is important but also

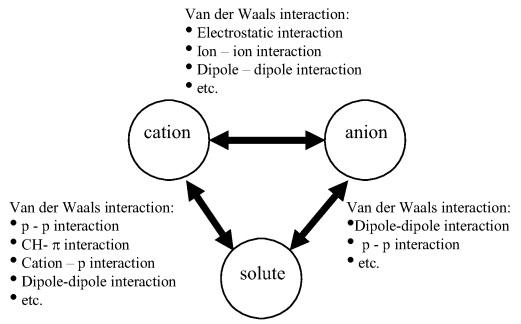

Figure 2. Interaction between ionic liquid and solutes.

the interactions between cation and anion as well as between anion and solute. However, the main interaction forces are derived from the cation (Figure 2).

This can be explained by the nature of the molecules implicating complex forming between cation and solute, whereas the interaction is based on van der Waals forces, namely π-π-interaction, ion-ion interaction, dipole-dipole forces [7]. It is assumed that all these different types of interactions contribute to the extraction mechanism, whereas π-π interaction is considered to have the greatest influence [8]. Therefore, arenic solutes, due to their π-system, interact with the π-system of the aromatic cations, whereas the naturally rather electron-rich aromatic hydrocarbons tend to be attracted by the positive charge of the nitrogen atom. This leads to a sandwich structure where cations and solutes are arranged alternately. The cations form a cage structure in which the solute is enclosed. This phenomenon is also described by Holbrey et al. [9]. Within this sandwich structure, the anions are arranged around the cation aromatic hydrocarbon packing, whereas the type and shape of the anion is important. However, as it can be seen in Figures 1 and 2, the combination of anion and cation plays an important role, and concerning molecule interactions, they cannot be considered apart from each other, since there are interaction forces between cation-anion, cation-solute, and anion-solute [10].

Influence of the Cation

In Figure 1, several ionic liquids consisting of different cations with the same anion are compared. It can be seen that pyridinium ionic liquids outperform imidazolium ionic liquids. Imidazolium contains two nitrogen atoms and, therewith, the positive charge is delocalized, which makes it less strong per nitrogen. Hence, pyridine, which has only one positively charged nitrogen atom, has a stronger interaction potential and, therewith, forms easier π-interactions with an aromatic ring.

The shown ionic liquids based on the aliphatic pyrrolidinium cation provide comparable results to the aromatic-based ionic liquids. Since aliphatic molecules do not have the possibility for π-π interaction, probably other van der Waals forces, like cation-π interaction and dipole-dipole interaction, become more important.

Influence of the Anion

A second observation that is made is that the same cation with different anions can have tremendous differences in capacity. Hence, the size and shape of the different types of anions seems to have a big influence [10]. In general, it can be seen that, except for $[AlCl_4]^-$, rather flat anions with a delocalized charge like

[{bis(trifluoromethyl)sulfonyl}imide]$^-$, [Tf_2N]$^-$, or [dicyanamide]$^-$, [DCA]$^-$, perform better than spherical anions like [BF_4]$^-$.

The strength, size, shape, and flexibility of the anion can have an impact on the extraction behavior. As an example, [Tf_2N]$^-$ has a more flexible structure due to the possibility to form cis- and trans-isomers, which could have an advantage in terms of the packing structure [11]. The anion [DCA]$^-$ has a similar structure but is less complex than [Tf_2N]$^-$. On the other hand, it is a small, almost flat anion, which can have an advantage for packing compared with spherical anions. An exception is formed by the anion [$AlCl_4$]$^-$; it is a spherical molecule like [BF_4]$^-$; however, [$AlCl_4$]$^-$ is a little bit bigger molecule, which leads to the hypothesis that the anion size is important. AlsoZhang et al. mentioned that the anion size has most likely influence on the extraction capacity of an ionic liquid [12]. It is assumed that the anion should not be too big but also not too small. Moreover, the influence of the anion can also have a significant effect. Nevertheless, more research is needed to explain those effects in more detail.

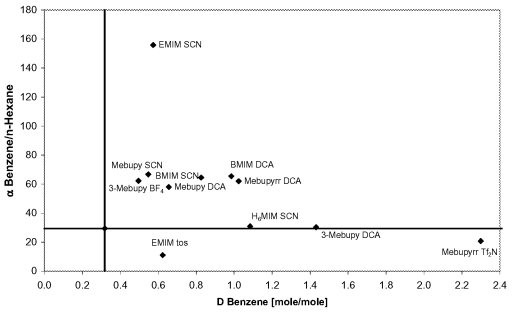

Figure 3. Comparison of selectivity and capacity of different ionic liquids for benzene/*n*-hexane at $T = 303$ K.

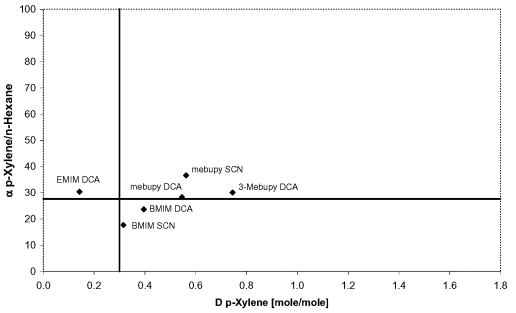

Figure 4. Comparison of selectivity and capacity of different ionic liquids for p-xylene/*n*-hexane at $T = 303$ K.

Simplified Naphtha Model Feed

Nevertheless, not only for binary mixtures, the above mentioned water-stable ionic liquid performs better than first-generation ionic liquids [3]. Several ionic liquids have been evaluated with a simplified naphtha feed consisting of benzene, toluene, *p*-xylene, and hexane. The results of these LLE-measurements are shown in Figures 3 and 4. Also, for more complex mixtures, the same trend as for toluene/*n*-heptane mixtures can be shown. As it is visible, except for [Mebupyrr][Tf_2N], [3-Mebupy][DCA] performs better here as well. Additionally, Figure 3 and 4 confirm that ionic liquids that contain the anions dicyanamide [DCA]$^-$ or thiocyanate [SCN]$^-$ outperform other ionic liquids.

It can be observed that the capacity for the extraction of arenes with the same ionic liquids decreases in the following order: benzene > toluene > *p*-xylene. Therefore, two mechanisms are possible. On one hand side, it is assumed that all aromatic hydrocarbons have π-π-interactions with the cations of the ionic liquid. However, the more side chains an aromatic solute has, here methyl groups, the higher the steric hindering. This means that the lesser the interaction between cation and solute becomes the more difficult it is to organize in a proper sandwich packing structure. On the other

hand, the more side chains an arene has, the lower the activity coefficient for the aliphatic phase, and therewith the higher the solubility is in the raffinate phase.

Comparison of Mole Fractions and Mass Fractions (Engineering Aspects)

From an engineering aspect, the mass fraction of a solvent is an important parameter for the operation of a separation unit. Hence, a solvent that seems excellent on a mole basis can be less efficient on mass basis, because a high molar mass causes a high need of solvent, which is economically unfavorable.

Table 1. Comparison of mole- and weight-based capacity of different ionic liquids for the mixtures toluene/*n*-heptane at $T = 313$ K and benzene/*n*-hexane and *p*-xylene/*n*-hexane at $T = 303$ K

	D_i [mole/mole]			D_i [g/g]		
IL	Benzene	Toluene	*p*-Xylene	Benzene	Toluene	*p*-Xylene
EMIM $AlCl_4$	-	1.80	-	-	0.69	-
BMIM $AlCl_4$	-	1.65	-	-	0.59	-
BMIM DCA	0.99	0.55	0.40	0.75	0.24	0.30
BMIM SCN	0.83	0.47	0.32	0.64	0.21	0.24
EMM SCN	0.57	0,27	-	0.31	0.18	-
3-Mebupy DCA	1.43	0.95	0.75	0.87	0.59	0.56
Mebupy SCN	0.55	0.48	0.56	0.28	0.24	0.44
Mebupyrr Tf_2N*	2.30	1.57	-	0.39	0.27	-
Sulfolane	0.32	0.33	0.29	0.25	0.21	0.19

*Tested for toluene/*n*-hexane.

Table 1 compares the molar and mass capacities of the ionic liquids shown in Figure 1. It becomes apparent that ionic liquids that have a high molar extraction capacity do not necessarily provide high mass-based capacities. For example, the capacity of the ionic liquid [Mebupyrr][Tf_2N] decreases almost by a factor of 6 when the values are expressed in weight fractions. For [EMIM][$AlCl_4$], the decrease is a factor of 2.6. This deviation is caused by the high molecular weight of the anions, because ions like $[Tf_2N]^-$ and $[AlCl_4]^-$ are large. Therefore, theses ionic liquids have a high molar density. However, ionic liquids containing small, linear anions like $[DCA]^-$ and $[SCN]^-$, which have considerably lower molar capacities, provide comparable mass-related capacities. Especially, the ionic liquid [3-Mebupy][DCA], which is on molar basis significantly worse than [EMIM][$AlCl_4$], is on a mass basis as good as [BMIM][$AlCl_4$]. Moreover, [3-Mebupy][DCA] is comparable with [EMIM][$AlCl_4$]. Furthermore, based on weight fractions, [3-Mebupy][DCA] is three times as good as Sulfolane.

CONCLUSIONS

It can be concluded that very promising, but water-unstable, first-generation ionic liquids can be replaced by new and improved ionic liquids. These improved ionic liquids consist of aromatic-type cations and small linear anions. It was shown that the extraction feasibility (i.e. capacity) is determined by the cation supported by small anions with

delocalized charge. It could be observed that pyridinium based ionic liquids in combination with a small linear anion, perform better than imidazolium based ionic liquids in combination with small linear anions, because the reactivity of the pyridine molecule tends to be slightly higher than the reactivity of imidazole. The ionic liquid [3-Mebupy][DCA] has been found to be the best one in terms of mass-based capacity and can outperform Sulfolane by a factor of 3 for the separation of toluene/*n*-heptane.

ACKNOWLEDGMENTS

We acknowledge BP for financial support and BASF for the support with ionic liquids.

REFERENCES

1. W. A. Sweeny and P. F. Bryan, Kirk-Othmer Encyclopedia of Chemical Technology (electronic version), John Wiley & Sons, 1992.
2. A. Heintz, "Recent Developments in Thermodynamics and Thermophysics of non-aqueous Mixtures containing ionic liquids. A Review," *J. Chem. Thermodyn.*, **37**, 525-535 (2005).
3. G. W. Meindersma, "Extraction of Aromatics from Naphtha with Ionic Liquids," Ph.D. Thesis, University of Twente, Enschede, The Netherlands, 2005. (http://doc.utwente.nl/50805)
4. C. Jork, C. Kristen, D. Pieraccini, A. Stark, C. Chiappe, Y. A. Beste, and W. Arlt, "Tailor-made Ionic Liquids," *J. Chem. Thermodyn.*, **37**, 537-558 (2005).
5. U. Domanska, A. Pobudkowska, and M. Krolikowski, "Separation of Aromatic Hydrocarbons from Alkanes using Ammonium Ionic Liquid C_2NTf_2 at T = 298.15 K," *Fluid Phase Equilib.*, **259**, 173-179 (2007).
6. Y. Liu, Z. Zhang, G. Zhang, Z. Liu, Y. Hu, S. Quan, and D. Ji, "Effect of the Structure of Cations and Anions of Ionic Liquids on Separation of Aromatics from Hydrocarbon Mixtures," *Pet. Sci.*, **3**(3), 73-78 (2006).
7. C. Reichardt, Solvents and Solvent Effects in Organic Chemistry, Wiley, Weinheim, 5-56, (2003).
8. P. Stepnowski, J. Nichthauser, W. Mrozik, and B. Buszewski, "Usefulness of π…π Aromatic Interactions in the Selective Separation and Analysis of Imidazolium and Pyridinium Ionic Liquid Cations," *Anal. Bioanal. Chem.*, **385**, 1483-1491 (2006).
9. J. D. Holbrey, W. M. Reichert, M. Nieuwenhuyzen, O. Sheppard, C. Hardacre, and R. D. Rogers, "Liquid Clathrate Formation in Ionic Liquid-Aromatic Mixtures," *Chem. Commun.*, 476-477 (2003).
10. C. G. Hanke, A. Johansson, J. B. Harper, and R. M. Lynden-Bell, "Why are Aromatic Compounds more Soluble than Aliphatic Compounds in Dimethylimidazolium Ionic Liquids? A Simulation Study," *Chem. Phys. Lett.*, **374**, 85-90 (2003).
11. M. Deetlefs, C. Hardacre, M. Nieuwenhyzen, A. A. H. Padua, O. Sheppard, and A. K. Soper, "Liquid Structure of the Ionic Liquid 1,3-Dimethylimidazolium Bis{(trifluoromethyl)sulfonyl}amide," *J. Phys. Chem. B*, **110**, 12055–12061 (2006).
12. J. Zhang, C. Huang, B. Chen, P. Ren, and Z. Lei, "Extraction of Aromatic Hydrocarbons from Aromatic/Aliphatic Mixtures using Chloroaluminate Room-Temperature Ionic Liquids as Extractants," *Energy Fuels*, **21**, 1724-1730 (2007).

IONIC LIQUIDS IN EXTRACTION OPERATIONS: COMPARISON OF ROTATING DISC CONTACTOR PERFORMANCE BETWEEN [4-MEBUPY]BF_4 AND SULFOLANE® FOR AROMATICS EXTRACTION

S. A. F. Onink, G. W. Meindersma, and A. B. De Haan

Technische Universiteit Eindhoven, Den Dolech 2, P. O. Box 513, 5600 MB Eindhoven, The Netherlands. Corresponding author email address: s.a.f.onink@tue.nl

ABSTRACT

Using nonvolatile ionic liquids instead of solvents as N-methylpyrrolidone (NMP) or Sulfolane in extraction provides the advantage of a simple solvent recovery as flash distillation or stripping. Successful introduction of RTILs into extractions requires knowledge on their hydrodynamic and mass-transfer characteristics. Extraction of aromatics from aliphatics with 4-methyl-N-butylpyridinium tetrafluoroborate as solvent in a pilot-plant rotating-disc contactor was compared to Sulfolane. From a hydrodynamic point of view, [4-mebupy]BF_4 is a better solvent, but the mass-transfer performance of Sulfolane was superior due to its lower viscosity. ILs can extract feeds containing high (>65%) aromatics, which is not possible with current solvents.

INTRODUCTION

In previous studies, we have demonstrated that Room Temperature Ionic Liquids (RTIL) are promising solvents for the extraction of aromatic hydrocarbons [1]. However, successful introduction of RTILs into extraction operations also requires knowledge on their hydrodynamic and mass-transfer characteristics. Therefore, this research presents the results of a study on the extraction of aromatics from aliphatics in a pilot-plant rotating-disc contactor (RDC) with 4-methyl-N-butylpyridinium tetrafluoroborate ([4-mebupy]BF_4) as the solvent. The RDC was selected since it is the most commonly used extractor for aromatics extraction in the petrochemical industry. In the extraction process, hydrodynamics (drop size, hold-up, and operational window) and mass-transfer efficiency determine the column performance [2]. As model components for aromatic/aliphatic separation, toluene/*n*-heptane mixtures were chosen, in which the toluene content is varied from 10 to 75 wt %. The results regarding the hydrodynamic behavior of the column and mass-transfer profiles over the column are benchmarked against the commonly used solvent Sulfolane [3]. The investigated parameters concern the total flux, the rotating speed of the RDC [4,5], and the concentration of toluene in the organic (*n*-heptane) phase.

EXPERIMENTAL

Chemicals

The ionic liquid 4-methyl-N-butylpyridinium tetrafluoroborate (>97%), *n*-heptane (>99.9%) and toluene (>99.9%) were purchased from Merck. Sulfolane (>99%) was purchased from Sigma Aldrich.

Experimental Setup

The pilot RDC extraction column is schematically shown in Figure 1. The column consisted of five jacketed glass segments each of 360 mm in length and an inside diameter 60 mm, each with eight stirred compartments. Every glass segment had attached sample ports either for measuring the hold-up or for determining the concentration profile. Settlers of 240 mm (bottom) and 210 mm (top) with an internal diameter of 90 mm enclosed the stirred segments. The internals of the stirred segments consisted of alternating discs, and doughnuts and were made of SS material. The outside and inner diameters of the doughnuts were 60 mm and 22 mm, respectively, and the thickness was 1.5 mm. The discs had a diameter of 40 mm and a thickness of 1.5 mm. The distance between two doughnuts was 32 mm, the same as the distance between two discs. The solvent was fed to the top of the column, and the extract phase was collected from the bottom settler. This phase (ionic liquid or Sulfolane) was dispersed. The heptane/toluene phase was fed from the bottom, and the raffinate phase was collected from the top settler. The solvents were regenerated in the extraction column at 80 °C by bubbling nitrogen through the column for 24 h. Total heptane removal was possible, but total toluene removal was not: 0.78 mole % was left in the Sulfolane and 0.70 mole % in [4-mebupy]BF_4. The regenerated ionic liquid was used in the extraction experiments.

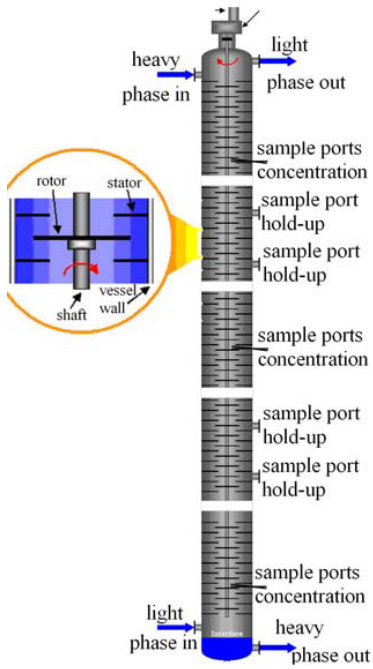

Figure 1. Schematic representation of the rotating disc column.

Hydrodynamics and Operational Region

For determination of the operational regions, the total flux is varied while keeping the solvent-to-feed (S/F) ratio constant. When performing these experiments, the system has to be operated in steady state, and the phases must be in equilibrium. The flux (m^3/m^2.hr) is defined as the volume that passes through the cross-section of the column in a certain time period. In order to find the flooding point, the rotor speed is increased at constant flux. When the rotor speed increases, the dispersed-phase droplets become

smaller, and the droplets are slowed down, and consequently, the hold-up increases until the drop size becomes too small or the hold-up becomes too large and flooding or phase inversion occurs. Flooding of the extractor is manifested by the appearance of a second interface at the opposite end to the main interface. Phase inversion is a phenomenon caused by a change in mixing conditions such that the dispersed and continuous phases interchange. Until the maximum rotor speed at which flooding occurs for a certain flux, the dispersed phase hold-up and drop size can be determined at each rotor speed. The drop sizes in the column were determined by taking digital photos of the column contents. The drop size was determined as the Sauter mean diameter. For determination of the hold-up, 250 mL samples were taken through the different sample ports and collected in a separation funnel.

Number of Equilibrium Stages

The number of equilibrium stages (N_S) was determined graphically with an equilibrium line and an operating line in an extraction diagram. The results for the extraction of 10 wt % toluene were confirmed by means of the well-known Kremser equation. Since the operating and equilibrium lines are not straight, this equation can only be used at low concentrations. The results for the extraction of 50 and 75 wt % toluene are confirmed by means of stage wise extraction calculations carried out with ternary equilibrium diagrams.

RESULTS AND DISCUSSION

Drop Size

Figure 2 shows the results for drop size for the extraction of 10 and 75 wt % toluene from *n*-heptane. For both experiments, the drop size decreases with increasing rotor speed. Drop sizes determined at extraction of 75 wt % toluene are smaller than those measured at extraction of 10 wt %. The differences in drop size can be explained by the higher concentration of toluene in [4-mebupy]BF_4 when extracting 75 wt % toluene than when extracting 10 wt % toluene. This higher concentration reduces the viscosity of [4-mebupy]BF_4, which results in easier break-up and therefore smaller droplets.

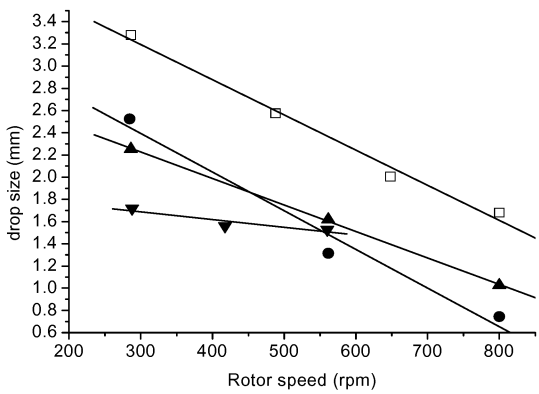

Figure 2. Drop sizes for extraction of 10 wt % toluene from *n*-heptane with [4-mebupy]BF_4 (flux = 2.8 m/hr, □) and of 75 wt % toluene with flux varying from 3.7 (●), 8.2 (▲), to 10.5 (▼) m^3/m^2 hr.

Hold-up

The experimental hold-up fraction for constant flow rates of both phases is shown in Figures 3. At low fluxes, the hold-up decreases with increasing rotor speed when [4-mebupy]BF_4 is used as solvent. This is not expected, since an increase in rotor speed should result in a greater torroidal motion of the dispersed phase, which results in a greater residence time of the dispersed phase. This was also found by others [6]. The explanation for this is that cohesion of droplets at the stator rings causes an increase in the hold-up at lower fluxes. At higher fluxes, there is less cohesion, which is confirmed by the decrease in drop size at increasing flux (Figure 2). Because Sulfolane has a much lower viscosity (8 mPas at T = 313 K) than [4-mebupy]BF_4 (80 mPas at T = 313 K), there is less cohesion when Sulfolane is used and so the Sulfolane hold-up increases with increasing rotor speed as expected.

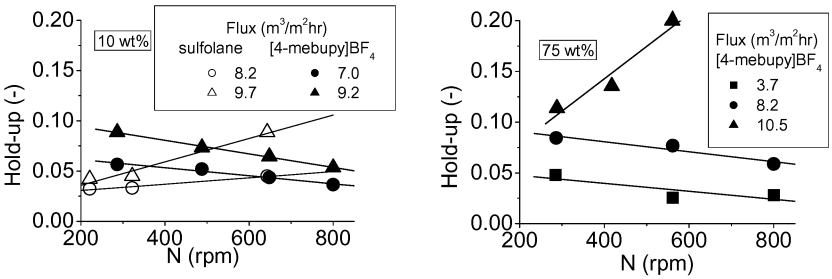

Figure 3. Hold-up for Sulfolane (open symbols, S/F = 4) and [4-mebupy]BF_4 (closed symbols, S/F = 6) extraction for 10 wt % toluene (left) and for [4-mebupy]BF_4 extraction 75 wt % toluene (right, S/F = 7.5).

Operational Region

The performances of Sulfolane and [4-mebupy]BF_4 as dispersed solvent phase were compared for the extractive removal of toluene from a mixture of 10 to 75 wt % toluene in *n*-heptane at 40 °C. For Sulfolane, a S/F ratio of 4 (10 wt %) resp. 6 (50 wt %), and for [4-mebupy]BF_4 a S/F ratio of 6 (10 wt %) resp 7.5 (50 and 75 wt %) were used. In Figures 4a-c, two areas can be discerned: flooding and the normal operating area. From Figures 4a-b, it can be concluded that, for extraction of 10 wt % toluene as well for extraction of 50 wt % toluene in the RDC, the maximum achievable flux is higher for [4-mebupy]BF_4 than for Sulfolane.

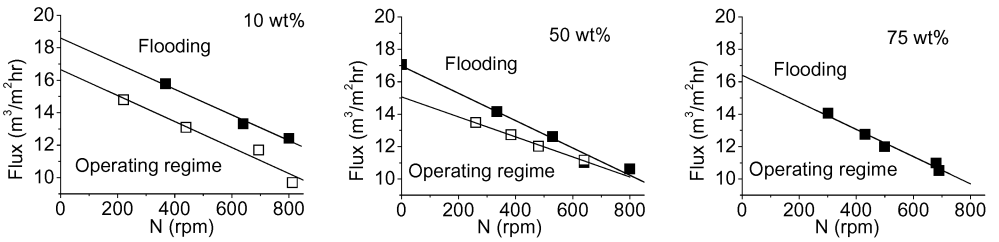

Figures 4 a-c. Operational region for extraction of toluene from *n*-heptane in RDC at T = 313K with Sulfolane (open symbols) and [4-mebupy]BF_4 (closed symbols).

The difference in maximum flux can be explained by the difference in drop size. The viscosity of [4-mebupy]BF_4 is much higher than the viscosity of Sulfolane. Therefore, [4-mebupy]BF_4 has larger drop sizes than Sulfolane, and consecutively a higher gravitational force and less resistance cause the [4-mebupy]BF_4 droplets to fall faster through the heptane, and higher counteracting forces at higher fluxes can be overcome. Extraction of more than 65 wt % toluene from *n*-heptane is not possible with Sulfolane, since the compositions approach the plait point in the ternary diagram, so separation is not possible anymore [7,8].

Mass Transfer

Figures 5a-b show the concentration profiles of toluene over the column length. In Table 1, an overview of the calculated and graphically determined number of equilibrium stages and H_{ets} (height equivalent to a theoretical stage, calculated from $H_{ets} = H_{column}/N_s$) is given. In Figure 6, the method of determining N_s is shown.

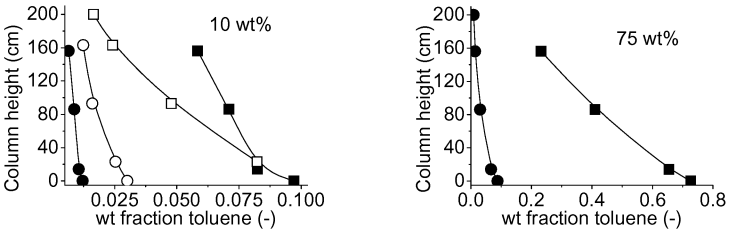

Figures 5a-b. Concentration profile of toluene over the column. $T = 313$ K; $N = 640$ rpm; closed symbols for [4-mebupy]BF_4 as solvent; open symbols for Sulfolane; raffinate (■,□), extract (♦,◊).

The calculated value for N_s at extraction of 10 wt % toluene differs slightly from the graphically determined value. This is due to the fact that, in the Kremser equation, the solvent-to-feed ratio is assumed constant. This ratio, however, is not constant because of mass transfer throughout the column. From Figure 5a and Table 1, it can be concluded that, with Sulfolane as solvent, more toluene is extracted than with [4-mebupy]BF_4, although the distribution ratios of toluene in Sulfolane and [4-mebupy]BF_4 are comparable on weight basis (0.22 wt/wt for [4-mebupy]BF4 vs. 0.26 wt/wt for Sulfolane [6]. The value of N_s for Sulfolane is higher than when [4-mebupy]BF_4 is used. In line with the results for N_s, H_{ets} is much smaller for Sulfolane. This can be explained by the much lower viscosity for Sulfolane. In Figure 3, it can be seen that the hold-up for Sulfolane at 640 rpm is larger than for [4-mebupy]BF_4, which causes better mass transfer for Sulfolane and, therefore, H_{ets} is smaller for Sulfolane. So, although the distribution ratios for Sulfolane as well for [4-mebupy]BF_4 are almost the same on a weight basis, fluid dynamics cause the difference in these extraction experiments.

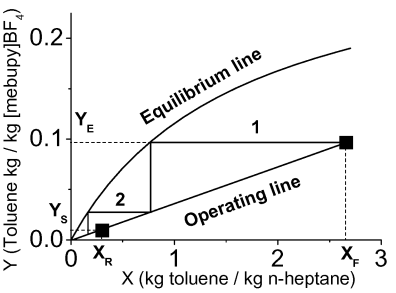

Figure 6. Determination of N_s, extraction of 75 wt % toluene.

Extraction of more then 65 wt % toluene is not possible with Sulfolane [7,8], but from Figure 5b, it can be concluded that with [4-mebupy]BF_4 a rapid decrease of toluene concentration in the raffinate phase occurred.

Table 1. Calculated and graphically determined number of equilibrium stages for extraction of 10–75 wt % toluene with Sulfolane and [4-mebupy]BF_4 in RDC at 313 K

Toluene wt %	Solvent	N_s calc	N_s graph	H_{ets} (m)
10	Sulfolane® [1]	4.1	NA	0.5
	[4-mebupy]BF_4	1.6	1.2	1.7
50	[4-mebupy]BF_4	NA	1.5	1.3
75	[4-mebupy]BF_4	NA	1.5	1.3

CONCLUSIONS

From a hydrodynamic point of view, [4-mebupy]BF_4 is a better solvent than Sulfolane; the operational region is larger. However, based on mass-transfer characteristics, it can be concluded that Sulfolane outperforms [4-mebupy]BF_4. This is due to the large difference in viscosity of the two compared solvents. ILs such as [4-mebupy]BF_4 offer the advantage to extract feeds containing high (>65%) aromatic content, which is not possible with the currently used solvents.

ACKNOWLEDGMENTS

BASF, Ludwigshafen is kindly acknowledged for their financial support.

REFERENCES

1. G. W. Meindersma, J. G. Podt, M. B. Klaren, and A. B. de Haan, "Separation of Aromatic and Aliphatic Hydrocarbons with Ionic Liquids," *Chem. Eng. Commun.,* **193** (10-12), 1384-1396 (2006).
2. J. C. Godfrey and M. J. Slater, Liquid-Liquid Extraction Equipment, John Wiley & Sons, Inc. New York, NY USA, 1994.
3. http://www.uop.com/objects/55%20Sulfolane.pdf.
4. T. C. Lo, M. H. I. Baird, and C. Hanson, Handbook of Solvent Extraction, John Wiley & Sons, New York, NY USA, 1983.
5. F. Ullmann, Ullmann's Encyclopedia of Industrial Chemistry, Wiley-Interscience, New York, electronic version, 2004.
6. M. S. Kamath, K. Laxminarayana Rao, and R. Jayabalou, "Hold-up Studies in a Rotary Disc Contactor," *Indian J. Technol.,* **14**, 1-5 (1976).
7. G. W. Meindersma, J. G. Podt, and A. B. de Haan, "Selection of Ionic Liquids for the Extraction of Aromatic Hydrocarbons from Aromatic/Aliphatic Mixtures," *Fuel Process. Technol.*, **87**, 59-70 (2005).
8. G. W. Meindersma, J. G. Podt, and A. B. de Haan, "Ternary Liquid-Liquid Equilibria for Mixtures of Toluene + *n*-Heptane + an Ionic Liquid," *Fluid Phase Equilib.*, **247**, 158-168 (2006).

SOLVENT IMPREGNATED RESIN FOR ISOLATION OF U(VI) FROM INDUSTRIAL WASTES

M. Karve and R. V. Rajgor

Department of Chemistry, University of Mumbai, Vidyanagari, Mumbai- 400098. India.
Corresponding author e-mail address: mkarve@yahoo.com and manjusha@chem.mu.ac.in

ABSTRACT

A solid-phase extraction method based upon impregnation of Cyanex 302 (bis(2,4,4-trimethylpentyl)monothiophosphinic acid) on Amberlite XAD-2 resin is proposed for isolation of U(VI) from uranmicrolite ore tailing samples and industrial effluent samples. U(VI) was sorbed from nitric acid media on the solvent-impregnated resin (SIR) and was recovered completely with 1.0 M HCl. Based upon sorption behavior of U(VI) with Cyanex 302, it was quantitatively sorbed on the SIR in a dynamic method, while the other metal ions were not sorbed by the modified resin. The preparation of impregnated resin is simple, based upon physical interaction of the extractant and solid support, has good sorption capacity for U(VI), and is also reliable for detection of traces of U(VI).

INTRODUCTION

Uranium is a toxic element and is also used in nuclear-energy programs. Hence, its separation from environmental samples as well as from other rare earth elements and thorium has significance. Solid-phase extraction (SPE) has emerged as a technological alternative to conventional separation techniques like solvent extraction due to the clean methodologies it offers. SPE methods for preconcentration of uranium from samples like soil, sediments, and water have been reported using polymeric resins, silica, or naphthalene as solid supports [1]. Most of these methods were based upon chemical binding of chelating ligands or anchoring of a chelating group on these supports. Although different types of sorbents have been reported for isolation of uranium [2], the impregnation of a liquid cation exchanger involving its physical interaction with a polymeric resin is simple compared to the rather tedious chemical reactions involved for the synthesis of chelating resins. Moreover it combines the advantages of high distribution ratios with the extractant and the multistage character of a chromatographic process.

In the present work, Amberlite XAD-2 was selected due to its characteristic structural properties [3] for impregnating with Cyanex 302. This (SIR) permitted recovery of traces of U(VI) and its separation from other associated elements.

EXPERIMENTAL

Apparatus, Reagents, and Solutions

A Digispec 110-D visible spectrophotometer, Feedback India Ltd., Perkin Elmer atomic absorption spectrophotometer, AAnalyst200, and an inductively coupled plasma atomic emission spectrophotometer, ICP-AES JY JOBIN YVON HORIBA ULTIMA 2 were employed for determining metal ion concentration.

A stock solution of U(VI), 2.0 mg cm^{-3}, was prepared by dissolving an appropriate quantity of uranyl nitrate hexahydrate (British Drug House Ltd.) in slightly acidified distilled water. The solution was standardized gravimetrically [4], and a working solution containing 30 μg cm^{-3} U(VI) was prepared by appropriate dilution. Arsenazo(III) (S. D. Fine chemicals) was prepared as a 0.100% w/v aqueous solution. Amberlite XAD-2 (20-60 mesh size, 330 m^2 g^{-1} average surface area) was obtained from Supelco, Sigma Aldrich Co. It was pretreated prior to use,n as reported earlier [3]. Cyanex 302 obtained from Cytec Canada as a gift sample was used without purification. All chemicals and reagents used were of A.R. grade.

General Procedure for Sorption of U(VI)

Cyanex 302 was impregnated on XAD-2 as per the earlier procedure [5]. A 0.1 g of impregnated resin (SIR) was equilibrated with 50 cm^3 solution containing 0.6 μg cm^{-3} U(VI) in 1×10^{-3} M HNO_3 on a mechanical shaker for 10.0 min. U(VI) was eluted with 10.0 cm^3 of 1.0 M HCl and determined spectrophotometrically with Arsenazo(III) at 650 nm [6]. Six replicate determinations of U(VI) using the same experimental conditions resulted in its quantitative sorption (99.2%) and gave a relative standard deviation not greater than 0.4%.

Effect of Aqueous Phase Acidity

The effect of different concentrations (1×10^{-4} M to 1.0 M) of HNO_3 and HCl on sorption of U(VI) was studied using 0.1 g of SIR. The amount of U(VI) sorbed was determined from the aqueous phase. The sorption of U(VI) was at a maximum (99.2 ± 0.4%) when the aqueous phase acidity was 1×10^{-3} M HNO_3. Its sorption continuously decreased beyond 1×10^{-2} M HNO_3 and in HCl. The sorption of U(VI) was only 3.1% from 1.0 M HNO_3 and 2.8% from 1.0 M HCl. This decrease in sorption with increase in aqueous phase acidity is a consequence of an effective cation-exchange mechanism. Hence, the aqueous-phase acidity used throughout the studies was 1×10^{-3} M HNO_3.

Adsorption Kinetics

The amount of U(VI) adsorbed (mg g−1 of SIR) as a function of time was evaluated. U(VI) (10 mg) was shaken for 1.0, 2.0, 5.0, 10.0, 15.0, and 20.0 min. with the SIR and the amount adsorbed (q) was determined. At an equilibrium time of 25

min., the amount of U(VI) adsorbed was q_e. The time required for the SIR to attain 50% sorption of U(VI) under the experimental conditions is the loading half-time ($t_{1/2}$). From Figure 1, it is clear that the $t_{1/2} < 1.0$ min.

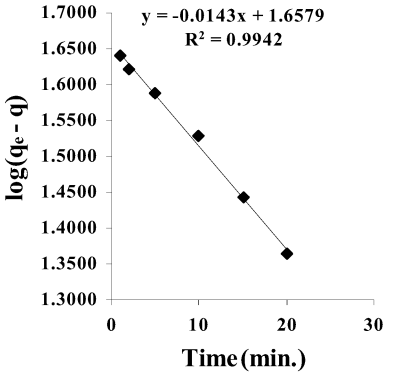

Figure 1. Adsorption kinetics.

Adsorption Isotherm

A 20 cm^3 solution containing 50-2500 mg dm^{-3} of U(VI) and SIR was shaken in a stoppered bottle on a mechanical shaker for an equilibrium time of 10 min. The resin was then filtered, and the residual solution was analyzed for U(VI).

The experimental data were treated using both Langmuir and Freundlich models for adsorption isotherms. The rearranged Langmuir equation is

$$\frac{C_e}{q_e} = \frac{1}{q_o^b} + \frac{C_e}{q_o}$$

where C_e is the equilibrium concentration (mg dm^{-3}), q_e is the amount adsorbed at equilibrium, and q_0 and b are Langmuir constants related to adsorption capacity and energy of adsorption, respectively. The Freundlich equation is represented as follows:

$$\log\left(\frac{x}{m}\right) = \log K_f + \left(\frac{1}{n}\right)\log C_e$$

where x/m is the amount of metal adsorbed per unit mass of solid support, Freundlich's constants K_f is the measure of adsorption capacity, and $1/n$ is adsorption intensity. The plots of C_e/q_e vs. C_e and $\log(x/m)$ vs. $\log C_e$ indicated that the adsorption of U(VI) on Cyanex 302 impregnated XAD-2 resin obeys Langmuir as well as Freundlich adsorption models (Figures 2 and 3). The correlation coefficients (R^2) for the linear regression fit of the Langmuir and Freundlich plots were 0.9944 and 0.9942 respectively while the values for q_0, b, K_f, and n were 11.82, 0.4437, 1.97, and 4.2, respectively.

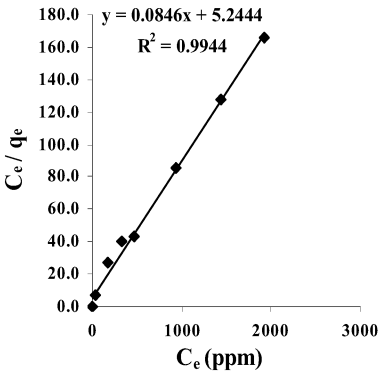

Figure 2. Langmuir isotherm.

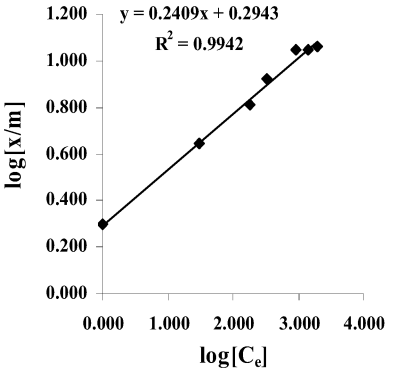

Figure 3. Freundlich isotherm.

Sorption Capacity of SIR

A 20 cm^3 sample of aqueous phase containing 1-50 mg U(VI) was shaken with 100 mg of SIR. The amount of U(VI) sorbed was evaluated from analysis of the aqueous phase for U(VI). Maximum sorption capacity for U(VI) was 116 mg g^{-1}, which is much higher than that obtained with other modified XAD series resins [1] (Figure 4).

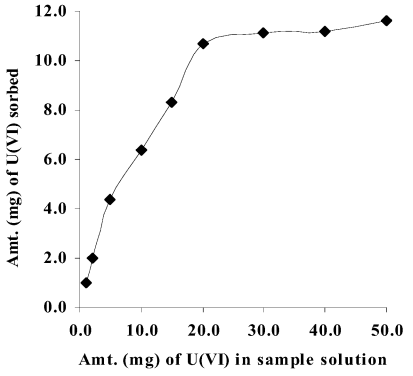

Figure 4. Sorption capacity of modified support for U(VI).

Sorption of U(VI) by Column or Dynamic Method

A glass column was packed with impregnated resin as reported earlier [4]. A 50 cm^3 sample solution containing U(VI) in 1 x 10^{-3} M HNO_3 was passed through the column at an aqueous phase flow rate of 10.0 cm^3 $min.^{-1}$ and eluted with 10.0 cm^3 of 1.0 M HCl.

Amberlite XAD-2 impregnated with Cyanex 302 (SIR) had good stability and reusability as reported earlier [5]. A column containing the SIR was checked for leakage of Cyanex 302 after using it continuously for a certain number of runs. Cyanex 302 loaded resin was then completely eluted and its amount was determined

as described in the literature [7]. Using the column 35 times, resulted in 99.1% sorption of U(VI). After 65 runs, the amount of Cyanex 302 loaded on column decreased by 8.8 mg, and consequently, the resulting sorption of U(VI) was also lower (97.8%).

These studies indicate that the same column can be used several times. Hence, under these dynamic conditions, the SIR was applied for the recovery of U(VI) from real samples.

Analytical Applications

Uranmicrolite Ore Tailings

A sample of 0.5 g of the dried uranmicrolite tailings was fused with 3 g of KOH pellets in a nickel crucible for 20 minutes. The fused mass was cooled and extracted with dilute HNO_3, filtered, and diluted to 100 cm^3 [8]. After appropriate dilution, a known aliquot of this sample, which also contained 195.0, 232.5, and 206.5 µg of Nb^{5+}, Ta^{5+}, and Sb^{3+}, respectively, when passed through the column, resulted in 99.4% recovery of U(VI). During the sorption of U(VI) under its optimum sorption conditions, the amount of these matrix elements was much below their tolerance limit, defined as the amount of element causing ±2.0% change in the recovery of U(VI). As Nb^{5+}, Ta^{5+}, and Sb^{3+} were tolerated up to 500, 500, and 1000 µg respectively, they were not detected in the stripped phase and thus separated from U(VI). The amount of U(VI) found by proposed method was 51.3 ± 0.3 mg g^{-1} as against 51.6 mg g^{-1} present in the tailings.

Industrial Effluent

A sample of industrial effluent was first passed through a 0.45 µm membrane filter and an aliquot (0.5 cm^3) from this filtered sample was treated to eliminate interference of iron by extraction [9] and thorium by masking with EDTA. The sample when passed through the column as per the general procedure for sorption of U(VI) resulted in 99.6% recovery of U(VI). Rare earth elements (REEs), namely, Dy^{3+}, Gd^{3+}, Nd^{3+}, La^{3+}, Pr^{3+}, Yb^{3+}, and Ce^{4+} detected in the aqueous phase were 24.2, 4.5, 2.1, 3.0, 0.6, 65.4, and 5.0 µg, respectively. Dy^{3+}, Gd^{3+}, Nd^{3+}, La^{3+}, Pr^{3+}, Yb^{3+}, and Ce^{4+} were not sorbed on the column, as Nd^{3+}, Pr^{3+}, Yb^{3+}, and Ce^{4+} could be tolerated at the same concentration as that of U(VI), while Dy^{3+}, La^{3+}, and Gd^{3+} were tolerated up to 0.1, 0.1, and 0.06 mg level, respectively. This may be attributed to the better complexing ability of Cyanex 302 for U(VI) in comparison to the REEs. Consequently, the REEs which were present in the sample well below their tolerance limits for U(VI), were separated from it during its sorption. These results were crosschecked with ICP-AES, which confirmed that the REEs were quantitatively present in the aqueous phase, while in the stripped phase, they were below detection limits. U(VI) recovered was 58.6 ± 0.1 mg dm^{-3} by the proposed method as against 58.8 mg dm^{-3} present in the effluent sample. These results compare well when crosschecked with those obtained by ICP-AES determination.

CONCLUSIONS

The solid phase based upon the impregnation of Cyanex 302 on XAD-2 is simple, selective, and reliable for separation of traces of U(VI) from other associated elements. The recovery of U(VI) was achieved using 1.0 M HCl. The modified resin has fast sorption kinetics, high sorption capacity for U(VI), and applicability for isolation of U(VI) from rare earths and wastes.

REFERENCES

1. T. P. Rao, P. Metilda, and J. M. Gladis, "Preconcentration techniques for uranium(VI) and thorium(IV) prior to analytical determination-an overview," *Talanta*, **68**, 1047-1064 (2006).
2. S. Seyhan, M. Colak, M. Merdivan, and N. Demirel, "Solid phase extractive preconcentration of trace metals using *p-tert*-butylcalix[4]arene-1,2-crown-4-anchored chloromethylated polymeric resin beads," *Anal. Chim. Acta*, **584**, 462-468 (2007).
3. H. Matsunaga, A. A. Ismail, Y. Wakui, and T. Yokoyama, "Extraction of rare earth elements with 2-ethylhexyl hydrogen 2-ethylhexyl phosphonate impregnated resins having different morphology and reagent content," *React. Funct. Polym.*, **49**, 189-195 (2001).
4. A. I. Vogel, A text book of Quantitative Inorganic Analysis, 3rd ed. Longman, London, 1962; p. 540.
5. M. Karve and R. V. Rajgor, "Amberlite XAD-2 Impregnated with Cyanex 302 for Separation of Traces of Thorium(IV)," *Sep. Sci. Technol.*, **42**, 2255-2273 (2007).
6. F. D. Snell, Photometric and Fluorimetric Method of Analysis, Part II, John Wiley and Sons, New York, 1978; p. 1356.
7. J. L. Cortina, N. Miralles, A. Sastre, M. Aguilar, A. Profumo, and M. Pesavento, "Solvent-impregnated resins containing di-(2,4,4-trimethylpentyl)phosphinic acid I. Comparative study of di-(2,4,4-trimethylpentyl)phosphinic acid adsorbed into Amberlite XAD-2 and dissolved in toluene," *React. Polym.,* **21**, 89-101 (1993).
8. W. F. Hillebrand and G. E. F. Lundell, Applied Inorganic Analysis of Metal, Minerals and Rocks, John Wiley and Sons, New York, 1953; p. 593.
9. A. K. De, S. M. Khopkar, and R. A. Chalmers, Solvent Extraction of Metals, Van Nostrand Reinhold, London, 1970; p. 259.

HOLLOW-FIBER SUPPORTED LIQUID MEMBRANE (HFSLM) FOR THE SEPARATION OF LANTHANIDES AND ACTINIDES

P. K. Mohapatra,[1] C. B. Patil,[2] S. A. Ansari,[1] A. Bhattacharyya,[1] and V. K. Manchanda[1]

[1]*Radiochemistry Division, B.A.R.C., Trombay, Mumbai-400085, INDIA.*
[2]*PREFRE Lab, N.R.G., B.A.R.C., Tarapur, Maharashtra-401502, INDIA.*
Corresponding author email address: vkm@barc.gov.in

ABSTRACT

The transport behavior of Nd(III) was investigated using hollow-fiber supported liquid membranes (HFSLM) from an acidic feed solution using N,N,N'N'-tetraoctyldiglycolamide (TODGA) in normal paraffinic hydrocarbon (NPH) as the carrier. Near quantitative transport (>99%) of Nd(III) from 500 mL of feed containing 1 g/L Nd in 3.5 M HNO_3 was possible in about 45 minutes. Quantitative transport time increased when the volume or Nd(III) concentration in the feed was increased. The liquid membrane had excellent stability as indicated by eight consecutive runs that gave consistent transport rates. The HFSLM data using Cyanex-301 in *n*-dodecane as carrier extractant for the lanthanide–actinide separation with the feed solution 1 M $NaNO_3$ at pH 3.5 and stripping solution 0.01 M EDTA at a pH 3.5 were promising.

INTRODUCTION

Though solvent extraction has a wider acceptability due to its rapidity, ease of operation, and large throughputs, it requires high solvent inventory and large-size contactors and is power intensive. Moreover, the use of toxic and inflammable solvents causes a great deal of concern towards industrial and personnel safety. Separation methods with low solvent inventory are rapidly gaining popularity over the past few decades. Amongst them, liquid membrane (LM) based techniques are particularly attractive, as they involve much lower inventory of organic extractants and solvents [1]. Among the LM methods, the one involving microporous hollow-fiber supported liquid membranes (HFSLM) is particularly popular due to advantages like large surface-to-volume ratio, faster mass-transfer rates (as compared to flat-sheet SLMs), continuous flow, and possibility of simultaneous extraction and stripping [2-4]. The major disadvantage of the HFSLM method is its stability [5], which prompted many research groups to carry out studies in the nondispersive extraction mode [6,7]. However, our recent studies involving flat-sheet supported liquid membranes have indicated diluent properties to be one of the major factors deciding the membrane stability [8,9]. In studies that involved *n*-dodecane as the diluent, exceptionally high stability of the SLM was observed. It was therefore imperative to extend such studies to the HFSLM mode and to

investigate both the transport efficiency as well as membrane stability. TODGA (N,N,N'N'-tetraoctyldiglycolamide) and Cyanex-301 ((bis(2,4,4-trimethylpentyl) dithiophosphinic acid) have been reported to be very effective for actinide partitioning and Ln-An separation, relevant in radioactive waste management [10,11]. In the present paper, two HFSLMs were examined using TODGA and Cyanex-301 as carriers for the transport of Nd(III) from nitric acid and selective transport of Am(III) from a mixture of lanthanide(III) ions, respectively.

EXPERIMENTAL

Materials

N,N,N′,N′-tetraoctyl-3-oxapentane diamide (TODGA) was synthesized following a reported procedure [11] and was characterized by elemental analysis and NMR as well as IR spectroscopy. Commercial Cyanex-301 (Cytec Canada Inc.) was purified by the reported method [12], and the purity (>99.9%) was checked by ^{31}P-NMR, GC-MS, and elemental analysis. Sulphanilic acid was procured from Sisco Research Laboratory (SRL), Mumbai and was used as received. Rare earth oxides (>99.99%), obtained from Alpha Biochem, were used in the studies involving macro concentrations of the lanthanides. All the other reagents were of AR grade and were used without further purification.

^{152,154}Eu was procured from the Board of Radiation and Isotope Technology (BRIT), Mumbai, India. All other lanthanide tracers were prepared by neutron activation of the respective spec-pure oxides. Concentrations of radiotracers ^{241}Am, ^{140}La, ^{152,154}Eu, ^{160}Tb, ^{166}Ho, ^{175}Yb, and ^{177}Lu were measured using HPGe gamma ray spectrometry.

Hollow-Fiber Supported Liquid Membrane Studies

A 28.25 cm long Liqui-Cel® hollow-fiber module (procured from Alting, France) with 6.65 cm diameter was employed in the present studies. The total effective surface area was 1.4 square meters with ~10,000 fibers. The specifications of the hollow-fiber module used in the present work are summarized in Table 1. The HFSLM was prepared by pumping the ligand solution (0.1 M TODGA or 0.5 M Cyanex-301 in NPH; ~20 mL volume held in the pores) through the lumen side of module for 30 minutes at a pressure of 3 psi in recycling mode. The leftover TODGA solution was flushed out by passing distilled water through both the shell as well as the lumen side. The feed solution was passed through lumen side, while the receiver solution was passed through the shell side of the module in all the experiments. The flow rates of the feed and receiver solutions were maintained constant at 200 mL/min with the help of gear pumps equipped with precise flow control (Cole-Parmer, USA). A schematic of the HFSLM set up is shown in Figure 1.

Table 1. Specifications of the hollow-fiber Liqui-Cel X50 (2.5 x 8 Membrane Contactor)

Parameter	Specification
Fiber type	Polypropylene
Number of fibers	9950
Fiber internal diameter (μm)	240
Fiber outer diameter (μm)	300
Fiber wall thickness (μm)	30
Effective pore size (μm)	0.03
Porosity (%)	40
Tortuosity	2.5
Effective fiber length (cm)	15
Effective surface area (m^2)	1.4

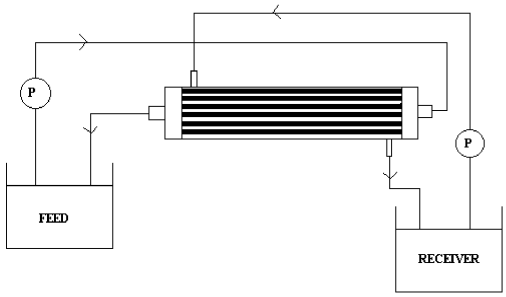

Figure 1. Schematic representation of the HFSLM set-up used in the present work.

RESULTS AND DISCUSSION

Transport of Neodymium from HNO_3 Solution

Transport of Nd(III) from nitric acid solution was studied on the liter scale (feed volume varying in the range 0.5–6.5 L, while the receiver phase volume was 0.5 L) using the HFSLM made from TODGA in NPH while operating in the recycling mode. The transport efficiency was the highest (quantitative transport was achieved in <45 minutes) when the feed as well as the receiver phase volumes were equal at 0.5 L (Figure 2). Increasing the feed volume (at a constant receiver phase volume of 0.5 L) to 1, 2, and 6.5 L resulted in lower transport (viz. 84%, 80%, and 20%, respectively) after 45 minutes. In all cases, a plateau was observed (Figure 2), and quantitative (>99%) mass transfer was not possible. This was ascribed to significant acid transport from the feed to the receiver side. As evident from Table 2, the acid-transport rate increased with increasing feed acidity. Though the receiver phase acidity was about 0.7 M after 60 minutes of operation for a feed acidity of 3.5 M at a feed:receiver volume ratio of 1, the same was found to be >2.5 M when the volume ratio increased to 13. Increasing Nd concentration also resulted in a decrease in transport rates.

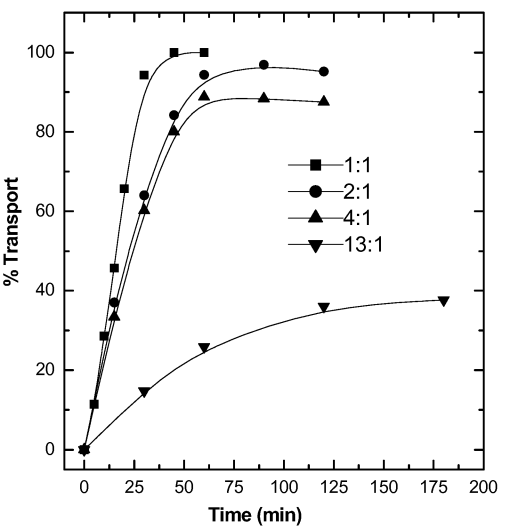

Figure 2. Nd(III) transport (in %) as a function of feed:receiver phase ratio. Carrier: 0.1 M TODGA in NPH. Feed: 1 g/L Nd in 3.5 M HNO_3. Receiver: distilled water.

Table 2. Permeation of acid from feed to the receiver side through HFSLM module*

Time (min.)	Nitric acid transport (M)				
	Feed: 0.5 M	Feed: 1 M	Feed: 2 M	Feed: 3.5 M	Feed: 6 M
0	0.00	0.00	0.00	0.00	0.00
5	0.01	0.01	0.07	0.03	0.15
10	0.01	0.03	0.11	0.20	0.21
20	0.01	0.05	0.13	0.34	0.34
30	0.02	0.06	0.21	0.54	0.50
45	0.02	0.07	0.25	0.63	0.66
60	0.03	0.09	0.32	0.70	0.95

*Feed: 1 g/L Nd. Receiver: distilled water. Volume ratio = 1.

Lanthanide-Actinide Separation

We have reported the separation of lanthanides from actinides using flat-sheet SLMs containing Cyanex-301 in *n*-dodecane as the organic carrier [13]. However, in order to increase the throughput, an attempt was made in the present work using the HFSLM method. The transport of Am(III) and some lanthanides was measured by spiking tracers such as ^{241}Am, ^{140}La, ^{152,154}Eu, ^{160}Tb, ^{166}Ho, ^{175}Yb, and ^{177}Lu into the feed solution containing 1 g/L rare earth carriers. Table 3 shows the increase in Am transport at 2 and 10 minutes. It also showed the relatively insignificant transport of the rare earth elements. Amongst the lanthanides, Eu had the lowest transport (0.17% in 10 minutes) compared to the others (< 2% in 10 minutes). Exact reasons for low transport rates for Eu are not known. The receiver solution sampled after 10 minutes indicated near quantitative transport (>99%) of Am with almost negligible presence of the rare earth tracers. The DF values for Am with respect to the corresponding rare earth elements were comparable to those reported earlier for the flat-sheet SLM studies [13]. DF values invariably increased with the transport time. An average DF value of 90 was obtained after 10 minutes. From the transport data obtained as a function of time (Table 3 lists % transport at 2 and 10 minutes), it is clear that better decontamination may be achieved at low contact times.

Table 3. Transport data of trivalent actinide (Am^{3+})/lanthanide ions and the respective decontamination factors (DFs) with respect to the lanthanide ions*

M^{3+}	%*T* (2 min.)	%*T* (10 min.)
Am^{3+}	46.7	98.9
La^{3+}	0.82	1.2
Eu^{3+}	0.11	0.17
Ho^{3+}	1.36	1.41
Yb^{3+}	0.87	1.94
Lu^{3+}	0.99	1.2

*Note: [Cyanex-301] = 0.5 M; [Am] ~ 7-10 M; [lanthanides] = 1 g/L.

Stability of HFSLM

The long-term stability of the HFSLM is important from the standpoint of its industrial application. For such a stability test, the module was impregnated once with the carrier solution, and the system was run continuously for the transport of Nd(III) from a solution containing 1 g/L Nd at 3.5 M HNO_3 in eight successive cycles. The permeability of Nd^{3+} was measured for 45 min., and after this period of time, the depleted feed and enriched receiver solutions were replaced with fresh ones. From the data reported in Figure 3, it can be observed that the Nd transport was reproducible within the error limit in all the eight runs. In the present work, TODGA being a weakly surface-active carrier, a prerequisite for stability of HFSLM is that the inside and outside hydraulic pressure are balanced, though our study was restricted to only several successive cycles of continuous operation.

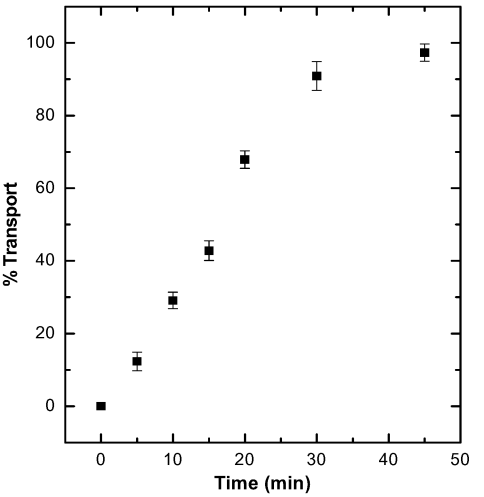

Figure 3. Plot of mean transport rate (in %) for Nd(III) for eight successive runs. Carrier: 0.1 M TODGA in NPH. Feed: 1 g/L Nd in 3.5 M HNO_3. Receiver: distilled water. Volume ratio = 1.

CONCLUSIONS

The hollow-fiber supported liquid membrane technique appears promising for metal ion recovery and separation at the back end of the nuclear fuel cycle. Both actinide partitioning as well as lanthanide–actinide separation, key steps in radioactive waste management, were successfully carried out in lab scale. It will be interesting to devise a simultaneous separation process combining both these processes and also to scale up to pilot scale.

REFERENCES

1. P. K. Mohapatra and V. K. Manchanda, "Liquid Membrane Based Separations of Actinides and Fission Products," *Ind. J. Chem.,* **42A**, 2529-2538 (2003).
2. P. R. Alexander and R. W. Callahan, "Liquid-liquid extraction and stripping of gold with microporous hollow-fibers," *J. Membr. Sci*., **35**, 57-71 (1987). C. H. Yun, R. Prasad, A. H. Guha, and K. K. Sirkar, "Hollow-fiber solvent extraction removal of toxic heavy metals from aqueous waste streams," *Ind. Eng. Chem. Res*., **32**, 1186-1195 (1993).
3. A. K. Pabby, R. Haddad, F. J. Alguacil, and A. M. Sastre, "Improved kinetics-based gold cyanide extraction with mixture of LIX79 + TOPO utilizing hollow-fiber membrane contactors," *Chem. Eng. J.*, **100**, 11-22 (2004).

4. I. J. Youri, P. J. Harrington, and G. W. Stevens, "Long-term performance of hollow-fiber membrane solvent extraction modules used for Cr(VI) recovery from electroplating rinse water," *Solvent Extr. Ion Exch*., **18,** 933-951 (2000).
5. A. Geist, M. Weigl, and K. Gompper, "Minor actinide partitioning by liquid-liquid extraction: Using a synergistic mixture of bis(chlorophenyl)-dithiophosphinic acid and TOPO in a hollow-fiber module for americium(II)-lanthanides (III) separation," *Sep. Sci. Technol.,* **37**, 3369-3390 (2002).
6. A. Geist, M. Weigl U. Muellich, and K. Gompper, "Application of novel extractants for actinide (III)/lanthanide (III) separation in hollow-fiber modules," *Membr. Technol*., **5**, 5-7 (2003).
7. P. K. Mohapatra, D. S. Lakshmi, D. Mohan, and V. K. Manchanda, "Selective Membrane Transport of Cesium Using Di-*t*-butyl benzo 18 crown 6 as the carrier," *J. Membr. Sci*., **232,** 133-140 (2004).
8. S. A. Ansari, P. K. Mohapatra, and V. K. Manchanda, "Transport of americium(III) through a supported liquid membrane containing N,N,N',N'-tetraoctyl-3-oxapentanediamide (TODGA) in dodecane as the carrier," *J. Membr. Sci*., **282,** 133-141(2006).
9. Y. Zhu, J. Chen, and R. Jiao, "Extraction of Am(III) and Eu(III) from nitrate solution with purified Cyanex-301," *Solvent Extr. Ion Exch.*, **14**, 61-67 (1996).
10. Y. Sasaki, Y. Sugo, S. Suzuki, and S. Tachimori, "The novel extractants diglycolamides for the extraction of lanthanides and actinides in HNO_3-*n*-dodecane system," *Solvent Extr. Ion Exch*., **19,** 91-103 (2001).
11. Y. Zhu, J. Chen, and R. Jiao, *Solvent Extr. Ion Exch*., **14,** 61 – 69 (1996).
12. A. Bhattacharyya, P. K. Mohapatra, and V. K. Manchanda, "Separation of Trivalent Actinides and Lanthanides Using a Flat Sheet Supported Liquid Membrane Containing Cyanex-301 as the Carrier," *Sep. Purif. Technol*., **50**, 278–281(2006).

CARRIER-MEDIATED TRANSPORT OF ACTINIDE IONS USING SUPPORTED LIQUID MEMBRANES CONTAINING TODGA AS THE CARRIER EXTRACTANT

S. Panja,[1] P. K. Mohapatra,[2] A. Dakshinamoorthy,[1] S. K. Munshi,[1] P. K. Dey,[1] and V. K. Manchanda[2]

[1]*Fuel Reprocessing Division, B.A.R.C., Trombay, Mumbai-400085, INDIA.*
[2]*Radiochemistry Division, B.A.R.C., Trombay, Mumbai-400085, INDIA.*
Corresponding author email address: vkm@barc.gov.in

ABSTRACT

The transport behavior of Pu^{3+} under varying reducing conditions was investigated from a feed containing 3.0 M HNO_3 into a receiver phase containing 0.1 M HNO_3 using TODGA (N,N,N'N'-tetraoctyldiglycolamide) as the carrier ligand. A mixture of 0.2 M hydroxyl ammonium nitrate and 0.2 M hydrazinium nitrate (used in the feed as the reducing agent) has been found to be effective for quantitative (>99%) transport of the trivalent Pu in about 3 h. Transport of trivalent plutonium in 3 h (>99%) was higher as compared to that of the tetravalent plutonium (94%), though their *D* values followed an opposite trend. The permeability coefficient (*P*) of Pu^{3+} was $(4.63 \pm 0.26) \times 10^{-3}$ cm/s as compared to $(2.10 \pm 0.14) \times 10^{-3}$ cm/s for Pu^{4+} and $(3.67 \pm 0.06) \times 10^{-3}$ cm/s Am^{3+}. *P* values of trivalent actinide ions such as Am^{3+}, Pu^{3+}, and Cm^{3+} are compared with their distribution data.

INTRODUCTION

"Actinide partitioning" is emerging as the strategy for the removal of minor actinides from high level waste (HLW) prior to the burial of the latter in the form of vitrified blocks. Several processes for actinide partitioning (viz., TRUEX, TRPO, DIDPA, and DIAMEX) utilizing the reagents such as octyl(phenyl)*N*,*N*-diisobutylcarbamoylmethylphosphine oxide (CMPO), trialkylphosphine oxide (TRPO), diisodecylphosphoric acid (DIDPA), and N,N′,N,N′-dimethyldibutyltetradecylmalonamide (DMDBTDMA), respectively, have been developed and tested at various laboratories [1-4]. Though all these extractants have shown great promise, tetraalkylmalonamides (or diamides) have been found to be particularly promising in view of their improved back-extraction properties towards Am^{3+}/Cm^{3+}, their complete incinerability, and the innocuous

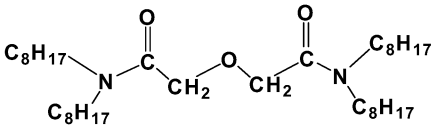

Figure 1. N,N,N',N'-Tetraoctyldiglycolamide (TODGA).

nature of their radiolytic degradation products (mainly carboxylic acids and amines) that can be easily washed out [5-7]. To increase the efficiency of the diamide-based extractants, several structural modifications have been attempted. One such modification leading to the introduction of one etheric oxygen in between the two amide groups (diglycolamide) caused significant enhancement in the extraction efficiency of minor actinides due to their tridentate nature [8]. Amongst the various extractants suggested for actinide partitioning, TODGA (N,N,N',N'-tetraoctyldiglycolamide, Figure 1) appears to be one of the most promising, due to its exceptional ability to extract trivalent actinides from the nitric acid medium. However, in order to reduce ligand inventory, membrane-based methods are becoming increasingly popular. Supported liquid membranes using TODGA as the carrier have been evaluated for Am^{3+} transport from acidic solutions as well as from synthetic HLW [9,10]. The present work deals with the transport behaviour of Pu in different oxidation states such as tri-, tetra-, as well as hexa-valent states from the HNO_3 medium. A comparison is also made with the transport behaviour of Am^{3+} and Cm^{3+}.

EXPERIMENTAL

N,N,N',N'-tetraoctyl diglycolamide (TODGA) was synthesized by slight modification of an earlier method [11]. Characterization of TODGA was done by elemental analysis and NMR and IR spectroscopy. PTFE membranes used in the present study were procured from Sartorius, Germany. All the other reagents were of AR grade and were used without further purification.

Solvent Extraction Studies

In the solvent-extraction studies, solutions of desired concentration of TODGA prepared in *n*-dodecane were employed after pre-equilibration at respective acidities. The oxidation states of Pu (mainly ^{239}Pu) were maintained as reported earlier [12,13]. The oxidation states of Pu^{4+} and PuO_2^{2+} were adjusted using $NaNO_2$ and AgO, respectively [12,13], while reduction to Pu^{3+} was carried out using several reducing agents, as discussed below. Equal volumes of the organic and aqueous phases (containing the requisite quantity of Pu tracer) were equilibrated in a rotary thermostated water bath for an hour at 25.0 ± 0.2 ^{o}C. The two phases were then centrifuged and assayed by taking suitable aliquots from both the phases. The distribution ratio (*D*) is defined as the ratio of concentration of metal ion in the organic phase to that in the aqueous phase.

Transport Studies

The SLM studies were carried out at ambient temperature using 25 mL glass transport cells with feed and strip solutions stirred at 200 rpm [14] using a high-speed magnetic stirrer equipped with precise speed control. The stirring rate of 200 rpm was set to ensure minimal thickness of the aqueous boundary layers without obstructing the membrane phase. The microporous PTFE membrane filters (pore size, 0.2 micron; porosity, 64%; thickness, 80 microns; tortuosity, 1.48) were soaked in the carrier solution

(0.1 M TODGA in *n*-dodecane) for about 10 minutes prior to use. Effective transport area was 3.12 cm^2, which was used for permeability calculations.

Assay of Pu, Am, and Cm in the feed as well as in the receiver side was done at different time intervals using alpha liquid scintillation counting to calculate the permeability coefficients as per our earlier report [14] using the following equation:

$$\ln(C_{f,t}/C_{f,o}) = -(Q/V)\,P\,t \quad (1)$$

where $C_{f,t}$ and $C_{f,o}$ are the concentrations of metal ion in the feed side at a given time interval and at the start of the experiment, respectively. Q is the effective membrane area, V is the volume of the feed solution in cm^3, and t is the permeation time. The cumulative percent transport ($\%T$) at a given time is determined by the following equation,

$$\%T = 100 \cdot (C_{f,o} - C_{f,t}) / C_{f,o} \quad (2)$$

The material balance in these studies was found to be within ±5%.

RESULTS AND DISCUSSION

Solvent-Extraction Studies

Extraction of Pu^{4+} and PuO_2^{2+} from nitric acid medium using 0.1 M TODGA was carried out, and the respective D values were found to be 56 and 1.62. In order to adjust the valency state to +3, several reducing agents (viz., ascorbic acid, hydroxylammonium nitrate (HAN), hydrazinium nitrate (HN), and phenylhydrazine) were evaluated at two different concentrations (0.01 M and 0.1 M). The D_{Pu} values obtained using 0.1 M TODGA in *n*-dodecane are listed in Table 1. As evident from the data, L-ascorbic acid was found to be a far superior reductant (D value for Am^{3+} is reported to be close to 200 [9] for 3 M HNO_3 and 0.1 M TODGA, and a similar value is expected for Pu^{3+}) as compared to the other three. However, as will be seen below, ascorbic acid has a poor stability in nitric acid, and phenyl hydrazine was used for best transport results.

Transport Studies

Figure 2 shows the effect of several reducing agents on Pu^{3+} transport (reducing agent was added one hour prior the transport experiments) from 3 M nitric acid using 0.1 M TODGA as the carrier. In contrast to the data obtained from the extraction studies, the transport studies have indicated poor transport with ascorbic acid. This was ascribed to the instability of the reducing agent under the feed 3 M nitric acid concentration. On the other hand, phenyl hydrazine was found to result in faster transport, indicating its usefulness as the reducing agent. The transport rates for Pu^{3+} were comparable to those reported by us for Am^{3+} transport under identical conditions [10]. The permeability coefficient values were calculated and are listed in Table 2. As expected from the transport data presented in Figure 2, the P values were the highest when phenyl hydrazine was used as the reducing agent (Table 2).

Table 1. Distribution ratio of Pu^{3+} using different reducing agents at 0.1 M and 0.01 M.

Reducing agent	D_{Pu}	
	Concentration (0.01 M)	Concentration (0.1 M)
L-Ascorbic Acid	78	150
Hydroxyl ammonium nitrate	64	96
Hydrazinium nitrate	75	91
Phenyl Hydrazine	79	94

Note: Organic phase: 0.1 M TODGA in *n*-dodecane. Aqueous phase: 3 M HNO_3.
Contact time: 1 h.

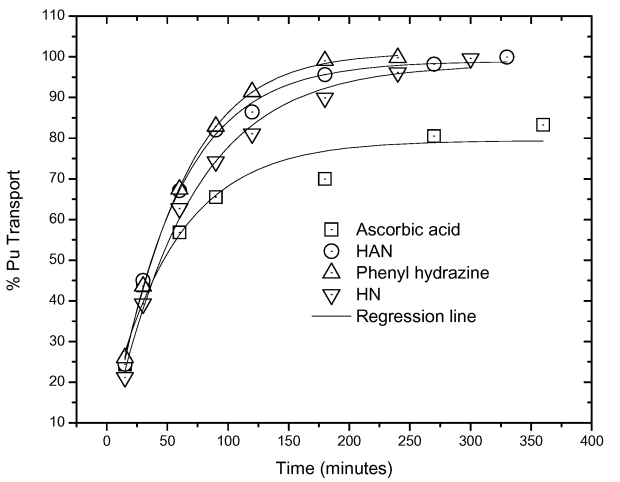

Figure 2. Effect of various reducing agents on Pu3+ transport.
Carrier: 0.1 M TODGA in dodecane. Feed: 3 M nitric acid. Receiver: water.

Table 2. Permeability coefficient data for Am^{3+}, Cm^{3+}, Pu^{3+}, Pu^{4+}, and PuO_2^{2+} from 3 M nitric acid using 0.1 M TODGA in *n*-dodecane

Reducing agent	*P* (cm/s) for Pu^{3+}	Metal ion	*P* (cm/s)
Ascorbic acid	$(1.67 \pm 0.24) \times 10^{-3}$	Pu^{3+}	$(4.63 \pm 0.26) \times 10^{-3}$
HAN	$(3.19 \pm 0.32) \times 10^{-3}$	Am^{3+*}	$(3.67 \pm 0.06) \times 10^{-3}$
Phenyl hydrazine	$(4.63 \pm 0.26) \times 10^{-3}$	Cm^{3+}	$(6.69 \pm 0.27) \times 10^{-3}$
HN	$(2.12 \pm 0.07) \times 10^{-3}$	Pu^{4+}	$(2.10 \pm 0.14) \times 10^{-3}$
--	--	PuO_2^{2+}	$(2.05 \pm 0.06) \times 10^{-4}$

*Data taken from ref. [9].

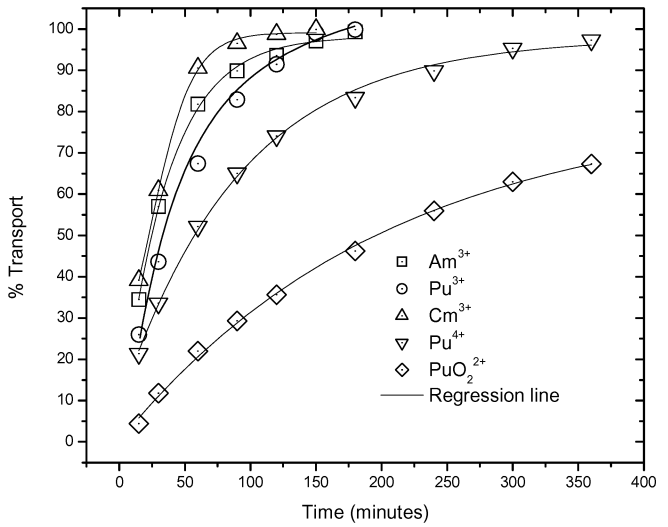

Figure 3. Transport rates of several actinide ions at different oxidation states. Carrier: 0.1 M TODGA in *n*-dodecane. Feed: 3 M nitric acid. Receiver: water

Figure 3 shows the percentage transport data for Pu^{3+}, Pu^{4+}, and PuO_2^{2+} from 3 M nitric acid feed solutions using 0.1 M TODGA in *n*-dodecane as the carrier ligand. Transport data for Am^{3+} as well as Cm^{3+} are also included in the figure for comparison purposes. As shown in the figure, the transport rates follow the order Cm^{3+} > Am^{3+} > Pu^{3+} > Pu^{4+} > PuO_2^{2+}. The transport rates of the trivalent ions such as Cm^{3+}, Am^{3+}, and Pu^{3+} follow their ionic potentials (defined as the ratio of charge to ionic radius for the given ion), which is also the order of their extractability with TODGA. However, Pu^{4+} extraction is reported here to be lower compared to Pu^{3+} extraction, and hence, the transport rates are lower. The permeability coefficients are calculated and listed in Table 2. Data on Am^{3+} and Cm^{3+} transport is also shown along with those obtained with Pu^{3+} for comparison purposes. As indicated in Table 2 and Figure 2, the valency state of Pu^{3+} was maintained satisfactorily. This was evident from *P* of Pu^{3+} which was comparable with that for Am^{3+}. It was reported earlier that quantitative Am^{3+} transport (in tracer scale) across an SLM containing TODGA in *n*-dodecane required nearly 3 hours. In the present study, quantitative (>99%) Pu^{3+} transport in the tracer scale required nearly 3 hours as well when phenyl hydrazine was used as the reducing agent. While Pu^{4+} required >6h for quantitative transport, only about 68% transport of PuO_2^{2+} was observed after a comparable time period. The slow transport of PuO_2^{2+} was ascribed to the lower extractability of the hexavalent actinide ions in a manner similar to UO_2^{2+}, reported earlier [10].

CONCLUSIONS

The transport data for trivalent plutonium obtained during the present studies compared well with those for Cm^{3+} (reported here) and Am^{3+} (reported earlier). The role of reducing agent assumes significance, as its stability and concentration play a very important role in Pu^{3+} transport. PuO_2^{2+} transport was much slower as compared to Pu^{3+} and Pu^{4+}, suggesting its similarity with the transport behaviour of UO_2^{2+} reported by us earlier.

REFERENCES

1. W. W. Schulz and E. P. Horwitz, "TRUEX process and the management of liquid TRU waste," *Sep. Sci. Techol.,* **23**, 1191-1210 (1988).
2. J. N. Mathur, M. S. Murali, P. R. Natarajan, L. P. Badheka, A. Banerji, A. Ramanujam, P. S. Dhami, V. Gopalkrishnan, R. K. Dhumwad, and M. K. Rao, "Partitioning of actinides from high-level waste streams of Purex process using mixtures of CMPO and TBP in dodecane," *Waste Manag.,* **13**, 317-325 (1993).
3. J. N. Mathur and M.S. Murali, "Use of a mixture of trpo and tbp for the partitioning of actinides from high-level waste solutions of purex origin and its comparison with cmpo and other phosphorus-based extractants," *Solvent Extr. Ion Exch.,* **19**, 61-77 (2001).
4. C. Cuillerdier, C. Musikas, P. Hoel, L. Nigond, and X. Vitart, "Malonamides as new extractants for nuclear waste solutions," *Sep. Sci. Techol.,* **26**, 1229-1244 (1991).
5. G. R. Mahajan, D. R. Prabhu, V. K. Manchanda, and L. P. Badheka, "Substituted malonamides as extractants for partitioning of actinides from nuclear waste solutions," *Waste Manag.,* **18**, 125-133 (1998).
6. C. Musikas, "Solvent extraction for the chemical separations of 5f elements," *Inorg. Chim. Acta*, **140**, 197-206 (1987).
7. C. Musikas and H. Hubart, "Extraction by N,N'-tetraalkylmalonamides. II. Extraction of metallic ions," *Solvent Extr. Ion Exch*., **5**, 877-893 (1987**)**.
8. H. Narita, T. Yaita, and S. Tachimori, "Extraction Behavior for Trivalent Lanthanides with Amides and EXAFS Study of their Complexes," In Solvent Extraction for the 21st Century, Proceedings of ISEC'99, Barcelona, Spain, July, 1999; Vol. 1 M. Cox, M. Hidalgo, and M. Valiente, Eds., Society of Chemical Industry, London, 2001; pp. 693-696.
9. S. A. Ansari, P. K. Mohapatra, D. R. Prabhu, and V. K. Manchanda, "Transport of Americium(III) through a supported liquid membrane containing N,N,N′,N′-tetraoctyl-3-oxapentane diamide (TODGA) in n-dodecane as the carrier," *J. Membr. Sci.,* **282**, 133-141 (2006).
10. S. A. Ansari, P. K. Mohapatra, D. R. Prabhu, and V. K. Manchanda, "Evaluation of N,N,N′,N′-tetraoctyl-3-oxapentane-diamide (TODGA) as a mobile carrier in remediation of nuclear waste using supported liquid membrane," *J. Membr. Sci.,* **298**, 169-174 (2007).
11. Y. Sasaki, Y. Sugo, S. Suzuki, and S. Tachimori, "The novel extractants diglycolamides for the extraction of lanthanides and actinides in HNO_3-n-dodecane system," *Solvent Extr. Ion Exch*., **19,** 91-103 (2001).
12. P. K. Mohapatra and V. K. Manchanda, "Role of ligand basicity and stereochemistry in the extraction of plutonium(IV) isoxazolonates," *Radiochim. Acta*, **91**, 705-712 (2003).
13. P. N. Pathak, D. R. Prabhu, and V. K. Manchanda, "The role of oxidants in Pu-Th separation studies employing di(2-ethylhexyl)isobutyramide (D2EHIBA) as extractant," *Radiochim. Acta*, **91**, 141-146 (2003).
14. S. Sriram, P. K. Mohapatra, A. K. Pandey, V. K. Manchanda, and L. P. Badheka, "Facilitated transport of americium(III) from nitric acid media using dimethyldibutyltetradecyl-1,3-malonamide," *J. Membr. Sci*., **177**, 163-171 (2000).

RECOVERY OF URANIUM FROM DILUTE SOLUTION USING LIQUID EMULSION MEMBRANE SYSTEM

S. Mukhopadhyay,[1] S. K. Ghosh,[1] and V. A. Juvekar[2]

[1]*Chemical Engineering Division, BARC, Mumbai, India 400085.*
[2]*Chemical Engineering, Department, IIT Bombay, Mumbai, India 400019.*
Corresponding author email address: sulekha@barc.gov.in

ABSTRACT

The liquid emulsion membrane (LEM) technique has great potential for application in the nuclear industry for large interfacial area, low consumption of organics, and high recovery from dilute streams. A LEM system composed DEHPA-kerosene-SPAN80-HNO_3 has been developed for recovery of uranium from dilute nitrate solution, which gives 98% extraction and 88% stripping in a single stage. An attempt has been made to understand the mechanism of the LEM process, in which phenomena like pertraction, occlusion, swelling, and leakage occur simultaneously. The effect of various parameters on these phenomena has been described with a mathematical model, which is able to explain the experimental findings.

INTRODUCTION

The field of liquid emulsion membrane (LEM) technology is currently undergoing a rapid expansion in the areas of research and industrial separation, which include isolation and concentration of substances, both valued and harmful, in the fields of separation processes, analytical processes, environmental remediation, detoxification in biological fields, etc. LEM process has been utilized in the separation of heavy metals, actinides, and rare earths from aqueous streams.

The LEM extraction process is carried out in four steps: i) emulsification/preparation of the primary emulsion, ii) extraction/pertraction, iii) settling/phase separation of the secondary emulsion, and iv) demulsification. Large interfacial area (1000-3000 m^2/m), high treat ratio (feed to *p*-emulsion), and high driving force due to simultaneous extraction and stripping leads to low inventory of solvents and high enrichment of the recovered solute. These are particularly impressive for recovery of solutes from low-concentration feed streams such as solvent-extraction raffinate for recovery of uranium and thorium.

The LEM technique has been tried by various workers for recovery of uranium, plutonium, and lanthanides from dilute secondary solutions [1-2]. Various carriers have been used for various feed streams. Hirato [3] has studied uranium extraction from

sulfate solution using TOA (tri-*n*-octylamine) as a carrier. TOPO has been used [4] for recovery of uranium from nitrate medium with sodium carbonate as strip.

Macasek et al. [5] used LEMs for concentration of uranium. It is important to note that none of these workers have used nitric acid as the stripping agent, which is the focus of the present experimental study, so that the concentrated uranyl nitrate can be directly recycled in the plant. In spite of encouraging potential in recovery and isolation of materials, LEM systems are limited by poor stability of the system under shear. Phenomena such as leakage, breakage, occlusion, and osmotic swelling of the emulsions results in contamination of the outer phase and dilution of the inner phase [6]. Understanding of the mechanism of the extraction, solute transport, swelling, and breakage are important in order to have an insight into the process based on which a system with high efficiency can be designed.

MATHEMATICAL MODEL

An attempt has been made to develop a mathematical model for the process of transfer of uranium though a LEM system composed of 1% v/v DEHPA and 3% v/v surfactant in kerosene emulsified in 2 M nitric acid at 3000 rpm speed. The composition of the system has been developed through experimental studies on LLX and pertraction of uranium.

The mathematical model is based on the following assumptions.

1. A globule is viewed as a sphere with the internal phase as core surrounded by the membrane layer in the form of a shell, assuming substantial circulation of the droplets inside the emulsion globules and also a significant coalescence.
2. The volume of the internal phase changes with time due to occlusion of the external phase and the leakage of the internal phase, while the volume of the membrane phase is constant. This results in variation of the membrane thickness with time. This affects both the rate of occlusion as well as leakage.
3. Occlusion occurs due to deformation of the membrane. The rate of occlusion is assumed to be directly proportional to the thickness of the membrane.
4. Leakage occurs due to rupture of the membrane covering cavities. The rate of leakage is assumed to be inversely proportional to the thickness of the membrane.
5. The concentration gradients of DEHPA and DEHPA-uranium complex exist only in the membrane phase. Both the core and the external phases are assumed to be well mixed and do not offer mass-transfer resistance.

The rate of change of uranium in the internal phase is caused by three modes: permeation mediated by DEHPA, occlusion, and leakage. The rate of permeation of uranium across the membrane can be written as

$$r_U = k_u \left(\frac{t^0}{t} \right) \left([U]_{me} - [U]_{mi} \right) A \qquad (1)$$

The rate of occlusion and leakage are, respectively

$$r_a = k_a\left(\frac{t}{t^0}\right)[U]_e A \tag{2}$$

$$r_\ell = -k_\ell\left(\frac{t^0}{t}\right)[U]_a A \tag{3}$$

The equation describing the buildup of uranium in the internal phase can therefore be written in terms of rate of change of uranium concentration in the external phase (U_e) as

$$-V_e\frac{d}{d\theta}\left([U]_e\right) = k_u A\left(\frac{t^0}{t}\right)\left([U]_{me} - [U]_{mi}\right) - k_\ell A\left(\frac{t^0}{t}\right)[U]_i + k_a A\left(\frac{t}{t^0}\right)[U]_e \tag{4}$$

Equation 4 can be derived as

$$-\frac{dU_e}{d\theta} = \left(\frac{3}{R^0}\right)\frac{\psi_s^{2/3}}{T_r(1-\varphi_m)}\left[\begin{array}{l} k_u\left[\frac{\psi_s^{1/3}-(\psi_s-\varphi_m)^{1/3}}{1-(1-\varphi_m)^{1/3}}\right]^{-1}(U_{me}-U_{mi}) + k_a\left[\frac{\psi_s^{1/3}-(\psi_s-\varphi_m)^{1/3}}{1-(1-\varphi_m)^{1/3}}\right]U_e \\ -k_\ell T_r\frac{(1-\varphi_m)}{(\psi_s-\varphi_m)}\left[\frac{\psi_s^{1/3}-(\psi_s-\varphi_m)^{1/3}}{1-(1-\varphi_m)^{1/3}}\right]^{-1}(1-U_e)\end{array}\right] \tag{5}$$

The initial condition is

$$U_e = 1 \text{ at } t = 0 \tag{6}$$

Variation of the extent of swelling of the inner phase, ψ_s, with time can be expressed as

$$\frac{d\psi_s}{d\theta} = \left(\frac{3}{R^0}\right)\psi_s^{2/3}\left[\begin{array}{l} k_p^0\left[\frac{\psi_s^{1/3}-(\psi_s-\varphi_m)^{1/3}}{1-(1-\varphi_m)^{1/3}}\right]^{-1}\left\{p - p_e^0 - \frac{1}{T_r}\left[1-\frac{(\psi_s-\varphi_m)}{(1-\varphi_m)}p\right]\right\} \\ + k_a\left[\frac{\psi_s^{1/3}-(\psi_s-\varphi_m)^{1/3}}{1-(1-\varphi_m)^{1/3}}\right] - k_\ell\left[\frac{\psi_s^{1/3}-(\psi_s-\varphi_m)^{1/3}}{1-(1-\varphi_m)^{1/3}}\right]^{-1}\end{array}\right] \tag{7}$$

where $p = \frac{[HNO_3]_i}{[HNO_3]_i^0}$ & $p_e^0 = \frac{[HNO_3]_e^0}{[HNO_3]_i^0}$, and $k_p^0 = k_p[HNO_3]_i^0$.

The initial condition for Equation 7 is $\psi_s = 1$ at $t = 0$. Variation of p with time can be obtained from the following equation

$$\begin{aligned}\frac{dp}{d\theta} = -\left(\frac{3}{R^0}\right)\frac{\psi_s^{2/3}}{(\psi_s-\phi_m)}\left\{p - p_e^0 - \frac{1}{T_r}\left[1-\frac{(\psi_s-\phi_m)}{(1-\phi_m)}p\right]\right\} \\ \times\left[k_p^0\left[\frac{\psi_s^{1/3}-(\psi_s-\phi_m)^{1/3}}{1-(1-\phi_m)^{1/3}}\right]^{-1}p + k_a\left[\frac{\psi_s^{1/3}-(\psi_s-\phi_m)^{1/3}}{1-(1-\phi_m)^{1/3}}\right]\right]\end{aligned} \tag{8}$$

The initial condition for Equation 8 is $p = 1$ at $t = 0$.

Equations 5, 7, and 8 should be solved simultaneously, along with the equilibrium conditions to yield the variation of uranium concentration in the external phase.

EXPERIMENTAL

A laboratory-scale facility was set up for conducting experimental studies. It consists of four parts: (1) primary emulsifier, (2) pertractor, (3) phase separator, and (4) de-emulsifier. The procedure is described in detail by Mukhopadhyay [7].

RESULTS AND DISCUSSION

Experiments have been conducted to study extent of pertraction of uranium with simultaneous measurement of leakage and swelling under various operating conditions. The experimental results have been compared with the prediction of the model.

Figure 1 presents the effect of impeller speed of pertractor on rate of pertraction of uranium. The values of k_a, k_l, and k_p, used in the model are those obtained from independent experiments. The value of k_u has been regressed from the experiment at N_p = 300 and is used in the rest two experiments. The model fits the experiments fairly well.

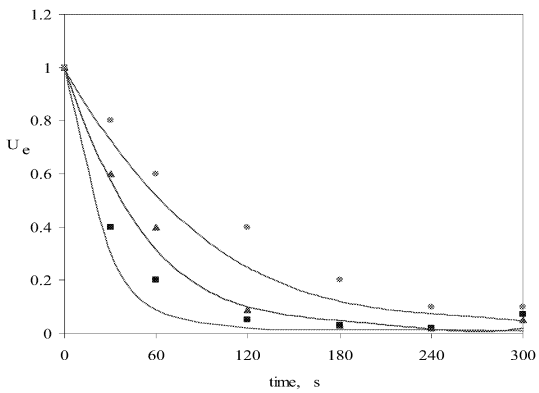

Figure 1: Rate of pertraction of uranium as a function of impeller speed. ■ N_p = 500, ▲ N_p = 300, ● N_p = 200. The solid lines represent the model fits. TR = 10, $[D]^0_m$ = 30, [S] = 69, $[U]^0_e$ = 2.1, $[U]^0_e$ = 10 mol m^{-3}, $[HNO_3]^0_i$ = 2000 mol m^{-3}, N_e = 3000, $R^0 \times 10^5$ m = 7.5 (200 N_p), 5.8 (300 N_p), and 5.0 (200 N_p). Parameters: $k_a = 1.5 \times 10^{-8}$ m s^{-1}, $k_l = 1.5 \times 10^{-9}$ m s^{-1}, $k_p = 1.0 \times 10^{-8}$ m^4 mol^{-1} s^{-1}, $k_u = 1.8 \times 10^{-6}$ m s^{-1}.

Effect of internal strip concentration on rate of pertraction of uranium has been presented in Figure 2. With regressed values of parameters, the model explains the experimental findings satisfactorily. The predictions are done using the same set of the model parameters used in Figure 1.

Figure 3 presents the effect of various carrier (DEHPA) concentration in the membrane on pertraction of uranium. Increase in concentration of DEHPA increases the viscosity of the membrane phase, reducing diffusivity of uranium and water while resisting deformation and leakage.

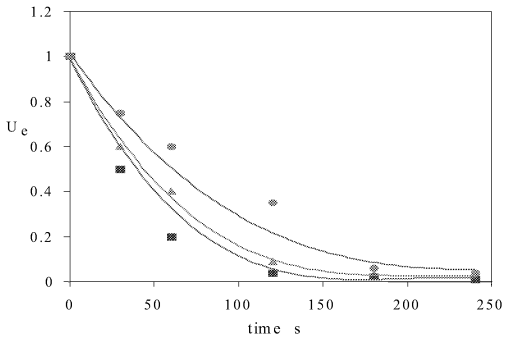

Figure 2: Rate of pertraction of uranium as a function of strip concentration.

■ $[HNO_3]_i^0$ = 4000, ▲ $[HNO_3]_i^0$ = 2000, ● $[HNO_3]_i^0$ = 1000. The solid lines are the model fits. TR = 10, N_p = 300 ($R^0 = 5.8 \times 10^{-5}$m), [S] = 69, $[U]_e^0$ = 2.1, $[H]_e^0$ = 10 mol m^{-3}, $[D]_m^0$ = 30 mol m^{-3}, N_e = 3000 rpm. Parameters: $k_a = 1.5 \times 10^{-8}$ m s^{-1}, $k_l = 1.5 \times 10^{-9}$ m s^{-1}, $k_p = 1.0 \times 10^{-8}$ m^4 mol^{-1} s^{-1}, $k_u = 1.8 \times 10^{-6}$ m s^{-1}.

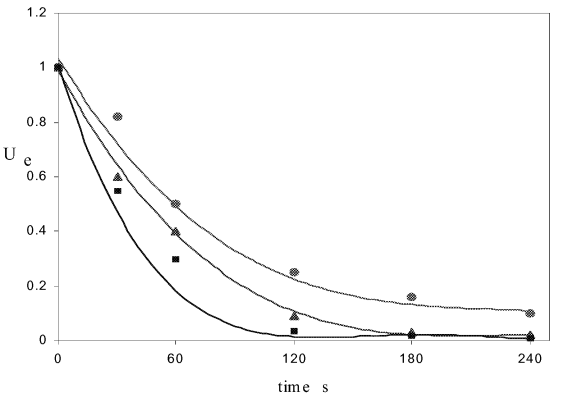

Figure 3: Rate of pertraction as a function of concentration of DEHPA. ■ $[D]_m^0$ = 60, ▲ $[D]_m^0$ = 30, ● $[D]_m^0$ = 15. The model fits are represented by the solid lines. TR = 10, Np = 300 ($R^0 = 5.8 \times 10^{-5}$ m), [S] = 69, $[U]_e^0$ = 2.1, $[H]_e^0$ = 10, $[HNO_3]_i^0$ = 2000, N_e = 3000. $[D]_m^0$ = initial concentration of carrier DEHPA in mol m^{-3}.

Parameters:

$[D]_m^0$ mol m^{-3}	$k_a \times 10^8$ m s^{-1}	$k_l \times 10^9$ m s^{-1}	$k_p \times 10^8$ m^4 mol^{-1} s^{-1}	$k_u \times 10^6$ m s^{-1}
15	1.55	1.65	1.05	1.85
30	1.50	1.50	1.00	1.80
60	1.46	1.38	0.90	1.75

CONCLUSIONS

The work has resulted in the following understanding about the LEM system.

1. For extraction of uranium from dilute nitric acid stream and its recovery as concentrated nitrate solution, DEHPA is a suitable carrier.
2. The assumption of core-shell model is able to represent the present system satisfactorily. By fitting the model to the data, four transport coefficients were regressed: k_a, the occlusion coefficient; k_P, the osmotic coefficient; k_l the leakage coefficient; and k_u, the uranium permeation coefficient. It is important to note that k_a, k_l, and k_p were determined using independent experiment not involving pertraction and then used in pertraction.
3. Development of suitable surfactant is the key for better stability of LEM system.

NOMENCLATURE

$[D]_m^0$ = initial concentration of DEHPA (di-2-ethylhexylphosphoric acid) in membrane, mol m^{-3}. N_e = impeller speed during emulsification, rpm. N_p = impeller speed during pertraction, rpm. [S] = concentration of surfactant (SPAN80), mol m^{-3}. [U] = concentration of uranium, mol m^{-3}. R = radius of emulsion globule, m. T_r = volume ratio of external to internal phase. V = volume, m^3. A = interfacial area of globule. $[HNO_3]$ = concentration of nitric acid, mol m^{-3}. k_a = occlusion coefficient, m s^{-1}. k^0_p = osmotic coefficient, m s^{-1}. k_p = osmotic coefficient, m^4 mol^{-1} s^{-1}. k_l = leakage coefficient, ms^{-1}. k_u = uranium transfer coefficient, ms^{-1}. p = ratio of concentration of nitric acid in the internal phase to its initial value. p_e = ratio of nitric acid concentration in the external phase to initial nitric acid concentration in the internal phase. r_a = volume rate of occlusion, m^3 s^{-1}. r_l = volume rate of leakage, m^3 s^{-1}. r_p = volume rate of osmosis, m^3 s^{-1}. r_u = rate of transfer of uranium, mol s^{-1}. t = thickness of the membrane in globule, m. ϕ_m = membrane-to-strip phase ratio in the primary emulsion. θ = time, s. ψ = ratio of emulsion globule volume to its initial volume. Prefix/Suffix: ^{0} = initial condition, $_e$ = external phase, $_m$ = membrane phase, $_i$ = internal phase.

REFERENCES

1. J. Bock and P. L. Valint, "Uranium extraction from wet process phosphoric acid. A liquid membrane approach," *Ind. Eng. Chem. Fundam.*, **21**, 417 (1982).
2. H. C. Hayworth, W. S. Ho, W. A. Burns, and N. N. Li, "Extraction of uranium from wet process phosphoric acid by liquid membranes," *Sep. Sci. Technol.*, **18**(6), 493 (1983).
3. T. Hirato, I. Kishigamin, Y. Awakura, and H. Majima, "Concentration of uranyl sulfate solution by an emulsion type liquid membrane process," *Hydrometallurgy*, **26**, 19 (1991).
4. P. S. Kulkarni, S. Mukhopadhyay, M. P. Bellary, and S. K. Ghosh, "Studies on membrane stability and recovery of uranium (VI) from aqueous solutions using liquid emulsion membrane process," *Hydrometallurgy*, **64**, 49 (2002).
5. F. Macasek, P. Rajec, V. Rahacek, V. N. Anh, and T. Popovnakova, "Emulsion membrane systems for preconcentration of uranium," *J. Radioanal. Nucl. Chem. Lett.*, **96**(5), 529 (1985).
6. H. J. Bart, C. Ramsedar, T. Haselgrubler, and R. Marr, "The investigation of osmosis in liquid membrane technology: influence of key parameters," *Hydrometallurgy*, **28**, 253 (1992).
7. S. Mukhopadhyay, Application of liquid emulsion membrane to extraction of uranium from dilute aqueous streams, PhD thesis, Indian Institute of Technology Bombay, India (2005).

IMPROVING THE PERFORMANCE OF SUPPORTED LIQUID MEMBRANES

M. Fritz, M. Siebenhofer, and R. Marr

Department of Chemical Engineering and Environmental Technology, University of Technology Graz, Inffeldgasse 25C, 8010 Graz.
Corresponding authoremail address: marlene.fritz@tugraz.at

ABSTRACT

The present project deals with supported-liquid-membrane permeation and the development and construction of a new type of mass-transfer apparatus. The aim of the project is to find suitable membrane modules with minimum solvent bleeding. Therefore, a membrane screening was made and the influences of pressure, surface tension, pore-size distribution, and thickness of the membrane on the flow rate was investigated. The project started with the investigation of axial flux and bleed flux of aqueous mobile phase. The experiments were performed with hydrophilic PE membranes. The flux of the mobile phase was modelled with the Darcy equation.

INTRODUCTION

Rising commodity prizes and growing importance of environmental affairs support research in recycling and upgrading of valuable substances like metal ions from aqueous effluents [1]. Therefore, improvement of liquid membrane technology has become subject of our investigations.

Supported liquid membranes can be employed in many different applications, for example analytical, inorganic and organic chemistry, chemical engineering, biotechnology, and biomedical engineering [2]. Several configurations of supported liquid membranes (SLM) such as flat-sheet supported liquid membranes, or hollow-fiber supported liquid membranes have been investigated but have still not achieved state-of-the-art status. Liquid membranes are highly efficient, but because of problems in handling and stability, liquid membranes have yet achieved successful industrial application [3]. Hence, a new approach that might help overcome the problem of membrane bleeding has become the subject of investigation. The basic idea of our project is to avoid phase break through and, as a consequence, short circuiting between the feed and the strip phase by applying a constant axial flux of the mobile phase through the membrane perpendicular to the direction of mass transfer. This measure is assumed to support repair solvent leaks from the membrane. The experimental setup is similar to the assembling of a filter press enabling mass-transfer areas of 100 m^2/m^3.

Mass-transfer investigations were carried out with the standard test system for reactive extraction Zn^{2+}/DEHPA/H^+ [4-7, 7-11] which is well known and easy to handle.

Application of the system Zn^{2+}/DEHPA/H^{+} in supported-liquid-membrane permeation makes use of simultaneous extraction and re-extraction with the rate-limiting step being diffusion of the DEHPA/metal ion complex through membrane phase [3]. Membrane screening and modeling of the axial mobile phase flux is the focus of current research activities.

EXPERIMENTAL PROCEDURE

Figure 1 shows the experimental set up for a representative mass-transfer experiment carried out with the test system Zn^{2+}/DEHPA/H^{+}.

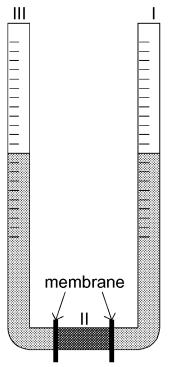

Figure 1. Experimental set-up used to investigate Zn^{2+} permeation by supported-liquid-membrane permeation. Temperature: 20 °C; membrane: Cellgard 2400Microporous Membranes; mobile phase: 25 wt% DEHPA in dodecane; Zn^{2+} start concentration in phase III (feed phase): 400mg/L; H_2SO_4 start concentration in phase I (strip phase): 1 mol/L.

The experiment was carried out with a Cellgard 2400 microporous membrane with a porosity of 37%, membrane thickness of 25 μm and pore size of 0.117 x 0.042 μm. The result of a representative mass-transfer experiment is shown in Figure 2.

From this experiment, which could be performed without membrane failure, the diffusion coefficient of Zn^{2+} was determined to be $D_{Zn2+} = 2.5 \cdot 10^{-10}$ m² s^{-1}. Mass-transfer experiments were repeated 3 times with an experimental error of ±5% including errors of analysis, performance of the experiment, and sampling error.

Membrane failure will cause a rather rapid depletion of Zn^{2+} concentration in the strip phase. To avoid membrane failures due to break-up and to repair membrane leaks, the membrane module is equipped with a mobile-phase reservoir enabling a steady-state axial flux of the mobile phase perpendicular to the mass-transfer direction based on static pressure.

After mass-transfer experiments, phase flow in hydrophilic polyethylene membranes was investigated. In principle, we were looking at the relative volumes of circulating phase that bleeds through the membrane as a function of physical properties and pressure. Therefore, we used hydrophilic polyethylene membranes (type: porous polyethylene membranes Porex, Germany) with a porosity of 35%, a membrane

thickness of 1-5 mm, and a pore size distribution of 7-12 µm and 20-60 µm were investigated.

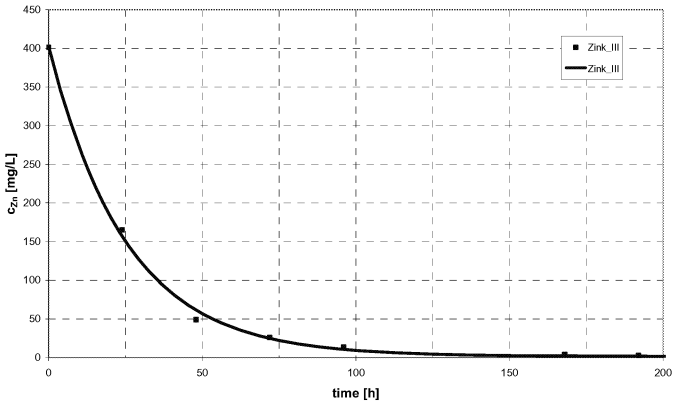

Figure 2. Results of Zn^{2+} permeation by supported-liquid-membrane permeation. Operation conditions: Temperature: 20 °C; membrane, Cellgard 2400Microporous Membranes; mobile phase, 25 wt% DEHPA in dodecane; Zn^{2+} start concentration in phase III (feed phase), 400 mg/L; H_2SO_4 start concentration in phase I (strip phase), 1 mol/L.

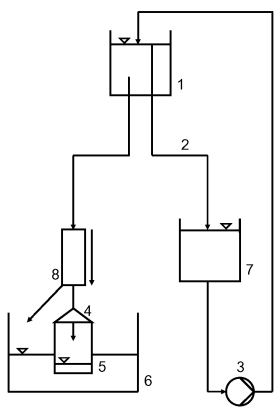

1. Feed tank with level control
2. Liquid phase overflow
3. Circulation pump
4. Cone for separate collection of bleed and membrane flux
5/6 Liquid phase storage vessels for bleed phase and axial flux
7. Circulation liquid phase storage
8. Membrane module

Figure 3: Experimental Set up

The experimental setup used for investigation of axial mobile phase flow is shown in Figure 3. To study the hydraulics of the membranes, experiments were performed with deionized water, isopropyl alcohol (technical grade), and a 0.2% water/tenside mixture using the tenside Silwet® L-7600 (polydimethyl siloxane, modified with polyethylene oxide) in p.a. quality.

To ensure constant liquid level on top of the membrane, a liquid-phase circuit that includes a constant liquid-level storage vessel (1), the liquid overflow (2), the circulation pump (3), and a storage tank for the circulation liquid (7) was installed. The funnel (4) separates the bleed phase from the membrane flux. In vessel (5), the membrane flux phase is collected, and in vessel (6), the bleed phase flux phase is collected. Depending on membrane thickness and pore size, the experiments lasted about 5 to 60 minutes. Membrane equipment ensured that the bleeding phase and membrane flux were separated, where at the end of the membrane, the funnel was placed. The funnel ensured that both phases could not come together after the membrane.

RESULTS AND DISCUSSION

Experiments were carried out with feed solutions of different physical properties: (Surface tension: $\sigma_{water/tenside}$ = 27.2 mN/m; $\sigma_{isopropyl\ alcohol}$ = 23.1 mN/m; σ_{water} = 72.75 mN/m. Density: ρ_{water} = 0.998 kg/m³; $\rho_{water/tenside}$ = 0.998 kg/m³; $\rho_{isopropyl\ alcohol}$ = 0.847 kg/m³. Dynamic viscosity: η_{water} = 1.0 mPa s $\eta_{isopropyl\ alcohol}$ = 3.21 mPa s $\eta_{water/tenside}$ = 1.003 mPa s.

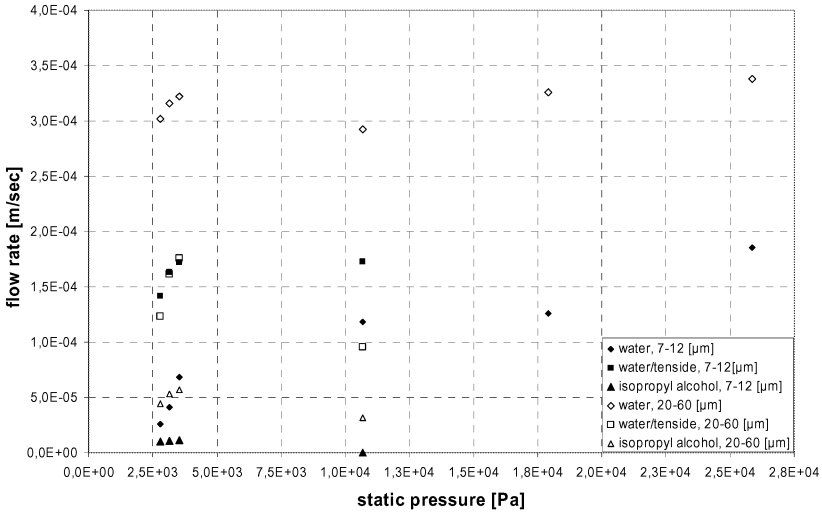

Figure 4. Flow rate versus static pressure at ambient temperature for membranes with a pore size distribution of 7-12 µm and 20-60 µm and a membrane thickness of 1 mm.

Figure 4 shows the effect of pore-size distribution, static pressure, and physical properties of the liquid phase on the flow rate. The static pressure was varied between 2.6 x 10^4 and 2.8 x 10^3 Pa. As shown in Figure 4, the lowest flow rate was found for isopropyl alcohol. Possible reasons therefore are, on the one hand, the high dynamic viscosity of isopropyl alcohol and, on the other hand, the hydrophobic character of isopropyl alcohol versus the hydrophilic character of the PE-membrane**.**

For any pore-size distribution, the flow rate was highest for water and the water/tenside mixture. Expectedly the highest flow rate was found for membranes with pore size distribution of 20-60 µm and a membrane thickness of 1.5 mm. The bleed-

phase flux (V_{Bleed}) and the axial membrane flux phase ($V_{Membrane}$) were collected in separate beakers. From these data, the phase ratio (P) was calculated.

$$P = \frac{V_{membrane}}{V_{Bleed}} \tag{1}$$

The highest phase ratio was found for the membrane with a pore-size distribution of 7-12 μm and a membrane thickness of 1 mm.

The permeability B was determined with the Darcy correlation according to Equation 2. The value of B was calculated from the axial phase flux via $V_{Membrane}$, the cross section of the membrane and the time recorded for each experiment, the static pressure Δp, and the length of the modules L. B was determined with $10^{-12} \pm 10^{-1}$ m².

$$\frac{\Delta p}{L} = \frac{\eta * u}{B} \tag{2}$$

The effect of the static pressure, pore-size distribution, liquid phase and surface tension on the flow rate of the axial flux in hydrophilic PE-membranes was determined. According to Equation 2, it was expected that the mobile-phase velocity would increase with increasing static pressure. But actually the static pressure has little effect on the axial flow rate while membrane bleeding increases. The effect of pore-size distribution on the flow rate, was determined. Flow rate varies with the physical properties of the liquid phase. Flow rate rises with pore-size distribution for a surface tension of σ = 72 $mN \cdot m^{-1}$. For low surface tension, investigated with a water/tenside mixture, the axial flow rate will break down rapidly. The lowest flow rate was detected for isopropyl alcohol.

Membranes with a small pore-size distribution of 7-12 μm show a different flow characteristic. The flow rate rises with falling surface tension, and the highest flow rate was found for the water/tenside mixture.

CONCLUSIONS

Water permeability of membranes of different thickness and a pore size of 7-12 μm increases with increasing static pressure, passing through a maximum and then decreasing because of increasing bleed flux.

Permeability increases with decreasing membrane thickness. Membranes with pore size of 20-60 μm and membrane thickness of 1, 1.5, 2, 3, and 5 mm undergo an immediate tendency to bleed. Permeability decreases with increasing static pressure. Permeability depends on membrane thickness and passes a maximum at a membrane thickness of 2 mm.

Decreasing surface tension does not change the trend of results but affects the absolute flux values.

Based on the results of these membrane phase flow experiments, mass-transfer experiments will be investigated with the following membranes. For both aqueous phases, hydrophilic membranes with a pore-size distribution of 20-60 μm and a

membrane thickness of 2 mm, and for the solvent phase, hydrophobic membranes with a pore-size distribution of 7-12 mm and a membrane thickness of 1 mm will be used.

ACKNOWLEDGMENTS

The work was carried out at the Department of Chemical Engineering and Environmental Technology at the University of Technology Graz. Membranes were sponsored by POREX. Christian Morales De Csaky carried out most of the experimental work which was incorporated into his diploma thesis.

REFERENCES

1. G. Leon and M. A. Guzmàn, "Facilitated transport of cobalt through bulk liquid membranes containing diethylhexyl phosphoric acid," *Desalination*, **162**, 211-215 (2004).
2. N. M. Kocherginsky, Q. Yang, and L. Seelam, "Recent advances in supported liquid membrane technology," *Sep. Purif. Technol.*, **53**, 171-177 (2007).
3. Ch. Huber, R. Marr, and M. Siebenhofer, "A new approach of modelling mass transfer of Zinc through supported liquid membranes," *Proc. Int. Solv. Extr. Conf., (ISEC2005), Beijing*, 2005; pp. 1479-1483.
4. O. N. Ata, A. V. Bese, S. Colak, B. Dönmez, and A.Cakici, "Effect of parameters on the transport of zinc ion through supported liquid membranes," *Chem. Eng. Process.,* **43**, 895-903 (2004).
5. M. Mörters and H.-J. Bart, "Mass transfer into droplets undergoing reactive extraction," *Chem. Eng. Process.,* **42,** 801-809 (2003).
6. K. Takeshita, K. Watanabe, Y. Nakano, and M. Watanabe, "Solvent extraction separation of Cd(II) and Zn(II) with the organophosphorus extractant D2EHPA and the aqueous nitrogen-donor ligand TPEN," *Hydrometallurgy,* **70,** 63-71 (2003).
7. M. T. A. Reis and J. M. R. Carvalho, "Modelling of zinc extraction from sulphate solutions with bis(2-ethylhexyl)thiophosphoric acid by emulsion liquid membranes," *J. Membr. Sci.,* **237**, 97-107 (2004).
8. H.-J. Bart and H.-P. Rouselle, "Microkinetics and reaction equilibria in the system $ZnSO_4$/D2EHPA/isododecane," *Hydrometallurgy,* **51**, 285-298 (1999).
9. C. I. Sainz-Diaz, H. Klocker, R. Marr, and H.-J. Bart, "New approach in the modelling of the extraction equilibrium of zinc with bis-(2-ethylhexyl)phosphoric acid," *Hydrometallurgy,* **42**, 1-11 (1996).
10. J. P. Simonin, H. Hendrawan, F. Dardoize, and G. Clodic, "Study of salt effects on the kinetics of extraction of cobalt(II) and zinc(II) at trace level by D2EHPA in n-dodecane," *Hydrometallurgy*, **69**, 23-38 (2003).
11. M. Mörters and H.-J. Bart, "Extraction equilibria of zinc with bis(2-ethylhexyl)-phosphoric acid," *J. Phys. Chem. Ref. Data*, **45**, 82-85 (2000).

SEPARATION OF Co(II) AND Li(I) BY SUPPORTED LIQUID MEMBRANE AND SOLVENT EXTRACTION USING CYANEX 272 AS AN EXTRACTANT

B. Swain,[1,2] J. Jeong,[1] J-C. Lee,[1] K. Yoo,[1] and M-S. Kim[1]

[1]Minerals and Materials Processing Division, Korea Institute of Geoscience and Mineral Resources (KIGAM), Daejeon, 305-350, Korea. [2]Department of Chemistry, Chungnam National University, Daejeon, Korea.
Corresponding author email address: jinkiz@kigam.re.kr

ABSTRACT

Co(II) and Li(I) have been recovered from dilute sulfate solutions using a flat-sheet supported liquid membrane (SLM) and solvent extraction (SX). A microporous hydrophobic PVDF film was used as the solid support for the liquid membrane. Cyanex 272 was used as the extractant for SX and the mobile carrier in the SLM. Sulfuric acid was used as the stripping agent. In both of the separation processes, the effect of parameters such as the pH of the feed solution, Cyanex 272 concentrations, metal ion concentration in the feed solution, and H_2SO_4 concentration in the strip solution on the Co(II) flux ($J_{Co(II)}$), Li(I) flux ($J_{Li(I)}$), and the distribution ratio (D_{sx}) for both of the metals was investigated and compared.

INTRODUCTION

The tremendous growth in the use of the rechargeable lithium ion battery (LIB) and recent legislation such as the European Union's Waste of Electrical, Electronic Equipment (WEEE), and Restriction of Hazardous Substances (RoHS) [Directive 2002/96/EC] has stimulated efforts to recycle valuable components from spent LIBs. The recovery of Co(II) in the presence of different metals like nickel, zinc, manganese, etc. by SLMs and SX has been reported [1-5]. Although much work has been done investigating the recovery of Co(II) from either two-metal or multi metal systems by SLM and SX, a comparative study regarding the separation of Co(II) and Li(I) using Cyanex 272 by SLM and SX has not yet been reported. This investigation compares SLM and SX as techniques to achieve the separation of Co(II) and Li(I) from dilute H_2SO_4 solutions. SX studies were carried out by varying parameters such as pH and the relative concentrations of Cyanex 272, Co(II), and H_2SO_4. SLM studies investigated the effect of various process variables such as the stirring speed, pH of feed solution, and relative concentrations of extractant, Co(II), and H_2SO_4. The metal ion flux in both the SX and SLM studies was compared.

EXPERIMENTAL

Chemicals and Reagents

All chemicals used in this study, $CoSO_4 \cdot 7H_2O$, $Li_2SO_4 \cdot H_2O$, H_2SO_4, NaOH, NH_4OH, CH_3CO_2Na, and CH_3CO_2H, were of analytical reagent grade. The commercial extractant Cyanex 272 was supplied by Cytec Korea Inc. and was used as received. Kerosene and tri-*n*-butyl-phosphate (TBP) were used as diluent and phase modifier respectively.

Membrane Specifications

Durapore disc membrane, a microporous hydrophobic PVDF film, was used as the solid support for the liquid membrane as specified by the supplier. The membrane has 75% porosity, pore size of 0.45 μm, refractive index of 1.42, membrane diameter of 47 mm, and membrane thickness of 125 μm.

Procedure for Supported Liquid Membrane Experiments

A two-compartment cell with an effective membrane area of 9.42×10^{-4} m^2 was used for the liquid-membrane experiment. The volumes of the strip and feed solutions were 200 cm^3. A buffer solution of CH_3COOH-CH_3COONa was used to maintain the required pH of the feed solution in the range of 4.00 to 6.75. The feed solution was kept under agitation using a mechanical stirrer. Equal volumes of samples (1 cm^3) were withdrawn from both of the solutions after a time interval of 30 minutes. The samples were analyzed for Co(II) and Li(I) concentrations using an atomic absorption spectrophotometer. The following experimental conditions for SLM studies were maintained unless otherwise stated: feed pH = 6.00, $[CoSO_4]_{feed}$ = 10 mol/m^3, $[Li_2SO_4]_{feed}$ = 10 mol/m^3, $[H_2SO_4]_{strip}$ = 100 mol/m^3, and stirring speed = 350 rpm.

Liquid-liquid Extraction Experiments

The aqueous solutions for the solvent-extraction experiments contained 100 mol/m^3 Na_2SO_4 in order to maintain a constant ionic strength and buffering in the aqueous phase. The initial pH of the solutions was adjusted to the desired value using dilute H_2SO_4 and NH_4OH. The volume of the aqueous phase was 20 cm^3 and contained 10 mol/m^3 Co(II) and Li(I) sulfate and 100 mol/m^3 Na_2SO_4. The aqueous phase was contacted in separatory funnels with an equal volume of organic phase containing 30 mol/m^3 of extractant for 10 min. After phase separation, the equilibrium pH of the raffinate was measured. All of the extraction and stripping experiments were carried out at ambient temperature (25 ± 2°C). The samples were analyzed for Co(II) and Li(I) concentration using an atomic absorption spectrophotometer. The following experimental conditions for SX studies were maintained unless otherwise stated: $[CoSO_4]_{feed}$ = 10 mol/m^3, $[Li_2SO_4]_{feed}$ = 10 mol/m^3, and feed pH = 6.00.

RESULTS AND DISCUSSION

The Effect of pH on Co(II) and Li(I) Recovery

For the SLM studies, the recovery of Co(II) and Li(I) from sulfate media containing 10 mol/m^3 of each metal was studied using Cyanex 272 concentrations of 500 and 30 mol/m^3 within a pH range of 4.00–6.75. As the pH was increased from 4.00 to 6.00, the flux for Co(II) increased from 11.17 x 10^{-6} mol/m^{2}s to 82.17 x 10^{-6} mol/m^{2}s, after which it decreased to 75.68 x 10^{-6} mol/m^{2}s at a pH 6.75 (Figure 1). No flux was detected below pH 4.00.

In the SX studies, as the pH was increased from 4.00 to 6.00 (corresponding to an equilibrium pH of 6.50 to 6.90), the percentage extraction of Co(II) increased from 79.14% to 84.19%, whereas only about 8% of Li(I) was extracted. In this pH range, the distribution ratio (D_{sx}) for Co(II) increased from 4.00 to 4.909, but D_{sx} for Li(I) remained constant at 0.086.

Figure 1 shows that, in the SLM study for the separation of Co(II) and Li(I), a pH of 6 in the feed solution is optimum whereas, in the SX study, a pH of 5 in the feed solution is optimum. In the SX process, the distribution ratio D_{sx} depends on the equilibrium pH whereas, in the SLM process, the flux $J_{Co(II)}$ and $J_{Li(I)}$ is independent of equilibrium pH. The separation factor β_{SX} (obtained by SX) was compared with separation factor β_{SLM} (obtained by SLM) as a function of pH. Figure 1 shows that β_{SLM} increases from 24.34 to 180.00 as the pH in the feed solution increases from 4.00 to 6.00, then it decreases to 164.9 as the feed pH increases to 6.75. β_{SX} increases from 46.52 to 57.08 as the pH in the feed solution increases from 4.00 to 6.75. At the optimum pH, β_{SLM} is 3 times β_{SX}.

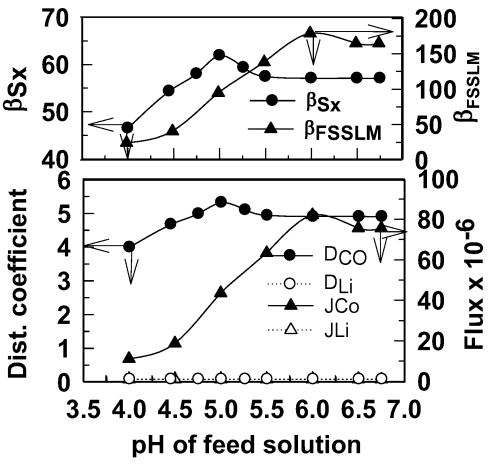

Figure 1. Effect of feed pH on flux J_M and extraction of metal.

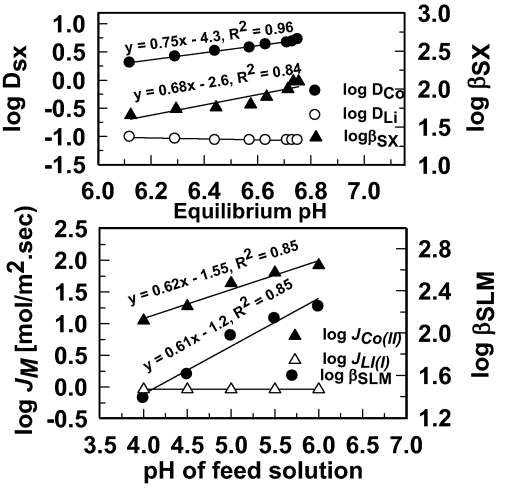

Figure 2. Effect of pH on log J_M log D_{sx} and log β.

Figure 2 shows log J_{Co} and log J_{Li} versus the feed pH at a constant Cyanex 272 concentration of 750 mol/m^3 for SLM studies and log D_{SX} versus equilibrium pH and log β_{SX} versus the equilibrium pH at a constant Cyanex 272 concentration of 30 mol/m^3 for

SX studies. The plots are linear with slopes of 0.67 for SLM and 0.75, for SX. The least-square slope value of the line for Co(II) SX is 0.75, and for Co(II) SLM it is 0.67, indicating the exchange of one mole of H^+ per mole of Co(II).

The Effect of Extractant Concentration on Co(II) and Li(I) Recovery

To study the effect of Cyanex 272 concentration on the separation of Co(II) and Li(I) in both SX and SLM systems, the concentration of the extractant was varied from 2.5 to 1250 mol/m^3 for SX and 30 to 1250 mol/m^3 for the SLM. The pH of the feed solutions for both the SLM and SX processes was kept constant at 6.00 and 5.00, respectively.

In the SLM study, the strip solution concentration was 100 mol/m^3. Figure 3 shows that, in the SLM study, as the Cyanex 272 concentration increases from 30 mol/m^3 to 750 mol/m^3, the flux $J_{Co(II)}$ increases steadily from 9.73 x 10^{-6} mol/m^2 s to 82.17 x 10^{-6} mol/m^2 s. Above a Cyanex 272 concentration of 750 mol/m^3, the flux $J_{Co(II)}$ decreases to 35.32 x 10^{-6} mol/m^2 s. In all cases, the flux $J_{Li(I)}$ remains constant at 0.918 x 10^{-6} mol/m^2 s.

In the SX study, as the concentration of Cyanex 272 varies from 2.5 to 100 mol/m^3, the distribution ratio D_{SX} for Co(II) varies from 0.14 (7.15% Co(II) extraction) to 7784 (99.99% Co(II) extraction). In the same Cyanex 272 concentration range, the distribution ratio D_{SX} for Li(I) varies from 0.013 (1.36% Li(I) extraction) to 1.178 (54.08% Li(I) extraction).

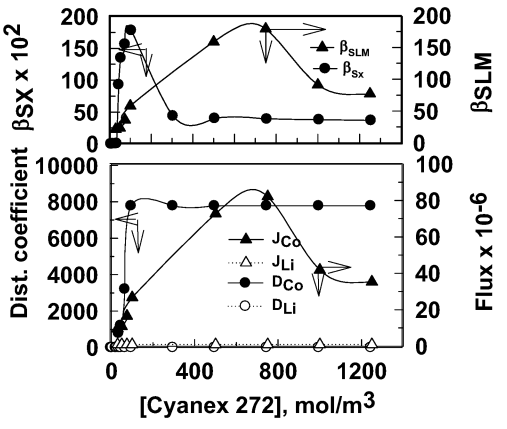

Figure 3. Effect of [Cyanex 272] on flux J_M, and metal extraction.

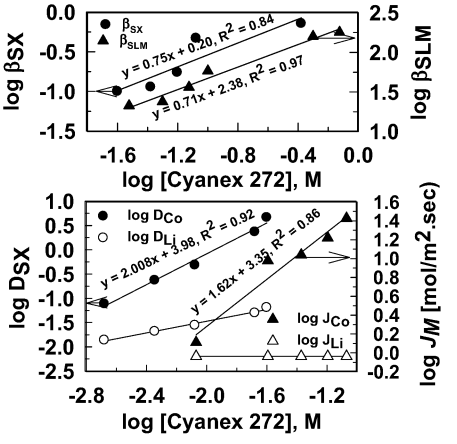

Figure 4. Effect of [Cyanex 272] on flux J_M, and log Dsx.

The optimum permeability for the SLM study was obtained at 750 mol/m^3 of Cyanex 272, whereas the best distribution ratio for the SX study was obtained at 100 mol/m^3 of Cyanex 272. The best quantitative extraction of Co(II) was obtained at 100 mol/m^3. The optimum Cyanex 272 concentration for the SLM process is about 7.5 times more than for the SX process, although solvent inventory is significantly less.

In Figure 4, log D_{SX} versus log [Cyanex 272] for the SX study and log J_M versus log[Cyanex 272] for the SLM study are plotted and compared. For Co(II) extraction, the least-square slope value for log D_{SX} versus log[Cyanex 272] in the SX study is 2, and the

least-square slope for log $J_{Co(II)}$ versus log[Cyanex 272] in the SLM study is 1.62. This indicates that 2 moles of extractant is associated with the extracted metal species for both the SX and SLM process, and thus, a similar kind of stochiometry in reaction mechanism for extraction of metal in both SX and SLM is indicated. In Figure 4 the plots for log β_{SLM} and β_{SX} versus log[Cyanex 272] have been drawn. The linear least square values for the separation factors are 0.75 for the SLM study and 0.71 for the SX study, indicating a similar kind of mechanism.

The Effect of $[CoSO_4]_{feed}$ Concentrations in Feed on Co(II) and Li(I) Recovery

The effect of $[CoSO_4]_{feed}$ concentration on the flux and extraction behavior of Co(II) and Li(I) was studied in the range of 2.5 mol/m^3 to 300 mol/m^3 for both SLM and SX studies. In the case of the SLM study, the Cyanex 272 concentration in the membrane phase was 750 mol/m^3, and the pH of the solution was 6.00. The strip acid concentration was kept constant at 100 mol/m^3. In the case of the SX study, the Cyanex 272 concentration was 30 mol/m^3, and the pH of the solution was 5.00. The results obtained are presented in Figure 5.

In the SLM study, with increasing concentration of $[CoSO_4]_{feed}$ from 2.5 mol/m^3 to 300 mol/m^3, the flux value of Co(II) $J_{Co(II)}$ increases from 27.03 x 10^{-6} to 94.43 x 10^{-6} mol/m^2 s. The flux value of Li(I) $J_{Li(I)}$ remained constant at 0.918 x 10^{-6} mol/m^2 s. Within this $[CoSO_4]_{feed}$ concentration range, the availability of Co(II) ions at the feed side of the membrane interface increases with increasing Co(II) concentration so that the interfacial chemical reaction shifts towards the products, leading to an increase in $J_{Co(II)}$ from 27.03 x 10^{-6} to 94.43 x 10^{-6} mol/m^2 s (Figure 5).

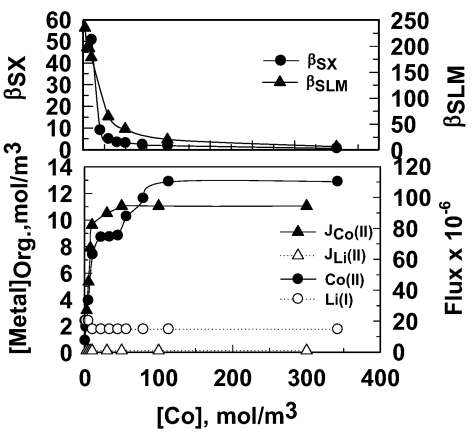

Figure 5. Effect of [Co(II)] on the metal flux J_M and $[Co]_{org.}$

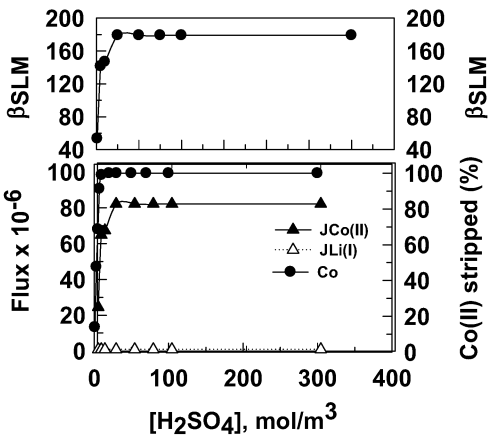

Figure 6. Effect of strip acid on flux J_M and Co(II) stripping.

In the SX study, with increasing $[CoSO_4]_{feed}$ from 1 mol/m^3 to 100 mol/m^3, the Co(II) loading in the organic phase increases from 0.91 mol/m^3 to 12.89 mol/m^3. The maximum Co(II) loading in the organic phase at pH 5.00 and 30 mol/m^3 of Cyanex 272 is 12.89 mol/m^3. Hence, the SX process is limited by the loading capacity of the extractant.

Effect of Strip Acid Concentration

The stripping kinetics were studied with different concentrations of acid solutions ranging from 1 to 300 mol/m^3. All other parameters, such as the pH of the feed at 6.00, Cyanex 272 concentration in the membrane phase at 750 mol/m^3, and Co(II) and Li(I) sulfate each at 10 mol/m^3 were kept constant. Figure 6 indicates that $J_{Co(II)}$ increased from 24.50 x 10^{-6} mol/m^2 s to 82.20 x 10^{-6} mol/m^2 s with an increase of strip acid concentration from 1 mol/m^3 to 25 mol/m^3. A further increase of acid concentration to 300 mol/m^3 has no significant effect on metal ion flux. The stripping behavior of Co(II) in acid concentrations ranging from 1 mol/m^3 to 300 mol/m^3 for SX was also studied. The percentage stripping of Co(II) into the aqueous phase for the SX studies increases from 13.95% to 99.99% as strip acid concentration increases from 1 mol/m^3 to 30 mol/m^3. In the SLM study, the extraction and stripping were combined in a single step, whereas in the SX study, extraction and stripping are two different stages. Figure 5 shows that the separation factor of Co(II) over Li(I) varies from 53.38 to 180.00.

CONCLUSIONS

The dependence of log D or log J on log[Cyanex 272] indicates that 2 moles of the extractant were involved with 1 mole of the extracted metal species for both the SX and SLM processes. The flux of Co(II) and distribution ratio of Co(II) depends on H^+ ion concentration in the feed phase in the pH range of 4.00 to 6.75. In the SX process, D_{SX} increases as the pH increases from 4.00 to 6.00. Above pH 6.00, both flux and distribution ratio decrease. The H_2SO_4 concentration of 25 mol/m^3 provides enough protons to break the metal-Cyanex 272 complex and displace the equilibrium toward the uncoordinated species for both the SLM process and SX process.

ACKNOWLEDGMENTS

This research was supported by the Basic Research Project of the Korea Institute of Geosciences and Mineral Resources (KIGAM) funded by the Ministry of Science and Technology of Korea.

REFERENCES

1. M. Lofti and A. Nafaa, "Modified activated carbon for the removal of copper, zinc, chromium and cyanide from wastewater," *Sep. Purif. Technol.,* **26,** 137-146 (2002).
2. S. Yabe, M. Josefa, and E. Oliveira, "Heavy metals removal in industrial effluents by sequential adsorbent treatment," *Adv. Environ. Res.*, **7**, 263-272 **(**2003).
3. D. Seog, "The removal by crab shell of mixed heavy metal ions in aqueous solution," *Bioresource Technol.*, **87**, 355-357 (2003).
4. B. Purnendu, A. Bose, and K. Sunil, "Critical evaluation of treatment strategies involving adsorption and chelation for wastewater containing copper, zinc and cyanide," *Adv. Environ. Res.*, **7**, 179-195 (2002).
5. B. Swain, K. Sarangi, and R. P. Das, "Effect of different anions on separation of cadmium and zinc by supported liquid membrane using TOPS-99 as mobile carrier," *J. Membr. Sci.*, **277**(1-2), 240-248 (2006).

EVALUATION OF THE DEPENDENCY OF PHASE COMPOSITION ON INDIUM(III) PERMEABILITY IN CYANEX 272 / NPOE PIM-BASED SYSTEMS

E. Rodríguez de San Miguel,[1] J. C. Aguilar[1], M. Muñoz,[2] and J. de Gyves[1]

[1]Departamento de Química Analítica, Facultad de Química, UNAM. Ciudad Universitaria, 04510, México, D.F. México. [2]Unitat de Química Analítica. Universidad Autónoma de Barcelona, 08193, Bellaterra (Barcelona), España.
Corresponding author email address: erdsmg@servidor.unam.mx

ABSTRACT

Optimum conditions for In(III) permeation using polymer inclusion membranes (PIMs) with CYANEX 272 as the carrier, 2-nitrophenyloctylether (NPOE) as the plasticizer, and cellulose triacetate as the support are reported. The effects of modifying the composition of the phases (aqueous pH of the feed solution and HCl concentration of the strip solution; NPOE and CYANEX 272 concentrations in the membrane) on metal ion permeability were analyzed. Additionally, both the selectivity towards variable amounts of Fe(III) and Zn(II) and the stability of the system were evaluated. Preliminary SX experiments were used to characterize extraction affinity and behavior of the system.

INTRODUCTION

Continuous technological developments in the electronic industry, especially in the applications of indium in LCDs, semiconductor materials, low-temperature solders, and high definition television, make recovery of this metal using solvent extraction (SX) attractive for industry [1]. Although the main production of indium is as a by-product of the processing of zinc ores, indium recovery from secondary sources is expected to increase with the increase in recycling of electronic waste. For this reason research in indium SX systems continues [2].

Several avenues for SX implementation using membranes have been proposed [3]. Indium recovery using supported liquid membranes (SLMs) represents an interesting alternative [4-6]. However, despite their advantages, the major concern for SLM use is their stability. Recently, membranes in which the carrier is trapped in a polymeric matrix in the presence of a plasticizer (i.e., polymer inclusion membranes or PIMs), have shown extraction capabilities better or comparable to those of SLMs with other carriers [7] so that their application with organophosphorus carriers is promising.

In this work, we continue our research on PIM transport [8,9] with an optimization study of the aqueous and organic phase compositions to improve In(III) transport using membranes with 2-nitrophenyloctylether (NPOE) as a plasticizer,

CYANEX 272 as the carrier, and cellulose triacetate as the support. The efficiency factors (permeability, selectivity and stability) for this system are reported.

EXPERIMENTAL

Reagents and Equipment

$Fe(NO_3)_3.9H_2O$ A. R. (Merck), In_2O_3 A. R., and a 1000 mg L^{-1} Zn(II) solution in HNO_3 were used as reagents for the aqueous solutions. A 25 mmol L^{-1} sodium acetate/ acetic acid (Merck, A.R.) buffer solution was used to control pH. CYANEX 272, used as received, has the active component bis(2,4,4-trimethylpentyl)phosphinic acid (R_2PO_2H, 87-88%) and was kindly supplied by CYTEC Industries. Cellulose triacetate (CTA, Aldrich), 2-nitrophenyloctylether (NPOE, Aldrich), and chloroform (Merck) were used in PIM preparation using a standard procedure [8,9]. Metal ion concentrations as a function of time were determined using F-AAS (3100 Perkin Elmer spectrophotometer) under the conditions recommended by the producer. The same extraction cell employed in other experiments [6] was used at 650 (feed) and 600 (strip) rpm using 200 mL of aqueous phases and a total exposed membrane area of 11×10^{-4} m^2. SEM photographs were taken with a JEOL 35CF scanning electron microscope. Energy-dispersion analysis of X-rays was performed using an energy-dispersive X-ray spectrometer (EDAX-Link Isis 200) to analyze metal content on the membrane surface after transport.

Procedure

Standard solutions of the metals (0.01 mol L^{-1}) were prepared from which portions were diluted as appropriate with deionized water and HNO_3 (Fisher A. R.) or NaOH (Merck A. R.) to adjust the pH. HCl (1 mol L^{-1}) was used as strip solution, except when the influence of HCl concentration was studied. No metal ion transfer was observed when no extracting reagent was present in the membrane phase. Temperature was kept constant at 20 ± 1 °C. The results reported correspond to the average of at least three replicates with observed deviation within ±5%. Two different values of the permeability coefficients were determined: one was measured from the decrease of the metal concentration in the feed solution (P_f) and the other was determined from the increase of the metal ion concentration in the strip solution (P_s). P_f was evaluated from the slope of the graph $\log \frac{[In^{3+}]_f}{[In^{3+}]_{0,f}}$ vs. time, and P_s from the slope of the graph $\log \frac{[In^{3+}]_{0,f} - [In^{3+}]_s}{[In^{3+}]_{0,f}}$ vs. time. Permeabilities were obtained considering the data taken over 4 h.

RESULTS

Membrane Experiments

Permeability: Influence of the pH of the Feed Phase

P_f and P_s are plotted as a function of pH in Figure 1, which shows both permeability values decrease as pH increases. Retention (difference between P_f and P_s) is practically constant with pH. An explanation for the reduction of permeability may involve the presence of instabilities at the feed solution-membrane interface due to emulsion formation. Liquid-liquid extraction experiments showed that it takes more time to separate the phases as the pH becomes more basic. Gaonkar and Neuman [10] observed that micelle development, a prior step in emulsion formation, depends on extractant concentration and pH when using D2EHPA, an organophosphorus compound similar to CYANEX 272. Thus, it is possible that microemulsion formation develops with increasing pH, causing a blocking effect. At pH 5, precipitation of indium hydroxide takes place (p*K*s ~33) contributing to total metal ion entrapping.

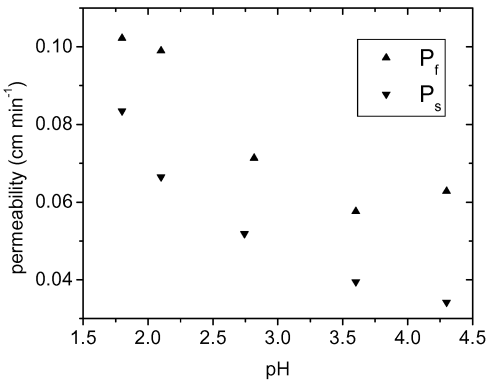

Figure 1. Permeability as a function of pH of the feed solution.

Permeability: Influence of HCl Concentration in the Strip Phase

It was observed that further increase in HCl concentration (above 1 mol L^{-1}) in the strip solution does not improve metal ion transport but rather diminishes it. The possible protonation of the carrier in concentrated acid media may be the cause for this effect, as previously reported for the Co(II)/D2EHPA system in SLMs [11].

Permeability: Influence of NPOE and CYANEX 272 Concentrations

The modification of the plasticizer content showed a maximum in the permeability at about 1 mmol g^{-1} concentration with increasing amounts of NPOE, probably caused by plasticization effects and changes in the characteristics of the membrane matrix [12]. When varying the extractant content, the presence of a percolation threshold suggested a chained-carrier transport process with reduced mobility caused by the plasticization properties of the system and interactions between membrane components [12].

Selectivity

Fe(III) and Zn(II) were tested as representative interfering ions. Fe(III) concentration in the feed solution was varied (0.1–2.4 mmol L^{-1}) at constant In(III) concentration (0.1 mmol L^{-1}). It was observed that above an In:Fe ratio of 1:4, indium retention in the membrane does not depend on iron concentration in the feed solution; indium retention was approximately 2.3×10^{-6} m s^{-1} at 33% w/w of CYANEX and $1.5 \times$

10^{-5} m s^{-1} at 50% w/w. A 10-fold excess of Fe(III) reduces by 60% In(III) permeability at 33% w/w of CYANEX and 43% at 50% w/w of extractant. Fe(III) was not transported during these experiments.

The independence of indium retention on iron concentration in the feed solution and the absence of iron permeation indicates that an interfacial phenomenon is responsible for the decrease in indium permeability and this phenomenon is dependant on the iron concentration. Figures 2a-c show feed-side SEM micrographs of the PIM after indium transport at pH ≈ 2.0 when a) only In is present and b) In and Fe are both present. In Figure 2a, a clean membrane surface is observed. In contrast, 2b shows the presence of a deposit on the membrane surface. EDAX revealed the presence of large amounts of iron over indium (3:1 percent ratio), so that the possible formation of an interfacial compound of iron with the extractant may be responsible for the obstruction, as no precipitation of iron hydroxide is expected under the pH ≈ 2.0 working conditions, (a SEM micrograph of this precipitate taken at more basic medium is shown in Figure 2c).

Selectivity over Zn(II) was also tested with the presence of 40-fold and 80-fold excess of Zn(II) over In(III). As the pH interval over which this separation may be accomplished is about one unit and In(III) flux decreases as pH increases, experiments were performed under compromise conditions to allow high indium fluxes with small amount of Zn(II) transport. For a membrane composition of 50% w/w CYANEX 272, 25% w/w CTA, and 25% w/w NPOE and adjusting the pH of the feed phase at 2.0, the selectivity factor, S_{Zn}^{In}, defined as

$$S_{Zn}^{In} = \frac{[In(III)]_s [Zn(II)]_{0,f}}{[In(III)]_{0,f} [Zn(II)]_s}$$

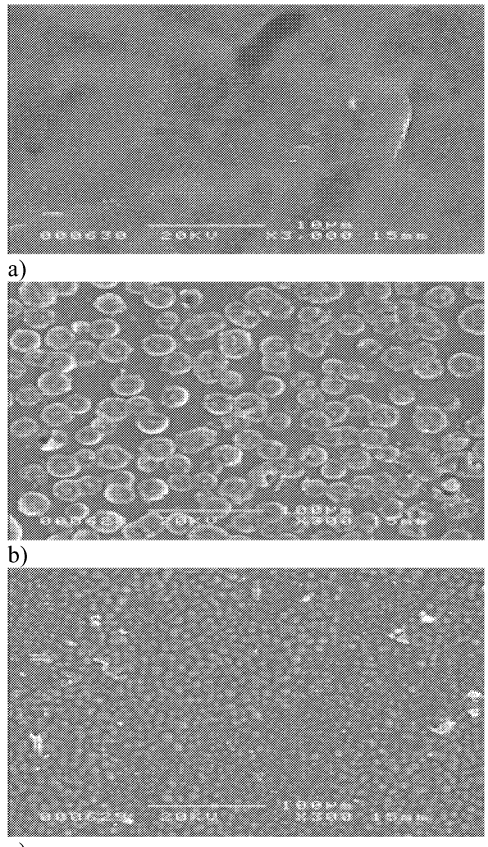

Figure 2. SEM micrographs of the PIM surfaces. a) In alone in the feed solution at pH = 2; b) In in presence of Fe at pH = 2.2; and c) In in presence of Fe at pH = 4.5.

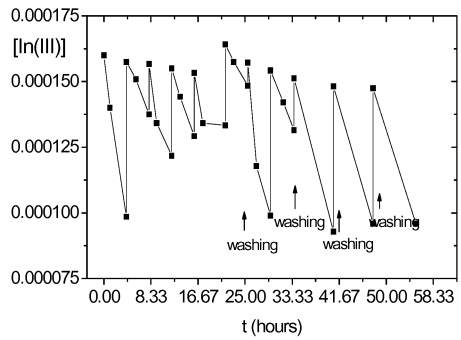

Figure 3. PIM stability during continuous operation.

measured after 320 min. was equal to 72 and 35 for 0.004 and 0.008 mol L^{-1} of Zn(II), respectively. These results indicate that only 1% of the initial zinc concentration migrates to the strip phase, which is surprisingly good considering that $pH_{0.5}$ (Zn) = 2.0 in SX experiments.

Stability

The feed solution indium concentration profile under PIM continuous use is shown in Figure 3, beginning with fresh aqueous solutions contacting the membrane. After about 4 h use, the feed solution was replaced by a fresh one. In(III) transport continued for another 4 h, and after this period of time, the feed solution was replaced once again. This procedure was repeated four times. As observed from the Figure, the transport performance of the system decayed as the number of runs increased. After several runs, the feed solution was changed to 1 mol L^{-1} HCl solution, and the cell was stirred for 40 min. This procedure allowed removal of the possible accumulated indium in the membrane. The HCl solution was removed and water used to wash the membrane. Then a new indium-containing feed solution was added to the feed compartment and the transport experiment continued. Using this washing procedure, the membrane recovered its initial flux value. It was observed, that as long as the membrane was washed, transport performance remained constant (see the 33–55 h use interval). Thus, it was possible to use the membrane under these conditions for about 130 h. After this, the membrane mechanical strength was considerably reduced, and the membrane broke.

CONCLUSIONS

The PIM systems studied were fruitful for In(III) transport from a nitrate medium. Optimization of the composition of the phases indicated that the best recovery of the metal is obtained using pH = 1.8 (feed), 1 mol L^{-1} (HCl strip), 1.2–1.8 mmol g^{-1} NPOE/0.8 mmol g^{-1} CYANEX 272 (membrane). Such PIMs allow In(III) separation from Fe(III) and Zn(II). Although in competitive experiments Fe(III) hinders In(III) permeation, extremely high selectivity for the separation was accomplished. Using a membrane composition of 25% CTA, 25% NPOE, and 50% CYANEX 272, the P_s value was 1.08×10^{-5} m s^{-1} (0.065 cm min^{-1}) in the presence of a 10-fold excess of iron(III) and 1.83×10^{-5} m s^{-1} (0.11 cm min^{-1}) with both cations in equimolar quantities under optimal transport conditions. The extent of reduction in the indium permeability is conditioned by the iron concentration. A membrane interface destabilizing effect by Fe(III) is the possible cause for iron obstruction. The selectivity factors of In(III) over Zn(II) under the selected compromised transport conditions were 72 and 35, respectively, for a 40-fold and 80-fold excess of Zn(II). It was possible to operate the PIM system satisfactorily for 130 h. However, indium-retention in the membrane produced a flux reduction as the membrane was repeatedly used with fresh feed solution. Washing the membrane with HCl to completely strip the indium retained in the membrane allowed recovery of the original flux values; however, the mechanical strength of the membrane was considerably reduced.

ACKNOWLEDGMENTS

The authors wish to thank DGAPA-UNAM (projects IN106802 and IN211405) and CONACyT (projects 38061U and 47417).

REFERENCES

1 A. P. Paiva, "Recovery of indium from aqueous solutions by solvent extraction," *Sep. Sci. Technol.*, **36**(7), 1395-1419 (2001).

2 C. Lupi, M. Morgana, D. Pilone, and V. Siepe, "Solvent extraction of indium by Ionquest 801," Proc. Global Symposium on Recycling, Waste Treatment and Clean Technology, REWAS 2004, Vol. III; I. Gaballah, B. Mishra, R. Solozabal, and M. Tanaka, Eds., TMS-INASMET, Spain, 2004; pp. 2205-2211.

3 A. M. Sastre, A. Kumar, J. P. Shukla, and R. K. Singh, "Improved techniques in liquid membrane separations: An overview," *Sep. Purif. Methods,* **27**(2), 213-298 (1998).

4 H. Okushita and T. Shimidzu, "Selective and active transport of In^{3+} through N-nitroso-N-p-octadecylphenylhydroxylamine ammonium salt," *Bull. Chem. Soc. Jpn.*, **63**, 920-925 (1990).

5 K. Kondo, Y. Yamamoto, and M. Matsumoto, "Separation of indium(III) and gallium(III) by a supported liquid membrane containing diisostearylphosphoric acid as carrier," *J. Membr. Sci.,* **137**, 9-15 (1997).

6 E. Rodríguez de San Miguel, J. C. Aguilar, and J. de Gyves, "An SLM system for the extraction of In(III) from concentrated HCl media using ADOGEN 364 as carrier," *J. Chem. Technol. Biotechnol.*, **66**, 56-64 (1996).

7 L. D. Nghiem, P. Mornane, I. D. Potter, J. M. Perera, R. W. Cattrall, and S D. Kolev, "Extraction and transport of metal ions and small organic compounds using polymer inclusion membranes (PIMs)," *J. Membr. Sci.,* **281**, 7-41 (2006).

8 G. Salazar-Alvarez, A. N. Bautista-Flores, E. Rodríguez de San Miguel, M. Muhammed, and J. de Gyves, "Transport characterisation of a PIM system used for the extraction of Pb(II) using D2EHPA as carrier," *J. Membr. Sci.,* **250**, 247-257 (2005).

9 E. Rodríguez de San Miguel, A. V. Garduño-García, J. C. Aguilar, and J. de Gyves, "Gold(III) transport through polymer inclusion membranes: efficiency factors and pertraction mechanism using KELEX 100 as carrier," *Ind. Eng. Chem. Res.,* **46**, 2861-2869 (2007).

10 A. G. Gaonkar and R. D. Neuman, "Purity considerations and interfacial behavior of solvent extraction systems," *Sep. Purif. Methods*, **13**, 141-152, (1984).

11 M. Ashraf Chaudry, M. Tayyib Malik, and Ali Azmat, "Transport of Co(II) ions through Di(2-ethylhexyl)phosphoric acid-CCl_4 supported liquid membranes," *Sep. Sci. Technol.*, **25**(11&12), 1161-1174 (1990).

12 E. Rodríguez de San Miguel, J. C. Aguilar, and J. de Gyves, "Structural effects on metal ion migration across polymer inclusion membranes: Dependence of transport profiles on nature of active plasticizer," *J. Membr. Sci.,* **307**, 105-116 (2008).

PHENOL REMOVAL FROM DILUTE AQUEOUS STREAMS USING SOLVENT-IMPREGNATED RESINS

B. Burghoff, E. L. V. Goetheer, and A. B. de Haan

Eindhoven University of Technology, Den Dolech 2, 5600 MB Eindhoven, Netherlands.
Corresponding author email address: b.burghoff@tue.nl

ABSTRACT

Phenol removal from dilute aqueous streams with solvent-impregnated resins (SIRs) is investigated. After extractant selection comprising a literature review, quantum chemical molecular modelling, and experiments, the alkylphosphine oxide compound Cyanex 923 is determined to be the most promising extractant to impregnate macro porous polymer (MPP) particles. At low phenol concentrations (<0.02 mol L^{-1}), the prepared SIRs exhibit better performance than ion exchangers and synthetic adsorbents. Furthermore, SIRs can also be advantageous over active carbon due to their facile regeneration using an alkaline solution. Overall Cyanex 923 containing SIRs are a promising technique for phenol removal.

INTRODUCTION

Phenol is contained in process waters and waste waters of the chemical industry. Therefore, it is important to have an efficient phenol separation technology. Solvent-impregnated resin (SIR) technology is investigated as an alternative separation technology. A SIR consists of a macro porous resin impregnated with an extractant. Advantages are low solvent loss and prevention of emulsification [1]. The whole pore volume is filled with the extractant and thus incorporated in the extraction. A suitable extractant for SIR applications is, of course, crucial. The quality of an extractant is determined by its distribution ratio K_D, which describes the equilibrium partitioning of a component between two liquid phases.

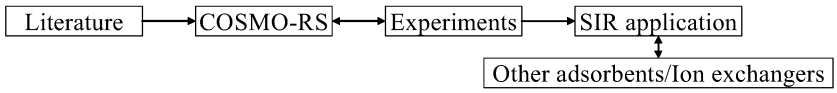

Figure 1. Approach of the investigation.

The approach of the project is depicted in Figure 1. The starting point is the selection of different phenol extractants based on a literature study. In Table 1, a selection of extractants found in references including their respective K_D values for phenol are given. Octanol [2] serves as a reference point. One of the possible extractants found in references is a combination of trioctylamine/trioctylamine salt dissolved in

octanol [3]. Also alkylphosphates, like tributylphosphate, are used in chromatography, mainly as a means to preconcentrate phenolic solutions [4]. Phosphine oxides like trioctylphosphine oxide (TOPO) [5] are also suggested. Due to its melting point of 50–55 ºC, TOPO needs to be diluted [6]. A different phosphine oxide compound than TOPO, namely Cyanex 923 is investigated amongst others by Watson et al. for phenol extraction [7]. It shows a high K_D value for phenol and can be used undiluted, as it is liquid at ambient temperature.

Table 1. Potential phenol extractants according to references

Substance	Distribution ratio $[(\text{mol L}^{-1})\ (\text{mol L}^{-1})^{-1}]$
Cyanex 923 (trialkyl–(C6, C8)–phosphine oxide) [7]	1034
Trioctylamine (TOA) salts and TOA in octanol [3]	800
Tri-n-octylphosphine oxide in diisobutyl ketone [5]	660
Tributylphosphate [4]	450
Octanol [2]	30

Quantum-chemical continuum models can be used as extractant-screening methods. Unlike empirical models, they do not depend on experimentation but dependonly on quantum chemical calculations. One of these continuum models is the conductor-like screening model for real solvents COSMO-RS [8]. Since it provides fast calculations, it is used to screen for a suitable phenol extractant for application in an SIR. The simulation of K_D values with COSMO-RS is based on activity-coefficient estimations. The K_D of phenol between the extractants and water are evaluated based on this screening technique. Subsequent experiments are carried out to validate the simulation.

Based on the screening described above, an extractant is selected, which is used for the impregnation of macro porous polymer (MPP) particles. This SIR is experimentally evaluated in terms of its applicability and regenerability. Finally, the performance of the SIR during phenol extraction is compared with other synthetic resins as well as activated carbon and ion exchangers.

MATERIALS AND METHODS

The substances that are examined are trioctylamine (≥93%, Merck KGaA, Germany), toluene (analysis grade, Merck KGaA, Germany), 1-octanol (~99%, Acros Chemicals, Belgium), tributylphosphate (>99%, Merck KGaA, Germany), tri-n-octylphosphine oxide (≥99%, Sigma Aldrich, Germany), tri-(C6,C8)-alkylphosphine oxide (Cyanex 923) (93%, Cytec Industries Inc., Netherlands) and phenol (≥99%, Merck KGaA, Germany). The reason why pure trioctylamine is used instead of a combination of trioctylamine/trioctylamine salt as suggested by Braun et al. [3] is that the trioctylamine salt is unstable during multiple cycles, as the regeneration is done with alkaline solution. Each substance is used without further purification. The liquid-liquid equilibria are determined in closed stirred glass vessels. The aqueous phase spiked with phenol 1 g kg^{-1} is mixed with the respective undiluted extractant in a 10:1 ratio at ambient pressure and

temperature for approximately 16 hours. After the extraction, the two phases are separated. Samples from the aqueous phase are taken and analyzed via aminoantipyrine complexation and detection at 510 nm (Cary 300 Conc UV/VIS spectrophotometer, Varian, Netherlands). The phenol content of the organic phase in equilibrium is determined by a simple mass balance.

The particles for impregnation consist of semicrystalline macro porous polypropylene polymer MPP (Akzo MPP Systems, Netherlands), washed with acetone prior to use. Cyanex 923 is diluted with *n*-hexane, and the particles are contacted with this solution during impregnation. The impregnation takes place at 25 ºC and standard pressure for 16 hours to ensure complete impregnation of the particles with the solution. The *n*-hexane is then slowly evaporated at 60 ºC and 10 kPa for 16 hours. Pure Cyanex 923 remains inside the pores. The prepared SIR is completely impregnated and has a Cyanex 923 content of 1.57 mol kg^{-1} SIR.

The stability tests of the SIR are carried out batchwise by determining the isotherms in a concentration range up to 8 g kg^{-1} phenol. The phenol content of the aqueous phase is determined as described above. The SIR is regenerated with barium hydroxide (≥98%, Fluka, Italy) solution of pH = 13. Isotherms for Amberlite XAD7, Amberlite XAD16 (Rohm and Haas Company, France), AquaSorb 202 (Jacobi Carbons, Germany), and ion exchangers Amberlyst A21 and Amberlite IRA-900 (Rohm and Haas Company, France) are determined in a concentration range up to 8 g kg^{-1}.

RESULTS AND DISCUSSION

Simulations with COSMO-RS are performed for different component groups such as alcohols, alkylamines, alkylphosphates, and alkylphosphine oxides. However, for the sake of simplicity, only the results of substances also found in the literature are explained. As illustrated by comparing the datapoints along the vertical axis in Figure 2, COSMO-RS predicts Cyanex 923 to be the most efficient phenol extractant of the evaluated substances, which is in agreement with the literature review. Trioctylphosphine oxide, which is quite similar to Cyanex 923, is the second best followed by tributylphosphate, 1-octanol, trioctylamine, and toluene in decreasing order. In line with the simulations, liquid-liquid equilibrium experiments show that the phosphorous-containing substances have a higher phenol K_D than the others investigated. The experiments confirm Cyanex 923 as the most efficient phenol extractant. Moreover, the experiments show that trioctylphosphine oxide is slightly less effective than Cyanex 923 in terms of the experimentally determined distribution ratio, which is also in line with the simulation trend. The experimentally determined distribution ratio decreases further in the order of tributylphosphate, 1-octanol, trioctylamine, and the diluent toluene, which has a low phenol capacity. Strikingly, the K_D of trioctylamine is not as good as expected from the high value in Table 1 for trioctylamine/trioctylamine salt. Pure trioctylamine has an experimental K_D 100 times lower than the respective salt. Nonetheless, trioctylamine performs better during the experiments than predicted by COSMO-RS.

Comparing the simulated distribution ratio $K_D^{sim.}$ and the experimental distribution ratio K_D^{exp}, a qualitative trend for the investigated extractants can be observed (Figure 2). The simulated values of K_D^{sim} are qualitatively accurate. The

disagreement between the simulated and experimental results of trioctylamine can be attributed to the fact that trioctylamine, like amines in general, are very hard to simulate in quantum-chemical continuum models and apt to erroneous results. The otherwise qualitatively accurate description of the distribution ratio corroborates that COSMO-RS is a suitable tool for quick extractant screening.

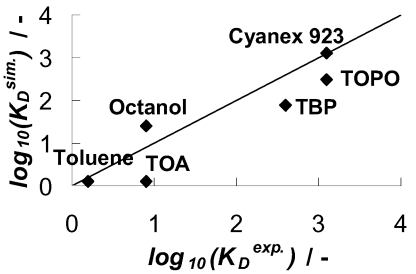

Figure 2. Parity plot of simulated and experimental distribution ratios.

In the next step the most suitable phenol extractant Cyanex 923 is used for the impregnation of macro porous polymer (MPP). The completely impregnated particles are supposed to be used during multiple cycles, and the capacity isdesired to remain constant. This is why a suitable regeneration method has to be found. Regeneration at high temperature is possible, but MPP particles are stable up to 120 ºC, and in this temperature range the regeneration is not complete. Another efficient method for the regeneration of phenol-containing extractants is possible at high pH [9]. However, the use of a sodium hydroxide solution causes leaching of Cyanex 923 from the pores. This emulsification effect also occurs with potassium hydroxide, strontium hydroxide, and aqueous ammonia solution. Only barium hydroxide $Ba(OH)_2$ was found not to cause emulsification. In Figure 3, the stability of the Cyanex 923 containing SIR during seven cycles of repeated phenol extraction and regeneration with $Ba(OH)_2$ is shown. The isotherms depicted are from the first, fourth, and seventh extraction cycle in order to maintain clarity of the graph.

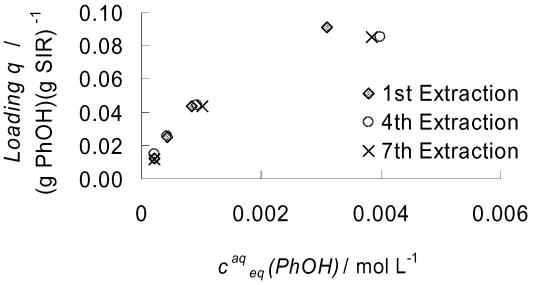

Figure 3. Regeneration of SIR's with $Ba(OH)_2$ solution during multiple cycles.

After the first cycle, the extraction performance of the SIR decreases as a result of two contributing mechanisms. These mechanisms are the extractant wash-off due to the expansion of the organic phase during phenol uptake and the wash-off of residual extractant from the outside surface of the SIR. This leaching only occurs during the first

cycle. Afterwards, the SIR shows a stable performance up to the seventh cycle, which was the last one measured. This shows that the prepared SIR is stable and can be used successfully for the extraction of phenol.

The prepared SIR is compared with other resins in order to evaluate its competitiveness. For this comparison, the unimpregnated MPP, two synthetic adsorbents, two ion exchangers, and active carbon were used. The two ion exchangers are the weakly basic Amberlyst A21 and the strongly basic Amberlite IRA-900. Both resins are modified *tert*-amine divinylbenzenestyrene copolymers. The active carbon used is AquaSorb 202, a steam-activated granulate of bituminous coal. Additionally, the unimpregnated polypropylene polymer MPP and the nonionic aliphatic acrylic polymer Amberlite XAD7 and crosslinked polystyrene divinylbenzene Amberlite XAD16 are investigated. These three resins do not have additional functional groups.

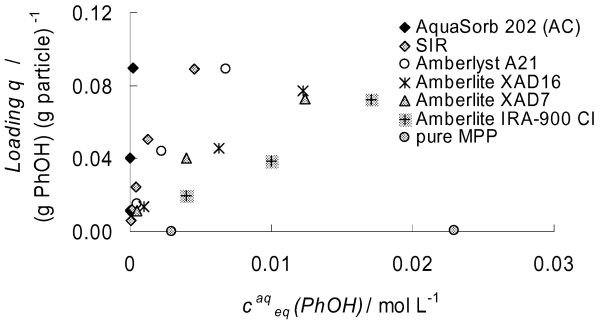

Figure 4. Comparison of SIR with synthetic adsorbents, ion exchangers, and activated carbon.

In Figure 4, the results of phenol extraction experiments for the above-mentioned resins are depicted. The SIR shows a better performance than the two basic ion exchangers, Amberlyst A21 and Amberlite IRA-900, and the adsorbents, Amberlite XAD7, XAD16, and unimpregnated MPP. The latter has no significant phenol capacity. Evidently, active carbon is the best phenol adsorbent in this case. There are nonetheless several drawbacks in its application. Although active carbon performs better than the SIR, its use in a recovery unit is only economic at a bed size larger than 30 m^3. Below a bed size of 30 m^3, the loaded active carbon is preferably burnt. At higher bed sizes, harsh regeneration conditions are needed under which more than 10% of the particles are lost. The prepared MPP-based SIR is the second best phenol remover. As was already shown, it can be easily regenerated and reused. This is why in spite of the superior phenol capacity of active carbon, the MPP based SIR with an extractant loading of 1.57 mol Cyanex 923 kg^{-1} can become more attractive than active carbon. Based on the above presented experimental results, it can be stated that SIR technology is a promising alternative to other phenol removal technologies such as ion exchange and adsorption.

CONCLUSIONS

The distribution ratios simulated with COSMO-RS show a reliable qualitative trend. During simulations and experiments, the compound Cyanex 923 is determined to be the best phenol extractant out of the investigated substances, which is in agreement

with the literature. Except for the problematic description of amines, COSMO-RS can be used as a quick screening tool for extractant selection.

The SIR, which is prepared using MPP as a matrix and Cyanex 923 as extractant, is applicable for the phenol extraction during multiple cycles. Furthermore, it is competitive to the evaluated synthetic resins. The main advantage compared to active carbon is its easy regeneration. The regeneration can be done with barium hydroxide. This indicates that a SIR is a promising alternative for the conventional phenol removal technologies at low concentration levels.

ACKNOWLEDGMENTS

This work is financially supported by the Technology Foundation STW, Akzo Nobel, INEOS Phenol, and Vitens. Support by our colleagues ir. Cuypers and Prof. Dr. Zuilhof at University of Wageningen and Prof. Dr. Sudhölter at Delft University is also acknowledged. The supply of Cyanex 923 by Cytec Industries Inc., Netherlands, and the support of COSMOlogic GmbH, Germany is gratefully acknowledged.

REFERENCES

1. K. Babić, L. van der Ham, and A. de Haan, "Recovery of benzaldehyde from aqueous streams using extractant impregnated resins," *React. Funct. Polym.*, **66**(12), 1494–1505 (2006).
2. E. Bekou, D. D. Dionysiou, R. Y. Qian, and G. D. Botsaris, "Extraction of Chlorophenols from Water Using Room Temperature Ionic Liquids," ACS Symposium Series, 856, 544–562 (2003).
3. G. Braun, W. Grünbein, M. Mayer, and B. Wojtech, "A Simple and Complete Recovery of Phenol from Waste Water by Tertiary Amines in Form of Sulfates – A New Powerful Extractant," International Solvent Extraction Conference, München, Germany, 1986; pp. 885–891.
4. V. G. Torgov, Y. I. Korenman, M. K. Drozdova, V. V. Rebristaya, and R. P. Lisitskaya, "Extraction of phenol from aqueous media with trioctylamine oxide," *Russ. J. Appl. Chem.*, **66**(1), 182–183 (1993).
5. J. D. MacGlashan, J. L. Bixby, and C. J. King, "Separation of Phenols from Dilute Aqueous Solution by Use of Tri-*n*-octyl phosphine Oxide as Extractant," *Solvent Extr. Ion Exch.*, **3**(1&2), 1–25 (1985).
6. A. M. Urtiaga and I. Ortiz, "Extraction of Phenol Using Trialkylphosphine Oxides (Cyanex 923) in Kerosene," *Sep. Sci. Technol.*, **32**(6), 1157–1162 (1997).
7. E. K. Watson, W. A. Rickelton, A. J. Robertson, and J. T. Brown, "A Liquid Phosphine Oxide: Solvent Extraction of Phenol, Acetic Acid and Ethanol," *Solvent Extr. Ion Exch.*, **6**(2), 207–220 (1988).
8. F. Eckert and A. Klamt, "Fast Solvent Screening via Quantum Chemistry: COSMO-RS Approach," *AIChE Journal*, **48**(2), 369–385 (2002).
9. W. Cichy, S. Schlosser, and J. Szymanowski, "Recovery of Phenol with Cyanex(R) 923 in Membrane Extraction-Stripping Systems," *Solvent Extr. Ion Exch.*, **19**(5), 905–923 (2001).

EXTRACTANT IMPREGNATED RESIN TECHNOLOGY FOR THE RECOVERY OF ALDEHYDES FROM AQUEOUS STREAMS

K. Babić,[1] A. G. J. van de Ham,[1] and A. B. de Haan[2]

[1]University of Twente, P.O. Box 217, 7500 AE Enschede, the Netherlands. [2]Eindhoven University of Technology, P.O. Box 513, 5600 MB Eindhoven, The Netherlands.
Corresponding author e-mail address: Katarina.Babic@SABIC-Europe.com

ABSTRACT

Extractant Impregnated Resin technology, a synergistic combination of adsorption and reactive extraction, is proposed for the removal of aldehydes from aqueous streams. As complexing agent, the primary amine Primene JM-T was used. The extraction capability towards several aldehydes, in both liquid-liquid and impregnated-resin systems was tested and corresponding equilibrium isotherms determined. An equilibrium model was developed for the prediction of isotherms in impregnated systems based on the known liquid-liquid behavior. Subsequently, the sorption kinetics was investigated. Results show a strong dependency on the molecular structure of the aldehyde as well as on the polymeric support material.

INTRODUCTION

Extractant Impregnated Resin (EIR) technology [1] is a process that combines the characteristics of adsorption and reactive liquid-liquid extraction, offering high capacity and selectivity together with the ease of operation of a fixed bed for processing dilute or viscous solutions. Moreover, it minimizes the problems of emulsion formation and extractant losses. In EIRs, the extractant is physically immobilized in the adsorbent particle (Figure 1). When contacted with an aqueous solution, the reagent forms a complex with a solute. Both reagent and the formed complex remain in the resin phase, as they are insoluble in the aqueous phase. Preparation of such particles by soaking the adsorbent in the extractant solution is rather simple, yielding a relatively inexpensive separation medium. Additionally, by changing the extractant liquid inside the pores, this technique can be tuned to meet the requirements of a specific separation problem.

EIR technology was proposed by us for the removal of aldehydes from aqueous streams down to the ppb level [2], either to protect the environment or to obtain a valuable product. As complexing agent, the primary amine Primene JM-T was used. It shows a reversible yet sufficiently strong reaction with aldehydes, increasing the aldehydes affinity for the organic phase by several orders of magnitude. In the present work, the extraction performance of JM-T towards aldehydes of different molecular structure is investigated. The influence of different polymeric supports was also studied.

The comparison was made based on liquid-liquid and sorption equilibria as well as kinetic performance.

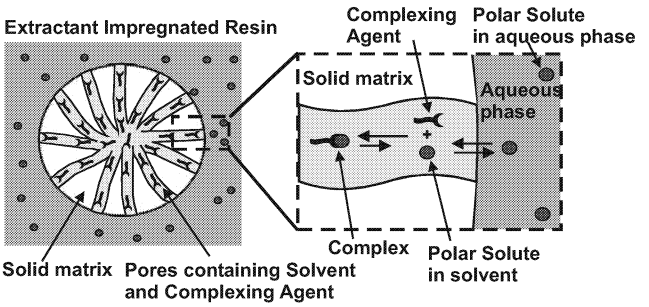

Figure 1. Extractant impregnated resin particle.

EXPERIMENTAL

Reagents

The chemicals were obtained from the following suppliers: benzaldehyde and furfural from Merck, Germany; pentanal, 3-methylbutanal, and 2-methyl-2-butenal from Fluka, Germany; and Amberlite XAD-16 and XAD-4 (polystyrene divinyl benzene copolymer) from Sigma Aldrich, Germany. A sample of Primene® JM-T was donated by Rohm and Haas, Europe; macroporous polypropylene (MPP) particles by Akzo Nobel, the Netherlands; and macroporous polyethylene (Stamypor) particles by Sabic-Europe. All chemicals were used as received. All aqueous solutions were made using MiliQ water.

Experimental Procedures

Liquid-liquid equilibrium experiments were conducted on a fully automated workstation, as described elsewhere [2,3]. The extraction was done in closed 2-ml glass vials that were agitated for 24 h at 25 ^{o}C to ensure equilibrium. After agitation, the vials were transferred into thermostated (25 ^{o}C) trays, and a settling time of at least 2 h was allowed and shown to be sufficient. After settling, a sample of the aqueous phase was taken and placed in a separate vial together with the precalculated amounts of ethanol and internal standard solution (dibenzofuran in ethanol). Quantitative analysis was done using a gas chromatograph, Varian CP-3800 system equipped with a capillary VF-5ms column (30 m, 0.25 mm; 0.50 μm packing) and a FID detector. Accuracy of the analytical method was determined to hold within 2.5%. The concentration of aldehydes in the organic phase was calculated from the mass balance.

Resins were impregnated with Primene JM-T using the dry impregnation method according to the procedure described in our previous work [2]. The loading of the resin with extractant was determined by measuring the increase of the mass.

The experimental procedure as well as the analytical method was described in more detail in our previous work [2]. Different amounts of impregnated resins were placed in a flask. Then 15 mL of aqueous solution of an aldehyde was added. The system

was allowed to equilibrate in a thermostated shaking bath for 24 h before a sample of the aqueous phase was taken and the concentration of aldehyde determined. The concentration of aldehyde in the particle was calculated via a mass balance.

Kinetics was investigated using a shallow bed [4]. For the on-line detection of aldehydes, a UV/Vis detector was used. The volume of the impregnated particles placed in the column was 0.21 mL in all experiments yielding a packed layer thickness of about 2 mm and bed porosity of 0.61. Experiments were performed at sufficiently high flow rates to eliminate the effect of external mass transfer and axial dispersion. Prior to the experiments, the set-up was calibrated as described elsewhere [5]. The dead volume of the set-up used in these experiments was determined to be 3.2 ± 0.1 mL.

RESULTS AND DISCUSSION

Liquid-Liquid Equilibrium

For the description of the reactive extraction of aldehydes with Primene JM-T, a simple equilibrium model is developed. The extraction occurs due to both the physical partitioning and the chemical reaction (Equation 1). To keep the model as simple as possible, it was assumed that activities could be replaced with concentrations, the concentration of water is constant, these can therefore be incorporated in the conditional equilibrium constant K_r and the physical partitioning ratio P remains constant through the whole range of concentrations. The reaction equilibrium constant and the physical partitioning ratio are defined by Equation 2. By combining Equations 2 and the mass balances for the species present in the system, the total concentration of aldehyde in the organic phase can be calculated as a function of the concentration of aldehyde in the aqueous phase at equilibrium and the initial concentration of amine in the organic phase (Equation 3). For the prediction of the equilibrium isotherm, the model parameters, the reaction equilibrium constant K_r and physical partitioning coefficient P need to be known. In these equations, C is the concentration in mol/L. Subscripts *Ald* and *Am* stand for aldehyde and amine, while *AldAm* stands for the formed complex. Superscripts *org* and *aq* indicate the organic and aqueous phase, and subscript *o* denotes the initial value.

$$R_1R_2CO + R_3NH_2 \leftrightarrow R_1R_2C{=}NR_3 + H_2O \tag{1}$$

$$K_r = \frac{C_{AldAm}^{org}}{C_{Ald}^{org} \cdot C_{Am}^{org}} \quad ; \quad P = \frac{C_{Ald}^{org}}{C_{Ald}^{aq}} \tag{2}$$

$$C_{total}^{org} = P \cdot C_{Ald}^{aq} \cdot \left(1 + \frac{K_r \cdot C_{Am,o}^{org}}{1 + P \cdot K_r \cdot C_{Ald}^{aq}} \right) \tag{3}$$

The extraction capability of Primene JM-T towards different aldehydes was compared in Figure 2 including the values of the model parameters [3]. Primene JMT shows the best extraction performance towards straight-chain aliphatic aldehydes (pentanal and 3-methylbutanal). They are the most accessible to the nucleophilic attack by the amine, because there is no steric hindrance. 3-Methylbutanal is slightly more soluble in water then pentanal; thus, the value of P is somewhat lower as well as the

overall extraction. Due to its aromatic ring, benzaldehyde has a rather rigid structure, reducing the number of steric conformations it can take and possibly causing poor solvation by a bulky and intermolecularly hydrogen-bonded molecule like JM-T. The reaction between benzaldehyde and JM-T is also stericaly hindered, and upon reaction, a complex containing both an aromatic ring and a double bond next to each other is formed, which is even more rigid and probably less capable of solvating additional benzaldehyde molecules. The extraction of furfural with JM-T is somewhat low due to the hydrogen bonds furfural forms with water molecules and the delocalization of its electrons. 2-Methyl-2-butenal exhibits a very low complexation with the amine, largely due to the considerable steric hindrance caused by the methyl group at the α position and also due to the delocalization of its electrons.

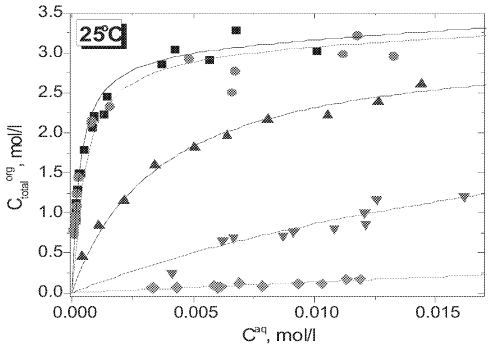

symbol	aldehyde	P [-]	K_r [l/mol]
■ ; —	pentanal	15.8	198.6 ± 10.9
● ; —	3-methylbutanal	11.6	182.9 ± 11.3
▲ ; —	benzaldehyde	1.7	168
▼ ; —	furfural	0.65	58.6 ± 1.9
♦ ; —	2-methyl-2-butenal	2.22	1.7 ± 0.1

Figure 2. Equilibrium isotherms for liquid-liquid extraction at 25 °C (points – experimental data; lines – model) and corresponding values of model parameters [3].

Sorption Equilibrium

The basic assumption of the sorption equilibrium model is that the reaction takes place in the liquid organic phase, only and thus, the polymeric backbone can be considered to be inert. In that case, the Equation 3 can be used to describe the sorption equilibrium isotherm. Nevertheless, this assumption is valid only in the case that the adsorption on the particle surface is negligible. Therefore, this approach allows an insight into the influence of the polymeric backbone material on the overall sorption.

To highlight this influence, the performance of EIRs is compared with the reactive liquid-liquid extraction. The equilibrium isotherms of pentanal are presented in Figure 3a. It can be noticed that the experimental points for all the impregnated particles studied are spread around the theoretically calculated curve (Equation 3). The same is observed for 3-methylbutanal and furfural (not shown). Thus, it can be concluded that the particle material does not influence the sorption of these aldehydes. However, different behavior is observed for benzaldehyde (Figure 3b). In the case that there would be no particle influence, all the points would lay on the theoretically predicted curve model line (Equation 3) as this is the case for pentanal. However, it is shown that, for all the impregnated resins there is an increase in the total organic concentration compared with the liquid-liquid isotherm, which is probably caused by additional adsorption on the particle surface. The increase is especially large in the low concentration region. If different polymeric supports are compared, the additional capacity increases in the order Stamypor < MPP < XAD16 < XAD4. Taking into account resin properties, it can be

concluded that the two least polar particles, Stamypor and MPP, increase the overall capacity less than the two slightly more polar ones. Moreover, XAD16 and XAD4 are aromatic resins and have some affinity towards aromatic components. XAD4 has a larger surface area than XAD16 and therefore a higher adsorption capacity.

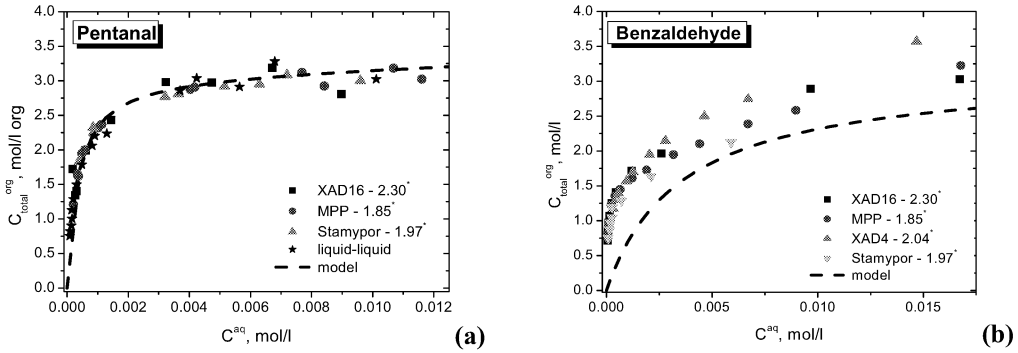

Figure 3. Comparison between reactive liquid-liquid extraction and extractant impregnated resins at 25 °C for the recovery of a) pentanal and b) benzaldehyde. Particle loadings are expressed in mol_{JMT}/L_{EIR}.

Sorption Kinetics

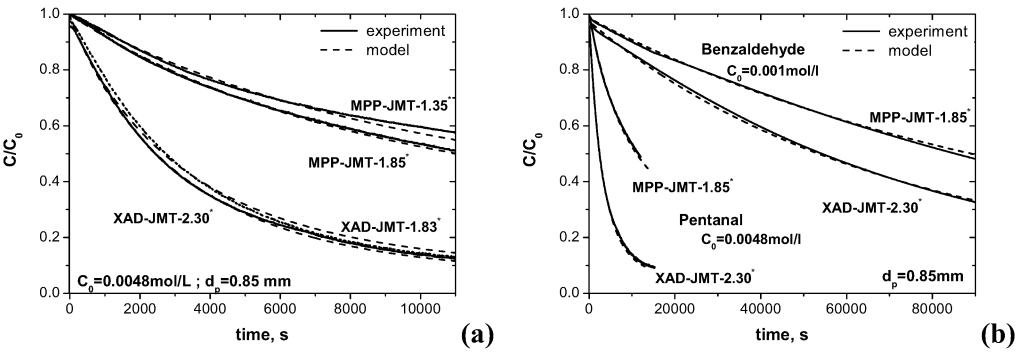

Figure 4. Influence of the a) particle material and extractant loading on the particle for pentanal and b) molecular structure of aldehyde on the sorption kinetics. Particle loadings are expressed in mol_{JMT}/L_{EIR}; all particles have the same mean diameter of 0.85 mm.

Kinetics of the aldehydes sorption with resins impregnated with Primene JM-T is shown in Figure 4. It is influenced by both intraparticle diffusion and chemical reaction. This was proven with a modified shrinking-core model and a rigorous model based on the analogy to diffusion and reaction in a stagnant liquid sphere corrected for the porosity and particle properties [2,5]. Figure 4a shows that the particle properties strongly influence the sorption kinetics. Even though MPP has larger pores, the more polar XAD16 promotes the diffusion of the polar molecules. It can also be noticed that the sorption rate slightly increases with the increase of the extractant loading (and thus, the volume of the organic phase), which suggests that the chemical reaction is slow and occurs in the bulk organic phase [6]. As shown in Figure 4b, the sorption of

benzaldehyde is much slower than the sorption of pentanal, possibly due to the steric hindrances. Additionally, it is observed and explained by several authors [7] that the complex-formation mechanism is different for aromatic and aliphatic compounds. Unlike the sorption of pentanal, the sorption of benzaldehyde with impregnated resins is influenced by both reactive extraction and surface adsorption. Therefore it can not be assumed that the polymeric support is inert. However, even though the surface diffusion is not included in the model it fits the experimental data rather well, suggesting that the surface diffusion is negligible [8].

CONCLUSIONS

The molecular structure of an aldehyde strongly influences the extraction capability of Primene JM-T. The extraction capacity in both liquid-liquid and impregnated systems decreases in the order pentanal > 3-methylbutanal > benzaldehyde > furfural > 2-methyl-2-butenal. A simple model based on the known liquid-liquid equilibrium can be used for extractant impregnated resins to predict the sorption equilibrium for all the investigated aldehydes except benzaldehyde, where additional adsorption on the particle surface is observed. Sorption kinetics is influenced by both chemical reaction and diffusion, that is, by molecular structure of the aldehyde (faster for pentanal than for benzaldehyde) and particle support material (diffusion is promoted by slightly more polar particle).

REFERENCES

1. J. L. Cortina and A. Warshawsky, "Developments in Solid-Liquid Extraction by Solvent-Impregnated Resins," Ion Exchange and Solvent Extraction, Vol. 13, J. A. Marinsky and Y. Marcus, Eds., Dekker, New York, 1997; pp.195-293.
2. K. Babić, A. G. J. van der Ham, and A. B. de Haan, "Recovery of benzaldehyde from aqueous streams using extractant impregnated resins," *React. Funct. Polym.*, **66**(12), 1494-1505 (2006).
3. K. Babić, A. G. J. van der Ham, and A. B. de Haan, "Reactive Extraction of Aldehydes from Aqueous Solutions with Primene JM-T," *submitted.*
4. M. Eić and D. M. Ruthven, "A new experimental technique for measurement of intercrystalline diffusivity," *Zeolites*, **8**, 40-45 (1988).
5. K. Babić, A. G. J. van der Ham, and A. B. de Haan, "Sorption Kinetics for the Removal of Aldehydes from Aqueous Streams with Extractant Impregnated Resins", *Adsorption,* accepted for publication.
6. B. P. Nikhade and V. G. Pangarkar, "Equilibria and kinetics of extraction of citric acid from aqueous solutions in Alamine 336-cyclohexanone system," *Sep. Sci. Technol.*, **40**(12), 2539-2554 (2005).
7. B. Martin, "Reactions of Carbonyl Compounds with Amines and Derivatives", *J. Phys. Chem.,* **68**(6), 1369-1377 (1964).
8. J. A. Hoogendoorn, G. F. Versteeg, and W. P. M. van Swaaij, "Experimental study of the absorption of acid gases in porous particles impregnated with aqueous alkanolamine solutions," *Chem. Eng. Sci.*, **49**(20), 3421-3438 (1994).

DISPLAYED "END EFFECTS" FOR EXTRACTION WITH EMULSION LIQUID MEMBRANES: MASS-TRANSFER MODEL OF EXTRACTION OF ZINC WITH D2EHPA IN SINGLE-DROP APPARATUS

J. F. le Bon, A. Buch, D. Pareau, C. Leroi, J. El Bekri, and M. Stambouli

Ecole Centrale Paris, LGPM, 92295 Chatenay Malabry, France.
Corresponding author email address: arnaud.buch@ecp.fr

ABSTRACT

We state that mass-transfer experiments in ELM extraction with the single-drop apparatus offer an original result from the kinetics point of view during the drop-formation step, namely the "end effects". To characterize this phenomenon, we have developed a mass-transfer model for carrier-facilitated transport in emulsion-liquid membranes. The model is based on the diffusion flux in the external aqueous phase and on the extraction reaction at the interface between the Zn^{2+} ions and the carrier molecules for the recovery of zinc from an aqueous solution by the di-(2-ethylhexyl)phosphoric acid (D2EHPA) carrier with water/oil/water emulsion-liquid membranes.

INTRODUCTION

The goal of current research on Emulsion Liquid Membrane (ELM) systems is to take benefit of the large mass-transfer areas offered by such systems, leading to high transfer rates. In addition, these systems may provide high separation factors thanks to the choice of carrier molecule. Indeed, ELM allows one to improve the mass-transfer efficiency compared to the classical solvent extraction. The "end effects" have been first observed by S. Perocheau [1] in the kinetic study of ELM extraction of Zn by trioctylamine (TOA). They correspond to a large extraction during drop-formation. The interest of this result is kinetic because of the short drop-formation time compared to the large drop rising-up time in the column. The goal of this paper is to study ELM extraction of Zn with the single-drop apparatus for another extractant family, the Zn/D2EHPA system.

EXPERIMENTAL

Reagents and Solutions

The extractant D2EHPA (Sigma, >95%) was dissolved in dodecane (VWR). The internal aqueous phase was composed of H_2SO_4 solutions (5×10^{-1} mol L^{-1}). The external aqueous solution is composed of $ZnSO_4$ (VWR, 99%, 1.2×10^{-2} mol L^{-1}). The emulsion

was prepared by mixing, at 25 °C, the stripping aqueous phase and the organic phase containing a surfactant (Abil EM 90 from Goldschmidt GmbH, 3%) with a rotor/stator emulsifier (ultra-turrax T25, Janke and Kunnel) at a high speed (13500 rpm).

End Effect and Single-Drop Procedure

The single-drop method has been chosen as the experimental method to measure the extraction kinetics.

In a single drop apparatus, the life-time of an emulsion drop is divided into three steps: (1) drop-formation, (2) drop rise-up, and (3) drop coalescence. End effects correspond to the extracted amount during drop-formation. They are quantified by the intercept at zero of the plot of the zinc concentration in the emulsion internal phase (C_I) versus the drop rising-up time (t_r). To understand the end-effects phenomenon, we have modelled mass-transfer for the Zn/D2EHPA system. For this chemical study, the thermodynamic study allowed us to establish:

$$Zn^{2+} + 3.\left(\overline{AH}\right) \Leftrightarrow \overline{ZnA_2\left(AH\right)} + 2.H^+ \quad (1)$$

$\overline{AH}$ is the monomer of D2EHPA, and the overbar denotes species in the organic phase.

MODELING

Modeling of Mass-transfer for the Zn/D2EHPA System

The mass-transfer of Zn^{2+} can be subdivided into the five following steps:

a. Transfer of Zn^{2+} from the external phase bulk (III) to the surface of the emulsion globule (external interface).
b. Reaction of Zn^{2+} with (AH) at the external interface releasing the counterion H^+.
c. Diffusion of the zinc organic complex across the organic phase.
d. Stripping of zinc at the internal interface
e. Back-diffusion of the free carrier to the external interface.

The two diffusion steps (c and e) and the Zn stripping of (step d) are assumed to be fast.

Mass-transfer Model for Drop Rising-Up

For step a, the transfer flux of Zn^{2+} in phase III can be written as follows:

$$N_r = k_{IIIr}.(C_{III} - C_{III}^{\ i}) \text{ (m.mol/L/s)} \quad (2)$$

with k_{IIIr} the diffusional transfer coefficient of Zn in the bulk external phase (m/s), C_{III}:Zn^{2+} concentration in the external phase (III) and C_{III}^{i}:Zn^{2+} concentration at the external interface.

The amount extracted by the emulsion could be neglected when compared to the amount contained in the whole external phase. Then $C_{III} = C_{III}^{\circ}$, where C_{III}° is the initial concentration of Zn in the external phase.

The transfer coefficient k_{IIIr} has been deduced from different correlations [2-4]. It is nearly constant in the diameter range of the study with k_{IIIr} = 2.14 (± 1.01) x 10^{-4} m/s.

Interfacial reaction (step b) could be represented by the following steps :

1. $Zn_i^{2+} + AH_{ad} \Leftrightarrow \left(ZnA^+\right)_{ad} + H^+$ K_1 (fast)
2. $\left(ZnA^+\right)_{ad} + \overline{AH} \Leftrightarrow \left(ZnA_2\right)_{ad} + H^+$ K_2 (fast)
3. $\left(ZnA_2\right)_{ad} + \overline{AH} \Leftrightarrow \overline{ZnA_2} + AH_{ad}$ k_3, k_3 (slow)
4. $\overline{ZnA_2} + \overline{AH} \Leftrightarrow \overline{ZnA_2(AH)}$ K_4 (fast)

K_1, K_2, and K_4 are the equilibrium constants. k_3 ,k_3 are the direct and opposite kinetic constants of Step 3 respectively. The desorption reaction of Zn loaded carrier is considered the rate-determining step. The stripping reaction in ELM process is considered as quantitative and fast. Therefore, it is possible to neglect the opposite reaction:

$$R_r = k_c . \frac{C_{III}^{\ i} . [\overline{AH}]^2 . [AH]_{(ad)r}}{[H^+]^2} \quad \text{(m.mol/L/s)} \tag{3}$$

with: $k_c = k_3 . K_1 . K_2$ (m^3/mol/s). During the drop rising-up, the interfacial concentration of $[AH]_{(ad)r}$ can be considered as constant, and the variation of the interfacial tension (γ), is given by the Langmuir isotherm:

$$[AH]_{(ad)r} = \frac{K_{ad} . \Gamma_0 . [\overline{AH}]}{1 + K_{ad} . [\overline{AH}]} \tag{4}$$

Γ_0 is the interfacial concentration at saturation (mol/m^2) and K_{ad} is the adsorption constant (L/mol).

Under pseudo-steady state conditions, there is no mass accumulation at interface; thus: $N_r = R_r$, then $k_{IIIr} . (C_{III}^{\ \circ} - C_{III}^{\ i}) = k_{cr} . C_{III}^{\ i}$ with: $k_{cr} = k_c . \left([\overline{AH}]^2 / [H^+]^2\right) [AH]_{(ad)r}$; k_{IIIr} and k_{cr} are the diffusional transfer coefficient and the chemical transfer coefficient, respectively. It comes the following expression of the transfer flux:

$$N_r = k_{gr} . C_{III}^{\ \circ} \tag{5}$$

with $k_{gr} = k_{IIIr} . k_{cr} / (k_{IIIr} + k_{cr})$. k_{gr} is the global transfer coefficient.

By assuming there is no mass accumulation in the organic membrane, we can write:

$$V_I . d(C_I(t)) = N_r . S_{III} . dt \tag{6}$$

where V_I is the internal-phase volume (m^3), C_I is the internal-phase concentration of Zn^{2+} (mol/L), and S_{III} is the emulsion-drop surface (m^2).

From experimental value, $2V_I = V_{III}$, where V_{III} is the emulsion-drop volume. By assuming the emulsion-drop spherical, then, from the Equations 5 and 6 and after integration of d$C1$ we obtain:

$$C_I = \left((12/d).C_{III}^{\circ}\right).k_{gr}.t_r + C_f \quad (7)$$

C_f is the extracted quantity during drop formation. Two cases could be considered depending on the nature of the rate-determining step:

- $k_{III\,r} << k_{cr}$: diffusional regime. The external diffusion of Zn is the rate-determining step. Thus, $k_{gr} = k_{III\,r}$. k_{gr} would not depend on the chemical parameters:

$$C_I = \left((12/d)C_{III}^{\circ}\right).k_{III\,r}.t_r + C_f \quad (8)$$

- $k_{IIIr} >> k_{cr}$: chemical regime. The interfacial reaction is the rate-determining step: $k_{gr} = k_{cr}$. Then k_{gr} would depend on the chemical conditions:

$$C_I = \left(\frac{12}{d}.C_{III}^{\circ}\right).k_c.\frac{[\overline{AH}]^2}{[H^+]^2}.[AH]_{(ad)\,r}.t_r + C_f \quad (9)$$

Mass-transfer Model for Drop Formation

For Step a, due to the short contact times, we used the penetration theory of Higbie [5] under constant renewal of the interface:

$$k_{III\,f} = 2.\sqrt{D_{III}/(\pi.\tau)} \quad (10)$$

τ(s), is the time necessary for the emulsion globule to rise a length equal to its diameter.

For Step b, we think that the desorption step is occurring later compared to extraction sequential steps of the drop rising-up due to the "viscosity" change.

(1')	$Zn_i^{2+} + AH_{ad} \Leftrightarrow ZnA_{ad}^{+} + H^+$	K'_1	(fast)
(2')	$ZnA_{ad}^{+} + \overline{AH} \Leftrightarrow ZnA_{2ad} + H^+$	K'_2	(fast)
(3')	$ZnA_{2ad} + \overline{AH} \Leftrightarrow ZnA_2(AH)_{ad}$	K'_3	(fast)
(4')	$ZnA_2(AH)_{ad} + \overline{AH} \Leftrightarrow \overline{ZnA_2(AH)} + AH_{ad}$	$\overrightarrow{k_{4f}}, \overleftarrow{k_{4f}}$	(slow)

In this case, the reaction rate is:

$$R_f = k'_c.([\overline{AH}]^3/[H^+]^2).[AH]_{(ad)\,f}.C_{III}^{i} \quad (12)$$

During drop formation, the interfacial concentration of extractant is not constant. By assuming there is no mass accumulation in the organic membrane and after mathematical treatment and integration of dC_I, then the mass-transfer model for drop formation is:

$$C_f = \left(\frac{12}{d}.C_{III}^{\circ}\right).\int_0^{t_f} \frac{\left(2.\sqrt{\frac{D_{III}}{\pi t_f}}\right).\left(\frac{\alpha_n.k'_c.[\overline{AH}]^3}{d^n.[H^+]^2}.\left(\frac{t_f}{t}\right)^{\frac{n}{3}}\right)}{\left(2.\sqrt{\frac{D_{III}}{\pi t_f}}\right)+\left(\frac{\alpha_n.k'_c.[\overline{AH}]^3}{d^n.[H^+]^2}.\left(\frac{t_f}{t}\right)^{\frac{n}{3}}\right)}.\left(\frac{t}{t_f}\right)^{\frac{2}{3}}.dt \quad (13)$$

Two limit cases are possible as a function of the nature of the mass-transfer regime:

- $k_{III\,f} << k_{c\,f}$: Diffusional regime $C_{f(diff)} = (72/d).C^{0}_{III}.\sqrt{D_{III}/\pi}.\sqrt{t_f}$
- $k_{III\,f} >> k_{c\,f}$: Chemical regime $(0 \le n \le 2)$

$$C_{f(chem)} = \frac{36}{5-n}.C^{0}_{III}.k'_{c}.\frac{\alpha_n}{d^{1+n}}.\frac{\left[\overline{AH}\right]^3}{[H^+]^2}.t_f \qquad (14)$$

RESULTS AND VALIDATION

Rising-up Model Validation

The linearity of C_I with t_r has been verified. We have studied the influence of d, $\left|\overline{AH}\right|$, and $[H^+]$ on C_I, by plotting logarithm of (C_I - C_f) versus logarithm of the considered parameter keeping others parameters constant. Experimental results have showed that the orders of t_r, d, $\left|\overline{AH}\right|$, and $[H^+]$ are 1, -1, 2, and -2 respectively. Consequently, the proposed mass-transfer model is validated, and we prove that mass-transfer regime is chemically limited in the experimental conditions of study. From experimental results, the reaction rate constant is then calculated to be k_c = 6.13 (± 0.92) (m^3/mol/s).

Then we can express C_I as following:

$$C_I = \frac{12}{d}.C^{\circ}_{III}.k_c.\frac{\left|\overline{AH}\right|^2}{[H^+]^2}.[AH]_{(ad)r}.t_r + C_f \qquad (15)$$

A plot of C_I theoretical versus C_I experimental shows good agreement between theoretical and experimental values of C_I.

Formation Model Validation

We have studied the influence of t_f, d, $[\overline{AH}]$, and $[H^+]$ on C_f. The experimental measure of C_f is possible by reducing the rising-up time at about 0.3 s., then: $C_I = C_f$. The linear variation of C_f with pH proves that mass-transfer regime is chemical. Moreover, the slope of log C_f = f(-pH) is equal to -2 according to Equation 14. The slope of the log C_f = f(log(d)) is equal to -2.3, that is to say, between -1 and -3 according to the chemical formation model Equation 14.

The influence of t_f and $[\overline{AH}]$ on C_f can't be easily read. Consequently, we have to determine the following relationships: $n = f(t_f, [\overline{AH}])$ and $\alpha_n = f(t_f, [\overline{AH}])$ for a drop-formation time between 0.9 and 2.3 s and for a total bulk D2EHPA concentration between 0.01 and 0.05 mol/L. The results are in good agreement with the chemical formation model. Moreover, we prove that the mass-transfer regime is chemically limited

during drop formation. The comparison of experimental and theoretical values of C_f is in good agreement with a mean deviation of 18% (Figure 1).

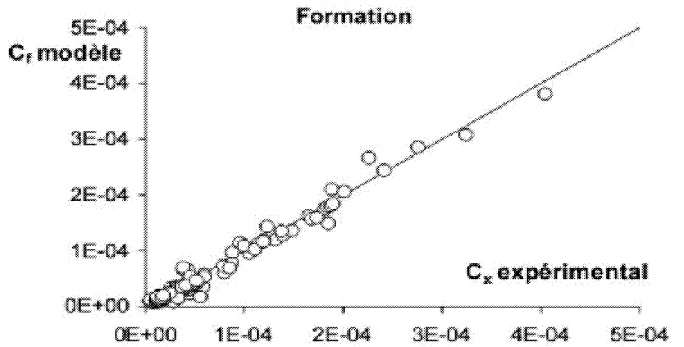

Figure 1. Comparison between experimental and theoretical values of C_f.

CONCLUSIONS

We have verified the presence of end effects in ELM extraction with the Zn/D2EHPA systems. We can assume that end effects are inherent to emulsion properties. The developed mass-transfer models for drop formation and for drop rising-up take into account the external diffusion of solute and interfacial reaction between solute and extractant. The major difference between drop formation and drop rising-up resides in the sequential steps of interfacial reaction due to the shear thinning properties of emulsion. With this assumption, the experimental and theoretical values are in good agreement.

REFERENCE

1. S. Pepocheau, "Cinétique de transfert de matière dans le procédé d'extraction par MLE," Ph.D. Thesis, Ecole Centrale Paris, 1999, pp. 1-160.
2. G. Thorsen and S. G. Tergesen, "On the mechanism of mass-transfer in liquid–liquid extraction," *Chem. Eng. Sci.*, **17**, 137-148 (1962).
3. A. C. Lochiel and P. H. Calderbank, "Mass-transfer in the continuous phase around axisymmetric bodies of revolution," *Chem. Eng. Sci.,* **19**, 471-484 (1964).
4. E. M. Weber, "Mass-transfer from Spherical Drops at High Reynolds Numbers," *Ind. Eng. Chem. Fundam,* **14**(4), 365-366 (1975).
5. A. H. P. Skelland, "Diffusional Mass-transfer," Wiley Interscience, 1974.

REMOVAL AND SEPARATION OF ORGANIC ACIDS BY MEMBRANE-FACILITATED SOLVENT-EXTRACTION TECHNIQUES

Zdravka Lazarova[1] and Stanislava Boyadzhieva[2]

[1]Austrian Research Centers GmbH-ARC, Biogenetics-Natural Resources-Water, 2444 Seibersdorf, Austria. [2]Institute of Chemical Engineering – Bulgarian Academy of Sciences, Acad. G. Bontchev Str., Bl. 103, 1113 Sofia, Bulgaria.
Corresponding author email address: Zdravka.Lazarova@arcs.ac.at

ABSTRACT

The application of two membrane-facilitated extraction techniques, Double Emulsion Membranes (DEM) and Hollow Fiber Membranes (HFM), for separation of binary mixtures of maleic and fumaric acid is studied. Based on experiments with Aliquat® 336 as a selective extractant, the effect of important process parameters on the removal of maleic acid from its mixtures with fumaric acid is determined. In the case of DEM, efficient separation is reached with a liquid membrane containing 5% extractant and 10% surfactant, and 4 M NaCl as a stripping solution. An improvement of the separation efficiency in HFM is achieved by increasing the aqueous-phase flow rate.

INTRODUCTION

Low energy-consuming and efficient methods for separation and purification of organic compounds are needed in biotechnology, as well as in industrial chemistry. A number of studies on the recovery of organic acids from aqueous solutions by liquid-liquid extraction have been published [1-4]. There have been, however, fewer studies on the extractive separation of multi-acid mixtures, and especially of organic acid isomers [2,5-10]. In this work, the separation of binary mixtures of maleic (MA) and fumaric (FA) acids was studied using membrane-based extraction methods. These acids represent stereo (geometric) isomers of 2-butenedioic acid with MA the *cis*- and FA the trans-isomer

MA and FA belong to the most important group of unsaturated dicarboxylic acids. Fumaric acid is derived from maleic acid by catalytic heat isomerisation followed by purification from the residual unconverted maleic acid. The separation of MA from a liquid mixture of MA and FA has been studied using an electrically activated polyelectrolyte gel membrane [11]. There is no information about the application of liquid membrane separation for this purpose. In this study the separation of MA and FA was performed using the extractant Aliquat 336, and two different membrane-based extraction techniques: Double Emulsion Membranes (DEM) and Hollow Fiber

Membrane (HFM). HFM is a nondispersive technique that uses porous synthetic membranes as inert barriers between the organic and aqueous phases, whereas DEM is a surfactant-based three-liquid system with an active intermediate phase (a liquid membrane) that contains a selective extractant-carrier. In DEM, the extraction and stripping processes run simultaneously.

EXPERIMENTAL

Materials and Analytical Methods

Organic acids: maleic acid (Reachim, purity 99%, Russia), fumaric acid (Sigma-Aldrich, 99%, Germany) Extractant: Aliquat 336 (Cognis Corp.). The active components of Aliquat 336 comprise a mixture of quaternary ammonium salts containing C8 (octyl) and C10 (capryl) chains with C8 predominating. Modifier: 1-octanol (Fluka Chemie GmbH, Switzerland, purity 99%). Surfactant: SPAN® 80 (Atlas Europol, Italy). Diluent: undecane (domestic product, Neftochim, BG).

The concentration of the organic acids in the aqueous solutions was determined by liquid chromatography (HPLC Perkins Elmer, Series 10) using a column for organic acid analysis (Aminex®, HPX-87H, 300 x 7.8 mm), and a UV-Spectrophotometer (Knauer No 40901, Germany). As an eluent, 0.01 mol/L H_2SO_4 with velocity of 0.6 mL/min was used. The pH values were measured on a pH meter (Radelkis, OP-265-1, Hungary).

RESULTS AND DISCUSSION

DEM Separation of Maleic/Fumaric Acid Binary Mixtures

The effect of the following concentration parameters on the separation efficiency was studied: a) concentration of the extractant-carrier Aliquat 336 (2-15% v/v.); b) concentration of the surfactant SPAN 80 (5-10% v/v); c) concentration of the stripping reagent NaCl (0.8-4 mol/L). The total organic acid concentration in the feed aqueous solution was kept constant at 7 g/L (1:1 ratio FA/MA); the initial pH value of the feed solution was 1.7. The volume of the three phases in the DEM system was as follows: 30 cm^3 feed aqueous phase, 3 cm^3 organic membrane, and 3 cm^3 stripping aqueous phase. All experimental data are shown graphically as kinetic curves of the normalized concentration C/C^0 of both acids (MA and FA) in the treated aqueous solution. The relationship between the ratio C/C^0 and the extraction efficiency E is $E = (1 - C/C^0)$ x 100%.

In Figure 1 the effect of the carrier (Aliquat 336) concentration is shown. It is seen that separation of both acids is possible, because this carrier removes more MA than FA from the feed solution under the given experimental conditions.

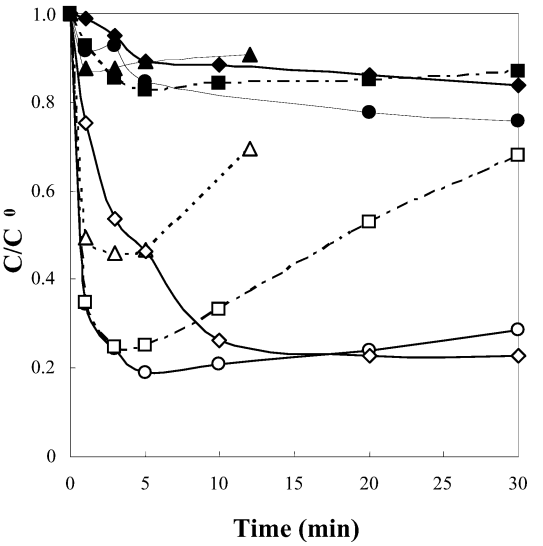

Figure 1. Effect of carrier (Aliquat 336) concentration on the dimensionless concentration of both organic acids (FA, closed symbols; MA, open symbols).
◆ ◇, 2 % carrier; ● ○, 5 % carrier; ■ □, 10% carrier; ▲ △, 15% carrier.
Outer phase: C^0_{FA+MA} = 7 g/L; C_{FA}/C_{MA} = 1:1, pH^0 = 1.7; Organic phase: undecane, Aliquat 336, 10% SPAN 80. Inner phase: 4 M NaCl.

The reason for this separation is that both acids have different dissociation characteristics: for MA, pK_{a1} = 1.92 and pK_{a2} = 6.32, and forFA, pK_{a1} = 3.02 and pK_{a2} = 4.38. Thus, the degree of dissociation (or the ionic conditions) of MA and FA varies with the pH [11]. At pH ~ 1, neither MA nor FA are dissociated, but at pH ~ 2, one of the two COOH groups in MA is dissociated forming the anion MA^-, while most of the FA exists in the feed solution as neutral molecules. Aliquat 336 is a quaternary salt and behaves as a typical anion exchanger, removing MA anions from the feed solution by an ion-pairing mechanism. The best results are achieved with 5% v/v carrier in undecane, and SPAN 80 (sorbitan monooleate) as a nonionic surfactant in the liquid membrane. The use of higher carrier concentrations (e.g., 10% or 15%) is disadvantageous. At 10% carrier, the concentration of MA in the treated aqueous solution increases sharply after 5 minutes, respectively the removal efficiency of MA decreases substantially (from E ~ 75% to E ~ 30% at the end of the experiment). In the case of 15% carrier, the DEM system becomes increasingly unstable after 3 minutes, and the emulsion droplets break down. The reason for emulsion breakdown is that there is co-transport of water molecules accompanying the transportation of MA anion complexes with the Aliquat cation through the liquid membrane. The higher carrier concentration leads to a greater transport of water, increasing the volume of the inner stripping aqueous phase. In the last case (with 15% carrier), the volume of the inner aqueous phase increases from 3 to 9 cm^3; the inner microdrops swell and break, releasing stripped MA^- into the outer feed solution. The influence of the surfactant (SPAN 80) in the concentration range from 5 to 10% v/v is

illustrated in Figure 2. The best separation is achieved using 10% v/v surfactant. All experiments were carried out with this concentration.

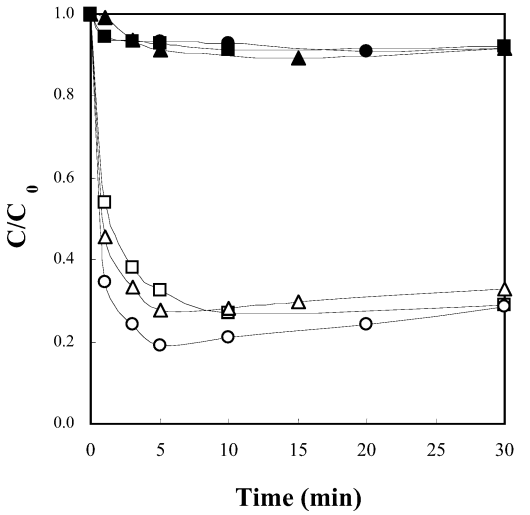

Figure 2. Effect of surfactant (SPAN 80) on the dimensionless concentration of both organic acids (FA, closed symbols; MA, open symbols). ■ □, 5 % surfactant; ▲ △, 7% surfactant; ● ○, 10 % surfactant. Outer phase: C^0_{FA+MA} = 7 g/L; C_{FA}/C_{MA} = 1:1, pH^0 = 1.7. Organic phase: undecane, 5% Aliquat 336, SPAN 80. Inner phase: 4M NaCl.

The importance of the concentration of the stripping reagent NaCl can be seen in Figure 3 where kinetic curves for two NaCl concentrations (0.8 and 4.0 mol/L) are compared. The results show that the removal of MA is substantially improved by the higher NaCl concentration, whereas the extraction of FA from the treated aqueous solution remains low and unchanged. This means that the driving force for the removal of MA^- from the feed aqueous solution depends sharply on the Cl^- concentration in the stripping phase.

HFM Separation of Maleic/Fumaric Acid Mixtures

In the framework of this study, only one hollow-fiber module is used. A HF module contained a bundle of polypropylene hollow fibers (Enka S6/2, Germany) with the following characteristics: $Di_{(HF)}$ 2 mm; $\delta_{(HF)}$, 0.5 mm; porosity, 30%; $L_{(HF)}$, 160 mm; $D_{(module)}$ 23 mm; $L_{(module)}$ 195 mm; $N_{(HF)}$ 30. The aqueous phase containing a mixture of maleic and fumaric acids was passed through the inside of the hollow fibers, whereas the organic phase (5% v/v Aliquat 336, 5% v/v 1-octanol, and undecane) was fed co-currently into the shell side of the module. The separation of the binary mixture containing MA and FA was examined as a function of the flow rates, respectively, the linear velocities of both phases, aqueous and organic. The experimental results (Figure 4) indicate that there is little effect of either flow rate on the transport of fumaric acid through the porous membrane; the extraction remaining low and practically constant.

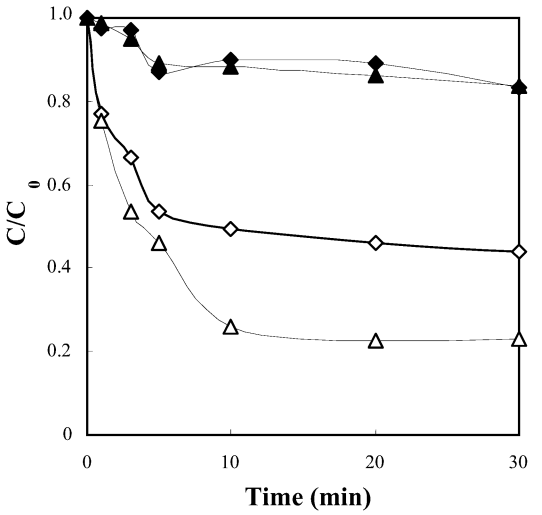

Figure 3. Effect of stripping agent (NaCl) concentration on the dimensionless concentration of both organic acids (FA closed symbols; MA, open symbols). ▲ △, 4.0 NaCl; ◆ ◇, 0.8 M NaCl. Outer phase C^0_{FA+MA} = 7 g/L; C_{FA}/C_{MA} = 1:1, pH^0 = 1.7.
Organic phase: undecane, 2% Aliquat 336, 10% SPAN 80. Inner phase: NaCl-solution.

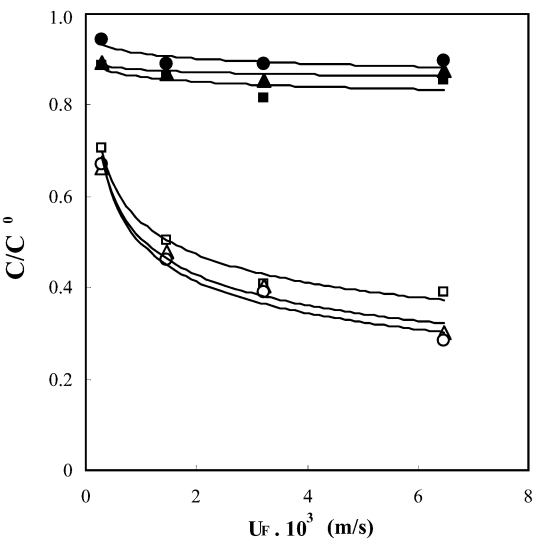

Figure 4. Effect of linear velocity of the feed aqueous phase U_{aq} on the dimensionless concentration of both acids (FA, closed symbols; MA, open symbols) at different U_{org} (velocity of the organic phase). ■ □, U_{org} = 0.678.10^{-3} m.s^{-1}; ▲ △, U_{org} = 1.357.10^{-3} m.s^{-1};
● ○, U_{org} = 3,393.10^{-3} m.s^{-1}. Aqueous feed phase: C^0_{FA+MA} = 7 g/L; C_{FA}/C_{MA} =1:1, pH^0 = 2.2.
Organic phase: 5% vol. Aliquat 336, 5% vol. octanol; undecane

The aqueous-phase flow rate influences substantially the removal efficiency of the maleic acid at the lowest U_F, where E_{MA} is about 30%; whereas at the highest U_F value, E_{MA} increases to more than 70%. At the same time, E_{FA} is no more than 10%.

CONCLUSIONS

The experimental results show that maleic acid can be successfully removed from mixtures containing fumaric acid using Aliquat 336 as a selective extractant in DEM and HFM systems. The most important parameter in the case of DEM is the concentration of the extractant-carrier and of the stripping reagent (NaCl), whereas the efficiency of the separation process in the HFM is determined by the aqueous-phase flow rate. Further experiments are needed to optimize the experimental conditions for the effective separation of MA from FA by both methods. Two coupled hollow-fiber modules will be used to study the simultaneous extraction and stripping nondisperse operation.

REFERENCES

1. S. T. Yang, S. A. White, and S. T. Hsu, "Extraction of Carboxylic Acids with Tertiary and Quaternary Amines: Effect of pH," *Ind. Eng. Chem. Res.*, **30**, 1335-1342 (1991).
2. K. Schuegerl, Solvent Extraction in Biotechnology: Recovery of Primary and Secondary Metabolites, Springer-Verlag, Berlin Heidelberg, 1994.
3. G. Malmary, J. Albet, A. Putranto, and J. Molinier, "Recovery of Carboxylic Acids from Aqueous Solutions by Liquid-Liquid Extraction with a Triisooctylamine Diluent System," *Braz. J. Chem. Eng.*, **18**(4), 441-447 (2001).
4. N. Syzova, A. Eyal, A. Vitner, and B. Hazan, "Extraction of Dicarboxylic Acids by ABC Extractants," *Solvent Extr. Ion Exch.*, **22**, 51-67 (2004).
5. R. S. Juang, R. H. Huang, and R. T. Wu, "Separation of Citric and Lactic Acids in Aqueous Solutions by Solvent Extraction and Liquid Membrane Processes," *J. Membr Sci.*, **136**, 89-99 (1997).
6. R. Wodzki, J. Nowaczyk, and M. Kujawski, "Separation of Propionic and Acetic Acid by Pertraction in a Multimembrane Hybrid System," *Sep. Purif. Technol.*, **21**, 39-54 (2000).
7. D. Cascaval, C. Oniscu, and A. I. Galaction, "Selective Separation of Amino Acids by Reactive Extraction," *Biochem. Eng. J.*, 171-176 (2001).
8. K. Abe, M. Goto, and F. Nakashio, "Novel Optical Resolution of Phenylalanine Racemate Utilizing Enzyme Reaction and Membrane Extraction," *Sep. Sci. Technol.*, **32**(11), 1921-1935 (1997).
9. P. Hadik, L. Szabo, E. Nagy, and Zs. Farkas, "Enantioseparation of D,L-Lactic Acid by Membrane Technique," *J. Membr. Sci.,* **251**, 223-232 (2005).
10. P. Hadik, L. Szabo, and E. Nagy, "D,L-Lactic Acid and D,L-Alanine Enantioseparation by Membrane Process," *Desalination*, **148,** 193-198 (2002).
11. E. Kokufuta, T. Yamauchi, and Y. Osada, "Electrically Controlled Separation of Maleic Acid and Fumaric Acid through a Poly(Vinyl Alcohol)/Poly(Acrylic Acid) Composite Membrane," *Polymer Gels and Networks*, **3**, 397-406 (1995).

MEMBRANE-BASED SOLVENT EXTRACTION AS AN ALTERNATIVE TO CONVENTIONAL PROCESSES IN THE TREATMENT OF HOT-DIP GALVANIZING PROCESSES

J. A. Carrera, E. Bringas, M. F. San Román, and I. Ortiz

Departments of Chemical Engineering and Inorganic Chemistry, University of Cantabria, ETSIIyT. Avda. los Castros s/n (39005), Santander, Spain.
Corresponding author email address: ortizi@unican.es

ABSTRACT

Acidic effluents from spent pickling effluents contain high quantities of iron and zinc. These effluents need to be treated before disposal due to their strongly hazardous character, allowing the recovery of zinc because of its added value. Membrane-based solvent extraction technologies, in particular Emulsion Pertraction Technology (EPT) and Non-Dispersive Solvent Extraction (NDSX) with Hollow-Fiber Modules (HFM) are suitable technologies to carry out the separation of valuable compounds and at the same time to make the recovery of electrolytic-grade metal possible. In this work, the comparison of both configurations and analysis of the influence of the operation variables on the process efficiency was performed. It was observed that, working under the same experimental conditions, similar extraction (EX) and back-extraction (BEX) kinetics were obtained for both technologies. Consequently, EPT offers the capacity to achieve similar separation and concentration efficiencies with half the membrane area.

INTRODUCTION

Hot-dip galvanizing processes with molten zinc are commonly used to protect steel goods from corrosion. The hydrochloric acid effluents generated in this process contain appreciable quantities of both iron and zinc, which are considered pollutants [1]. On the other hand, the treatment of these effluents—for reuse in some industrial applications—is an interesting alternative in order to minimize the environmental impact and to compensate the costs associated with the cleaning processes.

Conventional treatment methods such as effluent neutralization and hydrochloric acid evaporation are less effective at high zinc concentrations due to the physicochemical complexity usually encountered in waste effluents, where the target species are present in a heterogeneous mixture with different amounts of undesirable compounds. Thus, membrane-based solvent-extraction technologies have been proven as feasible alternatives to the conventional ones [2].

In this work, two different membrane-based solvent-extraction technologies for the separation of zinc from iron and its recovery from spent pickling effluents using

hollow-fiber modules (HFM) are compared: (i) Non Dispersive Solvent Extraction (NDSX) and (ii) Emulsion Pertraction Technology (EPT).

EXPERIMENTAL SET UP

The two membrane-based solvent-extraction technologies proposed used HFM as membrane contactors, and the extraction of the pollutants was carried out using a selective extractant as carrier.

In NDSX technology, for the simultaneous extraction (EX) and back-extraction (BEX) processes, two HFM were used, flowing the organic phase from the EX module to the BEX one. In the first module, the target species was transferred from the aqueous feed phase to the organic phase, and in the second module, the solute was transported to the BEX phase. The organic phase left the BEX module and flowed to the homogenization tank of the organic phase and then to the EX module again.

In EPT, the aqueous phase with the target species is put into contact in one HFM with an emulsion formed by dispersing the stripping phase into an organic phase containing the selective extractant and a BEX agent; for this purpose, an emulsifier (Ultraturrax T25, IKA A.G.) able to provide high stirring speed (8,000–20,500 rpm) was used. The solute was transferred from the aqueous feed phase to the organic phase and then transported to the internal BEX solution. Therefore, in the EPT technology, EX and BEX operations are efficiently combined in a single membrane-contactor unit. Figures 1 and 2 show the EPT and NDSX systems, respectively. The systems includes the HFMs, the stirred tanks for the fluid phases, and accessories.

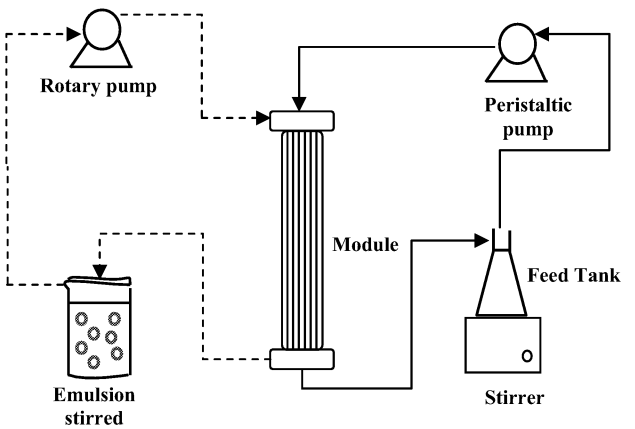

Figure 1. Experimental set-up (EPT).

Hollow-fiber modules (Liqui-Cel® Extra-Flow 2.5 × 8, Hoechst Celanese) were the contactors, with an effective contact area of 1.4 m^2 and an effective mass-transfer length of 0.15 m. These contactors contained 10,200 fibers of polypropylene (X-30 fibers) with a nominal porosity of 40%, an internal diameter of 240 μm, and a wall thickness of 30 μm. The tortuosity factor was 2.6.

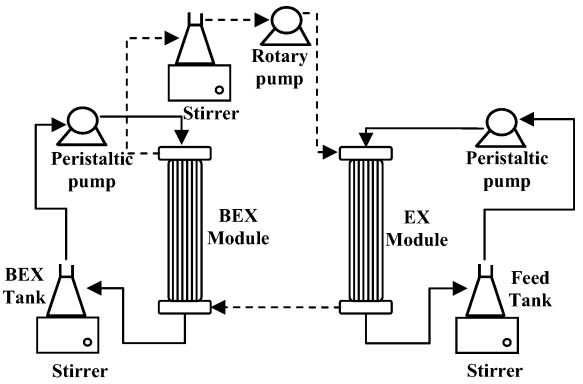

Figure 2. Experimental set-up (NDSX).

Analysis of feed solutions gave average concentrations of the metals, $[Zn^{+2}]$ = 1254 mol/m^3, $[Fe^{+2}]$ = 1718 mol/m^3, and $[Cl^-]$ = 6403 mol/m^3 along with small amounts of other heavy metals (Mn, Pb, Al, Cr, etc.). The pH of the feed was approximately zero. The system under study has a very high chloride concentration, and consequently zinc ions form chlorocomplex species.

Pure TBP (tributyl phosphate, MERCK) and service water were the solvating extractant and the BEX agent, respectively, that were selected in both technologies. TBP was chosen after a literature survey into the characteristics of feed solutions, giving importance to the fact that the BEX could be simply and satisfactorily achieved using service water as the BEX agent [1,3].

RESULTS AND DISCUSSION

The viability of the separation-concentration process from the solution with composition given above was analyzed working with both membrane configurations. The results have been reported in a previous work [4].

Influence of the Initial Zinc Concentration in the Aqueous Feed Solution

In order to study the influence of initial zinc concentration in the aqueous feed phase for both technologies, and starting with an initial concentration of zinc of 1200 mol/m^3 (EXP1), two batches were prepared by dilution of the effluent to obtain initial zinc concentrations of 600 and 300 mol/m^3 (EXP2 and 3). On the other hand, the ratio TBP/Water (EXP4 and 5) and the volume of emulsion phase (EXP6 to 8) were studied in the EPT configuration. Table 1 shows the experimental conditions of the realized experiments for 1 L of aqueous feed solution. Figure 3 shows the EX and BEX kinetic results corresponding to EXP1 in both cases, with dimensionless Zn defined as $[Zn]_{Aq}/[Zn]_{Aq,0}$.

Table 1. Experimental conditions for EPT and NDSX

Tech.	EXP	$[Zn]_0$ (mol/m^3)	Q_A (m^3/h)	Q_{Em} (m^3/h)	Q_O (m^3/h)	Q_S (m^3/h)	V_O (L)	V_S (L)	V_{Em} (L)
NDSX	1	1200	0.036		0.033	0.036	1	1	
	2	600	0.036		0.033	0.036	1	1	
	3	300	0.036		0.033	0.036	1	1	
EPT	1	1200	0.027	0.024			0.8	0.2	1
	2	600	0.027	0.024			0.8	0.2	1
	3	300	0.027	0.024			0.8	0.2	1
	4	1200	0.027	0.024			0.6	0.4	1
	5	1200	0.027	0.024			0.5	0.5	1
	6	1200	0.027	0.024			1.6	0.4	2
	7	1200	0.027	0.024			1.2	0.8	2
	8	1200	0.027	0.024			1	1	2

V_O, organic phase volume; V_S, BEX phase volume; V_{Em}, emulsion volume; $[Zn]_0$, initial zinc concentration in the aqueous feed solution; Q_A, aqueous feed flow rate; Q_O, organic phase flow rate; Q_S, BEX phase flow rate; Q_{Em}, emulsion flow rate.

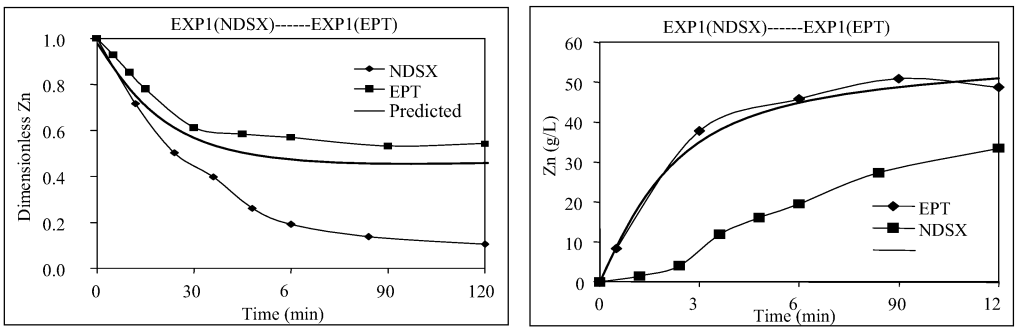

Figure 3. EX and BEX kinetic results for EXP1 in EPT and NDSX.

It can be seen that NDSX reaches a higher EX percentage (approx. 90%) than EPT (approx. 60%). Also, EPT reaches a higher BEX concentration than NDSX. These phenomena are a consequence of the lower BEX phase volume in EPT than in NDSX. Solid lines represent a mathematical model described in another work [5], which describes the kinetic behavior of the EPT process. Table 2 shows the EX and BEX percentages for EXP1 to EXP3. In order to compare the results obtained working with both configurations, the same experimental conditions were selected. Figure 4 shows the kinetic results for EXP1 (NDSX) and EXP8 (EPT).

Table 2. EX and BEX percentages in EXP1 to EXP3 for EPT and NDSX

Experiment	EX % (EPT)	EX % (NDSX)	BEX % (EPT)	BEX % (NDSX)
EXP1	46	92	19	61
EXP2	63	88	19	57
EXP3	59	85	25	80

As shown in Figure 4, the EX and BEX kinetics are similar for the same experimental conditions in both technologies; consequently, similar extraction and back-extraction percentages were obtained.

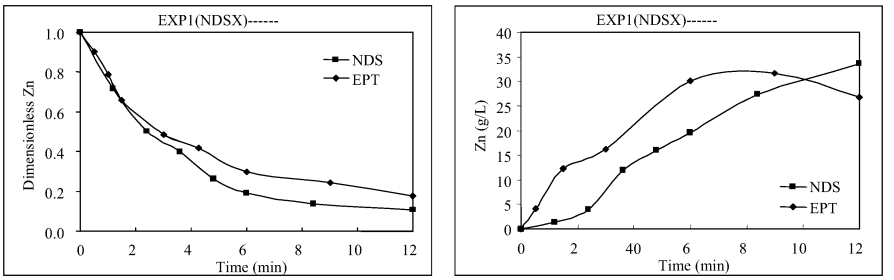

Figure 4. EX and BEX kinetics for EXP1 (NDSX) and EXP8 (EPT).

Influence of TBP/Water Volume Ratio

Figure 5 shows the evolution of dimensionless zinc concentration with the time in the aqueous feed phase and the mass of zinc in the stripping phase in EXP1, EXP4, and EXP5 of EPT technology.

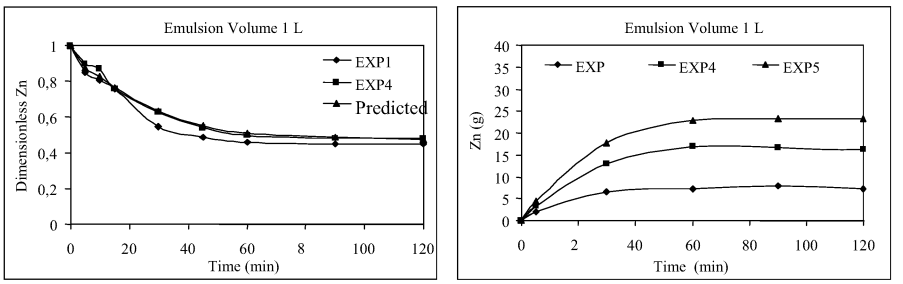

Figure 5. EX kinetic and mass in BEX Phase in EXP1, EXP4 and EXP5.

It can be seen that the influence of TBP/Water volume ratio in the EX phase can be considered negligible, due to the fact that in all the experiments, the carrier concentration was higher than the stoichiometric value required for the total extraction of zinc. Also, in relation to the BEX phase, the lower the TBP/Water volume ratio is, the higher is the mass of back-extracted zinc. This behavior can be explained by two reasons: i) working with a lower extractant concentration, the BEX reaction shifts to the right, and ii) the higher the volume of water in the emulsion phase is, the higher is the mass of zinc back-extracted before reaching the solubility equilibrium.

Influence of Emulsion Volume

Table 3 shows the EX and BEX percentages in EXP1 and EXP4—EXP8. It can be observed that the higher the emulsion volume is, the higher is the amount of zinc extracted for the same TBP/Water volume ratio. Also, with respect to the BEX phase, the

higher the emulsion volume is, the higher the mass of zinc back-extracted. These behaviors can be explained through the same reasons given above.

Table 3. EX and BEX percentages in EXP1 and EXP4 to EXP8

Experiment	% TBP / % Water	V_{Em} (L)	% EX	% BEX
EXP1	80/20	1	50	19
EXP4	60/40	1	50	21
EXP5	50/50	1	50	29
EXP6	80/20	2	75	24
EXP7	60/40	2	75	49
EXP8	50/50	2	75	60

CONCLUSIONS

It has been shown that NDSX and EPT configurations allow the separation and recovery of zinc from spent pickling effluents, achieving a range of separation from 60% to 90% in the separation step and from 30% to 60% in the recovery step. In order to compare both configurations, the same experimental conditions were selected, and similar EX and BEX kinetics were obtained; as a result similar EX (75%) and BEX (60%) percentages were obtained.

It was observed that the influence of the TBP/water ratio on the EX phase is negligible, while in the BEX phase the lower the TBP/Water volume ratio is, the higher is the mass of back-extracted zinc. On the other hand, the higher the emulsion volume, the higher is the mass of zinc in the EX and BEX phases for the same TBP/Water volume ratio.

ACKNOWLEDGMENTS

Financial support from projects CTQ2005-02583/PPQ and CTQ2006-14360/PPQ (MEyC), Spain) is gratefully acknowledged.

REFERENCES

1. R. Cierpiszweski, I. Miesiac, M. Regel-Rosocka, A. M. Sastre, and J. Szymanowski, "Removal of Zinc(II) from Spent Hydrochloric Acid Solutions from Hot Galvanizing Plants," *Ind. Eng. Chem. Res*., **41**, 598-603 (2002).
2. I. Ortiz, E. Bringas, H. Samaniego, M. F. San Román, and A. M. Urtiaga, "Membrane processes for the efficient recovery of anionic pollutants," *Desalination*, **193**, 375-380 (2006).
3. I. Ortiz, E. Bringas, M. F. San Román, and A. M. Urtiaga, "Selective Separation of Zinc and Iron from Spent Pickling Solutions by Membrane-Based Solvent Extraction: Process Viability," *Sep. Sci. Technol.*, **39,** 2441-2455 (2004).
4. H. Samaniego, M. F. San Román, and I. Ortiz, "Kinetics of Zinc Recovery from Spent Pickling Effluents," *Ind. Eng. Chem. Res.,* **46**, 907-912 (2007).
5. J. A. Carrera, M. F. San Román, E. Bringas, and I. Ortiz, "Kinetics and Modelling of Zinc Recovery from Spent Pickling Effluents by means of Emulsion Pertraction Technology," *J. Membr. Sci.*, Manuscript accepted.

CONVERTING MEMBRANE-BASED SOLVENT-EXTRACTION NETWORKS INTO SUSTAINABLE PROCESSES: REMEDIATION OF GROUNDWATER POLLUTED WITH Cr(VI) AS CASE STUDY

E. Bringas, M. F. San Román, and I. Ortiz

Dept. Chemical Engineering and Inorganic Chemistry. University of Cantabria. ETSIIyT. Avda. los Castros s/n (39005). Santander, Spain
Corresponding author email address: ortizi@unican.es

ABSTRACT

This work provides the guidelines to carry out the optimal synthesis of membrane-based solvent-extraction (MBSX) networks according to the principles of the sustainable-development strategy, which searches for technologies able to meet environmental objectives with minimum cost and minimum risk. MBSX technologies allow both the selective removal of the contaminants to meet disposal requirements and the valorization of the metals for reuse. Cost and risk minimization calls for the determination of the optimal process configuration. Starting with the fundamentals of solvent extraction based separation-concentration processes, the technical evaluation is carried out followed by the use of optimization techniques that are efficient tools for the design of sustainable processes. As case study, the remediation of polluted groundwater containing hexavalent chromium by means of the emulsion pertraction technology using hollow-fiber contactors has been analyzed.

INTRODUCTION

The widespread use of metallic compounds such us chromium or zinc in the surface-treatment industry has caused contamination of surface and groundwater. These polluted streams should be treated before release into the environment, to remove contaminants to meet disposal requirements and to assure the valorization of the metals by the recovery of the contaminants selectively for sale or reuse in industry.

Although different processes exist for the treatment of aqueous streams containing metallic contaminants, one of the sustainable technological alternatives that allows both the efficient removal and selective recovery of the contaminants is a membrane-based solvent-extraction (MBSX) process using microporous hollow-fiber contactors.

MBSX technologies allow the simultaneous separation and concentration of the metallic pollutants in the aqueous feed solution by means of hollow-fiber contactors that avoid the mixing of the fluid phases involved in the process.

In particular, emulsion pertraction technology (EPT) has been selected in this work as an alternative for the remediation of polluted streams containing heavy metals. EPT uses an emulsion prepared by dispersion of the aqueous stripping solution (dispersed phase) into the organic phase (continuous phase) that contains the extractant agent able to selectively remove a target species from the aqueous feed.

In addition to the viability of MBSX technologies to efficiently meet environmental objectives, the definition of sustainable processes implies the determination of the process configuration with minimum cost and minimum risk. Although the viability of the MBSX technology and the phenomena involved in the separation process have been extensively studied [1], there is still limited information on the procedure required to perform the optimal design of MBSX networks that contain multiple membrane modules. This work therefore provides the guidelines to achieve this goal according to the principles of sustainable development.

METHODOLOGY FOR THE OPTIMAL SYNTHESIS OF MBSX NETWORKS

A novel approach for the optimal design of MBSX networks is proposed. Figure 1 shows a scheme of the design methodology.

<table>
<tr><td colspan="3">1. FUNDAMENTALS</td></tr>
<tr><td>Problem Statement
- Effluent characterisation
- Objectives</td><td>Selection of Extraction (EX) and Back-Extraction (BEX) Agents
- Proposal of EX and BEX reactions
- Kinetic or equilibrium Pattern
- Obtention of the equilibrium/kinetic parameters</td><td>MBSX Technology Selection
- Process configuration
- Operational conditions</td></tr>
<tr><td colspan="3">2. TECHNICAL EVALUATION</td></tr>
<tr><td colspan="2">Kinetic Analysis of the Separation - Concentration Process
- Process Viability
- Analysis of the influence of the operation variables on the EX and BEX kinetics</td><td>Mathematical Modeling of the Separation-Concentration Process
- Mass transfer hypothesis
- Solute mass balances in the different fluid phases
- Mass transfer coefficients
- Model validation</td></tr>
<tr><td colspan="2">3. PROCESS DESIGN</td><td>4. ECONOMICAL EVALUATION</td></tr>
<tr><td colspan="2">- Removal and recovery requirements (Constrains)
- Preliminary capital cost definition (Objective Function)
- Proposal of design alternatives (Network Superestructures)
- Mathematical modeling of the network superestructures (Optimization Model)
- Application of the mathematical optimization techniques to select the alternative with minimum total cost</td><td>Detailed cost evaluation of the selected alternative
- Capital cost evaluation
- Operation cost evaluation
- Analysis of the investment recovery</td></tr>
</table>

Figure 1. Schematic representation of the methodology for optimal design of MBSX networks.

As a case study, the proposed methodology has been applied to the remediation of polluted groundwater that contains hexavalent chromium, and competitive species like sulfate and chloride anions are present because of the specific location of the groundwater reservoir.

FUNDAMENTALS

The widespread use of chromium in industrial applications such as leather tanning, metallurgy, and electroplating processes has caused chromium contamination of surface and groundwater. Aqueous solutions containing heavy metals are traditionally treated using a combination of physicochemical and biological processes. They, however, often fail to reduce the concentration of heavy metals below permissible limits. Furthermore, these technologies usually do not provide the selectivity necessary to create valuable product streams suitable for recycle or reuse. As a consequence, the by-product sludge can itself become a disposal problem. MBSX technologies are promising alternatives to conventional processes.

Problem Statement: Effluent Characterization and Objectives

The average composition of the polluted groundwater is shown in Table 1.

Table 1. Composition of the polluted groundwater

Component	Concentration (mol/m^3)
Cr(VI)	26.1
SO_4^{2-}	33.5
Cl^-	29.1
Ca^{+2}	13.6
pH	7.3

The presence of high concentrations of calcium required the elimination of the cations prior to the separation of anions to avoid precipitation of calcium compounds and fouling of the microporous hollow-fiber membranes.

This works aims at the design of a MBSX process to i) reduce the chromium concentration below the disposal limit (0.0961 mol/m^3), and ii) obtain a concentrated chromium solution (>380 mol/m^3) with negligible concentrations of sulfate and chloride anions.

Selection of the Extraction and Stripping Agents

Hexavalent chromium species in aqueous solution are present as anions for all concentration and pH values. The Cr(VI) extraction should therefore be performed with an extraction agent capable of extracting anions.

The efficiency of the extraction process depends on the affinity of the selective extractant for the target species and can be determined by analyzing the extraction isotherms. An anionic extractant selective for Cr(VI) over sulfate and chloride anions is

required. The selection of the extractant should also take into account cost and commercial availability.

From the literature, it was concluded that tertiary and quaternary amines are the most efficient reagents for the selective extraction of hexavalent chromium [2]. According to criteria of affinity for Cr(VI) and product availability, a commercial tertiary amine Alamine®336 (Cognis) was chosen. Alamine 336 is a mixture of tri-octyl and decyl amines. For the system Alamine 336/Cr(VI) extraction efficiency increases with increasing acid strength. The pH of the aqueous phase solution was therefore adjusted to 1.5 with H_2SO_4. NaOH was selected as the stripping agent.

Extraction systems involving ionic species are generally thought to reach chemical equilibrium at the interface, and thus, equilibrium models of the chemical reactions are proposed. In prior work [3], the equilibrium parameters for the system Alamine 336/chromium/sulfate/chloride were determined. The extraction mechanism and the equilibrium parameters obtained are shown in Table 2.

Table 2. Equilibrium parameters for extraction system

Extraction Reaction	Equilibrium Parameter
$HCrO_4^- + H^+ + \overline{R_3N} \Leftrightarrow \overline{(R_3NH)HCrO_4}$	$K_1 = 4.83\ mol^{-2}\ m^6$
$Cr_2O_7^{2-} + 2H^+ + 2\overline{R_3N} \Leftrightarrow \overline{(R_3NH)_2Cr_2O_7}$	$K_2 = 0.741\ mol^{-4}\ m^{12}$
$HSO_4^- + H^+ + \overline{R_3N} \Leftrightarrow \overline{(R_3NH)HSO_4}$	$K_3 = 1.37\ 10^{-3}\ mol^{-2}\ m^6$
$\overline{(R_3NH)HSO_4} + Cl^- \Leftrightarrow \overline{(R_3NH)Cl} + HSO_4^-$	$K_4 = 1.52$

The reaction between the organo metallic complexes formed in the extraction step and the stripping agent is totally shifted to the right, since the concentration of stripping agent is much higher than the concentrations of the other species taking part in the reaction.

MBSX Technology Selection

The most widely used MBSX technologies using hollow-fiber contactors are: hollow-fiber supported-liquid membranes, hollow-fiber contained liquid membranes, nondispersive solvent extraction, and more recently, emulsion pertraction technology (EPT). EPT was selected for the present study.

In EPT, the simultaneous extraction and stripping reactions are carried out in a single hollow-fiber (HF) module. The stripping agent is dispersed into the organic phase to form an emulsion. Aqueous feed solution flow is through the inner side of the microporous HF membranes, and the stripping emulsion flow is countercurrent through the shell side of the HF modules. The solute is transferred from the aqueous feed solution to the organic phase that is embedded in the pores of the hollow fibers. It is then transported to the inner side of the droplets, where the stripping solution is situated. The solute is recovered from the internal aqueous phase after emulsion breakage. The aqueous feed solution flowed in a single-pass mode whereas the emulsion phase is

recycled to achieve a high concentration strip solution. Figure 2 shows the experimental set-up used.

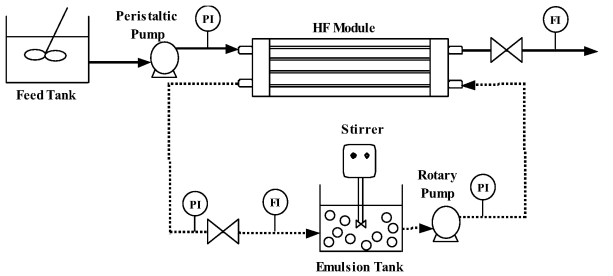

Figure 2. Experimental set-up (EPT).

The organic phase was prepared using 10% v/v Alamine336 and Isopar L Fluid (ExxonMobile Chemical), an isoparaffinic hydrocarbon as diluent. A 3% v/v solution of Pluronic PE 3100 (BASF), a block copolymer of ethylene oxide and propylene oxide, was added to enhance the phase separation of the aqueous stripping solution from the organic phase in the absence of agitation for the recovery of the stripping solution. 1% 1-Dodecanol (Merck) v/v was added to the organic phase to avoid the segregation of a third phase. NaOH (Panreac) at a concentration range of 3000-6000 mol/m^3 was used as the stripping solution. The emulsion was prepared by dispersing the stripping agent in the organic phase at a ratio of 1:4 by volume.

TECHNICAL EVALUATION

The application of a new technology like EPT requires the use of a reliable mathematical model and the model parameters (mass transport coefficients and interfacial equilibrium parameters). To this end, an analysis of the kinetics and development of a multicomponent mathematical model of the EPT process were performed.

Kinetic Analysis of the EPT Process

Various kinetic experiments were performed to analyze the influence of the operating variables on the process kinetics and to obtain kinetic data for the validation of the mathematical model. The detailed kinetic analysis performed is reported elsewhere [4].

Mathematical Modelling of the EPT Process

The multicomponent mathematical modelling of the process requires the establishment of the mass-transport hypotheses and the development of the solute mass balances in both the aqueous feed solution and the emulsion streams. The system of differential partial equations obtained was integrated using a commercial software package gPROMS (general Process Modelling System). The parameter estimation was

carried out by means of the estimation tool gEST that applied the least-square technique to find the numerical values of the parameters that minimize the difference between experimental kinetic data and simulated values. Further information about the mass-transport hypothesis, the values of the mass transport coefficients, and the model validation are reported elsewhere [4].

PROCESS DESIGN

The mathematical model obtained was employed in the process design that was performed using mathematical optimization techniques. Network superstructures that incorporate all possible design alternatives were proposed, and then an optimization procedure was followed to obtain the minimum-cost process configuration that was able to meet the disposal and valorization requirements. Further details of the optimization procedure are reported elsewhere [5].

CONCLUSIONS

This works deals with the methodology to carry out the optimal design of MBSX networks for the treatment of effluents containing metallic pollutants. As a case study, the procedure was applied to the remediation of polluted groundwater containing hexavalent chromium using the EPT. As further work, the detailed economical evaluation and the risk minimization of the selected design alternative will be performed.

ACKNOWLEDGMENTS

Financial support from projects CTQ2005-02583/PPQ and CTQ2006-14360/PPQ (MEC, Spain) is gratefully acknowledged.

REFERENCES

1. R. Klaassen and A. E. Jansen, “The Membrane Contactor: Environmental Applications and Possibilities,” *Environ. Prog.*, **20**(1), 37-43 (2001).
2. A. Senol, “Amine Extraction of Chromium(VI) from Aqueous Acidic Solutions,” *Sep. Purif. Technol.* **36**, 63-75 (2004).
3. E. Bringas, M. F. San Román, and I. Ortiz, “Removal of Anionic Pollutants from Groundwaters using Alamine 336: Chemical Equilibrium Modelling,” *J. Chem. Technol. Biotechnol.*, **81**, 1829-1835 (2006).
4. E. Bringas, M. F. San Román, and I. Ortiz, “Separation and Recovery of Anionic Pollutants by the Emulsion Pertraction Technology. Remediation of Polluted Groundwaters with Cr(VI),” *Ind. Eng. Chem. Res.*, **45**(12), 4295-4303 (2006).
5. E. Bringas, R. Karuppiah, M. F. San Román, I. Ortiz, and I. E. Grossmann, “Optimal Groundwater Remediation Network using Selective Membranes,” *Ind. Eng. Chem. Res.*, **45**, 5555-5569 (2007).

SYNERGISTIC EXTRACTION OF RARE EARTHS WITH A MIXTURE OF CALIX[4]ARENE CARBOXYLIC ACID AND PRIMARY AMINE N1923

W. W. He,[1,2] W. P. Liao,[1] D. Q. Li,[1] and C. J. Niu[1]

[1]State Key Laboratory of Rare Earth Resources and Application, Changchun Institute of applied Chemistry, Changchun, P.R. China. [2]Graduate University of Chinese Academy of Sciences, Beijing, P.R. China. Corresponding author email address: ldq@ciac.jl.cn

ABSTRACT

Polyatomic carboxylic acid 5,11,17,23-tetra-*tert*-butyl-25,26,27,28-tetrakis(carboxymethoxy) calix[4]arene (^{t}Bu[4]CH$_2$COOH or H$_4$A) was used to extract rare earths (RE) from chloride solutions. The preorganization of ^{t}Bu[4]CH$_2$COOH in the uptake of different alkali metal ions induced a dimensional "rigidification" in the lower rim of the calixarene and facilitated the extractability towards RE. The synergistic extraction of Pr^{3+}, Eu^{3+}, and Yb^{3+} from chloride medium using a mixture of ^{t}Bu[4]CH$_2$COOH and primary amine N1923 in chloroform was investigated. The extraction mechanism was investigated by the slope-analysis method.

INTRODUCTION

Recently, the employment of calixarenes as molecular scaffolds has attracted considerable interest in the chemistry separation field for such species as bioactive molecules, metal ions, and neutral molecules [1-3]. For the purpose of higher separation efficiency and perfect purity of materials, much effort has been devoted to the development of appropriate functional groups in calixarene derivatives such as carboxylic acid, ketone, ester, and amine. COOH-substituted calixarenes were among the first ones investigated for rare earth cation-exchange extraction in a search for intragroup separation [4-6].

Synergistic extraction is an important method to enhance the extraction efficiency, and several synergistic extraction systems have been researched for the purification of RE. However, there have few reports on the synergistic extraction with calixarene derivatives and other extractants. Zhu et al. [7] found the synergistic extraction of Fe^{3+} with a calix[8]arene carboxylic acid and tributyl phosphate. Mikulasek et al. [8] discovered an "intramolecular" synergistic effect between the ligating functions and the ionic functions prearranged on a calix[4]arene in the extraction of Eu^{3+} or Am^{3+}.

In this study, we compared the extraction behavior difference of the preorganized ^{t}Bu[4]CH$_2$COOH using alkali metal ions to induce preorganization. In order to seek for more advantageous extraction behavior of ^{t}Bu[4]CH$_2$COOH, a synergistic extraction system of

^{t}Bu[4]CH_2COOH and primary amine N1923 was exploited in the form of more stable calixarene carboxylic RE complexes.

EXPERIMENTAL

Reagents and Apparatus

^{t}Bu[4]CH_2COOH was synthesized according to the literature [9] and identified by FT-IR, ^{1}H-NMR, and elemental-analysis measurements. A commercial extractant primary amine N1923 (RNH_2) was purified [10] and acidified by an equal molar amount of hydrochloric acid to convert it into the ammonium salt, and then the remainder of the acid must be washed off with deionized water. Stock solutions of RE(III) were prepared by dissolving their oxides (≥ 99.9%) in concentrated hydrochloric acid, diluting to required volume, and then standardizing by titration using EDTA standard solution at pH 5.5 with xylenol orange as indicator. All the other reagents were of analytical grade.

A model 720 digital pH meter made by Orion Research Inc. (U.S.A.) was used for pH measurement. The concentration of RE was determined using a spectrophotometer made by Shanghai Precision & Instrument Co. Ltd. A Perkin-Elmer Analyst 800 atomic absorption Spectrometer was used to determine the concentration of alkali metal ions.

Extraction Procedure

Equal volumes of aqueous and organic phases were shaken in an equilibrium tube for 30 min. at 298 ± 1 K, which was sufficient for equilibrium attainment. The concentration of the metal ion in the aqueous phase was analyzed by spectrophotometry (the maximum absorption at 654 nm with Arsenazo(III) as an indicator) and that in the organic phase was obtained by mass balance. These concentrations were used to calculate the distribution ratio *D*. The pH value of aqueous solution was adjusted with hydrochloric acid and glycine solution.

RESULTS AND DISCUSSION

Extraction Behavior of RE Using ^{t}Bu[4]CH_2COOH without Alkali Metal Ions

Inoue et al. [4] have studied the extraction behavior of RE(III) using ^{t}Bu[4]CH_2COOH in the toluene-perchlorate system. However, the extraction mechanism of RE by ^{t}Bu[4]CH_2COOH in chloroform-chloride medium has not been discussed in detail. The slope-analysis method was adopted to study the Pr^{3+} and Eu^{3+} extraction equilibrium in this experiment. The plots of log *D vs.* pH_{eq} give a straight line with a slope of about 3.0, and the plots of log *D*-3pH *vs.* log[H_4A] are linear with a slope of about 1.0. So the extraction equilibrium of RE without maintaining the ionic strength constant by alkali metal ions can be expressed according to a cation-exchange mechanism:

$$RE^{3+}_{(a)} + H_4A_{(o)} \longleftrightarrow REHA_{(o)} + 3H^{+}_{(a)} \quad (1)$$

where a and o denote aqueous and organic phase, respectively.

Extraction Behavior of Alkali Metal Ions Using ^{t}Bu[4]CH$_2$COOH

Goto et al. [11] used ^{t}Oct[4]CH$_2$COOH as the extractant to investigate the extraction behavior of alkali metal ions. As the homologous compound, ^{t}Bu[4]CH$_2$COOH can also extract alkali metal ions to a different extent. Both the plots of log D *vs.* pH_{eq} and the plots of log D-pH *vs.* log[H_4A] show a slope about 1.0 in the pH range of 2.8 and 5.5, indicating the complex formation between the ^{t}Bu[4]CH$_2$COOH and alkali metal ions proceeds with the following extraction equilibrium equation:

$$M^+_{(a)} + H_4A_{(o)} \longleftrightarrow MH_3A_{(o)} + H^+_{(a)} \quad (2)$$

where M^+ denotes the alkali metal ion. The degree of alkali metal extraction by ^{t}Bu[4]CH$_2$COOH increased in the order $Li^+ < K^+ < Na^+$, in which the sodium ions were extracted dramatically and the lithium ions were hardly extracted.

Extraction Behavior of RE Using the Preorganized ^{t}Bu[4]CH$_2$COOH with Alkali Metal Ions

Ohto et al. [12] found that the preorganization of sodium ions enhances the extraction of RE(III) by a calix[4]arene carboxylic acid. Similarly, the other alkali metal ions can also be complexed in the cavity of the calix[4]arene and change the extraction behavior. However, the preorganized ^{t}Bu[4]CH$_2$COOH with Li^+, Na^+, or K^+ has a different extractability for RE. The extractability effect of "preorganization" promotion for RE(III) followed the order of extractability ($Na^+ > K^+ > Li^+$). When 0.1 mol/L NaCl was used to maintain the ionic strength constant, the extractability for RE by ^{t}Bu[4]CH$_2$COOH differed much from that in the system without sodium ions. In the absence of sodium ions, the extractability of Eu^{3+} was characterized by a $pH_{0.5}$ of 3.40 at which 50% extraction of Eu^{3+} was achieved. While in the presence of 0.1 mol/L sodium ions to maintain the ionic strength, the $pH_{0.5}$ value was 2.70. But the promoter action of sodium ions for the extraction of Pr^{3+} was not obvious. Moreover, the enhancement effect of equal molar lithium ions in the preorganized ^{t}Bu[4]CH$_2$COOH is so unprominent that it can be neglected. The slope of log D vs. pH_{eq} is about 1.5 for the system of ^{t}Bu[4]CH$_2$COOH using sodium ions to keep the ionic strength constant and the slope of log D - 1.5pH vs. log[H_4A] is about 1.5, suggesting the extracted species has an apparent composition of about $1.5NaH_3A$, which may be caused by the co-extraction of a 1: 1 and a 1: 2 (metal:extractant) complex.

Synergistic Extraction of Pr^{3+}, Eu^{3+}, and Yb^{3+} with the Mixture of the Preorganized ^{t}Bu[4]CH$_2$COOH and N1923

In this study, the effect of alkali metal ions was investigated initially in the mixture system of ^{t}Bu[4]CH$_2$COOH and N1923. Results indicated that this mixture has no prominent synergistic extractability for RE when alkali metal ions were not added to maintain the ionic strength. However, the addition of sodium ions obviously enhances the extraction of RE.

To obtain insight into the synergistic effect of Pr^{3+}, Eu^{3+}, and Yb^{3+} observed with the mixture of preorganized ^{t}Bu[4]CH$_2$COOH and primary amine N1923, a continuous-variation X_{N1923} experiment was performed. The distribution ratios of RE (Figure 1) varied with mole

fraction of N1923 when the total concentration of ^{t}Bu[4]CH$_2$COOH and N1923 was fixed to 2×10^{-3} mol/L.

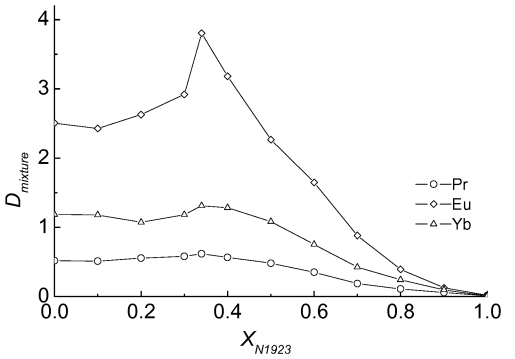

Figure 1. Synergistic extraction of Pr^{3+}, Eu^{3+}, and Yb^{3+} by the mixture of ^{t}Bu[4]CH$_2$COOH and N1923. $[RE^{3+}]_{(a)} = 1 \times 10^{-4}$ mol/L, $\mu = 0.1$ mol/L (NaCl); $[^t\text{Bu[4]CH}_2\text{COOH} + \text{N1923}]_{(o)} = 2 \times 10^{-3}$ mol/L; pH = 3.20.

Figure 1 shows that $D_{mixture}$ varied with the mole fraction of N1923. It can be seen from the figure that the "preorganized" ^{t}Bu[4]CH$_2$COOH exhibits different extractability for the three RE elements, while N1923 hardly extracts the them under the same experimental conditions. The most prominent synergistic effect was obtained at the mole fraction of $X_{N1923} = 0.35$, indicating the association of extractants with a ratio of 2:1 (^{t}Bu[4]CH$_2$COOH: N1923) in the extracted species.

Synergistic Extraction Mechanism of Pr^{3+}, Eu^{3+}, and Yb^{3+} with the Mixture of Preorganized ^{t}Bu[4]CH$_2$COOH and N1923

In order to determine the extracted complexes in the ^{t}Bu[4]CH$_2$COOH and N1923 system, a series of experiments was carried out.

As shown in Figure 2, the plots of log D_{12} vs. pH_{eq} in the ratio of 2:1 of ^{t}Bu[4]CH$_2$COOH and N1923 give a straight line with a slope of about 2.0. Similarly, at fixed aqueous acidity and concentration of the other extractant, the plots are linear with slopes of about 2.0 for preorganized

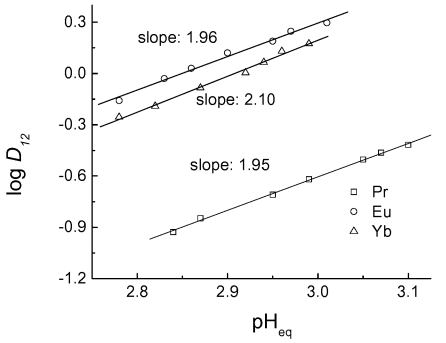

Figure 2. Plots of the distribution ratio D_{12} vs. pH_{eq}. $[RE^{3+}]_{(a)} = 1 \times 10^{-4}$ mol/L, $\mu = 0.1$ mol/L(NaCl); $[^t\text{Bu[4]CH}_2\text{COOH}]_{(o)} = 1.33 \times 10^{-3}$ mol/L, $[\text{N1923}]_{(o)} = 0.67 \times 10^{-3}$ mol/L.

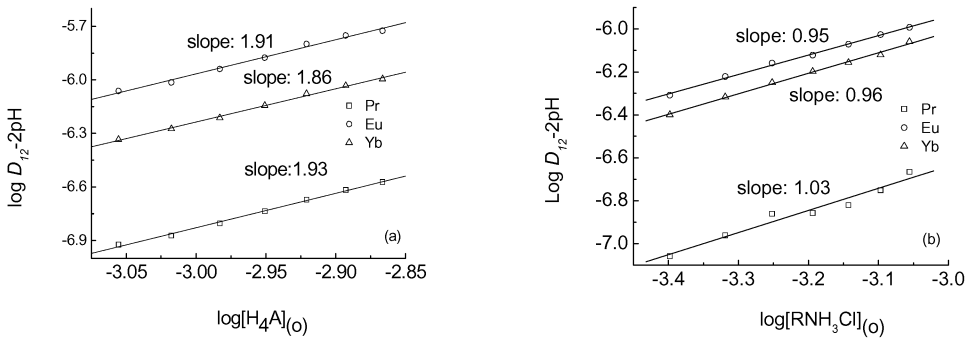

Figure 3. Plots of the distribution ratio D_{12} vs. the concentration of ^{t}Bu[4]CH_2COOH or N1923. $[RE^{3+}]_{(a)} = 1 \times 10^{-4}$ mol/L, $\mu = 0.1$ mol/L (NaCl), pH = 3.20; (a) $[N1923]_{(o)} = 0.67 \times 10^{-3}$ mol/L, (b) $[^t\text{Bu[4]CH}_2\text{COOH}]_{(o)} = 1.33 \times 10^{-3}$ mol/L.

^{t}Bu[4]CH_2COOH (Figure 3(a)) and about 1.0 for N1923 (Figure 3(b)), respectively, indicating two NaH_3A molecules and one RNH_3Cl molecule in the extracted complex of RE(III). The extractant ratio in the synergistic system by the slope-analysis method is consistent with that obtained by the continuous-variation method. Therefore, the synergistic extraction reaction can thus be deduced as

$$RE^{3+}_{(a)} + Cl^-_{(a)} + 2NaH_3A_{(o)} + RNH_3Cl_{(o)} \xleftrightarrow{K_{12}} RECl Na_2H_4A_2(RNH_3Cl)_{(o)} + 2H^+_{(a)} \qquad (3)$$

In the synergistic extraction mechanism mentioned above, the final complex $RECl Na_2H_4A_2(RNH_3Cl)$ is chemically stable in that the single preorganized species ^{t}Bu[4]CH_2COOH is prone to react with N1923, suggesting the single preorganized species ^{t}Bu[4]CH_2COOH is a more reactive complex and favors the formation reaction. Therefore, the increase of the extractability might be due to a kind of intermolecular cooperative effect of the -CH_2COOH and RNH_3Cl that facilitates the more stable complex $RECl Na_2H_4A_2(RNH_3Cl)$.

Stripping Behavior of the Synergistic Extraction of preorganized ^{t}Bu[4]CH_2COOH and N1923

An organic phase (with a total concentration of preorganized ^{t}Bu[4]CH_2COOH and N1923 being 2×10^{-3} mol/L) loaded with Pr^{3+}, Eu^{3+}, and Yb^{3+} (1×10^{-4} mol/L) was back-extracted with hydrochloric acid. It indicated that the majority of Pr^{3+}, Eu^{3+}, and Yb^{3+} can be stripped by one single stage of stripping when the concentration of hydrochloric acid is more than 0.01 mol/L. The lower stripping acidity in the mixture system will benefit the application of this system in the hydrometallurgical industry.

CONCLUSIONS

This paper deals wtihe the extraction, of Pr^{3+}, Eu^{3+}, and Yb^{3+} from chloride medium using the mixture of ^{t}Bu[4]CH_2COOH and primary amine N1923 in chloroform. A possible extraction

mechanism was proposed. The complex extracted by the mixture is determined to be $RECl Na_2H_4A_2(RNH_3Cl)$.

ACKNOWLEDGMENTS

The authors thank Tianjin Chemical Plant for supplying primary amine N1923. This project was supported by National Natural Science Foundation of China (No.50704029).

REFERENCES

1. R. Ludwig, "Calixarenes in Analytical and Separation Chemistry," *Fresenius J. Anal. Chem.*, **367**, 103-128 (2000).
2. R. Ludwig, "Calixarenes for Biochemical Recognition and Separation," *Microchim. Acta*, **152,** 1-19 (2005).
3. W. Sliwa, "Calixarene Complexes with Transition Metal Ions," *J. Inclusion. Phenom. Macrocyclic Chem.*, **52**, 13-37 (2005).
4. R. Ludwig, K. Inoue, and T. Yamato, "Solvent Extraction Behaviour of Calixarene-type Cyclophanes towards Trivalent La, Nd, Eu, Er and Yb," *Solvent Extr. Ion Exc.*, **11**(2), 311-330 (1993).
5. R. Ludwig, K. Kunogi, N. Dung, and S. Tachimori, "A Calixarene-based Extractant with Selectivity for Am^{III} over Ln^{III}," *Chem. Commun.*, **20**, 1985-1986 (1997).
6. K. Ohto, M. Yano, K. Inoue, T. Yamamoto, M. Goto, F. Nakashio, S.Shinkai, and T. Nagasaki, "Solvent Extraction of Trivalent Rare Earth Metal Ions with Carboxylate Derivatives of Calixarenes," *Anal. Sci.*, **11**, 893-902 (1995).
7. Z. L. Zhu, J. Ye, J. Y. Gu, G. D. Lu, and Y. D. Chen, "The Extraction of Fe^{3+} and La^{3+} by Synergetic Effects of TBP and P-tert-buytlcalix[8]arene Octacarboxylic Acid," *Sep. Sci. Technol.*, **36**(12), 2761-2772 (2001).
8. L. Mikulasek, B. Gruner, C. Danila, V. Bohmer, J. Caslavsky, and P. Selucky, "Synergistic Effect of Ligating and Ionic Functions, Prearranged on a Calix[4]arene," *Chem. Commun.*, **38**, 4001-4003 (2006).
9. C. D. Gutsche, B. Dhawan, K. H. No, and R. Muthukrishnan, "Calixarenes. 4. The Synthesis, Characterization, and Properties of the Calixarenes from p-tert-Butylphenol," *J. Am. Chem. Soc.*, **103**, 3782-3792 (1981).
10. J. J. Liu, Y. L. Wang, and D. Q. Li, "Extraction Kinetics of Cerium(IV) from Sulfuric Acid Medium by the Primary Amine N1923 Using a Constant Interfacial Area Cell with Flow," *J. Chem. Technol. Biotechnol.* **82**(10), 949-955 (2007).
11. T. Kakoi, T. Toh, F. Kubota, M. Goto, S. Shinkai, and F. Nakashio, "Liquid-Liquid Extraction of Metal Ions with a Cyclic Ligand Calixarene Carboxyl Derivative," *Anal. Sci.*, **14**, 501-506 (1998).
12. K. Ohto, M. Yano, K. Inoue, T. Nagasaki, M. Goto, F. Nakashio, and S. Shinkai, "Effect of Coexisting Alkaline Metal ions on the Extraction Selectivity of Lanthanide Ions with Calixarene Carboxylate Derivatives," *Polyhedron*, **16**(10), 1655-1661 (1997).

SEPARATION OF MINOR ACTINIDES FROM LANTHANIDES BY DITHIOPHOSPHINIC ACID EXTRACTANTS

D. R. Peterman,[1] M. R. Greenhalgh,[1] R. D. Tillotson,[1] J. R. Klaehn,[1] M. K. Harrup,[1] T. A. Luther,[1] J. D. Law,[1] and L. M. Daniels[2]

[1]Idaho National Laboratory, P. O. Box 1625, Idaho Falls, ID 83415-7113. [2]Rigaku Americas Corp., 9009 New Trails Dr., The Woodlands, TX 77381.
Corresponding author email address: Dean.Peterman@inl.gov

ABSTRACT

The selective extraction of the minor actinides (Am(III) and Cm(III)) from the lanthanides is an important part of advanced reprocessing of spent nuclear fuel. This separation would allow the Am/Cm to be fabricated into targets and recycled to a reactor and the lanthanides to be dispositioned. This separation is difficult to accomplish due to the similarities in the chemical properties of the trivalent actinides and lanthanides. Research efforts at the Idaho National Laboratory have identified an innovative synthetic pathway yielding new regiospecific dithiophosphinic acid (DPAH) extractants. The synthesis provides DPAH derivatives that can address the issues concerning minor actinide separation and extractant stability. For this work, two new symmetric DPAH extractants have been prepared. The use of these extractants for the separation of minor actinides from lanthanides will be discussed.

INTRODUCTION

The minor actinides (MA) Am and Cm and other transplutonium elements represent a significant, long-term hazard found in spent nuclear fuel (SNF). The hazards of the MA elements are mainly related to the heat produced by their radioactive decay and the inherent radiotoxicity of the MA elements. The removal of these elements from SNF will reduce the overall hazards of the remaining material. Unfortunately, Am/Cm and Ln ions are most stable in the trivalent oxidation state and, as a result, have quite similar chemical behavior. Separation of the MA from the lanthanides is recognized as one of the most difficult challenges in separation science.

An important approach to the realization of an effective An(III)/Ln(III) separation is the incorporation of softer donor atoms (e.g., N or S) into ligands of suitable geometries. It has been argued that increased covalency in the interaction of An(III) with the soft donor atom and/or changes in coordination geometries account for these effects [1-6]. While there are many examples in the literature reporting the use of ligands incorporating either S [2,7,8] or N [9-12] donor atoms for the separation of An(III) from Ln(III) species, the largest An(III)/Ln(III) selectivities reported used the

dialkyldithiophosphinic acid, bis(2,4,4-dimethylpentyl)-dithiophosphinic acid, the active component of the commercial extractant Cyanex 301. Using Cyanex 301, Chen et al. [13], reported a separation factor of Am(III) from Eu(III) of ~4700 in nitrate media.

Recent work at our laboratory has led to the development of a new synthetic pathway for the preparation of a more diverse series of dithiophosphinic acid (DPAH) extractants. In this work, the extraction behavior of two DPAH derivatives prepared in our laboratory will be contrasted. One of the first DPAH extractants developed (ortho-trifluoromethylphenyl dithiophosphinic acid, referred to as **1**, exhibits significantly better separation efficiency and extractant stability relative to commercially available examples [14]. The second DPAH derivative (bis(3,5-bis(trifluoromethyl)phenyl) dithiophosphinic acid, referred to as **2**, exhibits markedly less separation efficiency (relative to **1**). This serves to illustrate how a seemingly minor structural variation can have significant impacts on the observed extraction behavior.

EXPERIMENTAL

Materials

The DPAH extractants (see Figure 1 for structures) were prepared according to published procedures [15]. The DPAH derivatives are isolated as the ammonium salt and converted to the corresponding acid prior to use. Extractant purity was verified by multinuclear (^{31}P, ^{19}F, ^{13}C, ^{1}H) NMR spectroscopy. All reagents (HNO_3 and $NaNO_3$, etc.) utilized in these experiments were of reagent grade quality and used as received. The trifluoromethylphenyl sulfone (FS-13) was obtained from Marshallton Research Laboratories Inc. (King, NC) and used as received. All aqueous solutions were prepared using filtered, high-resistivity water (Barnstead Nanopure). The ^{241}Am and ^{244}Cm radiotracers were obtained from laboratory stocks. The ^{152,154}Eu radiotracer was obtained from Isotope Products Laboratories (Burbank, CA). Aliquots of these nuclides were adjusted to 0.001M HNO_3 to ensure no acid interference in the subsequent experiments.

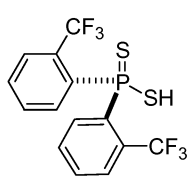

Bis(o-trifluoromethylphenyl)-dithiophosphinic acid
"**1**"

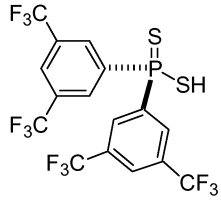

Bis-(3,5-bis(trifluoromethyl)phenyl)-dithiophosphinic acid
"**2**"

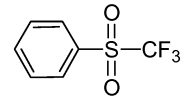

Trifluoromethylphenyl sulfone (FS-13)

Figure 1. Structures of DPAH studied in this work and the diluent.

Radioanalytical Methods

Distribution ratios for ^{241}Am and ^{154}Eu ($D_M = [M]_{org} / [M]_{aq}$) were measured by equilibrium batch contacts between the organic and aqueous phases at an organic-to-

aqueous phase ratio of unity (O/A = 1). In all experiments, the organic phase was pre-equilibrated by contacting three times with fresh aqueous containing the appropriate concentration of HNO_3 and $NaNO_3$, thus insuring all matrix components were present at equilibrium concentrations in the organic phase. In all radioactive experiments, the aqueous phase was of the appropriate HNO_3, $NaNO_3$, and stable $Eu(NO_3)_3$ concentrations spiked with the radionuclides of interest (^{241}Am, ^{244}Cm, $^{152,154}Eu$) in trace quantities (typically, less than 10^{-7} M each). The phases were mixed by vortexing for two minutes, sufficient time to ensure equilibrium is attained, and separated by centrifugation.

Each separated phase was sampled and the ^{241}Am and $^{152,154}Eu$ activities determined by gamma spectroscopy. The activity of ^{244}Cm in each phase was determined by subtracting the activity due to ^{241}Am (determined by gamma spectroscopy) from the total alpha emitter activity in the sample (determined by liquid scintillation).

Prior to the experimental determination of ^{244}Cm distribution ratios, the liquid scintillation counting techniques were developed and validated. A quench curve was determined for the organic phase to correct for any quenching effects caused by FS-13. The aqueous phase did not indicate any negative effects from quenching in the liquid scintillation counting techniques.

RESULTS AND DISCUSSION

Acid Dependence of Extraction

The distribution ratios for the partitioning of Am, Cm, and Eu between a 0.1 M solutions of **1** and **2** in FS-13 solvent as a function of varying [HNO_3] are shown in Figure 2. The negative slope (m ~ -3.0) of the Am acid dependence at >~0.003 M HNO_3 is consistent with an acidic cation-exchange extraction mechanism in which three protons are exchanged to the aqueous phase for each metal cation complex formed in the organic phase. The slope of the Cm acid dependence (triangles in Figure 1) is similar to that for Am. The apparent plateau that is seen in D_{Am} at the lower limit of acidity is not explained at present but could indicate limits in the solubility of **1** in the diluent under high pH conditions or possibly aggregation of the extractant under these conditions. The latter effect is known to reduce selectivity. The significantly different slope in the case of the Eu acid dependence indicates the Eu complex has a dramatically different stoichiometry or a fundamentally different interaction mode with this extractant. In fact, the D_{Eu} values are likely an "optimistic" estimate of very low Eu partitioning in this system.

The separation factors (S_{Eu}^{Am}) observed for **1** are $>10^5$ at 0.005 M HNO_3. The observed values of S_{Eu}^{Am} far exceed those previously reported for ligands of this type [13], including similarly structured reagents. The implicit difference in free energy of the phase-transfer reaction for Am^{3+} vs. Eu^{3+} of approximately 28 kJ/mol ($\Delta(\Delta G) = -RT \ln D_{Am}/D_{Eu}$) is not readily explained based on present understanding of lanthanide-actinide coordination chemistry. In the case of extraction by **2**, the acid dependency is strikingly different in that little to no selectivity for Am or Cm over Eu is observed.

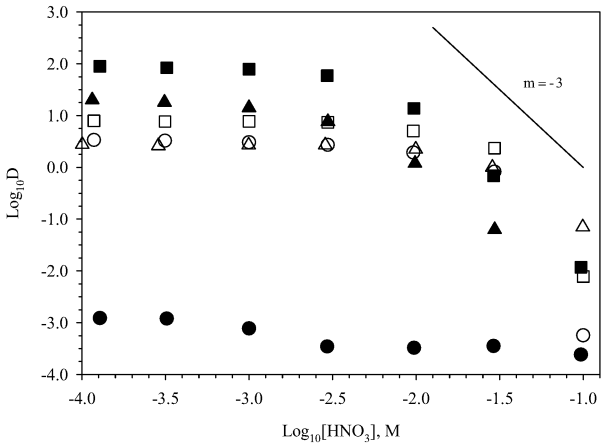

Figure 2. Nitric acid dependence of the extraction of Am (squares), Cm (triangles), and Eu (circles) by 0.1 M **1** (solid markers) and 0.1 M **2** (open markers) in FS-13 diluent. Aqueous phases contained 0.001 M $Eu(NO_3)_3$ and 1.0 M $NaNO_3$. The solid line depicts a slope of m = -3.

Solutions of varying concentrations of the DPAH extractants **1** and **2** in FS-13 diluent were used to investigate the partitioning of Am, Cm, and Eu between the organic phase and an aqueous phase containing 0.010 M HNO_3 (Figure 3). This acid concentration was chosen to minimize the possible impact of the partitioning of the extractant molecule to the aqueous phase, which may occur at lower acid concentrations as mentioned above. The slope (m = 3.0) of the D_{Am} and D_{Cm} dependence is consistent with the proposed formation of an ML_3 complex in the organic phase for both **1** and **2** extractants. The significantly different slope (m = 1.0) of the best-fit line in the case of the Eu distribution ratios indicates the Eu complex has a dramatically different stoichiometry.

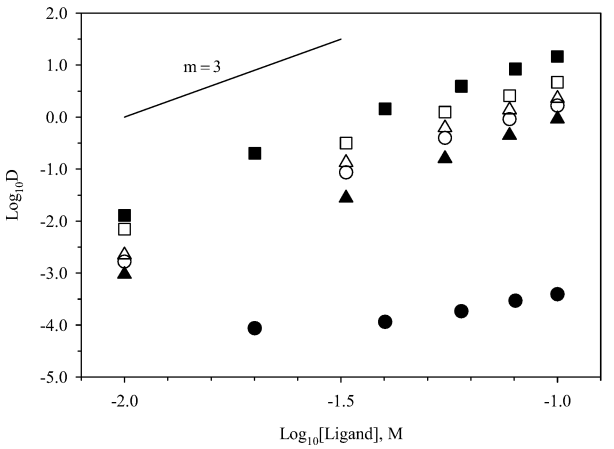

Figure 3. The ligand concentration dependence of the extraction of Am (squares), Cm (triangles), and Eu (circles) by **1** (solid markers) and **2** (open markers) in FS-13 diluent. Aqueous phases contained 0.001 M $Eu(NO_3)_3$ and 1.0 M $NaNO_3$. The solid line depicts a slope of m = 3.

The extraction of Am, Cm, and Eu by **1** was found to be independent of the concentration of added $NaNO_3$, as indicated in Figure 4. This result indicates that nitrate ions do not accompany the metal cation into the organic phase, thus confirming that cation exchange is the most important mechanism of cation phase transfer. The lack of a salting-out effect indicates that cation/complex/organic solvent hydration effects are complex in this system and play an integral role in the apparent separation efficiency. The slight dependence of the extraction of Am, Cm, and Eu by **2** is likely due to varying extents of Eu(III) complexation by nitrate anion.

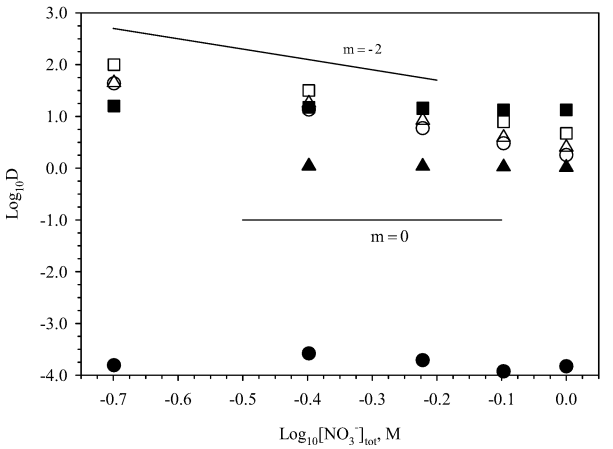

Figure 4. The total nitrate concentration dependence of the extraction of Am (squares), Cm (triangles), and Eu (circles) by 0.1 M **1** (solid markers) and 0.1 M **2** (open markers) in FS-13. Aqueous phases contained 0.001 M $Eu(NO_3)_3$ and 0.010 M HNO_3. The solid lines depict slopes of m = 0 and -2, respectively.

CONCLUSIONS

A novel synthetic pathway to an array of dithiophosphinic acid extractants has produced two derivatives which were used to study the selective extraction of Am and Cm from Eu. These data show that a cation exchange mechanism is operating in these complexes with no nitrate co-extraction. In the course of this work, two striking features of the behavior of these extractants were noted. First, (for **1**) the separation factors for the Am/Eu extraction are in excess of 10^5, much higher than the separation factors for any previously known DPAH. Second, a very minor structural change, moving a $–CF_3$ group over by only one carbon remote from the metal coordination site, completely alters the efficiency of the An/Ln separation. Work continues in our labs to better understand the behavior of these and other structurally similar DPAH extractants.

ACKNOWLEDGMENTS

This work was supported by the United States Department of Energy and the Laboratory Directed Research and Development (LDRD) program at the Idaho National Laboratory (INL) through contract DE-AC07-05ID14517.

REFERENCES

1. R. M. Diamond, K. Street, and G. T. Seaborg, "An Ion-exchange Study of Possible Hybridized 5f Bonding in the Actinides," *J. Am. Chem. Soc.*, **76**(6), 1461-1469 (1954).
2. M. P. Jensen and A. H. Bond, "Comparison of covalency in the complexes of trivalent actinide and lanthanide cations," *J. Am. Chem. Soc.*, **124**(33), 9870-9877 (2002).
3. T. Mehdoui, J. C. Berther, P. Thuery, and M. Ephritikhine, "The distinct affinity of cyclopentadienyl ligands towards trivalent uranium over lanthanide ions. Evidence for cooperative ligation and back-bonding in the actinide complexes," *Dalton Trans.*, (7), 1263-1272 (2005).
4. M. Miguirditchian, D. Guillaneus, D. Guillaumont, P. Moisy, C. Madic, M. P. Jensen, and K. L. Nash, "Thermodynamic study of the complexation of trivalent actinide and lanthanide cations by ADPTZ, a tridentate N-donor ligand," *Inorg. Chem.*, **44**(5), 1404-1412 (2005).
5. L. Petit, C. Adamo, and P. Maldivi, "Toward a clear-cut vision on the origin of 2,6-di(1,2,4-triazin-3-yl)pyridine selectivity for trivalent actinides: Insights from theory," *Inorg. Chem.*, **45**(21), 8517-8522 (2006).
6. J. N. Mathur, M. S. Murali, and K. L. Nash, "Actinide Partitioning -- A Review," *Solvent Extr. Ion Exch.*, **19**(3), 357-390 (2001).
7. G. Modolo and S. Nabet, "Thermodynamic study on the synergistic mixture of bis(chlorophenyl)dithiophosphinic acid and tris(2-ethylhexyl)phosphate for separation of actinides(III) from lanthanides(III)," *Solvent Extr. Ion Exch.*, **23,** 359-373 (2005).
8. Y. Zhu, "The separation of americium from light lanthanides by Cyanex 301 extraction," *Radiochim. Acta*, **68**(2), 95-98 (1995).
9. A. Giest, C. Hill, G. Modolo, M. Foreman, M. Weigl, K. Gompper, and M. Hudson, "6,6'-bis(5,5,8,8-tetramethyl-5,6,7,8-tetrahydro-benzo[1,2,4]triazin-3-yl) [2,2']bipyridine, and effective extracting agent for the separation of americium(III) and curium(III) from the lanthanides," *Solvent Extr. Ion Exch.*, **24,** 463-483 (2006).
10. M. P. Jensen, J. V. Beitz, R. D. Rogers, and K. L. Nash, "Thermodynamics and hydration of the europium complexes of a nitrogen heterocycle methane-1,1-diphosphonic acid," *Dalton Trans.*, **18,** 3058-3064 (2000).
11. M. G. B. Drew, P. B. Iveson, M. J. Hudson, J. O. Liljenzin, L. Spjuth, P. V. Cordier, A. Enarsson, C. Hill, and C. Madic, "Separation of americium(III) from europium(III) with tridentate heterocyclic nitrogen ligands and crystallographic studies of complexes formed by 2,2 ': 6 ',2-terpyridine with the lanthanides," *Dalton Trans.*, **5,** 821-830 (2000).
12. Z. Kolarik, U. Mullich, and F. Gassner, "Extraction of Am(III) and Eu(III) nitrates by 2,6-di-(5,6-dipropyl-1,2,4-triazin-3-yl)pyridines," *Solvent Extr. Ion Exch.*, **17**(5), 1155-1170 (1999).
13. J. Chen, Y. Zhu, and R. Jiao, "The separation of Am from lanthanides by purified Cyanex 301 extraction," *Sep. Sci. Technol.*, **31**(19), 2723-2731 (1996).
14. D. R. Peterman, J. R. Klaehn, M. K. Harrup, M. R. Greenhalgh, R. D. Tillotson, and T. A. Luther, Submitted to *Solvent Extr. Ion Exch.*, 2007.
15. J. R. Klaehn, D. R. Peterman, R. D.Tillotson, T. A. Luther, M. K. Harrup, J. D. Law, and L. M. Daniels, *Inorg. Chim. Acta*, Submitted 2007.

SELECTIVE EXTRACTION OF U(VI) AND SOME OTHER METALS FROM NITRIC ACID MEDIA BY POLYPHOSPHINE POLYOXIDES

M. Nogami,[1] K. Maruyama,[2] Y. Sugiyama,[1] and Y. Ikeda[1]

[1]Research Laboratory for Nuclear Reactors, Tokyo Institute of Technology, 2-12-1-N1-34 O-okayama, Meguro-ku, Tokyo 152-8550, Japan. [2]Mitsubishi Chemical Corp., 1000 Kamoshida-cho, Aoba-ku, Yokohama 227-8502, Japan.
Corresponding author email address: mnogami@nr.titech.ac.jp

ABSTRACT

For the selective extraction of radionuclides from nitrate media, the extractabilities of organopolyphosphine polyoxides were examined in the form of impregnated resins. It was found that the extractability of 1,1,3,5,5-pentaphenyl-1,3,5-triphosphapentane trioxide (PPTPT) for U(VI) is quite unusual with very high values at both low and high concentrations of nitric acid, which is not observed for other types of extractants. Thus, this extractant might be promising for the selective extraction of U(VI) in very high concentrations of HNO_3.

INTRODUCTION

In the treatment of radioactive liquid wastes, a lot of extractants have been developed for the extraction of actinide and lanthanide species from nitrate media [1-3]. Recently, extractants not containing phosphorus have been receiving attention because of their easy disposal after use [1]. However, phosphine oxide extractants have a number of advantages for this application:

(i) They have strong affinities for actinide species.
(ii) Extraction from highly concentrated nitrate media and back-extraction with diluted HNO_3 may be expected as they have aprotic properties.
(iii) In principle, they do not undergo acid hydrolysis unlike nitrogen compounds such as diamides and ester phosphates such as tri-*n*-butylphosphate.

Ether bonds, which are used to increase extractability for actinide species, decrease the stability of extractants in acid media [1]. Therefore, extractants like phosphine oxides without ether bonds are expected to be chemically stable in acid media.

From these viewpoints, phosphine oxide extractants have a number of benefits over those without phosphorus, especially if in addition they have some specific advantages in their extractability and chemical stability.

Generally, an increase in number of phosphoryl groups in extractants enhances the extractability of metal ions, because of a stronger chelating effect with oxygen

coordination of phosphine oxides to metal ions. Thus, we focused on triphosphine trioxides and tetraphosphine tetraoxides. In this study, 1,1,3,5,5-pentaphenyl-1,3,5-triphosphapentane trioxide (PPTPT) and 1,1,5,5,2',2'-hexa-phenyl-1,3,5,2'-tetraphospha-3-ethylpentane tetraoxide (HPTEPT) were studied (Figure 1).

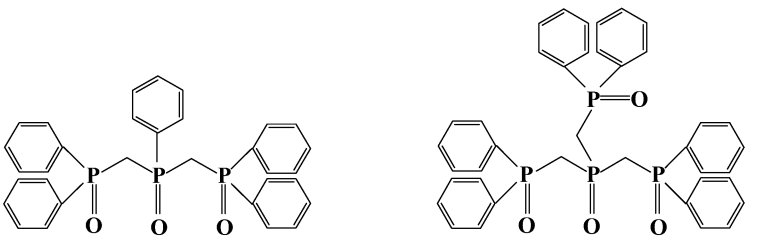

Figure 1. Chemical structures of PPTPT (left) and HPTEPT (right).

Earlier, Cristau et al. [4] had examined the extractability of these two extractants for Pu, Am, and Np using a liquid-liquid extraction system at a tracer level for the recovery of these radionuclides from high-activity liquid wastes, and found that they extracted more than 99% of both Pu and Am from the solution consisting of 4 mol/dm^3 $NaNO_3$ and 1 mol/dm^3 HNO_3. However, the medium studied was limited to that mentioned above, and uncommon diluents such as nitrophenylhexylether and nitrophenyloctylether were used in their experiments. Organochlorine solvents such as dichloromethane and chloroform are frequently used as diluents for extractants with high polarity, but the use of such solvents must be restricted from an environmental point of view. Thus finding an appropriate and more common diluent would be another tough task.

In this study, therefore, we examined the extractabilities of PPTPT and HPTEPT under a wide range of solution conditions in the form of an impregnated resin to avoid the problem of diluents.

EXPERIMENTAL

Preparation of Impregnated Resins

For the PPTPT resin, formylstyrene and divinylbenzene (Aldrich, purity 80%) were firstly copolymerized with organic diluents on a porous silica support by a similar method as described earlier [5]. The porous silica support has a uniform particle diameter of 50 μm with a pore size of 600 nm, and the synthesized resins also have uniform particle diameters of ca. 50 μm. PPTPT (from Shiratori Pharmaceutical Co., Ltd., Chiba, Japan) was dissolved in dichloromethane and mixed at a ratio of 2 g of the dried silica-supported polymer to 1 g PPTPT. Dichloromethane was then removed under reduced pressure at 333 K.

HPTEPT resin was prepared in a similar way except for the use of chloromethylstyrene instead of formylstyrene in the polymerization step. HPTEPT was purchased from Koyo Chemical Co., Ltd., Hyogo, Japan.

Adsorption Experiments

The adsorption rate for PPTPT was measured by a batch method using Zr(IV). Samples of the resin (0.25 g) and 5 cm^3 of the sample solution containing 10 $mmol/dm^3$ Zr(IV) and 0.1 mol/dm^3 HNO_3 were shaken at 298 K in a thermostatic shaking bath. Samples of the supernatant liquid were taken after appropriate contact times and the concentrations of Zr measured by ICP-AES.

Adsorptivities of PPTPT and HPTEPT resins for metal ions at equilibrium were obtained by a batch method using the same procedure as for the rate of adsorption. That is, the initial concentration of each metal ion was 10 $mmol/dm^3$, and contact time was 24 h. Adsorptivities were evaluated by the distribution ratio, K_d, defined as,

$$K_d = \frac{C_0 - C}{C} \times \frac{V}{W} \ (cm^3/g) \qquad (1)$$

where, C_0 and C denote the concentrations of the nuclide in the solution before and after contact with the resin, respectively; V and W represent the volume of the solution and the weight of the resin including silica, respectively. The values of C_0 and C for each metal ion were determined by ICP-AES.

RESULTS AND DISCUSSION

Adsorption Rate

The adsorptivity of the PPTPT resin for Zr(IV) as a function of time is shown in Figure 2. As shown by this figure, approximately 6 h is required to attain equilibrium in spite of a small size of the resin (50 μm). This is probably because PPTPT exists as a solid at room temperature. The rates for other metal ions including U(VI) will be examined in the near future.

Adsorption Equilibrium

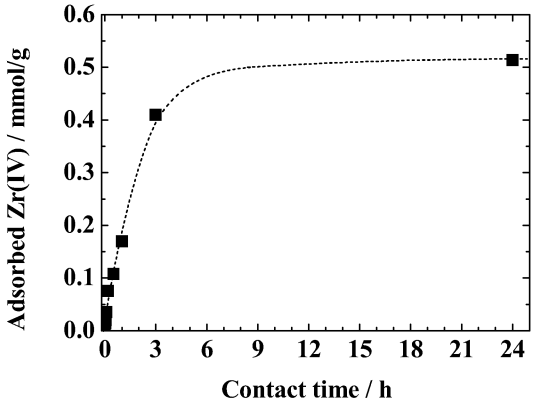

Figure 2. Adsorption of Zr(IV) onto PPTPT resin as a function of time.

Adsorptivities of PPTPT and HPTEPT resins for U(VI) and Nd(III) in solutions of varying HNO_3 concentration are shown in Figure 3. The K_d values of HTPEPT for U(VI) and PPTPT for Nd(III) are almost identical. They increase with increasing concentration of HNO_3. This phenomenon is consistent with the common tendencies observed for many neutral extractants in HNO_3 media. The K_d values of HTPEPT for Nd(III) are found to be almost flat in the range of 0.5 to 6 mol/dm^3 HNO_3 and to decrease both above and below this concentration range. Similar behavior is found for many neutral extractants in HNO_3 media. These tendencies can be explained by the combination of the change in concentrations of NO_3^- and H^+, that is, K_d values increase with increasing concentration of NO_3^- and decrease with increasing concentration of H^+.

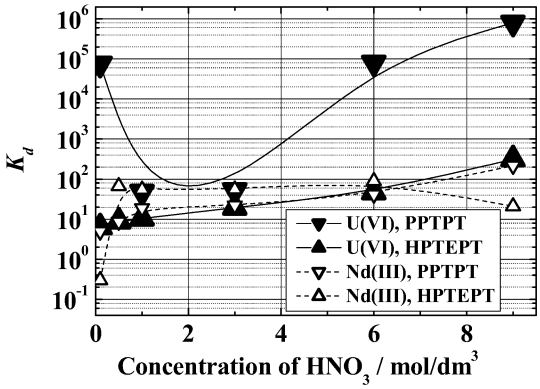

Figure 3. Adsorptivity of PPTPT and HPTEPT resins for U(VI) and Nd(III) in HNO_3 solutions.

However, the dependence of the K_d values of PPTPT for U(VI) on HNO_3 concentration seems most unusual, with a minimum at around 2–3 mol/dm^3 HNO_3 and very much higher than HTPEPT in both the lower and higher concentration ranges. The same tendency was found for PPTPT when the initial concentration of U(VI) in the sample solution was 100 mmol/dm^3. The reason for this remains unclear.

These results indicate that the triphosphine trioxide (PPTPT) is a much better extractant for U(VI) in high concentrations of HNO_3 than the tetraphosphine tetraoxide (HTPEPT). The lower adsorptivity of HTPEPT suggests that at least one oxygen atom of HTPEPT does not participate in the coordination to U(VI) due to the constraint of the conformation.

To investigate the wider possibilities for the PPTPT resin, the variation of K_d values for Zr(IV), Mo(VI), and Sr(II) with HNO_3 concentration were examined. The results are shown in Figure 4. Unlike U(VI), the Zr(IV) and Mo(VI) species are both efficiently adsorbed regardless of the concentration of HNO_3. Although both these two ions are strongly adsorbed onto the resin, U(VI) species are more strongly adsorbed from HNO_3 solutions stronger than 5 mol/dm^3. This means that PPTPT has high selectivity for U(VI) in HNO_3 solutions of high concentrations not observed for other types of extractants. The adsorptivities for actinide(IV) will be examined in the near future. Sr(II)

ions are found to be slightly adsorbed with a K_d maximum around 0.5 mol/dm^3 HNO_3. On the other hand, Sr(II) was not adsorbed onto the HTPEPT resin. These results suggest that PPTPT produces a very negative electron field.

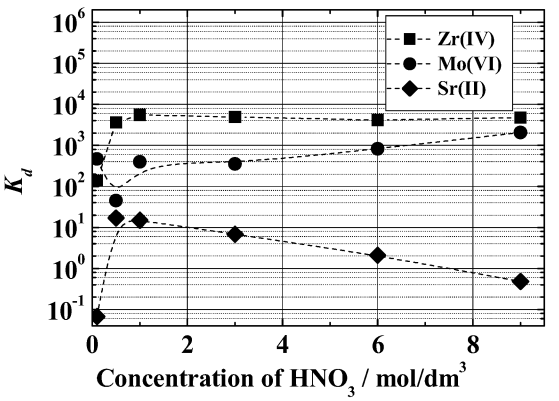

Figure 4. Adsorptivity of PPTPT resin for Zr(IV), Mo(VI), and Sr(II) in HNO_3 solutions.

The dependence of the adsorption of PPTPT resin on the nature of the solution was examined using Nd(III) (Figure 5). It was found that Nd(III) is adsorbed in similar way from both HCl and HNO_3 solutions. It was also found that, unlike more common extraction systems, the adsorptivity in acid media is higher than that in the presence of salts.

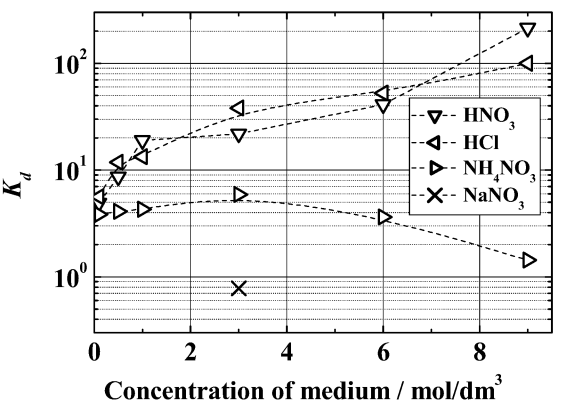

Figure 5. Adsorptivity of PPTPT resin for Nd(III) in various media.

CONCLUSIONS

It has been shown that the triphosphine trioxide (PPTPT) has a remarkable affinity and selective extractability for U(VI) from very high concentrations of HNO_3. Adsorptivities for actinide(IV) species should be examined in the near future.

REFERENCES

1. C. Madic, et al., "New partitioning techniques for minor actinides," Nuclear science and technology, Final report, EUR19149, European Commission, 2000.
2. K. L. Nash, C. Lavallette, M. Borkowski, R. T. Paine, and X. Gan, "Features of the Thermodynamics of Two-Phase Distribution Reactions of Americium(III) and Europium(III) Nitrates into Solutions of 2,6-Bis[(bis(2-ethylhexyl)phosphono)methyl]pyridine *N,P,P'*-Trioxide," *Inorg. Chem.*, **41**, 5849-5858 (2001).
3. A. N. Turanov, V. K. Karandashev, and V. E. Baulin, "Extraction of Rare-Earth and Americium from Nitric Acid Solutions with Polyphosphine Oxides," *Radiochem.,* **44**(1), 26-34 (2002).
4. H. J. Cristau, D. Virieux, J. F. Dozol, and H. Rouquette, "Selective extraction of actinides by polyphosphine polyoxides through supported liquid membrane," *J. Radioanal. Nucl. Chem.*, **241**(3), 543-547(1999).
5. M. Nogami, T. Ishihara, K. Suzuki, and Y. Ikeda, "Syntheses and Adsorption Behavior of Monoamide Resins with Porous Silica Support for Selective Recovery of Uranium(VI) from Nitric Acid Media," *J. Radioanal. Nucl. Chem.*, **273**(1), 37-41 (2007).

EXTRACTION OF METAL IONS FROM CHLORIDE MEDIA: CAN MALONAMIDE DERIVATIVES BE USEFUL?

A. P. Paiva,[1] P. Malik,[1] A. M. Rosa,[2] C. Castro,[2] and M. C. Costa[2*]

[1] *DQB-FCUL, CQB, Rua Ernesto de Vasconcelos, C8 1749-016 Lisboa, Portugal,*
[*]*CCMAR,* [2]*Universidade do Algarve, 8005-139 Faro, Portugal.*
Corresponding author email address: appaiva@fc.ul.pt

ABSTRACT

This paper presents a selection and discussion of some of the most remarkable results that have been achieved regarding the use of a series of specific *N,N'*-tetrasubstituted malonamides to extract metal ions from chloride media. In addition to the literature information concerning the extraction of some lanthanide and actinide ions, some new results involving *N,N'*-dimethyl-*N,N'*-dicyclohexyltetradecylmalonamide (DMDCHTDMA) towards iron(III) recovery are presented and discussed, as well as some promising data obtained for the extraction of a few platinum-group metals by *N,N'*-dimethyl-*N,N'*-diphenyltetradecylmalonamide (DMDPHTDMA).

INTRODUCTION

N,N'-tetrasubstituted malonamides caused a marked impact in the solvent-extraction (SX) world when they were proposed as the basis of the DIAMEX process. This project, developed in the late 1980s, has shown the utility of malonamide derivatives to recover lanthanides and actinides from irradiated nuclear fuels, claiming to be a viable alternative to replace tributylphosphate (TBP) in the PUREX process. Since then, several research efforts have been carried out to apply malonamides in specific metal ion extraction purposes, particularly for lanthanides and actinides, usually from nitric acid media (for example, [1]).

The application of several pentaalkylpropanediamides to extract actinides from chloride media (HCl or its mixture with Li, Ca, Mg, or K chloride salts) has been reported [2]. Pu(IV) was easily recovered, but the Am(III) extraction was only effective when a salting-out agent such as LiCl was used. Details regarding metal stripping have also been provided [2]. The extraction of trivalent lanthanide ions from HCl solutions by *N,N'*-dimethyl-*N,N'*-diphenyl-3-oxapentanediamide (DMDPhOPDA, a diglycolamide derivative) has been attempted, the overall results obtained pointing to a much better performance towards Ln(III) extraction from HNO_3 than from HCl media [3]. The related Ln(III) distribution ratios, obtained when HCl solutions were involved, decreased with increasing atomic number [3].

A systematic research regarding the application of malonamide derivatives to recover Fe(III) from chloride media has been carried out [4,5]. In fact, several distinct structural features such as different *N,N'*-alkyl groups besides the methyl ones [5], the absence or presence of a central alkyl chain on the carbon atom within the carbonyl functional groups [4,5] and the effects caused by that central alkyl chain when exhibiting different sizes [5] have been investigated. Generally, it can be said that all malonamide derivatives studied until now exhibit good extractive properties towards Fe(III) recovery at >4 M HCl, with the exception of *N,N*'-dimethyl-*N,N'*-diphenylmalonamide, DMDPHMA, which needs a ~6 M HCl medium to be efficient [4]. The good selectivity patterns shown by the extractants towards Fe(III) when in presence of In(III), Cr(III), Cu(II), Zn(II), Pb(II), Ni(II), Co(II), Cd(II), and Ag(I) [4], as well as the easy and efficient stripping of the metal ion through a simple contact with water, have been highlighted. In addition, the influence of the malonamide structure on the type of chemical reaction involved in the metal ion extraction [4,5] has also been discussed and clarified.

More recently, *N,N'*-dimethyl-*N,N'*-diphenyltetradecylmalonamide (DMDPHTDMA) has been employed to recover Pt-group metals from concentrated HCl media. Hence, the recovery of Rh(III) when in presence of an adequate concentration of tin(II) chloride as a labilizing agent has been reported [6], including a flowsheet proposal demonstrating the viability of the selective separation of Rh and Sn from a 5 M HCl solution.

Contrary to the situation involving nitric acid media, papers focusing on the research of the surface-activity phenomena occurring in malonamide derivatives/HCl systems are still rare [7]. In fact, the metal ion extraction from HNO_3 media exhibited by malonamides is crucially determined by superficial phenomena and supramolecular aggregation [8], but this situation seems not to apply to the chloride media. Although a molecular dynamics study with three different malonamide derivatives, for a water-chloroform interface, evidenced that the uncomplexed malonamide ligands are surface active [9], a detailed research performed with a tetraalkylglycolamide (*N,N,N',N'*-tetraoctyl-3-oxapentane-1,5-diamide) revealed that the scattering data for a 4 M HCl system resembled that of the low acidity of the HNO_3 samples, reflecting a lack of oligomers, a simple monomer-dimer equilibrium and insignificant interparticle scattering [7]. However, the investigation of the malonamide surface-activity properties for chloride media deserves further developments.

In this work, some preliminary results regarding the use of *N,N*'-dimethyl-*N,N'*-dicyclohexyltetradecylmalonamide (DMDCHTDMA) to recover Fe(III) from chloride media are presented, in sequence to the work performed with the derivative without the tetradecyl chain [5]. Furthermore, the potentialities of DMDPHTDMA to separate some Pt-group metals (Pt, Pd, and Rh) from concentrated HCl media are studied and discussed.

EXPERIMENTAL

The syntheses of DMDCHTDMA and DMDPHTDMA were carried out according to a procedure previously described [4,6]. Their characterization was

performed using adequate spectroscopic techniques, the results obtained being in agreement with the expected ones.

For the iron(III) extraction studies, 0.05 M DMDCHTDMA solutions were prepared in toluene. Aqueous phases consisted of ~0.01 M $FeCl_3.6H_2O$ dissolved in aqueous HCl. For the extraction and stripping experiments, equal volumes of aqueous and organic phases (A/O = 1) were shaken at 1000 rpm for 15 minutes [4,5], at room temperature. In the stripping experiments, the Fe(III) loaded organic phases were singly contacted with distilled water. The iron content in the aqueous phases was analyzed before and after extraction by flame atomic absorption spectroscopy (AAS) using a Shimatzu equipment, model AA 680.

For the platinum, palladium, and rhodium extraction studies, solutions of Pt(IV) and Pd(II) were prepared from their atomic absorption standard solutions, whereas those of Rh(III) were prepared from an analytical reagent grade $RhCl_3$ salt. The diluent used for DMDPHTDMA was 1,2-dichloroethane (1,2-DCE). The different Rh solutions were freshly prepared from an aged mother solution. Extraction and stripping experiments were carried out at 25 ± 3 °C for 10 minutes [6], with the help of a water bath. Different compositions of aqueous solutions and multiple A/O ratios were used for stripping purposes. The different metal ion contents were determined in the aqueous phases by both AAS (Unicam SP9) and UV-visible spectrophotometry (Shimatzu, model 1603). Pt-Sn and Pd-Sn complex solutions were prepared at room temperature, while the Rh-Sn complex solutions were heated to 70 °C for 15 minutes. Three replicate experiments were carried out for each condition; a precision of ± 5% was achieved for all cases.

RESULTS AND DISCUSSION

Iron(III) recovery

Figure 1 presents the profile of DMDCHTDMA to extract Fe(III) from HCl solutions, this data being compared with the results obtained for DMDCHMA under similar conditions.

As already verified [4,5], iron extraction is dependent on the HCl concentration of the aqueous phases, since Fe(III) extraction increases as the HCl concentration also increases. With both malonamides, the extraction of Fe(III) can be considered quantitative when the concentration of HCl is 6 M or higher. Although presenting a similar extraction behavior in the range 1 to 6 M HCl, DMDCHTDMA extracts less Fe(III) than DMDCHMA for a given HCl concentration. An opposite situation has been found for DMDPHMA and DMDPHTDMA [4], this new result showing the determinant dependence of the extractive profile of malonamides on their structures, particularly for intermediate HCl concentrations.

Data on Fe(III) stripping from the loaded DMDCHTDMA is shown in Figure 2.

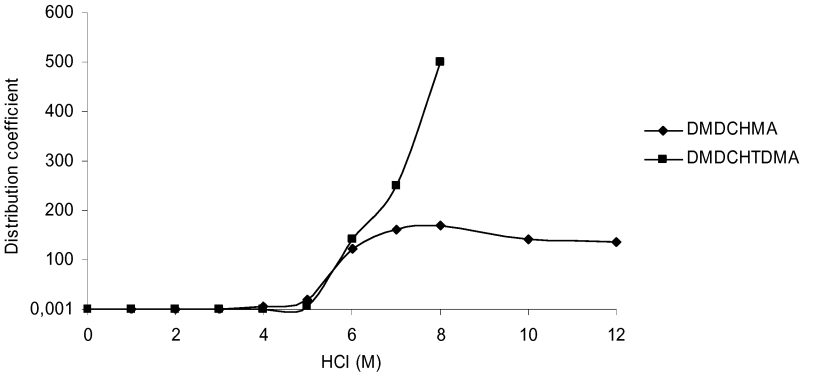

Figure 1. Extraction of ~0.01 M Fe(III) by DMDCHTDMA and DMDCHMA (0.05 M in toluene) from HCl solutions.

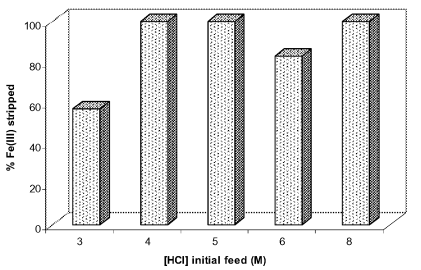

Figure 2. Fe(III) stripping from the loaded organic phases with distilled water (DMDCHTDMA in toluene).

The results obtained demonstrate that Fe(III) can be quantitatively removed by water from the loaded organic phases, depending on the HCl concentration of the initial aqueous feed solutions. A complete Fe(III) stripping was observed for initial aqueous phases with HCl concentrations of 4, 5, or 8 M. A 100% iron(III) recovery was achieved from an 8 M HCl solution.

Platinum, Palladium, and Rhodium Recovery

The effect of the HCl concentration (1 to 9 M) on the separate extraction of Pt, Pd, and Rh has been studied by keeping DMDPHTDMA concentration to 0.1 M. In the absence of tin(II) chloride, the extraction of all those metal ions decreased with increasing acid concentrations (for an equilibration time of 1 hour). In the presence of tin(II) chloride, the metal ions extraction increased and remained quantitative until ~5 M HCl. Afterwards, a slight decrease in the extraction of Rh and Pd was noticed (Figure 3).

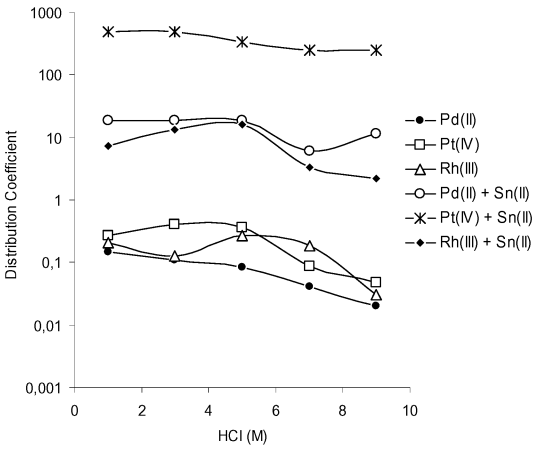

Figure 3. Effect of [HCl] on the extraction of Pt, Pd and Rh in the absence and presence of $SnCl_2$. Sn:(Pt, Pd or Rh) = 10:1.

For studying the use of different stripping reagents, the extraction of these three metal ions has been carried out separately using 10:1 Sn-(Pt, Pd, or Rh) proportions, from 5 M HCl, by a 0.1 M DMDPHTDMA solution. Under these conditions, all the metal ions suffered more than 90% extraction. The results indicate that a 5 M or more highly concentrated HCl solution can be a selective stripping reagent for Pd with respect to Pt and Rh. Both Pt and Rh can be stripped easily by an oxidizing mixture of 4 M HCl and 0.05 M $NaClO_3$.

The possibility to achieve the mutual separation of the three metal ions has been explored using a synthetic mixture, where Pd, Pt, and Rh were in a 1:1:1 proportion and the amount of tin was ten times higher than the total metal ion contents. This complex solution was prepared at room temperature. After its contact with 0.1 M DMDPHTDMA, only Pt and Pd were extracted; the major part of Rh remained in the aqueous phase. From the organic phase, both Pt and Pd were selectively separated, firstly using 7 M HCl to strip Pd and, afterwards, 4 M HCl + 0.05 M $NaClO_3$ to strip Pt. The results are shown in Table 1.

Table 1. Separation of Pt, Pd, and Rh from a synthetic mixture using DMDPHTDMA

Element	Initial Conc. (mg/L)	Conc. in the Organic Phase (mg/L)	Conc. in the Aqueous Phase (mg/L)	Stripping with 7 M HCl (3 times) (mg/L)	Stripping with 4 M HCl + 0.05 M $NaClO_3$ (3 times) (mg/L)
Pt	50.0	49.9	0.05	<0.10	49.7
Pd	55.0	44.5	5.50	44.1	0.2
Rh	60.0	5.0	55.0	<0.10	4.8

CONCLUSIONS

Malonamide derivatives can surely be useful to carry out the SX of different metal ions from chloride media. Their efficiency to recover Fe(III) from concentrated chloride solutions has once again been evidenced for a new derivative, DMDCHTDMA, and particularly the potential shown by DMDPHTDMA to mutually separate some Pt-group metals from 5 M HCl solutions is somehow encouraging. The development of suitable processing schemes to individually separate Pt-group metals from several base ones such as Fe(III), Cu(II), Co(II), Ni(II), Zn(II), Mn(II), and In(III) is currently underway.

ACKNOWLEDGMENTS

The post-doc grant kindly offered by FCT (Lisbon, Portugal) to P. Malik is gratefully acknowledged.

REFERENCES

1. Y. Sasaki and S. Tachimori, "Extraction of Actinides (III), (V), (VI) and Lanthanides (III) by Structurally Tailored Diamides," *Solvent Extr. Ion Exch.*, **20**(1), 21-34 (2002).
2. C. Cuillerdier and C. Musikas, "Extraction of Actinides from a Chloride Medium Using Pentaalkylpropanediamides," *Sep. Sci. Technol.*, **28**(1-3), 115-126 (1993).
3. H. Narita, T. Yaita, K. Tamura, and S. Tachimori, "Solvent Extraction of Trivalent Lanthanoid Ions with N,N'-dimethyl-N,N'-diphenyl-3-oxapentanediamide," *Radiochim. Acta*, **81**(4), 223-226 (1998).
4. M. C. Costa, A. Carvalho, A. Uryga, and A. P. Paiva, "Solvent Extraction of Iron(III) from HCl Solutions Using N,N'-dimethyl-N,N'-diphenylmalonamide and N,N'-dimethyl-N,N'-diphenyltetradecylmalonamide," *Solvent Extr. Ion Exch.,* **21**(5), 653-686 (2003).
5. M. C. Costa, I. Pêczek, Z. Sadowski, S. Natu, and A. P. Paiva, "The Solvent Extraction of Iron(III) from Chloride Solutions by N,N'-tetrasubstituted Malonamides: Structure-Activity Relationships," *Solvent Extr. Ion Exch.*, **25**(4), 463-484 (2007).
6. P. Malik and A. P. Paiva, "Solvent Extraction of Rhodium from Chloride Media by N,N'-dimethyl-N,N'-diphenyltetradecylmalonamide," *Solvent Extr. Ion Exch.*, accepted for publication (2008).
7. M. P. Jensen, T. Yaita, and R. Chiarizia, "Reverse-Micelle Formation in the Partitioning of Trivalent f-Element Cations by Biphasic Systems Containing a Tetraalkyldiglycolamide," *Langmuir*, **23**, 4765-4774 (2007).
8. C. Erlinger, L. Belloni, Th. Zemb, and C. Madic, "Attractive Interactions Between Reverse Aggregates and Phase Separation in Concentrated Malonamide Extractant Solutions," *Langmuir*, **15**, 2290-2300 (1999).
9. R. Diss and G. Wipff, "Lanthanide Cation Extraction by Malonamide Ligands: From Liquid-liquid Interfaces to Microemulsions. A Molecular Dynamics Study," *Phys. Chem. Chem. Phys.*, **7**, 264-272 (2005).

SEPARATION OF PALLADIUM IN HYDROCHLORIC ACID SOLUTION WITH SULFIDE-CONTAINING AMIDE COMPOUNDS

H. Narita, M. Tanaka, and K. Morisaku

Research Institute for Environmental Management Technology, National Institute of Advanced Industrial Science and Technology (AIST), 16-1 Onogawa, Tsukuba, Ibaraki 305-8569, Japan. Corresponding author email address: hirokazu-narita@aist.go.jp

ABSTRACT

The extraction and separation properties of palladium from hydrochloric acid solutions with sulfide-containing monoamide and diamide compounds were investigated. *N*,*N*-di-*n*-octyl-3-thiapentanamide (DO3TPA) and *N*,*N*,*N*′,*N*′-tetra-*n*-octylthiodiglycolamide (TOTDGA) were synthesized as a monoamide and a diamide, respectively. Both of them rapidly extracted Pd(II) compared to the conventional Pd(II) extractant, di-*n*-hexylsulfide (DHS); in particular, it took <2 min to achieve ~100% extraction in the DO3TPA system. The high selectivity for Pd(II) over Pt(IV) was obtained at ≤5 M HCl for DO3TPA and at ≤3 M HCl for TOTDGA. The Pd(II) extracted in the DO3TPA or TOTDGA phase was back-extracted with ammonia solutions.

INTRODUCTION

The demand for autocatalysts that contain a significant amount of platinum group metals (PGMs) has been enhanced worldwide with the tightening of regulations regarding the emissions from automobiles [1]. Hence, their wastes have recently increased, and the improvement of the PGM recovery from them, along with metal refining from ores, has become more important. In general, the separation and purification of the PGMs in hydrometallurgical processes is carried out by solvent extraction [2,3]. The development of a successful solvent-extraction process depends on the choice of the appropriate extractants, while practical extractants have been limited over the past several decades, as they have some problems. As for the palladium extraction, dialkylsulfide compounds (DAS) (e.g., di-*n*-octylsulfide (DOS) and di-*n*-hexylsulfide (DHS)) have been extensively introduced for practical use. DAS can selectively extract Pd(II) from an acidic chloride solution, and the loaded Pd(II) can be back-extracted with an ammonia solution; however, the Pd(II) extraction is very slow, and the sulfide is readily oxidized, which decreases the Pd(II) extractability [3].

Solvent extraction using *N*-disubstituted amide compounds has been widely studied in spent nuclear fuel treatment processes [4-6]. They are relatively stable against acids [7]; therefore, we have focused on their use as extractants for precious metals. So

far, we have found that the monoamide [8,9], thiodiglycolamide [10], and diglycolamide compounds [11] show a high extractability for gold, palladium, and platinum, respectively. Among them, *N,N'*-dimethyl-*N,N'*-di-*n*-octyl-thiodiglycolamide (MOTDGA) has good Pd(II) extraction properties compared to DHS, especially in terms of the extraction rate [10]. In order to clarify the dominant factor regarding its extraction properties, knowledge of structural effects such as changes in the *N*-substituents and the number of amide groups seems to be very useful. In this study, therefore, we synthesized *N,N*-di-*n*-octyl-3-thiapentanamide (DO3TPA) and *N,N,N',N'*-tetra-*n*-octyl-thiodiglycolamide (TOTDGA) (Figure 1), then investigated their extractability for Pd(II).

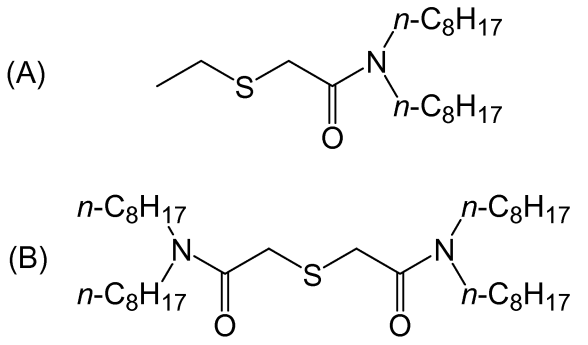

Figure 1. Structures of the extractants (A) DO3TPA and (B) TOTDGA.

EXPERIMENTAL

Reagents

Stock solutions of each metal ion were prepared by dissolving the metal chlorides ($PdCl_2$, H_2PtCl_6, and $RhCl_3 \cdot 3H_2O$ from Soekawa Chemical Co., Ltd.; $CuCl_2 \cdot 2H_2O$, $FeCl_3 \cdot 6H_2O$, $NiCl_2 \cdot 6H_2O$, and $ZnCl_2$ from Wako Pure Chemical Industries, Ltd.) into HCl solutions. TOTDGA and DO3TPA were synthesized using a procedure similar to the synthesis of MOTDGA [10] (purity 91.4% for TOTDGA, 98.6% for DO3TPA). All the other chemicals used in this study were of reagent grade.

Solvent Extraction

DO3TPA or TOTDGA diluted by 80 vol % *n*-dodecane/20 vol % 2-ethylhexanol was pre-equilibrated with the same volume of an HCl solution in the absence of the metal ions. One milliliter aliquots of the pre-equilibrated organic phase and the same volume of the HCl solution containing 0.1 g/L each of mixed metal ions (Pd(II), Pt(IV), Rh(III), Fe(III), Cu(II), Ni(II), and Zn(II)), were vertically shaken in a 10 mL glass tube at an amplitude of 100 mm and a frequency of 200 $min.^{-1}$, then centrifuged. A portion of the organic phase and the same volume of a 28% ammonia solution were shaken, and the metal ions in the organic phase were back-extracted to the aqueous phase. The volume ratio (*O*/*A*) of the organic and aqueous phases was 1 during all the experiments. All the

extractions were carried out at room temperature (23 ± 2 °C). The concentrations of the metal ions in the aqueous phase were measured by ICP-AES (Horiba ULTIMA2); those in the organic phase were calculated on the basis of the mass balance of the metal ions before and after the extraction.

RESULTS AND DISCUSSION

Effect of Extraction Time

Figure 2 shows the dependence of the extraction percentages (*E*%) of Pd(II) and Pt(IV) on the extraction (shaking) time in which the extractant and HCl concentrations were 0.1 M and 1 M, respectively. Platinum(IV) is barely extracted during this extraction time in all the systems. In addition, none of the extractants extract Rh(III) and the base metals under these conditions; thus, the selectivity for Pd(II) is high. In the DHS system, the Pd(II) extraction is very slow as previously reported [3]; it takes about 240 min to reach >99% extraction. In contrast, DO3TPA and TOTDGA rapidly extract Pd(II). Taking into account the structural difference between these amide compounds and DHS, the amide group plays an important role in the promotion of the extraction rate. In particular, an almost 100% extraction is attained within 2 min. in the DO3TPA system. This immediate extraction is comparable to that with MOTDGA [10]. On the other hand, in the TOTDGA system, ~15 min. is required to reach >99% extraction. The longer alkyl chain attached to the N atom in the TOTDGA molecule (four *n*-octyl groups) than that in the MOTDGA (2 methyl and 2 *n*-octyl groups) could produce a steric hindrance during the coordination to the Pd(II), though we need further studies to prove this hypothesis. As for DO3TPA, the part of di-*n*-octyl would not disturb the coordination to Pd(II), because DO3TPA is a monoamide.

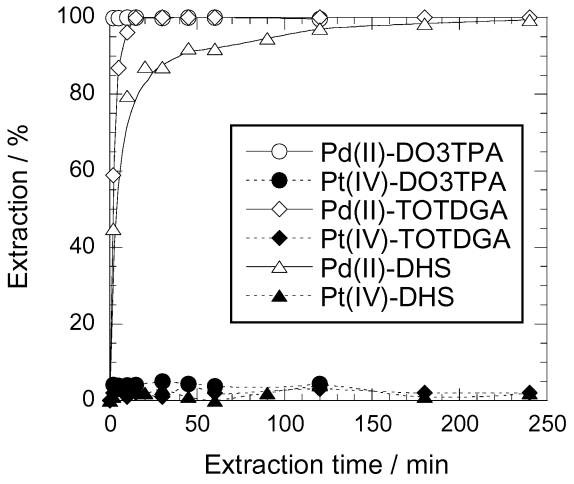

Figure 2. Effect of extraction time on the *E*% of Pd(II) and Pt(IV).
[DO3TPA] = [TOTDGA] = [DHS] = 0.1 M, [HCl] = 1 M.

Effect of HCl Concentration

Figure 3 shows the effect of the HCl concentration on the *E*% of Pd(II) and Pt(IV) using 0.1 M DO3TPA or TOTDGA. In both systems, the *E*% of Pd(II) shows ~100% in the studied HCl concentration range of 0.2-7 M. In contrast, Pt(IV) is hardly extracted at ≤5 M HCl in the DO3TPA system and at ≤3 M HCl in the TOTDGA one. Accordingly, a high selectivity for Pd(II) over Pt(IV) can be obtained over a wide range of HCl concentrations. The *E*% of Pt(IV) drastically increases at the higher HCl concentrations. This indicates that ion-pair extraction is probably dominant (i.e., extraction of $PtCl_6^{2-}$ by protonated extractants), as suggested in the literature [11]. On the other hand, the high *E*% of Pd(II) in the lower HCl concentration range means that Pd(II) could be predominantly extracted by the coordinative mechanism (substitution of the Cl^- in $PdCl_4^{2-}$ by the S of the extractant like the DOS system [12]).

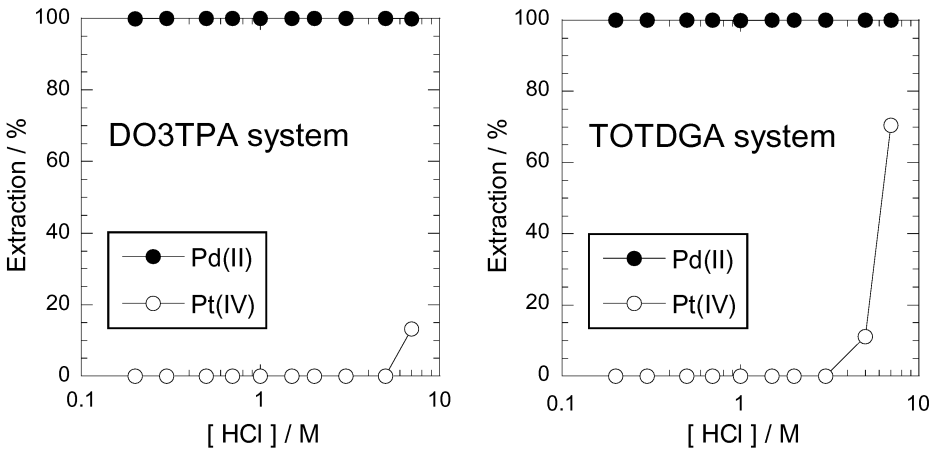

Figure 3. Effect of HCl concentration on the *E*% of Pd(II) and Pt(IV). [DO3TPA] = [TOTDGA] = 0.1 M; extraction time, 30 min.

Back-Extraction

The back-extraction of Pd(II) in the DO3TPA or TOTDGA phase was carried out using a 28% ammonia solution. In the TOTDGA system, Pd(II) (0.1 g/L) in the 0.1 M TOTDGA extracted from the 1 M HCl solution is transferred to the ammonia solution with the back-*E* of 70–80%. Under the same condition, the back-*E*% in the DO3TPA system is ~90%. Using the higher concentration of Pd(II) (5 g/L) in the organic phase extracted from the 1 M HCl solution, the back-*E*% decreases to ~50% for TOTDGA and ~70% for DO3TPA. The DO3TPA system shows a better back-extractability than the TOTDGA system, suggesting that fewer donor atoms in the DO3TPA molecule can provide a higher flexibility regarding the coordination of Pd(II).

CONCLUSIONS

We synthesized two types of sulfide-containing amide compounds, DO3TPA (monoamide) and TOTDGA (diamide), and then investigated their extraction properties for Pd(II), while comparing them to the conventional extractant DHS. The order of the extraction rates of Pd(II) from 1 M HCl using the 0.1 M extractants is as follows: DO3TPA > TOTDGA >> DHS. Both DO3TPA and TOTDGA selectively extract Pd(II) over Pt(IV) in a wide range of HCl concentration. Palladium(II) in the DO3TPA or TOTDGA phase can be back-extracted using ammonia solution. DO3TPA provides better properties regarding the extraction rate, selectivity, and back-extractability for Pd(II) than TOTDGA.

ACKNOWLEDGMENTS

This work was financially supported in part by the Industrial Technology Research Grant Program in '06 from the New Energy and Industrial Technology Development Organization (NEDO) of Japan.

REFERENCES

1. D. Jollie, Platinum 2006 Interim Review, Johnson Matthey, London, 2006.
2. R. I. Edward and W. A. M. te Riele, "Commercial Processes for Precious Metals," Handbook of Solvent Extraction, T. C. Lo, M. H. I. Baird, and C. Hanson, Eds., John Wiley & Sons, New York, 1983; pp. 725-732.
3. M. Cox, "Solvent Extraction in Hydrometallurgy," Principles and Practices of Solvent Extraction, J. Rydberg, M. Cox, C. Musikas, and G. R. Choppin, Eds., Marcel Dekker, New York, 2004; pp. 455-505.
4. C. Musikas, "Potentiality of Nonorganophosphorus Extractants in Chemical Separations of Actinides," *Sep. Sci. Technol.*, **23**, 1211-1226 (1988).
5. C. Madic and M. J. Hudson, "High-Level Liquid Waste Partitioning by Means of Completely Incinerable Extractants," Nuclear Science and Technology Series, European Commission, Luxembourg, 1998.
6. H. Narita, T. Yaita, K. Tamura, and S. Tachimori, "Solvent Extraction of Trivalent Lanthanoid Ions with *N,N'*-Dimethyl-*N,N'*-diphenyl-3-oxapentanediamide," *Radiochim. Acta*, **81**, 223-226 (1998).
7. Y. Sugo, Y. Sasaki, and S. Tachimori, "Studies on Hydrolysis and Radiolysis of *N,N,N',N'*-Tetraoctyl-3-oxapentane-1,5-diamide," *Radiochim. Acta*, **90,** 161-165 (2002).
8. H. Narita, M. Tanaka, K. Morisaku, T. Yaita, S. Suzuki, Y. Isomae, and T. Abe, "Structural Effect of Monoamide Compounds on the Extraction of Gold," *Solvent Extr. Res. Dev., Jpn.*, **12**, 123-130 (2005).
9. H. Narita, M. Tanaka, K. Morisaku, and T. Abe, "Extraction of Gold(III) in Hydrochloric Acid Solution Using Monoamide Compounds," *Hydrometallurgy*, **81**, 153-158 (2006).
10. H. Narita, M. Tanaka, K. Morisaku, and T. Abe, "Rapid Separation of Palladium(II) from Platinum(IV) in Hydrochloric Acid Solution with Thiodiglycolamide," *Chem. Lett.*, **33,** 1144-1145 (2004).

11. H. Narita, M. Tanaka, K. Morisaku, and K. Tamura, “Extraction of Platinum(IV) in Hydrochloric Acid Solution Using Diglycolamide and Thiodiglycolamide,” *Solvent Extr. Res. Dev., Jpn.*, **13**, 101-106 (2006).
12. S. J. Al-Bazi and H. Freiser, “Mechanistic Studies on the Extraction of Palladium(II) with Dioctyl Sulfide,” *Solvent Extr. Ion Exch.*, **5**, 265-275 (1987).

POLYTOPIC SALICYLALDIMINE LIGANDS FOR THE RECOVERY OF ZINC CHLORIDE

T. Lin, V. Gasperov, K. J. Smith, C. C. Tong, and P. A. Tasker

School of Chemistry, University of Edinburgh, Edinburgh, EH9 3JJ, UK.
Corresponding author email address: p.a.tasker@ed.ac.uk

ABSTRACT

Attaching amine groups to salicylaldehyde precursors for the conventional oxime extractants has allowed us to develop a new class of reagents which is very efficient in recovery of $ZnCl_2$ from high-tenor feeds. The new reagents are polytopic, providing separated binding sites for the Zn^{2+} cation and the anions Cl^- or $[ZnCl_4]^{2-}$. They operate in a zwitterionic form in which protons released from phenol groups of the salicylaldimine units become attached to the pendant amines to generate overall charge-neutral complexes such as $[ZnLCl_2]$ and $[ZnL(ZnCl_4)]$. Under forcing conditions, one of the ligands loads more than two moles of $ZnCl_2$ per mole of reagent, and water stripping gives ca. 150% recovery of $ZnCl_2$ per cycle.

INTRODUCTION

Global zinc consumption grew by ca. 20% between 2002 and 2005 [1], and processes based on hydrometallurgical flowsheets are being developed to extract the metal from a variety of ores [2]. Oxidative ferric chloride leaching can be employed to generate $ZnCl_2$ feed solutions and yields sulfur as a by-product from sulfidic ores, rather than SO_2 or sulfuric acid, which have little commercial value [3]. Several other leaching technologies generating high-tenor chloride streams have been developed recently to recover base metals from primary sources [4]. Also, as much of the global zinc usage is for galvanized steel, which results in chloride-rich secondary sources, there is a driving force to develop novel and efficient reagents to recover zinc chloride. A few *solvating extractants* [3] have already been developed in which neutral ligands form uncharged dichlorozinc(II) complexes (see Equation 1) or dinuclear analogues, $[Zn_2L_2Cl_4]$.

$$Zn^{2+} + 2Cl^- + L_{(org)} \rightleftharpoons [ZnLCl_2]_{(org)} \quad (1)$$

$$Zn^{2+} + 2Cl^- + 2[R_3NH]Cl_{(org)} \rightleftharpoons [R_3NH]_{2\,(org)} \quad (2)$$

Anion exchange extractants, such as trilaurylammonium chloride or the Alamine® reagents, have also been used to recover zinc chloride as $[ZnCl_4]^{2-}$ (see Equation 2) [5]. In this paper, we describe new salicylaldimine reagents that can perform both cation- and

anion-exchanger roles and can be prepared from the precursors used in the manufacture of the conventional phenolic oxime extractants for copper [6].

RESULTS AND DISCUSSION

In earlier work, we have described the use of polytopic ligands to transport metal salts where the cations and anion(s) are bound in separated sites [7]. A ditopic system of this type is displayed schematically as **I** in Figure 1, and an example based on a bis-salicylaldiminato unit to bind the metal cation and two pendant ammonium groups to carry the attendant dianion X^{2-} is shown as **II**.

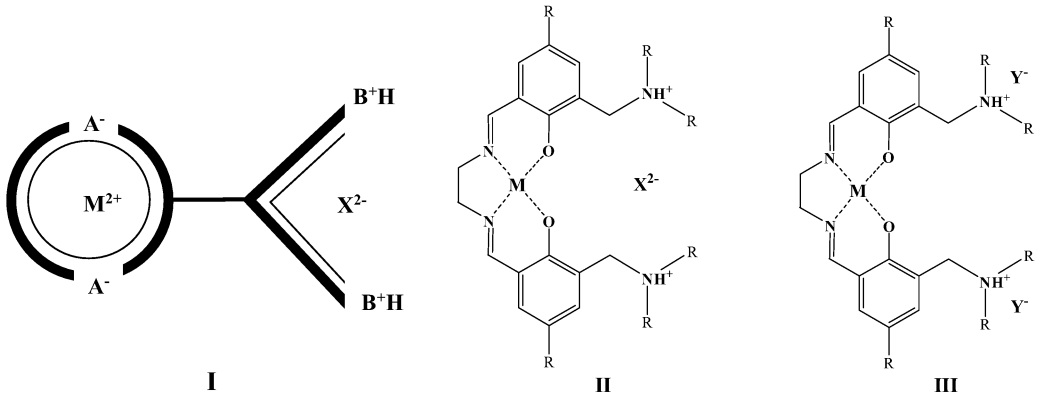

Figure 1. Ditopic systems **I** and **II** to recover divalent metal salts $M^{II}X$ and a tritopic arrangement, **III**, for salts of monoanions.

For the purposes of solvent extraction, a key feature is that the metal salt complex **II** carries no overall charge, because the M^{2+} and X^{2-} components are bound in a zwitterionic form of the ligand. This feature also allows the cation and anion to be stripped separately by adjustment of the pH of the aqueous phase [7]. When recovering metals from high-tenor chloride streams, it is possible that the anion-binding site could be loaded with a chlorometallate anion, MCl_x^{y-}, which would double the metal transport efficiency. In the case of zinc, two moles could be transported (as Zn^{2+} and $[ZnCl_4]^{2-}$) by one mole of extractant. We have investigated this possibility using the reagents in Scheme 1. The *tert*-butyl derivative **1** of the well-known tetradentate Schiff base ligand (salen) should provide an $N_2O_2^{2-}$ donor set for a metal dication. Ligand **2** has the salen unit substituted with dihexylaminomethyl units adjacent to the phenol groups to provide an anion-binding site. It is ditopic when a dianion is enclosed between the pendant arms as in **II** in Figure 1 and tritopic when each pendant arm complexes a monoanion as in **III**. The dihexyl groups were incorporated to ensure good solubility in water-immiscible solvents. The piperidin-1-ylmethyl analogue (ligand **3**) was prepared to facilitate the isolation of crystalline complexes. For **2** and **3**, the precursors were prepared by modification of literature procedures [8,9].

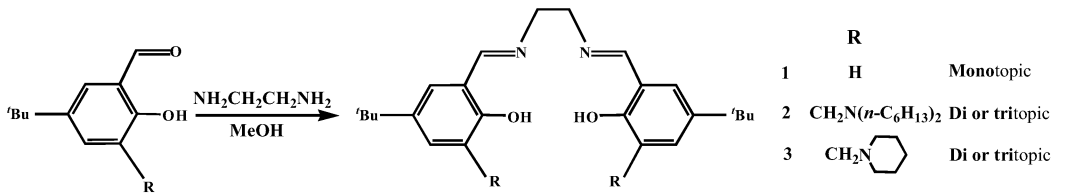

Scheme 1. Synthesis of the ligands.

The uptake of zinc by 0.01 M chloroform solutions of extractants **1–3** after contacting with equal volumes of 1 M zinc chloride/sulfate solutions is shown in Figure 2. Zinc concentrations were determined by inductively coupled plasma optical emission spectroscopy (ICP-OES) after evaporation and making up to a known volume in butan-1-ol. Complete (100%) Zn loading in Figure 2 corresponds to one mole of zinc per mole of extractant. The uptakes of zinc are much greater from chloride solutions than sulfate solutions, which in the cases of **1** and **3** are zero within the limits of error.

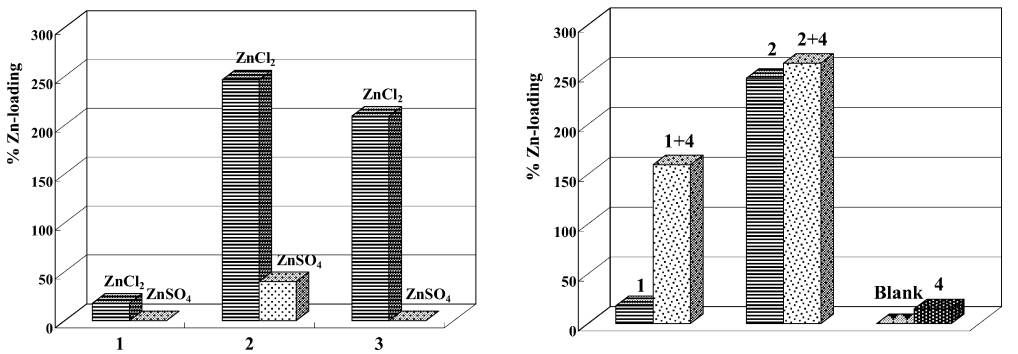

Figure 2. Equilibrium uptake of zinc by 0.01 M chloroform solutions of reagents. Left: use of **1**, **2**, or **3** from an equal volume of 1 M aqueous $ZnCl_2$ or $ZnSO_4$. Right: use of **1** or **2** in the presence or absence of **4** (0.02 M) from an equal volume of 1 M aqueous $ZnCl_2$.

The polytopic ligands **2** and **3** show much higher zinc uptake from chloride media than the monotopic analogue **1**. This and the observation that 246% and 209% loadings were achieved support the proposition that the inclusion of the pendant amine groups into **2** and **3** does indeed allow the uptake of both Zn^{2+} and $[ZnCl_4]^{2-}$. The much lower loading of zinc from sulfate media is also consistent with this loading mechanism, because anionic sulfato complexes of zinc such as $[Zn(SO_4)_2]^{2-}$ are not very stable, whereas in 1 M $ZnCl_2$ solution, the dominant species is $[ZnCl_4]^{2-}$ [10]. The Hofmeister bias also suggests that it will be much more difficult to transfer anions with very high hydration energies such as sulfate into water-immiscible solvents [7].

A key issue in the development of new polytopic reagents is whether they are more effective than the sum of their parts, that is, dual host systems [11] in which a *mixture* of cation and anion exchange reagents is used to transport a salt. For our systems, we have assessed this by using **4**, which is structurally related to the pendant arms of **2**,

as an anion-exchange reagent of the Alamine type [5] for recovery of chlorometallates from acidic solution as in Equation 2. Ligand **4** was prepared by modification of a literature procedure [12], as described in Scheme 2.

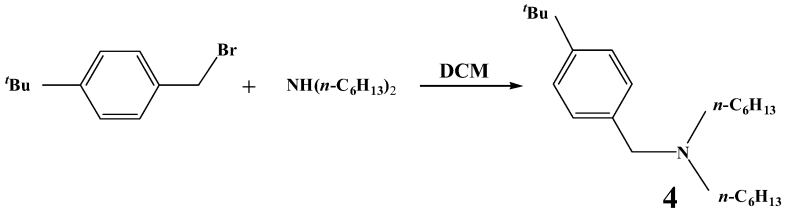

Scheme 2. The preparation of 1-*tert*-butyl-4-(dihexylamino)methylbenzene, ligand **4**.

Neither the monotopic cation exchanger **1** nor the anion exchanger **4** on their own transports significant quantities of zinc (Figure 2, right). The dual-host formulation of **1** and **4** transports 1.60 moles Zn per mole of **1** but is much less efficient than the polytopic reagent **2**, which loads 2.46 moles under the same conditions. The boosting of Zn-uptake by adding **4** to a solution of **1** to create the dual host system implies that a benefit arises from the assembly of complexes which contain deprotonated form of **1**, $[\mathbf{1}\text{-H}]^-$ or $[\mathbf{1}\text{-2H}]^{2-}$, and the protonated form of **4**. These complexes could have a range of structures analogous to those in the preorganized polytopic reagent **2** in Figure 3. Chloride analysis of the loaded organic phases indicates that two moles of Cl^- are present per mole of Zn, confirming uptake as $ZnCl_2$. Consequently, the Zn-loading efficiency of **2** will depend on the activity of Cl^- in the aqueous feed, and indeed, addition of NaCl to 0.030 M $ZnCl_2$ solutions was shown to give substantial increases in Zn uptake, with a 200% loading being observed when the NaCl concentration was increased to 0.94 M.

As zinc is diamagnetic, ^{1}H NMR spectroscopy could be used to study the spectra of **2** and its complexes at different levels of $ZnCl_2$ loading. The ligand exchange is slow on the NMR timescale, and thus, chemical shifts from the same proton in different species are distinct instead of being the weighted-average peaks. The spectra show that two different complexes are formed as the ligand to zinc stoichiometry is increased to 1L:2$ZnCl_2$. The azomethine proton appears at δ 8.42 in a 0.01 M solution of the free ligand in $CDCl_3$. A new signal appears at δ 8.31 when $ZnCl_2$ is loaded, reaching a maximum intensity at 100% Zn loading, corresponding to complete disappearance of the signal at δ 8.42. Higher zinc loadings are accompanied by the loss of the peak at δ 8.31, which is replaced by a new signal at δ 8.65, reaching maximum intensity at 200% $ZnCl_2$ loading. No further changes to the azomethine signal are observed when $CDCl_3$ solutions are contacted with very large excesses of $ZnCl_2$ in D_2O. The ^{1}H NMR data are consistent with the formation of first the tritopic and then the ditopic assemblies (Figure 3) as the $ZnCl_2$ loading is increased. These mechanisms for uptake of $ZnCl_2$ can be adapted to account for cases where more than two moles of $ZnCl_2$ are loaded per mole of **2**. When the zinc content of the aqueous feed is very high, some $[ZnCl_3]^-$ monoanions could replace the chloride ions in the tritopic assembly, giving some $[Zn(\mathbf{2})(ZnCl_3)_2]$. Stripping the $ZnCl_2$-loaded solutions of **2** with water liberates much of the $ZnCl_2$ and gives a 150% recovery of $ZnCl_2$ from one cycle of extraction and stripping.

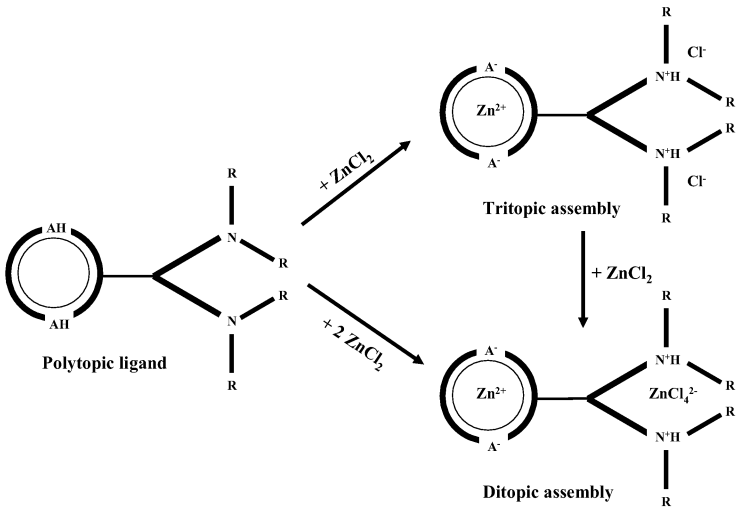

Figure 3. Tritopic and ditopic assemblies to account for the ^{1}H NMR spectra of 1:1 and 1:2 loading of $ZnCl_2$ by **2**.

CONCLUSIONS

The polytopic ligand **2** shows much higher transport efficiency of Zn from chloride media than its monotopic analogue **1** and the dual-host combination of **1** and **4**. ^{1}H NMR studies suggest that the mechanism of loading involves the formation of complexes [Zn(**2**)Cl_2] and [Zn(**2**)($ZnCl_4$)] at low and high Zn-loading, respectively. Current work is being focused on determining cation selectivity, for example, Zn^{2+}/Fe^{3+}, and on establishing efficient protocols for stripping and recycling this new type of reagent.

ACKNOWLEDGMENT

We thank EaStCHEM for a studentship (TL), and the EPSRC and the Crystal Faraday Partnership, UK for funding.

REFERENCES

1. C. Zhang, Y. Zhao, C. Guo, X. Huang, and H. Li, "Leaching of zinc sulfide in alkaline solution via chemical conversion with lead carbonate," *Hydrometallurgy*, In press (2007).
2. K. C. Sole, R. J. Stewart, R. F. Maluleke, A. Rampersad, and A. E. Mavhungu, "Removal of Entrained Organic Phase from Zinc Electrolyte: Pilot Plant Comparison of CoMatrix and Carbon Filtration," *Hydrometallurgy*, **89**, 11-20 (2007).
3. P. A. Tasker, P. G. Plieger, and L. C. West, Comprehensive Coordination Chemistry II, Elsevier Ltd., Oxford, 2004.

4. "Leaching and Solution Purification", Proceedings of Hydrometallurgy, 2003, C. Young, A. Alfantazi, C. Anderson, A. James, D. Dreisinger, and B. Harris, Eds., TMS, Warrendale, Pennsylvania, 2003; pp. 501-700.
5. M. K. Jha, V. Kumar, and R. J. Singh, "Solvent Extraction of Zinc from Chloride Solutions," *Solvent Extr. Ion Exch.*, **20**(3), 389-405 (2002).
6. J. Szymanowski, Hydroxyoximes and Copper Hydrometallurgy, CRC Press, London, 1993.
7. S. G. Galbraith, Q. Wang, L. Li, A. J. Blake, C. Wilson, S. R. Collinson, L. F. Lindoy, P. G. Plieger, M. Schroder, and P. A. Tasker, "Anion Selectivity in Zwitterionic Amide-Functionalised Metal Salt Extractants," *Chem. Eur. J.,* **13**(21), 6091-6107 (2007).
8. R. Aldred, R. Johnston, D. Levin, and J. Neilan, "Magnesium-mediated ortho-Specific Formylation and Formaldoximation," *J. Chem. Soc. Perkin Trans. 1*, **13**, 1823-1831 (1994).
9. H. Adams, N. A. Bailey, D. E. Fenton, and G. Papageorgiou, "A Mononuclear Copper(II) Complex of an Unsymmetrical Dinucleating Ligand," *J. Chem. Soc., Dalton Trans.*, **11**, 1883-1886 (1995).
10. J. A. Tossell, "Calculations of the Structures, Stabilities, and Raman and Zn NMR Spectra of $ZnCl_n(OH_2)_a^{2-n}$ Species in Aqueous Solution," *J. Phys. Chem.*, **95**, 366-371 (1991).
11. K. Kavallieratos, R. A. Sachleben, G. J. Van Berkel, and B. A. Moyer, "Novel dual-host approach in ion pair extraction," *Chem. Commun.*, 187-188 (2000).
12. T. Jerphagnon, G. P. M. van Klink, J. G. de Vries, and G. van Koten, "Aminoarenethiolate-Copper(I)-catalyzed Amination of Aryl Bromides," *Org. Lett.*, **7**(23), 5241-5244 (2005).

ANION RECOGNITION: THE SELECTIVE EXTRACTION OF $[PtCl_6]^{2-}$

K. J. Bell,[1] J. Chartres,[2] R. J. Ellis,[2] D. J. Robinson,[3] C. C. Tong,[2] R. J. Warr,[1]
A. N. Westra,[2] M. Schröder,[1] and P. A. Tasker[2]

[1] *School of Chemistry, The University of Nottingham, Nottingham, NG7 2RD, UK.*
[2] *School of Chemistry, The University of Edinburgh, Edinburgh, EH9 3JJ, UK.*
[3] *CSIRO Minerals, PO Box 7229, Karawara, WA 6152, Australia.*
Corresponding author email address: Peter.Tasker@ed.ac.uk

ABSTRACT

A series of new anion-binding ligands has been shown to be very effective for the recovery of $PtCl_6^{2-}$ from acidic chloride media. These new ionophores have a tripodal structure incorporating amido and urea groups, and these hydrogen-bond to the $[PtCl_6]^{2-}$ anion via the faces and edges of the octahedron, where the greatest electron density on the anion is located. The metal value is extracted into the organic phase as a $[(PtCl_6)(LH)_2]$ complex, and the loading and stripping of the metallate anion is controlled by "pH swing":

$$\text{Loading: } 2H^+ + [PtCl_6]^{2-} + 2L_{(org)} \rightarrow [(LH)_2(PtCl_6)]_{(org)}$$
$$\text{Stripping: } 2OH^- + [(LH)_2(PtCl_6)]_{(org)} \rightarrow [PtCl_6]^{2-} + 2L_{(org)} + 2H_2O$$

The new reagents show much greater selectivity for $[PtCl_6]^{2-}$ over chloride than trioctylamine (TOA), which was used as a model for the Alamine® reagents.

INTRODUCTION

Solvent extraction is an effective method to achieve concentration and separation of platinum in hydrometallurgical flowsheets based on chloride streams in which the platinum is present as the hexachloroplatinate dianion, $[PtCl_6]^{2-}$ (Figure 1). Since this dianion shows high kinetic inertness and ligand exchange is slow [1], it is not practical to use solvent extractants that replace chloride ions in the inner sphere to generate neutral organic-soluble complexes. Consequently, anion-exchange reagents of the Alamine type that form organic-soluble ion pairs are preferred [2]. The latter can be used to transfer the chlorometallate to a water-immiscible solvent in a pH-dependent equilibrium [3]:

$$n R_3N_{(org)} + nH^+ + MCl_x^{n-} \rightleftharpoons [(R_3NH)_nMCl_x]_{(org)} \quad (1)$$

We report herein the development of new anion-exchange reagents that contain hydrogen-bond donor groups to recognize the outer-coordination spheres of

chlorometallate anions such as $[PtCl_6]^{2-}$ and thus give enhanced extractant strength and selectivity over chloride compared to the trialkylamines of the Alamine type.

RESULTS AND DISCUSSION

The new extractants have been designed to bind strongly and selectively to $[PtCl_6]^{2-}$ and take advantage of the difference in charge distribution and size of Cl^- and $[PtCl_6]^{2-}$ anions. Single-crystal X-ray diffraction structures containing $[PtCl_6]^{2-}$, DFT calculations, and NMR studies indicate that electron density on the $[PtCl_6]^{2-}$ anion resides mainly on its octahedral faces and edges [4,5]. It is important for their end use that extractants resist decomposition at low pH and incorporate a protonatable site to afford a pH-swing mechanism to control the uptake and release of the metallate ion:

$$2H^+ + [PtCl_6]^{2-} + 2L_{(org)} \rightarrow [(LH)_2(PtCl_6)]_{(org)}$$

The new tripodal ionophores incorporate amide or urea functional groups radiating from a central amine N-centre, which also acts as a protonatable site. The N-H hydrogen-bond donor groups on the ammonium, amide, and urea units may address the electron density on the $[PtCl_6]^{2-}$ octahedron as shown in Figure 1. Hydrophobic benzyl and methoxyphenyl groups were incorporated into the tripodal ligands to enhance the solubility of anion–ligand complexes in water-immiscible solvents.

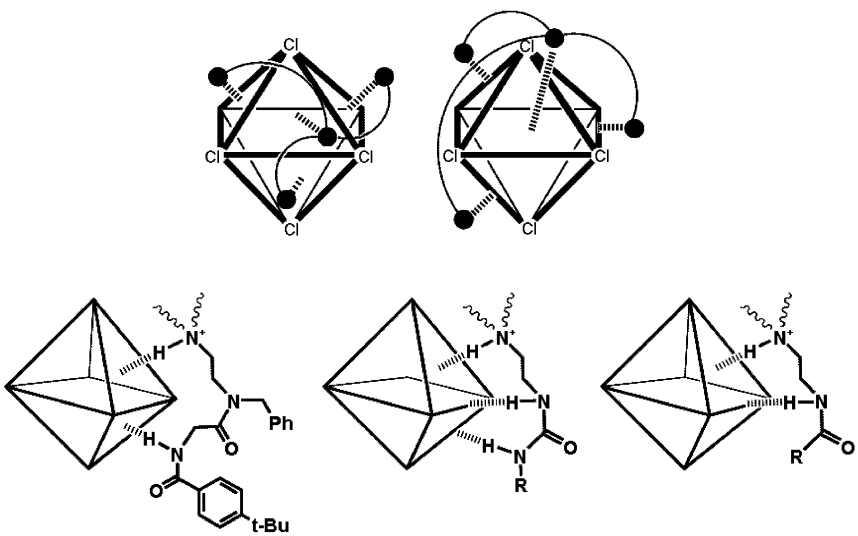

Figure 1. Binding modes of the amide and urea arms of the tripodal reagents L^1-L^9.

Of the new extractants shown in Scheme 1, those with amide arms, L^1 and L^6–L^9, can provide a total of four hydrogen-bond donor groups in their protonated form, whilst the urea derivatives, L^2–L^5, can provide seven. Ligands L^2-L^9 were prepared directly from tris(2-aminoethyl)amine in a one-step process. Ligand L^1 was designed with a longer spacer between the protonatable amine bridgehead and the neutral hydrogen-bond

donors, and was prepared in three steps from tris(N-benzyl-2-aminoethyl)amine, **1** (Scheme 1) [6].

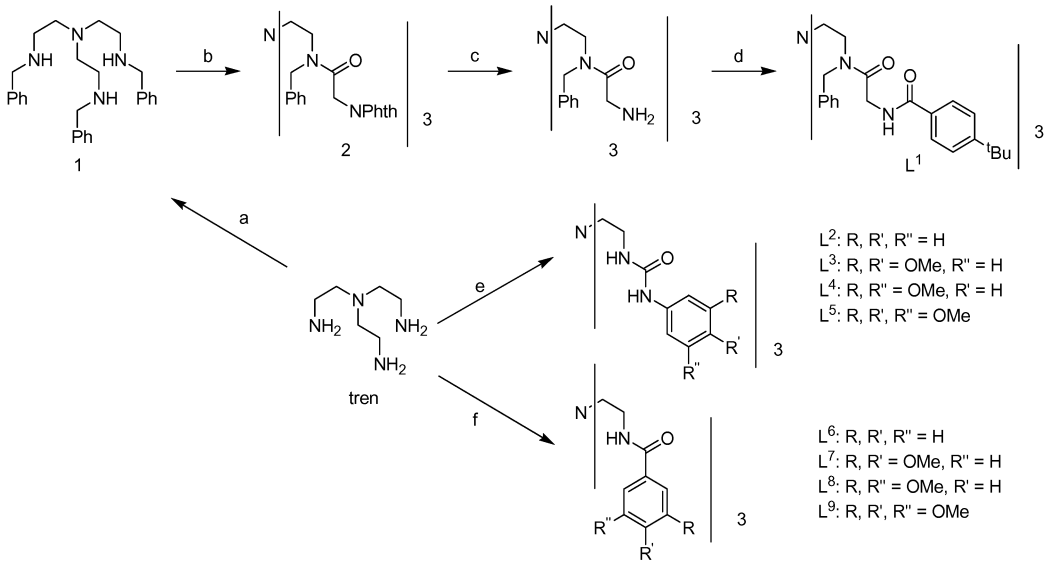

Scheme 1. Preparation of the extractants L^1-L^9. Conditions: a) benzaldehyde, MeOH, r.t. then $NaBH_4$ [6]; b) 2-phthalimidoacetyl chloride, Et_3N, $CHCl_3$, 0 °C then r.t.; c) NH_2NH_2, EtOH, $CHCl_3$, reflux; d) *t*-butylbenzoyl chloride, Et_3N, $CHCl_3$, 0 °C then r.t.; e) phenyl or 3,4-dimethoxy-, 3,5-dimethoxy-, or 3,4,5-trimethoxy-phenyl isocyanate, THF, r.t. [7]; f) benzoyl or 3,4-dimethoxy-, 3,5-dimethoxy-, or 3,4,5-trimethoxy-benzoyl chloride, NaOH, CH_2Cl_2, r.t. [8,9].

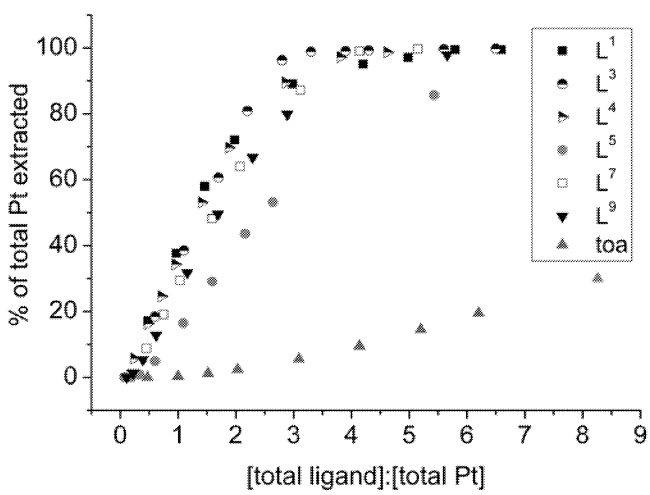

Figure 2. The percent of the total platinum extracted as a function of [L]:[Pt] ratios by chloroform solutions of L^1, L^3, L^4, L^5, L^7, L^9, and TOA.

The uptake of $[PtCl_6]^{2-}$ into chloroform solutions containing between 0.0005 and 0.01 M ligand was determined by contacting with 0.001 M H_2PtCl_6 in 0.6 M HCl. After 4 hours, the phases were allowed to separate, and the "loaded" organic was treated with 2 equivalents of NaOH to strip platinum back into an aqueous solution. The concentration of Pt in the latter solution was determined by ICP-OES. Ligands L^1, L^3–L^5, L^7, and L^9 were found (Figure 2) to be more effective extractants in 0.6 M HCl than trioctylamine (TOA) which is a model for the Alamines [3,6].

Extraction data for the phenylurea and phenylamido ligands, L^2, L^6, and L^8 were not obtained, because precipitation of the complex salts was observed when these were contacted with H_2PtCl_6 solutions. We did not observe any evidence for inner-sphere substitution of $[PtCl_6]^{2-}$ during the course of extraction procedures, although the ligands are capable, in principle, of coordinating to Pt through the amine. Incorporation of the urea group into our ionophores leads to stronger extraction of $[PtCl_6]^{2-}$. The longer spacing group between the bridgehead nitrogen atom in L^1 may be beneficial in allowing the amide N-H donors to position themselves more favorably than the amide donors in L^7 and L^9 (Figure 1). There are considerable differences between the extraction behavior of the reagents L^6–L^9, which vary only in the nature of the methoxy substitution patterns on the pendant arene rings. It is possible that the differing abilities of the tripodal arms of the two ligands to interdigitate when forming a 2:1 ionophore:$[PtCl_6]^{2-}$ complex may significantly influence the thermodynamic stability of the assembly and its solvation enthalpy. However, detailed modelling and nmr spectroscopic studies are required to substantiate this proposition. Both interdigitation of arms of the ligands and the preorganization of amido groups to recognize sites of high electron density on the surface of chlorometallate anions are likely to be key factors in the design of reagents that show selectivity in precious-metal recovery from chloride streams. Work on reagents which can separate $[PtCl_6]^{2-}$ and $[PdCl_4]^{2-}$ is in progress.

Figure 3 shows that Pt-loading by ligand L^1 is much less sensitive to chloride concentration than that by TOA and that the selectivity for $PtCl_6^{2-}$ over Cl^- is greater over the whole range of ligand:$PtCl_6^{2-}$ ratios studied.

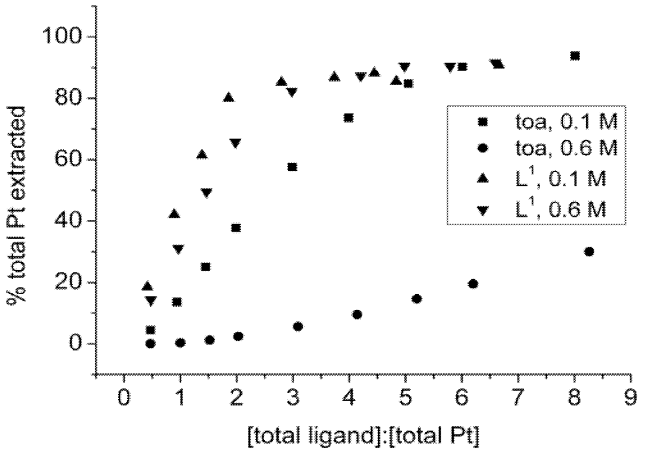

Figure 3. The percent of the total Pt extracted at varying ligand:Pt ratios for TOA and L^1 from solutions containing 0.1 or 0.6 M HCl.

The expected 2:1 stoichiometry of the receptor-anion complex, as in $[(LH)_2(PtCl_6)]$, was confirmed using the procedure reported by Yoshizawa and co-workers [3]. Under acidic conditions and with high chloride concentrations in the aqueous phase, the extraction equilibrium can be represented as

$$PtCl_6^{2-} + 2[(LH)Cl]_{(org)} \overset{K_{PtCl_6^{2-}}}{\rightleftharpoons} [(LH)_2PtCl_6]_{(org)} + 2Cl^-$$

$$\text{with } K_{PtCl_6^{2-}} = \frac{[(LH)_2PtCl_6]\cdot[Cl^-]^2}{[PtCl_6^{2-}]\cdot[(LH)Cl]^2}$$

The distribution ratio for Pt is $D_{Pt} = [(LH)_2PtCl_6]/[PtCl_6^{2-}]$. Substitution of D_{Pt} into the equation defining $K_{PtCl_6^{2-}}$, followed by rearrangement gives:

$$\log D_{Pt} = \log K_{PtCl_6^{2-}} + 2\log\left\{\frac{[(LH)Cl]}{[Cl^-]}\right\}$$

At low ligand concentrations, plots of log D_{Pt} against log{[(LH)Cl]/[Cl]} for L^1, L^4, and TOA (Figure 4) show slopes close to 2 and thus support the formation of 2:1 assemblies, $[(LH)_2(PtCl_6)]$, in the organic phase. For other ligands and for TOA at high ligand concentrations, the plots show some deviation from linearity. This variation from the expected stoichiometry may be caused by formation of species that include hydronium ions as in $[(LH)(H_3O)(PtCl_6)]$ at low ligand concentrations. Alternatively, 3:1 $(LH)^+$:$[PtCl_6]^{2-}$ species such as $[(LH)_3(PtCl_6)Cl]$ may be formed at high extractant concentrations. The data in Figure 4 confirm that the tri-amide, L^1, and tri-urea ligand, L^4, show much higher selectivity for $[PtCl_6]^{2-}$ over Cl^- than TOA.

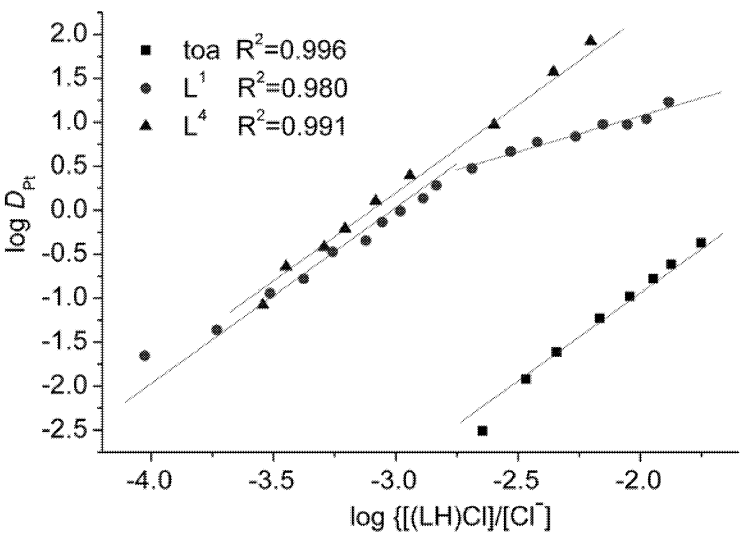

Figure 4. Plots of log D_{Pt} vs. log{[(LH)Cl]/[Cl$^-$]} for L^1, L^4, and TOA.

CONCLUSIONS

The incorporation of amido groups into the arms of trialkylamines leads to extractants that have much higher selectivity for $[PtCl_6]^{2-}$ over chloride ions than the Alamine reagents and show quantitative recovery of platinum from feed solutions with a 60-fold excess of chloride.

ACKNOWLEDGMENTS

We thank the EPSRC, the Crystal Faraday Partnership Scheme (UK) and the National Research Foundation (S. Africa) for financial support and the EPSRC National Mass Spectrometry Service, Swansea (UK) for mass spectra. MS gratefully acknowledges receipt of a Royal Society Wolfson Merit Award and of a Royal Society Leverhulme Trust Senior Research Fellowship.

REFERENCES

1. N. N. Greenwood and A. Earnshaw, Chemistry of the Elements, Pergamon Press, Oxford, 1984.
2. P. A. Tasker, P. G. Plieger, and L. C. West, Metal Complexes for Hydrometallurgy and Extraction, J. A. McCleverty and T. J. Meyer, Eds, Comprehensive Coordination Chemistry II, Elsevier, London, 2004.
3. H. Yoshizawa, K. Shiomori, S. Yamada, Y. Baba, Y. Kawano, K. Kondo, I. Kazuo, K. Ijichi, and Y. Hatate, "Solvent extraction of platinum(IV) from aqueous acidic chloride media with tri-*n*-octylaniline in toluene," *Solvent Extr. Res. Dev. Jpn.*, **4**, 157-166 (1997).
4. L. Brammer, J. K. Swearingen, E. A. Bruton, and P. Sherwood, "Hydrogen bonding and perhalometal late ions," *Proc. Nat. Acad. Sci. U.S.A.*, **99**, 4956–4961 (2002).
5. K. J. Naidoo, A. S. Lopis, A. N. Westra, D. J. Robinson, and K. R. Koch, "Contact ion pair between Na^+ and $PtCl_6^{2-}$ favored in methanol," *J. Am. Chem. Soc.*, **125** 13330–13331 (2003).
6. K. J. Bell, A. N. Westra, R. J. Warr, J. Chartres, R. J. Ellis, C. C. Tong, A. J. Blake, P. A. Tasker, and M. Schröder, "Outer-sphere co-ordination chemistry: selective extraction and transport of the $PtCl_6]^{2-}$ anion," *Angew. Chem. Int. Ed.*, **47**, 1745-1748 (2008).
7. C. Raposo, M. Almaraz, M. Martin, V. Weinrich, M. L. Mussons, V. Alcazar, M. C. Caballero, and J. R. Moran, "Tris(2-aminoethyl)amine, a suitable spacer for phosphate and sulfate receptors," *Chem. Lett.*, 759–760 (1995).
8. P. D. Beer, P. K. Hopkins, and J. D. McKinney, "Cooperative halide, perrhenate anion-sodium cation binding and pertechnetate extraction and transport by a novel tripodal tris(amidobenzo-15-crown-5) ligand," *Chem. Commun.* 1253–1254 (1999).
9. S. Valiyayeettil, J. F. J. Engbersen, W. Verboom, and D. N. Reinhoudt, "Synthesis and complexation studies of neutral anion receptors," *Angew. Chem. Int. Ed.*, **32**, 900–901 (1993).

DESIGN OF EXTRACTION REAGENTS OF HIGH SELECTIVITY BASED ON STERIC FACTORS

S. Umetani,[1] Y. Fukui,[1] and K. Uezu[2]

[1]Institute for Chemical Research, Kyoto University, Uji, Kyoto 611-0011, Japan.
[2]Department of Chemical Processes and Environments, University of Kitakyushu, Hibikino, Kitakyushu 808-0135, Japan.
Corresponding author email address: umetani@scl.kyoto-u.ac.jp

ABSTRACT

Some novel acylpyrazolone derivatives having bulky substituents at the 4-position have been prepared, and the extractions of Group 13 metal ions were examined. The structures of the acylpyrazolone derivatives were evaluated by semi-empirical MNDO/H molecular orbital calculation and ^{1}H-NMR. The extraction of Al^{3+} and Ga^{3+} was found to be greatly influenced by the interligand contact and that of the In^{3+} bite size. Although the ionic radius of Al^{3+} is smaller than that of Ga^{3+}, the extraction of Al^{3+} was made in the higher pH region and reduced as the 4-acyl group became bulkier. The extraction of In^{3+} was much lowered with the 4-adamanthanecarbonyl and 4-pivaloyl derivatives, which narrow the distance between the two donating oxygens by the steric repulsion with the 3-methyl group.

INTRODUCTION

β-Diketones are well known as versatile chelating reagents for metal ions. A large number of studies have been done using chelating reagents, especially in the field of the solvent extraction of metal ions, for the purpose of separation and concentration [1,2]. Much attention has been also paid to structural chemistry of ß-diketones involving keto-enol tautomerism and the intramolecular hydrogen bond [3,4]. In the course of the studies on the solvent extraction of metal ions with acylpyrazolones or acylisoxazolones, the authors have noticed that improved extraction with strongly acidic extractants is usually accompanied by poor selectivity [5-8]. Examination of ligand structures by molecular-orbital calculations suggested a relationship between the O…O donor-atom distance and the acidity of the ligands and their performance as metal extractants for Group 13 [9] and lanthanide ions [10]. In the work described in this paper some novel acylpyrazolone derivatives were synthesized (Figure 1), and the extractions of Group 13 metal ions were examined.

EXPERIMENTAL

Materials

Acylpyrazolone derivatives were prepared as described in the literature [11].

1-Phenyl-3-methyl-4-anthracenecarbonyl-5-pyrazolone (**1**). Yellow powder. Yield: 70.6%. M.p. 147.6-147.8 °C. Calc. for $C_{25}H_{18}O_2N_2$: C, 79.43; H, 4.79; N, 7.37. Found: C, 79.43; H, 4.66; N, 7.37%. ^{1}H-NMR ($CDCl_3$, 200 MHz): δ 2.45 (3H,CH_3) and 7.20-8.10 (9H,$C_{14}H_9$).

1-Phenyl-3-methyl-4-(3.5-dimethyl)benzoyl-5-pyrazolone (**2**). Yellow powder. Yield: 56%. M.p. 138.8-139.1 °C. Calc. for $C_{19}H_{18}O_2N_2$: C, 74.49; H, 5.92; N, 9.14. Found: C, 74.47; H, 5.83; N, 9.15%. ^{1}H-NMR ($CDCl_3$, 200 MHz): δ 2.10 (3H,CH_3), 2.39 (6H,CH_3) and 7.15-7.90 (5H,C_6H_5).

1-Phenyl-3-methyl-4-adamanthanecarbonyl-5-pyrazolone (**3**). White powder. Yield: 25%. M.p. 76.7-77.0 °C. Calc. for $C_{21}H_{24}O_2N_2$: C, 74.97; H, 7.19; N, 8.32. Found: C, 74.71; H, 7.32; N, 7.55%. ^{1}H-NMR ($CDCl_3$, 200MHz): δ 1.70 (6H,CH_2), 1.91 (6H,CH_2), 2.01 (3H,CH), 2.31 (3H,CH_3) and 7.20-7.55 (5H,C_6H_5).

The analytical data for **4-6** matched those reported [12-14].

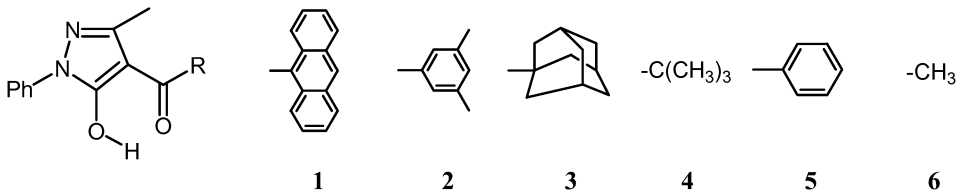

Figure 1. Acylpyrazolone derivatives

Apparatus

Metal ion concentrations were measured with a Japan Jarrell Ash Model ICAP-500 inductively coupled argon plasma atomic emission spectrophotometer. pH measurements were made with a Hitachi-Horiba F-8L pH meter equipped with a glass electrode. ^{1}H-NMR spectra were measured with a Varian VXR-200 spectrometer (200 MHz) at 25 °C in $CDCl_3$. The extractions were performed in 30 cm^3 centrifuge tubes with the aid of Taitek Bio-shaker type BR-30L thermostated at 25 °C. Semi-empirical MNDO/H calculation was performed on fully optimized molecular geometries on a Cray T94/4128 using MNDO94 (Cray Research, Inc.).

Extraction of Metal Ions

A 10 mL aliquot of an aqueous phase containing 1 x 10^{-4} M of metal ion, 0.1 M sodium perchlorate, and 0.01 M sodium acetate or 2-morpholinoethanesulfonic acid, monohydrate (MES) as buffering component was adjusted to the desired pH with hydrochloric acid or sodium hydroxide solution. The aqueous phase was shaken with an equal volume of benzene containing the required amount of ligand at 25 ˚C Due to the

slow extraction rate, a fairly long shaking time was required. The shaking time was 72 h for Al^{3+}, 48 h for Ga^{3+}, and 3 h for In^{3+}. After centrifugation, the pH of the aqueous phase was measured and taken as the equilibrium value. The metal concentration in the aqueous phase was determined by inductively coupled plasma atomic emission spectrometry. Metal in the organic phase was measured in the same way after back-extraction with hydrochloric acid solution. The sum of the metal concentrations in the two phases agrees well with the initial concentration.

RESULTS AND DISCUSSION

Molecular Structure of the Ligands

The molecular structure of the ligands was evaluated by semi-empirical MNDO/H calculation, which takes the hydrogen bond into consideration. The O…O distances found by MNDO/H are shown in Table 2.

The distance between the oxygen donor atoms, calculated by MNDO/H, shortens as the 4-acyl group becomes bulkier. The steric repulsion between the 3-methyl group and the 4-acyl group in the structure of the acylpyrazolone derivatives results in a shortening of this distance. Such structural changes were also seen in the 2-trifluoroacetylcycloalkanones [9] and α-substituted β-diketones [10]. This structural change is consistent with ^{1}H-NMR data. As a consequence of their five-membered heterocyclic groups, acylpyrazolones have a longer O…O distance than the conventional β-diketones. No enolic ^{1}H-NMR proton peak is usually observed for acylpyrazolones, although they exist quantitatively in the enol form in the organic solvents. This is the case for the compounds in Table 1, with the exception of **4,** which shows a fairly sharp OH signal at 14.9 ppm. The absence of a peak for the methyne proton at the 4-position confirms the occurrence of the enolic form for all. The intramolecular hydrogen bond energy (E_{OH}) can be estimated as the energy difference between the hydrogen-bonded structure and the open structure in which the O-H is rotated by 180° in order to minimize the hydrogen-bond energy; these values are shown in Table 2. E_{OH} increases as the O…O distance decreases.

Table 1. Comparison of Acylpyrazolones

	1	2	3	4	5	6
O...O distance (Å) [a]						
HA	2.63	2.65	2.45	2.46	2.65	2.60
A^- [b]	3.05	3.06	2.81	2.84	3.06	3.04
E_{OH} (kcal/mol) [a]	12.88	12.43	18.63	18.38	12.43	13.74
^{1}H-NMR (-OH, ppm)	—	—	—	14.9	—	—
pK_a [c]	—	—	—	4.26	3.92	3.94

[a]MNDO/H. [b]Fixed at planar. [c]Taken from reference [12].

Extraction of Group 13 Metal Ions

The extractions of M^{3+} (Al^{3+}, Ga^{3+}, and In^{3+}) from a 0.1 M sodium perchlorate aqueous phase into a 5 x 10^{-3} M acylpyrazolone benzene phase have been examined. To

clarify the composition of the extracted species, the effects of pH and log $[HA]_o$ on log D ($D = [M^{3+}]_o/[M^{3+}]$) were also examined. Here, HA stands for the ligand, and the subscript o denotes the species in the organic phase. The log D *vs.* pH and log D *vs.* log $[HA]_o$ plots are straight lines with a slope of 3, indicating that the extracted species is MA_3. Based on these slope analyses, the extraction equilibrium can be expressed as follows:

$$M3+ + 3HAo \rightleftharpoons MA3,o + 3H+ \quad (1)$$

The extraction constant, K_{ex}, is defined in Equations 2 and 3.

$$K_{ex} = [MA_3]_o[H^+]^3 /[M^{3+}][HA]^3_o = D[H^+]^3 /[HA]^3_o \quad (2)$$

$$\log K_{ex} = \log D - 3pH - 3\log [HA]_o \quad (3)$$

The log K_{ex} values are obtained by substituting the $pH_{1/2}$ values, the pH read from log D *vs.* pH plots at which half of the metal ion is extracted (log D = 0), in Equation 3 and are summarized in Table 2.

As seen in Table 2, Al^{3+} is extracted in higher pH regions than Ga^{3+} and In^{3+}, although the ionic radii increase in the order, $Al^{3+} < Ga^{3+} < In^{3+}$. The intracomplex interligand contacts should have great influence on the stability of Al β-diketonates, which can be deduced from the extraction order of Al^{3+} and In^{3+} with β-diketones [1,2]. In general, simple organic ligands such as the β-diketones form more stable complexes with metal ions having smaller ionic radii when their valency is the same. However, in the extraction of Al^{3+} and In^{3+}, the reverse order is frequently seen as a consequence of the bulk of the ligands, and for bulky β-diketones, such as dibenzoylmethane and thenoyltrifluoroacetone, the steric crowding around Al^{3+} greatly destabilizes the complexes because of the latter's very small ionic radius, while this is not a serious issue in the case of In^{3+}. As a result, In^{3+} is more efficiently extracted than Al^{3+} with bulky β-diketones. The effect of the interligand contact is also seen for the extraction of Ga^{3+} in the literature [1,2] however, it is less serious than that for Al^{3+}.

Table 2. Extraction constants for Group 13 metal ions

	Al^{3+}		Ga^{3+}		In^{3+}	
Ligand	$pH_{1/2}$ [a]	log K_{ex}	$pH_{1/2}$ [a]	log K_{ex}	$pH_{1/2}$ [a]	log K_{ex}
1	3.62	4.85	2.17	0.52	2.00	0.00
2	3.43	4.28	1.20	2.40	1.58	1.26
3	4.63	7.89	3.22	3.66	—	—
4	4.30	6.01	2.43	0.39	4.04	5.21
5	3.12	2.47	1.39	2.74	1.65	1.96
6	2.56	0.78	1.04	3.78	1.75	1.64

[a] $[HA]_o = 1 \times 10^{-2}$ M for **1-3** and $[HA]_o = 5 \times 10^{-3}$ M for **4-5** in benzene.

Considering that the acylpyrazolones themselves are bulkier than β-diketones, as mentioned above, and their acidities are similar, it is clear that the extraction of Al^{3+} is influenced by interligand contacts. As seen in Table 2, the extraction of Al^{3+} reduces as the substituent at the 4-position becomes bulkier. Similar influences of the interligand contacts are also seen in the extraction of Ga^{3+}.

The extraction behavior of **3** and **4** is different from the other acylpyrazolones shown in Table 2. Extraction of In^{3+} by **4** occurs only at a much higher pH, and In^{3+} was not extracted at all by **3**. The lower recovery of Al^{3+} and Ga^{3+} with **3** and **4** can be ascribed to the interligand contacts caused by their bulky adamanthanecarbonyl and pivaloyl groups. The much greater reduction in the extraction of In^{3+} is remarkable.

A comparison of some X-ray crystal structures of aluminium and indium ß-diketonates was undertaken to investigate the role of the adamanthanecarbonyl and pivaloyl groups. The O…O bite distances of the β-diketones in $Al(AA)_3$ [15], $In(AA)_3$ [16], and $In(TTA)_3$ [17] have been reported to be 2.726, 2.905, and 2.905 Å, respectively, where AA and TTA denote acetylacetonate and thenoyltrifluoroacetonate. The O…O bite distances in Al β-diketonates are among the shortest, while those in In β-diketonates are among the longest. The poor extraction of In^{3+} by **3** and **4** could be ascribed to the bulky 4-acyl groups, which prevents the O…O bite distances expanding to fit a favorable configuration in the In complex.

All the acylpyrazolones examined give a quantitative separation of Al^{3+} and Ga^{3+}, and, with the exception of **4** and **6**, a quantitative separation of Al^{3+} and In^{3+}. Owing to the shortened O…O bite distances in **3** and **4**, it is possible to use these ligands to separate Ga^{3+} and In^{3+}.

CONCLUSIONS

This work has confirmed that there are two major factors governing the stability of Group 13 metal ion complexes with β-diketones, the bite distance of the two oxygen donor atoms and the interligand interactions in the coordination sphere. The balance between these two factors defines the extraction order and metal separation and provides a strategy for developing novel extractants showing high selectivity by fine-tuning the structures of well-known types of ligands.

REFERENCES

1. J. Rydberg, C. Musikas, and G. R. Choppin, Principles and Practices of Solvent Extraction, Marcel Dekker, New York, 1992.
2. T. Sekine and Y. Hasegawa, Solvent Extraction Chemistry, Marcel Dekker, New York, 1977.
3. J. Emsley, “The composition, structure and hydrogen bonding of the β-diketones,” *Struct. Bonding (Berlin)*, **57,** 147-191 (1984).
4. G. Gilli, F. Bellucci, V. Ferretti, and V. Bertolasi, “Evidence for resonance-assisted hydrogen bonding from crystal-structure correlations on the enol form of the β-diketone fragment,” *J. Am. Chem. Soc*., **111**, 1023-1028 (1989).
5. A. Roy and K. Nag, “Solvent extraction behavior of rare earth ions with 1-phenyl-3-methyl-4-benzoyl-5-pyrazolone. II. An examination of gadolinium break, tetrad effect, double-double effect and the relevance of "inclined-W" plot,” *J. Inorg. Nucl. Chem*., **40**, 331-334 (1978).
6. S. Umetani and H. Freiser, “Mixed ligand chelate extraction of lanthanides with 1-phenyl-3-methyl-4-trifluoroacetyl-5-pyrazolone and some phosphine oxide compounds,” *Inorg. Chem*., **26**, 3179-3181 (1987).

7. S. Umetani and M. Matsui, "Solvent extraction of alkaline earth metals with 4-acyl-5-pyrazolones and polydentate phosphine oxides," *Anal. Chem.*, **64**, 2288-2292 (1992).
8. Q. T. H. Le, S. Umetani, H. Takahara, and M. Matsui, "Liquid-liquid extraction of lanthanides with a highly acidic extractant, 3-phenyl-4-benzoyl-5-isoxazolone, in the presence or absence of tri-n-octylphosphine oxide," *Anal. Chim. Acta*, **272**, 293-299 (1993).
9. Q. T. H. Le, S. Umetani, and M. Matsui, "Ion-size recognition of Group 13 metals (Al^{3+}, In^{3+}) with modified ß-Diketones," *J. Chem. Soc., Dalton Trans*., 3835-3840 (1997).
10. S. Umetani, Y. Kawase, Q. T. H. Le, and M. Matsui, "Role of the intramolecular hydrogen bond and the ligand rigidity in the complexation of trifluoroacetylcycloalkanones with lanthanides: Novel strategy for the design of organic ligands of high selectivity," *Inorg. Chim. Acta*, **267**, 201-207 (1998).
11. B. S. Jensen, "Synthesis of 1-phenyl-3-methyl-4-acyl-5-pyrazolones," *Acta Chem. Scand*., **13**, 1668-70 (1959).
12. S. Umetani and M. Matsui, "Liquid-liquid distribution of 4-acyl-3-methyl-1-phenyl-5-pyrazolones and their zinc complexes," *Bull. Chem. Soc. Japan*., **56**, 3426-3429 (1983).
13. M. Matsui, J. Tôei, S. Umetani, and T. Shigematsu, "4-Acyl-5-pyrazolones as an analytical reagent (II). Applicability of halogen substituted 4-acyl-5-pyrazolones to the solvent Extraction of metals," *Bull. Inst. Chem. Res., Kyoto Univ.*, **57**, 337-342 (1979).
14. S. Umetani, Q. T. H. Le, M. Matsui, and K. Uezu, to be published.
15. P. K. Hon and C. E. Pfluger, "Crystal and molecular structure of tris(acetylacetonato)aluminum(III) and -cobalt(III)," *J. Coord. Chem.*, **3**, 67-76 (1973).
16. G. J. Palenik and K. R. Dymock, "The structure of tris(2,4-pentanedionato)indium(III)," *Acta Cryst.*, **B36**, 2059-2063 (1980).
17. H. Soling, "The crystal and molecular structure of indium and iron(III) complexes with 1-(2-thienyl)-4,4,4-trifluoro-1,3-butanedione," *Acta Chem. Scand.*, **A30**, 163-170 (1976).

A SEARCH FOR NEW COPPER SOLVENT-EXTRACTION REAGENTS: ACYLPYRAZOLONES AND PHENOXYPYRAZOLES

J. Campbell,[1] R. M. Swart,[1] S. Owens,[1] P. A. Tasker,[2] and L. J. Stewart[2]

[1]*Cytec Industries UK Ltd, P.O. Box 42, Blackley, Manchester, M9 8ZS, UK.*
[2]*School of Chemistry, University of Edinburgh, Edinburgh, EH9 3JJ, UK.*
Corresponding author email address: ron.swart@cytec.com

ABSTRACT

Current copper extractants based on aldoxime and ketoxime chemistry have proven very reliable and flexible in the formulation of reagents to treat the great majority of mixed-metal feeds from most leaching operations. A research project has been completed to review and assess other chemistries which might extend the properties of the reagents. Two types of chemistry were chosen for further investigation, acylpyrazolones and phenoxypyrazoles. This paper will outline the positive and negative properties of these chemistries, highlighting some of the surprising characteristics of the extractants. Although some significant improvements could be achieved, the overall behavior could not meet all the technical and economic requirements of modern-day extractants.

INTRODUCTION

In the hydrometallurgical extraction of metals, the process of solvent extraction is well known [1]. The extraction and concentration of the desired metal is achieved through the use of a selective reagent that extracts the metal under moderately acidic conditions and then can be stripped of the metal by stronger acid. The solvent-extraction step is the key link between leaching of ore and electrowinning of the metal and has to meet the changing requirements of these two processes. Most commonly, the aqueous metal-containing solutions for extraction are the result of the acid-leaching of ores. However, it is known that some metals, especially copper, can be leached from certain ores with ammoniacal solutions [1,2]. This has the advantage that solutions containing especially high concentrations of copper are derived and that there is little contamination of the solution with iron.

Several types of organic solvent extractants have been proposed for use in the recovery of metals from aqueous solutions. Whilst many of the proposed reagents have been found to work well under laboratory conditions and exhibit affinity for the recovery of copper or other metals from solutions, there are often problems encountered with the application of such reagents in commercial systems. Even the most well known of the commercial agents, the oxime reagents (*o*-hydroxyaryloximes and *o*-

hydroxyarylketoximes), are known to suffer from some defects. Although the aldoxime and ketoxime reagents show good stability under strip acid conditions, they can, under certain circumstances, undergo some acid hydrolysis [3], which can result in a build-up of degradation products in the organic phase. Reagents that can resist degradation under these conditions will enhance the metallurgical properties of the ligand.

In this paper, we report the coordination chemistry and extraction properties of two classes of reagents: (i) acyl pyrazolones and (ii) phenoxy pyrazoles; these provide an insight into how reagents can be designed to attempt to overcome some of the challenges seen in the industry today.

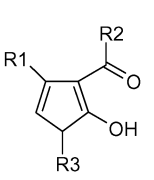

Acyl Pyrazolones

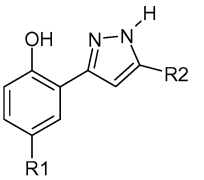

Phenoxy Pyrazoles

EXPERIMENTAL

Preparation of 2-Phenyl-4-(2-hexyldecan-1-oyl)-5-methyl–(3H)-pyrazol-3-one

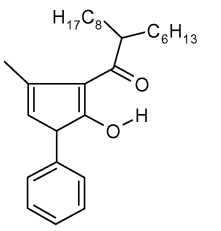

A mixture of 2-phenyl-5-methyl-(3H)-pyrazol-3-one (164 g, 1 M) and dioxane (700 mL) was heated to 60 °C until complete dissolution was obtained. Calcium hydroxide (148 g, 2 M) was added and the mixture stirred for 30 minutes; 2-hexyldecanoyl chloride (274.5 g, 1 M) was added drop-wise over 30 minutes. The temperature was raised to 95-100 °C and held at this temperature, with stirring, overnight. After cooling to RT, the reaction mixture was drowned out into 2 N hydrochloric acid solution (3 liters). The brown oil was extracted into hexane and washed with methanol/water. The organic phase was separated off, dried over magnesium sulphate, and the solvent removed under reduced pressure. Yield = 85% (strength 91.4%, calculated by copper uptake). Mass Spec: Mol wt: 412; found: 411 $(M\text{-}H)^-$, 413 $(M\text{-}H)^+$. ^1H NMR ($CDCl_3$, 300Hz): δ0.85 (triplet, 2 × CH_3), δ1.25 (multiplet, alkyl 20H), δ1.50 (multiplet, CH_2), δ1.80 (multiplet, CH_2), δ2.50 (singlet, CH_3), δ2.95 (multiplet, CH), δ7.30 (triplet, aryl H), δ7.50 (triplet, aryl 2H), δ7.90 (doublet, aryl 2H).

Preparation of 4-Nonyl-2-(5-nonyl-1H-pyrazol-3-yl)-phenol

A solution of 2-hydroxy-5-nonylacetophenone (0.3 M) in toluene (50 mL) was added drop-wise to a stirred slurry of sodium hydride (0.3 M) in toluene (150 mL) at 30 °C over 30 minutes. The reaction mixture was stirred at 30 °C for 1 hour before versatic acid chloride (0.3 M) was added drop wise over 1 hour. After the acid chloride addition was complete, the reaction mixture was heated to 80 °C and held at this temperature for 1 hour. After cooling to RT, potassium hydroxide flake (0.6 M) was added, and the mixture

was heated to 80 °C and held at this temperature for 2 hours. After cooling to RT, the reaction mass was neutralized with aqueous acetic acid solution (25%). The toluene phase was washed with water (3 × 25 mL) and then vacuum evaporated to leave a brown oil. ^{1}H NMR ($CDCl_3$, 300Hz): δ0.5–1.8 (multiplets, alkyl 38H), δ6.4 (singlet, CH), δ6.9 (doublet, aryl H), δ7.1 (multiplet, aryl H), δ7.5 (multiplet, aryl H), δ9.8 & 10.8 (2 × singlets, phenol OH & enol OH).

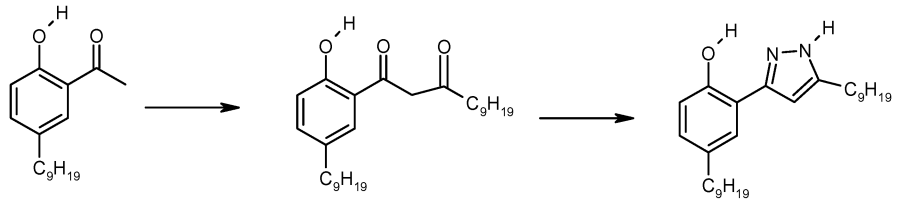

1-(2-Hydroxy-5-nonyl-phenyl)dodecane-1,3-dione (0.1 M) was dissolved in toluene (50 mL), hydrazine hydrate (0.105 M) added, and the reaction solution heated to reflux. After refluxing for 2 hours, the reaction was cooled to RT and the organic phase washed with water (2 × 25 mL). Toluene was removed by vacuum evaporation to produce a brown oil. Mass Spec: Mol wt: 412; found: 411 $(M-H)^-$, 413 $(M-H)^+$. ^{1}H NMR ($CDCl_3$, 300Hz): δ0.5–1.8 (multiplets, alkyl 38H), δ6.2 (singlet, CH), δ6.9 (doublet, aryl H), δ7.5 (multiplet, 2 × aryl H), δ11.9 & 15.6 (phenol OH & pyrazole NH).

RESULTS AND DISCUSSION

Acyl Pyrazolones

Although acyl pyrazolones have been known as metal chelators for some time, the two hard oxygen atoms in the donor set would be expected to be very good for extraction of iron. However, choice of the correct analogue significantly improved the reagent's selectivity for copper. Increasing both the branching and chain length of an alkyl group in the R2 position increased the copper/iron selectivity from 10:1 to >2000:1 (Table 1) and also improved the solubility of the ligand/metal complex by >3000%.

Table 1. Effect of structure on copper/iron selectivity

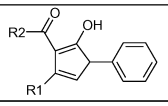	R2 = C_7H_{15} α-branched			R2 = $C_{11}H_{23}$ α-branched			R2 = $C_{15}H_{31}$ α-branched		
Contact time (mins)	Cu (ppm)	Fe (ppm)	Ratio Cu:Fe	Cu (ppm)	Fe (ppm)	Ratio Cu:Fe	Cu (ppm)	Fe (ppm)	Ratio Cu:Fe
0.5	2583	2		1890	1		1580	0	
1	2792	3		2400	1		2090	1	
2	2787	8	350:1	2750	2	1375:1	2620	1	2620:1
3	2795	10		2840	2		2840	2	
5	2781	18	155:1	2830	3	943:1	2990	2	1495:1

Commercial copper extractants (salicylaldoximes/ketoximes), although showing good resistance to degradation, can, under certain conditions, undergo hydrolysis. With the trend towards higher copper tenors and hotter feed solutions, reagents with a higher metal capacity and a greater resistance to degradation may be required. Acyl pyrazolones have been shown to have total stability (Figure 1) under aggressive acidic conditions compared with commercial extractants and to exhibit a similar viscosity at 100 vol % reagent (no diluent) to that of current reagents at 40 vol %.

Although these reagents have been shown to possess some significant advantages over existing reagents and to fall between the strong salicylaldoxime and weaker ketoximes in extraction strength, they exhibited some properties that were detrimental to their use as solvent extractants. Firstly, the kinetics of extraction of the pure compound were slow, and the addition of a selective kinetics booster was required; secondly, although the copper:iron selectivity was acceptable, any iron that did load onto the ligand could be difficult to strip.

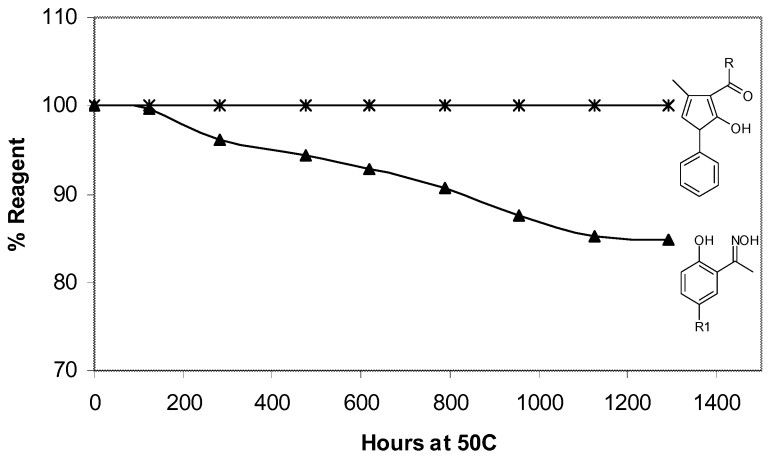

Figure 1. Reagent stability in contact with strip acid (30 g/L Cu, 150 g/L H_2SO_4 at 50 °C).

Phenoxy Pyrazoles

Phenoxy pyrazoles are similar to the commercial oxime extractants both having mixed nitrogen and oxygen donors. However, the phenoxy pyrazole system is hydrolytically stabilized as a result of the nitrogen chelator being provided by heterocyclic ring system rather than an oxime functionality. Crystallographic data has shown that the coordination plane of the central copper atom (O-Cu-N) in the phenoxy pyrazole copper complex (Figure 2) was closer to 90° than that found in the salicylaldoxime copper complex, therefore providing an ideal geometry for the formation of a copper (II) square planar complex. The Cu-O and Cu-N bond lengths were very similar in the pyrazole complex (whereas in the salicyladoxime complex, the Cu-O bonds were significantly shorter). Due to the restriction of the heterocyclic ring, the intermolecular H-bonds between the phenolic oxygen and the pyrazole N-H were longer than those seen in the oxime complex. From the similarities between the crystal

structures, it was expected that ligands of this type would have similar metallurgical properties to those of commercial extractants.

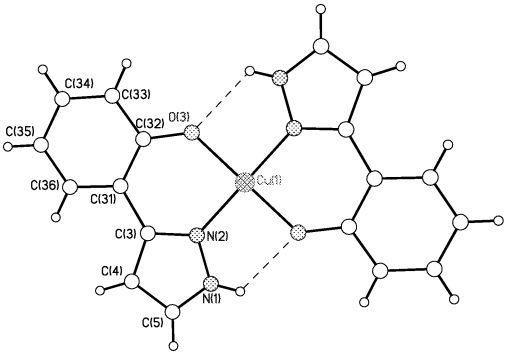

Copper Complex	Angle O-Cu-N /°	Cu-O /Å	Cu-N /Å	Inter H-Bonds /Å
Phenoxy pyrazole	90.89	1.915	1.919	2.23
Salicylald-oxime	91.40	1.893	1.955	1.90

Figure 2. Crystal structure data of a model phenoxy pyrazole copper complex.

The extraction and strip profiles of the phenoxy pyrazole ligand indicated the reagent was a weaker extractant than the commercial salicylaldoximes but had a greatly enhanced ability to strip copper in comparison to commercial extractants (Figure 3). With a reagent of this type, it could be envisaged that either the copper transfer across a circuit could be advanced, thus increasing production, or the acid strength in the tankhouse could be lowered, potentially reducing problems associated with acid misting.

The enhanced stripping profile observed was also seen in the acid stripping of both copper and nickel when loaded from ammoniacal feeds. To ensure the stripping profile was not due to reagent degradation, long-term stability tests were completed in contact with both acidic and ammoniacal strip media. Results showed excellent stability of the phenoxy pyrazole as compared to a commercial extractant under aggressive acidic and basic conditions. It was also observed that, under basic conditions, ammonia transfer into the organic phase was dramatically reduced in comparison to the commercial nonyl hydroxyacetophenone oximes.

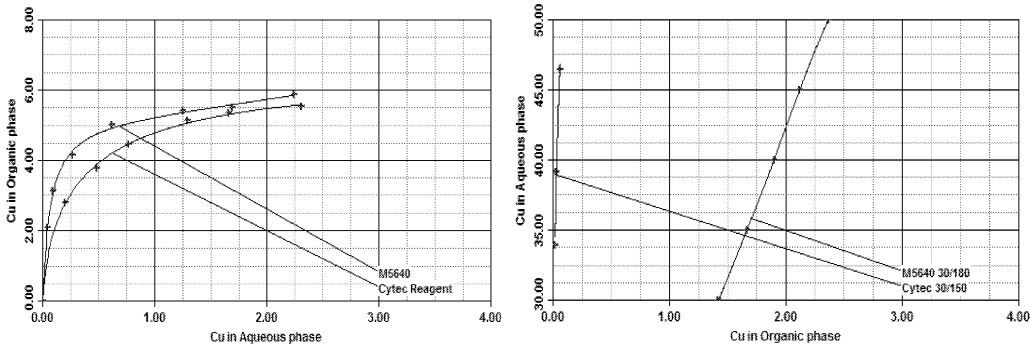

Figure 3. Copper extract/strip isotherms of phenoxy pyrazole compared with a commercial reagent.

Table 2. Percentage of reagents[1,2] remaining after contact with strip solutions

Reagents in contact with acidic strip solution* at 50 °C			Reagents in contact with ammoniacal strip soln.† at 40 °C			Ammonia transfer in contact with ammoniacal strip solution††		
Time /h	Comm. reagent[1]	Phenoxy pyrazole[2]	Time /h	Comm. reagent[1]	Phenoxy pyrazole[2]		Comm. reagent[1]	Phenoxy pyrazole[2]
						Org:Aq Ratio	Org. Phase (NH_3 ppm)	Org. Phase (NH_3 ppm)
0	100	100	0	100	100			
66	95.6	100	476	93.5	100	1:1	2033	35
162	70.6	100	1004	91.2	100	1:4	763	24
306	32.5	100	1822	83.4	100			

*(30 g/L Cu, 180 g/L H_2SO_4). †(280 g/L NH_3, 220 g/L CO_2). ††(280 g/L NH_3, 220 g/L CO_2).
[1]2-Hydroxy-5-nonyl-acetophenone-oxime. [2]2-(5-Nonyl-1H-pyrazol-3-yl)-phenol.

Although this ligand-type has been shown to possess considerable advantages over commercial reagents for the extraction of metals from both acidic and ammoniacal feeds, the cost and difficulty of manufacturing would be significantly greater than reagents seen in the market today.

REFERENCES

1. J. Szymanowski, Hydroxyoximes and Copper Hydrometallurgy, CRC Press, London, 1993.
2. R. G. Reddy and R. N. Weizenbach, "Fundamental Aspects," The Paul Queneau International Symposium on Extractive Hydrometallurgy of Copper, Nickel, and Cobalt, Vol. 1, 1993; pp. 881-910.
3. R. Swart, K. Cramer, O. Castro, P. Tasker, and R. Forgan, Evolution of Copper SX Reagents: Hydrocopper, 2007; pp. 41-47.

POLYACIDIC EXTRACTANTS TO IMPROVE MASS TRANSPORT EFFICIENCIES OF BASE METALS

R. J. Gordon,[1] J. Campbell,[2] D. C. R. Henry,[1] R. M. Swart,[2] P. A. Tasker,[1] F. J. White,[1] J. L. Wood,[1] and L. J. Yellowlees[1]

[1]School of Chemistry, The University of Edinburgh, Edinburgh, UK, EH9 3JJ. [2]Cytec Industries Inc, P.O. Box 42, Blackley, Manchester, UK, M9 8ZS.
Corresponding author email address: Peter.Tasker@ed.ac.uk

ABSTRACT

The molar transport efficiency of copper extraction by salicylaldimine reagents with structures similar to those of the commercial phenolic oximes can be doubled or trebled by incorporating one or two acidic groups into the ligand structure. In these new extractants, deprotonation of the added acid groups allows for the formation of neutral di- and tri-nuclear complexes.

$$2LH_{2(org)} + 2Cu^{2+} \rightleftharpoons [Cu_2L_2]_{(org)} + 4H^+ \text{ and}$$

$$2LH_{3(org)} + 3Cu^{2+} \rightleftharpoons [Cu_3L_2]_{(org)} + 6H^+$$

Extracted species have stoichiometries of 2Cu:2L and 3Cu:2L, respectively, accounting for higher molar transport efficiencies than the conventional phenolic oximes, which give complexes with 1Cu:2L stoichiometry,

$$2LH_{(org)} + Cu^{2+} \rightleftharpoons [CuL_2]_{(org)} + 2H^+$$

Issues relating to exploiting these new extractants in commercial operations, multistep loading and their strength and solubility, are discussed.

INTRODUCTION

Solvent extraction has proved to be very successful in certain metal recovery operations and now accounts for approximately 20 to 30% of the world's annual copper production [1]. For circuits that are based on acidic leaching, a good overall materials balance is obtained when an acid reagent is used to effect separation and extraction, because this regenerates the acid needed in leaching [2,3].

The use of modifiers [2,4] to tune the "strength" of extractants to meet the requirements of such "pH-swing" processes has meant that pregnant leach solutions in a wide range of operations can be processed efficiently using a single class of extractant, the phenolic oximes [4]. These show very high selectivity for copper over other metals, allowing high-purity electrolytes to be generated, yielding conductivity-grade copper. Whilst the commercial oxime reagents such as 5-nonylsalicylaldoxime (P50) meet most criteria for efficient recovery of copper from acid leach/solvent extraction/electowinning circuits [3], mass-transport efficiency is limited by the stoichiometry of the extraction

equation because two moles of extractant are required to transfer one mole of Cu(II) into the organic phase.

In light of the development of several new leaching processes that are capable of delivering pregnant leach solutions with high copper tenors [5], we have considered how to design classes of extractants which operate with more favorable metal:ligand stoichiometries and thus enhance mass-transport efficiencies. Instead of using *mono*-acidic extractants of the phenolic oxime type, we have developed *di*- and *tri*-acidic reagents that are capable of forming neutral *di*- and *tri*-nuclear complexes (Figure 1). As these new extractants complex more moles of copper per mole of reagent, they should give higher mass-transport efficiencies than the conventional oximes, provided that their molecular masses are not significantly higher.

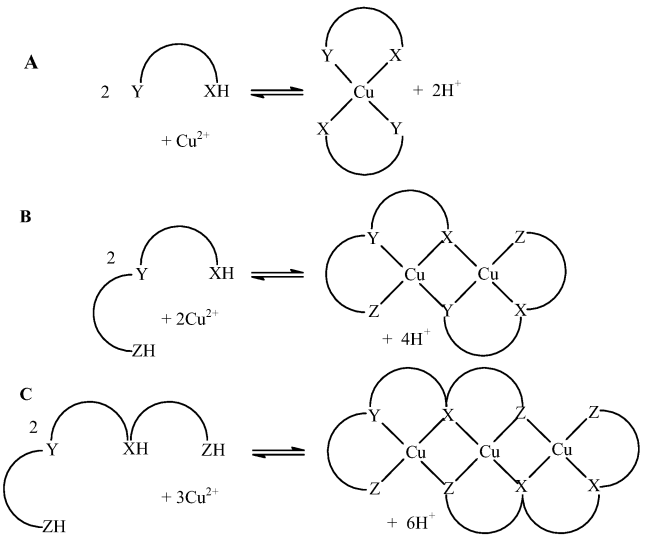

Figure 1. Neutral di- and tri-nuclear Cu-complexes (**B** and **C**) formed by addition of 1 or 2 anionic bridging donors (Z^-) to conventional monoacidic extractants (**A**).

RESULTS AND DISCUSSION

The new *di*- and *tri*-acidic reagents were prepared from salicylaldehyde precursors similar to those used in the manufacture of the commercial phenolic oximes. Our strategy to obtain neutral, organic soluble, copper complexes involved the formation of polynuclear assemblies by incorporating anionic donor atoms derived from acidic groups (ZH in Figure 1) that bridge Cu(II) cations. Adding an acidic group to the conventional bidentate structure (**A**) creates a ligand that can generate a dinuclear complex as in **B**. The molar extraction efficiency is doubled, because one mole of copper is transferred to the organic phase per mole of extractant. Ligands with two pendant acidic groups give a molar extraction efficiency three times that of the conventional bidentate extractants when trinuclear complexes are formed in **C**.

The literature has many examples of phenolate groups forming bridged copper complexes [6]. Consequently fifteen new di- and tri-nucleating extractants were prepared

as shown in Scheme 1 from the appropriate salicylaldehydes and either an acyl hydrazide or an *o*-aminophenol. The Cu-extraction properties of four new ligands, $\mathbf{L}^{1\text{-}3}H_2$ and $\mathbf{L}^4H_3$, which represent the main classes of structure and have good solubilities in chloroform, are reported in this paper. The new ligands were characterized by spectroscopic methods, and single-crystal X-ray structure determinations were undertaken for $\mathbf{L}^3H_2$ and $\mathbf{L}^4H_3$. The former has a conformation to provide an NO_2^{2-} donor set to three vertices of a square-planar Cu^{2+} cation. $\mathbf{L}^4H_3$, crystallizes in a conformation that optimizes *inter*molecular hydrogen bonding in the solid state, but it is apparent from Figure 2 that rotation about two bonds will generate the arrangement of the donor set shown in Scheme 1, which could form trinuclear complexes of the type **C** in Figure 1.

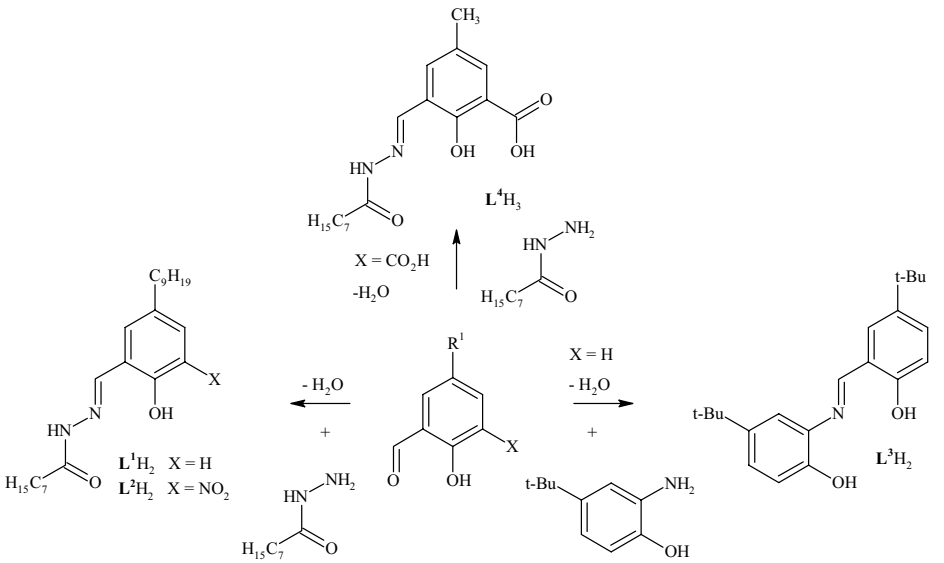

Scheme 1. Preparation of the ligands $\mathbf{L}^1H_2$, $\mathbf{L}^2H_2$ and $\mathbf{L}^3H_2$ from 5-alkyl-salicylaldehydes and $\mathbf{L}^4H_3$ from 5-methyl-salicylaldehyde-3-carboxylic acid.

Methanolic solutions of $\mathbf{L}^{1\text{-}3}H_2$ and $\mathbf{L}^4H_3$ containing an excess of copper(II) acetate, in some cases in the presence of excess base, gave complexes with mass spectra consistent with formation of di- or trinuclear complexes, $[(L)_2Cu_2]$ or $[(L)_2Cu_3]$. This encouraged us to investigate whether such multi-loading could be obtained in solvent extraction. Experiments were carried out initially to compare the pH dependence of Cu-uptake from aqueous sulfate solutions by chloroform solutions of four of the ligands. Results are compared in Figure 3, in which a 100% loading corresponds to the formation of a 1:2 copper:ligand assembly, that is, the maximum loading possible for the conventional reagents (**A** in Figure 1). Maximum theoretical uptake by the dinucleating ligands involves formation of 2:2 copper:ligand complexes (**B**) and corresponds to a 200% loading, and maximum uptake by the trinucleating ligands gives 3:2 complexes (**C**) and is recorded as a 300% loading. In general, for the dinucleating ligands (e. g., for $\mathbf{L}^1H_2$ and $\mathbf{L}^3H_2$), the pH-profiles for Cu-loading showed a single-step process (Figure 3) and are fully (doubly) loaded once the pH of the aqueous phase has increased to 3.5.

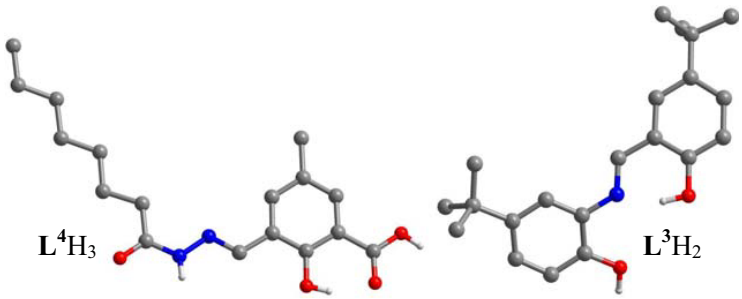

Figure 2. The X-ray crystal structures of L^3H_2 and L^4H_3.

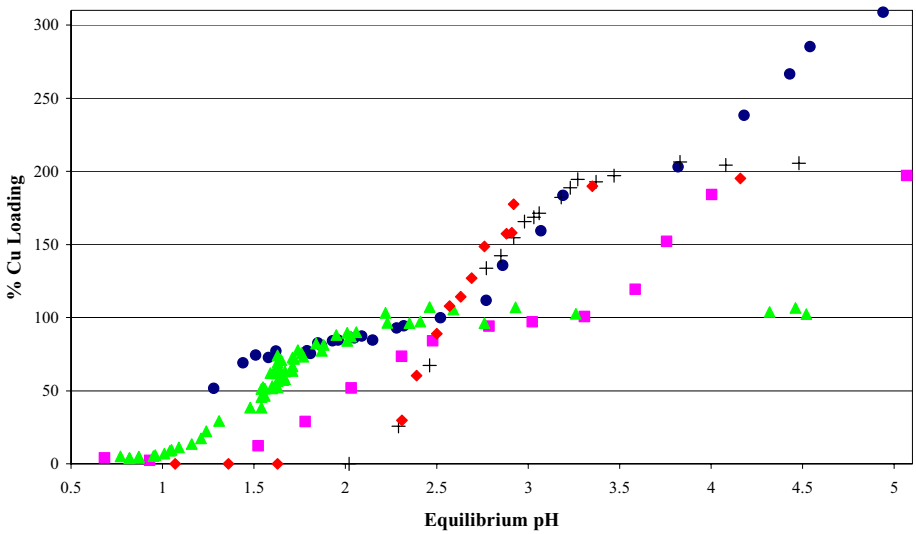

Figure 3. Comparison of Cu-loading by chloroform solutions of P50 (▲), $\mathbf{L^1}H_2$ (♦), $\mathbf{L^2}H_2$(■), $\mathbf{L^3}H_2$(+), and $\mathbf{L^4}H_3$(●) as a function of pH. Loading of 100, 200, and 300% correspond to Cu:2L, 2Cu:2L, and 3Cu:2L molar ratios.

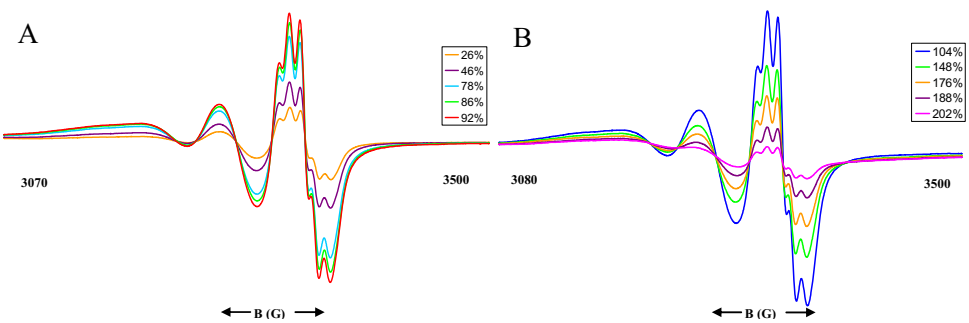

Figure 4. Variation of the EPR spectra of a chloroform solution of $\mathbf{L^2}H_2$ as Cu-loading increases from 0-100% (curves A) and from 100-200% (curves B).

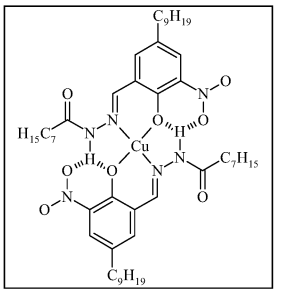

The pH-profile of the 3-nitro-substituted hydrazone ligand, $\mathbf{L^2}H_2$, indicates a two-step loading process (Figure 3). In this instance, the 2:1 complex appears significantly more stable than the 2:2 species ($pH_{½}$ values of ca. 2.0 and 3.7, respectively). A plausible explanation is that the 2:1 assembly is stabilized by the 3-nitro-substituents, which "buttress" the intra-complex hydrogen bonding between the hydrazone NH group and the complexed phenolate oxygen atom (see drawing at right). Similar buttressing of hydrogen-bonding by 3-substituents has been shown recently [7] to have a major effect on the strength of the phenolic oxime extractants similar to the commercial reagents.

The formation of the above mononuclear copper complex was followed by recording EPR spectra. As the pH was raised and copper taken up by the ligand increased, the intensity of the EPR increased to a maximum at 100% loading (**A**, Figure 4) when the mononuclear 1:2 species shown above predominates. The hyperfine coupling constants are consistent with the copper atom having the centrosymmetric N_2O_2 donor set. At higher loadings, the intensity of the EPR signal diminishes, and virtually no signal is detected when the loading reaches 200% (**B**, Figure 1). This is consistent with the dinuclear 2Cu:2L complex showing antiferromagnetic spin-coupling of unpaired electrons on the copper atoms. The potentially trinucleating ligand $\mathbf{L^4}H_3$ shows evidence for three-step loading (Figure 3), and at pH > 5 the 300% loading is consistent with the formation of a 3Cu:2L complex via mechanism **C** in Figure 1.

The results displayed in Figure 4 demonstrate that it is indeed possible to double and triple the *molar* metal-transport efficiency by the addition of one or two acidic groups to a conventional monoacidic extractant. However, toward more efficient reagents for commercial operations, the *mass*-transport efficiency will depend on the molecular weight of the extractants. Table 1 compares the mass-transport efficiency of the commercial P50 oxime reagent with the three dinucleating reagents, $\mathbf{L^{1\text{-}3}}H_2$, and the trinucleating ligand $\mathbf{L^4}H_3$ for which extraction data are reported in Figure 3. These results are encouraging; the trinucleating reagent $\mathbf{L^4}H_3$ transports 2.47 times the mass of copper transported by the conventional reagent P50.

A major practical consideration for the development of formulated reagents is the solubility of the extractants and their metal complexes in hydrocarbon solvents of the types used in commercial operations. In general the new classes of reagent listed in Table 1 have significantly lower solubility in hydrocarbon solvents than conventional phenolic oxime extractants such as P50. Some variations of the structures reported in Scheme 1 were undertaken to increase hydrocarbon solubility. In practice, this could only be achieved by increasing the size and complexity of the alkyl substituents, which increases the molecular weight of the reagents and consequently reduces the benefit of the increased *molar* transport efficiency.

Another important factor is the "strength" of the new reagents. Taking advantage of the improved transport efficiency in processing high-tenor copper feeds will only be possible if maximum loading can be obtained at the low pH values generated by release of protons from the loaded extractant. None of the extractants have $pH_{½}$ values as low as the conventional phenolic oxime, P50. Interstage adjustment of pH to ensure maximum

loading by addition of base is not a practicable option, as this will have an adverse effect on the materials balance of an acid leach/solvent extraction/electrowinning flowsheet.

Table 1. Comparison of the mass-transport efficiencies of 5-nonylsalicylaldoxime (P50), $\mathbf{L}^{1\text{-}3}H_2$, and $\mathbf{L}^4H_3$ and their percentage efficiencies relative to P50

Reagent	Molecular weight	Stoichiometry of loading	Mass of Cu(II)/g transported per kg reagent	% Relative to P50
P50	263	1Cu:2L	121	100
$\mathbf{L}^1H_2$	388	2Cu:2L	163	136
$\mathbf{L}^2H_2$	433	2Cu:2L	147	122
$\mathbf{L}^3H_2$	325	2Cu:2L	195	162
$\mathbf{L}^4H_3$	320	3Cu:2L	298	247

CONCLUSIONS

We have shown that adding acidic groups to the salicylaldehyde building block of the conventional phenolic oxime reagents gives ligands that can form di- and trinuclear complexes. Whilst these show double and triple the *molar* transport efficiency of the conventional copper extractants, higher solubility and strength will be needed to exploit the new systems in commercial operations.

ACKNOWLEDGMENTS

We thank the Engineering and Physical Sciences Research Council (UK), Cytec Industries Inc. and EaStCHEM for PhD studentship funding.

REFERENCES

1. P. J. Mackey, "The Changing Landscape in Copper in 2007," *CIM Mag.*, **2**(2), 35-42 (2007).
2. J. Szymanowski, Hydroxyoximes and Copper Hydrometallurgy, CRC Press, London, 1993.
3. P. A. Tasker, P. G. Plieger, and L. C. West, "Metal complexes for hydrometallurgy and extraction," *Comprehensive Coordin. Chem. II*, **9**, 759-808 (2004).
4. A. M. Sastre and J. Szymanowski, "Discussion of the physicochemical effects of modifiers on the extraction properties of hydroxyoximes. A review," *Solvent Extr. Ion Exch.*, **22**(5), 737-759 (2004).
5. D. Dreisinger, "Copper leaching from primary sulfides: Options for biological and chemical extraction of copper," *Hydrometallurgy*, **83**(1-4), 10-20 (2006).
6. C. R. Choudhury, S. K. Dey, R. Karmakar, C. D. Wu, C. Z. Lu, M. S. El Fallah, and S. Mitra, "First report of singly phenoxo-bridged copper(II) dimeric complexes: synthesis, crystal structure and low-temperature magnetic behaviour study," *New J. Chem.*, **27**(9), 1360-1366 (2003).
7. R. S. Forgan, P. A. Wood, J. Campbell, D. K. Henderson, F. E. McAllister, S. Parsons, E. Pidcock, R. M. Swart, and P. A. Tasker, "Supramolecular chemistry in metal recovery; H-bond buttressing to tune extractant strength," *Chem. Commun.*, 4940-4942 (2007).

SOLVENT EXTRACTION OF SEVERAL METAL IONS WITH A NOVEL TRIPODAL TYPE OF CARBOXYLIC ACID

K. Ohto, Y. Fujimoto, H. Furugou, H. Kawakita, H. Harada, and K. Inoue

Honjo, Saga 840-8502, Japan, Faculty of Science and Engineering, Department of Chemistry and Applied Chemistry, Saga University.
Corresponding author email address: ohtok@cc.saga-u.ac.jp

ABSTRACT

A novel tripodal carboxylic acid compound with a three-dimensionally oriented, narrow, and rigid coordination site with C_3 symmetry has been prepared. In solvent extractions of trivalent Group 3 ions and divalent base metal ions, the extractant shows a significantly higher extraction efficiency compared with a commercial carboxylic acid extractant, Versatic Acid 10. The extractive selectivity sequence of Group 3 ions is different for the present extractant than for the commercial extractant. The coordination site of the present extractant is suitable for Ga(III), whereas In(III) is too large to be effectively extracted. The stoichiometry of the extraction process with gallium and indium has also been investigated.

INTRODUCTION

In past years, a large number of metal extractions with a carboxylic acid type of extractant have been reported, including some reviews [1]. Only a few papers have been published on structure-extractability relationships, that is, the length of alkyl chains, the kind of lipophilic side chains, and their steric effects on the metal extraction behavior [2]. As alternatives to conventional carboxylic acid types of extractant, macrocyclic host compounds, such as crown ethers [3] and three-dimensionally molecularly-designed calixarenes [4], have lately been used as parent compounds followed by modification to carboxylic acid. In metal extraction, those extractants with three-dimensional metal-ion recognition sites have demonstrated high effective separation abilities. Tripodal alkyltrimethylol compounds are very attractive and interesting host compounds, since they also provide three-dimensionally designed, narrow, and rigid structures for metal uptake; some characteristics were introduced in the previous paper [5]. Although several carboxylic-type tripodal compounds with short alkyl chains have been reported [6], only a few papers [7] have been published on metal extraction due to the poor lipophilicity of the compounds.

In the present work, 1,1,1-tris(carboxymethoxymethyl)-9-decene has been prepared as an extractant to investigate trivalent Group 3 and divalent base metal extractions.

EXPERIMENTAL

Reagents

The synthetic scheme for the reported extractant is shown in Figure 1. Compound **1**, 1,1,1-tris(hydroxymethyl)-9-decene, has been prepared by a similar procedure reported by Dermer et al. [8]. 1,1,1-Tris(ethoxycarbonylmethoxymethyl)-9-decene, **2**, and 1,1,1-tris(carboxymethoxymethyl)-9-decene, **3**, have been prepared by a similar procedure reported by Viguier et al. [6]. The other reagents were of reagent grade, and a commercial extractant, Versatic Acid 10 (VA-10) was used without further purification.

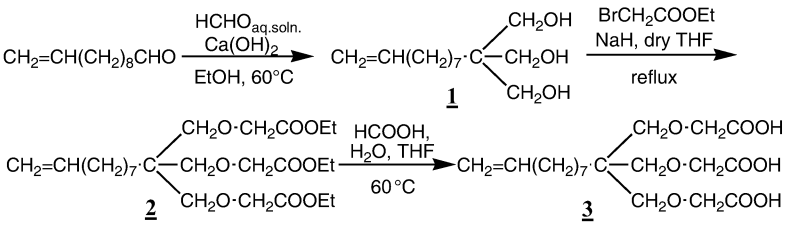

Figure 1. Synthetic scheme for the extractant.

1,1,1-Tris(ethoxycarbonylmethoxymethyl)-9-decene (**2**)

To compound **1** (8.57 g, 37.2 mmol) was added 400 cm^3 dry THF. Sodium hydride (22.2 g, 561 mmol) was carefully added to the solution at -15 °C under a nitrogen flow for an hour. Ethyl bromoacetate (114 g, 683 mmol) was added dropwise to the mixture at room temperature. The mixture was refluxed for 48 h. After cooling, ethanol and water were carefully added to the mixture to deactivate the sodium hydride. After drying in vacuo, chloroform was added to the extract. The organic solution was washed with dilute hydrochloric acid and distilled water three times each and then was dried over anhydrous magnesium sulfate. After filtration, the solvent was removed in vacuo. The crude residue was purified by column chromatography (SiO_2, chloroform:ethyl acetate = 4:1 v/v) to give a brown liquid; 6.18 g (34.0%); R_f = 0.82; IR (KBr) $\nu_{C\text{-}H}$ 2926 cm^{-1}, $\nu_{C=O}$ 1736 cm^{-1}; ^{1}H-NMR (300 MHz, $CDCl_3$, TMS, 25 °C) δ 1.28 (21H, m, $(CH_2)_6CH_2CH=CH_2$ + OCH_2CH_3), 2.05 (2H, m, $CH_2CH=CH_2$), 3.49 (6H, s, CH_2OCH_2O), 4.07 (6H, s, OCH_2CO), 4.19 (6H, q, OCH_2CH_3), 5.01 (2H, m, $CH=CH_2$), 5.83 (1H, m, $CH=CH_2$).

1,1,1-Tris(carboxymethoxymethyl)-9-decene (**3**)

To compound **2** (2.16 g, 5.34 mmol) were added 100 cm^3 formic acid and 3 cm^3 water. The mixture was heated at 60 °C for 2 days. After drying in vacuo, chloroform was added to the residue. The organic solution was washed with distilled water, and then dried over anhydrous magnesium sulfate. After filtration, the solvent was removed in vacuo to give an umber viscous liquid; 1.59 g (89.0%); IR (KBr) $\nu_{O\text{-}H}$ 3200 cm^{-1} (br); $\nu_{C\text{-}H}$ 2931 cm^{-1}, $\nu_{C=O}$ 1733 cm^{-1}; ^{1}H-NMR (300 MHz, $CDCl_3$, TMS, 25 °C) δ 1.26 (12H, m,

$(CH_2)_6CH_2CH=CH_2$), 2.03 (2H, m, $CH_2CH=CH_2$), 3.54 (6H, s, CH_2OCH_2COO), 4.13 (6H, s, OCH_2CO), 5.01 (2H, m, $CH=CH_2$), 5.83 (1H, m, $CH=CH_2$), 8.75 (3H, s(br), OH).

Distribution Study of Metal Ions

An organic solution was prepared by diluting each extractant with analytical-grade chloroform to desired concentrations. An aqueous solution was prepared by dissolving metal salts in analytical-grade 0.1 M HEPES or by diluting 0.1 M nitric acid to 0.1 mM. For trivalent Group 3 ions, the aqueous solution contained Al, Ga, and In ions; for divalent base metals, it contained Pb, Cu, Zn, Co, and Ni ions. Both solutions (0.1 M HEPES and 0.1 M nitric acid) were arbitrarily mixed to adjust the pH of the solutions. Equal volumes (3 cm^3) of both phases were mixed and gently shaken (130 rpm at 303 K for more than 4 h. After phase separation, the pH values and the metal concentrations in the aqueous solutions were measured by pH meter (Orion 720A) and ICP-AES (Shimadzu ICPS-8100), respectively. The extracted metal concentrations were calculated from the differences of the aqueous metal concentrations before and after the equilibration.

RESULTS AND DISCUSSION

Distribution Study of Metal Ions

Extraction Equilibrium Time of Group 3

The effect of shaking time on the percentage extraction of Group 3 ions with the present tripodal carboxylic acid extractant is shown in Figure 2. Extraction of trivalent aluminum, gallium, and indium together with the new extractant reaches equilibrium within 4 h, although the extraction rate of aluminum is known to be slow.

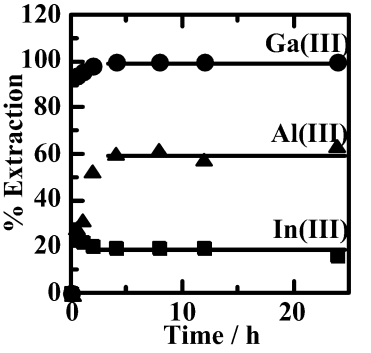

Figure 2. Effect of shaking time on % extraction of Group 3 metals. [Extractant] = 5 mM, [metal ion] = 0.1 mM, initial pH = 3.23.

pH Dependency of Trivalent Group 3 and Divalent Base Metal Extraction

The effects of pH on the percentage extraction of divalent metals, Pb(II), Cu(II), Zn(II), Ni(II), and Co(II) with the present tripodal extractant and commercial VA-10, are shown in Figures 3(a) and 3(b), respectively. The % extraction of all metals with **3** decreases at high pH (over 3.7) due to leakage of the extractant to the aqueous phase, which was confirmed by TOC analysis (Shimadzu TOC-V_{CPH}). Although no leakage of the extractant into the aqueous phase is required from a practical point of view, the extractant leakage was observed due to poor lipophilicity. The selectivity sequence for extractant **3** among the metals examined is as follows: Pb > Cu > Ni > Zn ≈ Co, while that for VA-10 is Pb >> Cu >> Zn ≈ Ni ≈ Co. The different separation efficiency between **3** and VA-10 would be attributed to the narrow coordination site of **3**. Ionic radii of Cu (II), with coordination number (CN) 4, Ni (II, CN

6), Zn (II, CN 4), and Co (II, CN 6) are 62, 69, 60, and 75 pm, respectively, whereas Pb (II, CN 6) is 118 pm. In particular, a remarkably poor separation efficiency between Pb(II) and Cu(II) with **3** is observed by adverse influence of the extractant structure compared with VA-10.

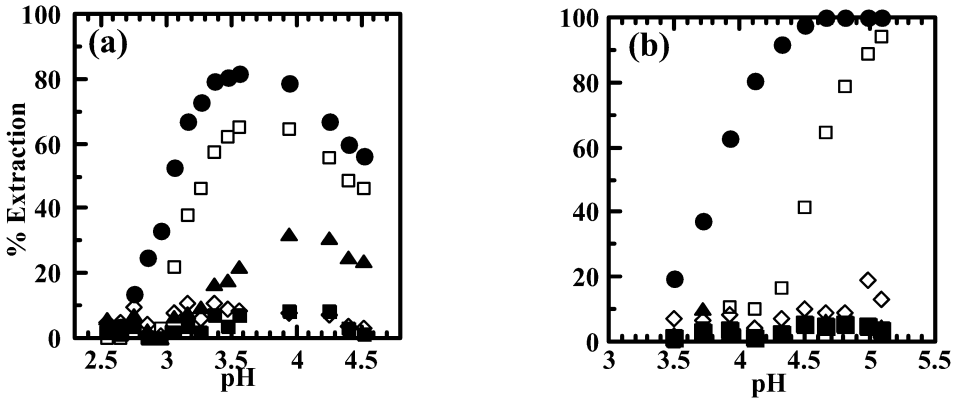

Figure 3. Effect of pH on percentage extraction of divalent metal ions. (a) Present extractant (5 mM), (b) VA-10 (20 vol % ≈ 1.05 M). Close circles, Pb(II); open squares, Cu(II); close triangle, Ni(II); open diamond, Zn(II); close square, Co(II). [metal ion] = 0.1 mM each.

The effects of pH on the percentage extraction of trivalent Group 3 ions, Al(III), Ga(III), and In(III) with the extractant **3** and VA-10 are shown in Figures 4(a) and 4(b), respectively. At low pH (below 3.5), the extractant leakage of **3** does not take place; the percentage extractions of all metals increase with increasing pH.

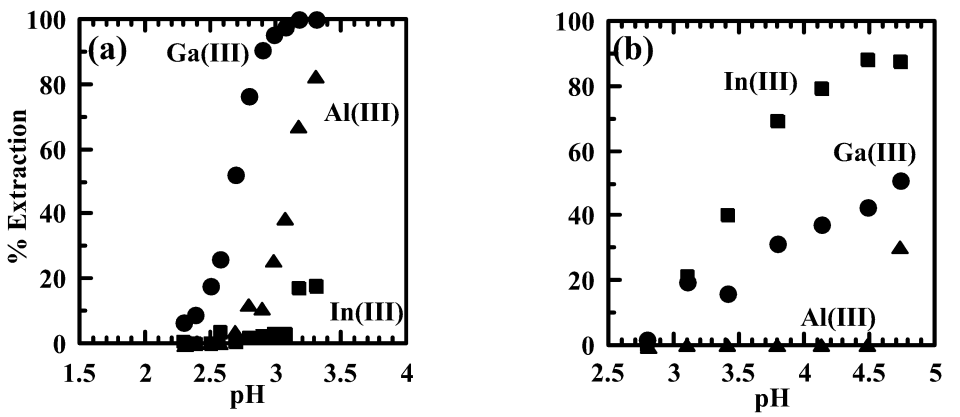

Figure 4. Effect of pH on percentage extraction of aluminum-group metal ions.
(a) Present Extractant **3** (5 mM), (b) VA-10 (150 mM); [metal ion] = 0.1 mM each.

The selectivity sequence for **3** among Group 3 metals is as follows: Ga > Al >> In, while that for VA-10 is In > Ga >> Al. The drastic change in the selectivity can also be caused by the structural effect of **3** with the three-dimensionally oriented, narrow, and rigid coordination site as described above for divalent metal extraction. Ionic radii of trivalent Group 3 ions with coordination number 6, Al, Ga, and In are 53, 62, and 80 pm,

respectively. From the data of Figures 3(a) and 4(a), the size of the coordination site of **3** was roughly estimated to be 120 pm.

Extractant **3** displays a vastly higher extraction ability than VA-10, because the concentrations of VA-10 in Figure 3(b) and 4(b) are 210 and 30 times as much as those of **3**, respectively. (Since **3** has three carboxylic acid groups, the numbers of carboxylic acids for VA-10 are respectively 70 and 10 times as much as those for **3**.) It can be attributed to size-fitting and aggregation effects of functional groups.

Extraction Reaction of Group 3

The effects of equilibrium pH and equilibrium extractant concentration on the distribution ratio of gallium and aluminum ions with **3** are shown in Figures 5 and 6, respectively. The experimental points in Figure 5 lie on straight lines with slopes of 3.3, which means trivalent metal extraction takes place by an ion-exchange mechanism. The experimental points for Al, Ga, and In in Figure 6 respectively lie on straight lines with slopes of 0.88, 0.88, and 2.0, which means Al and Ga form 1:1 complexes with **3**, while the large In forms 1:2 complex with **3**. (The carboxylic acid extractant does not dimerize in chloroform.) Different stoichiometry can also be attributed to the coordination site size of the extractant. The extraction reactions of Group 3 ions with **3** are as follows:

$$Al^{3+}\ (\text{or } Ga^{3+}) + H_3R_{(org)} \rightleftharpoons Al(\text{or } Ga)R_{(org)} + 3H^+ \quad (1)$$

$$In^{3+} + H_3R_{(org)} \rightleftharpoons InR_{(org)} + 3H^+ \quad (2)$$

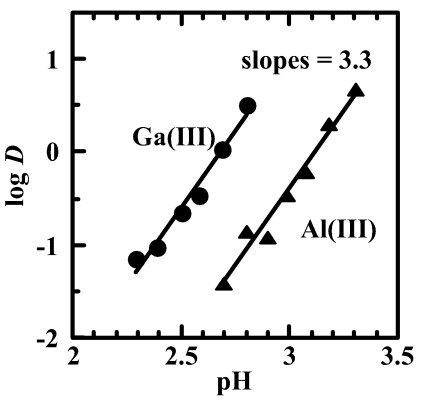

Figure 5. Effect of pH on the distribution ratio of gallium and aluminum ions. [Extractant] = 5 mM, [Al(III)] = [Ga(III)] = 0.1 mM.

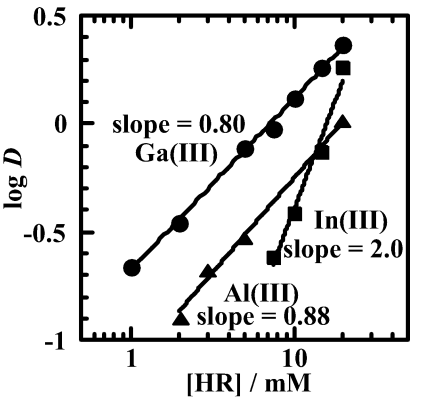

Figure 6. Effect of extractant concentration on the distribution ratio of Group 3 metals. [Extractant] = 5 mM, [metal ion] = 0.1 mM.

CONCLUSIONS

A novel tripodal carboxylic acid extractant has been prepared to investigate extraction behavior on trivalent Group 3 and divalent base metals. The extractant shows significantly higher extraction ability compared with a commercial extractant. The

specific coordination site affects the selectivity sequence and the stoichiometry of extraction.

REFERENCES

1. (a) D. S. Flett and M. J. Jaycock, "Extraction of metals by carboxylic acids," *Ion Exch. Solvent Extr.*, **3**, 1-50 (1973); (b) A. W. Ashbrook, "Review of the use of carboxylic acids as extractants for the separation of metals in commercial liquid-liquid extraction operations," *Minerals Sci., Eng.*, **5**(3), 169-80 (1973); (c) B. Weaver, "Solvent extraction in the separation of rare earths and trivalent actinides," *Ion Exch. Solvent Extr.*, **6**, 189-277 (1974); (d) N. M.Rice, "Recent developments and potential uses for carboxylic acid extractants—a review," *Hydrometallurgy*, **3**(2), 111-133 (1978); (e) R. Brzozka and C. Rozycki, "Application of monocarboxylic acids for the extraction of metal ions—literature survey," *Chemia Analityczna*, **25**(1), 3-24 (1980); (f) B. Gupta, D. Singh, and S. N. Tandon, "Extraction of metals by carboxylic acids—a review," *J. Sci. Ind. Res.*, **52**(12), 808-832 (1993).
2. (a) R. Piesch and H. Sinic, "Solvent extraction of metal cations with homologous aliphatic carboxylic acids," *Anal. Chim. Acta.*, **49**(1), 51-6 (1970); (b) J. S.Preston, "Solvent extraction of metals by carboxylic acids," *Hydrometallugy*, **14**(2), 171-188 (1985); (c) D. Zheng, N. B. Gray, and G. W. Stevens, "Comparison of naphthenic acid, versatic acid and D2EHPA for the separation of rare earths," *Solvent Extr. Ion Exch.*, **9**(1), 85-102 (1991); (d) J. S. Preston and A. C. du Preez, "The solvent extraction of europium(II) by some organophosphorus and carboxylic acids," *Solvent Extr. Ion Exch.*, **9**(2), 237-57 (1991); (e) A. C. du Preez and J. S. Preston, "The solvent extraction of rare earth metals by carboxylic acids," *Solvent Extr. Ion Exch.*, **10**(2), 207-230 (1992); (f) H. Yamada, C. Kato, and M. Mizuta, "Comparison of 2,4-hexadienoic with 1-hexanoic acids as extractant for copper(II)," *Bull. Chem. Soc. Jpn.*, 65(1), 186-190 (1992).
3. (a) J. Strzelbicki and R. A.Bartsch, "Extraction of alkali metal cations from aqueous solutions by a crown ether carboxylic acid," *Anal. Chem.*, **53**(12), 1894-1899 (1981); (b) J. Tang and C. M. Wai, "Enhanced extraction of lanthanides with crown ether carboxylic acids of increasing lipophilicity," *Analyst*, **114**, 451-453 (1989).
4. (a) R. Ludwig, K. Inoue, and T. Yamato, "Solvent extraction behavior of calixarene-type cyclophanes towards trivalent La, Nd, Eu, Er, and Yb," *Solvent Extr. Ion Exch.*, **11**(2), 311-330 (1993); (b) K. Ohto, M. Yano, K. Inoue, T. Yamamoto, M. Goto, F. Nakashio, S. Shinkai, and T. Nagasaki, "Solvent extraction of trivalent rare earth metal ions with carboxylate derivatives of calixarenes," *Anal. Sci.*, **11**(6), 893-902 (1995).
5. K. Ohto, H. Nakagawa, H. Furutsuka, T. Shinohara, T. Nakamura, T. Oshima, and K. Inoue, "Solvent extraction of rare earths with a novel phosphonate extractant providing a narrow coordination site," *Solvent Extr. Res. Dev. Jpn.*, **11**, 121-134 (2004).
6. R. Viguier, G. Serrartice, A. Dupraz, and C. Dupuy, "New polypodal polycarboxylic ligands-complexation of rare earth ions in aqueous solution," *Eur. J. Inorg. Chem.*, 1789-1795 (2001).
7. T. Nakamura, K. Ohto, T. Oshima, and K. Inoue, "Preparation of a novel broom phthalamic acid extractant and the extraction behavior of rare earth metals," *Solvent Extr. Res. Dev. Jpn.,* **13**, 89-99 (2006).
8. O. C. Dermer and P. W. Solomon, "Extensions of the Tollens condensation," *J. Am. Chem. Soc.*, **76**, 1697-1699 (1954).

NEXT GENERATION EXTRACTANTS FOR SEPARATION OF CESIUM FROM HIGH-LEVEL WASTE

R. A. Bartsch,[1] H. Zhou,[1] L. H. Delmau,[2] and B. A. Moyer[2]

[1]*Department of Chemistry and Biochemistry, Texas Tech University, Lubbock, Texas, 79409-1061, USA.* [2]*Chemical Sciences Division, Oak Ridge National Laboratory, P.O. Box 2008, Oak Ridge, Tennessee 37830-6119.*
Corresponding author email address: richard.bartsch@ttu.edu

ABSTRACT

Using calix[4]arene as a scaffold, lipophilic, proton-ionizable ligands for cesium ion extraction have been synthesized. In the 1,3-alternate conformation, lipophilic octyl groups are attached to distal oxygens on one side of the calix[4]arene molecule, and an alkylated benzocrown-6 unit is connected to distal oxygens on the other side. One phenyl octyl ether unit bears an acidic group in the para-position which orients it directly over the polyether ring. Solvent extractions of trace cesium ion from aqueous solutions into toluene have been performed. The efficiency of cesium ion extraction as a function of the aqueous phase pH and the identity of the acidic group have been assessed. Promising results are obtained for this new series of cesium ion extractants.

INTRODUCTION

The current best technology for removal of cesium from high-level waste HLW at the US-DOE Savannah River Site (SRS) is the Caustic-Side Solvent Extraction (CSSX) process. Highly selective cesium salt extraction is accomplished with a combination of calix[4]arene-bis(4-*tert*-octylbenzocrown-6, (abbreviated "BOBCalixC6", Figure 1), trioctylamine, and an alkyl-phenoxyalcohol modifier (Cs-7SB) in Isopar® L [1]. The process has achieved a decontamination factor of >40,000 for cesium in actual high-level waste.

Based upon the experience gained in this earlier work, a second generation of lipophilic calix[4]arene-benzocrown-6 extractants was proposed in which an incorporated proton-ionizable function would facilitate stripping of extracted cesium ion upon contact with aqueous acid. Furthermore, the new extractants would contain single crown ether rings to eliminate possible complications with concomitant extraction of another alkali metal cation by the second polyether ring in BOBCalixC6. We now report the preparation of these "next generation" cesium extractants and results from initial evaluation of their cesium ion extraction behavior.

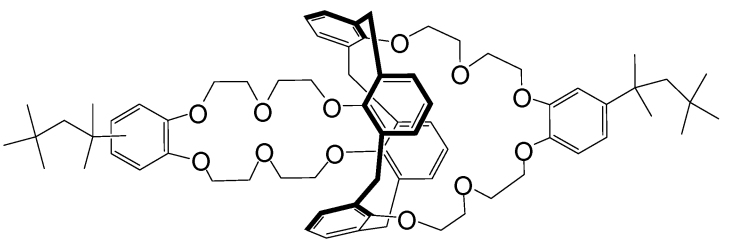

Figure 1. Structure of BOBCalix6 Cesium Extractant.

EXPERIMENTAL

Synthesis of Next-Generation Cesium Extractants

Preparation of the new, lipophilic, proton-ionizable calix[4]arene-benzocrown-6 ligands will be described in detail elsewhere.

Cesium Ion Extraction by Next-Generation Extractants in Toluene

The ^{137}Cs used for spiking the aqueous phases was obtained as $^{137}CsNO_3$ in water from Isotope Products Laboratories in Burbank, California.

The pH-variation experiments were performed with 13 different buffered aqueous solutions containing 0.20 mM cesium with the maximum concentration of sodium of 0.60 M. Compositions are given in Table 1. Spike volumes of ^{137}Cs radiotracer were chosen to give activities of 0.2 μCi/mL per sample. The diluent was a 0.10 mM solution of the cesium extractant in toluene.

Batch-equilibrium liquid-liquid contacting experiments were performed in polypropylene tubes. Appropriate volumes of the aqueous and organic phases were contacted for 30-90 minutes at 25 °C by end-over-end rotation at 60 ± 5 rpm using a Glass-Col laboratory rotator placed inside a 25 ± 0.2 °C constant-temperature airbox. Complete phase separation was aided by centrifugation for 5 minutes at 2060 X *g* in a Beckman Coulter Allegra 6R refrigerated centrifuge at 25 ± 1 °C. Aliquots of the separated phases were pipetted into counting vials for determination of the ^{137}Cs activities by standard gamma counting using a Packard Cobra Quantum Model 5003 gamma counter equipped with a 3" NaI (Tl) crystal through-hole detector. Counting times varied with the activity of the samples, and sufficient counts were recorded such that the distribution ratios were obtained with a standard deviation within ±5%.

The cesium distribution ratios (D_{Cs}) were determined as the ratio of the volumetric count rates of the radioisotope in each phase at equilibrium. Uncertainty in the results is estimated at ±5% due to handling (pipetting, preparation) error. Counting errors were all below ±1%, since all results exhibited a significant number of counts in both organic and aqueous phases.

Table 1. Aqueous-phase compositions for cesium extraction studies

pH	$[HNO_3]$ (M)	$[NaNO_3]$ (M)	[NaOH] (M)	[NaAc] (M)	[Borax] (M)	$[NaH_2PO_4]$ (M)	$[Na_2HPO_4]$ (M)
1	0.1	0.4	0	0	0	0	0
2	0.01	0.5	0	0	0	0	0
3	0.0484	0.5	0	0.05	0	0	0
11	0	0.5	0.0041	0	0	0	0.025
4	0.0376	0.5	0	0.05	0	0	0
5	0.0116	0.5	0	0.05	0	0	0
6	0	0.5	0.0056	0	0	0.05	0
7	0	0.5	0.0291	0	0	0.05	0
8	0	0.5	0.0461	0	0	0.05	0
9	0.0046	0.5	0	0	0.0125	0	0
10	0	0.5	0.0183	0	0.0125	0	0
12	0	0.5	0.0269	0	0	0	0.025
13	0	0.5	0.1	0	0	0	0

RESULTS AND DISCUSSION

New Lipophilic, Proton-Ionizable Calix[4]arene-benzocrown-6 Extractants

Structures of the new cesium extractants are presented in Figure 2.

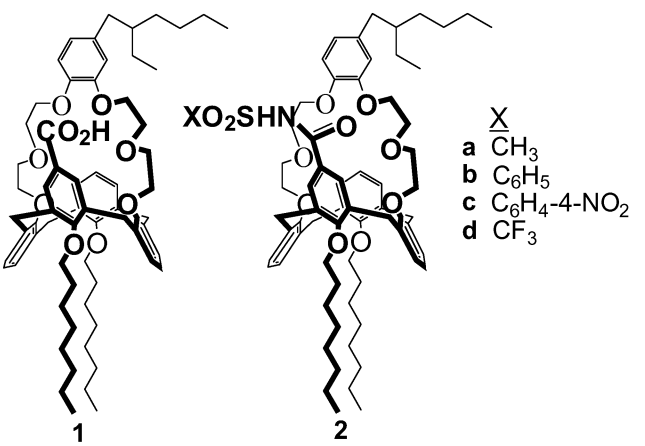

Figure 2. Structures of next generation cesium extractants.

To promote solubility in organic diluents of low polarity, each extractant bears octyl groups attached to two phenolic oxygens of the 1,3-alternate calix[4]arene scaffold, as well as a 2-ethylhexyl group on the benzo group of the crown ether ring on the opposite side of the molecule. Each extractant has a proton-ionizable group positioned

directly over the polyether ring [2]. In **1**, this group is a carboxylic acid functionality. In **2a-d**, acidity is provided by *N*-(X)sulfonyl carboxamide groups for which the acidity of the N-H unit may be "tuned" by variation in the electron-withdrawing ability of X [3]. Due to their proton-ionizable groups, ligands **1** and **2a-d** can extract cesium ion by an ion-exchange mechanism.

The synthetic route to extractants **1** and **2a-d** is shown in Scheme 1. Thus, refluxing lipophilic 4-bromo-substituted calix[4]arene **3**, lipophilic dimesylate **4**, and cesium carbonate in acetonitrile gave the 1,3-alternate calix[4]arene-benzocrown-6 **5**. Reaction of **5** with butyllithium in tetrahydrofuran followed by carbon dioxide produced the carboxylic acid extractant **1**. Treatment of **1** with oxalyl chloride in benzene gave the corresponding acid chloride, which without purification was reacted with the appropriate commercially available sulfonamide and sodium hydride in tetrahydrofuran. New extractants **1** and **2a-d** were fully characterized by IR and NMR spectroscopy and by combustion analysis.

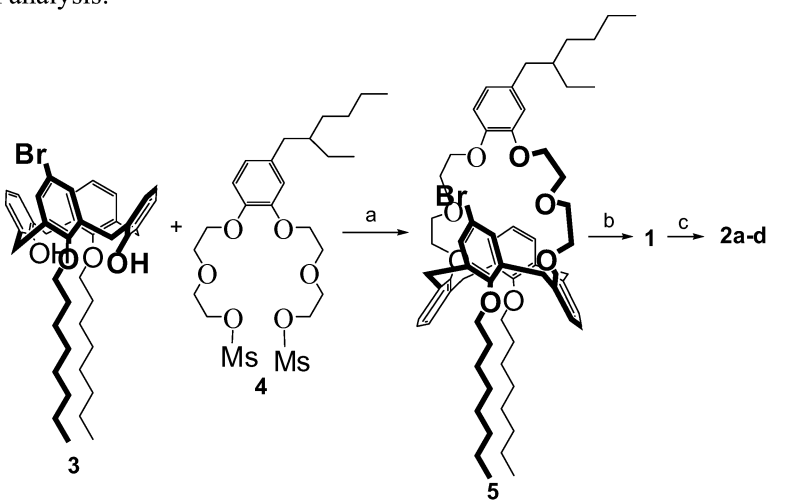

Scheme 1. Formation of the calix[4]arene-benzocrown-6 extractants.

Effect of pH on Cesium Ion Extraction by the Next Generation Extractants

Liquid-liquid extractions of cesium ion from buffered solutions at pH values of 1-13 by toluene solutions of extractants **1** and **2a-d** were performed using ^{137}Cs radiotracer. Cesium distribution ratios as a function of pH of the aqueous phase are presented graphically in Figure 3 for which the symbols for the five different extractants are designated in the figure caption.

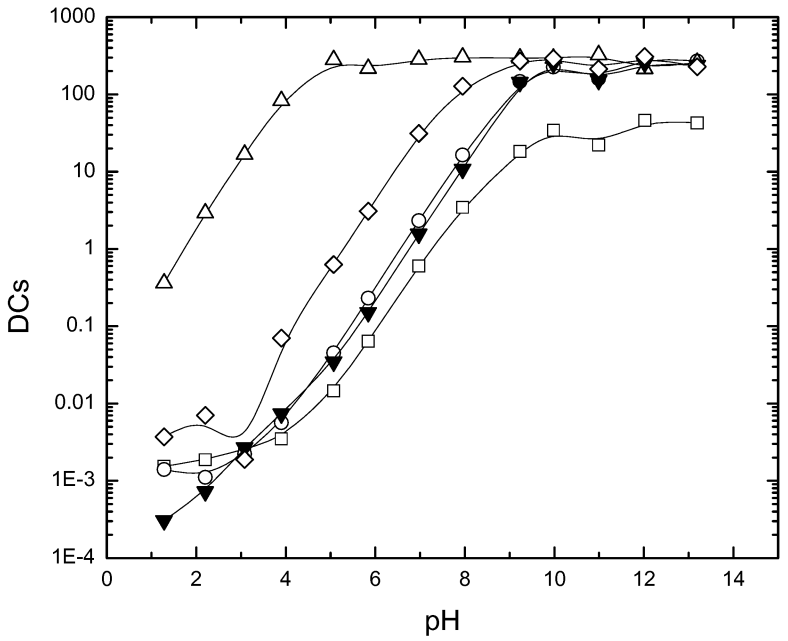

Figure 3. D_{Cs} as a function of pH for cesium extractions by **1** (open squares), **2a** (filled inverted triangles), **2b** (open circles), **2c** (open tilted squares), and **2d** (open triangles).

Immediately apparent is a pronounced dependence of the distribution ratio on the pH of the aqueous phase. Thus, the ligands exhibit strong cesium ion extraction ability from highly alkaline aqueous solutions, such as those at SRS, and marked diminutions in the extraction propensity from acidic aqueous solutions. Thus, cesium ion can be efficiently extracted from strongly basic aqueous solutions and then stripped from the loaded diluent by contact with acidic aqueous solution.

For the series of *N*-(X)sulfonyl ligands **2a-d**, all four have approximately the same cesium distribution ratios at pH 10 and greater. However, an effect of extractant acidity upon the identity of the X group is evident, as would be expected if only the ionized form of the ligand is the effective extractant.

CONCLUSIONS

This study has produced "next generation" extractants for removal of cesium ion from high-level waste. They feature high lipophilicity, high cesium ion extraction from strongly basic aqueous solutions, and low cesium ion extraction from acidic aqueous solutions. This would allow stripping of loaded organic diluent by a pH switch.

ACKNOWLEDGMENTS

This research was supported at Texas Tech University by the Office of Biological and Environmental Research of the U.S. Department of Energy (Grant Number FG02-03ER63676). This research was supported at Oak Ridge National Laboratory by the Environmental Management Science Program of the Offices of Science and Environmental Management of the U.S. Department of Energy (Contract Number DE-AC05-00OR22725.

REFERENCES

1. L. H. Delmau, P. V. Bonnesen, and B. A. Moyer, "A Solution to Stripping Problems Caused by Organophilic Anion Impurities in Crown-Ether Based Solvent Extraction Systems: A Case Study of Cesium Removal from Radioactive Wastes," *Hydrometallurgy*, **74**, 9-19, 2004.
2. V. S. Talanov, G. G. Talanova, and R. A. Bartsch, "New Proton-Ionizable, Cesium-Selective Calix 4 arene-bis(crown- 6-ethers) with Markedly Enhanced extraction Dfficiency," *Tetrahedron Lett*., **41**, 8221-8224.
3. V. J. Huber, S. N. Ivy, J. Lu, and R. A. Bartsch, "Lariat Ethers with a Novel Proton-Ionizable Group. Synthesis and Solvent Extraction of Alkali Metal Cations," *J. Chem. Soc., Chem. Commun.*, 1499-1500 (1997).

LIQUID-LIQUID EXTRACTION STUDIES WITH BIS-β-DIKETONES

Marco Wenzel,[1] David J. Bray,[2] Jack K. Clegg,[2] Kerstin Gloe,[1] Karsten Gloe,[1] Leonard F. Lindoy,[2] and George V. Meehan[3]

[1]Department of Chemistry and Food Chemistry, TU Dresden, 01062 Dresden, Germany. [2]School of Chemistry, University of Sydney, Sydney, NSW 2006, Australia. [3]School of Pharmacy and Molecular Sciences, James Cook University, Townsville QLD 4811, Australia. Corresponding author email address: karsten.gloe@chemie.tu-dresden.de

ABSTRACT

1,4- (H_2L^1) and 1,3-phenylene (H_2L^2) linked bis-β-diketone ligands as well as corresponding metal complexes of composition $M_3(L^1)_3B_6$ and $M_2(L^2)_2B_2$ with B = pyridine (Py) or 4-ethylpyridine (EtPy) have been synthesized. Extraction studies involving the systematic variation of the metal, bis-β-diketone, and 4-ethylpyridine concentrations have been performed for Co(II) and Zn(II) in order to probe the solution stoichiometries of the extracted species. Significant synergistic effects were observed when EtPy was present along with the bis-β-diketone ligand in the organic ($CHCl_3$) phase. Competitive extraction studies (water/chloroform) demonstrated a clear uptake preference for Cu(II) over Co(II), Ni(II), Zn(II), and Cd(II).

INTRODUCTION

β-Diketones represent a versatile class of chelating ligands whose utility for metal extraction has been appreciated for many years [1,2]. However, bis-β-diketones, where two such chelating functions are linked by different spacer groups, have received considerably less attention, even though individual examples of the latter have been known for a considerable time. Further, it is only recently that such ditopic systems have been used as building blocks for new metallo-supramolecular assemblies [3].

The studies reported here are focussed on both the extraction of the metal ions Co(II), Ni(II), Cu(II), Zn(II), and Cd(II) with the aryl-linked bis-β-diketone ligands H_2L^1 and H_2L^2 (with R = Me, Et, *t*-Bu, hexyl, octyl, and nonyl) and on the structural aspects of the complexes with both ligand types. The goal of these experiments was to probe preferred structure-extraction relationships and synergistic effects for the ligand/metal ion systems investigated.

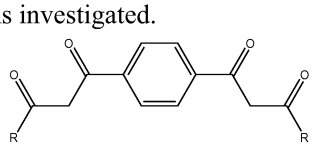

H_2L^1

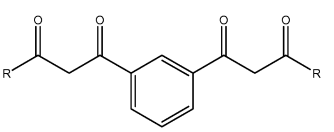

H_2L^2

EXPERIMENTAL

Ligands of types H_2L^1 and H_2L^2 with R = Me, Et, Pr, *t*-Bu, hexyl, octyl, nonyl and Ph were prepared using the previously reported method [4]. The crystalline metal complexes $[Ni_3(L^1)_3(Py)_6]\cdot 3.5Py$ (R = *t*-Bu; Py = pyridine) and $[Zn_2(L^2)_2(EtPy)_2]$ (R = Me; EtPy = 4-ethylpyridine) were also synthesized as reported previously [4-6]. All structural data were collected on a Bruker-Nonius APEX2-X8-FR591 diffractometer employing graphite-monochromated Mo-Kα radiation.

The extraction experiments were performed at 24 ± 1 °C in microcentrifuge tubes (2 mL) with a 1:1 phase ratio $V_{(org)}$:$V_{(aq)}$ (500 μL each). The aqueous phases contained the metal perchlorate and a selected zwitterionic buffer system (TAPS/NaOH, HEPES/NaOH, or MES/NaOH). The $CHCl_3$ phase contained a known concentration of H_2L^1 or H_2L^2 and in some experiments also EtPy. All extraction experiments involved the mechanical shaking of the two-phase system until equilibrium had been established. In the case of the single-metal ion experiments, a shaking time of 3 h was used for the Co(II) experiments and 30 min. for the Zn(II) experiments. The phases were separated, centrifuged, and then duplicate 100 μL samples were removed for analysis.

Concentrations were measured in both phases radiometrically using ^{60}Co and ^{65}Zn radioisotopes (ROTOP Pharmaka) by means of a NaI (TI) scintillation counter (Cobra II/Canberra-Packard) [7,8]. The competitive extraction experiments employed a shaking time of 24 h, and the depletion of the metal ion concentrations in the aqueous phase was measured using an ICP-MS (ELAN 9000/Perkin Elmer) spectrometer. Ligand-dependence studies were performed in which the concentrations of H_2L^1 or H_2L^2 were varied (5×10^{-4} to 1.5×10^{-3} M) while the Zn(II) concentration (1×10^{-4} M) was maintained constant. Similar experiments were carried out in the presence of EtPy (2×10^{-3} M) for both Co(II) and Zn(II). In each case, log D_M was plotted against log $[H_2L^1]_{org}$ or log $[H_2L^2]_{org}$ and the slope determined. EtPy dependence studies (2×10^{-4} to 2×10^{-3} M) were also carried out. Log D_M was then plotted against log $[EtPy]_{org}$ and the slope determined. A series of experiments were also performed in which the metal ion concentration (1×10^{-4} to 5×10^{-3} M) was varied both in the absence and presence of EtPy (2×10^{-3} M) while maintaining the ligand concentration (1×10^{-3} M) constant. From the observed maximum metal loading of the organic phase, the stoichiometry of the extracted complex can be deduced [9]. Multi-metal competitive extractions were also performed using an equimolar mixture of Co(II), Ni(II), Cu(II), Zn(II), and Cd(II).

RESULTS AND DISCUSSION

Extraction Studies

The extraction of Co(II) and Zn(II) using H_2L^1 with R = Pr, *t*-Bu, hexyl, octyl and nonyl has been performed. Parallel sets of extractions were carried out both in the absence and presence of EtPy, and the results are summarized in Figure 1a. At pH 8.7 in the absence of EtPy, Co(II) extraction is negligible (≤2%) for each member of the above ligand series, while the range towards Zn(II) falls between 2 and 35%. As expected, the more lipophilic ligand derivatives give rise to enhanced extraction. On addition of two

equivalents (relative to H_2L^1) of EtPy, the extraction of Co(II) was markedly enhanced (from ~2 to 26%) in the case of H_2L^1 (R = nonyl) and also enhanced from 35 to 61% for Zn(II) with this ligand. Further, the time for equilibrium to be reached in the case of Co(II) was also approximately halved (from three to one and a half hours). Parallel "control" experiments with EtPy in the absence of H_2L^1 gave a metal extraction ≤1%. Similar graded extraction results for Co(II) and Zn(II) were obtained with H_2L^2 (R = Pr, *t*-Bu, octyl and nonyl) (Figure 1b) under identical conditions. However, the extraction of both metal ions with the more lipophilic derivatives of H_2L^2 (namely, with R = octyl, nonyl) is significantly higher, as also occurs for the analogous H_2L^1 ligands.

These systems show no significant metal extraction below pH 6, both in the presence and absence of EtPy, and thus, stripping may be achieved at aqueous pH < 6.

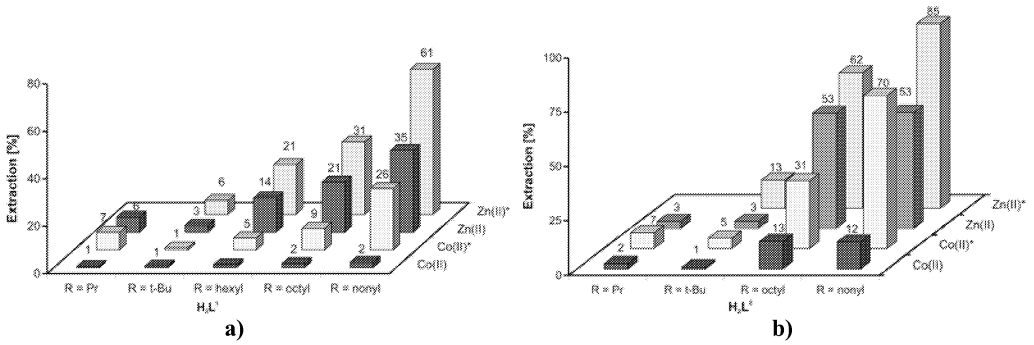

Figure 1. Percentage of metal ion extracted by a) H_2L^1 (R= Pr, *t*-Bu, hexyl, octyl, nonyl); b) H_2L^2 (R= Pr, *t*-Bu, octyl, nonyl), and on the addition of EtPy(*). $[M(ClO_4)_2] = 1 \times 10^{-4}$ M, pH = 8.7 (TAPS/NaOH buffer); $[H_2L^1] = 1 \times 10^{-3}$ M, [EtPy] = 2×10^{-3} M in $CHCl_3$ (*).

To probe the composition of the extracted complexes, three sets of experiments were performed. Studies to investigate the extraction dependence on the concentration of the bis-β-diketone ligand (with and without EtPy present) or on the concentration of EtPy in the organic phase were undertaken. The stoichiometries of the extracted species were then deduced from the slopes of the plots of log D_M vs. log $[H_2L]_{(org)}$ and log D_M vs. log $[EtPy]_{(org)}$, respectively. The slopes obtained for the Zn(II) extraction with the two bis-β-diketone ligands and EtPy are given in Table 1. The data show only small difference between the two sets of conditions. In the absence of EtPy, H_2L^1 forms only a 1:2 (M:L) complex in the organic phase, whereas for H_2L^2, the evidence appears consistent with the likely formation of both 1:1 and 1:2 (M:L) species. In contrast, the presence of EtPy clearly favors the formation of 1:2:1 (M:L:EtPy) complexes for both ligands.

Table 1. Slopes for the variable H_2L^1, H_2L^2 (R = nonyl), and EtPy extraction of Zn(II).

Concentration varied	Slopes in different systems			
	H_2L^1	H_2L^1 + EtPy	H_2L^2	H_2L^2 + EtPy
Ligand	2.0	1.9	1.6	1.9
EtPy	0.8	-	0.7	-

In order to gain further information about complex composition, organic-phase loading experiments at varying metal concentrations in the aqueous phase were carried

out both in the presence and absence of EtPy. Under these conditions, maximum metal-to-ligand ratios of 1.0 and 0.6 in respectively the absence and presence of EtPy were obtained for both ligands H_2L^1 and H_2L^2 (R = nonyl). Clearly, each of these ligand types prefers a 1:1 (M:L) stoichiometry in the absence of EtPy (more likely with an actual stoichiometry of $M_3(L^1)_3$ in the case of H_2L^1 and $M_2(L^2)_2$ in the case H_2L^2, as observed in the corresponding X-ray structures). In the presence of EtPy, the observed metal-to-ligand ratio of 0.6 points to a significant change in the stoichiometry of the extracted species. Thus, the coordination of the EtPy co-ligand apparently leads to the extraction of 1:2:1 (M:L:EtPy) species into the organic phase. A summary of the different types of Zn(II) species extracted by H_2L^1 and H_2L^2, based on the present extraction and structural results (see the next section), is given in Figure 2. In competitive extraction experiments of Co(II), Ni(II), Cu(II), Zn(II), and Cd(II) (each 1×10^{-4} M) with H_2L^1 and H_2L^2 (1×10^{-3} M; R = *t*-Bu, octyl, nonyl), a pronounced selectivity for Cu(II) ($E > 95\%$) over the remaining metal ions ($E < 35\%$) was observed.

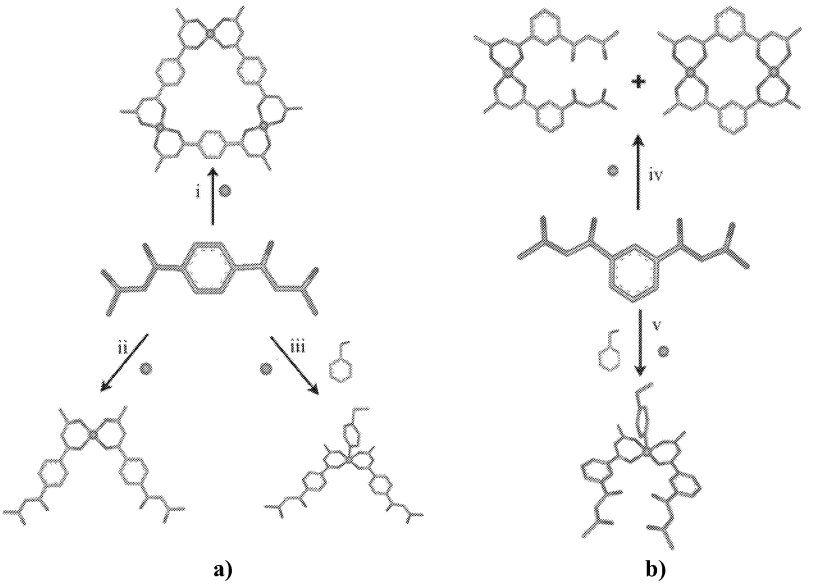

Figure 2. Proposed major species formed in the liquid-liquid extraction studies a) by H_2L^1 (i) on metal ion saturation of the organic phase; (ii) with excess ligand present in the organic phase; and (iii) in the presence of EtPy when ether an excess of ligand is present or metal ion saturation has occurred in the organic phase; b) by H_2L^2 (iv) in the absence of 4-ethylpyridine, both 1:1 and 1:2 (M:L) complexes occur (v) in the presence of 4-ethylpyridine a 1:2 (M:L) complex appears to be the major extracted species in all cases.

Structural Studies

The X-ray structure of H_2L^1 (R = *t*-Bu) is shown in Figure 3 and reveals that the β-diketone fragments are essentially in the same plane as the central phenylene core. The β-diketone groups exist in their enol form, which favors metal ion binding. In contrast to the structure of H_2L^2 (R = *t*-Bu), in which the hydrogens were located on the oxygens

closest to the phenylene ring [10], in the present structure, the enol hydrogen atoms are located on the oxygens (O(1)) farthest from the central phenylene ring.

As observed previously for a related system [11], the X-ray structure of the Ni(II) complex $[Ni_3(L^1)_3(Py)_3]\cdot 3.5Py$ (R = *t*-Bu) is characterized by a triangular arrangement and shows that each nickel center adopts a tetragonally-distorted octahedral geometry in which the pyridine ligands occupy axial sites (Figure 3b). In contrast, the Zn(II) complex $[Zn_2(L^2)_2(EtPy)_2]$ (R = Me) possesses a dinuclear arrangement in which each metal center is five-coordinated, with the Zn(II) centers exhibiting distorted trigonal-bipyramidal geometries (Figure 3c); the axial 4-ethylpyridine groups on the zinc centers lie on opposite sides of the metallocycle.

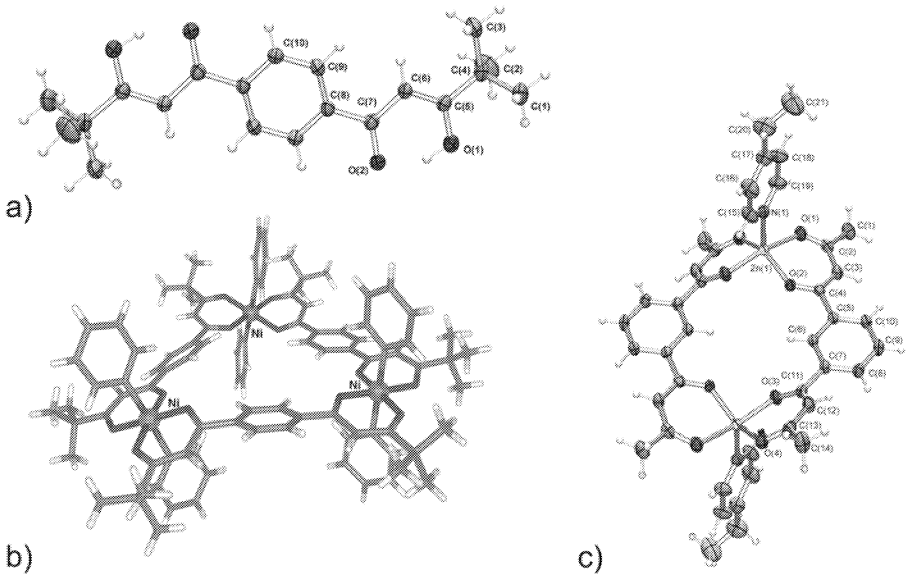

Figure 3. Molecular Structures of a) H_2L^1 (R = *t*-Bu), b) $[Ni_3(L^1)_3(Py)_6]\cdot 3.5Py$ (R = *t*-Bu) and c) $[Zn_2(L^2)_2(EtPy)_2]$ (R = Me) shown with 50% probability ellipsoids.

CONCLUSIONS

The results from the present investigations are consistent with the present bis-β-diketone reagents forming neutral tri- (with H_2L^1) and dinuclear (with H_2L^2) complexes with some or all of Co(II), Ni(II), Cu(II), and Zn(II), where additional pyridine molecules are bound in axial sites to complete the coordination spheres of the corresponding metal ions. This appears to be a characteristic of these systems that yields enhanced extraction of the metal ions investigated.

The liquid-liquid extraction studies collectively show that the stoichiometries of the extracted species clearly depend on both the relative concentrations of the metal and ligand species as well as on their respective natures. As expected, enhanced metal extraction efficiencies in general occur for the more lipophilic ligand derivatives. For these, the extraction of Co(II) and Zn(II) is slightly improved in the case of the 1,3-phenylene linked ligands in comparison with the 1,4-phenylene ones. It is interesting to

note that, under comparable conditions, both significantly exceed the extraction efficiency of structurally related mono-β-diketones.

An interesting feature of the present results is that for both lipophilic H_2L^1 and H_2L^2, substantial extraction synergism is obtained on addition of 4-ethylpyridine to the respective ligand/metal ion systems.

Finally, it is noted that competitive metal ion studies (water/chloroform) indicate a clear preference for Cu(II) extraction over Co(II), Ni(II), Zn(II), and Cd(II) when equal concentrations of these ions are also present in the aqueous phase.

ACKNOWLEDGMENTS

The authors thank the Deutsche Forschungsgemeinschaft and the Australian Research Council for support.

REFERENCES

1. P. A. Tasker, P. G. Plieger, and L. C. West, in Comprehensive Coordination Chemistry II, J. A. McCleverty and T. J. Meyer, Eds., Elsevier, Oxford, Vol. 9, 2004; pp. 759-808.
2. J. Rydberg, G. R. Choppin, C. Musikas, and T. Sekine, in Solvent Extraction Principles and Practices, J. Rydberg, M. Cox, C. Musikas, and G. R. Choppin, Eds., Marcel Dekker, New York, 2004; pp. 109-201.
3. D. J. Bray, J. K. Clegg, L. F. Lindoy, and D. Schilter, *Adv. Inorg. Chem.,* **59**, 1-57 (2006).
4. J. K. Clegg, L. F. Lindoy, B. Moubouraki, K. S. Murray, and J. C. McMurtrie, *Dalton Trans.*, 2417-2423 (2004).
5. J. K. Clegg, K. Gloe, M. J. Hayter, O. Kataeva, L. F. Lindoy, B. Moubaraki, J. C. McMurtrie, K. S. Murray, and D. Schilter, *Dalton Trans.*, 3977-3984 (2006).
6. J. K. Clegg, D. J. Bray, K. Gloe, K. Gloe, M. J. Hayter, K. A. Jolliffe, G. A. Lawrance, G. V. Meehan, J. C. McMurtrie, L. F. Lindoy, and M. Wenzel, *Dalton Trans.*, 1719-1730 (2007).
7. K. Gloe and P. Mühl, *Isotopenpraxis,* **19**, 257-26 (1983).
8. H. Stephan, S. Juran, B. Antonioli, K. Gloe, and K. Gloe, in Analytical Methods in Supramolecular Chemistry, Ch. Schalley, Ed., Wiley-VCH, Weinheim, 2006; pp. 79-103.
9. Y. Marcus and A. S. Kertes, Ion Exchange and Solvent Extraction of Metal Complexes, Wiley, London, 1969; pp. 480-487.
10. J. K. Clegg, L. F. Lindoy, J. C. McMurtrie, and D. Schilter, *Dalton Trans.*, 857-864 (2005).
11. D. V. Soldatov, A. S. Zanina, G. D. Enright, C. I. Ratcliffe, and J. A. Ripmeester, *Cryst. Growth Des.*, **3**, 1005-1013 (2003).

4,5-BIS(DIPHENYLPHOSPHINOYL)-1,2,3-TRIAZOLE: A NOVEL LIGAND FOR METAL EXTRACTION

H. Mukai,[1] S. Kobayashi,[1] S. Butoh,[1] S. Ikegami,[1] A. Minami,[1] Y. Maruyama,[1] Y. Matsuo,[1] J. Murakami,[1] S. Mae,[1] T. Sasamori,[2] N. Tokitoh,[2] and S. Trofimenko[3]

[1]Department of Chemistry, Kyoto University of Education, Fukakusa-Fujinomori, Fushimi, Kyoto, Japan, 612-8522. [2]Institute for Chemical Research, Kyoto University Uji, Kyoto, Japan, 611-0011. [3]Department of Chemistry and Biochemistry, University of Delaware, Newark, DE, USA, 19716.
Corresponding author email address: mukai@kyokyo-u.ac.jp

ABSTRACT

4,5-Bis(diphenylphosphinoyl)-1,2,3-triazole (BDPPTA) is a new chelating agent with the N,O or O,O chelating donor atoms. The extraction behaviors of the divalent metal ions of Mn, Co, Ni, Cu, Zn, Cd, and Pb into chloroform with BDPPTA have been investigated. The metal ions examined are extracted quantitatively in the region of relatively low pH. The pH half values and extraction constants of these systems were collected. The extracted species were estimated to be a binuclear or mononuclear complex with N,O coordination, which is also supported by the X-ray structural analyses of single crystals.

INTRODUCTION

The nitrogen atoms in azole rings such as imidazole and pyrazole are potential donor atoms for complex formation with metal ions. Poly(pyrazolyl)borates which have 1,2-diazolyl rings in their structures are known to be versatile ligands [1]. The use of the compounds as chelating agents for metal ions in solvent extractions is also successful [2]. In particular, an extractant with isopropyl groups at the 3-position of the 1,2-diazolyl rings has displayed very high selectivity for Cu(II) and Zn(II) due to the interligand steric repulsion between the bulky isopropyl groups [3].

A novel azole compound, 4,5-bis(diphenylphosphinoyl)-1,2,3-triazole (BDPPTA), which has a 1,2,3-triazole ring as a main body in its structure, was synthesized [4]. As this azole compound has two $P(O)Ph_2$ groups at the 4- and 5-positons of the 1,2,3-triazole ring, it can combine with a metal ion by either an N,O- or an O,O-chelation mode. Therefore, BDPPTA is a distinctive chelating agent with two chelation modes. Although poly(pyrazolyl)borates always behave as anions, BDPPTA behaves as a monoprotic weak acid by the dissociation of its proton at the 2-position of the 1,2,3-triazole ring. BDPPTA can be used as an extractant even under harsh conditions, because it is thermally, oxidatively, and hydrolytically very stable.

In order to evaluate the usefulness of this novel reagent as an extractant, the extraction behaviors of divalent metal ions into chloroform with BDPPTA have been investigated for Mn, Co, Ni, Cu, Zn, Cd, and Pb. The fraction extracted (*%E*) of the metal ions, the compositions of the extracted complexes, and their extraction constants (K_{ex}) were examined. The structures of the ligand and its metal complexes in single crystals were investigated by X-ray crystallography in order to estimate the donor atoms and the chelation mode of the extracted complexes.

EXPERIMENTAL

Reagents and Apparatus

BDPPTA ($C_{26}H_{21}N_3O_2P_2$) was synthesized and refined as white crystals from bis(diphenylphosphinoyl)acetylene and NaN_3 by the literature method [4]. All other chemicals were of reagent grade. Water was distilled and demineralized.

The concentrations of BDPPTA were measured with a Shimadzu UV-160A UV-visible recording spectrophotometer. Metal concentrations were measured with a Hitachi Z-6100 polarized Zeeman atomic absorption spectrophotometer. The pH measurement was made with a TOA HM-60S pH meter equipped with a glass electrode. The aqueous and organic phases were shaken with a TAITEC Bio-Shaker BR-40L.

The lattice parameters and intensity data were measured on a Rigaku Saturn70 CCD system with VariMax Mo Optic using Mo Kα radiation (λ = 0.71070 Å). The structure was solved by direct method (SHELXS-97) and refined by full-matrix least-squares procedures on F2 for all reflections (SHELXL-97). All non-hydrogen atoms were refined anisotropically. All hydrogen atoms were placed using AFIX instructions.

Distribution of the Ligand

An aqueous solution containing 0.01 mol dm^{-3} sodium acetate or a Good's buffer (MOPS, MES, or TAPS) as a pH buffer and 0.1 mol dm^{-3} potassium chloride to give an ionic strength of 0.1 was prepared. A 10 mL aliquot of the aqueous solution was adjusted to the desired pH (pH > 6) with hydrochloric acid or sodium hydroxide and shaken with an equal volume of a chloroform solution containing 2×10^{-4} mol dm^{-3} BDPPTA in a 30 mL glass-stoppered centrifuge tube for 30 min. by a thermostatic mechanical shaker at 25 ± 1 °C. The shaking time of 30 min. was found to be long enough for equilibration. After centrifugation, the pH of the aqueous phase was measured and taken as the equilibrium values. The concentrations of the ligands in both the aqueous and the organic phases were determined by spectrophotometry.

If the pH levels of aqueous phases were less than 6, the following procedure to concentrate BDPPTA in an aqueous phase was adopted. A 110 mL aliquot of the aqueous solution was shaken with a 10 mL aliquot of a chloroform solution containing 1×10^{-2} mol dm^{-3} BDPPTA in a 200 mL separatory funnel for 30 min. After centrifugation in centrifuge tubes, a 50 mL or 100 mL aliquot of the aqueous phase, after being acidified, was shaken with a 10 mL or 5 mL aliquot of chloroform to transfer all of the ligand into the chloroform. The concentration of the ligand in the chloroform solution was to be 5,

10, or 20 times higher than that in the aqueous phase at equilibrium. The concentration in the organic phase was determined after a 25-fold dilution by chloroform.

Extraction of Metal Ions

Aqueous solutions containing 2×10^{-5} mol dm^{-3} divalent metal ions, 0.01 mol dm^{-3} sodium acetate as a buffer component, and 0.1 mol dm^{-3} potassium chloride for Mn, Co, Ni, Cu, and Zn, or 0.1 mol dm^{-3} sodium perchlorate for Cd and Pb to make the ionic strength constant were prepared. A 10 mL aliquot of each aqueous solution was adjusted to the desired pH with a hydrochloric acid or sodium hydroxide solution and shaken with an equal volume of chloroform containing the 5.0×10^{-5} mol dm^{-3} BDPPTA in a 30 mL glass-stoppered centrifuge tube at 25 ± 1 °C. After centrifugation, the pH of the aqueous phase was measured and taken as an equilibrium value. The concentrations of metal ions in the aqueous phase and in a 0.1 mol dm^{-3} hydrochloric acid (1 mol dm^{-3} HCl for Ni) solution by which the metal ions in the organic phase had been stripped were determined. The shaking times for the extraction and stripping were 0.5 h in extractions and 0.5 h in stripping for Mn, Zn, and Pb, 1 h and 0.5 h for Co, Cu, and Cd, and 4 h and 2 h for Ni, which were found to be long enough for equilibration. The sum of the metal concentrations in the two phases agreed well with the initial concentration in each case.

Syntheses of the Complexes

Twenty mL of ethanol containing 8.0×10^{-3} mol dm^{-3} BDPPTA was mixed with the same volume of the aqueous solution containing 1.0×10^{-2} mol dm^{-3} $Co(NO_3)_2$, $Ni(NO_3)_2$, or $Cu(NO_3)_2$. To the mixed solution, 1.0×10^{-3} mol dm^{-3} KOH was added to precipitate the complex. The precipitations were refined by recrystallization from mixed solutions of dichloromethane and cyclohexane. The single crystals of the Co and Ni complexes for X-ray diffraction were obtained by the slow recrystallization from dichloromethane-xylene mixed solutions at room temperature. The single crystal of the Cu complex was from a 2-propanol-1,2-dichloroethane mixed solution. That of BDPPTA was obtained from a mixed solution of dichloromethane and benzene.

RESULTS AND DISCUSSION

Properties of BDPPTA

The molar absorption coefficients of BDPPTA were found to be 2870 mol^{-1} dm^3 cm^{-1} (267.6 nm) in chloroform, 2622 (267.3 nm) in dichloromethane, 2480 (266.7 nm) in ethanol, and 1826 (273.0 nm) at pH 11.6 in water. The saturated concentrations at 25 °C were 1.6×10^{-2} mol dm^{-3} in chloroform, 1.0×10^{-2} in dichloromethane, and 9.4×10^{-3} in ethanol. Figure 1 shows the pH dependence of the logarithms of the distribution ratios of BDPPTA between chloroform and water. The acid dissociation constant, K_a, and partition constant of BDPPTA(HL), P_{HL}, were obtained as $pK_a = 3.75 \pm 0.02$ and $\log P_{HL} = 3.39 \pm 0.01$ by curve fitting of Equation 1 to the experimental plot by a least-square method as shown in Figure 1. BDPPTA is a weak acid with a relatively low pK_a value.

$$\log D = \log P_{HL} - pH - \log (10^{-pH} + K_a) \quad (1)$$

As shown in Figure 2, BDPPTA can coordinate to a metal ion by an N,O-chelation mode. The N-O distance and the torsion angle of N-C-P-O were observed to be 2.839 Å and 4.3°, respectively. An O,O-chelation mode might be also possible by the rotation around a C-P bond axis that binds a phosphinoyl group to an azole ring.

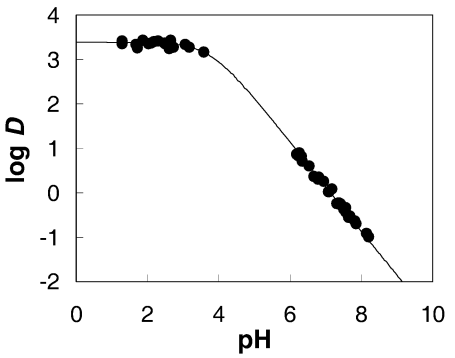

Figure 1. The pH dependence of log *D* of BDPPTA between $CHCl_3$ and H_2O.

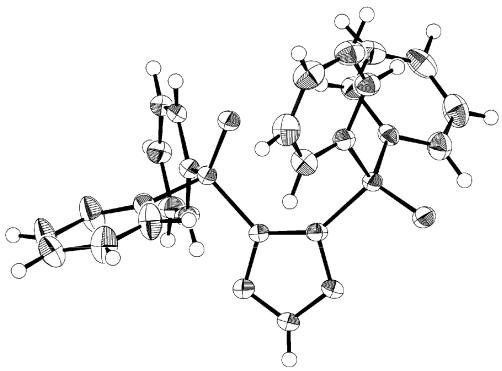

Figure 2. ORTEP plot of the structure of BDPPTA.

Extraction of MetalS

The dependence of the fraction of the metal ions extracted (*%E*) on pH was examined for the seven divalent metal ions of Mn, Co, Ni, Cu, Zn, Cd, and Pb (Figure 3).

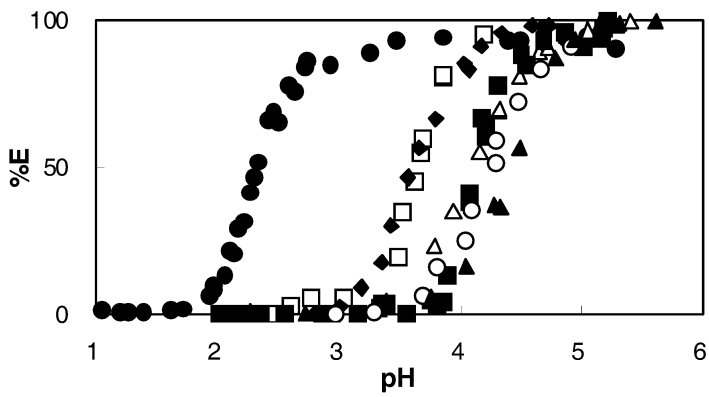

Figure 3. The fraction extracted of metal ions as a function of pH. Black circles, Cu^{2+}; open squares, Ni^{2+}; black rhombuses, Cd^{2+}; open triangles, Pb^{2+}; black squares, Co^{2+}; open circles, Mn^{2+}; black triangles, Zn^{2+}.

Quantitative extractions were achieved below pH 5 for all metal ions. A high selectivity for Cu was observed as usual. For transition elements, the order of the

extractability is Cu > Ni > Co > Mn, which follows the Irving-Williams series in stability constants. For typical elements, the order is Cd (109 pm) > Pb (133 pm) > Zn (88 pm), in which the values in the parentheses show the ionic radii of divalent ions in crystals with the coordination number of 6 [5]. The ionic radius does not seem to be the main determinant of the extractability.

The extracted species in each system were elucidated by the slope analysis of the dependence of the logarithm of the distribution ratio, log D, on pH and the concentrations of metal ions, the ligand, and a hydroxide ion in the aqueous phase. Three types of the extracted species, ML_2, ML_2HL, and M_2L_3OH, were found.

The experiments of the dependences on metal concentrations show that, in the case of Cu and Co, binuclear complexes exist in the organic phase, because the slopes of log D vs. log $[M^{2+}]$ plots are about 1. It suggests that at least one ligand molecule is a bridge between the two metal ions using its donor N or O atoms. For Cu and Co, the following equations are concluded. The slope analysis concerning the dependence on the ligand concentration and pOH were consistent with Equation 2.

$$2M^{2+} + 3HL_o + H_2O \rightleftharpoons M_2L_3OH_o + 4H^+ \quad (2)$$

$$\log K_{ex} = \log D - \log [M^{2+}] - 4\,\mathrm{pH} - 3 \log [HL]_o \quad (3)$$

$$[HL]_o = C_{HL}P_{HL}/(1 + P_{HL} + K_a 10^{pH}) \quad (4)$$

where C_{HL} is the initial concentration of HL in the organic phase, and subscript o denotes the species in the organic phase. From Equations 3 and 4 the extraction constants, K_{ex}, were obtained for these metal ions.

Mononuclear complexes were observed as usual in other extraction systems except for those of Cu and Co. From the dependence of log D on the ligand concentration, the extracted species of Cd was concluded to be ML_2HL_o, the reaction formula of which is expressed by Equation 5.

$$M^{2+} + 3HL_o \rightleftharpoons ML_2HL_o + 2H^+ \quad (5)$$

$$\log K_{ex} = \log D - 2\,\mathrm{pH} - 3 \log [HL]_o \quad (6)$$

Table 1. The summary of pH half-values and extraction constants

Metal Ion	Extraction Time/h	Stripping Time/h	Ionic Strength	$pH_{1/2}$*	Extracted Species	log K_{ex}
Mn^{2+}	0.5	0.5	0.1 (KCl)	4.22	ML_2	-3.78 ± 0.15
Co^{2+}	1	0.5	0.1 (KCl)	4.13	M_2L_3OH	-4.59 ± 0.13
Ni^{2+}	4	2	0.1 (KCl)	3.63	ML_2	-2.55 ± 0.16
Cu^{2+}	1	0.5	0.1 (KCl)	2.35	M_2L_3OH	2.69 ± 0.20
Zn^{2+}	0.5	0.5	0.1 (KCl)	4.40	ML_2	-4.29 ± 0.13
Cd^{2+}	1	0.5	0.1 ($NaClO_4$)	3.65	ML_2HL	-0.45 ± 0.08
Pb^{2+}	0.5	0.5	0.1 ($NaClO_4$)	4.12	ML_2	-3.65 ± 0.15

*5.0×10^{-5} mol dm^{-3} BDPPTA in chloroform.

For other metal ions, popular 1:2 metal-ligand complexes were observed.

$$M^{2+} + 2HL_o \rightleftharpoons ML_{2,o} + 2H^+ \quad (7)$$

$$\log K_{ex} = \log D - 2\,pH - 2 \log [HL]_o \quad (8)$$

Structures of the Complexes

For Cu(II), Co(II), and Ni(II), single crystals were obtained. The structures of these complexes were examined by X-ray diffraction methods. The complexes examined are all multinuclear: an M_2L_4-type complex for Cu and M_3L_6-type for Co and Ni, as shown in Figure 4. Only the N,O-chelation mode was observed in the crystals examined. Water molecules are attached to metal ions in Co and Ni complexes as shown in Figure 4. These results seem to support the possibility of the existence of binuclear complexes with OH^- in the organic phase that were observed in the solvent extraction systems.

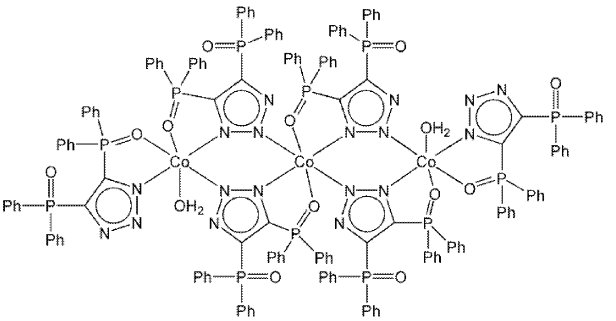

Figure 4. Molecular structure of $Co_3L_6(H_2O)_4$. Two water molecules are omitted for clarity.

CONCLUSIONS

The divalent metal ions of Mn, Co, Ni, Cu, Zn, Cd, and Pb can be quantitatively extracted into chloroform with BDPPTA below pH 5, which indicates that this reagent is effective for the extraction of metal ions from acidic media. For Cu, Co, and Ni, N,O coordination was suggested by X-ray crystallographic results. For Cu and Co, multinuclear complexes were observed in both solvent extraction systems and crystals.

REFERENCES

1. S. Trofimenko, Scorpionates—The Coordination Chemistry of Polypyrazolylborate Ligands, Imperial College Press, London, 1999.
2. T. Kitano, H. Wada, H. Mukai, K. Ueda, and Y. Sohrin, "Separation of Transition Metals with Poly(pyrazolyl)borates by Solvent Extraction Technique," *Anal. Sci.*, **17**(Supplement), i1113-i1116 (2001).
3. T. Kitano, Y. Sohrin, Y. Hata, H. Mukai, H. Wada, and K. Ueda, "Highly selective extraction of Cu(II) and Zn(II) using $[B(3\text{-iPrpz})_4]^-$ (iPrpz=isopropylpyrazolyl)", *Polyhedron*, **23**(2-3), 283-289 (2004).
4. A. L. Rheingold, L. M. Liable-Sands, and S. Trofimenko, "4,5-Bis(diphenylphosphinoyl)-1,2,3-triazole: A Powerful New Ligand That Uses Two Different Modes of Chelation," *Angew. Chem. Int. Ed.*, **39**(18), 3321-3324 (2000).
5. R. D. Shannon, "Revised Effective Ionic Radii and Systematic Studies of Interatomic Distances in Halides and Chalcogenides," *Acta Crystallogr.*, **A32**, 751-767 (1976).

OPTICAL-RESPONSE EXTRACTION OF GOLD(III) BY *cis-trans* PHOTOISOMERIZATION OF BIS(2,2'-DIPYRIDINYL-6-YL)DIAZENE

K. Takeshita, N. Sawai, and Y. Okada

Chemical Resources Laboratory, Tokyo Institute of Technology,
4259 Nagatsuta, Midori-ku,Yokohama 226-8503, Japan.
Corresponding author email address: takeshit@res.titech.ac.jp

ABSTRACT

Optical-response extraction of Au(III) with an azopyridine compound, bis(2,2'-dipyridyl-6-yl)diazene (BDPDA), was studied. The distribution ratio of Au(III) was increased by the configuration change of BDPDA from *trans* to *cis* under UV irradiation (340 nm). However, the distribution ratios under the UV irradiation were less than 3 times those under visible-light (VIS) irradiation (465nm). The difference of distribution ratios under the UV and VIS irradiation is insufficient for practical use. For the further improvement of optical-response extraction, synergistic extraction of Au using a carboxylic acid as a synergist was tested. Octanoic acid was very effective for improving the extraction performance of *cis*-BDPDA and was coordinated mainly with the complex of Au and *cis*-BDPDA, $AuCl_3$(*cis*-BDPDA). In the presence of more than 3 mol/L octanoic acid, the distribution ratio of Au under the UV irradiation reached 10 times that under the VIS irradiation.

INTRODUCTION

Solvent extraction is an important separation technique in the chemical industry and is applied widely to metal recovery, separation of biochemistry materials, removal of environmental pollutants, etc. In industrial-scale solvent-extraction processes, a large amount of chemicals are consumed by the recovery of target materials. The used chemicals are disposed of finally as secondary wastes. If a solvent-extraction process is controlled by external energies, such as heat, light, and ultrasonic waves, instead of chemicals, the amount of chemicals consumed can be reduced. In this study, an optical-response extraction system, in which the extraction performance is changed by the irradiation by UV and VIS (visible) light, is proposed. This extraction system is very useful to suppress the consumption of chemicals.

Figure 1 shows the concept of an optical-response extraction. An optical-response material, whose molecular configuration is changed reversibly by the irradiation of light with different wavelengths, is used as an extractant. The complex formation between the extractant and a target metal is controlled by the induced

configuration change of the extractant. For example, an azo-pyridine compound with functional ligands extracts a metal ion effectively by the configuration change from *trans* to *cis* under the irradiation of UV light and elutes the target metal by the configuration change from *cis* to *trans* under the VIS irradiation. If the target metal is eluted effectively by the VIS irradiation, a large quantity of chemicals is not required in the stripping process. The target metal can be recovered by slightly acidic solution. As a result, the consumption of chemicals will be suppressed largely by the application of the proposed system.

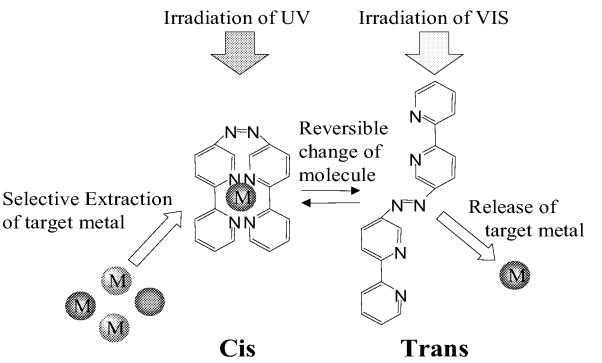

Figure 1. Concept of optical-response extraction.

A similar concept was studied previously by Shinkai and co-workers [1-2]. They synthesized photoresponsive azobis(benzocrown ether)s and tested the selective adsorption of alkaline metals with different ionic diameters. These results indicate that the optical-response extraction is realized principally as a separation technique. However, it is very difficult to apply this concept directly to a metal-separation process, because the change of stability constants by the irradiation of UV and VIS is small. Therefore, these compounds were applicable to functional membranes and chemical sensors such as a light-switched electrode [3]. If the optical-response extraction is considered as a separation technique, new ideas to promote the change of extractability by the photoirradiation are required.

The object of this study is to develop an optical-response extraction system that is applicable as a practical metal separation technique. The optical-response extraction of Au(III) with an azo compound, bis(2,2'-dipyridyl-6-yl)diazene (BDPDA), was examined, and the distribution ratios of Au were measured under UV and VIS irradiation. Four nitrogen donors in BDPDA coordinate selectively with soft metals such as precious metals. The selective extraction of precious metals with BDPDA is expected by the photoirradiation. Furthermore, we tried to promote the optical-response extractability of BDPDA by the introduction of asynergistic extraction system. The synergistic extraction systems using carboxylic acids, heptanoic acid, octanoic acid, and nonanoic acid, as synergists were tested.

EXPERIMENTAL

Synthesis of Optical-Response Extractant

BDPDA was synthesized by an azo-coupling reaction with 6-amino-2,2'-bipyridine (BBPA) in NaClO solution at 2 °C [4-5]. The synthesis scheme is very simple, as shown in Equation 1.

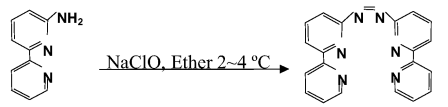

Bis[2,2']bipyridinyl-6-yl-amine(BBPA) BDPDA 1)

BDPDA formed in NaClO solution was extracted into diethylether and purified by recrystallization. BDPDA ($C_{20}H_{14}N_6$) obtained was identified by ES-MS and elementary analysis. ES-MS: *m/z* 339.3. $C_{20}H_{14}N_6$ ($[M + H]^+$) requires 339.37. Anal. Calc. for $C_{20}H_{14}N_6$ (Mw = 338.37): C, 70.94; H,4.17; N,24.84. Found: C, 71.10; H, 4.33; N, 24.57.

Extraction Tests of Au(III) with BDPDA

BDPDA was diluted with chloroform and used as an organic phase. The concentration of BDPDA was adjusted in the range of 10^{-3} to 10^{-5} mol/L. A 5 x 10^{-5} mol/L chloroauric acid ($HAuCl_4$) solution, adjusting the ionic strength and pH with NaCl and HCl, was used as an aqueous phase. A 3 mL sample of the organic solution was placed in a quartz glass cell and exposed to the UV light (340 nm). Then, the same volume of the chloroauric acid solution was added to the cell. The cell temperature was adjusted to 25 ± 1 °C. The organic and aqueous phases were agitated vigorously for 3 h under the UV irradiation. In the preliminary tests, it was confirmed that the agitating time was sufficient for attaining the extraction equilibrium complex. After agitating, the organic and aqueous phases were phase-separated and sampled. The concentration of Au in the aqueous phase was measured by ICP-OES (inductively-coupled plasma optical emission spectrometry). The concentration of Au extracted into the organic phase was evaluated from the mass balance, and the distribution ratio of Au was calculated. The same procedure was done under the VIS irradiation (465 nm), and the extraction of Au was tested.

RESULTS AND DISCUSSION

***Cis-trans* Transformation of BDPDA**

Photoisomerization of BDPDA in chloroform was tested by the irradiation of UV (340 nm) and VIS (465 nm) to a quartz cell. Figure 2 shows the UV-VIS spectra of BDPDA. As shown in Figure 2(a), UV-VIS spectra of BDPDA were measured, and a clear peak was observed at 340 nm. This absorption peak is identified as the UV absorption of pyridyl rings in BDPDA. When BDPDA was

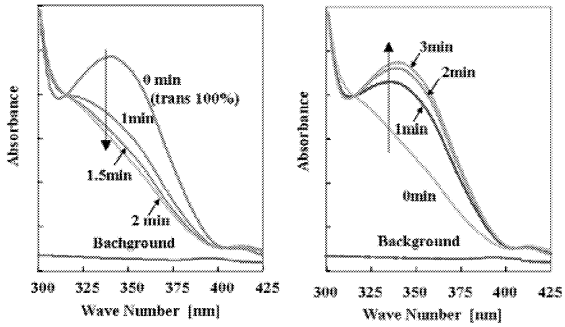

(a) UV irradiation (b) VIS irradiation

Figure 2. UV-VIS spectra of BDPDA under UV and VIS irradiation.

exposed to the UV light, the decrease of peak height was observed for 3 min. Next, when BDPDA is exposed to the visible light, the peak at 340 nm was also recovered completely within 2 min., as shown in Figure 2(b). The change of UV adsorption peak is caused by the photoisomerization of BDPDA, called the *cis-trans* transformation [5]. The *cis-trans* transformation rate of BDPDA is sufficient for practical use. These procedures were repeated 3 times. The photoisomerization of BDPDA was repeated reversibly. From the peak heights at 340 nm before and after the UV irradiation, the isomer ratio of *cis* and *trans* after the UV irradiation was evaluated. The peak height at 340 nm before UV irradiation was assumed as 100% *trans*-BDPDA. These results suggest that half of the *trans*-BDPDA molecules are transformed to the *cis*-isomer by the UV irradiation for 3 min.

Determination of Appropriate pH Value

Before the extraction tests, we evaluated the appropriate pH range for the extraction operation using BDPDA. BDPDA is protonated in a lower pH range and dissolved in the water phase. The distribution of BDPDA between the organic phase and aqueous phase was measured. An organic solution of 10.5 mg/L BDPDA in chloroform was contacted with an aqueous solution adjusted to pH 0 to 4. The volume ratio of the organic solution to the aqueous solution was kept at 1:1. Figure 3 shows the solubility loss of BDPDA to the aqueous solution in the pH range of 1 to 4. The vertical axis corresponds to the concentration of BDPDA in the organic solution. The concentration of BDPDA in the organic solution remained at the initial concentration in the pH range above 2 and decreased with increasing the acidity of aqueous solution in the pH range below 2. The decrease in the BDPDA concentration is due to the protonation of BDPDA. On the other hand, we used chloroauric acid as trivalent gold ion. The chemical structure of chloroauric acid in an aqueous solution can change with pH. In the pH range above 4, chloroauric acid ($HAuCl_4$) is hydrolyzed, and chloride ions in chloroauric acid are replaced with OH^- ions. From these results, the pH value in aqueous solution was adjusted to 3.0 ± 0.1 in all extraction tests. The extraction can be operated simply under the conditions of no dissolution loss of BDPDA to the aqueous solution and no formation of hydrolyzed species of $AuCl_4^-$.

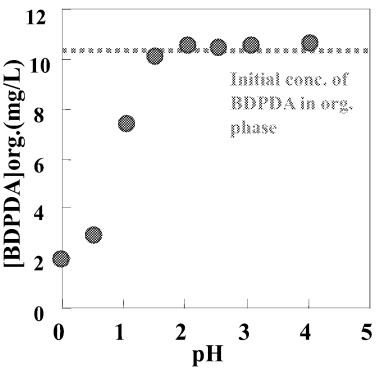

Figure 3. Solubility loss of BDPDA to the aqueous solutions adjusted to pH 0 to 4.

Extraction of Au(III) with BDPDA

Figure 4 shows the results of the extraction tests of Au(III) with BDPDA. The distribution ratio of Au was increased by the configuration change of BDPDA from *trans* to *cis* under the UV irradiation (340 nm); however, the distribution ratios under the UV irradiation were less than 3 times those under the VIS irradiation (465 nm). The number

of BDPDA molecules coordinated with an Au(III) ion was evaluated by slope-analysis technique. A stoichiometric relation for the complex formation of Au with BDPDA is assumed as

$$AuCl_4^-{}_{(a)} + m\ BDPDA_{(o)} \rightleftharpoons AuCl_3(BDPDA)_{m\,(o)} + Cl^-{}_{(a)} \quad (2)$$

where "*m*" denotes the number of coordinated BDPDA molecules. When a relation between log *D* + log [Cl^-] and log [BDPDA] is plotted, the slope represents the m-value, where *D* denotes the distribution ratio of Au(III). From the results of Figure 3, the slopes for the UV and VIS irradiation were evaluated as about 1.1 and 1.4, respectively. These results mean that a 1:1 complex of Au and BDPDA, $AuCl_3$(BDPDA), is formed mainly for the *cis* isomer of BDPDA in the organic phase. On the other hand, for the *trans* isomer, the formation of 1:1 and 1:2 complexes, $AuCl_3$(BDPDA) and $AuCl_3(BDPDA)_2$, should be considered. Furthermore, the relation of the distribution ratio of Au(III) and the concentration of Cl^- in the aqueous phase was shown in Ref. [6]. The slope for the relation between *D* and the activity of Cl^- calculated by the Debye-Huckel equation was evaluated as about −0.8 from the experimental data in Ref. [6]. These results indicate that a Cl^- ion is released from an $AuCl_4^-$ ion, and neutral compounds, $AuCl_3$(BDPDA) and $AuCl_3(BDPDA)_2$, are formed in the organic phase.

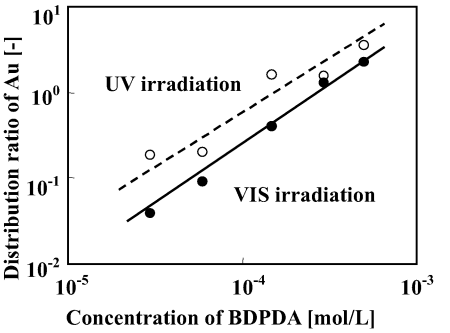

Figure 4. Relation between the distribution ratio of Au(III) and the concentration of BDPDA under UV and VIS irradiation.

Promotion of Optical response Extraction by the Introduction of Synergist

Since the difference between the distribution ratios under the UV and VIS irradiation is not so large, it is difficult to design a practical optical-response system based on the direct extraction of Au with BDPDA. The improvement of the optical-response extractability of BDPDA is therefore required for practical use. Use of hydrophobic anion as a synergist was considered. If a hydrophobic anion instead of chloride ion is coordinated with Au ion, the hydrophobicity of Au-BDPDA complex will be enhanced. As a result, the extraction of Au with BDPDA may be at least in part promoted by the introduction of synergist.

In this study, some carboxylic acids (heptanoic acid, octanoic acid, and nonanoic acid) were tested as synergists. Figure 5 shows the results of optical-response extraction tests using these synergists. The ionic strength was kept at 0.001 m for all experiments. The initial concentration of BDPDA was adjusted to 5 x 10^{-4} mol/L. The effect of the length of alkyl chain on the optical-response extraction is shown in this figure. In the case that chloroform was used as a diluent, octanoic acid alone was effective for improving the extraction performance. As shown in Figure 5(b), the distribution ratio of Au under the UV irradiation increased with increasing concentration of octanoic acid,

especially in the high concentration range over 3 mol/L. The difference between distribution ratios under the UV and VIS irradiation was extended by the addition of octanoic acid. These results indicate that the synergistic effect acts strongly for the complex of Au and *cis*-BDPDA formed under the UV irradiation. As a result, in the presence of more than 3 mol/L octanoic acid, the distribution ratio under the UV irradiation increased to 10 times that under the VIS irradiation. These results indicate that a practical optical-response extraction system of Au can be designed by the introduction of synergistic extraction using a hydrophobic carboxylic acid such as octanoic acid.

CONCLUSIONS

1. *Cis-trans* transformation rate of BDPDA by the irradiation of UV and VIS was fas,t and the equilibrium state for the *cis-trans* transformation was attained within 3 min. The photoisomerization of BDPDA was repeated reversibly. The *cis-trans* transformation rate of BDPDA is sufficient for the practical use. Azo-pyridine compounds such as BDPDA are applicable for optical-response extraction shown in Figure 1.
2. The extraction of Au(III) with BDPDA was promoted by the configuration change of BDPDA from *trans* to *cis* under UV irradiation. The distribution ratios under UV irradiation were larger than those under VIS irradiation. However, the difference between distribution ratios under UV and VIS irradiation was less than 3 times.
3. The optical-response extraction of Au with BDPDA was improved by the introduction of a synergistic extraction system using octanoic acid. In the presence of more than 3mol/L octanoic acid, the distribution ratio of Au under UV irradiation was increased to 10 times that under VIS irradiation. A practical optical-response extraction system can be designed by the introduction of synergistic extraction system using hydrophobic carboxylic acid such as octanoic acid.

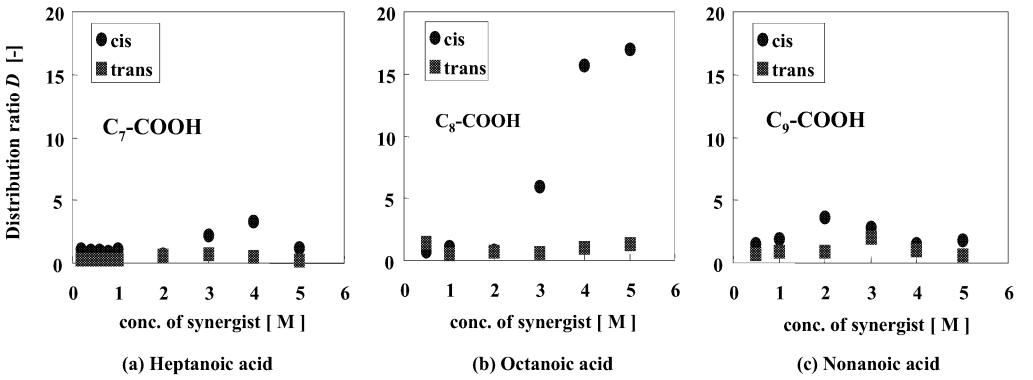

Figure 6. Optical-response extraction tests using carboxylic acids as synergists.

REFERENCES

1. S. Shinkai, T. Mitani, Y. Kusano, and O. Manabe, "Photoresponsive Crown Ethers. 8. Azobenzenophane- Type "Switched-On" Crown Ethers Which Exhibit an All-or-Nothing Change in Ion-Binding Ability," *J. Am. Chem. Soc.*, **105**, 1851-1856 (1983).
2. S. Shinkai, T. Yoshida, O. Manabe, and Y. Fuchita, "Photoresponsive crown ethers. Part 20. Reversible photocontrol of association dissociation equilibria between azobis(benzo-18-crown-6) and diammonium cations," *J. Chem. Soc. Perkin Trans. 1*, 1431-1437 (1988).
3. G. Deng, T Sakaki, Y. Kawahara, and S. Shinkai, "Tunable chemical sensors: Light-switched ion selective electrodes on the basis of a photoresponsive calix[4]arene," *Supramol. Chem.*, **2**, 71-76 (1993).
4. T. F. Chung, Y. M. Wu, and C. H. Cheng, "Reduction of Aromatic Nitro Compounds by Ethylenediamine. A New Selective Reagent for the Synthesis of Symmetric Azo Compounds," *J. Org. Chem.*, **49**, 1215-1217 (1984).
5. S. B. Park and R. F.Standaert, "A Photoregulated Ligand for the Nuclear Import Receptor Karyopherin α," *Bioorg. Med. Chem.*, **9**, 3215-3223 (2001).
6. Y. Okada "Optical-response Extraction of Gold(III) with Bis(2,2'-dipyridinyl-6-yl)diazene," (in Japanese) Masters Thesis, Department of Environmental Science and Engineering, Tokyo Institute of Technology, 2006.

THE POTENTIAL USE OF HYDROCARBON MAGNETIC LIQUIDS IN SOLVENT EXTRACTION

L. L. Vatta,[1] K. R. Koch,[2] and K. C. Sole[1]

[1]*Anglo Research, a division of Anglo Operations Ltd, Johannesburg, South Africa.*
[2]*Department of Chemistry and Polymer Science, University of Stellenbosch, South Africa. Corresponding author email address: lvatta@angloresearch.com*

ABSTRACT

The rate of disengagement of the aqueous and organic phases directly affects throughput time and capital costs of solvent-extraction systems. Using an organic phase containing a magnetic liquid (a stable colloidal suspension of magnetizable nanoparticles in a carrier liquid), an externally applied magnetic field effects more rapid phase disengagement with potentially lower entrainment losses than could be achieved by natural settling under gravitational force alone. The phase-separation rates and chemical properties of systems using a hydrocarbon magnetic liquid containing an extractant (CYANEX 272, D2EHPA, or LIX 984N) are compared with those of conventional systems.

INTRODUCTION

Magnetic liquids comprise a stable colloidal suspension of single-domain ferro- or ferrimagnetic particles (*e.g.*, magnetite, iron, cobalt) in a carrier liquid such as kerosene [1]. Stabilization is imparted to the particles from their size (<10 nm) and by use of a surfactant that prevents them settling out. Magnetic liquids are superparamagnetic: they can be magnetized by an external applied magnetic field but exhibit no hysteresis in their magnetization curve and have zero magnetization at zero applied field [2-3]. This property allows these materials to be used as conventional "unmagnetized" materials, but with the advantage that they can be controlled and transported as required by application of an external applied magnetic field.

In solvent extraction (SX), the rate of disengagement of the aqueous and organic phases directly affects throughput time and capital costs. In most conventional contactors, phase disengagement occurs by gravitational settling. By adding a magnetic component to the organic phase, it was envisaged that phase disengagement time (PDT) could be reduced by application of an external magnetic field. The superparamagnetic property of magnetic liquids allows them to behave as a liquid during extraction but be responsive when exposed to a magnetic field, allowing efficient removal of the magnetic phase from the mixed phases.

Although a magnetic SX process has been patented, only preliminary investigations into the extraction of Cu^{2+} from sulfate and UO_2^{2+} from nitrate media are reported [4-5]. Potential extractants identified for use in combination with a magnetic liquid for more rapid phase separation included oximes, phosphine oxides, and tertiary and quaternary amines [4]. Although little information was given regarding extraction efficiencies, a reduced PDT (60 to 120 times faster than gravitational separation) was observed in the presence of a permanent magnet. Our study of the extraction of $[Co(SCN)_4]^{2-}$ from an aqueous phase onto the surface of bare magnetite and into a magnetic organic phase (magnetic liquid or Aliquat 336 in magnetic liquid) by ion-pair formation, showed that extraction of the cobalt complex increased with an increase in volume of magnetite or magnetic liquid, indicating some interaction of these components (as well as the extractant) with the extracted species [6].

The potential enhancement of PDT was investigated by comparing conventional SX systems with those in which the extractant was incorporated into a magnetic liquid, thereby conferring magnetic properties to the organic phase. The extraction efficiency, selectivity, kinetics, and rate of phase separation were compared in three systems: CYANEX® 272 was used for separation of cobalt and nickel, di(2-ethylhexyl)phosphoric acid (D2EHPA) for zinc extraction, and LIX® 984N for copper extraction.

EXPERIMENTAL METHODS

All reagents and solvents were purchased from commercial sources and were used without further purification. CYANEX 272, D2EHPA, and LIX 984N were supplied by Cytec, Rhodia, and Cognis, respectively. Selected properties of the diluents are given in Table 1. The preparation of the magnetic liquids has been described elsewhere [7].

The three systems investigated are shown in Table 2. Extraction studies were performed in triplicate and were carried out at room temperature. Equal volumes of each phase (50 mL) were contacted in a baffled vessel by overhead stirring for 15 min. under aqueous- and organic-continuous mixing conditions. The phases were allowed to separate (under the influence of an external magnetic field provided by a NdFeB permanent magnet for those samples containing magnetic liquid) and the aqueous fraction analyzed for metal ion concentration by inductively coupled plasma atomic emission spectroscopy. The solution pH was controlled by addition of NaOH for the CYANEX 272 system.

Table 1. Properties of diluents used in this study

Diluent	Abbreviation	Density (g/mL)	Flash point (°C)	Aromatic content (vol %)
Shellsol 2325 (Shell Chemicals)	SS	0.81	87	18
Magnetic liquid prepared using kerosene as the carrier liquid	ML	0.84	38	<5

Table 2. Aqueous- and organic-phase compositions of the three systems studied

System	Aqueous phase[a]	Organic phase[b]
A	5.4 g/L Co, 1.1 g/L Ni	10 vol % CYANEX 272
B	5.2 g/L Zn, 0.9 g/L Ca, 1.1 g/L Co, 1.0 g/L Cu, 1.1 g./L Ni	10 vol % D2EHPA
C	4.8 g/L Cu, 1.1 g/L Co, 1.1 g/L Zn, 1.0 g/L Mn	10 vol % LIX 984N

[a]Made up from the respective sulfate salts. [b]Made up in each of the diluents shown in Table 1.

Conventional techniques for PDT determination rely on optical observation of emulsion band height as a function of time. PDT was determined (after 15 min. stirring) by visually monitoring the time required to achieve clarity of the aqueous phase and was recorded as a function of the interface height. After a 5 min. interval, the phases were remixed for 3 min. and the rate of phase separation remeasured. This was repeated four times to obtain six readings in total. To eliminate potential errors in parallax and possible bias, the PDT was also determined by two alternative methods. For UV-visible absorbance studies, using an Agilent 8453E single-beam diode-array UV-visible spectrophotometer, the organic (1 mL) and aqueous (2 mL) phases were agitated in plastic tubes for 10 s using a vortex mixer. Absorbance measurements of four replicates (repeated five times each) were recorded during phase separation. A second alternative method determined the PDT by inductance, performed with an inductance measuring device manufactured by De Beers Consolidated Mines. Equal volumes of each phase (0.5 mL) were agitated for 20 s in a glass vial using a vortex mixer. Inductance measurements were taken at a fixed sample height after agitation.

RESULTS AND DISCUSSION

Efficiency and Selectivity of Metal Ion Extraction

Table 3 compares metal ion extractions in ML or SS diluents for the three systems under aqueous- and organic-continuous mixing conditions using the mixer-settler system. The magnetic and nonmagnetic extraction systems showed similar extractions of the major metal and selectivity of extraction over the impurity elements. The extraction of Co by CYANEX 272 was in the range 60–76%, Zn by D2EHPA at 42–56%, and Cu(II) by LIX 984N, 68–78%. The CYANEX 272 and LIX 984N ML systems showed a lower, while the D2EHPA system a higher, degree of extraction of the main element compared to the corresponding SS systems. These differences are attributed to an interaction of the extractant molecules with the magnetite surface or coating (similar to that observed previously [6]) and the consequent neutralization of liberated H^+ ions in a complex, and as yet not fully understood, mechanism [7].

Analogous studies of the kinetics and loading capacity of metal extractions showed no measurable differences in the rates or extents of extraction of the main elements in the three systems in the presence of a magnetic diluent compared to the conventional diluent.

Table 3. Influence of magnetic diluent on efficiency and selectivity of extraction

Extractant	Metal	Extraction by SS system (%)		Extraction by ML system (%)	
		Aq. cont.	Org. cont.	Aq. cont.	Org. cont.
CYANEX 272	Co(II)	74 ± 3	76 ± 5	60 ± 4	62 ± 4
	Ni(II)	<2	<6	<1	<1
D2EHPA	Zn(II)	42 ± 1	43 ± 4	50 ± 4	56 ± 2
	Co(II)	<1	<4	<1	17 ± 7
	Ca(II)	6 ± 7	8 ± 6	<12	9 ± 6
	Cu(II)	<1	<1	<1	9 ± 6
	Ni(II)	<1	<1	<1	25 ± 8
LIX 984N	Cu(II)	78 ± 0.2	78 ± 0.1	68 ± 1	69 ± 0.2
	Co(II)	<1	<1	<1	<1
	Zn(II)	<1	<2	<1	<1
	Mn(II)	<3	<3	<1	<1

Rate of Phase Disengagement

Figure 1 shows PDTs determined using the conventional method. In the nonmagnetic (SS) systems, phase separation is shown by decreasing emulsion-band height with time. In the ML systems, no clear emulsion band occurred during phase separation, as the ML was pulled towards the base of the vessel by an external magnetic field. PDT is represented as a single dashed line; for example, in System A (Figure 1a and 1d), the SS PDT was ~60 s, while the ML PDT was ~30 s. PDT was found to improve by 48–86% on the introduction of the magnetic liquid. While the magnitude of the improvement is dependent on specific vessel geometry and magnetic-field strength, proof-of-concept of reduced PDT is validated.

For the PDT studies performed using UV-visible absorbance, 94 and 84% improvements in phase separation were found for CYANEX 272 (Figure 2a) and LIX 984N (Figure 2b), respectively, in ML in contact with water when an externally applied magnetic field was used to effect separation. There was, however, no statistically significant difference in PDT when the magnetic and nonmagnetic phases were contacted with the metal-containing solutions. This was attributed to bubble formation from agitation in the ML systems, which influenced absorbance readings. Inductance measurements were therefore used to further investigate the phase-separation rate in the presence of magnetic liquids.

For the inductance study, samples were placed concentric to a coil through which an electric current was passed, thereby generating a magnetic field. The change in resonance frequency as a result of changes in the coil inductance indicated relative density changes with time; that is, a decrease in induced current indicated that the magnetic phase had settled, allowing for the determination of the PDT. The ML PDT was compared with the SS PDT determined by UV-visible absorbance measurements. An example of the results is given in Figure 3, where the PDT was found to be lower in the LIX 984N ML system by 91%.

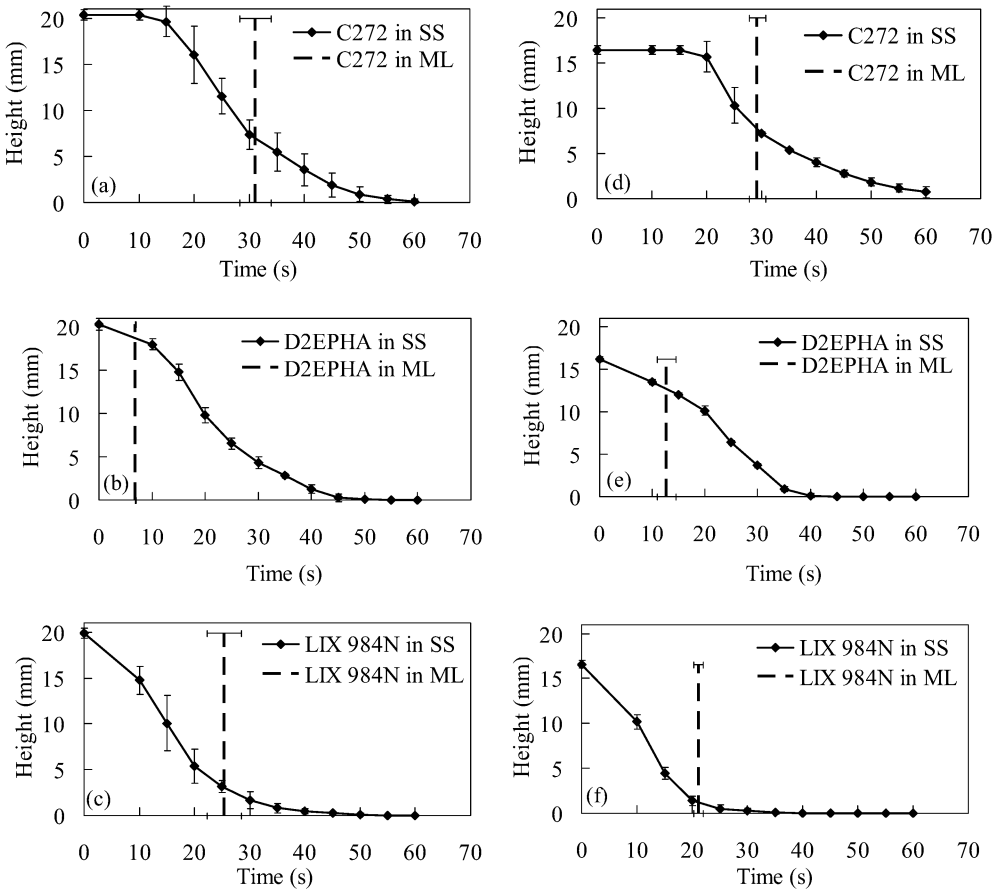

Figure 1. PDT for SS (solid lines) and ML system (dashed lines) for phase separation following aqueous- (a-c) and organic-continuous (d-f) extraction.

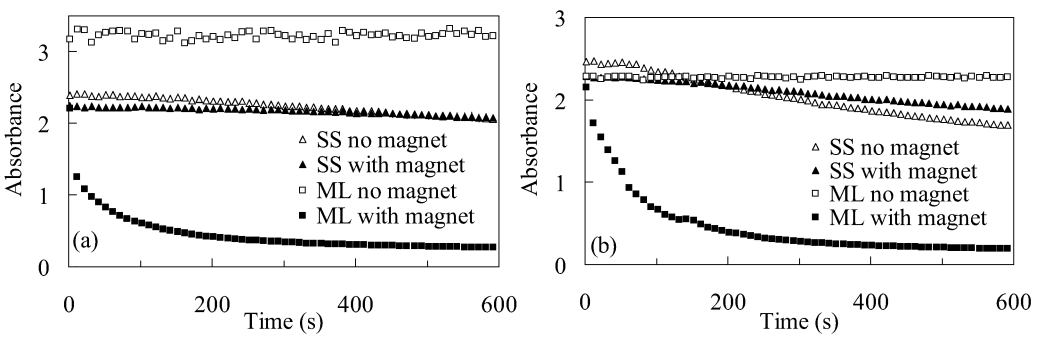

Figure 2. PDT determined by absorbance for (a) 10% CYANEX 272 and (b) 10% LIX 984N in SS and ML contacted with water.

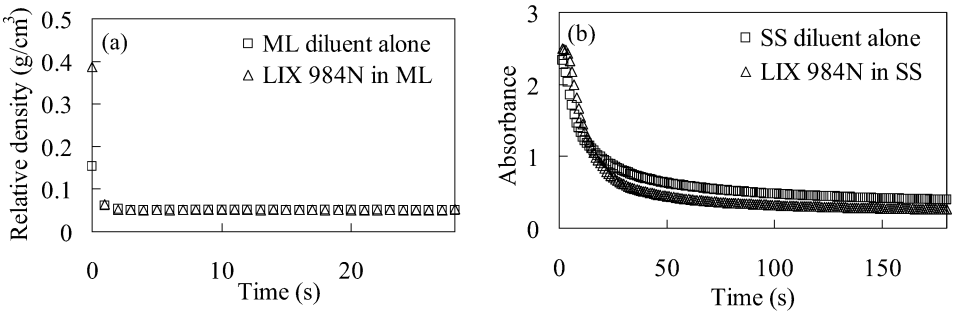

Figure 3. Change in (a) relative density for magnetic diluent and (b) absorbance (nonmagnetic diluent) for System C.

CONCLUSIONS

Using novel methods of monitoring phase disengagement rates, it has been demonstrated that addition of a magnetic component to the diluent of a conventional SX system promotes rapid phase separation without loss of extraction ability, selectivity, or kinetics. While development of this concept could potentially reduce capital costs, residence times, and entrainment losses, its possible limitations may include suspension of magnetite in the aqueous phase and chemical compatibility with various process streams because of the magnetite solubility below pH 4. The system may also behave differently to conventional SX diluents as a consequence of the amphoteric magnetite surface charge.

ACKNOWLEDGMENTS

Financial support was from the Anglo American Innovation Fund, Harry Crossley Foundation (University of Stellenbosch), and South African National Research Foundation is acknowledged. This paper is published by permission of Anglo Research.

REFERENCES

1. R. E. Rosensweig, Ferrohydrodynamics, Cambridge University, Cambridge, 1985.
2. D. Craik, Magnetism: principles and applications, John Wiley, Chichester, 1995.
3. D. L. Leslie-Pelecky and R. D. Rieke, "Magnetic properties of nanostructured materials," *Chem. Mater.*, **8**, 1770-1783 (1996).
4. J. Y. Hwang, "Magnetic solvent extraction," US Patent 5 043 070, 27 August 1991.
5. W. Palyska and A. G. Chmielewski, "Solvent extraction and emulsion separation in magnetic fields," *Sep. Sci. Technol.*, **28**, 127 (1993).
6. L. L. Vatta, R. D. Sanderson, and K. R. Koch, "Magnetic nanoparticles: Properties and potential applications," *Pure Appl. Chem.*, **78**(9), 1791-1799 (2006).
7. L. L. Vatta, "Synthesis of magnetite nanoparticles and their potential application in transition and platinum group metal ion extraction," Ph.D. Thesis, Stellenbosch, South Africa, 2007.

STUDY AND APPLICATION OF MODIFIED ROTATING-DISC CONTACTORS

Weiyang Fei and Yundong Wang

The State Key Laboratory of Chemical Engineering, Department of Chemical Engineering, Tsinghua University, Beijing 100084, P. R. China.
Corresponding author email address: fwy-dce@tsinghua.edu.cn

ABSTRACT

The Rotating Disc Contactor (RDC) is widely used in Industry. However, the performance of commercial RDCs is often much lower than those of experimental ones, especially for large-diameter columns and low interfacial-tension systems, because of the very complex two-phase transfer phenomena inside the column. In response to urgent demands from industry, the flow patterns of two phases inside the columns were simulated by computational fluid dynamics (CFD) and verified by laser doppler velocimetry (LDV) and particle image velocimetry (PIV). A modified RDC (MRDC) is proposed to control the axial mixing and improve column performance. The advantage of the MRDC is verified by experiments and case studies.

INTRODUCTION

The rotating disc contactor (RDC) has been studied intensively in laboratories and is widely used in petroleum refining and chemical industries all over the world [1-6]. It was shown from the laboratory and pilot-plant tests that the RDC has high throughput, reasonable mass-transfer efficiency, low investment needs, and easy maintenance. However, the mass-transfer efficiencies of commercial RDC are often much lower than those of experimental ones, especially for low interfacial-tension systems and large-diameter columns. Different approaches were studied [7-10], but the results were not good enough, and there is no report on their commercial applications.

The RDC was popular in China 30 years ago. However, many RDCs for lube-oil refining by furfural, propane de-asphalting, and caprolactam extraction in refineries and petrochemical plants suffered from problems such as low efficiency and limited capacity [11-14]. Most of them have been revamped with packed extraction columns using Super Mine Rings and other high-efficiency packings. The columns after revamping usually have much higher efficiency and capacity, but the cost is relative high, and sometimes the columns suffer from plugging and coke problems. It seems wasteful to throw away

the original rotating-disc cartridge and to use a large volume of new and expensive packing.

Systematic studies were carried out in the State Key Laboratory of Chemical Engineering (Tsinghua University), therefore, to search for new approaches to improve the RDC performance substantially. The flow patterns of the two phases inside the columns were simulated by computational fluid dynamics (CFD) and verified by laser doppler velocimetry (LDV) and particle image velocimetry (PIV). A new patent on a modified rotating-disc contactor (MRDC) was proposed to control the serious axial mixing between the compartments and improve the column performance [15]. The advantage of the MRDC was verified by experiments, and the new designs were applied for commercial columns successfully. Several parts of the experimental data have been reported in the last few years [16-18]. Additional information is described in this paper.

STUDIES OF FLOW PATTERNS BY CFD, LDV, AND PIV MEASUREMENTS

Numerical simulations were performed to study the flow patterns inside a pilot-scale RDC by using the commercial CFD software PHEONICS 1.4 [19]. Figure 1 shows a typical single-phase pattern inside the RDC compartments. On the left are the rotating discs, and on the right the stator rings. It is clear from Figure 1 that the vortices between the compartments are serious, and the mixing inside the compartments is poor. This is consistent with CFD simulated results reported recently [20,21] but totally different from earlier RDC literature [2].

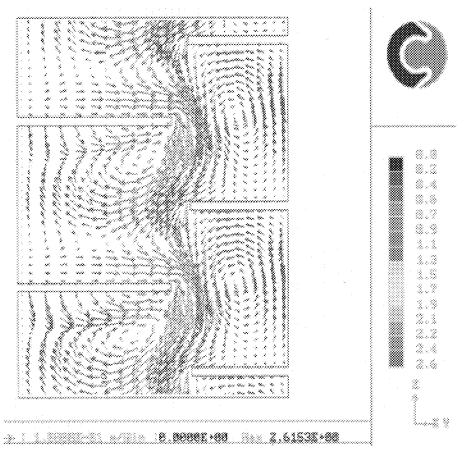

Figure 1. Typical flow pattern inside a RDC.

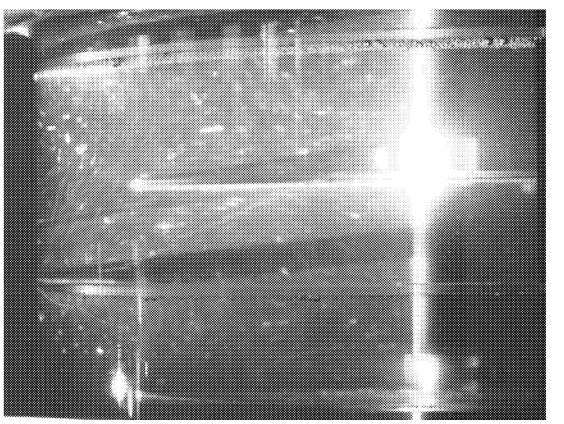

Figure 2. A PIV visible flow pattern of a RDC.

In order to verify the CFD simulated results, a 300 mm glass RDC model for velocity-field measurements was designed and constructed. A TSI9100-3 Laser Doppler Velocimeter (model 1980B) and a QSP LDA processor were used for 3D flow-field measurements. Systematic studies show that the measured results by LDV are consistent with the simulation ones [17,18]. Additional PIV measurements were completed in the

Hydrodynamic Lab, Tsinghua University to get the flow-pattern image. A typical picture for single-phase flow at zero rotating speed is shown in Figure 2, in which the vortices between the compartments can be seen.

The flow-pattern studies by CFD, LDV, and PIV measurements demonstrated that serious axial mixing exists inside the RDC. Further CFD simulation indicated that the larger the RDC diameter, the heavier the impacts of axial mixing. It seems essential to improve the structure of the RDC to control the axial mixing between the compartments. Therefore, a modified rotating-disc contactor (MRDC) was proposed to improve performance by installing additional perforated discs between the rotating discs and at the same level of stator rings (as shown in Figure 3) [15]. The additional perforated discs have as large a free area as possible and elegant design to control the axial mixing between the compartments and allow two phases across it fluently. The function of additional perforated plates for control of the axial mixing has been demonstrated by CFD simulation and LDV measurements, too [18].

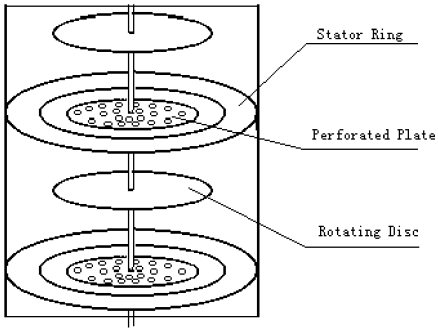

Figure 3. The scheme of MRDC.

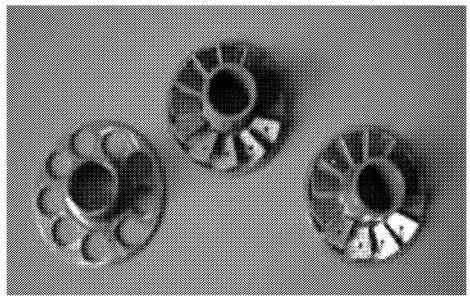

Figure 4. Experimental additional perforated discs.

Experimental Comparisons of RDC and MRDC

The hydrodynamic and mass-transfer performance of RDC and MRDC were compared in a 100 mm i.d. experimental column using the *n*-butanol-succinic acid-water system as recommended by the European Federation of Chemical Engineering (EFCE). Three kinds of additional perforated discs were used in the experiments (Figure 4).

The details of the experimental rig and the main results have been reported [18]. In comparison with the RDC, the MRDC has a 21–35% higher apparent number of transfer units N_{oxp}, while the capacities decrease only a few percent.

In order to confirm the advantage of the MRDC, more experiments were carried out to measure the concentration profiles of the two phases. The apparent number of transfer units N_{oxp}, true number of transfer units N_{ox}, and number of dispersion units N_{oxd} were estimated based on the back-flow model and Ricker-King algorithm [19,22]. The apparent height of transfer units H_{oxp}, true height of transfer units H_{ox}, and height of dispersion units H_{oxd} can then be calculated respectively, and the following equation is well known: $H_{oxp} = H_{ox} + H_{oxd}$. The relationships between H_{oxp}, H_{ox}, H_{oxd} and the rotating

speed N for the RDC (at two phases flow rate $V_c = V_d = 60$ L/h) are shown in Figure 5. It is clear that, even for small experimental RDC columns, the H_{oxd} is high and the axial mixing still plays an important role.

The comparison of H_{oxd} for RDC and two kinds of MRDC are shown in Figure 6. It can be seen that MRDCs have much lower H_{oxd}, which indicates that MRDCs have lower axial mixing than a normal RDC. This characteristic could explain why the MRDC has much higher mass-transfer efficiency than the RDC.

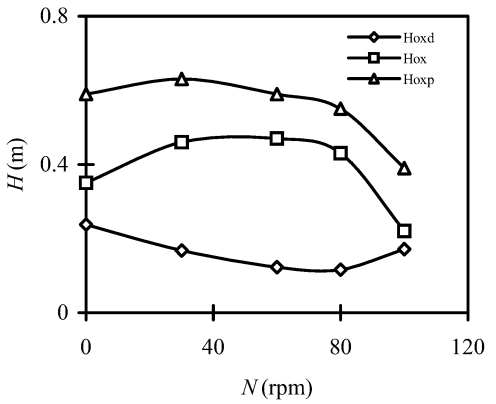

Figure 5. Relationships between H_{oxp}, H_{ox}, H_{oxd} and rotating speed N (at $V_c = V_d = 60$ L/h).

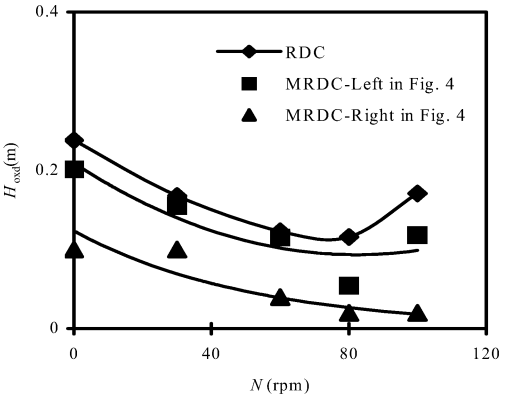

Figure 6. Relationship between H_{oxd} and N for RDC and MRDC (at $V_c = V_d = 60$ L/h).

Applications

The MRDC has been used in Chinese petrochemical plants successfully since 1998. These commercial applications verified the advantage of the MRDC. Two examples are described in this paper:

1. Case one: An existing RDC column with an inner diameter of 1.9 m for the caprolactam extraction suffered from low mass-transfer efficiency and limited capacity. After revamping, using a MRDC, the capacity increased more than 40%, and the caprolactam concentration in the raffinate decreased significantly.
2. Case two: A newly designed MRDC with an inner diameter of 2.4 m for a caprolactam unit with 100,000 tons p.a. capacity was put into operation in 2004. The caprolactam concentration in the raffinate was reduced from 0.5 wt % to 0.1–0.2 wt %.

CONCLUSIONS

1. The advantages of the MRDC in controlling serious axial mixing and improving the column performance have been proved by CFD simulations, LDV, PIV measurements, and experiments.

2. It is shown from two case studies that the commercial application of the MRDC for caprolactam extraction is successful. In comparison with the traditional RDC, the MRDC has advantages in both capacity and mass-transfer efficiency.
3. Further pilot-plant tests are necessary for new MRDC applications in fields of lube-oil refining by furfural, propane, de-asphalting, etc.

ACKNOWLEDGMENTS

This research was carried out under Grant No. 29836130 of the National Natural Science Foundation of China, and Grant No. X598026 of China National Petrochemical Corporation, in the State Key Laboratory of Chemical Engineering (Tsinghua University), Beijing, P. R. China. The authors gratefully acknowledge these grants.

REFERENCES

1. G. H. Reman and R. B. Olney, "The Rotating Disk Contactor—A New Tool for Liquid-liquid Extraction," *Chem. Eng. Prog.*, **51**, 141-146 (1955).
2. W. C. G. Kosters, "Rotating-disk Contactor," in Handbook of Solvent Extraction, T. C. Lo, M. H. I. Baird, and C. Hansen, Eds., Wiley, New York, 1983.
3. W. J. Korchinsky, "Rotating Disc Contactor," in Liquid-liquid Extraction Equipment, J. C. Godfrey and M. J. Slater, Eds., John Wiley and Sons, Chichester, 1994; pp. 247-276.
4. W. Y. Fei and M. J. Slater, "New Look at the Hydrodynamic Behavior of Rotating Disc Contactor," Proceedings of ISEC' 83, AIChE, New York, USA, 1983; p. 174.
5. D. K. Chang-Kakoti, W. Y. Fei, J. Godfrey, and M. Slater, "Drop Sizes and Distributions in Rotating Disc Contactors used for Liquid-Liquid Extraction," *J. Sep. Process Technol.*, **6**, 40-48 (1985).
6. W. Y. Fei, Z. Y. Shen, and J. D. Wang, "The Liquid-liquid Extraction Characteristics and Design of Rotating Disc Contactor (part 1)," *Petroleum Proc. (China)*, **10**(10), 10-16 (1980).
7. L. Steiner and S. Hartland, "A New Type of Agitated Liquid/liquid Extraction Column with Enhanced Coalescence Plates," *Sep. Sci. Technol.*, **15**, 907-923 (1980).
8. W. Gaubinger, G. Husung, and R. Marr, "Operating Behaviour of the Self-stabilizing High Performance Extractor 'SHE'," *German Chem. Eng.*, **6**(2), 74-79 (1983).
9. J. W. Zhu, S. H. Zhang, X. K. Zhou, X. X. Chen, Y. F. Su, and A. Vogelpohl, "Hydrodynamics, Axial Mixing and Mass Transfer in Open Turbine Rotating Disc Contactor (OTRDC)," *Chem. Eng. Technol.*, **14**, 167-177 (1991).
10. M. M. Krishnaiah, M. U. Pai, M. V. R. Rao, and S. R. S. Sastri, "Performance of a Rotating Disk Contactor with Perforated Rotors," *Br. Chem. Eng.*, **12**, 719-721 (1967).
11. W. Y. Fei, "Proposals on the Innovation of Lube Oil Refining by Furfural," *Lubricating Oil (China)*, **6**(2), 10-13 (1991).
12. W. Y. Fei, D. H. Chen, and X. M. Wen, "The Characteristics and Application Prospects of Super Mini Ring," *Chem. Ind. Eng. Progr. (China)*, **16**(2), 36-40 (1997).
13. W. Y. Fei, "Recent Advances on the Intensification of Extraction Columns in China," ISEC' 2005, Beijing, China, 19-23 Sept. 2005; pp. 35-44.

14. Y. D. Wang, W. Y. Fei, Y. Y. Dai, and J. D. Wang, "Numerical Simulation and Experimental Investigation of Velocity Fields in a Rotating Disc Contactor," *Tsinghua Sci. Technol.*, **1**(4), 323-326 (1996).
15. W. Y. Fei and Y. D. Wang, "A Rotating Disc Contactor Extraction Column with Perforated Plates between Compartments," Chinese Patent No. ZL99208868.2, 1999.
16. H. Q. Xu and W. Y. Fei, "The Measurement of Flow Field in a Rotating Disc Contactor with LDV," *J. Exper. Mech. (China)*, **10**(4), 316-322 (1995).
17. W. Y. Fei, Y. D. Wang, and Y. K. Wan, "Physical Modelling and Numerical Simulation of Velocity Fields in Rotating Disc Contactor via CFD Simulation and LDV Measurement," *Chem. Eng. J.*, **78**(2-3), 131-139 (2000).
18. Y. D. Wang, W. Y. Fei, J. H. Sun, and Y. K. Wan, "Hydrodynamics and Mass Transfer Performance of A Modified Rotating Disc Contactor (MRDC)," *Trans IChemE*, Part A, *Chem. Eng. Res. Des.*, **80** (A4), 392-400 (2002).
19. Y. K. Wan, "Study on Velocity Fields and Structure Modification of Rotating Disc Contactor (RDC)," Ph.D. Thesis, Tsinghua University, Beijing, P. R. China, 1998.
20. R. Rieger, C. Weiss, G. Wigley, H.-J. Bart, and R. Marr, "Investigating the process of liquid-liquid extraction by means of computational fluid dynamics," *Computers Chem. Eng.*, **20**, 1467-1476 (1996).
21. C. Weiss and H.-J. Bart, "Calculation of flow patterns in an RDC based on computational fluid dynamics," in Solvent extraction in process industry - Proceedings of ISEC'93, D. H. Logsdail, and M. J. Slater, Eds., Elsevier Applied Science Pub. Ltd., New York, Vol. 2, 1995; pp. 1191-1197.
22. V. Rod, W. Y. Fei, and C. Hanson, "Evaluation of Mass Transfer and Backmixing Parameters in Extraction Columns from Measured Solute Concentrations," *Chem. Eng. Res. Des.*, **61**(4), 290-295 (1983).

THIN-LAYER EXTRACTION

R. Lavie

Chemical Engineering, Technion – Israel Institute of Technology, Technion City, Haifa 32000 Israel. Corresponding author email address: lavie@tx.technion.ac.il

ABSTRACT

The overall task of a solvent extraction process consists of selectively transferring solutes from a donor solution to a recipient solution through a liquid extractant. Thin-layer extraction (TLX) is a novel method to carry out this task, using specialized equipment and temporal modes of operation. In TLX, a thin layer of extractant is firmly attached to a solid substrate. Relatively thin films of the donor and recipient solutions are alternately, intimately, and frequently brought into contact with the thin extractant layer thereby optimizing mass transfer. TLX incorporates the complete extraction/stripping scheme in one single device.

INTRODUCTION

Liquid-Liquid extraction addresses the recovery or purification of a desired substance through the selective transfer of dissolved species from one liquid solution to another. This transfer is done through an intermediary substance, an extractant, which is usually diluted by a diluent, together forming a solvent that is insoluble in the liquid solutions. The process involves an extraction step, where the donor solution is brought into contact with the solvent at conditions that favor the selective transfer of the desired species from the donor solution to the extractant, and a stripping step, where the recipient solution is brought into contact with the same solvent at conditions that favor the transfer of the desired species from the extractant to the recipient solution. In cases where there is a limited amount transferred in a single contact instance, the effect is multiplied by carrying out each of the extraction and stripping steps in countercurrent trains of contacting stages (Figure 1).

Each of the extraction and stripping steps entails, at each contact instance, two elements: mass transfer and phase separation. In conventional liquid-liquid extraction, with the solution and the solvent flowing in bulk, dispersion of one phase into the other is the mode of attaining enough transfer area for mass transfer, therefore requiring recoalescence of droplets to permit phase separation. This generates a contradiction in what concerns the desirable size of the dispersed droplets: small droplets provide a high mass-transfer surface but make the phase separation more difficult. Every compromise on this count inevitably leads to bulky equipment and a large inventory of solvents [1].

Initially, liquid-liquid extraction was carried only in mixer-settler trains. Over the years, processes have been refined that reduced inventory to some extent, notably extraction columns, centrifugal extractors, and more recently membranes. A major motivation behind the development of thin layer extraction concerns the elimination of mixing of the phases and their separation [2] while optimizing mass transfer. An early attempt [3] failed to provide a practical method, because it missed important facets of the problem.

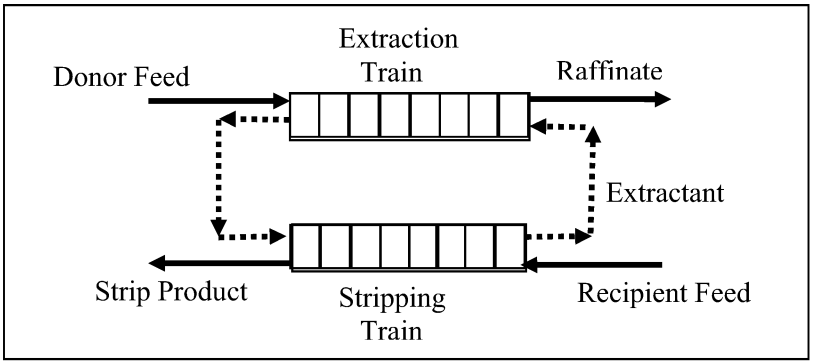

Figure 1. Basic conventional liquid-liquid extraction scheme.

The Thin-Layer Extraction (TLX) Concept

In TLX, we replace the solvent by a microporous solid substrate to which a thin layer of the liquid extractant is attached [4]. A relatively thin film of the donor or recipient solution flows past the extractant layer (Figure 2). This constitutes ideal conditions for mass transfer between the solution and the extractant, because it maximizes the diffusion cross-section surface and minimizes the length of the diffusion path of the absorbed species between the solution and the extractant. With the extractant layer firmly attached to the solid substrate, separation of the phases is trivialized. This leaves mass transfer as the sole consideration determining the necessary time of contact between the solution and the extractant. Fast mass transfer permits frequent switching between extraction and stripping modes of operation such that the accumulated amount of solutions processed over time may compare to those processed in alternative conventional liquid-liquid extraction processes. In this context, it is interesting to note that, because in conventional liquid-liquid extraction, the diffusion from/to the interior of each phase to their interface constitutes most of the resistance to mass-transfer and this resistance accrues exponentially with the depth of penetration into the body of fluid, the TLX approach gains almost exponentially in mass transfer rate while forfeiting linearly in the capacity of the extractant layer. This makes a thin layer beneficial. In addition, the thin layer, possibly composed of the pure extractant without recourse to a solvent, will mostly contain more solute than would an extractant-containing solvent. Finally, in conventional liquid-liquid extraction, entrainment of some solvent into the processed solutions often necessitates further purification of the product solutions while also constituting a loss of costly materials. In thin layer extraction, with the entrained

extractant firmly attached to the solid substrate, contamination of the solutions by the extractant is practically eliminated.

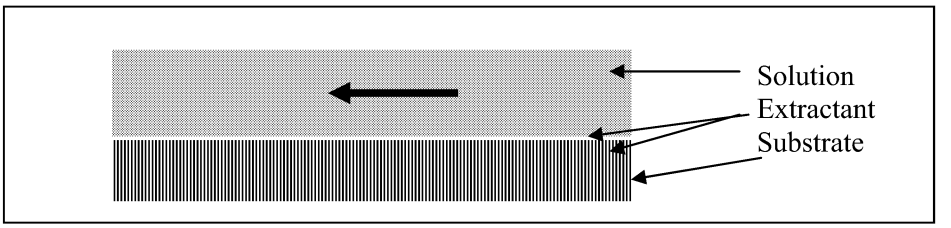

Figure 2. Enlarged view of the contact zone in TLX.

The TLX technology translates the TLX concept into closed extraction/stripping schemes, using devices and temporal modes of operation that rely on a proper choice of materials, structures, and timing.

The TLX Process Sructure - the TLX Cell

The basic element in a TLX process is the TLX cell that consists of a container, a cartridge, a flow arrangement, and a timed program of operation. The ***cartridge*** is an open-cell macroporous matrix made of a solid microporous substrate, with a thin layer of a liquid extractant coating the substrate and firmly attached to it, as depicted in Figure 2. The ***flow arrangement*** provides for the donor and the recipient solutions to alternate in being brought into contact with the TLX cartridge. This may be achieved by rotating the cartridge through regions containing the respective donor or recipient solutions or by letting the donor and recipient streams reciprocate in contacting a fixed cartridge. ***The program of operation*** determines when and for how long each of the participating solutions is brought into contact with the cartridge. Figure 3 depicts a conceptual TLX cell with the cartridge changing position in time through constant-position streams.

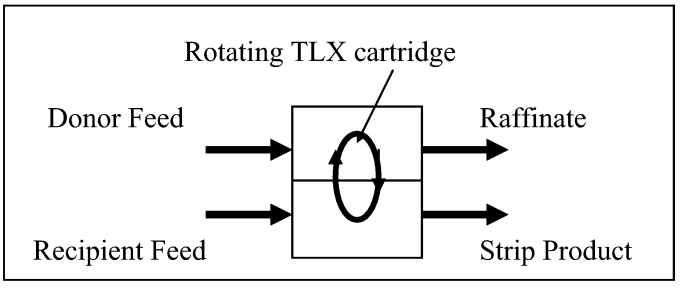

Figure 3. Conceptual TLX cell.

Each TLX cell constitutes a microcosm of the entire extraction/ stripping scheme (such as the one depicted in figure 1). TLX cells may be stacked to form a countercurrent multistage TLX where each cell becomes a stage, as shown in Figure 4.

The Multistage TLX Process Structure

Like in any other extraction process, when a single contacting stage fails to provide the desired extent of solute transfer from the donor solution to the recipient solution, one resorts to countercurrent multistage processing. However, the structure of a multistage countercurrent TLX plant differs from that in the familiar extraction and back-extraction trains, where an extractant-bearing-solvent is circulated in a countercurrent direction to each of the donor and the recipient solutions, as shown in Figure 1. In TLX, each stage performs a single cycle of the entire process (extraction, scrubbing, stripping, etc.). When stacking together several TLX stages to form a multistage TLX process, countercurrent flow between the donor solution and the recipient solution can be maintained with the products of one stage serving as the feeds to neighboring stages. However, the extractant can be recognized as "flowing" in a crosscurrent direction to both as depicted in Figure 4.

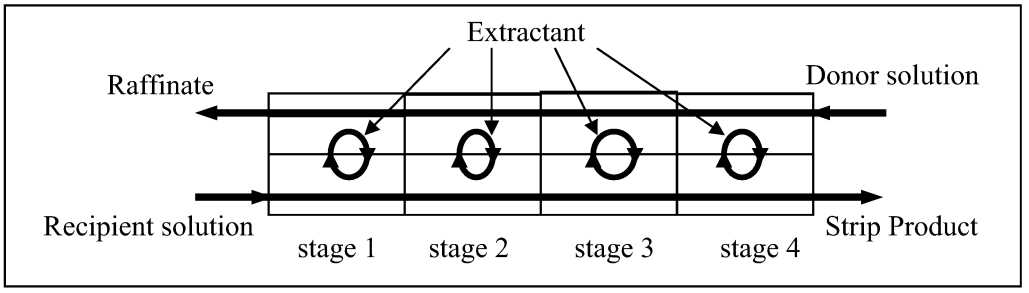

Figure 4. The multistage countercurrent TLX structure.

TLX Embodiments

TLX has been implemented in several different forms. To mention only two of them:

a. The rotating cartridge TLX, an example of which is described below, and
b. The Micro TLX consisting of a single or a set of parallel, cartridge-containing tubes along which small batches of the solutions are made to travel in opposing directions at different times. Each tube represents a full multistage TLX plant.

EXPERIMENTAL RESULTS

Results pertaining to an experiment on the Rotating Cartridge embodiment are provided as an example. A vertical cylindrical container contains a vertical cylindrical cartridge that may be rotated on its vertical axis. The cartridge consists of multiple vertical leaflets made of a stretched polypropylene microporous Celgard 2500 membrane with a micro-porosity of 0.55 and a thickness of 25 microns, provided by Celgard Inc., forming together a cylindrical matrix 7 cm high and 12.6 cm diameter, an accessible top surface of 100 cm^2, an accessible membrane surface of 0.42 m^2, and a macro porosity of

0.93. The container is divided into virtual halves. Two sets of fine spraying nozzles are installed on top of the cartridge, one sprays the donor feed solution onto a region containing half the cartridge and the other sprays the recipient feed solution onto the other half. At any particular moment, half a cartridge is exposed to the donor solution while the other half is exposed to the recipient solution, changing roles each half cycle. The container bottom is subdivided into two pans, each collecting one of the raffinate or the strip product.

The cartridge was initially soaked with an Alamine 336 extractant and then washed generously under a stream of water until the wash effluent was free of any entrained extractant, leaving the cartridge loaded with 4.6 g of the extractant, which indicates an extractant layer thickness of 0.0025 cm. The donor solution was a citric acid solution in water of composition varying in different runs from 0.1% to 8% w/w The recipient solution in all runs was pure water. The temperature of both feeds was 25 ^{o}C. Compositions were measured by means of a calibrated conductivity electrode. After some tests intended to determine optimal timing, the operation program was set to consist of a periodic cycle during which (1) the donor and recipient solutions were simultaneously sprayed onto respective halves of the cartridge at a constant rate for t_{spr} seconds, then (2) came a wait period of 1 second, then (3) the cartridge was gently shaken for 1.5 seconds to clear any solution clinging onto the cartridge, and then (4) the cartridge was rapidly rotated by 180° to its new position ready to restart the program. Two program cycles constitute one process cycle. The spray time t_{spr} varied in different runs from 1 to 8 seconds, translating into an average solution film thickness of 0.002 to 0.016 cm. Figure 5 depicts typical results for a set of runs, in comparison to expected equilibrium compositions (dotted lines). The average solution flow rate of each of the solutions was calculated as equal to the spraying flow rate times spraying time/cycle time. The flow rate is essentially proportional to the thickness of the solution layer in each run.

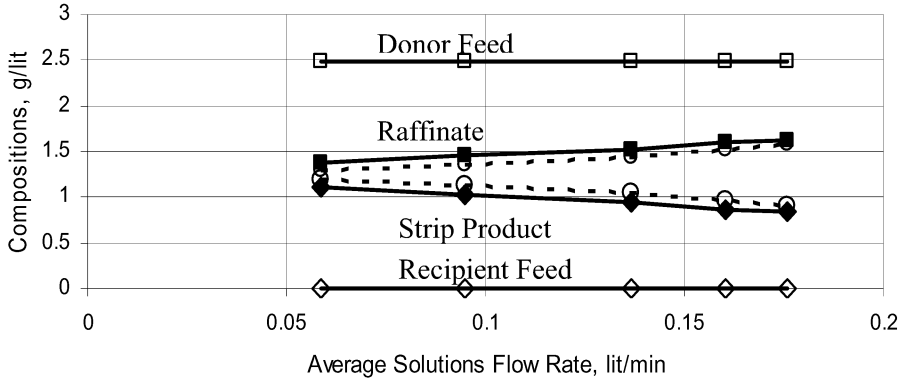

Figure 5. Sample experimental results for a rotating cartridge TLX.

DISCUSSION

It is striking to observe that indeed, by reducing the thickness of the contacting layers of extractant and solvent, we manage to equilibrate the phases to substantial

completion within a few seconds. In all experimental runs, 92-95% of the equilibrium value was reached. Frequent cycling also leads to a short start-up time, another useful characteristic of TLX. While the above example addresses an extraction plant configuration consisting of a single extraction and a single stripping step, it is possible to apply TLX to an extraction flowsheet, where the extractant undergoes more than two steps per cycle.

TLX provides a tool to carry out selective transfer of a solute from one solution to another using a minute amount of extractant. The elimination of solvent inventories, together with the prevention of organic entrainment into the products, begets significant safety and environmental advantages as well as cost savings.

It may be argued that TLX is akin to ion exchange (IX) in beds of resin. There is, however, a significant difference in the cycle period. While in IX the active ingredient is dispersed in hard-to-reach pores leading to long cycles of operation that often translate into a limitation on the economic concentration of the feed, the relatively high TLX frequency combined with its structure and mode of operation allows TLX to process a feed of any concentration for long stretches of time. Pressure drop through the TLX equipment is low. TLX is applicable at any scale, from the micro- to full-size plant-scale. The scale-up of a plant is simple due to modularity and simple hydraulics. TLX is limited to the processing of clear or filtered solutions because of the relatively narrow passages in the cartridge.

CONCLUSIONS

TLX promises to be an efficient tool for liquid-liquid extraction. It uses efficiently the extractant (usually an expensive compound). It is applicable at any scale. It may be applied to process feeds of any concentration. It avoids, or at least minimizes, solvent inventories with significant safety and environmental benefits. It has no observable organic entrainment (losses), thereby further establishing its standing as an inherently safe and environment-friendly process.

ACKNOWLEDGMENTS

Thanks are due to Celgard Inc. for providing the Celgard membrane samples and to Bateman Advanced Technologies Ltd. for a fruitful cooperation.

REFERENCES

1. B. Grinbaum, “An Integrated Method for Development and Scaling Up of Extraction Processes,” Ion Exchange and Solvent Extraction, A Series of Advances, Volume 15, Y. Marcus, CRC, 2001.
2. R. Blumberg, *Liquid-Liquid Extraction*, Academic Press, 1988.
3. A. Dolev, E. Kehat and R. Lavie, “Intensive Periodic liquid-Liquid Extraction in a thin Extractant Layer,” *Ind. Eng. Chem. Res.*, **38**,(4), 1618-1624 (1999).
4. R. Lavie, “Method and apparatus for Liquid-Liquid Extraction,” PCT/IL2007/000707, 12 June 2007.

CONTROLLABLE PREPARATION OF NANOPARTICLES BY DROPS AND PLUGS FLOW IN A MICROCHANNEL DEVICE

S. Li, J. Xu, Y. Wang and G. Luo

State Key Lab of Chemical Engineering, Department of Chemical Engineering, Tsinghua University, Beijing, 100084, China.
Corresponding author email address: gsluo@tsinghua.edu.cn

ABSTRACT

Well-controlled two-liquid phase flows in a T-junction microchannel device have been realized, and $BaSO_4$ nanoparticles with narrow size and good dispersibility were produced through drops or plugs flow in the microdevice. As a novel work, the influence of mass transfer and chemical reaction on flow patterns is discussed based on the experimental investigation of flow patterns under different operating conditions. Meanwhile, the effect of the two-phase flow patterns on the nanoparticle size was discussed. It was found that the increase of the amount of mass transfer and chemical reaction could change the flow patterns from plugs flow to drops flow. The drop diameter or plug length could be changed in a wide range. The prepared nanoparticles ranged from 10 to 40 nm. Apparently, the particle size decreased with an increase of the drop diameter or plug length.

INTRODUCTION

Recently, the rapid development of microreaction and micromixing technology has led to a considerable variety of microfluidic devices. These devices have been used in many fields for their high efficiency, safety, repeatability, and facile controllability [1]. In particular, significant advances have been made in the use of microfluidic devices for controlling multiphase flow patterns. Cross-flow and focusing flow are two main methods for controlling different multiphase flow patterns, which can be suspended drops flow, channel-spanning slugs flow, or wall-wetting films flow [2]. Well-controlled multiphase flows in microdevices have been widely used in chemical reaction [3], liquid-liquid extraction [4], crystallization [5], and nanoparticle synthesis [6,7]. Especially, in nanoparticle synthesis, particle-size control is just one of the key issues in the production of nanoparticles, because many properties of the solid particles are sensitive to the particle size and particle-size distribution [8]. Drops or plugs flow can provide high mixing efficiency, which is very important for particle-size control [9,10]. Moreover, well-controlled multiphase flows can also prevent a liquid from direct contact with microchannel walls and thereby eliminate or reduce undesired clogging of channels due to deposition of material on wall surfaces [2,6].

Most of the works on nanoparticle preparation with multiphase flows in microdevices are not closely connected with multiphase reactions. The reactants exist in either phase only. The other phase is inert and only provides an isolated reaction environment on the micro-scale. Obtaining high mixing performance for homogeneous reaction systems is the main application. But for heterogeneous reaction systems, there has been little research on how the mass transfer and chemical reaction affect the multiphase flows in microdevices, and the preparation of nanoparticles with heterogeneous reaction systems in microdeveices is also little mentioned in the previous work. In this work, a T-junction microchannel device was used to produce liquid-liquid drops flow and plugs flow with different size. And $BaSO_4$ nanoparticles were produced by the interphase reaction of reactants in liquid-liquid phases. The influence of mass transfer and chemical reaction on two-phase flow patterns in the T-junction microchannel device was investigated. Meanwhile, the effects of the operating conditions and the droplet size on the particle size was also investigated and discussed.

EXPERIMENTAL

Figure 1 shows the experimental setup. Nanoparticles were produced in a T-junction microchannel device fabricated on a polymethyl methacrylate (PMMA) sample plate (60 × 40 × 5 mm) using an end mill. The main channel dimensions were about 1000 × 1000 μm (width × height). The dispersed channel was about 200 × 200 μm (width × height) and perpendicular to the main channel. The microfluidic device was sealed using another PMMA thin plate (1 mm in thickness) by curing at 105 °C using high-pressure thermal sealing techniques. Two microsyringe pumps and two gastight microsyringes were used to pump the two phases into the microfluidic device, respectively.

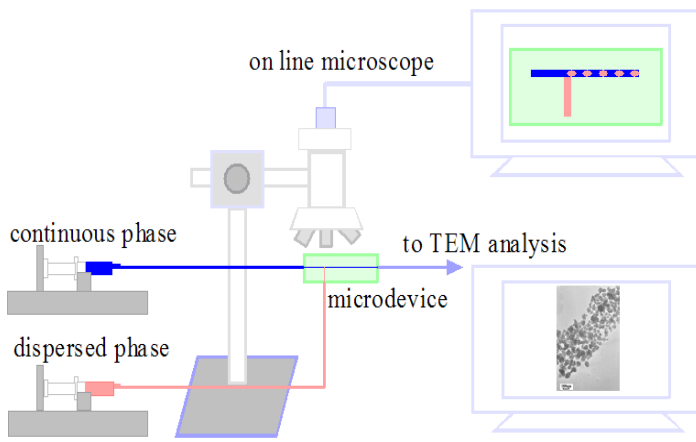

Figure 1. The experimental setup.

Butyl alcohol solutions, hexyl alcohol solution, or octyl alcohol solutions with sulfuric acid concentration of 0.1 mol/L, 0.2 mol/L, 0.4 mol/L, and 0.8 mol/L were used as the continuous phase, respectively. Aqueous solutions with barium chloride concentration of 0.02 mol/L, 0.05 mol/L, 0.1 mol/L, 0.2 mol/L, 0.4 mol/L, and 0.8 mol/L were used as the dispersed phase. Droplets of aqueous solution were formed by the crossflowing rupture in the main channel. The reaction of sulfuric acid with barium chloride took place at the droplet interface, and nanoparticles of barium sulfate were produced.

A microscope at magnifications from 20× to 200× with a high-speed CCD video camera was used to measure the drop diameter and the plug length. The images were recorded at a frequency of 600 images/s and then analyzed using a custom-made image-analysis software. The produced nanoparticles were characterized by TEM pictures on JEM2010 (Japan), and the particle size was analyzed using the TEM pictures.

RESULTS AND DISCUSSION

Two-Phase Flow Patterns

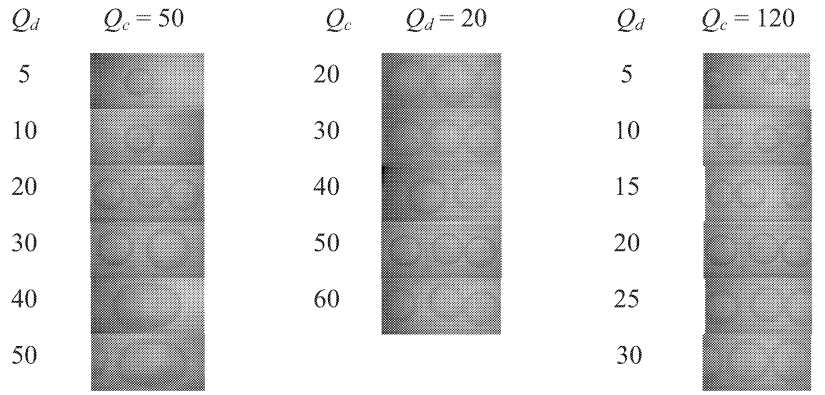

Figure 2. Micrographs of droplet flow with the butyl alcohol solution as the continuous phase and aqueous solution as the dispersed phase. Q in μL/min, C_c = 0.4 mol/L, C_d = 0.4 mol/L.

Figure 2 shows some of the droplet shapes and sizes in different experimental conditions. Based on the experimental data, we could distinguish the different flow regions by defining a new parameter of Ca/Q_d, as shown in Figure 3. Here Ca = $\mu_0 u_c/\gamma_0$ is the capillary number of reaction-free system. μ_0 and u_c are viscosity and mean velocity of the continuous phase, respectively. γ_0 is the interfacial tension and Q_d is the flow rate of the dispersed phase. We could see that the flow patterns can be distinguished as plugs flow and drops flow very well with the new defined parameter.

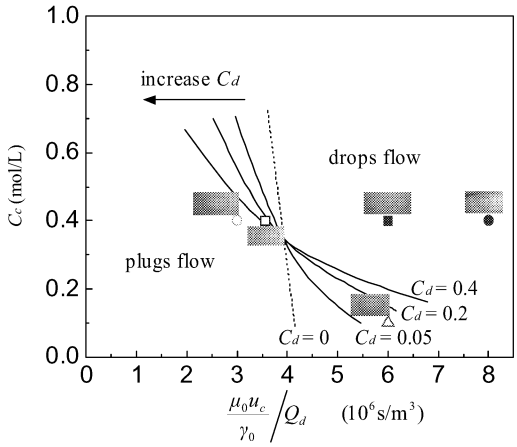

Figure 3. Two-phase flow patterns. C_d in mol/L and Q in μL/min.

Particle Size

$BaSO_4$ nanoparticles with size between 10 and 40 nm were successfully produced with the two-phase flow described above. Some of the TEM pictures are listed in Figure 4. The particle size varies obviously when the experimental conditions are changed.

In order to know about the relationship between the droplet size and the nanoparticle size, we plot all the results of particle size and droplet size in one picture, as shown in Figure 5. We call this figure the particle-size diagram.

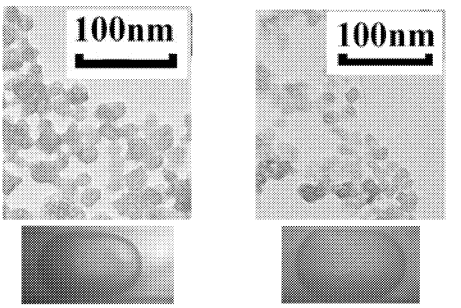

(b).C_d = 0.1mol/L (d).C_d = 0.8mol/L

Figure 4. Particle and corresponding droplet pictures in the butyl alcohol system with C_c = 0.1mol/L, Q_c = 50μL/min, and Q_d = 20μL/min.

In the particle-size diagram, the abscissa is droplet size, which is the drop diameter (below 1000 μm) or plug length (above 1000 μm). The ordinate is the particle size. We can see clearly that the particle size decreases with the increase of drop diameter or plug length within a narrow belt marked in the diagram. The slope of the belts characterizes the effect of the droplet size on particle size, while the width of the belts characterizes the effect of the initial ion product of Ba^{2+} and SO_4^{2-}. Of course, as shown in Figure 3, the initial concentration of both phases has a great influence on the flow patterns and the segment size.

The initial concentration affects the flow pattern because of the changes of the interfacial tension. The increase of the sulfuric acid concentration leads to the increase of the mass transfer, which results in the decrease of the interfacial tension. Therefore, the droplet size is decreased. When the sulfuric acid concentration is high, the mass transfer plays a key role, and the dispersed-phase concentration has relatively less influence. But because of the mass-transfer enhancement due to the chemical reaction, the dispersed-phase size is decreased a little when the dispersed-phase concentration is increased. When the sulfuric acid concentration is low, the mass transfer and chemical reaction will have little influence on the two-phase flow. At this condition, the increase of the dispersed-phase concentration may lead to the increase of the interfacial tension due to the salting-out effect, causing the increase of the dispersed-phase size.

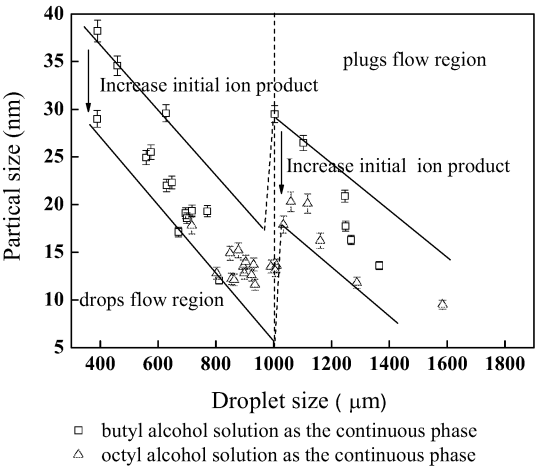

Figure 5. Particle size diagram.

Sulfuric acid is usually excessive in drops flow, and the supersaturation ratio is controlled by the mass-transfer speed inside drops. At the drop-generating stage, there is a strong inner circulatory flow inside drops because of the action of the shear force of the continuous phase, and the mass-transfer speed inside drops is very high. Nucleation will mainly take place at this stage, and a large amount of reactants will react at this stage too. After the drops are formed and flow in the mcirochannel, the inner circulatory flow will be very weak, and the mass-transfer inside drops just provides the materials for the particle growth. Therefore, the nucleation process persists a little longer time in a bigger drop. The materials left for the later growth stage become less, and the finally produced particles are smaller. Most of the plug flows are in low continuous-phase concentration. The phase ratio of the continuous phase to the dispersed phase is also much lower than that of the drops flow. The mass-transport speed in the continuous phase may become a determining factor on the particle size. Short segment of the continuous phase will benefit the rapid mixing and cause high supersaturation ratio. Therefore, opposite to the segment length of the continuous phase, longer plug length of the dispersed phase will be helpful for the preparation of small nanoparticles.

CONCLUSIONS

Nanoparticles with size between 10 and 40 nm were produced through the two-phase flow in a T-junction microchannel device. By adjusting the experimental conditions, including the two-phase concentrations and flow rates, droplets with different shapes and sizes were generated in the microdevice, and the size of $BaSO_4$ nanoparticles was controlled. We found that mass transfer and chemical reaction could affect the flow patterns seriously. With a new parameter of Ca/Q_d as the horizontal axis and C_c as the vertical axis, two-phase flow patterns can be distinguished. The experimental results showed that the particle size decreased with an increase in drop diameter or plug length.

ACKNOWLEDGMENTS

We gratefully acknowledge the support of the National Natural Science Foundation of China (20490200 and 20525622) and of the National Basic Research Program of China (2007CB714302).

REFERENCES

1. W. Ehrfeld, V. Hessel, and H. Löwe, Microreactors: New Technology for Modern Chemistry, Wiley-VCH, Weinheim, 2000.
2. A. Günther and K. F. Jensen, "Multiphase microfluidics: from flow characteristics to chemical and materials synthesis," *Lab Chip*, **6**, 1487-1503 (2006).
3. J. R. Burns and C. Ramshaw, "The intensification of rapid reactions in multiphase systems using slug flow in capillaries," *Lab Chip*, **1**, 10-15 (2001).
4. J. H. Xu, G. S. Luo, G. G. Chen, and B. Tan, "Mass transfer performance and two-phase flow characteristic in membrane dispersion mini-extractor," *J. Membr. Sci.*, **249**, 75-81 (2005).

5. B. Zheng, J. D. Tice, and R. F. Ismagilov, "Formation of droplets of in microfluidic channels alternating composition and applications to indexing of concentrations in droplet-based assays," *Anal. Chem.*, **76**, 4977-4982 (2004).
6. E. M. Chan, A. P. Alivisatos, and R. A. Mathies, "High-Temperature Microfluidic Synthesis of CdSe Nanocrystals in Nanoliter Droplets," *J. Am. Chem. Soc.*, **127**, 13854-13861 (2005).
7. B. K. H. Yen, A. Günther, M. A. Schmidt, K. F. Jensen, and M. G. Bawendi, "A Microfabricated Gas–Liquid Segmented Flow Reactor for High-Temperature Synthesis: The Case of CdSe Quantum Dots," *Angew. Chem. Int. Ed.*, **44**, 5447-5451 (2005).
8. R. W. Siegel, "Creating nanophase materials," *Sci. Am.*, **275**, 74-79 (1996).
9. S. W. Li, J. H. Xu, and G. S.Luo, "Control of crystal morphology through supersaturation ratio and mixing conditions," *J. Cryst. Growth*, **304**, 219-224 (2007).
10. H. C. Schwarzer and W. Peukert, "Tailoring particle size through nanoparticle precipitation," *Chem. Eng. Commun.*, **191**, 580-606 (2004).

PRELIMINARY EXPERIMENTAL STUDY OF BUTYL ACETATE SEPARATION BY AIR-ASSISTED SOLVENT EXTRACTION

Y. Ma,[1,2] Z.Chang,[1] B. Xiao,[1,2] S. Shen,[1,2] and H. Liu[1]

[1]Laboratory of Separation Science and Engineering, State Key Laboratory of Biochemical Engineering, Chinese Academy of Sciences, Beijing 100080, China. [2]Graduate University of the Chinese Academy of Sciences, Beijing 100080, China.
Corresponding authors' email addresses: hzliu@home.ipe.ac.cn, yinchen.ma@gmail.com

ABSTRACT

A new kind of process named air-assisted solvent extraction is studied, and some preliminary experimental work is reported in this paper. The effects of air flow rate, the height ratio of extraction section to enrichment section, frequency of reciprocating, and column diameter on the overall plate extraction efficiency in a gas-agitated sieve-plate column of 50 mm in diameter with air, butyl acetate working solution, and *n*-nonane as the experimental system have been investigated. Some of our supposition was confirmed by the experimental results.

INTRODUCTION

Butyl acetate (BA) dissolves into the aqueous phase with a content of about 1% by weight during the extraction operation of penicillin from the filtered fermentation broth. Separation and recovery of BA from aqueous solution is of paramount importance from ecological, environmental, and economical points of view. Solvent sublation, which is a nonfoaming adsorptive bubble separation process, has been widely used in the treatment and separation of various hydrophobic substances from their dilute solutions [1]. Separation of BA from the aforementioned wastewater by solvent sublation and bubble separation has been explored by our group [2-6] with *n*-nonane as the extractant, and acceptable efficiency has been achieved. However, there exists the problem of low throughput, even with two columns operated in series. But using solvent extraction alone will lead to the loss of solvent, and separation efficiency is limited by thermodynamics. Otherwise, solvent extraction is not economical for treating dilute solutions.

To solve this problem, a novel solvent-extraction process named air-assisted

solvent extraction, in which solvent-extraction and solvent-sublation processes are integrated into an equipment and carried out in the upper and lower section, respectively, has been developed [7]. This new process, combining the merits of both processes, has a number of advantages in terms of simple equipment configuration and reduction of solvent loss, while providing a sufficiently large interfacial area for mass transfer. Our process, which uses the reciprocating plate and air agitation to intensify extraction, is different from that of Chen [8] and Tarkan [9-11], which use solvent-coated bubbles to intensify extraction and fulfill the separation.

The aim of this work was to check and demonstrate the feasibility of this new process. Some preliminary experimental studies were conducted. To find optimal conditions, the effect of gas flow rate, the height ratio of extraction section to enrichment section, frequency of reciprocating, and column diameter was investigated.

EXPERIMENTAL WORK

Materials and Equipment

Butyl acetate, *n*-nonane, and *n*-hexane were purchased from Beijing Chemical Reagent Company (China) and were all of analytical grade. The experimental work was mainly conducted in the self-made reciprocating plate column with the diameter of 50.5 mm (RPC) and a compartmental height of 2000 mm. The column consisted of two glass cylindrical tubes along which five sampling ports equally distributed. These ports can be also used as the solvent inlet. A scheme of the experimental setup and the details of the setup are described elsewhere [7].

Description of the Process

The feed solution to the column is BA saturated solution, and *n*-nonane was used as extractant. Air from a compressor was used as the dispersed gas phase in a one-pass-through mode and introduced at the bottom of the column through a sintered glass disk (G4 Porosity) at a constant pressure with an adequate pressure regulator. The gas flow rate was adjusted by a valve and measured by a rotameter.

During the extraction process, BA saturated solution was filled into the column by peristaltic pump, and *n*-nonane was carefully added to the top of the water in the column according to the ratio of oil to water. The volume flow rate ratio of oil to water was kept 1:50 in all the experiments. The air was adjusted at the desired value and introduced when the water and solvent pumps were operated for a while until the steady-state condition was established. The extraction was operated countercurrent in both semi-continuous and continuous mode. In each experiment, the column was operated for long enough for steady state to be reached. Details of the procedure used to

analyze the sample and the calculating method of separation efficiency can be found in Sun [3]. For the sake of comparing the results, the separation efficiency is defined as

$$E = \frac{C_{wi} - C_w}{C_{wi}} \times 100\% \quad (1)$$

where C_{wi} and C_w is initial concentration of the solute and solute concentration in the aqueous phase after extraction, respectively.

RESULTS AND DISCUSSION

Effect of Gas Flow Rate

Figure 1 demonstrates the dependency of the separation efficiency on the flow rate of the gaseous phase. Under the same gas flow rate, E increases with the increase of time and approaches asymptotically its maximum value. Moreover, at the same operating time, the higher the gas flow rate becomes, the bigger is the separation efficiency. This trend is similar to that of solvent sublation. Higher flow rate will produce more bubbles and provide more surface areas for mass transfer of solute and improve the separation efficiency. Also, this behavior may be attributed to the increase in the population density of the dispersed-phase droplets within the chambers between the plates and a decrease in the size of dispersed-phase droplets. Such a phenomenon promotes the droplets to break up and consequently increases the interfacial area between dispersed and continuous phases and surface-renewal mechanism [12]. However, under very high gas flow rate, there will be the intensive back-mixing of solvent in the lower section, where solute is concentrated by solvent sublation, leading to the upset of operation and decreasing of separation efficiency. The desired gas flow rate was chosen to be 400 mL/min.

Effect of Reciprocating Frequency

The presence of gas-phase in a RPC increases the axial mixing of the aqueous phase [14]. The mass transfer between the organic and aqueous phase increases with increasing reciprocating frequency, which is desirable, but so does dispersion, which is only desired to a certain extent. Five reciprocating frequencies were used, and their effect on the separation is demonstrated in Figure 2. It can be seen that the extraction efficiency of 100 Hz was higher than others during most of the extraction time except that in the first 15 minutes. There was no obvious back-mixing of bubble and extractant in sight in the column. The surge on the plot may be due to the introduction of air suddenly at the beginning of the experiment. So the optimal reciprocating frequency is set at 100 Hz.

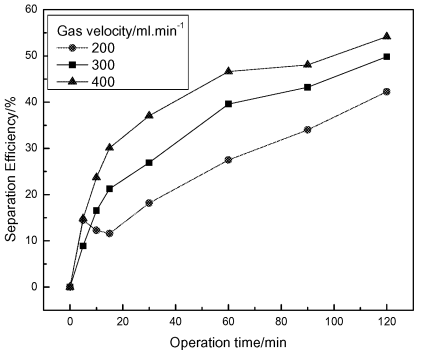

Figure 1. Effect of gas velocity.

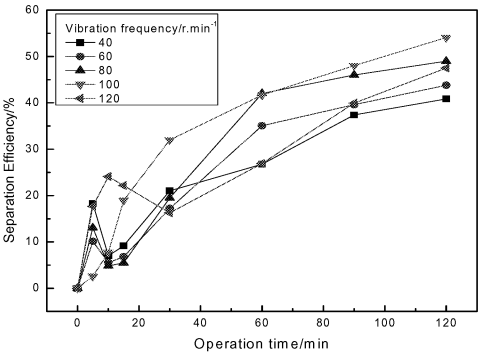

Figure 2. Effect of reciprocating frequency.

Effect of Length Ratio of Extraction Section to Sublation Section

Air-assisted solvent extraction includes the concentrating section of solvent sublation and extraction section of solvent extraction, in which solvent sublation is thought to be the most important in this process for its concentration effect because of the low concentration of BA in influent. The length ratio of extraction section to that of sublation $R_{SE/SS}$ plays an important role in the whole process, because extraction efficiency can be improved only when the concentration of BA in water is enriched.

Three different lengths of reciprocating plates (300, 550, and 800 mm) were used in the experiment, and the length ratios were 3:17, 11:29, and 2:3 correspondingly. The effect of $R_{SE/SS}$ on the separation efficiency is shown in Figure 3. It can be seen that the efficiency is higher when the length of the sublation section is longer. To demonstrate the concentration effect of sublation in the whole process, we took samples from two different ports that are at the lower part of the reciprocating plate and above the air inlet, respectively. The concentration profiles are plotted in Figure 4. From the figure, we can see that the concentration of the upper sampling port is higher than that of the lower one, which shows the concentration effect of sublation. However, the extractant is not distributed evenly, and the oil/water phase interface will decrease when the length of extraction section is short, because of the decrease of the reciprocating plate. So the length of extraction section was chosen as 550 mm in our experiment.

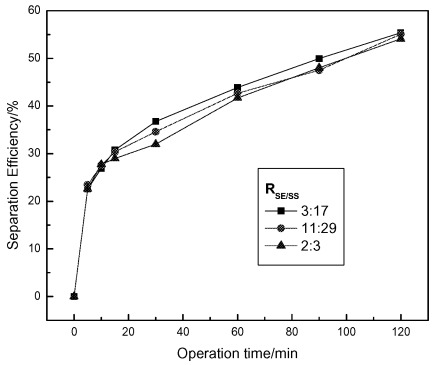

Figure 3. Effect of $R_{SE/S}$.

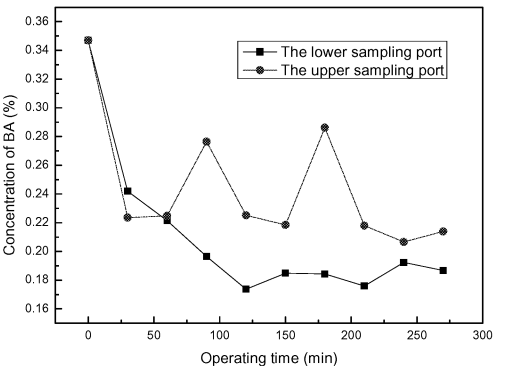

Figure 4. Concentrating effect of solvent sublation.

Effect of Column Diameter

To study the effect of the column diameter on the separation efficiency, another set of extraction columns with diameters of 25 mm was used to carry out a similar study of the process, and the experimental results were compared with that of 50 mm. The comparison is shown in Figure 5. It can be seen from the figure that the separation efficiency decreases with increasing column diameter. The experimental results were similar to that of solvent sublation. The decrease of the efficiency may be due to the decreasing of holdup and the uneven distribution of extractant in the column chamber and the decreasing of axial dispersion of the continuous phase.

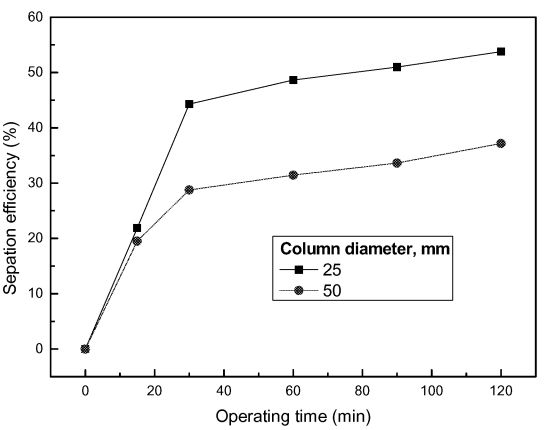

Figure 5. Effect of column diameter.

CONCLUSIONS

The new process of air-assisted solvent extraction has been examined and some of the affecting parameters were investigated. The experimental results show that this process can be used to separate partly soluble chemicals from their dilute solutions.

However, it can be seen from our experimental results that the overall separation efficiency is not high, which may be due to the very small ratio of oil to water, the big plate spacing, or some other reasons. Moreover, the loss of extractant was not focused in this paper, which is the greatest advantage of this new process. Further investigations need to be done to check the feasibility of this process in wastewater treatment.

REFERENCE

1. K. T. Valsaraj, G. L. Thoma, L. J. Thibodeaux, and D. J. Wilson, "Nonfoaming Adsorptive Bubble Separation Processes," *Sep. Technol.*, **1**(5), 234-244 (1991).
2. X. H. Sun, "Bubble Separation and Air-Assisted Solvent Extraction For Recovery of Organics in Wastewater of Penicillin Plant," Ph.D. Thesis, Institute of Process Engineering, Chinese Academy of Science, Beijing, China, 2006.
3. X. H. Sun, Z. D. Chang, and H. Z. Liu, "Recovery of Butyl Acetate in Wastewater of Penicillin Plant by Solvent Sublation I. Experimental Study," *Sep. Sci. Technol.*, **40**(4), 927-940 (2005).
4. X. H. Sun, Z. D. Chang, and H. Z. Liu, "Recovery of Butyl Acetate in Wastewater of Penicillin Plant by Solvent Sublation II. Theoretical Modeling," *Sep. Sci. Technol.*, **40**(4), 941-957 (2005).
5. X. Hu, Z. D. Chang, X. H. Sun, S. F. Shen, and Z. Xie, "Enrichment of Butyl Acetate in Discharged Water from Penicillin Production by Solvent Extraction Through Bubble Separation," *Chin. J. Antibiotics* (in Chinese), **30**(1), 38-41 (2005).
6. X. H. Sun, Z. D. Chang, X. Hu, S. F. Shen, and H. Z. Liu, "Nonfoaming Bubble Separation for Recovery of Butyl Acetate from Discharged Wastewater During Penicillin Production," *Chin. J. Chem. Eng.*, **13(3)**, 329-333 (2005).
7. X. H. Sun, Z. D. Chang, Z. T. An, and H. Z. Liu, "A Method and Apparatus of Air-Assisted Solvent Extraction," Chinese Patent, No.200510115735.X, 16 October 2005.
8. F. Chen, J. A. Finch, P. A. Distin, and C. A. Gomez, "Air-Assisted Solvent Extraction," *Can. Metall. Q.*, **42**(3), 277-280 (2003).
9. H. M. Tarkan and J. A. Finch, "Air-Assisted Solvent Extraction: Towards a Novel Extraction Process," *Miner. Eng.*, **18**(1), 83-88 (2005).
10. H. M. Tarkan and J. A. Finch, "Foaming Properties of Solvent for Use in Air-Assisted Solvent Extraction," *Colloids Surf., A,* **264**(1-3), 126-132 (2005).
11. H. M. Tarkan, S. Gélinas, and J. A. Finch, "Measurement of Thickness and Composition of a Solvent Film on a Bubble," *J. Colloid Interface Sci.*, **297**(2), 732-737 (2006).
12. A. M. Dehkordi, "Novel Type of Impinging Streams Contactor for Liquid-Liquid Extraction," *Ind. Eng. Chem. Res.*, **40**(2), 681-688 (2001).

ULTRA-FAST EXTRACTION OF AN ETHYL ESTER OF DOCOSAHEXAENOIC ACID WITH SILVER ION USING SLUG FLOW

E. Kamio, Y. Seike, H. Yoshizawa, and T. Ono

Department of Environmental Chemistry and Materials, Okayama University, 3-1-1, Tsushima-naka, Okayama-shi, Okayama, 700-8530, Japan.
Corresponding author email address: tono@cc.okayama-u.ac.jp

ABSTRACT

The liquid-liquid extraction dynamics of docosahexaenoic acid ethyl ester (DHA-Et) with silver ion was investigated with a slug flow prepared by microreactor. The extraction mechanism and kinetic parameters were determined using a Lewis cell. A rate equation containing the diffusion and the complex-formation resistances was proposed, and the uptake curves of DHA-Et extraction for the slug-flow system were predicted. Comparing the calculated and experimental uptake curves, the characteristics of slug flow were defined, and the most influential parameters in the ultra-fast extraction of slug flow system were identified.

INTRODUCTION

With growing public interest in the considerable impact on health of N-3 polyunsaturated fatty acids (PUFA), various products such as food additives and medical supplies have been developed. Docosahexaenoic acid (DHA) is the representative N-3 PUFA, which is contained in fish oils with many other fatty acids. There is a great demand for an effective separation and purification technique of PUFA. Separation of PUFA ethyl ester (PUFA-Et) by liquid-liquid extraction with silver ion is one of the effective methods [1]. Recently, we demonstrated the effective extraction of DHA-Et with silver ion by utilizing slug flow prepared with a T-shape microchip [2].

In this study, we carried out a kinetic investigation of DHA-Et extraction dynamics with silver ion. The aims of this study were the determination of the kinetic parameters and the modeling the extraction of DHA-Et with slug flow. A Lewis cell was used to determine the kinetic parameters, and an overall rate equation containing the diffusion resistances as well as the complex-formation reaction resistance was proposed to predict the uptakes of DHA-Et with slug flow. We also discuss the characteristics of the slug flow and evaluate the influential parameters on the ultra-fast extraction.

EXPERIMENTAL

DHA-Et with >98 % purity was kindly supplied by Bizen Chemical Co. Ltd. Other chemicals, such as silver nitrate, sodium nitrate, and *n*-heptane were of guaranteed grade. The organic phase was prepared by dissolving DHA-Et in *n*-heptane. The aqueous phase was prepared by dissolving silver nitrate and sodium nitrate in ultra-pure water. The ionic strength of aqueous solutions was adjusted to 4.0×10^3 mol m^{-3}.

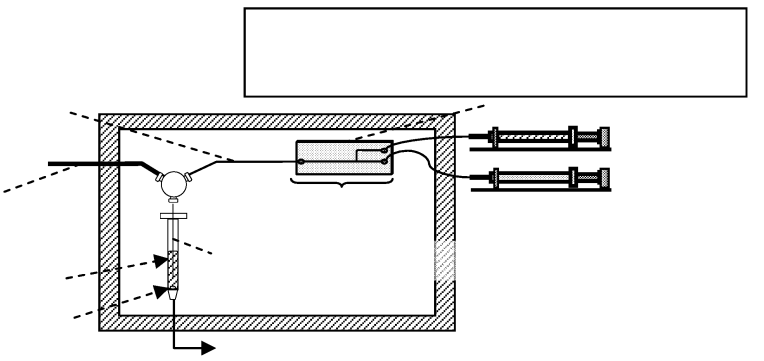

Experimental Procedure

Measurement of Extraction Rate with Lewis Cell

The initial extraction rate was measured by using a Lewis cell with an interface area of 3.14×10^{-4} m^2 immersed in a thermostatic bath. An aliquot (1.25×10^{-4} m^3) of an aqueous solution was first introduced, and then 1.16×10^{-4} m^3 of an organic solution was quickly but carefully introduced in the cell. The mixture was immediately stirred by four flat-blade stirrers in order not to disturb the interface. Samples of the organic phase (3.5×10^{-7} m^3) were taken at desired intervals. The DHA-Et concentration in the sample was measured by a gas chromatograph equipped with a flame ionization detector (GC-14A, Shimadzu Co., Ltd.). The initial extraction rates were measured under various experimental conditions: stirring speed 0.583–1.083 s^{-1}, DHA-Et concentration 5–50 mol m^{-3}, and Ag^+ concentration 1.4×10^3 to 2.9×10^3 mol m^{-3}. We also measured the temperature dependence of the initial extraction rate in order to determine the activation energy and frequency factor. Temperature was varied in the range of 278–313 K.

Extraction of DHA-Et with Slug Flow Prepared with a Microreactor

The experimental set-up for DHA-Et extraction with slug flow is shown in Figure 1. A glass chip with a T-shaped microchannel (MP4B-15, Toso Co. Ltd.) was used to prepare the slug flow. The aqueous and organic phases were fed with syringe pumps (BS-MD1001, Bioanalytical Systems, Inc.). Behind the glass chip, PTFE tubes of internal diameter 5×10^{-4} m with various lengths were connected. In the PTFE tube, DHA-Et was extracted from the organic division to the aqueous division of the slug flow. At steady state, the slug flow was introduced into a syringe wherein organic and aqueous

phases quickly separated from each other and the aqueous phase was continuously removed from the syringe with an HPLC pump to prevent the extraction of DHA-Et in the syringe. After a desired time passed, 5×10^{-7} m^3 of the organic phase was collected, and the concentration of DHA-Et was measured by using gas chromatography. All experiments were carried out twice, and the reproducibility was confirmed.

THEORETICAL SECTION

Determination of the Apparent Rate Constant for Complex Formation Reactions

The apparent rate constant for complex-formation reactions between DHA-Et and silver ion, k_1, was determined as follows. It should be noted that the theory described below is only applicable for the case in which diffusion resistance is ignored. Such condition can be realized by using a Lewis cell. The complex formation rate of DHA-Et with silver ion near the interface, W_{com}, can be expressed as Eq. (1). In the case that the diffusion resistance is considered negligible, W_{com} is the overall mass transfer rate:

$$W_{com} = -\frac{\mathrm{d}\overline{[\text{DHA-Et}]}_b}{\mathrm{d}t} = \frac{A}{V_{org}} \frac{k_1 [\mathrm{Ag}^+]_{b,0}{}^m \overline{[\text{DHA-Et}]}_{b,0}}{\overline{[\text{DHA-Et}]}_{b,0} - \overline{[\text{DHA-Et}]}_{b,eq}} \left(\overline{[\text{DHA-Et}]}_b - \overline{[\text{DHA-Et}]}_{b,eq} \right) \quad (1)$$

where A and V denote the area of the liquid-liquid interface and the volume of the liquid phase, respectively, m and t are the apparent reaction order for Ag^+ concentration and time, respectively, and subscripts "org", "b", "0", and "eq" mean the organic phase, bulk, initial state, and equilibrium state, respectively. The over-bar denotes organic phase. Integrating Equation 1 under the initial condition; $\overline{[\text{DHA-Et}]}_b = \overline{[\text{DHA-Et}]}_{b,0}$ at $t = 0$,

$$-\ln \frac{\overline{[\text{DHA-Et}]}_b - \overline{[\text{DHA-Et}]}_{b,eq}}{\overline{[\text{DHA-Et}]}_{b,0} - \overline{[\text{DHA-Et}]}_{b,eq}} = \frac{A}{V_{org}} \frac{k_1 [\mathrm{Ag}^+]_{b,0}{}^m \overline{[\text{DHA-Et}]}_{b,0}}{\overline{[\text{DHA-Et}]}_{b,0} - \overline{[\text{DHA-Et}]}_{b,eq}} t \quad (2)$$

Therefore, from the slope of the plot based on Equation 2, k_1 was determined.

Derivation of the Theoretical Model for the Process Utilizing Slug Flow

In order to predict the uptake of DHA-Et extraction with slug flow, a theoretical model was derived considering the diffusion resistance in the both aqueous and organic phases and the reaction resistance of complex formation on the liquid-liquid interface. The derivation of the theoretical model is presented below.

Diffusion of DHA-Et Through the Organic Film to the Interface

With a linear driving-force approximation, the mass-transfer rate of DHA-Et through the organic film, W_{org}, can be expressed as follows:

$$W_{org} = A \frac{D_{org}}{\delta_{org}} \left(\overline{[\text{DHA-Et}]}_b - \overline{[\text{DHA-Et}]}_i \right) \quad (3)$$

where D and δ denote the diffusion coefficient and liquid laminar-film thickness, respectively, and subscript "i" denotes near the interface.

Complex Formation Reaction of DHA-Et with Silver Ion Near the Interface

Considering the stepwise complex formation reaction, the complex-formation rate of DHA-Et with silver ion near the interface, W_{com}, can be written as follows:

$$W_{com} = A\left(k_1[\overline{\text{DHA-Et}}]_i[\text{Ag}^+]_i^{\,m} - k_2[\text{com}]_i\right) \tag{4}$$

where "com" is the extracted complex. $[\overline{\text{DHA-Et}}]_i$ can be replaced by $[\overline{\text{DHA-Et}}]_{b,eq}$ and $[\text{Ag}^+]_{b,0}$ with the extraction equilibrium constant of DHA-Et with silver ion. Therefore, Equation 4 is rewritten as follows:

$$W_{com} = Ak_1[\text{Ag}^+]_{b,0}^{\,m}\left([\overline{\text{DHA-Et}}]_i - \frac{[\text{com}]_i}{K_{ex}[\text{Ag}^+]_{b,0}^{\,n}}\right) \tag{5}$$

Diffusion of Extracted Complex Through the Aqueous Film to the Aqueous Bulk

The mass transfer rate of extracted complex, com, through the aqueous laminar film, W_{aq}, can be expressed with a linear driving force approximation as follows:

$$W_{aq} = A\frac{D_{aq}}{\delta_{aq}}([\text{com}]_i - [\text{com}]_b) \tag{6}$$

Rate Equation for the Overall Process of DHA-Et Extraction

By assuming a quasi-steady-state for the overall process, it is considered that Equations 3, 5, and 6 are equal to the reaction rate of DHA-Et, $-r_{DHA\text{-}Et}$. In addition, considering the mass-balance of DHA-Et, $-r_{DHA\text{-}Et}$ can be expressed as:

$$-r_{DHA\text{-}Et} = -V_{org}\frac{\mathrm{d}[\overline{\text{DHA-Et}}]_b}{\mathrm{d}t} = \frac{(1+\beta)[\overline{\text{DHA-Et}}]_b - \beta[\overline{\text{DHA-Et}}]_{b,0}}{\alpha} \tag{7}$$

where $\alpha = \frac{\delta_{org}}{AD_{org}} + \frac{1}{Ak_1[\text{Ag}^+]_{b,0}^{\,m}} + \frac{\delta_{aq}}{AD_{aq}}\frac{1}{K_{ex}[\text{Ag}^+]_{b,0}^{\,n}}$ and $\beta = \frac{1}{K_{ex}[\text{Ag}^+]_{b,0}^{\,n}}\frac{V_{org}}{V_{aq}}$.

Integrating Equation 7 under the initial condition, $[\overline{\text{DHA-Et}}]_b = [\overline{\text{DHA-Et}}]_{b,0}$ at $t = 0$, Equation 8 can be derived.

$$[\overline{\text{DHA-Et}}]_b = \frac{\beta + \exp\{-(1+\beta)t/(\alpha \cdot V_{org})\}}{1+\beta}[\overline{\text{DHA-Et}}]_{b,0} \tag{8}$$

RESULTS AND DISCUSSION

Determination of Kinetic Parameters for Complex Formation with a Lewis Cell

At first, the effect of stirring speed on the initial extraction rate was investigated so as to determine the experimental conditions in which the mass-transfer resistance of diffusion can be considered negligible. It was confirmed that the mass-transfer resistance of diffusion is negligible with a stirring speed over 0.833 s^{-1}. Therefore, subsequent experiments were carried out with stirring speeds of 1.0 s^{-1}. The initial extraction rates for various DHA-Et concentrations and silver ion concentrations were measured. From these experiments, the reaction order was confirmed to be 1, and the value of m was found to be 2.5. Subsequently, in order to determine k_1, a graph based on Equation 2 for different temperatures was plotted. The results are given in Figure 2. The plots show a proportional relationship, and k_1 was determined from the slopes. With the determined k_1, an Arrhenius plot was made. The Arrhenius plot shows a linear relationship, and the activation energy E_a and frequency factor k_0 were determined as -54.29 kJ mol^{-1} and 2.88 $\times$ 10^{-23} $m^{8.5}$ mol^{-2} s^{-1}, respectively. The negative activation energy indicates that some 1:1–1:6 complex formation reactions are the rate-controlling steps [3]. With the determined parameters and Equation 8, the uptakes determined from the Lewis cell were calculated for various experimental conditions. The calculated results show reasonable agreement to the experimental data when δ is taken as 5 $\times$ 10^{-6} m. This reasonable δ shows that the proposed model and determined kinetic parameters are adequate.

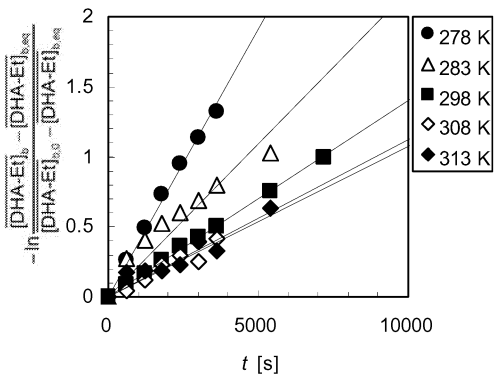

Figure 2. Plots based on Equation (2).

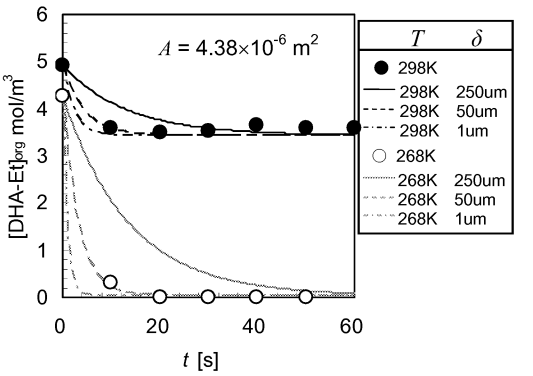

Figure 3. Uptakes for slug-flow system.

Simulating the Uptake Curves of DHA-Et Extraction with the Slug Flow

Figure 3 shows the experimental results of DHA-Et extraction at 298 and 268 K. The experiments were carried out by using the aqueous phases containing 2.0 $\times$ 10^3 mol m^{-3} of Ag^+. The flow rates of both phases were 1.67 $\times$ 10^{-9} m^3 s^{-1}. As shown in Figure 3, equilibration was completed within 20 s by utilizing the slug flow. We tried to elucidate the reason for the ultra-fast extraction with slug flow from the theoretical calculation. The solid, broken and dash-dotted lines in Figure 3 are the calculated uptake curves using

Equation 8 with the determined kinetic parameters. In the calculation, three different values of liquid laminar film thickness and two different interfacial areas were used to discuss the characteristics of the slug flow. At first, the interfacial area is considered. The calculated uptakes shown in Figure 3 were obtained when the columnar area of the unit slug was used as the interfacial area. The calculated lines fit well to the experimental data for δ = 50 μm. We also calculated the uptakes with the sum of the circular area of both ends of the unit slug as the interfacial area; however, the results did not fit the experimental data even for values of δ between 100 nm and 250 μm. The results for the two different interfacial areas indicate that the side of either aqueous or organic phases of the slug as well as in front and behind the slug take part in the mass transfer and the complex-formation reaction. Secondly, the thickness of the liquid laminar film is considered. Comparing the experimental results with those calculated in Figure 3, it is found that the reasonable liquid film thickness is less than 50 μm. Although there is insuffucient experimental data for early periods of extraction to discuss the effect of liquid-film thickness, it can be concluded that the liquid laminar film thickness is less than half of the inner diameter of the channel (2.5×10^{-4} m), which corresponds to the liquid laminar film thickness in the slug created under stillness conditions. It is suggested that the reduction of the liquid film thickness is due to internal circulation.

CONCLUSIONS

The extraction dynamics of DHA-Et with Ag^+ were investigated with the Lewis cell. The DHA-Et extraction was found to be first order with respect to DHA-Et and 2.5th order with respect to Ag^+. Based on the proposed model, the apparent rate constant for complex-formation reaction between DHA-Et and Ag^+ was determined for different temperatures. The overall rate equation containing the diffusion resistances and complex-formation resistance was proposed, and the DHA-Et extraction for the slug flow system was predicted. The calculated uptakes corresponded well to the experimental data. Comparing the experimental uptake curves with the calculated values, we conclude that the influential parameter on the ultra-fast extraction of the slug-flow system is the large specific interfacial area caused by the presence of wall film and the thin liquid film caused by internal circulation.

REFERENCES

1. M. Teramoto, H. Matsuyama, N. Ohnishi, S. Uwagawa, and K. Nakai, “Extraction of Ethyl and Methyl Esters of Polyunsaturated Fatty Acids with Aqueous Silver Nitrate Solutions,” *Ind. Eng. Chem. Res.*, **33**, 341 (1994).
2. Y. Seike, E. Kamio, T. Ono, and H. Yoshizawa, “Extraction of Ethyl Ester of Polyunsaturated Fatty Acids by Utilizing Slug Flow Prepared by Microreactor,” *J. Chem. Eng. Jpn.*, in press.
3. T. Shimomura, K. J. Toile, J. Smid, and M. Szwarc, “Energy and Entropy of Activation of Propagation by the Free Polystyryl Anions and Their Ion Pairs. The Phenomenon of ‘Negative’ Activation Energy,” *J. Am. Chem. Soc.*, **89**, 796 (1967).

FUNDAMENTALS AND POTENTIAL APPLICATIONS OF CLOUD-POINT EXTRACTION

M. A. Ensor and K. L. Nash

Chemistry Department, Washington State University, Pullman, WA 99163.
Corresponding author email address: mensor@wsu.edu

ABSTRACT

Cloud Point Extraction (CPE) is a separation process which uses a surfactant in an aqueous system to preconcentrate metal-ligand complexes into a surfactant-rich phase (SRP). Interest has been shown in the application of this process to f-elements. The mechanisms of extraction into the SRP and its structure have yet to be elucidated. The objective of this investigation is to better understand the mechanism of formation of the SRP and the driving forces attendant to f-element partitioning between phases. Spectroscopic techniques as well as additives have been used to explore effects on extraction efficiency and structure.

INTRODUCTION

As nuclear reactors become a more significant contributor to energy generation in the United States, a separations process needs to be put in place to minimize storage of spent nuclear fuel. Several processes have been developed and have demonstrated the capabilities for such separations. However, there is still a desire to improve and/or simplify the separations processes. A crucial part of spent-fuel reprocessing is the separation of lanthanides and trivalent actinides, which is notoriously difficult. If the trivalent actinides could be stabilized in a higher oxidation state, separation from the lanthanides could be achieved with greater ease.

In a classical solvent-extraction system it may be problematic to keep some actinides in an unusual oxidation state, partly due to redox interference from the organic phase. One possibility is to use a system without a "classic" organic phase. An example of such a system is cloud point extraction (CPE), a relatively new separation technique. The technique potentially offers many advantages over traditional solvent extraction, including the possibility of stabilizing unusual oxidation states of actinides in the "organic phase." The separation process uses a surfactant to selectively concentrate metal-ligand complexes into a smaller-volume "organic phase" called the surfactant-rich phase (SRP). Both phases are predominantly aqueous, thus eliminating complications associated with the use of organic solvents. The SRP partitions from the mixture of surfactant and water by means of either a temperature shift or electrolyte addition, resulting in separation and preconcentration [1]. The key to the preconcentration of a

metal is that the metal-ligand complex has higher affinity for the SRP than the bulk aqueous phase. While CPE has been applied successfully to transition metals [2], only limited interest has been shown in its application to the f-elements [3].

Analytical applications of CPE have been exploited but with little understanding of the physical properties of the separation process and subsequent SRP. A more thorough understanding of the system would allow for better separation designs and more efficient extraction. One way to help elucidate the mechanism of extraction and structure of the SRP is to monitor the effect of additives on the system. There have been literature reports on the effect of electrolytes in surfactant systems [4]; however, the effects of these electrolytes on the extraction efficiency and structure of the surfactant-rich phase are mostly unknown, and understanding the effects of electrolytes on the system will provide insight into the mechanism of extraction and phase formation.

For a CPE system, electrolytes are known to either "salt-in" or "salt-out." In CPE the effect of an electrolyte on the system can easily be determined by the change in the cloud-point temperature (CPT). For electrolytes that "salt-in," the CPT is raised and for those which "salt-out," the temperature is lowered [1]. Electrolytes which salt-in typically contain large anions with low charge density, such as ClO_4^-, I^-, and SCN^-. They salt-in by extending the solubility of the surfactant in the aqueous phase. This is done by complexation of the electrolyte with the ether groups on the surfactant or by the destructuring of water [4]. Electrolytes which are known to salt-out typically have anions with a high charge density, such as CO_3^{2-}, Cl^-, and F^-. They salt-out by reducing the solubility of the surfactant in the aqueous phase. This is done by increased water-molecule association or dehydration of the surfactant [4]. The effect of an electrolyte and the cation and anion components may be quantified using the change in the CPT [5].

The aim of this study was to examine CPE as a potential method of separation for lanthanides and actinides as well as to develop a better fundamental understanding of the system using spectroscopic techniques. A new separation system using 1-phenyl-3-methyl-4-benzoyl-5-pyrazolone (PMBP) with Eu was investigated, and the effect of electrolytes on extraction efficiency was examined. In addition, the influence of electrolytes on the CPT and IR spectra are reported and discussed.

EXPERIMENTAL

All chemicals, including all salts, were used as received. Triton X-114 came from Fluka Biochemika and contained <1% H_2O and <0.001% peroxides. PMBP came from Acros Organics. A stock solution of 20 wt % Triton X-114 was prepared and used for all experiments. All experiments were performed using 2 wt % surfactant.

For determination of the cloud-point temperature of various electrolyte solutions, the samples all had a total volume of 12 mL with 2 wt % Triton X-114 and salt concentrations from 0.01 M to 1 M. The solutions were homogenized and placed in a VWR digital thermostated water bath at a temperature at which the samples were clear, indicating they were below their CPT. Cloud-point determination was accomplished by increasing the temperature until the solutions were visibly cloudy. The temperature was raised 1° C every 40 minutes, allowing for a CPT determination of ± 1 °C.

A Thermo Nicolet 6700 FT-IR with diamond 30,000–200 cm^{-1} and equipped with single-reflection attenuated total reflection feature was used for this study with 10 mL total volume used for all samples. The salt concentrations ranged from 0.01 M to 6 M depending upon the solubility of the individual salts. The samples were then placed in a 60 °C water bath for 20 min., removed, and placed on ice. After cooling, the SRP became very viscous, and separation could be achieved by simply decanting the aqueous phase off. The SRP was used for the IR analysis.

For the distribution study, $^{152/154}Eu$ was used as a tracer. PMBP was the ligand used and was present in a concentration of 10^{-4} M. A total volume of 4.5 mL and incubation at 60 °C for 20 min. were used for all samples. Aliquots of 200 µL were taken from both phases and counted for gross gamma on a NaI (Tl) solid scintillation counter, a Packard Cobra II Auto Gamma.

RESULTS AND DISCUSSION

CPT Study

The cloud-point of Triton X-114 can be affected by salts. In Figures 1 and 2 the effect of different salts on the CPT is shown. Most salts change the CPT, but some salts have little or no effect. The CPT for a 2 wt % solution of Triton X-114 without any salt is 26 °C. The addition of Br^- and NO_3^- salts result in CPTs which do not vary from 26 °C by more than 3 °C. This indicates not only that the NO_3^- and Br^- anions have little to no effect on the CPT but also that the cations in this study associated with these anions (K^+, NH_4^+, Na^+, and $(CH_3)_4N^+$) have little or no effect on the CPT.

Other salts changed the CPT of the Triton X-114 solution quite dramatically as shown in Figures 1 and 2. Figure 1 shows the salts that raised the CPT, salting-in while Figure 2 shows the salts which lowered the CPT, salting-out. ClO_4^-, I^-, and SCN^- are anions which strongly salt-in due to their destructuring nature, and the dramatic increases in the CPT are expected.

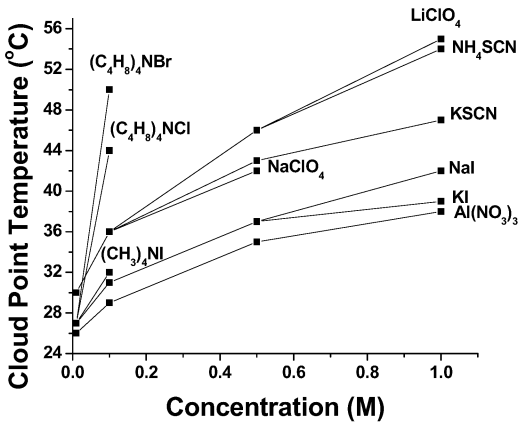

Figure 1. Effect of salting-in electrolytes on CPT.

However, $(C_4H_8)_4NBr$, $(C_4H_8)_4NCl$, and $Al(NO_3)_3$ salts, which contain anions that either have no effect on the CPT (NO_3^- and Br^-) or are known to salt-out (Cl^-), decrease the CPT. This indicates that the cation of these salts may be controlling the salting-in effect. This is unexpected, since anions typically dominate any effect a salt may have in solution [6]. In particular $(C_4H_8)_4N^+$ very strongly salts in as the CPT of the 0.5 M and 1 M solutions were well above 75 °C and have not yet been accurately determined.

Figure 2 shows those electrolytes which salt-out and these include CO_3^{2-}, Cl^-, F^-, and SO_4^{2-} salts. No cation effects are observed here indicating the dominance of the anion effect. All the salts observed to lower the CPT contain anions with a high charge density and which are known to structure water.

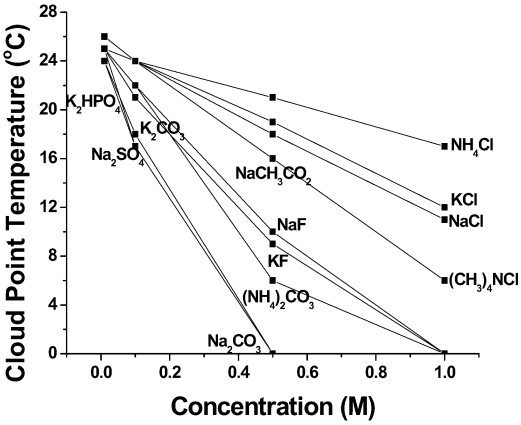

Figure 2. The effect of salting-out electrolytes on CPT.

Distribution Study

PMBP was found to have a Eu extraction efficiency into the SRP of >92% in the pH range 2.5 to 3.5. A pH of 3 was chosen for all subsequent distribution experiments. Distribution studies were done in the presence of 0.5 M salt with and without PMBP. Figure 3 shows the increase in the distribution ratio of Eu that is observed with salts which increase the CPT. Overall there appears to be a trend. Those salts which salt-in most strongly have the highest distribution ratio of Eu, which may be an effect of higher water solubility in the SRP observed in the IR study presented below.

In the presence of ligand the D values are significantly higher. However, any trend is not clearly seen as shown in Figure 4. How PMBP affects the system and the effect of additives on the system is not yet clear.

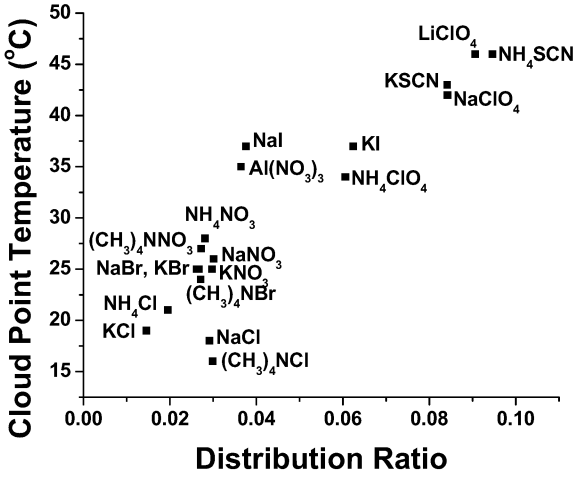

Figure 3. Distribution ratio of salts as a function of CPT without PMBP.

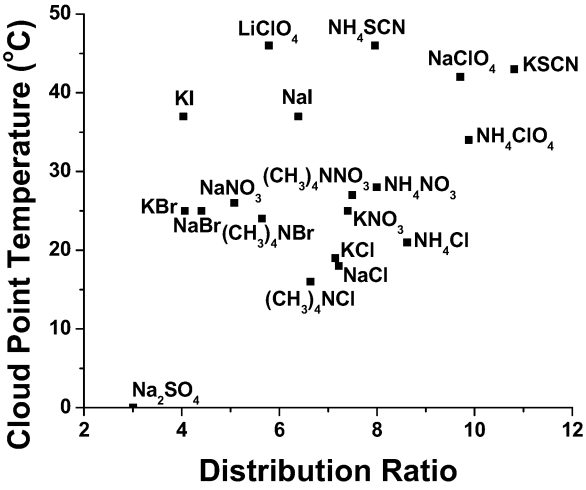

Figure 4. Distribution ratio of salts in the presence of PMBP.

IR Study

As the salt concentration was increased, changes are visible in the IR spectra of the SRP of most salts. The predominant changes occurred in the O-H stretches around 3300 cm^{-1} and 1600 cm^{-1} and in the surfactant fingerprint region. For salts such as $(CH_3)_4NCl$ that salt-out, there is a dramatic decrease in the intensity of the O-H stretching with increasing salt concentration and a dramatic increase in the intensity of the surfactant fingerprint region. For KSCN, which salts-in, there is less effect on the IR spectra, as the decrease in the O-H stretching intensity and increase in intensity in the surfactant fingerprint region are both significantly less dramatic. These results seem to

indicate more water is present in the SRP for the salts that salt-in and less water present in the SRP for salts that salt-out.

CONCLUSIONS

From the studies conducted thus far, it appears that water and/or salt content in the SRP plays a vital role in the extraction of Eu. It is necessary to quantify salt and water content in both phases to gain further evidence for their roles, which will be done using a Karl Fischer titrator and ion selective electrodes.

REFERENCES

1. W. Hinze and E. Pramauro, "Critical Review of Surfactant-Mediated Phase Separations (Cloud-Point Extractions): Theory and Applications," *Crit. Rev. Anal. Chem.*, **24**(2), 133-177 (1993).
2. H. Watanabe and H. Tanaka, "A Non-Ionic Surfactant as a New Solvent for Liquid-Liquid Extraction of Zinc (II) with 1-(2-Pyridylazo)-2-Naphthol," *Talanta*, **25**(10), 585-589 (1978).
3. N. De Jong, M. Draye, A. Favre-Reguillon, G. LeBuzit, G. Cote, and J. Foos, "Lanthanum (III) and Gadolinium (III) Separation by Cloud Point Extraction," *J. Colloid Interf. Sci.*, **291**, 303-306 (2005).
4. M. Morini, P. Messina, and P. Schulz, "The Interaction of Electrolytes with Non-Ionic Surfactant Micelles," *Colloid Polym. Sci.*, **283**, 1206-1218 (2005).
5. H. Schott, A. Royce, and S. Han, "Effect of Inorganic Additives on Solutions of Nonionic Surfactants. VII. Cloud Point Shift Values of Individual Ions," *J. Colloid Interf. Sci.*, **98**(1), 196-201 (1984).
6. H. Schott, "Effect of Inorganic Additives on Solutions of Nonionic Surfactants. XIV. Effect of Chaotropic Anions on the Cloud Point of Octoxynol (Triton X-100)," *J. Colloid Interf. Sci.*, **189**, 117-122 (1997).

CLOUD POINT (TWO-AQUEOUS PHASE) EXTRACTION OF HEAVY METAL SALTS

L. J. Nogueira Duarte[1] and J. P. Canselier[2]

[1]Centro Federal de Educação Tecnológica da Bahia (CEFET-BA), Via Universitária, s/n, Pitanguinhas, Simões Filho, Bahia - Cep: 43.700-000. [2]Laboratoire de Génie Chimique (UMR CNRS 5503, ENSIACET- INPT/UPS) BP 1301, F31106 Toulouse Cedex 01, France.
Corresponding author email address: JeanPaul.Canselier@ensiacet.fr

ABSTRACT

Above a temperature called the "cloud point" (T_c), the aqueous solutions of most polyethoxylated nonionic surfactants separate into two equilibrium phases: a surfactant-rich one (coacervate) and a dilute one. Micellar solubilization allows two-aqueous phase extraction and concentration of hydrophobic or amphiphilic compounds into the small volume of coacervate. For electrolytes (e.g., heavy metal salts), the use of ionic/nonionic mixed micelles makes a chelating agent unnecessary. Such a cloud-point extraction may be applied to the decontamination of industrial effluents containing metal or organic compounds (soluble or dispersed pollution) or to the concentration or even the separation of high value-added substances. This is therefore a "green chemistry" process, that is, environmentally friendly and energy-saving. Cloud-point extraction of metal ions (Ni^{2+}, Cd^{2+}, Pb^{2+}, and Cr^{3+}) with mixed micelles of polyethoxylated alcohols (C_iE_j) and anionic surfactants (sodium dodecylsulfate "SDS" or dodecylbenzenesulfonates "SDBS") is achieved from model solutions of metal nitrates, possibly mixed with organics. The results are promising, due to extraction percentages lying between 50 and 90% and small volume fractions of coacervate, the best performances being obtained for Pb^{2+}, whose hydration enthalpy is the lowest. Moreover, the ability of those mixed micelles to extract both organic (phenol and 2,4-dimethylaniline) and heavy metal pollutants from model solutions is shown.

INTRODUCTION

The respect of environment is nowadays a worldwide requirement, which implies the development of new curative processes and the design of intrinsically clean processes. Among others, these processes apply to wastewater treatment (water polluted by organics or heavy metals). The criteria of water quality (compliance with regulations) and economy are decisive; in order to take into account the physical and chemical specificities of the effluents, tests with real wastewaters are necessary.

Surfactant adsorption at interfaces makes them useful auxiliaries in several types of extraction processes. On the other hand, volatile organic solvents, commonly used in

liquid-liquid extraction, are subject to more and more severe regulations, due to their toxicity and ecotoxicity. Since the phase diagrams of many polyethoxylated surfactant/water binary systems show a lower consolute point curve, the existence of the corresponding two-phase region can be turned to account to extract metal ions, small organic molecules or biological macromolecules from their dilute aqueous solutions. This operation, known as liquid-coacervate or cloud-point extraction (CPE), consists of two steps: (1) organic solute or metal-chelate complex solubilization into the extractant (aqueous solution of nonionic surfactant) and (2) cloud-point phase separation of this solution into a dilute phase and a surfactant-rich one, called coacervate. Whether the dilute phase or the coacervate is of interest, two main types of applications may be considered: removal of pollutants from aqueous effluents and concentration, recovery, and possibly separation of high added-value substances [1-6].

Since the CPE technique has been proposed, a lot of applications in wastewater treatment have been published. However, previous studies on the removal of dissolved contaminants by CPE were mainly based on the use of single surfactant systems and restricted to some types of organic solutes [4-8]. Few studies have been conducted on the applications of mixed surfactants on the simultaneous removal of metal ions and organic solutes in a CPE process [9]. One of the most important properties of these organized structures is their good capacity to solubilize solutes of different character and nature. These solutes may interact with surfactant aggregates electrostatically, hydrophobically, or a combination of both effects.

This work involves the extraction of soluble electrolytes (Ni^{2+}, Cd^{2+}, Pb^{2+}, and Cr^{3+}), from model solutions with polyethoxylated alcohols (C_iE_j) mixed with anionic surfactants (sodium dodecylsulfate “SDS” or dodecylbenzenesulfonates “SDBS”). The nonionic surfactant, along with its cloud-point property, is responsible for phase separation; the anionic species plays the role of a complexing agent. The CPE technique thus offers a convenient alternative to conventional liquid-liquid extraction that uses organic solvents, with another major interest: the absence of classical but expensive chelating agents for metal ions.

EXPERIMENTAL

Materials

The two anionic surfactants used were sodium dodecylsulfate (SDS 98.5% purity, Aldrich) and sodium dodecylbenzenesulfonate (SDBS 97.5% purity, kindly supplied by Rhodia France). The nonionic surfactant was an oxo-alcohol (Oxo-$C_{10}E_3$). About 20% of the oxo-alcohol chains are branched. This sample was kindly supplied by SEPPIC (Castres, France). The Oxo-$C_{10}E_3$ sample was freed from residual polyols by washing with water at 95 °C. The inorganic salts used were $Pb(NO_3)_2.4H_2O$ (99%, Aldrich), $Cd(NO_3)_2.4H_2O$ (99%, Aldrich), $Ni(NO_3)_2.6H_2O$ (99%, Aldrich), and $Cr(NO_3)_3.9H_2O$ (99%, Aldrich). Reagent-grade phenol, C_6H_5OH, and 2,4-dimethylaniline, $(CH_3)_2C_6H_3NH_2$, were used as received from Aldrich. The water was distilled and deionized.

Procedure

The concentrations of phenol and 2,4-dimethylaniline were measured by a reversed-phase HPLC system consisting of one SpectraSystem P-1000-XR pump, an AS-1000-XR auto injector, a RP18 (ODS) column, and a SpectraSystem UV-2000. The conditions used for the determination of aromatic solute concentrations were as follows: column temperature, 25 °C; pressure, 80 bar; flow rate 1 mL/min of 67/37 (v/v) of H_2O/CH_3CN eluant. Phenol and 2,4-dimethylaniline concentrations were obtained from data processed with the Chromquest 3.0 software.

Inductively coupled plasma, ICP (Jobin Yvon–Ultima 2R), was used to measure the concentration of metal ions in the following conditions: plasma temperature, 8000 °C; air flow rate 20 mL/min; nebulizer pressure, 3.10 bar. The concentration of heavy metal was measured by UV absorption at the relevant wavelength (λ, nm): λ_{Pb} = 220.353; λ_{Cd} = 228.802; λ_{Ni} = 221.647; λ_{Cr} = 283.563.

The polluted aqueous phase and the surfactant solution were mixed together and separated at room temperature or after heating according to the cloud-point curve of the surfactant [10].

RESULTS AND DISCUSSION

Figure 1 represents the ratio, *E*%, of metal ions (Ni^{2+}, Cd^{2+}, Pb^{2+}, and Cr^{3+}) extracted as a function of anionic surfactant (SDS and SDBS) concentration. From zero for pure nonionic micelles, this ratio increases with anionic surfactant concentration. Only for Cr^{3+} is the variation linear in the concentration range studied. The incorporation of an anionic surfactant into nonionic micelles involves Coulombic interactions with metal ions. In other words, the negatively charged micelles cause the cations to bind or adsorb onto the micelle surface; however, the coacervate volume fraction, ϕ_C, increases with surfactant concentration. The main issue is to obtain the best compromise between *E*% (maximum) and ϕ_C (minimum).

The maximum extraction ratios are summarized in Table 1. Extraction efficiency increases in the following order: $E\%_{Pb} > E\%_{Cd} > E\%_{Ni} > E\%_{Cr}$. This order seems to be correlated with those of ionic radii, RI_M ($RI_{Pb} > RI_{Cd} > RI_{Ni} > RI_{Cr}$), hydration enthalpies, $\Delta_h H_M$, and hydration radii, RH_M ($\Delta_h H_{Pb} < \Delta_h H_{Cd} < \Delta_h H_{Ni} < \Delta_h H_{Cr}$; $RH_{Pb} < RH_{Cd} < RH_{Ni} < RH_{Cr}$).

The case of Cr^{3+}, a trivalent cation, is slightly different from those of the other three metal cations, and it makes sense that, although the attraction of Cr^{+3} ions towards the micelle surface is strong, for a given density of micellar charge, Cr^{+3} extraction is less efficient, probably due to the reduction of the charged micelle binding sites for Cr^{+3} to be adsorbed onto the micelle surface. So, to obtain the same performance as with the divalent cations, it is likely that a mixed micelle richer in anionic species should be required. In fact, at least with Oxo-$C_{10}E_3$, the use of higher ratios of anionic surfactant comes up against the precipitation of chromium dodecylsulfate or dodecylbenzenesulfonates.

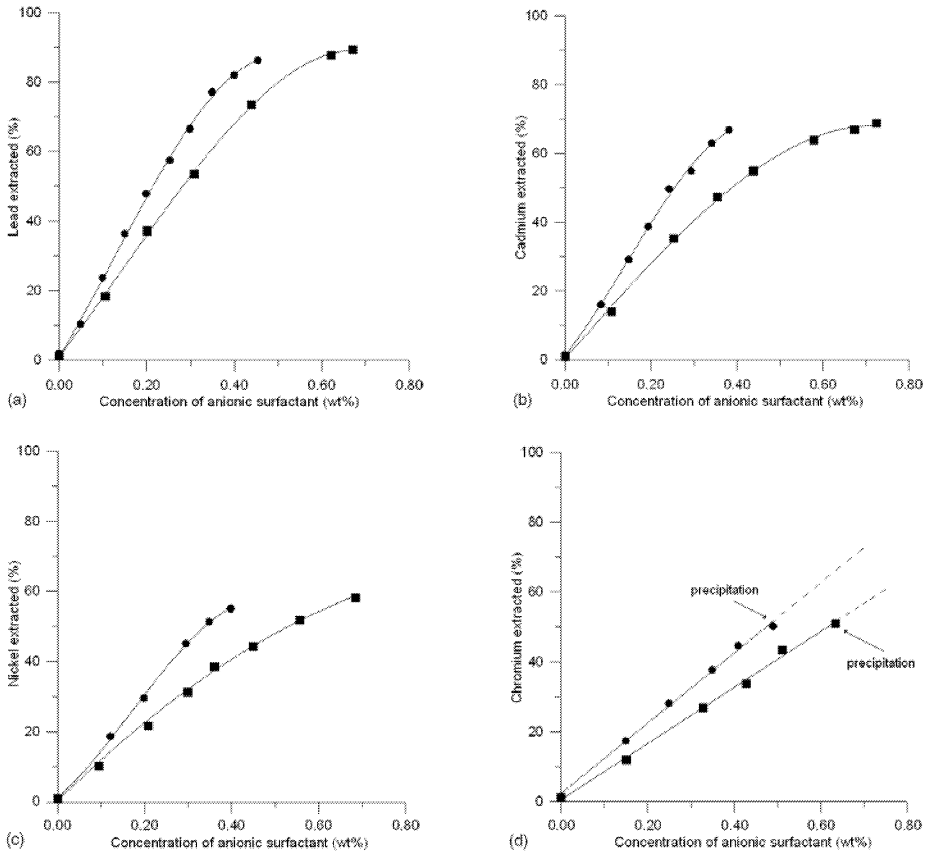

Figure 1. Effect of anionic surfactant concentration on heavy-metal pollutant recovery. (●) SDS, (■) SDBS. Oxo-$C_{10}E_3$ = 2.0%; $[M^{n+}]$ = 1.5 g/L; T = 45 °C. (a) Pb^{2+}, (b) Cd^{2+}, (c) Ni^{2+}, (d) Cr^{3+}.

Table 1. E% maximum for the metal ions

Anionic surfactant	E% (M^{n+})			
	Pb^{2+}	Cd^{2+}	Ni^{2+}	Cr^{3+}
SDS	86	68	55	49
SDBS	90	70	59	51

Figure 2 shows that the recoveries of phenol and 2,4-dimethylaniline are strongly improved when the nonionic surfactant (Oxo-$C_{10}E_3$) concentration increases. Thus, in a 8 wt % Oxo-$C_{10}E_3$ solution, the extents of phenol and 2,4-dimethylaniline recovery are about 90% and 86%, respectively. However, for lead, the effect of the nonionic surfactant concentration is relatively insignificant. The recovery of lead is about 80% in a 4 wt % surfactant solution.

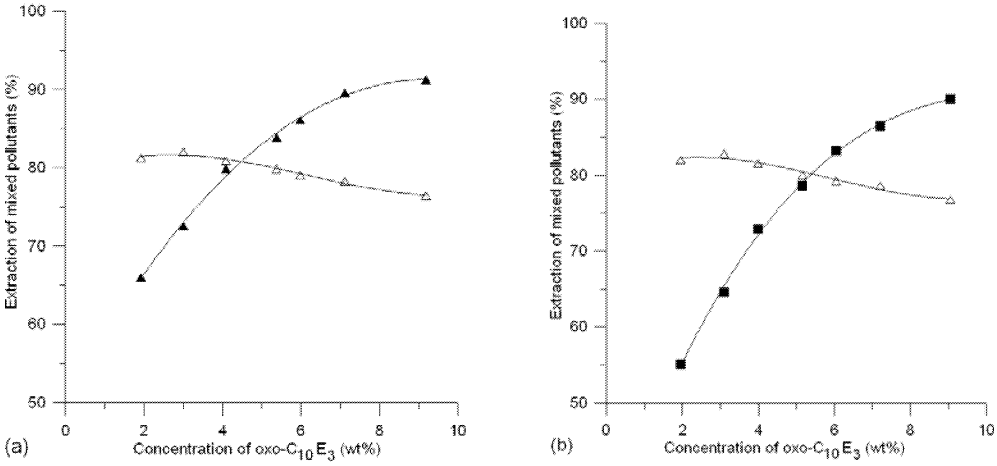

Figure 2. Effect of surfactant concentration on organic and heavy-metal pollutant recovery. SDS = 0.38%, SDBS = 0.60%, [Pb^{2+}] = 1.5 g/L, [Ph] = 2.0 g/L, [DMA] = 1.3 g/L, T = 45 °C. (▲) Phenol, (■) DMA, (Δ) lead,
(a) SDS, (b) SDBS

These results suggest that mixed micelles can form hydrogen bonds between hydroxyl or amino groups and the most available ether oxygen atoms of the polyoxyethylene chain (reducing surfactant solubility) [11]. The rate of recovery in such systems can be correlated to the log P (octanol/H_2O partition coefficient) of the aromatic solutes but not to their aqueous solubility [12]. On the other hand, metal ions bind to the negatively charged surface of anionic surfactant micelles by Coulombic interactions. In summary, metal ions bind or adsorb on the surface of oppositely charged micelles, while organic solutes are solubilized within the micelles.

CONCLUSIONS

A new possibility for the application of CPE involves the use of mixed surfactants as extractants. The combination of the surfactant capacity to solubilize different species can be applied to the extraction of organic and heavy metal pollutants from model solutions. The results are promising, due to extraction percentages lying between 50 and 90%, the best performances being obtained for Pb^{2+}, whose hydration enthalpy is the lowest. Moreover, the ability of those mixed micelles to extract both organic (e.g., phenol and 2,4-dimethylaniline) and heavy-metal pollutants from model solutions is shown. Further studies on the extraction of metals under anionic form or both cationic and anionic forms are currently in progress, affording encouraging results. A compromise is always to be found between E% (maximum) and coacervate volume fraction (minimum). These results all the prediction of a possible treatment of more complex media. In addition, CPE offers the benefit of low cost, easy handling, and reduced toxic effects. Finally, a continuous, multistage process should be developed rather soon.

ACKNOWLEDGMENTS

One of the authors (L.J.N. Duarte) gratefully acknowledges financial support from the CNPq - Brazil.

REFERENCES

1. F. H. Quina and W. L. Hinze, "Surfactant-Mediated Cloud Point Extractions: An Environmentally-Benign Alternative Separation Approach," *Ind. Eng. Chem. Res*., **38**, 4150-4168 (1999).
2. Z. S. Ferrera, C. P. Sanz, C. M. Santana, and J. J. S. Rodriguez, "The Use of Micellar Systems in the Extraction and Pre-concentration of Organic Pollutants in Environmental Samples," *Trends Anal. Chem.,* **23**(7), 479-489 (2004).
3. W. Kimchuwanit, S. Osuwan, J. F. Scamehorn, J. H. Harwell, and K. J. Haller, "Use of a Micellar-Rich Coacervate Phase to Extract Trichloroethylene from Water," *Sep. Sci. Technol*., **35**(13), 1991-2002 (2000).
4. S. Sakulwongyai, P. Trakultamupatam, J. F. Scamehorn, S. Osuwan, and S. D. Christian, "Use of Surfactant Coacervate Phase to Extract Chlorinated Aliphatic Compounds from Water: Extraction of Chlorinated Ethanes and Quantitative Comparison to Solubilization in Micelles," *Langmuir*, **16**, 8226-8230 (2000).
5. P. Trakultamupatam, J. F. Scamehorn, and S. Osuwan, "Removal of Volatile Aromatic Contaminants from Wastewater by Cloud Point Extraction," *Sep. Sci. Technol*., **37**(6), 1291-1305 (2002).
6. R. Carabias-Martinez, E. Rodriguez-Gonzalo, J. Dominguez-Alvarez, C. Garcia-Pinto, and J. Hernandez-Mendez, "Prediction of the Behavior of Organic Pollutants Using Cloud Point Extraction," *J. Chromatogr*., A, 1005, 23-34 (2003).
7. B. Haddou, J. P. Canselier, and C. Gourdon, "Purification of Effluents by Two-Aqueous Phase Extraction," *Trans IChemE (Chem. Eng. Res. Des*.), **81A**, 1185-1192 (2003).
8. B. Haddou, J. P. Canselier, and C. Gourdon, "Cloud Point Extraction of Phenol and Benzyl Alcohol from Aqueous Stream," *Sep. Purif. Technol*., **50**(1), 114-121 (2006).
9. L. Gotlieb, J. W. Bozzelli, and E. Gotlieb, "Soil and water decontamination by extraction with surfactants," *Sep. Sci. Technol*., **28**(1-3), 793-204 (1993).
10. L. J. N. Duarte and J. P. Canselier, **"**Oxo-alcohol Ethoxylates: Surface and Thermodynamic Properties and Effect of Various Additives on the Cloud Point," *Tenside Surf. Deterg*., **42**(5), 299-306 (2005).
11. D. Bai, J. Li, S. B. Chen, and B. H. Chen, "A Novel Cloud-Point Extraction Process for Preconcentrating Selected Polycyclic Aromatic Hydrocarbons in Aqueous Solution," *Environ. Sci. Technol*., **35**, 3936-3940 (2001).
12. L. J. N. Duarte and J. P. Canselier, "Extração de Compostos Orgânicos Homólogos e Isômeros em um Sistema de Duas Fases Aquosas," *Quím. Nova*, **28**(3), 426-432 (2005).

A MEMBRANE PROCESS TO RECOVER EXTRACTANTS FROM RESIDUAL PHASES

S. Wang, W. Qin, and Y. Y. Dai

State Key Laboratory of Chemical Engineering, Department of Chemical Engineering, Tsinghua University, Beijing 100084, China.
Corresponding author email address: qinwei@tsinghua.edu.cn

ABSTRACT

A membrane adsorption and extraction process to recover extractants from residual phases is proposed. D2EHPA and heptane were used as extractant and diluent, respectively, and the emulsion with D2EHPA:*n*-heptane:surfactant (1:1.64:0.062) was used as simulated residual. A hollow-fiber membrane was used as the membrane adsorption and extraction device. The results show that the process provides an effective and relatively simple way to recover extractant from aqueous phase. The tube-side flow rate was found to be an important factor in determining efficiency, whilst other conditions, such as shell-side flow rate and transmembrane pressure difference, have only minor effects.

INTRODUCTION

Oil/water separation plays a crucial role in many technological processes as well as in environmental engineering [1]. One important application concerns phase separation at the end of solvent-extraction processes [2]. In solvent extraction, some kinds of secondary liquid-liquid droplets, emulsions, droplet-film structures, or double emulsions, occur as an undesirable consequence, and these droplets or droplet-film structures are small and stable [3]. Therefore, they are mechanically entrained by the residual phase, and secondary phase separation and recovery of the entrained extractant has an economic as well as environmental significance.

Various apparatus, such as gravity settlers [4-5], adsorption columns [6-8], air flotation units [9], lamellar coalescers [3], and fibrous beds, etc. [10], have been applied for this secondary phase separation in the extraction process. A pilot plant was examined by Spasic [3], and the overall efficiency of the entrained light-phase separation was 92%.

Membrane processes, such as membrane filtration [11-13] and membrane-induced coalescence [14-17], have also been investigated as phase-separation techniques. Daiminger [14] proved that the enlarged droplets could be removed when the dispersion was led through the lumen of hollow fibers. In a membrane process, membrane affinity for substances is very important, and so membranes used in pervaporation have to be highly selective [18]. Furthermore, membrane adsorption in filtration processes was

discussed [19-20]. Adsorption was considered by Comerton [20] to be one of the main mechanisms contributing to compound removal by membrane filtration, in addition to size exclusion and charge repulsion. It is known that the diluent used as a coadjutor in solvent extraction has a better solvency for the extractant in the residual phase than water. It should therefore be possible to remove extractant from the residual phase by mixing it with the diluent [21]; however, direct contact may lead to problems such as phase separation, entrainment of diluent, etc. In recent years, membrane extraction as an alternative to traditional solvent extraction has been widely studied, because it can avoid the problems of entrainment and secondary pollution [22]. At the same time, membrane surface adsorption may play an important role because of its affinity for organic reagents. In this paper, a membrane adsorption and extraction process where the residual phase is contacted with diluent via a hydrophobic membrane is investigated.

EXPERIMENTAL

An emulsion of di-(2-ethylhexyl)phosphate (D2EHPA):*n*-heptane:surfactant (Triton X-114) (1:1.64:0.062) was used as simulating residual phase, with the original concentration of D2EHPA (C_0) being 87.0 mg/L. The critical micelle concentration (CMC) of Triton X-114 at room temperature is about 109 mg/L [23], which is above the experimental concentration, indicating the solution is indeed an emulsion.

The required amounts of D2EHPA and *n*-heptane were added to distilled water, and the mixture was put into a magnetic mixer for 1 h. Finally, the emulsion was stabilized via energy added by an ultrasound system (200 W, 50 kHz). All of our experiments were carried out at 20 °C, which was maintained by air conditioning.

D2EHPA and *n*-heptane were supplied by Sinopharm Chemical Reagent Co. (China), and Triton X-114 was supplied by Aldrich. All reagents were chemically pure and used without further purification.

Steady Process of Membrane Adsorption-Extraction

The emulsion flowed in from the tube side, and *n*-heptane from the shell side. Samples were collected from the outlet of the tube at certain time intervals, and the concentration of D2EHPA (C_W) was analyzed. The hollow fiber membrane module consisted of 254 hollow membrane fibers made of polyvinylidene fluoride, giving an effective length of 313 mm, inner diameter of 42 mm and total membrane area of 0.2 m^2. The inner diameter of each fiber was 0.8 mm, with 0.3 mm wall thickness, and 0.1 μm effective pore size. The concentration of D2EHPA in the aqueous phase was measured by the Ammonium Molybdate Spectrophotometric Method (GB 11893-89, China), and an ultraviolet spectrometer (HP8453, Agilent, USA) was used. Figure 1 shows a schematic view of the experimental unit.

Unsteady Process of Membrane Adsorption-Extraction

In this experiment, both emulsion (0.4 L) and *n*-heptane (0.5 L) were recycled from the module outlet to the respective tank. Other operations stayed the same as above.

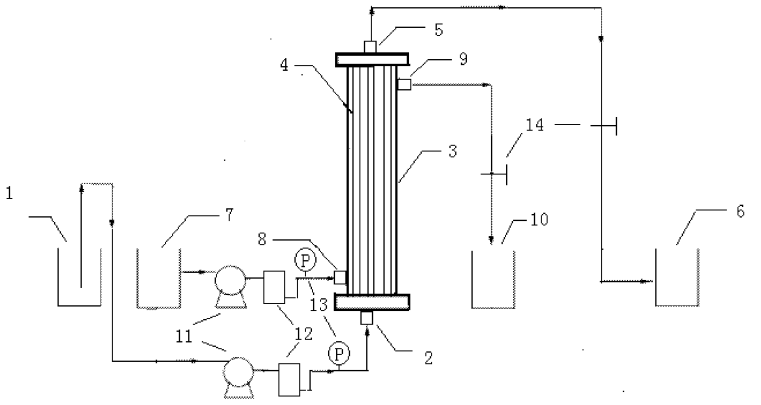

Figure 1. Schematic view of experimental unit: (1) emulsion tank, (2) inlet of tube, (3) hollow-membrane module, (4) hollow-membrane fibers, (5) outlet of tube, (6) treated emulsion tank, (7) diluent tank, (8) inlet of shell, (9) outlet of shell, (10) enriched diluent tank, (11) pump, (12) flux buffer, (13) pressure gauge, and (14) valve.

RESULTS AND DISCUSSION

Membrane Adsorption-Extraction of D2EHPA

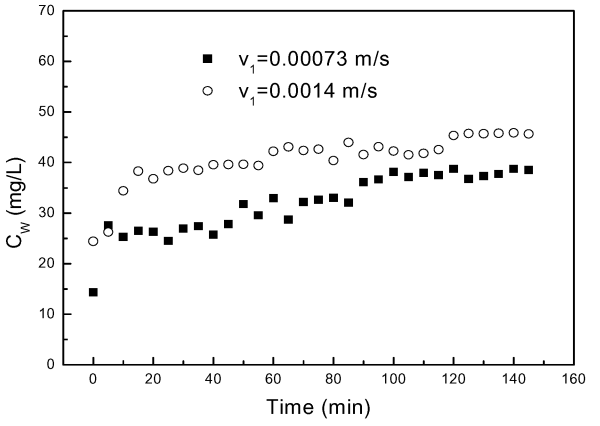

Figure 2. The concentration of D2EHPA at outlet of tube side.
ΔP = 0.4 kPa, v_2 = 0.0004 m/s.

Figure 2 shows the D2EHPA concentration from the outlet with time. The C_W rises first and slowly stabilizes at a steady point. The membrane used is highly hydrophobic, so oil droplets in the emulsion can be adsorbed on the surface. At the beginning, the membrane surface is fresh and has a larger adsorption capacity, but as time goes by, the main adsorption is imposed by the wetted oil on the membrane, and the adsorption capacity slows down. The contemporaneous solvent extraction of D2EHPA with *n*-heptane in the shell side can be considered to be constant. It should be noted that a larger v_1 corresponds to a higher $C_{W,}$ which means the adsorption-extraction capacity

decreases. As the length of membrane module is constant, a larger v_1 results a smaller contact time, although an increase in velocity can improve the mass-transfer processes.

Unsteady Process of Membrane Adsorption-Extraction

In order to simulate the best removal efficiency of D2EHPA for this process, the feed was recycled from the module export to the feed container. Figure 3 shows the concentration of D2EHPA from the outlet with time, demonstrating that the concentration increases at first, then goes through a decline, and finally stabilizes at a low steady point about 9 mg/L (in 80 min.). This trend can be explained by the larger adsorption rate of membrane surface at the beginning of the experiment and the decrease of the D2EHPA concentration at the inlet with time.

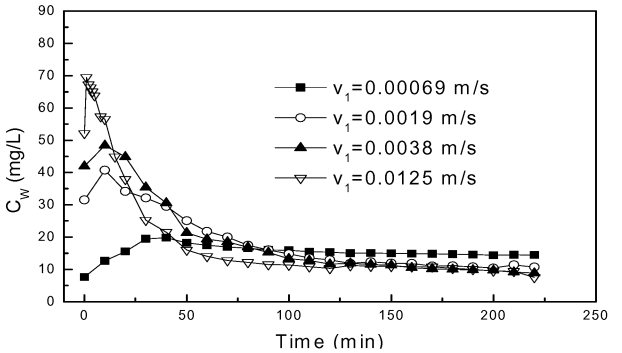

Figure 3. Influence of tube-side velocity on the C_W. C_0 = 87 mg/L, v_2 = 0.0004 m/s, △P = 0.4 kPa.

Thermodynamic equilibrium limits the removal efficiency of D2EHPA. In this experiment, 0.4 L of emulsion through the tube side and 0.5 L n-heptane through the shell side are both recycled, therefore, the final removal efficiency should depend on the equilibrium for one contact. A higher R can be obtained by using multiple contact stages. In order to gain a better understanding of the processes involved in the experiment, the operational factors that might have an effect on the D2EHPA separation, including tube and shell side velocities, and also the transmembrane pressure difference, were investigated. As shown in Figures 3 and 4, a higher tube side velocity results in a higher value of C_W at the beginning but a more rapid decrease, and also a lower steady point within 4 hrs, while the flow rate in the shell side does not apparently affect C_W. It can be concluded that the flow rate on the tube side is a sensitive factor to affect the mass-transfer process. This is because the membrane pores are filled with organic phase, meaning the adsorption and extraction take place in the tube side, and conditions here play a much more important role.

Figure 5 shows the influence of transmembrane pressure difference on separation of D2EHPA. The △P, which mainly determines the interface position of the aqueous and organic stream, has to be controlled within an appropriate range in order to prevent the permeation between two phases. It can be seen that $\triangle P$ plays a negligible role on the process within the selected range.

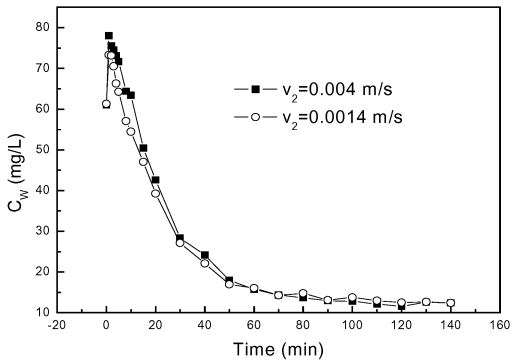

Figure 4. Influence of shell-side velocity. C_0 = 87 mg/L, v_1 = 0.0125 m/s, △P = 0.4 kPa.

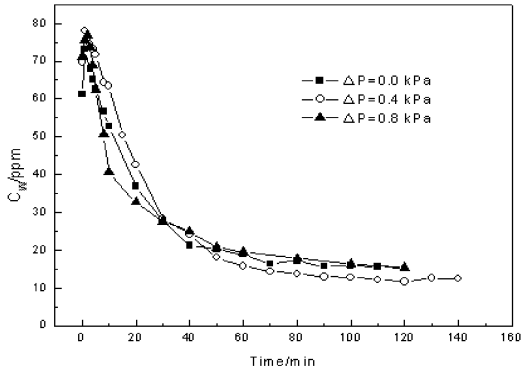

Figure 5. Influence of transmembrane pressure. C_0 = 87 mg/L, v_1 = 0.0125 m/s, v_2 = 0.0004 m/s.

CONCLUSIONS

A new method for secondary phase separation in solvent extraction and membrane adsorption-extraction processes has been developed. Both the affinity of the membrane to the oil droplet of extractant and the extraction of diluent to the soluble extractant in the residual phase contribute to the method. In this experiment, an efficient removal of D2EHPA was achieved via recycling the feed. Several factors were investigated, and it was found that the tube-side velocity has a strong effect on the process, while the shell-side velocity and transmembrane pressure difference are significantly less important factors. The mechanism of the process merits more detailed study.

REFERENCES

1. K. J. Lissant, Demulsification: industrial applications, M. Dekker, New York, 1983.
2. R. E. Treybal, Liquid Extraction, McGraw-Hill, New York, 1963.
3. A. M. Spasic, N. N. Djokovic, M. D. Babic, M. M. Marinko, and G. N. Jovanovic, "Performance of demulsions: entrainment problems in solvent extraction," *Chem. Eng. Sci.*, **52**, 657-675 (1997).

4. J. Golob and R. Modic, "Coalescence of liquid/liquid dispersions in gravity settlers," *Trans. Inst. Chem. Eng.*, **55**, 207-211 (1977).
5. R. Padilla, M. C. Ruiz, and W. Trujillo, "Separation of liquid-liquid dispersions in a deep-layer gravity settler: Part I. Experimental study of the separation process," *Hydrometallurgy*, **42**, 267-279 (1996).
6. M. Seredych and A. Gierak, "Influence of water on adsorption of organic compounds from its aqueous solutions on surface of synthetic active carbons," *Colloid Surf.*, **245**, 61-67 (2004).
7. S. H. Lin and C. P. Huang, "Adsorption of hydrazoic acid from aqueous solution by macroreticular resin," *J. Hazard. Mater.*, **84**, 217-228 (2001).
8. O. Bouras, J. C. Bollinger, M. Baudu, and H. Khalaf, "Adsorption of diuron and its degradation products from aqueous solution by surfactant-modified pillared clays," *Appl. Clay. Sci.*, **37**, 240-250 (2007).
9. A. A. Al-Shamrani, A. James, and H.Xiao, "Separation of oil from water by dissolved air flotation," *Colloid Surf.*, **209**, 15-26 (2002).
10. R. Magiera and E. Blass, "Separation of liquid-liquid dispersion by flow through fibre beds," *Filtr. Separat*, **34**, 369-376 (1997).
11. N. Nabi, P. Aimar, and M. Meireles, "Ultrafiltration of an olive oil emulsion stabilized by an anionic surfactant," *J. Membr. Sci*., **166**, 177–188 (2000).
12. P. Wang, N. Xu, and J. Shi, "A pilot study of the treatment of waste rolling emulsion using zirconia microfiltration membranes," *J. Membr. Sci.*, **173**, 159-166 (2000).
13. I. W. Cumming, R. G. Holdich, and I. D. Smith, "The rejection of oil by microfiltration of a stabilized kerosene/water emulsion," *J. Membr. Sci*, **169**, 147-155 (2000).
14. U. Daiminger, W. Nitsch, P. Plucinski, and S. Hoffmann, "Novel techniques for oil/water separation," *J. Membr. Sci.*, **99**. 197–203 (1995).
15. M. Hlavacek, "Break-up of oil-in-water emulsions induced by permeation through a microfiltration membrane," *J. Membr.Sci.*, **102**, 1-7 (1995).
16. T. Kawakatsu, R. M. Boom, H. Navetani, Y. Kikuchi, and M. Nakajima, "Emulsion breakdown: mechanisms and development of multilayer membrane," *AIChE J.*, **45**, 967–975 (1999).
17. G. Hong, A. Fane, and R. Burford, "Factors affecting membrane coalescence of stable oil-in-water emulsions," *J. Membr. Sci.*, **222**, 19–39 (2003).
18. P. Shao and R.Y.M. Huang, "Polymeric membrane pervaporation," *J. Membr. Sci.*, **287**, 162-179 (2007).
19. K. Kimura, G. Amy, J. Drewes, and Y. Watanabe, "Adsorption of hydrophobic compounds onto NF/RO membranes:an artifact leading to overestimation of rejection," *J. Membr. Sci.*, **221**, 89-101 (2003).
20. A. M. Comerton, R. C. Andrews, D. M. Bagley, and P. Yang, "Membrane adsorption of endocrine disrupting compounds and pharmaceutically active compounds," *J. Membr. Sci.*, **303**, 267-277 (2007).
21. H. C. Hein, "Recovery of extractant from effluent of a solvent extraction circuit," US patent, No. 5879556-A, 1996.
22. P. B. Kosaraju and K. K. Sirkar, "Novel solvent-resistant hydrophilic hollow fiber membranes for efficient membrane solvent back extraction," *J. Membr. Sci.*, **288**, 41-50 (2007).
23. E. D. Kille and C. T. Chiou, "Water solubility enhancements of DDT and trichlorobenzene by some surfactants below and above the critical micelle concentration," *Environ. Sci. Technol.*, **23**, 832-838 (1989).

POTENTIAL OF LIQUID MEMBRANES FOR THE TREATMENT OF A PHENOLIC-RESIN PLANT EFFLUENT

Shiva Agarwal, M. Teresa A. Reis, Licínio M. Ferreira, Paulo F. M. M. Correia, and Jorge M. R. Carvalho

Centre of Chemical Processes, Department of Chemical and Biological Engineering, Instituto Superior Técnico, Av. Rovisco Pais, 1049-001 Lisboa, Portugal.
Corresponding author email address: jcarv@ist.utl.pt

ABSTRACT

The detoxification of a phenolic-resin plant effluent was studied by applying liquid membranes. The first step was the selective removal and recovery of phenol from the aqueous stream. Two configurations of liquid membranes were tested: emulsion liquid membranes (ELM) and nondispersive solvent extraction using hollow fibers as contactors (NDSX). The second step was the processing of the raffinate containing formaldehyde. Formaldehyde was oxidized to formate with hydrogen peroxide in alkaline medium, and its removal and recovery was then tried by applying the ELM technique. The effect of the composition of the membrane on the recovery of formate ion was examined.

INTRODUCTION

Phenol and formaldehyde are the main reagents in the phenolic resin production process. One of the reaction products is water, which has to be removed from the resin mixture before further processing. Water is usually removed by distillation, thus generating a condensate stream containing phenol. The content of phenol in the condensate increases with distillation temperature, and all the fractions containing a phenol concentration in the range of 5-80 g/kg are usually collected together [1]. There are two phenolic effluents commonly generated in phenolic resin plants: the latter, which contains typically 50 g/L of phenol and another one with a low concentration of phenol resulting from the initial fraction of the distillate and rinse waters.

A possible method for the removal and recovery of phenol from aqueous solution is the solvent-extraction process. However, if the concentration of solute in the effluent is as low as 1 g/L, a large inventory of solvent ought to be required. This drawback can be overcome by using liquid membranes, such as emulsion liquid membranes (ELM) and nondispersive solvent extraction (NDSX) using hollow fibers as contactors.

ELM is a liquid membrane based process, where a primary emulsion is dispersed in the feed phase to be treated. During permeation, the solute is transported through the membrane into the droplets of stripping phase. ELM exhibits a high interfacial area of

mass transfer, and the kinetics of stripping is particularly favored due to the small size of the internal droplets of receiving phase. However, there are some deleterious phenomena, such as the break-up of the emulsion and water transport, which decrease the efficiency of the process, and their occurrence should be, therefore, minimized.

NDSX has been developed to avoid many of the problems associated with conventional liquid-liquid extraction including solvent losses, formation of stable emulsions, the need of an appropriate density difference between the phases, and the shortcomings due to flooding and loading limits in conventional contactors. The basic principle of NDSX is the immobilization of the interface in the pores of membranes due to wetting by one phase and overpressure applied to the other phase. The solute is thus transported from the feed to the organic phase through the membrane without phase dispersion. The use of microporous hollow fibers modules as liquid/liquid phase contactors is very attractive, because these devices present several advantages such as a very large contact area, the capability of treating a large amount of dilute solutions, and the reduction in equipment volume and space [2].

Several works concerning the recovery and concentration of organic acids, including phenol, by membrane-based solvent extraction and pertraction are extensively reviewed elsewhere [3]. Nevertheless, there is still a lack of data related to the processing of industrial effluents. The present work was thus focused on the treatment of a phenolic-resin plant effluent, which contained 400 mg/L of phenol and 400 mg/L of formaldehyde. The first step was the selective removal of phenol from the effluent by using liquid membranes with different configurations, ELM and NDSX in hollow fibers. Previous studies showed that formaldehyde could be removed from aqueous solutions by liquid-liquid extraction using 1-decanol as solvent, but the kinetics of the process was very slow [4]. Thus, it was decided to oxidize formaldehyde to formate ion with hydrogen peroxide in alkaline medium [5], and its recovery was then tried by applying the ELM technique. It is worth mentioning that sodium formate, as well as formic acid, is widely used in tanning industry, and its recovery is therefore of particular interest.

EXPERIMENTAL

The organic phases were prepared by diluting the extractant in a paraffinic solvent (Shellsol T, Shell Chemical Ltd.). In the ELM tests, a nonionic surfactant (polyamine ECA 4360J, Essochem Europe Inc.) was used to stabilize the emulsion.

The extractant Cyanex 923 (Cytec) contained four trialkyl(C_6,C_8)phosphine oxides as the active substance. The tertiary amines Alamine 308 (triisooctylamine) and Alamine 336 (tricaprylamine), both from Cognis, and Hostarex A327 (mixture of tri-*n*-octylamine and tri-*n*-decylamine, Clariant Chemical Co.) were also tested. The modifiers 1-decanol and isodecanol (Riedel-de-Haën) were used in some organic phases. The solvent phase containing the alkyl amine was equilibrated with an H_2SO_4 aqueous solution and washed with water until the aqueous pH was ~5. The solvent containing the sulfate salt was then used for extracting formic acid from the aqueous solution after the oxidation step. All organic reagents were used without further purification.

The emulsion was prepared by mixing the stripping aqueous solution (0.5 M NaOH) with the organic membrane phase using a rotor-stator type high-speed disperser

(IKA Ultra Turrax T50) at 7000 rpm during 1200 s. The organic phase contained 2 wt % of surfactant, 1-2 wt % of modifier, and 2 wt % of carrier. A predetermined volume ratio of 2:1 was maintained for organic phase to the internal stripping phase. The emulsion was dispersed in the feed aqueous phase in a baffled glass reactor (84 mm internal diameter) immersed in a water bath with temperature control. The three-phase dispersion (1 L) was stirred at 280 rpm during at least 180 s with a stainless-steel paddle (45 × 45 × 1 mm) at 298 K. After permeation, the phases were settled, and the emulsion was broken down by applying a 1-2 kV and 3-6 kHz electric field in a coaxial electrocoalescer.

Nondispersive solvent extraction (NDSX) was carried out using two Liqui-Cel® Extra-Flow 2.5" × 8" membrane contactors (Celgard, USA). Each hollow-fiber membrane module had 10,800 polypropylene fibers. Each fiber was 15.6 cm length with an external diameter of 300 μm and a pore size of 0.03 μm, the porosity being 40%. The aqueous phases flowed through the lumen side (tube side), whereas the organic phase flowed through the shell side of the fibers. The flow rates of the phases were kept at 400 mL/min. All the experiments were carried out at 298 K. The apparatus and procedure for carrying out NDSX experiments are described with detail in a previous work [6].

The aqueous concentration of phenol was measured with a double-beam ultra-violet/visible spectrophotometer (Hitachi U2000) at 270 nm under acidic medium. Formate ion was analyzed by potentiometric titration in a Metrohm 682 Titroprocessor.

RESULTS AND DISCUSSION

Recovery of Phenol from Effluent

Experiments were performed to check the feasibility of ELM for the separation and recovery of phenol from effluent. The concentrations of phenol achieved in the effluent phase and stripping phase under various operating conditions are presented in Table 1. The net swelling of the emulsion, which was estimated by measuring the emulsion volume before and after permeation, is also listed in the Table 1.

Table 1. Results of the ELM experiments.[a]

Extractant	V_{aq}/V_{str}	$[PhOH]_{aq}$ (mg/L)					$[PhOH]_{str}$ (g/L)	Net swelling
		30 s	60 s	120 s	180 s	300 s	180 s/300 s	180 s/300 s
---	20	165	110	40	19	8.0	---/7.4	---/–5%
Cyanex 923[b]	20	29	9.1	6.4	6.6	10	7.0/6.7	0%/2%
Cyanex 923[c]	10	7.4	6.7	6.0	7.0	---	3.4/---	1%/---
	20	12	8.3	6.6	6.0	13	6.7/5.8	2%/7%
	40	60	24	12	11	---	13.1/---	0%/---

[a]Initial aqueous phase: [PhOH] = 400 mg/L, [HCHO] = 400 mg/L, pH 6.3. Subscripts aq and str respectively denote feed effluent phase and stripping phase. [b]1 wt % (0.02 M) of Cyanex 923. [c]2 wt % (0.04 M) of Cyanex 923.

The results showed that the use of Cyanex 923 as carrier allowed removing 97-99% of the phenol content in 3 min. As expected, the concentration in the stripping phase rose

with the volume ratio of feed to receiving phase, but recovery decreased to 82-93%. The increase of permeation time from 3 to 5 min. made the process less efficient due to nonideal phenomena, which increased after 3 min. As observed, the net swelling was kept low when the permeation time was 3 min. It is worth noting that formaldehyde extraction of from the effluent was confirmed to be negligible for all the tests carried out.

NDSX experiments were also carried out to assess the effect of volume ratio of feed phase to stripping phase on the recovery of phenol. Figure 1 shows representative concentration profiles in the aqueous feed phase and stripping phase. Values of phenol recovery and the concentration ratio reached in several experiments are summarized in Table 2. The results obtained by using the ELM technique are also tabulated for comparing the performance of liquid membranes with different configurations.

Table 2. ELM versus NDSX using Cyanex 923 (0.04 M)—removal, recovery, and concentration ratio*

Technique	Volume ratio feed:stripping	Phenol removal	Phenol recovery	Concentration ratio
ELM	10	98.3%	93%	8.6
	20	98.5%	84%	17
	40	97.3%	82%	33
NDSX	10	99.7%	98%	9.8
	20	99.5%	96%	19
	40	99.0%	94%	38

*Initial feed phase: [PhOH] = 400 mg/L, [HCHO] = 400 mg/L. ELM permeation time, 180 s.

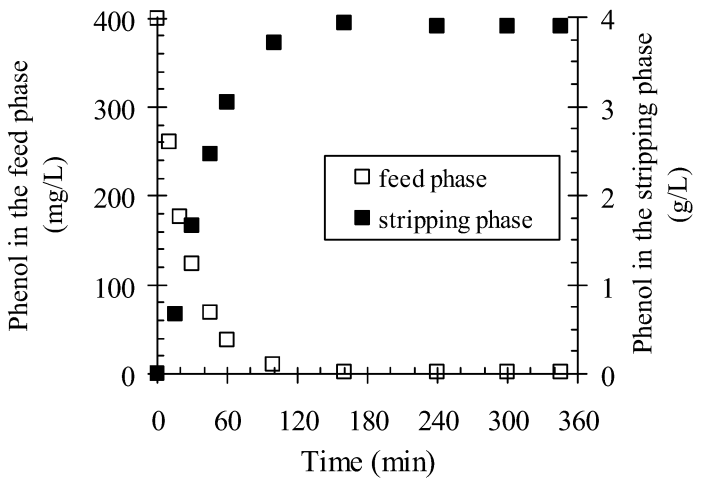

Figure 1. Phenol concentration profiles during extraction-stripping experiments (NDSX). Initial feed phase: [PhOH] = 400 mg/L, [HCHO] = 400 mg/L. Organic phase: 0.04 M Cyanex 923. Volumes of the feed, organic, and stripping (0.5 M NaOH) phases: 5, 0.9, and 0.5 L, respectively.

As observed in Figure 1, the extraction step was faster than the stripping step. For instance, the removal of phenol from the effluent was found to be about 70% after 30

min., whereas the corresponding recovery only achieved a level of 42%. The maximum extraction rate and stripping rate per unit of interfacial area were then calculated from the slope of the linear part of the time dependence of the concentration in the feed phase and stripping phase. The initial extraction rate of phenol per unit of interfacial area was evaluated to be 2.4×10^{-5} mol/m^2 s, whereas the maximum stripping rate per unit of interfacial area was estimated to be 1.2×10^{-5} mol/m^2 s. As expected, the stripping step controlled the overall rate of the process because of a large affinity of solute to the stripping phase and hydrophobic membrane. Besides, the chemical reaction of stripping contributed to the augment of the overall resistance to mass transfer. These results are in agreement with the ones previously obtained using a feed phase with phenol only [6]. Concerning the removal and recovery of phenol reached in ELM and NDSX tests, it was found that NDSX in hollow fibers allowed obtaining a raffinate with a very low content of phenol, the recovery being very high. The recovery was slightly lower in the case of ELM due to the break-up of the emulsion and osmosis.

Recovery of Formate Ion from Effluent

Formaldehyde was totally oxidized to formate ion in the presence of the corresponding stoichiometric amounts of hydrogen peroxide and sodium hydroxide. The recovery of formate ion was then tried by using ELM. Several compositions of the membrane were tested to assess its effect on the recovery and concentration achieved in the stripping phase. Figure 2 shows the results obtained. It is worth mentioning that the pH (~ 2) of the effluent was adjusted with H_2SO_4 to allow the extraction of formic acid (pK_a = 3.56) in its neutral form. The results showed that membrane additives, besides ECA 4360J, improved formate recovery. The highest recovery was obtained with 1-decanol. However, the swelling of the emulsion was found to be promoted, thus

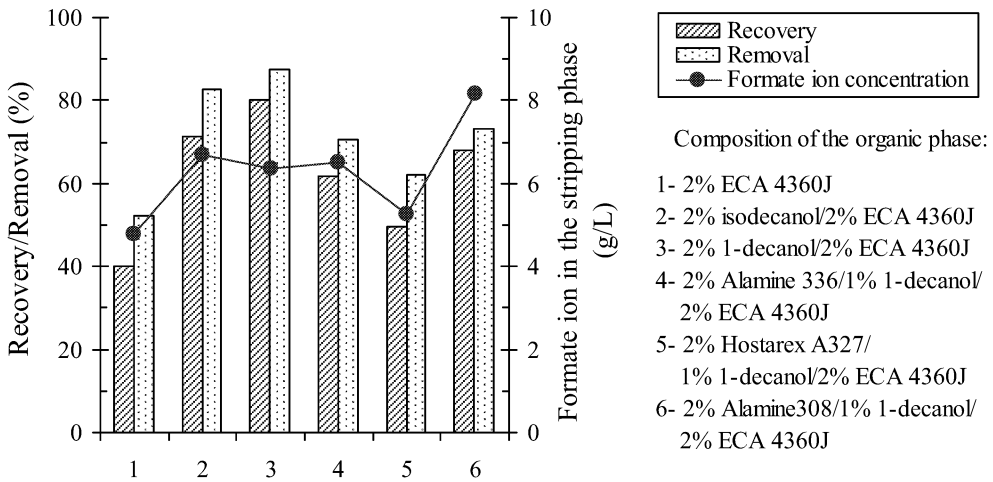

Figure 2. Influence of the composition of the organic phase on the recovery of formate and concentration achieved in the stripping phase. Initial feed phase: [HCOOH] = 600 mg/L, pH ~ 2. Permeation time in ELM, 10 min.; volume ratio of feed phase to stripping phase, 20.

decreasing the enrichment in the stripping phase. The system Alamine 308/1-decanol led to the highest concentration ratio. The removal of solute was achieved in the range 60-85% in one stage. Some more studies are still necessary to optimize the process.

CONCLUSIONS

Liquid membranes using Cyanex 923 as a carrier were found to be adequate for separating and recovering phenol from a phenolic-resin plant effluent. Two configurations of liquid membranes were used: emulsion liquid membranes and nondispersive solvent extraction in hollow fibers. High efficiencies of removal and recovery of phenol were attained in both processes. Nondispersive solvent extraction yielded the highest degree of phenol removal (99.7%) and recovery (98%). The second step of the treatment of the effluent was the oxidation of formaldehyde to formate ion. The recovery of formate ion was then tried by applying the emulsion liquid membranes technique. The use of additives such as 1-decanol and the alkylamine Alamine 308 in the membrane allowed obtaining significant recoveries of formate ion.

ACKNOWLEDGMENTS

Financial support by "Fundação para a Ciência e a Tecnologia" (FCT) and the European Community (FEDER), through the project POCTI/EQU/33207/2000, is gratefully acknowledged. The financial support of AdI/PRIME trough the AMBIRES project is also acknowledged. Shiva Agarwal acknowledges FCT for her post Ph.D. financial assistance (SFRH/BPD/32429/2006).

REFERENCES

1. F. C. Ferreira, L. Peeva, A. Boam, S. Zhang, and A. Livingston, "Pilot Scale Application of the Membrane Aromatic System (MARS) for Recovery of Phenol from Resin Production Condensates," *J. Membr. Sci.*, **257**, 120-133 (2005).
2. R. -S. Juang and I. -P. Huang, "Hollow-Fiber Membrane Extraction of Copper(II) from Aqueous Ethylenediaminetetraacetic Acid Solutions with Aliquat 336," *Ind. Eng. Chem. Res.*, **39**(5), 1409-1415 (2000).
3. Š. Schlosser, R. Kertész, and J. Marták, "Recovery and Separation of Organic Acids by Membrane-Based Solvent Extraction and Pertraction," *Sep. Purif. Technol.*, **41**, 237-266 (2005).
4. P. F. M. M. Correia, L. M. Ferreira, M. T. A. Reis, and J. M. R. Carvalho, "A Study on the Recovery of Phenol from Phenolic Resin Plant Effluents by Solvent Extraction," *Solvent Extr. Ion Exch.*, **25**(4), 485-501 (2007).
5. J. F. Walker, Formaldehyde, 3rd ed., Robert E. Krieger Publishing Co., New York, 1975; pp. 483-660.
6. M. T. A., Reis, O. M. F. Freitas, M. R. C. Ismael, and J. M. R. Carvalho, "Recovery of Phenol from Aqueous Solutions Using Liquid Membranes with CYANEX 923," *J. Membr. Sci.*, **305**, 313-324 (2007).

SEPARATION AND PURIFICATION OF EOPO2500 COPOLYMER IN THREE-LIQUID-PHASE EXTRACTION SYSTEMS

S.F. Shen,[1,2] Z.D. Chang,[1] H.Z. Liu,[1] Y.C. Ma,[1,2] and X. Hu[1,2]

[1]Laboratory of Separation Science and Engineering, Institute of Process Engineering, Chinese Academy of Sciences, P. O. Box 353, Beijing, 100080, P.R. China. [2]Graduate University of the Chinese Academy of Sciences, Beijing, 100080, P.R. China. Corresponding author email address: hzliu@home.ipe.ac.cn; sfshen@home.ipe.ac.cn

ABSTRACT

Poly(ethylene glycol-ran-propylene glycol) copolymer, EOPO2500, is an important phase-forming component in some three-liquid-phase extraction systems and will be enriched in the aqueous middle phase. A recycling process for separation and purification of EOPO2500 copolymer has been proposed by integration of thermal phase separation and solvent extraction. After temperature-induced phase separation at 70 ºC, EOPO2500 could be concentrated greatly, and its recovery was above 94.5%. EOPO2500 could be extracted into the dichloromethane phase, while soluble impurities were partitioned into the aqueous phase. One-step extraction recovery could be greater than 90%.

INTRODUCTION

A three-liquid-phase extraction system is composed of organic solvent, polymer, inorganic salt, and water and could offer new possibilities of separating two or more compounds by a single-step extraction due to different physicochemical properties among three equilibrated phases. In the last few years, there have been a number of articles published describing its applications in the fields of pharmaceutical industry, natural products, and lab-scale wastewater treatment [1-4].

Poly(ethyleneglycol) (PEG) and random copolymers of ethylene oxide (EO) and propylene oxide (PO), EOPO2500, were considered as excellent phase-forming chemicals [4]. The polymer was always enriched in the middle phase in these systems and would play a very important role for separation or differential partition. However, it also makes up the most of the cost of these systems. The recycling of these polymers is an attractive alternative to reduce significantly the system costs [1,4,5]. Difficulties arise when considering the complex phase compositions in the middle phase after three-liquid-phase extraction. Two major issues should be solved in order to recycle the polymer. The one is that the polymer solution needs to be concentrated. After extraction, the concentration of polymer is always below 40 wt %, which can not be reused directly as phase-forming components (stock solution, 50 wt %). The other is to remove the soluble

and insoluble impurities, which probably influence the following extraction and partition behavior and the quality of objective products.

The recycling of PEG has been extensively studied by adding more salt to cause the phase splitting again at the extra cost of salt consumption and environmental issues, or by thermo-separation over its cloud point temperature (above 100 ºC) [5,6]. Therefore, economics associated with these promising extraction technologies was relatively low, and few have discussed the purification aspects of the polymer solution. Some preliminary studies have showed EOPO copolymer with higher PO content (>50 wt %) would have an efficient thermo-separation and yield at lower temperature, but these copolymers could not form stable three-liquid-phase systems with extractants [4,6-8].

The focus in this paper is to investigate the concentration of EOPO2500 with 25 wt % PO content by thermal phase separation and try to offer an integrated recycling scheme with its purification by conventional solvent extraction.

EXPERIMENTAL

Chemicals and Materials

Poly (ethylene glycol-ran-propylene glycol), Average Mn. ca.2500 (EOPO2500), a random copolymer of 75% ethylene oxide (EO) and 25% propylene oxide (PO), was purchased from Sigma-Aldrich Inc. Acetonitrile, methanol and water were of HPLC grade. Tri-butyl phosphate (TBP), dichloromethane, ammonium sulfate ($(NH_4)_2SO_4$) and other chemicals were of analytical reagent grade. All the concentrations of compositions were calculated as percentage of weight (w/w). Stock solutions of ammonium sulfate 40% and the copolymer 50% were previously prepared to be used in the three-liquid-phase systems.

Preparation of Aqueous Copolymer Middle Phase

Aqueous copolymer solution was obtained from the three-liquid-phase extraction systems. Their system compositions in these systems were as follows: 24.52 wt % TBP, 10.59 wt % EOPO2500, and 9.06 wt % $(NH_4)_2SO_4$ and about 50.0 wt % aqueous extract of liquorice or penicillin fermentation broths. Extraction experiments were described in detail in the references [3,4]. Phase separation was enhanced by centrifugation. Finally, three liquid phases were formed. The middle phase was separated and investigated.

Concentration of EOPO2500 in the Middle Phase by Thermal Phase Separation

The copolymer-rich phase from the three-liquid-phase extraction system containing EOPO2500 was removed and transferred to 10 mL graduated glass tubes. These tubes were put in a water bath at different temperature for 30 min. After temperature-induced phase separation, phase volumes were measured accurately again. The phase compositions were analyzed using the developed HPLC-ELSD method. The recovery of the copolymer was calculated by knowing the volume and compositions of the copolymer phase.

Separation and Purification of EOPO2500

The purification studies were performed in 50 mL graduated glass vessels. The primary copolymer-rich phase and extractant, dichloromethane, were mixed adequately at different volume ratios, and the separation into two phases was enhanced by centrifugation, 2000 rpm for 5 min. In these studies, the residual copolymer phase was obtained in the top phase. The volume and copolymer concentration in the original phase and the top aqueous phase were determined. The recovery of copolymer was calculated by knowing the total mass in the original and the residual mass in the top phase after solvent extraction.

Determination of Phase Composition

Chromatographic separations were carried out on HP1100 liquid chromatography (Agilent Technologies, USA) and a Luna C18 (2) column (250 × 4.6 mm, 5.0 μm, Phenomenex, USA) was used. Alltech ELSD2000ES (Alltech, USA) and an Agilent 35900E signal transmitter (Agilent Technologies, USA) were equipped. The copolymer in the aqueous phase was analyzed by an optimized HPLC-ELSD method. A mixture containing 70% v/v acetonitrile and 30% v/v water was used as the mobile phase with a flow rate of 1.0mL/min; the drift-tube temperature of ELSD was set at 85 ºC; and the gas flow-rate was 2.2 L/min [4]. The concentration of EOPO2500 over 10% w/v was analyzed by diluting 1000 times and others by diluting 100 times.

RESULTS AND DISCUSSION

Concentration of EOPO2500 by Thermal Phase Separation

EOPO2500 is a thermo-separating copolymer in aqueous solution. After three-liquid-phase extraction, the EOPO2500-rich phase was transferred into graduated pipettes. The concentration of copolymer and ammonium sulfate was 38.22 g/L and 3.30 wt % respectively (39.25 g/L and 1.40 wt % respectively for the liquorice system). Experiments have shown that a two-phase system can be formed with an EOPO2500-rich top phase and a small aqueous bottom phase when above 40 ºC. However, when increasing the operating temperature in the range of 50-60 ºC, phase separation was quite slow, and the interphase was not stable and clear. Interestingly, the bottom phase became the copolymer-rich phase at 60 ºC for 30 min. This phenomena can be ascribed to the increasing concentration of EOPO2500, resulting in higher phase density than the other phase.

The volume of the EOPO2500-rich bottom phase decreased, and its concentration increased greatly when increasing the temperature, as shown in Table 1. At about 70 ºC, the recovery of copolymer would be above 94%, and its concentration could reach 50 wt %, which was close to that of stock solution, but only about 5 wt % in the top phase. Ammonium sulfate was enriched in the top phase (about 7.0-10.0 wt %). Some insoluble impurities, for example, cell or mycelial fragments and microparticles, were partitioned or transferred to the interphase. However, some soluble impurities, such as pigments,

were still kept in the copolymer-rich phase as depicted in Figure 1. Phase separation could speed up by adding small amount of sulfates (the results were not shown). The similar trends of thermo-separation have also been found for the liquorice systems.

Table 1. Effect of temperature on recovery of EOPO2500 by thermal phase separation

T, ºC	Phase volumes, mL		Concentrations, g/mL		Recovery, %
	Top	Bottom	Top	Bottom	
40	7.20	0.80	0.3912	-	92.12
50	6.75	1.41	0.4106	-	90.64
60	1.56	6.62	-	0.4406	95.39
70	2.35	5.85	0.0664	0.4959	94.88
80	2.90	5.30	0.0573	0.5495	95.25
70*	1.90	6.30	0.0482	0.5052	97.87

* The middle phase from three-liquid-phase extraction of liquorice.

Purification of EOPO2500 by Dichloromethane Extraction

Although the concentrated copolymer-rich phase by thermal separation might be applied as phase-forming component in new three-liquid-phase systems, soluble impurities could accumulate to such an extent that affect greatly the extraction behaviors. Based on the principles of similar polarity and solubility parameter (SP), dichloromethane and chloroform with poor polarity were selected as extractants for EOPO2500 [4,9,10]. The primary investigation and feasibility was performed on the purification of EOPO2500 by dichloromethane in this paper.

Effect of phase ratio (organic/aqueous phase, *R*) between dichloromethane and aqueous solution on the recovery of EOPO2500 was investigated as shown in Figure 1 (Left). It can be seen that the recovery decreased gradually as decreasing the *R*. When the *R* was not less than 1.0, the recovery could be above 90% by one-step extraction, and the concentration of EOPO2500 was about 5 wt % in the top phase. When further decreasing the *R*, the recovery decreased sharply and the copolymer concentration increased markedly in the top phase. The recovery and the concentration of EOPO2500 in the aqueous phase were about 65% and 16 wt %, respectively, when *R* was 0.25.

Typical photographs of EOPO2500 purification (R = 1.0) are also shown in Figure 1 (Right). It can be found that EOPO2500 was extracted into the bottom dichloromethane phase, and most of impurities were still partitioned into the top phase (Figure 1 Right, b). The volume of aqueous phase was decreased greatly, and no emulsion took place in this particle-free system from thermal separation. The purified copolymer could be back-extracted into water, which was integrated with rotary evaporation. The copolymer concentration could also be adjusted by the volume of water added.

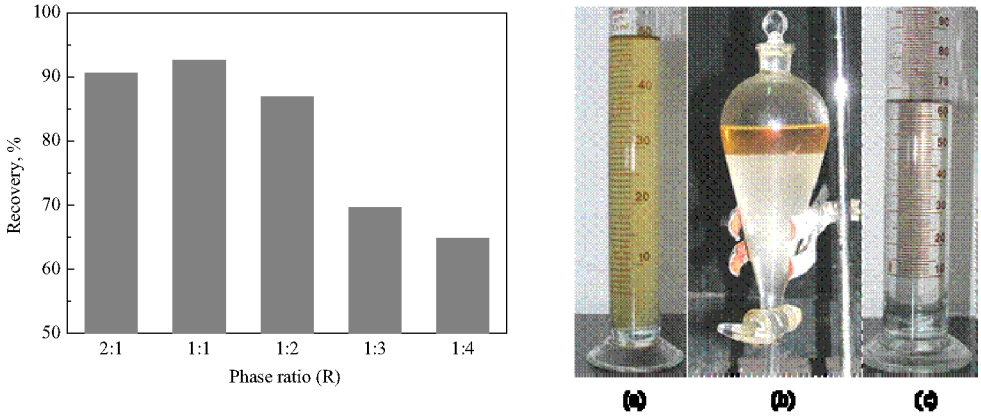

Figure 1. Left: effect of phase ratio (*R*) on the recovery of EOPO2500. Right: typical photographs of EOPO2500 purification. (a) Middle phase. (b) Extraction by dichloromethane. (c) The purified aqueous copolymer solution.

Separation and Purification Scheme for EOPO2500 Recycling

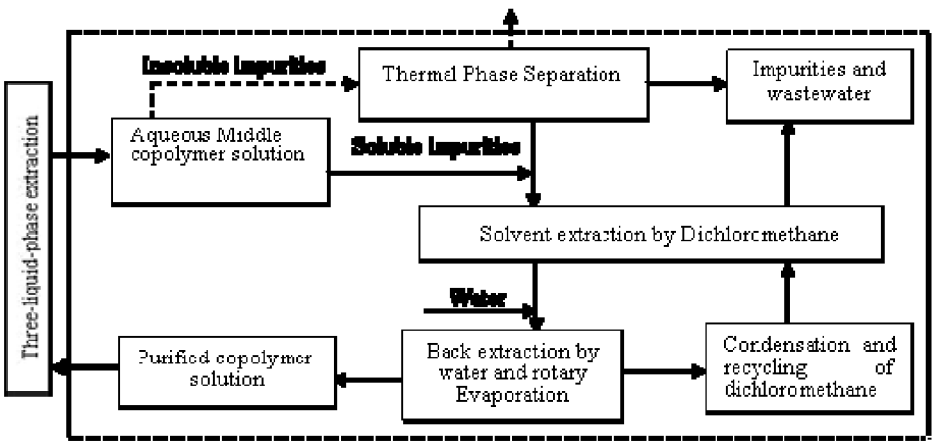

Figure 2. Schematic diagram of the proposed scheme for EOPO2500 recycling.

Primary results have shown the excellent efficiency in concentrating and purifying EOPO2500 by thermal separation and extraction steps. Based on these results and the characteristics of the middle phase, a separation and purification process for EOPO2500 recycling was proposed, as shown in Figure 2 [4,8]. In the early stages, as the insoluble-particle impurities predominated in the middle phase, the copolymer can be recycled only by thermal phase separation. After several extraction recycles, soluble impurities accumulated and predominated. The recycling process would consist of three steps, thermo-separation to remove the insoluble impurities, dichloromethane extraction, and back-extraction with water. Moreover, dichloromethane could also be condensed and recycled. The possibility for recycling of copolymer means that the costs for three-liquid-phase extraction in some novel processes can be significantly reduced.

CONCLUSIONS

The EOPO2500-rich middle phase from three-liquid-phase extraction systems could be concentrated and purified by thermal phase separation and dichloromethane extraction. The proposed recycling process for EOPO2500 copolymer was feasible and promising.

ACKNOWLEDGMENTS

This work was financially supported by Innovative Research Group Science Fund (No. 20221603) National Natural Science Fund (No. 20406021) and National Natural Science Key Fund (No. 20236050), P.R. China.

REFERENCES

1. S. F. Shen, Z. D. Chang, X. H. Sun, X. Hu, and H. Z. Liu, "Application and Recycling of Tri-block Copolymer in Three-Phase Extraction System," Proc. Int. Solvent Extr. Conf. *(ISEC' 2005)*, Beijing, 2005; pp. 1360-1365.
2. S. F. Shen, Z. D. Chang, and H. Z. Liu, "Three-Liquid-Phase Extraction Systems for Separation of Phenol and p-Nitrophenol from Wastewater," *Sep. Purif. Technol.,* **49**(3), 217-222 (2006).
3. S. F. Shen, Z. D. Chang, J. Liu, X. H. Sun, X. Hu, and H. Z. Liu, "Separation of Glycyrrhizic Acid and Liquiritin from Glycyrrhiza Uralensis Fisch Extract by Three-Liquid-Phase Extraction Systems," *Sep. Purif. Technol.*, **53**(3), 216-223(2007).
4. S. F. Shen, "Study on Phase-Forming Theory of Three-Liquid-Phase Systems and Its Extraction Application," Ph.D. Thesis, Institute of Process Engineering, Chinese Academy of Sciences, Beijing, China, 2007.
5. K. S. M. S. Raghavarao, T. V. Ranganathan, N. D. Srinivas, and R. S. Barhate, "Aqueous Two Phase Extraction—An Environmentally Benign Technique," *Clean Technol. Environ. Policy*, **5**, 136-141(2003).
6. M. Pereira, Y. T. Wu, A. Venancio, and J. Teixeira, "Aqueous Two-Phase Extraction Using Thermoseparating Polymer: A New System for the Separation of Endo-Polygalacturonase," *Biochem. Eng. J.*, **15**, 131-138(2003).
7. J. Persson, H-O. Johansson, and F. Tjerneld, "Purification of Protein and Recycling of Polymers in a New Aqueous Two-Phase System Using Two Thermoseparating Polymers," *J. Chromatogr., A*, **864**, 31-48(1999).
8. J. Persson, A. Kaul, and F. Tjerneld, "Polymer Recycling in Aqueous Two-Phase Extractions Using Thermoseparating Ethylene Oxide-Propylene Oxide Copolymers," *J. Chromat., B*, **743**, 115-126(2000)
9. M. Spitzer, L. H. M. da Silva, and W. Loh, "Liquid Biphase Systems Formed in Ternary Mixtures of Two Organic Solvents and Ethylene Oxide Oligomers or Polymers," *J. Braz. Chem. Soc.*, **11**, 375-380(2000).
10. M. Spitzer, E. Sabadini, and W. Loh, "Entropically Driven Partitioning of Ethylene Oxide Oligomers and Polymers in Aqueous/Organic Biphasic Systems," *J. Phys. Chem., B*, **106**, 12448-12452(2002).

FUNCTIONALIZED ORGANO-CERAMIC ADSORBENTS FOR GERMANIUM SEPARATIONS

H. J. Park and L. L. Tavlarides

Department of Biomedical and Chemical Engineering, Syracuse University, Syracuse, NY 13244, USA. Corresponding author email address: lltavlar@syr.edu

ABSTRACT

The removal of germanium from acid solution systems using a Kelex-100 (7-(4-ethyl-1-methyloctyl)-8-hydroxyquinoline) functional sol-gel adsorbent is investigated. Kelex-100 has been used for separating some metals like Ga(III), Co(II), Cd(II), Pb(II), and Cu(II) from aqueous solution by solvent extraction and liquid membranes. The goal of the work is to demonstrate that elutable mesoporous organo-ceramic adsorbents based on Kelex-100 can be synthesized for selective separation of germanium from simulated leachate solution. This approach allowed us to develop nanostructure organoceramic materials by synthesizing appropriate precursors and developing sol-gel processing conditions to obtain adsorbents with high capacity. Several functional precursor silanes were screened as silica gels and the most promising tested. Characterization studies, such as adsorption isotherms, breakthrough curves for fixed-bed operation, and kinetics showed that this organo-ceramic adsorbent has potential applications in germanium recovery.

INTRODUCTION

Germanium is a scarce, but not an extremely rare, element in the Earth's crust (6.7 ppm worldwide overall) [1]. Its compounds have been widely used in various fields of industry such as semiconductors, special optical glasses, alloys, and catalyst in the production of polyesters and organometallic compounds. Germanium occurs as a by-product of hydrometallurgical zinc-processing operations [2] and is also found as an oxide, mainly tetragonal GeO_2, usually substituting for SiO_2 in silicates [3]. The separation and recovery of germanium(IV) are important because of the high price of refined germanium ($1700/kg) [4]. The separation of the element from acidic leach solutions has attracted much attention because of the economic implications, especially in zinc production [5].

The literature contains a variety of methods for separation, such as solvent extraction [5,6,7], membrane separation [7], and resin adsorption [8]. However, each of these can only be applied under restricted conditions and comes with a high cost of purification as a result of the lack of selectivity and capacity of the materials used. The reagent studied in this paper, Kelex-100, has been used for separation of metals such as Cu(II), Ga(III), and Ge(IV) from aqueous solution in liquid membranes and solvent

extraction [5,9,10]. The, syntheses of adsorbents by sol-gel processing and their adsorptive characteristics for germanium separation in aqueous solutions are discussed.

EXPERIMENTAL

Material and Reagents

SOL-KELEX adsorbents were synthesized by the sol-gel processing techniques as reported in our application [11]. Kelex-100 was kindly supplied by the Cognis Corporation, Tuscon, Arizona. As received, it was of low purity and required extensive purification before being used in the experiments reported in this paper. Details of the purification of Kelex-100 are reported elsewhere [12].

In the first step according to standard methods, 5-chloromethyl-Kelex-100 was synthesized by modification of the reported method [13]. A mixture of 29.9 g (0.1 mol) of Kelex-100, 50 mL of 32% HCl, and 16 mL (0.1 mol) of 37% HCHO at room temperature was treated with hydrogen chloride gas for 10 h and the solution allowed to stand at room temperature for 2 h without stirring. The resulting chemical was filtered, washed with ethanol, and dried under vacuum to give 5-chloromethyl-Kelex-100. Yield, 94.3%.

In the second step, aminopropyltriethoxysilane (APTES) and tetraethoxysilane (TEOS) were used as a functional precursor and a cross-linking silane, respectively. Two sol-gel processing routes were used for the synthesis of an adsorbent, depending on hydrolysis and co-condensation of both silanes. The molar ratio between APTES and TEOS studied in this work is 1 to 3. APTES was hydrolyzed and homo-condensed for 15 min. at room temperature with the molar ratio of APTES:EtOH:H_2O:HCl = 1:4:1:10^{-5}. Similarly, TEOS was hydrolyzed and homo-condensed for 15 min. at room temperature with the molar ratio of TEOS:EtOH:H_2O:HCl = 1:3:1:3 x 10^{-5}. These two partially condensed silanes were mixed to co-condense, and gelation of the sol occurred after two to five minutes of mixing. The gelled materials were aged for 24 h at 25 °C and dried for 24 h at 80 °C.

In the third step, gelled material and 5-chloromethyl-Kelex-100 was synthesized with 1 to 1 molar ratio. 1.0 g of gelled material was suspended in 30 mL of ethanol, then 2 mmol of 5-chloromethyl-Kelex-100 added. The mixture was kept at 45 °C for 72 h, then an excess of $NaBH_4$ (0.11g, 2.91 mmol) added at room temperature for 12 h [14]. The resulting solid was filtered and washed with ethanol.

The dried adsorbents were crushed into the desired particle size ranges of 75~125 μm and 125~180 μm for characterization. A thermostatically controlled shaker bath (Precision Scientific model 50) was used in batch adsorption experiments. Analyses of total germanium concentration were measured with ICP-MS (Perkin-Elmer model Elan 6100). Batch adsorption experiments were conducted in a temperature-controlled shaker water bath. pH measured using a Chemcadet pH meter. Fixed-bed experiments studied with a 0.7 cm ID column and cartridge pump (Master Flex model 7519-20) to control flow rate. A 5000 mg/L germanium stock solution was prepared from 9898 μg/mL of germanium standard solution (Sigma Aldrich). All other chemicals used in this study were of reagent grade.

Characterization

Equilibrium uptake capacities of SOL-KELEX were determined using 0.1 g of adsorbent with 15 mL of germanium solution buffered by 0.05M acetate at various initial concentrations (1-1000 mg/L) and pH (2, 4, and 6) at room temperature. The amount of adsorbed germanium ions was calculated by a mass balance between the initial and equilibrium concentrations. Kinetic experiments were performed in a batch mode with 100 mg/L of initial germanium concentrations at 25 °C. Samples were withdrawn at determined intervals to plot C/C_0 versus time. The column adsorption performance was carried out using 250 mL solution of initial germanium concentration (50 mg/L) at a flow rate of 0.69 mL/min through a 0.7 cm ID column packed with 0.53 g of adsorbent. Effluent concentrations were collected at volume intervals for analyses. Based on preliminary stripping studies, 1 M hydrochloric acid solution was chosen as the stripping agent. The volume of stripping agents used was 100 mL. A 5 mL of DI water was used to wash the column before and after stripping steps to ensure discharge of remaining metal ions.

RESULTS AND DISCUSSION

Equilibrium Studies

Aqueous-phase equilibrium concentrations of germanium species were evaluated using an appropriate chemical reaction equilibrium analysis to understand the distribution of various forms of germanium ions in solution. The proposed reaction mechanism following [15, 16] is:

$$GeO_2 + 2H_2O \leftrightarrow Ge(OH)_4 \qquad \log K = -5.02 \pm 0.13 \qquad (1)$$

$$Ge(OH)_4 \leftrightarrow GeO(OH)_3^- + H^+ \qquad \log K = -9.32 \pm 0.05 \qquad (2)$$

$$GeO(OH)_3^- \leftrightarrow GeO_2(OH)_2^{2-} + H^+ \qquad \log K = -12.72 \qquad (3)$$

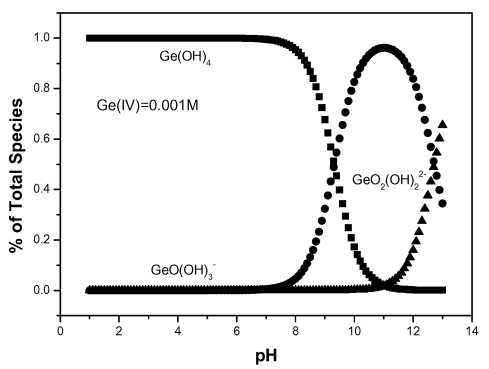

Figure 1. Speciation of germanium in aqueous solution using Equations 1 and 2.

Germanium ion species in the aqueous solution evaluated using the analyses show that $Ge(OH)_4$ and $GeO(OH)_3^-$ are the predominant species in the total germanium concentration, but the distribution of each species depends on total concentration of germanium and pH value. From Figure 1, the predominant germanium species is $Ge(OH)_4$ at acidic and neutral pH, whereas at alkalinity of $9 \leq pH \leq 11$, $GeO(OH)_3^-$ predominates.

Batch Adsorption Studies

Equilibrium adsorption isotherms conducted batchwise at four pH values (2, 4, and 6) are shown in Figure 2. The maximum germanium adsorption capacity observed at pH 6 was found to be 0.33 mmol/g, whereas that at acidic pH value was 0.30 mmol/g.

The following balance exists when Kelex-100 extracts germanium from sulfuric acid solutions [7]. The results of the developed analytical isotherm expression are also plotted in Figure 2.

$$Ge(OH)_4 + 3\overline{HQ} + HSO_4^- + H^+ \leftrightarrow \overline{GeQ_3HSO_4} + 4H_2O \qquad (4)$$

Batch kinetics experiments were conducted with 100 mg/L of germanium solution at pH values of 4 and 6. As shown in Figure 3, equilibrium is reached within 1 minute of contact time for the 100 mg/L solution. The rapid adsorption equilibrium is an indication that the surface of the SOL-KELEX is readily available for adsorption. In addition, this may also be due to the large open-pore channels accompanied by hydrophilic pore surfaces. After rapid decrease in concentration, a slight increase is observed. This result may be due to the instability of the material, which leads to a leaching out of ligand from the matrix during the series of experiments. Also, it may be due to experimental error.

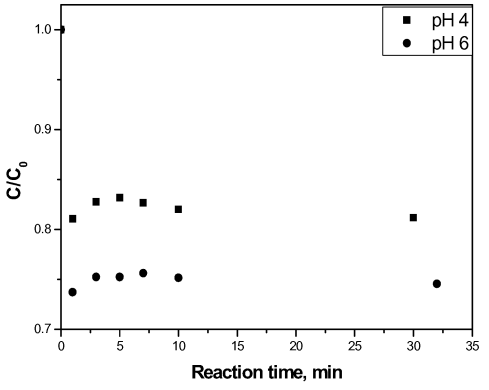

Figure 2. Equilibrium adsorption isotherms of SOL-KELEX at pH 2, 4, and 6. Solid lines represent predictions of the isotherm equation developed from Equation 4.

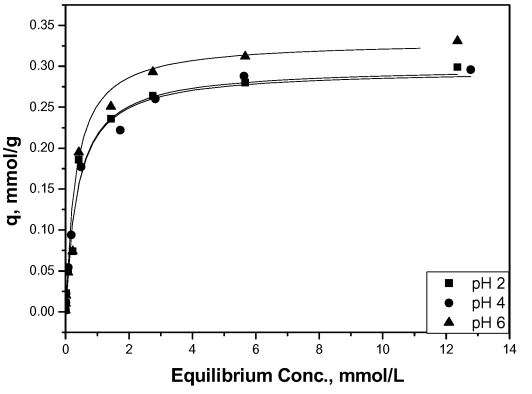

Figure 3. Adsorption kinetics of germanium on SOL-KELEX. Loading concentration = 100 mg/L; weight of SOL-KELEX = 0.2 g; volume = 100 mL; pH_i = 4 and 6.

Fixed-Bed Adsorption Studies

The breakthrough experiment was performed with a 0.7 cm ID column packed with 0.5 g of SOL-KELEX to evaluate the performance of this adsorbent in a fixed-bed column adsorption. This experiment was conducted using a germanium concentration of 50 mg/L, which meets the concentration range of leachate solution [3]. As shown in Figure 4 (a), the sharp effluent concentration of the breakthrough curve shows that the adsorption of germanium ions by adsorbent is fast and that there exists minimal mass-

transfer resistance in the adsorbent pores. The effluent concentrations are observed to be below 0.05 mg/L up to 190 bed volumes before breakthrough that occurs at 230 bed volumes.

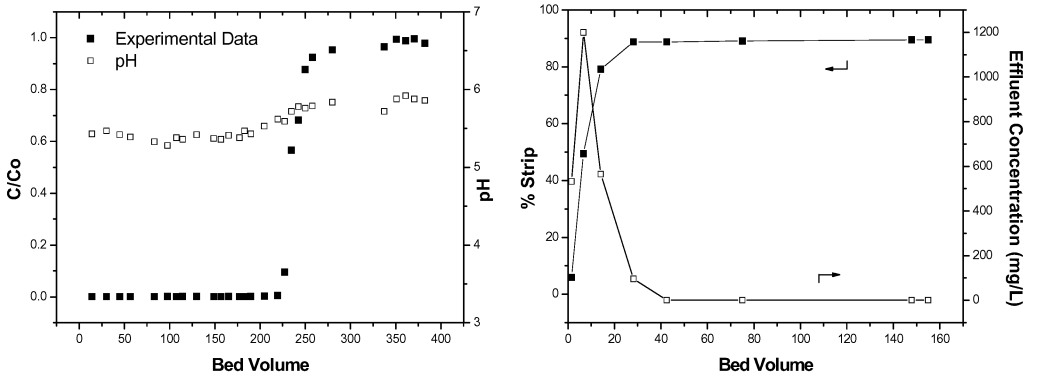

Figure 4. (a) Breakthrough curve of germanium on a SOL-KELEX adsorbent. 1 bed volume = 0.654 mL; $[Ge]_{feed}$ = 50 mg/L at pH 6.11; volume = 250 mL; weight of SOL-KELEX = 0.53 g; Q = 0.69 mL/min ; capacity = 14.9 mg/g. (b) Stripping of germanium using 1 M HCl.

Although, sodium hydroxide is typically used as the stripping agent in several germanium sorption studies, in this work, due to the instability of the adsorbent under basic conditions, acid solutions were used as stripping agents. Based on preliminary stripping studies, 1 M HCl solutions were chosen as the stripping agent for germanium. The subsequent stripping of the loaded germanium using 1 M HCl is shown in Figure 4 (b). A stripping efficiency of 89% was obtained at 28 bed volumes. The percent recovery from the total loaded amounts was 89.5%.

CONCLUSIONS

The organoceramic adsorbent functionalized with Kelex-100 (SOL-KELEX) synthesized by sol-gel processing technology to separate germanium at acidic and neutral pH. SOL-KELEX has high uptake capacity and rapid kinetics for germanium extraction. The breakthrough experiment showed that a 0.05 mg/L effluent concentration was maintained up to 190 bed volumes. Consequently, this adsorbent has a high potential for application in the separation and recovery of germanium from leachate solutions. Additional studies on selectivity in multimetal ion solutions, and modeling the kinetics and breakthrough curves are in progress.

ACKNOWLEDGMENT

Laboratory facilities provided for the Tavlarides' Team at Syracuse University are gratefully acknowledged.

REFERENCES

1. Ullman's Encyclopedia of Industrial Chemistry, Germanium and Germanium Compounds, Wiley-VCH Verlag GmbH & Co., KgaA, 1987.
2. V. Vojkovic, I. Juranovic, and B. Tamhina, "Extraction and separation of germanium (IV) with 4-pyridone derivatives," *Croat. Chem. Acta*, **74**, 467-477 (2001).
3. A. H. Exposito, J. M. Chimenos, A. I. Fernandez, O. Font, X. Querol, P. Coca, and F. G. Pena, "Ion flotation of germanium from fly ash aqueous leachates," *Chem. Eng. J.*, **118**, 69-75 (2006).
4. R. D. Brown, Jr., "Volume I. Metals and Minerals," *U.S. Geological Survey, Minerals Yearbook*, 2004.
5. G. Cote and D. Bauer, "Liquid liquid extraction of germanium with oxine derivatives," *Hydrometallurgy*, **5**, 149-160 (1980).
6. A. de Schepper., "Liquid liquid extraction of germanium by LIX 63," *Hydrometallurgy*, **1**, 291-298 (1976).
7. O. Tukun, N. Demircan, and R. A. Kumbasar, "Extraction of germanium from acid leach solutions by liquid membrane technique," *Clean Products and Processes*, **1**, 148-153 (1999).
8. Y. Inukai, Y. Tanaka, Y. Shiraishi, T. Matsuda, N. Mihara, K. Yamada, N. Nambu, O. Itho, T. Doi, Y. Kaida, and S. Yasuda, "Selective separation of germanium(IV) by di-(2-hydroxyethyl) amine-type cellulose derivative," *Anal. Sci.,* **1**, 1117-1120 (2001).
9. G. V. K. Puvvada, "Liquid–liquid extraction of gallium from Bayer process liquor using Kelex100 in the presence of surfactants," *Hydrometallurgy*, **52**, 9-19 (1999).
10. G. Kyuchoukov, S. Zhivkova, A. B. Resterna, and J. Szymanowski, "Separation of copper(II) and zinc(II) from chloride solutions with alkyl-8-hydroxyquinoline in various stages of extraction: stripping process," *Ind. Eng. Chem. Res*., **39**, 3896-3900 (2000).
11. L. L. Tavlarides, N. V. Deorkar, and J. S. Lee, "High performance adsorbent ceramic compositions synthesized by sol-gel method," US Pat. Appl. No. 09/574405, 18 May 2000
12. N. Agarwal, "Characterization of sol-gel adsorbents for cesium and germanium separation from acidic solutions," Master's Thesis, Syracuse University, Syracuse, NY, USA, 2005
13. G. R. Clemo and R. Howe, "5-formyl-8-hydroxy-quinoline," *J. Chem. Soc*., 3552 (1955).
14. H. Wang, J. Huang, S. Wu, C. Xu, L. Xing, L. Xu and Q. Kan, "Design and synthesis of Alq3-functionalized SBA-15 mesoporous material," *Mat. Lett.*, **60**, 2662-2665 (2006).
15. G. S. Pokrovski and J. Schott, "Thermodynamic properties of aqueous Ge(IV) hydroxide complexes from 25 to 350 °C: Implications for the behavior of germanium and the Ge/Si ratio in hydrothermal fluids," *Geochim. Cosmochim. Acta*, **62**, 1631-1642 (1998).
16. S. A. Wood and I. M. Samson, "The aqueous geochemistry of gallium, germanium, indium and scandium," *Ore Geol. Rev.*, **28**, 57-102 (2006).

POLY-N-ISOPROPYLACRYLAMIDE WITH INCORPORATED THIOETHER UNITS AS AN EXTRACTION MEDIA FOR SOFT METAL IONS

K. Chayama, Y. Morita, and S. Iwatsuki

Department of Chemistry, Faculty of Science and Engineering, Konan University, Okamoto 8-9-1, Higashinada, Kobe 658-8501 Japan.
Corresponding author email address: chayama@konan-u.ac.jp

ABSTRACT

New temperature-sensitive copolymers of *N*-isopropylacrylamide and monoaza-tetrathioether derivatives have been synthesized successfully. The ratio of *N*-isopropylacrylamide and monoaza-tetrathioether groups was determined by ICP-AES to calculate the sulfur atom concentration of the polymer solution. Extraction using the copolymer for soft metal ions and counter anions such as the picrate ion has been examined. Soft metal ions such as silver(I), copper(I), and palladium(II) were extracted efficiently into the polymer phase above the lower critical solution temperature. Extraction efficiency of silver ion increased as the ratio of monoaza-tetrathioether groups to *N*-isopropylacrylamide groups in the polymer was increased.

INTRODUCTION

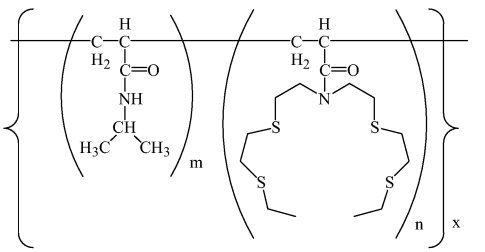

Thioether ligands have been developed since 1970. Macrocyclic thioethers, thio-crown ethers are known to be highly selective, soft-metal extractants. Acyclic analogues also react selectively with soft metal ions such as silver, copper, mercury, and palladium ions [1]. As reagents containing thio-ether groups are soluble in the organic solvents, especially halogenated hydrocarbons such as chloroform or 1,2-dichloroethane, they are often used as solvent extractants for soft metal ions. However, the use of such organic solvents has certain ecological problems. On the other hand, a thermosensitive gel, poly(*N*-isopropylacrylamide) has a lower critical solution temperature (LCST), is soluble in water, dehydrates when the solution temperature increases above the LCST, and forms a polymer phase of small volume [2-4]. During the formation of the polymer phase, some hydrophobic species are collected into the polymer phase as well as liquid-liquid extraction. This polymer extracts some hydrophobic compounds such as ion-paired complexes of metal ions, aromatic hydrocarbons, and some environmental hormones such as alkylphenols and phthalic esters when the solution is heated above the lower

critical solution temperature. The authors examined the extraction behavior of the ion pair of silver-monoazadithioether derivative complexes with picrate ion into the polymer phase. Results indicated the possibility of the preconcentration of silver by means of an extraction medium of the neutral ligand, the counter anion, and the poly(*N*-isopropylacrylamide). Such a hydrophobic ligand was necessary to be solvated by acetone prior to addition to the aqueous solution containing the polymer. To avoid the use of acetone, the ligand could be incorporated into the polymer chain. In this study, the polymer extraction using a copolymer of poly(*N*-isopropylacrylamide) and monoaza-tetrathioether derivatives for noble metal ions and counter anions such as picrate ion were examined.

EXPERIMENTAL

The reagent, 9-aza-3,6,12,15-tetrathiaheptadecane (ATH), was obtained from the reaction of bis(2-chloroethyl)amine hydrochloride and ethylthioethanethiol, and the monomer unit 9-acryloyl-9-aza-3,6,12,15-tetrathiaheptadecane was synthesized as shown in Scheme 1.

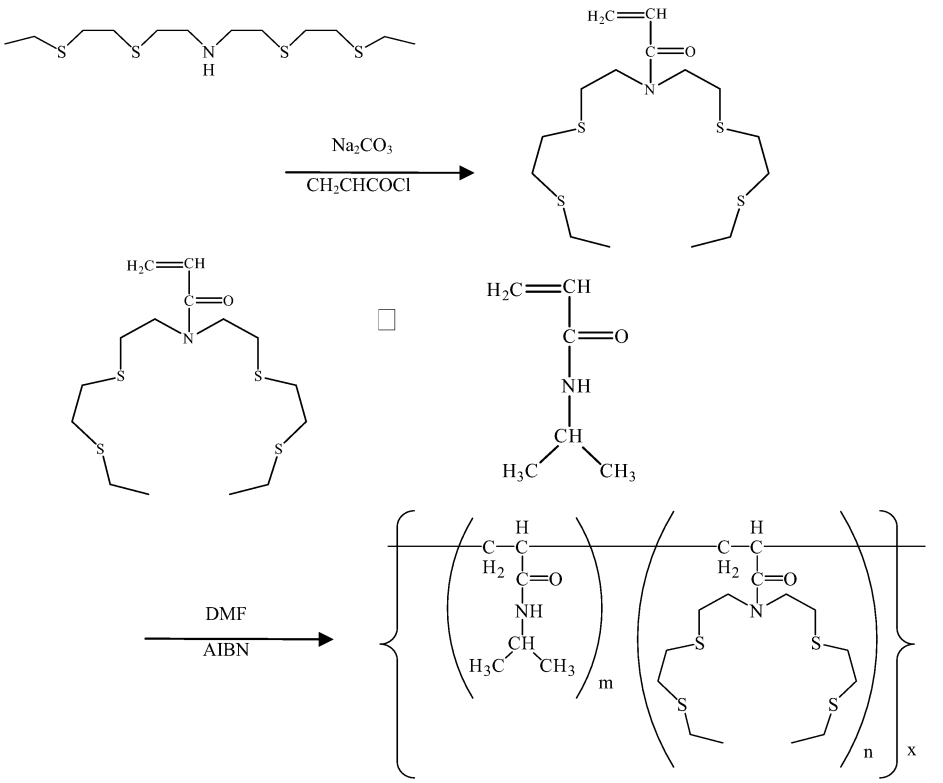

Scheme 1. Synthetic route to the ATH-NIPAAm copolymer.

Reagents were characterized by NMR spectroscopy. The polymerization reaction was performed with *N*,*N*-dimethylformamide as a solvent and *α,α'*-azobisisobutyronitrile

as the initiator. The molar ratio of the monomers *N*-isopropylacrylamide and 9-acryloyl-ATH was varied between 20:1 and 150:1 in the feed. The resulting products were precipitated in doubly-distilled water and washed for two or three days, then evaporated to dryness. The polymers synthesized (ATH-NIPAAm) were dissolved in aliquot volumes of water. The sulfur atom concentration of the solution was determined by ICP-AES.

Lower Critical Solution Temperature

The LCST was determined spectrophotometrically with a Hitachi U-3200 spectrophotometer using the relative absorbance change at 750 nm with temperature of the solution.

Extraction of Soft Metal Ions

An aliquot of aqueous solution containing 5.0×10^{-5} M metal ion, 3.3×10^{-2} M sodium sulfate, 1×10^{-3} M counter anion such as picrate ion, and 1×10^{-2} M buffer solution in a stoppered cylindrical tube was shaken at 298 K for 10 minutes and then 343 K for 20 minutes. After the two phases were separated, metal ion concentrations in the aqueous phase and in the polymer phase dissolved in 0.1 M nitric acid were determined using a Hitachi Z-5310 atomic absorption spectrometer. The pH of the aqueous phase was measured with a Horiba M-12 pH meter.

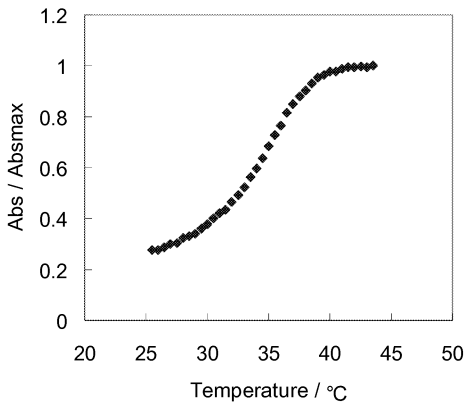

Figure 2. Plots of the relative absorbance at 750 nm against The temperature of the solution. The ratio ATH to PNIPAAm in the polymer was 1:31 in the 0.05% w/v solution.

RESULTS AND DISCUSSION

Synthesis of the Copolymer

Copolymers of various ratios of ATH to NIPAAm were synthesized successfully. The thioether content in each copolymer solution was determined by ICP-AES to measure the emission intensity of the sulfur atoms. After the synthesis of the copolymers, the determined ratio of ATH:NIPAAm slightly decreased relative to the feed. The lower critical solution temperature (LCST) was determined spectrophotometrically using a Hitachi U-3200 spectrophotometer. The LCST of the ATH-NIPAAm copolymer (1:31) was 307.5 K, almost the same as the LCST of poly-*N*-isopropylacrylamide (PNIPPAm). Therefore, the ATH-NIPAAm copolymer showed phase-transition phenomena, in which the copolymer was swollen at lower than 307.5 K and shrunken at temperatures higher than the LCST.

Table 1. The determination of the ratio of ATH to NIPAAm in the polymer

ATH to NIPAAm in feed	Sulfur content of the copolymer (ppm)	ATH to NIPAAm determined
1:20	16.4	1:31
1:50	8.23	1:66
1:70	6.50	1:84
1:100	3.98	1:139
1:150	2.98	1:187

Extraction Behavior of Soft Metal Ions

Effect of Counter-Anion on Silver (I) Ion Extraction

When the temperature of the solution containing the copolymer is increased, phase transfer occurs, and lipophilic species can be absorbed into the polymer phase and separated from the aqueous phase. As the polymer contains the monoaza-tetra- thioether unit, metal ions can coordinate with the thioether groups in the polymer chain. Then, the metal ion can be transferred into the polymer phase with an appropriate anion to compensate the charge. As shown in Figure 3, the use of anions such as picrate, nitrate, and perchlorate was effective for the extraction of silver ion from the aqueous phase into the polymer phase. When in the presence of picrate ion, more than 98% of the silver ion was extracted. In this study, picrate ion was used for the examination of extraction conditions.

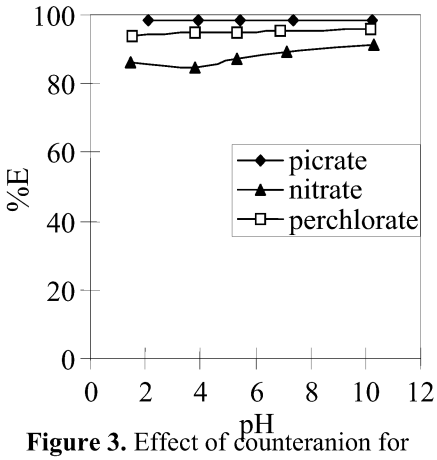

Figure 3. Effect of counteranion for silver(I) ion extraction efficiency against pH of the polymer solution.

The Ratio of ATH to NIPPAm in the Polymer

Figure 4 shows the extraction behavior of silver ion with the use of several polymers containing ATU units and/or NIPPAm units. The extraction of silver(I) with PNIPPAm without ATH indicates that silver(I) ion was not extracted at all at the range of pH 2 to 5. Silver(I) ion was slightly extracted into PNIPPAm phase from the alkaline solution. It is thought that neutral silver

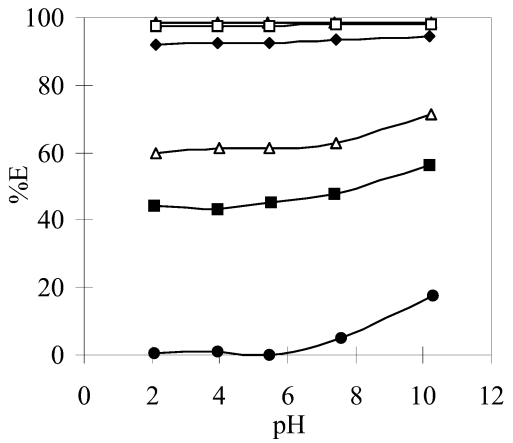

Figure 4. Effect of the ratio of ATH to NIPPAm in the polymer for the Ag(I) ion. Each ratio shows the composition of ATH to NIPPAm. PNIPPAm does not contain any ATH units. ATH:NIPAAm = 1:31 (▲), 1:66 (□), 1:84 (◆), 1:139 (△), 1:187 (■). PNIPAAm (●).

oxide is precipitated in that pH region, may be extracted by the solid polymer phase. On the other hand, the polymer containing both ATH and NIPPAm groups extracts silver(I) well. The percentage extraction of silver(I) ion increases with increasing ratio of ATH to NIPPAm. The copolymer with the ratio 1:66 is sufficient to bind more than 99% of silver(I) ion in the solution. The results indicate that the sulfur-containing ATH reacts with silver(I) ion and extracts it into the polymer phase.

Copper(I) Ion Extraction

Liquid-liquid extractions of copper(I), using monoazapolythioether derivatives in the organic solvents such as 1,2-dichloroethane, proceed as well as for silver(I) ion. Hydroxylamine was added into the solution containing copper(II) sulfate to convert the copper(II) to copper (I). Figure 5 shows the extraction behavior of copper(I) ion with the ATH-NIPPAm copolymer. The results indicate that increasing the proton concentration causes a decrease in the extraction efficiency. This phenomenon might be due to the decrease in the reducing power of hydroxylamine, which permits the copper(II) ion to exist as the predominant species in highly acidic solutions. However, copper(I) was extracted well in the pH range 3 to 6, with polymers with ratios of ATH to NIPPAm more than 1:66. It is thought monovalent metal ions such as silver(I) or copper(I) form a 1:1 complex with the ATH units in the polymer chain. The order of the extraction efficiency of copper(I) ion is consistent with the order of the ratio of ATH to NIPPAm as with silver ion.

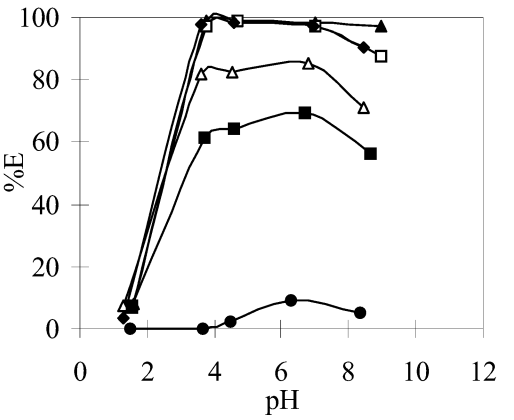

Figure 5. Effect of the ratio of ATH to NIPPAm for Cu(I). Symbols, which indicate ATH to NIPPAm ratio, are as in Figure 4. PNIPPAm does not contain any ATH units. ATH:NIPAAm = 1:31 (▲), 1:66 (□), 1:84 (◆), 1:139 (△), 1:187 (■). PNIPAAm (●).

Effect of Coagulation Temperature for Extraction of Silver(I) Ion

Temperature-sensitive copolymers are shrunken at temperatures higher than the LCST, which is 307.5 K for the 1:31 (ATH to NIPPAm) copolymer. The temperature of the solution was varied, and the effect of the coagulation temperature was examined. The results in Figure 6 indicate that the extraction efficiency decreases slightly at 65 °C. It is thought that for a liquid-liquid extraction of metal ion with a tetrathioether, the extraction efficiency of metal ion decreases according to the increase of temperature of the aqueous and organic phase.

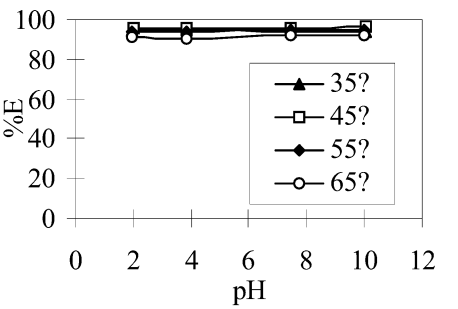

Figure 6. Effect of the temperature of the solution on the extraction efficiency of silver(I) ion.

CONCLUSIONS

The results obtained show that there is a possibility of separating noble metal ions such as silver, copper, and gold from transition metals such as nickel, cobalt, iron, manganese, and cadmium without using organic solvents which are volatile or toxic.

Silver ion was not extracted at all by PNIPAAm, which contains no thioether units. As the concentration of ATH units in the polymer is increased, the extraction efficiency of silver ion increased. It is thought when the polymer containing ATH units in the chain and hydrated under the temperature of LCST, ATH units coordinate with silver ion, and after the temperature increases over the LCST, silver ion is included in the solid polymer phase with picrate ion for the charge compensation. The results obtained have been compared with those of liquid-liquid extraction using 1,2-dichloroethane [5]. As the affinity of ATH for noble metal ions such as silver(I), gold(III), and palladium(II) is superior to that of classical reagents containing O- or N-donor atoms, a thermo-sensitive polymer containing such thioether units may prove to be useful for selective metal recovery.

REFERENCES

1. K. Chayama and E. Sekido, "Liquid-Liquid Extraction of Copper with Cyclic and Acyclic Tetrathioethers," *Anal. Chim. Acta*, **248**, 511-515 (1991).
2. T. Saitoh, T. Ohyama, K. Takamura, T. Sakurai, T. Kaise, and C. Matsubara, "Extraction of Iron(II)-Tris(1,10-phenanthrolinato) Chelate into the Polymer Phase Formed from an Aqueous Solution of Poly(*N*-isopropylacrylamide)," *Anal. Sci.*, **13**, 1 (1997).
3. J. Zhang and N. A. Peppas, "Synthesis and Characterization of pH- and Temperature Sensitive Poly(methacrylic acid) / Poly(*N*-isopropylacrylamide) Interpenetrating Polymeric Networks," *Macromolecules*, **33**, 102 (2000).
4. S. R. Lustig, G. J. Everlof and G.. D. Jaycox, "Stimuli-Responsive Polymers. 5. Azobenzene Modified Polyaramides Containing Atropisomeric Binaphthyl Linkages: Tuning Chiroptical Behavior with Light and Heat," *Macromolecules*, **34**, 2364 (2001).
5. K. Chayama, K. Adachi, T. Mori, and H. Tsuji, "Extraction Behavior of Soft Metal Ions with Polythioether Derivatives Containing O or N Donor Atoms," International Solvent Extraction Conference, 2002; pp. 576-580.

EXTRACTION OF COPPER FROM PHOSPHORIC ACID SOLUTIONS USING ALGINATE BEADS CONTAINING LIX 622

F. Mijangos, A. Ocio, M. P. Elizalde, and A. Almela

Departments of Analytical Chemistry and Chemical Engineering, Faculty of Science and Technology, University of The Basque Country, P.O. Box 644, 48080 Bilbao, Spain.
Corresponding author email address: federico.mijangos@ehu.es

ABSTRACT

A new methodology based on the encapsulation of organic solutions of LIX 622 (5–dodecylsalicylaldoxime) into calcium alginate gels has been developed. Composite beads are able to recover copper from aqueous 0.4–2.5 M phosphoric acid as well as from H_3PO_4/KH_2PO_4 buffer solutions. The influence of the aqueous acidity and the extractant concentration has been studied. Retention data have been fitted to a theoretical physicochemical model that takes into account a Donnan diffusion between aqueous and alginate phases as well as the formation of the complex CuL_2, L being 5-dodecylsalicylaldoximate, in the organic microdrops.

INTRODUCTION

Liquid–liquid extraction processes have been widely focused on the elimination of heavy metals from industrial wastes. In order to improve operating performance and extractant reutilization, unconventional techniques such as supported or emulsion liquid membranes have been tested. Recently, several works concerning the encapsulation of organophosphorus extractants into calcium alginate gels have been published.

The efficiency of alginate gels containing Cyanex 302 or Cyanex 301 for the recovery of Pd, Am, Cu, Cd, Zn, and Ag from HNO_3 or HCl solutions has been proved.

Regarding metal retention from phosphoric acid, copper and cadmium from 1.0–7.5 M H_3PO_4 as well as from WPA solutions can be extracted using alginate gels containing Cyanex 302 [1] or Cyanex 301 [2]. The latter also allows the extraction of zinc.

LIX 622 (5–dodecylsalicylaldoxime), which extracts copper from synthetic H_3PO_4 solutions [3], has not been used encapsulated into alginate gels. For these reasons, in the present work alginate gels enclosing LIX 622 have been prepared and applied to diluted phosphoric acid solutions.

EXPERIMENTAL

Reagents and Solutions

Synthetic solutions of Cu(II) in phosphoric acid were prepared by weighing appropriate amounts of phosphoric acid (Carlo Erba p.a.), potassium dihydrogenphosphate (Merck p.a.) and 1000 mg/L standard solutions of the metal ion (Merck p.a.). Four phosphoric acid solutions (0.4, 0.7, 1.0, and 2.5 M) and a 0.5 M H_3PO_4/0.5 M KH_2PO_4 buffer solution were prepared. Copper concentration was varied between 5 and 150 mg/L.

LIX 622, kindly supplied by Cognis Ireland, was used without further purification. It contains 67.7% 5–dodecylsalicylaldoxime (HL) [4] and 15.9% isotridecanol [5]. Solutions containing 0.5, 0.8, and 0.9 M HL were prepared in toluene (Fluka p.a.). The density of the organic solutions was measured yielding the value of 900 kg/m^3.

Dry sodium alginate (Carlo Erba) was used for the preparation of the beads. A 0.05 M calcium nitrate solution was used as gelation medium.

Alginate Bead Preparation

Sodium alginate hydrosol was prepared by dissolving 2 g of dry sodium alginate in 96 g of deionized water at room temperature. 2 g of the organic solution containing the extractant in toluene were mechanically stirred with the sodium alginate solution and then dropped into a magnetically stirred 0.05 M calcium nitrate solution. As a consequence of an ion-exchange process [6], a hydrogel is formed as free sodium ions are removed from the alginate structure by the calcium ions. Approximately 50% of the initial water in the hydrosol is reported to be released in this process [7]. The physicochemical parameters of the beads are summarized in Table 1.

Mixed alginate beads were kept in the calcium solution for 14 h before the experiments of metal retention. When calcium alginate beads are immersed in phosphoric acid solutions simultaneously to metal retention, and due to the high hydrogen ion concentration, a new ion exchange between hydrogen and calcium takes places. Furthermore, the spheres shrink, and water is released. Table 1 also shows the estimated gel composition once the beads are immersed in phosphoric acid solutions.

Metal Loading Experiments

Volumes of 10 mL of aqueous solutions containing Cu(II) in phosphoric acid were shaken with 1.00 g of calcium alginate gels for 14 h. After phase separation, the metal concentration in the aqueous phase was measured by atomic absorption spectroscopy (Perkin Elmer Aanalyst 100). Values of relative standard deviation of the results were always lower than 4%. The amount of metal loaded into the mixed gel was calculated from the mass balance of the metal ion.

Table 1. Weight composition of the mixed alginate gels containing LIX 622

Component	Conditions						
	Initial solution	0.05 M $Ca(NO_3)_2$	H_3PO_4/ KH_2PO_4	0.4 M H_3PO_4	0.7 M H_3PO_4	1.0 M H_3PO_4	2.5 M H_3PO_4
Sodium alginate (g)	2.00	–	–	–	–	–	–
Imbibed phase (g)	96.00	44.30	29.48	30.41	30.74	31.33	30.05
Organic solution (g)	2.00	2.00	2.00	2.00	2.00	2.00	2.00
Calcium alginate	–	1.99*	–	–	–	–	–
Alginic acid	–	–	1.83*	1.83*	1.83*	1.83*	1.83*
Total weight (g)	100.00	48.29	33.31	34.24	34.57	35.16	33.88
Density (g/mL)	1.01	1.03	1.02	1.01	1.03	1.05	1.13

*Estimated values.

RESULTS AND DISCUSSION

Figure 1 illustrates the amount of copper, q, expressed as mmol/kg $_{gel}$ loaded into mixed alginate gels containing 0.89 M LIX 622 in toluene at several phosphoric acid concentrations. As expected, copper uptake decreases when aqueous phase acidity increases. Metal uptake (q) by mixed alginate gels containing organic solutions of extractant is due to the sum of both alginate (q_{alg}) and organic (q_{org}) contributions.

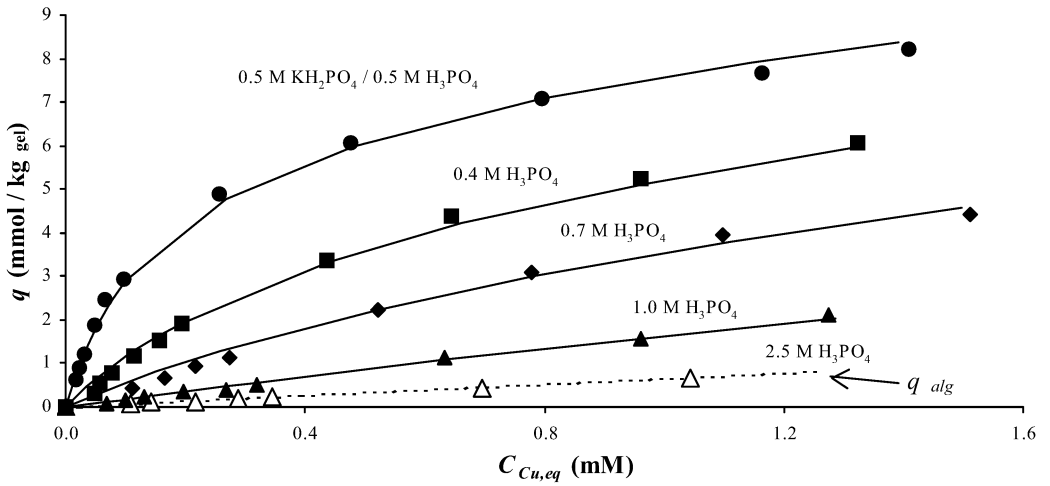

Figure 1. Experimental retention of copper into mixed alginate beads enclosing organic solutions of 0.89 M LIX 622.

Calcium alginate behaves as an ion exchanger when the pH is higher than 3 [6,8], and consequently, the carboxylic groups of the alginate polymer are expected to be protonated under the experimental conditions of this work. However, some amount will remain imbibed in the polymeric matrix. This concentration can be expressed as a function of a Donnan–type by

$$\lambda = \frac{C_{H,a\lg}}{C_{H,aq}} = \sqrt{\frac{C_{Cu,a\lg}}{C_{Cu,aq}}} = \sqrt{\frac{C_{Ca,a\lg}}{C_{Ca,aq}}} \quad (1)$$

Assuming a partition factor of 1.0, the copper retention coefficient due to the alginate phase is:

$$q_{a\lg} = \frac{V_{a\lg} C_{Cu,a\lg}}{m_{gel}} = \frac{V_{a\lg}}{m_{gel}} \lambda^2 \cdot C_{Cu,aq} = \frac{V_{a\lg}}{m_{gel}} \cdot C_{Cu,aq} \quad (2)$$

The function $q_{alg} = f\,(C_{Cu,\,aq})$, drawn also in Figure 1 (dash line), acceptably fits the retention data corresponding to 2.5 M phosphoric acid, thus indicating that, under those conditions, metal retention is only due to the alginate phase.

Concerning the liquid–liquid extraction process, copper extraction from phosphoric acid by LIX 622 has been explained [3] by the reaction

$$Cu^{2+}{}_{aq} + 2\ HL_{org} \rightleftharpoons CuL_{2\ org} + 2\ H^{+}{}_{aq} \quad (3)$$

It can be assumed that copper ion diffused in the alginate phase goes into the organic microdrops by this type of reaction. The corresponding conditional equilibrium constant can be defined as

$$k' = \frac{C_{Cu,org} \left[H^+\right]^2_{aq-a\lg}}{C_{Cu,aq-a\lg} \left[HL\right]^2_{org}} = \frac{q_{Cu,org} \left[H^+\right]^2_{aq-a\lg}}{C_{Cu,aq-a\lg} \left[HL\right]^2_{org}} \cdot \frac{m_{gel}}{V_{org}} \quad (4)$$

where C denotes total molar concentration in the corresponding phase, m the mass of mixed gel, and V_{org} the volume of the organic microdrops.

Equation 4 has been used as starting point to look for the best fit to the data. Theoretical values of q_{org} as a function of copper concentration in aqueous phase have been obtained by means of the Letagrop–Distr program [9]. It has been also taken into account that 5–dodecylsalicilaldoxime dimerizes in toluene [10], and that forms a 1:1 adduct with isotridecanol [11]. Nevertheless, taking into account the high extractant concentration used in the experiments, the total concentration of oxime has been corrected according to the parameter γ, defined as the quotient between the effective extractant concentration and the total one.

Figure 2 illustrates, together with metal retention data at different phosphoric acid and LIX 622 concentrations, the theoretical functions obtained in the fit to the data. The corresponding parameters are summarized in Table 2.

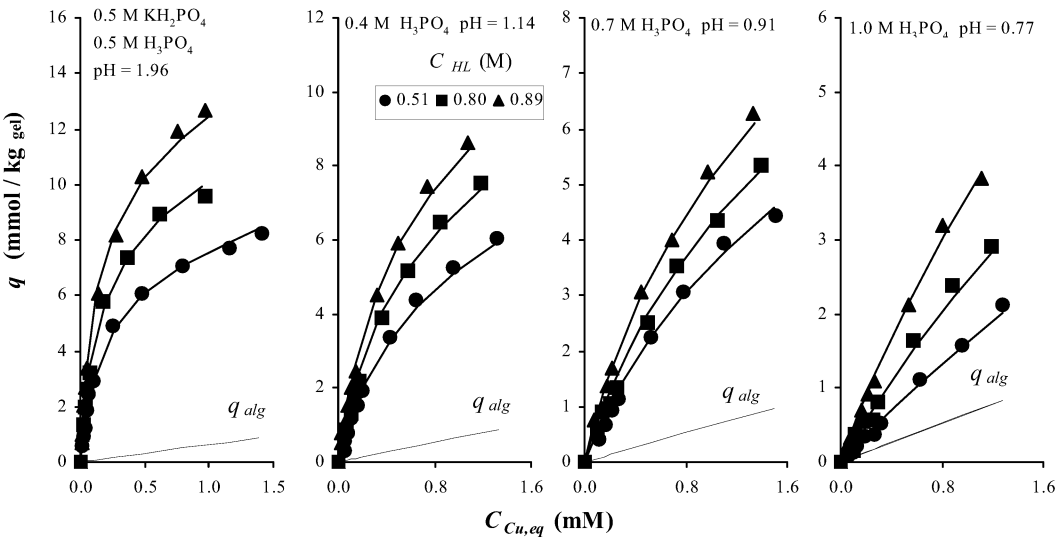

Figure 2. Experimental retention of copper into mixed alginate beads enclosing toluene solutions of LIX 622. Curved lines correspond to the proposed retention model.

CONCLUSIONS

Copper uptake from diluted phosphoric acid solutions by calcium alginate gels containing toluene solutions of LIX 622 is produced both in alginate and in the organic phase. In the less acidic conditions (H_3PO_4 / $H_2PO_4^-$), the retention is mainly due to the extraction in the organic phase. In 1 M H_3PO_4, the retention in both phases is similar. However, alginate is the only responsible for the weak copper retention obtained at 2.5 M phosphoric acid.

A model of copper retention based on the contribution of liquid–liquid extraction and diffusion into the alginate phase, which acceptably explains the experimental results, is proposed. Values of the fitting parameter γ, which accounts for the effective extractant concentration compared with the total one obtained, reveal that interactions between the components of the commercial extractant are stronger than those in diluted solutions [10,11], although it is also possible that the presence of the alginate phase can decrease the free concentration of 5-dodecylsalicylaldoxime.

Table 2. Values of the conditional equilibrium constants and fitting parameters of copper retention by mixed alginate gels containing LIX 622

Aqueous solution	log k'	γ		
		0.51 M HL	0.80 M HL	0.89 M HL
0.5 M H_3PO_4 / 0.5 M KH_2PO_4	0.00	1.00	0.97	0.95
0.4 M H_3PO_4	1.15	1.00	0.95	0.90
0.7 M H_3PO_4	1.20	1.00	0.90	0.85
1.0 M H_3PO_4	1.00	0.85	0.92	1.00

REFERENCES

1. A. Ocio, F. Mijangos, and M. P. Elizalde, "Copper and Cadmium Extraction from Highly Concentrated Phosphoric Acid Solutions using Calcium Alginate Gels Enclosing bis(2, 4, 4-trimethylpentyl)dithiophosphinic Acid," *J. Chem. Technol. Biotechnol.*, **81**, 1409–1418 (2006).
2. A. Ocio, F. Mijangos, and M. Elizalde, "Application of Calcium Alginate Gels Enclosing Cyanex 301 for Metal Extraction from Highly Concentrated Phosphoric Solutions. Analysis of Equilibrium Data," *Book of Abstracts IEX 2006, 153.*
3. A. Ocio and M. P. Elizalde, "Copper(II) Extraction from Phosphoric Acid Media by 5-dodecylsalicylaldoxime (LIX 622)," *Solvent Extr. Ion Exch.*, **24**, 861–875 (2006).
4. A. Ocio, M. Elizalde, and J. A. Prieto, "Determination of 5-dodecylsalicylaldoxime and 5-nonylsalicylaldoxime in Commercial Extractants by HPLC with Photometric Detection," *J. Chromatogr., A*, **1032**, 129–132 (2004).
5. A. Ocio, B. Menoyo, and M. Elizalde, "Identification and Quantification of Alkylsalicylaldoximes and Alcoholic Modifiers in Commercial Extractants by Gas Chromatography–Mass Spectrometry," *Book of Abstracts Euroanalysis XIII PS2-231, Salamanca (Spain) 2004.*
6. Y. Jodra and F. Mijangos, "Ion-Exchange Selectivities of Calcium Alginate Gels for Heavy Metals," *Water Sci. Technol.*, **43**, 237–244 (2001).
7. Y. Jodra, "Intercambio Iónico sobre Hidrogeles de Ácidos Poliurónicos," Ph.D. Thesis, University of the Basque Country, Bilbao, Spain, 2000; pp. 415–418.
8. F. Mijangos and Y. Jodra, "Feasibility of Alginates as Ionic Exchangers for Wastewater Treatment. Equilibrium Studies," *Afinidad.*, **52**, 313–318 (1995).
9. D. H. Liem, "High–speed Computers as a Suplement to Graphical Methods," *Acta Chem. Scand.*, **25**, 1521–1534 (1971).
10. M. S. Rúa, A. Almela, and M. P. Elizalde, "Aggregation Equilibria of the Components of the Commercial Extractants LIX 622 and LIX 622N in Toluene and *n*-heptane," *Fluid Phase Equilib.*, **244**, 111–116 (2006).
11. M. S. Rúa, A. Almela, and M. P. Elizalde, "Interactions between Components of the Commercial Extractants LIX 622 and LIX 622N in Toluene," *Fluid Phase Equilib.*, **258**, 186–190 (2007).

MICROEMULSION LEACHING OF METALS

E. V. Yurtov and N. M. Murashova

Mendeleev University of Chemical Technology of Russia, 125047 Miusskaya sq., 9, Moscow, Russia. Corresponding author e-mail address: yurtov@muctr.ru

ABSTRACT

The possibility of nonferrous metals leaching from ore and secondary raw materials by means of direct sodium bis(2-ethylhexyl)phosphate microemulsion is demonstrated. The recovery of Fe, Co, Ni, and Cu from the sample of the cobalt-copper concentrate and was studied. The influence of various factors on rate of the microemulsion leaching of Cu was investigated.

INTRODUCTION

Recently the attention of researchers has turned to the possible use of nanoparticles and nanostructures to overcome the problems of chemical technology, including extraction and separation of substances. The variant of liquid extraction with such nanoparticles, as in reverse-micelle and microemulsion-micelle extraction, are known. Application of micelles and microemulsions allows for the recovery of both organic and inorganic substances.

In this work, extractant-containing microemulsions are used for the recovery of metals directly from a solid phase (microemulsion leaching). This method combines leaching and extraction processes.

Special interest from the technological point of view is represented by direct microemulsions in which the volume of an organic phase is approximately equal to volume of a water phase. It allows to lower extractant losses on wetting of solid particles and consequently to reduce environmental contamination by components of the organic phase. It is possible to use in microemulsions extractants of various classes and also their mixtures. As an external phase of direct microemulsions is the water phase; such microemulsions are considerably less combustible and toxic than extractant solutions in organic solvents or reverse microemulsions.

As an example we have considered the use for the leaching microemulsions based on salts of the widely known extractant bis(2-ethylhexyl)phosphoric acid (DEHPA), namely sodium bis(2-ethylhexyl)phosphate (NaDEHP). NaDEHP microemulsions can find application for recovery of metals that are favorably extracted by DEHPA.

Formation of microemulsions of various types in the systems containing NaDEHP, organic solvent, and water is well known. Formation of reverse microemulsion in the system water solution of sodium or ammonium hydroxide/DEHPA and secondary

octyl alcohol in kerosene [1], bicontinuous and direct microemulsion in the system NaDEHP-heptane/water [2], reverse microemulsion in thesystem NaDEHP-heptane-water solution of NaCl [3]. The formation of microemulsion and two or three phases equilibria in system NaDEHP-decane/water, containing both pure DEHPA, and technical extractant are reported [4].

The purpose of this work is to demonstrate the possibility of nonferrous metals leaching from ore and secondary raw materials by means of direct NaDEHP microemulsion.

EXPERIMENTAL

DEHPA (Merck, Germany) with purity of more than 98%, octanol and NaOH of pure grade, twice-distilled water, and kerosene were used for preparation of microemulsions. NaDEHP microemulsions were prepared by mixing the required amounts of aqueous NaOH solution and DEHPA (and octanol in some cases) solution in kerosene. Microemulsions used in this work are presented in Table 1.

Table 1. Composition of microemulsions used for the leaching of metals

Micro-emulsion	Composition of organic phase			Water phase content, vol %
	C_{NaDEHP}, mol/L	C_{DEHPA}, mol/L	$C_{octanol}$, vol %	
ME1	1.60	0.06	3.1	47
ME2	1.65	0.50	0	40
ME3	1.65	0.50	0	30
ME4	1.60	0	3.3	50

Cobalt-copper ore concentrate and samples of galvanic sludge were used. Composition of the ore concentrate is shown in the Table 2. Fraction of the concentrate with particles less 0.2 mm was used.

Table 2. Composition of the cobalt-copper concentrate

Element	Co	Cu	Fe	Si	Al	Ni	Mn	Zn	Pb	As	S
Concentration, mass %	8.3	1.1	10.0	32.4	0.6	0.7	0.4	0.04	0.03	0.01	0.3

The leaching was carried out in a closed flask with mechanical agitation (rotary movement with amplitude of 4 mm and frequency of 200 rpm) in a water bath-shaker at a solid-liquid phase ratio of 1:100. After the leaching, a solid phase was separated and metals were re-extracted from the microemulsion by 10% sulfuric acid. Copper concentration was determined by photometrical method (cuprizon coloring). Iron, cobalt, nickel, and copper concentrations were analyzed by the atom absorption spectroscopy method.

RESULTS AND DISCUSSION

The recovery of iron, cobalt, nickel, and copper from the sample of the cobalt-copper concentrate containing significant amounts of iron and silicon (Table 2) by direct NaDEHP microemulsion was investigated. Results are shown in Table 3.

Table 3. Metal leaching from cobalt-copper concentrate by microemulsion 1 (ME1) at 80 ºC

Duration of the leaching, hours	Metal concentration in the microemulsion, mmol/L				Recovery factor, %			
	Fe	Co	Ni	Cu	Fe	Co	Ni	Cu
8	0.273	2.372	0.073	0.647	3.2	14.3	18.8	44.0
80	0.395	6.055	0.238	1.140	4.6	36.4	61.0	77.5

Apparently from Table 3, application of NaDEHP microemulsion allows the selective extraction of nonferrous metals with very low iron extraction. Selectivity of extraction of nonferrous metals (nickel, cobalt, copper) and iron from the sample of a cobalt-copper concentrate in the microemulsion corresponds to the selectivity of the extractant, bis(2-ethylhexyl)phosphoric acid. The ratio of recovery factors of nonferrous metals and iron in 80 hours leaching are Cu/Fe 16.8, Ni/Fe 13.3, and Co/Fe 7.9. As the water phase in NaDEHP microemulsion is at neutral pH, silicon is not extractable and separates with a solid phase.

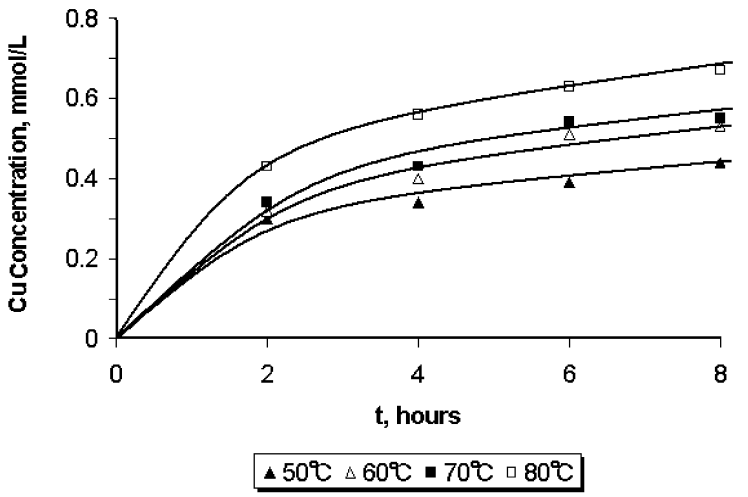

Figure 1. Effect of temperature on copper leaching from cobalt-copper concentrate by microemulsion 1 (ME1).

Influence of various factors on rate of the microemulsion leaching was studied on an example of extraction of copper from the cobalt-copper concentrate. Kinetic curves of the microemulsion leaching in the range of temperatures 50-80 ºC are presented in Figure 1.

At temperature above 80 ºC, it is not efficient to carry out the microemulsion leaching, as the stability of the microemulsion decreases. At a temperature of 90 ºC, the microemulsion used for the leaching breaks onto organic and water-rich phases.

The rate of the microemulsion leaching can be increased, having raised the extractant content (free, that is, not neutralized DEHPA) in the microemulsion. The influence of "free" DEHPA content in the microemulsion on the rate of the microemulsion leaching of copper is shown in Figure 2. At approximately equal NaDEHP concentration (1.60-1.65 mol/L) the increase of "free" DEHPA content leads to appreciable increase of the leaching rate. At the same time, it has been established that change of the water-phase volume in the microemulsion in the range from 20 to 40% does not influence the leaching rate.

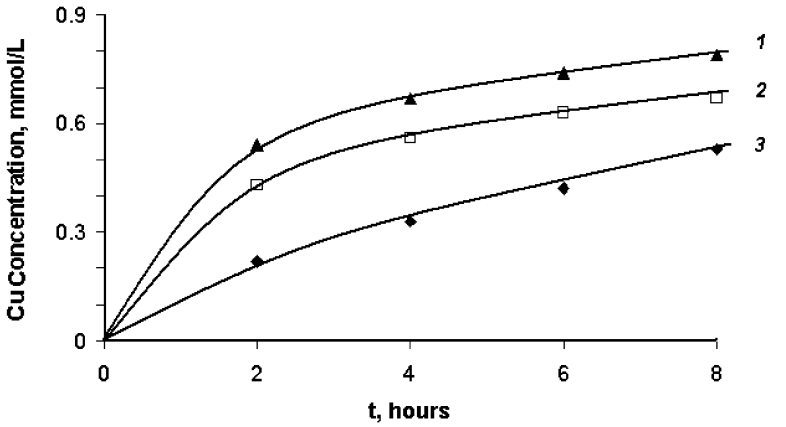

Figure 2. Effect of the microemulsion composition on the rate of copper leaching from cobalt-copper concentrate at 80 ºC. Microemulsions: 1 – ME2, 2 – ME1, 3 – ME4.

The rate of the microemulsion leaching can be raised considerably by ultrasonic activation and additional grinding of ore (Figure 3). The combination of additional grinding of the sample and ultrasound agitation allows reaching in 2 hours the same degrees of extraction of copper from the cobalt-copper concentrate that are reached in 8 hours of mechanical agitation.

Direct NaDEHP microemulsion allows recovering nonferrous metals not only from ores but also from secondary raw materials, for example, from galvanic sludge (Figure 4). The rate of extraction of metals from secondary raw materials can be considerably higher than from natural ores. This may be due to the finely divided nature of the secondary raw material and a more leachable metal compound being present.

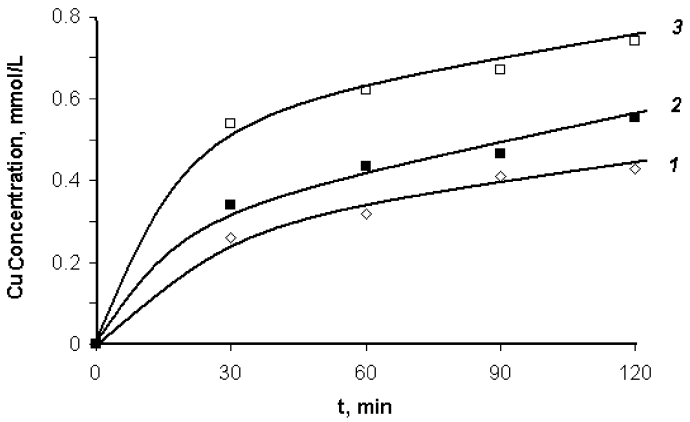

Figure 3. Effect of ultrasound activation on copper leaching from cobalt-copper concentrate by microemulsion 2 at 80 ºC. 1—mechanical agitation, 2—ultrasound agitation, 3—additional grinding and ultrasound agitation.

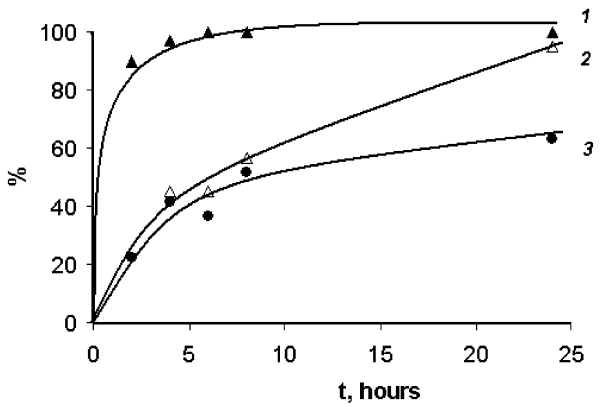

Figure 4. Copper leaching from different samples by microemulsion 3 (ME3) at 80 ºC. Samples: 1—galvanic copper sludge, prepared by NaOH precipitation; copper content 161.4 g/kg; 2—galvanic copper sludge, prepared by $Ca(OH)_2$ precipitation; copper content 92.2 g/kg; 3—cobalt-copper concentrate.

Based of the data obtained in this work, it is possible to offer the principal technological scheme of microemulsion leaching (Figure 5). Such a scheme allows combining the processes of leaching and extraction. During the leaching, the valuable metals are selectively extracted in the microemulsion, and components that are not or are poorly extractable by DEHPA, such as Si, Al, Fe, Ca, etc., remain as a part of the solid phase and have to be separated by filtration. The extracted metals in the microemulsion, after the re-extraction (stripping) remain in the water phase and are subject to additional separation and purification. The organic phase after the re-extraction is returned to the microemulsion preparation.

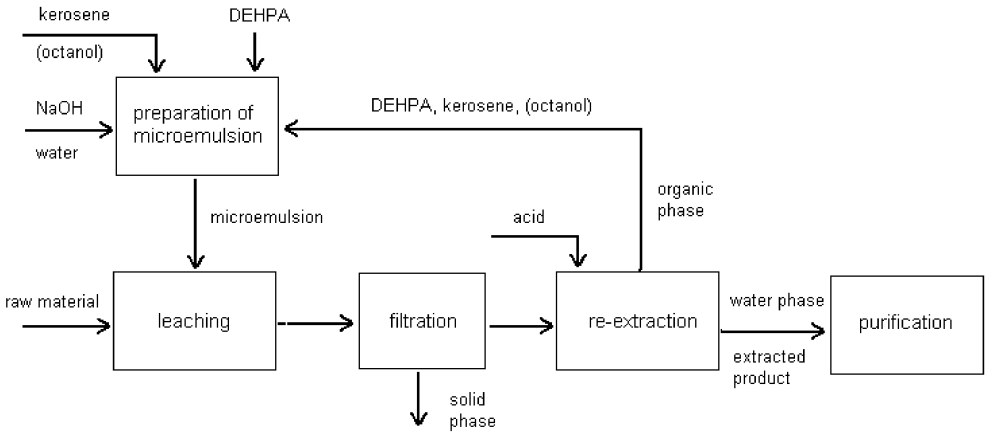

Figure 5. Principal process of microemulsion leaching of metals.

CONCLUSIONS

The use of extractant-containing microemulsion opens the possibility of combined leaching and extraction processes. Microemulsion leaching has been demonstrated to extract metals from a solid phase selectively without strong acids and bases. Silicon and other nonextractable components will remain in the solid-phase residue.

Direct *(O/W)* NaDEHP microemulsion is a promising system for nonferrous metal recovery from solid particles—ore concentrates, sludges, ashes, dusts, etc. The results obtained in this study are considered as the basis for the elaboration of the process of nonferrous metal leaching from complex ores and secondary raw material by means of NaDEHP microemulsion.

REFERENCES

1. C.-K. Wu, H.-C. Kao, T. Chen, et al. "Microemulsion Formation in the Organic Phase of Some Important Extractants and its Effects on the Extraction Mechanism," Int. Solvent Extraction Conference ISEC'80 Proc., Liege. Belgium, 1980; Vol. 1., pp.185-195.
2. Z.-J. Yu and R. D. Neuman, "Reversed Micellar Solution-to-Bicontinuous Microemulsion Transition in Sodium Bis(2-ethylhexyl) phosphate/*n*-Heptane/Water System," *Langmuir*, **11**(4), 1081-1086 (1995).
3. A. Shioi, M. Harada, and K. Matsumoto, "Phase Structure of Organized Assembly Composed of Amphiphilic Compounds," *Bull. Inst. Atom. Energy Kyoto Univ.*, **77**, 57-57 (1990).
4. E. V. Yurtov and N. M. Murashova, "Phase Equilibria and Nonequilibrium Structures in the Sodium Di-2-Ethylhexyl Phosphate – Decane – Water System," *Colloid J.*, **66**(5), 629-634 (2004). Translated from *Kolloidnyi Zhurnal* (Russ.) **66**(5), 702-707 (2004).

NOVEL DEXTRAN GEL FORMATION BY ENZYMATIC REACTION TO USE FOR SOLID-PHASE EXTRACTION

H. Kawakita, H. Seto, K. Ohto, H. Harada, and K. Inoue

Dept. of Applid Chemistry, Saga University, Saga 840-8502, Japan.
Corresponding author email address:kawakita@cc.saga-u.ac.jp

ABSTRACT

Novel solid-extraction material was prepared using functional dextran gel generated enzymatically on the membrane surface. Dextransucrase was immobilized on the membrane pore, and then ketone-introduced sucrose solution was permeated to DSase-immobilized membrane to generate the ketone-introduced dextran membrane at 21 mg/g. Copper ion solution, used as a probe, was again permeated to the membrane, indicating that ketone-introduced dextran exhibited higher solid-extraction capacity to copper ion.

INTRODUCTION

Solid-phase extraction is an analytical method to bind target analytes selectively to use for preconcentration. To prepare the solid-phase extraction material, it is necessary to design the recognition site for the target molecule, preventing the unselective binding to the material. The trunk molecule, polymer, and material to prevent unselective binding should be selected as a main matrix, and the functional group to recognize the analyte is to be introduced to the main matrix.

Dextran is a polysaccharide with an α-(1,6) pyranose ring linkage and has the following unique characteristics: 1) flexibility of the random structure due to the free rotation of glycosyl bonding and 2) high solubility due to the plural hydroxyl groups. The hydroxyl group of dextran reduces the unselective binding of the molecules because of less interaction. To introduce the specific binding site to dextran enables us to prepare the high-performance solid-extraction material.

The method to introduce the recognition site, namely, the functional group, to dextran polymer is mainly chemical [1,2]. The functional groups can be introduced to the plural hydroxyl groups of dextran. However, due to the equal reactivity of the hydroxyl groups and due to the steric hinderance of the functional group molecule, it is difficult to introduce the functional group to the intended-designed site. Possibly, the glycoside bonding of dextran is cleaved during the introduction reaction.

Dextransucrase (DSase), a kind of transferase, produces dextran and fructose using sucrose as a substrate. The product dextran forms a complex with DSase at the active site. By using this characteristic, the dextran was formed on the pore surface of the

membrane to use for the membrane-pore-size control and the adsorption site of lectin in our previous researches [3-5].

To introduce the functional group to dextran, the functional group was preliminarily introduced to sucrose, and subsequently the functional sucrose was reacted with DSase to produce the designed functional dextran. During the reaction of sucrose with DSase, it is known that DSase recognizes the C3 position of glucose unit in sucrose. Due to this, the functional group should be introduced to C2 or C4 position of glucose unit in sucrose to maintain DSase's activity to sucrose.

In this study, by utilizing the DSase reaction in which dextran forms a complex with the active site of DSase, the preliminary functionalized sucrose is reacted with DSase immobilized on the membrane pore to generate the functional dextran gel on the pore surface, as shown in Figure 1. Sucrose was reacted with pyranose-2-oxidase (POase) to introduce the ketone group at C2 position of glucose unit in sucrose. In order to investigate the potential of ketone-dextran generated to the membrane pore surface as a solid-phase extraction, copper ion solution was permeated through the ketone-dextran-containing membrane.

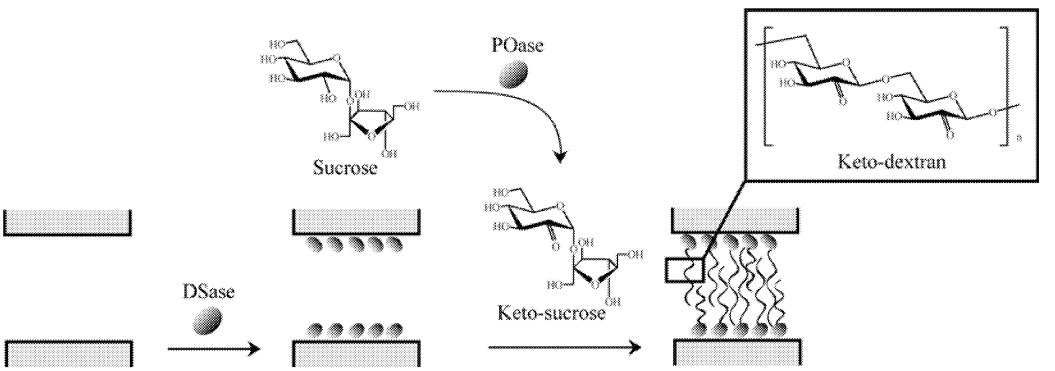

Figure 1. Preparation of keto-dextran-containing membrane by enzymatic reaction on pore surface.

EXPERIMENTAL

Materials

Dextransucase (EC 2.4.1.5, Lot No. 067K4164), pyranose-2-oxidase (EC 1.1.3.10 Lot No. 056K1489), and catalase (EC 1.11.1.6, Lot No. 096K7035) were purchased from Sigma Co. Shirasu porous membrane (SPG Technology Co., Ltd.,) was used as a trunk inorganic material. This membrane had inner and outer diameter of 4 and 5 mm, respectively, with an average pore size of 2000 nm. Other reagents were of analytical grade or higher.

Synthesis of Ketone-Introduced Sucrose Using POase's Reaction

Sucrose (5 g/L) was reacted with POase to introduce aketone group to the C2 position of glucose of sucrose at 303 K. Sucrose was dissolved in 200 mL pure water as a solvent, and POase (50 U) and catalase (5000 U) were added to the solution with aeration. Catalase functions to eliminate hydrogen peroxide because it inhibits the POase's activity. After 24 h, the enzyme was inactivated and filtered using the ultrafiltration membrane (MW cut 50,000, Millipore). The filtrate was dried in vacuum to obtain a white powder. The resultant powder was referred to as a keto-sucrose. The amount of carbonyl group in keto-sucrose was determined by colorimetric assay using dinitrophenylhidrazine [6] in which the standard reagent used was ketone-introduced glucose.

Generation of Ketone-Introduced Dextran by Immobilized DSase on the Membrane Pore

DSase solution (0.1 U/mL, 10 mM acetate buffer, pH 5.5) was permeated through the pore of the SPG membrane at a flowrate of 30 mL/h. The effluent penetrating the outside surface of the SPG membrane was continuously collected, and the activity of DSase in the effluent was determined. An activity of 1 U was defined as the amount of enzyme required to produce 1 μmol of fructose for 1 min.

Keto-sucrose solution (25 g/L, 10 mM acetate buffer, pH 5.5) was permeated radially outward from the inside surface of a DSase-immobilized membrane at 30 mL/h to generate keto-dextran on the membrane pore. The effluent was continuously collected, and the fructose concentration produced by DSase was determined by the Somogyi-Nelson method [7,8]. For comparison, sucrose solution was permeated through DSase-immobilized membrane to generate dextran. Generated functional dextran was referred to as a keto-dextran.

Permeation of Copper Ion Solution through the Membranes

Copper ion solution (0.1 mM, pH 5.5) was permeated through SPG membrane, dextran-containing membrane, and keto-dextran-containing membrane. Space velocity of the solution was set at 23 h^{-1}. The effluent was collected, and the concentration of copper ion in it was determined by atomic absorption spectrophotometry (AA-6650, Shimadzu).

RESULTS AND DISCUSSION

Generation of Keto-Dextran on the Membrane Pore Surface

To polymerize keto-dextran, keto-sucrose was synthesized from sucrose via POase's reaction. POase can introduce a ketone group to thebC2 position of glucose unit in sucrose. As a result, sucrose was perfectly converted to keto-sucrose enzymatically, determined by colorimetirc assay.

DSase solution was permeated through the SPG membrane to immobilize DSase on the membrane pore, as shown in Figure 2. In permeating DSase solution, the amount

of DSase immobilized increased exponentially. As shown in our previous paper [3], the interaction between DSase and the pore surface was hydrophilic or ionic interaction. Subsequently, keto-sucrose solution was permeated through the DSase-immobilized membrane to generate keto-dextran on the pore surface shown in Figure 3. The slope of the amount of keto-dextran produced was a straight line. When sucrose was used as a substrate to generate dextran, the reactivity of the immobilized DSase was higher due to the recognition of DSase at the active site to the substrate. The obtained functional dextran would form a gel structure on the membrane pore, because the ketone group in dextran possibly interacted with hydroxyl groups of dextran via hydrogen bonding.

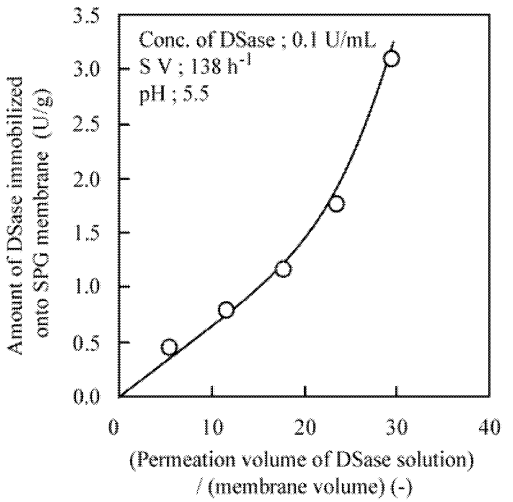

Figure 2. DSase immobilization on the SPG membrane.

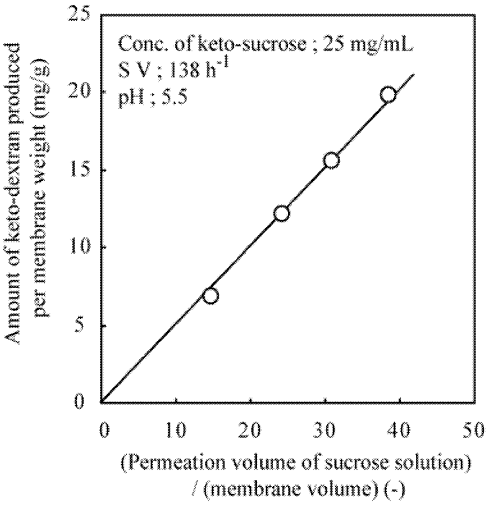

Figure 3. Keto-dextran formation on the pore surface of the membrane.

Solid-Phase Extraction of Copper Ion with Keto-Dextran

Dextran has no specific interaction to the molecule due to plural hydroxyl groups. By introducing the functional group to dextran, the specific interaction was expressed to the target molecule to use for the solid-phase extraction material. The probe used to investigate the performance of keto-dextran as a solid-phase extraction was copper ion. Copper ion solution was permeated through the membranes at SV 23 h^{-1}, as shown in Figure 4. Keto-dextran-containing membrane represented higher copper adsorption capacity than other membranes, indicating that keto-dextran has the potential as a solid-extraction material.

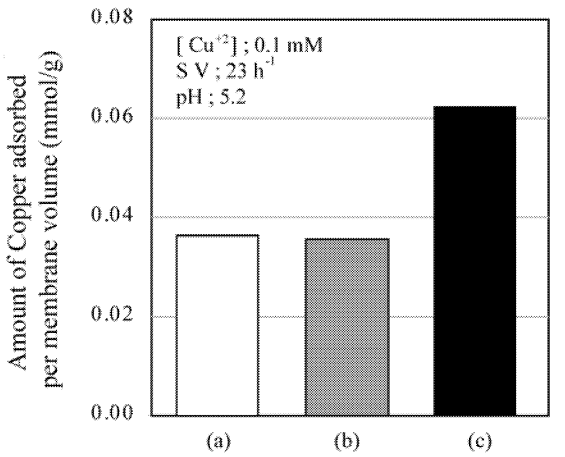

Figure 4. Solid-phase extraction of copper ion to (a) SPG membrane, (b) dextran-containing membrane, and (c) keto-dextran-containing membrane.

CONCLUSIONS

To prepare novel solid-phase extraction material, the functional dextran was generated on the pore surface of the membrane by using dextransucrase's reaction. Prior to functional dextran synthesis, a ketone group was introduced to sucrose enzymatically, resulting in perfect introduction of ketone group at the C2 position of the glucose unit in sucrose. After immobilizing DSase on the membrane pore, ketone-introduced sucrose solution was permeated through DSase-immobilized membrane to generate the functional dextran on the membrane pore. To discuss the potential of ketone-introduced dextran as a solid-phase extractant, copper ion solution was permeated through the ketone-introduced dextran membrane. Copper ion was more captured by ketone-dextran than dextran, indicating that specific interaction was incorporated into the functional dextran. More regulation of functional dextran enables us to prepare a high-performance solid-phase extraction material.

REFERENCES

1. K. I. Shingel, "Current Knowledge on Biosynthesis, Biological Activity, and Chemical Modification of the Exopolysaccharide, Pullulan," *Carbohydr. Res.*, **339**, 447–460 (2004).
2. S. Tanna, T. S. Sahota, K. Sawicka, and M. J. Taylor, "The Effect of Degree of Acrylic Derivatisation on Dextran and Concanavalin A Glucose-Responsive Materials for Closed-Loop Insulin Delivery," *Biomaterials*, **27**, 4498–4507 (2006).
3. H. Kawakita, H. Seto, K. Ohto, K. Inoue, and H. Harada, "Pore Control with Dextran Generated from Immobilized Dextransucrase," *Biochem. Eng. J.*, **36**, 190–193 (2007).
4. H. Seto, H. Kawakita, K. Ohto, H. Harada, and K. Inoue, "Membrane Porosity Control with Dextran Produced by Immobilized Dextransucrase," *J. Chem. Technol. Biotechnol.*, **82**, 248–252 (2007).

5. H. Kawakita, K. Hamamoto, H. Seto, K. Ohto, H. Harada, and K. Inoue, "Bioseparation of Lectin by Dextran Produced by Dextranscurase," *J. Ion Exch.*, **18**, 324-327 (2007).
6. A. Huwig, H.-J. Danneel, and F. Giffhorn, "Laboratory Procedures for Producing 2-Keto-D-Glucose, 2-Keto-D-xylose and 5-Keto-D-Fructose from D-Glucose, D-Xylose and L-Sorbose with Immobilized Pyranose Oxidase of *Peniophora Gigantea*," *J. Biotechnol*., **32**, 309-315 (1994).
7. M. Somogyi, "Notes on Sugar Determination," *J. Biol. Chem*., **195**, 19-23 (1952).
8. N. Nelson, "A Photometric Adaptation of the Somogyi Method for the Determination of Glucose," *J. Biol. Chem*., **153**, 375-380 (1944).

PARTITIONING OF MODIFIED MERRIFIELD RESINS MICROPARTICLES IN AQUEOUS BIPHASIC SYSTEMS

Y. F. Deng, D. L. Zhang, L. L. Zhu, and J. Chen

Key Laboratory of Rare Earth Chemistry and Physics, Changchun Institute of Applied Chemistry, Chinese Academy of Sciences, Changchun, 130022, People's Republic of China. Corresponding author email address: jchen@ciac.jl.cn

ABSTRACT

Aqueous biphasic systems (ABS) have shown interesting applications in the separation of solid microparticles. We have studied the partitioning of Merrifield resin and modified Merrifield resin microparticles in PEG-4000/Dextran-20000, PEG-4000/K_2CO_3, and [C_4mim]Cl/K_2CO_3, and demonstrated that the substituted functional group of the modified Merrifield resins and the types of ABS can change the partitioning behavior of the particles in the ABS. PEG-4000/Dextran-20000 showed a satisfactory separation for the Merrifield resins and the modified Merrifield resins into different phases, and the other ABS showed useful interface partitioning.

INTRODUCTION

Aqueous biphasic systems (ABS) are formed when two mutually incompatible polymer/polymer, polymer/salt, or salt/salt components are dissolved in water above a certain critical concentration. These systems comprise a mass fraction of water of 80-90% in equilibrium phases, and each phase mainly contains one of the compounds and a small amount of the other. ABS have been widely used in the separation, concentration and fractionation of biological solutes and particles, such as cells and proteins [1,2]. They have also been studied for applications in the separation of metal ion species [3] and small organic molecules [4] for use and as green media [5-7]. Recently, the use of ABS has been broadened to separate nano- and micro-solid particles. Zeng et al. studied how the pH and surfactant influenced the partition behavior of SiO2 particles in an ABS [8], and Baxter and co-workers have shown that the partitioning of an acrylic latex and inorganic particles (TiO2) depended on both the size and surface character of the particles [9]. ABS are potentially attractive alternatives to particles and functionalized particles due to their low and tunable interfacial tensions.

Ionic liquids (ILs) have been gaining great exposure due to their potential use as green solvents and as possible replacements for traditional volatile organic compounds (VOCs). Rogers et al. first reported a new type of ABS consisting of ILs and salt that 1-butyl-3-methylimidazolium chloride ([C4mim]Cl) + K_3PO_4 + water can be used to form an ABS [10]. Li and co-workers studied the extraction of biochemical compounds and drugs using [C_4mim]Cl + K_2HPO_4 + water ABS [11].

In our previous work, phase diagrams of salt ([C_4mim]Cl, [C_6mim]Cl, and [C_8mim]Cl) + salt (K_2CO_3, K_3PO_4) ABS were determined [12]. In this paper, we studied the partitioning of microparticles, such as Merrifield resin (Ps), poly[1-(p-vinylbenzyl)-3-butylimidazolium chloride (PsmimCl) in PEG-4000/Dextran-20000, PEG-4000/K_2CO_3, and [C_4mim]Cl/K_2CO_3 ABS, and discussed the surface character of the particles and the types of ABS, which affected the partitioning behavior in the ABS.

EXPERIMENTAL PROCEDURE

PEG-4000 was purchased from Tianjin Tiantai Fine Chemical Reagent Co. Ltd., China. Dextran-20000 was purchased from Sinopharm Chemical Reagent Co. Ltd., China. K_2CO_3 and K_3PO_4 were analytical-grade reagents and purchased from Beijing chemical Reagent Co. Ltd., China. All the solutions were prepared from pure water. Merrifield resin (Ps, 3.5 mmol Cl/g, 1% DVB, 200-400 mesh) was purchased from Tianjin Nankai Hecheng Science & Technology Co. Ltd., China. 1-Methyl imidazole was purchased from Linhai Kaile Chemical factory. 1-Butyl-3- methylimidazolium chloride ([C4mim]Cl) was synthesized according to the literature [12]. Analysis of [C4mim]Cl by H NMR (DMSO, ppm) resulted in a spectrum containing the following peaks: δ (ppm) = 0.88 (3H, t), 1.24 (2H, m), 1.75 (2H, m), 3.87(3H, 0s), 4.18 (2H, t, J = 3.2Hz), 7.77(1H, s), 7.85 (1H, s), 9.45 (1H, s). The corresponding ^{13}C NMR (DMSO, ppm) is δ (ppm) =13.21, 18.69, 31.33, 35.63, 48.31, 122.21, 123.49, 136.71. Poly[1-(p-vinylbenzyl)-3-butylimidazolium chloride (PsmimCl) was prepared according to the literature [13]. Energy dispersive spectrometry shows 58.14% C, 31.39% N, 4.05% O, and 7.33% Cl for PsmimCl. The chemical structures of the particles are shown in Figure 1. The other chemicals were analytical-grade reagents.

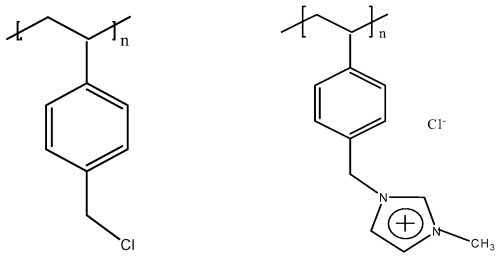

Figure 1. The chemical structures of the Ps (left) and PsmimCl (right).

The binodal curve was determined by the cloud-point method at room temperature, and the binodal curve of [C_4mim]Cl/salt ABS was refered to the reference [12]. The same procedure was used to determine the binodal curve of the PEG-4000/Dextran-20000 and PEG-4000/salt ABS.

The aqueous biphasic phase systems were prepared by weighing mixed amounts of polymer/polymer, polymer/salt, or salt/salt into a known volume of water. The composition of PEG-4000/Dextran-20000 ABS was 7.8 wt % PEG-4000, 14 wt % Dextran-20000, and 78.2 wt % water. In this system, the top phase was the PEG-rich phase, and the bottom phase was the Dextran-rich phase. The composition of PEG-

4000/K2CO3 ABS was 20 wt % PEG-4000, 15 wt % K_2CO_3, and 65 wt % water. In this system, the top phase was the PEG-rich phase, and the bottom phase was the salt-rich phase. The composition of $[C_4mim]Cl/K_2CO_3$ ABS was 25 wt %$[C_4mim]Cl$, 21 wt % K2CO3, and 54 wt % water. In this system, the top phase was the $[C_4mim]Cl$-rich phase, and the bottom phase was the salt-rich phase. The particles were thoroughly mixed in small vials with the ABS at about 1 wt % solid on total system weight. The samples were mixed with a vorticity mixture apparatus for ten minutes; then the samples were allowed to stand until the phases separated; finally, the phase preference of the particles was recorded.

RESULTS AND DISCUSSION

A phase diagram of the ABS is a unique "fingerprint" under a given set of conditions, such as the temperature, the concentration of each component, and the pH of the ABS. The phase diagram shows the concentration of phase-forming components, the equilibrium components concentration in the top and bottom phases, and the ratio of phase mass. Phase diagram data of the PEG/Dextran and PEG/salt ABS have appeared in the literature, but phase diagrams of the new type salt/salt ABS are not generally available. We assumed that the formation of salt/salt ABS occurs because water-structuring salts "salt-out" the IL ions from aqueous solution. Figure 2 illustrates the binodal curves for PEG-4000/Dextran-20000, PEG-4000/salt (K_3PO_4 and K_2CO_3), and $[C_4mim]Cl$/salt (K_3PO_4 and K_2CO_3) ABS. It shows that the binodal curves for the same $[C_4mim]Cl$ or PEG-4000 with different salts ABS, and the K_3PO_4 results are closer than K_2CO_3 to the origin in the binodal curve, meaning less salt is needed to form an ABS. It indicated that the salting-out ability of the anions follows the ordering $PO_4^{3-} > CO_3^{2-}$. This ordering directly follows the anions, ΔG_{hyd} values (PO_4^{3-}, -2835 kJ/mol > CO_3^{2-}, -1300 kJ/mol) [12]. It also shows that the binodal curves for the same salt with PEG-4000 and $[C_4mim]Cl$ ABS, and PEG-4000 results are closer than $[C_4mim]Cl$ to the origin in the binodal curve, meaning PEG-4000 forms an ABS more easily than $[C_4mim]Cl$. This is because the space steric hindrance of PEG is greater than the $[C_4mim]Cl$ IL', and the kosmotropic salts can salt-out PEG more easily than IL from aqueous solution. The phase diagrams of ABS would be desirable in partitioning experiments to better quantify the degree of cross-miscibility and to establish its importance in partitioning [9].

Table 1 shows the partitioning behavior of the Ps and PsmimCl in the PEG-4000/Dextran-20000, PEG-4000/K_2CO_3, and C_4mimCl/K_2CO_3 ABS. It has been found that the Ps resin mainly stayed in the top phase, and PsmimCl resin mainly stayed in the bottom phase in PEG-4000/Dextran-20000, and in the top phase and interface in PEG-4000/K_2CO_3 and C_4mimCl/K_2CO_3 respectively. Figure 3 was the picture of partitioning of the Ps and PsmimCl in PEG-4000/Dextran-20000 ABS. Although the Ps and PsmimCl resin diameter is about 80 μm, the resin can be partitioned into the ,ABS because of the hollow structure and lower density of the resin.

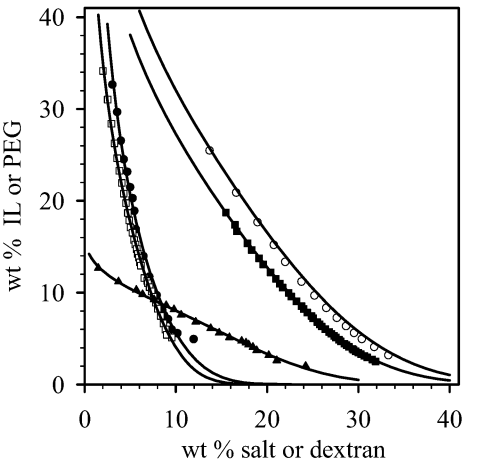

Figure 2. The binodal curves for different ABS. □, PEG-4000/K_3PO_4 ; ●, PEG-4000/K_2CO_3 ; ▲, PEG-4000/Dextran-20000; ■, [C_4mim]Cl/K_3PO_4; ○, [C_4mim]Cl/K_2CO_3.

Table 1. The results of Ps and PsmimCl partitioning in ABS

Particles	ABS	Partitioning results
Ps	7.8% PEG/14% Dextran	In the top phase
PsmimCl	7.8% PEG/14% Dextran	In the bottom phase
Ps	20% PEG/15% K_2CO_3	In the top phase
PsmimCl	20% PEG/15% K_2CO_3	Mainly in top phase, and some at interface
Ps	25% C_4mimCl/21% K_2CO_3	In the top phase
PsmimCl	25% C_4mimCl/21% K_2CO_3	Mainly in top phase, and some at interface

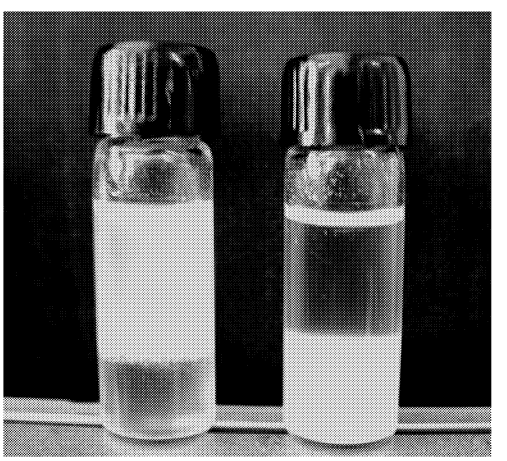

Figure 3. The partitioning of the Ps (left) and PsmimCl (right) in PEG-4000/Dextran-20000 ABS.

The partition relied on the surface properties of the solids and the interfacial interactions between the particles and the surrounding molecules. The partition is affected by the surface character of the particles, diameter, composition, temperature, concentration of each component, and pH of the ABS. Ps was preferentially partitioned into the top phase, which was due to the surface of Ps being hydrophobic and partitioned in the hydrophobic top phase, such as PEG-rich and IL-rich phase. The PsmimCl was modified by immobilizing the IL fragments on the Ps surface. The surface of PsmimCl was both hydrophobic and hydrophilic. So it was mainly partitioned at the interface. It was interesting that the PsmimCl was partitioned in the bottom phase in the PEG/Dextran ABS. There is higher O-H functionality in the Dextran than PEG, and strong hydrogen-bonding interactions are formed between the Cl^- of PsmimCl and O-H of Dextran. Thus, it is apparent that Dextran has a stronger interaction with PsmimCl than PEG. As a result, the PsmimCl particles are expected to prefer the bottom Dextran-rich phase.

CONCLUSIONS

In this study, Merrifield resin and surface-functionality Merrifield resin were partitioned into the ABS. ABS have shown useful applications in partitioning the surface functionality particles from the material and in reactive extractions as green reaction media. Consequently ABS might find potential applications in the extractive preparation of micro-particles.

ACKNOWLEDGMENTS

This work was supported by the Natural Science Foundation of China (50574080), the Hundred of Talent Program of Chinese Academy of Sciences and the Distinguished Young Scholar Foundation of Jilin Province (20060114).

REFERENCES

1. P. Å. Albertsson, Partition of Cell Particles and Macromolecules, 3rd ed., Wiley, New York, 1986.
2. J. Chen, G. X. Ma, and D. Q. Li, "HPCPC Separation of Protein Using Polyethylene Glycol-Potassium Phosphate Aqueous Two-Phase," *Pre. Biochem. Biotechnol.*, **29**(4), 371-383 (1999).
3. R. D. Rogers and C. B. Bauer, "Partitioning Behavior of Group 1 and Group 2 Cations in Poly(ethylene glycol)-Based Aqueous Biphasic System," *J. Chromatogr., B*, **680**, 237-241 (1996).
4. R. D. Rogers, H. D. Willauer, S. T. Griffin, and J. G. Huddleston, "Partitioning of Small Organic Molecules in Aqueous Biphasic Systems," *J. Chromatogr., B*, **711**, 255-263 (1998).
5. J. Chen, S. K. Spear, J. G. Huddleston, and R. D. Rogers, "Polyethylene Glycol and Solutions of Polyethylene Glycol as Green Reaction Media," *Green Chem.*, **7**, 64-82 (2005).

6. J. Chen, S. K. Spear, J. G. Huddleston, J. D. Holbrey, R. P. Swatloski, and R. D. Rogers, "Application of Poly(ethylene glycol)-Based Aqueous Biphasic Systems as Reaction and Reactive Extraction Media," *Ind. Eng. Chem. Res.*, **43**(17), 5358-5364 (2004).
7. J. Chen, S. K. Spear, J. G. Huddleston, J. D. Holbrey, and R. D. Rogers, "Application of Polyethylene Glycol-Based Aqueous Biphasic Reactive Extraction to the Catalytic Oxidation of Cyclic Olefins," *J. Chromatogr., B*, **807**, 145-149 (2004).
8. X. Zeng and K. Osseo-Asare, "Partitioning behavior of silica in the Trion X-100/ Dextran/water aqueous biphasic system," *J. Colloid Interface Sci.*, **272**, 298-307 (2004).
9. S. M. Baxter, P. R. Sperry, and Z. W. Fu, "Partitioning of Polymer and Inorganic Colloids in Two-Phase Aqueous Polymer Systems," *Langmuir*, **13**(15), 3948-3952 (1997).
10. K. E. Gutowski, G. A. Broker, H. D. Willauer, J. G. Huddleston, R. P. Swatloski, J. D. Holbrey, and R. D. Rogers, "Controlling the Aqueous Miscibility of Ionic Liquids: Aqueous Biphasic Systems of Water-Miscible Ionic Liquids and Water-Structuring Salts for Recycle, Metathesis, and Separations," *J. Am. Chem. Soc.*, **125**(22), 6632-6633 (2003).
11. S. H. Li, C. Y. He, H. W. Liu, K. Li, and F. Liu, "Ionic Liquid-based Aqueous Two-phase System, a Sample Pretreatment Procedure Prior to High-performance Liquid Chromatography of Opium Alkaloids," *J. Chromatogr., B*, **826**, 58-62 (2005).
12. Y. F. Deng, J. Chen, and D. L. Zhang, "Phase Diagram Data for Several Salt + Salt Aqueous Biphasic Systems at 298.15 K," *J. Chem. Eng. Data*, **52**(4), 1332-1335 (2007).
13. Z. T. Wang, S. C. Wang, and L. W. Xu, "Polymer-Supported Ionic-Liquid- Catalyzed Synthesis of 1,2,3,4-Tetrahydro-2-oxopyrimidine-5- carboxylates via Biginelli Reaction," *Helv. Chim. Acta.*, **88**, 986-989 (2005).

TARTARIC ACID-BASED COMPLEXING SURFACTANTS FOR MICELLAR ENHANCED ULTRAFILTRATION: A GREEN WAY FOR METAL REMOVAL

L. Dupont-Leclercq, S. Giroux, S. Parant, B. Henry, and P. Rubini

Groupe C2M2, Laboratoire SRSMC (UMR CNRS-Université Henri Poincaré Nancy 1), Nancy Université, BP 239, F-54506 Vandœuvre-lès-Nancy Cedex, France.
Corresponding author email address: laurence.leclercq@lesoc.uhp-nancy.fr

ABSTRACT

This study deals with the removal of Cu(II) from water by micellar-enhanced ultrafiltration (MEUF). The extracting system is composed of octylamidotartaric acid (C_8T) incorporated in Brij 58 micelles. The complexation of Cu(II) in the presence of micelles is characterized by pHmetry, UV-vis, and circular dichroism spectroscopy. MEUF experiments are carried out from pH 3.0 to 11.0. The efficiency of this system to remove Cu(II) is proved. The agreement between the experimental extraction yields and those predicted from the distribution curves is very good. The Cu(II) complexes are totally incorporated in the micelles whatever their structure and their charge.

INTRODUCTION

Solvent extraction is the conventional process used to perform metal ion separation and extraction. However, this technique presents several drawbacks insofar as it requires great volumes of volatile organic solvents that are often expensive, toxic, and flammable. Micellar extraction has emerged over the last decade as an interesting, green, solvent-free alternative to traditional liquid-liquid extraction [1]. Indeed, the hydrophobic core of the micelles can be used to solubilize lipophilic species (ligands, complexes). The separation of this micellar pseudophase from the aqueous phase can be achieved by micellar-enhanced ultrafiltration (MEUF) using membranes with pore diameter smaller than the size of the micelles. The advantage of this technique is that it requires little energy [2] compared to other separation processes such as cloud-point extraction. Many MEUF systems have been studied, and the role played by various chemical factors, such as the pH or the concentration of the complexing agent, on the extraction yield has been demonstrated [1]. However, few authors establish a link between the structure and the distribution of the species in the medium on one hand and the results of extraction on the another hand.

This study deals with the MEUF of Cu(II). This cation has been chosen for its spectroscopic properties in UV-vis and can be considered as a model of divalent cations (for example, Ni^{2+}, Pb^{2+}). The extracting system is composed of an original amphiphilic

complexing agent [3], called octylamidotartaric acid (C_8T), solubilized in nonionic micelles of Brij 58 (B58). This system presents various advantages for MEUF: (i) it has been previously demonstrated that Brij 58 micelles present high solubilization capacities towards C_8T [4], and (ii) Brij 58 has a very low critical micellar concentration (CMC = 3.5×10^{-6} mol/L), so that little surfactant is wasted in the filtrate, which improves the green aspect of this process.

Initially, the structures and the distribution of the complexes formed according to the pH are established in the presence of micelles. Then, the evolution of the MEUF extraction yields as a function of pH is studied: a correlation between these yields and the distribution curves permits the identification of the extracted complexes and the prediction of the performance of MEUF.

EXPERIMENTAL

Materials

Octylamidotartaric acid (2,3-dihydroxy-4-(octylamino)-4-oxobutanoic acid), called C_8T, was prepared from tartaric acid and octylamine according to a procedure described earlier [3]. Its purity was checked by NMR spectroscopy. Polyethyleneglycol(20)-hexadecyl-ether a.k.a. Brij 58 (Fluka), copper(II) nitrate trihydrate (Prolabo), and potassium chloride (BDH, 99.5%) were used as received.

Procedure and Apparatus

pHmetric Measurements

The protonation and coordination equilibria were investigated by pHmetric titrations by NaOH (0.100 mol/L) at 298.1 ± 0.1 K under argon atmosphere and at constant ionic strength (0.10 mol/L, KCl). pH was measured by using an automatic titration set (Metrohm 716 titrator and Thermo Orion combined glass electrode, model Ross 8103SC). The species formed in the system were characterized by the following general equilibrium process:

$$pM + qL + rH \rightleftharpoons M_pL_qH_r \qquad \beta_{pqr} = \frac{\left|M_pL_qH_r\right|}{\left|M\right|^p\left|L\right|^q\left|H\right|^r} \qquad (1)$$

where M denotes the Cu(II) cation and L, the nonprotonated ligand molecule (carboxylate form of C_8T). A detailed description of the experimental procedure and the data evaluation (using the PSEQUAD program [5]) has been reported earlier [4].

Spectroscopic Measurements

The UV-vis spectra were recorded simultaneously with the pHmetric titration using a USB4000 miniature fiber optic spectrometer from Ocean Optics equipped with a charge-coupled device. The circular dichroism (CD) spectra were recorded on a MOS-450 spectrometer from Bio-Logic, coupled with a Metrohm 716 titrator combined with a Fisher Bioblock electrode for pH adjustments.

Micellar Enhanced Ultrafiltration Experiments

MEUF was performed with an Amicon stirred cell of 10 mL volume, at room temperature. Regenerated cellulose membranes (Millipore) with a nominal molecular weight limit of 30,000 D were used. The pressure was 3.8 bar. The filtration was stopped when half of the initial volume was collected. Atomic absorption measurements were carried out on a Varian 220FS apparatus, using an air-acetylene flame, in order to analyze the metal content of the filtrate and of the retentate.

RESULTS AND DISCUSSION

Speciation and Structure of the Cu(II) Complexes

The speciation and structure of the Cu(II) complexes were investigated by pHmetry, UV-vis, and CD spectroscopy. The UV-vis and CD spectra recorded for the Cu(II)-C_8T-B58 system are represented in Figure 1.

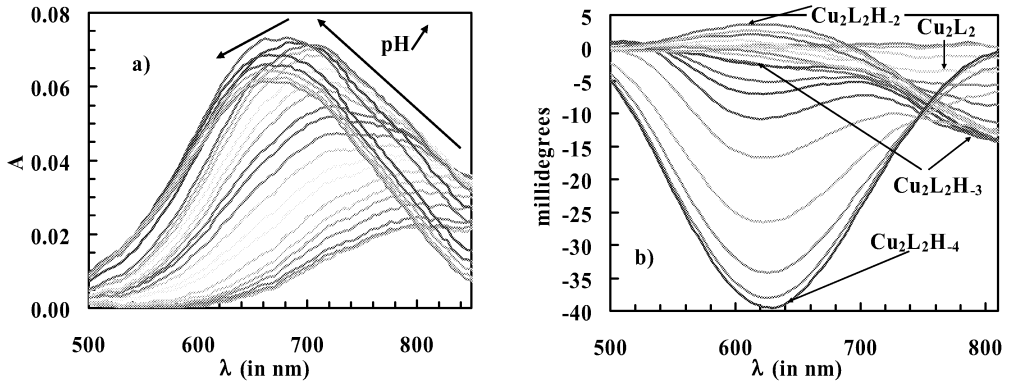

Figure 1. Evolution of UV-vis spectra (a) and CD spectra (b) of Cu(II)-C_8T-B58 system from pH = 2 to 12; [B58] = 4.0×10^{-2} mol/L, [C_8T] = 4.01×10^{-3} mol/L, [Cu(II)] = 2.00×10^{-3} mol/L.

The PSEQUAD program [5] allowed fitting of the pHmetric titration curves, and the pHAB program [6] allowed fitting the UV-vis data.

Table 1. Set of complexes and their log β for the Cu(II)-C_8T-B58 system determined from pHmetry by PSEQUAD and from UV-vis by pHAB. Statistical errors are indicated.

	M_2L_2	$M_2L_2H_{-2}$	$M_2L_2H_{-3}$	$M_2L_2H_{-4}$
pHmetry	8.4 ± 0.1	–0.03 ± 0.08	–5.42 ± 0.09	–15.7 ± 0.1
UV-vis	8.77 ± 0.02	–0.22 ± 0.03	–5.64 ± 0.04	–14.02 ± 0.06

The existence of dimers (M_2L_2 type) is coherent with the analysis of pHmetric data: *i*n the pH range 6–9, the number of hydroxide ions needed to complex one cation is close to 1.5. It probably corresponds to the $M_2L_2H_{-3}$ complex. The existence of dimers with Cu(II)-tartaric acid system [7] or with Cu(II)-gluconic acid system [8] has been previously reported in the literature.

The set of complexes that can describe the system is indicated in Table 1. This set is common to both methods, and the log β values are quite similar. Some distribution curves established from the log β values are represented in Figure 2. Figure 2a corresponds to the conditions of the pHmetric and spectroscopic measurements. Figure 2b corresponds to the conditions of MEUF experiments, described in the next part.

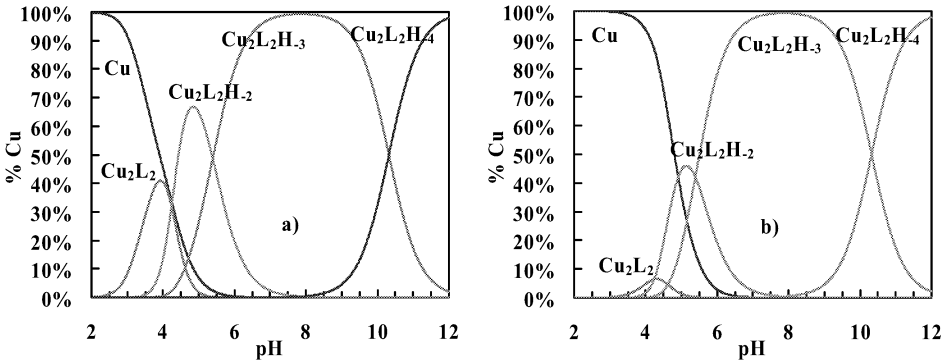

Figure 2. Distribution curves of Cu(II) as a function of the pH; a) [B58] = 4.0×10^{-2} mol/L, [C_8T] = 4.01×10^{-3} mol/L, [Cu(II)] = 2.00×10^{-3} mol/L; b) [B58] = 1.0×10^{-2} mol/L, [C_8T] = 1.00×10^{-3} mol/L, [Cu(II)] = 5.0×10^{-4} mol/L.

CD spectra are in good agreement with this set of complexes and can be described according to the complex distribution (Figure 2a). M_2L_2 corresponds to a weak negative band around 800 nm (Figure 1b). $M_2L_2H_{-2}$ corresponds to a more intense negative band around 800 nm and to a weak positive band around 620 nm. $M_2L_2H_{-3}$ corresponds to a quite intense negative band around 800 nm and to a weak negative band around 620 nm. $M_2L_2H_{-4}$ corresponds to an intense negative band around 630 nm.

Micellar Enhanced Ultrafiltration

The extraction of Cu(II) by the system composed of C_8T incorporated in the Brij 58 nonionic micelles was investigated. The results of MEUF experiments are reported in Figure 3. The yield of metal ion extraction in the micelles is expressed as:

$$R(\%) = \frac{n^R - n^F}{n_0} \times 100 = \frac{n^R_{micelle}}{n_0} \times 100 \qquad (2)$$

where n_0 represents the total amount of Cu(II) in the solution before MEUF; n^R and n^F are the amount of Cu(II) (free or complexed metal ion) in the retentate and in the filtrate, respectively. In the retentate, two types of species including Cu(II) must be taken into account: the species incorporated in the micelles ($n^R_{micelle}$) and the species soluble in the aqueous bulk phase (n^R_{free}). If we consider an equality of the amount of Cu(II) species soluble in the bulk on both sides of the membrane ($n^R_{free} = n^F$), the quantity $n^R - n^F$

represents the amount of Cu(II) species incorporated in the micelles ($n^{R}_{micelle}$), as indicated in Equation 2. Such an assumption is correct if the Donnan ion expulsion effect is negligible, as generally reported in the literature with nonionic surfactants [9].

The extraction in the micelles starts between pH = 3.0 and pH = 4.1. The yields of extraction reach 100% at pH higher than 7.6. Then the yields of extraction do not decrease up to pH = 11.0. These results demonstrate the efficiency of this extracting system to remove Cu(II) from aqueous environment. Moreover, by decreasing the pH from above 8.0 to below 3.0, the release of free Cu(II) in the bulk occurs. This can be interesting for metal preconcentration or de-extraction.

These MEUF results can be correlated with the speciation study to predict the yields of extraction. From the distribution curves (see Figure 2b), the coefficient α, corresponding to the ratio of n_0 to the amount of free Cu(II) in the solution before MEUF, can be calculated. Formulating the hypothesis that 100% of the complexes are extracted in the micelles and that no free Cu(II) is incorporated in the micelles:

$$R(\%) = \left(1 - \frac{1}{\alpha}\right) \times 100 \qquad (3)$$

In Figure 3, the solid curve represents the extraction yields calculated from Equation 3.

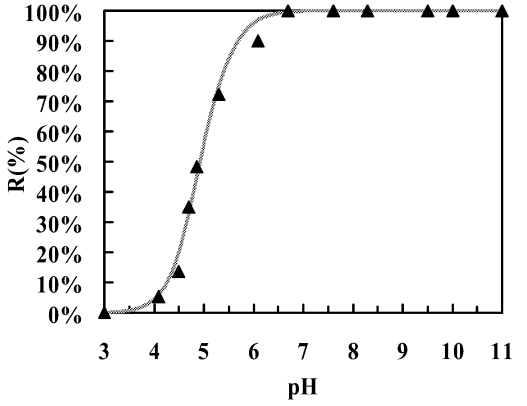

Figure 3. Experimental (▲) and calculated (solid line) yields of MEUF as a function of the pH; [B58] = 1.0×10^{-2} mol/L, [C_8T] = 1.00×10^{-3} mol/L, [Cu(II)] = 5.0×10^{-4} mol/L.

A very good agreement between the experimental and calculated *R* values is observed. This confirms the hypothesis that no free Cu(II) is incorporated in the micelles and that 100% of the complexes are extracted in the micelles, whatever their charge. This could be explained by the structures of the complexes containing two C_8T ligands. These species are quite hydrophobic with two octyl chains and are preferentially solubilized in the micelles. The incorporation of charged species in nonionic micelles has been previously reported [4,9]. Such a phenomenon can be explained dealing with the role of the counterions in the structure of the complexes. Moreover, incorporation of these charged entities at the interface between the inner hydrophobic core and the hydrophilic region of the micelles can be proposed [4].

CONCLUSION

In this paper, the distribution and the structure of the Cu(II) complexes formed with the amphiphilic ligand C_8T in the presence of Brij 58 nonionic micelles were investigated. This system was used to remove Cu(II) from water by MEUF and was proved to be very efficient (100% of the complexes are extracted whatever their charge). We gave evidence that the speciation of the complexes is a precious tool to interpret and predict the yields of MEUF. The dimeric structure of the complexes must be confirmed by complementary techniques as EPR, NMR, or ESI-MS. This original approach is being applied to the study of the removal by MEUF of Ni(II) or Pr(III) (particularly interesting for nuclear fuel reprocessing).

ACKNOWLEDGMENTS

We would like to thank Dr. Christian Tondre who has provided valuable assistance and precious help in performing this work.

REFERENCES

1. C. Tondre, Surfactant-Based Separation, Science and Technology, ACS Symposium Series 740, Washington, DC, 2000, Chapter 10.
2. J. F. Scamehorn and J. H. Harwell, Surfactants in Chemical/Process Engineering, Marcel Dekker, New York, 1988, Chapter 3.
3. S. Giroux, P. Rubini, C. Gérardin, C. Selve, and B. Henry, "Hydrophobic Tartaric Acid Monoamides as Complexing and Tensioactive Agents," *New J. Chem.*, **24**, 173–178 (2000).
4. L. Dupont-Leclercq, S. Giroux, B. Henry, and P. Rubini, "Solubilization of Amphiphilic Carboxylic Acids in Nonionic Micelles: Determination of Partition Coefficients from pK_a Measurements and NMR Experiments," *Langmuir*, **23**, 10463–10470 (2007).
5. L. Zékány and L. Nagypál, Computational Methods for the Determination of Stability Constants, D. Legget, Plenum Press: New York, 1985, Chapter 8.
6. P. Gans, A. Sabatini, and A. Vacca, "Investigation of Equilibria in Solution. Determination of Equilibrium Constants with the Hyperquad Suite of Programs," *Talanta*, **43**, 1739–1753 (1996).
7. K. Blomqvist and E. R. Still, "Solution Studies of Systems with Polynuclear Complex Formation. 5. Copper(II) and Cadmium(II) D-(+)-Tartrate Systems," *Inorg. Chem.*, **23**, 3730–3734 (1984).
8. T. Gajda, B. Gyurcsik, T. Jakusch, K. Burger, B. Henry, and J.-J. Delpuech, "Coordination Chemistry of Polyhydroxy Acids: Role of the Hydroxy Groups," *Inorg. Chim. Acta*, **275–276**, 130–140 (1998).
9. M. Hébrant, N. François, and C. Tondre, "Comparison of Micellar Ultrafiltration and Solvent Extraction for the Removal of Copper Ions from Aqueous Solutions," *Colloids Surf. A*, **143**, 77–88 (1998).

STABILIZED METAL AND METAL SULFIDE NANOPARTICLES PREPARED BY THE TWO-PHASE LIQUID-LIQUID METHOD

G. Sánchez,[1] R. Tovar,[1] J. Aguilera,[1] F. Ruiz,[2] and G. Martínez[2]

[1]Institute of Metallurgy, [2]Faculty of Sciences, Universidad Autónoma de San Luis Potosí, Sierra Leona 550, 78210 San Luis Potosí, Mexico.
Corresponding author email address: msanchez@uaslp.mx

ABSTRACT

The preparation of Ag, Ag_2S, CdS, and ZnS nanoparticles (NPs) from loaded organic media is reported. The method involves the phase transfer of metal species from aqueous to organic solution, followed by reductive or precipitation stripping. Cyanex®471x, Cyanex®272, and D2EHPA were used for extraction from Ag(I) nitrate or Cd(II) or Zn(II) sulphate solutions. Silver NPs were obtained using borohydride ions and the semiconductor particles using ammonium sulfide. Under some conditions, the extractants were effective in stabilizing the colloids; in other cases, surfactants were added. The particles were characterized structurally and optically.

INTRODUCTION

Several approaches are used to prepare dispersed ultrafine particles. Among them, precipitation from solution is commonly used because it offers the possibility to control the particle characteristics by changing the experimental parameters. If preparation occurs from aqueous media, short-chain organic ligands are normally used as stabilizers, which passivate the surface and control growth [1].

A modification of the extraction process is the addition of a crystallization step, where low-solubility metals salts are precipitated. Precipitation-stripping of yttrium oxalate powders from loaded D2EHPA has been reported [2]. Metal oxalates can be decomposed by heat-treatment to become the corresponding oxides [3]. Preparation of cobalt ferrite from Versatic Acid was studied by Konishi et al. [4], and Fu and co-workers [5-7] have reported the preparation of organic fluids containing Ag, Ag_2S, Bi_2S_3 and CdS from organophosphorus extractant solutions.

The use of reducing agents has been proposed as an alternative to conventional stripping in solvent-extraction technology [8]. Au can be recovered directly from the solvent by a precipitation method called hydrolytic stripping [9]. The first report of stabilized gold nanoparticles (NPs) of good quality synthesized by the two-phase approach appeared in 1993, and a year later a simple but successful method for preparing larger amounts of NPs appeared, involving the transfer of an anionic Au(III) complex in a two-phase system, followed by reduction with borohydride ions in the presence of a long-chain thiol [10]. Similar procedures for the preparation of silver NPs were reported,

but the mechanism of the phase transfer was not clear, since silver was present in the aqueous phase as a cation [11].

We report here the synthesis and characterization of Ag, Ag_2S, CdS, and ZnS NPs obtained from organic phases containing the organophosphorus Cyanex and D2EHPA reagents, using reductive and precipitation stripping.

EXPERIMENTAL

The aqueous media were nitrates (0.01 M Ag^+ in water) and sulfates (0.02 M Zn(II) and Cd(II)). Cyanex 471x and Cyanex 272 were kindly donated by Cytec Industries. The phase-transfer was carried out at room temperature in separating funnels shaken mechanically at a fixed frequency of 90 min^{-1}. The loading was performed by shaking 0.2 L of a metal solution with 0.2 L of the organic phase (0.005 M Cyanex 471x in *p*-xylene or 0.1-0.5 M Cyanex 272 or D2EHPA in kerosene). After 30 minutes shaking, the phases were allowed to separate. Metal concentration of the aqueous phase before and after extraction was determined using an atomic absorption spectrometer, Varian Spectra AA 220, with graphite furnace GTA-110. The organic-phase metal content was calculated by mass balance. The loaded organic phase was transferred into a reaction vessel, and the precipitates were obtained by adding 0.2 L of a freshly prepared stripping solution (0.1 M $NaBH_4$ or $(NH_4)_2S$). After 30 minutes stirring, the two phases were allowed to separate and filtered. The powders were washed with acetone and dried. Dispersions were characterized as obtained. In some experiments, Span 80 or Triton X-100 (concentration 0.0004 M) were added to the sulfide solutions before stripping.

X-ray diffraction patterns were recorded with a GBC-Difftech MMA diffractometer, using Ni filtered CuK_α (λ=1.54Å) radiation. Particle-size determination was carried out using the MAUD (Materials Analysis Using Diffraction) software, an analysis program based on the Rietveld method [12,13]. The morphology and size were observed by transmission electron microscopy (TEM) using a Jeol 1230 electron microscope (120 kV). Chemical composition was determined by energy-dispersive X-ray spectrometry (EDS), carried out using an X-ray microanalyzer (DX-4I, EDAX) built on a XL-30 scanning electron microscope (Philips). The optical properties were measured in an OceanOptics S2000 UV/vis spectrophotometer and an OceanOptics NIR spectrophotometer NIR512.

RESULTS AND DISCUSSION

Reductive Stripping

Attempts to precipitate silver or silver sulfide from loaded organic solutions have already been reported [14]. In general, precipitation was possible from solutions containing Cyanex 471x, Cyanex 272, and Cyanex 302, but the synthesis resulted in uncontrolled growth, with material precipitating after injection of the strip solution. In the work reported in this paper, loading experiments were carried out varying metal and extractant concentrations and maintaining the strip reagent concentration constant. Interesting results were obtained using a higher Ag/Cyanex 471x ratio. Reduction

produced stable dispersions in the aqueous phase, together with some powders. This was surprising, as normally an excess of stabilizing ligand is necessary for efficient capping of the growing particles. For the powder, an XRD pattern with peaks corresponding to metallic Ag was obtained, with reflections indexed to an fcc sublattice (JCPDS 04-0783). TEM images of the powder and dispersion products are shown in Figure 1.

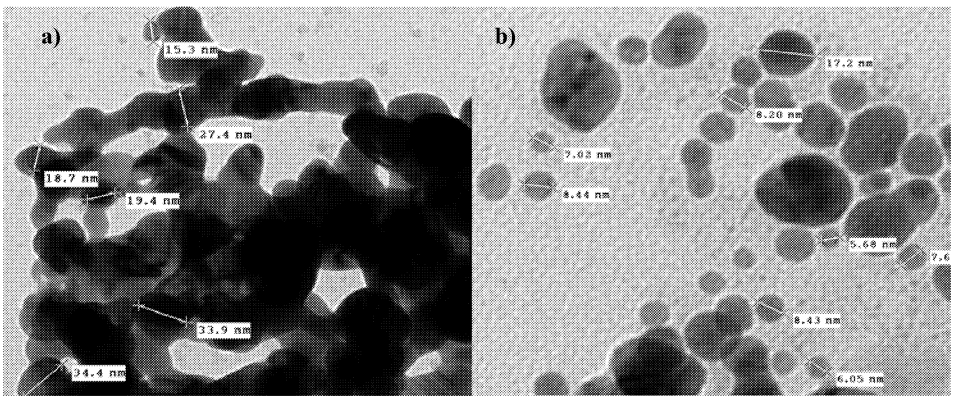

Figure 1. TEM images of Ag prepared from Cyanex 471x in *p*-xylene, powders (a) and as a dispersion (b).

The average size of the measured particles was 24 nm and 13 nm for the colloids. Figure 1a shows that most particles are twinned. The particles in the dispersion are almost spherical and show less imperfections. It was speculated that the extractant molecules were adsorbed onto the particles surface to form a stabilizing layer. Some images show the presence of organic layers surrounding the nanocrystals. To study the presence of quantum-confined effects on the colloid, the UV/vis spectrum was recorded. The spectrum exhibits a peak (plasmon band) with a noticeable blue shift (392 nm) compared with the bulk value. The position of the plasmon absorption of silver nanoparticles is strongly dependent on the particle size and adsorbed species [15].

Precipitation Stripping

For the Ag_2S particles synthesized from Cyanex 471x solution, the diffraction pattern (Figure 2a) matches that of monoclinic acanthite (ICSD44507), the stable form at room temperature. A significant mass loss of about 15% was observed, probably due to loss of organics. The XRD pattern of the ZnS NPs (Figure 2b) corresponds to wurtzite (JCPDS 39-1363), and the CdS NPs (not shown) to the hexagonal system (JCPDS 41-1049). EDS analysis showed that the spectra of the samples of CdS and ZnS can be assigned to the corresponding sulfides, but the phosphorous content from the extractant was about 3.0 At %. Figure 3 shows images of the NPs obtained. The Ag_2S powders are ellipsoidal with other irregular particles; their average size is 61 nm. Particle sizes for CdS and ZnS, obtained from TEM images and the Rietveld refinement method, are shown in Table 1.

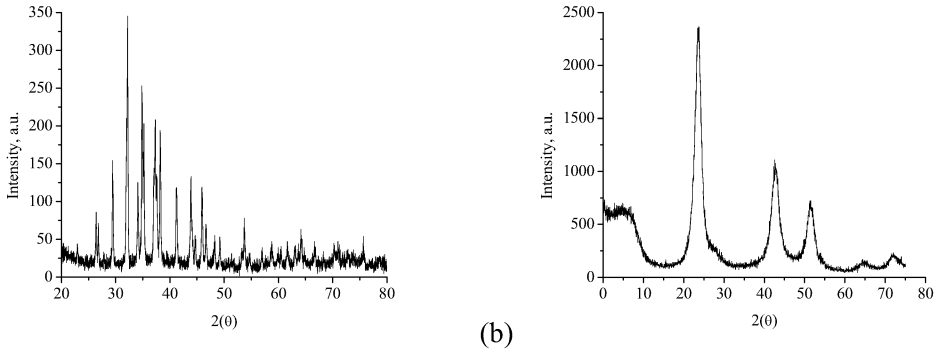

Figure 2. X-ray diffraction patterns of (a) silver sulfide synthesized from Cyanex 471x solutions in *p*-xylene and (b) zinc sulfide synthesized from Cyanex 272 in kerosene.

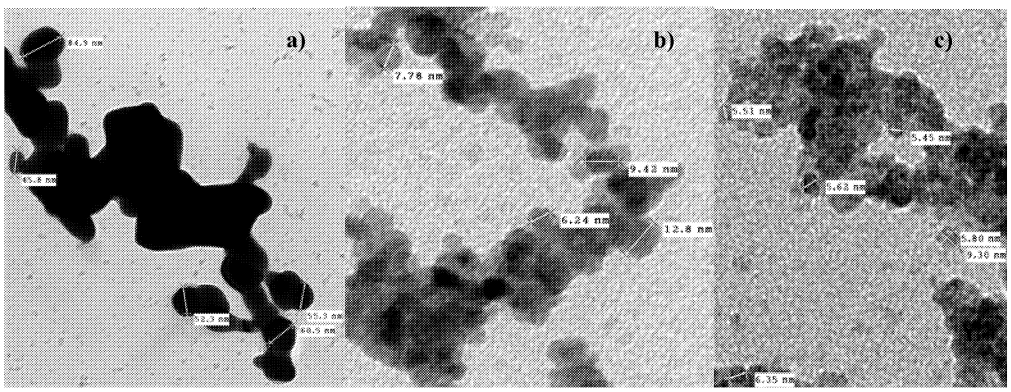

Figure 3. TE micrographs of metallic sulfide nanoparticles (a) Ag_2S from Cyanex 471 in *p*-xylene, (b) CdS from Cyanex 272 in kerosene, and (c) ZnS from D2EHPA in kerosene.

A fundamental property of semiconductor compounds is the band gap, the energy separation between the filled valence band and the empty conduction band. Nanometer-sized ultrafine semiconductors have band gaps greater than those of the bulk semiconductors owing to a quantum size effect. Ag_2S is a direct band gap semiconductor with a band gap value of 1 eV (near infrared region) in the bulk form. We determined the optical band gap using simple diffuse reflectance spectroscopy in order to determine if there was a "size quantization" effect in the synthesized materials [16]. The band gap value obtained for Ag_2S was close to 1 eV, indicating an absence of any "quantization" effect, probably as a result of the relative large size of the NPs obtained. ZnS and CdS absorb the part of the UV/vis spectrum. The band gaps for bulk CdS and ZnS are 517 nm and 340 nm [17]. The absorption threshold wavelength obtained for most of our particles were red-shifted compared to the bulk (Table 1). This red-shift could be due to the influence of the capping ligands on the optical properties or to structural defects of the materials. As evident from Table 1, the different experimental conditions and capping ligands show in general little influence over particle size and optical band gap of the obtained materials.

Table 1. Particle size and optical band gaps of the obtained ZnS and CdS NPs.

Name	Extractant, M	Surfactant	Particle size, nm	Band gap, nm
ZnSCy1	Cyanex 272, 0.1	-	7.9*	342
ZnSCy2	0.5	-	6.1	358
ZnSCyT		Triton X-100		342
ZnSCyS		Span 80	7.7	361
ZnSD21	D2EHPA, 0.1	-	5.8*	344
ZnSD22	0.5	-	6.1	356
ZnSD2T		Triton X-100		342
ZnSD2S		Span 80	9.1	364
CdSCy1	Cyanex 272, 0.1	-	14.0*	540
CdSCy2	0.5	-	12.5	538
CdSCyT		Triton X-100	8.4	542
CdSCyS		Span 80	9.4	544
CdSD21	D2EHPA 0.1	-	13.8*	536
CdSD22	0.5	-	9.1	537
CdSD2T		Triton X-100		539
CdSD2S		Span 80		523

*Calculated from diffraction data by the Rietveld refinement method

CONCLUSIONS

Characterization of the silver and metal sulfide NPs prepared by the two-phase method has revealed that the organophosphorus extractants can act as capping agents. Preparation of nanoparticulate silver from Cyanex 471x/*p*-xylene under excess-silver conditions exhibited controlled growth in solution with only a small amount of bulk waste by-product. Reduction in particle size gives a significant blue shift in the absorption spectra of the dispersion. In contrast, the Ag_2S particles were not small enough to change the optical properties. The strength of the interaction of the extractant with the growing particles of CdS and ZnS was not always sufficient to prevent uncontrolled precipitation, but the addition of surfactants favored the formation of dispersions in some cases. In most cases, optical spectra of the materials were red-shifted compared with the bulk values.

ACKNOWLEDGMENTS

Cytec Industries Canada are thanked for providing the extractants. G. Martínez is grateful for receipt of a CONACyT scholarship. This work was supported by grants from the FAI-UASLP and Fondos Mixtos CONACyT-SLP (2002-5630). We thank M.Sc. I. Esparza, UASLP, for TEM characterisation.

REFERENCES

1. A. Eychmüller, "Structure and photophysics of semiconductor nanocrystals," *J. Phys. Chem.,* **B104**, 6514-6528 (2000).

2. E. Combes, C. Sella, D. Bauer, and J. L. Sabot, "Precipitation-stripping of yttrium oxalate powders from yttrium-loaded HDEHP organic solutions using an ultrasonic stirrer," *Hydromet.,* **46**, 1-12 (1997).
3. J. Shibata and H. Yamamoto, "Application of solvent extraction to production of multicomponent composite powders," Proceedings of the International Solvent Extraction Conference 2002, K. C. Sole, P. M. Cole, J. S. Preston and D.J . Robinson, Eds., South African Institute of Mining and Metallurgy, Johannesburg, 2002; pp. 543-547.
4. Y. Konishi, T. Nomura, K. Mizoe, and K. Nakata, "Preparation of cobalt ferrite nanoparticles by hydrolysis of cobalt-iron (III) carboxylate dissolved in organic solvent," *Mater. Trans.,* **45**(1), 81-85 (2004).
5. X. Fu, Z.-S. Hu, G.-H. Gu, D.-B. Wang, H.-T. Zhu, and X.-D. Zhou, "Study on the preparation of nanomaterials with extractant and extraction systems," International Solvent Extraction Conference 2005, China Academic Journal Electronic Publishing House, Beijing, 2005; pp. 852-857.
6. H.-Q. Shi, X. Fu, X.-D. Zhou and Z.-S. Hu, "Preparation of organic fluids containing Ag_2S nanoparticles with the extractant Cyanex 301," International Solvent Extraction Conference 2005, China Academic Journal Electronic Publishing House, Beijing, 2005; pp. 874-880.
7. S.-L. Zhang, H.-Q. Shi, X. Fu, and Z.-S. Hu, "Preparation and characterisation of organic fluids containing Bi_2S_3 nanoparticles," International Solvent Extraction Conference 2005, China Academic Journal Electronic Publishing House, Beijing, China, 2005; pp. 858-863.
8. G. P. Demopoulos, "Solvent extraction in precious metals refining," *J. Metals,* **38**(6), 13-17 (1986).
9. G. P. Demopoulos and G. Pouskouleli, "Hydrochemical preparation of fine precious metal powders," *J. Metals,* **40**(6), 46-50 (1998).
10. M. Brust, M. Walker, D. Bethell, D. J. Schiffrin, and R. Whyman, "Synthesis of thiol-derivatised gold nanoparticles in a two-phase liquid–liquid system," *Chem. Commun.*, 801-802 (1994).
11. M. Brust and C. J. Kiely, "Some recent advances in nanostructure preparation from gold and silver particles: a short topical review," *Colloids Surf., A,* **202**, 175-186 (2002).
12. http://www.ing.unitn.it/luttero/maud/
13. R. A. Young, The Rietveld Method, ed. by the International Union of Crystallography, Oxford University Press, New York, 1993.
14. M. G. Sánchez-Loredo, R. L. Tovar-Tovar, F. Ruiz, J. R. Martínez-Mendoza, G. Ortega-Zarzosa, and G. A. Martínez-Castañón, "Two-phase systems involving commercial organophosphorus extractants for the preparation of silver and silver sulfide nanoparticles," International Solvent Extraction Conference 2005, China Academic Journal Electronic Publishing House, Beijing, 2005; pp. 828-833.
15. D. L. Van Hyning, W. G. Klemperer, and C. F. Zukoski, "Characterization of colloidal stability during precipitation reactions," *Langmuir* **17**, 3120-3127 (2001).
16. G. A. Martínez-Castañón, M. G. Sánchez-Loredo, J. R. Martínez-Mendoza, and F. Ruiz, "Synthesis of CdS nanoparticles: a simple method in aqueous media," *Adv. Tech. Mater. & Mater. Proc. J.,* **7**(2), 171-174 (2005).
17. H. Sato, T. Hirai, and I. Komasawa, "Mechanism of formation of composite CdS-ZnS ultrafine particles in reversed micelles," *Ind. Eng. Chem. Res.,* **34**, 2493-2498 (1995).

BACK-EXTRACTION OF METAL SPECIES FROM SUPERCRITICAL CARBON DIOXIDE MODIFIED WITH TRI-*n*-BUTYL PHOSPHATE

Y. Enokida, K. Sawada, and Y. Katakami

EcoTopia Science Institute, Nagoya University, 1-Furo-cho, Chikusa-ku, Nagoya-shi 464-8603, Japan. Corresponding author email address: yenokida@nagoya-u.jp

ABSTRACT

A method is proposed for directly extracting heavy metals from solid matrices using supercritical carbon dioxide modified with tri-*n*-butyl phosphate (TBP) in the form of its nitric acid complex and has been shown to be effective for the recovery of uranium and plutonium from the solid powder of nuclear fuel for fast breeder reactors. The back extraction of uranium from supercritical carbon dioxide modified with TBP into an aqueous phase at ambient pressure or onto porous silica beads at high pressure is reported. For the back-extraction onto the silica beads, neodymium was used as a simulant for uranium. The back extraction of uranium into an aqueous solution from supercritical carbon dioxide modified with tri-*n*-butyl phosphate complexed with uranyl nitrate was successfully performed using a high-pressure experimental column in which a single droplet fell from the nozzle and the overall mass-transfer coefficients were evaluated to be 1.5×10^{-9} ms^{-1} on the aqueous phase side and 0.94×10^{-3} ms^{-1} on the CO_2 phase side. The latter value is two orders of magnitude greater than that normally evaluated in 30% TBP-70% *n*-dodecane (v/v).

INTRODUCTION

The direct extraction of uranium and plutonium into supercritical CO_2 from solid nuclear fuel has several advantages when applied to nuclear fuel reprocessing. If we could reduce the amounts of high-level liquid waste by omitting an aqueous dissolution process using a large amount of nitric acid, this would reduce the plant's operating costs. Supercritical CO_2 extraction has already been demonstrated on a laboratory scale to recover uranium and plutonium from the solid powder of nuclear fuel for fast breeder reactors [1-4]. Back-extraction into an aqueous solution is necessary to complete the nuclear fuel reprocessing [5], and in this paper, we report studies of the back-extraction of heavy metal species from supercritical CO_2 modified with TBP.

Currently, during commercial reprocessing, back-extraction from a loaded organic phase containing TBP is performed using diluted nitric acid. A similar approach to the recovery of heavy metals from the high-pressure fluid is considered in this paper. For the stripping of the heavy metals from the high-pressure fluid into the aqueous nitric acid solution, the mass-transfer coefficient should be evaluated for the design of processing equipment.

In the study described below, we investigated the transfer of uranium from a CO_2 phase into an aqueous phase in the form of a single aqueous droplet falling from the top of the high-pressure column through the CO_2-phase containing a TBP nitrate complex and obtained a mass-transfer coefficient based on the double thin film theory [6] from the concentration change in the aqueous droplets.

As the TBP molecule has a P = O double bond, the negative charge located on the O atom is likely to have an affinity for the surface of polar solids such as SiO_2. Recently, many types of porous silica beads have become commercially available. Such beads can have high specific surface areas and many tiny pores under a micrometer in diameter, where capillary condensation and the trapping effect on the silica surface are expected. Consequently, we undertook a study using porous silica beads for the back-extraction of heavy metal ions complexed with TBP in supercritical carbon dioxide. The results are reported below.

EXPERIMENTAL

Back-Extraction by Aqueous Nitric Acid

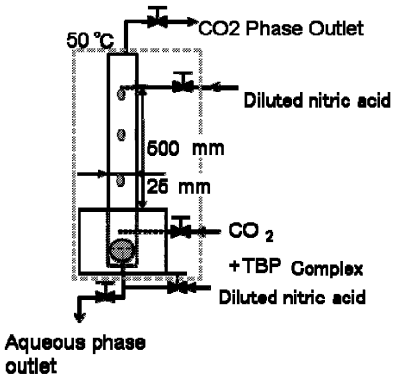

Figure 1. Schematic diagram of experimental set-up for back-extraction by aqueous solution.

The experimental set-up for a single-droplet falling experiment is illustrated in Figure 1 in which a counter-current extraction column for a high-pressure fluid was employed. For the continuous phase, we used a single phase fluid of supercritical CO_2 containing TBP complexed with uranyl nitrate, $UO_2(NO_3)\cdot 2TBP$ at 15.5 MPa and 323 K. Liquid CO_2 (>99.999%, Japan Fine Products, Japan) was passed through a heat exchanger at 323 K and pumped by a syringe pump (260D ISCO, PA) at the flow rate of 3.00 cm^3/min and mixed with the organic solution, which was fed by an HPLC pumping system (DP-8020, TOSO Corp., Japan) at the flow rate of 0.20 cm^3/min. The prepared initial concentration of uranium in the high-pressure fluid was determined to be 7.4×10^{-5} mol dm^{-3} (M) by an inductively coupled plasma atomic emission spectrometer (ICP-AES, ICPS-7000E, Shimadzu Co. Ltd., Japan) followed by sampling a fraction of the fluid into 50 cm^3 of a 0.1 M HNO_3 solution. A single droplet was formed through the nozzle of a stainless steel pipe whose outer diameter was 3 mm (2 mm internal diameter) by feeding a 0.01 M nitric acid solution at the flow rate of 1.00 cm^3/min for 300 min. The aqueous phase settled at the bottom of the column and was continuously removed. Part of

the aqueous effluent was used for the determination of uranium by the ICP-AES. The CO_2 phase was taken from the top of the column through a pressure regulating valve system (SCF-GETS, JASCO, Japan) followed by contact with distilled water for back-extraction in order to obtain aqueous samples for the ICP-AES measurement. A time-series of the measurement data for the uranium concentrations in the aqueous and CO_2 phases was used for calculating of the mass-transfer coefficients. The effective height of the column was defined as the distance between the nozzle for the aqueous droplets and the surface of the aqueous settler at the column bottom, which was regulated at a constant position by manually manipulating the valve opening. The effective height was 500 mm. The internal diameter of the column was 25 mm, which was sufficient to ignore the fluid-dynamic effect due to the falling droplets and the column wall.

Back-Extraction by Porous Silica Beads

The experimental set-up for the absorption of heavy-metal species in the high-pressure fluid on porous silica beads is illustrated in Figure 2. The silica beads were purchased from GL Science Corp., Ltd, Japan (1001-15308) and washed with a 0.1 N HCl solution, ethanol, and distilled water. The beads were dried and then vibrationally packed in a stainless steel column whose internal diameter was 4.4 mm and length was 250 mm. The nominal value of their diameter was 160 micrometers. An organic solution of the TBP complex with $Nd(NO_3)$ was prepared by dissolving $Nd(NO_3)_3 \cdot 6H_2O$ in neat TBP which was purchased from Sigma Aldrich, Japan and used as received. At pressures higher than 20 MPa, the organic solution of the TBP complex with $Nd(NO_3)_3$ dissolves in supercritical CO_2 and forms a single-phase solution for any fraction of the organic solution in CO_2. A view-cell was employed so as to confirm the formation of a single fluid. At 20 MPa, the high-pressure fluid was fed from the view-cell, using the high-pressure pumping system, into the packed column at the flow rates of 1.00 cm^3/min. for CO_2 and 0.04 cm^3/min. for the organic solution.

The eluants from the packed column were fractioned and collected every two minutes into a test tube that contained *n*-dodecane for the trapping organic solution.

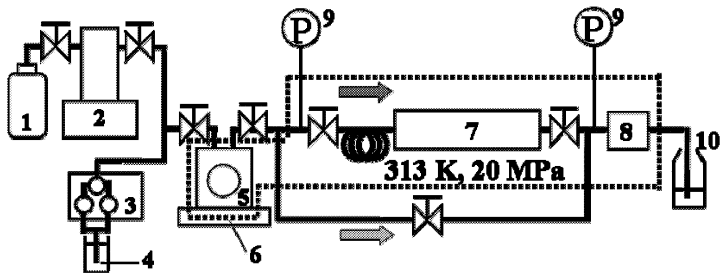

Figure 2. Schematic diagram of experimental set-up for back-extraction on silica beads.
1. Liquid CO_2 cylinder. 2. Syringe pump. 3. HPLC pump. 4. Organic solution of TBP complex with Neodymium nitrate. 5. High-pressure vessel with view window. 6. Magnetic stirrer. 7. Packed column. 8. Back pressure regulator. 9. Pressure gauges. 10. Collecting vessel containing *n*-dodecane.

RESULTS AND DISCUSSION

Stripping Heavy Metals into Aqueous Solution

The uranium concentrations in the aqueous and CO_2 phases illustrated in Figure 3 reached a steady state in about 150 min. after starting the falling aqueous droplets, and the concentrations were 3.2×10^{-4} M and 1.1×10^{-5} M, respectively. The average diameter of the droplets was 4.0 mm, determined by pictured image of droplets through the window of sapphire. After taking into account the mass transfer over the aqueous settling surface at the bottom of the high-pressure column shown in Figure 1, we evaluated the local and overall mass-transfer coefficients by assuming the double-film theory. From the experimental results, the overall mass-transfer coefficients on the dispersed phase side and continuous phase side were determined to be 1.5×10^{-9} ms^{-1} and 0.94×10^{-3} ms^{-1}, respectively. For comparison with the literature values, we applied the correlations by A. E. Handlos [6] and Ranz-Marshall [7]. The values calculated by the correlations are shown in Table 1.

The values obtained in our experiment are the same order of magnitude for the calculated values, being two orders of magnitude greater than that evaluated in the 30% TBP-70% *n*-dodecane v/v.

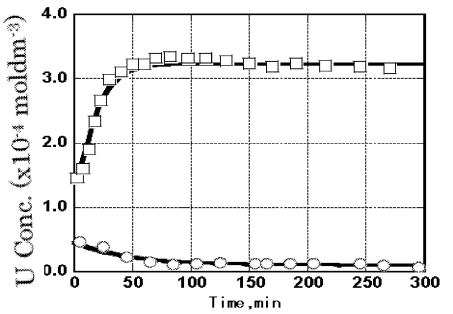

Figure 3. Uranium concentration change in the aqueous phase (rectangles) and CO_2 phase (circles) in the column effluents.

Table1. Overall and local mass-transfer coefficients for back-extraction of uranyl nitrate.

Mass transfer coefficient type	For 30% TBP	For supercritical CO_2
Local at dispersion phase side / ms^{-1}	4.6×10^{-5}	4.2×10^{-5}
Local at continuous phase side / ms^{-1}	2.2×10^{-5}	4.8×10^{-3}
Overall at dispersion phase side / ms^{-1}	3.6×10^{-11}	7.7×10^{-9}
Overall at continuous phase side / ms^{-1}	2.2×10^{-5}	4.8×10^{-3}

Stripping Heavy Metals onto Porous Silica Beads

A result of the break-through experiment for CO_2 containing $Nd(NO_3)_3 \cdot 3TBP$ through a packed column filled with porous silica beads compared to that for an empty column is shown in Figure 4(a). The flow rate of the organic solution was 0.040 ± 0.001 cm^3 min^{-1}. The value was gravimetrically determined by a calibration experiment. A time

delay due to the adsorption of $Nd(NO_3)_3 \cdot 3TBP$ by the silica beads was observed. If we assume a one-dimensional diffusion process in the packed column, the following equation may be used to describe the curves found in Figure 4, where t is time, and a, b and t_0 are fitted parameters.

$$F(x) = b\int_0^x f(t)dt = b\int_0^x \exp\left[-\left\{(t-t_0)/a\right\}^2\right]dt$$

The parameters were computed using software for a nonlinear least-square fitting. The values of t_0 were 4.76 and 19.61 for the two results. By using these values, the specific adsorption amount was evaluated to be 0.20 g $Nd(NO_3)_3 \cdot 3TBP$/g-silica beads.

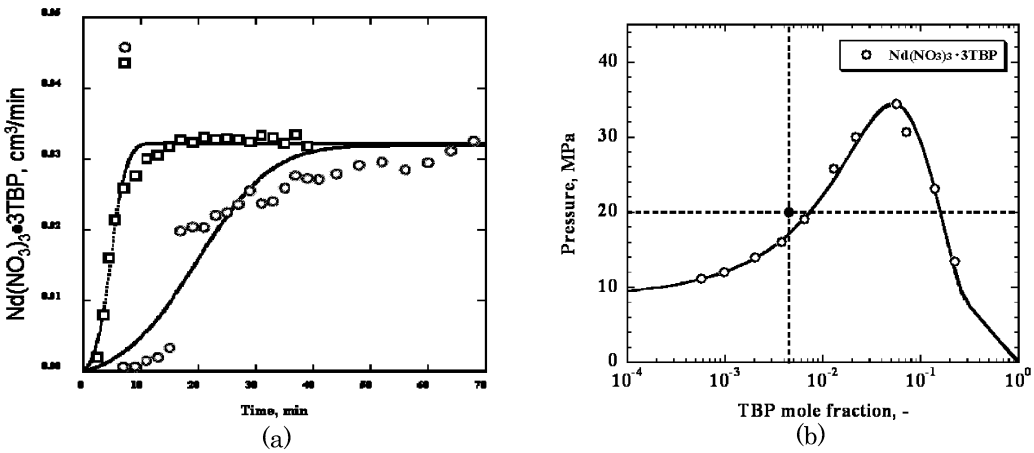

Figure 4. (a) Break-through curve for CO_2 containing $Nd(NO_3)_3 \cdot 3TBP$ through a packed column filled with porous silica beads (open circle) compared to that for an empty column (open rectangle). The curves are plotted on the basis of a least-squares fitting.
(b) Phase diagram observed for a mixture of CO_2 and $Nd(NO_3)_3 \cdot 3TBP$. At the upper region of the curve, the fluid exists in a single phase, whereas below the curve, in two phases.

After the break-through experiment, all the beads in the column whose total dry weight was 2.90 g with the adsorbed TBP complex were leached with 0.01M HNO_3, and we found that almost all (>99.85%) the Nd was recovered from the silica beads; the total recovery yield exceeds 99%.

The nominal diameter of the pores in the silica beads was 2.5 nm, for which we can expect capillary condensation. Figure 4(b) illustrates the transition between a single phase and two phases for CO_2 and $Nd(NO_3)_3 \cdot 3TBP$, which was originally obtained in this study by the method described in the literature [9] for a high-pressure mixture of CO_2 and $Nd(NO_3)_3 \cdot 3TBP$. In the back-extraction experiment using silica beads, the pressure was maintained at 20 MPa, and at this pressure the fluid was a single phase, but when we apply the Kelvin formula of capillary condensation [8] for a concave structure whose curvature was 25 nm in diameter, the condensation pressure was reduced from the saturated pressure of 17.1 MPa to approximately 1.9 MPa in the pores. At this pressure range, the fluid exists in two phases, as shown in Figure 4(b). Therefore, $Nd(NO_3)_3 \cdot 3TBP$ was split from the single-phase fluid in the pores and trapped. The surface of the silica beads has an affinity for the TBP complex, but water molecules have

a stronger affinity so that dilute nitric acid may work very well to strip TBP complex from the surface of silica, which explains the experimental results.

CONCLUSIONS

The back-extraction of uranium into an aqueous solution from supercritical carbon dioxide modified with tri-*n*-butyl phosphate complexed with uranyl nitrate was successfully performed using a high-pressure experimental column in which a single droplet fell from the nozzle and the overall mass transfer coefficients were evaluated to be 1.5×10^{-9} ms^{-1} on the aqueous phase side and 0.94×10^{-3} ms^{-1} on the CO_2 phase side. The latter value is two orders of magnitude greater than that normally evaluated in 30% TBP-70% *n*-dodecane v/v. Therefore, we may conclude that the back-extraction of uranyl nitrate, as described, proceeds efficiently.

The back-extraction of neodymium nitrate complexed with TBP in supercritical CO_2 onto porous silica beads in a packed column at 20 MPa was also successfully performed. This new result may lead to the easy regeneration of the extractant and recycling of CO_2 in the process.

REFERENCES

1. O. Tomioka, Y. Enokida, et al., "Solvent extraction of lanthanides from their oxides with TBP in supercritical carbon dioxide," *J. Nucl. Sci. Technol.*, **35**(7), 515-516 (1989).
2. Y. Enokida et al., "Ultrasound-enhanced dissolution of UO_2 in supercritical CO_2 containing a CO_2-philic complexant of tri-*n*-butylphosphate and nitric acid," *Ind. Eng. Chem. Res.*, **41**(9), 2282-2286 (2002).
3. Y. Enokida et al., "Characterization of a tri-*n*-butyl phosphate-nitric acid complex: A CO_2-soluble extractant for dissolution of uranium dioxide," *Ind. Eng. Chem. Res.*, **42**(21), 5037-5041 (2003).
4. Y. Enokida et al., "An option making for nuclear fuel reprocessing by using supercritical carbon dioxide," Proceedings of the International Conference on Advanced Nuclear Fuel Cycle and Systems, American Nuclear Society, CD-ROM (2007).
5. T. Shimada et al., "Selective extraction of uranium from a mixture of metal or metal oxides by a tri-*n*-butylphosphate complex with HNO_3 and H_2O in supercritical CO_2," *Anal. Sci.*, **22**(11) 1387-1391 (2006).
6. A. A. E. Handlos and T. Baron, "Mass and heat transfer from drops in liquid-liquid extraction," *AICHE J.*, **3**(1) 127-136 (1957).
7. W. E. Ranz and W. R. Marshall, "Evaporation from drops .1," *Chem. Eng. Progr.*, **48**(3), 141-146 (1952).
8. S. J. Gregg and K. S. W. Sing, "Adsorption, surface area and porosity," 2nd edition, Academic Press, New York, 1982.
9. Y. Enokida, I. Yamamoto, and C. M. Wai, "Extraction of uranium and lanthanides from their oxides with a high-pressure mixture of TBP-HNO_3-H_2O-CO_2," ACS Symposium Series, **860**, 10-22 (2003).

Author Index

Abdel Rahman, N. 629
Agarwal, S. 367, 1567
Aguilar, J.C. 1379
Aguilera, J. 1621
Alamdari, E.K. 233, 239
Alexová, J. 653
Alguacil, F.J. 287
Allard, S. 1113
Almaraz, M. 575
Almela, A. 353, 903, 1591
Alonso, M. 287
Alvarado, R.J. 843
Aly, H.F. 629
Alyapyshev, M. 665
Ansari, S.A. 1349
Antonio, M.R. 799
Arias, L.A. 1313
Arm, S.T. 709
Arnaud, F. 1043
Arunachalam, R. 1165
Ashtari, K. 885
Ashtari, P. 885
Atmakidis, T. 1213
Attarakih, M.M. 1177
Auger, F. 251
Avila Rodriguez, M. 293
Avila, M. 1313
Avila-Rodriguez, M. 299, 1145

Baba, Y. 879
Babain, V. 623, 647, 665
Babain, V.A. 533
Babic, D. 1243
Babić, K. 1391
Bahri, P.A. 459
Bai, Y. 1195
Balamurugan, M. 763
Bara, J.E. 1301
Barnard, K.R. 113, 119, 125, 459, 909
Baron, P. 581, 587, 715, 721
Bart, H.-J. 17, 961, 1177, 1231, 1289
Bartsch, R.A. 689, 1487
Bazelaire, E. 689
Becquart, E.T. 263
Belair, S.C. 1087
Bélanger, S. 209
Bell, K.J. 1457
Belova, V.V. 347
Benchikouhne-Ranchoux, M. 581
Bender, J.T. 101
Berthon, L. 1017
Bhattacharyya, A. 1349
Birdwell, J.F. Jr. 923
Bisel, I. 721
Blaauw, C. 485
Bonnesen, P.V. 689
Boubals, N. 1043
Boullis, B. 29
Bourget, C. 447
Bowser, T. 1165
Boyadzhieva, S. 1403
Brahman, R.K. 751
Brass, E.A. 739
Bray, D.J. 1493
Bringas, E. 1409, 1415
Brown, S.J. 739
Bryson, L.J. 341
Buch, A. 293, 1003, 1397
Bukunkwe, D. 139
Bunio, P. 1307
Burghoff, B. 1385
Butoh, S. 1499
Bwalya, E. 139

Calor, J-N. 581
Camès, B. 721
Campbell, J. 1469, 1475
Campbell, S.G. 739
Campos, K. 1307
Canselier, J.P. 1555

Cao, H-B. 1159
Cao, P. 703
Carlisle, T. 1301
Carrera, J.A. 1409
Carvalho, D.H. 215
Carvalho, J.M.R. 227, 367, 567
Castro, C. 1439
Chagnes, A. 275, 1057
Chang, Z. 1537
Chang, Z.D. 1573
Charbonnel, M-C. 1043
Chartres, J. 1457
Chaumont, A. 43
Chavez, F. 287
Chayama, K. 1585
Chekmarev, A.M. 1127
Chelbina, Y.V. 943
Chen, J. 611, 1195, 1277, 1609
Cheng, C.Y. 163, 177, 183
Chernyak, M.Y. 967
Chevrot, G. 43
Chiarizia, R. 1029
Chirkov, A.V. 533
Chisakuta, G.C. 145
Chocron, M. 263
Choppin, G.R. 527
Cieszyńska, A. 1295
Clegg, J.K. 1493
Cocalia, V.A. 1263
Cole, P.M. 131
Corona, I. 287
Correia, P.F.M.M. 1567
Costa, M.C. 1439
Cote, G. 275, 1057
Courtaud, B. 251, 275
Courtijn, E. 1151
Couston, L. 1043
Cronje, I. 453
Crozes, X 1017
Cui, S. 1069

Dai, Y. 949
Dai, Y.Y. 1561
Dakshinamoorthy, A. 1355
Daniels, L.M. 1427
Dann, M. 829
Dannus, P. 1087
Daoud, J.A. 629
Darvishi, D. 233, 239
Davenport, W. 435
de Almeida, V. 1069
de Gyves, J. 1379
de Haan, A.B. 1331, 1337, 1385, 1391
de M. Fábrega, F. 323
de Mendoza, J. 575
de Morais, C.A. 215
Deep, A. 227
Delmau, L.H. 689, 1487
Demetrio, S. 435
Deng, Y.F. 1609
Dey, P.K. 1355
Díaz, G. 201
Dietz, M.L. 799
Dinh, B. 581, 587
Dobson, A. 709
Doi, T. 787
Domic, E. 435
Donegan, S. 169
Dormidonova, A. 647
Drain, F. 587
Draye, M. 1057
Dreisinger, D.B. 107
Drumm, C. 1177
du Preez, R. 169
Duan, W. 611, 703
Duhamet, J. 587
Dupont-Leclercq, L. 1615
Dutton, D.F. 329

Efraim, A. 257, 385
Eiswirth, R.T. 1231
Eivazi Hollagh, A.R. 233
Ekberg, C. 189, 545, 551, 1133
Ekman, E. 473
El Bekri, J. 293, 1003, 1397
Elias, G. 671
Elizalde, M.P. 353, 903, 1591
Ellis, R.J. 1457
Engle, N.L. 689
Enokida, Y. 1627

Ensor, D.D. 557, 689
Ensor, M.A. 1549
Espartero, A.G. 575
Espinoux, D. 581, 715
Etemadi, S. 239
Evans, H.A. 459

Falling, S.N. 937
Famehsari, D.H. 239
Favre-Réguillon, A. 1057, 1325
Feather, A. 269, 497
Feather, A.M. 131
Fei, W. 1519
Fermvik, A. 545, 551
Fernandes, W.E. Jr. 479
Ferreira, B.K. 341
Ferreira, L.M. 1567
Field, K. 329
Fijimoto, Y. 1481
Finotello, A. 1301
Firestone, M.A. 799
Fiúza, A.M.A. 421
Foos, J. 1057
Foreman, M.R.S. 545, 551
Frades, M. 427
Fritz, M. 1367
Fujinaga, K. 817, 823
Fukui, Y. 1463
Fuls, H.F. 485
Furugou, H. 1481

Galand, N. 43
Galvão, E.L. 955
Gameiro, M.L.F. 367
Gamino Arroyo, Z. 293
Garn, T.G. 727, 733
Gasperov, V. 1451
Geeting, M.W. 739
Gerlach, K. 973
Ghosh, S.K. 1171, 1361
Gin, D.L. 1301
Giroux, S. 1615
Glasson, S. 1201
Glatz, D.J. 361
Gloe, J.K. 1049, 1493
Gloe, K. 1049, 1493
Gnoinski, J. 201
Godleski, S.A. 937
Goetheer, E.L.V. 1385
Golubina, E.N. 1255
Gomes, E.F. 409
Gomiero, L.A. 245
Gonçalves, L.A.G. 955
Gonzalez, P. 1145
Górak, A. 931
Gorbunova, M.G. 689
Gordon, R.J. 1475
Gorri, D. 1319
Goto, M. 873
Gouvea, L.R. 221
Grant, R.A. 281, 415
Greenhalgh, M.R. 1427
Grimes, T.S. 563
Grinbaum, B. 257, 373, 379
Grosber-Manon, M. 1003
Gross, Z. 467
Grossiord, J-L. 1003
Grote, M. 1049
Grüner, B. 539
Guibal, E. 1307, 1313
Guimarães, G.C. 311
Guimarães, M.M.L. 409, 421
Gulevich, A.L. 1093
Gupta, B. 305
Gurau, G. 1263
Gurker, T. 403
Guțu, O.A. 1075

Haderer, T. 403
Hano, T. 997
Hansmeier, A.R. 1331
Harada, H. 317, 1481, 1603
Harlamovs, J.R. 209, 441
Harmon, B.W. 689
Harrington, R.C. 593
Harrup, M.K. 1427
Hartmann, T. 503
Hasegawa, Y. 891
Hashimoto, T. 811
Haverlock, T.J. 689

Hay, B.P. 1011
Haywood, R. 453
He, W.W. 1421
Heeres, H.J. 979
Hennessy, W.P. 751
Henry, B. 1615
Henry, D.C.R. 1475
Herbst, R.S. 665, 677
Hinoue, T. 835
Hirata, M. 653, 745, 997
Hoch, C. 569
Holdt, H.-J. 1049
Hori, T. 811
Horwitz, E.P. 1099
Hu, X. 1573
Hudlow, S.L. 617
Huebra, M. 903

Ibana, D.C. 391
Iglesias-Sánchez, J.C. 575
Ikeda, Y. 1433
Ikegami, S. 1499
Ikuta, A. 793
Imura, H. 811
Inaba, K. 787
Inoue, K. 317, 879, 891, 1481, 1603
Ireland, N. 169
Irie, A. 879
Ishii, T. 879
Ismael, M.R.C. 367
Iwai, T. 623
Iwatsuki, S. 1585

Jakovljevic, B. 447
Jalhoom, M.G. 769
Jennings, H.L. 923
Jensen, M.P. 1029, 1081
Jeong, J. 157, 1373
Jiao, R.Z. 641
Jolsterå, R. 1133
Joshi, J.M. 849
Juvekar, V.A. 1361

Kalem, M. 397
Kamachev, V. 647
Kamio, E. 1105, 1543
Kanekar, A.S. 897
Kanel, J.S. 937
Kapambwe, C. 139
Karcas, G. 435, 473
Karve, M. 1343
Katakami, Y. 1627
Kavallieratos, K. 843
Kawakita, H. 317, 1481, 1603
Kaygorodov, K.L. 943
Kelling, A. 1049
Kenig, E.Y. 1213
Khalaf, J.S. 769
Khanchi, A. 885
Kholkin, A.I. 347
Khomami, B. 1069
Khopkar, S.M. 915
Kim, M-S. 1373
Kimoto, T. 835
Kimura, T. 653, 745
Kitatsuji, Y. 745
Kiyko, T.N. 1093
Kizim, N.F. 1255
Klaehn, J.R. 1421
Knutsson, A. 1133
Kobayashi, S. 1499
Koch, K.R. 1513
Kodama, H. 879
Koganti, S.B. 635, 757, 763
Kokusen, H. 817
Komatsu, Y. 805, 817, 823
Kondo, K. 1105
Kordosky, G.A. 3, 93
Koropachinskaya, N.V. 943
Kosogorov, A.V. 985
Kotze, M. 169
Kovalevich, V.A. 1093
Kramer, E.P. 491
Krebs, J.F. 599
Kubota, F. 873
Kuhnert, J. 1177
Kulichenkov, S.A. 347
Kumar, R. 757, 763
Kumar, S. 635, 757, 763
Kuvaeva, Z.I. 985

Kuznetsov, G.I. 985
Kvíčalová, M. 539
Kyser, E.A. 617

La Gamma, A.M.G. 263
Lagrave, S. 1017
Laidler, J.J. 695
Laitala, H. 473
Langton, M. 485
Lapidus, G.T. 299
Larsson, K. 189
Latruwe, K. 1151
Lavenu, A. 587
Lavie, R. 1525
Law, J.D. 659, 665, 727, 733, 1427
Lazarova, Z. 991, 1403
le Bon, J.F. 1397
Lee, J-C. 157, 1373
Lee, R. 1119
Lemaire, M. 1325
Lerner, O. 467
Leroi, C. 1397
Li, D.Q. 1195, 1277, 1421
Li, S. 1531
Li, S.W. 861, 867
Li, Y-P. 1159
Liang, J.F. 641
Liao, W.P. 1421
Lin, T. 1451
Lin, X. 1159
Lindoy, L.F. 1493
Liu, H. 1537
Liu, H.Z. 1573
Liu, X.G. 641
Lopez, F. 287
Lopez-Delgado, A. 287
Lorrain, B. 581, 715
Lu, P. 1219
Lučaníková, M. 539
Luo, G. 1531
Luo, G.S. 861, 867
Luther, T.A. 1427

Ma, Y.C. 1537, 1573
Machado, R.M. 227
Mae, S. 1499
Magnusson, D. 521
Mahajani, S.M. 1171
Malik, P. 1439
Malkhede, D.D. 915
Malmbeck, R. 521
Maluleke, R.F. 201, 329
Manchanda, V.K. 849, 897, 1349, 1355
Mann, N.R. 727, 733
Mansur, M.B. 215, 311, 323
Mao, Z-S. 1183, 1219
Marr, R. 403, 1367
Martín, D. 427
Martin, L.R. 605, 671
Martínez, G. 1621
Martins, A.H. 311
Martinson, B. 485
Maruyama, K. 1433
Maruyama, Y. 1499
Masiiwa, H. 169
Mathe, O. 169
Matsumoto, M. 1105
Matsuo, Y. 1499
McAlister, D.R. 1099
McFarlane, J. 923
Meadors, V.M. 689
Medeiros, G.S. 479
Meehan, G.V. 1493
Meier, G.P. 569, 1063
Meikrantz, D.A. 659
Meikrantz, D.H. 727, 733
Meindersma, G.W. 1331, 1337
Mejías, A.B. 427
Mendoza-Muñoz, P. 299
Menoyo, B. 353
Meridiano, Y. 1017
Meze, F. 587
Mezyk, S.P. 671, 677
Micović, J. 973
Miguirditchian, M. 721
Mijangos, F. 1591
Mikulich, A.V. 985
Miller, G. 145
Minami, A. 1499
Minango, R. 139

Mincher, B.J. 605, 671, 677
Miroshnichenko, S. 1207
Moats, M. 435
Modolo, G. 521
Mohammed, D.A. 769
Mohapatra, P.K. 1349, 1355
Moisy, P. 581
Moldovan, B. 257
Monnier, J.R. 937
Montuir, M. 715
Moradkhani, D. 233
Moraes, N.A. 479
Morais, C.A. 221, 245
Moreira, A.V.B. 955
Morel, P. 251
Morisaku, K. 1445
Morita, Y. 1585
Motomizu, S. 793
Movsowitz, R. 385
Moyer, B.A. 689, 1487
Mudring, A.V. 1271
Mukai, H. 1499
Mukhopadhyay, S. 1361
Mukutuma, A. 497
Muñoz, M. 1379
Munshi, S.K. 1355
Munyungano, B. 269
Murakami, J. 1499
Murashova, N.M. 1597
Murat, D. 1057
Muraviova, O.V. 1249
Murillo, M.T. 575
Murzin, A. 647
Mwakila, B. 145

Naganawa, H. 787
Narbutt, J. 1035
Narendranathan, R. 183
Narita, H. 195, 1445
Nash, K.L. 511, 563, 569, 593, 1063, 1111, 1549
Navarro, R. 1145, 1313
Naydenov, D. 1289
Nazarenko, A.Y. 855
Nel, G. 169
Nilsson, M. 563, 569
Nisbett, A. 93
Nishiura, M. 317
Niu, C.J. 1421
Noble, R.D. 1301
Nogami, M. 1433
Nogueira Duarte, L.J. 1555
Noro, J. 787, 805, 817

Ocio, A. 353, 1591
Ödegaard-Jensen, A. 1133
Ogden, M.D. 1063
Ohashi, A. 811
Ohashi, K. 811
Ohto, K. 317, 879, 1481, 1505, 1603
Okumura, M. 823
Oliveira, H.N.M. 955
Onink, S.A.F. 1337
Ono, T. 1543
Oprea, F. 1075
Ortiz, I. 1319, 1409, 1415
Oshima, S. 817
Oshima, T. 879
Otu, C.G. 1139
Otu, E.O. 1139
Owens, S. 1469
Ozawa, M. 623

Paiva, A.P. 1439
Palacios, E.G. 287
Pandey, A.K. 849
Panja, S. 1355
Parant, S. 1615
Pareau, D. 293, 1003, 1145, 1397
Park, H.J. 1579
Parker, W.L. 361
Pathak, P.N. 849, 897
Patil, C.B. 1349
Paulenova, A. 599, 665
Paulo, J.B.A. 479
Paviet-Hartmann, P. 751
Peabody, S. 93
Perera, J.M. 1201
Peterman, D.R. 659, 1427
Pfennig, A. 397, 1207, 1237, 1243

Phillips, C. 709
Phillips, G.W. 937
Pinoy, L. 1151
Pinto, G.A. 409
Pitner, W. 931
Poulter, S. 453
Prabhu, D.R. 897
Prados, P. 575
Pranolo, Y. 163, 177, 183
Pushkov, A.A. 985

Qin, W. 949, 1561

Rais, J. 539, 653
Rajgor, R.V. 1343
Rampersad, A. 485
Raventos, M. 973
Regel-Rosocka, M. 1283, 1295
Reis, M.T.A. 1567
Retegan, T. 545, 551
Reznik, A.M. 1189
Ribeiro, L.M. 409
Ribeiro, M.M.M. 421
Rice, N.M. 1119
Richert, P.G. 799
Riddle, C.L. 659
Rizk, S.E. 629
Robinson, D.J. 1457
Robinson, T. 435
Robles, E. 453
Rocha, S.D.F. 215
Rodríguez de San Miguel, E. 1379
Rodriguez, M. 177
Rogers, R.D. 1263
Rosa, A.M. 1439
Rosenberg, J.M. 843
Rúa, M.S. 903
Rubini, P. 1615
Ruiz, A. 1319
Ruiz, F. 1621
Ruiz, P. 1319
Rumball, J.A. 459

Saiki, Y. 195
San Román, M.F. 1409, 1415
Sánchez, F. 201, 427
Sánchez, G. 1621
Sánchez-Loredo, M.G. 1049
Sánchez-Quesada, J. 575
Sanoussi, M. 251
Santangelo, F. 931
Santos, S.M.C. 227
Sasaki, Y. 745
Sasamori, T. 1499
Sato, Y. 195
Saucedo, I. 1313
Saucedo, T.I. 1145
Sawada, K. 1627
Sawai, N. 1505
Schmidt, M. 961
Schmidtchen, F.P. 59
Schmitt, N.C. 605
Schröder, M. 1457
Schulte, M. 931
Schulze-Messing, J. 329
Schurhammer, R. 43
Schuur, S. 979
Schwarz, N. 497
Scott, S.A. 151
Segura, M. 575
Seike, Y. 823, 1543
Seiller, M. 1003
Selucky, P. 539
Semenov, S.A. 1189
Seto, H. 1603
Shadrin, A. 623, 647
Shafer, J.C. 593
Shafikov, D. 647
Shen, S. 1537
Shen, S.F. 1573
Shenoy, K.T. 1171
Shimojo, K. 873
Siebenhofer, M. 1367
Sieffert, N. 43
Silwamba, R. 145
Sinegribova, O.A. 1249
Singh Gaur, R.P. 335
Singh, H.P. 139
Singh, I. 305
Singh, K.K. 1171

Sinkov, S.I. 527
Širová, M. 653
Sivakumar, D. 763
Skarnemark, G. 189, 551, 545
Slavinskiy, K.A. 1127
Smirnov, I. 665
Smirnov, I.V. 533
Smirnova, M.A. 967
Smith, K.H. 1225
Smith, K.J. 1451
Soares, E.V. 421
Sohn, J-S. 157
Sole, K.C. 201, 329, 341, 485, 829, 1513
Song, C. 683
Song, C.L. 641
Songo, M.B. 829
Sorel, C. 521, 715, 721, 1017
Sousa, E.M.B.D. 955
Stambouli, M. 293, 1003, 1145, 1397
Steffens, M.J. 391
Stepanov, S.I. 1127
Stevens, G. 373
Stevens, G.W. 1165, 1201, 1225
Stewart, L.J. 1469
Sugiyama, Y. 1433
Surowiec, M.A. 689
Suzuki, S. 653
Swain, B. 157, 1373
Swart, D.R. 201
Swart, R.M. 1469, 1475
Szreder, T. 799

Tachimori, S. 653
Takayanagi, T. 793
Takeshita, K. 1505
Takimoto, Y. 793
Tamaki, S. 891
Tan, J. 861, 867
Tanaka, M. 195, 1445
Tarabanko, N.V. 943
Tarabanko, V.E. 943, 967
Tasker, P.A. 1451, 1457, 1469, 1475
Tavlarides, L.L. 1579
Taylor, R.J. 527
Testard, F. 1017
Thakare, Y.S. 915
Thiry, J. 275
Thumberg, M.A. 491
Tillotson, R.D. 677, 1427
Tiwari, S. 1177
Tkac, P. 599
Todd, T.A. 659, 665, 727, 733
Tokitoh, N. 1499
Tong, C.C. 1451, 1457
Tonova, K. 991
Toorisaka, E. 997
Tovar, R. 1621
Trochimczuk, A. 1307
Trofimenko, S. 1449
Tsouris, C. 923
Tsurubou, S. 817
Turner, N.L. 119, 125
Turriza Cruz, R.G. 1145

Uezu, K. 1463
Umetani, S. 1463

van de Ham, A.G.J. 1391
Van de Voorde, I. 1151
Vandegrift, G.F. 599
Vargas, C. 287
Varnek, A. 1023
Vatta, L.L. 1513
Verpoort, F. 1151
Vijgen, H. 521
Viljoen, K. 329, 341
Vincent, T. 1307
Virnig, M. 101, 269
Voshkin, A.A. 347
Voss, B. 1301
Vu, T-H. 1043

Wang, J. 611, 683, 1183
Wang, K. 861, 885
Wang, S. 1561
Wang, Y. 1519, 1531
Warr, R.J. 1457
Watanabe, T. 1105
Watarai, H. 83, 779
Wentink, A.E. 931, 973

Wenzel, M. 1049, 1493
Westra, A.N. 1457
White, F.J. 1475
Win, K.T. 1249
Winkelman, J.G.M. 979
Wipff, G. 43
Wishart, J.F. 799
Wiśniewski, M. 1283, 1295
Wood, J.L. 1475
Woollam, S.F. 281, 415

Xiao, B. 1537
Xie, F. 107
Xie, L-L. 1325
Xu, J. 1531
Xu, J.H. 861, 867

Yaita, T. 1029
Yajima, H. 891
Yamauchi, A. 823
Yang, C. 1183, 1219
Yang, H.L. 1277
Yang, X.H. 885
Yellowlees, L.J. 1475
Yoo, K. 1373
Yoshizawa, H. 1543
Yoshizuka, K. 745
Yurtov, E.V. 1597

Zalupski, P.R. 1111
Zemb, T. 1017
Zhang, D.L. 1609
Zhang, G. 1219
Zhang, W. 163, 177, 183
Zhang, Y. 1159
Zhidkova, T.I. 347
Zhou, H. 689, 1487
Zhou, Z. 949
Zhu, L.L. 1609
Zimmerman, M.H. 557
Zorz, N. 1017
Zuo, Y. 1195

Keyword Index

Abil EM 90 surfactant 1003
Acetic acid 1183
Acetohydroxamic acid 527, 665
Acetone 1231
Acetylacetonate complexes....1035
Acid dissociation constants....1063
Acidity, effect of....1343, 1439
Acorga M5640 367
Acorga P....101
Acrylamide, poly-N-isopropyl....1585
Actinides 521, 563, 605, 641, 703, 721, 1043, 1087, 1271, 1427
Actinium 1099
Activity coefficients....721, 1127
Acyloin, as degradation product 125
Advanced Fuel Cycle Initiative 563
Aggregation....293, 793, 1119
Air-assisted SX 1537
Alamine 336....3, 263, 329, 829, 1567
Alcohols, analysis of....855
Alcohols, as modifiers 101
Aldoxime....101
Alginate gel beads....1591
Aliquat 336....107, 1403
Alkali metal cations 1421
Alkyl groups, effect of....745
Aluminum 131, 201, 335, 915, 1549
Amberlite IRA-900 1385
Amberlite XAD16....1391
Amberlite XAD7....1385
Americium 29, 527, 545, 563, 599, 623, 659, 709, 745, 897, 1087, 1349
Amide type extractant....521, 745, 1355
Amides, mono 1295
Amides, as modifiers 101
Amine, octyl....943
Amine, primary 1189, 1421
Amine, quaternary....347, 849, 991, 1403
Amine, tertiary 257, 275, 467, 703, 1119, 1451, 1567
Amino acids 879, 985
Aminodiphenylamine....835
Ammonia, as stripping agent 257
Ammonium hydroxide, as stripping agent....1445
Amylase 991
An/Ln partitioning 539, 557, 715, 1081, 1349

Aniline....83
Anion exchange....3, 1093
Anion recognition....1457
Anode....189
Antimony....209
Aqueous biphasic systems....1609
Aromatics, removal of....1325
Arrhenius equation....1277
Arsenic....209
ASPEN software....1075
ATPs....533
Axial mixing....367
Aza podand, thioether....1585

Backmixing....17
Baja Mining....125
Barium....43, 521, 653, 817
Barium sulfate nanoparticles....861
Batteries....189
Benzaldehyde....1391
Benzene....1075, 1331
Benzoylacetone....787
Betulinic acid....961
Binary extractants....347
Biocide....421
Biofuels....923
Biomass....961
Biopharmaceuticals....985
Bis(aryltetrazolyl)pyridines....533
Bis(triazinyl)bipyridines....533
Bis(triazinyl)pyridines....29, 545
Bis(trifluoromethylsulfonyl)imide....799, 1271, 1331
Bismuth....915
Bispyridinyltriazines....29
BOBCalixC6....653, 689
Bond distance, ...1463
Boric acid, impurity....341
Breakthrough curve....317
Brij 35 surfactant....793
Brij 78 surfactant....793
BTBPs, see Bis(triazinyl)bipyridines
BTPs, see Bis(triazinyl)pyridines
Buffers, effect of....511
Butanol....867
Butanol, as extraction solvent....967
Butene, 3,4-epoxy-1-....937

Butyl acetate, as extractant 943
tert-Butylamine, analysis of....855

Cadmium 139, 221, 485, 823, 1313, 1579
Calcium 3, 125, 151, 183, 233, 817, 885
Calcium hydrogen phosphate nanoparticles 861
Caleflonum....985
Calixarene 653, 677
Calixarene, acetyl derivative....915
Calixarenes, carboxylic acid 879
Calixarenes, proton ionizable....1487
Calix-crown....659, 683
Calorimetry, micro 1043
Camphor....961
Carbamoylmethylphosphine oxide 521, 623, 727
Carbazole, extraction of....1325
Carbon adsorption, for solvent recovery....453
Carbon disulfide....823
Carbon tetrachloride....1159
Carbonate media 849
Carboxylates, as ligands....1133
Carboxylic acid, as synergist 119
Carboxylic acids....1403
Carboxylic acids, extraction by....1421
Cartridge, membrane....1561
Catalysis, base....923
Cathode 151, 485
Caustic-Side Solvent Extraction process 689
CCD 43
CCD-PEG process 709
Cellgard 2400 membrane....1367
Central African copper belt....131
Centrifugal contactor 979
Centrifugal contactors....611, 727
Centrifugal extractor 985
Centrifugal partition chromatography....817
Centrifugation, 2- or 3-phase 503
Centrifuge 497
Cerium....189, 521, 659, 1081
Cesium 43, 533, 653, 671, 683, 709, 1487
CFD....403, 1171
CFX software....1213
Chambishi Metals 139
Chiral separation 979
Chloride....43, 201, 849
Chloride media....1151, 1439, 1505

Chlorinated cobalt dicarbollide....533, 709
Chlorocomplexes....1049
Chloroform....305, 805, 891, 1057, 1457, 1493
Chloroquine, extraction of....1003
CHON principle....653
Chromate....1159
Chromium....215, 329, 653, 897, 1555
CINC centrifugal contactor....733
Circular dichroism....83, 779
Clarifier....473
Clay treatment....497
Clay, as entrained solids....503
Cloud-point extraction....1549
CMPO....511, 539, 703, 1263
Coal tar....949
Coalescence....361, 479, 1177
Coalescers....435
Cobalt....3, 119, 139, 157, 177, 201, 233, 335, 447, 473, 885, 1481
Cobalt bis(dicarbollide), derivatives of....539
CODESSA PRO software....1023
Column, design of....361
Column, Karr....1225
Column, pulsed....373, 581
Column, rotating disc....403
Column, sieve plate....1537
Commercial extractants, analysis of....903
Complexants....511, 623
Complexants, soft-donor....569
Complexation....1043
Computational fluid dynamics....403, 1171, 1213
Computational molecular modeling....1011
Computer simulation....43
Conformation....59
Constant, extraction....569
Contactor, rotating disk....1177
Continuous variation method....1151
Copper....3, 101, 119, 139, 163, 183, 221, 239, 347, 435, 653, 829, 915, 1151, 1469, 1493, 1579, 1597
Copper cathode....497
COSMOS-RS model....1385
Column, pulsed....385
CPC, see Centrifugal partition chromatography
Critical micelle concentration....787
Cross-contamination, extractant....453
Crown ether....43, 659, 769
14-Crown-4....1011

Crud....201, 263, 447, 829
Crud, treatment of....497
Cryptands....43
Cs-7SB modifier....659, 1487
CSSX process....1487
Curium....29, 563, 695, 721, 1355
CYANEX 272....139, 177, 293, 473, 1373, 1621
CYANEX 301....305, 1151, 293, 1151
CYANEX 471X....1621
CYANEX 923....317, 1385
Cyanide....703
Cyclitols, purification of....973
Cyclohexane....1319
Cyclohexanone....551
Cyphos IL-101....1295
Cyphos IL-104....1295

D2EHPA, see Di-2-ethylhexylphosphoric acid
Dansyl group....843
Decane....287
Decanter....479
Degradation....113, 269, 467, 551, 1159
Degradation, of diluent....447
Degradation, radiolytic....677
DEHPA, see Di-2-ethylhexylphosphoric acid
Density, of diluent....623
Design, molecular....1023
Design, of refineries....453
Design, SX plant....453
Di(2-ethylhexyl)amine....195
Di(isodecyl)phosphoric acid....511
Di-2-ethylhexylphosphoric acid....3, 201, 233, 373, 447, 563, 829, 1111, 1151, 1367, 1561
Di-2-ethylhexylphosphoric acid, recovery of....1561
Diameter, column, effect of....1225
DIAMEX process....29, 581, 1439
Diamide....665, 1439
Diamides, synthesis of....745
Dibenzo-18-crown-6....769
Dicarbollide....653, 709
Dichloroethane....557, 843
Dichloromethane....1573
Dicyclopentadiene impurities, removal of....1319
Diesel fuel, purification of....1325
Differential scanning calorimetry....799
Diffusion....1397

Diffusion regime 1277
Diffusion, intraparticle 1391
Diglycolamide 1349
Diglycolic acids, synthesis of 575
Diimine, bis(salicylidine)cyclohexyl 891
beta-Diketone 787, 1035
beta-Diketones 1469
Diketone, degradation product 113
Diluent wash 453
Diluent, effect of 533, 623, 915
Dimethyl-3-oxa-glutaramic acid 611
Dinitrophenolate, in anion exchange 1093
4,7-Diphenyl-1,10-phenanthroline 557
Dispersion 17
Dispersion forces 1263
Dithiocarbamates 823
Dithiophosphinic acid 557
Dithizone 83
Docosahexaenoic acid, ethyl ester 1543
Dodecane 275, 569, 605, 727, 757, 1069, 1355
Dodecanol 101
Donnan diffusion 1591
Drop size 861, 1337
Droplet population balance 1177
Droplet, behavior 397
Droplet, coalescence of 409
Droplet, formation of 397
Droplet, size 17
Droplet, size distribution 379, 763
DTPA 511, 665
Dye 83
Dysprosium 527, 1271

Economics 453
EDTA 569
EDTA, as masking reagent 1343
El Boleo project 113, 163
Electroless nickel plating 195
Electrospray mass spectrometry 843
Electrowinning 3, 145, 209, 427
Emulsification 1003
Emulsion liquid membrane 1597
Emulsion pertraction 1415
Encapsulation, of extractants 1591
Enthalpy 1111
Entrainment 169, 281, 727

Entrainment, analysis of....909
Entropy, of ion transfer....835
EOPO2500 Copolymer, purification of....1573
Equilibria....769, 811, 1003, 1099, 1127, 1145, 1201, 1283, 1421, 1579
Equilibrium constant....293, 459, 569, 787, 811, 1093, 1145, 1499, 1591
Erbium....1255
Escaid 100....829
ESI-MS, see Electrospray mass spectrometry
Ethanol....1289
Ethanol, as extraction solvent....961
Ethyl ether....955
2-Ethylhexanol....287
EUROPART....545
Europium....511, 539, 557, 593, 647, 665, 811, 1017, 1099, 1349, 1549
EXAFS....1263
Explosion hazard....757
EXTREQ-2 software....1127
Exxsol D-100....215
Exxsol D-80 diluent....323

Fatty acids....955
Fermentation broth....973
Ferrous sulfamate....617
Filtration....473
Filtration, for solvent recovery....453
Fission products....647, 695
Flocculants....829
Flooding....385
Flotation cells, for solvent recovery....453
Flow patterns, in rotating disc contactor....1519
Flowrate, effect of....733
Flowsheet....93, 145, 195, 245, 341, 521, 587, 641, 695, 721, 1597
FLUENT simulation code....403
Fluorescence microscopy....421
Fluoride....201
Fluorometry....83
Foaming....739
Formate, extraction of....1567
FPEX process....671
Free energy....59
Freundlich isotherm....1343
FS-13 diluent....677
Fumaric acid....1403

Gadolinium....891
Gallium....751, 1579
Galvanizing, hot dip....1409
Gas chromatography....113, 269, 671, 923
Gas sorption, by ILs....1301
Geologic repository....659
Germanium....703
Glass waste form....29
Glycerol, as byproduct....923
Glycolamide....1029
GNEP....659, 733
Gold....287, 311, 703, 1585
Groundwater, remediation of....1415
Guanidinium cation....59

Hafnium....1119
Halides....1049
Harjavalta plant....473
HCl....769
HCl media....1313
HCl, as catalyst....967
HCl, as stripping acid....415, 1343
HCl, leach solution....317
HDEHP, see Di-2-ethylhexylphosphoric acid
Headspace analysis....855
Heap leaching....251
HEDTA complexant....29, 521
Heptane....83, 973, 1195, 1543
Heptanol....973
Hexafluorophosphate, as IL anion....931, 1301
Hexane....973, 1537
Hexanol....1531
Hexylmethylketone....539
High-level liquid waste....511, 551, 623, 659, 695, 745, 1487
Hofmeister, order or bias....59
Holdup....367, 1237, 1337
Holmium....1349
Host-guest chemistry....59
HPLC....119, 961
HTTA, see 2-Thenoyltrifluoroacetone
HTP diluent....721
Hydration....1043
Hydration, entropy of....59
Hydraulics....385
Hydrazine....623
Hydrazinium nitrate....1355

Hydrodynamics 17, 409, 763, 1183, 1225
Hydrogen 3
Hydrogen bonding 101, 1263
Hydrogen peroxide 751
Hydrogen sulfate, as catalyst 967
Hydrolysis, of hydroxyoxime 281
Hydrophobicity 59
Hydroxyketone, degradation product 113
Hydroxylamine, as reductant 897
Hydroxyoxime type extractant 3, 119, 221, 447
Hydroxyquinoline type extractant 1579
Hyfane diluent 721

Ibuprofen 1093
ICP, see Inductively coupled plasma
Idaho National Laboratory 659
Imidizolium 873
Imidizolium, IL cations 1263, 1301, 1331
Imine, formation of 1391
In silico design 1023
Indium 703, 1463
Infrared spectroscopy 269, 855, 1159
Intensification, process 867
Interface between two immiscible electrolyte solutions 835
Interface, liquid-liquid 43
Interfacial activity 43
Interfacial instability 1183
Interfacial phenomena 779, 1207, 1277
Interfacial vibration 1255
Iodide, as IL anion 937
Ion exchange 131
Ion-pair extractant 1451
Ionic liquids 43, 931, 1263, 1283, 1301, 1319, 1337
Ionquest 290 131
Iron 3, 145, 169, 201, 227, 293, 347, 435, 623, 787, 885, 1099, 1343, 1439
Iron, as reductant 897
Isobutyrate, modifier 227
Isodecanol 227, 269
Isododecane 397
Isopar L 659, 1415
Isosaccharinate as ligand 1133

Kapustinskii equation 1301
Karl Fischer titration 1283
Karr reciprocating column 1165
Kelex-100 1579

Kerosene 949, 1361
Keto-dextran 1603
Ketones, as solvating agents 1093
Keto-oxime, degradation product 125
Kinetics 83
Kinetics, AHA decomposition 635
Kinetics, degradation 275, 677
Kinetics, extraction 177, 897, 1283
Kinetics, oxidation 605
Kinetics, sorption 1307
Kinetics, stripping 177
Kokkola plant 473
KREBS CycloClean 491
Krypton 709

Lactate 511
Lactic acid, partitioning of 563
Langmuir-Schaefer film 779
Lanthanides 189, 539, 569, 611, 659, 703, 721, 891, 1043, 1087, 1195, 1349
Lanthanum 521, 653, 897, 1349
Laser Doppler anemometry 403
Launder, organic or aqueous 453
Leaching 139, 157, 317
Leaching, by microemulsion 1597
Lead 201, 843, 1481, 1579
Leonard-Jones potential 59
Levulinic acid 967
Light water reactors, see Reactor
Linoleic acid, extraction of 955
Linseed oil, extraction of 955
Lithium 157, 1373
Lithium chloride 769
LIX 622 1591
LIX 63 ....119, 183
LIX 64 3
LIX 65N 83
LIX 84 177
LIX 84-I 909
LIX 860N-I, analysis of 903
LIX 984N 151, 829
LLECMOD 17
Lonshi ore 497
Losses, of organic 497
Lutetium 201, 1035
LWR fuel 659

Macrocycles 1011
Magnesium 3, 125, 151, 183, 275, 385, 817
Magnetic microparticles 885
Magnetically assisted chemical separation 885
Magnetite 1513
Malaria, treatment of 1003
Malonamide, design of 1011
Malonamides 745
Manganese 119, 139, 169, 201, 233, 335, 617, 1499
Marangoni effect 1219
Mass spectrometry 677
Mass spectrometry, electrospray 1017
Mass transfer 367, 391, 763, 1165, 1207, 1237, 1277, 1519, 1627
Materials of construction 453
McCabe-Thiele diagram 215, 441
MD simulation, see molecular dynamics
Mechanism, complexation 1201
Mechanism, extraction 329, 1249
Mechanism, kinetic 269
MELOX plant 29
Membrane, adsorption-extraction 1561
Membrane, emulsion liquid 1597
Membrane, hollow fiber 1409, 1567
Membrane, liquid emulsion 1397
Membrane, optode 849
Membrane, stability of 1349
Membrane, supported liquid 1349, 1373
Membrane-facilitated SX 1567
Mercury 323
Methane, sorption of 1301
Methanol, in transesterification 923
MIBK 335
Mica 503
Micelles 1201, 1615
Micelles, reverse 1017
Michaelis-Menten mechanism 873
Microemulsion leaching 1597
Microfluidics 867
Microparticles, magnetic 885
Microscopy, fluorescence 421
Mikulin equation 721
Mineral acid, extraction of 347
Minor actinides 29
Mixer, helical coil 763
Mixer-settlers 145, 385, 421, 453, 581, 721, 1237
Model, discrete phase 403

Model, equilibrium 323, 459, 715, 1133
Model, mixer-settlers 415
Model, process 581
Model, transport 1361
Modeling, flowsheet 251
Modeling, molecular 1207
Modifiers 101
Molecular design 1011
Molecular mechanics 1011
Molybdenum 245, 335, 623, 885
Mono(2-ethylhexyl)phosphoric acid 239
Monolayer 83
Monte Carlo simulation 1237
MOX fuel 29
MSDS 751

Nanodroplets 1207
Nanoparticles 1301
Nanoparticles, preparation of 861
Naproxen 1093
Neodymium 189, 521, 653, 849, 1081, 1271, 1627
Neptunium 527, 605, 623, 695, 721, 897
NEWPART 521
NEXT reprocessing system 511
Nickel 113, 151, 183, 201, 221, 341, 391, 467, 653, 829, 897, 1499, 1597
Niobium 335
Nitrate media 1379
Nitrate, as matrix anion 1017
Nitrate, counteranion 1585
Nitrate, in uranium ore leach liquor 275
Nitration, of Cs-7SB 671
Nitric acid 527, 551, 575, 617, 647, 665, 683, 715, 757, 1087, 1343, 1361, 1481
Nitric acid, as stripping agent 1313
Nitric acid, effect of 799
Nitrilotriacetic acid 665
Nitrobenzene 539, 689
Nitrogen compounds, removal of 1325
Nitronium ion 269
Nitrosamines, as degradation products 269
Nitrous acid 581
NMR spectroscopy 1159
Nonane 1537
Nondispersive SX 1567
4-Nonylphenol 101
Nonylsalicylaldoxime 367
Nylon plate material 1165

Octane 107, 1075
Octanol 43, 575, 683, 943, 1043, 1597
Oleanolic acid 961
Optical chirality 779
Optimization, circuit configuration 93
Optode 849
Ore 131, 353, 485
ORGA process 623
Organophosphorous extractant 511
Oxalate 849
Oxalic acid 521, 751
Oxime type extractant 101, 125, 221, 353, 829, 1451
Oxoanions 1049

P50, 5-nonylsalicylaldoxime extractant 1475
Palladium 521, 715, 1295, 1445
PAREX code 521, 715
Particle size, effect on sorption 1307
PARTNEW 545
PEG 709, 1201
PEG-4000 1609
2,4-Pentanedione 787
Perchlorate media 1049, 1499
Perchlorate, as counteranion 1585
Perchloric acid 533
Perchloric acid, extraction of 347
Permeability coefficient 1355
Perrhenate 769
pH, effect of 107, 221, 239, 299, 459, 805, 823, 915, 961, 1057, 1145, 1255, 1421, 1487, 1585
Pharmaceuticals 979, 1003
Phase disengagement 169, 453
Phase disengagement, measurement of 829
Phase ratio, effect of 629
Phenol compound, as chromophore 849
Phenol, as system component 1165
Phenol, removal of 1385
Phenyltrifluoromethylsulfone 653, 709
Phosphate, in uranium ore leach liquor 275
Phosphine oxide, bis, triazole-linked 1499
Phosphine oxide, trialkyl 973, 1385
Phosphine oxides 317, 641
Phosphinic acid type extractant 157, 467
Phosphinic acid, dialkyl 1151
Phosphite ions, removal of 195

Phosphonium, tetraalkyl 799, 1283, 1313
Phosphoric acid, dialkyl....1105, 1397
Phosphoric acid, wet 385
Photodiode 83
Phthalocyanine, thioether derivative....779
Picket fence....453
Pickling solution, spent....1283
Picrate 59
Pilot plant....17, 177, 251, 341, 385, 421, 485, 611, 1237
Piperidine 823
Plating, zinc....215
Platinum 415, 1445
Pluronic PE 3100 surfactant....1415
Plutonium....521, 581, 611, 635, 665, 709, 751, 1099
Plutonium, purification cycle....587
Polarity....101
Polyamine ECA 4360J surfactant 1567
Polyaminocarboxylic acid complexants 569
Polyethylene glycol....665, 1201
Polymeric ionic liquids 1301
Polyoxyethylene, see PEG or polyethylene glycol
Polysaccharide 1603
Porphryin....779
Potassium 275, 689, 1549
Pourbaix diagram 329
Praseodymium....653, 1421
Precipitation 145
Preorganization 1011
Pressure, effect of on transport 1367
Primene JM-T 1159
Proliferation risk 695
Promethium....1099
Protactinium....769
Protonation constants....1063
Pulsed columns 215, 385, 581
PUREX process 521, 551, 599, 751
PUREX raffinate....521, 715
Pyridine ligands, tetradentate....1063
2,6-Pyridinedipicolinic acid....665
Pyridinium, IL cations 1331

QSPR....1023
Quantum mechanics....1463
Quaternary amine, see Amine
Quinine, derivative as extractant....979
Quinolinol 83

Radiolysis, effect of 511
Radiolysis, products and mechanism of....677
Radiolysis, resistance to....533
Raman spectroscopy 779
Ranchers Bluebird plant....3
Rare earth metals....703, 1343
Rate constants 1397
Reactor, chemical....757
Reactor, fast neutron 29
Reactor, light water....695
Reactor, two-phase....923
Recognition, molecular 59
Redox control....269
Repository 1133
Reprocessing 641, 695, 721
Resin, aminophosphonic chelating 131
Resin, Merrifield....1609
Resin, solvent-impregnated....1343, 1433
Reynolds number 379
Rhodium....521, 1049
Ricinolate, tetraglycerin-condensed....997
RTILs, see Ionic liquids
Roasting 145
Rotating disc column 361
Rotating disc contactor 1519
Ruashi project 131
Rubidium....659
Ruthenium....551, 1049

Sage, extraction of....961
Salicylaldoxime type extractant....101, 367
Salting out....593
Samarium 83, 659, 1105
SANEX process 29, 581
Savannah River Site....617
Scaleup....385
Scaleup, of column....379
Scanning electron microscopy 189, 1389
Schlieren technique....1231
Sea nodules 3
Sedimentation, of drops 397
SEM, see Scanning electron microscopy
Semiconductor band gap....1621
Sergievskii-Dannus theory....1017
SETFICS process 511

Settler 479
ShellSol 2046 ..... 263, 909
ShellSol 2325 1513
ShellSol A150 829
ShellSol D70 ..... 163, 183
Shikimic acid 973
Sieve-plate column 367, 1537
Silica 209, 335
Silicate ore 201
Silver 299, 1585
Silver nitrate 751
SIMPSEX code 635
Simulation, Monte Carlo 1207
Simulation, of settler dynamics 409
Simulation, process 385
Single-drop microextraction 855
Skorpion Zinc plant 201, 485
Slope analysis 299, 557, 769, 1003, 1139, 1481
Sludge 485
Smart-Level Solvex 275, 653, 829, 885, 1549
Sodium dodecyl sulfate 1555
Sodium nitrate, as medium 805
Sodium, as impurity 617
Soft-donor extractants 1081
Sol-gel process 1579
Solids, effect of 473
Solids, removal of 473
SOL-KELEX adsorbents 1579
Solvation 1035
Solvation shell 1043
Solvent impregnated resin 1343, 1433
Solvent, recovery of 491
Solvesso 150 diluent 281
Sorption, of gold on resin 1307
Span-80 surfactant 1361
Speciation 287, 769, 1579
Spectropolarimeter 779
Spent fuel 581, 647, 695, 1427
Spherand 59
SSX 210 diluent 829
Stability constant 1043
Stability, of pyrazole extractant 1469
Stability, of solvent 467
Stargo plant 491
Steric factors 1463
Stoichiometry 293, 347, 545, 629, 879, 1057, 1145, 1277, 1475, 1499

Stripping....101, 221, 299, 329, 623, 1439
Stripping, from SCF....1627
Stripping, reductive....629
Strontium....139, 641, 659, 677, 709, 1099
Succinimide, as modifier....101
Sulfate, in nickel electrolyte....341
Sulfate, sodium dodecyl....1555
Sulfate media....151, 233, 391, 459, 1373
Sulfide ore....3
Sulfide smelter product....341
Sulfolane....1337
Sulfonate, dodecylbenzene....1555
Sulfonic acid media....1463
Sulfur dioxide....131
Sulfuric acid....131, 177, 209, 227, 275, 335, 391, 441
Sulfuric acid, as stripping agent....915, 1313
Supercritical carbon dioxide....43, 961
Suppressor....689
Surfactant....997, 1555
Surfactant, nonionic....1615
Swelling, variation with time....1361
Synergism....163, 533, 1105
Synthesis, of diazene type extractant....1505
Synthesis, of functionalized adsorbents....1579
Synthesis, of salicylaldimines....1475
Synthesis, of thioether monoaza podand....1585

TALSPEAK process....511, 599
Tamiflu....973
Tartaric acid, octylamido....1615
TBP, see Tributylphosphate
Technetium....695, 721
Temperature, effect of....59, 233 ,459, 769, 1277, 1597
Tenke-Fungurume project....131
Terbium....1271
Tetrachloroaluminate, as IL anion....1331
Tetraethylammonium....835
Tetrafluoroborate, as IL anion....1319
Tetramethylammonium....835
Tetraoctyldiglycolamide....575, 1099
Tetraoctyldiglycolamide, thia ether analog....1445
2-Thenoyltrifluoroacetone....83, 811, 891, 1463
Thermodynamics....233, 1043, 1111
Thin-layer extraction....1525
Thioether type extractants....1585
Thiophosphinic acid, dialkyl....353

Thiosulfate, as leachant....299
Thiourea, leaching with....293
Third-phase formation....257
Thorium....527, 617, 745, 849, 1195
Time, of adsorption....1433
Time, reaction....923
Time, swelling, effect of....961
Tin slag....335
Titanium dioxide nanoparticles....861
TODGA, see Tetraoctyldiglycolamide
Toluene....107, 317, 557, 943, 1093, 1231, 1325, 1439
TOPO, see Tri-*n*-octylphosphine oxide
TPH diluent....521
Transfer, Gibbs energy of....793
Transmission electron microscopy....1621
Transport....1349, 1367, 1409
Transuranics....659
Tren....1457
TBP, nitric acid adducts....647
Tributylphosphate....43, 139, 215, 293, 521, 599, 623, 647, 727, 757, 817, 943, 1133, 1385, 1573
Tributylphosphine oxide....973
Tridecanol....3, 909
Trifluoromethanesulfonate....1301
Triglyceride....923
Trioctylamine....275, 689, 1385
Tri-*n*-octylphosphine oxide....311, 1035
Tris(2-ethylhexyl)amine....341
Triterpenes....961
Triton X-100....653
Triton X-114....1057, 1621
TRPO process....703
TRUEX process....563, 709
Tungsten carbide scrap....335

UNEX process....665
Uranium....3, 251, 269, 527, 605, 635, 695, 745, 769, 849, 1081, 1263, 1433
Uranium, carbonate complexes....849
Uranous nitrate....587
Urea, tripodal anion receptors....1457
UREX process....563, 659, 727
Ursolic acid....961
UV/vis irradiation....1505
UV/vis spectrophotometry....527, 849, 1063, 1271

van der Waals interactions....59

Vanadium....275
Vanillin, extraction of....943
van't Hoff analysis....1111
Versatic acid....3, 125, 183, 1481
Viscosity....367
Viscosity, emulsion....1003
Voltammetry, photomodulation....835
Vortex flow in drops....867

Water activity....1087
Water, organic-phase content....909
Wet phosphoric acid....385

Xenon....695
X-ray crystal structure....1263, 1469, 1499
Xylene....287, 915, 1139

Yellow cake....3
Ytterbium....527, 1421
Yttrium....521, 703, 1277

Zinc....3, 119, 151, 177, 201, 221, 239, 335, 373, 427, 485, 829, 891, 1307, 1397, 1481, 1513
Zinc, as reductant....119
Zincex process....427
Zirconium....275, 623, 659, 885, 1249

ANGLO AMERICAN

The Global Leader in Mining

Anglo's Product Diversity

Platinum	Anglo Platinum (74%) - the world's leading primary producer of platinum
Gold	AngloGold (18%) - one of the world's leading gold producers
Diamonds	De Beers (45%) - largest producer by value of gem diamonds
Coal	One of the world's leading private sector coal producers
Base Metals	Growing presence in copper, nickel and zinc markets
Industrial Minerals	UK market leader in aggregates, asphalt and concrete blocks
Ferrous Metals	Producer of iron ore and value-added niche ferrous metals products

Spread of Anglo Operations

*Including investment in JVs and associates

ANGLO AMERICAN

The Global Leader in Mining

Researching Opportunities

Anglo Research is an integrated and strategic technology partner within the Anglo American Group providing world-class solutions and expertise.

We focus on partnering with Group companies

- to add value to the Anglo American Group globally as an extension of the operating divisions and to be the strategic technology partner of choice
- to pioneer breakthrough technologies and develop incremental technology innovations that improve the efficiencies of Anglo American
- to support continuous improvement thrusts and generate significant competitive advantage for our partners
- to secure the sustainability of global resources
- to entrench a culture of innovation, flexibility and creativity in Anglo Research, and to attract, retain and develop passionate and brilliant people
- to create an integrated, world-class facility and team at Anglo Research

Key technical departments include:

Extractive Metallurgy

The strength of this department lies in their ability to take a process concept from scouting and optimisation testwork, to mini-plant testwork, and finally to pilot-plant scale in an integrated circuit.

Minerals Processing

Providing clients with innovative, cost-effective and pragmatic solutions in the areas of comminution, flotation, solid-liquid separation, ore upgrading and physical separation. This team works closely with operating divisions, providing them with survey work, plant modelling and consulting. Operational continuous improvement is their main goal.

Mineralogical Research

This department provides applied mineralogical information to Group Companies, from the initial geological exploration stage through to the final refining stage. Investigations include long term research (to increase the understanding of ore bodies and processes), optimisation studies, troubleshooting investigations and routine monitoring tasks.

ANGLO AMERICAN

The Global Leader in Mining

Chemistry

This is the largest department in Anglo Research and aims to serve the Group in a cost-effective and efficient way, whilst providing our partners with a powerful tool in terms of qualitative and quantitative outputs. Sections include metal accounting, minerals technology, analytical services, PGM projects, quality, specialist services, and geochemistry.

Technology

This diverse group of scientists aims to identify, secure and develop potential breakthrough technologies. Activities cover high risk conceptual studies of emerging technology and technical viability testing, and radical research aimed at creating an understanding of knowledge new to the Group (possibly the world).

Refining Research

This is a highly specialised team which provides a service to Anglo Platinum operations in the fields of Platinum Group Metal refining and in chemical analysis technology.

CAREERS AT ANGLO RESEARCH

We seek motivated self-starters who have a keen interest in being at the cutting-edge of technology development and innovation.

Being part of the Anglo American Group of Companies offers staff the benefit of inter-divisional and global employment opportunities. Our technical departments require graduates from a variety of degree disciplines, including Chemical Engineering, Metallurgy, Geology and Chemistry.

We also offer a limited number of bursaries for approved studies and these bursaries are currently administered by Careerwise. They can be contacted on (011) 484-7505 for further details.

Visit our website at
http://www.angloresearch.com

Anglo Research (a division of Anglo Operations Limited)
8 Schonland Street, Theta, Johannesburg, South Africa
P.O. Box 106, Crown Mines 2025
Tel +27 (0)11 377 4600 Fax +27 (0)11 835 1314

The SX unit provides:

- Optimal SX processes tailored to meet customers' requirements
- Efficient SX plants – on time and within budget
- Plant commissioning led by experienced teams of process engineers
- Project financing facilitation
- Superior HSE and Quality Control standards
- Minimization of environmental risks

Bateman Litwin Headquarters

Haaksbergweg 59
1101 BR Amsterdam,
The Netherlands
Tel: +31 20 564 0491
Fax: +31 20 564 0490

Litwin

13-15, rue Edouard Manet
92504 Rueil Malmaison
Cedex, France
Tel: +33 (0)1 72 25 52 52
Fax: +33 (0)1 72 25 52 90

Regional offices:

Chile, Kazakhstan, Morocco, Nigeria, Russia, Romania, Switzerland, Israel, Italy, USA

Selected Case Studies

Olympic Dam expansion, Australia

Following a successful pilot, done in 1995, Bateman Litwin continued working with the Olympic Dam uranium production facility and performed several expansion projects to the SX plant. This facility is currently utilizing 14 Bateman Pulsed Columns.

WengFu PPA plant, China

Bateman Litwin's Advanced Technologies Division supplied Guizhou Hongfu Industry & Commerce Development Co. Ltd, (WengFu) with a purified phosphoric acid (PPA) plant. The project included the process development, design and supply of an SX section, which utilizes six Bateman Pulsed Columns and two mixer settlers.

Mantos De La Luna copper SX project, Chile

Bateman Litwin provided its proprietary BATEMAN SETTLER™ technology for the copper SX plant. The Company also performed the detailed process, FRP (fiber-reinforced polymers) and mechanical design of the SX plant.

Bateman Litwin at a glance

Bateman Litwin focuses on mid-sized Energy EPC contracts, principally executed on a lump sum turnkey (LSTK) basis. Bateman Litwin also provides technology solutions to the Phosphate Sector and Solvent Extraction Applications.

Backed by an impressive track record of hundreds of projects in more than 40 countries, Bateman Litwin has established a reputation for excellence and on-time, on-price project delivery, which maximize customer profitability.

www.bateman-litwin.com

BATEMAN Litwin

From Concept to Turnkey

Solvent Extraction

Advanced solutions for:

- Minerals & metals industry
- Petrochemical industry
- Chemical process industry
- Environmental protection

Bateman Litwin's Solvent Extraction (SX) unit develops advanced solvent extraction technologies and provides comprehensive solvent extraction solutions for the hydrometallurgical, chemical, petrochemical, fertilizer, minerals, food and pharmaceutical industries.

Bateman Litwin's SX processes are taken from the preliminary stages of defining the customer's needs and conducting research and feasibility studies, through to plant modification, expansion and new facility construction. The projects are fully covered by process guarantees and mechanical warranties.

SX solutions and services are backed by Bateman Litwin's research and development center, utilizing advanced SX systems and equipment.

Solvent Extraction - The optimal solution for your process plant

BATEMAN Pulsed Column technology

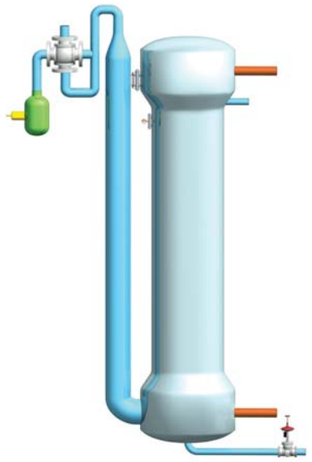

The BATEMAN pulsed column technology provides a highly efficient, cost-effective and safe contactor, which enhances solvent extraction processes during the extraction, stripping and scrubbing or washing stages.

SX Project Development

Over the years Bateman Litwin (BNLN) has cultivated a comprehensive step-by-step approach for project development, ensuring the all-around fulfillment of the project requirements and the successful delivery of the project.

Pre - Feasibility
Go/no go decision, evaluating optional process schemes & costs

Feasibility
Confirms/revises earlier conclusions, enhances accuracy of cost evaluation

Definitive Feasibility
Formal documentation reporting process details, estimation of capital & operating costs

Finance
Facilitating the optimum, most cost - effective financing packages. For certain solutions equity investment may be considered.

Need
Defining processing goals, optimization of capital and operating costs, safety and environmental issues

Lab
Evaluating potential extractants, utilizing synthetic/authentic samples, determininig materials for construction, identifying recovery procedures

Mini Pilot
At BNLN research center/on site: SX process on a small scale in operation, utilizing equipment, mini pilot plant, samples for testing, market assessment

Pilot
At BNLN research center/client facility: integrating the plant into the process stream, authentic process solutions, validating previous data for scale up purposes

Demonstration
Produces authentic marketable samples on a small - scale simulation plant which, provides conclusive evidence of project viability.

Design, Supply & Construction
Best equipment for the process, industrial SX plant designed, supplied & constructed by BNLN

Commissioning & Start-up
Full training provided for the plant operation team as well as technical and operational support services. BOO skills available if required

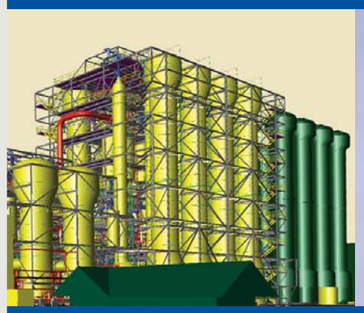

Selected Projects

- Olympic Dam Operations, Australia, Uranium
- Bulong Nickel, Australia, Nickel/Cobalt/Zinc
- Mantos de la Luna, Chile, Copper
- Piedras Verdes, Mexico, Copper
- Cananea SX/EW plant No.2, Mexico, Copper
- Weng Fu, China, Phosphoric Acid
- Goro Nickel, New Caledonia, Nickel/Cobalt
- Dominion Reefs, South Africa, Uranium
- Gaby-Codelco, Chile, Copper (ongoing project)
- Project 118-CVRD, Brazil, Copper (ongoing project)

Lump-Sum Turnkey and EPCM solutions for:

- Minerals and metals industry – processing uranium, copper, nickel, cobalt, gold, zinc, rare earth elements and vanadium
- Specialized SX processes for the mineral industry including sulfuric acid, halides and cyanide removal
- Chemical industry – processing nitric, phosphoric, hydrochloric and citric acids, inorganic salts and organic solvents
- Petrochemical industry – processing lubricant oils, caprolactam, etc
- Environmental protection – effluent treatment, removal of nitrates and heavy metals

BATEMAN SETTLER™ Reverse Flow technology

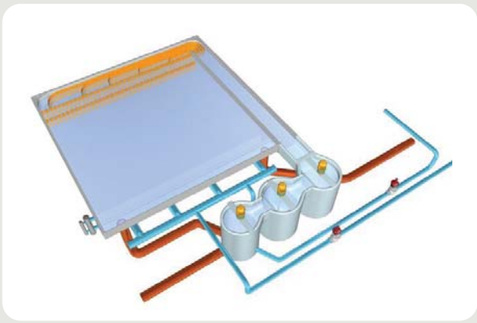

The BATEMAN SETTLER™ with its advanced design, unique Reverse-Flow technology and enhanced efficiency provides many advantages compared to conventional settlers used in SX circuits.

Cognis is the world leader in the SX/EW production of copper. Because our reagents are simply more productive – in total copper produced and in efficiency. (The fact is, you'll need less of our reagents, and more of theirs, to produce the same tonne of copper.) We also provide sophisticated MSP™ technical support to help you make your plant work more efficiently.

That's real leadership. That's innovation, teamwork and value. That's Cognis.

To contact the world leader in SX/EW copper recovery, please call:
Cognis Corporation • 2430 North Huachuca Drive • Tucson, Arizona USA 85745-1273
Telephone (520) 622-8891 • FAX (520) 624-0912 • www.cognis.com

cognis.
we know how

COPPER SOLVENT EXTRACTION – 2007 WORLD OPERATING DATA

T. Robinson,[1] M. Moats,[2] W. Davenport,[3] G. Karcas,[4] S. Demetrio,[5] and E. Domic[6]

[1]Freeport McMoran, Phoenix, AZ, USA . [2]University of Utah, Salt Lake City, UT, USA. [3]University of Arizona, Tucson, AZ, USA. [4]Outokumpu Technology, Metals processing, Athens, Greece. [5]Smeltec S.A. Las Condes, Santiago, Chile. [6]Domic S.A, Providencia, Santiago,Chile. Corresponding author email address: tim_robinson@fmi.com

ABSTRACT

World copper solvent extraction (SX) plant practices have been surveyed. This survey is a supplement to previous surveys that were carried out in 1997 and 1999. On a world basis, process technology trends include higher process flows, new mixer settler materials of construction, reverse flow mixer settlers and advanced mixer technology and designs. These changes have resulted in reduced capital and operating costs. Most greenfield copper SX projects are occurring in South America and Central Africa.

INTRODUCTION

This manuscript is an update of the world copper solvent extraction surveys performed in 1997 and 1999 [1-3]. This paper presents operating data and plant practices from 24 copper solvent extraction operations from around the world. The present survey includes respondents from Australia (1), Chile (6), Laos (1), Myanmar (1), Peru (1), USA (13) and Zambia (1). Copper solvent extraction plants that are not included in the survey include many of the Chilean plants. Several recent African projects such as Kansanshi are also not included. The detailed survey results are presented "as received" on the CD-ROM version of these proceedings. This paper will summarize the results of the survey and discuss process technology trends and greenfield developments.

SURVEY SUMMARY AND ANALYSIS

The survey data was analyzed to determine most common practices and ranges of values. In the analysis of numerical values, if a range was given then the average of the two values was used. If a response was questionable in the authors' opinions then it was excluded from the analysis.

Plant Design

Summaries of plant design are given in Tables 1-3. All plants in the survey either operate two or three extraction stages per train with about an equal percentage for each value. Of those plants operating three extractions, 75% operated in series-parallel. Of the two plants that operate in parallel, both use three extraction stages. Most plants, 75%, use one stripping stage per train. The use of an organic wash is fairly evenly split with slightly more plants using them than not.

Settlers are specifically designed for each plants' flow rate. Most settlers are 15-30 m in length and width with a length to width ratio around 1. Settler depth is typically 1 m. Settling velocities range from 2 to 8 m^3/m^2 with a median value of 4.4. All plants surveyed use picket fences with most employing two per settler.

There is a wide range in the style of impellers used. They range in size from 1.3 to 2.9 m in diameter. The mixers operate at 37 to 69 RPM with most using 10-40 kW of power.

Table 1. Summary of Copper Solvent Extraction Train Design

Category	Data Summary
Extraction Stages Per Train	2 (52%), 3 (48%)
Extraction Operation	Series (46%), Parallel (8%), Series-Parallel (46%)
Stripping Stages Per Train	1 (75%), 2 (25%)
Organic Wash	Yes (55%), No (45%)

Table 2. Summary of Settler Design

Category	Data Summary
Settler Length:Width Ratio	Min. – 0.6, Median – 1.0, Max. – 2.6
Settler Depth (m)	Min. – 0.8, Median – 1.0, Max. – 9.9
Settling Velocity (m^3/m^2 per hour)	Min. – 1.95, Median – 4.4, Max. – 8
# of Picket Fences per Settler	1 (29%), 2 (57%), 3 (10%), 4 (5%)

Table 3. Summary of Mixer Designs

Category	Data Summary
Extraction Mixers	
Impeller Dia. (m)	Min. – 1.27, Median – 1.9, Max. – 2.9
RPM	Min. – 36.4, Median – 48, Max. – 69
Power (kW)	Min. – 10, Median – 19, Max. – 134 (?)
Stripping Mixers	
Impeller Dia. (m)	Min. – 1.22, Median – 1.8, Max. – 2.9
RPM	Min. – 36.4, Median – 49, Max. – 69
Power (kW)	Min. – 10, Median – 19, Max. – 134 (?)

Flow Rates and Phase Continuity

A summary of flow rates is presented in Table 4. PLS flow rates ranged from small plants of 266 m^3/hr to very large plants of 10,000 m^3/hr with most treating less than 2000 m^3/hr. The ratio of PLS to organic flow rates ranged from 0.2 to 4.2 with 70% of the plants between 0.75 and 3. The ratio of organic to electrolyte flow rates was between 0.6 and 47 with 2/3 of the plants between 2 and 10. The percentage of electrolyte flowing to solvent extraction was typically between 20% and 40%.

Table 4. Summary of Flow Rates

Category	Data Summary
PLS per train (m^3/hr)	Min. – 266, Median – 1200, Max. – 10000
Electrolyte per train (m^3/hr)	Min. – 7.5, Median – 327, Max. – 1249
% of electrolyte flow to SX	Min. – 1, Median – 25, Max. – 100
Organic from ext. to strip (m^3/hr)	Min. – 64, Median – 1055, Max. – 4000

The use of aqueous and organic phase continuity for each stage appears to be very plant specific. A summary of phase continuity by stage is given in Table 5. The most consensus way to operate appears to be aqueous continuous in first stage extraction especially for trains in series and organic continuous first stage stripping. Otherwise, the plants are most evenly split on phase continuity in second and third stage extraction, washing and second stage stripping.

Table 5. Summary of Phase Continuity

Stage	Data Summary
E1 (all)	Aqueous (76%), Organic (24%)
E1 (series)	Aqueous (87%), Organic (13%)
E1P (parallel)	Aqueous (50%), Organic (50%)
E2	Aqueous (52%), Organic (48%)
E3	Aqueous (50%), Organic (50%)
W	Aqueous (55%), Organic (45%)
S1	Aqueous (16%), Organic (84%)
S2	Aqueous (60%), Organic (40%)

Solution Compositions

Summaries of PLS, raffinate, organic and electrolyte compositions are presented in Tables 6-9, respectively. The median PLS composition is 2.75 g/L Cu, 2.6 g/L Fe (2.0 g/L Fe^{3+}), 2.5 g/L H_2SO_4, 0.65 g/L Mn at a pH of 2.0 with 20 ppm of suspended solids. There is a considerable range of values for every PLS variable except pH which only ranged from 1.3 to 2.15. The median raffinate composition is 0.2 g/L Cu, 7.2 g/L H_2SO_4 at a pH of 1.66 with an organic loss of 40 ppm. The median copper concentrations of the loaded organic and barren organic are 6.45 g/L and 2.1 g/L, respectively. While the

specific extractant is highly variable, all of the plants report using either LIX (Cognis) or Acorga (Cytec) extractant with more in this survey using LIX. Eight different suppliers of diluent were listed with the most common being Penerco and Shellsol. The median spent electrolyte sent to the solvent extraction trains is 34 g/L Cu, 184 g/L H_2SO_4 and 151 ppm Co. The median rich electrolyte returned to electrowinning is 48 g/L Cu, 165 g/L H_2SO_4 and some organic (many plants report ≤ 10 ppm).

Table 6. Summary of PLS Composition

Component (unit)	Data Summary
Cu^{2+} (g/L)	Min. – 0.24, Median – 2.75, Max. – 41
pH	Min. – 1.3, Median – 2.0, Max. – 2.15
Total Fe (g/L)	Min. – 0.06, Median – 2.6, Max. – 32.4
Fe^{3+} (g/L)	Min. – 0.12, Median – 2.0, Max. – 25.3
H_2SO_4 (g/L)	Min. – 0.69, Median – 2.5, Max. – 20
Mn (g/L)	Min. – 0.09, Median – 0.65, Max. – 3.4
Solids (ppm)	Min. – 1.5, Median – 20, Max. – 60

Table 7. Summary of Raffinate Composition

Component (unit)	Data Summary
Cu^{2+} (g/L)	Min. – 0.015, Median – 0.2, Max. – 11
pH	Min. – 0.7, Median – 1.66, Max. – 1.9
H_2SO_4 (g/L)	Min. – 1.75, Median – 7.2, Max. – 65
Organic loss to raffinate (ppm)	Min. – 20, Median – 40, Max. – 89

Table 8. Summary of Organic Composition

Component (unit)	Data Summary
Cu^{2+} (g/L) in Loaded Organic	Min. – 1.05, Median – 6.45, Max. – 20
Cu^{2+} (g/L) in Barren Organic	Min. – 0.25, Median – 2.1, Max. – 6.5
Extractant Family (% of Data)	LIX (74%), Acorga (26%)
Diluent Supplier (% of Data)	Penreco (30%), Shellsol (30%), 6 others (40%)

Table 9. Summary of Electrolyte Composition

Component (unit)	Data Summary
Spent Electrolyte	
Cu^{2+} (g/L)	Min. – 28, Median – 34, Max. – 43
H_2SO_4 (g/L)	Min. – 165, Median – 184, Max. – 195
Co (ppm)	Min. – 50, Median – 151, Max. – 200
Rich Electrolyte	
Cu^{2+} (g/L)	Min. – 37, Median – 48, Max. – 55
H_2SO_4 (g/L)	Min. – 140, Median – 165, Max. – 186
Organic Loss in Electrolyte	43% of plants ≤10 ppm

Operational Variables and Methods

Most process variables reported in the survey indicate a wide range of operating conditions utilized by the various plants as indicated in Table 10. The median values indicate perhaps what a "typical" plant would be, if one actually existed.

The most common operation methods were the use of interfacial pumping to remove crud and dual media filters for electrolyte treatment as show in Table 10. The majority of plants do not operate organic coalescers or organic filters.

Table 10. Summary of Operational Variables and Methods

Component (unit)	Data Summary
Extraction Efficiency (%)	Min. – 85.0, Median – 92.5, Max. – 95.6
Extraction Mixer Residence Time (min)	Min. – 1.6, Median – 2.5, Max. – 3.0
Organic Depth in Settler (mm)	Min. – 12, Median – 268, Max. – 500
Aqueous Depth in Settler (mm)	Min. – 24, Median – 498, Max. – 2140
Extractant in Organic Vol%	Min. – 3, Median – 15.4, Max. – 34
Net Cu Transference (Cu g/L per % Extractant)	Min. – 0.15, Median – 0.25, Max. – 0.36
Stripping Efficiency (%)	Min. – 34, Median – 69, Max. – 97.5
Stripping Mixer Residence Time (min)	Min. – 0.13, Median – 3, Max. – 4.8
Phase Disengagement Time	92% between 40-120 seconds
Organic Coalescers	Yes (32%), No (68%)
Organic Filters	Yes (40%), No (60%)
Crud Removal	Pump from Interface (74%)
Crud Treatment	Clay and Filter (41%)
Electrolyte Coalescer	Yes (44%), No (56%)
Electrolyte Treatment	Dual Media Filter (91%), Jameson Cell (28%)

Materials of Construction

Materials of construction for copper solvent extraction plants are becoming more standardized as shown in Table 11. A majority of plants use stainless steel for settlers, mixers (each as a liner or complete vessel), piping and tanks. High density polyethylene (HDPE) is also used extensively in piping. Gratings are typically fibre-reinforced plastic (FRP) or fibreglass.

Table 11. Summary of Materials Construction

Component (unit)	Most Common Material
Settlers	Stainless Steel (60%)
Mixers	Stainless Steel or Stainless Steel Liner (70%)
Piping	Stainless Steel (79%), HDPE (67%)
Tanks	Stainless Steel (71%)
Grating	FRP (50%), Fiberglass (32%)

PROCESS TECHNOLOGY TRENDS

Copper solvent extraction plant practices and design where reviewed in 2003 [4]. Recent process technology and design trends are:

- New and improved copper SX extractant reagents that do not transfer iron and in some cases are modified mixtures of aldoxime and ketoximes

- New and improved SX diluents that have higher flash points

- Conventional SX mixer settler design trends include:

    - SX Circuits that are now designed up front with pipe work for multiple configurations between series and series parallel and other combinations. The purpose of this is for operations flexibility.
    - Reverse flow mixer settlers
    - Deeper settlers
    - Advanced conventional mixer designs that reduce shear and small droplet generation
    - Advanced and multiple picket fence designs for enhanced settling
    - Advanced in-settler coalescer designs and installation for enhanced settling
    - Going more to stainless steel material of construction due to fire safety reasons
    - Separating SX trains for fire retardation purposes
    - Higher specific flows
    - CFD modelling of SX mixer and settling technology for further enhancement

- As yet no copper SX circuit has installed a multi-stage settler column(as used in uranium extraction) or

- No copper SX circuit has installed an in-line plug flow mixer settler such as proposed by Koch but Zinc SX is investigating this technology

GREENFIELD DEVELOPMENTS AND POSSIBLE FUTURE SX PROJECTS

Future copper SX projects are centered in Central Africa. In Africa, the projects are associated with cobalt (from tailings and ore), gold and concentrate (through pressure leaching) production. The major copper SX projects include:

*Tenke Fungurume, DRC
*Kolwesi Tailings, DRC
*Kinsevre, DRC
*Nikanor, DRC
*Chambishi, Zambia

CONCLUSIONS

It is clear from our latest 2007 copper SX survey that recent copper SX projects and expansions are implementing and the world's latest and best practice process technologies. These technologies include the latest mixer and settler designs and Copper SX circuits are being designed for enhanced operational flexibility.

ACKNOWLEDGMENTS

The authors would like to thank the plant personnel who kindly provided the data for the surveys. Without them this paper would have been impossible.

REFERENCES

1. J. Jenkins, W. G. Davenport, B. Kennedy, and T. Robinson, "Electroytic Copper - Leach, Solvent Extraction and Electrowinning World Operating Data, " Copper 99-Cobre 99, Volume 4, Hydrometallurgy of Copper, Young, S.K., Dreisinger, D.B., Hackl, R.P. and Dixon, D.G., Eds., The Minerals, Metals & Materials Society, Warrendale, PA, 1999, pp. 493-566.
2. T. Robinson, W. G. Davenport, and J. Jenkins, “Electrolytic Copper Electrowinning and Solvent Extraction World Operating Data,” ALTA 1997 Copper Hydrometallrugy Forum, Brisbane, Australia, 1997.
3. T. Robinson, W. G. Davenport, and J. Jenkins, “Electrolytic Copper Electrowinning and Solvent Extraction World Operating Data,” Randol Copper Hydromet Roundtable, Vancouver, BC Canada, 1997.
4. T. Robinson, S. Sandoval, and P. Cook, “World Copper Solvent Extraction Plants: Practices and Design”, *JOM*, **55**(7), 24-26 (2003).

COPPER SOLVENT EXTRACTION – 2007 WORLD OPERATING DATA

T. Robinson,1 M. Moats,2 W. Davenport,3 G. Karcas,4 S. Demetrio,5 and E. Domic6

	Port Pirie	Escondida oxide	Codelco Chile Salvador	Compania Minera Quebrada Blanca	Sociedad Contractuel Minera El Abra
status	2006 Data	2006 Data	2006 Data	2006 Data	2006 Survey
location	Port Pirie, SA, AUSTRALIA	Antofagasta-Chile	III Región Chile	Region I CHILE	Region II CHILE
contact person	Terry Deed	Ramon Robles T.	Enrique Molina Jara	Hector Yáñez, Plt. Sup	Percy Mayta
e-mail address		Ramon.o.robles@ bhpbilliton.com		hyanez@qblanca.cl	55-818676
phone number	08 86381758	56-55-203706 / 203701	52-474942	56-57-528-220	55-818675
fax number	08 86381568	56 55 248389		56-57-528-562	1996
date of commissioning					
longitude and latitude		3150 m.s.n.m.		Longitude W 68°47'53" Latitude S 21° 00' 50"	
PLANT DESCRIPTION					
cathode production rate, tonnes per year	5000	150000	25000	80000	225 000
number of solvent extraction trains	1	3	2	3	4
number of extraction mixer-settlers per train	2	2	2	2	3
series or parallel	series	series	series	series	serie-paralelo
number of strip mixer-settlers per train	2	1	1	1	1
series or parallel	series		series		series
washing of organic	1 mixer-settler wash with 35 to 40 gpl acid	yes	yes	no	yes
SETTLERS					
settler dimensions, length x width x depth	7.8 x 4.1 x 0.99	24,7 x 26,4 x 1,06 (Overall depth)	12,5 x 12,5 x 1,0 m	23.3 x 24.5 x 0.8	28 x 29 x 1.1
number of picket fences, per settler	1 + 5 up-&-over fences	1	2	2	2
settling velocity, m3/m2 per hour		3.8	3.9	4	3.7
EXTRACTION MIXERS					
principal extraction mixer	conventional	2 stage	2	Lightnin, R301 (37kW) & A310 (5kw), both normally used	1 pump mixer, 2 auxiliary
impeller diameter, m		261 m/minute tip speed	1.473	2.3 (six blades)	1.905
RPM			47	48RPM	55
power, kW				37kW	37
normal operation		all mixers in use	all mixers in use		pump mixer only
STRIPPING MIXERS					
principal strip mixer	conventional	1 stage x train	1	Lightnin R301 & A310, both normally used	1 pump mixer, 1 auxiliary
impeller diameter, m			1.473	2.3 (six blades)	1.905
RPM			47	48RPM	47
power, kW				37kW	37
normal operation			all mixers in use		pump mixer only

COPPER SOLVENT EXTRACTION – 2007 WORLD OPERATING DATA

T. Robinson,1 M. Moats,2 W. Davenport,3 G. Karcas,4 S. Demetrio,5 and E. Domic6

	Port Pirie	Escondida oxide	Codelco Chile Salvador	Compania Minera Quebrada Blanca	Sociedad Contractuel Minera El Abra
FLOW RATES					
pregnant leach solution per train, m3 per hour	320	1123	280	1200	1 200 - 1 450
electrolyte per train, m3 per hour	520	450	105	290	500-540
percent of total electrolyte flow going to SX				30	20
organic between extraction and strip per train, m3/h	1300	1250	340	1060	1 400 - 1 650
aqueous-continuous	all	E-1 series, E-1 parallel	no	E1	E-1, W
organic continuous		E-2, S-1	E-1,E-2, S, W	E2 and S	E-2,E-1P, S-1
PREGNANT LEACH SOLUTION (gpl)					
Cu	41	7	6	3	2.4-2.6
pH		1,6 to 1,8	1.8-2.0	1.9	2-2.1
FeT	0.06	2.5	8.86	1.3	2.9-3.1
Fe+3		0.5	6.94	0.3	2.6-2.8
H2SO4	20	3	3 - 5	2.5	2.7-2.9
Mn	0.1	0.45	3.3	0.09	0.6-0.7
Cl-, ppm	18gpl	0.25	2.55	30	1100
solids, ppm	silica (removed with Polyox coagulant)	10	< 30 ppm	20	8
RAFFINATE (gpl)					
Cu	11	0.5	0.6	0.3	0.17-0.18
H2SO4	65	12	10 a 12	6.7	6-7
pH		1.1	1.3	0.7	1.6
organic loss to raffinate, ppm		40		45	15-25
organic-from-raffinate recovery method		6 Wemco Pacesetters coalescers	post decantador - cinta oleofílica	Mop Wringers and pumping orgánic in surface of raffinate pond	Wemco Pacesetters coalescers Cintas recuperadoras
extraction efficiency per train, %		93 - 96	93	90	93
extraction mixer retention time, minutes		3	3	three mix stages, one minute each	2 - 3
ORGANIC					
Cu concentration in loaded organic, gpl	20	8.1	8.8	4.4	6.6
Cu concentration in barren organic, gpl		3.5	3.2	1.2	2
organic depth in settlers, mm		300	300	275	270 - 320
aqueous depth in settlers, mm		600	450	525	730 - 680
extractant name	LIX 860-1 / LIX984	Acorga M5640 HS	Lix 860 NIC- Lix 84 IC	LIX 984	LIX 84 IC+ LIX 612 NLV
solvent name	Shellsol	Shellsol 2046 AR	Scaid100	Orform SX 12	Shellsol 2046 AR
extractant concentration in organic, volume %	20	17	20	9.5	16.2-16.6
net copper transference, gpl per % extractant		0.24	0.25	0.27	0.27
stripping efficiency per train, %		70	63	70	68-70
strip mixer retention time, minutes		4.8	2	2 (2 mix stages, 1 min each)	3
phase disengagement time, seconds	<0.75	< 120	60 - 90	2	120 - 150
organic coalescer		none	yes	none	Wemco Pacesetters
organic filters	none	none	coalescer	no	yes

COPPER SOLVENT EXTRACTION – 2007 WORLD OPERATING DATA

T. Robinson,1 M. Moats,2 W. Davenport,3 G. Karcas,4 S. Demetrio,5 and E. Domic6

	Port Pirie	Escondida oxide	Codelco Chile Salvador	Compania Minera Quebrada Blanca	Sociedad Contractuel Minera El Abra
crud removal system	settler is taken offline and crud is physically drained	pump from interface	lavado de decantadores	batch diaphragm pumping	pneumatic pump
crud treatment system	none	none	ruptura mecánica	collection tank, centrifuge, solids storage	system with centrifuge
organic cleaning technique	bentonite clay treatment then filtering	Perrin Filter	filtro sparkler-TF1000	organic is mixed with clay then pressure filtered in Sparkler filter	Zeolita, clay treatment
SPENT ELECTROLYTE					
Cu, gpl	31	37-39	33	34	40-41
sulfuric acid, gpl	175	180	180	195	185-190
cobalt, ppm	80	160	140	135	180
RICH ELECTROLYTE					
Cu, gpl	46	50	45	45	54
sulfuric acid, gpl	140	170	160	180	170
organic loss in electrolyte, ppm	8	<10	5 - 10 ppm.	55	3-5
electrolyte coalescer				none	Wemco Pacesetters
electrolyte treatment before tankhouse	none	anthracite/garnet - Disep	Filtros chuqui o Demister	2 parallel column flotation cells followed by 4 garnet/anthracite filters	Spintek - sand, anthracite, garnet
DESIGN AND BUILDING MATERIALS					
mixers	mild steel, fiberglass lined	stainless steel	FRP	316L stainless steel	polymer concrete
settlers	mild steel, flake lined	stainless steel	FRP	concrete, HDPE lined	HDPE lined concrete
piping		HDPE/stainless steel	HDPE	316L and HDPE	HDPE
tanks		stainless steel	FRP	316L and FRP	HDPE lined concrete
gratings		FRP	FRP	FRP	FRP

COPPER SOLVENT EXTRACTION – 2007 WORLD OPERATING DATA

T. Robinson,1 M. Moats,2 W. Davenport,3 G. Karcas,4 S. Demetrio,5 and E. Domic6

	Xstrata Copper Lomas Bayas	Codelco Chile Gaby CHILE	Sociedad Minera Cerro Verde		Lane Xang Minerals	MICCL Myanmar
status	2006 data		2006 Data		2006 Data	2006 Data
location	Antofagasta-Chile	Region II (Calama) CHILE	Arequipa, Perú		Sapon, Laos PDR	Monywa, Myanmar
contact person	Miguel Monrroy		Javier Guevara		Brenden Weekes Tony Moore	Aung Law Ha
e-mail address	mmonroy@altonorte.xstratacopper.cl				bweekes@lxmlmine.com tmoore@lxmlmine.com	alha@miccl.com.mm
phone number	(56)055200600		51-54-381515-2200		61 8 6263 2109	0951-514194 to 7
fax number	(56)055229387					951-514208
date of commissioning			June 1977		38412	1998 October
longitude and latitude	Longitude S 23°25'51" Latitude O 69° 31' 1"					
			SX1	SX2		
PLANT DESCRIPTION						
cathode production rate, tonnes per year	64320	150000	90520		60000	39000
number of solvent extraction trains	1	2	4	1	1	1
number of extraction mixer-settlers per train	2 series / 1 parallel	2	3	2	3	2
series or parallel	serie/paralelo optimizado	series	series/parallel	series	Series	series 25 000tpa / series-parallel 39 000 tpa
number of strip mixer-settlers per train	2	2	2	2	2	1
series or parallel	serie	series	series/parallel	series	Series	see above comment
washing of organic	1 mixer-settler wash w/ 10 (verano)-18 (invierno) gpl acid	wash stage with slightly acidic water	no	no	yes	1 washing stage
SETTLERS						
settler dimensions, length x width x depth	26 x 18 x 1,1	26500x30000x1200	24 x 9.12 x 0.8	22 x 27 x 1.0	20.35 x 17.7 x 2.0	18 x 24.25 x 0.85
number of picket fences, per settler	1	2	2	2	4	1
settling velocity, m3/m2 per hour	4.8	5 / 4,2	3.4	4.9	4.7	5
EXTRACTION MIXERS						
principal extraction mixer	conventional		single Turbine	1 pump mixer + 2 impellers	3 stage, 1*DOP, 2*VSF Mixer	3 stages
impeller diameter, m	1.6	1.676	1.753		1.8	1.525 m
RPM	66	70 max.	47		50	69
power, kW	22.5		17.89		30-37	18.5
normal operation	yes		single turbine	1 pump mixer + 1 auxiliary impeller	all mixers in use	all mixers in use
STRIPPING MIXERS						
principal strip mixer	conventional		single turbine	1 pump mixer + 1 impellers	3 stage, 1*DOP, 2*VSF Mixer	3 stages
impeller diameter, m	1.6	1.676	1.753		1.8	1.525
RPM	63	70 max.	47		50	69
power, kW	22.5		17.89		30-37	18.5
normal operation	yes		single turbine	1 pump mixer + 1 auxiliary	Organic Continuous	

COPPER SOLVENT EXTRACTION – 2007 WORLD OPERATING DATA

T. Robinson,1 M. Moats,2 W. Davenport,3 G. Karcas,4 S. Demetrio,5 and E. Domic6

	Xstrata Copper Lomas Bayas	Codelco Chile Gaby CHILE	Sociedad Minera Cerro Verde		Lane Xang Minerals	MICCL Myanmar
FLOW RATES						
pregnant leach solution per train, m3 per hour	1150 E1-E3 // 1150 E2	1500 / 1750	750	1690	600	1150
electrolyte per train, m3 per hour	720	613 / 740	125	330	570	260
percent of total electrolyte flow going to SX			100	100	1	23
organic between extraction and strip per train, m3/h	1100		480	1350	1000-1100	1000
aqueous-continuous	E1, E2, E3, S2, W		E-1, R-1	E-1 S-1	Nil	Stripping and scrubbing
organic continuous	S1		E-2, EP1	E-2, S-1	ALL	Extraction stage E1 & E2
PREGNANT LEACH SOLUTION (gpl)						
Cu	4.07	6.6	2.80	2.80	14-17	5
pH	2.12	1.3	1.9 - 2.0	1.9 - 2.1	1.8-2.5	1.4
FeT	1.48	9.3	5.50	5.50	30 to 35	1.1
Fe+3	0.42	8.3	0.60	0.60	10 to 15	25.3
H2SO4	0.69	6.6	3.60	3.60	8 to 16	7
Mn	3.41	0.31	0.50	0.50	2	650 ppm
Cl-, ppm	10.6	2500	0.309	0.309		1500 ppm
solids, ppm	<5	20	40	40	40 to 80ppm	30
RAFFINATE (gpl)						
Cu	0.65	0.65	0.38	0.2	0.6-1.5	1.2
H2SO4	6	15.6	8.4	8.4	30-35	13
pH	1.26		1.54	1.54		1.3
organic loss to raffinate, ppm	30	<30			20-30	50
organic-from-raffinate recovery method	cinta oleofilica		poly mop	poly mop	Nil, recover from pond and clay treat.	skimming and pumping
extraction efficiency per train, %	85	93	92.3	95.6	0.93	95
extraction mixer retention time, minutes	2	3	2.0	1.7	3	3
ORGANIC						
Cu concentration in loaded organic, gpl	8.3	11.9	5.8	5.8	13 to 16	6.3
Cu concentration in barren organic, gpl	1	5.7	2.1	2.1	5 to 8	2.7
organic depth in settlers, mm	30		400	500	350	250
aqueous depth in settlers, mm	60		400	500	1650	600
extractant name	Lix 84-IC		Lix 984 NC	Lix 984 NC	Lix 974NLVS	LIX 946
solvent name	Shellsol 2046AR		Kerosene	Kerosene	Shellsol 2046TH	Shellsol 2046
extractant concentration in organic, volume %	21	24	15	13	32-36	15
net copper transference, gpl per % extractant	0.36		0.30	0.30	0.22-0.25	0.23
stripping efficiency per train, %	84	37.5	95	92		95
strip mixer retention time, minutes	1.65	3	2.1	2.3	3	3
phase disengagement time, seconds			45	45	60-80	50
organic coalescer	none		no	no	none	yes in all settlers
organic filters	none		Press Filter		none	one

COPPER SOLVENT EXTRACTION – 2007 WORLD OPERATING DATA

T. Robinson,1 M. Moats,2 W. Davenport,3 G. Karcas,4 S. Demetrio,5 and E. Domic6

	Xstrata Copper Lomas Bayas	Codelco Chile Gaby CHILE	Sociedad Minera Cerro Verde		Lane Xang Minerals	MICCL Myanmar
crud removal system	pump from interface		pumped daily from interphase	pumped daily from interphase	pump from interface	pumping
crud treatment system	ruptura mecánica		Drum Vacuum Filter (use diatomite		plate and frame filter press	clay treatment and filtration
organic cleaning technique	Zeolita, clay treatment		Plates Press Filter		Engelhard clay treatment	clay treatment and filtration
SPENT ELECTROLYTE						
Cu, gpl	43	35	40	40	33-36	35-42
sulfuric acid, gpl	182	180	170	170	180-190	180
cobalt, ppm	195	120	200	200	200	150
RICH ELECTROLYTE						
Cu, gpl	53	50	55	55	49-53	45-50
sulfuric acid, gpl	165	157	146	146	165	150
organic loss in electrolyte, ppm	13	<30	<50	< 50	<15	<10
electrolyte coalescer	none		no	no	None	
electrolyte treatment before tankhouse	2 column flotation, 4 filters Spintek		6 Disep filters (316L stainless steel) and one backwash		Spintek Duel media filter	Multimedia filter (anthracite/garnet)
DESIGN AND BUILDING MATERIALS						
mixers	steel	FRP	316 stainless Steel	316 stainless Steel	Stainless steel	904 L stainless steel
settlers	concrete, HDPE lined	HDPE lined concrete	316 stainless Steel	concrete, HDPE lined	Stainless steel	HDPE lined concrete and FRP lined concrete
piping	HDPE	HDPE	316 stainless Steel & polietilene	316 stainless Steel	Stainless steel/HDPE	HDPE
tanks	FRP	HDPE lined concrete	316 stainless Steel	concrete, HDPE lined	Stainless steel lined concrete	HDPE lined concrete
gratings	FRP		iron & fiberglass	iron & fiberglass	FRP	Wood

COPPER SOLVENT EXTRACTION – 2007 WORLD OPERATING DATA

T. Robinson,1 M. Moats,2 W. Davenport,3 G. Karcas,4 S. Demetrio,5 and E. Domic6

	BHP Billiton Pinto Valley	Phelps Dodge Miami Mining Corp	Phelps Dodge Morenci Central SX Plant	Phelps Dodge Morenci Metcalf SX Plant	Phelps Dodge Morenci Modoc SX Plant
status	2006 Data	2006 Survey	2006 Data	2006 Data	2006 Data
location	Miami AZ USA	Miami AZ USA	Morenci, AZ, USA	Morenci, AZ, USA	Morenci, AZ, USA
contact person	Paul Thomas	Troy Pool	Ochirbal Boolokhuu	Jackie Leaf	Jarred Larson
e-mail address		1 928 473 7086	928 865 6535	928 865 6526	928 865 6737
phone number	1 928 473 6427	1 928 473 7248	928 865 2234	928 865 2234	928 865 2234
fax number	1 928 473 6437		1987	1987	1991
date of commissioning	1981				
longitude and latitude					
PLANT DESCRIPTION					
cathode production rate, tonnes per year	3 500	8 620	39400	129209	113800
number of solvent extraction trains	2	2	1	2	2
number of extraction mixer-settlers per train	2	3	3	2	3
series or parallel	series	series/parallel	1EP + 2E + 1S	both modified series/parallel: A - 2E + 1W + 1S, B - 2E + 1S	1 x 2
number of strip mixer-settlers per train	1	1	1	1	1
series or parallel		series			
washing of organic	no	no	no	Wash Stage on A train	Wash Stage
SETTLERS					
settler dimensions, length x width x depth	12 x 20.7 x 9.9	82 X 65 X 3	21 x 25 x 1	21 x 25 x 1 (S1A) 20.42 x 25 x 1 (all others)	21 x 25 x 1
number of picket fences, per settler	1 stationary, 3 portable	3	(2 EP, 2 E2, 2 E1,) (2 S1)	4 in E1B, all 2 on S1A, S1B and W1A, 3 all others	(3 EP, E1, E2G, W1), (2 S1), (4 E2F)
settling velocity, m3/m2 per hour	7.9	1.95	6.576 on CP, 6.32 on E1&2, 3.02 on S1.	E1=6.79, E2=7.1, W1A=4.24, S1=3.61	EP - 6.4; E1S - 7.22; E2S - 8.0
EXTRACTION MIXERS					
principal extraction mixer	Philadelphia Terro 16 plus auxiliary mixers (used only in warm weather)	2 stage	Lightnin straight-vaned pump impellers (on series), Philadelphia Mixers curve vaned impellers (on parallels).	Lightnin straight-vaned pump impellers (series)	Lightnin straight-vaned pump impellers (series), Philadelphia Mixers curve vaned impellers (parallels).
impeller diameter, m	2.1	260 m/minute tip speed	2.18	2.18	2.18
RPM	42	1800	51	51	51
power, kW	19		40	17.6	E1S, E2S, & W1 - 45; E1P & S1 - 15
normal operation		primaries	All mixers usually in use.	All Primaries; Typically no Aux. run for E1 or E2; No Aux typically run for W1A; Aux 1 & Aux 2 for S1A, Aux 1 for S1B (No Aux 2 in place)	all Primaries, Aux just on parallels,
STRIPPING MIXERS					
principal strip mixer	Philadelphia Terro 16 plus auxiliary mixers		Lightnin straight-vaned pump impellers (series), Philadelphia Mixers curve vaned impellers (parallels).	A Train - Double impeller: Lightnin straight-vaned and additional curved blade above. B Train - Lighnin straight-vaned pump impellers	Double impeller: Lightnin straight-vaned impellers and additional curved blade above
impeller diameter, m	2.1	260 m/minute tip speed	2.18	A: 1.22/B: 2.18	1.22
RPM	42		51RPM	A: 51RPM/B: 51RPM	51RPM
power, kW	19		40	A: 15/B: 40	15
normal operation		primaries	All mixers are used.	all mixers run	all mixers run maxed

COPPER SOLVENT EXTRACTION – 2007 WORLD OPERATING DATA

T. Robinson,1 M. Moats,2 W. Davenport,3 G. Karcas,4 S. Demetrio,5 and E. Domic6

	BHP Billiton Pinto Valley	Phelps Dodge Miami Mining Corp	Phelps Dodge Morenci Central SX Plant	Phelps Dodge Morenci Metcalf SX Plant	Phelps Dodge Morenci Modoc SX Plant
FLOW RATES					
pregnant leach solution per train, m3 per hour	547	10000	4233	3861	4200
electrolyte per train, m3 per hour	27	850	468	418	647
percent of total electrolyte flow going to SX	8	100	13	22	34.3
organic between extraction and strip per train, m3/h	770	4000	1035	1421	1680
aqueous-continuous	E1, E2	E-1-E2 series, E-1-E-2 parallel	E1,E2,EP	E1S, E2S	E1, E2
organic continuous	S	S-1	S1	W1, S1	W1, S1, EP
PREGNANT LEACH SOLUTION (gpl)					
Cu	0.35	0.24	1.21	1.47	1.53
pH	2.1	2	1.92	2	1.97
FeT	1.8	0.10	2.67	2.31	0.31
Fe+3	1.7	0.32	2.61	2.28	1.98
H2SO4	0.9	1.6	2.57	2.31	2.26
Mn			0.77	0.82	0.81
Cl-, ppm			NA	NA	NA
solids, ppm		2	NA	NA	5 - 30
RAFFINATE (gpl)					
Cu	0.03	0.015	0.14	0.15	0.09
H2SO4	2.6	2	4.36	4.92	4.47
pH	1.7	1.9	1.72	1.66	1.66
organic loss to raffinate, ppm	50	89	39	36	50
organic-from-raffinate recovery method	Skimmers on raffinate pond	6 Wemco Pacesetters coalescers and ALPHA skimmer	floated in one organic recovery tank; also 3 belt mops used on raff pond.	skimmed from organic recovery tanks; also use organic containment booms and 3 rope mop skimmers	skimmed from organic recovery tanks and use organic absorbant rope mops on the raff pond
extraction efficiency per train, %	90	92	90	A: 92.3% B:90%	95
extraction mixer retention time, minutes	3	2.3	1.98	1.93	1.6
ORGANIC					
Cu concentration in loaded organic, gpl	1.1 to 1.3	1.05	7.03	8.73	7.74
Cu concentration in barren organic, gpl	0.2 to 0.3	0.6	2.59	4.56	3.67
organic depth in settlers, mm	127 to 203	12	262	283	268
aqueous depth in settlers, mm	380	24	500.1	479	494
extractant name	LIX 984N	Cytec/Acorga m5850	LIX 616N-LV	LIX 616N-LV	LIX 616N-LV
solvent name	Phillips SX-12	Penreco 170es	Penreco 170ES	Penreco 170ES	Penreco 170ES
extractant concentration in organic, volume %	3	3	13.7	18.5	15.4
net copper transference, gpl per % extractant	0.17	0.147	0.327	0.225	0.24
stripping efficiency per train, %	96 to 99	93	63.2	47.8	55
strip mixer retention time, minutes	3	2.1	2.55	3.51	2.07
phase disengagement time, seconds	<1	70-80	44-93 on Extractors, 50 - 135 on Stripper	E1 & E2:60-100 S1: 45-70	50-90
organic coalescer	none	6	none	none	PVC Grid Packing in the E2s and EPs
organic filters	none	none	Filter Press	Pacific Press-Filter Press	Filter Press

COPPER SOLVENT EXTRACTION – 2007 WORLD OPERATING DATA

T. Robinson,1 M. Moats,2 W. Davenport,3 G. Karcas,4 S. Demetrio,5 and E. Domic6

	BHP Billiton Pinto Valley	Phelps Dodge Miami Mining Corp	Phelps Dodge Morenci Central SX Plant	Phelps Dodge Morenci Metcalf SX Plant	Phelps Dodge Morenci Modoc SX Plant
crud removal system	external pumping (also set up for flooding from settlers, not now done)	pump from interface	Interface pumping	interface pumping	interface pumping on the strippers
crud treatment system	Cone Tank	none	Mix with DE and Clay filter through filter press until Phase Break is 75 sec or less.	Mix with DE and/or Clay, filter through filter press (until phase break is 75 sec or less for recovered organic).	Mix with DE and/or Clay, filter through filter press (until phase break is 60 sec or less for recovered organic).
organic cleaning technique	Clay Filter	none	Clay treatment & Filter press	Clay treatment & Filter press	Clay treatment & Filter press
SPENT ELECTROLYTE					
Cu, gpl	32	30	32.29	32.5	32
sulfuric acid, gpl	190	165	193.08	190	195
cobalt, ppm	50	150	160	162	154
RICH ELECTROLYTE					
Cu, gpl	44 to 48	37	41.4	46.9	43.3
sulfuric acid, gpl	170	165	177	167.7	179.2
organic loss in electrolyte, ppm	50	<10	NA	36	50
electrolyte coalescer	none		1 coalesing tank and organic is skimmed off from the top of the tank	none	organic is skimmed from rich booster tank
electrolyte treatment before tankhouse	dual media filter, garnet and anthracite	anthracite/garnet - Disep	1 Jameson cell and (4) 12, (3)-13 ft diameter Dicep Sand/Garnet/Anthracite filters	Jameson cell and Dicep sand/anthracite/garnet filters, and tank skimming	Jameson cell and Dicep sand/anthracite/garnet filters
DESIGN AND BUILDING MATERIALS					
mixers	concrete, lined with 316L stainless steel	stainless steel	concrete with 12 gauge 316L stainless steel liner	extractors and wash stages - concrete with 12 gauge 316L stainless steel liner, strippers- 316L stainless steel	extractors and wash stages - concrete with 12 gauge 316L stainless steel liner, strippers- 316L stainless steel
settlers	concrete, lined with 316L stainless steel	stainless steel	316L stainless steel	316L stainless steel	316L stainless steel
piping	316L stainless steel	HDPE/stainless steel	316L stainless steel	316L stainless steel	316L stainless steel
tanks	316L stainless steel	stainless steel	316L stainless steel	316L stainless steel	316L stainless steel
gratings	fiberglass	FRP	Dur-A-Deck fiberglass	Sea Fab fiberglass	Dur-A-Deck fiberglass

COPPER SOLVENT EXTRACTION – 2007 WORLD OPERATING DATA

T. Robinson,1 M. Moats,2 W. Davenport,3 G. Karcas,4 S. Demetrio,5 and E. Domic6

	Phelps Dodge Morenci Stargo SX Plant	Phelps Dodge Sierrita		Burro Chief Copper Co Phelps Dodge Chino Mines Co.	Phelps Dodge Tyrone
status	2006 Data	2006 Data	2006 Data	2006 Data	2006 Survey
location	Morenci, AZ, USA	Green Valley AZ USA	Green Valley AZ USA	Santa Rita NM USA	Tyrone NM USA
contact person	Melissa Thumberg	Tim Fisher	Tim Fisher		Philippa Killian
e-mail address	928 865 6077	1 502 648 8872	1 502 648 8872	505 537 4283	1 505 538 7236
phone number	928 865 2234	1 520 648 8685	1 520 648 8685	505 537 2645	1 505 537 8059
fax number	1998	1978, moved 1987	1974, moved 1994	July 1988 (Mine 1912)	1984
date of commissioning					
longitude and latitude					
PLANT DESCRIPTION					
cathode production rate, tonnes per year	125372	7700		66200	28960
number of solvent extraction trains	1	5	1	2	2
number of extraction mixer-settlers per train	3	3	2	2	2
series or parallel	1 x 2	parallel		series	series/parallel
number of strip mixer-settlers per train	1	1		1	1
series or parallel		-		series	series
washing of organic	Wash stage	wash stage with water @ pH 1.2			no
		SX 1	SX 2		
SETTLERS					
settler dimensions, length x width x depth	31.7 x 28.7 x 1.25	13.5 x 3.7 x 0.9	34.5 x 13.8 x 1.08	23 x 25 x 1.0	28.7x20.4x1
number of picket fences, per settler	2	1	2	1 S, 2E1, 3 E2 with media	2
settling velocity, m3/m2 per hour	3.31 on EH1, EH2, EHP and 3.62 on S1H	3.7	3.7	143	104 in Ext, 42 in Strip
EXTRACTION MIXERS					
principal extraction mixer	Outokumpu Spirok mixer and DOP pump mixers	Lightnin	Davy	Lightnin R320 D	Lightnin straight-vaned pump impellers
impeller diameter, m	2.9	1.37	2.72	2.2	2.173.26
RPM	40	46	36.4	50 - 60	46
power, kW	37	10	134	18	30
normal operation	All mixers normally are in use.	all mixers in use - single stage		pump mixer only - aux mixers on/off depending on phase stability	primaries
STRIPPING MIXERS					
principal strip mixer	Outokumpu Spirok mixer and DOP pump mixers	Lightnin	Davy	Lightnin R320 D	Lightnin straight-vaned pump impellers
impeller diameter, m	2.9	1.52	2.72	2.1	2.173.26
RPM	40	46	36.4	50 - 60	
power, kW	37	10	134	18	
normal operation	All mixers used.	all mixers in use - single stage		pump mixer only	primaries

COPPER SOLVENT EXTRACTION – 2007 WORLD OPERATING DATA

T. Robinson,1 M. Moats,2 W. Davenport,3 G. Karcas,4 S. Demetrio,5 and E. Domic6

	Phelps Dodge Morenci Stargo SX Plant	Phelps Dodge Sierrita		Burro Chief Copper Co Phelps Dodge Chino Mines Co.	Phelps Dodge Tyrone
FLOW RATES					
pregnant leach solution per train, m3 per hour	6041	266	1660	1 987	3179
electrolyte per train, m3 per hour	1249	7.5	37.2	273	317
percent of total electrolyte flow going to SX	10.86			25	21
organic between extraction and strip per train, m3/h	2043	64	532	1 408	794
aqueous-continuous	E1, E2, EP	E1, wash	E1, E2, wash	E1, E2	E-1-E2 series, parallel
organic continuous	S1, W1	E2, strip	strip	strip	S-0
PREGNANT LEACH SOLUTION (gpl)					
Cu	2.7	0.4		1.2 - 1.5	0.59
pH	1.9	2		2.1	2.14
FeT	3.1	0.2		7	2.69
Fe+3	0.12	0.2		3.2	2.22
H2SO4	2.6	1		1.4	1.06
Mn	0.547	trace		1.3	1.61
Cl-, ppm	NA	3.4 gpl		100 - 200	0.029
solids, ppm	NA	4.5		5 - 50	NA
RAFFINATE (gpl)					
Cu	0.2	0.02		0.10 - 0.12	0.06
H2SO4	7.2	2		8	2.8
pH	1.37	1.75		1.6 - 1.8	1.85
organic loss to raffinate, ppm	40	47		35 - 50	39.9
organic-from-raffinate recovery method	Skimming of Organic Recovery Tank, Hydrocyclones	mop-wringer from raffinate pond			Skimmer on Raffinate tank(Jamesons also -but shut down)
extraction efficiency per train, %	94	93		90 - 95	90-95
extraction mixer retention time, minutes	2.5	2		2	2
ORGANIC					
Cu concentration in loaded organic, gpl	11.2	3.5	4.1	3.6	3.6
Cu concentration in barren organic, gpl	4.1	2.1	2.75	1.5	1.4
organic depth in settlers, mm	355	190	190	250	267
aqueous depth in settlers, mm	610	710	890	450	495
extractant name	LIX 616	Cytec 5774		Acora M5640	Cytec/Acorga m5774
solvent name	Penrico 170ES	Penreco 170 ES		Conosol 170	Penreco 170es
extractant concentration in organic, volume %	28	6		10 - 11 (by weight)	6.95
net copper transference, gpl per % extractant	0.3	0.23		0.25 - 0.30	0.32
stripping efficiency per train, %	63	40	34		96-99
strip mixer retention time, minutes	0.125	3		<2	3
phase disengagement time, seconds	70-90	90 - 120		E1/E2 90 - 120, S1 15	E1/E2/PS 75-110; S1 90-130
organic coalescer	none	none			Eimco pacesetter coalescers
organic filters	Filter Press	filter press for reclaimed organic and crud processing			Pacific Press-Filter Press

COPPER SOLVENT EXTRACTION – 2007 WORLD OPERATING DATA

T. Robinson,1 M. Moats,2 W. Davenport,3 G. Karcas,4 S. Demetrio,5 and E. Domic6

	Phelps Dodge Morenci Stargo SX Plant	Phelps Dodge Sierrita		Burro Chief Copper Co Phelps Dodge Chino Mines Co.	Phelps Dodge Tyrone
crud removal system	Interface pumping.	scheduled shutdowns & cleanout		pneumatic pump from interface	Interface pumping
crud treatment system	Mix with DE and/or Clay, filter through filter press (until phase break is 75 sec or less for recovered organic).	clay treatment and filtration		filter press	Mix with DE and/or Clay, filter through filter press
organic cleaning technique	Clay treatment & Filter press	clay treatment and filtration			clay treatment
SPENT ELECTROLYTE					
Cu, gpl	31-33	30		34	34
sulfuric acid, gpl	193-197	180		185	192
cobalt, ppm	150-160	55		140	0.134
RICH ELECTROLYTE					
Cu, gpl	44.9	50		45 - 50	40
sulfuric acid, gpl	172	160		150 - 160	186
organic loss in electrolyte, ppm	10	~5		not determined	<10
electrolyte coalescer	Coalescing media in the Filter Feed Tank.	6,400 cu. m. surge tank			None
electrolyte treatment before tankhouse	Sand/Garnet/Anthracite Dicep filters	Natco stainless steel dual media filter		4 Disep garnet/anthracite filters	anthracite - Disep
DESIGN AND BUILDING MATERIALS		SX 1	SX 2		
mixers	316L stainless steel	FRP	316 stainless steel	316SS	stainless steel
settlers	316L stainless steel	FRP	316 stainless steel	316 stainless steel	stainless steel
piping	316L stainless steel	FRP/SS/HDPE	FRP/SS/HDPE	316 stainless steel	HDPE/stainless steel
tanks	316L stainless steel	FRP/SS/lined steel	FRP/SS/lined steel	316SS/FRP	stainless steel
gratings	Dur-A-Deck fiberglass	steel	steel	FRP	FRP

COPPER SOLVENT EXTRACTION – 2007 WORLD OPERATING DATA

T. Robinson,1 M. Moats,2 W. Davenport,3 G. Karcas,4 S. Demetrio,5 and E. Domic6

	Phelps Dodge Safford Project	Mineral Park	Silver Bell Mining L.L.C.	Bwana Mkubwa EW Lonshi Expansion
status		2006 Data	2006 Data	2006 Data
location	Safford AZ, USA	Kingman, AZ, USA	Marana AZ USA	Ndola, Zambia
contact person		Cesar Romero	Damon Fisbeck	Anthony Mukutuma
e-mail address		cromero@mineralparkinc.com		anthony.mukutuma@fqml.com
phone number		(928) 565-2226	2 520 682 2420	260 02 655 121
fax number		(928) 565-9239	2 520 682 2347	260 02 655 399
date of commissioning	2008	11/6/2006	July 1997	Jun-05
longitude and latitude				
PLANT DESCRIPTION				
cathode production rate, tonnes per year	109000	7000	21410.62091	51 000
number of solvent extraction trains	1	1	2	2 (split circuit)
number of extraction mixer-settlers per train	3	3	2	3
series or parallel	series/parallel	parallell	series	Both series parallel
number of strip mixer-settlers per train	1	1	1	1
series or parallel			series	series
washing of organic		none	none	none
SETTLERS				
settler dimensions, length x width x depth		19.8x10.5x2.1	23 x 20 x 1.2	10.7 x 17.25 x 1.2
number of picket fences, per settler	3	1	2	2
settling velocity, m3/m2 per hour	5.99	2.5	4.4	4.9
EXTRACTION MIXERS				
principal extraction mixer	shrouded curved vane axial flow turbine for up pumping	3 stage	pump mixer Lightnin R-320	Mixtec pump mixers
impeller diameter, m		1.98	1.27	1.38
RPM		48	80 - 84 (VFD)	69
power, kW			15	11
normal operation		secondary mixer off	all mixers in use	all mixers in use
STRIPPING MIXERS				
principal strip mixer	shrouded curved vane axial flow turbine for up pumping	1 stage	pump mixer Lightnin R-320	pump mixers
impeller diameter, m		1.98	1.27	1.38
RPM		50	80 - 84 (VFD)	69
power, kW			15	11
normal operation		seconday miser off	pump mixer only	

COPPER SOLVENT EXTRACTION – 2007 WORLD OPERATING DATA

T. Robinson,1 M. Moats,2 W. Davenport,3 G. Karcas,4 S. Demetrio,5 and E. Domic6

	Phelps Dodge Safford Project	Mineral Park	Silver Bell Mining L.L.C.	Bwana Mkubwa EW Lonshi Expansion
FLOW RATES				
pregnant leach solution per train, m3 per hour	450	1000	795 - 1000	700-750
electrolyte per train, m3 per hour		327	114	300/180
percent of total electrolyte flow going to SX		40 m3/hr	26	32
organic between extraction and strip per train, m3/h		410	875 - 1000	550/650
aqueous-continuous	E1	E-1, E-2, E-3	E1 stage	non
organic continuous	E2, EP, S1	S-1	E2 and stripping stages	all
PREGNANT LEACH SOLUTION (gpl)				
Cu	5.2 max	0.8-1.2	1.4	8 & 13
pH	2	2.0-2.1	2	2.00
FeT	3 g/L max	0.9-1.6	5	
Fe+3		0.7-1.3	4	
H2SO4		0.75-2.0	2	0.1 - 5
Mn			0.46	0.3 - 0.8
Cl-, ppm	< 25ppm	none	125	
solids, ppm	suspended solids 50 ppm	5-20	2 - 3 TSS	30 - 60
RAFFINATE (gpl)				
Cu	0.5	0.06-0.15	0.13	<0.6/<1.5
H2SO4	5 to 10	1.5-2.5	2	11 and 17
pH		1.6-1.9	1.8	<1.2
organic loss to raffinate, ppm	33	25-50	20	
organic-from-raffinate recovery method		skimmers	Eimco Pacesetters coalescers	Skimmers on raffinate pond
extraction efficiency per train, %		86.0-91.0	90 - 94	
extraction mixer retention time, minutes		3	3	2.5 - 3
ORGANIC				
Cu concentration in loaded organic, gpl	0 - 14	2.6-3.1	2.0 - 2.20	11.4
Cu concentration in barren organic, gpl		0.9-1.2	0.7 - 0.8	5.6
organic depth in settlers, mm		200	300	
aqueous depth in settlers, mm		2140	450	200 - 380
extractant name	LIX 612N-LV or LIX 984N-C	Cytec Acorga M5774	LIX 984N	LIX 984NC
solvent name	Orform SX80	Conoco 170	Phillips SX-7	Shellsol 2325
extractant concentration in organic, volume %	30	5.5-6.7	5	28/25
net copper transference, gpl per % extractant		0.25	0.26 - 0.30	0.2 - 0.26
stripping efficiency per train, %		95	65	65 - 68
strip mixer retention time, minutes		3	2	3
phase disengagement time, seconds		60-110	50	90 (O.C)
organic coalescer		none	loaded organic tank bottom baffled with raised pump suction	1st Loaded Organic Tank packed with 2 & 4inch ID coalescer rings
organic filters		none	none	none

COPPER SOLVENT EXTRACTION – 2007 WORLD OPERATING DATA

T. Robinson,1 M. Moats,2 W. Davenport,3 G. Karcas,4 S. Demetrio,5 and E. Domic6

	Phelps Dodge Safford Project	Mineral Park	Silver Bell Mining L.L.C.	Bwana Mkubwa EW Lonshi Expansion
crud removal system	pump from interface	pump from interface	pneumatic pump from interface	online pumping of surface and interface crud with peristatic pumps.
crud treatment system	diatomaceous earth pretreat follwed by filter press or drum	filter press	centrifuge	Flottweg Tricanter
organic cleaning technique		clay treatment	clay treated and filtered	clay treatment
SPENT ELECTROLYTE				
Cu, gpl	38	26-30	36.4	37 -38
sulfuric acid, gpl	180	180-184	190	185 - 190
cobalt, ppm	120	80-120	152 mg/l	180
RICH ELECTROLYTE				
Cu, gpl	48	46-50	48.5	49 - 50
sulfuric acid, gpl	165	160-167	175	178
organic loss in electrolyte, ppm	0.039 g/L	5-10	not determined	
electrolyte coalescer		none	2 Magma design column cells	electrolyte after-settler
electrolyte treatment before tankhouse	multimedia filter	sparkler filters	3 Disep dual media downflow pressure filters	Jameson cell
DESIGN AND BUILDING MATERIALS				
mixers		FRP	316 stainless steel	FRP being replaced with stainless steel
settlers	316L SS	FRP & HDPE	316 stainless steel	stainless steel
piping	316L SS or HDPE	FRP, HDPE, stainless steel	HDPE/stainless steel	HDPE/stainless
tanks	316L SS	FRP	316 stainless steel	316 stainless steel
gratings		FRP	steel and FRP	stainless steel

The Most Innovative Mines Use Cytec Reagents

For nearly a century, some of mining's greatest discoveries have taken place above ground, not below it. Cytec specialty reagents such as MAX HT® (sodalite scale control for alumina refining), MAXGOLD™ (collector blends for gold and PGM containing ores) and ACORGA OPT (novel solvent extraction blends for copper), pioneered by Cytec laboratories, have led the way. Cytec research scientists on three continents continue to develop imaginative solutions to address today's operational challenges. With the mining chemical industry's highest investment in R&D, the future has never looked brighter.

CYTEC

Alumina Refining | Mineral Processing | Solvent Extraction

Email: custinfo@cytec.com | Worldwide Contact info: www.cytec.com | US Toll Free: 800-652-6013 | Tel: 973-357-3193

©2008 Cytec Industries Inc. All Rights Reserved.

CYT8170inn.indd 1 4/8/08 2:25:14 PM

The Most Profitable Mines Use Cytec Reagents

For nearly a century, Cytec specialty reagents have been at the forefront of technologies designed to optimize recoveries under the most challenging conditions. Our experienced team of metallurgists and engineers will work with you to develop process applications tailored to your unique needs and operational objectives, your ore types and your plant conditions. Our goal is to help you achieve the highest levels of recovery – resulting in maximum yields and greater returns. As the world's largest supplier of specialty mining reagents, Cytec has the global reach to help you succeed, wherever your search for profitability takes you.

CYTEC

Alumina Refining | Mineral Processing | Solvent Extraction

Email: custinfo@cytec.com | Worldwide Contact info: www.cytec.com | US Toll Free: 800-652-6013 | Tel: 973-357-3193

©2008 Cytec Industries Inc. All Rights Reserved.

FREEPORT-McMoRan COPPER & GOLD

A World of Commitments

Working Toward Sustainable Development

FREEPORT-McMoRan COPPER & GOLD INC.

2007 Working Toward Sustainable Development Report

To Our Stakeholders

Freeport-McMoRan Copper & Gold Inc.'s acquisition of Phelps Dodge Corporation combined two companies with strong core values concerning environmental protection and mitigation and the support of local communities where we operate.

The new Freeport-McMoRan Copper & Gold Inc. – created by our acquisition in March 2007 of Phelps Dodge Corporation – is the world's largest publicly traded copper company. We now have major mining operations in North America, South America and Indonesia, and a development project in Africa. We also have significant, geographically diverse reserves and development projects. This is reflected in our 2007 Freeport-McMoRan Copper & Gold Inc. Annual Report, titled "A World of Assets/A World of Opportunities."

We recognize that success in our global operations and development projects is dependent on attaining a "social license" – our ability to earn and maintain the goodwill of local communities wherever we operate. To accomplish this, we engage with local communities to identify their needs and concerns and commit to programs to help address them. Some of these commitments are site-specific, while others are global. For that reason, we have titled this report, "A World of Commitments."

The world needs the metals we produce to sustain and expand economies and to build infrastructure in developing nations. Fulfilling this need for our products must be balanced with the social and environmental concerns of the local communities so that, in meeting the needs of the current generation, we do not compromise the ability of future generations to meet their own needs. This is the core concept of "sustainable development" and the underlying premise of our commitments.

We are dedicated to working toward sustainable development by mitigating our environmental impacts and providing beneficial economic and social results wherever we operate. We realize that sustainable development is particularly challenging for the mining industry because mining operations have significant environmental and social impacts and are focused on a finite resource at each location that will eventually be depleted, although in some cases this would be in the distant future. We embrace sustainable development as our duty as a responsible corporate citizen and because we consider it a prudent business practice.

We have in place Environmental and Social, Employment & Human Rights policies. We have updated and broadened our Principles of Business Conduct – a system of shared values and consistent principles that guides our management and employees in the conduct of our business. We are taking steps to ensure that our commitments detailed in these policies are fully implemented throughout our worldwide operations. As part of the integration of the two companies, we have set in motion a management review of our sustainable development programs and performance to identify an effective management structure to fulfill our commitments.

The integration of our combined companies provides the opportunity to draw upon the strengths of both. For example, the lessons Freeport-McMoRan Copper & Gold Inc. learned about dealing with complex social issues at its Grasberg mine in Papua, Indonesia, are being applied to the development of community programs at the new Tenke Fungurume mine in the Democratic Republic of Congo (DRC). The cutting-edge scientific work under way at the Freeport-McMoRan Process Technology Center in Arizona is now helping develop cost-effective, environmentally sound and less energy intensive processes we can apply company-wide.

Our efforts to fulfill our commitment to sustainable development are carried out through numerous programs globally. Examples include assisting communities in economic development and capacity building, facilitating open dialogue to solve problems, and supporting schools and scholarships; training the first female heavy equipment operators in Papua and training Congolese engineers at our U.S. and South American mining operations; applying the human rights training, health care and small business development programs we established in Papua to our operations in the DRC; bringing entrepreneurial training to members of 11 indigenous communities

near our El Abra operations in Chile; assisting with a water treatment plant for communities in Peru, and helping build bridges and airstrips to end the isolation of remote communities in Papua; protecting and repatriating threatened land kangaroos in Papua and bighorn sheep in Arizona; abiding by environmental regulations, including long-term reclamation projects, wherever we operate; and shouldering the responsibility of environmental remediation at legacy U.S. sites that ceased operations long before these companies were acquired by Freeport-McMoRan Copper & Gold Inc.

Ours is not a static commitment through rigid programs. We are committed to continuous improvement in our sustainable development performance. We assess our programs annually in search of better ways to achieve our goals and conduct recurring third-party audits to gain fresh insight and ideas.

One of the most important areas where we seek continual improvement is the safety of our employees. We know that the strength of our operations and programs depends on the hard work of our employees and their safety is our highest priority. Our 2007 safety statistics are better than the U.S. average, but, regrettably, our company recorded five worker fatalities during the year. Our commitment is to zero workplace fatalities. We have ordered a top-to-bottom review of our safety programs globally to find ways to improve our performance. Partly as a result of this refocus and recommitment, PT Freeport Indonesia achieved its first-ever company-wide 5-Star Rating for 2007, the highest rating achievable under the National Occupational Safety Association (NOSA) standards. Despite this fine achievement, we are saddened by the loss of co-workers and are committed more strongly than ever to our goal of zero workplace fatalities.

This 2007 Working Toward Sustainable Development Report is the first such report for the new Freeport-McMoRan Copper & Gold Inc., reflecting the combination of Freeport-McMoRan and Phelps Dodge. Similarly, our 2007 Global Reporting Initiative Report – which will be posted on our web site, www.fcx.com, when it has been completed and undergone third-party verification – will be the first GRI report as a combined company.

We look forward to bringing you many such reports as the new Freeport-McMoRan Copper & Gold Inc. continues on the path to sustainable development and a promising future.

Respectfully yours,

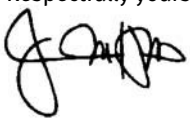

James R. Moffett
Chairman of the Board

Richard C. Adkerson
President and Chief Executive Officer

Our commitment to sustainable development is demonstrated through programs to assist communities in economic development, education, health and human resource development.

Photo: A company-supported school near the Cerro Verde operations in Peru.

Introduction to the New Freeport-McMoRan Copper & Gold Inc.

The global economy needs the metals we produce to manufacture goods and to build infrastructure.

Freeport-McMoRan Copper & Gold Inc. is a leading global mining company with headquarters in Phoenix, Arizona. We operate large, long-lived, geographically diverse assets with significant proven and probable reserves of copper, gold and molybdenum, a metal used in high-strength steel alloys and the production of lubricants. We have a dynamic portfolio of operating, expansion and growth projects in the copper industry and are the world's largest producer of molybdenum. The company's portfolio of assets includes the Grasberg minerals district in Papua, Indonesia; significant mining operations in the Americas; and the potential world-class Tenke Fungurume development project in the Democratic Republic of Congo.

The principal asset of our operating subsidiary PT Freeport Indonesia is the Grasberg mine discovered in 1988, at a site where we have operated since 1972. The Grasberg minerals district contains the world's largest single copper reserve and the world's largest single gold reserve. PT Freeport Indonesia is also a 25 percent owner of PT Smelting, which operates a copper smelter and refinery in Gresik, Indonesia.

SUSTAINABILITY POLICIES AND COMMITMENTS

Freeport-McMoRan Copper & Gold Inc. has adopted the principles of the Sustainable Development Framework of the International Council on Mining and Metals (ICMM), of which we are a member. We are reporting our company-wide performance related to these principles according to the Global Reporting Initiative (GRI) for the reporting year 2007. Our full reporting of GRI indicators, including performance data, is available on our web site www.fcx.com/envir/gri.htm.

Major Mine Operations & Development Projects

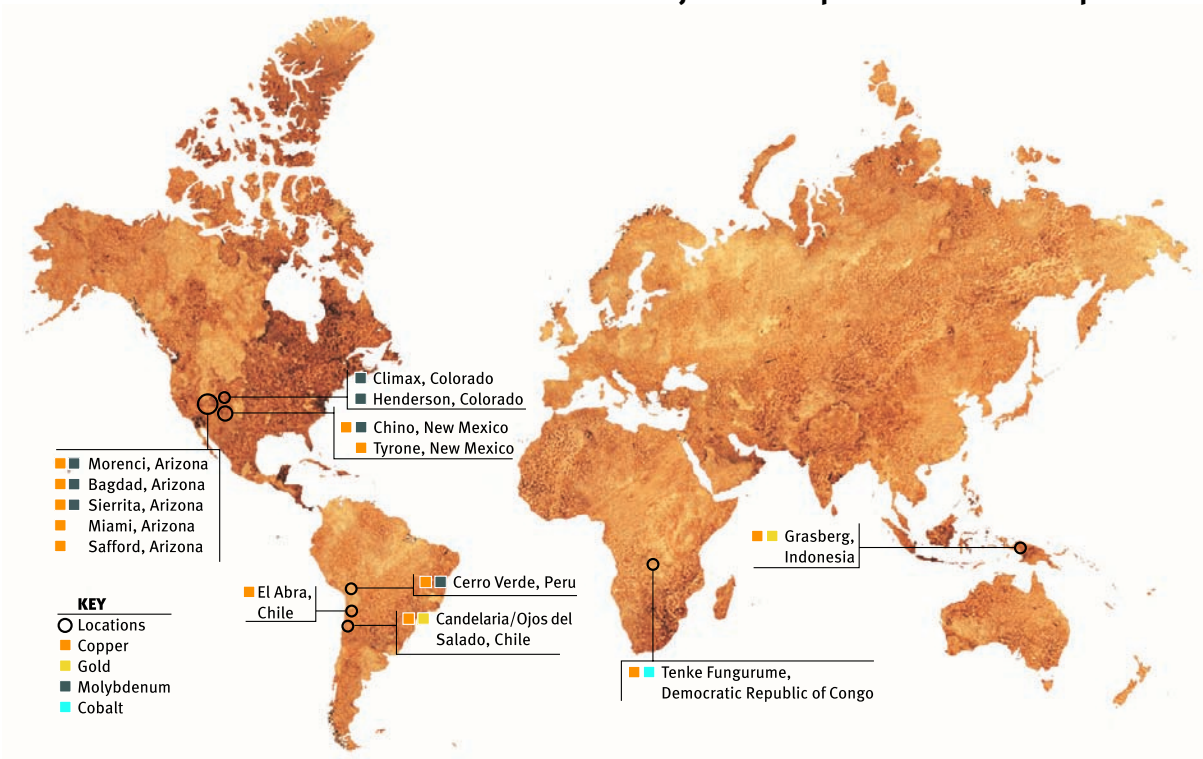

Our 2006 report is available on our web site and our 2007 GRI Report will be posted during the second half of 2008. The 2006 report includes reporting detail prior to the 2007 acquisition of Phelps Dodge and contains information for our operations in Indonesia and Spain. This Working Toward Sustainable Development report is designed to complement the GRI data by providing discussion, context and illustrations of our commitment to sustainable development and responsible mining practices.

Freeport-McMoRan Copper & Gold Inc. has recently endorsed the Extractive Industries Transparency Initiative (EITI), making a company-wide commitment to disclose all revenues and payments in the countries in which we operate. FCX's commitments and policies are also aligned with IFC performance standards.

The merger between Freeport-McMoRan Copper & Gold Inc. and Phelps Dodge Corporation combines not only our businesses, but also our respective commitments to the communities and local environments in which we operate. We are establishing a global team responsible for ensuring that we live up to our commitment to sustainable development. We have formally adopted new environmental, health and safety policies and are updating our Social, Employment & Human Rights Policy to apply across our entire organization. The current text of all these policies is available on our web site at www.fcx.com/envir/policies.htm.

ENVIRONMENTAL POLICY
updated July 2007

This policy outlines our guidelines to minimize and mitigate environmental impacts, to protect and enhance the quality of the environment wherever we operate, to comply with all applicable regulations and to seek continuous improvement in environmental performance. The policy also includes commitments to achieve ISO 14001 certification at all operating facilities, recognize and protect biodiversity, and protect and remediate sites for which we are responsible.

ENVIRONMENTAL AUDITING POLICY
updated July 2007

An effective corporate environmental auditing program increases environmental management effectiveness and our confidence that the risks of potential exposure to adverse environmental issues are being addressed. Our Environmental Auditing Policy requires all major properties worldwide to be audited at least every two years and provides additional details on auditing procedures.

CORPORATE SAFETY & HEALTH POLICY
updated July 2007

This policy lays out our objective of zero workplace injuries and occupational illnesses and provides for the establishment of benchmarks to evaluate our performance in achieving that objective. The policy also strengthens and re-emphasizes the implementation of safety and industrial health audits at all facilities.

SOCIAL, EMPLOYMENT & HUMAN RIGHTS POLICY

As part of the integration of Phelps Dodge operations into the new Freeport-McMoRan Copper & Gold Inc., we are updating our Social, Employment & Human Rights Policy to be applicable to our increased global scope of operations. In the meantime, all of our sites will adhere to the commitments that existed before the merger, which commit us to being a responsible corporate citizen by fostering positive social and employment relationships, as well as ensuring that operations are conducted in a manner consistent with the Universal Declaration of Human Rights.

PRINCIPLES OF BUSINESS CONDUCT

The cornerstone of our commitment to integrity is our Principles of Business Conduct. They are designed to be a tool to reinforce what is important in our everyday work life – hard work, honesty, treating people fairly and working safely. Our commitment to these principles is the bond that binds us all in pursuing our common vision, from top-level management to entry-level employees. More discussion of the Principles of Business Conduct is included in the Corporate Governance portion of this report, or visit our web site at www.fcx.com/envir/compliance.htm.

Technical Bulletin

DEHPA

Di (2-ethylhexyl) Phosphoric Acid

CHEMICAL STRUCTURE

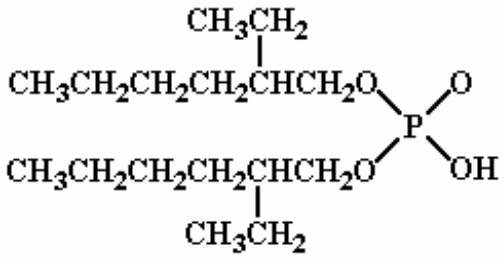

Application Information

DEHPA is a highly effective extractant used commercially to recover uranium, vanadium, beryllium, yttrium, cobalt, zinc, rare earths, and other valuable metals. DEHPA, registered trade name for Di (2-ethylhexyl) Phosphoric Acid, may be used alone or in combination with other synergistic extractants including trioctylphosphine oxide, tributyl phosphate, and dibutyl butyl phosphonate.

Extraction Mechanism

DEHPA is described as an acidic extractant, which can deprotonate to form an anion.

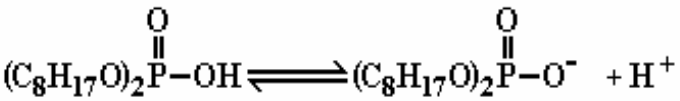

This hydrophobic anion can chelate a cation from an aqueous phase, the chelate being soluble in the organic phase.

Several studies have suggested that chelation by the DEHPA anion is assisted by coordination with the non-deprotonated species. The extraction of Zn^{+2} is a typical example of DEHPA chelation and coordination.

Rhodia, Inc. believes that any information, instruction or advice given by its personnel in response to this request for technical assistance is accurate based on the information made available by your company. We offer such information, instruction or advice in good faith, BUT WITHOUT ANY REPRESENTATION OR WARRANTY WHATSOEVER, EXPRESSED OR IMPLIED, AS TO THE ACCURACY, COMPLETENESS OR SUFFICIENCY THEREOF.

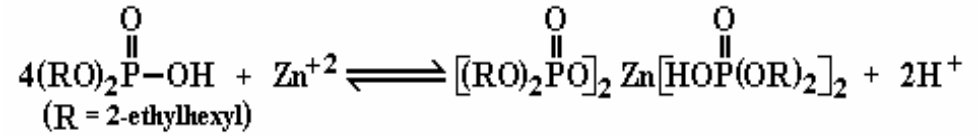

As shown by the equation above, the extraction is an equilibrium, which can shift in either direction dependent on the [H^+]. E.g., as the hydrogen ion concentration decreases, the formation of the DEHPA:Zn complex is favored. Consequently, DEHPA is a pH dependent extractant. Yet, the pH alone is not the only consideration. Structure and valence also play an important part in extraction.

Typical Properties

Molecular Weight	**322.4**
Composition (Wt%)	
Di (2-ethylhexyl) Phosphoric Acid (DEHPA)	**95 min**
Mono (2-ethylhexyl) Phosphoric Acid (MEHPA)	**3 max**
Water	**0.5 max**
Phosphorus Content	**9.8**
Physical Data	
Appearance	**Clear, colorless to pale yellow liquid**
Color, APHA	**<100**
Gardner	**<5**
Flash Point	
Open Cup, °C	**171**
Closed Cup, °C	**150**
Refractive Index, 25°C	**1.440-1.444**
Density, g/cc	
25°C	**0.974**
40°C	**0.952**
60°C	**0.937**
Viscosity, CPS	
-30°C	**1710**
0°C	**160**
20°C	**56**
40°C	**21**
100°C	**4.4**
Melting Point, °C	**< -60**
Acid Number, mg KOH/gm	**174**
Autoignition Temp, °C	**327**
Vapor Pressure, mm @ 125°C	**< 1**
Solubility in Water, %	**< 0.01**
Water in, %	**2.4**
pKa	**3.95**

Rhodia

IONQUEST® 290

Version: 120104-4 Date 04/06

Bis (2,4,4-Trimethylpentyl)Phosphinic Acid

Formula-$C_{16}H_{35}O_2P$ Molecular Weight – 290.4 CAS No.83411-71-6

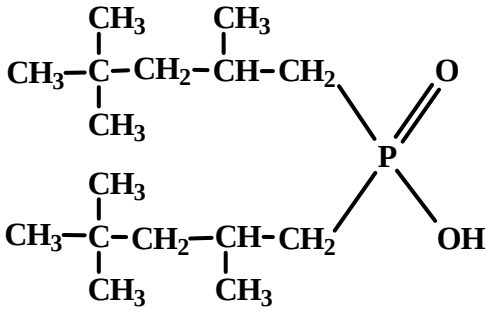

Specification:

	Typical
Assay, %	95% min.
Appearance	Clear colorless to pale yellow liquid
Viscosity, cps (25ºC)	88-90
Specific Gravity, 25°C	0.918
Phosphorus, %	10.5 - 11
Refractive Index, 25°C	1.456
Freezing point °C	< -30ºC
Flash Point, Closed Cup	>108ºC

TYPICAL APPLICATIONS

IONQUEST 290 is a solvent extraction reagent capable of extracting several metals via a cation exchange mechanism similar to Rhodia's DEHPA®. It is miscible with common solvent extraction diluents and is very stable to both heat and hydrolysis.

Although it is used primarily for the separation of Cobalt from Nickel it is also suitable for extracting other cations such as Zinc, Cadmium, Manganese and Magnesium. Metal extraction is achieved mainly by pH control.

The Distribution Coefficients for extracting these metals are affected by many things such as the Phase Ratio, Concentrations, Kinetics, pH and Temperature. Please contact Rhodia's Technical personnel to discuss specific systems.

® IONQUEST and DEHPA are registered trademarks of Rhodia

IONQUEST® 290

Safety and Handling

Customers should satisfy themselves that their facilities and arrangements are suitable for handling or using this product and must take into account the product label and any associated material safety data sheets.

Avoid contact with skin and eyes. Do not breathe vapors. Do not ingest.

In case of spill wear appropriate PPE, as noted in the MSDS, and absorb with an inert absorbent. Place the absorbed material in an appropriate container.

Transport Information

IONQUEST 290 can be shipped as “Not Regulated”.

NFPA Hazard Rating: Fire 1 – Health 2 – Reactivity 0

Rhodia

CONSUMER AND INDUSTRIAL SOLUTIONS

www.rhodia-ppd.com

Europe

Oak House
Reeds Crescent
Watford
Hertfordshire
WD24 4QP United Kingdom

Customer Service
Tel. +44 (0)1215413717
Fax +44 (0) 121 5413853

United States

Rhodia Inc.
259 Prospect Plains Rd.
C7500
Cranbury,
NJ 08512-7500

Customer Services
Tel.+1-888-776 7337
Fax 1-609-395-7155

The information contained in this document is to the best of Rhodia's knowledge and belief, correct based on general industrial experience. Rhodia's Technical Services will be pleased to give further advice and assistance but customers must satisfy themselves (by appropriate testing if necessary) that the product is suitable for their purposes and conditions of use. Accordingly, Rhodia is not liable for any loss, injury or damage, consequential or otherwise, which may result from the use of the product, the information contained in this brochure or from such advice and assistance save as may be expressly agreed under its terms of sale or disclosure.

Rhodia, Inc believes that any information, instruction or advice given by its personnel in response to this request for technical assistance is accurate based on the information made available by your company. BUT WITHOUT ANY REPRESENTATION OR WARRANTY WHATSOEVER EXPRESSED OR IMPLIED, AS TO THE ACCURACY, COMPLETENESS, OR SUFFICIENCY THEREOF

Customers are also reminded that there may be uses or applications for the product which are protected by Rhodia's or third parties' patent rights and nothing herein may be construed as an authority or encouragement to use or apply the product in contravention of such rights.